CERN-LPCC-2018-03
December 23, 2019

Standard Model Physics at the HL-LHC and HE-LHC

Report from Working Group 1 on the Physics of the HL-LHC, and Perspectives at the HE-LHC

Editors:
P. Azzi[1], S. Farry[2], P. Nason[3,4], A. Tricoli[5], D. Zeppenfeld[6]

Contributors:
R. Abdul Khalek[7,8], J. Alimena[9], N. Andari[10], L. Aperio Bella[11], A.J. Armbruster[11], J. Baglio[12], S. Bailey[13], E. Bakos[14], A. Bakshi[15], C. Baldenegro[16], F. Balli[10], A. Barker[15], W. Barter[17], J. de Blas[18,1], F. Blekman[19], D. Bloch[20], A. Bodek[21], M. Boonekamp[10], E. Boos[22], J.D. Bossio Sola[23], L. Cadamuro[24], S. Camarda[11], F. Campanario[25], M. Campanelli[26], J.M. Campbell[27], Q.-H. Cao[28,29,30], V. Cavaliere[5], A. Cerri[31], G.S. Chahal[17,32], B. Chargeishvili[33], C. Charlot[34], S.-L. Chen[35], T. Chen[36], L. Cieri[3], M. Ciuchini[37], G. Corcella[38], S. Cotogno[34], R. Covarelli[39,40], J.M. Cruz-Martinez[41], M. Czakon[42], A. Dainese[1], N.P. Dang[43], L. Darmé[44], S. Dawson[5], H. De la Torre[45], M. Deile[11], F. Deliot[10], S. Demers[46], A. Denner[47], F. Derue[48], L. Di Ciaccio[49], W.K. Di Clemente[50], D. Dominguez Damiani[51], L. Dudko[22], A. Durglishvili[33], M. Dünser[11], J. Ebadi[52], R.B. Ferreira De Faria[53], G. Ferrera[41,54], A. Ferroglia[55], T.M. Figy[36], K.D. Finelli[56], M.C.N. Fiolhais[57,53], E. Franco[58], R. Frederix[59], B. Fuks[60,61], B. Galhardo[53,62], J. Gao[63], J.R. Gaunt[11], T. Gehrmann[64], A. Gehrmann-De Ridder[65], D. Giljanovic[66,34], F. Giuli[67], E.W.N. Glover[32], M.D. Goodsell[68], E. Gouveia[53], P. Govoni[3,4], C. Goy[49], M. Grazzini[64], A. Grohsjean[51], J.F. Grosse-Oetringhaus[11], P. Gunnellini[69], C. Gwenlan[70], L.A. Harland-Lang[13], P.F. Harrison[71], G. Heinrich[72], C. Helsens[11], M. Herndon[73], O. Hindrichs[21], V. Hirschi[65], A. Hoang[74], K. Hoepfner[42], J.M. Hogan[75,76], A. Huss[11], S. Jahn[72], Sa. Jain[77], S.P. Jones[11], A.W. Jung[15], H. Jung[51], S. Kallweit[4], D. Kar[78], A. Karlberg[64], T. Kasemets[79], M. Kerner[64], M.K. Khandoga[10], H. Khanpour[80], S. Khatibi[81], A. Khukhunaishvili[82], J. Kieseler[11], J. Kretzschmar[2], J. Kroll[50], E. Kryshen[83], V.S. Lang[51], L. Lechner[84], C.A. Lee[5], M. Leigh[85], D. Lelas[58], R. Les[86], I.M. Lewis[16], B. Li[87], Q. Li[28], Y. Li[88], J. Lidrych[51], Z. Ligeti[89], J.M. Lindert[90,32], Y. Liu[91], K. Lohwasser[92], K. Long[73], D. Lontkovskyi[19], G. Majumder[77], M. Mancini[19], P. Mandrik[93], M.L. Mangano[11], I. Marchesini[19], C. Mayer[94], K. Mazumdar[77], J.A. McFayden[11], P.M. Mendes Amaral Torres Lagarelhos[53], A.B. Meyer[51], S. Mikhalcov[95], S. Mishima[96], A. Mitov[97], M. Mohammadi Najafabadi[52], M. Moreno Llácer[11], M. Mulders[11], M. Myska[98], M. Narain[76], A. Nisati[58,99], T. Nitta[100], A. Onofre[101], S. Pagan Griso[89,102], D. Pagani[59], E. Palencia Cortezon[103], A. Papanastasiou[97], K. Pedro[27], M. Pellen[97], M. Perfilov[22], L. Perrozzi[65], B.A. Petersen[11], M. Pierini[11], J. Pires[104], M.-A. Pleier[5], S. Plätzer[74], K. Potamianos[88], S. Pozzorini[64], A.C. Price[90], M. Rauch[6], E. Re[11,105], L. Reina[106], J. Reuter[51], T. Robens[107], J. Rojo[8], C. Royon[16], S. Saito[77], A. Savin[73], S. Sawant[77], B. Schneider[27], R. Schoefbeck[84], M. Schoenherr[32,11], H. Schäfer-Siebert[6], M. Seidel[11], M. Selvaggi[11], T. Shears[2], L. Silvestrini[58,11], M. Sjodahl[108], K. Skovpen[19], N. Smith[27], D. Spitzbart[84], P. Starovoitov[109], C.J.E. Suster[110], P. Tan[27], R. Taus[21], D. Teague[73], K. Terashi[111], J. Terron[112], S. Uplap[77], F. Veloso[53], M. Verzetti[64], M.A. Vesterinen[71], V.E. Vladimirov[71], P. Volkov[22], G. Vorotnikov[22], M. Vranjes Milosavljevic[14], N. Vranjes[14], E. Vryonidou[11], D. Walker[90], M. Wiesemann[11], Y. Wu[113], T. Xu[10], S. Yacoob[85], E. Yazgan[114], J. Zahreddine[48], G. Zanderighi[11,72], M. Zaro[8], O. Zenaiev[51], G. Zevi Della

Porta[115], *C. Zhang*[114], *W. Zhang*[76], *H.L. Zhu*[113,5], *R. Zlebcik*[51], *F.N. Zubair*[11]

[1] INFN Sezione di Padova, Padova, Italy
[2] Oliver Lodge Laboratory, University of Liverpool, Liverpool, United Kingdom
[3] INFN Sezione di Milano-Bicocca, Milano, Italy
[4] Università degli Studi di Milano-Bicocca, Dipartimento di Fisica "G.Occhialini", Piazza della Scienza 3, 20126 Milan, Italy
[5] Brookhaven National Laboratory (BNL), USA
[6] Karlsruher Institut für Technologie (KIT), Institut für Theoretische Physik (TP), Wolfgang-Gaede-Str. 1, 76131 Karlsruhe, Germany
[7] Department of Physics and Astronomy, VU University, NL-1081 HV Amsterdam, Netherlands
[8] Nikhef National Institute for Subatomic Physics, Amsterdam, Netherlands
[9] The Ohio State University, Columbus, USA
[10] IRFU, CEA, Université Paris-Saclay, France
[11] European Laboratory for Particle Physics, CERN, Geneva, Switzerland
[12] Institut for Theoretical Physics, Eberhard Karls University Tübingen, Auf der Morgenstelle 14, D-72076 Tübingen, Germany
[13] Rudolf Peierls Centre, Beecroft Building, Parks Road, Oxford, OX1 3PU, United Kingdom
[14] Institute of Physics, University of Belgrade, Belgrade, Serbia
[15] Purdue University, West Lafayette, USA
[16] The University of Kansas, Lawrence, USA
[17] Imperial College, London, United Kingdom
[18] Università di Padova, Padova, Italy
[19] Vrije Universiteit Brussel, Brussel, Belgium
[20] Université de Strasbourg, CNRS, IPHC UMR 7178, Strasbourg, France
[21] University of Rochester, Rochester, NY, USA
[22] Skobeltsyn Institute of Nuclear Physics, Lomonosov Moscow State University, Moscow, Russia
[23] Universidad de Buenos Aires, Buenos Aires, Argentina
[24] University of Florida, Gainesville, USA
[25] Theory Division, IFIC, University of Valencia-CSIC, E-46980 Paterna, Valencia, Spain
[26] Department of Physics and Astronomy, University College London, London, United Kingdom
[27] Fermi National Accelerator Laboratory, P.O. Box 500 Batavia, 60510 USA
[28] Department of Physics and State Key Laboratory of Nuclear Physics and Technology, Peking University, Beijing 100871, China
[29] Collaborative Innovation Center of Quantum Matter, Beijing 100871, China
[30] Center for High Energy Physics, Peking University, Beijing 100871, China
[31] Department of Physics and Astronomy, University of Sussex, Brighton, United Kingdom
[32] Institute for Particle Physics Phenomenology, University of Durham, Durham, UK
[33] High Energy Physics Institute of Tbilisi State University, Tbilisi, Georgia
[34] LLR, Ecole polytechnique, CNRS/IN2P3, Université Paris-Saclay, Palaiseau, France
[35] Key Laboratory of Quark and Lepton Physics (MoE) and Institute of Particle Physics, Central China Normal University, China
[36] Department of Mathematics, Statistics, and Physics, Wichita State University, Wichita KS, USA
[37] INFN Sezione di Roma Tre, Via della Vasca Navale 84, I-00146 Roma, Italy
[38] INFN, Laboratori Nazionali di Frascati, Frascati, Italy
[39] Istituto Nazionale di Fisica Nucleare (INFN) Sezione di Torino , Italy
[40] Università di Torino, Torino, Italy
[41] Universita' di Milano, Dipartimento di Fisica, Milano, Italy

[42] RWTH Aachen University, III. Physikalisches Institut A, Aachen, Germany
[43] University of Louisville, Louisville, Kentucky, USA
[44] Narodowe Centrum Badań Jądrowych (NCBJ), Hoża 69, 00-681 Warszawa, Poland
[45] Department of Physics and Astronomy, Michigan State University, East Lansing, Michigan, USA
[46] Department of Physics, Yale University, New Haven CT, USA
[47] Universität Würzburg, Institut für Theoretische Physik und Astrophysik, Emil-Hilb-Weg 22, 97074 Würzburg, Germany
[48] Laboratoire de Physique Nucléaire et de Hautes Energies (LPNHE), Sorbonne Université, Paris-Diderot Sorbonne Paris Cité, CNRS/IN2P3, France
[49] LAPP, Univ. Grenoble Alpes, Univ. Savoie Mont Blanc, CNRS/IN2P3, Annecy, France
[50] Department of Physics and Astronomy, University of Pennsylvania, Philadelphia, Pennsylvania, USA
[51] Deutsches Elektronen-Synchrotron, Hamburg, Germany
[52] School of Physics, Institute for Research in Fundamental Sciences (IPM), P.O. Box 19395-5531, Tehran, Iran
[53] Laboratório de Instrumentação e Física Experimental de Partículas - LIP, Lisboa, Portugal
[54] INFN, Sezione di Milano, Via Celoria 16, I-20133 Milan, Italy
[55] Physics Department, New York City College of Technology, CUNY, 300 Jay Street, Brooklyn, NY 11201 USA
[56] Boston University, Department of Physics, Boston, Massachusetts, USA
[57] Science Department, Borough of Manhattan Community College, New York, NY 10007, USA
[58] INFN, Sezione Roma I, Roma, Italy
[59] Technische Universität München, München, Germany
[60] Laboratoire de Physique Théorique et Hautes Énergies (LPTHE), Boite 126, T13-14 4ème étage, 4 place Jussieu, F-75252 Paris CEDEX 05, France
[61] Institut Universitaire de France, 103 boulevard Saint-Michel, 75005 Paris, France
[62] Laboratório de Instrumentação e Física Experimental de Partículas - LIP, Coimbria, Portugal
[63] School of Physics and Astronomy, Shanghai Jiao Tong University, Shanghai, China
[64] Physik-Institut, Universitaet Zurich, 8057 Zurich, Switzerland
[65] Department of Physics, ETH Zurich, CH-8093 Zurich, Switzerland
[66] University of Split, Split, Croatia
[67] Università di Roma Tor Vergata, Dipartimento di Fisica, Roma, Italy
[68] Laboratoire de Physique Theorique et Hautes Energies, UMR 7589, Sorbonne Université et CNRS, Boîte 126, T13-14 4ème étage, 4 place Jussieu, F-75252 Paris CEDEX 05, France
[69] University of Hamburg, Hamburg, Germany
[70] Denys Wilkinson Building, University of Oxford, Oxford, OX1 3RH, United Kingdom
[71] Department of Physics, University of Warwick, Coventry, United Kingdom
[72] Max Planck Institute for Physics, Foehringer Ring 6, 80805 Munich, Germany
[73] University of Wisconsin - Madison, Madison, USA
[74] University of Vienna, Vienna, Austria
[75] Bethel University, St. Paul, USA
[76] Brown University, Providence, USA
[77] Tata Institute of Fundamental Research, Mumbai, India
[78] School of Physics, University of the Witwatersrand, South Africa
[79] PRISMA Cluster of Excellence and Institute for Physics (THEP), Johannes Gutenberg University Mainz, D-55099 Mainz, Germany
[80] Department of Physics, University of Science and Technology of Mazandaran, P.O.Box 48518-78195, Behshahr, Iran
[81] Department of Physics, University of Tehran, North Karegar Ave., Tehran 14395-547, Iran

[82] Cornell University, Physics Department, Ithaca, NY, USA
[83] Petersburg Nuclear Physics Institute (PNPI), Gatchina, Russia
[84] Institut für Hochenergiephysik, Wien, Austria
[85] University of Cape Town, South Africa
[86] Department of Physics, University of Toronto, Toronto, Canada
[87] Department of Physics, University of Michigan, Ann Arbor, Michigan, USA
[88] DESY, Hamburg and Zeuthen, Germany
[89] Lawrence Berkeley National Laboratory, 1 Cyclotron Road, Berkeley CA 94720 USA
[90] Durham University, Institute for Particle Physics Phenomenology, Ogden Centre for Fundamental Physics, South Road, Durham DH1 3LE, United Kingdom
[91] College of Nuclear Science and Technology,Beijing Normal University,100875 Beijing, China, Beijing Radiation Center, Beijing 100875, China
[92] University of Sheffield, Sheffield, United Kingdom
[93] Institute for High Energy Physics of National Research Centre 'Kurchatov Institute', Protvino, Russia
[94] Henryk Niewodniczanski Institute of Nuclear Physics Polish Academy of Sciences, Kraków, Poland
[95] Research Institute for Nuclear Problems of Byelorussian State University, Minsk, Belarus
[96] Institute of Particle and Nuclear Studies, High Energy Accelerator Research Organization (KEK), Tsukuba 305-0801, Japan
[97] Cavendish Laboratory, University of Cambridge, Cambridge, United Kingdom
[98] Czech Technical University in Prague, Prague, Czech Republic
[99] Sapienza Universita' di Roma, Dipartimento di Fisica
[100] Waseda University, Waseda Research Institute for Science and engineering (WISE), Tokyo, Japan
[101] Physics Department, University of Minho, 4710 - 057, Braga, Portugal
[102] University of California, Berkeley, California, USA
[103] Universidad de Oviedo, Oviedo, Spain
[104] CFTP, Instituto Superior Técnico, Universidade de Lisboa, Avenida Rovisco Pais 1, 1049 Lisboa, Portugal
[105] LAPTh, 9 Chemin de Bellevue, F-74941 Annecy Cedex, France
[106] Physics Department, Florida State University, Tallahassee, Florida, USA
[107] Rudjer Boskovic Institute, Bijenicka cesta 54, P.O. Box 180, 10002 Zagreb, Croatia
[108] Department of Astronomy and Theoretical Physics, Lund University, Lund, Sweden
[109] Kirchhoff-Institut für Physik, Heidelberg, Germany
[110] University of Sydney, Sydney, Australia
[111] International Center for Elementary Particle Physics and Department of Physics, The University of Tokyo, Japan
[112] Physics Department, Universidad Autonoma de Madrid, Spain
[113] University of Science and Technology of China, Hefei, China
[114] Institute of High Energy Physics, Chinese Academy of Sciences, Beijing, China
[115] University of California, San Diego, La Jolla, USA

Abstract

The successful operation of the Large Hadron Collider (LHC) and the excellent performance of the ATLAS, CMS, LHCb and ALICE detectors in Run-1 and Run-2 with pp collisions at center-of-mass energies of 7, 8 and 13 TeV as well as the giant leap in precision calculations and modeling of fundamental interactions at hadron colliders have allowed an extraordinary breadth of physics studies including precision measurements of a variety physics processes. The LHC results have so far confirmed the validity of the Standard Model of particle physics up to unprecedented energy scales and with great precision in the sectors of strong and electroweak interactions as well as flavour physics, for instance in top quark physics. The upgrade of the LHC to a High Luminosity phase (HL-LHC) at 14 TeV center-of-mass energy with 3 ab^{-1} of integrated luminosity will probe the Standard Model with even greater precision and will extend the sensitivity to possible anomalies in the Standard Model, thanks to a ten-fold larger data set, upgraded detectors and expected improvements in the theoretical understanding. This document summarises the physics reach of the HL-LHC in the realm of strong and electroweak interactions and top quark physics, and provides a glimpse of the potential of a possible further upgrade of the LHC to a 27 TeV pp collider, the High-Energy LHC (HE-LHC), assumed to accumulate an integrated luminosity of 15 ab^{-1}.

Contents

1 Introduction

The Large Hadron Collider (LHC) is one of largest scientific instruments ever built. To extend its discovery potential, the LHC will undergo a major upgrade in the 2020s, the High-Luminosity LHC (HL-LHC). The HL-LHC will collide protons against protons at 14 TeV centre-of-mass energy with an instantaneous luminosity a factor of five greater than the LHC and will accumulate ten times more data, resulting in an integrated luminosity of 3 ab^{-1}.

The LHC results have so far confirmed the validity of the Standard Model of particle physics up to unprecedented energy scales and with great precision in the sectors of strong and electroweak interactions, Higgs boson as well as flavour physics including top quark properties. The HL-LHC program, thanks to a ten-fold larger data set, upgraded detectors and expected improvements in the theoretical understanding, will extend the sensitivity to new physics in direct and indirect searches for processes with low production cross sections and harder signatures. In addition, a considerable improvement is expected in precise measurements of properties of the Higgs boson, e.g. couplings measurements at the percent level, and of Standard Model (SM) production processes. Several of these measurements will be limited by the uncertainties on the knowledge of the partonic inner structure of the proton, i.e. Parton Denstity Functions (PDFs). Global PDF fits of several HL-LHC measurements will allow a significant improvement in PDF uncertainties and, in turn, in measurements of SM parameters, e.g. the weak mixing angle and the W boson mass. Anomalies in precision measurements in the SM sector can become significant when experimental measurements and theoretical predictions reach the percent level of precision, and when probing unprecedented energy scales in the multi-TeV regime. These anomalies could give insights to new physics effects from higher energy scales.

Additional studies on the potential of a possible further upgrade of the LHC to a 27 TeV pp collider, the High-Energy LHC (HE-LHC), assumed to accumulate an integrated luminosity of 15 ab^{-1}, have also been carried out.

A year long Workshop organized at CERN in 2017-2018 brought together experimentalists from the ATLAS, CMS, LHCb, and ALICE Collaborations and theorists to study the expected physics reach of the HL-LHC project and its possible upgrade to the HE-LHC. Studies of the Workshop in the sectors of electroweak and strong interactions as well as top physics were carried out within the Working Group 1 (WG1) and the results are summarized in this report that constitutes a chapter of the HL/HE-LHC Yellow Report volume to be submitted to the European Strategy Group.

The report first introduces the theoretical tools used for the following theoretical projections and their expected future improvements as well as the experimental performance assumed in the following experimental analyses. Dedicated sections summarize the results of the studies in the areas of electroweak processes, strong interactions, top physics including effective coupling interpretations, and proposes studies of forward physics that are possible with new forward detectors. The sections focus on physics projections for the HL-LHC and the expected improvements in measurement precision or kinematic reach compared to LHC. In some cases the studies are extended to HE-LHC highlighting the larger statistics and energy reach of HE-LHC compared to HL-LHC. In the following sections the authors of the theoretical contributions are listed in footnotes to the section titles. Where the authors are not explicitly indicated, they are the experimental LHC Collaborations.

2 Theoretical tools

2.1 High Order QCD calculations[1]

In order to exploit the full potential of the High-Luminosity LHC physics program, the high precision of experimental data must be compared to theoretical predictions that have the same accuracy. Precision calculations in QCD are typically classified into fixed-order expansions in the coupling constant α_s, and into predictions that resum large logarithms to all orders in α_s. The latter are usually also subdivided into numerical parton-shower approaches and analytic resummed calculations. In recent years, a lot of work has been devoted also to matching and merging fixed-order and resummed calculations, so as to have an improved accuracy in all regions of phase space.

The technical ingredients required for a fixed-order calculation to higher orders are the computation of real, virtual or, from two loop on, mixed real-virtual amplitudes, the calculations of the required master integrals and a procedure to regularize intermediate soft and collinear divergences. The first non-trivial contribution is of next-to-leading order (NLO). Here, the basis of master integrals required to compute any process at one-loop in QCD had been known for a long time, and is now available in public codes [1, 2]. In addition, two general subtraction methods (FKS [3] and CS [4]), well suited for automation, were developed. The tensor reduction of virtual amplitudes (i.e. the reduction of virtual amplitude into a combination of master integrals) proved to be the most difficult problem, since the most straightforward approaches yielded too complex results for generic processes. Around ten to fifteen years ago, a number of breakthrough ideas [5–10] led to algorithms for tensor reduction that can be automatized efficiently. With all ingredients in place, a number of tools to compute NLO cross sections for generic LHC processes in an automated way were developed. These tools are today heavily used at the LHC and will be indispensable for future phenomenology. The most widely used tools include GOSAM [11], MADLOOP [12], or OPENLOOPS [10]. It is interesting to note that, in the early days of NLO calculations, also slicing approaches were suggested to handle intermediate divergences (see e.g. [13]). They were however soon abandoned in favour of subtraction approaches.

While NLO tools are certainly more appropriate then leading-order (LO) generators to accurately predict LHC distributions, already with Run-2 data it is clear that an even better perturbative accuracy is required to match the precision of data. One of the first explicit demonstrations of this fact was given by the WW cross section [14–16], that raised interest because of discrepancies in the extrapolated total cross section between theory and data both at 7 TeV and 8 TeV, and both at ATLAS and CMS. The discrepancy could be resolved thanks to the inclusion of next-to-next-to-leading (NNLO) corrections and thanks to the observation that the extrapolation from the fiducial to the inclusive cross section had a larger uncertainty than the estimated one. This example highlights the importance of quoting also fiducial cross sections, prior to any Monte Carlo based extrapolation, and of including NNLO corrections when comparing to high-precision data.

Current years are seeing an incredibly fast progress in the calculation of NNLO cross sections (for recent short reviews see e.g. Ref. [17, 18]). The current status is that all non-loop induced $2 \to 2$ SM processes are known at NNLO, including dijet production [19] that has the most complicated subprocess and singularity structure. This breakthrough was possible thanks to the development of new methods to compute two-loop integrals. One idea that was exploited to a great extent is the fact that polylogarithmic integrals can be calculated by means of differential equations [20–23]. Currently, the processes that are more difficult to compute are those that involve internal masses, since they lead not only to polylogarithms but also to elliptic integrals. Examples include loop-induced processes like gluon-fusion Higgs or di-Higgs production with full top-mass dependence, or gluon induced di-boson production.

With the High-Luminosity run of the LHC, it will be possible to explore the Higgs transverse

[1] Contributed by G. Zanderighi.

momentum spectrum up to almost 1 TeV, where the large-m_t approximation is well-known to fail. Recently, two-loop NLO results for the Higgs transverse momentum spectrum became available [24,25], but genuine NNLO predictions for these loop-induced processes are still out of reach.

The calculations of multi-scale two-loop amplitudes with massive internal particles relevant for Higgs-, top- and vector-boson production, and in particular the mathematical structures beyond multiple polylogarithms that appear in these amplitudes, is a very active area of research today [26–39]. The developments of yet new ideas and computational methods are eagerly needed. Approaches for the full numerical calculation of master integrals also exist (see e.g. Ref. [40–43] and references therein), requiring however considerable computing power as the complexity increases.

As far as the problem of canceling divergences, quite a number of different approaches are being pursued now. They can be broadly divided into subtractions methods (antenna subtraction [44], sector-improved residue subtraction [45–48], nested subtraction [49], colourful subtraction [50], projection to Born [51]) or slicing methods (q_T-subtraction [52], N-jettiness [53,54]). These methods are being scrutinized, compared, and refined, and while it is not clear yet which method will prevail, it seems realistic to assume that, by the beginning of the High-Luminosity phase, the issue of handling intermediate divergences in NNLO calculations will be considered solved. An ambitious goal is in fact to have $2 \to 3$ NNLO results by the beginning of the High-Luminosity phase. A milestone would be certainly to have NNLO prediction for ttH production. Motivated by the success at one-loop, a lot of effort is devoted to extending generalized unitarity and the OPP methods beyond one loop (see e.g. Ref. [55]). Currently, $2 \to 3$ processes are a very active subject of study, with initial results of 3-jet amplitudes starting to appear [56–62].

Beyond NNLO, two calculations of LHC processes exist today at N^{3}LO for inclusive Higgs production in the large m_t approximation [63, 64] and for vector-boson-fusion (VBF) Higgs production in the structure function approximation [65]. The complexity of these calculations suggest that it will be very hard to extend this level of accuracy to more complicated processes, since the technology they use explicitly exploits the simplicity of these two processes, and cannot be easily extended to more complex ones.

Besides fixed-order, also resummed calculations have seen a leap in recent years. The accuracy with which particular observables can be resummed analytically reaches N^{3}LL (see e.g. Ref, [66–68]), which means three towers of logarithmic terms down compared to the leading logarithms that arise when only soft and collinear gluons are correctly accounted for. These results are properly matched to fixed order NNLO calculations.

Resummed calculations rely either on methods based upon coherent branching [69, 70] or upon Soft Collinear Effective Theory (SCET) [71]. So far, the two approaches have also been considered as complementary, in fact both methods proceed by performing a systematic expansion of the contributions to the cross section. Recent work highlights the connection between the two methods [72].

While the logarithmic accuracy of resummed calculations is impressive, the formal accuracy of parton showers is much less advanced. Unlike resummed calculations, that are targeted to a well defined cross section or distribution, Monte Carlo generators make predictions for several kind of observables at the same time, and, at present, a rigorous way to qualify their accuracy is missing. First studies in this direction can be found in [73]. Nevertheless, attempts to improve some aspects of the shower algorithms are the focus of recent work. Different approaches are taken: one can incorporate the spin-color interference into showers [74], include higher-order splitting functions and $1 \to 3$ splitting kernels into showers [75, 76] or consider different shower evolution variables [77, 78]. It seems likely that by the start of the High-Luminosity program we will have a much better theoretical control on the parton shower evolution and the uncertainty associated to it.

In the same way as the progress in NLO went hand in hand with the development of matching

procedures of NLO and parton shower, a number of approaches have been suggested recently to match NNLO calculations and parton showers [79–81]. The bottleneck in these approaches is currently the fact that they rely on a reweighing procedure that is differential in the Born phase space. Such a reweighing is possible for relatively simple processes but becomes numerically unfeasible for more complicated ones. It seems reasonable to expect that in the next years better NNLOPS approaches will be developed that do not rely on any reweighing to the NNLO. This would make it possible to have NNLO predictions matched to parton shower (PS), also called NNLOPS, to more generic processes for which an NNLO calculation is available, as is currently the case at NLO.

2.2 Electroweak corrections[2]

Existing tools

In the last few years, the automation of electroweak (EW) NLO corrections has witnessed an impressive progress, for what concerns both one-loop and real-emission contributions (and their combination), by collaborations such as RECOLA [82, 83] with SHERPA [84, 85], OPENLOOPS [10] with SHERPA, GOSAM [11, 86] with either MADDIPOLE [87, 88] or SHERPA, and MadGraph5_aMC@NLO [12, 89]. For most of these codes tuned comparisons have also been published [90, 91], displaying excellent agreement among them. Although the capabilities and reach in process complexity can differ from one computer program to another, recent results obtained with these tools [92–117] clearly demonstrate how automation has made it possible to tackle problems whose complexity is too great to justify their solutions through traditional approaches.

Stemming from these advances, newer applications have become possible, one of these is the computation of the so-called "complete-NLO" corrections. In general, a given scattering processes can proceed through n different coupling combinations at LO (for example, $t\bar{t}$ or dijet production receives contributions at order α_s^2, $\alpha_s\alpha$ and α^2); typically only the term with the largest power of α_s is retained, owing to the fact that $\alpha_s \gg \alpha$. This structure generates a similar one at N^{p}LO, with $n+p$ contributions, and the term "complete-NLO" means the (simultaneous) computation of all the terms entering at LO and NLO. Among the computer programs cited above, some have been employed for the computation of the complete-NLO corrections. In most of the cases the impact of the various contributions closely follows the pattern one would expect from the coupling powers, as it is the case for dijet production [106], top-pair [113] possibly with one extra jet [116]. However, there exist processes for which the coupling hierarchy is violated, or even flipped. Examples are same-sign W production with two jets [111], top-pair production in association with a W boson and four-top production [115].

Corrections beyond NLO

Similarly to the NLO case, also NNLO corrections can be organized in powers of α and α_s. At the moment, $\mathcal{O}(\alpha_s^2)$ NNLO QCD calculations have been performed for many production processes at the LHC. Conversely, complete NNLO mixed QCD-EW calculations of $\mathcal{O}(\alpha_s\alpha)$ have not been performed for any process yet. These calculations are essential in order to pin down the theoretical uncertainties for processes that at the HL- and HE-LHC will be measured with very high precision. For this reason a great effort has been already invested for achieving this result and great progress can be expected in the next years. We recall the calculations that have been performed for Drell-Yan production [118, 119] in the resonance region via the pole approximation. For this kind of calculations two-loop amplitudes [120–124] as well as regularized double-real emissions [125] are necessary ingredients. Similarly, NNLO mixed QCD-EW corrections to gluon-gluon-fusion (ggF) Higgs production, which are induced by three-loop diagrams, have been estimated in ref. [126]. Further recent calculations [127, 128] support those

[2] Contributed by D. Pagani, M. Zaro and M. Schönherr.

results and, in particular, support the fact that they can be correctly approximated via the so-called multiplicative approach. In short: NNLO mixed QCD-EW $\sim$ NLO QCD $\times$ NLO EW.

The aforementioned multiplicative approach is in general a very good approximation when the bulk of QCD and EW corrections at NLO is dominated by soft effects and Sudakov logarithms, respectively. Given the current lack of exact NNLO mixed QCD-EW calculations, this approximation is already being used for estimating these corrections and/or missing higher orders uncertainties of different processes. First (N)NNLO QCD calculations including NLO EW corrections via the multiplicative approach have already appeared [63, 113, 129] and are already necessary for a correct interpretation of current data; this level of accuracy will be mandatory for more processes at HL and HE-LHC.

Besides NNLO mixed QCD-EW corrections of $\mathcal{O}(\alpha_s\alpha)$, non-negligible contributions can emerge also from large $\mathcal{O}(\alpha^n)$ corrections with $n > 1$. These typically involve final-state radiation (FSR) from massless/light particles and Sudakov logarithms. Both effects can be resummed, (at LL) via shower simulations (see the following sections on matching with QED showers and with EW showers), or analytically. In the case of Sudakov logarithms, general methods for their calculation [130, 131] and techniques for resumming them [132, 133] are already known since quite some time. Based on the study already performed for 100 TeV proton–proton collisions [134], at the HE-LHC, the resummation of Sudakov effects may be relevant in the tail of distributions.

Matching with QED shower

Fixed order computations need to be matched to parton showers, which compute a fully differential numerical resummation and implement the evolution of both QCD and EW particles from the hard scale to low scales, connecting it to the non-perturbative hadronization stage to arrive at fully differential particle level that can be subjected to detector level data. This matching has been fully automated for NLO QCD calculations. At NLO EW accuracy only selected process specific solutions exist [135–139]. As all parton showers incorporate a joint QCD+QED parton evolution, general matching procedures, which are still lacking at the moment, will become available in the near future. This will enable precise particle level predictions that can be subjected to detector simulations for highly realistic and detailed studies.

Additionally, first solutions exist to incorporate approximate electroweak corrections in multijet merged calculations [98, 116, 140]. In these approximations, the universal nature of EW corrections in the high energy limit, where they are dominated by Sudakov-type logarithms of virtual origin, is exploited. Thus, these methods will form the cornerstone of precise particle-level predictions at large transverse momenta, which are at the basis of the increased reach of both the HL– and HE–LHC new physics search program.

Weak showers

All parton showers publicly available in the major Monte-Carlo event generators HERWIG, PYTHIA and SHERPA contain both QCD and QED splitting functions to numerically resum the respective logarithms at (N)LL accuracy. First steps towards parton showers incorporating also weak effects in their splitting functions have been taken recently [141, 142]. The now complete electroweak splitting functions suffer from their strong dependence on the helicity of the propagating parton. These parton showers, however, operate in the spin-averaged approximation, neglecting all spin-correlations. The current effort to understand the full spin dependence of the electroweak part of the evolution of partons [143, 144] in analytic resummations is complemented by efforts to keep the full colour and spin structure, including non-diagonal parts of the (now matrix-valued) evolution equations, in the parton shower community. In time for the High Luminosity Upgrade fully spin-dependent parton evolution will then be incorporated in fully differential parton shower resummations that can then produce accurate predictions for the

emission probabilities of secondary weakly interacting particles and gauge bosons.

2.3 Monte Carlo generators[3]

The complexity of the final states, together with the complexity of the detectors that analyse them, are such that a full simulation of an event, yielding a realistic multi-particle final state distribution, is an indispensable theoretical tool for the physics of high-energy hadron colliders. Driven by the needs of the Tevatron and LHC, the physics of Monte Carlo (MC) generators has seen steady progress from its inception to the present, and is, at the moment, a field in active development. The current LHC physics program, as well as the requirements for its HL-LHC and eventually its HE-LHC phases, has evidenced several areas of development that need to be addressed by theorists. These are mainly driven by the quest for higher precision and accuracy, but also by practical issues, such as the need for generating very large samples for the most abundant LHC processes, and for the efficient handling of the variations of the input parameters needed in order to study uncertainties.

Much progress in this field takes place within the main collaborations that maintain the widely used general purpose Monte Carlo generators, i.e. HERWIG [145–147], PYTHIA [148,149] and SHERPA [84], but there is also a large theoretical community that works on more specialised aspects of Monte Carlo generators, such as formal/theoretical advances to improve the resummation accuracy, and to improve the fixed-order accuracy in the generation of the primary event and of the hardest radiations accompanying it.

In spite of the several challenges ahead of us, considering the evolution of the field in the last twenty years, it can be anticipated that considerable progress will be made from now up to the beginning (around 2025) and in the following ten-fifteen years of the high luminosity program. This progress will take place in particularly favourable conditions, as the running of the LHC and the data accumulated will provide continuous feedback to the theoretical work in the field.

It can be can anticipated major developments in the following directions: precision for inclusive observables, logarithmic accuracy, technical improvements for fast and efficient generation of events, and improvements in the modeling of hadronization and underlying event.

Precision for inclusive observables

In this context, let us generically refer to “precision" as a measure of the accuracy of the result as well as of the size of the left-over uncertainties that can be achieved in the computation of inclusive quantities, i.e. those that can be computed directly in fixed-order calculations. Fixed-order calculation have always been, and are now, ahead of the precision that Monte Carlo generators can provide for inclusive observables. Since their wide use started, and up to about twenty years ago, shower MC’s had typically leading order precision for inclusive observables, while the state of the art for fixed order computations was at the Next-to-Leading-Order (NLO) level. Thanks to the introduction of general methods for interfacing shower Monte Carlo to fixed-order NLO calculations, like AMC@NLO [150], POWHEG [151], and more recently the KRK-NLO method [152], the state of the art for shower MC’s precision has reached the NLO level. On the other hand, progress in fixed-order computations, including the evaluation of two-loop amplitudes and the development of several subtraction methods, allowed NNLO calculations to become available for a rather large set of processes. It is therefore natural to wonder whether *general methods for interfacing Shower generators to NNLO calculation will be available at the start of the High Luminosity program.* NNLO-PS methods have already appeared for relatively simple processes, typically in the production of massive colourless final states [79, 80, 153–155]. However, the methods used so far do not seem to have the generality needed to handle processes of increasing complexity, and it is very likely that new theoretical breakthroughs will be needed.

[3] Contributed by F. Maltoni, M. Schönherr and P. Nason.

Achieving NNLO accuracy for a given final state, for example for Higgs production, implies also the NLO accuracy for the the same final state in association with a jet, i.e. the HJ process in the Higgs example. In practical applications, the less ambitious goal of having NLO accuracy for inclusive result, and also achieve NLO accuracy for the final states that also include associated production of jets, thus achieving an extension of the CKKW [156] method to NLO order, can be extremely useful.

The availability of automated NLO corrections for arbitrary processes including a relatively large number of associated jets has paved the way to important developments in this direction. Several proposals to merge samples with different jet multiplicity computed at the NLO, usually called "NLO-PS matrix-element merging", have been put forward. These are the FxFx method [157], implemented in the aMC@NLO framework; the UNLOPS method [158], implemented in Pythia and the MePSNLO method [159], implemented in Sherpa. All methods introduce a separation scale that defines the jet multiplicity for a given event, and allows to generate inclusive samples out of non-overlapping samples with different jet multiplicity. Whether these procedures really achieve NLO accuracy for observables involving different jet multiplicity also when generic (i.e. different from those used at the generation level) separation scales are chosen, is a delicate question, which is still a matter of debate. Alternative merging procedures, that consider more carefully the problems that may arise at the boundary of the merging regions and also aim at improving the resummation accuracy , have been proposed in the GENEVA approach [160], and presently applied to Drell-Yan production [155,161]. The goal of achieving NLO accuracy for different jet multiplicity has also been achieved without the use of merging with the so called MiNLO procedure [162, 163].

While NLO-PS generators for standard QCD processes can be obtained with a fairly high level of automation, there are processes that require particular attention, typically the loop induced ones. An example of one such process is Higgs-pair production, that has been implemented first in aMC@NLO [164] using an approximation for the yet unknown two-loop contributions and then in POWHEG and aMC@NLO [165] as soon as the results of the two-loop computation has become available. [166, 167]. There are several other gg loop-induced processes for which a full NLO+PS implementation is still missing which, thanks to the quick developments in computation of two-loop amplitudes, are expected to become available in the coming years.

Another important direction where there has been considerable progress recently is the automation of the computation of EW corrections [83, 85, 89, 95] to the point that fixed-order NLO QCD and EW corrections are readily available for virtually all processes of interest. Details can be found in Section 2.2. An general interface of these calculations to shower generators that correctly account for QED radiation for these computations, however, is not yet available. The problem in this case is the consistent handling of photon radiation, that can arise both from the shower and from the fixed-order calculation. These pose new problems compared to the production of coloured partons, where the presence of individual partons cannot be required in the final state, and thus showers develop inclusively generating jets from partons. Photons, on the other hand, can be explicitly detected in the final state, and an NLO+PS scheme should take care of handling both shower generated photons and those originating in the NLO calculation in a consistent way, in order to give a reliable description of both collinear photons embedded in jets and highly energetic isolated ones. A scheme for achieving this in the Drell-Yan case has been presented in Ref. [136, 137] in the context of the POWHEG method. A scheme using fragmentation functions has been introduced in Ref. [89].

Finally, it is to be noted that the progress achieved recently to account for intermediate resonant states in the NLO+PS context [168–170] will likely be essential in the framework of electro-weak corrections. In this case, weak vector bosons are part of the electroweak corrections and their presence entail a correct handling of their decays also in presence of extra QED radiation. It is expected that interfacing complete NLO EW-QCD calculations with a shower approach (QED+QCD) will become standard procedure by the beginning of HL-LHC.

Accuracy in resummation

As current state of the art, shower generators rely upon the first order Altarelli-Parisi splitting kernels, together with some appropriate scheme to handle soft emissions, either by angular ordering in parton shower cascades or using dipole shower algorithms. Several studies have appeared recently aiming at improving parton showers by increasing the accuracy of specific ingredients, either by developing novel shower schemes that remain within the standard parton or dipole branching, such as DIRE [77] and Vincia [78, 171]; by going beyond the typical probabilistic cascade of the shower algorithms and handling directly the quantum density matrix [172]; and by incorporating higher order splitting functions [76, 152, 173–175].

While fixed order improvements in shower MC generators have the clear goal of reaching the same fixed order accuracy as the corresponding computations for inclusive observables, it is less straightforward to quantify how improvements in the shower algorithms impact the precision of the description of observables that require resummation. In a recent study [73], some criteria were proposed in order to address this problem. In particular, two criteria were examined: the first refers to the ability of a shower algorithm to correctly reproduce the singularity structure of n-parton matrix elements, while the second measures the level of accuracy of a shower algorithm in the computation of a general class of observables that require resummation. It was found that there are regions where commonly used shower algorithms fail to reproduce the correct singularity structure of the matrix elements, and that this affects the logarithmic resummation accuracy of the shower already in the leading term, yet at subleading number of colours, and in the next-to-leading term at leading colour.

Thus, the current trend of research moves along parallel directions, not only by seeking improvements in the shower algorithms in particular areas, but also by critical examination of the shower formalism in an attempt to qualify their accuracy in a more solid way.

Technical improvements

The pressing requirements of the LHC physics program have already had an impact in driving technical improvements in Monte Carlo generators. In particular, the need to study uncertainties, corresponding to a large set of combination of parameter variations when generating a sample, often leading to several hundreds variations, has led to the development of procedures to implement the variation of parameters by reweighting the same event, rather than generating independent samples. Besides the obvious simplification of having to deal with a single event sample, this has also the advantage that the effects of variations of the input parameters are affected by smaller theoretical errors, since they all apply to the same generated event. A method for reweigthing the full shower development was presented in Ref. [176] and implemented in HERWIG in Ref. [177]. A similar method was presented in [178] for PYTHIA, and in Ref. [179] for SHERPA. Reweighting techniques to evaluate uncertainties as well as for other applications are available in MADGRAPH5_AMC@NLO [12, 180] and in POWHEG.

For certain common Standard Model processes, a large statistics is often required, and is especially needed to populate the kinematic tails at large transverse momenta. The most advanced generators usually suffer from poor performance, especially in such areas of the phase space, and thus the need for more accurate tools must be balanced with the practical needs for large samples. These problems will need to be addressed on a case by case basis, depending upon the process that is been considered, and the specific purpose that a generator for that process should serve. The presence of negative weights, for example, should be minimised for generators that must produce large samples to be fed through detector simulators. The sampling of suppressed tails of phase space, on the other hand, may be easily increased by suitable bias functions. It is also apparent that attention should be given to whether new computer architectures may be advantageously explored for Monte Carlo generators, such as MPIs and GPU architectures, and that new software techniques making use of Boosted Decision Trees or Deep Neural Networks may provide advantages over traditional techniques of Monte Carlo integration and

phase space generation [181].

Hadronization and underlying event

A recent fascinating direction in parton shower MC's is towards establishing a unified picture in the description of multi-parton dynamics in pp, pA, and AA collisions [182]. Traditionally, pp collisions have been described through the picture of double-, single- and non-diffractive interactions of partons in a vacuum in pp collisions. AA collisions, on the other hand, are typically described in terms of the dynamics of a quark gluon plasma, with a formalism more related to hydrodynamics than particle physics. A series of observations in high-multiplicity pp events at the LHC, however, have exposed remarkable similarities and features in common with those observed in pA and AA collisions, at least with respect to flavour composition and flow. The question therefore arises whether a new state of matter, the quark gluon plasma, is actually formed in high-multiplicity pp events and how this could be tested quantitatively. Efforts and new ideas have recently emerged towards having a unified MC description of such events. This has started with a simple stacking of (soft and hard) pp events [183]. A recent proposal, Angantyr [184], has been inspired by the old Fritiof model [185] and the notion of wounded nucleons. While more elaborated than a stacking approach, it does not yet feature a description of collective effects. In the coming years, progress will be achieved by first identifying the experimental features that are genuine signatures of the formation of a quark gluon plasma, and those which could be associated to other effects. Alternative explanations would likely also be of a collective character, yet without requiring a phase transition.

The intense ongoing theoretical and experimental work in this framework is likely to lead to new breakthrough in the modeling of the hadronization phase and the underlying event before the beginning of the HL-LHC running.

In the description of the underlying event in pp collisions, a key role is played by multi-parton interactions (MPI, see Sec. 5.3). There has been recent progress in the theoretical understanding of double parton scattering that has been summarised in Sec. 5.3.2. There it is also shown that at the HL-LHC it may be possible to find evidence of correlations in double parton interactions. This opens the possibility of constructing improved models of MPI in MC generators, to be eventually refined in the first few years of running of the HL-LHC.

2.4 PDF calculations and tools[4]

At the HL-LHC, a precise knowledge of the quark and gluon structure of the proton will be essential for many analyses. These include the profiling of the Higgs boson sector [186], direct searches for new heavy BSM states [187], indirect BSM searches by e.g. means of the SMEFT [188], and the measurement of fundamental SM parameters such as the W boson mass [189], the Weinberg mixing angle [190] or the strong coupling constant [191] and its running.

This section gives a brief review the PDF tools that will be used in this Report for the studies of the SM chapter. Those aspects of modern PDF fits that are more relevant for studies at the HL-LHC will be also highlighted. The end of this section will provide some perspectives about the role of PDFs at the HE-LHC. It must be stressed that this document is not intended to be a review of recent developments on PDFs, and the reader is referred to [192–194] and reference therein, for further details in this sense.

The studies presented in this Report will be based mostly on the PDF4LHC15 set [195], constructed from the statistical combination and subsequent reduction [196–198] of the CT14 [199], MMHT14 [200], and NNPDF3.0 [201] global analyses. The PDF4LHC15 set is interfaced to matrix-elements calculators and Monte Carlo shower programs by means of the LHAPDF6 package [202].

[4] Contributed by L. Harland-Lang, J. Gao and J. Rojo.

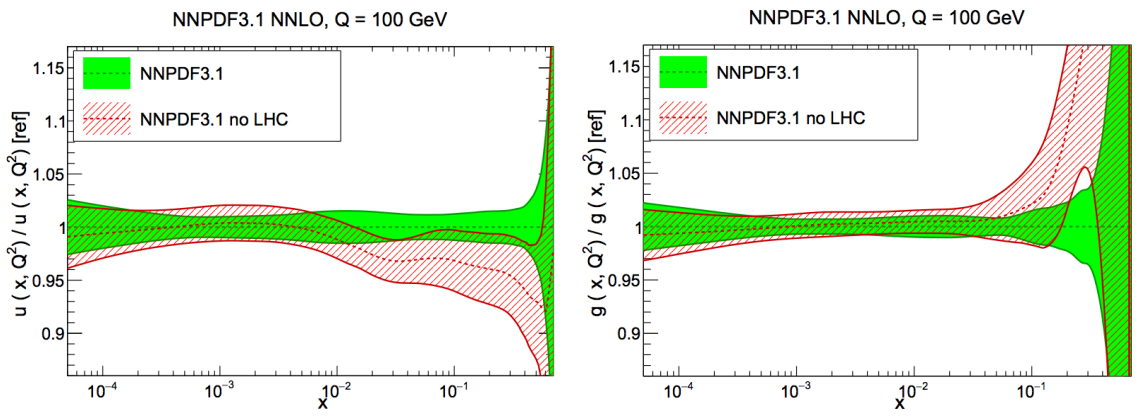

Fig. 1: Comparison of the NNPDF3.1NNLO fits with and without LHC data, normalized to the central value of the former at $Q = 100$ GeV. The up quark (left) and the gluon (right plot) are shown. The bands indicate the 68% confidence level PDF uncertainty.

Quantifying the impact of LHC measurements.

In recent years, one of the main developments in global PDF fits has been the increasingly significant role played by LHC processes in providing stringent PDF constraints. The combination of high precision LHC data with state-of-the art NNLO theory calculations for such hadronic processes as top-quark pair production [203], the transverse momentum spectrum of Z bosons [204], direct photon production [205], and inclusive jet production [206] is having an important impact on precision PDF fits. To illustrate this, Fig. 1 compares the recent NNPDF3.1 fit [207] with and without the LHC data at $Q = 100$ GeV for the up quark and gluon PDFs. The marked impact of the LHC data for $x \gtrsim 0.005$ can be observed both for central values and for the PDF uncertainties. It is of particular note that only Run-1 data has been included in these fits. Thus, it is clear that the addition of data from Run-2 and -3 first and then from the HL-LHC, for which the precision and reach will be greatly increased, should lead to further improvements in the determination of the proton structure. A subsequent section of this report will quantify the impact of HL-LHC measurements, demonstrating that a significant reduction can be expected and providing a public PDF set including the expected constraints from the final HL-LHC dataset.

Fast interfaces to (N)NLO calculations

To avoid the direct evaluation of the lengthy (N)NLO hadronic cross sections during the fit itself, a method of fast interfaces is generally applied, whereby the CPU time intensive part of the higher–order calculation is pre–computed once using a complete interpolation basis for the input PDFs. For a number of years, the APPLGRID [208] and FASTNLO [209] tools have been available for a range of NLO processes. The former is interfaced to the MCFM [210] and NLOJET++ [211] programs. More recently, the AMCFAST interface [212] to MADGRAPH5_AMC@NLO [12] has also been developed. Results within the FASTNLO framework for differential top quark production at NNLO are already available [213, 214], while work is ongoing within the APPLFAST project to extend the FASTNLO and APPLGRID technology to NNLO. This will be interfaced by default to the NNLOJET program [206], but will be reusable for other theory codes. Thus, for future PDF fits, relevant to HL and HE-LHC running, fast interface implementations of NNLO theory calculations are expected to be the standard.

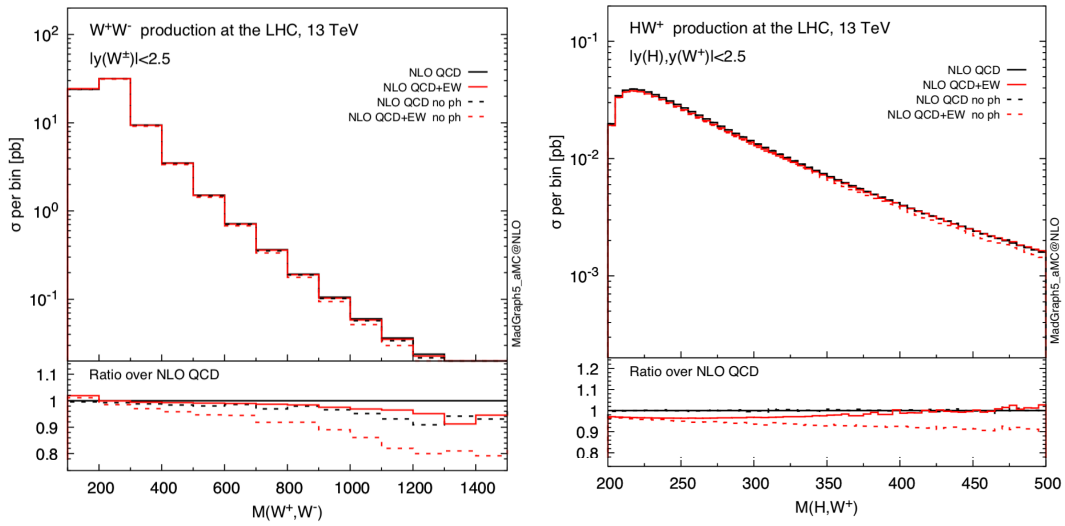

Fig. 2: Photon-initiated contributions partially cancel the NLO EW corrections in the TeV region, as shown for the case of W^+W^- production (left) and hW^+ production (right plot) at 13 TeV.

Theoretical uncertainties

Given the high precision expected for HL-LHC data, it will be crucial to include all sources of experimental, methodological, and theoretical uncertainties associated with PDFs in order to ensure robust predictions. An important issue in this context is to estimate the theoretical uncertainties in PDFs due to missing higher orders (MHOU) in the perturbative expansion for the theory prediction [215], which are so far ignored in all global fits. There is by now some evidence that MHOUs can be comparable, if not larger, than the nominal PDF uncertainties based on the propagation of experimental and methodological uncertainties. In this context, HL-LHC projections should ideally be based on PDFs that consistently account for MHOUs in addition to other sources of uncertainties.

To keep such uncertainties to a minimum, global PDF fits will need to include higher-order perturbative corrections either at fixed-order or at all-orders using some form of resummation. In the former case, encouraging recent progress with N^{3}LO splitting functions [216] suggest that an (approximate) N^{3}LO fit might be within the reach of the HL-LHC era, to match the precision of partonic cross-sections for processes such as Higgs production in gluon fusion [63,217]. In the latter case, one can use threshold (BFKL) resummation [218, 219] to reduce theoretical uncertainties at the large-x (small-x) kinematic regions. Indeed, several state-of-the-art predictions for LHC processes include threshold resummation, such as for example top quark pair production [220].

Electroweak effects and photon-initiated contributions

The enhanced coverage of the TeV region at the HL-LHC requires not only higher-order QCD corrections to be accounted for, but also electroweak ones, which can be enhanced due to Sudakov logarithms [221]. In the context of PDF studies, there are two main considerations to take into account. First of all, exploiting the constraints from the HL-LHC measurements for PDF fits will require systematically accounting for NLO EW corrections. Secondly, PDFs with QED effects and thus with photon-initiated contributions should become the baseline. It has now been demonstrated [222, 223] (see Ref. [224] for a recent implementation within a global fit) that the photon PDF can be determined with percent–level uncertainties and carry up to $\simeq 0.5\%$ of the proton's momentum. For certain processes, in the TeV region the photon-initiated contributions can have a comparable size but opposite sign to the NLO virtual

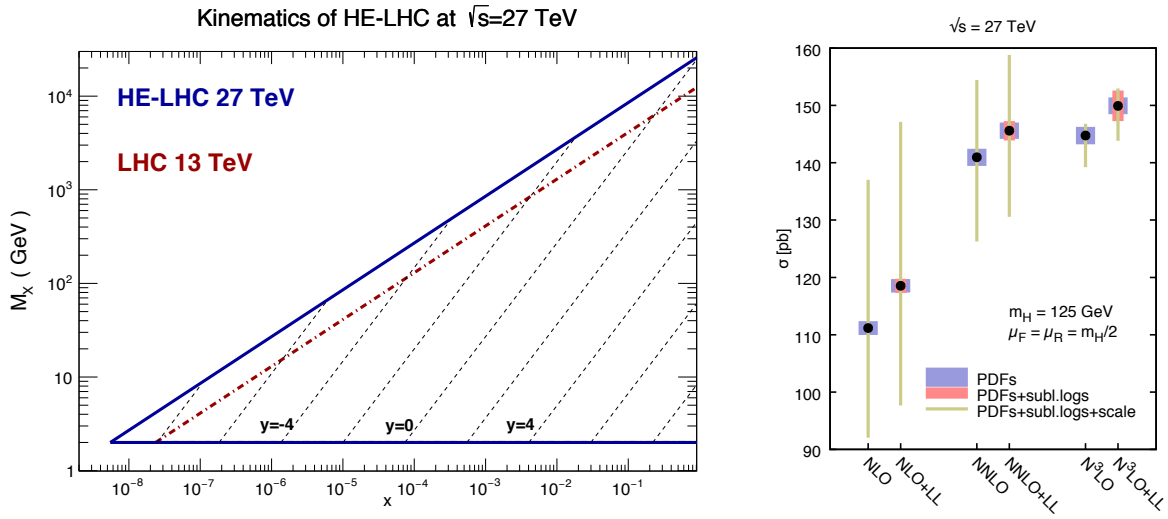

Fig. 3: Left: kinematic coverage of the HE-LHC at $\sqrt{s} = 27$ TeV compared to 13 TeV. Right: the Higgs cross section at the HE-LHC, for different orders and with/without (LL) low–x resummation, and with uncertainty bands from PDF, subleading logarithms, and scale variations [226].

EW corrections, and therefore it is crucial to include both consistently. This is illustrated in Fig. 2 in the specific cases of W^+W^- and hW^+ production at 13 TeV. A more detailed discussion of EW corrections for HL-LHC studies is presented later in the report.

Perspectives at the High Energy LHC

At a centre-of-mass energy of $\sqrt{s} = 27$ GeV, a number of novel phenomena are expected to arise, due to the increased phase space available. Much of this has already been discussed in the context of the Future Circular Collider (FCC) studies at $\sqrt{s} = 100$ TeV [134,225]. To begin with, as illustrated in Fig. 3, when going to higher energies one becomes more sensitive to the small-x region, even for electroweak-scale observables, implying that BFKL resummation effects could become relevant.

Indeed, for $M_X \simeq 100$ GeV the NNPDF3.1sx results [219] at NNLO and at NNLO+NLLx for the gg luminosities are found to differ at the $\simeq 5\%$ level at the HE–LHC. In Ref. [226] a detailed study of SM Higgs boson production via gluon fusion has been performed, consistently including BFKL resummation in the PDFs (see Ref. [219]) and coefficient functions. The role of the former is found to be dominant, and while the impact is mild at the LHC, for the HE–LHC a larger increase is seen relative to the N^{3}LO result with fixed–order NNLO PDFs, that lies outside the fixed–order PDF uncertainty bands, see Fig. 3 (right). This highlights the important role such effects will play at high energies and precision.

Another effect that might become relevant at the HE-LHC are the electroweak PDFs [143, 227] from the resummation of large collinear logarithms of the masses of the W and Z bosons, which become effectively massless at high energies. Related to this is the top quark PDF, which can be (and is) straightforwardly generated within the standard PDF framework. When included with a suitably matched flavour scheme, this may provide a more accurate description of processes involving top quarks [228,229]. In addition, at $\sqrt{s} = 27$ TeV, knowledge of the small-x PDFs will be also required for the modeling of soft and semi-hard QCD dynamics in Monte Carlo event generators [134, 230]. In turn, an improved understanding of the PDFs in the ultra-low-x regime will have implications in high-energy astrophysics, for processes such as cosmic ray detection and for signal and background event rates in neutrino telescopes [231].

2.5 Effective Field Theory calculations and tools[5]

State of the art

The success of the Standard Model Effective Theory (SMEFT) programme at the LHC relies on the availability of public tools for calculations in this framework. Among the most important of these are Monte Carlo (MC) tools for providing realistic predictions for collider processes both for phenomenological studies and experimental analyses. In this respect, significant efforts are being made to implement the effects of dimension-6 operators in MC event generators. Concerning Leading Order (LO) predictions, recent progress includes SMEFTSIM, a complete implementation of the dimension-6 operators in the Warsaw basis [232], an alternative implementation of the Warsaw basis in the R_ξ gauge [233], DIM6TOP, an implementation of top quark operators under various flavour assumptions [234] and the Higgs Effective Lagrangian (HEL) [235] implementation of SILH basis operators. Complementary to SMEFT implementations, there also exist several models of anomalous couplings such as the Higgs Characterisation [236–238] and BSM Characterisation models [239]. These models are all made available in the Universal FEYNRULES Output (UFO) format that can be imported into general purpose Monte Carlo tools, such as MADGRAPH5_AMC@NLO or SHERPA, to generate events and interface them to parton shower generators (PS). A powerful aspect of this workflow is that, once implemented, the model is generic enough to enable event generation for any desired process.

Implementations of particular processes in the presence of dimension-6 operators exist also in other frameworks. An example is the weak production of Higgs in association with a vector boson in POWHEG based on the NLO computation of [240], the implementation of Higgs pair production in the EFT in HPAIR (including approximate NLO corrections) [241] and in HERWIG [147, 242]. Two well-known tools for calculating cross sections for Higgs production via gluon fusion including higher order QCD corrections, HIGLU [243, 244] and SUSHI [245], can also include the effects of modified top and bottom quark Yukawas and the dimension-5 Higgs-gluon-gluon operator. The latter code also permits event generation at NLOQCD+PS accuracy via AMCSUSHI [246] including modified top and bottom quark Yukawa couplings. For a variety of processes with electroweak and Higgs bosons in the final state (VBF H, W and Z production, weak boson pair production, vector-boson-scattering processes, triboson production) the VBFNLO program [247, 248] provides NLO QCD corrections together with implementations of dimension-6 operators and, in the case of VBS and triboson production, dimension-8 operators.

There are also EFT-specific tools providing a number of useful interfaces and calculations. EHDECAY [249, 250] is a package for the calculation of Higgs boson branching fractions including SMEFT effects parametrised by SILH basis operators. The freedom of basis choice in the SMEFT implies that arbitrarily many equivalent descriptions of the model can be formulated. This has important consequences for the development of EFT tools given that any numerical implementation of EFT effects requires choosing a specific basis. A SMEFT basis translation tool, ROSETTA [239], can be used to numerically transform points in parameter space from one basis to another. It adopts the SLHA convention for model parameter specification and provides an interface to Monte Carlo event generation tools through the aforementioned BSMC model. Furthermore, additional interfaces exist to other programs such as EHDECAY, internal routines testing compatibility of Higgs signal-strength and EW precision measurements as well as providing predictions for di-Higgs production cross sections in the SMEFT. Rosetta provides SMEFT basis-independent access to these functionalities. A related tool is DEFT [251], a python code that can check if a set of operators forms a basis, generate a basis and change between bases. A similar implementation based on FEYNRULES is ALLYOURBASES, that performs the reduction of an arbitrary dimension-6 operator into the Warsaw basis operator set. Efforts are also underway to establish a common format for the Wilson coefficients [252], which will allow interfacing various programs computing the matching and running of the operators such as DIM6TOOLS [253] and

[5] Contributed by E. Vryonidou.

WILSON [254]. A public fitting framework that can be used to obtain constraints on the EFT is HEPFIT, which is based on the Bayesian Analysis Toolkit, and includes Higgs and electroweak precision observables.

Future Developments

There is significant progress in computing NLO QCD corrections for the EFT, in both the top and Higgs sector [240, 255–262]. This progress, now on a process-by-process basis, will eventually lead to a full automation of QCD corrections for the SMEFT. As experimental measurements become increasingly systematics dominated, the importance of higher order calculations grows. The complete implementation of dimension-6 operators at NLO, including some flavour symmetry assumptions, is in preparation. This implementation will enable the computation of NLO-QCD corrections to any tree-level process, bringing the Monte Carlo automation to the same level as the Standard Model.

Another direction in which progress is expected over the coming years is the computation of weak corrections in the SMEFT. A small sample of computations has been done, e.g. weak corrections to Higgs production and decay due to top quark loops [263] and due to modified trilinear Higgs coupling [264–266] as well as Higgs and Z-boson decays [267–272]. Due to the behaviour of the Sudakov logarithms, weak corrections are typically important for high transverse momentum regions. Therefore at HE/HL-LHC their impact is expected to be enhanced. It can be expected that the recent progress on a process-by-process basis will eventually lead to the automation of the computation of weak loops in the EFT, as in the Standard Model.

Finally progress is expected in linking tools which compute the running and mixing of the operators with Monte Carlo tools. This will allow the automatic computation of cross-sections and differential distributions taking into account the mixing and running of the operator coefficients.

3 Experimental environment at HL-LHC

3.1 Analysis methods, particle reconstruction and identification

Different approaches have been used by the experiments and in theoretical prospect studies, hereafter named projections, to assess the sensitivity in searching for new physics at the HL-LHC and HE-LHC. For some of the projections, a mix of the approaches described below is used, in order to deliver the most realistic result. The total integrated luminosity for the HL-LHC dataset is assumed to be 3000 fb^{-1} at a centre-of-mass energy of 14 TeV. For HE-LHC studies the dataset is assumed to be 15 ab^{-1} at a centre-of-mass of 27 TeV. The effect of systematic uncertainties is taken into account based on the studies performed for the existing analyses and using common guidelines for projecting the expected improvements that are foreseen thanks to the large dataset and upgraded detectors, as described in Section 3.2.

Detailed-simulations are used to assess the performance of reconstructed objects in the upgraded detectors and HL-LHC conditions, as described in Sections 3.1.1,3.1.2. For some of the projections, such simulations are directly interfaced to different event generators, parton showering (PS) and hadronisation generators. Monte Carlo (MC) generated events are used for Standard Model (SM) and beyond-the-Standard-Model (BSM) processes, and are employed in the various projections to estimate the expected contributions of each process.

Extrapolations of existing results rely on the existent statistical frameworks to estimate the expected sensitivity for the HL-LHC dataset. The increased centre-of-mass energy and the performance of the upgraded detectors are taken into account for most of the extrapolations using scale factors on the individual processes contributing to the signal regions. Such scale factors are derived from the expected cross sections and from detailed simulation studies.

Fast-simulations are employed for some of the projections in order to produce a large number of Monte Carlo events and estimate their reconstruction efficiency for the upgraded detectors. The upgraded CMS detector performance is taken into account encoding the expected performance of the upgraded detector in DELPHES [273], including the effects of pile-up interactions. Theoretical contributions use DELPHES [273] with the commonly accepted HL-LHC card corresponding to the upgraded ATLAS and CMS detectors.

Parametric-simulations are used for some of the projections to allow a full re-optimization of the analysis selections that profit from the larger available datasets. Particle-level definitions are used for electrons, photons, muons, taus, jets and missing transverse momentum. These are constructed from stable particles of the MC event record with a lifetime larger than 0.3×10^{-10} s within the observable pseudorapidity range. Jets are reconstructed using the anti-k_{T} algorithm [274] implemented in the Fastjet [275] library, with a radius parameter of 0.4. All stable final-state particles are used to reconstruct the jets, except the neutrinos, leptons and photons associated to W or Z boson or τ lepton decays. The effects of an upgraded ATLAS detector are taken into account by applying energy smearing, efficiencies and fake rates to generator level quantities, following parameterisations based on detector performance studies with the detailed simulations. The effect of the high pileup at the HL-LHC is incorporated by overlaying pileup jets onto the hard-scatter events. Jets from pileup are randomly selected as jets to be considered for analysis with $\sim 2\%$ efficiency, based on studies of pile-up jet rejection and current experience.

3.1.1 ATLAS and CMS performance

The expected performance of the upgraded ATLAS and CMS detectors has been studied in detail in the context of the Technical Design Reports and subsequent studies; the assumptions used for this report and a more detailed description are available in Ref. [276, 277]. For CMS, the object performance in the central region assumes a barrel calorimeter aging corresponding to an integrated luminosity of

1000 fb^{-1}.

The triggering system for both experiments will be replaced and its impact on the triggering abilities of each experiment assessed; new capabilities will be added, and, despite the more challenging conditions, most of the trigger thresholds for common objects are expected to either remain similar to the current ones or to even decrease [278, 279].

The inner detector is expected to be completely replaced by both experiments, notably extending its coverage to $|\eta| < 4.0$. The performance for reconstructing charged particles has been studied in detail in Ref. [280–282].

Electrons and photons are reconstructed from energy deposits in the electromagnetic calorimeter and information from the inner tracker [283–286]. Several identification working points have been studied and are employed by the projection studies as most appropriate.

Muons are reconstructed combining muon spectrometer and inner tracker information [287, 288].

Jets are reconstructed by clustering energy deposits in the electromagnetic and hadronic calorimeters [283, 284, 289] using the anti-k_{T} algorithm [274]. B-jets are identified via b-tagging algorithms. B-tagging is performed if the jet is within the tracker acceptance ($|\eta| < 4.0$). Multivariate techniques are employed in order to identify $b-$jets and $c-$jets, and were fully re-optimized for the upgraded detectors [280, 282]. An 70% $b-$jet efficiency working point is used, unless otherwise noted.

High p_{T} boosted jets are reconstructed using large-radius anti-k_{T} jets with a distance parameter of 0.8. Various jet substructure variables are employed to identify boosted W/Z/Higgs boson and top quark jets with good discrimination against generic QCD jets.

Missing transverse energy is reconstructed following similar algorithms as employed in the current data taking. Its performance has been evaluated for standard processes, such as top pair production [280, 290].

The addition of new precise-timing detectors and its effect on object reconstruction has also been studied in Ref. [286, 291], although its results are only taken into account in a small subset of the projections in this report.

3.1.2 LHCb performance

The LHCb upgrades are shifted with respect to those of ATLAS and CMS. A first upgrade will happen at the end of Run-2 of the LHC, to run at a luminosity five times larger (2×10^{33}cm^{-2}s^{-1}) in LHC Run-3 compared to those in Runs-1 and-2, while maintaining or improving the current detector performance. This first upgrade (named Upgrade I) will be followed by by the so-called Upgrade II (planned at the end of Run-4) to run at a luminosity of $\sim 2 \times 10^{34}$cm^{-2}s^{-1}.

The LHCb MC simulation used in this document mainly relies on the PYTHIA 8 generator [292] with a specific LHCb configuration [293], using the CTEQ6 leading-order set of parton density functions [294]. The interaction of the generated particles with the detector, and its response, are implemented using the GEANT toolkit [295, 296], as described in Ref. [297].

The reconstruction of jets is done using a particle flow algorithm, with the output of this clustered using the anti-k_{T} algorithm as implemented in FASTJET, with a distance parameter of 0.5. Requirements are placed on the candidate jet in order to reduce the background formed by particles which are either incorrectly reconstructed or produced in additional pp interactions in the same event.

Concerning the increased pile-up, different assumptions are made, but in general the effect is assumed to be similar to the one in Run-2.

3.2 Treatment of systematic uncertainties

It is a significant challenge to predict the expected systematic uncertainties of physics results at the end of HL-LHC running. It is reasonable to anticipate improvements to techniques of determining systematic uncertainties over an additional decade of data-taking. To estimate the expected performance, experts in the various physics objects and detector systems from ATLAS and CMS have looked at current limitations to systematic uncertainties in detail to determine which contributions are limited by statistics and where there are more fundamental limitations. Predictions were made taking into account the increased integrated luminosity and expected potential gains in technique. These recommendations were then harmonized between the experiments to take advantage of a wider array of expert opinions and to allow the experiments to make sensitivity predictions on equal footing [276, 277]. For theorists' contributions, a simplified approach is often adopted, loosely inspired by the improvements predicted by experiments.

General guide-lining principles were defined in assessing the expected systematic uncertainties. Theoretical uncertainties are assumed to be reduced by a factor of two with respect to the current knowledge, thanks to both higher-order calculation as well as reduced PDF uncertainties [298]. All the uncertainties related to the limited number of simulated events are neglected, under the assumption that sufficiently large simulation samples will be available by the time the HL-LHC becomes operational. For all scenarios, the intrinsic statistical uncertainty in the measurement is reduced by a factor $1/\sqrt{\mathrm{L}}$, where L is the projection integrated luminosity divided by that of the reference Run-2 analysis. Systematics driven by intrinsic detector limitations are left unchanged, or revised according to detailed simulation studies of the upgraded detector. Uncertainties on methods are kept at the same value as in the latest public results available, assuming that the harsher HL-LHC conditions will be compensated by method improvements.

The uncertainty in the integrated luminosity of the data sample is expected to be reduced down to 1% by a better understanding of the calibration methods and their stability employed in its determination, and making use of the new capabilities of the upgraded detectors.

In addition to the above scenario (often referred to as "YR18 systematics uncertainties" scenario), results are often compared to the case where the current level of understanding of systematic uncertainties is assumed ("Run-2 systematic uncertainties") or to the case of statistical-only uncertainties.

3.3 Precision Luminosity

Motivation

Measurements of production cross sections provide fundamental tests of theoretical predictions. Ultimate precision both of the experimental measurements and the theoretical predictions is required in order to determine fundamental parameters of the Standard Model and to constrain or discover beyond-the-Standard-Model phenomena. At the LHC, the precision of cross section measurements is limited by the uncertainty of the integrated luminosity, currently about 2%. The impact of all other experimental uncertainties combined is smaller than $\sim$ 1% (2–3%) for Drell-Yan ($t\bar{t}$) cross section measurements, respectively [299, 300]. For the HL-LHC [301], significant improvements of the luminosity measurement are being planned. A target uncertainty of 1% has been set, and this is also assumed for many of the results presented in this report. Such improvement is expected to be achieved by combination of improved luminosity detector instrumentation, currently in the design phase, and refined analysis techniques, rapidly developing during the analysis of Run-2 data. In the following, we provide a short description of the general plan towards the 1% target for the integrated luminosity at the HL-LHC.

Van der Meer Scans

At hadron colliders, the precision of theoretical predictions for inclusive cross sections, e.g. for Z/γ^* production, is limited by the knowledge of the parton density functions (PDFs) in the proton, and the

uncertainty is of the order of 3–5% [302]. A more precise, and purely experimental method to determine the luminosity is based on the Van der Meer (VdM) scan technique [303]. In VdM scans, beam axes are moved in the transverse planes, x and y, across each other such that the beam overlap integral can be determined. From the measured overlap integral, and the beam currents, the instantaneous luminosity during the VdM scan is determined [304].

In practice, VdM scan data are typically recorded with a small number of low pile-up bunches well separated in time, with special interaction-region optics optimised for the measurement of the luminous-region parameters [304–306], and with the bunch intensity lowered to about 3/4 of that during physics runs so as to reduce beam-beam biases while retaining adequate statistics in the luminometers. To transfer the luminosity information from VdM scans to high pileup operation, rate measurements are performed during the VdM scan, in several detectors. The absolute scale, i.e. the relation between the measured rate in a given detector and the luminosity measurement is a detector-specific calibration constant, usually referred to as visible cross section σ_{vis}, relating the measured event rate $\mathrm{d}N/\mathrm{d}t$ to the instantaneous luminosity through the relation $\mathrm{d}N/\mathrm{d}t = L \cdot \sigma_{\text{vis}}$. The integrated luminosity for a complete data taking period, e.g. a full year of data taking is then obtained by continuous rate measurements throughout the year. The integrated normalized rate measurement then corresponds to the integrated luminosity.

Systematic Uncertainties

The uncertainty in the integrated luminosity consists of three components [306, 307]: the absolute-scale uncertainty, i.e. that on the measured visible cross-sections extracted from the VdM-scan analysis; the calibration-transfer uncertainty, which affects the extrapolation of the visible cross-section from the low pile-up, low luminosity VdM regime to the high pile-up, high luminosity physics regime; and the stability uncertainty, that arises from possible time-dependencies and degradations of the detector response affecting the rate measurement over time. Improved analysis techniques, better detectors and extended data takings dedicated to precision luminosity measurements are required to reduce the current uncertainty towards the 1% goal.

Absolute Scale Uncertainty

Dominant uncertainties in the luminosity scale arise from the modeling of, and the potential non-linear correlations between, the horizontal and vertical beam profiles; from inconsistencies between equivalent visible cross-section measurements carried out during the same calibration session or using different luminometers; from the absolute displacement scale of the beams during the scans; and from beam-orbit stability. In Run-2, these and other uncertainties have been reduced using refined methods and dedicated additional data have been recorded for such specific purposes. Improvements of the uncertainty can be achieved by combination of different complementary approaches, of results obtained using different detectors, and of datasets obtained from different VdM scans.

An alternative technique, complementary to VdM scans, was established by the LHCb experiment [308]. The shape of a single beam is measured as the distribution of beam-gas interactions. For this purpose a gas is injected into the interaction region during the VdM fill. The combination of VdM-scan and beam-gas imaging measurements leads to further reduction of the uncertainty, at least for LHCb, thanks to the exquisite performance of the VELO vertex detector.

Calibration-transfer Uncertainty

In the HL-LHC area, the VdM calibration will typically be carried out under similar conditions as in Run-2, i.e. at a pile-up level of about 0.5 interactions per bunch crossing, and with a luminosity of a few Hz/μbarn. In contrast, the physics running during the HL-LHC, will be characterized by pile-up

parameters of up to 200 interactions per bunch crossing, and by average instantaneous luminosities of 50 Hz/nb, two to three times the peak instantaneous luminosity achieved so far. This will lead to an increase of the uncertainties associated with non-linearities in luminometer response. Most luminosity detectors for HL-LHC are still being designed. Drawing on Run-1 and Run-2 experience with precision luminosity measurements, the design of the future detectors aims to reduce the associated systematic uncertainties. HL-LHC detectors are required to behave linearly over several orders of magnitude in their track, energy or hit rate measurements, with residual non-linearities that are reproducible and monitorable. Special runs with scans at intermediate instantaneous luminosity can be used to pin down nonlinear behaviour further.

Long-term stability and consistency of luminosity measurements

In the past, one obvious way to determine stability and linearity effects has been to devise and compare the luminosity measurements by several detectors, using different technologies, with uncorrelated systematics. Since 2016, experiments started to exploit so-called emittance scans. These are short VdM scans (duration of minutes) performed at standard physics optics and currents, regularly at the beginning and at the end of fills [309–312]. While the emittance scans are not primarily designed for the precision determination of σ_{vis}, trends over time, or as a function of instantaneous luminosity, can be used to determine stability effects, such as aging, independently for each given detector. The combination of emittance scans and of rate comparisons between redundant and independent detector systems has been successfully used to discover and control drifts and trends throughout Run-2, the longest LHC data-taking period so far, during which 150 fb^{-1} worth of data were recorded. As a result, the uncertainty in the integrated luminosity in recent years remained at around 2-2.5% even though the pile-up extrapolation range and the duration of the integration periods increased significantly.

Recent Ideas

Additional methods are being discussed among luminosity experts of the LHC experiments and machine. One method recently developed is to use the rate measurement of $Z \to \mu\mu$ production [313]. This is a high-rate physics process with in-situ calibration capabilities. Luminosity and Z boson rate are experimentally related through the following formula: $\sigma_Z = N_Z/(L \times \epsilon_{Z\to\mu\mu})$ where N_Z is the number of reconstructed Z bosons, L the integrated luminosity, and $\epsilon_{Z\to\mu\mu}$ the $Z \to \mu\mu$ event reconstruction efficiency. If $\epsilon_{Z\to\mu\mu}$ and L are known, then the fiducial Z boson production cross section σ_Z can directly be determined from the measured event rate. To minimize the uncertainties associated with luminometer non-linearities and long-term stability, the fiducial Z boson cross section is measured from data recorded during an extended proton–proton production run at low pileup. This run should be close in time to one or two extended VdM scans. The efficiency $\epsilon_{Z\to\mu\mu}$ can be determined in situ, using the tag-and-probe method on the same event sample [313]. Once the cross section is measured at sub-percent level precision, the continuous rate measurement can be used to transfer the calibration to the high pileup dataset. The integrated luminosity will be given by the total number of produced Z bosons, corrected by the time-integrated muon identification efficiency with an uncertainty consisting of the absolute scale uncertainty from the VdM scan (or, in LHCb, beam-gas imaging scan), and a remaining uncertainty in the pileup dependency of the muon identification efficiency.

Conclusions Towards HL-LHC

The aim for HL-LHC is to measure luminosity with substantially improved precision. This aim can be achieved by combination of three ingredients:

1. High precision luminosity detectors are needed to provide high-granularity bunch-by-bunch luminosity measurements, with very good linearity and stability.

2. Advanced, multiple and redundant VdM scans and refined VdM analysis techniques can lead to substantial improvements.

3. Novel techniques, such as the measurement of fiducial Z boson production rates exploiting in-situ efficiency determination, provide handles for advancement of the integrated luminosity uncertainty towards the 1% target.

In order to achieve these goals during HL-LHC, a suite of tests and proof-of-concept measurements is being developed which should be carried out already during Run-3.

4 Electroweak processes

The study of electroweak processes is a central topic of SM tests. Given the small electroweak couplings, high luminosity provides a crucial handle for gaining precision in these measurements, in particular for complex final states with relatively small cross sections. Prospects for those measurements and for their theoretical description are considered in the following for vector boson fusion (VBF) and vector boson scattering (VBS) processes, for di-boson and tri-boson production, and for single weak boson production processes, which promise unprecedented precision on W-mass and weak mixing angle measurements.

4.1 Vector boson fusion[6]

This sub-section discusses the prospects for vector boson fusion Higgs production at the HL-LHC and the HE-LHC, respectively. A particular focus is to investigate how hard and how forward the two tag jets are expected to be at 27 TeV. The efficiency of VBF cuts will be discussed, and fiducial cross sections and differential distributions for a set of typical analysis cuts will be determined. Finally, the quality of the VBF approximation will be considered, in particular when extra jet activity in addition to the two tag jets is required.

The relevant parameters used for the calculations in this chapter are reported here. More details can be found in LHC Higgs Cross Section Working Group report [186]. The gauge boson masses and widths are set to

$$m_W = 80.385 \text{ GeV}, \qquad \Gamma_W = 2.085\text{GeV}. \tag{1}$$

$$m_Z = 91.1876 \text{ GeV}, \qquad \Gamma_Z = 2.4952 \text{ GeV}. \tag{2}$$

and the Fermi constant is

$$G_F = 1.16637 \cdot 10^{-5} \text{ GeV}^{-2}. \tag{3}$$

The Higgs is described in the narrow width approximation with mass $m_H = 125$ GeV. The parton distribution function PDF4LHC15_nnlo_100_pdfas is used and the central renormalization and factorization scale is set to $\mu_0 = m_W$, unless otherwise specified.

Detector requirements

VBF production is characterized by two hard and forward jets accompanying the two bosons. The requirement of two such jets can significantly reduce the QCD induced background along with the electroweak production stemming from s-channel processes. The transverse hardness of the VBF jets is fundamentally set by the mass scale of the virtual vector bosons. It is therefore expected that the jet spectrum is not very sensitive to the collider centre-of-mass energy, and in particular that the jets do not get appreciably harder when increasing the energy.

Figure 4 shows the fraction of total VBF cross sections that survives the cut on the transverse momentum of the two tag jets for the three collider energies 14, 27, and 100 TeV. As can be seen, the cross section drops rapidly as the p_{T}-cut is increased. In particular, at 27 TeV, roughly 60% survive for $p_{\mathrm{T,tag}} > 30$ GeV, which diminishes to 30% of the total VBF cross section for $p_{\mathrm{T,tag}} > 50$ GeV. It will therefore be of great importance to the VBF program to be able to keep the jet definition not too hard.

Given that the two tag jets tend to be forward in the detector volume, it is of interest to study how many jets are lost above a certain rapidity threshold. Figure 5 shows the fraction of events with $\max\left(\left|y_{j_1}\right|, \left|y_{j_2}\right|\right)$ above some threshold at $\sqrt{s} = 27$ TeV for various jet p_{T} definitions. As can be seen

[6] Contribution by F. Campanario, T. Chen, J. M. Cruz-Martinez, T. Figy, A. Karlberg, S. Plätzer and M. Sjödahl.

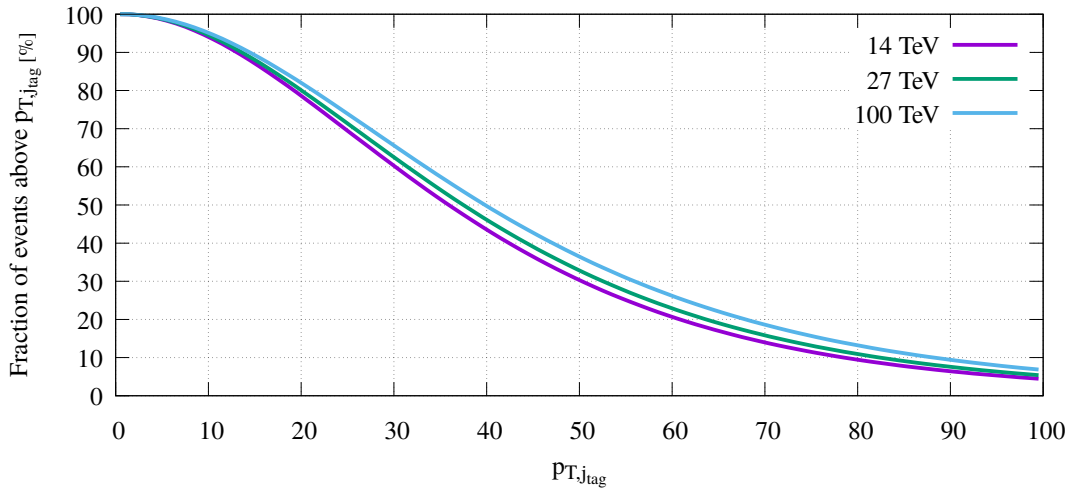

Fig. 4: Fraction of the total VBF cross section surviving a p_{T} cut on the two hardest jets of $p_{\mathrm{T,j_{tag}}}$ for three different collider energies. The results shown here are computed at LO.

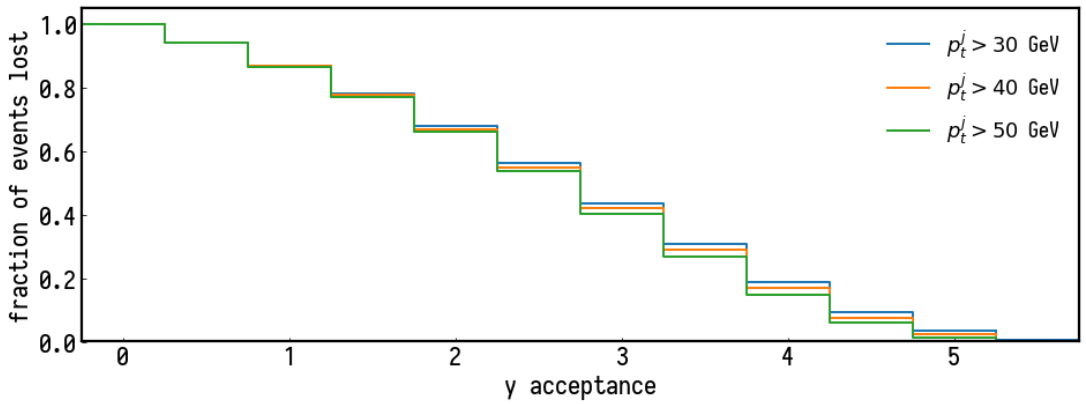

Fig. 5: Fraction of events lost as a function of the rapidity acceptance of the detector at a collider energy of $\sqrt{s} = 27$ TeV. Results shown for three different tag jet transverse momentum cuts. The results shown here are computed at LO.

from the plot, about 20% of the cross section has $\max\left|y_{j_1}\right|, \left|y_{j_2}\right| > 4$. For comparison, this number is $\sim$ 5% at 14 TeV. Additionally one finds that these losses increase to $\sim$ 30% when imposing the dedicated VBF cuts for 27 TeV defined below. Hence, in order to maximize the potential of VBF analyses at the HE-LHC it will be highly desirable that the detectors have a rapidity reach beyond 4.0.

HL-LHC

For VBF production with a centre of mass energy of $\sqrt{s} = 14$ TeV, VBF cuts as in Ref. [186] are used, with two anti-k_{T} jets with $R = 0.4$ and

$$p_{\mathrm{T}}^j > 20 \text{ GeV}, \qquad |y_j| < 5.0, \qquad |y_{j_1} - y_{j_2}| > 3.0, \qquad M_{jj} > 130 \text{ GeV}. \tag{4}$$

The requirement on the rapidity separation and invariant mass significantly reduces background contributions to the process $pp \to Hjj$.

Table 1 reports the fiducial VBF cross section under the above cuts. The cross section includes

Table 1: Fiducial VBF cross sections including QCD and EW corrections and their uncertainties for collider energy $\sqrt{s} = 14$ TeV and for a Higgs-boson mass $m_H = 125$ GeV. The QCD corrections have been updated compared to those reported in Ref. [186].

σ^{VBF}[fb]	Δ_{scale}[%]	$\Delta_{\text{PDF}\oplus\alpha_s}$[%]	$\sigma^{\text{DIS}}_{\text{NNLOQCD}}$[fb]	δ_{EW}[%]	σ_γ[fb]	$\sigma_{s\text{-channel}}$[fb]
2259	$^{+1.5}_{-1.3}$	$\pm 2.1 / \pm 0.4 / \pm 2.1$	2401	-6.9	23.6	32.9

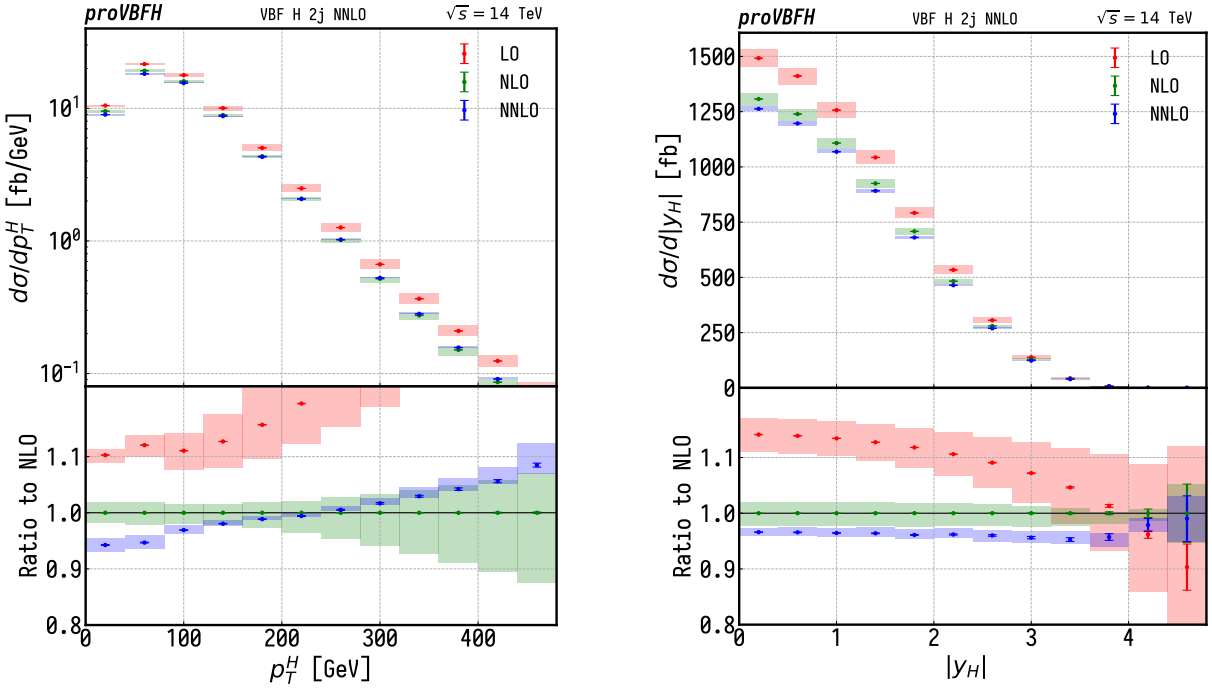

Fig. 6: Transverse momentum and rapidity of the Higgs boson after the cuts of eq. (4) and at a collider energy $\sqrt{s} = 14$ TeV.

NNLO-QCD corrections in the DIS approximation and NLO-EW corrections including photon induced contributions. Shown separately is the s-channel contribution which is not included in the total number. The NNLO-QCD corrections have been computed with PROVBFH-1.1.0 [51, 65, 314–316] and the electroweak contributions with HAWK-2.0 [317–320].

HE-LHC

For fiducial cross sections at a centre-of-mass energy of $\sqrt{s} = 27$ TeV, all physical parameters are kept unchanged with respect to the previous sections. The contributions of the gluon fusion (ggF) and VBF channels to Hjj production are compared, and results are presented for the effects of the NLO and NNLO QCD corrections to VBF Hjj production as computed in NNLOJET [321] with a redefined set of VBF cuts for the new energy choice.

For the comparison of VBF to the ggF background, any kind of VBF cut is omitted, requiring only two jets with

$$p_{\text{T}}^j > 30 \text{ GeV}, \qquad |y_j| < 5.0, \tag{5}$$

defined using the anti-k_{T} algorithm [322] with $R = 0.4$. The total cross section for ggF and VBF is shown in Table 2. Both the ggF and VBF contributions are computed with the parton-level Monte Carlo

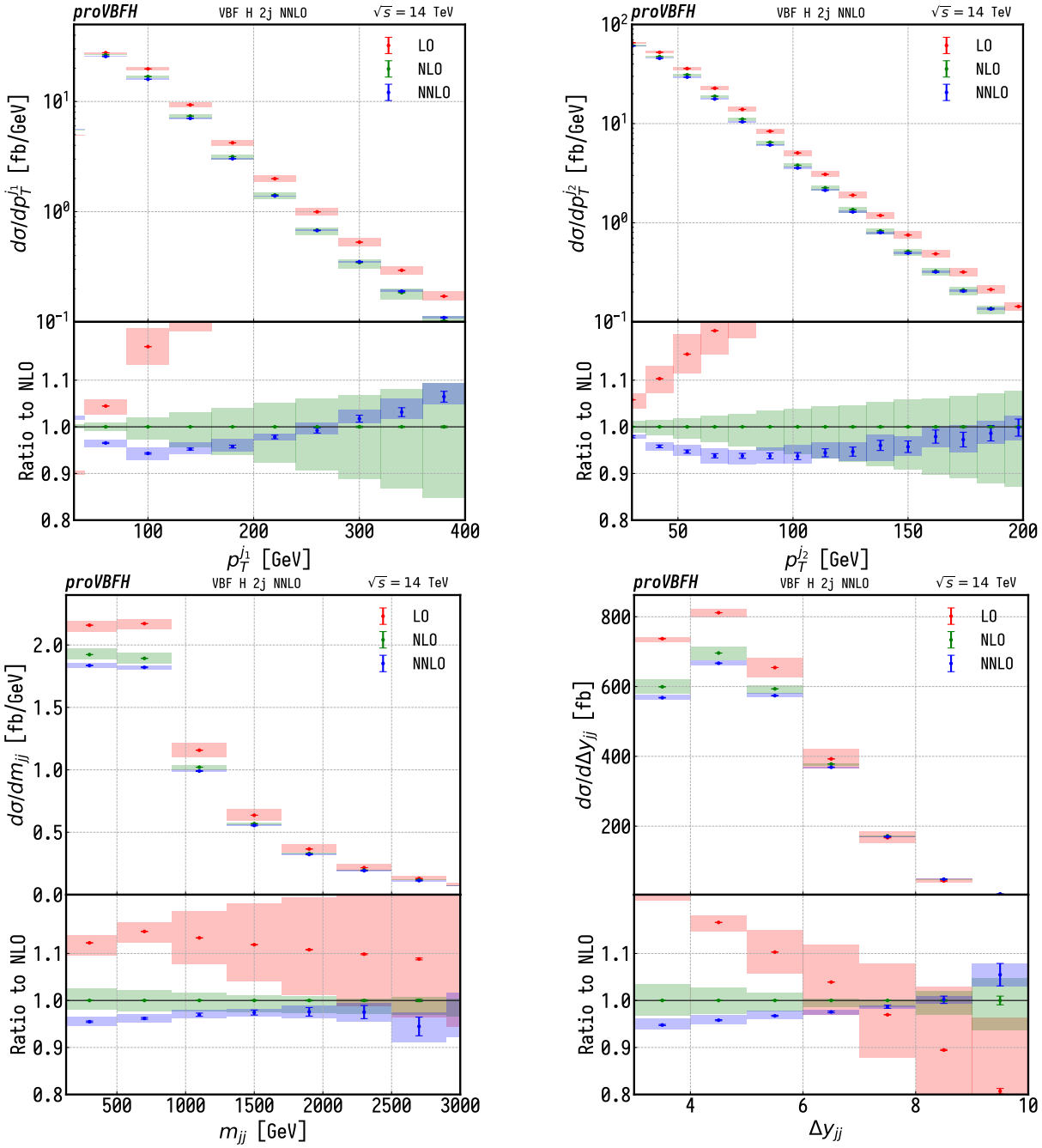

Fig. 7: In the top row the transverse momentum the two hardest jet after the cuts of eq. (4) and at collider energy $\sqrt{s} = 14$ TeV. In the bottom row the invariant mass and absolute rapidity gap between the two hardest jets.

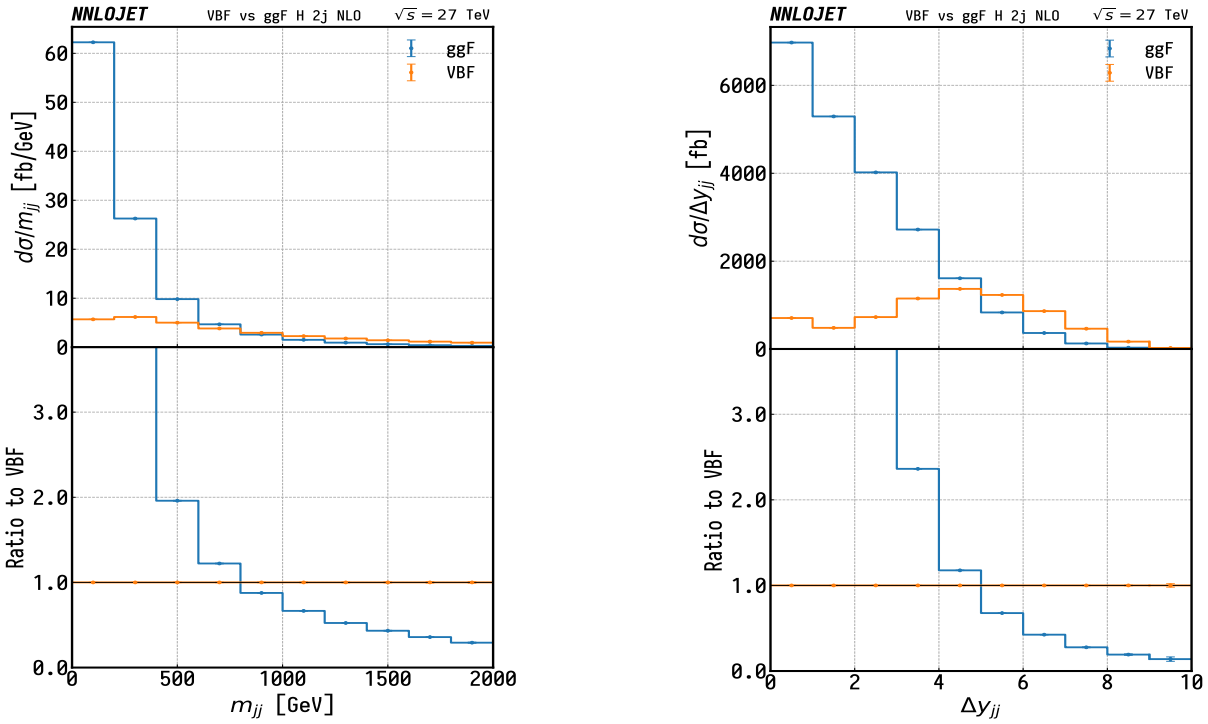

Fig. 8: Differential distributions for the invariant mass (left) and spatial distribution (right) of the dijet system. At lower values of m_{jj} and Δy_{jj} one observes a strong dominance of the ggF channel. For larger values of both observables, however, the VBF channel gains importance.

NNLOJET which includes ggF Higgs production in the heavy top limit (HTL) [67,68,323–325] among other processes [19,206,326–332]. The comparison of Table 2 is done at NLO QCD since Higgs plus two jets in gluon fusion is only available at this accuracy level.

In order to define a set of cuts which enhance the VBF contribution, the invariant mass (m_{jj}) and the spacial distribution (through the rapidity gap between both jets, Δy_{jj}) of the dijet system formed by the two leading jets is considered. The VBF production mode dominates over ggF in the large rapidity separation region ($\Delta y_{jj} > 4.5$) as well as for moderate and high values of the dijet invariant mass ($m_{jj} > 700$ GeV).

Table 2: Comparison between Higgs production by gluon fusion and vector boson fusion for a centre-of-mass energy $\sqrt{s} = 27$ TeV, at NLO QCD. Errors correspond to Monte Carlo statistics.

Production mode	Total cross section (fb)	% of Total
ggF (HTL)	21984 ± 10	75.32 ± 0.04
VBF	7203 ± 2	24.68 ± 0.01

Fiducial cross sections for VBF at $\sqrt{s} = 27$ TeV are defined with a set of tight VBF cuts,

$$\Delta y_{jj} > 4.5, \qquad m_{jj} > 600 \text{ GeV}, \tag{6}$$

requiring the two leading jets to be found in opposite rapidity hemispheres with a maximum rapidity of $|y_j| < 5.0$. In Table 3 the fiducial cross section is computed for three choices of the cut on the transverse momentum of the two leading jets: $p_{\mathrm{T}}^j > \{30, 40, 50\}$ GeV while differential distributions for $p_{\mathrm{T}}^j > 30$ GeV are shown in Figs. 9 and 10. The Hjj contribution in the VBF approximation as well as plots in this section are calculated at NNLO QCD accuracy with NNLOJET, electroweak corrections

Table 3: Fiducial VBF cross sections including QCD and EW corrections and their uncertainties for collider energy $\sqrt{s} = 27$ TeV ($m_H = 125$ GeV). For completeness the s-channel contribution (corresponding to $pp \to HV \to q\bar{q}$) is also included.

σ^{VBF}[fb]	Δ_{scale}[%]	$\sigma^{\text{DIS}}_{\text{NNLOQCD}}$[fb]	δ_{EW}[%]	σ_γ[fb]	$\sigma_{s\text{-channel}}$[fb]	p_{T}^j cut [GeV]
2805	$^{+1.05}_{-0.02}$	3059	−9.6	39.8	5.9	30
2087	$^{+1.13}_{-1.05}$	2283	−10.0	32.3	4.4	40
1442	$^{+1.43}_{-1.61}$	1586	−10.5	22.3	3.0	50

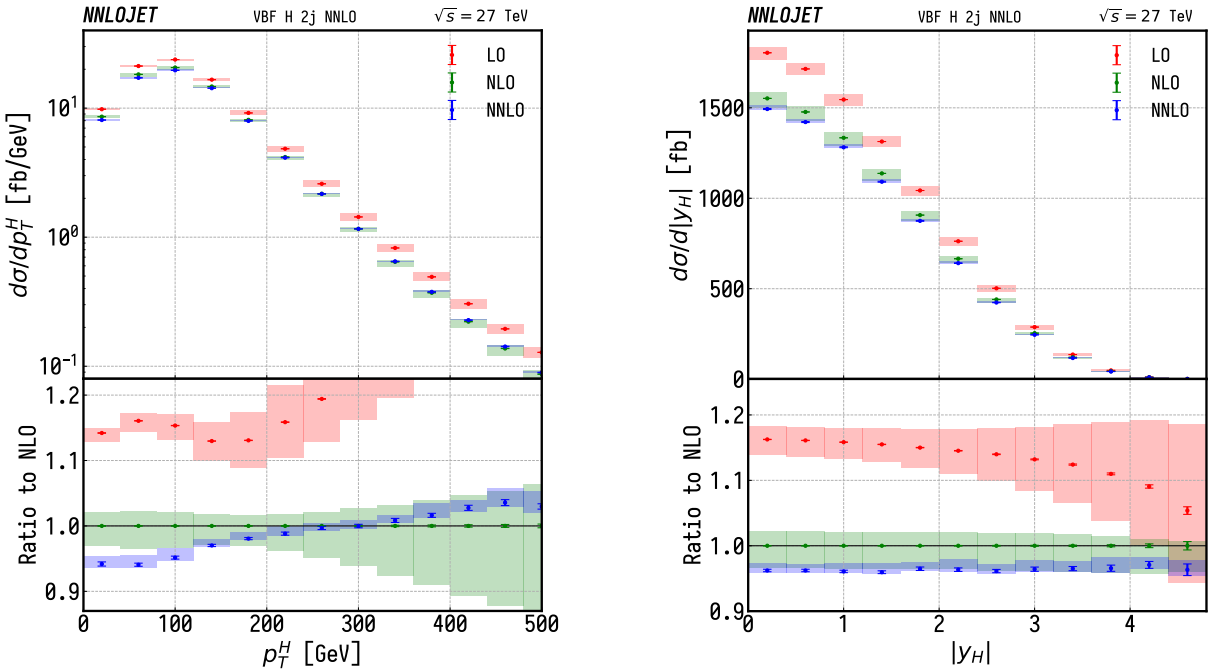

Fig. 9: Kinematical variables for the Higgs boson at $\sqrt{s} = 27$ TeV for tight VBF cuts. The NLO corrections are of more than -10 % across the whole considered range. The NNLO corrections, much smaller than NLO, show good convergence of the perturbative series. The NNLO corrections changes sign for high transverse momentum (left). For the rapidity distribution (right) they remain stable across the entire range of the observable.

and the s-channel contribution shown in Table 3 are again computed with HAWK-2.0. Shaded boxes in all plots represent scale variations with $\mu_R = \mu_F = \{0.5, 2\}\mu_0$ with the central scale $\mu_0 = m_W$ and error bars represent statistical uncertainties from the Monte Carlo integration. In Fig. 9 the transverse momentum and rapidity distribution of the Higgs boson is shown. The kinematical variables for the system formed by the two leading jets are shown in Fig. 10.

Comparison of HJETS++ *and* VBFNLO *for Higgs boson production*

The HJETS++ 1.1 module implements [333–336] electroweak Higgs boson plus two and three jet production. The one-loop integrals are computed using the techniques discussed in Ref. [337] and the colour algebra is performed using COLORFULL [338]. For the VBF approximation, the matrix elements encoded in VBFNLO version 3.0 beta 5 [247, 248, 339, 340] are used, with HERWIG 7 as the event generator [146, 147, 341, 342]. Jet reconstruction is performed on final state partons using the

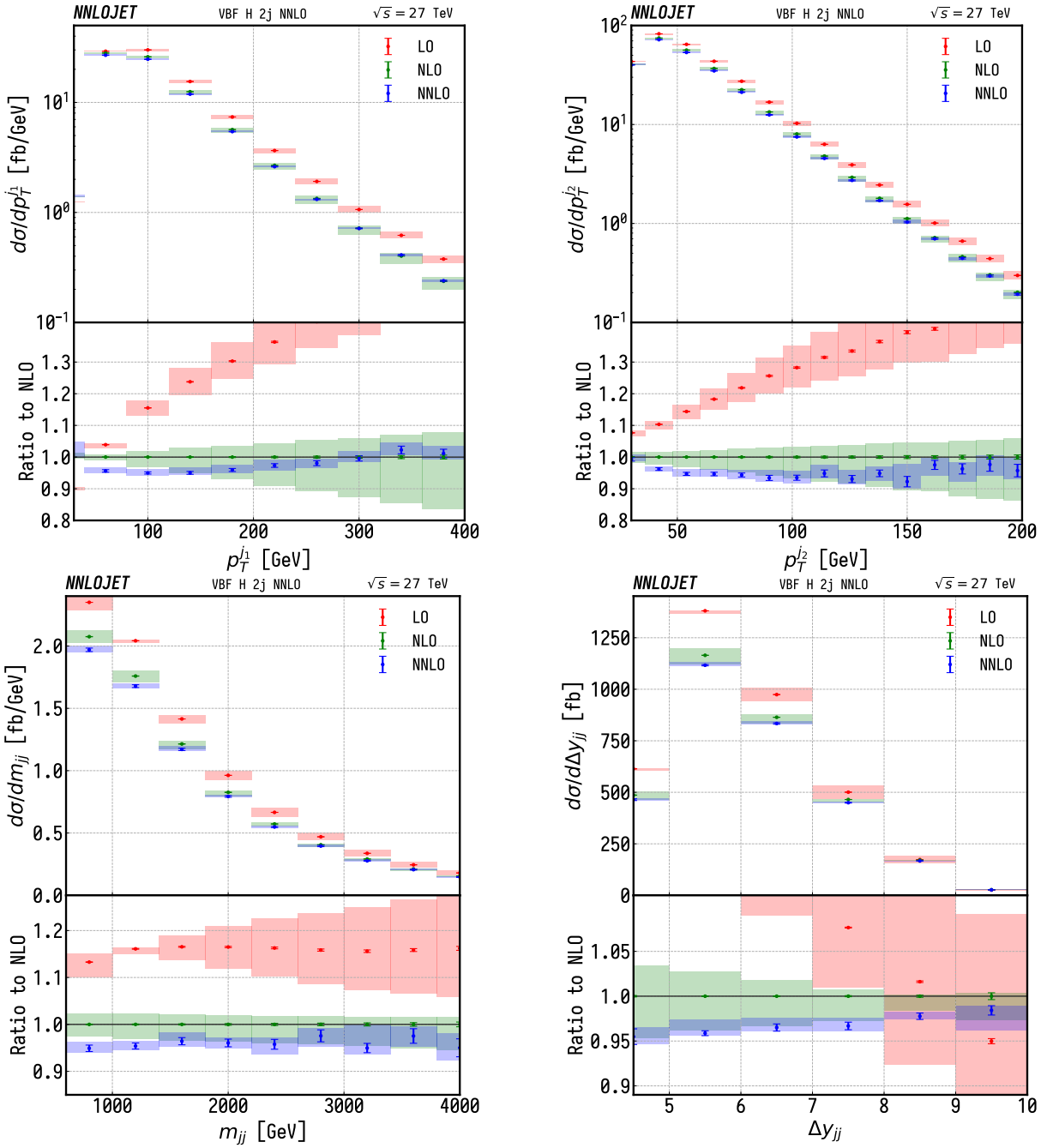

Fig. 10: The top row shows the transverse momentum of the two leading jets ordered in rapidity at $\sqrt{s} = 27$ TeV for tight VBF cuts. The bottom row depicts the kinematical variables for the dijet system they form. Note that NNLO corrections noticeably reduce the scale uncertainties for both observables over the entire range considered. NLO corrections are big for moderate and high transverse momentum with a scale uncertainty that grows with the transverse momentum. This behaviours is softened by the NNLO corrections.

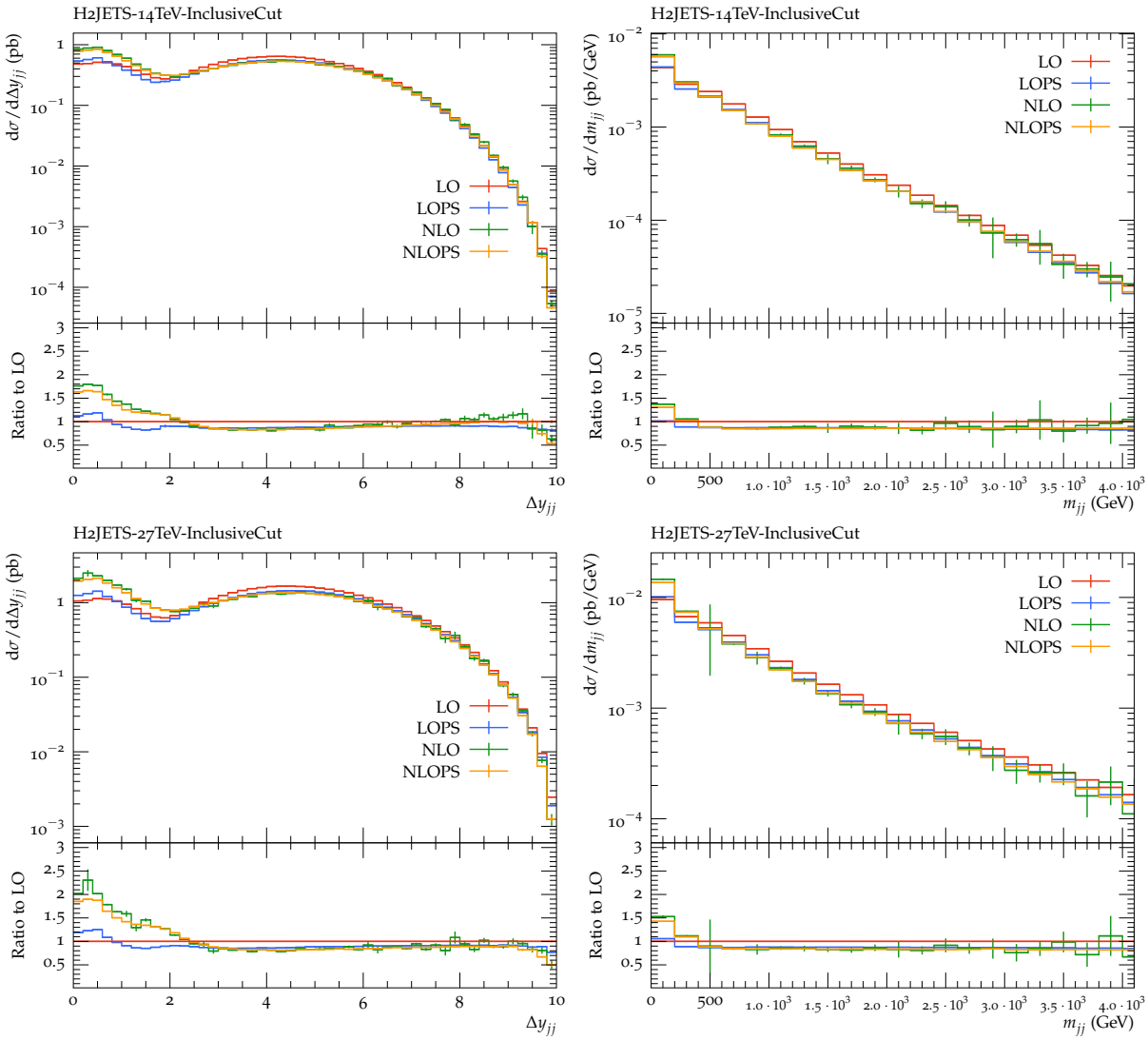

Fig. 11: Differential distributions of Δy_{jj} and m_{jj} at $\sqrt{s} = 14$ TeV (top row) and $\sqrt{s} = 27$ TeV (bottom row). HJETS++ matrix elements and inclusive cuts are used in the $H + 2$ jets calculations.

anti-k_T algorithm [322] in the FASTJET library [343]. Simulated events are analyzed via RIVET [344].

For comparison plots of Higgs plus two jet calculations, collider energies of $\sqrt{s} = 14$ TeV and $\sqrt{s} = 27$ TeV are considered. Two kinematic variables, namely the invariant mass, m_{jj}, and the spatial distribution, Δy_{jj}, of the two tag jets are chosen to present their differential distributions. Parton distribution functions PDF4_LHC15_nlo_100 are used, while all other input parameters are the same as given at the beginning of Section 4.1. Differential distributions for leading order, leading order plus parton shower, next-to-leading order, and next-to-leading order plus parton shower are shown in Fig. 11, with the inclusive cuts defined in eq. (5). Comparison plots between two different matrix elements, HJETS++ and VBFNLO are shown in Fig. 12. VBFNLO uses the VBF approximation throughout, i.e. s-channel contributions such as $pp \to VH \to jjH$ production need to be added as separate processes. The comparison between HJETS++ and VBFNLO thus also serves to highlight the phase space regions where the VBF approximation is warranted.

The tight VBF cuts applied for $\sqrt{s} = 14$ TeV are defined as

$$p_T^j > 30 \text{ GeV}, \qquad |y_j| < 5.0, \qquad |y_{j_1} - y_{j_2}| > 3.0, \qquad M_{jj} > 130 \text{ GeV}. \tag{7}$$

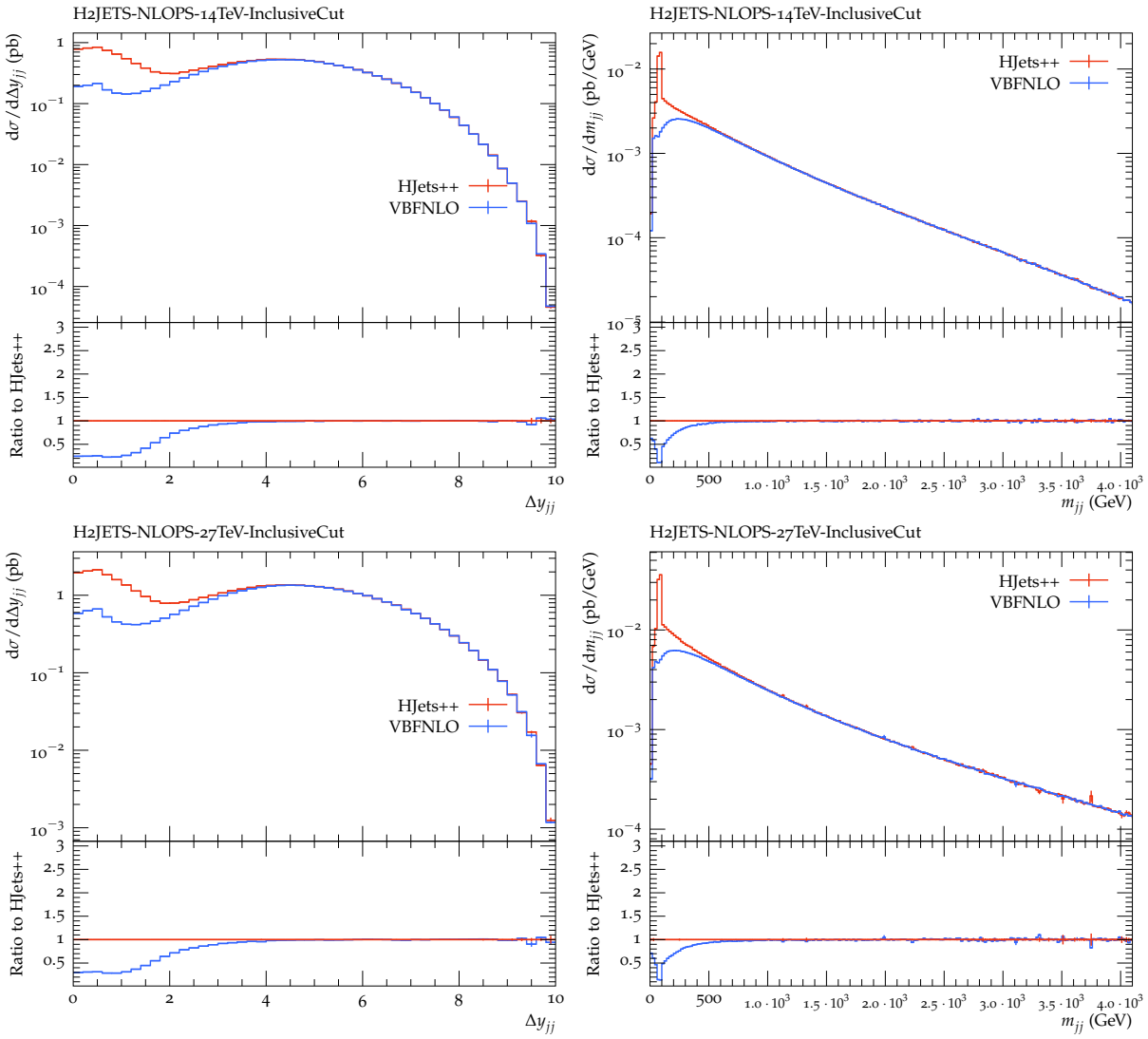

Fig. 12: The distributions of kinematic variables in $H + 2$ jets at $\sqrt{s} = 14$ TeV (top row) and $\sqrt{s} = 27$ TeV (bottom row). Comparisons are between the HJETS++ matrix elements and the VBFNLO matrix elements at NLO plus parton shower. Plots indicate that both HJETS++ and VBFNLO calculations agree once the tight VBF cuts are applied.

For $\sqrt{s} = 27$ TeV comparison plots, the tight VBF cuts defined in eq. (6) are used. The VBFNLO calculation is consistent with the HJETS++ calculation after applying the tight VBF cut.

Fig. 13 shows differential distributions of kinematics variables for the NLO full and approximate results at $\sqrt{s} = 14$ TeV and $\sqrt{s} = 27$ TeV. The comparison of the full and approximate calculations are shown in the second and third rows of Fig. 13 for tight VBF cuts for the transverse momentum of the third jet $p_{\mathrm{T}}^{j_3}$ and the centrality of the third jet $y^{\star}_{j_3} = (y_{j_3} - \frac{1}{2}(y_{j_1} + y_{j_2}))/|y_{j_1} - y_{j_2}|$. For the $\sqrt{s} = 27$ TeV tight VBF cuts ($\Delta y_{jj} > 4.5$, $m_{jj} > 600$ GeV, and $y_{j_1} \cdot y_{j_2} < 0$), one observes excellent agreement between the full and approximate calculation. For the $\sqrt{s} = 14$ TeV tight VBF cuts ($\Delta y_{jj} > 3.0$, $m_{jj} > 130$ GeV, and $y_{j_1} \cdot y_{j_2} < 0$), the full and approximate calculations still do not converge. However, for $\Delta y_{jj} > 4.0$ or $m_{jj} > 600$ GeV the full and approximate calculations would compare quite well.

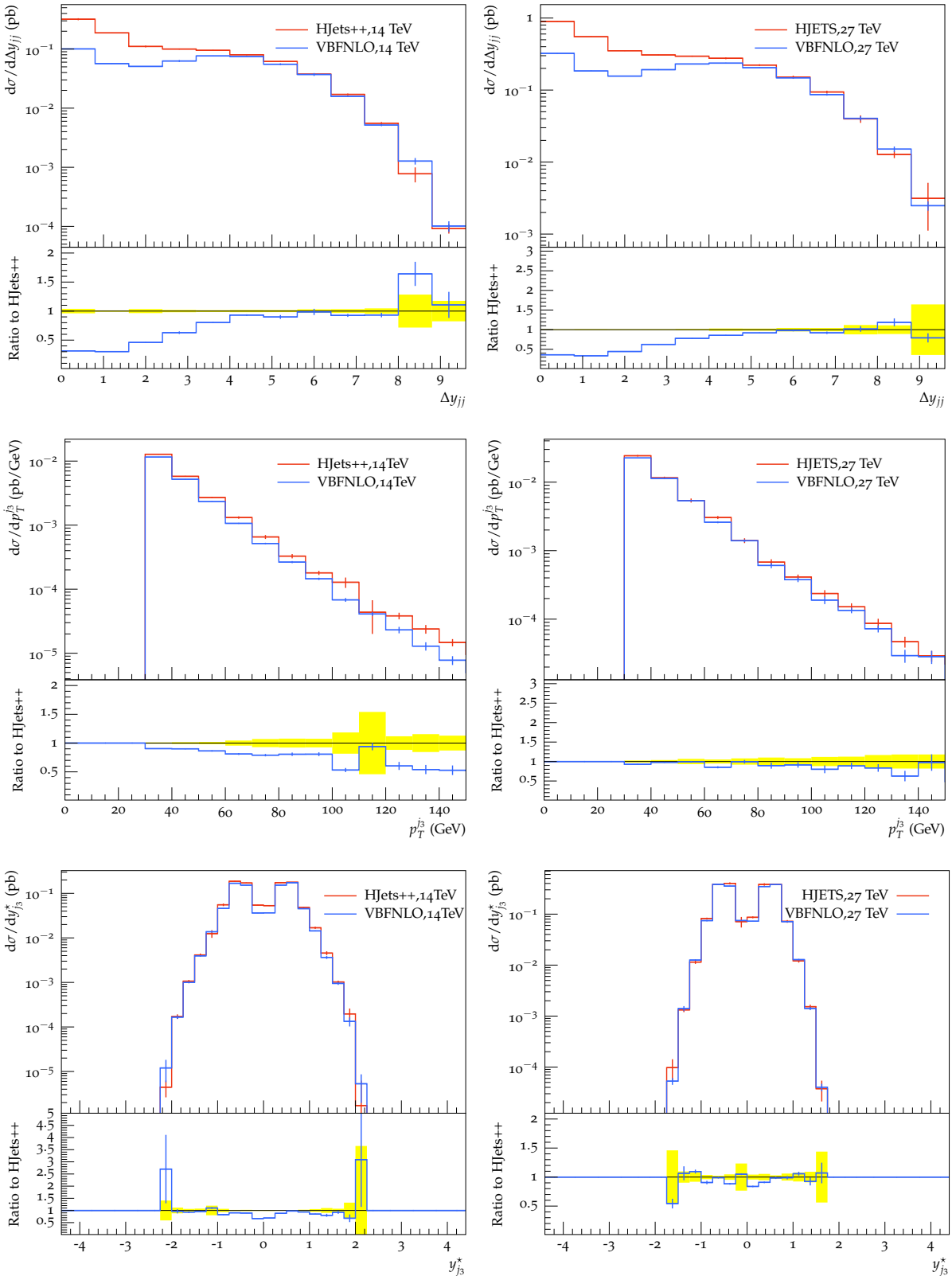

Fig. 13: Kinematics distributions for $H + 3$ jet production at NLO for the full result (HJETS++) and the approximate result (VBFNLO) for $\sqrt{s} = 14$ TeV (first column) and $\sqrt{s} = 27$ TeV (second column). The kinematic distribution Δy_{jj} (top row) is shown for inclusive selection cuts. The kinematic distributions for $p_{\mathrm{T}}^{j_3}$ and $y^{\star}_{j_3}$ are shown for VBF tight selection cuts.

4.2 Vector boson scattering processes

The study of the scattering of two massive vector bosons $V = W, Z$ (vector boson scattering, VBS) provides a key opportunity to probe the nature of the electroweak symmetry breaking (EWSB) mechanism as well as physics beyond the Standard Model (SM) [345, 346]. It is still unknown whether the discovered Higgs boson [347] preserves unitarity of the longitudinal VV scattering amplitude at all energies, or if other new physics processes are involved [348–352]. In the VBS topology, two incoming quarks radiate bosons which interact, yielding a final state of two jets from the outgoing quarks, and two massive bosons which decay into fermions. This final state can be the result of $VVjj$ electroweak (EW) production with and without a scattering topology, or of processes involving the strong interaction.

4.2.1 Measurements of $W^{\pm}W^{\pm}$ scattering and extraction of the longitudinal scattering component

With the largest cross section ratio of electroweak to strong production [353, 354], events with $W^{\pm}W^{\pm}$ plus two jets ($W^{\pm}W^{\pm}jj$) provide one of the best opportunities to study the scattering of two vector bosons. ATLAS and CMS have both observed the EW process at 13 TeV with significances of 6.9 σ and 5.5 σ, respectively [355, 356].

This section describes the prospects for the study of $W^{\pm}W^{\pm}jj$ at $\sqrt{s} = 14$ TeV at the HL-LHC, with the HL-LHC upgraded ATLAS and CMS detectors [357, 358]. Results are presented for a range of integrated luminosities $\mathcal{L}$, from 300 fb^{-1}through 8000 fb^{-1}, where the first value corresponds to one year of data taking, and the latter to 10 years of combined data sets collected by the ATLAS and CMS experiments in the most optimistic scenario.

In both ATLAS and CMS analyses, the signal (VBS and non-VBS EW) and background (QCD) $W^{\pm}W^{\pm}jj$ events are simulated at leading order using MADGRAPH5_AMC@NLO [12, 150] with the NNPDF3.0 set [201, 359], interfaced with PYTHIA V8 [149] for parton showering, hadronization and underlying event modelling. The information about the polarization of the individual W bosons in the signal process is extracted by generating a separate set of events using the DECAY package of MADGRAPH(v1.5.14). The other backgrounds – top ($t\bar{t}$ + jets, single-top), Drell-Yan, diboson ($W\gamma$, $W^{\pm}W^{\pm}$ and WZ) and triboson ($WW\gamma$, $WZ\gamma$, WWW, WWZ, WZZ, ZZZ) – are generated with either MADGRAPH5_AMC@NLO, POWHEG [360], or PYTHIA V8. The analyses use generated events obtained either using a fully simulated description of the HL-LHC CMS detector, implemented using the GEANT4 package [296] (CMS) or using a parameterised description of the detector response [276] (ATLAS). Additional details for each analysis are provided in the relevant reports from CMS [358] and ATLAS [357].

The experimental signature of the $W^{\pm}W^{\pm}jj$ scattering process consists of exactly two isolated leptons (electrons or muons) with the same electric charge, two jets well-separated in rapidity, and moderate E_{T}^{miss}. The event selection requirements for the two experiments are listed in Table 4. A minimum requirement on the dilepton mass reduces the contamination from low-mass Drell-Yan processes, with an additional restriction excluding the Z mass in the dielectron channel where the likelihood of charge misidentification is higher. A requirement on E_{T}^{miss} further reduces the background from charge misidentified events, and events containing any b-tagged jets[7] are vetoed to suppress background contribution from $t\bar{t}$ production. A veto on additional preselected leptons significantly reduces background from WZ events. The two leading jets are required to have a large invariant mass, and large angular separation, to satisfy the expected VBS topology. Since leptons in the EW $W^{\pm}W^{\pm}jj$ process are expected to be located in the central region defined by the forward-backward jets, non-VBS background can be suppressed with a requirement on the centrality of the two leptons. CMS uses the Zeppenfeld variable

[7] The b-tagging of jets in CMS is performed with the Deep Combined Secondary Vertex discriminator based on a deep neural network [363].

Table 4: ATLAS and CMS event selection criteria for $W^{\pm}W^{\pm}jj$ candidate events, with $\ell = e, \mu$ and j as the leading(sub-leading) lepton or jet.

Selection requirement	ATLAS Selection	CMS Selection
Signal lepton p_{T}	p_{T}> 28(25) GeV	p_{T}> 20 GeV
Signal lepton η	$\lvert\eta\rvert \leq 4.0$	$\lvert\eta\rvert \leq 3.0$
Tag jet p_{T}	p_{T}> 90(45) GeV	p_{T}> 50 GeV
Tag jet η	$\lvert\eta\rvert \leq 4.5$	$\lvert\eta\rvert \leq 4.7$
Dilepton mass	$m_{\ell\ell} > 28$ GeV	$m_{\ell\ell} > 20$ GeV
Z_{ee} veto	$\lvert m_{ee} - m_Z\rvert > 10$ GeV	$\lvert m_{ee} - m_Z\rvert > 15$ GeV
E_{T}^{miss}	E_{T}^{miss}> 40 GeV	E_{T}^{miss}> 40 GeV
Number of b-tagged jets	0	0
Jet selection	Anti-k_{T} [361] jets with $\Delta R_{\ell,j} > 0.3$	Anti-k_{T} PUPPI [362] jets with $\Delta R_{\ell,j} > 0.4$
Preselected lepton veto	p_{T}> 7(6) GeV	p_{T}> 10 GeV
Dijet rapidity separation	$\Delta\eta_{j,j} > 2.5$	$\Delta\eta_{j,j} > 2.5$
Dijet mass	$m_{jj} > 520$ GeV	$m_{jj} > 500$ GeV
Lepton centrality	ζ > -0.5	Z_{MAX} < 0.75

[364], defined for a given lepton with pseudorapidity η_ℓ as

$$Z_\ell = \frac{[\eta_\ell - 0.5(\eta_1 + \eta_2)]}{|(\eta_1 - \eta_2)|},$$

where η_1, η_2 refer to the pseudorapidities of the leading and subleading jets. The maximum value of this variable, Z_{MAX}, for any of the leptons is required to be less than 0.75. ATLAS uses a requirement on the function ζ, where $\zeta = \min[\min(\eta_{\ell 1}, \eta_{\ell 2}) - \min(\eta_{j1}, \eta_{j2}), \max(\eta_{j1}, \eta_{j2}) - \max(\eta_{\ell 1}, \eta_{\ell 2})]$

The event selections are optimized to maximize signal acceptance (CMS) or minimize fake background (ATLAS). ATLAS uses tight electron requirements, which have a lower efficiency (around 50% [276]).

The expected event yields are summarized in Table 5 for CMS, and Table 6 for ATLAS. The m_{jj} distributions after the full event selection for $\mathcal{L} = 3000\,\mathrm{fb}^{-1}$ are presented in Fig. 14 . The main background contributions in the final signal region are due to inclusive $t\bar{t}$ and WZ productions, where the third lepton in the event was not reconstructed within the detector acceptance. ATLAS explicitly models the background contributions from jets faking electrons and lepton charge misidentification, which also contribute significantly in the signal region, while CMS includes the fake contribution under $t\bar{t}$ and does not consider the charge-misidentified or triboson backgrounds in this study, since their contributions were found to be negligible. The integrated number of signal and background events as a function of the dilepton invariant mass is shown in Figure 16 for the ATLAS selection.

The uncertainty of the expected cross section measurement as a function of integrated luminosity is measured by fitting the m_{jj} distribution, using a binned maximum likelihood approach with all systematic uncertainties in the form of nuisance parameters with log- normal distributions. The correlations among different sources of uncertainties are taken into account while different final states are considered as independent channels in the fit. CMS considers three channels categorised by lepton flavour (ee, eμ

Table 5: CMS expected yields for signal and background contributions for $\mathcal{L} = 3000\,\text{fb}^{-1}$.

Process	Expected yield, $\mathcal{L} = 3000\,\text{fb}^{-1}$
$W^{\pm}W^{\pm}$ (QCD)	196
$t\bar{t}$	5515
WZ	1421
$W\gamma$	406
Total Background	7538
Signal $W^{\pm}W^{\pm}$ (EW)	5368

Table 6: The ATLAS expected signal and background event yields after the optimised full event selection for a corresponding integrated luminosity of $\mathcal{L}$=3000 fb^{-1}. Events tagged as either "charge misidentification" or "jets faking leptons" are summed for all background samples and combined into a single entry each in the table. Remaining events are listed separately per process. Both QCD and EW production of WZ processes are included in the diboson background.

Process	All channels	$\mu^{\pm}\mu^{\pm}$	$e^{\pm}e^{\pm}$	$\mu^{\pm}e^{\pm}$	$e^{\pm}\mu^{\pm}$
$W^{\pm}W^{\pm}jj$(QCD)	168.7	74.6	19.7	32.2	42.2
Charge Misidentification	200	0.0	11	30	160
Jets faking electrons	460	0.0	130	260	70
$WZ + ZZ$	1286	322	289	271	404
Tribosons	76	30.1	9.6	15.1	21.6
Other non-prompt	120	29	16.6	50	19
Total Background	2310	455	480	660	710
Signal $W^{\pm}W^{\pm}jj$(EW)	2958	1228	380	589	761

and $\mu\mu$), while ATLAS uses eight channels by lepton flavour and charge ($e^{+}e^{+}$, $e^{-}e^{-}$, $e^{+}\mu^{+}$, $e^{-}\mu^{-}$, $\mu^{+}e^{+}$, $\mu^{-}e^{-}$, $\mu^{+}\mu^{+}$, $\mu^{-}\mu^{-}$).

The experimental uncertainties, statistical and systematic, in the CMS analysis contribute to a total uncertainty on the signal strength of 3.2% for 3000 fb^{-1}. Including a theoretical uncertainty of 3% and an uncertainty on the luminosity of 1%, the total uncertainty reaches a value of 4.5% for 3000 fb^{-1}. For the ATLAS analysis experimental systematics on the trigger, leptons, jets, and flavour tagging are taken from the 13 TeV analysis unchanged, while for the baseline estimation, rate uncertainties on the backgrounds are halved. An "optimistic" set of uncertainties is also presented, where the uncertainties on the non-data-driven backgrounds are aggressively reduced. The total uncertainty is presented in Fig. 15 as a function of the integrated luminosity. The values of $\mathcal{L}$ exceeding 3000 fb^{-1} are an estimation of a combination of the measurements from CMS and ATLAS, effectively doubling the total integrated luminosity.

The total $W^{\pm}W^{\pm}jj$ VBS cross section can be decomposed into the polarized components based on the decays of the individual W bosons. Either or both can be longitudinally (L) or transversely (T) polarized, giving rise to final states of LL, TT as well as the mixed state LT (with TL combination implied). The LL component, $W^{\pm}_{\text{L}}W^{\pm}_{\text{L}}jj$, is expected to be only about 6-7% of the total VBS cross

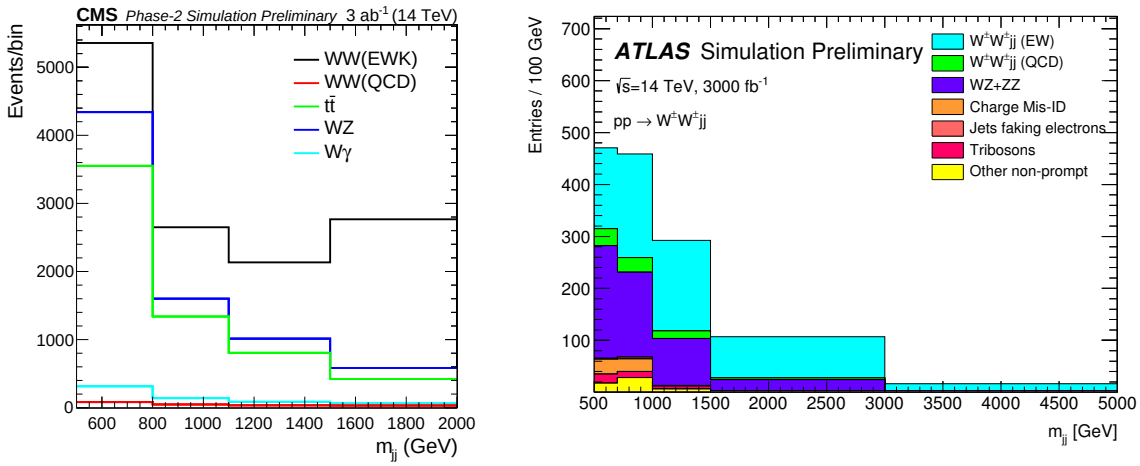

Fig. 14: The distribution of the invariant mass of the two leading jets after the selection requirements for an integrated luminosity of 3000 fb^{-1}, for CMS (left) and ATLAS (right).

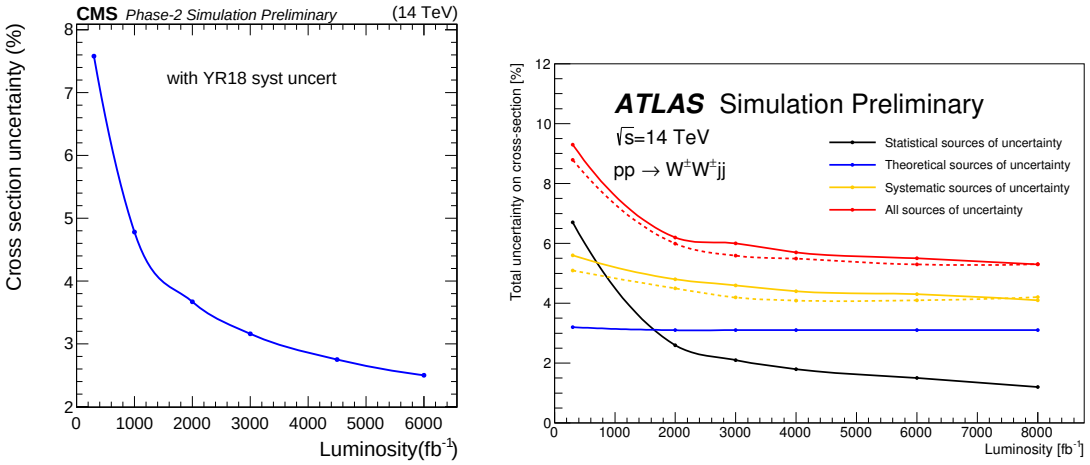

Fig. 15: The estimated uncertainty of the EW $W^{\pm}W^{\pm}$ cross section measurement as a function of the integrated luminosity, for CMS (left), only statistical and experimental systematic uncertainties are considered, and ATLAS (right).

section for jet $p_{\mathrm{T}} > 50$ GeV. The difference in azimuthal angle between the two leading jets, $\Delta\phi_{jj}$, has the potential for discriminating the LL component of the VBS scattering from TT and LT contributions. Since the signal-to-background separation for the EW $W^{\pm}W^{\pm}jj$ process improves with increasing m_{jj} as shown in Fig. 14 (left), the $\Delta\phi_{jj}$ distributions are studied in two ranges of m_{jj}: for 500-1100 GeV and above 1100 GeV. Figure 17 shows the combination of signal and background yields as a function of $\Delta\phi_{jj}$ for high m_{jj} regions. Using a simultaneous fit to two mass regions[8], the significance for the observation of the LL process is estimated as a function of integrated luminosity. The significance is found to be up to 2.7 standard deviations for $\mathcal{L} = 3000\,\mathrm{fb}^{-1}$. The gradual improvement of signal significance as a function of integrated luminosity is shown in Fig. 18 right. A combination of ATLAS and CMS results, using fully simulated ATLAS events and improved electron efficiency, is expected to reach an expected significance of 3 standard deviations with 2000 fb^{-1} per experiment. In addition,

[8]The low m_{jj} region serves to constrain the $t\bar{t}$/fake background.

recent studies [365] have shown that advances in machine learning can also improve the prospects for the measurement of the $W_{\mathrm{L}}^{\pm}W_{\mathrm{L}}^{\pm}jj$ process.

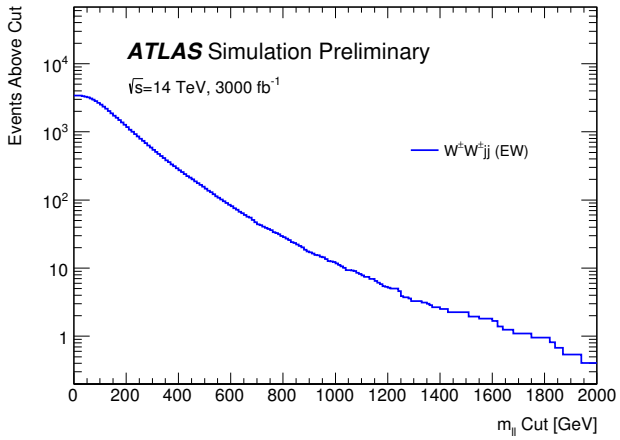

Fig. 16: Integrated number of events as a function of dilepton invariant mass for events passing all selection criteria of the ATLAS signal region.

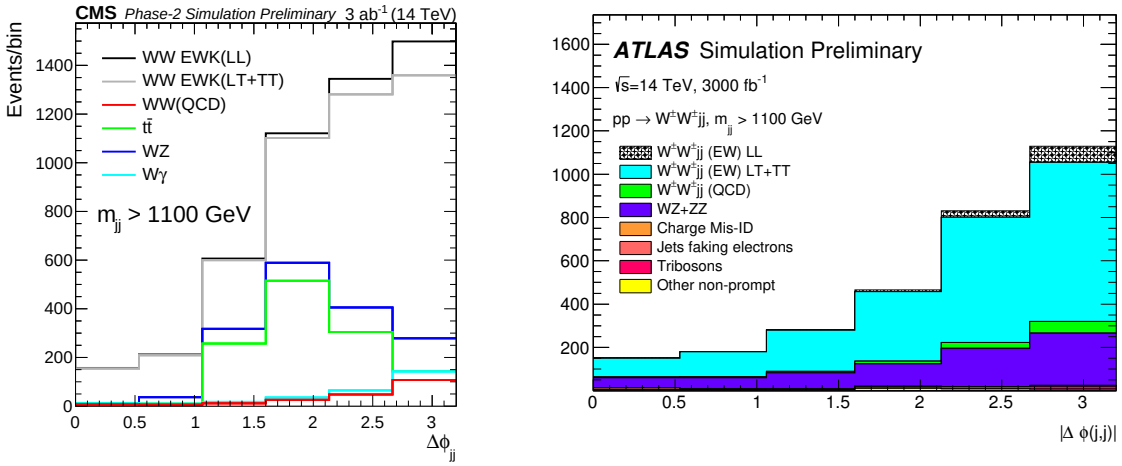

Fig. 17: Distribution of the azimuthal angle difference between two leading jets for dijet invariant mass above 1100 GeV.

4.2.2 High Order corrections in VBS $W^{\pm}W^{\pm}$ production[9]

The expected experimental precision in the measurement of VBS processes offers great opportunities to probe the electroweak (EW) sector and its associated symmetry breaking mechanism (see Refs. [134, 366, 367] for 100 TeV-collider studies). Therefore, it is of prime importance to make precise theoretical predictions available for the future operation of the LHC. In this contribution, predictions for NLO EW corrections are provided for the LHC running in its high-luminosity and high-energy configurations. The HL set-up corresponds to a centre-of-mass energy of 14 TeV while the HE one refers to 27 TeV.

[9] Contribution by A. Denner and M. Pellen.

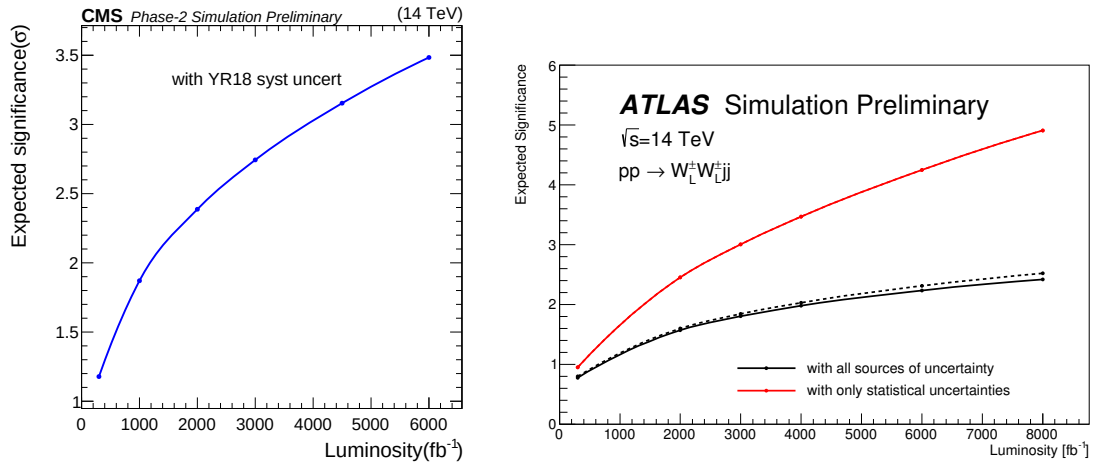

Fig. 18: Significance of the observation of the scattering of a pair of longitudinally polarized W bosons as a function of the integrated luminosity at CMS (left) and ATLAS (right).

For both centre-of-mass energies the same type of event selections has been used. These predictions represent important benchmarks as they indicate the expected rates when accounting for NLO EW corrections. The NLO EW corrections have been shown to be very large for VBS processes [103] and even the dominating NLO contribution for same-sign WW scattering [111]. Nonetheless, the inclusion of NLO QCD corrections is necessary as they can significantly distort the shape of jet-related observables [111,368–376]. In addition, they drastically reduce theoretical uncertainties. The QCD corrections for all VBS signatures can be obtained from public programs such as MADGRAPH5_AMC@NLO [12], POWHEG [151,314,377], SHERPA [84,378], or VBFNLO [247,248,339].

In this study, the NLO EW corrections have been obtained from MOCANLO+RECOLA [82,82, 91] based on a full NLO computation [111] for the same-sign WW signature. While the exact value of the corrections is expected to be different for other signatures, their magnitudes and nature should be similar.

The hadronic scattering processes are simulated at the LHC with a centre-of-mass energies $\sqrt{s} = 14\,\text{TeV}$ and $\sqrt{s} = 27\,\text{TeV}$. The NNNPDF 3.1 LUXQED parton distribution functions (PDFs) [224] with five massless flavours,[10] NLO-QCD evolution, and a strong coupling constant $\alpha_s(M_Z) = 0.118$ are employed.[11] Initial-state collinear singularities are factorised according to the $\overline{\text{MS}}$ scheme, consistently with the conventions in the NNPDF set.

The other input parameters have been chosen as in Ref. [375]. For the massive particles, the following masses and decay widths are used:

$$\begin{aligned} m_t &= 173.21\,\text{GeV}, & \Gamma_t &= 0\,\text{GeV}, \\ M_Z^{\text{OS}} &= 91.1876\,\text{GeV}, & \Gamma_Z^{\text{OS}} &= 2.4952\,\text{GeV}, \\ M_W^{\text{OS}} &= 80.385\,\text{GeV}, & \Gamma_W^{\text{OS}} &= 2.085\,\text{GeV}, \\ M_H &= 125.0\,\text{GeV}, & \Gamma_H &= 4.07 \times 10^{-3}\,\text{GeV}. \end{aligned} \tag{8}$$

The measured on-shell (OS) values for the masses and widths of the W and Z bosons are converted into

[10] For the process considered, no bottom (anti-)quarks appear in the initial or final state at LO and NLO, as they would lead to top quarks rather than light jets in the final state.

[11] The corresponding identifier `lhaid` in the program LHAPDF6 [202] is 324900.

pole values for the gauge bosons ($V = W, Z$) according to Ref. [379],

$$\begin{aligned} M_V &= M_V^{\text{OS}} / \sqrt{1 + (\Gamma_V^{\text{OS}} / M_V^{\text{OS}})^2}\,, \\ \Gamma_V &= \Gamma_V^{\text{OS}} / \sqrt{1 + (\Gamma_V^{\text{OS}} / M_V^{\text{OS}})^2}. \end{aligned} \tag{9}$$

The EW coupling is fixed in the G_μ scheme [380] according to

$$\alpha = \frac{\sqrt{2}}{\pi} G_\mu M_{\text{W}}^2 \left(1 - \frac{M_{\text{W}}^2}{M_{\text{Z}}^2}\right), \tag{10}$$

with

$$G_\mu = 1.16637 \times 10^{-5}\,\text{GeV}^{-2}, \tag{11}$$

and M_V^2 corresponds to the real part of the squared pole mass. The complex-mass scheme [381–383] is used throughout to treat unstable intermediate particles in a gauge-invariant manner.

The central value of the renormalisation and factorisation scales is set to

$$\mu_{\text{R}} = \mu_{\text{F}} = \sqrt{p_{\text{T,j}_1}\, p_{\text{T,j}_2}}. \tag{12}$$

The transverse momenta are those of the two hardest jets. This choice of scale has been shown to provide stable NLO-QCD predictions [373].

Following experimental measurements [354, 384–386] and prospect studies [387], the event selection used in the present study is:

- The two same-sign charged leptons are required to fulfill cuts on transverse momentum, rapidity, separation in the rapidity–azimuthal-angle, and the lepton-pair invariant mass,

$$p_{\text{T},\ell} > 20\,\text{GeV}, \qquad |y_\ell| < 4.0, \qquad \Delta R_{\ell\ell} > 0.3, \qquad m_{\ell\ell} > 20\,\text{GeV}. \tag{13}$$

- The total missing transverse momentum, computed from the vectorial sum of the transverse momenta of the two neutrinos, is required to be

$$p_{\text{T,miss}} > 40\,\text{GeV}\,. \tag{14}$$

- QCD partons (light quarks and gluons) are clustered using the anti-k_{T} algorithm [274] with jet-resolution parameter $R = 0.4$. Cuts on the jets' transverse momenta and rapidities are imposed,

$$p_{\text{T},j} > 30\,\text{GeV}, \qquad |y_j| < 4.0. \tag{15}$$

  VBS cuts are applied to the two jets with largest transverse momentum, specifically on the invariant mass of the di-jet system, as well as on the rapidity separation of the two jets and their separation from leptons,

$$m_{jj} > 500\,\text{GeV}, \qquad |\Delta y_{jj}| > 2.5, \qquad \Delta R_{j\ell} > 0.3. \tag{16}$$

- Finally, the centrality of the leptons is enforced according to Ref. [387]:

$$\zeta = \min\left[\min\left(y_{\ell_1}, y_{\ell_2}\right) - \min\left(y_{j_1}, y_{j_2}\right), \max\left(y_{j_1}, y_{j_2}\right) - \max\left(y_{\ell_1}, y_{\ell_2}\right)\right] > 0. \tag{17}$$

- For EW corrections, real photons and charged fermions are clustered using the anti-k_{T} algorithm with radius parameter $R = 0.1$. In this case, leptons and quarks are understood as *dressed fermions*.

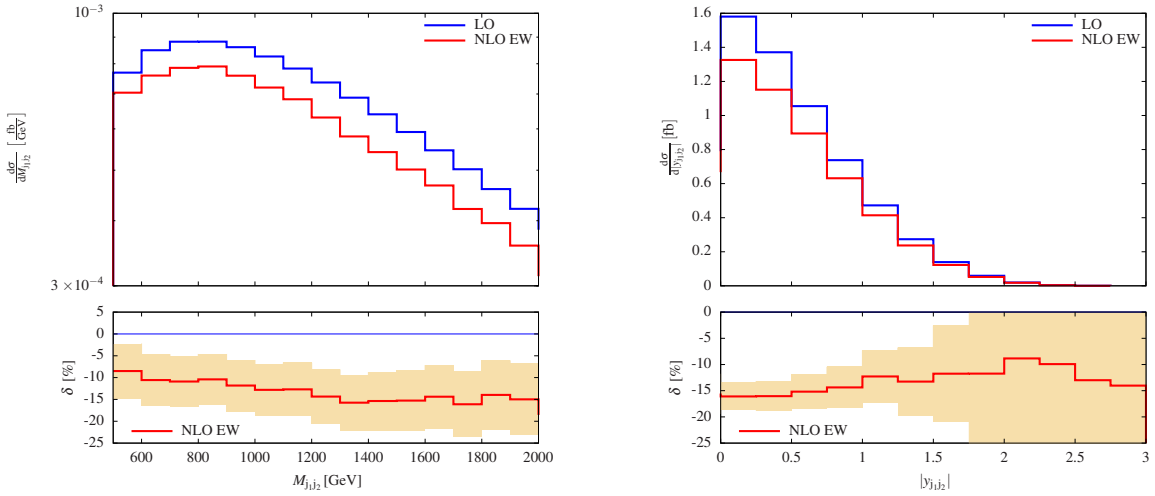

Fig. 19: Differential distributions in the invariant mass of the two jets (left) and their rapidity (right) in $pp \to \mu^+\nu_\mu e^+\nu_e jj$ at 14 TeV including NLO EW corrections (upper panel) and relative NLO EW corrections (lower panel). The yellow band describes the expected statistical uncertainty for a high-luminosity LHC collecting 3000 fb^{-1} and represents a relative variation of $\pm 1/\sqrt{N_{\text{obs}}}$ where N_{obs} is the number of observed events in each bin.

In the following discussion of SM predictions for the HL- and HE-LHC both QCD and EW corrections have been combined. For VBS processes EW corrections are particularly large and therefore of prime importance. The leading contributions originate from the exchange of massive gauge bosons in the virtual corrections. They tend to grow large and negative in the high-energy limit owing to so-called Sudakov double logarithms. As shown in Ref. [103], large EW corrections are an intrinsic feature of VBS at the LHC. While this study is based on the same-sign W channel, it has been further confirmed recently by the computation of large EW corrections to the WZ channel [388, 389].

Given their size and the foreseen experimental precision, these corrections are actually measurable. Because they involve interactions of the EW sector, their measurement would constitute a further test of the SM. On the left hand-side of Fig. 19, the distribution in the invariant mass of the two leading jets is shown at LO and NLO EW for the process $pp \to \mu^+\nu_\mu e^+\nu_e jj$ at 14 TeV. The yellow band describes the expected statistical uncertainty for a HL LHC collecting 3000 fb^{-1}. On the right hand-side for Fig. 19, a similar plot for the absolute rapidity of the jet pair is shown. It is thus clear that with the expected luminosity, one is not only sensitive to the VBS process but also to its EW corrections.

In Fig. 20, the distributions in the invariant mass of the visible system ($e^+\mu^+jj$) at both 14 TeV (left) and 27 TeV (right) are shown. As expected, the corrections are larger for higher centre-of-mass energy due to the higher representative scale of the process. In the tail of the distribution where new physics could play an important role, the corrections are particularly large and reach about 25% for the 27 TeV set-up. Note that in the present predictions, the real radiation of massive gauge bosons is not taken into account. This effect has been estimated to be of the order of few percent for the HL set-up when considering the total cross section. While this effect is for now negligible, for the HL and HE mode of the LHC, it will become relevant in the same way as the use of VBS approximations in theoretical predictions [375]. These observations are further confirmed via the cross sections for the two centre-of-mass energies at LO (using full matrix element) and NLO EW given in Table 7. At 27 TeV the EW corrections are a few percent larger than at 14 TeV (-18.9% against -15.1%, respectively). Note that the jump in energy from 14 TeV to 27 TeV is accompanied by an increase by more than a factor 3 in

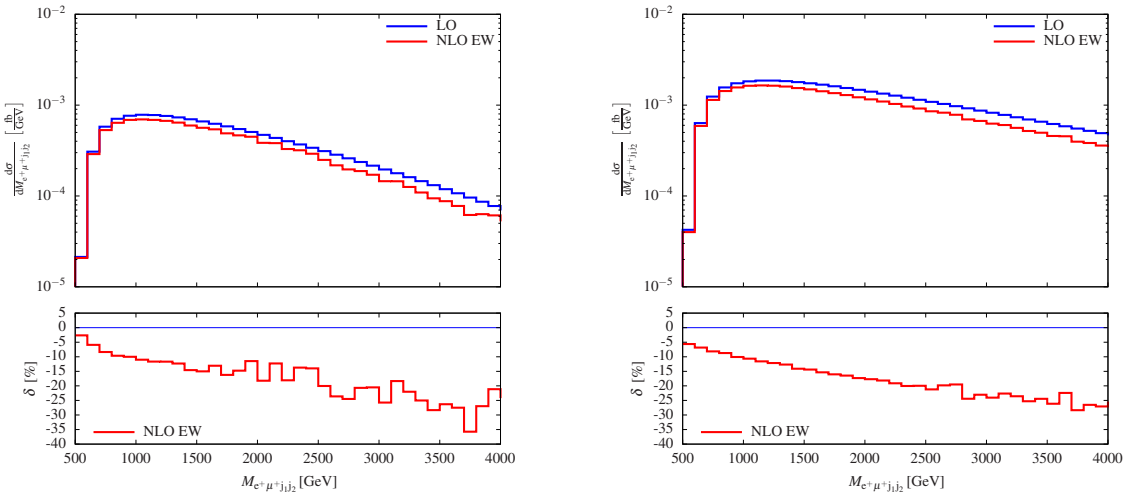

Fig. 20: Differential distribution in the invariant mass of the visible system ($e^+\mu^+jj$) in $pp \to \mu^+\nu_\mu e^+\nu_e jj$ at 14 TeV (left) and 27 TeV (right) including NLO EW corrections (upper panel) and relative NLO EW corrections (lower panel).

Table 7: Cross sections at LO ($\mathcal{O}\left(\alpha^6\right)$) and NLO EW ($\mathcal{O}\left(\alpha^7\right)$) for $pp \to \mu^+\nu_\mu e^+\nu_e jj$ at both 14 TeV and 27 TeV at the LHC. The relative EW corrections are given in percent, and the digits in parentheses indicate the integration error.

	σ^{LO} [fb]	$\sigma^{\text{NLO}}_{\text{EW}}$ [fb]	δ_{EW} [%]
14 TeV	1.4282(2)	1.213(5)	−15.1
27 TeV	4.7848(5)	3.881(7)	−18.9

the cross section at LO.

4.2.3 Measurements of W Z scattering at the HL-HLC

Prospects are presented for measuring the WZ electroweak production in fully leptonic final state at the HL-LHC. This work includes studies of the polarised WZ production: measurements of the vector bosons in longitudinally polarized states are of particular importance, since they give direct access to the nature of the electroweak symmetry breaking via the exchange of a Higgs bosons in the t-channel as shown in Fig. 21. Another relevant aspect of WZ production lies in the probe of the non-abelian structure of the Standard Model via sensitive tests to triple and quartic gauge couplings, a topic which is partially addressed in the next subsection. Measurements of the electroweak production using 36 $\text{fb}^{-1}$of the proton-proton collisions at 13 TeV were reported by both the ATLAS [390] and CMS [391] collaborations. The existing results are strongly limited by the statistical uncertainties of the data samples, therefore the integrated luminosity expected at the end of the HL-LHC operation is mandatory to fully exploit the physics behind VBS in WZ production via measurement of differential distributions and the polarization of the final state bosons.

In proton-proton collisions, the VBS process results from the interaction of two bosons radiated by the initial quarks leading to a final state with two centrally produced bosons and two forward jets. The main irreducible background is represented by events in which the same final state is mediated by strong interactions (QCD$-WZ$) and where the two bosons are not the direct result of a scattering

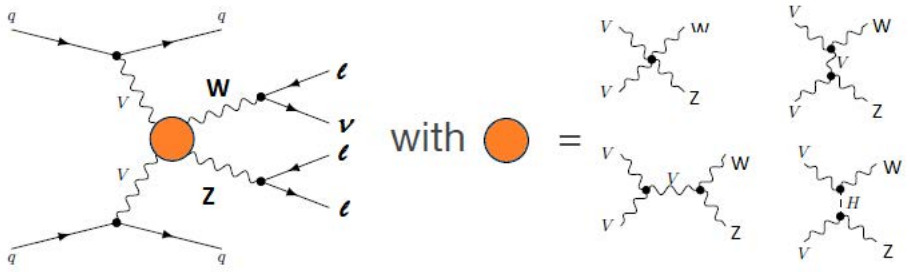

Fig. 21: Feymann diagrams contributing to VBS WZ production.

process. Other backgrounds consist of different di-boson final states (ZZ, $Z\gamma$), tri-bosons and tV or $t\bar{t}V$ production, where V is a Z or a W boson. The amount of the non-prompt backgrounds, where one or more lepton candidates are coming from jets misidentified as leptons, ultimately depends on the detector geometry, reconstruction technique and event selection requirements.

The signal selection requires events with three isolated leptons with $\mathrm{p_T}$ > 15 GeV with $|\eta| < 4$ for ATLAS and $|\eta| < 2.8$ (3.0) for muons (electrons) for CMS. In addition, at least one lepton should pass the single lepton trigger (ATLAS). In order to suppress the background from ZZ processes, events containing four or more lepton candidates are discarded. At least one of the three lepton candidates is required to have $\mathrm{p_T}$ > 25 GeV. The event must have at least one pair of leptons of the same flavor and opposite charge, with an invariant mass that is consistent with the nominal Z boson mass at $M_Z = 91.188$ GeV within 10 GeV for ATLAS and 15 GeV for CMS. This pair is considered as a Z boson candidate. The third lepton is assigned to the W boson and its $\mathrm{p_T}$ is required to be greater than 20 GeV. Finally, E_T^{miss} (CMS) or the transverse mass of the W candidate computed using E_T^{miss} and the $\mathrm{p_T}$ of the third lepton (ATLAS) is required to be above 30 GeV. The VBS signature is characterized by the presence of two forward jets. Jets are reconstructed with the anti-k_T algorithm with distance parameter 0.4. For ATLAS, the event is selected if it contains two jets in opposite hemispheres with $\mathrm{p_T^{jet}}$ greater than 30 GeV and $|\eta^{\mathrm{jet}}|$ < 3.8. For CMS, the event is selected if it contains two jets with $\mathrm{p_T^{jet}}$ > 50 GeV and $|\eta^{\mathrm{jet}}|$ < 4.7. In addition, the pseudorapidity separation between jets, $\Delta\eta_{jj}$, is requested to be greater than 2.5. Finally, the dijet mass m_{jj} is required to be greater than 500 GeV. The full list of selection requirements is summarized in Table 8.

Distinct approaches are used by ATLAS and CMS, respectively based on simulation at 14 TeV and on extrapolation from Run-2 results. ATLAS uses Monte Carlo samples generated with a fast simulation based on the parameteriation of the performance of the HL-LHC detector and where jets from pileup (PU) interactions corresponding to <μ> = 200 are added to the event record; a loose event selection and a conservative background hypothesis is used. The signal events are generated at LO with SHERPA 2.2.2 [84] and the QCD$-WZ$ background is simulated at NLO with SHERPA 2.2.0: in Ref. [390], it was shown that the QCD$-WZ$ background predictions might be overestimated by 40% in certain regions of the phase-space. And with a $\mathrm{p_T^{jet}}$cut as low as 30 GeV, an $|\eta^{jet}|$ cut less than 3.8, corresponding to the HL-LHC tracker acceptance, was found necessary to maintain the contamination of PU jets in signal (resp. QCD$-WZ$) events from 18% (resp. 69%) to 2% (resp. 11%).

The CMS projection is based on MC samples with full simulation of the CMS detector at 13 TeV and data driven background estimates, see Ref. [392]. The cross sections of samples are scaled for this projection from 13 to 14 TeV using SM predictions, for the data-driven backgrounds the scaling is done using appropriate mixture of simulated events. The performance of the CMS detector at the HL-LHC at pileup 200 is simulated using DELPHES. It is proven that lepton and PUPPI [362] jet reconstruction allow to keep the same or better level of reconstruction efficiency and background rejection as in existing data; no additional corrections are applied in the projection. An additional scaling factor is applied to

Table 8: Summary of event selection requirements.

Variables	ATLAS	CMS
$\mathrm{p_T}(\ell)$ [GeV]	> 15	> 15
$\mathrm{p_T}(\ell_{lead})$	> 25	–
$\mathrm{p_T}(\ell_{Z,1})$, $\mathrm{p_T}(\ell_{Z,2})$ [GeV]		$> 25, > 15$
$\mathrm{p_T}(\ell_W)$ [GeV]	> 20	> 20
$\lvert\eta(\mu)\rvert$	< 4.0	< 2.8
$\lvert\eta(\mathrm{e})\rvert$	< 4.0	< 3.0
$\lvert m_Z - m_Z^{\mathrm{PDG}}\rvert$ [GeV]	< 10	< 15
$m_{3\ell}$ [GeV]	–	> 100
$m_{\ell\ell}$ [GeV]	–	> 4
E_{T}^{miss} [GeV]	–	> 30
M_{T}^{W} [GeV]	> 30	–
n_{j}	≥ 2	≥ 2
$\lvert\eta(j)\rvert$	< 3.8	< 4.7
$\mathrm{p_T^{jet}}$ [GeV]	> 30	> 50
$\Delta R(j, \ell)$	–	> 0.4
$\mathrm{p_T}(b)$ [GeV]	–	> 30
$n_{b-\mathrm{jet}}$	–	$= 0$
m_{jj}	> 500	> 500
$\Delta\eta_{jj}$	Opp. hemis.	> 2.5
$\lvert\eta_{3\ell} - \frac{1}{2}(\eta_{j_1} + \eta_{j_2})\rvert$	–	< 2.5

Table 9: Expected signal and background yields corresponding to the event selection listed in Table 8 for 3000 fb^{-1}. Background contributions are grouped differently for ATLAS and CMS.

Process	ATLAS	CMS
EW$-WZjj$	3889	2757
QCD$-WZ$	29754	3486
$t\bar{t}V$	3145	–
tZ	2221	–
tV/VVV	–	1374
Non prompt	–	1192
ZZ	1970	–
VV	–	398
Zγ	–	296

account for the increased pseudorapidity coverage of the HL-LHC CMS detector. The ATLAS and CMS signal and background yields are summarized in Table 9 for the total integrated luminosity of 3000 fb^{-1}.

To extract the electroweak signal, ATLAS uses nominally a final m_{jj} cut optimised at 600 GeV or a multivariate analysis (BDT) based on 25 variables that are shown to best separate the signal and background events. The shape of the BDT output is shown in Fig. 22 left. In the CMS case, a 2D distribution of dijet invariant mass in bins of dijet angular separation is used, as shown in Fig. 22 right. The measurement of the EW$-WZjj$ production cross section results from a maximum likelihood fit of this distribution performed simultaneously for four different lepton combinations in the final states,

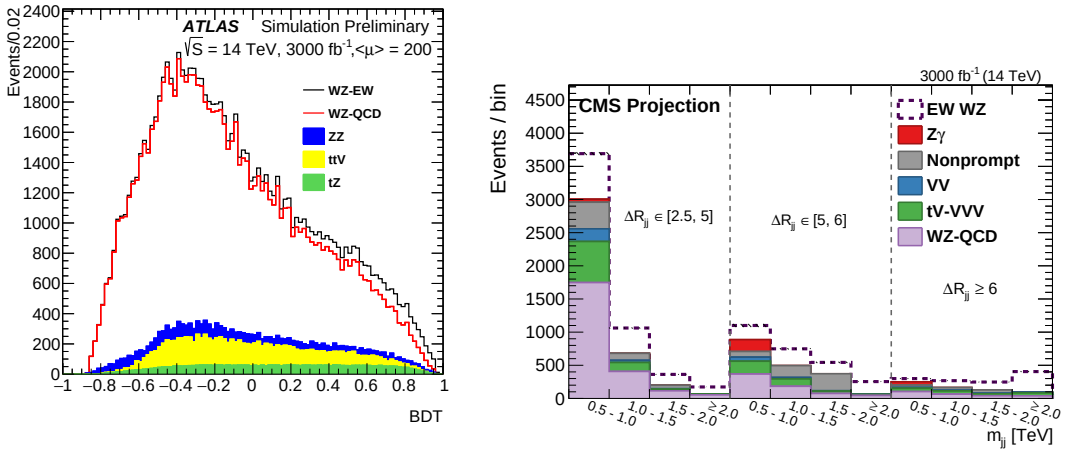

Fig. 22: Example of BDT distribution for 3000 fb^{-1}(left). The m_{jj} distributions in bins of ΔR_{jj} for 3000 fb^{-1}(right).

each combination being considered as independent decay channel. The systematic uncertainties are represented by nuisance parameters in the fit and are allowed to vary according to their probability density functions. The correlations across bins, between different sources of uncertainty and decay channels are taken into account. The background contributions are allowed to vary within the estimated uncertainties.

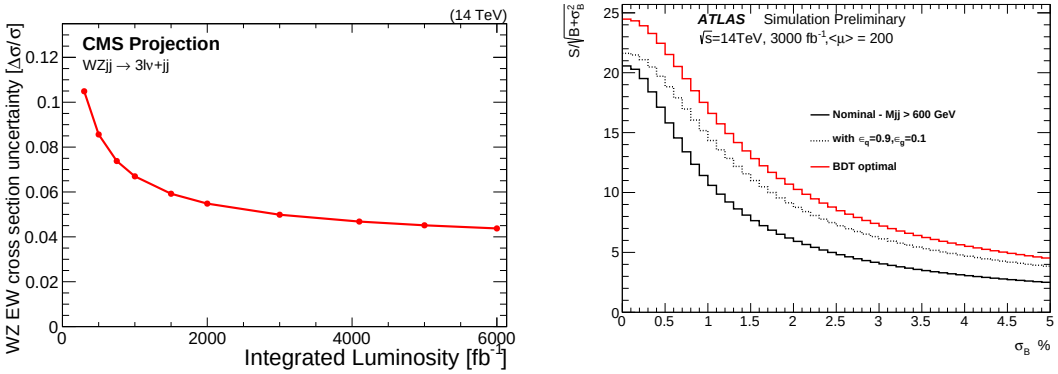

Fig. 23: Expected uncertainty on the cross section measurement as a function of the integrated luminosity for the CMS projection (left). Signal significance versus the total background uncertainty for the ATLAS simulation (right), presented for the nominal selection, along with two alternative selections meant to mitigate the QCD$-WZ$ background.

The experimental systematic error will be dominated by the jet energy related uncertainties, and amounts to a maximum of 5%. The non-prompt background uncertainty may also be significant depending on the final state. Depending on the level of QCD$-WZ$ background, the theoretical error affecting its modeling will eventually dominate. However it is expected that the impact of these uncertainties can be controlled to less that 5% using refined and diverse control regions allowed by the large statistics at HL-LHC. The total uncertainty of the electroweak cross section measurement as a function of luminosity is shown in Fig. 23 left for the CMS projection, while the signal significance as a function of the projected total uncertainty on background is presented in Fig. 23 right for the ATLAS simulation as it is

arguable whether the theoretical uncertainty can be precisely predicted at this stage.

The polarisation of the final state bosons can be measured inclusively for each boson in two different final state configurations, ZW^+ and ZW^- or combined in a doubly longitudinally polarised final state. The $\cos\theta^*_Z$ ($\cos\theta^*_W$), where θ^*_Z represents the angle of the lepton with the Z (W) direction in the WZ rest frame, is the most sensitive differential distribution to the polarisation of the Z (W) boson. An example of the $\cos\theta^*_Z$ distribution is shown in Fig. 24 left for the EW$-WZjj$ signal and the sum of backgrounds for $Z(W^+)$ final state; the distribution is fitted with three parameters: the longitudinal polarised fraction F0, the left-handed minus right-handed contributions and the number of EW$-WZjj$ events using three polarisation templates plus the two background contributions. The result of the fit is shown in Fig. 24 left, where the fraction of EW$-WZjj$ events where the Z-boson is longitudinally, left or right polarised are represented, while the log-likelihood profile corresponding to F0 is presented in Fig. 24 right. The significance to measure F0, computed as $\sqrt{-2log(\lambda(F0=0))}$, is estimated to be between 1.5 and 2.5 σ for $Z(W^+)$ and 0.7 and 1.5 σ for W^- depending on the final selection that affects the signal purity, and systematic assumptions on the total background normalisation.

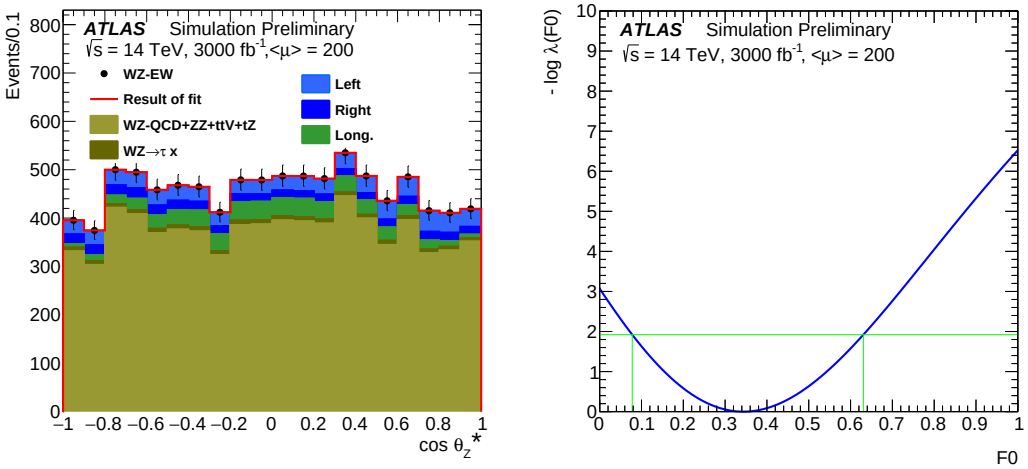

Fig. 24: Distribution of $\cos\theta^*_Z$ for 3000 fb^{-1}and result of the fit of the long, polarised contribution (F0), left- and right-handed contributions on top of the sum of backgrounds and of the $WZ \to x\tau$ background, both contributions taken into account with a normalisation error of 2.5% (left). Shape of the log-likelihood profile for the F0 parameter around its minimum (right) .

To measure the doubly longitudinal (LL) process, an approach based on the jets kinematics similar to this for the total EW$-WZjj$ cross section is used by CMS. The LL fraction is expected to be of the order of 5% of the total EW$-WZjj$ production ([393]) and its unrolled 2D distribution is shown in Fig. 25 left for 3000 fb^{-1}. It can be observed that the LL contribution is increasing from 2-3% to 7-8% for high angular separation between jets and for high invariant mass of the dijet system. In the fit, the LL fraction is considered as signal, while the rest of the EW$-WZjj$ process is considered as an additional background. The systematic uncertainties of the LL and non-LL fractions are considered as fully correlated within the total electroweak cross section. The significance of the LL observation as a function of integrated luminosity is shown in Fig. 25 right: the red curve presents the significance if only statistical uncertainties of the measurement are taken into account and the black line presents the results including the systematics as discussed above.

The results presented in this section confirm that the EW$-WZjj$ cross section can be measured with accuracy at the HL-LHC if the jets from pileup collisions in the events are well separated from the jets produced in the hard interactions. Increased pseudorapidity coverage of the detectors should

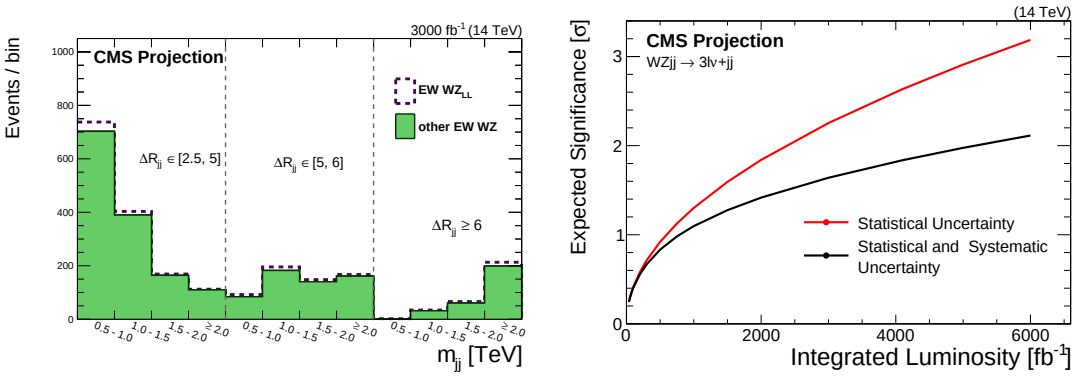

Fig. 25: Unrolled 2D $(\Delta R_{jj}; m_{jj})$ LL and non-LL distribution for 3000 fb^{-1}(left). Significance of the LL observation with and without systematic error (right).

improve precision of such measurement. The single polarized cross sections can also be measured and the double polarized measurement requires more sophisticated methods, including development of multivariate discriminants for better separation of the signal from background. Systematic uncertainties also start to play a significant role at the HL-LHC, in particular those affecting the theoretical prediction.

4.2.4 Prospects for quartic gauge coupling measurements in VBS[12]

Due to the strong gauge theory cancellations between the different Feynman graphs present in VBS (Fig. 21) the various VBS processes provide excellent probes for the structure of gauge boson interactions, in particular for the quartic gauge couplings. Deviations from SM predictions can conveniently be parameterised by an effective Lagrangian, $\mathcal{L}_{\mathrm{EFT}} = \sum_i f_i/\Lambda^{d_i-4}\,\mathcal{O}_i^{(d_i)}$, where the operators $\mathcal{O}_i^{(d_i)}$ of energy dimension d_i are built with the covariant derivative of the SM Higgs doublet field, $D_\mu\Phi$, and the $SU(2)_L$ and $U(1)_Y$ field strength tensors $\widehat{W}_{\mu\nu}$ and $\widehat{B}_{\mu\nu}$ (normalized according to $[D_\mu, D_\nu] = \widehat{W}_{\mu\nu} + \widehat{B}_{\mu\nu}$). At the dimension six level, all allowed operators in $\mathcal{L}_{\mathrm{EFT}}$ also contribute to trilinear couplings of electroweak gauge bosons or to hVV couplings, which are better measured in $q\bar{q} \to VV$ processes or in Higgs boson decay. Thus, operators of energy dimension eight, which do not give rise to anomalous trilinear couplings, are used for a parameterisation of anomalous quartic gauge couplings (aQGC), which is sufficiently general for the present purpose. In the following, the operator basis of Ref. [394, 395] with VBFNLO normalization [374, 396, 397] is used to assess the sensitivity of VBS $W^\pm W^\pm jj$ and $WZjj$ production to aQGC, with the subset of operators

$$\mathcal{O}_{S_0} = \left[\left(D_\mu\Phi\right)^\dagger D_\nu\Phi\right] \times \left[\left(D^\mu\Phi\right)^\dagger D^\nu\Phi\right] , \tag{18a}$$

$$\mathcal{O}_{S_1} = \left[\left(D_\mu\Phi\right)^\dagger D^\mu\Phi\right] \times \left[\left(D_\nu\Phi\right)^\dagger D^\nu\Phi\right] \tag{18b}$$

$$\mathcal{O}_{T_0} = \mathrm{Tr}\left[\widehat{W}_{\mu\nu}\widehat{W}^{\mu\nu}\right] \times \mathrm{Tr}\left[\widehat{W}_{\alpha\beta}\widehat{W}^{\alpha\beta}\right] , \tag{18c}$$

$$\mathcal{O}_{T_1} = \mathrm{Tr}\left[\widehat{W}_{\alpha\nu}\widehat{W}^{\mu\beta}\right] \times \mathrm{Tr}\left[\widehat{W}_{\mu\beta}\widehat{W}^{\alpha\nu}\right] \tag{18d}$$

$$\mathcal{O}_{M_0} = \mathrm{Tr}\left[\widehat{W}_{\mu\nu}\widehat{W}^{\mu\nu}\right] \times \left[\left(D_\beta\Phi\right)^\dagger D^\beta\Phi\right] , \tag{18e}$$

$$\mathcal{O}_{M_1} = \mathrm{Tr}\left[\widehat{W}_{\mu\nu}\widehat{W}^{\nu\beta}\right] \times \left[\left(D_\beta\Phi\right)^\dagger D^\mu\Phi\right] . \tag{18f}$$

in $\mathcal{L}_{\mathrm{EFT}} = \sum_i \frac{f_i}{\Lambda^4}\,\mathcal{O}_i$. At high invariant masses, $\sqrt{s}$, of the $VV \to VV$ subprocess, the tree level insertions of the dimension eight operators lead to matrix elements which grow like s^2 and violate

[12] Contribution by H. Schäfer-Siebert and D. Zeppenfeld.

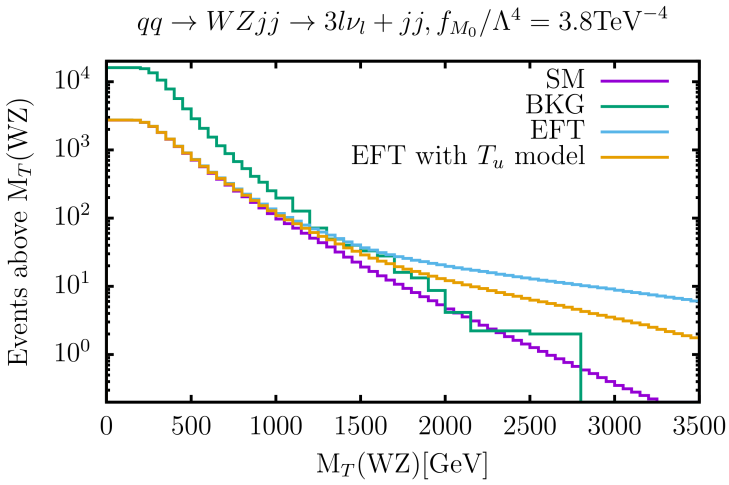

Fig. 26: Integrated WZ transverse mass distribution for $f_{M_0}/\Lambda^4 = 3.8$ TeV^{-4} within the pure EFT, the unitarization of the T_u-model as well as the SM VBS signal and the background predictions based on the ATLAS $WZjj$ analysis.

unitarity within the accessible energy range of the LHC. This unphysical behaviour is avoided below by using the unitarization scheme of Ref. [397], dubbed T_u-model, which is a variant of K-matrix unitarization, producing close to maximal absolute values of the partial wave amplitudes at high energies.

In the presence of aQGC which signify strong interactions in the bosonic sector, VBS cross sections are enhanced at high VV invariant masses, which feeds into observables correlated to m_{VV} such as the integrated dilepton invariant mass distribution for $W^\pm W^\pm jj$ events shown in Fig. 16 or the integrated WZ transverse mass distribution shown in Fig. 26. The $m_{\text{T}}(WZ)$-distribution is obtained from the ATLAS $WZjj$ analysis (see Table 8) with the additional cuts $m_{jj} > 600$ GeV, $\Delta\eta_{jj} > 3.0$ on the invariant mass and the rapidity separation of the tagging jets, and $|\eta_\mu| < 2.7$ on muon rapidity. Also shown in Fig. 26 are $m_{\text{T}}(WZ)$-distributions for $f_{M_0}/\Lambda^4 = 3.8$ TeV^{-4} within the pure EFT and including the unitarization of the T_u-model for the VBS $WZjj$ signal. Detector effects are included by assuming the same efficiencies in each $m_{\text{T}}(WZ)$ bin as for the SM EW signal. The processes contributing to the background distribution in Fig. 26 are listed in Table 9. The aQGC leads to an excess of events at very high $m_{\text{T}}(WZ)$. Assuming that no significant excess is observed in the high energy tail, one finds the expected 95% CL bounds on aQGC listed in Table 10. Also shown in the Table are bounds expected from $W^\pm W^\pm jj$ production, based on the dilepton invariant mass distribution of Fig. 16. The expected bounds for the HE-LHC are obtained in a similar fashion, assuming the same signal to background ratio as at 14 TeV for the SM case, and generating VBS $W^\pm W^\pm jj$ and $WZjj$ events with VBFNLO at LO QCD.

The above procedure provides conservative estimates for the sensitivity to aQGC in VBS: The experimental VBS analyses focused on the significance of the various SM VBS signals and did not try to optimize sensitivity to deviations at highest VV invariant masses, as would be favorable for aQGC measurements. Taking into account weak boson rapidity and transverse momentum distributions and correlations, the sensitivity to aQGC could be improved somewhat. On the other hand, dedicated analyses including Sudakov suppression at high invariant mass, as discussed in Section 4.2.2, which is expected to slightly decrease sensitivity to aQGC, have not been performed yet in the above setting.

Table 10: Expected bounds (in TeV^{-4}) on the coefficients of dimension-8 operators, assuming no significant excess in the integrated $m_{\mathrm{T}}(WZ)$ ($WZjj$) or m_{ll} ($W^{\pm}W^{\pm}jj$) distributions at high mass.

	14 TeV		27 TeV	
	$WZjj$	$W^{\pm}W^{\pm}jj$	$WZjj$	$W^{\pm}W^{\pm}jj$
f_{S_0}/Λ^4	[-8,8]	[-6,6]	[-1.5,1.5]	[-1.5,1.5]
f_{S_1}/Λ^4	[-18,18]	[-16,16]	[-3,3]	[-2.5,2.5]
f_{T_0}/Λ^4	[-0.76,0.76]	[-0.6,0.6]	[-0.04,0.04]	[-0.027,0.027]
f_{T_1}/Λ^4	[-0.50,0.50]	[-0.4,0.4]	[-0.03,0.03]	[-0.016,0.016]
f_{M_0}/Λ^4	[-3.8,3.8]	[-4.0,4.0]	[-0.5,0.5]	[-0.28,0.28]
f_{M_1}/Λ^4	[-5.0,5.0]	[-12,12]	[-0.8,0.8]	[-0.90,0.90]

4.2.5 Measurements of ZZ scattering

This section presents the studies performed for VBS in the ZZ fully leptonic decay channel for HL-LHC and HE-LHC. Despite the very low cross section times branching fraction, the reconstruction of all final state leptons allows to precisely measure the angular distributions of the Z decays to optimally separate the longitudinal from the dominating transverse polarizations. In addition, a precise measurement of the hard scattering centre-of-mass energy is possible from the reconstructed four-leptons invariant mass. Last but not least, the reducible background in this channel is very small, making it an ideal case for high statistics measurement since the impact of associated experimental systematics uncertainties is expected to be very small.

The ATLAS analysis is performed with simulated events at generator level at 14 TeV, where the detector effects of lepton and jet reconstruction and identification were estimated by corrections, assuming a mean number of interactions per bunch crossing of 200. The CMS analysis is based on the experimental investigation of VBS in the ZZ channel using 36 fb^{-1} of data collected in 2016 [398] which showed an observed significance of 2.7 standard deviations. This analysis is projected to HL-LHC conditions [399] by scaling the expected yields for the signal and background processes, taking into account the increase in luminosity and scattering energy as well as the changes in acceptance and selection efficiencies between the LHC Phase-1 (13 TeV) and the HL-LHC (14 TeV) configurations. The DELPHES simulation [273] is then used to assess the sensitivity to VBS $Z_{\mathrm{L}}Z_{\mathrm{L}}$. The HL-LHC result is further projected to the HE-LHC configuration.

Several Monte Carlo event generators were used to simulate the signal and background contributions. In the ATLAS analysis, both the EW-$ZZjj$ and QCD-$ZZjj$ processes with the $ZZ \to 4\ell$ decays are modeled using SHERPA v2.2.2 [84] with the NNPDF3.0NNLO [400] parton distribution functions (PDFs) set. The signal sample is generated with two jets at Matrix Element (ME) level. The background process is modeled with next-to-leading order (NLO) QCD accuracy for events with up to one outgoing parton and with leading order (LO) accuracy for the case with two and three partons, in a phase space of $m_{\ell\ell} > 4$ GeV and at least two leptons with $p_{\mathrm{T}} > 5$ GeV. Other backgrounds have minor contributions to the 4ℓ channel and therefore are not included. The CMS analysis uses MADGRAPH5_AMC@NLO v2.3.3 [401] to simulate the EW-$ZZjj$ signal and QCD-$ZZjj$ background samples with zero, one, and two outgoing partons at Born level at NLO. The different jet multiplicities are merged using the FxFx scheme [157] with a merging scale of 30 GeV, and leptonic Z boson decays were simulated using MADSPIN [402]. The gluon loop-induced production of two Z bosons ($ggZZ$) is simulated at LO with MCFM v.7.0.1 [403], and checked with a dedicated simulation of the loop-induced $\mathrm{gg} \to ZZjj$ process using MADGRAPH5_AMC@NLO. The NNPDF3.0 PDF set is also used. The interference between EW-$ZZjj$ and QCD-$ZZjj$ processes is found to be small and is neglected in both analyses. Simulated samples with polarization information on the outgoing Z bosons

are generated using MADGRAPH5_AMC@NLO v1.5.14 and the DECAY package from this version.

The selections are based on Run-2 analyses and have been modified according to the expected changes for the detectors at HL-LHC. The foreseen forward lepton coverage is up to $|\eta| = 4.0$ for both electrons and muons in ATLAS, while it is is up to $|\eta| = 3.0(2.8)$ for electrons (muons) in the CMS upgrade, with an option for an extension of up to $|\eta| = 4.0$ for electrons. Candidate events should contain two pairs of oppositely charged isolated leptons (electrons or muons), consistent with the decays of two on-shell Z bosons. The VBS topology is ensured by requiring at least two jets with large invariant mass and η separation in the cut based analysis, whereas an inclusive selection is used when the signal extraction is performed with a multivariate discriminant (BDT). Table 11 summarizes the details of the selection criteria used by the ATLAS and CMS collaborations.

Table 11: Event selections used in ATLAS and CMS analyses. For the leptons η and p_{T} in CMS the first number refers to electrons and the second, in parenthesis, to muons.

	ATLAS	CMS
lepton η	$\|\eta\| < 4.0$	$\|\eta\| < 3.0(2.8)$ ($\|\eta\| < 4.0(2.8)$, extended option)
lepton p_{T}	$p_{\mathrm{T}} > 20, 20, 10, 7$ GeV	$p_{\mathrm{T}} > 20, 12(10), 10, 7(5)$ GeV
N leptons	exactly 4	≥ 4
Z mass	$60 < m_{ll} < 120$ GeV	$60 < m_{ll} < 120$ GeV
Z_1 definition	m_{ll} closest to PDG [404] value	p_{T}-leading Z
jet η	$\|\eta\| < 4.5$	$\|\eta\| < 4.7$
jet p_{T}	$p_{\mathrm{T}} > 30(70)$ GeV for $\|\eta\| < 3.8(> 3.8)$	$p_{\mathrm{T}} > 30$ GeV
N jets	≥ 2, with $\eta^{j_1} \times \eta^{j_2} < 0$	≥ 2
VBS cuts	$m_{jj} > 600$ GeV and $\|\Delta\eta_{jj}\| > 2$	$m_{jj} > 100$ GeV, signal extraction from BDT

The distributions of the ZZ invariant mass (m_{ZZ}) and the azimuthal angular difference between the two Z bosons ($|\Delta\phi(ZZ)|$) are shown in Fig. 27, after the ATLAS event selection. The numbers of selected signal and background events are quoted in Table 12, normalized to 3000 fb^{-1} of integrated luminosity. In addition to the baseline selection, two alternative selections are also studied to compare different detector scenarios at the HL-LHC. Uncertainties in the table refer to expected data statistical

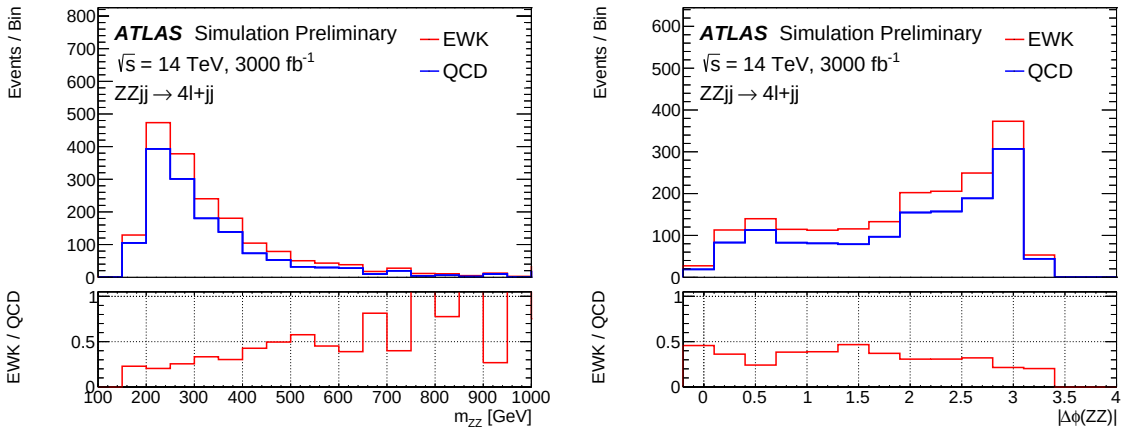

Fig. 27: Detector level distributions of m_{ZZ} and $|\Delta\phi(ZZ)|$ for the EW and QCD $ZZjj$ processes after the cut-based event selection, normalized to 3000 fb^{-1}.

uncertainty at 14 TeV with 3000 fb^{-1}. The benefit of the extension for the rejection of PU jets is

Table 12: Comparison of event yields for the signal ($N_{\mathrm{EW}-ZZjj}$) and background ($N_{\mathrm{QCD}-ZZjj}$) processes, and expected significance of EW-$ZZjj$ processes, normalized to 3000 fb^{-1} data at 14 TeV, for baseline and alternative selections.

Selection	$N_{\mathrm{EW}-ZZjj}$	$N_{\mathrm{QCD}-ZZjj}$	$N_{\mathrm{EW}-ZZjj}$ / $\sqrt{N_{\mathrm{QCD}-ZZjj}}$
Baseline	432 ± 21	1402 ± 37	11.5 ± 0.6
Leptons with $\|\eta\| < 2.7$	373 ± 19	1058 ± 33	11.5 ± 0.6
PU jet suppression only in $\|\eta\| < 2.4$	536 ± 23	15470 ± 124	4.3 ± 0.2

clear. The extended tracking coverage improves the lepton detection efficiency and increases the number of signal events, providing larger event yield for differential cross section measurements and for the longitudinal scattering. However, the overall significance of observing the EW-$ZZjj$ process does not improve as much, due to larger increase of the QCD-$ZZjj$ background contribution. This is due to the ZZ system being more centrally produced in EW processes than in QCD processes. These results, however, do not include the gluon-induced contribution, for which the ZZ system is found to be more centrally produced than for the leading quark-induced contribution. Moreover, in the case of the longitudinal scattering, the η distribution of longitudinally polarized Z bosons is peaked in the forward region, therefore extended coverage is beneficial in this case as will be shown in the following.

The dominant systematics for 4ℓ channel are from theoretical modeling of the QCD-$ZZjj$ background processes. The ATLAS analysis considers different sizes of systematic uncertainty in the background modeling of 5, 10 and 30%. The 30% uncertainty is a conservative estimation from direct calculation by comparing different choices of PDF sets and QCD renormalization and factorization scales, following recommendation from PDF4LHC [195]. The 5% one is an optimistic estimation where enough data events from QCD enriched control region at the HL-LHC could be used to provide constraints on the theoretical modeling of QCD-$ZZjj$ processes. For the experimental sources, the jet uncertainties have been checked following the studies in Ref. [405] and the effect is within fluctuation of the simulated events, which is at the 5% level. Thus a 5% uncertainty is used as a conservative estimate of the experimental uncertainties. In this analysis these uncertainties are treated as uncorrelated and summed up quadratically. The CMS analysis considers two scenarios for the systematic uncertainties. The first scenario ('Run-2 scenario') consists in using the same systematic uncertainties as those used for the Run-2 analysis, apart from the uncertainty in the gluon-induced background contribution for which a 10% uncertainty is considered. In the second scenario ('YR18 scenario'), improved systematic uncertainties are assumed to be obtained from the more data and better understanding of the detector. In this scenario, the theory systematic uncertainties (PDF and QCD scales) are halved with respect to the Run-2 scenario. In this analysis the systematic uncertainties are considered as nuisances in the fit and profiled.

Figure 28 (left) shows the result of a scan over different m_{jj} cuts in addition to the ATLAS baseline selection, for an integrated luminosity of 3000 fb^{-1}. The expected significance of EW-$ZZjj$ production processes is calculated as $\mathrm{Significance} = S/\sqrt{\sigma(B)^2_{stat.} + \sigma(B)^2_{syst.}}$, where S denotes the number of signal events after the selection, and $\sigma(B)_{stat.}$ and $\sigma(B)_{syst.}$ refer to the statistical and systematic uncertainties in background yield. The statistical uncertainty is estimated from expected data yield at 14 TeV with 3000 fb^{-1}.

The CMS analysis employs a multivariate discriminant based on a boosted decision tree (BDT) to extract the EW-$ZZjj$ signal from the QCD-$ZZjj$ background processes. Seven observables are used in the BDT, including m_{jj}, $|\Delta\eta_{\mathrm{jj}}|$, m_{ZZ}, as well as the Zeppenfeld variables [364] $\eta^*_{Z_{1,2}} = \eta_{Z_{1,2}} - (\eta_{\mathrm{jet}_1} + \eta_{\mathrm{jet}_2})/2$ of the two Z bosons, and the ratio between the p_{T} of the tagging jet system and the scalar sum

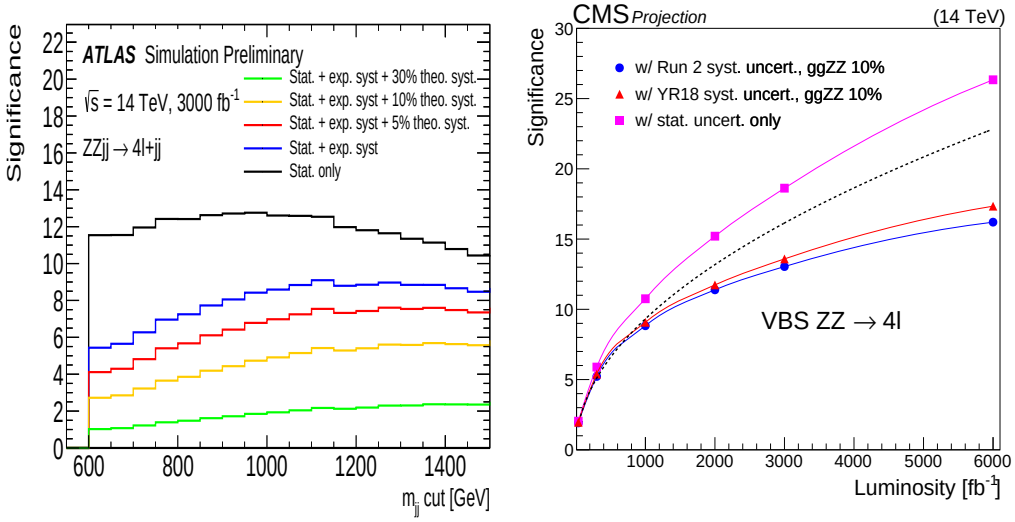

Fig. 28: Expected significance of EW-$ZZjj$ processes as a function of different m_{jj} cuts for 3000 fb^{-1}, for different sizes of theoretical uncertainties in the QCD-$ZZjj$ background modeling (left). Projected significance in the multivariate analysis as a function of the integrated luminosity for the two considered scenario and a 10% uncertainty in the loop-induced $ggZZ$ background yield, as well as with only the statistical uncertainties included (right).

of p_{T} of the tagging jets ($R(p_{\mathrm{T}})^{\mathrm{jets}}$). The BDT also exploits the event balance $R(p_{\mathrm{T}})^{\mathrm{hard}}$, defined as the transverse component of the vector sum of the Z bosons and tagging jets momenta, normalized to the scalar p_{T} sum of the same objects [406]. The modeling of all these observables was checked with Run-2 data in a background-enriched region [398]. A maximum likelihood fit of the BDT distributions for signal and backgrounds is used to extract the signal strength. The shape and normalization of each distribution are allowed to vary within their respective uncertainties. Figure 28 (right) shows the projected significance for a 10% uncertainty in the loop-induced $ggZZ$ background yield, as a function of the integrated luminosity and for the two scenarios described above, as well as for a scenario with only the statistical uncertainty included. The dashed line shows the projected significance as obtained scaling the 2016 result with statistical uncertainty only by the luminosity ratio. The impact of a multivariate analysis is clear for such small signal. The expected significance is 13.0σ (13.6σ) for the Run-2 (YR18) systematic scenario, with a 10% uncertainty in the loop-induced $ggZZ$ background yield and an integrated luminosity of 3000 fb^{-1}.

A fiducial phase space is defined at generator level with the same kinematic selections as listed in Table 11, and is used to study the expected precision of the cross section measurements. Table 13 shows the expected cross section measurement in this phase space for 3000 fb^{-1}, with the statistical only case, and the cases with different sizes of theoretical uncertainties. The statistical uncertainty is at 10% level and the integrated cross section measurement becomes dominated by experimental and modeling uncertainty in the QCD-$ZZjj$ background. For the possible extension of the HL-LHC run to 4000 fb^{-1}, the statistical uncertainty will be further reduced to 8% level.

Table 13: Summary of expected cross section measurements for different theoretical uncertainties. The statistical uncertainty is estimated from expected data yield at 14 TeV with 3000 fb^{-1}. Different uncertainties are summed up quadratically.

	Cross section [fb]	Stat. only	Plus exp.	Plus 5% theo.	Plus 10% theo.	Plus 30% theo.
EW-$ZZjj$	0.21	$\pm$0.02	$\pm$0.04	$\pm$0.05	$\pm$0.08	$\pm$0.21

The projected measurement uncertainty from the CMS analysis is 9.8% (8.8%) for the Run-2 (YR18) scenario and for a 10% uncertainty in the loop-induced $ggZZ$ background yield, for an integrated luminosity of 3000 fb^{-1}and a coverage of up to $|\eta| = 3$ for electrons. Extending the coverage up to $|\eta| = 4$ for electrons, the expected measurement uncertainty becomes 9.5% and 8.5%, respectively. In these estimates it is assumed that a fiducial cross section close to the detector volume is used, such that the measurement is to first order insensitive to theoretical uncertainties in the signal cross section.

In addition, the expected differential cross section measurements of the EW-$ZZjj$ processes at 14 TeV have been studied in the defined phase space, as a function of m_{jj}, and m_{ZZ}, as shown in Fig. 29. The expected differential cross section measurements are calculated bin by bin as

$$\sigma = \frac{N_{\mathrm{pseudo-data}} - N_{\mathrm{QCD}-ZZjj}}{L * C_{\mathrm{EW}-ZZjj}},\ C_{\mathrm{EW}-ZZjj} = \frac{N^{det.}_{\mathrm{EW}-ZZjj}}{N^{part.}_{\mathrm{EW}-ZZjj}}, \tag{19}$$

where $N_{\mathrm{pseudo-data}}$ is the expected number of data events with 3000 fb^{-1} luminosity, and $N_{\mathrm{QCD}-ZZjj}$ and $N_{\mathrm{EW}-ZZjj}$ are the number of predicted events from QCD-$ZZjj$ and EW-$ZZjj$ processes, respectively. The $C_{\mathrm{EW}-ZZjj}$ factor refers to the detector efficiency for EW-$ZZjj$ processes, calculated as number of selected signal events at detector level ($N^{det.}_{\mathrm{EW}-ZZjj}$), divided by number of selected events at particle level in the fiducial phase space ($N^{part.}_{\mathrm{EW}-ZZjj}$). Both the statistical only case (statistical uncertainty is estimated from expected data yield at 14 TeV with 3000 fb^{-1}) and the ones with different sizes of theoretical uncertainties on the background modeling are shown in Fig. 29.

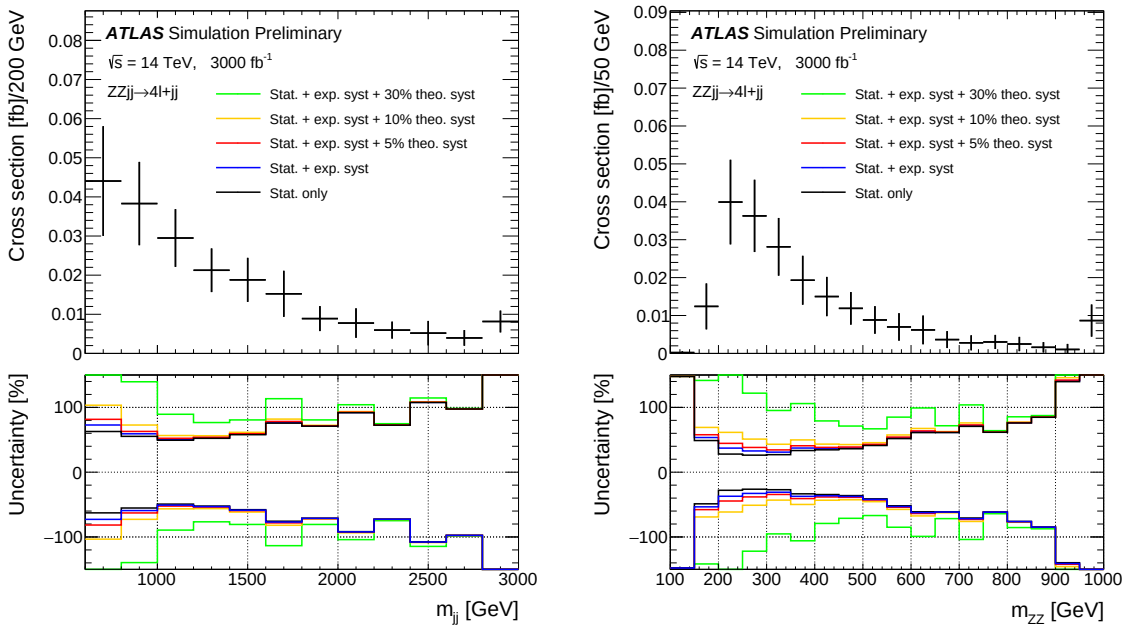

Fig. 29: Expected differential cross sections at 14 TeV for the EW-$ZZjj$ processes as a function of m_{jj}(left) and m_{ZZ} (right). Results are shown with different sizes of systematic uncertainties.

The decay angle $\cos\theta^*$ of the lepton direction in the Z decay rest frame with respect to the Z momentum direction in the laboratory frame is the most distinctive feature of longitudinal Z bosons (Z_{L}). The Z boson p_{T} and η distributions also carry information on $Z_{\mathrm{L}}Z_{\mathrm{L}}$ production, in particular longitudinal Z bosons are produced with a lower p_{T} and more forward, compared to transverse polarizations (Z_{T}). The distributions of $\cos\theta^*$, p_{T} and η of both Z bosons, together with the distributions of all observables used to separate VBS processes from QCD backgrounds and described above are employed as input to a BDT to separate the VBS $Z_{\mathrm{L}}Z_{\mathrm{L}}$ signal from all backgrounds. The BDT is trained separately

to discriminate the VBS $Z_{\mathrm{L}}Z_{\mathrm{L}}$ signal from the QCD backgrounds (QCD BDT) and to discriminate the VBS $Z_{\mathrm{L}}Z_{\mathrm{L}}$ signal from the VBS background (VBS BDT). Cut values are defined on the QCD BDT and on the VBS BDT output values, which maximizes the overall significance estimator $S/\sqrt{B}$ for the selected events. The corresponding signal efficiency is 14.1% and the VBS, leading QCD-$ZZjj$ and loop-induced $ggZZ$ background efficiencies are 1.6%, 0.03% and 0.05%, respectively. It is assumed that the VBS $Z_{\mathrm{L}}Z_{\mathrm{L}}$ fraction, defined as VBS $Z_{\mathrm{L}}Z_{\mathrm{L}}$ / VBS ($Z_{\mathrm{L}}Z_{\mathrm{L}} + Z_{\mathrm{L}}Z_{\mathrm{T}} + Z_{\mathrm{T}}Z_{\mathrm{T}}$) will be measured, rather than the absolute VBS Z_{L} Z_{L} cross section. In such ratio measurement, the systematic uncertainties from luminosity, and selection efficiency, as well as theoretical uncertainties on the VBS and VBS background cross section cancel out, such that only the uncertainties in the QCD backgrounds yields are considered.

Figure 30 shows the expected significance for the VBS $Z_{\mathrm{L}}Z_{\mathrm{L}}$ fraction as a function of the integrated luminosity and for the two scenarios described above and a 10% uncertainty in the loop-induced $ggZZ$ background yield, as well as for a scenario with only the statistical uncertainty included. A significance of 1.4σ is reached for 3000 fb^{-1}. As expected from the ratio measurement, the effect of systematic uncertainties is very small. Results are also shown for an integrated luminosity of 6000 fb^{-1}, which would approximately correspond to combining ATLAS and CMS after 3000 fb^{-1}. Table 14

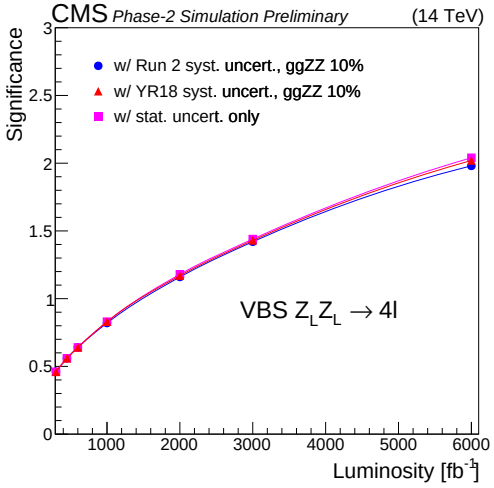

Fig. 30: Expected significance for the VBS $Z_{\mathrm{L}}Z_{\mathrm{L}}$ fraction as a function of the integrated luminosity and for systematic uncertainties according to the Run-2 and YR18 scenario, as well as with only the statistical uncertainties included.

presents the expected significance and relative uncertainty in the VBS $Z_{\mathrm{L}}Z_{\mathrm{L}}$ fraction for various η coverage configurations. The foreseen coverage extension of up to $|\eta| = 3\ (2.8)$ for electrons (muons) leads to a $\sim 13\%$ improvement for the significance and precision on the VBS $Z_{\mathrm{L}}Z_{\mathrm{L}}$ fraction. An extension of up to $|\eta| = 4$ for electrons would allow to further improve by $\sim 4\%$ both significance and cross section measurement uncertainty.

Finally, a simple scaling of the signal and background cross sections is performed to assess the sensitivity to the VBS $Z_{\mathrm{L}}Z_{\mathrm{L}}$ fraction at HE-LHC. An integrated luminosity of 15 ab^{-1} is considered, together with a c.o.m energy of 27 TeV. The cross section ratios $\sigma_{27\,\mathrm{TeV}}$ / $\sigma_{14\,\mathrm{TeV}}$ are evaluated at LO with MADGRAPH(v5.4.2) [393] for the EW signal and the leading QCD-$ZZjj$ background, and with MCFM(v.7.0.1) [403] for the $ggZZ$ loop-induced background. Table 15 shows the expected significance and relative uncertainty for the VBS $Z_{\mathrm{L}}Z_{\mathrm{L}}$ fraction at HE-LHC, compared to HL-LHC. The HE-LHC machine would allow to bring the sensitivity (uncertainty) for the measurement of the VBS $Z_{\mathrm{L}}Z_{\mathrm{L}}$ frac-

Table 14: Significance and measurement uncertainty for the VBS $Z_{\mathrm{L}}Z_{\mathrm{L}}$ fraction for different acceptance configurations at HL-LHC. In the quoted η coverages, the first number corresponds to electrons while the number in parentheses corresponds to muons.

η coverage	significance	VBS $Z_{\mathrm{L}}Z_{\mathrm{L}}$ fraction uncertainty (%)
$\|\eta\| < 2.5$ (2.4)	1.22σ	88
$\|\eta\| < 3.0$ (2.8)	1.38σ	78
$\|\eta\| < 4.0$ (2.8)	1.43σ	75

tion to the level of $\sim 5\sigma$ ($\sim 20\%$).

Table 15: Expected significance and measurement uncertainty for the VBS $Z_{\mathrm{L}}Z_{\mathrm{L}}$ fraction at HL-LHC and HE-LHC with and without systematic uncertainties included.

	significance		precision (%)	
	w/ syst. uncert.	w/o syst. uncert.	w/ syst. uncert.	w/o syst. uncert.)
HL-LHC	1.4σ	1.4σ	75%	75%
HE-LHC	5.2σ	5.7σ	20%	19%

4.2.6 The production of WW / WZ via vector boson scattering with semi-leptonic final states

The existing Run-2 VBS measurements and the above analyses have focused on channels involving the fully leptonic boson decays, or decay modes involving photons. The semileptonic channels can however offer some interesting advantages: the $V \to q\bar{q}$ branching fractions are much larger than the leptonic ones and the use of jet substructure techniques with large-radius jet reconstruction allows to reconstruct and identify the V-boson produced in the high-p_{T} region, which is the most sensitive to new physics effects. This section presents the sensitivity of the ATLAS experiment to VBS in the $V(qq)W(\ell\nu)$ final state, assuming an integrated luminosity of 300 or 3000 fb^{-1} of pp collisions at $\sqrt{s}$= 14 TeV.

This analyses uses generator-level samples of the main signal and background processes, combined with the parameterisations of the detector performance (muon and jet reconstruction and selection efficiencies and momentum resolutions) expected at the HL-LHC from fully simulated samples. The parametrized detector resolutions are used to smear the generator-level particle transverse momenta, while the parametrized efficiencies are used to reweigh the selected events. All generated samples were produced at $\sqrt{s}$= 14 TeV and normalized to luminosities of 300 or 3000 fb^{-1} when the results are presented.

The electroweak (EW) $VVjj$ production is modeled using MADGRAPH5_AMC@NLO v2.3.3 [12], plus PYTHIA8 [292] for fragmentation. The main background sources are W bosons produced in association with jets (W+jets), with significant contributions from top-quark production (both $t\bar{t}$ pair and single-top), non-resonant vector-boson pair production (ZZ, WZ and WW) and Z bosons produced in association with jets (Z+jets). Background originating from multi-jet processes are expected to be negligible due to the event selection requirements. Details about the samples generation can be found in Ref. [407].

To increase the purity of considered events, several requirements are placed on the constituents of an event. Events are required to have exactly one lepton. Generator-level electrons or muons are required to be isolated and pass the tight identification criteria [405] and to have $p_{\mathrm{T}} > 27$ GeV. Events are required to contain a hadronically-decaying W/Z candidate, reconstructed either from two small-R

jets, defined as the resolved channel, or from one large-R jet, designated the boosted channel. Small-R jets are defined using the anti-k_{T} algorithm [408] with a radius parameter of R = 0.4. The identification of jets originating from b-quarks is done by finding jets with generator-level b-hadron within a cone of $\Delta R < 0.4$ around the jet direction. Similarly, the anti-k_{T} algorithm with a radius parameter of R = 1.0 is used to reconstruct large-R jets. The large-R jets are trimmed using the standard ATLAS trimming parameters [409]. It is assumed that the performance of a future W/Z-boson tagger at the HL-LHC conditions will have similar, if not better, performance as existing boson taggers. To simulate the effect of Run-2 W/Z-boson tagging performance [410, 411] events which contain a large-R jet are scaled by the expected boson tagging efficiency for the $V \rightarrow qq$ with kinematics corresponding to the large-R jet, calculated from fully-simulated 13 TeV Monte-Carlo (MC) samples. The missing transverse energy E_{T}^{miss} is required to be greater than 60 GeV, which suppresses the expected multijet background to a negligible level. By constraining the E_{T}^{miss} + lepton system to be consistent with the W mass, the z component of the neutrino (ν) momentum can be reconstructed by solving a quadratic equation.

Experimentally, VBS is characterized by the presence of a pair of vector bosons and two forward jets with a large separation in pseudorapidity and a large dijet invariant mass. Therefore the VBS search is required to have 2 additional forward VBS-topology tagging jets in the event in addition to jets associated with the boson decay, similar to the resonant VBF search. The VBS tagging jets are required to be non-b-tagged, be in the opposite hemispheres, $\eta(j_1^{\mathrm{tag}}) \cdot \eta(j_2^{\mathrm{tag}}) < 0$, and to have the highest dijet invariant mass among all pairs of jets remaining in the event after the $V \rightarrow jj$ jet selection. After the tagging jet pair are selected, it is required that both tagging jets should have p_{T} >30 GeV, and that the invariant mass of the two tagging jets system is greater than 400 GeV . In the merged selection, events are required to have at least one large-R jet with $p_{\mathrm{T}}(J) > 200$ GeV and $|\eta(J)| < 2$. From those candidate large-R jets, the one with the smallest $|m(J) - m(W/Z)|$ is selected as the signal large-R jet. Mass window cuts and boson tagging efficiencies are applied as described above. To suppress backgrounds with top quarks, an event is rejected if any of the reconstructed jets outside the large R jet, is identified as containing a b-quark. If events fail the merged VBS selection, the resolved selection is then applied. Signal jets are chosen as the pair with $m(jj)$ closest to the W/Z mass. The signal jet pairs are then required to have $|m(jj) - m(W/Z)| < 15$ GeV. To suppress backgrounds with top quarks, an event is rejected if any of the reconstructed jets is identified as containing a b-quark.

To optimize the signal sensitivity, Boosted Decision Trees (BDT) for the resolved and merged searches were trained on the background and signal MC samples in the respective regions. Four variables are included in the merged BDT: the invariant mass of the $l\nu J$ system, the lepton η, the second tag jet p_{T} and the boson centrality ζ_V. The boson centrality is defined as $\zeta_V = min(\Delta\eta_+, \Delta\eta_-)$ where $\Delta\eta_+ = max(\eta(j_1^{\mathrm{tag}}), \eta(j_2^{\mathrm{tag}})) - max(\eta(\ell\nu), \eta(J))$ and $\Delta\eta_- = min(\eta(\ell\nu), \eta(J)) - min(\eta(j_1^{\mathrm{tag}}), \eta(j_2^{\mathrm{tag}}))$. In the resolved BDT, eight variables were used: the invariant mass of the $WVjj$ system , the lepton η, the p_{T} of both VBS-tagging jets and sub-leading signal jet, the boson centrality defined similarly to above, the $\Delta\eta$ between signal jets, and the ΔR between the lepton and neutrino candidate. These variables were chosen as they are the minimal subset of variables with the greatest separation between the signal and background, that provide significant improvement when added during the training. The BDT were trained using a gradient descent BDT algorithm, maximizing the Gini index, in the TMVA package [412]. The BDT are chosen as the discriminants and their distributions are used in the final fit for the VBS search shown in Figure 31.

If an event fails either a mass-window cut or a b-veto but passes all other events then the event is categorized as a W or top control region. These regions are used to constrain the normalization and shape systematics of the background.

The results are extracted by performing a simultaneous binned maximum-likelihood fit to the BDT distributions in the signal regions and the W+jets and $t\bar{t}$ control regions. A test statistic based on the profile likelihood ratio [413] is used to test hypothesized values of the signal cross section. The

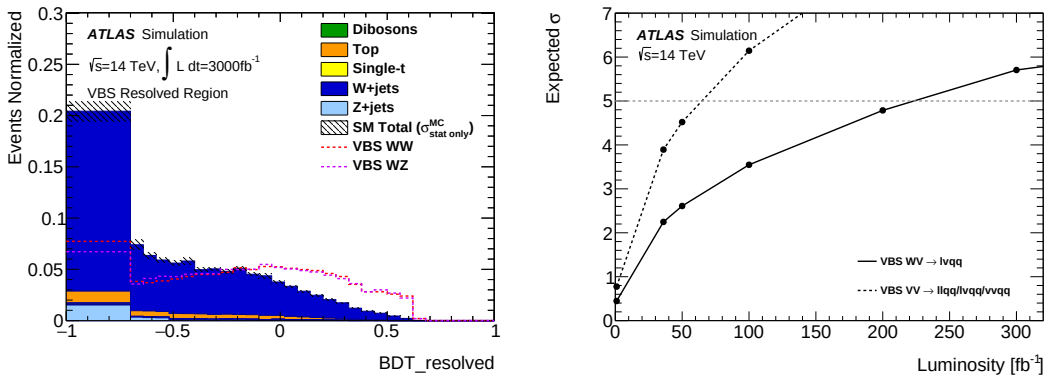

Fig. 31: Final signal and background distributions for the VBS search in the respective resolved signal region for the normalized BDT response. Background distributions are separated into production type. VBS signals in WW and WZ mode are overlaid as dashed curves where appropriate. Both background and signal BDT distributions are normalized to unity (left). Expected signal significance as a function of integrated luminosity up to 300 fb^{-1}. The solid black curve is the significance from the $\ell\nu qq$channel, while the black dashed curve shows the expected significance from all semi-leptonic channels assuming equal sensitivity (right).

likelihood is defined as the product of the Poisson likelihoods for all signal and control regions for a given production mechanism category and channel. Systematic uncertainties are taken into account as constrained nuisance parameters with Gaussian or log-normal distributions. The main background modelling systematics, namely the W+jets and $t\bar{t}$ shape uncertainties, are constrained by the corresponding control regions and are treated as uncorrelated among the resolved and merged signal regions.

The expected significance for the SM VBS process is 5.7σ at 300 fb^{-1} as shown in Fig. 31. The expected cross section uncertainties are 18% at 300 fb^{-1} and 6.5% at 3000 fb^{-1}. The effects of unfolding were not considered for the cross section estimates. If control regions are not used to constrain the systematics the expected significance is reduced to 3.6σ at 300 fb^{-1}. Likewise the cross section uncertainty are increased to 28% at 300 fb^{-1} and 10% at 3000 fb^{-1} when control regions are ignored.

4.2.6.1 Electroweak WW / WZ production analysis at HE-LHC

The prospect analysis at HE-LHC [414] mimics the analysis at HL-LHC but the DELPHES simulation is used [415]. VBS signal samples are produced in the same manner as the HL-LHC analysis. The major backgrounds W+jets and $t\bar{t}$ production are simulated with MADGRAPH and aMC@NLO respectively, interfaced with PYTHIA. Z+jets, single top and diboson contribution are not simulated and are expected to contribute at most 10% to the total background.

The unprecedented energy of pp collisions at the HE-LHC will significantly improve sensitivity to new multi-TeV particles over LHC and HL-LHC. However, the experimental environment is expected to be challenging at the HE-LHC, primarily due to a significant increase of the number of pp collisions in a same and nearby bunch crossings (pile-up). The HE-LHC is planned to be operated at a centre-of-mass energy of 27 TeV with 800 pile-up collisions at the peak luminosity. Such extreme pile-up conditions are expected to be particularly challenging for identifying hadronically decaying W/Z boson as the extra contribution of particles produced from pile-up collisions into jets could degrade the performance of W/Z boson tagger significantly. It is therefore important to assess the performance of pile-up mitigation technique at the HE-LHC in order to have a reliable estimate of the search sensitivity.

The study presented here focuses on the performance of pile-up mitigation techniques and W/Z

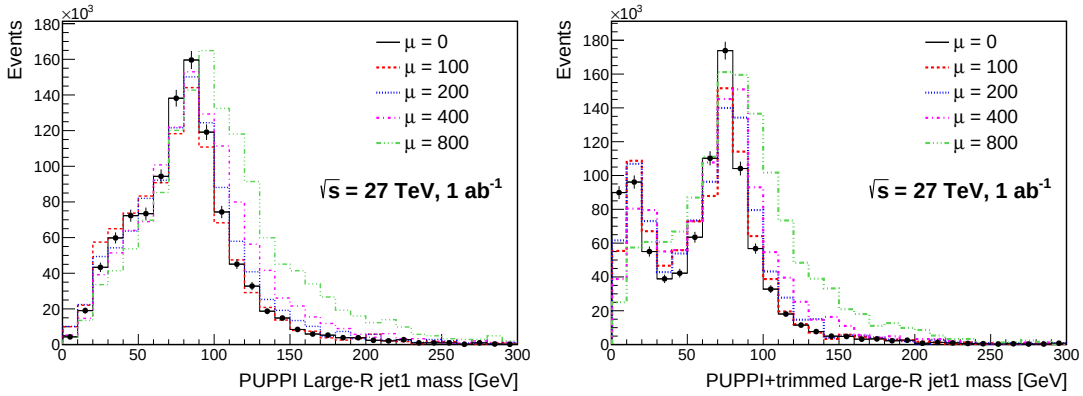

Fig. 32: Leading large-R jet mass (left) after applying the PUPPI algorithm at an integrated luminosity of 1 ab^{-1} at $\sqrt{s} = 27$ TeV with five different pile-up overlay conditions of $\mu_{\text{pileup}} = 0$, 100, 200, 400 and 800. The right plots shows the same distribution but after additionally requiring that the jets are trimmed with the conditions described in the text.

boson tagging. The VBS signal events are produced with the overlay of minimum-bias pp interactions generated using PYTHIA 8. The minimum-bias interactions are overlaid onto hard scattering event using Poisson probability distribution with the mean number of interactions (μ_{pileup}) varied from 0 to 100, 200, 400 and 800. Furthermore, the minimum-bias interactions are distributed randomly in z and timing using Gaussian profiles of $\sigma_z = 5.3$ cm and $\sigma_t = 160$ ps, respectively (z=0 at the detector centre and t=0 for hard scattering event). The overlaid VBS signal events are processed through DELPHES with two pile-up mitigation techniques: the Pile-up Per Particle Identification (PUPPI) algorithm [362] used in CMS and the trimming procedure used in ATLAS. The trimming parameters of the p_{T} fraction cut and the sub-jet reclustering radius are chosen to be the same as those used in ATLAS. For the PUPPI algorithm the standard DELPHES implementation is used.

Figure 32 shows the leading large-R jet mass (m_J) for the PUPPI-only jets and the PUPPI+trimmed jets, both required to have $p_{\text{T}} > 200$ GeV. The m_J distribution get shifted towards lower values with the trimming applied, enhancing the peak around m_W . The residual pile-up effect is still visible as a shift towards larger values with increasing μ_{pileup}, but the overall signal yield after the mass-window and D_2 requirements (e.g, $D_2 < 1.5$) is largely stable. This indicates that an impact to the W/Z-boson tagging performance from expected pile-up collisions at the HE-LHC can be mitigated to the level where the tagging performance is similar to what is expected at Run-2 or the HL-LHC. Therefore, the study presented in the rest of this note is based on the W/Z-boson tagging performance at Run-2.

The sensitivity to the VBS signal at 27 TeV is extracted in the same manner as the HL-LHC analysis. The event selection is similar and a BDT is built using the same variables both in the resolved and boosted channel. For more details about the BDT and the setup used please refer to citation. Figure 33 shows the expected cross section uncertainty as function of integrated luminosity at 27 TeV compared to the one obtained at 14 TeV. The results are very consistent and show that given the same luminosity the same uncertainty can be reached at 27 TeV. Prospects are also presented for the extraction of the longitudinal component of the WW scattering. For the extraction of the longitudinal component in VBS processes, the electroweak $WWjj$ samples are generated with the DECAY program to identify the polarization state of the produced V bosons. The generated events are then classified according to the polarization state: both V bosons are longitudinally (LL) or transversely (TT) polarized, or in the mixed state (LT). Each event is showered using PYTHIA and then processed through the DELPHES simulation.

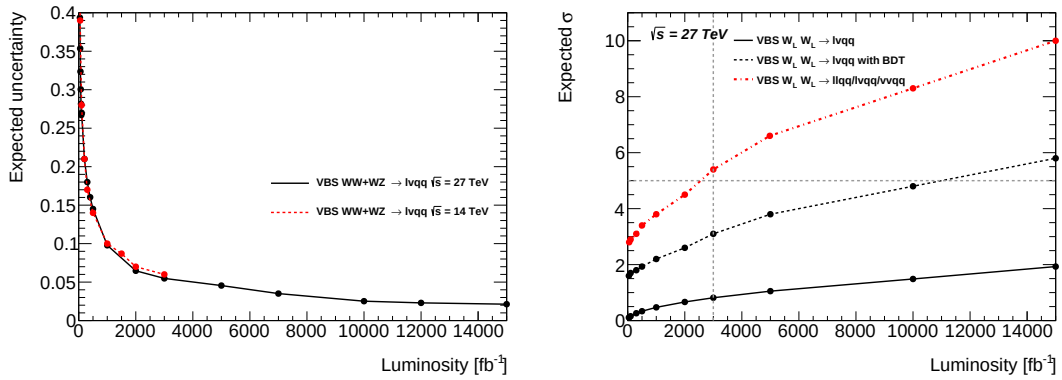

Fig. 33: The expected cross section uncertainty as function of integrated luminosity at 27 TeV compared to the one obtained at 14 TeV (left). Right: Observed significance as a function of the luminosity and expected uncertainty for the EW W_LW_L signal assuming a 10% fraction predicted by MADGRAPH (right). One line shows the results obtained by fitting a single variable, the total invariant mass of the system and the other one shows the expected significance using the BDT. The third line shows the expected significance assuming the combination of all three semi-leptonic channels with the same sensitivity.

In this case a BDT is built training the signal samples ($WW\ LL$) against the sum of the backgrounds which include the TT and LT component of the electroweak $WWjj$ samples. The observed significance expected with this simple setup is shown in the right figure of Fig. 33. One line shows the results obtained by fitting a single variable, the total invariant mass of the system and the other one shows the expected significance using the BDT. The third line shows the expected significance assuming the combination of all three semi-leptonic channels with the same sensitivity. It is expected to reach 5σ sensitivities with 3000 fb^{-1} combining all the semileptonic channels.

4.3 Tri-boson production

The production of multiple heavy gauge bosons V (= $W^{\pm}, Z$) opens up a multitude of potential decay channels categorised according to the number of charged leptons in the final state. The sensitivity prospect studies have been performed related to the production of $W^{\pm}W^{\pm}W^{\mp}$, $W^{\pm}W^{\mp}Z$ or $W^{\pm}ZZ$ followed by the fully leptonic or semi-hadronic[13] decays: $W^{\pm}W^{\pm}W^{\mp} \rightarrow \ell^{\pm}\nu\ell^{\pm}\nu\ell^{\mp}\nu$, $W^{\pm}W^{\pm}W^{\mp} \rightarrow \ell^{\pm}\nu\ell^{\pm}\nu jj$, $W^{\pm}W^{\mp}Z \rightarrow \ell^{\pm}\nu\ell^{\pm}\nu\ell^{+}\ell^{-}$, $W^{\pm}W^{\mp}Z \rightarrow \ell^{\pm}\nu jj\ell^{+}\ell^{-}$, $W^{\pm}ZZ \rightarrow \ell^{\pm}\nu\ell^{+}\ell^{-}\ell^{+}\ell^{-}$, $W^{\pm}ZZ \rightarrow \ell^{\pm}\nu\ell^{+}\ell^{-}\nu\nu$, $W^{\pm}ZZ \rightarrow jj\ell^{+}\ell^{-}\ell^{+}\ell^{-}$ and $W^{\pm}ZZ \rightarrow \ell^{\pm}\nu\ell^{+}\ell^{-}jj$, with $\ell = e$ or μ. Prospect studies have been performed, using a cut-based analysis, corresponding to an integrated luminosity of 3000 fb^{-1} and 4000 fb^{-1} of proton–proton collisions at a centre-of-mass energy of $\sqrt{s}$ = 14 TeV, expected to be collected by the ATLAS detector at the HL-LHC [301]. In this section we summarize only results that are expected to provide the best sensitivity according to the full prospect studies documented in [416].

Monte Carlo (MC) simulated event samples are used to predict the background from SM processes and to model the multi-boson signal production. The effects of an upgraded ATLAS detector are taken into account by applying energy smearing, efficiencies and fake rates to generator level quantities, following parameterisations based on detector performance studies with full simulation and HL-LHC conditions. The most relevant MC samples have equivalent luminosities (at 14 TeV) of at least 3000 fb^{-1}. Several MC generators are used to model the production of signal and dominant SM background

[13] In case of semi-hadronic channels we assume that one of the vector bosons decays hadronically while the other two decay leptonically.

processes relevant for the analysis.

For the generation of triboson signal events, matrix elements for all combinations of $pp \to VV$ ($V = W^{\pm}, Z$) have been generated using SHERPA v2.2.2 [84] with up to two additional partons in the final state, including full next-to-leading-order calculations (NLO) [417–419] accuracy for the inclusive process. All diagrams with three electroweak couplings are taken into account, including diagrams involving Higgs propagators. However, since these samples use factorised decays with on-shell vector bosons, the resonant contribution from those diagrams can not be reached from the 125 GeV Higgs. In order to account for the contribution coming from these diagrams the corresponding production of VH ($V = W, Z$) bosons is added to the signal. Electroweak NLO corrections to the signal production cross sections are not considered in this analysis. The diboson processes are generated with SHERPA event generator following the approach described in [420]. For the simulation of the top quark pair and the production of VH ($V = W, Z$) bosons POWHEG [151, 314, 377]+PYTHIA [148] was used as described in [421], while for the $t\bar{t}$ + V ($V = W, Z, H$) MADGRAPH5_aMC@NLO [12] interfaced to PYTHIA was used as in [422].

The expected multi-boson yields are normalised to the SHERPA predictions, while the $t\bar{t}$ + V ($V = W, Z, H$) yields are normalized to NLO. The top quark pair-production contribution is normalised to approximate NNLO+NNLL accuracy [41, 423].

Experimental signatures

The experimental signature of the triboson processes considered in these studies consists of at least three charged leptons, moderate $E_{\mathrm{T}}^{\mathrm{miss}}$ originating from the leptonic decay of W bosons, and jets in case one of the vector bosons decays hadronically. The event selection starts from the one used in the published analysis in Ref. [424], but considers tighter selection criteria in terms of transverse momentum of the selected objects and missing transverse momentum of the event, in order to suppress higher pile-up contributions expected at the HL-LHC. The selection requirements used to define the signal regions are obtained from an optimization to maximize the sensitivity to $W^{\pm}W^{\pm}W^{\mp}$, $W^{\pm}W^{\mp}Z$ and $W^{\pm}ZZ$ processes and to reduce the contributions from SM background processes. In the case of $W^{\pm}W^{\pm}W^{\mp} \to \ell^{\pm}\nu\ell^{\pm}\nu\ell^{\mp}\nu$ channel, three separate signal regions are defined based on the number of same-flavour opposite-sign (SFOS) lepton pairs in the event: 0SFOS ($e^{\pm}e^{\pm}\mu^{\mp}$, $\mu^{\pm}\mu^{\pm}e^{\mp}$), 1SFOS ($e^{\pm}e^{\mp}\mu^{\pm}$, $e^{\pm}e^{\mp}\mu^{\mp}$, $\mu^{\pm}\mu^{\mp}e^{\pm}$, $\mu^{\pm}\mu^{\mp}e^{\mp}$) and 2SFOS ($e^{\pm}e^{\pm}e^{\mp}$, $\mu^{\pm}\mu^{\pm}\mu^{\mp}$). Similarly, in $W^{\pm}W^{\mp}Z \to \ell^{\pm}\nu\ell^{\pm}\nu\ell^{+}\ell^{-}$ channel, two signal regions are defined based on the selection of SFOS or different-flavour opposite-sign (DFOS) lepton-pair events: SFOS ($e^{\pm}e^{\mp}\mu^{\mp}\mu^{\pm}$, $e^{\pm}e^{\mp}e^{\pm}e^{\mp}$, $\mu^{\mp}\mu^{\pm}\mu^{\mp}\mu^{\pm}$) and DFOS ($e^{\pm}e^{\mp}\mu^{\mp}e^{\pm}$, $\mu^{\mp}\mu^{\pm}\mu^{\mp}e^{\pm}$). To select $W^{\pm}W^{\pm}W^{\mp} \to \ell^{\pm}\nu\ell^{\pm}\nu jj$ candidates, events are required to have exactly two leptons with the same electric charge, and at least two jets. Three different final states are considered based on the lepton flavour, namely $e^{\pm}e^{\pm}$, $e^{\pm}\mu^{\pm}$ and $\mu^{\pm}\mu^{\pm}$. In the case of $W^{\pm}ZZ$ process, separate set of selection criteria are defined in order to select events in which vector bosons undergo either fully leptonic of semi-hadronic decay. In all channels, events are rejected if they have identified b-jets. This selection requirement suppresses background involving top quarks, with marginal impact on the signal efficiency. Full description to the optimized selection criteria, estimated systematic uncertainties and expected signal and background event yields for all channels considered in the study are available in Ref. [416]. Three channels, 0SFOS $W^{\pm}W^{\pm}W^{\mp} \to 3\ell\,3\nu$, DFOS $W^{\pm}W^{\mp}Z \to 4\ell\,2\nu$ and $W^{\pm}ZZ \to 5\ell\,1\nu$, for which we give details in the following, are estimated to provide best sensitivities. Tables 16 to 18 show the kinematic selection criteria used to select signal events in these channels.

Results

The SM processes that mimic the multi-boson signal signatures by producing at least three prompt leptons or two prompt leptons with the same electric charge, can be grouped into the following categories:

Table 16: Event selection criteria for $W^{\pm}W^{\pm}W^{\mp} \to 3\ell\ 3\nu$ candidate events.

$W^{\pm}W^{\pm}W^{\mp} \to \ell^{\pm}\nu\ell^{\pm}\nu\ell^{\mp}\nu$	0SFOS events: $e^{\pm}e^{\pm}\mu^{\mp}$, $\mu^{\pm}\mu^{\pm}e^{\mp}$
Preselection	Exactly 3 charged *tight* leptons with $p_{\mathrm{T}} > 30$ GeV and $\lvert\eta\rvert < 4$
SFOS dilepton mass	$m_{\ell\ell}^{\mathrm{SFOS}} > 20$ GeV
Angle between the trilepton system and $\overrightarrow{E}_{\mathrm{T}}^{miss}$	$\lvert\varphi^{3\ell} - \varphi^{\overrightarrow{E}_{\mathrm{T}}^{miss}}\rvert > 2.5$
Z boson veto	$\lvert m_{\mathrm{ee}} - m_{\mathrm{Z}}\rvert > 15$ GeV
Jet veto	At most one jet with $p_{\mathrm{T}} > 30$ GeV and $\lvert\eta\rvert < 2.5$
b-jet veto	No identified b-jets with $p_{\mathrm{T}} > 30$ GeV

Table 17: Event selection criteria for $W^{\pm}W^{\mp}Z \to 4\ell\ 2\nu$ candidate events. The four-lepton mass $m_{4\ell}$ is calculated as invariant mass of the four-lepton system.

$W^{\pm}W^{\mp}Z \to \ell^{\pm}\nu\ell^{\pm}\nu\ell^{+}\ell^{-}$	DFOS events: $e^{\pm}e^{\mp}\mu^{\mp}e^{\pm}$, $\mu^{\mp}\mu^{\pm}\mu^{\mp}e^{\pm}$
Preselection	Exactly 4 charged *loose* (3^{rd} and 4^{th} *tight*) leptons with $p_{\mathrm{T}}(1,2) > 30$ GeV, $p_{\mathrm{T}}(3,4) > 25$ GeV and $\lvert\eta\rvert < 4$
SFOS dilepton mass	$\lvert m_{\ell\ell}^{\mathrm{SFOS}} - 91\ \mathrm{GeV}\rvert < 15$ GeV
DFOS dilepton mass	$m_{\ell\ell}^{\mathrm{DFOS}} > 40$ GeV
Four-lepton mass	$m_{4\ell} > 250$ GeV
b-jet veto	No identified b-jets with $p_{\mathrm{T}} > 30$ GeV

Table 18: Event selection criteria for $W^{\pm}ZZ \to 5\ell\ 1\nu$ candidate events. Two-lepton pairs of the same flavour and opposite charge have to satisfy same-flavour dilepton mass selection requirement. The transverse mass is calculated from the $E_{\mathrm{T}}^{\mathrm{miss}}$ and the lepton that does not pass dilepton mass requirement.

$W^{\pm}ZZ \to \ell^{\pm}\nu\ell^{+}\ell^{-}\ell^{+}\ell^{-}$	$5\ell 1\nu$
Preselection	Exactly 5 charged *loose* (4^{rd} and 5^{th} *tight*) leptons with $p_{\mathrm{T}}(1,2,3) > 30$ GeV, $p_{\mathrm{T}}(4,5) > 25$ GeV and $\lvert\eta\rvert < 4$
SFOS dilepton mass	$\lvert m_{\ell\ell}^{\mathrm{SFOS}} - 91\ \mathrm{GeV}\rvert < 15$ GeV
Transverse mass	$m_{\mathrm{T}} > 40$ GeV
b-jet veto	No identified b-jets with $p_{\mathrm{T}} > 30$ GeV

- The WZ and ZZ processes, referred to as "diboson background";
- The WWW, WWZ, WZZ, ZZZ processes, excluding the signal process under study, referred to as "triboson background";
- The VH and $t\bar{t}H$ processes, excluding the processes which are added to the signal, referred to as "Higgs+X background";
- The production of four top quarks, top quark associated with WZ bosons or $t\bar{t}$ associated with W, Z, WZ or $W^{\pm}W^{\mp}$ bosons, referred to as "top background";
- Processes that have non-prompt leptons (electrons) originating from misidentified jets (referred to as "fake-lepton background");
- Processes that produce prompt charged leptons, but the charge of one lepton is misidentified (referred to as "charge-flip background").

The contributions from the WW and $t\bar{t}$ processes are accounted for in the fake-lepton and charge-flip backgrounds. The diboson, triboson, Higgs+X and top background sources are estimated using simulated events, with the dominant irreducible background in most of the channels originating from the diboson processes. In some channels the contribution of the fake-lepton background, which is derived by applying the pre-defined (p_{T}, η)-dependent likelihood as described in Section 3, becomes significant.

The charge-flip background has been investigated and found to be negligible in all considered processes.

In $W^{\pm}W^{\pm}W^{\mp} \to 3\ell\ 3\nu$ channel, the background is dominated by the irreducible diboson background and fake-lepton contribution. The contribution of signal events containing Higgs decays are at the level of 40%. In $W^{\pm}W^{\mp}Z \to 4\ell\ 2\nu$ channel with two leptons being of different flavour, this requirement suppresses a large fraction of the diboson background. Contribution of Higgs decays is quite smaller with respect to the one in $W^{\pm}W^{\pm}W^{\mp} \to 3\ell\ 3\nu$ due to smaller lepton p_{T} and invariant mass requirement $m_{\ell\ell}^{\mathrm{DFOS}} > 40$ GeV. In the $W^{\pm}ZZ$ channel, the most promising signal region is the one with five charged leptons. In this case, the fake-lepton contribution becomes significant. The background is dominated by rare top production of $t\bar{t}ZW$.

Figure 34 shows relevant distributions in the three channels: the $m_{\mathrm{T}}^{3\ell}$ distribution for the $W^{\pm}W^{\pm}W^{\mp} \to 3\ell\ 3\nu$ channel, the distribution of transverse momenta of the two-lepton system $p_{\mathrm{T}}^{\ell\ell}$ in $W^{\pm}W^{\mp}Z \to 4\ell\ 2\nu$ channel and the distribution of two lepton invariant mass $p_{\mathrm{T}}^{\ell\ell}$ selected to give the mass closest to the mass of the Z boson in $W^{\pm}ZZ \to 5\ell\ 1\nu$ channel.

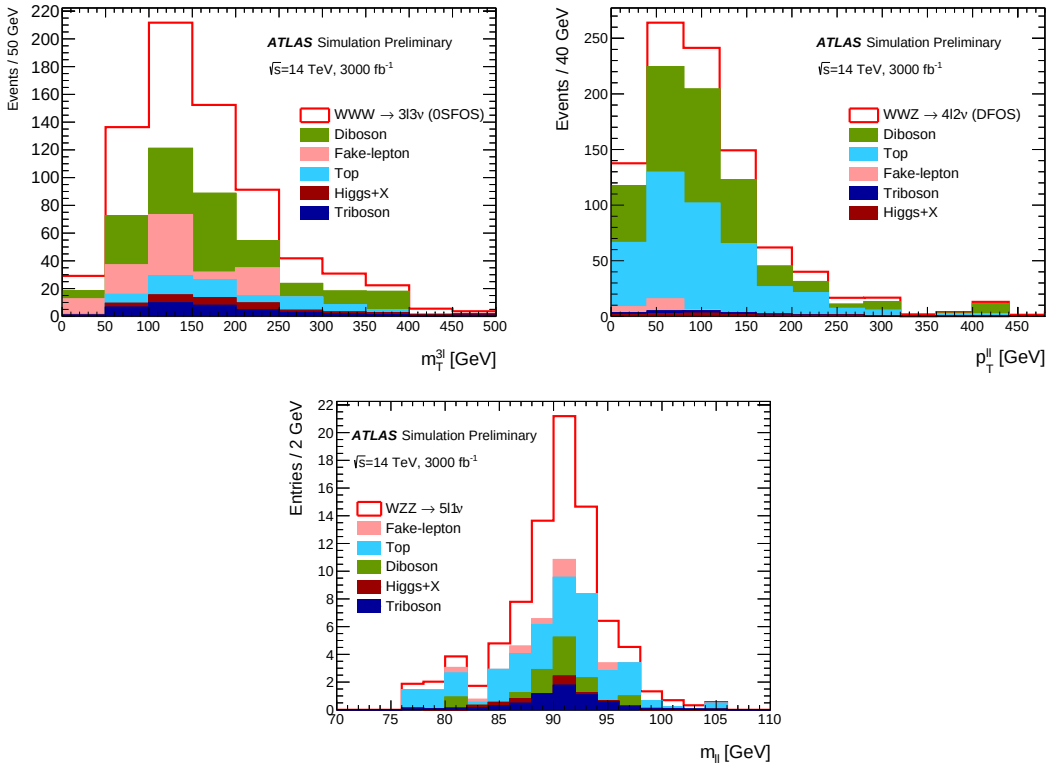

Fig. 34: The distribution of $m_{\mathrm{T}}^{3\ell}$ for the $W^{\pm}W^{\pm}W^{\mp} \to 3\ell\ 3\nu$ channel (top left), the distribution of transverse momenta of the two-lepton system $p_{\mathrm{T}}^{\ell\ell}$ in $W^{\pm}W^{\mp}Z \to 4\ell\ 2\nu$ channel (top right) and the distribution of two lepton invariant mass $p_{\mathrm{T}}^{\ell\ell}$ selected to give the mass closest to the mass of the Z boson in $W^{\pm}ZZ \to 5\ell\ 1\nu$ channel (bottom) as expected from the signal and background processes at 3000 fb^{-1} after applying the selection criteria from Tables 16 to 18.

Systematic uncertainties in the signal and background predictions arise from the uncertainties in the measurement of the integrated luminosity, from the experimental modelling of the signal acceptance and detection efficiency, and from the background normalisation. With the much larger integrated luminosity and a sophisticated understanding of the detector performance and backgrounds at the HL-LHC, we expect experimental uncertainties related to the lepton reconstruction and identification efficiencies as well as lepton energy/momentum resolution and scale modelling of 1%, to the $E_{\mathrm{T}}^{\mathrm{miss}}$ modelling of

1%, to the jet energy scale and resolution of 1.5% and 5% in the fully leptonic and leptons+jets channels, respectively, to the luminosity measurement of 1% and to the expected pileup of 1% [276]. Based on the extrapolations of current ATLAS measurements and assuming a reduction of the uncertainty at the level of 15–80%, depending on the process and the origin of the systematics, the following systematic uncertainties on the cross section normalisation for each of the background processes are assumed: 4% on σ_{diboson}, 30% on σ_{triboson}, 3% on $\sigma_{t\bar{t}}$, 20% on $\sigma_{t\bar{t}H}$, 6% on $\sigma_{t\bar{t}Z}$, and 11% on $\sigma_{t\bar{t}W}$. The uncertainty on the level of the fake-lepton background is estimated to be 10%. Taking these assumptions into account, we estimate the total systematic uncertainty on the background of 9% for $W^{\pm}W^{\pm}W^{\mp} \to 3\ell 3\nu$ and $W^{\pm}ZZ \to 5\ell 1\nu$ channels and 6% in $W^{\pm}W^{\mp}Z \to 4\ell 2\nu$ channel. Assuming that the number of signal events follows a Poissonian distribution and taking into account an estimated systematic uncertainty on the background, the signal significance Z_{σ} and the estimated precision on the signal strength measurement, $\frac{\Delta\mu}{\mu}$ are calculated using the asymptotic formula from Ref. [413]. Only experimental uncertainties are taken into account for the signal. Uncertainties related to the limited number of MC events are neglected. The total number of signal and background events expected after applying the full set of selection requirements from Tables 16 to 18 in three selected channels, the corresponding signal significance and the expected precision on the signal strength measurement, for an integrated luminosity of 3000 fb^{-1} are shown in Table 19.

Table 19: Expected number of signal and background events, the expected signal significance Z_{σ} and the estimated precision on the signal strength measurement, $\frac{\Delta\mu}{\mu}$ in $W^{\pm}W^{\pm}W^{\mp} \to 3\ell 3\nu$, $W^{\pm}W^{\mp}Z \to 4\ell 2\nu$ and $W^{\pm}ZZ \to 5\ell 1\nu$ channels after applying the selection criteria from Tables 16 to 18.

	$W^{\pm}W^{\pm}W^{\mp} \to 3\ell 3\nu$	$W^{\pm}W^{\mp}Z \to 4\ell 2\nu$	$W^{\pm}ZZ \to 5\ell 1\nu$
Signal	312	168	19
Diboson	208	357	4.0
Triboson	37	11	3.0
Higgs+X	25	10	0.3
Top	60	390	15
fake-lepton	97	16	3.0
Total:	427	784	25
Significance Z_{σ}	6.7	3.0	3.0
Significance Z_{σ} (4000 fb^{-1})	7.0	3.1	3.4
Precision $\frac{\Delta\mu}{\mu}$	11%	27%	36%
Precision $\frac{\Delta\mu}{\mu}$ (4000 fb^{-1})	10%	25%	31%

The HL-LHC offers a large improvement to multi-boson production, where this simple cut-and-count approach provides sensitivities larger than 3σ in the three channels considered in this analysis. It should be noted that more mature analysis techniques such as MVA, would likely improve these results further. However, high level of background control, mainly diboson background as well as instrumental background arising from fake-leptons, will be needed in order to maintain desired level of precision.

4.4 Precision electroweak measurements

4.4.1 NNLO predictions for Z-boson pair production[14]

The results presented in this section are produced using the program described in Ref. [425] with the NNPDF3.0 [201] set of parton distribution functions. The parton densities and α_s are evaluated at each corresponding order (i.e. $(n{+}1)$-loop α_s is used at N^{n}LO, with $n = 0, 1, 2$) and $N_f = 5$ massless quark flavours are considered. For the renormalisation (μ_R) and factorisation (μ_F) scales two choices are investigated: $\mu_R = \mu_F = m_Z$ and the dynamic scale $\mu_R = \mu_F = m_{ZZ}/2$. The G_{μ} EW scheme is

[14] Contribution by G. Heinrich, S. Jahn, S. Jones, M. Kerner and J. Pires.

used where the EW input parameters have been set to $G_F = 1.16639 \times 10^{-5}$, $m_W = 80.399$ GeV and $m_Z = 91.1876$ GeV. The top quark and Higgs boson masses that are included in the real-virtual one-loop contributions and in the loop-induced gg channel have been set to $m_t = 173.2$ GeV and $m_H = 125$ GeV, respectively. The one-loop contributions are calculated with the program GoSam [11, 86]. For the NNLO real radiation the N-jettiness subtraction scheme [53, 54, 426, 427] is employed. The process dependent hard function has been extracted from the two-loop amplitude computed in Ref. [428] and cross-checked with an in-house calculation. The top quark contributions in the double virtual two-loop diagrams are not included in the results below. Table 20 shows cross section results for the central scale $\mu_R = \mu_F = m_Z$, including 7-point scale variations. In Table 21 results for the dynamic scale $\mu_R = \mu_F = m_{ZZ}/2$ are given.

Table 20: Inclusive cross section for ZZ production at the LHC for $\sqrt{s}$ =14 TeV and $\sqrt{s}$ =27 TeV at LO, NLO and NNLO with $\mu_R = \mu_F = m_Z$. The uncertainties are obtained by varying the renormalisation and factorisation scales in the range $m_Z/2 < \mu_R, \mu_F < 2m_Z$ with the constraint $0.5 < \mu_F/\mu_R < 2$.

	σ_{LO} [pb]	σ_{NLO} [pb]	σ_{NNLO} [pb]	$gg \to ZZ$ [pb]
14 TeV	$10.80^{+5.7\%}_{-6.7\%}$	$15.55^{+3.0\%}_{-2.4\%}$	$18.50^{+3.0\%}_{-3.2\%}$	$1.56^{+25\%}_{-18\%}$
27 TeV	$23.59^{+10.0\%}_{-10.9\%}$	$35.59^{+3.2\%}_{-4.2\%}$	$44.52^{+3.7\%}_{-4.1\%}$	$4.81^{+25\%}_{-18\%}$

Table 21: Inclusive cross section for ZZ production at the LHC for $\sqrt{s}$ =14 TeV and $\sqrt{s}$ =27 TeV at LO, NLO and NNLO with the dynamic scale choice $\mu_R = \mu_F = m_{ZZ}/2$. The uncertainties are obtained by varying the renormalisation and factorisation scales in the range $m_{ZZ}/4 < \mu_R, \mu_F < m_{ZZ}$ with the constraint $0.5 < \mu_F/\mu_R < 2$.

	σ_{LO} [pb]	σ_{NLO} [pb]	σ_{NNLO} [pb]	$gg \to ZZ$ [pb]
14 TeV	$11.03^{+5.2\%}_{-6.1\%}$	$15.38^{+2.5\%}_{-2.0\%}$	$18.20^{+3.3\%}_{-2.3\%}$	$1.41^{+23\%}_{-18\%}$
27 TeV	$24.68^{+9.0\%}_{-9.8\%}$	$35.43^{+2.6\%}_{-3.7\%}$	$43.71^{+3.3\%}_{-3.2\%}$	$4.41^{+23\%}_{-17\%}$

Figures 35 and 36 show largely non-overlapping scale uncertainty bands between NLO and NNLO, both for a fixed central scale choice $\mu = m_Z$ as well as for a dynamic central scale choice $\mu = m_{ZZ}/2$. This demonstrates that for this process, the scale variations are insufficient to estimate missing higher order terms in the perturbative expansion. This is mostly due to the fact that at NNLO, the loop-induced gluon fusion channel $gg \to ZZ$ opens up, and due to the large gluon flux it represents a numerically significant contribution, about 8% at $\sqrt{s} = 14$ TeV and 11% at $\sqrt{s} = 27$ TeV of the total NNLO cross section, for both central scale choices. Further studies of the gluon channel can be seen in Refs. [429,430]. Since this new channel contributes for the first time at NNLO its contribution cannot be captured by the scale variations of the NLO cross section. Therefore, with increasing perturbative order, a systematic reduction of the factorisation scale dependence of the cross section is observed (indicated by the thickness of the scale uncertainty band), while there is no significant reduction of the renormalisation scale dependence. To show that this effect can be attributed to the gluon fusion channel opening up at NNLO, the NNLO result excluding this channel is also shown in Figs. 35 and 36.

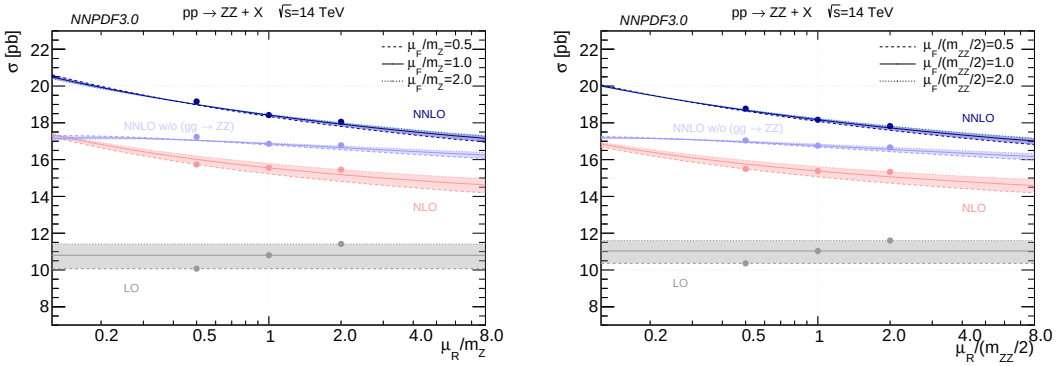

Fig. 35: Renormalisation and factorisation scale dependence of the ZZ cross section for $\sqrt{s} = 14\,\text{TeV}$ at LO, NLO and NNLO for the fixed central scale choice $\mu_R = \mu_F = m_Z$ (left) and for the dynamic central scale choice $\mu_R = \mu_F = m_{ZZ}/2$ (right). The NNLO result without the gluon fusion contributions is shown in light blue. The thickness of the bands show the variation with the factorisation scale, while the slope shows the renormalisation scale dependence. The scale uncertainties are the envelope of scale variations by a factor of two up and down with the constraint $0.5 < \mu_F/\mu_R < 2$, i.e. 7-point scale variations.

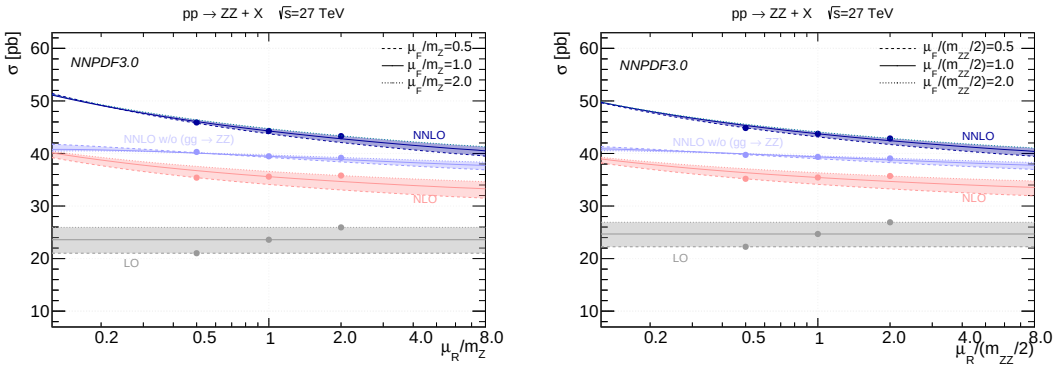

Fig. 36: Renormalisation and factorisation scale dependence of the ZZ cross section for $\sqrt{s} = 27\,\text{TeV}$ at LO, NLO and NNLO for the fixed central scale choice $\mu_R = \mu_F = m_Z$ (left) and for the dynamic central scale choice $\mu_R = \mu_F = m_{ZZ}/2$ (right). The NNLO result without the gluon fusion contributions is shown in light blue, and the bands are produced in the same way as in Fig. 35.

4.4.2 *Gauge-boson pair production with MATRIX*[15]

NNLO QCD predictions for W^+W^-, $W^\pm Z$ and ZZ production in proton–proton collisions are presented in this section. Two LHC upgrade scenarios are considered, namely the HL-LHC running at $\sqrt{s} = 14\,\text{TeV}$ with an assumed integrated luminosity of $3\,\text{ab}^{-1}$, and the HE-LHC at $\sqrt{s} = 27\,\text{TeV}$ with $15\ \text{ab}^{-1}$. More precisely, the following inclusive hard-scattering processes are considered

$$
\begin{aligned}
pp &\to \ell^+\nu_\ell\,\ell'^-\bar{\nu}_{\ell'} + X\,,\\
pp &\to \ell\nu_\ell\,\ell'^+\ell'^- + X\,,\\
pp &\to \ell^+\ell^-\ell'^+\ell'^- + X\,,
\end{aligned}
$$

where all off-shell effects and interference contributions are fully accounted for.

[15] Contribution by S. Kallweit, M. Grazzini and M. Wiesemann.

All results are obtained with the public parton-level NNLO framework MATRIX. This program, and earlier versions of it, have been used to compute state-of-the-art QCD predictions for gauge-boson pair production processes [431–439].[16] All tree-level and one-loop amplitudes are evaluated with OPENLOOPS[17] [10,444]. At two-loop level the $q\bar{q} \to VV'$ amplitudes of Ref. [428] are used.

The complex mass scheme [382] is applied throughout, i.e. complex W- and Z-boson masses are used and the EW mixing angle is defined as $\cos\theta_W^2 = (m_W^2 - i\Gamma_W m_W)/(m_Z^2 - i\Gamma_Z m_Z)$. For the input of the weak parameters the G_μ scheme is employed with $\alpha = \sqrt{2}\, G_\mu |(m_W^2 - i\Gamma_W m_W)\sin^2\theta_W|/\pi$. The following parameters are set, $G_F = 1.16639\times10^{-5}\,\text{GeV}^{-2}$, $m_W = 80.399\,\text{GeV}$, $\Gamma_W = 2.1054\,\text{GeV}$, $m_Z = 91.1876\,\text{GeV}$, $\Gamma_Z = 2.4952\,\text{GeV}$, $m_H = 125\,\text{GeV}$ and $\Gamma_H = 0.00407\,\text{GeV}$. Furthermore, a diagonal CKM matrix is used.

The number of light quarks is chosen differently for the processes under consideration: all W^+W^- results are obtained by applying the four-flavour scheme (4FS) with massive top and bottom quarks in order to consistently remove top-quark contamination by omitting the (separately IR finite) partonic processes with real bottom-quark emissions. In the 4FS, the on-shell bottom mass $m_b = 4.92\,\text{GeV}$ is used. For all other processes the five-flavour scheme (5FS) is applied with a vanishing bottom mass $m_b = 0$. The top quark is treated as massive and unstable throughout, and m_t is set to $173.2\,\text{GeV}$ as well as $\Gamma_t = 1.44262\,\text{GeV}$.[18]

The MMHT2014 [200] sets of parton distribution functions (PDFs) are used with $n_f = 4$ or $n_f = 5$ active quark flavours, consistently with the flavour scheme under consideration. N^{n}LO ($n = 0, 1, 2$) predictions are obtained by using PDFs at the same perturbative order and the evolution of α_S at $(n+1)$-loop order, as provided by the corresponding PDF set. To be precise, in the 5FS MMHT2014lo68cl, MMHT2014nlo68cl, and MMHTnnlo68cl at LO, NLO, and NNLO are used. In the 4FS MSTW2008lo68cl_nf4, MMHT2014nlo68cl_nf4, and MMHT2014nnlo68cl_nf4 at LO, NLO, and NNLO are used.

The central predictions are obtained by setting the factorization and renormalization scales to $\mu_F = \mu_R = \mu_0 \equiv E_{\text{T},V_1} + E_{\text{T},V_2}$, with $E_{\text{T},V_i} = \sqrt{M_{V_i}^2 + p_{\text{T},V_i}^2}$, where M_{V_i} is the invariant mass and p_{T,V_i} the transverse momentum of the respective vector boson. Uncertainties from missing higher-order contributions are estimated in the usual way by independently varying μ_F and μ_R in the range $0.5\mu_0 < \mu_F, \mu_R < 2\mu_0$ with the constraint $0.5 < \mu_F/\mu_R < 2$.

In Table 22 cross sections are presented for W^+W^-, $W^\pm Z$ and ZZ production, inclusive over the phase space of the final-state leptons, for pp collisions at $\sqrt{s} = 14\,\text{TeV}$ and $\sqrt{s} = 27\,\text{TeV}$. Throughout, only a basic selection cut on Z bosons is applied, by requiring the invariant masses of all opposite-sign same-flavour lepton pairs to be within a Z-mass window of $66\,\text{GeV} < m_{\ell^-\ell^+} < 116\,\text{GeV}$, which is necessary to avoid divergencies induced by soft intermediate photons. The gain in the inclusive cross section at $\sqrt{s} = 27\,\text{TeV}$ is roughly a factor of 2.5 for all processes under consideration, see last column of Table 22. The importance of QCD corrections is seen: Higher-order contributions are huge, especially for $W^\pm Z$ production. The NLO corrections range from about $+36\%$ to $+82\%$ depending on process and collider energy, while NNLO QCD corrections are still sizeable and induce a further increase of the cross sections of 13% to 20%. The cross-section ratio for W^+Z/W^-Z production is about 1.55 at NNLO for $\sqrt{s} = 14\,\text{TeV}$, changes to 1.42 for $\sqrt{s} = 27\,\text{TeV}$, and is essentially independent on the perturbative order.

[16] It was also used in the NNLL+NNLO computation for W^+W^- and ZZ production of Ref. [440], and in the NNLOPS computation for W^+W^- production of Ref. [153].

[17] OPENLOOPS which relies on the fast and stable tensor reduction of COLLIER [441,442], supported by a rescue system based on quad-precision CUTTOOLS [443] with ONELOOP [2] to deal with exceptional phase-space points.

[18] Massive top-quark contributions are neglected in the virtual two-loop corrections, but are kept everywhere else in the computations.

Table 22: Inclusive cross sections for W^+W^-, $W^\pm Z$ and ZZ production where the leptonic decays of the bosons are included.

σ [fb] (correction)		LO	NLO (NLO/LO−1)	NLO′+gg (NLO′+gg/NLO−1)	NNLO (NNLO/NLO−1)	$\frac{\sigma_{\rm NNLO}(27\,\text{TeV})}{\sigma_{\rm NNLO}(14\,\text{TeV})}$
W^+W^-	$\sqrt{s} = 14\,\text{TeV}$	$897.27(9)^{+4.3\%}_{-5.3\%}$	$1303.3(1)^{+2.7\%}_{-2.2\%}$ (+45.3%)	$1386.1(2)^{+3.7\%}_{-2.9\%}$ (+6.4%)	$1485.(1)^{+2.4\%}_{-2.2\%}$ (+13.9%)	2.33
	$\sqrt{s} = 27\,\text{TeV}$	$2091.5(2)^{+7.6\%}_{-8.6\%}$	$2988.4(3)^{+2.8\%}_{-2.9\%}$ (+42.9%)	$3213.0(4)^{+4.1\%}_{-3.2\%}$ (+7.0%)	$3457.(4)^{+2.8\%}_{-2.4\%}$ (+15.6%)	
W^+Z	$\sqrt{s} = 14\,\text{TeV}$	$60.322(6)^{+3.4\%}_{-4.3\%}$	$106.15(1)^{+3.6\%}_{-3.0\%}$ (+76.0%)	—	$120.5(1)^{+2.0\%}_{-1.9\%}$ (+13.5%)	2.35
	$\sqrt{s} = 27\,\text{TeV}$	$136.66(1)^{+6.8\%}_{-7.8\%}$	$248.51(2)^{+4.0\%}_{-3.3\%}$ (+81.8%)	—	$283.4(3)^{+2.1\%}_{-2.1\%}$ (+14.0%)	
W^-Z	$\sqrt{s} = 14\,\text{TeV}$	$39.182(4)^{+3.7\%}_{-4.7\%}$	$68.430(7)^{+3.7\%}_{-3.0\%}$ (+74.6%)	—	$77.63(7)^{+1.9\%}_{-1.9\%}$ (+13.4%)	2.57
	$\sqrt{s} = 27\,\text{TeV}$	$96.70(1)^{+7.2\%}_{-8.2\%}$	$175.44(2)^{+4.0\%}_{-3.3\%}$ (+81.4%)	—	$199.7(2)^{+2.0\%}_{-2.0\%}$ (+13.8%)	
ZZ	$\sqrt{s} = 14\,\text{TeV}$	$24.500(2)^{+4.3\%}_{-5.3\%}$	$34.201(3)^{+2.0\%}_{-1.8\%}$ (+39.6%)	$37.531(4)^{+3.3\%}_{-2.6\%}$ (+9.7%)	$39.64(4)^{+2.4\%}_{-2.1\%}$ (+15.9%)	2.40
	$\sqrt{s} = 27\,\text{TeV}$	$58.622(6)^{+7.9\%}_{-8.9\%}$	$79.757(8)^{+2.2\%}_{-3.0\%}$ (+36.1%)	$89.89(1)^{+3.7\%}_{-3.0\%}$ (+12.7%)	$95.20(9)^{+2.9\%}_{-2.4\%}$ (+19.4%)	

It should be stressed that QCD radiative corrections may change quite significantly as soon as fiducial cuts on the leptonic final state are applied, or when kinematical distributions are considered. The corrections for the inclusive cross sections in Table 22 should therefore be understood as illustrative, and the use of inclusive K-factors to obtain NNLO predictions from lower order results with different sets of cuts should be avoided in general.

It is interesting to quantify the size of the loop-induced gluon fusion contribution of the charge-neutral processes, which is part of the NNLO QCD corrections. By NLO′+gg its sum is denoted with the NLO cross section computed with NNLO PDFs. The NLO′+gg result for W^+W^- production is 6.4% (7.0%) larger than the NLO result at $\sqrt{s} = 14\,(27)$ TeV, while their difference is even 9.7% (12.7%) for ZZ production. These numbers amount to roughly half of the full NNLO correction of the W^+W^- process, and even about two-thirds for ZZ production. However, one has to bear in mind that under typical fiducial selection requirements on the leptons and missing transverse energy, the impact of the loop-induced contribution decreases significantly, especially for W^+W^- production. Furthermore, its relative contribution is strongly suppressed as far as the tails of the kinematical distributions are concerned, due to the large-x suppression of the gluon density.

To illustrate how strongly the radiative corrections may depend on the fiducial cuts, in Table 23 cross sections are shown with a minimum $p_{\rm T,min} = 100\,\text{GeV}$ cut on the transverse momentum of the charged leptons and the missing energy. More precisely, depending on the process the following cuts have been applied, as shown in Table 24.

As can be read from Tables 22 and 23, radiative corrections at NLO can be enormous for some processes with $p_{\rm T,min} = 100\,\text{GeV}$, ranging from +51% to even +281%. Also the NNLO corrections are significantly increased with respect to the inclusive case, and can be as large as +27%. It is also apparent that the importance of the loop-induced gluon fusion contribution is significantly reduced. For W^+W^- production, due to the applied $p_{\rm T,miss}$ cut the NLO′+gg contribution is even smaller than the NLO cross

Table 23: Cross sections with a $p_{\mathrm{T,min}} = 100\,\mathrm{GeV}$ cut on the transverse momentum of the charged leptons and the missing energy for W^+W^-, $W^\pm Z$ and ZZ production.

σ [fb] (correction)		LO	NLO (NLO/LO−1)	NLO′+gg (NLO′+gg/NLO−1)	NNLO (NNLO/NLO−1)	$\frac{\sigma_{\mathrm{NNLO}}(27\,\mathrm{TeV})}{\sigma_{\mathrm{NNLO}}(14\,\mathrm{TeV})}$
W^+W^-	$\sqrt{s} = 14\,\mathrm{TeV}$	$0.920(1)^{+2.7\%}_{-2.7\%}$	$2.827(5)^{+9.7\%}_{-8.0\%}$ (+207.1%)	$2.793(7)^{+9.9\%}_{-8.1\%}$ (−1.2%)	$3.51(1)^{+5.2\%}_{-5.0\%}$ (+24.3%)	3.93
	$\sqrt{s} = 27\,\mathrm{TeV}$	$2.847(3)^{+0.08\%}_{-0.5\%}$	$10.83(2)^{+8.2\%}_{-6.9\%}$ (+280.5%)	$10.66(2)^{+8.4\%}_{-7.1\%}$ (−1.6%)	$13.80(4)^{+5.3\%}_{-4.8\%}$ (+27.3%)	
W^+Z	$\sqrt{s} = 14\,\mathrm{TeV}$	$0.06524(8)^{+3.3\%}_{-3.2\%}$	$0.1273(3)^{+7.1\%}_{-5.8\%}$ (+95.2%)	—	$0.1485(9)^{+3.4\%}_{-3.3\%}$ (+16.6%)	3.82
	$\sqrt{s} = 27\,\mathrm{TeV}$	$0.1919(2)^{+0.1\%}_{-0.5\%}$	$0.4642(8)^{+7.0\%}_{-5.8\%}$ (+141.9%)	—	$0.568(3)^{+3.8\%}_{-3.6\%}$ (+22.5%)	
W^-Z	$\sqrt{s} = 14\,\mathrm{TeV}$	$0.03289(4)^{+3.1\%}_{-3.1\%}$	$0.0641(2)^{+7.5\%}_{-6.0\%}$ (+94.9%)	—	$0.0767(5)^{+3.4\%}_{-3.5\%}$ (+19.7%)	4.34
	$\sqrt{s} = 27\,\mathrm{TeV}$	$0.1121(1)^{+0.\%}_{-0.3\%}$	$0.2719(5)^{+7.2\%}_{-5.9\%}$ (+142.7%)	—	$0.333(2)^{+3.7\%}_{-3.5\%}$ (+22.5%)	
ZZ	$\sqrt{s} = 14\,\mathrm{TeV}$	$0.02108(3)^{+3.1\%}_{-3.1\%}$	$0.0318(1)^{+3.8\%}_{-3.2\%}$ (+50.6%)	$0.0342(1)^{+5.4\%}_{-4.3\%}$ (+7.7%)	$0.0371(3)^{+3.6\%}_{-3.0\%}$ (+16.9%)	3.70
	$\sqrt{s} = 27\,\mathrm{TeV}$	$0.0675(1)^{+0.\%}_{-0.2\%}$	$0.1100(3)^{+3.5\%}_{-2.8\%}$ (+62.9%)	$0.1235(3)^{+5.4\%}_{-4.3\%}$ (+12.3%)	$0.1371(7)^{+4.3\%}_{-3.5\%}$ (+24.7%)	

Table 24: Selection cuts applied in the analysis for the different processes.

	W^+W^-	$W^\pm Z$	ZZ
lepton cuts	$p_{\mathrm{T},\ell_{1/2}} > p_{\mathrm{T,min}}$	$p_{\mathrm{T},\ell_{1/2/3}} > p_{\mathrm{T,min}}$	$p_{\mathrm{T},\ell_{1/2/3/4}} > p_{\mathrm{T,min}}$
neutrino cuts	$p_{\mathrm{T,miss}} > p_{\mathrm{T,min}}$	$p_{\mathrm{T,miss}} > p_{\mathrm{T,min}}$	—

section by -1.2% (-1.6%) at $\sqrt{s} = 14\,(27)\,\mathrm{TeV}$ (i.e. the positive impact of the gg channel is smaller than the negative effect from using NNLO PDFs instead of NLO PDFs in the NLO′+gg prediction). For ZZ production, it is still sizeable with 7.7% (12.3%), but its relative contribution at $\mathcal{O}(\alpha_{\mathrm{S}}^2)$ has decreased from roughly two-thirds in the inclusive case to less than half of the NNLO corrections for $p_{\mathrm{T,min}} = 100\,\mathrm{GeV}$. Furthermore, compared to the inclusive results an even more substantial increase of the cross sections is observed from $\sqrt{s} = 14\,\mathrm{TeV}$ to $\sqrt{s} = 27\,\mathrm{TeV}$ of roughly a factor of four. This can be understood by the fact, that the additional energy enlarges the available phase-space, especially at high momentum transfer.

From the results in Table 22 and 23 it is clear that the perturbative uncertainties at NLO cannot account for the additional loop-induced gluon fusion contribution that appears at NNLO. Besides that, also the genuine NNLO corrections to the quark–antiquark production mechanism cannot be anticipated from NLO scale variations, which in turn means that the NLO uncertainties are underestimated. The inclusion of NNLO corrections is therefore crucial. At this order all partonic channels are included for the first time, and scale variations can be used to obtain an estimate of the actual size of missing higher-order terms. However, the NLO corrections to the loop-induced gluon fusion contribution are relevant and should be included when possible, especially at $\sqrt{s} = 27\,\mathrm{TeV}$ where gluons with smaller x are

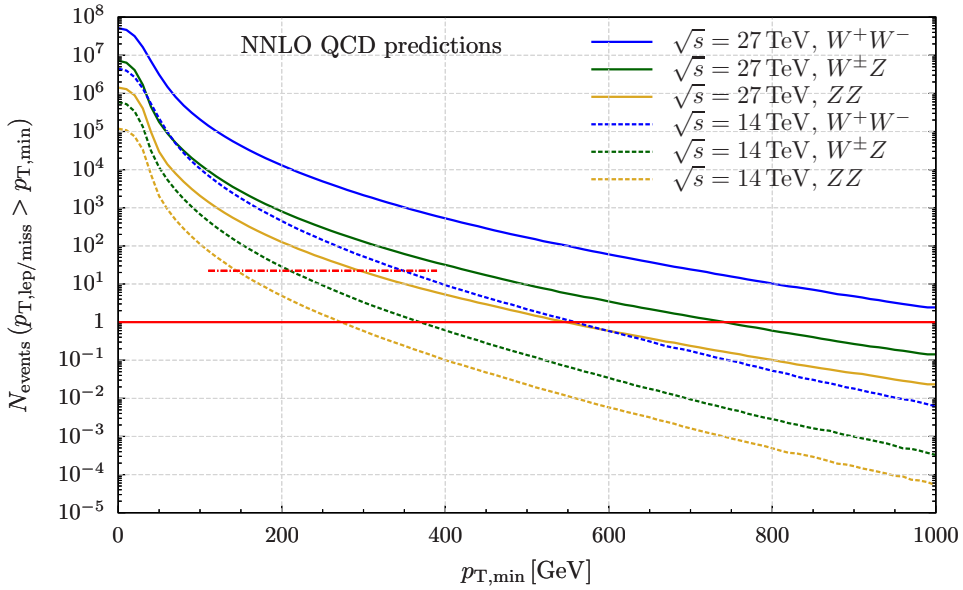

Fig. 37: Cumulative number of events as a function of $p_{\text{T,min}}$ for the following production processes: W^+W^- (blue), $W^\pm Z$ (green), and ZZ (orange); at 14 TeV (dashed) and 27 TeV (solid).

probed. In particular in tails of high-energy observables, the inclusion of NLO EW corrections and their interplay with QCD corrections will also need to be investigated. Nevertheless NNLO QCD results are presented in the following, but the above-mentioned extensions will become available well before the start of the HL-LHC.

The differential results in diboson processes in light of the HL and HE upgrades of the LHC are now discussed. Since the importance of highest-order predictions is evident from the previous discussion, only NNLO QCD accurate results are presented here. The cumulative cross section with a minimum $p_{\text{T,min}}$ cut, as introduced above is considered first. In order to analyse the number of expected events as a function of $p_{\text{T,min}}$, the cross sections have been translated into event numbers by assuming an integrated luminosity of $3\,\text{ab}^{-1}$ at 14 TeV and of $15\,\text{ab}^{-1}$ at 27 TeV.

Figure 37 shows the expected number of events as a function of $p_{\text{T,min}}$. Since the transverse momentum of all leptonic final states are restricted simultaneously, the reach in the tails may appear smaller than expected, and would be significantly larger if a cut on the transverse momentum of only the leading lepton or the missing energy were to be considered. However, the toy scenario considered is well suited to compare the three diboson production processes, and to quantify the relative gain of the additional energy and luminosity.

The curves in Fig. 37 show all production processes under consideration: W^+W^- (blue), $W^\pm Z$ (green), and ZZ (orange); at 14 TeV (dashed) and 27 TeV (solid). The horizontal red line shows the one-event threshold, below which no events are expected anymore. The following features are evident in the plot: At $\sqrt{s} = 14\,\text{TeV}$ events up to $p_{\text{T,min}}$ values of roughly 550 GeV, 370 GeV, and 270 GeV are expected for W^+W^-, $W^\pm Z$, and ZZ production, respectively. At $\sqrt{s} = 27\,\text{TeV}$ these values read >1000 GeV, 740 GeV, and 550 GeV. To put these numbers into perspective, a dash-dotted red line for the present status at the end of Run-2 is added, which represents the one-event threshold for $150\,\text{fb}^{-1}$ at 13 TeV (14 TeV $\to$ 13 TeV conversion approximated by a constant cross-section correction factor of 0.9). Its intersection points with the $\sqrt{s} = 14\,\text{TeV}$ curves indicates the current reach of the LHC, which is roughly up to 350 GeV, 210 GeV, and 140 GeV for W^+W^-, $W^\pm Z$, and ZZ production, respectively. The improved reach in the tails at 27 TeV is not only related to the larger inclusive cross section and

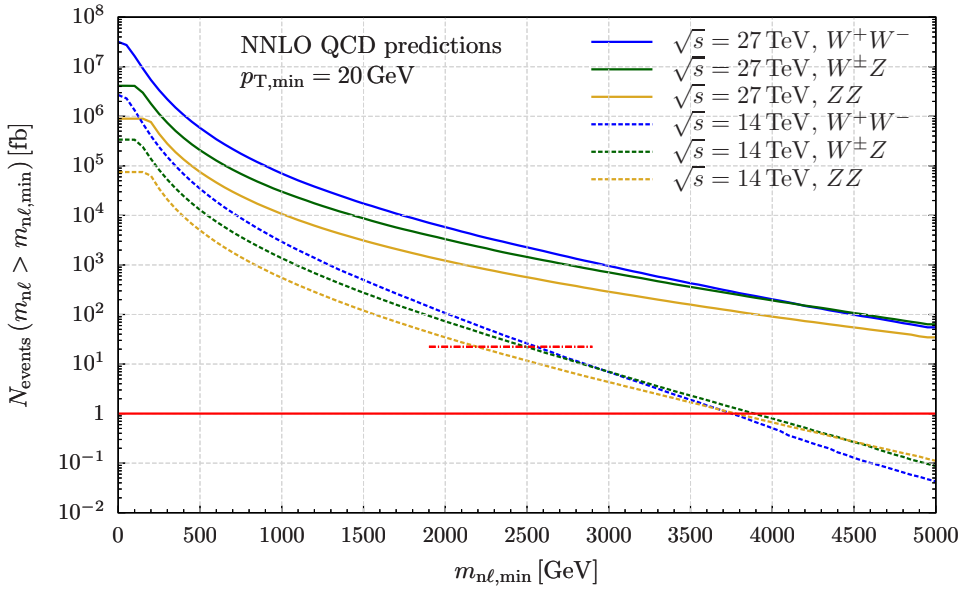

Fig. 38: Cumulative number of events as a function of $m_{n\ell,\mathrm{min}}$ for the following production processes: W^+W^- (blue), $W^\pm Z$ (green), and ZZ (orange); at 14 TeV (dashed) and 27 TeV (solid).

higher luminosity, but also the enlarged phase-space available with higher energies plays an important role: Whereas the solid curves fall only by $7-8$ orders of magnitude in the range of $0\,\mathrm{GeV} \leq p_{\mathrm{T,min}} \leq 1000\,\mathrm{GeV}$, the dashed 14 TeV curves fall by more than 9 orders of magnitude in the same region. This also explains why the 14 TeV W^+W^- result, which has a much larger inclusive cross section, crosses the red one-event line at almost the same point as the 27 TeV ZZ result.

In Fig. 38 the reach of the three vector-boson pair production processes is considered for future LHC upgrades in the invariant-mass distributions of all produced charged leptons. A scenario is chosen where $p_{\mathrm{T,min}}$, defined as before in the three processes, is 20 GeV in order to have at least a rough definition of the fiducial phase-space. The expected number of events, assuming the same integrated luminosities as stated above, is shown for $\sqrt{s} = 14\,\mathrm{TeV}$ (dashed) and $\sqrt{s} = 27\,\mathrm{TeV}$ (solid) with a lower cut $m_{n\ell} > m_{n\ell,\mathrm{min}}$, where n is the number of leptons in the respective process, i.e., for W^+W^- production it is the distribution in $m_{2\ell}$ (blue), for $W^\pm Z$ it is the one in $m_{3\ell}$ (green), and for ZZ in $m_{4\ell}$ (orange). The significant reach in energy for both the HL run of the LHC and a potential HE upgrade is evident, where “reach" refers to the point where the curves cross the red horizontal one-event threshold. A resonance in the tails of the invariant masses of two leptons (plus missing transverse momentum) or of four leptons is indeed a realistic signature predicted by many BSM theories. While with the current Run-2 data (red, dash-dotted line crossing the 14 TeV results) searches can hardly pass the two TeV frontier, future LHC upgrades will probe mass scales of a few TeV at 14 TeV with $3\,\mathrm{ab}^{-1}$, or potentially even up to ten TeV at 27 TeV with $15\,\mathrm{ab}^{-1}$. It is also apparent that despite $\sigma_{W^+W^-} \gg \sigma_{W^\pm Z} \gg \sigma_{ZZ}$ holding inclusively, the point where the three lines fall below one event is much closer. This is simply caused by the fact that the phase space of the four-lepton system in ZZ production is larger than the one of the three-lepton system in $W^\pm Z$ production, where some energy is taken by the additional neutrino. An analogous interpretation applies to W^+W^- production. Furthermore, also here the significantly enlarged phase space induced by the increase in energy at 27 TeV is evident: The 27 TeV results drop by roughly $4-5$ orders of magnitude in the displayed range, while the 14 TeV ones drop by more than 6 orders.

The study is continued by analysing the importance of the additional fiducial phase space that

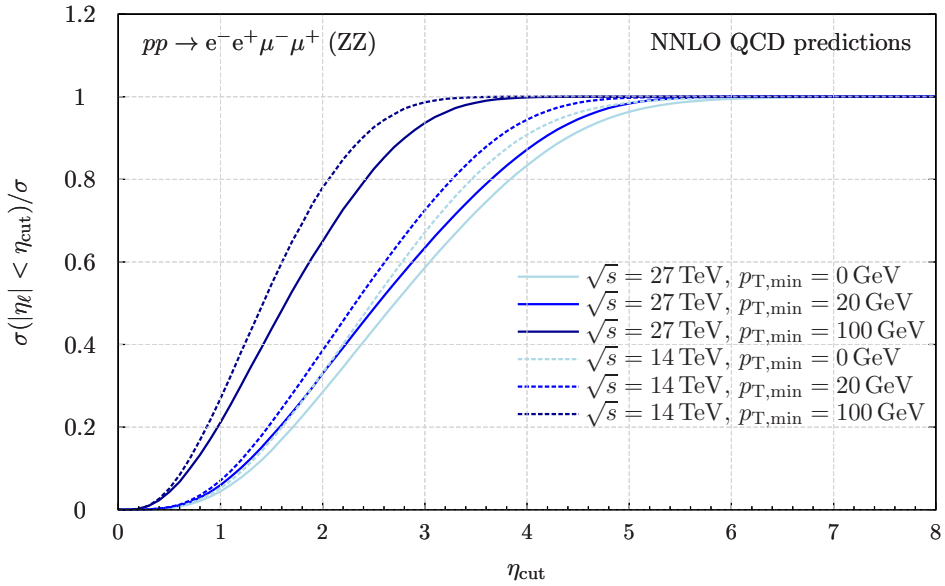

Fig. 39: Rapidity efficiency of the charged leptons.

becomes available with detector upgrades to enlarge the accessible rapidity range of charged leptons. Since very similar results were found for W^+W^-, $W^\pm Z$ and ZZ production in that respect, in Fig. 39 the rapidity efficiency of the four-lepton signature for ZZ production only is shown. The rapidity efficiency is defined as the ratio of the cross section with an absolute-rapidity cut η_{cut} on all four charged leptons, divided by the inclusive cross section. As for $\eta_{\text{cut}} \to \infty$ no cut is applied, the ratio tends to unity for large η_{cut} values. The efficiency as a function of η_{cut} is studied for three $p_{\text{T,min}}$ scenarios: inclusive (light blue), $p_{\text{T,min}} = 20\,\text{GeV}$ (blue), and $p_{\text{T,min}} = 100\,\text{GeV}$ (dark blue); at 14 TeV (dashed) and 27 TeV (solid). It is directly observed that the efficiency decreases with the machine energy. In other words, a small rapidity threshold at 27 TeV results in a much larger (relative) reduction of the cross section than at 14 TeV. This is because the additional energy induces more forward (and boosted) leptons, and it shows that detector upgrades that enlarge the measurable rapidity range become even more important at the HE LHC. Requiring minimum transverse-momentum cuts, on the other hand, has the effect of increasing the rapidity efficiency, which is particularly striking for $p_{\text{T,min}} = 100\,\text{GeV}$. The reason for this is simple: Leptons with high transverse momentum are predominantly produced at central rapidities.

The scenario with $p_{\text{T,min}} = 20\,\text{GeV}$ provides the most realistic fiducial setup, which is actually not much different from the fully inclusive case, and is discussed here. Typical rapidity cuts on charged leptons with the current LHC detectors are of the order of $\eta_\ell = 2.5$. Future detector upgrades for the HL phase of the LHC can be expected to reach rapidities at the level of $\eta_\ell = 4$. At 14 (27) TeV this would allow us to improve measurements of fiducial cross from a $<60\%$ ($\sim 50\%$) efficiency for $\eta_{\text{cut}} = 2.5$ to a $>90\%$ ($\lesssim 90\%$) efficiency for $\eta_{\text{cut}} = 4$. This implies that the available inclusive cross section will be hardly reduced by fiducial rapidity requirements anymore once the detectors have been upgraded. This statement holds even more when considering scenarios with boosted leptons: For $p_{\text{T,min}} = 100\,\text{GeV}$ the efficiency is practically 100% for $\eta_{\text{cut}} = 4$.

4.4.3 *Projections for measurements of anomalous 3-gauge boson couplings*[19]

The sensitivity of the production of W^+W^- pairs to anomalous gauge boson and anomalous fermion couplings at future LHC upgrades is now discussed. The $SU(2) \times U(1)$ structure of the electroweak sector of the Standard Model determines the W^+W^-V interactions ($V = \gamma, Z$). The amplitudes for the production of W^+W^- pairs involve subtle cancellations between contributions that grow with energy, so the pair production of gauge bosons is extremely sensitive to new physics interactions. Assuming C and P conservation, the most general Lorentz invariant $3-$gauge boson couplings can be written as in Ref. [445, 446]

$$\begin{aligned}\mathcal{L}_V &= -ig_{WWV}\Big\{(1+\delta g_1^V)\left(W^+_{\mu\nu}W^{-\mu}V^\nu - W^-_{\mu\nu}W^{+\mu}V^\nu\right) + (1+\delta\kappa^V)W^+_\mu W^-_\nu V^{\mu\nu}) \\ &\quad + \frac{\lambda^V}{M_W^2}W^+_{\rho\mu}W^{-\mu}{}_\nu V^{\nu\rho}\Big\}, \end{aligned} \tag{20}$$

where $V = \gamma, Z$, $g_{WW\gamma} = e$, $g_{WWZ} = g\cos\theta_W$, $s_W \equiv \sin\theta_W$, $c_W \equiv \cos\theta_W$, and in the SM, $\delta g_1^V = \delta\kappa^V = \lambda^V = 0$. Because of gauge invariance, this form can be translated into the language of effective field theory, where δg_1^V , $\delta\kappa^V$, $\lambda^V \sim \frac{v^2}{\Lambda^2}$, with Λ the scale of BSM physics, $\Lambda \gg v$.

The effective couplings of fermions to gauge fields are parameterised as,

$$\begin{aligned}\mathcal{L} &= \frac{g}{c_W}Z_\mu\left[g_L^{Zq} + \delta g_L^{Zq}\right]\overline{q}_L\gamma_\mu q_L + g_Z Z_\mu\left[g_R^{Zq} + \delta g_R^{Zq}\right]\overline{q}_R\gamma_\mu q_R \\ &\quad + \frac{g}{\sqrt{2}}\left\{W_\mu\left[(1+\delta g_L^W)\overline{q}_L\gamma_\mu q'_L + \delta g_R^W\,\overline{q}_R\gamma_\mu q'_R\right] + h.c.\right\}, \end{aligned} \tag{21}$$

where Q_q is the electric charge of the quarks, and q denotes up-type or down-type quarks. The anomalous fermion couplings also scale as $\delta g_{L,R}^{Zq}, \delta g_{L,R}^W \sim \frac{v^2}{\Lambda^2}$. The SM quark couplings are $g_R^{Zq} = -s_W^2 Q_q$ and $g_L^{Zq} = T_3^q - s_W^2 Q_q$ with $T_3^q = \pm\frac{1}{2}$. $SU(2)$ invariance relates the coefficients, $\delta g_L^W = \delta g_L^{Zf} - \delta g_L^{Zf'}$, $\delta g_1^Z = \delta\kappa^Z + \frac{s_W^2}{c_W^2}\delta\kappa^\gamma$ and $\lambda^\gamma = \lambda^Z$, where f denotes up-type quarks and f' down-type quarks.

The anomalous 3-gauge boson and fermion couplings have been implemented into the POWHEG BOX framework [447–449] for W^+W^- production and samples of events are generated with $pp \to W^+W^- \to \mu^\pm e^\mp \nu\nu$. Fits to 8 TeV data [450, 451] illustrate the importance of including both anomalous fermion and 3-gauge boson couplings. The sensitivity to anomalous couplings results almost entirely from contributions quadratic in the anomalous couplings and the effects of anomalous 3-gauge boson and fermion couplings are numerically similar.

To probe the sensitivity to anomalous couplings, events are generated using the cuts

$$p_{\rm T}^l > 30\ {\rm GeV},\ |\,\eta^l\,| < 2.5,\ m_{ll} > 10\ {\rm GeV}, E_{\rm T}^{\rm miss} > 20\ {\rm GeV}\,. \tag{22}$$

These cuts are similar to those applied in the ATLAS [452] and CMS [453] extractions of anomalous coupling limits using the 8 TeV data. A hypothetical future systematic uncertainty of $\delta_{sys} = 16\%$ is postulated and a cut on the $p_{\rm T}$ of the leading lepton applied such that the systematic error is smaller than the statistical error, $\delta_{stat} = \frac{1}{\sqrt{L\sigma(p_{l,T}^{lead} > p_{\rm T}^{cut})}} > \delta_{sys}$,where L is the integrated luminosity. The integrated cross section above a $p_{\rm T}^{cut}$ is evaluated, assuming a 50 % efficiency and the cuts set as

$$27\ {\rm TeV\ with}\ 15\,{\rm ab}^{-1}: \quad p_{\rm T}^{cut} = 750\ {\rm GeV}, \qquad 14\ {\rm TeV\ with}\ 3\,{\rm ab}^{-1}: p_{\rm T}^{cut} = 1350\ {\rm GeV}\,. \tag{23}$$

[19] Contribution by J. Baglio, S. Dawson and I. M. Lewis.

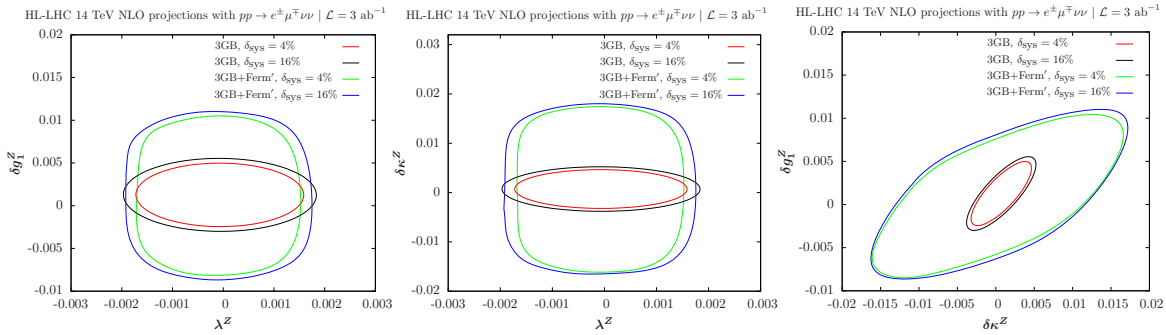

Fig. 40: Projections for 14 TeV with 3 ab^{-1}. $p_{\mathrm{T},cut} = 750$ GeV, corresponding to $\delta_{stat} = 16\%$ with $\delta_{sys} = 4\%$ and $\delta_{sys} = 16\%$. The curves labelled 3GB have SM Z-fermion couplings, while the curves labelled 3GB +Ferm' allow the Z-fermion couplings to vary around a central value of 0.

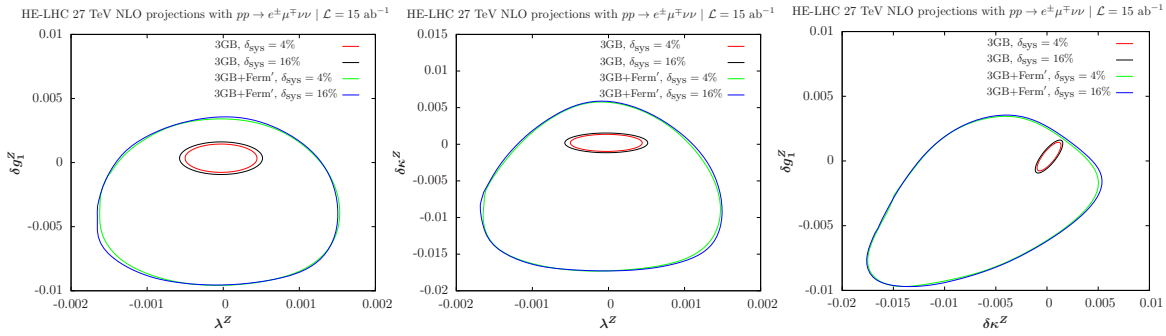

Fig. 41: Projections for 27 TeV with 15 ab^{-1}. $p_{\mathrm{T},cut} = 1350$ GeV, corresponding to $\delta_{stat} = 16\%$ with $\delta_{sys} = 4\%$ and $\delta_{sys} = 16\%$. The curves labelled 3GB have SM Z-fermion couplings, while the curves labelled 3GB +Ferm' allow the Z-fermion couplings to vary around a central value of 0.

The calculations are performed at NLO QCD, using CT14qed-inc-proton PDFs, and the renormalisation/factorisation scales are taken to be to be $M_{WW}/2$. It is assumed the $Wl\nu$ couplings in the decays are SM-like.

The results of the scans are shown in Figs. 40 and 41; the allowed regions are within the ellipses. A significant improvement going from 14 TeV to 27 TeV is seen, while the improvement from reducing the systematic error, $\delta_{sys} = 0.16 \to 0.04$, is marginal. The fermion couplings are allowed to vary around 0, assuming the 2σ errors from fits to LEP data. As can be seen, by including the anomalous fermion couplings, the sensitivity of the scan is significantly reduced [449, 450, 454]. This effect is quite pronounced at 27 TeV and implies that global fits to both anomalous fermion and 3 gauge boson couplings are necessary.

4.4.4 Prospects for the measurement of the W-boson mass

Special low pile-up proton-proton collision data at the HL-LHC (and HE-LHC) will be of large interest for W boson physics. At $\sqrt{s} = 14$ TeV and for an instantaneous luminosity of $\mathcal{L} \sim 5 \times 10^{32}$ cm^{-2}s^{-1}, corresponding to two collisions per bunch crossing on average, about $2{\times}10^6$ W boson events can be collected in one week. Such a sample provides a statistical sensitivity at the permille level for cross section measurements, at the percent level for measurements of the W boson transverse momentum distribution, and of about 10 MeV for a measurement of m_W. The increased acceptance provided by the new inner detector in ATLAS, the ITk [281], extends the coverage in pseudorapidity from $|\eta| < 2.5$ to

$|\eta| < 4$ and allows further constraints on the parton density functions (PDFs) from cross section measurements, reducing the corresponding uncertainties in the measurement of m_W. An energy increase at the HE-LHC to $\sqrt{s} = 27$ TeV [455] could play a similar role. A first quantitative study of the potential improvement in the W-boson mass using low pile-up data at the HL-LHC and HE-LHC is discussed in [456] considering only statistical and PDF uncertainties. Experimental systematic uncertainties can be maintained at a level similar to the statistical uncertainty, since they are largely dominated by the statistics of the low pile-up samples. Other theoretical uncertainties in the modelling of the W-boson production, like the description of the boson transverse momentum distribution, will also be constrained by measurements using these data.

Leptonic W boson decays are characterised by an energetic, isolated electron or muon, and significant missing transverse momentum reflecting the decay neutrino. The hadronic recoil, u_{T}, is defined from the vector sum of the transverse momenta of all reconstructed particles in the event excluding the charged lepton, and provides a measure of the W boson transverse momentum. The lepton transverse momentum, p_{T}^{ℓ}, the missing transverse momentum, $E_{\mathrm{T}}^{\mathrm{miss}}$, and the hadronic recoil are related through $\vec{E}_{\mathrm{T}}^{\mathrm{miss}} = -(\vec{p}_{\mathrm{T}}^{\ell} + \vec{u}_{\mathrm{T}})$. The p_{T}^{ℓ} and $E_{\mathrm{T}}^{\mathrm{miss}}$ distributions have sharp peaks at $p_{\mathrm{T}}^{\ell} \sim E_{\mathrm{T}}^{\mathrm{miss}} \sim m_W/2$. The transverse mass m_{T}, defined as $m_{\mathrm{T}} = \sqrt{2p_{\mathrm{T}}^{\ell} E_{\mathrm{T}}^{\mathrm{miss}} \cos(\phi_{\ell} - \phi_{\mathrm{miss}})}$, peaks at $m_{\mathrm{T}} \sim m_W$.

Events are generated at $\sqrt{s} = 14$ and 27 TeV using the W_EW_BMNNP process [136] of the POWHEG v1 event generator [314], with electroweak corrections switched off. The CT10 PDF set [457] is used, and parton shower effects are included using the PYTHIA v8 event generator [149] with parameters set according to the AZNLO tune [458]. Final-state QED corrections are applied using PHOTOS [459]. The energy resolutions of the lepton and hadronic recoil are parameterised as a function of the truth-related observables in order to emulate detector effects. These parameterised resolutions are checked against simulated distributions at the reconstructed level, and they agree at the level of a few percent.

Events are selected by applying the following cuts to the object kinematics, after resolution corrections: $p_{\mathrm{T}}^{\ell} > 25$ GeV, $E_{\mathrm{T}}^{\mathrm{miss}} > 25$ GeV, $m_{\mathrm{T}} > 50$ GeV and $u_{\mathrm{T}} < 15$ GeV; $|\eta_{\ell}| < 2.4$ or $2.4 < |\eta_{\ell}| < 4$. The first set of cuts selects the range of the kinematic peaks of the W boson decay products, restricting to the region of small p_{T}^{W} to maximise the sensitivity of the distributions to m_W. Two pseudorapidity ranges are considered, corresponding to the central region accessible with the current ATLAS detector, and to the forward region accessible in the electron channel with the ITk.

The Monte Carlo samples are produced using the CT10 PDF set, $m_W^{\mathrm{ref}} = 80.399$ GeV, and the corresponding Standard Model prediction for Γ_W. Kinematic distributions for the different values of m_W are obtained by applying an event weight to the reference samples based on the ratio of the Breit–Wigner densities corresponding to m_W and m_W^{ref}, for a given value of the final state invariant mass. A similar event weight, calculated internally by POWHEG and corresponding to the ratio of the event cross sections predicted by CT10 and several alternate PDFs, is used to obtain final state distributions corresponding to the CT14 [199], MMHT2014 [200], HL-LHC [298] and LHeC [460] PDF sets and their associated uncertainties. Compared to current sets such as CT14 and MMHT2014, the HL-LHC set incorporates the expected constraints from present and future LHC data; it starts from the PDF4LHC convention [195] and comes in three scenarios corresponding to more or less optimistic projections of the experimental uncertainties. The LHeC PDF set represents the impact of a proposed future high-energy, high-luminosity ep scattering experiment [461] on the uncertainties in the proton structure, using the theoretically best understood process for this purpose.

The shift in the measured value of m_W resulting from a change in the assumed PDF set is estimated as follows. Considering a set of template distributions obtained for different values of m_W and a given reference PDF set, and "pseudo-data" distributions obtained for $m_W = m_W^{\mathrm{ref}}$ and an alternate set i (representing, for example, uncertainty variations with respect to the reference set), the preferred value

of m_W for this set is determined by minimising the χ^2 between the pseudo-data and the templates. The preferred value is denoted m_W^i, and the corresponding variation is defined as $\delta m_W^i = m_W^i - m_W^{\text{ref}}$. The statistical uncertainty on the measurement is estimated from the half width of the χ^2 function one unit above the minimum.

The present study considers measurements of m_W in separate categories, corresponding to W^+ and W^- events; five pseudorapidity bins, $|\eta_\ell| < 0.6$, $0.6 < |\eta_\ell| < 1.2$, $1.2 < |\eta_\ell| < 1.8$, $1.8 < |\eta_\ell| < 2.4$, and $2.4 < |\eta_\ell| < 4$; p_{T}^ℓ and m_{T} distribution fits; and two centre-of-mass energies ($\sqrt{s} = 14$ and 27 TeV). For each category α and for the PDF sets considered here, the Hessian uncertainty corresponding to a given set is estimated as $\delta m_{W\alpha}^+ = \left[\sum_i \left(\delta m_{W\alpha}^i\right)^2\right]^{1/2}$, if $\delta m_{W\alpha}^i > 0$, and as $\delta m_{W\alpha}^- = \left[\sum_i \left(\delta m_{W\alpha}^i\right)^2\right]^{1/2}$, if $\delta m_{W\alpha}^i < 0$, where i runs over the uncertainty sets, and $\delta m_{W\alpha}^i$ is calculated with respect to the reference PDF set. For CT10 and CT14, the uncertainties are divided by a factor 1.645 to match the 68% CL. Only symmetrised uncertainties, $\delta m_{W\alpha} = (\delta m_{W\alpha}^+ + \delta m_{W\alpha}^-)/2$, are considered for simplicity. The correlation of PDF uncertainties between different measurement categories is calculated as $\rho_{\alpha\beta} = \frac{\sum_i \delta m_{W\alpha}^i \delta m_{W\beta}^i}{\delta m_{W\alpha} \delta m_{W\beta}}$.

PDF variations generate correlated variations in the p_{T}^W and p_{T}^Z distributions, while the latter are strongly constrained by experimental data [458, 462]. These constraints were used in the ATLAS measurement of m_W [189], bringing significant reduction in the PDF uncertainties. The uncertainties estimated here are thus conservative from this perspective, and partly account for uncertainties in the p_{T}^W distribution.

The overall measurement precision is evaluated by combining the results obtained in the different categories using the BLUE prescription [463]. Only statistical and PDF uncertainties are considered. The former are assigned assuming an integrated luminosity of 200 pb^{-1}, and normalising the samples to the expected cross-sections. The expected measurement uncertainties, together with their statistical and PDF components, are summarised in Fig. 42 (a) for CT10. The numbers quoted for $0 < |\eta_\ell| < 2.4$ correspond to the combination of the four pseudorapidity bins in this range. Moderate or negative PDF uncertainty correlations, leading to reduced combined uncertainties, are observed between categories of different W-boson charges, and between central and forward pseudorapidities, at given $\sqrt{s}$. On the other hand, PDF uncertainty correlations tend to be large and positive between $\sqrt{s} = 14$ and 27 TeV, for a given boson charge and lepton pseudorapidity range. With 200 pb^{-1} of data collected at each energy, a total uncertainty of about 10 MeV is obtained.

Table 25 and Fig. 42 (b) compare the uncertainties obtained for different PDF sets. The CT10 and CT14 sets display similar uncertainty correlations, leading to similar improvements under combination of categories, and yielding comparable final PDF uncertainties. The MMHT2014 uncertainties are about 30% lower. The three projected HL-LHC PDF sets give very similar uncertainties; the most conservative one is shown here. Compared to CT10 and CT14, a reduction in PDF uncertainty of about a factor of two is obtained. The LHeC projection results from a QCD fit to 1 ab^{-1} of ep scattering pseudodata, with $E_e = 60$ GeV and $E_p = 7$ TeV. Such a sample could be collected in about five years, synchronously with the HL-LHC operation. In this configuration, the neutral- and charged-current DIS samples are sufficient to disentangle the first and second generation parton densities without ambiguity, and reduce the PDF uncertainty below 2 MeV, a factor 5–6 compared to present knowledge. Also in this case the m_W measurement will benefit from the large W boson samples collected at the LHC, and from the anti-correlation between central and forward categories. In this context, PDF uncertainties would still be sub-leading with 1 fb^{-1} of low pile-up data.

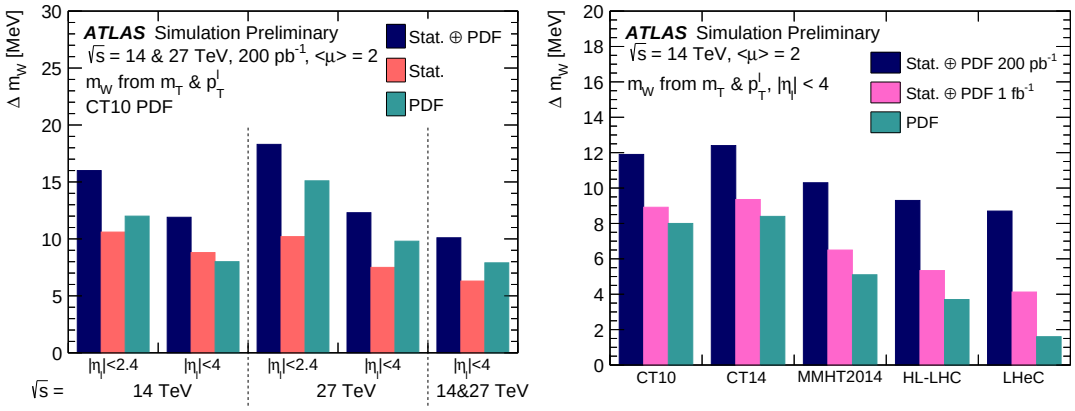

(a) (b)

Fig. 42: Measurement uncertainty for combined fits to the p_{T}^{ℓ} and m_{T} distributions (a) in different lepton acceptance regions and for different centre-of-mass energies, using the CT10 PDF set and for 200 pb^{-1}collected at each energy and (b) for different PDF sets in $|\eta_{\ell}| < 4$, for 200 pb^{-1}and 1 fb^{-1}collected at $\sqrt{s} = 14$ TeV. The numbers quoted for $0 < |\eta_{\ell}| < 2.4$ correspond to the combination of the four pseudorapidity bins in this range.

Table 25: Measurement uncertainty for different lepton acceptance regions, centre-of-mass energies and PDF sets, combined fits to the p_{T}^{ℓ} and m_{T} distributions, and for 200 pb^{-1}collected at each energy. The numbers quoted for $0 < |\eta_{\ell}| < 2.4$ correspond to the combination of the four pseudorapidity bins in this range. In each case, the first number corresponds to the sum of statistical and PDF uncertainties, and the numbers between parentheses are the statistical and PDF components, respectively.

$\sqrt{s}$ [TeV]	Lepton acceptance	Uncertainty in m_W [MeV]		
		CT10	CT14	MMHT2014
14	$\|\eta_{\ell}\| < 2.4$	16.0 (10.6 $\oplus$ 12.0)	17.3 (11.4 $\oplus$ 13.0)	15.4 (10.7 $\oplus$ 11.1)
14	$\|\eta_{\ell}\| < 4$	11.9 (8.8 $\oplus$ 8.0)	12.4 (9.2 $\oplus$ 8.4)	10.3 (9.0 $\oplus$ 5.1)
27	$\|\eta_{\ell}\| < 2.4$	18.3 (10.2 $\oplus$ 15.1)	18.8 (10.5 $\oplus$ 15.5)	16.5 (9.4 $\oplus$ 13.5)
27	$\|\eta_{\ell}\| < 4$	12.3 (7.5 $\oplus$ 9.8)	12.7 (8.2 $\oplus$ 9.7)	11.4 (7.9 $\oplus$ 8.3)
14+27	$\|\eta_{\ell}\| < 4$	10.1 (6.3 $\oplus$ 7.9)	10.1 (6.9 $\oplus$ 7.4)	8.6 (6.5 $\oplus$ 5.5)

$\sqrt{s}$ [TeV]	Lepton acceptance	Uncertainty in m_W [MeV]	
		HL-LHC	LHeC
14	$\|\eta_{\ell}\| < 2.4$	11.5 (10.0 $\oplus$ 5.8)	10.2 (9.9 $\oplus$ 2.2)
14	$\|\eta_{\ell}\| < 4$	9.3 (8.6 $\oplus$ 3.7)	8.7 (8.5 $\oplus$ 1.6)

4.4.5 Prospects for the measurement of the effective weak mixing angle

At leading order dilepton pairs are produced through the annihilation of a quark and antiquark via the exchange of a Z boson or a virtual photon: $q\bar{q} \rightarrow Z/\gamma^{*} \rightarrow \ell^{+}\ell^{-}$. The definition of the forward-backward asymmetry, $\mathrm{A_{FB}}$, is based on the angle θ^{*} of the lepton (ℓ^{-}) in the Collins-Soper [464, 465] frame of the dilepton system:

$$\mathrm{A_{FB}} = \frac{\sigma_{\mathrm{F}} - \sigma_{\mathrm{B}}}{\sigma_{\mathrm{F}} + \sigma_{\mathrm{B}}}, \tag{24}$$

where σ_{F} and σ_{B} are the cross sections in the forward ($\cos\theta^* > 0$) and backward ($\cos\theta^* < 0$) hemispheres, respectively. In this frame the θ^* is the angle of the ℓ^- direction with respect to the axis that bisects the angle between the direction of the quark and opposite direction of the anti-quark. In pp collisions the direction of the quark is assumed to be in the boost direction of the dilepton pair. Here, $\cos\theta^*$ is calculated using laboratory-frame quantities as follows:

$$\cos\theta^* = \frac{2(p_1^+ p_2^- - p_1^- p_2^+)}{\sqrt{M^2(M^2 + P_{\mathrm{T}}^2)}} \times \frac{P_{\mathrm{z}}}{|P_{\mathrm{z}}|}, \tag{25}$$

where M, P_{T}, and P_{z} are the mass, transverse momentum, and longitudinal momentum, respectively, of the dilepton system, and $p_1(p_2)$ are defined in terms of energy, $e_1(e_2)$, and longitudinal momentum, $p_{\mathrm{z},1}(p_{\mathrm{z},2})$, of the negatively (positively) charged lepton as $p_{\mathrm{i}}^{\pm} = (e_i \pm p_{\mathrm{z},i})/\sqrt{2}$ [464].

A non-zero $\mathrm{A_{FB}}$ in dilepton events arises from the vector and axial-vector couplings of electroweak bosons to fermions. At tree level, the vector v_{f} and axial-vector a_{f} couplings of Z bosons to fermions (f) are:

$$v_{\mathrm{f}} = T_3^{\mathrm{f}} - 2Q_{\mathrm{f}} \sin^2\theta_{\mathrm{W}}, \tag{26}$$

$$a_{\mathrm{f}} = T_3^{\mathrm{f}}, \tag{27}$$

where T_3^{f} and Q_{f} are the third component of the weak isospin and the charge of the fermion, respectively, and $\sin^2\theta_{\mathrm{W}}$ is the weak mixing angle, which is related to the masses of the W and Z bosons by the relation $\sin^2\theta_{\mathrm{W}} = 1 - M_{\mathrm{W}}^2/M_{\mathrm{Z}}^2$. Electroweak radiative corrections affect these leading-order relations. An effective weak mixing angle, $\sin^2\theta_{\mathrm{eff}}^{\mathrm{f}}$, is defined based on the relation between these couplings: $v_{\mathrm{f}}/a_{\mathrm{f}} = 1 - 4|Q_{\mathrm{f}}|\sin^2\theta_{\mathrm{eff}}^{\mathrm{f}}$, with $\sin^2\theta_{\mathrm{eff}}^{\mathrm{f}} = \kappa_{\mathrm{f}}\sin^2\theta_{\mathrm{W}}$, where flavour-dependent κ_{f} is determined by electroweak corrections. Consequently, precise measurements of $\mathrm{A_{FB}}$ can be used to extract the effective leptonic weak mixing angle ($\sin^2\theta_{\mathrm{eff}}^{\mathrm{lept}}$).

The most precise previous measurements of $\sin^2\theta_{\mathrm{eff}}^{\mathrm{lept}}$ were performed by the LEP and SLD experiments [466]. There is, however, a known tension of about 3 standard deviations between the two most precise measurements. Measurements of $\sin^2\theta_{\mathrm{eff}}^{\mathrm{lept}}$ have also been performed by the LHC and Tevatron experiments [467–472].

In measurements of $\mathrm{A_{FB}}$ (or associated angular variables) in leptonic decays of Z bosons at a pp collider, the assignment of the z-axis is crucial. At low rapidities, there is a two-fold ambiguity in the direction of the initial state quark and anti-quark; the colliding quark is equally likely to be in either proton and the parton level asymmetry is diluted. However, at higher rapidities, the Z boson tends to be produced in the direction of travel of the quark, since the (valence) quark tends to be at higher Bjorken-x than the anti-quark. This means that the dilution between parton level and proton level quantities is significantly smaller at larger rapidities, illustrated in Fig. 43, and a larger forward-backward asymmetry is induced. Consequently, the forward acceptance of LHCb, in addition to the increased forward coverage of the ATLAS and CMS detectors, will be crucial to achieving the most precise measurement of $\sin^2\theta_{\mathrm{eff}}^{\mathrm{lept}}$ possible at the HL-LHC.

The uncertainties on the parton distribution functions translate into sizeable variations in the observed $\mathrm{A_{FB}}$ values, which have limited the precision of current measurements of $\sin^2\theta_{\mathrm{eff}}^{\mathrm{lept}}$ at the LHC. However, the changes in PDFs affect the $\mathrm{A_{FB}}(M_{\ell\ell}, Y_{\ell\ell})$ distribution in a different way from changes in $\sin^2\theta_{\mathrm{eff}}^{\mathrm{lept}}$. Because of this behaviour, the distribution of $\mathrm{A_{FB}}$ can itself be used to constrain the PDF uncertainties on the extraction of $\sin^2\theta_{\mathrm{eff}}^{\mathrm{lept}}$ using either a Bayesian χ^2 reweighting method [473–475] (in the case of PDFs with Monte Carlo replicas) or through a profiling procedure [476] (in the case of PDFs with Hessian error sets).

Prospects for the measurement of the effective weak mixing angle using the forward-backward asymmetry, $\mathrm{A_{FB}}$, in Drell-Yan di-lepton events at the HL-LHC at ATLAS [477], CMS [478] and LHCb [479]

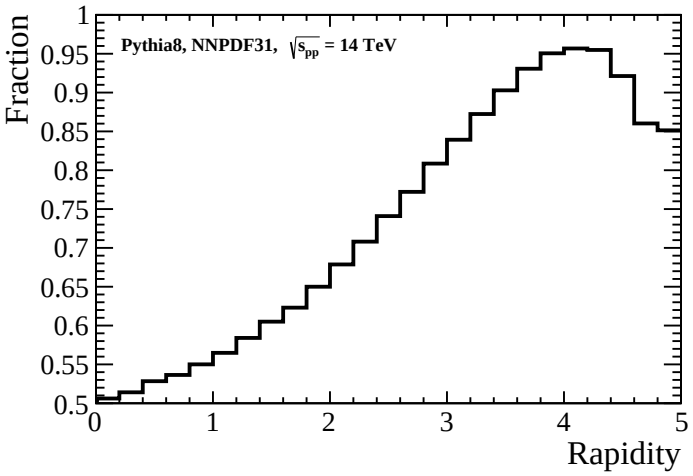

Fig. 43: The fraction of events where the Z boson travels in the same direction along the z-axis as the colliding quark, in proton-proton collisions with $\sqrt{s} = 14$ TeV. This increases as the event becomes more forward, reaching a maximum in the region probed by LHCb. The decrease once the rapidity is greater than 4 is because the fraction of collisions involving valence quarks decreases (the Bjorken-x value of the high momentum quark in these collisions is typically greater than 0.3). No detector effects are simulated for this figure.

have been performed and are reported here. The leptonic effective weak mixing angle is extracted from measurements of $\mathrm{A_{FB}}$ in dilepton events by minimising the χ^2 value between the simulated data and template $\mathrm{A_{FB}}$ distributions representing different $\sin^2\theta^{\mathrm{lept}}_{\mathrm{eff}}$ values and PDF variations. The LHCb and CMS analyses consider the dimuon final state, while the ATLAS analysis considers the dielectron final state. For CMS and LHCb the samples and different $\sin^2\theta^{\mathrm{lept}}_{\mathrm{eff}}$ templates are generated at next-to-leading order using the POWHEG event generator [480–483], where the NNPDF3.0 [484] PDF set is used in the case of the CMS analysis, and the NNPDF3.1 PDF set [207] for LHCb. For CMS, the analysis is performed at generator level without the effect of smearing due to detector effects[20] while for LHCb, a smearing is performed where the momentum resolution and reconstruction efficiency is assumed to be similar to the performance of the current detector [485]. In the case of ATLAS, events are generated with POWHEG and overlaid with additional inelastic pp collisions per bunch-crossing simulated with PYTHIA. Parameterisations of the expected ATLAS detector performances during the HL-LHC runs [486] are then applied on particle-level objects to emulate the detector response. Lepton trigger and identification efficiencies are derived as a function of η and p_{T} and used to estimate the likelihood of a given lepton to fulfil either the trigger or identification requirements, which have been optimised for the level of pile-up expected at the HL-LHC [405]. The $\mathrm{A_{FB}}$ distributions are generated, at leading order (LO) in QCD, with DYTURBO, an optimised version of DYRES/DYNNLO [487] with NNLO CT14 PDF and the world average value for $\sin^2\theta^{\mathrm{lept}}_{\mathrm{eff}} = 0.23153$.

The HL-LHC CMS detector will extend the pseudorapidity, η, coverage of the muon reconstruction from the current configuration of 2.4 to 2.8. In the CMS analysis an event is selected if there are at least two muons with $|\eta| < 2.8$ and with the leading p_{T} muon $p_{\mathrm{T}} > 25$ GeV and the second leading muon $p_{\mathrm{T}} > 15$ GeV. Figure 44 shows the $\mathrm{A_{FB}}$ distributions in bins of dimuon mass and rapidity for different energies and pseudorapidity acceptances. As expected, at higher centre-of-mass energies the observed $\mathrm{A_{FB}}$ is smaller because the interacting partons have smaller x-values which results in a smaller fraction of dimuon events produced by the valence quarks, which also means more dilution. The samples are normalised to the integrated luminosities of 19 fb^{-1} for $\sqrt{s} = 8$ TeV and to 10 – 3000 fb^{-1}

[20] A comparison of 8 TeV predictions and measured values suggests the effect is not significant.

for $\sqrt{s} = 14$ TeV samples and the simulated data are shown for $\sqrt{s} = 8$ TeV and $\sqrt{s} = 14$ TeV for two different selection requirements, $|\eta| < 2.4$ and 2.8. Extending the pseudorapidity acceptance significantly increases the coverage for larger x-values in the production and reduces both the statistical and PDF uncertainties, as shown below.

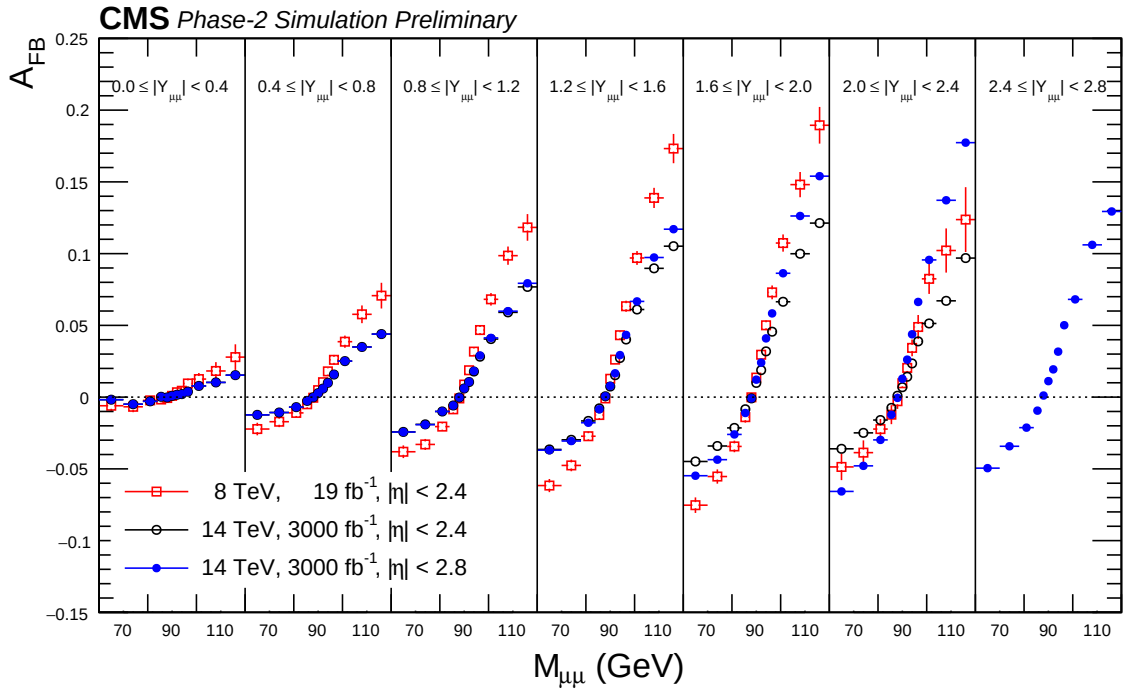

Fig. 44: Forward-backward asymmetry distribution, $\mathrm{A_{FB}}(M_{\mu\mu}, Y_{\mu\mu})$, in dimuon events at $\sqrt{s} = 8$ TeV and 14 TeV. The distributions are made with POWHEG event generator using NNPDF3.0 PDFs and interfaced with PYTHIA v8 for parton-showering, QED final-state radiation (FSR) and hadronization. Following acceptance selections are applied to the generated muons after FSR: $|\eta| < 2.4$ (or $|\eta| < 2.8$), $p_{\mathrm{T}}^{\mathrm{lead}} > 25$ GeV, $p_{\mathrm{T}}^{\mathrm{trail}} > 15$ GeV. The error bars represent the statistical uncertainties for the integrated luminosities corresponding to 19 fb^{-1} at $\sqrt{s} = 8$ TeV and 3000 fb^{-1} at $\sqrt{s} = 14$ TeV.

In the case of the 14 TeV analysis with a large number of events (> 200 fb^{-1}), the pseudo-data are too precise to estimate the PDF uncertainties with the Bayesian reweighting approach because the replica distributions are too sparse compared to the statistical uncertainties. Therefore, the PDF uncertainties after the Bayesian reweighting are estimated by extrapolating from the lower values of integrated luminosities.

The corresponding values for various luminosities at CMS are summarized in Table 26. One can see from the table that with the extended pseudorapidity coverage of $|\eta| < 2.8$, the statistical uncertainties are reduced by about 30% and the PDF uncertainties are reduced by about 20%, compared to $|\eta| < 2.4$ regardless of the target integrated luminosity and for both nominal and constrained PDF uncertainties.

The LHCb detector has coverage in the pseudorapidity range $2 < \eta < 5$ and expects to install its 'Upgrade II' in Long Shutdown 4. Following this upgrade, LHCb will collect at least 300 fb^{-1} of data, allowing high precision measurements. The forward acceptance of LHCb brings a number of benefits in measurements of $\sin^2\theta_{\mathrm{eff}}^{\mathrm{lept}}$ at the LHC. The lower level of dilution in the forward region results in a larger sensitivity to $\sin^2\theta_{\mathrm{eff}}^{\mathrm{lept}}$ and the PDF effects are (in relative terms) smaller, providing both statistical precision in measurements of the weak mixing angle and a reduction in PDF uncertainties. In addition, LHCb does not simply probe forward rapidities of the Z boson: the leptons themselves are located over

Table 26: Statistical, nominal NNPDF3.0, and constrained NNPDF3.0 uncertainties of the extracted $\sin^2\theta^{\text{lept}}_{\text{eff}}$ value at CMS at 14 TeV for muon acceptances of $|\eta| < 2.4$ and $|\eta| < 2.8$ and for different values of integrated luminosity. For comparison, results of the 8 TeV estimate of this analysis are compared to the results obtained from 8 TeV measurement [488].

L_{int}	$\delta_{\text{stat}}[10^{-5}]$		$\delta^{\text{nominal}}_{\text{nnpdf3.0}}[10^{-5}]$		$\delta^{\text{constrained}}_{\text{nnpdf3.0}}[10^{-5}]$	
(fb^{-1})	$\|\eta\| < 2.4$	$\|\eta\| < 2.8$	$\|\eta\| < 2.4$	$\|\eta\| < 2.8$	$\|\eta\| < 2.4$	$\|\eta\| < 2.8$
10	76	51	75	57	39	29
100	24	16	75	57	27	20
500	11	7	75	57	20	16
1000	8	5	75	57	18	14
3000	4	3	75	57	15	12
19	43		49		27	
19 (from [488])	44		54		32	

a significant range of rapidities, allowing extremal values of $\cos\theta^*$ to be probed, increasing sensitivity to the weak mixing angle. Finally, LHCb has the ability to select events at low momentum using a flexible full software trigger and real time analysis scheme (from Run-3 onwards). It is therefore foreseen that the LHCb Upgrade II will be able to select Z boson decays where one lepton has transverse momentum above 20 GeV, while the other lepton has a transverse momentum above 5 GeV. Such low thresholds again increase the sensitivity to asymmetric events at high $|\cos\theta^*|$. In addition to the advantages of the extended forward acceptance for such measurements, as part of Upgrade II LHCb is expected to undergo a significant calorimeter upgrade[21] allowing similar precision to be achieved in both the dielectron and dimuon final states.

LHCb has performed a study of projected sensitivities, considering the dimuon final state. The experiment is assumed to have coverage in the region $2.0 < \eta < 5$. Toy measurements of the forward-backward asymmetry are used to determine the sensitivity of measurements at LHCb Upgrade II to the weak mixing angle. Only statistical uncertainties are considered alongside the effects of knowledge of PDFs. The statistical uncertainty on $\sin^2\theta^{\text{lept}}_{\text{eff}}$ is expected to be below 5×10^{-5} with 300 fb^{-1} of data. The expected PDF uncertainty from current PDF knowledge is $\sim 20 \times 10^{-5}$, but with Bayesian reweighting this can be reduced to the level of about 10×10^{-5} (with analysis of a dataset corresponding to an integrated luminosity of 300 fb^{-1}). This reduction assumes systematic effects are negligible in comparison to statistical uncertainties, though the current knowledge of PDFs means that any measurement in the forward region is expected to offer a smaller PDF uncertainty than the total uncertainties in the previous best measurements of the weak mixing angle. The main challenge of such measurements at LHCb Upgrade II will therefore be to control systematic uncertainties in order to ensure the overall measurement also achieves high precision; however, the large dataset of J/ψ and Υ mesons to be recorded is expected to aid the understanding of effects such as the momentum scale (which introduced the largest systematic uncertainty in the Run-1 analysis at LHCb). This should enable a measurement at LHCb Upgrade II with a precision similar to or better than that achieved in the combination of measurements at LEP and SLD.

In the ATLAS analysis di-electron candidates are selected where each electron has p_{T} in excess of 25 GeV and the combined invariant mass is in the region of the Z pole. A new inner tracking system (ITk) will extend the tracking coverage of the ATLAS detector from $|\eta| \leq 2.5$ up to $|\eta| \leq 4.0$ at the HL-LHC, providing the ability to reconstruct forward charged particle tracks, which can be matched to calorimeter clusters for forward electron reconstruction. The selected data sample is split into three

[21] This upgrade will offer an extended dynamic range within the ECAL, offering improved electron momentum resolution.

channels, where both electrons are in the central region, satisfying $|\eta| < 2.47$ (the CC channel), where one electron is central and the other is forward, satisfying $2.5 < \eta < 4.2$ (the CF channel), and finally where both electrons are forward (the FF channel). Events are selected by requiring at least one electron firing the single electron trigger, except in the FF channel, where a dielectron trigger is required.

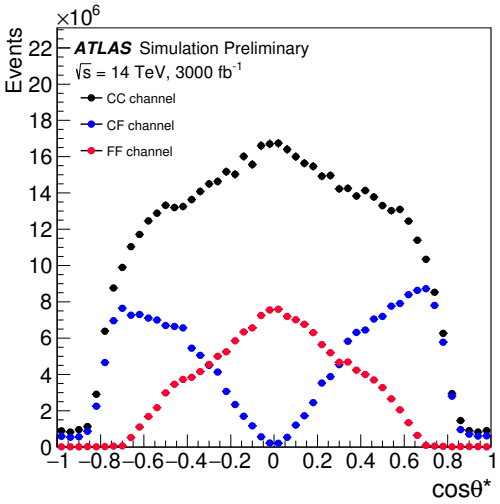

Fig. 45: The $\cos\theta^*$ distribution for CC, CF and FF channels for selected Drell-Yan di-electron events expected for 3000 fb^{-1} of data at $\sqrt{s} = 14$ TeV.

As Fig. 45 shows, the CF channel selects events at high $\cos\theta^*$ values where the forward-backward asymmetry is more pronounced, and consequently the sensitivity to $\sin^2\theta^{\text{lept}}_{\text{eff}}$ is higher in this channel. While the LHCb and CMS analyses consider only uncertainties due to statistics and PDFs, the ATLAS analysis considers also various sources of experimental uncertainty which affect the precision of the extraction of A_{FB}. The main contributions arise from the limited knowledge of the momentum scale and resolution of the electrons, and the background contributions, which are mostly relevant in the CF and FF channels.

The extraction of $\sin^2\theta^{\text{lept}}_{\text{eff}}$ is performed by minimising the χ^2 value comparing particle-level A_{FB} distributions with different weak mixing angle hypotheses in invariant mass and rapidity bins combining the CC, CF and FF channels. A global fit is performed where $\sin^2\theta^{\text{lept}}_{\text{eff}}$ is extracted while constraining the PDF uncertainties using a profiling procedure following that used in a previous ATLAS publication [489] and implemented in the xFitter package [490].

With this analysis, a significant reduction of the light quark uncertainties at low x is seen and combining the three channels together, the measurement reaches a precision of $18{\cdot}10^{-5}$ ($\pm 16{\cdot}10^{-5}$ (PDF) $\pm 9{\cdot}10^{-5}$ (exp.)). The uncertainty of the results remains dominated by the limited knowledge of the PDFs.

In the context of the Yellow Report for the HL-LHC, prospect PDF fits including HL-LHC pseudo-data of future PDF-sensitive measurements from ATLAS, CMS and LHCb were performed (see Sec. 5.2). Three prospect PDF scenarios were considered and compared with the reference PDF set PDF4LHC15 [195]. The expected sensitivity of the $\sin^2\theta^{\text{lept}}_{\text{eff}}$ measurements with 3000 fb^{-1} at $\sqrt{s} = 14$ TeV is improved by 10-25% depending on the prospect PDFs scenario considered. In Table 27 the precision on $\sin^2\theta^{\text{lept}}_{\text{eff}}$ obtained with the "ultimate" HL-LHC PDF set is compared with the with the one obtained with CT14NNLO PDF set.

The sensitivity of the analysis to the $\sin^2\theta^{\text{lept}}_{\text{eff}}$ extraction is also estimated with a prospect PDF set including expected data from the LHeC collider [460]. In this case the PDF uncertainty is reduced by an additional factor of 5 with respect to the one obtained with the HL-LHC prospect PDFs.

Table 27: The value of $\sin^2\theta^{\text{lept}}_{\text{eff}}$ with the breakdown of uncertainties from the ATLAS preliminary results at $\sqrt{s} = 8$ TeV with $20\,\text{fb}^{-1}$ [491] is compared to the projected $\sin^2\theta^{\text{lept}}_{\text{eff}}$ measurements with $3000\,\text{fb}^{-1}$ of data at $\sqrt{s} = 14$ TeV for two PDF sets considered in this note. All the numbers values are given in units of 10^{-5}. Note that other sources of systematic uncertainties, such as the impact of the MC statistical uncertainty, evaluated in Ref. [491] are not considered in this prospect analysis. For the HL-LHC prospect PDFs the "ultimate" scenario is chosen.

	ATLAS $\sqrt{s} = 8$ TeV	ATLAS $\sqrt{s} = 14$ TeV	ATLAS $\sqrt{s} = 14$ TeV
$\mathcal{L}$ [fb^{-1}]	20	3000	3000
PDF set	MMHT14	CT14	PDF4LHC15$_{HL-LHC}$
$\sin^2\theta^{\text{lept}}_{\text{eff}}$ [$\times 10^{-5}$]	23140	23153	23153
Stat.	$\pm$ 21	$\pm$ 4	$\pm$ 4
PDFs	$\pm$ 24	$\pm$ 16	$\pm$ 13
Experimental Syst.	$\pm$ 9	$\pm$ 8	$\pm$ 6
Other Syst.	$\pm$ 13	-	-
Total	$\pm$ 36	$\pm$ 18	$\pm$ 15

To conclude, the accuracy of measurements of the weak mixing angle obtained with an analysis of A_{FB} in Z events at $\sqrt{s} = 14$ TeV with $3000\,\text{fb}^{-1}$ at ATLAS and CMS and $300\,\text{fb}^{-1}$ at LHCb at the HL-LHC exceed the precision achieved in all previous single-experiment results to date and the measurements are dominated by PDF uncertainties. To explore the full potential of the HL-LHC data it will be therefore essential to reduce PDF uncertainties. A significant improvement of the sensitivity of the measurement is observed in the ATLAS analysis when using prospect PDF sets including ancillary Drell-Yan measurements performed with the data collected during the high luminosity phase of the LHC and at the LHeC collider.

4.4.6 The global EW fit[22]

The measurement of the Higgs Boson mass (M_H) at the Large Hadron Collider (LHC) has provided the last input to the global fit of electroweak (EW) precision observables (EWPO), which can now be used to effectively constrain new physics. Moreover, the measurement of Higgs-boson production and decay rates that is at the core of the physics program of the LHC Run-2 will further constrain those interactions that directly affect Higgs-boson physics.

The HL-LHC will have the potential to provide more constraining bounds on new physics via the global fit to EWPO and Higgs data, thanks to the higher precision it will reach both in the measurement of some of the crucial input parameters of global EW fits (e.g. M_W, m_t, M_H, and $\sin^2\theta^{\text{lept}}_{\text{eff}}$), and in the measurement of Higgs-boson total and differential rates. In this study the reach of the HL-LHC in constraining new physics is explored via a global fit to EWPO. Earlier studies on the prospects for the LHC were performed in [492, 493].

In the following, details are provided first on the parameters and procedure of the global EW fit. Next the results are interpreted within the Standard Model (SM). Finally, the EW fit is used to constrain new physics beyond the SM. The results are presented for both the current data and the projections in the HL-LHC scenario.

The global fit of EWPO is performed using the HEPFIT package [494], a general tool to combine direct and indirect constraints on the SM and its extensions in any statistical framework. The default fit proce-

[22] Contribution by J. de Blas, M. Ciuchini, E. Franco, S. Mishima, M. Pierini, L. Reina, and L. Silvestrini.

dure, used here, follows a Bayesian statistical approach and uses BAT (Bayesian Analysis Toolkit) [495]. Flat priors are used for all input parameters, and the likelihoods are built assuming Gaussian distributions for all experimental measurements. The output of the fit is therefore given as the posterior distributions for each input parameters and observables, calculated using a Markov Chain Monte Carlo method.

All EWPO are calculated as a SM core plus corrections. The SM core includes all available higher-order corrections, including the latest theoretical developments in the calculation of radiative corrections to the EWPO of [496, 497].[23] New physics corrections are computed at the leading order. The HEPFIT code allows for the implementation of different models of new physics. In particular, as explained below, the study is specialised in the general framework of the so called SM effective field theory (SMEFT), where the SM Lagrangian is extended by the addition of operators of canonical mass dimension higher than four (limited to the basis of operators of canonical dimension six in this study).

As far as EWPO are concerned, this study updates the EWPO fit of Refs. [493, 498, 499], including recent updates on the theory calculations [497] and experimental measurements [190, 491, 500–506]. The uncertainties on some input parameters that have been obtained by including hadron collider data are further reduced, in order to account for the level of accuracy expected for the HL-LHC. In all these projections it is assumed that the central values for the HL-LHC measurements will not change with respect to current data. In particular the following assumptions are made:

1. The W mass, whose uncertainty obtained by combining ATLAS and Tevatron+LEP2 measurements is currently around 12 MeV [189, 507–509] could be measured at the HL-LHC with a precision of 7 MeV. This number is derived from the current estimate of the statistical plus PDF uncertainty using 1 fb^{-1} of data reported in Sec. 4.4.4, and assuming systematic errors to be of similar size to the statistical ones. In this fit a measurement of $M_W = 80.379 \pm 0.007$ GeV is therefore added to the current combination.

2. An aggressive estimate of the current uncertainty on the top-quark mass, obtained by combining current Tevatron and LHC measurements, puts the uncertainty on m_t at the level of 0.4 GeV. It will be difficult to further reduce this number at the HL-LHC, since the remaining uncertainty is mainly of systematic and theoretical origin. In the current fit $m_t = 172.8 \pm 0.4$ GeV is used.

3. The measurements of the effective angle $\sin^2\theta^{\rm lept}_{\rm eff}$ can also be improved at the HL-LHC. Currently, a combination of the latest LHC and Tevatron results returns a precision for this observable of $\sim 0.00022 - 0.00027$, depending on the assumptions made in combining common uncertainties. For the HL-LHC fit, the combination is repeated using the ATLAS projections outlined in Sec. 4.4.5 where the HL-LHC PDF set is used, corresponding to the value $\sin^2\theta^{\rm lept}_{\rm eff} = 0.23143 \pm 0.00015$.

4. The error on the Higgs-boson mass, currently around 0.20 GeV, can be reduced to 0.05 GeV [510, 511].

5. The HL-LHC should also be able to improve the current knowledge on the W width, whose precision of 42 MeV is currently given by the combination of LEP2 and Tevatron measurements. This uncertainty is dominated by the hadron collider measurement. While there is no available information about a possible determination of this quantity at the (HL-)LHC, the conservative assumption that the HL-LHC can achieve a precision on Γ_W at least as good as the one on the current average is used. An independent HL-LHC measurement of $\Gamma_W = 2.085 \pm 0.042$ GeV is therefore added. This gives a 30 MeV uncertainty when combined with the current average.

[23] The uncertainties associated to missing higher-order corrections to the SM predictions for the EWPO are also taken into account in the fits, via nuisance parameters with Gaussian priors.

Finally, apart from the improved precision of the HL-LHC measurements, the assumption is made that, by the end of the HL-LHC run, better measurements of some of the SM input parameters are possible from other experiments. In particular, following Ref. [493, 498], it is assumed that: 1) the uncertainty on $\Delta\alpha^{(5)}_{\rm had}(M_Z)$ can be reduced to $\pm 5 \times 10^{-5}$ by using data from currently ongoing and future experiments that measure the cross section for $e^+e^- \to$ hadrons, and 2) future lattice QCD measurements will provide a determination of the strong coupling constant with accuracy $\delta\alpha_S(M_Z) = \pm 0.0002$. The measurements of all other EWPO and input parameters have been kept to their currently available values. The current values of all EWPO measurements, as well as the corresponding HL-LHC projected uncertainties, are listed in the second and third columns of Table 28, respectively.

Table 28: Current experimental measurement, HL-LHC projected uncertainty, posterior, and pull for the five input parameters ($\alpha_s(M_Z)$, $\Delta\alpha^{(5)}_{\rm had}(M_Z)$, M_Z, m_t, M_H), and for the main EWPO considered in the SM fit. The pulls in the last column are obtained comparing the experimental measurements with the predictions from a fit *removing* the corresponding observable(s) (See for e.g. Ref. [493] for details.).

	Measurement	HL-LHC uncertainty	Posterior		Pull
			Current	HL-LHC	Current/HL-LHC
$\alpha_s(M_Z)$	0.1180 ± 0.0010	± 0.0002	0.1180 ± 0.0009	0.1180 ± 0.0002	$0/0.5$
$\Delta\alpha^{(5)}_{\rm had}(M_Z)$	0.027611 ± 0.000111	± 0.00005	0.02758 ± 0.00011	0.02759 ± 0.00005	$1.1/2.1$
M_Z [GeV]	91.1875 ± 0.0021		91.1880 ± 0.0020	91.1890 ± 0.0020	$-1.3/-2.6$
m_t [GeV]	172.8 ± 0.7	± 0.4	173.2 ± 0.66	173.1 ± 0.38	$-1.7/-2.9$
M_H [GeV]	125.13 ± 0.17	± 0.05	125.13 ± 0.17	125.13 ± 0.05	$1.4/3$
M_W [GeV]	80.379 ± 0.012	± 0.007	80.362 ± 0.006	80.367 ± 0.004	$1.6/2.7$
Γ_W [GeV]	2.085 ± 0.042	± 0.042	2.0885 ± 0.0006	2.0889 ± 0.0003	-0.1
$\mathrm{BR}_{W\to\ell\nu}$	0.1086 ± 0.0009		0.10838 ± 0.00002	0.10838 ± 0.000005	0.2
$\mathrm{BR}_{W\to\mathrm{had}}$	0.6741 ± 0.0027		0.67486 ± 0.00007	0.67486 ± 0.00001	-0.3
$\sin^2\theta^{\rm lept}_{\rm eff}(Q^{\rm had}_{\rm FB})$	0.2324 ± 0.0012		0.23151 ± 0.00006	0.23150 ± 0.00005	0.7
$P^{\rm pol}_\tau = A_\ell$	0.1465 ± 0.0033		0.14711 ± 0.0005	0.14713 ± 0.0004	-0.2
Γ_Z [GeV]	2.4952 ± 0.0023		2.4946 ± 0.0007	2.4947 ± 0.0005	0.3
σ^0_h [nb]	41.540 ± 0.037		41.492 ± 0.008	41.491 ± 0.006	1.3
R^0_ℓ	20.767 ± 0.025		20.749 ± 0.008	20.749 ± 0.006	0.7
$A^{0,\ell}_{\rm FB}$	0.0171 ± 0.0010		0.01623 ± 0.0001	0.016247 ± 0.00008	0.9
A_ℓ (SLD)	0.1513 ± 0.0021		0.14711 ± 0.0005	0.14718 ± 0.0004	1.9
R^0_b	0.21629 ± 0.00066		0.21586 ± 0.0001	0.21586 ± 0.0001	$0.7/0.6$
R^0_c	0.1721 ± 0.0030		0.17221 ± 0.00005	0.17221 ± 0.00005	0
$A^{0,b}_{\rm FB}$	0.0992 ± 0.0016		0.10313 ± 0.00032	0.10319 ± 0.00026	$-2.4/-2.5$
$A^{0,c}_{\rm FB}$	0.0707 ± 0.0035		0.07369 ± 0.00024	0.07373 ± 0.0002	-0.9
A_b	0.923 ± 0.020		0.93475 ± 0.00004	0.93476 ± 0.00004	-0.6
A_c	0.670 ± 0.027		0.66792 ± 0.0002	0.66794 ± 0.0002	0.1
$\sin^2\theta^{\rm lept}_{\rm eff(Had.coll.)}$	0.23143 ± 0.00027	± 0.00015	0.23151 ± 0.00006	0.23150 ± 0.00005	$-0.5/-0.9$

The results of the SM global fit to EWPO for both the present (LHC) and future (HL-LHC) scenarios are collected in Table 28. These are given in the form of the mean and standard deviation for each of the observables, as derived from the posterior of the fits. For each EWPO the "pull" is also computed, defined as the difference between the experimental value and the SM prediction computed by removing each observable from the fit (not shown in the table), normalized to the total uncertainty. As it is apparent, the differences in the posteriors between both fits are quite small. However, looking at the pulls one can see that, should the central values of the SM input parameters remain the same, the expected improvements in their experimental uncertainties, combined with the more precise measurements of some EWPO at the HL-LHC, would significantly increase the tension between the indirect determinations of M_Z, m_t, and M_H from the EW fit and the corresponding experimental measurements, pushing them to the 3σ

level. The improvement in the precision on m_t would also reduce the parametric uncertainty on some observables, e.g. the W mass, bringing the total residual error very close to the intrinsic uncertainty associated to missing higher-order corrections in the calculation of M_W. As in the case of some of the SM inputs, the expected improvement on the experimental precision of M_W, without a significant deviation on the central value, would add some tension between theory and experiment, pushing the pull for this observable well beyond the 2σ level. The impact of the HL-LHC measurements on the EW fit is well illustrated in Fig. 46 where one can see the comparison between direct (i.e. experimental) and indirect constraints on the fit input parameters given for both the current and HL-LHC scenarios in the M_W vs. m_t and the M_W vs. $\sin^2\theta^{\rm lept}_{\rm eff}$ planes respectively.

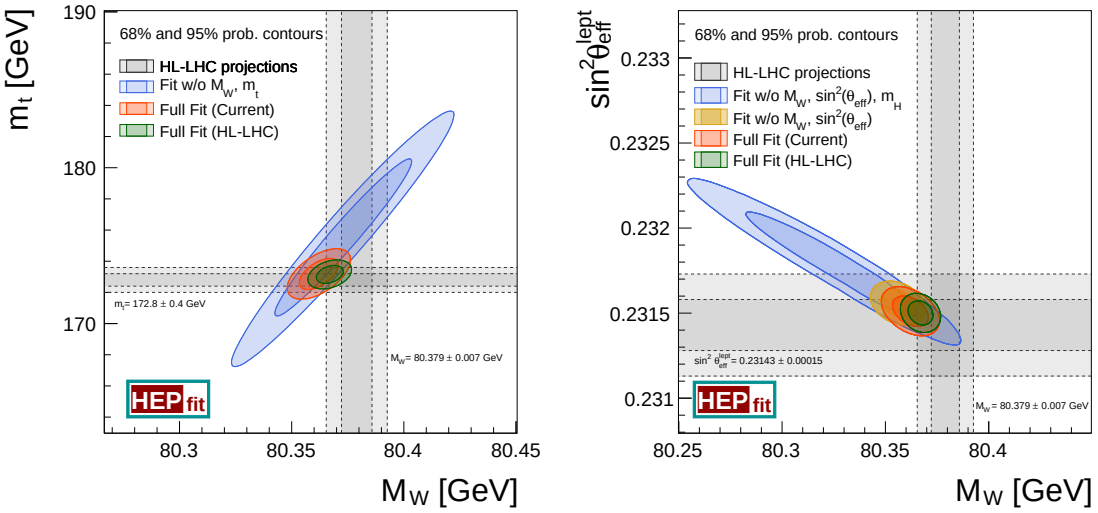

Fig. 46: Comparison of the indirect constraints on M_W and m_t with the current experimental measurements and the expected improvements at the HL-LHC (left). The same in the M_W-$\sin^2\theta^{\rm lept}_{\rm eff}$ plane (right).

The EWPO, being measured in processes mediated by the exchange of a Z or W boson, are extremely sensitive to any new physics that modifies the propagation of such particles. This results in a universal modification of the interactions between the EW gauge bosons and the SM fermions, which, from the point of view of EWPO, can be described in terms of only three parameters: the well-known S, T, and U oblique parameters [512]. The study of the constraints on the S, T, and U parameters is one of the classical benchmarks in the study of EW precision constraints on new physics, and it is well motivated from a theory point of view, within the context of universal theories. The results of the fit to the S, T, and U parameters are given in Table 29. The results are presents in terms of the full (S,T,U) fit and also assuming $U = 0$, which is motivated in theories where EW symmetry breaking is realised linearly, since in that case $U \ll S, T$. In both cases the current constraints are compared with the expected precision at the HL-LHC, which, in some cases, could improve the sensitivity to such new physics effects by up to $\sim 30\%$. The results for the ST fit ($U = 0$) are shown in Fig. 47, illustrating also the constraints imposed by the different EWPO.

As stressed above, the STU parameterisation only describes universal deformations with respect to the SM predictions. In order to systematically explore the impact of global EW precision fits on new physics, the framework of the SMEFT is adopted in what follows. In this formalism, the SM Lagrangian is extended via operators of dimension five and higher, i.e.

$$\mathcal{L}_{\rm eff} = \mathcal{L}_{\rm SM} + \sum_{d>4} \frac{1}{\Lambda^{d-4}} \mathcal{L}_d, \quad \text{with} \quad \mathcal{L}_d = \sum_i C_i \mathcal{O}_i^{(d)}, \quad \left[\mathcal{O}_i^{(d)}\right] = d\,, \tag{28}$$

Table 29: Results of the fit for the oblique parameters S, T, U; and S, T ($U = 0$). Projections for the uncertainties at the HL-LHC are given in the last column.

	Result	Correlation Matrix			Precision at HL-LHC
S	0.04 ± 0.10	1.00			0.09
T	0.08 ± 0.12	0.90	1.00		0.12
U	0.00 ± 0.09	-0.62	-0.84	1.00	0.08
S	0.04 ± 0.08	1.00			0.06
T	0.08 ± 0.06	0.90	1.00		0.05
($U = 0$)					

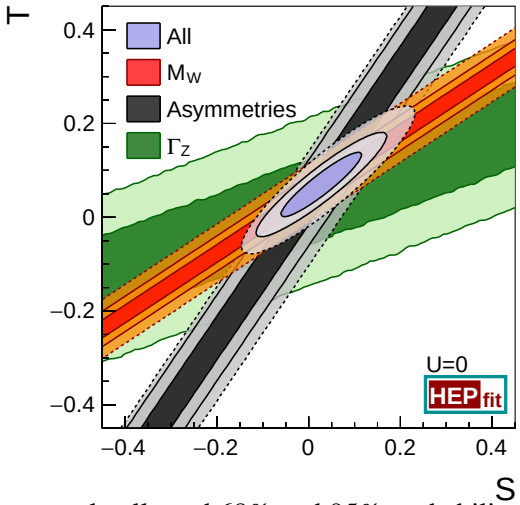

Fig. 47: Comparison of the currently allowed 68% and 95% probability regions in the S, T fit ($U = 0$) (dashed contours) with the HL-LHC projections (solid contours). The different bands illustrate the bounds from the different EWPO included in the fit and the projected improvements at the HL-LHC.

where Λ denotes the cut-off scale of the SMEFT. This new physics scale introduces a first hierarchical ordering between contributions of operators of lower versus higher dimension, where higher-dimension operators are suppressed by inverse powers of Λ. Each term in $\mathcal{L}_d$ is a linear combination of d-dimensional operators $O_i^{(d)}$ built in terms of SM fields, with Wilson coefficients C_i that can depend on both SM masses and couplings, as well as new physics parameters. For the analysis of EWPO the leading new physics corrections come from dimension-six operators ($\mathcal{L}_6$). The study is limited to this order in the effective theory expansion. Using the complete basis of dimension-six interactions presented in Ref. [513], the Z-pole and W observables in Table 28 are corrected at the leading order by 10 different operators. The bosonic operators

$$\mathcal{O}_{\phi D} = |\phi^\dagger D^\mu \phi|^2 \quad \text{and} \quad \mathcal{O}_{\phi WB} = (\phi^\dagger \sigma_a \phi) W^a_{\mu\nu} B^{\mu\nu},$$

modify the gauge-boson propagators in a way similar to the T and S parameters, respectively. Among the remaining operators,

$$\mathcal{O}^{(1)}_{\phi\psi} = (\phi^\dagger \overleftrightarrow{D^\mu} \phi)(\overline{\psi}\gamma_\mu \psi) \quad \text{and} \quad \mathcal{O}^{(3)}_{\phi F} = (\phi^\dagger \sigma_a \overleftrightarrow{D^\mu} \phi)(\overline{F}\gamma_\mu \sigma_a F),$$

with $\psi = l,\ e,\ q,\ u\ , d$ and $F = l, q$ (where l and q denote the SM left-handed fermion doublets, e, u, d the SM right-handed fermion singlets, and flavour universality is assumed), correct, upon EW symmetry

breaking, the EW couplings of the Z and W bosons to quarks and leptons. Finally, the four-lepton operator $\mathcal{O}_{ll} = \left(\bar{l}\gamma_\mu l\right)\left(\bar{l}\gamma^\mu l\right)$ modifies the muon decay amplitude and, by affecting the extraction of the Fermi constant, propagates its effect to all the different observables considered in the EW global fit.

The aim of a global fit to EWPO data is to constrain the corresponding Wilson coefficients. Of the ten operators considered, only eight combinations can be constrained using EW precision data in the case of flavour universal couplings. This means that in the basis of [513] there are two flat directions which, for simplicity are lifted by performing a field redefinition to exchange $C_{\phi D}$ and $C_{\phi WB}$ with two interactions that do not enter in EWPO. The results of the fit to EWPO using the projected HL-LHC data are shown in Fig. 48, both for the case in which the eight remaining coefficients are active and fitted simultaneously and for the case in which only one coefficient at a time is active and independently fitted. The results of both fits are also summarised in Table 30 where the HL-LHC bounds are additionally compared to current bounds. It can be seen that the HL-LHC could improve the current bounds on some of the considered Wilson coefficients by up to a 10-30%, although for most coefficients the effect is much milder both when different effective interactions are fitted simultaneously and individually.

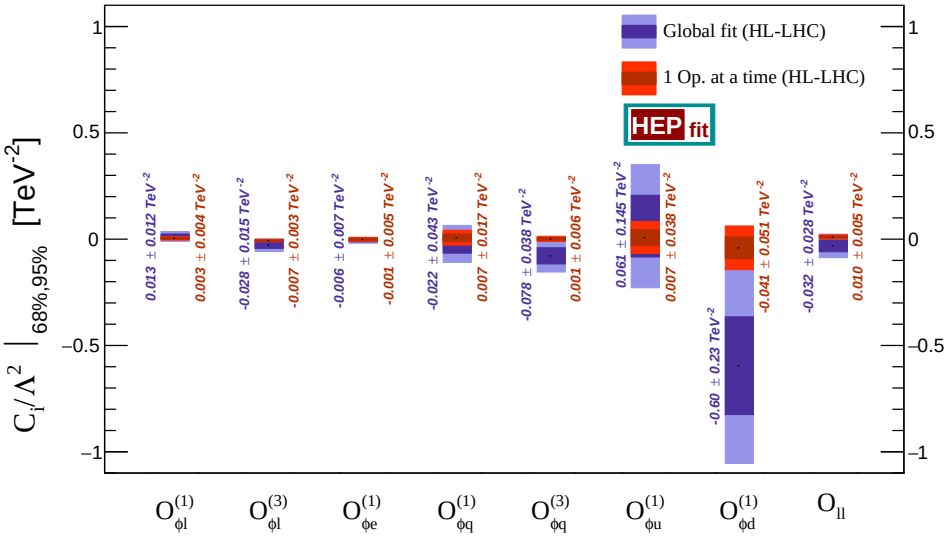

Fig. 48: 68% and 95% probability limits on the dimension-six operator coefficients C_i/Λ^2 [TeV^{-2}] from the global fit to EWPO at HL-LHC including all operators (in blue), compared with the limits obtained assuming only one operator at a time (in red). See Table 30 for the comparison with current uncertainties.

Table 30: Results of the fit to the coefficients of the SMEFT dimension-six Lagrangian. The uncertainties shown refer to the fit performed assuming the presence of only one effective operator at a time and to the case when all (eight) operators are active at the same time (global fit). Projections for the uncertainties at the HL-LHC are given in the last two columns. Result shown for the ratios $\overline{C}_i \equiv C_i/\Lambda^2$. See text for details.

	Current uncertainty [TeV^{-2}]		Precision at HL-LHC [TeV^{-2}]	
Operator Coefficient	1 op. at a time	Global fit	1 op. at a time	Global fit
$\overline{C}_{\phi l}^{(1)}$	0.004	0.012	0.004	0.012
$\overline{C}_{\phi q}^{(1)}$	0.018	0.044	0.017	0.043
$\overline{C}_{\phi e}$	0.005	0.009	0.005	0.007
$\overline{C}_{\phi u}$	0.040	0.146	0.038	0.145
$\overline{C}_{\phi d}$	0.054	0.237	0.051	0.230
$\overline{C}_{\phi l}^{(3)}$	0.004	0.017	0.003	0.015
$\overline{C}_{\phi q}^{(3)}$	0.007	0.040	0.006	0.038
$\overline{C}_{ll}$	0.007	0.028	0.005	0.028
$\overline{C}_{\phi WB}$	0.003	–	0.002	–
$\overline{C}_{\phi D}$	0.007	–	0.005	–

5 Strong interactions

This section presents studies at the HL-LHC and HE-LHC conditions for jet and photon production, parton density functions, underlying event and multi/double-parton interactions. Thanks to the larger integrated luminosity at the HL-LHC and HE-LHC and the jump in centre-of-mass energy at the HE-LHC, an increase in the kinematic reach is expected for light- and heavy-flavour jet production as well as photon production. An improvement is also expected in the experimental systematic uncertainty on the jet calibration. The measurements of jet and photon production cross sections in addition to other processes, e.g. Drell-Yan and top quark, at the HL-LHC will help improve the understanding of the parton density functions. The level of the underlying event activity is not expected to change significantly at the HL-LHC given the small increase in centre-of-mass energy from $\sqrt{s} = 13$ TeV at the LHC Run-2 to $\sqrt{s} = 14$ TeV at the HL-LHC, however a significant increase is expected at the HE-LHC energy of $\sqrt{s} = 27$ TeV. Multi-parton interactions are expected to play a more significant role at higher energies and, thanks to the large statistics available at both the HL- and HE-LHC, new measurements can be carried out to test more precisely the current theoretical models.

5.1 Jet and photon production [24]

This section presents phenomenological studies of inclusive jet, dijet, heavy-flavour jet production as well as inclusive photon, diphoton, and associated photon and jet production at future upgrades at the HL and HE stages of the LHC. In particular the reach in yields for these processes is investigated. A comparison between the results expected at the future design centre-of-mass energies of $\sqrt{s} = 14$ TeV and $\sqrt{s} = 27$ TeV is presented.

5.1.1 Inclusive jet production

Jets are reconstructed using the anti-k_{T} algorithm [274] with distance parameter R=0.4 as implemented in the FastJet software package [343], and calibrated following the procedure described in [514]. The total jet energy scale (JES) uncertainty in ATLAS Run-2 measurements comprises of 88 sources, and all need to be propagated through the analysis in order to correctly account for uncertainty correlations in the jet calibration in the final result. Here follows a summary of the analysis detailed in Ref. [515].

A reduced set of uncertainty components (nuisance parameters) is derived from eigenvectors and eigenvalues of the diagonalised total JES covariance matrix on the jet level. The globally reduced configuration with 19 nuisance parameters (NPs) is used in this study. Eight NPs coming from the in situ techniques are related to the detector description, physics modelling and measurements of the Z/γ energies in the ATLAS calorimeters. Three describe the physics modelling, the statistics of the dijet MC sample and the non-closure of the method used to derive the η-intercalibration [514]. Single-hadron response studies [516] are used to describe the JES uncertainty in the high-p_{T} jet regions, where the in situ studies have limited statistics. Four NPs are due to the pile-up corrections of the jet kinematics that take into account mis-modelling of N_{PV} and $\langle\mu\rangle$ distributions, the average energy density ρ, and the residual p_{T} dependence. Finally, two uncertainty components take into account the difference in the calorimeter response to the quark- and gluon-initiated jets (flavour response) and the jet flavour composition, and one uncertainty estimates the correction for the energy leakage beyond the calorimeter, the "punch-through" effect.

In order to estimate the precision in the jet cross section measurements at the HL-LHC, three scenarios of possible uncertainties in the jet energy scale calibration are defined.

In all three scenarios, the high-p_{T} uncertainty, the punch-through uncertainty and the flavour composition uncertainty are considered to be negligible. The JES uncertainty in the high-p_{T} range will be accessed using the multi-jet balance (MJB) method, rather than single hadron response measurements,

[24] Contributed by the experimental collaborations, and by L. Cieri, G. Ferrera, A. Huss, and J. Pires.

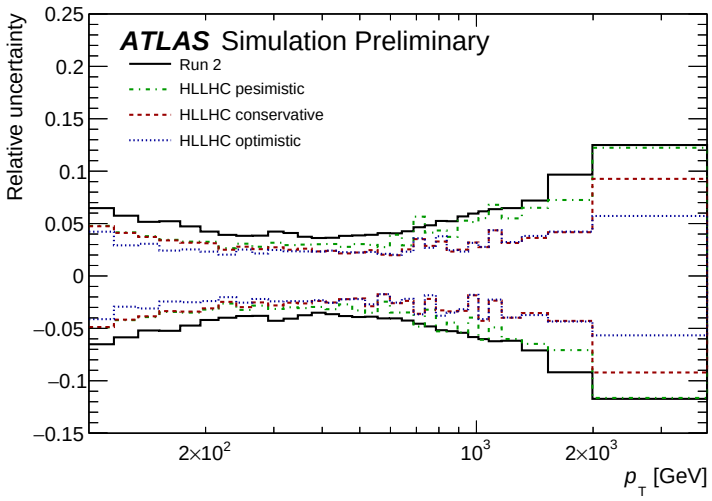

Fig. 49: Relative uncertainties in the inclusive jet cross section measurements at the HL-LHC due the JES uncertainties. Three HL-LHC scenarios are compared to the Run-2 performance. Black line corresponds to the Run-2 performance. Green, red and blue lines represent pessimistic, conservative and optimistic scenarios, respectively.

since the high statistics at the HL-LHC will allow precision JES measurements in the high-p_{T} region. Flavour composition and flavour response uncertainties are derived from the MC generators. With the advances in the MC modelling and development of tunes, these uncertainties could be significantly reduced. The flavour composition uncertainties are set to zero to highlight the maximal impact of possible future improvements in the understanding of parton shower and hadronisation modeling on the precision of the jet energy measurements. The flavour response uncertainties are kept the same as in Run-2 or reduced by a factor of two in conservative and optimistic scenarios, respectively.

The pile-up uncertainties, except the ρ topology uncertainty, are considered to be negligible. Current small uncertainties in the JES due to mis-modelling of N_{PV} and $\langle\mu\rangle$ distributions and the residual p_{T} dependence lead to a very small uncertainties at the HL-LHC conditions. With the advances of new pile-up rejection techniques, the ρ topology uncertainty could be maintained at a level comparable to the one in Run-2 or reduced by a factor of two. This is addressed in conservative and optimistic scenarios.

Since the Run-2 jet energy resolution (JER) uncertainty estimation is conservative, the final Run-2 JER uncertainty is expected (based on Run-1 experience) to be about twice as small as the current one. Therefore, the JER uncertainty is estimated to be half of that in Run-2.

The remaining uncertainty sources are fixed in different scenarios as follows:

- Conservative scenario:
  - All in situ components are kept the same as in Run-2, except the uncertainties related to the photon energy measurement in the high-E_{T} range and the MJB method uncertainties whose uncertainties are reduced by a factor of two, since those are expected to be improved at the HL-LHC;
  - The MC modelling uncertainty in the η-intercalibration is reduced by a factor of two while the other two are neglected. Currently, the MC modelling uncertainty is derived through a comparison of leading-order (LO) pQCD generators. With future advances in next-to-leading-order MC generators this uncertainty is expected to improve;
  - The flavour response uncertainty is set to the Run-2 value;

  - The ρ-topology uncertainty is unchanged compared to Run-2 results;
- Optimistic scenario:
  - All in situ components are treated identically to the conservative scenario;
  - All three uncertainty sources in the η-intercalibration method are set to zero;
  - The flavour response uncertainty is reduced by a factor of two compared to Run-2 results;
  - ρ-topology uncertainty is two times smaller as in Run-2;
- Pessimistic scenario:
  - Same as the optimistic scenario, but all uncertainty sources of in situ methods are retained from Run-2.

All components of the JES uncertainty are propagated from the jet-level to the cross section level as follows. The jet p_{T} is scaled up and down by one standard deviation of each source of uncertainty. The difference between the nominal detector-level spectrum and the systematically shifted one is taken as a systematic uncertainty. All JES uncertainties are treated as bin-to-bin correlated and independent from each other in this procedure. The unfolding of the detector-level distributions to the particle-level spectrum is not performed is this study. A possible modification of the shapes of uncertainty components during the unfolding procedure is expected to be small and neglected in this study.

The inclusive jet cross-sections are studied as a function of the jet transverse momentum for jets with $p_{\mathrm{T}} > 100$ GeV and within $|y| < 3$. The total JES uncertainty in the inclusive jet cross section measurement for the three HL-LHC scenarios is depicted in Fig. 49 and is compared to the total JES uncertainty estimate for the Run-2 jet cross section measurements. The total JES uncertainty in the low p_{T} range is the same as in Run-2 and is about 2% better in the high-p_{T} region. In the conservative and pessimistic scenarios the JES uncertainties in the cross section are very similar in the intermediate and high-p_{T} range, while the JES uncertainty is about 1% better in the low-p_{T} range for the optimistic scenario.

The predicted number of events estimated using the program NNLOJET [326], which includes next-to-next-to-leading order QCD calculations for both single jet inclusive [206] and dijet inclusive [19] production, is shown in Fig. 50 (left and right respectively). In the dijet analysis, a second jet with $p_{\mathrm{T}} >$ 75 GeV is required in the event. The lower panels show the ratios of events yields at 27 TeV and 14 TeV. This plot shows an enhancement of the cross section growing with the jet p_{T} (left) and dijet mass (right). In summary, assuming $\mathcal{L}_{int} = 3$ ab^{-1} of pp collision data at $\sqrt{s} = 14$ TeV the p_{T} reach of the measurement is 5 TeV with the observation of dijet events of mass up to 9 TeV. At the HE-LHC upgrade, an increase in cross section by a factor between 10^3 and 10^6 in the tails of the distributions extends the p_{T} range of the measurement by a factor of 2 up to 9 TeV, allowing the observation of dijet events of mass up to 16 TeV.

The increase in cross section in these scenarios will allow for a very precise multi-differential measurement of inclusive jet production. Working at a fixed centre-of-mass energy, the high-p_{T} the high-x and the large Q^2 region are probed and the sensitivity to higher order QCD/EW effects and BSM signals is increased. On the other hand, at fixed-p_{T}, an increase in the collider energy and the inclusion of the forward detector regions increase the coverage to the low-x regime, which is highly sensitive to small-x resummation effects. For these reasons, it will be necessary to have accurate jet predictions covering both regions.

To this end Fig. 51 presents the double-differential k-factors at $\sqrt{s} = 14$ TeV (left) and $\sqrt{s} =$ 27 TeV (right) for the inclusive jet p_{T} (top), differentially in p_{T} and rapidity $|y|$ and dijet mass (bottom) differentially in dijet mass m_{jj} and rapidity difference $y^* = 1/2\,|y_{j1} - y_{j2}|$. The shaded bands assess the scale uncertainty at different perturbative orders, LO, NLO and NNLO. As for the value of the renormalization (μ_R) and factorization (μ_F) scales $\mu = \hat{H}_T$ is used, i.e. the scalar sum of the p_{T} of all

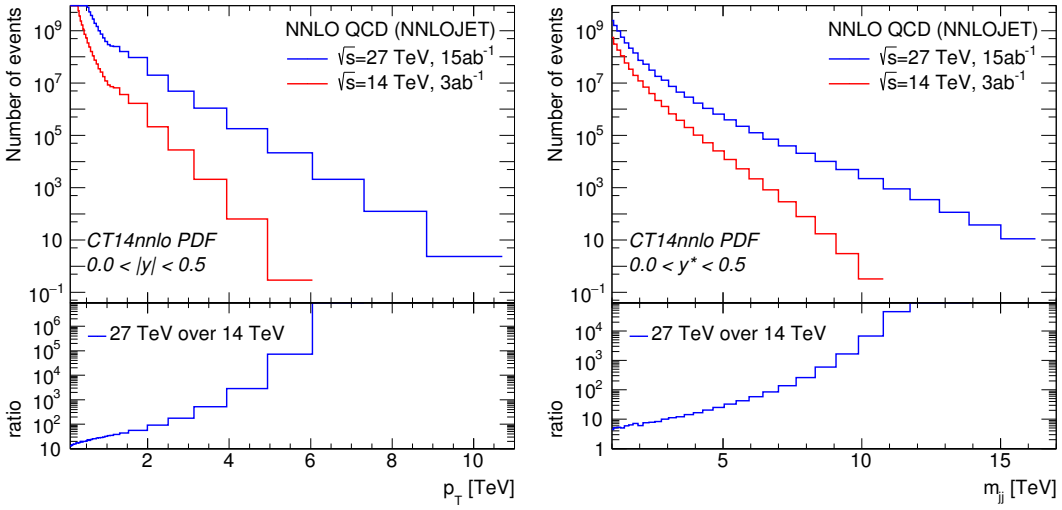

(a) (b)

Fig. 50: Predicted number of inclusive jet events as a function of the jet p_{T} (left) and dijet events as a function of dijet mass m_{jj} (right) at NNLO, assuming an integrated luminosity of 3 ab^{-1} (15 ab^{-1}) of pp collision data at $\sqrt{s}$=14 TeV ($\sqrt{s}$=27 TeV).

partons in the event, as recommended in [332] for the inclusive jet p_{T}, and the dijet mass $\mu = m_{jj}$ for the dijet mass distribution, as recommended in [19].

For the inclusive jet p_{T} large NLO effects at high-p_{T} and central rapidity of approximately 90% (14 TeV) and 50% (27 TeV) are observed with large NLO scale uncertainties of $\mathcal{O}(20-30\%)$. At NNLO moderate corrections across the entire p_{T} and rapidity range are observed, except at high-p_{T} in the central rapidity slices where the NNLO effects can reach between 10 to 30%. An excellent convergence of the perturbative result is observed as well as a significant reduction in the scale uncertainty of the cross section when going from NLO to NNLO. The NNLO scale uncertainties are estimated at the $< 5\%$ level. Similarly to the inclusive jet p_{T} case, an excellent convergence of the perturbative result for the dijet mass is observed. The NNLO/NLO k-factors are typically $< 10\%$ and alter the shape of the prediction at low m_{jj} and low y^*. A large reduction is observed in the scale variation and NNLO scale uncertainties are estimated to be below the 5% level, even at large m_{jj}. Scale uncertainties at this level are well below the PDF uncertainty, highlighting the huge potential to constrain PDFs with inclusive jet data.

Measurements of weak bosons [517], top quarks [518], photon and jet production [519] (and many others) performed by the LHC Collaborations have been already used by the global PDF groups [199, 200, 207, 520] in the determination of the proton structure. Comparisons of inclusive jet and dijet production cross sections using different PDF sets at $\sqrt{s} = 14$ and 27 TeV, show 5–10% differences respectively between central values in the low and intermediate p_{T} and m_{jj} regions, consistent with current PDF uncertainties. Larger differences between the predictions of the various PDF sets in the high-p_{T} and m_{jj} range highlight the expected constraining power of future measurements at the HL-LHC and HE-LHC.

A study to estimate the impact of future PDF-sensitive measurements at the HL-LHC on PDFs determination was performed in [298] and reported in Sec. 5.2. Three possible scenarios for the experimental systematic uncertainties were considered. This study concluded that HL-LHC measurements will further reduce the PDF uncertainties, and published dedicated PDF sets, PDF4LHC HL-LHC, with

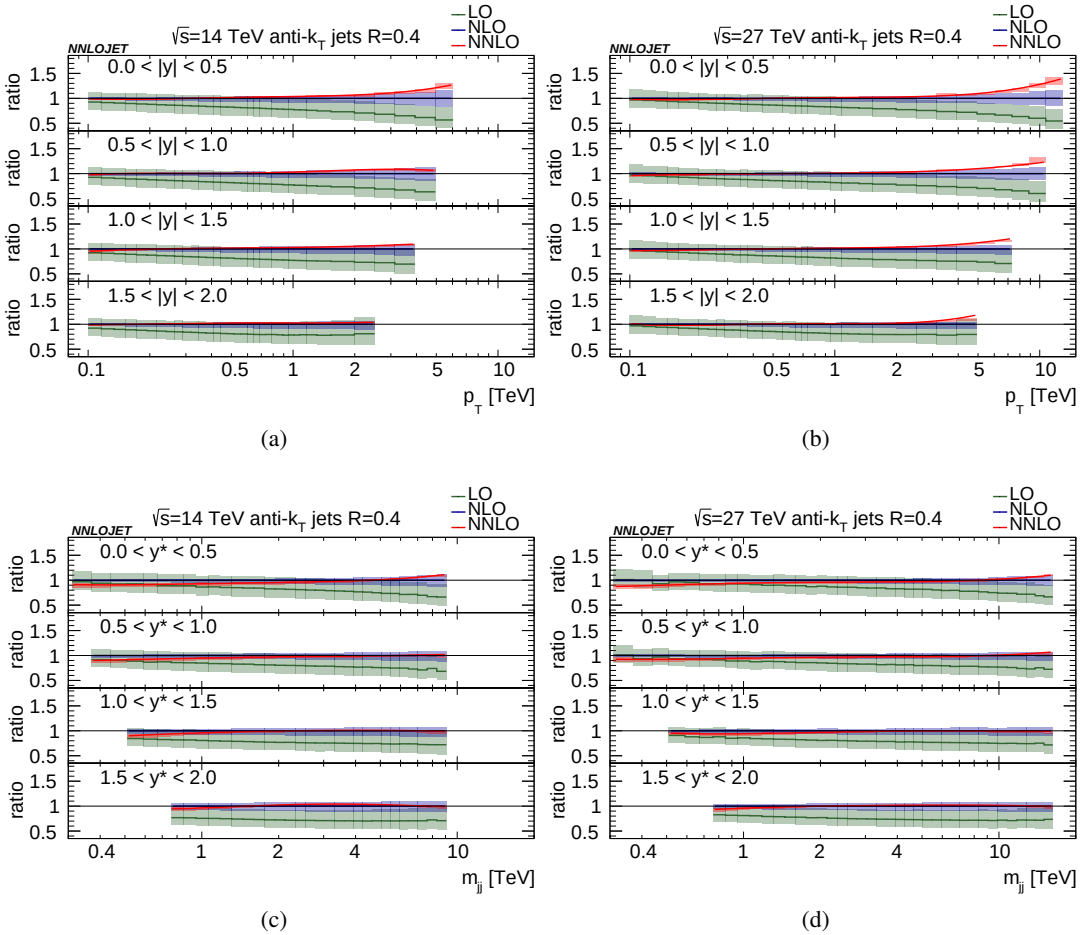

Fig. 51: Predictions for the inclusive jet p_{T} (top) and dijet mass m_{jj} (bottom) at LO (green), NLO (blue) and NNLO (red) at (a and c) $\sqrt{s} = 14$ TeV and (b and d) $\sqrt{s} = 27$ TeV normalised to the NLO result.

the inclusion of HL-LHC pseudo-data in the fits. Figure 52 depicts the comparison of PDF uncertainties in the inclusive jet and dijet production cross sections for CT14 and PDF4LHC HL-LHC (conservative scenario) in pp collisions at $\sqrt{s} = 14$ and 27 TeV. A significant reduction in the PDF uncertainty is expected with the inclusion of PDF-sensitive measurements in HL-LHC PDF fits.

5.1.2 High–p_{T} light– and heavy–flavour jet measurements at the HL–LHC

The program of jet physics will substantially profit from the HL-LHC data since higher scales can be reached and the region of very low partonic momentum fractions x can be accessed, where the parton density becomes large. Measurements of jets originating from b quarks are important to investigate the heavy-flavor contribution to the total jet cross section and to study the agreement of the measurement with available theoretical predictions. In particular, inclusive b-jet production is very sensitive to higher-order corrections and to parton showers. In top quark production processes, top jets can be defined when the top quark decays hadronically and all decay products can be clustered into a single jet. The production of W bosons is studied in the high-p_{T} region, where the W bosons decay hadronically and are reconstructed as jets. Jet substructure techniques are applied to discriminate the jets originating from top quarks and W bosons from the QCD background.

Higher order QCD radiation affects the distribution of the angular correlation, and the region

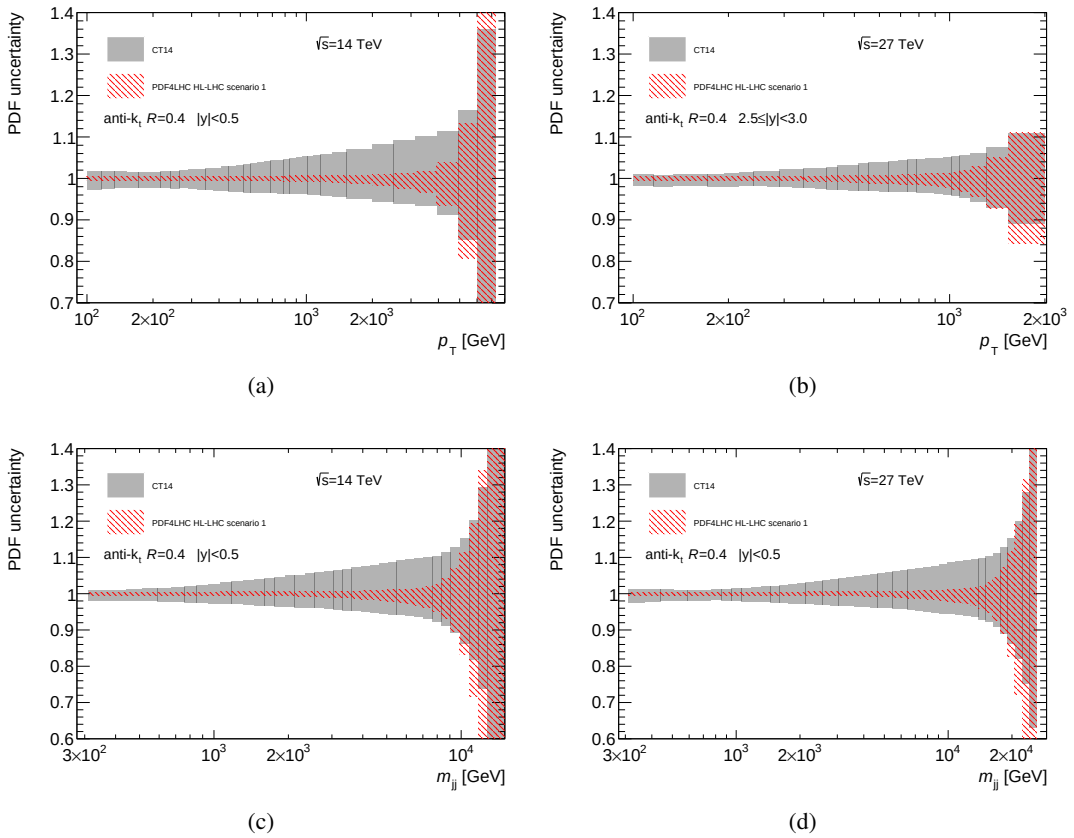

Fig. 52: Comparison of PDF uncertainty in the inclusive jet (a,b) and dijet (c,d) cross sections calculated using the CT14 PDF set and the conservative PDF4LHC HL-LHC scenario 1 (i.e. scenario C in Sec. 5.2) [298] set at $\sqrt{s} = 14$ TeV (left) and $\sqrt{s} = 27$ TeV (right).

where the jets are back-to-back in the transverse plane is particularly sensitive to multiple "soft" gluon contributions, treated by all-order resummation and parton showers. This region is of particular interest since soft-gluon interference effects between the initial and final state can be significant [521, 522]. The azimuthal correlations $\Delta\phi = |\phi_2 - \phi_1|$ between the two leading p_{T} jets and their dependency on the production process is of particular interest because of color interference effects [523, 524].

Compared to Run-2 measurements at $\sqrt{s} = 13$ TeV the increase of the centre-of-mass energy leads to about twice larger cross section at highest p_{T}. Taking into account the much higher luminosity and the higher cross section, the statistical uncertainty is expected to be around six times smaller, compared to the analysis of the Run-2 data [525].

Measurements of high-p_{T} jets originated from b-quarks are sensitive to the higher-order corrections, parton shower modeling and the parton densities of the proton. In Fig. 53 (left), the inclusive b-jet cross section differential in p_{T} is shown for centre-of-mass energy of 13 and 14 TeV and rapidity $|y| < 0.5$. The depicted statistical uncertainties correspond to the luminosity $300\,\mathrm{fb}^{-1}$ (13 TeV) and $3\,\mathrm{ab}^{-1}$ (14 TeV). The systematic uncertainty of the measurement is dominated by the jet energy scale uncertainty, which is of similar size as for inclusive jets, and the b-tagging uncertainty, which is expected to play a role mainly at higher p_{T} where it is about 10%. It can be seen that the p_{T} reach at HL-LHC for the inclusive b-jets is about 3 TeV, where about 30 events with $p_{\mathrm{T}} > 3\,\mathrm{TeV}$ are expected.

It is worth noticing that at high-p_{T} the mass of the b-quark is nearly negligible with respect to

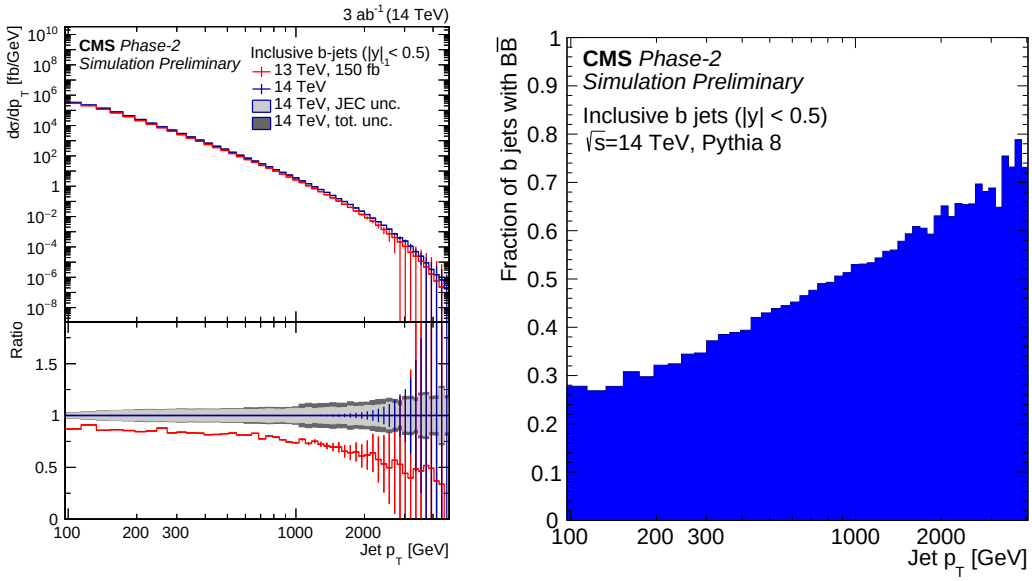

Fig. 53: The inclusive b-jet cross section differential in the p_{T} (left). The error bars show the statistical uncertainty corresponding to the given luminosity, while the gray band represent the systematic uncertainty from the jet-energy-scale and the total systematic uncertainty. The fraction of b-jets containing both B and $\bar{B}$ hadrons as a function of p_{T} (right).

the jet momentum. This leads to the high probability that the b-quark is not produced in the hard subprocess, but in the parton shower. As the mass of the b-quark becomes negligible, the probability of gluon splitting into $b\bar{b}$-pairs is similar to any other flavour (excluding top). In this case, the pair of the B-hadrons is expected to be found inside the b-jet, where one consists of a b-quark, the second a $\bar{b}$-quark. The fraction of such jets as a function of p_{T} as predicted by PYTHIA v8 MC is shown on Fig. 53 (right). In the future, it will be crucial to disentangle between b-jets with b-quarks produced in the shower, and b-jets with b-quarks produced in the hard sub-process.

Figure 54 shows a comparison of the jet cross sections as a function of p_{T} and as a function of $\Delta\phi$ for the different processes applying the anti-k_{T} clustering algorithm [526] with $R = 0.8$. In Fig. 54 (left) the inclusive b-jet cross section is shown (for comparison with the inclusive jet cross section), while in Fig. 54 (right) the two-b-jet cross section is shown. Except for the cross section for W production, the statistical uncertainties shown correspond to an integrated luminosity of 3 ab^{-1} including efficiencies due to b-tagging and selection at the detector level, estimated using the DELPHES simulation. Details of the studies can be found in Ref. [525].

It can be seen that the shapes of the p_{T} spectra are comparable but the top-jet cross section is about ten thousand times smaller than the inclusive jet cross section. The ratio to the inclusive dijet cross section as a function of $\Delta\phi$ illustrates the differences in shape of the $\Delta\phi$ distribution of the different processes (all processes are normalized at $\Delta\phi = \pi$), which depend on the partonic configuration of the initial state.

5.1.3 Inclusive photon production

Here follows a summary of the studies detailed in Ref. [515] of inclusive isolated photon production and photon production in association with at least one jet. In both analyses the photon is required to have a transverse energy in excess of 400 GeV and the pseudorapidity to lie in the range $|\eta^{\gamma}| < 2.37$ excluding the region $1.37 < |\eta^{\gamma}| < 1.56$. The photon is required to be isolated by imposing an upper limit on

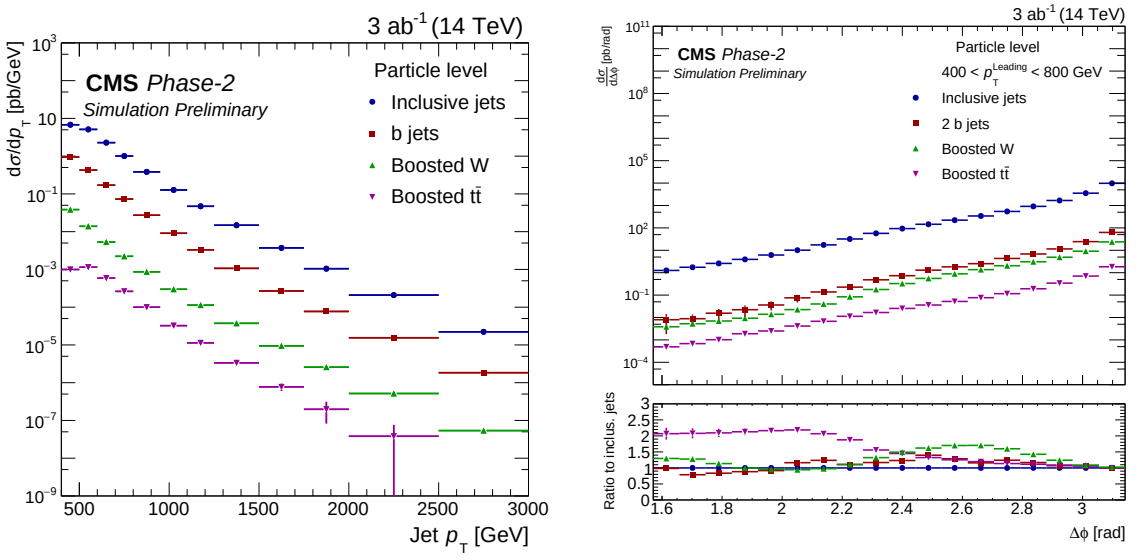

Fig. 54: The particle-level differential jet cross sections (with anti-k_{T} $R = 0.8$) as a function of the jet p_{T} (left) and dijet $\Delta\phi$ (right) for various processes. In the left plot the inclusive b jet cross section is shown (for comparison with the inclusive jet cross section), while for $\Delta\phi$ the two-b-jet cross section is shown. For the ratio the normalization is fixed arbitrarily at $\Delta\phi = \pi$. The cross section of W production does not include statistical uncertainties corrected for efficiencies and background subtraction.

the amount of transverse energy inside a cone of size $\Delta R = 0.4$ in the η–ϕ plane around the photon, excluding the photon itself: $E_{\mathrm{T}}^{\mathrm{iso}} < E_{\mathrm{T,max}}^{\mathrm{iso}}$.

In the inclusive photon analysis, the goal is the measurement of the differential cross section as a function of E_{T}^{γ} in four regions of the photon pseudorapidity: $|\eta^{\gamma}| < 0.6$, $0.6 < |\eta^{\gamma}| < 1.37$, $1.56 < |\eta^{\gamma}| < 1.81$ and $1.81 < |\eta^{\gamma}| < 2.37$. Photon isolation is enforced by requiring $E_{\mathrm{T}}^{\mathrm{iso}} < 4.2 \cdot 10^{-3} \cdot E_{\mathrm{T}}^{\gamma} + 4.8$ GeV.

In the photon+jet analysis, jets are reconstructed using the anti-k_{T} algorithm [274] with a radius parameter $R = 0.4$. Jets overlapping with the photon are not considered if the jet axis lies within a cone of size $\Delta R = 0.8$. The leading jet is required to have transverse momentum above 300 GeV and rapidity in the range $|y^{\mathrm{jet}}| < 2.37$. No additional condition is used for the differential cross section as a function of $p_{\mathrm{T}}^{\mathrm{jet}}$. For the differential cross section as a function of the invariant mass of the photon+jet system additional constraints are imposed: $m^{\gamma-\mathrm{jet}} > 1.45$ TeV, $|\cos\theta^{*}| < 0.83$ and $|\eta^{\gamma} \pm y^{\mathrm{jet}}| < 2.37$. These additional constraints are imposed to remove the bias due to the rapidity and transverse-momentum requirements on the photon and the leading jet [527, 528]. Photon isolation is enforced by requiring $E_{\mathrm{T}}^{\mathrm{iso}} < 4.2 \cdot 10^{-3} \cdot E_{\mathrm{T}}^{\gamma} + 10$ GeV.

The yields of inclusive isolated photons and of photon+jet events are estimated using the program JETPHOX 1.3.1_2 [529, 530]. This program includes a full next-to-leading-order QCD calculation of both the direct-photon and fragmentation contributions to the cross sections for the $pp \to \gamma + \mathrm{X}$ and $pp \to \gamma + \mathrm{jet} + \mathrm{X}$ reactions. The number of massless quark flavours is set to five. The renormalisation (μ_{R}), factorisation (μ_{F}) and fragmentation (μ_{f}) scales are chosen to be $\mu_{\mathrm{R}} = \mu_{\mathrm{F}} = \mu_{\mathrm{f}} = E_{\mathrm{T}}^{\gamma}$. The calculations are performed using the MMHT2014 [531] parameterisations of the proton parton distribution functions (PDFs) and the BGF set II of parton-to-photon fragmentation functions at NLO [532]. The strong coupling constant $\alpha_{\mathrm{s}}(m_{\mathrm{Z}})$ is set to the value assumed in the fit to determine the PDFs. The reliability of the estimated yields using the program JETPHOX is supported by the high purity of the signal photons, the mild unfolding corrections and the fact that the NLO QCD predictions describe adequately

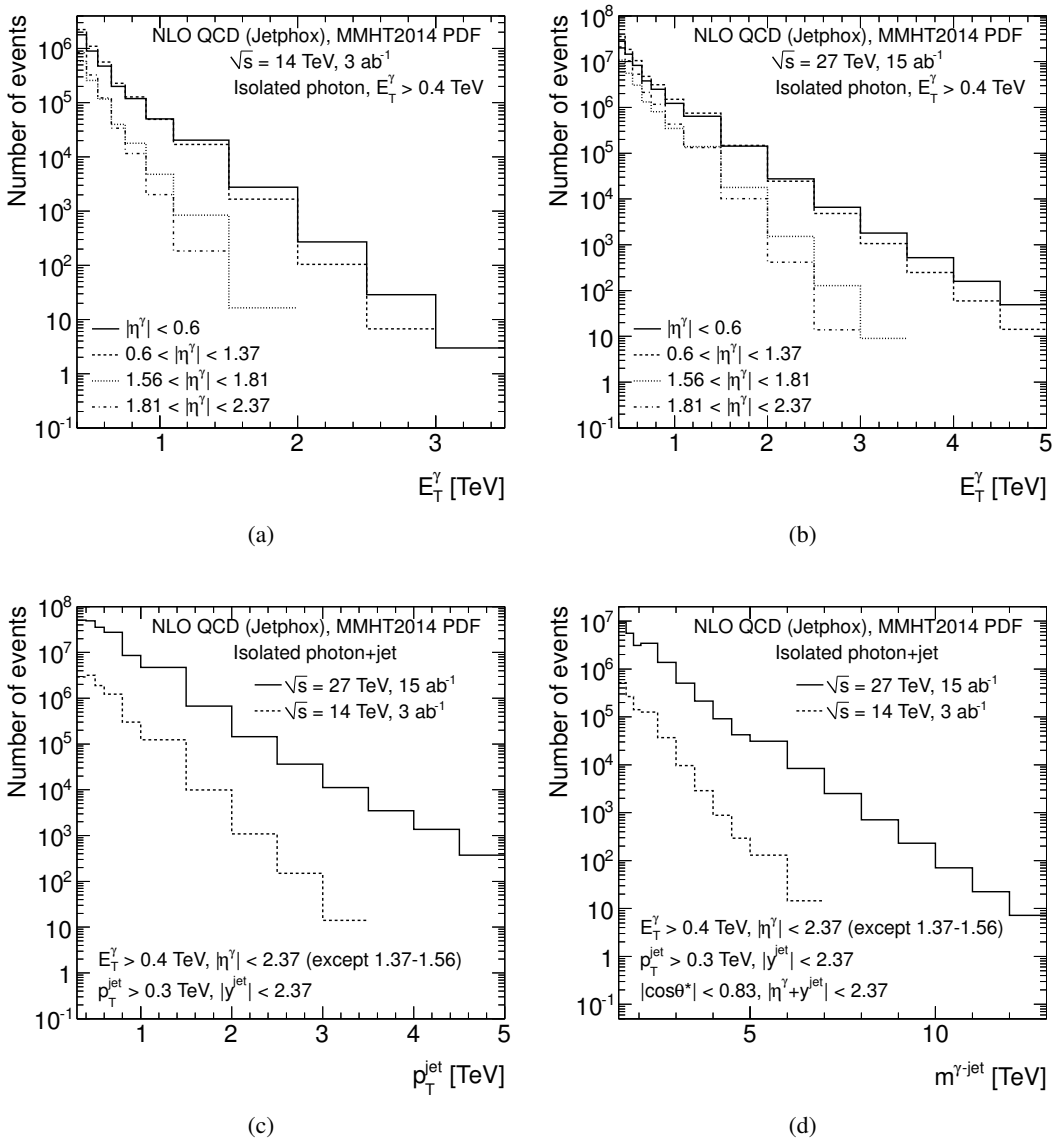

Fig. 55: (a,b) Predicted number of inclusive isolated photon events as a function of E_{T}^{γ} assuming an integrated luminosity of 3 ab^{-1} (15 ab^{-1}) of pp collision data at $\sqrt{s} = 14$ TeV (27 TeV) in different ranges of photon pseudorapidity: $|\eta^{\gamma}| < 0.6$ (solid histogram), $0.6 < |\eta^{\gamma}| < 1.37$ (dashed histogram), $1.56 < |\eta^{\gamma}| < 1.81$ (dotted histogram) and $1.81 < |\eta^{\gamma}| < 2.37$ (dot-dashed histogram). (c,d) Predicted number of photon+jet events assuming an integrated luminosity of 3 ab^{-1} (15 ab^{-1}) of pp collision data at $\sqrt{s} = 14$ TeV (27 TeV) as a function of (c) $p_{\mathrm{T}}^{\mathrm{jet}}$ and (d) $m^{\gamma-\mathrm{jet}}$.

the measurements of these processes using pp collisions at $\sqrt{s} = 13$ TeV [533, 534].

The predicted number of inclusive isolated photon events as a function of E_{T}^{γ} in the different ranges of $|\eta^{\gamma}|$ assuming an integrated luminosity of 3 ab^{-1} (15 ab^{-1}) of pp collision data at $\sqrt{s} = 14$ TeV (27 TeV) is shown in Figure 55(a) and 55(b). For the HL-LHC (HE-LHC), the reach in E_{T}^{γ} is (a) 3–3.5 (5) TeV for $|\eta^{\gamma}| < 0.6$, (b) 2.5–3 (5) TeV for $0.6 < |\eta^{\gamma}| < 1.37$, (c) 1.5–2 (3–3.5) TeV for $1.56 < |\eta^{\gamma}| < 1.81$ and (d) 1–1.5 (2.5–3) TeV for $1.81 < |\eta^{\gamma}| < 2.37$. This represents a significant extension of the region measured so far with pp collisions at $\sqrt{s} = 13$ TeV [533]; as an example, at the

HL-LHC (HE-LHC) the $E_{\rm T}^{\gamma}$ reach is extended from 1.5 TeV to 3–3.5 (5) TeV for $|\eta^{\gamma}| < 0.6$.

The predicted number of photon+jet events as a function of $p_{\rm T}^{\rm jet}$ and $m^{\gamma-{\rm jet}}$ assuming an integrated luminosity of 3 ab^{-1} (15 ab^{-1}) of pp collision data at $\sqrt{s} = 14$ TeV (27 TeV) is shown in Figs. 55(c) and 55(d). In comparison with the latest measurements at $\sqrt{s} = 13$ TeV [534], the expectations obtained at the HL-LHC (HE-LHC) extend significantly the reach in $p_{\rm T}^{\rm jet}$ from 1.5 TeV to 3.5 (5) TeV and $m^{\gamma-{\rm jet}}$ from 3.3 TeV to 7 (12) TeV.

5.1.4 Diphoton production

The production of photon pairs (diphotons) with high invariant mass is a very important process for physics studies at high-energy hadron colliders. Photons are very clean final states and photon energies and momenta can be measured with high precision in modern electromagnetic calorimeters. Therefore *prompt* photons represent ideal probes to test the properties of the Standard Model (SM) [535]– [536] and they are also important in searches for new-physics signals (see, e.g., Refs. [537]– [538]). Owing to the above reasons, it is important to provide accurate theoretical predictions for diphoton production at LHC energies. This task requires in particular, the calculation of QCD and EW radiative corrections at high perturbative orders.

This contribution considers diphoton production in pp collisions at the $\sqrt{s} = 14$ GeV and $\sqrt{s} = 27$ GeV energies, and presents perturbative QCD results up to the NNLO by using the smooth cone isolation criterion [25]. Within the smooth cone isolation criterion [539] (see also Refs. [540,541]) photons are selected by fixing the size R of the isolation cone and imposing a maximal amount of hadronic energy ($E_{\rm T}^{had}(r)$) allowed inside the cone

$$E_{\rm T}^{had}(r) \leq E_{\rm T\,max}\,\chi(r;R)\,, \quad \text{in } \textit{all} \text{ cones with } r \leq R\,, \tag{29}$$

with a suitable choice of the r dependence of the isolation function $\chi(r;R)$. The smooth isolation function $\chi(r;R)$ used is [26]

$$\chi(r;R) = \left(\frac{1-\cos(r)}{1-\cos(R)}\right)^{n}\,, \tag{30}$$

and the value of the power n is set to the $n = 1$. This value of n avoids the sensitivity of the cross section to soft (collinear) photons for large (small) value of n [544]. The radius of the photon isolation cone is set at the value $R = 0.4$ and $E_{\rm T\,max} = 10$ GeV. Detailed comparisons between standard and smooth cone isolation criteria have been presented in Refs. [90, 544–546].

The following kinematic cuts are applied:

$$p_{\rm T}^{\gamma;\,hard} > 40\ GeV, \qquad p_{\rm T}^{\gamma;\,soft} > 30\ GeV, \qquad |y_{\gamma}| < 2.8\,, \tag{31}$$

where $p_{\rm T}^{\gamma;\,hard}$ and $p_{\rm T}^{\gamma;\,soft}$ are respectively the transverse momenta of the harder and softer photon and $|y_{\gamma}|$ is the photon rapidity. The minimum angular distance between the two photons is $R_{\gamma\gamma}^{\rm min} = 0.4$.

A lower limit $r_{\rm cut}$ is implemented on the ratio $p_{{\rm T}\gamma\gamma}/M_{\gamma\gamma}$ ($p_{{\rm T}\gamma\gamma} > r_{\rm cut} M_{\gamma\gamma}$) [547], and values in the range $r_{\rm cut} = 0.08\%$–0.15% are used. The perturbative uncertainty is computed as the envelope of three-point scale variation by considering the two asymmetric scale configurations with $\{\mu_R = \mu_0/2,\ \mu_F = 2\mu_0\}$ and $\{\mu_R = 2\mu_0\,,\ \mu_F = \mu_0/2\}$ and the central scale $\{\mu_R = \mu_F = \mu_0\}$.

This study begins by considering the invariant mass ($M_{\gamma\gamma}$) distribution up to value of 2 TeV. The LO, NLO and NNLO QCD results for a centre–of–mass energy of $\sqrt{s} = 14$ TeV are presented in Fig.56 (left). It is first observed the presence of a LO threshold at an invariant mass $M^{LO} = 2p_{\rm T}^{\gamma;\,hard}$. The

[25] The NNLO QCD calculation within the standard cone isolation criterion has not been performed yet.

[26] The same form of the isolation function is used in the NNLO predictions reported in Refs. [536, 542, 543].

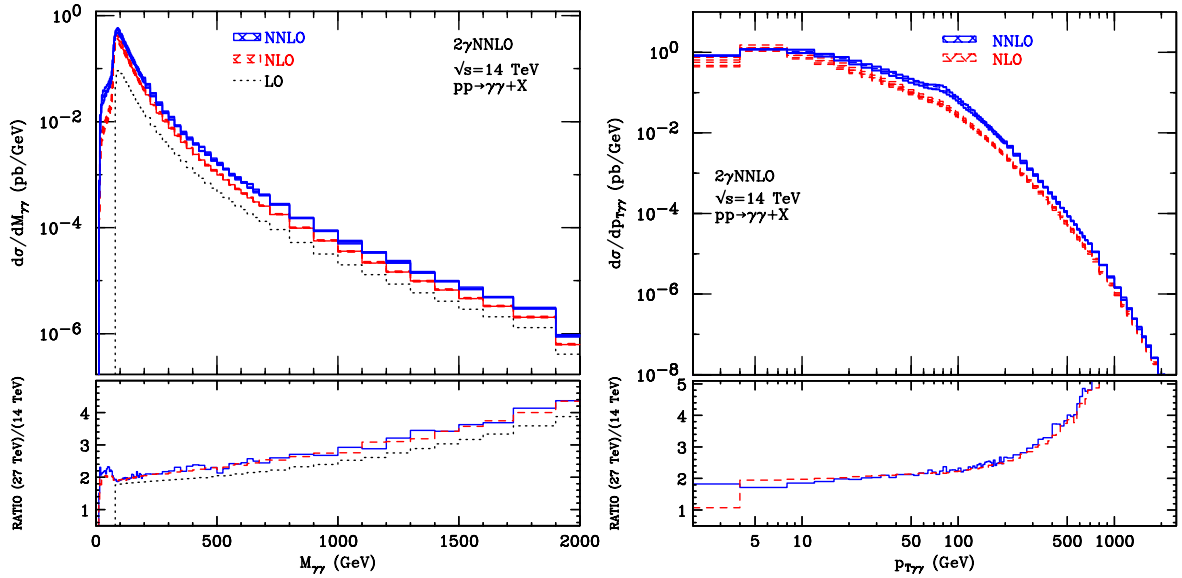

Fig. 56: The differential cross sections $d\sigma/dM_{\gamma\gamma}$ (left) and $d\sigma/dp_{\mathrm{T}\gamma\gamma}$ (right) at $\sqrt{s} = 14$ TeV are shown in the upper panel at LO (black dotted), NLO (red dashed) and NNLO (blue solid). The NLO and NNLO scale variation bands are obtained as detailed in the text. In the lower subpanels the ratio between cross sections at two different centre–of–mass energies ($\sqrt{s} = 27$ TeV and $\sqrt{s} = 14$ TeV) is also shown. The selection cuts are described in the text.

bulk of the cross section is concentrated in the region around M^{LO} while for large values of $M_{\gamma\gamma}$ the distribution rapidly decreases. At high invariant mass, $M_{\gamma\gamma} > 1$ TeV, the cross section is dominated by the quark annihilation ($q\bar{q}$) partonic subprocess (the other partonic subprocesses are suppressed by one order of magnitude or more). The NNLO K factor, $K^{NNLO} = \sigma^{NNLO}/\sigma^{NLO}$, is flat at large values of $M_{\gamma\gamma}$ and it is roughly equal to the NNLO K factor of the $q\bar{q}$ channel. The lower subpanel of Figure 56 (left) presents results for the ratio (R) between the invariant mass distribution at $\sqrt{s} = 27$ TeV and $\sqrt{s} = 14$ TeV. At LO the dynamic enhancement of the ratio can be described roughly as $\mathcal{G}(M^2_{\gamma\gamma}/27^2\ \mathrm{TeV}^2)/\mathcal{G}(M^2_{\gamma\gamma}/(14^2\ \mathrm{TeV}^2)$, where $\mathcal{G}(\tau) = \log(\tau) \times \mathcal{L}_{q\bar{q}}(\tau, \mu_f)$ and $\mathcal{L}$ are the integrated parton luminosities. The ratio at NLO and NNLO is numerically similar to the corresponding LO one. The enhancement of the ratio R at large values of invariant mass is directly related to the increasing the centre–of–mass energy and it reaches the value $R \sim 4$ at $M_{\gamma\gamma} \simeq 1$ TeV.

Finally theoretical results are presented for the transverse momentum ($p_{\mathrm{T}\gamma\gamma}$) distribution. The NLO and NNLO predictions with a centre–of–mass energy of $\sqrt{s} = 14$ TeV are shown in the upper panel of Figure 56 (right). Given the LO kinematical constraint $p_{\mathrm{T}\gamma\gamma} = 0$, the (N)NLO correction represent *effectively* an (N)LO prediction. Moreover, in the small $p_{\mathrm{T}\gamma\gamma}$ region, the convergence of the fixed order expansion is spoiled by the presence of large logarithmic corrections. Reliable perturbative results require an all order resummation of these enhanced logarithmic contributions.

The lower subpanel of Figure 56 (right) presents results for the ratio (R) between the transverse momentum distribution at $\sqrt{s} = 27$ TeV and $\sqrt{s} = 14$ TeV. The ratio increases at large value of $p_{\mathrm{T}\gamma\gamma}$, reaching $R \sim 4$ for $p_{\mathrm{T}\gamma\gamma} \simeq 1$ TeV.

It is observed that the uncertainty bands for the NLO and NNLO results fail to overlap in most of the kinematical regions. This suggests that the computed scale dependence at NNLO cannot be considered a reliable estimate of the true perturbative uncertainty. As an alternative approach the perturbative uncertainty of the NNLO result can be estimated by considering half of the difference between the NNLO and NLO results at central values of the scales [544].

It is finally observed that the photon fragmentation component (which is absent in the case of smooth cone isolation) mainly affects the the low invariant mass region, where the cross section is strongly suppressed. Conversely, the intermediate and high invariant mass region, the transverse momentum distribution and the value of total cross section, are less sensitive to photon fragmentation effects. In particular, for isolation parameters commonly used in the experimental analysis at the LHC, the quantitative differences between smooth and standard isolation predictions are much smaller than the corresponding perturbative uncertainties. This observation justifies the use of the smooth cone criterion in the theoretical calculations.

5.2 Ultimate Parton Densities[27]

The goal of this study is to quantify the precision that can be expected in the determination of the parton distribution functions (PDFs) of the proton in the HL-LHC era. Such "ultimate PDFs" will provide an important ingredient for the physics projections at the HL-LHC with a robust estimate of theoretical uncertainties, including some of those presented in other chapters of this Yellow Report. With this motivation, HL-LHC pseudo-data have been generated for a number of PDF-sensitive measurements such as top-quark, Drell-Yan, isolated photon, and W+charm production, and then studied the constraints that these pseudo-data impose on the global PDF analysis by means of the Hessian profiling method. While such studies have been performed in the context of future lepton-hadron colliders, see e.g. [461, 548] for the LHeC, this is the first time that such a systematic effort has been directed to the projections for a future hadron collider. The study below is described in further detail in [549].

5.2.1 HL-LHC measurements for PDF studies

The PDF-sensitive processes that will be considered in this study are listed here first. In all cases, pseudo-data is generated for a centre-of-mass energy of $\sqrt{s} = 14$ TeV assuming a total integrated luminosity of $\mathcal{L} = 3$ ab^{-1} for the CMS and ATLAS experiments, and of $\mathcal{L} = 0.3$ ab^{-1} for the LHCb experiment. With these settings, HL-LHC pseudo-data has been generated for the following processes:

- High-mass Drell-Yan, specifically the dilepton invariant mass differential distributions $d\sigma(pp \to ll)/dm_{ll}$ for $m_{ll} \gtrsim 110$ GeV for a central rapidity acceptance, $|\eta^l| \leq 2.4$. This process is particularly useful for quark flavour separation, in particular of the poorly known large-x sea quarks.
- Differential distributions in top-quark pair production, providing direct information on the large x gluon [203]. Specifically, pseudo-data has been generated for the top-quark transverse momentum $p_{\rm T}^t$ and rapidity y_t as well as for the top-quark pair rapidity $y_{t\bar{t}}$ and invariant mass $m_{t\bar{t}}$.
- The transverse momentum distribution of the Z bosons in the large $p_{\rm T}^Z$ region for central rapidity $|y_Z| \leq 2.4$ and different bins of the dilepton invariant mass m_{ll}. This process is relevant to constrain the gluon and the antiquarks at intermediate values of x [204].
- The production of W bosons in association with charm quarks (both in the central and forward region). This process provides a sensitive handle to the strangeness content of the proton [550, 551]. The pseudo-data for this process has been generated as function of the pseudorapidity η_l of the charged lepton from the W boson decay.
- Prompt isolated photon production, which represents a complementary probe of the gluon PDF at intermediate values of x [205, 552]. Here the pseudo-data have been generated as differential distributions in the photon transverse momentum $p_{\rm T}^\gamma$ for different bins in the photon pseudorapidity η^γ.
- Differential distributions for on-peak W and Z boson production in the forward region, $2.0 \leq \eta_l \leq 4.5$, covered by detectors with large acceptance, including forward rapidity. These measure-

[27] Contribution by R. Abdul Khalek, S. Bailey, J. Gao, L. Harland-Lang and J. Rojo.

ments constrain quark flavour separation, including the strange and charm content of the proton, in the large and small x region [553].

– The inclusive production of jets in different bins of rapidity (both in the central and forward region) as a function of $p_{\rm T}^{\rm jet}$. Jets have been reconstructed using the anti–k_t algorithm [274] with $R = 0.4$, and provide information on the large-x gluon and valence quarks [554].

In all cases, the binning and kinematic cuts from the most recent $\sqrt{s} = 13$ TeV analyses or the corresponding 8 TeV analyses if the former are not available, are taken as the baseline. The binning has been suitably extended to account for the extended kinematic coverage achieved with $\mathcal{L} = 3$ (0.3) ab^{-1}. The statistical uncertainties are computed from the number of events per bin, while systematic errors are rescaled as compared to the 13 (or 8) TeV baseline analysis, see below. Various scenarios for the reduction of systematic errors are considered, from a more conservative one to a more optimistic one. The overall acceptance of the selection cuts (which affects the final event yield per bin) is estimated globally again based on the reference experimental analysis.

As mentioned above, this list of processes is not exhaustive: several other important processes will provide useful information on the parton distributions in the HL-LHC era, from inclusive dijet production [19] to single top quark [555] and D meson production [231], see also [193]. In addition, progress may be expected from both the experimental and theory sides leading to novel processes, not considered so far, being added to the PDF fitting toolbox. Even with these caveats, the list above is extensive enough to provide a reasonable snapshot of the PDF-constraining potential of the HL-LHC.

It is worth emphasising that the projections are based on pseudo-data which have been generated specifically for this study. They are thus not endorsed by the LHC experiments, although the feedback received from the ATLAS, CMS, and LHCb contact persons have been taken into account.

Generation of HL-LHC pseudo-data and fitting procedure

For each of the HL-LHC processes listed above, theoretical predictions have been generated at next-to-leading order (NLO) using MCFM [210] interfaced to APPLGRID [208] to produce the corresponding fast grids. The central value of the pseudo-data is first produced according the central prediction of the PDF4LHC15 NNLO set [195], and then fluctuations as expected by the corresponding experimental uncertainties are included. Since the present study is based on pseudo-data, it does not account for higher-order QCD effects or electroweak corrections. As in the case of PDF closure tests [201], here only the relative reduction of PDF uncertainties once the HL-LHC data are added are of interest, while by construction the central value will be mostly unaffected.

To be more specific, if $\sigma_i^{\rm th}$ is the theoretical cross-section for bin i of a given process, computed with PDF4LHC15 NNLO, then the central value of the HL-LHC pseudo-data $\sigma_i^{\rm exp}$ is constructed by means of

$$\sigma_i^{\rm exp} = \sigma_i^{\rm th} \times \left(1 + r_i \cdot \delta_{{\rm tot},i}^{\rm exp} + \lambda \cdot \delta_{\mathcal{L}}^{\rm exp}\right) , \tag{32}$$

where r_i, λ are univariate Gaussian random numbers, $\delta_{{\rm tot},i}^{\rm exp}$ is the total (relative) experimental uncertainty corresponding to this specific bin, and $\delta_{\mathcal{L}}^{\rm exp}$ is the luminosity uncertainty related to the experiment. The latter are taken to be 1.5% for each of the CMS, ATLAS, and LHCb experiments. The motivation for adding the fluctuations on top of the central theoretical predictions is to simulate the statistical and systematic uncertainties of an actual experimental measurement. In eq. (32) the total experimental error is defined as

$$\delta_{{\rm tot},i}^{\rm exp} \equiv \left(\left(\delta_{{\rm stat},i}^{\rm exp}\right)^2 + \left(f_{\rm corr} \times f_{\rm red} \times \delta_{{\rm sys},i}^{\rm exp}\right)^2 \right)^{1/2} . \tag{33}$$

In this expression, the relative statistical error $\delta_{{\rm stat},i}^{\rm exp}$ is computed as

$$\delta_{{\rm stat},i}^{\rm exp} = \left(f_{\rm acc} \times N_{{\rm ev},i}\right)^{-1/2} , \tag{34}$$

where $N_{\mathrm{ev},i} = \sigma_i^{\mathrm{th}} \times \mathcal{L}$ is the expected number of events in bin i at the HL-LHC with $\mathcal{L} = 3\ (0.3)\ \mathrm{ab}^{-1}$, and $f_{\mathrm{acc}} \leq 1$ is an acceptance correction which accounts for the fact that, for some of the processes considered, such as top quark pair production, there is a finite experimental acceptance and/or one needs to include the effects of branching fractions. The value of f_{acc} is then determined by extrapolation using the reference dataset. The one exception to this is the case of forward W+charm production, for which no baseline measurement has so far been performed by LHCb; here the acceptance is set to $f_{\mathrm{acc}} = 0.3$ to account for the anticipated c–jet tagging efficiency. In eq. (33), $\delta_{\mathrm{sys},i}^{\mathrm{exp}}$ indicates the total systematic error of bin i taken from the reference LHC measurement at either 8 TeV or 13 TeV. The correction factor $f_{\mathrm{red}} \leq 1$ accounts for the expected improvement in the average systematic uncertainties at the HL-LHC in comparison to Run-2, due to both detector improvements and the enlarged dataset for calibration.

With the exception of the luminosity in eq. (33) the systematic uncertainties have simply been added in quadrature with the statistical ones. That is, correlations between systematic errors are not taken into account. The full inclusion of such correlations goes beyond the scope of the closure tests being pursued in this exercise, which aim simply to provide a reasonable extrapolation of the expected PDF reach at the HL-LHC. In particular, the expected improvements in the overall size of the systematic uncertainties can only be based on the estimates and expectations provided by the LHC collaborations, and cannot be predicted with absolute certainty. The situation is certainly even more challenging in the case of the specific mutual correlations of the systematic uncertainties, which will be sensitive to the precise experimental setup in the future. However, simply excluding the effects of correlations would artificially reduce the impact of the pseudo-data into the fit.

For this reason, an effective correction factor f_{corr} is introduced to accounts for the fact that data with correlated systematic uncertainties is more constraining than the same data where all errors are added in quadrature. The value of f_{corr} has been checked against the available $\sqrt{s} = 8$ TeV top quark [556,557] and the 13 TeV W+charm [558] differential distributions, that is f_{corr} is varied until the PDF impact is in line with the result including full experimental correlations. This turns out to have a value of between $f_{\mathrm{corr}} \simeq 1.0$ and 0.3 depending on the data set and observable. A factor of $f_{\mathrm{corr}} = 0.5$ is taken in what follows.

In Table 31 a summary of the features of the HL-LHC pseudo-data generated for the present study is collected. For each process, the kinematic coverage, the number of pseudo-data points used N_{dat}, the values of the correction factors f_{acc}, f_{corr}, and f_{red}; and finally the reference from the 8 TeV or 13 TeV measurement used as baseline to define the binning and the systematic uncertainties of the HL-LHC pseudo-data are indicated. A total of $N_{\mathrm{dat}} = 768$ pseudo-data points are then used in the PDF profiling. The values of the reduction factor for the systematic errors f_{red} are varied between 1 (0.5) and 0.4 (0.2) in the conservative and optimistic scenarios for a 8 TeV (13 TeV) baseline measurement. This choice is motivated because available 13 TeV measurements are based on a relatively small $\mathcal{L}$ and therefore cannot be taken as representative of the systematic errors expected at the HL-LHC, even in the most conservative scenario.

Hessian profiling

There exist a number of techniques that can be used to quantify the impact on PDFs of the pseudo-data listed in Table 31. In the case of Monte Carlo sets such as NNPDF, the Bayesian reweighting method [564,565] reproduces the result of a direct fit, but it is restricted by the fact that information loss limits its reliability when the measurements provide significant new information. For Hessian sets such as PDF4LHC15_100 instead, the profiling technique [476] is more suitable to achieve the same purpose.

Table 31: Summary of the features of the HL-LHC pseudo-data generated for the present study. For each process the kinematic coverage, the number of pseudo-data points used $N_{\rm dat}$ across all detectors, the values of the correction factors $f_{\rm corr}$ and $f_{\rm red}$; and finally the reference from the 8 TeV or 13 TeV measurement used as baseline to define the binning and the systematic uncertainties of the HL-LHC pseudo-data, as discussed in the text, are indicated.

Process	Kinematics	$N_{\rm dat}$	$f_{\rm corr}$	$f_{\rm red}$	Baseline
Z $p_{\rm T}$	$20\,{\rm GeV} \leq p_{\rm T}^{ll} \leq 3.5$ TeV $12\,{\rm GeV} \leq m_{ll} \leq 150$ GeV $\lvert y_{ll}\rvert \leq 2.4$	338	0.5	$(0.4, 1)$	[559] (8 TeV)
high-mass Drell-Yan	$p_{\rm T}^{l1(2)} \geq 40(30)\,{\rm GeV}$ $\lvert\eta^l\rvert \leq 2.5, m_{ll} \geq 116\,{\rm GeV}$	32	0.5	$(0.4, 1)$	[560] (8 TeV)
top quark pair	$\lvert y_t\rvert \leq 2.4$	110	0.5	$(0.4, 1)$	[557] (8 TeV)
W+charm (central)	$p_{\rm T}^{\mu} \geq 26\,{\rm GeV}, p_{\rm T}^{c} \geq 5\,{\rm GeV}$ $\lvert\eta^{\mu}\rvert \leq 2.4$	12	0.5	$(0.2, 0.5)$	[558] (13 TeV)
W+charm (forward)	$p_{\rm T}^{\mu} \geq 20\,{\rm GeV}, p_{\rm T}^{c} \geq 20\,{\rm GeV}$ $p_{\rm T}^{\mu+c} \geq 20\,{\rm GeV}$ $2 \leq \eta^{\mu} \leq 5, 2.2 \leq \eta^{c} \leq 4.2$	10	0.5	$(0.4, 1)$	LHCb projection
Direct photon	$E_{\rm T}^{\gamma} \lesssim 3$ TeV, $\lvert\eta_{\gamma}\rvert \leq 2.5$	118	0.5	$(0.2, 0.5)$	[561] (13 TeV)
Forward W, Z	$p_{\rm T}^{l} \geq 20\,{\rm GeV}, 2.0 \leq \eta^{l} \leq 4.5$ $2.0 \leq y_{ll} \leq 4.5$ $60 \leq m_{ll} \leq 120\,{\rm GeV}$	90	0.5	$(0.4, 1)$	[562] (8 TeV)
Inclusive jets	$\lvert y\rvert \leq 3, R = 0.4$	58	0.5	$(0.2, 0.5)$	[563] (13 TeV)
Total		712			

This Hessian profiling is based on the minimization of

$$\chi^2\left(\beta_{\rm exp}, \beta_{\rm th}\right) = \sum_{i=1}^{N_{\rm dat}} \frac{1}{\left(\delta_{{\rm tot},i}^{\rm exp}\sigma_i^{\rm th}\right)^2}\left(\sigma_i^{\rm exp} + \sum_j \Gamma_{ij}^{\rm exp}\beta_{j,{\rm exp}} - \sigma_i^{\rm th} + \sum_k \Gamma_{ik}^{\rm th}\,\beta_{k,{\rm th}}\right)^2 + \sum_j \beta_{j,{\rm exp}}^2 + T^2\sum_k \beta_{k,{\rm th}}^2\,, \tag{35}$$

with $\sigma_i^{\rm exp}$ ($\sigma_i^{\rm th}$) are the central values of a given experimental measurement (theory prediction), $\beta_{j,{\rm exp}}$ are the nuisance parameters corresponding to the set of fully correlated experimental systematic uncertainties, $\beta_{k,{\rm th}}$ are the nuisance parameters corresponding to the PDF Hessian eigenvectors, $N_{\rm dat}$ is the number of data points and T is the tolerance factor. The matrices $\Gamma_{ij}^{\rm exp}$ and $\Gamma_{ik}^{\rm th}$ encode the effects of the corresponding nuisance parameters on the experimental data and on the theory predictions, respectively.

As mentioned above, in this study the statistical and experimental uncertainties are added in quadrature excluding the luminosity, and then the effects of the missing correlations are accounted for

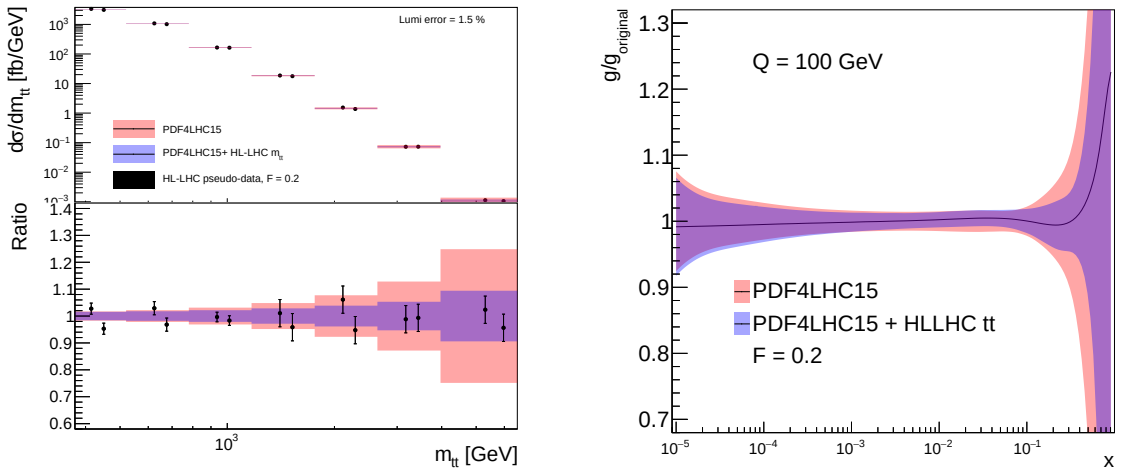

Fig. 57: Comparison of the predictions for the $m_{t\bar{t}}$ distribution in top-quark pair production at the HL-LHC using PDF4LHC15 with the associated pseudo-data and with the profiled results with $F \equiv f_{\rm corr} \cdot f_{\rm red} = 0.2$ (left). The corresponding differences at the level of the gluon PDF at $Q = 100$ GeV before and after profiling all top-quark pair production observables (right).

by means of the factor $f_{\rm corr}$. For this reason there are only nuisance parameters for the luminosity errors, and for an overall normalization uncertainty of 5% in forward W+charm production due to charm-jet tagging. If eq. (35) is minimised with respect to these nuisance parameters, this gives:

$$\chi^2\left(\beta_{\rm th}\right) = \sum_{i,j=1}^{N_{\rm dat}} \left(\sigma_i^{\rm exp} - \sigma_i^{\rm th} + \sum_k \Gamma_{ik}^{\rm th}\,\beta_{k,\rm th}\right) \left(\rm cov\right)_{ij}^{-1} \left(\sigma_j^{\rm exp} - \sigma_j^{\rm th} + \sum_m \Gamma_{jm}^{\rm th}\,\beta_{m,\rm th}\right) + T^2 \sum_k \beta_{k,\rm th}^2 \,, \tag{36}$$

where:

$$\left(\rm cov\right)_{ij} = \delta_{ij} \left(\delta_{{\rm tot},i}^{\rm exp} \sigma_i^{\rm th}\right)^2 + \sum \Gamma_{i,\rm lumi/norm}^{\rm exp} \Gamma_{j,\rm lumi/norm}^{\rm exp}. \tag{37}$$

eq. (36) is then minimised with respect to the Hessian PDF nuisance parameters $\beta_{k,\rm th}$, which can be interpreted as leading to PDFs that have been optimised to describe this new dataset. The resulting Hessian matrix on $\beta_{k,\rm th}$ at the minimum can be diagonalised to construct the new eigenvector directions. Finally, the PDF uncertainties are determined from the $\Delta\chi^2 = T^2$ criteria. In the studies presented here, a global $T = 3$ is used which approximately corresponds to the average tolerance determined dynamically in the CT14 and MMHT14 analyses.

Results for individual processes

The results of the Hessian profiling of PDF4LHC15 from individual processes are now presented, and subsequently the corresponding results from the combination of all the HL-LHC processes are considered in different scenarios. First, the top-quark pair production case listed in Table 31 is considered. In Fig. 57 the comparison of the predictions for the $m_{t\bar{t}}$ distribution in top-quark pair production at the HL-LHC using PDF4LHC15 is shown with the associated pseudo-data for ATLAS and CMS experiments, and with the profiled results with $F \equiv f_{\rm corr} \cdot f_{\rm red} = 0.2$. The corresponding impact at the level of the gluon PDF at $Q = 100$ GeV is also presented before and after profiling with all $t\bar{t}$ data in Table 31. It is clear that the HL-LHC pseudo-data in this scenario will have much smaller uncertainties than the PDF uncertainties, so there is a marked reduction on the PDF errors on the gluon at large-x. Note that the two points in each of the bins in Fig. 57 (left) correspond to the ATLAS and CMS pseudo-data.

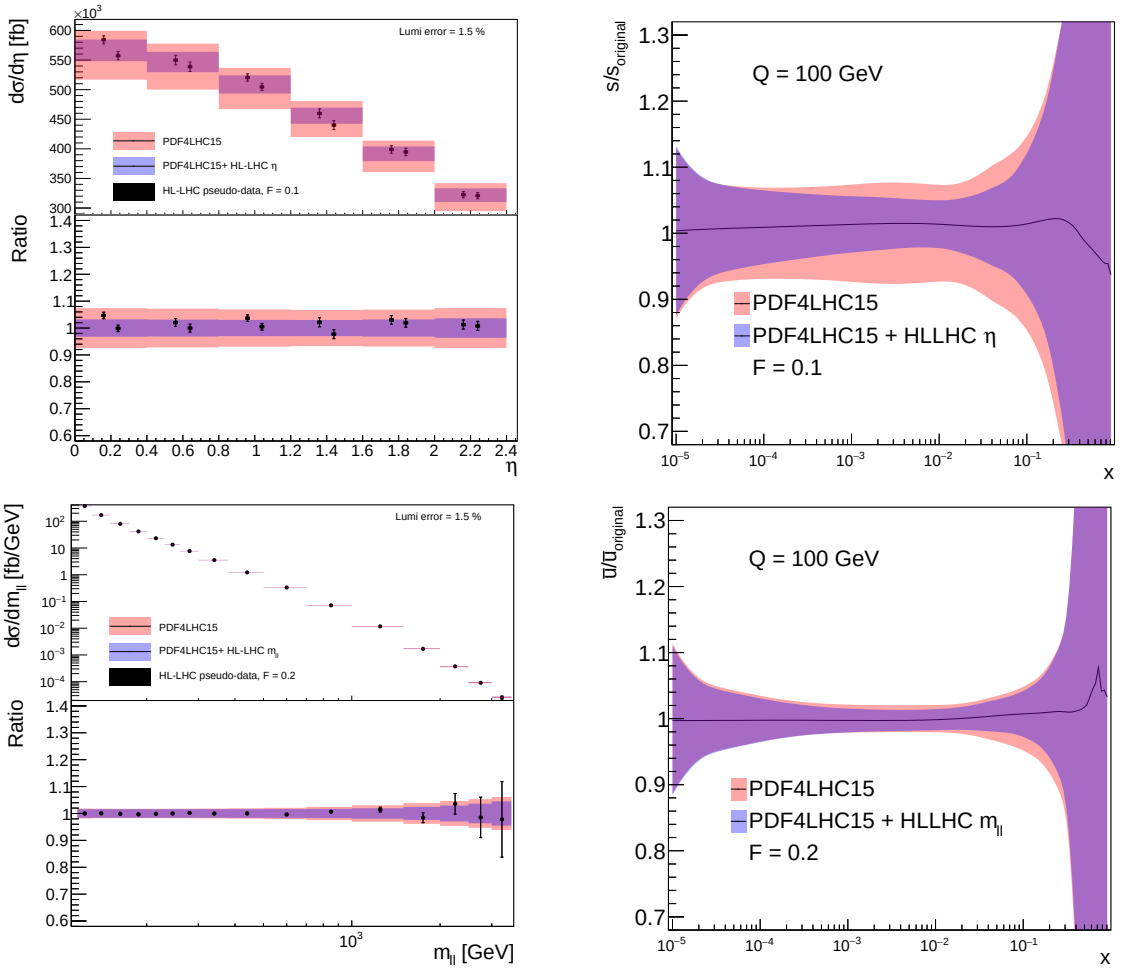

Fig. 58: Same as Fig. 57 for W+charm quark production with impact on strange quark PDF (upper) and the high-mass Drell-Yan process with impact on $\bar{u}$ PDF (lower).

Two other representative processes are considered next: W+charm quark production in central rapidity region and the high-mass Drell-Yan process. In Fig. 58 the same comparison is shown as in Fig. 57 for these two processes. In the case of the W+charm quark production, a clear reduction of PDF errors is observed in the strangeness, $s+\bar{s}$, at intermediate values of x, highlighting the sensitivity of this measurement to the strange content of the proton. For the case of high-mass Drell-Yan, the uncertainties on the $\bar{u}$ quark PDF are reduced at large x region. Here the impact is rather moderate, as experimental and PDF errors are comparable even in the high m_{ll} region.

5.2.2 Ultimate PDFs from HL-LHC data

The final profiled PDF sets are based on the combined datasets listed in Table 31; these provide an estimate of the impact of future HL-LHC measurements into our knowledge of the quark and gluon structure of the proton. In Table 32 the three scenarios for the systematic uncertainties of the HL-LHC pseudo-data assumed in the present exercise are listed. These scenarios, ranging from more conservative to more optimistic, differ among them in the reduction factor $f_{\rm red}$, eq. (33), applied to the systematic errors of the reference 8 TeV or 13 TeV measurements. In particular, in the optimistic scenario a reduction of the systematic errors by a factor 2.5 compared to the reference 8 TeV measurements is assumed. A

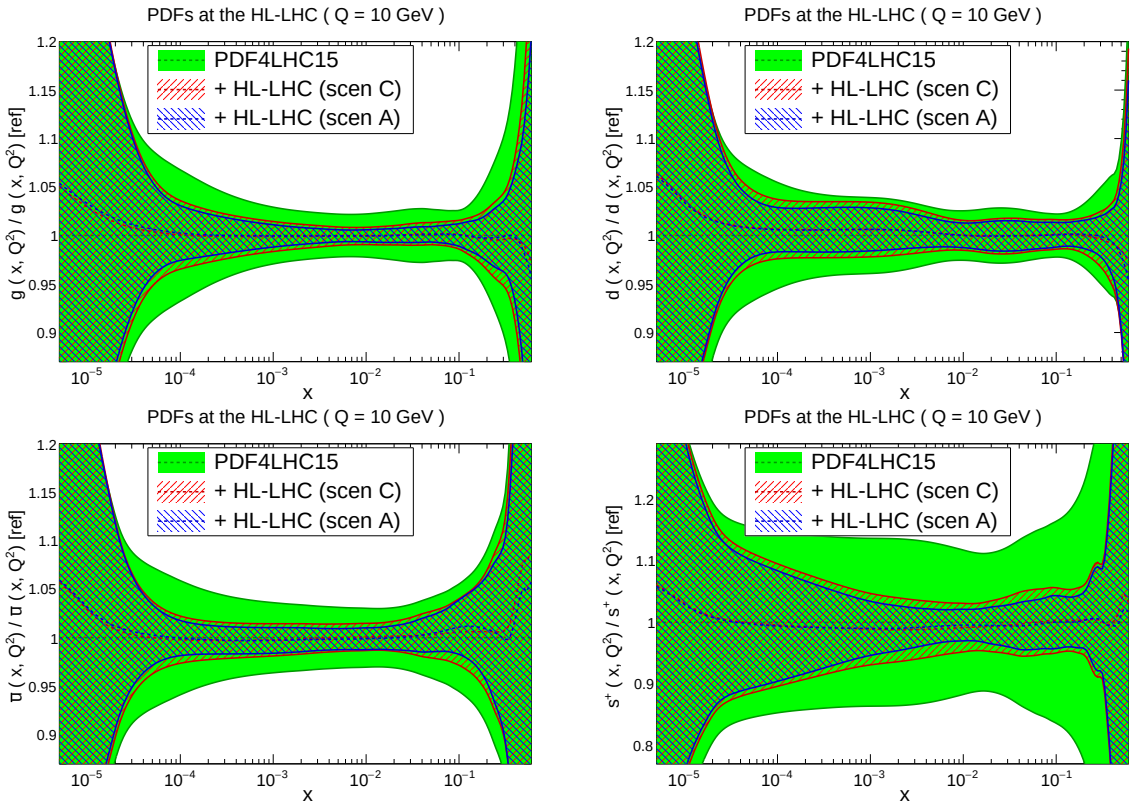

Fig. 59: Comparison of PDF4LHC15 with the profiled sets with HL-LHC data in scenarios A and C (see text). The gluon, down quark, up anti-quark, and total strangeness at $Q = 10$ GeV are shown, normalized to the central value of the baseline.

large factor of 5 for the 13 TeV measurements is assumed, correcting for the fact that these are based in the initial datasets which generally have larger systematic errors in comparison to the 8 TeV case. The name of the corresponding `LHAPDF` grid is also indicated in each case.

Table 32: The three scenarios for the systematic uncertainties of the HL-LHC pseudo-data assumed in the present exercise. These scenarios, ranging from conservative to optimistic, differ among them in the reduction factor $f_{\rm red}$, eq. (33), applied to the systematic errors of the reference 8 TeV or 13 TeV measurements. The name of the corresponding `LHAPDF` grid is also indicated in each case.

Scenario	$f_{\rm red}$ (8 TeV)	$f_{\rm red}$ (13 TeV)	`LHAPDF` set	Comments
A	0.4	0.2	`PDF4LHC_nnlo_hllhc_scen3`	Optimistic
B	0.7	0.36	`PDF4LHC_nnlo_hllhc_scen2`	Intermediate
C	1	0.5	`PDF4LHC_nnlo_hllhc_scen1`	Conservative

Then in Fig. 59 a comparison of the baseline PDF4LHC15 set is presented with the profiled sets based on HL-LHC pseudo-data from scenarios A and C in Table 32. Specifically, the gluon, down quark, up anti-quark, and total strangeness at $Q = 10$ GeV are shown, normalized to the central value of the baseline. The predictions of scenarios A and C (optimistic and conservative respectively) are observed to be reasonably similar. This demonstrates that the results are relatively robust against the projections of how experimental errors will be reduced in HL-LHC measurements. A marked reduction of PDF

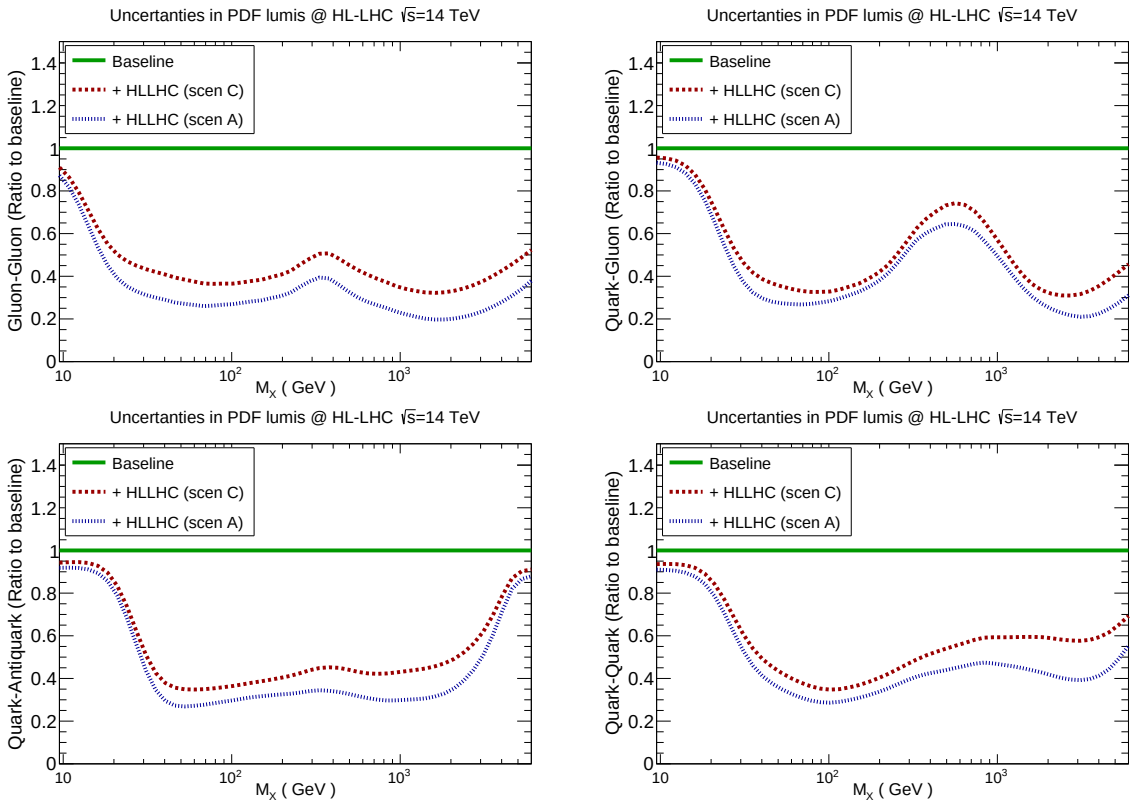

Fig. 60: The reduction of PDF uncertainties in the gg, qg, $q\bar{q}$, and qq luminosities at $\sqrt{s} = 14$ TeV due to the HL-LHC pseudo-data (in scenarios A and C) with respect to the PDF4HC15 baseline.

uncertainties is visible in all cases, and is particularly significant for the gluon and the sea quarks, which are worse known than the valence quarks.

Next, the partonic luminosities are investigated, in particular by quantifying the improvement in the PDF uncertainties in different initial-state partonic combinations from the HL-LHC pseudo-data. In Fig. 60 the reduction of PDF uncertainties are shown in the gg, qg, $q\bar{q}$, and qq luminosities at $\sqrt{s} = 14$ TeV due to the HL-LHC pseudo-data (in scenarios A and C) with respect to the PDF4HC15 baseline. The average values of this PDF error reduction for three different invariant mass bins (low, medium, and high values of M_X) is shown in the table in Fig. 61.[28] The value outside (inside) brackets correspond to scenario C (A). Note that in this table the us luminosity is also listed, which contributes to processes such as inclusive W^+ production.

From the comparisons in Fig. 60 and in Fig. 61 it is observed the overall error reduction is not too sensitive to the specific projections assumed for the experimental systematic uncertainties. In the intermediate mass bin, $40\ \text{GeV} \leq M_X \leq 1\ \text{TeV}$, the reduction of PDF uncertainties ranges roughly between a factor of 2-4, depending on the partonic channel and the scenario for the systematic errors. For example, for the gg luminosity in the range relevant for Higgs production, a reduction by a factor $\simeq 3$ in scenario A is found. A similar improvement is found in the high mass region, $M_X \geq 1$ TeV, directly relevant for beyond-SM (BSM) searches. In the optimistic scenario, the PDF error reduction at high masses ranges between a factor 4 for the gg luminosity to around a factor 2 for the qq and $q\bar{q}$ ones. On the other hand, the PDF error reduction is more moderate in the low mass region, $M_X \lesssim 20$ GeV, since none of the processes in Table 31 is directly sensitive to it.

[28] The average is computed from 10 points per mass bin, log-spaced in M_X.

PDF uncertainties HLLHC / Current	10 GeV < M_X < 40 GeV	40 GeV < M_X < 1 TeV	1 TeV < M_X < 6 TeV
g-g luminosity	0.58 (0.49)	0.41 (0.29)	0.38 (0.24)
q-g luminosity	0.71 (0.65)	0.49 (0.42)	0.39 (0.29)
quark-quark luminosity	0.78 (0.73)	0.46 (0.37)	0.60 (0.45)
quark-antiquark luminosity	0.73 (0.70)	0.40 (0.30)	0.61 (0.50)
up-strange luminosity	0.73 (0.67)	0.38 (0.27)	0.42 (0.38)

Fig. 61: The uncertainties associated to different PDF luminosities, normalised to the uncertainties of the current baseline (PDF4LHC15). The average for three different invariant mass M_X bins is computed. The numbers outside (inside) brackets correspond to the conservative (optimistic) scenario.

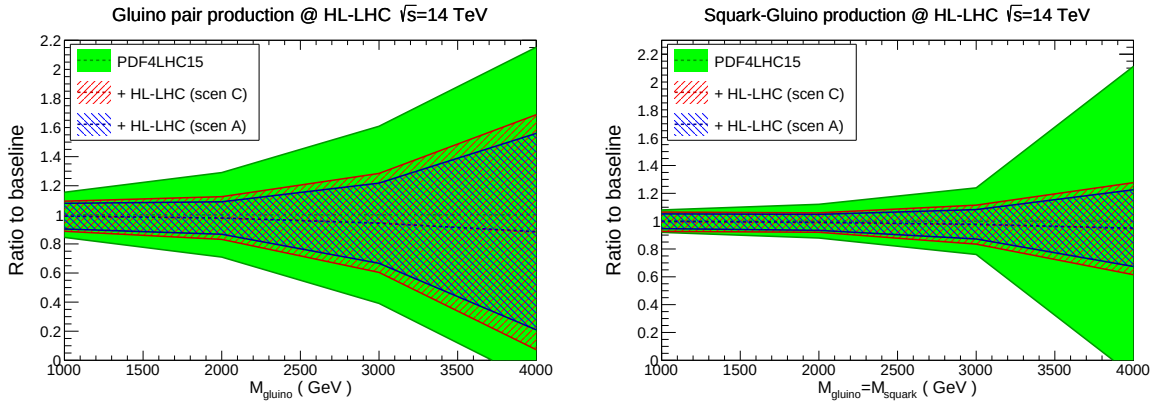

Fig. 62: Comparison between the baseline PDF4LHC15 predictions for high-mass supersymmetric particle production at the HL-LHC with the corresponding HL-LHC projections corresponding to scenarios C and A, normalised to the central value of the baseline. The results for gluino-gluino and squark-gluino production cross-sections are shown at $\sqrt{s} = 14$ TeV.

Implications for LHC phenomenology

Now some selected phenomenological implications of these "ultimate" PDFs at the HL-LHC are presented for a variety of processes, both within the SM and beyond. First high-mass supersymmetric (SUSY) particle production at the HL-LHC is considered, where sparticles masses up to $\simeq 3$ TeV can be searched for. While this SUSY scenario is considered for concreteness, similar results will hold for the production of new BSM states within other models. In Fig. 62 the comparison between the baseline PDF4LHC15 predictions with the corresponding HL-LHC results is shown corresponding to scenarios C and A (conservative and optimistic respectively), normalised to the central value of the former. Specifically, the cross-sections for gluino-gluino and squark-gluino are shown at $\sqrt{s} = 14$ TeV. Theoretical predictions have been computed at leading order (LO) using PYTHIA8.235 [292] with the SLHA2 benchmark point [566] for a range of sparticle masses. For simplicity, underlying event and multiple interactions have been ignored.

From the comparisons in Fig. 62, the constraints on the PDFs from the HL-LHC pseudo-data

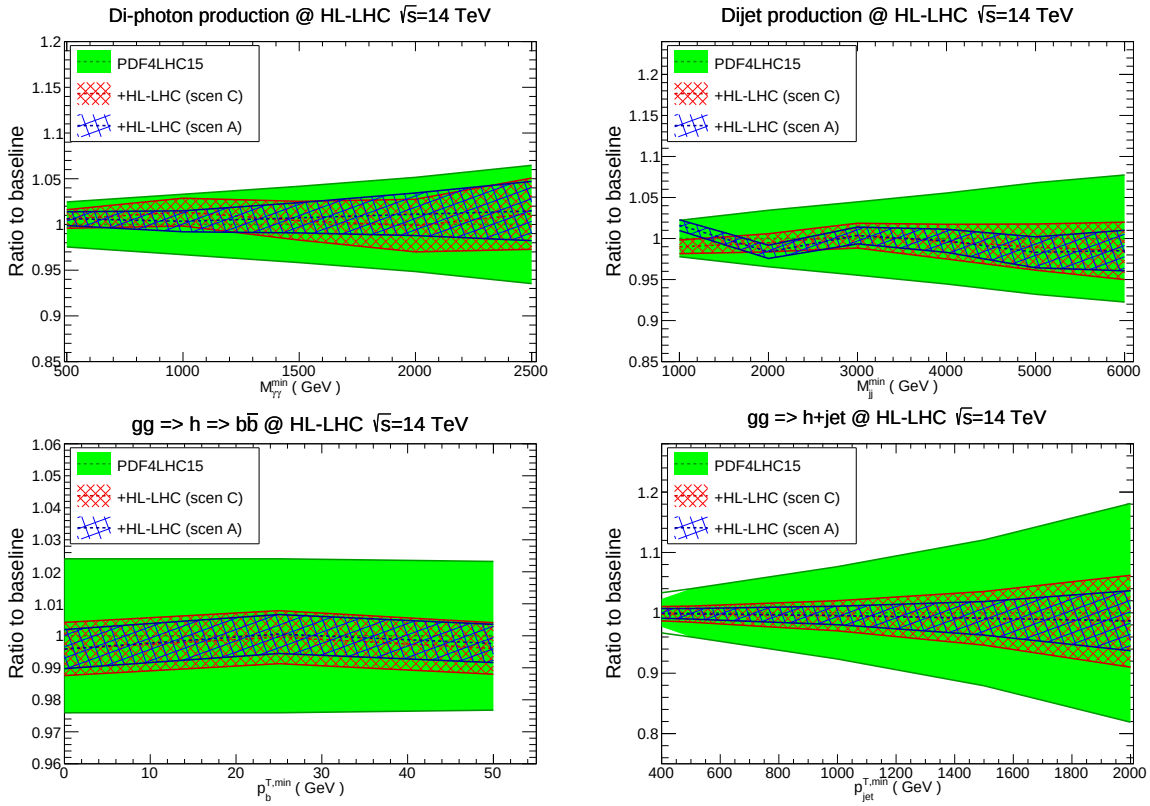

Fig. 63: Same as Fig. 62 for Standard Model processes. The upper plots show diphoton (dijet) production as a function of the minimum invariant mass $M_{\gamma\gamma}^{\rm min}$ ($M_{jj}^{\rm min}$). The bottom plots show Higgs boson production in gluon fusion, first inclusive and decaying into $b\bar{b}$ as a function of $p_b^{\rm T,min}$, and then in association with a hard jet as a function of $p_{\rm jet}^{\rm T,min}$.

lead to a marked reduction to the uncertainties in the high-mass SUSY cross-sections, consistent with the corresponding reduction at the level of luminosities reported in Fig. 60. For instance, for gluino pair-production with $M_{\tilde{g}} = 3$ TeV, the PDF uncertainties are reduced from $\simeq 60\%$ to $\simeq 25\%$ in the optimistic scenario. An even more marked reduction is found for the squark-gluino cross-section, specially at large sparticle masses. More moderate improvements are found in the case of squark-antisquark production, due to the limited constraints that the HL-LHC provides on the large-x antiquarks, at least for the processes considered here. In this case, an error reduction of a factor of $\simeq 25\%$ is found for $M_{\tilde{q}} = 3$ TeV.

Next, in Fig. 63 a similar comparison is presented as that of Fig. 62, now for various SM processes. The upper plots display diphoton (dijet) production as a function of the minimum invariant mass $M_{\gamma\gamma}^{\rm min}$ ($M_{jj}^{\rm min}$). The bottom plots show Higgs boson production in gluon fusion, first inclusive and decaying into $b\bar{b}$ as a function of $p_b^{\rm T,min}$, and then in association with a hard jet as a function of $p_{\rm jet}^{\rm T,min}$. These cross-sections have been computed at LO with `MCFMv8.2` [210] with the basic ATLAS and CMS acceptance cuts. The use of leading-order theory is justified as only the relative impact of the PDF error reduction is of interest, rather than providing state-of-the-art predictions for the rates.

From the comparisons in Fig. 63, the two scenarios, A and C, give similar results. In the case of dijet production, which at large masses is dominated by the qq and qg luminosities, PDF errors are expected to reduce down to $\simeq$2% even for invariant masses as large as $M_{jj} = 6$ TeV. A similar conclusion can be drawn for diphoton production, also sensitive to the qq partonic initial state. Concerning

Higgs boson production in gluon fusion, in the inclusive case the HL-LHC constraints should lead to PDF errors below the percent level. For Higgs boson production in association with a hard jet, a marked error reduction is found, suggesting that PDF uncertainties in the $p_{\rm T}^h$ distribution should be down to at most the $\simeq$2% level at the HL-LHC in the entire relevant kinematical range.

Summary and outlook

In this study, the constraints that HL-LHC measurements are expected to impose on the quark and gluon structure of the proton have been quantified. The impact of a range of physical processes have been assessed, from weak gauge boson and jet production to top quark and photon production, and the robustness of the results has been studied with respect to different projections for the experimental systematic uncertainties. It is found that, in the invariant mass region $M_X \gtrsim 100$ GeV, the HL-LHC measurements can be expected to reduce the PDF uncertainties in processes such as Higgs boson or SUSY particle production by a factor between 2 and 4, depending on the dominant partonic luminosity and on the scenario for the systematic errors. Therefore, the exploitation of the HL-LHC constraints on PDFs will feed into improved theoretical predictions for a range of phenomenologically relevant processes both within and beyond the SM.

Two caveats are relevant at this point. First, only a non–exhaustive subset of all possible measurements of relevance for PDF fits has been considered. Other processes not considered here, due to currently anticipated measurements and those not foreseen but which may well added to the PDF toolbox in the future, will certainly increase the PDF impact in some regions. Second, any possible issues such as data incompatibility, theoretical limitations, or issues with the data correlation models, which may limit the PDF impact in some cases have been ignored. All these issues can only be tackled once the actual measurements are presented.

The results of this study are made publicly available in the `LHAPDF6` format [202], with the grid names listed in Table 32. This way, the "ultimate" PDFs produced here can be straightforwardly applied to related physics projections of HL-LHC processes taking into account our improved knowledge of the partonic structure of the proton which is expected by then.

5.3 Underlying Event and Multiple Parton Interactions

Underlying event (UE), defined as a accompanying activity to hard proton-proton scattering process, is an unavoidable background to collider observables for most measurements and searches. The UE activity is not constant on an event-by-event basis, so the contribution from UE cannot be subtracted. However by using measurements sensitive to UE activity, the modelling of it in Monte Carlo (MC) event generators is *tuned*.

Multiple parton interactions (MPI) are one of the most important contributors to UE. The dependence of MPI on the centre-of-mass energy ($\sqrt{s}$) cannot be derived from first principles, rather modelled by looking at data at different centrer-of-mass energies, from Tevatron to LHC. At the start of the LHC, it was found that the this energy extrapolation of MPI based in Tevatron Run-1 and -2 data (at $\sqrt{s} = 1.8$ TeV and $\sqrt{s} = 1.96$ TeV) did not describe the LHC data at $\sqrt{s} = 900$ GeV and at $\sqrt{s} = 7$ TeV [567], and predictions of different MC generators varied significantly. These generators were then tuned using LHC Run-1 and Run-2 ($\sqrt{s} = 13$ TeV) data.

5.3.1 Underlying Event at 27 TeV[29]

The level of UE activity at the HL-LHC centre-of-mass energy of $\sqrt{s} = 14$ TeV is expected to be very similar to the one measured at $\sqrt{s} = 13$ TeV in Run-2. Given such a small increment in centre-of-mass

[29] Contribution by D. Kar.

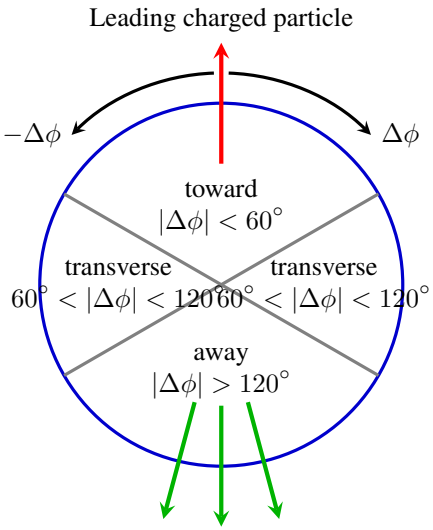

Fig. 64: Definition of UE regions in the azimuthal angle with respect to the leading charged particle

energy, it is expected that the current MC tunes will be generally valid at HL-LHC too. On the other hand, to get a sense of the UE activity at HE-LHC, two state-of-the-art MC generators, PYTHIA8 [292] (v235) with Monash tune [230] and HERWIG7 [146, 147] (v713) with default tune were used. As the first measurements at a new centre-of-mass energy data are easiest to perform in inclusive (i.e minimum-bias) events, 5 million such events were generated in each case. The UE activity is measured using the leading charged particle as the reference object, and defining the usual UE regions with respect to it, as shown in Fig. 64.

In Fig. 65, the scalar sum (density in per unit η-ϕ area) of charged particles and charged particle multiplicity (density) as a function of leading charged particle p_{T} are shown. The data is from the ATLAS measurement at $\sqrt{s} = 13$ TeV [568], while MC predictions both at $\sqrt{s} = 13$ TeV and $\sqrt{s} = 27$ TeV are shown. A few conclusions can be drawn. The activity increases by about 25 - 30% by roughly doubling the centre-of-mass energy, and the predictions by both generators are extremely consistent. The typical plateau-like behaviour of the activity with increasing leading charged particle p_{T} can be seen at $\sqrt{s} = 27$ TeV as well.

The similarity in predictions by two different generators is a welcoming sign, and perhaps indicates that the modelling of MPI evolution with centre-of-mass energy is mature enough. Of course at $\sqrt{s} = 27$ TeV, the events will be very active, and disentangling the effect of MPI in even typical UE observables will be a challenge, and innovative topologies and observables will be have to be devised in order perform UE measurements.

The analysis and plots are done using the Rivet [344] analysis framework.

5.3.2 Double Parton Scattering[30]

An instance of MPI is the double parton scattering (DPS) that occurs when one has two distinct hard parton-parton collisions in a single proton-proton interaction. In terms of the total cross section to produce a final state AB that may be divided into two subsets A and B, DPS is formally power suppressed by $\sim \Lambda^2_{QCD}/\min(Q^2_A, Q^2_B)$ compared to the more-familiar single parton scattering (SPS) mechanism. However, in practice there are various processes and kinematic regions where DPS contributes at a similar (or greater) level than SPS. Processes include those in which the SPS is suppressed by small/multiple

[30] Contribution by S. Cotogno, M. Dunser, J. R. Gaunt, T. Kasemets, and M. Myska.

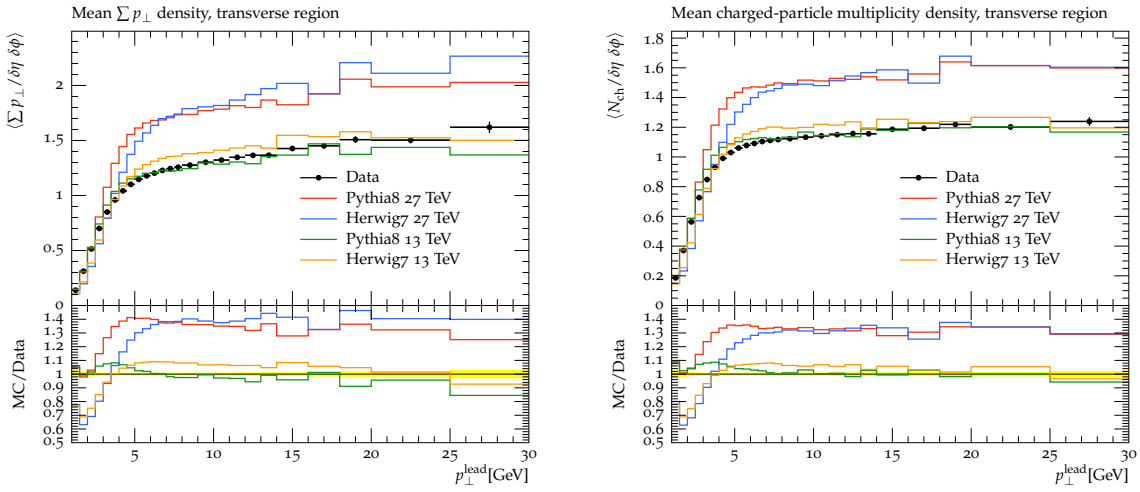

Fig. 65: Comparison of the UE activities in different centre-of-mass energies.

coupling constants, such as same-sign WW production, and processes where at least one part of the final state can be produced via a comparatively low scale scattering – e.g. those involving a charm/bottom quark pair.

The full theoretical description of DPS in QCD is rather complex, and many of the steps towards its formulation were achieved only recently [569–574]. As a result, many past studies of DPS have taken a strongly simplified approach in which it is assumed that the two colliding partons from each proton are entirely uncorrelated with one another, and that the (single) parton density in momentum fraction x and impact parameter $\mathbf{b}$ may be factorised into the PDF and a transverse profile depending only on $\mathbf{b}$. In this case the DPS cross section simplifies into the so-called 'pocket formula':

$$\sigma_{\text{DPS}}^{AB} \simeq \frac{\sigma_{\text{SPS}}^{A}\sigma_{\text{SPS}}^{B}}{\sigma_{\text{eff}}} \tag{38}$$

The quantity σ_{eff} is a geometrical factor of order of the proton radius squared. The modelling of more general multiple parton interactions (MPI) in Monte Carlo event generators such as HERWIG and PYTHIA is based on similar approximations.

The eq. (38) does not take into account the possibility that the two partons from either or both protons may have arisen as the result of a perturbative $1 \to 2$ splitting of a single parton into two. It also does not take into account a multitude of possible correlations between two partons in a proton, in spin, colour, and momentum fraction x_i, correlations between x_i and the transverse separation between partons $\mathbf{y}$, as well as potential interference contributions in parton type. These correlations and QCD effects can result in a DPS cross section differing from the prediction of eq. (38), both in terms of overall rate and also, crucially, in distributions.

Studies of DPS at the LHC and earlier colliders have essentially been restricted to extractions of a single number, the DPS rate, for several processes. From these early studies, in which the error bars are large and multiple factors change between measurements (x values, parton channels, scales...), nothing conclusive can be determined thus far concerning correlations. However, the increased luminosity of the HL-LHC will provide the statistics needed to study differential distributions with sufficiently small uncertainties that it will be possible to probe quantum correlations between partons in the proton and the dynamics of the $1 \to 2$ splitting for the first time. The results of these studies can be fed back and used to improve the theoretical modelling of DPS (and more general MPI), yielding improved DPS signal or background predictions.

As can be inferred from eq. (38), DPS roughly scales as the fourth power of a parton distribution, whilst SPS only scales as the second power. This means that for given hard scales Q_A, Q_B, the DPS cross section grows faster than the SPS one as the collider energy increases (and decrease x), meaning that at a HE-LHC DPS will be more prominent and easily measurable than at the LHC. At the same time, at the lower x values involved the effects of the correlations and $1 \to 2$ splittings will be different - a combination of measurements of different processes at both the HL-LHC and HE-LHC should help us to separate out the effects of the different correlations.

Let us illustrate the general points above using a concrete process – namely same-sign WW production, where both Ws decay leptonically into e or μ. A simple correlation-sensitive observable for this process is the asymmetry a_{η_l}:

$$a_{\eta_l} = \frac{\sigma(\eta_1 \cdot \eta_2 < 0) - \sigma(\eta_1 \cdot \eta_2 > 0)}{\sigma(\eta_1 \cdot \eta_2 < 0) + \sigma(\eta_1 \cdot \eta_2 > 0)}, \tag{39}$$

where $\eta_{1,2}$ are the rapidities of the two leptons. This quantity measures the discrepancy between the number of times the produced leptons emerge into opposite hemispheres of the detector and the number of times they emerge into the same hemisphere, normalised by the total number of lepton pairs produced. In the absence of parton correlations, it is found that $a_{\eta_l} = 0$; any departure from this value indicates the presence of correlations. A more differential version of this asymmetry is the cross section differential in the product $\eta_1 \cdot \eta_2$. Here an absence of correlations yields a symmetric distribution under $\eta_1 \cdot \eta_2 \leftrightarrow -\eta_1 \cdot \eta_2$, and an asymmetric distribution indicates correlations. In the below studies a cut of $|\eta_i| < 2.4$ is always applied.

One type of correlation that will clearly affect these observables are correlations in momentum fraction x between the partons. This type of effect was investigated in [575]. Here, the double parton distributions (DPDs) were calculated at an input scale of $Q_0^2 = 0.26\,\text{GeV}^2$ from a constituent quark model calculation where the proton is taken as being composed only from the three quarks uud. At this scale there are necessarily strong correlations in x space from the fact that there are only three quarks and due to the constraint $\sum_i x_i = 1$. These inputs were then evolved up to the W mass scale via the double DGLAP equations, with effects of $1 \to 2$ splittings being ignored. In Fig. 66, the green band represents their result at $\sqrt{s} = 14\,\text{TeV}$ for a quantity equal to $\sigma(\eta_1 \cdot \eta_2 < 0)/\sigma(\eta_1 \cdot \eta_2 > 0)$ – their result corresponds to $a_{\eta_l} \sim 0.05$. On the same plot is given the anticipated sensitivity of the CMS experiment at the HL-LHC ($3\,\text{ab}^{-1}$) [576] and the lowest values of this ratio that would allow one to reject the hypothesis of eq. (38) at the 95% confidence level. These results indicate good prospects of the HL-LHC measuring a_{η_l} values on the few per cent level for this process.

One simple feature that must necessarily be present in the true DPDs, and is taken into account by the DPDs of [575] but not by eq. (38), is the fact that removing one valence u quark from the proton halves the probability to find another, and there is no chance to find two valence d quarks (this requirement is formally expressed in the number sum rules of [577]). This effect is highly relevant to a_{η_l} as it results in a reduction of cross section for large $\eta_1 \cdot \eta_2$ (which probes the 'double valence' region in one DPD) whilst leaving the cross section elsewhere unchanged. To investigate the size of a_{η_l} resulting from this effect only, DPD inputs are constructed at $Q_0 = 1\,\text{GeV}$ based on a factorised ansatz of a product of MSTW2008LO PDFs times a transverse factor, except that in the uu and dd cases the PDF part is given by $D^u(x_1)D^u(x_2) - \frac{1}{2}D^{u_v}(x_1)D^{u_v}(x_2)$ and $D^d(x_1)D^d(x_2) - D^{d_v}(x_1)D^{d_v}(x_2)$ respectively. Evolving these inputs and using them to calculate the W^+W^+ cross section at $\sqrt{s} = 13\,\text{TeV}$, an asymmetry of ~ 0.017 is observed, indicating that these simple 'valence number effects' are at least one important driving force in the asymmetry of [575].

Correlations in (longitudinal) spin can affect the rapidity distributions of the produced leptons [578] and result in a nonzero a_{η_l}. The potential size of effects from spin correlations was investigated recently in [579]. In this study the unpolarised double parton distributions were constructed according to

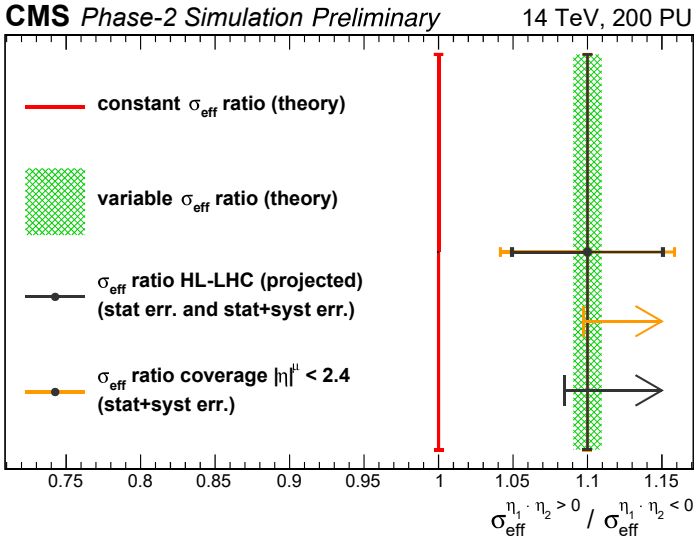

Fig. 66: Ratio of σ_{eff} for $\eta_1 \cdot \eta_2 > 0$ and $\eta_1 \cdot \eta_2 < 0$, which is equal to the inverse ratio for σ_{DPS}. The value of this in the absence of parton correlations is 1 (red line), whilst the prediction of [575] is given by the green band. The black error bars indicate systematic uncertainty attainable by the CMS experiment at 3 ab^{-1}, the orange bars include systematic uncertainties assuming a conservative correlation of 0.8 between them for $\eta_1 \cdot \eta_2 > 0$ and $\eta_1 \cdot \eta_2 < 0$. The vertical line on the arrows indicates the lowest measured value of the ratio that would allow the exclusion of the uncorrelated parton hypothesis (i.e. eq. (38) with constant σ_{eff}) at 95% CL. The black arrow corresponds to muon rapidity coverage $|\eta| < 2.8$, and the orange arrow $|\eta| < 2.4$.

an uncorrelated ansatz at an initial scale of 1 GeV. The polarised double parton distributions, encoding parton spin correlations, were chosen at the initial scale to correspond to the maximal possible spin correlations (technically, saturate the positivity bounds [580]), in such a way that the effects on the cross section would be maximal. These distributions were evolved to the W mass and used to compute polarised and unpolarised W^+W^+ cross sections at $\sqrt{s} = 13$ TeV. The resulting $\eta_1 \cdot \eta_2$ distribution is shown in Fig. 67(a) – the corresponding value of a_{η_l} is 0.07, which is even larger than that resulting from x correlations. One should, however, bear in mind that this is a maximal value, and that there are possibilities for the polarised distributions at the input scale, compatible with the positivity bounds, that also ultimately yield negative values for a_{η_l} [581]. Figure 67(b) shows the expected significance of a measured non-zero asymmetry as a function of luminosity L, using a rapidity cut $|\eta_i| > 0.6$ imposed such that the asymmetry a_{η_l} rises to 0.11 (but overall W^+W^+ cross section reduces from 0.51 fb to 0.29 fb). The blue band shows the sensitivity achievable using the $\mu^+\mu^+$ channel only, whilst the red band shows the sensitivity attainable using $\mu^+\mu^+$, μ^+e^+, and e^+e^+ assuming a similar sensitivity can be achieved for electrons as for muons. This plot reinforces the notion that a few per cent level asymmetry can be measured at the HL-LHC.

To investigate how $1 \to 2$ splittings may affect the asymmetry a_{η_l}, the code discussed in section 9 of [571] was upgraded to include charm and bottom quarks above the appropriate mass thresholds (chosen here to be equal to the MSTW 2008 values of 1.40 GeV and 4.75 GeV respectively). The 'intrinsic' and 'splitting' part of the DPDs were initialised as in [571] – in particular, the intrinsic part was initialised according to an uncorrelated ansatz, up to a suppression factor near the phase space boundary $x_1 + x_2 = 1$, that does not have a strong impact on a_{η_l}. Then, any nonzero value of a_{η_l} will be almost entirely due to $1 \to 2$ splitting effects. Computing W^+W^+ cross sections at $\sqrt{s} = 13$ TeV it

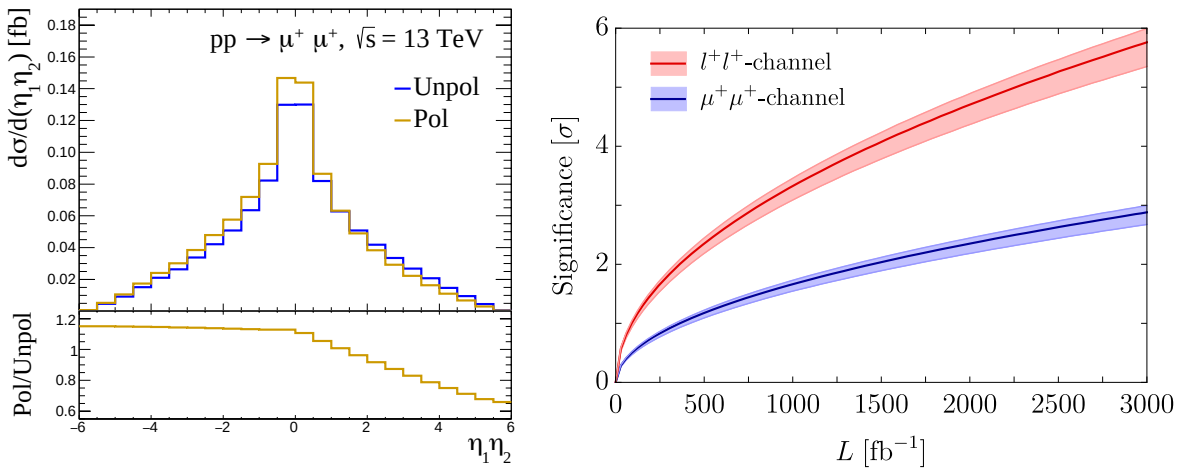

Fig. 67: Distribution in product of rapidities for two positively charged muons arising from W^+W^+ DPS. The blue plot includes only the unpolarised contribution, whilst the yellow also includes longitudinally polarised contributions (left). Estimated significance of a nonzero asymmetry as the distance in standard deviations of a measured asymmetry from zero, when the W^+W^+ cross section is 0.29 fb and asymmetry is 0.11 (right). This corresponds to the calculation of [579] with polarised contributions, and a cut on muon $|\eta| > 0.6$. The uncertainty bands indicate dependence of the sensitivity on assumptions regarding the subtraction of SPS backgrounds. More details regarding the set-up for both panels may be found in [579].

is found that $a_{\eta_l} \sim 0.028$, which is of similar size to the asymmetry arising from other sources.

Note that the asymmetries from x correlations, valence number effects and $1 \to 2$ splitting are in the same direction (favouring $\eta_1 \cdot \eta_2 < 0$ over $\eta_1 \cdot \eta_2 > 0$), whilst polarisation effects can potentially either favour a positive or negative asymmetry.

At the HE-LHC, the asymmetry should be smaller for the same cuts on $|\eta_i|$ – as x is lowered, we move away from the 'double valence' region where valence number effects are important, and the ratio of polarised to unpolarised quark distributions reduces (see Fig. 6 of [582]). Repeating the study above where a minimal modification of the uncorrelated ansatz at the input scale is made to take account of number effects, but at $\sqrt{s} = 27$ TeV, it is found that $a_{\eta_l} \sim 0.008$. Including instead the effects of the $1 \to 2$ splittings yields $a_{\eta_l} \sim 0.013$ at $\sqrt{s} = 27$ TeV. At the HE-LHC (and the HL-LHC) it could be interesting to compare same-sign WW, which is comparatively weakly affected by $1 \to 2$ parton splitting (due to the fact there is no direct LO splitting yielding, for example uu), with processes that should receive stronger contributions from parton splitting, such as low mass Drell-Yan or $b\bar{b}b\bar{b}$ production, to probe in detail the effects of the $1 \to 2$ parton splitting and compare to theoretical predictions. More detailed studies in this direction are needed.

In conclusion, the HL-LHC offers the opportunity to measure the effects of correlations between partons, via measurements of DPS processes, for the first time. In same-sign WW production a good observable to probe correlations is the lepton pseudorapidity asymmetry a_{η_l}, which can only be nonzero in the presence of correlations – theoretical calculations indicate values of a_{η_l} at LHC energies on the order of a few per cent, which should be measurable at the HL-LHC. By combining measurements of various processes sensitive to DPS at the HL-LHC, and later and the HE-LHC, it will be ultimately possible to build up a picture of the various correlatons existing between partons in the proton.

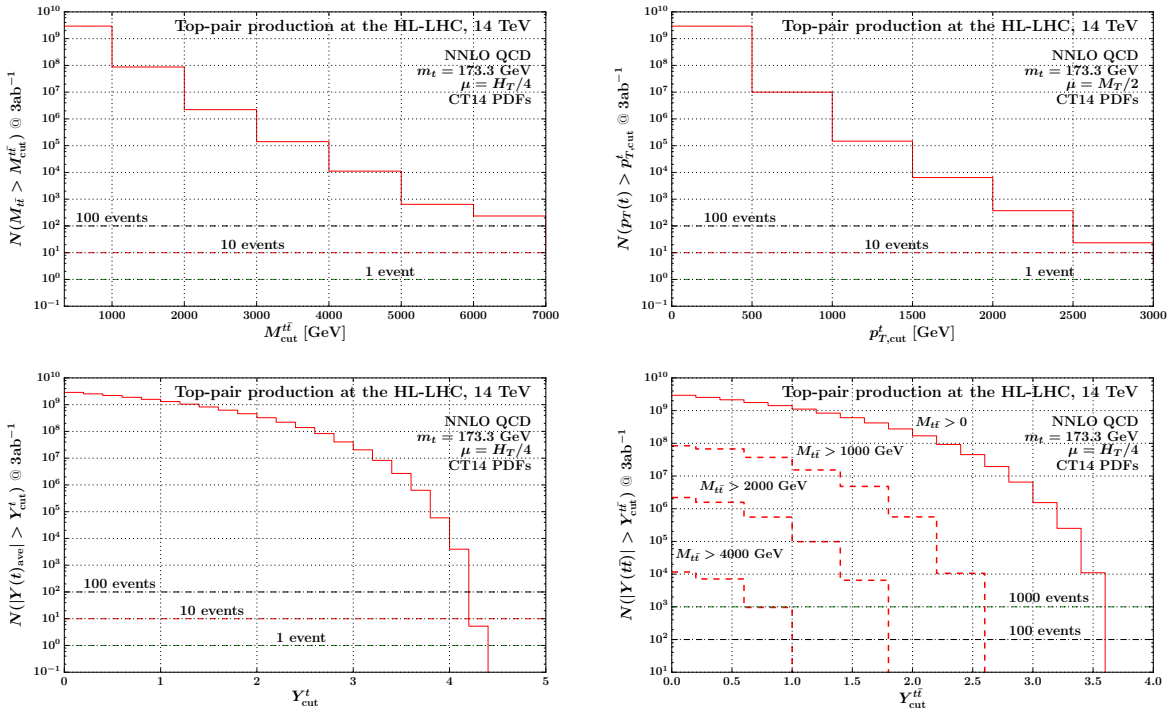

Fig. 68: Cumulative differential distributions for HL-LHC at 14 TeV.

6 Top quark physics

Precision measurements of top quark properties present an important test of the SM. As the heaviest particle in the SM, the top quark plays an important role for the electroweak symmetry breaking and becomes a sensitive probe for physics beyond the SM.

6.1 Top quark cross section

6.1.1 The $t\bar{t}$ production cross section: theoretical results[31]

This sub-section provides a quick reference for the kinematic reach of the main $t\bar{t}$ differential distributions for both HL and HE-LHC. Figures 68 and 69 are given in terms of expected events for the proposed ultimate luminosities for both colliders: 3 ab^{-1} for the HL-LHC running at 14 TeV and 15 ab^{-1} for the 27 TeV HE-LHC. The results are presented as plots of cumulative differential distributions and should be interpreted as follows: the histograms show the numbers of expected events (for the luminosities given above) above a given cut in any one of the four kinematic variables: $m_{t\bar{t}}, p_{\rm T,avt}, y_{\rm avt}$ and $y_{t\bar{t}}$. Note that the cut corresponds to the left edge of a bin. The predictions are based on the CT14 parton distributions [199] with value of the top quark mass $m_t = 173.3$ GeV which is close to the current world average. The calculation is based on Ref. [583] and uses the dynamical scales of Ref. [213].

Figure 68 presents predictions for the four cumulative distributions specified above in the case of the $t\bar{t}$ production at the HL-LHC (14 TeV), computed in NNLO QCD. In conclusion the HL-LHC allows detailed studies of top quark pair production with $m_{t\bar{t}}$ of up to about 7 TeV. Events with even larger values of $m_{t\bar{t}}$ are kinematically accessible and one expects about 10 events with $m_{t\bar{t}} > 7$ TeV. Therefore, the region $m_{t\bar{t}} > 7$ TeV provides a low SM background for, for example, searches for decays of BSM heavy particles to $t\bar{t}$ pairs. A detailed understanding of the SM background - at the level of one expected event - will require a dedicated future effort due to the significant MC error in that region.

[31] Contributed by M. Czakon, A. Mitov, and A. Papanastasiou.

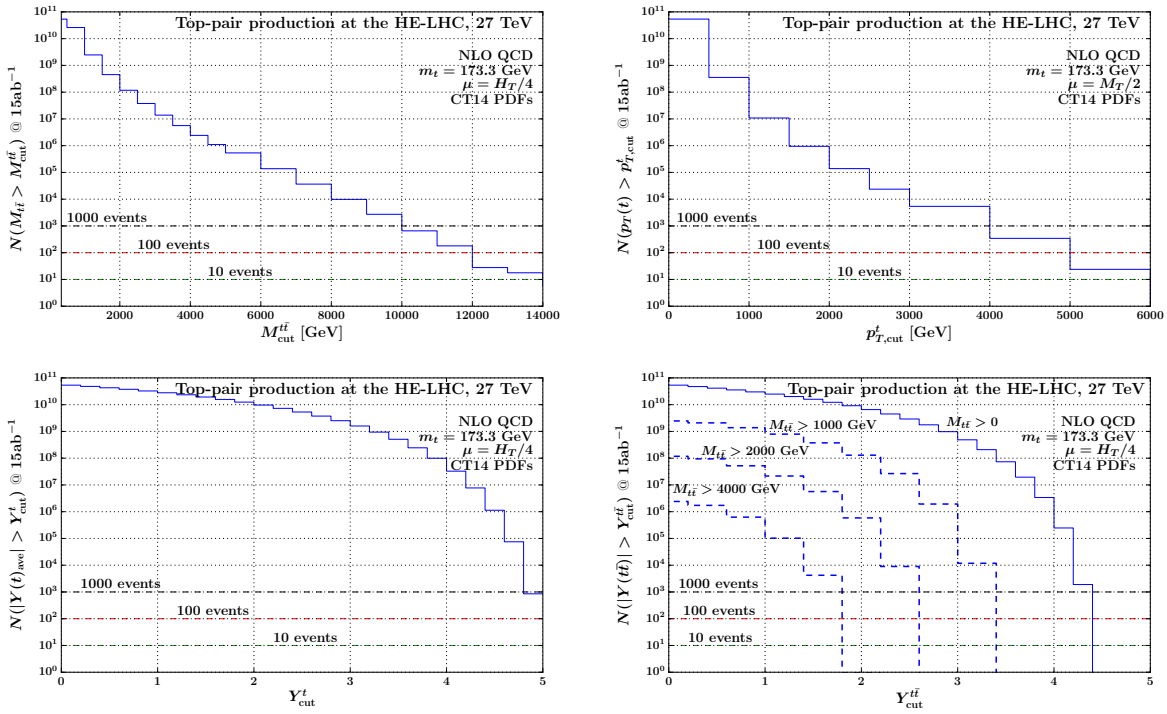

Fig. 69: Cumulative differential distributions for HE-LHC at 27 TeV.

The top quark $p_{\rm T}$ distribution can probe $p_{\rm T}$ values as high as 2.5 TeV, with a total of about 30 events expected beyond that value.

The HL-LHC offers the possibility to access top production at high rapidity which might provide a link between top measurements at LHCb on one hand and ATLAS and CMS on the other. Indeed, in Fig. 68 it can be observed that top quarks with rapidity $y_{\rm avt}$ as large as 4 will be copiously produced. The cross-section is a steeply falling function at large rapidity with a maximum attainable value of around 4.2 or so. Similarly, the rapidity of top quark pairs can be measured in detail up to values exceeding 3.4 with the maximum reach at about $y_{t\bar{t}} \sim 3.6$. In Fig. 68 it is shown the $y_{t\bar{t}}$ distribution for a set of cuts on the top pair invariant mass. One should bear in mind that the NNLO $y_{t\bar{t}}$ calculation has significant MC error in the bins with 10 events or less.

Figure 69 presents the predictions for the same four cumulative distributions but in NLO QCD for the case of $t\bar{t}$ production at the HE-LHC (27 TeV). From this figure one can easily conclude that the increase in the kinematic reach over the HL-LHC is very substantial. There will be few hundred events with $m_{t\bar{t}}$ above 11 TeV and a similar number of events can be measured with $p_{\rm T}$ above 4 TeV. For the reliable description of such kinematics the inclusion of EW corrections as well as yet higher order soft and or collinear radiation will be essential; see Ref. [113, 220].

Very large rapidities can be attained at the HE-LHC. In particular, the top quark rapidity $y_{\rm avt}$ distribution can be measured to values as high as 4.8 with excellent statistics. Indeed, about 1000 events are expected above $y_{\rm avt} = 4.8$. The top pair rapidity can reach values as high as 4.4 and, if no additional cuts are applied, few thousand events will be produced with $y_{t\bar{t}} > 4.2$. As for the case of 14 TeV it is also show in Fig. 69 the expected number of events as a function of $y_{t\bar{t}}$ for several cuts in $m_{t\bar{t}}$.

6.1.2 *Prospects in the measurement of differential $t\bar{t}$ cross sections*

A study is presented for the resolved reconstruction of top quark pairs in the e/μ+jets channels and a projection of differential $t\bar{t}$ cross sections measurements with an integrated luminosity of 3 ab^{-1} at 14 TeV [584]. The analysis techniques are based on previous measurements of differential $t\bar{t}$ cross sections at 13 TeV [585, 586]. It is shown that such a measurement is feasible at the HL-LHC despite the expected large number of pileup interactions. The precision of the differential cross section can profit from the enormous amount of data and the extended η-range of the HL-LHC CMS detector. The results are used to estimate the improvement of measurements of parton distribution functions.

This study is based on a DELPHES simulation of the HL-LHC CMS detector [587–590] using the Monte Carlo program POWHEG [151, 314, 360, 377] (v2,hvq) in combination with PYTHIA [148, 292] (v8.219) for the generation of $t\bar{t}$ events at NLO accuracy. Events with a single isolated electron or muon with $p_{\mathrm{T}} > 30$ GeV and $|\eta| < 2.8$ are selected. Events with additional isolated electrons or muons with $p_{\mathrm{T}} > 15$ GeV and $|\eta| < 2.8$ are rejected. At least 4 jets with $p_{\mathrm{T}} > 30$ GeV and $|\eta| < 4.0$ are required, where at least 2 of the jets have to be identified as b jets. It is essential that the PUPPI algorithm [591] is used for the mitigation of pileup contribution when the jets are clustered and the $\vec{p}_{\mathrm{T}}^{\,\mathrm{miss}}$ is calculated.

A detailed description of the $t\bar{t}$ reconstruction is presented in [585,586]. For the reconstruction all possible permutations of assigning detector-level jets to the corresponding $t\bar{t}$ decay products are tested and a likelihood that a certain permutation is correct is evaluated. In each event, the permutation with the highest likelihood is selected. The likelihood is constructed from the 2 dimensional m_t–m_{W} distribution of correctly assigned jets for the hadronically decaying top quark and the distribution of $D_{\nu,\mathrm{min}}$ obtained when calculating the neutrino momentum [592] for the leptonically decaying top quark. A comparison of the expected event yields and the migration matrices together with their properties are shown in Fig. 70 for the HL-LHC expectation. Despite the high pileup a performance of the $t\bar{t}$ reconstruction similar to the one in 2016 [586] can be reached, while the portion of the direct measurable phase space is increased due to the extended η-range.

The following experimental uncertainties are estimated based on the expected performance of the HL-LHC CMS detector [277]: electron and muon identification, b-tagging efficiencies, jet energy and $\vec{p}_{\mathrm{T}}^{\,\mathrm{miss}}$ calibration, and luminosity. All theoretical and modelling uncertainties have been reduced by a factor two.

The unfolded results of the differential $t\bar{t}$ cross section measurements as a function of p_{T} and rapidity y of the hadronically decaying top quark ($\mathrm{t_h}$) are shown in Fig. 71. In Fig. 72 the normalized double-differential cross section as a function of $M(t\bar{t})$ vs $|y(t\bar{t})|$ is shown. The strong impact of these measurement on PDF constraints is studied in Section 6.1.3. The high amount of data and the extended η-range of the HL-LHC detector allow for fine-binned measurements in phase-space regions — especially at high rapidity — that are not accessible in current measurements. The most significant reduction of uncertainty is expected due to an improved jet energy calibration.

6.1.3 *PDF constraints from double-differential $t\bar{t}$ cross sections*

The impact of differential $t\bar{t}$ cross section measurements at the HL-LHC on the proton PDFs is quantitatively estimated using a profiling technique [476], which is based on minimizing χ^2 function between data and theoretical predictions taking into account both experimental and theoretical uncertainties arising from PDF variations. The analysis is performed using the XFITTER program [490], with the theoretical predictions for the $t\bar{t}$ cross sections calculated at NLO QCD using the MG5_AMC@NLO [12] framework, interfaced with the AMCFAST [593] and APPLGRID [208] programs. Three NLO PDF sets were chosen for this study: ABMP16 [594], CT14 [199], and NNPDF3.1 [207]. The normalized double-differential $t\bar{t}$ production cross sections as a function of $M(t\bar{t})$ vs $|y(t\bar{t})|$ are used which are expected to impose stringent constraints on the gluon distribution [595]. The χ^2 value is calculated using

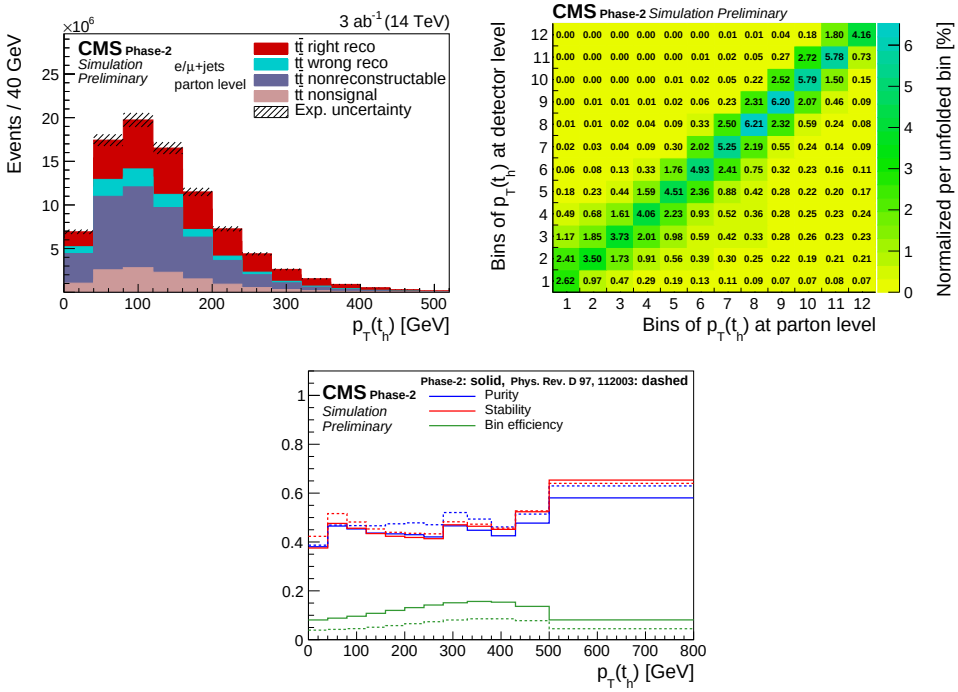

Fig. 70: Expected signal yields (top-left), migration matrices (top-right), and its properties (bottom) for measurements of $p_{\mathrm{T}}(\mathrm{t_h})$ for the HL-LHC (Phase-2) simulation. The purity is defined as the fraction of parton-level top quarks in the same bin at the detector level, the stability as the fraction of detector-level top quarks in the same bin at the parton level, and the bin efficiency as the ratio of the number of events found in a certain bin at detector level and the number of events found at parton-level in the same bin.

the full covariance matrix representing the statistical and systematic uncertainties of the data, while the PDF uncertainties are treated through nuisance parameters. The values of these nuisance parameters at the minimum are interpreted as optimized or profiled PDFs, while their uncertainties determined using the tolerance criterion of $\Delta\chi^2 = 1$ correspond to the new PDF uncertainties. The profiling approach assumes that the new data are compatible with theoretical predictions using the existing PDFs, such that no modification of the PDF fitting procedure is needed. Under this assumption, the central values of the measured cross sections are set to the central values of the theoretical predictions. The original and profiled ABMP16, CT14, and NNPDF3.1 uncertainties of the gluon distribution at the scale $\mu_{\mathrm{f}}^2 = 30\,000\,GeV^2 \simeq m_{\mathrm{t}}^2$ are shown in Fig. 73. A consistent impact of the $t\bar{t}$ data on the PDFs is observed for the three PDF sets. The uncertainties of the gluon distribution are drastically reduced once the $t\bar{t}$ data are included in the fit.

6.1.4 Forward top quark physics

Three measurements of top production have been performed by LHCb during Run-1 and -2 of the LHC with a precision of (20-40)%, limited by the available data samples. As LHCb collects data at a lower rate than ATLAS and CMS, and has a limited acceptance, the measurements have focused on a partial reconstruction of the $t\bar{t}$ final state in order to make optimal use of statistics. Additionally, as no estimate of missing energy is available, the measurements are performed at the level of the lepton and jets only, with no full top quark reconstruction performed. The first observation in the forward region was made in the μb final state, where the top quark is identified by the presence of a muon and a b-jet [596]. This final state has the highest signal yield, but suffers from the largest backgrounds, in particular from W boson production in association with a b-jet. It also cannot separate single top and top pair production,

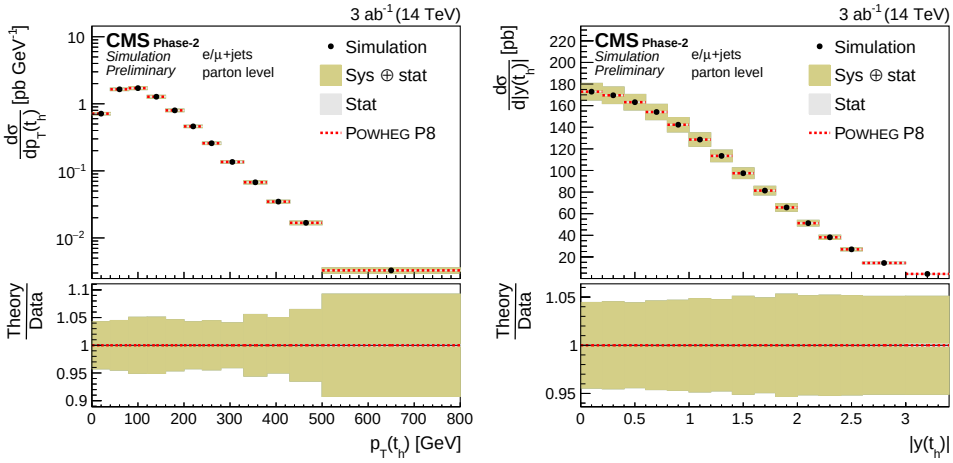

Fig. 71: Projections of the differential cross sections as a function of $p_{\mathrm{T}}(\mathrm{t_h})$ (right) and $|y(\mathrm{t_h})|$ (left).

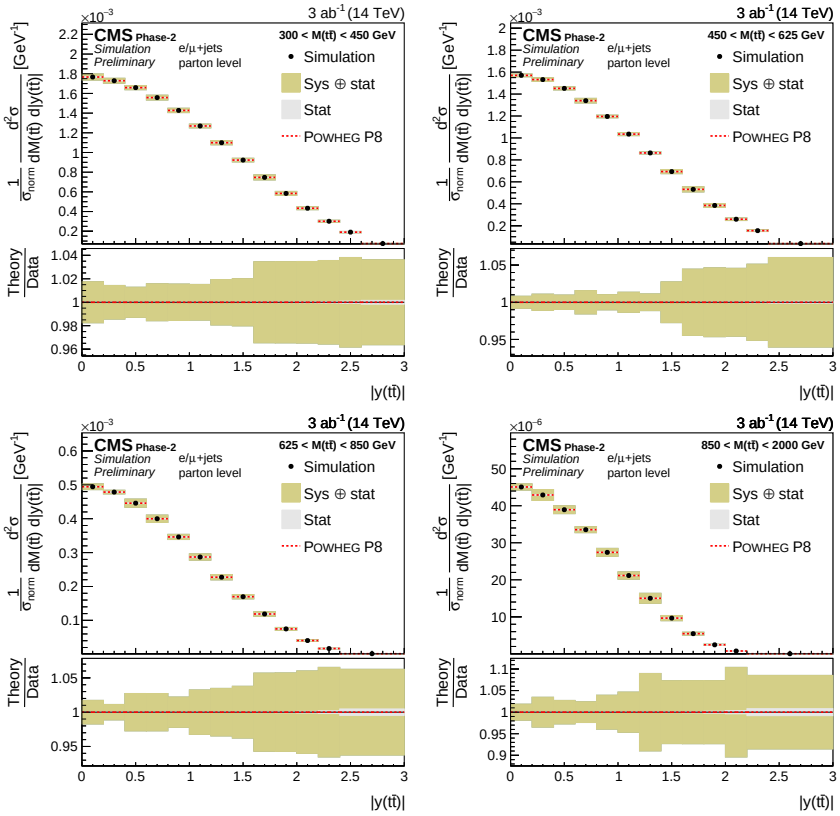

Fig. 72: Projections of the double-differential cross section as a function of $|y(t\bar{t})|$.

which both contribute to the final state. Measurements were also performed in the ℓbb final state [597] and μeb final state [598], which suffer from lower statistics but select the signal with a higher purity.

While current measurements in the top sector at LHCb have been statistically limited, the available dataset at the HL-LHC, where LHCb is expected to collect 300 fb^{-1}, will permit precision measurements of the top quark pair production cross-section in the forward region, providing complementary information to ATLAS and CMS. The expected number of top pair events to be reconstructed at LHCb are given in Table 33, where the yields are obtained using next-to-leading predictions from the AMC@NLO gen-

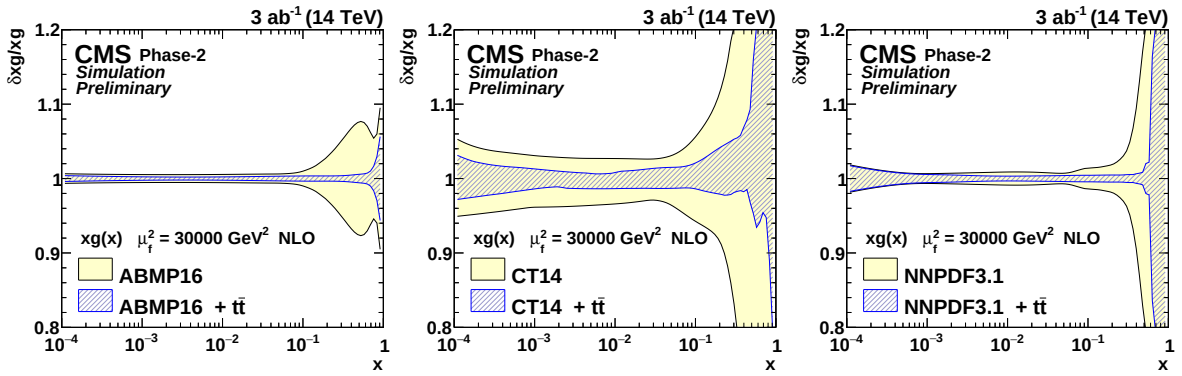

Fig. 73: The relative gluon PDF uncertainties of the original and profiled ABMP16 (left), CT14 (middle) and NNPDF3.1 (right) sets.

Table 33: The number of $t\bar{t}$ events expected to be reconstructed at LHCb per final state using a dataset corresponding to an integrated luminosity of 300 fb^{-1}. The mean value of Bjorken-x of the most energetic initiating parton is also shown for each final state.

Final state	300 fb^{-1}	$< x >$
ℓb	830k	0.295
$\ell b\bar{b}$	130k	0.368
μeb	12k	0.348
$\mu eb\bar{b}$	1.5k	0.415

erator interfaced with PYTHIA v8, with electroweak corrections approximated as described in Ref. [599]. Leptons are required to satisfy $2.0 < \eta < 4.5$ and $p_{\mathrm{T}} > 20$ GeV, while jets are required to satisfy $2.2 < \eta < 4.2$ and $p_{\mathrm{T}} > 20$ GeV in all final states except the ℓb final state, where the p_{T} threshold is raised to 60 GeV to combat the increased background. The detector efficiency is extrapolated from current measurements, where increases of between 10 and 50% are expected due to to improvements in the b-tagging algorithm and analysis techniques. Both muons and electrons are assumed to be employed for all analyses with similar efficiencies due to anticipated improvements in electron performance at LHCb during the HL-LHC. Measurements are expected to be made at sub-percent statistical precision in the ℓb final state, and at the percent level in the μeb and μebb final states. The dominant systematic uncertainties are expected to arise from the purity determination, particularly for the single lepton final states, and the knowledge of the b-tagging efficiency, which are both expected to be at the level of a few percent.

As $t\bar{t}$ production in the LHCb acceptance probes very large values of Bjorken-x, it has the potential to provide significant constraints on the gluon PDF in this region. The potential of the μeb final state was evaluated in Ref. [600], where reductions of 20% were found for a cross-section measurement with a precision of 4%. Even more stringent constraints can be obtained through precise differential cross-section measurements, and measurements in the μebb final state, both of which will only be possible with the data available at the HL-LHC.

6.1.5 *Single top cross section: theoretical results*[32]

Although top quarks are predominantly produced in $t\bar{t}$ pairs through strong interactions, a substantial fraction of them is also produced through the exchange of electroweak bosons. In the latter case, only a single (anti-)top is produced per collision, hence one refers to these processes as "single-top" production. Despite their smaller rates with respect to pair production, single-top processes offer unique opportunities to study the electroweak structure of top interactions.

The purpose of this section is to summarize the state-of-the-art for the computation of single-top production cross sections, and highlight what type of studies could be performed with an HL/HE-LHC upgrade.

It is customary to categorize single-top production in the SM according to the virtuality of the W-boson involved in the leading-order $2 \to 2$ partonic process: the s-channel processes ($q\bar{q}' \to t\bar{b}$) involve the exchange of a time-like W boson, the t-channel processes $bq \to tq'$ involve the exchange of a space-like W, while associated Wt-production ($bg \to tW^-$) involves the production of a top quark in association with a W boson.

Although convenient, the above characterization suffers two theoretical issues:

- a classification in terms of underlying $2 \to 2$ processes implicitly assumes that the b-quark is treated as massless, i.e. the computations are performed in the so-called five-flavour number scheme (5FNS). This framework effectively resums large logarithms of the form $\ln m_b/Q$, where Q is a typical transverse scale of the process and as such it is particularly appropriate for observables that are only sensitive to large $p_{\rm T} \gg m_b$ scales, like for example total cross sections. However, especially in the t-channel case, there are important observables which are sensitive to small transverse scales $p_{\rm T} \sim m_b$ (e.g. the kinematics of the "spectator" b-jet which originates from initial state $g \to b\bar{b}$ splitting, particularly at small $p_{\rm T}$). In this case, the 5FNS is not appropriate and it is important to treat the b-quark as massive, i.e. to work in four-flavour mass scheme (4FNS). In this scheme, the t-channel LO process becomes $2 \to 3$: $gq \to t\bar{b}q'$. The 4FNS and 5FNS are formally equivalent, but differences can arise when the perturbative expansion is truncated, and in practice these effects might be relevant for some observables [601–603]. Within this context, the advantages of a HL/HE upgrade is twofold. On the one hand, the larger dataset and increased energy would allow for more harsh selection cuts that would effectively remove regions of the phase space sensitive to small transverse scales. This would allow for a clean theoretical description using the 5FNS, which does not suffer from large logarithmic contaminations. On the other hand, it would allow one to explore with high accuracy the transition region between the range of validity of the 4FNS and 5FNS, thus providing important information on their interplay.
- once higher-order corrections are included, the distinction between s and t channels does not hold, due to interference effects. These interference effects first appear at order $\mathcal{O}(\alpha_s^2\alpha^2)$, i.e. at NNLO in the 5FNS, or at NLO in the 4FNS, and are color and (typically) kinematic suppressed. Given the large hierarchy and small kinematic overlap between t- and s- channels, interference effects are typically very small in pp collisions, but may in principle play a role if very high accuracy is required for specific observables. Moreover, once the W and top decay products are included, interferences arise also between $t\bar{t}$, single-top (with Wt-production, as well as t-channel in the 4FNS) and $WWb\bar{b}$ production, unless the narrow-width limit $\Gamma_t \to 0$ is taken. These effects can play a role for high precision studies, see e.g. [169, 604].

In spite of the above issues, as long as only NLO QCD corrections are considered, it is possible to compute well-defined cross-sections for s and t-channel in the 5FNS, and, by imposing a jet-veto on b-jets, to suppress the contamination of $t\bar{t}$ to the Wt process, thereby allowing for a sensible definition

[32] Contributed by F. Caola and E. Re.

of the cross section for the latter channel as well. In Table 34 the NLO cross sections are reported for the 3 channels at the LHC, for centre-of-mass energies of 14 and 27 TeV. Scale and PDF uncertainties are also reported. At both energies, the t-channel is the dominant production mechanism. The relative importance of the s-channel decreases with the collider energy, while it increases for Wt associated production.

Table 34: Single-top inclusive cross sections at NLO for the LHC at 14 and 27 TeV, in the 5FNS. All results were obtained using PDF4LHC15_nlo_mc, the central value for the renormalization and factorizations scales (μ_R, μ_F) have been set equal to $m_t = 173.2$ GeV and varied by a factor of two, with the constraint $1/2 \leq \mu_R/\mu_F \leq 2$. For these predictions, V_{tb} has been set to one. For Wt-channel only, a jet-veto on b-jets has been used ($p_{\mathrm{T,b_j}} < 50$ GeV), and the central value for μ_R and μ_F has been set to 50 GeV too.

	14 TeV			27 TeV		
	σ [pb]	Δ_{μ_R,μ_F}	Δ_{PDF}	σ [pb]	Δ_{μ_R,μ_F}	Δ_{PDF}
t-channel (t)	156	$^{+3\%}_{-2.2\%}$	$\pm$ 2.3 %	447	$^{+3\%}_{-2.6\%}$	$\pm$ 2%
t-channel ($\bar{t}$)	94	$^{+3.1\%}_{-2.1\%}$	$\pm$ 3.1%	299	$^{+3.1\%}_{-2.5\%}$	$\pm$ 2.6%
s-channel (t)	6.8	$^{+2.7\%}_{-2.2\%}$	$\pm$ 1.7%	14.8	$^{+2.7\%}_{-3.2\%}$	$\pm$ 1.8%
s-channel ($\bar{t}$)	4.3	$^{+2.7\%}_{-2.2\%}$	$\pm$ 1.8%	10.4	$^{+2.7\%}_{-3.3\%}$	$\pm$ 1.8%
Wt-channel (t or $\bar{t}$)	36	$^{+2.9\%}_{-4.4\%}$	$\pm$ 5%	137	$^{+3.8\%}_{-6.1\%}$	$\pm$ 4%

Figure 74 also shows, for the t-channel case, the cumulative cross section with a minimum $p_{\mathrm{T,min}}$ cut on the top, or antitop, transverse momentum, obtained at NLO in the 5FNS. The two horizontal bars

Fig. 74: Cumulative cross section for t-channel single-(anti)top production in the 5FNS at 14 and 27 TeV as a function of $p_{\mathrm{T,min}}$. The same settings used to obtain results in Table 34 were used here.

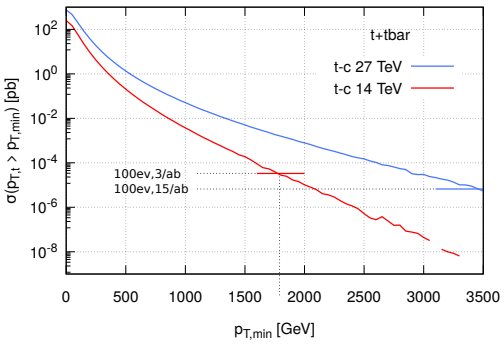

in the plot correspond to the cross sections for which one has 100 events, by assuming an integrated luminosity of 3 ab^{-1} at 14 TeV (red) and of 15 ab^{-1} at 27 TeV (blue).

For t-channel production, NNLO QCD corrections have also been computed in Refs. [555, 605, 606].[33] These corrections have been obtained in the structure function approximations, where higher-order corrections to the light and heavy-quark lines ($q \to q'W$ and $b \to tW$, respectively) are computed separately. Within this approximation, the terms which are not included at NNLO are color suppressed

[33] NNLO QCD results were also obtained for s-channel, see Ref. [607].

($1/N_c^2$), and hence estimated to be negligible for phenomenology, given the moderate size of NNLO effects. Moreover, when working in these approximations, interference effects between s and t-channel are also absent. The results obtained in Refs [605, 606] indicate that NNLO QCD corrections are small: the total cross sections at NNLO increase by at most 2% with respect to the NLO result (when the latter is obtained with NLO PDFs), whereas the relative scale uncertainty is reduced by at least $\sim 50\%$. Moreover, the NNLO result is contained within the NLO uncertainty band, showing extremely good convergence for the perturbative expansion.[34] Despite the fact that the total cross section shows excellent perturbative stability, more sizeable effects can be noticed in some differential distributions, where NNLO/NLO corrections can reach $\mathcal{O}(10\%)$ in certain regions of the transverse momentum distributions of the top (anti-)quark and the pseudo-rapidity distributions of the leading jet. In these cases, scale variation may underestimate the actual theoretical uncertainty.

NNLO corrections to the top quark decay are also known [608, 609], and they can be combined with the NNLO corrections to production using the "on-shell top-quark approximation" where the top width Γ_t is kept finite, but tree-level interference effects between the single top production and decay stage are neglected, as well as loop diagrams with a virtual gluon connecting the production and decay stages. This is an excellent approximation for inclusive-enough quantities, since omitted corrections are suppressed by a factor $\Gamma_t/m_t < 1\%$ [35]. More details can be found in Ref. [555].

In presence of fiducial cuts, it is important to stress that QCD corrections are more pronounced, with NNLO effects amounting about 5% on total rates as well as differential distributions. In this case, corrections from pure decay are typically half of those from pure production. Finally, it should be noted that NLO EW corrections to on-shell single top production are small, $\sim$ few permille, see e.g. [89]. The EW effect can become more relevant in tails of distributions, or for observables highly sensitive to off-shell effects.

Single-top can also be produced in association with a Z boson (tZq). Although the cross section is smaller than in the aforementioned channels, a HL/HE upgrade at the LHC will allow one to measure well this production process too. QCD NLO corrections to tZq-production are known [611]. Table 35 reports the total cross sections at NLO in the SM, for centre-of-mass energies of 14 and 27 TeV.

Table 35: Single-top production cross section in association with a Z boson, at NLO for the LHC at 14 and 27 TeV, in the 5FNS. All results were obtained using PDF4LHC15_nlo_mc, the renormalization and factorizations scales have been set equal to $m_t = 173.2$ GeV.

	σ [fb] @14 TeV	σ [fb] @27 TeV
tZq-channel (t)	639	2536
tZq-channel ($\bar{t}$)	350	1543

As far as phenomenology is concerned, single-top offers the possibility to perform several studies within and beyond the SM. Within the "SM only" hypothesis, one can use it to extract information about the SM V_{tb} matrix element, as discussed for instance in Ref. [612]. Setting constraints on the b-quark PDF might also be possible, by looking at charge ratios, i.e. ratios of $t/\bar{t}$ cross sections. These ratios depend in general upon the PDFs used, and notably, in the t-channel case, on the b-quark PDF. Moreover, they can be predicted quite accurately, as most of the theoretical uncertainties cancel out in the ratio, leaving a residual theoretical uncertainty from scale variation (at NNLO) of few percent for each PDF set, as shown for instance in Fig. 29 of Ref. [555]. Although the charge ratio for total

[34] When NLO corrections are computed with NNLO PDFs, the NNLO/NLO ratio is instead slightly smaller than one, but the conclusions remain the same.

[35] This is not the case for exclusive observables, which are sensitive to off-shell effects in the reconstructed top mass M_{Wb}, and beyond kinematic edges, see Ref. [610] for a thorough analysis.

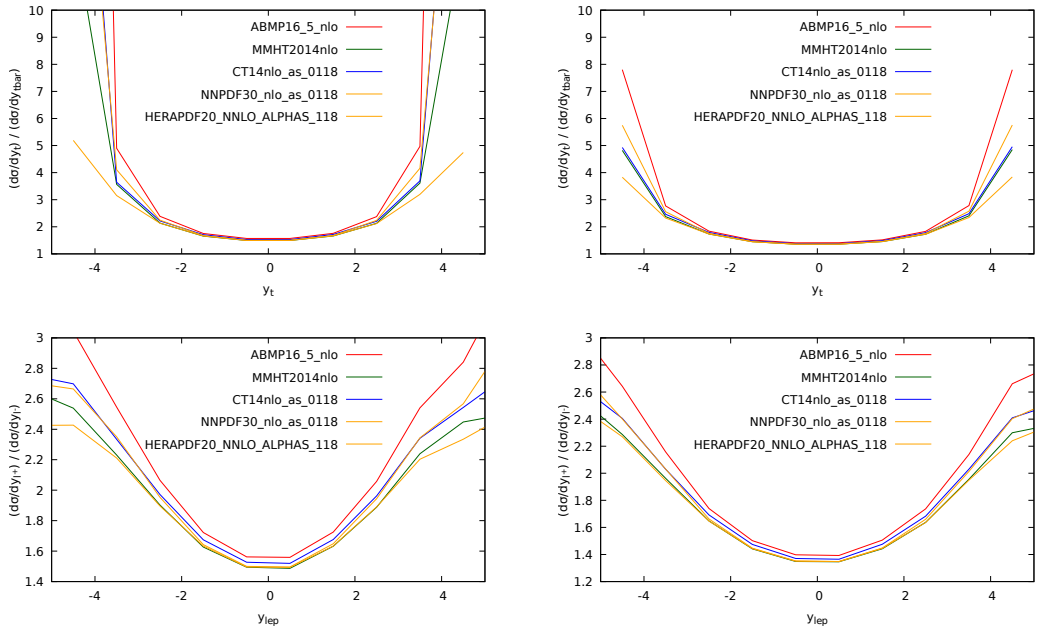

Fig. 75: Differential charge ratios $\mathcal{O}_t/\mathcal{O}_{\bar{t}}$ at 14 (left panels) and 27 (right panels) TeV for the top quark and charged lepton rapidities, in t-channel single-top production.

cross sections $\sigma_t/\sigma_{\bar{t}}$ exhibits a dependence upon the PDF set [613, 614], slightly more pronounced sensitivity might be obtained by looking at differential distributions, such as $(d\sigma/dy_t)/(d\sigma/dy_{\bar{t}})$ and $(d\sigma/dy_{\ell^+})/(d\sigma/dy_{\ell^-})$, which also allow one to constrain the u/d ratio in the proton. In Fig. 75 such a comparison among different PDF sets is shown, for LHC collisions at 14 and 27 TeV: differences among different PDF sets can be observed, especially at large rapidities. It is clear that a HL upgrade will allow one to reduce the statistical uncertainty at large rapidities, giving the chance to discriminate among different PDF sets. As the available phase space opens up, further sensitivity might be expected at 27 TeV.

Single-top processes offer also several opportunities to probe some new-physics scenarios[36]. In order to systematically interpret potential deviations from the SM, it is particularly convenient to work in the SM Effective Field Theory (SMEFT) [615, 616], where the SM is augmented by a set of higher-dimension operators. If the discussion is limited to dimension-6 operators, the SMEFT Lagrangian has the form

$$\mathcal{L}_{\rm SMEFT} = \mathcal{L}_{\rm SM} + \sum_i \frac{C_i}{\Lambda^2}\mathcal{O}_i + \mathcal{O}(\Lambda^{-4}). \tag{40}$$

where the sum runs over all the dimension-6 operators that maintain the SM symmetries. The remarkable virtue of t-channel single-top production is that its cross section only depends upon a limited number of dimension-6 operators, thereby allowing to set bounds on them relatively easily. At LO and in the 5FNS only three operators contribute:

$$\mathcal{O}_{tW} = i\left(\bar{Q}\sigma^{\mu\nu}\tau_I\, t\right)\tilde{\phi}\, W^I_{\mu\nu} + \text{h.c.}\,, \tag{41}$$

$$\mathcal{O}^{(3)}_{\phi q} = i\left(\phi^\dagger \overleftrightarrow{D}_\mu \tau_I \phi\right)\left(\bar{q}_i\,\gamma^\mu\,\tau^I\, q_i\right) + \text{h.c.}\,, \tag{42}$$

$$\mathcal{O}^{(3,1)}_{Qq} = \left(\bar{q}_i\,\gamma_\mu\,\tau_I q_i\right)\left(\bar{Q}\,\gamma^\mu\,\tau^I Q\right), \tag{43}$$

[36] In the following the discussion is limited to the t-channel case, and the production in association with a Z boson.

in agreement with the notation of [234]. The operators of eq. (41)-eq. (42) modify the Wtb interaction in the following way

$$\begin{aligned}\mathcal{L}_{Wtb}^{\dim-6} &= -\frac{g}{\sqrt{2}}\bar{b}(x)\gamma^{\mu}P_L t(x)\,W_{\mu}(x)\left(1+\frac{C_{\varphi Q}^{(3)}v^2}{\Lambda^2}\right)\\ &+ \frac{2\,v\,C_{tW}}{\Lambda^2}\bar{b}(x)\sigma^{\mu\nu}P_R t(x)\,\partial_{\nu}W_{\mu}(x) + \text{h. c.}\,, \end{aligned} \tag{44}$$

where $v = 246$ GeV is the Higgs doublet vacuum expectation value, and y_t the top quark Yukawa coupling. Here and below it is assumed $V_{tb} = 1$. Note that the four-fermion operator of eq. (43) introduces a contact $udtb$ interaction. From eq. (44) it is clear that setting bounds on the SMEFT using single-top measurements allows to probe in detail the structure of the Wtb coupling. A comprehensive discussion can be found in Ref. [262], where a NLO study of the effect of these operators on total and differential distributions in single top production and decay is performed.

In the SMEFT, the single top cross section can be parameterised as

$$\sigma = \sigma_{SM} + \sum_i \frac{1\text{TeV}^2}{\Lambda^2}C_i\sigma_i + \sum_{i\leq j}\frac{1\text{TeV}^4}{\Lambda^4}C_iC_j\sigma_{ij}. \tag{45}$$

To establish the impact of the operators on single top production at HL/HE-LHC, Table 36 shows the ratio $r_i = \sigma_i/\sigma_{SM}$ for 14 TeV and 27 TeV both for the inclusive cross section and the high transverse momentum region. Results are obtained in the 5FNS with NNPDF3.0 LO PDFs [201]. Central scales for μ_R, μ_F are chosen as m_t. It is found that the impact of the operator in eq. (42) remains unchanged when going from 14 to 27 TeV, as its effect is to only rescale the SM coupling. The impact of the dipole operator in eq. (41) is only mildly affected by going to the HE-LHC, whereas the sensitivity to the four-fermion operator is the one which benefits most by probing the high p_{T} tail and by the HE-LHC.

Table 36: Comparison among the LO sensitivities of $t-$ channel single-top to the three operators described in eq. (41)-(43), for the inclusive cross-section and with a cut $p_{\text{T}}^t > 350$ GeV, at 14 and 27 TeV. Results are obtained in the 5FNS with NNPDF3.0 LO PDFs [201], the renormalization and factorizations scales have been set equal to $m_t = 173.2$ GeV. The interference term $r_i = \sigma_i/\sigma_{SM}$ (when non-zero) and the square $r_{i,i} = \sigma_{i,i}/\sigma_{SM}$ are given for each operator. σ_i and $\sigma_{i,i}$ are defined in eq. (45).

	t-channel 14 TeV		t-channel 27 TeV	
		($p_{\text{T}}^t > 350$ GeV)		($p_{\text{T}}^t > 350$ GeV)
σ_{SM}	225 pb	0.746 pb	640 pb	3.40 pb
r_{tW}	0.025	0.052	0.022	0.040
$r_{tW,tW}$	0.014	0.31	0.016	0.34
$r_{\phi Q^{(3)}}$	0.12	0.12	0.12	0.12
$r_{\phi Q^{(3)},\phi Q^{(3)}}$	0.0037	0.0037	0.0037	0.0037
$r_{Qq^{(3,1)}}$	-0.36	-6.45	-0.39	-6.79
$r_{Qq^{(3,1)},Qq^{(3,1)}}$	0.135	18.8	0.222	26.8

Production in association with a Z boson is also important in the BSM context. A complete study of its sensitivity to BSM effects was performed in Ref. [261], where the interplay with t-channel single-top, as well as single-top production in association with a Higgs boson, is discussed thoroughly, and at NLO. Table 6 of [261] reports a comparison among the sensitivity of these processes to various

operators. Current limits from other processes, as well as current and future projections for bounds that can be achieved looking into tZj production are also discussed (e.g. in Fig. 6 of Ref. [261]). For some operators, notably $\mathcal{O}_{tW}$ and $\mathcal{O}_{\phi q}^{(3)}$, the improvement due to considering tZj measurements at HL are remarkable, especially when tails of distributions are considered. It is likely that even more promising results could be obtained at HE.

Another goal of a HL/HE upgrade is to extract bounds on (or find evidence of) WWZ anomalous gauge couplings, or FCNC. In this context, tZq is quite important both because it is sensitive to these effects, as well as because it's an irreducible background, as its production rate is competitive with $t\bar{t}Z$ production, where these effects are typically looked for.

6.2 Four top production at the HL/HE-LHC

The production of four top quarks is one of the rare processes in top quark physics that has large sensitivity to variety of new physics effects (including effective field theory sensitivity and sensitivity to anomalous top-Higgs couplings), while at the same time it is interesting in the Standard Model context as a complex QCD process. The cross section at 13 TeV is about fifty times smaller than $t\bar{t}$H production, with multiple precision calculations predicting values of $\sigma_{t\bar{t}t\bar{t}} = 9.2^{+2.9}_{-2.4}$fb (NLO) and $\sigma_{t\bar{t}t\bar{t}} = 11.97^{+2.15}_{-2.51}$fb (NLO+EW) [12, 115, 617].

ATLAS and CMS have published multiple papers where limits on $t\bar{t}t\bar{t}$ production were presented as SM-oriented searches [618–620] and/or derived as a side product of searches for new physics, typically coming from searches for vector-like quarks or MSSM SUSY signatures [621–625].

The production of $t\bar{t}t\bar{t}$ is a rare SM process that is expected to be discovered by future LHC runs, including HL-LHC and HE-LHC. The increase in collision energy is important for $t\bar{t}t\bar{t}$ production because the cross section is largely induced by gluons in the initial state, leading to a substantial improvement in the signal-to-background ratio when the collision energy of the LHC is increased. Analyses looking for the production of $t\bar{t}t\bar{t}$ also are well-suited for interpretation in SMEFT [234].

The $t\bar{t}t\bar{t}$ process has not yet been observed at the LHC. Once closer to observation, and considering the sensitivity of $t\bar{t}t\bar{t}$ production to new physics scenarios in the top quark and scalar section, it is prudent to instead consider how accurately the cross section can be measured. Of course in the future analysis techniques are also expected to improve, and dedicated analyses will surely improve this sensitivity, but this is beyond the scope of this study. It is however important to keep in mind that such a study is less sensitive to systematic uncertainties on the background determination, while being more sensitive to the signal modelling uncertainties and overall branching fraction and acceptance of the selection.

6.2.1 The complete NLO corrections to four-top production[37]

In this section the so-called "complete"-NLO corrections to four-top production at the HE and HL-LHC is computed. Four-top production can proceed through different terms of order $\alpha_s^p \alpha^q$ with $p+q = 4,\ 5$ at LO and at NLO respectively. The term complete-NLO refers to computation of all terms with $p+q \leq 5$, which has been performed for the first time in Ref. [115] by employing the newly-released version of MG5_aMC@NLO [12] capable of computing mixed QCD and electroweak corrections [89]. Among the various contributions, the NLO QCD corrections ($p = 5$, $q = 0$) are also included, which have been known for some years [617, 626]. Despite that power-counting arguments suggest that the larger q the more suppressed a contribution is, it has been shown in Ref. [115] that this is not the case for $t\bar{t}t\bar{t}$ production. In fact, terms with up to two powers of α still contribute to several 10%s with respect to the $\mathcal{O}(\alpha_s^4)$ LO contribution. One of the reasons why this happens is because of the large Higgs-top Yukawa coupling; furthermore, important cancellations appear among these terms, which may be spoiled by non-SM effects.

[37] Contributed by R. Frederix, D. Pagani and M. Zaro.

This short paragraph reports inclusive predictions for the HL and HE-LHC, with a centre-of-mass energy of respectively 14 TeV and 27 TeV. For differential distributions, the qualitative and quantitative behaviour is very similar to the predictions at 13 TeV reported in Ref. [115]. The same setup and notation of Ref. [115], is used, where the interested reader can find more details as well as predictions for 13 and 100 TeV.

Table 37: Cross section for four-top production at the HL and HE-LHC, in various approximations, for $\mu = H_{\mathrm{T}}/4$. See Ref. [115] for details.

σ[fb]	$\mathrm{LO}_{\mathrm{QCD}}$	$\mathrm{LO}_{\mathrm{QCD}} + \mathrm{NLO}_{\mathrm{QCD}}$	LO	LO + NLO	$\frac{\mathrm{LO(+NLO)}}{\mathrm{LO}_{\mathrm{QCD}}\mathrm{(+NLO}_{\mathrm{QCD}})}$
14 TeV	$9.04^{+69\%}_{-38\%}$	$14.72^{+19\%}_{-23\%}$	$10.04^{+63\%}_{-35\%}$	$15.83^{+18\%}_{-21\%}$	1.11 (1.08)
27 TeV	$81.87^{+62\%}_{-36\%}$	$135.19^{+19\%}_{-21\%}$	$91.10^{+56\%}_{-33\%}$	$143.93^{+17\%}_{-20\%}$	1.11 (1.06)

Table 37 reports the total-cross section for $t\bar{t}t\bar{t}$ production in different approximations, and Table 38 the breakdown of the different orders contributing at LO and NLO, as fraction of the $\mathcal{O}(\alpha_s^4)$ LO contribution, LO_1. It is observed that the pattern of relative corrections is rather similar between 14 and 27 TeV. In particular, besides NLO_1 which is entirely of QCD origin, and thus displays a strong dependence on the renormalisation and factorisation scales, such a feature is present also for NLO_2 and NLO_3, which witnesses the fact that they receive an important contribution through QCD corrections from LO_2 and LO_3 respectively, on top of the electroweak corrections from LO_1 and LO_2. Furthermore, NLO_2 and NLO_3 tend to cancel each other almost exactly, leading to a complete-NLO prediction well within the uncertainty band of the one at NLO QCD accuracy. Such a feature may be spoiled by effects beyond the Standard Model, such as anomalous Higgs-top couplings. Thus, NLO corrections cannot be neglected when similar studies are performed, such as those presented in Sec. 6.3.2.

6.2.2 Prospect for experimental measurements

ATLAS has studied the potential to measure the Standard Model $t\bar{t}t\bar{t}$ cross section using 3000 fb^{-1} of HL-LHC data in the channel with several leptons [627]. Events are selected if they contain at least two isolated leptons with the same charge or at least three isolated leptons. At least six jets among which at least three are b-tagged are required. In addition the scalar sum of the p_{T} of all selected jets and leptons (H_{T}) is requested to be $H_{\mathrm{T}} > 500$ GeV and the missing transverse momentum $E_{\mathrm{T}}^{miss} > 40$ GeV. In order to extract the measured $t\bar{t}t\bar{t}$ cross section a fit is performed to the H_{T} distributions in several signal regions according to the jets and b-jets multiplicities: at least 6 jets and exactly 3 b-jets, or at least 6 jets and at least 4 b jets. These regions are further split in events with two same-charge leptons or with at least three leptons leading to 4 signal regions.

The background arises from $t\bar{t}V$ process, multiboson and $t\bar{t}H$ events as well as events with fake, non prompt or charge mis-identified leptons. The rate of this difficult instrumental background is computed from the ATLAS 36 fb^{-1} analysis [625] in the relevant regions with different lepton and b-tagged jet multiplicities. The number of events selected in the different signal regions are shown in Fig. 76.

The main sources of systematic uncertainties taken into account come from uncertainties on the fake lepton background and on the SM background and signal normalisations. A maximum-likelihood fit is performed simultaneously in the four signal regions to extract the $t\bar{t}t\bar{t}$ signal cross section normalised to the prediction from the SM. The impact of systematic uncertainties on the background expectations is described by nuisance parameters. As a result of the fit, the expected uncertainty on the measured $t\bar{t}t\bar{t}$ cross section is found to be 11%. The systematic uncertainty that impacts the precision the most is uncertainty in the normalisation of the $t\bar{t}V$ and instrumental background in the region with at least 6 jets

Table 38: $t\bar{t}t\bar{t}$: $\sigma_{(\mathrm{N})\mathrm{LO}_i}/\sigma_{\mathrm{LO}_{\mathrm{QCD}}}$ ratios at 14 and 27 TeV, for different values of $\mu = \mu_R = \mu_F$. See Ref. [115] for details.

$\delta[\%]$	14 TeV			27 TeV		
	$\mu = H_{\mathrm{T}}/8$	$\mu = H_{\mathrm{T}}/4$	$\mu = H_{\mathrm{T}}/2$	$\mu = H_{\mathrm{T}}/8$	$\mu = H_{\mathrm{T}}/4$	$\mu = H_{\mathrm{T}}/2$
LO_2	-25.8	-28.1	-30.4	-23.6	-25.9	-28.2
LO_3	32.5	38.9	45.8	30.7	37.0	43.8
LO_4	0.2	0.3	0.4	0.1	0.2	0.2
LO_5	0.0	0.0	0.1	0.0	0.0	0.1
NLO_1	14.7	62.9	103.3	21.7	65.1	101.9
NLO_2	8.1	-3.5	-15.1	5.0	-4.4	-13.9
NLO_3	-10.0	1.8	15.8	-7.8	1.6	13.2
NLO_4	2.2	2.7	3.4	1.6	2.0	2.4
NLO_5	0.1	0.2	0.2	0.1	0.2	0.2
NLO_6	< 0.1	< 0.1	< 0.1	< 0.1	< 0.1	< 0.1
$\mathrm{NLO}_2 + \mathrm{NLO}_3$	-1.9	-1.7	0.7	-2.8	-2.8	-0.7

and exactly 3 b-jets. Overall the impact of the systematic uncertainties remain limited as a fit without systematic uncertainties leads to a precision of 9% on the extracted $t\bar{t}t\bar{t}$ cross section.

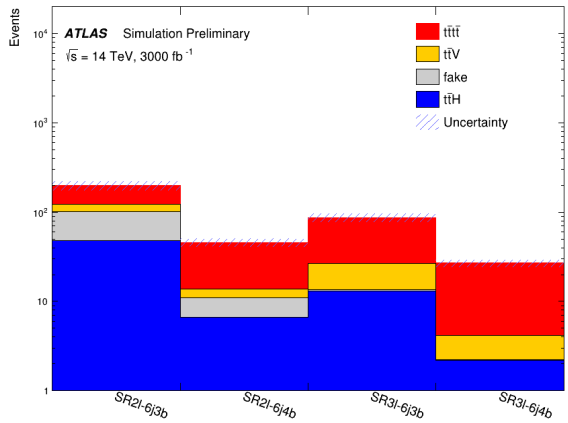

Fig. 76: Event yields of signal and background processes in the different signal regions used to extract the $t\bar{t}t\bar{t}$ cross section for an integrated luminosity of 3000 fb^{-1} [627].

The most sensitive result of the CMS collaboration on the Standard Model $t\bar{t}t\bar{t}$ process [618] is based on an integrated luminosity of 35.9 fb^{-1}and a centre-of-mass energy of 13 TeV, and relies on events with 2 same-sign leptons or 3 or more leptons. This Run-2 analysis sets an expected 95% CL upper limit on the $t\bar{t}t\bar{t}$ production cross section of $20.8^{+11.2}_{-6.9}$ fb, and an expected significance (based on a cross section of 9.2 fb) of 1.0 standard deviations above the background-only hypothesis.

The result of Ref. [618] is used to derive extrapolations for HL and HE-LHC, which are described in Ref. [628] and summarized below. The extrapolations rely on a simple rescaling of the signal and background cross sections, and make different assumptions on the systematic uncertainties. First, the statistical uncertainties are considered, then the same systematic uncertainties as the Run-2 published result are used, and finally these systematics are progressively reduced as a function of the integrated luminosity.

The expected sensitivity on the $t\bar{t}t\bar{t}$ cross section for different HL and HE-LHC scenarios is listed in Table 39. Based on these results, evidence for $t\bar{t}t\bar{t}$ production will become possible with around 300 fb^{-1} of HL-LHC data at $\sqrt{s} = 14$ TeV, at which point the statistical uncertainty on the measured cross section will be of the order of 30% and the measurement will have a total uncertainty of around 33-43%, depending on the systematic uncertainty scenario considered. For larger datasets at HL-LHC, all scenarios considered become dominated by systematic uncertainties. With 3 ab^{-1} the cross section can be constrained to 9% statistical uncertainty, and the total uncertainty of a measurement ranges between 18% and 28% depending on the considered systematic uncertainties. At HE-LHC the $t\bar{t}t\bar{t}$ cross section is expected to be constrained to within a 1-2% statistical uncertainty, and the systematic uncertainties also decrease due to the improved signal to background ratio at $\sqrt{s} = 27$ TeV. Future changes to the analysis strategy might allow improvements based on optimizing the interplay between statistical and systematic uncertainties.

The $t\bar{t}t\bar{t}$ cross section measurements can also be used to constrain the Wilson coefficients of the $\mathcal{O}_R$, $\mathcal{O}_L^{(1)}$, $\mathcal{O}_B^{(1)}$ and $\mathcal{O}_B^{(8)}$ dimension-6 operators of the Effective-Field-Theory (EFT) Lagrangian. These constraints are included in Ref. [628] for both HL-LHC and HE-LHC scenarios.

Table 39: Expected sensitivity for the production cross section of $t\bar{t}t\bar{t}$ production, in percent, at 68% confidence level. The fractional uncertainty on the cross section signal strength is given for various LHC upgrade scenarios. Cross sections are corrected for the changes expected by $\sqrt{s}$. For the 15 ab^{-1} 27 TeV scenario, the systematic uncertainty extrapolation is no longer valid, so only the statistical uncertainty is provided.

Int. Luminosity	$\sqrt{s}$	*Stat. only* (%)	*Run-2* (%)	*YR18* (%)	*YR18+* (%)
300 fb^{-1}	14 TeV	$+30, -28$	$+43, -39$	$+36, -34$	$+36, -33$
3 ab^{-1}	14 TeV	± 9	$+28, -24$	$+20, -19$	± 18
3 ab^{-1}	27 TeV	± 2	$+15, -12$	$+9, -8$	$+8, -7$
15 ab^{-1}	27 TeV	± 1			

6.3 Four top quarks as a probe of new physics

Heavy coloured resonances decaying into a pair of top quarks are present in many new physics theories [629–633]. Such particles are typically pair-produced at large rate and their decay then leads to a substantial enhancement of four-top production. Current bounds on such a setup are driven by a recent CMS analysis of four-top events [618], using 35.9 fb^{-1} of LHC collisions at a centre-of-mass energy of 13 TeV. Those bounds however are expected to strongly improve in the upcoming years, as illustrated in following contributions, with the example of a scalar colour-octet field O, traditionally dubbed a sgluon.

6.3.1 Limits on pseudoscalar colour-octets[38]

The effective Lagrangian describing the couplings of such a sgluon to the Standard Model is given by [634]

$$\mathcal{L} \supset g_8 d_{abc} O^a G^b_{\mu\nu} G^{\mu\nu c} + \tilde{g}_8 d_{abc} O^a G^b_{\mu\nu} \tilde{G}^{\mu\nu c} + \left\{ \bar{q} \left[\mathbf{y_8^L} P_L + \mathbf{y_8^R} P_R \right] O^a T_a q + \text{h.c.} \right\} , \qquad (46)$$

where T^a and d_{abc} are respectively the fundamental representation matrices and symmetric structure constants of $SU(3)$. Moreover, flavour and fundamental colour indices are understood for simplicity and the gluon field strength (dual field strength) tensor is denoted by $G^a_{\mu\nu}$ ($\tilde{G}^a_{\mu\nu}$). The focus here is on the case of a pseudoscalar sgluon with $g_8 = 0$ and purely imaginary $\mathbf{y_8}$ matrices, and it is additionally enforced

[38] Contributed by B. Fuks, L. Darmé and M.D. Goodsell.

$\tilde{g}_8 = 0$ as in Dirac gaugino supersymmetric scenarios. A non-vanishing $\tilde{g}_8$ coupling would however weaken the bounds by reducing the sgluon branching ratio into top quarks. In order to assess the impact of future search on the potential discovery of a sgluon, recasting strategy is followed here, as detailed in Ref. [635]. An NLO UFO module [636] is generated through FEYNRULES [637], NLOCT [638] and FEYNARTS [639] and it is used to generate events within the MG5_aMC@NLO framework [12], the hard-scattering matrix elements being convolved with the NNPDF3.0 NLO set of parton densities [201] and the sgluon decays being achieved with MADSPIN [402] and MADWIDTH [640]. Parton showering and hadronisation are performed by PYTHIA 8 [149] and the response of the CMS detector is simulated with DELPHES 3 [273] and FASTJET [343]. Finally, the four-top selection strategy of CMS [618] is mimicked by using the MADANALYSIS 5 [641–643] framework.

The best signal region (SR6) from Ref. [618], in terms of constraints, focuses on a topology featuring one pair of same-sign leptons, at least 4 b-jets and at least 5 hard jets. It is shown the observed and expected limits on the pseudoscalar octet cross section times the corresponding branching ration into four top quarks in Fig. 77 (left). While the analysis of Ref. [618] targeted a Standard Model four-top signal, future studies adopting a new physics signal selection strategy relying on the large differences in the final-state kinematics could be more adapted and lead to sizeable improvement in the reach [635].

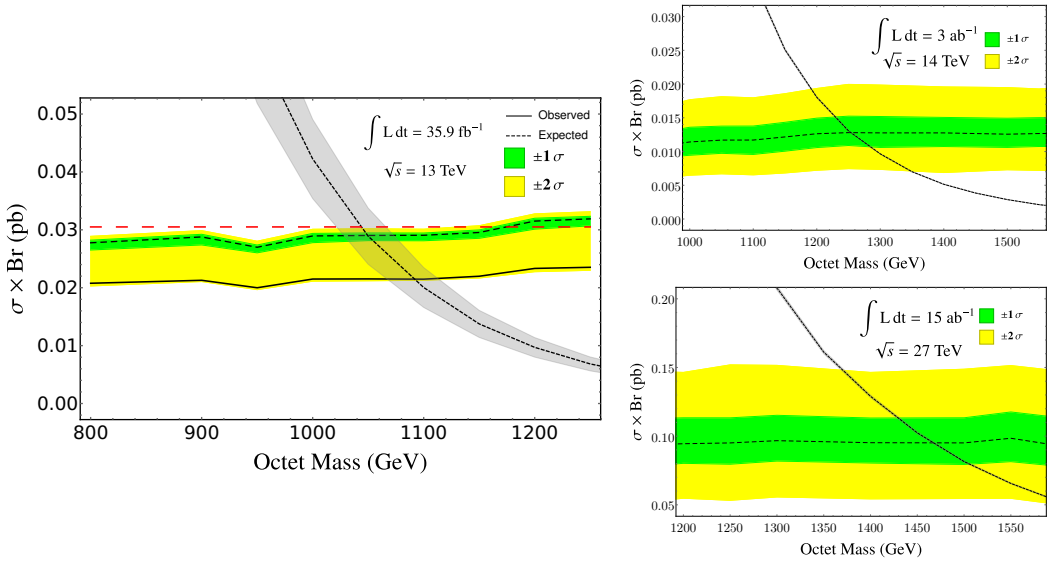

Fig. 77: Left: Expected (dashed) and observed (solid) pseudoscalar sgluon pair-production cross section excluded at the 95% confidence level when making use of the results associated with the SR6 region of the four-top CMS analysis of Ref. [618]. Theoretical predictions for the signal rate are indicated by the grey band. Right: expected limits for proton-proton collisions at centre-of-mass energies of 14 (top) and 27 (bottom) TeV, with the sgluon cross-section as the fine dotted line.

To calculate the projected sensitivity of the HL/HE-LHC, it is assumed that the current selection efficiencies at 13 TeV are similar to the future ones, and moreover rescale the four-top and other SM backgrounds by the appropriate partonic luminosities relative to those at 13 TeV. The rescaling factor for the non-four-top SM background is taken to be the largest ratio of the ttZ and ttW background component, using the projected cross-sections reported in Sec. 6.8. Factors of 1.3 and 12 are obtained for the 14 and 27 TeV cases, respectively. According to Sec. 6.2.1, the four-top cross section is then set to 15.83 fb and 144 fb at 14 and 27 TeV, respectively, recalling that the 13 TeV cross section is of 11.97 fb. The results for the projected mass limits are then given in the following Table 40, together with the 13 TeV value for reference.

Table 40: Results for the projected mass limits on pseudo-scalar color octets.

	$35.9\,\text{fb}^{-1}$, 13 TeV	$3\,\text{ab}^{-1}$, 14 TeV	$15\,\text{ab}^{-1}$, 27 TeV
Octet mass (GeV)	1060	1260	1470

6.3.2 Limits on top-Higgs interaction from multi-top final state[39]

Four top-quark ($t\bar{t}t\bar{t}$) production provides a powerful tool to probe the Top-quark Yukawa coupling (y_t) [644]. In the SM the $t\bar{t}t\bar{t}$ production can be induced either by the pure gauge interaction (involving the gluon, Z-boson or photon in the intermediate state) [645] or by the Higgs boson mediation [644]. Defining the general top-Higgs coupling as $y_t \equiv \kappa_t y_t^{\rm SM}$ with $y_t^{\rm SM}$ the top-Yukawa coupling in the SM, the leading-order cross section of $t\bar{t}t\bar{t}$ production can be parameterised as

$$\sigma(t\bar{t}t\bar{t}) = \sigma(t\bar{t}t\bar{t})^{\rm SM}_{g/Z/\gamma} + \kappa_t^2\sigma(t\bar{t}t\bar{t})^{\rm SM}_{\rm int} + \kappa_t^4\sigma(t\bar{t}t\bar{t})^{\rm SM}_{H}, \tag{47}$$

where $\sigma(t\bar{t}t\bar{t})^{\rm SM}_{g/Z,\gamma,\ H,\ \rm int}$ denotes the cross section induced by the pure gauge interaction, Higgs-boson mediation and the interfere effect, respectively. Note that $\sigma^{\rm SM}_{H,\rm int}$ is comparable to $\sigma(t\bar{t}t\bar{t})^{\rm SM}_{g/Z,\gamma}$ as $y_t^{\rm SM} \sim 1$ in the SM. For example, the leading order calculation with the renormalization/factorization scale (μ) fixed to the dynamics scale [12] yields

$$\begin{aligned}
&\text{HL}-\text{LHC}\ (\sqrt{s}=14\ \text{TeV}) \quad : \quad \sigma(t\bar{t}t\bar{t}) = \ 13.14 - \ \ 2.01\kappa_t^2 + \ 1.52\kappa_t^4 \ \ [\text{fb}] \\
&\text{HE}-\text{LHC}\ (\sqrt{s}=27\ \text{TeV}) \quad : \quad \sigma(t\bar{t}t\bar{t}) = 115.10 - 15.57\kappa_t^2 + 11.73\kappa_t^4 \ \ [\text{fb}]
\end{aligned} \tag{48}$$

Clearly, $\sigma(t\bar{t}t\bar{t})$ depends only on κ_t such that it directly probes y_t without any assumption on Higgs boson. The above values suffer from a large μ dependence; when varying the scale by a factor 2, the cross section varies by about 50%. It is crucial to take the full next-to-leading order corrections [115,617] into account to get a realistic simulation. Here, the tree level events are generated and the cross section rescaled to the NLO.

A special signature of the $t\bar{t}t\bar{t}$ events is the same-sign charged leptons (SSL) from the two same-sign top quarks. The other two top quarks are demanded to decay hadronically to maximize the event rate. Therefore, the topology of the signal event consists of two same-sign charged leptons, four b-quarks, four light-flavor quarks, and two invisible neutrinos. In practice it is challenging to identify four b-jets. Instead, it is required for at least 5 (6) jets to be tagged and three of them to be identified as b-jets at the HL(HE)-LHC, respectively. The two invisible neutrinos appear as a missing transverse momentum $E_{\rm T}^{miss}$ in the detector. The SM backgrounds contain $t\bar{t}+X$, $W^{\pm}W^{\pm}jj$ and $W^{\pm}W^{\pm}jj$ processes. See Ref. [644] for the details of those kinematic cuts used to disentangle the $t\bar{t}t\bar{t}$ signal from the huge backgrounds. It is demanded that $E_{\rm T}^{miss} > 100$ GeV at the HL-LHC and $E_{\rm T}^{miss} > 150$ GeV at the HE-LHC. Table 41 displays the numbers of signal and background events after applying the kinematics cuts listed in each row sequentially. In Table 41, at the HL-LHC the $t\bar{t}t\bar{t}$ production cross section is multiplied by a constant K-factor of 1.27 with uncertainty 27% (see Ref. [617]), while at the HE-LHC the cross section is rescaled to NLO order of $143.93^{+17\%}_{-20\%}$ fb (see Table 37 in Sec. 6.2.1).

The MC simulation shows that the $t\bar{t}t\bar{t}$ production ($\kappa_t = 1$) can be discovery at a 5σ confidence level with an integrated luminosity of 2075 fb^{-1} at the HL-LHC and 146 fb^{-1} at the HE-LHC, respectively. The event rate is not enough for measuring y_t precisely at the HL/HE-LHC but it is good for bounding y_t; for example, a direct bound $\kappa_t \leq 1.41\ [1.37, 1.47]$ is obtained at the HL-LHC and $\kappa_t \leq 1.15\ [1.12, 1.17]$ ($1.12\ [1.10, 1.13]$, $1.10\ [1.08, 1.12]$) with an luminosity of 10 (20, 30) ab^{-1} at the HE-LHC, respectively.

[39] Contributed by Qing-Hong Cao, Shao-Long Chen and Yandong Liu.

A few words of care on the interpretation of results from this study are however necessary: as it has been discussed in Sec. 6.2.1, the complete-NLO corrections to $t\bar{t}t\bar{t}$ are large and can involve terms proportional to y_t^3, y_t^5 and y_t^6 (on top of y_t^2 and y_t^4 already present at LO). However, since in such corrections y_t is renormalised, an extension of our study will not be immediately possible at NLO.

Table 41: The numbers of signal and background events at the HL-LHC with an integrated luminosity of 300 fb^{-1} (left) and at the HE-LHC with an integrated luminosity of 1 ab^{-1}. The cuts listed in the row are applied sequentially [644].

HL-LHC	Basic	SSL	Jets	$\not{E}_{\text{T}}$	m_{T}	H_{T}
$t\bar{t}t\bar{t}_H$	577.22	9.82	4.68	2.43	1.33	1.21
$t\bar{t}t\bar{t}_{g/Z/\gamma}$	5006.34	78.15	37.02	19.25	11.09	10.16
$t\bar{t}t\bar{t}_{\text{int}}$	-764.67	-12.79	-6.19	-3.23	-1.93	-1.77
$t\bar{t}$	2.5×10^8	28802.4	44.1	18.9	0	0
$t\bar{t}W^+$	32670	2359.5	36.9	17.7	12.3	8.7
$t\bar{t}W^-$	16758	1397.1	49.5	9.9	4.5	4.5
$t\bar{t}Z$	24516	2309.4	20.1	10.8	10.8	9.3
$W^\pm W^\pm jj$	4187.7	1147.5	0.11	0	0	0

HE-LHC	Basic	SSL	Jets	$\not{E}_{\text{T}}$	m_{T}	H_{T}
$t\bar{t}t\bar{t}_H$	15174.4	260.09	84.61	27.92	15.42	15.17
$t\bar{t}t\bar{t}_{g/Z/\gamma}$	148898.	2421.08	814.77	268.02	168.55	166.77
$t\bar{t}t\bar{t}_{\text{int}}$	-20141.9	-347.81	-117.95	-36.17	-20.14	-19.66
$t\bar{t}$	3.3×10^7	130207	291.9	0	0	0
$t\bar{t}W^+$	1.3×10^6	11488.5	171.0	39.6	27.1	27.1
$t\bar{t}W^-$	7.6×10^5	7387.1	99.5	19.9	9.9	9.9
$t\bar{t}Z$	3.9×10^6	20748.7	507.2	129.7	70.8	70.8
$W^\pm W^\pm jj$	888700	7947.0	4.7	3.5	0	0

6.3.3 Constraining four-fermion operators in the EFT[40]

The four-top total cross section measurement can be interpreted within the SMEFT framework [646][41]. Following the notation in Refs. [646] and [234], the relevant operators consist of four independent four-top-quark operator coefficients, $\tilde{C}_{\text{tt}}$, $\tilde{C}_{\text{QQ}}^{(+)}$, $\tilde{C}_{\text{Qt}}^{(1)}$, $\tilde{C}_{\text{Qt}}^{(8)}$, and fourteen independent two-light-two-top-quark ($qqtt$) operator coefficients, $\tilde{C}_{\text{td}}^{(8)}$, $\tilde{C}_{\text{td}}^{(1)}$, $\tilde{C}_{\text{Qd}}^{(8)}$, $\tilde{C}_{\text{Qd}}^{(1)}$, $\tilde{C}_{\text{tu}}^{(8)}$, $\tilde{C}_{\text{tu}}^{(1)}$, $\tilde{C}_{\text{Qu}}^{(8)}$, $\tilde{C}_{\text{Qu}}^{(1)}$, $\tilde{C}_{\text{Qq}}^{(8,1)}$, $\tilde{C}_{\text{Qq}}^{(1,1)}$, $\tilde{C}_{\text{Qq}}^{(8,3)}$, $\tilde{C}_{\text{Qq}}^{(1,3)}$, $\tilde{C}_{\text{tq}}^{(8)}$, $\tilde{C}_{\text{tq}}^{(1)}$. Here $\tilde{C}_i \equiv C_i/\Lambda^2$. O_{tG} is relevant but better constrained by other processes.

To estimate the projected limits on these coefficients, a few simple assumptions are made: 1) the effective operators do not significantly change the distribution of events, so the sensitivity mainly comes from inclusive measurements; 2) a kinematic cut M_{cut} of a few TeV can be applied to the total mass of the four tops to make sure the SMEFT can be matched to BSM models with scales larger than this energy (i.e. following Ref. [647]); and 3) M_{cut} does not significantly change the projected sensitivity on cross section measurements. By combining the expected experimental sensitivity discussed in Sec. 6.2.2 and the theoretical predictions presented in Sec. 6.2.1 it is estimated that the total cross section can be

[40] Contributed by Cen Zhang.

[41] This interpretation is also present in Ref. [628].

determined with an uncertainty of 102%, 58%, and 40%, at 95% CL level, for the 13, 14 and 27 TeV runs respectively. The corresponding integrated luminosities are 300 fb^{-1}, 3 ab^{-1} and 15 ab^{-1}.

For illustration, Fig. 78 shows the signal strength dependence on two operator coefficients: one four-top coefficient (left) and one $qqtt$ coefficient (right), assuming a 3 TeV M_{cut}. The cross section becomes more sensitive to the four-top operator coefficient at larger energies. Together with smaller uncertainties, the limit on this coefficient is significantly improved with the 27 TeV run. On the other hand, the cross section becomes less sensitive to the $qqtt$ operator coefficient as the energy increases. The limits are thus not very much affected by energy. Table 42 presents individual limits on all 18 operator coefficients, assuming $M_{cut} = 3$ TeV.

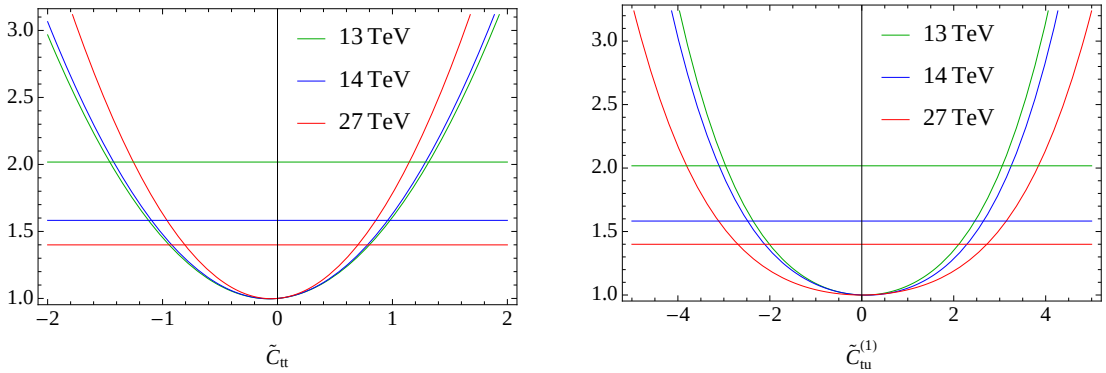

Fig. 78: Four-top signal strength as a function of operator coefficients, $\tilde{C}_{tt}$ (left) and $\tilde{C}_{tu}^{(1)}$ (right). Horizontal lines represent the expected measurements at each energy. $M_{cut} = 3$ TeV is applied.

6.3.4 Top quark dipole moment in multi-top production[42]

This paragraph presents the study of the sensitivity of the four top quark production on the strong dipole moments of the top quark [648]. Within the SM framework, the top quark dipole moments are zero at tree level, however, higher-order corrections could generate non-zero strong dipole moments for the top quark. The top quark strong dipole moments have very small values in the SM, so that they would not be observable at the LHC experiments. However, there are extensions of the SM in which sizable contributions to these dipole moments arise, making them accessible by the experiments at the LHC [649, 650]. As a result, observation of any significant deviation of dipole moments from zero would point to beyond the SM physics. The most general effective Lagrangian describing the $gt\bar{t}$ coupling considering dimension-6 operators can be parametrized as [651]:

$$\mathcal{L}_{gt\bar{t}} = -g_s \bar{t}\frac{\lambda^a}{2}\gamma^\mu t G_\mu^a - g_s \bar{t}\lambda^a \frac{i\sigma^{\mu\nu}q_\nu}{m_t}(d_V^g + id_A^g\gamma_5)tG_\mu^a,$$

where the chromomagnetic and chromoelectric dipole moments of the top quark are denoted by d_V^g and d_A^g (both are zero in the SM at leading order). Direct bounds on both d_V^g and d_A^g were obtained from the top quark pair cross section measurements at the LHC and the Tevatron. The bounds on the dipole moments using the $t\bar{t}$ cross section at the LHC and Tevatron were found to be: $-0.012 \leq d_V^g \leq 0.023$, $|d_A^g| \leq 0.087$ [652]. Four-top quark production is also affected by the $gt\bar{t}$ effective coupling and provides a powerful way to probe the chromomagnetic and chromoelectric dipole moments of the top quark. The representative Feynman diagrams with the effective $gt\bar{t}$ coupling denoted by filled red circles are shown in Fig. 79. The contribution of the top quark dipole moments to the $t\bar{t}t\bar{t}$ production cross section is determined with the MG5_aMC@NLO package [12]. By taking into account at most

[42] Contributed by J. Ebadi, H. Khanpour, S. Khatibi and M. Mohammadi Najafabadi.

Table 42: Limits on 14 $qqtt$ operator coefficients and 4 four-top operator coefficients, expected at the 13, 14 and 27 TeV scenarios, at the 95% CL level.

	13 TeV	14 TeV	27 TeV
$\tilde{C}^{(8)}_{\mathrm{td}}$	[-9.8, 6.4]	[-8.8, 5.4]	[-6.6, 5.4]
$\tilde{C}^{(1)}_{\mathrm{td}}$	[-3.9, 4.1]	[-3.3, 3.4]	[-3.3, 3.3]
$\tilde{C}^{(8)}_{\mathrm{Qd}}$	[-9.6, 6.2]	[-8.8, 5.2]	[-7.6, 5.2]
$\tilde{C}^{(1)}_{\mathrm{Qd}}$	[-4., 4.]	[-3.3, 3.3]	[-3.4, 3.3]
$\tilde{C}^{(8)}_{\mathrm{tu}}$	[-8.2, 4.8]	[-6.4, 4.3]	[-9.6, 4.5]
$\tilde{C}^{(1)}_{\mathrm{tu}}$	[-3., 3.1]	[-2.5, 2.6]	[-2.7, 2.7]
$\tilde{C}^{(8)}_{\mathrm{Qu}}$	[-7.8, 4.6]	[-7.8, 4.]	[-5.8, 4.2]
$\tilde{C}^{(1)}_{\mathrm{Qu}}$	[-3., 3.]	[-2.6, 2.6]	[-2.7, 2.7]
$\tilde{C}^{(8,1)}_{\mathrm{Qq}}$	[-7.5, 4.2]	[-6., 3.6]	[-6.5, 3.7]
$\tilde{C}^{(1,1)}_{\mathrm{Qq}}$	[-2.5, 2.7]	[-2.1, 2.3]	[-2.2, 2.3]
$\tilde{C}^{(8,3)}_{\mathrm{Qq}}$	[-5.8, 4.8]	[-4.7, 4.2]	[-5.4, 4.]
$\tilde{C}^{(1,3)}_{\mathrm{Qq}}$	[-2.6, 2.6]	[-2.1, 2.2]	[-2.2, 2.2]
$\tilde{C}^{(8)}_{\mathrm{tq}}$	[-7.1, 3.9]	[-6.9, 3.3]	[-5.1, 3.4]
$\tilde{C}^{(1)}_{\mathrm{tq}}$	[-2.6, 2.6]	[-2.2, 2.2]	[-2.3, 2.2]
$\tilde{C}_{\mathrm{tt}}$	[-1.5, 1.3]	[-1.1, 0.96]	[-0.81, 0.7]
$\tilde{C}^{(+)}_{\mathrm{QQ}}$	[-1.5, 1.3]	[-1.1, 0.96]	[-0.81, 0.7]
$\tilde{C}^{(1)}_{\mathrm{Qt}}$	[-2.4, 2.4]	[-1.8, 1.8]	[-1.3, 1.3]
$\tilde{C}^{(8)}_{\mathrm{Qt}}$	[-5.3, 4.4]	[-4.1, 3.1]	[-3., 2.3]

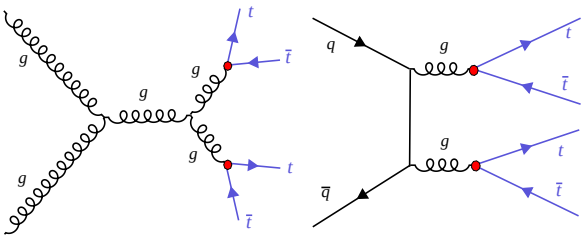

Fig. 79: Representative Feynman diagrams for the $t\bar{t}t\bar{t}$ production where the effects of the strong dipole moments are shown as filled red circles.

an effective vertex in each diagram, the total four top cross section at $\sqrt{s} = 14$ TeV has the following form:

$$\begin{aligned} \sigma(pp \to t\bar{t}t\bar{t})(\mathrm{fb}) &= \sigma_{\mathrm{SM}} + 154.8 \times d_V^g + 3404.4 \times (d_V^g)^2, \\ \sigma(pp \to t\bar{t}t\bar{t})(\mathrm{fb}) &= \sigma_{\mathrm{SM}} + 2731.3 \times (d_A^g)^2, \end{aligned} \tag{49}$$

where the SM four top quark cross section is denoted by σ_{SM}. The linear terms are due to the interference between the new physics and SM with the contribution of the order of Λ^{-2}. The quadratic terms suppressed by Λ^{-4} power are the pure contributions of the strong dipole moments. To estimate the sensitivity of the four top process to dipole moments, the same-sign dilepton channel is the focus here due to its clean signature and very low background contribution. The main background contributions

Table 43: Limits at 95% CL on the chromoelectric and chromomagnetic dipole moments $d_V^{g,Z}$ at 95% CL for the HL-LHC and HE-LHC.

Coupling	HL-LHC, 14 TeV, 3 ab^{-1}	HE-LHC, 27 TeV, 15 ab^{-1}
d_V^g	[-0.084, 0.009]	[-0.063, 0.001]
d_A^g	[-0.030, 0.030]	[-0.011, 0.011]

come from the $t\bar{t}W$ and $t\bar{t}Z$ processes. Signal and the background processes are generated with the MG5_aMC@NLO package at leading order. PYTHIA v6 [653] is used for hadronization, showering and decay of unstable particles. Jets are reconstructed using the anti-k_{T} algorithm [274]. Signal events are selected by requiring exactly two same-sign charged leptons with $p_{\mathrm{T}}^{\ell} > 25$ GeV and $|\eta^{\ell}| < 2.5$. The missing transverse energy has to be larger than 30 GeV. Each event is required to have at least eight jets with $p_{\mathrm{T}} > 30$ GeV and $|\eta| < 2.5$ from which at least three should be b-tagged jets. All objects in the final state are required to be well isolated objects by requiring $\Delta R(i,j) > 0.4$. Table 43 presents limits at 95% CL on the chromoelectric (d_A^g) and chromomagnetic (d_V^g) dipole moments for the HL-LHC and HE-LHC. The HE-LHC improves the HL-LHC bound on d_A^g by about a factor of three and the upper bound on d_V^g by one order of magnitude. The four top-quark production at the HE-LHC would be able to tighten the upper limit on d_A^g (d_V^g) by a factor of two (eight) with respect to the top pair production at the HL-LHC [652].

6.4 The $t\bar{t}V$ production at the HL/HE-LHC

6.4.1 $t\bar{t}Z$ cross sections at NLO QCD and EW[43]

This section provides the cross section for $t\bar{t}Z$ production at the HL and HE-LHC. The results are accurate up to NLO QCD and NLO EW accuracy [99]. NLO QCD and EW corrections are computed simultaneously with MG5_aMC@NLO [12], more specifically by using the recently-released version capable of mixed-coupling expansions [89]. The same setup as in Ref. [186] is used (see in particular Sec. 1.6.7.a), except for the PDF set, for which the PDF4LHC15_nlo_30_pdfas set [195] is employed. In fact, at variance with the predictions in Ref. [186], photon-initiated contributions are not included, since recent studies on the photon distribution became available [222, 223], and the corresponding photon density gives negligible contributions for $t\bar{t}Z$. The quoted EW corrections include the LO term at $\mathcal{O}(\alpha^2\alpha_s)$ and the NLO one at $\mathcal{O}(\alpha^2\alpha_s^2)$. At variance with $t\bar{t}W$ production, for which other contributions, subleading in the couplings, turn instead to be relevant (see Sec. 6.4.2), it has been shown in Ref. [89] that such contributions can be safely neglected for $t\bar{t}Z$.

Cross-sections for $t\bar{t}Z$ are quoted in Table 44, together with the NLO/LO QCD K-factor, the relative impact of EW corrections, and the theory uncertainties. For the latter, the uncertainty coming from scale variations, the PDF uncertainty and the α_s one are quoted separately.

Table 44: Cross section, in pb, for $t\bar{t}Z$ production at the HL and HE-LHC. Uncertainties on the cross sections are at the per-mil level.

$\sqrt{s}$	$\sigma_{\mathrm{QCD}}^{\mathrm{NLO}}$	$\sigma_{\mathrm{QCD+EW}}^{\mathrm{NLO}}$	K_{QCD}	δ_{EW} [%]	scale [%]		PDF [%]	α_s [%]
14 TeV	1.018	1.015	1.40	-0.3	+9.6	-11.2	±2.7	± 2.8
27 TeV	4.90	4.81	1.45	-2.0	+9.9	-10.4	±2.0	± 2.0

[43] Contributed by R. Frederix, D. Pagani and M. Zaro.

6.4.2 *The complete-NLO corrections to $t\bar{t}W$*[44]

This section presents the so-called "complete"-NLO corrections to $t\bar{t}W^{\pm}$ production. This process can proceed through different terms of order $\alpha_s^p \alpha^{q+1}$ with $p+q = 2,\ 3$ at LO and at NLO respectively. The term complete-NLO refers to computation of all terms with $p+q \leq 3$, which has been performed for the first time in Ref. [115] by employing the newly-released version of MG5_aMC@NLO [12] capable of computing mixed QCD and electroweak corrections [89]. Among the various contributions, the complete-NLO corrections include the NLO QCD ones ($p = 3$, $q = 0$) [418, 419, 654, 655], and the NLO EW corrections ($p = 2$, $q = 2$) [99]. This short paragraph reports inclusive predictions for the HL and HE-LHC, with a centre-of-mass energy of respectively 14 TeV and 27 TeV. The same setup and notation of Ref. [115] is used, where the interested reader can find more details as well as predictions for 13 and 100 TeV.

Table 45: Cross section for $t\bar{t}W^{\pm}$ production at the HL and HE-LHC, in various approximations, for $\mu = H_{\rm T}/2$. Number in parentheses are computed with a jet veto. See Ref. [115] for details.

σ[fb]	LO_{QCD}	$\text{LO}_{\text{QCD}} + \text{NLO}_{\text{QCD}}$	LO	LO + NLO	$\frac{\text{LO(+NLO)}}{\text{LO}_{\text{QCD}}\text{(+NLO}_{\text{QCD}})}$
14 TeV	$414^{+23\%}_{-18\%}$	$628^{+11\%}_{-11\%}$ $(521^{+5\%}_{-7\%})$	$418^{+23\%}_{-17\%}$	$670^{+12\%}_{-11\%}$ $(548^{+6\%}_{-7\%})$	1.07 (1.05)
27 TeV	$1182^{+21\%}_{-16\%}$	$2066^{+14\%}_{-11\%}$ $(1561^{+7\%}_{-7\%})$	$1194^{+21\%}_{-16\%}$	$2329^{+14\%}_{-11\%}$ $(1750^{+7\%}_{-7\%})$	1.13 (1.12)

Table 45 reports the total-cross section for $t\bar{t}W^{\pm}$ production in different approximations, and Table 46 the breakdown of the different orders contributing at LO and NLO, as fraction of the $\mathcal{O}(\alpha_s^2\alpha)$ LO contribution, LO_1. Number in parentheses are computed by vetoing hard central jets, with $p_{\rm T} > 100\,\text{GeV}$ and $\eta < 2.5$. As it can be gathered from the tables, the jet veto is beneficial in order to reduce the NLO QCD corrections, in particular the large contribution coming from hard real emissions with a soft or collinear W boson. It can be appreciated how the NLO_3 contribution is actually larger than the NLO_2 (the EW corrections) despite the extra power of α, and how such a contribution grows with the collider energy. As explained in Ref. [115], this is due to the $t-W$ scattering process [656]. Since the size of NLO_3 is not much affected by the jet veto, a measurement of the $t-W$ scattering from the $t\bar{t}W$ cross section should be possible.

6.5 Top mass

6.5.1 *Theoretical issues*[45]

The currently most precise methods for top mass measurements at the LHC are the so called "direct measurements" which are obtained exploiting information from the kinematic reconstruction of the measured top quark decay products, and their corresponding combinations. The typical errors currently quoted for the direct LHC top mass measurements are of the order of 500-600 MeV, and with the prospect of the high luminosity operations, as can be seen from Fig. 80 of the following section, the projected future experimental uncertainty is around 200 MeV. Such a high precision entails also a high level of scrutiny concerning the extracted top mass value. In direct measurements, the measured top mass is the value of the top mass parameter in the Monte Carlo generator that is used to fit top-mass sensitive distributions, because the complexity of the measurement is such that the extraction of these distributions corrected for detector effects, to be compared with analytic calculations, is not feasible. In this respect, the scrutiny must also regard theoretical aspects dealing with how the Monte Carlo models

[44] Contributed by R. Frederix, D. Pagani and M. Zaro.

[45] Contribution by G. Corcella, P. Nason, A. Hoang and H. Yokoya.

Table 46: $t\bar{t}W$: $\sigma_{(\mathrm{N})\mathrm{LO}_i}/\sigma_{\mathrm{LO}_{\mathrm{QCD}}}$ ratios at 14 and 27 TeV, for different values of $\mu = \mu_r = \mu_f$. LO_2 is identically zero and is not quoted in the table. Number in parentheses are computed with a jet veto. See Ref. [115] for details.

$\delta[\%]$	14 TeV			27 TeV		
	$\mu = H_{\mathrm{T}}/4$	$\mu = H_{\mathrm{T}}/2$	$\mu = H_T$	$\mu = H_{\mathrm{T}}/4$	$\mu = H_{\mathrm{T}}/2$	$\mu = H_{\mathrm{T}}$
LO_3	0.8	1.0	1.1	0.9	1.0	1.2
NLO_1	37.4 (7.7)	51.8 (25.9)	64.7 (41.9)	67.4 (18.4)	74.8 (32.0)	82.0 (44.3)
NLO_2	−4.5 (−4.7)	−4.3 (−4.5)	−4.1 (−4.3)	−5.1 (−5.4)	−5.0 (−5.2)	−4.8 (−5.1)
NLO_3	13.0 (9.7)	13.3 (9.9)	13.6 (10.1)	25.5 (19.8)	26.1 (20.2)	26.6 (20.6)
NLO_4	0.02 (−0.00)	0.03 (0.00)	0.05 (0.01)	0.06 (0.01)	0.08 (0.02)	0.10 (0.03)

the relevant mass sensitive distributions, keeping in mind that all effects that can lead to variations of the result in the 100 MeV range should be considered.

The top mass parameter, as all coupling constants characterizing the underlying field theory, requires renormalization, and its precise value depends upon the adopted renormalization scheme. The differences in the top mass in different renormalization prescriptions used in the theoretical community are parametrically of order $R\,\alpha_s(R)$, with R between about 1 GeV and m_t, and thus can amount from a few hundred MeV to several GeV. It is thus clear that an experimental result, in order to be of any use, must specify to which scheme the measured value corresponds to.

At present, the experimental collaborations have renounced to qualify direct mass measurements by also specifying a renormalization scheme. This is a consequence of the fact that no full agreement has been reached among theorists on this issue. Some authors have argued that, in view of the inherent leading-order nature of the Monte Carlo generators, no scheme can be specified for the mass measured in direct measurements, since at leading order all schemes are equivalent. This argument was also used as part of the motivation in favour of alternative measurements where the mass-sensitive observable is directly computed in perturbation theory at NLO or NNLO accuracy, and is compared to experimental distributions already corrected for detector effects [657, 658]. For example, the total cross section for $t\bar{t}$ production is sensitive to the top mass, it has been computed up to the NNLO order in QCD [41], and can be used to extract a top mass value [659–661]. Similarly, in Ref. [657, 658], shape observables constructed out of the $t\bar{t} + \mathrm{jet}$ kinematics are used.

Several theoretical works have appeared proposing alternative techniques to measure the top mass, partly to provide predictions with at least NLO precision to allow for a mass determination in a well-defined mass scheme, and partly to circumvent other aspects of direct measurements that may be considered problematic. The authors of Ref. [662] presented a method, based upon the charged-lepton energy spectrum, that is not sensitive to top production kinematics, but only to top decay, and does not make use of jets. Since top decays have been computed at NNLO accuracy [608, 609], they argue that a very accurate measurement may be achieved in this way. Other authors have advocated using the invariant mass of boosted top jets supplemented by light grooming (see Ref. [663] and references therein). In Ref. [664], the b-jet energy peak position is proposed as mass-sensitive observable, that is claimed to have a reduced sensitivity to production dynamics. In Ref. [665], the use of lowest Mellin moments of lepton kinematic distributions is discussed. In the leptonic channel, it is also possible to use distributions based on the "transverse" mass variable [666], which generalizes the concept of transverse mass for a system with two identical decay branches [667, 668]. Some of these methods have been effectively exploited by the experimental collaborations [666, 669–672] to yield alternative determinations of m_t. They are consistent within errors with direct measurements, and thus provide valuable checks. It turns out, however, that at the moment their errors are not competitive with direct measurements, mostly be-

cause the (less direct) observables of the alternative methods do not have the top mass discriminating power of the direct method. Furthermore, in view of the larger errors, the assessment of their eventual theoretical uncertainties is a less demanding task in comparison to the case of direct measurements.

The notion that the Monte Carlo mass parameter cannot be qualified as a field theoretical mass has extensively permeated the discussions regarding the interpretation of top mass measurements. This notion, however, oversimplifies the situation, because more precise statements on the Monte Carlo mass parameter can be made. In reality, the accuracy of Shower Monte Carlo's depends upon the observables one considers. As a trivial example, the total cross section for the production of top quarks is predicted at leading order by standard Shower Monte Carlo's, so that the value of the top mass extracted by fitting it to the measured total production cross section would indeed carry a scheme ambiguity of order $m_t\alpha_s$, because the pole or the $\overline{\rm MS}$ schemes can be used for computing the total cross section at higher orders. Such measurement cannot be qualified by specifying any particular scheme.[46] This is not the case if one considers as an observable the mass of the top decay products. In Ref. [673], for example, it is pointed out that, in the narrow width limit, a perturbative calculation of the mass of the top decay products performed in the pole mass scheme yields the pole mass at any perturbative order. Since Monte Carlo generators, when performing heavy particle decay, strictly conserve the mass of the decaying particle, it can be inferred that the Monte Carlo mass parameter should be identified with the pole mass up to non-perturbative effects[47] as far as the mass of the decay products is concerned. From a different point of view, in Ref. [674] it is argued that since the top-quark decay is treated with a Breit-Wigner form in the Monte Carlo generators, and due to the infrared shower cutoff $Q_0 \approx 1\,\text{GeV}$, the top mass parameter should be close to top mass schemes that are compatible with the Breit-Wigner form. In turn, these schemes yield mass values that differ from the pole mass by terms of order $\alpha_s(R)R$, with $R \approx \Gamma_t \approx Q_0$. In a subsequent work [675], it is argued that, in the narrow width limit, one can relate the Monte Carlo mass parameter to a running mass (such as the MSR mass [676]) evaluated at the scale of the Monte Carlo shower cutoff Q_0, as long as $Q_0 \gtrsim 1\,\text{GeV}$. These arguments entail that the Monte Carlo mass parameter differs from the top pole mass by several hundred MeV. It must also be noted that theoretical papers that make use of the direct top mass (noticeably those on electroweak precision fits [404, 492], and calculations inherent to the issue of the SM vacuum stability [677–679]) interpret the direct measurement results as being close to the pole mass, up to a theoretical error of few hundred MeV.

A problem that has received much attention is the presence of an infrared renormalon in the pole mass definition. The QCD perturbative series for the difference of the pole mass and the $\overline{\rm MS}$ mass has factorially divergent coefficients [680, 681]. This is related to an ambiguity of the order of a typical hadronic scale in the pole mass. Estimates of this inherent ambiguity vary from 110 to 250 MeV [682–685]. It should be stressed, however, that the finite width of the top screens the effects of soft radiation, so that this ambiguity *does not affect the physics* of top production and decay. This mean that the pole mass ambiguity does not represent in principle a limitation on the precision of top quark mass measurements, since short-distance mass schemes that are free of the pole mass ambiguity can be adopted. So in view of the considerable time to the start of the LHC HL program, the pole mass ambiguity, if it becomes a limiting factor, can be easily avoided, and is thus not discussed further here.

Accepting the fact that the difference between the top mass in direct measurements and the top pole mass is of the order of few hundred MeV, and in view of the current and projected accuracy of the direct measurements, several works have appeared in the literature to better quantify the difference. In [686] numerical relations between the Monte Carlo mass parameter and the pole mass as well as the

[46] In fact, at the moment, Monte Carlo generators that achieve NLO accuracy for sufficiently inclusive cross section are routinely used in top mass studies.

[47] In the narrow width limit the top can propagate a long time before decay, and long-distance non-perturbative effects can manifest themselves there, and affect the mass by a few hundred MeV.

MSR mass [676] were determined from comparing hadron level resummed analytic NNLL calculations performed in SCET factorization and Monte Carlo output (using PYTHIA v8.2) for the 2-Jettiness distribution at the top mass resonance for boosted top jets in e^+e^- annihilation.[48] In the work of Ref. [675], exploiting the fact that soft emission effects both in shower Monte Carlo and in full QCD can be computed as long as the shower cut Q_0 is a perturbative scale, the analytic structure of angular ordered shower algorithms was examined in detail and compared to the one of resummed calculations in SCET factorization for hemisphere masses for boosted top jets in e^+e^- annihilation. From the analysis an analytic relation at $\mathcal{O}(\alpha_s)$ between the shower mass parameter and the pole mass was calculated which is proportional to $Q_0\,\alpha_s(Q_0)$.

The results of Ref. [675, 686] are obtained in the context of global event-shape-type top jets observables in e^+e^- annihilation, which are different from observables involving jets of the top decay product that enter the direct measurements. Furthermore, the findings of Ref. [675] represent parton level results and refer exclusively to angular ordered parton showers. Future work should be aimed to lift these limitations and to extend studies of this sort to observables that enter the direct measurements at the LHC. Such studies are also valuable to expose effects that should be included to eventually match the experimental accuracy.

Direct measurements are not the only context where theoretical effects in the top mass that are linear in the strong interaction scale, i.e. of the order of few hundred MeV, do arise. In Ref. [688], the production and decay of a top quark is considered in a very simplified context, and in a particular approximation, such that non-perturbative corrections can be examined in relation to the factorial growth of the coefficients of the perturbative expansions. Linear power corrections are found to affect all observables that make use of jets. But it was also found that typical leptonic observables are also affected by linear power corrections. Notice that this implies that the total cross section is also affected by linear power corrections, as soon as selection cuts are imposed. These kind of studies can also be extended to more complex measurement procedures, eventually making use of jet calibration, in order to understand to what extent these theoretical limitations to the precision can be removed.

The discussion carried out so far has highlighted theoretical issues that should be studied in more depth in order to advance our understanding of the theoretical precision of the measurements. In essence these issues are related to the physics of different stages of soft emission, where a deeper insight would allow to draw conclusions motivated by perturbation theory, that may be extrapolated to low scales. There are also aspects of the event simulations that on the one hand only have to do with relatively hard scales, and can be reliably computed, and on the other hand are more related to the modeling of hadronization effects that currently cannot be computed from first principles. There is a current research effort, aimed at improving the simulation of top production and decay, in both these directions. It includes both the improvement of perturbative accuracy, and the improvement in the overall shower-hadronization aspects. Regarding the perturbative accuracy, recent progress has been achieved in the Monte Carlo implementation of finite width and off-resonance effects [169], whose impact has also been investigated in Ref. [689]. Regarding the hadronization aspects, the importance of the colour reconnection models has been recognized and investigated in Ref. [690,691]. Furthermore, studies of the sensitivity of top-mass sensitive observables to the perturbative accuracy, to the shower implementation and to the hadronization model, are being carried out. In one such study [692], significant differences were found when comparing HERWIG v7 and PYTHIA v8, where the former adopts an angular ordered shower, and the latter has a dipole shower, in the description of top-mass sensitive observables. In general, there is a range of equally plausible simulation models than can be used to describe heavy quark

[48] This procedure is often quoted as a form of calibration of the Monte Carlo top mass parameter. It must be noted that the same terminology has also been used in a different context in Ref. [687], where it is suggested that the Monte Carlo mass parameter can be constrained by fitting it from kinematic normalized distributions predicted from the Monte Carlo generator, simultaneously with an inclusive cross section measurement, that is then compared to a fixed order calculation.

production and decay, that will include different Monte Carlo generators, different Monte Carlo tunes in a given generator, and different implementations of some component of a generator, like for example the colour reconnection model. As more work is done by exploring different options for simulation models, the range of models may enlarge, and potentially also the error in mass measurement may increase. This increase in the error should be contrasted by limiting the range of models, typically by requiring that some key observables are in reasonable agreement with data, or by scrutiny concerning the models themselves. An example of a study in this direction is given in Ref. [693], where the sensitivity of the top-mass error upon the uncertainties in key Monte Carlo tuning parameters is studied, and a set of calibration observables strongly sensitive to the Monte Carlo parameters, but with very mild sensitivity to the top mass, is considered in order to reduce the parametric uncertainties.

A complementary way of reducing the error is to find variants of measurement methods that reduce the dependence of the extracted mass from the range of models. In situ jet calibration is routinely used by the experimental collaborations in top mass measurement. This procedure not only reduces the experimental error associated with the jet energy scale, but it may also reduces the theoretical error, by reducing the sensitivity of the measurements from features of jet simulations in the generators. More specific proposals in this direction have appeared in Ref. [694], where the impact of adopting jet grooming techniques to the jets in direct top mass measurements is examined.

As mentioned earlier, alternative techniques for mass measurements are currently explored, and will become more precise at the HL-LHC. As shown in Fig. 80 in the following subsection, the mass measurement from single top production will acquire a precision similar to the one available today from direct measurements. The end-point measurement using the J/Ψ will also reach a precision near 600 MeV. Thus, at the HL-LHC there will likely be one highly precise measurement technique, plus a number of independent methods supporting its results. It should not be forgotten however, that high luminosity and/or high energy may also offer opportunities for new techniques. In Ref. [663], the use of grooming techniques applied to boosted top jets is studied, with the goal of directly extracting a short distance mass. To what extent the high luminosity phase can make this technique feasible is a matter for future studies. Another example is given in the work of Ref. [695], where it is argued that a glitch in the dilepton spectrum should be visible for a dilepton invariant mass near twice the top mass. This effect is due to the diphoton production subprocess $gg \to \gamma\gamma$ mediated by a top loop. The projected statistical error for the mass determination using this method is of 2-3 GeV for the High Luminosity LHC, and 0.3-0.6 GeV for the 27 TeV High Energy option. A 1 GeV error systematic from the EM calorimeter calibration should also accounted for. Furthermore, a complete study of the projected theoretical error is not yet available. It is nevertheless interesting to remember that "out of the box" thinking may lead to progress in this area.

In summary, from a theoretical point of view, much work is still needed to put the top mass measurements at the HL-LHC on a solid ground. Such work should comprise more thorough experimental work aimed at understanding and reduce the sources of errors; theoretical work in the framework of Monte Carlo studies and simulation; and formal theoretical work aimed at understanding conceptual aspects. Such work is already under way, and it is expected that much more will be understood by the time the High Luminosity program starts. Thus, in spite of the many challenges, one can expect that a theoretical precision matching the foreseeable experimental errors for top mass measurements at the HL-HLC can be achieved.

6.5.2 Experimental projections

The input material for the experimental summary is collected in Ref [696, 697]. The measurement of the top quark mass $m_t$with high precision is a crucial task for the expected 3000 fb^{-1}of pp collision data expected in HL-LHC. The top quark mass is one of the free parameters within the Standard Model and its Yukawa coupling is predicted to be close to unity. Therefore it may play a special role in the electroweak

symmetry breaking. The top quark mass dominantly contributes to the quantum corrections of the Higgs field, which become important for any extrapolation of the Standard Model to extremely high energies, from a few hundred GeV and above. At these high energies some of the fundamental deficiencies of the Standard Model can be further investigated, such as the stability of the electroweak vacuum state in the Higgs potential. Thus, precise measurements of the top quark mass allow for consistency tests of the Standard Model and to look for signs of new physics beyond.

The top quark mass is measured using various techniques and in different decays channels by the ATLAS and CMS experiments following two different approaches. Firstly, direct $m_t$measurements are obtained exploiting information from the kinematic reconstruction of the measured top quark decay products, and their corresponding combinations. This information is obtained from Monte Carlo (MC) simulated events using different assumed values for the top quark mass parameter in the program. Therefore, such results relate to measurements of the input parameter of MC event generators, and differences between different MC are covered by a specific systematic uncertainty. The relation between the measured Monte-Carlo top quark mass parameter and theoretical mass schemes such as the pole mass is discussed in detail in Section 6.5.1. Secondly, indirect determinations of m_t are obtained based on the comparison of inclusive or differential $t\bar{t}$ production cross-section to the corresponding theory calculations, thus sensitive to m_t^{pole}.

The methods exploited for the measurement of m_t directly using the kinematic properties of the $t\bar{t}$ (or single-top quark) decay products are the template, the matrix element and the ideogram methods. In the template method, based on a full ($t\bar{t}$ $\rightarrow$lepton+jets, $t\bar{t}$ $\rightarrow$all-jets) or partial ($t\bar{t}$ $\rightarrow$dilepton and single-top quark) reconstruction of the kinematics underlying the top-quark(s) decay, probability density functions (templates) for observables sensitive to the underlying m_t, and to additional parameters, are constructed based on MC simulation. These templates are fitted to functions interpolating between the different input values of m_t, fixing all other parameters of the functions. Finally, an unbinned likelihood fit to the observed data distribution of the observable is used to obtain the value of m_t describing the data best. Typically, for single top and dilepton events the $m(lb)$ variable is used, whereas for the lepton+jets events the m_t^{reco} obtained from a kinematic fit is more appropriate. The ideogram method can be considered as a computational effective approximation of a matrix element method. After a kinematic fit of the decay products to a $t\bar{t}$ hypothesis, MC-based likelihood functions are exploited for each event (ideograms) that depend only on the parameters to be determined from the data. The ideograms reflect the compatibility of the kinematics of the event with a given decay hypothesis. As in the case of the template method, ideograms can be generalised in multiple dimensions depending on the number of input observables used.

The latest ATLAS combination of direct m_t measurements leads to of top quark mass value of $m_t = 172.69 \pm 0.48$ TeV with a total precision of $\sim 0.28\%$ [698]. The latest CMS combination of direct m_t measurements leads to of top quark mass value of $m_t = 172.44 \pm 0.48$ TeV with a total precision of $\sim 0.28\%$ [arXiv:1509.04044]. The precision in each of these analyses is primarily limited by systematic effects, in particular by the modelling of top quark production and decay and by the jet energy scale. Analysis techniques have been developed to use in-situ constraints from the data on a global jet energy scale factor or light jet and b-jet energy scale (3D fits) [698], which still suffer from statistical uncertainties, which will be reduced strongly at the HL-LHC. The total amount of 3000 fb^{-1}of 14 TeV data would clearly decrease the statistical uncertainty in these analyses. Therefore, the statistical precision in each analysis should be traded in various ways for a reduced total systematic uncertainty by cutting into phase space regions where the systematic uncertainties are high.

A variety of alternative methods are exploited to supplement the top quark mass measurements from direct mass reconstruction based on jet observables. One source of alternative observables is the usage of the b-jet information in the $t\bar{t}$ decay, e.g. via final states featuring J/ψ produced in the b-hadron decays or secondary vertices in b-jets. With the alternative approaches, a large variety of other

m_t^{MC} measurements can be done, which have different sensitivities to the top quark production and decay mechanisms and making therefore different contributions to the systematic uncertainties. Compared to the template method with the standard final states, the sensitivity to the light-jet and b-jet energy scale (respectively JES and b-JES) is expected to be reduced. One of the limiting factors of this approach is the small branching fraction, $\mathcal{B}(t\bar{t} \to (W^+b)(W^-b) \to (\ell\nu_\ell J/\psi(\to \mu^+\mu^-)X)(qq'b) \sim 4.1 \times 10^{-4}$, where $\ell = e, \mu$. On the other hand the modelling of b-fragmentation and b-decay are expected to be among the dominating sources of systematic uncertainties of these two analyses and need to be studied extensively in a dedicated study to reduce the signal modelling uncertainties. Both measurements can contribute in different ways to the final combination to improve the precision measurement of m_t. Individual m_t results resting on various techniques and $t\bar{t}$ (or single-top quark) decay channels, have different sensitivities to statistical and systematic effects, and to the details of the MC simulation. To exploit the full physics potential of the available measurements, and to profit from their diversity and complementarity, they are combined, thereby further increasing our knowledge on m_t.

In some alternative techniques the top quark mass is extracted by comparing cross sections or distributions that can be calculated directly in QCD at either NLO or NNLO, to corresponding distributions extracted from data. The mass parameter used in the NLO or NNLO calculation (either the $\overline{\mathrm{MS}}$ or the Pole top mass) is obtained by fitting the theoretical cross-section or distribution to the measured one. In this framework, mass measurements have been performed using as observables the inclusive $t\bar{t}$ cross-section, the differential decay rate in $t\bar{t}$+1 jet events, lepton and dilepton differential cross-sections.

Due to the changes of the detector performance for the HL-LHC, it is difficult to estimate precisely the effects of systematic uncertainties. The sources of uncertainty are assumed to be the same as the current ones. The estimated Run-2 uncertainties are scaled to align with HL-LHC extrapolations developed by the ATLAS and CMS Collaborations and documented in Ref. [699]. The impact of the experimental systematic uncertainties will likely be reduced relative to their effect on the Run-2 analysis given the large datasets available, allowing precise performance studies to be conducted. The jet reconstruction uncertainties on m_t are expected to be divided by a factor up to two, while uncertainties related to the reconstruction of electrons and muons remain the same as in Run-2. The theory modelling uncertainties are expected to be divided by a factor two compared to existing values. The larger HL-LHC dataset will allow for dedicated tuning and good understanding of NLO MC generators matched to parton showers, as already started with Run-2 data [421]. Another large contribution to the uncertainties stems from the modelling of QCD interactions, which can be investigated and constrained using differential measurements of the mass parameter itself or other ancillary measurements in parts of the phase space not yet accessible. These measurements are partially already being performed [700–702], but will benefit from more statistics, therefore strong constraints from the high statistics at the HL-LHC are expected.

For this report, ATLAS Collaboration presents projections for the top quark mass measurement accuracy using $t\bar{t} \to$ lepton+jets events with $J/\psi \to \mu^+\mu^-$ in the final state [697]. Samples of simulated events for signal and background processes are produced at 14 TeV centre-of-mass energy. They include the production of $t\bar{t}$ pairs, single-top quarks and W/Z bosons in association with jets. After the event generation step, a fast simulation of the trigger and detector effects is added with the dedicated ATLAS software framework. The event selection follows the analysis done at 8 TeV [703]. Events are required to have at least one charged isolated lepton with $p_{\mathrm{T}} > 25$ GeV and $|\eta| < 4$ and at least 4 jets with $p_{\mathrm{T}} > 25$ GeV and $|\eta| < 4.5$. No requirement is applied on the number of b-tagged jets. J/ψ candidates are reconstructed using all pairs of opposite charge sign soft muons with $p_{\mathrm{T}} > 4$ GeVand $|\eta| < 4.5$ The top quark mass is obtained from a template method with unbinned likelihood maximisation approach. A statistical uncertainty of 0.14 GeVis expected, with a systematic uncertainty of 0.48 GeV.

This paragraph discusses the potential of selected top quark mass measurements at the HL-LHC done by the CMS Collaboration, as described in detail in Ref [696]. The extrapolations are based on measurements performed at 7 and 8 TeV centre-of-mass energy using 5 fb^{-1}and 19.7 fb^{-1}, respectively.

The numbers presented here do not include the possible ambiguity in the interpretation of the measured value with respect to a well defined renormalisation scheme. However, also the measurement of the pole mass from the inclusive $\mathrm{t\bar{t}}$ cross-section cross section is extrapolated to HL-LHC conditions.

Typically, the jet energy scale uncertainties play a dominant role for top quark mass measurements. The contribution from background processes, important only for the measurement using single top events, is expected to be well under control. For the extrapolation of the extraction of m_t from the total cross-section, the cross-section measurement is assumed to be ultimately limited by the luminosity uncertainty, here assumed to be 1.5%. For the prediction, no predictions beyond NNLO are assumed, such that the uncertainty due to scale variations is constant.

The resulting extrapolated uncertainties on the top quark mass measurements are summarised in Fig. 80. The measurement using J/ψ mesons and using in general secondary vertices benefit the most from higher statistics. But also the other measurements improve significantly, mostly from more precise understanding of systematic uncertainties, as discussed above, such that ultimately, the precision will range between 0.1% (which is of the order of Λ_{QCD}) and 0.7%.

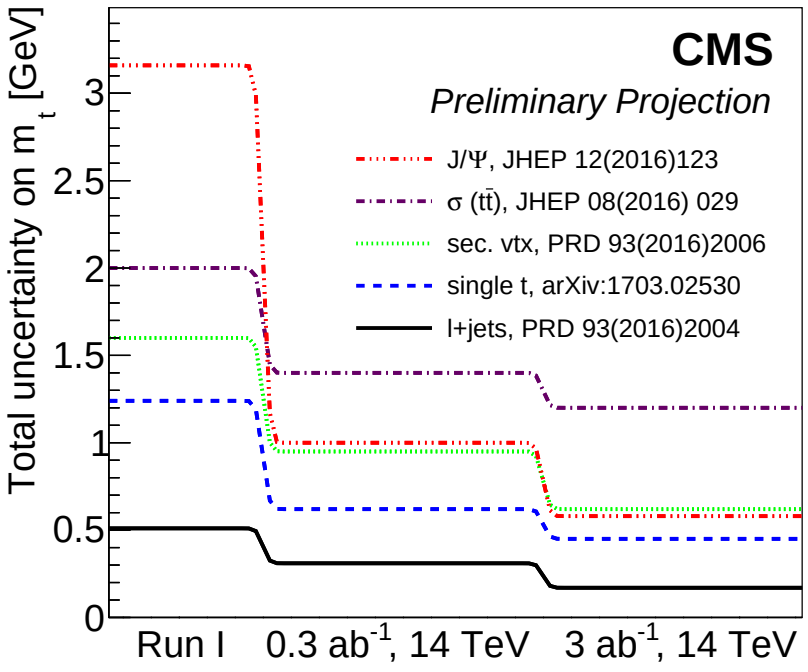

Fig. 80: The top mass measurement uncertainty for different methods as a function of integrated luminosity as obtained by CMS.

6.6 Top quark properties and couplings

6.6.1 Top quark charge asymmetries at LHCb

The top quark charge asymmetry present in quark-initiated production is diluted by the presence of gluon-gluon fusion and the increased quark content in the proton at forward rapidities gives LHCb additional sensitivity to this observable. As LHCb takes data at a lower rate than ATLAS and CMS, and has a limited acceptance, a partial reconstruction of the $t\bar{t}$ final state is anticipated in order to make

Table 47: Projected total uncertainties on the top quark mass for 3 ab^{-1} and $\sqrt{s}$=14 TeV obtained with different methods as obtained by CMS.

Method	Statistical	Systematic	Total (GeV)
$t\bar{t}$ lepton+jets	0.17	0.02	0.17
single-t t-channel	0.45	0.06	0.45
$m_{sv\ell}$	0.62	0.02	0.62
J/ψ	0.24	0.53	0.58
$\sigma_{t\bar{t}}$	0.4% (exp)	0.4% (theory)	1.2

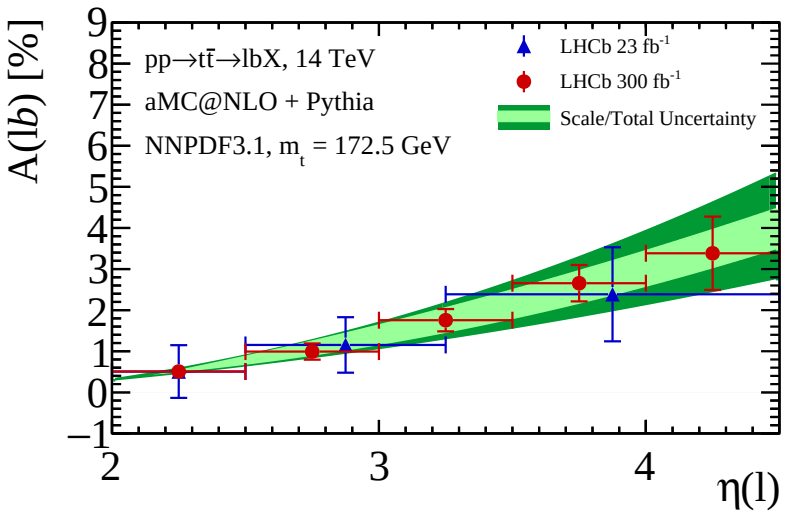

Fig. 81: The predicted SM asymmetry at LHCb as a function of lepton pseudorapidity in the ℓb final state at 14 TeV. The bands show the uncertainty on the theoretical predictions due to scale variations (light green) and due to combined scale, PDF and α_s variations (dark green). The expected statistical precision on measurements performed by LHCb using 23 and 300 fb^{-1} of data is indicated by the error bars on the points.

optimal use of statistics, as described in Sec. 6.1.4. The expected differential single lepton asymmetry at LHCb, inferred from the rate of $\ell^+ b$ and $\ell^- b$ production as a function of lepton pseudorapidity, is shown in Fig. 81 [704]. The expected statistical precision of a dataset corresponding to 300 fb^{-1} of integrated luminosity, the total expected at LHCb during the HL-LHC, is shown, along with the theoretical uncertainties due to scale, α_s and PDF uncertainties. The projection indicates that LHCb will have sufficient statistics to make a non-zero observation of the $t\bar{t}$ charge asymmetry at the HL-LHC. The dominant systematic uncertainty on the measurement is expected to come from the knowledge of the background contributions, particularly from W production in association with b-jets. Other final states, where an additional b-jet or lepton are required to be present will provide additional information as, despite the lower statistical precision, they probe larger values of Bjorken-x and select the data sample with a higher purity.

6.6.2 *A method to determine $|V_{cb}|$ at the weak scale in top quark decays*

In a recent paper [705], a new method was proposed to measure the $|V_{cb}|$ element of the Cabibbo Kobayashi Maskawa (CKM) quark mixing matrix at the scale $q \simeq m_W$, using top decays at the LHC. To date, $|V_{cb}|$ has always been measured in B decays, i.e. at an energy scale $q \simeq \frac{m_b}{2}$, far below the weak scale, and it is currently known to an uncertainty of about 2% [509]:

$$|V_{cb}| = (42.2 \pm 0.8) \times 10^{-3}. \tag{50}$$

In the proposed measurement at the LHC, $|V_{cb}|$ will be measured at the scale $q \simeq m_W$, more representative of the weak scale. The motivation for such a measurement is that the traditional extraction of $|V_{cb}|$ in B decays relies heavily on the operator product expansion, and its sensitivity is significantly affected by theoretical uncertainties [509]. In contrast, in dealing with decays of on-shell Ws, as here, the theoretical situation is likely to be much cleaner and the systematic uncertainties will be very different. Moreover, there could be significant evolution of $|V_{cb}|$ between $q \simeq \frac{m_b}{2}$ and $q \simeq m_W$ due to radiative corrections: e.g. the application (somewhat inappropriately) of the Standard Model (SM) six-quark evolution equations [706] at two-loop order [707] to the CKM matrix between $q \simeq \frac{m_b}{2}$ and $q \simeq m_W$ yields a fractional increase in $|V_{cb}|$ of $\simeq 5\%$, see Fig. 82. While the correct treatment for SM evolution at such

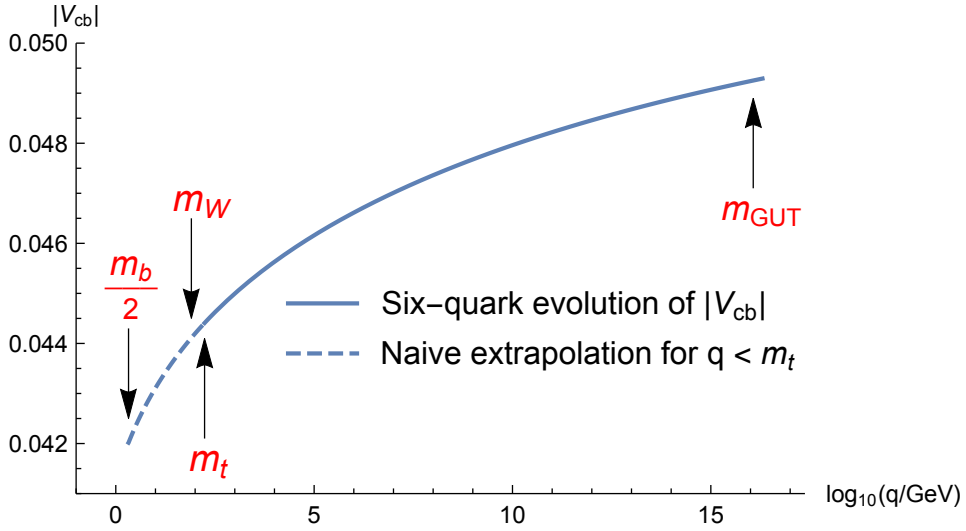

Fig. 82: Renomalisation Group evolution of $|V_{cb}|$ using the six-quark running scheme [706–708] between m_{GUT} and $\frac{m_b}{2}$. Previous publications stop at m_t, while a correct procedure would use a five-quark scheme for $q \lesssim m_t$. This naive procedure at least suggests the possibility of significant low-energy evolution of $|V_{cb}|$.

low energies is rather to use an effective field theory, integrating out the top quark below $q \sim m_t$ [708], such a calculation of the $|V_{cb}|$ running has not yet appeared in the literature. Thus the low-energy evolution of $|V_{cb}|$ is currently completely uncertain, while the naive calculation outlined above at least opens the possibility that its running might be observable, if $|V_{cb}|$ can be measured at or above the weak scale.

The proposed method uses the decays of tagged $t\bar{t}$ pairs with one semileptonic top decay, (the tag), $\bar{t} \to \bar{b}W^- \to \bar{b}\ell^-\bar{\nu}_\ell$, and the other a hadronic decay, $t \to bW \to b\bar{q}c$, where $\bar{q}$ is a charge $\frac{1}{3}$ anti-quark (charge-conjugate decays will be assumed everywhere unless otherwise stated). The fraction of these in which $\bar{q} = \bar{b}$ is (up to negligible phase-space factors), exactly $|V_{cb}|^2$. Using this ratio, otherwise leading experimental uncertainties in most of the tagging efficiencies are cancelled. Thus the required signal will contain three tagged b-jets and a tagged c-jet, in addition to a charged lepton and missing transverse momentum.

Taking as a starting point, efficiencies from existing ATLAS and CMS $t\bar{t}$ cross-section analyses, already-achieved experimental tagging performances [709–714], and reasonable assumptions about backgrounds, it is estimated [705], that the fractional uncertainty on $|V_{cb}|$ which can be obtained at a single experiment using the Run-2 dataset is:

$$\frac{\Delta|V_{cb}|}{|V_{cb}|} \sim 0.07, \tag{51}$$

which is statistics-limited. Averaging the two experiments would give a fractional error of $\sim 5\%$.

Since the values of the systematic uncertainties on the tagging performances used to calculate eq. (51) were based roughly on their present determinations, the result is generalised in Fig. 83, to show

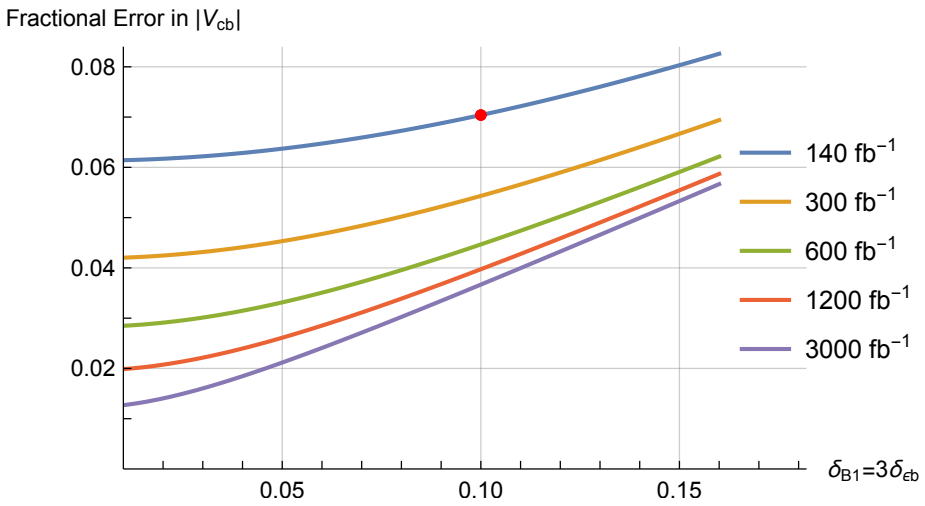

Fig. 83: Estimated fractional error in $|V_{cb}|^2$ as a function of the systematic uncertainties δ_{ϵ_b} in the b-jet tagging efficiency and $\delta_{\mathcal{B}_1}$ in the light-to-b jet flavour mis-tag probability, and integrated luminosity. For ease of presentation, we assume $\delta_{\mathcal{B}_1} \simeq 3\delta_{\epsilon_b}$ as it is at the time of writing. The top curve represents the Run-2 statistics and the red point on it indicates the illustrative values used to obtain eq. (51). The second curve corresponds to luminosity projections for Run-3, while the bottom curve is for the projected integrated luminosity for HL-LHC. We have allowed for a 15% increase in the $t\bar{t}$ cross section in the lower three curves, corresponding to an increase in beam collision energy to 14 TeV.

the dependence of the obtained fractional error on the systematic uncertainties as they vary. Also shown in Fig. 83 are the results using larger datasets, corresponding to various future LHC luminosity scenarios. The systematics-limited regime is represented by the linear-sloping region towards the bottom-right part of the figure, while the statistics-limited regime lies close to the y-axis, where the benefit of more statistics is most marked. The figure shows that making the measurement with future LHC data promises further improvements from both increased statistics and if tagging performance uncertainties can be reduced. E.g. if $\delta_{\mathcal{B}_1} = 3\delta_{\epsilon_b}$ can be reduced to $\simeq 0.05$, then at the end of Run-3, the uncertainty on $|V_{cb}|$ per experiment using this method could be as low as 4.5%, giving a fractional uncertainty on the average of the two $|V_{cb}|$ measurements of $\sim 3\%$. HL-LHC would then deliver a further reduction in the measurement uncertainty of better than a factor of 2. Either of these higher statistics measurements could give sensitivity for the first time to the renormalisation group running of $|V_{cb}|$.

6.7 Flavour changing neutral current

Processes with flavour-changing neutral currents (FCNC) are forbidden at tree level and are strongly suppressed in higher orders by the Glashow-Iliopoulos-Maiani (GIM) mechanism [715]. The SM predicts the branching fractions for top quark FCNC decays of $\mathcal{O}(10^{-12}$–$10^{-16})$ [716–718]. However, various extensions of the SM allow a significant enhancement of the FCNC top quark decay rates arising from possible contributions of new particles [718–720]. Any deviations from heavily suppressed top FCNC rates would be a clear sign of new physics. The FCNC interactions of the top quark with the SM gauge and Higgs bosons can be described through the following anomalous coupling Lagrangian:

$$\begin{aligned}\mathcal{L} = \sum_{q=u,c} [\sqrt{2} g_s \frac{\kappa_{gqt}}{\Lambda} \bar{t}\sigma^{\mu\nu} T_a (f^L_{Gq} P_L + f^R_{Gq} P_R) q G^a_{\mu\nu} + \\ + \frac{g}{\sqrt{2} c_W} \frac{\kappa_{zqt}}{\Lambda} \bar{t}\sigma^{\mu\nu} (f^L_{Zq} P_L + f^R_{Zq} P_R) q Z_{\mu\nu} + \frac{g}{4 c_W} \zeta_{zqt} \bar{t}\gamma^{\mu} (f^L_{Zq} P_L + f^R_{Zq} P_R) q Z_{\mu} - \\ - e \frac{\kappa_{\gamma qt}}{\Lambda} \bar{t}\sigma^{\mu\nu} (f^L_{\gamma q} P_L + f^R_{\gamma q} P_R) q A_{\mu\nu} + \\ + \frac{g}{\sqrt{2}} \bar{t} \kappa_{Hqt} (f^L_{Hq} P_L + f^R_{Hq} P_R) q H] + h.c.,\end{aligned} \tag{52}$$

where P_L and P_R are chiral projection operators in spin space, κ_{Xqt} is the anomalous coupling for tXq vertex ($X = g, Z, \gamma, H$), ζ_{Zqt} is the additional anomalous coupling for tZq vertex, f^L_{Xq} and f^R_{Xq} are the left and right-handed complex chiral parameters with an unitarity constraint of $|f^L_{Xq}|^2 + |f^R_{Xq}|^2 = 1$. Each of the anomalous couplings can be probed in events with the top quark pair production where one of the top quark decays via FCNC interaction, as well as in events with the associated production of the single top quark with a gluon, Z boson, γ, or Higgs boson.

Top-gluon

The gqt FCNC process was studied by CMS [721] in single top quark events. The event signature includes the requirement of one isolated lepton and exactly one b and one non-b jet to be present in the final state with the dominant background arising from the $t\bar{t}$+jets and W+jets production. The signal events are simulated in the SINGLETOP Monte-Carlo (MC) generator [722] based on the COMPHEP v4.5.2 package [723]. The backgrounds processes are estimated with the MG5_AMC@NLO v2.5.2 [393] package, showered and hadronized with PYTHIA v8.230 [149]. The full detector simulation has been performed for the signal and background events. A Bayesian neural network technique is used to separate signal from background events. The shape of the neural networks discriminants are used in the statistical analysis to estimate the expected sensitivity to the contribution from FCNC. Bayesian inference is used to obtain the posterior probabilities based on an Asimov data set of the background-only model. We assume the same systematic scenario as in Ref. [724]. To obtain the individual exclusion limits on $|\kappa_{tug}|/\Lambda$ and $|\kappa_{tcg}|/\Lambda$ we assume the presence of only one corresponding FCNC parameter in the FCNC signal Monte Carlo model. These individual limits can be used to calculate the upper limits on the branching fractions $\mathcal{B}(t \to ug)$ and $\mathcal{B}(t \to cg)$ [725]. The expected exclusion limits at 95% C.L. on the FCNC couplings and the corresponding branching fractions are given in Table 48. In addition the two-dimensional contours that reflect the possible simultaneous presence of both FCNC parameters are shown in Fig. 84. In this case both FCNC couplings are implemented in the FCNC signal Monte Carlo model. The expected limits can be compared with the recent CMS results [726] for the upper limits on the branching fractions of 2.0×10^{-5} and 4.1×10^{-4} for the decays $t \to ug$ and $t \to cg$, respectively.

Table 48: The expected exclusion 1D limits at 95% C.L. on the FCNC couplings and the corresponding branching fractions for an integrated luminosity of 300 fb^{-1} and 3000 fb^{-1}. In addition, a comparison with statistic-only uncertainties is shown.

Integrated luminosity	$\mathcal{B}(t \to ug)$	$\lvert\kappa_{tug}\rvert/\Lambda$	$\mathcal{B}(t \to cg)$	$\lvert\kappa_{tcg}\rvert/\Lambda$
300 fb^{-1}	$9.8 \cdot 10^{-6}$	0.0029 TeV^{-1}	$99 \cdot 10^{-6}$	0.0091 TeV^{-1}
3000 fb^{-1}	$3.8 \cdot 10^{-6}$	0.0018 TeV^{-1}	$32 \cdot 10^{-6}$	0.0052 TeV^{-1}
3000 fb^{-1} Stat. only	$1.0 \cdot 10^{-6}$	0.0009 TeV^{-1}	$4.9 \cdot 10^{-6}$	0.0020 TeV^{-1}

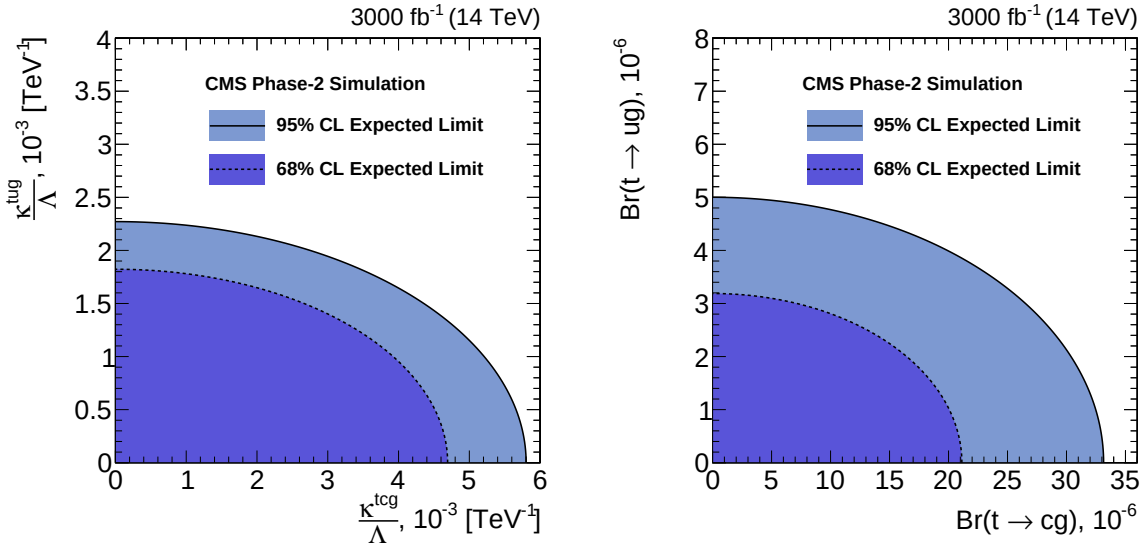

Fig. 84: Two-dimensional expected limits on the FCNC couplings and the corresponding branching fractions at 68% and 95% C.L. for an integrated luminosity of 3000 fb^{-1}.

Top-Z

The ATLAS Collaboration studied the sensitivity to the tqZ interaction, by performing an analysis, detailed in Ref. [727], based on simulated samples and following the strategy detailed in Ref [728] for the analysis of Run-2 data at 13 TeV centre-of-mass energy and the general recommendations for HL-LHC studies for this report. The study is performed in the three charged lepton final state of $t\bar{t}$ events, in which one of the top quarks decays to qZ, $(q = u, c)$ and the other one decays to bW ($t\bar{t} \to bWqZ \to b\ell\nu q\ell\ell$). The kinematics of the events are reconstructed through a χ^2 minimisation and dedicated control regions are used to normalize the main backgrounds and constrain systematic uncertainties. The main uncertainties, in both the background and signal estimations, are expected to come from theoretical normalization uncertainties and uncertainties in the modeling of background processes in the simulation. Different scenarios for the systematic uncertainties are considered, ranging from the conservative estimations obtained with the 13 TeV data analysis, to those that assume a factor two improvement due to expected advances in theoretical predictions. Figure 85 shows the χ^2 distribution for the events reconstructed in the signal region, after the combined fit of signal and control regions under the background-only hypothesis. A binned likelihood function $L(\mu, \theta)$ is used to extract the signal normalisation. An improvement by a factor of five is expected with respect to the current 13 TeV data analysis results. The limits on the branching ratio are at the level of 4 to 5 $\times 10^{-5}$ depending on the considered scenarios assumed for the systematic uncertainties.

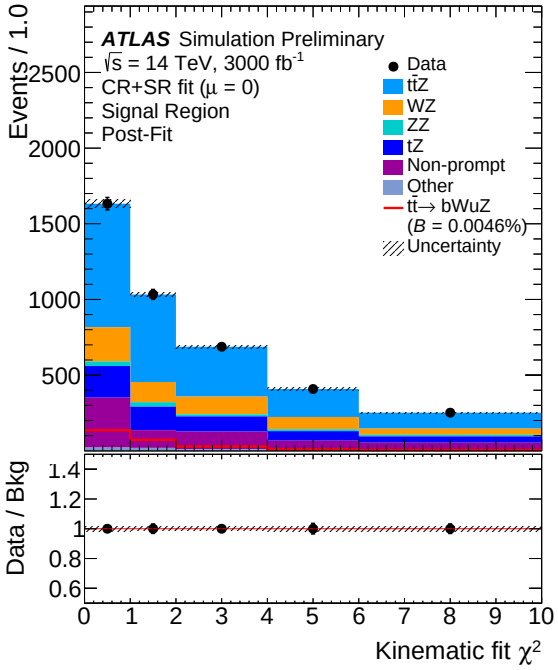

Fig. 85: The distributions for the χ^2 for events reconstructed in the signal region, after the combined fit of signal and control regions under the background-only hypothesis. The data points are from the "Asimov dataset", defined as a total expected pre-fit background. The number of signal events is normalized to the expected branching ratio limit of $B(t \to uZ) = 4.6 \cdot 10^{-5}$. The dashed area represents the systematic uncertainty on the background prediction.

Top-γ

The $t\gamma q$ anomalous interactions have been probed by CMS at 8 TeV in events with single top quarks produced in association with a photon [729] and the resulting exclusion limits are $\mathcal{B}(t \to \gamma u) < 1.3\ (1.9) \times 10^{-4}$ and $\mathcal{B}(t \to \gamma c) < 2.0\ (1.7) \times 10^{-3}$.

In this section, the sensitivity of the upgraded CMS detector to $tq\gamma$ FCNC transitions is estimated for integrated luminosities of 300 and 3000 fb^{-1} using single top quark production via $q \to q\gamma$, with q being a u or a charm quark [724]. This analysis focuses on subsequent SM decays of the top quark in a W boson and bottom quark, with the W boson decays leptonically to a muon or electron and a neutrino. The finale state signature is the presence of a single muon or electron, large missing transverse momentum, a b-jet, and an isolated high energy photon, with a broad η spectrum. The photon properties themselves provide good separation with respect to the dominant background processes from W+jets, and single top or top quark pair production in association with photons. For the discrimination of signal and background events, and to set the limits on the FCNC couplings, the events are split into two categories depending on the pseudo-rapidity of the photon (central region with $|\eta_\gamma| < 1.4$ and forward region with $1.6 < |\eta_\gamma| < 2.8$). In the central (forward) region the photon p_{T} (energy) is used as a discriminating distribution: the low p_{T} (energy) is background dominated, while the high p_{T} (energy) region is populated by signal events. The distributions are shown in Fig. 86.

The limits on the cross section for the single top quark production via $tq\gamma$ are obtained considering systematic uncertainties from variations of the renormalization and factorization scale, b-tagging and jet energy scale corrections and their effects as propagated to missing transverse energy, lepton efficiency

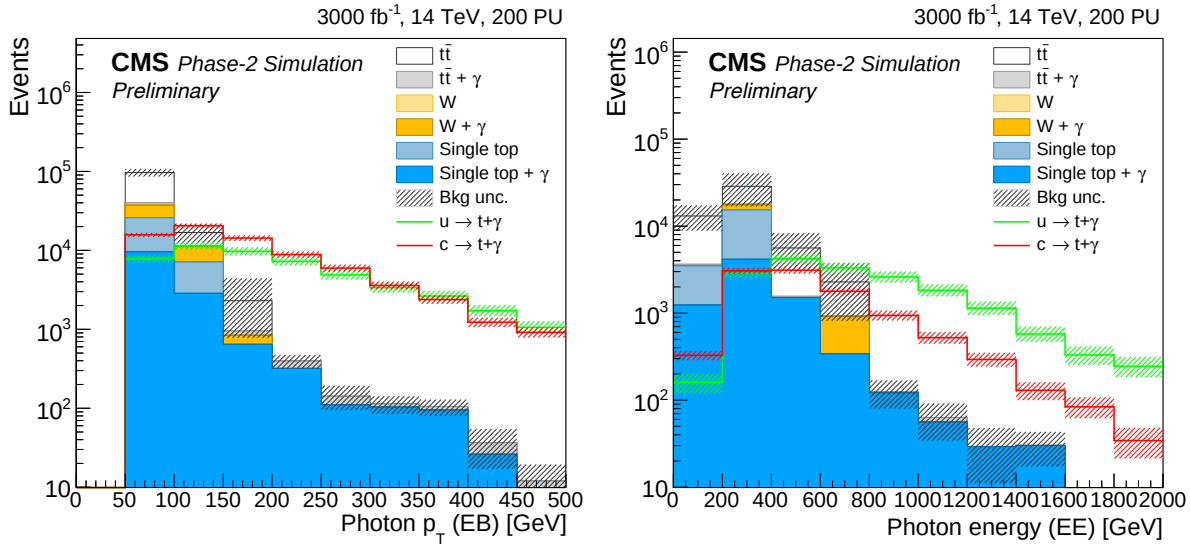

Fig. 86: Transverse momentum of photon candidates for the central η region (left) and energy of photon candidates in the forward region (right).

and luminosity.

These studies yield the following upper limite on the branching ratios at 95%C.L.: $\mathcal{B}(t \to \gamma u) < 8.6 \times 10^{-6}$, $\mathcal{B}(t \to \gamma c) < 7.4 \times 10^{-5}$.

Top-Higgs

The tHq interactions are studied by ATLAS in top quark pair events with $t \to qH, H \to \gamma\gamma$ [730] and $H \to WW$ [731] at 13 TeV. The former analysis explores the final state with two isolated photons. For leptonic top quark decays the selection criteria includes the requirement of one isolated lepton, exactly one b jet, and at least one non-b jet. In case of hadronic top quark decays the analysis selects events with no isolated leptons, at least one b jet, and at least three additional non-b jets. The dominant background processes are associated with the production of non-resonant $\gamma\gamma$+jets, $t\bar{t}$+jets and W+$\gamma\gamma$ events. The resultant limits are $\mathcal{B}(t \to Hu) < 2.4\ (1.7) \times 10^{-3}$ and $\mathcal{B}(t \to Hc) < 2.2\ (1.6) \times 10^{-3}$. The search for FCNC in $H \to WW$ includes the analysis of multilepton final states with either two same-sign or three leptons. The dominant backgrounds arising from the ttW, ttZ and non-prompt lepton production are suppressed with a BDT. The obtained limits are $\mathcal{B}(t \to Hu) < 1.9\ (1.5) \times 10^{-3}$ and $\mathcal{B}(t \to Hc) < 1.6\ (1.5) \times 10^{-3}$. The tHq anomalous couplings are probed by CMS in $H \to b\bar{b}$ channel in top quark pair events, as well as in single top associated production with a Higgs boson, at 13 TeV [732]. The event selection includes the requirement of one isolated lepton, at least two b jets, and at least one additional non-b jet. The dominant $t\bar{t}$ background is suppressed with a BDT discriminant to set the exclusion limits of $\mathcal{B}(t \to Hu) < 4.7\ (3.4) \times 10^{-3}$ and $\mathcal{B}(t \to Hc) < 4.7\ (4.4) \times 10^{-3}$. Preliminary projections suggest $\mathcal{B}(t \to Hq) < \mathcal{O}(10^{-4})$ [733, 734].

Table 49: Summary of the projected reach for the 95% C.L. limits on the branching ratio for anomalous flavor changing top couplings.

$\mathcal{B}$ limit at 95%C.L.	3 ab^{-1}, 14 TeV	15ab^{-1}, 27 TeV	Ref.
$t \to gu$	3.8×10^{-6}	5.6×10^{-7}	[721]
$t \to gc$	32.1×10^{-6}	19.1×10^{-7}	[721]
$t \to Zq$	$2.4 - 5.8 \times 10^{-5}$		[733]
$t \to \gamma u$	8.6×10^{-6}		[724]
$t \to \gamma c$	7.4×10^{-5}		[724]
$t \to Hq$	10^{-4}		[733]

6.8 Effective coupling interpretations for top quark cross sections and properties[49]

Effective Field Theory (SMEFT) [615, 616], where the SM is augmented by a set of higher-dimension operators

$$\mathcal{L}_{\text{SMEFT}} = \mathcal{L}_{\text{SM}} + \sum_i \frac{C_i}{\Lambda^2}\mathcal{O}_i + \mathcal{O}(\Lambda^{-4}). \tag{53}$$

As an example the relevant operators for the tWb vertex are:

$$\mathcal{O}_{tW} = i\left(\bar{Q}\sigma^{\mu\nu}\,\tau_I\,t\right)\tilde{\phi}\,W^I_{\mu\nu} + \text{h.c.} \tag{54}$$

$$\mathcal{O}^{(3)}_{\phi q} = i\left(\phi^\dagger \overleftrightarrow{D}_\mu\,\tau_I\phi\right)\left(\bar{q}_i\,\gamma^\mu\,\tau^I q_i\right) + \text{h.c.} \tag{55}$$

in agreement with the notation of [234].

The operators of eq. (54)-(55) modify the Wtb interaction in the following way

$$\begin{aligned}\mathcal{L}^{\text{dim}-6}_{Wtb} &= -\frac{g}{\sqrt{2}}\bar{b}(x)\gamma^\mu P_L t(x)\,W_\mu(x)\left(1 + \frac{C^{(3)}_{\varphi Q}v^2}{\Lambda^2}\right)\\ &+ \frac{2\,v\,C_{tW}}{\Lambda^2}\bar{b}(x)\sigma^{\mu\nu}P_R t(x)\,\partial_\nu W_\mu(x) + \text{h. c.}\,,\end{aligned} \tag{56}$$

where $v = 246$ GeV is the Higgs doublet vacuum expectation value, and y_t the top quark Yukawa coupling. Here and below it is assumed $V_{tb} = 1$. It must be noted that a slightly different approach [735–739], not using operators but anomalous couplings, has also been used in the literature. It is straightforward to connect the operator coefficients with the anomalous couplings description. The connection between the operator coefficients to the anomalous couplings is discussed in Ref. [651]. The Wtb vertex can be probed in single top production ($t-, Wt, s-$channel top production), W helicity fractions and forward-backward asymmetries.

Similarly the coupling of the top to the Z and photon can be parameterised by the dimension-6 operators as discussed in Ref. [234], where the relevant degrees of freedom are discussed. The relevant degrees of freedom for the top-Z interaction $c^-_{\phi Q}, c^3_{\phi Q}, c_{\phi t}, c^{[I]}_{tZ}$ whilst the photon-top interaction depends on $c^{[I]}_{tA}$ as defined in Ref. [234]. Phenomenological studies of top production in association with a vector boson or a photon exist in the literature [258, 259, 740, 741] including NLO QCD corrections.

This section examines the prospects of probing top charged and neutral couplings at the HL-LHC.

[49] Contributed by L. Lechner, D. Spitzbart, R. Schöfbeck, D. Azevedo,F. Déliot, A. Ferroglia, M. C. N. Fiolhais, E. Gouveia, A. Onofre, E. Vryonidou, and M. Moreno Llacer.

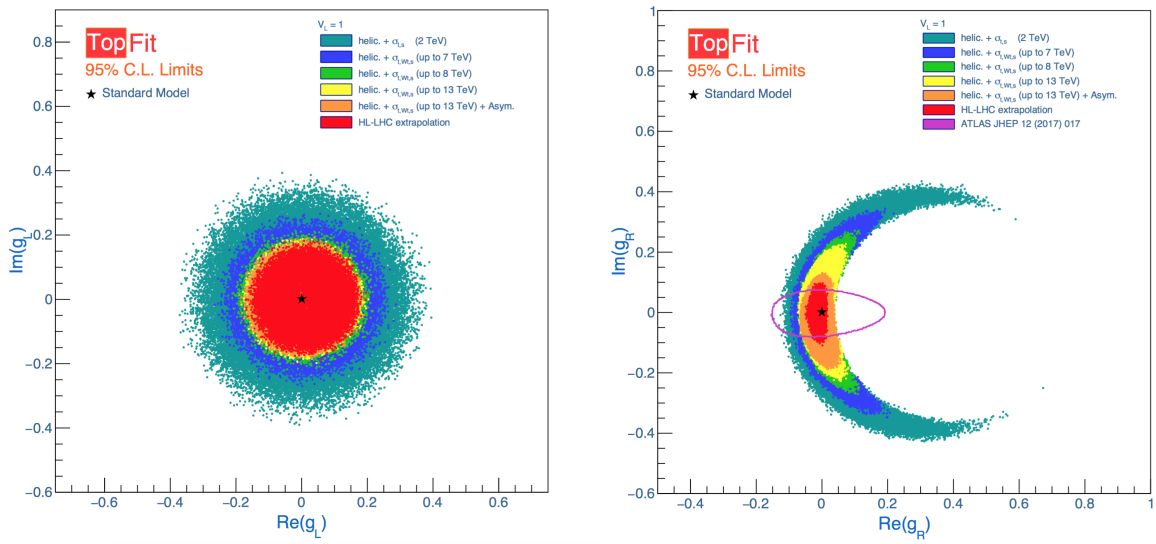

Fig. 87: Limits at 95% CL on the allowed regions for anomalous couplings [752]. The two-dimensional distributions of the Re versus the Im components of g_{L} (left) and g_{R} (right), are shown.

6.8.1 The top quark couplings to the W boson

The latest and most precise measurements on single top quark production cross sections ($t-, Wt-$ and $s-$channels) [614, 742–748], W boson helicity fractions (F_0,F_{L} and F_{R}) [749, 750] and forward-backward asymmetries (A_{FB}^{ℓ},A_{FB}^{N},A_{FB}^{T}) [751], measured at different centre-of-mass energies i.e., 2 TeV at Tevatron and 7, 8 and 13 TeV at the LHC, were used to set stringent 95% CL limits on possible new physics that affect the Wtb vertex structure. The results were extrapolated to the HL-LHC phase of the LHC, by assuming the full expected luminosity (3000 fb^{-1}) and scaling the uncertainties obtained at the LHC for $\sqrt{s} = 13$ TeV (the central value of the observables were assumed to be the Standard Model prediction at 14 TeV). The statistical and simulation related uncertainties were scaled according to the total integrated luminosity at the HL-LHC. All generator and signal modelling related systematic uncertainties of these observables were extrapolated to be half of their current value, in accordance with the recent ATLAS and CMS official recommendations for the High-Luminosity studies. All experimental performance related uncertainties (leptons and jets, efficiencies, energy resolutions, etc.) were considered to maintain the current value at 13 TeV, at the exception of the efficiency of tagging jets from the hadronization of $b-$quarks (b-tagging), which is expected to be reduced by half. These extrapolated measurements were included in the global fit, in combination with the current measurements, in order to estimate expected limits on the real and imaginary components of the top quark couplings. The allowed regions of the new couplings are presented in Figure 87 and Table 50. Figure 87 allows also for a comparison between current LHC results and the HL-LHC projections.

Table 50: Allowed regions for anomalous couplings.

HL-LHC	g_{R}	g_{L}	V_{R}
Allowed Region (Re)	[-0.05 , 0.02]	[-0.17 , 0.19]	[-0.28 , 0.32]
Allowed Region (Im)	[-0.11 , 0.10]	[-0.19 , 0.18]	[-0.30 , 0.30]

6.8.2 *The $t\bar{t}\gamma$ production*

Measurements of $t\bar{t}\gamma$ production at the HL-LHC are studied by ATLAS in terms of the expected precision for the measurements of fiducial and differential cross sections in leptonic final states and the expected limits that can be imposed on the Wilson coefficients of operators relevant to $t\bar{t}\gamma$ production [753]. These operators are the O_{tB}, O_{tG}, and O_{tW} in Ref. [234]. The analysis is performed in the same way as the 13 TeV $t\bar{t}\gamma$ analysis [754], by selecting leptonic decay final states of the $t\bar{t}$ pair with an isolated high-p_{T} photon. Compared to the 13 TeV analysis, data statistical uncertainty is scaled down according to the integrated luminosity at the HL-LHC. Monte Carlo (MC) statistical uncertainty is ignored as it is expected to have enough MC events generated. Theoretical uncertainties are reduced by a factor of two due to the expected improvement in the theoretical tools and background estimation and experimental uncertainties are in general kept the same, with respect to the uncertainties in the 13 TeV analysis. The fiducial cross-section measurement can reach an uncertainty as low as 3% (8%) in the channel with two (one) leptons and requiring a photon candidate with p_{T} larger than 20 (500) GeV. The expected uncertainties of differential cross-section measurements, normalised to unity, for several typical observables like the photon p_{T} and η, are found to be in general below 5%. The expected uncertainty of the absolute differential cross-section as a function of the photon p_{T} is interpreted as 95% CL limits for the relevant EFT operators, as shown in Table 51 for single-lepton and dilepton final states.

Table 51: Expected 95 % CL intervals for the three Wilson coefficients relevant to $t\bar{t}\gamma$ production.

Operator	$\mathcal{O}_{tB}$	$\mathcal{O}_{tG}$	$\mathcal{O}_{tW}$
Single lepton	[-0.5,0.3]	[-0.1,0.1]	[-0.3,0.5]
Dilepton	[-0.6,0.4]	[-0.1,0.1]	[-0.4,0.3]

6.8.3 *The $t\bar{t}Z$ production*

Many beyond the Standard Model (BSM) predictions include anomalous couplings of the top quark to the electroweak gauge bosons [649, 755–760]. While this study is restricted to the $t\bar{t}Z$ channel and the CMS HL-LHC detector with a luminosity scenario of 3 ab^{-1}, it goes beyond earlier work [741] and studies the sensitivity of the $t\bar{t}Z$ process using differential cross section data [761]. The results are interpreted in terms of the SM effective field theory [234] and limits are set on the relevant Wilson coefficients of the Warsaw basis [513] C_{tZ}, $C_{tZ}^{[\mathrm{Im}]}$, $C_{\phi t}$ and $C_{\phi Q}$ [762, 763].

Events are generated at the parton level at LO using MG5_aMC@NLO v2.3.3 [12], and decay them using MadSpin [402, 764]. Parton showering and hadronization are done using Pythia v8.2 [149, 292]. Fast detector simulation was performed using Delphes [273], with the CMS reconstruction efficiency parameterisation for the HL-LHC upgrade. The mean number of interactions per bunch crossing (pileup, PU) is varied from 0 to 200. Jets are reconstructed with the FastJet package [343] and using the anti-k_{T} algorithm [274] with a cone size $R = 0.4$. Besides the signals, the main backgrounds are also generated in the leptonic final states in order to achieve a realistic background prediction. The WZ, tZq, tWZ, $t\bar{t}\gamma$ and $t\bar{t}Z$ processes are normalized to cross sections calculated up to next-to-leading order (NLO) in perturbative QCD.

The results on the inclusive $t\bar{t}Z$ cross section from ATLAS [765, 766] and CMS [767–770] show that the three lepton channel, where the Z and one of the W bosons originating from a top quark decay leptonically is the most sensitive. Thus, it is required to have three reconstructed leptons (e or μ) with $\mathrm{p_T}(l)$ thresholds of 10, 20, and 40 GeV, respectively, and $|\eta(l)| < 3.0$. It is furthermore required that there is among them a pair of opposite-sign same-flavor leptons consistent with the Z boson by requiring $|m(ll) - m_{\mathrm{Z}}| < 10$ GeV. Reconstructed leptons are removed within a cone of $\Delta R < 0.3$

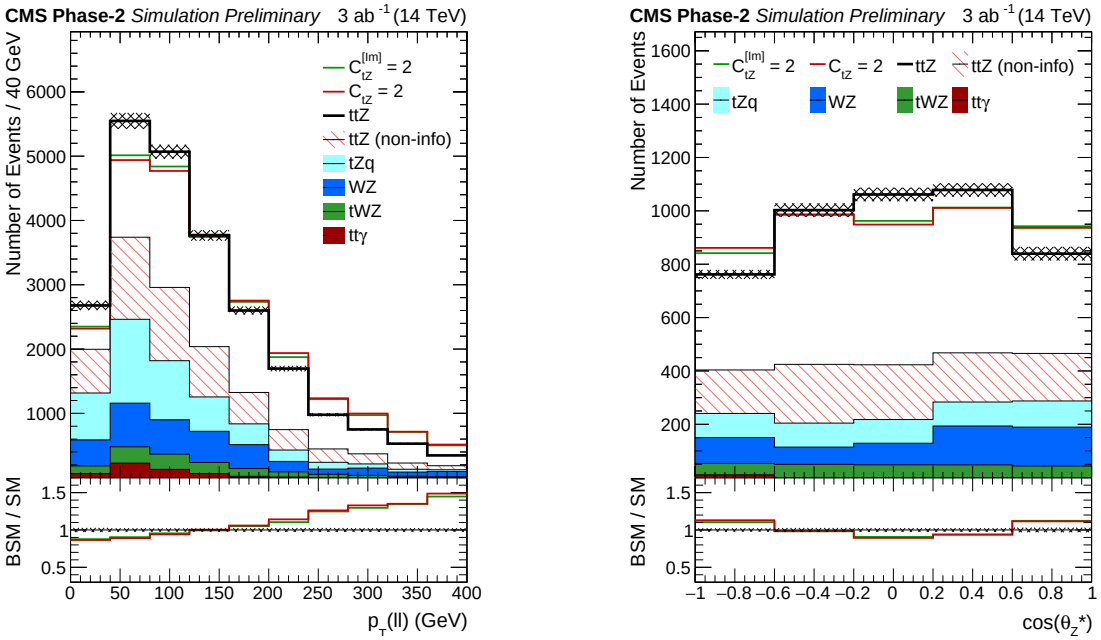

Fig. 88: Differential cross sections of $p_T(Z)$ (left) and $\cos\theta^*_Z$ (right) for the in the text mentioned selection and the HL-LHC scenario. For $\cos\theta^*_Z$, additionally $p_T(Z) > 200$ GeV is applied.

to any reconstructed jet satisfying $p_T(j) > 30$ GeV. Furthermore, at least 3 jets are required with $p_T(j) > 30$ GeV and $|\eta(j)| < 4.0$, where one of the jets has been identified as a b-tag jet according to the DELPHES specification.

The distributions of the above-mentioned observables are considered in equally sized bins of the transverse Z boson momenta $p_T(Z)$ [740] and $\cos\theta^*_Z$, the relative angle of the negatively charged lepton to the Z boson direction of flight in the rest frame of the boson. The differential cross sections for the SM (black) and BSM (colored lines) interpretations in $t\bar{t}Z$ with respect to $p_T(Z)$ and $\cos\theta^*_Z$ are shown in Fig. 88 for $C_{tZ} = 2$ $(\Lambda/\text{TeV})^2$ and $C_{tZ}^{[\text{Im}]} = 2$ $(\Lambda/\text{TeV})^2$. The BSM distributions are normalized to the SM yield in the plots to visualize the discriminating features of the parameters. The part of the signal which does not contain information on the Wilson coefficients is shown hatched, backgrounds are shown in solid colors.

The predicted yields are estimated for the 3 ab^{-1} HL-LHC scenario at $\sqrt{s} = 13$ TeV and scaled to 14 TeV, where an additional small background from non-prompt leptons is taken from Ref. [770] and scaled to 3 ab^{-1}. A profiled maximum likelihood fit of the binned likelihood function $L(\theta)$ is performed and it is considered $q(r) = -2\log(L(\hat{\theta})/L(\hat{\theta}_{\text{SM}}))$, where $\hat{\theta}$ and $\hat{\theta}_{\text{SM}}$ are the set of nuisance parameters maximizing $L(\theta)$ at the BSM and SM point, respectively. Experimental uncertainties are estimated based on the expected performance of the HL-LHC CMS detector. In Table 52, the 68% and 95% CL intervals of the likelihood scan for the $t\bar{t}Z$ process are shown, where one non-zero Wilson coefficient is considered at a time, and all others are set to zero.

Table 53 shows the 68% and 95% CL intervals of the likelihood ratios for two pairs of Wilson coefficients corresponding to modified neutral current interactions ($C_{\phi t}$ and $C_{\phi Q}$) and dipole moment interactions (C_{tZ} and $C_{tZ}^{[\text{Im}]}$). The corresponding second Wilson coefficient is included in the profiling of nuisance parameters.

In Fig. 89, the log-likelihood scan for the $t\bar{t}Z$ process is shown in the $C_{\phi Q}/C_{\phi t}$ parameter plane (left) and the dipole moment parameter plane $C_{tZ}/C_{tZ}^{[\text{Im}]}$ (right). The green (red) lines show the 68% (95%) CL contour line and the SM parameter point corresponds to $C_{\phi t} = C_{\phi Q} = 0$ and $C_{tZ} = C_{tZ}^{[\text{Im}]} = 0$.

Table 52: Expected 68 % and 95 % CL intervals, where one Wilson coefficient at a time is considered non-zero.

Wilson coefficient	68 % CL $(\Lambda/\text{TeV})^2$	95 % CL $(\Lambda/\text{TeV})^2$
$C_{\phi t}$	[-0.47, 0.47]	[-0.89, 0.89]
$C_{\phi Q}$	[-0.38, 0.38]	[-0.75, 0.73]
C_{tZ}	[-0.37, 0.36]	[-0.52, 0.51]
$C_{tZ}^{[\text{Im}]}$	[-0.38, 0.36]	[-0.54, 0.51]

Table 53: Expected 68 % and 95 % CL intervals for the selected Wilson coefficients in a profiled scan over the 2D parameter planes $C_{\phi Q}/C_{\phi t}$ and $C_{tZ}/C_{tZ}^{[\text{Im}]}$. The respective second parameter of the scan is left free.

Wilson coefficient	68 % CL $(\Lambda/\text{TeV})^2$	95 % CL $(\Lambda/\text{TeV})^2$
$C_{\phi t}$	[-1.65, 3.37]	[-2.89, 6.76]
$C_{\phi Q}$	[-1.35, 2.92]	[-2.33, 6.69]
C_{tZ}	[-0.37, 0.36]	[-0.52, 0.51]
$C_{tZ}^{[\text{Im}]}$	[-0.38, 0.36]	[-0.54, 0.51]

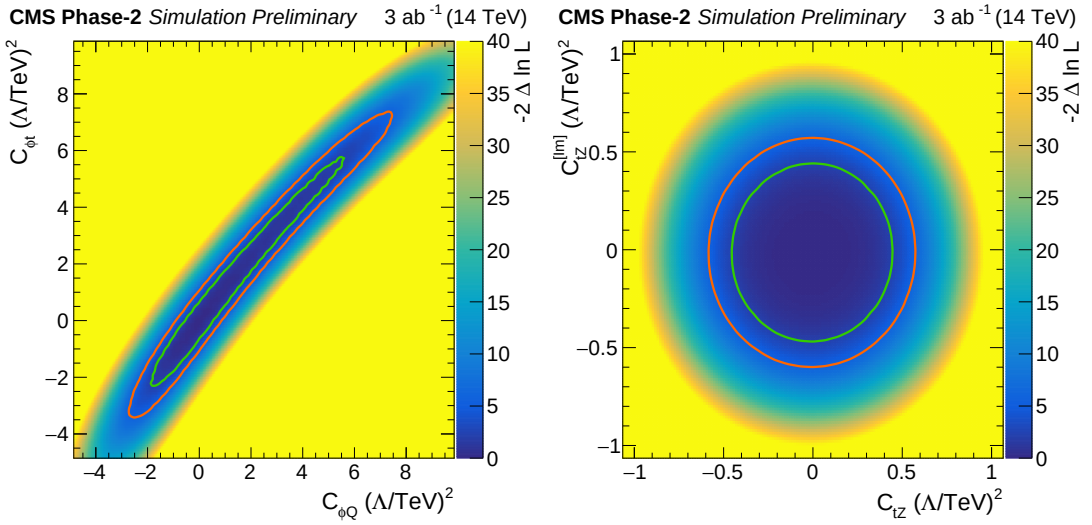

Fig. 89: Scan of the negative likelihood in the $C_{\phi Q}/C_{\phi t}$ (left) and $C_{tZ}/C_{tZ}^{[\text{Im}]}$ parameter planes (right) for the $t\bar{t}Z$ process under the SM hypothesis. The 68% (95%) CL contour lines are given in green (red).

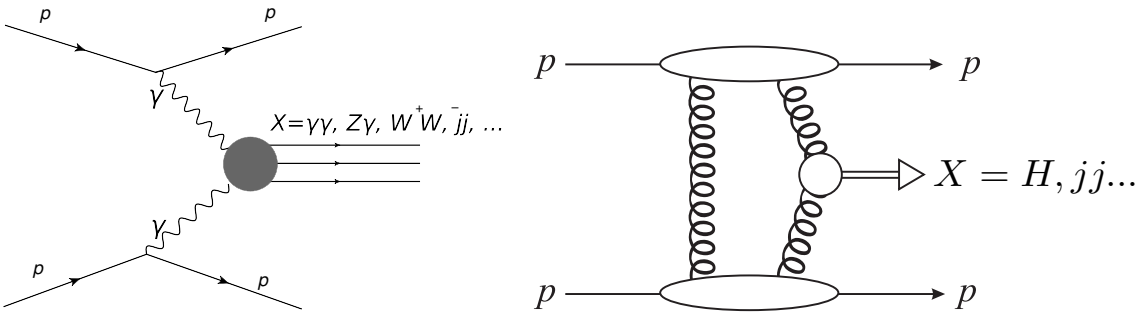

Fig. 90: Schematic diagram of the production of a system X in (left) two–photon (right) QCD–initiated central exclusive production.

7 Forward physics

7.1 Photon-induced collisions at the HL–LHC[50]

Central exclusive production (CEP) corresponds to the production of a central system X, and nothing else, with two outgoing intact protons:

$$pp \to p \; + \; X \; + \; p \; . \tag{57}$$

Such a process may be mediated by photon exchange, with the elastic photon emission vertex leaving the protons intact, see Fig. 90 (left). A range of SM (e.g. $X = \gamma\gamma$, $Z\gamma$, ZZ, $\ell\bar{\ell}$) and BSM states (e.g. $X =$ axion–like particles, monopoles, SUSY particles) may be produced in this way. These have the benefit of:

- The theoretical framework to model the underlying production mechanism, based on the equivalent photon approximation [771], is very well understood. Moreover, due to the peripheral nature of the interaction the possibility for additional inelastic proton–proton interactions (in other words of multiple–particle interactions) is very low.
- As the mass of the central system increases, the relative size of any contribution from QCD–initiated production, see section 7.2, becomes increasingly small [772], due to the strong Sudakov suppression in vetoing on additional QCD radiation.

CEP therefore offers a unique opportunity at the LHC to observe the purely photon–initiated production of electromagnetically charged objects at the LHC in a clean and well understood environment; in this context the LHC is effectively used as a photon–photon collider. The cross sections for such processes can be relatively small, in particular at higher mass, and therefore to select such events it is essential to run during nominal LHC running with tagged protons. The increased statistics available during the HL–LHC stage will allow these studies to push to higher masses and lower cross sections, increasing the discovery potential. A detailed study for the example case of anomalous quartic gauge couplings is discussed below.

7.1.1 Anomalous quartic gauge couplings with proton tagging at the HL–LHC[51]

This section discusses the discovery potential of anomalous quartic gauge interactions at the LHC via the measurement of central exclusive production (see Refs. [773–780]). The central system X is reconstructed in the central detector (CMS, ATLAS) while the outgoing protons, which remain intact due to

[50] Section edited by L. Harland-Lang.
[51] Contribution by C. Baldenegro and C. Royon.

the coherent photon exchange, can be reconstructed with dedicated tracking detectors located in the very forward region at about $\pm$ 210 m (220 m) with respect to the interaction point of the CMS (ATLAS) experiment. The fractional momentum loss of the outgoing protons $\xi = \Delta p/p$ is reconstructed offline. Central exclusive production processes satisfy $m_X = m_X^{\text{fwd}} = \sqrt{\xi_1 \xi_2 s}$ and $y_X = y_X^{\text{fwd}} = \frac{1}{2}\log\left(\frac{\xi_1}{\xi_2}\right)$, where m_X and y_X are the mass and rapidity of the system X reconstructed with the central detector, m_X^{fwd} and y_X^{fwd} are the mass and rapidity of the system X reconstructed with the forward detectors and $\sqrt{s}$ is the proton-proton centre-of-mass energy. This relationship sets a powerful offline selection tool for background suppression, since non-exclusive events are not correlated to the forward protons.

In these projections, it is assumed that a similar set-up as with the CT-PPS and AFP detectors is possible at the HL-LHC. An overview of the physics case for light-by-light scattering is given as the prototype example, and the quartic $\gamma\gamma\gamma Z$ coupling is given as an instance of other gauge couplings that could be studied at the HL-LHC. These projections consider also the impact of the difference of the measured time-of-flight for the intact protons with various timing precisions (on the order of 10 ps), which can be used to determine the longitudinal coordinate of the event vertex down to $\sim$ 2 mm. Time-of-flight measurements can help further reduce the background, especially at the HL-LHC where the number of interactions per bunch crossing will range from 140-200.

Scattering of light-by-light in p-p collisions

Under the assumption that there exists a New Physics energy scale Λ much heavier than the experimentally accessible energy E, new physics manifestations can be described using an effective Lagrangian valid for $\Lambda \gg E$. Among these operators, the pure photon dimension-eight operators $\mathcal{L}_{4\gamma} = \zeta_1^{4\gamma} F_{\mu\nu}F^{\mu\nu}F_{\rho\sigma}F^{\rho\sigma} + \zeta_2^{4\gamma} F_{\mu\nu}F^{\nu\rho}F_{\rho\lambda}F^{\lambda\mu}$ induce the $\gamma\gamma\gamma\gamma$ interaction. This coupling can be probed in $pp \to p(\gamma\gamma \to \gamma\gamma)p$ reactions. This sub-process and the SM light-by-light scattering one are implemented in the Forward Physics Monte Carlo (FPMC) [781] event generator. The Equivalent Photon Approximation is used to calculate the emitted coherent photon flux off the protons.

With proton tagging, one can probe $\gamma\gamma \to \gamma\gamma$ collisions from about 300 GeV to 2 TeV. The mass acceptance on the photon pair is limited mainly by the acceptance of ξ of the proton taggers ($0.015 \leq \xi \leq 0.15$). The background is dominated by non-exclusive diphoton production events overlapped with uncorrelated events with intact protons coming from the secondary collisions occurring in the same bunch crossing. This background can be suppressed by looking at the central and forward systems kinematic correlations (the aforementioned mass and rapidity matching). The irreducible background coming from the SM exclusive diphoton production is negligible at large invariant masses. The background can be further suppressed if the time-of-flight difference of each of the scattered protons is measured. The precision of the event vertex longitudinal position determined with the time-of-flight measurement is given by $\delta z = c\,\delta t/\sqrt{2}$, where c is the speed of light and δt is the timing precision. In these projections, the average pileup of 200 collisions per bunch crossing was considered.

The expected bounds on the anomalous couplings $\zeta_{1,2}^{4\gamma}$ at 95% CL are calculated based on the total expected background rate and can be seen in Fig. 91. The reach on the quartic couplings $\zeta_{1,2}^{4\gamma}$ down

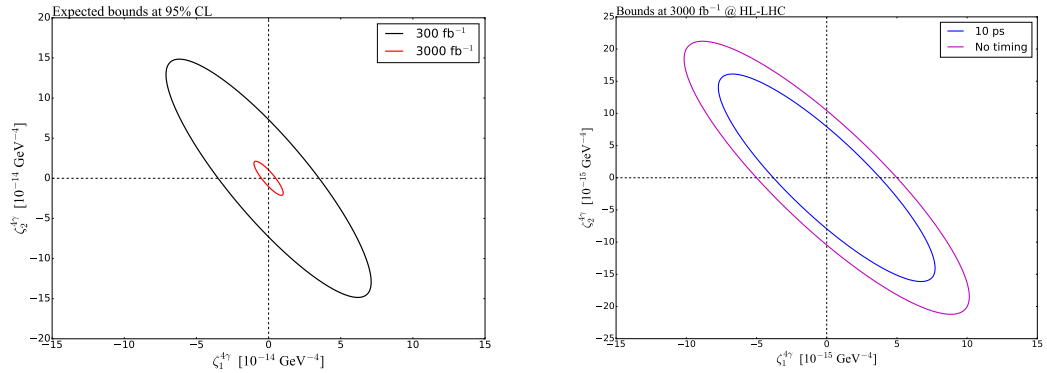

Fig. 91: Expected bounds at 95% CL on the anomalous quartic coupling for 300 fb^{-1} and at the HL-LHC with 3000 fb^{-1} (no time-of-flight measurement) (left). Expected bounds at 95% CL on the anomalous couplings at the HL-LHC with time-of-flight measurement with precision of 10 ps and without time-of-flight measurement (right).

to $5 \cdot 10^{-14}$ GeV^{-4} with 300 fb^{-1} at 14 TeV, and down to $1 \cdot 10^{-14}$ GeV^{-4} at the HL-LHC with a luminosity of 3000 fb^{-1} without using time-of-flight information. The last bound can be improved by a factor of ~ 1.2 if the timing precision is of 10 ps.

Constraining $\gamma\gamma\gamma Z$ coupling via $pp \to p(\gamma\gamma \to \gamma Z)p$

The $\gamma\gamma\gamma Z$ interaction is induced at one-loop level in the SM via loops of fermions and $W^{\pm}$ bosons. Loops of heavy particles charged under SU(2)$_L \times$ U(1)$_Y$ contribute to the $\gamma\gamma\gamma Z$ couplings. The dimension-eight effective operators are $\mathcal{L}_{\gamma\gamma\gamma Z} = \zeta_1^{3\gamma Z} F^{\mu\nu} F_{\mu\nu} F^{\rho\sigma} Z_{\rho\sigma} + \zeta_2^{3\gamma Z} F^{\mu\nu} \tilde{F}_{\mu\nu} F^{\rho\sigma} \tilde{Z}_{\rho\sigma}$, which induce the $\gamma\gamma\gamma Z$ interaction. This induces the anomalous $\gamma\gamma \to \gamma Z$ scattering and generates the rare SM decay $Z \to \gamma\gamma\gamma$. This coupling can be probed in $pp \to p(\gamma\gamma \to \gamma Z)p$ reactions. The sub-process was implemented in the FPMC event generator as well.

Since the exclusive channel is very clean, it allows the possibility of studying exclusive $Z\gamma$ production with the Z boson decaying into a charged lepton pair or to hadrons (dijet or large radius jet signature). The signature $(Z \to \ell\bar{\ell}) + \gamma$ is much cleaner, but has vastly fewer events than $(Z \to \text{hadrons}) + \gamma$ final states. A similar event selection is applied on the exclusive $Z\gamma$ production as in the exclusive $\gamma\gamma$ case. The sensitivity on the anomalous coupling at 95% CL combining both channels at 14 TeV with 300 fb^{-1} of data is on the order of $1 \cdot 10^{-13}$ GeV $^{-4}$ (see Fig. 92). For the HL-LHC with 3000 fb^{-1} it scales down to $1 \cdot 10^{-14}$ GeV^{-4} when combining both channels. The time-of-flight measurement can improve the expected bounds by a factor of ~ 2 .

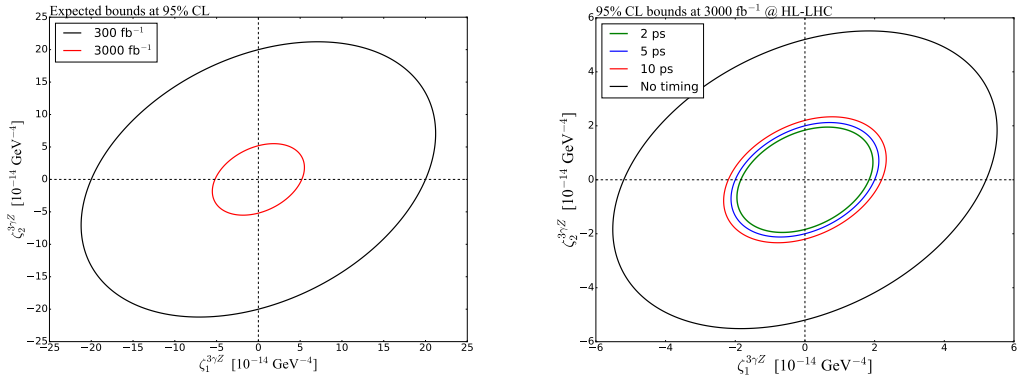

Fig. 92: Expected bounds on the anomalous couplings at 95% CL with 300 fb^{-1} and 3000 fb^{-1} at the HL-LHC (no time-of-flight measurement) (left). Expected bounds at 95%CL for timing precisions of $\delta t = 2,\ 5,\ 10$ ps at the HL-LHC (right).

7.2 Central exclusive production: QCD prospects[52]

The CEP process may be mediated purely by the strong interaction, and in such a case if the mass of the central system is large enough a perturbative approach may be applied, via the diagram shown in Fig. 90 (right), see [782, 783] for reviews. As well as probing QCD in a novel regime, the exclusive nature of this process has the benefit that the produced object obeys a quantum number selection rule. Namely the object must be C even, while the production of P even states with $J_z = 0$ angular momentum projection on the beam axis is strongly dominant. From the point of view of the production of new BSM states or the understanding of existing QCD bound states (e.g. exotic quarkonia) this therefore has the benefit of identifying the produced object quantum numbers. The $J_z = 0$ selection implies that only certain helicity configurations in the underlying $gg \to X$ production process contribute, which also leads to unique phenomenological consequences. A detailed discussion of this selection rule can be found in [783] and the references therein. Two example processes, namely exclusive jet and Higgs boson production, are discussed briefly below. These represent higher mass test cases relevant to HL–LHC running with tagged protons at ATLAS or CMS. The possibilities for the observation of lower mass objects with the ALICE detector will be addressed in section 7.4.

The exclusive production of jets provides a new and unexplored area of QCD phenomenology. This process has been first observed at the Tevatron [784, 785]. The quantum number selection rule discussed above has a number of consequences that are quite distinct from the standard inclusive channels. In particular, the production of purely gluonic dijets is predicted to be strongly dominant, allowing a study of purely gg jets from a colour–singlet initial state. In the three–jet case the presence of 'radiation zeros' [786], that is a complete vanishing in the leading order amplitudes for certain kinematic configurations, is expected. This phenomena is well known in electroweak processes, but this is the only known example of a purely QCD process where this occurs. Some representative predictions for the HL–LHC are shown in Table 54. These are calculated using the SUPERCHIC 2.5 MC generator [787], which provides the most up to date predictions for CEP processes. The cross sections are suppressed

[52] Contribution by L. Harland-Lang.

Table 54: Parton–level predictions for exclusive two and three jet production cross sections (in pb) at the LHC for different cuts on the minimum central system invariant mass M_X at $\sqrt{s} = 14$ TeV. The jets are required to have transverse momentum $p_{\rm T} > 20$ GeV for $M_X(\min) = 75, 150$ GeV and $p_{\rm T} > 40$ GeV for $M_X(\min) = 250$ GeV and pseudorapidity $|\eta| < 2.5$. The anti-$k_{\rm T}$ algorithm with jet radius $R = 0.6$ is used in the three jet case and the $q\bar{q}$ cross sections correspond to one massless quark flavour.

$M_X(\min)$	gg	$q\bar{q}$	$b\bar{b}$	ggg	$gq\bar{q}$
75	130	0.032	0.082	5.0	0.11
150	4.5	6.1×10^{-4}	1.1×10^{-3}	0.70	0.019
250	0.15	2.2×10^{-5}	2.7×10^{-5}	0.016	4.3×10^{-4}

relative to the inclusive case, but are nonetheless relatively large. On the other hand, in the three jet case, in particular in the invariant mass region that may be relevant for the acceptance of proton tagging detectors, the cross sections are lower and would clearly benefit from as large a data sample as possible for studies of novel features, such as radiation zeros and other jet shape variables.

The production of the Higgs boson through exclusive gg fusion would represent a completely new observation channel. As discussed in more detail in [783], this has the potential to shed light on the CP properties of the state, as well as its coupling to b quarks in a distinct way to inclusive channels. The cross section for a SM Higgs, as predicted by SUPERCHIC 2.5 [787], is $\sigma(|y_H| < 2.5) = (1 \overset{\times}{\div} 2)$ fb, where the dominant uncertainties are due to PDFs and modelling of the soft gap survival probability. The predicted rate is therefore relatively small, and would again benefit both from the increased statistics available in HL running, and even more crucially from the potential installation of new tagging detectors at a larger distance from the ATLAS or CMS interaction points (IPs), see section 7.3, which would extend the existing mass acceptance into the Higgs region.

7.3 Tagged proton at the HL–LHC: experimental prospects

This section discusses possible locations for movable near-beam detectors along the outgoing beam lines near IP5, designed for detecting the leading protons from central production processes (Fig. 90, eq. (57)). While the results which follow consider the possibilities for detectors in association with the CMS experiment, similar qualitative prospects are expected in the case of the ATLAS detector, although this is not discussed explicitly here. After identifying the best-suited positions, the proton detection acceptance and hence the central-mass tagging reach is calculated for each of these positions as a function of beam parameters and based on present-day assumptions on optics, collimation scheme and near-beam-detector insertion rules from machine protection arguments. Given that at the time of this report the crossing-angle plane in IP5 (horizontal as until LS3, or vertical) has not yet been decided, both options have been investigated. It has to be pointed out that the crossing planes of IP1 and IP5 have to be different: one will be horizontal, the other vertical.

While in the CT-PPS (later PPS) project [788] in Run-2 the near-beam detectors were Roman Pots inherited from the TOTEM experiment [789, 790] and upgraded for high-luminosity operation [791], no technological assumptions are made at this early stage of preparation for HL-LHC. The highly demanding engineering and detector physics challenges are not addressed here.

Possible Locations for Near-Beam Detectors

The search for suitable detector locations around IP5 is driven by the goal to cover the widest possible range of central masses M to be measured via the fractional momentum losses

$$\xi_{1/2} = \frac{\Delta p_{1/2}}{p} \tag{58}$$

of the two surviving protons using the relation

$$M^2 = \xi_1 \, \xi_2 \, s \, , \tag{59}$$

where $\sqrt{s} = 14\,\text{TeV}$ is the centre-of-mass energy.

The minimum accessible ξ of leading protons at a location z [53] along the beam line is given by

$$\xi_{\text{min}}(\alpha, \beta^*, z) = \frac{[n_{\text{TCT}}(\beta^*) + \Delta n]\sigma_{\text{XRP}}(\beta^*, z) + \Delta d + \delta}{D_{x,\text{XRP}}(\alpha, \xi_{\text{min}}, z)} \, , \tag{60}$$

where σ_x is the horizontal beam width depending on the optics (characterised by β^*), D_x is the horizontal dispersion depending on the crossing-angle α, n_{TCT} is the half-gap of the tertiary collimators (TCT) as defined by the collimation scheme, $\Delta n = 3$ is the retraction of the near-beam detector housings (e.g. Roman Pots) relative to the TCT position in terms of σ_x, $\Delta d = 0.3\,\text{mm}$ is an additional safety retraction to allow for beam orbit fluctuations, and the constant δ, typically 0.5 mm, accounts for any distance between the outer housing surface closest to the beam and the sensitive detector. The dependence of the dispersion on ξ implies that eq. (60) has to be resolved for ξ_{min} after parameterising $D_x(\xi)$.

The first step of the study is to plot the z-dependent quantities, σ_x and D_x, along the outgoing beam line for one typical HL-LHC optics configuration (Fig. 93, left). The resulting ξ_{min} is shown in Fig. 93 (right). Note that for vertical crossing smaller values are reached. The locations most suitable for the measurement of small $|\xi|$ values are marked in red. Closer layout inspection of the region around the minimum at 232 m (inside the quadrupole Q6) indicated two promising locations: at 220 m (just before the collimator TCL6) and at 234 m (after the exit of Q6). Even smaller momentum losses can be reached at 420 m (the "missing magnet" region already studied previously by the FP420 project [792]).

The apparent sign change of ξ_{min} at $z \approx 270\,\text{m}$ reflects the sign change of the dispersion at that location (as seen in the left panel of the figure). It means that the diffractive proton trajectories transition from $x > 0$ to $x < 0$. The implication for the potential detector location at 420 m is that detectors need to be placed in the confined space between the incoming and the outgoing beam pipes, excluding conventional Roman Pot technology. A further complication is that in this location the beam pipes are in a cryostat, necessitating more involved engineering changes.

A region of interest for the detection of higher masses lies at 196 m just upstream of the collimator TCL5 that intercepts protons with large $|\xi|$ (section 7.3). Locations even further upstream, before TCLX4, would give an even higher upper mass cut but are excluded due to the prohibitively high low-mass limit leaving no acceptance interval.

In summary, for the more detailed discussions in the following sections, four detector locations have been retained: 196 m, 220 m, 234 m, 420 m.

[53] In this article the variable z is used for the longitudinal coordinate instead of s to avoid confusion with the Mandelstam s.

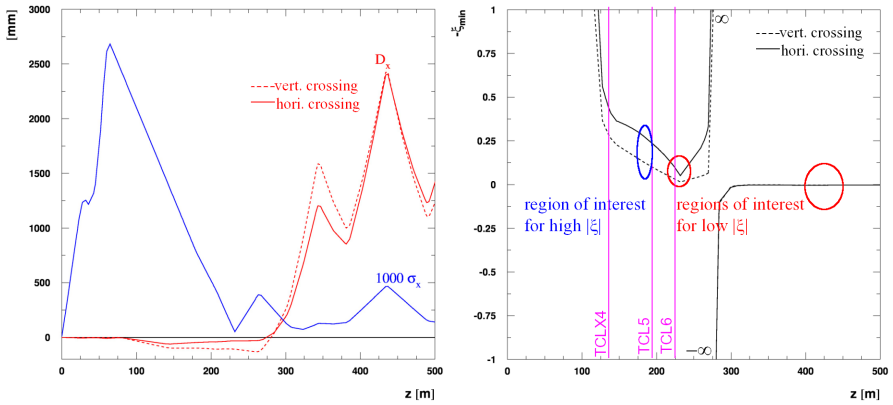

Fig. 93: Horizontal dispersion and beam width (scaled by 1000) as a function of the distance s from IP5 for Beam 1, i.e. in LHC Sector 5-6 (left). Minimum accepted ξ as a function of z according to eq. (60) for $(\alpha/2, \beta^*) = (250\,\mu\text{rad}, 15\,\text{cm})$ and $n_{\text{TCT}} = 12.9$ (right). The TCL collimator positions are indicated. In both pictures the continuous and dashed lines represent horizontal and vertical crossing in IP5, respectively.

Crossing-Angle and Optics Dependence of the Mass Acceptance Limits

In the previous section, only one specific combination of crossing-angle α and beam optics (β^*) was considered. However, at HL-LHC luminosity levelling will be performed in all fills by changing α and β^* in a pre-defined sequence. For the present study the $(\alpha/2, \beta^*)$ trajectories envisaged in [793] were used.

Minimum Mass

The minimum mass accepted at a location z for given α and β^* can be calculated using eq. (59) and (60). For simplicity, symmetric optics in the two beams, i.e. equal ξ_{min}, are assumed:

$$M_{\text{min}} = |\xi_{\text{min}}|\,\sqrt{s}\,. \tag{61}$$

The α and ξ dependencies of D_x can be parameterised based on simulations with MAD-X [794]. The α dependence is linear, and the ξ-dependence can be linearly approximated within the ξ-ranges relevant in practice.

The β^* dependence of σ_{XRP} was calculated analytically, profiting from invariance properties of the presently planned family of ATS optics. This is likely to change in the future and will need to be adapted.

The β^* dependence of n_{TCT} follows the presently foreseen collimation strategy [795] of keeping the TCT gap constant at $d_{\text{TCT}} = 12.9\,\sigma_{\text{TCT}}(\beta^* = 15\,\text{cm})$ (for nominal emittance $\varepsilon_n = 2.5\,\mu\text{m rad}$), implying $n_{\text{TCT}}(\beta^*) = \frac{d_{\text{TCT}}}{\sigma_{\text{TCT}}(\beta^*)}$, where an analytical expression for $\sigma_{\text{TCT}}(\beta^*)$ can be derived.

The result of this calculation, contour lines of M_{min} in the beam parameter space $(\alpha/2, \beta^*)$, is shown in Fig. 94 for the four detector locations chosen in the previous section. Some possible luminosity-levelling trajectories are drawn, too. The start point at the beginning of the fill is always at the maximum β^* value.

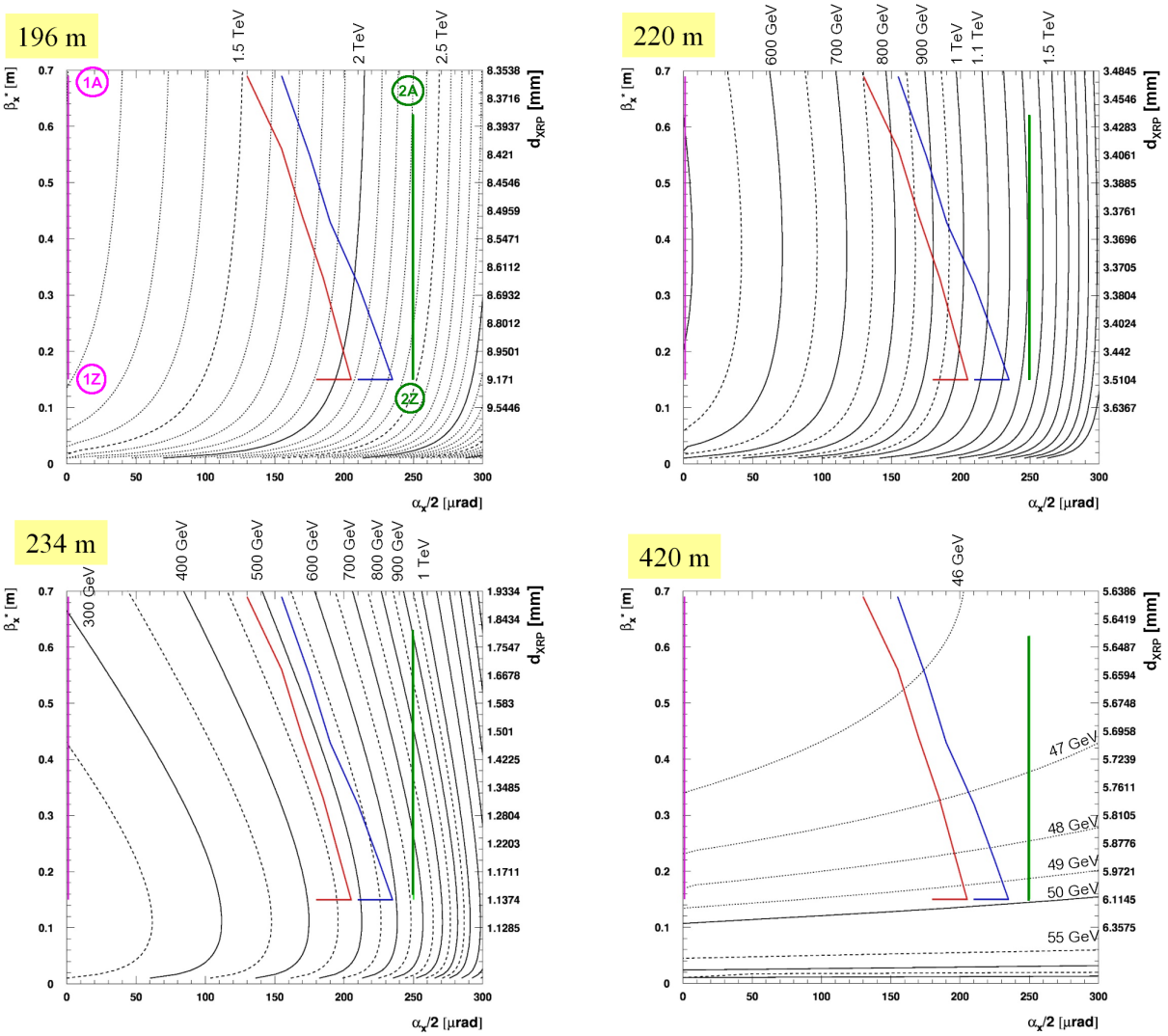

Fig. 94: Contour lines for the minimum accepted mass $M_{\text{min}} = |\xi|_{\text{min}}\sqrt{s}$ in the crossing-angle/optics parameter space $(\alpha/2, \beta^*)$. On the right-hand ordinate the XRP approach distance is calculated from β^*. The coloured lines represent possible luminosity-levelling trajectories [793]. For horizontal crossing: green corresponds to "baseline", blue to "relaxed adaptive", red to "aggressive adaptive"; for vertical crossing: violet corresponds to any trajectory. The labels (1A) – (2Z) in the first panel define the trajectory start and end points used in Figs. 96 and 97.

From these graphs the following conclusions are drawn:

- The main driving factor for the minimum mass is the dispersion which in turn is fully determined by the crossing-angle. The optics (via β^*) plays a minor role.
- If the 420 m location can be instrumented, the minimum mass is about 50 GeV with only a very weak dependence on the optics, the crossing-angle and its plane (horizontal or vertical).
- Without the 420 m location, the vertical crossing gives a much better low-mass acceptance (210 GeV)

than the horizontal crossing (660 GeV).

Maximum Mass

The maximum mass accepted at a location z is determined by the tightest aperture restriction d_A upstream of z and the dispersion there:

$$M_{\max} = |\xi_{\max}|\sqrt{s} = \frac{d_A}{D_A(\alpha, \xi_{\max})} \,. \tag{62}$$

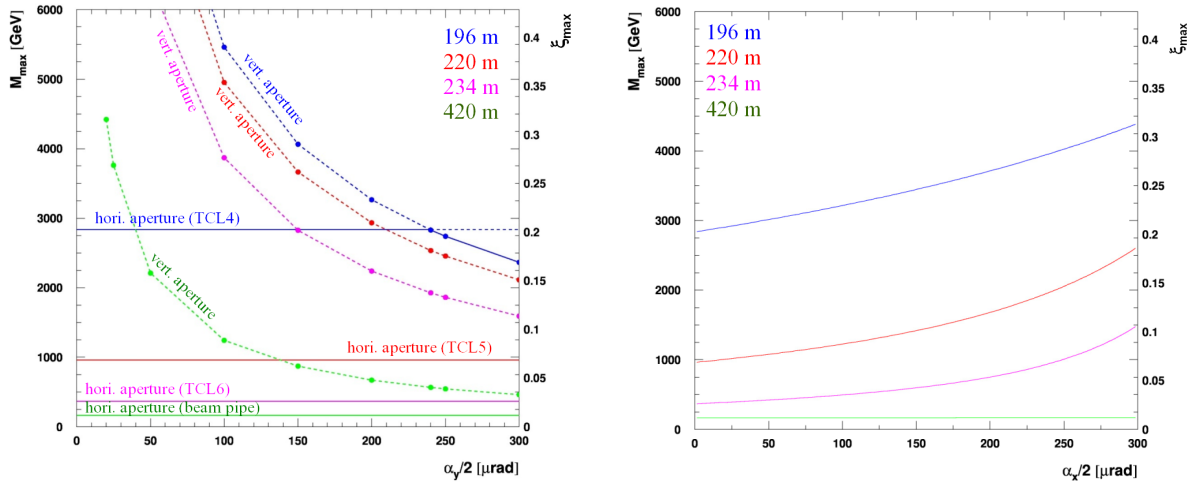

Fig. 95: Maximum accepted diffractive mass for each detector location as a function of the crossing-angle. Vertical crossing (left): both horizontal and vertical apertures contribute to the mass limits. The continuous lines denote the most restrictive, i.e. dominant, limitations. Horizontal crossing (right): only the horizontal apertures contribute.

In the case of the vertical beam crossing in IP5, both the horizontal and vertical apertures may impose limitations, whereas in the case of the horizontal crossing there is no substantial vertical dispersion and hence no acceptance loss from the vertical aperture. Figure 95 shows the results of a complete aperture study. It was concluded that even for vertical crossing most limitations come from the horizontal aperture and that for all locations, except 420 m, this horizontal aperture is limited by the TCL collimators. At 420 m, on the other hand, the beam-pipe absorbs diffractive protons with $|\xi| > 0.012$. The highest masses are accepted by the unit at 196 m: up to 2.7 TeV for vertical crossing and up to 4 TeV for horizontal crossing.

Mass-Rapidity Acceptance

The CEP acceptance for a given point in the beam parameter space (α, β^*) can be visualised by drawing for every instrumented detector location the $|\xi|$-acceptance bands – whose limits are calculated according to the previous section – in the mass-rapidity plane

$$\left(\ln\frac{M}{\sqrt{s}}, y\right) = \left(\frac{1}{2}(\ln\xi_1 + \ln\xi_2), \frac{1}{2}(\ln\xi_1 - \ln\xi_2)\right) \,. \tag{63}$$

Figure 96 shows these (M, y) contour plots for the start and end points of the two extreme levelling cases defined in Fig. 94: points (1A) and (1Z) for any trajectory with vertical crossing in IP5, points (2A) and (2Z) for the "Baseline" trajectory with horizontal crossing. The projections on the mass axis, under the approximation of flat rapidity distributions, are given in Fig. 97.

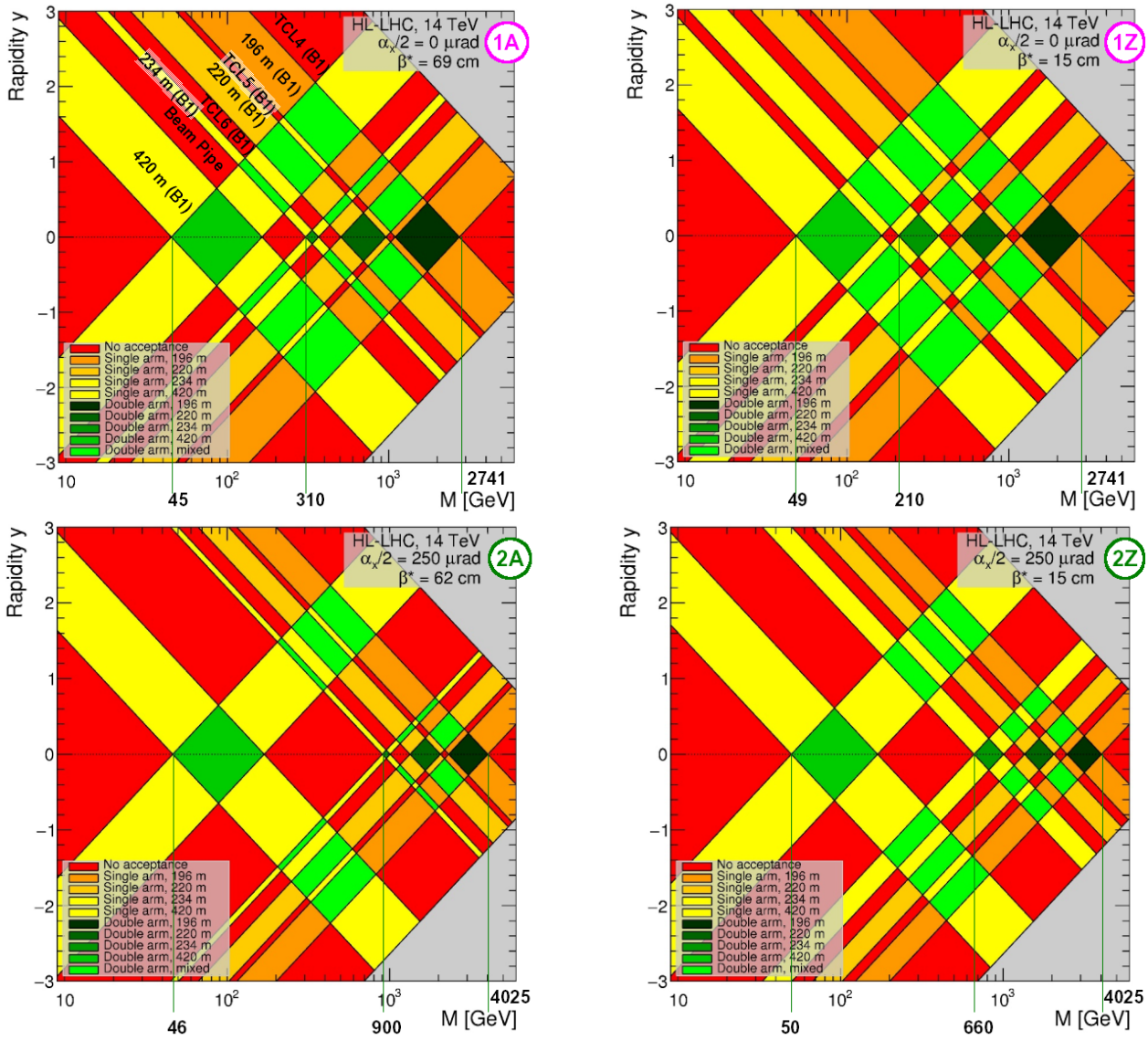

Fig. 96: Acceptance for the protons from central diffraction in the mass-rapidity plane. The yellow/orange colour tones mark single-arm proton acceptance, the green tones mark double-arm acceptance. Top: start and end point of any levelling trajectory for vertical crossing, bottom: start and end point of the baseline levelling trajectory for horizontal crossing.

The following observations are made:

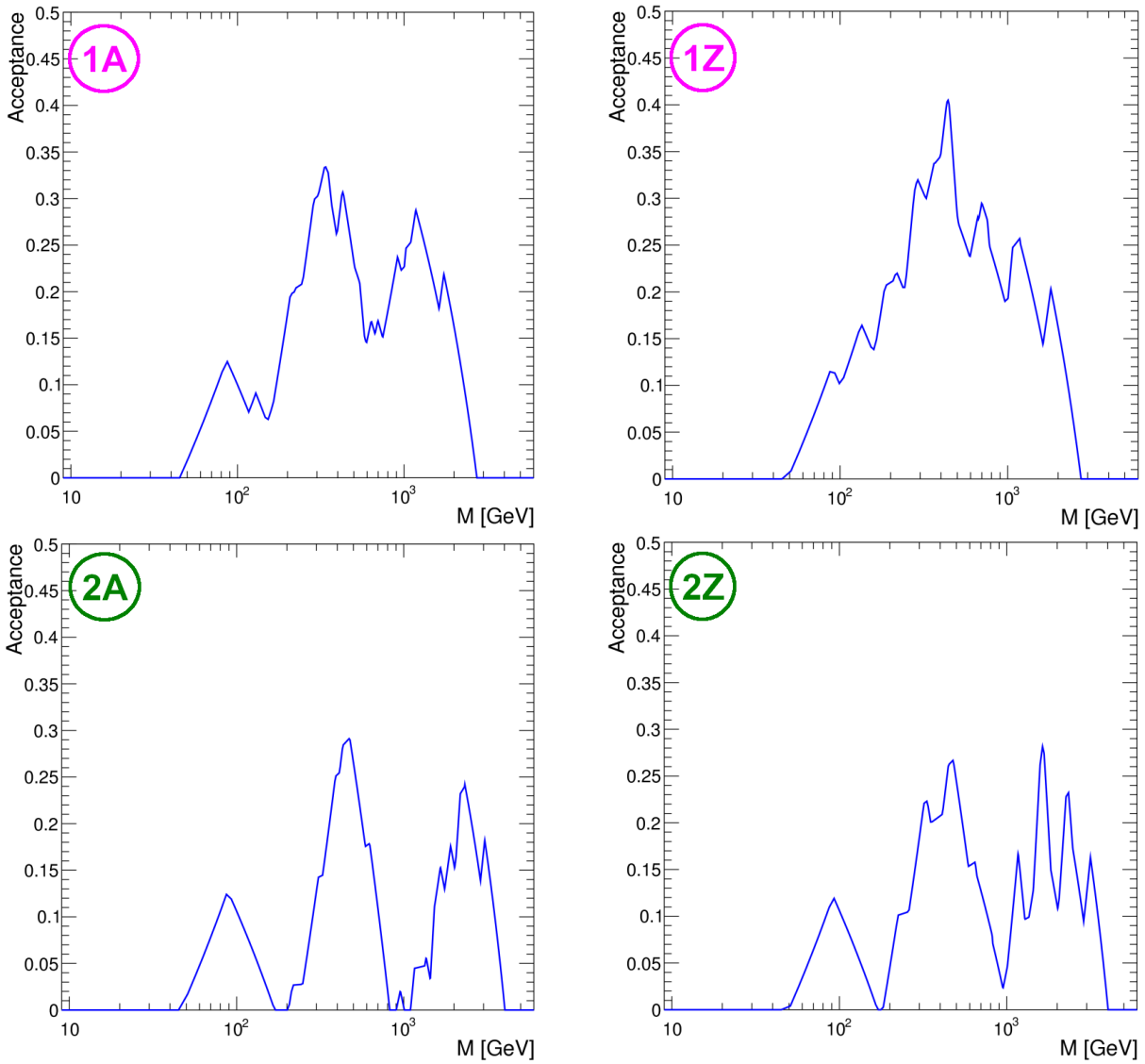

Fig. 97: Projection of the (M, y) acceptance on the mass axis, adding up all the double-arm areas of Fig. 96 for the same points in the (α, β^*) beam parameter space.

– The acceptance zones of the four detector locations are non-overlapping and separated by gaps. For horizontal crossing the gaps are wider than for vertical crossing.
– Although the double-arm acceptance has mass gaps at central rapidities, the mixed acceptance zones combining different detector units in the two arms of the experiment (e.g. 420 m left + 234 m right) fill some of these mass gaps by providing acceptance at forward rapidities.
– The gaps between the acceptances of 196 m, 220 m and 234 m can potentially be closed by opening TCL5 and TCL6 a little further if allowable from machine protection arguments. On the other

hand, the gap between 234 m and 420 m is caused by the beam pipe at $z > 300$ m limiting the aperture. It could only be closed by adding a detector unit near 300 m.

7.4 Low-mass central exclusive production

Central exclusive production of low-mass diffractive states in pp collisions at the LHC may serve as a valuable source of information on the non-perturbative aspects of strong interaction. At low masses, CEP is usually described in terms of a double pomeron exchange (DPE) mechanism. DPE is expected to be an ideal process for the investigation of meson resonances with $I^G(J^{PC}) = 0^+(0^{++}, 2^{++}, \ldots)$ quantum numbers and gluonic bound states. Glueball searches in CEP are of particular interest because lattice QCD calculations predict the lightest glueballs to have masses $M_G(0^{++}) = 1710$ MeV and $M_G(2^{++}) = 2390$ MeV [796]. Pure glueballs are predicted to decay equally well into pair of pions, kaons or η mesons with suppressed two photon decays. However this simple signature is spoiled by the fact that glueballs are expected to mix with nearby $q\bar{q}$ states.

Central-exclusive production of low-mass resonances in $\pi\pi$ and KK channels has been extensively studied in fixed target experiments at CERN and Fermilab (see review in [782]) and recent collider experiments at RHIC [797], Tevatron [798] and the LHC [799]. The partial-wave analysis (PWA) has been performed in several experiments to investigate the spin-parity nature of the centrally produced system [800–802]. There is a clear evidence of supernumerous light scalar meson states, not fitting well into the conventional groundstate $q\bar{q}$ nonet and suggesting that some of these states have significant gluonic component. The $f_0(1370)$, $f_0(1500)$ and $f_0(1710)$ mesons are considered as most promising glueball-meson mixing state candidates but the nature of all these states is still open for discussion [803]. In the tensor sector, the lightest isoscalar $q\bar{q}$ states $f_2(1270)$ and $f_2'(1525)$ are well established however there are at least four additional reported tensor resonances requiring confirmation.

CEP can be also used to investigate the spin structure of the Pomeron and its coupling to hadrons. Historically, the Pomeron was considered as effective spin 1 quasiparticle supported by successful fits of total and differential pp cross sections [804]. Recently, an alternative approach based on the tensorial Pomeron has been developed [805] providing definitive predictions and restrictions of spin-parity, polarization and rapidity of the produced diffractive system in CEP at the LHC [806–808].

Multidifferential measurements and PWA of $\pi\pi$, KK and $p\bar{p}$ final states in a wide range of invariant masses in CEP at the LHC would also allow one to constrain poorly known Pomeron-meson couplings and form-factors in various phenomenological models [806, 809] and also build a transition to perturbative QCD models of hadron pair production in CEP [810] valid at high invariant masses and transverse momenta of the produced pair. Another important outcome of CEP measurements would be a determination of the absorptive corrections, the probability that the rapidity gaps would be filled with particles from accompanying initial- or final-state interactions. The central exclusive production of meson pairs therefore represents a process of much phenomenological interest, which can shed light on both perturbative and non-perturbative aspects of QCD.

Perturbative aspects of QCD can be also investigated in CEP of heavy quarkonium states [783]. Detailed studies of χ_c resonances in CEP at the LHC would provide a valuable input to test the ideas and methods of the QCD physics of bound states. Measurements of the outgoing proton momentum distributions, cross sections and relative abundances of χ_{c0}, χ_{c1} and χ_{c2} states would be important for the test of the overall theoretical formalism.

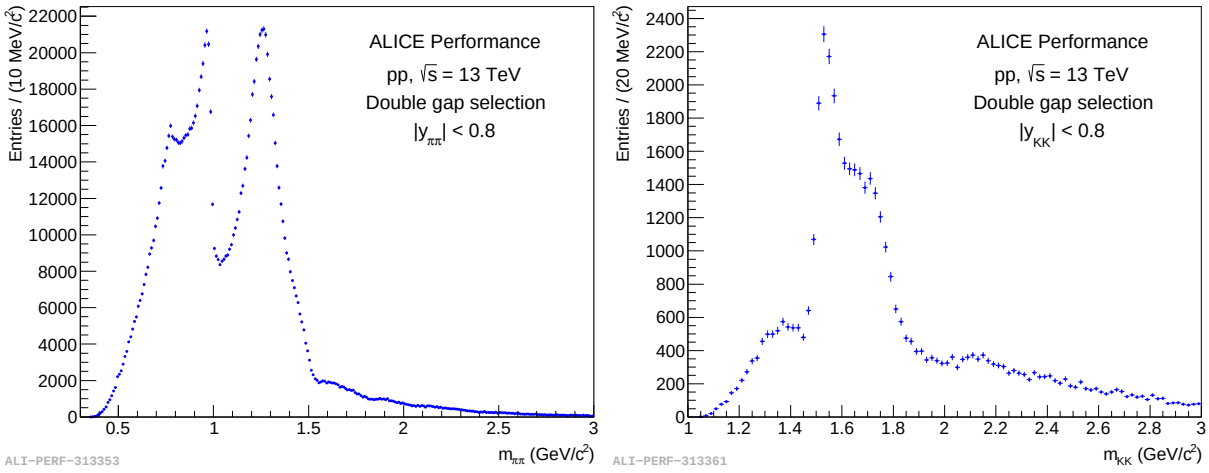

Fig. 98: Raw invariant mass spectra of $\pi^+\pi^-$ (left) and K^+K^- (right) pairs in CEP events collected by ALICE in proton-proton collisions at $\sqrt{s} = 13$ TeV.

Measurements of CEP processes rely on the selection of events with only few tracks in an otherwise empty detector, therefore large pseudorapidity coverage and low pileup conditions are essential to guarantee the event emptiness. The ALICE detector nicely matches these requirements. Low material budget, access to low transverse momenta and excellent particle identification capabilities in ALICE serve as additional advantages. First CEP measurements have been already performed by ALICE in the LHC Run-1 and -2. Figure 98 illustrates raw invariant mass spectra of $\pi^+\pi^-$ and K^+K^- pairs in CEP events collected by ALICE in proton-proton collisions at $\sqrt{s} = 13$ TeV, where one can easily identify several resonance structures. ALICE is going to collect a much larger sample of central exclusive events and significantly extend the scope of the CEP program in proton-proton collisions in LHC Run-3 with expected integrated luminosity of about 200 pb^{-1} at $\sqrt{s} = 14$ TeV and 6 pb^{-1} at $\sqrt{s} = 5.5$ TeV profiting from much better efficiency in the continuous readout mode. The CEP program includes glueball searches and precision hadron spectroscopy in $\pi^+\pi^-$, K^+K^-, $p\bar{p}$, $2\pi2K$, 4π and other channels. The expected high integrated luminosity will also allow ALICE to measure the spectrum of heavy quarkonium states in various decay channels, e.g. a yield of at least 50,000 $\chi_{c0} \to \pi^+\pi^-$ decays is expected in CEP events by the end of Run-3 based on cross section estimates from SUPERCHIC generator [811].

The LHCb experiment can extend the CEP program to forward rapidities. High luminosity at moderate pileup and good hadron PID capabilities would be particularly useful for the studies of heavy quarkonium states in central exclusive events. Measurements of low-mass central exclusive production processes with proton tagging might be also possible with the ATLAS and CMS detectors during low pile-up runs at high β^*.

Acknowledgements

We would like to thank the LHC experimental Collaborations and the WLCG for their essential support. We are especially grateful for the efforts by the computing, generator and validation groups who were instrumental for the creation of large simulation samples. We thank the detector upgrade groups as well as the physics and performance groups for their input. Not least, we thank the many colleagues who have provided useful comments on the analyses.

References

[1] R. K. Ellis and G. Zanderighi, *Scalar one-loop integrals for QCD*, JHEP **02** (2008) 002, arXiv:0712.1851 [hep-ph].

[2] A. van Hameren, *OneLOop: For the evaluation of one-loop scalar functions*, Comput. Phys. Commun. **182** (2011) 2427–2438, arXiv:1007.4716 [hep-ph].

[3] S. Frixione, Z. Kunszt, and A. Signer, *Three jet cross-sections to next-to-leading order*, Nucl. Phys. **B467** (1996) 399–442, arXiv:hep-ph/9512328 [hep-ph].

[4] S. Catani and M. H. Seymour, *A General algorithm for calculating jet cross-sections in NLO QCD*, Nucl. Phys. **B485** (1997) 291–419, arXiv:hep-ph/9605323 [hep-ph]. [Erratum: Nucl. Phys.B510,503(1998)].

[5] R. Britto, F. Cachazo, and B. Feng, *Generalized unitarity and one-loop amplitudes in N=4 super-Yang-Mills*, Nucl. Phys. **B725** (2005) 275–305, arXiv:hep-th/0412103 [hep-th].

[6] G. Ossola, C. G. Papadopoulos, and R. Pittau, *Reducing full one-loop amplitudes to scalar integrals at the integrand level*, Nucl. Phys. **B763** (2007) 147–169, arXiv:hep-ph/0609007 [hep-ph].

[7] R. K. Ellis, W. T. Giele, Z. Kunszt, and K. Melnikov, *Masses, fermions and generalized D-dimensional unitarity*, Nucl. Phys. **B822** (2009) 270–282, arXiv:0806.3467 [hep-ph].

[8] W. T. Giele, Z. Kunszt, and K. Melnikov, *Full one-loop amplitudes from tree amplitudes*, JHEP **04** (2008) 049, arXiv:0801.2237 [hep-ph].

[9] R. K. Ellis, Z. Kunszt, K. Melnikov, and G. Zanderighi, *One-loop calculations in quantum field theory: from Feynman diagrams to unitarity cuts*, Phys. Rept. **518** (2012) 141–250, arXiv:1105.4319 [hep-ph].

[10] F. Cascioli, P. Maierhofer, and S. Pozzorini, *Scattering Amplitudes with Open Loops*, Phys. Rev. Lett. **108** (2012) 111601, arXiv:1111.5206 [hep-ph].

[11] G. Cullen et al., *GOSAM-2.0: a tool for automated one-loop calculations within the Standard Model and beyond*, Eur. Phys. J. **C74** (2014) no. 8, 3001, arXiv:1404.7096 [hep-ph].

[12] J. Alwall, R. Frederix, S. Frixione, V. Hirschi, F. Maltoni, O. Mattelaer, H. S. Shao, T. Stelzer, P. Torrielli, and M. Zaro, *The automated computation of tree-level and next-to-leading order differential cross sections, and their matching to parton shower simulations*, JHEP **07** (2014) 079, arXiv:1405.0301 [hep-ph].

[13] T. O. Eynck, E. Laenen, L. Phaf, and S. Weinzierl, *Comparison of phase space slicing and dipole subtraction methods for gamma* —> anti-Q*, Eur. Phys. J. **C23** (2002) 259–266, arXiv:hep-ph/0109246 [hep-ph].

[14] ATLAS Collaboration, G. Aad et al., *Measurement of W^+W^- production in pp collisions at $\sqrt{s} = 7$ TeV with the ATLAS detector and limits on anomalous WWZ and WWγ couplings*, Phys. Rev. **D87** (2013) no. 11, 112001, arXiv:1210.2979 [hep-ex]. [Erratum: Phys. Rev.D88,no.7,079906(2013)].

[15] CMS Collaboration, S. Chatrchyan et al., *Measurement of the W^+W^- Cross section in pp Collisions at $\sqrt{s} = 7$ TeV and Limits on Anomalous $WW\gamma$ and WWZ couplings*, Eur. Phys. J. **C73** (2013) no. 10, 2610, arXiv:1306.1126 [hep-ex].

[16] CMS Collaboration, S. Chatrchyan et al., *Measurement of W+W- and ZZ production cross sections in pp collisions at sqrt(s) = 8 TeV*, Phys. Lett. **B721** (2013) 190–211, arXiv:1301.4698 [hep-ex].

[17] G. Heinrich, *QCD calculations for the LHC: status and prospects*, in *5th Large Hadron Collider Physics Conference (LHCP 2017) Shanghai, China, May 15-20, 2017*. 2017. arXiv:1710.04998 [hep-ph].

[18] S. Dittmaier, *Standard Model Theory*, in *Proceedings, 2017 European Physical Society Conference on High Energy Physics (EPS-HEP 2017): Venice, Italy, July 5-12, 2017*. 2017. arXiv:1709.08564 [hep-ph]. https://pos.sissa.it/314/581/pdf.

[19] J. Currie, A. Gehrmann-De Ridder, T. Gehrmann, E. W. N. Glover, A. Huss, and J. Pires, *Precise predictions for dijet production at the LHC*, Phys. Rev. Lett. **119** (2017) no. 15, 152001, arXiv:1705.10271 [hep-ph].

[20] A. V. Kotikov, *Differential equations method: The Calculation of vertex type Feynman diagrams*, Phys. Lett. **B259** (1991) 314–322.

[21] A. V. Kotikov, *Differential equation method: The Calculation of N point Feynman diagrams*, Phys. Lett. **B267** (1991) 123–127. [Erratum: Phys. Lett.B295,409(1992)].

[22] J. M. Henn, *Multiloop integrals in dimensional regularization made simple*, Phys. Rev. Lett. **110** (2013) 251601, arXiv:1304.1806 [hep-th].

[23] C. G. Papadopoulos, *Simplified differential equations approach for Master Integrals*, JHEP **07** (2014) 088, arXiv:1401.6057 [hep-ph].

[24] S. P. Jones, M. Kerner, and G. Luisoni, *Next-to-Leading-Order QCD Corrections to Higgs Boson Plus Jet Production with Full Top-Quark Mass Dependence*, Phys. Rev. Lett. **120** (2018) no. 16, 162001, arXiv:1802.00349 [hep-ph].

[25] J. M. Lindert, K. Kudashkin, K. Melnikov, and C. Wever, *Higgs bosons with large transverse momentum at the LHC*, Phys. Lett. **B782** (2018) 210–214, arXiv:1801.08226 [hep-ph].

[26] L. Adams, C. Bogner, and S. Weinzierl, *The two-loop sunrise graph in two space-time dimensions with arbitrary masses in terms of elliptic dilogarithms*, J. Math. Phys. **55** (2014) no. 10, 102301, arXiv:1405.5640 [hep-ph].

[27] J. M. Henn, K. Melnikov, and V. A. Smirnov, *Two-loop planar master integrals for the production of off-shell vector bosons in hadron collisions*, JHEP **05** (2014) 090, arXiv:1402.7078 [hep-ph].

[28] F. Caola, J. M. Henn, K. Melnikov, and V. A. Smirnov, *Non-planar master integrals for the production of two off-shell vector bosons in collisions of massless partons*, JHEP **09** (2014) 043, arXiv:1404.5590 [hep-ph].

[29] T. Gehrmann, A. von Manteuffel, L. Tancredi, and E. Weihs, *The two-loop master integrals for* $q\bar{q} \to VV$, JHEP **06** (2014) 032, arXiv:1404.4853 [hep-ph].

[30] C. G. Papadopoulos, D. Tommasini, and C. Wever, *Two-loop Master Integrals with the Simplified Differential Equations approach*, JHEP **01** (2015) 072, arXiv:1409.6114 [hep-ph].

[31] C. G. Papadopoulos, D. Tommasini, and C. Wever, *The Pentabox Master Integrals with the Simplified Differential Equations approach*, JHEP **04** (2016) 078, arXiv:1511.09404 [hep-ph].

[32] E. Remiddi and L. Tancredi, *An Elliptic Generalization of Multiple Polylogarithms*, Nucl. Phys. **B925** (2017) 212–251, arXiv:1709.03622 [hep-ph].

[33] R. Bonciani, V. Del Duca, H. Frellesvig, J. M. Henn, F. Moriello, and V. A. Smirnov, *Two-loop planar master integrals for Higgs→ 3 partons with full heavy-quark mass dependence*, JHEP **12** (2016) 096, arXiv:1609.06685 [hep-ph].

[34] L. Adams, E. Chaubey, and S. Weinzierl, *Analytic results for the planar double box integral relevant to top-pair production with a closed top loop*, JHEP **10** (2018) 206, arXiv:1806.04981 [hep-ph].

[35] L. Adams, E. Chaubey, and S. Weinzierl, *Simplifying Differential Equations for Multiscale Feynman Integrals beyond Multiple Polylogarithms*, Phys. Rev. Lett. **118** (2017) no. 14, 141602, arXiv:1702.04279 [hep-ph].

[36] L. Adams, C. Bogner, A. Schweitzer, and S. Weinzierl, *The kite integral to all orders in terms of elliptic polylogarithms*, J. Math. Phys. **57** (2016) no. 12, 122302, arXiv:1607.01571 [hep-ph].

[37] J. Ablinger, J. Blümlein, A. De Freitas, M. van Hoeij, E. Imamoglu, C. G. Raab, C. S. Radu, and C. Schneider, *Iterated Elliptic and Hypergeometric Integrals for Feynman Diagrams*, J. Math. Phys. **59** (2018) no. 6, 062305, arXiv:1706.01299 [hep-th].

[38] A. von Manteuffel and L. Tancredi, *A non-planar two-loop three-point function beyond multiple polylogarithms*, JHEP **06** (2017) 127, arXiv:1701.05905 [hep-ph].

[39] J. Broedel, C. Duhr, F. Dulat, B. Penante, and L. Tancredi, *Elliptic symbol calculus: from elliptic polylogarithms to iterated integrals of Eisenstein series*, JHEP **08** (2018) 014, arXiv:1803.10256 [hep-th].

[40] S. Becker and S. Weinzierl, *Direct numerical integration for multi-loop integrals*, Eur. Phys. J. **C73** (2013) no. 2, 2321, arXiv:1211.0509 [hep-ph].

[41] M. Czakon, P. Fiedler, and A. Mitov, *Total Top-Quark Pair-Production Cross Section at Hadron Colliders Through $O(\alpha_S^4)$*, Phys. Rev. Lett. **110** (2013) 252004, arXiv:1303.6254 [hep-ph].

[42] C. Bogner, A. Schweitzer, and S. Weinzierl, *Analytic continuation and numerical evaluation of the kite integral and the equal mass sunrise integral*, Nucl. Phys. **B922** (2017) 528–550, arXiv:1705.08952 [hep-ph].

[43] S. Borowka, G. Heinrich, S. Jahn, S. P. Jones, M. Kerner, J. Schlenk, and T. Zirke, *pySecDec: a toolbox for the numerical evaluation of multi-scale integrals*, Comput. Phys. Commun. **222** (2018) 313–326, arXiv:1703.09692 [hep-ph].

[44] A. Gehrmann-De Ridder, T. Gehrmann, and E. W. N. Glover, *Antenna subtraction at NNLO*, JHEP **09** (2005) 056, arXiv:hep-ph/0505111 [hep-ph].

[45] G. Heinrich, *A numerical method for NNLO calculations*, Nucl. Phys. Proc. Suppl. **116** (2003) 368–372, arXiv:hep-ph/0211144 [hep-ph]. [,368(2002)].

[46] M. Czakon, *A novel subtraction scheme for double-real radiation at NNLO*, Phys. Lett. **B693** (2010) 259–268, arXiv:1005.0274 [hep-ph].

[47] R. Boughezal, K. Melnikov, and F. Petriello, *A subtraction scheme for NNLO computations*, Phys. Rev. **D85** (2012) 034025, arXiv:1111.7041 [hep-ph].

[48] M. Czakon and D. Heymes, *Four-dimensional formulation of the sector-improved residue subtraction scheme*, Nucl. Phys. **B890** (2014) 152–227, arXiv:1408.2500 [hep-ph].

[49] F. Caola, K. Melnikov, and R. Röntsch, *Nested soft-collinear subtractions in NNLO QCD computations*, Eur. Phys. J. **C77** (2017) no. 4, 248, arXiv:1702.01352 [hep-ph].

[50] V. Del Duca, C. Duhr, A. Kardos, G. Somogyi, and Z. Trócsányi, *Three-Jet Production in Electron-Positron Collisions at Next-to-Next-to-Leading Order Accuracy*, Phys. Rev. Lett. **117** (2016) no. 15, 152004, arXiv:1603.08927 [hep-ph].

[51] M. Cacciari, F. A. Dreyer, A. Karlberg, G. P. Salam, and G. Zanderighi, *Fully Differential Vector-Boson-Fusion Higgs Production at Next-to-Next-to-Leading Order*, Phys. Rev. Lett. **115** (2015) no. 8, 082002, arXiv:1506.02660 [hep-ph]. [Erratum: Phys. Rev. Lett.120,no.13,139901(2018)].

[52] S. Catani, L. Cieri, G. Ferrera, D. de Florian, and M. Grazzini, *Vector boson production at hadron colliders: a fully exclusive QCD calculation at NNLO*, Phys. Rev. Lett. **103** (2009) 082001, arXiv:0903.2120 [hep-ph].

[53] R. Boughezal, C. Focke, X. Liu, and F. Petriello, *W-boson production in association with a jet at next-to-next-to-leading order in perturbative QCD*, Phys. Rev. Lett. **115** (2015) no. 6, 062002, arXiv:1504.02131 [hep-ph].

[54] J. Gaunt, M. Stahlhofen, F. J. Tackmann, and J. R. Walsh, *N-jettiness Subtractions for NNLO QCD Calculations*, JHEP **09** (2015) 058, arXiv:1505.04794 [hep-ph].

[55] S. Badger, H. Frellesvig, and Y. Zhang, *Hepta-Cuts of Two-Loop Scattering Amplitudes*, JHEP **04** (2012) 055, arXiv:1202.2019 [hep-ph].

[56] S. Badger, H. Frellesvig, and Y. Zhang, *A Two-Loop Five-Gluon Helicity Amplitude in QCD*, JHEP **12** (2013) 045, arXiv:1310.1051 [hep-ph].

[57] S. Badger, G. Mogull, A. Ochirov, and D. O'Connell, *A Complete Two-Loop, Five-Gluon Helicity Amplitude in Yang-Mills Theory*, JHEP **10** (2015) 064, arXiv:1507.08797 [hep-ph].

[58] T. Gehrmann, J. M. Henn, and N. A. Lo Presti, *Analytic form of the two-loop planar five-gluon all-plus-helicity amplitude in QCD*, Phys. Rev. Lett. **116** (2016) no. 6, 062001, arXiv:1511.05409 [hep-ph]. [Erratum: Phys. Rev. Lett.116,no.18,189903(2016)].

[59] S. Badger, G. Mogull, and T. Peraro, *Local integrands for two-loop all-plus Yang-Mills amplitudes*, JHEP **08** (2016) 063, arXiv:1606.02244 [hep-ph].

[60] D. C. Dunbar, G. R. Jehu, and W. B. Perkins, *Two-loop six gluon all plus helicity amplitude*, Phys. Rev. Lett. **117** (2016) no. 6, 061602, arXiv:1605.06351 [hep-th].

[61] S. Badger, C. Brønnum-Hansen, H. B. Hartanto, and T. Peraro, *First look at two-loop five-gluon scattering in QCD*, Phys. Rev. Lett. **120** (2018) no. 9, 092001, arXiv:1712.02229 [hep-ph].

[62] S. Abreu, F. Febres Cordero, H. Ita, B. Page, and M. Zeng, *Planar Two-Loop Five-Gluon Amplitudes from Numerical Unitarity*, Phys. Rev. **D97** (2018) no. 11, 116014, arXiv:1712.03946 [hep-ph].

[63] C. Anastasiou, C. Duhr, F. Dulat, E. Furlan, T. Gehrmann, F. Herzog, A. Lazopoulos, and B. Mistlberger, *High precision determination of the gluon fusion Higgs boson cross-section at the LHC*, JHEP **05** (2016) 058, arXiv:1602.00695 [hep-ph].

[64] B. Mistlberger, *Higgs boson production at hadron colliders at N^3LO in QCD*, JHEP **05** (2018) 028, arXiv:1802.00833 [hep-ph].

[65] F. A. Dreyer and A. Karlberg, *Vector-Boson Fusion Higgs Production at Three Loops in QCD*, Phys. Rev. Lett. **117** (2016) no. 7, 072001, arXiv:1606.00840 [hep-ph].

[66] W. Bizon, P. F. Monni, E. Re, L. Rottoli, and P. Torrielli, *Momentum-space resummation for transverse observables and the Higgs $p_\perp$ at N^3LL+NNLO*, JHEP **02** (2018) 108, arXiv:1705.09127 [hep-ph].

[67] X. Chen, T. Gehrmann, E. W. N. Glover, A. Huss, Y. Li, D. Neill, M. Schulze, I. W. Stewart, and H. X. Zhu, *Precise QCD Description of the Higgs Boson Transverse Momentum Spectrum*, Phys. Lett. **B788** (2019) 425–430, arXiv:1805.00736 [hep-ph].

[68] W. Bizoń, X. Chen, A. Gehrmann-De Ridder, T. Gehrmann, N. Glover, A. Huss, P. F. Monni, E. Re, L. Rottoli, and P. Torrielli, *Fiducial distributions in Higgs and Drell-Yan production at N^3LL+NNLO*, JHEP **12** (2018) 132, arXiv:1805.05916 [hep-ph].

[69] J. C. Collins, D. E. Soper, and G. F. Sterman, *Transverse Momentum Distribution in Drell-Yan Pair and W and Z Boson Production*, Nucl. Phys. **B250** (1985) 199–224.

[70] S. Catani, L. Trentadue, G. Turnock, and B. R. Webber, *Resummation of large logarithms in e+ e- event shape distributions*, Nucl. Phys. **B407** (1993) 3–42.

[71] C. W. Bauer, D. Pirjol, and I. W. Stewart, *Soft collinear factorization in effective field theory*, Phys. Rev. **D65** (2002) 054022, arXiv:hep-ph/0109045 [hep-ph].

[72] C. W. Bauer and P. F. Monni, *A numerical formulation of resummation in effective field theory*, arXiv:1803.07079 [hep-ph].

[73] M. Dasgupta, F. A. Dreyer, K. Hamilton, P. F. Monni, and G. P. Salam, *Logarithmic accuracy of parton showers: a fixed-order study*, JHEP **09** (2018) 033, arXiv:1805.09327 [hep-ph].

[74] Z. Nagy and D. E. Soper, *Effects of subleading color in a parton shower*, JHEP **07** (2015) 119, arXiv:1501.00778 [hep-ph].

[75] S. Jadach, A. Kusina, W. Placzek, and M. Skrzypek, *On the dependence of QCD splitting functions on the choice of the evolution variable*, JHEP **08** (2016) 092, arXiv:1606.01238 [hep-ph].

[76] S. Höche and S. Prestel, *Triple collinear emissions in parton showers*, Phys. Rev. **D96** (2017) no. 7, 074017, arXiv:1705.00742 [hep-ph].

[77] S. Höche and S. Prestel, *The midpoint between dipole and parton showers*, Eur. Phys. J. **C75** (2015) no. 9, 461, arXiv:1506.05057 [hep-ph].

[78] N. Fischer, S. Prestel, M. Ritzmann, and P. Skands, *Vincia for Hadron Colliders*, Eur. Phys. J. **C76** (2016) no. 11, 589, arXiv:1605.06142 [hep-ph].

[79] S. Alioli, C. W. Bauer, C. Berggren, F. J. Tackmann, J. R. Walsh, and S. Zuberi, *Matching Fully Differential NNLO Calculations and Parton Showers*, JHEP **06** (2014) 089, arXiv:1311.0286 [hep-ph].

[80] K. Hamilton, P. Nason, E. Re, and G. Zanderighi, *NNLOPS simulation of Higgs boson production*, JHEP **10** (2013) 222, arXiv:1309.0017 [hep-ph].

[81] S. Höche, Y. Li, and S. Prestel, *Drell-Yan lepton pair production at NNLO QCD with parton showers*, Phys. Rev. **D91** (2015) no. 7, 074015, arXiv:1405.3607 [hep-ph].

[82] S. Actis, A. Denner, L. Hofer, J.-N. Lang, A. Scharf, and S. Uccirati, *RECOLA: REcursive Computation of One-Loop Amplitudes*, Comput. Phys. Commun. **214** (2017) 140–173, arXiv:1605.01090 [hep-ph].

[83] S. Actis, A. Denner, L. Hofer, A. Scharf, and S. Uccirati, *Recursive generation of one-loop amplitudes in the Standard Model*, JHEP **04** (2013) 037, arXiv:1211.6316 [hep-ph].

[84] T. Gleisberg, S. Hoeche, F. Krauss, M. Schonherr, S. Schumann, F. Siegert, and J. Winter, *Event generation with SHERPA 1.1*, JHEP **02** (2009) 007, arXiv:0811.4622 [hep-ph].

[85] M. Schönherr, *An automated subtraction of NLO EW infrared divergences*, Eur. Phys. J. **C78** (2018) no. 2, 119, arXiv:1712.07975 [hep-ph].

[86] G. Cullen, N. Greiner, G. Heinrich, G. Luisoni, P. Mastrolia, G. Ossola, T. Reiter, and F. Tramontano, *Automated One-Loop Calculations with GoSam*, Eur. Phys. J. **C72** (2012) 1889, arXiv:1111.2034 [hep-ph].

[87] R. Frederix, T. Gehrmann, and N. Greiner, *Automation of the Dipole Subtraction Method in MadGraph/MadEvent*, JHEP **09** (2008) 122, arXiv:0808.2128 [hep-ph].

[88] T. Gehrmann and N. Greiner, *Photon Radiation with MadDipole*, JHEP **12** (2010) 050, arXiv:1011.0321 [hep-ph].

[89] R. Frederix, S. Frixione, V. Hirschi, D. Pagani, H. S. Shao, and M. Zaro, *The automation of next-to-leading order electroweak calculations*, JHEP **07** (2018) 185, arXiv:1804.10017 [hep-ph].

[90] J. R. Andersen et al., *Les Houches 2015: Physics at TeV Colliders Standard Model Working Group Report*, in *9th Les Houches Workshop on Physics at TeV Colliders (PhysTeV 2015) Les Houches, France, June 1-19, 2015*. 2016. arXiv:1605.04692 [hep-ph]. http://lss.fnal.gov/archive/2016/conf/fermilab-conf-16-175-ppd-t.pdf.

[91] J. R. Andersen et al., *Les Houches 2017: Physics at TeV Colliders Standard Model Working Group Report*, in *10th Les Houches Workshop on Physics at TeV Colliders (PhysTeV 2017) Les Houches, France, June 5-23, 2017*. 2018. arXiv:1803.07977 [hep-ph]. http://lss.fnal.gov/archive/2018/conf/fermilab-conf-18-122-cd-t.pdf.

[92] A. Denner, L. Hofer, A. Scharf, and S. Uccirati, *Electroweak corrections to lepton pair production in association with two hard jets at the LHC*, JHEP **01** (2015) 094, arXiv:1411.0916 [hep-ph].

[93] A. Denner, R. Feger, and A. Scharf, *Irreducible background and interference effects for Higgs-boson production in association with a top-quark pair*, JHEP **04** (2015) 008, arXiv:1412.5290 [hep-ph].

[94] A. Denner and R. Feger, *NLO QCD corrections to off-shell top-antitop production with leptonic decays in association with a Higgs boson at the LHC*, JHEP **11** (2015) 209, arXiv:1506.07448 [hep-ph].

[95] S. Kallweit, J. M. Lindert, P. Maierhöfer, S. Pozzorini, and M. Schönherr, *NLO electroweak automation and precise predictions for W+multijet production at the LHC*, JHEP **04** (2015) 012, arXiv:1412.5157 [hep-ph].

[96] S. Frixione, V. Hirschi, D. Pagani, H. S. Shao, and M. Zaro, *Weak corrections to Higgs hadroproduction in association with a top-quark pair*, JHEP **09** (2014) 065, arXiv:1407.0823 [hep-ph].

[97] M. Chiesa, N. Greiner, and F. Tramontano, *Automation of electroweak corrections for LHC processes*, J. Phys. **G43** (2016) no. 1, 013002, arXiv:1507.08579 [hep-ph].

[98] S. Kallweit, J. M. Lindert, P. Maierhofer, S. Pozzorini, and M. Schönherr, *NLO QCD+EW predictions for V + jets including off-shell vector-boson decays and multijet merging*, JHEP **04** (2016) 021, arXiv:1511.08692 [hep-ph].

[99] S. Frixione, V. Hirschi, D. Pagani, H. S. Shao, and M. Zaro, *Electroweak and QCD corrections to top-pair hadroproduction in association with heavy bosons*, JHEP **06** (2015) 184, arXiv:1504.03446 [hep-ph].

[100] B. Biedermann, M. Billoni, A. Denner, S. Dittmaier, L. Hofer, B. Jäger, and L. Salfelder, *Next-to-leading-order electroweak corrections to $pp \to W^+W^- \to 4$ leptons at the LHC*, JHEP **06** (2016) 065, arXiv:1605.03419 [hep-ph].

[101] B. Biedermann, A. Denner, S. Dittmaier, L. Hofer, and B. Jäger, *Electroweak corrections to $pp \to \mu^+\mu^- e^+ e^- + X$ at the LHC: a Higgs background study*, Phys. Rev. Lett. **116** (2016) no. 16, 161803, arXiv:1601.07787 [hep-ph].

[102] A. Denner and M. Pellen, *NLO electroweak corrections to off-shell top-antitop production with leptonic decays at the LHC*, JHEP **08** (2016) 155, arXiv:1607.05571 [hep-ph].

[103] B. Biedermann, A. Denner, and M. Pellen, *Large electroweak corrections to vector-boson scattering at the Large Hadron Collider*, Phys. Rev. Lett. **118** (2017) no. 26, 261801, arXiv:1611.02951 [hep-ph].

[104] B. Biedermann, A. Denner, S. Dittmaier, L. Hofer, and B. Jager, *Next-to-leading-order electroweak corrections to the production of four charged leptons at the LHC*, JHEP **01** (2017) 033, arXiv:1611.05338 [hep-ph].

[105] A. Denner, J.-N. Lang, M. Pellen, and S. Uccirati, *Higgs production in association with off-shell top-antitop pairs at NLO EW and QCD at the LHC*, JHEP **02** (2017) 053, arXiv:1612.07138 [hep-ph].

[106] R. Frederix, S. Frixione, V. Hirschi, D. Pagani, H.-S. Shao, and M. Zaro, *The complete NLO corrections to dijet hadroproduction*, JHEP **04** (2017) 076, arXiv:1612.06548 [hep-ph].

[107] D. Pagani, I. Tsinikos, and M. Zaro, *The impact of the photon PDF and electroweak corrections on $t\bar{t}$ distributions*, Eur. Phys. J. **C76** (2016) no. 9, 479, arXiv:1606.01915 [hep-ph].

[108] B. Biedermann, S. Bräuer, A. Denner, M. Pellen, S. Schumann, and J. M. Thompson, *Automation of NLO QCD and EW corrections with Sherpa and Recola*, Eur. Phys. J. **C77** (2017) 492, arXiv:1704.05783 [hep-ph].

[109] S. Kallweit, J. M. Lindert, S. Pozzorini, and M. Schönherr, *NLO QCD+EW predictions for $2\ell 2\nu$ diboson signatures at the LHC*, JHEP **11** (2017) 120, arXiv:1705.00598 [hep-ph].

[110] M. Chiesa, N. Greiner, M. Schönherr, and F. Tramontano, *Electroweak corrections to diphoton plus jets*, JHEP **10** (2017) 181, arXiv:1706.09022 [hep-ph].

[111] B. Biedermann, A. Denner, and M. Pellen, *Complete NLO corrections to W^+W^+ scattering and its irreducible background at the LHC*, JHEP **10** (2017) 124, arXiv:1708.00268 [hep-ph].

[112] B. Biedermann, A. Denner, and L. Hofer, *Next-to-leading-order electroweak corrections to the production of three charged leptons plus missing energy at the LHC*, JHEP **10** (2017) 043, arXiv:1708.06938 [hep-ph].

[113] M. Czakon, D. Heymes, A. Mitov, D. Pagani, I. Tsinikos, and M. Zaro, *Top-pair production at the LHC through NNLO QCD and NLO EW*, JHEP **10** (2017) 186, arXiv:1705.04105 [hep-ph].

[114] N. Greiner and M. Schönherr, *NLO QCD+EW corrections to diphoton production in association with a vector boson*, JHEP **01** (2018) 079, arXiv:1710.11514 [hep-ph].

[115] R. Frederix, D. Pagani, and M. Zaro, *Large NLO corrections in $t\bar{t}W^{\pm}$ and $t\bar{t}t\bar{t}$ hadroproduction from supposedly subleading EW contributions*, JHEP **02** (2018) 031, arXiv:1711.02116 [hep-ph].

[116] C. Gütschow, J. M. Lindert, and M. Schönherr, *Multi-jet merged top-pair production including electroweak corrections*, Eur. Phys. J. **C78** (2018) no. 4, 317, arXiv:1803.00950 [hep-ph].

[117] M. Schönherr, *Next-to-leading order electroweak corrections to off-shell WWW production at the LHC*, JHEP **07** (2018) 076, arXiv:1806.00307 [hep-ph].

[118] S. Dittmaier, A. Huss, and C. Schwinn, *Mixed QCD-electroweak $O(\alpha_s\alpha)$ corrections to Drell-Yan processes in the resonance region: pole approximation and non-factorizable corrections*, Nucl. Phys. **B885** (2014) 318–372, arXiv:1403.3216 [hep-ph].

[119] S. Dittmaier, A. Huss, and C. Schwinn, *Dominant mixed QCD-electroweak $O(\alpha_s\alpha)$ corrections to Drell–Yan processes in the resonance region*, Nucl. Phys. **B904** (2016) 216–252, arXiv:1511.08016 [hep-ph].

[120] A. Kotikov, J. H. Kuhn, and O. Veretin, *Two-Loop Formfactors in Theories with Mass Gap and Z-Boson Production*, Nucl. Phys. **B788** (2008) 47–62, arXiv:hep-ph/0703013 [HEP-PH].

[121] W. B. Kilgore and C. Sturm, *Two-Loop Virtual Corrections to Drell-Yan Production at order $\alpha_s\alpha^3$*, Phys. Rev. **D85** (2012) 033005, arXiv:1107.4798 [hep-ph].

[122] R. Bonciani, *Two-loop mixed QCD-EW virtual corrections to the Drell-Yan production of Z and W bosons*, PoS **EPS-HEP2011** (2011) 365.

[123] R. Bonciani, S. Di Vita, P. Mastrolia, and U. Schubert, *Two-Loop Master Integrals for the mixed EW-QCD virtual corrections to Drell-Yan scattering*, JHEP **09** (2016) 091, arXiv:1604.08581 [hep-ph].

[124] A. von Manteuffel and R. M. Schabinger, *Numerical Multi-Loop Calculations via Finite Integrals and One-Mass EW-QCD Drell-Yan Master Integrals*, JHEP **04** (2017) 129, arXiv:1701.06583 [hep-ph].

[125] R. Bonciani, F. Buccioni, R. Mondini, and A. Vicini, *Double-real corrections at $\mathcal{O}(\alpha\alpha_s)$ to single gauge boson production*, Eur. Phys. J. **C77** (2017) no. 3, 187, arXiv:1611.00645 [hep-ph].

[126] C. Anastasiou, R. Boughezal, and F. Petriello, *Mixed QCD-electroweak corrections to Higgs boson production in gluon fusion*, JHEP **04** (2009) 003, arXiv:0811.3458 [hep-ph].

[127] M. Bonetti, K. Melnikov, and L. Tancredi, *Higher order corrections to mixed QCD-EW contributions to Higgs boson production in gluon fusion*, Phys. Rev. **D97** (2018) no. 5, 056017, arXiv:1801.10403 [hep-ph]. [Erratum: Phys. Rev.D97,no.9,099906(2018)].

[128] C. Anastasiou, V. Del Duca, E. Furlan, B. Mistlberger, F. Moriello, A. Schweitzer, and C. Specchia, *Mixed QCD-electroweak corrections to Higgs production via gluon fusion in the small mass approximation*, arXiv:1811.11211 [hep-ph].

[129] J. M. Lindert et al., *Precise predictions for $V+$ jets dark matter backgrounds*, Eur. Phys. J. **C77** (2017) no. 12, 829, arXiv:1705.04664 [hep-ph].

[130] A. Denner and S. Pozzorini, *One loop leading logarithms in electroweak radiative corrections. 1. Results*, Eur. Phys. J. **C18** (2001) 461–480, arXiv:hep-ph/0010201 [hep-ph].

[131] A. Denner and S. Pozzorini, *One loop leading logarithms in electroweak radiative corrections. 2. Factorization of collinear singularities*, Eur. Phys. J. **C21** (2001) 63–79, arXiv:hep-ph/0104127 [hep-ph].

[132] J.-y. Chiu, F. Golf, R. Kelley, and A. V. Manohar, *Electroweak Sudakov corrections using effective field theory*, Phys. Rev. Lett. **100** (2008) 021802, arXiv:0709.2377 [hep-ph].

[133] J.-y. Chiu, R. Kelley, and A. V. Manohar, *Electroweak Corrections using Effective Field Theory: Applications to the LHC*, Phys. Rev. **D78** (2008) 073006, arXiv:0806.1240 [hep-ph].

[134] M. L. Mangano et al., *Physics at a 100 TeV pp Collider: Standard Model Processes*, CERN Yellow Report (2017) no. 3, 1–254, arXiv:1607.01831 [hep-ph].

[135] C. Bernaciak and D. Wackeroth, *Combining NLO QCD and Electroweak Radiative Corrections to W boson Production at Hadron Colliders in the POWHEG Framework*, Phys. Rev. **D85** (2012) 093003, arXiv:1201.4804 [hep-ph].

[136] L. Barze, G. Montagna, P. Nason, O. Nicrosini, and F. Piccinini, *Implementation of electroweak corrections in the POWHEG BOX: single W production*, JHEP **04** (2012) 037, arXiv:1202.0465 [hep-ph].

[137] L. Barze, G. Montagna, P. Nason, O. Nicrosini, F. Piccinini, and A. Vicini, *Neutral current Drell-Yan with combined QCD and electroweak corrections in the POWHEG BOX*, Eur. Phys. J. **C73** (2013) no. 6, 2474, arXiv:1302.4606 [hep-ph].

[138] A. Mück and L. Oymanns, *Resonace-improved parton-shower matching for the Drell-Yan process including electroweak corrections*, JHEP **05** (2017) 090, arXiv:1612.04292 [hep-ph].

[139] F. Granata, J. M. Lindert, C. Oleari, and S. Pozzorini, *NLO QCD+EW predictions for HV and HV +jet production including parton-shower effects*, JHEP **09** (2017) 012, arXiv:1706.03522 [hep-ph].

[140] M. Chiesa, G. Montagna, L. Barze, M. Moretti, O. Nicrosini, F. Piccinini, and F. Tramontano, *Electroweak Sudakov Corrections to New Physics Searches at the LHC*, Phys. Rev. Lett. **111** (2013) no. 12, 121801, arXiv:1305.6837 [hep-ph].

[141] J. R. Christiansen and T. Sjöstrand, *Weak Gauge Boson Radiation in Parton Showers*, JHEP **04** (2014) 115, arXiv:1401.5238 [hep-ph].

[142] F. Krauss, P. Petrov, M. Schoenherr, and M. Spannowsky, *Measuring collinear W emissions inside jets*, Phys. Rev. **D89** (2014) no. 11, 114006, arXiv:1403.4788 [hep-ph].

[143] C. W. Bauer, N. Ferland, and B. R. Webber, *Standard Model Parton Distributions at Very High Energies*, JHEP **08** (2017) 036.

[144] J. Chen, T. Han, and B. Tweedie, *Electroweak Splitting Functions and High Energy Showering*, JHEP **11** (2017) 093, arXiv:1611.00788 [hep-ph].

[145] G. Corcella, I. G. Knowles, G. Marchesini, S. Moretti, K. Odagiri, P. Richardson, M. H. Seymour, and B. R. Webber, *HERWIG 6: An Event generator for hadron emission reactions with interfering gluons (including supersymmetric processes)*, JHEP **01** (2001) 010, arXiv:hep-ph/0011363 [hep-ph].

[146] M. Bahr et al., *Herwig++ Physics and Manual*, Eur. Phys. J. **C58** (2008) 639–707, arXiv:0803.0883 [hep-ph].

[147] J. Bellm et al., *Herwig 7.0/Herwig++ 3.0 release note*, Eur. Phys. J. **C76** (2016) no. 4, 196, arXiv:1512.01178 [hep-ph].

[148] T. Sjostrand, S. Mrenna, and P. Z. Skands, *PYTHIA 6.4 Physics and Manual*, JHEP **05** (2006) 026, arXiv:0603175 [hep-ph].

[149] T. Sjöstrand, S. Ask, J. R. Christiansen, R. Corke, N. Desai, P. Ilten, S. Mrenna, S. Prestel, C. O. Rasmussen, and P. Z. Skands, *An Introduction to PYTHIA 8.2*, Comput. Phys. Commun. **191** (2015) 159–177, arXiv:1410.3012 [hep-ph].

[150] S. Frixione and B. R. Webber, *Matching NLO QCD computations and parton shower simulations*, JHEP **06** (2002) 029, arXiv:hep-ph/0204244 [hep-ph].

[151] P. Nason, *A New Method for Combining NLO QCD with Shower Monte Carlo Algorithms*, JHEP **11** (2004) 040, arXiv:0409146 [hep-ph].

[152] S. Jadach, W. Płaczek, S. Sapeta, A. Siódmok, and M. Skrzypek, *Matching NLO QCD with parton shower in Monte Carlo scheme — the KrkNLO method*, JHEP **10** (2015) 052, arXiv:1503.06849 [hep-ph].

[153] E. Re, M. Wiesemann, and G. Zanderighi, *NNLOPS accurate predictions for W^+W^- production*, JHEP **12** (2018) 121, arXiv:1805.09857 [hep-ph].

[154] S. Höche, Y. Li, and S. Prestel, *Higgs-boson production through gluon fusion at NNLO QCD with parton showers*, Phys. Rev. **D90** (2014) no. 5, 054011, arXiv:1407.3773 [hep-ph].

[155] S. Alioli, C. W. Bauer, C. Berggren, F. J. Tackmann, and J. R. Walsh, *Drell-Yan production at NNLL'+NNLO matched to parton showers*, Phys. Rev. **D92** (2015) no. 9, 094020, arXiv:1508.01475 [hep-ph].

[156] S. Catani, F. Krauss, R. Kuhn, and B. R. Webber, *QCD matrix elements + parton showers*, JHEP **11** (2001) 063, arXiv:hep-ph/0109231 [hep-ph].

[157] R. Frederix and S. Frixione, *Merging meets matching in MC@NLO*, JHEP **12** (2012) 061, arXiv:1209.6215 [hep-ph].

[158] L. Lönnblad and S. Prestel, *Merging Multi-leg NLO Matrix Elements with Parton Showers*, JHEP **03** (2013) 166, arXiv:1211.7278 [hep-ph].

[159] S. Hoeche, F. Krauss, M. Schonherr, and F. Siegert, *QCD matrix elements + parton showers: The NLO case*, JHEP **04** (2013) 027, arXiv:1207.5030 [hep-ph].

[160] S. Alioli, C. W. Bauer, C. J. Berggren, A. Hornig, F. J. Tackmann, C. K. Vermilion, J. R. Walsh, and S. Zuberi, *Combining Higher-Order Resummation with Multiple NLO Calculations and Parton Showers in GENEVA*, JHEP **09** (2013) 120, arXiv:1211.7049 [hep-ph].

[161] S. Alioli, C. W. Bauer, S. Guns, and F. J. Tackmann, *Underlying event sensitive observables in Drell-Yan production using GENEVA*, Eur. Phys. J. **C76** (2016) no. 11, 614, arXiv:1605.07192 [hep-ph].

[162] K. Hamilton, P. Nason, C. Oleari, and G. Zanderighi, *Merging H/W/Z + 0 and 1 jet at NLO with no merging scale: a path to parton shower + NNLO matching*, JHEP **05** (2013) 082, arXiv:1212.4504 [hep-ph].

[163] R. Frederix and K. Hamilton, *Extending the MINLO method*, JHEP **05** (2016) 042, arXiv:1512.02663 [hep-ph].

[164] F. Maltoni, E. Vryonidou, and M. Zaro, *Top-quark mass effects in double and triple Higgs production in gluon-gluon fusion at NLO*, JHEP **11** (2014) 079, arXiv:1408.6542 [hep-ph].

[165] G. Heinrich, S. P. Jones, M. Kerner, G. Luisoni, and E. Vryonidou, *NLO predictions for Higgs boson pair production with full top quark mass dependence matched to parton showers*, JHEP **08** (2017) 088, arXiv:1703.09252 [hep-ph].

[166] S. Borowka, N. Greiner, G. Heinrich, S. Jones, M. Kerner, J. Schlenk, U. Schubert, and T. Zirke, *Higgs Boson Pair Production in Gluon Fusion at Next-to-Leading Order with Full Top-Quark Mass Dependence*, Phys. Rev. Lett. **117** (2016) no. 1, 012001, arXiv:1604.06447 [hep-ph]. [Erratum: Phys. Rev. Lett.117,no.7,079901(2016)].

[167] S. Borowka, N. Greiner, G. Heinrich, S. P. Jones, M. Kerner, J. Schlenk, and T. Zirke, *Full top quark mass dependence in Higgs boson pair production at NLO*, JHEP **10** (2016) 107, arXiv:1608.04798 [hep-ph].

[168] T. Ježo and P. Nason, *On the Treatment of Resonances in Next-to-Leading Order Calculations Matched to a Parton Shower*, JHEP **12** (2015) 065, arXiv:1509.09071 [hep-ph].

[169] T. Ježo, J. M. Lindert, P. Nason, C. Oleari, and S. Pozzorini, *An NLO+PS generator for $t\bar{t}$ and Wt production and decay including non-resonant and interference effects*, Eur. Phys. J. **C76** (2016) no. 12, 691, arXiv:1607.04538 [hep-ph].

[170] R. Frederix, S. Frixione, A. S. Papanastasiou, S. Prestel, and P. Torrielli, *Off-shell single-top production at NLO matched to parton showers*, JHEP **06** (2016) 027, arXiv:1603.01178 [hep-ph].

[171] W. T. Giele, D. A. Kosower, and P. Z. Skands, *A simple shower and matching algorithm*, Phys. Rev. **D78** (2008) 014026, arXiv:0707.3652 [hep-ph].

[172] Z. Nagy and D. E. Soper, *Jets and threshold summation in Deductor*, Phys. Rev. **D98** (2018) no. 1, 014035, arXiv:1711.02369 [hep-ph].

[173] S. Jadach, A. Kusina, M. Skrzypek, and M. Slawinska, *Monte Carlo modelling of NLO DGLAP QCD evolution in the fully unintegrated form*, Nucl. Phys. Proc. Suppl. **205-206** (2010) 295–300, arXiv:1007.2437 [hep-ph].

[174] S. Höche, F. Krauss, and S. Prestel, *Implementing NLO DGLAP evolution in Parton Showers*, JHEP **10** (2017) 093, arXiv:1705.00982 [hep-ph].

[175] F. Dulat, S. Höche, and S. Prestel, *Leading-Color Fully Differential Two-Loop Soft Corrections to QCD Dipole Showers*, Phys. Rev. **D98** (2018) no. 7, 074013, arXiv:1805.03757 [hep-ph].

[176] J. Bellm, S. Plätzer, P. Richardson, A. Siódmok, and S. Webster, *Reweighting Parton Showers*, Phys. Rev. **D94** (2016) no. 3, 034028, arXiv:1605.08256 [hep-ph].

[177] J. Bellm, G. Nail, S. Plätzer, P. Schichtel, and A. Siódmok, *Parton Shower Uncertainties with Herwig 7: Benchmarks at Leading Order*, Eur. Phys. J. **C76** (2016) no. 12, 665, arXiv:1605.01338 [hep-ph].

[178] S. Mrenna and P. Skands, *Automated Parton-Shower Variations in Pythia 8*, Phys. Rev. **D94** (2016) no. 7, 074005, arXiv:1605.08352 [hep-ph].

[179] E. Bothmann, M. Schönherr, and S. Schumann, *Reweighting QCD matrix-element and parton-shower calculations*, Eur. Phys. J. **C76** (2016) no. 11, 590, arXiv:1606.08753 [hep-ph].

[180] O. Mattelaer, *On the maximal use of Monte Carlo samples: re-weighting events at NLO accuracy*, Eur. Phys. J. **C76** (2016) no. 12, 674, arXiv:1607.00763 [hep-ph].

[181] J. Bendavid, *Efficient Monte Carlo Integration Using Boosted Decision Trees and Generative Deep Neural Networks*, arXiv:1707.00028 [hep-ph].

[182] T. Sjöstrand, *Collective Effects: the viewpoint of HEP MC codes*, Nucl. Phys. **A982** (2019) 43–49, arXiv:1808.03117 [hep-ph].

[183] J. Bellm and C. Bierlich, *PISTA: Posterior Ion STAcking*, arXiv:1807.01291 [hep-ph].

[184] C. Bierlich, G. Gustafson, L. Lönnblad, and H. Shah, *The Angantyr model for Heavy-Ion Collisions in PYTHIA8*, JHEP **10** (2018) 134, arXiv:1806.10820 [hep-ph]. [JHEP18,134(2020)].

[185] B. Andersson, G. Gustafson, and B. Nilsson-Almqvist, *A Model for Low p(t) Hadronic Reactions, with Generalizations to Hadron - Nucleus and Nucleus-Nucleus Collisions*, Nucl. Phys. **B281** (1987) 289–309.

[186] LHC Higgs Cross Section Working Group Collaboration, D. de Florian et al., *Handbook of LHC Higgs Cross Sections: 4. Deciphering the Nature of the Higgs Sector*, arXiv:1610.07922 [hep-ph].

[187] W. Beenakker, C. Borschensky, M. Kramer, A. Kulesza, E. Laenen, S. Marzani, and J. Rojo, *NLO+NLL squark and gluino production cross-sections with threshold-improved parton distributions*, Eur. Phys. J. **C76** (2016) no. 2, 53.

[188] S. Alioli, M. Farina, D. Pappadopulo, and J. T. Ruderman, *Precision Probes of QCD at High Energies*, JHEP **07** (2017) 097.

[189] ATLAS Collaboration, M. Aaboud et al., *Measurement of the W-boson mass in pp collisions at $\sqrt{s} = 7$ TeV with the ATLAS detector*, Eur. Phys. J. **C78** (2018) no. 2, 110, arXiv:1701.07240 [hep-ex]. [Erratum: Eur. Phys. J.C78,no.11,898(2018)].

[190] CDF, D0 Collaboration, T. A. Aaltonen et al., *Tevatron Run II combination of the effective leptonic electroweak mixing angle*, Phys. Rev. **D97** (2018) no. 11, 112007, arXiv:1801.06283 [hep-ex].

[191] R. D. Ball, S. Carrazza, L. Del Debbio, S. Forte, Z. Kassabov, J. Rojo, E. Slade, and M. Ubiali, *Precision determination of the strong coupling constant within a global PDF analysis*, Eur. Phys. J. **C78** (2018) no. 5, 408.

[192] J. Gao, L. Harland-Lang, and J. Rojo, *The Structure of the Proton in the LHC Precision Era*, Phys. Rept. **742** (2018) 1–121.

[193] J. Rojo et al., *The PDF4LHC report on PDFs and LHC data: Results from Run I and preparation for Run II*, J. Phys. **G42** (2015) 103103.

[194] S. Forte and G. Watt, *Progress in the Determination of the Partonic Structure of the Proton*, Ann. Rev. Nucl. Part. Sci. **63** (2013) 291–328, arXiv:1301.6754 [hep-ph].

[195] J. Butterworth et al., *PDF4LHC recommendations for LHC Run II*, J. Phys. **G43** (2016) 023001, arXiv:1510.03865 [hep-ph].

[196] J. Gao and P. Nadolsky, *A meta-analysis of parton distribution functions*, JHEP **1407** (2014) 035.

[197] S. Carrazza, J. I. Latorre, J. Rojo, and G. Watt, *A compression algorithm for the combination of PDF sets*, Eur. Phys. J. **C75** (2015) 474.

[198] S. Carrazza, S. Forte, Z. Kassabov, J. I. Latorre, and J. Rojo, *An Unbiased Hessian Representation for Monte Carlo PDFs*, Eur. Phys. J. **C75** (2015) no. 8, 369.

[199] S. Dulat, T.-J. Hou, J. Gao, M. Guzzi, J. Huston, P. Nadolsky, J. Pumplin, C. Schmidt, D. Stump, and C. P. Yuan, *New parton distribution functions from a global analysis of quantum chromodynamics*, Phys. Rev. D **93** (2016) no. 3, 033006, arXiv:1506.07443 [hep-ph].

[200] L. A. Harland-Lang, A. D. Martin, P. Motylinski, and R. S. Thorne, *Parton distributions in the LHC era: MMHT 2014 PDFs*, Eur. Phys. J. C **75** (2015) no. 5, 204, arXiv:1412.3989 [hep-ph].

[201] NNPDF Collaboration, R. D. Ball et al., *Parton distributions for the LHC Run II*, JHEP **04** (2015) 040, arXiv:1410.8849 [hep-ph].

[202] A. Buckley, J. Ferrando, S. Lloyd, K. Nordström, B. Page, M. Rüfenacht, M. Schönherr, and G. Watt, *LHAPDF6: parton density access in the LHC precision era*, Eur. Phys. J. **C75** (2015) 132, arXiv:1412.7420 [hep-ph].

[203] M. Czakon, N. P. Hartland, A. Mitov, E. R. Nocera, and J. Rojo, *Pinning down the large-x gluon with NNLO top-quark pair differential distributions*, JHEP **04** (2017) 044.

[204] R. Boughezal, A. Guffanti, F. Petriello, and M. Ubiali, *The impact of the LHC Z-boson transverse momentum data on PDF determinations*, JHEP **07** (2017) 130.

[205] J. M. Campbell, J. Rojo, E. Slade, and C. Williams, *Direct photon production and PDF fits reloaded*, Eur. Phys. J. **C78** (2018) no. 6, 470.

[206] J. Currie, E. W. N. Glover, and J. Pires, *Next-to-Next-to Leading Order QCD Predictions for Single Jet Inclusive Production at the LHC*, Phys. Rev. Lett. **118** (2017) no. 7, 072002, arXiv:1611.01460 [hep-ph].

[207] NNPDF Collaboration, R. D. Ball et al., *Parton distributions from high-precision collider data*, Eur. Phys. J. C **77** (2017) 663, arXiv:1706.00428 [hep-ph].

[208] T. Carli, D. Clements, A. Cooper-Sarkar, C. Gwenlan, G. P. Salam, F. Siegert, P. Starovoitov, and M. Sutton, *A posteriori inclusion of parton density functions in NLO QCD final-state calculations at hadron colliders: The* APPLGRID *project*, Eur. Phys. J. C **66** (2010) 503, arXiv:0911.2985 [hep-ph].

[209] fastNLO Collaboration, M. Wobisch, D. Britzger, T. Kluge, K. Rabbertz, and F. Stober, *Theory-Data Comparisons for Jet Measurements in Hadron-Induced Processes*, arXiv:1109.1310 [hep-ph].

[210] R. Boughezal, J. M. Campbell, R. K. Ellis, C. Focke, W. Giele, X. Liu, F. Petriello, and C. Williams, *Color singlet production at NNLO in MCFM*, Eur. Phys. J. **C77** (2017) no. 1, 7.

[211] Z. Nagy, *Three jet cross-sections in hadron hadron collisions at next-to-leading order*, Phys. Rev. Lett. **88** (2002) 122003, arXiv:hep-ph/0110315 [hep-ph].

[212] V. Bertone, R. Frederix, S. Frixione, J. Rojo, and M. Sutton, *aMCfast: automation of fast NLO computations for PDF fits*, JHEP **1408** (2014) 166.

[213] M. Czakon, D. Heymes, and A. Mitov, *Dynamical scales for multi-TeV top-pair production at the LHC*, JHEP **04** (2017) 071, arXiv:1606.03350 [hep-ph].

[214] M. Czakon, D. Heymes, and A. Mitov, *fastNLO tables for NNLO top-quark pair differential distributions*, arXiv:1704.08551 [hep-ph].

[215] E. Bagnaschi, M. Cacciari, A. Guffanti, and L. Jenniches, *An extensive survey of the estimation of uncertainties from missing higher orders in perturbative calculations*, JHEP **02** (2015) 133.

[216] S. Moch, B. Ruijl, T. Ueda, J. A. M. Vermaseren, and A. Vogt, *Four-Loop Non-Singlet Splitting Functions in the Planar Limit and Beyond*, JHEP **10** (2017) 041.

[217] F. Dulat, B. Mistlberger, and A. Pelloni, *Differential Higgs production at N^3LO beyond threshold*, JHEP **01** (2018) 145.

[218] M. Bonvini, S. Marzani, J. Rojo, L. Rottoli, M. Ubiali, R. D. Ball, V. Bertone, S. Carrazza, and N. P. Hartland, *Parton distributions with threshold resummation*, JHEP **09** (2015) 191.

[219] R. D. Ball, V. Bertone, M. Bonvini, S. Marzani, J. Rojo, and L. Rottoli, *Parton distributions with small-x resummation: evidence for BFKL dynamics in HERA data*, Eur. Phys. J. **C78** (2018) no. 4, 321.

[220] M. Czakon, A. Ferroglia, D. Heymes, A. Mitov, B. D. Pecjak, D. J. Scott, X. Wang, and L. L. Yang, *Resummation for (boosted) top-quark pair production at NNLO+NNLL' in QCD*, JHEP **05** (2018) 149, arXiv:1803.07623 [hep-ph].

[221] K. Mishra et al., *Electroweak Corrections at High Energies*, in *Proceedings, 2013 Community Summer Study on the Future of U.S. Particle Physics: Snowmass on the Mississippi (CSS2013): Minneapolis, MN, USA, July 29-August 6, 2013*. 2013. arXiv:1308.1430 [hep-ph]. http://lss.fnal.gov/archive/2013/conf/fermilab-conf-13-514-cms.pdf.

[222] A. Manohar, P. Nason, G. P. Salam, and G. Zanderighi, *How bright is the proton? A precise determination of the photon parton distribution function*, Phys. Rev. Lett. **117** (2016) no. 24, 242002, arXiv:1607.04266 [hep-ph].

[223] A. V. Manohar, P. Nason, G. P. Salam, and G. Zanderighi, *The Photon Content of the Proton*, JHEP **12** (2017) 046, arXiv:1708.01256 [hep-ph].

[224] NNPDF Collaboration, V. Bertone, S. Carrazza, N. P. Hartland, and J. Rojo, *Illuminating the photon content of the proton within a global PDF analysis*, SciPost Phys. **5** (2018) no. 1, 008, arXiv:1712.07053 [hep-ph].

[225] J. Rojo, *Parton Distributions at a 100 TeV Hadron Collider*, PoS **DIS2016** (2016) 275, arXiv:1605.08302 [hep-ph].

[226] M. Bonvini, *Small-x phenomenology at the LHC and beyond: HELL 3.0 and the case of the Higgs cross section*, Eur. Phys. J. **C78** (2018) no. 10, 834, arXiv:1805.08785 [hep-ph].

[227] B. Fornal, A. V. Manohar, and W. J. Waalewijn, *Electroweak Gauge Boson Parton Distribution Functions*, JHEP **05** (2018) 106.

[228] T. Han, J. Sayre, and S. Westhoff, *Top-Quark Initiated Processes at High-Energy Hadron Colliders*, JHEP **04** (2015) 145.

[229] V. Bertone, A. Glazov, A. Mitov, A. Papanastasiou, and M. Ubiali, *Heavy-flavor parton distributions without heavy-flavor matching prescriptions*, JHEP **04** (2018) 046.

[230] P. Skands, S. Carrazza, and J. Rojo, *Tuning PYTHIA 8.1: the Monash 2013 Tune*, European Physical Journal C **74** (2014) 3024, arXiv:1404.5630 [hep-ph].

[231] R. Gauld and J. Rojo, *Precision determination of the small-x gluon from charm production at LHCb*, Phys. Rev. Lett. **118** (2017) no. 7, 072001, arXiv:1610.09373 [hep-ph].

[232] I. Brivio, Y. Jiang, and M. Trott, *The SMEFTsim package, theory and tools*, JHEP **12** (2017) 070, arXiv:1709.06492 [hep-ph].

[233] A. Dedes, W. Materkowska, M. Paraskevas, J. Rosiek, and K. Suxho, *Feynman rules for the Standard Model Effective Field Theory in R_x -gauges*, JHEP **06** (2017) 143, arXiv:1704.03888 [hep-ph].

[234] D. Barducci et al., *Interpreting top-quark LHC measurements in the standard-model effective field theory*, arXiv:1802.07237 [hep-ph].

[235] A. Alloul, B. Fuks, and V. Sanz, *Phenomenology of the Higgs Effective Lagrangian via FEYNRULES*, JHEP **04** (2014) 110, arXiv:1310.5150.

[236] F. Maltoni, K. Mawatari, and M. Zaro, *Higgs characterisation via vector-boson fusion and associated production: NLO and parton-shower effects*, Eur. Phys. J. **C74** (2014) no. 1, 2710, arXiv:1311.1829 [hep-ph].

[237] F. Demartin, F. Maltoni, K. Mawatari, B. Page, and M. Zaro, *Higgs characterisation at NLO in QCD: CP properties of the top-quark Yukawa interaction*, Eur. Phys. J. **C74** (2014) no. 9, 3065, arXiv:1407.5089 [hep-ph].

[238] F. Demartin, F. Maltoni, K. Mawatari, and M. Zaro, *Higgs production in association with a single top quark at the LHC*, Eur. Phys. J. **C75** (2015) no. 6, 267, arXiv:1504.00611 [hep-ph].

[239] A. Falkowski, B. Fuks, K. Mawatari, K. Mimasu, F. Riva, and V. Sanz, *Rosetta: an operator basis translator for Standard Model effective field theory*, Eur. Phys. J. **C75** (2015) no. 12, 583, arXiv:1508.05895 [hep-ph].

[240] K. Mimasu, V. Sanz, and C. Williams, *Higher Order QCD predictions for Associated Higgs production with anomalous couplings to gauge bosons*, JHEP **08** (2016) 039, arXiv:1512.02572 [hep-ph].

[241] R. Grober, M. Muhlleitner, and M. Spira, *Higgs Pair Production at NLO QCD for CP-violating Higgs Sectors*, Nucl. Phys. **B925** (2017) 1–27, arXiv:1705.05314 [hep-ph].

[242] F. Goertz, A. Papaefstathiou, L. L. Yang, and J. Zurita, *Higgs boson pair production in the D=6 extension of the SM*, JHEP **04** (2015) 167, arXiv:1410.3471 [hep-ph].

[243] M. Spira, *HIGLU: A program for the calculation of the total Higgs production cross-section at hadron colliders via gluon fusion including QCD corrections*, arXiv:hep-ph/9510347 [hep-ph].

[244] M. Spira, *HIGLU and HDECAY: Programs for Higgs boson production at the LHC and Higgs boson decay widths*, Nucl. Instrum. Meth. **A389** (1997) 357–360, arXiv:hep-ph/9610350 [hep-ph].

[245] R. V. Harlander, S. Liebler, and H. Mantler, *SusHi Bento: Beyond NNLO and the heavy-top limit*, Comput. Phys. Commun. **212** (2017) 239–257, arXiv:1605.03190 [hep-ph].

[246] H. Mantler and M. Wiesemann, *Hadronic Higgs production through NLO + PS in the SM, the 2HDM and the MSSM*, Eur. Phys. J. **C75** (2015) no. 6, 257, arXiv:1504.06625 [hep-ph].

[247] K. Arnold et al., *VBFNLO: A Parton level Monte Carlo for processes with electroweak bosons*, Comput. Phys. Commun. **180** (2009) 1661–1670, arXiv:0811.4559 [hep-ph].

[248] K. Arnold et al., *VBFNLO: A Parton Level Monte Carlo for Processes with Electroweak Bosons – Manual for Version 2.5.0*, arXiv:1107.4038 [hep-ph].

[249] A. Djouadi, J. Kalinowski, and M. Spira, *HDECAY: A Program for Higgs boson decays in the standard model and its supersymmetric extension*, Comput. Phys. Commun. **108** (1998) 56–74, arXiv:hep-ph/9704448 [hep-ph].

[250] R. Contino, M. Ghezzi, C. Grojean, M. Mühlleitner, and M. Spira, *eHDECAY: an Implementation of the Higgs Effective Lagrangian into HDECAY*, Comput. Phys. Commun. **185** (2014) 3412–3423, arXiv:1403.3381 [hep-ph].

[251] B. Gripaios and D. Sutherland, *DEFT: A program for operators in EFT*, arXiv:1807.07546 [hep-ph].

[252] J. Aebischer et al., *WCxf: an exchange format for Wilson coefficients beyond the Standard Model*, Comput. Phys. Commun. **232** (2018) 71–83, arXiv:1712.05298 [hep-ph].

[253] A. Celis, J. Fuentes-Martin, A. Vicente, and J. Virto, *DsixTools: The Standard Model Effective Field Theory Toolkit*, Eur. Phys. J. **C77** (2017) no. 6, 405, arXiv:1704.04504 [hep-ph].

[254] J. Aebischer, J. Kumar, and D. M. Straub, *Wilson: a Python package for the running and matching of Wilson coefficients above and below the electroweak scale*, Eur. Phys. J. **C78** (2018) no. 12, 1026, arXiv:1804.05033 [hep-ph].

[255] C. Degrande, B. Fuks, K. Mawatari, K. Mimasu, and V. Sanz, *Electroweak Higgs boson production in the standard model effective field theory beyond leading order in QCD*, Eur. Phys. J. **C77** (2017) no. 4, 262, arXiv:1609.04833 [hep-ph].

[256] S. Alioli, W. Dekens, M. Girard, and E. Mereghetti, *NLO QCD corrections to SM-EFT dilepton and electroweak Higgs boson production, matched to parton shower in POWHEG*, JHEP **08** (2018) 205, arXiv:1804.07407 [hep-ph].

[257] D. Buarque Franzosi and C. Zhang, *Probing the top-quark chromomagnetic dipole moment at next-to-leading order in QCD*, Phys. Rev. **D91** (2015) no. 11, 114010, arXiv:1503.08841 [hep-ph].

[258] C. Zhang, *Single Top Production at Next-to-Leading Order in the Standard Model Effective Field Theory*, Phys. Rev. Lett. **116** (2016) no. 16, 162002, arXiv:1601.06163 [hep-ph].

[259] O. Bessidskaia Bylund, F. Maltoni, I. Tsinikos, E. Vryonidou, and C. Zhang, *Probing top quark neutral couplings in the Standard Model Effective Field Theory at NLO in QCD*, JHEP **05** (2016) 052, arXiv:1601.08193 [hep-ph].

[260] F. Maltoni, E. Vryonidou, and C. Zhang, *Higgs production in association with a top-antitop pair in the Standard Model Effective Field Theory at NLO in QCD*, JHEP **10** (2016) 123, arXiv:1607.05330 [hep-ph].

[261] C. Degrande, F. Maltoni, K. Mimasu, E. Vryonidou, and C. Zhang, *Single-top associated production with a Z or H boson at the LHC: the SMEFT interpretation*, JHEP **10** (2018) 005, arXiv:1804.07773 [hep-ph].

[262] M. de Beurs, E. Laenen, M. Vreeswijk, and E. Vryonidou, *Effective operators in t-channel single top production and decay*, Eur. Phys. J. **C78** (2018) no. 11, 919, arXiv:1807.03576 [hep-ph].

[263] E. Vryonidou and C. Zhang, *Dimension-six electroweak top-loop effects in Higgs production and decay*, JHEP **08** (2018) 036, arXiv:1804.09766 [hep-ph].

[264] G. Degrassi, P. P. Giardino, F. Maltoni, and D. Pagani, *Probing the Higgs self coupling via single Higgs production at the LHC*, JHEP **12** (2016) 080, arXiv:1607.04251 [hep-ph].

[265] W. Bizon, M. Gorbahn, U. Haisch, and G. Zanderighi, *Constraints on the trilinear Higgs coupling from vector boson fusion and associated Higgs production at the LHC*, JHEP **07** (2017) 083, arXiv:1610.05771 [hep-ph].

[266] S. Di Vita, C. Grojean, G. Panico, M. Riembau, and T. Vantalon, *A global view on the Higgs self-coupling*, JHEP **09** (2017) 069, arXiv:1704.01953 [hep-ph].

[267] C. Hartmann and M. Trott, *Higgs Decay to Two Photons at One Loop in the Standard Model Effective Field Theory*, Phys. Rev. Lett. **115** (2015) no. 19, 191801, arXiv:1507.03568 [hep-ph].

[268] C. Hartmann and M. Trott, *On one-loop corrections in the standard model effective field theory; the $\Gamma(h \to \gamma\,\gamma)$ case*, JHEP **07** (2015) 151, arXiv:1505.02646 [hep-ph].

[269] C. Hartmann, W. Shepherd, and M. Trott, *The Z decay width in the SMEFT: y_t and λ corrections at one loop*, JHEP **03** (2017) 060, arXiv:1611.09879 [hep-ph].

[270] S. Dawson and P. P. Giardino, *Higgs decays to ZZ and $Z\gamma$ in the standard model effective field theory: An NLO analysis*, Phys. Rev. **D97** (2018) no. 9, 093003, arXiv:1801.01136 [hep-ph].

[271] A. Dedes, M. Paraskevas, J. Rosiek, K. Suxho, and L. Trifyllis, *The decay $h \to \gamma\gamma$ in the Standard-Model Effective Field Theory*, JHEP **08** (2018) 103, arXiv:1805.00302 [hep-ph].

[272] S. Dawson and P. P. Giardino, *Electroweak corrections to Higgs boson decays to $\gamma\gamma$ and W^+W^- in standard model EFT*, Phys. Rev. **D98** (2018) no. 9, 095005, arXiv:1807.11504 [hep-ph].

[273] DELPHES 3 Collaboration, J. de Favereau, C. Delaere, P. Demin, A. Giammanco, V. Lemaître, A. Mertens, and M. Selvaggi, *DELPHES 3, A modular framework for fast simulation of a generic collider experiment*, JHEP **02** (2014) 057, arXiv:1307.6346 [hep-ex].

[274] M. Cacciari, G. P. Salam, and G. Soyez, *The Anti-k_t Jet Clustering Algorithm*, JHEP **04** (2008) 063, arXiv:0802.1189 [hep-ph].

[275] M. Cacciari, G. P. Salam, and G. Soyez, *FastJet User Manual*, Eur. Phys. J. **C72** (2012) 1896, arXiv:1111.6097 [hep-ph].

[276] ATLAS Collaboration, *Expected performance of the ATLAS detector at the High-Luminosity LHC*, ATL-PHYS-PUB-2019-005, CERN, Geneva, Jan, 2019. http://cds.cern.ch/record/2655304.

[277] CMS Collaboration, *Expected performance of the physics objects with the upgraded CMS detector at the HL-LHC*, CERN-CMS-NOTE-2018-006, CERN, Geneva, Dec, 2018. https://cds.cern.ch/record/2650976.

[278] ATLAS Collaboration, *Technical Design Report for the Phase-II Upgrade of the ATLAS TDAQ System*, CERN-LHCC-2017-020. ATLAS-TDR-029, CERN, Geneva, Sep, 2017. http://cds.cern.ch/record/2285584.

[279] CMS Collaboration, *The Phase-2 Upgrade of the CMS L1 Trigger Interim Technical Design Report*, CERN-LHCC-2017-013. CMS-TDR-017, CERN, Geneva, Sep, 2017. https://cds.cern.ch/record/2283192. This is the CMS Interim TDR devoted to the upgrade of the CMS L1 trigger in view of the HL-LHC running, as approved by the LHCC.

[280] ATLAS Collaboration, *Technical Design Report for the ATLAS Inner Tracker Pixel Detector*, CERN-LHCC-2017-021. ATLAS-TDR-030, CERN, Geneva, Sep, 2017. http://cds.cern.ch/record/2285585.

[281] ATLAS Collaboration, *Technical Design Report for the ATLAS Inner Tracker Strip Detector*, CERN-LHCC-2017-005. ATLAS-TDR-025, CERN, Geneva, Apr, 2017. http://cds.cern.ch/record/2257755.

[282] CMS Collaboration, *The Phase-2 Upgrade of the CMS Tracker*, CERN-LHCC-2017-009. CMS-TDR-014, CERN, 2017. https://cds.cern.ch/record/2272264.

[283] ATLAS Collaboration, *Technical Design Report for the Phase-II Upgrade of the ATLAS LAr Calorimeter*, CERN-LHCC-2017-018. ATLAS-TDR-027, CERN, Geneva, Sep, 2017. http://cds.cern.ch/record/2285582.

[284] CMS Collaboration, *The Phase-2 Upgrade of the CMS Barrel Calorimeters Technical Design Report*, CERN-LHCC-2017-011. CMS-TDR-015, CERN, 2017. https://cds.cern.ch/record/2283187.

[285] CMS Collaboration, *The Phase-2 Upgrade of the CMS Endcap Calorimeter*, CERN-LHCC-2017-023. CMS-TDR-019, 2017. https://cds.cern.ch/record/2293646.

[286] CMS Collaboration, *Technical Proposal for a MIP Timing Detector in the CMS Experiment Phase-2 Upgrade*, CERN-LHCC-2017-027. LHCC-P-009, 2017. https://cds.cern.ch/record/2296612.

[287] ATLAS Collaboration, *Technical Design Report for the Phase-II Upgrade of the ATLAS Muon Spectrometer*, CERN-LHCC-2017-017. ATLAS-TDR-026, CERN, Geneva, Sep, 2017. http://cds.cern.ch/record/2285580.

[288] CMS Collaboration, *The Phase-2 Upgrade of the CMS Muon Detectors*, CERN-LHCC-2017-012. CMS-TDR-016, 2017. https://cds.cern.ch/record/2283189.

[289] ATLAS Collaboration, *Technical Design Report for the Phase-II Upgrade of the ATLAS Tile Calorimeter*, CERN-LHCC-2017-019. ATLAS-TDR-028, CERN, Geneva, Sep, 2017. http://cds.cern.ch/record/2285583.

[290] CMS Collaboration, *Technical Proposal for the Phase-II Upgrade of the CMS Detector*, Cern-lhcc-2015-010, Geneva, Jun, 2015. https://cds.cern.ch/record/2020886.

[291] ATLAS Collaboration, *Technical Proposal: A High-Granularity Timing Detector for the ATLAS Phase-II Upgrade*, CERN-LHCC-2018-023. LHCC-P-012, CERN, Geneva, Jun, 2018. http://cds.cern.ch/record/2623663.

[292] T. Sjostrand, S. Mrenna, and P. Z. Skands, *A Brief Introduction to PYTHIA 8.1*, Comput. Phys. Commun. **178** (2008) 852–867, arXiv:0710.3820 [hep-ph].

[293] I. Belyaev et al., *Handling of the generation of primary events in Gauss, the LHCb simulation framework*, J. Phys. Conf. Ser. **331** (2011) 032047.

[294] J. Pumplin, D. Stump, J. Huston, H. Lai, P. M. Nadolsky, et al., *New generation of parton distributions with uncertainties from global QCD analysis*, JHEP **07** (2002) 012, arXiv:hep-ph/0201195 [hep-ph].

[295] J. Allison et al., *Geant4 developments and applications*, IEEE Trans. Nucl. Sci. **53** (2006) 270. SLAC-PUB-11870.

[296] S. Agostinelli et al., *GEANT4: A Simulation Toolkit*, Nucl. Instrum. Meth. **A 506** (2003) 250. SLAC-PUB-9350.

[297] M. Clemencic et al., *The LHCb simulation application, Gauss: Design, evolution and experience*, J. Phys. Conf. Ser. **331** (2011) 032023.

[298] R. Abdul Khalek, S. Bailey, J. Gao, L. Harland-Lang, and J. Rojo, *Towards Ultimate Parton Distributions at the High-Luminosity LHC*, Eur. Phys. J. **C78** (2018) no. 11, 962, arXiv:1810.03639 [hep-ph].

[299] ATLAS Collaboration, G. Aad et al., *Measurement of $W^{\pm}$ and Z-boson production cross sections in pp collisions at $\sqrt{s} = 13$ TeV with the ATLAS detector*, Phys. Lett. **B759** (2016) 601–621, arXiv:1603.09222 [hep-ex].

[300] CMS Collaboration, A. M. Sirunyan et al., *Measurement of the $t\bar{t}$ production cross section using events with one lepton and at least one jet in pp collisions at $\sqrt{s}$ = 13 TeV*, JHEP **09** (2017) 051, arXiv:1701.06228 [hep-ex].

[301] G. Apollinari, I. Béjar Alonso, O. Brüning, P. Fessia, M. Lamont, L. Rossi, and L. Tavian, *High-Luminosity Large Hadron Collider (HL-LHC): Technical Design Report V. 0.1*. CERN Yellow Reports: Monographs. CERN, Geneva, 2017. https://cds.cern.ch/record/2284929.

[302] H. Ogul and K. Dilsiz, *Cross Section Prediction for Inclusive Production of Z Boson in pp Collisions at $\sqrt{s} = 14$ TeV: A Study of Systematic Uncertainty Due to Scale Dependence*, Adv. High Energy Phys. **2017** (2017) 8262018, arXiv:1702.07206 [hep-ph].

[303] S. van der Meer, *Calibration of the effective beam height in the ISR*, CERN-ISR-PO-68-31. ISR-PO-68-31, CERN, Geneva, 1968. https://cds.cern.ch/record/296752.

[304] P. Grafström and W. Kozanecki, *Luminosity determination at proton colliders*, Prog. Part. Nucl. Phys. **81** (2015) 97–148.

[305] H. Bartosik and G. Rumolo, *Production of single Gaussian bunches for Van der Meer scans in the LHC injector chain*, CERN-ACC-NOTE-2013-0008, 2013. https://cds.cern.ch/record/1590405.

[306] CMS Collaboration, *CMS luminosity measurement for the 2017 data-taking period at* $\sqrt{s} = 13$ TeV, CMS-PAS-LUM-17-004, CERN, Geneva, 2018. https://cds.cern.ch/record/2621960.

[307] ATLAS Collaboration, M. Aaboud et al., *Luminosity determination in pp collisions at* $\sqrt{s} = 8$ *TeV using the ATLAS detector at the LHC*, Eur. Phys. J. **C76** (2016) no. 12, 653, arXiv:1608.03953 [hep-ex].

[308] LHCb Collaboration, R. Aaij et al., *Precision luminosity measurements at LHCb*, JINST **9** (2014) no. 12, P12005, arXiv:1410.0149 [hep-ex].

[309] M. Hostettler and G. Papotti, *Beam Size Estimation from Luminosity Scans at the LHC During 2015 Proton Physics Operation*, in *Proceedings, 7th International Particle Accelerator Conference (IPAC 2016): Busan, Korea, May 8-13, 2016*, p. MOPMR025. 2016.

[310] O. Karacheban and T. Peter, *CMS emittance scans for luminosity calibration in 2017*, AYSS-2018: XXII International Scientific Conference of Young Scientists and Specialists , https://indico.jinr.ru/contributionDisplay.py?contribId=348&confId=436.

[311] M. Hostettler, K. Fuchsberger, G. Papotti, Y. Papaphilippou, and T. Pieloni, *Luminosity Scans for Beam Diagnostics*, Phys. Rev. Accel. Beams **21** (2018) no. 10, 102801, arXiv:1804.10099 [physics.acc-ph].

[312] CMS Collaboration, O. Karacheban, *CMS emittance scans for luminosity calibration in 2017*, CMS-CR-2018-062, CERN, Geneva, Jun, 2018. https://cds.cern.ch/record/2630628.

[313] J. Salfeld-Nebgen and D. Marlow, *Data-Driven Precision Luminosity Measurements with Z Bosons at the LHC and HL-LHC*, JINST **13** (2018) no. 12, P12016, arXiv:1806.02184 [hep-ex].

[314] S. Alioli, P. Nason, C. Oleari, and E. Re, *A General Framework for Implementing NLO Calculations in Shower Monte Carlo Programs: the POWHEG BOX*, JHEP **06** (2010) 043, arXiv:1002.2581 [hep-ph].

[315] P. Nason and C. Oleari, *NLO Higgs boson production via vector-boson fusion matched with shower in POWHEG*, JHEP **02** (2010) 037, arXiv:0911.5299 [hep-ph].

[316] B. Jager, F. Schissler, and D. Zeppenfeld, *Parton-shower effects on Higgs boson production via vector-boson fusion in association with three jets*, JHEP **07** (2014) 125, arXiv:1405.6950 [hep-ph].

[317] M. Ciccolini, A. Denner, and S. Dittmaier, *Electroweak and QCD corrections to Higgs production via vector-boson fusion at the LHC*, Phys. Rev. **D77** (2008) 013002, arXiv:0710.4749 [hep-ph].

[318] M. Ciccolini, A. Denner, and S. Dittmaier, *Strong and electroweak corrections to the production of Higgs + 2jets via weak interactions at the LHC*, Phys. Rev. Lett. **99** (2007) 161803, arXiv:0707.0381 [hep-ph].

[319] A. Denner, S. Dittmaier, S. Kallweit, and A. Muck, *Electroweak corrections to Higgs-strahlung off W/Z bosons at the Tevatron and the LHC with HAWK*, JHEP **03** (2012) 075, arXiv:1112.5142 [hep-ph].

[320] Denner, Ansgar and Dittmaier, Stefan and Kallweit, Stefan and Mück, Alexander, *HAWK 2.0: A Monte Carlo program for Higgs production in vector-boson fusion and Higgs strahlung at hadron colliders*, Comput. Phys. Commun. **195** (2015) 161–171, arXiv:1412.5390 [hep-ph].

[321] J. Cruz-Martinez, T. Gehrmann, E. Glover, and A. Huss, *Second-order QCD effects in Higgs boson production through vector boson fusion*, Physics Letters B **781** (2018) 672 – 677.

[322] M. Cacciari and G. P. Salam, *Dispelling the* N^3 *Myth for the* k_t *Jet-Finder*, Phys. Lett. **B 641** (2006) 57, arXiv:0512210 [hep-ph].

[323] X. Chen, T. Gehrmann, E. W. N. Glover, and M. Jaquier, *Precise QCD predictions for the production of Higgs + jet final states*, Phys. Lett. **B740** (2015) 147–150, arXiv:1408.5325 [hep-ph].

[324] X. Chen, J. Cruz-Martinez, T. Gehrmann, E. W. N. Glover, and M. Jaquier, *NNLO QCD corrections to Higgs boson production at large transverse momentum*, JHEP **10** (2016) 066, arXiv:1607.08817 [hep-ph].

[325] L. Cieri, X. Chen, T. Gehrmann, E. W. N. Glover, and A. Huss, *Higgs boson production at the LHC using the q_T subtraction formalism at N^3LO QCD*, JHEP **02** (2019) 096, arXiv:1807.11501 [hep-ph].

[326] T. Gehrmann et al., *Jet cross sections and transverse momentum distributions with NNLOJET*, in *13th International Symposium on Radiative Corrections: Application of Quantum Field Theory to Phenomenology (RADCOR 2017) St. Gilgen, Austria, September 24-29, 2017*. 2018. arXiv:1801.06415 [hep-ph].

[327] A. Gehrmann-De Ridder, T. Gehrmann, E. W. N. Glover, A. Huss, and T. A. Morgan, *Precise QCD predictions for the production of a Z boson in association with a hadronic jet*, Phys. Rev. Lett. **117** (2016) no. 2, 022001, arXiv:1507.02850 [hep-ph].

[328] J. Currie, T. Gehrmann, and J. Niehues, *Precise QCD predictions for the production of dijet final states in deep inelastic scattering*, Phys. Rev. Lett. **117** (2016) no. 4, 042001, arXiv:1606.03991 [hep-ph].

[329] A. Gehrmann-De Ridder, T. Gehrmann, E. W. N. Glover, A. Huss, and D. M. Walker, *Next-to-Next-to-Leading-Order QCD Corrections to the Transverse Momentum Distribution of Weak Gauge Bosons*, Phys. Rev. Lett. **120** (2018) no. 12, 122001, arXiv:1712.07543 [hep-ph].

[330] J. Currie, T. Gehrmann, E. W. N. Glover, A. Huss, J. Niehues, and A. Vogt, *N^3LO corrections to jet production in deep inelastic scattering using the Projection-to-Born method*, JHEP **05** (2018) 209, arXiv:1803.09973 [hep-ph].

[331] J. Niehues and D. Walker, *NNLO QCD corrections to jet production in charged current deep inelastic scattering*, Physics Letters B **788** (2019) 243 – 248.

[332] J. Currie, A. Gehrmann-De Ridder, T. Gehrmann, E. W. N. Glover, A. Huss, and J. Pires, *Infrared sensitivity of single jet inclusive production at hadron colliders*, JHEP **10** (2018) 155, arXiv:1807.03692 [hep-ph].

[333] F. Campanario, T. M. Figy, S. Plätzer, and M. Sjodahl, *Electroweak Higgs Boson Plus Three Jet Production at Next-to-Leading-Order QCD*, Phys. Rev. Lett. **111** (2013) no. 21, 211802, arXiv:1308.2932 [hep-ph].

[334] F. Campanario, T. M. Figy, S. Plätzer, and M. Sjodahl, *NLO QCD Corrections to Electroweak Higgs Boson Plus Three Jet Production at the LHC*, PoS **RADCOR2013** (2013) 042, arXiv:1311.5455 [hep-ph].

[335] F. Campanario, T. M. Figy, S. Plätzer, and M. Sjodahl, *Beyond the t-channel Approximation: Next-to-Leading Order QCD Corrections to Electroweak Higgs Boson Production Plus Three Jets Production at the LHC*, PoS **LL2014** (2014) 025, arXiv:1407.5050 [hep-ph].

[336] F. Campanario, T. M. Figy, S. Plätzer, M. Rauch, P. Schichtel, and M. Sjödahl, *Stress testing the vector-boson-fusion approximation in multijet final states*, Phys. Rev. D **98** (Aug, 2018) 033003.

[337] F. Campanario, *Towards pp -> VVjj at NLO QCD: Bosonic contributions to triple vector boson production plus jet*, JHEP **10** (2011) 070, arXiv:1105.0920 [hep-ph].

[338] M. Sjodahl, *ColorFull – a C++ library for calculations in SU(Nc) color space*, Eur. Phys. J. **C75** (2015) no. 5, 236, arXiv:1412.3967 [hep-ph].

[339] J. Baglio et al., *Release Note - VBFNLO 2.7.0*, arXiv:1404.3940 [hep-ph].

[340] T. Figy, V. Hankele, and D. Zeppenfeld, *Next-to-leading order QCD corrections to Higgs plus three jet production in vector-boson fusion*, JHEP **02** (2008) 076, arXiv:0710.5621 [hep-ph].

[341] S. Platzer and S. Gieseke, *Dipole Showers and Automated NLO Matching in Herwig++*, Eur. Phys. J. **C72** (2012) 2187, arXiv:1109.6256 [hep-ph].

[342] J. Bellm et al., *Herwig 7.1 Release Note*, arXiv:1705.06919 [hep-ph].

[343] M. Cacciari, G. P. Salam, and G. Soyez, *FastJet User Manual*, Eur. Phys. J. **C72** (2012) 1896, arXiv:1111.6097 [hep-ph].

[344] A. Buckley, J. Butterworth, L. Lonnblad, D. Grellscheid, H. Hoeth, J. Monk, H. Schulz, and F. Siegert, *Rivet user manual*, Comput. Phys. Commun. **184** (2013) 2803–2819, arXiv:1003.0694 [hep-ph].

[345] J. Bagger, V. D. Barger, K.-m. Cheung, J. F. Gunion, T. Han, G. A. Ladinsky, R. Rosenfeld, and C. P. Yuan, *The Strongly interacting WW system: Gold plated modes*, Phys. Rev. D **49** (1994) 1246–1264, arXiv:hep-ph/9306256.

[346] J. Bagger, V. D. Barger, K.-m. Cheung, J. F. Gunion, T. Han, G. A. Ladinsky, R. Rosenfeld, and C. P. Yuan, *CERN LHC analysis of the strongly interacting WW system: Gold plated modes*, Phys. Rev. D **52** (1995) 3878–3889, arXiv:hep-ph/9504426.

[347] CMS Collaboration, *Observation of a new boson at a mass of 125 GeV with the CMS experiment at the LHC*, Phys. Lett. B **716** (2012) 30–61, arXiv:1207.7235 [hep-ex].

[348] M. J. G. Veltman, *Second Threshold in Weak Interactions*, Acta Phys. Polon. B **8** (1977) 475. Print-77-0040 (UTRECHT).

[349] B. W. Lee, C. Quigg, and H. B. Thacker, *The Strength of Weak Interactions at Very High-Energies and the Higgs Boson Mass*, Phys. Rev. Lett. **38** (1977) 883–885. FERMILAB-PUB-77-022-THY.

[350] B. W. Lee, C. Quigg, and H. B. Thacker, *Weak Interactions at Very High-Energies: The Role of the Higgs Boson Mass*, Phys. Rev. D **16** (1977) 1519. FERMILAB-PUB-77-030-THY.

[351] HEPAP Subcommittee Collaboration, HEPAP Subcommittee Collaboration, *Building for Discovery: Strategic Plan for U.S. Particle Physics in the Global Context*, . https://inspirehep.net/record/1299183/files/FINAL_P5_Report_053014.pdf.

[352] R. Aleksan et al., *Physics Briefing Book: Input for the Strategy Group to draft the update of the European Strategy for Particle Physics*, . https://cds.cern.ch/record/1628377. Open Symposium held in Cracow from 10th to 12th of September 2012.

[353] E. Accomando, A. Ballestrero, S. Bolognesi, E. Maina, and C. Mariotti, *Boson-boson scattering and Higgs production at the LHC from a six fermion point of view: Four jets + l nu processes at* $\mathcal{O}(\alpha_{em}^6)$, JHEP **03** (2006) 093, arXiv:hep-ph/0512219.

[354] B. Zhu, P. Govoni, Y. Mao, C. Mariotti, and W. Wu, *Same Sign WW Scattering Process as a Probe of Higgs Boson in pp Collision at* $\sqrt{s} = 10$ *TeV*, Eur. Phys. J. C **71** (2011) 1514, arXiv:1010.5848 [hep-ex].

[355] ATLAS Collaboration, *Observation of electroweak production of a same-sign* W *boson pair in association with two jets in pp collisions at* $\sqrt{s} = 13$ *TeV with the ATLAS detector*, ATLAS-CONF-2018-030, CERN, Geneva, Jul, 2018. https://cds.cern.ch/record/2629411.

[356] CMS Collaboration, A. M. Sirunyan et al., *Observation of electroweak production of same-sign W boson pairs in the two jet and two same-sign lepton final state in proton-proton collisions at* $\sqrt{s} = 13$ *TeV*, Phys. Rev. Lett. **120** (2018) no. 8, 081801, arXiv:1709.05822 [hep-ex].

[357] ATLAS Collaboration, *Prospects for the measurement of the $W^{\pm}W^{\pm}$ scattering cross section and extraction of the longitudinal scattering component in pp collisions at the High-Luminosity LHC with the ATLAS experiment*, ATL-PHYS-PUB-2018-052, CERN, Geneva, 2018. https://cds.cern.ch/record/2652447.

[358] CMS Collaboration, *Study of $W^{\pm}W^{\pm}$ production via vector boson scattering at the HL-LHC with the upgraded CMS detector*, CMS-PAS-FTR-18-005, CERN, Geneva, 2018. https://cds.cern.ch/record/2646870.

[359] R. D. Ball et al., *Parton distributions with LHC data*, Nucl. Phys. B **867** (2013) 244, arXiv:1207.1303 [hep-ph].

[360] J. M. Campbell, R. K. Ellis, P. Nason, and E. Re, *Top-Pair Production and Decay at NLO Matched with Parton Showers*, JHEP **04** (2015) 114, arXiv:1412.1828 [hep-ph].

[361] M. Cacciari, G. P. Salam, G. Soyez, *The anti-k_t jet clustering algorithm*, JHEP **04** (2008) 063, arXiv:0802.1189 [hep-ph].

[362] D. Bertolini, P. Harris, M. Low, and N. Tran, *Pileup Per Particle Identification*, JHEP **10** (2014) 059, arXiv:1407.6013 [hep-ph].

[363] D. Guest, J. Collado, P. Baldi, S.-C. Hsu, G. Urban, and D. Whiteson, *Jet flavor classification in high-energy physics with deep neural networks*, Phys. Rev. D **94** (Dec, 2016) 112002. https://link.aps.org/doi/10.1103/PhysRevD.94.112002.

[364] D. L. Rainwater, R. Szalapski, and D. Zeppenfeld, *Probing color singlet exchange in Z + two jet events at the CERN LHC*, Phys. Rev. **D54** (1996) 6680–6689, arXiv:hep-ph/9605444 [hep-ph].

[365] J. Searcy, L. Huang, M.-A. Pleier, and J. Zhu, *Determination of the WW polarization fractions in $pp \to W^{\pm}W^{\pm}jj$ using a deep machine learning technique*, Phys. Rev. D **93** (2016) no. 9, 094033, arXiv:1510.01691 [hep-ph].

[366] D. Gonçalves, T. Plehn, and J. M. Thompson, *Weak boson fusion at 100 TeV*, Phys. Rev. **D95** (2017) no. 9, 095011, arXiv:1702.05098 [hep-ph].

[367] B. Jäger, L. Salfelder, M. Worek, and D. Zeppenfeld, *Physics opportunities for vector-boson scattering at a future 100 TeV hadron collider*, Phys. Rev. **D96** (2017) no. 7, 073008, arXiv:1704.04911 [hep-ph].

[368] B. Jäger, C. Oleari, and D. Zeppenfeld, *Next-to-leading order QCD corrections to W^+W^- production via vector-boson fusion*, JHEP **07** (2006) 015, arXiv:hep-ph/0603177 [hep-ph].

[369] B. Jäger, C. Oleari, and D. Zeppenfeld, *Next-to-leading order QCD corrections to Z boson pair production via vector-boson fusion*, Phys. Rev. **D73** (2006) 113006, arXiv:hep-ph/0604200 [hep-ph].

[370] G. Bozzi, B. Jäger, C. Oleari, and D. Zeppenfeld, *Next-to-leading order QCD corrections to W^+Z and W^-Z production via vector-boson fusion*, Phys. Rev. **D75** (2007) 073004, arXiv:hep-ph/0701105 [hep-ph].

[371] B. Jäger, C. Oleari, and D. Zeppenfeld, *Next-to-leading order QCD corrections to W^+W^+jj and W^-W^-jj production via weak-boson fusion*, Phys. Rev. **D80** (2009) 034022, arXiv:0907.0580 [hep-ph].

[372] B. Jäger and G. Zanderighi, *NLO corrections to electroweak and QCD production of W^+W^+ plus two jets in the POWHEGBOX*, JHEP **11** (2011) 055, arXiv:1108.0864 [hep-ph].

[373] A. Denner, L. Hošeková, and S. Kallweit, *NLO QCD corrections to W^+W^+jj production in vector-boson fusion at the LHC*, Phys. Rev. **D86** (2012) 114014, arXiv:1209.2389 [hep-ph].

[374] M. Rauch, *Vector-Boson Fusion and Vector-Boson Scattering*, arXiv:1610.08420 [hep-ph].

[375] A. Ballestrero et al., *Precise predictions for same-sign W-boson scattering at the LHC*, Eur. Phys. J. **C78** (2018) no. 8, 671, arXiv:1803.07943 [hep-ph].

[376] B. Jager, A. Karlberg, and J. Scheller, *Parton-shower effects in electroweak $WZjj$ production at the next-to-leading order of QCD*, Eur. Phys. J. **C79** (2019) no. 3, 226, arXiv:1812.05118 [hep-ph].

[377] S. Frixione, P. Nason, and C. Oleari, *Matching NLO QCD Computations with Parton Shower Simulations: the POWHEG Method*, JHEP **11** (2007) 070, arXiv:0709.2092 [hep-ph].

[378] T. Gleisberg, S. Höche, F. Krauss, A. Schälicke, S. Schumann, and J.-C. Winter, *SHERPA 1.α: A Proof of concept version*, JHEP **02** (2004) 056, arXiv:hep-ph/0311263 [hep-ph].

[379] D. Yu. Bardin, A. Leike, T. Riemann, and M. Sachwitz, *Energy-dependent width effects in e^+e^--annihilation near the Z-boson pole*, Phys. Lett. **B206** (1988) 539–542.

[380] A. Denner, S. Dittmaier, M. Roth, and D. Wackeroth, *Electroweak radiative corrections to $e^+e^- \to WW \to$ 4 fermions in double-pole approximation: The RACOONWW approach*, Nucl. Phys. **B587** (2000) 67–117, arXiv:hep-ph/0006307 [hep-ph].

[381] A. Denner et al., *Predictions for all processes $e^+e^- \to 4$ fermions $+\gamma$*, Nucl. Phys. **B560** (1999) 33–65, arXiv:hep-ph/9904472.

[382] A. Denner et al., *Electroweak corrections to charged-current $e^+e^- \to 4$ fermion processes: Technical details and further results*, Nucl. Phys. **B724** (2005) 247–294, arXiv:hep-ph/0505042.

[383] A. Denner and S. Dittmaier, *The complex-mass scheme for perturbative calculations with unstable particles*, Nucl. Phys. Proc. Suppl. **160** (2006) 22–26, arXiv:hep-ph/0605312 [hep-ph]. [,22(2006)].

[384] ATLAS Collaboration, G. Aad et al., *Evidence for Electroweak Production of $W^\pm W^\pm jj$ in pp Collisions at $\sqrt{s} = 8$ TeV with the ATLAS Detector*, Phys. Rev. Lett. **113** (2014) no. 14, 141803, arXiv:1405.6241 [hep-ex].

[385] ATLAS Collaboration, M. Aaboud et al., *Measurement of $W^\pm W^\pm$ vector-boson scattering and limits on anomalous quartic gauge couplings with the ATLAS detector*, Phys. Rev. **D96** (2017) 012007, arXiv:1611.02428 [hep-ex].

[386] CMS Collaboration, V. Khachatryan et al., *Study of vector boson scattering and search for new physics in events with two same-sign leptons and two jets*, Phys. Rev. Lett. **114** (2015) no. 5, 051801, arXiv:1410.6315 [hep-ex].

[387] ATLAS Collaboration, *Studies on the impact of an extended Inner Detector tracker and a forward muon tagger on $W^\pm W^\pm$ scattering in pp collisions at the High-Luminosity LHC with the ATLAS experiment*, . https://cds.cern.ch/record/2298958.

[388] C. Schwan, *NLO EW corrections for W and Z scattering at the LHC*, 2018. https://indico.cern.ch/event/702614/.

[389] A. Denner, S. Dittmaier, P. Maierhöfer, M. Pellen, and C. Schwan, *QCD and electroweak corrections to WZ scattering at the LHC*, arXiv:1904.00882 [hep-ph].

[390] ATLAS Collaboration, *Observation of electroweak $W^\pm Z$ boson pair production in association with two jets in pp collisions at $\sqrt{s} = 13$ TeV with the ATLAS detector*, Submitted to: Phys. Lett. (2018) , arXiv:1812.09740 [hep-ex].

[391] CMS Collaboration, *Measurement of electroweak WZ production and search for new physics in pp collisions at sqrt(s) = 13 TeV*, CMS-PAS-SMP-18-001, CERN, Geneva, 2018. https://cds.cern.ch/record/2629457.

[392] CMS Collaboration, *Prospects for the measurement of electroweak and polarized WZ to 3lv production cross sections at the High-Luminosity LHC* , CMS-PAS-FTR-18-038, CERN, Geneva, 2018. https://cds.cern.ch/record/2650774.

[393] J. Alwall, M. Herquet, F. Maltoni, O. Mattelaer, and T. Stelzer, *MadGraph 5: going beyond*, JHEP **06** (2011) 128, arXiv:1106.0522 [hep-ph].

[394] O. J. P. Éboli, M. C. Gonzalez-Garcia, and J. K. Mizukoshi, *$pp \to jje^{\pm}\mu^{\pm}\nu\nu$ and $jje^{\pm}\mu^{\mp}\nu\nu$ at $\mathcal{O}(\alpha_{\rm em}^6)$ and $\mathcal{O}(\alpha_{\rm em}^4\alpha_s^2)$ for the study of the quartic electroweak gauge boson vertex at CERN LHC*, Phys. Rev. D **74** (Oct, 2006) 073005. https://link.aps.org/doi/10.1103/PhysRevD.74.073005.

[395] O. J. P. Éboli and M. C. Gonzalez–Garcia, *Classifying the bosonic quartic couplings*, Phys. Rev. **D93** (2016) no. 9, 093013, arXiv:1604.03555 [hep-ph].

[396] M. Baak et al., *Working Group Report: Precision Study of Electroweak Interactions*, in *Proceedings, Community Summer Study 2013: Snowmass on the Mississippi (CSS2013): Minneapolis, MN, USA, July 29-August 6, 2013*. 2013. arXiv:1310.6708 [hep-ph].

[397] G. Perez, M. Sekulla, and D. Zeppenfeld, *Anomalous quartic gauge couplings and unitarization for the vector boson scattering process $pp \to W^+W^+jjX \to \ell^+\nu_\ell\ell^+\nu_\ell jjX$*, Eur. Phys. J. **C78** (2018) no. 9, 759, arXiv:1807.02707 [hep-ph].

[398] CMS Collaboration, T. Sirunyan et al., *Measurement of vector boson scattering and constraints on anomalous quartic couplings from events with four leptons and two jets in proton-proton collisions at sqrt(s) = 13 TeV.*, Phys. Lett. B **774** (Aug, 2017) 682–705. 24 p, arXiv:1708.02812.

[399] CMS Collaboration, *Vector Boson Scattering prospective studies in the ZZ fully leptonic decay channel for the High-Luminosity and High-Energy LHC upgrades*, CMS-PAS-FTR-18-014, CERN, Geneva, 2018. https://cds.cern.ch/record/2650915.

[400] NNPDF Collaboration, R. D. Ball et al., *Parton distributions for the LHC Run II*, JHEP **04** (2015) 040, arXiv:1410.8849 [hep-ph].

[401] J. Alwall, R. Frederix, S. Frixione, V. Hirschi, F. Maltoni, O. Mattelaer, H.-S. Shao, T. Stelzer, P. Torielli, and M. Zaro, *The automated computation of tree-level and next-to-leading order differential cross sections, and their matching to parton shower simulations*, JHEP **07** (2014) 079, arXiv:1405.0301 [hep-ph].

[402] P. Artoisenet, R. Frederix, O. Mattelaer, and R. Rietkerk, *Automatic spin-entangled decays of heavy resonances in Monte Carlo simulations*, JHEP **03** (2013) 015, arXiv:1212.3460 [hep-ph].

[403] J. M. Campbell and R. K. Ellis, *MCFM for the Tevatron and the LHC*, Nucl. Phys. B Proc. Suppl. **205-206** (2010) 10, arXiv:1007.3492 [hep-ph].

[404] Particle Data Group Collaboration, C. Patrignani et al., *Review of Particle Physics*, Chin. Phys. **C40** (2016) no. 10, 100001.

[405] ATLAS Collaboration, *Expected performance for an upgraded ATLAS detector at High-Luminosity LHC*, ATL-PHYS-PUB-2016-026, CERN, Geneva, Oct, 2016. https://cds.cern.ch/record/2223839.

[406] CMS Collaboration, V. Khachatryan et al., *Measurement of electroweak production of two jets in association with a Z boson in proton–proton collisions at $\sqrt{s} = 8$ TeV*, Eur. Phys. J. C **75** (2015) 66, arXiv:1410.3153 [hep-ex].

[407] ATLAS Collaboration, *HL-LHC prospects for diboson resonance searches and electroweak vector boson scattering in the $WW/WZ \to \ell\nu qq$ final state*, ATL-PHYS-PUB-2018-022, CERN, Geneva, Oct, 2018. https://cds.cern.ch/record/2645269.

[408] M. Cacciari, C. P. Salam and G. Soyez, *The anti-k_t jet clustering algorithm*, JHEP **04** (2008) 063.

[409] D. Krohn, J. Thaler, and L.-T. Wang, *Jet Trimming*, JHEP **02** (2010) 084, arXiv:0912.1342 [hep-ph].

[410] ATLAS Collaboration, G. Aad et al., *Identification of boosted, hadronically decaying W bosons and comparisons with ATLAS data taken at $\sqrt{s} = 8$ TeV*, Eur. Phys. J. **C76** (2016) no. 3, 154, arXiv:1510.05821 [hep-ex].

[411] ATLAS Collaboration, *Identification of boosted, hadronically-decaying W and Z bosons in $\sqrt{s} = 13$ TeV Monte Carlo Simulations for ATLAS*, ATL-PHYS-PUB-2015-033, CERN, Geneva, Aug, 2015. https://cds.cern.ch/record/2041461.

[412] A. Hocker et al., *TMVA - Toolkit for Multivariate Data Analysis*, arXiv:physics/0703039 [physics.data-an].

[413] G. Cowan, K. Cranmer, E. Gross, and O. Vitells, *Asymptotic formulae for likelihood-based tests of new physics*, Eur. Phys. J. **C71** (2011) 1554, arXiv:1007.1727 [physics.data-an]. [Erratum: Eur. Phys. J.C73,2501(2013)].

[414] V. Cavaliere, R. Les, T. Nitta, and K. Terashi, *HE-LHC prospects for diboson resonance searches and electroweak WW/WZ production via vector boson scattering in the semi-leptonic final states*, arXiv:1812.00841 [hep-ex].

[415] The DELPHES 3 Collaboration, de Favereau, J., Delaere, C. *et al.*, *DELPHES 3: a modular framework for fast simulation of a generic collider experiment*, JHEP **02** (2014) 057, arXiv:1307.6346 [hep-ex].

[416] ATLAS Collaboration, *Prospect studies for the production of three massive vector bosons with the ATLAS detector at the High-Luminosity LHC*, ATL-PHYS-PUB-2018-030, CERN, Geneva, Nov, 2018. https://cds.cern.ch/record/2647220.

[417] A. Lazopoulos, T. McElmurry, K. Melnikov, and F. Petriello, *Next-to-Leading Order QCD Corrections to $t\bar{t}Z$ Production at the LHC*, Phys. Lett. **B 666** (2008) 62, arXiv:0804.2220 [hep-ph].

[418] M. Garzelli, A. Kardos, C. Papadopoulos, and Z. Trocsanyi, *$t\bar{t}W^{\pm}$ and $t\bar{t}Z$ Hadroproduction at NLO Accuracy in QCD with Parton Shower and Hadronization Effects*, JHEP **11** (2012) 056, arXiv:1208.2665 [hep-ph].

[419] J. M. Campbell and R. K. Ellis, *$t\bar{t}W^{\pm}$ Production and Decay at NLO*, JHEP **07** (2012) 052, arXiv:1204.5678 [hep-ph].

[420] ATLAS Collaboration, *Multi-Boson Simulation for 13 TeV ATLAS Analyses*, ATL-PHYS-PUB-2017-005, 2017. https://cds.cern.ch/record/2261933.

[421] ATLAS Collaboration, *Improvements in $t\bar{t}$ modelling using NLO+PS Monte Carlo generators for Run 2*, ATL-PHYS-PUB-2018-009, 2018. https://cds.cern.ch/record/2630327.

[422] ATLAS Collaboration, *Modelling of the $t\bar{t}H$ and $t\bar{t}V(V = W, Z)$ processes for $\sqrt{s} = 13$ TeV ATLAS analyses*, ATL-PHYS-PUB-2016-005, 2016. https://cds.cern.ch/record/2120826.

[423] M. Czakon and A. Mitov, *Top++: A Program for the Calculation of the Top-Pair Cross-Section at Hadron Colliders*, Comput. Phys. Commun. **185** (2014) 2930, arXiv:1112.5675 [hep-ph].

[424] ATLAS Collaboration, M. Aaboud et al., *Search for triboson $W^{\pm}W^{\pm}W^{\mp}$ production in pp collisions at $\sqrt{s} = 8$ TeV with the ATLAS detector*, Eur. Phys. J. **C77** (2017) no. 3, 141, arXiv:1610.05088 [hep-ex].

[425] G. Heinrich, S. Jahn, S. P. Jones, M. Kerner, and J. Pires, *NNLO predictions for Z-boson pair production at the LHC*, JHEP **03** (2018) 142, arXiv:1710.06294 [hep-ph].

[426] I. W. Stewart, F. J. Tackmann, and W. J. Waalewijn, *Factorization at the LHC: From PDFs to Initial State Jets*, Phys. Rev. **D81** (2010) 094035, arXiv:0910.0467 [hep-ph].

[427] R. Boughezal, C. Focke, W. Giele, X. Liu, and F. Petriello, *Higgs boson production in association with a jet at NNLO using jettiness subtraction*, Phys. Lett. **B748** (2015) 5–8, arXiv:1505.03893 [hep-ph].

[428] T. Gehrmann, A. von Manteuffel, and L. Tancredi, *The two-loop helicity amplitudes for $q\bar{q}' \to V_1 V_2 \to 4$ leptons*, JHEP **09** (2015) 128, arXiv:1503.04812 [hep-ph].

[429] S. Alioli, F. Caola, G. Luisoni, and R. Röntsch, *ZZ production in gluon fusion at NLO matched to parton-shower*, Phys. Rev. **D95** (2017) no. 3, 034042, arXiv:1609.09719 [hep-ph].

[430] M. Grazzini, S. Kallweit, M. Wiesemann, and J. Y. Yook, *ZZ production at the LHC: NLO QCD corrections to the loop-induced gluon fusion channel*, JHEP **03** (2019) 070, arXiv:1811.09593 [hep-ph].

[431] M. Grazzini, S. Kallweit, D. Rathlev, and A. Torre, *$Z\gamma$ production at hadron colliders in NNLO QCD*, Phys. Lett. **B731** (2014) 204–207, arXiv:1309.7000 [hep-ph].

[432] M. Grazzini, S. Kallweit, and D. Rathlev, *$W\gamma$ and $Z\gamma$ production at the LHC in NNLO QCD*, JHEP **07** (2015) 085, arXiv:1504.01330 [hep-ph].

[433] F. Cascioli, T. Gehrmann, M. Grazzini, S. Kallweit, P. Maierhöfer, A. von Manteuffel, S. Pozzorini, D. Rathlev, L. Tancredi, and E. Weihs, *ZZ production at hadron colliders in NNLO QCD*, Phys. Lett. **B735** (2014) 311–313, arXiv:1405.2219 [hep-ph].

[434] M. Grazzini, S. Kallweit, and D. Rathlev, *ZZ production at the LHC: fiducial cross sections and distributions in NNLO QCD*, Phys. Lett. **B750** (2015) 407–410, arXiv:1507.06257 [hep-ph].

[435] T. Gehrmann, M. Grazzini, S. Kallweit, P. Maierhöfer, A. von Manteuffel, S. Pozzorini, D. Rathlev, and L. Tancredi, *W^+W^- Production at Hadron Colliders in Next to Next to Leading Order QCD*, Phys. Rev. Lett. **113** (2014) no. 21, 212001, arXiv:1408.5243 [hep-ph].

[436] M. Grazzini, S. Kallweit, S. Pozzorini, D. Rathlev, and M. Wiesemann, *W^+W^- production at the LHC: fiducial cross sections and distributions in NNLO QCD*, JHEP **08** (2016) 140, arXiv:1605.02716 [hep-ph].

[437] M. Grazzini, S. Kallweit, D. Rathlev, and M. Wiesemann, *$W^\pm Z$ production at hadron colliders in NNLO QCD*, Phys. Lett. **B761** (2016) 179–183, arXiv:1604.08576 [hep-ph].

[438] M. Grazzini, S. Kallweit, D. Rathlev, and M. Wiesemann, *$W^\pm Z$ production at the LHC: fiducial cross sections and distributions in NNLO QCD*, JHEP **05** (2017) 139, arXiv:1703.09065 [hep-ph].

[439] S. Kallweit and M. Wiesemann, *ZZ production at the LHC: NNLO predictions for $2\ell 2\nu$ and 4ℓ signatures*, Phys. Lett. **B786** (2018) 382–389, arXiv:1806.05941 [hep-ph].

[440] M. Grazzini, S. Kallweit, D. Rathlev, and M. Wiesemann, *Transverse-momentum resummation for vector-boson pair production at NNLL+NNLO*, JHEP **08** (2015) 154, arXiv:1507.02565 [hep-ph].

[441] A. Denner, S. Dittmaier, and L. Hofer, *COLLIER - A fortran-library for one-loop integrals*, PoS **LL2014** (2014) 071, arXiv:1407.0087 [hep-ph].

[442] A. Denner, S. Dittmaier, and L. Hofer, COLLIER*: a fortran-based Complex One-Loop LIbrary in Extended Regularizations*, Comput. Phys. Commun. **212** (2017) 220–238, arXiv:1604.06792 [hep-ph].

[443] G. Ossola, C. G. Papadopoulos, and R. Pittau, *CutTools: A Program implementing the OPP reduction method to compute one-loop amplitudes*, JHEP **03** (2008) 042, arXiv:0711.3596 [hep-ph].

[444] F. Buccioni, S. Pozzorini, and M. Zoller, *On-the-fly reduction of open loops*, Eur. Phys. J. **C78** (2018) no. 1, 70, arXiv:1710.11452 [hep-ph].

[445] K. J. F. Gaemers and G. J. Gounaris, *Polarization Amplitudes for e+ e- —> W+ W- and e+ e- —> Z Z*, Z. Phys. **C1** (1979) 259. CERN-TH-2548.

[446] K. Hagiwara, R. D. Peccei, D. Zeppenfeld, and K. Hikasa, *Probing the Weak Boson Sector in e+ e- —> W+ W-*, Nucl. Phys. **B282** (1987) 253–307. DESY-86-058.

[447] T. Melia et al., *W^+W^-, WZ and ZZ production in the POWHEG BOX*, JHEP **11** (2011) 078, arXiv:1107.5051 [hep-ph].

[448] P. Nason and G. Zanderighi, *W^+W^- , WZ and ZZ production in the POWHEG-BOX-V2*, Eur. Phys. J. **C74** (2014) no. 1, 2702, arXiv:1311.1365 [hep-ph].

[449] J. Baglio, S. Dawson, and I. M. Lewis, *NLO effects in EFT fits to W^+W^- production at the LHC*, Phys. Rev. **D99** (2019) no. 3, 035029, arXiv:1812.00214 [hep-ph].

[450] J. Baglio, S. Dawson, and I. M. Lewis, *An NLO QCD effective field theory analysis of W^+W^- production at the LHC including fermionic operators*, Phys. Rev. **D96** (2017) no. 7, 073003, arXiv:1708.03332 [hep-ph].

[451] A. Alves, N. Rosa-Agostinho, O. J. P. Éboli, and M. C. Gonzalez-Garcia, *Effect of Fermionic Operators on the Gauge Legacy of the LHC Run I*, Phys. Rev. **D98** (2018) no. 1, 013006, arXiv:1805.11108 [hep-ph].

[452] ATLAS Collaboration, G. Aad et al., *Measurement of total and differential W^+W^- production cross sections in proton-proton collisions at $\sqrt{s} = 8$ TeV with the ATLAS detector and limits on anomalous triple-gauge-boson couplings*, JHEP **09** (2016) 029, arXiv:1603.01702 [hep-ex].

[453] CMS Collaboration, V. Khachatryan et al., *Measurement of the $\mathrm{W^+W^-}$ cross section in pp collisions at $\sqrt{s} = 8$ TeV and limits on anomalous gauge couplings*, Eur. Phys. J. **C76** (2016) no. 7, 401, arXiv:1507.03268 [hep-ex].

[454] C. Grojean, M. Montull, and M. Riembau, *Diboson at the LHC vs LEP*, JHEP **03** (2019) 020, arXiv:1810.05149 [hep-ph].

[455] F. Zimmermann, *HE-LHC Overview, Parameters and Challenges*, ICFA Beam Dyn. Newslett. **72** (2017) 138–141. http://inspirehep.net/record/1647471/files/9999999_138-141.pdf.

[456] ATLAS Collaboration, *Prospects for the measurement of the W-boson mass at the HL- and HE-LHC*, . https://cds.cern.ch/record/2645431. ATL-PHYS-PUB-2018-026.

[457] H.-L. Lai, M. Guzzi, J. Huston, Z. Li, P. M. Nadolsky, et al., *New parton distributions for collider physics*, Phys. Rev. D **82** (2010) 074024, arXiv:1007.2241 [hep-ph].

[458] ATLAS Collaboration, *Measurement of the Z/γ^* boson transverse momentum distribution in pp collisions at $\sqrt{s} = 7$ TeV with the ATLAS detector*, JHEP **09** (2014) 145, arXiv:1406.3660 [hep-ex].

[459] N. Davidson, T. Przedzinski, and Z. Was, *PHOTOS interface in C++: Technical and Physics Documentation*, Comput. Phys. Commun. **199** (2016) 86–101, arXiv:1011.0937 [hep-ph].

[460] M. Klein and V. Radescu, *Partons from the LHeC*, . https://cds.cern.ch/record/1564929.

[461] LHeC Study Group Collaboration, J. L. Abelleira Fernandez et al., *A Large Hadron Electron Collider at CERN: Report on the Physics and Design Concepts for Machine and Detector*, J. Phys. **G39** (2012) 075001, arXiv:1206.2913 [physics.acc-ph].

[462] ATLAS Collaboration, *Measurement of the transverse momentum and ϕ^*_η distributions of Drell-Yan lepton pairs in proton–proton collisions at $\sqrt{s} = 8$ TeV with the ATLAS detector*, Eur. Phys. J. C **76** (2016) 291, arXiv:1512.02192 [hep-ex].

[463] A. Valassi, *Combining correlated measurements of several different physical quantities*, Nucl. Instrum. Meth. A **500** (2003) 391–405.

[464] J. C. Collins and D. E. Soper, *Angular Distribution of Dileptons in High-Energy Hadron Collisions*, Phys. Rev. **D16** (1977) 2219.

[465] M. Chaichian, M. Hayashi, and K. Yamagishi, *Angular Distributions of High Mass Dileptons With Finite Transverse Momentum in High-energy Hadronic Collisions*, Phys. Rev. **D25** (1982) 130. [Erratum: Phys. Rev.D26,2534(1982)], HU-TFT-81-13.

[466] SLD Electroweak Group, DELPHI, ALEPH, SLD, SLD Heavy Flavour Group, OPAL, LEP Electroweak Working Group, L3 Collaboration, S. Schael et al., *Precision electroweak measurements on the Z resonance*, Phys. Rept. **427** (2006) 257, arXiv:hep-ex/0509008 [hep-ex].

[467] CMS Collaboration, S. Chatrchyan et al., *Measurement of the weak mixing angle with the Drell-Yan process in proton-proton collisions at the LHC*, Phys. Rev. D **84** (2011) 112002, arXiv:1110.2682 [hep-ex].

[468] ATLAS Collaboration, G. Aad et al., *Measurement of the forward-backward asymmetry of electron and muon pair-production in pp collisions at $\sqrt{s}$ = 7 TeV with the ATLAS detector*, JHEP **09** (2015) 049, arXiv:1503.03709 [hep-ex].

[469] LHCb Collaboration, R. Aaij et al., *Measurement of the forward-backward asymmetry in $Z/\gamma^* \to \mu^+\mu^-$ decays and determination of the effective weak mixing angle*, JHEP **11** (2015) 190, arXiv:1509.07645 [hep-ex].

[470] CDF Collaboration, T. A. Aaltonen et al., *Indirect measurement of $\sin^2\theta_W$ (or M_W) using $\mu^+\mu^-$ pairs from γ^*/Z bosons produced in $p\bar{p}$ collisions at a center-of-momentum energy of 1.96 TeV*, Phys. Rev. D **89** (2014) 072005, arXiv:1402.2239 [hep-ex].

[471] CDF Collaboration, T. A. Aaltonen et al., *Measurement of $\sin^2\theta^{\rm lept}_{\rm eff}$ using e^+e^- pairs from γ^*/Z bosons produced in $p\bar{p}$ collisions at a center-of-momentum energy of 1.96 TeV*, Phys. Rev. D **93** (2016) 112016, arXiv:1605.02719 [hep-ex].

[472] D0 Collaboration, V. M. Abazov et al., *Measurement of the effective weak mixing angle in $p\bar{p} \to Z/\gamma^* \to e^+e^-$ events*, Phys. Rev. Lett. **115** (2015) 041801, arXiv:1408.5016 [hep-ex].

[473] W. T. Giele and S. Keller, *Implications of hadron collider observables on parton distribution function uncertainties*, Phys. Rev. D **58** (1998) 094023, arXiv:hep-ph/9803393 [hep-ph].

[474] N. Sato, J. F. Owens, and H. Prosper, *Bayesian Reweighting for Global Fits*, Phys. Rev. D **89** (2014) 114020, arXiv:1310.1089 [hep-ph].

[475] A. Bodek, J. Han, A. Khukhunaishvili, and W. Sakumoto, *Using Drell-Yan forward-backward asymmetry to reduce PDF uncertainties in the measurement of electroweak parameters*, Eur. Phys. J. C **76** (2016) 115, arXiv:1507.02470 [hep-ex].

[476] H. Paukkunen and P. Zurita, *PDF reweighting in the Hessian matrix approach*, JHEP **12** (2014) 100, arXiv:1402.6623 [hep-ph].

[477] ATLAS Collaboration, *Prospect for a measurement of the Weak Mixing Angle in $pp \to Z/\gamma^* \to e^+e^-$ ATLAS detector at the High Luminosity Large Hadron Collider*, ATL-PHYS-PUB-2018-037, CERN, Geneva, Nov, 2018. https://cds.cern.ch/record/2649330.

[478] CMS Collaboration, *A proposal for the measurement of the weak mixing angle at the HL-LHC*, CMS-PAS-FTR-17-001, CERN, Geneva, 2017. https://cds.cern.ch/record/2294888.

[479] W. J. Barter, *Prospects for measurement of the weak mixing angle at LHCb*, LHCb-PUB-2018-013. CERN-LHCb-PUB-2018-013, CERN, Geneva, Nov, 2018. https://cds.cern.ch/record/2647836.

[480] S. Alioli, P. Nason, C. Oleari, and E. Re, *NLO vector-boson production matched with shower in POWHEG*, JHEP **07** (2008) 060, arXiv:0805.4802 [hep-ph].

[481] P. Nason, *A new method for combining NLO QCD with shower Monte Carlo algorithms*, JHEP **11** (2004) 040, arXiv:hep-ph/0409146 [hep-ph].

[482] S. Frixione, P. Nason, and C. Oleari, *Matching NLO QCD computations with parton shower simulations: the POWHEG method*, JHEP **11** (2007) 070, arXiv:0709.2092 [hep-ph].

[483] S. Alioli, P. Nason, C. Oleari, and E. Re, *A general framework for implementing NLO calculations in shower Monte Carlo programs: the POWHEG BOX*, JHEP **06** (2010) 043, arXiv:1002.2581 [hep-ph].

[484] NNPDF Collaboration, R. D. Ball et al., *Parton distributions for the LHC Run II*, JHEP **04** (2015) 040, arXiv:1410.8849 [hep-ph].

[485] LHCb Collaboration, R. Aaij et al., *LHCb Detector Performance*, Int. J. Mod. Phys. **A30** (2015) no. 07, 1530022, arXiv:1412.6352 [hep-ex].

[486] ATLAS Collaboration, *ATLAS Phase-II Upgrade Scoping Document*, CERN-LHCC-2015-020, Geneva, Sep, 2015. http://cds.cern.ch/record/2055248.

[487] S. Catani, L. Cieri, G. Ferrera, D. de Florian, and M. Grazzini, *Vector Boson Production at Hadron Colliders: A Fully Exclusive QCD Calculation at Next-to-Next-to-Leading Order*, Phys. Rev. Lett. **103** (Aug, 2009) 082001. https://link.aps.org/doi/10.1103/PhysRevLett.103.082001.

[488] CMS Collaboration, *Measurement of the weak mixing angle with the forward-backward asymmetry of Drell-Yan events at 8 TeV*, CMS-PAS-SMP-16-007, CERN, Geneva, 2017. http://cds.cern.ch/record/2273392.

[489] ATLAS Collaboration, M. Aaboud et al., *Measurement of the Drell-Yan triple-differential cross section in pp collisions at $\sqrt{s} = 8$ TeV*, JHEP **12** (2017) 059, arXiv:1710.05167 [hep-ex].

[490] S. Alekhin et al., *HERAFitter*, Eur. Phys. J. **C75** (2015) no. 7, 304, arXiv:1410.4412 [hep-ph].

[491] ATLAS Collaboration, *Measurement of the effective leptonic weak mixing angle using electron and muon pairs from Z-boson decay in the ATLAS experiment at $\sqrt{s} = 8$ TeV*, ATLAS-CONF-2018-037, CERN, Geneva, Jul, 2018. https://cds.cern.ch/record/2630340.

[492] Gfitter Group Collaboration, M. Baak, J. Cúth, J. Haller, A. Hoecker, R. Kogler, K. Mönig, M. Schott, and J. Stelzer, *The global electroweak fit at NNLO and prospects for the LHC and ILC*, Eur. Phys. J. **C74** (2014) 3046, arXiv:1407.3792 [hep-ph].

[493] J. de Blas, M. Ciuchini, E. Franco, S. Mishima, M. Pierini, L. Reina, and L. Silvestrini, *Electroweak precision observables and Higgs-boson signal strengths in the Standard Model and beyond: present and future*, JHEP **12** (2016) 135, arXiv:1608.01509 [hep-ph].

[494] HEPfit *Collaboration*, https://web.archive.org/web/20181110113242/http://hepfit.roma1.infn.it, Archived 10 November 2018.

[495] A. Caldwell, D. Kollar, and K. Kroninger, *BAT: The Bayesian Analysis Toolkit*, Comput. Phys. Commun. **180** (2009) 2197–2209, arXiv:0808.2552 [physics.data-an].

[496] I. Dubovyk, A. Freitas, J. Gluza, T. Riemann, and J. Usovitsch, *The two-loop electroweak bosonic corrections to* $\sin^2\theta^b_{eff}$, Phys. Lett. **B762** (2016) 184–189, arXiv:1607.08375 [hep-ph].

[497] I. Dubovyk, A. Freitas, J. Gluza, T. Riemann, and J. Usovitsch, *Complete electroweak two-loop corrections to Z boson production and decay*, Phys. Lett. **B783** (2018) 86–94, arXiv:1804.10236 [hep-ph].

[498] J. de Blas, M. Ciuchini, E. Franco, S. Mishima, M. Pierini, L. Reina, and L. Silvestrini, *Electroweak precision constraints at present and future colliders*, PoS **ICHEP2016** (2017) 690, arXiv:1611.05354 [hep-ph].

[499] J. de Blas, M. Ciuchini, E. Franco, S. Mishima, M. Pierini, L. Reina, and L. Silvestrini, *The Global Electroweak and Higgs Fits in the LHC era*, PoS **EPS-HEP2017** (2017) 467, arXiv:1710.05402 [hep-ph].

[500] A. Keshavarzi, D. Nomura, and T. Teubner, *Muon* $g-2$ *and* $\alpha(M_Z^2)$*: a new data-based analysis*, Phys. Rev. **D97** (2018) no. 11, 114025, arXiv:1802.02995 [hep-ph].

[501] CMS Collaboration, A. M. Sirunyan et al., *Measurement of the top quark mass using single top quark events in proton-proton collisions at* $\sqrt{s} = 8$ *TeV*, Eur. Phys. J. **C77** (2017) no. 5, 354, arXiv:1703.02530 [hep-ex].

[502] ATLAS Collaboration, *Measurement of the top quark mass in the* $t\bar{t}$ *lepton+jets channel from* $\sqrt{s}$*=8 TeV ATLAS data*, ATLAS-CONF-2017-071, CERN, Geneva, 2017.

[503] CMS Collaboration, A. M. Sirunyan et al., *Measurement of the top quark mass with lepton+jets final states using* p p *collisions at* $\sqrt{s} = 13$ *TeV*, Eur. Phys. J. **C78** (2018) no. 11, 891, arXiv:1805.01428 [hep-ex].

[504] CMS Collaboration, A. M. Sirunyan et al., *Measurements of properties of the Higgs boson decaying into the four-lepton final state in pp collisions at* $\sqrt{s} = 13$ *TeV*, JHEP **11** (2017) 047, arXiv:1706.09936 [hep-ex].

[505] ATLAS Collaboration, M. Aaboud et al., *Measurement of the Higgs boson mass in the* $H \to ZZ^* \to 4\ell$ *and* $H \to \gamma\gamma$ *channels with* $\sqrt{s} = 13$ *TeV pp collisions using the ATLAS detector*, Phys. Lett. **B784** (2018) 345–366, arXiv:1806.00242 [hep-ex].

[506] CMS Collaboration, *Measurement of the weak mixing angle using the forward-backward asymmetry of Drell-Yan events in pp collisions at 8 TeV*, Eur. Phys. J. **C78** (2018) 701, arXiv:1806.00863 [hep-ex].

[507] ALEPH, DELPHI, L3, OPAL, LEP Electroweak Collaboration, S. Schael et al., *Electroweak Measurements in Electron-Positron Collisions at W-Boson-Pair Energies at LEP*, Phys. Rept. **532** (2013) 119–244, arXiv:1302.3415 [hep-ex].

[508] CDF Collaboration, T. A. Aaltonen et al., *Precise measurement of the W -boson mass with the Collider Detector at Fermilab*, Phys. Rev. **D89** (2014) no. 7, 072003, arXiv:1311.0894 [hep-ex].

[509] Particle Data Group Collaboration, M. Tanabashi et al., *Review of Particle Physics*, Phys. Rev. **D98** (2018) no. 3, 030001.

[510] S. Dawson et al., *Working Group Report: Higgs Boson*, in *Proceedings, 2013 Community Summer Study on the Future of U.S. Particle Physics: Snowmass on the Mississippi (CSS2013): Minneapolis, MN, USA, July 29-August 6, 2013*. 2013. arXiv:1310.8361 [hep-ex]. http://www.slac.stanford.edu/econf/C1307292/docs/EnergyFrontier/Higgs-18.pdf.

[511] M. Cepeda et al., *Higgs Physics at the HL-LHC and HE-LHC*, arXiv:1902.00134 [hep-ph].

[512] M. E. Peskin and T. Takeuchi, *Estimation of oblique electroweak corrections*, Phys. Rev. **D46** (1992) 381–409. SLAC-PUB-5618.

[513] B. Grzadkowski, M. Iskrzynski, M. Misiak, and J. Rosiek, *Dimension-Six Terms in the Standard Model Lagrangian*, JHEP **10** (2010) 085, arXiv:1008.4884 [hep-ph].

[514] ATLAS Collaboration, *Jet energy scale measurements and their systematic uncertainties in proton–proton collisions at $\sqrt{s}$=13 TeV with the ATLAS detector*, Phys. Rev. D **96** (2017) 072002, arXiv:1703.09665 [hep-ex].

[515] ATLAS Collaboration, *Prospects for jet and photon physics at the HL-LHC and HE-LHC*, ATL-PHYS-PUB-2018-051, CERN, Geneva, Dec, 2018. http://cds.cern.ch/record/2652285.

[516] ATLAS Collaboration, *A measurement of the calorimeter response to single hadrons and determination of the jet energy scale uncertainty using LHC Run-1 pp-collision data with the ATLAS detector*, Eur. Phys. J. C **77** (2017) 26, arXiv:1607.08842 [hep-ex].

[517] ATLAS Collaboration, *Measurement of the inclusive $W^{\pm}$ and Z/gamma cross sections in the electron and muon decay channels in pp collisions at $\sqrt{s} = 7$ TeV with the ATLAS detector*, Phys. Rev. **D85** (2012) 072004, arXiv:1109.5141 [hep-ex].

[518] ATLAS Collaboration, *Measurement of the cross section for top-quark pair production in pp collisions at $\sqrt{s} = 7$ TeV with the ATLAS detector using final states with two high-pt leptons*, JHEP **05** (2012) 059, arXiv:1202.4892 [hep-ex].

[519] ATLAS Collaboration, *Measurement of inclusive jet and dijet production in pp collisions at $\sqrt{s} = 7$ TeV using the ATLAS detector*, Phys. Rev. **D86** (2012) 014022, arXiv:1112.6297 [hep-ex].

[520] S. Alekhin, J. Blümlein, S. Moch, and R. Placakyte, *Parton distribution functions, α_s, and heavy-quark masses for LHC Run II*, Phys. Rev. **D96** (2017) no. 1, 014011, arXiv:1701.05838 [hep-ph].

[521] P. Sun, C. P. Yuan, and F. Yuan, *Transverse Momentum Resummation for Dijet Correlation in Hadronic Collisions*, Phys. Rev. **D92** (2015) no. 9, 094007, arXiv:1506.06170 [hep-ph].

[522] J. Collins and J.-W. Qiu, *k_T factorization is violated in production of high-transverse-momentum particles in hadron-hadron collisions*, Phys. Rev. D **75** (2007) 114014, arXiv:0705.2141 [hep-ph].

[523] S. Catani, M. Grazzini, and H. Sargsyan, *Transverse-momentum resummation for top-quark pair production at the LHC*, JHEP **11** (2018) 061, arXiv:1806.01601 [hep-ph].

[524] S. Catani, M. Grazzini, and A. Torre, *Transverse-momentum resummation for heavy-quark hadroproduction*, Nucl.Phys. B **890** (2015) 518–538, arXiv:1408.4564 [hep-ph].

[525] CMS Collaboration, *High-p_{T} jet measurements at HL-LHC*, CMS Physics Analysis Summary CMS-PAS-FTR-18-032, 2018. http://cds.cern.ch/record/2651219.

[526] M. Cacciari, G. P. Salam, and G. Soyez, *The anti-k_{t} jet clustering algorithm*, JHEP **04** (2008) 063, 0802.1189.

[527] ATLAS Collaboration, *Dynamics of isolated-photon plus jet production in pp collisions at $\sqrt{s} = 7$ TeV with the ATLAS detector*, Nucl. Phys. B **875** (2013) 483, arXiv:1307.6795 [hep-ex].

[528] ATLAS Collaboration, *High-E_T isolated-photon plus jets production in pp collisions at $\sqrt{s} = 8$ TeV with the ATLAS detector*, Nucl. Phys. B **918** (2017) 257, arXiv:1611.06586 [hep-ex].

[529] S. Catani, M. Fontannaz, J. Ph. Guillet and E. Pilon, *Cross section of isolated prompt photons in hadron-hadron collisions*, JHEP **0205** (2002) 028, arXiv:hep-ph/0204023 [hep-ph].

[530] P. Aurenche, M. Fontannaz, J. Ph. Guillet, E. Pilon and M. Werlen, *A new critical study of photon production in hadronic collisions*, Phys. Rev. D **73** (2006) 094007, arXiv:hep-ph/0602133 [hep-ph].

[531] L.A. Harland-Lang, A.D. Martin, P. Motylinski and R.S. Thorne, *Parton distributions in the LHC era: MMHT 2014 PDFs*, Eur. Phys. J. **C 75** (2015) 204, arXiv:1412.3989 [hep-ph].

[532] L. Bourhis, M. Fontannaz and J.Ph. Guillet, *Quark and gluon fragmentation functions into photons*, Eur. Phys. J. C **2** (1998) 529, arXiv:hep-ph/9704447 [hep-ph].

[533] ATLAS Collaboration, *Measurement of the cross section for inclusive isolated-photon production in pp collisions at $\sqrt{s}$=13 TeV using the ATLAS detector*, Phys. Lett. B **770** (2017) 473, arXiv:1701.06882 [hep-ex].

[534] ATLAS Collaboration, *Measurement of the cross section for isolated-photon plus jet production in pp collisions at $\sqrt{s}$=13 TeV using the ATLAS detector*, Phys. Lett. B **780** (2018) 578, arXiv:1801.00112 [hep-ex].

[535] CDF Collaboration, T. Aaltonen et al., *Measurement of the Cross Section for Prompt Isolated Diphoton Production in $p\bar{p}$ Collisions at $\sqrt{s} = 1.96$ TeV*, Phys. Rev. **D84** (2011) 052006, arXiv:1106.5131 [hep-ex].

[536] ATLAS Collaboration, M. Aaboud et al., *Measurements of integrated and differential cross sections for isolated photon pair production in pp collisions at $\sqrt{s} = 8$ TeV with the ATLAS detector*, Phys. Rev. **D95** (2017) no. 11, 112005, arXiv:1704.03839 [hep-ex].

[537] ATLAS Collaboration, G. Aad et al., *Search for diphoton events with large missing transverse momentum in 7 TeV proton-proton collision data with the ATLAS detector*, Phys. Lett. **B718** (2012) 411–430, arXiv:1209.0753 [hep-ex].

[538] CMS Collaboration, V. Khachatryan et al., *Search for diphoton resonances in the mass range from 150 to 850 GeV in pp collisions at $\sqrt{s} = 8$ TeV*, Phys. Lett. **B750** (2015) 494–519, arXiv:1506.02301 [hep-ex].

[539] S. Frixione, *Isolated photons in perturbative QCD*, Phys. Lett. **B429** (1998) 369–374, arXiv:hep-ph/9801442 [hep-ph].

[540] S. Frixione and W. Vogelsang, *Isolated photon production in polarized pp collisions*, Nucl. Phys. **B568** (2000) 60–92, arXiv:hep-ph/9908387 [hep-ph].

[541] S. Catani et al., *QCD*, in *1999 CERN Workshop on standard model physics (and more) at the LHC, CERN, Geneva, Switzerland, 25-26 May: Proceedings*. 2000. arXiv:hep-ph/0005025 [hep-ph]. http://weblib.cern.ch/abstract?CERN-TH-2000-131.

[542] ATLAS Collaboration, G. Aad et al., *Measurement of isolated-photon pair production in pp collisions at $\sqrt{s} = 7$ TeV with the ATLAS detector*, JHEP **01** (2013) 086, arXiv:1211.1913 [hep-ex].

[543] CMS Collaboration, S. Chatrchyan et al., *Measurement of differential cross sections for the production of a pair of isolated photons in pp collisions at $\sqrt{s} = 7$ TeV*, Eur. Phys. J. **C74** (2014) no. 11, 3129, arXiv:1405.7225 [hep-ex].

[544] S. Catani, L. Cieri, D. de Florian, G. Ferrera, and M. Grazzini, *Diphoton production at the LHC: a QCD study up to NNLO*, JHEP **04** (2018) 142, arXiv:1802.02095 [hep-ph].

[545] L. Cieri, *Diphoton isolation studies*, Nucl. Part. Phys. Proc. **273-275** (2016) 2033–2039, arXiv:1510.06873 [hep-ph].

[546] J. R. Andersen et al., *Les Houches 2013: Physics at TeV Colliders: Standard Model Working Group Report*, arXiv:1405.1067 [hep-ph].

[547] M. Grazzini, S. Kallweit, and M. Wiesemann, *Fully differential NNLO computations with MATRIX*, Eur. Phys. J. **C78** (2018) no. 7, 537, arXiv:1711.06631 [hep-ph].

[548] LHeC Study Group Collaboration, J. L. Abelleira Fernandez et al., *On the Relation of the LHeC and the LHC*, arXiv:1211.5102 [hep-ex].

[549] L. A. Harland-Lang, V. A. Khoze, and M. G. Ryskin, *Exclusive LHC physics with heavy ions: SuperChic 3*, Eur. Phys. J. **C79** (2019) no. 1, 39, arXiv:1810.06567 [hep-ph].

[550] W. J. Stirling and E. Vryonidou, *Charm production in association with an electroweak gauge boson at the LHC*, Phys. Rev. Lett. **109** (2012) 082002, arXiv:1203.6781 [hep-ph].

[551] CMS Collaboration, *Measurement of the muon charge asymmetry in inclusive pp to WX production at $\sqrt{s}$ = 7 TeV and an improved determination of light parton distribution functions*, Phys.Rev. **D90** (2014) 032004.

[552] D. d'Enterria and J. Rojo, *Quantitative constraints on the gluon distribution function in the proton from collider isolated-photon data*, Nucl. Phys. **B860** (2012) 311–338, arXiv:1202.1762 [hep-ph].

[553] NNPDF Collaboration, J. Rojo, *Improving quark flavor separation with forward W and Z production at LHCb*, PoS **DIS2017** (2018) 198, arXiv:1705.04468 [hep-ph].

[554] J. Rojo, *Constraints on parton distributions and the strong coupling from LHC jet data*, Int. J. Mod. Phys. **A30** (2015) 1546005, arXiv:1410.7728 [hep-ph].

[555] E. L. Berger, J. Gao, and H. X. Zhu, *Differential Distributions for t-channel Single Top-Quark Production and Decay at Next-to-Next-to-Leading Order in QCD*, JHEP **11** (2017) 158, arXiv:1708.09405 [hep-ph].

[556] CMS Collaboration, *Measurement of the differential cross section for top quark pair production in pp collisions at $\sqrt{s} = 8$ TeV*, Eur. Phys. J. **C75** (2015) no. 11, 542.

[557] ATLAS Collaboration, *Measurements of top-quark pair differential cross-sections in the lepton+jets channel in pp collisions at $\sqrt{s} = 8$ TeV using the ATLAS detector*, Eur. Phys. J. **C76** (2016) no. 10, 538.

[558] CMS Collaboration, *Measurement of associated production of W bosons with charm quarks in proton-proton collisions at $\sqrt{s} = 13$ TeV with the CMS experiment at the LHC*, CMS-PAS-SMP-17-014, CERN, Geneva, 2018. https://cds.cern.ch/record/2314570.

[559] ATLAS Collaboration, *Measurement of the transverse momentum and ϕ^*_η distributions of Drell-Yan lepton pairs in proton-proton collisions at $\sqrt{s} = 8$ TeV with the ATLAS detector*, Eur. Phys. J. **C76** (2016) no. 5, 291.

[560] ATLAS Collaboration, *Measurement of the double-differential high-mass Drell-Yan cross section in pp collisions at $\sqrt{s} = 8$ TeV with the ATLAS detector*, JHEP **08** (2016) 009.

[561] ATLAS Collaboration, *Measurement of the cross section for inclusive isolated-photon production in pp collisions at $\sqrt{s} = 13$ TeV using the ATLAS detector*, Phys. Lett. **B770** (2017) 473–493.

[562] LHCb Collaboration, *Measurement of forward W and Z boson production in pp collisions at $\sqrt{s} = 8$ TeV*, JHEP **01** (2016) 155.

[563] CMS Collaboration, V. Khachatryan et al., *Measurement of the double-differential inclusive jet cross section in proton–proton collisions at $\sqrt{s} = 13$ TeV*, Eur. Phys. J. **C76** (2016) no. 8, 451, arXiv:1605.04436 [hep-ex].

[564] R. D. Ball, V. Bertone, F. Cerutti, L. Del Debbio, S. Forte, et al., *Reweighting and Unweighting of Parton Distributions and the LHC W lepton asymmetry data*, Nucl.Phys. **B855** (2012) 608–638.

[565] NNPDF Collaboration, R. D. Ball, V. Bertone, F. Cerutti, L. Del Debbio, S. Forte, A. Guffanti, J. I. Latorre, J. Rojo, and M. Ubiali, *Reweighting NNPDFs: the W lepton asymmetry*, Nucl. Phys. B **849** (2011) 112–143, arXiv:1012.0836 [hep-ph]. [Erratum: Nucl. Phys.B855,927(2012)].

[566] B. C. Allanach et al., *SUSY Les Houches Accord 2*, Comput. Phys. Commun. **180** (2009) 8–25, arXiv:0801.0045 [hep-ph].

[567] ATLAS Collaboration, *Measurement of underlying event characteristics using charged particles in pp collisions at $\sqrt{s} = 900GeV$ and 7 TeV with the ATLAS detector*, Phys. Rev. **D83** (2011) 112001, arXiv:1012.0791 [hep-ex].

[568] ATLAS Collaboration, *Measurement of charged-particle distributions sensitive to the underlying event in $\sqrt{s} = 13$ TeV proton-proton collisions with the ATLAS detector at the LHC*, JHEP **03** (2017) 157, arXiv:1701.05390 [hep-ex].

[569] M. Diehl, D. Ostermeier, and A. Schafer, *Elements of a theory for multiparton interactions in QCD*, JHEP **03** (2012) 089, arXiv:1111.0910 [hep-ph]. [Erratum: JHEP03,001(2016)].

[570] M. Diehl, J. R. Gaunt, D. Ostermeier, P. Plößl, and A. Schäfer, *Cancellation of Glauber gluon exchange in the double Drell-Yan process*, JHEP **01** (2016) 076, arXiv:1510.08696 [hep-ph].

[571] M. Diehl, J. R. Gaunt, and K. Schönwald, *Double hard scattering without double counting*, JHEP **06** (2017) 083, arXiv:1702.06486 [hep-ph].

[572] M. G. A. Buffing, M. Diehl, and T. Kasemets, *Transverse momentum in double parton scattering: factorisation, evolution and matching*, JHEP **01** (2018) 044, arXiv:1708.03528 [hep-ph].

[573] B. Blok, Yu. Dokshitser, L. Frankfurt, and M. Strikman, *pQCD physics of multiparton interactions*, Eur. Phys. J. **C72** (2012) 1963, arXiv:1106.5533 [hep-ph].

[574] A. V. Manohar and W. J. Waalewijn, *A QCD Analysis of Double Parton Scattering: Color Correlations, Interference Effects and Evolution*, Phys. Rev. **D85** (2012) 114009, arXiv:1202.3794 [hep-ph].

[575] F. A. Ceccopieri, M. Rinaldi, and S. Scopetta, *Parton correlations in same-sign W pair production via double parton scattering at the LHC*, Phys. Rev. **D95** (2017) no. 11, 114030, arXiv:1702.05363 [hep-ph].

[576] CMS Collaboration, *The Phase-2 Upgrade of the CMS Muon Detectors*, CERN-LHCC-2017-012. CMS-TDR-016, CERN, Geneva, Sep, 2017. https://cds.cern.ch/record/2283189.

[577] J. R. Gaunt and W. J. Stirling, *Double Parton Distributions Incorporating Perturbative QCD Evolution and Momentum and Quark Number Sum Rules*, JHEP **03** (2010) 005, arXiv:0910.4347 [hep-ph].

[578] T. Kasemets and M. Diehl, *Angular correlations in the double Drell-Yan process*, JHEP **01** (2013) 121, arXiv:1210.5434 [hep-ph].

[579] S. Cotogno, T. Kasemets, and M. Myska, *A spin on same-sign W-boson pair production*, arXiv:1809.09024 [hep-ph].

[580] M. Diehl and T. Kasemets, *Positivity bounds on double parton distributions*, JHEP **05** (2013) 150, arXiv:1303.0842 [hep-ph].

[581] S. Cotogno, *Polarized partons in hadrons at high energy - The structure of hadrons from single and double parton interactions*. PhD thesis, Vrije U., Amsterdam, 2018-09. http://inspirehep.net/record/1725056/.

[582] M. Diehl, T. Kasemets, and S. Keane, *Correlations in double parton distributions: effects of evolution*, JHEP **05** (2014) 118, arXiv:1401.1233 [hep-ph].

[583] M. Czakon, D. Heymes, and A. Mitov, *High-precision differential predictions for top-quark pairs at the LHC*, Phys. Rev. Lett. **116** (2016) no. 8, 082003, arXiv:1511.00549 [hep-ph].

[584] CMS Collaboration, *Projection of measurements of differential ttbar production cross sections in the e/u+jets channels in pp collisions at the HL-LHC*, CMS-PAS-FTR-18-015, CERN, Geneva, 2018. https://cds.cern.ch/record/2651195.

[585] CMS Collaboration, V. Khachatryan et al., *Measurement of differential cross sections for top quark pair production using the lepton+jets final state in proton-proton collisions at 13 TeV*, Phys. Rev. D **95** (2017) 092001, arXiv:1610.04191 [hep-ex].

[586] CMS Collaboration, A. M. Sirunyan et al., *Measurement of differential cross sections for the production of top quark pairs and of additional jets in lepton+jets events from pp collisions at* $\sqrt{s} = 13$ *TeV*, Phys. Rev. D **97** (2018) 112003, arXiv:1803.08856 [hep-ex].

[587] CMS Collaboration, *The Phase-2 Upgrade of the CMS Tracker*, Technical Report CERN-LHCC-2017-009, 2017. https://cds.cern.ch/record/2272264.

[588] CMS Collaboration, *The Phase-2 Upgrade of the CMS Barrel Calorimeters Technical Design Report*, Technical Report CERN-LHCC-2017-011, 2017. https://cds.cern.ch/record/2283187.

[589] CMS Collaboration, *The Phase-2 Upgrade of the CMS Endcap Calorimeter*, Technical Report CERN-LHCC-2017-023, 2017. https://cds.cern.ch/record/2293646.

[590] CMS Collaboration, *The Phase-2 Upgrade of the CMS Muon Detectors*, Technical Report CERN-LHCC-2017-012, 2017. https://cds.cern.ch/record/2283189.

[591] D. Bertolini, P. Harris, M. Low, and N. Tran, *Pileup Per Particle Identification*, JHEP (2014) 059, arXiv:1407.6013 [hep-ph].

[592] B. A. Betchart, R. Demina, and A. Harel, *Analytic solutions for neutrino momenta in decay of top quarks*, Nucl. Instrum. Meth. **A736** (2014) 169–178, arXiv:1305.1878 [hep-ph].

[593] V. Bertone, R. Frederix, S. Frixione, J. Rojo, and M. Sutton, *aMCfast: automation of fast NLO computations for PDF fits*, JHEP **08** (2014) 166, arXiv:1406.7693 [hep-ph].

[594] S. Alekhin, J. Blümlein, and S. Moch, *NLO PDFs from the ABMP16 fit*, Eur. Phys. J. **C78** (2018) no. 6, 477, arXiv:1803.07537 [hep-ph].

[595] CMS Collaboration, A. M. Sirunyan et al., *Measurement of double-differential cross sections for top quark pair production in pp collisions at* $\sqrt{s} = 8$ *TeV and impact on parton distribution functions*, Eur. Phys. J. **C77** (2017) no. 7, 459, arXiv:1703.01630 [hep-ex].

[596] LHCb collaboration, R. Aaij et al., *First observation of top quark production in the forward region*, Phys. Rev. Lett. **115** (2015) 112001 LHCb-PAPER-2015-022, CERN-PH-EP-2015-132, arXiv:1506.00903 [hep-ex].

[597] LHCb collaboration, R. Aaij et al., *Measurement of the* $t\bar{t}$*,* $W + b\bar{b}$ *and* $W + c\bar{c}$ *production cross sections in pp collisions at* $\sqrt{s} = 8$ *TeV*, Phys. Lett. **B767** (2017) 110 LHCb-PAPER-2016-038, CERN-EP-2016-232, arXiv:1610.08142 [hep-ex].

[598] LHCb collaboration, R. Aaij et al., *Measurement of forward top pair production in the dilepton channel in pp collisions at* $\sqrt{s} = 13$ *TeV*, LHCb-PAPER-2017-050, CERN-EP-2018-022, arXiv:1803.05188 [hep-ex]. submitted to JHEP.

[599] R. Gauld, *Leptonic top-quark asymmetry predictions at LHCb*, Phys. Rev. **D91** (2015) 054029, arXiv:1409.8631 [hep-ph].

[600] R. Gauld, *Feasibility of top quark measurements at LHCb and constraints on the large-*x *gluon PDF*, JHEP **02** (2014) 126, arXiv:1311.1810 [hep-ph].

[601] J. M. Campbell, R. Frederix, F. Maltoni, and F. Tramontano, *NLO predictions for t-channel production of single top and fourth generation quarks at hadron colliders*, JHEP **10** (2009) 042, arXiv:0907.3933 [hep-ph].

[602] J. M. Campbell, R. Frederix, F. Maltoni, and F. Tramontano, *Next-to-Leading-Order Predictions for t-Channel Single-Top Production at Hadron Colliders*, Phys. Rev. Lett. **102** (2009) 182003, arXiv:0903.0005 [hep-ph].

[603] R. Frederix, E. Re, and P. Torrielli, *Single-top t-channel hadroproduction in the four-flavour scheme with POWHEG and aMC@NLO*, JHEP **09** (2012) 130, arXiv:1207.5391 [hep-ph].

[604] F. Cascioli, S. Kallweit, P. Maierhöfer, and S. Pozzorini, *A unified NLO description of top-pair and associated Wt production*, PoS **LL2014** (2014) 026.

[605] M. Brucherseifer, F. Caola, and K. Melnikov, *On the NNLO QCD corrections to single-top production at the LHC*, Phys. Lett. **B736** (2014) 58–63, arXiv:1404.7116 [hep-ph].

[606] E. L. Berger, J. Gao, C. P. Yuan, and H. X. Zhu, *NNLO QCD Corrections to t-channel Single Top-Quark Production and Decay*, Phys. Rev. **D94** (2016) no. 7, 071501, arXiv:1606.08463 [hep-ph].

[607] Z. L. Liu and J. Gao, *s -channel single top quark production and decay at next-to-next-to-leading-order in QCD*, Phys. Rev. **D98** (2018) no. 7, 071501, arXiv:1807.03835 [hep-ph].

[608] J. Gao, C. S. Li, and H. X. Zhu, *Top Quark Decay at Next-to-Next-to Leading Order in QCD*, Phys. Rev. Lett. **110** (2013) no. 4, 042001, arXiv:1210.2808 [hep-ph].

[609] M. Brucherseifer, F. Caola, and K. Melnikov, *$\mathcal{O}(\alpha_s^2)$ corrections to fully-differential top quark decays*, JHEP **04** (2013) 059, arXiv:1301.7133 [hep-ph].

[610] A. S. Papanastasiou, R. Frederix, S. Frixione, V. Hirschi, and F. Maltoni, *Single-top t-channel production with off-shell and non-resonant effects*, Phys. Lett. **B726** (2013) 223–227, arXiv:1305.7088 [hep-ph].

[611] J. Campbell, R. K. Ellis, and R. Röntsch, *Single top production in association with a Z boson at the LHC*, Phys. Rev. **D87** (2013) 114006, arXiv:1302.3856 [hep-ph].

[612] J. Alwall, R. Frederix, J. M. Gerard, A. Giammanco, M. Herquet, S. Kalinin, E. Kou, V. Lemaitre, and F. Maltoni, *Is $V_{(tb)} \simeq 1$?*, Eur. Phys. J. **C49** (2007) 791–801, arXiv:hep-ph/0607115 [hep-ph].

[613] ATLAS Collaboration, M. Aaboud et al., *Measurement of the inclusive cross-sections of single top-quark and top-antiquark t-channel production in pp collisions at $\sqrt{s}$ = 13 TeV with the ATLAS detector*, JHEP **04** (2017) 086, arXiv:1609.03920 [hep-ex].

[614] CMS Collaboration, A. M. Sirunyan et al., *Cross section measurement of t-channel single top quark production in pp collisions at $\sqrt{s} = 13$ TeV*, Phys. Lett. **B772** (2017) 752–776, arXiv:1610.00678 [hep-ex].

[615] S. Weinberg, *Phenomenological Lagrangians*, Physica **A96** (1979) no. 1-2, 327–340.

[616] W. Buchmuller and D. Wyler, *Effective Lagrangian Analysis of New Interactions and Flavor Conservation*, Nucl. Phys. **B268** (1986) 621–653. CERN-TH-4254/85.

[617] G. Bevilacqua and M. Worek, *Constraining BSM Physics at the LHC: Four top final states with NLO accuracy in perturbative QCD*, JHEP **07** (2012) 111, arXiv:1206.3064 [hep-ph].

[618] CMS Collaboration, A. M. Sirunyan et al., *Search for standard model production of four top quarks with same-sign and multilepton final states in proton–proton collisions at $\sqrt{s} = 13$ TeV*, Eur. Phys. J. **C78** (2018) no. 2, 140, arXiv:1710.10614 [hep-ex].

[619] CMS Collaboration, A. M. Sirunyan et al., *Search for standard model production of four top quarks in proton-proton collisions at $\sqrt{s}$ = 13 TeV*, Phys. Lett. **B772** (2017) 336–358, arXiv:1702.06164 [hep-ex].

[620] CMS Collaboration, V. Khachatryan et al., *Search for Standard Model Production of Four Top Quarks in the Lepton + Jets Channel in pp Collisions at $\sqrt{s}$ = 8 TeV*, JHEP **11** (2014) 154, arXiv:1409.7339 [hep-ex].

[621] CMS Collaboration, V. Khachatryan et al., *Search for new physics in same-sign dilepton events in proton–proton collisions at $\sqrt{s} = 13$ TeV*, Eur. Phys. J. **C76** (2016) no. 8, 439, arXiv:1605.03171 [hep-ex].

[622] ATLAS Collaboration, G. Aad et al., *Search for supersymmetry at $\sqrt{s}$=8 TeV in final states with jets and two same-sign leptons or three leptons with the ATLAS detector*, JHEP **06** (2014) 035, arXiv:1404.2500 [hep-ex].

[623] ATLAS Collaboration, G. Aad et al., *Search for production of vector-like quark pairs and of four top quarks in the lepton-plus-jets final state in pp collisions at $\sqrt{s} = 8$ TeV with the ATLAS detector*, JHEP **08** (2015) 105, arXiv:1505.04306 [hep-ex].

[624] ATLAS Collaboration, M. Aaboud et al., *Search for pair production of up-type vector-like quarks and for four-top-quark events in final states with multiple b-jets with the ATLAS detector*, JHEP **07** (2018) 089, arXiv:1803.09678 [hep-ex].

[625] ATLAS Collaboration, M. Aaboud et al., *Search for new phenomena in events with same-charge leptons and b-jets in pp collisions at $\sqrt{s} = 13$ TeV with the ATLAS detector*, JHEP **12** (2018) 039, arXiv:1807.11883 [hep-ex].

[626] F. Maltoni, D. Pagani, and I. Tsinikos, *Associated production of a top-quark pair with vector bosons at NLO in QCD: impact on $\mathrm{t\bar{t}H}$ searches at the LHC*, JHEP **02** (2016) 113, arXiv:1507.05640 [hep-ph].

[627] ATLAS Collaboration, *HL-LHC prospects for the measurement of the Standard Model four-top-quark production cross-section*, ATL-PHYS-PUB-2018-047, 2018. https://cds.cern.ch/record/2651870.

[628] CMS Collaboration, *Projections of sensitivities for tttt production at HL-LHC and HE-LHC*, CMS-PAS-FTR-18-031, CERN, Geneva, 2018. http://cds.cern.ch/record/2650211.

[629] P. J. Fox, A. E. Nelson, and N. Weiner, *Dirac gaugino masses and supersoft supersymmetry breaking*, JHEP **08** (2002) 035, arXiv:hep-ph/0206096 [hep-ph].

[630] G. Burdman, B. A. Dobrescu, and E. Ponton, *Resonances from two universal extra dimensions*, Phys. Rev. **D74** (2006) 075008, arXiv:hep-ph/0601186 [hep-ph].

[631] G. D. Kribs, E. Poppitz, and N. Weiner, *Flavor in supersymmetry with an extended R-symmetry*, Phys. Rev. **D78** (2008) 055010, arXiv:0712.2039 [hep-ph].

[632] K. Benakli and M. D. Goodsell, *Dirac Gauginos in General Gauge Mediation*, Nucl. Phys. **B816** (2009) 185–203, arXiv:0811.4409 [hep-ph].

[633] C. Kilic, T. Okui, and R. Sundrum, *Vectorlike Confinement at the LHC*, JHEP **02** (2010) 018, arXiv:0906.0577 [hep-ph].

[634] S. Calvet, B. Fuks, P. Gris, and L. Valery, *Searching for sgluons in multitop events at a center-of-mass energy of 8 TeV*, JHEP **04** (2013) 043, arXiv:1212.3360 [hep-ph].

[635] L. Darmé, B. Fuks, and M. Goodsell, *Cornering sgluons with four-top-quark events*, Phys. Lett. **B784** (2018) 223–228, arXiv:1805.10835 [hep-ph].

[636] C. Degrande, C. Duhr, B. Fuks, D. Grellscheid, O. Mattelaer, and T. Reiter, *UFO - The Universal FeynRules Output*, Comput. Phys. Commun. **183** (2012) 1201–1214, arXiv:1108.2040 [hep-ph].

[637] A. Alloul, N. D. Christensen, C. Degrande, C. Duhr, and B. Fuks, *FeynRules 2.0 - A complete toolbox for tree-level phenomenology*, Comput. Phys. Commun. **185** (2014) 2250–2300, arXiv:1310.1921 [hep-ph].

[638] C. Degrande, *Automatic evaluation of UV and R2 terms for beyond the Standard Model Lagrangians: a proof-of-principle*, Comput. Phys. Commun. **197** (2015) 239–262, arXiv:1406.3030 [hep-ph].

[639] T. Hahn, *Generating Feynman diagrams and amplitudes with FeynArts 3*, Comput. Phys. Commun. **140** (2001) 418–431, arXiv:hep-ph/0012260 [hep-ph].

[640] J. Alwall, C. Duhr, B. Fuks, O. Mattelaer, D. G. Öztürk, and C.-H. Shen, *Computing decay rates for new physics theories with FeynRules and MadGraph5_aMC@NLO*, Comput. Phys. Commun. **197** (2015) 312–323, arXiv:1402.1178 [hep-ph].

[641] E. Conte, B. Fuks, and G. Serret, *MadAnalysis 5, A User-Friendly Framework for Collider Phenomenology*, Comput. Phys. Commun. **184** (2013) 222–256, arXiv:1206.1599 [hep-ph].

[642] E. Conte, B. Dumont, B. Fuks, and C. Wymant, *Designing and recasting LHC analyses with MadAnalysis 5*, Eur. Phys. J. **C74** (2014) no. 10, 3103, arXiv:1405.3982 [hep-ph].

[643] B. Dumont, B. Fuks, S. Kraml, S. Bein, G. Chalons, E. Conte, S. Kulkarni, D. Sengupta, and C. Wymant, *Toward a public analysis database for LHC new physics searches using MADANALYSIS 5*, Eur. Phys. J. **C75** (2015) no. 2, 56, arXiv:1407.3278 [hep-ph].

[644] Q.-H. Cao, S.-L. Chen, and Y. Liu, *Probing Higgs Width and Top Quark Yukawa Coupling from $t\bar{t}H$ and $t\bar{t}t\bar{t}$ Productions*, Phys. Rev. **D95** (2017) no. 5, 053004, arXiv:1602.01934 [hep-ph].

[645] V. D. Barger, A. L. Stange, and R. J. N. Phillips, *Four heavy quark hadroproduction*, Phys. Rev. **D44** (1991) 1987–1996.

[646] C. Zhang, *Constraining $qqtt$ operators from four-top production: a case for enhanced EFT sensitivity*, Chin. Phys. **C42** (2018) no. 2, 023104, arXiv:1708.05928 [hep-ph].

[647] R. Contino, A. Falkowski, F. Goertz, C. Grojean, and F. Riva, *On the Validity of the Effective Field Theory Approach to SM Precision Tests*, JHEP **07** (2016) 144, arXiv:1604.06444 [hep-ph].

[648] M. Malekhosseini, M. Ghominejad, H. Khanpour, and M. Mohammadi Najafabadi, *Constraining top quark flavor violation and dipole moments through three and four-top quark productions at the LHC*, Phys. Rev. **D98** (2018) no. 9, 095001, arXiv:1804.05598 [hep-ph].

[649] T. Ibrahim and P. Nath, *The Top quark electric dipole moment in an MSSM extension with vector like multiplets*, Phys. Rev. **D82** (2010) 055001, arXiv:1007.0432 [hep-ph].

[650] B. Yang, J. Han, and X. Zhang, *Production of $Zt\bar{t}$ and $Zt\bar{T}$ in the littlest Higgs model with T-parity at High Energy Colliders*, Eur. Phys. J. **C73** (2013) no. 12, 2639.

[651] J. A. Aguilar-Saavedra, *A Minimal set of top anomalous couplings*, Nucl. Phys. **B812** (2009) 181–204, arXiv:0811.3842 [hep-ph].

[652] J. A. Aguilar-Saavedra, B. Fuks, and M. L. Mangano, *Pinning down top dipole moments with ultra-boosted tops*, Phys. Rev. **D91** (2015) 094021, arXiv:1412.6654 [hep-ph].

[653] T. Sjostrand, L. Lonnblad, S. Mrenna, and P. Z. Skands, *Pythia 6.3 physics and manual*, arXiv:hep-ph/0308153 [hep-ph].

[654] V. Hirschi, R. Frederix, S. Frixione, M. V. Garzelli, F. Maltoni, and R. Pittau, *Automation of one-loop QCD corrections*, JHEP **05** (2011) 044, arXiv:1103.0621 [hep-ph].

[655] F. Maltoni, M. L. Mangano, I. Tsinikos, and M. Zaro, *Top-quark charge asymmetry and polarization in $t\bar{t}W^{\pm}$ production at the LHC*, Phys. Lett. **B736** (2014) 252–260, arXiv:1406.3262 [hep-ph].

[656] J. A. Dror, M. Farina, E. Salvioni, and J. Serra, *Strong tW Scattering at the LHC*, JHEP **01** (2016) 071, arXiv:1511.03674 [hep-ph].

[657] S. Alioli, P. Fernandez, J. Fuster, A. Irles, S.-O. Moch, P. Uwer, and M. Vos, *A new observable to measure the top-quark mass at hadron colliders*, Eur. Phys. J. **C73** (2013) 2438, arXiv:1303.6415 [hep-ph].

[658] G. Bevilacqua, H. B. Hartanto, M. Kraus, M. Schulze, and M. Worek, *Top quark mass studies with $t\bar{t}j$ at the LHC*, JHEP **03** (2018) 169, arXiv:1710.07515 [hep-ph].

[659] CMS Collaboration, V. Khachatryan et al., *Measurement of the t-tbar production cross section in the e-mu channel in proton-proton collisions at sqrt(s) = 7 and 8 TeV*, JHEP **08** (2016) 029, arXiv:1603.02303 [hep-ex].

[660] ATLAS Collaboration, G. Aad et al., *Measurement of the $t\bar{t}$ production cross-section using $e\mu$ events with b-tagged jets in pp collisions at $\sqrt{s}$ = 7 and 8* TeV *with the ATLAS detector*, Eur. Phys. J. **C74** (2014) no. 10, 3109, arXiv:1406.5375 [hep-ex]. [Addendum: Eur. Phys. J.C76,no.11,642(2016)].

[661] U. Langenfeld, S. Moch, and P. Uwer, *Measuring the running top-quark mass*, Phys. Rev. **D80** (2009) 054009, arXiv:0906.5273 [hep-ph].

[662] S. Kawabata, Y. Shimizu, Y. Sumino, and H. Yokoya, *Weight function method for precise determination of top quark mass at Large Hadron Collider*, Phys. Lett. **B741** (2015) 232–238, arXiv:1405.2395 [hep-ph].

[663] A. H. Hoang, S. Mantry, A. Pathak, and I. W. Stewart, *Extracting a Short Distance Top Mass with Light Grooming*, arXiv:1708.02586 [hep-ph].

[664] K. Agashe, R. Franceschini, D. Kim, and M. Schulze, *Top quark mass determination from the energy peaks of b-jets and B-hadrons at NLO QCD*, Eur. Phys. J. **C76** (2016) no. 11, 636, arXiv:1603.03445 [hep-ph].

[665] S. Frixione and A. Mitov, *Determination of the top quark mass from leptonic observables*, JHEP **09** (2014) 012, arXiv:1407.2763 [hep-ph].

[666] CMS Collaboration, A. M. Sirunyan et al., *Measurement of the top quark mass in the dileptonic $t\bar{t}$ decay channel using the mass observables $M_{b\ell}$, M_{T2}, and $M_{b\ell\nu}$ in pp collisions at $\sqrt{s} = 8$ TeV*, Phys. Rev. **D96** (2017) no. 3, 032002, arXiv:1704.06142 [hep-ex].

[667] C. G. Lester and D. J. Summers, *Measuring masses of semiinvisibly decaying particles pair produced at hadron colliders*, Phys. Lett. **B463** (1999) 99–103, arXiv:hep-ph/9906349 [hep-ph].

[668] A. J. Barr, B. Gripaios, and C. G. Lester, *Transverse masses and kinematic constraints: from the boundary to the crease*, JHEP **11** (2009) 096, arXiv:0908.3779 [hep-ph].

[669] CMS Collaboration, *Determination of the normalised invariant mass distribution of $\mathrm{t\bar{t}}$+jet and extraction of the top quark mass*, CMS-PAS-TOP-13-006, CERN, Geneva, 2016. https://cds.cern.ch/record/2153653.

[670] CMS Collaboration, *Measurement of the top-quark mass from the b jet energy spectrum*, CMS-PAS-TOP-15-002, CERN, Geneva, 2015. https://cds.cern.ch/record/2053086.

[671] ATLAS Collaboration, G. Aad et al., *Determination of the top-quark pole mass using $t\bar{t}$ + 1-jet events collected with the ATLAS experiment in 7 TeV pp collisions*, JHEP **10** (2015) 121, arXiv:1507.01769 [hep-ex].

[672] ATLAS Collaboration, M. Aaboud et al., *Measurement of lepton differential distributions and the top quark mass in $t\bar{t}$ production in pp collisions at $\sqrt{s} = 8$ TeV with the ATLAS detector*, Eur. Phys. J. **C77** (2017) no. 11, 804, arXiv:1709.09407 [hep-ex].

[673] P. Nason, *The Top Mass in Hadronic Collisions*, in *From My Vast Repertoire ...: Guido Altarelli's Legacy*, A. Levy, S. Forte, and G. Ridolfi, eds., pp. 123–151. 2019. arXiv:1712.02796 [hep-ph].

[674] A. H. Hoang and I. W. Stewart, *Top Mass Measurements from Jets and the Tevatron Top-Quark Mass*, Nucl. Phys. Proc. Suppl. **185** (2008) 220–226, arXiv:0808.0222 [hep-ph].

[675] A. H. Hoang, S. Plätzer, and D. Samitz, *On the Cutoff Dependence of the Quark Mass Parameter in Angular Ordered Parton Showers*, JHEP **10** (2018) 200, arXiv:1807.06617 [hep-ph].

[676] A. H. Hoang, A. Jain, C. Lepenik, V. Mateu, M. Preisser, I. Scimemi, and I. W. Stewart, *The MSR mass and the $\mathcal{O}\left(\Lambda_{\rm QCD}\right)$ renormalon sum rule*, JHEP **04** (2018) 003, arXiv:1704.01580 [hep-ph].

[677] G. Degrassi, S. Di Vita, J. Elias-Miro, J. R. Espinosa, G. F. Giudice, G. Isidori, and A. Strumia, *Higgs mass and vacuum stability in the Standard Model at NNLO*, JHEP **08** (2012) 098, arXiv:1205.6497 [hep-ph].

[678] D. Buttazzo, G. Degrassi, P. P. Giardino, G. F. Giudice, F. Sala, A. Salvio, and A. Strumia, *Investigating the near-criticality of the Higgs boson*, JHEP **12** (2013) 089, arXiv:1307.3536 [hep-ph].

[679] A. Andreassen, W. Frost, and M. D. Schwartz, *Scale Invariant Instantons and the Complete Lifetime of the Standard Model*, Phys. Rev. **D97** (2018) no. 5, 056006, arXiv:1707.08124 [hep-ph].

[680] I. I. Y. Bigi, M. A. Shifman, N. G. Uraltsev, and A. I. Vainshtein, *The Pole mass of the heavy quark. Perturbation theory and beyond*, Phys. Rev. **D50** (1994) 2234–2246, arXiv:hep-ph/9402360 [hep-ph].

[681] M. Beneke and V. M. Braun, *Heavy quark effective theory beyond perturbation theory: Renormalons, the pole mass and the residual mass term*, Nucl. Phys. **B426** (1994) 301–343, arXiv:hep-ph/9402364 [hep-ph].

[682] M. Beneke, P. Marquard, P. Nason, and M. Steinhauser, *On the ultimate uncertainty of the top quark pole mass*, Phys. Lett. **B775** (2017) 63–70, arXiv:1605.03609 [hep-ph].

[683] A. H. Hoang, C. Lepenik, and M. Preisser, *On the Light Massive Flavor Dependence of the Large Order Asymptotic Behavior and the Ambiguity of the Pole Mass*, JHEP **09** (2017) 099, arXiv:1706.08526 [hep-ph].

[684] A. Pineda, *Determination of the bottom quark mass from the Upsilon(1S) system*, JHEP **06** (2001) 022, arXiv:hep-ph/0105008 [hep-ph].

[685] G. S. Bali, C. Bauer, A. Pineda, and C. Torrero, *Perturbative expansion of the energy of static sources at large orders in four-dimensional SU(3) gauge theory*, Phys. Rev. **D87** (2013) 094517, arXiv:1303.3279 [hep-lat].

[686] M. Butenschoen, B. Dehnadi, A. H. Hoang, V. Mateu, M. Preisser, and I. W. Stewart, *Top Quark Mass Calibration for Monte Carlo Event Generators*, Phys. Rev. Lett. **117** (2016) no. 23, 232001, arXiv:1608.01318 [hep-ph].

[687] J. Kieseler, K. Lipka, and S.-O. Moch, *Calibration of the Top-Quark Monte Carlo Mass*, Phys. Rev. Lett. **116** (2016) no. 16, 162001, arXiv:1511.00841 [hep-ph].

[688] S. Ferrario Ravasio, P. Nason, and C. Oleari, *All-orders behaviour and renormalons in top-mass observables*, JHEP **01** (2019) 203, arXiv:1810.10931 [hep-ph].

[689] G. Heinrich, A. Maier, R. Nisius, J. Schlenk, M. Schulze, L. Scyboz, and J. Winter, *NLO and off-shell effects in top quark mass determinations*, JHEP **07** (2018) 129, arXiv:1709.08615 [hep-ph].

[690] S. Argyropoulos and T. Sjöstrand, *Effects of color reconnection on $t\bar{t}$ final states at the LHC*, JHEP **11** (2014) 043, arXiv:1407.6653 [hep-ph].

[691] J. R. Christiansen and P. Z. Skands, *String Formation Beyond Leading Colour*, JHEP **08** (2015) 003, arXiv:1505.01681 [hep-ph].

[692] S. Ferrario Ravasio, T. Ježo, P. Nason, and C. Oleari, *A theoretical study of top-mass measurements at the LHC using NLO+PS generators of increasing accuracy*, Eur. Phys. J. **C78** (2018) no. 6, 458, arXiv:1801.03944 [hep-ph].

[693] G. Corcella, R. Franceschini, and D. Kim, *Fragmentation Uncertainties in Hadronic Observables for Top-quark Mass Measurements*, Nucl. Phys. **B929** (2018) 485–526, arXiv:1712.05801 [hep-ph].

[694] A. Andreassen and M. D. Schwartz, *Reducing the Top Quark Mass Uncertainty with Jet Grooming*, JHEP **10** (2017) 151, arXiv:1705.07135 [hep-ph].

[695] S. Kawabata and H. Yokoya, *Top-quark mass from the diphoton mass spectrum*, Eur. Phys. J. **C77** (2017) no. 5, 323, arXiv:1607.00990 [hep-ph].

[696] CMS Collaboration, *ECFA 2016: Prospects for selected standard model measurements with the CMS experiment at the High-Luminosity LHC*, CMS PAS-FTR-16-006, 2017. https://cds.cern.ch/record/2262606.

[697] ATLAS Collaboration, *Projection of the top quark mass measurement accuracy using $J/\psi \to \mu^+\mu^-$ in $t\bar{t}$ events in proton-proton collisions with 3000 fb^{-1} at the HL-LHC*, ATL-PHYS-PUB-2018-042, 2018. http://cdsweb.cern.ch/record/2649882.

[698] ATLAS Collaboration, *Measurement of the top quark mass in the $t\bar{t} \to$lepton+jets channel from $\sqrt{s} = 8$TeV ATLAS data and combination with previous results*, subm. Eur. Phys. J. C , arXiv:1810.01772 [hep-ex].

[699] *Recommendations on systematic uncertainties for HL-LHC*, https://web.archive.org/https://twiki.cern.ch/twiki/bin/view/LHCPhysics/HLHELHCCommonSystematics.

[700] CMS Collaboration, *Study of the underlying event, b-quark fragmentation and hadronization properties in tbart events*, CMS-PAS-TOP-13-007, CERN, Geneva, 2013. https://cds.cern.ch/record/1600599.

[701] CMS Collaboration, *Measurement of the top quark mass using the B-hadron lifetime technique*, CMS-PAS-TOP-12-030, CERN, Geneva, 2013. https://cds.cern.ch/record/1563140.

[702] CMS Collaboration, *Underlying event measurement with ttbar+X events with p-p collision data at sqrt(s)=13 TeV*, CMS-PAS-TOP-15-017, CERN, Geneva, 2015. https://cds.cern.ch/record/2114809.

[703] ATLAS Collaboration, *Reconstruction of J/ψ mesons in $t\bar{t}$ final states in proton–proton collisions at $\sqrt{s} = 8$ TeV with the ATLAS detector*, ATLAS-CONF-2015-040, 2015. https://cds.cern.ch/record/2046216.

[704] LHCb collaboration, *Physics case for an LHCb Upgrade II — Opportunities in flavour physics, and beyond, in the HL-LHC era*, CERN-LHCC-2018-027 LHCb-PUB-2018-009, CERN, Geneva, 2018. arXiv:1808.08865 [hep-ex].

[705] P. F. Harrison and V. E. Vladimirov, *A Method to Determine $|V_{cb}|$ at the Weak Scale in Top Decays at the LHC*, JHEP **01** (2019) 191, arXiv:1810.09424 [hep-ph].

[706] T. P. Cheng, E. Eichten, and L.-F. Li, *Higgs Phenomena in Asymptotically Free Gauge Theories*, Phys. Rev. **D9** (1974) 2259. SLAC-PUB-1340.

[707] M. E. Machacek and M. T. Vaughn, *Two Loop Renormalization Group Equations in a General Quantum Field Theory. 2. Yukawa Couplings*, Nucl. Phys. **B236** (1984) 221–232. NUB-2611.

[708] C. Balzereit, T. Mannel, and B. Plumper, *The Renormalization group evolution of the CKM matrix*, Eur. Phys. J. **C9** (1999) 197–211, arXiv:hep-ph/9810350 [hep-ph].

[709] ATLAS Collaboration, *Optimisation of the ATLAS b-tagging performance for the 2016 LHC Run*, ATL-PHYS-PUB-2016-012, CERN, Geneva, Jun, 2016. https://cds.cern.ch/record/2160731.

[710] ATLAS Collaboration, M. Aaboud et al., *Measurements of b-jet tagging efficiency with the ATLAS detector using $t\bar{t}$ events at $\sqrt{s} = 13$ TeV*, JHEP **08** (2018) 089, arXiv:1805.01845 [hep-ex].

[711] ATLAS Collaboration, *Measurement of b-tagging Efficiency of c-jets in $t\bar{t}$ Events Using a Likelihood Approach with the ATLAS Detector*, ATLAS-CONF-2018-001, CERN, Geneva, Mar, 2018. https://cds.cern.ch/record/2306649.

[712] ATLAS Collaboration, *Calibration of light-flavour jet b-tagging rates on ATLAS proton-proton collision data at $\sqrt{s} = 13$ TeV*, ATLAS-CONF-2018-006, CERN, Geneva, Apr, 2018. https://cds.cern.ch/record/2314418.

[713] ATLAS Collaboration, M. Aaboud et al., *Search for the Decay of the Higgs Boson to Charm Quarks with the ATLAS Experiment*, Phys. Rev. Lett. **120** (2018) no. 21, 211802, arXiv:1802.04329 [hep-ex].

[714] CMS Collaboration, A. M. Sirunyan et al., *Identification of heavy-flavour jets with the CMS detector in pp collisions at 13 TeV*, JINST **13** (2018) no. 05, P05011, arXiv:1712.07158 [physics.ins-det].

[715] S. L. Glashow, J. Iliopoulos, and L. Maiani, *Weak Interactions with Lepton-Hadron Symmetry*, Phys. Rev. D **2** (Oct, 1970) 1285–1292.

[716] G. Eilam, J. L. Hewett, and A. Soni, *Rare decays of the top quark in the standard and two-Higgs-doublet models*, Phys. Rev. D **44** (Sep, 1991) 1473–1484.

[717] B. Mele, S. Petrarca, and A. Soddu, *A New evaluation of the $t \to cH$ decay width in the standard model*, Phys. Lett. **B435** (1998) 401–406, arXiv:hep-ph/9805498 [hep-ph].

[718] J. A. Aguilar-Saavedra, *Top flavor-changing neutral interactions: Theoretical expectations and experimental detection*, Acta Phys. Polon. **B35** (2004) 2695–2710, arXiv:hep-ph/0409342 [hep-ph].

[719] F. Larios, R. Martinez, and M. A. Perez, *New physics effects in the flavor-changing neutral couplings of the top quark*, Int. J. Mod. Phys. **A21** (2006) 3473–3494, arXiv:hep-ph/0605003 [hep-ph].

[720] Top Quark Working Group Collaboration, K. Agashe et al., *Working Group Report: Top Quark*, in *Proceedings, 2013 Community Summer Study on the Future of U.S. Particle Physics: Snowmass on the Mississippi (CSS2013): Minneapolis, MN, USA, July 29-August 6, 2013*. 2013. arXiv:1311.2028 [hep-ph]. http://www.slac.stanford.edu/econf/C1307292/docs/Top-21.pdf.

[721] CMS Collaboration, *Prospects for the search for gluon-mediated FCNC in top quark production with the CMS Phase-2 detector at the HL-LHC*, CMS-PAS-FTR-18-004, CERN, Geneva, 2018. https://cds.cern.ch/record/2638815.

[722] E. E. Boos, V. E. Bunichev, L. V. Dudko, V. I. Savrin, and A. V. Sherstnev, *Method for simulating electroweak top-quark production events in the NLO approximation: SingleTop event generator*, Phys. Atom. Nucl. **69** (2006) 1317.

[723] CompHEP Collaboration, E. Boos, V. Bunichev, M. Dubinin, L. Dudko, V. Ilyin, A. Kryukov, V. Edneral, V. Savrin, A. Semenov, and A. Sherstnev, *CompHEP 4.4: Automatic computations from Lagrangians to events*, Nucl. Instrum. Meth. **A534** (2004) 250–259, arXiv:hep-ph/0403113 [hep-ph].

[724] CMS Collaboration, *The Phase-2 Upgrade of the CMS Endcap Calorimeter*, CERN-LHCC-2017-023. CMS-TDR-019, CERN, Geneva, Nov, 2017. https://cds.cern.ch/record/2293646.

[725] J. J. Zhang, C. S. Li, J. Gao, H. Zhang, Z. Li, et al., *Next-to-leading order QCD corrections to the top quark decay via model-independent FCNC couplings*, Phys. Rev. Lett. **102** (2009) 072001, arXiv:0810.3889 [hep-ph].

[726] CMS Collaboration, V. Khachatryan et al., *Search for anomalous Wtb couplings and flavour-changing neutral currents in t-channel single top quark production in pp collisions at $\sqrt{s} = 7$ and 8 TeV*, JHEP **02** (2017) 028, arXiv:1610.03545 [hep-ex].

[727] ATLAS Collaboration, *Sensitivity of searches for the flavour-changing neutral current decay $t \to qZ$ using the upgraded ATLAS experiment at the High Luminosity LHC*, ATL-PHYS-PUB-2019-001, 2019. https://cds.cern.ch/record/2653389.

[728] ATLAS Collaboration, M. Aaboud et al., *Search for flavour-changing neutral current top-quark decays $t \to qZ$ in proton-proton collisions at $\sqrt{s} = 13$ TeV with the ATLAS detector*, JHEP **07** (2018) 176, arXiv:1803.09923 [hep-ex].

[729] CMS Collaboration, V. Khachatryan et al., *Search for Anomalous Single Top Quark Production in Association with a Photon in pp Collisions at $\sqrt{s} = 8$ TeV*, JHEP **04** (2016) 035, arXiv:1511.03951 [hep-ex].

[730] ATLAS Collaboration, M. Aaboud et al., *Search for top quark decays $t \to qH$, with $H \to \gamma\gamma$, in $\sqrt{s} = 13$ TeV pp collisions using the ATLAS detector*, JHEP **10** (2017) 129, arXiv:1707.01404 [hep-ex].

[731] ATLAS Collaboration, M. Aaboud et al., *Search for flavor-changing neutral currents in top quark decays $t \to Hc$ and $t \to Hu$ in multilepton final states in proton-proton collisions at $\sqrt{s} = 13$ TeV with the ATLAS detector*, Phys. Rev. **D98** (2018) no. 3, 032002, arXiv:1805.03483 [hep-ex].

[732] CMS Collaboration, A. M. Sirunyan et al., *Search for the flavor-changing neutral current interactions of the top quark and the Higgs boson which decays into a pair of b quarks at $\sqrt{s} =$ 13 TeV*, JHEP **06** (2018) 102, arXiv:1712.02399 [hep-ex].

[733] ATLAS Collaboration, *Expected sensitivity of ATLAS to FCNC top quark decays $t \to Zu$ and $t \to Hq$ at the High Luminosity LHC*, ATL-PHYS-PUB-2016-019, CERN, Geneva, Aug, 2016. https://cds.cern.ch/record/2209126.

[734] ATLAS Collaboration, *Sensitivity of ATLAS at HL-LHC to flavour changing neutral currents in top quark decays $t \to cH$, with $H \to \gamma\gamma$*, ATL-PHYS-PUB-2013-012, CERN, Geneva, Sep, 2013. http://cds.cern.ch/record/1604506.

[735] J. A. Aguilar-Saavedra, J. Carvalho, N. F. Castro, F. Veloso, and A. Onofre, *Probing anomalous Wtb couplings in top pair decays*, Eur. Phys. J. **C50** (2007) 519–533, arXiv:hep-ph/0605190 [hep-ph].

[736] J. A. Aguilar-Saavedra, *Single top quark production at LHC with anomalous Wtb couplings*, Nucl. Phys. **B804** (2008) 160–192, arXiv:0803.3810 [hep-ph].

[737] J. A. Aguilar-Saavedra and S. Amor Dos Santos, *New directions for top quark polarization in the t-channel process*, Phys. Rev. **D89** (2014) no. 11, 114009, arXiv:1404.1585 [hep-ph].

[738] A. Prasath V, R. M. Godbole, and S. D. Rindani, *Longitudinal top polarisation measurement and anomalous Wtb coupling*, Eur. Phys. J. **C75** (2015) no. 9, 402, arXiv:1405.1264 [hep-ph].

[739] A. Jueid, *Probing anomalous Wtb couplings at the LHC in single t-channel top quark production*, Phys. Rev. **D98** (2018) no. 5, 053006, arXiv:1805.07763 [hep-ph].

[740] R. Röntsch and M. Schulze, *Constraining couplings of top quarks to the Z boson in $t\bar{t}$ + Z production at the LHC*, JHEP **07** (2014) 091, arXiv:1404.1005 [hep-ph]. [Erratum: JHEP09,132(2015)].

[741] R. Röntsch and M. Schulze, *Probing top-Z dipole moments at the LHC and ILC*, JHEP **08** (2015) 044, arXiv:1501.05939 [hep-ph].

[742] CDF, D0 Collaboration, T. A. Aaltonen et al., *Tevatron Combination of Single-Top-Quark Cross Sections and Determination of the Magnitude of the Cabibbo-Kobayashi-Maskawa Matrix Element $\mathbf{V_{tb}}$*, Phys. Rev. Lett. **115** (2015) no. 15, 152003, arXiv:1503.05027 [hep-ex].

[743] CDF, D0 Collaboration, T. A. Aaltonen et al., *Observation of s-channel production of single top quarks at the Tevatron*, Phys. Rev. Lett. **112** (2014) 231803, arXiv:1402.5126 [hep-ex].

[744] ATLAS Collaboration, M. Aaboud et al., *Fiducial, total and differential cross-section measurements of t-channel single top-quark production in pp collisions at 8 TeV using data collected by the ATLAS detector*, Eur. Phys. J. **C77** (2017) no. 8, 531, arXiv:1702.02859 [hep-ex].

[745] ATLAS Collaboration, G. Aad et al., *Evidence for single top-quark production in the s-channel in proton-proton collisions at $\sqrt{s}$ =8 TeV with the ATLAS detector using the Matrix Element Method*, Phys. Lett. **B756** (2016) 228–246, arXiv:1511.05980 [hep-ex].

[746] CMS Collaboration, S. Chatrchyan et al., *Measurement of the single-top-quark t-channel cross section in pp collisions at $\sqrt{s} = 7$ TeV*, JHEP **12** (2012) 035, arXiv:1209.4533 [hep-ex].

[747] CMS Collaboration, S. Chatrchyan et al., *Evidence for associated production of a single top quark and W boson in pp collisions at $\sqrt{s}$ = 7 TeV*, Phys. Rev. Lett. **110** (2013) 022003, arXiv:1209.3489 [hep-ex].

[748] CMS Collaboration, V. Khachatryan et al., *Search for s channel single top quark production in pp collisions at $\sqrt{s} = 7$ and 8 TeV*, JHEP **09** (2016) 027, arXiv:1603.02555 [hep-ex].

[749] CDF, D0 Collaboration, T. Aaltonen et al., *Combination of CDF and D0 measurements of the W boson helicity in top quark decays*, Phys. Rev. **D85** (2012) 071106, arXiv:1202.5272 [hep-ex].

[750] ATLAS Collaboration, M. Aaboud et al., *Measurement of the W boson polarisation in $t\bar{t}$ events from pp collisions at $\sqrt{s}$ = 8 TeV in the lepton + jets channel with ATLAS*, Eur. Phys. J. **C77** (2017) no. 4, 264, arXiv:1612.02577 [hep-ex].

[751] ATLAS Collaboration, M. Aaboud et al., *Analysis of the Wtb vertex from the measurement of triple-differential angular decay rates of single top quarks produced in the t-channel at $\sqrt{s}$ = 8 TeV with the ATLAS detector*, JHEP **12** (2017) 017, arXiv:1707.05393 [hep-ex].

[752] F. Déliot, M. C. N. Fiolhais, and A. Onofre, *Top Quark Anomalous Couplings at the High-Luminosity Phase of the LHC*, Mod. Phys. Lett. **A34** (2019) 1950142, arXiv:1811.02492 [hep-ph].

[753] ATLAS Collaboration, *Prospects for the measurement of $t\bar{t}\gamma$ with the upgraded ATLAS detector at the High-Luminosity LHC*, ATL-PHYS-PUB-2018-049, 2018. http://cdsweb.cern.ch/record/2652168.

[754] ATLAS Collaboration, M. Aaboud et al., *Measurements of inclusive and differential fiducial cross-sections of $t\bar{t}\gamma$ production in leptonic final states at $\sqrt{s}$ = 13 TeV in ATLAS*, arXiv:1812.01697 [hep-ex].

[755] W. Hollik, J. I. Illana, S. Rigolin, C. Schappacher, and D. Stockinger, *Top dipole form-factors and loop induced CP violation in supersymmetry*, Nucl. Phys. **B551** (1999) 3–40, arXiv:hep-ph/9812298 [hep-ph]. [Erratum: Nucl. Phys.B557,407(1999)].

[756] K. Agashe, G. Perez, and A. Soni, *Collider Signals of Top Quark Flavor Violation from a Warped Extra Dimension*, Phys. Rev. **D75** (2007) 015002, arXiv:hep-ph/0606293 [hep-ph].

[757] A. L. Kagan, G. Perez, T. Volansky, and J. Zupan, *General Minimal Flavor Violation*, Phys. Rev. **D80** (2009) 076002, arXiv:0903.1794 [hep-ph].

[758] T. Ibrahim and P. Nath, *The Chromoelectric Dipole Moment of the Top Quark in Models with Vector Like Multiplets*, Phys. Rev. **D84** (2011) 015003, arXiv:1104.3851 [hep-ph].

[759] C. Grojean, O. Matsedonskyi, and G. Panico, *Light top partners and precision physics*, JHEP **10** (2013) 160, arXiv:1306.4655 [hep-ph].

[760] F. Richard, *Can LHC observe an anomaly in $t\bar{t}Z$ production?*, arXiv:1304.3594 [hep-ph].

[761] CMS Collaboration, *Anomalous couplings in the tt+Z final state at the HL-LHC*, CMS-PAS-FTR-18-036, CERN, Geneva, 2018. https://cds.cern.ch/record/2652018.

[762] J. Brehmer, K. Cranmer, F. Kling, and T. Plehn, *Better Higgs boson measurements through information geometry*, Phys. Rev. **D95** (2017) no. 7, 073002, arXiv:1612.05261 [hep-ph].

[763] J. Brehmer, *New Ideas for Effective Higgs Measurements*. PhD thesis, U. Heidelberg (main), 2017. http://inspirehep.net/record/1624219.

[764] S. Frixione, E. Laenen, P. Motylinski, and B. R. Webber, *Angular correlations of lepton pairs from vector boson and top quark decays in Monte Carlo simulations*, JHEP **04** (2007) 081, arXiv:hep-ph/0702198 [HEP-PH].

[765] ATLAS Collaboration, G. Aad et al., *Measurement of the $t\bar{t}W$ and $t\bar{t}Z$ production cross sections in pp collisions at $\sqrt{s} = 8$ TeV with the ATLAS detector*, JHEP **11** (2015) 172, arXiv:1509.05276 [hep-ex].

[766] ATLAS Collaboration, *Measurement of the $t\bar{t}Z$ and $t\bar{t}W$ production cross sections in multilepton final states using 3.2 fb^{-1} of pp collisions at $\sqrt{s} = 13$ TeV with the ATLAS detector*, Eur. Phys. J. C **77** (2017) 40, arXiv:1609.01599 [hep-ex].

[767] CMS Collaboration, S. Chatrchyan et al., *Measurement of associated production of vector bosons and ttbar in pp collisions at $\sqrt{s} = 7TeV$*, Phys. Rev. Lett. **110** (2013) 172002, 1303.3239.

[768] CMS Collaboration, V. Khachatryan et al., *Measurement of top quark-antiquark pair production in association with a W or Z boson in pp collisions at $\sqrt{s} = 8$ TeV*, Eur. Phys. J. C **74** (2014) 3060, arXiv:1406.7830 [hep-ex].

[769] CMS Collaboration, V. Khachatryan et al., *Observation of top quark pairs produced in association with a vector boson in pp collisions at $\sqrt{s} = 8$ TeV*, JHEP **01** (2016) 096, arXiv:1510.01131 [hep-ex].

[770] CMS Collaboration, A. M. Sirunyan et al., *Measurement of the cross section for top quark pair production in association with a W or Z boson in proton-proton collisions at $\sqrt{s} = 13$ TeV*, JHEP **08** (2018) 011, arXiv:1711.02547 [hep-ex].

[771] V. M. Budnev, I. F. Ginzburg, G. V. Meledin, and V. G. Serbo, *The Two photon particle production mechanism. Physical problems. Applications. Equivalent photon approximation*, Phys. Rept. **15** (1975) 181–281.

[772] V. A. Khoze, A. D. Martin, and M. G. Ryskin, *Prospects for new physics observations in diffractive processes at the LHC and Tevatron*, Eur.Phys.J. **C23** (2002) 311–327, arXiv:hep-ph/0111078 [hep-ph].

[773] C. Baldenegro, S. Fichet, G. von Gersdorff, and C. Royon, *Searching for axion-like particles with proton tagging at the LHC*, JHEP **06** (2018) 131, arXiv:1803.10835 [hep-ph].

[774] C. Baldenegro, S. Fichet, G. von Gersdorff, and C. Royon, *Probing the anomalous $\gamma\gamma\gamma Z$ coupling at the LHC with proton tagging*, JHEP **06** (2017) 142, arXiv:1703.10600 [hep-ph].

[775] S. Fichet, G. von Gersdorff, and C. Royon, *Measuring the Diphoton Coupling of a 750 GeV Resonance*, Phys. Rev. Lett. **116** (2016) no. 23, 231801, arXiv:1601.01712 [hep-ph].

[776] S. Fichet, G. von Gersdorff, and C. Royon, *Scattering light by light at 750 GeV at the LHC*, Phys. Rev. **D93** (2016) no. 7, 075031, arXiv:1512.05751 [hep-ph].

[777] S. Fichet, G. von Gersdorff, B. Lenzi, C. Royon, and M. Saimpert, *Light-by-light scattering with intact protons at the LHC: from Standard Model to New Physics*, JHEP **02** (2015) 165, arXiv:1411.6629 [hep-ph].

[778] S. Fichet, G. von Gersdorff, O. Kepka, B. Lenzi, C. Royon, and M. Saimpert, *Probing new physics in diphoton production with proton tagging at the Large Hadron Collider*, Phys. Rev. **D89** (2014) 114004, arXiv:1312.5153 [hep-ph].

[779] E. Chapon, C. Royon, and O. Kepka, *Anomalous quartic W W gamma gamma, Z Z gamma gamma, and trilinear WW gamma couplings in two-photon processes at high luminosity at the LHC*, Phys. Rev. **D81** (2010) 074003, arXiv:0912.5161 [hep-ph].

[780] O. Kepka and C. Royon, *Anomalous $WW\gamma$ coupling in photon-induced processes using forward detectors at the LHC*, Phys. Rev. **D78** (2008) 073005, arXiv:0808.0322 [hep-ph].

[781] M. Boonekamp, A. Dechambre, V. Juranek, O. Kepka, M. Rangel, C. Royon, and R. Staszewski, *FPMC: A Generator for forward physics*, arXiv:1102.2531 [hep-ph].

[782] M. G. Albrow, T. D. Coughlin, and J. R. Forshaw, *Central Exclusive Particle Production at High Energy Hadron Colliders*, Prog.Part.Nucl.Phys. **65** (2010) 149–184, arXiv:1006.1289 [hep-ph].

[783] L. A. Harland-Lang, V. A. Khoze, M. G. Ryskin, and W. Stirling, *Central exclusive production within the Durham model: a review*, Int.J.Mod.Phys. **A29** (2014) 1430031, arXiv:1405.0018 [hep-ph].

[784] CDF Collaboration, T. Aaltonen et al., *Observation of Exclusive Dijet Production at the Fermilab Tevatron $p^{-}\bar{p}$ Collider*, Phys. Rev. **D77** (2008) 052004, arXiv:0712.0604 [hep-ex].

[785] D0 Collaboration, V. M. Abazov et al., *High mass exclusive diffractive dijet production in $\mathbf{p\bar{p}}$ collisions at $\sqrt{\mathbf{s}}$ = 1.96 TeV*, Phys.Lett. **B705** (2011) 193–199, arXiv:1009.2444 [hep-ex].

[786] L. A. Harland-Lang, *Planar radiation zeros in five-parton QCD amplitudes*, JHEP **1505** (2015) 146, arXiv:1503.06798 [hep-ph].

[787] L. A. Harland-Lang, V. A. Khoze, and M. G. Ryskin, *Exclusive physics at the LHC with SuperChic 2*, Eur. Phys. J. **C76** (2016) no. 1, 9, arXiv:1508.02718 [hep-ph].

[788] The CMS and TOTEM Collaborations, *CMS-TOTEM Precision Proton Spectrometer Technical Design Report*, CERN-LHCC-2014-021. https://cds.cern.ch/record/1753795.

[789] TOTEM Collaboration, *Technical Design Report*, CERN-LHCC-2004-002; addendum CERN-LHCC-2004-020. http://cds.cern.ch/record/704349.

[790] TOTEM Collaboration, G. Anelli et al., *The TOTEM experiment at the CERN Large Hadron Collider*, JINST **3** (2008) S08007.

[791] TOTEM Collaboration, *TOTEM Upgrade Proposal*, CERN-LHCC-2013-009. https://cds.cern.ch/record/1554299.

[792] FP420 R, D Collaboration, M. G. Albrow et al., *The FP420 & Project: Higgs and New Physics with forward protons at the LHC*, JINST **4** (2009) T10001, arXiv:0806.0302 [hep-ex].

[793] N. Karastathis et al., *Field quality to achieve the required lifetime goals (with beam-beam)*, 7th HL-LHC Collaboration Meeting, 15.11.2017, https://indico.cern.ch/event/647714/contributions/2646093.

[794] CERN, *The MAD-X Program*. https://web.archive.org/web/https://www.cern.ch/madx/, accessed April 2019.

[795] D. Mirarchi et al., *TCL/TCTs setting scenarios for HL-LHC*, Collimation Upgrade Specification Meeting #83, 24.02.2017, https://indico.cern.ch/event/614887/.

[796] C. J. Morningstar and M. J. Peardon, *The Glueball spectrum from an anisotropic lattice study*, Phys. Rev. **D60** (1999) 034509, arXiv:hep-lat/9901004 [hep-lat].

[797] STAR Collaboration, R. Sikora, *Recent results on Central Exclusive Production with the STAR detector at RHIC*, in *Diffraction and Low-x 2018 (Difflowx2018) Reggio Calabria, Italy, August 26-September 1, 2018*. 2018. arXiv:1811.03315 [hep-ex].

[798] CDF Collaboration, T. A. Aaltonen et al., *Measurement of central exclusive $\pi^+\pi^-$ production in $p\bar{p}$ collisions at $\sqrt{s} = 0.9$ and 1.96 TeV at CDF*, Phys. Rev. **D91** (2015) no. 9, 091101, arXiv:1502.01391 [hep-ex].

[799] CMS Collaboration, V. Khachatryan et al., *Exclusive and semi-exclusive pi+pi- production in proton-proton collisions at sqrt(s) = 7 TeV*, arXiv:1706.08310 [hep-ex].

[800] E690 Collaboration, M. A. Reyes et al., *Partial wave analysis of the centrally produced K(s) K(s) system at 800-GeV/c*, Phys. Rev. Lett. **81** (1998) 4079–4082. FERMILAB-PUB-97-223-E.

[801] WA102 Collaboration, D. Barberis et al., *A Partial wave analysis of the centrally produced K+ K- and K0(S) K0(S) systems in p p interactions at 450-GeV/c and new information on the spin of the f(J)(1710)*, Phys. Lett. **B453** (1999) 305–315, arXiv:hep-ex/9903042 [hep-ex].

[802] WA102 Collaboration, D. Barberis et al., *A Partial wave analysis of the centrally produced pi0 pi0 system in p p interactions at 450-GeV/c*, Phys. Lett. **B453** (1999) 325–332, arXiv:hep-ex/9903044 [hep-ex].

[803] V. Crede and C. A. Meyer, *The Experimental Status of Glueballs*, Prog. Part. Nucl. Phys. **63** (2009) 74–116, arXiv:0812.0600 [hep-ex].

[804] F. E. Close and G. A. Schuler, *Evidence that the pomeron transforms as a nonconserved vector current*, Phys. Lett. **B464** (1999) 279–285, arXiv:hep-ph/9905305 [hep-ph].

[805] P. Lebiedowicz, O. Nachtmann, and A. Szczurek, *Exclusive central diffractive production of scalar and pseudoscalar mesons tensorial vs. vectorial pomeron*, Annals Phys. **344** (2014) 301–339, arXiv:1309.3913 [hep-ph].

[806] P. Lebiedowicz, O. Nachtmann, and A. Szczurek, *Central exclusive diffractive production of $\pi^+\pi^-$ continuum, scalar and tensor resonances in pp and $p\bar{p}$ scattering within tensor pomeron approach*, Phys. Rev. **D93** (2016) no. 5, 054015, arXiv:1601.04537 [hep-ph].

[807] P. Lebiedowicz, O. Nachtmann, and A. Szczurek, *Towards a complete study of central exclusive production of K^+K^- pairs in proton-proton collisions within the tensor Pomeron approach*, Phys. Rev. **D98** (2018) 014001, arXiv:1804.04706 [hep-ph].

[808] P. Lebiedowicz, O. Nachtmann, and A. Szczurek, *Central exclusive diffractive production of $p\bar{p}$ pairs in proton-proton collisions at high energies*, Phys. Rev. **D97** (2018) no. 9, 094027, arXiv:1801.03902 [hep-ph].

[809] L. A. Harland-Lang, V. A. Khoze, and M. G. Ryskin, *Modelling exclusive meson pair production at hadron colliders*, Eur. Phys. J. **C74** (2014) 2848, arXiv:1312.4553 [hep-ph].

[810] L. A. Harland-Lang, V. A. Khoze, M. G. Ryskin, and W. J. Stirling, *Central exclusive meson pair production in the perturbative regime at hadron colliders*, Eur. Phys. J. **C71** (2011) 1714, arXiv:1105.1626 [hep-ph].

[811] L. A. Harland-Lang, V. A. Khoze, and M. G. Ryskin, SuperChic2*: a New Monte Carlo for Central Exclusive Production*, Acta Phys. Polon. Supp. **8** (2015) 751–756.

RECENT PRECISION W/Z MEASUREMENTS AT THE LHC

N. VRANJEŠ, on behalf of ATLAS, CMS and LHCb Collaborations
Institute of Physics, University of Belgrade,
Pregrevica 118, Zemun, Serbia

Recent precision measurements of W and Z bosons obtained at the Large Hadron Collider with the ATLAS, CMS and LHCb experiments are reviewed.

ATL-PHYS-PROC-2019-154
09 November 2019

1 Introduction

In proton-proton collisions at the Large Hadron Collider (LHC), electroweak bosons (W and Z) are produced via Drell-Yan (DY) process. The DY process was proposed in the paper from 1970[1], and served as a milestone in building of the quantum chromodynamics (QCD) as the theory of the strong interaction. Even now, after 50 years we are still interested in studying it. It is a cornerstone of the LHC program, crucial for a detailed understanding of LHC data collected by the ATLAS[2], CMS[3] and LHCb[4] experiments. It allows us to (i) probe the structure of the proton, determining the valence and sea quark parton distribution functions (PDFs), including placing constraints on the proton strangeness; (ii) improve Monte Carlo tools, of which a prominent example is the modelling of the production and decay of these bosons in a regime dominated by soft gluon radiation; (iii) test the self-consistency of the Standard Model (SM) by measuring fundamental electroweak parameters: the W-boson mass, m_W, and the effective leptonic weak mixing angle, $\sin^2\theta^{\ell}_{\text{eff}}$; (iv) search for new physics, for example measuring high dilepton mass final states and probing rare decays (though the latter, strictly speaking, is not DY); and (v) establish detector performance *in situ* and control the delivered luminosity by exploiting the clean leptonic final states of these bosons.

2 Probing proton structure via Drell-Yan production

Hadron collider data together with Deep Inelastic Scattering data (DIS) are used to constrain PDFs and DY cross sections (integrated and differential) and are an important input to global fits[5]. The range of Bjorken-x and Q^2 that can be probed depends on center of mass energy, $\sqrt{s}$, and rapidity, y, of electroweak bosons. Improved sensitivity to PDFs is achieved by measuring ratios where correlations suppress many sources of uncertainty. Measuring the production of W and Z bosons constrains the strange-quark distribution, while the W^+/W^- ratio and charge asymmetry are sensitive to u_v and d_v. Inclusive and differential W and Z cross sections measured at $\sqrt{s} = 7$ TeV by ATLAS collaboration[6] are included in global PDF fits. The statistical uncertainty of the measurement is at the 0.5% level, while the systematic uncertainty is dominated by the luminosity (1.9%), out of which the experimental uncertainty is at the 1% level. Results are compared to predictions using different PDFs, which broadly describe the data. However

the ATLAS measurement prefers a non-suppressed strange, in contrast to the expectation from fits to neutrino induced DIS data. Another important example of a measurement sensitive to PDFs is the ratio of the cross sections for the production of top-quark pairs to the Z boson. Single cross section ratios as well as double ratios have been measured at $\sqrt{s}$ = 13, 8, 7 TeV energies [7]. Data demonstrate significant power to constrain the gluon distribution function for x values near 0.1 and the light-quark sea for $x < 0.02$. Results are compared to predictions at NNLO QCD + NLO EW (Z) and NNLO+NNLL ($t\bar{t}$) accuracy[a].

A measurement of the associated production of a W boson and a charm quark ($W + c$) at $\sqrt{s} = 13$ TeV has been performed using data collected by the CMS experiment [8]. The W bosons are identified by their decay into a muon and a neutrino, while the charm quarks are tagged via the full reconstruction of $D^*(2010)^{\pm}$ mesons via $D^*(2010)^{\pm} \to D^0 + \pi^{\pm} \to K^{\mp} + \pi^{\pm} + \pi^{\pm}$. The cross section is measured in the fiducial region defined by the muon transverse momentum $p_{\mathrm{T}}^{\mu} > 26$ GeV, muon pseudorapidity $|\eta_{\mu}| < 2.4$, and charm quark transverse momentum $p_{\mathrm{T}}^{\mathrm{c}} > 5$ GeV. The inclusive cross section for this kinematic range is measured along with the differential cross section as a function of pseudorapidity of the muon from the W boson decay, Figure 1 (left). These measurements are compared with theoretical predictions and are used to probe the strange quark content of the proton.

Recently, cross sections and the associated charge asymmetry of $W^+ \to \mu^+\nu$ and $W^+ \to \mu^-\nu$ as a function of the absolute pseudorapidity of the muon have been published [9]. The asymmetry versus lepton η can provide information on the d/u ratio and sea (anti)quarks (including strangeness). The data were collected in proton–proton collisions at a centre-of-mass energy of 8 TeV. The precision of the cross section measurements varies between 0.8% to 1.5% as a function of pseudorapidity (excluding the 1.9% uncertainty on the integrated luminosity). The charge asymmetry is measured with an absolute uncertainty of between 0.002 and 0.003. The results are compared with predictions based on NNLO calculations with various PDFs and have the sensitivity to discriminate between them as shown in Figure 1 (right).

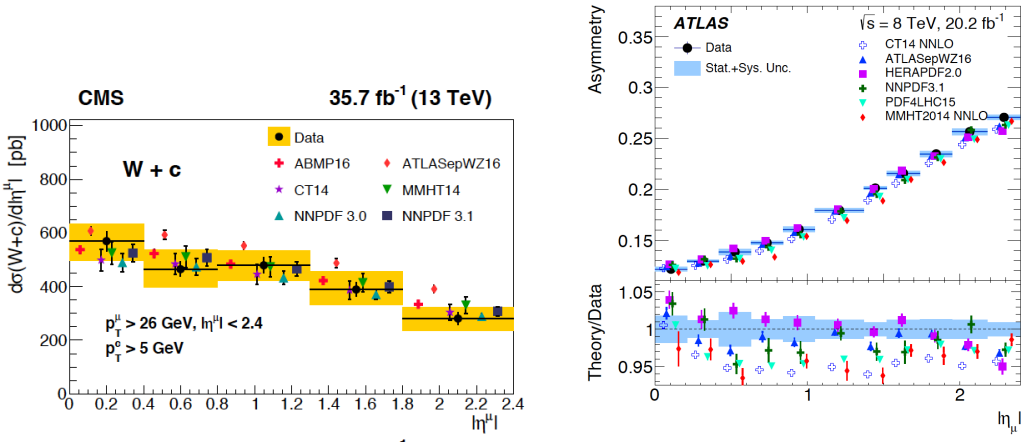

Figure 1 – *Left*: Differential cross sections of $W + c$ production at 13 TeV as a function of absolute muon pseudorapidity [8]. The measurements are compared to the QCD predictions calculated at NLO using different PDF sets. The error bars represent theoretical uncertainties, which include the PDF and scale variation uncertainties. *Right*: The W boson charge asymmetry at 8 TeV as a function of absolute muon pseudorapidity [9]. The data are compared with the central prediction at NNLO produced using a selection of PDFs. The statistical uncertainties of the predictions are indicated by the error bars. The ratios of the data to the predictions are shown in the lower panel.

Measurements of W and Z cross sections at different $\sqrt{s}$ is important for constraining PDFs. Measurements of fiducial integrated and differential cross sections for inclusive W^+, W^- and Z

[a] Details of all calculations are given in the relevant measurement publications.

boson production at $\sqrt{s} = 5.02$ TeV are reported by ATLAS [10]. The electron and muon channels are analysed, and combined integrated W^+, W^- and Z cross sections have been measured and found to be in good agreement with NNLO QCD cross section calculations. The results are compared with several PDF predictions and, in general, agreement is found for most of the PDFs. Significant tension with all PDF sets at very low η (low x) for W^- and Z is observed. The production cross sections for $W^\pm$ and Z bosons have been measured using ATLAS data at $\sqrt{s} = 2.76$ TeV [11]. The cross sections are presented for a fiducial region defined by the detector acceptance and are also extrapolated to the full phase space for the total inclusive production cross section. Measured ratios and asymmetries constructed using these cross sections are also presented. The results obtained, and the ratios and charge asymmetries constructed from them, are in agreement with theoretical calculations based on NNLO QCD based on a selection of different PDF sets.

Measurements of the differential cross section for the DY process in the dimuon and dielectron channels, at $\sqrt{s} = 13$ TeV, have been performed with data collected by the CMS experiment [12]. The total and fiducial cross section measurements are presented as a function of the dilepton invariant mass in the range 15 GeV$< m_{\ell\ell} <$ 3000 GeV. The result is extrapolated to the full phase space including Final State Radiation (FSR). For $m_{\ell\ell}$ <400 GeV the statistical uncertainty is subleading, and the main systematic uncertainty arises from the lepton efficiencies. The results are in good agreement with the theoretical predictions at NLO (including PDFs at the same level of accuracy). Full phase space cross sections are in good agreement with NNLO QCD + NLO EW predictions. The photon-initiated production of same-flavour lepton pairs is estimated with an NNLO simulation code with photon PDFs. It is shown that photon-induced contribution has a sizable effect in the high $m_{\ell\ell}$ region.

The W+jets process provides a novel source of input to PDF fits that is sensitive to partons at higher x than can be accessed by inclusive W and Z data. ATLAS 8 TeV data, have been used to perform measurements of unfolded cross sections of $W \to e\nu$+jets and relevant ratios [13]. Jets are reconstructed using the anti-k_{T} algorithm with $p_{\mathrm{T}}^{\mathrm{jet}}$ >30 GeV and $|y^{\mathrm{jet}}|$ <4.4. Top background is suppressed by vetoing events containing b-jets. Achieved precision of the measurement is $5 - 16\%$ for W+0/1/2 jets and is limited by the jet energy scale and resolution, and unfolding uncertainties. Precision for the ratio is $0.7 - 4\%$ for 0/1/2 jets. The results are compared with various models and various versions of the `CTEQ`, `CT` and `NNPDF` PDFs. A QCD analysis of this ATLAS measurement has also been performed [14]. These data are fitted together with ATLAS inclusive $W^\pm$ production measurements at $\sqrt{s} = 7$ TeV data [6] and HERA deep-inelastic scattering data [15]. The parton distribution functions extracted from the resulting fit show an improved determination of the high-x sea-quark densities, while confirming the unsuppressed strange-quark density at lower $x < 0.023$ found by previous ATLAS analyses (Figure 2 (left)). A better constraint on the $d - u$ distribution is also achieved. The resulting PDF set is labelled `ATLASepWZWjet19`.

Similarly to the ATLAS W+jets study, CMS has published a measurement of the production of $Z \to \ell\ell$ in association with jets in proton-proton collisions at $\sqrt{s} = 13$ TeV [16]. The cross section has been measured as a function of the jet multiplicity and its dependence on the transverse momentum of the Z boson, the jet kinematic variables (transverse momentum and rapidity), the scalar sum of the jet momenta, which quantifies the hadronic activity, and the balance in transverse momentum between the reconstructed jet recoil and the Z. The measurements are compared with predictions from four different calculations including fully differential NNLO + parton shower in the final state and an NNLO+NNLL model without parton showering. A multiparton NLO prediction provides a very good description for jet multiplicities computed with NLO accuracy. The NNLO+NNLL predictions fail to describe observables sensitive to extra jets (N_{jets} >1). At low p_{T}^Z, the NLO multiparton calculation is better than the NNLO+NNLL one, while both calculations provide a similar description at high p_{T}^Z.

Measurements of W and Z boson cross sections at $\sqrt{s}$= 7, 8, 13 TeV, the W boson charge

asymmetry, as well as the production of electroweak bosons in association with jets have been performed at LHCb [17], [18], [19], [20], exploiting complementary rapidity coverage with respect to ATLAS and CMS. In addition, differential cross sections are measured as functions of p_{T}^{Z}, boson rapidity and the angular variable ϕ_{η}^{*}. Measurements are compared to fixed-order QCD calculations, and various state of the art PDFs. Typically good agreement with predictions is observed as demonstrated in Figure 2 (right).

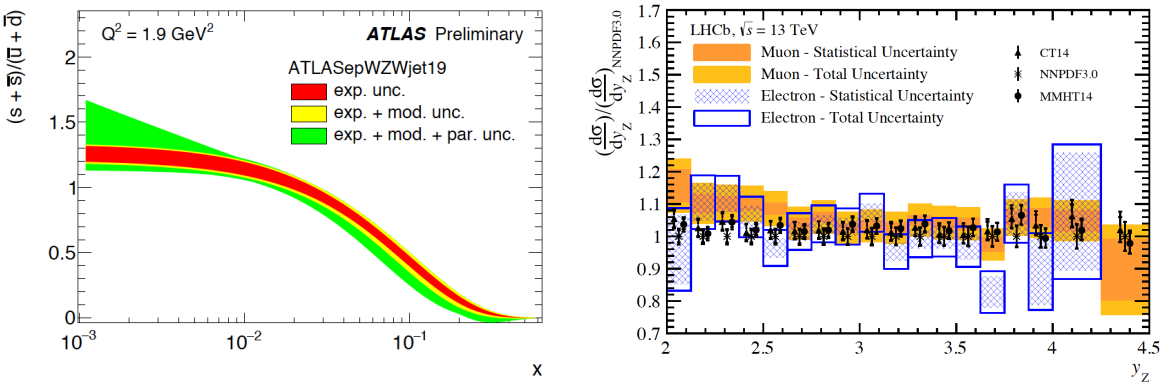

Figure 2 – *Left*: The $R_s = \frac{s+\bar{s}}{\bar{u}+\bar{d}}$ distribution, evaluated at $Q^2 = 1.9$ GeV^2, obtained with the `ATLASepWZWjet19` PDF [14]. The uncertainty bands are displayed separated in to the experimental, model and parameterisation uncertainties. *Right*: The differential cross section as a function of the Z boson rapidity compared to the theory based on $O(\alpha_s^2)$ predictions with different PDF sets, normalised to the central value of the `NNPDF3.0` evaluated at NLO [20].

3 Improving QCD tools

Precision measurements of specific variables lead to improvement in tools employed to model the production of electroweak bosons. Notable examples are the boson transverse momentum and the angular variable ϕ_{η}^{*}. The W and Z bosons have non-zero p_{T} due to the intrinsic transverse momentum of the initial state partons and initial-state radiation of gluons and quarks. Measurements of the p_{T} distributions of W and Z bosons probe various aspects of the strong interaction. The low $p_{\mathrm{T}}^{W,Z}$ can be described using soft-gluon resummation plus a non-perturbative contribution from the parton intrinsic k_{T}, while the high p_{T} spectrum should be described by fixed order perturbative QCD. Parton-shower models are used to compensate for missing higher-order corrections in the fixed-order QCD calculations. Measurements of the p_{T}^{Z} and ϕ_{η}^{*} are possible with high precision due to well-measured leptons in the final states. CMS and ATLAS have published these results [21], [22] around the Z-boson peak, $|y^{Z}|$ <2.4, with an uncertainty dominated by the lepton reconstruction (not counting luminosity). The measurement is compared to the predictions of NNLO QCD calculations and using parton shower modeling (`MADGRAPH5_aMC@NLO` [23], `POWHEG` [24] , `POWHEG + MiNLO` [25]) as well as resummed prediction of `Resbos` [26] and `Geneva` [27], see Figure 3. Measurement of the p_{T}^{W} distribution is a key ingredient for a precise m_W measurement, however it is more difficult than p_{T}^{Z} due to the neutrino escaping reconstruction. The resolution of the hadronic recoil is much worse than that of the lepton momentum. It is planned to directly measure p_{T}^{W} in events with low-$\langle\mu\rangle$ data with a target precision of 1% precision in 5 GeV-bins at low p_{T} [28]. Promising results are expected from NNLO+ N3LL calculations although still far from 1% precision.

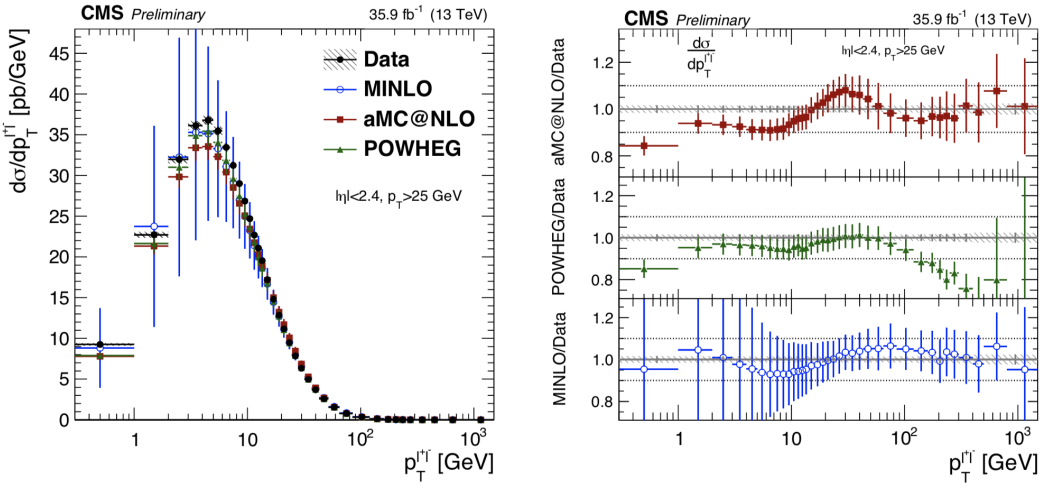

Figure 3 – *Left*: The measured absolute Z-boson cross sections in bins of p_{T}^{Z} [21]. The shaded band around the data points correspond to the total experimental uncertainty. The measurement is compared to predictions with `MADGRAPH5_aMC@NLO` [23], `POWHEG` [24] and `POWHEG-MINLO` [25]. The error bars around the predictions correspond to the statistical, PDF, and scale uncertainties. *Right*: The ratios of the predictions to the unfolded data.

4 Measuring fundamental electroweak parameters

The consistency of the SM can be tested through higher precision measurements of its fundamental parameters such as m_W and $\sin^2\theta_{\mathrm{eff}}^{\ell}$. To achieve ultimate precision in the measurement of these parameters at the LHC, specific efforts in both the experimental and theory community are needed. Precision DY measurements require ultimate performance of the detector for electrons and muons (including high $|y^{\ell\ell}|$ events to enhance sensitivity to $\sin^2\theta_{\mathrm{eff}}^{\ell}$), as well as the best possible measurement of the hadronic recoil (to measure directly p_{T}^{W}). On the theory side improvement is needed in predictions and on the uncertainties on $p_{\mathrm{T}}^{W}/p_{\mathrm{T}}^{Z}$ and the PDFs. A challenging measurement of m_W at the LHC has been reported by ATLAS some time ago [29], with a precision matching that from the Tevatron experiments. Recently, both CMS [30] and ATLAS [31] reported measurements of $\sin^2\theta_{\mathrm{eff}}^{\ell}$ using data collected at $\sqrt{s} = 8$ TeV. At hadron colliders $\sin^2\theta_{\mathrm{eff}}^{\ell}$ is measured via the asymmetry in lepton angular distributions in Z decays induced by the V-A coupling structure of Z bosons to fermions. In the case of CMS, $\sin^2\theta_{\mathrm{eff}}^{\ell}$ is extracted from a template fit to the forward-backward asymmetry using dielectron and dimuon events, with $|y^{\ell\ell}|$ <2.4. Templates are built from the `POWHEG` Monte Carlo [24] and the `NNPDF3.0` NLO PDF [32] in 12 $m_{\ell\ell}\times 6$ $y^{\ell\ell}$ bins. Experimental systematics are dominated by statistics, including limited MC (the situation is similar in ATLAS). The PDFs are constrained by Bayesian χ^2 reweighting and thereby their uncertainties are reduced in the extracted value of $\sin^2\theta_{\mathrm{eff}}^{\ell}$. In the Bayesian χ^2 reweighting method, PDF replicas that offer good descriptions of the observed forward-backward distribution are assigned large weights, and those that poorly describe the asymmetry are given small weights. Figure 4 (left) shows a scatter plot of χ^2_{min} versus the best-fit $\sin^2\theta_{\mathrm{eff}}^{\ell}$ for 100 `NNPDF` replicas. The extreme PDF replicas from either side are disfavoured. After the reweighting, the PDF uncertainties are reduced by about a factor of 2. It should be noted that the Bayesian χ^2 reweighting technique works well when the replicas span the optimal value on both sides. PDFs represented by Hessian eigenvectors using `CT10`, `CT14`, and `MMHT2014`, are also studied, and the contribution from these uncertainties has been found to be subleading with respect to the `NNPDF3.0` PDF set. The combined result from the dielectron and dimuon channels is:

$$\sin^2\theta_{\mathrm{eff}}^{\ell} = 0.23101 \pm 0.00036(\mathrm{stat}) \pm 0.00018(\mathrm{syst}) \pm 0.00016(\mathrm{theo}) \pm 0.00031(\mathrm{PDF}), \qquad (1)$$

or summing the uncertainties in quadrature,

$$\sin^2\theta^{\ell}_{\rm eff} = 0.23101 \pm 0.00053. \quad (2)$$

The ATLAS measurement is based on a methodology of angular coefficients $A_{\rm i}(m_{\ell\ell}, p^{\ell}_{\rm T}, y^{\ell\ell})$ [31]. Here, the $pp \to Z \to \ell\ell$ cross section in the full lepton phase space is determined by 5 variables that separate Z production from its decay kinematics. Angular coefficients encapsulate all QCD production dynamics at all orders. Direct measurement of the angular coefficients A_4 and A_3 leads to the measurement of $\sin^2\theta^{\ell}_{\rm eff}$, based on the effective linear relation: $A_4 = a \times \sin^2\theta^{\ell}_{\rm eff} + b$ predicted in each measurement bin[b]. Technically this is more challenging than the classical approach employed by CMS, but with some advantages: (i) angular variables can constrain experimental systematics, and (ii) measurements in the full phase space via analytical extrapolation reduces theory uncertainties. Possibly this is more sensitive to NLO EW effects that can break harmonic decomposition compared to the extraction from the forward-backward asymmetry. Results are based on three analysis channels: 6 million dielectron central-central events ($ee_{\rm CC}$, both electrons satisfy $0 < |\eta| < 2.4$), 7.5 million dimuon central-central events ($\mu\mu_{\rm CC}$, both muons satisfy $0 < |\eta| < 2.4$) and 1.5 million dielectron central-forward events ($ee_{\rm CF}$, one electron $0 < |\eta| < 2.5$ and the other one in $2.5 < |\eta| < 4.9$). Results are binned in $m_{\ell\ell}$ and $y^{\ell\ell}$, and the background is found to be small even in the ee_{CF} analysis channel. A test of the compatibility of all measurement bins (19 bins plus the reference one) have been performed and an overall p-value of 3.4% is obtained (due to the 3σ pull from the lowest $y^{\ell\ell}$ $\mu\mu_{\rm CC}$ channel which has small weight in the final result). In the full combination, the expected statistical uncertainty is of the same size as the total systematic uncertainty, which arises predominantly from the PDF uncertainties in the predictions. The fit using `MMHT14` provides the best overall result, i.e. the best fit χ^2 and also the smallest uncertainties from PDFs after profiling. The results are quite close for `CT14` and `NNPDF31` while their uncertainties are a bit larger compared to `MMHT14` . `CT10nnlo` is also shown since it fits best the ensemble of ATLAS W/Z precision data at 7 TeV used for the measurement of m_W. The overall range of $\sin^2\theta^{\ell}_{\rm eff}$ spanned by all PDF sets is 28×10^{-5} and it comes predominantly from the `CT10` set. This range of values is consistent with the uncertainty band arising from the uncertainties in the chosen `MMHT14` PDF set and is not considered as an additional uncertainty. The next dominant uncertainty is from limited MC statistics: 12×10^{-5}. The combined result is measured to be:

$$\sin^2\theta^{\ell}_{\rm eff} = 0.23140 \pm 0.00021({\rm stat}) \pm 0.00024({\rm PDF}) \pm 0.00016({\rm syst}), \quad (3)$$

where the first uncertainty corresponds to the data statistical uncertainty, the second to the PDF uncertainties in the `MMHT14` PDF set, and the third to all other systematic uncertainties affecting the measurement and its interpretation. This result agrees within its total uncertainty of ± 0.00036 with the current value of 0.23150 ± 0.00006 from global electroweak fits. Figure 4 (right) compares the ATLAS measurements to previous measurements from the LHC experiments, to the recently published combined legacy measurement from the CDF and D0 experiments at the Tevatron, and to the most precise legacy individual measurements from LEP and SLC. The combined ATLAS result has similar precision to that of the most precise LEP/SLC measurements shown in the plot, and to that of the overall combined legacy result from the Tevatron. It is also interesting to note that the ATLAS combined result for the $ee_{\rm CC}$ and $\mu\mu_{\rm CC}$ channels has a very similar precision to that of the CMS 8 TeV result which did not include the channel with forward electrons.

5 Prospects at the HL-LHC and HE-LHC

ATLAS prospects for a measurement of m_W at the High Luminosity-LHC and the High Energy-LHC have been evaluated, as well as ATLAS, CMS and LHCb prospects for the measurement

[b] A_3 is sensitive only at high $p^{Z}_{\rm T}$, not used in the measurement.

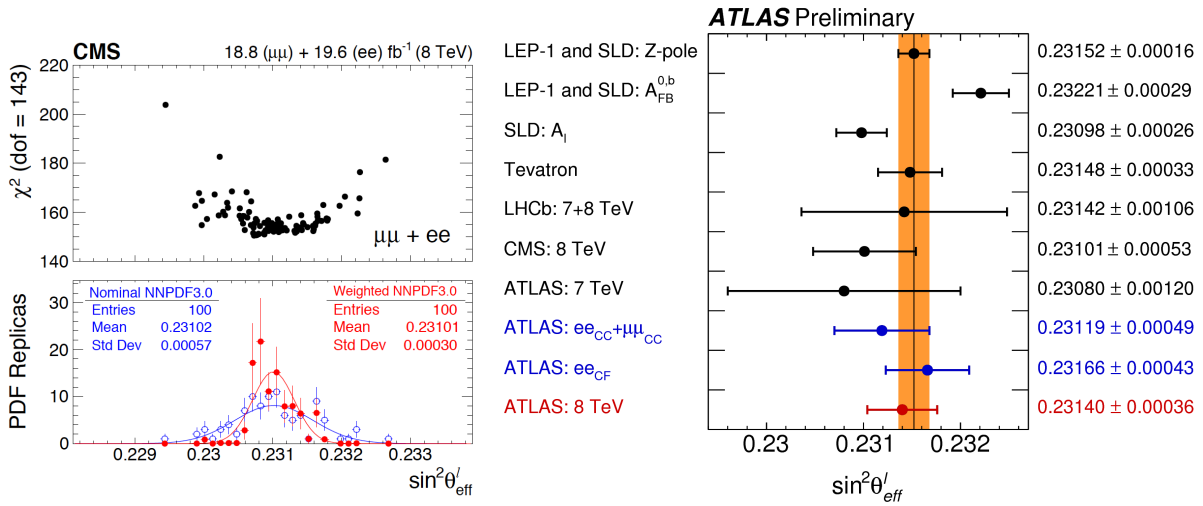

Figure 4 – *Left*: Plot of $\chi^2_{\rm min}$ versus the best-fit $\sin^2\theta^\ell_{\rm eff}$ for 100 NNPDF replicas [30]. The lower panel shows the projected distributions in the best-fit $\sin^2\theta^\ell_{\rm eff}$ for the nominal (open circles) and weighted (solid circles) replicas. *Right*: Comparison of the ATLAS $\sin^2\theta^\ell_{\rm eff}$ measurement to previous measurements at LEP/SLC, at the Tevatron, and at the LHC [31]. The overall LEP-1/SLD average is represented together with its uncertainty as a vertical band. The ATLAS combined result for all channels is shown, together with the results for the $ee_{\rm CF}$ channel alone and for the combined $ee_{\rm CC}$ and $\mu\mu_{\rm CC}$ channels.

of $\sin^2\theta^\ell_{\rm eff}$ at the HL-LHC [33]. The increased acceptance provided by the new inner tracker extends the coverage up to $|\eta|$ <4 and allows further constraints on PDFs from cross section measurements, reducing the corresponding uncertainties in m_W. Results are obtained assuming low pile-up data (1 week of $\langle\mu\rangle$ =2 leads to a statistical precision of $\delta^{\rm stat}m_W$ ≈10 MeV) with reference PDF CT10 reweighted to various different existing, as well as projected HL-LHC [34] and LHeC [35] PDFs. The LHeC PDF set represents the impact of a proposed future high-energy and high-luminosity ep scattering experiment. In the scenario with an extended tracker without an LHeC, the PDF uncertainty of m_W could be halved with respect to the "central only" selection, while in the LHeC scenario another factor of ≈3 could be achieved in reducing PDF uncertainties. ATLAS, CMS and LHCb considered prospects for the $\sin^2\theta^\ell_{\rm eff}$ measurement at the at HL-LHC. In these studies $\sin^2\theta^\ell_{\rm eff}$ is extracted from the measurements of forward-backward asymmetry in dilepton events at the Z-pole. With the extended rapidity coverage (ATLAS and CMS) or selection of low-$p_{\rm T}$ events due to flexible full software trigger and real time analysis scheme (LHCb), as well as improvements in PDFs (from *in situ* constraint, e.g. ATLAS exploiting CC, CF and FF configurations), each of the experiments could reach the precision of LEP/SLD. Including LHeC data, the PDF uncertainty could be reduced by a factor of 5, leading to a total uncertainty of $\sin^2\theta^\ell_{\rm eff}$ of 8×10^{-5} (half of the LEP/SLD).

Conclusions

Recent precision measurements of W and Z bosons obtained with the ATLAS, CMS and LHCb experiments are reviewed. There is a very rich experimental program at all these experiments exploiting large samples of W and Z bosons in their leptonic decay final states. It is a cornerstone of the LHC program allowing the structure of the proton to be probed, improvements to MC tools, and tests of the self-consistency of the Standard Model by measuring fundamental electroweak parameters such as m_W and $\sin^2\theta^\ell_{\rm eff}$.

References

1. S. D. Drell and T. M. Yan, Phys. Rev. Lett. **25** (1970) 316 Erratum: [Phys. Rev. Lett. **25** (1970) 902].
2. ATLAS Collaboration, JINST **3** (2008) S08003.
3. CMS Collaboration, JINST **3** (2008) S08004.
4. LHCb Collaboration, JINST **3** (2008) S08005.
5. M. Tanabashi *et al.* [Particle Data Group], Phys. Rev. D **98** (2018) no.3, 030001.
6. ATLAS Collaboration, Eur. Phys. J. C **77** (2017) no.6, 367 [arXiv:1612.03016 [hep-ex]].
7. ATLAS Collaboration, JHEP **1702** (2017) 117 [arXiv:1612.03636 [hep-ex]].
8. CMS Collaboration, Eur. Phys. J. C **79** (2019) no.3, 269 [arXiv:1811.10021 [hep-ex]].
9. ATLAS Collaboration, Eur. Phys. J. C **79** (2019) no.9, 760 [arXiv:1904.05631 [hep-ex]].
10. ATLAS Collaboration, Eur. Phys. J. C **79** (2019) no.2, 128 Erratum: [Eur. Phys. J. C **79** (2019) no.5, 374] [arXiv:1810.08424 [hep-ex]].
11. ATLAS Collaboration, arXiv:1907.03567 [hep-ex].
12. CMS Collaboration, [arXiv:1812.10529 [hep-ex]].
13. ATLAS Collaboration, JHEP **1805** (2018) 077 [arXiv:1711.03296 [hep-ex]].
14. ATLAS Collaboration, ATL-PHYS-PUB-2019-016, http://cdsweb.cern.ch/record/2670662/
15. H1 and ZEUS Collaborations, Eur. Phys. J. C **75** (2015) no.12, 580 [arXiv:1506.06042 [hep-ex]].
16. CMS Collaboration, Eur. Phys. J. C **78** (2018) no.11, 965 [arXiv:1804.05252 [hep-ex]].
17. LHCb Collaboration, JHEP **1605** (2016) 131 [arXiv:1605.00951 [hep-ex]].
18. LHCb Collaboration, JHEP **1601** (2016) 155 [arXiv:1511.08039 [hep-ex]].
19. LHCb Collaboration, JHEP **1609** (2016) 136 [arXiv:1607.06495 [hep-ex]].
20. LHCb Collaboration, JHEP **1610** (2016) 030 [arXiv:1608.01484 [hep-ex]].
21. CMS Collaboration, CMS-PAS-SMP-17-010, https://cds.cern.ch/record/2675022/
22. ATLAS Collaboration, Eur. Phys. J. C **76** (2016) no.5, 291 [arXiv:1512.02192 [hep-ex]].
23. J. Alwall *et al.*, JHEP **1407** (2014) 079 [arXiv:1405.0301 [hep-ph]].
24. S. Alioli, P. Nason, C. Oleari and E. Re, JHEP **0807** (2008) 060 [arXiv:0805.4802 [hep-ph]].
25. K. Hamilton, P. Nason, C. Oleari and G. Zanderighi, JHEP **1305** (2013) 082 [arXiv:1212.4504 [hep-ph]].
26. F. Landry, R. Brock, P. M. Nadolsky and C. P. Yuan, Phys. Rev. D **67** (2003) 073016 [hep-ph/0212159].
27. S. Alioli, C. W. Bauer, C. Berggren, F. J. Tackmann and J. R. Walsh, Phys. Rev. D **92** (2015) no.9, 094020 [arXiv:1508.01475 [hep-ph]].
28. ATLAS Collaboration, ATL-PHYS-PUB-2017-021, https://cds.cern.ch/record/2298152/
29. ATLAS Collaboration, Eur. Phys. J. C **78** (2018) no.2, 110 Erratum: [Eur. Phys. J. C **78** (2018) no.11, 898] [arXiv:1701.07240 [hep-ex]].
30. CMS Collaboration, Eur. Phys. J. C **78** (2018) no.9, 701 [arXiv:1806.00863 [hep-ex]].
31. ATLAS Collaboration, ATLAS-CONF-2018-037, http://cds.cern.ch/record/2630340/
32. R. D. Ball *et al.* [NNPDF Collaboration], JHEP **1504** (2015) 040 [arXiv:1410.8849 [hep-ph]].
33. P. Azzi *et al.* [HL-LHC Collaboration and HE-LHC Working Group], arXiv:1902.04070 [hep-ph].
34. R. Abdul Khalek, S. Bailey, J. Gao, L. Harland-Lang and J. Rojo, Eur. Phys. J. C **78** (2018) no.11, 962 [arXiv:1810.03639 [hep-ph]].
35. M. Klein and V. Radescu, CERN-LHeC-Note-2013-002, https://cds.cern.ch/record/1564929

Published for SISSA by Springer

Received: October 17, 2017
Accepted: November 3, 2017
Published: December 12, 2017

Measurement of the Drell-Yan triple-differential cross section in pp collisions at $\sqrt{s} = 8$ TeV

The ATLAS collaboration

E-mail: atlas.publications@cern.ch

Abstract: This paper presents a measurement of the triple-differential cross section for the Drell-Yan process $Z/\gamma^* \to \ell^+\ell^-$ where ℓ is an electron or a muon. The measurement is performed for invariant masses of the lepton pairs, $m_{\ell\ell}$, between 46 and 200 GeV using a sample of 20.2 fb^{-1} of pp collisions data at a centre-of-mass energy of $\sqrt{s} = 8$ TeV collected by the ATLAS detector at the LHC in 2012. The data are presented in bins of invariant mass, absolute dilepton rapidity, $|y_{\ell\ell}|$, and the angular variable $\cos\theta^*$ between the outgoing lepton and the incoming quark in the Collins-Soper frame. The measurements are performed in the range $|y_{\ell\ell}| < 2.4$ in the muon channel, and extended to $|y_{\ell\ell}| < 3.6$ in the electron channel. The cross sections are used to determine the Z boson forward-backward asymmetry as a function of $|y_{\ell\ell}|$ and $m_{\ell\ell}$. The measurements achieve high-precision, below the percent level in the pole region, excluding the uncertainty in the integrated luminosity, and are in agreement with predictions. These precision data are sensitive to the parton distribution functions and the effective weak mixing angle.

Keywords: Hadron-Hadron scattering (experiments)

ArXiv ePrint: 1710.05167

https://doi.org/10.1007/JHEP12(2017)059

JHEP12(2017)059

Contents

JHEP12(2017)059

JHEP12(2017)059

1 Introduction

In the Drell-Yan process [1, 2] $q\bar{q} \to Z/\gamma^* \to \ell^+\ell^-$, parity violation in the neutral weak coupling of the mediator to fermions induces a forward-backward asymmetry, A_{FB}, in the decay angle distribution of the outgoing lepton (ℓ^-) relative to the incoming quark direction as measured in the dilepton rest frame. This decay angle depends on the sine of the weak mixing angle, $\sin^2\theta_{\mathrm{W}}$, which enters in the fermionic vector couplings to the Z boson. At leading order in electroweak (EW) theory it is given by $\sin^2\theta_{\mathrm{W}} = 1 - m_W^2/m_Z^2$, where m_W and m_Z are the W and Z boson masses, respectively. Higher-order loop corrections modify this relation depending on the renormalisation scheme used, and so experimental measurements are often given in terms of the sine of the effective weak mixing angle, $\sin^2\theta^{\mathrm{eff}}$ [3]. High-precision cross-section measurements sensitive to the asymmetry, and therefore to the effective weak mixing angle, provide a testing ground for EW theory and could offer some insight into physics beyond the Standard Model (SM).

Previous measurements by ATLAS and CMS of the Drell-Yan (DY) process include measurements of fiducial cross sections [4–7], and one-dimensional differential cross sections as a function of rapidity [8, 9], transverse momentum [9–12], and invariant mass [13–15]. Double-differential cross-section measurements as a function of invariant mass and either rapidity or transverse momentum [16–21] have also been published, as well as Z boson polarisation coefficients [22, 23] and the forward-backward asymmetry [24, 25]. Extraction of the effective weak mixing angle in leptonic Z boson decays, $\sin^2\theta^{\mathrm{eff}}_{\mathrm{lept}}$, from A_{FB} measurements has been performed by ATLAS using $5\,\mathrm{fb}^{-1}$ of proton-proton collision data at $\sqrt{s} = 7$ TeV [24] — a result in which the largest contribution to the uncertainty was due to limited knowledge of the parton distribution functions (PDFs) of the proton.

A complete description of the Drell-Yan cross section to all orders in quantum chromodynamics (QCD) depends on five kinematic variables of the Born-level leptons, namely $m_{\ell\ell}$, the invariant mass of the lepton pair; $y_{\ell\ell}$, the rapidity of the dilepton system; θ and ϕ, the lepton decay angles in the rest frame of the two incident quarks; and $p_{\mathrm{T},Z}$, the transverse momentum of the vector boson. In this paper, measurements of the triple-differential Drell-Yan cross section, $\mathrm{d}^3\sigma/\mathrm{d}m_{\ell\ell}\mathrm{d}|y_{\ell\ell}|\mathrm{d}\cos\theta^*$, are reported as a function of $m_{\ell\ell}$, $|y_{\ell\ell}|$, and $\cos\theta^*$, where the lepton decay angle is defined in the Collins-Soper (CS) reference frame [26]. These cross-section measurements are designed to be simultaneously sensitive to $\sin^2\theta^{\mathrm{eff}}_{\mathrm{lept}}$ and to the PDFs, therefore allowing a coherent determination of both. A simultaneous extraction has the potential to reduce the PDF-induced uncertainty in the extracted value of the effective weak mixing angle.

At leading order (LO) in perturbative electroweak and QCD theory, the Drell-Yan triple-differential cross section can be written as

$$\frac{\mathrm{d}^3\sigma}{\mathrm{d}m_{\ell\ell}\mathrm{d}y_{\ell\ell}\mathrm{d}\cos\theta^*} = \frac{\pi\alpha^2}{3m_{\ell\ell}s}\sum_q P_q\left[f_q(x_1,Q^2)f_{\bar{q}}(x_2,Q^2)+(q\leftrightarrow\bar{q})\right], \tag{1.1}$$

where s is the squared proton-proton (pp) centre-of-mass energy; the incoming parton momentum fractions are $x_{1,2} = (m_{\ell\ell}/\sqrt{s})\mathrm{e}^{\pm y_{\ell\ell}}$; and $f_q(x_1,Q^2)$ are the PDFs for parton flavour q. Here, Q^2 is the four-momentum transfer squared and is set to the dilepton centre-of-mass energy, $m_{\ell\ell}$, which is equal to the partonic centre-of-mass energy. The $q\leftrightarrow\bar{q}$ term accounts for the case in which the parent protons of the q and $\bar{q}$ are interchanged. The function P_q in equation (1.1) is given by

$$\begin{aligned} P_q = {} & e_\ell^2 e_q^2(1+\cos^2\theta^*) \\ & + e_\ell e_q \frac{2m_{\ell\ell}^2(m_{\ell\ell}^2-m_Z^2)}{\sin^2\theta_{\mathrm{W}}\cos^2\theta_{\mathrm{W}}\left[(m_{\ell\ell}^2-m_Z^2)^2+\Gamma_Z^2m_Z^2\right]}\left[v_\ell v_q(1+\cos^2\theta^*)+2a_\ell a_q\cos\theta^*\right] \\ & + \frac{m_{\ell\ell}^4}{\sin^4\theta_{\mathrm{W}}\cos^4\theta_{\mathrm{W}}\left[(m_{\ell\ell}^2-m_Z^2)^2+\Gamma_Z^2m_Z^2\right]}\left[(a_\ell^2+v_\ell^2)(a_q^2+v_q^2)(1+\cos^2\theta^*)+8a_\ell v_\ell a_q v_q\cos\theta^*\right]. \end{aligned} \tag{1.2}$$

In this relation m_Z and Γ_Z are the Z boson mass and width, respectively; e_ℓ and e_q are the lepton and quark electric charges; and $v_\ell = -\frac{1}{4}+\sin^2\theta_{\mathrm{W}}$, $a_\ell = -\frac{1}{4}$, $v_q = \frac{1}{2}I_q^3 - e_q\sin^2\theta_{\mathrm{W}}$, and $a_q = \frac{1}{2}I_q^3$ are the vector and axial-vector lepton and quark couplings, respectively where I_q^3 is the third component of the weak isospin.

The first term in equation (1.2) corresponds to pure virtual photon, γ^*, exchange in the scattering process, the second corresponds to the interference of γ^* and Z exchange, and the last term corresponds to pure Z exchange. Thus the DY invariant mass spectrum is characterized by a $1/m_{\ell\ell}^2$ fall-off from γ^* exchange contribution, an $m_{\ell\ell}$-dependent Breit-Wigner peaking at the mass of the Z boson, and a Z/γ^* interference contribution which changes sign from negative to positive as $m_{\ell\ell}$ increases across the m_Z threshold.

The terms which are linear in $\cos\theta^*$ induce the forward-backward asymmetry. The largest contribution comes from the interference term, except at $m_{\ell\ell} = m_Z$ where the interference term is zero, and only the Z exchange term contributes to the asymmetry. The resulting asymmetry is, however, numerically small due to the small value of v_ℓ. The

JHEP12(2017)059

net effect is an asymmetry which is negative for $m_{\ell\ell} < m_Z$ and increases, becoming positive for $m_{\ell\ell} > m_Z$. The point of zero asymmetry occurs slightly below $m_{\ell\ell} = m_Z$.

The forward-backward asymmetry varies with $|y_{\ell\ell}|$. The incoming quark direction can only be determined probabilistically: for increasing $|y_{\ell\ell}|$ the momentum fraction of one parton reaches larger x where the valence quark PDFs dominate because the valence quarks typically carry more momentum than the antiquarks. Therefore, the Z/γ^* is more likely to be boosted in the quark direction. Conversely, at small boson rapidity, $|y_{\ell\ell}| \sim 0$, it becomes almost impossible to identify the direction of the quark since the quark and antiquark have nearly equal momenta.

The sensitivity of the cross section to the PDFs arises primarily from its dependence on $y_{\ell\ell}$ (and therefore x_1 and x_2) in equation (1.1). Further sensitivity is gained by analysing the cross section in the $m_{\ell\ell}$ dimension, since in the Z resonance peak the partons couple through the weak interaction and off-peak the electric couplings to the γ^* dominate. Therefore, the relative contributions of up-type and down-type quarks vary with $m_{\ell\ell}$. Finally, the $\cos\theta^*$ dependence of the cross section provides sensitivity to terms containing $a_\ell a_q$ and $v_\ell v_q a_\ell a_q$ in equation (1.2). Three different combinations of couplings to the incident quarks contribute to the LO cross section. The magnitude of the asymmetry is proportional to the valence quark PDFs and offers direct sensitivity to the corresponding PDF component.

The full five-dimensional cross section can also be decomposed into harmonic polynomials for the lepton decay angle scattering amplitudes and their corresponding coefficients A_{0-7} [22]. Higher-order QCD corrections to the LO $q\bar{q}$ process involve $qg + \bar{q}g$ terms at next-to-leading order (NLO), and gg terms at next-to-next-to-leading order (NNLO). These higher-order terms modify the decay angle dependence of the cross section. Measuring the $|\cos\theta^*|$ distribution provides additional sensitivity to the gluon versus sea-quark PDFs and is related to the measurements of the angular coefficients as a function of the Z boson transverse momentum [22, 23].

Initial-state QCD radiation can introduce a non-zero transverse momentum for the final-state lepton pair, leading to quark directions which may no longer be aligned with the incident proton directions. Hence, in this paper, the decay angle is measured in the CS reference frame [26] in which the decay angle is measured from an axis symmetric with respect to the two incoming partons. The decay angle in the CS frame (θ^*) is given by

$$\cos\theta^* = \frac{p_{\mathrm{z},\ell\ell}}{m_{\ell\ell}|p_{\mathrm{z},\ell\ell}|}\frac{p_1^+ p_2^- - p_1^- p_2^+}{\sqrt{m_{\ell\ell}^2 + p_{\mathrm{T},\ell\ell}^2}},$$

where $p_i^\pm = E_i \pm p_{\mathrm{z},i}$ and $i = 1$ corresponds to the negatively-charged lepton and $i = 2$ to the positively-charged antilepton. Here, E and p_z are the energy and longitudinal z-components of the leptonic four-momentum, respectively; $p_{\mathrm{z},\ell\ell}$ is the dilepton z-component of the momentum; and $p_{\mathrm{T},\ell\ell}$ the dilepton transverse momentum.

The triple-differential cross sections are measured using $20.2\,\mathrm{fb}^{-1}$ of pp collision data at $\sqrt{s} = 8$ TeV. The measurements are performed in the electron and muon decay channels for $|y_{\ell\ell}| < 2.4$. The electron channel analysis is extended to high rapidity in the region $1.2 < |y_{\ell\ell}| < 3.6$. The measured cross sections cover the kinematic range $46 < m_{\ell\ell} <$

JHEP12(2017)059

200 GeV, $0 < |y_{\ell\ell}| < 3.6$, and $-1 < \cos\theta^* < +1$. For convenience the notation

$$\mathrm{d}^3\sigma \equiv \frac{\mathrm{d}^3\sigma}{\mathrm{d}m_{\ell\ell}\mathrm{d}|y_{\ell\ell}|\mathrm{d}\cos\theta^*}$$

is used. The cross sections are classified as either *forward* ($\cos\theta^* > 0$) or *backward* ($\cos\theta^* < 0$) and used to obtain an experimental measurement of A_{FB} differentially in $m_{\ell\ell}$ and $|y_{\ell\ell}|$:

$$A_{\mathrm{FB}} = \frac{\mathrm{d}^3\sigma(\cos\theta^* > 0) - \mathrm{d}^3\sigma(\cos\theta^* < 0)}{\mathrm{d}^3\sigma(\cos\theta^* > 0) + \mathrm{d}^3\sigma(\cos\theta^* < 0)} \,. \tag{1.3}$$

2 ATLAS detector

The ATLAS detector [27] consists of an inner tracking detector (ID) surrounded by a thin superconducting solenoid, electromagnetic and hadronic calorimeters, and a muon spectrometer (MS). Charged particles in the pseudorapidity[1] range $|\eta| < 2.5$ are reconstructed with the ID, which consists of layers of silicon pixel and microstrip detectors and a straw-tube transition-radiation tracker having a coverage of $|\eta| < 2.0$. The ID is immersed in a 2 T magnetic field provided by the solenoid. The latter is surrounded by a hermetic calorimeter that covers $|\eta| < 4.9$ and provides three-dimensional reconstruction of particle showers. The electromagnetic calorimeter is a liquid-argon sampling calorimeter, which uses lead absorbers for $|\eta| < 3.2$. The hadronic sampling calorimeter uses plastic scintillator tiles as the active material and steel absorbers in the region $|\eta| < 1.7$. In the region $1.5 < |\eta| < 3.2$, liquid argon is used as the active material, with copper absorbers. A forward calorimeter covers the range $3.2 < |\eta| < 4.9$ which also uses liquid argon as the active material, and copper and tungsten absorbers for the EM and hadronic sections of the subdetector, respectively.

Outside the calorimeters, air-core toroids supply the magnetic field for the MS. There, three layers of precision chambers allow the accurate measurement of muon track curvature in the region $|\eta| < 2.7$. The majority of these precision chambers is composed of drift tubes, while cathode-strip chambers provide coverage in the inner layers of the forward region $2.0 < |\eta| < 2.7$. The muon trigger in the range $|\eta| < 2.4$ uses resistive-plate chambers in the central region and thin-gap chambers in the forward region. A three-level trigger system [28] selects events to be recorded for offline analysis.

3 Simulated event samples

Monte Carlo (MC) simulation samples are used to model the expected signal and background yields, with the exception of certain data-driven background estimates. The MC samples are normalised using the highest-order cross-section predictions available in perturbation theory.

[1] ATLAS uses a right-handed coordinate system with its origin at the nominal interaction point in the centre of the detector and the z-axis along the beam pipe. The x-axis points from the interaction point to the centre of the LHC ring, and the y-axis points upward. Cylindrical coordinates (r, ϕ) are used in the transverse plane, ϕ being the azimuthal angle around the beam pipe. The pseudorapidity is defined in terms of the polar angle θ as $\eta = -\ln\tan(\theta/2)$.

JHEP12(2017)059

The DY process was generated at NLO using Powheg-Box (referred to as Powheg in the following) [29–32] and the CT10 PDF set [33], with Pythia 8 [34] to model parton showering, hadronisation, and the underlying event (UEPS). The $Z/\gamma^* \to \ell^+\ell^-$ differential cross section as a function of mass has been calculated at NNLO in perturbative QCD (pQCD) using FEWZ 3.1 [35–37] with the MSTW2008NNLO PDF set [38]. The renormalisation, μ_{r}, and factorisation, μ_{f}, scales were both set equal to $m_{\ell\ell}$. The calculation includes NLO EW corrections beyond final-state photon radiation (FSR) using the G_μ EW scheme [39]. A mass-dependent K-factor used to scale the $Z/\gamma^* \to \ell^+\ell^-$ MC sample is obtained from the ratio of the calculated total NNLO pQCD cross section with the additional EW corrections, to the total cross section from the Powheg sample. This one-dimensional (and therefore partial) NNLO K-factor is found to vary from 1.035 at the lowest invariant mass values considered in this analysis to 1.025 at the highest. This factor also improves the modelling of the Z boson lineshape. The DY production of τ pairs was modelled using Powheg in the same way as the signal simulation.

The scattering amplitude coefficients describing the distributions of lepton decay angles are known to be not accurately modelled in Powheg particularly A_0 at low $p_{\mathrm{T},Z}$ [22]. For this reason, the signal MC events are reweighted as a function of $p_{\mathrm{T},Z}$ and $y_{\ell\ell}$ to improve their modelling. These weights were calculated using the cross-section calculator DYNNLO [40].

The photon-induced process, $\gamma\gamma \to \ell\ell$, is simulated at LO using Pythia 8 and the MRST2004qed PDF set [41]. The expected yield for this process also accounts for NLO QED/EW corrections from references [42, 43], which decrease the yield by approximately 30%.

The production of top quark pairs with prompt isolated leptons from electroweak boson decays constitutes a dominant background. It is estimated at NLO in QCD using Powheg and the CT10 PDF set, with Pythia 6 [44] for UEPS. The $t\bar{t}$ sample is normalized using a cross section calculated at NNLO in QCD including resummation effects [45–50]. Small compared to the $t\bar{t}$ contribution, single-top production in association with a W boson (Wt) is also modelled by Powheg and the CT10 PDF set, with Pythia 6 for UEPS. Both the $t\bar{t}$ and Wt contributions are summed and collectively referred to as the top quark background.

Further small background contributions are due to diboson (WW, WZ and ZZ) production with decays to final states with at least two leptons. The diboson processes were generated at LO with Herwig, using the CTEQ6L1 PDF set [51]. The samples are scaled to NLO calculations [52, 53] or to ATLAS measurements as described in reference [17]. Additionally, the background arising from W boson production in association with jets (W+jets) is studied with MC samples generated with Powheg under identical conditions as the DY signal samples.

All MC samples used in the analysis include the effects of QED FSR, multiple interactions per bunch crossing ("pile-up"), and detector simulation. QED FSR was simulated using Photos [54], while the effects of pile-up were accounted for by overlaying simulated minimum-bias events [55] generated with Pythia8 [34]. The interactions of particles with the detector were modelled using a full ATLAS detector simulation [55] based on Geant4 [56]. Finally, several corrections are applied to the simulated samples, ac-

JHEP12(2017)059

Process	Generator	Parton shower & underlying event	Generator PDF	Model parameters ("Tune")
$Z/\gamma^* \to \ell\ell$	Powheg v1(r1556)	Pythia 8.162	CT10	AU2 [62]
$Z/\gamma^* \to \tau\tau$	Powheg v1(r1556)	Pythia 8.162	CT10	AU2
$\gamma\gamma \to \ell\ell$	Pythia 8.170	Pythia 8.170	MRST2004qed	4C [63]
$t\bar{t}$	Powheg v1(r1556)	Pythia 6.427.2	CT10	AUET2 [64]
Wt	Powheg v1(r1556)	Pythia 6.427.2	CT10	AUET2
Diboson	Herwig 6.520	Herwig 6.520	CTEQ6L1	AUET2
$W \to \ell\nu$	Powheg v1(r1556)	Pythia 8.162	CT10	AU2

Table 1. Overview of the Monte Carlo samples used in this analysis.

counting for differences between data and simulation in the lepton trigger, reconstruction, identification, and isolation efficiencies as well as lepton resolution and muon momentum scale [57–61, 61]. The electron energy scale corrections are applied to the data.

An overview of the simulated event samples is given in table 1.

4 Event selection

Events are required to have been recorded during stable beam condition periods and must pass detector and data-quality requirements. This corresponds to an integrated luminosity of $20.2\,\text{fb}^{-1}$ for the muon channel. Small losses in the data processing chain lead to an integrated luminosity of $20.1\,\text{fb}^{-1}$ for the electron channel. Due to differences in the detector response to electrons and muons the selection is optimised separately for each channel and is described in the following.

4.1 Central rapidity electron channel

The electron data were collected using a dilepton trigger which uses calorimetric and tracking information to identify compact electromagnetic energy depositions. Identification algorithms use calorimeter shower shape information and the energy deposited in the vicinity of the electron candidates to find candidate electron pairs with a minimum transverse energy of 12 GeV for both the leading and subleading electron.

Electrons are reconstructed by clustering energy deposits in the electromagnetic calorimeter using a sliding-window algorithm. These clusters are then matched to tracks reconstructed in the inner detector. The calorimeter provides the energy measurement and the track is used to determine the angular information of the electron trajectory. An energy scale correction determined from $Z \to e^+e^-$, $W \to e\nu$, and $J/\psi \to e^+e^-$ decays [57] is applied to data. Central electron candidates are required to have $|\eta^e| < 2.4$. Furthermore, candidates reconstructed within the transition region between the barrel and endcap calorimeters, $1.37 < |\eta^e| < 1.52$, are excluded from the measurement. Each candidate is required to satisfy the "medium" electron identification [58, 59] criteria, based on calorimetric shower shapes and track parameters. To ensure the selected electrons are on the efficiency plateau of the trigger, electrons are required to have $E_{\text{T}}^e > 20\,\text{GeV}$. Candidate events are

JHEP12(2017)059

required to have exactly one pair of oppositely-charged electrons and their invariant mass is required to be in the range $46 < m_{ee} < 200\,\text{GeV}$.

4.2 High rapidity electron channel

In this channel, the rapidity range of the measurement is extended by selecting one central electron and one forward electron. Forward electrons are defined as having pseudorapidities in the range $2.5 < |\eta^e| < 4.9$, reconstructed by the endcap or forward calorimeters. The data were collected using two single-electron triggers in the central calorimeter region with $E_{\text{T}}^e > 24\,\text{GeV}$ or $E_{\text{T}}^e > 60\,\text{GeV}$. The lower-threshold trigger has additional criteria for the shower shape and energy deposited in the vicinity of the electron candidate. The reconstructed central electrons are required to have $E_{\text{T}}^e > 25\,\text{GeV}$, $|\eta^e| < 2.4$, and must satisfy the "tight" identification criteria. Electrons in the calorimeter transition regions $1.37 < |\eta^e| < 1.52$ are rejected. Leptons produced in the Drell-Yan process are expected to be well isolated from other particles not associated with the lepton. This provides a good discriminant against the multijet background arising from the semileptonic decays of heavy quarks or hadrons faking electrons. The track isolation is defined as the scalar sum of the transverse momenta, $\sum p_{\text{T}}$, of the additional tracks contained in a cone of size $\Delta R = \sqrt{(\Delta\phi)^2 + (\Delta\eta)^2} = 0.2$ around the electron (omitting the contribution from the electron track). Central electrons are required to have a track isolation less than 14% of E_{T}^e.

The forward electron is required to satisfy "tight" identification criteria, $E_{\text{T}}^e > 20\,\text{GeV}$, and $2.5 < |\eta^e| < 4.9$, excluding the transition region between the endcap and forward calorimeters, $3.00 < |\eta^e| < 3.35$. Due to insufficient accuracy in the modelling of the material in front of the endcap calorimeter, forward electrons in the region $2.70 < |\eta^e| < 2.80$ are also rejected.

A dedicated calibration procedure is performed for the forward electrons. Energy scale and Gaussian resolution corrections are derived in bins of η^e by comparing the peak position and the width of the m_{ee} distributions in data and simulation. The scale and resolution corrections are the values that bring the peak regions, $80 < m_{ee} < 100\,\text{GeV}$, of the data and simulation into the best agreement.

No isolation criteria are applied to the forward electron and due to the absence of tracking information in the forward region, no charge requirements are placed on the selected electron pair. Lastly, events in the high rapidity electron channel are required to have exactly one central-forward pair of electrons with an invariant mass in the range $66 < m_{ee} < 150\,\text{GeV}$. Events with more than one possible central-forward pair are not used in this measurement channel.

4.3 Central rapidity muon channel

Candidate events in the muon channel were collected using two sets of triggers with the set of triggers used depending on the p_{T}^μ of the muon with the larger transverse momentum. For $p_{\text{T}}^\mu > 25\,\text{GeV}$, two single-muon triggers are used, with transverse momentum thresholds of 24 GeV and 36 GeV. The low-threshold trigger requires the muon to be isolated. This combination of triggers collected the majority of the events in the data sample. For $p_{\text{T}}^\mu <$

JHEP12(2017)059

25 GeV, a dimuon trigger is used which requires two muons with transverse momentum thresholds of 18 GeV for one muon and 8 GeV for the other.

Muons are identified by tracks reconstructed in the muon spectrometer matched to tracks reconstructed in the inner detector, and are required to have $p_{\mathrm{T}}^{\mu} > 20\,\mathrm{GeV}$ and $|\eta^{\mu}| < 2.4$. Additionally, they must satisfy identification criteria based on the number of hits in the inner detector and muon spectrometer, and on the consistency between the charge and momentum measurements in both systems [60]. Backgrounds from multijet events are efficiently suppressed by imposing an isolation condition requiring that the sum of the transverse momentum, $\sum p_{\mathrm{T}}$, of the tracks contained in a cone of size $\Delta R = 0.2$ around the muon (omitting the contribution from the muon track) to be less than 10% of p_{T}^{μ}. A small contribution of cosmic muons is removed by requiring the magnitude of the longitudinal impact parameter with respect to the primary interaction vertex z_0 to be less than 10 mm. Events are selected if they contain exactly two oppositely-charged muons satisfying the isolation and impact parameter requirements. Finally, the dilepton invariant mass must be in the range $46 < m_{\mu\mu} < 200\,\mathrm{GeV}$.

In order to minimise the influence of residual misalignments between the ID and MS, muon kinematic variables are measured using the ID only. A small residual η^{μ}- and charge-dependent bias in the muon momentum was observed, most likely arising from residual rotational misalignments of the inner detector. Such ID misalignments bias the measurement of the muon track sagitta and have an opposite effect on the momentum of positively- and negatively-charged muons. Hence, the reconstructed invariant mass or rapidity of muon pairs are not affected, in contrast to measurements of $\cos\theta^*$ which are charge-dependent. These residual inner detector misalignments are corrected for based on two methods, one which uses $Z \to \mu^+\mu^-$ events, and another using $Z \to e^+e^-$ events as described in reference [65]. Together with a χ^2 minimisation technique, the dimuon data sample is used to determine the corrections binned finely, which are however insensitive to the η-independent component of the track curvature bias. This bias is corrected for using dielectron data by comparing the ratio of the calorimeter energy to the track momentum for electrons and positrons.

4.4 Measurement bins

The measurement bins are chosen by taking into consideration several competing demands on the analysis such as its sensitivity to the underlying physics, the statistical precision in each bin, and detector resolution effects particularly in the $m_{\ell\ell}$ dimension. The binning must also match those used in recent ATLAS cross section measurements [13, 18].

The measurement is performed in seven bins of $m_{\ell\ell}$ from 46 GeV to 200 GeV with edges set at 66, 80, 91, 102, 116, and 150 GeV; 12 equidistant bins of $|y_{\ell\ell}|$ from 0 to 2.4; and bins of $\cos\theta^*$ from -1 to $+1$, separated at -0.7, -0.4, 0.0, $+0.4$, $+0.7$ giving 6 bins. In total, 504 measurement bins are used for the central rapidity electron and muon channel measurements.

For the high rapidity electron channel the measurement is restricted to the 5 invariant mass bins in the region $66 < m_{\ell\ell} < 150\,\mathrm{GeV}$. The $|y_{\ell\ell}|$ region measured in this channel ranges from 1.2 to 3.6 in 5 bins with boundaries at 1.6, 2.0, 2.4, 2.8. The $\cos\theta^*$ binning is

JHEP12(2017)059

identical to the binning of the central analyses. A total of 150 measurement bins is used in this channel.

5 Background estimation

The background from processes with two isolated final-state leptons of the same flavour is estimated using MC simulation. The processes with non-negligible contributions are $Z/\gamma^* \to \tau\tau$, diboson (WW, WZ and ZZ), and photon-induced dilepton production — together termed the *electroweak* background sources. The top quark background arising from $t\bar{t}$ and Wt production is also estimated using MC simulation. The samples used for these estimates are listed in table 1.

Background contributions from events where at least one final state jet satisfies the electron or muon selection criteria, hereafter referred to as the *fake lepton* background, are determined using a combination of data-driven methods and MC simulation. By far the largest contribution to the fake lepton background comes from light- and heavy-flavour multijet production, referred to as the *multijet* background, which is determined from data. Descriptions on the fake background estimations used in each of the three channels are given in the following subsections.

5.1 Fake lepton background estimation in the central rapidity electron channel

To separate the signal from the multijet background, the analysis relies on the electron relative transverse energy isolation distribution (I^e). This is a good discriminant for the multijet contribution, which has larger values of I^e than the signal process. It is defined as the ratio of the summed calorimetric transverse energy contained in a cone of size $\Delta R = 0.2$ around the electron to the electron transverse energy: $I^e = \sum E_{\mathrm{T}}(\Delta R = 0.2)/E^e_{\mathrm{T}}$. The smaller of the I^e values of the two electron candidates is chosen to represent each event, as it was found to provide optimal discrimination.

The multijet fraction is then estimated from data by fitting this distribution using a template method. The background template is selected with inverted electron identification requirements and the signal, electroweak, and W+jet templates are taken from simulation. The non-isolated sample where the smaller I^e of the two electrons exceeds a certain value is found to be dominated by multijet background and is used to adjust the normalization of the background template, taking into account the small signal contamination. Since the multijet background is not expected to exhibit any parity violating effects and the $\cos\theta^*$ background templates in data were found not to show any asymmetry about $\cos\theta^* = 0$, the method is symmetrised in bins of $|\cos\theta^*|$, resulting in a doubling of the sample sizes and therefore more stable results.

The multijet contribution is found to be largest at low m_{ee} and also at large $|\cos\theta^*|$ for $|y_{ee}| \sim 0$, where it reaches 15% of the expected number of signal events. In the pole region, $80 < m_{ee} < 102\,\mathrm{GeV}$, the contribution is less than 0.1%.

The contribution of W+jet production to the fake lepton background is estimated from MC simulation. It is small compared to the multijet background for all kinematic regions, and therefore does not introduce any significant charge asymmetry.

JHEP12(2017)059

5.2 Fake lepton background estimation in the high rapidity electron channel

The multijet background in the high rapidity electron channel is estimated using a template method similar to the one used in the central electron channel with, however, some small adjustments. The isolation variable is used for the normalisation of the multijet background only for the mass bins in the range $80 < m_{ee} < 102\,\text{GeV}$. The size of the isolation cone in this case is increased to $\Delta R = 0.3$, which was found to improve the stability of the fits. For the off-peak mass bins, the transverse energy of the forward electron is used as an alternative discriminating variable, where the multijet background contributes mostly at low E_{T}. This decreases the statistical uncertainty of the estimation and reduces its dependence on the W+jet background modelling, as discussed below.

The multijet background is the dominant contribution to the background in this measurement channel and is typically about 5–10% of the expected signal, but increases rapidly at large $|\cos\theta^*|$. It can be as large as 30–60% in some bins at large $|y_{ee}|$ where the $|A_{\text{FB}}|$ is large and the signal cross section is suppressed, i.e. $\cos\theta^* < 0$ for $m_{ee} > m_Z$.

The W+jet background is estimated using MC simulation. As was the case in the central electron analysis, it is found to be small under the peak of the Z resonance. It is found to be more significant off peak, reaching 30% of the fake lepton background.

5.3 Fake lepton background estimation in the central rapidity muon channel

The multijet background remaining after event selection in the muon channel is largely due to heavy-flavour b- and c-quark decays, and is estimated in two steps. First, the shape as a function of $|y_{\mu\mu}|$ and $|\cos\theta^*|$ is estimated in each $m_{\mu\mu}$ bin. Next its overall normalisation is then determined in each invariant mass region.

Three orthogonal control regions with inverted muon isolation requirements defined by $I^\mu = \sum p_{\text{T}}(\Delta R = 0.2)/p_{\text{T}}^\mu > 0.1$, and/or inverted muon pair charge requirements are used to determine the multijet background. In each control region the contamination from signal and electroweak background is subtracted using simulation.

A comparison of the shape of the I^μ distributions for muons in events with same-charge and opposite-charge muon pairs shows a small linear deviation from unity of up to +10% when extrapolated into the isolated signal region $I^\mu < 0.1$. This is found to be independent of $m_{\mu\mu}$, and is accounted for in the extrapolation. The $|y_{\mu\mu}|$ and $|\cos\theta^*|$ dependence of the background in each $m_{\mu\mu}$ bin is obtained in the multijet enriched data control region in which pairs of same-charge and opposite-charge muons satisfy $I^\mu > 0.1$. Finally, the resulting $|y_{\mu\mu}|$ and $|\cos\theta^*|$ spectra are normalised in the signal region using the constraint that the yield ratio of opposite-charge to same-charge muon pairs is similar in the isolated and non-isolated control regions.

This method does not account for a potential W+jets background contribution. This component is estimated from simulation and found to be negligible.

The estimated fake lepton background contribution in the muon channel is everywhere smaller than its contribution in the central electron channel, and never more than 5% of the expected signal yield.

JHEP12(2017)059

5.4 Top quark and electroweak backgrounds

These sources of background arise from QCD and EW processes in which two prompt isolated leptons are produced. Their contributions are estimated using MC simulation.

Background events from top quark processes increase with $m_{\ell\ell}$ and are typically below 2% of the expected signal yields. The contribution is largest at the extremes of $\cos\theta^*$ where it can reach 10–20% of the expected signal in the central channels. At high rapidity, this background source is typically below 5% everywhere.

The diboson background increases with invariant mass and reaches about 6% of the expected signal yield at large $|\cos\theta^*|$ in both the central electron and muon channels. In the high rapidity electron channel it reaches about 3% at moderate $|y_{\ell\ell}|$.

The background from $Z \to \tau\tau$ is significant only at low $m_{\ell\ell}$, where it can reach 7% in the central rapidity channels and 3% in the high rapidity channel.

Photon-induced production of dilepton pairs gives a small background contribution of 2% or less in all channels. However, for large values of $m_{\ell\ell}$, this contribution can reach about 5%.

6 Cross-section measurement

As defined in section 4.4, the binning scheme used for the triple-differential measurements consists of 504 bins for the central rapidity electron and muon channels, and 150 bins in the high rapidity electron channel. The Drell-Yan cross section is measured in the central rapidity channels within the fiducial region defined by $p_{\mathrm{T}}^{\ell} > 20\,\mathrm{GeV}$, $|\eta^{\ell}| < 2.4$, and $46 < m_{\ell\ell} < 200\,\mathrm{GeV}$. In the high rapidity electron channel the fiducial region of the measurement is defined by $p_{\mathrm{T}}^{\ell} > 25\,\mathrm{GeV}$ and $|\eta^{\ell}| < 2.4$ for the central electron, $p_{\mathrm{T}}^{\ell} > 20\,\mathrm{GeV}$ and $2.5 < |\eta^{\ell}| < 4.9$ for the forward electron, and $66 < m_{\ell\ell} < 150\,\mathrm{GeV}$.

The cross-section results are first unfolded to the "dressed"-level, defined at the particle-level using leptons after FSR recombined with radiated photons within a cone of $\Delta R = 0.1$. The unfolded data are then corrected to the Born-level, before final-state QED radiation at the particle-level, using a correction factor obtained from the Powheg MC sample. This procedure neglects the bin migrations between the dressed- and Born-level kinematics, an approximation which was verified to have a negligible impact on the central values and uncertainties of the results presented in this paper.

The triple-differential cross section is calculated as

$$\left.\frac{\mathrm{d}^3\sigma}{\mathrm{d}m_{\ell\ell}\,\mathrm{d}|y_{\ell\ell}|\,\mathrm{d}\cos\theta^*}\right|_{l,m,n} = \mathcal{M}_{ijk}^{lmn} \cdot \frac{N_{ijk}^{\mathrm{data}} - N_{ijk}^{\mathrm{bkg}}}{\mathcal{L}_{\mathrm{int}}} \frac{1}{\Delta_{m_{\ell\ell}} \cdot 2\Delta_{|y_{\ell\ell}|} \cdot \Delta_{\cos\theta^*}}\,, \tag{6.1}$$

where i, j, k are the bin indices for reconstructed final-state kinematics; l, m, n are the bin indices for the generator-level kinematics; and $\mathcal{L}_{\mathrm{int}}$ is the integrated luminosity of the data set. Quantity N^{data} is the number of candidate signal events observed in a given bin of width $\Delta_{m_{\ell\ell}}$, $\Delta_{|y_{\ell\ell}|}$, and $\Delta_{\cos\theta^*}$, while N^{bkg} is the number of background events in the same bin. The factor of two in the denominator accounts for the modulus in the rapidity bin

JHEP12(2017)059

width. Integrated single- and double-differential cross sections are measured by summing over the corresponding indices of equation (6.1).

The factor $\mathcal{M}$ is the inverted response matrix and takes into account the efficiency of the signal selection and bin migration effects. It gives the probability that a selected event reconstructed in some measurement bin was originally generated in a given fiducial (generator-level) bin. The factor $\mathcal{M}$ is obtained from the Drell-Yan signal samples after correcting for differences in the reconstruction, identification, trigger, and isolation efficiencies between data and simulation, as well as for momentum scale and resolution mismodelling effects. It also accounts for events originally outside of the fiducial selection that migrate into the reconstructed event sample. Finally, $\mathcal{M}$ also includes extrapolations over the regions that are excluded from the electron selection ($1.37 < |\eta^e| < 1.52$, $2.70 < |\eta^e| < 2.80$, and $3.00 < |\eta^e| < 3.35$).

The quality of the simulation and its ability to describe the data are checked in figures 1–4, comparing data and prediction for the $y_{\ell\ell}$, $\cos\theta^*$, and $m_{\ell\ell}$ distributions in selected regions of the measured kinematic range, as indicated in the figure captions. The expected number of events is calculated as the sum of expected signal and background yields. Acceptable agreement is found in all channels, given that the simulation is only accurate to NLO for the observables shown in figures 1–3, and to NNLO accuracy for the $m_{\ell\ell}$ distribution shown in figure 4.

The background-subtracted data are unfolded to fiducial cross sections using the inverse of the response matrix obtained using an iterative Bayesian unfolding method [66] in which the prior is improved at each iteration. When using such methods the statistical and systematic uncertainties (discussed in section 7) increase with each unfolding iteration, while the residual bias from the initial prior decreases. A balance between these two competing effects must be struck when deciding on the number of iterations to be used to unfold the measurement. Only small changes to the prior are expected, however, since the lineshape of the Z boson resonance and the PDFs are known to high-precision. Moreover, the prior (Powheg) is enhanced using QCD and EW corrections and describes the data within experimental uncertainties. An optimum was found using two iterations in this analysis.

Finally, measurement bins which are predicted by signal MC simulation to have fewer than 25 signal events are expected to have large statistical uncertainties and therefore these bins are removed from the analysis. Approximately 50 bins are discarded in each of the central electron and muon channels. They typically lie at large $|y_{\ell\ell}|$ and large $|\cos\theta^*|$. In the high rapidity electron channel, 27 bins are removed, all corresponding to small $|\cos\theta^*|$. In all cases the discarded bins correspond to ones for which the signal prediction at LO in QCD is consistent with zero.

JHEP12(2017)059

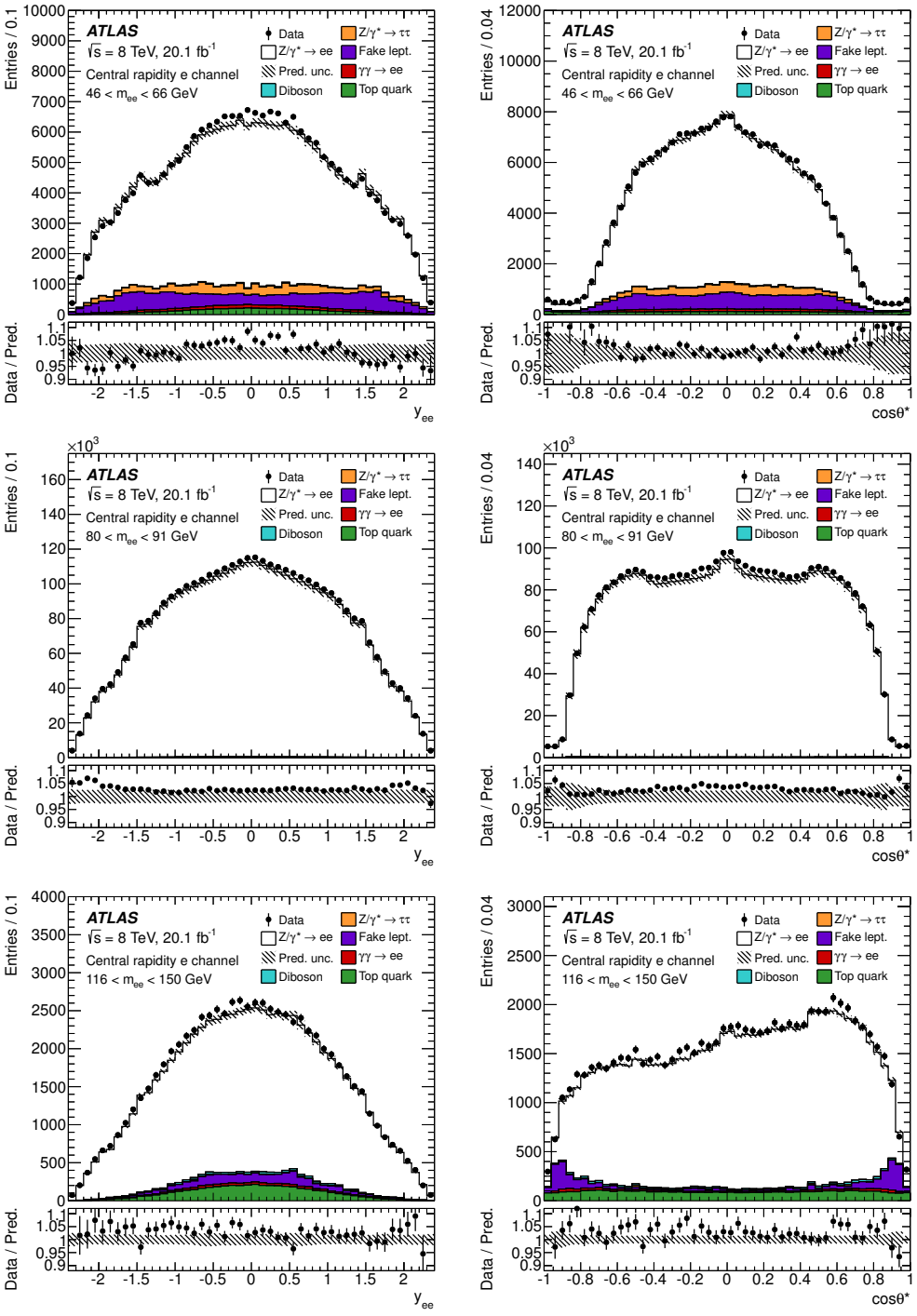

Figure 1. Distributions of dilepton rapidity (left) and $\cos\theta^*$ (right) in the central rapidity electron channel for m_{ee} bins 46–66 GeV (top row), 80–91 GeV (middle), and 116–150 GeV (bottom). The data (solid markers) and the prediction (stacked histogram) are shown after event selection. The lower panels in each plot show the ratio of data to prediction. The error bars represent the data statistical uncertainty while the hatched band represents the systematic uncertainty in the prediction.

JHEP12(2017)059

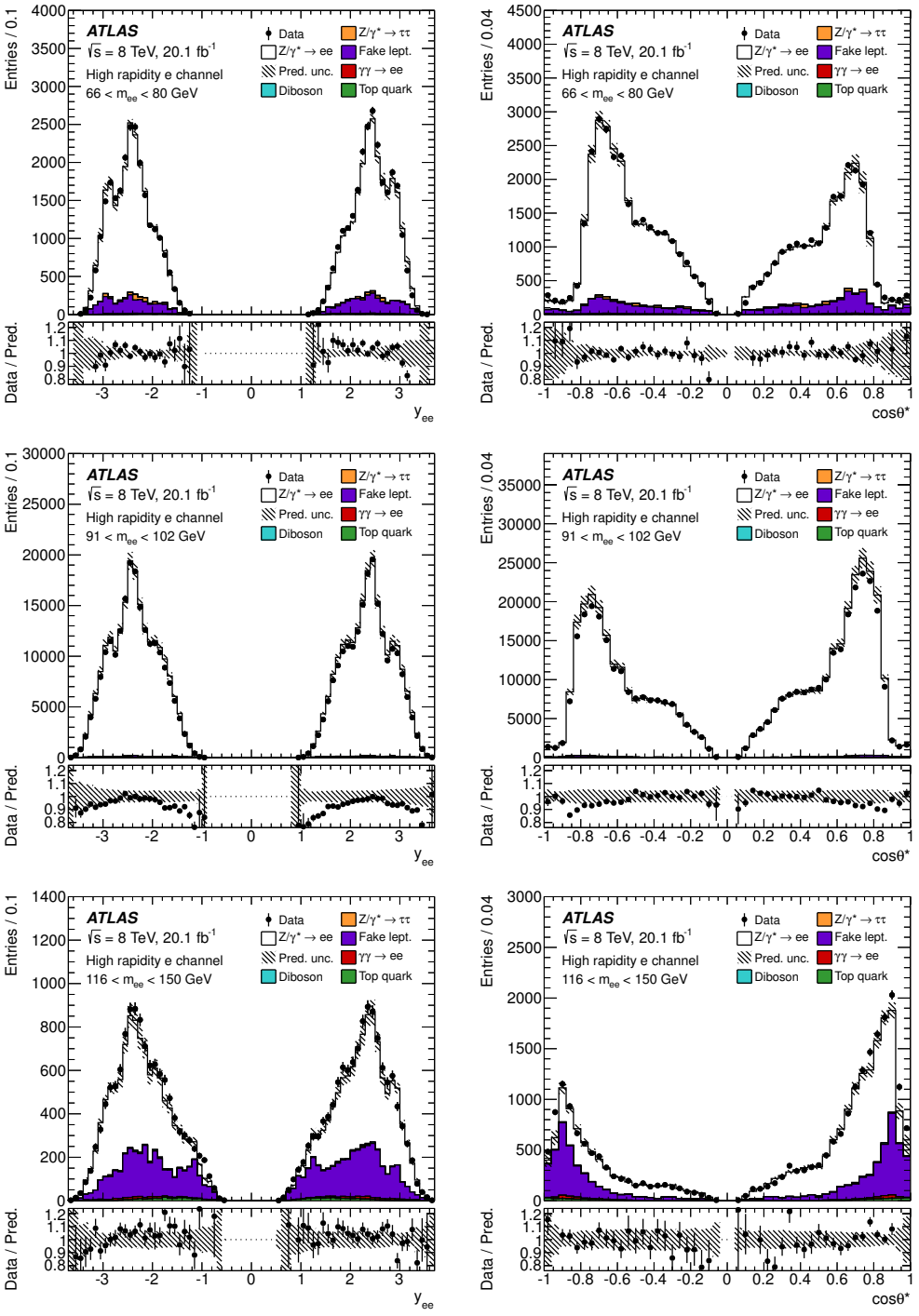

Figure 2. Distributions of dilepton rapidity (left) and $\cos\theta^*$ (right) in the high rapidity electron channel for m_{ee} bins 66–80 GeV (top row), 91–102 GeV (middle), and 116–150 GeV (bottom). The data (solid markers) and the prediction (stacked histogram) are shown after event selection. The lower panels in each plot show the ratio of data to prediction. The error bars represent the data statistical uncertainty while the hatched band represents the systematic uncertainty in the prediction.

JHEP12(2017)059

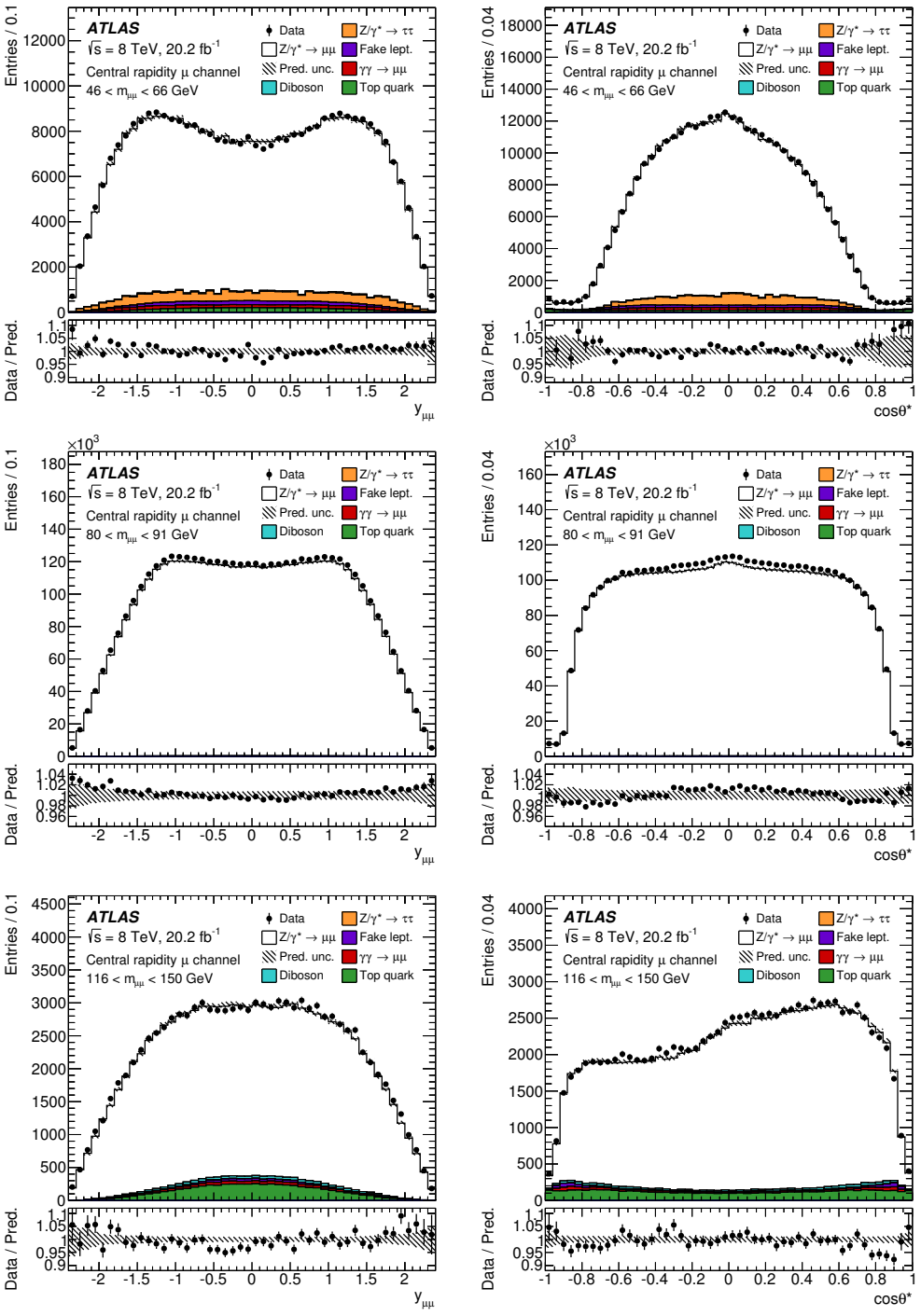

Figure 3. Distributions of dilepton rapidity (left) and $\cos\theta^*$ (right) in the central rapidity muon channel for $m_{\mu\mu}$ bins 46–66 GeV (top row), 80–91 GeV (middle), and 116–150 GeV (bottom). The data (solid markers) and the prediction (stacked histogram) are shown after event selection. The lower panels in each plot show the ratio of data to prediction. The error bars represent the data statistical uncertainty while the hatched band represents the systematic uncertainty in the prediction.

JHEP12(2017)059

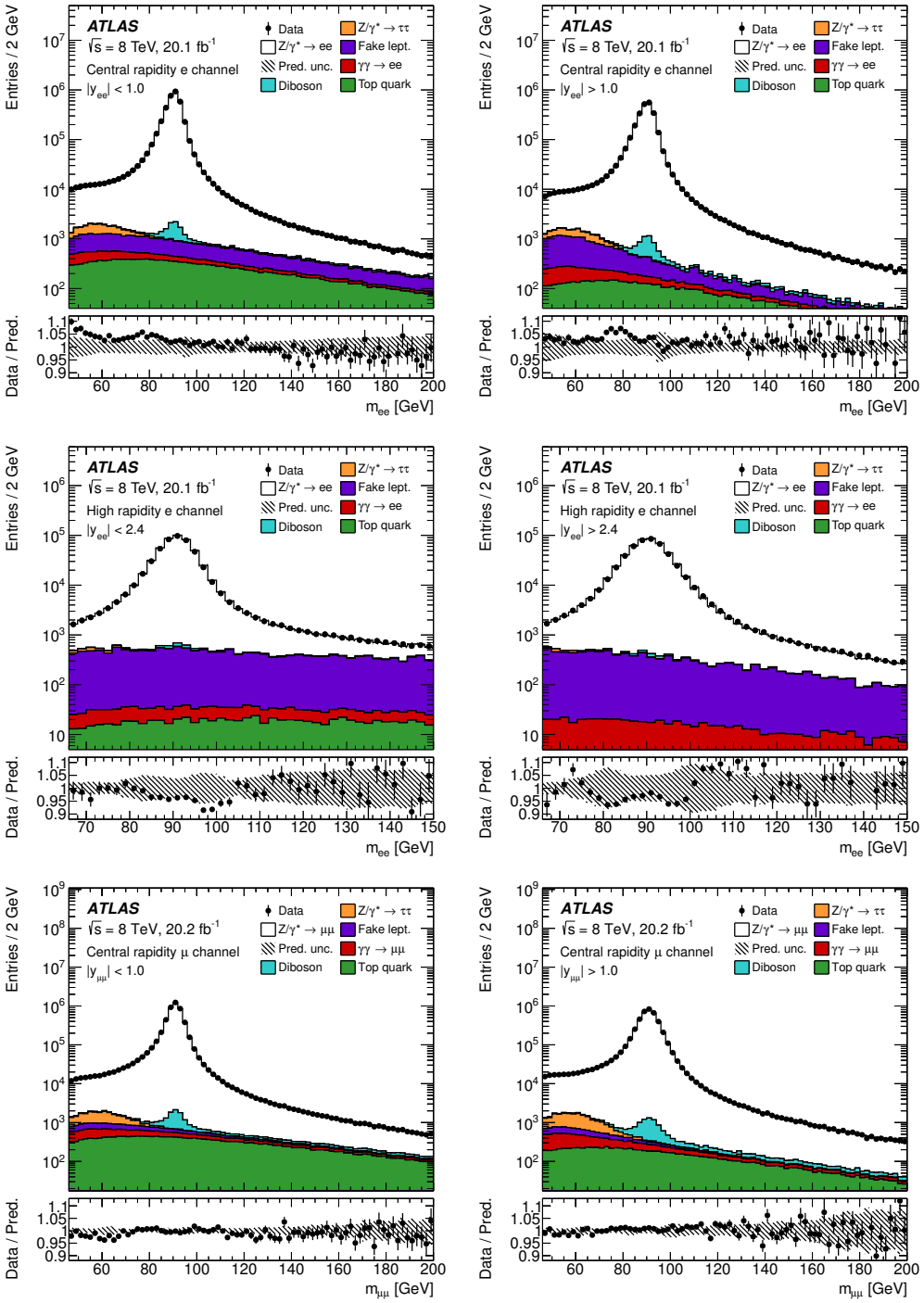

Figure 4. Distributions of invariant mass for all three measurements: the central rapidity electron (top row), the high rapidity electron channel (middle), and the central rapidity muon (bottom) channels. For the central measurements, the distributions are plotted for $|y_{\ell\ell}| < 1.0$ (left) and $|y_{\ell\ell}| > 1.0$ (right) while for the high rapidity measurement, regions $|y_{ee}| < 2.4$ (left) and $|y_{ee}| > 2.4$ (right) are shown. The data (solid markers) and the prediction (stacked histogram) are shown after event selection. The lower panels in each plot show the ratio of data to prediction. The error bars represent the data statistical uncertainty while the hatched band represents the systematic uncertainty in the prediction.

JHEP12(2017)059

7 Measurement uncertainties

The uncertainties in the measurements are discussed separately starting with the sources relevant to both electron channels, then the sources only appearing in the high rapidity electron channel. Next, sources of uncertainty specific to the muon channel are given followed by the sources common to all three measurements. Uncertainties due to statistical sources from both the data and MC samples, the modelling of the energy and momentum response to leptons, lepton selection efficiencies, background subtraction, and theoretical uncertainties are covered in this section. Each source is classified as being correlated or uncorrelated between measurement bins in a single channel. The sources are propagated using one of three techniques: the bootstrap method [67], the pseudo-experiment method, or the offset method.

7.1 Statistical uncertainties

The impact of the statistical uncertainty in the number of events in the data and MC simulations on the cross-section measurement is quantified using the bootstrap method, a statistical resampling technique in which each event is reweighted with a random number drawn from a Poisson distribution with a mean of unity. This reweighting procedure is done 1000 times producing 1000 replicas of the measurement. All replicas are then unfolded and the uncertainty is taken as the standard deviation of the measured cross sections. In the case of the signal MC sample the bootstrap replicas are used to produce an ensemble of 1000 response matrices which are used to unfold the measurement. The standard deviation of the unfolded cross sections is used as the signal MC statistical uncertainty.

7.2 Systematic uncertainties

The pseudo-experiment method is used for correction factors determined in bins of lepton kinematics, typically η and transverse energy/momentum. These correction factors have statistical and systematic uncertainties which are fluctuated randomly using 1000 pseudo-experiments according to a Gaussian distribution whose mean and standard deviation are set to the value and uncertainty of the correction factor, respectively. For correlated sources, a single set of varied correction factors is used for all measurement bins, whereas for uncorrelated sources the random shifts are applied separately for each bin. The uncertainties are propagated via the unfolding procedure yielding 1000 cross-section results which are used to determine a covariance matrix.

In the offset method the correction factor values from each source are coherently shifted upwards and downwards by one standard deviation and the measurement is remade using the varied values. The uncertainty is taken as half the difference between the two unfolded measurements.

7.3 Central and high rapidity electron channels

The systematic uncertainties in the cross section that are unique to the electron channels are dominated by the uncertainties in the electron energy scale, and the electron reconstruction and identification efficiency uncertainties. In addition, a large contribution to the

JHEP12(2017)059

uncertainty arises from the electron energy resolution uncertainty in the two neighbouring m_{ee} bins at the Z-peak, $80 < m_{ee} < 91\,\text{GeV}$ and $91 < m_{ee} < 102\,\text{GeV}$.

7.3.1 Energy scale and resolution

The electron energy scale and resolution and their corresponding uncertainties are determined using $Z \to e^+e^-$, $W \to e\nu$, and $J/\psi \to e^+e^-$ decays. The uncertainty in the energy scale is separated into a statistical component and 14 uncorrelated systematic sources. Some of these sources are split into fine η^e bins, while others are coarsely binned into barrel and endcap regions as described in reference [57]. These sources are found to be strongly anti-correlated between the regions $m_{ee} < m_Z$ and $m_{ee} > m_Z$. The statistical uncertainty in the energy scale is found to be negligible. Adding the effects of the 14 sources of uncertainty in the energy scale in quadrature after propagating to the measured cross sections, the combined uncertainty is 1–2% for the mass bins $80 < m_{ee} < 91\,\text{GeV}$ and $91 < m_{ee} < 102\,\text{GeV}$, but is less than 1% at low and high m_{ee}. However, in the integrated m_{ee} cross-section measurement the effect of these sources is strongly reduced as a result of the anti-correlation between these two m_{ee} bins.

The uncertainty in the energy resolution is separated into seven uncorrelated systematic sources which are propagated to the cross-section measurements individually. This combined uncertainty is typically 0.1–0.5% except in the invariant mass regions neighbouring the Z-peak where it reaches 1%.

7.3.2 Reconstruction and identification efficiencies

The reconstruction and identification efficiencies of electrons are determined from data using various tag-and-probe methods in Z and J/ψ decays, following the prescription in reference [58] with certain improvements and adjustments for the 2012 conditions [68]. The uncertainties arise from variations in the tag-and-probe selection and the background subtraction methods. The correlated systematic uncertainty is taken from the RMS of all variations, separately for the reconstruction and identification efficiency sources, and propagated using the pseudo-experiment method.

The influence of the identification efficiency uncertainty is found to be 0.2–0.4% increasing for larger $|\cos\theta^*|$, and up to 2% at low m_{ee}. The reconstruction efficiency uncertainty translates into a variation of the measured cross section which is generally below 0.2% but as large as 0.4% at low m_{ee}.

7.3.3 Trigger efficiency

The trigger efficiency is measured in both the data and MC simulation using a tag-and-probe method in $Z \to e^+e^-$ decays and is composed of a statistical uncorrelated component which is small, and a correlated piece which is propagated using the pseudo-experiment method. The resulting uncertainty in the cross section amounts to approximately 0.5% at low m_{ee} but decreases to approximately 0.1% for $m_{ee} > 116\,\text{GeV}$.

JHEP12(2017)059

7.3.4 Charge misidentification

The electron charge is determined from the sign of the curvature of the associated ID track. Bremsstrahlung radiation and subsequent conversion of the radiated photons can lead to misidentification of the charge. This is measured in Z boson decays in which one lepton has an incorrectly reconstructed charge. Such events are selected by requiring the electron pair to possess the same electric charge and an invariant mass to be near m_Z, consistent with a Z boson decay. The resulting correlated uncertainty is propagated with the offset method and found to be less than 0.2% everywhere.

7.3.5 Multijet background

Uncertainties in the multijet estimation arise from the sample size used in the method, the subtracted signal and EW contamination, the shape of the multijet distribution, and the range of the isolation distribution used. The subtracted top quark and diboson contamination is varied coherently within the theoretical cross-section uncertainties. The subtracted signal contamination is varied by ±5%. The shape of the multijet distribution is varied by relaxing the same-sign charge requirement in the case of the central electron channel, and using the transverse energy E_{T}^{e} of the forward electron as an alternative discriminant in the high rapidity electron channel. The range of the isolation distribution used is varied by ±15%.

The variations made to account for systematic uncertainties in the method lead to changes in the estimated multijet yield in the central electron channel. The variations in the multijet yields range from about 10% at low m_{ee} and $\cos\theta^* \sim 0$, to more than 100% in regions where the nominal multijet yield is small, e.g. at large $|\cos\theta^*|$ and high m_{ee}.

The uncorrelated statistical component is propagated to the measured cross sections with the bootstrap replica method. The remaining two correlated components are propagated with the offset method, which when summed in quadrature amount to a measurement uncertainty of less than 0.1% of the cross section, except at low m_{ee} and large $|\cos\theta^*|$ where it grows to almost 1% in the central electron channel.

In the high rapidity channel the multijet yields range from 15% to more than 100% due to systematic uncertainties in the method. At small $\cos\theta^*$ and high invariant masses where the signal contribution is suppressed, the expected multijet background can be very large, as noted in section 5.2. Here, the systematic uncertainty in the multijet background is 20–70% depending on $|y_{ee}|$, resulting in a measurement uncertainty of 30% or greater when propagated to the triple-differential cross section.

7.4 High rapidity electron channel

The high rapidity electron analysis differs from the central electron channel measurement by requiring one electron to be in the forward region $2.5 < |\eta^e| < 4.9$ where there is no tracking system, which leads to larger background contamination. This is compensated for by the addition of an isolation requirement on the central electron, and more restrictive identification requirements (see section 4.2) on the central and forward electrons. The technique used to calibrate the forward calorimeters is also different, and the impact of

JHEP12(2017)059

potential charge misidentification is different. Since the charge can be measured only for the central electron, the impact of misidentification is to swap the sign of $\cos\theta^*$. Each of these leads to additional sources of systematic uncertainty which are discussed in the following.

The energy scale and resolution corrections for forward electrons lead to correlated sources of uncertainty propagated using the offset method. They arise from changes in the event selection used to perform the calibration as well as variations of the methodology. The influence of the scale uncertainty on the measurement is about 1% but can reach 5% at high $|\cos\theta^*|$. The resolution uncertainty amounts to 0.1–0.3% increasing to 3–5% at large $|\cos\theta^*|$ and off-peak mass bins.

The uncertainty in the cross-section measurement due to the identification efficiency of forward electrons is considered to be correlated across the measurement bins and is estimated using the pseudo-experiment method. It amounts to about 1% uncertainty in the cross section.

The efficiency of the isolation selection for central electrons is derived using a tag-and-probe method in central $Z \to e^+e^-$ decays and is well described by the simulation. The resulting uncertainty in the cross section is negligible.

To verify that the modelling of the W+jet background does not affect the estimation of the total fake lepton background in the high rapidity channel, its normalisation is varied by 60% (as motivated by reference [18]) and the fit of the multijet background is repeated. Since the shape of the E_{T} distribution is similar for the W+jet and multijet backgrounds, the total fake lepton background remains almost invariant for the off-peak regions while for the peak mass bins the variation is small compared to the multijet background uncertainty.

7.5 Central rapidity muon channel

Uncertainties related to the muon momentum scale and resolution, and the efficiencies of the muon trigger, reconstruction, and isolation and impact parameter selections are all studied using $Z \to \mu^+\mu^-$ events, and in some cases $J/\psi \to \mu^+\mu^-$ events are also used. The efficiencies are determined using a tag-and-probe method. The largest contributions to the systematic uncertainty in the measurements typically arise from the reconstruction efficiency and isolation efficiency modelling, and from the muon momentum scale calibration.

7.5.1 Momentum scale and resolution

Corrections to the muon momentum scale and resolution are obtained from fits to the $Z \to \mu^+\mu^-$ and $J/\psi \to \mu^+\mu^-$ lineshapes with scale and resolution parameters derived in local detector regions [60]. These sources are separated into 12 correlated components for the resolution in fine η^μ bins and one correlated component for the momentum scale. Uncertainties in the momentum scale arising from the methodology, and uncertainties in the ID material simulation, muon angle reconstruction, and alignment are propagated using the offset method. They result in a systematic uncertainty correlated in η^μ bins of the measured cross sections of typically 0.3%, increasing for larger $|y_{\mu\mu}|$, $|\cos\theta^*|$, and $m_{\mu\mu}$

JHEP12(2017)059

to 2%. The correlated resolution uncertainty has a small influence on the measurement and is also propagated with the offset method.

The influence of residual misalignments is estimated from two sources. The first arises from the statistical uncertainty of the alignment corrections derived using $Z \to \mu^+\mu^-$ data and is considered uncorrelated. This component is propagated to the cross section using the pseudo-experiment method, and is separated into 84 uncorrelated components. The second source accounts for biases in the correction method, and is defined as the difference between the corrections derived for data and simulation in bins of η^μ. This uncertainty is separated into 40 correlated components. After propagating this correlated source to the cross section using the pseudo-experiment method, the resulting uncertainty is found to be about 0.2%, increasing significantly with $|\cos\theta^*|$ at large $|y_{\mu\mu}|$.

7.5.2 Reconstruction efficiency

The uncertainty due to the muon reconstruction efficiency is parameterised as a function of η^μ and p_{T}^μ [60] and is decomposed into correlated and uncorrelated parts. The uncertainty is propagated to the cross section using the offset and pseudo-experiment methods for the correlated and uncorrelated components, respectively. The correlated component has an uncertainty of 0.1%, which corresponds to an uncertainty in the measured cross section of 0.2–0.4%.

7.5.3 Trigger efficiency

The efficiency corrections for single-muon and dimuon triggers are obtained using the tag-and-probe method as described in reference [61]. They are parameterised in terms of muon pseudorapidity η^μ, azimuthal angle ϕ^μ, and electric charge. The correlated uncertainty components arise from the background contamination, a possible residual dependence on muon p_{T}^μ, and an uncertainty based on the event topology, which are propagated using the offset method. The uncorrelated statistical uncertainty is propagated to the cross section using the pseudo-experiment method. Events selected with the single-muon triggers ($p_{\mathrm{T}}^\mu > 25\,\mathrm{GeV}$) cover most of the kinematic range of the measurement, whereas the dimuon triggers supplement the selection at low $m_{\mu\mu}$ and have somewhat larger uncertainties. This translates into a correlated uncertainty in the measured cross section which is typically 0.1% where the single-muon triggers are used, and can reach 0.6% at large $|\cos\theta^*|$ in the lowest $m_{\mu\mu}$ bin.

7.5.4 Isolation and impact parameter efficiency

Muon isolation and impact parameter selection efficiencies give rise to additional systematic uncertainties and are estimated together. The sources considered include the remaining background contamination, the residual variation in η^μ, and a possible bias from the event topology estimated by varying the azimuthal opening angle between the two muons used in the tag-and-probe method. The resulting correlated cross-section uncertainty determined with the pseudo-experiment method is found to be typically 0.2%, rising to 0.5% at high $m_{\mu\mu}$.

JHEP12(2017)059

7.5.5 Multijet background

The uncertainty in the multijet background estimate comes from several sources. The uncorrelated statistical uncertainty of the control regions is propagated using the bootstrap replica method and can be significant, in particular from the isolated same-charge control sample. The subtracted top quark and diboson contamination in the control regions is varied coherently within the theoretical cross-section uncertainties given in section 3. The subtracted signal contamination is varied by ±5%. The correlated uncertainty in the shape of the $|y_{\mu\mu}|$ and $|\cos\theta^*|$ spectra is determined from the RMS of these distributions in five regions of increasing non-isolation of the muon pairs obtained from the control regions. The final contribution comes from the fit extrapolation of the background estimate into the signal region and is assessed by varying the range of the fit. Systematic components lead to changes in the multijet yields of 15% to 30% of the expected signal contribution. This is largest in the regions of large $|\cos\theta^*|$. The variations can be up to 60% for large $|\cos\theta^*|$ and large $|y_{\ell\ell}|$.

Both the shape and extrapolation uncertainties are propagated to the cross section using the offset method and dominate the total uncertainty. The combined uncertainty in the background estimate when propagated to the cross-section measurement is below 0.1% in all measurement bins except in the lowest $m_{\mu\mu}$ bin where it reaches 1% at large $|\cos\theta^*|$ and small $|y_{\mu\mu}|$.

7.6 Systematic uncertainties common to all channels

The systematic uncertainties common to all three channels are derived using identical methods. With the exception of the statistical uncertainties arising from the MC samples used, which are uncorrelated between the measurement channels, common systematic uncertainties are assumed to be fully correlated between the channels. The dominant common uncertainty is the uncertainty in the luminosity measurement.

7.6.1 Top, diboson, W+jet, $Z/\gamma^* \to \tau\tau$, and photon-induced background normalisation

The normalisation uncertainties considered for these background sources arise from variations in the PDFs, α_S, and the QCD scales used in the theoretical predictions. The normalisation uncertainty in the top quark background, which is dominated by $t\bar{t}$ production, is taken to be 6% following the PDF4LHC prescription [69]. The uncertainty includes scale and α_S variations and also takes into account the uncertainty in the top-quark mass. Diboson (WW, WZ and ZZ) production is another important background source for which the normalisation uncertainties are about 10%. See reference [17] for additional information on the normalisation uncertainties of the various Monte Carlo samples used.

The background contributions from W+jet processes are assigned a normalisation uncertainty of 5% for the central rapidity measurements. For the high rapidity electron channel, where W+jet is a dominant background, a variation of 60% is considered (see section 7.4).

The background contribution from $Z/\gamma^* \to \tau\tau$ decays is assigned a normalisation uncertainty of 5%. The photon-induced background is assigned an uncertainty of 40%,

JHEP12(2017)059

derived by calculating the photon-induced contribution in a constituent and a current mass scheme for the quark [41], and taking the magnitude of the difference between either scheme and their average [13]. In all cases the normalisation uncertainties are propagated to the final cross sections using the offset method.

7.6.2 Unfolding bias

The simulation used as an initial prior in the unfolding process could lead to a potential bias in the measured cross sections. This potential bias is quantified by varying the predictions within theoretical uncertainties. The PDF bias is probed using signal MC events reweighted to each of the 26 different eigenvector variations of the CT10 PDF set in the determination of $\mathcal{M}$. For each variation the change in the unfolded cross section is found to be much smaller than the change in the predicted cross section using each eigenvector PDF set. Changing the PDF set can alter the predicted cross section by up to a few percent but the influence on the unfolded result is less than 0.1%. Furthermore, the change in the unfolded result, using one to five iterations of unfolding, is much smaller than the total uncertainty in the data. This study is repeated by reweighting the signal MC events to different values of the scattering amplitude coefficient $A_4 = \frac{8}{3}A_{\mathrm{FB}}$, which is proportional to $\sin^2\theta_W$. A variation of ± 0.01 is used, corresponding to a maximum change of 0.5% in the cross-section prior, which results in a change in the unfolded cross section of less than 0.1%. These studies show that potential biases are small for five iterations or less.

A potential overestimate or underestimate of the statistical and systematic uncertainties of the measurement due to the chosen number of unfolding iterations is also studied. Tests of the statistical uncertainty are performed using pseudo-data generated using an alternative PDF. Ultimately, two unfolding iterations are used for the final cross-section determination. This number has a negligible bias due to the initial prior and produces a negligible bias in the data statistical and systematic uncertainties.

7.6.3 MC modelling

The Z boson p_{T} distribution is not well modelled in MC simulation and could influence the measurement. The potential bias is estimated by reweighting the signal MC events to the observed data spectrum at reconstruction-level. This reweighted MC sample is used to unfold the cross section and the difference to the nominal measurement is taken as the uncertainty, which is typically below 0.1%, rising to about 1% at large $|\cos\theta^*|$ and large $|y_{\ell\ell}|$.

Adjustments to the reweighting of the scattering amplitude coefficients in the Powheg MC sample are found to have negligible impact on the measured cross sections.

The MC simulations used for modelling the underlying event and parton shower processes are not explicitly studied here, but are only expected to influence this measurement via the lepton isolation selection efficiencies. Studies presented in reference [18] indicate that such effects are small.

JHEP12(2017)059

7.6.4 PDF uncertainty

As discussed in section 6, the response matrix $\mathcal{M}$ also includes a small acceptance interpolation from the measured region to the fiducial region. These acceptance corrections differ in each of the three measurement channels due to $\eta^{e,\mu}$ gaps in the detector. The corrections are 5–10% but can be larger in certain bins of the triple-differential cross-section measurement. The PDF uncertainties due to these acceptance corrections are estimated using the CT10 PDF eigenvector set at 68% confidence level. They are found to be small, with uncertainties on the order of 0.1% or below for most cross-section measurement bins in the electron channel. In the high rapidity electron channel the uncertainty is also found to be small, except at large $|\cos\theta^*|$ where it can reach 0.6%. The uncertainty evaluated in the muon channel is found to be about 0.5% at low $m_{\mu\mu}$, negligible for $m_{\mu\mu}$ at m_Z, and reaches 0.6% for large $|\cos\theta^*|$ and large $|y_{\mu\mu}|$.

7.6.5 Luminosity

The uncertainty in the integrated luminosity is 1.9%, which is derived following the methodology detailed in reference [70]. This is fully correlated across all measurement bins and analysis channels.

7.7 Summary of measurement uncertainties

Tables 2–4 present the contributions of the individual uncertainties discussed above for each channel in selected analysis bins. The influence of the experimental systematic uncertainties on the measurements of $\mathrm{d}^3\sigma$ can be divided into three regions of $m_{\ell\ell}$ — below the resonance peak, on the peak region, and above the resonance. In the electron channels, the largest measurement uncertainties arise from background and efficiency correction uncertainties at low and high $m_{\ell\ell}$. In the peak region the uncertainty is dominated by the energy scale sources. The muon channel precision is limited by the background uncertainty at low $m_{\ell\ell}$, and by both the momentum scale and misalignment uncertainties in the peak region. At larger invariant mass the uncertainties related to the muon reconstruction and isolation efficiency also become important.

JHEP12(2017)059

Bin	m_{ee} [GeV]	$\lvert y_{ee}\rvert$	$\cos\theta^*$	$\delta^{\text{stat}}_{\text{unc}}$ [%]	$\delta^{\text{sig}}_{\text{unc}}$ [%]	$\delta^{\text{bkg}}_{\text{unc}}$ [%]	$\delta^{\text{mj}}_{\text{unc}}$ [%]	$\delta^{\text{bkg}}_{\text{cor}}$ [%]	$\delta^{\text{mj}}_{\text{cor}}$ [%]	$\delta^{\text{scl}}_{\text{cor}}$ [%]	$\delta^{\text{res}}_{\text{cor}}$ [%]	$\delta^{\text{rec}}_{\text{cor}}$ [%]	$\delta^{\text{id}}_{\text{cor}}$ [%]	$\delta^{\text{trig}}_{\text{cor}}$ [%]	$\delta^{\text{qmid}}_{\text{cor}}$ [%]	$\delta^{\text{kfac}}_{\text{cor}}$ [%]	$\delta^{\text{zpt}}_{\text{cor}}$ [%]	$\delta^{\text{pdf}}_{\text{cor}}$ [%]	δ^{tot} [%]
1	46, 66	0.0, 0.2	−1.0, −0.7	6.7	2.4	3.4	3.1	1.9	5.2	0.5	0.7	0.5	2.5	0.7	0.2	0.0	0.9	0.2	10.6
2	46, 66	0.0, 0.2	−0.7, −0.4	2.3	0.8	1.2	0.9	1.1	2.0	0.2	0.2	0.5	2.7	0.9	0.0	0.0	0.0	0.1	4.7
3	46, 66	0.0, 0.2	−0.4, 0.0	1.4	0.5	0.9	0.4	0.9	0.9	0.3	0.1	0.3	1.9	0.3	0.0	0.0	0.0	0.0	2.9
4	46, 66	0.0, 0.2	0.0, +0.4	1.4	0.5	0.8	0.5	0.9	0.9	0.3	0.1	0.3	1.9	0.3	0.0	0.0	0.0	0.1	3.0
5	46, 66	0.0, 0.2	+0.4, +0.7	2.2	0.8	0.9	0.9	1.1	2.0	0.2	0.1	0.5	2.6	0.8	0.0	0.0	0.0	0.1	4.5
6	46, 66	0.0, 0.2	+0.7, +1.0	6.7	2.3	4.8	3.1	1.8	4.9	0.9	0.5	0.5	2.6	0.7	0.1	0.0	0.9	0.2	10.9
79	66, 80	0.2, 0.4	−1.0, −0.7	2.7	1.3	0.5	0.7	0.5	1.6	1.5	1.1	0.6	3.7	1.2	0.1	0.0	0.3	0.2	5.6
80	66, 80	0.2, 0.4	−0.7, −0.4	1.3	0.6	0.4	0.3	0.3	0.3	0.4	0.4	0.3	1.7	0.4	0.1	0.0	0.0	0.0	2.5
81	66, 80	0.2, 0.4	−0.4, 0.0	1.3	0.4	0.4	0.3	0.3	0.1	0.3	0.1	0.1	0.7	0.2	0.0	0.0	0.0	0.0	1.6
82	66, 80	0.2, 0.4	0.0, +0.4	1.2	0.5	0.3	0.4	0.3	0.1	0.3	0.1	0.1	0.7	0.2	0.1	0.0	0.0	0.0	1.7
83	66, 80	0.2, 0.4	+0.4, +0.7	1.4	0.6	0.3	0.3	0.3	0.3	0.6	0.2	0.3	1.7	0.4	0.1	0.0	0.1	0.0	2.6
84	66, 80	0.2, 0.4	+0.7, +1.0	2.7	1.4	0.4	0.7	0.4	1.6	2.8	1.0	0.6	3.8	1.2	0.2	0.0	0.3	0.1	6.1
157	80, 91	0.4, 0.6	−1.0, −0.7	0.6	0.3	0.0	0.1	0.0	0.1	1.4	0.3	0.3	3.2	0.4	0.1	0.0	0.0	0.1	3.6
158	80, 91	0.4, 0.6	−0.7, −0.4	0.4	0.2	0.0	0.0	0.0	0.0	1.0	0.1	0.1	0.5	0.2	0.1	0.0	0.1	0.0	1.2
159	80, 91	0.4, 0.6	−0.4, 0.0	0.4	0.1	0.0	0.0	0.0	0.0	1.0	0.1	0.0	0.3	0.1	0.1	0.0	0.0	0.0	1.1
160	80, 91	0.4, 0.6	0.0, +0.4	0.4	0.1	0.0	0.0	0.0	0.0	1.0	0.0	0.0	0.3	0.1	0.1	0.0	0.0	0.0	1.2
161	80, 91	0.4, 0.6	+0.4, +0.7	0.4	0.2	0.0	0.0	0.0	0.0	1.0	0.1	0.1	0.5	0.2	0.1	0.0	0.1	0.0	1.2
162	80, 91	0.4, 0.6	+0.7, +1.0	0.6	0.3	0.0	0.0	0.0	0.1	1.6	0.2	0.3	3.2	0.4	0.1	0.0	0.0	0.1	3.7
235	91, 102	0.6, 0.8	−1.0, −0.7	0.5	0.2	0.0	0.1	0.0	0.0	2.1	0.2	0.3	2.6	0.5	0.0	0.0	0.2	0.0	3.5
236	91, 102	0.6, 0.8	−0.7, −0.4	0.4	0.2	0.0	0.0	0.0	0.0	1.3	0.0	0.1	0.5	0.2	0.0	0.0	0.1	0.0	1.5
237	91, 102	0.6, 0.8	−0.4, 0.0	0.4	0.1	0.0	0.0	0.0	0.0	1.0	0.1	0.0	0.2	0.1	0.0	0.0	0.0	0.0	1.1
238	91, 102	0.6, 0.8	0.0, +0.4	0.3	0.1	0.0	0.0	0.0	0.0	1.0	0.0	0.0	0.2	0.1	0.0	0.0	0.0	0.0	1.1
239	91, 102	0.6, 0.8	+0.4, +0.7	0.4	0.2	0.0	0.0	0.0	0.0	1.2	0.0	0.1	0.5	0.2	0.0	0.0	0.1	0.0	1.4
240	91, 102	0.6, 0.8	+0.7, +1.0	0.5	0.2	0.0	0.1	0.0	0.1	2.1	0.1	0.3	2.6	0.5	0.0	0.0	0.2	0.0	3.4
313	102, 116	0.8, 1.0	−1.0, −0.7	2.8	1.2	0.6	0.8	0.5	0.7	2.1	0.9	0.2	1.4	0.3	0.1	0.0	0.1	0.0	4.3
314	102, 116	0.8, 1.0	−0.7, −0.4	2.6	1.2	0.2	0.5	0.2	0.9	2.3	1.0	0.0	0.4	0.2	0.0	0.0	0.1	0.1	4.0
315	102, 116	0.8, 1.0	−0.4, 0.0	2.0	0.8	1.6	0.3	0.2	0.2	1.0	0.3	0.1	0.3	0.1	0.1	0.0	0.0	0.0	2.9
316	102, 116	0.8, 1.0	0.0, +0.4	1.8	0.7	0.1	0.2	0.2	0.1	0.9	0.5	0.1	0.3	0.1	0.0	0.0	0.1	0.1	2.2
317	102, 116	0.8, 1.0	+0.4, +0.7	2.3	1.0	0.5	0.4	0.2	0.7	1.7	1.3	0.0	0.4	0.2	0.1	0.0	0.0	0.1	3.5
318	102, 116	0.8, 1.0	+0.7, +1.0	2.3	1.0	0.2	0.6	0.3	0.6	2.1	0.6	0.2	1.4	0.3	0.0	0.0	0.0	0.1	3.8
391	116, 150	1.0, 1.2	−1.0, −0.7	4.8	1.0	2.8	1.8	1.3	5.1	0.2	0.4	0.1	0.4	0.2	0.1	0.0	0.0	0.1	8.0
392	116, 150	1.0, 1.2	−0.7, −0.4	3.5	0.9	0.4	0.7	0.7	0.6	0.6	0.1	0.1	0.3	0.2	0.1	0.0	0.2	0.1	3.9
393	116, 150	1.0, 1.2	−0.4, 0.0	3.1	0.8	1.3	0.4	0.5	0.8	0.6	0.1	0.1	0.4	0.2	0.1	0.0	0.0	0.2	3.7
394	116, 150	1.0, 1.2	0.0, +0.4	3.0	0.8	0.6	0.5	0.4	0.9	0.6	0.2	0.1	0.4	0.2	0.1	0.0	0.1	0.0	3.5
395	116, 150	1.0, 1.2	+0.4, +0.7	2.8	0.7	0.5	0.5	0.5	0.4	0.6	0.4	0.1	0.3	0.2	0.1	0.0	0.1	0.1	3.2
396	116, 150	1.0, 1.2	+0.7, +1.0	3.7	0.8	2.2	1.1	0.8	3.4	0.4	0.2	0.1	0.4	0.2	0.1	0.0	0.0	0.1	5.7
469	150, 200	1.2, 1.4	−1.0, −0.7	11.9	1.4	2.0	3.6	2.2	1.5	0.4	0.3	0.1	0.5	0.3	0.1	0.0	0.0	0.2	12.9
470	150, 200	1.2, 1.4	−0.7, −0.4	6.6	0.8	1.0	5.9	1.6	0.9	0.9	0.2	0.1	0.5	0.3	0.1	0.0	0.0	0.1	9.2
471	150, 200	1.2, 1.4	−0.4, 0.0	6.6	1.0	3.1	1.9	1.0	0.4	1.0	0.1	0.2	0.6	0.3	0.2	0.0	0.0	0.1	7.8
472	150, 200	1.2, 1.4	0.0, +0.4	5.3	0.9	0.8	0.9	0.6	0.2	0.6	0.2	0.2	0.6	0.3	0.2	0.0	0.1	0.0	5.6
473	150, 200	1.2, 1.4	+0.4, +0.7	4.4	0.6	0.5	1.9	0.7	0.4	0.9	0.2	0.1	0.5	0.3	0.1	0.0	0.0	0.0	5.0
474	150, 200	1.2, 1.4	+0.7, +1.0	7.6	0.9	1.1	2.3	1.1	0.7	0.3	0.2	0.1	0.5	0.3	0.2	0.0	0.0	0.1	8.3

Table 2. Central rapidity electron channel uncertainties in selected bins. All uncertainties quoted are in units of percent, relative to the measured differential cross section. The uncertainties are separated into those which are bin-to-bin correlated within a single channel (marked "cor") and those which are uncorrelated (marked "unc"). The sources are the uncertainties arising from the data sample size ($\delta^{\text{stat}}_{\text{unc}}$); the signal MC sample size ($\delta^{\text{sig}}_{\text{unc}}$); the sizes of the background MC samples ($\delta^{\text{bkg}}_{\text{unc}}$); the statistical component of the multijet estimation ($\delta^{\text{mj}}_{\text{unc}}$); the combined correlated (normalisation) component of all background MC samples ($\delta^{\text{bkg}}_{\text{cor}}$); the multijet estimation ($\delta^{\text{mj}}_{\text{cor}}$); the electron energy scale ($\delta^{\text{scl}}_{\text{cor}}$) and resolution ($\delta^{\text{res}}_{\text{cor}}$); the reconstruction ($\delta^{\text{rec}}_{\text{cor}}$), identification ($\delta^{\text{id}}_{\text{cor}}$), and trigger efficiencies ($\delta^{\text{trig}}_{\text{cor}}$); the electron charge misidentification ($\delta^{\text{qmid}}_{\text{cor}}$); the K-factors ($\delta^{\text{kfac}}_{\text{cor}}$); the Z boson p_{T} modelling ($\delta^{\text{zpt}}_{\text{cor}}$); the PDF variation ($\delta^{\text{pdf}}_{\text{cor}}$); and the total measurement uncertainty (δ^{tot}). The luminosity uncertainty is not included in these tables.

JHEP12(2017)059

Bin	m_{ee} [GeV]	$\lvert y_{ee}\rvert$	$\cos\theta^*$	$\delta^{\text{stat}}_{\text{unc}}$ [%]	$\delta^{\text{sig}}_{\text{unc}}$ [%]	$\delta^{\text{bkg}}_{\text{unc}}$ [%]	$\delta^{\text{mj}}_{\text{unc}}$ [%]	$\delta^{\text{bkg}}_{\text{cor}}$ [%]	$\delta^{\text{mj}}_{\text{cor}}$ [%]	$\delta^{\text{scl}}_{\text{cor}}$ [%]	$\delta^{\text{res}}_{\text{cor}}$ [%]	$\delta^{\text{fscl}}_{\text{cor}}$ [%]	$\delta^{\text{fres}}_{\text{cor}}$ [%]	$\delta^{\text{rec}}_{\text{cor}}$ [%]	$\delta^{\text{id}}_{\text{cor}}$ [%]	$\delta^{\text{trig}}_{\text{cor}}$ [%]	$\delta^{\text{iso}}_{\text{cor}}$ [%]	$\delta^{\text{fid}}_{\text{cor}}$ [%]	$\delta^{\text{qmid}}_{\text{cor}}$ [%]	$\delta^{\text{kfac}}_{\text{cor}}$ [%]	$\delta^{\text{zpt}}_{\text{cor}}$ [%]	$\delta^{\text{pdf}}_{\text{cor}}$ [%]	δ^{tot} [%]
1	66, 80	1.2, 1.6	−1.0, −0.7	6.4	3.0	6.0	4.5	0.9	11.5	0.4	0.6	3.1	2.1	0.2	0.8	0.3	0.0	0.7	0.0	0.0	0.8	0.6	16.0
2	66, 80	1.2, 1.6	−0.7, −0.4	16.4	8.7	8.0	9.9	0.5	11.4	0.5	1.2	5.8	2.5	0.1	0.2	0.1	0.0	0.8	0.0	0.0	0.8	0.3	26.0
3	66, 80	1.2, 1.6	−0.4, 0.0	—	—	—	—	—	—	—	—	—	—	—	—	—	—	—	—	—	—	—	—
4	66, 80	1.2, 1.6	0.0, +0.4	—	—	—	—	—	—	—	—	—	—	—	—	—	—	—	—	—	—	—	—
5	66, 80	1.2, 1.6	+0.4, +0.7	15.7	8.0	6.7	7.9	0.5	10.7	0.9	0.8	3.8	5.5	0.1	0.1	0.1	0.0	0.8	0.0	0.0	1.6	1.4	24.1
6	66, 80	1.2, 1.6	+0.7, +1.0	7.9	3.3	8.8	5.8	1.6	15.3	0.7	0.7	2.3	2.9	0.2	0.8	0.3	0.0	0.7	0.0	0.0	0.9	0.3	20.9
19	66, 80	2.4, 2.8	−1.0, −0.7	3.4	2.2	1.4	2.8	0.3	3.4	2.5	0.7	4.3	5.2	0.2	1.6	0.4	0.1	1.4	0.0	0.0	2.4	0.2	10.1
20	66, 80	2.4, 2.8	−0.7, −0.4	2.2	1.3	0.8	1.6	0.3	1.1	1.2	0.6	3.1	3.9	0.1	0.8	0.2	0.0	1.3	0.0	0.0	0.5	0.1	6.4
21	66, 80	2.4, 2.8	−0.4, 0.0	2.3	1.0	0.8	1.4	0.2	1.5	0.4	0.2	0.9	0.3	0.1	0.5	0.2	0.0	0.8	0.0	0.0	0.1	0.0	3.6
22	66, 80	2.4, 2.8	0.0, +0.4	2.8	1.2	1.5	1.9	0.4	2.0	0.4	0.5	1.3	0.3	0.1	0.5	0.2	0.0	0.7	0.0	0.0	0.3	0.1	4.7
23	66, 80	2.4, 2.8	+0.4, +0.7	2.7	1.6	1.3	2.3	0.4	1.7	1.6	0.2	4.0	6.0	0.1	0.8	0.2	0.0	1.4	0.1	0.0	1.1	0.2	8.8
24	66, 80	2.4, 2.8	+0.7, +1.0	4.2	2.7	3.4	3.7	0.7	5.5	2.8	0.9	4.9	6.5	0.2	1.6	0.4	0.1	1.4	0.0	0.0	3.6	0.3	13.2
73	91, 102	2.0, 2.4	−1.0, −0.7	0.9	0.6	0.2	0.3	0.0	0.8	0.8	0.1	1.9	0.1	0.2	0.8	0.2	0.0	1.2	0.0	0.0	0.8	0.1	2.9
74	91, 102	2.0, 2.4	−0.7, −0.4	0.5	0.3	0.0	0.2	0.0	0.7	0.9	0.1	1.5	0.2	0.0	0.4	0.1	0.0	0.8	0.0	0.0	0.1	0.1	2.1
75	91, 102	2.0, 2.4	−0.4, 0.0	0.7	0.3	0.1	0.4	0.0	0.6	0.6	0.1	1.7	0.1	0.0	0.2	0.1	0.0	0.7	0.0	0.0	0.1	0.0	2.2
76	91, 102	2.0, 2.4	0.0, +0.4	0.6	0.3	0.1	0.4	0.0	0.5	0.5	0.1	1.5	0.1	0.0	0.2	0.1	0.0	0.7	0.0	0.0	0.1	0.1	2.0
77	91, 102	2.0, 2.4	+0.4, +0.7	0.5	0.3	0.1	0.1	0.0	0.5	0.9	0.2	1.3	0.3	0.0	0.4	0.1	0.0	0.8	0.0	0.0	0.2	0.1	2.0
78	91, 102	2.0, 2.4	+0.7, +1.0	0.9	0.5	0.2	0.3	0.0	0.3	0.7	0.2	1.6	0.2	0.2	0.7	0.2	0.0	1.2	0.0	0.0	0.8	0.0	2.6
97	102, 116	1.6, 2.0	−1.0, −0.7	3.8	1.8	2.0	2.9	0.7	4.2	0.6	0.3	2.4	2.2	0.1	0.3	0.1	0.0	0.8	0.0	0.0	1.5	0.1	7.9
98	102, 116	1.6, 2.0	−0.7, −0.4	4.4	2.1	2.0	3.4	0.3	3.6	1.2	0.6	2.1	1.2	0.0	0.2	0.0	0.0	0.7	0.0	0.0	1.5	0.2	8.0
99	102, 116	1.6, 2.0	−0.4, 0.0	—	—	—	—	—	—	—	—	—	—	—	—	—	—	—	—	—	—	—	—
100	102, 116	1.6, 2.0	0.0, +0.4	—	—	—	—	—	—	—	—	—	—	—	—	—	—	—	—	—	—	—	—
101	102, 116	1.6, 2.0	+0.4, +0.7	3.3	1.5	1.6	2.1	0.2	2.2	1.0	0.7	1.7	1.0	0.0	0.2	0.0	0.0	0.7	0.0	0.0	1.1	0.1	5.6
102	102, 116	1.6, 2.0	+0.7, +1.0	2.6	1.4	1.3	1.5	0.3	1.9	0.3	0.1	2.1	1.0	0.1	0.3	0.1	0.0	0.8	0.0	0.0	0.9	0.2	4.9
109	102, 116	2.4, 2.8	−1.0, −0.7	3.7	2.2	2.3	3.4	0.8	6.2	3.3	1.2	6.7	6.6	0.1	0.6	0.1	0.0	1.4	0.0	0.0	3.3	0.3	13.7
110	102, 116	2.4, 2.8	−0.7, −0.4	4.2	2.3	1.0	3.7	0.3	3.3	1.4	1.2	5.5	4.2	0.0	0.2	0.1	0.0	1.2	0.0	0.0	2.0	0.2	10.2
111	102, 116	2.4, 2.8	−0.4, 0.0	3.9	1.9	1.5	4.5	0.2	4.6	0.7	0.9	2.3	1.2	0.1	0.3	0.2	0.0	0.7	0.0	0.0	0.9	0.2	8.5
112	102, 116	2.4, 2.8	0.0, +0.4	3.1	1.5	0.7	2.9	0.1	3.2	0.6	0.4	2.3	1.3	0.1	0.3	0.1	0.0	0.8	0.0	0.0	0.9	0.1	6.3
113	102, 116	2.4, 2.8	+0.4, +0.7	2.7	1.6	1.1	1.7	0.2	1.6	1.2	0.8	4.0	2.1	0.0	0.2	0.1	0.0	1.2	0.0	0.0	1.4	0.2	6.5
114	102, 116	2.4, 2.8	+0.7, +1.0	2.2	1.4	1.3	1.5	0.3	2.4	2.0	0.8	3.3	3.2	0.1	0.6	0.1	0.0	1.3	0.0	0.0	2.2	0.1	7.0
127	116, 150	1.6, 2.0	−1.0, −0.7	8.4	1.7	8.7	7.1	2.9	29.0	0.2	0.4	1.8	1.2	0.0	0.1	0.0	0.0	0.6	0.0	0.0	0.7	0.2	32.5
128	116, 150	1.6, 2.0	−0.7, −0.4	7.6	2.0	4.2	9.0	1.3	8.6	0.6	0.2	0.3	0.5	0.0	0.1	0.0	0.0	0.6	0.0	0.0	0.5	0.2	15.4
129	116, 150	1.6, 2.0	−0.4, 0.0	—	—	—	—	—	—	—	—	—	—	—	—	—	—	—	—	—	—	—	—
130	116, 150	1.6, 2.0	0.0, +0.4	—	—	—	—	—	—	—	—	—	—	—	—	—	—	—	—	—	—	—	—
131	116, 150	1.6, 2.0	+0.4, +0.7	4.4	1.2	3.1	3.8	0.5	3.1	0.2	0.1	0.3	0.2	0.0	0.1	0.0	0.0	0.6	0.0	0.0	0.3	0.1	7.4
132	116, 150	1.6, 2.0	+0.7, +1.0	3.9	0.9	5.5	2.5	1.2	9.8	0.2	0.1	0.9	0.2	0.0	0.1	0.0	0.0	0.7	0.0	0.0	0.5	0.1	12.3
139	116, 150	2.4, 2.8	−1.0, −0.7	16.3	2.9	11.4	14.0	5.4	29.3	1.3	0.5	5.4	1.7	0.1	0.3	0.1	0.0	1.1	0.1	0.0	1.3	0.3	39.1
140	116, 150	2.4, 2.8	−0.7, −0.4	7.5	3.0	7.5	7.3	1.2	10.7	0.2	0.2	1.2	1.4	0.0	0.2	0.1	0.0	0.9	0.0	0.0	1.6	0.3	17.2
141	116, 150	2.4, 2.8	−0.4, 0.0	6.0	1.7	3.8	5.6	0.5	6.8	0.2	0.1	1.8	0.5	0.1	0.4	0.1	0.0	0.6	0.1	0.0	0.9	0.1	11.6
142	116, 150	2.4, 2.8	0.0, +0.4	4.5	1.4	3.1	3.2	0.5	3.4	0.1	0.5	0.8	0.2	0.1	0.4	0.1	0.0	0.6	0.0	0.0	0.5	0.1	7.4
143	116, 150	2.4, 2.8	+0.4, +0.7	3.8	1.4	2.4	2.4	0.4	3.3	0.3	0.3	0.9	0.7	0.0	0.2	0.1	0.0	1.0	0.0	0.0	0.9	0.1	6.5
144	116, 150	2.4, 2.8	+0.7, +1.0	3.3	1.0	1.7	2.0	0.7	3.8	0.7	0.2	1.8	0.6	0.1	0.3	0.1	0.0	1.1	0.0	0.0	0.2	0.1	6.3

Table 3. High rapidity electron channel uncertainties in selected bins. All uncertainties quoted are in units of percent, relative to the measured differential cross section. Bins with blank entries ("—") are those that have been omitted from the measurement due to a lack of expected events. The uncertainties are separated into those which are bin-to-bin correlated within a single channel (marked "cor") and those which are uncorrelated (marked "unc"). The sources are the uncertainties arising from the data sample size ($\delta^{\text{stat}}_{\text{unc}}$); the signal MC sample size ($\delta^{\text{sig}}_{\text{unc}}$); the sizes of the background MC samples ($\delta^{\text{bkg}}_{\text{unc}}$); the statistical component of the multijet estimation ($\delta^{\text{mj}}_{\text{unc}}$); the combined correlated (normalisation) component of all background MC samples ($\delta^{\text{bkg}}_{\text{cor}}$); the multijet estimation ($\delta^{\text{mj}}_{\text{cor}}$); the electron energy scale ($\delta^{\text{scl}}_{\text{cor}}$) and resolution ($\delta^{\text{res}}_{\text{cor}}$); the forward electron energy scale ($\delta^{\text{fscl}}_{\text{cor}}$) and resolution ($\delta^{\text{fres}}_{\text{cor}}$); the reconstruction ($\delta^{\text{rec}}_{\text{cor}}$), identification ($\delta^{\text{id}}_{\text{cor}}$), trigger ($\delta^{\text{trig}}_{\text{cor}}$), isolation ($\delta^{\text{iso}}_{\text{cor}}$), and forward identification efficiencies ($\delta^{\text{fid}}_{\text{cor}}$); the electron charge misidentification ($\delta^{\text{qmid}}_{\text{cor}}$); the K-factors ($\delta^{\text{kfac}}_{\text{cor}}$); the Z boson p_{T} modelling ($\delta^{\text{zpt}}_{\text{cor}}$); the PDF variation ($\delta^{\text{pdf}}_{\text{cor}}$); and the total measurement uncertainty (δ^{tot}). The luminosity uncertainty is not included in these tables.

JHEP12(2017)059

Bin	$m_{\mu\mu}$ [GeV]	$\lvert y_{\mu\mu}\rvert$	$\cos\theta^*$	$\delta^{\text{stat}}_{\text{unc}}$ [%]	$\delta^{\text{sig}}_{\text{unc}}$ [%]	$\delta^{\text{bkg}}_{\text{unc}}$ [%]	$\delta^{\text{bkg}}_{\text{cor}}$ [%]	$\delta^{\text{mj}}_{\text{cor}}$ [%]	$\delta^{\text{scl}}_{\text{cor}}$ [%]	$\delta^{\text{sag}}_{\text{cor}}$ [%]	$\delta^{\text{res}}_{\text{cor}}$ [%]	$\delta^{\text{rec}}_{\text{cor}}$ [%]	$\delta^{\text{id}}_{\text{cor}}$ [%]	$\delta^{\text{trig}}_{\text{cor}}$ [%]	$\delta^{\text{kfac}}_{\text{cor}}$ [%]	$\delta^{\text{zpt}}_{\text{cor}}$ [%]	$\delta^{\text{pdf}}_{\text{cor}}$ [%]	δ^{tot} [%]
1	46, 66	0.0, 0.2	−1.0, −0.7	5.4	2.0	2.1	1.5	0.5	0.2	0.5	0.6	0.3	0.3	0.7	0.0	0.5	0.3	6.6
2	46, 66	0.0, 0.2	−0.7, −0.4	1.8	0.7	1.1	1.2	0.0	0.0	0.1	0.1	0.2	0.2	0.5	0.2	0.3	0.2	2.7
3	46, 66	0.0, 0.2	−0.4, 0.0	1.5	0.6	0.8	0.9	0.5	0.0	0.1	0.0	0.5	0.4	0.0	0.2	0.4	0.2	2.3
4	46, 66	0.0, 0.2	0.0, +0.4	1.5	0.6	0.9	0.9	0.5	0.0	0.1	0.1	0.5	0.4	0.0	0.2	0.5	0.2	2.3
5	46, 66	0.0, 0.2	+0.4, +0.7	1.9	0.6	1.2	1.2	0.0	0.1	0.1	0.4	0.2	0.2	0.5	0.2	0.3	0.2	2.8
6	46, 66	0.0, 0.2	+0.7, +1.0	5.7	2.0	3.6	1.8	0.5	0.1	1.0	0.1	0.3	0.3	0.8	0.2	0.6	0.8	7.7
79	66, 80	0.2, 0.4	−1.0, −0.7	2.3	1.1	0.5	0.6	0.7	0.1	0.7	0.4	0.2	0.2	0.3	0.0	0.0	0.1	3.0
80	66, 80	0.2, 0.4	−0.7, −0.4	1.3	0.7	0.3	0.4	0.1	0.1	0.2	0.1	0.3	0.3	0.0	0.0	0.0	0.1	1.7
81	66, 80	0.2, 0.4	−0.4, 0.0	1.4	0.7	0.4	0.3	0.2	0.1	0.2	0.2	0.4	0.4	0.0	0.1	0.1	0.3	1.8
82	66, 80	0.2, 0.4	0.0, +0.4	1.4	0.7	0.3	0.3	0.2	0.1	0.1	0.2	0.4	0.4	0.1	0.1	0.1	0.2	1.8
83	66, 80	0.2, 0.4	+0.4, +0.7	1.4	0.7	0.4	0.4	0.1	0.1	0.2	0.2	0.3	0.3	0.0	0.1	0.1	0.1	1.8
84	66, 80	0.2, 0.4	+0.7, +1.0	2.2	1.1	0.4	0.6	0.8	0.2	0.7	0.1	0.2	0.2	0.3	0.0	0.0	0.3	3.0
157	80, 91	0.4, 0.6	−1.0, −0.7	0.4	0.2	0.0	0.0	0.0	0.1	1.0	0.1	0.3	0.3	0.0	0.0	0.0	0.1	1.4
158	80, 91	0.4, 0.6	−0.7, −0.4	0.4	0.2	0.0	0.0	0.0	0.2	0.6	0.1	0.4	0.4	0.1	0.0	0.0	0.0	1.1
159	80, 91	0.4, 0.6	−0.4, 0.0	0.3	0.1	0.0	0.0	0.0	0.2	0.3	0.1	0.3	0.3	0.0	0.0	0.0	0.0	0.9
160	80, 91	0.4, 0.6	0.0, +0.4	0.3	0.1	0.0	0.0	0.0	0.2	0.3	0.1	0.3	0.3	0.0	0.0	0.0	0.0	0.9
161	80, 91	0.4, 0.6	+0.4, +0.7	0.4	0.2	0.0	0.0	0.0	0.2	0.6	0.0	0.4	0.4	0.1	0.0	0.0	0.0	1.1
162	80, 91	0.4, 0.6	+0.7, +1.0	0.4	0.2	0.0	0.0	0.0	0.2	1.1	0.1	0.3	0.3	0.1	0.0	0.1	0.0	1.4
235	91, 102	0.6, 0.8	−1.0, −0.7	0.4	0.2	0.0	0.0	0.0	0.1	0.5	0.0	0.3	0.3	0.1	0.0	0.1	0.0	1.0
236	91, 102	0.6, 0.8	−0.7, −0.4	0.3	0.2	0.0	0.0	0.0	0.1	1.0	0.0	0.4	0.4	0.2	0.0	0.0	0.0	1.3
237	91, 102	0.6, 0.8	−0.4, 0.0	0.3	0.1	0.0	0.0	0.0	0.1	0.3	0.0	0.2	0.2	0.0	0.0	0.0	0.0	0.8
238	91, 102	0.6, 0.8	0.0, +0.4	0.3	0.1	0.0	0.0	0.0	0.2	0.3	0.0	0.3	0.2	0.0	0.0	0.0	0.0	0.8
239	91, 102	0.6, 0.8	+0.4, +0.7	0.3	0.2	0.0	0.0	0.0	0.2	1.0	0.0	0.4	0.4	0.1	0.0	0.0	0.0	1.3
240	91, 102	0.6, 0.8	+0.7, +1.0	0.4	0.2	0.0	0.0	0.0	0.1	0.5	0.0	0.3	0.3	0.1	0.0	0.1	0.1	1.0
313	102, 116	0.8, 1.0	−1.0, −0.7	2.1	1.0	0.1	0.4	0.0	0.2	0.9	1.4	0.4	0.4	0.2	0.0	0.0	0.1	3.0
314	102, 116	0.8, 1.0	−0.7, −0.4	1.8	0.8	0.0	0.2	0.1	0.2	1.8	0.3	0.3	0.3	0.2	0.0	0.0	0.0	2.8
315	102, 116	0.8, 1.0	−0.4, 0.0	1.7	0.7	0.0	0.1	0.0	0.1	0.4	0.6	0.3	0.3	0.1	0.0	0.0	0.0	2.0
316	102, 116	0.8, 1.0	0.0, +0.4	1.6	0.6	0.0	0.1	0.0	0.2	0.4	0.5	0.3	0.3	0.0	0.0	0.0	0.0	2.0
317	102, 116	0.8, 1.0	+0.4, +0.7	1.6	0.7	0.0	0.2	0.1	0.2	2.0	0.8	0.4	0.3	0.1	0.0	0.0	0.1	2.8
318	102, 116	0.8, 1.0	+0.7, +1.0	2.0	0.9	0.1	0.3	0.0	0.2	0.8	1.5	0.4	0.4	0.0	0.0	0.0	0.0	2.7
391	116, 150	1.0, 1.2	−1.0, −0.7	4.1	1.2	0.3	1.3	0.0	0.1	0.5	0.3	0.5	0.5	0.2	0.1	0.0	0.1	4.8
392	116, 150	1.0, 1.2	−0.7, −0.4	2.9	0.7	0.2	0.7	0.1	0.1	0.7	0.4	0.4	0.3	0.2	0.0	0.1	0.1	3.4
393	116, 150	1.0, 1.2	−0.4, 0.0	2.5	0.6	0.1	0.5	0.1	0.1	0.5	0.1	0.3	0.3	0.2	0.0	0.1	0.1	2.8
394	116, 150	1.0, 1.2	0.0, +0.4	2.2	0.6	0.1	0.4	0.0	0.0	0.5	0.0	0.3	0.3	0.1	0.0	0.1	0.1	2.5
395	116, 150	1.0, 1.2	+0.4, +0.7	2.3	0.6	0.2	0.5	0.0	0.0	0.4	0.3	0.3	0.3	0.0	0.0	0.1	0.0	2.6
396	116, 150	1.0, 1.2	+0.7, +1.0	3.2	0.9	0.3	0.7	0.1	0.1	0.8	0.1	0.5	0.5	0.0	0.0	0.0	0.1	3.8
469	150, 200	1.2, 1.4	−1.0, −0.7	11.1	1.5	1.2	2.9	0.1	0.3	2.7	0.5	0.7	0.5	0.2	0.1	0.0	0.1	13.6
470	150, 200	1.2, 1.4	−0.7, −0.4	5.6	0.8	0.5	1.4	0.0	0.1	1.3	0.1	0.5	0.4	0.2	0.0	0.0	0.1	6.2
471	150, 200	1.2, 1.4	−0.4, 0.0	4.6	0.6	0.3	0.9	0.1	0.0	1.0	0.2	0.4	0.4	0.2	0.0	0.0	0.1	5.1
472	150, 200	1.2, 1.4	0.0, +0.4	4.1	0.5	0.2	0.7	0.1	0.0	1.1	0.0	0.4	0.4	0.1	0.0	0.0	0.0	4.5
473	150, 200	1.2, 1.4	+0.4, +0.7	4.0	0.5	0.2	0.8	0.0	0.1	0.8	0.2	0.4	0.4	0.0	0.0	0.0	0.1	4.3
474	150, 200	1.2, 1.4	+0.7, +1.0	6.6	0.9	0.5	1.2	0.1	0.0	1.7	0.0	0.6	0.5	0.0	0.0	0.1	0.1	8.0

Table 4. Central rapidity muon channel uncertainties in selected bins. All uncertainties quoted are in units of percent, relative to the measured differential cross section. The uncertainties are separated into those which are bin-to-bin correlated within a single channel (marked "cor") and those which are uncorrelated (marked "unc"). The sources are the uncertainties arising from the data sample size ($\delta^{\text{stat}}_{\text{unc}}$); the signal MC sample size ($\delta^{\text{sig}}_{\text{unc}}$); the sizes of the background MC samples ($\delta^{\text{bkg}}_{\text{unc}}$); the combined correlated (normalisation) component of all background MC samples ($\delta^{\text{bkg}}_{\text{cor}}$); the multijet estimation ($\delta^{\text{mj}}_{\text{cor}}$); the muon momentum scale ($\delta^{\text{scl}}_{\text{cor}}$); the sagitta bias corrections ($\delta^{\text{sag}}_{\text{cor}}$); the muon momentum resolution ($\delta^{\text{res}}_{\text{cor}}$); the reconstruction ($\delta^{\text{rec}}_{\text{cor}}$), identification ($\delta^{\text{id}}_{\text{cor}}$), and trigger efficiencies ($\delta^{\text{trig}}_{\text{cor}}$); the K-factors ($\delta^{\text{kfac}}_{\text{cor}}$); the Z boson p_{T} modelling ($\delta^{\text{zpt}}_{\text{cor}}$); the PDF variation ($\delta^{\text{pdf}}_{\text{cor}}$); and the total measurement uncertainty (δ^{tot}). The luminosity uncertainty is not included in these tables.

JHEP12(2017)059

8 Results

In the two invariant mass bins in the region $80 < m_{\ell\ell} < 102\,\text{GeV}$, the measurement of $\mathrm{d}^3\sigma$ in the central electron channel achieves a total uncertainty (excluding the luminosity contribution) of 1–2% per bin. In the muon channel the precision is better than 1%. In both cases the measurement precision is dominated by the experimental systematic uncertainties, compared to a data statistical uncertainty of about 0.5% per bin in this high-precision region. In the high rapidity electron channel, the precision of the measurement reaches 2–3% per bin, of which the statistical uncertainty is about 0.5%.

The data tables provided in this paper contain compact summaries of the measurement uncertainties; however, complete tables with the full breakdown of all systematic uncertainties and their correlated components are provided in HEPData [71, 72]. These complete tables also include the correction factors used to translate the unfolded measurements from the dressed-level to the Born-level as discussed in section 6.

8.1 Combination of the central rapidity electron and muon channels

The central rapidity electron and muon measurement channels are defined with a common fiducial region given in section 6 and therefore are combined to further reduce the experimental uncertainties. A χ^2-minimisation technique is used to combine the cross sections [73–75]. This method introduces a nuisance parameter for each systematic error source which contributes to the total χ^2. The sources of uncertainty considered are discussed in section 7. Correlated sources of uncertainty which are propagated with the pseudo-experiment or bootstrap resampling methods can be represented in covariance matrix form for each source. The covariance matrices are decomposed into eigenvector representations as input to the χ^2-minimisation function. For each covariance matrix the eigenvectors are sorted by the magnitude of their corresponding eigenvalues. The largest of the eigenvalues are added in order of decreasing value until their sum exceeds a certain fraction of the sum of all eigenvalues, f_{eig}. At which point the correlation information for the eigenvectors whose eigenvalues were not included in the sum is ignored and the eigenvectors are added in quadrature to form a diagonal uncorrelated uncertainty matrix. The resulting numbers of nuisance parameters depends on the complexity of the correlation pattern and on f_{eig}, for which values between 99% and 20% are chosen depending on the source.

This method of decomposition can accurately describe the full covariance matrix, and simultaneously reduce the number of nuisance parameters. The method preserves the total uncertainty and marginally enhances the uncorrelated component of the uncertainty by construction. The original and decomposed covariance matrices are compared and found to agree well such that the combined results are found to be stable in terms of χ^2 and the central values and their uncertainties when f_{eig} is varied around the chosen value in a wide range.

Bin-to-bin correlated sources of uncertainty which are also correlated between the two measurement channels share common nuisance parameters, and are listed in section 7.6. In total, 275 nuisance parameters are used in the procedure. The behaviour of the uncertainties with respect to the combined cross-section values can lead to non-Gaussian

JHEP12(2017)059

distributions of the nuisance parameters. For example, sources related to the selection efficiencies are expected to be proportional to the combined cross-section value, i.e. have multiplicative behaviour; sources related to background subtraction are expected to be independent of the combined cross section and therefore have an additive behaviour. Finally, data statistical sources are expected to be proportional to the square-root of the combined cross section, and have Poisson-like behaviour even after unfolding.

The combination of the central electron and muon channels introduces shifts and constraints to the nuisance parameters. These shifts are propagated to high rapidity electron channel measurement but only have a small impact on this channel since it is dominated by the forward calorimeter uncertainties. The combination of the electron and muon channel cross-section measurements results in a χ^2 per degree of freedom (dof) of 489/451 (p-value of 10%). The pulls of the individual channel measurements to the combined data are found to be Gaussian-distributed about zero with unit RMS. They do not indicate any trends as a function of the kinematic variables. The pulls of the nuisance parameters are similarly found to be Gaussian-distributed about zero with a somewhat larger width of 1.18. Only six nuisance parameters have shifts exceeding three standard deviations, which are sources related to the calibration of the electromagnetic calorimeter, and the source describing the normalisation of the $Z \to \tau\tau$ background MC sample. These particular sources have negligible impact on the measurement.

8.2 Compatibility tests and integrated measurements

In the following subsections, the triple-differential cross sections measured in each of the three channels are compared to one another. The compatibility of the combined data with published ATLAS DY measurements made using the same 2012 dataset is briefly discussed. Moreover, the combined triple-differential cross section is integrated to produce single- and double-differential cross sections which are then compared to theoretical predictions.

8.2.1 Compatibility of the central and high rapidity measurements

The measurements performed in the central electron and muon channels are compared with the high rapidity analysis to test for compatibility. The measurements are made in two different fiducial regions and therefore a common fiducial volume is defined within which the comparison is made. This volume is chosen to be $66 < m_{\ell\ell} < 150\,\text{GeV}$, $p_{\text{T}}^{\ell} > 20\,\text{GeV}$, and no requirement is made on the pseudorapidity of the lepton. The comparison is performed in the overlapping $|y_{\ell\ell}|$ bins of the central and high rapidity analyses.

The corresponding acceptance corrections are obtained from the Powheg simulation for each individual measurement bin. Bins with extrapolation factors smaller than 0.1 are excluded from this test, since they correspond to very restricted regions of phase space. Such regions are subject to large modelling uncertainties, in particular the uncertainty associated with modelling the Z boson transverse momentum. In each bin, the sum of the extrapolation factors for the central and high rapidity channels are found to be close to 80%, indicating that the two sets of measurements cover most of the phase space for $66 < m_{\ell\ell} < 150\,\text{GeV}$ and $p_{\text{T}}^{\ell} > 20\,\text{GeV}$. A second calculation of the extrapolation factors to the full phase space (i.e. $p_{\text{T}}^{\ell} > 0\,\text{GeV}$) has an uncertainty of 1.5%. This is assumed to be

JHEP12(2017)059

strongly anti-correlated between the factors for the central and high rapidity channels since the sum of factors is close to unity. Therefore, an additional 1% anti-correlated uncertainty in the extrapolation factors is used.

The uncertainties arising from electron efficiency corrections are taken to be uncorrelated between the central and high rapidity electron channels since they use different identification criteria and triggers. The multijet uncertainty is also taken to be uncorrelated. The χ^2/dof of the compatibility test is found to be 32/30 (p-value of 37%) for the electron channel and 39/30 (p-value of 13%) for the muon channel.

8.2.2 Compatibility with published data

The cross-section measurements in the central electron and muon channels partially overlap with published DY measurements from ATLAS using the same data set. They are differential measurements of the Z boson transverse momentum spectrum [16] and of the high-mass DY cross section for $m_{\ell\ell} > 116\,\text{GeV}$ [17]. The compatibility of the data presented here with these two published measurements has been tested in identical fiducial regions, separately for the electron and muon channels. The measurements are in good agreement with each other.

The reader is referred to [16] where the most precise measurements of integrated and p_{T}-differential Z cross sections were made in the fiducial region $p_{\text{T}}^{\ell} > 20\,\text{GeV}$ and $|\eta^{\ell}| < 2.4$.

For cross sections differential in $m_{\ell\ell}$ and $|y_{\ell\ell}|$ in the region $m_{\ell\ell} > 116\,\text{GeV}$, see the results presented in reference [17]. These measurements are given in the fiducial region of $p_{\text{T}}^{\ell} > 40, 30\,\text{GeV}$ for leading and subleading leptons, and $|\eta^{\ell}| < 2.5$. Note that the published cross sections include the $\gamma\gamma \to \ell^+\ell^-$ process.

For cross sections measured in the region $m_{\ell\ell} < 116\,\text{GeV}$ and differential in $m_{\ell\ell}$ and $|y_{\ell\ell}|$, the data presented in this paper should be used.

8.2.3 Integrated cross sections

The combined measurements are integrated over the kinematic variables $\cos\theta^*$ and $y_{\ell\ell}$ in order to determine the cross section $\mathrm{d}\sigma/\mathrm{d}m_{\ell\ell}$. Similarly, the integration is performed in $\cos\theta^*$ to determine the cross section $\mathrm{d}^2\sigma/\mathrm{d}m_{\ell\ell}\mathrm{d}|y_{\ell\ell}|$. The integration is firstly performed for the electron and muon channels separately to allow a χ^2-test for compatibility of the two channels. The measurements are simply summed in the e and μ channels for the bins in which both electron and muon measurements are present. Statistical and uncorrelated uncertainties are added in quadrature, whereas correlated systematic uncertainties are propagated linearly. The compatibility tests return $\chi^2/\text{dof} = 12.8/7$ (p-value of 7.7%) for the one-dimensional cross section, and 103/84 (p-value of 7.4%) for the two-dimensional cross section.

The integrated cross sections $\mathrm{d}\sigma/\mathrm{d}m_{\ell\ell}$ and $\mathrm{d}^2\sigma/\mathrm{d}m_{\ell\ell}\mathrm{d}|y_{\ell\ell}|$ are determined from the combined Born-level fiducial triple-differential cross sections. The one-dimensional result is shown in figure 5. The corresponding table of measurements is given in table 5 located in the appendix. The data shows that the combined Born-level fiducial cross section falls by three orders of magnitude in the invariant mass region from the resonant peak to 200 GeV. The data have an uncertainty of about 2%, dominated by the luminosity uncertainty of

JHEP12(2017)059

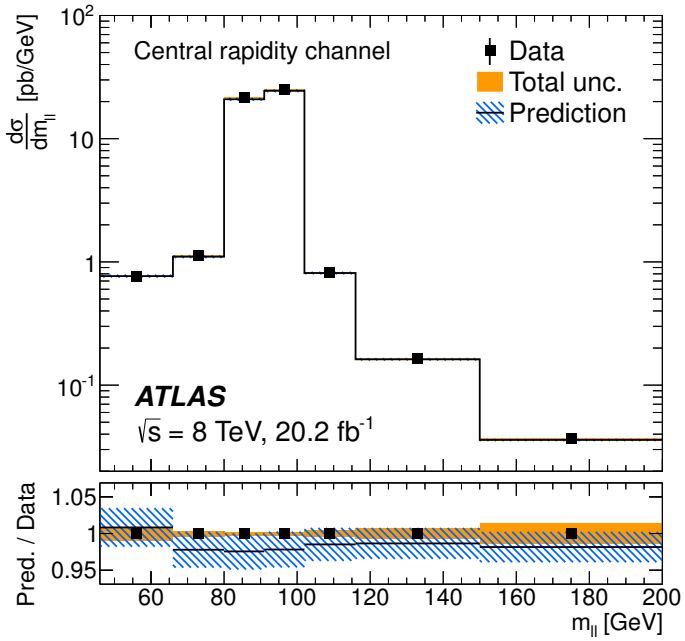

Figure 5. The combined Born-level fiducial cross section $\mathrm{d}\sigma/\mathrm{d}m_{\ell\ell}$. The data are shown as solid markers and the prediction from Powheg including NNLO QCD and NLO EW K-factors is shown as the solid line. The lower panel shows the ratio of prediction to measurement. The inner error bars represent the data statistical uncertainty and the solid band shows the total experimental uncertainty. The contribution to the uncertainty from the luminosity measurement is excluded. The hatched band represents the statistical and PDF uncertainties in the prediction.

1.9%, while uncertainties from the experimental systematic sources can be as low as 0.5% for the peak region. The statistical precision is 0.5% or better, even for the highest invariant mass bin. The fiducial measurements are well predicted by the NLO QCD and parton shower simulation from Powheg partially corrected for NNLO QCD and NLO EW effects, and scattering amplitude coefficients as described in section 3. The uncertainties in the predictions include those arising from the sample size and the PDF variations. No renormalization, factorisation and matching scale variation uncertainties are included although they can be sizeable — as large as 5% for NLO predictions. Except in the lowest mass bin, the predictions underestimate the cross section by about 1–2% (smaller than the luminosity uncertainty), as seen in the lower panel of the figure which shows the ratio of prediction to the measurement.

The two-dimensional Born-level fiducial cross section, $\mathrm{d}^2\sigma/\mathrm{d}m_{\ell\ell}\mathrm{d}|y_{\ell\ell}|$, is illustrated in figure 6 and listed in table 6 of the appendix. In each measured invariant mass bin, the shape of the rapidity distribution shows a plateau at small $|y_{\ell\ell}|$ leading to a broad shoulder followed by a cross section falling to zero at the highest accessible $|y_{\ell\ell}|$. The width of the plateau narrows with increasing $m_{\ell\ell}$. In the two high-precision Z-peak mass bins, the measured cross-section values have a total uncertainty (excluding the common luminosity uncertainty) of 0.4% for $|y_{\ell\ell}| < 1$ rising to 0.7% at $|y_{\ell\ell}| = 2.4$. At high invariant mass, the statistical and experimental uncertainty components contribute equally

JHEP12(2017)059

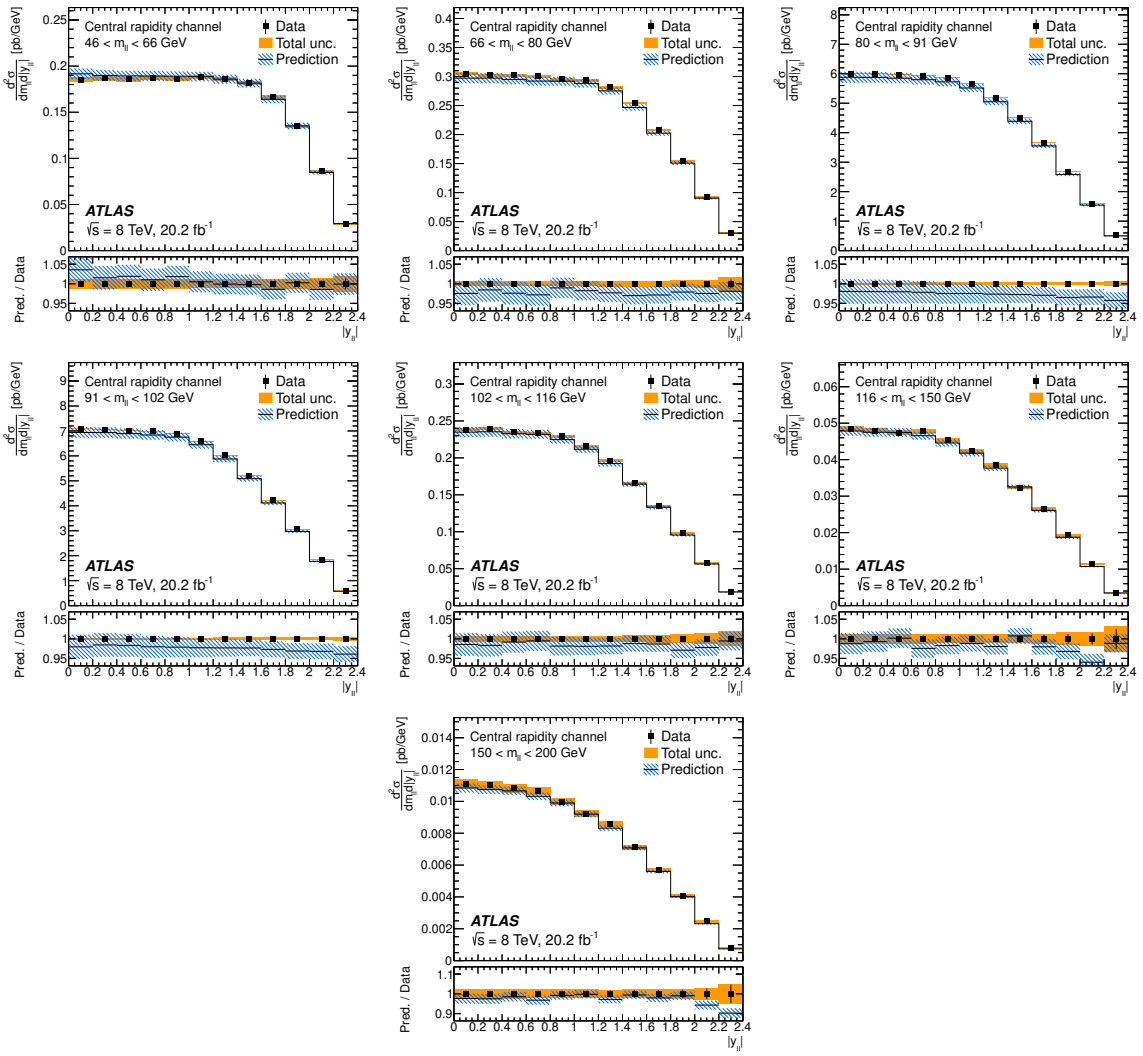

Figure 6. The combined Born-level fiducial cross section $\mathrm{d}^2\sigma/\mathrm{d}m_{\ell\ell}\mathrm{d}|y_{\ell\ell}|$ in the seven invariant mass bins of the central measurements. The data are shown as solid markers and the prediction from Powheg including NNLO QCD and NLO EW K-factors is shown as the solid line. The lower panel shows the ratio of prediction to measurement. The inner error bars represent the data statistical uncertainty and the solid band shows the total experimental uncertainty. The contribution to the uncertainty from the luminosity measurement is excluded. The hatched band represents the statistical and PDF uncertainties in the prediction.

to the total measurement precision in the plateau region, increasing from 0.5% to 1.8%. The theoretical predictions replicate the features in the data well. The lower panel of each figure shows the ratio of the prediction to the measurement. Here, in addition to overall rate difference already observed in the one-dimensional distribution, a small tendency of the data to exceed the predictions at the highest $|y_{\ell\ell}|$ can be seen in some of the mass bins.

JHEP12(2017)059

8.3 Triple-differential cross sections

The combined triple-differential Born-level cross section is shown in figures 7–10. For each invariant mass bin, the data are presented as a function of $|y_{\ell\ell}|$, with each of the six $\cos\theta^*$ regions overlaid in the main panel of the figures. The lower panels show in more detail the ratio of the prediction to the data for each $\cos\theta^*$ bin in turn. The statistical and total, excluding the contribution from the luminosity, uncertainties in the data are shown in the ratio panels.

The accessible range of the $|y_{\ell\ell}|$ distribution is largest for the region close to $\cos\theta^* \simeq 0$, and smallest at the extremes of $\cos\theta^*$. In the lowest invariant mass bin, the cross-section measurements in $\cos\theta^*$ bins with the same absolute value, e.g. bins $-1.0 < \cos\theta^* < -0.7$ and $+0.7 < \cos\theta^* < +1.0$, are consistent with each other at low $|y_{\ell\ell}| \simeq 0$, but exhibit an asymmetry which increases with $|y_{\ell\ell}|$. At large $|y_{\ell\ell}|$, the cross sections for $\cos\theta^* < 0$ are up to 35% larger than the corresponding measurements at $\cos\theta^* > 0$. In the $66 < m_{\ell\ell} < 80\,\text{GeV}$ bin, all cross sections are larger, for large $|\cos\theta^*|$ in particular, due to reduced influence of the fiducial selection on p_{T}^{ℓ}.

The next two invariant mass bins show the peak of the cross section where the asymmetry is smallest. In fact, for $80 < m_{\ell\ell} < 91\,\text{GeV}$ the difference between $\cos\theta^* > 0$ and $\cos\theta^* < 0$ is close to zero. The dramatic improvement in the overall precision of the measurements in this region is also apparent. For the $91 < m_{\ell\ell} < 102\,\text{GeV}$ region, the small asymmetry is observed to change sign, yielding larger cross sections for the $\cos\theta^* < 0$ part of the phase space. This behaviour is expected from the interference effects between the Z and γ^* contributions to the scattering amplitudes. For bins of higher invariant mass the asymmetry increases albeit with larger uncertainties due to the limited statistical precision of the data. The combined measurement is listed in table 7 with its uncertainties.

The predictions describe the data very well, as can be seen from the ratio panels, apart from some bins at large $|y_{\ell\ell}|$ and $|\cos\theta^*|$. These bins correspond to edges of the fiducial acceptance and may be affected by the $p_{\text{T},\ell\ell}$ modelling uncertainties which are not shown for the predictions.

In figures 11–15 the measured triple differential Born-level cross section for the high rapidity electron channel analysis is presented as a function of $\cos\theta^*$. In this channel the region of small $|\cos\theta^*|$ is experimentally accessible only for moderate values of rapidity, i.e. $|y_{\ell\ell}| \simeq 2.0$–$2.8$. Nevertheless the same features of the cross section are observed: the cross sections are largest for the region $m_{\ell\ell} \sim m_Z$; an asymmetry in the $\cos\theta^*$ spectrum is observed with larger cross sections at negative $\cos\theta^*$ for $m_{\ell\ell} < m_Z$, and larger cross sections at positive $\cos\theta^*$ for $m_{\ell\ell} > m_Z$; the magnitude of the asymmetry is smallest for $80 < m_{\ell\ell} < 91\,\text{GeV}$ and increases with $m_{\ell\ell}$. The triple-differential measurement is listed in table 8 with its uncertainties.

JHEP12(2017)059

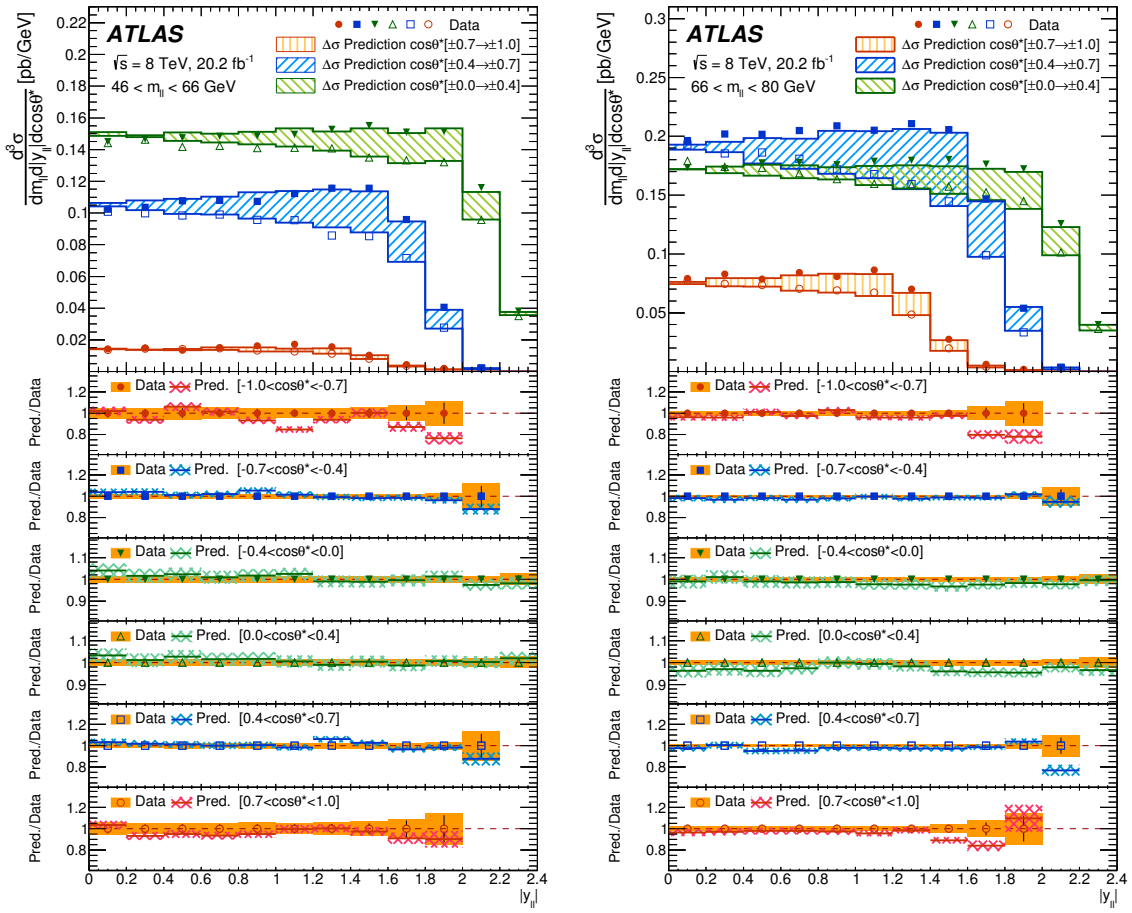

Figure 7. The combined Born-level fiducial cross sections $\mathrm{d}^3\sigma$. The kinematic region shown is labelled in each plot. The data are shown as solid ($\cos\theta^* < 0$) and open ($\cos\theta^* > 0$) markers and the prediction from Powheg including NNLO QCD and NLO EW K-factors is shown as the solid line. The difference, $\Delta\sigma$, between the predicted cross sections in the two measurement bins at equal $|\cos\theta^*|$ symmetric around $\cos\theta^* = 0$ is represented by the hatched shading. In each plot, the lower panel shows the ratio of prediction to measurement. The inner error bars represent the statistical uncertainty of the data and the solid band shows the total experimental uncertainty. The contribution to the uncertainty from the luminosity measurement is excluded. The crosshatched band represents the statistical and PDF uncertainties in the prediction.

JHEP12(2017)059

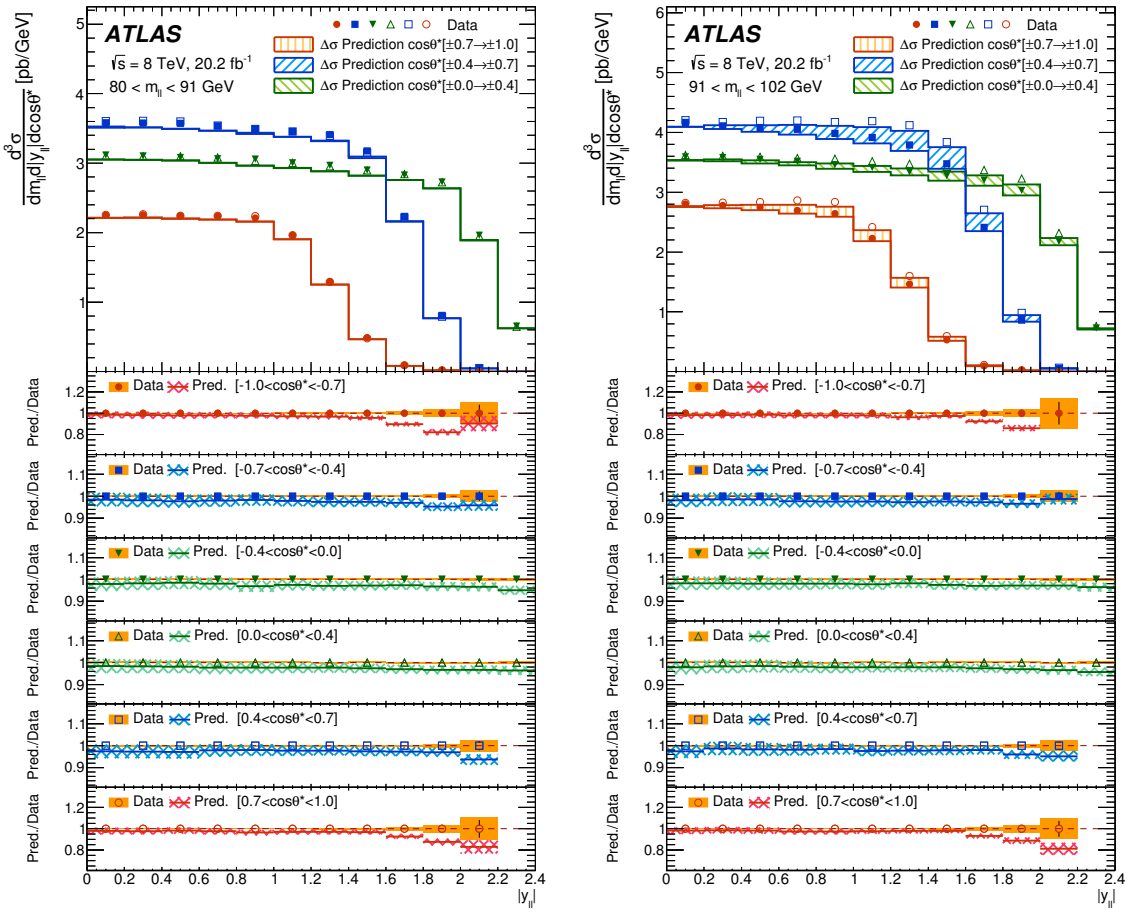

Figure 8. The combined Born-level fiducial cross sections $\mathrm{d}^3\sigma$. The kinematic region shown is labelled in each plot. The data are shown as solid ($\cos\theta^* < 0$) and open ($\cos\theta^* > 0$) markers and the prediction from Powheg including NNLO QCD and NLO EW K-factors is shown as the solid line. The difference, $\Delta\sigma$, between the predicted cross sections in the two measurement bins at equal $|\cos\theta^*|$ symmetric around $\cos\theta^* = 0$ is represented by the hatched shading. In each plot, the lower panel shows the ratio of prediction to measurement. The inner error bars represent the statistical uncertainty of the data and the solid band shows the total experimental uncertainty. The contribution to the uncertainty from the luminosity measurement is excluded. The crosshatched band represents the statistical and PDF uncertainties in the prediction.

JHEP12(2017)059

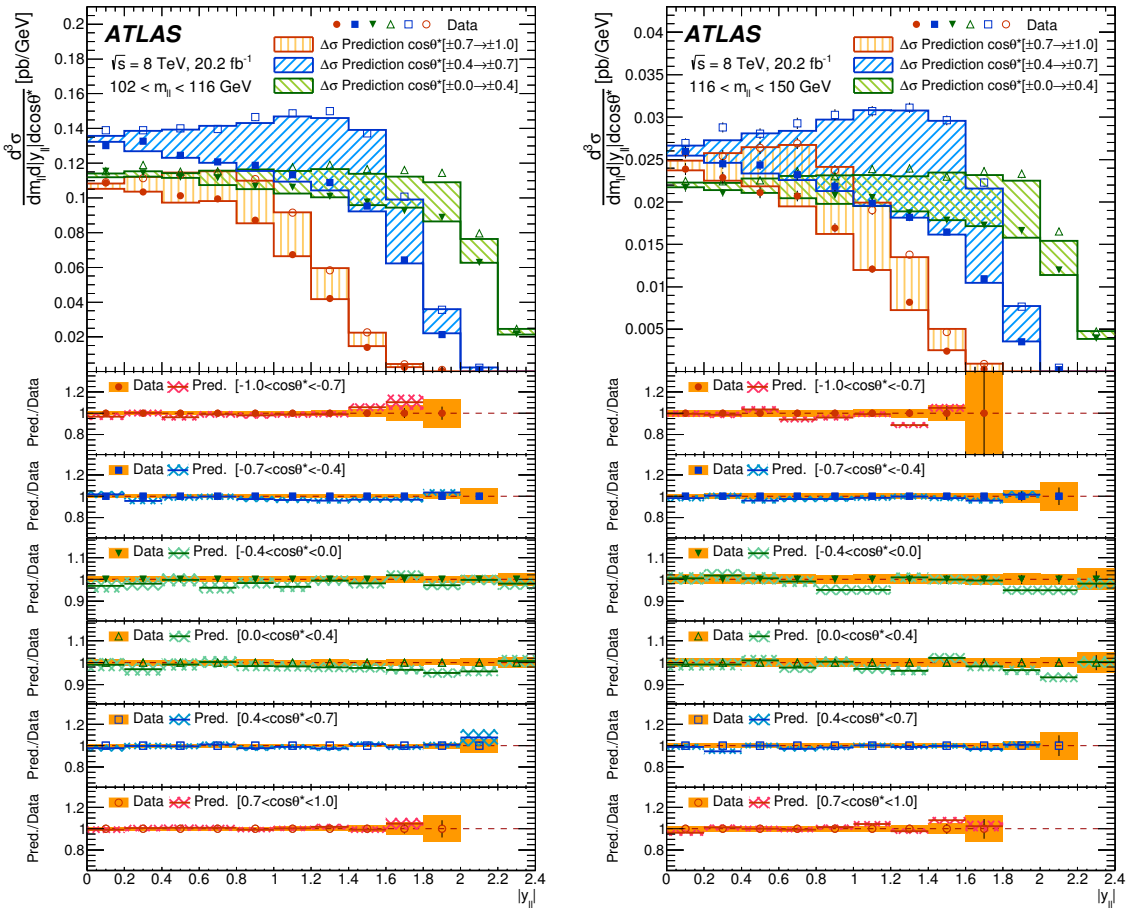

Figure 9. The combined Born-level fiducial cross sections $\mathrm{d}^3\sigma$. The kinematic region shown is labelled in each plot. The data are shown as solid ($\cos\theta^* < 0$) and open ($\cos\theta^* > 0$) markers and the prediction from Powheg including NNLO QCD and NLO EW K-factors is shown as the solid line. The difference, $\Delta\sigma$, between the predicted cross sections in the two measurement bins at equal $|\cos\theta^*|$ symmetric around $\cos\theta^* = 0$ is represented by the hatched shading. In each plot, the lower panel shows the ratio of prediction to measurement. The inner error bars represent the statistical uncertainty of the data and the solid band shows the total experimental uncertainty. The contribution to the uncertainty from the luminosity measurement is excluded. The crosshatched band represents the statistical and PDF uncertainties in the prediction.

JHEP12(2017)059

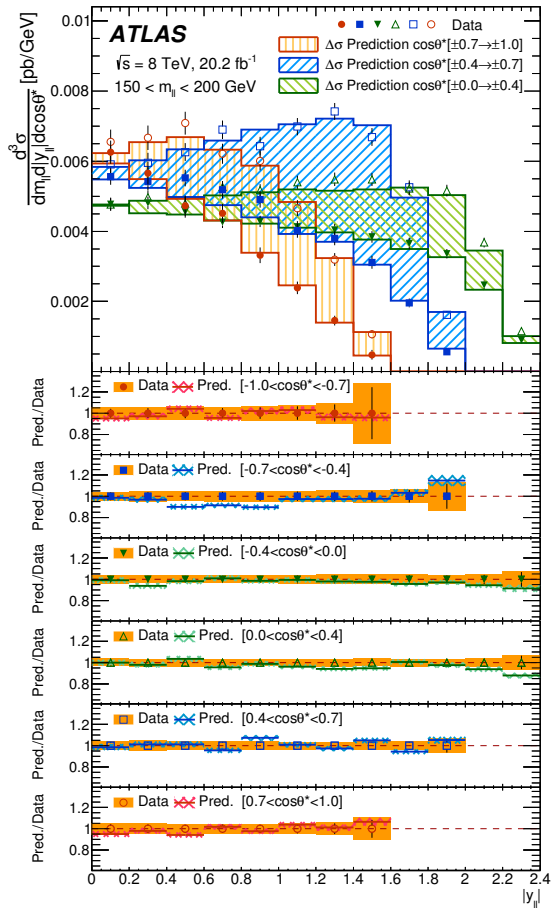

Figure 10. The combined Born-level fiducial cross sections $\mathrm{d}^3\sigma$. The kinematic region shown is labelled in each plot. The data are shown as solid ($\cos\theta^* < 0$) and open ($\cos\theta^* > 0$) markers and the prediction from Powheg including NNLO QCD and NLO EW K-factors is shown as the solid line. The difference, $\Delta\sigma$, between the predicted cross sections in the two measurement bins at equal $|\cos\theta^*|$ symmetric around $\cos\theta^* = 0$ is represented by the hatched shading. In each plot, the lower panel shows the ratio of prediction to measurement. The inner error bars represent the statistical uncertainty of the data and the solid band shows the total experimental uncertainty. The contribution to the uncertainty from the luminosity measurement is excluded. The crosshatched band represents the statistical and PDF uncertainties in the prediction.

JHEP12(2017)059

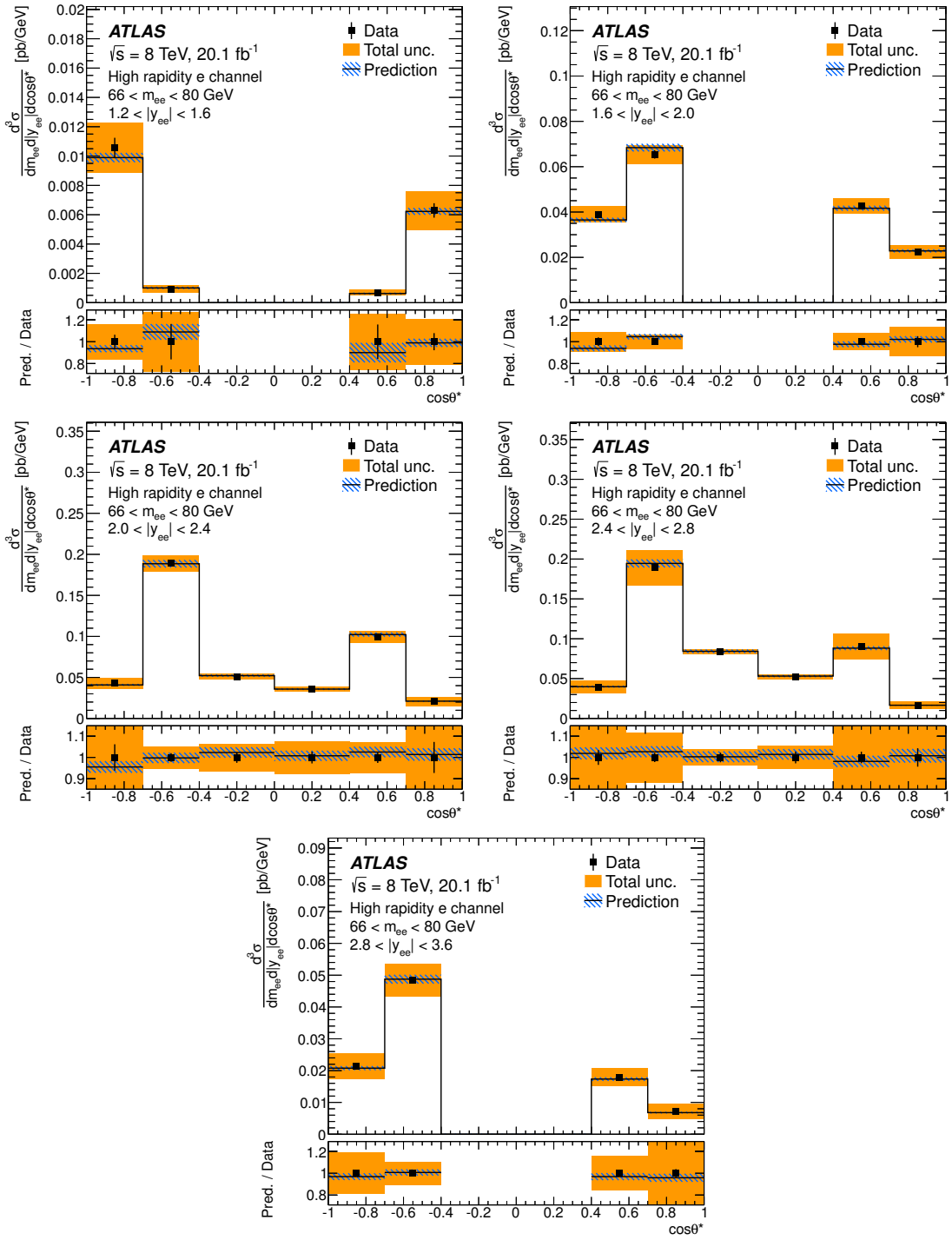

Figure 11. The high rapidity electron channel Born-level fiducial cross section $d^3\sigma$. The kinematic region shown is labelled in each plot. The data are shown as solid markers and the prediction from Powheg including NNLO QCD and NLO EW K-factors is shown as the solid line. In each plot, the lower panel shows the ratio of prediction to measurement. The inner error bars represent the statistical uncertainty of the data and the solid band shows the total experimental uncertainty. The contribution from the uncertainty of the luminosity measurement is excluded. The hatched band represents the statistical and PDF uncertainties in the prediction.

JHEP12(2017)059

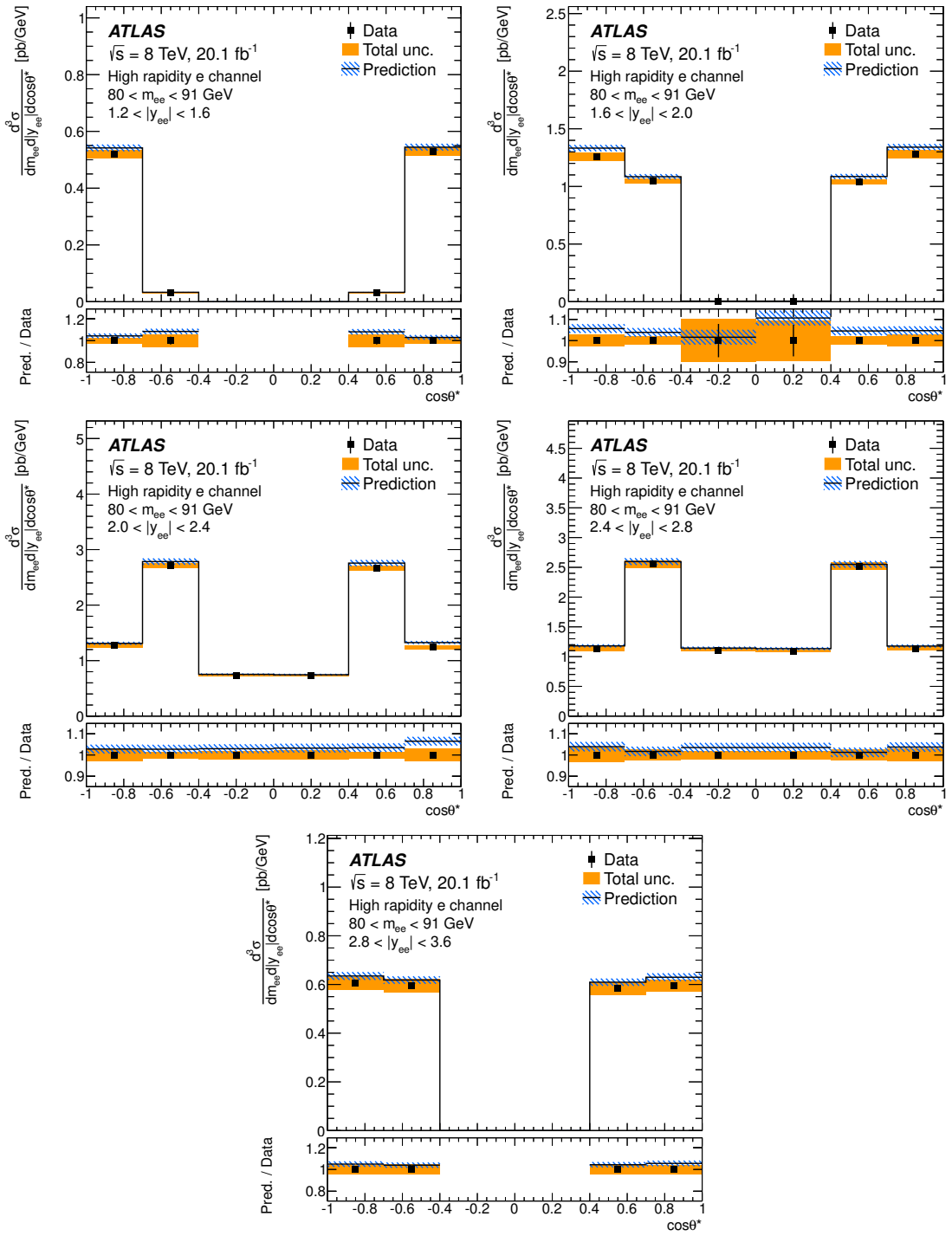

Figure 12. The high rapidity electron channel Born-level fiducial cross section $d^3\sigma$. The kinematic region shown is labelled in each plot. The data are shown as solid markers and the prediction from Powheg including NNLO QCD and NLO EW K-factors is shown as the solid line. In each plot, the lower panel shows the ratio of prediction to measurement. The inner error bars represent the statistical uncertainty of the data and the solid band shows the total experimental uncertainty. The contribution from the uncertainty of the luminosity measurement is excluded. The hatched band represents the statistical and PDF uncertainties in the prediction.

JHEP12(2017)059

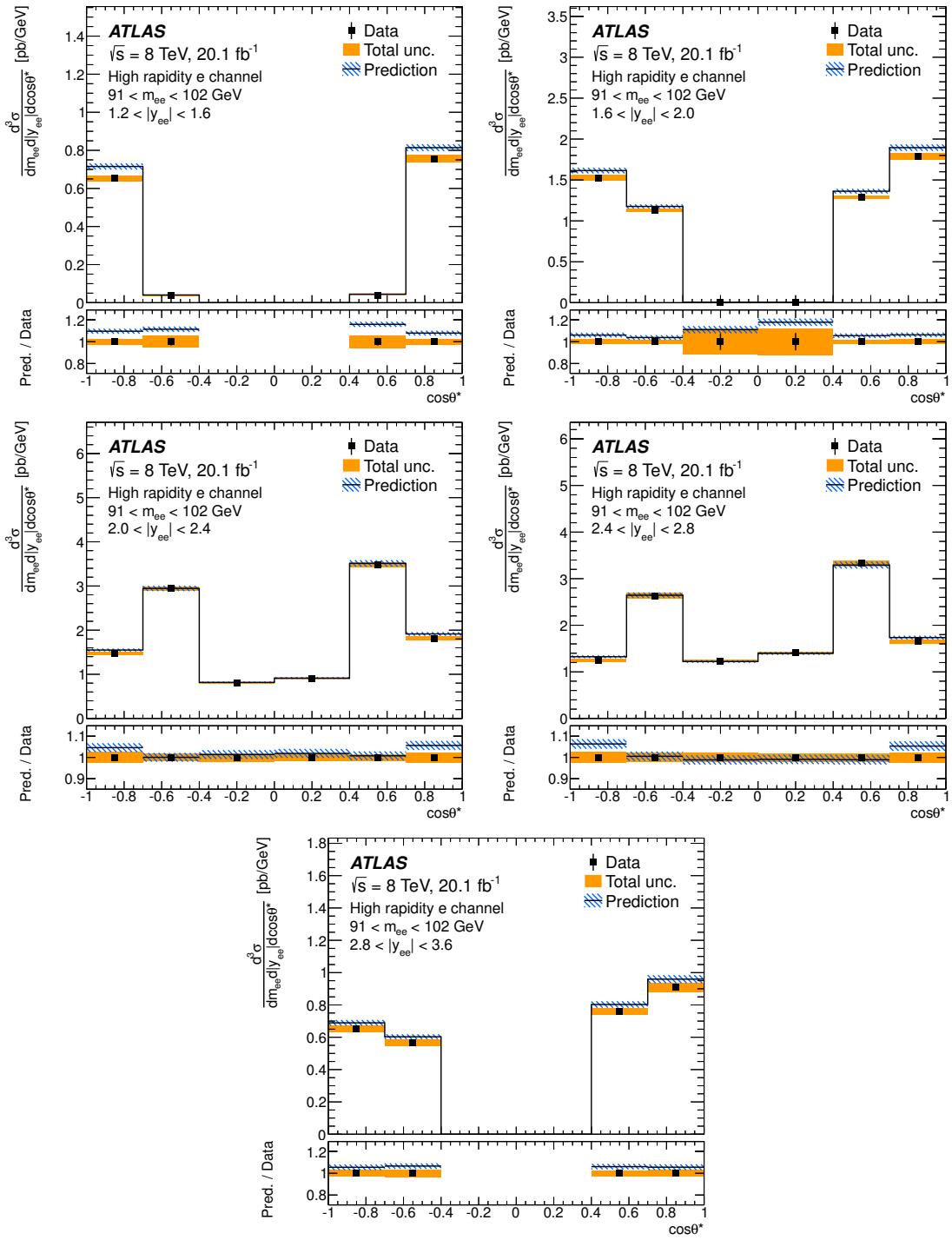

Figure 13. The high rapidity electron channel Born-level fiducial cross section $d^3\sigma$. The kinematic region shown is labelled in each plot. The data are shown as solid markers and the prediction from Powheg including NNLO QCD and NLO EW K-factors is shown as the solid line. In each plot, the lower panel shows the ratio of prediction to measurement. The inner error bars represent the statistical uncertainty of the data and the solid band shows the total experimental uncertainty. The contribution from the uncertainty of the luminosity measurement is excluded. The hatched band represents the statistical and PDF uncertainties in the prediction.

JHEP12(2017)059

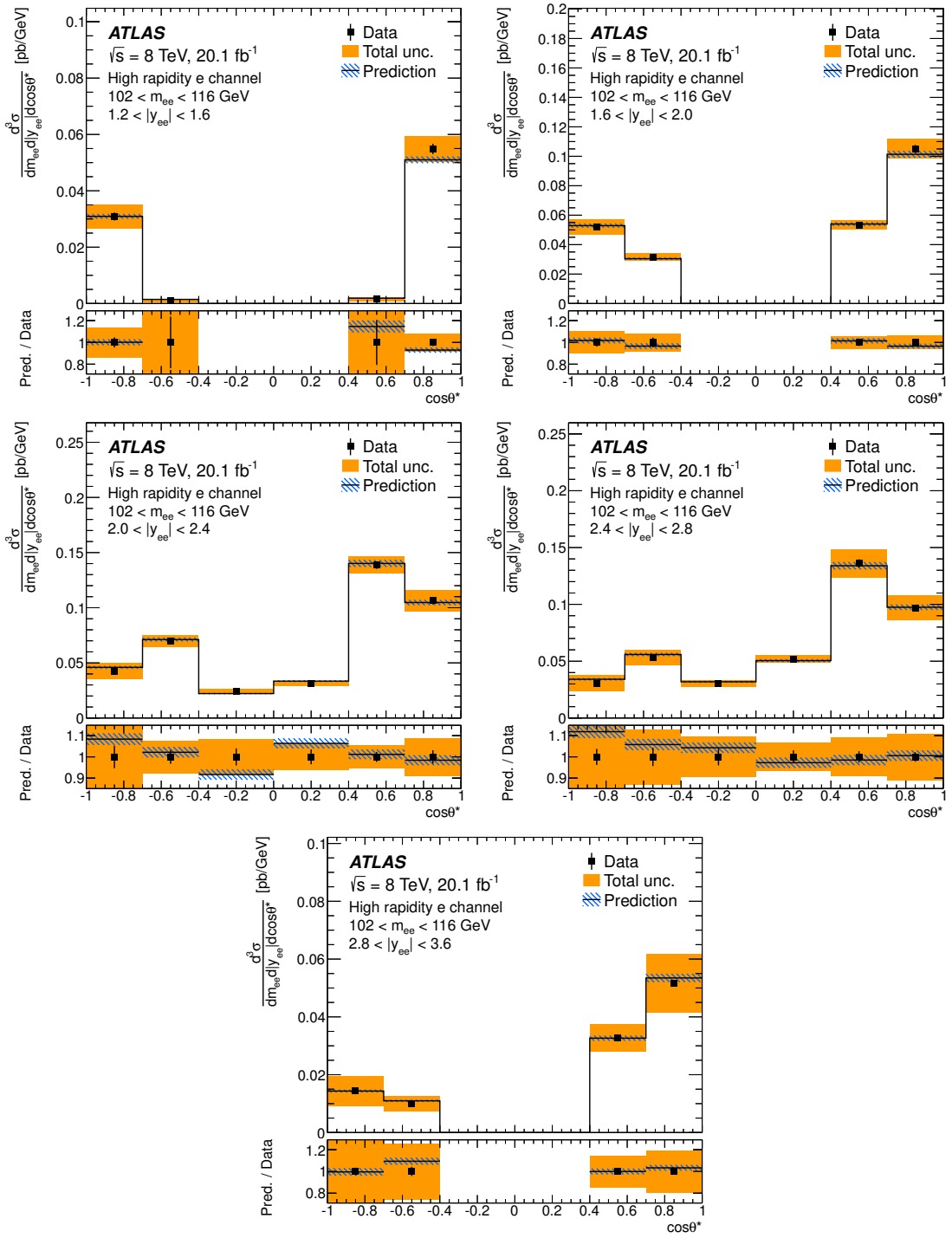

Figure 14. The high rapidity electron channel Born-level fiducial cross section $d^3\sigma$. The kinematic region shown is labelled in each plot. The data are shown as solid markers and the prediction from Powheg including NNLO QCD and NLO EW K-factors is shown as the solid line. In each plot, the lower panel shows the ratio of prediction to measurement. The inner error bars represent the statistical uncertainty of the data and the solid band shows the total experimental uncertainty. The contribution from the uncertainty of the luminosity measurement is excluded. The hatched band represents the statistical and PDF uncertainties in the prediction.

JHEP12(2017)059

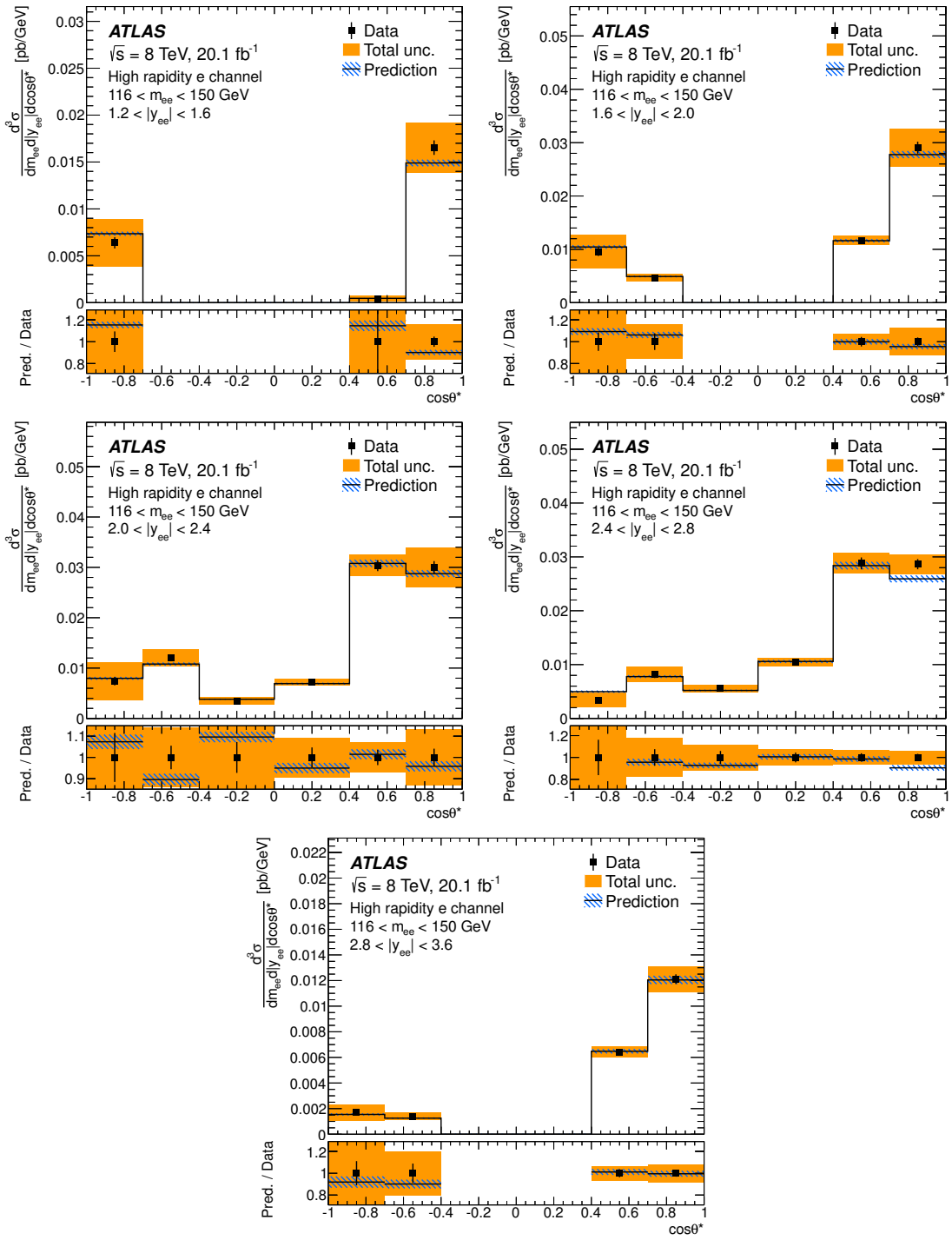

Figure 15. The high rapidity electron channel Born-level fiducial cross section $d^3\sigma$. The kinematic region shown is labelled in each plot. The data are shown as solid markers and the prediction from Powheg including NNLO QCD and NLO EW K-factors is shown as the solid line. In each plot, the lower panel shows the ratio of prediction to measurement. The inner error bars represent the statistical uncertainty of the data and the solid band shows the total experimental uncertainty. The contribution from the uncertainty of the luminosity measurement is excluded. The hatched band represents the statistical and PDF uncertainties in the prediction.

JHEP12(2017)059

8.4 Forward-backward asymmetry

The effect of parity violation in Z boson decays is more clearly visible in the forward-backward asymmetry, A_{FB}, derived from the cross-section measurements of $\mathrm{d}^3\sigma$. The combined Born-level cross sections are used to determine A_{FB} in the region $0 < |y_{\ell\ell}| < 2.4$ by summing the measurement bins for $\cos\theta^* > 0$ and for $\cos\theta^* < 0$ and calculating the asymmetry according to equation (1.3).

The uncorrelated uncertainty in A_{FB} is determined using standard error propagation. The correlated uncertainty is determined for each source in turn by coherently shifting $\mathrm{d}^3\sigma$ by the associated correlated uncertainty and calculating the difference to the nominal value of A_{FB}. Finally, the total uncertainty in A_{FB} is taken as the sum in quadrature of the correlated and uncorrelated components. The uncertainties in A_{FB} are significantly reduced, especially the correlated uncertainties such as the electron energy scale and resolution. The total uncertainty is dominated by the data statistical uncertainty everywhere. An experimental uncertainty of 1×10^{-3} is reached for the combined measurement, and 4×10^{-3} for the high rapidity electron channel measurement. In the high-precision region of $80 < m_{\ell\ell} < 102\,\mathrm{GeV}$ the largest systematic uncertainty contributions are from the MC sample size (which are a factor two smaller than the data statistical uncertainty) and the lepton scale contributions, which are an order of magnitude smaller. At low $m_{\ell\ell}$ the uncorrelated and statistical contributions from the background sources are also of comparable size. Summary tables of these measurements are given in tables 9 and 10 in the appendix.

The measurements of A_{FB} are shown in figure 16 for the combined data. The data are compared to a Born-level prediction from Powheg including K-factors for NNLO QCD and NLO EW corrections. The value of $\sin^2\theta^{\mathrm{eff}}_{\mathrm{lept}}$ used in the simulation is 0.23113 [76]. The measured asymmetry is found to generally increase with $m_{\ell\ell}$ from a negative to a positive asymmetry which is close to zero near $m_{\ell\ell} = m_Z$. The magnitude of A_{FB} is smallest for $|y_{\ell\ell}| = 0$ and increases to a maximum in the region $1.0 < |y_{\ell\ell}| < 2.0$, before decreasing at larger rapidity. This is expected from the effect of dilution and the unknown direction of the incident q on an event-by-event basis. At larger $|y_{\ell\ell}|$, and hence larger x, the influence of the higher-momentum valence u- and d-quarks becomes increasingly apparent through the longitudinal boost in the valence direction. This allows a correct determination of the q direction to be made on average and is well modelled by the Powheg prediction. At even larger $|y_{\ell\ell}|$ in the combined measurements the maximum of $|A_{\mathrm{FB}}|$ decreases again due to the limited acceptance of the detector in $\eta^{e,\mu}$.

The measurements of A_{FB} in the high rapidity electron channel analysis, which is expected to be more sensitive to the asymmetry, are presented in figure 17. Qualitatively, the asymmetry shows behaviour similar to that seen in the combined measurement: the asymmetry increases with m_{ee} and values of $|A_{\mathrm{FB}}|$ reaching 0.7 are observed at the highest $|y_{ee}|$ where the influence of dilution is smallest. As was the case in the combined measurement, the high rapidity A_{FB} measurement is well-described by the Powheg prediction.

JHEP12(2017)059

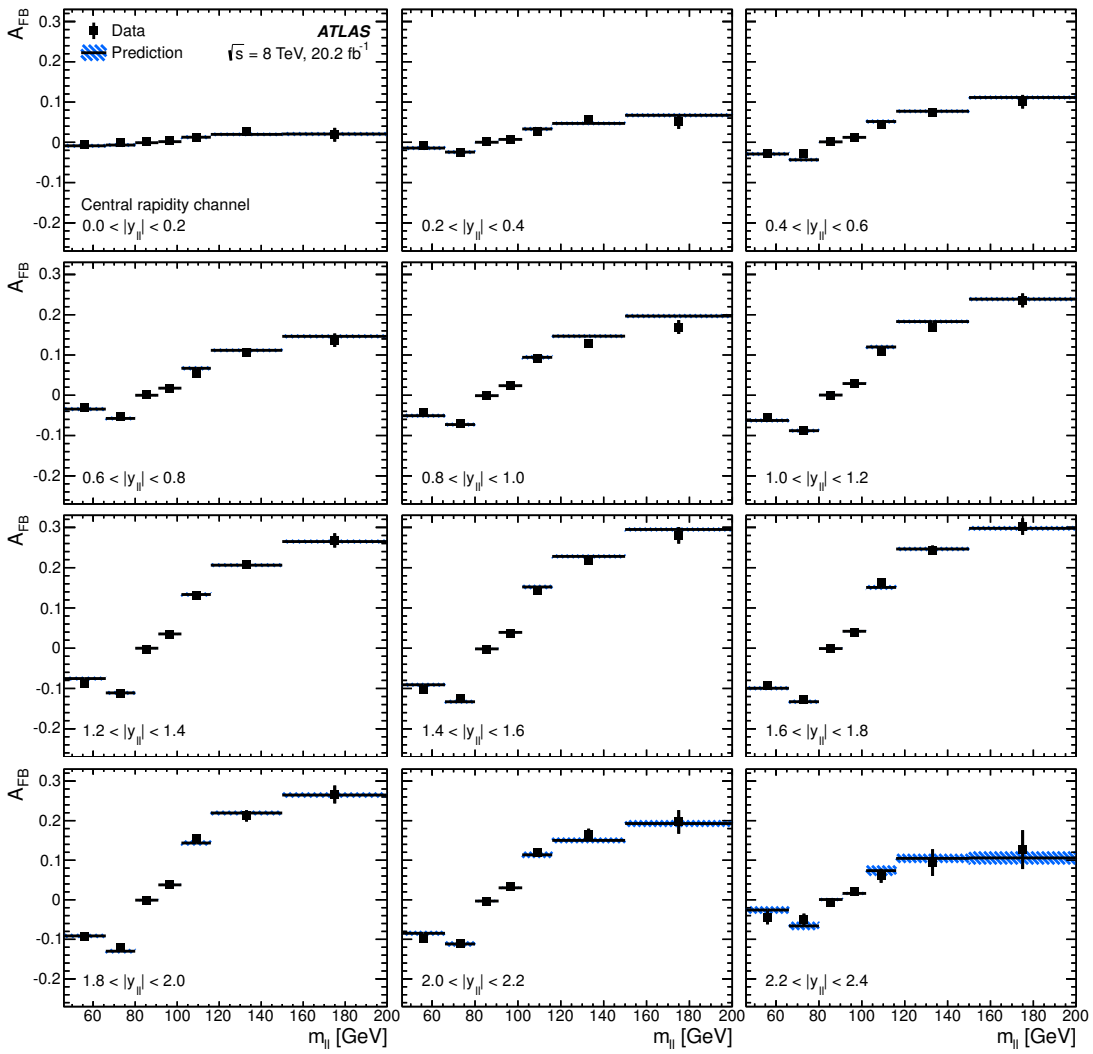

Figure 16. Forward-backward asymmetry, A_{FB}, determined from the combined Born-level fiducial cross section. The kinematic region shown is labelled in each plot. The data are shown as solid markers and the error bars represent the total experimental uncertainty. The prediction from Powheg including NNLO QCD and NLO EW K-factors is shown as the solid line and the hatched band represents the statistical and PDF uncertainties in the prediction.

JHEP12(2017)059

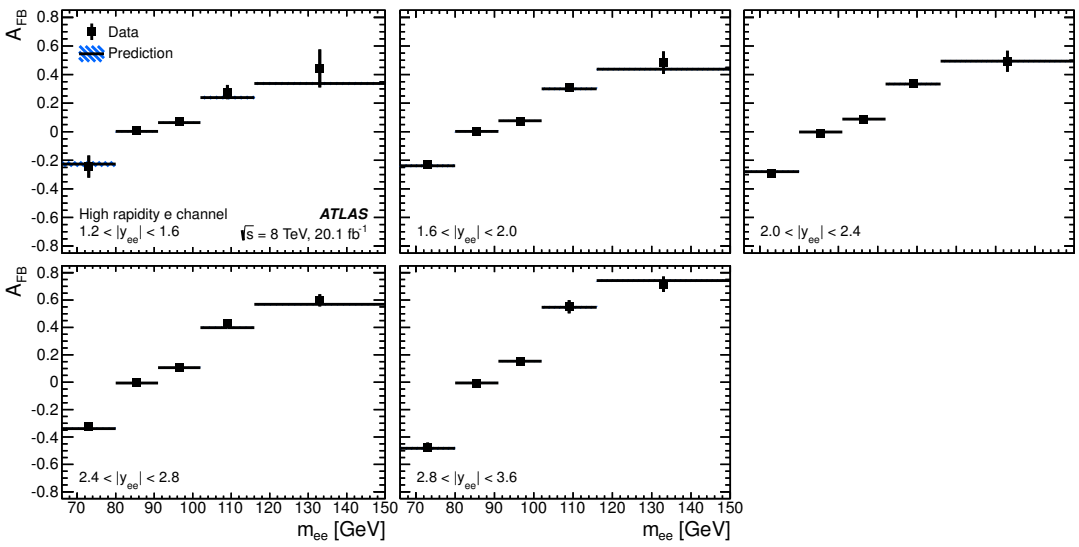

Figure 17. Forward-backward asymmetry, A_{FB}, determined from the high rapidity electron Born-level fiducial cross section. The kinematic region shown is labelled in each plot. The data are shown as solid markers and the error bars represent the total experimental uncertainty. The prediction from Powheg including NNLO QCD and NLO EW K-factors is shown as the solid line and the hatched band represents the statistical and PDF uncertainties in the prediction.

9 Conclusion

The triple-differential Drell-Yan production cross section $\mathrm{d}^3\sigma/\mathrm{d}m_{\ell\ell}\mathrm{d}|y_{\ell\ell}|\mathrm{d}\cos\theta^*$ is measured in the range $46 < m_{\ell\ell} < 200\,\mathrm{GeV}$ and $|y_{\ell\ell}| < 2.4$ for electron and muon pairs. The measurements are extended to high rapidity in the electron channel up to $|y_{ee}| = 3.6$ in the mass range $66 < m_{\ell\ell} < 150\,\mathrm{GeV}$. The analysis uses $20.2\,\mathrm{fb}^{-1}$ of pp collision data at $\sqrt{s} = 8$ TeV collected in 2012 by the ATLAS detector at the LHC. The central rapidity measurement channels are combined taking into account the systematic uncertainty correlations. Their combination achieves an experimental precision of better than 0.5%, excluding the overall uncertainty in the luminosity measurement of 1.9%.

The combined cross sections are integrated to produce the single- and double-differential cross sections $\mathrm{d}\sigma/\mathrm{d}m_{\ell\ell}$ and $\mathrm{d}^2\sigma/\mathrm{d}m_{\ell\ell}\mathrm{d}|y_{\ell\ell}|$. The fiducial cross sections are compared to a theoretical prediction calculated using Powheg at NLO with matched leading-logarithm parton showers. The calculation is approximately corrected for NNLO QCD effects and for additional higher-order electroweak effects applied as a function of $m_{\ell\ell}$. The single- and double-differential measurements are well described by the prediction. Having applied corrections to the scattering amplitude coefficients in Powheg the prediction also provides a good description of the triple-differential measurements.

The measured cross sections are used to determine the forward-backward asymmetry A_{FB} as a function of dilepton invariant mass and rapidity. The Powheg predictions enhanced with NNLO QCD and NLO EW K-factors describe the observed behaviour of A_{FB} well.

Acknowledgments

We thank CERN for the very successful operation of the LHC, as well as the support staff from our institutions without whom ATLAS could not be operated efficiently.

We acknowledge the support of ANPCyT, Argentina; YerPhI, Armenia; ARC, Australia; BMWFW and FWF, Austria; ANAS, Azerbaijan; SSTC, Belarus; CNPq and FAPESP, Brazil; NSERC, NRC and CFI, Canada; CERN; CONICYT, Chile; CAS, MOST and NSFC, China; COLCIENCIAS, Colombia; MSMT CR, MPO CR and VSC CR, Czech Republic; DNRF and DNSRC, Denmark; IN2P3-CNRS, CEA-DSM/IRFU, France; SRNSF, Georgia; BMBF, HGF, and MPG, Germany; GSRT, Greece; RGC, Hong Kong SAR, China; ISF, I-CORE and Benoziyo Center, Israel; INFN, Italy; MEXT and JSPS, Japan; CNRST, Morocco; NWO, Netherlands; RCN, Norway; MNiSW and NCN, Poland; FCT, Portugal; MNE/IFA, Romania; MES of Russia and NRC KI, Russian Federation; JINR; MESTD, Serbia; MSSR, Slovakia; ARRS and MIZŠ, Slovenia; DST/NRF, South Africa; MINECO, Spain; SRC and Wallenberg Foundation, Sweden; SERI, SNSF and Cantons of Bern and Geneva, Switzerland; MOST, Taiwan; TAEK, Turkey; STFC, United Kingdom; DOE and NSF, United States of America. In addition, individual groups and members have received support from BCKDF, the Canada Council, CANARIE, CRC, Compute Canada, FQRNT, and the Ontario Innovation Trust, Canada; EPLANET, ERC, ERDF, FP7, Horizon 2020 and Marie Skłodowska-Curie Actions, European Union; In-

JHEP12(2017)059

vestissements d'Avenir Labex and Idex, ANR, Région Auvergne and Fondation Partager le Savoir, France; DFG and AvH Foundation, Germany; Herakleitos, Thales and Aristeia programmes co-financed by EU-ESF and the Greek NSRF; BSF, GIF and Minerva, Israel; BRF, Norway; CERCA Programme Generalitat de Catalunya, Generalitat Valenciana, Spain; the Royal Society and Leverhulme Trust, United Kingdom.

The crucial computing support from all WLCG partners is acknowledged gratefully, in particular from CERN, the ATLAS Tier-1 facilities at TRIUMF (Canada), NDGF (Denmark, Norway, Sweden), CC-IN2P3 (France), KIT/GridKA (Germany), INFN-CNAF (Italy), NL-T1 (Netherlands), PIC (Spain), ASGC (Taiwan), RAL (U.K.) and BNL (U.S.A.), the Tier-2 facilities worldwide and large non-WLCG resource providers. Major contributors of computing resources are listed in ref. [77].

A Data tables

Summary tables of $\mathrm{d}^3\sigma/\mathrm{d}m_{\ell\ell}\mathrm{d}|y_{\ell\ell}|\mathrm{d}\cos\theta^*$ cross sections and A_{FB} are given in this appendix. Tables containing the complete breakdown of systematic uncertainties are available in HEPData [71, 72].

A.1 Integrated cross-section tables

$m_{\ell\ell}$ [GeV]	$\mathrm{d}\sigma/\mathrm{d}m_{\ell\ell}$ [pb/GeV]	δ^{stat} [%]	$\delta^{\mathrm{syst}}_{\mathrm{unc}}$ [%]	$\delta^{\mathrm{syst}}_{\mathrm{cor}}$ [%]	δ^{total} [%]
46, 66	7.61×10^{-1}	0.2	0.1	0.9	0.9
66, 80	1.13	0.1	0.1	0.4	0.4
80, 91	21.4	0.0	0.0	0.2	0.2
91, 102	25.0	0.0	0.0	0.2	0.2
102, 116	8.25×10^{-1}	0.2	0.1	0.4	0.4
116, 150	1.64×10^{-1}	0.3	0.1	0.7	0.7
150, 200	3.66×10^{-2}	0.5	0.2	1.3	1.4

Table 5. The combined Born-level single-differential cross section $\mathrm{d}\sigma/\mathrm{d}m_{\ell\ell}$. The measurements are listed together with the statistical (δ^{stat}), uncorrelated systematic ($\delta^{\mathrm{syst}}_{\mathrm{unc}}$), correlated systematic ($\delta^{\mathrm{syst}}_{\mathrm{cor}}$), and total ($\delta^{\mathrm{total}}$) uncertainties. The luminosity uncertainty of 1.9% is not shown and not included in the overall systematic and total uncertainties.

JHEP12(2017)059

$m_{\ell\ell}$ [GeV]	$\lvert y_{\ell\ell}\rvert$	$\mathrm{d}^2\sigma/\mathrm{d}m_{\ell\ell}\mathrm{d}\lvert y_{\ell\ell}\rvert$ [pb/GeV]	δ^{stat} [%]	$\delta^{\mathrm{syst}}_{\mathrm{unc}}$ [%]	$\delta^{\mathrm{syst}}_{\mathrm{cor}}$ [%]	δ^{total} [%]	m_{ee} [GeV]	$\lvert y_{\ell\ell}\rvert$	$\mathrm{d}^2\sigma/\mathrm{d}m_{\ell\ell}\mathrm{d}\lvert y_{\ell\ell}\rvert$ [pb/GeV]	δ^{stat} [%]	$\delta^{\mathrm{syst}}_{\mathrm{unc}}$ [%]	$\delta^{\mathrm{syst}}_{\mathrm{cor}}$ [%]	δ^{total} [%]
46, 66	0.0, 0.2	1.85×10^{-1}	0.6	0.4	1.0	1.2	46, 66	1.2, 1.4	1.86×10^{-1}	0.6	0.4	0.9	1.1
46, 66	0.2, 0.4	1.87×10^{-1}	0.6	0.5	1.0	1.2	46, 66	1.4, 1.6	1.82×10^{-1}	0.6	0.4	0.9	1.1
46, 66	0.4, 0.6	1.86×10^{-1}	0.6	0.4	0.9	1.2	46, 66	1.6, 1.8	1.66×10^{-1}	0.6	0.5	0.9	1.2
46, 66	0.6, 0.8	1.87×10^{-1}	0.6	0.4	0.9	1.2	46, 66	1.8, 2.0	1.35×10^{-1}	0.7	0.5	0.8	1.2
46, 66	0.8, 1.0	1.86×10^{-1}	0.6	0.4	0.9	1.2	46, 66	2.0, 2.2	8.60×10^{-2}	0.8	0.6	0.8	1.3
46, 66	1.0, 1.2	1.88×10^{-1}	0.6	0.4	0.9	1.1	46, 66	2.2, 2.4	2.93×10^{-2}	1.4	1.1	0.9	2.0
66, 80	0.0, 0.2	3.05×10^{-1}	0.4	0.2	0.4	0.6	66, 80	1.2, 1.4	2.82×10^{-1}	0.4	0.2	0.4	0.6
66, 80	0.2, 0.4	3.02×10^{-1}	0.4	0.2	0.4	0.6	66, 80	1.4, 1.6	2.54×10^{-1}	0.5	0.3	0.4	0.6
66, 80	0.4, 0.6	3.02×10^{-1}	0.4	0.2	0.4	0.6	66, 80	1.6, 1.8	2.08×10^{-1}	0.5	0.3	0.4	0.7
66, 80	0.6, 0.8	3.01×10^{-1}	0.4	0.2	0.4	0.6	66, 80	1.8, 2.0	1.54×10^{-1}	0.6	0.3	0.5	0.8
66, 80	0.8, 1.0	2.95×10^{-1}	0.4	0.2	0.4	0.6	66, 80	2.0, 2.2	9.27×10^{-2}	0.7	0.4	0.6	1.0
66, 80	1.0, 1.2	2.93×10^{-1}	0.4	0.2	0.4	0.6	66, 80	2.2, 2.4	3.05×10^{-2}	1.2	0.7	0.9	1.7
80, 91	0.0, 0.2	6.00	0.1	0.0	0.2	0.2	80, 91	1.2, 1.4	5.19	0.1	0.1	0.2	0.3
80, 91	0.2, 0.4	6.00	0.1	0.0	0.2	0.2	80, 91	1.4, 1.6	4.51	0.1	0.1	0.2	0.3
80, 91	0.4, 0.6	5.97	0.1	0.1	0.2	0.2	80, 91	1.6, 1.8	3.66	0.1	0.1	0.3	0.3
80, 91	0.6, 0.8	5.93	0.1	0.0	0.2	0.3	80, 91	1.8, 2.0	2.67	0.1	0.1	0.3	0.3
80, 91	0.8, 1.0	5.87	0.1	0.1	0.2	0.3	80, 91	2.0, 2.2	1.60	0.2	0.1	0.3	0.4
80, 91	1.0, 1.2	5.66	0.1	0.1	0.2	0.3	80, 91	2.2, 2.4	5.20×10^{-1}	0.3	0.2	0.4	0.5
91, 102	0.0, 0.2	7.08	0.1	0.1	0.2	0.2	91, 102	1.2, 1.4	6.02	0.1	0.0	0.2	0.3
91, 102	0.2, 0.4	7.04	0.1	0.1	0.2	0.2	91, 102	1.4, 1.6	5.21	0.1	0.1	0.2	0.3
91, 102	0.4, 0.6	7.01	0.1	0.1	0.2	0.2	91, 102	1.6, 1.8	4.23	0.1	0.1	0.3	0.3
91, 102	0.6, 0.8	6.98	0.1	0.0	0.2	0.2	91, 102	1.8, 2.0	3.07	0.2	0.1	0.3	0.3
91, 102	0.8, 1.0	6.90	0.1	0.0	0.2	0.2	91, 102	2.0, 2.2	1.83	0.2	0.1	0.3	0.4
91, 102	1.0, 1.2	6.60	0.1	0.1	0.2	0.3	91, 102	2.2, 2.4	5.96×10^{-1}	0.3	0.2	0.4	0.5
102, 116	0.0, 0.2	2.38×10^{-1}	0.5	0.2	0.3	0.7	102, 116	1.2, 1.4	1.96×10^{-1}	0.5	0.3	0.5	0.7
102, 116	0.2, 0.4	2.39×10^{-1}	0.5	0.2	0.4	0.7	102, 116	1.4, 1.6	1.66×10^{-1}	0.5	0.3	0.5	0.8
102, 116	0.4, 0.6	2.35×10^{-1}	0.5	0.2	0.4	0.7	102, 116	1.6, 1.8	1.35×10^{-1}	0.6	0.4	0.7	1.0
102, 116	0.6, 0.8	2.33×10^{-1}	0.5	0.3	0.4	0.7	102, 116	1.8, 2.0	9.84×10^{-2}	0.6	0.4	0.8	1.1
102, 116	0.8, 1.0	2.29×10^{-1}	0.5	0.3	0.4	0.7	102, 116	2.0, 2.2	5.76×10^{-2}	0.7	0.5	1.0	1.3
102, 116	1.0, 1.2	2.16×10^{-1}	0.5	0.3	0.4	0.7	102, 116	2.2, 2.4	1.85×10^{-2}	1.0	0.9	1.3	1.9
116, 150	0.0, 0.2	4.84×10^{-2}	0.8	0.3	0.8	1.2	116, 150	1.2, 1.4	3.84×10^{-2}	0.9	0.4	0.6	1.1
116, 150	0.2, 0.4	4.79×10^{-2}	0.8	0.3	0.8	1.2	116, 150	1.4, 1.6	3.23×10^{-2}	0.9	0.4	0.5	1.1
116, 150	0.4, 0.6	4.74×10^{-2}	0.8	0.3	0.8	1.2	116, 150	1.6, 1.8	2.66×10^{-2}	1.0	0.5	0.5	1.2
116, 150	0.6, 0.8	4.77×10^{-2}	0.8	0.3	0.8	1.2	116, 150	1.8, 2.0	1.93×10^{-2}	1.2	0.7	0.6	1.5
116, 150	0.8, 1.0	4.54×10^{-2}	0.8	0.3	0.7	1.1	116, 150	2.0, 2.2	1.14×10^{-2}	1.4	0.7	0.7	1.7
116, 150	1.0, 1.2	4.23×10^{-2}	0.8	0.4	0.6	1.1	116, 150	2.2, 2.4	3.48×10^{-3}	2.6	1.7	1.2	3.3
150, 200	0.0, 0.2	1.11×10^{-2}	1.6	0.6	1.8	2.4	150, 200	1.2, 1.4	8.56×10^{-3}	1.6	0.6	1.0	2.0
150, 200	0.2, 0.4	1.10×10^{-2}	1.5	0.7	1.8	2.4	150, 200	1.4, 1.6	7.12×10^{-3}	1.8	0.9	0.9	2.2
150, 200	0.4, 0.6	1.08×10^{-2}	1.5	0.6	1.7	2.3	150, 200	1.6, 1.8	5.72×10^{-3}	1.9	0.7	0.8	2.2
150, 200	0.6, 0.8	1.07×10^{-2}	1.5	0.5	1.5	2.2	150, 200	1.8, 2.0	4.06×10^{-3}	2.2	0.7	0.7	2.4
150, 200	0.8, 1.0	9.98×10^{-3}	1.6	0.5	1.3	2.1	150, 200	2.0, 2.2	2.46×10^{-3}	2.8	1.0	0.7	3.0
150, 200	1.0, 1.2	9.22×10^{-3}	1.6	0.6	1.2	2.1	150, 200	2.2, 2.4	8.20×10^{-4}	4.7	1.3	1.0	5.0

Table 6. The combined Born-level double-differential cross section $\mathrm{d}^2\sigma/\mathrm{d}m_{\ell\ell}\mathrm{d}|y_{\ell\ell}|$. The measurements are listed together with the statistical (δ^{stat}), uncorrelated systematic ($\delta^{\mathrm{syst}}_{\mathrm{unc}}$), correlated systematic ($\delta^{\mathrm{syst}}_{\mathrm{cor}}$), and total ($\delta^{\mathrm{total}}$) uncertainties. The luminosity uncertainty of 1.9% is not shown and not included in the overall systematic and total uncertainties.

JHEP12(2017)059

A.2 Triple-differential cross-section tables

Bin	$m_{\ell\ell}$ [GeV]	$\lvert y_{\ell\ell}\rvert$	$\cos\theta^*$	$\mathrm{d}^3\sigma$ [pb/GeV]	δ^{stat} [%]	$\delta^{\text{syst}}_{\text{unc}}$ [%]	$\delta^{\text{syst}}_{\text{cor}}$ [%]	δ^{total} [%]	Bin	$m_{\ell\ell}$ [GeV]	$\lvert y_{\ell\ell}\rvert$	$\cos\theta^*$	$\mathrm{d}^3\sigma$ [pb/GeV]	δ^{stat} [%]	$\delta^{\text{syst}}_{\text{unc}}$ [%]	$\delta^{\text{syst}}_{\text{cor}}$ [%]	δ^{total} [%]
1	46, 66	0.0, 0.2	−1.0, −0.7	1.42×10^{-2}	4.0	2.5	1.8	5.1	6	46, 66	0.0, 0.2	+0.7, +1.0	1.37×10^{-2}	4.2	3.4	2.0	5.7
2	46, 66	0.0, 0.2	−0.7, −0.4	1.02×10^{-1}	1.4	1.1	1.2	2.1	5	46, 66	0.0, 0.2	+0.4, +0.7	1.01×10^{-1}	1.4	1.1	1.2	2.1
3	46, 66	0.0, 0.2	−0.4, 0.0	1.45×10^{-1}	1.0	0.8	0.9	1.5	4	46, 66	0.0, 0.2	0.0, +0.4	1.44×10^{-1}	1.0	0.8	0.9	1.6
7	46, 66	0.2, 0.4	−1.0, −0.7	1.48×10^{-2}	3.9	2.1	1.8	4.8	12	46, 66	0.2, 0.4	+0.7, +1.0	1.46×10^{-2}	3.9	1.9	1.8	4.7
8	46, 66	0.2, 0.4	−0.7, −0.4	1.03×10^{-1}	1.4	1.3	1.2	2.2	11	46, 66	0.2, 0.4	+0.4, +0.7	9.99×10^{-2}	1.4	1.1	1.2	2.2
9	46, 66	0.2, 0.4	−0.4, 0.0	1.47×10^{-1}	1.0	0.8	0.9	1.5	10	46, 66	0.2, 0.4	0.0, +0.4	1.46×10^{-1}	1.0	0.9	0.9	1.6
13	46, 66	0.4, 0.6	−1.0, −0.7	1.35×10^{-2}	4.5	3.3	1.9	5.9	18	46, 66	0.4, 0.6	+0.7, +1.0	1.43×10^{-2}	4.2	2.5	1.8	5.2
14	46, 66	0.4, 0.6	−0.7, −0.4	1.08×10^{-1}	1.4	1.1	1.0	2.1	17	46, 66	0.4, 0.6	+0.4, +0.7	9.84×10^{-2}	1.6	1.3	1.2	2.3
15	46, 66	0.4, 0.6	−0.4, 0.0	1.47×10^{-1}	0.9	0.7	0.9	1.5	16	46, 66	0.4, 0.6	0.0, +0.4	1.42×10^{-1}	1.0	0.8	0.9	1.5
19	46, 66	0.6, 0.8	−1.0, −0.7	1.50×10^{-2}	4.0	2.8	1.8	5.2	24	46, 66	0.6, 0.8	+0.7, +1.0	1.46×10^{-2}	4.1	3.0	1.9	5.5
20	46, 66	0.6, 0.8	−0.7, −0.4	1.08×10^{-1}	1.4	1.0	1.1	2.1	23	46, 66	0.6, 0.8	+0.4, +0.7	9.90×10^{-2}	1.5	1.1	1.2	2.2
21	46, 66	0.6, 0.8	−0.4, 0.0	1.48×10^{-1}	0.9	0.7	0.8	1.4	22	46, 66	0.6, 0.8	0.0, +0.4	1.42×10^{-1}	0.9	0.8	0.9	1.5
25	46, 66	0.8, 1.0	−1.0, −0.7	1.63×10^{-2}	4.1	2.7	1.5	5.1	30	46, 66	0.8, 1.0	+0.7, +1.0	1.33×10^{-2}	4.4	3.2	2.0	5.8
26	46, 66	0.8, 1.0	−0.7, −0.4	1.07×10^{-1}	1.5	1.1	1.1	2.1	29	46, 66	0.8, 1.0	+0.4, +0.7	9.57×10^{-2}	1.6	1.1	1.3	2.3
27	46, 66	0.8, 1.0	−0.4, 0.0	1.49×10^{-1}	0.9	0.7	0.8	1.4	28	46, 66	0.8, 1.0	0.0, +0.4	1.41×10^{-1}	1.0	0.8	0.8	1.5
31	46, 66	1.0, 1.2	−1.0, −0.7	1.71×10^{-2}	3.5	2.2	1.4	4.4	36	46, 66	1.0, 1.2	+0.7, +1.0	1.27×10^{-2}	4.2	2.5	1.8	5.2
32	46, 66	1.0, 1.2	−0.7, −0.4	1.12×10^{-1}	1.4	1.0	1.1	2.0	35	46, 66	1.0, 1.2	+0.4, +0.7	9.56×10^{-2}	1.5	1.1	1.2	2.2
33	46, 66	1.0, 1.2	−0.4, 0.0	1.50×10^{-1}	1.0	0.8	0.8	1.5	34	46, 66	1.0, 1.2	0.0, +0.4	1.41×10^{-1}	1.0	0.8	0.8	1.5
37	46, 66	1.2, 1.4	−1.0, −0.7	1.57×10^{-2}	3.8	2.3	1.6	4.7	42	46, 66	1.2, 1.4	+0.7, +1.0	1.13×10^{-2}	4.4	3.3	1.9	5.8
38	46, 66	1.2, 1.4	−0.7, −0.4	1.16×10^{-1}	1.3	0.9	1.0	1.9	41	46, 66	1.2, 1.4	+0.4, +0.7	8.57×10^{-2}	1.6	1.2	1.4	2.4
39	46, 66	1.2, 1.4	−0.4, 0.0	1.53×10^{-1}	1.0	0.7	0.8	1.4	40	46, 66	1.2, 1.4	0.0, +0.4	1.41×10^{-1}	1.0	0.8	0.8	1.5
43	46, 66	1.4, 1.6	−1.0, −0.7	1.04×10^{-2}	4.4	2.4	1.5	5.3	48	46, 66	1.4, 1.6	+0.7, +1.0	8.25×10^{-3}	5.0	3.9	1.7	6.6
44	46, 66	1.4, 1.6	−0.7, −0.4	1.16×10^{-1}	1.3	0.9	0.9	1.8	47	46, 66	1.4, 1.6	+0.4, +0.7	8.55×10^{-2}	1.6	1.3	1.3	2.5
45	46, 66	1.4, 1.6	−0.4, 0.0	1.55×10^{-1}	1.0	0.7	0.7	1.4	46	46, 66	1.4, 1.6	0.0, +0.4	1.35×10^{-1}	1.1	0.8	0.9	1.6
49	46, 66	1.6, 1.8	−1.0, −0.7	4.44×10^{-3}	6.6	3.2	1.8	7.5	54	46, 66	1.6, 1.8	+0.7, +1.0	3.58×10^{-3}	7.8	4.2	2.3	9.1
50	46, 66	1.6, 1.8	−0.7, −0.4	9.59×10^{-2}	1.4	1.0	1.0	2.0	53	46, 66	1.6, 1.8	+0.4, +0.7	7.16×10^{-2}	1.7	1.4	1.3	2.6
51	46, 66	1.6, 1.8	−0.4, 0.0	1.51×10^{-1}	1.0	0.8	0.8	1.5	52	46, 66	1.6, 1.8	0.0, +0.4	1.33×10^{-1}	1.1	0.8	0.9	1.6
55	46, 66	1.8, 2.0	−1.0, −0.7	1.97×10^{-3}	10.0	4.7	2.4	11.4	60	46, 66	1.8, 2.0	+0.7, +1.0	1.38×10^{-3}	12.8	6.6	2.7	14.7
56	46, 66	1.8, 2.0	−0.7, −0.4	4.05×10^{-2}	2.3	1.4	1.0	2.9	59	46, 66	1.8, 2.0	+0.4, +0.7	2.76×10^{-2}	2.8	2.0	1.3	3.6
57	46, 66	1.8, 2.0	−0.4, 0.0	1.51×10^{-1}	1.0	0.8	0.8	1.5	58	46, 66	1.8, 2.0	0.0, +0.4	1.32×10^{-1}	1.1	0.8	0.9	1.6
61	46, 66	2.0, 2.2	−1.0, −0.7	—	—	—	—	—	66	46, 66	2.0, 2.2	+0.7, +1.0	—	—	—	—	—
62	46, 66	2.0, 2.2	−0.7, −0.4	2.48×10^{-3}	9.7	7.1	3.0	12.3	65	46, 66	2.0, 2.2	+0.4, +0.7	1.64×10^{-3}	11.1	6.4	5.2	13.8
63	46, 66	2.0, 2.2	−0.4, 0.0	1.16×10^{-1}	1.1	0.8	0.7	1.6	64	46, 66	2.0, 2.2	0.0, +0.4	9.58×10^{-2}	1.2	1.0	0.9	1.8
67	46, 66	2.2, 2.4	−1.0, −0.7	—	—	—	—	—	72	46, 66	2.2, 2.4	+0.7, +1.0	—	—	—	—	—
68	46, 66	2.2, 2.4	−0.7, −0.4	—	—	—	—	—	71	46, 66	2.2, 2.4	+0.4, +0.7	—	—	—	—	—
69	46, 66	2.2, 2.4	−0.4, 0.0	3.82×10^{-2}	1.9	1.5	0.9	2.6	70	46, 66	2.2, 2.4	0.0, +0.4	3.50×10^{-2}	2.0	1.4	1.0	2.6
73	66, 80	0.0, 0.2	−1.0, −0.7	7.92×10^{-2}	1.6	0.9	0.8	2.0	78	66, 80	0.0, 0.2	+0.7, +1.0	7.70×10^{-2}	1.6	0.9	0.8	2.0
74	66, 80	0.0, 0.2	−0.7, −0.4	1.96×10^{-1}	0.9	0.5	0.4	1.1	77	66, 80	0.0, 0.2	+0.4, +0.7	1.93×10^{-1}	1.0	0.5	0.4	1.1
75	66, 80	0.0, 0.2	−0.4, 0.0	1.74×10^{-1}	0.9	0.6	0.3	1.1	76	66, 80	0.0, 0.2	0.0, +0.4	1.79×10^{-1}	0.9	0.4	0.3	1.0
79	66, 80	0.2, 0.4	−1.0, −0.7	8.29×10^{-2}	1.7	0.9	0.8	2.0	84	66, 80	0.2, 0.4	+0.7, +1.0	7.47×10^{-2}	1.6	0.9	0.8	2.0
80	66, 80	0.2, 0.4	−0.7, −0.4	2.02×10^{-1}	0.9	0.5	0.4	1.1	83	66, 80	0.2, 0.4	+0.4, +0.7	1.85×10^{-1}	1.0	0.5	0.4	1.2
81	66, 80	0.2, 0.4	−0.4, 0.0	1.72×10^{-1}	0.9	0.5	0.3	1.0	82	66, 80	0.2, 0.4	0.0, +0.4	1.74×10^{-1}	0.9	0.5	0.3	1.0
85	66, 80	0.4, 0.6	−1.0, −0.7	7.86×10^{-2}	1.6	0.9	0.9	2.0	90	66, 80	0.4, 0.6	+0.7, +1.0	7.37×10^{-2}	1.7	0.9	0.9	2.1
86	66, 80	0.4, 0.6	−0.7, −0.4	2.02×10^{-1}	1.0	0.5	0.4	1.2	89	66, 80	0.4, 0.6	+0.4, +0.7	1.86×10^{-1}	1.0	0.5	0.4	1.2
87	66, 80	0.4, 0.6	−0.4, 0.0	1.77×10^{-1}	0.8	0.4	0.3	1.0	88	66, 80	0.4, 0.6	0.0, +0.4	1.73×10^{-1}	0.8	0.4	0.3	1.0
91	66, 80	0.6, 0.8	−1.0, −0.7	8.41×10^{-2}	1.6	0.8	0.8	2.0	96	66, 80	0.6, 0.8	+0.7, +1.0	7.03×10^{-2}	1.6	1.0	0.8	2.1
92	66, 80	0.6, 0.8	−0.7, −0.4	2.05×10^{-1}	1.0	0.5	0.4	1.2	95	66, 80	0.6, 0.8	+0.4, +0.7	1.81×10^{-1}	1.0	0.7	0.5	1.3
93	66, 80	0.6, 0.8	−0.4, 0.0	1.78×10^{-1}	0.8	0.4	0.3	1.0	94	66, 80	0.6, 0.8	0.0, +0.4	1.69×10^{-1}	0.9	0.4	0.3	1.0
97	66, 80	0.8, 1.0	−1.0, −0.7	8.08×10^{-2}	1.7	1.0	0.8	2.1	102	66, 80	0.8, 1.0	+0.7, +1.0	6.90×10^{-2}	1.8	1.0	0.9	2.2
98	66, 80	0.8, 1.0	−0.7, −0.4	2.09×10^{-1}	1.0	0.5	0.4	1.2	101	66, 80	0.8, 1.0	+0.4, +0.7	1.72×10^{-1}	1.0	0.6	0.5	1.3
99	66, 80	0.8, 1.0	−0.4, 0.0	1.76×10^{-1}	0.8	0.4	0.3	1.0	100	66, 80	0.8, 1.0	0.0, +0.4	1.63×10^{-1}	0.9	0.5	0.3	1.0
103	66, 80	1.0, 1.2	−1.0, −0.7	8.63×10^{-2}	1.6	0.9	0.7	2.0	108	66, 80	1.0, 1.2	+0.7, +1.0	6.71×10^{-2}	1.7	1.0	0.8	2.1
104	66, 80	1.0, 1.2	−0.7, −0.4	2.05×10^{-1}	0.9	0.5	0.4	1.1	107	66, 80	1.0, 1.2	+0.4, +0.7	1.68×10^{-1}	1.0	0.6	0.5	1.2
105	66, 80	1.0, 1.2	−0.4, 0.0	1.79×10^{-1}	0.9	0.5	0.3	1.0	106	66, 80	1.0, 1.2	0.0, +0.4	1.60×10^{-1}	0.9	0.5	0.4	1.1
109	66, 80	1.2, 1.4	−1.0, −0.7	7.00×10^{-2}	1.6	1.0	0.8	2.1	114	66, 80	1.2, 1.4	+0.7, +1.0	4.86×10^{-2}	1.9	1.0	1.0	2.3
110	66, 80	1.2, 1.4	−0.7, −0.4	2.11×10^{-1}	0.9	0.5	0.4	1.1	113	66, 80	1.2, 1.4	+0.4, +0.7	1.59×10^{-1}	1.0	0.6	0.5	1.2
111	66, 80	1.2, 1.4	−0.4, 0.0	1.79×10^{-1}	0.9	0.5	0.4	1.1	112	66, 80	1.2, 1.4	0.0, +0.4	1.58×10^{-1}	0.9	0.5	0.4	1.2
115	66, 80	1.4, 1.6	−1.0, −0.7	2.74×10^{-2}	2.6	1.5	0.8	3.1	120	66, 80	1.4, 1.6	+0.7, +1.0	1.97×10^{-2}	2.9	2.3	1.1	3.9
116	66, 80	1.4, 1.6	−0.7, −0.4	2.06×10^{-1}	0.9	0.5	0.4	1.1	119	66, 80	1.4, 1.6	+0.4, +0.7	1.45×10^{-1}	1.0	0.6	0.5	1.3
117	66, 80	1.4, 1.6	−0.4, 0.0	1.80×10^{-1}	0.9	0.5	0.4	1.1	118	66, 80	1.4, 1.6	0.0, +0.4	1.57×10^{-1}	0.9	0.5	0.4	1.1
121	66, 80	1.6, 1.8	−1.0, −0.7	6.28×10^{-3}	5.1	3.5	1.8	6.5	126	66, 80	1.6, 1.8	+0.7, +1.0	4.06×10^{-3}	6.1	4.2	1.8	7.7
122	66, 80	1.6, 1.8	−0.7, −0.4	1.47×10^{-1}	1.0	0.6	0.5	1.3	125	66, 80	1.6, 1.8	+0.4, +0.7	9.89×10^{-2}	1.2	0.8	0.6	1.6
123	66, 80	1.6, 1.8	−0.4, 0.0	1.76×10^{-1}	0.9	0.5	0.4	1.1	124	66, 80	1.6, 1.8	0.0, +0.4	1.52×10^{-1}	0.9	0.5	0.5	1.1
127	66, 80	1.8, 2.0	−1.0, −0.7	1.90×10^{-3}	9.4	5.8	3.5	11.6	132	66, 80	1.8, 2.0	+0.7, +1.0	8.82×10^{-4}	11.9	7.4	4.3	14.7
128	66, 80	1.8, 2.0	−0.7, −0.4	5.38×10^{-2}	1.8	1.2	0.9	2.3	131	66, 80	1.8, 2.0	+0.4, +0.7	3.34×10^{-2}	2.1	1.3	1.0	2.7
129	66, 80	1.8, 2.0	−0.4, 0.0	1.72×10^{-1}	0.8	0.5	0.5	1.1	130	66, 80	1.8, 2.0	0.0, +0.4	1.45×10^{-1}	0.9	0.5	0.5	1.2
133	66, 80	2.0, 2.2	−1.0, −0.7	—	—	—	—	—	138	66, 80	2.0, 2.2	+0.7, +1.0	—	—	—	—	—
134	66, 80	2.0, 2.2	−0.7, −0.4	3.68×10^{-3}	6.5	4.8	3.0	8.6	137	66, 80	2.0, 2.2	+0.4, +0.7	2.62×10^{-3}	7.8	5.4	3.9	10.2
135	66, 80	2.0, 2.2	−0.4, 0.0	1.26×10^{-1}	1.0	0.5	0.6	1.3	136	66, 80	2.0, 2.2	0.0, +0.4	1.01×10^{-1}	1.0	0.6	0.7	1.4
139	66, 80	2.2, 2.4	−1.0, −0.7	—	—	—	—	—	144	66, 80	2.2, 2.4	+0.7, +1.0	—	—	—	—	—
140	66, 80	2.2, 2.4	−0.7, −0.4	—	—	—	—	—	143	66, 80	2.2, 2.4	+0.4, +0.7	—	—	—	—	—
141	66, 80	2.2, 2.4	−0.4, 0.0	4.01×10^{-2}	1.6	1.0	1.1	2.2	142	66, 80	2.2, 2.4	0.0, +0.4	3.62×10^{-2}	1.7	1.1	1.1	2.3

JHEP12(2017)059

Bin	$m_{\ell\ell}$ [GeV]	$\lvert y_{\ell\ell}\rvert$	$\cos\theta^*$	$\mathrm{d}^3\sigma$ [pb/GeV]	δ^{stat} [%]	$\delta^{\mathrm{syst}}_{\mathrm{unc}}$ [%]	$\delta^{\mathrm{syst}}_{\mathrm{cor}}$ [%]	δ^{total} [%]	Bin	$m_{\ell\ell}$ [GeV]	$\lvert y_{\ell\ell}\rvert$	$\cos\theta^*$	$\mathrm{d}^3\sigma$ [pb/GeV]	δ^{stat} [%]	$\delta^{\mathrm{syst}}_{\mathrm{unc}}$ [%]	$\delta^{\mathrm{syst}}_{\mathrm{cor}}$ [%]	δ^{total} [%]
145	91, 102	0.0, 0.2	−1.0, −0.7	2.25	0.3	0.2	0.3	0.5	150	91, 102	0.0, 0.2	+0.7, +1.0	2.26	0.3	0.2	0.3	0.5
146	91, 102	0.0, 0.2	−0.7, −0.4	3.58	0.3	0.1	0.2	0.3	149	91, 102	0.0, 0.2	+0.4, +0.7	3.60	0.3	0.1	0.2	0.3
147	91, 102	0.0, 0.2	−0.4, 0.0	3.12	0.3	0.1	0.2	0.4	148	91, 102	0.0, 0.2	0.0, +0.4	3.10	0.3	0.1	0.2	0.4
151	91, 102	0.2, 0.4	−1.0, −0.7	2.26	0.3	0.2	0.3	0.5	156	91, 102	0.2, 0.4	+0.7, +1.0	2.27	0.3	0.2	0.3	0.5
152	91, 102	0.2, 0.4	−0.7, −0.4	3.58	0.3	0.1	0.2	0.3	155	91, 102	0.2, 0.4	+0.4, +0.7	3.61	0.3	0.1	0.2	0.4
153	91, 102	0.2, 0.4	−0.4, 0.0	3.10	0.3	0.1	0.2	0.4	154	91, 102	0.2, 0.4	0.0, +0.4	3.10	0.2	0.1	0.2	0.4
157	91, 102	0.4, 0.6	−1.0, −0.7	2.24	0.3	0.2	0.3	0.5	162	91, 102	0.4, 0.6	+0.7, +1.0	2.24	0.3	0.2	0.3	0.5
158	91, 102	0.4, 0.6	−0.7, −0.4	3.57	0.3	0.1	0.2	0.4	161	91, 102	0.4, 0.6	+0.4, +0.7	3.60	0.3	0.1	0.2	0.4
159	91, 102	0.4, 0.6	−0.4, 0.0	3.08	0.2	0.1	0.2	0.3	160	91, 102	0.4, 0.6	0.0, +0.4	3.10	0.2	0.1	0.2	0.3
163	91, 102	0.6, 0.8	−1.0, −0.7	2.24	0.3	0.2	0.3	0.5	168	91, 102	0.6, 0.8	+0.7, +1.0	2.24	0.3	0.2	0.3	0.5
164	91, 102	0.6, 0.8	−0.7, −0.4	3.54	0.3	0.1	0.3	0.4	167	91, 102	0.6, 0.8	+0.4, +0.7	3.54	0.3	0.1	0.3	0.4
165	91, 102	0.6, 0.8	−0.4, 0.0	3.06	0.2	0.1	0.2	0.3	166	91, 102	0.6, 0.8	0.0, +0.4	3.08	0.2	0.1	0.2	0.3
169	91, 102	0.8, 1.0	−1.0, −0.7	2.21	0.3	0.2	0.3	0.5	174	91, 102	0.8, 1.0	+0.7, +1.0	2.24	0.3	0.2	0.3	0.5
170	91, 102	0.8, 1.0	−0.7, −0.4	3.50	0.3	0.1	0.3	0.4	173	91, 102	0.8, 1.0	+0.4, +0.7	3.49	0.3	0.1	0.3	0.4
171	91, 102	0.8, 1.0	−0.4, 0.0	3.06	0.2	0.1	0.2	0.3	172	91, 102	0.8, 1.0	0.0, +0.4	3.03	0.2	0.1	0.2	0.3
175	91, 102	1.0, 1.2	−1.0, −0.7	1.96	0.4	0.2	0.3	0.5	180	91, 102	1.0, 1.2	+0.7, +1.0	1.96	0.3	0.2	0.3	0.5
176	91, 102	1.0, 1.2	−0.7, −0.4	3.45	0.3	0.1	0.3	0.4	179	91, 102	1.0, 1.2	+0.4, +0.7	3.46	0.2	0.1	0.3	0.4
177	91, 102	1.0, 1.2	−0.4, 0.0	3.01	0.2	0.1	0.3	0.4	178	91, 102	1.0, 1.2	0.0, +0.4	3.00	0.2	0.1	0.3	0.4
181	91, 102	1.2, 1.4	−1.0, −0.7	1.29	0.4	0.2	0.4	0.6	186	91, 102	1.2, 1.4	+0.7, +1.0	1.29	0.4	0.2	0.4	0.6
182	91, 102	1.2, 1.4	−0.7, −0.4	3.41	0.3	0.1	0.3	0.4	185	91, 102	1.2, 1.4	+0.4, +0.7	3.39	0.2	0.1	0.2	0.4
183	91, 102	1.2, 1.4	−0.4, 0.0	2.97	0.3	0.1	0.3	0.4	184	91, 102	1.2, 1.4	0.0, +0.4	2.95	0.2	0.1	0.3	0.4
187	91, 102	1.4, 1.6	−1.0, −0.7	4.87×10^{-1}	0.7	0.4	0.4	0.8	192	91, 102	1.4, 1.6	+0.7, +1.0	4.80×10^{-1}	0.6	0.4	0.4	0.8
188	91, 102	1.4, 1.6	−0.7, −0.4	3.18	0.2	0.1	0.3	0.4	191	91, 102	1.4, 1.6	+0.4, +0.7	3.16	0.2	0.1	0.3	0.4
189	91, 102	1.4, 1.6	−0.4, 0.0	2.90	0.2	0.1	0.3	0.4	190	91, 102	1.4, 1.6	0.0, +0.4	2.90	0.2	0.1	0.3	0.4
193	91, 102	1.6, 1.8	−1.0, −0.7	9.17×10^{-2}	1.5	0.9	0.5	1.8	198	91, 102	1.6, 1.8	+0.7, +1.0	9.08×10^{-2}	1.5	0.9	0.6	1.8
194	91, 102	1.6, 1.8	−0.7, −0.4	2.24	0.3	0.2	0.3	0.5	197	91, 102	1.6, 1.8	+0.4, +0.7	2.22	0.3	0.2	0.3	0.5
195	91, 102	1.6, 1.8	−0.4, 0.0	2.83	0.2	0.1	0.3	0.4	196	91, 102	1.6, 1.8	0.0, +0.4	2.84	0.2	0.1	0.3	0.4
199	91, 102	1.8, 2.0	−1.0, −0.7	2.11×10^{-2}	2.9	1.9	0.7	3.5	204	91, 102	1.8, 2.0	+0.7, +1.0	2.02×10^{-2}	2.9	1.9	1.1	3.6
200	91, 102	1.8, 2.0	−0.7, −0.4	8.08×10^{-1}	0.5	0.3	0.4	0.7	203	91, 102	1.8, 2.0	+0.4, +0.7	7.92×10^{-1}	0.5	0.3	0.4	0.7
201	91, 102	1.8, 2.0	−0.4, 0.0	2.73	0.2	0.1	0.3	0.4	202	91, 102	1.8, 2.0	0.0, +0.4	2.73	0.2	0.1	0.3	0.4
205	91, 102	2.0, 2.2	−1.0, −0.7	2.53×10^{-3}	7.9	6.1	2.2	10.3	210	91, 102	2.0, 2.2	+0.7, +1.0	2.74×10^{-3}	8.3	5.6	3.4	10.6
206	91, 102	2.0, 2.2	−0.7, −0.4	4.99×10^{-2}	2.1	1.5	0.7	2.7	209	91, 102	2.0, 2.2	+0.4, +0.7	5.03×10^{-2}	2.1	1.5	0.7	2.7
207	91, 102	2.0, 2.2	−0.4, 0.0	1.96	0.3	0.2	0.3	0.5	208	91, 102	2.0, 2.2	0.0, +0.4	1.95	0.3	0.2	0.3	0.5
211	91, 102	2.2, 2.4	−1.0, −0.7	—	—	—	—	—	216	91, 102	2.2, 2.4	+0.7, +1.0	—	—	—	—	—
212	91, 102	2.2, 2.4	−0.7, −0.4	—	—	—	—	—	215	91, 102	2.2, 2.4	+0.4, +0.7	—	—	—	—	—
213	91, 102	2.2, 2.4	−0.4, 0.0	6.54×10^{-1}	0.4	0.3	0.4	0.7	214	91, 102	2.2, 2.4	0.0, +0.4	6.46×10^{-1}	0.4	0.3	0.4	0.7
217	91, 102	0.0, 0.2	−1.0, −0.7	2.80	0.3	0.2	0.3	0.4	222	91, 102	0.0, 0.2	+0.7, +1.0	2.82	0.3	0.2	0.3	0.4
218	91, 102	0.0, 0.2	−0.7, −0.4	4.17	0.2	0.1	0.2	0.3	221	91, 102	0.0, 0.2	+0.4, +0.7	4.21	0.2	0.1	0.2	0.3
219	91, 102	0.0, 0.2	−0.4, 0.0	3.59	0.2	0.1	0.2	0.4	220	91, 102	0.0, 0.2	0.0, +0.4	3.62	0.2	0.1	0.2	0.4
223	91, 102	0.2, 0.4	−1.0, −0.7	2.78	0.3	0.2	0.3	0.4	228	91, 102	0.2, 0.4	+0.7, +1.0	2.83	0.3	0.2	0.3	0.4
224	91, 102	0.2, 0.4	−0.7, −0.4	4.11	0.3	0.1	0.2	0.3	227	91, 102	0.2, 0.4	+0.4, +0.7	4.17	0.2	0.1	0.2	0.3
225	91, 102	0.2, 0.4	−0.4, 0.0	3.58	0.2	0.1	0.2	0.4	226	91, 102	0.2, 0.4	0.0, +0.4	3.61	0.2	0.1	0.2	0.3
229	91, 102	0.4, 0.6	−1.0, −0.7	2.75	0.3	0.2	0.3	0.5	234	91, 102	0.4, 0.6	+0.7, +1.0	2.84	0.3	0.2	0.3	0.5
230	91, 102	0.4, 0.6	−0.7, −0.4	4.07	0.3	0.1	0.2	0.4	233	91, 102	0.4, 0.6	+0.4, +0.7	4.19	0.3	0.1	0.2	0.4
231	91, 102	0.4, 0.6	−0.4, 0.0	3.55	0.2	0.1	0.2	0.3	232	91, 102	0.4, 0.6	0.0, +0.4	3.59	0.2	0.1	0.2	0.3
235	91, 102	0.6, 0.8	−1.0, −0.7	2.70	0.3	0.2	0.3	0.4	240	91, 102	0.6, 0.8	+0.7, +1.0	2.86	0.3	0.1	0.3	0.4
236	91, 102	0.6, 0.8	−0.7, −0.4	4.05	0.3	0.1	0.3	0.4	239	91, 102	0.6, 0.8	+0.4, +0.7	4.20	0.3	0.1	0.3	0.4
237	91, 102	0.6, 0.8	−0.4, 0.0	3.52	0.2	0.1	0.2	0.3	238	91, 102	0.6, 0.8	0.0, +0.4	3.57	0.2	0.1	0.2	0.3
241	91, 102	0.8, 1.0	−1.0, −0.7	2.64	0.3	0.2	0.3	0.5	246	91, 102	0.8, 1.0	+0.7, +1.0	2.83	0.3	0.2	0.3	0.5
242	91, 102	0.8, 1.0	−0.7, −0.4	3.98	0.3	0.1	0.3	0.4	245	91, 102	0.8, 1.0	+0.4, +0.7	4.17	0.3	0.1	0.3	0.4
243	91, 102	0.8, 1.0	−0.4, 0.0	3.46	0.2	0.1	0.2	0.3	244	91, 102	0.8, 1.0	0.0, +0.4	3.56	0.2	0.1	0.2	0.3
247	91, 102	1.0, 1.2	−1.0, −0.7	2.23	0.3	0.2	0.3	0.5	252	91, 102	1.0, 1.2	+0.7, +1.0	2.42	0.3	0.2	0.3	0.5
248	91, 102	1.0, 1.2	−0.7, −0.4	3.91	0.2	0.1	0.3	0.4	251	91, 102	1.0, 1.2	+0.4, +0.7	4.19	0.2	0.1	0.2	0.4
249	91, 102	1.0, 1.2	−0.4, 0.0	3.41	0.2	0.1	0.3	0.4	250	91, 102	1.0, 1.2	0.0, +0.4	3.52	0.2	0.1	0.2	0.4
253	91, 102	1.2, 1.4	−1.0, −0.7	1.46	0.4	0.2	0.3	0.5	258	91, 102	1.2, 1.4	+0.7, +1.0	1.60	0.4	0.2	0.3	0.5
254	91, 102	1.2, 1.4	−0.7, −0.4	3.79	0.3	0.1	0.2	0.4	257	91, 102	1.2, 1.4	+0.4, +0.7	4.12	0.2	0.1	0.2	0.3
255	91, 102	1.2, 1.4	−0.4, 0.0	3.34	0.2	0.1	0.3	0.4	256	91, 102	1.2, 1.4	0.0, +0.4	3.48	0.2	0.1	0.3	0.4
259	91, 102	1.4, 1.6	−1.0, −0.7	5.29×10^{-1}	0.6	0.3	0.4	0.8	264	91, 102	1.4, 1.6	+0.7, +1.0	5.95×10^{-1}	0.6	0.3	0.4	0.8
260	91, 102	1.4, 1.6	−0.7, −0.4	3.48	0.2	0.1	0.3	0.4	263	91, 102	1.4, 1.6	+0.4, +0.7	3.84	0.2	0.1	0.2	0.4
261	91, 102	1.4, 1.6	−0.4, 0.0	3.27	0.2	0.1	0.3	0.4	262	91, 102	1.4, 1.6	0.0, +0.4	3.42	0.2	0.1	0.3	0.4
265	91, 102	1.6, 1.8	−1.0, −0.7	9.80×10^{-2}	1.5	1.0	0.7	1.9	270	91, 102	1.6, 1.8	+0.7, +1.0	1.13×10^{-1}	1.3	0.9	0.6	1.7
266	91, 102	1.6, 1.8	−0.7, −0.4	2.41	0.3	0.1	0.3	0.5	269	91, 102	1.6, 1.8	+0.4, +0.7	2.70	0.3	0.1	0.3	0.4
267	91, 102	1.6, 1.8	−0.4, 0.0	3.20	0.2	0.1	0.3	0.4	268	91, 102	1.6, 1.8	0.0, +0.4	3.37	0.2	0.1	0.3	0.4
271	91, 102	1.8, 2.0	−1.0, −0.7	2.17×10^{-2}	3.0	1.8	0.9	3.7	276	91, 102	1.8, 2.0	+0.7, +1.0	2.36×10^{-2}	2.8	1.7	0.8	3.4
272	91, 102	1.8, 2.0	−0.7, −0.4	8.61×10^{-1}	0.5	0.3	0.5	0.7	275	91, 102	1.8, 2.0	+0.4, +0.7	9.82×10^{-1}	0.5	0.3	0.4	0.7
273	91, 102	1.8, 2.0	−0.4, 0.0	3.03	0.2	0.1	0.3	0.4	274	91, 102	1.8, 2.0	0.0, +0.4	3.23	0.2	0.1	0.3	0.4
277	91, 102	2.0, 2.2	−1.0, −0.7	2.30×10^{-3}	10.6	8.0	5.2	14.3	282	91, 102	2.0, 2.2	+0.7, +1.0	3.47×10^{-3}	7.6	5.2	2.6	9.6
278	91, 102	2.0, 2.2	−0.7, −0.4	5.15×10^{-2}	2.0	1.3	1.0	2.6	281	91, 102	2.0, 2.2	+0.4, +0.7	6.30×10^{-2}	1.9	1.2	1.0	2.5
279	91, 102	2.0, 2.2	−0.4, 0.0	2.17	0.3	0.1	0.3	0.4	280	91, 102	2.0, 2.2	0.0, +0.4	2.32	0.3	0.1	0.3	0.4
283	91, 102	2.2, 2.4	−1.0, −0.7	—	—	—	—	—	288	91, 102	2.2, 2.4	+0.7, +1.0	—	—	—	—	—
284	91, 102	2.2, 2.4	−0.7, −0.4	—	—	—	—	—	287	91, 102	2.2, 2.4	+0.4, +0.7	—	—	—	—	—
285	91, 102	2.2, 2.4	−0.4, 0.0	7.30×10^{-1}	0.4	0.2	0.4	0.7	286	91, 102	2.2, 2.4	0.0, +0.4	7.59×10^{-1}	0.4	0.2	0.4	0.6

JHEP12(2017)059

Bin	$m_{\ell\ell}$ [GeV]	$\lvert y_{\ell\ell}\rvert$	$\cos\theta^*$	$\mathrm{d}^3\sigma$ [pb/GeV]	δ^{stat} [%]	$\delta^{\mathrm{syst}}_{\mathrm{unc}}$ [%]	$\delta^{\mathrm{syst}}_{\mathrm{cor}}$ [%]	δ^{total} [%]	Bin	$m_{\ell\ell}$ [GeV]	$\lvert y_{\ell\ell}\rvert$	$\cos\theta^*$	$\mathrm{d}^3\sigma$ [pb/GeV]	δ^{stat} [%]	$\delta^{\mathrm{syst}}_{\mathrm{unc}}$ [%]	$\delta^{\mathrm{syst}}_{\mathrm{cor}}$ [%]	δ^{total} [%]
289	102, 116	0.0, 0.2	−1.0, −0.7	1.09×10^{-1}	1.4	0.8	0.6	1.7	294	102, 116	0.0, 0.2	+0.7, +1.0	1.09×10^{-1}	1.4	0.8	0.6	1.7
290	102, 116	0.0, 0.2	−0.7, −0.4	1.30×10^{-1}	1.2	0.6	0.4	1.4	293	102, 116	0.0, 0.2	+0.4, +0.7	1.39×10^{-1}	1.2	0.5	0.3	1.4
291	102, 116	0.0, 0.2	−0.4, 0.0	1.15×10^{-1}	1.2	0.5	0.3	1.4	292	102, 116	0.0, 0.2	0.0, +0.4	1.15×10^{-1}	1.2	0.5	0.4	1.4
295	102, 116	0.2, 0.4	−1.0, −0.7	1.03×10^{-1}	1.5	0.8	0.6	1.8	300	102, 116	0.2, 0.4	+0.7, +1.0	1.11×10^{-1}	1.5	0.8	0.6	1.7
296	102, 116	0.2, 0.4	−0.7, −0.4	1.33×10^{-1}	1.2	0.6	0.4	1.4	299	102, 116	0.2, 0.4	+0.4, +0.7	1.39×10^{-1}	1.2	0.5	0.4	1.4
297	102, 116	0.2, 0.4	−0.4, 0.0	1.14×10^{-1}	1.2	0.5	0.4	1.3	298	102, 116	0.2, 0.4	0.0, +0.4	1.19×10^{-1}	1.2	0.5	0.4	1.3
301	102, 116	0.4, 0.6	−1.0, −0.7	1.01×10^{-1}	1.5	0.8	0.6	1.8	306	102, 116	0.4, 0.6	+0.7, +1.0	1.13×10^{-1}	1.4	0.7	0.6	1.7
302	102, 116	0.4, 0.6	−0.7, −0.4	1.25×10^{-1}	1.3	0.7	0.4	1.5	305	102, 116	0.4, 0.6	+0.4, +0.7	1.40×10^{-1}	1.2	0.6	0.4	1.4
303	102, 116	0.4, 0.6	−0.4, 0.0	1.12×10^{-1}	1.1	0.5	0.4	1.3	304	102, 116	0.4, 0.6	0.0, +0.4	1.15×10^{-1}	1.1	0.5	0.3	1.3
307	102, 116	0.6, 0.8	−1.0, −0.7	9.95×10^{-2}	1.4	0.8	0.7	1.8	312	102, 116	0.6, 0.8	+0.7, +1.0	1.14×10^{-1}	1.4	0.7	0.7	1.7
308	102, 116	0.6, 0.8	−0.7, −0.4	1.21×10^{-1}	1.4	0.7	0.5	1.6	311	102, 116	0.6, 0.8	+0.4, +0.7	1.40×10^{-1}	1.3	0.7	0.5	1.6
309	102, 116	0.6, 0.8	−0.4, 0.0	1.12×10^{-1}	1.1	0.5	0.4	1.3	310	102, 116	0.6, 0.8	0.0, +0.4	1.15×10^{-1}	1.1	0.5	0.3	1.3
313	102, 116	0.8, 1.0	−1.0, −0.7	8.72×10^{-2}	1.6	0.9	0.6	1.9	318	102, 116	0.8, 1.0	+0.7, +1.0	1.11×10^{-1}	1.4	0.8	0.6	1.7
314	102, 116	0.8, 1.0	−0.7, −0.4	1.19×10^{-1}	1.3	0.7	0.5	1.6	317	102, 116	0.8, 1.0	+0.4, +0.7	1.47×10^{-1}	1.2	0.6	0.5	1.4
315	102, 116	0.8, 1.0	−0.4, 0.0	1.07×10^{-1}	1.1	0.7	0.4	1.4	316	102, 116	0.8, 1.0	0.0, +0.4	1.18×10^{-1}	1.0	0.5	0.4	1.2
319	102, 116	1.0, 1.2	−1.0, −0.7	6.74×10^{-2}	1.7	1.0	0.7	2.1	324	102, 116	1.0, 1.2	+0.7, +1.0	9.14×10^{-2}	1.5	0.8	0.6	1.8
320	102, 116	1.0, 1.2	−0.7, −0.4	1.13×10^{-1}	1.2	0.7	0.5	1.5	323	102, 116	1.0, 1.2	+0.4, +0.7	1.49×10^{-1}	1.1	0.6	0.5	1.3
321	102, 116	1.0, 1.2	−0.4, 0.0	1.06×10^{-1}	1.1	0.6	0.5	1.4	322	102, 116	1.0, 1.2	0.0, +0.4	1.18×10^{-1}	1.1	0.5	0.5	1.3
325	102, 116	1.2, 1.4	−1.0, −0.7	4.21×10^{-2}	1.9	1.2	1.1	2.5	330	102, 116	1.2, 1.4	+0.7, +1.0	5.84×10^{-2}	1.7	1.0	0.8	2.1
326	102, 116	1.2, 1.4	−0.7, −0.4	1.09×10^{-1}	1.2	0.6	0.6	1.5	329	102, 116	1.2, 1.4	+0.4, +0.7	1.50×10^{-1}	1.0	0.6	0.5	1.3
327	102, 116	1.2, 1.4	−0.4, 0.0	1.01×10^{-1}	1.1	0.6	0.6	1.4	328	102, 116	1.2, 1.4	0.0, +0.4	1.19×10^{-1}	1.1	0.7	0.7	1.5
331	102, 116	1.4, 1.6	−1.0, −0.7	1.39×10^{-2}	2.5	1.9	1.5	3.5	336	102, 116	1.4, 1.6	+0.7, +1.0	2.25×10^{-2}	2.2	1.6	1.5	3.1
332	102, 116	1.4, 1.6	−0.7, −0.4	9.53×10^{-2}	1.2	0.7	0.6	1.5	335	102, 116	1.4, 1.6	+0.4, +0.7	1.37×10^{-1}	1.1	0.6	0.6	1.3
333	102, 116	1.4, 1.6	−0.4, 0.0	9.77×10^{-2}	1.1	0.6	0.7	1.5	334	102, 116	1.4, 1.6	0.0, +0.4	1.17×10^{-1}	1.0	0.6	0.6	1.3
337	102, 116	1.6, 1.8	−1.0, −0.7	2.35×10^{-3}	4.6	4.9	2.8	7.3	342	102, 116	1.6, 1.8	+0.7, +1.0	4.19×10^{-3}	4.2	3.8	2.2	6.1
338	102, 116	1.6, 1.8	−0.7, −0.4	6.43×10^{-2}	1.2	0.9	1.0	1.8	341	102, 116	1.6, 1.8	+0.4, +0.7	1.01×10^{-1}	1.1	0.7	0.9	1.6
339	102, 116	1.6, 1.8	−0.4, 0.0	9.25×10^{-2}	1.1	0.7	1.0	1.6	340	102, 116	1.6, 1.8	0.0, +0.4	1.16×10^{-1}	1.0	0.7	0.8	1.5
343	102, 116	1.8, 2.0	−1.0, −0.7	4.34×10^{-4}	6.1	11.4	3.4	13.4	348	102, 116	1.8, 2.0	+0.7, +1.0	8.65×10^{-4}	8.2	9.1	2.9	12.6
344	102, 116	1.8, 2.0	−0.7, −0.4	2.13×10^{-2}	1.7	1.5	1.6	2.8	347	102, 116	1.8, 2.0	+0.4, +0.7	3.56×10^{-2}	1.5	1.3	1.5	2.5
345	102, 116	1.8, 2.0	−0.4, 0.0	8.89×10^{-2}	1.0	0.6	0.9	1.5	346	102, 116	1.8, 2.0	0.0, +0.4	1.14×10^{-1}	0.9	0.6	0.9	1.4
349	102, 116	2.0, 2.2	−1.0, −0.7	—	—	—	—	—	354	102, 116	2.0, 2.2	+0.7, +1.0	—	—	—	—	—
350	102, 116	2.0, 2.2	−0.7, −0.4	1.39×10^{-3}	3.3	5.6	3.5	7.4	353	102, 116	2.0, 2.2	+0.4, +0.7	2.22×10^{-3}	3.6	4.9	2.2	6.5
351	102, 116	2.0, 2.2	−0.4, 0.0	6.28×10^{-2}	1.0	0.8	1.3	1.8	352	102, 116	2.0, 2.2	0.0, +0.4	7.95×10^{-2}	0.9	0.7	1.1	1.6
355	102, 116	2.2, 2.4	−1.0, −0.7	—	—	—	—	—	360	102, 116	2.2, 2.4	+0.7, +1.0	—	—	—	—	—
356	102, 116	2.2, 2.4	−0.7, −0.4	—	—	—	—	—	359	102, 116	2.2, 2.4	+0.4, +0.7	—	—	—	—	—
357	102, 116	2.2, 2.4	−0.4, 0.0	2.17×10^{-2}	1.4	1.4	1.9	2.7	358	102, 116	2.2, 2.4	0.0, +0.4	2.45×10^{-2}	1.3	1.3	1.6	2.5
361	116, 150	0.0, 0.2	−1.0, −0.7	2.39×10^{-2}	2.4	1.1	1.4	3.0	366	116, 150	0.0, 0.2	+0.7, +1.0	2.59×10^{-2}	2.2	1.0	1.3	2.7
362	116, 150	0.0, 0.2	−0.7, −0.4	2.59×10^{-2}	1.9	0.6	0.8	2.1	365	116, 150	0.0, 0.2	+0.4, +0.7	2.69×10^{-2}	1.9	0.6	0.7	2.1
363	116, 150	0.0, 0.2	−0.4, 0.0	2.16×10^{-2}	1.9	0.9	0.6	2.2	364	116, 150	0.0, 0.2	0.0, +0.4	2.25×10^{-2}	1.8	0.7	0.6	2.0
367	116, 150	0.2, 0.4	−1.0, −0.7	2.29×10^{-2}	2.3	1.2	1.5	3.0	372	116, 150	0.2, 0.4	+0.7, +1.0	2.54×10^{-2}	2.3	1.2	1.3	2.8
368	116, 150	0.2, 0.4	−0.7, −0.4	2.45×10^{-2}	2.1	0.8	0.8	2.4	371	116, 150	0.2, 0.4	+0.4, +0.7	2.88×10^{-2}	1.9	0.6	0.7	2.1
369	116, 150	0.2, 0.4	−0.4, 0.0	2.10×10^{-2}	1.9	0.6	0.7	2.1	370	116, 150	0.2, 0.4	0.0, +0.4	2.25×10^{-2}	1.8	0.5	0.6	2.0
373	116, 150	0.4, 0.6	−1.0, −0.7	2.11×10^{-2}	2.4	1.0	1.6	3.1	378	116, 150	0.4, 0.6	+0.7, +1.0	2.64×10^{-2}	2.3	1.1	1.3	2.8
374	116, 150	0.4, 0.6	−0.7, −0.4	2.44×10^{-2}	2.1	0.7	0.8	2.4	377	116, 150	0.4, 0.6	+0.4, +0.7	2.81×10^{-2}	2.0	0.7	0.7	2.2
375	116, 150	0.4, 0.6	−0.4, 0.0	2.10×10^{-2}	1.8	0.7	0.6	2.0	376	116, 150	0.4, 0.6	0.0, +0.4	2.26×10^{-2}	1.7	0.5	0.6	1.9
379	116, 150	0.6, 0.8	−1.0, −0.7	2.07×10^{-2}	2.4	1.0	1.5	3.0	384	116, 150	0.6, 0.8	+0.7, +1.0	2.69×10^{-2}	2.0	0.8	1.1	2.4
380	116, 150	0.6, 0.8	−0.7, −0.4	2.32×10^{-2}	2.3	0.8	0.9	2.5	383	116, 150	0.6, 0.8	+0.4, +0.7	2.93×10^{-2}	2.0	0.8	0.7	2.3
381	116, 150	0.6, 0.8	−0.4, 0.0	2.06×10^{-2}	1.8	0.6	0.6	2.0	382	116, 150	0.6, 0.8	0.0, +0.4	2.36×10^{-2}	1.7	0.5	0.5	1.9
385	116, 150	0.8, 1.0	−1.0, −0.7	1.69×10^{-2}	2.6	1.2	1.5	3.3	390	116, 150	0.8, 1.0	+0.7, +1.0	2.37×10^{-2}	2.1	0.9	1.1	2.6
386	116, 150	0.8, 1.0	−0.7, −0.4	2.18×10^{-2}	2.3	0.9	0.8	2.6	389	116, 150	0.8, 1.0	+0.4, +0.7	3.03×10^{-2}	1.9	0.7	0.6	2.1
387	116, 150	0.8, 1.0	−0.4, 0.0	2.08×10^{-2}	1.8	0.6	0.6	2.0	388	116, 150	0.8, 1.0	0.0, +0.4	2.30×10^{-2}	1.7	0.6	0.5	1.9
391	116, 150	1.0, 1.2	−1.0, −0.7	1.21×10^{-2}	3.1	1.6	1.3	3.7	396	116, 150	1.0, 1.2	+0.7, +1.0	1.90×10^{-2}	2.4	1.2	1.1	2.9
392	116, 150	1.0, 1.2	−0.7, −0.4	1.99×10^{-2}	2.2	0.9	0.8	2.5	395	116, 150	1.0, 1.2	+0.4, +0.7	3.07×10^{-2}	1.8	0.6	0.6	2.0
393	116, 150	1.0, 1.2	−0.4, 0.0	2.05×10^{-2}	1.9	0.8	0.6	2.1	394	116, 150	1.0, 1.2	0.0, +0.4	2.39×10^{-2}	1.7	0.6	0.6	1.9
397	116, 150	1.2, 1.4	−1.0, −0.7	8.16×10^{-3}	3.6	1.5	1.3	4.1	402	116, 150	1.2, 1.4	+0.7, +1.0	1.38×10^{-2}	2.7	1.0	0.8	3.0
398	116, 150	1.2, 1.4	−0.7, −0.4	1.82×10^{-2}	2.2	1.1	0.8	2.6	401	116, 150	1.2, 1.4	+0.4, +0.7	3.11×10^{-2}	1.7	0.7	0.6	1.9
399	116, 150	1.2, 1.4	−0.4, 0.0	1.87×10^{-2}	2.0	0.8	0.6	2.2	400	116, 150	1.2, 1.4	0.0, +0.4	2.39×10^{-2}	1.8	0.7	0.6	2.0
403	116, 150	1.4, 1.6	−1.0, −0.7	2.40×10^{-3}	6.3	2.9	2.0	7.2	408	116, 150	1.4, 1.6	+0.7, +1.0	4.68×10^{-3}	4.4	2.5	1.2	5.2
404	116, 150	1.4, 1.6	−0.7, −0.4	1.64×10^{-2}	2.2	0.9	0.8	2.6	407	116, 150	1.4, 1.6	+0.4, +0.7	2.96×10^{-2}	1.7	0.7	0.6	1.9
405	116, 150	1.4, 1.6	−0.4, 0.0	1.79×10^{-2}	2.0	0.9	0.7	2.3	406	116, 150	1.4, 1.6	0.0, +0.4	2.30×10^{-2}	1.7	0.8	0.5	2.0
409	116, 150	1.6, 1.8	−1.0, −0.7	3.00×10^{-4}	70.7	18.8	4.6	73.3	414	116, 150	1.6, 1.8	+0.7, +1.0	9.12×10^{-4}	9.2	7.6	2.1	12.2
410	116, 150	1.6, 1.8	−0.7, −0.4	1.09×10^{-2}	2.8	1.2	0.9	3.1	413	116, 150	1.6, 1.8	+0.4, +0.7	2.23×10^{-2}	2.0	0.9	0.7	2.3
411	116, 150	1.6, 1.8	−0.4, 0.0	1.72×10^{-2}	2.0	0.9	0.7	2.3	412	116, 150	1.6, 1.8	0.0, +0.4	2.36×10^{-2}	1.8	0.9	0.6	2.0
415	116, 150	1.8, 2.0	−1.0, −0.7	—	—	—	—	—	420	116, 150	1.8, 2.0	+0.7, +1.0	—	—	—	—	—
416	116, 150	1.8, 2.0	−0.7, −0.4	3.51×10^{-3}	4.7	2.7	1.8	5.7	419	116, 150	1.8, 2.0	+0.4, +0.7	7.66×10^{-3}	3.5	2.0	1.3	4.2
417	116, 150	1.8, 2.0	−0.4, 0.0	1.66×10^{-2}	2.1	1.2	0.8	2.6	418	116, 150	1.8, 2.0	0.0, +0.4	2.33×10^{-2}	1.8	1.0	0.7	2.2
421	116, 150	2.0, 2.2	−1.0, −0.7	—	—	—	—	—	426	116, 150	2.0, 2.2	+0.7, +1.0	—	—	—	—	—
422	116, 150	2.0, 2.2	−0.7, −0.4	2.20×10^{-4}	8.3	8.9	6.0	13.5	425	116, 150	2.0, 2.2	+0.4, +0.7	4.66×10^{-4}	9.7	7.6	3.8	12.9
423	116, 150	2.0, 2.2	−0.4, 0.0	1.20×10^{-2}	2.1	1.0	0.9	2.5	424	116, 150	2.0, 2.2	0.0, +0.4	1.65×10^{-2}	1.9	0.9	0.8	2.2
427	116, 150	2.2, 2.4	−1.0, −0.7	—	—	—	—	—	432	116, 150	2.2, 2.4	+0.7, +1.0	—	—	—	—	—
428	116, 150	2.2, 2.4	−0.7, −0.4	—	—	—	—	—	431	116, 150	2.2, 2.4	+0.4, +0.7	—	—	—	—	—
429	116, 150	2.2, 2.4	−0.4, 0.0	3.94×10^{-3}	3.8	2.5	1.9	4.9	430	116, 150	2.2, 2.4	0.0, +0.4	4.75×10^{-3}	3.5	2.2	1.9	4.5

JHEP12(2017)059

Bin	$m_{\ell\ell}$ [GeV]	$\lvert y_{\ell\ell}\rvert$	$\cos\theta^*$	$\mathrm{d}^3\sigma$ [pb/GeV]	δ^{stat} [%]	$\delta^{\mathrm{syst}}_{\mathrm{unc}}$ [%]	$\delta^{\mathrm{syst}}_{\mathrm{cor}}$ [%]	δ^{total} [%]	Bin	$m_{\ell\ell}$ [GeV]	$\lvert y_{\ell\ell}\rvert$	$\cos\theta^*$	$\mathrm{d}^3\sigma$ [pb/GeV]	δ^{stat} [%]	$\delta^{\mathrm{syst}}_{\mathrm{unc}}$ [%]	$\delta^{\mathrm{syst}}_{\mathrm{cor}}$ [%]	δ^{total} [%]
433	150, 200	0.0, 0.2	−1.0, −0.7	6.26×10^{-3}	4.2	1.6	2.8	5.3	438	150, 200	0.0, 0.2	+0.7, +1.0	6.55×10^{-3}	4.3	1.7	2.8	5.4
434	150, 200	0.0, 0.2	−0.7, −0.4	5.56×10^{-3}	3.7	1.2	1.6	4.2	437	150, 200	0.0, 0.2	+0.4, +0.7	5.91×10^{-3}	3.6	1.3	1.6	4.1
435	150, 200	0.0, 0.2	−0.4, 0.0	4.77×10^{-3}	3.4	1.3	1.2	3.8	436	150, 200	0.0, 0.2	0.0, +0.4	4.76×10^{-3}	3.5	0.7	1.1	3.7
439	150, 200	0.2, 0.4	−1.0, −0.7	5.66×10^{-3}	4.6	1.7	3.2	5.8	444	150, 200	0.2, 0.4	+0.7, +1.0	6.67×10^{-3}	4.0	2.0	2.7	5.2
440	150, 200	0.2, 0.4	−0.7, −0.4	5.41×10^{-3}	3.9	1.9	1.6	4.7	443	150, 200	0.2, 0.4	+0.4, +0.7	5.96×10^{-3}	3.6	1.9	2.5	4.8
441	150, 200	0.2, 0.4	−0.4, 0.0	4.81×10^{-3}	3.4	0.9	1.2	3.7	442	150, 200	0.2, 0.4	0.0, +0.4	4.97×10^{-3}	3.2	1.0	1.2	3.6
445	150, 200	0.4, 0.6	−1.0, −0.7	4.73×10^{-3}	4.8	2.2	3.3	6.2	450	150, 200	0.4, 0.6	+0.7, +1.0	7.08×10^{-3}	3.7	1.3	2.3	4.6
446	150, 200	0.4, 0.6	−0.7, −0.4	5.52×10^{-3}	3.9	1.0	1.6	4.3	449	150, 200	0.4, 0.6	+0.4, +0.7	6.26×10^{-3}	3.6	1.2	1.4	4.0
447	150, 200	0.4, 0.6	−0.4, 0.0	4.56×10^{-3}	3.4	0.8	1.1	3.7	448	150, 200	0.4, 0.6	0.0, +0.4	4.79×10^{-3}	3.4	1.9	1.1	4.1
451	150, 200	0.6, 0.8	−1.0, −0.7	4.51×10^{-3}	4.7	1.9	3.0	5.9	456	150, 200	0.6, 0.8	+0.7, +1.0	6.21×10^{-3}	3.8	1.3	2.2	4.6
452	150, 200	0.6, 0.8	−0.7, −0.4	5.18×10^{-3}	4.2	1.5	1.7	4.8	455	150, 200	0.6, 0.8	+0.4, +0.7	6.90×10^{-3}	3.5	0.8	1.2	3.8
453	150, 200	0.6, 0.8	−0.4, 0.0	4.26×10^{-3}	3.4	1.2	1.2	3.8	454	150, 200	0.6, 0.8	0.0, +0.4	5.26×10^{-3}	3.1	0.6	1.0	3.3
457	150, 200	0.8, 1.0	−1.0, −0.7	3.32×10^{-3}	5.4	2.3	3.2	6.7	462	150, 200	0.8, 1.0	+0.7, +1.0	6.01×10^{-3}	3.8	1.5	1.8	4.5
458	150, 200	0.8, 1.0	−0.7, −0.4	4.91×10^{-3}	4.3	1.1	1.7	4.8	461	150, 200	0.8, 1.0	+0.4, +0.7	6.43×10^{-3}	3.7	1.3	1.3	4.1
459	150, 200	0.8, 1.0	−0.4, 0.0	4.28×10^{-3}	3.5	0.8	1.1	3.7	460	150, 200	0.8, 1.0	0.0, +0.4	5.18×10^{-3}	3.1	0.7	0.9	3.3
463	150, 200	1.0, 1.2	−1.0, −0.7	2.39×10^{-3}	6.4	2.4	3.0	7.5	468	150, 200	1.0, 1.2	+0.7, +1.0	4.66×10^{-3}	4.2	1.8	1.8	4.9
464	150, 200	1.0, 1.2	−0.7, −0.4	4.03×10^{-3}	4.4	1.7	1.8	5.1	467	150, 200	1.0, 1.2	+0.4, +0.7	6.99×10^{-3}	3.2	1.1	1.0	3.5
465	150, 200	1.0, 1.2	−0.4, 0.0	4.13×10^{-3}	3.7	1.2	1.3	4.1	466	150, 200	1.0, 1.2	0.0, +0.4	5.40×10^{-3}	3.1	1.2	0.9	3.5
469	150, 200	1.2, 1.4	−1.0, −0.7	1.46×10^{-3}	8.1	4.1	2.8	9.5	474	150, 200	1.2, 1.4	+0.7, +1.0	3.19×10^{-3}	5.0	2.4	1.5	5.7
470	150, 200	1.2, 1.4	−0.7, −0.4	3.80×10^{-3}	4.4	2.1	1.8	5.2	473	150, 200	1.2, 1.4	+0.4, +0.7	7.42×10^{-3}	3.0	1.0	0.9	3.3
471	150, 200	1.2, 1.4	−0.4, 0.0	4.04×10^{-3}	3.8	1.3	1.2	4.2	472	150, 200	1.2, 1.4	0.0, +0.4	5.48×10^{-3}	3.3	0.8	0.9	3.5
475	150, 200	1.4, 1.6	−1.0, −0.7	4.78×10^{-4}	24.4	14.5	3.2	28.6	480	150, 200	1.4, 1.6	+0.7, +1.0	1.06×10^{-3}	8.4	5.8	2.2	10.4
476	150, 200	1.4, 1.6	−0.7, −0.4	3.12×10^{-3}	4.9	2.4	2.0	5.9	479	150, 200	1.4, 1.6	+0.4, +0.7	6.69×10^{-3}	3.1	2.0	0.9	3.8
477	150, 200	1.4, 1.6	−0.4, 0.0	3.84×10^{-3}	3.8	1.4	1.2	4.2	478	150, 200	1.4, 1.6	0.0, +0.4	5.48×10^{-3}	3.1	1.1	0.8	3.4
481	150, 200	1.6, 1.8	−1.0, −0.7	—	—	—	—	—	486	150, 200	1.6, 1.8	+0.7, +1.0	—	—	—	—	—
482	150, 200	1.6, 1.8	−0.7, −0.4	1.96×10^{-3}	5.9	2.0	2.0	6.5	485	150, 200	1.6, 1.8	+0.4, +0.7	5.25×10^{-3}	3.5	1.2	0.9	3.8
483	150, 200	1.6, 1.8	−0.4, 0.0	3.65×10^{-3}	3.9	1.6	1.5	4.5	484	150, 200	1.6, 1.8	0.0, +0.4	5.22×10^{-3}	3.2	1.1	0.8	3.5
487	150, 200	1.8, 2.0	−1.0, −0.7	—	—	—	—	—	492	150, 200	1.8, 2.0	+0.7, +1.0	—	—	—	—	—
488	150, 200	1.8, 2.0	−0.7, −0.4	5.67×10^{-4}	11.8	4.8	4.4	13.4	491	150, 200	1.8, 2.0	+0.4, +0.7	1.62×10^{-3}	6.4	1.9	1.6	6.9
489	150, 200	1.8, 2.0	−0.4, 0.0	3.36×10^{-3}	3.8	0.9	1.0	4.0	490	150, 200	1.8, 2.0	0.0, +0.4	5.16×10^{-3}	3.0	0.9	0.7	3.2
493	150, 200	2.0, 2.2	−1.0, −0.7	—	—	—	—	—	498	150, 200	2.0, 2.2	+0.7, +1.0	—	—	—	—	—
494	150, 200	2.0, 2.2	−0.7, −0.4	—	—	—	—	—	497	150, 200	2.0, 2.2	+0.4, +0.7	—	—	—	—	—
495	150, 200	2.0, 2.2	−0.4, 0.0	2.47×10^{-3}	4.4	1.7	1.3	4.9	496	150, 200	2.0, 2.2	0.0, +0.4	3.68×10^{-3}	3.5	1.2	0.8	3.8
499	150, 200	2.2, 2.4	−1.0, −0.7	—	—	—	—	—	504	150, 200	2.2, 2.4	+0.7, +1.0	—	—	—	—	—
500	150, 200	2.2, 2.4	−0.7, −0.4	—	—	—	—	—	503	150, 200	2.2, 2.4	+0.4, +0.7	—	—	—	—	—
501	150, 200	2.2, 2.4	−0.4, 0.0	8.93×10^{-4}	7.0	2.0	1.7	7.5	502	150, 200	2.2, 2.4	0.0, +0.4	1.15×10^{-3}	6.3	1.8	1.3	6.6

Table 7. The combined Born-level triple-differential cross section $\mathrm{d}^3\sigma/\mathrm{d}m_{\ell\ell}\mathrm{d}|y_{\ell\ell}|\mathrm{d}\cos\theta^*$. The measurements are listed together with the statistical (δ^{stat}), uncorrelated systematic ($\delta^{\mathrm{syst}}_{\mathrm{unc}}$), correlated systematic ($\delta^{\mathrm{syst}}_{\mathrm{cor}}$), and total ($\delta^{\mathrm{total}}$) uncertainties. The luminosity uncertainty of 1.9% is not shown and not included in the overall systematic and total uncertainties.

JHEP12(2017)059

Bin	m_{ee} [GeV]	$\lvert y_{ee}\rvert$	$\cos\theta^*$	$\mathrm{d}^3\sigma$ [pb/GeV]	δ^{stat} [%]	$\delta^{\mathrm{syst}}_{\mathrm{unc}}$ [%]	$\delta^{\mathrm{syst}}_{\mathrm{cor}}$ [%]	δ^{total} [%]	Bin	m_{ee} [GeV]	$\lvert y_{ee}\rvert$	$\cos\theta^*$	$\mathrm{d}^3\sigma$ [pb/GeV]	δ^{stat} [%]	$\delta^{\mathrm{syst}}_{\mathrm{unc}}$ [%]	$\delta^{\mathrm{syst}}_{\mathrm{cor}}$ [%]	δ^{total} [%]
1	66, 80	1.2, 1.6	−1.0, −0.7	1.06×10^{-2}	6.4	8.1	12.4	16.1	6	66, 80	1.2, 1.6	+0.7, +1.0	6.29×10^{-3}	7.8	11.0	16.1	21.0
2	66, 80	1.2, 1.6	−0.7, −0.4	9.24×10^{-4}	16.2	15.4	15.3	27.1	5	66, 80	1.2, 1.6	+0.4, +0.7	6.97×10^{-4}	15.7	13.1	15.5	25.7
3	66, 80	1.2, 1.6	−0.4, 0.0	—	—	—	—	—	4	66, 80	1.2, 1.6	0.0, +0.4	—	—	—	—	—
7	66, 80	1.6, 2.0	−1.0, −0.7	3.89×10^{-2}	3.9	3.8	7.0	8.9	12	66, 80	1.6, 2.0	+0.7, +1.0	2.24×10^{-2}	5.1	6.7	10.4	13.3
8	66, 80	1.6, 2.0	−0.7, −0.4	6.54×10^{-2}	2.8	2.6	5.1	6.4	11	66, 80	1.6, 2.0	+0.4, +0.7	4.27×10^{-2}	3.2	3.5	6.1	7.8
9	66, 80	1.6, 2.0	−0.4, 0.0	—	—	—	—	—	10	66, 80	1.6, 2.0	0.0, +0.4	—	—	—	—	—
13	66, 80	2.0, 2.4	−1.0, −0.7	4.28×10^{-2}	6.2	6.6	13.1	16.0	18	66, 80	2.0, 2.4	+0.7, +1.0	2.08×10^{-2}	7.3	8.6	25.4	27.8
14	66, 80	2.0, 2.4	−0.7, −0.4	1.89×10^{-1}	2.0	2.1	4.4	5.2	17	66, 80	2.0, 2.4	+0.4, +0.7	9.97×10^{-2}	2.6	3.4	6.0	7.3
15	66, 80	2.0, 2.4	−0.4, 0.0	5.10×10^{-2}	2.5	2.5	5.4	6.5	16	66, 80	2.0, 2.4	0.0, +0.4	3.55×10^{-2}	2.8	3.2	6.3	7.6
19	66, 80	2.4, 2.8	−1.0, −0.7	3.91×10^{-2}	3.5	3.8	19.5	20.2	24	66, 80	2.4, 2.8	+0.7, +1.0	1.65×10^{-2}	4.3	5.7	26.9	27.9
20	66, 80	2.4, 2.8	−0.7, −0.4	1.89×10^{-1}	2.2	2.2	11.3	11.8	23	66, 80	2.4, 2.8	+0.4, +0.7	8.98×10^{-2}	2.7	3.1	17.5	18.0
21	66, 80	2.4, 2.8	−0.4, 0.0	8.40×10^{-2}	2.3	1.9	2.4	3.8	22	66, 80	2.4, 2.8	0.0, +0.4	5.24×10^{-2}	2.8	2.7	3.9	5.5
25	66, 80	2.8, 3.6	−1.0, −0.7	2.14×10^{-2}	3.0	3.1	18.4	18.9	30	66, 80	2.8, 3.6	+0.7, +1.0	7.09×10^{-3}	3.8	7.4	32.7	33.8
26	66, 80	2.8, 3.6	−0.7, −0.4	4.84×10^{-2}	2.1	1.9	10.3	10.7	29	66, 80	2.8, 3.6	+0.4, +0.7	1.79×10^{-2}	2.8	3.2	15.2	15.7
27	66, 80	2.8, 3.6	−0.4, 0.0	—	—	—	—	—	28	66, 80	2.8, 3.6	0.0, +0.4	—	—	—	—	—
31	80, 91	1.2, 1.6	−1.0, −0.7	5.20×10^{-1}	0.9	0.7	2.4	2.7	36	80, 91	1.2, 1.6	+0.7, +1.0	5.29×10^{-1}	0.9	0.7	2.6	2.8
32	80, 91	1.2, 1.6	−0.7, −0.4	3.07×10^{-2}	3.6	2.6	3.4	5.6	35	80, 91	1.2, 1.6	+0.4, +0.7	3.07×10^{-2}	3.5	2.8	3.6	5.8
33	80, 91	1.2, 1.6	−0.4, 0.0	—	—	—	—	—	34	80, 91	1.2, 1.6	0.0, +0.4	—	—	—	—	—
37	80, 91	1.6, 2.0	−1.0, −0.7	1.26	0.7	0.4	2.7	2.8	42	80, 91	1.6, 2.0	+0.7, +1.0	1.28	0.6	0.4	2.6	2.7
38	80, 91	1.6, 2.0	−0.7, −0.4	1.04	0.7	0.5	1.7	1.9	41	80, 91	1.6, 2.0	+0.4, +0.7	1.04	0.7	0.5	1.7	1.9
39	80, 91	1.6, 2.0	−0.4, 0.0	5.59×10^{-3}	7.9	4.4	4.4	10.0	40	80, 91	1.6, 2.0	0.0, +0.4	5.05×10^{-3}	7.4	4.6	3.5	9.4
43	80, 91	2.0, 2.4	−1.0, −0.7	1.28	0.9	0.8	2.7	2.9	48	80, 91	2.0, 2.4	+0.7, +1.0	1.24	0.9	0.7	2.6	2.9
44	80, 91	2.0, 2.4	−0.7, −0.4	2.71	0.5	0.4	1.4	1.5	47	80, 91	2.0, 2.4	+0.4, +0.7	2.66	0.5	0.4	1.5	1.6
45	80, 91	2.0, 2.4	−0.4, 0.0	7.32×10^{-1}	0.6	0.6	1.8	2.0	46	80, 91	2.0, 2.4	0.0, +0.4	7.23×10^{-1}	0.6	0.6	1.9	2.1
49	80, 91	2.4, 2.8	−1.0, −0.7	1.14	0.7	0.6	3.2	3.4	54	80, 91	2.4, 2.8	+0.7, +1.0	1.14	0.6	0.6	2.7	2.9
50	80, 91	2.4, 2.8	−0.7, −0.4	2.55	0.6	0.5	2.4	2.5	53	80, 91	2.4, 2.8	+0.4, +0.7	2.52	0.6	0.5	2.5	2.6
51	80, 91	2.4, 2.8	−0.4, 0.0	1.10	0.6	0.5	1.7	1.9	52	80, 91	2.4, 2.8	0.0, +0.4	1.10	0.6	0.5	1.7	1.9
55	80, 91	2.8, 3.6	−1.0, −0.7	6.05×10^{-1}	0.6	0.6	4.1	4.2	60	80, 91	2.8, 3.6	+0.7, +1.0	5.97×10^{-1}	0.6	0.6	4.0	4.1
56	80, 91	2.8, 3.6	−0.7, −0.4	5.95×10^{-1}	0.5	0.5	4.6	4.6	59	80, 91	2.8, 3.6	+0.4, +0.7	5.84×10^{-1}	0.5	0.5	4.5	4.5
57	80, 91	2.8, 3.6	−0.4, 0.0	—	—	—	—	—	58	80, 91	2.8, 3.6	0.0, +0.4	—	—	—	—	—
61	91, 102	1.2, 1.6	−1.0, −0.7	6.53×10^{-1}	0.8	0.6	2.2	2.4	66	91, 102	1.2, 1.6	+0.7, +1.0	7.55×10^{-1}	0.8	0.6	2.3	2.5
62	91, 102	1.2, 1.6	−0.7, −0.4	3.64×10^{-2}	3.5	2.8	2.7	5.2	65	91, 102	1.2, 1.6	+0.4, +0.7	3.88×10^{-2}	3.5	3.0	3.2	5.6
63	91, 102	1.2, 1.6	−0.4, 0.0	—	—	—	—	—	64	91, 102	1.2, 1.6	0.0, +0.4	—	—	—	—	—
67	91, 102	1.6, 2.0	−1.0, −0.7	1.52	0.6	0.4	2.2	2.3	72	91, 102	1.6, 2.0	+0.7, +1.0	1.78	0.6	0.4	2.1	2.3
68	91, 102	1.6, 2.0	−0.7, −0.4	1.13	0.7	0.5	1.5	1.7	71	91, 102	1.6, 2.0	+0.4, +0.7	1.29	0.7	0.4	1.4	1.6
69	91, 102	1.6, 2.0	−0.4, 0.0	6.15×10^{-3}	7.6	6.1	6.4	11.6	70	91, 102	1.6, 2.0	0.0, +0.4	5.73×10^{-3}	8.0	6.7	6.3	12.2
73	91, 102	2.0, 2.4	−1.0, −0.7	1.48	0.9	0.7	2.3	2.6	78	91, 102	2.0, 2.4	+0.7, +1.0	1.81	0.8	0.6	2.2	2.4
74	91, 102	2.0, 2.4	−0.7, −0.4	2.94	0.5	0.3	1.6	1.7	77	91, 102	2.0, 2.4	+0.4, +0.7	3.48	0.4	0.3	1.5	1.6
75	91, 102	2.0, 2.4	−0.4, 0.0	8.06×10^{-1}	0.7	0.6	1.6	1.9	76	91, 102	2.0, 2.4	0.0, +0.4	8.97×10^{-1}	0.6	0.6	1.5	1.7
79	91, 102	2.4, 2.8	−1.0, −0.7	1.25	0.7	0.6	2.3	2.5	84	91, 102	2.4, 2.8	+0.7, +1.0	1.65	0.6	0.5	2.3	2.4
80	91, 102	2.4, 2.8	−0.7, −0.4	2.63	0.6	0.5	2.0	2.1	83	91, 102	2.4, 2.8	+0.4, +0.7	3.33	0.5	0.5	1.8	2.0
81	91, 102	2.4, 2.8	−0.4, 0.0	1.24	0.6	1.0	1.7	2.1	82	91, 102	2.4, 2.8	0.0, +0.4	1.41	0.6	0.8	1.5	1.8
85	91, 102	2.8, 3.6	−1.0, −0.7	6.54×10^{-1}	0.6	0.6	3.0	3.1	90	91, 102	2.8, 3.6	+0.7, +1.0	9.09×10^{-1}	0.5	0.6	2.9	3.0
86	91, 102	2.8, 3.6	−0.7, −0.4	5.66×10^{-1}	0.6	0.5	3.3	3.4	89	91, 102	2.8, 3.6	+0.4, +0.7	7.57×10^{-1}	0.5	0.4	2.5	2.6
87	91, 102	2.8, 3.6	−0.4, 0.0	—	—	—	—	—	88	91, 102	2.8, 3.6	0.0, +0.4	—	—	—	—	—
91	102, 116	1.2, 1.6	−1.0, −0.7	3.09×10^{-2}	4.6	6.3	11.4	13.8	96	102, 116	1.2, 1.6	+0.7, +1.0	5.49×10^{-2}	3.3	4.0	6.5	8.3
92	102, 116	1.2, 1.6	−0.7, −0.4	1.06×10^{-3}	23.7	22.9	33.4	46.9	95	102, 116	1.2, 1.6	+0.4, +0.7	1.64×10^{-3}	20.6	29.7	24.2	43.5
93	102, 116	1.2, 1.6	−0.4, 0.0	—	—	—	—	—	94	102, 116	1.2, 1.6	0.0, +0.4	—	—	—	—	—
97	102, 116	1.6, 2.0	−1.0, −0.7	5.20×10^{-2}	3.8	4.0	8.5	10.1	102	102, 116	1.6, 2.0	+0.7, +1.0	1.05×10^{-1}	2.6	2.4	5.0	6.2
98	102, 116	1.6, 2.0	−0.7, −0.4	3.15×10^{-2}	4.4	4.4	4.9	8.0	101	102, 116	1.6, 2.0	+0.4, +0.7	5.32×10^{-2}	3.3	3.0	3.5	5.7
99	102, 116	1.6, 2.0	−0.4, 0.0	—	—	—	—	—	100	102, 116	1.6, 2.0	0.0, +0.4	—	—	—	—	—
103	102, 116	2.0, 2.4	−1.0, −0.7	4.24×10^{-2}	5.3	5.0	15.5	17.1	108	102, 116	2.0, 2.4	+0.7, +1.0	1.06×10^{-1}	3.2	3.1	7.8	9.0
104	102, 116	2.0, 2.4	−0.7, −0.4	6.96×10^{-2}	3.2	3.5	5.9	7.6	107	102, 116	2.0, 2.4	+0.4, +0.7	1.38×10^{-1}	2.4	2.2	4.4	5.4
105	102, 116	2.0, 2.4	−0.4, 0.0	2.42×10^{-2}	4.0	4.4	5.9	8.4	106	102, 116	2.0, 2.4	0.0, +0.4	3.15×10^{-2}	3.5	3.5	4.0	6.3
109	102, 116	2.4, 2.8	−1.0, −0.7	3.05×10^{-2}	3.8	4.6	22.0	22.8	114	102, 116	2.4, 2.8	+0.7, +1.0	9.69×10^{-2}	2.2	2.4	10.5	11.0
110	102, 116	2.4, 2.8	−0.7, −0.4	5.28×10^{-2}	4.3	4.5	11.4	12.9	113	102, 116	2.4, 2.8	+0.4, +0.7	1.36×10^{-1}	2.7	2.6	8.4	9.2
111	102, 116	2.4, 2.8	−0.4, 0.0	3.06×10^{-2}	4.0	5.1	6.9	9.5	112	102, 116	2.4, 2.8	0.0, +0.4	5.19×10^{-2}	3.1	3.3	4.8	6.6
115	102, 116	2.8, 3.6	−1.0, −0.7	1.44×10^{-2}	3.4	3.9	35.9	36.3	120	102, 116	2.8, 3.6	+0.7, +1.0	5.18×10^{-2}	2.0	1.8	19.3	19.4
116	102, 116	2.8, 3.6	−0.7, −0.4	1.00×10^{-2}	4.2	4.6	24.8	25.5	119	102, 116	2.8, 3.6	+0.4, +0.7	3.27×10^{-2}	2.4	2.1	14.2	14.6
117	102, 116	2.8, 3.6	−0.4, 0.0	—	—	—	—	—	118	102, 116	2.8, 3.6	0.0, +0.4	—	—	—	—	—

JHEP12(2017)059

Bin	m_{ee} [GeV]	$\lvert y_{ee}\rvert$	$\cos\theta^*$	$\mathrm{d}^3\sigma$ [pb/GeV]	δ^{stat} [%]	$\delta^{\mathrm{syst}}_{\mathrm{unc}}$ [%]	$\delta^{\mathrm{syst}}_{\mathrm{cor}}$ [%]	δ^{total} [%]	Bin	m_{ee} [GeV]	$\lvert y_{ee}\rvert$	$\cos\theta^*$	$\mathrm{d}^3\sigma$ [pb/GeV]	δ^{stat} [%]	$\delta^{\mathrm{syst}}_{\mathrm{unc}}$ [%]	$\delta^{\mathrm{syst}}_{\mathrm{cor}}$ [%]	δ^{total} [%]
121	116, 150	1.2, 1.6	−1.0, −0.7	6.38×10^{-3}	9.4	13.8	36.2	39.9	126	116, 150	1.2, 1.6	+0.7, +1.0	1.65×10^{-2}	4.7	5.6	14.4	16.1
122	116, 150	1.2, 1.6	−0.7, −0.4	—	—	—	—	—	125	116, 150	1.2, 1.6	+0.4, +0.7	4.05×10^{-4}	33.3	55.4	43.5	78.0
123	116, 150	1.2, 1.6	−0.4, 0.0	—	—	—	—	—	124	116, 150	1.2, 1.6	0.0, +0.4	—	—	—	—	—
127	116, 150	1.6, 2.0	−1.0, −0.7	9.56×10^{-3}	8.4	11.4	29.7	32.9	132	116, 150	1.6, 2.0	+0.7, +1.0	2.91×10^{-2}	3.9	6.2	9.9	12.3
128	116, 150	1.6, 2.0	−0.7, −0.4	4.62×10^{-3}	7.6	10.1	9.1	15.6	131	116, 150	1.6, 2.0	+0.4, +0.7	1.16×10^{-2}	4.4	5.1	3.3	7.5
129	116, 150	1.6, 2.0	−0.4, 0.0	—	—	—	—	—	130	116, 150	1.6, 2.0	0.0, +0.4	—	—	—	—	—
133	116, 150	2.0, 2.4	−1.0, −0.7	7.42×10^{-3}	11.5	16.3	46.1	50.3	138	116, 150	2.0, 2.4	+0.7, +1.0	3.00×10^{-2}	4.1	5.2	11.3	13.1
134	116, 150	2.0, 2.4	−0.7, −0.4	1.21×10^{-2}	5.5	6.4	11.2	14.0	137	116, 150	2.0, 2.4	+0.4, +0.7	3.03×10^{-2}	3.6	3.8	4.7	7.0
135	116, 150	2.0, 2.4	−0.4, 0.0	3.48×10^{-3}	7.2	12.2	14.1	20.1	136	116, 150	2.0, 2.4	0.0, +0.4	7.29×10^{-3}	4.7	5.9	5.6	9.4
139	116, 150	2.4, 2.8	−1.0, −0.7	3.36×10^{-3}	16.2	18.3	30.4	39.0	144	116, 150	2.4, 2.8	+0.7, +1.0	2.87×10^{-2}	3.3	3.0	4.3	6.2
140	116, 150	2.4, 2.8	−0.7, −0.4	8.13×10^{-3}	7.6	10.9	11.6	17.6	143	116, 150	2.4, 2.8	+0.4, +0.7	2.88×10^{-2}	3.8	3.8	3.9	6.7
141	116, 150	2.4, 2.8	−0.4, 0.0	5.61×10^{-3}	5.9	7.0	7.1	11.6	142	116, 150	2.4, 2.8	0.0, +0.4	1.05×10^{-2}	4.5	4.7	3.8	7.5
145	116, 150	2.8, 3.6	−1.0, −0.7	1.68×10^{-3}	11.1	13.6	32.3	36.8	150	116, 150	2.8, 3.6	+0.7, +1.0	1.21×10^{-2}	3.1	3.6	6.8	8.3
146	116, 150	2.8, 3.6	−0.7, −0.4	1.39×10^{-3}	8.8	11.4	14.1	20.1	149	116, 150	2.8, 3.6	+0.4, +0.7	6.41×10^{-3}	3.7	4.0	3.8	6.6
147	116, 150	2.8, 3.6	−0.4, 0.0	—	—	—	—	—	148	116, 150	2.8, 3.6	0.0, +0.4	—	—	—	—	—

Table 8. The high rapidity electron channel Born-level triple-differential cross section $\mathrm{d}^3\sigma/\mathrm{d}m_{\ell\ell}\mathrm{d}|y_{\ell\ell}|\mathrm{d}\cos\theta^*$. The measurements are listed together with the statistical (δ^{stat}), uncorrelated systematic ($\delta^{\mathrm{syst}}_{\mathrm{unc}}$), correlated systematic ($\delta^{\mathrm{syst}}_{\mathrm{cor}}$), and total ($\delta^{\mathrm{total}}$) uncertainties. The luminosity uncertainty of 1.9% is not shown and not included in the overall systematic and total uncertainties.

JHEP12(2017)059

A.3 Forward-backward asymmetry tables

$\lvert y_{\ell\ell}\rvert$	$m_{\ell\ell}$ [GeV]	A_{FB}	Δ^{stat}	$\Delta^{\mathrm{syst}}_{\mathrm{unc}}$	$\Delta^{\mathrm{syst}}_{\mathrm{cor}}$	Δ^{total}	$\lvert y_{\ell\ell}\rvert$	$m_{\ell\ell}$ [GeV]	A_{FB}	Δ^{stat}	$\Delta^{\mathrm{syst}}_{\mathrm{unc}}$	$\Delta^{\mathrm{syst}}_{\mathrm{cor}}$	Δ^{total}
0.0, 0.2	46, 66	-5.97×10^{-3}	5.6×10^{-3}	4.5×10^{-3}	7.2×10^{-4}	7.3×10^{-3}	0.2, 0.4	46, 66	-8.12×10^{-3}	5.7×10^{-3}	4.7×10^{-3}	8.7×10^{-4}	7.4×10^{-3}
0.0, 0.2	66, 80	-2.48×10^{-4}	4.2×10^{-3}	2.3×10^{-3}	7.5×10^{-4}	4.8×10^{-3}	0.2, 0.4	66, 80	-2.61×10^{-2}	4.2×10^{-3}	2.3×10^{-3}	6.7×10^{-4}	4.9×10^{-3}
0.0, 0.2	80, 91	8.26×10^{-4}	1.1×10^{-3}	5.6×10^{-4}	3.5×10^{-4}	1.3×10^{-3}	0.2, 0.4	80, 91	1.85×10^{-3}	1.1×10^{-3}	5.5×10^{-4}	5.5×10^{-4}	1.4×10^{-3}
0.0, 0.2	91, 102	3.78×10^{-3}	1.1×10^{-3}	5.1×10^{-4}	3.2×10^{-4}	1.2×10^{-3}	0.2, 0.4	91, 102	6.49×10^{-3}	1.1×10^{-3}	5.0×10^{-4}	5.1×10^{-4}	1.3×10^{-3}
0.0, 0.2	102, 116	1.29×10^{-2}	5.3×10^{-3}	2.5×10^{-3}	9.1×10^{-4}	5.9×10^{-3}	0.2, 0.4	102, 116	2.59×10^{-2}	5.3×10^{-3}	2.5×10^{-3}	1.1×10^{-3}	5.9×10^{-3}
0.0, 0.2	116, 150	2.60×10^{-2}	8.3×10^{-3}	3.3×10^{-3}	1.3×10^{-3}	9.0×10^{-3}	0.2, 0.4	116, 150	5.69×10^{-2}	8.4×10^{-3}	3.6×10^{-3}	1.5×10^{-3}	9.2×10^{-3}
0.0, 0.2	150, 200	1.88×10^{-2}	1.6×10^{-2}	5.8×10^{-3}	2.9×10^{-3}	1.7×10^{-2}	0.2, 0.4	150, 200	5.11×10^{-2}	1.6×10^{-2}	6.9×10^{-3}	4.2×10^{-3}	1.8×10^{-2}
0.4, 0.6	46, 66	-2.71×10^{-2}	5.9×10^{-3}	4.5×10^{-3}	9.1×10^{-4}	7.5×10^{-3}	0.6, 0.8	46, 66	-2.96×10^{-2}	5.7×10^{-3}	4.3×10^{-3}	9.5×10^{-4}	7.2×10^{-3}
0.4, 0.6	66, 80	-2.76×10^{-2}	4.3×10^{-3}	2.3×10^{-3}	7.6×10^{-4}	4.9×10^{-3}	0.6, 0.8	66, 80	-5.27×10^{-2}	4.4×10^{-3}	2.5×10^{-3}	9.2×10^{-4}	5.1×10^{-3}
0.4, 0.6	80, 91	2.61×10^{-3}	1.1×10^{-3}	5.5×10^{-4}	6.0×10^{-4}	1.4×10^{-3}	0.6, 0.8	80, 91	1.48×10^{-3}	1.1×10^{-3}	5.6×10^{-4}	6.6×10^{-4}	1.4×10^{-3}
0.4, 0.6	91, 102	1.23×10^{-2}	1.1×10^{-3}	5.2×10^{-4}	5.7×10^{-4}	1.3×10^{-3}	0.6, 0.8	91, 102	1.74×10^{-2}	1.1×10^{-3}	5.1×10^{-4}	6.4×10^{-4}	1.4×10^{-3}
0.4, 0.6	102, 116	4.39×10^{-2}	5.2×10^{-3}	2.6×10^{-3}	1.2×10^{-3}	6.0×10^{-3}	0.6, 0.8	102, 116	5.37×10^{-2}	5.2×10^{-3}	2.7×10^{-3}	1.7×10^{-3}	6.1×10^{-3}
0.4, 0.6	116, 150	7.39×10^{-2}	8.5×10^{-3}	3.3×10^{-3}	1.7×10^{-3}	9.3×10^{-3}	0.6, 0.8	116, 150	1.06×10^{-1}	8.3×10^{-3}	3.1×10^{-3}	1.8×10^{-3}	9.1×10^{-3}
0.4, 0.6	150, 200	1.01×10^{-1}	1.6×10^{-2}	5.8×10^{-3}	2.7×10^{-3}	1.7×10^{-2}	0.6, 0.8	150, 200	1.37×10^{-1}	1.6×10^{-2}	5.3×10^{-3}	3.2×10^{-3}	1.7×10^{-2}
0.8, 1.0	46, 66	-4.28×10^{-2}	5.8×10^{-3}	4.4×10^{-3}	8.9×10^{-4}	7.3×10^{-3}	1.0, 1.2	46, 66	-5.60×10^{-2}	5.7×10^{-3}	4.2×10^{-3}	1.2×10^{-3}	7.2×10^{-3}
0.8, 1.0	66, 80	-7.03×10^{-2}	4.4×10^{-3}	2.4×10^{-3}	9.0×10^{-4}	5.1×10^{-3}	1.0, 1.2	66, 80	-8.76×10^{-2}	4.3×10^{-3}	2.4×10^{-3}	9.5×10^{-4}	5.0×10^{-3}
0.8, 1.0	80, 91	-7.42×10^{-5}	1.1×10^{-3}	5.7×10^{-4}	7.5×10^{-4}	1.5×10^{-3}	1.0, 1.2	80, 91	8.90×10^{-5}	1.1×10^{-3}	5.7×10^{-4}	7.8×10^{-4}	1.5×10^{-3}
0.8, 1.0	91, 102	2.33×10^{-2}	1.1×10^{-3}	5.2×10^{-4}	6.9×10^{-4}	1.4×10^{-3}	1.0, 1.2	91, 102	2.88×10^{-2}	1.1×10^{-3}	5.1×10^{-4}	7.4×10^{-4}	1.4×10^{-3}
0.8, 1.0	102, 116	9.15×10^{-2}	5.2×10^{-3}	2.8×10^{-3}	1.6×10^{-3}	6.1×10^{-3}	1.0, 1.2	102, 116	1.10×10^{-1}	5.1×10^{-3}	2.7×10^{-3}	1.7×10^{-3}	6.0×10^{-3}
0.8, 1.0	116, 150	1.28×10^{-1}	8.4×10^{-3}	3.4×10^{-3}	1.8×10^{-3}	9.2×10^{-3}	1.0, 1.2	116, 150	1.68×10^{-1}	8.4×10^{-3}	3.6×10^{-3}	2.0×10^{-3}	9.3×10^{-3}
0.8, 1.0	150, 200	1.69×10^{-1}	1.6×10^{-2}	5.3×10^{-3}	4.0×10^{-3}	1.7×10^{-2}	1.0, 1.2	150, 200	2.36×10^{-1}	1.6×10^{-2}	5.9×10^{-3}	4.2×10^{-3}	1.7×10^{-2}
1.2, 1.4	46, 66	-8.88×10^{-2}	5.7×10^{-3}	4.2×10^{-3}	1.4×10^{-3}	7.2×10^{-3}	1.4, 1.6	46, 66	-1.03×10^{-1}	5.8×10^{-3}	4.3×10^{-3}	1.7×10^{-3}	7.5×10^{-3}
1.2, 1.4	66, 80	-1.14×10^{-1}	4.2×10^{-3}	2.4×10^{-3}	1.1×10^{-3}	5.0×10^{-3}	1.4, 1.6	66, 80	-1.25×10^{-1}	4.4×10^{-3}	2.6×10^{-3}	1.3×10^{-3}	5.3×10^{-3}
1.2, 1.4	80, 91	-2.23×10^{-3}	1.1×10^{-3}	5.7×10^{-4}	8.7×10^{-4}	1.5×10^{-3}	1.4, 1.6	80, 91	-2.59×10^{-3}	1.2×10^{-3}	6.2×10^{-4}	9.2×10^{-4}	1.6×10^{-3}
1.2, 1.4	91, 102	3.38×10^{-2}	1.1×10^{-3}	5.2×10^{-4}	8.5×10^{-4}	1.5×10^{-3}	1.4, 1.6	91, 102	3.77×10^{-2}	1.1×10^{-3}	5.7×10^{-4}	8.9×10^{-4}	1.6×10^{-3}
1.2, 1.4	102, 116	1.30×10^{-1}	5.0×10^{-3}	2.8×10^{-3}	2.0×10^{-3}	6.1×10^{-3}	1.4, 1.6	102, 116	1.44×10^{-1}	5.1×10^{-3}	3.0×10^{-3}	2.2×10^{-3}	6.3×10^{-3}
1.2, 1.4	116, 150	2.09×10^{-1}	8.5×10^{-3}	3.7×10^{-3}	2.6×10^{-3}	9.6×10^{-3}	1.4, 1.6	116, 150	2.19×10^{-1}	8.9×10^{-3}	3.9×10^{-3}	2.8×10^{-3}	1.0×10^{-2}
1.2, 1.4	150, 200	2.68×10^{-1}	1.6×10^{-2}	6.6×10^{-3}	4.3×10^{-3}	1.8×10^{-2}	1.4, 1.6	150, 200	2.80×10^{-1}	1.8×10^{-2}	9.0×10^{-3}	4.5×10^{-3}	2.1×10^{-2}
1.6, 1.8	46, 66	-9.35×10^{-2}	6.1×10^{-3}	4.6×10^{-3}	1.4×10^{-3}	7.8×10^{-3}	1.8, 2.0	46, 66	-9.23×10^{-2}	6.7×10^{-3}	4.9×10^{-3}	1.5×10^{-3}	8.5×10^{-3}
1.6, 1.8	66, 80	-1.26×10^{-1}	4.9×10^{-3}	2.8×10^{-3}	1.5×10^{-3}	5.8×10^{-3}	1.8, 2.0	66, 80	-1.20×10^{-1}	5.6×10^{-3}	3.3×10^{-3}	2.0×10^{-3}	6.8×10^{-3}
1.6, 1.8	80, 91	-7.79×10^{-4}	1.3×10^{-3}	7.0×10^{-4}	1.0×10^{-3}	1.8×10^{-3}	1.8, 2.0	80, 91	-2.65×10^{-3}	1.5×10^{-3}	8.1×10^{-4}	1.1×10^{-3}	2.0×10^{-3}
1.6, 1.8	91, 102	3.96×10^{-2}	1.3×10^{-3}	6.3×10^{-4}	9.6×10^{-4}	1.7×10^{-3}	1.8, 2.0	91, 102	3.97×10^{-2}	1.5×10^{-3}	7.4×10^{-4}	1.1×10^{-3}	2.0×10^{-3}
1.6, 1.8	102, 116	1.63×10^{-1}	5.3×10^{-3}	3.6×10^{-3}	2.8×10^{-3}	7.0×10^{-3}	1.8, 2.0	102, 116	1.54×10^{-1}	5.6×10^{-3}	3.9×10^{-3}	3.5×10^{-3}	7.7×10^{-3}
1.6, 1.8	116, 150	2.43×10^{-1}	1.0×10^{-2}	4.6×10^{-3}	2.6×10^{-3}	1.2×10^{-2}	1.8, 2.0	116, 150	2.12×10^{-1}	1.2×10^{-2}	6.8×10^{-3}	3.9×10^{-3}	1.4×10^{-2}
1.6, 1.8	150, 200	3.02×10^{-1}	1.8×10^{-2}	6.8×10^{-3}	5.6×10^{-3}	2.0×10^{-2}	1.8, 2.0	150, 200	2.66×10^{-1}	2.1×10^{-2}	6.3×10^{-3}	4.2×10^{-3}	2.3×10^{-2}
2.0, 2.2	46, 66	-9.82×10^{-2}	8.3×10^{-3}	6.2×10^{-3}	2.6×10^{-3}	1.1×10^{-2}	2.2, 2.4	46, 66	-4.44×10^{-2}	1.4×10^{-2}	1.1×10^{-2}	3.1×10^{-3}	1.8×10^{-2}
2.0, 2.2	66, 80	-1.10×10^{-1}	6.9×10^{-3}	4.2×10^{-3}	3.0×10^{-3}	8.6×10^{-3}	2.2, 2.4	66, 80	-5.03×10^{-2}	1.2×10^{-2}	7.5×10^{-3}	6.1×10^{-3}	1.5×10^{-2}
2.0, 2.2	80, 91	-3.33×10^{-3}	1.9×10^{-3}	1.1×10^{-3}	1.5×10^{-3}	2.7×10^{-3}	2.2, 2.4	80, 91	-6.44×10^{-3}	3.1×10^{-3}	1.9×10^{-3}	2.1×10^{-3}	4.2×10^{-3}
2.0, 2.2	91, 102	3.33×10^{-2}	1.9×10^{-3}	9.8×10^{-4}	1.5×10^{-3}	2.6×10^{-3}	2.2, 2.4	91, 102	1.99×10^{-2}	3.1×10^{-3}	1.6×10^{-3}	2.3×10^{-3}	4.2×10^{-3}
2.0, 2.2	102, 116	1.20×10^{-1}	6.5×10^{-3}	5.1×10^{-3}	6.3×10^{-3}	1.0×10^{-2}	2.2, 2.4	102, 116	6.06×10^{-2}	9.7×10^{-3}	9.3×10^{-3}	1.2×10^{-2}	1.8×10^{-2}
2.0, 2.2	116, 150	1.64×10^{-1}	1.4×10^{-2}	6.6×10^{-3}	3.9×10^{-3}	1.6×10^{-2}	2.2, 2.4	116, 150	9.40×10^{-2}	2.6×10^{-2}	1.6×10^{-2}	1.5×10^{-2}	3.4×10^{-2}
2.0, 2.2	150, 200	1.97×10^{-1}	2.7×10^{-2}	1.0×10^{-2}	7.7×10^{-3}	3.0×10^{-2}	2.2, 2.4	150, 200	1.27×10^{-1}	4.6×10^{-2}	1.3×10^{-2}	1.0×10^{-2}	4.9×10^{-2}

Table 9. The asymmetry A_{FB} determined from the combined triple-differential cross-section measurements. The measurements are listed together with the statistical (Δ^{stat}), uncorrelated systematic ($\Delta^{\mathrm{syst}}_{\mathrm{unc}}$), correlated systematic ($\Delta^{\mathrm{syst}}_{\mathrm{cor}}$), and total ($\Delta^{\mathrm{total}}$) uncertainties.

JHEP12(2017)059

$\lvert y_{ee}\rvert$	m_{ee} [GeV]	A_{FB}	Δ^{stat}	$\Delta^{\mathrm{syst}}_{\mathrm{unc}}$	$\Delta^{\mathrm{syst}}_{\mathrm{cor}}$	Δ^{total}
1.2, 1.6	66, 80	-2.44×10^{-1}	4.4×10^{-2}	5.9×10^{-2}	2.5×10^{-2}	7.8×10^{-2}
1.2, 1.6	80, 91	8.57×10^{-3}	6.2×10^{-3}	4.6×10^{-3}	3.6×10^{-3}	8.5×10^{-3}
1.2, 1.6	91, 102	7.03×10^{-2}	5.7×10^{-3}	4.1×10^{-3}	4.9×10^{-3}	8.6×10^{-3}
1.2, 1.6	102, 116	2.78×10^{-1}	2.6×10^{-2}	3.4×10^{-2}	2.6×10^{-2}	5.0×10^{-2}
1.2, 1.6	116, 150	4.43×10^{-1}	4.2×10^{-2}	6.0×10^{-2}	1.1×10^{-1}	1.3×10^{-1}
1.6, 2.0	66, 80	-2.32×10^{-1}	1.7×10^{-2}	1.9×10^{-2}	1.1×10^{-2}	2.7×10^{-2}
1.6, 2.0	80, 91	3.08×10^{-3}	3.3×10^{-3}	2.3×10^{-3}	2.5×10^{-3}	4.7×10^{-3}
1.6, 2.0	91, 102	7.30×10^{-2}	3.2×10^{-3}	2.1×10^{-3}	1.8×10^{-3}	4.2×10^{-3}
1.6, 2.0	102, 116	3.09×10^{-1}	1.6×10^{-2}	1.6×10^{-2}	1.3×10^{-2}	2.6×10^{-2}
1.6, 2.0	116, 150	4.83×10^{-1}	2.6×10^{-2}	3.7×10^{-2}	6.5×10^{-2}	7.9×10^{-2}
2.0, 2.4	66, 80	-2.89×10^{-1}	1.2×10^{-2}	1.4×10^{-2}	1.3×10^{-2}	2.3×10^{-2}
2.0, 2.4	80, 91	-9.15×10^{-3}	2.8×10^{-3}	2.1×10^{-3}	1.7×10^{-3}	3.9×10^{-3}
2.0, 2.4	91, 102	8.43×10^{-2}	2.7×10^{-3}	1.9×10^{-3}	2.7×10^{-3}	4.3×10^{-3}
2.0, 2.4	102, 116	3.40×10^{-1}	1.3×10^{-2}	1.3×10^{-2}	1.6×10^{-2}	2.5×10^{-2}
2.0, 2.4	116, 150	4.93×10^{-1}	2.1×10^{-2}	2.7×10^{-2}	6.5×10^{-2}	7.3×10^{-2}
2.4, 2.8	66, 80	-3.26×10^{-1}	1.1×10^{-2}	1.1×10^{-2}	1.7×10^{-2}	2.3×10^{-2}
2.4, 2.8	80, 91	-4.68×10^{-3}	2.6×10^{-3}	2.2×10^{-3}	2.4×10^{-3}	4.2×10^{-3}
2.4, 2.8	91, 102	1.11×10^{-1}	2.6×10^{-3}	2.5×10^{-3}	2.1×10^{-3}	4.1×10^{-3}
2.4, 2.8	102, 116	4.29×10^{-1}	1.2×10^{-2}	1.3×10^{-2}	1.8×10^{-2}	2.6×10^{-2}
2.4, 2.8	116, 150	5.98×10^{-1}	1.8×10^{-2}	2.3×10^{-2}	3.3×10^{-2}	4.4×10^{-2}
2.8, 3.6	66, 80	-4.73×10^{-1}	1.1×10^{-2}	1.4×10^{-2}	2.7×10^{-2}	3.2×10^{-2}
2.8, 3.6	80, 91	-8.07×10^{-3}	2.8×10^{-3}	2.7×10^{-3}	2.3×10^{-3}	4.5×10^{-3}
2.8, 3.6	91, 102	1.55×10^{-1}	2.7×10^{-3}	2.7×10^{-3}	5.0×10^{-3}	6.2×10^{-3}
2.8, 3.6	102, 116	5.51×10^{-1}	1.1×10^{-2}	1.1×10^{-2}	4.5×10^{-2}	4.8×10^{-2}
2.8, 3.6	116, 150	7.15×10^{-1}	1.9×10^{-2}	2.3×10^{-2}	4.8×10^{-2}	5.7×10^{-2}

Table 10. The asymmetry A_{FB} determined from the high rapidity electron channel triple-differential cross-section measurement. The measurement is listed together with the statistical (Δ^{stat}), uncorrelated systematic ($\Delta^{\mathrm{syst}}_{\mathrm{unc}}$), correlated systematic ($\Delta^{\mathrm{syst}}_{\mathrm{cor}}$), and total ($\Delta^{\mathrm{total}}$) uncertainties.

JHEP12(2017)059

References

[1] S.D. Drell and T.-M. Yan, *Massive Lepton Pair Production in Hadron-Hadron Collisions at High-Energies*, *Phys. Rev. Lett.* **25** (1970) 316 [*Erratum ibid.* **25** (1970) 902] [INSPIRE].

[2] S.D. Drell and T.-M. Yan, *Partons and their Applications at High-Energies*, *Annals Phys.* **66** (1971) 578 [INSPIRE].

[3] SLD Electroweak Group, DELPHI, ALEPH, SLD, SLD Heavy Flavour Group, OPAL, LEP Electroweak Working Group and L3 collaborations, S. Schael et al., *Precision electroweak measurements on the Z resonance*, *Phys. Rept.* **427** (2006) 257 [hep-ex/0509008] [INSPIRE].

[4] ATLAS collaboration, *Measurement of $W^{\pm}$ and Z-boson production cross sections in pp collisions at $\sqrt{s} = 13$ TeV with the ATLAS detector*, *Phys. Lett.* **B 759** (2016) 601 [arXiv:1603.09222] [INSPIRE].

[5] ATLAS collaboration, *Measurements of top-quark pair to Z-boson cross-section ratios at $\sqrt{s} = 13$, 8, 7 TeV with the ATLAS detector*, *JHEP* **02** (2017) 117 [arXiv:1612.03636] [INSPIRE].

[6] CMS collaboration, *Measurement of the Inclusive W and Z Production Cross sections in pp Collisions at $\sqrt{s} = 7$ TeV*, *JHEP* **10** (2011) 132 [arXiv:1107.4789] [INSPIRE].

[7] CMS collaboration, *Measurement of inclusive W and Z boson production cross sections in pp collisions at $\sqrt{s} = 8$ TeV*, *Phys. Rev. Lett.* **112** (2014) 191802 [arXiv:1402.0923] [INSPIRE].

[8] ATLAS collaboration, *Measurement of the inclusive $W^{\pm}$ and Z/gamma cross sections in the electron and muon decay channels in pp collisions at $\sqrt{s} = 7$ TeV with the ATLAS detector*, *Phys. Rev.* **D 85** (2012) 072004 [arXiv:1109.5141] [INSPIRE].

[9] CMS collaboration, *Measurement of the Rapidity and Transverse Momentum Distributions of Z Bosons in pp Collisions at $\sqrt{s} = 7$ TeV*, *Phys. Rev.* **D 85** (2012) 032002 [arXiv:1110.4973] [INSPIRE].

[10] ATLAS collaboration, *Measurement of angular correlations in Drell-Yan lepton pairs to probe Z/gamma* boson transverse momentum at $\sqrt{s} = 7$ TeV with the ATLAS detector*, *Phys. Lett.* **B 720** (2013) 32 [arXiv:1211.6899] [INSPIRE].

[11] ATLAS collaboration, *Measurement of the Z/γ^* boson transverse momentum distribution in pp collisions at $\sqrt{s} = 7$ TeV with the ATLAS detector*, *JHEP* **09** (2014) 145 [arXiv:1406.3660] [INSPIRE].

[12] CMS collaboration, *Measurement of the transverse momentum spectra of weak vector bosons produced in proton-proton collisions at $\sqrt{s} = 8$ TeV*, *JHEP* **02** (2017) 096 [arXiv:1606.05864] [INSPIRE].

[13] ATLAS collaboration, *Measurement of the high-mass Drell-Yan differential cross-section in pp collisions at $\sqrt{s} = 7$ TeV with the ATLAS detector*, *Phys. Lett.* **B 725** (2013) 223 [arXiv:1305.4192] [INSPIRE].

JHEP12(2017)059

[14] ATLAS collaboration, *Measurement of the low-mass Drell-Yan differential cross section at $\sqrt{s} = 7$ TeV using the ATLAS detector*, *JHEP* **06** (2014) 112 [arXiv:1404.1212] [INSPIRE].

[15] CMS collaboration, *Measurement of the Drell-Yan Cross section in pp Collisions at $\sqrt{s} = 7$ TeV*, *JHEP* **10** (2011) 007 [arXiv:1108.0566] [INSPIRE].

[16] ATLAS collaboration, *Measurement of the transverse momentum and ϕ^*_η distributions of Drell-Yan lepton pairs in proton-proton collisions at $\sqrt{s} = 8$ TeV with the ATLAS detector*, *Eur. Phys. J.* **C 76** (2016) 291 [arXiv:1512.02192] [INSPIRE].

[17] ATLAS collaboration, *Measurement of the double-differential high-mass Drell-Yan cross section in pp collisions at $\sqrt{s} = 8$ TeV with the ATLAS detector*, *JHEP* **08** (2016) 009 [arXiv:1606.01736] [INSPIRE].

[18] ATLAS collaboration, *Precision measurement and interpretation of inclusive W^+, W^- and Z/γ^* production cross sections with the ATLAS detector*, *Eur. Phys. J.* **C 77** (2017) 367 [arXiv:1612.03016] [INSPIRE].

[19] CMS collaboration, *Measurement of the Z boson differential cross section in transverse momentum and rapidity in proton-proton collisions at 8 TeV*, *Phys. Lett.* **B 749** (2015) 187 [arXiv:1504.03511] [INSPIRE].

[20] CMS collaboration, *Measurements of differential and double-differential Drell-Yan cross sections in proton-proton collisions at 8 TeV*, *Eur. Phys. J.* **C 75** (2015) 147 [arXiv:1412.1115] [INSPIRE].

[21] CMS collaboration, *Measurement of the differential and double-differential Drell-Yan cross sections in proton-proton collisions at $\sqrt{s} = 7$ TeV*, *JHEP* **12** (2013) 030 [arXiv:1310.7291] [INSPIRE].

[22] ATLAS collaboration, *Measurement of the angular coefficients in Z-boson events using electron and muon pairs from data taken at $\sqrt{s} = 8$ TeV with the ATLAS detector*, *JHEP* **08** (2016) 159 [arXiv:1606.00689] [INSPIRE].

[23] CMS collaboration, *Angular coefficients of Z bosons produced in pp collisions at $\sqrt{s} = 8$ TeV and decaying to $\mu^+\mu^-$ as a function of transverse momentum and rapidity*, *Phys. Lett.* **B 750** (2015) 154 [arXiv:1504.03512] [INSPIRE].

[24] ATLAS collaboration, *Measurement of the forward-backward asymmetry of electron and muon pair-production in pp collisions at $\sqrt{s} = 7$ TeV with the ATLAS detector*, *JHEP* **09** (2015) 049 [arXiv:1503.03709] [INSPIRE].

[25] CMS collaboration, *Forward-backward asymmetry of Drell-Yan lepton pairs in pp collisions at $\sqrt{s} = 7$ TeV*, *Phys. Lett.* **B 718** (2013) 752 [arXiv:1207.3973] [INSPIRE].

[26] J.C. Collins and D.E. Soper, *Angular Distribution of Dileptons in High-Energy Hadron Collisions*, *Phys. Rev.* **D 16** (1977) 2219 [INSPIRE].

[27] ATLAS collaboration, *The ATLAS Experiment at the CERN Large Hadron Collider*, 2008 *JINST* **3** S08003 [INSPIRE].

[28] ATLAS collaboration, *Performance of the ATLAS Trigger System in 2010*, *Eur. Phys. J.* **C 72** (2012) 1849 [arXiv:1110.1530] [INSPIRE].

[29] P. Nason, *A new method for combining NLO QCD with shower Monte Carlo algorithms*, *JHEP* **11** (2004) 040 [hep-ph/0409146] [INSPIRE].

JHEP12(2017)059

[30] S. Frixione, P. Nason and C. Oleari, *Matching NLO QCD computations with Parton Shower simulations: the POWHEG method*, *JHEP* **11** (2007) 070 [arXiv:0709.2092] [INSPIRE].

[31] S. Alioli, P. Nason, C. Oleari and E. Re, *NLO vector-boson production matched with shower in POWHEG*, *JHEP* **07** (2008) 060 [arXiv:0805.4802] [INSPIRE].

[32] S. Alioli, P. Nason, C. Oleari and E. Re, *A general framework for implementing NLO calculations in shower Monte Carlo programs: the POWHEG BOX*, *JHEP* **06** (2010) 043 [arXiv:1002.2581] [INSPIRE].

[33] H.-L. Lai et al., *New parton distributions for collider physics*, *Phys. Rev.* **D 82** (2010) 074024 [arXiv:1007.2241] [INSPIRE].

[34] T. Sjöstrand, S. Mrenna and P.Z. Skands, *A Brief Introduction to PYTHIA 8.1*, *Comput. Phys. Commun.* **178** (2008) 852 [arXiv:0710.3820] [INSPIRE].

[35] K. Melnikov and F. Petriello, *Electroweak gauge boson production at hadron colliders through* $\mathcal{O}(\alpha_s^2)$, *Phys. Rev.* **D 74** (2006) 114017 [hep-ph/0609070] [INSPIRE].

[36] R. Gavin, Y. Li, F. Petriello and S. Quackenbush, *FEWZ 2.0: A code for hadronic Z production at next-to-next-to-leading order*, *Comput. Phys. Commun.* **182** (2011) 2388 [arXiv:1011.3540] [INSPIRE].

[37] Y. Li and F. Petriello, *Combining QCD and electroweak corrections to dilepton production in FEWZ*, *Phys. Rev.* **D 86** (2012) 094034 [arXiv:1208.5967] [INSPIRE].

[38] A.D. Martin, W.J. Stirling, R.S. Thorne and G. Watt, *Parton distributions for the LHC*, *Eur. Phys. J.* **C 63** (2009) 189 [arXiv:0901.0002] [INSPIRE].

[39] W.F.L. Hollik, *Radiative Corrections in the Standard Model and their Role for Precision Tests of the Electroweak Theory*, *Fortsch. Phys.* **38** (1990) 165 [INSPIRE].

[40] S. Catani, L. Cieri, G. Ferrera, D. de Florian and M. Grazzini, *Vector boson production at hadron colliders: a fully exclusive QCD calculation at NNLO*, *Phys. Rev. Lett.* **103** (2009) 082001 [arXiv:0903.2120] [INSPIRE].

[41] A.D. Martin, R.G. Roberts, W.J. Stirling and R.S. Thorne, *Parton distributions incorporating QED contributions*, *Eur. Phys. J.* **C 39** (2005) 155 [hep-ph/0411040] [INSPIRE].

[42] D. Bardin et al., *SANC integrator in the progress: QCD and EW contributions*, *JETP Lett.* **96** (2012) 285 [arXiv:1207.4400] [INSPIRE].

[43] S.G. Bondarenko and A.A. Sapronov, *NLO EW and QCD proton-proton cross section calculations with mcsanc-v1.01*, *Comput. Phys. Commun.* **184** (2013) 2343 [arXiv:1301.3687] [INSPIRE].

[44] T. Sjöstrand, S. Mrenna and P.Z. Skands, *PYTHIA 6.4 Physics and Manual*, *JHEP* **05** (2006) 026 [hep-ph/0603175] [INSPIRE].

[45] M. Cacciari, M. Czakon, M. Mangano, A. Mitov and P. Nason, *Top-pair production at hadron colliders with next-to-next-to-leading logarithmic soft-gluon resummation*, *Phys. Lett.* **B 710** (2012) 612 [arXiv:1111.5869] [INSPIRE].

[46] P. Bärnreuther, M. Czakon and A. Mitov, *Percent Level Precision Physics at the Tevatron: First Genuine NNLO QCD Corrections to* $q\bar{q} \to t\bar{t} + X$, *Phys. Rev. Lett.* **109** (2012) 132001 [arXiv:1204.5201] [INSPIRE].

JHEP12(2017)059

[47] M. Czakon and A. Mitov, *NNLO corrections to top-pair production at hadron colliders: the all-fermionic scattering channels*, *JHEP* **12** (2012) 054 [arXiv:1207.0236] [INSPIRE].

[48] M. Czakon and A. Mitov, *NNLO corrections to top pair production at hadron colliders: the quark-gluon reaction*, *JHEP* **01** (2013) 080 [arXiv:1210.6832] [INSPIRE].

[49] M. Czakon, P. Fiedler and A. Mitov, *Total Top-Quark Pair-Production Cross section at Hadron Colliders Through* $O(\alpha_S^4)$, *Phys. Rev. Lett.* **110** (2013) 252004 [arXiv:1303.6254] [INSPIRE].

[50] M. Czakon and A. Mitov, *Top++: A Program for the Calculation of the Top-Pair Cross-Section at Hadron Colliders*, *Comput. Phys. Commun.* **185** (2014) 2930 [arXiv:1112.5675] [INSPIRE].

[51] J. Pumplin, D.R. Stump, J. Huston, H.L. Lai, P.M. Nadolsky and W.K. Tung, *New generation of parton distributions with uncertainties from global QCD analysis*, *JHEP* **07** (2002) 012 [hep-ph/0201195] [INSPIRE].

[52] J.M. Campbell and R.K. Ellis, *An update on vector boson pair production at hadron colliders*, *Phys. Rev.* **D 60** (1999) 113006 [hep-ph/9905386] [INSPIRE].

[53] J.M. Campbell, R.K. Ellis and C. Williams, *Vector boson pair production at the LHC*, *JHEP* **07** (2011) 018 [arXiv:1105.0020] [INSPIRE].

[54] P. Golonka and Z. Was, *PHOTOS Monte Carlo: A precision tool for QED corrections in Z and W decays*, *Eur. Phys. J.* **C 45** (2006) 97 [hep-ph/0506026] [INSPIRE].

[55] ATLAS collaboration, *The ATLAS Simulation Infrastructure*, *Eur. Phys. J.* **C 70** (2010) 823 [arXiv:1005.4568] [INSPIRE].

[56] GEANT4 collaboration, S. Agostinelli et al., *GEANT4: A simulation toolkit*, *Nucl. Instrum. Meth.* **A 506** (2003) 250 [INSPIRE].

[57] ATLAS collaboration, *Electron and photon energy calibration with the ATLAS detector using LHC Run 1 data*, *Eur. Phys. J.* **C 74** (2014) 3071 [arXiv:1407.5063] [INSPIRE].

[58] ATLAS collaboration, *Electron reconstruction and identification efficiency measurements with the ATLAS detector using the 2011 LHC proton-proton collision data*, *Eur. Phys. J.* **C 74** (2014) 2941 [arXiv:1404.2240] [INSPIRE].

[59] ATLAS collaboration, *Electron efficiency measurements with the ATLAS detector using 2012 LHC proton-proton collision data*, *Eur. Phys. J.* **C 77** (2017) 195 [arXiv:1612.01456] [INSPIRE].

[60] ATLAS collaboration, *Measurement of the muon reconstruction performance of the ATLAS detector using 2011 and 2012 LHC proton-proton collision data*, *Eur. Phys. J.* **C 74** (2014) 3130 [arXiv:1407.3935] [INSPIRE].

[61] ATLAS collaboration, *Performance of the ATLAS muon trigger in pp collisions at* $\sqrt{s} = 8$ *TeV*, *Eur. Phys. J.* **C 75** (2015) 120 [arXiv:1408.3179] [INSPIRE].

[62] ATLAS collaboration, *Summary of ATLAS Pythia 8 tunes*, ATL-PHYS-PUB-2012-003 (2012).

[63] R. Corke and T. Sjöstrand, *Interleaved Parton Showers and Tuning Prospects*, *JHEP* **03** (2011) 032 [arXiv:1011.1759] [INSPIRE].

[64] ATLAS collaboration, *New ATLAS event generator tunes to 2010 data*, ATL-PHYS-PUB-2011-008 (2011).

JHEP12(2017)059

[65] ATLAS collaboration, *Measurement of the W-boson mass in pp collisions at $\sqrt{s} = 7$ TeV with the ATLAS detector*, arXiv:1701.07240 [INSPIRE].

[66] G. D'Agostini, *A multidimensional unfolding method based on Bayes' theorem*, *Nucl. Instrum. Meth.* **A 362** (1995) 487 [INSPIRE].

[67] B. Efron, *Bootstrap methods: Another look at the jackknife*, *Ann. Statist.* **7** (1979) 1.

[68] ATLAS collaboration, *Electron efficiency measurements with the ATLAS detector using the 2012 LHC proton-proton collision data*, ATLAS-CONF-2014-032 (2014).

[69] M. Botje et al., *The PDF4LHC Working Group Interim Recommendations*, arXiv:1101.0538 [INSPIRE].

[70] ATLAS collaboration, *Luminosity determination in pp collisions at $\sqrt{s} = 8$ TeV using the ATLAS detector at the LHC*, *Eur. Phys. J.* **C 76** (2016) 653 [arXiv:1608.03953] [INSPIRE].

[71] *The durham high energy physics database*, https://www.hepdata.net.

[72] E. Maguire, L. Heinrich and G. Watt, *HEPData: a repository for high energy physics data*, arXiv:1704.05473 [INSPIRE].

[73] A. Glazov, *Averaging of DIS cross section data*, *AIP Conf. Proc.* **792** (2005) 237 [INSPIRE].

[74] H1 collaboration, F.D. Aaron et al., *Measurement of the Inclusive ep Scattering Cross section at Low Q^2 and x at HERA*, *Eur. Phys. J.* **C 63** (2009) 625 [arXiv:0904.0929] [INSPIRE].

[75] ZEUS and H1 collaborations, F.D. Aaron et al., *Combined Measurement and QCD Analysis of the Inclusive e+- p Scattering Cross sections at HERA*, *JHEP* **01** (2010) 109 [arXiv:0911.0884] [INSPIRE].

[76] Particle Data Group collaboration, C. Patrignani et al., *Review of Particle Physics*, *Chin. Phys.* **C 40** (2016) 100001 [INSPIRE].

[77] ATLAS collaboration, *ATLAS Computing Acknowledgements 2016-2017*, ATL-GEN-PUB-2016-002 (2016).

JHEP12(2017)059

The ATLAS collaboration

M. Aaboud[137d], G. Aad[88], B. Abbott[115], O. Abdinov[12,*], B. Abeloos[119], S.H. Abidi[161], O.S. AbouZeid[139], N.L. Abraham[151], H. Abramowicz[155], H. Abreu[154], R. Abreu[118], Y. Abulaiti[148a,148b], B.S. Acharya[167a,167b,a], S. Adachi[157], L. Adamczyk[41a], J. Adelman[110], M. Adersberger[102], T. Adye[133], A.A. Affolder[139], Y. Afik[154], T. Agatonovic-Jovin[14], C. Agheorghiesei[28c], J.A. Aguilar-Saavedra[128a,128f], S.P. Ahlen[24], F. Ahmadov[68,b], G. Aielli[135a,135b], S. Akatsuka[71], H. Akerstedt[148a,148b], T.P.A. Åkesson[84], E. Akilli[52], A.V. Akimov[98], G.L. Alberghi[22a,22b], J. Albert[172], P. Albicocco[50], M.J. Alconada Verzini[74], S.C. Alderweireldt[108], M. Aleksa[32], I.N. Aleksandrov[68], C. Alexa[28b], G. Alexander[155], T. Alexopoulos[10], M. Alhroob[115], B. Ali[130], M. Aliev[76a,76b], G. Alimonti[94a], J. Alison[33], S.P. Alkire[38], B.M.M. Allbrooke[151], B.W. Allen[118], P.P. Allport[19], A. Aloisio[106a,106b], A. Alonso[39], F. Alonso[74], C. Alpigiani[140], A.A. Alshehri[56], M.I. Alstaty[88], B. Alvarez Gonzalez[32], D. Álvarez Piqueras[170], M.G. Alviggi[106a,106b], B.T. Amadio[16], Y. Amaral Coutinho[26a], C. Amelung[25], D. Amidei[92], S.P. Amor Dos Santos[128a,128c], S. Amoroso[32], G. Amundsen[25], C. Anastopoulos[141], L.S. Ancu[52], N. Andari[19], T. Andeen[11], C.F. Anders[60b], J.K. Anders[77], K.J. Anderson[33], A. Andreazza[94a,94b], V. Andrei[60a], S. Angelidakis[37], I. Angelozzi[109], A. Angerami[38], A.V. Anisenkov[111,c], N. Anjos[13], A. Annovi[126a,126b], C. Antel[60a], M. Antonelli[50], A. Antonov[100,*], D.J. Antrim[166], F. Anulli[134a], M. Aoki[69], L. Aperio Bella[32], G. Arabidze[93], Y. Arai[69], J.P. Araque[128a], V. Araujo Ferraz[26a], A.T.H. Arce[48], R.E. Ardell[80], F.A. Arduh[74], J-F. Arguin[97], S. Argyropoulos[66], M. Arik[20a], A.J. Armbruster[32], L.J. Armitage[79], O. Arnaez[161], H. Arnold[51], M. Arratia[30], O. Arslan[23], A. Artamonov[99,*], G. Artoni[122], S. Artz[86], S. Asai[157], N. Asbah[45], A. Ashkenazi[155], L. Asquith[151], K. Assamagan[27], R. Astalos[146a], M. Atkinson[169], N.B. Atlay[143], K. Augsten[130], G. Avolio[32], B. Axen[16], M.K. Ayoub[35a], G. Azuelos[97,d], A.E. Baas[60a], M.J. Baca[19], H. Bachacou[138], K. Bachas[76a,76b], M. Backes[122], P. Bagnaia[134a,134b], M. Bahmani[42], H. Bahrasemani[144], J.T. Baines[133], M. Bajic[39], O.K. Baker[179], P.J. Bakker[109], E.M. Baldin[111,c], P. Balek[175], F. Balli[138], W.K. Balunas[124], E. Banas[42], A. Bandyopadhyay[23], Sw. Banerjee[176,e], A.A.E. Bannoura[178], L. Barak[155], E.L. Barberio[91], D. Barberis[53a,53b], M. Barbero[88], T. Barillari[103], M-S Barisits[32], J.T. Barkeloo[118], T. Barklow[145], N. Barlow[30], S.L. Barnes[36c], B.M. Barnett[133], R.M. Barnett[16], Z. Barnovska-Blenessy[36a], A. Baroncelli[136a], G. Barone[25], A.J. Barr[122], L. Barranco Navarro[170], F. Barreiro[85], J. Barreiro Guimarães da Costa[35a], R. Bartoldus[145], A.E. Barton[75], P. Bartos[146a], A. Basalaev[125], A. Bassalat[119,f], R.L. Bates[56], S.J. Batista[161], J.R. Batley[30], M. Battaglia[139], M. Bauce[134a,134b], F. Bauer[138], H.S. Bawa[145,g], J.B. Beacham[113], M.D. Beattie[75], T. Beau[83], P.H. Beauchemin[165], P. Bechtle[23], H.P. Beck[18,h], H.C. Beck[57], K. Becker[122], M. Becker[86], C. Becot[112], A.J. Beddall[20e], A. Beddall[20b], V.A. Bednyakov[68], M. Bedognetti[109], C.P. Bee[150], T.A. Beermann[32], M. Begalli[26a], M. Begel[27], J.K. Behr[45], A.S. Bell[81], G. Bella[155], L. Bellagamba[22a], A. Bellerive[31], M. Bellomo[154], K. Belotskiy[100], O. Beltramello[32], N.L. Belyaev[100], O. Benary[155,*], D. Benchekroun[137a], M. Bender[102], N. Benekos[10], Y. Benhammou[155], E. Benhar Noccioli[179], J. Benitez[66], D.P. Benjamin[48], M. Benoit[52], J.R. Bensinger[25], S. Bentvelsen[109], L. Beresford[122], M. Beretta[50], D. Berge[109], E. Bergeaas Kuutmann[168], N. Berger[5], J. Beringer[16], S. Berlendis[58], N.R. Bernard[89], G. Bernardi[83], C. Bernius[145], F.U. Bernlochner[23], T. Berry[80], P. Berta[86], C. Bertella[35a], G. Bertoli[148a,148b], I.A. Bertram[75], C. Bertsche[45], D. Bertsche[115], G.J. Besjes[39], O. Bessidskaia Bylund[148a,148b], M. Bessner[45], N. Besson[138], A. Bethani[87], S. Bethke[103], A.J. Bevan[79], J. Beyer[103], R.M. Bianchi[127], O. Biebel[102], D. Biedermann[17], R. Bielski[87], K. Bierwagen[86], N.V. Biesuz[126a,126b], M. Biglietti[136a], T.R.V. Billoud[97], H. Bilokon[50], M. Bindi[57], A. Bingul[20b], C. Bini[134a,134b], S. Biondi[22a,22b], T. Bisanz[57], C. Bittrich[47], D.M. Bjergaard[48], J.E. Black[145], K.M. Black[24], R.E. Blair[6], T. Blazek[146a], I. Bloch[45], C. Blocker[25], A. Blue[56],

JHEP12(2017)059

W. Blum[86,*], U. Blumenschein[79], S. Blunier[34a], G.J. Bobbink[109], V.S. Bobrovnikov[111,c], S.S. Bocchetta[84], A. Bocci[48], C. Bock[102], M. Boehler[51], D. Boerner[178], D. Bogavac[102], A.G. Bogdanchikov[111], C. Bohm[148a], V. Boisvert[80], P. Bokan[168,i], T. Bold[41a], A.S. Boldyrev[101], A.E. Bolz[60b], M. Bomben[83], M. Bona[79], M. Boonekamp[138], A. Borisov[132], G. Borissov[75], J. Bortfeldt[32], D. Bortoletto[122], V. Bortolotto[62a,62b,62c], D. Boscherini[22a], M. Bosman[13], J.D. Bossio Sola[29], J. Boudreau[127], J. Bouffard[2], E.V. Bouhova-Thacker[75], D. Boumediene[37], C. Bourdarios[119], S.K. Boutle[56], A. Boveia[113], J. Boyd[32], I.R. Boyko[68], A.J. Bozson[80], J. Bracinik[19], A. Brandt[8], G. Brandt[57], O. Brandt[60a], F. Braren[45], U. Bratzler[158], B. Brau[89], J.E. Brau[118], W.D. Breaden Madden[56], K. Brendlinger[45], A.J. Brennan[91], L. Brenner[109], R. Brenner[168], S. Bressler[175], D.L. Briglin[19], T.M. Bristow[49], D. Britton[56], D. Britzger[45], F.M. Brochu[30], I. Brock[23], R. Brock[93], G. Brooijmans[38], T. Brooks[80], W.K. Brooks[34b], J. Brosamer[16], E. Brost[110], J.H Broughton[19], P.A. Bruckman de Renstrom[42], D. Bruncko[146b], A. Bruni[22a], G. Bruni[22a], L.S. Bruni[109], S. Bruno[135a,135b], BH Brunt[30], M. Bruschi[22a], N. Bruscino[127], P. Bryant[33], L. Bryngemark[45], T. Buanes[15], Q. Buat[144], P. Buchholz[143], A.G. Buckley[56], I.A. Budagov[68], F. Buehrer[51], M.K. Bugge[121], O. Bulekov[100], D. Bullock[8], T.J. Burch[110], S. Burdin[77], C.D. Burgard[51], A.M. Burger[5], B. Burghgrave[110], K. Burka[42], S. Burke[133], I. Burmeister[46], J.T.P. Burr[122], E. Busato[37], D. Büscher[51], V. Büscher[86], P. Bussey[56], J.M. Butler[24], C.M. Buttar[56], J.M. Butterworth[81], P. Butti[32], W. Buttinger[27], A. Buzatu[153], A.R. Buzykaev[111,c], S. Cabrera Urbán[170], D. Caforio[130], H. Cai[169], V.M. Cairo[40a,40b], O. Cakir[4a], N. Calace[52], P. Calafiura[16], A. Calandri[88], G. Calderini[83], P. Calfayan[64], G. Callea[40a,40b], L.P. Caloba[26a], S. Calvente Lopez[85], D. Calvet[37], S. Calvet[37], T.P. Calvet[88], R. Camacho Toro[33], S. Camarda[32], P. Camarri[135a,135b], D. Cameron[121], R. Caminal Armadans[169], C. Camincher[58], S. Campana[32], M. Campanelli[81], A. Camplani[94a,94b], A. Campoverde[143], V. Canale[106a,106b], M. Cano Bret[36c], J. Cantero[116], T. Cao[155], M.D.M. Capeans Garrido[32], I. Caprini[28b], M. Caprini[28b], M. Capua[40a,40b], R.M. Carbone[38], R. Cardarelli[135a], F. Cardillo[51], I. Carli[131], T. Carli[32], G. Carlino[106a], B.T. Carlson[127], L. Carminati[94a,94b], R.M.D. Carney[148a,148b], S. Caron[108], E. Carquin[34b], S. Carrá[94a,94b], G.D. Carrillo-Montoya[32], D. Casadei[19], M.P. Casado[13,j], M. Casolino[13], D.W. Casper[166], R. Castelijn[109], V. Castillo Gimenez[170], N.F. Castro[128a,k], A. Catinaccio[32], J.R. Catmore[121], A. Cattai[32], J. Caudron[23], V. Cavaliere[169], E. Cavallaro[13], D. Cavalli[94a], M. Cavalli-Sforza[13], V. Cavasinni[126a,126b], E. Celebi[20d], F. Ceradini[136a,136b], L. Cerda Alberich[170], A.S. Cerqueira[26b], A. Cerri[151], L. Cerrito[135a,135b], F. Cerutti[16], A. Cervelli[22a,22b], S.A. Cetin[20d], A. Chafaq[137a], D. Chakraborty[110], S.K. Chan[59], W.S. Chan[109], Y.L. Chan[62a], P. Chang[169], J.D. Chapman[30], D.G. Charlton[19], C.C. Chau[31], C.A. Chavez Barajas[151], S. Che[113], S. Cheatham[167a,167c], A. Chegwidden[93], S. Chekanov[6], S.V. Chekulaev[163a], G.A. Chelkov[68,l], M.A. Chelstowska[32], C. Chen[36a], C. Chen[67], H. Chen[27], J. Chen[36a], S. Chen[35b], S. Chen[157], X. Chen[35c,m], Y. Chen[70], H.C. Cheng[92], H.J. Cheng[35a], A. Cheplakov[68], E. Cheremushkina[132], R. Cherkaoui El Moursli[137e], E. Cheu[7], K. Cheung[63], L. Chevalier[138], V. Chiarella[50], G. Chiarelli[126a,126b], G. Chiodini[76a], A.S. Chisholm[32], A. Chitan[28b], Y.H. Chiu[172], M.V. Chizhov[68], K. Choi[64], A.R. Chomont[37], S. Chouridou[156], Y.S. Chow[62a], V. Christodoulou[81], M.C. Chu[62a], J. Chudoba[129], A.J. Chuinard[90], J.J. Chwastowski[42], L. Chytka[117], A.K. Ciftci[4a], D. Cinca[46], V. Cindro[78], I.A. Cioara[23], A. Ciocio[16], F. Cirotto[106a,106b], Z.H. Citron[175], M. Citterio[94a], M. Ciubancan[28b], A. Clark[52], B.L. Clark[59], M.R. Clark[38], P.J. Clark[49], R.N. Clarke[16], C. Clement[148a,148b], Y. Coadou[88], M. Cobal[167a,167c], A. Coccaro[52], J. Cochran[67], L. Colasurdo[108], B. Cole[38], A.P. Colijn[109], J. Collot[58], T. Colombo[166], P. Conde Muiño[128a,128b], E. Coniavitis[51], S.H. Connell[147b], I.A. Connelly[87], S. Constantinescu[28b], G. Conti[32], F. Conventi[106a,n], M. Cooke[16], A.M. Cooper-Sarkar[122], F. Cormier[171], K.J.R. Cormier[161], M. Corradi[134a,134b], F. Corriveau[90,o], A. Cortes-Gonzalez[32], G. Costa[94a], M.J. Costa[170], D. Costanzo[141], G. Cottin[30],

JHEP12(2017)059

G. Cowan[80], B.E. Cox[87], K. Cranmer[112], S.J. Crawley[56], R.A. Creager[124], G. Cree[31], S. Crépé-Renaudin[58], F. Crescioli[83], W.A. Cribbs[148a,148b], M. Cristinziani[23], V. Croft[112], G. Crosetti[40a,40b], A. Cueto[85], T. Cuhadar Donszelmann[141], A.R. Cukierman[145], J. Cummings[179], M. Curatolo[50], J. Cúth[86], S. Czekierda[42], P. Czodrowski[32], G. D'amen[22a,22b], S. D'Auria[56], L. D'eramo[83], M. D'Onofrio[77], M.J. Da Cunha Sargedas De Sousa[128a,128b], C. Da Via[87], W. Dabrowski[41a], T. Dado[146a], T. Dai[92], O. Dale[15], F. Dallaire[97], C. Dallapiccola[89], M. Dam[39], J.R. Dandoy[124], M.F. Daneri[29], N.P. Dang[176], A.C. Daniells[19], N.S. Dann[87], M. Danninger[171], M. Dano Hoffmann[138], V. Dao[150], G. Darbo[53a], S. Darmora[8], J. Dassoulas[3], A. Dattagupta[118], T. Daubney[45], W. Davey[23], C. David[45], T. Davidek[131], D.R. Davis[48], P. Davison[81], E. Dawe[91], I. Dawson[141], K. De[8], R. de Asmundis[106a], A. De Benedetti[115], S. De Castro[22a,22b], S. De Cecco[83], N. De Groot[108], P. de Jong[109], H. De la Torre[93], F. De Lorenzi[67], A. De Maria[57], D. De Pedis[134a], A. De Salvo[134a], U. De Sanctis[135a,135b], A. De Santo[151], K. De Vasconcelos Corga[88], J.B. De Vivie De Regie[119], R. Debbe[27], C. Debenedetti[139], D.V. Dedovich[68], N. Dehghanian[3], I. Deigaard[109], M. Del Gaudio[40a,40b], J. Del Peso[85], D. Delgove[119], F. Deliot[138], C.M. Delitzsch[7], A. Dell'Acqua[32], L. Dell'Asta[24], M. Dell'Orso[126a,126b], M. Della Pietra[106a,106b], D. della Volpe[52], M. Delmastro[5], C. Delporte[119], P.A. Delsart[58], D.A. DeMarco[161], S. Demers[179], M. Demichev[68], A. Demilly[83], S.P. Denisov[132], D. Denysiuk[138], D. Derendarz[42], J.E. Derkaoui[137d], F. Derue[83], P. Dervan[77], K. Desch[23], C. Deterre[45], K. Dette[161], M.R. Devesa[29], P.O. Deviveiros[32], A. Dewhurst[133], S. Dhaliwal[25], F.A. Di Bello[52], A. Di Ciaccio[135a,135b], L. Di Ciaccio[5], W.K. Di Clemente[124], C. Di Donato[106a,106b], A. Di Girolamo[32], B. Di Girolamo[32], B. Di Micco[136a,136b], R. Di Nardo[32], K.F. Di Petrillo[59], A. Di Simone[51], R. Di Sipio[161], D. Di Valentino[31], C. Diaconu[88], M. Diamond[161], F.A. Dias[39], M.A. Diaz[34a], E.B. Diehl[92], J. Dietrich[17], S. Díez Cornell[45], A. Dimitrievska[14], J. Dingfelder[23], P. Dita[28b], S. Dita[28b], F. Dittus[32], F. Djama[88], T. Djobava[54b], J.I. Djuvsland[60a], M.A.B. do Vale[26c], D. Dobos[32], M. Dobre[28b], D. Dodsworth[25], C. Doglioni[84], J. Dolejsi[131], Z. Dolezal[131], M. Donadelli[26d], S. Donati[126a,126b], P. Dondero[123a,123b], J. Donini[37], J. Dopke[133], A. Doria[106a], M.T. Dova[74], A.T. Doyle[56], E. Drechsler[57], M. Dris[10], Y. Du[36b], J. Duarte-Campderros[155], A. Dubreuil[52], E. Duchovni[175], G. Duckeck[102], A. Ducourthial[83], O.A. Ducu[97,p], D. Duda[109], A. Dudarev[32], A.Chr. Dudder[86], E.M. Duffield[16], L. Duflot[119], M. Dührssen[32], C. Dulsen[178], M. Dumancic[175], A.E. Dumitriu[28b], A.K. Duncan[56], M. Dunford[60a], A. Duperrin[88], H. Duran Yildiz[4a], M. Düren[55], A. Durglishvili[54b], D. Duschinger[47], B. Dutta[45], D. Duvnjak[1], M. Dyndal[45], B.S. Dziedzic[42], C. Eckardt[45], K.M. Ecker[103], R.C. Edgar[92], T. Eifert[32], G. Eigen[15], K. Einsweiler[16], T. Ekelof[168], M. El Kacimi[137c], R. El Kosseifi[88], V. Ellajosyula[88], M. Ellert[168], S. Elles[5], F. Ellinghaus[178], A.A. Elliot[172], N. Ellis[32], J. Elmsheuser[27], M. Elsing[32], D. Emeliyanov[133], Y. Enari[157], O.C. Endner[86], J.S. Ennis[173], M.B. Epland[48], J. Erdmann[46], A. Ereditato[18], M. Ernst[27], S. Errede[169], M. Escalier[119], C. Escobar[170], B. Esposito[50], O. Estrada Pastor[170], A.I. Etienvre[138], E. Etzion[155], H. Evans[64], A. Ezhilov[125], M. Ezzi[137e], F. Fabbri[22a,22b], L. Fabbri[22a,22b], V. Fabiani[108], G. Facini[81], R.M. Fakhrutdinov[132], S. Falciano[134a], R.J. Falla[81], J. Faltova[32], Y. Fang[35a], M. Fanti[94a,94b], A. Farbin[8], A. Farilla[136a], C. Farina[127], E.M. Farina[123a,123b], T. Farooque[93], S. Farrell[16], S.M. Farrington[173], P. Farthouat[32], F. Fassi[137e], P. Fassnacht[32], D. Fassouliotis[9], M. Faucci Giannelli[49], A. Favareto[53a,53b], W.J. Fawcett[122], L. Fayard[119], O.L. Fedin[125,q], W. Fedorko[171], S. Feigl[121], L. Feligioni[88], C. Feng[36b], E.J. Feng[32], M.J. Fenton[56], A.B. Fenyuk[132], L. Feremenga[8], P. Fernandez Martinez[170], S. Fernandez Perez[13], J. Ferrando[45], A. Ferrari[168], P. Ferrari[109], R. Ferrari[123a], D.E. Ferreira de Lima[60b], A. Ferrer[170], D. Ferrere[52], C. Ferretti[92], F. Fiedler[86], A. Filipčič[78], M. Filipuzzi[45], F. Filthaut[108], M. Fincke-Keeler[172], K.D. Finelli[152], M.C.N. Fiolhais[128a,128c,r], L. Fiorini[170], A. Fischer[2], C. Fischer[13], J. Fischer[178], W.C. Fisher[93], N. Flaschel[45], I. Fleck[143], P. Fleischmann[92], R.R.M. Fletcher[124], T. Flick[178], B.M. Flierl[102],

JHEP12(2017)059

L.R. Flores Castillo[62a], M.J. Flowerdew[103], G.T. Forcolin[87], A. Formica[138], F.A. Förster[13], A. Forti[87], A.G. Foster[19], D. Fournier[119], H. Fox[75], S. Fracchia[141], P. Francavilla[83], M. Franchini[22a,22b], S. Franchino[60a], D. Francis[32], L. Franconi[121], M. Franklin[59], M. Frate[166], M. Fraternali[123a,123b], D. Freeborn[81], S.M. Fressard-Batraneanu[32], B. Freund[97], D. Froidevaux[32], J.A. Frost[122], C. Fukunaga[158], T. Fusayasu[104], J. Fuster[170], O. Gabizon[154], A. Gabrielli[22a,22b], A. Gabrielli[16], G.P. Gach[41a], S. Gadatsch[32], S. Gadomski[80], G. Gagliardi[53a,53b], L.G. Gagnon[97], C. Galea[108], B. Galhardo[128a,128c], E.J. Gallas[122], B.J. Gallop[133], P. Gallus[130], G. Galster[39], K.K. Gan[113], S. Ganguly[37], Y. Gao[77], Y.S. Gao[145,g], F.M. Garay Walls[34a], C. García[170], J.E. García Navarro[170], J.A. García Pascual[35a], M. Garcia-Sciveres[16], R.W. Gardner[33], N. Garelli[145], V. Garonne[121], A. Gascon Bravo[45], K. Gasnikova[45], C. Gatti[50], A. Gaudiello[53a,53b], G. Gaudio[123a], I.L. Gavrilenko[98], C. Gay[171], G. Gaycken[23], E.N. Gazis[10], C.N.P. Gee[133], J. Geisen[57], M. Geisen[86], M.P. Geisler[60a], K. Gellerstedt[148a,148b], C. Gemme[53a], M.H. Genest[58], C. Geng[92], S. Gentile[134a,134b], C. Gentsos[156], S. George[80], D. Gerbaudo[13], G. Geßner[46], S. Ghasemi[143], M. Ghneimat[23], B. Giacobbe[22a], S. Giagu[134a,134b], N. Giangiacomi[22a,22b], P. Giannetti[126a,126b], S.M. Gibson[80], M. Gignac[171], M. Gilchriese[16], D. Gillberg[31], G. Gilles[178], D.M. Gingrich[3,d], M.P. Giordani[167a,167c], F.M. Giorgi[22a], P.F. Giraud[138], P. Giromini[59], G. Giugliarelli[167a,167c], D. Giugni[94a], F. Giuli[122], C. Giuliani[103], M. Giulini[60b], B.K. Gjelsten[121], S. Gkaitatzis[156], I. Gkialas[9,s], E.L. Gkougkousis[13], P. Gkountoumis[10], L.K. Gladilin[101], C. Glasman[85], J. Glatzer[13], P.C.F. Glaysher[45], A. Glazov[45], M. Goblirsch-Kolb[25], J. Godlewski[42], S. Goldfarb[91], T. Golling[52], D. Golubkov[132], A. Gomes[128a,128b,128d], R. Gonçalo[128a], R. Goncalves Gama[26a], J. Goncalves Pinto Firmino Da Costa[138], G. Gonella[51], L. Gonella[19], A. Gongadze[68], S. González de la Hoz[170], S. Gonzalez-Sevilla[52], L. Goossens[32], P.A. Gorbounov[99], H.A. Gordon[27], I. Gorelov[107], B. Gorini[32], E. Gorini[76a,76b], A. Gorišek[78], A.T. Goshaw[48], C. Gössling[46], M.I. Gostkin[68], C.A. Gottardo[23], C.R. Goudet[119], D. Goujdami[137c], A.G. Goussiou[140], N. Govender[147b,t], E. Gozani[154], I. Grabowska-Bold[41a], P.O.J. Gradin[168], J. Gramling[166], E. Gramstad[121], S. Grancagnolo[17], V. Gratchev[125], P.M. Gravila[28f], C. Gray[56], H.M. Gray[16], Z.D. Greenwood[82,u], C. Grefe[23], K. Gregersen[81], I.M. Gregor[45], P. Grenier[145], K. Grevtsov[5], J. Griffiths[8], A.A. Grillo[139], K. Grimm[75], S. Grinstein[13,v], Ph. Gris[37], J.-F. Grivaz[119], S. Groh[86], E. Gross[175], J. Grosse-Knetter[57], G.C. Grossi[82], Z.J. Grout[81], A. Grummer[107], L. Guan[92], W. Guan[176], J. Guenther[32], F. Guescini[163a], D. Guest[166], O. Gueta[155], B. Gui[113], E. Guido[53a,53b], T. Guillemin[5], S. Guindon[32], U. Gul[56], C. Gumpert[32], J. Guo[36c], W. Guo[92], Y. Guo[36a], R. Gupta[43], S. Gupta[122], S. Gurbuz[20a], G. Gustavino[115], B.J. Gutelman[154], P. Gutierrez[115], N.G. Gutierrez Ortiz[81], C. Gutschow[81], C. Guyot[138], M.P. Guzik[41a], C. Gwenlan[122], C.B. Gwilliam[77], A. Haas[112], C. Haber[16], H.K. Hadavand[8], N. Haddad[137e], A. Hadef[88], S. Hageböck[23], M. Hagihara[164], H. Hakobyan[180,*], M. Haleem[45], J. Haley[116], G. Halladjian[93], G.D. Hallewell[88], K. Hamacher[178], P. Hamal[117], K. Hamano[172], A. Hamilton[147a], G.N. Hamity[141], P.G. Hamnett[45], L. Han[36a], S. Han[35a], K. Hanagaki[69,w], K. Hanawa[157], M. Hance[139], B. Haney[124], P. Hanke[60a], J.B. Hansen[39], J.D. Hansen[39], M.C. Hansen[23], P.H. Hansen[39], K. Hara[164], A.S. Hard[176], T. Harenberg[178], F. Hariri[119], S. Harkusha[95], P.F. Harrison[173], N.M. Hartmann[102], Y. Hasegawa[142], A. Hasib[49], S. Hassani[138], S. Haug[18], R. Hauser[93], L. Hauswald[47], L.B. Havener[38], M. Havranek[130], C.M. Hawkes[19], R.J. Hawkings[32], D. Hayakawa[159], D. Hayden[93], C.P. Hays[122], J.M. Hays[79], H.S. Hayward[77], S.J. Haywood[133], S.J. Head[19], T. Heck[86], V. Hedberg[84], L. Heelan[8], S. Heer[23], K.K. Heidegger[51], S. Heim[45], T. Heim[16], B. Heinemann[45,x], J.J. Heinrich[102], L. Heinrich[112], C. Heinz[55], J. Hejbal[129], L. Helary[32], A. Held[171], S. Hellman[148a,148b], C. Helsens[32], R.C.W. Henderson[75], Y. Heng[176], S. Henkelmann[171], A.M. Henriques Correia[32], S. Henrot-Versille[119], G.H. Herbert[17], H. Herde[25], V. Herget[177], Y. Hernández Jiménez[147c], H. Herr[86], G. Herten[51], R. Hertenberger[102], L. Hervas[32], T.C. Herwig[124], G.G. Hesketh[81], N.P. Hessey[163a], J.W. Hetherly[43], S. Higashino[69],

JHEP12(2017)059

E. Higón-Rodriguez[170], K. Hildebrand[33], E. Hill[172], J.C. Hill[30], K.H. Hiller[45], S.J. Hillier[19], M. Hils[47], I. Hinchliffe[16], M. Hirose[51], D. Hirschbuehl[178], B. Hiti[78], O. Hladik[129], X. Hoad[49], J. Hobbs[150], N. Hod[163a], M.C. Hodgkinson[141], P. Hodgson[141], A. Hoecker[32], M.R. Hoeferkamp[107], F. Hoenig[102], D. Hohn[23], T.R. Holmes[33], M. Homann[46], S. Honda[164], T. Honda[69], T.M. Hong[127], B.H. Hooberman[169], W.H. Hopkins[118], Y. Horii[105], A.J. Horton[144], J-Y. Hostachy[58], A. Hostiuc[140], S. Hou[153], A. Hoummada[137a], J. Howarth[87], J. Hoya[74], M. Hrabovsky[117], J. Hrdinka[32], I. Hristova[17], J. Hrivnac[119], T. Hryn'ova[5], A. Hrynevich[96], P.J. Hsu[63], S.-C. Hsu[140], Q. Hu[36a], S. Hu[36c], Y. Huang[35a], Z. Hubacek[130], F. Hubaut[88], F. Huegging[23], T.B. Huffman[122], E.W. Hughes[38], G. Hughes[75], M. Huhtinen[32], R.F.H. Hunter[31], P. Huo[150], N. Huseynov[68,b], J. Huston[93], J. Huth[59], R. Hyneman[92], G. Iacobucci[52], G. Iakovidis[27], I. Ibragimov[143], L. Iconomidou-Fayard[119], Z. Idrissi[137e], P. Iengo[32], O. Igonkina[109,y], T. Iizawa[174], Y. Ikegami[69], M. Ikeno[69], Y. Ilchenko[11,z], D. Iliadis[156], N. Ilic[145], F. Iltzsche[47], G. Introzzi[123a,123b], P. Ioannou[9,*], M. Iodice[136a], K. Iordanidou[38], V. Ippolito[59], M.F. Isacson[168], N. Ishijima[120], M. Ishino[157], M. Ishitsuka[159], C. Issever[122], S. Istin[20a], F. Ito[164], J.M. Iturbe Ponce[62a], R. Iuppa[162a,162b], H. Iwasaki[69], J.M. Izen[44], V. Izzo[106a], S. Jabbar[3], P. Jackson[1], R.M. Jacobs[23], V. Jain[2], K.B. Jakobi[86], K. Jakobs[51], S. Jakobsen[65], T. Jakoubek[129], D.O. Jamin[116], D.K. Jana[82], R. Jansky[52], J. Janssen[23], M. Janus[57], P.A. Janus[41a], G. Jarlskog[84], N. Javadov[68,b], T. Javůrek[51], M. Javurkova[51], F. Jeanneau[138], L. Jeanty[16], J. Jejelava[54a,aa], A. Jelinskas[173], P. Jenni[51,ab], C. Jeske[173], S. Jézéquel[5], H. Ji[176], J. Jia[150], H. Jiang[67], Y. Jiang[36a], Z. Jiang[145], S. Jiggins[81], J. Jimenez Pena[170], S. Jin[35a], A. Jinaru[28b], O. Jinnouchi[159], H. Jivan[147c], P. Johansson[141], K.A. Johns[7], C.A. Johnson[64], W.J. Johnson[140], K. Jon-And[148a,148b], R.W.L. Jones[75], S.D. Jones[151], S. Jones[7], T.J. Jones[77], J. Jongmanns[60a], P.M. Jorge[128a,128b], J. Jovicevic[163a], X. Ju[176], A. Juste Rozas[13,v], M.K. Köhler[175], A. Kaczmarska[42], M. Kado[119], H. Kagan[113], M. Kagan[145], S.J. Kahn[88], T. Kaji[174], E. Kajomovitz[154], C.W. Kalderon[84], A. Kaluza[86], S. Kama[43], A. Kamenshchikov[132], N. Kanaya[157], L. Kanjir[78], V.A. Kantserov[100], J. Kanzaki[69], B. Kaplan[112], L.S. Kaplan[176], D. Kar[147c], K. Karakostas[10], N. Karastathis[10], M.J. Kareem[163b], E. Karentzos[10], S.N. Karpov[68], Z.M. Karpova[68], K. Karthik[112], V. Kartvelishvili[75], A.N. Karyukhin[132], K. Kasahara[164], L. Kashif[176], R.D. Kass[113], A. Kastanas[149], Y. Kataoka[157], C. Kato[157], A. Katre[52], J. Katzy[45], K. Kawade[70], K. Kawagoe[73], T. Kawamoto[157], G. Kawamura[57], E.F. Kay[77], V.F. Kazanin[111,c], R. Keeler[172], R. Kehoe[43], J.S. Keller[31], E. Kellermann[84], J.J. Kempster[80], J Kendrick[19], H. Keoshkerian[161], O. Kepka[129], B.P. Kerševan[78], S. Kersten[178], R.A. Keyes[90], M. Khader[169], F. Khalil-zada[12], A. Khanov[116], A.G. Kharlamov[111,c], T. Kharlamova[111,c], A. Khodinov[160], T.J. Khoo[52], V. Khovanskiy[99,*], E. Khramov[68], J. Khubua[54b,ac], S. Kido[70], C.R. Kilby[80], H.Y. Kim[8], S.H. Kim[164], Y.K. Kim[33], N. Kimura[156], O.M. Kind[17], B.T. King[77], D. Kirchmeier[47], J. Kirk[133], A.E. Kiryunin[103], T. Kishimoto[157], D. Kisielewska[41a], V. Kitali[45], O. Kivernyk[5], E. Kladiva[146b], T. Klapdor-Kleingrothaus[51], M.H. Klein[92], M. Klein[77], U. Klein[77], K. Kleinknecht[86], P. Klimek[110], A. Klimentov[27], R. Klingenberg[46], T. Klingl[23], T. Klioutchnikova[32], E.-E. Kluge[60a], P. Kluit[109], S. Kluth[103], E. Kneringer[65], E.B.F.G. Knoops[88], A. Knue[103], A. Kobayashi[157], D. Kobayashi[73], T. Kobayashi[157], M. Kobel[47], M. Kocian[145], P. Kodys[131], T. Koffas[31], E. Koffeman[109], N.M. Köhler[103], T. Koi[145], M. Kolb[60b], I. Koletsou[5], A.A. Komar[98,*], T. Kondo[69], N. Kondrashova[36c], K. Köneke[51], A.C. König[108], T. Kono[69,ad], R. Konoplich[112,ae], N. Konstantinidis[81], R. Kopeliansky[64], S. Koperny[41a], A.K. Kopp[51], K. Korcyl[42], K. Kordas[156], A. Korn[81], A.A. Korol[111,c], I. Korolkov[13], E.V. Korolkova[141], O. Kortner[103], S. Kortner[103], T. Kosek[131], V.V. Kostyukhin[23], A. Kotwal[48], A. Koulouris[10], A. Kourkoumeli-Charalampidi[123a,123b], C. Kourkoumelis[9], E. Kourlitis[141], V. Kouskoura[27], A.B. Kowalewska[42], R. Kowalewski[172], T.Z. Kowalski[41a], C. Kozakai[157], W. Kozanecki[138], A.S. Kozhin[132], V.A. Kramarenko[101], G. Kramberger[78], D. Krasnopevtsev[100], M.W. Krasny[83],

JHEP12(2017)059

A. Krasznahorkay[32], D. Krauss[103], J.A. Kremer[41a], J. Kretzschmar[77], K. Kreutzfeldt[55], P. Krieger[161], K. Krizka[16], K. Kroeninger[46], H. Kroha[103], J. Kroll[129], J. Kroll[124], J. Kroseberg[23], J. Krstic[14], U. Kruchonak[68], H. Krüger[23], N. Krumnack[67], M.C. Kruse[48], T. Kubota[91], H. Kucuk[81], S. Kuday[4b], J.T. Kuechler[178], S. Kuehn[32], A. Kugel[60a], F. Kuger[177], T. Kuhl[45], V. Kukhtin[68], R. Kukla[88], Y. Kulchitsky[95], S. Kuleshov[34b], Y.P. Kulinich[169], M. Kuna[134a,134b], T. Kunigo[71], A. Kupco[129], T. Kupfer[46], O. Kuprash[155], H. Kurashige[70], L.L. Kurchaninov[163a], Y.A. Kurochkin[95], M.G. Kurth[35a], E.S. Kuwertz[172], M. Kuze[159], J. Kvita[117], T. Kwan[172], D. Kyriazopoulos[141], A. La Rosa[103], J.L. La Rosa Navarro[26d], L. La Rotonda[40a,40b], F. La Ruffa[40a,40b], C. Lacasta[170], F. Lacava[134a,134b], J. Lacey[45], D.P.J. Lack[87], H. Lacker[17], D. Lacour[83], E. Ladygin[68], R. Lafaye[5], B. Laforge[83], T. Lagouri[179], S. Lai[57], S. Lammers[64], W. Lampl[7], E. Lançon[27], U. Landgraf[51], M.P.J. Landon[79], M.C. Lanfermann[52], V.S. Lang[45], J.C. Lange[13], R.J. Langenberg[32], A.J. Lankford[166], F. Lanni[27], K. Lantzsch[23], A. Lanza[123a], A. Lapertosa[53a,53b], S. Laplace[83], J.F. Laporte[138], T. Lari[94a], F. Lasagni Manghi[22a,22b], M. Lassnig[32], T.S. Lau[62a], P. Laurelli[50], W. Lavrijsen[16], A.T. Law[139], P. Laycock[77], T. Lazovich[59], M. Lazzaroni[94a,94b], B. Le[91], O. Le Dortz[83], E. Le Guirriec[88], E.P. Le Quilleuc[138], M. LeBlanc[172], T. LeCompte[6], F. Ledroit-Guillon[58], C.A. Lee[27], G.R. Lee[34a], S.C. Lee[153], L. Lee[59], B. Lefebvre[90], G. Lefebvre[83], M. Lefebvre[172], F. Legger[102], C. Leggett[16], G. Lehmann Miotto[32], X. Lei[7], W.A. Leight[45], M.A.L. Leite[26d], R. Leitner[131], D. Lellouch[175], B. Lemmer[57], K.J.C. Leney[81], T. Lenz[23], B. Lenzi[32], R. Leone[7], S. Leone[126a,126b], C. Leonidopoulos[49], G. Lerner[151], C. Leroy[97], R. Les[161], A.A.J. Lesage[138], C.G. Lester[30], M. Levchenko[125], J. Levêque[5], D. Levin[92], L.J. Levinson[175], M. Levy[19], D. Lewis[79], B. Li[36a,af], Changqiao Li[36a], H. Li[150], L. Li[36c], Q. Li[35a], Q. Li[36a], S. Li[48], X. Li[36c], Y. Li[143], Z. Liang[35a], B. Liberti[135a], A. Liblong[161], K. Lie[62c], J. Liebal[23], W. Liebig[15], A. Limosani[152], K. Lin[93], S.C. Lin[182], T.H. Lin[86], R.A. Linck[64], B.E. Lindquist[150], A.E. Lionti[52], E. Lipeles[124], A. Lipniacka[15], M. Lisovyi[60b], T.M. Liss[169,ag], A. Lister[171], A.M. Litke[139], B. Liu[67], H. Liu[92], H. Liu[27], J.K.K. Liu[122], J. Liu[36b], J.B. Liu[36a], K. Liu[88], L. Liu[169], M. Liu[36a], Y.L. Liu[36a], Y. Liu[36a], M. Livan[123a,123b], A. Lleres[58], J. Llorente Merino[35a], S.L. Lloyd[79], C.Y. Lo[62b], F. Lo Sterzo[43], E.M. Lobodzinska[45], P. Loch[7], F.K. Loebinger[87], A. Loesle[51], K.M. Loew[25], T. Lohse[17], K. Lohwasser[141], M. Lokajicek[129], B.A. Long[24], J.D. Long[169], R.E. Long[75], L. Longo[76a,76b], K.A. Looper[113], J.A. Lopez[34b], I. Lopez Paz[13], A. Lopez Solis[83], J. Lorenz[102], N. Lorenzo Martinez[5], M. Losada[21], P.J. Lösel[102], X. Lou[35a], A. Lounis[119], J. Love[6], P.A. Love[75], H. Lu[62a], N. Lu[92], Y.J. Lu[63], H.J. Lubatti[140], C. Luci[134a,134b], A. Lucotte[58], C. Luedtke[51], F. Luehring[64], W. Lukas[65], L. Luminari[134a], O. Lundberg[148a,148b], B. Lund-Jensen[149], M.S. Lutz[89], P.M. Luzi[83], D. Lynn[27], R. Lysak[129], E. Lytken[84], F. Lyu[35a], V. Lyubushkin[68], H. Ma[27], L.L. Ma[36b], Y. Ma[36b], G. Maccarrone[50], A. Macchiolo[103], C.M. Macdonald[141], B. Maček[78], J. Machado Miguens[124,128b], D. Madaffari[170], R. Madar[37], W.F. Mader[47], A. Madsen[45], N. Madysa[47], J. Maeda[70], S. Maeland[15], T. Maeno[27], A.S. Maevskiy[101], V. Magerl[51], C. Maiani[119], C. Maidantchik[26a], T. Maier[102], A. Maio[128a,128b,128d], O. Majersky[146a], S. Majewski[118], Y. Makida[69], N. Makovec[119], B. Malaescu[83], Pa. Malecki[42], V.P. Maleev[125], F. Malek[58], U. Mallik[66], D. Malon[6], C. Malone[30], S. Maltezos[10], S. Malyukov[32], J. Mamuzic[170], G. Mancini[50], I. Mandić[78], J. Maneira[128a,128b], L. Manhaes de Andrade Filho[26b], J. Manjarres Ramos[47], K.H. Mankinen[84], A. Mann[102], A. Manousos[32], B. Mansoulie[138], J.D. Mansour[35a], R. Mantifel[90], M. Mantoani[57], S. Manzoni[94a,94b], L. Mapelli[32], G. Marceca[29], L. March[52], L. Marchese[122], G. Marchiori[83], M. Marcisovsky[129], C.A. Marin Tobon[32], M. Marjanovic[37], D.E. Marley[92], F. Marroquim[26a], S.P. Marsden[87], Z. Marshall[16], M.U.F Martensson[168], S. Marti-Garcia[170], C.B. Martin[113], T.A. Martin[173], V.J. Martin[49], B. Martin dit Latour[15], M. Martinez[13,v], V.I. Martinez Outschoorn[169], S. Martin-Haugh[133], V.S. Martoiu[28b], A.C. Martyniuk[81], A. Marzin[32], L. Masetti[86], T. Mashimo[157], R. Mashinistov[98],

JHEP12(2017)059

J. Masik[87], A.L. Maslennikov[111,c], L.H. Mason[91], L. Massa[135a,135b], P. Mastrandrea[5], A. Mastroberardino[40a,40b], T. Masubuchi[157], P. Mättig[178], J. Maurer[28b], S.J. Maxfield[77], D.A. Maximov[111,c], R. Mazini[153], I. Maznas[156], S.M. Mazza[94a,94b], N.C. Mc Fadden[107], G. Mc Goldrick[161], S.P. Mc Kee[92], A. McCarn[92], R.L. McCarthy[150], T.G. McCarthy[103], L.I. McClymont[81], E.F. McDonald[91], J.A. Mcfayden[32], G. Mchedlidze[57], S.J. McMahon[133], P.C. McNamara[91], C.J. McNicol[173], R.A. McPherson[172,o], S. Meehan[140], T.J. Megy[51], S. Mehlhase[102], A. Mehta[77], T. Meideck[58], K. Meier[60a], B. Meirose[44], D. Melini[170,ah], B.R. Mellado Garcia[147c], J.D. Mellenthin[57], M. Melo[146a], F. Meloni[18], A. Melzer[23], S.B. Menary[87], L. Meng[77], X.T. Meng[92], A. Mengarelli[22a,22b], S. Menke[103], E. Meoni[40a,40b], S. Mergelmeyer[17], C. Merlassino[18], P. Mermod[52], L. Merola[106a,106b], C. Meroni[94a], F.S. Merritt[33], A. Messina[134a,134b], J. Metcalfe[6], A.S. Mete[166], C. Meyer[124], J-P. Meyer[138], J. Meyer[109], H. Meyer Zu Theenhausen[60a], F. Miano[151], R.P. Middleton[133], S. Miglioranzi[53a,53b], L. Mijović[49], G. Mikenberg[175], M. Mikestikova[129], M. Mikuž[78], M. Milesi[91], A. Milic[161], D.A. Millar[79], D.W. Miller[33], C. Mills[49], A. Milov[175], D.A. Milstead[148a,148b], A.A. Minaenko[132], Y. Minami[157], I.A. Minashvili[54b], A.I. Mincer[112], B. Mindur[41a], M. Mineev[68], Y. Minegishi[157], Y. Ming[176], L.M. Mir[13], A. Mirto[76a,76b], K.P. Mistry[124], T. Mitani[174], J. Mitrevski[102], V.A. Mitsou[170], A. Miucci[18], P.S. Miyagawa[141], A. Mizukami[69], J.U. Mjörnmark[84], T. Mkrtchyan[180], M. Mlynarikova[131], T. Moa[148a,148b], K. Mochizuki[97], P. Mogg[51], S. Mohapatra[38], S. Molander[148a,148b], R. Moles-Valls[23], M.C. Mondragon[93], K. Mönig[45], J. Monk[39], E. Monnier[88], A. Montalbano[150], J. Montejo Berlingen[32], F. Monticelli[74], S. Monzani[94a,94b], R.W. Moore[3], N. Morange[119], D. Moreno[21], M. Moreno Llácer[32], P. Morettini[53a], S. Morgenstern[32], D. Mori[144], T. Mori[157], M. Morii[59], M. Morinaga[174], V. Morisbak[121], A.K. Morley[32], G. Mornacchi[32], J.D. Morris[79], L. Morvaj[150], P. Moschovakos[10], M. Mosidze[54b], H.J. Moss[141], J. Moss[145,ai], K. Motohashi[159], R. Mount[145], E. Mountricha[27], E.J.W. Moyse[89], S. Muanza[88], F. Mueller[103], J. Mueller[127], R.S.P. Mueller[102], D. Muenstermann[75], P. Mullen[56], G.A. Mullier[18], F.J. Munoz Sanchez[87], W.J. Murray[173,133], H. Musheghyan[32], M. Muškinja[78], A.G. Myagkov[132,aj], M. Myska[130], B.P. Nachman[16], O. Nackenhorst[52], K. Nagai[122], R. Nagai[69,ad], K. Nagano[69], Y. Nagasaka[61], K. Nagata[164], M. Nagel[51], E. Nagy[88], A.M. Nairz[32], Y. Nakahama[105], K. Nakamura[69], T. Nakamura[157], I. Nakano[114], R.F. Naranjo Garcia[45], R. Narayan[11], D.I. Narrias Villar[60a], I. Naryshkin[125], T. Naumann[45], G. Navarro[21], R. Nayyar[7], H.A. Neal[92], P.Yu. Nechaeva[98], T.J. Neep[138], A. Negri[123a,123b], M. Negrini[22a], S. Nektarijevic[108], C. Nellist[57], A. Nelson[166], M.E. Nelson[122], S. Nemecek[129], P. Nemethy[112], M. Nessi[32,ak], M.S. Neubauer[169], M. Neumann[178], P.R. Newman[19], T.Y. Ng[62c], T. Nguyen Manh[97], R.B. Nickerson[122], R. Nicolaidou[138], J. Nielsen[139], N. Nikiforou[11], V. Nikolaenko[132,aj], I. Nikolic-Audit[83], K. Nikolopoulos[19], J.K. Nilsen[121], P. Nilsson[27], Y. Ninomiya[157], A. Nisati[134a], N. Nishu[36c], R. Nisius[103], I. Nitsche[46], T. Nitta[174], T. Nobe[157], Y. Noguchi[71], M. Nomachi[120], I. Nomidis[31], M.A. Nomura[27], T. Nooney[79], M. Nordberg[32], N. Norjoharuddeen[122], O. Novgorodova[47], M. Nozaki[69], L. Nozka[117], K. Ntekas[166], E. Nurse[81], F. Nuti[91], K. O'connor[25], D.C. O'Neil[144], A.A. O'Rourke[45], V. O'Shea[56], F.G. Oakham[31,d], H. Oberlack[103], T. Obermann[23], J. Ocariz[83], A. Ochi[70], I. Ochoa[38], J.P. Ochoa-Ricoux[34a], S. Oda[73], S. Odaka[69], A. Oh[87], S.H. Oh[48], C.C. Ohm[149], H. Ohman[168], H. Oide[53a,53b], H. Okawa[164], Y. Okumura[157], T. Okuyama[69], A. Olariu[28b], L.F. Oleiro Seabra[128a], S.A. Olivares Pino[34a], D. Oliveira Damazio[27], A. Olszewski[42], J. Olszowska[42], A. Onofre[128a,128e], K. Onogi[105], P.U.E. Onyisi[11,z], H. Oppen[121], M.J. Oreglia[33], Y. Oren[155], D. Orestano[136a,136b], N. Orlando[62b], R.S. Orr[161], B. Osculati[53a,53b,*], R. Ospanov[36a], G. Otero y Garzon[29], H. Otono[73], M. Ouchrif[137d], F. Ould-Saada[121], A. Ouraou[138], K.P. Oussoren[109], Q. Ouyang[35a], M. Owen[56], R.E. Owen[19], V.E. Ozcan[20a], N. Ozturk[8], K. Pachal[144], A. Pacheco Pages[13], L. Pacheco Rodriguez[138], C. Padilla Aranda[13], S. Pagan Griso[16], M. Paganini[179], F. Paige[27], G. Palacino[64], S. Palazzo[40a,40b], S. Palestini[32],

JHEP12(2017)059

M. Palka[41b], D. Pallin[37], E.St. Panagiotopoulou[10], I. Panagoulias[10], C.E. Pandini[52], J.G. Panduro Vazquez[80], P. Pani[32], S. Panitkin[27], D. Pantea[28b], L. Paolozzi[52], Th.D. Papadopoulou[10], K. Papageorgiou[9,s], A. Paramonov[6], D. Paredes Hernandez[179], A.J. Parker[75], M.A. Parker[30], K.A. Parker[45], F. Parodi[53a,53b], J.A. Parsons[38], U. Parzefall[51], V.R. Pascuzzi[161], J.M. Pasner[139], E. Pasqualucci[134a], S. Passaggio[53a], Fr. Pastore[80], S. Pataraia[86], J.R. Pater[87], T. Pauly[32], B. Pearson[103], S. Pedraza Lopez[170], R. Pedro[128a,128b], S.V. Peleganchuk[111,c], O. Penc[129], C. Peng[35a], H. Peng[36a], J. Penwell[64], B.S. Peralva[26b], M.M. Perego[138], D.V. Perepelitsa[27], F. Peri[17], L. Perini[94a,94b], H. Pernegger[32], S. Perrella[106a,106b], R. Peschke[45], V.D. Peshekhonov[68,*], K. Peters[45], R.F.Y. Peters[87], B.A. Petersen[32], T.C. Petersen[39], E. Petit[58], A. Petridis[1], C. Petridou[156], P. Petroff[119], E. Petrolo[134a], M. Petrov[122], F. Petrucci[136a,136b], N.E. Pettersson[89], A. Peyaud[138], R. Pezoa[34b], F.H. Phillips[93], P.W. Phillips[133], G. Piacquadio[150], E. Pianori[173], A. Picazio[89], E. Piccaro[79], M.A. Pickering[122], R. Piegaia[29], J.E. Pilcher[33], A.D. Pilkington[87], M. Pinamonti[135a,135b], J.L. Pinfold[3], H. Pirumov[45], M. Pitt[175], L. Plazak[146a], M.-A. Pleier[27], V. Pleskot[86], E. Plotnikova[68], D. Pluth[67], P. Podberezko[111], R. Poettgen[84], R. Poggi[123a,123b], L. Poggioli[119], I. Pogrebnyak[93], D. Pohl[23], I. Pokharel[57], G. Polesello[123a], A. Poley[45], A. Policicchio[40a,40b], R. Polifka[32], A. Polini[22a], C.S. Pollard[56], V. Polychronakos[27], K. Pommès[32], D. Ponomarenko[100], L. Pontecorvo[134a], G.A. Popeneciu[28d], D.M. Portillo Quintero[83], S. Pospisil[130], K. Potamianos[45], I.N. Potrap[68], C.J. Potter[30], H. Potti[11], T. Poulsen[84], J. Poveda[32], M.E. Pozo Astigarraga[32], P. Pralavorio[88], A. Pranko[16], S. Prell[67], D. Price[87], M. Primavera[76a], S. Prince[90], N. Proklova[100], K. Prokofiev[62c], F. Prokoshin[34b], S. Protopopescu[27], J. Proudfoot[6], M. Przybycien[41a], A. Puri[169], P. Puzo[119], J. Qian[92], G. Qin[56], Y. Qin[87], A. Quadt[57], M. Queitsch-Maitland[45], D. Quilty[56], S. Raddum[121], V. Radeka[27], V. Radescu[122], S.K. Radhakrishnan[150], P. Radloff[118], P. Rados[91], F. Ragusa[94a,94b], G. Rahal[181], J.A. Raine[87], S. Rajagopalan[27], C. Rangel-Smith[168], T. Rashid[119], S. Raspopov[5], M.G. Ratti[94a,94b], D.M. Rauch[45], F. Rauscher[102], S. Rave[86], I. Ravinovich[175], J.H. Rawling[87], M. Raymond[32], A.L. Read[121], N.P. Readioff[58], M. Reale[76a,76b], D.M. Rebuzzi[123a,123b], A. Redelbach[177], G. Redlinger[27], R. Reece[139], R.G. Reed[147c], K. Reeves[44], L. Rehnisch[17], J. Reichert[124], A. Reiss[86], C. Rembser[32], H. Ren[35a], M. Rescigno[134a], S. Resconi[94a], E.D. Resseguie[124], S. Rettie[171], E. Reynolds[19], O.L. Rezanova[111,c], P. Reznicek[131], R. Rezvani[97], R. Richter[103], S. Richter[81], E. Richter-Was[41b], O. Ricken[23], M. Ridel[83], P. Rieck[103], C.J. Riegel[178], J. Rieger[57], O. Rifki[115], M. Rijssenbeek[150], A. Rimoldi[123a,123b], M. Rimoldi[18], L. Rinaldi[22a], G. Ripellino[149], B. Ristić[32], E. Ritsch[32], I. Riu[13], F. Rizatdinova[116], E. Rizvi[79], C. Rizzi[13], R.T. Roberts[87], S.H. Robertson[90,o], A. Robichaud-Veronneau[90], D. Robinson[30], J.E.M. Robinson[45], A. Robson[56], E. Rocco[86], C. Roda[126a,126b], Y. Rodina[88,al], S. Rodriguez Bosca[170], A. Rodriguez Perez[13], D. Rodriguez Rodriguez[170], S. Roe[32], C.S. Rogan[59], O. Røhne[121], J. Roloff[59], A. Romaniouk[100], M. Romano[22a,22b], S.M. Romano Saez[37], E. Romero Adam[170], N. Rompotis[77], M. Ronzani[51], L. Roos[83], S. Rosati[134a], K. Rosbach[51], P. Rose[139], N.-A. Rosien[57], E. Rossi[106a,106b], L.P. Rossi[53a], J.H.N. Rosten[30], R. Rosten[140], M. Rotaru[28b], J. Rothberg[140], D. Rousseau[119], A. Rozanov[88], Y. Rozen[154], X. Ruan[147c], F. Rubbo[145], F. Rühr[51], A. Ruiz-Martinez[31], Z. Rurikova[51], N.A. Rusakovich[68], H.L. Russell[90], J.P. Rutherfoord[7], N. Ruthmann[32], Y.F. Ryabov[125], M. Rybar[169], G. Rybkin[119], S. Ryu[6], A. Ryzhov[132], G.F. Rzehorz[57], A.F. Saavedra[152], G. Sabato[109], S. Sacerdoti[29], H.F-W. Sadrozinski[139], R. Sadykov[68], F. Safai Tehrani[134a], P. Saha[110], M. Sahinsoy[60a], M. Saimpert[45], M. Saito[157], T. Saito[157], H. Sakamoto[157], Y. Sakurai[174], G. Salamanna[136a,136b], J.E. Salazar Loyola[34b], D. Salek[109], P.H. Sales De Bruin[168], D. Salihagic[103], A. Salnikov[145], J. Salt[170], D. Salvatore[40a,40b], F. Salvatore[151], A. Salvucci[62a,62b,62c], A. Salzburger[32], D. Sammel[51], D. Sampsonidis[156], D. Sampsonidou[156], J. Sánchez[170], V. Sanchez Martinez[170], A. Sanchez Pineda[167a,167c], H. Sandaker[121], R.L. Sandbach[79], C.O. Sander[45], M. Sandhoff[178],

JHEP12(2017)059

C. Sandoval[21], D.P.C. Sankey[133], M. Sannino[53a,53b], Y. Sano[105], A. Sansoni[50], C. Santoni[37], H. Santos[128a], I. Santoyo Castillo[151], A. Sapronov[68], J.G. Saraiva[128a,128d], B. Sarrazin[23], O. Sasaki[69], K. Sato[164], E. Sauvan[5], G. Savage[80], P. Savard[161,d], N. Savic[103], C. Sawyer[133], L. Sawyer[82,u], J. Saxon[33], C. Sbarra[22a], A. Sbrizzi[22a,22b], T. Scanlon[81], D.A. Scannicchio[166], J. Schaarschmidt[140], P. Schacht[103], B.M. Schachtner[102], D. Schaefer[33], L. Schaefer[124], R. Schaefer[45], J. Schaeffer[86], S. Schaepe[23], S. Schaetzel[60b], U. Schäfer[86], A.C. Schaffer[119], D. Schaile[102], R.D. Schamberger[150], V.A. Schegelsky[125], D. Scheirich[131], M. Schernau[166], C. Schiavi[53a,53b], S. Schier[139], L.K. Schildgen[23], C. Schillo[51], M. Schioppa[40a,40b], S. Schlenker[32], K.R. Schmidt-Sommerfeld[103], K. Schmieden[32], C. Schmitt[86], S. Schmitt[45], S. Schmitz[86], U. Schnoor[51], L. Schoeffel[138], A. Schoening[60b], B.D. Schoenrock[93], E. Schopf[23], M. Schott[86], J.F.P. Schouwenberg[108], J. Schovancova[32], S. Schramm[52], N. Schuh[86], A. Schulte[86], M.J. Schultens[23], H.-C. Schultz-Coulon[60a], H. Schulz[17], M. Schumacher[51], B.A. Schumm[139], Ph. Schune[138], A. Schwartzman[145], T.A. Schwarz[92], H. Schweiger[87], Ph. Schwemling[138], R. Schwienhorst[93], J. Schwindling[138], A. Sciandra[23], G. Sciolla[25], M. Scornajenghi[40a,40b], F. Scuri[126a,126b], F. Scutti[91], J. Searcy[92], P. Seema[23], S.C. Seidel[107], A. Seiden[139], J.M. Seixas[26a], G. Sekhniaidze[106a], K. Sekhon[92], S.J. Sekula[43], N. Semprini-Cesari[22a,22b], S. Senkin[37], C. Serfon[121], L. Serin[119], L. Serkin[167a,167b], M. Sessa[136a,136b], R. Seuster[172], H. Severini[115], T. Sfiligoj[78], F. Sforza[165], A. Sfyrla[52], E. Shabalina[57], N.W. Shaikh[148a,148b], L.Y. Shan[35a], R. Shang[169], J.T. Shank[24], M. Shapiro[16], P.B. Shatalov[99], K. Shaw[167a,167b], S.M. Shaw[87], A. Shcherbakova[148a,148b], C.Y. Shehu[151], Y. Shen[115], N. Sherafati[31], P. Sherwood[81], L. Shi[153,am], S. Shimizu[70], C.O. Shimmin[179], M. Shimojima[104], I.P.J. Shipsey[122], S. Shirabe[73], M. Shiyakova[68,an], J. Shlomi[175], A. Shmeleva[98], D. Shoaleh Saadi[97], M.J. Shochet[33], S. Shojaii[94a,94b], D.R. Shope[115], S. Shrestha[113], E. Shulga[100], M.A. Shupe[7], P. Sicho[129], A.M. Sickles[169], P.E. Sidebo[149], E. Sideras Haddad[147c], O. Sidiropoulou[177], A. Sidoti[22a,22b], F. Siegert[47], Dj. Sijacki[14], J. Silva[128a,128d], S.B. Silverstein[148a], V. Simak[130], Lj. Simic[68], S. Simion[119], E. Simioni[86], B. Simmons[81], M. Simon[86], P. Sinervo[161], N.B. Sinev[118], M. Sioli[22a,22b], G. Siragusa[177], I. Siral[92], S.Yu. Sivoklokov[101], J. Sjölin[148a,148b], M.B. Skinner[75], P. Skubic[115], M. Slater[19], T. Slavicek[130], M. Slawinska[42], K. Sliwa[165], R. Slovak[131], V. Smakhtin[175], B.H. Smart[5], J. Smiesko[146a], N. Smirnov[100], S.Yu. Smirnov[100], Y. Smirnov[100], L.N. Smirnova[101,ao], O. Smirnova[84], J.W. Smith[57], M.N.K. Smith[38], R.W. Smith[38], M. Smizanska[75], K. Smolek[130], A.A. Snesarev[98], I.M. Snyder[118], S. Snyder[27], R. Sobie[172,o], F. Socher[47], A. Soffer[155], A. Søgaard[49], D.A. Soh[153], G. Sokhrannyi[78], C.A. Solans Sanchez[32], M. Solar[130], E.Yu. Soldatov[100], U. Soldevila[170], A.A. Solodkov[132], A. Soloshenko[68], O.V. Solovyanov[132], V. Solovyev[125], P. Sommer[51], H. Son[165], A. Sopczak[130], D. Sosa[60b], C.L. Sotiropoulou[126a,126b], S. Sottocornola[123a,123b], R. Soualah[167a,167c], A.M. Soukharev[111,c], D. South[45], B.C. Sowden[80], S. Spagnolo[76a,76b], M. Spalla[126a,126b], M. Spangenberg[173], F. Spanò[80], D. Sperlich[17], F. Spettel[103], T.M. Spieker[60a], R. Spighi[22a], G. Spigo[32], L.A. Spiller[91], M. Spousta[131], R.D. St. Denis[56,*], A. Stabile[94a], R. Stamen[60a], S. Stamm[17], E. Stanecka[42], R.W. Stanek[6], C. Stanescu[136a], M.M. Stanitzki[45], B.S. Stapf[109], S. Stapnes[121], E.A. Starchenko[132], G.H. Stark[33], J. Stark[58], S.H Stark[39], P. Staroba[129], P. Starovoitov[60a], S. Stärz[32], R. Staszewski[42], M. Stegler[45], P. Steinberg[27], B. Stelzer[144], H.J. Stelzer[32], O. Stelzer-Chilton[163a], H. Stenzel[55], G.A. Stewart[56], M.C. Stockton[118], M. Stoebe[90], G. Stoicea[28b], P. Stolte[57], S. Stonjek[103], A.R. Stradling[8], A. Straessner[47], M.E. Stramaglia[18], J. Strandberg[149], S. Strandberg[148a,148b], M. Strauss[115], P. Strizenec[146b], R. Ströhmer[177], D.M. Strom[118], R. Stroynowski[43], A. Strubig[49], S.A. Stucci[27], B. Stugu[15], N.A. Styles[45], D. Su[145], J. Su[127], S. Suchek[60a], Y. Sugaya[120], M. Suk[130], V.V. Sulin[98], DMS Sultan[162a,162b], S. Sultansoy[4c], T. Sumida[71], S. Sun[59], X. Sun[3], K. Suruliz[151], C.J.E. Suster[152], M.R. Sutton[151], S. Suzuki[69], M. Svatos[129], M. Swiatlowski[33], S.P. Swift[2], I. Sykora[146a], T. Sykora[131], D. Ta[51],

JHEP12(2017)059

K. Tackmann[45], J. Taenzer[155], A. Taffard[166], R. Tafirout[163a], E. Tahirovic[79], N. Taiblum[155], H. Takai[27], R. Takashima[72], E.H. Takasugi[103], K. Takeda[70], T. Takeshita[142], Y. Takubo[69], M. Talby[88], A.A. Talyshev[111,c], J. Tanaka[157], M. Tanaka[159], R. Tanaka[119], S. Tanaka[69], R. Tanioka[70], B.B. Tannenwald[113], S. Tapia Araya[34b], S. Tapprogge[86], S. Tarem[154], G.F. Tartarelli[94a], P. Tas[131], M. Tasevsky[129], T. Tashiro[71], E. Tassi[40a,40b], A. Tavares Delgado[128a,128b], Y. Tayalati[137e], A.C. Taylor[107], A.J. Taylor[49], G.N. Taylor[91], P.T.E. Taylor[91], W. Taylor[163b], P. Teixeira-Dias[80], D. Temple[144], H. Ten Kate[32], P.K. Teng[153], J.J. Teoh[120], F. Tepel[178], S. Terada[69], K. Terashi[157], J. Terron[85], S. Terzo[13], M. Testa[50], R.J. Teuscher[161,o], T. Theveneaux-Pelzer[88], F. Thiele[39], J.P. Thomas[19], J. Thomas-Wilsker[80], P.D. Thompson[19], A.S. Thompson[56], L.A. Thomsen[179], E. Thomson[124], Y. Tian[38], M.J. Tibbetts[16], R.E. Ticse Torres[88], V.O. Tikhomirov[98,ap], Yu.A. Tikhonov[111,c], S. Timoshenko[100], P. Tipton[179], S. Tisserant[88], K. Todome[159], S. Todorova-Nova[5], S. Todt[47], J. Tojo[73], S. Tokár[146a], K. Tokushuku[69], E. Tolley[59], L. Tomlinson[87], M. Tomoto[105], L. Tompkins[145,aq], K. Toms[107], B. Tong[59], P. Tornambe[51], E. Torrence[118], H. Torres[47], E. Torró Pastor[140], J. Toth[88,ar], F. Touchard[88], D.R. Tovey[141], C.J. Treado[112], T. Trefzger[177], F. Tresoldi[151], A. Tricoli[27], I.M. Trigger[163a], S. Trincaz-Duvoid[83], M.F. Tripiana[13], W. Trischuk[161], B. Trocmé[58], A. Trofymov[45], C. Troncon[94a], M. Trottier-McDonald[16], M. Trovatelli[172], L. Truong[147b], M. Trzebinski[42], A. Trzupek[42], K.W. Tsang[62a], J.C-L. Tseng[122], P.V. Tsiareshka[95], G. Tsipolitis[10], N. Tsirintanis[9], S. Tsiskaridze[13], V. Tsiskaridze[51], E.G. Tskhadadze[54a], I.I. Tsukerman[99], V. Tsulaia[16], S. Tsuno[69], D. Tsybychev[150], Y. Tu[62b], A. Tudorache[28b], V. Tudorache[28b], T.T. Tulbure[28a], A.N. Tuna[59], S. Turchikhin[68], D. Turgeman[175], I. Turk Cakir[4b,as], R. Turra[94a], P.M. Tuts[38], G. Ucchielli[22a,22b], I. Ueda[69], M. Ughetto[148a,148b], F. Ukegawa[164], G. Unal[32], A. Undrus[27], G. Unel[166], F.C. Ungaro[91], Y. Unno[69], K. Uno[157], C. Unverdorben[102], J. Urban[146b], P. Urquijo[91], P. Urrejola[86], G. Usai[8], J. Usui[69], L. Vacavant[88], V. Vacek[130], B. Vachon[90], K.O.H. Vadla[121], A. Vaidya[81], C. Valderanis[102], E. Valdes Santurio[148a,148b], M. Valente[52], S. Valentinetti[22a,22b], A. Valero[170], L. Valéry[13], S. Valkar[131], A. Vallier[5], J.A. Valls Ferrer[170], W. Van Den Wollenberg[109], H. van der Graaf[109], P. van Gemmeren[6], J. Van Nieuwkoop[144], I. van Vulpen[109], M.C. van Woerden[109], M. Vanadia[135a,135b], W. Vandelli[32], A. Vaniachine[160], P. Vankov[109], G. Vardanyan[180], R. Vari[134a], E.W. Varnes[7], C. Varni[53a,53b], T. Varol[43], D. Varouchas[119], A. Vartapetian[8], K.E. Varvell[152], J.G. Vasquez[179], G.A. Vasquez[34b], F. Vazeille[37], D. Vazquez Furelos[13], T. Vazquez Schroeder[90], J. Veatch[57], V. Veeraraghavan[7], L.M. Veloce[161], F. Veloso[128a,128c], S. Veneziano[134a], A. Ventura[76a,76b], M. Venturi[172], N. Venturi[32], A. Venturini[25], V. Vercesi[123a], M. Verducci[136a,136b], W. Verkerke[109], A.T. Vermeulen[109], J.C. Vermeulen[109], M.C. Vetterli[144,d], N. Viaux Maira[34b], O. Viazlo[84], I. Vichou[169,*], T. Vickey[141], O.E. Vickey Boeriu[141], G.H.A. Viehhauser[122], S. Viel[16], L. Vigani[122], M. Villa[22a,22b], M. Villaplana Perez[94a,94b], E. Vilucchi[50], M.G. Vincter[31], V.B. Vinogradov[68], A. Vishwakarma[45], C. Vittori[22a,22b], I. Vivarelli[151], S. Vlachos[10], M. Vogel[178], P. Vokac[130], G. Volpi[13], H. von der Schmitt[103], E. von Toerne[23], V. Vorobel[131], K. Vorobev[100], M. Vos[170], R. Voss[32], J.H. Vossebeld[77], N. Vranjes[14], M. Vranjes Milosavljevic[14], V. Vrba[130], M. Vreeswijk[109], R. Vuillermet[32], I. Vukotic[33], P. Wagner[23], W. Wagner[178], J. Wagner-Kuhr[102], H. Wahlberg[74], S. Wahrmund[47], J. Walder[75], R. Walker[102], W. Walkowiak[143], V. Wallangen[148a,148b], C. Wang[35b], C. Wang[36b,at], F. Wang[176], H. Wang[16], H. Wang[3], J. Wang[45], J. Wang[152], Q. Wang[115], R.-J. Wang[83], R. Wang[6], S.M. Wang[153], T. Wang[38], W. Wang[153,au], W. Wang[36a,av], Z. Wang[36c], C. Wanotayaroj[45], A. Warburton[90], C.P. Ward[30], D.R. Wardrope[81], A. Washbrook[49], P.M. Watkins[19], A.T. Watson[19], M.F. Watson[19], G. Watts[140], S. Watts[87], B.M. Waugh[81], A.F. Webb[11], S. Webb[86], M.S. Weber[18], S.M. Weber[60a], S.W. Weber[177], S.A. Weber[31], J.S. Webster[6], A.R. Weidberg[122], B. Weinert[64], J. Weingarten[57], M. Weirich[86],

JHEP12(2017)059

C. Weiser[51], H. Weits[109], P.S. Wells[32], T. Wenaus[27], T. Wengler[32], S. Wenig[32], N. Wermes[23], M.D. Werner[67], P. Werner[32], M. Wessels[60a], T.D. Weston[18], K. Whalen[118], N.L. Whallon[140], A.M. Wharton[75], A.S. White[92], A. White[8], M.J. White[1], R. White[34b], D. Whiteson[166], B.W. Whitmore[75], F.J. Wickens[133], W. Wiedenmann[176], M. Wielers[133], C. Wiglesworth[39], L.A.M. Wiik-Fuchs[51], A. Wildauer[103], F. Wilk[87], H.G. Wilkens[32], H.H. Williams[124], S. Williams[109], C. Willis[93], S. Willocq[89], J.A. Wilson[19], I. Wingerter-Seez[5], E. Winkels[151], F. Winklmeier[118], O.J. Winston[151], B.T. Winter[23], M. Wittgen[145], M. Wobisch[82,u], T.M.H. Wolf[109], R. Wolff[88], M.W. Wolter[42], H. Wolters[128a,128c], V.W.S. Wong[171], N.L. Woods[139], S.D. Worm[19], B.K. Wosiek[42], J. Wotschack[32], K.W. Wozniak[42], M. Wu[33], S.L. Wu[176], X. Wu[52], Y. Wu[92], T.R. Wyatt[87], B.M. Wynne[49], S. Xella[39], Z. Xi[92], L. Xia[35c], D. Xu[35a], L. Xu[27], T. Xu[138], B. Yabsley[152], S. Yacoob[147a], D. Yamaguchi[159], Y. Yamaguchi[159], A. Yamamoto[69], S. Yamamoto[157], T. Yamanaka[157], F. Yamane[70], M. Yamatani[157], Y. Yamazaki[70], Z. Yan[24], H. Yang[36c], H. Yang[16], Y. Yang[153], Z. Yang[15], W-M. Yao[16], Y.C. Yap[45], Y. Yasu[69], E. Yatsenko[5], K.H. Yau Wong[23], J. Ye[43], S. Ye[27], I. Yeletskikh[68], E. Yigitbasi[24], E. Yildirim[86], K. Yorita[174], K. Yoshihara[124], C. Young[145], C.J.S. Young[32], J. Yu[8], J. Yu[67], S.P.Y. Yuen[23], I. Yusuff[30,aw], B. Zabinski[42], G. Zacharis[10], R. Zaidan[13], A.M. Zaitsev[132,aj], N. Zakharchuk[45], J. Zalieckas[15], A. Zaman[150], S. Zambito[59], D. Zanzi[91], C. Zeitnitz[178], G. Zemaityte[122], A. Zemla[41a], J.C. Zeng[169], Q. Zeng[145], O. Zenin[132], T. Ženiš[146a], D. Zerwas[119], D. Zhang[36b], D. Zhang[92], F. Zhang[176], G. Zhang[36a,av], H. Zhang[119], J. Zhang[6], L. Zhang[51], L. Zhang[36a], M. Zhang[169], P. Zhang[35b], R. Zhang[23], R. Zhang[36a,at], X. Zhang[36b], Y. Zhang[35a], Z. Zhang[119], X. Zhao[43], Y. Zhao[36b,ax], Z. Zhao[36a], A. Zhemchugov[68], B. Zhou[92], C. Zhou[176], L. Zhou[43], M. Zhou[35a], M. Zhou[150], N. Zhou[35c], C.G. Zhu[36b], H. Zhu[35a], J. Zhu[92], Y. Zhu[36a], X. Zhuang[35a], K. Zhukov[98], A. Zibell[177], D. Zieminska[64], N.I. Zimine[68], C. Zimmermann[86], S. Zimmermann[51], Z. Zinonos[103], M. Zinser[86], M. Ziolkowski[143], L. Živković[14], G. Zobernig[176], A. Zoccoli[22a,22b], R. Zou[33], M. zur Nedden[17], L. Zwalinski[32].

[1] *Department of Physics, University of Adelaide, Adelaide, Australia*
[2] *Physics Department, SUNY Albany, Albany NY, United States of America*
[3] *Department of Physics, University of Alberta, Edmonton AB, Canada*
[4] [(a)] *Department of Physics, Ankara University, Ankara;* [(b)] *Istanbul Aydin University, Istanbul;* [(c)] *Division of Physics, TOBB University of Economics and Technology, Ankara, Turkey*
[5] *LAPP, CNRS/IN2P3 and Université Savoie Mont Blanc, Annecy-le-Vieux, France*
[6] *High Energy Physics Division, Argonne National Laboratory, Argonne IL, United States of America*
[7] *Department of Physics, University of Arizona, Tucson AZ, United States of America*
[8] *Department of Physics, The University of Texas at Arlington, Arlington TX, United States of America*
[9] *Physics Department, National and Kapodistrian University of Athens, Athens, Greece*
[10] *Physics Department, National Technical University of Athens, Zografou, Greece*
[11] *Department of Physics, The University of Texas at Austin, Austin TX, United States of America*
[12] *Institute of Physics, Azerbaijan Academy of Sciences, Baku, Azerbaijan*
[13] *Institut de Física d'Altes Energies (IFAE), The Barcelona Institute of Science and Technology, Barcelona, Spain*
[14] *Institute of Physics, University of Belgrade, Belgrade, Serbia*
[15] *Department for Physics and Technology, University of Bergen, Bergen, Norway*
[16] *Physics Division, Lawrence Berkeley National Laboratory and University of California, Berkeley CA, United States of America*
[17] *Department of Physics, Humboldt University, Berlin, Germany*
[18] *Albert Einstein Center for Fundamental Physics and Laboratory for High Energy Physics, University of Bern, Bern, Switzerland*
[19] *School of Physics and Astronomy, University of Birmingham, Birmingham, United Kingdom*

JHEP12(2017)059

[20] [(a)] Department of Physics, Bogazici University, Istanbul; [(b)] Department of Physics Engineering, Gaziantep University, Gaziantep; [(d)] Istanbul Bilgi University, Faculty of Engineering and Natural Sciences, Istanbul; [(e)] Bahcesehir University, Faculty of Engineering and Natural Sciences, Istanbul, Turkey
[21] Centro de Investigaciones, Universidad Antonio Narino, Bogota, Colombia
[22] [(a)] INFN Sezione di Bologna; [(b)] Dipartimento di Fisica e Astronomia, Università di Bologna, Bologna, Italy
[23] Physikalisches Institut, University of Bonn, Bonn, Germany
[24] Department of Physics, Boston University, Boston MA, United States of America
[25] Department of Physics, Brandeis University, Waltham MA, United States of America
[26] [(a)] Universidade Federal do Rio De Janeiro COPPE/EE/IF, Rio de Janeiro; [(b)] Electrical Circuits Department, Federal University of Juiz de Fora (UFJF), Juiz de Fora; [(c)] Federal University of Sao Joao del Rei (UFSJ), Sao Joao del Rei; [(d)] Instituto de Fisica, Universidade de Sao Paulo, Sao Paulo, Brazil
[27] Physics Department, Brookhaven National Laboratory, Upton NY, United States of America
[28] [(a)] Transilvania University of Brasov, Brasov; [(b)] Horia Hulubei National Institute of Physics and Nuclear Engineering, Bucharest; [(c)] Department of Physics, Alexandru Ioan Cuza University of Iasi, Iasi; [(d)] National Institute for Research and Development of Isotopic and Molecular Technologies, Physics Department, Cluj Napoca; [(e)] University Politehnica Bucharest, Bucharest; [(f)] West University in Timisoara, Timisoara, Romania
[29] Departamento de Física, Universidad de Buenos Aires, Buenos Aires, Argentina
[30] Cavendish Laboratory, University of Cambridge, Cambridge, United Kingdom
[31] Department of Physics, Carleton University, Ottawa ON, Canada
[32] CERN, Geneva, Switzerland
[33] Enrico Fermi Institute, University of Chicago, Chicago IL, United States of America
[34] [(a)] Departamento de Física, Pontificia Universidad Católica de Chile, Santiago; [(b)] Departamento de Física, Universidad Técnica Federico Santa María, Valparaíso, Chile
[35] [(a)] Institute of High Energy Physics, Chinese Academy of Sciences, Beijing; [(b)] Department of Physics, Nanjing University, Jiangsu; [(c)] Physics Department, Tsinghua University, Beijing 100084, China
[36] [(a)] Department of Modern Physics and State Key Laboratory of Particle Detection and Electronics, University of Science and Technology of China, Anhui; [(b)] School of Physics, Shandong University, Shandong; [(c)] Department of Physics and Astronomy, Key Laboratory for Particle Physics, Astrophysics and Cosmology, Ministry of Education; Shanghai Key Laboratory for Particle Physics and Cosmology, Shanghai Jiao Tong University, Shanghai(also at PKU-CHEP), China
[37] Université Clermont Auvergne, CNRS/IN2P3, LPC, Clermont-Ferrand, France
[38] Nevis Laboratory, Columbia University, Irvington NY, United States of America
[39] Niels Bohr Institute, University of Copenhagen, Kobenhavn, Denmark
[40] [(a)] INFN Gruppo Collegato di Cosenza, Laboratori Nazionali di Frascati; [(b)] Dipartimento di Fisica, Università della Calabria, Rende, Italy
[41] [(a)] AGH University of Science and Technology, Faculty of Physics and Applied Computer Science, Krakow; [(b)] Marian Smoluchowski Institute of Physics, Jagiellonian University, Krakow, Poland
[42] Institute of Nuclear Physics Polish Academy of Sciences, Krakow, Poland
[43] Physics Department, Southern Methodist University, Dallas TX, United States of America
[44] Physics Department, University of Texas at Dallas, Richardson TX, United States of America
[45] DESY, Hamburg and Zeuthen, Germany
[46] Lehrstuhl für Experimentelle Physik IV, Technische Universität Dortmund, Dortmund, Germany
[47] Institut für Kern- und Teilchenphysik, Technische Universität Dresden, Dresden, Germany
[48] Department of Physics, Duke University, Durham NC, United States of America
[49] SUPA - School of Physics and Astronomy, University of Edinburgh, Edinburgh, United Kingdom
[50] INFN e Laboratori Nazionali di Frascati, Frascati, Italy
[51] Fakultät für Mathematik und Physik, Albert-Ludwigs-Universität, Freiburg, Germany

JHEP12(2017)059

[52] Departement de Physique Nucleaire et Corpusculaire, Université de Genève, Geneva, Switzerland
[53] [(a)] INFN Sezione di Genova; [(b)] Dipartimento di Fisica, Università di Genova, Genova, Italy
[54] [(a)] E. Andronikashvili Institute of Physics, Iv. Javakhishvili Tbilisi State University, Tbilisi; [(b)] High Energy Physics Institute, Tbilisi State University, Tbilisi, Georgia
[55] II Physikalisches Institut, Justus-Liebig-Universität Giessen, Giessen, Germany
[56] SUPA - School of Physics and Astronomy, University of Glasgow, Glasgow, United Kingdom
[57] II Physikalisches Institut, Georg-August-Universität, Göttingen, Germany
[58] Laboratoire de Physique Subatomique et de Cosmologie, Université Grenoble-Alpes, CNRS/IN2P3, Grenoble, France
[59] Laboratory for Particle Physics and Cosmology, Harvard University, Cambridge MA, United States of America
[60] [(a)] Kirchhoff-Institut für Physik, Ruprecht-Karls-Universität Heidelberg, Heidelberg; [(b)] Physikalisches Institut, Ruprecht-Karls-Universität Heidelberg, Heidelberg, Germany
[61] Faculty of Applied Information Science, Hiroshima Institute of Technology, Hiroshima, Japan
[62] [(a)] Department of Physics, The Chinese University of Hong Kong, Shatin, N.T., Hong Kong; [(b)] Department of Physics, The University of Hong Kong, Hong Kong; [(c)] Department of Physics and Institute for Advanced Study, The Hong Kong University of Science and Technology, Clear Water Bay, Kowloon, Hong Kong, China
[63] Department of Physics, National Tsing Hua University, Taiwan, Taiwan
[64] Department of Physics, Indiana University, Bloomington IN, United States of America
[65] Institut für Astro- und Teilchenphysik, Leopold-Franzens-Universität, Innsbruck, Austria
[66] University of Iowa, Iowa City IA, United States of America
[67] Department of Physics and Astronomy, Iowa State University, Ames IA, United States of America
[68] Joint Institute for Nuclear Research, JINR Dubna, Dubna, Russia
[69] KEK, High Energy Accelerator Research Organization, Tsukuba, Japan
[70] Graduate School of Science, Kobe University, Kobe, Japan
[71] Faculty of Science, Kyoto University, Kyoto, Japan
[72] Kyoto University of Education, Kyoto, Japan
[73] Research Center for Advanced Particle Physics and Department of Physics, Kyushu University, Fukuoka, Japan
[74] Instituto de Física La Plata, Universidad Nacional de La Plata and CONICET, La Plata, Argentina
[75] Physics Department, Lancaster University, Lancaster, United Kingdom
[76] [(a)] INFN Sezione di Lecce; [(b)] Dipartimento di Matematica e Fisica, Università del Salento, Lecce, Italy
[77] Oliver Lodge Laboratory, University of Liverpool, Liverpool, United Kingdom
[78] Department of Experimental Particle Physics, Jožef Stefan Institute and Department of Physics, University of Ljubljana, Ljubljana, Slovenia
[79] School of Physics and Astronomy, Queen Mary University of London, London, United Kingdom
[80] Department of Physics, Royal Holloway University of London, Surrey, United Kingdom
[81] Department of Physics and Astronomy, University College London, London, United Kingdom
[82] Louisiana Tech University, Ruston LA, United States of America
[83] Laboratoire de Physique Nucléaire et de Hautes Energies, UPMC and Université Paris-Diderot and CNRS/IN2P3, Paris, France
[84] Fysiska institutionen, Lunds universitet, Lund, Sweden
[85] Departamento de Fisica Teorica C-15, Universidad Autonoma de Madrid, Madrid, Spain
[86] Institut für Physik, Universität Mainz, Mainz, Germany
[87] School of Physics and Astronomy, University of Manchester, Manchester, United Kingdom
[88] CPPM, Aix-Marseille Université and CNRS/IN2P3, Marseille, France
[89] Department of Physics, University of Massachusetts, Amherst MA, United States of America
[90] Department of Physics, McGill University, Montreal QC, Canada
[91] School of Physics, University of Melbourne, Victoria, Australia
[92] Department of Physics, The University of Michigan, Ann Arbor MI, United States of America

JHEP12(2017)059

[93] *Department of Physics and Astronomy, Michigan State University, East Lansing MI, United States of America*
[94] [(a)] *INFN Sezione di Milano;* [(b)] *Dipartimento di Fisica, Università di Milano, Milano, Italy*
[95] *B.I. Stepanov Institute of Physics, National Academy of Sciences of Belarus, Minsk, Republic of Belarus*
[96] *Research Institute for Nuclear Problems of Byelorussian State University, Minsk, Republic of Belarus*
[97] *Group of Particle Physics, University of Montreal, Montreal QC, Canada*
[98] *P.N. Lebedev Physical Institute of the Russian Academy of Sciences, Moscow, Russia*
[99] *Institute for Theoretical and Experimental Physics (ITEP), Moscow, Russia*
[100] *National Research Nuclear University MEPhI, Moscow, Russia*
[101] *D.V. Skobeltsyn Institute of Nuclear Physics, M.V. Lomonosov Moscow State University, Moscow, Russia*
[102] *Fakultät für Physik, Ludwig-Maximilians-Universität München, München, Germany*
[103] *Max-Planck-Institut für Physik (Werner-Heisenberg-Institut), München, Germany*
[104] *Nagasaki Institute of Applied Science, Nagasaki, Japan*
[105] *Graduate School of Science and Kobayashi-Maskawa Institute, Nagoya University, Nagoya, Japan*
[106] [(a)] *INFN Sezione di Napoli;* [(b)] *Dipartimento di Fisica, Università di Napoli, Napoli, Italy*
[107] *Department of Physics and Astronomy, University of New Mexico, Albuquerque NM, United States of America*
[108] *Institute for Mathematics, Astrophysics and Particle Physics, Radboud University Nijmegen/Nikhef, Nijmegen, Netherlands*
[109] *Nikhef National Institute for Subatomic Physics and University of Amsterdam, Amsterdam, Netherlands*
[110] *Department of Physics, Northern Illinois University, DeKalb IL, United States of America*
[111] *Budker Institute of Nuclear Physics, SB RAS, Novosibirsk, Russia*
[112] *Department of Physics, New York University, New York NY, United States of America*
[113] *Ohio State University, Columbus OH, United States of America*
[114] *Faculty of Science, Okayama University, Okayama, Japan*
[115] *Homer L. Dodge Department of Physics and Astronomy, University of Oklahoma, Norman OK, United States of America*
[116] *Department of Physics, Oklahoma State University, Stillwater OK, United States of America*
[117] *Palacký University, RCPTM, Olomouc, Czech Republic*
[118] *Center for High Energy Physics, University of Oregon, Eugene OR, United States of America*
[119] *LAL, Univ. Paris-Sud, CNRS/IN2P3, Université Paris-Saclay, Orsay, France*
[120] *Graduate School of Science, Osaka University, Osaka, Japan*
[121] *Department of Physics, University of Oslo, Oslo, Norway*
[122] *Department of Physics, Oxford University, Oxford, United Kingdom*
[123] [(a)] *INFN Sezione di Pavia;* [(b)] *Dipartimento di Fisica, Università di Pavia, Pavia, Italy*
[124] *Department of Physics, University of Pennsylvania, Philadelphia PA, United States of America*
[125] *National Research Centre "Kurchatov Institute" B.P.Konstantinov Petersburg Nuclear Physics Institute, St. Petersburg, Russia*
[126] [(a)] *INFN Sezione di Pisa;* [(b)] *Dipartimento di Fisica E. Fermi, Università di Pisa, Pisa, Italy*
[127] *Department of Physics and Astronomy, University of Pittsburgh, Pittsburgh PA, United States of America*
[128] [(a)] *Laboratório de Instrumentação e Física Experimental de Partículas - LIP, Lisboa;* [(b)] *Faculdade de Ciências, Universidade de Lisboa, Lisboa;* [(c)] *Department of Physics, University of Coimbra, Coimbra;* [(d)] *Centro de Física Nuclear da Universidade de Lisboa, Lisboa;* [(e)] *Departamento de Fisica, Universidade do Minho, Braga;* [(f)] *Departamento de Fisica Teorica y del Cosmos, Universidad de Granada, Granada;* [(g)] *Dep Fisica and CEFITEC of Faculdade de Ciencias e Tecnologia, Universidade Nova de Lisboa, Caparica, Portugal*
[129] *Institute of Physics, Academy of Sciences of the Czech Republic, Praha, Czech Republic*

JHEP12(2017)059

[130] Czech Technical University in Prague, Praha, Czech Republic
[131] Charles University, Faculty of Mathematics and Physics, Prague, Czech Republic
[132] State Research Center Institute for High Energy Physics (Protvino), NRC KI, Russia
[133] Particle Physics Department, Rutherford Appleton Laboratory, Didcot, United Kingdom
[134] [(a)] INFN Sezione di Roma; [(b)] Dipartimento di Fisica, Sapienza Università di Roma, Roma, Italy
[135] [(a)] INFN Sezione di Roma Tor Vergata; [(b)] Dipartimento di Fisica, Università di Roma Tor Vergata, Roma, Italy
[136] [(a)] INFN Sezione di Roma Tre; [(b)] Dipartimento di Matematica e Fisica, Università Roma Tre, Roma, Italy
[137] [(a)] Faculté des Sciences Ain Chock, Réseau Universitaire de Physique des Hautes Energies - Université Hassan II, Casablanca; [(b)] Centre National de l'Energie des Sciences Techniques Nucleaires, Rabat; [(c)] Faculté des Sciences Semlalia, Université Cadi Ayyad, LPHEA-Marrakech; [(d)] Faculté des Sciences, Université Mohamed Premier and LPTPM, Oujda; [(e)] Faculté des sciences, Université Mohammed V, Rabat, Morocco
[138] DSM/IRFU (Institut de Recherches sur les Lois Fondamentales de l'Univers), CEA Saclay (Commissariat à l'Energie Atomique et aux Energies Alternatives), Gif-sur-Yvette, France
[139] Santa Cruz Institute for Particle Physics, University of California Santa Cruz, Santa Cruz CA, United States of America
[140] Department of Physics, University of Washington, Seattle WA, United States of America
[141] Department of Physics and Astronomy, University of Sheffield, Sheffield, United Kingdom
[142] Department of Physics, Shinshu University, Nagano, Japan
[143] Department Physik, Universität Siegen, Siegen, Germany
[144] Department of Physics, Simon Fraser University, Burnaby BC, Canada
[145] SLAC National Accelerator Laboratory, Stanford CA, United States of America
[146] [(a)] Faculty of Mathematics, Physics & Informatics, Comenius University, Bratislava; [(b)] Department of Subnuclear Physics, Institute of Experimental Physics of the Slovak Academy of Sciences, Kosice, Slovak Republic
[147] [(a)] Department of Physics, University of Cape Town, Cape Town; [(b)] Department of Physics, University of Johannesburg, Johannesburg; [(c)] School of Physics, University of the Witwatersrand, Johannesburg, South Africa
[148] [(a)] Department of Physics, Stockholm University; [(b)] The Oskar Klein Centre, Stockholm, Sweden
[149] Physics Department, Royal Institute of Technology, Stockholm, Sweden
[150] Departments of Physics & Astronomy and Chemistry, Stony Brook University, Stony Brook NY, United States of America
[151] Department of Physics and Astronomy, University of Sussex, Brighton, United Kingdom
[152] School of Physics, University of Sydney, Sydney, Australia
[153] Institute of Physics, Academia Sinica, Taipei, Taiwan
[154] Department of Physics, Technion: Israel Institute of Technology, Haifa, Israel
[155] Raymond and Beverly Sackler School of Physics and Astronomy, Tel Aviv University, Tel Aviv, Israel
[156] Department of Physics, Aristotle University of Thessaloniki, Thessaloniki, Greece
[157] International Center for Elementary Particle Physics and Department of Physics, The University of Tokyo, Tokyo, Japan
[158] Graduate School of Science and Technology, Tokyo Metropolitan University, Tokyo, Japan
[159] Department of Physics, Tokyo Institute of Technology, Tokyo, Japan
[160] Tomsk State University, Tomsk, Russia
[161] Department of Physics, University of Toronto, Toronto ON, Canada
[162] [(a)] INFN-TIFPA; [(b)] University of Trento, Trento, Italy
[163] [(a)] TRIUMF, Vancouver BC; [(b)] Department of Physics and Astronomy, York University, Toronto ON, Canada
[164] Faculty of Pure and Applied Sciences, and Center for Integrated Research in Fundamental Science and Engineering, University of Tsukuba, Tsukuba, Japan

JHEP12(2017)059

[165] Department of Physics and Astronomy, Tufts University, Medford MA, United States of America
[166] Department of Physics and Astronomy, University of California Irvine, Irvine CA, United States of America
[167] [(a)] INFN Gruppo Collegato di Udine, Sezione di Trieste, Udine; [(b)] ICTP, Trieste; [(c)] Dipartimento di Chimica, Fisica e Ambiente, Università di Udine, Udine, Italy
[168] Department of Physics and Astronomy, University of Uppsala, Uppsala, Sweden
[169] Department of Physics, University of Illinois, Urbana IL, United States of America
[170] Instituto de Fisica Corpuscular (IFIC), Centro Mixto Universidad de Valencia - CSIC, Spain
[171] Department of Physics, University of British Columbia, Vancouver BC, Canada
[172] Department of Physics and Astronomy, University of Victoria, Victoria BC, Canada
[173] Department of Physics, University of Warwick, Coventry, United Kingdom
[174] Waseda University, Tokyo, Japan
[175] Department of Particle Physics, The Weizmann Institute of Science, Rehovot, Israel
[176] Department of Physics, University of Wisconsin, Madison WI, United States of America
[177] Fakultät für Physik und Astronomie, Julius-Maximilians-Universität, Würzburg, Germany
[178] Fakultät für Mathematik und Naturwissenschaften, Fachgruppe Physik, Bergische Universität Wuppertal, Wuppertal, Germany
[179] Department of Physics, Yale University, New Haven CT, United States of America
[180] Yerevan Physics Institute, Yerevan, Armenia
[181] Centre de Calcul de l'Institut National de Physique Nucléaire et de Physique des Particules (IN2P3), Villeurbanne, France
[182] Academia Sinica Grid Computing, Institute of Physics, Academia Sinica, Taipei, Taiwan

[a] Also at Department of Physics, King's College London, London, United Kingdom
[b] Also at Institute of Physics, Azerbaijan Academy of Sciences, Baku, Azerbaijan
[c] Also at Novosibirsk State University, Novosibirsk, Russia
[d] Also at TRIUMF, Vancouver BC, Canada
[e] Also at Department of Physics & Astronomy, University of Louisville, Louisville, KY, United States of America
[f] Also at Physics Department, An-Najah National University, Nablus, Palestine
[g] Also at Department of Physics, California State University, Fresno CA, United States of America
[h] Also at Department of Physics, University of Fribourg, Fribourg, Switzerland
[i] Also at II Physikalisches Institut, Georg-August-Universität, Göttingen, Germany
[j] Also at Departament de Fisica de la Universitat Autonoma de Barcelona, Barcelona, Spain
[k] Also at Departamento de Fisica e Astronomia, Faculdade de Ciencias, Universidade do Porto, Portugal
[l] Also at Tomsk State University, Tomsk, and Moscow Institute of Physics and Technology State University, Dolgoprudny, Russia
[m] Also at The Collaborative Innovation Center of Quantum Matter (CICQM), Beijing, China
[n] Also at Universita di Napoli Parthenope, Napoli, Italy
[o] Also at Institute of Particle Physics (IPP), Canada
[p] Also at Horia Hulubei National Institute of Physics and Nuclear Engineering, Bucharest, Romania
[q] Also at Department of Physics, St. Petersburg State Polytechnical University, St. Petersburg, Russia
[r] Also at Borough of Manhattan Community College, City University of New York, New York City, United States of America
[s] Also at Department of Financial and Management Engineering, University of the Aegean, Chios, Greece
[t] Also at Centre for High Performance Computing, CSIR Campus, Rosebank, Cape Town, South Africa
[u] Also at Louisiana Tech University, Ruston LA, United States of America
[v] Also at Institucio Catalana de Recerca i Estudis Avancats, ICREA, Barcelona, Spain

JHEP12(2017)059

[w] Also at Graduate School of Science, Osaka University, Osaka, Japan
[x] Also at Fakultät für Mathematik und Physik, Albert-Ludwigs-Universität, Freiburg, Germany
[y] Also at Institute for Mathematics, Astrophysics and Particle Physics, Radboud University Nijmegen/Nikhef, Nijmegen, Netherlands
[z] Also at Department of Physics, The University of Texas at Austin, Austin TX, United States of America
[aa] Also at Institute of Theoretical Physics, Ilia State University, Tbilisi, Georgia
[ab] Also at CERN, Geneva, Switzerland
[ac] Also at Georgian Technical University (GTU),Tbilisi, Georgia
[ad] Also at Ochadai Academic Production, Ochanomizu University, Tokyo, Japan
[ae] Also at Manhattan College, New York NY, United States of America
[af] Also at Department of Physics, The University of Michigan, Ann Arbor MI, United States of America
[ag] Also at The City College of New York, New York NY, United States of America
[ah] Also at Departamento de Fisica Teorica y del Cosmos, Universidad de Granada, Granada, Portugal
[ai] Also at Department of Physics, California State University, Sacramento CA, United States of America
[aj] Also at Moscow Institute of Physics and Technology State University, Dolgoprudny, Russia
[ak] Also at Departement de Physique Nucleaire et Corpusculaire, Université de Genève, Geneva, Switzerland
[al] Also at Institut de Física d'Altes Energies (IFAE), The Barcelona Institute of Science and Technology, Barcelona, Spain
[am] Also at School of Physics, Sun Yat-sen University, Guangzhou, China
[an] Also at Institute for Nuclear Research and Nuclear Energy (INRNE) of the Bulgarian Academy of Sciences, Sofia, Bulgaria
[ao] Also at Faculty of Physics, M.V.Lomonosov Moscow State University, Moscow, Russia
[ap] Also at National Research Nuclear University MEPhI, Moscow, Russia
[aq] Also at Department of Physics, Stanford University, Stanford CA, United States of America
[ar] Also at Institute for Particle and Nuclear Physics, Wigner Research Centre for Physics, Budapest, Hungary
[as] Also at Giresun University, Faculty of Engineering, Turkey
[at] Also at CPPM, Aix-Marseille Université and CNRS/IN2P3, Marseille, France
[au] Also at Department of Physics, Nanjing University, Jiangsu, China
[av] Also at Institute of Physics, Academia Sinica, Taipei, Taiwan
[aw] Also at University of Malaya, Department of Physics, Kuala Lumpur, Malaysia
[ax] Also at LAL, Univ. Paris-Sud, CNRS/IN2P3, Université Paris-Saclay, Orsay, France
[*] Deceased

JHEP12(2017)059

Eur. Phys. J. C (2018) 78:898
https://doi.org/10.1140/epjc/s10052-018-6354-3

THE EUROPEAN PHYSICAL JOURNAL C

Erratum

Erratum to: Measurement of the W-boson mass in pp collisions at $\sqrt{s} = 7$ TeV with the ATLAS detector

ATLAS Collaboration[⋆]

CERN, 1211 Geneva 23, Switzerland

Received: 16 October 2018 / Accepted: 17 October 2018 / Published online: 5 November 2018

Erratum to:
Eur. Phys. J. C (2018) 78:110
https://doi.org/10.1140/epjc/s10052-017-5475-4

It has been found that Fig. 30 shows the 68% and 99% confidence-level contours for the W boson and top quark mass measurements, instead of the 68% and 95% confidence-level contours, as stated in the legend. The corrected error ellipses, corresponding to 68% and 95% confidence level, are shown in Fig. 1.

Funded by SCOAP[3].

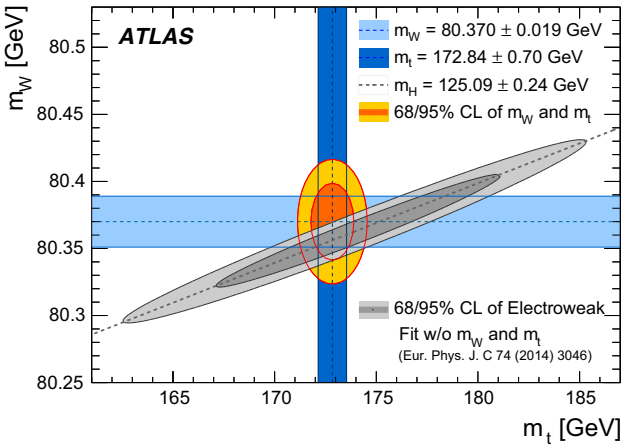

Fig. 1 Replacement of Fig. 30: The 68% and 95% confidence-level contours of the m_W and m_t indirect determination from the global electroweak fit [1] are compared to the 68 and 95% confidence-level contours of the ATLAS measurements of the top-quark and W-boson masses. The determination from the electroweak fit uses as input the LHC measurement of the Higgs-boson mass, $m_H = 125.09 \pm 0.24$ GeV [2]

References

1. M. Baak et al., The global electroweak fit at NNLO and prospects for the LHC and ILC. Eur. Phys. J. C **74**, 3046 (2014). arXiv:1407.3792 [hep-ph]
2. ATLAS and CMS Collaborations, Combined measurement of the Higgs Boson mass in pp collisions at $\sqrt{s} = 7$ and 8 TeV with the ATLAS and CMS experiments. Phys. Rev. Lett. **114**, 191803 (2015). arXiv:1503.07589 [hep-ex]

The original article can be found online at https://doi.org/10.1140/epjc/s10052-017-5475-4.

⋆ e-mail: atlas.publications@cern.ch

ATLAS Collaboration

M. Aaboud[137d], G. Aad[88], B. Abbott[115], J. Abdallah[8], O. Abdinov[12], B. Abeloos[119], S. H. Abidi[161], O. S. AbouZeid[139], N. L. Abraham[151], H. Abramowicz[155], H. Abreu[154], R. Abreu[118], Y. Abulaiti[148a,148b], B. S. Acharya[167a,167b,a], S. Adachi[157], L. Adamczyk[41a], D. L. Adams[27], J. Adelman[110], M. Adersberger[102], T. Adye[133], A. A. Affolder[139], T. Agatonovic-Jovin[14], C. Agheorghiesei[28b], J. A. Aguilar-Saavedra[128a,128f], S. P. Ahlen[24], F. Ahmadov[68,b], G. Aielli[135a,135b], S. Akatsuka[71], H. Akerstedt[148a,148b], T. P. A. Åkesson[84], A. V. Akimov[98], G. L. Alberghi[22a,22b], J. Albert[172], M. J. Alconada Verzini[74], M. Aleksa[32], I. N. Aleksandrov[68], C. Alexa[28b], G. Alexander[155], T. Alexopoulos[10], M. Alhroob[115], B. Ali[130], M. Aliev[76a,76b], G. Alimonti[94a], J. Alison[33], S. P. Alkire[38], B. M. M. Allbrooke[151], B. W. Allen[118], P. P. Allport[19], A. Aloisio[106a,106b], A. Alonso[39], F. Alonso[74], C. Alpigiani[140], A. A. Alshehri[56], M. Alstaty[88], B. Alvarez Gonzalez[32], D. Álvarez Piqueras[170], M. G. Alviggi[106a,106b], B. T. Amadio[16], Y. Amaral Coutinho[26a], C. Amelung[25], D. Amidei[92], S. P. Amor Dos Santos[128a,128c], A. Amorim[128a,128b], S. Amoroso[32], G. Amundsen[25], C. Anastopoulos[141], L. S. Ancu[52], N. Andari[19], T. Andeen[11], C. F. Anders[60b], J. K. Anders[77], K. J. Anderson[33], A. Andreazza[94a,94b], V. Andrei[60a], S. Angelidakis[9], I. Angelozzi[109], A. Angerami[38], F. Anghinolfi[32], A. V. Anisenkov[111,c], N. Anjos[13], A. Annovi[126a,126b], C. Antel[60a], M. Antonelli[50], A. Antonov[100,*], D. J. Antrim[166], F. Anulli[134a], M. Aoki[69], L. Aperio Bella[32], G. Arabidze[93], Y. Arai[69], J. P. Araque[128a], V. Araujo Ferraz[26a], A. T. H. Arce[48], R. E. Ardell[80], F. A. Arduh[74], J-F. Arguin[97], S. Argyropoulos[66], M. Arik[20a], A. J. Armbruster[145], L. J. Armitage[79], O. Arnaez[32], H. Arnold[51], M. Arratia[30], O. Arslan[23], A. Artamonov[99], G. Artoni[122], S. Artz[86], S. Asai[157], N. Asbah[45], A. Ashkenazi[155], L. Asquith[151], K. Assamagan[27], R. Astalos[146a], M. Atkinson[169], N. B. Atlay[143], K. Augsten[130], G. Avolio[32], B. Axen[16], M. K. Ayoub[119], G. Azuelos[97,d], A. E. Baas[60a], M. J. Baca[19], H. Bachacou[138], K. Bachas[76a,76b], M. Backes[122], M. Backhaus[32], P. Bagiacchi[134a,134b], P. Bagnaia[134a,134b], J. T. Baines[133], M. Bajic[39], O. K. Baker[179], E. M. Baldin[111,c], P. Balek[175], T. Balestri[150], F. Balli[138], W. K. Balunas[124], E. Banas[42], Sw. Banerjee[176,e], A. A. E. Bannoura[178], L. Barak[32], E. L. Barberio[91], D. Barberis[53a,53b], M. Barbero[88], T. Barillari[103], M-S. Barisits[32], T. Barklow[145], N. Barlow[30], S. L. Barnes[36c], B. M. Barnett[133], R. M. Barnett[16], Z. Barnovska-Blenessy[36a], A. Baroncelli[136a], G. Barone[25], A. J. Barr[122], L. Barranco Navarro[170], F. Barreiro[85], J. Barreiro Guimarães da Costa[35a], R. Bartoldus[145], A. E. Barton[75], P. Bartos[146a], A. Basalaev[125], A. Bassalat[119,f], R. L. Bates[56], S. J. Batista[161], J. R. Batley[30], M. Battaglia[139], M. Bauce[134a,134b], F. Bauer[138], H. S. Bawa[145,g], J. B. Beacham[113], M. D. Beattie[75], T. Beau[83], P. H. Beauchemin[165], P. Bechtle[23], H. P. Beck[18,h], K. Becker[122], M. Becker[86], M. Beckingham[173], C. Becot[112], A. J. Beddall[20d], A. Beddall[20b], V. A. Bednyakov[68], M. Bedognetti[109], C. P. Bee[150], T. A. Beermann[32], M. Begalli[26a], M. Begel[27], J. K. Behr[45], A. S. Bell[81], G. Bella[155], L. Bellagamba[22a], A. Bellerive[31], M. Bellomo[89], K. Belotskiy[100], O. Beltramello[32], N. L. Belyaev[100], O. Benary[155,*], D. Benchekroun[137a], M. Bender[102], K. Bendtz[148a,148b], N. Benekos[10], Y. Benhammou[155], E. Benhar Noccioli[179], J. Benitez[66], D. P. Benjamin[48], M. Benoit[52], J. R. Bensinger[25], S. Bentvelsen[109], L. Beresford[122], M. Beretta[50], D. Berge[109], E. Bergeaas Kuutmann[168], N. Berger[5], J. Beringer[16], S. Berlendis[58], N. R. Bernard[89], G. Bernardi[83], C. Bernius[112], F. U. Bernlochner[23], T. Berry[80], P. Berta[131], C. Bertella[86], G. Bertoli[148a,148b], F. Bertolucci[126a,126b], I. A. Bertram[75], C. Bertsche[45], D. Bertsche[115], G. J. Besjes[39], O. Bessidskaia Bylund[148a,148b], M. Bessner[45], N. Besson[138], C. Betancourt[51], A. Bethani[87], S. Bethke[103], A. J. Bevan[79], R. M. Bianchi[127], O. Biebel[102], D. Biedermann[17], M. Bianco[32], R. Bielski[87], N. V. Biesuz[126a,126b], M. Biglietti[136a], J. Bilbao De Mendizabal[52], T. R. V. Billoud[97], H. Bilokon[50], M. Bindi[57], A. Bingul[20b], C. Bini[134a,134b], S. Biondi[22a,22b], T. Bisanz[57], C. Bittrich[47], D. M. Bjergaard[48], C. W. Black[152], J. E. Black[145], K. M. Black[24], D. Blackburn[140], R. E. Blair[6], J.-B. Blanchard[138], T. Blazek[146a], I. Bloch[45], C. Blocker[25], A. Blue[56], W. Blum[86,*], U. Blumenschein[79], S. Blunier[34a], G. J. Bobbink[109], V. S. Bobrovnikov[111,c], S. S. Bocchetta[84], A. Bocci[48], C. Bock[102], M. Boehler[51], D. Boerner[178], D. Bogavac[102], A. G. Bogdanchikov[111], C. Bohm[148a], V. Boisvert[80], P. Bokan[168,i], T. Bold[41a], A. S. Boldyrev[101], M. Bomben[83], M. Bona[79], M. Boonekamp[138], A. Borisov[132], G. Borissov[75], J. Bortfeldt[32], D. Bortoletto[122], V. Bortolotto[62a,62b,62c], K. Bos[109], D. Boscherini[22a], M. Bosman[13], J. D. Bossio Sola[29], J. Boudreau[127], J. Bouffard[2], E. V. Bouhova-Thacker[75], D. Boumediene[37], C. Bourdarios[119], S. K. Boutle[56], A. Boveia[113], J. Boyd[32], I. R. Boyko[68], J. Bracinik[19], A. Brandt[8], G. Brandt[57], O. Brandt[60a], U. Bratzler[158], B. Brau[89], J. E. Brau[118], W. D. Breaden Madden[56], K. Brendlinger[45], A. J. Brennan[91], L. Brenner[109], R. Brenner[168], S. Bressler[175], D. L. Briglin[19], T. M. Bristow[49], D. Britton[56], D. Britzger[45], F. M. Brochu[30], I. Brock[23], R. Brock[93], G. Brooijmans[38], T. Brooks[80], W. K. Brooks[34b], J. Brosamer[16], E. Brost[110], J. H Broughton[19], P. A. Bruckman de Renstrom[42], D. Bruncko[146b], A. Bruni[22a], G. Bruni[22a], L. S. Bruni[109], B H Brunt[30], M. Bruschi[22a], N. Bruscino[23], P. Bryant[33], L. Bryngemark[84], T. Buanes[15], Q. Buat[144], P. Buchholz[143], A. G. Buckley[56], I. A. Budagov[68], F. Buehrer[51], M. K. Bugge[121], O. Bulekov[100], D. Bullock[8], H. Burckhart[32], S. Burdin[77], C. D. Burgard[51], A. M. Burger[5], B. Burghgrave[110], K. Burka[42], S. Burke[133], I. Burmeister[46], J. T. P. Burr[122], E. Busato[37], D. Büscher[51], V. Büscher[86], P. Bussey[56], J. M. Butler[24], C. M. Buttar[56], J. M. Butterworth[81], P. Butti[32], W. Buttinger[27],

A. Buzatu[35c], A. R. Buzykaev[111,c], S. Cabrera Urbán[170], D. Caforio[130], V. M. Cairo[40a,40b], O. Cakir[4a], N. Calace[52], P. Calafiura[16], A. Calandri[88], G. Calderini[83], P. Calfayan[64], G. Callea[40a,40b], L. P. Caloba[26a], S. Calvente Lopez[85], D. Calvet[37], S. Calvet[37], T. P. Calvet[88], R. Camacho Toro[33], S. Camarda[32], P. Camarri[135a,135b], D. Cameron[121], R. Caminal Armadans[169], C. Camincher[58], S. Campana[32], M. Campanelli[81], A. Camplani[94a,94b], A. Campoverde[143], V. Canale[106a,106b], M. Cano Bret[36c], J. Cantero[116], T. Cao[155], M. D. M. Capeans Garrido[32], I. Caprini[28b], M. Caprini[28b], M. Capua[40a,40b], R. M. Carbone[38], R. Cardarelli[135a], F. Cardillo[51], I. Carli[131], T. Carli[32], G. Carlino[106a], B. T. Carlson[127], L. Carminati[94a,94b], R. M. D. Carney[148a,148b], S. Caron[108], E. Carquin[34b], G. D. Carrillo-Montoya[32], J. Carvalho[128a,128c], D. Casadei[19], M. P. Casado[13,j], M. Casolino[13], D. W. Casper[166], R. Castelijn[109], A. Castelli[109], V. Castillo Gimenez[170], N. F. Castro[128a,k], A. Catinaccio[32], J. R. Catmore[121], A. Cattai[32], J. Caudron[23], V. Cavaliere[169], E. Cavallaro[13], D. Cavalli[94a], M. Cavalli-Sforza[13], V. Cavasinni[126a,126b], E. Celebi[20a], F. Ceradini[136a,136b], L. Cerda Alberich[170], A. S. Cerqueira[26b], A. Cerri[151], L. Cerrito[135a,135b], F. Cerutti[16], A. Cervelli[18], S. A. Cetin[20c], A. Chafaq[137a], D. Chakraborty[110], S. K. Chan[59], W. S. Chan[109], Y. L. Chan[62a], P. Chang[169], J. D. Chapman[30], D. G. Charlton[19], A. Chatterjee[52], C. C. Chau[161], C. A. Chavez Barajas[151], S. Che[113], S. Cheatham[167a,167c], A. Chegwidden[93], S. Chekanov[6], S. V. Chekulaev[163a], G. A. Chelkov[68,l], M. A. Chelstowska[32], C. Chen[67], H. Chen[27], S. Chen[35b], S. Chen[157], X. Chen[35c,m], Y. Chen[70], H. C. Cheng[92], H. J. Cheng[35a], Y. Cheng[33], A. Cheplakov[68], E. Cheremushkina[132], R. Cherkaoui El Moursli[137e], V. Chernyatin[27,*], E. Cheu[7], L. Chevalier[138], V. Chiarella[50], G. Chiarelli[126a,126b], G. Chiodini[76a], A. S. Chisholm[32], A. Chitan[28b], Y. H. Chiu[172], M. V. Chizhov[68], K. Choi[64], A. R. Chomont[37], S. Chouridou[159], B.K.B. Chow[102], V. Christodoulou[81], D. Chromek-Burckhart[32], M. C. Chu[62a], J. Chudoba[129], A. J. Chuinard[90], J. J. Chwastowski[42], L. Chytka[117], A. K. Ciftci[4a], D. Cinca[46], V. Cindro[78], I. A. Cioara[23], C. Ciocca[22a,22b], A. Ciocio[16], F. Cirotto[106a,106b], Z. H. Citron[175], M. Citterio[94a], M. Ciubancan[28b], A. Clark[52], B. L. Clark[59], M. R. Clark[38], P. J. Clark[49], R. N. Clarke[16], C. Clement[148a,148b], Y. Coadou[88], M. Cobal[167a,167c], A. Coccaro[52], J. Cochran[67], L. Colasurdo[108], B. Cole[38], A. P. Colijn[109], J. Collot[58], T. Colombo[166], P. Conde Muiño[128a,128b], E. Coniavitis[51], S. H. Connell[147b], I. A. Connelly[87], V. Consorti[51], S. Constantinescu[28b], G. Conti[32], F. Conventi[106a,n], M. Cooke[16], B. D. Cooper[81], A. M. Cooper-Sarkar[122], F. Cormier[171], K. J. R. Cormier[161], T. Cornelissen[178], M. Corradi[134a,134b], F. Corriveau[90,o], A. Cortes-Gonzalez[32], G. Cortiana[103], G. Costa[94a], M. J. Costa[170], D. Costanzo[141], G. Cottin[30], G. Cowan[80], B. E. Cox[87], K. Cranmer[112], S. J. Crawley[56], R. A. Creager[124], G. Cree[31], S. Crépé-Renaudin[58], F. Crescioli[83], W. A. Cribbs[148a,148b], M. Crispin Ortuzar[122], M. Cristinziani[23], V. Croft[108], G. Crosetti[40a,40b], A. Cueto[85], T. Cuhadar Donszelmann[141], J. Cummings[179], M. Curatolo[50], J. Cúth[86], H. Czirr[143], P. Czodrowski[32], G. D'amen[22a,22b], S. D'Auria[56], M. D'Onofrio[77], M. J. Da Cunha Sargedas De Sousa[128a,128b], C. Da Via[87], W. Dabrowski[41a], T. Dado[146a], T. Dai[92], O. Dale[15], F. Dallaire[97], C. Dallapiccola[89], M. Dam[39], J. R. Dandoy[124], N. P. Dang[51], A. C. Daniells[19], N. S. Dann[87], M. Danninger[171], M. Dano Hoffmann[138], V. Dao[150], G. Darbo[53a], S. Darmora[8], J. Dassoulas[3], A. Dattagupta[118], T. Daubney[45], W. Davey[23], C. David[45], T. Davidek[131], M. Davies[155], P. Davison[81], E. Dawe[91], I. Dawson[141], K. De[8], R. de Asmundis[106a], A. De Benedetti[115], S. De Castro[22a,22b], S. De Cecco[83], N. De Groot[108], P. de Jong[109], H. De la Torre[93], F. De Lorenzi[67], A. De Maria[57], D. De Pedis[134a], A. De Salvo[134a], U. De Sanctis[151], A. De Santo[151], K. De Vasconcelos Corga[88], J. B. De Vivie De Regie[119], W. J. Dearnaley[75], R. Debbe[27], C. Debenedetti[139], D. V. Dedovich[68], N. Dehghanian[3], I. Deigaard[109], M. Del Gaudio[40a,40b], J. Del Peso[85], T. Del Prete[126a,126b], D. Delgove[119], F. Deliot[138], C. M. Delitzsch[52], A. Dell'Acqua[32], L. Dell'Asta[24], M. Dell'Orso[126a,126b], M. Della Pietra[106a,106b], D. della Volpe[52], M. Delmastro[5], P. A. Delsart[58], D. A. DeMarco[161], S. Demers[179], M. Demichev[68], A. Demilly[83], S. P. Denisov[132], D. Denysiuk[138], D. Derendarz[42], J. E. Derkaoui[137d], F. Derue[83], P. Dervan[77], K. Desch[23], C. Deterre[45], K. Dette[46], P. O. Deviveiros[32], A. Dewhurst[133], S. Dhaliwal[25], A. Di Ciaccio[135a,135b], L. Di Ciaccio[5], W. K. Di Clemente[124], C. Di Donato[106a,106b], A. Di Girolamo[32], B. Di Girolamo[32], B. Di Micco[136a,136b], R. Di Nardo[32], K. F. Di Petrillo[59], A. Di Simone[51], R. Di Sipio[161], D. Di Valentino[31], C. Diaconu[88], M. Diamond[161], F. A. Dias[49], M. A. Diaz[34a], E. B. Diehl[92], J. Dietrich[17], S. Díez Cornell[45], A. Dimitrievska[14], J. Dingfelder[23], P. Dita[28b], S. Dita[28b], F. Dittus[32], F. Djama[88], T. Djobava[54b], J. I. Djuvsland[60a], M. A. B. do Vale[26c], D. Dobos[32], M. Dobre[28b], C. Doglioni[84], J. Dolejsi[131], Z. Dolezal[131], M. Donadelli[26d], S. Donati[126a,126b], P. Dondero[123a,123b], J. Donini[37], J. Dopke[133], A. Doria[106a], M. T. Dova[74], A. T. Doyle[56], E. Drechsler[57], M. Dris[10], Y. Du[36b], J. Duarte-Campderros[155], E. Duchovni[175], G. Duckeck[102], O. A. Ducu[97,p], D. Duda[109], A. Dudarev[32], A. Chr. Dudder[86], E. M. Duffield[16], L. Duflot[119], M. Dührssen[32], M. Dumancic[175], A. E. Dumitriu[28b], A. K. Duncan[56], M. Dunford[60a], H. Duran Yildiz[4a], M. Düren[55], A. Durglishvili[54b], D. Duschinger[47], B. Dutta[45], M. Dyndal[45], C. Eckardt[45], K. M. Ecker[103], R. C. Edgar[92], T. Eifert[32], G. Eigen[15], K. Einsweiler[16], T. Ekelof[168], M. El Kacimi[137c], V. Ellajosyula[88], M. Ellert[168], S. Elles[5], F. Ellinghaus[178], A. A. Elliot[172], N. Ellis[32], J. Elmsheuser[27], M. Elsing[32], D. Emeliyanov[133], Y. Enari[157], O. C. Endner[86], J. S. Ennis[173], J. Erdmann[46], A. Ereditato[18], G. Ernis[178], M. Ernst[27], S. Errede[169], E. Ertel[86], M. Escalier[119], H. Esch[46], C. Escobar[127], B. Esposito[50], A. I. Etienvre[138], E. Etzion[155], H. Evans[64], A. Ezhilov[125], F. Fabbri[22a,22b], L. Fabbri[22a,22b], G. Facini[33], R. M. Fakhrutdinov[132],

S. Falciano[134a], R. J. Falla[81], J. Faltova[32], Y. Fang[35a], M. Fanti[94a,94b], A. Farbin[8], A. Farilla[136a], C. Farina[127], E. M. Farina[123a,123b], T. Farooque[93], S. Farrell[16], S. M. Farrington[173], P. Farthouat[32], F. Fassi[137e], P. Fassnacht[32], D. Fassouliotis[9], M. Faucci Giannelli[80], A. Favareto[53a,53b], W. J. Fawcett[122], L. Fayard[119], O. L. Fedin[125,q], W. Fedorko[171], S. Feigl[121], L. Feligioni[88], C. Feng[36b], E. J. Feng[32], H. Feng[92], A. B. Fenyuk[132], L. Feremenga[8], P. Fernandez Martinez[170], S. Fernandez Perez[13], J. Ferrando[45], A. Ferrari[168], P. Ferrari[109], R. Ferrari[123a], D. E. Ferreira de Lima[60b], A. Ferrer[170], D. Ferrere[52], C. Ferretti[92], F. Fiedler[86], A. Filipčič[78], M. Filipuzzi[45], F. Filthaut[108], M. Fincke-Keeler[172], K. D. Finelli[152], M. C. N. Fiolhais[128a,128c,r], L. Fiorini[170], A. Fischer[2], C. Fischer[13], J. Fischer[178], W. C. Fisher[93], N. Flaschel[45], I. Fleck[143], P. Fleischmann[92], R. R. M. Fletcher[124], T. Flick[178], B. M. Flierl[102], L. R. Flores Castillo[62a], M. J. Flowerdew[103], G. T. Forcolin[87], A. Formica[138], A. Forti[87], A. G. Foster[19], D. Fournier[119], H. Fox[75], S. Fracchia[113], P. Francavilla[83], M. Franchini[22a,22b], D. Francis[32], L. Franconi[121], M. Franklin[59], M. Frate[166], M. Fraternali[123a,123b], D. Freeborn[81], S. M. Fressard-Batraneanu[32], B. Freund[97], D. Froidevaux[32], J. A. Frost[122], C. Fukunaga[158], E. Fullana Torregrosa[86], T. Fusayasu[104], J. Fuster[170], C. Gabaldon[58], O. Gabizon[154], A. Gabrielli[22a,22b], A. Gabrielli[16], G. P. Gach[41a], S. Gadatsch[32], S. Gadomski[80], G. Gagliardi[53a,53b], L. G. Gagnon[97], P. Gagnon[64], C. Galea[108], B. Galhardo[128a,128c], E. J. Gallas[122], B. J. Gallop[133], P. Gallus[130], G. Galster[39], K. K. Gan[113], S. Ganguly[37], J. Gao[36a], Y. Gao[77], Y. S. Gao[145,g], F. M. Garay Walls[49], C. García[170], J. E. García Navarro[170], M. Garcia-Sciveres[16], R. W. Gardner[33], N. Garelli[145], V. Garonne[121], A. Gascon Bravo[45], K. Gasnikova[45], C. Gatti[50], A. Gaudiello[53a,53b], G. Gaudio[123a], I. L. Gavrilenko[98], C. Gay[171], G. Gaycken[23], E. N. Gazis[10], C. N. P. Gee[133], M. Geisen[86], M. P. Geisler[60a], K. Gellerstedt[148a,148b], C. Gemme[53a], M. H. Genest[58], C. Geng[36a,s], S. Gentile[134a,134b], C. Gentsos[156], S. George[80], D. Gerbaudo[13], A. Gershon[155], S. Ghasemi[143], M. Ghneimat[23], B. Giacobbe[22a], S. Giagu[134a,134b], P. Giannetti[126a,126b], S. M. Gibson[80], M. Gignac[171], M. Gilchriese[16], D. Gillberg[31], G. Gilles[178], D. M. Gingrich[3,d], N. Giokaris[9,*], M. P. Giordani[167a,167c], F. M. Giorgi[22a], P. F. Giraud[138], P. Giromini[59], D. Giugni[94a], F. Giuli[122], C. Giuliani[103], M. Giulini[60b], B. K. Gjelsten[121], S. Gkaitatzis[156], I. Gkialas[9], E. L. Gkougkousis[139], L. K. Gladilin[101], C. Glasman[85], J. Glatzer[13], P. C. F. Glaysher[45], A. Glazov[45], M. Goblirsch-Kolb[25], J. Godlewski[42], S. Goldfarb[91], T. Golling[52], D. Golubkov[132], A. Gomes[128a,128b,128d], R. Gonçalo[128a], R. Goncalves Gama[26a], J. Goncalves Pinto Firmino Da Costa[138], G. Gonella[51], L. Gonella[19], A. Gongadze[68], S. González de la Hoz[170], S. Gonzalez-Sevilla[52], L. Goossens[32], P. A. Gorbounov[99], H. A. Gordon[27], I. Gorelov[107], B. Gorini[32], E. Gorini[76a,76b], A. Gorišek[78], A. T. Goshaw[48], C. Gössling[46], M. I. Gostkin[68], C. R. Goudet[119], D. Goujdami[137c], A. G. Goussiou[140], N. Govender[147b,t], E. Gozani[154], L. Graber[57], I. Grabowska-Bold[41a], P. O. J. Gradin[58], J. Gramling[52], E. Gramstad[121], S. Grancagnolo[17], V. Gratchev[125], P. M. Gravila[28f], H. M. Gray[32], Z. D. Greenwood[82,u], C. Grefe[23], K. Gregersen[81], I. M. Gregor[45], P. Grenier[145], K. Grevtsov[5], J. Griffiths[8], A. A. Grillo[139], K. Grimm[75], S. Grinstein[13,v], Ph. Gris[37], J.-F. Grivaz[119], S. Groh[86], E. Gross[175], J. Grosse-Knetter[57], G. C. Grossi[82], Z. J. Grout[81], L. Guan[92], W. Guan[176], J. Guenther[65], F. Guescini[163a], D. Guest[166], O. Gueta[155], B. Gui[113], E. Guido[53a,53b], T. Guillemin[5], S. Guindon[2], U. Gul[56], C. Gumpert[32], J. Guo[36c], W. Guo[92], Y. Guo[36a], R. Gupta[43], S. Gupta[122], G. Gustavino[134a,134b], P. Gutierrez[115], N. G. Gutierrez Ortiz[81], C. Gutschow[81], C. Guyot[138], M. P. Guzik[41a], C. Gwenlan[122], C. B. Gwilliam[77], A. Haas[112], C. Haber[16], H. K. Hadavand[8], A. Hadef[88], S. Hageböck[23], M. Hagihara[164], H. Hakobyan[180,*], M. Haleem[45], J. Haley[116], G. Halladjian[93], G. D. Hallewell[88], K. Hamacher[178], P. Hamal[117], K. Hamano[172], A. Hamilton[147a], G. N. Hamity[141], P. G. Hamnett[45], L. Han[36a], S. Han[35a], K. Hanagaki[69,w], K. Hanawa[157], M. Hance[139], B. Haney[124], P. Hanke[60a], R. Hanna[138], J. B. Hansen[39], J. D. Hansen[39], M. C. Hansen[23], P. H. Hansen[39], K. Hara[164], A. S. Hard[176], T. Harenberg[178], F. Hariri[119], S. Harkusha[95], R. D. Harrington[49], P. F. Harrison[173], F. Hartjes[109], N. M. Hartmann[102], M. Hasegawa[70], Y. Hasegawa[142], A. Hasib[49], S. Hassani[138], S. Haug[18], R. Hauser[93], L. Hauswald[47], L. B. Havener[38], M. Havranek[130], C. M. Hawkes[19], R. J. Hawkings[32], D. Hayakawa[159], D. Hayden[93], C. P. Hays[122], J. M. Hays[79], H. S. Hayward[77], S. J. Haywood[133], S. J. Head[19], T. Heck[86], V. Hedberg[84], L. Heelan[8], K. K. Heidegger[51], S. Heim[45], T. Heim[16], B. Heinemann[45,x], J. J. Heinrich[102], L. Heinrich[112], C. Heinz[55], J. Hejbal[129], L. Helary[32], A. Held[171], S. Hellman[148a,148b], C. Helsens[32], J. Henderson[122], R. C. W. Henderson[75], Y. Heng[176], S. Henkelmann[171], A. M. Henriques Correia[32], S. Henrot-Versille[119], G. H. Herbert[17], H. Herde[25], V. Herget[177], Y. Hernández Jiménez[147c], G. Herten[51], R. Hertenberger[102], L. Hervas[32], T. C. Herwig[124], G. G. Hesketh[81], N. P. Hessey[163a], J. W. Hetherly[43], S. Higashino[69], E. Higón-Rodriguez[170], E. Hill[172], J. C. Hill[30], K. H. Hiller[45], S. J. Hillier[19], I. Hinchliffe[16], M. Hirose[51], D. Hirschbuehl[178], B. Hiti[78], O. Hladik[129], X. Hoad[49], J. Hobbs[150], N. Hod[163a], M. C. Hodgkinson[141], P. Hodgson[141], A. Hoecker[32], M. R. Hoeferkamp[107], F. Hoenig[102], D. Hohn[23], T. R. Holmes[16], M. Homann[46], S. Honda[164], T. Honda[69], T. M. Hong[127], B. H. Hooberman[169], W. H. Hopkins[118], Y. Horii[105], A. J. Horton[144], J-Y. Hostachy[58], S. Hou[153], A. Hoummada[137a], J. Howarth[45], J. Hoya[74], M. Hrabovsky[117], I. Hristova[17], J. Hrivnac[119], T. Hryn'ova[5], A. Hrynevich[96], P. J. Hsu[63], S.-C. Hsu[140], Q. Hu[36a], S. Hu[36c], Y. Huang[35a], Z. Hubacek[130], F. Hubaut[88], F. Huegging[23], T. B. Huffman[122], E. W. Hughes[38], G. Hughes[75], M. Huhtinen[32], P. Huo[150], N. Huseynov[68,b], J. Huston[93], J. Huth[59], G. Iacobucci[52], G. Iakovidis[27], I. Ibragimov[143], L. Iconomidou-Fayard[119], P. Iengo[32], O. Igonkina[109,x], T. Iizawa[174],

Y. Ikegami[69], M. Ikeno[69], Y. Ilchenko[11,y], D. Iliadis[156], N. Ilic[145], G. Introzzi[123a,123b], P. Ioannou[9,*], M. Iodice[136a], K. Iordanidou[38], V. Ippolito[59], N. Ishijima[120], M. Ishino[157], M. Ishitsuka[159], C. Issever[122], S. Istin[20a], F. Ito[164], J. M. Iturbe Ponce[87], R. Iuppa[162a,162b], H. Iwasaki[69], J. M. Izen[44], V. Izzo[106a], S. Jabbar[3], P. Jackson[1], V. Jain[2], K. B. Jakobi[86], K. Jakobs[51], S. Jakobsen[32], T. Jakoubek[129], D. O. Jamin[116], D. K. Jana[82], R. Jansky[65], J. Janssen[23], M. Janus[57], P. A. Janus[41a], G. Jarlskog[84], N. Javadov[68,b], T. Javůrek[51], M. Javurkova[51], F. Jeanneau[138], L. Jeanty[16], J. Jejelava[54a,aa], A. Jelinskas[173], P. Jenni[51,ab], C. Jeske[173], S. Jézéquel[5], H. Ji[176], J. Jia[150], H. Jiang[67], Y. Jiang[36a], Z. Jiang[145], S. Jiggins[81], J. Jimenez Pena[170], S. Jin[35a], A. Jinaru[28b], O. Jinnouchi[159], H. Jivan[147c], P. Johansson[141], K. A. Johns[7], C. A. Johnson[64], W. J. Johnson[140], K. Jon-And[148a,148b], R. W. L. Jones[75], S. Jones[7], T. J. Jones[77], J. Jongmanns[60a], P. M. Jorge[128a,128b], J. Jovicevic[163a], X. Ju[176], A. Juste Rozas[13,v], M. K. Köhler[175], A. Kaczmarska[42], M. Kado[119], H. Kagan[113], M. Kagan[145], S. J. Kahn[88], T. Kaji[174], E. Kajomovitz[48], C. W. Kalderon[84], A. Kaluza[86], S. Kama[43], A. Kamenshchikov[132], N. Kanaya[157], S. Kaneti[30], L. Kanjir[78], V. A. Kantserov[100], J. Kanzaki[69], B. Kaplan[112], L. S. Kaplan[176], D. Kar[147c], K. Karakostas[10], N. Karastathis[10], M. J. Kareem[57], E. Karentzos[10], M. Karnevskiy[86], S. N. Karpov[68], Z. M. Karpova[68], K. Karthik[112], V. Kartvelishvili[75], A. N. Karyukhin[132], K. Kasahara[164], L. Kashif[176], R. D. Kass[113], A. Kastanas[149], Y. Kataoka[157], C. Kato[157], A. Katre[52], J. Katzy[45], K. Kawade[105], K. Kawagoe[73], T. Kawamoto[157], G. Kawamura[57], E. F. Kay[77], V. F. Kazanin[111,c], R. Keeler[172], R. Kehoe[43], J. S. Keller[45], J. J. Kempster[80], H. Keoshkerian[161], O. Kepka[129], B. P. Kerševan[78], S. Kersten[178], R. A. Keyes[90], M. Khader[169], F. Khalil-zada[12], A. Khanov[116], A. G. Kharlamov[111,c], T. Kharlamova[111,c], A. Khodinov[160], T. J. Khoo[52], V. Khovanskiy[99,*], E. Khramov[68], J. Khubua[54b,ac], S. Kido[70], C. R. Kilby[80], H. Y. Kim[8], S. H. Kim[164], Y. K. Kim[33], N. Kimura[156], O. M. Kind[17], B. T. King[77], D. Kirchmeier[47], J. Kirk[133], A. E. Kiryunin[103], T. Kishimoto[157], D. Kisielewska[41a], K. Kiuchi[164], O. Kivernyk[138], E. Kladiva[146b], T. Klapdor-Kleingrothaus[51], M. H. Klein[38], M. Klein[77], U. Klein[77], K. Kleinknecht[86], P. Klimek[110], A. Klimentov[27], R. Klingenberg[46], T. Klioutchnikova[32], E.-E. Kluge[60a], P. Kluit[109], S. Kluth[103], J. Knapik[42], E. Kneringer[65], E. B. F. G. Knoops[88], A. Knue[103], A. Kobayashi[157], D. Kobayashi[159], T. Kobayashi[157], M. Kobel[47], M. Kocian[145], P. Kodys[131], T. Koffas[31], E. Koffeman[109], N. M. Köhler[103], T. Koi[145], M. Kolb[60b], I. Koletsou[5], A. A. Komar[98,*], Y. Komori[157], T. Kondo[69], N. Kondrashova[36c], K. Köneke[51], A. C. König[108], T. Kono[69,ad], R. Konoplich[112,ae], N. Konstantinidis[81], R. Kopeliansky[64], S. Koperny[41a], A. K. Kopp[51], K. Korcyl[42], K. Kordas[156], A. Korn[81], A. A. Korol[111,c], I. Korolkov[13], E. V. Korolkova[141], O. Kortner[103], S. Kortner[103], T. Kosek[131], V. V. Kostyukhin[23], A. Kotwal[48], A. Koulouris[10], A. Kourkoumeli-Charalampidi[123a,123b], C. Kourkoumelis[9], V. Kouskoura[27], A. B. Kowalewska[42], R. Kowalewski[172], T. Z. Kowalski[41a], C. Kozakai[157], W. Kozanecki[138], A. S. Kozhin[132], V. A. Kramarenko[101], G. Kramberger[78], D. Krasnopevtsev[100], M. W. Krasny[83], A. Krasznahorkay[32], D. Krauss[103], A. Kravchenko[27], J. A. Kremer[41a], M. Kretz[60c], J. Kretzschmar[77], K. Kreutzfeldt[55], P. Krieger[161], K. Krizka[33], K. Kroeninger[46], H. Kroha[103], J. Kroll[124], J. Kroseberg[23], J. Krstic[14], U. Kruchonak[68], H. Krüger[23], N. Krumnack[67], M. C. Kruse[48], M. Kruskal[24], T. Kubota[91], H. Kucuk[81], S. Kuday[4b], J. T. Kuechler[178], S. Kuehn[51], A. Kugel[60c], F. Kuger[177], T. Kuhl[45], V. Kukhtin[68], R. Kukla[88], Y. Kulchitsky[95], S. Kuleshov[34b], Y. P. Kulinich[169], M. Kuna[134a,134b], T. Kunigo[71], A. Kupco[129], O. Kuprash[155], H. Kurashige[70], L. L. Kurchaninov[163a], Y. A. Kurochkin[95], M. G. Kurth[35a], V. Kus[129], E. S. Kuwertz[172], M. Kuze[159], J. Kvita[117], T. Kwan[172], D. Kyriazopoulos[141], A. La Rosa[103], J. L. La Rosa Navarro[26d], L. La Rotonda[40a,40b], C. Lacasta[170], F. Lacava[134a,134b], J. Lacey[45], H. Lacker[17], D. Lacour[83], E. Ladygin[68], R. Lafaye[5], B. Laforge[83], T. Lagouri[179], S. Lai[57], S. Lammers[64], W. Lampl[7], E. Lançon[27], U. Landgraf[51], M. P. J. Landon[79], M. C. Lanfermann[52], V. S. Lang[60a], J. C. Lange[13], A. J. Lankford[166], F. Lanni[27], K. Lantzsch[23], A. Lanza[123a], A. Lapertosa[53a,53b], S. Laplace[83], J. F. Laporte[138], T. Lari[94a], F. Lasagni Manghi[22a,22b], M. Lassnig[32], P. Laurelli[50], W. Lavrijsen[16], A. T. Law[139], P. Laycock[77], T. Lazovich[59], M. Lazzaroni[94a,94b], B. Le[91], O. Le Dortz[83], E. Le Guirriec[88], E. P. Le Quilleuc[138], M. LeBlanc[172], T. LeCompte[6], F. Ledroit-Guillon[58], C. A. Lee[27], S. C. Lee[153], L. Lee[1], B. Lefebvre[90], G. Lefebvre[83], M. Lefebvre[172], F. Legger[102], C. Leggett[16], A. Lehan[77], G. Lehmann Miotto[32], X. Lei[7], W. A. Leight[45], A. G. Leister[179], M. A. L. Leite[26d], R. Leitner[131], D. Lellouch[175], B. Lemmer[57], K. J. C. Leney[81], T. Lenz[23], B. Lenzi[32], R. Leone[7], S. Leone[126a,126b], C. Leonidopoulos[49], G. Lerner[151], C. Leroy[97], A. A. J. Lesage[138], C. G. Lester[30], M. Levchenko[125], J. Levêque[5], D. Levin[92], L. J. Levinson[175], M. Levy[19], D. Lewis[79], M. Leyton[44], B. Li[36a,s], C. Li[36a], H. Li[150], L. Li[48], L. Li[36c], Q. Li[35a], S. Li[48], X. Li[36c], Y. Li[143], Z. Liang[35a], B. Liberti[135a], A. Liblong[161], K. Lie[169], J. Liebal[23], W. Liebig[15], A. Limosani[152], S. C. Lin[153,af], T. H. Lin[86], B. E. Lindquist[150], A. E. Lionti[52], E. Lipeles[124], A. Lipniacka[15], M. Lisovyi[60b], T. M. Liss[169], A. Lister[171], A. M. Litke[139], B. Liu[153,ag], H. Liu[92], H. Liu[27], J. Liu[36b], J. B. Liu[36a], K. Liu[88], L. Liu[169], M. Liu[36a], Y. L. Liu[36a], Y. Liu[36a], M. Livan[123a,123b], A. Lleres[58], J. Llorente Merino[35a], S. L. Lloyd[79], C. Y. Lo[62b], F. Lo Sterzo[153], E. M. Lobodzinska[45], P. Loch[7], F. K. Loebinger[87], K. M. Loew[25], A. Loginov[179,*], T. Lohse[17], K. Lohwasser[45], M. Lokajicek[129], B. A. Long[24], J. D. Long[169], R. E. Long[75], L. Longo[76a,76b], K. A. Looper[113], J. A. Lopez[34b], D. Lopez Mateos[59], I. Lopez Paz[13], A. Lopez Solis[83], J. Lorenz[102], N. Lorenzo Martinez[64], M. Losada[21], P. J. Lösel[102], X. Lou[35a], A. Lounis[119], J. Love[6],

P. A. Love[75], H. Lu[62a], N. Lu[92], Y. J. Lu[63], H. J. Lubatti[140], C. Luci[134a,134b], A. Lucotte[58], C. Luedtke[51], F. Luehring[64], W. Lukas[65], L. Luminari[134a], O. Lundberg[148a,148b], B. Lund-Jensen[149], P. M. Luzi[83], D. Lynn[27], R. Lysak[129], E. Lytken[84], V. Lyubushkin[68], H. Ma[27], L. L. Ma[36b], Y. Ma[36b], G. Maccarrone[50], A. Macchiolo[103], C. M. Macdonald[141], B. Maček[78], J. Machado Miguens[124,128b], D. Madaffari[88], R. Madar[37], H. J. Maddocks[168], W. F. Mader[47], A. Madsen[45], J. Maeda[70], S. Maeland[15], T. Maeno[27], A. Maevskiy[101], E. Magradze[57], J. Mahlstedt[109], C. Maiani[119], C. Maidantchik[26a], A. A. Maier[103], T. Maier[102], A. Maio[128a,128b,128d], S. Majewski[118], Y. Makida[69], N. Makovec[119], B. Malaescu[83], Pa. Malecki[42], V. P. Maleev[125], F. Malek[58], U. Mallik[66], D. Malon[6], C. Malone[30], S. Maltezos[10], S. Malyukov[32], J. Mamuzic[170], G. Mancini[50], L. Mandelli[94a], I. Mandić[78], J. Maneira[128a,128b], L. Manhaes de Andrade Filho[26b], J. Manjarres Ramos[163b], A. Mann[102], A. Manousos[32], B. Mansoulie[138], J. D. Mansour[35a], R. Mantifel[90], M. Mantoani[57], S. Manzoni[94a,94b], L. Mapelli[32], G. Marceca[29], L. March[52], G. Marchiori[83], M. Marcisovsky[129], M. Marjanovic[37], D. E. Marley[92], F. Marroquim[26a], S. P. Marsden[87], Z. Marshall[16], M. U. F Martensson[168], S. Marti-Garcia[170], C. B. Martin[113], T. A. Martin[173], V. J. Martin[49], B. Martin dit Latour[15], M. Martinez[13,v], V. I. Martinez Outschoorn[169], S. Martin-Haugh[133], V. S. Martoiu[28b], A. C. Martyniuk[81], A. Marzin[115], L. Masetti[86], T. Mashimo[157], R. Mashinistov[98], J. Masik[87], A. L. Maslennikov[111,c], L. Massa[135a,135b], P. Mastrandrea[5], A. Mastroberardino[40a,40b], T. Masubuchi[157], P. Mättig[178], J. Maurer[28b], S. J. Maxfield[77], D. A. Maximov[111,c], R. Mazini[153], I. Maznas[156], S. M. Mazza[94a,94b], N. C. Mc Fadden[107], G. Mc Goldrick[161], S. P. Mc Kee[92], A. McCarn[92], R. L. McCarthy[150], T. G. McCarthy[103], L. I. McClymont[81], E. F. McDonald[91], J. A. Mcfayden[81], G. Mchedlidze[57], S. J. McMahon[133], P. C. McNamara[91], R. A. McPherson[172,o], S. Meehan[140], T. J. Megy[51], S. Mehlhase[102], A. Mehta[77], T. Meideck[58], K. Meier[60a], C. Meineck[102], B. Meirose[44], D. Melini[170,ah], B. R. Mellado Garcia[147c], M. Melo[146a], F. Meloni[18], S. B. Menary[87], L. Meng[77], X. T. Meng[92], A. Mengarelli[22a,22b], S. Menke[103], E. Meoni[165], S. Mergelmeyer[17], P. Mermod[52], L. Merola[106a,106b], C. Meroni[94a], F. S. Merritt[33], A. Messina[134a,134b], J. Metcalfe[6], A. S. Meteınst166, C. Meyer[124], J-P. Meyer[138], J. Meyer[109], H. Meyer Zu Theenhausen[60a], F. Miano[151], R. P. Middleton[133], S. Miglioranzi[53a,53b], L. Mijović[49], G. Mikenberg[175], M. Mikestikova[129], M. Mikuž[78], M. Milesi[91], A. Milic[27], D. W. Miller[33], C. Mills[49], A. Milov[175], D. A. Milstead[148a,148b], A. A. Minaenko[132], Y. Minami[157], I. A. Minashvili[68], A. I. Mincer[112], B. Mindur[41a], M. Mineev[68], Y. Minegishi[157], Y. Ming[176], L. M. Mir[13], K. P. Mistry[124], T. Mitani[174], J. Mitrevski[102], V. A. Mitsou[170], A. Miucci[18], P. S. Miyagawa[141], A. Mizukami[69], J. U. Mjörnmark[84], M. Mlynarikova[131], T. Moa[148a,148b], K. Mochizuki[97], P. Mogg[51], S. Mohapatra[38], S. Molander[148a,148b], R. Moles-Valls[23], R. Monden[71], M. C. Mondragon[93], K. Mönig[45], J. Monk[39], E. Monnier[88], A. Montalbano[150], J. Montejo Berlingen[32], F. Monticelli[74], S. Monzani[94a,94b], R. W. Moore[3], N. Morange[119], D. Moreno[21], M. Moreno Llácer[57], P. Morettini[53a], S. Morgenstern[32], D. Mori[144], T. Mori[157], M. Morii[59], M. Morinaga[157], V. Morisbak[121], A. K. Morley[152], G. Mornacchi[32], J. D. Morris[79], L. Morvaj[150], P. Moschovakos[10], M. Mosidze[54b], H. J. Moss[141], J. Moss[145,ai], K. Motohashi[159], R. Mount[145], E. Mountricha[27], E. J. W. Moyse[89], S. Muanza[88], R. D. Mudd[19], F. Mueller[103], J. Mueller[127], R. S. P. Mueller[102], D. Muenstermann[75], P. Mullen[56], G. A. Mullier[18], F. J. Munoz Sanchez[87], W. J. Murray[173,133], H. Musheghyan[157], M. Muškinja[78], A. G. Myagkov[132,aj], M. Myska[130], B. P. Nachman[16], O. Nackenhorst[52], K. Nagai[122], R. Nagai[69,ad], K. Nagano[69], Y. Nagasaka[61], K. Nagata[164], M. Nagel[51], E. Nagy[88], A. M. Nairz[32], Y. Nakahama[105], K. Nakamura[69], T. Nakamura[157], I. Nakano[114], R. F. Naranjo Garcia[45], R. Narayan[11], D. I. Narrias Villar[60a], I. Naryshkin[125], T. Naumann[45], G. Navarro[21], R. Nayyar[7], H. A. Neal[92], P. Yu. Nechaeva[98], T. J. Neep[138], A. Negri[123a,123b], M. Negrini[22a], S. Nektarijevic[108], C. Nellist[119], A. Nelson[166], M. E. Nelson[122], S. Nemecek[129], P. Nemethy[112], A. A. Nepomuceno[26a], M. Nessi[32,ak], M. S. Neubauer[169], M. Neumann[178], R. M. Neves[112], P. Nevski[27], P. R. Newman[19], T. Y. Ng[62c], T. Nguyen Manh[97], R. B. Nickerson[122], R. Nicolaidou[138], J. Nielsen[139], V. Nikolaenko[132,aj], I. Nikolic-Audit[83], K. Nikolopoulos[19], J. K. Nilsen[121], P. Nilsson[27], Y. Ninomiya[157], A. Nisati[134a], N. Nishu[35c], R. Nisius[103], T. Nobe[157], Y. Noguchi[71], M. Nomachi[120], I. Nomidis[31], M. A. Nomura[27], T. Nooney[79], M. Nordberg[32], N. Norjoharuddeen[122], O. Novgorodova[47], S. Nowak[103], M. Nozaki[69], L. Nozka[117], K. Ntekas[166], E. Nurse[81], F. Nuti[91], D. C. O'Neil[144], A. A. O'Rourke[45], V. O'Shea[56], F. G. Oakham[31,d], H. Oberlack[103], T. Obermann[23], J. Ocariz[83], A. Ochi[70], I. Ochoa[38], J. P. Ochoa-Ricoux[34a], S. Oda[73], S. Odaka[69], H. Ogren[64], A. Oh[87], S. H. Oh[48], C. C. Ohm[16], H. Ohman[168], H. Oide[53a,53b], H. Okawa[164], Y. Okumura[157], T. Okuyama[69], A. Olariu[28b], L. F. Oleiro Seabra[128a], S. A. Olivares Pino[49], D. Oliveira Damazio[27], A. Olszewski[42], J. Olszowska[42], A. Onofre[128a,128e], K. Onogi[105], P. U. E. Onyisi[11,z], M. J. Oreglia[33], Y. Oren[155], D. Orestano[136a,136b], N. Orlando[62b], R. S. Orr[161], B. Osculati[53a,53b,*], R. Ospanov[87], G. Otero y Garzon[29], H. Otono[73], M. Ouchrif[137d], F. Ould-Saada[121], A. Ouraou[138], K. P. Oussoren[109], Q. Ouyang[35a], M. Owen[56], R. E. Owen[19], V. E. Ozcan[20a], N. Ozturk[8], K. Pachal[144], A. Pacheco Pages[13], L. Pacheco Rodriguez[138], C. Padilla Aranda[13], S. Pagan Griso[16], M. Paganini[179], F. Paige[27], P. Pais[89], G. Palacino[64], S. Palazzo[40a,40b], S. Palestini[32], M. Palka[41b], D. Pallin[37], E. St. Panagiotopoulou[10], I. Panagoulias[10], C. E. Pandini[83], J. G. Panduro Vazquez[80], P. Pani[32], S. Panitkin[27], D. Pantea[28b], L. Paolozzi[52], Th. D. Papadopoulou[10], K. Papageorgiou[9], A. Paramonov[6], D. Paredes Hernandez[179],

A. J. Parker[75], M. A. Parker[30], K. A. Parker[45], F. Parodi[53a,53b], J. A. Parsons[38], U. Parzefall[51], V. R. Pascuzzi[161], J. M. Pasner[139], E. Pasqualucci[134a], S. Passaggio[53a], Fr. Pastore[80], S. Pataraia[178], J. R. Pater[87], T. Pauly[32], J. Pearce[172], B. Pearson[103], L. E. Pedersen[39], S. Pedraza Lopez[170], R. Pedro[128a,128b], S. V. Peleganchuk[111,c], O. Penc[129], C. Peng[35a], H. Peng[36a], J. Penwell[64], B. S. Peralva[26b], M. M. Perego[138], D. V. Perepelitsa[27], L. Perini[94a,94b], H. Pernegger[32], S. Perrella[106a,106b], R. Peschke[45], V. D. Peshekhonov[68], K. Peters[45], R. F. Y. Peters[87], B. A. Petersen[32], T. C. Petersen[39], E. Petit[58], A. Petridis[1], C. Petridou[156], P. Petroff[119], E. Petrolo[134a], M. Petrov[122], F. Petrucci[136a,136b], N. E. Pettersson[89], A. Peyaud[138], R. Pezoa[34b], P. W. Phillips[133], G. Piacquadio[150], E. Pianori[173], A. Picazio[89], E. Piccaro[79], M. A. Pickering[122], R. Piegaia[29], J. E. Pilcher[33], A. D. Pilkington[87], A. W. J. Pin[87], M. Pinamonti[167a,167c,al], J. L. Pinfold[3], H. Pirumov[45], M. Pitt[175], L. Plazak[146a], M.-A. Pleier[27], V. Pleskot[86], E. Plotnikova[68], D. Pluth[67], P. Podberezko[111], R. Poettgen[148a,148b], L. Poggioli[119], D. Pohl[23], G. Polesello[123a], A. Poley[45], A. Policicchio[40a,40b], R. Polifka[32], A. Polini[22a], C. S. Pollard[56], V. Polychronakos[27], K. Pommès[32], L. Pontecorvo[134a], B. G. Pope[93], G. A. Popeneciu[28d], A. Poppleton[32], S. Pospisil[130], K. Potamianos[16], I. N. Potrap[68], C. J. Potter[30], C. T. Potter[118], G. Poulard[32], J. Poveda[32], M. E. Pozo Astigarraga[32], P. Pralavorio[88], A. Pranko[16], S. Prell[67], D. Price[87], L. E. Price[6], M. Primavera[76a], S. Prince[90], K. Prokofiev[62c], F. Prokoshin[34b], S. Protopopescu[27], J. Proudfoot[6], M. Przybycien[41a], D. Puddu[136a,136b], A. Puri[169], P. Puzo[119], J. Qian[92], G. Qin[56], Y. Qin[87], A. Quadt[57], W. B. Quayle[167a,167b], M. Queitsch-Maitland[45], D. Quilty[56], S. Raddum[121], V. Radeka[27], V. Radescu[122], S. K. Radhakrishnan[150], P. Radloff[118], P. Rados[91], F. Ragusa[94a,94b], G. Rahal[181], J. A. Raine[87], S. Rajagopalan[27], C. Rangel-Smith[168], M. G. Ratti[94a,94b], D. M. Rauch[45], F. Rauscher[102], S. Rave[86], T. Ravenscroft[56], I. Ravinovich[175], M. Raymond[32], A. L. Read[121], N. P. Readioff[77], M. Reale[76a,76b], D. M. Rebuzzi[123a,123b], A. Redelbach[177], G. Redlinger[27], R. Reece[139], R. G. Reed[147c], K. Reeves[44], L. Rehnisch[17], J. Reichert[124], A. Reiss[86], C. Rembser[32], H. Ren[35a], M. Rescigno[134a], S. Resconi[94a], E. D. Resseguie[124], S. Rettie[171], E. Reynolds[19], O. L. Rezanova[111,c], P. Reznicek[131], R. Rezvani[97], R. Richter[103], S. Richter[81], E. Richter-Was[41b], O. Ricken[23], M. Ridel[83], P. Rieck[103], C. J. Riegel[178], J. Rieger[57], O. Rifki[115], M. Rijssenbeek[150], A. Rimoldi[123a,123b], M. Rimoldi[18], L. Rinaldi[22a], B. Ristić[52], E. Ritsch[32], I. Riu[13], F. Rizatdinova[116], E. Rizvi[79], C. Rizzi[13], R. T. Roberts[87], S. H. Robertson[90,o], A. Robichaud-Veronneau[90], D. Robinson[30], J. E. M. Robinson[45], A. Robson[56], C. Roda[126a,126b], Y. Rodina[88], A. Rodriguez Perez[13], D. Rodriguez Rodriguez[170], S. Roe[32], C. S. Rogan[59], O. Røhne[121], J. Roloff[59], A. Romaniouk[100], M. Romano[22a,22b], S. M. Romano Saez[37], E. Romero Adam[170], N. Rompotis[77], M. Ronzani[51], L. Roos[83], S. Rosati[134a], K. Rosbach[51], P. Rose[139], N.-A. Rosien[57], V. Rossetti[148a,148b], E. Rossi[106a,106b], L. P. Rossi[53a], J. H. N. Rosten[30], R. Rosten[140], M. Rotaru[28b], I. Roth[175], J. Rothberg[140], D. Rousseau[119], A. Rozanov[88], Y. Rozen[154], X. Ruan[147c], F. Rubbo[145], F. Rühr[51], A. Ruiz-Martinez[31], Z. Rurikova[51], N. A. Rusakovich[68], A. Ruschke[102], H. L. Russell[140], J. P. Rutherfoord[7], N. Ruthmann[32], Y. F. Ryabov[125], M. Rybar[169], G. Rybkin[119], S. Ryu[6], A. Ryzhov[132], G. F. Rzehorz[57], A. F. Saavedra[152], G. Sabato[109], S. Sacerdoti[29], H. F-W. Sadrozinski[139], R. Sadykov[68], F. Safai Tehrani[134a], P. Saha[110], M. Sahinsoy[60a], M. Saimpert[45], M. Saito[157], T. Saito[157], H. Sakamoto[157], Y. Sakurai[174], G. Salamanna[136a,136b], J. E. Salazar Loyola[34b], D. Salek[109], P. H. Sales De Bruin[140], D. Salihagic[103], A. Salnikov[145], J. Salt[170], D. Salvatore[40a,40b], F. Salvatore[151], A. Salvucci[62a,62b,62c], A. Salzburger[32], D. Sammel[51], D. Sampsonidis[156], J. Sánchez[170], V. Sanchez Martinez[170], A. Sanchez Pineda[106a,106b], H. Sandaker[121], R. L. Sandbach[79], C. O. Sander[45], M. Sandhoff[178], C. Sandoval[21], D. P. C. Sankey[133], M. Sannino[53a,53b], A. Sansoni[50], C. Santoni[37], R. Santonico[135a,135b], H. Santos[128a], I. Santoyo Castillo[151], K. Sapp[127], A. Sapronov[68], J. G. Saraiva[128a,128d], B. Sarrazin[23], O. Sasaki[69], K. Sato[164], E. Sauvan[5], G. Savage[80], P. Savard[161,d], N. Savic[103], C. Sawyer[133], L. Sawyer[82,u], J. Saxon[33], C. Sbarra[22a], A. Sbrizzi[22a,22b], T. Scanlon[81], D. A. Scannicchio[166], M. Scarcella[152], V. Scarfone[40a,40b], J. Schaarschmidt[140], P. Schacht[103], B. M. Schachtner[102], D. Schaefer[32], L. Schaefer[124], R. Schaefer[45], J. Schaeffer[86], S. Schaepe[23], S. Schaetzel[60b], U. Schäfer[86], A. C. Schaffer[119], D. Schaile[102], R. D. Schamberger[150], V. Scharf[60a], V. A. Schegelsky[125], D. Scheirich[131], M. Schernau[166], C. Schiavi[53a,53b], S. Schier[139], C. Schillo[51], M. Schioppa[40a,40b], S. Schlenker[32], K. R. Schmidt-Sommerfeld[103], K. Schmieden[32], C. Schmitt[86], S. Schmitt[45], S. Schmitz[86], B. Schneider[163a], U. Schnoor[51], L. Schoeffel[138], A. Schoening[60b], B. D. Schoenrock[93], E. Schopf[23], M. Schott[86], J. F. P. Schouwenberg[108], J. Schovancova[8], S. Schramm[52], N. Schuh[86], A. Schulte[86], M. J. Schultens[23], H.-C. Schultz-Coulon[60a], H. Schulz[17], M. Schumacher[51], B. A. Schumm[139], Ph. Schune[138], A. Schwartzman[145], T. A. Schwarz[92], H. Schweiger[87], Ph. Schwemling[138], R. Schwienhorst[93], J. Schwindling[138], T. Schwindt[23], G. Sciolla[25], F. Scuri[126a,126b], F. Scutti[91], J. Searcy[92], P. Seema[23], S. C. Seidel[107], A. Seiden[139], J. M. Seixas[26a], G. Sekhniaidze[106a], K. Sekhon[92], S. J. Sekula[43], N. Semprini-Cesari[22a,22b], C. Serfon[121], L. Serin[119], L. Serkin[167a,167b], M. Sessa[136a,136b], R. Seuster[172], H. Severini[115], T. Sfiligoj[78], F. Sforza[32], A. Sfyrla[52], E. Shabalina[57], N. W. Shaikh[148a,148b], L. Y. Shan[35a], R. Shang[169], J. T. Shank[24], M. Shapiro[16], P. B. Shatalov[99], K. Shaw[167a,167b], S. M. Shaw[87], A. Shcherbakova[148a,148b], C. Y. Shehu[151], Y. Shen[115], P. Sherwood[81], L. Shi[153,an], S. Shimizu[70], C. O. Shimmin[179], M. Shimojima[104], S. Shirabe[73], M. Shiyakova[68,ao], J. Shlomi[175], A. Shmeleva[98], D. Shoaleh Saadi[97], M. J. Shochet[33], S. Shojaii[94a], D. R. Shope[115], S. Shrestha[113], E. Shulga[100],

M. A. Shupe[7], P. Sicho[129], A. M. Sickles[169], P. E. Sidebo[149], E. Sideras Haddad[147c], O. Sidiropoulou[177], D. Sidorov[116], A. Sidoti[22a,22b], F. Siegert[47], Dj. Sijacki[14], J. Silva[128a,128d], S. B. Silverstein[148a], V. Simak[130], Lj. Simic[14], S. Simion[119], E. Simioni[86], B. Simmons[81], M. Simon[86], P. Sinervo[161], N. B. Sinev[118], M. Sioli[22a,22b], G. Siragusa[177], I. Siral[92], S. Yu. Sivoklokov[101], J. Sjölin[148a,148b], M. B. Skinner[75], P. Skubic[115], M. Slater[19], T. Slavicek[130], M. Slawinska[109], K. Sliwa[165], R. Slovak[131], V. Smakhtin[175], B. H. Smart[5], L. Smestad[15], J. Smiesko[146a], S. Yu. Smirnov[100], Y. Smirnov[100], L. N. Smirnova[101,ap], O. Smirnova[84], J. W. Smith[57], M. N. K. Smith[38], R. W. Smith[38], M. Smizanska[75], K. Smolek[130], A. A. Snesarev[98], I. M. Snyder[118], S. Snyder[27], R. Sobie[172,o], F. Socher[47], A. Soffer[155], D. A. Soh[153], G. Sokhrannyi[78], C. A. Solans Sanchez[32], M. Solar[130], E. Yu. Soldatov[100], U. Soldevila[170], A. A. Solodkov[132], A. Soloshenko[68], O. V. Solovyanov[132], V. Solovyev[125], P. Sommer[51], H. Son[165], H. Y. Song[36a,aq], A. Sopczak[130], V. Sorin[13], D. Sosa[60b], C. L. Sotiropoulou[126a,126b], R. Soualah[167a,167c], A. M. Soukharev[111,c], D. South[45], B. C. Sowden[80], S. Spagnolo[76a,76b], M. Spalla[126a,126b], M. Spangenberg[173], F. Spanò[80], D. Sperlich[17], F. Spettel[103], T. M. Spieker[60a], R. Spighi[22a], G. Spigo[32], L. A. Spiller[91], M. Spousta[131], R. D. St. Denis[56,*], A. Stabile[94a], R. Stamen[60a], S. Stamm[17], E. Stanecka[42], R. W. Stanek[6], C. Stanescu[136a], M. M. Stanitzki[45], S. Stapnes[121], E. A. Starchenko[132], G. H. Stark[33], J. Stark[58], S. H Stark[39], P. Staroba[129], P. Starovoitov[60a], S. Stärz[32], R. Staszewski[42], P. Steinberg[27], B. Stelzer[144], H. J. Stelzer[32], O. Stelzer-Chilton[163a], H. Stenzel[55], G. A. Stewart[56], J. A. Stillings[23], M. C. Stockton[90], M. Stoebe[90], G. Stoicea[28b], P. Stolte[57], S. Stonjek[103], A. R. Stradling[8], A. Straessner[47], M. E. Stramaglia[18], J. Strandberg[149], S. Strandberg[148a,148b], A. Strandlie[121], M. Strauss[115], P. Strizenec[146b], R. Ströhmer[177], D. M. Strom[118], R. Stroynowski[43], A. Strubig[108], S. A. Stucci[27], B. Stugu[15], N. A. Styles[45], D. Su[145], J. Su[127], S. Suchek[60a], Y. Sugaya[120], M. Suk[130], V. V. Sulin[98], S. Sultansoy[4c], T. Sumida[71], S. Sun[59], X. Sun[3], K. Suruliz[151], C. J. E. Suster[152], M. R. Sutton[151], S. Suzuki[69], M. Svatos[129], M. Swiatlowski[33], S. P. Swift[2], I. Sykora[146a], T. Sykora[131], D. Ta[51], K. Tackmann[45], J. Taenzer[155], A. Taffard[166], R. Tafirout[163a], N. Taiblum[155], H. Takai[27], R. Takashima[72], T. Takeshita[142], Y. Takubo[69], M. Talby[88], A. A. Talyshev[111,c], J. Tanaka[157], M. Tanaka[159], R. Tanaka[119], S. Tanaka[69], R. Tanioka[70], B. B. Tannenwald[113], S. Tapia Araya[34b], S. Tapprogge[86], S. Tarem[154], G. F. Tartarelli[94a], P. Tas[131], M. Tasevsky[129], T. Tashiro[71], E. Tassi[40a,40b], A. Tavares Delgado[128a,128b], Y. Tayalati[137e], A. C. Taylor[107], G. N. Taylor[91], P. T. E. Taylor[91], W. Taylor[163b], P. Teixeira-Dias[80], D. Temple[144], H. Ten Kate[32], P. K. Teng[153], J. J. Teoh[120], F. Tepel[178], S. Terada[69], K. Terashi[157], J. Terron[85], S. Terzo[13], M. Testa[50], R. J. Teuscher[161,o], T. Theveneaux-Pelzer[88], J. P. Thomas[19], J. Thomas-Wilsker[80], P. D. Thompson[19], A. S. Thompson[56], L. A. Thomsen[179], E. Thomson[124], M. J. Tibbetts[16], R. E. Ticse Torres[88], V. O. Tikhomirov[98,ar], Yu. A. Tikhonov[111,c], S. Timoshenko[100], P. Tipton[179], S. Tisserant[88], K. Todome[159], S. Todorova-Nova[5], J. Tojo[73], S. Tokár[146a], K. Tokushuku[69], E. Tolley[59], L. Tomlinson[87], M. Tomoto[105], L. Tompkins[145,as], K. Toms[107], B. Tong[59], P. Tornambe[51], E. Torrence[118], H. Torres[144], E. Torró Pastor[140], J. Toth[88,at], F. Touchard[88], D. R. Tovey[141], C. J. Treado[112], T. Trefzger[177], A. Tricoli[27], I. M. Trigger[163a], S. Trincaz-Duvoid[83], M. F. Tripiana[13], W. Trischuk[161], B. Trocmé[58], A. Trofymov[45], C. Troncon[94a], M. Trottier-McDonald[16], M. Trovatelli[172], L. Truong[167a,167c], M. Trzebinski[42], A. Trzupek[42], K. W. Tsang[62a], J. C-L. Tseng[122], P. V. Tsiareshka[95], G. Tsipolitis[10], N. Tsirintanis[9], S. Tsiskaridze[13], V. Tsiskaridze[51], E. G. Tskhadadze[54a], K. M. Tsui[62a], I. I. Tsukerman[99], V. Tsulaia[16], S. Tsuno[69], D. Tsybychev[150], Y. Tu[62b], A. Tudorache[28b], V. Tudorache[28b], T. T. Tulbure[28a], A. N. Tuna[59], S. A. Tupputi[22a,22b], S. Turchikhin[68], D. Turgeman[175], I. Turk Cakir[4b,au], R. Turra[94a,94b], P. M. Tuts[38], G. Ucchielli[22a,22b], I. Ueda[69], M. Ughetto[148a,148b], F. Ukegawa[164], G. Unal[32], A. Undrus[27], G. Unel[166], F. C. Ungaro[91], Y. Unno[69], C. Unverdorben[102], J. Urban[146b], P. Urquijo[91], P. Urrejola[86], G. Usai[8], J. Usui[69], L. Vacavant[88], V. Vacek[130], B. Vachon[90], C. Valderanis[102], E. Valdes Santurio[148a,148b], N. Valencic[109], S. Valentinetti[22a,22b], A. Valero[170], L. Valéry[13], S. Valkar[131], A. Vallier[5], J. A. Valls Ferrer[170], W. Van Den Wollenberg[109], H. van der Graaf[109], N. van Eldik[154], P. van Gemmeren[6], J. Van Nieuwkoop[144], I. van Vulpen[109], M. C. van Woerden[109], M. Vanadia[134a,134b], W. Vandelli[32], R. Vanguri[124], A. Vaniachine[160], P. Vankov[109], G. Vardanyan[180], R. Vari[134a], E. W. Varnes[7], C. Varni[53a,53b], T. Varol[43], D. Varouchas[83], A. Vartapetian[8], K. E. Varvell[152], J. G. Vasquez[179], G. A. Vasquez[34b], F. Vazeille[37], T. Vazquez Schroeder[90], J. Veatch[57], V. Veeraraghavan[7], L. M. Veloce[161], F. Veloso[128a,128c], S. Veneziano[134a], A. Ventura[76a,76b], M. Venturi[172], N. Venturi[161], A. Venturini[25], V. Vercesi[123a], M. Verducci[136a,136b], W. Verkerke[109], J. C. Vermeulen[109], M. C. Vetterli[144,d], N. Viaux Maira[34a], O. Viazlo[84], I. Vichou[169,*], T. Vickey[141], O. E. Vickey Boeriu[141], G. H. A. Viehhauser[122], S. Viel[16], L. Vigani[122], M. Villa[22a,22b], M. Villaplana Perez[94a,94b], E. Vilucchi[50], M. G. Vincter[31], V. B. Vinogradov[68], A. Vishwakarma[45], C. Vittori[22a,22b], I. Vivarelli[151], S. Vlachos[10], M. Vlasak[130], M. Vogel[178], P. Vokac[130], G. Volpi[126a,126b], M. Volpi[91], H. von der Schmitt[103], E. von Toerne[23], V. Vorobel[131], K. Vorobev[100], M. Vos[170], R. Voss[32], J. H. Vossebeld[77], N. Vranjes[14], M. Vranjes Milosavljevic[14], V. Vrba[130], M. Vreeswijk[109], R. Vuillermet[32], I. Vukotic[33], P. Wagner[23], W. Wagner[178], H. Wahlberg[74], S. Wahrmund[47], J. Wakabayashi[105], J. Walder[75], R. Walker[102], W. Walkowiak[143], V. Wallangen[148a,148b], C. Wang[35b], C. Wang[36b,av], F. Wang[176], H. Wang[16], H. Wang[3], J. Wang[45], J. Wang[152], Q. Wang[115], R. Wang[6], S. M. Wang[153], T. Wang[38], W. Wang[153,aw], W. Wang[36a], C. Wanotayaroj[118], A. Warburton[90], C. P. Ward[30], D. R. Wardrope[81], A. Washbrook[49], P. M. Watkins[19], A. T. Watson[19], M. F. Watson[19],

G. Watts[140], S. Watts[87], B. M. Waugh[81], A. F. Webb[11], S. Webb[86], M. S. Weber[18], S. W. Weber[177], S. A. Weber[31], J. S. Webster[6], A. R. Weidberg[122], B. Weinert[64], J. Weingarten[57], C. Weiser[51], H. Weits[109], P. S. Wells[32], T. Wenaus[27], T. Wengler[32], S. Wenig[32], N. Wermes[23], M. D. Werner[67], P. Werner[32], M. Wessels[60a], K. Whalen[118], N. L. Whallon[140], A. M. Wharton[75], A. White[8], M. J. White[1], R. White[34b], D. Whiteson[166], F. J. Wickens[133], W. Wiedenmann[176], M. Wielers[133], C. Wiglesworth[39], L. A. M. Wiik-Fuchs[23], A. Wildauer[103], F. Wilk[87], H. G. Wilkens[32], H. H. Williams[124], S. Williams[109], C. Willis[93], S. Willocq[89], J. A. Wilson[19], I. Wingerter-Seez[5], F. Winklmeier[118], O. J. Winston[151], B. T. Winter[23], M. Wittgen[145], M. Wobisch[82,u], T. M. H. Wolf[109], R. Wolff[88], M. W. Wolter[42], H. Wolters[128a,128c], S. D. Worm[19], B. K. Wosiek[42], J. Wotschack[32], M. J. Woudstra[87], K. W. Wozniak[42], M. Wu[33], S. L. Wu[176], X. Wu[52], Y. Wu[92], T. R. Wyatt[87], B. M. Wynne[49], S. Xella[39], Z. Xi[92], L. Xia[35c], D. Xu[35a], L. Xu[27], B. Yabsley[152], S. Yacoob[147a], D. Yamaguchi[159], Y. Yamaguchi[120], A. Yamamoto[69], S. Yamamoto[157], T. Yamanaka[157], K. Yamauchi[105], Y. Yamazaki[70], Z. Yan[24], H. Yang[36c], H. Yang[16], Y. Yang[153], Z. Yang[15], W-M. Yao[16], Y. C. Yap[83], Y. Yasu[69], E. Yatsenko[5], K. H. Yau Wong[23], J. Ye[43], S. Ye[27], I. Yeletskikh[68], E. Yildirim[86], K. Yorita[174], K. Yoshihara[124], C. Young[145], C. J. S. Young[32], S. Youssef[24], D. R. Yu[16], J. Yu[8], J. Yu[67], L. Yuan[70], S. P. Y. Yuen[23], I. Yusuff[30,ax], B. Zabinski[42], G. Zacharis[10], R. Zaidan[13], A. M. Zaitsev[132,aj], N. Zakharchuk[45], J. Zalieckas[15], A. Zaman[150], S. Zambito[59], D. Zanzi[91], C. Zeitnitz[178], M. Zeman[130], A. Zemla[41a], J. C. Zeng[169], Q. Zeng[145], O. Zenin[132], T. Ženiš[146a], D. Zerwas[119], D. Zhang[92], F. Zhang[176], G. Zhang[36a,aq], H. Zhang[35b], J. Zhang[6], L. Zhang[51], L. Zhang[36a], M. Zhang[169], R. Zhang[23], R. Zhang[36a,av], X. Zhang[36b], Y. Zhang[35a], Z. Zhang[119], X. Zhao[43], Y. Zhao[36b,ay], Z. Zhao[36a], A. Zhemchugov[68], J. Zhong[122], B. Zhou[92], C. Zhou[176], L. Zhou[43], M. Zhou[35a], M. Zhou[150], N. Zhou[35c], C. G. Zhu[36b], H. Zhu[35a], J. Zhu[92], Y. Zhu[36a], X. Zhuang[35a], K. Zhukov[98], A. Zibell[177], D. Zieminska[64], N. I. Zimine[68], C. Zimmermann[86], S. Zimmermann[51], Z. Zinonos[103], M. Zinser[86], M. Ziolkowski[143], L. Živković[14], G. Zobernig[176], A. Zoccoli[22a,22b], R. Zou[33], M. zur Nedden[17], L. Zwalinski[32]

[1] Department of Physics, University of Adelaide, Adelaide, Australia
[2] Physics Department, SUNY Albany, Albany, NY, USA
[3] Department of Physics, University of Alberta, Edmonton, AB, Canada
[4] [(a)]Department of Physics, Ankara University, Ankara, Turkey; [(b)]Istanbul Aydin University, Istanbul, Turkey; [(c)]Division of Physics, TOBB University of Economics and Technology, Ankara, Turkey
[5] LAPP, CNRS/IN2P3 and Université Savoie Mont Blanc, Annecy-le-Vieux, France
[6] High Energy Physics Division, Argonne National Laboratory, Argonne, IL, USA
[7] Department of Physics, University of Arizona, Tucson, AZ, USA
[8] Department of Physics, The University of Texas at Arlington, Arlington, TX, USA
[9] Physics Department, National and Kapodistrian University of Athens, Athens, Greece
[10] Physics Department, National Technical University of Athens, Zografou, Greece
[11] Department of Physics, The University of Texas at Austin, Austin, TX, USA
[12] Institute of Physics, Azerbaijan Academy of Sciences, Baku, Azerbaijan
[13] Institut de Física d'Altes Energies (IFAE), The Barcelona Institute of Science and Technology, Barcelona, Spain
[14] Institute of Physics, University of Belgrade, Belgrade, Serbia
[15] Department for Physics and Technology, University of Bergen, Bergen, Norway
[16] Physics Division, Lawrence Berkeley National Laboratory, University of California, Berkeley, CA, USA
[17] Department of Physics, Humboldt University, Berlin, Germany
[18] Albert Einstein Center for Fundamental Physics, Laboratory for High Energy Physics, University of Bern, Bern, Switzerland
[19] School of Physics and Astronomy, University of Birmingham, Birmingham, UK
[20] [(a)]Department of Physics, Bogazici University, Istanbul, Turkey; [(b)]Department of Physics Engineering, Gaziantep University, Gaziantep, Turkey; [(c)]Faculty of Engineering and Natural Sciences, Istanbul Bilgi University, Istanbul, Turkey; [(d)]Faculty of Engineering and Natural Sciences, Bahcesehir University, Istanbul, Turkey
[21] Centro de Investigaciones, Universidad Antonio Narino, Bogotá, Colombia
[22] [(a)]INFN Sezione di Bologna, Bologna, Italy; [(b)]Dipartimento di Fisica e Astronomia, Università di Bologna, Bologna, Italy
[23] Physikalisches Institut, University of Bonn, Bonn, Germany
[24] Department of Physics, Boston University, Boston, MA, USA
[25] Department of Physics, Brandeis University, Waltham, MA, USA

[26] [(a)]Universidade Federal do Rio De Janeiro COPPE/EE/IF, Rio de Janeiro, Brazil; [(b)]Electrical Circuits Department, Federal University of Juiz de Fora (UFJF), Juiz de Fora, Brazil; [(c)]Federal University of Sao Joao del Rei (UFSJ), Sao Joao del Rei, Brazil; [(d)]Instituto de Fisica, Universidade de Sao Paulo, São Paulo, Brazil
[27] Physics Department, Brookhaven National Laboratory, Upton, NY, USA
[28] [(a)]Transilvania University of Brasov, Brasov, Romania; [(b)]Horia Hulubei National Institute of Physics and Nuclear Engineering, Bucharest, Romania; [(c)]Department of Physics, Alexandru Ioan Cuza University of Iasi, Iasi, Romania; [(d)]Physics Department, National Institute for Research and Development of Isotopic and Molecular Technologies, Cluj-Napoca, Romania; [(e)]University Politehnica Bucharest, Bucharest, Romania; [(f)]West University in Timisoara, Timisoara, Romania
[29] Departamento de Física, Universidad de Buenos Aires, Buenos Aires, Argentina
[30] Cavendish Laboratory, University of Cambridge, Cambridge, UK
[31] Department of Physics, Carleton University, Ottawa, ON, Canada
[32] CERN, Geneva, Switzerland
[33] Enrico Fermi Institute, University of Chicago, Chicago, IL, USA
[34] [(a)]Departamento de Física, Pontificia Universidad Católica de Chile, Santiago, Chile; [(b)]Departamento de Física, Universidad Técnica Federico Santa María, Valparaiso, Chile
[35] [(a)]Institute of High Energy Physics, Chinese Academy of Sciences, Beijing, China; [(b)]Department of Physics, Nanjing University, Nanjing, Jiangsu, China; [(c)]Physics Department, Tsinghua University, Beijing 100084, China
[36] [(a)]Department of Modern Physics, University of Science and Technology of China, Hefei, Anhui, China; [(b)]School of Physics, Shandong University, Jinan, Shandong, China; [(c)]Department of Physics and Astronomy, Key Laboratory for Particle Physics, Astrophysics and Cosmology, Ministry of Education, Shanghai Key Laboratory for Particle Physics and Cosmology, Shanghai Jiao Tong University, Shanghai (also at PKU-CHEP), Shanghai, China
[37] Université Clermont Auvergne, CNRS/IN2P3, LPC, Clermont-Ferrand, France
[38] Nevis Laboratory, Columbia University, Irvington, NY, USA
[39] Niels Bohr Institute, University of Copenhagen, Copenhagen, Denmark
[40] [(a)]INFN Gruppo Collegato di Cosenza, Laboratori Nazionali di Frascati, Frascati, Italy; [(b)]Dipartimento di Fisica, Università della Calabria, Rende, Italy
[41] [(a)]Faculty of Physics and Applied Computer Science, AGH University of Science and Technology, Kraków, Poland; [(b)]Marian Smoluchowski Institute of Physics, Jagiellonian University, Kraków, Poland
[42] Institute of Nuclear Physics, Polish Academy of Sciences, Kraków, Poland
[43] Physics Department, Southern Methodist University, Dallas, TX, USA
[44] Physics Department, University of Texas at Dallas, c, TX, USA
[45] DESY, Hamburg and Zeuthen, Germany
[46] Lehrstuhl für Experimentelle Physik IV, Technische Universität Dortmund, Dortmund, Germany
[47] Institut für Kern- und Teilchenphysik, Technische Universität Dresden, Dresden, Germany
[48] Department of Physics, Duke University, Durham, NC, USA
[49] SUPA-School of Physics and Astronomy, University of Edinburgh, Edinburgh, UK
[50] INFN Laboratori Nazionali di Frascati, Frascati, Italy
[51] Fakultät für Mathematik und Physik, Albert-Ludwigs-Universität, Freiburg, Germany
[52] Departement de Physique Nucleaire et Corpusculaire, Université de Genève, Geneva, Switzerland
[53] [(a)]INFN Sezione di Genova, Genoa, Italy; [(b)]Dipartimento di Fisica, Università di Genova, Genoa, Italy
[54] [(a)]E. Andronikashvili Institute of Physics, Iv. Javakhishvili Tbilisi State University, Tbilisi, Georgia; [(b)]High Energy Physics Institute, Tbilisi State University, Tbilisi, Georgia
[55] II Physikalisches Institut, Justus-Liebig-Universität Giessen, Giessen, Germany
[56] SUPA-School of Physics and Astronomy, University of Glasgow, Glasgow, UK
[57] II Physikalisches Institut, Georg-August-Universität, Göttingen, Germany
[58] Laboratoire de Physique Subatomique et de Cosmologie, Université Grenoble-Alpes, CNRS/IN2P3, Grenoble, France
[59] Laboratory for Particle Physics and Cosmology, Harvard University, Cambridge, MA, USA
[60] [(a)]Kirchhoff-Institut für Physik, Ruprecht-Karls-Universität Heidelberg, Heidelberg, Germany; [(b)]Physikalisches Institut, Ruprecht-Karls-Universität Heidelberg, Heidelberg, Germany; [(c)]ZITI Institut für technische Informatik, Ruprecht-Karls-Universität Heidelberg, Mannheim, Germany
[61] Faculty of Applied Information Science, Hiroshima Institute of Technology, Hiroshima, Japan

[62] [(a)]Department of Physics, The Chinese University of Hong Kong, Shatin, NT, Hong Kong; [(b)]Department of Physics, The University of Hong Kong, Hong Kong, China; [(c)]Department of Physics, Institute for Advanced Study, The Hong Kong University of Science and Technology, Clear Water Bay, Kowloon, Hong Kong, China
[63] Department of Physics, National Tsing Hua University, Taiwan, Taiwan
[64] Department of Physics, Indiana University, Bloomington, IN, USA
[65] Institut für Astro- und Teilchenphysik, Leopold-Franzens-Universität, Innsbruck, Austria
[66] University of Iowa, Iowa City, IA, USA
[67] Department of Physics and Astronomy, Iowa State University, Ames, IA, USA
[68] Joint Institute for Nuclear Research, JINR Dubna, Dubna, Russia
[69] KEK, High Energy Accelerator Research Organization, Tsukuba, Japan
[70] Graduate School of Science, Kobe University, Kobe, Japan
[71] Faculty of Science, Kyoto University, Kyoto, Japan
[72] Kyoto University of Education, Kyoto, Japan
[73] Department of Physics, Kyushu University, Fukuoka, Japan
[74] Instituto de Física La Plata, Universidad Nacional de La Plata and CONICET, La Plata, Argentina
[75] Physics Department, Lancaster University, Lancaster, UK
[76] [(a)]INFN Sezione di Lecce, Lecce, Italy; [(b)]Dipartimento di Matematica e Fisica, Università del Salento, Lecce, Italy
[77] Oliver Lodge Laboratory, University of Liverpool, Liverpool, UK
[78] Department of Experimental Particle Physics, Jožef Stefan Institute and Department of Physics, University of Ljubljana, Ljubljana, Slovenia
[79] School of Physics and Astronomy, Queen Mary University of London, London, UK
[80] Department of Physics, Royal Holloway University of London, Surrey, UK
[81] Department of Physics and Astronomy, University College London, London, UK
[82] Louisiana Tech University, Ruston, LA, USA
[83] Laboratoire de Physique Nucléaire et de Hautes Energies, UPMC and Université Paris-Diderot and CNRS/IN2P3, Paris, France
[84] Fysiska institutionen, Lunds universitet, Lund, Sweden
[85] Departamento de Fisica Teorica C-15, Universidad Autonoma de Madrid, Madrid, Spain
[86] Institut für Physik, Universität Mainz, Mainz, Germany
[87] School of Physics and Astronomy, University of Manchester, Manchester, UK
[88] CPPM, Aix-Marseille Université and CNRS/IN2P3, Marseille, France
[89] Department of Physics, University of Massachusetts, Amherst, MA, USA
[90] Department of Physics, McGill University, Montreal, QC, Canada
[91] School of Physics, University of Melbourne, Victoria, Australia
[92] Department of Physics, The University of Michigan, Ann Arbor, MI, USA
[93] Department of Physics and Astronomy, Michigan State University, East Lansing, MI, USA
[94] [(a)]INFN Sezione di Milano, Milan, Italy; [(b)]Dipartimento di Fisica, Università di Milano, Milan, Italy
[95] B.I. Stepanov Institute of Physics, National Academy of Sciences of Belarus, Minsk, Republic of Belarus
[96] Research Institute for Nuclear Problems of Byelorussian State University, Minsk, Republic of Belarus
[97] Group of Particle Physics, University of Montreal, Montreal, QC, Canada
[98] P.N. Lebedev Physical Institute of the Russian Academy of Sciences, Moscow, Russia
[99] Institute for Theoretical and Experimental Physics (ITEP), Moscow, Russia
[100] National Research Nuclear University MEPhI, Moscow, Russia
[101] D.V. Skobeltsyn Institute of Nuclear Physics, M.V. Lomonosov Moscow State University, Moscow, Russia
[102] Fakultät für Physik, Ludwig-Maximilians-Universität München, Munich, Germany
[103] Max-Planck-Institut für Physik (Werner-Heisenberg-Institut), Munich, Germany
[104] Nagasaki Institute of Applied Science, Nagasaki, Japan
[105] Graduate School of Science and Kobayashi-Maskawa Institute, Nagoya University, Nagoya, Japan
[106] [(a)]INFN Sezione di Napoli, Naples, Italy; [(b)]Dipartimento di Fisica, Università di Napoli, Naples, Italy
[107] Department of Physics and Astronomy, University of New Mexico, Albuquerque, NM, USA
[108] Institute for Mathematics, Astrophysics and Particle Physics, Radboud University Nijmegen/Nikhef, Nijmegen, The Netherlands
[109] Nikhef National Institute for Subatomic Physics, University of Amsterdam, Amsterdam, The Netherlands

[110] Department of Physics, Northern Illinois University, DeKalb, IL, USA
[111] Budker Institute of Nuclear Physics, SB RAS, Novosibirsk, Russia
[112] Department of Physics, New York University, New York, NY, USA
[113] Ohio State University, Columbus, OH, USA
[114] Faculty of Science, Okayama University, Okayama, Japan
[115] Homer L. Dodge Department of Physics and Astronomy, University of Oklahoma, Norman, OK, USA
[116] Department of Physics, Oklahoma State University, Stillwater, OK, USA
[117] Palacký University, RCPTM, Olomouc, Czech Republic
[118] Center for High Energy Physics, University of Oregon, Eugene, OR, USA
[119] LAL, Univ. Paris-Sud, CNRS/IN2P3, Université Paris-Saclay, Orsay, France
[120] Graduate School of Science, Osaka University, Osaka, Japan
[121] Department of Physics, University of Oslo, Oslo, Norway
[122] Department of Physics, Oxford University, Oxford, UK
[123] [(a)]INFN Sezione di Pavia, Pavia, Italy; [(b)]Dipartimento di Fisica, Università di Pavia, Pavia, Italy
[124] Department of Physics, University of Pennsylvania, Philadelphia, PA, USA
[125] National Research Centre "Kurchatov Institute" B.P. Konstantinov Petersburg Nuclear Physics Institute, St. Petersburg, Russia
[126] [(a)]INFN Sezione di Pisa, Pisa, Italy; [(b)]Dipartimento di Fisica E. Fermi, Università di Pisa, Pisa, Italy
[127] Department of Physics and Astronomy, University of Pittsburgh, Pittsburgh, PA, USA
[128] [(a)]Laboratório de Instrumentação e Física Experimental de Partículas-LIP, Lisbon, Portugal; [(b)]Faculdade de Ciências, Universidade de Lisboa, Lisbon, Portugal; [(c)]Department of Physics, University of Coimbra, Coimbra, Portugal; [(d)]Centro de Física Nuclear da Universidade de Lisboa, Lisbon, Portugal; [(e)]Departamento de Fisica, Universidade do Minho, Braga, Portugal; [(f)]Departamento de Fisica Teorica y del Cosmos and CAFPE, Universidad de Granada, Granada, Spain; [(g)]Dep Fisica and CEFITEC of Faculdade de Ciencias e Tecnologia, Universidade Nova de Lisboa, Caparica, Portugal
[129] Institute of Physics, Academy of Sciences of the Czech Republic, Prague, Czech Republic
[130] Czech Technical University in Prague, Prague, Czech Republic
[131] Faculty of Mathematics and Physics, Charles University, Prague, Czech Republic
[132] State Research Center Institute for High Energy Physics (Protvino), NRC KI, Protvino, Russia
[133] Particle Physics Department, Rutherford Appleton Laboratory, Didcot, UK
[134] [(a)]INFN Sezione di Roma, Rome, Italy; [(b)]Dipartimento di Fisica, Sapienza Università di Roma, Rome, Italy
[135] [(a)]INFN Sezione di Roma Tor Vergata, Rome, Italy; [(b)]Dipartimento di Fisica, Università di Roma Tor Vergata, Rome, Italy
[136] [(a)]INFN Sezione di Roma Tre, Rome, Italy; [(b)]Dipartimento di Matematica e Fisica, Università Roma Tre, Rome, Italy
[137] [(a)]Faculté des Sciences Ain Chock, Réseau Universitaire de Physique des Hautes Energies-Université Hassan II, Casablanca, Morocco; [(b)]Centre National de l'Energie des Sciences Techniques Nucleaires, Rabat, Morocco; [(c)]Faculté des Sciences Semlalia, Université Cadi Ayyad, LPHEA-Marrakech, Marrakech, Morocco; [(d)]Faculté des Sciences, Université Mohamed Premier and LPTPM, Oujda, Morocco; [(e)]Faculté des Sciences, Université Mohammed V, Rabat, Morocco
[138] DSM/IRFU (Institut de Recherches sur les Lois Fondamentales de l'Univers), CEA Saclay (Commissariat à l'Energie Atomique et aux Energies Alternatives), Gif-sur-Yvette, France
[139] Santa Cruz Institute for Particle Physics, University of California Santa Cruz, Santa Cruz, CA, USA
[140] Department of Physics, University of Washington, Seattle, WA, USA
[141] Department of Physics and Astronomy, University of Sheffield, Sheffield, UK
[142] Department of Physics, Shinshu University, Nagano, Japan
[143] Department Physik, Universität Siegen, Siegen, Germany
[144] Department of Physics, Simon Fraser University, Burnaby, BC, Canada
[145] SLAC National Accelerator Laboratory, Stanford, CA, USA
[146] [(a)]Faculty of Mathematics, Physics and Informatics, Comenius University, Bratislava, Slovak Republic; [(b)]Department of Subnuclear Physics, Institute of Experimental Physics of the Slovak Academy of Sciences, Kosice, Slovak Republic

147 (a)Department of Physics, University of Cape Town, Cape Town, South Africa; (b)Department of Physics, University of Johannesburg, Johannesburg, South Africa; (c)School of Physics, University of the Witwatersrand, Johannesburg, South Africa
148 (a)Department of Physics, Stockholm University, Stockholm, Sweden; (b)The Oskar Klein Centre, Stockholm, Sweden
149 Physics Department, Royal Institute of Technology, Stockholm, Sweden
150 Departments of Physics and Astronomy and Chemistry, Stony Brook University, Stony Brook, NY, USA
151 Department of Physics and Astronomy, University of Sussex, Brighton, UK
152 School of Physics, University of Sydney, Sydney, Australia
153 Institute of Physics, Academia Sinica, Taipei, Taiwan
154 Department of Physics, Technion: Israel Institute of Technology, Haifa, Israel
155 Raymond and Beverly Sackler School of Physics and Astronomy, Tel Aviv University, Tel Aviv, Israel
156 Department of Physics, Aristotle University of Thessaloniki, Thessaloníki, Greece
157 International Center for Elementary Particle Physics and Department of Physics, The University of Tokyo, Tokyo, Japan
158 Graduate School of Science and Technology, Tokyo Metropolitan University, Tokyo, Japan
159 Department of Physics, Tokyo Institute of Technology, Tokyo, Japan
160 Tomsk State University, Tomsk, Russia
161 Department of Physics, University of Toronto, Toronto, ON, Canada
162 (a)INFN-TIFPA, Trento, Italy; (b)University of Trento, Trento, Italy
163 (a)TRIUMF, Vancouver, BC, Canada; (b)Department of Physics and Astronomy, York University, Toronto, ON, Canada
164 Faculty of Pure and Applied Sciences, and Center for Integrated Research in Fundamental Science and Engineering, University of Tsukuba, Tsukuba, Japan
165 Department of Physics and Astronomy, Tufts University, Medford, MA, USA
166 Department of Physics and Astronomy, University of California Irvine, Irvine, CA, USA
167 (a)INFN Gruppo Collegato di Udine, Sezione di Trieste, Udine, Italy; (b)ICTP, Trieste, Italy; (c)Dipartimento di Chimica, Fisica e Ambiente, Università di Udine, Udine, Italy
168 Department of Physics and Astronomy, University of Uppsala, Uppsala, Sweden
169 Department of Physics, University of Illinois, Urbana, IL, USA
170 Instituto de Fisica Corpuscular (IFIC) and Departamento de Fisica Atomica, Molecular y Nuclear and Departamento de Ingeniería Electrónica and Instituto de Microelectrónica de Barcelona (IMB-CNM), University of Valencia and CSIC, Valencia, Spain
171 Department of Physics, University of British Columbia, Vancouver, BC, Canada
172 Department of Physics and Astronomy, University of Victoria, Victoria, BC, Canada
173 Department of Physics, University of Warwick, Coventry, UK
174 Waseda University, Tokyo, Japan
175 Department of Particle Physics, The Weizmann Institute of Science, Rehovot, Israel
176 Department of Physics, University of Wisconsin, Madison, WI, USA
177 Fakultät für Physik und Astronomie, Julius-Maximilians-Universität, Würzburg, Germany
178 Fakultät für Mathematik und Naturwissenschaften, Fachgruppe Physik, Bergische Universität Wuppertal, Wuppertal, Germany
179 Department of Physics, Yale University, New Haven, CT, USA
180 Yerevan Physics Institute, Yerevan, Armenia
181 Centre de Calcul de l'Institut National de Physique Nucléaire et de Physique des Particules (IN2P3), Villeurbanne, France

[a] Also at Department of Physics, King's College London, London, UK
[b] Also at Institute of Physics, Azerbaijan Academy of Sciences, Baku, Azerbaijan
[c] Also at Novosibirsk State University, Novosibirsk, Russia
[d] Also at TRIUMF, Vancouver, BC, Canada
[e] Also at Department of Physics and Astronomy, University of Louisville, Louisville, KY, USA
[f] Also at Physics Department, An-Najah National University, Nablus, Palestine
[g] Also at Department of Physics, California State University, Fresno, CA, USA
[h] Also at Department of Physics, University of Fribourg, Fribourg, Switzerland
[i] Also at II Physikalisches Institut, Georg-August-Universität, Göttingen, Germany

[j] Also at Department de Fisica de la Universitat Autonoma de Barcelona, Barcelona, Spain
[k] Also at Departamento de Fisica e Astronomia, Faculdade de Ciencias, Universidade do Porto, Porto, Portugal
[l] Also at Tomsk State University, Tomsk, Russia
[m] Also at The Collaborative Innovation Center of Quantum Matter (CICQM), Beijing, China
[n] Also at Universita di Napoli Parthenope, Napoli, Italy
[o] Also at Institute of Particle Physics (IPP), Canada
[p] Also at Horia Hulubei National Institute of Physics and Nuclear Engineering, Bucharest, Romania
[q] Also at Department of Physics, St. Petersburg State Polytechnical University, St. Petersburg, Russia
[r] Also at Borough of Manhattan Community College, City University of New York, New York, USA
[s] Also at Department of Physics, The University of Michigan, Ann Arbor MI, United States of America
[t] Also at Centre for High Performance Computing, CSIR Campus, Rosebank, Cape Town, South Africa
[u] Also at Louisiana Tech University, Ruston, LA, USA
[v] Also at Institucio Catalana de Recerca i Estudis Avancats, ICREA, Barcelona, Spain
[w] Also at Graduate School of Science, Osaka University, Osaka, Japan
[x] Also at Fakultät für Mathematik und Physik, Albert-Ludwigs-Universität, Freiburg, Germany
[y] Also at Institute for Mathematics, Astrophysics and Particle Physics, Radboud University Nijmegen/Nikhef, Nijmegen, The Netherlands
[z] Also at Department of Physics, The University of Texas at Austin, Austin, TX, USA
[aa] Also at Institute of Theoretical Physics, Ilia State University, Tbilisi, Georgia
[ab] Also at CERN, Geneva, Switzerland
[ac] Also at Georgian Technical University (GTU), Tbilisi, Georgia
[ad] Also at Ochadai Academic Production, Ochanomizu University, Tokyo, Japan
[ae] Also at Manhattan College, New York, NY, USA
[af] Also at Academia Sinica Grid Computing, Institute of Physics, Academia Sinica, Taipei, Taiwan
[ag] Also at School of Physics, Shandong University, Shandong, China
[ah] Also at Departamento de Fisica Teorica y del Cosmos and CAFPE, Universidad de Granada, Granada, Spain
[ai] Also at Department of Physics, California State University, Sacramento, CA, USA
[aj] Also at Moscow Institute of Physics and Technology State University, Dolgoprudny, Russia
[ak] Also at Departement de Physique Nucleaire et Corpusculaire, Université de Genève, Geneva, Switzerland
[al] Also at International School for Advanced Studies (SISSA), Trieste, Italy
[am] Also at Institut de Física d'Altes Energies (IFAE), The Barcelona Institute of Science and Technology, Barcelona, Spain
[an] Also at School of Physics, Sun Yat-sen University, Guangzhou, China
[ao] Also at Institute for Nuclear Research and Nuclear Energy (INRNE) of the Bulgarian Academy of Sciences, Sofia, Bulgaria
[ap] Also at Faculty of Physics, M.V. Lomonosov Moscow State University, Moscow, Russia
[aq] Also at Institute of Physics, Academia Sinica, Taipei, Taiwan
[ar] Also at National Research Nuclear University MEPhI, Moscow, Russia
[as] Also at Department of Physics, Stanford University, Stanford, CA, USA
[at] Also at Institute for Particle and Nuclear Physics, Wigner Research Centre for Physics, Budapest, Hungary
[au] Also at Faculty of Engineering, Giresun University, Giresun, Turkey
[av] Also at CPPM, Aix-Marseille Université and CNRS/IN2P3, Marseille, France
[aw] Also at Department of Physics, Nanjing University, Jiangsu, China
[ax] Also at Department of Physics, University of Malaya, Kuala Lumpur, Malaysia
[ay] Also at LAL, Univ. Paris-Sud, CNRS/IN2P3, Université Paris-Saclay, Orsay, France
*Deceased

Eur. Phys. J. C (2018) 78:110
https://doi.org/10.1140/epjc/s10052-017-5475-4

THE EUROPEAN PHYSICAL JOURNAL C

Regular Article - Experimental Physics

Measurement of the W-boson mass in pp collisions at $\sqrt{s} = 7$ TeV with the ATLAS detector

ATLAS Collaboration[⋆]

CERN, 1211 Geneva 23, Switzerland

Received: 26 January 2017 / Accepted: 18 December 2017 / Published online: 6 February 2018

Abstract A measurement of the mass of the W boson is presented based on proton–proton collision data recorded in 2011 at a centre-of-mass energy of 7 TeV with the ATLAS detector at the LHC, and corresponding to 4.6 fb^{-1} of integrated luminosity. The selected data sample consists of 7.8×10^6 candidates in the $W \to \mu\nu$ channel and 5.9×10^6 candidates in the $W \to e\nu$ channel. The W-boson mass is obtained from template fits to the reconstructed distributions of the charged lepton transverse momentum and of the W boson transverse mass in the electron and muon decay channels, yielding

$$\begin{aligned} m_W &= 80370 \pm 7\ (\text{stat.}) \pm 11 (\text{exp. syst.}) \\ &\quad \pm 14\ (\text{mod. syst.})\ \text{MeV} \\ &= 80370 \pm 19\,\text{MeV}, \end{aligned}$$

where the first uncertainty is statistical, the second corresponds to the experimental systematic uncertainty, and the third to the physics-modelling systematic uncertainty. A measurement of the mass difference between the W^+ and W^- bosons yields $m_{W^+} - m_{W^-} = -29 \pm 28$ MeV.

1 Introduction

The Standard Model (SM) of particle physics describes the electroweak interactions as being mediated by the W boson, the Z boson, and the photon, in a gauge theory based on the $\mathrm{SU(2)_L \times U(1)_Y}$ symmetry [1–3]. The theory incorporates the observed masses of the W and Z bosons through a symmetry-breaking mechanism. In the SM, this mechanism relies on the interaction of the gauge bosons with a scalar doublet field and implies the existence of an additional physical state known as the Higgs boson [4–7]. The existence of the W and Z bosons was first established at the CERN SPS in 1983 [8–11], and the LHC collaborations ATLAS and CMS reported the discovery of the Higgs boson in 2012 [12,13].

At lowest order in the electroweak theory, the W-boson mass, m_W, can be expressed solely as a function of the Z-boson mass, m_Z, the fine-structure constant, α, and the Fermi constant, G_μ. Higher-order corrections introduce an additional dependence of the W-boson mass on the gauge couplings and the masses of the heavy particles of the SM. The mass of the W boson can be expressed in terms of the other SM parameters as follows:

$$m_W^2 \left(1 - \frac{m_W^2}{m_Z^2}\right) = \frac{\pi\alpha}{\sqrt{2}G_\mu}(1 + \Delta r),$$

where Δr incorporates the effect of higher-order corrections [14,15]. In the SM, Δr is in particular sensitive to the top-quark and Higgs-boson masses; in extended theories, Δr receives contributions from additional particles and interactions. These effects can be probed by comparing the measured and predicted values of m_W. In the context of global fits to the SM parameters, constraints on physics beyond the SM are currently limited by the W-boson mass measurement precision [16]. Improving the precision of the measurement of m_W is therefore of high importance for testing the overall consistency of the SM.

Previous measurements of the mass of the W boson were performed at the CERN SPS proton–antiproton ($p\bar{p}$) collider with the UA1 and UA2 experiments [17,18] at centre-of-mass energies of $\sqrt{s} = 546$ GeV and $\sqrt{s} = 630$ GeV, at the Tevatron $p\bar{p}$ collider with the CDF and D0 detectors at $\sqrt{s} = 1.8$ TeV [19–21] and $\sqrt{s} = 1.96$ TeV [22–24], and at the LEP electron–positron collider by the ALEPH, DELPHI, L3, and OPAL collaborations at $\sqrt{s} = 161$–209 GeV [25–28]. The current Particle Data Group world average value of $m_W = 80385 \pm 15$ MeV [29] is dominated by the CDF and D0 measurements performed at $\sqrt{s} = 1.96$ TeV. Given the precisely measured values of α, G_μ and m_Z, and taking recent top-quark and Higgs-boson mass measurements, the SM prediction of m_W is $m_W = 80358 \pm 8$ MeV in Ref. [16] and $m_W = 80362 \pm 8$ MeV in Ref. [30]. The SM prediction uncertainty of 8 MeV represents a target for the precision of future measurements of m_W.

⋆ e-mail: atlas.publications@cern.ch

At hadron colliders, the W-boson mass can be determined in Drell–Yan production [31] from $W \to \ell\nu$ decays, where ℓ is an electron or muon. The mass of the W boson is extracted from the Jacobian edges of the final-state kinematic distributions, measured in the plane perpendicular to the beam direction. Sensitive observables include the transverse momenta of the charged lepton and neutrino and the W-boson transverse mass.

The ATLAS and CMS experiments benefit from large signal and calibration samples. The numbers of selected W- and Z-boson events, collected in a sample corresponding to approximately 4.6 fb^{-1} of integrated luminosity at a centre-of-mass energy of 7 TeV, are of the order of 10^7 for the $W \to \ell\nu$, and of the order of 10^6 for the $Z \to \ell\ell$ processes. The available data sample is therefore larger by an order of magnitude compared to the corresponding samples used for the CDF and D0 measurements. Given the precisely measured value of the Z-boson mass [32] and the clean leptonic final state, the $Z \to \ell\ell$ processes provide the primary constraints for detector calibration, physics modelling, and validation of the analysis strategy. The sizes of these samples correspond to a statistical uncertainty smaller than 10 MeV in the measurement of the W-boson mass.

Measurements of m_W at the LHC are affected by significant complications related to the strong interaction. In particular, in proton–proton (pp) collisions at $\sqrt{s} = 7$ TeV, approximately 25% of the inclusive W-boson production rate is induced by at least one second-generation quark, s or c, in the initial state. The amount of heavy-quark-initiated production has implications for the W-boson rapidity and transverse-momentum distributions [33]. As a consequence, the measurement of the W-boson mass is sensitive to the strange-quark and charm-quark parton distribution functions (PDFs) of the proton. In contrast, second-generation quarks contribute only to approximately 5% of the overall W-boson production rate at the Tevatron. Other important aspects of the measurement of the W-boson mass are the theoretical description of electroweak corrections, in particular the modelling of photon radiation from the W- and Z-boson decay leptons, and the modelling of the relative fractions of helicity cross sections in the Drell–Yan processes [34].

This paper is structured as follows. Section 2 presents an overview of the measurement strategy. Section 3 describes the ATLAS detector. Section 4 describes the data and simulation samples used for the measurement. Section 5 describes the object reconstruction and the event selection. Section 6 summarises the modelling of vector-boson production and decay, with emphasis on the QCD effects outlined above. Sections 7 and 8 are dedicated to the electron, muon, and recoil calibration procedures. Section 9 presents a set of validation tests of the measurement procedure, performed using the Z-boson event sample. Section 10 describes the analysis of the W-boson sample. Section 11 presents the extraction of m_W. The results are summarised in Sect. 12.

2 Measurement overview

This section provides the definition of the observables used in the analysis, an overview of the measurement strategy for the determination of the mass of the W boson, and a description of the methodology used to estimate the systematic uncertainties.

2.1 Observable definitions

ATLAS uses a right-handed coordinate system with its origin at the nominal interaction point (IP) in the centre of the detector and the z-axis along the beam pipe. The x-axis points from the IP to the centre of the LHC ring, and the y-axis points upward. Cylindrical coordinates (r, ϕ) are used in the transverse plane, ϕ being the azimuth around the z-axis. The pseudorapidity is defined in terms of the polar angle θ as $\eta = -\ln\tan(\theta/2)$.

The kinematic properties of charged leptons from W- and Z-boson decays are characterised by the measured transverse momentum, p_{T}^{ℓ}, pseudorapidity, η_ℓ, and azimuth, ϕ_ℓ. The mass of the lepton, m_ℓ, completes the four-vector. For Z-boson events, the invariant mass, $m_{\ell\ell}$, the rapidity, $y_{\ell\ell}$, and the transverse momentum, $p_{\mathrm{T}}^{\ell\ell}$, are obtained by combining the four-momenta of the decay-lepton pair.

The recoil in the transverse plane, $\vec{u}_{\mathrm{T}}$, is reconstructed from the vector sum of the transverse energy of all clusters reconstructed in the calorimeters (Sect. 3), excluding energy deposits associated with the decay leptons. It is defined as:

$$\vec{u}_{\mathrm{T}} = \sum_i \vec{E}_{\mathrm{T},i},$$

where $\vec{E}_{\mathrm{T},i}$ is the vector of the transverse energy of cluster i. The transverse-energy vector of a cluster has magnitude $E_{\mathrm{T}} = E/\cosh\eta$, with the energy deposit of the cluster E and its pseudorapidity η. The azimuth ϕ of the transverse-energy vector is defined from the coordinates of the cluster in the transverse plane. In W- and Z-boson events, $-\vec{u}_{\mathrm{T}}$ provides an estimate of the boson transverse momentum. The related quantities u_x and u_y are the projections of the recoil onto the axes of the transverse plane in the ATLAS coordinate system. In Z-boson events, $u_\parallel^Z$ and $u_\perp^Z$ represent the projections of the recoil onto the axes parallel and perpendicular to the Z-boson transverse momentum reconstructed from the decay-lepton pair. Whereas $u_\parallel^Z$ can be compared to $-p_{\mathrm{T}}^{\ell\ell}$ and probes the detector response to the recoil in terms of linearity and resolution, the $u_\perp^Z$ distribution satisfies $\langle u_\perp^Z \rangle = 0$ and its width provides an estimate of the recoil resolution. In W-boson events, $u_\parallel^\ell$ and $u_\perp^\ell$ are the projections of the recoil onto the

axes parallel and perpendicular to the reconstructed charged-lepton transverse momentum.

The resolution of the recoil is affected by additional event properties, namely the per-event number of pp interactions per bunch crossing (pile-up) μ, the average number of pp interactions per bunch crossing $\langle\mu\rangle$, the total reconstructed transverse energy, defined as the scalar sum of the transverse energy of all calorimeter clusters, $\Sigma E_{\mathrm{T}} \equiv \sum_i E_{\mathrm{T},i}$, and the quantity $\Sigma E_{\mathrm{T}}^{*} \equiv \Sigma E_{\mathrm{T}} - |\vec{u}_{\mathrm{T}}|$. The latter is less correlated with the recoil than ΣE_{T}, and better represents the event activity related to the pile-up and to the underlying event.

The magnitude and direction of the transverse-momentum vector of the decay neutrino, $\vec{p}_{\mathrm{T}}^{\,\nu}$, are inferred from the vector of the missing transverse momentum, $\vec{p}_{\mathrm{T}}^{\,\mathrm{miss}}$, which corresponds to the momentum imbalance in the transverse plane and is defined as:

$$\vec{p}_{\mathrm{T}}^{\,\mathrm{miss}} = -\left(\vec{p}_{\mathrm{T}}^{\,\ell} + \vec{u}_{\mathrm{T}}\right).$$

The W-boson transverse mass, m_{T}, is derived from $p_{\mathrm{T}}^{\mathrm{miss}}$ and from the transverse momentum of the charged lepton as follows:

$$m_{\mathrm{T}} = \sqrt{2 p_{\mathrm{T}}^{\ell} p_{\mathrm{T}}^{\mathrm{miss}} (1 - \cos\Delta\phi)},$$

where $\Delta\phi$ is the azimuthal opening angle between the charged lepton and the missing transverse momentum.

All vector-boson masses and widths are defined in the running-width scheme. Resonances are expressed by the relativistic Breit–Wigner mass distribution:

$$\frac{\mathrm{d}\sigma}{\mathrm{d}m} \propto \frac{m^2}{(m^2 - m_V^2)^2 + m^4\Gamma_V^2/m_V^2}, \tag{1}$$

where m is the invariant mass of the vector-boson decay products, and m_V and Γ_V, with $V = W, Z$, are the vector-boson masses and widths, respectively. This scheme was introduced in Ref. [35], and is consistent with earlier measurements of the W- and Z-boson resonance parameters [24,32].

2.2 Analysis strategy

The mass of the W boson is determined from fits to the transverse momentum of the charged lepton, p_{T}^{ℓ}, and to the transverse mass of the W boson, m_{T}. For W bosons at rest, the transverse-momentum distributions of the W decay leptons have a Jacobian edge at a value of $m/2$, whereas the distribution of the transverse mass has an endpoint at the value of m [36], where m is the invariant mass of the charged-lepton and neutrino system, which is related to m_W through the Breit–Wigner distribution of Eq. (1).

The expected final-state distributions, referred to as templates, are simulated for several values of m_W and include signal and background contributions. The templates are compared to the observed distribution by means of a χ^2 compatibility test. The χ^2 as a function of m_W is interpolated, and the measured value is determined by analytical minimisation of the χ^2 function. Predictions for different values of m_W are obtained from a single simulated reference sample, by reweighting the W-boson invariant mass distribution according to the Breit–Wigner parameterisation of Eq. (1). The W-boson width is scaled accordingly, following the SM relation $\Gamma_W \propto m_W^3$.

Experimentally, the p_{T}^{ℓ} and $p_{\mathrm{T}}^{\mathrm{miss}}$ distributions are affected by the lepton energy calibration. The latter is also affected by the calibration of the recoil. The p_{T}^{ℓ} and $p_{\mathrm{T}}^{\mathrm{miss}}$ distributions are broadened by the W-boson transverse-momentum distribution, and are sensitive to the W-boson helicity states, which are influenced by the proton PDFs [37]. Compared to p_{T}^{ℓ}, the m_{T} distribution has larger uncertainties due to the recoil, but smaller sensitivity to such physics-modelling effects. Imperfect modelling of these effects can distort the template distributions, and constitutes a significant source of uncertainties for the determination of m_W.

The calibration procedures described in this paper rely mainly on methods and results published earlier by ATLAS [38–40], and based on W and Z samples at $\sqrt{s} = 7$ TeV and $\sqrt{s} = 8$ TeV. The $Z \to \ell\ell$ event samples are used to calibrate the detector response. Lepton momentum corrections are derived exploiting the precisely measured value of the Z-boson mass, m_Z [32], and the recoil response is calibrated using the expected momentum balance with $p_{\mathrm{T}}^{\ell\ell}$. Identification and reconstruction efficiency corrections are determined from W- and Z-boson events using the tag-and-probe method [38,40]. The dependence of these corrections on p_{T}^{ℓ} is important for the measurement of m_W, as it affects the shape of the template distributions.

The detector response corrections and the physics modelling are verified in Z-boson events by performing measurements of the Z-boson mass with the same method used to determine the W-boson mass, and comparing the results to the LEP combined value of m_Z, which is used as input for the lepton calibration. The determination of m_Z from the lepton-pair invariant mass provides a first closure test of the lepton energy calibration. In addition, the extraction of m_Z from the p_{T}^{ℓ} distribution tests the p_{T}^{ℓ}-dependence of the efficiency corrections, and the modelling of the Z-boson transverse-momentum distribution and of the relative fractions of Z-boson helicity states. The $p_{\mathrm{T}}^{\mathrm{miss}}$ and m_{T} variables are defined in Z-boson events by treating one of the reconstructed decay leptons as a neutrino. The extraction of m_Z from the m_{T} distribution provides a test of the recoil calibration. The combination of the extraction of m_Z from the $m_{\ell\ell}$, p_{T}^{ℓ} and m_{T} distributions provides a closure test of the measurement procedure. The precision of this validation procedure is limited by the finite size of the Z-boson sample, which is approximately ten times smaller than the W-boson sample.

Table 1 Summary of categories and kinematic distributions used in the m_W measurement analysis for the electron and muon decay channels

Decay channel	$W \to e\nu$	$W \to \mu\nu$
Kinematic distributions	p_{T}^{ℓ}, m_{T}	p_{T}^{ℓ}, m_{T}
Charge categories	W^+, W^-	W^+, W^-
$\lvert\eta_\ell\rvert$ categories	[0, 0.6], [0.6, 1.2], [1.8, 2.4]	[0, 0.8], [0.8, 1.4], [1.4, 2.0], [2.0, 2.4]

The analysis of the Z-boson sample does not probe differences in the modelling of W- and Z-boson production processes. Whereas W-boson production at the Tevatron is charge symmetric and dominated by interactions with at least one valence quark, the sea-quark PDFs play a larger role at the LHC, and contributions from processes with heavy quarks in the initial state have to be modelled properly. The W^+-boson production rate exceeds that of W^- bosons by about 40%, with a broader rapidity distribution and a softer transverse-momentum distribution. Uncertainties in the modelling of these distributions and in the relative fractions of the W-boson helicity states are constrained using measurements of W- and Z-boson production performed with the ATLAS experiment at $\sqrt{s} = 7$ TeV and $\sqrt{s} = 8$ TeV [41–45].

The final measured value of the W-boson mass is obtained from the combination of various measurements performed in the electron and muon decay channels, and in charge- and $|\eta_\ell|$-dependent categories, as defined in Table 1. The boundaries of the $|\eta_\ell|$ categories are driven mainly by experimental and statistical constraints. The measurements of m_W used in the combination are based on the observed distributions of p_{T}^{ℓ} and m_{T}, which are only partially correlated. Measurements of m_W based on the $p_{\mathrm{T}}^{\mathrm{miss}}$ distributions are performed as consistency tests, but they are not used in the combination due to their significantly lower precision. The consistency of the results in the electron and muon channels provide a further test of the experimental calibrations, whereas the consistency of the results for the different charge and $|\eta_\ell|$ categories tests the W-boson production model.

Further consistency tests are performed by repeating the measurement in three intervals of $\langle\mu\rangle$, in two intervals of u_{T} and $u_{\parallel}^{\ell}$, and by removing the $p_{\mathrm{T}}^{\mathrm{miss}}$ selection requirement, which is applied in the nominal signal selection. The consistency of the values of m_W in these additional categories probes the modelling of the recoil response, and the modelling of the transverse-momentum spectrum of the W boson. Finally, the stability of the result with respect to the charged-lepton azimuth, and upon variations of the fitting ranges is verified.

Systematic uncertainties in the determination of m_W are evaluated using pseudodata samples produced from the nominal simulated event samples by varying the parameters corresponding to each source of uncertainty in turn. The differences between the values of m_W extracted from the pseudodata and nominal samples are used to estimate the uncertainty. When relevant, these variations are applied simultaneously in the W-boson signal samples and in the background contributions. The systematic uncertainties are estimated separately for each source and for fit ranges of $32 < p_{\mathrm{T}}^{\ell} < 45\,\mathrm{GeV}$ and $66 < m_{\mathrm{T}} < 99\,\mathrm{GeV}$. These fit ranges minimise the total expected measurement uncertainty, and are used for the final result as discussed in Sect. 11.

In Sects. 6, 7, 8, and 10, which discuss the systematic uncertainties of the m_W measurement, the uncertainties are also given for combinations of measurement categories. This provides information showing the reduction of the systematic uncertainty obtained from the measurement categorisation. For these cases, the combined uncertainties are evaluated including only the expected statistical uncertainty in addition to the systematic uncertainty being considered. However, the total measurement uncertainty is estimated by adding all uncertainty contributions in quadrature for each measurement category, and combining the results accounting for correlations across categories.

During the analysis, an unknown offset was added to the value of m_W used to produce the templates. The offset was randomly selected from a uniform distribution in the range $[-100, 100]$ MeV, and the same value was used for the W^+ and W^- templates. The offset was removed after the m_W measurements performed in all categories were found to be compatible and the analysis procedure was finalised.

3 The ATLAS detector

The ATLAS experiment [46] is a multipurpose particle detector with a forward-backward symmetric cylindrical geometry. It consists of an inner tracking detector surrounded by a thin superconducting solenoid, electromagnetic and hadronic calorimeters, and a muon spectrometer incorporating three large superconducting toroid magnets.

The inner-detector system (ID) is immersed in a 2 T axial magnetic field and provides charged-particle tracking in the range $|\eta| < 2.5$. At small radii, a high-granularity silicon pixel detector covers the vertex region and typically provides three measurements per track. It is followed by the silicon microstrip tracker, which usually provides eight measurement points per track. These silicon detectors are complemented by a gas-filled straw-tube transition radiation tracker, which enables radially extended track reconstruction up to

$|\eta| = 2.0$. The transition radiation tracker also provides electron identification information based on the fraction of hits (typically 35 in total) above a higher energy-deposit threshold corresponding to transition radiation.

The calorimeter system covers the pseudorapidity range $|\eta| < 4.9$. Within the region $|\eta| < 3.2$, electromagnetic (EM) calorimetry is provided by high-granularity lead/liquid-argon (LAr) calorimeters, with an additional thin LAr presampler covering $|\eta| < 1.8$ to correct for upstream energy-loss fluctuations. The EM calorimeter is divided into a barrel section covering $|\eta| < 1.475$ and two endcap sections covering $1.375 < |\eta| < 3.2$. For $|\eta| < 2.5$ it is divided into three layers in depth, which are finely segmented in η and ϕ. Hadronic calorimetry is provided by a steel/scintillator-tile calorimeter, segmented into three barrel structures within $|\eta| < 1.7$ and two copper/LAr hadronic endcap calorimeters covering $1.5 < |\eta| < 3.2$. The solid-angle coverage is completed with forward copper/LAr and tungsten/LAr calorimeter modules in $3.1 < |\eta| < 4.9$, optimised for electromagnetic and hadronic measurements, respectively.

The muon spectrometer (MS) comprises separate trigger and high-precision tracking chambers measuring the deflection of muons in a magnetic field generated by superconducting air-core toroids. The precision chamber system covers the region $|\eta| < 2.7$ with three layers of monitored drift tubes, complemented by cathode strip chambers in the forward region. The muon trigger system covers the range $|\eta| < 2.4$ with resistive plate chambers in the barrel, and thin gap chambers in the endcap regions.

A three-level trigger system is used to select events for offline analysis [47]. The level-1 trigger is implemented in hardware and uses a subset of detector information to reduce the event rate to a design value of at most 75 kHz. This is followed by two software-based trigger levels which together reduce the event rate to about 300 Hz.

4 Data samples and event simulation

The data sample used in this analysis consists of W- and Z-boson candidate events, collected in 2011 with the ATLAS detector in proton–proton collisions at the LHC, at a centre-of-mass energy of $\sqrt{s} = 7$ TeV. The sample for the electron channel, with all relevant detector systems operational, corresponds to approximately 4.6 fb^{-1} of integrated luminosity. A smaller integrated luminosity of approximately 4.1 fb^{-1} is used in the muon channel, as part of the data was discarded due to a timing problem in the resistive plate chambers, which affected the muon trigger efficiency. The relative uncertainty of the integrated luminosity is 1.8% [48]. This data set provides approximately 1.4×10^7 reconstructed W-boson events and 1.8×10^6 Z-boson events, after all selection criteria have been applied.

The POWHEG MC generator [49–51] (v1/r1556) is used for the simulation of the hard-scattering processes of W- and Z-boson production and decay in the electron, muon, and tau channels, and is interfaced to PYTHIA 8 (v8.170) for the modelling of the parton shower, hadronisation, and underlying event [52,53], with parameters set according to the AZNLO tune [44]. The CT10 PDF set [54] is used for the hard-scattering processes, whereas the CTEQ6L1 PDF set [55] is used for the parton shower. In the Z-boson samples, the effect of virtual photon production (γ^*) and Z/γ^* interference is included. The effect of QED final-state radiation (FSR) is simulated with PHOTOS (v2.154) [56]. Tau lepton decays are handled by PYTHIA 8, taking into account polarisation effects. An alternative set of samples for W- and Z-boson production is generated with POWHEG interfaced to HERWIG (v6.520) for the modelling of the parton shower [57], and to JIMMY (v4.31) for the underlying event [58]. The W- and Z-boson masses are set to $m_W = 80.399$ GeV and $m_Z = 91.1875$ GeV, respectively. During the analysis, the value of the W-boson mass in the $W \to \ell\nu$ and $W \to \tau\nu$ samples was blinded using the reweighting procedure described in Sect. 2.

Top-quark pair production and the single-top-quark processes are modelled using the MC@NLO MC generator (v4.01) [59–61], interfaced to HERWIG and JIMMY. Gauge-boson pair production (WW, WZ, ZZ) is simulated with HERWIG (v6.520). In all the samples, the CT10 PDF set is used. Samples of heavy-flavour multijet events ($pp \to b\bar{b} + X$ and $pp \to c\bar{c} + X$) are simulated with PYTHIA 8 to validate the data-driven methods used to estimate backgrounds with non-prompt leptons in the final state.

Whereas the extraction of m_W is based on the shape of distributions, and is not sensitive to the overall normalisation of the predicted distributions, it is affected by theoretical uncertainties in the relative fractions of background and signal. The W- and Z-boson event yields are normalised according to their measured cross sections, and uncertainties of 1.8% and 2.3% are assigned to the W^+/Z and W^-/Z production cross-section ratios, respectively [41]. The $t\bar{t}$ sample is normalised according to its measured cross section [62] with an uncertainty of 3.9%, whereas the cross-section predictions for the single-top production processes of Refs. [63–65] are used for the normalisation of the corresponding sample, with an uncertainty of 7%. The samples of events with massive gauge-boson pair production are normalised to the NLO predictions calculated with MCFM [66], with an uncertainty of 10% to cover the differences to the NNLO predictions [67].

The response of the ATLAS detector is simulated using a program [68] based on GEANT 4 [69]. The ID and the MS were simulated assuming an ideal detector geometry; alignment corrections are applied to the data during event reconstruction. The description of the detector material incorporates the results of extensive studies of the electron and photon calibration [39]. The simulated hard-scattering process

is overlaid with additional proton–proton interactions, simulated with PYTHIA 8 (v8.165) using the A2 tune [70]. The distribution of the average number of interactions per bunch crossing $\langle\mu\rangle$ spans the range 2.5–16.0, with a mean value of approximately 9.0.

Simulation inaccuracies affecting the distributions of the signal, the response of the detector, and the underlying-event modelling, are corrected as described in the following sections. Physics-modelling corrections, such as those affecting the W-boson transverse-momentum distribution and the angular decay coefficients, are discussed in Sect. 6. Calibration and detector response corrections are presented in Sects. 7 and 8.

5 Particle reconstruction and event selection

This section describes the reconstruction and identification of electrons and muons, the reconstruction of the recoil, and the requirements used to select W- and Z-boson candidate events. The recoil provides an event-by-event estimate of the W-boson transverse momentum. The reconstructed kinematic properties of the leptons and of the recoil are used to infer the transverse momentum of the neutrino and the transverse-mass kinematic variables.

5.1 Reconstruction of electrons, muons and the recoil

Electron candidates are reconstructed from clusters of energy deposited in the electromagnetic calorimeter and associated with at least one track in the ID [38,39]. Quality requirements are applied to the associated tracks in order to reject poorly reconstructed charged-particle trajectories. The energy of the electron is reconstructed from the energy collected in calorimeter cells within an area of size $\Delta\eta \times \Delta\phi = 0.075 \times 0.175$ in the barrel, and 0.125×0.125 in the endcaps. A multivariate regression algorithm, developed and optimised on simulated events, is used to calibrate the energy reconstruction. The reconstructed electron energy is corrected to account for the energy deposited in front of the calorimeter and outside the cluster, as well as for variations of the energy response as a function of the impact point of the electron in the calorimeter. The energy calibration algorithm takes as inputs the energy collected by each calorimeter layer, including the presampler, the pseudorapidity of the cluster, and the local position of the shower within the cell of the second layer, which corresponds to the cluster centroid. The kinematic properties of the reconstructed electron are inferred from the energy measured in the EM calorimeter, and from the pseudorapidity and azimuth of the associated track. Electron candidates are required to have $p_{\mathrm{T}} > 15\,\mathrm{GeV}$ and $|\eta| < 2.4$ and to fulfil a set of tight identification requirements [38]. The pseudorapidity range $1.2 < |\eta| < 1.82$ is excluded from the measurement, as the amount of passive material in front of the calorimeter and its uncertainty are largest in this region [39], preventing a sufficiently accurate description of non-Gaussian tails in the electron energy response. Additional isolation requirements on the nearby activity in the ID and calorimeter are applied to improve the background rejection. These isolation requirements are implemented by requiring the scalar sum of the p_{T} of tracks in a cone of size $\Delta R \equiv \sqrt{(\Delta\eta)^2 + (\Delta\phi)^2} < 0.4$ around the electron, $p_{\mathrm{T}}^{e,\mathrm{cone}}$, and the transverse energy deposited in the calorimeter within a cone of size $\Delta R < 0.2$ around the electron, $E_{\mathrm{T}}^{\mathrm{cone}}$, to be small. The contribution from the electron candidate itself is excluded. The specific criteria are optimised as a function of electron η and p_{T} to have a combined efficiency of about 95% in the simulation for isolated electrons from the decay of a W or Z boson.

The muon reconstruction is performed independently in the ID and in the MS, and a combined muon candidate is formed from the combination of a MS track with an ID track, based on the statistical combination of the track parameters [40]. The kinematic properties of the reconstructed muon are defined using the ID track parameters alone, which allows a simpler calibration procedure. The loss of resolution is small (10–15%) in the transverse-momentum range relevant for the measurement of the W-boson mass. The ID tracks associated with the muons must satisfy quality requirements on the number of hits recorded by each subdetector [40]. In order to reject muons from cosmic rays, the longitudinal coordinate of the point of closest approach of the track to the beamline is required to be within 10 mm of the collision vertex. Muon candidates are required to have $p_{\mathrm{T}} > 20\,\mathrm{GeV}$ and $|\eta| < 2.4$. Similarly to the electrons, the rejection of multijet background is increased by applying an isolation requirement : the scalar sum of the p_{T} of tracks in a cone of size $\Delta R < 0.2$ around the muon candidate, $p_{\mathrm{T}}^{\mu,\mathrm{cone}}$, is required to be less than 10% of the muon p_{T}.

The recoil, $\vec{u}_{\mathrm{T}}$, is reconstructed from the vector sum of the transverse energy of all clusters measured in the calorimeters, as defined in Sect. 2.1. The ATLAS calorimeters measure energy depositions in the range $|\eta| < 4.9$ with a topological clustering algorithm [71], which starts from cells with an energy of at least four times the expected noise from electronics and pile-up. The momentum vector of each cluster is determined by the magnitude and coordinates of the energy deposition. Cluster energies are initially measured assuming that the energy deposition occurs only through electromagnetic interactions, and are then corrected for the different calorimeter responses to hadrons and electromagnetic particles, for losses due to dead material, and for energy which is not captured by the clustering process. The definition of $\vec{u}_{\mathrm{T}}$ and the inferred quantities $p_{\mathrm{T}}^{\mathrm{miss}}$ and m_{T} do not involve the explicit reconstruction of particle jets, to avoid possible threshold effects.

Clusters located a distance $\Delta R < 0.2$ from the reconstructed electron or muon candidates are not used for the reconstruction of $\vec{u}_{\mathrm{T}}$. This ensures that energy deposits originating from the lepton itself or from accompanying photons (from FSR or Bremsstrahlung) do not contribute to the recoil measurement. The energy of any soft particles removed along with the lepton is compensated for using the total transverse energy measured in a cone of the same size $\Delta R = 0.2$, placed at the same absolute pseudorapidity as the lepton with randomly chosen sign, and at different ϕ. The total transverse momentum measured in this cone is rotated to the position of the lepton and added to $\vec{u}_{\mathrm{T}}$.

5.2 Event selection

The W-boson sample is collected during data-taking with triggers requiring at least one muon candidate with transverse momentum larger than 18 GeV or at least one electron candidate with transverse momentum larger than 20 GeV. The transverse-momentum requirement for the electron candidate was raised to 22 GeV in later data-taking periods to cope with the increased instantaneous luminosity delivered by the LHC. Selected events are required to have a reconstructed primary vertex with at least three associated tracks.

W-boson candidate events are selected by requiring exactly one reconstructed electron or muon with $p_{\mathrm{T}}^{\ell} > 30$ GeV. The leptons are required to match the corresponding trigger object. In addition, the reconstructed recoil is required to be $u_{\mathrm{T}} < 30$ GeV, the missing transverse momentum $p_{\mathrm{T}}^{\mathrm{miss}} > 30$ GeV and the transverse mass $m_{\mathrm{T}} > 60$ GeV. These selection requirements are optimised to reduce the multijet background contribution, and to minimise model uncertainties from W bosons produced at high transverse momentum. A total of 5.89×10^6 W-boson candidate events are selected in the $W \to e\nu$ channel, and 7.84×10^6 events in the $W \to \mu\nu$ channel.

As mentioned in Sect. 2, Z-boson events are extensively used to calibrate the response of the detector to electrons and muons, and to derive recoil corrections. In addition, Z-boson events are used to test several aspects of the modelling of vector-boson production. Z-boson candidate events are collected with the same trigger selection used for the W-boson sample. The analysis selection requires exactly two reconstructed leptons with $p_{\mathrm{T}}^{\ell} > 25$ GeV, having the same flavour and opposite charges. The events are required to have an invariant mass of the dilepton system in the range $80 < m_{\ell\ell} < 100$ GeV. In both channels, selected leptons are required to be isolated in the same way as in the W-boson event selection. In total, 0.58×10^6 and 1.23×10^6 Z-boson candidate events are selected in the electron and muon decay channels, respectively.

6 Vector-boson production and decay

Samples of inclusive vector-boson production are produced using the Powheg MC generator interfaced to Pythia 8, henceforth referred to as Powheg+Pythia 8. The W- and Z-boson samples are reweighted to include the effects of higher-order QCD and electroweak (EW) corrections, as well as the results of fits to measured distributions which improve the agreement of the simulated lepton kinematic distributions with the data. The effect of virtual photon production and Z/γ^* interference is included in both the predictions and the Powheg+Pythia 8 simulated Z-boson samples. The reweighting procedure used to include the corrections in the simulated event samples is detailed in Sect. 6.4.

The correction procedure is based on the factorisation of the fully differential leptonic Drell–Yan cross section [31] into four terms:

$$\frac{\mathrm{d}\sigma}{\mathrm{d}p_1\,\mathrm{d}p_2} = \left[\frac{\mathrm{d}\sigma(m)}{\mathrm{d}m}\right]\left[\frac{\mathrm{d}\sigma(y)}{\mathrm{d}y}\right]\left[\frac{\mathrm{d}\sigma(p_{\mathrm{T}},y)}{\mathrm{d}p_{\mathrm{T}}\,\mathrm{d}y}\left(\frac{\mathrm{d}\sigma(y)}{\mathrm{d}y}\right)^{-1}\right] \times \left[(1+\cos^2\theta)+\sum_{i=0}^{7} A_i(p_{\mathrm{T}},y)\,P_i(\cos\theta,\phi)\right], \tag{2}$$

where p_1 and p_2 are the lepton and anti-lepton four-momenta; m, p_{T}, and y are the invariant mass, transverse momentum, and rapidity of the dilepton system; θ and ϕ are the polar angle and azimuth of the lepton[1] in any given rest frame of the dilepton system; A_i are numerical coefficients, and P_i are spherical harmonics of order zero, one and two.

The differential cross section as a function of the invariant mass, $\mathrm{d}\sigma(m)/\mathrm{d}m$, is modelled with a Breit–Wigner parameterisation according to Eq. (1). In the case of the Z-boson samples, the photon propagator is included using the running electromagnetic coupling constant; further electroweak corrections are discussed in Sect. 6.1. The differential cross section as a function of boson rapidity, $\mathrm{d}\sigma(y)/\mathrm{d}y$, and the coefficients A_i are modelled with perturbative QCD fixed-order predictions, as described in Sect. 6.2. The transverse-momentum spectrum at a given rapidity, $\mathrm{d}\sigma(p_{\mathrm{T}},y)/(\mathrm{d}p_{\mathrm{T}}\,\mathrm{d}y)\cdot(\mathrm{d}\sigma(y)/\mathrm{d}y)^{-1}$, is modelled with predictions based on the Pythia 8 MC generator, as discussed in Sect. 6.3. An exhaustive review of available predictions for W- and Z-boson production at the LHC is given in Ref. [72].

Measurements of W- and Z-boson production are used to validate and constrain the modelling of the fully differential leptonic Drell–Yan cross section. The PDF central values and uncertainties, as well as the modelling of the differential cross section as a function of boson rapidity, are validated

[1] Here, lepton refers to the negatively charged lepton from a W^- or Z boson, and the neutrino from a W^+ boson.

by comparing to the 7 TeV W- and Z-boson rapidity measurements [41], based on the same data sample. The QCD parameters of the parton shower model were determined by fits to the transverse-momentum distribution of the Z boson measured at 7 TeV [44]. The modelling of the A_i coefficients is validated by comparing the theoretical predictions to the 8 TeV measurement of the angular coefficients in Z-boson decays [42].

6.1 Electroweak corrections and uncertainties

The dominant source of electroweak corrections to W- and Z-boson production originates from QED final-state radiation, and is simulated with PHOTOS. The effect of QED initial-state radiation (ISR) is also included through the PYTHIA 8 parton shower. The uncertainty in the modelling of QED FSR is evaluated by comparing distributions obtained using the default leading-order photon emission matrix elements with predictions obtained using NLO matrix elements, as well as by comparing PHOTOS with an alternative implementation based on the Yennie–Frautschi–Suura formalism [73], which is available in WINHAC [74]. The differences are small in both cases, and the associated uncertainty is considered negligible.

Other sources of electroweak corrections are not included in the simulated event samples, and their full effects are considered as systematic uncertainties. They include the interference between ISR and FSR QED corrections (IFI), pure weak corrections due to virtual-loop and box diagrams, and final-state emission of lepton pairs. Complete $O(\alpha)$ electroweak corrections to the $pp \to W + X$, $W \to \ell\nu$ process were initially calculated in Refs. [75,76]. Combined QCD and EW corrections are however necessary to evaluate the effect of the latter in presence of a realistic p_{T}^{W} distribution. Approximate $O(\alpha_{\mathrm{s}}\alpha)$ corrections including parton shower effects are available from WINHAC, SANC [77] and in the POWHEG framework [78–80]. A complete, fixed-order calculation of $O(\alpha_{\mathrm{s}}\alpha)$ corrections in the resonance region appeared in Ref. [81].

In the present work the effect of the NLO EW corrections are estimated using WINHAC, which employs the PYTHIA 6 MC generator for the simulation of QCD and QED ISR. The corresponding uncertainties are evaluated comparing the final state distributions obtained including QED FSR only with predictions using the complete NLO EW corrections in the $\alpha(0)$ and G_μ renormalisation schemes [82]. The latter predicts the larger correction and is used to assign the systematic uncertainty.

Final-state lepton pair production, through $\gamma^* \to \ell\ell$ radiation, is formally a higher-order correction but constitutes an significant additional source of energy loss for the W-boson decay products. This process is not included in the event simulation, and the impact on the determination of m_W is evaluated using PHOTOS and SANC.

Table 2 summarises the effect of the uncertainties associated with the electroweak corrections on the m_W measurements. All comparisons described above were performed at particle level. The impact is larger for the p_{T}^{ℓ} distribution than for the m_{T} distribution, and similar between the electron and muon decay channels. A detailed evaluation of these uncertainties was performed in Ref. [83] using POWHEG [78], and the results are in fair agreement with Table 2. The study of Ref. [83] also compares, at fixed order, the effect of the approximate $O(\alpha_{\mathrm{s}}\alpha)$ corrections with the full calculation of Ref. [81], and good agreement is found. The same sources of uncertainty affect the lepton momentum calibration through their impact on the $m_{\ell\ell}$ distribution in Z-boson events, as discussed in Sect. 7.

6.2 Rapidity distribution and angular coefficients

At leading order, W and Z bosons are produced with zero transverse momentum, and the angular distribution of the decay leptons depends solely on the polar angle of the lepton in the boson rest frame. Higher-order corrections give rise to sizeable boson transverse momentum, and to azimuthal asymmetries in the angular distribution of the decay leptons. The angular distribution of the W- and Z-boson decay leptons is determined by the relative fractions of helicity cross sections for the vector-boson production. The fully differential leptonic Drell–Yan cross section can be decomposed as a weighted sum of nine harmonic polynomials, with weights given by the helicity cross sections. The harmonic polyno-

Table 2 Impact on the m_W measurement of systematic uncertainties from higher-order electroweak corrections, for the p_{T}^{ℓ} and m_{T} distributions in the electron and muon decay channels

Decay channel	$W \to e\nu$		$W \to \mu\nu$	
Kinematic distribution	p_{T}^{ℓ}	m_{T}	p_{T}^{ℓ}	m_{T}
δm_W [MeV]				
FSR (real)	< 0.1	< 0.1	< 0.1	< 0.1
Pure weak and IFI corrections	3.3	2.5	3.5	2.5
FSR (pair production)	3.6	0.8	4.4	0.8
Total	4.9	2.6	5.6	2.6

mials depend on the polar angle, θ, and the azimuth, ϕ, of the lepton in a given rest frame of the boson. The helicity cross sections depend, in their most general expression, on the transverse momentum, p_{T}, rapidity, y, and invariant mass, m, of the boson. It is customary to factorise the unpolarised, or angular-integrated, cross section, $\mathrm{d}\sigma/(\mathrm{d}p_{\mathrm{T}}^2\,\mathrm{d}y\,\mathrm{d}m)$, and express the decomposition in terms of dimensionless angular coefficients, A_i, which represent the ratios of the helicity cross sections with respect to the unpolarised cross section [34], leading to the following expression for the fully differential Drell–Yan cross section:

$$\begin{aligned}\frac{\mathrm{d}\sigma}{\mathrm{d}p_{\mathrm{T}}^2\,\mathrm{d}y\,\mathrm{d}m\,\mathrm{d}\cos\theta\,\mathrm{d}\phi} = \frac{3}{16\pi}\frac{\mathrm{d}\sigma}{\mathrm{d}p_{\mathrm{T}}^2\,\mathrm{d}y\,\mathrm{d}m} \\ \times\Big[(1+\cos^2\theta)+A_0\,\frac{1}{2}(1-3\cos^2\theta) \\ +A_1\,\sin 2\theta\cos\phi+A_2\,\frac{1}{2}\sin^2\theta\cos 2\phi \\ +A_3\,\sin\theta\cos\phi+A_4\,\cos\theta \\ +A_5\,\sin^2\theta\sin 2\phi+A_6\,\sin 2\theta\sin\phi \\ +A_7\,\sin\theta\sin\phi\Big]. \end{aligned} \tag{3}$$

The angular coefficients depend in general on p_{T}, y and m. The A_5–A_7 coefficients are non-zero only at order $O(\alpha_{\mathrm{s}}^2)$ and above. They are small in the p_{T} region relevant for the present analysis, and are not considered further. The angles θ and ϕ are defined in the Collins–Soper (CS) frame [84].

The differential cross section as a function of boson rapidity, $\mathrm{d}\sigma(y)/\mathrm{d}y$, and the angular coefficients, A_i, are modelled with fixed-order perturbative QCD predictions, at $O(\alpha_{\mathrm{s}}^2)$ in the perturbative expansion of the strong coupling constant and using the CT10nnlo PDF set [85]. The dependence of the angular coefficients on m is neglected; the effect of this approximation on the measurement of m_W is discussed in Sect. 6.4. For the calculation of the predictions, an optimised version of DYNNLO [86] is used, which explicitly decomposes the calculation of the cross section into the different pieces of the q_{T}-subtraction formalism, and allows the computation of statistically correlated PDF variations. In this optimised version of DYNNLO, the Cuba library [87] is used for the numerical integration.

The values of the angular coefficients predicted by the POWHEG+PYTHIA 8 samples differ significantly from the corresponding NNLO predictions. In particular, large differences are observed in the predictions of A_0 at low values of $p_{\mathrm{T}}^{W,Z}$. Other coefficients, such as A_1 and A_2, are affected by significant NNLO corrections at high $p_{\mathrm{T}}^{W,Z}$. In Z-boson production, A_3 and A_4 are sensitive to the vector couplings between the Z boson and the fermions, and are predicted assuming the measured value of the effective weak mixing angle $\sin^2\theta_{\mathrm{eff}}^{\ell}$ [32].

6.3 Transverse-momentum distribution

Predictions of the vector-boson transverse-momentum spectrum cannot rely solely on fixed-order perturbative QCD. Most W-boson events used for the analysis have a low transverse-momentum value, in the kinematic region $p_{\mathrm{T}}^W < 30\,\mathrm{GeV}$, where large logarithmic terms of the type $\log(m_W/p_{\mathrm{T}}^W)$ need to be resummed, and non-perturbative effects must be included, either with parton showers or with predictions based on analytic resummation [88–92]. The modelling of the transverse-momentum spectrum of vector bosons at a given rapidity, expressed by the term $\mathrm{d}\sigma(p_{\mathrm{T}},y)/(\mathrm{d}p_{\mathrm{T}}\,\mathrm{d}y)\cdot(\mathrm{d}\sigma(y)/\mathrm{d}y)^{-1}$ in Eq. (2), is based on the PYTHIA 8 parton shower MC generator. The predictions of vector-boson production in the PYTHIA 8 MC generator employ leading-order matrix elements for the $q\bar{q}' \to W, Z$ processes and include a reweighting of the first parton shower emission to the leading-order V+jet cross section [93]. The resulting prediction of the boson p_{T} spectrum is comparable in accuracy to those of an NLO plus parton shower generator setup such as POWHEG+PYTHIA 8, and of resummed predictions at next-to-leading logarithmic order [94].

The values of the QCD parameters used in PYTHIA 8 were determined from fits to the Z-boson transverse momentum distribution measured with the ATLAS detector at a centre-of-mass energy of $\sqrt{s} = 7$ TeV [44]. Three QCD parameters were considered in the fit: the intrinsic transverse momentum of the incoming partons, the value of $\alpha_{\mathrm{s}}(m_Z)$ used for the QCD ISR, and the value of the ISR infrared cut-off. The resulting values of the PYTHIA 8 parameters constitute the AZ tune. The PYTHIA 8 AZ prediction was found to provide a satisfactory description of the p_{T}^Z distribution as a function of rapidity, contrarily to POWHEG+PYTHIA 8 AZNLO; hence the former is chosen to predict the p_{T}^W distribution. The good consistency of the m_W measurement results in $|\eta_\ell|$ categories, presented in Sect. 11, is also a consequence of this choice.

To illustrate the results of the parameters optimisation, the PYTHIA 8 AZ and 4C [95] predictions of the p_{T}^Z distribution are compared in Fig. 1a to the measurement used to determine the AZ tune. Kinematic requirements on the decay leptons are applied according to the experimental acceptance. For further validation, the predicted differential cross-section ratio,

$$R_{W/Z}(p_{\mathrm{T}}) = \left(\frac{1}{\sigma_W}\cdot\frac{\mathrm{d}\sigma_W(p_{\mathrm{T}})}{\mathrm{d}p_{\mathrm{T}}}\right)\left(\frac{1}{\sigma_Z}\cdot\frac{\mathrm{d}\sigma_Z(p_{\mathrm{T}})}{\mathrm{d}p_{\mathrm{T}}}\right)^{-1},$$

is compared to the corresponding ratio of ATLAS measurements of vector-boson transverse momentum [44,45]. The comparison is shown in Fig. 1b, where kinematic requirements on the decay leptons are applied according to the experimental acceptance. The measured Z-boson p_{T} distribution is

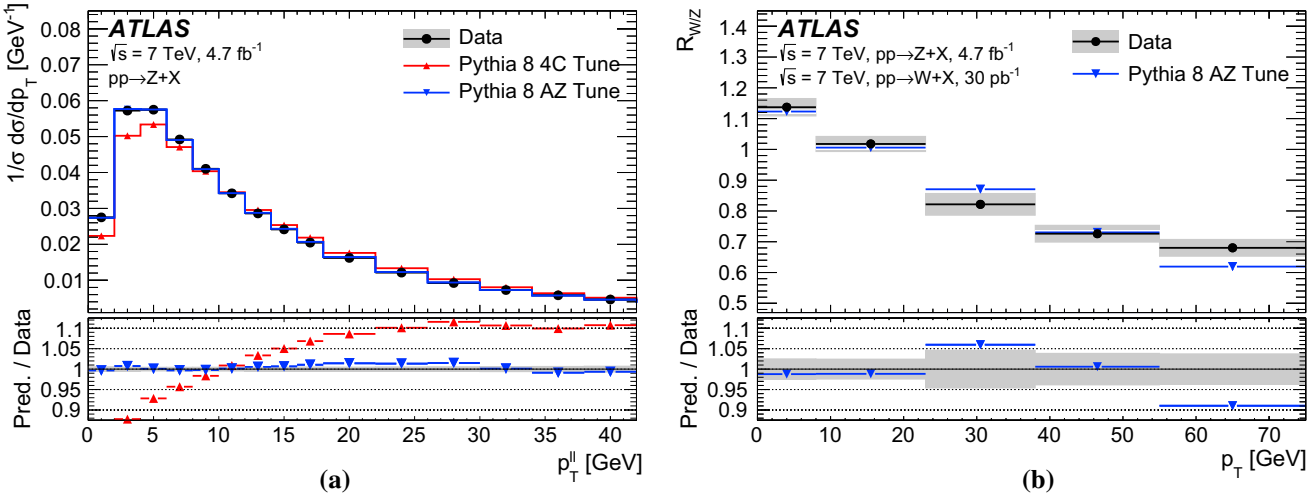

Fig. 1 **a** Normalised differential cross section as a function of $p_{\mathrm{T}}^{\ell\ell}$ in Z-boson events [44] and **b** differential cross-section ratio $R_{W/Z}(p_{\mathrm{T}})$ as a function of the boson p_{T} [44,45]. The measured cross sections are compared to the predictions of the PYTHIA 8 AZ tune and, in **a**, of the PYTHIA 8 4C tune. The shaded bands show the total experimental uncertainties

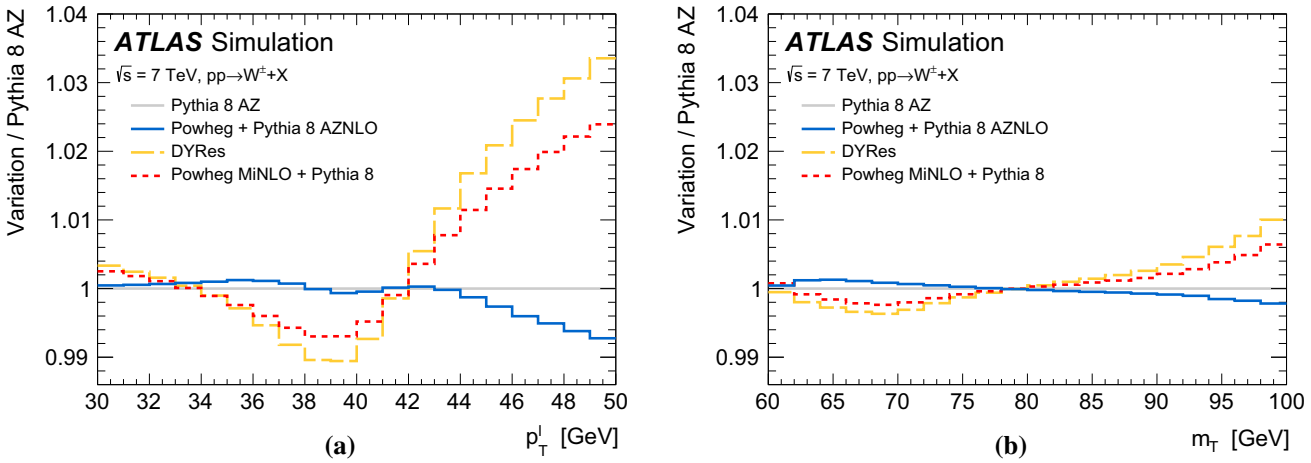

Fig. 2 Ratios of the reconstruction-level **a** p_{T}^{ℓ} and **b** m_{T} normalised distributions obtained using POWHEG+PYTHIA 8 AZNLO, DYRes and POWHEG MiNLO+PYTHIA 8 to the baseline normalised distributions obtained using PYTHIA 8 AZ

rebinned to match the coarser bins of the W-boson p_{T} distribution, which was measured using only 30 pb^{-1} of data. The theoretical prediction is in agreement with the experimental measurements for the region with $p_{\mathrm{T}} < 30$ GeV, which is relevant for the measurement of the W-boson mass.

The predictions of RESBOS [89,90], DYRes [91] and POWHEG MiNLO+PYTHIA 8 [96,97] are also considered. All predict a harder p_{T}^{W} distribution for a given p_{T}^{Z} distribution, compared to PYTHIA 8 AZ. Assuming the latter can be adjusted to match the measurement of Ref. [44], the corresponding p_{T}^{W} distribution induces a discrepancy with the detector-level u_{T} and $u_{\parallel}^{\ell}$ distributions observed in the W-boson data, as discussed in Sect. 11.2. This behaviour is observed using default values for the non-perturbative parameters of these programs, but is not expected to change significantly under variations of these parameters. These predictions are therefore not used in the determination of m_W or its uncertainty.

Figure 2 compares the reconstruction-level p_{T}^{ℓ} and m_{T} distributions obtained with POWHEG+PYTHIA 8 AZNLO, DYRes and POWHEG MiNLO+PYTHIA 8 to those of PYTHIA 8 AZ.[2] The effect of varying the p_{T}^{W} distribution is largest at high p_{T}^{ℓ}, which explains why the uncertainty due to the p_{T}^{W} modelling is reduced when limiting the p_{T}^{ℓ} fitting range as described in Sect. 11.3.

[2] Reconstruction-level distributions are obtained from the POWHEG+PYTHIA 8 signal sample by reweighting the particle-level p_{T}^{W} distribution according to the product of the p_{T}^{Z} distribution in PYTHIA 8 AZ, and of $R_{W/Z}(p_{\mathrm{T}})$ as predicted by POWHEG+PYTHIA 8 AZNLO, DYRes and POWHEG MiNLO+PYTHIA 8.

6.4 Reweighting procedure

The W and Z production and decay model described above is applied to the POWHEG+PYTHIA 8 samples through an event-by-event reweighting. Equation (3) expresses the factorisation of the cross section into the three-dimensional boson production phase space, defined by the variables m, p_{T}, and y, and the two-dimensional boson decay phase space, defined by the variables θ and ϕ. Accordingly, a prediction of the kinematic distributions of vector bosons and their decay products can be transformed into another prediction by applying separate reweighting of the three-dimensional boson production phase-space distributions, followed by a reweighting of the angular decay distributions.

The reweighting is performed in several steps. First, the inclusive rapidity distribution is reweighted according to the NNLO QCD predictions evaluated with DYNNLO. Then, at a given rapidity, the vector-boson transverse-momentum shape is reweighted to the PYTHIA 8 prediction with the AZ tune. This procedure provides the transverse-momentum distribution of vector bosons predicted by PYTHIA 8, preserving the rapidity distribution at NNLO. Finally, at given rapidity and transverse momentum, the angular variables are reweighted according to:

$$w(\cos\theta, \phi, p_{\mathrm{T}}, y) = \frac{1 + \cos^2\theta + \sum_i A'_i(p_{\mathrm{T}}, y)\, P_i(\cos\theta, \phi)}{1 + \cos^2\theta + \sum_i A_i(p_{\mathrm{T}}, y)\, P_i(\cos\theta, \phi)},$$

where A'_i are the angular coefficients evaluated at $O(\alpha_s^2)$, and A_i are the angular coefficients of the POWHEG+PYTHIA 8 samples. This reweighting procedure neglects the small dependence of the two-dimensional (p_{T},y) distribution and of the angular coefficients on the final state invariant mass. The procedure is used to include the corrections described in Sects. 6.2 and 6.3, as well as to estimate the impact of the QCD modelling uncertainties described in Sect. 6.5.

The validity of the reweighting procedure is tested at particle level by generating independent W-boson samples using the CT10nnlo and NNPDF3.0 [98] NNLO PDF sets, and the same value of m_W. The relevant kinematic distributions are calculated for both samples and used to reweight the CT10nnlo sample to the NNPDF3.0 one. The procedure described in Sect. 2.2 is then used to determine the value of m_W by fitting the NNPDF3.0 sample using templates from the reweighted CT10nnlo sample. The fitted value agrees with the input value within 1.5 ± 2.0 MeV. The statistical precision of this test is used to assign the associated systematic uncertainty.

The resulting model is tested by comparing the predicted Z-boson differential cross section as a function of rapidity, the W-boson differential cross section as a function of lepton pseudorapidity, and the angular coefficients in Z-boson events, to the corresponding ATLAS measurements [41,42]. The comparison with the measured W and Z cross sections is shown in Fig. 3. Satisfactory agreement between the measurements and the theoretical predictions is observed. A χ^2 compatibility test is performed for the three distributions simultaneously, including the correlations between the uncertainties. The compatibility test yields a χ^2/dof value of 45/34. Other NNLO PDF sets such as NNPDF3.0, CT14 [99], MMHT2014 [100], and ABM12 [101] are in worse agreement with these distributions. Based on the quantitative comparisons performed in

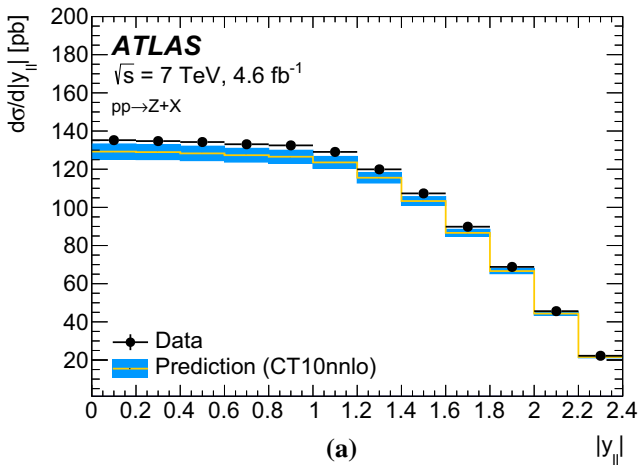

Fig. 3 **a** Differential Z-boson cross section as a function of boson rapidity, and **b** differential W^+ and W^- cross sections as a function of charged decay-lepton pseudorapidity at $\sqrt{s} = 7$ TeV [41]. The measured cross sections are compared to the POWHEG+PYTHIA 8 predictions, corrected to NNLO using DYNNLO with the CT10nnlo PDF set. The error bars show the total experimental uncertainties, including luminosity uncertainty, and the bands show the PDF uncertainties of the predictions

Ref. [41], only CT10nnlo, CT14 and MMHT2014 are considered further. The better agreement obtained with CT10nnlo can be ascribed to the weaker suppression of the strange quark density compared to the u- and d-quark sea densities in this PDF set.

The predictions of the angular coefficients in Z-boson events are compared to the ATLAS measurement at $\sqrt{s} = 8$ TeV [42]. Good agreement between the measurements and DYNNLO is observed for the relevant coefficients, except for A_2, where the measurement is significantly below the prediction. As an example, Fig. 4 shows the comparison for A_0 and A_2 as a function of p_{T}^{Z}. For A_2, an additional source of uncertainty in the theoretical prediction is considered to account for the observed disagreement with data, as discussed in Sect. 6.5.3.

6.5 Uncertainties in the QCD modelling

Several sources of uncertainty related to the perturbative and non-perturbative modelling of the strong interaction affect the dynamics of the vector-boson production and decay [33,102–104]. Their impact on the measurement of m_W is assessed through variations of the model parameters of the predictions for the differential cross sections as functions of the boson rapidity, transverse-momentum spectrum at a given rapidity, and angular coefficients, which correspond to the second, third, and fourth terms of the decomposition of Eq. (2), respectively. The parameter variations used to estimate the uncertainties are propagated to the simulated event samples by means of the reweighting procedure described in Sect. 6.4. Table 3 shows an overview of the uncertainties due to the QCD modelling which are discussed below.

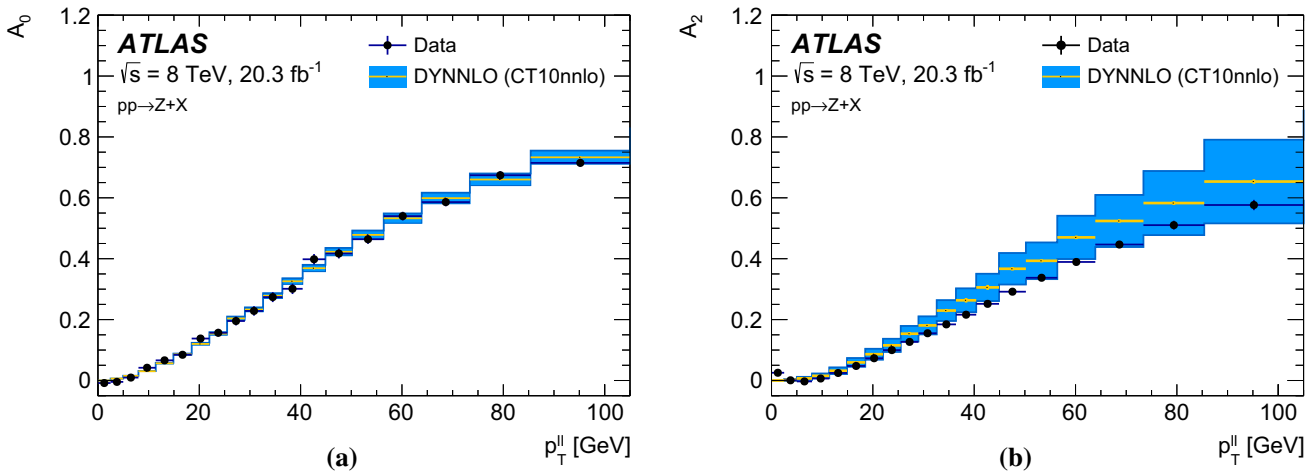

Fig. 4 The **a** A_0 and **b** A_2 angular coefficients in Z-boson events as a function of $p_{\mathrm{T}}^{\ell\ell}$ [42]. The measured coefficients are compared to the DYNNLO predictions using the CT10nnlo PDF set. The error bars show the total experimental uncertainties, and the bands show the uncertainties assigned to the DYNNLO predictions

Table 3 Systematic uncertainties in the m_W measurement due to QCD modelling, for the different kinematic distributions and W-boson charges. Except for the case of PDFs, the same uncertainties apply to W^+ and W^-. The fixed-order PDF uncertainty given for the separate W^+ and W^- final states corresponds to the quadrature sum of the CT10nnlo uncertainty variations; the charge-combined uncertainty also contains a 3.8 MeV contribution from comparing CT10nnlo to CT14 and MMHT2014

W-boson charge	W^+		W^-		Combined	
Kinematic distribution	p_{T}^{ℓ}	m_{T}	p_{T}^{ℓ}	m_{T}	p_{T}^{ℓ}	m_{T}
δm_W [MeV]						
Fixed-order PDF uncertainty	13.1	14.9	12.0	14.2	8.0	8.7
AZ tune	3.0	3.4	3.0	3.4	3.0	3.4
Charm-quark mass	1.2	1.5	1.2	1.5	1.2	1.5
Parton shower μ_{F} with heavy-flavour decorrelation	5.0	6.9	5.0	6.9	5.0	6.9
Parton shower PDF uncertainty	3.6	4.0	2.6	2.4	1.0	1.6
Angular coefficients	5.8	5.3	5.8	5.3	5.8	5.3
Total	15.9	18.1	14.8	17.2	11.6	12.9

6.5.1 Uncertainties in the fixed-order predictions

The imperfect knowledge of the PDFs affects the differential cross section as a function of boson rapidity, the angular coefficients, and the p_{T}^{W} distribution. The PDF contribution to the prediction uncertainty is estimated with the CT10nnlo PDF set by using the Hessian method [105]. There are 25 error eigenvectors, and a pair of PDF variations associated with each eigenvector. Each pair corresponds to positive and negative 90% CL excursions along the corresponding eigenvector. Symmetric PDF uncertainties are defined as the mean value of the absolute positive and negative excursions corresponding to each pair of PDF variations. The overall uncertainty of the CT10nnlo PDF set is scaled to 68% CL by applying a multiplicative factor of 1/1.645.

The effect of PDF variations on the rapidity distributions and angular coefficients are evaluated with DYNNLO, while their impact on the W-boson p_{T} distribution is evaluated using Pythia 8 and by reweighting event-by-event the PDFs of the hard-scattering process, which are convolved with the LO matrix elements. Similarly to other uncertainties which affect the p_{T}^{W} distribution (Sect. 6.5.2), only relative variations of the p_{T}^{W} and p_{T}^{Z} distributions induced by the PDFs are considered. The PDF variations are applied simultaneously to the boson rapidity, angular coefficients, and transverse-momentum distributions, and the overall PDF uncertainty is evaluated with the Hessian method as described above.

Uncertainties in the PDFs are the dominant source of physics-modelling uncertainty, contributing about 14 and 13 MeV when averaging p_{T}^{ℓ} and m_{T} fits for W^{+} and W^{-}, respectively. The PDF uncertainties are very similar when using p_{T}^{ℓ} or m_{T} for the measurement. They are strongly anti-correlated between positively and negatively charged W bosons, and the uncertainty is reduced to 7.4 MeV on average for p_{T}^{ℓ} and m_{T} fits, when combining opposite-charge categories. The anti-correlation of the PDF uncertainties is due to the fact that the total light-quark sea PDF is well constrained by deep inelastic scattering data, whereas the u-, d-, and s-quark decomposition of the sea is less precisely known [106]. An increase in the $\bar{u}$ PDF is at the expense of the $\bar{d}$ PDF, which produces opposite effects in the longitudinal polarisation of positively and negatively charged W bosons [37].

Other PDF sets are considered as alternative choices. The envelope of values of m_W extracted with the MMHT2014 and CT14 NNLO PDF sets is considered as an additional PDF uncertainty of 3.8 MeV, which is added in quadrature after combining the W^{+} and W^{-} categories, leading to overall PDF uncertainties of 8.0 MeV and 8.7 MeV for p_{T}^{ℓ} and m_{T} fits, respectively.

The effect of missing higher-order corrections on the NNLO predictions of the rapidity distributions of Z bosons, and the pseudorapidity distributions of the decay leptons of W bosons, is estimated by varying the renormalisation and factorisation scales by factors of 0.5 and 2.0 with respect to their nominal value $\mu_{\mathrm{R}} = \mu_{\mathrm{F}} = m_V$ in the DYNNLO predictions. The corresponding relative uncertainty in the normalised distributions is of the order of 0.1–0.3%, and significantly smaller than the PDF uncertainties. These uncertainties are expected to have a negligible impact on the measurement of m_W, and are not considered further.

The effect of the LHC beam-energy uncertainty of 0.65% [107] on the fixed-order predictions is studied. Relative variations of 0.65% around the nominal value of 3.5 TeV are considered, yielding variations of the inclusive W^{+} and W^{-} cross sections of 0.6 and 0.5%, respectively. No significant dependence as a function of lepton pseudorapidity is observed in the kinematic region used for the measurement, and the dependence as a function of p_{T}^{ℓ} and m_{T} is expected to be even smaller. This uncertainty is not considered further.

6.5.2 Uncertainties in the parton shower predictions

Several sources of uncertainty affect the Pythia 8 parton shower model used to predict the transverse momentum of the W boson. The values of the AZ tune parameters, determined by fits to the measurement of the Z-boson transverse momentum, are affected by the experimental uncertainty of the measurement. The corresponding uncertainties are propagated to the p_{T}^{W} predictions through variations of the orthogonal eigenvector components of the parameters error matrix [44]. The resulting uncertainty in m_W is 3.0 MeV for the p_{T}^{ℓ} distribution, and 3.4 MeV for the m_{T} distribution. In the present analysis, the impact of p_{T}^{W} distribution uncertainties is in general smaller when using p_{T}^{ℓ} than when using m_{T}, as a result of the comparatively narrow range used for the p_{T}^{ℓ} distribution fits.

Other uncertainties affecting predictions of the transverse-momentum spectrum of the W boson at a given rapidity, are propagated by considering relative variations of the p_{T}^{W} and p_{T}^{Z} distributions. The procedure is based on the assumption that model variations, when applied to p_{T}^{Z}, can be largely reabsorbed into new values of the AZ tune parameters fitted to the p_{T}^{Z} data. Variations that cannot be reabsorbed by the fit are excluded, since they would lead to a significant disagreement of the prediction with the measurement of p_{T}^{Z}. The uncertainties due to model variations which are largely correlated between p_{T}^{W} and p_{T}^{Z} cancel in this procedure. In contrast, the procedure allows a correct estimation of the uncertainties due to model variations which are uncorrelated between p_{T}^{W} and p_{T}^{Z}, and which represent the only relevant sources of theoretical uncertainties in the propagation of the QCD modelling from p_{T}^{Z} to p_{T}^{W}.

Uncertainties due to variations of parton shower parameters that are not fitted to the p_{T}^{Z} measurement include variations of the masses of the charm and bottom quarks, and variations of the factorisation scale used for the QCD ISR.

The mass of the charm quark is varied in PYTHIA 8, conservatively, by ± 0.5 GeV around its nominal value of 1.5 GeV. The resulting uncertainty contributes 1.2 MeV for the p_{T}^{ℓ} fits, and 1.5 MeV for the m_{T} fits. The mass of the bottom quark is varied in PYTHIA 8, conservatively, by ± 0.8 GeV around its nominal value of 4.8 GeV. The resulting variations have a negligible impact on the transverse-momentum distributions of Z and W bosons, and are not considered further.

The uncertainty due to higher-order QCD corrections to the parton shower is estimated through variations of the factorisation scale, μ_{F}, in the QCD ISR by factors of 0.5 and 2.0 with respect to the central choice $\mu_{\mathrm{F}}^2 = p_{\mathrm{T},0}^2 + p_{\mathrm{T}}^2$, where $p_{\mathrm{T},0}$ is an infrared cut-off, and p_{T} is the evolution variable of the parton shower [108]. Variations of the renormalisation scale in the QCD ISR are equivalent to a redefinition of $\alpha_{\mathrm{s}}(m_Z)$ used for the QCD ISR, which is fixed from the fits to the p_{T}^Z data. As a consequence, variations of the ISR renormalisation scale do not apply when estimating the uncertainty in the predicted p_{T}^W distribution.

Higher-order QCD corrections are expected to be largely correlated between W-boson and Z-boson production induced by the light quarks, u, d, and s, in the initial state. However, a certain degree of decorrelation between W- and Z-boson transverse-momentum distributions is expected, due to the different amounts of heavy-quark-initiated production, where heavy refers to charm and bottom flavours. The physical origin of this decorrelation can be ascribed to the presence of independent QCD scales corresponding to the three-to-four flavours and four-to-five flavours matching scales μ_c and μ_b in the variable-flavour-number scheme PDF evolution [109], which are of the order of the charm- and bottom-quark masses, respectively. To assess this effect, the variations of μ_{F} in the QCD ISR are performed simultaneously for all light-quark $q\bar{q} \to W, Z$ processes, with $q = u, d, s$, but independently for each of the $c\bar{c} \to Z$, $b\bar{b} \to Z$, and $c\bar{q} \to W$ processes, where $q = d, s$. The effect of the $c\bar{q} \to W$ variations on the determination of m_W is reduced by a factor of two, to account for the presence of only one heavy-flavour quark in the initial state. The resulting uncertainty in m_W is 5.0 MeV for the p_{T}^{ℓ} distribution, and 6.9 MeV for the m_{T} distribution. Since the μ_{F} variations affect all the branchings of the shower evolution and not only vertices involving heavy quarks, this procedure is expected to yield a sufficient estimate of the $\mu_{c,b}$-induced decorrelation between the W- and Z-boson p_{T} distributions. Treating the μ_{F} variations as correlated between all quark flavours, but uncorrelated between W- and Z-boson production, would yield a systematic uncertainty in m_W of approximately 30 MeV.

The predictions of the PYTHIA 8 MC generator include a reweighting of the first parton shower emission to the leading-order W+jet cross section, and do not include matching corrections to the higher-order W+jet cross section. As discussed in Sect. 11.2, predictions matched to the NLO W+jet cross section, such as POWHEG MiNLO+PYTHIA 8 and DYRes, are in disagreement with the observed $u_{\parallel}^{\ell}$ distribution and cannot be used to provide a reliable estimate of the associated uncertainty. The $u_{\parallel}^{\ell}$ distribution, on the other hand, validates the PYTHIA 8 AZ prediction and its uncertainty, which gives confidence that missing higher-order corrections to the W-boson p_{T} distribution are small in comparison to the uncertainties that are already included, and can be neglected at the present level of precision.

The sum in quadrature of the experimental uncertainties of the AZ tune parameters, the variations of the mass of the charm quark, and the factorisation scale variations, leads to uncertainties on m_W of 6.0 and 7.8 MeV when using the p_{T}^{ℓ} distribution and the m_{T} distribution, respectively. These sources of uncertainty are taken as fully correlated between the electron and muon channels, the positively and negatively charged W-boson production, and the $|\eta_{\ell}|$ bins.

The PYTHIA 8 parton shower simulation employs the CTEQ6L1 leading-order PDF set. An additional independent source of PDF-induced uncertainty in the p_{T}^W distribution is estimated by comparing several choices of the leading-order PDF used in the parton shower, corresponding to the CT14lo, MMHT2014lo and NNPDF2.3lo [110] PDF sets. The PDFs which give the largest deviation from the nominal ratio of the p_{T}^W and p_{T}^Z distributions are used to estimate the uncertainty. This procedure yields an uncertainty of about 4 MeV for W^+, and of about 2.5 MeV for W^-. Similarly to the case of fixed-order PDF uncertainties, there is a strong anti-correlation between positively and negatively charged W bosons, and the uncertainty is reduced to about 1.5 MeV when combining positive- and negative-charge categories.

The prediction of the p_{T}^W distribution relies on the p_{T}-ordered parton shower model of the PYTHIA 8 MC generator. In order to assess the impact of the choice of parton shower model on the determination of m_W, the PYTHIA 8 prediction of the ratio of the p_{T}^W and p_{T}^Z distributions is compared to the corresponding prediction of the HERWIG 7 MC generator [111,112], which implements an angular-ordered parton shower model. Differences between the PYTHIA 8 and HERWIG 7 predictions are smaller than the uncertainties in the PYTHIA 8 prediction, and no additional uncertainty is considered.

6.5.3 *Uncertainties in the angular coefficients*

The full set of angular coefficients can only be measured precisely for the production of Z bosons. The accuracy of the NNLO predictions of the angular coefficients is validated by comparison to the Z-boson measurement, and extrapolated to W-boson production assuming that NNLO predictions have similar accuracy for the W- and Z-boson processes. The ATLAS measurement of the angular coefficients in Z-boson

production at a centre-of-mass energy of $\sqrt{s} = 8$ TeV [42] is used for this validation. The $O(\alpha_s^2)$ predictions, evaluated with DYNNLO, are in agreement with the measurements of the angular coefficients within the experimental uncertainties, except for the measurement of A_2 as a function of Z-boson p_T.

Two sources of uncertainty affecting the modelling of the angular coefficients are considered, and propagated to the W-boson predictions. One source is defined from the experimental uncertainty of the Z-boson measurement of the angular coefficients which is used to validate the NNLO predictions. The uncertainty in the corresponding W-boson predictions is estimated by propagating the experimental uncertainty of the Z-boson measurement as follows. A set of pseudodata distributions are obtained by fluctuating the angular coefficients within the experimental uncertainties, preserving the correlations between the different measurement bins for the different coefficients. For each pseudoexperiment, the differences in the A_i coefficients between fluctuated and nominal Z-boson measurement results are propagated to the corresponding coefficient in W-boson production. The corresponding uncertainty is defined from the standard deviation of the m_W values as estimated from the pseudodata distributions.

The other source of uncertainty is considered to account for the disagreement between the measurement and the NNLO QCD predictions observed for the A_2 angular coefficient as a function of the Z-boson p_T (Fig. 4). The corresponding uncertainty in m_W is estimated by propagating the difference in A_2 between the Z-boson measurement and the theoretical prediction to the corresponding coefficient in W-boson production. The corresponding uncertainty in the measurement of m_W is 1.6 MeV for the extraction from the p_T^ℓ distribution. Including this contribution, total uncertainties of 5.8 and 5.3 MeV due to the modelling of the angular coefficients are estimated in the determination of the W-boson mass from the p_T^ℓ and m_T distributions, respectively. The uncertainty is dominated by the experimental uncertainty of the Z-boson measurement used to validate the theoretical predictions.

7 Calibration of electrons and muons

Any imperfect calibration of the detector response to electrons and muons impacts the measurement of the W-boson mass, as it affects the position and shape of the Jacobian edges reflecting the value of m_W. In addition, the p_T^ℓ and m_T distributions are broadened by the electron-energy and muon-momentum resolutions. Finally, the lepton-selection efficiencies depend on the lepton pseudorapidity and transverse momentum, further modifying these distributions. Corrections to the detector response are derived from the data, and presented below. In most cases, the corrections are applied to the simulation, with the exception of the muon sagitta bias corrections and electron energy response corrections, which are applied to the data. Backgrounds to the selected $Z \to \ell\ell$ samples are taken into account using the same procedures as discussed in Sect. 9. Since the Z samples are used separately for momentum calibration and efficiency measurements, as well as for the recoil response corrections discussed in Sect. 8, correlations among the corresponding uncertainties can appear. These correlations were investigated and found to be negligible.

7.1 Muon momentum calibration

As described in Sect. 5.1, the kinematic parameters of selected muons are determined from the associated inner-detector tracks. The accuracy of the momentum measurement is limited by imperfect knowledge of the detector alignment and resolution, of the magnetic field, and of the amount of passive material in the detector.

Biases in the reconstructed muon track momenta are classified as radial or sagitta biases. The former originate from detector movements along the particle trajectory and can be corrected by an η-dependent, charge-independent momentum-scale correction. The latter typically originate from curl distortions or linear twists of the detector around the z-axis [113], and can be corrected with η-dependent correction factors proportional to $q \times p_T^\ell$, where q is the charge of the muon. The momentum scale and resolution corrections are applied to the simulation, while the sagitta bias correction is applied to the data:

$$p_T^{\mathrm{MC,corr}} = p_T^{\mathrm{MC}} \times [1 + \alpha(\eta, \phi)] \times \left[1 + \beta_{\mathrm{curv}}(\eta) \cdot G(0, 1) \cdot p_T^{\mathrm{MC}}\right],$$

$$p_T^{\mathrm{data,corr}} = \frac{p_T^{\mathrm{data}}}{1 + q \cdot \delta(\eta, \phi) \cdot p_T^{\mathrm{data}}},$$

where $p_T^{\mathrm{data,MC}}$ is the uncorrected muon transverse momentum in data and simulation, $G(0, 1)$ are normally distributed random variables with mean zero and unit width, and α, β_{curv}, and δ represent the momentum scale, intrinsic resolution and sagitta bias corrections, respectively. Multiple-scattering contributions to the resolution are relevant at low p_T, and the corresponding corrections are neglected.

Momentum scale and resolution corrections are derived using $Z \to \mu\mu$ decays, following the method described in Ref. [40]. Template histograms of the dimuon invariant mass are constructed from the simulated event samples, including momentum scale and resolution corrections in narrow steps within a range covering the expected uncertainty. The optimal values of α and β_{curv} are determined by means of a χ^2 minimisation, comparing data and simulation in the

range of twice the standard deviation on each side of the mean value of the invariant mass distribution. In the first step, the corrections are derived by averaging over ϕ, and for 24 pseudorapidity bins in the range $-2.4 < \eta_\ell < 2.4$. In the second iteration, ϕ-dependent correction factors are evaluated in coarser bins of η_ℓ. The typical size of α varies from -0.0005 to -0.0015 depending on η_ℓ, while β_{curv} values increase from $0.2\,\text{TeV}^{-1}$ in the barrel to $0.6\,\text{TeV}^{-1}$ in the high η_ℓ region. Before the correction, the ϕ-dependence has an amplitude at the level of 0.1%.

The α and β_{curv} corrections are sensitive to the following aspects of the calibration procedure, which are considered for the systematic uncertainty: the choice of the fitting range, methodological biases, background contributions, theoretical modelling of Z-boson production, non-linearity of the corrections, and material distribution in the ID. The uncertainty due to the choice of fitting range is estimated by varying the range by $\pm 10\%$, and repeating the procedure. The uncertainty due to the fit methodology is estimated by comparing the template fit results with an alternative approach, based on an iterative χ^2 minimisation. Background contributions from gauge-boson pair and top-quark pair production are estimated using the simulation. The uncertainty in these background contributions is evaluated by varying their normalisation within the theoretical uncertainties on the production cross sections. The uncertainty in the theoretical modelling of Z-boson production is evaluated by propagating the effect of electroweak corrections to QED FSR, QED radiation of fermion pairs, and other NLO electroweak corrections described in Sect. 6.1. The experimental uncertainty in the value of the Z-boson mass used as input is also accounted for. These sources of uncertainty are summed in quadrature, yielding an uncertainty $\delta\alpha$ in the muon momentum scale correction of approximately 0.5×10^{-4}; these sources are considered fully correlated across muon pseudorapidity.

The systematic uncertainty in the muon momentum scale due to the extrapolation from the $Z \to \mu\mu$ momentum range to the $W \to \mu\nu$ momentum range is estimated by evaluating momentum-scale corrections as a function of $1/p_{\text{T}}$ for muons in various $|\eta|$ ranges. The extrapolation uncertainty $\delta\alpha$ is parameterised as follows:

$$\delta\alpha = p_0 + \frac{p_1}{\left\langle\, p_{\text{T}}^{\ell}(W)\,\right\rangle},$$

where $\left\langle\, p_{\text{T}}^{\ell}(W)\,\right\rangle$ is the average p_{T} of muons in W-boson events, and p_0 and p_1 are free parameters. If the momentum-scale corrections are independent of $1/p_{\text{T}}$, the fitting parameters are expected to be $p_0 = 1$ and $p_1 = 0$. Deviations of p_1 from zero indicate a possible momentum dependence. The fitted values of $\delta\alpha$ are shown in Fig. 5a, and are consistent with one, within two standard deviations of the statistical error. The corresponding systematic uncertainty in m_W is defined assuming, in each bin of $|\eta|$, a momentum non-linearity given by the larger of the fitted value of p_1 and its uncertainty. This source of uncertainty is considered uncorrelated across muon pseudorapidity given that p_1 is dominated by statistical fluctuations. The effect of the imperfect knowledge of the material in the ID is studied using simulated event samples including an increase of the ID material by 10%, according to the uncertainty estimated in Ref. [114]. The impact of this variation is found to be negligible in comparison with the uncertainties discussed above.

Two methods are used for the determination of the sagitta bias δ. The first method exploits $Z \to \mu\mu$ events. Muons are categorised according to their charge and pseudorapidity, and for each of these categories, the position of the peak in the dimuon invariant mass distribution is determined for data and simulation. The procedure allows the determination of the charge dependence of the momentum scale for p_{T} values of approximately 42 GeV, which corresponds to the average transverse momentum of muons from Z-boson decays. The second method exploits identified electrons in a sample of $W \to e\nu$ decays. It is based on the ratio of the measured electron energy deposited in the calorimeter, E, to the electron momentum, p, measured in the ID. A clean sample of $W \to e\nu$ events with tightly identified electrons [38] is selected. Assuming that the response of the electromagnetic calorimeter is independent of the charge of the incoming particle, charge-dependent ID track momentum biases are extracted from the average differences in E/p for electrons and positrons [113]. This method benefits from a larger event sample compared to the first method, and allows the determination of charge-dependent corrections for p_{T} values of approximately 38 GeV, which corresponds to the average transverse momentum of muons in W-boson decays. The sagitta bias correction factors are derived using both methods separately in 40 η bins and 40 ϕ bins. The results are found to agree within uncertainties and are combined, as illustrated in Fig. 5b. The combined correction uncertainty is dominated by the finite size of the event samples.

Figure 6 shows the dimuon invariant mass distribution of $Z \to \mu\mu$ decays in data and simulation, after applying all corrections. Table 4 summarises the effect of the muon momentum scale and resolution uncertainties on the determination of m_W. The dominant systematic uncertainty in the momentum scale is due to the extrapolation of the correction from the Z-boson momentum range to the W-boson momentum range. The extrapolation uncertainty $\delta\alpha$ is (2–5) $\times 10^{-5}$ for $|\eta_\ell| < 2.0$, and (4–7) $\times 10^{-4}$ for $|\eta_\ell| > 2.0$. Systematic uncertainties from other sources are relatively small. The systematic uncertainty of the resolution corrections is dominated by the statistical uncertainty of the Z-boson event sample, and includes a contribution from the imperfect closure of the method. The latter is defined from the residual difference between the standard deviations of the dimuon invariant mass in data and simulation, after applying resolution corrections.

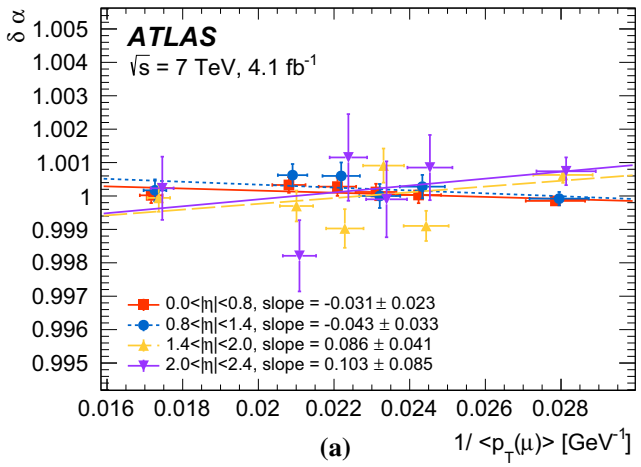

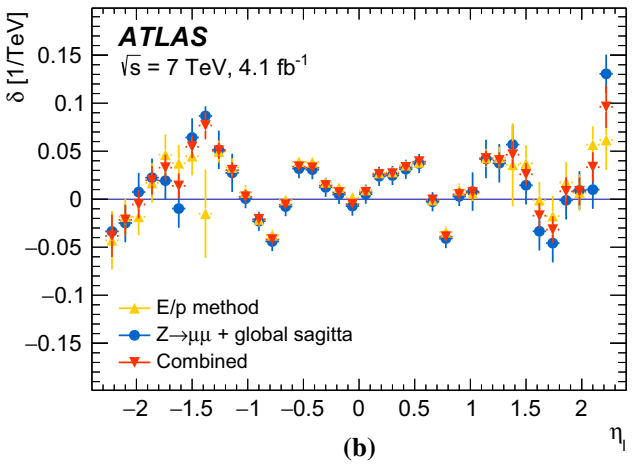

Fig. 5 **a** Residual muon momentum scale corrections as a function of muon $1/p_{\mathrm{T}}$ in four pseudorapidity regions, obtained with $Z \to \mu\mu$ events. The points are fitted using a linear function which parameterises the extrapolation of the muon momentum scale correction from Z to W events, as explained in the text. The error bars on the points show statistical uncertainties only. **b** Sagitta bias, δ, as a function of η_ℓ averaged over ϕ_ℓ. The results are obtained with the $Z \to \mu\mu$ and E/p methods and the combination of the two. The results obtained with the $Z \to \mu\mu$ method are corrected for the global sagitta bias. The E/p method uses electrons from $W \to e\nu$ decays. The two measurements are combined assuming they are uncorrelated. The error bars on the points show statistical uncertainties only

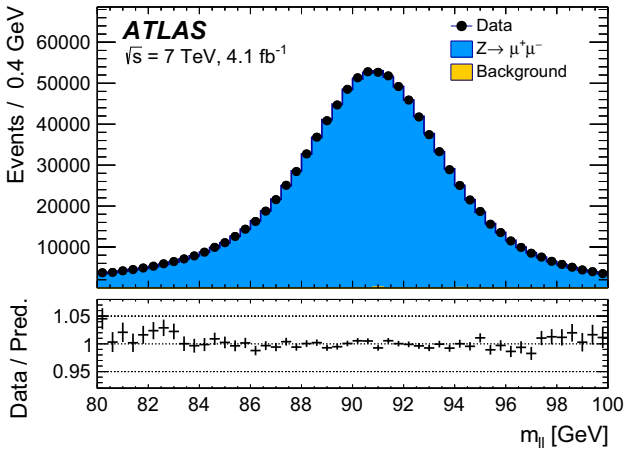

Fig. 6 Dimuon invariant mass distribution in $Z \to \mu\mu$ events. The data are compared to the simulation including signal and background contributions. Corrections for momentum scale and resolution, and for reconstruction, isolation, and trigger efficiencies are applied to the muons in the simulated events. Background events contribute less than 0.2% of the observed distribution. The lower panel shows the data-to-prediction ratio, with the error bars showing the statistical uncertainty

7.2 Muon selection efficiency

The selection of muon candidates in $W \to \mu\nu$ and $Z \to \mu\mu$ events requires an isolated track reconstructed in the inner detector and in the muon spectrometer. In addition, the events are required to pass the muon trigger selection. Differences in the efficiency of the reconstruction and selection requirements between data and simulation can introduce a systematic shift in the measurement of the W-boson mass, and have to be corrected. In particular, the extraction of m_W is sensitive to the dependence of the trigger, reconstruction and isolation efficiencies on the muon p_{T} and on the projection of the recoil on the lepton transverse momentum, $u_\parallel^\ell$.

For muons with p_{T} larger than approximately 15 GeV the detector simulation predicts constant efficiency as a function of p_{T}^ℓ, both for the muon trigger selection and the track reconstruction. In contrast, the efficiency of the isolation requirement is expected to vary as a function of p_{T}^ℓ and $u_\parallel^\ell$. The efficiency corrections also affect the muon selection inefficiency, and hence the estimation of the $Z \to \mu\mu$ background, which contributes to the $W \to \mu\nu$ selection when one of the decay muons fails the muon reconstruction or kinematic selection requirements.

Corrections to the muon reconstruction, trigger and isolation efficiencies are estimated by applying the tag-and-probe method [40] to $Z \to \mu\mu$ events in data and simulation. Efficiency corrections are defined as the ratio of efficiencies evaluated in data to efficiencies evaluated in simulated events. The corrections are evaluated as functions of two variables, p_{T}^ℓ and $u_\parallel^\ell$, and in various regions of the detector. The detector is segmented into regions corresponding to the η and ϕ coverage of the muon spectrometer. The subdivision accounts for the geometrical characteristics of the detector, such as the presence of uninstrumented or transition regions. The dependence of the efficiencies on $u_\parallel^\ell$ agree in data and simulation. Therefore, the muon efficiency corrections are evaluated only as a function of p_{T}^ℓ and η_ℓ, separately for positive and negative muon charges. The final efficiency correction factors are linearly interpolated as a function of muon p_{T}. No significant

Table 4 Systematic uncertainties in the m_W measurement from muon calibration and efficiency corrections, for the different kinematic distributions and $|\eta_\ell|$ categories, averaged over lepton charge. The momentum-scale uncertainties include the effects of both the momentum scale and linearity corrections. Combined uncertainties are evaluated as described in Sect. 2.2

$\|\eta_\ell\|$ range	[0.0, 0.8]		[0.8, 1.4]		[1.4, 2.0]		[2.0, 2.4]		Combined	
Kinematic distribution	p_{T}^ℓ	m_{T}	p_{T}^ℓ	m_{T}	p_{T}^ℓ	m_{T}	p_{T}^ℓ	m_{T}	p_{T}^ℓ	m_{T}
δm_W [MeV]										
Momentum scale	8.9	9.3	14.2	15.6	27.4	29.2	111.0	115.4	8.4	8.8
Momentum resolution	1.8	2.0	1.9	1.7	1.5	2.2	3.4	3.8	1.0	1.2
Sagitta bias	0.7	0.8	1.7	1.7	3.1	3.1	4.5	4.3	0.6	0.6
Reconstruction and isolation efficiencies	4.0	3.6	5.1	3.7	4.7	3.5	6.4	5.5	2.7	2.2
Trigger efficiency	5.6	5.0	7.1	5.0	11.8	9.1	12.1	9.9	4.1	3.2
Total	11.4	11.4	16.9	17.0	30.4	31.0	112.0	116.1	9.8	9.7

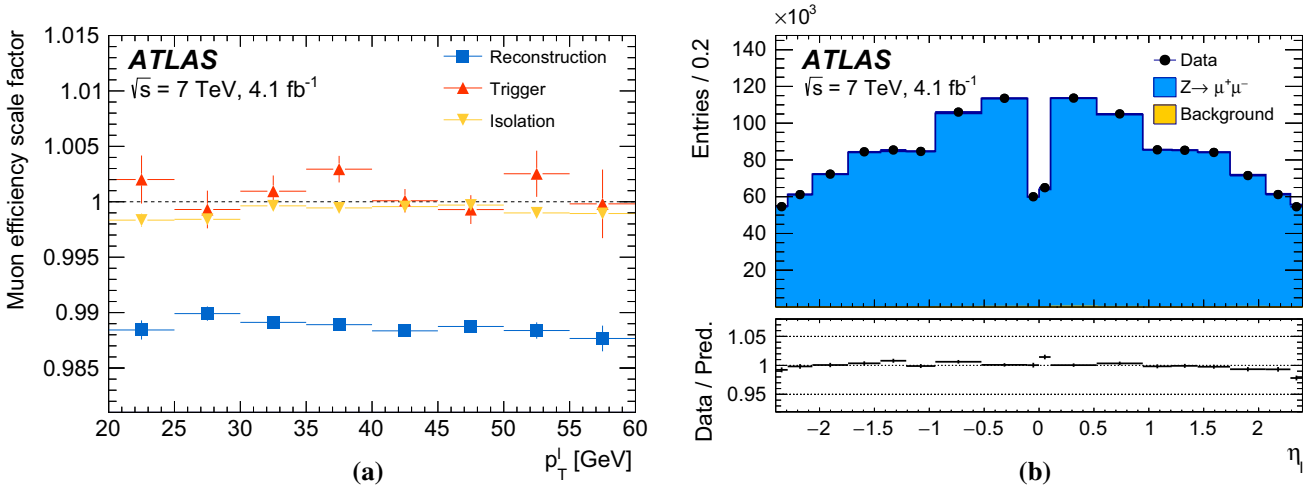

Fig. 7 **a** Scale factors for the muon reconstruction, trigger and isolation efficiency obtained with the tag and probe method as a function of the muon p_{T}. Scale factors for the trigger efficiency are averaged over two data-taking periods as explained in the text. The error bars on the points show statistical uncertainties only. **b** Distribution of the reconstructed muons η in $Z \to \mu\mu$ events. The data are compared to the simulation including signal and background contributions. Corrections for momentum scale and resolution, and for reconstruction, isolation, and trigger efficiencies are applied to the muons in the simulated events. Background events contribute less than 0.2% of the observed distribution. The lower panel shows the data-to-prediction ratio, with the error bars showing the statistical uncertainty

p_{T}-dependence of the corrections is observed in any of the detector regions.

The selection of tag-and-probe pairs from $Z \to \mu\mu$ events is based on the kinematic requirements described in Sect. 5.2. The tag muon is required to be a combined and energy-isolated muon candidate (see Sect. 5.1) which fulfils the muon trigger requirements. The selection requirements applied to the probe muon candidate differ for each efficiency determination: the selection requirement for which the efficiency is determined is removed from the set of requirements applied to the probe muon. All the efficiency corrections are derived inclusively for the full data set, with the exception of the trigger, for which they are derived separately for two different data-taking periods. The resulting scale factors are shown as a function of p_{T}^ℓ and averaged over η_ℓ in Fig. 7a. The trigger and isolation efficiency corrections are typically below 0.3%, while the reconstruction efficiency correction is on average about 1.1%. The corresponding impact on muon selection inefficiency reaches up to about 20%.

The quality of the efficiency corrections is evaluated by applying the corrections to the $Z \to \mu\mu$ simulated sample, and comparing the simulated kinematic distributions to the corresponding distributions in data. Figure 7b illustrates this procedure for the η_ℓ distribution. Further distributions are shown in Sect. 9.

The dominant source of uncertainty in the determination of the muon efficiency corrections is the statistical uncertainty of the Z-boson data sample. The largest sources of systematic uncertainty are the multijet background contribution and the momentum-scale uncertainty. The correspond-

ing uncertainty in the measurement of m_W is approximately 5 MeV. The ID tracking efficiencies for muon candidates are above 99.5% without any significant p_{T} dependence, and the associated uncertainties are not considered further. An overview of the uncertainties associated with the muon efficiency corrections is shown in Table 4.

7.3 Electron energy response

The electron-energy corrections and uncertainties are largely based on the ATLAS Run 1 electron and photon calibration results [39]. The correction procedure starts with the intercalibration of the first and second layers of the EM calorimeter for minimum-ionising particles, using the energy deposits of muons in $Z \to \mu\mu$ decays. After the intercalibration of the calorimeter layers, the longitudinal shower-energy profiles of electrons and photons are used to determine the presampler energy scale and probe the passive material in front of the EM calorimeter, leading to an improved description of the detector material distribution and providing estimates of the residual passive material uncertainty. Finally, a dependence of the cell-level energy measurement on the read-out gain is observed in the second layer and corrected for. After these preliminary corrections, an overall energy-scale correction is determined as a function of η_ℓ from $Z \to ee$ decays, by comparing the reconstructed mass distributions in data and simulation. Simultaneously, an effective constant term for the calorimeter energy resolution is extracted by adjusting the width of the reconstructed dielectron invariant mass distribution in simulation to match the distribution in data.

Uncertainties in the energy-response corrections arise from the limited size of the $Z \to ee$ sample, from the physics modelling of the resonance and from the calibration algorithm itself. Physics-modelling uncertainties include uncertainties from missing higher-order electroweak corrections (dominated by the absence of lepton-pair emissions in the simulation) and from the experimental uncertainty in m_Z; these effects are taken fully correlated with the muon channel. Background contributions are small and the associated uncertainty is considered to be negligible. Uncertainties related to the calibration procedure are estimated by varying the invariant mass range used for the calibration, and with a closure test. For the closure test, a pseudodata sample of $Z \to ee$ events is obtained from the nominal sample by rescaling the electron energies by known η-dependent factors; the calibration algorithm is then applied, and the measured energy corrections are compared with the input rescaling factors.

These sources of uncertainty constitute a subset of those listed in Ref. [39], where additional variations were considered in order to generalise the applicability of the Z-boson calibration results to electrons and photons spanning a wide energy range. The effect of these uncertainties is averaged within the different η_ℓ categories. The overall relative energy-scale uncertainty, averaged over η_ℓ, is 9.4×10^{-5} for electrons from Z-boson decays.

In addition to the uncertainties in the energy-scale corrections arising from the Z-boson calibration procedure, possible differences in the energy response between electrons from Z-boson and W-boson decays constitute a significant source of uncertainty. The linearity of the response is affected by uncertainties in the intercalibration of the layers and in the passive material and calorimeter read-out corrections mentioned above. Additional uncertainties are assigned to cover imperfect electronics pedestal subtraction affecting the energy measurement in the cells of the calorimeter, and to the modelling of the interactions between the electrons and the detector material in GEANT4. The contribution from these sources to the relative energy-scale uncertainty is (3–12) $\times 10^{-5}$ in each η bin, and 5.4×10^{-5} when averaged over the full η range after taking into account the correlation between the η bins.

Azimuthal variations of the electron-energy response are expected from gravity-induced mechanical deformations of the EM calorimeter, and are observed especially in the endcaps, as illustrated in Fig. 8. As the Z-boson calibration averages over ϕ_ℓ and the azimuthal distributions of the selected electrons differ in the two processes, a small residual effect from this modulation is expected when applying the calibration results to the $W \to e\nu$ sample. Related effects are discussed in Sect. 8. A dedicated correction is derived using the azimuthal dependence of the mean of the electron energy/momentum ratio, $\langle E/p \rangle$, after correcting p for the momentum scale and curvature bias discussed in Sect. 7.1. The effect of this correction is a relative change of the average energy response of 3.8×10^{-5} in W-boson events, with negligible uncertainty.

The E/p distribution is also used to test the modelling of non-Gaussian tails in the energy response. An excess of events is observed in data at low values of E/p, and interpreted as the result of the mismodelling of the lateral development of EM showers in the calorimeter. Its impact is evaluated by removing the electrons with E/p values in the region where the discrepancy is observed. The effect of this removal is compatible for electrons from W- and Z-boson decays within 4.9×10^{-5}, which corresponds to the statistical uncertainty of the test and is considered as an additional systematic uncertainty.

The result of the complete calibration procedure is illustrated in Fig. 9, which shows the comparison of the dielectron invariant mass distribution for $Z \to ee$ events in data and simulation. The impact of the electron-energy calibration uncertainties on the m_W measurement is summarised in Table 5.

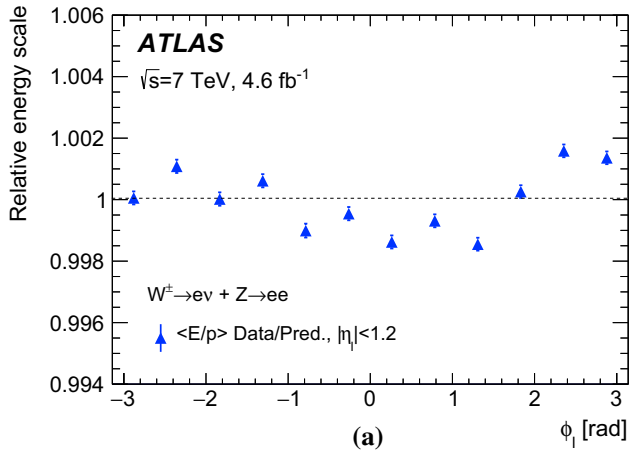

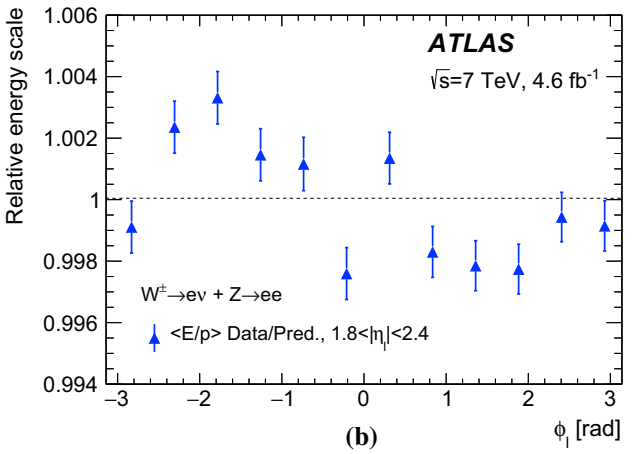

Fig. 8 Azimuthal variation of the data-to-prediction ratio of $\langle E/p \rangle$ in W and Z events, for electrons in **a** $|\eta_\ell| < 1.2$ and (b) $1.8 < |\eta_\ell| < 2.4$. The electron energy calibration based on $Z \to ee$ events is applied, and the track p is corrected for the momentum scale, resolution and sagitta bias. The mean for the E/p distribution integrated in ϕ is normalised to unity. The error bars are statistical only

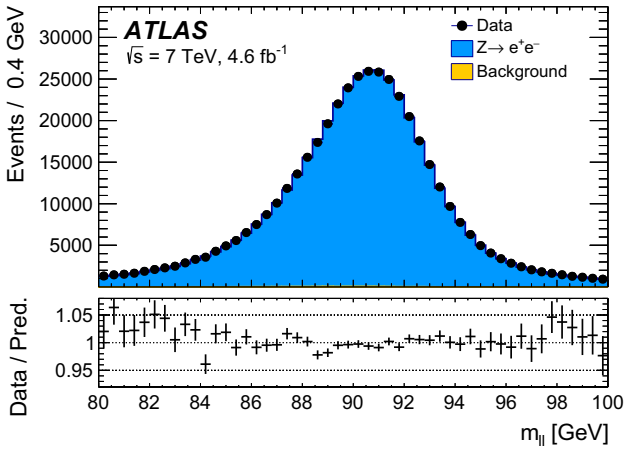

Fig. 9 Dielectron invariant mass distribution in $Z \to ee$ events. The data are compared to the simulation including signal and backgrounds. Corrections for energy resolution, and for reconstruction, identification, isolation and trigger efficiencies are applied to the simulation; energy-scale corrections are applied to the data. Background events contribute less than 0.2% of the observed distribution. The lower panel shows the data-to-prediction ratio, with the error bars showing the statistical uncertainty

7.4 Electron selection efficiency

Electron efficiency corrections are determined using samples of $W \to e\nu$, $Z \to ee$, and $J/\psi \to ee$ events, and measured separately for electron reconstruction, identification and trigger efficiencies [38], as a function of electron η and p_{T}. In the p_{T} range relevant for the measurement of the W-boson mass, the reconstruction and identification efficiency corrections have a typical uncertainty of 0.1–0.2% in the barrel, and 0.3% in the endcap. The trigger efficiency corrections have an uncertainty smaller than 0.1%, and are weakly dependent on p_{T}^{ℓ}.

For a data-taking period corresponding to approximately 20% of the integrated luminosity, the LAr calorimeter suffered from six front-end board failures. During this period, electrons could not be reconstructed in the region of $0 < \eta < 1.475$ and $-0.9 < \phi < -0.5$. The data-taking conditions are reflected in the simulation for the corresponding fraction of events. However, the trigger acceptance loss is not perfectly simulated, and dedicated efficiency corrections are derived as a function of η and ϕ to correct the mismodelling, and applied in addition to the initial corrections.

As described in Sect. 5, isolation requirements are applied to the identified electrons. Their efficiency is approximately 95% in the simulated event samples, and energy-isolation efficiency corrections are derived as for the reconstruction, identification, and trigger efficiencies. The energy-isolation efficiency corrections deviate from unity by less than 0.5%, with an uncertainty smaller than 0.2% on average.

Finally, as positively and negatively charged W-boson events have different final-state distributions, the W^+ contamination in the W^- sample, and vice versa, constitutes an additional source of uncertainty. The rate of electron charge mismeasurement in simulated events rises from about 0.2% in the barrel to 4% in the endcap. Estimates of charge mismeasurement in data confirm these predictions within better than 0.1%, apart from the high $|\eta|$ region where differences up to 1% are observed. The electron charge mismeasurement induces a systematic uncertainty in m_W of approximately 0.5 MeV in the regions of $|\eta_\ell| < 0.6$ and $0.6 < |\eta_\ell| < 1.2$, and of 5 MeV in the region of $1.8 < |\eta_\ell| < 2.4$, separately for W^+ and W^-. Since the W^+ and W^- samples contaminate each other, the effect

Table 5 Systematic uncertainties in the m_W measurement due to electron energy calibration, efficiency corrections and charge mismeasurement, for the different kinematic distributions and $|\eta_\ell|$ regions, averaged over lepton charge. Combined uncertainties are evaluated as described in Sect. 2.2

$\|\eta_\ell\|$ range	[0.0, 0.6]		[0.6, 1.2]		[1.8, 2.4]		Combined	
Kinematic distribution	p_{T}^{ℓ}	m_{T}	p_{T}^{ℓ}	m_{T}	p_{T}^{ℓ}	m_{T}	p_{T}^{ℓ}	m_{T}
δm_W [MeV]								
Energy scale	10.4	10.3	10.8	10.1	16.1	17.1	8.1	8.0
Energy resolution	5.0	6.0	7.3	6.7	10.4	15.5	3.5	5.5
Energy linearity	2.2	4.2	5.8	8.9	8.6	10.6	3.4	5.5
Energy tails	2.3	3.3	2.3	3.3	2.3	3.3	2.3	3.3
Reconstruction efficiency	10.5	8.8	9.9	7.8	14.5	11.0	7.2	6.0
Identification efficiency	10.4	7.7	11.7	8.8	16.7	12.1	7.3	5.6
Trigger and isolation efficiencies	0.2	0.5	0.3	0.5	2.0	2.2	0.8	0.9
Charge mismeasurement	0.2	0.2	0.2	0.2	1.5	1.5	0.1	0.1
Total	19.0	17.5	21.1	19.4	30.7	30.5	14.2	14.3

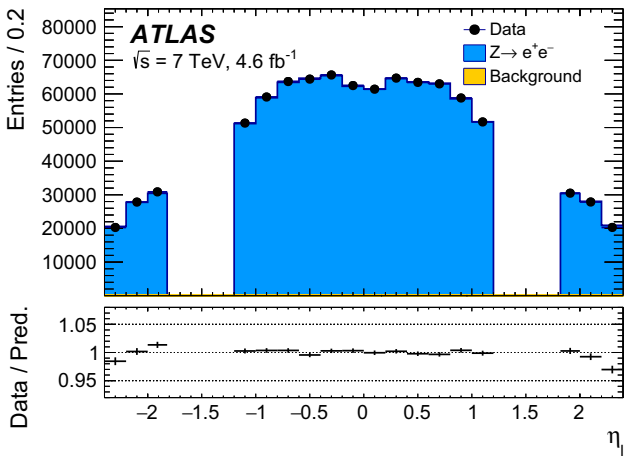

Fig. 10 Distribution of reconstructed electrons η in $Z \to ee$ events. The data are compared to the simulation including signal and background contributions. Corrections for energy resolution, and for reconstruction, identification, isolation and trigger efficiencies are applied to the simulation; energy-scale corrections are applied to the data. Background events contribute less than 0.2% of the observed distribution. The lower panel shows the data-to-prediction ratio, with the error bars showing the statistical uncertainty

is anti-correlated for the m_W measurements in the two different charge categories, and cancels in their combination, up to the asymmetry in the W^+/W^- production rate. After combination, the residual uncertainty in m_W is 0.2 MeV for $|\eta_\ell| < 1.2$, and 1.5 MeV for $1.8 < |\eta_\ell| < 2.4$, for both the p_{T}^{ℓ} and m_{T} distributions. The uncertainties are considered as uncorrelated across pseudorapidity bins.

Figure 10 compares the η_ℓ distribution in data and simulation for $Z \to ee$ events, after applying the efficiency corrections discussed above. The corresponding uncertainties in m_W due to the electron efficiency corrections are shown in Table 5.

8 Calibration of the recoil

The calibration of the recoil, u_{T}, affects the measurement of the W-boson mass through its impact on the m_{T} distribution, which is used to extract m_W. In addition, the recoil calibration affects the p_{T}^{ℓ} and m_{T} distributions through the $p_{\mathrm{T}}^{\mathrm{miss}}$, m_{T}, and u_{T} event-selection requirements. The calibration procedure proceeds in two steps. First, the dominant part of the u_{T} resolution mismodelling is addressed by correcting the modelling of the overall event activity in simulation. These corrections are derived separately in the W- and Z-boson samples. Second, corrections for residual differences in the recoil response and resolution are derived using Z-boson events in data, and transferred to the W-boson sample.

8.1 Event activity corrections

The pile-up of multiple proton–proton interactions has a significant impact on the resolution of the recoil. As described in Sect. 4, the pile-up is modelled by overlaying the simulated hard-scattering process with additional pp interactions simulated using PYTHIA 8 with the A2 tune. The average number of interactions per bunch crossing is defined, for each event, as $\langle\mu\rangle = \mathcal{L}\sigma_{\mathrm{in}}/f_{\mathrm{BC}}$, where $\mathcal{L}$ is the instantaneous luminosity, σ_{in} is the total pp inelastic cross section and f_{BC} is the average bunch-crossing rate. The distribution of $\langle\mu\rangle$ in the simulated event samples is reweighted to match the corresponding distribution in data. The distribution of $\langle\mu\rangle$ is affected in particular by the uncertainty in the cross section and properties of inelastic collisions. In the simulation, $\langle\mu\rangle$ is scaled by a factor α to optimise the modelling of observed data distributions which are relevant to the modelling of u_{T}. A value of $\alpha = 1.10 \pm 0.04$ is determined by minimising the χ^2 function of the compatibility test between data and simulation for the $\Sigma E_{\mathrm{T}}^{*}$ and $u_{\perp}^{Z}$ distributions, where the uncertainty accounts for differences in the values determined using the two distributions.

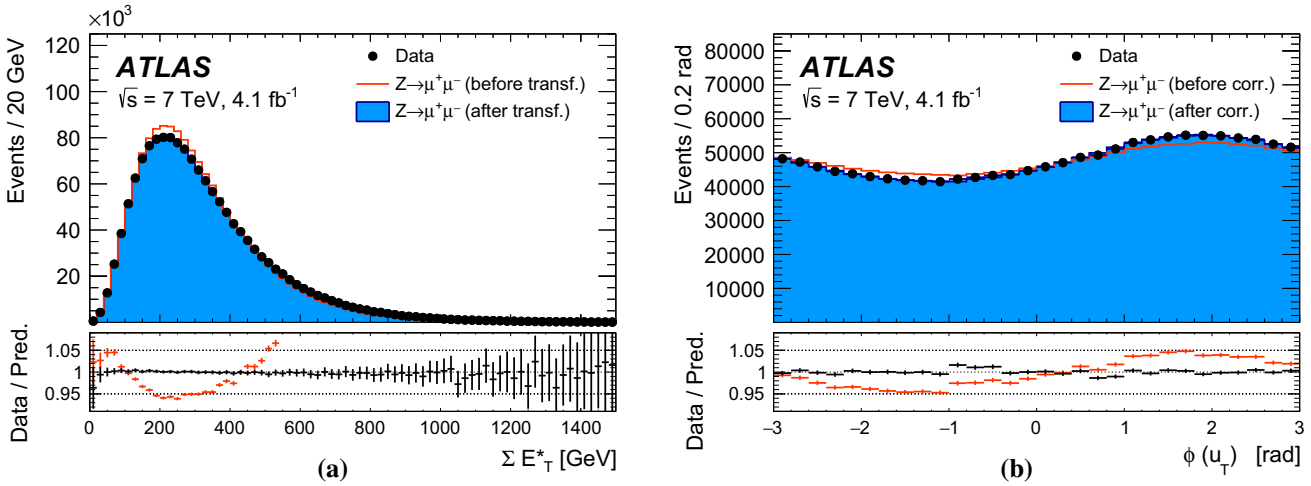

Fig. 11 Distributions of **a** $\Sigma E_{\mathrm{T}}^{*}$ and **b** azimuth ϕ of the recoil in data and simulation for $Z \to \mu\mu$ events. The $\Sigma E_{\mathrm{T}}^{*}$ distribution is shown before and after applying the Smirnov-transform correction, and the ϕ distribution is shown before and after the $u_{x,y}$ correction. The lower panels show the data-to-prediction ratios, with the vertical bars showing the statistical uncertainty

After the correction applied to the average number of pile-up interactions, residual data-to-prediction differences in the $\Sigma E_{\mathrm{T}}^{*}$ distribution are responsible for most of the remaining u_{T} resolution mismodelling. The $\Sigma E_{\mathrm{T}}^{*}$ distribution is corrected by means of a Smirnov transform, which is a mapping $x \to x'(x)$ such that a function $f(x)$ is transformed into another target function $g(x)$ through the relation $f(x) \to f(x') \equiv g(x)$ [115]. Accordingly, a mapping $\Sigma E_{\mathrm{T}}^{*} \to \Sigma E_{\mathrm{T}}^{*\prime}$ is defined such that the distribution of $\Sigma E_{\mathrm{T}}^{*}$ in simulation, $h_{\mathrm{MC}}(\Sigma E_{\mathrm{T}}^{*})$, is transformed into $h_{\mathrm{MC}}(\Sigma E_{\mathrm{T}}^{*\prime})$ to match the $\Sigma E_{\mathrm{T}}^{*}$ distribution in data, $h_{\mathrm{data}}(\Sigma E_{\mathrm{T}}^{*})$. The correction is derived for Z-boson events in bins of $p_{\mathrm{T}}^{\ell\ell}$, as the observed differences in the $\Sigma E_{\mathrm{T}}^{*}$ distribution depend on the Z-boson transverse momentum. The result of this procedure is illustrated in Fig. 11a. The modified distribution is used to parameterise the recoil response corrections discussed in the next section.

In W-boson events, the transverse momentum of the boson can only be inferred from u_{T}, which has worse resolution compared to $p_{\mathrm{T}}^{\ell\ell}$ in Z-boson events. To overcome this limitation, a p_{T}-dependent correction is defined assuming that the p_{T} dependence of differences between data and simulation in the $\Sigma E_{\mathrm{T}}^{*}$ distribution in W-boson events follows the corresponding differences observed in Z-boson events. The $\Sigma E_{\mathrm{T}}^{*}$ distribution to be matched by the simulation is defined as follows for W-boson events:

$$\tilde{h}^{W}_{\mathrm{data}}(\Sigma E_{\mathrm{T}}^{*}, p_{\mathrm{T}}^{W}) \equiv h^{Z}_{\mathrm{data}}(\Sigma E_{\mathrm{T}}^{*}, p_{\mathrm{T}}^{\ell\ell}) \left(\frac{h^{W}_{\mathrm{data}}(\Sigma E_{\mathrm{T}}^{*})}{h^{W}_{\mathrm{MC}}(\Sigma E_{\mathrm{T}}^{*})} \Big/ \frac{h^{Z}_{\mathrm{data}}(\Sigma E_{\mathrm{T}}^{*})}{h^{Z}_{\mathrm{MC}}(\Sigma E_{\mathrm{T}}^{*})} \right), \quad (4)$$

where p_{T}^{W} is the particle-level W-boson transverse momentum, and $p_{\mathrm{T}}^{\ell\ell}$ the transverse momentum measured from the decay-lepton pair, used as an approximation of the particle-level p_{T}^{Z}. The superscripts W and Z refer to W- or Z-boson event samples, and the double ratio in the second term accounts for the differences between the inclusive distributions in W- and Z-boson events. This correction is defined separately for positively and negatively charged W bosons, so as to incorporate the dependence of the p_{T}^{W} distribution on the charge of the W boson. Using $\tilde{h}^{W}_{\mathrm{data}}(\Sigma E_{\mathrm{T}}^{*}, p_{\mathrm{T}}^{W})$ defined in Eq. (4) as the target distribution, the p_{T}^{W}-dependent Smirnov transform of the $\Sigma E_{\mathrm{T}}^{*}$ distribution in W-boson events is defined as follows:

$$h^{W}_{\mathrm{MC}}(\Sigma E_{\mathrm{T}}^{*}; p_{\mathrm{T}}^{W}) \to h^{W}_{\mathrm{MC}}(\Sigma E_{\mathrm{T}}^{*\prime}; p_{\mathrm{T}}^{W}) \equiv \tilde{h}^{W}_{\mathrm{data}}(\Sigma E_{\mathrm{T}}^{*}; p_{\mathrm{T}}^{W}).$$

The validity of the approximation introduced in Eq. (4) is verified by comparing $h^{W}_{\mathrm{data}}(\Sigma E_{\mathrm{T}}^{*})/h^{W}_{\mathrm{MC}}(\Sigma E_{\mathrm{T}}^{*})$ and $h^{Z}_{\mathrm{data}}(\Sigma E_{\mathrm{T}}^{*})/h^{Z}_{\mathrm{MC}}(\Sigma E_{\mathrm{T}}^{*})$ in broad bins of u_{T}. The associated systematic uncertainties are discussed in Sect. 8.3.

8.2 Residual response corrections

In the ideal case of beams coinciding with the z-axis, the physical transverse momentum of W and Z bosons is uniformly distributed in ϕ. However, an offset of the interaction point with respect to the detector centre in the transverse plane, the non-zero crossing angle between the proton beams, and ϕ-dependent response of the calorimeters generate anisotropies in the reconstructed recoil distribution. Corresponding differences between data and simulation are addressed by effective corrections applied to u_x and u_y in simulation:

$$u'_x = u_x + \left(\langle u_x \rangle_{\mathrm{data}} - \langle u_x \rangle_{\mathrm{MC}} \right),$$
$$u'_y = u_y + \left(\langle u_y \rangle_{\mathrm{data}} - \langle u_y \rangle_{\mathrm{MC}} \right),$$

where $\langle u_{x,y} \rangle_{\text{data}}$ and $\langle u_{x,y} \rangle_{\text{MC}}$ are the mean values of these distributions in data and simulation, respectively. The corrections are evaluated in Z-boson events and parameterised as a function of ΣE_{T}^{*}. The effect of these corrections on the recoil ϕ distribution is illustrated in Fig. 11b.

The transverse momentum of Z bosons can be reconstructed from the decay-lepton pair with a resolution of 1–2 GeV, which is negligible compared to the recoil energy resolution. The recoil response can thus be calibrated from comparisons with the reconstructed $p_{\text{T}}^{\ell\ell}$ in data and simulation. Recoil energy scale and resolution corrections are derived in bins of ΣE_{T}^{*} and $p_{\text{T}}^{\ell\ell}$ at reconstruction level, and are applied in simulation as a function of the particle-level vector-boson momentum p_{T}^{V} in both the W- and Z-boson samples. The energy scale of the recoil is calibrated by comparing the $u_{\parallel}^{Z} + p_{\text{T}}^{\ell\ell}$ distribution in data and simulation, whereas resolution corrections are evaluated from the $u_{\perp}^{Z}$ distribution. Energy-scale corrections $b(p_{\text{T}}^{V}, \Sigma E_{\text{T}}^{*\prime})$ are defined as the difference between the average values of the $u_{\parallel}^{Z} + p_{\text{T}}^{\ell\ell}$ distributions in data and simulation, and the energy-resolution correction factors $r(p_{\text{T}}^{V}, \Sigma E_{\text{T}}^{*\prime})$ as the ratio of the standard deviations of the corresponding $u_{\perp}^{Z}$ distributions.

The parallel component of u_{T} in simulated events is corrected for energy scale and resolution, whereas the perpendicular component is corrected for energy resolution only. The corrections are defined as follows:

$$u_{\parallel}^{V,\text{corr}} = \left[u_{\parallel}^{V,\text{MC}} - \left\langle u_{\parallel}^{Z,\text{data}} \right\rangle (p_{\text{T}}^{V}, \Sigma E_{\text{T}}^{*\prime})\right] \cdot r(p_{\text{T}}^{V}, \Sigma E_{\text{T}}^{*\prime}) + \left\langle u_{\parallel}^{Z,\text{data}} \right\rangle (p_{\text{T}}^{V}, \Sigma E_{\text{T}}^{*\prime}) + b(p_{\text{T}}^{V}, \Sigma E_{\text{T}}^{*\prime}), \quad (5)$$

$$u_{\perp}^{V,\text{corr}} = u_{\perp}^{V,\text{MC}} \cdot r(p_{\text{T}}^{V}, \Sigma E_{\text{T}}^{*\prime}), \quad (6)$$

where $V = W, Z$, $u_{\parallel}^{V,\text{MC}}$ and $u_{\perp}^{V,\text{MC}}$ are the parallel and perpendicular components of u_{T} in the simulation, and $u_{\parallel}^{V,\text{corr}}$ and $u_{\perp}^{V,\text{corr}}$ are the corresponding corrected values. As for b and r, the average $\left\langle u_{\parallel}^{Z,\text{data}} \right\rangle$ is mapped as a function of the reconstructed $p_{\text{T}}^{\ell\ell}$ in Z-boson data, and used as a function of p_{T}^{V} in both W- and Z-boson simulation. Since the resolution of u_{T} has a sizeable dependence on the amount of pile-up, the correction procedure is defined in three bins of $\langle\mu\rangle$, corresponding to low, medium, and high pile-up conditions, and defined by the ranges of $\langle\mu\rangle \in [2.5, 6.5]$, $\langle\mu\rangle \in [6.5, 9.5]$, and $\langle\mu\rangle \in [9.5, 16.0]$, respectively. Values for $b(p_{\text{T}}^{V}, \Sigma E_{\text{T}}^{*\prime})$ are typically $O(100\,\text{MeV})$, and $r(p_{\text{T}}^{V}, \Sigma E_{\text{T}}^{*\prime})$ deviates from unity by 2% at most. The effect of the calibration is shown in Fig. 12 for $Z \to \mu\mu$ events. The level of agreement obtained after corrections is satisfactory, and similar performance is observed for $Z \to ee$ events.

A closure test of the applicability of Z-based corrections to W production is performed using W and Z samples simulated with POWHEG+HERWIG 6, which provide an alternative model for the description of hadronisation and the underlying event. The procedure described above is used to correct the recoil response from POWHEG+PYTHIA 8 to POWHEG+HERWIG 6, where the latter is treated as pseudo-data. As shown in Fig. 13, the corrected W recoil distributions in POWHEG+PYTHIA 8 match the corresponding distributions in POWHEG+HERWIG 6. For this study, the effect of the different particle-level p_{T}^{W} distributions in both samples is removed by reweighting the POWHEG+PYTHIA 8 prediction to POWHEG+HERWIG 6. This study is performed applying the standard lepton selection cuts, but avoiding further kinematic selections in order to maximize the statistics available for the test.

8.3 Systematic uncertainties

The recoil calibration procedure is sensitive to the following sources of systematic uncertainty: the uncertainty of the scale factor applied to the $\langle\mu\rangle$ distribution, uncertainties due to the Smirnov transform of the ΣE_{T}^{*} distribution, uncertainties in the correction of the average value of the $u_{x,y}$ distributions, statistical uncertainties in the residual correction factors and their p_{T} dependence, and expected differences in the recoil response between Z- and W-boson events.

The uncertainty from the $\langle\mu\rangle$ scale-factor α is evaluated by varying it by its uncertainty and repeating all steps of the recoil calibration procedure. These variations affect the determination of m_W by less than 1 MeV.

The systematic uncertainty related to the dependence of the ΣE_{T}^{*} correction on p_{T} is estimated by comparing with the results of a p_{T}-inclusive correction. This source contributes, averaging over W-boson charges, an uncertainty of approximately 1 MeV for the extraction of m_W from the p_{T}^{ℓ} distribution, and 11 MeV when using the m_{T} distribution.

The recoil energy scale and resolution corrections of Eqs. (5) and (6) are derived from the Z-boson sample and applied to W-boson events. Differences in the detector response to the recoil between W- and Z-boson processes are considered as a source of systematic uncertainty for these corrections. Differences between the $u_{\perp}^{W}$ and $u_{\perp}^{Z}$ distributions originating from different vector-boson kinematic properties, different ISR and FSR photon emission, and from different selection requirements are, however, discarded as they are either accurately modelled in the simulation or already incorporated in the correction procedure.

To remove the effect of such differences, the two-dimensional distribution $h_{\text{MC}}^{W}(p_{\text{T}}, \Sigma E_{\text{T}}^{*})$ in W-boson simulated events is corrected to match the corresponding distribution in Z-boson simulated events, treating the neutrinos in W-boson decays as charged leptons to calculate u_{T} as in Z-boson events. Finally, events containing a particle-level photon from final-state radiation are removed. After these corrections, the standard deviation of the $u_{\perp}$ distribution agrees within 0.03% between simulated W- and Z-boson

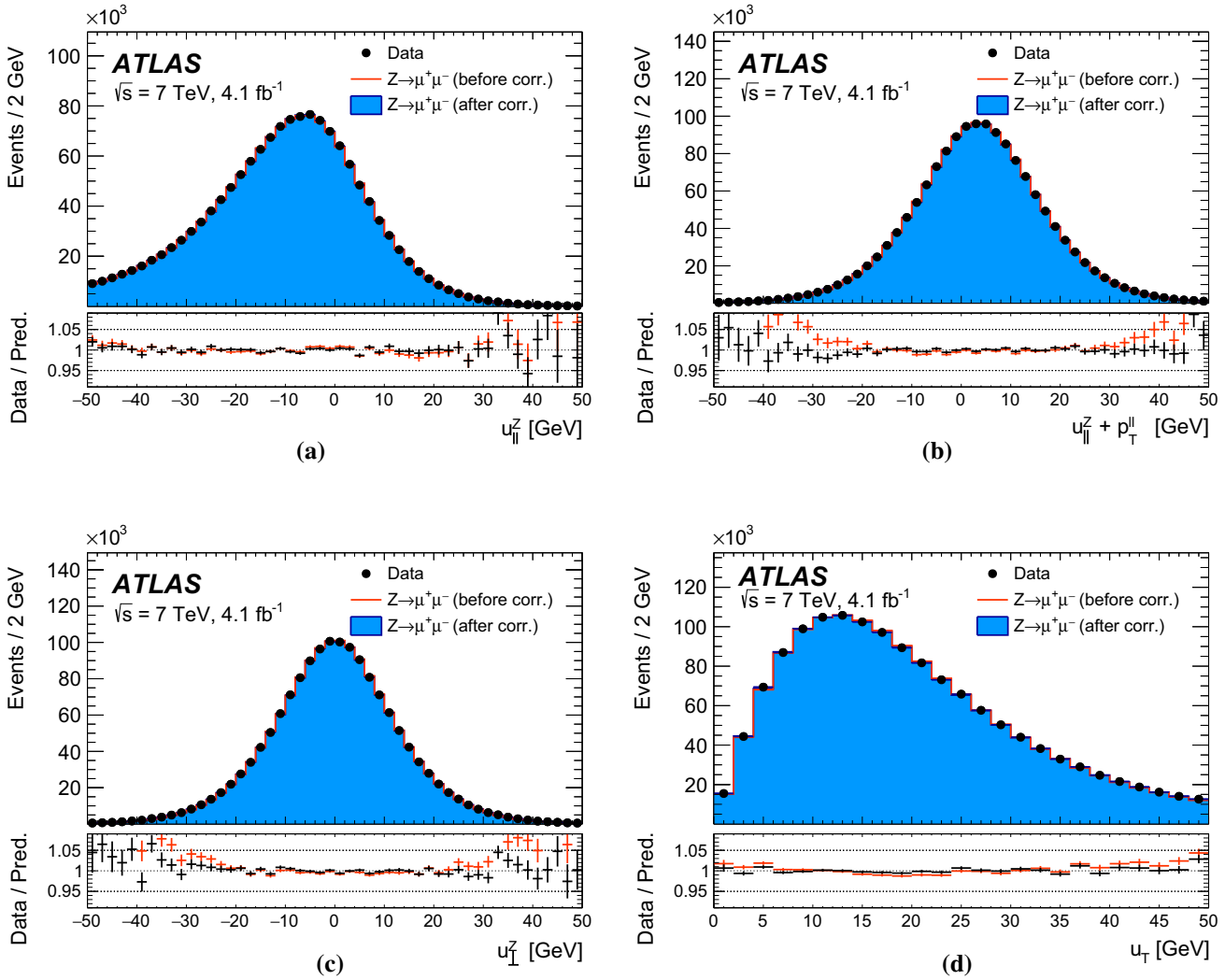

Fig. 12 Recoil distributions for **a** $u_{\parallel}^{Z}$, **b** $u_{\parallel}^{Z} + p_{\mathrm{T}}^{\ell\ell}$, (c) $u_{\perp}^{Z}$, and (d) u_{T} in $Z \to \mu\mu$ events. The data are compared to the simulation before and after applying the recoil corrections described in the text. The lower panels show the data-to-prediction ratios, with the vertical bars showing the statistical uncertainty

events. This difference is equivalent to 6% of the size of the residual resolution correction, which increases the standard deviation of the $u_{\perp}$ distribution by 0.5%. Accordingly, the corresponding systematic uncertainty due to the extrapolation of the recoil calibration from Z- to W-boson events is estimated by varying the energy resolution parameter r of Eqs. (5) and (6) by 6%. The impact of this uncertainty on the extraction of m_W is approximately 0.2 MeV for the p_{T}^{ℓ} distribution, and 5.1 MeV for the m_{T} distribution. The extrapolation uncertainty of the energy-scale correction b was found to be negligible in comparison.

In addition, the statistical uncertainty of the correction factors contributes 2.0 MeV for the p_{T}^{ℓ} distribution, and 2.7 MeV for the m_{T} distribution. Finally, instead of using a binned correction, a smooth interpolation of the correction values between the bins is performed. Comparing the binned and interpolated correction parameters $b(p_{\mathrm{T}}^{V}, \Sigma E_{\mathrm{T}}^{*\prime})$ and $r(p_{\mathrm{T}}^{V}, \Sigma E_{\mathrm{T}}^{*\prime})$ leads to a systematic uncertainty in m_W of 1.4 and 3.1 MeV for the p_{T}^{ℓ} and m_{T} distributions, respectively. Systematic uncertainties in the $u_{x,y}$ corrections are found to be small compared to the other systematic uncertainties, and are neglected.

The impact of the uncertainties of the recoil calibration on the extraction of the W-boson mass from the p_{T}^{ℓ} and m_{T} distributions are summarised in Table 6. The determination of m_W from the p_{T}^{ℓ} distribution is only slightly affected by the uncertainties of the recoil calibration, whereas larger uncertainties are estimated for the m_{T} distribution. The largest uncertainties are induced by the $\Sigma E_{\mathrm{T}}^{*}$ corrections and by the extrapolation of the recoil energy-scale and energy-resolution corrections from Z- to W-boson events. The systematic uncertainties are in general smaller for W^- events

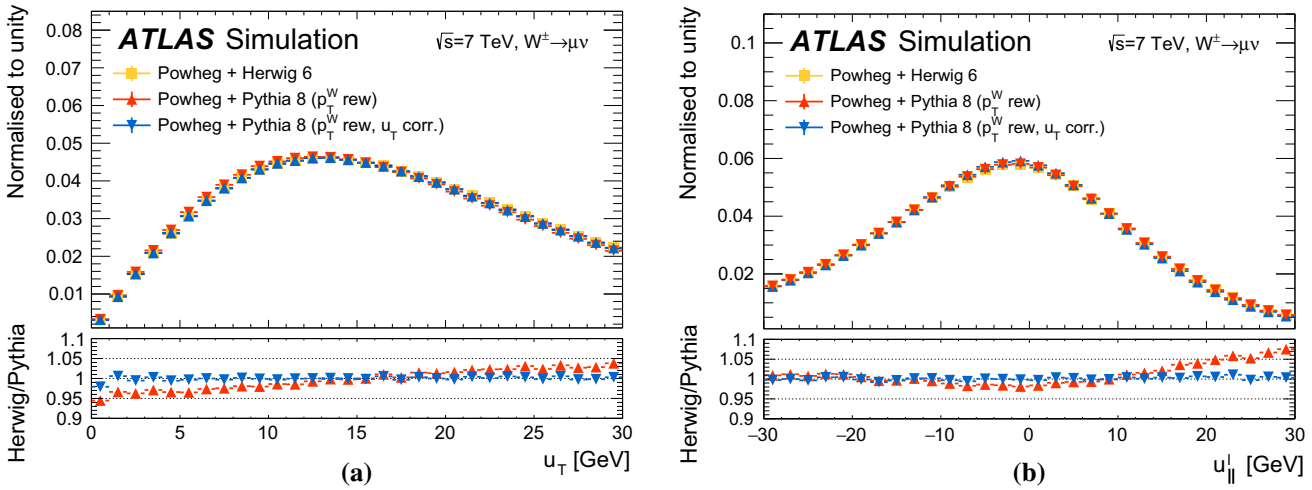

Fig. 13 Distributions of **a** u_{T} and **b** $u_{\parallel}^{\ell}$ in W events simulated using POWHEG+PYTHIA 8 and POWHEG+HERWIG 6. The recoil response in POWHEG+PYTHIA 8 is corrected to the POWHEG+HERWIG 6 response using simulated Z events following the method described in the text. The p_{T}^{W} distribution in POWHEG+PYTHIA 8 is reweighted to the POWHEG+HERWIG 6 prediction. The lower panels show the ratios of POWHEG+HERWIG 6 to POWHEG+PYTHIA 8, with and without the response correction in the POWHEG+PYTHIA 8 sample

Table 6 Systematic uncertainties in the m_W measurement due to recoil corrections, for the different kinematic distributions and W-boson charge categories. Combined uncertainties are evaluated as described in Sect. 2.2

W-boson charge	W^+		W^-		Combined	
Kinematic distribution	p_{T}^{ℓ}	m_{T}	p_{T}^{ℓ}	m_{T}	p_{T}^{ℓ}	m_{T}
δm_W [MeV]						
$\langle\mu\rangle$ scale factor	0.2	1.0	0.2	1.0	0.2	1.0
$\Sigma E_{\mathrm{T}}^{*}$ correction	0.9	12.2	1.1	10.2	1.0	11.2
Residual corrections (statistics)	2.0	2.7	2.0	2.7	2.0	2.7
Residual corrections (interpolation)	1.4	3.1	1.4	3.1	1.4	3.1
Residual corrections ($Z \to W$ extrapolation)	0.2	5.8	0.2	4.3	0.2	5.1
Total	2.6	14.2	2.7	11.8	2.6	13.0

than for W^+ events, as the $\Sigma E_{\mathrm{T}}^{*}$ distribution in W^- events is closer to the corresponding distribution in Z-boson events.

9 Consistency tests with Z-boson events

The $Z \to \ell\ell$ event sample allows several validation and consistency tests of the W-boson analysis to be performed. All the identification requirements of Sect. 5.1, the calibration and efficiency corrections of Sects. 7 and 8, as well as the physics-modelling corrections described in Sect. 6, are applied consistently in the W- and Z-boson samples. The Z-boson sample differs from the W-boson sample in the selection requirements, as described in Sect. 5.2. In addition to the event-selection requirements described there, the transverse momentum of the dilepton system, $p_{\mathrm{T}}^{\ell\ell}$, is required to be smaller than 30 GeV.

The missing transverse momentum in Z-boson events is defined by treating one of the two decay leptons as a neutrino and ignoring its transverse momentum when defining the event kinematics. This procedure allows the $p_{\mathrm{T}}^{\mathrm{miss}}$ and m_{T} variables to be defined in the Z-boson sample in close analogy to their definition in the W-boson sample. The procedure is repeated, removing the positive and negative lepton in turn.

In the Z-boson sample, the background contribution arising from top-quark and electroweak production is estimated using Monte Carlo samples. Each process is normalised using the corresponding theoretical cross sections, evaluated at NNLO in the perturbative expansion of the strong coupling constant. This background contributes a 0.12% fraction in each channel. In the muon channel, the background contribution from multijet events is estimated to be smaller than 0.05% using simulated event samples of $b\bar{b}$ and $c\bar{c}$ production, and neglected. In the electron channel, a data-driven estimate of the multijet background contributes about a 0.1% fraction, before applying the isolation selections, which reduce it to a negligible level.

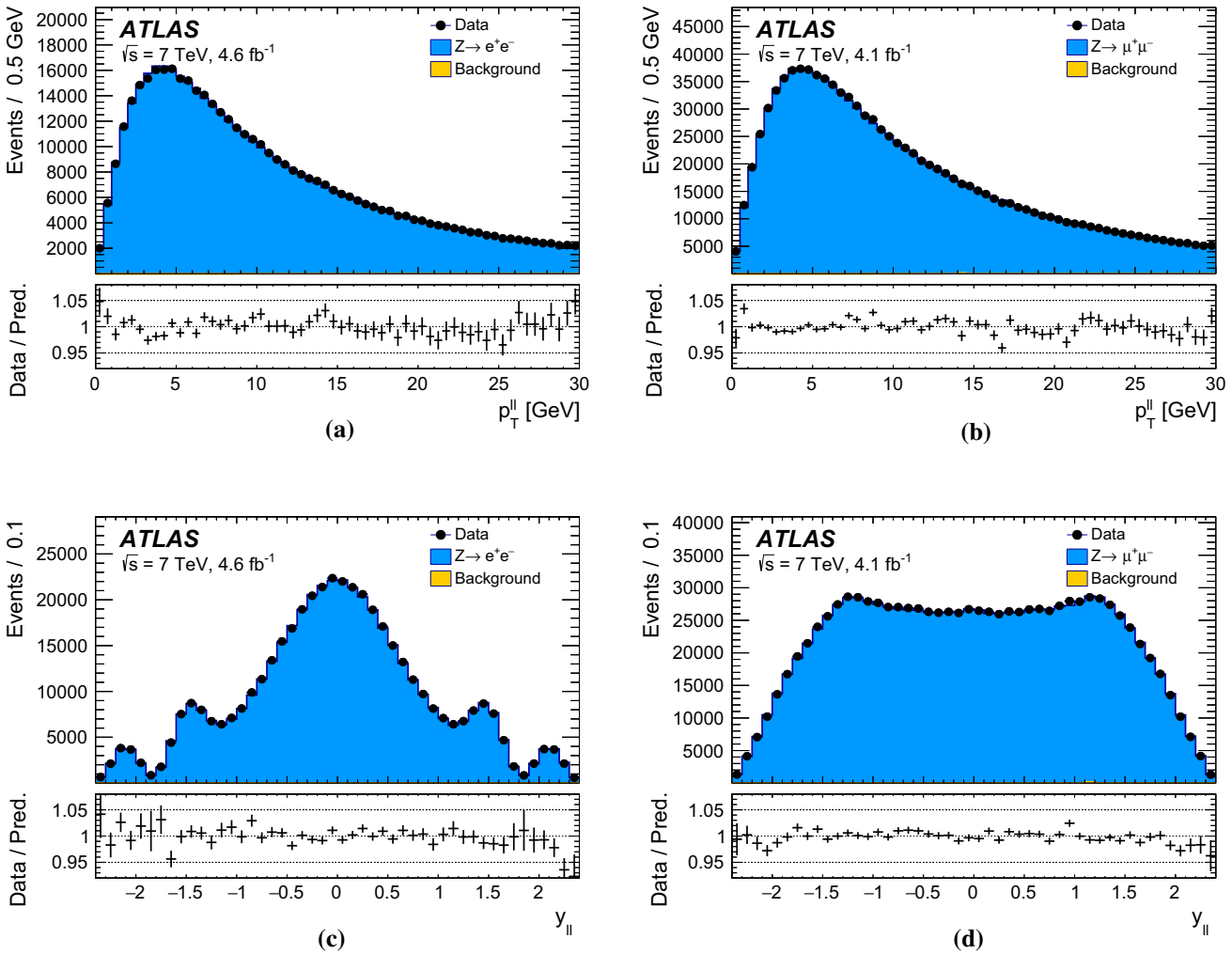

Fig. 14 The **a**, **b** $p_{\mathrm{T}}^{\ell\ell}$ and **c**, **d** $y_{\ell\ell}$ distributions in Z-boson events for the **a**, **c** electron and **b**, **d** muon decay channels. The data are compared to the simulation including signal and backgrounds. Detector calibration and physics-modelling corrections are applied to the simulated events. Background events contribute less than 0.2% of the observed distributions. The lower panels show the data-to-prediction ratios, with the error bars showing the statistical uncertainty

Figure 14 shows the reconstructed distributions of $p_{\mathrm{T}}^{\ell\ell}$ and $y_{\ell\ell}$ in selected Z-boson events; these distributions are not sensitive to the value of m_Z. Figure 15 shows the corresponding distributions for p_{T}^{ℓ} and m_{T}, variables which are sensitive to m_Z. Data and simulation agree at the level of 1–2% percent in all the distributions.

The mass of the Z boson is extracted with template fits to the $m_{\ell\ell}$, p_{T}^{ℓ}, and m_{T} kinematic distributions. The extraction of the Z-boson mass from the dilepton invariant mass distribution is expected to yield, by construction, the value of m_Z used as input for the muon-momentum and electron-energy calibrations, providing a closure test of the lepton calibration procedures. The p_{T}^{ℓ} distribution is very sensitive to the physics-modelling corrections described in Sect. 6. The comparison of the value of m_Z extracted from the p_{T}^{ℓ} distribution with the value used as input for the calibration tests the physics modelling and efficiency corrections. Finally, m_Z measurements from the m_{T} distribution provides a test of the recoil calibration.

Similarly to the W-boson mass, the value of m_Z is determined by minimising the χ^2 function of the compatibility test between the templates and the measured distributions. The templates are generated with values of m_Z in steps of 4 to 25 MeV within a range of ± 450 MeV, centred around a reference value corresponding to the LEP combined value, $m_Z = 91187.5$ MeV [32]. The χ^2 function is interpolated with a second order polynomial. The minimum of the χ^2 function yields the extracted value of m_Z, and the difference between the extracted value of m_Z and the reference value is defined as Δm_Z. The ranges used for the extraction are [80, 100] GeV for the $m_{\ell\ell}$ distributions, [30, 55] GeV for the p_{T}^{ℓ} distribution, and [40, 120] GeV for the m_{T} distribution.

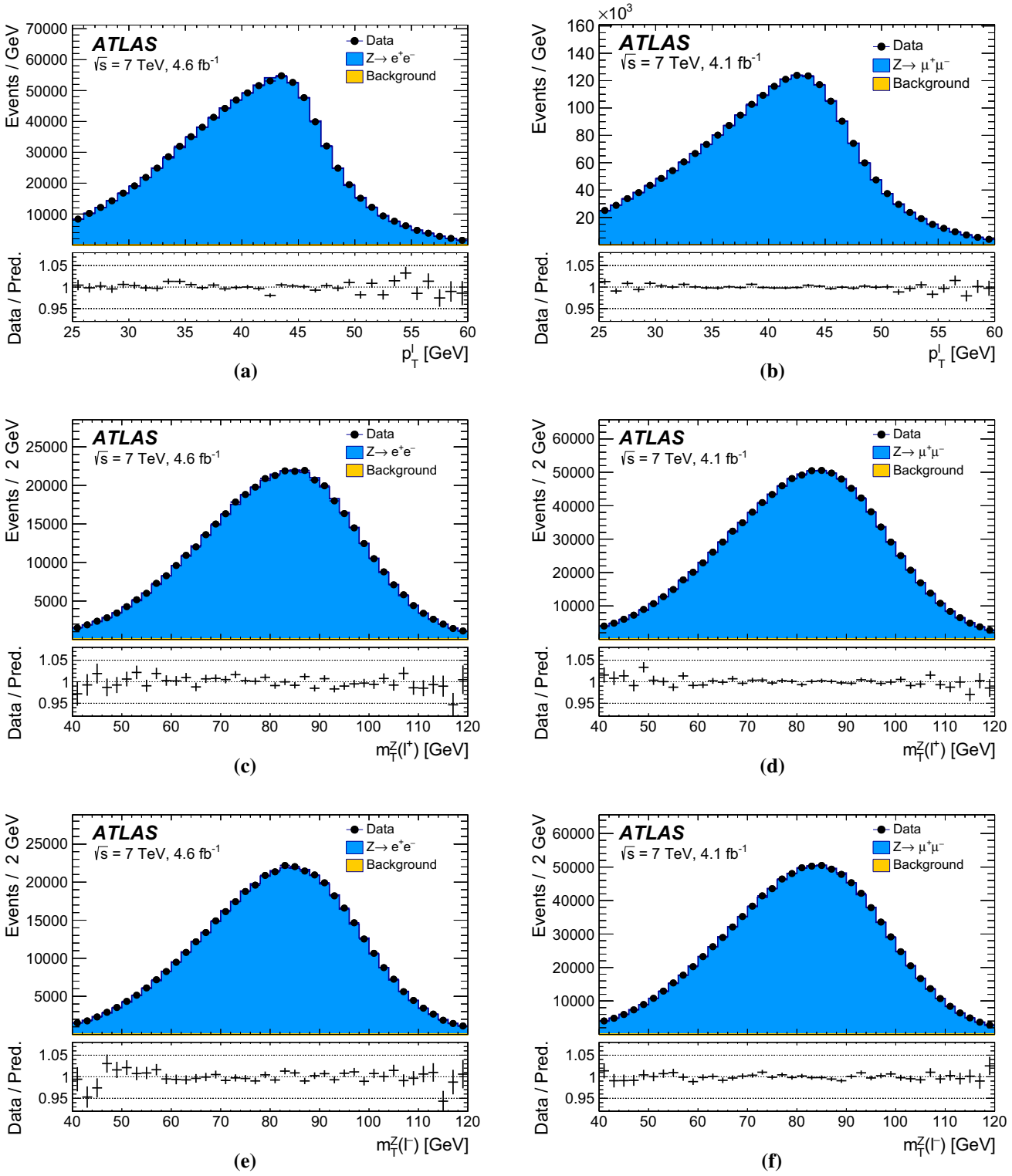

Fig. 15 The p_{T}^{ℓ} distribution in the **a** electron and **b** muon channels, and m_{T} distributions in the **c**, **e** electron and **d**, **f** muon decay channels for Z events when the **c**, **d** negatively charged, or **e**, **f** positively charged lepton is removed. The data are compared to the simulation including signal and backgrounds. Detector calibration and physics-modelling corrections are applied to the simulated events. Background events contribute less than 0.2% of the observed distributions. The lower panels show the data-to-prediction ratios, with the error bars showing the statistical uncertainty

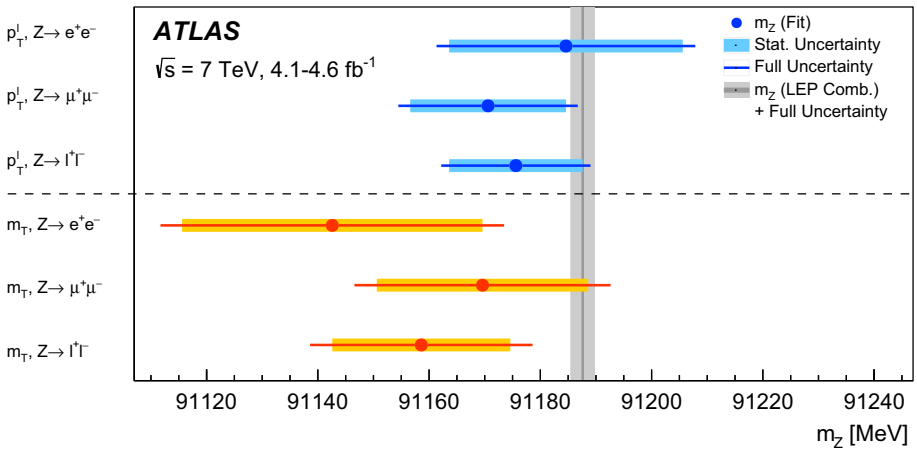

Fig. 16 Summary of the m_Z determinations from the p_{T}^{ℓ} and m_{T} distributions in the muon and electron decay channels. The LEP combined value of m_Z, which is used as input for the detector calibration, is also indicated. The horizontal and vertical bands show the uncertainties of the m_Z determinations and of the LEP combined value, respectively

Table 7 Difference between Z-boson mass, extracted from p_{T}^{ℓ} and m_{T} distributions, and the LEP combined value. The results are shown separately for the electron and muon decay channels, and their combination. The first quoted uncertainty is statistical, the second is the experimental systematic uncertainty, which includes lepton efficiency and recoil calibration uncertainties where applicable. Physics-modelling uncertainties are neglected

Lepton charge	ℓ^+		ℓ^-		Combined	
Kinematic distribution	p_{T}^{ℓ}	m_{T}	p_{T}^{ℓ}	m_{T}	p_{T}^{ℓ}	m_{T}
Δm_Z [MeV]						
$Z \to ee$	$13 \pm 31 \pm 10$	$-93 \pm 38 \pm 15$	$-20 \pm 31 \pm 10$	$4 \pm 38 \pm 15$	$-3 \pm 21 \pm 10$	$-45 \pm 27 \pm 15$
$Z \to \mu\mu$	$1 \pm 22 \pm 8$	$-35 \pm 28 \pm 13$	$-36 \pm 22 \pm 8$	$-1 \pm 27 \pm 13$	$-17 \pm 14 \pm 8$	$-18 \pm 19 \pm 13$
Combined	$5 \pm 18 \pm 6$	$-58 \pm 23 \pm 12$	$-31 \pm 18 \pm 6$	$1 \pm 22 \pm 12$	$-12 \pm 12 \pm 6$	$-29 \pm 16 \pm 12$

The extraction of m_Z from the m_{T} distribution is performed separately for positively and negatively charged leptons in the event, by reconstructing m_{T} from the kinematic properties of one of the two charged leptons and of the recoil reconstructed by treating the other as a neutrino.

Z-boson mass fits are performed using the m_{T} and p_{T}^{ℓ} distributions in the electron and muon decay channels, inclusively in η and separately for positively and negatively charged leptons. The results of the fits are summarised in Fig. 16 and Table 7. The p_{T}^{ℓ} fit results include all lepton reconstruction systematic uncertainties except the Z-based energy or momentum scale calibration uncertainties; the m_{T} fit results include recoil calibration systematic uncertainties in addition. Physics-modelling uncertainties are neglected.

The value of m_Z measured from positively charged leptons is correlated with the corresponding extraction from the negatively charged leptons. The p_{T}^{ℓ} distributions for positively and negatively charged leptons are statistically independent, but the m_{T} distributions share the same reconstructed recoil event by event, and are statistically correlated. In both cases, the decay of the Z-boson induces a kinematical correlation between the distributions of positively and negatively charged leptons. The correlation is estimated by constructing two-dimensional ℓ^+ and ℓ^- distributions, separately for p_{T}^{ℓ} and m_{T}, fluctuating the bin contents of these distributions within their uncertainties, and repeating the fits for each pseudodata sample. The correlation values are -7% for the p_{T}^{ℓ} distributions, and -12% for the m_{T} distributions.

Accounting for the experimental uncertainties as described above, the combined extraction of m_Z from the p_{T}^{ℓ} distribution yields a result compatible with the reference value within 0.9 standard deviations. The difference between the m_Z extractions from positively and negatively charged lepton distributions is compatible with zero within 1.4 standard deviations. For the extraction from the m_{T} distribution, the compatibility with the reference value of m_Z is at the level of 1.5 standard deviations. Fits using the lepton pair invariant mass distribution agree with the reference, yielding $\Delta m_Z = 1 \pm 3$ MeV in the muon channel and $\Delta m_Z = 3 \pm 5$ MeV in the electron channel, as expected from the calibration procedure. In summary, the consistency tests based on the Z-boson sample agree with the expectations within the experimental uncertainties.

10 Backgrounds in the W-boson sample

The W-boson event sample, selected as described in Sect. 5.2, includes events from various background processes. Background contributions from Z-boson, $W \to \tau\nu$, boson pair, and top-quark production are estimated using simulation.

Contributions from multijet production are estimated with data-driven techniques.

10.1 Electroweak and top-quark backgrounds

The dominant sources of background contribution in the $W \to \ell\nu$ sample are $Z \to \ell\ell$ events, in which one of the two leptons escapes detection, and $W \to \tau\nu$ events, where the τ decays to an electron or muon. These background contributions are estimated using the POWHEG+PYTHIA 8 samples after applying the modelling corrections discussed in Sect. 6, which include NNLO QCD corrections to the angular coefficients and rapidity distributions, and corrections to the vector-boson transverse momentum. The $Z \to ee$ background represents 2.9% of the $W^+ \to e\nu$ sample and 4.0% of the $W^- \to e\nu$ sample. In the muon channel, the $Z \to \mu\mu$ background represents 4.8 and 6.3% of the $W^+ \to \mu\nu$ and $W^- \to \mu\nu$ samples, respectively. The $W \to \tau\nu$ background represents 1.0% of the selected sample in both channels, and the $Z \to \tau\tau$ background contributes approximately 0.12%. The normalisation of these processes relative to the W-boson signal and the corresponding uncertainties are discussed in Sect. 4. A relative uncertainty of 0.2% is assigned to the normalisation of the $W \to \tau\nu$ samples with respect to the W-boson signal sample, to account for the uncertainty in the τ-lepton branching fractions to electrons and muons. In the determination of the W-boson mass, the variations of m_W are propagated to the $W \to \tau\nu$ background templates in the same way as for the signal.

Similarly, backgrounds involving top-quark (top-quark pairs and single top-quark) production, and boson-pair production are estimated using simulation, and normalisation uncertainties are assigned as discussed in Sect. 4. These processes represent 0.11 and 0.07% of the signal event selection, respectively.

Uncertainties in the distributions of the $W \to \tau\nu$ and $Z \to \ell\ell$ processes are described by the physics-modelling uncertainties discussed in Sect. 6, and are treated as fully correlated with the signal. Shape uncertainties for boson-pair production and top-quark production are considered negligible compared to the uncertainties in their cross sections, given the small contributions of these processes to the signal event selection.

10.2 Multijet background

Inclusive multijet production in strong-interaction processes constitutes a significant source of background. A fraction of multijet events contains semileptonic decays of bottom and charm hadrons to muons or electrons and neutrinos, and can pass the W-boson signal selection. In addition, inclusive jet production contributes to the background if one jet is misidentified as electron or muon, and sizeable missing transverse momentum is reconstructed in the event. In-flight decays of pions or kaons within the tracking region can mimic the W-boson signal in the muon channel. In the electron channel, events with photon conversions and hadrons misidentified as electrons can be selected as W-boson events. Due to the small selection probability for multijet events, their large production cross section, and the relatively complex modelling of the hadronisation processes, the multijet background contribution cannot be estimated precisely using simulation, and a data-driven method is used instead.

The estimation of the multijet background contribution follows similar procedures in the electron and muon decay channels, and relies on template fits to kinematic distributions in background-dominated regions. The analysis uses the distributions of $p_{\mathrm{T}}^{\mathrm{miss}}$, m_{T}, and the $p_{\mathrm{T}}^{\ell}/m_{\mathrm{T}}$ ratio, where jet-enriched regions are obtained by relaxing a subset of the signal event-selection requirements. The first kinematic region, denoted FR1, is defined by removing the $p_{\mathrm{T}}^{\mathrm{miss}}$ and m_{T} requirements from the event selection. A second kinematic region, FR2, is defined in the same way as FR1, but by also removing the requirement on u_{T}. Multijet background events, which tend to have smaller values of $p_{\mathrm{T}}^{\mathrm{miss}}$ and m_{T} than the signal, are enhanced by this selection. The $p_{\mathrm{T}}^{\ell}/m_{\mathrm{T}}$ distribution is sensitive to the angle between the p_{T}^{ℓ} and $p_{\mathrm{T}}^{\mathrm{miss}}$ vectors in the transverse plane. Whereas W-boson events are expected to peak at values of $p_{\mathrm{T}}^{\ell}/m_{\mathrm{T}} = 0.5$, relatively large tails are observed for multijet events.

Templates of the multijet background distributions for these observables are obtained from data by inverting the lepton energy-isolation requirements. Contamination of these control regions by electroweak and top production is estimated using simulation and subtracted. In the muon channel, the anti-isolation requirements are defined from the ratio of the scalar sum of the p_{T} of tracks in a cone of size $\Delta R < 0.2$ around the reconstructed muon to the muon p_{T}. The isolation variable $p_{\mathrm{T}}^{\mu,\mathrm{cone}}$, introduced in Sect. 5.1, is required to satisfy $c_1 < p_{\mathrm{T}}^{\mu,\mathrm{cone}}/p_{\mathrm{T}}^{\ell} < c_2$, where the anti-isolation boundaries c_1 and c_2 are varied as discussed below. In order to avoid overlap with the signal region, the lower boundary c_1 is always larger than 0.1. In the electron channel, the scalar sum of the p_{T} of tracks in a cone of size $\Delta R < 0.4$ around the reconstructed electron, defined as $p_{\mathrm{T}}^{e,\mathrm{cone}}$ in Sect. 5.1, is used to define the templates, while the requirements on the calorimeter isolation are omitted.

The multijet background normalisation is determined by fitting each of the $p_{\mathrm{T}}^{\mathrm{miss}}$, m_{T}, and $p_{\mathrm{T}}^{\ell}/m_{\mathrm{T}}$ distributions in the two kinematic regions FR1 and FR2, using templates of these distributions based on multijet events and obtained with several ranges of the anti-isolation variables. The multijet background in the signal region is determined by correcting the multijet fraction fitted in the FR1 and FR2 for the different

efficiencies of the selection requirements of the signal region. In the electron channel, c_1 is varied from 4 to 9 GeV in steps of 1 GeV, and c_2 is set to $c_2 = c_1 + 1\,\text{GeV}$. In the muon channel, c_1 is varied from 0.1 to 0.37 in steps of 0.03, and c_2 is set to $c_2 = c_1 + 0.03$. Example results of template fits in the electron and muon channels are shown in Fig. 17. The results corresponding to the various observables and to the different kinematic regions are linearly extrapolated in the isolation variables to the signal regions, denoted by $c_1 = 0$. Figure 18 illustrates the extrapolation procedure.

The systematic uncertainty in the multijet background fraction is defined as half of the largest difference between the results extrapolated from the different kinematic regions and observables. The multijet background contribution is estimated separately in all measurement categories. In the electron channel, the multijet background fraction rises from $0.58 \pm 0.08\%$ at low $|\eta_\ell|$ to $1.73 \pm 0.19\%$ in the last measurement bin, averaging the W^+ and W^- channels. In the muon channel, the charge-averaged multijet background fraction decreases from $0.72 \pm 0.07\%$ to $0.49 \pm 0.03\%$, when going from low to high $|\eta_\ell|$. The uncertainties in the multijet background fractions are sufficient to account for the observed residual discrepancies between the fitted distributions and the data (see Fig. 17). The estimated multijet background yields are consistent between W^+ and W^-, but the multijet background fraction is smaller in the W^+ channels due to the higher signal yield.

Corrections to the shape of the multijet background contributions and corresponding uncertainties in the distributions used to measure the W-boson mass are estimated with a similar procedure. The kinematic distributions in the control regions are obtained for a set of anti-isolation ranges, and parameterised with linear functions of the lower bound of the anti-isolation requirement. The distributions are extrapolated to the signal regions accordingly. Uncertainties in the extrapolated distributions are dominated by the statistical uncertainty, which is determined with a toy MC method by fluctuating within their statistical uncertainty the bin contents of the histograms in the various anti-isolation ranges. The resulting multijet background distribution is propagated to the templates, and the standard deviation of the determined values of m_W yields the estimated uncertainty due to the shape of the multijet background. Uncertainties due to the choice of parameterisation are small in comparison and neglected.

Uncertainties in the normalisation of multijet, electroweak, and top-quark background processes are considered correlated across decay channels, boson charges and rapidity bins, whereas the uncertainty in the shape of multijet background is considered uncorrelated between decay channels and boson charges. The impact of the background systematic uncertainties on the determination of m_W is summarised in Table 8.

11 Measurement of the W-boson mass

This section presents the determination of the mass of the W boson from template fits to the kinematic distributions of the W-boson decay products. The final measured value is obtained from the combination of measurements performed using the lepton transverse momentum and transverse mass distributions in categories corresponding to the electron and muon decay channels, positively and negatively charged W bosons, and absolute pseudorapidity bins of the charged lepton, as illustrated in Table 1. The number of selected events in each category is shown in Table 9.

11.1 Control distributions

The detector calibration and the physics modelling are validated by comparing data with simulated W-boson signal and backgrounds for several kinematic distributions that are insensitive to the W-boson mass. The comparison is based on a χ^2 compatibility test, including statistical and systematic uncertainties, and the bin-to-bin correlations induced by the latter. The systematic uncertainty comprises all sources of experimental uncertainty related to the lepton and recoil calibration, and to the background subtraction, as well as sources of modelling uncertainty associated with electroweak corrections, or induced by the helicity fractions of vector-boson production, the vector-boson transverse-momentum distribution, and the PDFs. Comparisons of data and simulation for the η_ℓ, u_T, and $u_\parallel^\ell$ distributions, in positively and negatively charged W-boson events, are shown in Figs. 19 and 20 for the electron and muon decay channels, respectively.

Data and simulation agree within uncertainties for all distributions, as confirmed by the satisfactory χ^2/dof values. The effect of the residual discrepancies in the u_T distributions for $W^- \to \ell\nu$, visible at low values in Figs. 19d and 20d, is discussed in Sect. 11.5.

11.2 Data-driven check of the uncertainty in the p_T^W distribution

The uncertainty in the prediction of the $u_\parallel^\ell$ distribution is dominated by p_T^W distribution uncertainties, especially at negative values of $u_\parallel^\ell$ in the kinematic region corresponding to $u_\parallel^\ell < -15\,\text{GeV}$. This is illustrated in Fig. 21, which compares the recoil distributions in the POWHEG+PYTHIA 8 and POWHEG+HERWIG 6 samples, before and after the corrections described in Sect. 8.2 (the p_T^W distribution predicted by POWHEG+PYTHIA 8 is not reweighted to that of POWHEG+HERWIG 6). As can be seen, the recoil corrections and the different p_T^W distributions have a comparable effect on the u_T distribution. In contrast, the effect of the recoil corrections is small at negative values of $u_\parallel^\ell$, whereas the

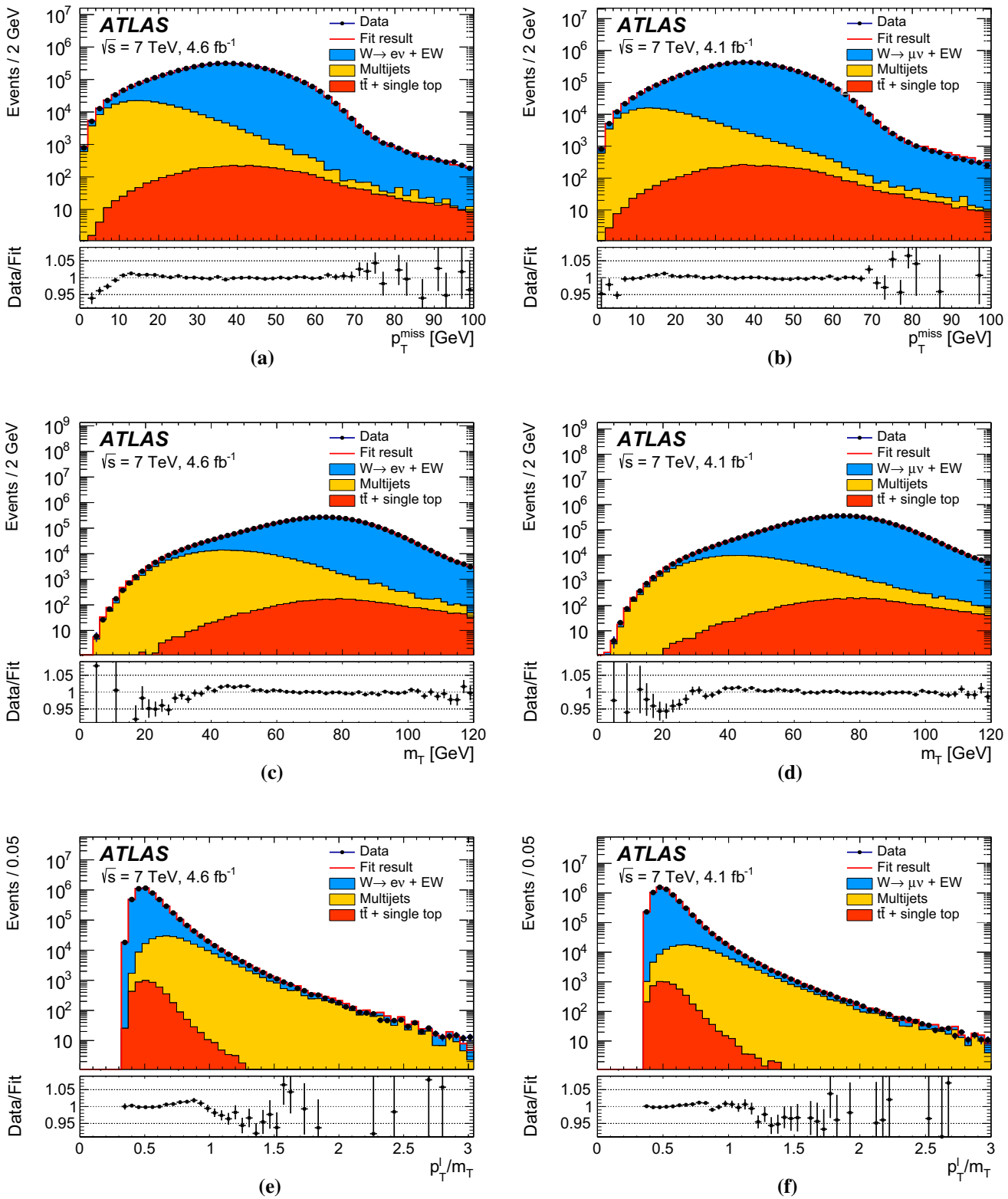

Fig. 17 Example template fits to the **a**, **b** $p_{\mathrm{T}}^{\mathrm{miss}}$, **c**, **d** m_{T}, and **e**, **f** $p_{\mathrm{T}}^{\ell}/m_{\mathrm{T}}$ distributions in the FR1 kinematic region, in the **a**, **c**, **e** electron and **b**, **d**, **f** muon decay channels. Multijet templates are derived from the data requiring $4\,\mathrm{GeV} < p_{\mathrm{T}}^{e,\mathrm{cone}} < 8\,\mathrm{GeV}$ in the electron channel, and $0.2 < p_{\mathrm{T}}^{\mu,\mathrm{cone}}/p_{\mathrm{T}}^{\ell} < 0.4$ in the muon channel. The data are compared to the simulation including signal and background contributions

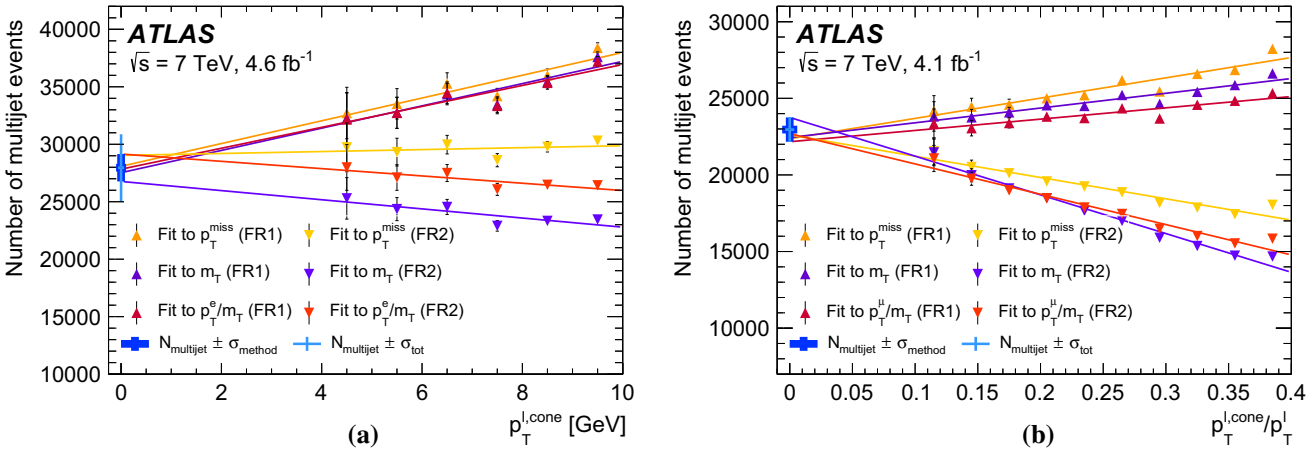

Fig. 18 Estimated number of multijet-background events as a function of the lower bound of the isolation-variable range used to define the control regions, for **a** electron and **b** muon decay channel. The estimation is performed for the two regions FR1 and FR2 and three distributions $p_{\mathrm{T}}^{\mathrm{miss}}$, m_{T}, and $p_{\mathrm{T}}^{\ell}/m_{\mathrm{T}}$, as described in the text. The linear extrapolations are indicated by the solid lines. The thick crosses show the results of the linear extrapolation of the background estimate to the signal region, including uncertainties from the extrapolation only. The thin crosses also include the uncertainty induced by the contamination of the control regions by EW and top-quark processes

Table 8 Systematic uncertainties in the m_W measurement due to electroweak, top-quark, and multijet background estimation, for fits to the p_{T}^{ℓ} and m_{T} distributions, in the electron and muon decay channels, with positively and negatively charged W bosons

Kinematic distribution	p_{T}^{ℓ}				m_{T}			
Decay channel	$W \to e\nu$		$W \to \mu\nu$		$W \to e\nu$		$W \to \mu\nu$	
W-boson charge	W^+	W^-	W^+	W^-	W^+	W^-	W^+	W^-
δm_W [MeV]								
$W \to \tau\nu$ (fraction, shape)	0.1	0.1	0.1	0.2	0.1	0.2	0.1	0.3
$Z \to ee$ (fraction, shape)	3.3	4.8	–	–	4.3	6.4	–	–
$Z \to \mu\mu$ (fraction, shape)	–	–	3.5	4.5	–	–	4.3	5.2
$Z \to \tau\tau$ (fraction, shape)	0.1	0.1	0.1	0.2	0.1	0.2	0.1	0.3
WW, WZ, ZZ (fraction)	0.1	0.1	0.1	0.1	0.4	0.4	0.3	0.4
Top (fraction)	0.1	0.1	0.1	0.1	0.3	0.3	0.3	0.3
Multijet (fraction)	3.2	3.6	1.8	2.4	8.1	8.6	3.7	4.6
Multijet (shape)	3.8	3.1	1.6	1.5	8.6	8.0	2.5	2.4
Total	6.0	6.8	4.3	5.3	12.6	13.4	6.2	7.4

Table 9 Numbers of selected W^+ and W^- events in the different decay channels in data, inclusively and for the various $|\eta_\ell|$ categories

$\lvert\eta_\ell\rvert$ range	0–0.8	0.8–1.4	1.4–2.0	2.0–2.4	Inclusive
$W^+ \to \mu^+\nu$	1 283 332	1 063 131	1 377 773	885 582	4 609 818
$W^- \to \mu^-\bar{\nu}$	1 001 592	769 876	916 163	547 329	3 234 960
$\lvert\eta_\ell\rvert$ range	0–0.6	0.6–1.2		1.8–2.4	Inclusive
$W^+ \to e^+\nu$	1 233 960	1 207 136		956 620	3 397 716
$W^- \to e^-\bar{\nu}$	969 170	908 327		610 028	2 487 525

difference in the p_{T}^{W} distributions has a large impact in this region.

The sensitivity of the $u_{\parallel}^{\ell}$ distribution is exploited to validate the modelling of the p_{T}^{W} distribution by PYTHIA 8 AZ, and its theory-driven uncertainty, described in Sect. 6.5.2, with a data-driven procedure. The parton-shower factorisation scale μ_{F} associated with the $c\bar{q} \to W$ processes constitutes the main source of uncertainty in the modelling of the p_{T}^{W} distribution. Variations of the $u_{\parallel}^{\ell}$ distribution induced by changes in the factorisation scale of the $c\bar{q} \to W$ processes are parameterised and fitted to the data. The $u_{\parallel}^{\ell}$ distribution is predicted for the two boundary values of μ_{F}, and assumed to vary linearly as a function of μ_{F}. Variations induced by changes in μ_{F} are parameterised using a variable

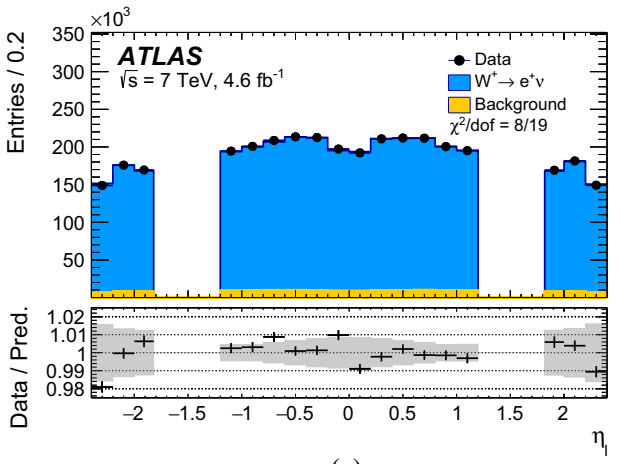

(a)

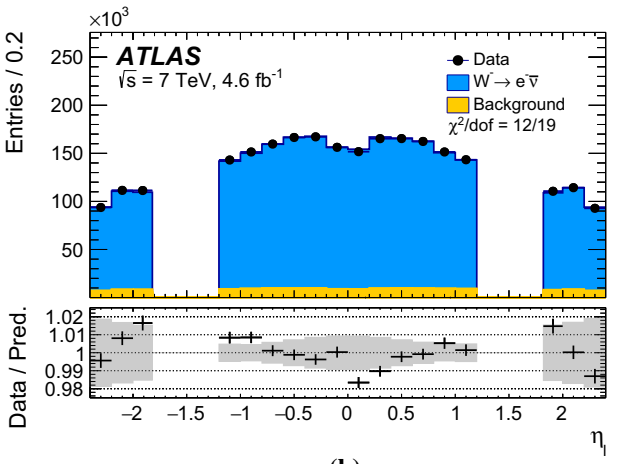

(b)

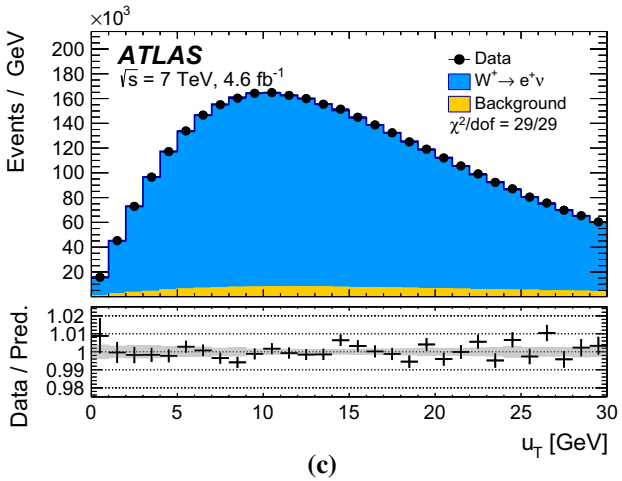

(c)

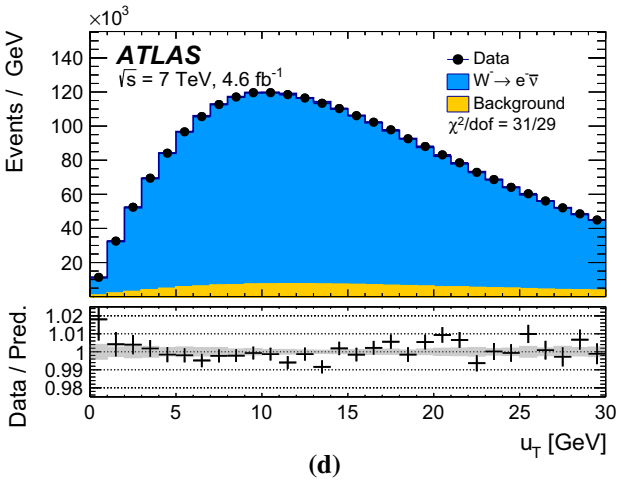

(d)

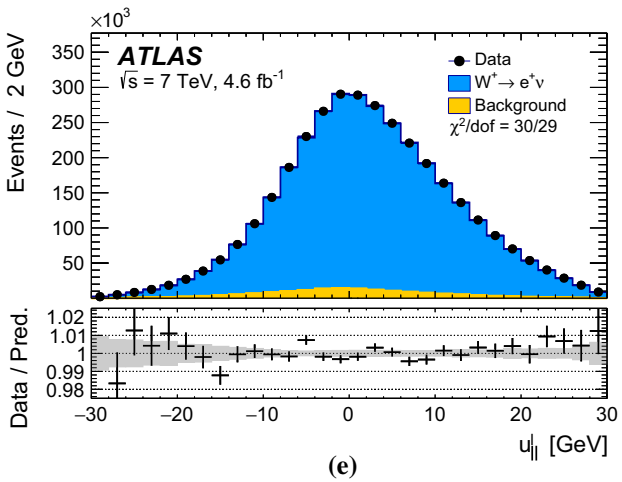

(e)

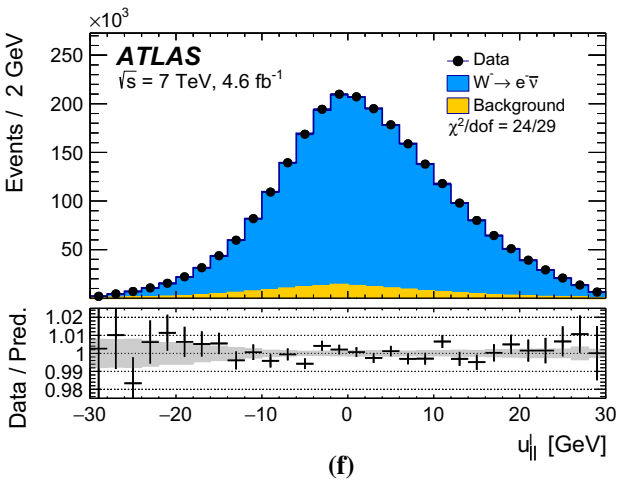

(f)

Fig. 19 The **a**, **b** η_ℓ, (c,d) u_{T}, and **e**, **f** $u_\parallel^\ell$ distributions for **a**, **c**, **e** W^+ events and **b**, **d**, **f** W^- events in the electron decay channel. The data are compared to the simulation including signal and background contributions. Detector calibration and physics-modelling corrections are applied to the simulated events. The lower panels show the data-to-prediction ratios, the error bars show the statistical uncertainty, and the band shows the systematic uncertainty of the prediction. The χ^2 values displayed in each figure account for all sources of uncertainty and include the effects of bin-to-bin correlations induced by the systematic uncertainties

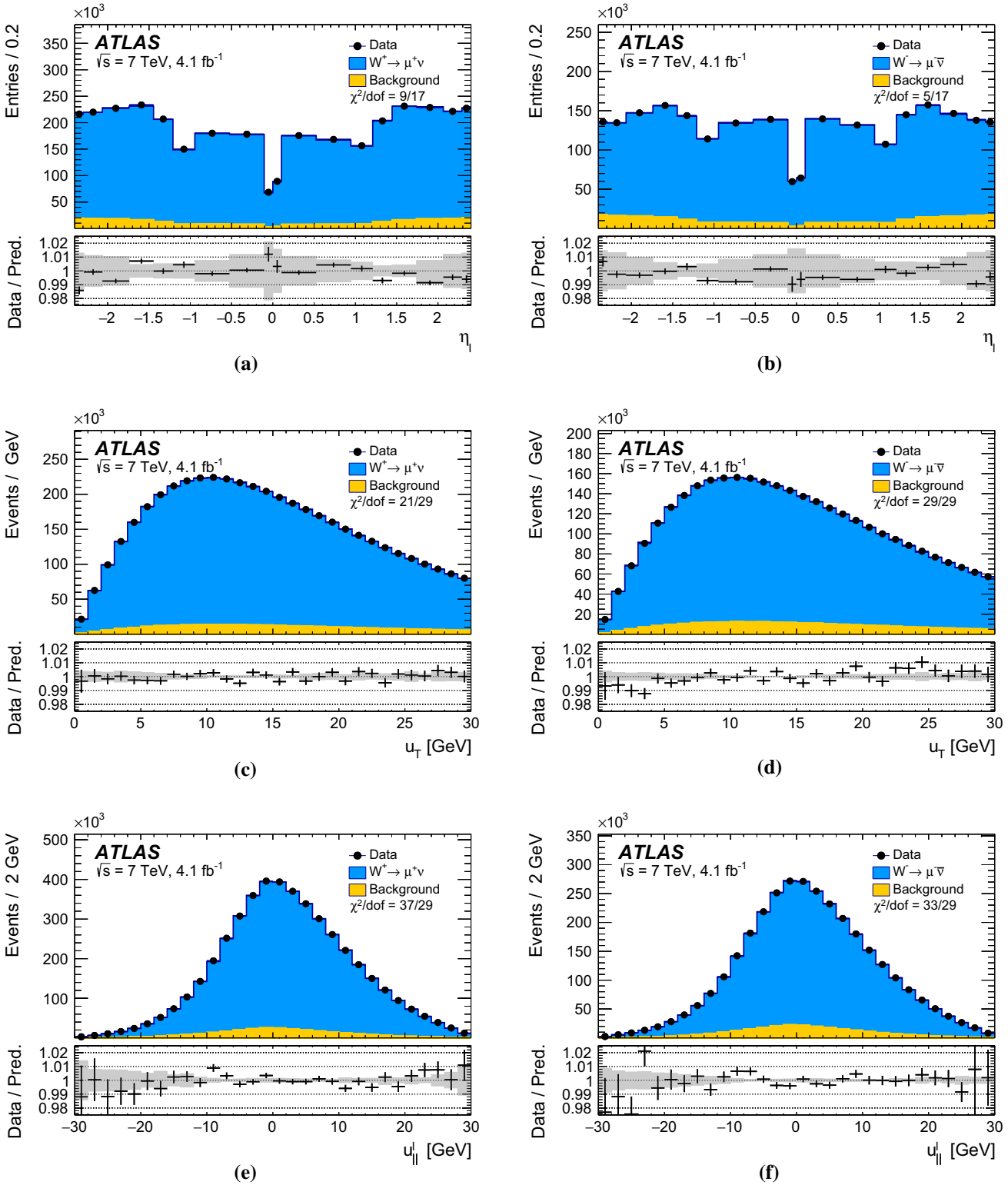

Fig. 20 The **a**, **b** η_ℓ, (c,d) u_{T}, and **e**, **f** $u_\parallel^\ell$ distributions for **a**, **c**, **e** W^+ events and **b**, **d**, **f** W^- events in the muon decay channel. The data are compared to the simulation including signal and background contributions. Detector calibration and physics-modelling corrections are applied to the simulated events. The lower panels show the data-to-prediction ratios, the error bars show the statistical uncertainty, and the band shows the systematic uncertainty of the prediction. The χ^2 values displayed in each figure account for all sources of uncertainty and include the effects of bin-to-bin correlations induced by the systematic uncertainties

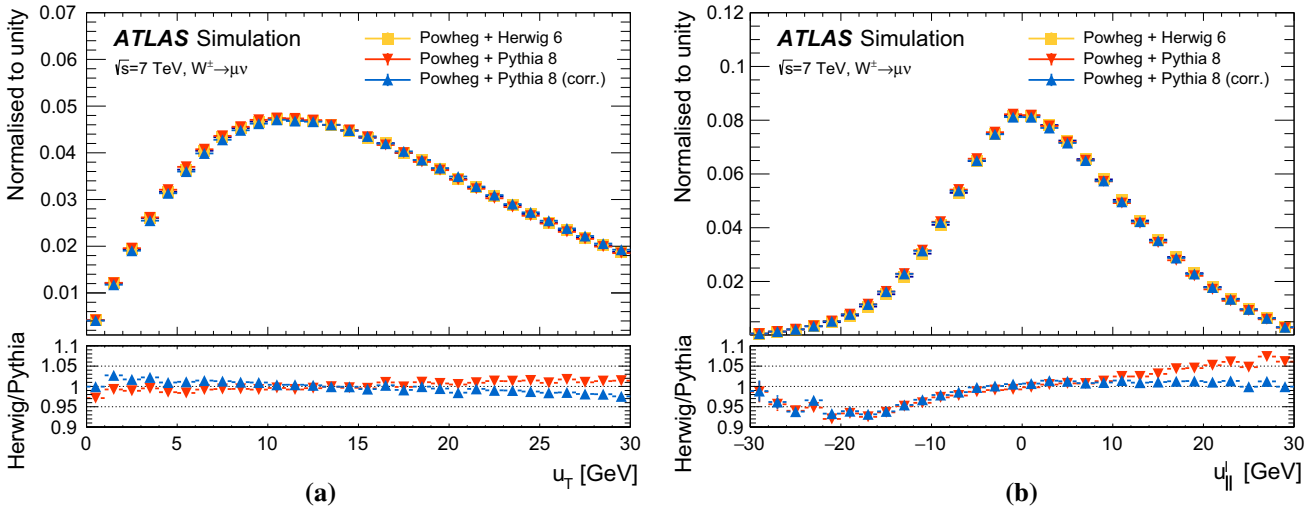

Fig. 21 Distributions of **a** u_{T} and **b** $u_{\parallel}^{\ell}$ in $W \to \mu\nu$ events simulated using POWHEG+PYTHIA 8 and POWHEG+HERWIG 6 after all analysis selection cuts are applied. The POWHEG+PYTHIA 8 distributions are shown before and after correction of the recoil response to that of POWHEG+HERWIG 6. The lower panels show the ratios of POWHEG+HERWIG 6 to POWHEG+PYTHIA 8, with and without the recoil response correction in the POWHEG+PYTHIA 8 sample. The discrepancy remaining after recoil corrections reflects the different p_{T}^{W} distributions

s defined in units of the initially allowed range, i.e. values of $s = -1, 0, +1$ correspond to half the effect[3] of changing from $\mu_{\mathrm{F}} = m_V$ to $\mu_{\mathrm{F}} = m_V/2, m_V, 2m_V$ respectively. The optimal value of s is determined by fitting the fraction of events in the kinematic region $-30 < u_{\parallel}^{\ell} < -15\,\mathrm{GeV}$. The fit accounts for all experimental and modelling uncertainties affecting the $u_{\parallel}^{\ell}$ distribution, and gives a value of $s = -0.22 \pm 1.06$. The best-fit value of s confirms the good agreement between the the PYTHIA 8 AZ prediction and the data; its uncertainty is dominated by PDF and recoil-calibration uncertainties, and matches the variation range of μ_{F} used for the initial estimation of the p_{T}^{W} distribution uncertainty.

This validation test supports the PYTHIA 8 AZ prediction of the p_{T}^{W} distribution and the theory-driven associated uncertainty estimate. On the other hand, as shown in Fig. 22, the data disagree with the DYRes and POWHEG MiNLO+PYTHIA 8 predictions. The latter are obtained reweighting the initial p_{T}^{W} distribution in POWHEG+PYTHIA 8 according to the product of the p_{T}^{Z} distribution of PYTHIA 8 AZ, which matches the measurement of Ref. [44], and $R_{W/Z}(p_{\mathrm{T}})$ as predicted by DYRes and POWHEG MiNLO+PYTHIA 8. The uncertainty bands in the DYRes prediction are calculated using variations of the factorisation, renormalisation and resummation scales μ_{F}, μ_{R} and μ_{Res} following the procedure described in Ref. [116,117]. The uncertainty obtained applying correlated scale variations in W and Z production does not cover the observed difference with the data. The potential effect of using $R_{W/Z}(p_{\mathrm{T}})$ as predicted by DYRes instead of PYTHIA 8 AZ for the determination of m_W is discussed in Sect. 11.5.

[3] Half the effect is used because only one of the two quarks in the initial state is heavy, as discussed in Sect. 6.5.2.

11.3 Results for m_W in the measurement categories

Measurements of m_W are performed using the p_{T}^{ℓ} and m_{T} distributions, separately for positively and negatively charged W bosons, in three bins of $|\eta_\ell|$ in the electron decay channel, and in four bins of $|\eta_\ell|$ in the muon decay channel, leading to a total of 28 m_W determinations. In each category, the value of m_W is determined by a χ^2 minimisation, comparing the p_{T}^{ℓ} and m_{T} distributions in data and simulation for different values of m_W. The templates are generated with values of m_W in steps of 1 to 10 MeV within a range of $\pm$ 400 MeV, centred around the reference value used in the Monte Carlo signal samples. The statistical uncertainty is estimated from the half width of the χ^2 function at the value corresponding to one unit above the minimum. Systematic uncertainties due to physics-modelling corrections, detector-calibration corrections, and background subtraction, are discussed in Sects. 6–8 and 10, respectively.

The lower and upper bounds of the range of the p_{T}^{ℓ} distribution used in the fit are varied from 30 to 35 GeV, and from 45 to 50 GeV respectively, in steps of 1 GeV. For the m_{T} distribution, the boundaries are varied from 65 to 70 GeV, and from 90 to 100 GeV. The total measurement uncertainty is evaluated for each range, after combining the measurement categories as described in Sect. 11.4 below. The

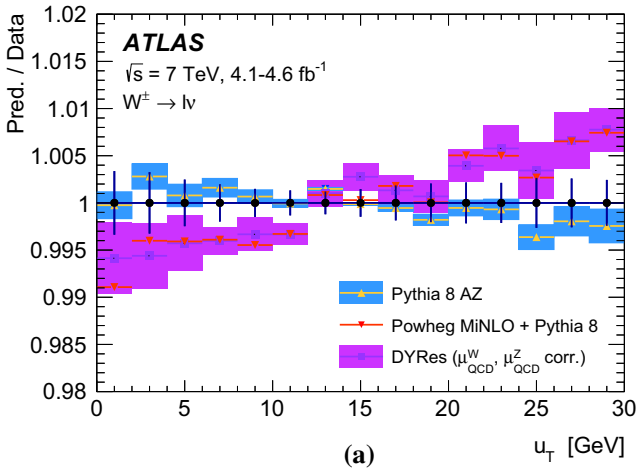

Fig. 22 Ratio between the predictions of PYTHIA 8 AZ, DYRes and POWHEG MINLO+PYTHIA 8 and the data for the **a** u_{T} and **b** $u_{\parallel}^{\ell}$ distributions in $W \to \ell\nu$ events. The W-boson rapidity distribution is reweighted according to the NNLO prediction. The error bars on the data points display the total experimental uncertainty, and the band around the PYTHIA 8 AZ prediction reflects the uncertainty in the p_{T}^{W} distribution. The uncertainty band around the DYRes prediction assumes that uncertainties induced by variations of the QCD scales μ_{F}, μ_{R} and μ_{Res}, collectively referred to as μ_{QCD}, are fully correlated in W and Z production

smallest total uncertainty in m_W is found for the fit ranges $32 < p_{\mathrm{T}}^{\ell} < 45\,\mathrm{GeV}$ and $66 < m_{\mathrm{T}} < 99\,\mathrm{GeV}$. The optimisation is performed before the unblinding of the m_W value and the optimised range is used for all the results described below.

The final measurement uncertainty is dominated by modelling uncertainties, with typical values in the range 25–35 MeV for the various charge and $|\eta_{\ell}|$ categories. Lepton-calibration uncertainties are the dominant sources of experimental systematic uncertainty for the extraction of m_W from the p_{T}^{ℓ} distribution. These uncertainties vary from about 15 MeV to about 35 MeV for most measurement categories, except the highest $|\eta|$ bin in the muon channel where the total uncertainty of about 120 MeV is dominated by the muon momentum linearity uncertainty. The uncertainty in the calibration of the recoil is the largest source of experimental systematic uncertainty for the m_{T} distribution, with a typical contribution of about 15 MeV for all categories. The determination of m_W from the p_{T}^{ℓ} and m_{T} distributions in the various categories is summarised in Table 10, including an overview of statistical and systematic uncertainties. The results are also shown in Fig. 23. No significant differences in the values of m_W corresponding to the different decay channels and to the various charge and $|\eta_{\ell}|$ categories are observed.

The comparison of data and simulation for kinematic distributions sensitive to the value of m_W provides further validation of the detector calibration and physics modelling. The comparison is performed in all measurement categories. The η-inclusive p_{T}^{ℓ}, m_{T} and $p_{\mathrm{T}}^{\mathrm{miss}}$ distributions for positively and negatively charged W bosons are shown in Figs. 24 and 25 for the electron and muon decay channels, respectively. The value of m_W used in the predictions is set to the overall measurement result presented in the next section. The χ^2 values quantifying the comparison between data and prediction are calculated over the full histogram range and account for all sources of uncertainty. The bin-to-bin correlations induced by the experimental and physics-modelling systematic uncertainties are also accounted for. Overall, satisfactory agreement is observed. The deficit of data visible for $p_{\mathrm{T}}^{\ell} \sim 40$–$42\,\mathrm{GeV}$ in the $W^+ \to e\nu$ channel does not strongly affect the mass measurement, as the observed effect differs from that expected from m_W variations. Cross-checks of possible sources of this effect were performed, and its impact on the mass determination was shown to be within the corresponding systematic uncertainties.

11.4 Combination and final results

The measurements of m_W in the various categories are combined accounting for statistical and systematic uncertainties and their correlations. The statistical correlation of the m_W values determined from the p_{T}^{ℓ} and m_{T} distributions is evaluated with the bootstrap method [118], and is approximately 50% for all measurement categories.

The systematic uncertainties have specific correlation patterns across the m_W measurement categories. Muon-momentum and electron-energy calibration uncertainties are uncorrelated between the different decay channels, but largely correlated between the p_{T}^{ℓ} and m_{T} distributions. Recoil-calibration uncertainties are correlated between electron and muon decay channels, and they are small for p_{T}^{ℓ} distributions. The PDF-induced uncertainties are largely cor-

Table 10 Results of the m_W measurements in the electron and muon decay channels, for positively and negatively charged W bosons, in different lepton-$|\eta|$ ranges, using the m_{T} and p_{T}^{ℓ} distributions in the optimised fitting range. The table shows the statistical uncertainties, together with all experimental uncertainties, divided into muon-, electron-, recoil- and background-related uncertainties, and all modelling uncertainties, separately for QCD modelling including scale variations, parton shower and angular coefficients, electroweak corrections, and PDFs. All uncertainties are given in MeV

Channel (m_{T} fits)	m_W [MeV]	Stat. Unc.	Muon Unc.	Elec. Unc.	Recoil Unc.	Bckg. Unc.	QCD Unc.	EW Unc.	PDF Unc.	Total Unc.
$W^+ \to \mu\nu, \lvert\eta\rvert < 0.8$	80371.3	29.2	12.4	0.0	15.2	8.1	9.9	3.4	28.4	47.1
$W^+ \to \mu\nu, 0.8 < \lvert\eta\rvert < 1.4$	80354.1	32.1	19.3	0.0	13.0	6.8	9.6	3.4	23.3	47.6
$W^+ \to \mu\nu, 1.4 < \lvert\eta\rvert < 2.0$	80426.3	30.2	35.1	0.0	14.3	7.2	9.3	3.4	27.2	56.9
$W^+ \to \mu\nu, 2.0 < \lvert\eta\rvert < 2.4$	80334.6	40.9	112.4	0.0	14.4	9.0	8.4	3.4	32.8	125.5
$W^- \to \mu\nu, \lvert\eta\rvert < 0.8$	80375.5	30.6	11.6	0.0	13.1	8.5	9.5	3.4	30.6	48.5
$W^- \to \mu\nu, 0.8 < \lvert\eta\rvert < 1.4$	80417.5	36.4	18.5	0.0	12.2	7.7	9.7	3.4	22.2	49.7
$W^- \to \mu\nu, 1.4 < \lvert\eta\rvert < 2.0$	80379.4	35.6	33.9	0.0	10.5	8.1	9.7	3.4	23.1	56.9
$W^- \to \mu\nu, 2.0 < \lvert\eta\rvert < 2.4$	80334.2	52.4	123.7	0.0	11.6	10.2	9.9	3.4	34.1	139.9
$W^+ \to e\nu, \lvert\eta\rvert < 0.6$	80352.9	29.4	0.0	19.5	13.1	15.3	9.9	3.4	28.5	50.8
$W^+ \to e\nu, 0.6 < \lvert\eta\rvert < 1.2$	80381.5	30.4	0.0	21.4	15.1	13.2	9.6	3.4	23.5	49.4
$W^+ \to e\nu, 1,8 < \lvert\eta\rvert < 2.4$	80352.4	32.4	0.0	26.6	16.4	32.8	8.4	3.4	27.3	62.6
$W^- \to e\nu, \lvert\eta\rvert < 0.6$	80415.8	31.3	0.0	16.4	11.8	15.5	9.5	3.4	31.3	52.1
$W^- \to e\nu, 0.6 < \lvert\eta\rvert < 1.2$	80297.5	33.0	0.0	18.7	11.2	12.8	9.7	3.4	23.9	49.0
$W^- \to e\nu, 1.8 < \lvert\eta\rvert < 2.4$	80423.8	42.8	0.0	33.2	12.8	35.1	9.9	3.4	28.1	72.3
Channel (p_{T}^{l} fits)										
$W^+ \to \mu\nu, \lvert\eta\rvert < 0.8$	80327.7	22.1	12.2	0.0	2.6	5.1	9.0	6.0	24.7	37.3
$W^+ \to \mu\nu, 0.8 < \lvert\eta\rvert < 1.4$	80357.3	25.1	19.1	0.0	2.5	4.7	8.9	6.0	20.6	39.5
$W^+ \to \mu\nu, 1.4 < \lvert\eta\rvert < 2.0$	80446.9	23.9	33.1	0.0	2.5	4.9	8.2	6.0	25.2	49.3
$W^+ \to \mu\nu, 2.0 < \lvert\eta\rvert < 2.4$	80334.1	34.5	110.1	0.0	2.5	6.4	6.7	6.0	31.8	120.2
$W^- \to \mu\nu, \lvert\eta\rvert < 0.8$	80427.8	23.3	11.6	0.0	2.6	5.8	8.1	6.0	26.4	39.0
$W^- \to \mu\nu, 0.8 < \lvert\eta\rvert < 1.4$	80395.6	27.9	18.3	0.0	2.5	5.6	8.0	6.0	19.8	40.5
$W^- \to \mu\nu, 1.4 < \lvert\eta\rvert < 2.0$	80380.6	28.1	35.2	0.0	2.6	5.6	8.0	6.0	20.6	50.9
$W^- \to \mu\nu, 2.0 < \lvert\eta\rvert < 2.4$	80315.2	45.5	116.1	0.0	2.6	7.6	8.3	6.0	32.7	129.6
$W^+ \to e\nu, \lvert\eta\rvert < 0.6$	80336.5	22.2	0.0	20.1	2.5	6.4	9.0	5.3	24.5	40.7
$W^+ \to e\nu, 0.6 < \lvert\eta\rvert < 1.2$	80345.8	22.8	0.0	21.4	2.6	6.7	8.9	5.3	20.5	39.4
$W^+ \to e\nu, 1, 8 < \lvert\eta\rvert < 2.4$	80344.7	24.0	0.0	30.8	2.6	11.9	6.7	5.3	24.1	48.2
$W^- \to e\nu, \lvert\eta\rvert < 0.6$	80351.0	23.1	0.0	19.8	2.6	7.2	8.1	5.3	26.6	42.2
$W^- \to e\nu, 0.6 < \lvert\eta\rvert < 1.2$	80309.8	24.9	0.0	19.7	2.7	7.3	8.0	5.3	20.9	39.9
$W^- \to e\nu, 1.8 < \lvert\eta\rvert < 2.4$	80413.4	30.1	0.0	30.7	2.7	11.5	8.3	5.3	22.7	51.0

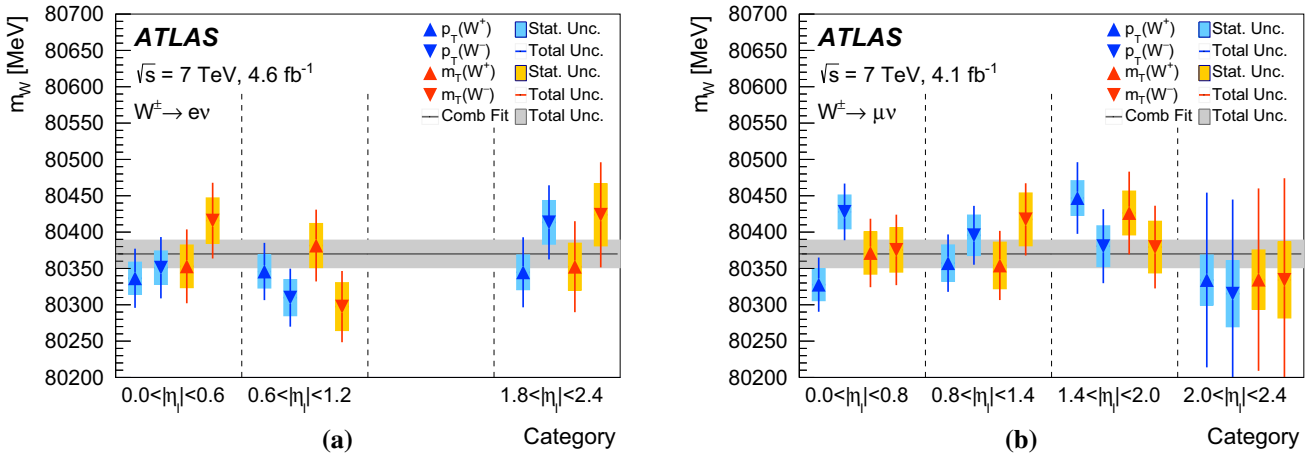

Fig. 23 Overview of the m_W measurements in the **a** electron and **b** muon decay channels. Results are shown for the p_{T}^{ℓ} and m_{T} distributions, for W^+ and W^- events in the different $|\eta_\ell|$ categories. The coloured bands and solid lines show the statistical and total uncertainties, respectively. The horizontal line and band show the fully combined result and its uncertainty

related between electron and muon decay channels, but significantly anti-correlated between positively and negatively charged W bosons, as discussed in Sect. 6. Due to the different balance of systematic uncertainties and to the variety of correlation patterns, a significant reduction of the uncertainties in the measurement of m_W is achieved by combining the different decay channels and the charge and $|\eta_\ell|$ categories.

As discussed in Sect. 2, the comparison of the results from the p_{T}^{ℓ} and m_{T} distributions, from the different decay channels, and in the various charge and $|\eta_\ell|$ categories, provides a test of the experimental and physics modelling corrections. Discrepancies between the positively and negatively charged lepton categories, or in the various $|\eta_\ell|$ bins would primarily indicate an insufficient understanding of physics-modelling effects, such as the PDFs and the p_{T}^{W} distribution. Inconsistencies between the electron and muon channels could indicate problems in the calibration of the muon-momentum and electron-energy responses. Significant differences between results from the p_{T}^{ℓ} and m_{T} distributions would point to either problems in the calibration of the recoil, or to an incorrect modelling of the transverse-momentum distribution of the W boson. Several measurement combinations are performed, using the best linear unbiased estimate (BLUE) method [119,120]. The results of the combinations are verified with the `HERAverager` program [121], which gives very close results.

Table 11 shows an overview of partial m_W measurement combinations. In the first step, determinations of m_W in the electron and muon decay channels from the m_{T} distribution are combined separately for the positive- and negative-charge categories, and together for both W-boson charges. The results are compatible, and the positively charged, negatively charged, and charge-inclusive combinations yield values of χ^2/dof corresponding to 2/6, 7/6, and 11/13, respectively. Compatibility of the results is also observed for the corresponding combinations from the p_{T}^{ℓ} distribution, with values of χ^2/dof of 5/6, 10/6, and 19/13, for positively charged, negatively charged, and charge-inclusive combinations, respectively. The χ^2 compatibility test validates the consistency of the results in the $W \to e\nu$ and $W \to \mu\nu$ decay channels. The precision of the determination of m_W from the m_{T} distribution is slightly worse than the result obtained from the p_{T}^{ℓ} distribution, due to the larger uncertainty induced by the recoil calibration. In addition, the impact of PDF- and p_{T}^{W}-related uncertainties on the p_{T}^{ℓ} fits is limited by the optimisation of the fitting range. In the second step, determinations of m_W from the p_{T}^{ℓ} and m_{T} distributions are combined separately for the electron and the muon decay channels. The results are compatible, with values of χ^2/dof of 4/5 and 8/5 in the electron channel for the p_{T}^{ℓ} and m_{T} distributions, respectively, and values of 7/7 and 3/7 in the muon channel for the p_{T}^{ℓ} and m_{T} distributions, respectively. The m_W determinations in the electron and in the muon channels agree, further validating the consistency of the electron and muon calibrations. Agreement between the m_W determinations from the p_{T}^{ℓ} and m_{T} distributions supports the calibration of the recoil, and the modelling of the transverse momentum of the W boson.

The results are summarised in Fig. 26. The combination of all the determinations of m_W reported in Table 10 has a value of χ^2/dof of 29/27, and yields a final result of

$$\begin{aligned} m_W &= 80369.5 \pm 6.8(\text{stat.}) \pm 10.6(\text{exp. syst.}) \\ &\quad \pm 13.6(\text{mod. syst.})\,\text{MeV} \\ &= 80369.5 \pm 18.5\,\text{MeV}, \end{aligned}$$

where the first uncertainty is statistical, the second corresponds to the experimental systematic uncertainty, and the

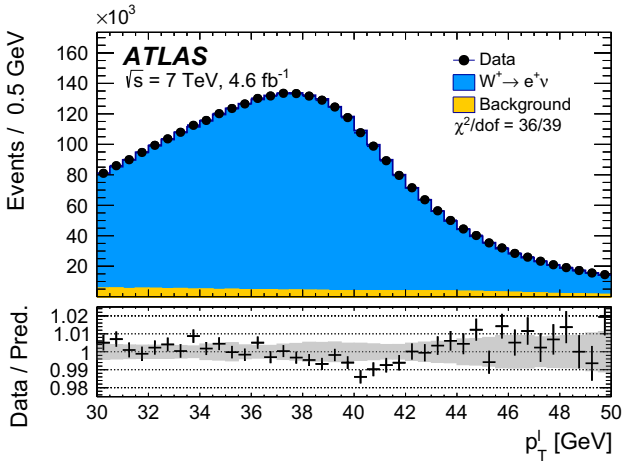

(a)

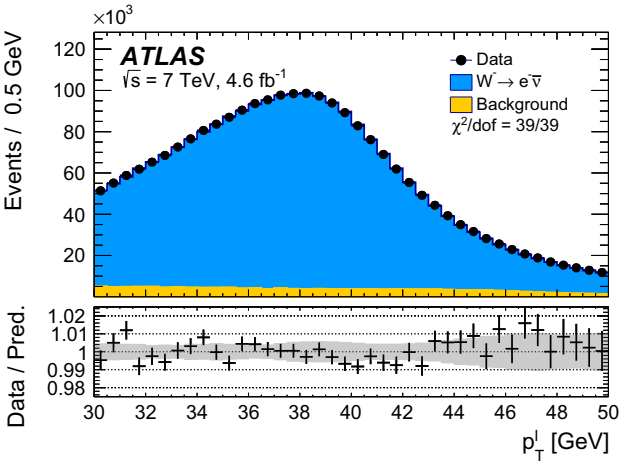

(b)

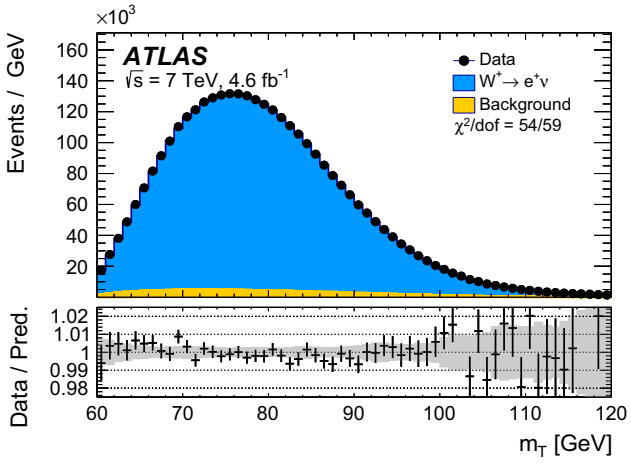

(c)

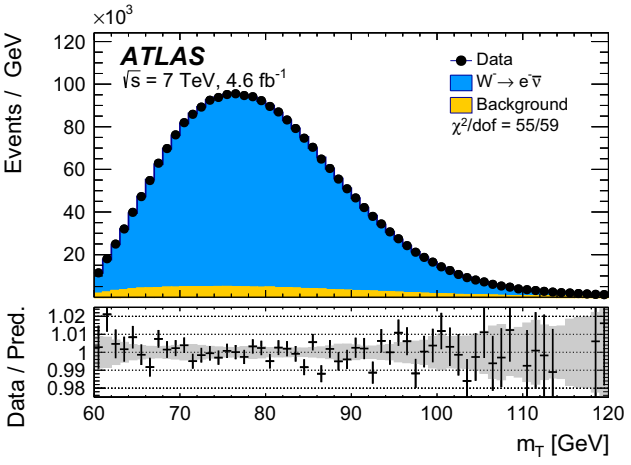

(d)

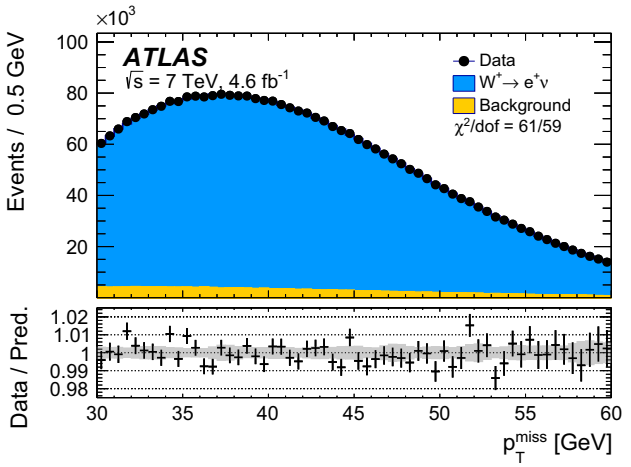

(e)

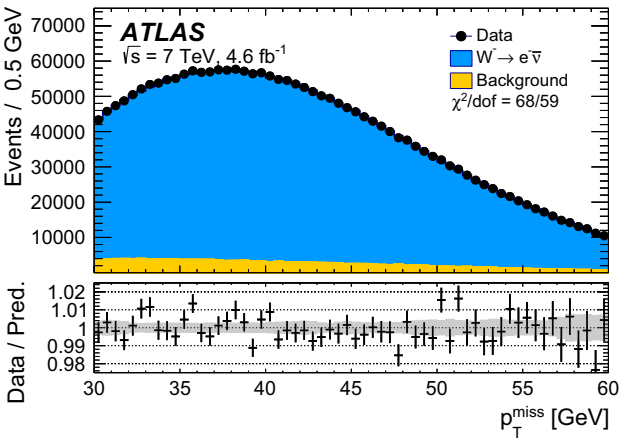

(f)

Fig. 24 The **a**, **b** p_{T}^{ℓ}, **c**, **d** m_{T}, and **e**, **f** $p_{\mathrm{T}}^{\mathrm{miss}}$ distributions for **a**, **c**, **e** W^+ events and **b**, **d**, **f** W^- events in the electron decay channel. The data are compared to the simulation including signal and background contributions. Detector calibration and physics-modelling corrections are applied to the simulated events. For all simulated distributions, m_W is set according to the overall measurement result. The lower panels show the data-to-prediction ratios, the error bars show the statistical uncertainty, and the band shows the systematic uncertainty of the prediction. The χ^2 values displayed in each figure account for all sources of uncertainty and include the effects of bin-to-bin correlations induced by the systematic uncertainties

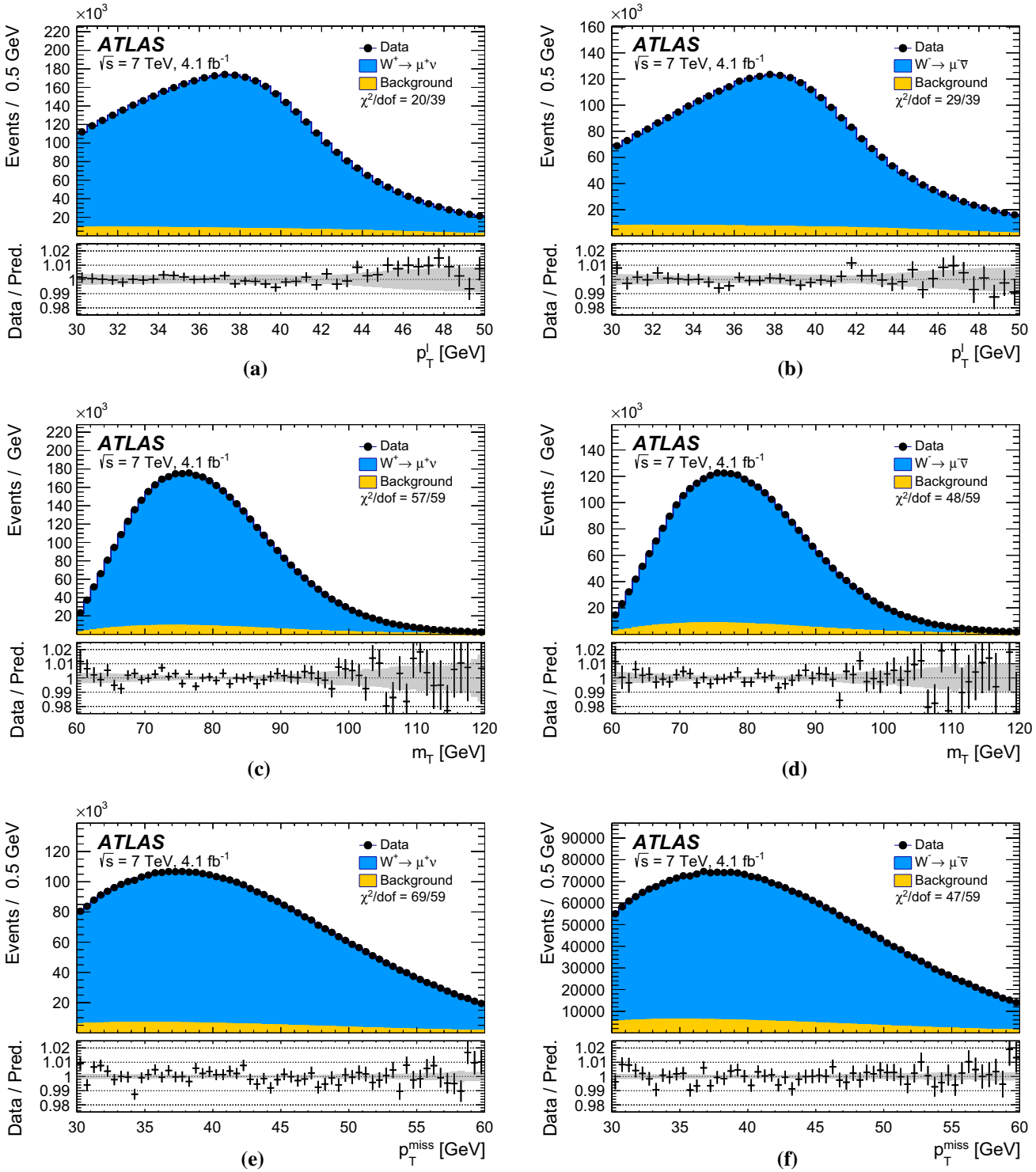

Fig. 25 The **a**, **b** p_{T}^{ℓ}, **c**, **d** m_{T}, and **e**, **f** $p_{\mathrm{T}}^{\mathrm{miss}}$ distributions for **a**, **c**, **e** W^+ events and **b**, **d**, **f** W^- events in the muon decay channel. The data are compared to the simulation including signal and background contributions. Detector calibration and physics-modelling corrections are applied to the simulated events. For all simulated distributions, m_W is set according to the overall measurement result. The lower panels show the data-to-prediction ratios, the error bars show the statistical uncertainty, and the band shows the systematic uncertainty of the prediction. The χ^2 values displayed in each figure account for all sources of uncertainty and include the effects of bin-to-bin correlations induced by the systematic uncertainties

Table 11 Results of the m_W measurements for various combinations of categories. The table shows the statistical uncertainties, together with all experimental uncertainties, divided into muon-, electron-, recoil- and background-related uncertainties, and all modelling uncertainties, separately for QCD modelling including scale variations, parton shower and angular coefficients, electroweak corrections, and PDFs. All uncertainties are given in MeV

Combined categories	m_w [MeV]	Stat. Unc.	Muon Unc.	Elec. Unc.	Recoil Unc.	Bckg. Unc.	QCD Unc.	EW Unc.	PDF Unc.	Total Unc.	χ^2/dof
m_{T}, W^+, e-μ	80370.0	12.3	8.3	6.7	14.5	9.7	9.4	3.4	16.9	30.9	2/6
m_{T}, W^-, e-μ	80381.1	13.9	8.8	6.6	11.8	10.2	9.7	3.4	16.2	30.5	7/6
m_{T}, $W^\pm$, e-μ	80375.7	9.6	7.8	5.5	13.0	8.3	9.6	3.4	10.2	25.1	11/13
p_{T}^ℓ, W^+, e-μ	80352.0	9.6	6.5	8.4	2.5	5.2	8.3	5.7	14.5	23.5	5/6
p_{T}^ℓ, W^-, e-μ	80383.4	10.8	7.0	8.1	2.5	6.1	8.1	5.7	13.5	23.6	10/6
p_{T}^ℓ, $W^\pm$, e-μ	80369.4	7.2	6.3	6.7	2.5	4.6	8.3	5.7	9.0	18.7	19/13
p_{T}^ℓ, $W^\pm$, e	80347.2	9.9	0.0	14.8	2.6	5.7	8.2	5.3	8.9	23.1	4/5
m_{T}, $W^\pm$, e	80364.6	13.5	0.0	14.4	13.2	12.8	9.5	3.4	10.2	30.8	8/5
m_{T}-p_{T}^ℓ, W^+, e	80345.4	11.7	0.0	16.0	3.8	7.4	8.3	5.0	13.7	27.4	1/5
m_{T}-p_{T}^ℓ, W^-, e	80359.4	12.9	0.0	15.1	3.9	8.5	8.4	4.9	13.4	27.6	8/5
m_{T}-p_{T}^ℓ, $W^\pm$, e	80349.8	9.0	0.0	14.7	3.3	6.1	8.3	5.1	9.0	22.9	12/11
p_{T}^ℓ, $W^\pm$, μ	80382.3	10.1	10.7	0.0	2.5	3.9	8.4	6.0	10.7	21.4	7/7
m_{T}, $W^\pm$, μ	80381.5	13.0	11.6	0.0	13.0	6.0	9.6	3.4	11.2	27.2	3/7
m_{T}-p_{T}^ℓ, W^+, μ	80364.1	11.4	12.4	0.0	4.0	4.7	8.8	5.4	17.6	27.2	5/7
m_{T}-p_{T}^ℓ, W^-, μ	80398.6	12.0	13.0	0.0	4.1	5.7	8.4	5.3	16.8	27.4	3/7
m_{T}-p_{T}^ℓ, $W^\pm$, μ	80382.0	8.6	10.7	0.0	3.7	4.3	8.6	5.4	10.9	21.0	10/15
m_{T}-p_{T}^ℓ, W^+, e-μ	80352.7	8.9	6.6	8.2	3.1	5.5	8.4	5.4	14.6	23.4	7/13
m_{T}-p_{T}^ℓ, W^-, e-μ	80383.6	9.7	7.2	7.8	3.3	6.6	8.3	5.3	13.6	23.4	15/13
m_{T}-p_{T}^ℓ, $W^\pm$, e-μ	80369.5	6.8	6.6	6.4	2.9	4.5	8.3	5.5	9.2	18.5	29/27

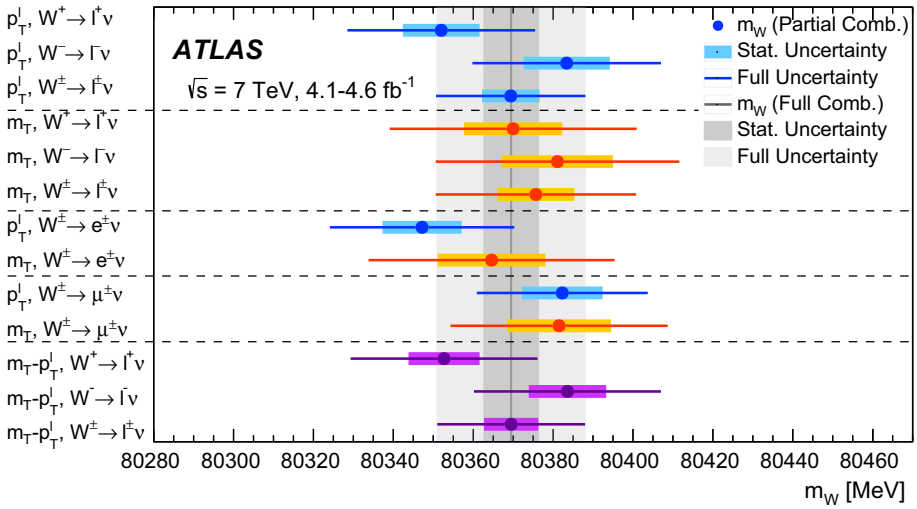

Fig. 26 Overview of the m_W determinations from the p_{T}^{ℓ} and m_{T} distributions, and for the combination of the p_{T}^{ℓ} and m_{T} distributions, in the muon and electron decay channels and for W^+ and W^- events. The horizontal lines and bands show the statistical and total uncertainties of the individual m_W determinations. The combined result for m_W and its statistical and total uncertainties are also indicated (vertical line and bands)

third to the physics-modelling systematic uncertainty. The latter dominates the total measurement uncertainty, and it itself dominated by strong interaction uncertainties. The experimental systematic uncertainties are dominated by the lepton calibration; backgrounds and the recoil calibration have a smaller impact. In the final combination, the muon decay channel has a weight of 57%, and the p_{T}^{ℓ} fit dominates the measurement with a weight of 86%. Finally, the charges contribute similarly with a weight of 52% for W^+ and of 48% for W^-.

The result is in agreement with the current world average of $m_W = 80385 \pm 15$ MeV [29], and has a precision comparable to the currently most precise single measurements of the CDF and D0 collaborations [22,23].

11.5 Additional validation tests

The final combination of m_W, presented above, depends only on template fits to the p_{T}^{ℓ} and m_{T} distributions. As a validation test, the value of m_W is determined from the $p_{\mathrm{T}}^{\mathrm{miss}}$ distribution, performing a fit in the range $30 < p_{\mathrm{T}}^{\mathrm{miss}} < 60$ GeV. Consistent results are observed in all measurement categories, leading to combined results of 80364 ± 26 (stat) MeV and 80367 ± 23 (stat) MeV for the electron and muon channels, respectively.

Several additional studies are performed to validate the stability of the m_W measurement. The stability of the result with respect to different pile-up conditions is tested by dividing the event sample into three bins of $\langle\mu\rangle$, namely [2.5, 6.5], [6.5, 9.5], and [9.5, 16]. In each bin, m_W measurements are performed independently using the p_{T}^{ℓ} and m_{T} distributions. This categorisation also tests the stability of m_W with respect to data-taking periods, as the later data-taking periods have on average more pile-up due to the increasing LHC luminosity.

The calibration of the recoil and the modelling of the p_{T}^{W} distribution are tested by performing m_W fits in two bins of the recoil corresponding to [0, 15] GeV and [15, 30] GeV, and in two regions corresponding to positive and negative values of $u_{\parallel}^{\ell}$. The analysis is also repeated with the $p_{\mathrm{T}}^{\mathrm{miss}}$ requirement removed from the signal selection, leading to a lower recoil modelling uncertainty but a higher multijet background contribution. The stability of the m_W measurements upon removal of this requirement is studied, and consistent results are obtained. All m_W determinations are consistent with the nominal result. An overview of the validation tests is shown in Table 12, where only statistical uncertainties are given. Fitting ranges of $30 < p_{\mathrm{T}}^{\ell} < 50$ GeV and $65 < m_{\mathrm{T}} < 100$ GeV are used for all these validation tests, to minimise the statistical uncertainty.

The lower and upper bounds of the range of the p_{T}^{ℓ} and m_{T} distributions are varied as in the optimisation procedure described in Sect. 11.3. The statistical and systematic uncertainties are evaluated for each range, and are only partially correlated between different ranges. Figure 27 shows measured values of m_W for selected ranges of the p_{T}^{ℓ} and m_{T} distributions, where only the uncorrelated statistical and systematic uncertainties with respect to the optimal range are shown. The observed variations are all within two standard deviations of the uncorrelated uncertainties, and small compared to the overall uncertainty of the measurement, which is illustrated by the band on Fig. 27. The largest dependence on the kinematic ranges used for the fits is observed for variations of the upper bound of the p_{T}^{ℓ} distribution in the $W^+ \to e\nu$ channel, and is related to the shape of the data-to-prediction ratio for this distribution in the region $40 < p_{\mathrm{T}}^{\ell} < 42$ GeV, as discussed in Sect. 11.3.

The effect of the residual discrepancies in the u_{T} distributions for $W^- \to \ell\nu$, visible at low values in Figs. 19-(d) and 20-(d), is estimated by adjusting, in turn, the particle-level p_{T}^{W} distribution and the recoil calibration

Table 12 Summary of consistency tests for the determination of m_W in several additional measurement categories. The Δm_W values correspond to the difference between the result for each category and the inclusive result for the corresponding observable (p_{T}^{ℓ} or m_{T}). The uncertainties correspond to the statistical uncertainty of the fit to the data of each category alone. Fitting ranges of $30 < p_{\mathrm{T}}^{\ell} < 50$ GeV and $65 < m_{\mathrm{T}} < 100$ GeV are used

Decay channel	$W \to e\nu$		$W \to \mu\nu$		Combined	
Kinematic distribution	p_{T}^{ℓ}	m_{T}	p_{T}^{ℓ}	m_{T}	p_{T}^{ℓ}	m_{T}
Δm_W [MeV]						
$\langle\mu\rangle$ in [2.5, 6.5]	8 ± 14	14 ± 18	-21 ± 12	0 ± 16	-9 ± 9	6 ± 12
$\langle\mu\rangle$ in [6.5, 9.5]	-6 ± 16	6 ± 23	12 ± 15	-8 ± 22	4 ± 11	-1 ± 16
$\langle\mu\rangle$ in [9.5, 16]	-1 ± 16	3 ± 27	25 ± 16	35 ± 26	12 ± 11	20 ± 19
u_{T} in [0, 15] GeV	0 ± 11	-8 ± 13	5 ± 10	8 ± 12	3 ± 7	-1 ± 9
u_{T} in [15, 30] GeV	10 ± 15	0 ± 24	-4 ± 14	-18 ± 22	2 ± 10	-10 ± 16
$u_{\parallel}^{\ell} < 0$ GeV	8 ± 15	20 ± 17	3 ± 13	-1 ± 16	5 ± 10	9 ± 12
$u_{\parallel}^{\ell} > 0$ GeV	-9 ± 10	1 ± 14	-12 ± 10	10 ± 13	-11 ± 7	6 ± 10
No $p_{\mathrm{T}}^{\mathrm{miss}}$-cut	14 ± 9	-1 ± 13	10 ± 8	-6 ± 12	12 ± 6	-4 ± 9

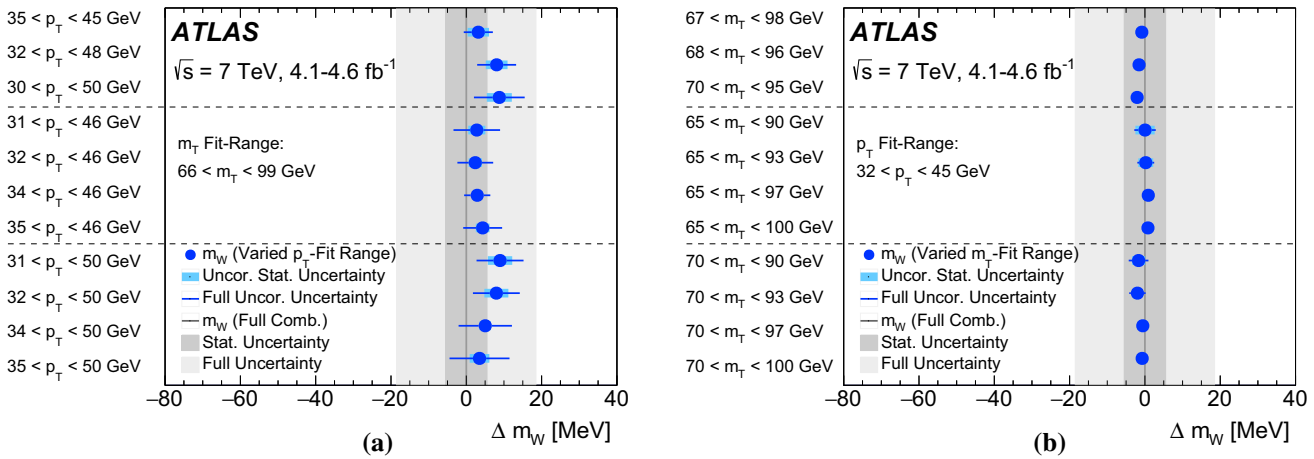

Fig. 27 Stability of the combined measurement of m_W with respect to variations of the kinematic ranges of **a** p_{T}^{ℓ} and **b** m_{T} used for the template fits. The optimal m_{T} range is used for the p_{T}^{ℓ} variations, and the optimal p_{T}^{ℓ} range is used for the m_{T} variations. The effect on the result of symmetric variations of the fitting range boundaries, and its dependence on variations of the lower (upper) boundary for two values of the upper (lower) boundary for p_{T}^{ℓ} (m_{T}) are shown. The bands and solid lines respectively show the statistical and total uncertainty on the difference with the optimal result

corrections to optimize the agreement between data and simulation. The impact of these variations on the determination of m_W is found to be small compared to the assigned p_{T}^{W} modelling and recoil calibration uncertainties, respectively.

When assuming $R_{W/Z}(p_{\mathrm{T}})$ as predicted by DYRes, instead of Pythia 8 AZ, to model the p_{T}^{W} distribution, deviations of about 3% appear in the distribution ratios of Figs. 24 and 25. This degrades the quality of the mass fits, and shifts the fitted values of m_W by about -20 to -90 MeV, depending on the channels, compared to the results of Table 11. Combining all channels, the shift is about -60 MeV. Since DYRes does not model the data distributions sensitive to p_{T}^{W}, as shown in Fig. 22, these shifts are given for information only and are not used to estimate the uncertainty in m_W.

11.6 Measurement of $m_{W^+} - m_{W^-}$

The results presented in the previous sections can be used to derive a measurement of the mass difference between the positively and negatively charged W bosons, $m_{W^+} - m_{W^-}$. Starting from the m_W measurement results in the 28 categories described above, 14 measurements of $m_{W^+} - m_{W^-}$ can be constructed by subtraction of the results obtained from the W^+ and W^- samples in the same decay channel and $|\eta|$ category. In practice, the m_W values measured in W^+ and W^- events are subtracted linearly, as are the effects of systematic uncertainties on these measurements, while the uncertainty contributions of a statistical nature are added in quadrature. Contrarily to the m_W measurement discussed above, no blinding procedure was applied for the measurement of $m_{W^+} - m_{W^-}$.

Table 13 Results of the $m_{W^+} - m_{W^-}$ measurements in the electron and muon decay channels, and of the combination. The table shows the statistical uncertainties; the experimental uncertainties, divided into muon-, electron-, recoil- and background-uncertainties; and the modelling uncertainties, separately for QCD modelling including scale variations, parton shower and angular coefficients, electroweak corrections, and PDFs. All uncertainties are given in MeV

Channel	$m_{W^+} - m_{W^-}$ [MeV]	Stat. Unc.	Muon Unc.	Elec. Unc.	Recoil Unc.	Bckg. Unc.	QCD Unc.	EW Unc.	PDF Unc.	Total Unc.
$W \to e\nu$	−29.7	17.5	0.0	4.9	0.9	5.4	0.5	0.0	24.1	30.7
$W \to \mu\nu$	−28.6	16.3	11.7	0.0	1.1	5.0	0.4	0.0	26.0	33.2
Combined	−29.2	12.8	3.3	4.1	1.0	4.5	0.4	0.0	23.9	28.0

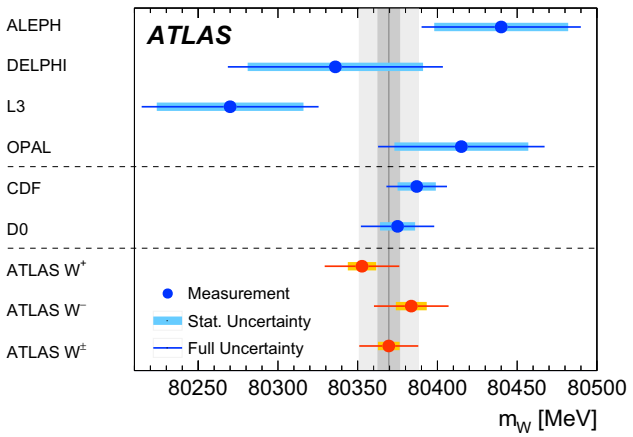

Fig. 28 The measured value of m_W is compared to other published results, including measurements from the LEP experiments ALEPH, DELPHI, L3 and OPAL [25–28], and from the Tevatron collider experiments CDF and D0 [22,23]. The vertical bands show the statistical and total uncertainties of the ATLAS measurement, and the horizontal bands and lines show the statistical and total uncertainties of the other published results. Measured values of m_W for positively and negatively charged W bosons are also shown

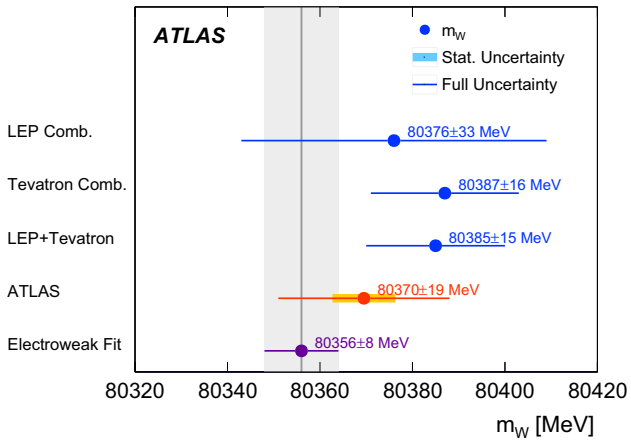

Fig. 29 The present measurement of m_W is compared to the SM prediction from the global electroweak fit [16] updated using recent measurements of the top-quark and Higgs-boson masses, $m_t = 172.84 \pm 0.70$ GeV [122] and $m_H = 125.09 \pm 0.24$ GeV [123], and to the combined values of m_W measured at LEP [124] and at the Tevatron collider [24]

In this process, uncertainties that are anti-correlated between W^+ and W^- and largely cancel for the m_W measurement become dominant when measuring $m_{W^+} - m_{W^-}$. On the physics-modelling side, the fixed-order PDF uncertainty and the parton shower PDF uncertainty give the largest contributions, while other sources of uncertainty only weakly depend on charge and tend to cancel. Among the sources of uncertainty related to lepton calibration, the track sagitta correction dominates in the muon channel, whereas several residual uncertainties contribute in the electron channel. Most lepton and recoil calibration uncertainties tend to cancel. Background systematic uncertainties contribute as the Z and multijet background fractions differ in the W^+ and W^- channels. The dominant statistical uncertainties arise from the size of the data and Monte Carlo signal samples, and of the control samples used to derive the multijet background.

The $m_{W^+} - m_{W^-}$ measurement results are shown in Table 13 for the electron and muon decay channels, and for the combination. The electron channel measurement combines six categories (p_{T}^{ℓ} and m_{T} fits in three $|\eta_\ell|$ bins), while the muon channel has four $|\eta_\ell|$ bins and eight categories in total. The fully combined result is

$$\begin{aligned} m_{W^+} - m_{W^-} &= -29.2 \pm 12.8(\text{stat.}) \\ &\quad \pm 7.0(\text{exp. syst.}) \\ &\quad \pm 23.9(\text{mod. syst.}) \text{ MeV} \\ &= -29.2 \pm 28.0 \text{ MeV}, \end{aligned}$$

where the first uncertainty is statistical, the second corresponds to the experimental systematic uncertainty, and the third to the physics-modelling systematic uncertainty.

12 Discussion and conclusions

This paper reports a measurement of the W-boson mass with the ATLAS detector, obtained through template fits to the kinematic properties of decay leptons in the electron and muon decay channels. The measurement is based on proton–proton collision data recorded in 2011 at a centre-of-mass energy of $\sqrt{s} = 7$ TeV at the LHC, and corresponding to an integrated luminosity of 4.6 fb^{-1}. The measurement relies

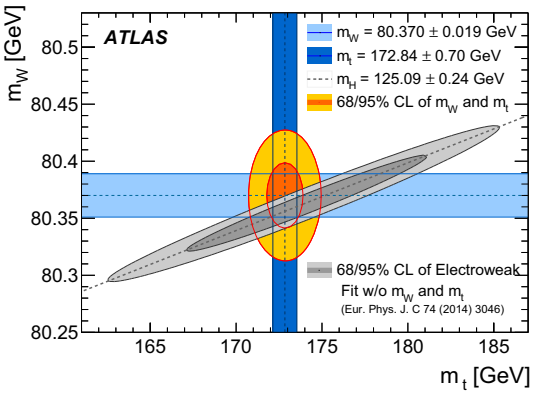

Fig. 30 The 68 and 95% confidence-level contours of the m_W and m_t indirect determination from the global electroweak fit [16] are compared to the 68 and 95% confidence-level contours of the ATLAS measurements of the top-quark and W-boson masses. The determination from the electroweak fit uses as input the LHC measurement of the Higgs-boson mass, $m_H = 125.09 \pm 0.24$ GeV [123]

on a thorough detector calibration based on the study of Z-boson events, leading to a precise modelling of the detector response to electrons, muons and the recoil. Templates for the W-boson kinematic distributions are obtained from the NLO MC generator POWHEG, interfaced to PYTHIA8 for the parton shower. The signal samples are supplemented with several additional physics-modelling corrections allowing for the inclusion of higher-order QCD and electroweak corrections, and by fits to measured distributions, so that agreement between the data and the model in the kinematic distributions is improved. The W-boson mass is obtained from the transverse-momentum distribution of charged leptons and from the transverse-mass distributions, for positively and negatively charged W bosons, in the electron and muon decay channels, and in several kinematic categories. The individual measurements of m_W are found to be consistent and their combination yields a value of

$$\begin{aligned} m_W &= 80370 \pm 7\ (\text{stat.}) \pm 11\ (\text{exp. syst.}) \\ &\quad \pm 14\ (\text{mod. syst.})\ \text{MeV} \\ &= 80370 \pm 19\ \text{MeV}, \end{aligned}$$

where the first uncertainty is statistical, the second corresponds to the experimental systematic uncertainty, and the third to the physics-modelling systematic uncertainty. A measurement of the W^+ and W^- mass difference yields $m_{W^+} - m_{W^-} = -29 \pm 28$ MeV.

The W-boson mass measurement is compatible with the current world average of $m_W = 80385 \pm 15$ MeV [29], and similar in precision to the currently leading measurements performed by the CDF and D0 collaborations [22,23]. An overview of the different m_W measurements is shown in Fig. 28. The compatibility of the measured value of m_W in the context of the global electroweak fit is illustrated in Figs. 29 and 30. Figure 29 compares the present measurement with earlier results, and with the SM prediction updated with regard to Ref. [16] using recent measurements of the top-quark and Higgs boson masses, $m_t = 172.84 \pm 0.70$ GeV [122] and $m_H = 125.09 \pm 0.24$ GeV [123]. This update gives a numerical value for the SM prediction of $m_W = 80356 \pm 8$ MeV. The corresponding two-dimensional 68 and 95% confidence limits for m_W and m_t are shown in Fig. 30, and compared to the present measurement of m_W and the average of the top-quark mass determinations performed by ATLAS [122].

The determination of the W-boson mass from the global fit of the electroweak parameters has an uncertainty of 8 MeV, which sets a natural target for the precision of the experimental measurement of the mass of the W boson. The modelling uncertainties, which currently dominate the overall uncertainty of the m_W measurement presented in this paper, need to be reduced in order to fully exploit the larger data samples available at centre-of-mass energies of 8 and 13 TeV. Better knowledge of the PDFs, as achievable with the inclusion in PDF fits of recent precise measurements of W- and Z-boson rapidity cross sections with the ATLAS detector [41], and improved QCD and electroweak predictions for Drell–Yan production, are therefore crucial for future measurements of the W-boson mass at the LHC.

Acknowledgements We thank CERN for the very successful operation of the LHC, as well as the support staff from our institutions without whom ATLAS could not be operated efficiently. We acknowledge the support of ANPCyT, Argentina; YerPhI, Armenia; ARC, Australia; BMWFW and FWF, Austria; ANAS, Azerbaijan; SSTC, Belarus; CNPq and FAPESP, Brazil; NSERC, NRC and CFI, Canada; CERN; CONICYT, Chile; CAS, MOST and NSFC, China; COLCIENCIAS, Colombia; MSMT CR, MPO CR and VSC CR, Czech Republic; DNRF and DNSRC, Denmark; IN2P3-CNRS, CEA-DSM/IRFU, France; SRNSF, Georgia; BMBF, HGF, and MPG, Germany; GSRT, Greece; RGC, Hong Kong SAR, China; ISF, I-CORE and Benoziyo Center, Israel; INFN, Italy; MEXT and JSPS, Japan; CNRST, Morocco; NWO, Netherlands; RCN, Norway; MNiSW and NCN, Poland; FCT, Portugal; MNE/IFA, Romania; MES of Russia and NRC KI, Russian Federation; JINR; MESTD, Serbia; MSSR, Slovakia; ARRS and MIZŠ, Slovenia; DST/NRF, South Africa; MINECO, Spain; SRC and Wallenberg Foundation, Sweden; SERI, SNSF and Cantons of Bern and Geneva, Switzerland; MOST, Taiwan; TAEK, Turkey; STFC, United Kingdom; DOE and NSF, United States of America. In addition, individual groups and members have received support from BCKDF, the Canada Council, CANARIE, CRC, Compute Canada, FQRNT, and the Ontario Innovation Trust, Canada; EPLANET, ERC, ERDF, FP7, Horizon 2020 and Marie Skłodowska-Curie Actions, European Union; Investissements d'Avenir Labex and Idex, ANR, Région Auvergne and Fondation Partager le Savoir, France; DFG and AvH Foundation, Germany; Herakleitos, Thales and Aristeia programmes co-financed by EU-ESF and the Greek NSRF; BSF, GIF and Minerva, Israel; BRF, Norway; CERCA Programme Generalitat de Catalunya, Generalitat Valenciana, Spain; the Royal Society and Leverhulme Trust, United Kingdom. The crucial computing support from all WLCG partners is acknowledged gratefully, in particular from CERN, the ATLAS Tier-1 facilities at TRIUMF (Canada), NDGF (Denmark, Norway, Sweden), CC-IN2P3 (France), KIT/GridKA (Germany), INFN-CNAF (Italy), NL-T1 (Netherlands), PIC (Spain), ASGC (Taiwan), RAL (UK) and BNL (USA), the Tier-2 facilities worldwide and large non-WLCG

resource providers. Major contributors of computing resources are listed in Ref. [125].

Funded by SCOAP[3].

References

1. S.L. Glashow, Partial symmetries of weak interactions. Nucl. Phys. **22**, 579–588 (1961)
2. A. Salam, J.C. Ward, Electromagnetic and weak interactions. Phys. Lett. **13**, 168–171 (1964)
3. S. Weinberg, A model of leptons. Phys. Rev. Lett. **19**, 1264–1266 (1967)
4. F. Englert, R. Brout, Broken symmetry and the mass of gauge vector mesons. Phys. Rev. Lett. **13**, 321–323 (1964)
5. P.W. Higgs, Broken symmetries and the masses of gauge bosons. Phys. Rev. Lett. **13**, 508–509 (1964)
6. P.W. Higgs, Broken symmetries, massless particles and gauge fields. Phys. Lett. **12**, 132–133 (1964)
7. G.S. Guralnik, C.R. Hagen, T.W.B. Kibble, Global conservation laws and massless particles. Phys. Rev. Lett. **13**, 585–587 (1964)
8. UA1 Collaboration, G. Arnison, et al., Experimental observation of isolated large transverse energy electrons with associated missing energy at $\sqrt{s}$ = 540 GeV. Phys. Lett. B **122**, 103–116 (1983)
9. UA1 Collaboration, G. Arnison, et al., Experimental observation of lepton pairs of invariant mass around 95 GeV/c^2 at the CERN SPS Collider. Phys. Lett. B **126**, 398–410 (1983)
10. UA2 Collaboration, M. Banner, et al., Observation of single isolated electrons of high transverse momentum in events with missing transverse energy at the CERN $\bar{p}p$ Collider. Phys. Lett. B **122**, 476–485 (1983)
11. UA2 Collaboration, P. Bagnaia, et al., Evidence for $Z^0 \to e^+e^-$ at the CERN $\bar{p}p$ Collider. Phys. Lett. B **129**, 130–140 (1983)
12. ATLAS Collaboration, Observation of a new particle in the search for the Standard Model Higgs boson with the ATLAS detector at the LHC. Phys. Lett. B **716**, 1 (2012). arXiv: 1207.7214 [hep-ex]
13. CMS Collaboration, Observation of a new boson at a mass of 125 GeV with the CMS experiment at the LHC. Phys. Lett. B **716**, 30 (2012). arXiv: 1207.7235 [hep-ex]
14. M. Awramik, M. Czakon, A. Freitas, G. Weiglein, Precise prediction for the W boson mass in the standard model. Phys. Rev. D **69**, 053006 (2004). arXiv:hep-ph/0311148
15. A. Sirlin, Radiative corrections in the $SU(2)_L \times U(1)$ theory: a simple renormalization framework. Phys. Rev. D **22**, 971–981 (1980)
16. M. Baak et al., The global electroweak fit at NNLO and prospects for the LHC and ILC. Eur. Phys. J. C **74**, 3046 (2014). arXiv:1407.3792 [hep-ph]
17. UA1 Collaboration, G. Arnison, et al., Intermediate vector boson properties at the CERN super proton synchrotron collider. Europhys. Lett. **1**, 327–345 (1986)
18. UA2 Collaboration, J. Alitti, et al., An Improved determination of the ratio of W and Z masses at the CERN $\bar{p}p$ collider. Phys. Lett. B **276**, 354–364 (1992)
19. CDF Collaboration, T. Affolder et al., Measurement of the W boson mass with the collider detector at fermilab. Phys. Rev. D **64**, 052001 (2001). arXiv: hep-ex/0007044
20. D0 Collaboration, V. M. Abazov, et al., Improved W boson mass measurement with the DØ detector. Phys. Rev. D **66**, 012001 (2002). arXiv: hep-ex/0204014
21. CDF and D0 collaborations, V. M. Abazov et al. Combination of CDF and D0 results on W boson mass and width. Phys. Rev. D **70**, 092008 (2004). arXiv: hep-ex/0311039
22. CDF Collaboration, T. Aaltonen et al. Precise measurement of the W-boson mass with the CDF II detector. Phys. Rev. Lett. **108**, 151803 (2012). arXiv: 1203.0275 [hep-ex]
23. D0 Collaboration, V. M. Abazov et al. Measurement of the W boson mass with the D0 detector. Phys. Rev. Lett. **108**, 151804 (2012). arXiv: 1203.0293 [hep-ex]
24. CDF and D0 Collaborations, T. Aaltonen et al. Combination of CDF and D0 W-boson mass measurements. Phys. Rev. D **88**, 052018 (2013). arXiv: 1307.7627 [hep-ex]
25. ALEPH Collaboration, S. Schael et al. Measurement of the W boson mass and width in e^+e^- collisions at LEP. Eur. Phys. J. C **47**, 309-335 (2006). arXiv: hep-ex/0605011
26. DELPHI Collaboration, J. Abdallah et al. Measurement of the mass and width of the W Boson in e^+e^- collisions at $\sqrt{s}$ = 161 – 209 GeV. Eur. Phys. J. C **55**, 1-38 (2008). arXiv: 0803.2534 [hep-ex]
27. L3 Collaboration, P. Achard, et al., Measurement of the mass and the width of the W boson at LEP. Eur. Phys. J. C **45**, 569–587 (2006). arXiv: hep-ex/0511049
28. OPAL Collaboration, G. Abbiendi et al., Measurement of the mass and width of the W boson. Eur. Phys. J. C **45**, 307–335 (2006). arXiv: hep-ex/0508060
29. Particle Data Group, K. A. Olive et al, Review of particle physics. Chin. Phys. C **38**, 090001 (2014)
30. J. de Blas, et al., Electroweak precision observables and Higgs-boson signal strengths in the Standard Model and beyond: present and future. JHEP **12**, 135. arXiv: 1608.01509 [hep-ph] (2016)
31. S. D. Drell, T.-M. Yan, Massive lepton pair production in hadron-hadron collisions at high-energies. Phys. Rev. Lett. **25**, 316-320 (1970) [Erratum: Phys. Rev. Lett. 25, 902(1970)]
32. S. Schael et al., Precision electroweak measurements on the Z resonance. Phys. Rept. **427**, 257–454 (2006). arXiv:hep-ex/0509008
33. M. Krasny, F. Dydak, F. Fayette, W. Placzek, A. Siodmok, $\Delta M_W \leq 10 MeV/c^2$ at the LHC: a forlorn hope?. Eur. Phys. J. C **69**, 379–397 (2010). arXiv: 1004.2597 [hep-ex]
34. E. Mirkes, Angular decay distribution of leptons from W bosons at NLO in hadronic collisions. Nucl. Phys. B **387**, 3–85 (1992)
35. D.Yu. Bardin, A. Leike, T. Riemann, M. Sachwitz, Energy dependent width effects in e^+e^- annihilation near the Z boson pole. Phys. Lett. B **206**, 539–542 (1988)
36. J. Smith, W.L. van Neerven, J.A.M. Vermaseren, The transverse mass and width of the W boson. Phys. Rev. Lett. **50**, 1738 (1983)
37. ATLAS Collaboration, Studies of theoretical uncertainties on the measurement of the mass of the W boson at the LHC. ATL-PHYS-PUB-2014-015 (2014). https://cdsweb.cern.ch/record/1956455
38. ATLAS Collaboration, Electron reconstruction and identification efficiency measurements with the ATLAS detector using the 2011 LHC proton–proton collision data. Eur. Phys. J. C **74**, 2941 (2014). arXiv: 1404.2240 [hep-ex]
39. ATLAS Collaboration, Electron and photon energy calibration with the ATLAS detector using LHC Run 1 data. Eur. Phys. J. C **74**, 3071 (2014). arXiv: 1407.5063 [hep-ex]
40. ATLAS Collaboration, Measurement of the muon reconstruction performance of the ATLAS detector using 2011 and 2012 LHC proton–proton collision data. Eur. Phys. J. C **74**, 3130 (2014). arXiv: 1407.3935 [hep-ex]
41. ATLAS Collaboration, Precision measurement and interpretation of inclusive W^+, W^- and Z/γ^* production cross sections with the ATLAS detector. Eur. Phys. J. C **77**, 367 (2017). arXiv: 1612.03016 [hep-ex]

42. ATLAS Collaboration, Measurement of the angular coefficients in Z-boson events using electron and muon pairs from data taken at $\sqrt{s} = 8$ TeV with the ATLAS detector. JHEP **08**, 159 (2016). arXiv: 1606.00689 [hep-ex]
43. ATLAS Collaboration, Measurement of angular correlations in Drell-Yan lepton pairs to probe Z/γ^* boson transverse momentum at $\sqrt{s} = 7$ TeV with the ATLAS detector. Phys. Lett. B **720**, 32 (2013). arXiv: 1211.6899 [hep-ex]
44. ATLAS Collaboration, Measurement of the Z/γ^* boson transverse momentum distribution in pp collisions at $\sqrt{s} = 7$ TeV with the ATLAS detector. JHEP **09**, 145 (2014). arXiv: 1406.3660 [hep-ex]
45. ATLAS Collaboration, Measurement of the transverse momentum distribution of W bosons in pp collisions at $\sqrt{s} = 7$ TeV with the ATLAS detector. Phys. Rev. D **85**, 012005 (2012). arXiv: 1108.6308 [hep-ex]
46. ATLAS Collaboration, The ATLAS Experiment at the CERN large hadron collider. JINST **3**, S08003 (2008)
47. ATLAS Collaboration, Performance of the ATLAS Trigger System in 2010. Eur. Phys. J. C **72**, 1849 (2012). arXiv: 1110.1530 [hep-ex]
48. ATLAS Collaboration, Improved luminosity determination in pp collisions at $\sqrt{s} = 7$ TeV using the ATLAS detector at the LHC. Eur. Phys. J. C **73**, 2518 (2013). arXiv: 1302.4393 [hep-ex]
49. P. Nason, A New method for combining NLO QCD with shower Monte Carlo algorithms. JHEP **11**, 040 (2004). arXiv:hep-ph/0409146
50. S. Frixione, P. Nason, C. Oleari, Matching NLO QCD computations with Parton Shower simulations: the POWHEG method. JHEP **11**, 070 (2007). arXiv:0709.2092 [hep-ph]
51. S. Alioli, P. Nason, C. Oleari, E. Re, A general framework for implementing NLO calculations in shower Monte Carlo programs: the POWHEG BOX. JHEP **06**, 043 (2010). arXiv:1002.2581 [hep-ph]
52. T. Sjöstrand, S. Mrenna, P.Z. Skands, PYTHIA 6.4 physics and manual. JHEP **05**, 026 (2006). arXiv:hep-ph/0603175
53. T. Sjöstrand, S. Mrenna, P. Skands, A brief introduction to PYTHIA 8.1. Comput. Phys. Commun. **178**, 852–867 (2008). arXiv:0710.3820 [hep-ph]
54. H.-L. Lai et al., New parton distributions for collider physics Phys. Rev. D **82**, 074024 (2010). arXiv:1007.2241 [hep-ph]
55. J. Pumplin et al., New generation of parton distributions with uncertainties from global QCD analysis. JHEP **07**, 012 (2002). arXiv:hep-ph/0201195
56. P. Golonka, Z. Was, PHOTOS Monte Carlo: a precision tool for QED corrections in Z and W decays. Eur Phys. J. C **45**, 97 (2006). arXiv:hep-ph/0506026
57. G. Corcella et al., HERWIG 6: An Event generator for hadron emission reactions with interfering gluons (including supersymmetric processes). JHEP **01**, 010 (2001). arXiv:hep-ph/0011363
58. J. Butterworth, J.R. Forshaw, M. Seymour, Multiparton interactions in photoproduction at HERA. Z. Phys. C **72**, 637–646 (1996). arXiv:hep-ph/9601371
59. S. Frixione, B.R. Webber, Matching NLO QCD computations and parton shower simulations. JHEP **06**, 029 (2002). arXiv:hep-ph/0204244
60. S. Frixione, P. Nason, B.R. Webber, Matching NLO QCD and parton showers in heavy flavor production. JHEP **08**, 007 (2003). arXiv:hep-ph/0305252 [hep-ph]
61. S. Frixione, E. Laenen, P. Motylinski, B.R. Webber, Single-top production in MC@NLO. JHEP **03**, 092 (2006). arXiv:hep-ph/0512250 [hep-ph]
62. ATLAS Collaboration, Measurement of the $t\bar{t}$ production cross-section using $e\mu$ events with b-tagged jets in pp collisions at $\sqrt{s} = 7$ and 8 TeV with the ATLAS detector. Eur. Phys. J. C **74**, 3109 (2014). arXiv: 1406.5375 [hep-ex]
63. N. Kidonakis, Next-to-next-to-leading-order collinear and soft gluon corrections for t-channel single top quark production. Phys. Rev. D **83**, 091503 (2011). arXiv:1103.2792 [hep-ph]
64. N. Kidonakis, NNLL resummation for s-channel single top quark production. Phys. Rev. D **81**, 054028 (2010). arXiv:1001.5034 [hep-ph]
65. N. Kidonakis, Two-loop soft anomalous dimensions for single top quark associated production with a W^- or H^-. Phys. Rev. D **82**, 054018 (2010). arXiv:1005.4451 [hep-ph]
66. J.M. Campbell, R.K. Ellis, An Update on vector boson pair production at hadron colliders. Phys. Rev. D **60**, 113006 (1999). arXiv:hep-ph/9905386 [hep-ph]
67. T. Gehrmann et al., W^+W^- Production at hadron colliders in next to next to leading order QCD. Phys. Rev. Lett. **113**, 212001 (2014). arXiv:1408.5243 [hep-ph]
68. ATLAS Collaboration, The ATLAS simulation infrastructure. Eur. Phys. J. C **70**, 823 (2010). arXiv: 1005.4568 [hep-ex]
69. S. Agostinelli et al., GEANT4: a simulation toolkit. Nucl. Instrum. Meth. A **506**, 250–303 (2003)
70. ATLAS Collaboration. Summary of ATLAS Pythia 8 tunes, ATL-PHYS-PUB-2012-003. (2012). https://cds.cern.ch/record/1474107
71. ATLAS Collaboration. Topological cell clustering in the ATLAS calorimeters and its performance in LHC Run 1. Eur. Phys. J. C **77**, 490 (2017). arXiv: 1603.02934 [hep-ex]
72. S. Alioli, et al., Precision studies of observables in $pp \to W \to \ell\nu$ and $pp \to \gamma, Z \to \ell^+\ell^-$ processes at the LHC working group report. Eur. Phys. J. C **77**, 280 (2017). arXiv: 1606.02330 [hep-ph]
73. S. Jadach, W. Placzek, B.F.L. Ward, BHWIDE 1.00: $\mathcal{O}(\alpha)$ YFS exponentiated Monte Carlo for Bhabha scattering at wide angles for LEP-1 / SLC and LEP-2. Phys. Lett. B **390**, 298–308 (1997). arXiv:hep-ph/9608412
74. W. Płaczek, S. Jadach, M.W. Krasny, Drell-Yan processes with WINHAC. Acta Phys. Polon. B **44**, 2171–2178 (2013). arXiv:1310.5994 [hep-ph]
75. S. Dittmaier, M. Krämer, Electroweak radiative corrections to W boson production at hadron colliders. Phys. Rev. D **65**, 073007 (2002). arXiv:hep-ph/0109062
76. U. Baur, D. Wackeroth, Electroweak radiative corrections to $p\bar{p} \to W^\pm \to \ell^\pm\nu$ beyond the pole approximation. Phys. Rev. D **70**, 073015 (2004). arXiv:hep-ph/0405191
77. Arbuzov, A. et al., One-loop corrections to the Drell-Yan process in SANC: the charged current case. Eur. Phys. J. C **46**, 407–412 (2006). arXiv: hep-ph/0506110 [Erratum: Eur. Phys. J.C50,505(2007)]
78. L. Barzè, G. Montagna, P. Nason, O. Nicrosini, F. Piccinini, Implementation of electroweak corrections in the POWHEG BOX: single W production. JHEP **04**, 037 (2012). arXiv:1202.0465 [hep-ph]
79. C. Bernaciak, D. Wackeroth, N.L.O. Combining, QCD and electroweak radiative corrections to W boson production at hadron colliders in the POWHEG framework. Phys. Rev. D **85**, 093003 (2012). arXiv:1201.4804 [hep-ph]
80. Mück A. Oymanns L., Resonance-improved parton-shower matching for the Drell-Yan process including electroweak corrections. JHEP **05**, 090 (2017). arXiv: 1612.04292 [hep-ph]
81. S. Dittmaier, A. Huss, C. Schwinn, Dominant mixed QCD-electroweak $O(\alpha_s\alpha)$ corrections to Drell-Yan processes in the resonance region. Nucl. Phys. B **904**, 216–252 (2016). arXiv:1511.08016 [hep-ph]
82. G. Altarelli, R. H. P. Kleiss, C. Verzegnassi (eds.) Workshop on Z physics at LEP1: standard physics. (1989). https://cds.cern.ch/record/116932
83. C.M. Carloni Calame, et al., Precision measurement of the W-boson mass: theoretical contributions and uncertainties. Phys. Rev. D **96**, 093005 (2017). arXiv: 1612.02841 [hep-ph]

84. J.C. Collins, D.E. Soper, Angular distribution of dileptons in high-energy hadron collisions. Phys. Rev. D **16**, 2219 (1977)
85. J. Gao, M. Guzzi, J. Huston, H.-L. Lai, Z. Li et al., CT10 next-to-next-to-leading order global analysis of QCD. Phys. Rev. D **89**, 033009 (2014). arXiv:1302.6246 [hep-ph]
86. S. Catani, L. Cieri, G. Ferrera, D. de Florian, M. Grazzini, Vector boson production at hadron colliders: a fully exclusive QCD calculation at NNLO. Phys. Rev. Lett. **103**, 082001 (2009). arXiv:0903.2120 [hep-ph]
87. T. Hahn, CUBA: a library for multidimensional numerical integration. Comput. Phys. Commun. **168**, 78–95 (2005). arXiv:hep-ph/0404043
88. J.C. Collins, D.E. Soper, G.F. Sterman, Transverse momentum distribution in Drell–Yan pair and W and Z boson production. Nucl. Phys. B **250**, 199 (1985)
89. G.A. Ladinsky, C.P. Yuan, The nonperturbative regime in QCD resummation for gauge boson production at hadron colliders. Phys. Rev. D **50**, R4239 (1994). arXiv:hep-ph/9311341
90. C. Balazs, P. Yuan, Soft gluon effects on lepton pairs at hadron colliders. Phys. Rev. D **56**, 5558–5583 (1997). arXiv:hep-ph/9704258
91. S. Catani, D. Florian, G. de Ferrera, M. Grazzini, Vector boson production at hadron colliders: transverse-momentum resummation and leptonic decay. JHEP **12**, 047 (2015). arXiv:1507.06937 [hep-ph]
92. T. Becher, M. Neubert, D. Wilhelm, Electroweak gauge-boson production at small q_T: infrared safety from the collinear anomaly. JHEP **02**, 124 (2012). arXiv:1109.6027 [hep-ph]
93. G. Miu, T. Sjöstrand, W production in an improved parton shower approach. Phys. Lett. B **449**, 313–320 (1999). arXiv:hep-ph/9812455
94. S. Catani, B.R. Webber, G. Marchesini, QCD coherent branching and semiinclusive processes at large x. Nucl. Phys. B **349**, 635–654 (1991)
95. R. Corke, T. Sjöstrand, Interleaved parton showers and tuning prospects. JHEP **03**, 032 (2011). arXiv:1011.1759 [hep-ph]
96. K. Hamilton, P. Nason, G. Zanderighi, MINLO: Multi-scale improved NLO. JHEP **10**, 155 (2012). arXiv:1206.3572 [hep-ph]
97. K. Hamilton, P. Nason, C. Oleari, G. Zanderighi, Merging H/W/Z + 0 and 1 jet at NLO with no merging scale: a path to parton shower + NNLO matching. JHEP **05**, 082 (2013). arXiv:1212.4504 [hep-ph]
98. R.D. Ball et al., Parton distributions for the LHC Run II. JHEP **04**, 040 (2015). arXiv:1410.8849 [hep-ph]
99. S. Dulat et al., New parton distribution functions from a global analysis of quantum chromodynamics. Phys. Rev. D **93**, 033006 (2016). arXiv: 1506.07443 [hep-ph]
100. L.A. Harland-Lang, A.D. Martin, P. Motylinski, R.S. Thorne, Parton distributions in the LHC era: MMHT 2014 PDFs Eur. Phys. J. C **75**, 204 (2015). arXiv:1412.3989 [hep-ph]
101. S. Alekhin, J. Blümlein,, S. Moch, The ABM parton distributions tuned to LHC data. Phys. Rev. D **89**, 054028 (2014). arXiv:1310.3059 [hep-ph]
102. M. Krasny, F. Fayette, W. Placzek, A. Siodmok, Z-boson as "the standard candle" for high precision W-boson physics at LHC. Eur. Phys. J. C **51**, 607–617 (2007). arXiv:hep-ph/0702251
103. F. Fayette, M. Krasny, W. Placzek, A. Siodmok, Measurement of $M_{W^+} - M_{W^-}$ at LHC. Eur. Phys. J. C **63**, 33–56 (2009). arXiv:0812.2571 [hep-ph]
104. G. Bozzi, L. Citelli, A. Vicini, Parton density function uncertainties on the W boson mass measurement from the lepton transverse momentum distribution. Phys. Rev. D **91**, 113005 (2015). arXiv:1501.05587 [hep-ph]
105. J. Pumplin et al., Uncertainties of predictions from parton distribution functions. II. The Hessian method. Phys. Rev. D. **65**, 014013 (2001). arXiv:hep-ph/0101032
106. H1 and ZEUS Collaborations, H. Abramowicz et al., Combination of measurements of inclusive deep inelastic $e^{\pm}p$ scattering cross sections and QCD analysis of HERA data. Eur. Phys. J. C **75**, 580 (2015). arXiv: 1506.06042 [hep-ex]
107. Wenninger J., Energy calibration of the LHC Beams at 4 TeV. CERN-ATS-2013-040 (2013). https://cdsweb.cern.ch/record/1546734
108. T. Sjöstrand, P.Z. Skands, Transverse-momentum-ordered showers and interleaved multiple interactions. Eur. Phys. J. C **39**, 129–154 (2005). arXiv:hep-ph/0408302
109. M. Bonvini, A.S. Papanastasiou, F.J. Tackmann, Matched predictions for the $b\bar{b}H$ cross section at the 13 TeV LHC. JHEP **10**, 053 (2016). arXiv:1605.01733 [hep-ph]
110. R.D. Ball et al., Parton distributions with LHC data. Nucl. Phys. B **867**, 244–289 (2013). arXiv:1207.1303 [hep-ph]
111. J. Bellm et al., Herwig 7.0/Herwig++ 3.0 release note. Eur. Phys. J. C **76**, 196 (2016). arXiv:1512.01178 [hep-ph]
112. M. Bahr et al., Herwig++ physics and manual. Eur. Phys. J. C **58**, 639–707 (2008). arXiv:0803.0883 [hep-ph]
113. ATLAS Collaboration, Study of alignment-related systematic effects on the ATLAS inner detector track reconstruction. ATLAS-CONF-2012-141 (2012). https://cdsweb.cern.ch/record/1483518
114. ATLAS Collaboration, A study of the material in the ATLAS inner detector using secondary hadronic interactions. JINST **7**, P01013. (2012). arXiv: 1110.6191 [hep-ex]
115. Devroye L., Non-Uniform Random Variate Generation. Springer, 1986. http://www.eirene.de/Devroye.pdf
116. G. Bozzi, S. Catani, G. Ferrera, D. de Florian, M. Grazzini, Transverse-momentum resummation: a perturbative study of Z production at the tevatron. Nucl. Phys. B **815**, 174–197 (2009). arXiv:0812.2862 [hep-ph]
117. G. Bozzi, S. Catani, G. Ferrera, D. de Florian, M. Grazzini, Production of Drell-Yan lepton pairs in hadron collisions: transverse-momentum resummation at next-to-next-to-leading logarithmic accuracy. Phys. Lett. B **696**, 207–213 (2011). arXiv:1007.2351 [hep-ph]
118. B. Efron, Bootstrap methods: another look at the jackknife. Ann. Statist. **7**, 1–26 (1979)
119. L. Lyons, D. Gibaut, P. Clifford, How to combine correlated estimates of a single physical quantity. Nucl. Instrum. Meth. A **270**, 110 (1988)
120. A. Valassi, Combining correlated measurements of several different physical quantities. Nucl. Instrum. Meth. A **500**, 391–405 (2003)
121. H1 Collaboration, F.D. Aaron et al., Measurement of the Inclusive ep Scattering Cross Section at Low Q^2 and x at HERA. Eur. Phys. J. C **63**, 625-678 (2009). arXiv: 0904.0929 [hep-ex]
122. ATLAS Collaboration, Measurement of the top quark mass in the $t\bar{t} \to$ dilepton channel from $\sqrt{s} = 8$ TeV ATLAS data. Phys. Lett. B **761**, 350-371 (2016) arXiv: 1606.02179 [hep-ex]
123. ATLAS and CMS Collaborations, Combined measurement of the Higgs Boson Mass in pp collisions at $\sqrt{s} = 7$ and 8 TeV with the ATLAS and CMS experiments. Phys. Rev. Lett. **114**, 191803 (2015). arXiv: 1503.07589 [hep-ex]
124. ALEPH, DELPHI, L3, OPAL Collaborations, LEP Electroweak Working Group, S. Schael et al., Electroweak Measurements in Electron-Positron Collisions at W-Boson-Pair Energies at LEP. Phys. Rept. **532**, 119-244 (2013) arXiv: 1302.3415 [hep-ex]
125. ATLAS Collaboration, ATLAS Computing Acknowledgements 2016–2017, ATL-GEN-PUB-2016-002. https://cds.cern.ch/record/2202407

ATLAS Collaboration

M. Aaboud[137d], G. Aad[88], B. Abbott[115], J. Abdallah[8], O. Abdinov[12], B. Abeloos[119], S. H. Abidi[161], O. S. AbouZeid[139], N. L. Abraham[151], H. Abramowicz[155], H. Abreu[154], R. Abreu[118], Y. Abulaiti[148a,148b], B. S. Acharya[167a,167b,a], S. Adachi[157], L. Adamczyk[41a], D. L. Adams[27], J. Adelman[110], M. Adersberger[102], T. Adye[133], A. A. Affolder[139], T. Agatonovic-Jovin[14], C. Agheorghiesei[28b], J. A. Aguilar-Saavedra[128a,128f], S. P. Ahlen[24], F. Ahmadov[68,b], G. Aielli[135a,135b], S. Akatsuka[71], H. Akerstedt[148a,148b], T. P. A. Åkesson[84], A. V. Akimov[98], G. L. Alberghi[22a,22b], J. Albert[172], M. J. Alconada Verzini[74], M. Aleksa[32], I. N. Aleksandrov[68], C. Alexa[28b], G. Alexander[155], T. Alexopoulos[10], M. Alhroob[115], B. Ali[130], M. Aliev[76a,76b], G. Alimonti[94a], J. Alison[33], S. P. Alkire[38], B. M. M. Allbrooke[151], B. W. Allen[118], P. P. Allport[19], A. Aloisio[106a,106b], A. Alonso[39], F. Alonso[74], C. Alpigiani[140], A. A. Alshehri[56], M. Alstaty[88], B. Alvarez Gonzalez[32], D. Álvarez Piqueras[170], M. G. Alviggi[106a,106b], B. T. Amadio[16], Y. Amaral Coutinho[26a], C. Amelung[25], D. Amidei[92], S. P. Amor Dos Santos[128a,128c], A. Amorim[128a,128b], S. Amoroso[32], G. Amundsen[25], C. Anastopoulos[141], L. S. Ancu[52], N. Andari[19], T. Andeen[11], C. F. Anders[60b], J. K. Anders[77], K. J. Anderson[33], A. Andreazza[94a,94b], V. Andrei[60a], S. Angelidakis[9], I. Angelozzi[109], A. Angerami[38], F. Anghinolfi[32], A. V. Anisenkov[111,c], N. Anjos[13], A. Annovi[126a,126b], C. Antel[60a], M. Antonelli[50], A. Antonov[100,*], D. J. Antrim[166], F. Anulli[134a], M. Aoki[69], L. Aperio Bella[32], G. Arabidze[93], Y. Arai[69], J. P. Araque[128a], V. Araujo Ferraz[26a], A. T. H. Arce[48], R. E. Ardell[80], F. A. Arduh[74], J-F. Arguin[97], S. Argyropoulos[66], M. Arik[20a], A. J. Armbruster[145], L. J. Armitage[79], O. Arnaez[32], H. Arnold[51], M. Arratia[30], O. Arslan[23], A. Artamonov[99], G. Artoni[122], S. Artz[86], S. Asai[157], N. Asbah[45], A. Ashkenazi[155], L. Asquith[151], K. Assamagan[27], R. Astalos[146a], M. Atkinson[169], N. B. Atlay[143], K. Augsten[130], G. Avolio[32], B. Axen[16], M. K. Ayoub[119], G. Azuelos[97,d], A. E. Baas[60a], M. J. Baca[19], H. Bachacou[138], K. Bachas[76a,76b], M. Backes[122], M. Backhaus[32], P. Bagiacchi[134a,134b], P. Bagnaia[134a,134b], J. T. Baines[133], M. Bajic[39], O. K. Baker[179], E. M. Baldin[111,c], P. Balek[175], T. Balestri[150], F. Balli[138], W. K. Balunas[124], E. Banas[42], Sw. Banerjee[176,e], A. A. E. Bannoura[178], L. Barak[32], E. L. Barberio[91], D. Barberis[53a,53b], M. Barbero[88], T. Barillari[103], M-S. Barisits[32], T. Barklow[145], N. Barlow[30], S. L. Barnes[36c], B. M. Barnett[133], R. M. Barnett[16], Z. Barnovska-Blenessy[36a], A. Baroncelli[136a], G. Barone[25], A. J. Barr[122], L. Barranco Navarro[170], F. Barreiro[85], J. Barreiro Guimarães da Costa[35a], R. Bartoldus[145], A. E. Barton[75], P. Bartos[146a], A. Basalaev[125], A. Bassalat[119,f], R. L. Bates[56], S. J. Batista[161], J. R. Batley[30], M. Battaglia[139], M. Bauce[134a,134b], F. Bauer[138], H. S. Bawa[145,g], J. B. Beacham[113], M. D. Beattie[75], T. Beau[83], P. H. Beauchemin[165], P. Bechtle[23], H. P. Beck[18,h], K. Becker[122], M. Becker[86], M. Beckingham[173], C. Becot[112], A. J. Beddall[20d], A. Beddall[20b], V. A. Bednyakov[68], M. Bedognetti[109], C. P. Bee[150], T. A. Beermann[32], M. Begalli[26a], M. Begel[27], J. K. Behr[45], A. S. Bell[81], G. Bella[155], L. Bellagamba[22a], A. Bellerive[31], M. Bellomo[89], K. Belotskiy[100], O. Beltramello[32], N. L. Belyaev[100], O. Benary[155,*], D. Benchekroun[137a], M. Bender[102], K. Bendtz[148a,148b], N. Benekos[10], Y. Benhammou[155], E. Benhar Noccioli[179], J. Benitez[66], D. P. Benjamin[48], M. Benoit[52], J. R. Bensinger[25], S. Bentvelsen[109], L. Beresford[122], M. Beretta[50], D. Berge[109], E. Bergeaas Kuutmann[168], N. Berger[5], J. Beringer[16], S. Berlendis[58], N. R. Bernard[89], G. Bernardi[83], C. Bernius[112], F. U. Bernlochner[23], T. Berry[80], P. Berta[131], C. Bertella[86], G. Bertoli[148a,148b], F. Bertolucci[126a,126b], I. A. Bertram[75], C. Bertsche[45], D. Bertsche[115], G. J. Besjes[39], O. Bessidskaia Bylund[148a,148b], M. Bessner[45], N. Besson[138], C. Betancourt[51], A. Bethani[87], S. Bethke[103], A. J. Bevan[79], R. M. Bianchi[127], O. Biebel[102], D. Biedermann[17], M. Bianco[32], R. Bielski[87], N. V. Biesuz[126a,126b], M. Biglietti[136a], J. Bilbao De Mendizabal[52], T. R. V. Billoud[97], H. Bilokon[50], M. Bindi[57], A. Bingul[20b], C. Bini[134a,134b], S. Biondi[22a,22b], T. Bisanz[57], C. Bittrich[47], D. M. Bjergaard[48], C. W. Black[152], J. E. Black[145], K. M. Black[24], D. Blackburn[140], R. E. Blair[6], J.-B. Blanchard[138], T. Blazek[146a], I. Bloch[45], C. Blocker[25], A. Blue[56], W. Blum[86,*], U. Blumenschein[79], S. Blunier[34a], G. J. Bobbink[109], V. S. Bobrovnikov[111,c], S. S. Bocchetta[84], A. Bocci[48], C. Bock[102], M. Boehler[51], D. Boerner[178], D. Bogavac[102], A. G. Bogdanchikov[111], C. Bohm[148a], V. Boisvert[80], P. Bokan[168,i], T. Bold[41a], A. S. Boldyrev[101], M. Bomben[83], M. Bona[79], M. Boonekamp[138], A. Borisov[132], G. Borissov[75], J. Bortfeldt[32], D. Bortoletto[122], V. Bortolotto[62a,62b,62c], K. Bos[109], D. Boscherini[22a], M. Bosman[13], J. D. Bossio Sola[29], J. Boudreau[127], J. Bouffard[2], E. V. Bouhova-Thacker[75], D. Boumediene[37], C. Bourdarios[119], S. K. Boutle[56], A. Boveia[113], J. Boyd[32], I. R. Boyko[68], J. Bracinik[19], A. Brandt[8], G. Brandt[57], O. Brandt[60a], U. Bratzler[158], B. Brau[89], J. E. Brau[118], W. D. Breaden Madden[56], K. Brendlinger[45], A. J. Brennan[91], L. Brenner[109], R. Brenner[168], S. Bressler[175], D. L. Briglin[19], T. M. Bristow[49], D. Britton[56], D. Britzger[45], F. M. Brochu[30], I. Brock[23], R. Brock[93], G. Brooijmans[38], T. Brooks[80], W. K. Brooks[34b], J. Brosamer[16], E. Brost[110], J. H Broughton[19], P. A. Bruckman de Renstrom[42], D. Bruncko[146b], A. Bruni[22a], G. Bruni[22a], L. S. Bruni[109], B H Brunt[30], M. Bruschi[22a], N. Bruscino[23], P. Bryant[33], L. Bryngemark[84], T. Buanes[15], Q. Buat[144], P. Buchholz[143], A. G. Buckley[56], I. A. Budagov[68], F. Buehrer[51], M. K. Bugge[121], O. Bulekov[100], D. Bullock[8], H. Burckhart[32], S. Burdin[77], C. D. Burgard[51], A. M. Burger[5], B. Burghgrave[110], K. Burka[42], S. Burke[133], I. Burmeister[46], J. T. P. Burr[122], E. Busato[37], D. Büscher[51], V. Büscher[86], P. Bussey[56], J. M. Butler[24], C. M. Buttar[56], J. M. Butterworth[81], P. Butti[32], W. Buttinger[27],

A. Buzatu[35c], A. R. Buzykaev[111,c], S. Cabrera Urbán[170], D. Caforio[130], V. M. Cairo[40a,40b], O. Cakir[4a], N. Calace[52], P. Calafiura[16], A. Calandri[88], G. Calderini[83], P. Calfayan[64], G. Callea[40a,40b], L. P. Caloba[26a], S. Calvente Lopez[85], D. Calvet[37], S. Calvet[37], T. P. Calvet[88], R. Camacho Toro[33], S. Camarda[32], P. Camarri[135a,135b], D. Cameron[121], R. Caminal Armadans[169], C. Camincher[58], S. Campana[32], M. Campanelli[81], A. Camplani[94a,94b], A. Campoverde[143], V. Canale[106a,106b], M. Cano Bret[36c], J. Cantero[116], T. Cao[155], M. D. M. Capeans Garrido[32], I. Caprini[28b], M. Caprini[28b], M. Capua[40a,40b], R. M. Carbone[38], R. Cardarelli[135a], F. Cardillo[51], I. Carli[131], T. Carli[32], G. Carlino[106a], B. T. Carlson[127], L. Carminati[94a,94b], R. M. D. Carney[148a,148b], S. Caron[108], E. Carquin[34b], G. D. Carrillo-Montoya[32], J. Carvalho[128a,128c], D. Casadei[19], M. P. Casado[13,j], M. Casolino[13], D. W. Casper[166], R. Castelijn[109], A. Castelli[109], V. Castillo Gimenez[170], N. F. Castro[128a,k], A. Catinaccio[32], J. R. Catmore[121], A. Cattai[32], J. Caudron[23], V. Cavaliere[169], E. Cavallaro[13], D. Cavalli[94a], M. Cavalli-Sforza[13], V. Cavasinni[126a,126b], E. Celebi[20a], F. Ceradini[136a,136b], L. Cerda Alberich[170], A. S. Cerqueira[26b], A. Cerri[151], L. Cerrito[135a,135b], F. Cerutti[16], A. Cervelli[18], S. A. Cetin[20c], A. Chafaq[137a], D. Chakraborty[110], S. K. Chan[59], W. S. Chan[109], Y. L. Chan[62a], P. Chang[169], J. D. Chapman[30], D. G. Charlton[19], A. Chatterjee[52], C. C. Chau[161], C. A. Chavez Barajas[151], S. Che[113], S. Cheatham[167a,167c], A. Chegwidden[93], S. Chekanov[6], S. V. Chekulaev[163a], G. A. Chelkov[68,l], M. A. Chelstowska[32], C. Chen[67], H. Chen[27], S. Chen[35b], S. Chen[157], X. Chen[35c,m], Y. Chen[70], H. C. Cheng[92], H. J. Cheng[35a], Y. Cheng[33], A. Cheplakov[68], E. Cheremushkina[132], R. Cherkaoui El Moursli[137e], V. Chernyatin[27,*], E. Cheu[7], L. Chevalier[138], V. Chiarella[50], G. Chiarelli[126a,126b], G. Chiodini[76a], A. S. Chisholm[32], A. Chitan[28b], Y. H. Chiu[172], M. V. Chizhov[68], K. Choi[64], A. R. Chomont[37], S. Chouridou[159], B.K.B. Chow[102], V. Christodoulou[81], D. Chromek-Burckhart[32], M. C. Chu[62a], J. Chudoba[129], A. J. Chuinard[90], J. J. Chwastowski[42], L. Chytka[117], A. K. Ciftci[4a], D. Cinca[46], V. Cindro[78], I. A. Cioara[23], C. Ciocca[22a,22b], A. Ciocio[16], F. Cirotto[106a,106b], Z. H. Citron[175], M. Citterio[94a], M. Ciubancan[28b], A. Clark[52], B. L. Clark[59], M. R. Clark[38], P. J. Clark[49], R. N. Clarke[16], C. Clement[148a,148b], Y. Coadou[88], M. Cobal[167a,167c], A. Coccaro[52], J. Cochran[67], L. Colasurdo[108], B. Cole[38], A. P. Colijn[109], J. Collot[58], T. Colombo[166], P. Conde Muiño[128a,128b], E. Coniavitis[51], S. H. Connell[147b], I. A. Connelly[87], V. Consorti[51], S. Constantinescu[28b], G. Conti[32], F. Conventi[106a,n], M. Cooke[16], B. D. Cooper[81], A. M. Cooper-Sarkar[122], F. Cormier[171], K. J. R. Cormier[161], T. Cornelissen[178], M. Corradi[134a,134b], F. Corriveau[90,o], A. Cortes-Gonzalez[32], G. Cortiana[103], G. Costa[94a], M. J. Costa[170], D. Costanzo[141], G. Cottin[30], G. Cowan[80], B. E. Cox[87], K. Cranmer[112], S. J. Crawley[56], R. A. Creager[124], G. Cree[31], S. Crépé-Renaudin[58], F. Crescioli[83], W. A. Cribbs[148a,148b], M. Crispin Ortuzar[122], M. Cristinziani[23], V. Croft[108], G. Crosetti[40a,40b], A. Cueto[85], T. Cuhadar Donszelmann[141], J. Cummings[179], M. Curatolo[50], J. Cúth[86], H. Czirr[143], P. Czodrowski[32], G. D'amen[22a,22b], S. D'Auria[56], M. D'Onofrio[77], M. J. Da Cunha Sargedas De Sousa[128a,128b], C. Da Via[87], W. Dabrowski[41a], T. Dado[146a], T. Dai[92], O. Dale[15], F. Dallaire[97], C. Dallapiccola[89], M. Dam[39], J. R. Dandoy[124], N. P. Dang[51], A. C. Daniells[19], N. S. Dann[87], M. Danninger[171], M. Dano Hoffmann[138], V. Dao[150], G. Darbo[53a], S. Darmora[8], J. Dassoulas[3], A. Dattagupta[118], T. Daubney[45], W. Davey[23], C. David[45], T. Davidek[131], M. Davies[155], P. Davison[81], E. Dawe[91], I. Dawson[141], K. De[8], R. de Asmundis[106a], A. De Benedetti[115], S. De Castro[22a,22b], S. De Cecco[83], N. De Groot[108], P. de Jong[109], H. De la Torre[93], F. De Lorenzi[67], A. De Maria[57], D. De Pedis[134a], A. De Salvo[134a], U. De Sanctis[151], A. De Santo[151], K. De Vasconcelos Corga[88], J. B. De Vivie De Regie[119], W. J. Dearnaley[75], R. Debbe[27], C. Debenedetti[139], D. V. Dedovich[68], N. Dehghanian[3], I. Deigaard[109], M. Del Gaudio[40a,40b], J. Del Peso[85], T. Del Prete[126a,126b], D. Delgove[119], F. Deliot[138], C. M. Delitzsch[52], A. Dell'Acqua[32], L. Dell'Asta[24], M. Dell'Orso[126a,126b], M. Della Pietra[106a,106b], D. della Volpe[52], M. Delmastro[5], P. A. Delsart[58], D. A. DeMarco[161], S. Demers[179], M. Demichev[68], A. Demilly[83], S. P. Denisov[132], D. Denysiuk[138], D. Derendarz[42], J. E. Derkaoui[137d], F. Derue[83], P. Dervan[77], K. Desch[23], C. Deterre[45], K. Dette[46], P. O. Deviveiros[32], A. Dewhurst[133], S. Dhaliwal[25], A. Di Ciaccio[135a,135b], L. Di Ciaccio[5], W. K. Di Clemente[124], C. Di Donato[106a,106b], A. Di Girolamo[32], B. Di Girolamo[32], B. Di Micco[136a,136b], R. Di Nardo[32], K. F. Di Petrillo[59], A. Di Simone[51], R. Di Sipio[161], D. Di Valentino[31], C. Diaconu[88], M. Diamond[161], F. A. Dias[49], M. A. Diaz[34a], E. B. Diehl[92], J. Dietrich[17], S. Díez Cornell[45], A. Dimitrievska[14], J. Dingfelder[23], P. Dita[28b], S. Dita[28b], F. Dittus[32], F. Djama[88], T. Djobava[54b], J. I. Djuvsland[60a], M. A. B. do Vale[26c], D. Dobos[32], M. Dobre[28b], C. Doglioni[84], J. Dolejsi[131], Z. Dolezal[131], M. Donadelli[26d], S. Donati[126a,126b], P. Dondero[123a,123b], J. Donini[37], J. Dopke[133], A. Doria[106a], M. T. Dova[74], A. T. Doyle[56], E. Drechsler[57], M. Dris[10], Y. Du[36b], J. Duarte-Campderros[155], E. Duchovni[175], G. Duckeck[102], O. A. Ducu[97,p], D. Duda[109], A. Dudarev[32], A. Chr. Dudder[86], E. M. Duffield[16], L. Duflot[119], M. Dührssen[32], M. Dumancic[175], A. E. Dumitriu[28b], A. K. Duncan[56], M. Dunford[60a], H. Duran Yildiz[4a], M. Düren[55], A. Durglishvili[54b], D. Duschinger[47], B. Dutta[45], M. Dyndal[45], C. Eckardt[45], K. M. Ecker[103], R. C. Edgar[92], T. Eifert[32], G. Eigen[15], K. Einsweiler[16], T. Ekelof[168], M. El Kacimi[137c], V. Ellajosyula[88], M. Ellert[168], S. Elles[5], F. Ellinghaus[178], A. A. Elliot[172], N. Ellis[32], J. Elmsheuser[27], M. Elsing[32], D. Emeliyanov[133], Y. Enari[157], O. C. Endner[86], J. S. Ennis[173], J. Erdmann[46], A. Ereditato[18], G. Ernis[178], M. Ernst[27], S. Errede[169], E. Ertel[86], M. Escalier[119], H. Esch[46], C. Escobar[127], B. Esposito[50], A. I. Etienvre[138], E. Etzion[155], H. Evans[64], A. Ezhilov[125], F. Fabbri[22a,22b], L. Fabbri[22a,22b], G. Facini[33], R. M. Fakhrutdinov[132],

S. Falciano[134a], R. J. Falla[81], J. Faltova[32], Y. Fang[35a], M. Fanti[94a,94b], A. Farbin[8], A. Farilla[136a], C. Farina[127], E. M. Farina[123a,123b], T. Farooque[93], S. Farrell[16], S. M. Farrington[173], P. Farthouat[32], F. Fassi[137e], P. Fassnacht[32], D. Fassouliotis[9], M. Faucci Giannelli[80], A. Favareto[53a,53b], W. J. Fawcett[122], L. Fayard[119], O. L. Fedin[125,q], W. Fedorko[171], S. Feigl[121], L. Feligioni[88], C. Feng[36b], E. J. Feng[32], H. Feng[92], A. B. Fenyuk[132], L. Feremenga[8], P. Fernandez Martinez[170], S. Fernandez Perez[13], J. Ferrando[45], A. Ferrari[168], P. Ferrari[109], R. Ferrari[123a], D. E. Ferreira de Lima[60b], A. Ferrer[170], D. Ferrere[52], C. Ferretti[92], F. Fiedler[86], A. Filipčič[78], M. Filipuzzi[45], F. Filthaut[108], M. Fincke-Keeler[172], K. D. Finelli[152], M. C. N. Fiolhais[128a,128c,r], L. Fiorini[170], A. Fischer[2], C. Fischer[13], J. Fischer[178], W. C. Fisher[93], N. Flaschel[45], I. Fleck[143], P. Fleischmann[92], R. R. M. Fletcher[124], T. Flick[178], B. M. Flierl[102], L. R. Flores Castillo[62a], M. J. Flowerdew[103], G. T. Forcolin[87], A. Formica[138], A. Forti[87], A. G. Foster[19], D. Fournier[119], H. Fox[75], S. Fracchia[113], P. Francavilla[83], M. Franchini[22a,22b], D. Francis[32], L. Franconi[121], M. Franklin[59], M. Frate[166], M. Fraternali[123a,123b], D. Freeborn[81], S. M. Fressard-Batraneanu[32], B. Freund[97], D. Froidevaux[32], J. A. Frost[122], C. Fukunaga[158], E. Fullana Torregrosa[86], T. Fusayasu[104], J. Fuster[170], C. Gabaldon[58], O. Gabizon[154], A. Gabrielli[22a,22b], A. Gabrielli[16], G. P. Gach[41a], S. Gadatsch[32], S. Gadomski[80], G. Gagliardi[53a,53b], L. G. Gagnon[97], P. Gagnon[64], C. Galea[108], B. Galhardo[128a,128c], E. J. Gallas[122], B. J. Gallop[133], P. Gallus[130], G. Galster[39], K. K. Gan[113], S. Ganguly[37], J. Gao[36a], Y. Gao[77], Y. S. Gao[145,g], F. M. Garay Walls[49], C. García[170], J. E. García Navarro[170], M. Garcia-Sciveres[16], R. W. Gardner[33], N. Garelli[145], V. Garonne[121], A. Gascon Bravo[45], K. Gasnikova[45], C. Gatti[50], A. Gaudiello[53a,53b], G. Gaudio[123a], I. L. Gavrilenko[98], C. Gay[171], G. Gaycken[23], E. N. Gazis[10], C. N. P. Gee[133], M. Geisen[86], M. P. Geisler[60a], K. Gellerstedt[148a,148b], C. Gemme[53a], M. H. Genest[58], C. Geng[36a,s], S. Gentile[134a,134b], C. Gentsos[156], S. George[80], D. Gerbaudo[13], A. Gershon[155], S. Ghasemi[143], M. Ghneimat[23], B. Giacobbe[22a], S. Giagu[134a,134b], P. Giannetti[126a,126b], S. M. Gibson[80], M. Gignac[171], M. Gilchriese[16], D. Gillberg[31], G. Gilles[178], D. M. Gingrich[3,d], N. Giokaris[9,*], M. P. Giordani[167a,167c], F. M. Giorgi[22a], P. F. Giraud[138], P. Giromini[59], D. Giugni[94a], F. Giuli[122], C. Giuliani[103], M. Giulini[60b], B. K. Gjelsten[121], S. Gkaitatzis[156], I. Gkialas[9], E. L. Gkougkousis[139], L. K. Gladilin[101], C. Glasman[85], J. Glatzer[13], P. C. F. Glaysher[45], A. Glazov[45], M. Goblirsch-Kolb[25], J. Godlewski[42], S. Goldfarb[91], T. Golling[52], D. Golubkov[132], A. Gomes[128a,128b,128d], R. Gonçalo[128a], R. Goncalves Gama[26a], J. Goncalves Pinto Firmino Da Costa[138], G. Gonella[51], L. Gonella[19], A. Gongadze[68], S. González de la Hoz[170], S. Gonzalez-Sevilla[52], L. Goossens[32], P. A. Gorbounov[99], H. A. Gordon[27], I. Gorelov[107], B. Gorini[32], E. Gorini[76a,76b], A. Gorišek[78], A. T. Goshaw[48], C. Gössling[46], M. I. Gostkin[68], C. R. Goudet[119], D. Goujdami[137c], A. G. Goussiou[140], N. Govender[147b,t], E. Gozani[154], L. Graber[57], I. Grabowska-Bold[41a], P. O. J. Gradin[58], J. Gramling[52], E. Gramstad[121], S. Grancagnolo[17], V. Gratchev[125], P. M. Gravila[28f], H. M. Gray[32], Z. D. Greenwood[82,u], C. Grefe[23], K. Gregersen[81], I. M. Gregor[45], P. Grenier[145], K. Grevtsov[5], J. Griffiths[8], A. A. Grillo[139], K. Grimm[75], S. Grinstein[13,v], Ph. Gris[37], J.-F. Grivaz[119], S. Groh[86], E. Gross[175], J. Grosse-Knetter[57], G. C. Grossi[82], Z. J. Grout[81], L. Guan[92], W. Guan[176], J. Guenther[65], F. Guescini[163a], D. Guest[166], O. Gueta[155], B. Gui[113], E. Guido[53a,53b], T. Guillemin[5], S. Guindon[2], U. Gul[56], C. Gumpert[32], J. Guo[36c], W. Guo[92], Y. Guo[36a], R. Gupta[43], S. Gupta[122], G. Gustavino[134a,134b], P. Gutierrez[115], N. G. Gutierrez Ortiz[81], C. Gutschow[81], C. Guyot[138], M. P. Guzik[41a], C. Gwenlan[122], C. B. Gwilliam[77], A. Haas[112], C. Haber[16], H. K. Hadavand[8], A. Hadef[88], S. Hageböck[23], M. Hagihara[164], H. Hakobyan[180,*], M. Haleem[45], J. Haley[116], G. Halladjian[93], G. D. Hallewell[88], K. Hamacher[178], P. Hamal[117], K. Hamano[172], A. Hamilton[147a], G. N. Hamity[141], P. G. Hamnett[45], L. Han[36a], S. Han[35a], K. Hanagaki[69,w], K. Hanawa[157], M. Hance[139], B. Haney[124], P. Hanke[60a], R. Hanna[138], J. B. Hansen[39], J. D. Hansen[39], M. C. Hansen[23], P. H. Hansen[39], K. Hara[164], A. S. Hard[176], T. Harenberg[178], F. Hariri[119], S. Harkusha[95], R. D. Harrington[49], P. F. Harrison[173], F. Hartjes[109], N. M. Hartmann[102], M. Hasegawa[70], Y. Hasegawa[142], A. Hasib[49], S. Hassani[138], S. Haug[18], R. Hauser[93], L. Hauswald[47], L. B. Havener[38], M. Havranek[130], C. M. Hawkes[19], R. J. Hawkings[32], D. Hayakawa[159], D. Hayden[93], C. P. Hays[122], J. M. Hays[79], H. S. Hayward[77], S. J. Haywood[133], S. J. Head[19], T. Heck[86], V. Hedberg[84], L. Heelan[8], K. K. Heidegger[51], S. Heim[45], T. Heim[16], B. Heinemann[45,x], J. J. Heinrich[102], L. Heinrich[112], C. Heinz[55], J. Hejbal[129], L. Helary[32], A. Held[171], S. Hellman[148a,148b], C. Helsens[32], J. Henderson[122], R. C. W. Henderson[75], Y. Heng[176], S. Henkelmann[171], A. M. Henriques Correia[32], S. Henrot-Versille[119], G. H. Herbert[17], H. Herde[25], V. Herget[177], Y. Hernández Jiménez[147c], G. Herten[51], R. Hertenberger[102], L. Hervas[32], T. C. Herwig[124], G. G. Hesketh[81], N. P. Hessey[163a], J. W. Hetherly[43], S. Higashino[69], E. Higón-Rodriguez[170], E. Hill[172], J. C. Hill[30], K. H. Hiller[45], S. J. Hillier[19], I. Hinchliffe[16], M. Hirose[51], D. Hirschbuehl[178], B. Hiti[78], O. Hladik[129], X. Hoad[49], J. Hobbs[150], N. Hod[163a], M. C. Hodgkinson[141], P. Hodgson[141], A. Hoecker[32], M. R. Hoeferkamp[107], F. Hoenig[102], D. Hohn[23], T. R. Holmes[16], M. Homann[46], S. Honda[164], T. Honda[69], T. M. Hong[127], B. H. Hooberman[169], W. H. Hopkins[118], Y. Horii[105], A. J. Horton[144], J-Y. Hostachy[58], S. Hou[153], A. Hoummada[137a], J. Howarth[45], J. Hoya[74], M. Hrabovsky[117], I. Hristova[17], J. Hrivnac[119], T. Hryn'ova[5], A. Hrynevich[96], P. J. Hsu[63], S.-C. Hsu[140], Q. Hu[36a], S. Hu[36c], Y. Huang[35a], Z. Hubacek[130], F. Hubaut[88], F. Huegging[23], T. B. Huffman[122], E. W. Hughes[38], G. Hughes[75], M. Huhtinen[32], P. Huo[150], N. Huseynov[68,b], J. Huston[93], J. Huth[59], G. Iacobucci[52], G. Iakovidis[27], I. Ibragimov[143], L. Iconomidou-Fayard[119], P. Iengo[32], O. Igonkina[109,x], T. Iizawa[174],

Y. Ikegami[69], M. Ikeno[69], Y. Ilchenko[11,y], D. Iliadis[156], N. Ilic[145], G. Introzzi[123a,123b], P. Ioannou[9,*], M. Iodice[136a], K. Iordanidou[38], V. Ippolito[59], N. Ishijima[120], M. Ishino[157], M. Ishitsuka[159], C. Issever[122], S. Istin[20a], F. Ito[164], J. M. Iturbe Ponce[87], R. Iuppa[162a,162b], H. Iwasaki[69], J. M. Izen[44], V. Izzo[106a], S. Jabbar[3], P. Jackson[1], V. Jain[2], K. B. Jakobi[86], K. Jakobs[51], S. Jakobsen[32], T. Jakoubek[129], D. O. Jamin[116], D. K. Jana[82], R. Jansky[65], J. Janssen[23], M. Janus[57], P. A. Janus[41a], G. Jarlskog[84], N. Javadov[68,b], T. Javůrek[51], M. Javurkova[51], F. Jeanneau[138], L. Jeanty[16], J. Jejelava[54a,aa], A. Jelinskas[173], P. Jenni[51,ab], C. Jeske[173], S. Jézéquel[5], H. Ji[176], J. Jia[150], H. Jiang[67], Y. Jiang[36a], Z. Jiang[145], S. Jiggins[81], J. Jimenez Pena[170], S. Jin[35a], A. Jinaru[28b], O. Jinnouchi[159], H. Jivan[147c], P. Johansson[141], K. A. Johns[7], C. A. Johnson[64], W. J. Johnson[140], K. Jon-And[148a,148b], R. W. L. Jones[75], S. Jones[7], T. J. Jones[77], J. Jongmanns[60a], P. M. Jorge[128a,128b], J. Jovicevic[163a], X. Ju[176], A. Juste Rozas[13,v], M. K. Köhler[175], A. Kaczmarska[42], M. Kado[119], H. Kagan[113], M. Kagan[145], S. J. Kahn[88], T. Kaji[174], E. Kajomovitz[48], C. W. Kalderon[84], A. Kaluza[86], S. Kama[43], A. Kamenshchikov[132], N. Kanaya[157], S. Kaneti[30], L. Kanjir[78], V. A. Kantserov[100], J. Kanzaki[69], B. Kaplan[112], L. S. Kaplan[176], D. Kar[147c], K. Karakostas[10], N. Karastathis[10], M. J. Kareem[57], E. Karentzos[10], M. Karnevskiy[86], S. N. Karpov[68], Z. M. Karpova[68], K. Karthik[112], V. Kartvelishvili[75], A. N. Karyukhin[132], K. Kasahara[164], L. Kashif[176], R. D. Kass[113], A. Kastanas[149], Y. Kataoka[157], C. Kato[157], A. Katre[52], J. Katzy[45], K. Kawade[105], K. Kawagoe[73], T. Kawamoto[157], G. Kawamura[57], E. F. Kay[77], V. F. Kazanin[111,c], R. Keeler[172], R. Kehoe[43], J. S. Keller[45], J. J. Kempster[80], H. Keoshkerian[161], O. Kepka[129], B. P. Kerševan[78], S. Kersten[178], R. A. Keyes[90], M. Khader[169], F. Khalil-zada[12], A. Khanov[116], A. G. Kharlamov[111,c], T. Kharlamova[111,c], A. Khodinov[160], T. J. Khoo[52], V. Khovanskiy[99,*], E. Khramov[68], J. Khubua[54b,ac], S. Kido[70], C. R. Kilby[80], H. Y. Kim[8], S. H. Kim[164], Y. K. Kim[33], N. Kimura[156], O. M. Kind[17], B. T. King[77], D. Kirchmeier[47], J. Kirk[133], A. E. Kiryunin[103], T. Kishimoto[157], D. Kisielewska[41a], K. Kiuchi[164], O. Kivernyk[138], E. Kladiva[146b], T. Klapdor-Kleingrothaus[51], M. H. Klein[38], M. Klein[77], U. Klein[77], K. Kleinknecht[86], P. Klimek[110], A. Klimentov[27], R. Klingenberg[46], T. Klioutchnikova[32], E.-E. Kluge[60a], P. Kluit[109], S. Kluth[103], J. Knapik[42], E. Kneringer[65], E. B. F. G. Knoops[88], A. Knue[103], A. Kobayashi[157], D. Kobayashi[159], T. Kobayashi[157], M. Kobel[47], M. Kocian[145], P. Kodys[131], T. Koffas[31], E. Koffeman[109], N. M. Köhler[103], T. Koi[145], M. Kolb[60b], I. Koletsou[5], A. A. Komar[98,*], Y. Komori[157], T. Kondo[69], N. Kondrashova[36c], K. Köneke[51], A. C. König[108], T. Kono[69,ad], R. Konoplich[112,ae], N. Konstantinidis[81], R. Kopeliansky[64], S. Koperny[41a], A. K. Kopp[51], K. Korcyl[42], K. Kordas[156], A. Korn[81], A. A. Korol[111,c], I. Korolkov[13], E. V. Korolkova[141], O. Kortner[103], S. Kortner[103], T. Kosek[131], V. V. Kostyukhin[23], A. Kotwal[48], A. Koulouris[10], A. Kourkoumeli-Charalampidi[123a,123b], C. Kourkoumelis[9], V. Kouskoura[27], A. B. Kowalewska[42], R. Kowalewski[172], T. Z. Kowalski[41a], C. Kozakai[157], W. Kozanecki[138], A. S. Kozhin[132], V. A. Kramarenko[101], G. Kramberger[78], D. Krasnopevtsev[100], M. W. Krasny[83], A. Krasznahorkay[32], D. Krauss[103], A. Kravchenko[27], J. A. Kremer[41a], M. Kretz[60c], J. Kretzschmar[77], K. Kreutzfeldt[55], P. Krieger[161], K. Krizka[33], K. Kroeninger[46], H. Kroha[103], J. Kroll[124], J. Kroseberg[23], J. Krstic[14], U. Kruchonak[68], H. Krüger[23], N. Krumnack[67], M. C. Kruse[48], M. Kruskal[24], T. Kubota[91], H. Kucuk[81], S. Kuday[4b], J. T. Kuechler[178], S. Kuehn[51], A. Kugel[60c], F. Kuger[177], T. Kuhl[45], V. Kukhtin[68], R. Kukla[88], Y. Kulchitsky[95], S. Kuleshov[34b], Y. P. Kulinich[169], M. Kuna[134a,134b], T. Kunigo[71], A. Kupco[129], O. Kuprash[155], H. Kurashige[70], L. L. Kurchaninov[163a], Y. A. Kurochkin[95], M. G. Kurth[35a], V. Kus[129], E. S. Kuwertz[172], M. Kuze[159], J. Kvita[117], T. Kwan[172], D. Kyriazopoulos[141], A. La Rosa[103], J. L. La Rosa Navarro[26d], L. La Rotonda[40a,40b], C. Lacasta[170], F. Lacava[134a,134b], J. Lacey[45], H. Lacker[17], D. Lacour[83], E. Ladygin[68], R. Lafaye[5], B. Laforge[83], T. Lagouri[179], S. Lai[57], S. Lammers[64], W. Lampl[7], E. Lançon[27], U. Landgraf[51], M. P. J. Landon[79], M. C. Lanfermann[52], V. S. Lang[60a], J. C. Lange[13], A. J. Lankford[166], F. Lanni[27], K. Lantzsch[23], A. Lanza[123a], A. Lapertosa[53a,53b], S. Laplace[83], J. F. Laporte[138], T. Lari[94a], F. Lasagni Manghi[22a,22b], M. Lassnig[32], P. Laurelli[50], W. Lavrijsen[16], A. T. Law[139], P. Laycock[77], T. Lazovich[59], M. Lazzaroni[94a,94b], B. Le[91], O. Le Dortz[83], E. Le Guirriec[88], E. P. Le Quilleuc[138], M. LeBlanc[172], T. LeCompte[6], F. Ledroit-Guillon[58], C. A. Lee[27], S. C. Lee[153], L. Lee[1], B. Lefebvre[90], G. Lefebvre[83], M. Lefebvre[172], F. Legger[102], C. Leggett[16], A. Lehan[77], G. Lehmann Miotto[32], X. Lei[7], W. A. Leight[45], A. G. Leister[179], M. A. L. Leite[26d], R. Leitner[131], D. Lellouch[175], B. Lemmer[57], K. J. C. Leney[81], T. Lenz[23], B. Lenzi[32], R. Leone[7], S. Leone[126a,126b], C. Leonidopoulos[49], G. Lerner[151], C. Leroy[97], A. A. J. Lesage[138], C. G. Lester[30], M. Levchenko[125], J. Levêque[5], D. Levin[92], L. J. Levinson[175], M. Levy[19], D. Lewis[79], M. Leyton[44], B. Li[36a,s], C. Li[36a], H. Li[150], L. Li[48], L. Li[36c], Q. Li[35a], S. Li[48], X. Li[36c], Y. Li[143], Z. Liang[35a], B. Liberti[135a], A. Liblong[161], K. Lie[169], J. Liebal[23], W. Liebig[15], A. Limosani[152], S. C. Lin[153,af], T. H. Lin[86], B. E. Lindquist[150], A. E. Lionti[52], E. Lipeles[124], A. Lipniacka[15], M. Lisovyi[60b], T. M. Liss[169], A. Lister[171], A. M. Litke[139], B. Liu[153,ag], H. Liu[92], H. Liu[27], J. Liu[36b], J. B. Liu[36a], K. Liu[88], L. Liu[169], M. Liu[36a], Y. L. Liu[36a], Y. Liu[36a], M. Livan[123a,123b], A. Lleres[58], J. Llorente Merino[35a], S. L. Lloyd[79], C. Y. Lo[62b], F. Lo Sterzo[153], E. M. Lobodzinska[45], P. Loch[7], F. K. Loebinger[87], K. M. Loew[25], A. Loginov[179,*], T. Lohse[17], K. Lohwasser[45], M. Lokajicek[129], B. A. Long[24], J. D. Long[169], R. E. Long[75], L. Longo[76a,76b], K. A. Looper[113], J. A. Lopez[34b], D. Lopez Mateos[59], I. Lopez Paz[13], A. Lopez Solis[83], J. Lorenz[102], N. Lorenzo Martinez[64], M. Losada[21], P. J. Lösel[102], X. Lou[35a], A. Lounis[119], J. Love[6], P. A. Love[75], H. Lu[62a], N. Lu[92],

Y. J. Lu[63], H. J. Lubatti[140], C. Luci[134a,134b], A. Lucotte[58], C. Luedtke[51], F. Luehring[64], W. Lukas[65], L. Luminari[134a], O. Lundberg[148a,148b], B. Lund-Jensen[149], P. M. Luzi[83], D. Lynn[27], R. Lysak[129], E. Lytken[84], V. Lyubushkin[68], H. Ma[27], L. L. Ma[36b], Y. Ma[36b], G. Maccarrone[50], A. Macchiolo[103], C. M. Macdonald[141], B. Maček[78], J. Machado Miguens[124,128b], D. Madaffari[88], R. Madar[37], H. J. Maddocks[168], W. F. Mader[47], A. Madsen[45], J. Maeda[70], S. Maeland[15], T. Maeno[27], A. Maevskiy[101], E. Magradze[57], J. Mahlstedt[109], C. Maiani[119], C. Maidantchik[26a], A. A. Maier[103], T. Maier[102], A. Maio[128a,128b,128d], S. Majewski[118], Y. Makida[69], N. Makovec[119], B. Malaescu[83], Pa. Malecki[42], V. P. Maleev[125], F. Malek[58], U. Mallik[66], D. Malon[6], C. Malone[30], S. Maltezos[10], S. Malyukov[32], J. Mamuzic[170], G. Mancini[50], L. Mandelli[94a], I. Mandić[78], J. Maneira[128a,128b], L. Manhaes de Andrade Filho[26b], J. Manjarres Ramos[163b], A. Mann[102], A. Manousos[32], B. Mansoulie[138], J. D. Mansour[35a], R. Mantifel[90], M. Mantoani[57], S. Manzoni[94a,94b], L. Mapelli[32], G. Marceca[29], L. March[52], G. Marchiori[83], M. Marcisovsky[129], M. Marjanovic[37], D. E. Marley[92], F. Marroquim[26a], S. P. Marsden[87], Z. Marshall[16], M. U. F Martensson[168], S. Marti-Garcia[170], C. B. Martin[113], T. A. Martin[173], V. J. Martin[49], B. Martin dit Latour[15], M. Martinez[13,v], V. I. Martinez Outschoorn[169], S. Martin-Haugh[133], V. S. Martoiu[28b], A. C. Martyniuk[81], A. Marzin[115], L. Masetti[86], T. Mashimo[157], R. Mashinistov[98], J. Masik[87], A. L. Maslennikov[111,c], L. Massa[135a,135b], P. Mastrandrea[5], A. Mastroberardino[40a,40b], T. Masubuchi[157], P. Mättig[178], J. Maurer[28b], S. J. Maxfield[77], D. A. Maximov[111,c], R. Mazini[153], I. Maznas[156], S. M. Mazza[94a,94b], N. C. Mc Fadden[107], G. Mc Goldrick[161], S. P. Mc Kee[92], A. McCarn[92], R. L. McCarthy[150], T. G. McCarthy[103], L. I. McClymont[81], E. F. McDonald[91], J. A. Mcfayden[81], G. Mchedlidze[57], S. J. McMahon[133], P. C. McNamara[91], R. A. McPherson[172,o], S. Meehan[140], T. J. Megy[51], S. Mehlhase[102], A. Mehta[77], T. Meideck[58], K. Meier[60a], C. Meineck[102], B. Meirose[44], D. Melini[170,ah], B. R. Mellado Garcia[147c], M. Melo[146a], F. Meloni[18], S. B. Menary[87], L. Meng[77], X. T. Meng[92], A. Mengarelli[22a,22b], S. Menke[103], E. Meoni[165], S. Mergelmeyer[17], P. Mermod[52], L. Merola[106a,106b], C. Meroni[94a], F. S. Merritt[33], A. Messina[134a,134b], J. Metcalfe[6], A. S. M ete[166], C. Meyer[124], J-P. Meyer[138], J. Meyer[109], H. Meyer Zu Theenhausen[60a], F. Miano[151], R. P. Middleton[133], S. Miglioranzi[53a,53b], L. Mijović[49], G. Mikenberg[175], M. Mikestikova[129], M. Mikuž[78], M. Milesi[91], A. Milic[27], D. W. Miller[33], C. Mills[49], A. Milov[175], D. A. Milstead[148a,148b], A. A. Minaenko[132], Y. Minami[157], I. A. Minashvili[68], A. I. Mincer[112], B. Mindur[41a], M. Mineev[68], Y. Minegishi[157], Y. Ming[176], L. M. Mir[13], K. P. Mistry[124], T. Mitani[174], J. Mitrevski[102], V. A. Mitsou[170], A. Miucci[18], P. S. Miyagawa[141], A. Mizukami[69], J. U. Mjörnmark[84], M. Mlynarikova[131], T. Moa[148a,148b], K. Mochizuki[97], P. Mogg[51], S. Mohapatra[38], S. Molander[148a,148b], R. Moles-Valls[23], R. Monden[71], M. C. Mondragon[93], K. Mönig[45], J. Monk[39], E. Monnier[88], A. Montalbano[150], J. Montejo Berlingen[32], F. Monticelli[74], S. Monzani[94a,94b], R. W. Moore[3], N. Morange[119], D. Moreno[21], M. Moreno Llácer[57], P. Morettini[53a], S. Morgenstern[32], D. Mori[144], T. Mori[157], M. Morii[59], M. Morinaga[157], V. Morisbak[121], A. K. Morley[152], G. Mornacchi[32], J. D. Morris[79], L. Morvaj[150], P. Moschovakos[10], M. Mosidze[54b], H. J. Moss[141], J. Moss[145,ai], K. Motohashi[159], R. Mount[145], E. Mountricha[27], E. J. W. Moyse[89], S. Muanza[88], R. D. Mudd[19], F. Mueller[103], J. Mueller[127], R. S. P. Mueller[102], D. Muenstermann[75], P. Mullen[56], G. A. Mullier[18], F. J. Munoz Sanchez[87], W. J. Murray[173,133], H. Musheghyan[157], M. Muškinja[78], A. G. Myagkov[132,aj], M. Myska[130], B. P. Nachman[16], O. Nackenhorst[52], K. Nagai[122], R. Nagai[69,ad], K. Nagano[69], Y. Nagasaka[61], K. Nagata[164], M. Nagel[51], E. Nagy[88], A. M. Nairz[32], Y. Nakahama[105], K. Nakamura[69], T. Nakamura[157], I. Nakano[114], R. F. Naranjo Garcia[45], R. Narayan[11], D. I. Narrias Villar[60a], I. Naryshkin[125], T. Naumann[45], G. Navarro[21], R. Nayyar[7], H. A. Neal[92], P. Yu. Nechaeva[98], T. J. Neep[138], A. Negri[123a,123b], M. Negrini[22a], S. Nektarijevic[108], C. Nellist[119], A. Nelson[166], M. E. Nelson[122], S. Nemecek[129], P. Nemethy[112], A. A. Nepomuceno[26a], M. Nessi[32,ak], M. S. Neubauer[169], M. Neumann[178], R. M. Neves[112], P. Nevski[27], P. R. Newman[19], T. Y. Ng[62c], T. Nguyen Manh[97], R. B. Nickerson[122], R. Nicolaidou[138], J. Nielsen[139], V. Nikolaenko[132,aj], I. Nikolic-Audit[83], K. Nikolopoulos[19], J. K. Nilsen[121], P. Nilsson[27], Y. Ninomiya[157], A. Nisati[134a], N. Nishu[35c], R. Nisius[103], T. Nobe[157], Y. Noguchi[71], M. Nomachi[120], I. Nomidis[31], M. A. Nomura[27], T. Nooney[79], M. Nordberg[32], N. Norjoharuddeen[122], O. Novgorodova[47], S. Nowak[103], M. Nozaki[69], L. Nozka[117], K. Ntekas[166], E. Nurse[81], F. Nuti[91], D. C. O'Neil[144], A. A. O'Rourke[45], V. O'Shea[56], F. G. Oakham[31,d], H. Oberlack[103], T. Obermann[23], J. Ocariz[83], A. Ochi[70], I. Ochoa[38], J. P. Ochoa-Ricoux[34a], S. Oda[73], S. Odaka[69], H. Ogren[64], A. Oh[87], S. H. Oh[48], C. C. Ohm[16], H. Ohman[168], H. Oide[53a,53b], H. Okawa[164], Y. Okumura[157], T. Okuyama[69], A. Olariu[28b], L. F. Oleiro Seabra[128a], S. A. Olivares Pino[49], D. Oliveira Damazio[27], A. Olszewski[42], J. Olszowska[42], A. Onofre[128a,128e], K. Onogi[105], P. U. E. Onyisi[11,z], M. J. Oreglia[33], Y. Oren[155], D. Orestano[136a,136b], N. Orlando[62b], R. S. Orr[161], B. Osculati[53a,53b,*], R. Ospanov[87], G. Otero y Garzon[29], H. Otono[73], M. Ouchrif[137d], F. Ould-Saada[121], A. Ouraou[138], K. P. Oussoren[109], Q. Ouyang[35a], M. Owen[56], R. E. Owen[19], V. E. Ozcan[20a], N. Ozturk[8], K. Pachal[144], A. Pacheco Pages[13], L. Pacheco Rodriguez[138], C. Padilla Aranda[13], S. Pagan Griso[16], M. Paganini[179], F. Paige[27], P. Pais[89], G. Palacino[64], S. Palazzo[40a,40b], S. Palestini[32], M. Palka[41b], D. Pallin[37], E. St. Panagiotopoulou[10], I. Panagoulias[10], C. E. Pandini[83], J. G. Panduro Vazquez[80], P. Pani[32], S. Panitkin[27], D. Pantea[28b], L. Paolozzi[52], Th. D. Papadopoulou[10], K. Papageorgiou[9], A. Paramonov[6], D. Paredes Hernandez[179], A. J. Parker[75], M. A. Parker[30], K. A. Parker[45], F. Parodi[53a,53b], J. A. Parsons[38], U. Parzefall[51],

V. R. Pascuzzi[161], J. M. Pasner[139], E. Pasqualucci[134a], S. Passaggio[53a], Fr. Pastore[80], S. Pataraia[178], J. R. Pater[87], T. Pauly[32], J. Pearce[172], B. Pearson[103], L. E. Pedersen[39], S. Pedraza Lopez[170], R. Pedro[128a,128b], S. V. Peleganchuk[111,c], O. Penc[129], C. Peng[35a], H. Peng[36a], J. Penwell[64], B. S. Peralva[26b], M. M. Perego[138], D. V. Perepelitsa[27], L. Perini[94a,94b], H. Pernegger[32], S. Perrella[106a,106b], R. Peschke[45], V. D. Peshekhonov[68], K. Peters[45], R. F. Y. Peters[87], B. A. Petersen[32], T. C. Petersen[39], E. Petit[58], A. Petridis[1], C. Petridou[156], P. Petroff[119], E. Petrolo[134a], M. Petrov[122], F. Petrucci[136a,136b], N. E. Pettersson[89], A. Peyaud[138], R. Pezoa[34b], P. W. Phillips[133], G. Piacquadio[150], E. Pianori[173], A. Picazio[89], E. Piccaro[79], M. A. Pickering[122], R. Piegaia[29], J. E. Pilcher[33], A. D. Pilkington[87], A. W. J. Pin[87], M. Pinamonti[167a,167c,al], J. L. Pinfold[3], H. Pirumov[45], M. Pitt[175], L. Plazak[146a], M.-A. Pleier[27], V. Pleskot[86], E. Plotnikova[68], D. Pluth[67], P. Podberezko[111], R. Poettgen[148a,148b], L. Poggioli[119], D. Pohl[23], G. Polesello[123a], A. Poley[45], A. Policicchio[40a,40b], R. Polifka[32], A. Polini[22a], C. S. Pollard[56], V. Polychronakos[27], K. Pommès[32], L. Pontecorvo[134a], B. G. Pope[93], G. A. Popeneciu[28d], A. Poppleton[32], S. Pospisil[130], K. Potamianos[16], I. N. Potrap[68], C. J. Potter[30], C. T. Potter[118], G. Poulard[32], J. Poveda[32], M. E. Pozo Astigarraga[32], P. Pralavorio[88], A. Pranko[16], S. Prell[67], D. Price[87], L. E. Price[6], M. Primavera[76a], S. Prince[90], K. Prokofiev[62c], F. Prokoshin[34b], S. Protopopescu[27], J. Proudfoot[6], M. Przybycien[41a], D. Puddu[136a,136b], A. Puri[169], P. Puzo[119], J. Qian[92], G. Qin[56], Y. Qin[87], A. Quadt[57], W. B. Quayle[167a,167b], M. Queitsch-Maitland[45], D. Quilty[56], S. Raddum[121], V. Radeka[27], V. Radescu[122], S. K. Radhakrishnan[150], P. Radloff[118], P. Rados[91], F. Ragusa[94a,94b], G. Rahal[181], J. A. Raine[87], S. Rajagopalan[27], C. Rangel-Smith[168], M. G. Ratti[94a,94b], D. M. Rauch[45], F. Rauscher[102], S. Rave[86], T. Ravenscroft[56], I. Ravinovich[175], M. Raymond[32], A. L. Read[121], N. P. Readioff[77], M. Reale[76a,76b], D. M. Rebuzzi[123a,123b], A. Redelbach[177], G. Redlinger[27], R. Reece[139], R. G. Reed[147c], K. Reeves[44], L. Rehnisch[17], J. Reichert[124], A. Reiss[86], C. Rembser[32], H. Ren[35a], M. Rescigno[134a], S. Resconi[94a], E. D. Resseguie[124], S. Rettie[171], E. Reynolds[19], O. L. Rezanova[111,c], P. Reznicek[131], R. Rezvani[97], R. Richter[103], S. Richter[81], E. Richter-Was[41b], O. Ricken[23], M. Ridel[83], P. Rieck[103], C. J. Riegel[178], J. Rieger[57], O. Rifki[115], M. Rijssenbeek[150], A. Rimoldi[123a,123b], M. Rimoldi[18], L. Rinaldi[22a], B. Ristić[52], E. Ritsch[32], I. Riu[13], F. Rizatdinova[116], E. Rizvi[79], C. Rizzi[13], R. T. Roberts[87], S. H. Robertson[90,o], A. Robichaud-Veronneau[90], D. Robinson[30], J. E. M. Robinson[45], A. Robson[56], C. Roda[126a,126b], Y. Rodina[88], A. Rodriguez Perez[13], D. Rodriguez Rodriguez[170], S. Roe[32], C. S. Rogan[59], O. Røhne[121], J. Roloff[59], A. Romaniouk[100], M. Romano[22a,22b], S. M. Romano Saez[37], E. Romero Adam[170], N. Rompotis[77], M. Ronzani[51], L. Roos[83], S. Rosati[134a], K. Rosbach[51], P. Rose[139], N.-A. Rosien[57], V. Rossetti[148a,148b], E. Rossi[106a,106b], L. P. Rossi[53a], J. H. N. Rosten[30], R. Rosten[140], M. Rotaru[28b], I. Roth[175], J. Rothberg[140], D. Rousseau[119], A. Rozanov[88], Y. Rozen[154], X. Ruan[147c], F. Rubbo[145], F. Rühr[51], A. Ruiz-Martinez[31], Z. Rurikova[51], N. A. Rusakovich[68], A. Ruschke[102], H. L. Russell[140], J. P. Rutherfoord[7], N. Ruthmann[32], Y. F. Ryabov[125], M. Rybar[169], G. Rybkin[119], S. Ryu[6], A. Ryzhov[132], G. F. Rzehorz[57], A. F. Saavedra[152], G. Sabato[109], S. Sacerdoti[29], H. F-W. Sadrozinski[139], R. Sadykov[68], F. Safai Tehrani[134a], P. Saha[110], M. Sahinsoy[60a], M. Saimpert[45], M. Saito[157], T. Saito[157], H. Sakamoto[157], Y. Sakurai[174], G. Salamanna[136a,136b], J. E. Salazar Loyola[34b], D. Salek[109], P. H. Sales De Bruin[140], D. Salihagic[103], A. Salnikov[145], J. Salt[170], D. Salvatore[40a,40b], F. Salvatore[151], A. Salvucci[62a,62b,62c], A. Salzburger[32], D. Sammel[51], D. Sampsonidis[156], J. Sánchez[170], V. Sanchez Martinez[170], A. Sanchez Pineda[106a,106b], H. Sandaker[121], R. L. Sandbach[79], C. O. Sander[45], M. Sandhoff[178], C. Sandoval[21], D. P. C. Sankey[133], M. Sannino[53a,53b], A. Sansoni[50], C. Santoni[37], R. Santonico[135a,135b], H. Santos[128a], I. Santoyo Castillo[151], K. Sapp[127], A. Sapronov[68], J. G. Saraiva[128a,128d], B. Sarrazin[23], O. Sasaki[69], K. Sato[164], E. Sauvan[5], G. Savage[80], P. Savard[161,d], N. Savic[103], C. Sawyer[133], L. Sawyer[82,u], J. Saxon[33], C. Sbarra[22a], A. Sbrizzi[22a,22b], T. Scanlon[81], D. A. Scannicchio[166], M. Scarcella[152], V. Scarfone[40a,40b], J. Schaarschmidt[140], P. Schacht[103], B. M. Schachtner[102], D. Schaefer[32], L. Schaefer[124], R. Schaefer[45], J. Schaeffer[86], S. Schaepe[23], S. Schaetzel[60b], U. Schäfer[86], A. C. Schaffer[119], D. Schaile[102], R. D. Schamberger[150], V. Scharf[60a], V. A. Schegelsky[125], D. Scheirich[131], M. Schernau[166], C. Schiavi[53a,53b], S. Schier[139], C. Schillo[51], M. Schioppa[40a,40b], S. Schlenker[32], K. R. Schmidt-Sommerfeld[103], K. Schmieden[32], C. Schmitt[86], S. Schmitt[45], S. Schmitz[86], B. Schneider[163a], U. Schnoor[51], L. Schoeffel[138], A. Schoening[60b], B. D. Schoenrock[93], E. Schopf[23], M. Schott[86], J. F. P. Schouwenberg[108], J. Schovancova[8], S. Schramm[52], N. Schuh[86], A. Schulte[86], M. J. Schultens[23], H.-C. Schultz-Coulon[60a], H. Schulz[17], M. Schumacher[51], B. A. Schumm[139], Ph. Schune[138], A. Schwartzman[145], T. A. Schwarz[92], H. Schweiger[87], Ph. Schwemling[138], R. Schwienhorst[93], J. Schwindling[138], T. Schwindt[23], G. Sciolla[25], F. Scuri[126a,126b], F. Scutti[91], J. Searcy[92], P. Seema[23], S. C. Seidel[107], A. Seiden[139], J. M. Seixas[26a], G. Sekhniaidze[106a], K. Sekhon[92], S. J. Sekula[43], N. Semprini-Cesari[22a,22b], C. Serfon[121], L. Serin[119], L. Serkin[167a,167b], M. Sessa[136a,136b], R. Seuster[172], H. Severini[115], T. Sfiligoj[78], F. Sforza[32], A. Sfyrla[52], E. Shabalina[57], N. W. Shaikh[148a,148b], L. Y. Shan[35a], R. Shang[169], J. T. Shank[24], M. Shapiro[16], P. B. Shatalov[99], K. Shaw[167a,167b], S. M. Shaw[87], A. Shcherbakova[148a,148b], C. Y. Shehu[151], Y. Shen[115], P. Sherwood[81], L. Shi[153,an], S. Shimizu[70], C. O. Shimmin[179], M. Shimojima[104], S. Shirabe[73], M. Shiyakova[68,ao], J. Shlomi[175], A. Shmeleva[98], D. Shoaleh Saadi[97], M. J. Shochet[33], S. Shojaii[94a], D. R. Shope[115], S. Shrestha[113], E. Shulga[100], M. A. Shupe[7], P. Sicho[129], A. M. Sickles[169], P. E. Sidebo[149], E. Sideras Haddad[147c], O. Sidiropoulou[177], D. Sidorov[116],

A. Sidoti[22a,22b], F. Siegert[47], Dj. Sijacki[14], J. Silva[128a,128d], S. B. Silverstein[148a], V. Simak[130], Lj. Simic[14], S. Simion[119], E. Simioni[86], B. Simmons[81], M. Simon[86], P. Sinervo[161], N. B. Sinev[118], M. Sioli[22a,22b], G. Siragusa[177], I. Siral[92], S. Yu. Sivoklokov[101], J. Sjölin[148a,148b], M. B. Skinner[75], P. Skubic[115], M. Slater[19], T. Slavicek[130], M. Slawinska[109], K. Sliwa[165], R. Slovak[131], V. Smakhtin[175], B. H. Smart[5], L. Smestad[15], J. Smiesko[146a], S. Yu. Smirnov[100], Y. Smirnov[100], L. N. Smirnova[101,ap], O. Smirnova[84], J. W. Smith[57], M. N. K. Smith[38], R. W. Smith[38], M. Smizanska[75], K. Smolek[130], A. A. Snesarev[98], I. M. Snyder[118], S. Snyder[27], R. Sobie[172,o], F. Socher[47], A. Soffer[155], D. A. Soh[153], G. Sokhrannyi[78], C. A. Solans Sanchez[32], M. Solar[130], E. Yu. Soldatov[100], U. Soldevila[170], A. A. Solodkov[132], A. Soloshenko[68], O. V. Solovyanov[132], V. Solovyev[125], P. Sommer[51], H. Son[165], H. Y. Song[36a,aq], A. Sopczak[130], V. Sorin[13], D. Sosa[60b], C. L. Sotiropoulou[126a,126b], R. Soualah[167a,167c], A. M. Soukharev[111,c], D. South[45], B. C. Sowden[80], S. Spagnolo[76a,76b], M. Spalla[126a,126b], M. Spangenberg[173], F. Spanò[80], D. Sperlich[17], F. Spettel[103], T. M. Spieker[60a], R. Spighi[22a], G. Spigo[32], L. A. Spiller[91], M. Spousta[131], R. D. St. Denis[56,*], A. Stabile[94a], R. Stamen[60a], S. Stamm[17], E. Stanecka[42], R. W. Stanek[6], C. Stanescu[136a], M. M. Stanitzki[45], S. Stapnes[121], E. A. Starchenko[132], G. H. Stark[33], J. Stark[58], S. H Stark[39], P. Staroba[129], P. Starovoitov[60a], S. Stärz[32], R. Staszewski[42], P. Steinberg[27], B. Stelzer[144], H. J. Stelzer[32], O. Stelzer-Chilton[163a], H. Stenzel[55], G. A. Stewart[56], J. A. Stillings[23], M. C. Stockton[90], M. Stoebe[90], G. Stoicea[28b], P. Stolte[57], S. Stonjek[103], A. R. Stradling[8], A. Straessner[47], M. E. Stramaglia[18], J. Strandberg[149], S. Strandberg[148a,148b], A. Strandlie[121], M. Strauss[115], P. Strizenec[146b], R. Ströhmer[177], D. M. Strom[118], R. Stroynowski[43], A. Strubig[108], S. A. Stucci[27], B. Stugu[15], N. A. Styles[45], D. Su[145], J. Su[127], S. Suchek[60a], Y. Sugaya[120], M. Suk[130], V. V. Sulin[98], S. Sultansoy[4c], T. Sumida[71], S. Sun[59], X. Sun[3], K. Suruliz[151], C. J. E. Suster[152], M. R. Sutton[151], S. Suzuki[69], M. Svatos[129], M. Swiatlowski[33], S. P. Swift[2], I. Sykora[146a], T. Sykora[131], D. Ta[51], K. Tackmann[45], J. Taenzer[155], A. Taffard[166], R. Tafirout[163a], N. Taiblum[155], H. Takai[27], R. Takashima[72], T. Takeshita[142], Y. Takubo[69], M. Talby[88], A. A. Talyshev[111,c], J. Tanaka[157], M. Tanaka[159], R. Tanaka[119], S. Tanaka[69], R. Tanioka[70], B. B. Tannenwald[113], S. Tapia Araya[34b], S. Tapprogge[86], S. Tarem[154], G. F. Tartarelli[94a], P. Tas[131], M. Tasevsky[129], T. Tashiro[71], E. Tassi[40a,40b], A. Tavares Delgado[128a,128b], Y. Tayalati[137e], A. C. Taylor[107], G. N. Taylor[91], P. T. E. Taylor[91], W. Taylor[163b], P. Teixeira-Dias[80], D. Temple[144], H. Ten Kate[32], P. K. Teng[153], J. J. Teoh[120], F. Tepel[178], S. Terada[69], K. Terashi[157], J. Terron[85], S. Terzo[13], M. Testa[50], R. J. Teuscher[161,o], T. Theveneaux-Pelzer[88], J. P. Thomas[19], J. Thomas-Wilsker[80], P. D. Thompson[19], A. S. Thompson[56], L. A. Thomsen[179], E. Thomson[124], M. J. Tibbetts[16], R. E. Ticse Torres[88], V. O. Tikhomirov[98,ar], Yu. A. Tikhonov[111,c], S. Timoshenko[100], P. Tipton[179], S. Tisserant[88], K. Todome[159], S. Todorova-Nova[5], J. Tojo[73], S. Tokár[146a], K. Tokushuku[69], E. Tolley[59], L. Tomlinson[87], M. Tomoto[105], L. Tompkins[145,as], K. Toms[107], B. Tong[59], P. Tornambe[51], E. Torrence[118], H. Torres[144], E. Torró Pastor[140], J. Toth[88,at], F. Touchard[88], D. R. Tovey[141], C. J. Treado[112], T. Trefzger[177], A. Tricoli[27], I. M. Trigger[163a], S. Trincaz-Duvoid[83], M. F. Tripiana[13], W. Trischuk[161], B. Trocmé[58], A. Trofymov[45], C. Troncon[94a], M. Trottier-McDonald[16], M. Trovatelli[172], L. Truong[167a,167c], M. Trzebinski[42], A. Trzupek[42], K. W. Tsang[62a], J. C-L. Tseng[122], P. V. Tsiareshka[95], G. Tsipolitis[10], N. Tsirintanis[9], S. Tsiskaridze[13], V. Tsiskaridze[51], E. G. Tskhadadze[54a], K. M. Tsui[62a], I. I. Tsukerman[99], V. Tsulaia[16], S. Tsuno[69], D. Tsybychev[150], Y. Tu[62b], A. Tudorache[28b], V. Tudorache[28b], T. T. Tulbure[28a], A. N. Tuna[59], S. A. Tupputi[22a,22b], S. Turchikhin[68], D. Turgeman[175], I. Turk Cakir[4b,au], R. Turra[94a,94b], P. M. Tuts[38], G. Ucchielli[22a,22b], I. Ueda[69], M. Ughetto[148a,148b], F. Ukegawa[164], G. Unal[32], A. Undrus[27], G. Unel[166], F. C. Ungaro[91], Y. Unno[69], C. Unverdorben[102], J. Urban[146b], P. Urquijo[91], P. Urrejola[86], G. Usai[8], J. Usui[69], L. Vacavant[88], V. Vacek[130], B. Vachon[90], C. Valderanis[102], E. Valdes Santurio[148a,148b], N. Valencic[109], S. Valentinetti[22a,22b], A. Valero[170], L. Valéry[13], S. Valkar[131], A. Vallier[5], J. A. Valls Ferrer[170], W. Van Den Wollenberg[109], H. van der Graaf[109], N. van Eldik[154], P. van Gemmeren[6], J. Van Nieuwkoop[144], I. van Vulpen[109], M. C. van Woerden[109], M. Vanadia[134a,134b], W. Vandelli[32], R. Vanguri[124], A. Vaniachine[160], P. Vankov[109], G. Vardanyan[180], R. Vari[134a], E. W. Varnes[7], C. Varni[53a,53b], T. Varol[43], D. Varouchas[83], A. Vartapetian[8], K. E. Varvell[152], J. G. Vasquez[179], G. A. Vasquez[34b], F. Vazeille[37], T. Vazquez Schroeder[90], J. Veatch[57], V. Veeraraghavan[7], L. M. Veloce[161], F. Veloso[128a,128c], S. Veneziano[134a], A. Ventura[76a,76b], M. Venturi[172], N. Venturi[161], A. Venturini[25], V. Vercesi[123a], M. Verducci[136a,136b], W. Verkerke[109], J. C. Vermeulen[109], M. C. Vetterli[144,d], N. Viaux Maira[34a], O. Viazlo[84], I. Vichou[169,*], T. Vickey[141], O. E. Vickey Boeriu[141], G. H. A. Viehhauser[122], S. Viel[16], L. Vigani[122], M. Villa[22a,22b], M. Villaplana Perez[94a,94b], E. Vilucchi[50], M. G. Vincter[31], V. B. Vinogradov[68], A. Vishwakarma[45], C. Vittori[22a,22b], I. Vivarelli[151], S. Vlachos[10], M. Vlasak[130], M. Vogel[178], P. Vokac[130], G. Volpi[126a,126b], M. Volpi[91], H. von der Schmitt[103], E. von Toerne[23], V. Vorobel[131], K. Vorobev[100], M. Vos[170], R. Voss[32], J. H. Vossebeld[77], N. Vranjes[14], M. Vranjes Milosavljevic[14], V. Vrba[130], M. Vreeswijk[109], R. Vuillermet[32], I. Vukotic[33], P. Wagner[23], W. Wagner[178], H. Wahlberg[74], S. Wahrmund[47], J. Wakabayashi[105], J. Walder[75], R. Walker[102], W. Walkowiak[143], V. Wallangen[148a,148b], C. Wang[35b], C. Wang[36b,av], F. Wang[176], H. Wang[16], H. Wang[3], J. Wang[45], J. Wang[152], Q. Wang[115], R. Wang[6], S. M. Wang[153], T. Wang[38], W. Wang[153,aw], W. Wang[36a], C. Wanotayaroj[118], A. Warburton[90], C. P. Ward[30], D. R. Wardrope[81], A. Washbrook[49], P. M. Watkins[19], A. T. Watson[19], M. F. Watson[19], G. Watts[140], S. Watts[87], B. M. Waugh[81], A. F. Webb[11], S. Webb[86], M. S. Weber[18], S. W. Weber[177], S. A. Weber[31],

J. S. Webster[6], A. R. Weidberg[122], B. Weinert[64], J. Weingarten[57], C. Weiser[51], H. Weits[109], P. S. Wells[32], T. Wenaus[27], T. Wengler[32], S. Wenig[32], N. Wermes[23], M. D. Werner[67], P. Werner[32], M. Wessels[60a], K. Whalen[118], N. L. Whallon[140], A. M. Wharton[75], A. White[8], M. J. White[1], R. White[34b], D. Whiteson[166], F. J. Wickens[133], W. Wiedenmann[176], M. Wielers[133], C. Wiglesworth[39], L. A. M. Wiik-Fuchs[23], A. Wildauer[103], F. Wilk[87], H. G. Wilkens[32], H. H. Williams[124], S. Williams[109], C. Willis[93], S. Willocq[89], J. A. Wilson[19], I. Wingerter-Seez[5], F. Winklmeier[118], O. J. Winston[151], B. T. Winter[23], M. Wittgen[145], M. Wobisch[82,u], T. M. H. Wolf[109], R. Wolff[88], M. W. Wolter[42], H. Wolters[128a,128c], S. D. Worm[19], B. K. Wosiek[42], J. Wotschack[32], M. J. Woudstra[87], K. W. Wozniak[42], M. Wu[33], S. L. Wu[176], X. Wu[52], Y. Wu[92], T. R. Wyatt[87], B. M. Wynne[49], S. Xella[39], Z. Xi[92], L. Xia[35c], D. Xu[35a], L. Xu[27], B. Yabsley[152], S. Yacoob[147a], D. Yamaguchi[159], Y. Yamaguchi[120], A. Yamamoto[69], S. Yamamoto[157], T. Yamanaka[157], K. Yamauchi[105], Y. Yamazaki[70], Z. Yan[24], H. Yang[36c], H. Yang[16], Y. Yang[153], Z. Yang[15], W-M. Yao[16], Y. C. Yap[83], Y. Yasu[69], E. Yatsenko[5], K. H. Yau Wong[23], J. Ye[43], S. Ye[27], I. Yeletskikh[68], E. Yildirim[86], K. Yorita[174], K. Yoshihara[124], C. Young[145], C. J. S. Young[32], S. Youssef[24], D. R. Yu[16], J. Yu[8], J. Yu[67], L. Yuan[70], S. P. Y. Yuen[23], I. Yusuff[30,ax], B. Zabinski[42], G. Zacharis[10], R. Zaidan[13], A. M. Zaitsev[132,aj], N. Zakharchuk[45], J. Zalieckas[15], A. Zaman[150], S. Zambito[59], D. Zanzi[91], C. Zeitnitz[178], M. Zeman[130], A. Zemla[41a], J. C. Zeng[169], Q. Zeng[145], O. Zenin[132], T. Ženiš[146a], D. Zerwas[119], D. Zhang[92], F. Zhang[176], G. Zhang[36a,aq], H. Zhang[35b], J. Zhang[6], L. Zhang[51], L. Zhang[36a], M. Zhang[169], R. Zhang[23], R. Zhang[36a,av], X. Zhang[36b], Y. Zhang[35a], Z. Zhang[119], X. Zhao[43], Y. Zhao[36b,ay], Z. Zhao[36a], A. Zhemchugov[68], J. Zhong[122], B. Zhou[92], C. Zhou[176], L. Zhou[43], M. Zhou[35a], M. Zhou[150], N. Zhou[35c], C. G. Zhu[36b], H. Zhu[35a], J. Zhu[92], Y. Zhu[36a], X. Zhuang[35a], K. Zhukov[98], A. Zibell[177], D. Zieminska[64], N. I. Zimine[68], C. Zimmermann[86], S. Zimmermann[51], Z. Zinonos[103], M. Zinser[86], M. Ziolkowski[143], L. Živković[14], G. Zobernig[176], A. Zoccoli[22a,22b], R. Zou[33], M. zur Nedden[17], L. Zwalinski[32]

[1] Department of Physics, University of Adelaide, Adelaide, Australia
[2] Physics Department, SUNY Albany, Albany, NY, USA
[3] Department of Physics, University of Alberta, Edmonton, AB, Canada
[4] [(a)]Department of Physics, Ankara University, Ankara, Turkey; [(b)]Istanbul Aydin University, Istanbul, Turkey; [(c)]Division of Physics, TOBB University of Economics and Technology, Ankara, Turkey
[5] LAPP, CNRS/IN2P3 and Université Savoie Mont Blanc, Annecy-le-Vieux, France
[6] High Energy Physics Division, Argonne National Laboratory, Argonne, IL, USA
[7] Department of Physics, University of Arizona, Tucson, AZ, USA
[8] Department of Physics, The University of Texas at Arlington, Arlington, TX, USA
[9] Physics Department, National and Kapodistrian University of Athens, Athens, Greece
[10] Physics Department, National Technical University of Athens, Zografou, Greece
[11] Department of Physics, The University of Texas at Austin, Austin, TX, USA
[12] Institute of Physics, Azerbaijan Academy of Sciences, Baku, Azerbaijan
[13] Institut de Física d'Altes Energies (IFAE), The Barcelona Institute of Science and Technology, Barcelona, Spain
[14] Institute of Physics, University of Belgrade, Belgrade, Serbia
[15] Department for Physics and Technology, University of Bergen, Bergen, Norway
[16] Physics Division, Lawrence Berkeley National Laboratory, University of California, Berkeley, CA, USA
[17] Department of Physics, Humboldt University, Berlin, Germany
[18] Albert Einstein Center for Fundamental Physics, Laboratory for High Energy Physics, University of Bern, Bern, Switzerland
[19] School of Physics and Astronomy, University of Birmingham, Birmingham, UK
[20] [(a)]Department of Physics, Bogazici University, Istanbul, Turkey; [(b)]Department of Physics Engineering, Gaziantep University, Gaziantep, Turkey; [(c)]Faculty of Engineering and Natural Sciences, Istanbul Bilgi University, Istanbul, Turkey; [(d)]Faculty of Engineering and Natural Sciences, Bahcesehir University, Istanbul, Turkey
[21] Centro de Investigaciones, Universidad Antonio Narino, Bogotá, Colombia
[22] [(a)]INFN Sezione di Bologna, Bologna, Italy; [(b)]Dipartimento di Fisica e Astronomia, Università di Bologna, Bologna, Italy
[23] Physikalisches Institut, University of Bonn, Bonn, Germany
[24] Department of Physics, Boston University, Boston, MA, USA
[25] Department of Physics, Brandeis University, Waltham, MA, USA

[26] [(a)]Universidade Federal do Rio De Janeiro COPPE/EE/IF, Rio de Janeiro, Brazil; [(b)]Electrical Circuits Department, Federal University of Juiz de Fora (UFJF), Juiz de Fora, Brazil; [(c)]Federal University of Sao Joao del Rei (UFSJ), Sao Joao del Rei, Brazil; [(d)]Instituto de Fisica, Universidade de Sao Paulo, São Paulo, Brazil
[27] Physics Department, Brookhaven National Laboratory, Upton, NY, USA
[28] [(a)]Transilvania University of Brasov, Brasov, Romania; [(b)]Horia Hulubei National Institute of Physics and Nuclear Engineering, Bucharest, Romania; [(c)]Department of Physics, Alexandru Ioan Cuza University of Iasi, Iasi, Romania; [(d)]Physics Department, National Institute for Research and Development of Isotopic and Molecular Technologies, Cluj-Napoca, Romania; [(e)]University Politehnica Bucharest, Bucharest, Romania; [(f)]West University in Timisoara, Timisoara, Romania
[29] Departamento de Física, Universidad de Buenos Aires, Buenos Aires, Argentina
[30] Cavendish Laboratory, University of Cambridge, Cambridge, UK
[31] Department of Physics, Carleton University, Ottawa, ON, Canada
[32] CERN, Geneva, Switzerland
[33] Enrico Fermi Institute, University of Chicago, Chicago, IL, USA
[34] [(a)]Departamento de Física, Pontificia Universidad Católica de Chile, Santiago, Chile; [(b)]Departamento de Física, Universidad Técnica Federico Santa María, Valparaiso, Chile
[35] [(a)]Institute of High Energy Physics, Chinese Academy of Sciences, Beijing, China; [(b)]Department of Physics, Nanjing University, Nanjing, Jiangsu, China; [(c)]Physics Department, Tsinghua University, Beijing 100084, China
[36] [(a)]Department of Modern Physics, University of Science and Technology of China, Hefei, Anhui, China; [(b)]School of Physics, Shandong University, Jinan, Shandong, China; [(c)]Department of Physics and Astronomy, Key Laboratory for Particle Physics, Astrophysics and Cosmology, Ministry of Education, Shanghai Key Laboratory for Particle Physics and Cosmology, Shanghai Jiao Tong University, Shanghai (also at PKU-CHEP), Shanghai, China
[37] Université Clermont Auvergne, CNRS/IN2P3, LPC, Clermont-Ferrand, France
[38] Nevis Laboratory, Columbia University, Irvington, NY, USA
[39] Niels Bohr Institute, University of Copenhagen, Copenhagen, Denmark
[40] [(a)]INFN Gruppo Collegato di Cosenza, Laboratori Nazionali di Frascati, Frascati, Italy; [(b)]Dipartimento di Fisica, Università della Calabria, Rende, Italy
[41] [(a)]Faculty of Physics and Applied Computer Science, AGH University of Science and Technology, Kraków, Poland; [(b)]Marian Smoluchowski Institute of Physics, Jagiellonian University, Kraków, Poland
[42] Institute of Nuclear Physics, Polish Academy of Sciences, Kraków, Poland
[43] Physics Department, Southern Methodist University, Dallas, TX, USA
[44] Physics Department, University of Texas at Dallas, c, TX, USA
[45] DESY, Hamburg and Zeuthen, Germany
[46] Lehrstuhl für Experimentelle Physik IV, Technische Universität Dortmund, Dortmund, Germany
[47] Institut für Kern- und Teilchenphysik, Technische Universität Dresden, Dresden, Germany
[48] Department of Physics, Duke University, Durham, NC, USA
[49] SUPA-School of Physics and Astronomy, University of Edinburgh, Edinburgh, UK
[50] INFN Laboratori Nazionali di Frascati, Frascati, Italy
[51] Fakultät für Mathematik und Physik, Albert-Ludwigs-Universität, Freiburg, Germany
[52] Departement de Physique Nucleaire et Corpusculaire, Université de Genève, Geneva, Switzerland
[53] [(a)]INFN Sezione di Genova, Genoa, Italy; [(b)]Dipartimento di Fisica, Università di Genova, Genoa, Italy
[54] [(a)]E. Andronikashvili Institute of Physics, Iv. Javakhishvili Tbilisi State University, Tbilisi, Georgia; [(b)]High Energy Physics Institute, Tbilisi State University, Tbilisi, Georgia
[55] II Physikalisches Institut, Justus-Liebig-Universität Giessen, Giessen, Germany
[56] SUPA-School of Physics and Astronomy, University of Glasgow, Glasgow, UK
[57] II Physikalisches Institut, Georg-August-Universität, Göttingen, Germany
[58] Laboratoire de Physique Subatomique et de Cosmologie, Université Grenoble-Alpes, CNRS/IN2P3, Grenoble, France
[59] Laboratory for Particle Physics and Cosmology, Harvard University, Cambridge, MA, USA
[60] [(a)]Kirchhoff-Institut für Physik, Ruprecht-Karls-Universität Heidelberg, Heidelberg, Germany; [(b)]Physikalisches Institut, Ruprecht-Karls-Universität Heidelberg, Heidelberg, Germany; [(c)]ZITI Institut für technische Informatik, Ruprecht-Karls-Universität Heidelberg, Mannheim, Germany
[61] Faculty of Applied Information Science, Hiroshima Institute of Technology, Hiroshima, Japan

[62] [(a)]Department of Physics, The Chinese University of Hong Kong, Shatin, NT, Hong Kong; [(b)]Department of Physics, The University of Hong Kong, Hong Kong, China; [(c)]Department of Physics, Institute for Advanced Study, The Hong Kong University of Science and Technology, Clear Water Bay, Kowloon, Hong Kong, China
[63] Department of Physics, National Tsing Hua University, Taiwan, Taiwan
[64] Department of Physics, Indiana University, Bloomington, IN, USA
[65] Institut für Astro- und Teilchenphysik, Leopold-Franzens-Universität, Innsbruck, Austria
[66] University of Iowa, Iowa City, IA, USA
[67] Department of Physics and Astronomy, Iowa State University, Ames, IA, USA
[68] Joint Institute for Nuclear Research, JINR Dubna, Dubna, Russia
[69] KEK, High Energy Accelerator Research Organization, Tsukuba, Japan
[70] Graduate School of Science, Kobe University, Kobe, Japan
[71] Faculty of Science, Kyoto University, Kyoto, Japan
[72] Kyoto University of Education, Kyoto, Japan
[73] Department of Physics, Kyushu University, Fukuoka, Japan
[74] Instituto de Física La Plata, Universidad Nacional de La Plata and CONICET, La Plata, Argentina
[75] Physics Department, Lancaster University, Lancaster, UK
[76] [(a)]INFN Sezione di Lecce, Lecce, Italy; [(b)]Dipartimento di Matematica e Fisica, Università del Salento, Lecce, Italy
[77] Oliver Lodge Laboratory, University of Liverpool, Liverpool, UK
[78] Department of Experimental Particle Physics, Jožef Stefan Institute and Department of Physics, University of Ljubljana, Ljubljana, Slovenia
[79] School of Physics and Astronomy, Queen Mary University of London, London, UK
[80] Department of Physics, Royal Holloway University of London, Surrey, UK
[81] Department of Physics and Astronomy, University College London, London, UK
[82] Louisiana Tech University, Ruston, LA, USA
[83] Laboratoire de Physique Nucléaire et de Hautes Energies, UPMC and Université Paris-Diderot and CNRS/IN2P3, Paris, France
[84] Fysiska institutionen, Lunds universitet, Lund, Sweden
[85] Departamento de Fisica Teorica C-15, Universidad Autonoma de Madrid, Madrid, Spain
[86] Institut für Physik, Universität Mainz, Mainz, Germany
[87] School of Physics and Astronomy, University of Manchester, Manchester, UK
[88] CPPM, Aix-Marseille Université and CNRS/IN2P3, Marseille, France
[89] Department of Physics, University of Massachusetts, Amherst, MA, USA
[90] Department of Physics, McGill University, Montreal, QC, Canada
[91] School of Physics, University of Melbourne, Victoria, Australia
[92] Department of Physics, The University of Michigan, Ann Arbor, MI, USA
[93] Department of Physics and Astronomy, Michigan State University, East Lansing, MI, USA
[94] [(a)]INFN Sezione di Milano, Milan, Italy; [(b)]Dipartimento di Fisica, Università di Milano, Milan, Italy
[95] B.I. Stepanov Institute of Physics, National Academy of Sciences of Belarus, Minsk, Republic of Belarus
[96] Research Institute for Nuclear Problems of Byelorussian State University, Minsk, Republic of Belarus
[97] Group of Particle Physics, University of Montreal, Montreal, QC, Canada
[98] P.N. Lebedev Physical Institute of the Russian Academy of Sciences, Moscow, Russia
[99] Institute for Theoretical and Experimental Physics (ITEP), Moscow, Russia
[100] National Research Nuclear University MEPhI, Moscow, Russia
[101] D.V. Skobeltsyn Institute of Nuclear Physics, M.V. Lomonosov Moscow State University, Moscow, Russia
[102] Fakultät für Physik, Ludwig-Maximilians-Universität München, Munich, Germany
[103] Max-Planck-Institut für Physik (Werner-Heisenberg-Institut), Munich, Germany
[104] Nagasaki Institute of Applied Science, Nagasaki, Japan
[105] Graduate School of Science and Kobayashi-Maskawa Institute, Nagoya University, Nagoya, Japan
[106] [(a)]INFN Sezione di Napoli, Naples, Italy; [(b)]Dipartimento di Fisica, Università di Napoli, Naples, Italy
[107] Department of Physics and Astronomy, University of New Mexico, Albuquerque, NM, USA
[108] Institute for Mathematics, Astrophysics and Particle Physics, Radboud University Nijmegen/Nikhef, Nijmegen, The Netherlands
[109] Nikhef National Institute for Subatomic Physics, University of Amsterdam, Amsterdam, The Netherlands

[110] Department of Physics, Northern Illinois University, DeKalb, IL, USA
[111] Budker Institute of Nuclear Physics, SB RAS, Novosibirsk, Russia
[112] Department of Physics, New York University, New York, NY, USA
[113] Ohio State University, Columbus, OH, USA
[114] Faculty of Science, Okayama University, Okayama, Japan
[115] Homer L. Dodge Department of Physics and Astronomy, University of Oklahoma, Norman, OK, USA
[116] Department of Physics, Oklahoma State University, Stillwater, OK, USA
[117] Palacký University, RCPTM, Olomouc, Czech Republic
[118] Center for High Energy Physics, University of Oregon, Eugene, OR, USA
[119] LAL, Univ. Paris-Sud, CNRS/IN2P3, Université Paris-Saclay, Orsay, France
[120] Graduate School of Science, Osaka University, Osaka, Japan
[121] Department of Physics, University of Oslo, Oslo, Norway
[122] Department of Physics, Oxford University, Oxford, UK
[123] [(a)]INFN Sezione di Pavia, Pavia, Italy; [(b)]Dipartimento di Fisica, Università di Pavia, Pavia, Italy
[124] Department of Physics, University of Pennsylvania, Philadelphia, PA, USA
[125] National Research Centre "Kurchatov Institute" B.P. Konstantinov Petersburg Nuclear Physics Institute, St. Petersburg, Russia
[126] [(a)]INFN Sezione di Pisa, Pisa, Italy; [(b)]Dipartimento di Fisica E. Fermi, Università di Pisa, Pisa, Italy
[127] Department of Physics and Astronomy, University of Pittsburgh, Pittsburgh, PA, USA
[128] [(a)]Laboratório de Instrumentação e Física Experimental de Partículas-LIP, Lisbon, Portugal; [(b)]Faculdade de Ciências, Universidade de Lisboa, Lisbon, Portugal; [(c)]Department of Physics, University of Coimbra, Coimbra, Portugal; [(d)]Centro de Física Nuclear da Universidade de Lisboa, Lisbon, Portugal; [(e)]Departamento de Fisica, Universidade do Minho, Braga, Portugal; [(f)]Departamento de Fisica Teorica y del Cosmos and CAFPE, Universidad de Granada, Granada, Spain; [(g)]Dep Fisica and CEFITEC of Faculdade de Ciencias e Tecnologia, Universidade Nova de Lisboa, Caparica, Portugal
[129] Institute of Physics, Academy of Sciences of the Czech Republic, Prague, Czech Republic
[130] Czech Technical University in Prague, Prague, Czech Republic
[131] Faculty of Mathematics and Physics, Charles University, Prague, Czech Republic
[132] State Research Center Institute for High Energy Physics (Protvino), NRC KI, Protvino, Russia
[133] Particle Physics Department, Rutherford Appleton Laboratory, Didcot, UK
[134] [(a)]INFN Sezione di Roma, Rome, Italy; [(b)]Dipartimento di Fisica, Sapienza Università di Roma, Rome, Italy
[135] [(a)]INFN Sezione di Roma Tor Vergata, Rome, Italy; [(b)]Dipartimento di Fisica, Università di Roma Tor Vergata, Rome, Italy
[136] [(a)]INFN Sezione di Roma Tre, Rome, Italy; [(b)]Dipartimento di Matematica e Fisica, Università Roma Tre, Rome, Italy
[137] [(a)]Faculté des Sciences Ain Chock, Réseau Universitaire de Physique des Hautes Energies-Université Hassan II, Casablanca, Morocco; [(b)]Centre National de l'Energie des Sciences Techniques Nucleaires, Rabat, Morocco; [(c)]Faculté des Sciences Semlalia, Université Cadi Ayyad, LPHEA-Marrakech, Marrakech, Morocco; [(d)]Faculté des Sciences, Université Mohamed Premier and LPTPM, Oujda, Morocco; [(e)]Faculté des Sciences, Université Mohammed V, Rabat, Morocco
[138] DSM/IRFU (Institut de Recherches sur les Lois Fondamentales de l'Univers), CEA Saclay (Commissariat à l'Energie Atomique et aux Energies Alternatives), Gif-sur-Yvette, France
[139] Santa Cruz Institute for Particle Physics, University of California Santa Cruz, Santa Cruz, CA, USA
[140] Department of Physics, University of Washington, Seattle, WA, USA
[141] Department of Physics and Astronomy, University of Sheffield, Sheffield, UK
[142] Department of Physics, Shinshu University, Nagano, Japan
[143] Department Physik, Universität Siegen, Siegen, Germany
[144] Department of Physics, Simon Fraser University, Burnaby, BC, Canada
[145] SLAC National Accelerator Laboratory, Stanford, CA, USA
[146] [(a)]Faculty of Mathematics, Physics and Informatics, Comenius University, Bratislava, Slovak Republic; [(b)]Department of Subnuclear Physics, Institute of Experimental Physics of the Slovak Academy of Sciences, Kosice, Slovak Republic

147 (a)Department of Physics, University of Cape Town, Cape Town, South Africa; (b)Department of Physics, University of Johannesburg, Johannesburg, South Africa; (c)School of Physics, University of the Witwatersrand, Johannesburg, South Africa
148 (a)Department of Physics, Stockholm University, Stockholm, Sweden; (b)The Oskar Klein Centre, Stockholm, Sweden
149 Physics Department, Royal Institute of Technology, Stockholm, Sweden
150 Departments of Physics and Astronomy and Chemistry, Stony Brook University, Stony Brook, NY, USA
151 Department of Physics and Astronomy, University of Sussex, Brighton, UK
152 School of Physics, University of Sydney, Sydney, Australia
153 Institute of Physics, Academia Sinica, Taipei, Taiwan
154 Department of Physics, Technion: Israel Institute of Technology, Haifa, Israel
155 Raymond and Beverly Sackler School of Physics and Astronomy, Tel Aviv University, Tel Aviv, Israel
156 Department of Physics, Aristotle University of Thessaloniki, Thessaloníki, Greece
157 International Center for Elementary Particle Physics and Department of Physics, The University of Tokyo, Tokyo, Japan
158 Graduate School of Science and Technology, Tokyo Metropolitan University, Tokyo, Japan
159 Department of Physics, Tokyo Institute of Technology, Tokyo, Japan
160 Tomsk State University, Tomsk, Russia
161 Department of Physics, University of Toronto, Toronto, ON, Canada
162 (a)INFN-TIFPA, Trento, Italy; (b)University of Trento, Trento, Italy
163 (a)TRIUMF, Vancouver, BC, Canada; (b)Department of Physics and Astronomy, York University, Toronto, ON, Canada
164 Faculty of Pure and Applied Sciences, and Center for Integrated Research in Fundamental Science and Engineering, University of Tsukuba, Tsukuba, Japan
165 Department of Physics and Astronomy, Tufts University, Medford, MA, USA
166 Department of Physics and Astronomy, University of California Irvine, Irvine, CA, USA
167 (a)INFN Gruppo Collegato di Udine, Sezione di Trieste, Udine, Italy; (b)ICTP, Trieste, Italy; (c)Dipartimento di Chimica, Fisica e Ambiente, Università di Udine, Udine, Italy
168 Department of Physics and Astronomy, University of Uppsala, Uppsala, Sweden
169 Department of Physics, University of Illinois, Urbana, IL, USA
170 Instituto de Fisica Corpuscular (IFIC) and Departamento de Fisica Atomica, Molecular y Nuclear and Departamento de Ingeniería Electrónica and Instituto de Microelectrónica de Barcelona (IMB-CNM), University of Valencia and CSIC, Valencia, Spain
171 Department of Physics, University of British Columbia, Vancouver, BC, Canada
172 Department of Physics and Astronomy, University of Victoria, Victoria, BC, Canada
173 Department of Physics, University of Warwick, Coventry, UK
174 Waseda University, Tokyo, Japan
175 Department of Particle Physics, The Weizmann Institute of Science, Rehovot, Israel
176 Department of Physics, University of Wisconsin, Madison, WI, USA
177 Fakultät für Physik und Astronomie, Julius-Maximilians-Universität, Würzburg, Germany
178 Fakultät für Mathematik und Naturwissenschaften, Fachgruppe Physik, Bergische Universität Wuppertal, Wuppertal, Germany
179 Department of Physics, Yale University, New Haven, CT, USA
180 Yerevan Physics Institute, Yerevan, Armenia
181 Centre de Calcul de l'Institut National de Physique Nucléaire et de Physique des Particules (IN2P3), Villeurbanne, France

[a] Also at Department of Physics, King's College London, London, UK
[b] Also at Institute of Physics, Azerbaijan Academy of Sciences, Baku, Azerbaijan
[c] Also at Novosibirsk State University, Novosibirsk, Russia
[d] Also at TRIUMF, Vancouver, BC, Canada
[e] Also at Department of Physics and Astronomy, University of Louisville, Louisville, KY, USA
[f] Also at Physics Department, An-Najah National University, Nablus, Palestine
[g] Also at Department of Physics, California State University, Fresno, CA, USA
[h] Also at Department of Physics, University of Fribourg, Fribourg, Switzerland
[i] Also at II Physikalisches Institut, Georg-August-Universität, Göttingen, Germany

[j] Also at Department de Fisica de la Universitat Autonoma de Barcelona, Barcelona, Spain
[k] Also at Departamento de Fisica e Astronomia, Faculdade de Ciencias, Universidade do Porto, Porto, Portugal
[l] Also at Tomsk State University, Tomsk, Russia
[m] Also at The Collaborative Innovation Center of Quantum Matter (CICQM), Beijing, China
[n] Also at Universita di Napoli Parthenope, Napoli, Italy
[o] Also at Institute of Particle Physics (IPP), Canada
[p] Also at Horia Hulubei National Institute of Physics and Nuclear Engineering, Bucharest, Romania
[q] Also at Department of Physics, St. Petersburg State Polytechnical University, St. Petersburg, Russia
[r] Also at Borough of Manhattan Community College, City University of New York, New York, USA
[s] Also at Department of Physics, The University of Michigan, Ann Arbor MI, United States of America
[t] Also at Centre for High Performance Computing, CSIR Campus, Rosebank, Cape Town, South Africa
[u] Also at Louisiana Tech University, Ruston, LA, USA
[v] Also at Institucio Catalana de Recerca i Estudis Avancats, ICREA, Barcelona, Spain
[w] Also at Graduate School of Science, Osaka University, Osaka, Japan
[x] Also at Fakultät für Mathematik und Physik, Albert-Ludwigs-Universität, Freiburg, Germany
[y] Also at Institute for Mathematics, Astrophysics and Particle Physics, Radboud University Nijmegen/Nikhef, Nijmegen, The Netherlands
[z] Also at Department of Physics, The University of Texas at Austin, Austin, TX, USA
[aa] Also at Institute of Theoretical Physics, Ilia State University, Tbilisi, Georgia
[ab] Also at CERN, Geneva, Switzerland
[ac] Also at Georgian Technical University (GTU), Tbilisi, Georgia
[ad] Also at Ochadai Academic Production, Ochanomizu University, Tokyo, Japan
[ae] Also at Manhattan College, New York, NY, USA
[af] Also at Academia Sinica Grid Computing, Institute of Physics, Academia Sinica, Taipei, Taiwan
[ag] Also at School of Physics, Shandong University, Shandong, China
[ah] Also at Departamento de Fisica Teorica y del Cosmos and CAFPE, Universidad de Granada, Granada, Spain
[ai] Also at Department of Physics, California State University, Sacramento, CA, USA
[aj] Also at Moscow Institute of Physics and Technology State University, Dolgoprudny, Russia
[ak] Also at Departement de Physique Nucleaire et Corpusculaire, Université de Genève, Geneva, Switzerland
[al] Also at International School for Advanced Studies (SISSA), Trieste, Italy
[am] Also at Institut de Física d'Altes Energies (IFAE), The Barcelona Institute of Science and Technology, Barcelona, Spain
[an] Also at School of Physics, Sun Yat-sen University, Guangzhou, China
[ao] Also at Institute for Nuclear Research and Nuclear Energy (INRNE) of the Bulgarian Academy of Sciences, Sofia, Bulgaria
[ap] Also at Faculty of Physics, M.V. Lomonosov Moscow State University, Moscow, Russia
[aq] Also at Institute of Physics, Academia Sinica, Taipei, Taiwan
[ar] Also at National Research Nuclear University MEPhI, Moscow, Russia
[as] Also at Department of Physics, Stanford University, Stanford, CA, USA
[at] Also at Institute for Particle and Nuclear Physics, Wigner Research Centre for Physics, Budapest, Hungary
[au] Also at Faculty of Engineering, Giresun University, Giresun, Turkey
[av] Also at CPPM, Aix-Marseille Université and CNRS/IN2P3, Marseille, France
[aw] Also at Department of Physics, Nanjing University, Jiangsu, China
[ax] Also at Department of Physics, University of Malaya, Kuala Lumpur, Malaysia
[ay] Also at LAL, Univ. Paris-Sud, CNRS/IN2P3, Université Paris-Saclay, Orsay, France
*Deceased

Physics Letters B 784 (2018) 345–366

Contents lists available at ScienceDirect

Physics Letters B

www.elsevier.com/locate/physletb

Measurement of the Higgs boson mass in the $H \to ZZ^* \to 4\ell$ and $H \to \gamma\gamma$ channels with $\sqrt{s} = 13$ TeV pp collisions using the ATLAS detector

The ATLAS Collaboration *

ARTICLE INFO

Article history:
Received 4 June 2018
Received in revised form 20 July 2018
Accepted 27 July 2018
Available online 2 August 2018
Editor: M. Doser

ABSTRACT

The mass of the Higgs boson is measured in the $H \to ZZ^* \to 4\ell$ and in the $H \to \gamma\gamma$ decay channels with 36.1 fb^{-1} of proton–proton collision data from the Large Hadron Collider at a centre-of-mass energy of 13 TeV recorded by the ATLAS detector in 2015 and 2016. The measured value in the $H \to ZZ^* \to 4\ell$ channel is $m_H^{ZZ^*} = 124.79 \pm 0.37$ GeV, while the measured value in the $H \to \gamma\gamma$ channel is $m_H^{\gamma\gamma} = 124.93 \pm 0.40$ GeV. Combining these results with the ATLAS measurement based on 7 and 8 TeV proton–proton collision data yields a Higgs boson mass of $m_H = 124.97 \pm 0.24$ GeV.

1. Introduction

The observation of a Higgs boson, H, by the ATLAS and CMS experiments [1,2] with the Large Hadron Collider (LHC) Run 1 proton–proton (pp) collision data at centre-of-mass energies of $\sqrt{s} = 7$ and 8 TeV was a major step towards understanding the mechanism of electroweak (EW) symmetry breaking [3–5]. The mass of the Higgs boson was measured to be 125.09 ± 0.24 GeV [6] based on the combined Run 1 data samples of the ATLAS and CMS Collaborations, who also reported individual mass measurements in Refs. [7,8]. Recently, the CMS Collaboration measured the Higgs boson mass in the $H \to ZZ^* \to 4\ell$ channel using 35.9 fb^{-1} of 13 TeV pp collision data [9]. The measured value of the mass is 125.26 ± 0.21 GeV.

This Letter presents a measurement of the Higgs boson mass, m_H, with 36.1 fb^{-1} of $\sqrt{s} = 13$ TeV pp collision data recorded with the ATLAS detector. The measurement is derived from a combined fit to the four-lepton and diphoton invariant mass spectra in the decay channels $H \to ZZ^* \to 4\ell$ ($\ell = e, \mu$) and $H \to \gamma\gamma$. A combination with the ATLAS Run 1 data is also presented.

2. ATLAS detector

The ATLAS experiment [10] at the LHC is a multi-purpose particle detector with nearly 4π coverage in solid angle.[1] It consists of an inner tracking detector (ID) surrounded by a 2 T superconducting solenoid, electromagnetic (EM) and hadronic calorimeters, and a muon spectrometer (MS) incorporating three large superconducting toroidal magnets. The ID provides tracking for charged particles for $|\eta| < 2.5$. The calorimeter system covers the pseudorapidity range $|\eta| < 4.9$. Its electromagnetic part is segmented into three shower-depth layers for $|\eta| < 2.5$ and includes a presampler for $|\eta| < 1.8$. The MS includes high-precision tracking chambers ($|\eta| < 2.7$) and fast trigger chambers ($|\eta| < 2.4$). Online event selection is performed by a first-level trigger with a maximum rate of 100 kHz, implemented in custom electronics, followed by a software-based high-level trigger with a maximum rate of 1 kHz.

3. Data and simulated samples

This measurement uses data from pp collisions with a centre-of-mass energy of 13 TeV collected during 2015 and 2016 using single-lepton, dilepton, trilepton and diphoton triggers, with looser identification, isolation and transverse momentum (p_{T}) requirements than those applied offline. The combined efficiency of the lepton triggers is about 98% for the $H \to ZZ^* \to 4\ell$ events (assuming $m_H = 125$ GeV) passing the offline selection. The diphoton trigger efficiency is higher than 99% for selected $H \to \gamma\gamma$ events (assuming $m_H = 125$ GeV). After trigger and data-quality requirements, the integrated luminosity of the data sample is 36.1 fb^{-1}.

* *E-mail address:* atlas.publications@cern.ch.

[1] ATLAS uses a right-handed coordinate system with its origin at the nominal interaction point (IP) in the centre of the detector and the z-axis along the beam pipe. The x-axis points from the IP to the centre of the LHC ring, and the y-axis points upwards. Cylindrical coordinates (r, ϕ) are used in the transverse plane, ϕ being the azimuthal angle around the z-axis. The pseudorapidity is defined in terms of the polar angle θ as $\eta = -\ln\tan(\theta/2)$. Angular distance is measured in units of $\Delta R \equiv \sqrt{(\Delta\eta)^2 + (\Delta\phi)^2}$.

https://doi.org/10.1016/j.physletb.2018.07.050

The mean number of proton–proton interactions per bunch crossing (integrated luminosity) is 14 (3.2 fb^{-1}) in the 2015 data set and 25 (32.9 fb^{-1}) in the 2016 data set.

Monte Carlo (MC) simulation is used in the analysis to model the detector response for signal and background processes. For the $H \to ZZ^* \to 4\ell$ measurement, a detailed list and description of the MC-simulated samples used can be found in Ref. [11] and only a few differences specific to the mass analysis are mentioned here. For the gluon–gluon fusion (ggF) signal, the NNLOPS sample generated at next-to-next-to-leading order (NNLO) in QCD [12] with $m_H = 123,\ 125,\ 126\,\text{GeV}$ and the PDF4LHC NLO parton distribution function (PDF) set [13] was used. Additional samples generated at different m_H values (120, 122, 124, 125, 126, 128, 130 GeV) at next-to-leading order (NLO) were also used. The NLO ggF simulation was performed with Powheg-Box v2 [14] interfaced to Pythia 8 [15] for parton showering and hadronisation, and to EvtGen [16] for the simulation of b-hadron decays. The CT10NLO [17] PDF set was used for the hard process and the CTEQ6L1 [18] set for the parton shower. The non-perturbative effects were modelled using the AZNLO set of tuned parameters [19].

The ZZ^* continuum background from quark–antiquark annihilation was modelled at NLO in QCD using Powheg-Box v2 and interfaced to Pythia 8 for parton showering and hadronisation, and to EvtGen for b-hadron decays. The PDF set used is the same as for the NLO ggF signal. NNLO QCD [20,21] and NLO EW corrections [22,23] were applied as a function of the invariant mass of the ZZ^* system (m_{ZZ^*}).

For the $H \to \gamma\gamma$ measurement, the same $H \to \gamma\gamma$ signal (generated for $m_H = 125$ GeV) and background simulated events used for the measurements of the Higgs boson couplings and fiducial cross-sections in the diphoton final state [24] were used. In addition, signal samples with alternative m_H values (110, 122, 123, 124, 126, 127, 130, 140 GeV) were produced, with the same generators and settings as the $m_H = 125$ GeV samples, but only for the four Higgs boson production modes with largest cross-section: gluon–gluon fusion, vector–boson fusion (VBF), and associated production with a vector boson $V = W, Z$ (VH), for $q\bar{q}' \to VH$ and $gg \to ZH$. For rarer processes, such as associated production of the Higgs boson with a top-quark pair ($t\bar{t}H$) or a single top-quark (tH), contributing to less than 2% of the total cross-section, only samples at $m_H = 125$ GeV were used.

Except for the $\gamma\gamma$ background sample, whose modelling requires a large MC sample obtained through a fast parametric simulation of the calorimeter response [25], the generated events for all processes were passed through a Geant4 [26] simulation of the response of the ATLAS detector [25]. For both detector emulation methods, events were reconstructed with the same algorithms as the data. Additional proton–proton interactions (pile-up) were included in both the parametric and the Geant4 simulations, matching the average number of interactions per LHC bunch crossing to the spectrum observed in the data.

The Standard Model (SM) expectations for the Higgs boson production cross-section times branching ratio, in the various production modes and final states under study and at each value of m_H, were taken from Refs. [27–30] and used to normalise the simulated samples, as described in Refs. [11,24].

4. Muon reconstruction, identification and calibration

Muon track reconstruction is first performed independently in the ID and the MS. Hit information from the individual subdetectors is then used in a combined muon reconstruction, which includes information from the calorimeters.

Corrections to the reconstructed momentum are applied in order to match the simulation to data precisely. These corrections to the simulated momentum resolution and momentum scale are parameterised as a power expansion in the muon p_{T}, with each coefficient measured separately for the ID and MS, as a function of η and ϕ, from large data samples of $J/\psi \to \mu^+\mu^-$ and $Z \to \mu^+\mu^-$ decays. The scale corrections range from 0.1% to 0.5% for the p_{T} of muons originating from $J/\psi \to \mu^+\mu^-$ and $Z \to \mu^+\mu^-$ decays and account for inaccurate measurement of the energy lost in the traversed material, local magnetic field inaccuracies and geometrical distortions. The corrections to the muon momentum resolution for muons from $J/\psi \to \mu^+\mu^-$ and $Z \to \mu^+\mu^-$ are at the percent level. After detector alignment, there are residual local misalignments that bias the muon track sagitta, leaving the track χ^2 invariant [31,32], and introduce a small charge-dependent resolution degradation. The bias in the measured momentum of each muon is corrected by an iterative procedure derived from $Z \to \mu^+\mu^-$ decays and checked against the E/p ratio measured in $Z \to e^+e^-$ decays. The residual effect after correction is reduced to the per mille level at the scale of the Z boson mass. This correction improves the resolution of the dimuon invariant mass in Z boson decays by 1% to 5%, depending on η and ϕ of the muon. The systematic uncertainty associated with this correction is estimated for each muon using simulation and is found to be about 0.4×10^{-3} for the average momentum of muons from $Z \to \mu^+\mu^-$ decays.

For muons from $Z \to \mu^+\mu^-$ decays, with momenta of about 45 GeV, the momentum scale is determined to a precision of 0.05% for muons with $|\eta| < 2$, and about 0.2% for muons with $|\eta| \geq 2$. Similarly, the resolution is known with a precision ranging from 1% to 2% for muons with $|\eta| < 2$ and around 10% for muons with $|\eta| \geq 2$ [33]. Both the momentum scale and momentum resolution uncertainties in the corrections to simulation are taken as fully correlated between the Run 1 and Run 2 measurements.

5. Photon and electron reconstruction, identification and calibration

Photon and electron candidates are reconstructed from clusters of electromagnetic calorimeter cells [34]. Clusters without a matching track or reconstructed conversion vertex in the inner detector are classified as unconverted photons. Those with a matching reconstructed conversion vertex or a matching track, consistent with originating from a photon conversion, are classified as converted photons [35]. Clusters matched to a track consistent with originating from an electron (based on transition radiation in the ID) produced in the beam interaction region are considered electron candidates.

The energy measurement for reconstructed electrons and photons is performed by summing the energies measured in the EM calorimeter cells belonging to the candidate cluster. The energy is measured from a cluster size of $\Delta\eta \times \Delta\phi = 0.075 \times 0.175$ in the barrel region of the calorimeter and $\Delta\eta \times \Delta\phi = 0.125 \times 0.125$ in the calorimeter endcaps. The procedure for the energy measurement of electrons and photons closely follows that used in Run 1 [36], with updates to reflect the 2015 and 2016 data-taking conditions:

- The different layers of the electromagnetic calorimeter are intercalibrated by applying methods similar to those described in Ref. [36]. The first and second calorimeter layers are intercalibrated using the energy deposited by muons from $Z \to \mu^+\mu^-$ decays, with a typical uncertainty of 0.7% to 1.5% (1.5% to 2.5%) as a function of η in the barrel (endcap) calorimeter, for $|\eta| < 2.4$. This uncertainty is added in quadrature to the uncertainty in the modelling of the muon ionisation in the simulation (1% to 1.5% depending on η). The energy scale of the presampler is estimated using electrons from Z boson

decays, after correcting the simulation on the basis of the correlations between the amount of detector material and the ratio of the energies deposited in the first and second layers of the calorimeter. The uncertainty in the presampler energy scale varies between 1.5% and 3% depending on η.

- The cluster energy is corrected for energy loss in the inactive materials in front of the calorimeter, the fraction of energy deposited outside the area of the cluster in the η–ϕ plane, the amount of energy lost behind the electromagnetic calorimeter, and to account for the variation of the energy response as a function of the impact point in the calorimeter. The calibration coefficients used to apply these corrections are obtained from a detailed simulation of the detector response to electrons and photons, and are optimised with a boosted decision tree (BDT). The algorithm, described in Ref. [37], has been trained on simulated samples corresponding to the data-taking conditions of 2015 and 2016. The response is calibrated separately for electron candidates, converted photon candidates and unconverted photon candidates. In data, small corrections are applied for the ϕ-dependent energy loss in the gaps between the barrel calorimeter modules (corrections up to 2%, in about 5% of the calorimeter acceptance) and for inhomogeneities due to sectors operated at non-nominal high voltage (corrections between 1% and 7%, in about 2% of the calorimeter acceptance).
- The global calorimeter energy scale is determined in situ with a large sample of $Z \to e^+e^-$ events selected in the 2015 and 2016 datasets. The energy response in data and simulation is equalised by applying η-dependent correction factors to match the invariant mass distributions of $Z \to e^+e^-$ events. The uncertainty in these energy scale correction factors ranges from 0.02% to 0.1% as a function of η, except for the barrel–endcap transition region ($1.37 < |\eta| < 1.52$), where it reaches a few per mille. In this procedure, the simulated width of the reconstructed Z boson mass distribution is matched to the width observed in data by adding in the simulation a contribution to the constant term c of the electron energy resolution, $\frac{\sigma_E}{E} = \frac{a}{\sqrt{E}} \oplus \frac{b}{E} \oplus c$. This constant term varies between 0.7% and 2% for $|\eta| < 2.4$ with an uncertainty of 0.03%–0.3%, except for the barrel–endcap transition region, where the constant term is slightly higher (2.5%–2.9%) with an uncertainty reaching 0.6%.

The main sources of systematic uncertainties in the calibration procedure discussed in Ref. [36] have been revisited. These sources include uncertainties in the method used to extract the energy scale correction factors, as well as uncertainties due to the extrapolation of the energy scale from $Z \to e^+e^-$ events to photons, and also to electrons with energies different from those produced in $Z \to e^+e^-$ decays. The latter arise from the uncertainties in the linearity of the response due to the relative calibration of the different gains used in the calorimeter readout, in the knowledge of the material in front of the calorimeter (inside and outside of the ID, referred to as ID and non-ID material in the following), in the intercalibration of the different calorimeter layers, in the modelling of the lateral shower shapes and in the reconstruction of photon conversions. The total calibration uncertainty for photons with transverse energy (E_{T}) around 60 GeV is 0.2%–0.3% in the barrel and 0.45%–0.8% in the endcap. These uncertainties are close to those quoted in Ref. [36], but typically about 10% larger. The small increase in the uncertainty arises mostly from a larger uncertainty in the relative calibration of the first and second calorimeter layers with muons because of a worse ratio of signal to pile-up noise in Run 2 data. In the case of electrons with E_{T} around 40 GeV, the total uncertainty ranges between 0.03% and 0.2% in most of the detector acceptance. For electrons with E_{T} around 10 GeV the uncertainty ranges between 0.3% and 0.8%.

The accuracy of the energy calibration for low-energy electrons (5–20 GeV) is checked by computing residual energy calibration corrections (after applying the corrections extracted from the $Z \to e^+e^-$ sample) for an independent sample of $J/\psi \to e^+e^-$ events. These residual correction factors are found to be compatible with one within uncertainties. A similar check is performed by computing residual corrections for photons in a sample of radiative Z boson decays. They are found to be compatible with one within uncertainties which are given by the combination of the statistical uncertainty of the radiative Z boson decays sample and of the systematic uncertainty from the extrapolation of the energy scale from electrons to photons.

Systematic uncertainties in the calorimeter energy resolution arise from uncertainties in the modelling of the sampling term $a/\sqrt{E}$ and in the measurement of the constant term in Z boson decays, in the amount of material in front of the calorimeter, which affects electrons and photons differently, and in the modelling of the contribution to the resolution from fluctuations in the pile-up from additional proton–proton interactions in the same or neighbouring bunch crossings. The uncertainty of the energy resolution for electrons and photons with transverse energy between 30 and 60 GeV varies between 5% and 10%.

The identification of photons and the rejection of background from hadrons is based primarily on shower shapes in the calorimeter. The two levels of selection, loose and tight, are described in Ref. [35]. To further reduce the background from jets, two complementary isolation selection criteria are used, based on topological clusters of energy deposits in the calorimeter and on reconstructed tracks in a direction close to that of the photon candidate, as described in Ref. [24].

Electrons are identified using a likelihood-based method combining information from the electromagnetic calorimeter and the ID. As in the case of photons, electrons are required to be isolated using both the calorimeter-based and track-based isolation variables as described in Ref. [38].

6. Statistical methods

The mass measurement is based on the maximisation of the profile likelihood ratio [39,40]

$$\Lambda(m_H) = \frac{L\big(m_H, \hat{\hat{\theta}}(m_H)\big)}{L\big(\hat{m}_H, \hat{\theta}\big)},$$

where the vectors $\hat{\theta}$ and $\hat{m}_H$ denote the unconditional-maximum likelihood estimates of the parameters of the likelihood function L, while $\hat{\hat{\theta}}$ is the conditional maximum-likelihood estimate of the parameters θ for a fixed value of the parameter m_H. Systematic uncertainties and their correlations are modelled by introducing nuisance parameters θ described by likelihood functions associated with the estimate of the corresponding effect [6].

The statistical uncertainty of m_H is estimated by fixing all nuisance parameters to their best-fit values, all remaining parameters are thus left unconstrained. This approach yields a lower bound on the statistical uncertainty, when the combination of the different event categories discussed in the next sections is performed neglecting the different impact of the systematic uncertainties in each category. The upper bound on the total systematic uncertainty is estimated by subtracting in quadrature the statistical uncertainty from the total uncertainty.

Alternatively, the decomposition of the uncertainty into statistical and systematic components is performed using the BLUE method [41–43]. The two approaches may lead to different results from the decomposition of the uncertainty for a combination of

measurements with significant and uncorrelated systematic uncertainties.

7. Mass measurement in the $H \to ZZ^* \to 4\ell$ channel

7.1. Event selection

Events are required to contain at least four isolated leptons ($\ell = e, \mu$) that emerge from a common vertex, form two pairs of oppositely charged same-flavour leptons. Electrons are required to be within the full pseudorapidity range of the inner tracking detector ($|\eta| < 2.47$) and have transverse energy $E_{\mathrm{T}} > 7$ GeV, while muons are required to be within the pseudorapidity range of the muon spectrometer ($|\eta| < 2.7$) and have transverse momentum $p_{\mathrm{T}} > 5$ GeV. The three higher-p_{T} (E_{T}) leptons in each quadruplet are required to pass thresholds of 20, 15, and 10 GeV, respectively. A detailed description of the event selection can be found in Refs. [11,44].

The lepton pair with an invariant mass closest to the Z boson mass in each quadruplet is referred to as the leading dilepton pair, while the remaining pair is referred to as the subleading dilepton pair. The selected events are split according to the flavour of the leading and subleading pairs; ordered according to the expected selection efficiency, they are 4μ, $2e2\mu$, $2\mu2e$, $4e$. Reconstructed photon candidates passing final-state radiation selections are searched for in all the events [45]. Such photons are found in 4% of the events and their energy is included in the mass computation. In addition, a kinematic fit is performed to constrain the invariant mass of the leading lepton pair to the Z boson mass, improving the $m_{4\ell}$ resolution by about 15% [7]. The improvement brought by the correction of the local tracker misalignments, as discussed in Section 4, is at the percent level for the $m_{4\ell}$ resolution of signal events. After event selection, the $m_{4\ell}$ resolution for the signal (at $m_H = 125$ GeV), estimated with a Gaussian fit around the peak, is expected to be about 1.6, 1.8, 2.2 and 2.4 GeV for the 4μ, $2e2\mu$, $2\mu2e$ and $4e$ channels respectively. In the fit range of $110 < m_{4\ell} < 135$ GeV, 123 candidate events are observed. The yield is in agreement with an expectation of 107 ± 6 events, 53% of which are expected to be from the signal, assuming $m_H = 125$ GeV.

The dominant contribution to the background is non-resonant ZZ^* production (about 84% of the total background yield). Events with hadrons, or hadron decay products, misidentified as prompt leptons also contribute (about 15%). Events originating from $t\bar{t}$+Z, ZZZ, WZZ, and WWZ production are estimated to contribute less than 1% of the total background. The residual combinatorial background, originating from events with additional prompt leptons, was found to be negligibly small [44].

The precision of the mass measurement is further improved by categorising events with a multivariate discriminant which distinguishes the signal from the ZZ^* background. The BDT described in Ref. [7], based on the same input variables, is trained on simulated signal events with different mass values simultaneously (124, 125 and 126 GeV) and ZZ^* background events that pass the event selection. For each final state, four equal-size exclusive bins in the BDT response are used. This improves the precision of the m_H measurement in the 4ℓ decay channel by about 6%.

7.2. Signal and background model

The invariant mass in each category is described by the sum of a signal and a background distribution.

Non-resonant ZZ^* production is estimated using simulation normalised to the most accurate predictions and validated in the sidebands of the selected 4ℓ mass range. Smaller contributions to the background from $t\bar{t}$+Z, ZZZ, WZZ and WWZ production are also estimated using simulation while the contributions from Z+jets, WZ, and $t\bar{t}$ production where one or more hadrons, or hadron decay products, are misidentified as a prompt lepton are estimated from data using minimal input from simulation following the methodology described in Ref. [11]. For each contribution to the background, the probability density function (pdf) is estimated with the kernel density estimation.

For the determination of the signal distribution, an approach based on the event-by-event response of the detector is employed. The measured $m_{4\ell}$ signal distribution is modelled as the convolution of a relativistic Breit–Wigner distribution, of 4.1 MeV width [27–30] and a peak at m_H, with a four-lepton invariant mass response distribution which is derived event-by-event from the expected response distributions of the individual leptons. The lepton energy response distributions are derived from simulation as a function of the lepton energy and detector region. The lepton energy response is modelled as a weighted sum of three Gaussian distributions. For an observed event, the $m_{4\ell}$ pdf is derived from the convolution of the response distributions of the four measured leptons. The direct convolution of the four leptons distributions, leading to $3^4 = 81$ Gaussian distributions, is simplified to a weighted sum of four Gaussian pdfs following an iterative merging procedure as performed with the Gaussian-sum filter procedure [46,47]. An additional correction is applied to remove the residual differences which arise from the correlation between the lepton energy measurements introduced by the kinematic constrained fit on the leading dilepton pair and the BDT categorisation of events. These are corrected by a fit of scaling modifiers of the reduced response parameters to the simulated four-lepton resolution. These modifiers are about 0.1% for the means and up to 10% for the widths of the Gaussians of the reduced response.

Finally, the mass of the Higgs boson m_H is determined by a simultaneous unbinned fit of signal-plus-background distributions to data over the sixteen categories.[2] The per-event component of the signal pdf is added to the background distribution which is integrated over all kinematic configurations of the four final state leptons. In each of the four BDT categories, the signal yield is factorised by a floating normalisation modifier independent for each BDT category. The measured Higgs boson mass depends on the lepton energy resolution and the lepton energy scale. Uncertainties in these quantities are accounted for in the fit by Gaussian-distributed penalty terms whose widths are obtained from auxiliary data or simulation control samples. The expected uncertainty, with $m_H = 125$ GeV and production rates predicted by the SM, for a data sample of the size of the experimental set, evaluated using simulation-based pseudo-experiments, is ± 0.35 GeV.

A validation with data is performed with $Z \to 4\ell$ events to test the performance of the method on a known resonance with similar topology. In this test, the peak and width of the relativistic Breit–Wigner function are set to those of the Z boson. The measured Z boson mass was found to be 91.62 ± 0.35 GeV including statistical and systematic uncertainty. The observed uncertainty is in agreement with the expectation of ± 0.34 GeV, as evaluated from simulation. The measured value is in agreement with the world average of 91.1876 ± 0.0021 GeV [48].

As an independent check, the template method [7] is also used to measure m_H. The simulated distributions of the samples generated for m_H values between 110 and 130 GeV are smoothed with a kernel density estimate technique, and then parametrised as a function of m_H by means of a B-spline interpolation to obtain the signal model for any value of m_H. The expected statistical uncertainty of m_H obtained with the per-event method from a

[2] Four per final state for each of the four BDT categories.

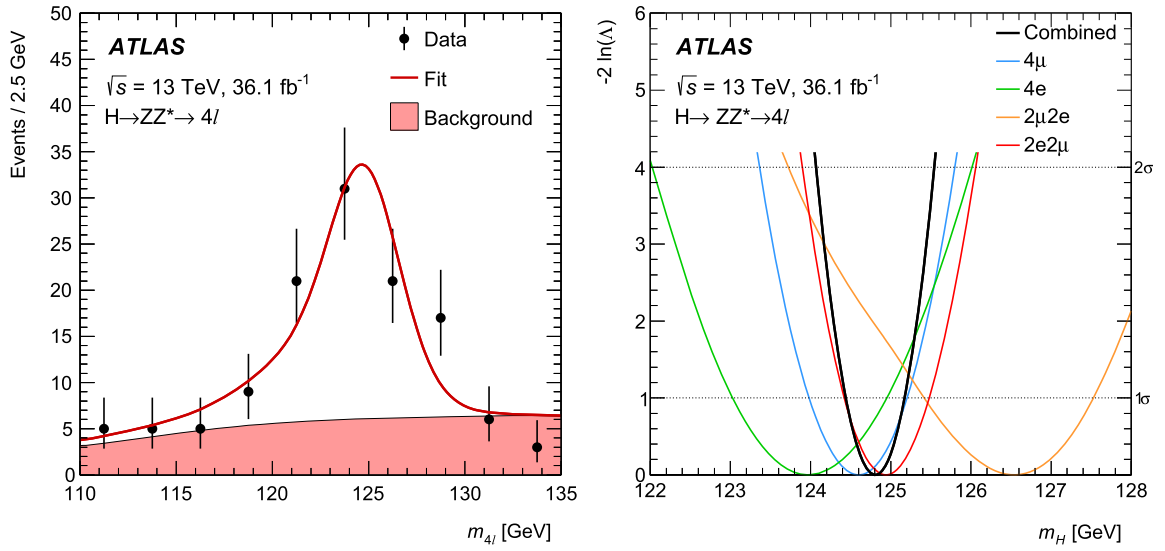

Fig. 1. (a) Invariant mass distribution for the data (points with error bars) shown together with the simultaneous fit result to $H \to ZZ^* \to 4\ell$ candidates (continuous line). The background component of the fit is also shown (filled area). The signal probability density function is evaluated per-event and averaged over the observed data. (b) Value of $-2\ln\Lambda$ as a function of m_H for the combined fit to all $H \to ZZ^* \to 4\ell$ categories. The intersection of the $-2\ln\Lambda$ curve with the horizontal lines labelled 1σ and 2σ provide the 68.3% and 95.5% confidence intervals.

sample equal in size to the experimental data set is, on average, 3% smaller than the statistical uncertainty obtained with the template method. Both methods are found to be unbiased within the statistical uncertainty of the simulated samples used of about 8 MeV on m_H.

7.3. Results

The estimate of m_H for the per-event and template methods is extracted with a simultaneous profile likelihood fit to the sixteen categories. The free parameters of the fit are m_H, the normalisation modifiers of each BDT category, and the nuisance parameters associated with systematic uncertainties. The measured value of m_H from the per-event method is found to be $m_H^{ZZ^*} = 124.79 \pm 0.36\ (\text{stat}) \pm 0.05\ (\text{syst})\ \text{GeV} = 124.79 \pm 0.37\ \text{GeV}$.

The total uncertainty is in agreement with the expectation and is dominated by the statistical component. The root-mean-square of the expected uncertainty due to statistical fluctuations in the event yields of each category was estimated to be 40 MeV. The p-value of the uncertainty being as high or higher than the observed value, estimated with pseudo-experiments, is found to be 0.47. The total systematic uncertainty is 50 MeV, the leading sources being the muon momentum scale (40 MeV) and the electron energy scale (26 MeV), with other sources (background modelling and simulation statistics) being smaller than 10 MeV.

For the template method, the total uncertainty is found to be $^{+0.41}_{-0.39}$ GeV, larger by 35 MeV than for the per-event method. The observed difference for the m_H estimates of the two methods is found to be 0.16 GeV, which is compatible with the expected variance estimated with pseudo-experiments and corresponds to a one sided p-value of 0.19. Fig. 1(a) shows the $m_{4\ell}$ distribution of the data together with the result of the fit to the $H \to ZZ^* \to 4\ell$ candidates when using the per-event method. The fit is also performed independently for each decay channel, fitting all BDT categories simultaneously; the resulting likelihood profile is compared with the combined fit in Fig. 1(b). The combined measured value of m_H is found to be compatible with the value measured independently for each channel, with the largest deviation being 1.4σ for the $2\mu 2e$ channel and the others being within 1σ.

The Higgs boson mass in the four-lepton channel is also measured by using a profile likelihood ratio to combine the information from the Run 1 analysis [6], where $m_H = 124.51 \pm 0.52$ GeV, and the Run 2 analysis, keeping each individual signal normalisation parameter independent. The systematic uncertainties taken to be correlated between the two runs are the muon momentum and electron energy scales, while all other systematic uncertainties are considered uncorrelated. The combined Run 1 and Run 2 result is $m_H^{ZZ^*} = 124.71 \pm 0.30\ (\text{stat}) \pm 0.05\ (\text{syst})\ \text{GeV} = 124.71 \pm 0.30\ \text{GeV}$. The difference between the measured values of m_H in the four-lepton channel in the two runs is $\Delta m_H^{ZZ^*} = 0.28 \pm 0.63$ GeV, with the two results being compatible, with a p-value of 0.84.

8. Mass measurement in the $H \to \gamma\gamma$ channel

In the diphoton channel, the Higgs boson mass is measured from the position of the narrow resonant peak in the $m_{\gamma\gamma}$ distribution due to the Higgs boson decay to two photons. Such a peak is observed over a large, monotonically decreasing, $m_{\gamma\gamma}$ distribution from continuum background events. The diphoton invariant mass is computed from the measured photon energies and from their directions relative to the diphoton production vertex, chosen among all reconstructed primary vertex candidates using a neural-network algorithm based on track and primary vertex information, as well as the directions of the two photons measured in the calorimeter and inner detector [49].

Events are selected and divided into categories with different mass resolutions and signal-to-background ratios, optimised for the measurement of simplified template cross-sections [30,50] and of production mode signal strengths of the Higgs boson in the diphoton decay channel. The event selection and classification are described in Ref. [24]. A potential reduction of the total expected uncertainty by 4% could have been obtained using the same event categories chosen for the mass measurement with the Run 1 data [7]. Given the small expected improvement, a choice was made to use the same categorisation for the measurement of the mass and of the production mode signal strengths.

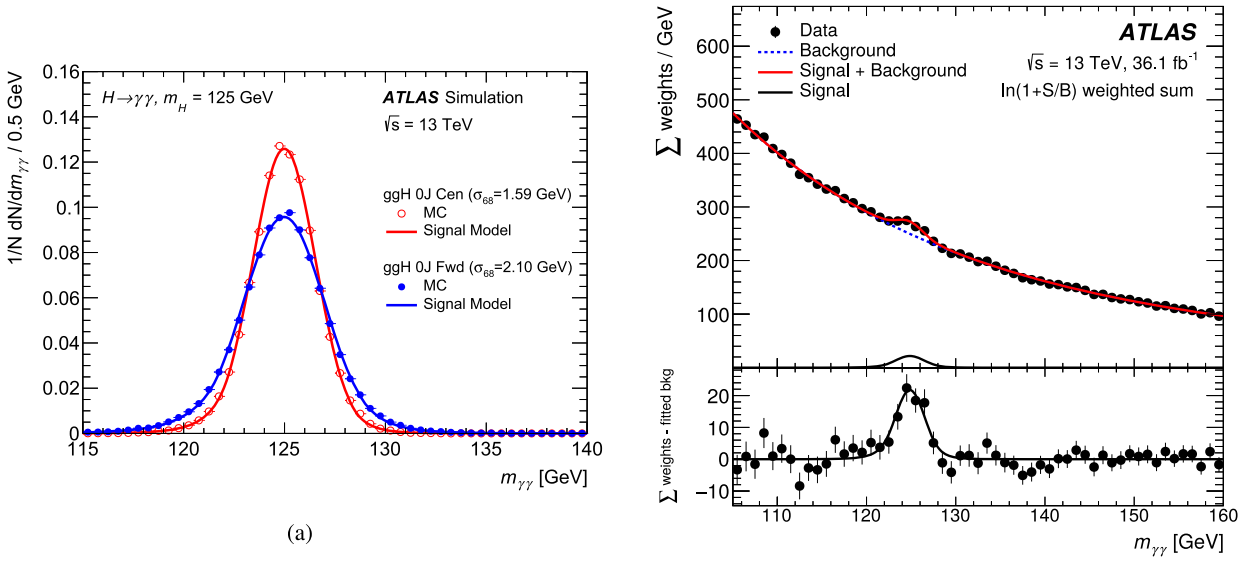

Fig. 2. (a) Invariant mass distributions (circles) of simulated $H \to \gamma\gamma$ events reconstructed in two categories with one of the best ("ggH 0J Cen": open circles) and one of the worst ("ggH 0J Fwd": solid circles) experimental resolutions. The signal model derived from a fit of the simulated events is superimposed (solid lines). (b) Diphoton invariant mass distribution of all selected data events, overlaid with the result of the fit (solid red line). Both for data and for the fit, each category is weighted by a factor $\ln(1+S/B)$, where S and B are the fitted signal and background yields in a $m_{\gamma\gamma}$ interval containing 90% of the expected signal. The dotted line describes the background component of the model. The bottom inset shows the difference between the sum of weights and the background component of the fitted model (dots), compared with the signal model (black line). (For interpretation of the colours in the figure(s), the reader is referred to the web version of this article.)

8.1. Event selection and categorisation

After an initial preselection, described in Ref. [24], requiring the presence of at least two loosely identified photon candidates with $|\eta| < 1.37$ or $1.52 < |\eta| < 2.37$, events are selected if the leading and the subleading photon candidates have $E_{\mathrm{T}}/m_{\gamma\gamma} > 0.35$ and 0.25 respectively, and satisfy the tight identification criteria and isolation criteria based on calorimeter and tracking information. Only events with invariant mass of the leading and subleading photon in the range $105\ \mathrm{GeV} < m_{\gamma\gamma} < 160\ \mathrm{GeV}$ are kept.

The events passing the previous selection are then classified, according to the properties of the two selected photons and of jets, electrons, muons and missing transverse momentum, into 31 mutually exclusive categories [24]. The most populated class, targeting gluon–gluon fusion production without reconstructed jets, is split into two categories of events with very different energy resolution: the first ("ggH 0J Cen") requires both photons to have $|\eta| < 0.95$, while the second ("ggH 0J Fwd") retains the remaining events.

8.2. Signal and background models

For each category, the shape of the diphoton invariant mass distribution of the signal is modelled with a double-sided Crystal Ball function [51], i.e. a Gaussian function in the peak region with power-law functions in both tails. The dependence of the parameters on the Higgs boson mass m_H is described by first-order polynomials, whose parameters are fixed by fitting simultaneously all the simulated signal samples generated for different values of m_H.

The quantity σ_{68}, defined as half of the smallest range containing 68% of the expected signal events, is an estimate of the signal $m_{\gamma\gamma}$ resolution and for $m_H = 125$ GeV it ranges between 1.41 GeV and 2.10 GeV depending on the category, while for the inclusive case its value is 1.84 GeV. Fig. 2(a) shows an example of the signal model for a category with one of the best invariant mass resolutions and for a category with one of the worst resolutions.

The expected signal yield is expressed as the product of integrated luminosity, production cross-section, diphoton branching ratio, acceptance and efficiency. The cross-section is parameterised as a function of m_H separately for each production mode. Similarly, the branching ratio is parameterised as a function of m_H. The product of acceptance and efficiency is evaluated separately for each production mode using only the samples with $m_H = 125$ GeV. Its dependence on the mass is weak (relative variation below 1% when varying the Higgs boson mass by ± 1 GeV) and is thus neglected. The cross-sections are fixed to the SM values multiplied by a signal modifier for each production mode: μ_{ggF}, μ_{VBF}, μ_{VH} and $\mu_{t\bar{t}H}$. The expected yield for $m_H = 125$ GeV varies between about one event in categories sensitive to rare production modes ($t\bar{t}H$, tH) to almost 500 events in the most populated event category ("ggH 0J Fwd").

The background invariant mass distribution of each category is parameterised with an empirical continuous function of the diphoton system invariant mass value. The parameters of these functions are fitted directly to data. The functional form used to describe the background in each category is chosen among several alternatives according to the three criteria described in Ref. [24]: (i) the fitted signal yield in a test sample representative of the data background, built by combining simulation and control regions in data, must be minimised; (ii) the χ^2 probability for the fit of this background control sample must be larger than a certain threshold; (iii) the quality of the fit to data sidebands must not improve significantly when adding an extra degree of freedom to the model. The models selected by this procedure are exponential or power-law functions with one degree of freedom for the categories with few events, while exponential functions of a second-order polynomial are used for the others.

From the extrapolation of a background-only fit to the sidebands of the $m_{\gamma\gamma}$ distribution in data, excluding events with $121\ \mathrm{GeV} < m_{\gamma\gamma} < 129\ \mathrm{GeV}$, the expected signal-to-background ratio in a $m_{\gamma\gamma}$ window containing 90% of the signal distribution for $m_H = 125$ GeV varies between 2% in the "ggH 0J Fwd" category and 100% in a high-purity, low-yield (about 12 events) category

targeting H+2jet, VBF-like events with low transverse momentum of the H+2jet system.

8.3. Systematic uncertainties

The main sources of systematic uncertainty in the measured Higgs boson mass in the diphoton channel are the uncertainties in the photon energy scale (PES), the uncertainty arising from the background model, and the uncertainty in the selection of the diphoton production vertex. They are described in detail in Ref. [24].

For each source of uncertainty in the PES described in Section 5, the diphoton invariant mass distribution for each category is recomputed after varying the photon energy by its uncertainty and is then compared with the nominal distribution. The sum in quadrature of the positive or negative shifts of the $m_{\gamma\gamma}$ peak position due to such variations ranges from ± 260 MeV in the "ggH 0J Cen" category to ± 470 MeV in the "jet BSM" category, which requires at least one jet with $p_{\mathrm{T}} > 200$ GeV. All the PES effects are considered as fully correlated across categories.

The uncertainty due to the background modelling is evaluated following the procedure described in Ref. [7]. The expected signal contribution as predicted by the signal model is added to the background control sample. The bias in the estimated Higgs boson mass from a signal-plus-background fit to the test sample relative to the injected mass is considered as a systematic uncertainty due to the background modelling. Its value is around ± 60 MeV for the most relevant categories for the mass measurement. In the other categories it can assume larger values, which are compatible with statistical fluctuations of the background control sample. For this reason this systematic uncertainty is ignored in the poorly populated $t\bar{t}H$ categories, which give a negligible contribution to the mass measurement. This systematic uncertainty is assumed to be uncorrelated between different categories.

The systematic uncertainty related to the selection of the diphoton production vertex is evaluated using $Z \to ee$ events, as described in Ref. [7]. An expected uncertainty of ± 40 MeV in m_H is used for all the categories and assumed to be fully correlated across different categories.

Systematic uncertainties in the diphoton mass resolution due to uncertainties in the photon energy resolution vary between $\pm 6\%$ (for the "ggH 0J Cen" category) and 11% (for the "jet BSM" category), and are expected to have a negligible impact on the mass measurement.

Systematic uncertainties in the yield and in the migration of events between categories described in Ref. [24] have a negligible impact on the mass measurement.

The uncertainty due to the signal modelling is evaluated similarly to that due to the background modelling. A sample is built using the expected background distribution and the simulated signal events at $m_H = 125$ GeV. The bias in the fitted Higgs boson mass is considered as a systematic uncertainty and is assumed to be correlated between different categories. The relative bias is below 10^{-4} in most of the categories, and at most a few times 10^{-4} in the other categories.

8.4. Results

The Higgs boson mass in the diphoton channel is estimated with a simultaneous binned maximum-likelihood fit to the $m_{\gamma\gamma}$ distributions of the selected event categories. In each category, the distribution is modelled with a sum of the background and signal models. The free parameters of the fit are m_H, the four signal strengths, the number of background events and the parameters describing the shape of the background invariant mass distribution in each category, and all the nuisance parameters associated with systematic uncertainties. Fig. 2(b) shows the distribution of the data overlaid with the result of the simultaneous fit. All event categories are included. For illustration purposes, events in each category are weighted by a factor $\ln(1 + S/B)$, where S and B are the fitted signal and background yields in a $m_{\gamma\gamma}$ interval containing 90% of the signal.

The measured mass of the Higgs boson in the diphoton channel is $m_H^{\gamma\gamma} = 124.93 \pm 0.21$ (stat) ± 0.34 (syst) GeV $= 124.93 \pm 0.40$ GeV where the first error is the statistical uncertainty while the second is the total systematic uncertainty, dominated by the photon energy scale uncertainty.

Assuming signal strengths as in the SM and the signal model determined from the simulation, the expected statistical uncertainty is 0.25 GeV and the expected total uncertainty is 0.41 GeV, with a root-mean-square, estimated from pseudo-experiments, of about 40 MeV. Compared to the expectation, the slightly larger systematic uncertainty and smaller statistical uncertainty observed in data are due to a lower than expected signal yield in some categories with large expected yield and small photon energy scale uncertainty, and to the fitted resolution in data being a few percent better than in the simulation (but still agreeing with it within one standard deviation).

To check if the measurement is sensitive to the assumption about the splitting of the production modes, the measurement is repeated using one common signal strength for all the processes. A small shift of the measured m_H by 20 MeV is observed. The mass measurement is also performed by allowing the overall signal yield in each analysis category to float independently in the fit. The measured value of m_H changes by less than 30 MeV.

Other checks targeting possible miscalibration due to detector effects for some specific category of photons are performed by partitioning the entire data sample into detector-oriented categories, different from those used for the nominal result, and determining the probability that m_H measured in one of these categories is compatible with the average m_H from the other categories. A first categorisation is based on whether the photons are reconstructed as converted or not, a second is based on the photons' impact points in the calorimeter (either in the barrel region, $|\eta| < 1.37$, or in the endcap region, $|\eta| > 1.52$), and a third is based on the number of interactions per bunch crossing. For each of these categories a new background model, a new signal model and new systematic uncertainty values are computed. For each category the compatibility of its m_H value with the combined m_H value is tested by considering as an additional likelihood parameter the quantity Δ_i equal to the difference between that category's m_H value and the combined value. No value of Δ_i significantly different from zero is found. A similar test is performed to assess the global compatibility of all the different categories with a common value of m_H. In the three categorisations considered the smallest global p-value is 12%. The same procedure is applied to the categories used in the analysis: the smallest p-value computed on single categories is 7% while the global p-value is 94%.

A combination of the Higgs boson mass measured in the diphoton channel by ATLAS in Run 1, 126.02 ± 0.51 GeV [6], and in Run 2 is performed using a profile likelihood ratio. The signal strengths are treated as independent parameters. The systematic uncertainties considered correlated between the two LHC run periods are most of the photon energy scale and resolution uncertainties and those in the pile-up modelling, while all the other systematic uncertainties are considered uncorrelated. The photon energy calibration uncertainties that are treated as uncorrelated between the two LHC data-taking periods are a few uncertainties included only in the Run 2 measurement, the uncertainty

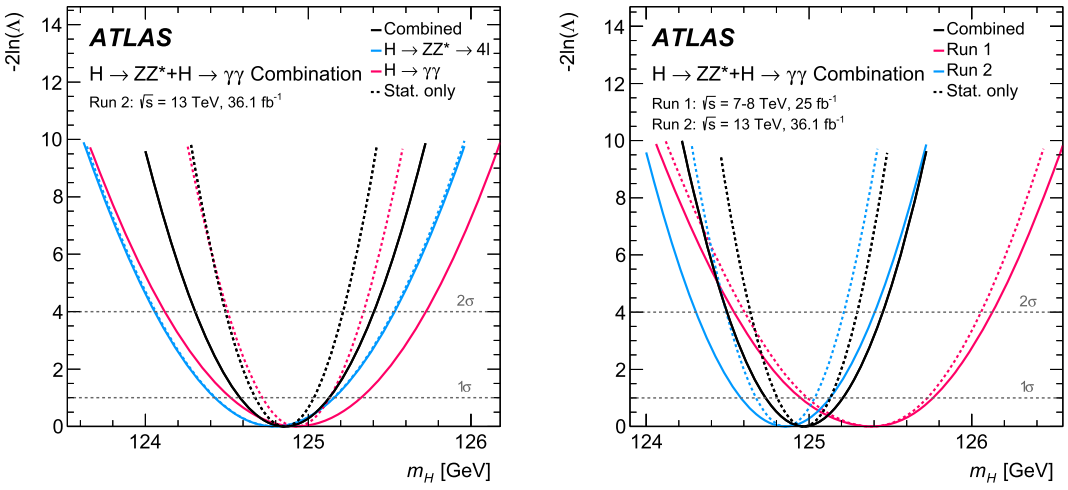

Fig. 3. The value of $-2\ln\Lambda$ as a function of m_H for (a) $H \to \gamma\gamma$, $H \to ZZ^* \to 4\ell$ channels and their combination (red, blue and black, respectively) using Run 2 data only and for (b) Run 1, Run 2 and their combination (red, blue and black, respectively). The dashed lines show the mass measurement uncertainties assuming statistical uncertainties only.

in the photon energy leakage outside the reconstructed cluster, whose measurement is limited by the statistical accuracy of $Z \to \ell\ell\gamma$, and the uncertainty in the electromagnetic calorimeter response non-linearity, which is estimated with different procedures in the two LHC run periods. The result is $m_H^{\gamma\gamma} = 125.32 \pm 0.19$ (stat) $\pm$ 0.29 (syst) GeV $= 125.32 \pm 0.35$ GeV. The difference between the measured values of m_H in the diphoton channel in the two LHC run periods is $\Delta m_H^{\gamma\gamma} = 1.09 \pm 0.46$ (stat) $\pm$ 0.34 (syst) GeV $= 1.09 \pm 0.57$ GeV. The probability that the two results are compatible is 5.1%.

9. Combined mass measurement

The Higgs boson mass is measured by combining information from both the $H \to ZZ^* \to 4\ell$ and $H \to \gamma\gamma$ channels. The correlations between the systematic uncertainties in the two channels are accounted for in the profile likelihood function. The main sources of correlated systematic uncertainty include the calibrations of electrons and photons, the pile-up modelling, and the luminosity. Signal yield normalisations are treated as independent free parameters in the fit to minimise model-dependent assumptions in the measurement of the Higgs boson mass.

The combined value of the mass measured using Run 2 data is $m_H = 124.86 \pm 0.27$ GeV. Assuming statistical uncertainties only, the uncertainty in the combined value is ± 0.18 GeV. The corresponding profile likelihood, for the two channels and for their combination, is shown in Fig. 3(a). This result is in good agreement with the ATLAS+CMS Run 1 measurement [6], $m_H = 125.09 \pm 0.24$ GeV.

The combined mass measurement from the ATLAS Run 1 ($m_H = 125.36 \pm 0.41$ GeV) and Run 2 results is $m_H = 124.97 \pm 0.24$ GeV. Assuming statistical uncertainties only, the measurement uncertainty amounts to 0.16 GeV. Fig. 3(b) shows the value of $-2\ln\Lambda$ as a function of m_H for the two channels combined, separately for the ATLAS Run 1 and Run 2 data sets, as well as for their combination.

The contributions of the main sources of systematic uncertainty to the combined mass measurement, using both ATLAS Run 1 and Run 2 data, are summarised in Table 1. The impact of each source of systematic uncertainty is evaluated starting from the contribution of each individual nuisance parameter to the total uncertainty. This contribution is defined as the mass shift δm_H observed when re-evaluating the profile likelihood ratio after fixing the nuisance parameter in question to its best-fit value increased or decreased by one standard deviation, while all remainder nuisance parameters remain free to float. The sum in quadrature of groups of nuisance parameter variations gives the impact of each category of systematic uncertainties. The nuisance parameter values from the unconditional maximum-likelihood fit are consistent with the pre-fit values within one standard deviation.

Table 1
Main sources of systematic uncertainty in the Higgs boson mass m_H measured with the 4ℓ and $\gamma\gamma$ final states using Run 1 and Run 2 data. The sum in quadrature of the individual contributions is not expected to reproduce the total systematic uncertainty due to the different methodologies employed to derive them.

Source	Systematic uncertainty in m_H [MeV]
EM calorimeter response linearity	60
Non-ID material	55
EM calorimeter layer intercalibration	55
$Z \to ee$ calibration	45
ID material	45
Lateral shower shape	40
Muon momentum scale	20
Conversion reconstruction	20
$H \to \gamma\gamma$ background modelling	20
$H \to \gamma\gamma$ vertex reconstruction	15
e/γ energy resolution	15
All other systematic uncertainties	10

The probability that the m_H results from the four measurements (in the 4ℓ and $\gamma\gamma$ final states, using Run 1 or Run 2 ATLAS data) are compatible is 12.3%. Due to the impact of the correlated systematic uncertainties, the correlation between m_H in the $H \to \gamma\gamma$ channel over the two runs is 23%. The residual correlation between $H \to ZZ^* \to 4\ell$ and $H \to \gamma\gamma$ is typically 1%. The results from each of the four individual measurements, as well as various combinations, along with the LHC Run 1 result, are summarised in Fig. 4.

The combination of the four ATLAS measurements using the BLUE approach as an alternative method, assuming two uncorrelated channels,[3] is found to be $m_H = 124.97 \pm 0.23$ GeV $=$

[3] The combination of the two LHC run periods for each channel was used as input.

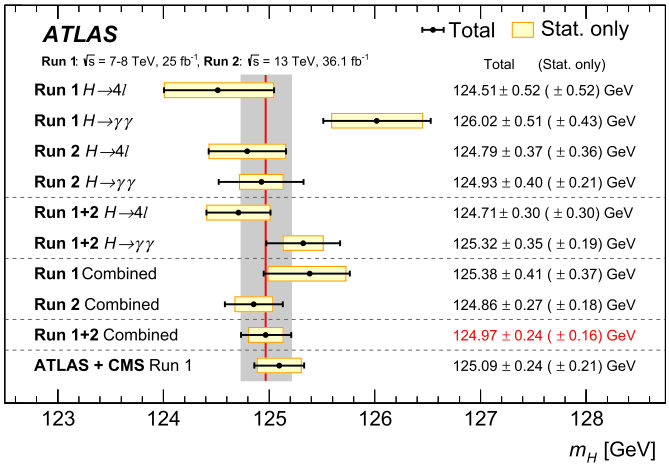

Fig. 4. Summary of the Higgs boson mass measurements from the individual and combined analyses performed here, compared with the combined Run 1 measurement by ATLAS and CMS [6]. The statistical-only (horizontal yellow-shaded bands) and total (black error bars) uncertainties are indicated. The (red) vertical line and corresponding (grey) shaded column indicate the central value and the total uncertainty of the combined ATLAS Run 1 + 2 measurement, respectively.

$124.97 \pm 0.19\,(\text{stat}) \pm 0.13\,(\text{syst})$ GeV. The splitting of the errors takes into account the relative weight of the two channels in the combined measurement.

10. Conclusion

The mass of the Higgs boson has been measured from a combined fit to the invariant mass spectra of the decay channels $H \to ZZ^* \to 4\ell$ and $H \to \gamma\gamma$. The results are obtained from a Run 2 pp collision data sample recorded by the ATLAS experiment at the CERN Large Hadron Collider at a centre-of-mass energy of 13 TeV, corresponding to an integrated luminosity of 36.1 fb^{-1}. The measurements are based on the latest calibrations of muons, electrons, and photons, and on improvements to the analysis techniques used to obtain the previous results from ATLAS Run 1 data.

The measured values of the Higgs boson mass for the $H \to ZZ^* \to 4\ell$ and $H \to \gamma\gamma$ channels are

$$m_H = 124.79 \pm 0.37 \text{ GeV},$$

$$m_H = 124.93 \pm 0.40 \text{ GeV}.$$

From the combination of these two channels, the mass is measured to be

$$m_H = 124.86 \pm 0.27 \text{ GeV}.$$

This result is in good agreement with the average of the ATLAS and CMS Run 1 measurements. The combination of the ATLAS Run 1 and Run 2 measurements yields

$$m_H = 124.97 \pm 0.24 \text{ GeV}.$$

Acknowledgements

We thank CERN for the very successful operation of the LHC, as well as the support staff from our institutions without whom ATLAS could not be operated efficiently.

We acknowledge the support of ANPCyT, Argentina; YerPhI, Armenia; ARC, Australia; BMWFW and FWF, Austria; ANAS, Azerbaijan; SSTC, Belarus; CNPq and FAPESP, Brazil; NSERC, NRC and CFI, Canada; CERN; CONICYT, Chile; CAS, MOST and NSFC, China; COLCIENCIAS, Colombia; MSMT CR, MPO CR and VSC CR, Czech Republic; DNRF and DNSRC, Denmark; IN2P3-CNRS, CEA-DRF/IRFU, France; SRNSFG, Georgia; BMBF, HGF, and MPG, Germany; GSRT, Greece; RGC, Hong Kong SAR, China; ISF, I-CORE and Benoziyo Center, Israel; INFN, Italy; MEXT and JSPS, Japan; CNRST, Morocco; NWO, Netherlands; RCN, Norway; MNiSW and NCN, Poland; FCT, Portugal; MNE/IFA, Romania; MES of Russia and NRC KI, Russian Federation; JINR; MESTD, Serbia; MSSR, Slovakia; ARRS and MIZŠ, Slovenia; DST/NRF, South Africa; MINECO, Spain; SRC and Wallenberg Foundation, Sweden; SERI, SNSF and Cantons of Bern and Geneva, Switzerland; MOST, Taiwan; TAEK, Turkey; STFC, United Kingdom; DOE and NSF, United States of America. In addition, individual groups and members have received support from BCKDF, the Canada Council, Canarie, CRC, Compute Canada, FQRNT, and the Ontario Innovation Trust, Canada; EPLANET, ERC, ERDF, FP7, Horizon 2020 and Marie Skłodowska-Curie Actions, European Union; Investissements d'Avenir Labex and Idex, ANR, Région Auvergne and Fondation Partager le Savoir, France; DFG and AvH Foundation, Germany; Herakleitos, Thales and Aristeia programmes co-financed by EU-ESF and the Greek NSRF; BSF, GIF and Minerva, Israel; BRF, Norway; CERCA Programme Generalitat de Catalunya, Generalitat Valenciana, Spain; the Royal Society and Leverhulme Trust, United Kingdom.

The crucial computing support from all WLCG partners is acknowledged gratefully, in particular from CERN, the ATLAS Tier-1 facilities at TRIUMF (Canada), NDGF (Denmark, Norway, Sweden), CC-IN2P3 (France), KIT/GridKA (Germany), INFN-CNAF (Italy), NL-T1 (Netherlands), PIC (Spain), ASGC (Taiwan), RAL (UK) and BNL (USA), the Tier-2 facilities worldwide and large non-WLCG resource providers. Major contributors of computing resources are listed in Ref. [52].

References

[1] ATLAS Collaboration, Observation of a new particle in the search for the Standard Model Higgs boson with the ATLAS detector at the LHC, Phys. Lett. B 716 (2012) 1, arXiv:1207.7214 [hep-ex].
[2] CMS Collaboration, Observation of a new boson at a mass of 125 GeV with the CMS experiment at the LHC, Phys. Lett. B 716 (2012) 30, arXiv:1207.7235 [hep-ex].
[3] F. Englert, R. Brout, Broken symmetry and the mass of gauge vector mesons, Phys. Rev. Lett. 13 (1964) 321.
[4] P.W. Higgs, Broken symmetries and the masses of gauge bosons, Phys. Rev. Lett. 13 (1964) 508.
[5] G. Guralnik, C. Hagen, T. Kibble, Global conservation laws and massless particles, Phys. Rev. Lett. 13 (1964) 585.
[6] ATLAS, CMS Collaborations, Combined measurement of the Higgs boson mass in pp collisions at $\sqrt{s} = 7$ and 8 TeV with the ATLAS and CMS experiments, Phys. Rev. Lett. 114 (2015) 191803, arXiv:1503.07589 [hep-ex].
[7] ATLAS Collaboration, Measurement of the Higgs boson mass from the $H \to \gamma\gamma$ and $H \to ZZ^* \to 4\ell$ channels in pp collisions at center-of-mass energies of 7 and 8 TeV with the ATLAS detector, Phys. Rev. D 90 (2014) 052004, arXiv:1406.3827 [hep-ex].
[8] CMS Collaboration, Precise determination of the mass of the Higgs boson and tests of compatibility of its couplings with the standard model predictions using proton collisions at 7 and 8 TeV, Eur. Phys. J. C 75 (2015) 212, arXiv:1412.8662 [hep-ex].
[9] CMS Collaboration, Measurements of properties of the Higgs boson decaying into the four-lepton final state in pp collisions at $\sqrt{s} = 13$ TeV, J. High Energy Phys. 11 (2017) 047, arXiv:1706.09936 [hep-ex].
[10] ATLAS Collaboration, The ATLAS experiment at the CERN Large Hadron Collider, J. Instrum. 3 (2008) S08003.
[11] ATLAS Collaboration, Measurement of inclusive and differential cross sections in the $H \to ZZ^* \to 4\ell$ decay channel in pp collisions at $\sqrt{s} = 13$ TeV with the ATLAS detector, J. High Energy Phys. 10 (2017) 132, arXiv:1708.02810 [hep-ex].
[12] K. Hamilton, P. Nason, E. Re, G. Zanderighi, NNLOPS simulation of Higgs boson production, J. High Energy Phys. 10 (2013) 222, arXiv:1309.0017 [hep-ph].
[13] J. Butterworth, et al., PDF4LHC recommendations for LHC Run II, J. Phys. G 43 (2016) 023001, arXiv:1510.03865 [hep-ph].
[14] S. Alioli, P. Nason, C. Oleari, E. Re, NLO Higgs boson production via gluon fusion matched with shower in POWHEG, J. High Energy Phys. 04 (2009) 002, arXiv:0812.0578 [hep-ph].

[15] T. Sjöstrand, S. Mrenna, P.Z. Skands, A brief introduction to PYTHIA 8.1, Comput. Phys. Commun. 178 (2008) 852, arXiv:0710.3820 [hep-ph].
[16] D.J. Lange, The EvtGen particle decay simulation package, Nucl. Instrum. Methods A 462 (2001) 152.
[17] H.-L. Lai, et al., New parton distributions for collider physics, Phys. Rev. D 82 (2010) 074024, arXiv:1007.2241 [hep-ph].
[18] J. Pumplin, et al., New generation of parton distributions with uncertainties from global QCD analysis, J. High Energy Phys. 07 (2002) 012, arXiv:hep-ph/0201195 [hep-ph].
[19] ATLAS Collaboration, Measurement of the Z/γ^* boson transverse momentum distribution in pp collisions at $\sqrt{s} = 7$ TeV with the ATLAS detector, J. High Energy Phys. 09 (2014) 145, arXiv:1406.3660 [hep-ex].
[20] F. Cascioli, et al., ZZ production at hadron colliders in NNLO QCD, Phys. Lett. B 735 (2014) 311, arXiv:1405.2219 [hep-ph].
[21] M. Grazzini, S. Kallweit, D. Rathlev, ZZ production at the LHC: fiducial cross sections and distributions in NNLO QCD, Phys. Lett. B 750 (2015) 407, arXiv:1507.06257 [hep-ph].
[22] B. Biedermann, A. Denner, S. Dittmaier, L. Hofer, B. Jäger, Electroweak corrections to $pp \to \mu^+\mu^- e^+ e^- + X$ at the LHC: a Higgs boson background study, Phys. Rev. Lett. 116 (2016) 161803, arXiv:1601.07787 [hep-ph].
[23] B. Biedermann, A. Denner, S. Dittmaier, L. Hofer, B. Jager, Next-to-leading-order electroweak corrections to the production of four charged leptons at the LHC, J. High Energy Phys. 01 (2017) 033, arXiv:1611.05338 [hep-ph].
[24] ATLAS Collaboration, Measurements of Higgs boson properties in the diphoton decay channel with 36 fb^{-1} of pp collision data at $\sqrt{s} = 13$ TeV with the ATLAS detector, arXiv:1802.04146 [hep-ex], 2018.
[25] ATLAS Collaboration, The ATLAS simulation infrastructure, Eur. Phys. J. C 70 (2010) 823, arXiv:1005.4568 [physics.ins-det].
[26] S. Agostinelli, et al., GEANT4 – a simulation toolkit, Nucl. Instrum. Methods A 506 (2003) 250.
[27] LHC Higgs Cross Section Working Group, S. Dittmaier, C. Mariotti, G. Passarino, R. Tanaka (Eds.), Handbook of LHC Higgs Cross Sections: 1. Inclusive Observables, CERN, Geneva, 2011, CERN-2011-002, arXiv:1101.0593 [hep-ph].
[28] LHC Higgs Cross Section Working Group, S. Dittmaier, C. Mariotti, G. Passarino, R. Tanaka (Eds.), Handbook of LHC Higgs Cross Sections: 2. Differential Distributions, CERN, Geneva, 2012, CERN-2012-002, arXiv:1201.3084 [hep-ph].
[29] LHC Higgs Cross Section Working Group, S. Heinemeyer, C. Mariotti, G. Passarino, R. Tanaka (Eds.), Handbook of LHC Higgs Cross Sections: 3. Higgs Properties, CERN, Geneva, 2013, CERN-2013-004, arXiv:1307.1347 [hep-ph].
[30] LHC Higgs Cross Section Working Group, D. de Florian, C. Grojean, F. Maltoni, C. Mariotti, A. Nikitenko, M. Pieri, P. Savard, M. Schumacher, R. Tanaka (Eds.), Handbook of LHC Higgs Cross Sections: 4. Deciphering the Nature of the Higgs Sector, CERN, Geneva, 2017, CERN-2017-002, arXiv:1610.07922 [hep-ph].
[31] ATLAS Collaboration, Early inner detector tracking performance in the 2015 data at $\sqrt{s} = 13$ TeV, ATL-PHYS-PUB-2015-051, URL: https://cds.cern.ch/record/2110140, 2015.
[32] ATLAS Collaboration, Study of alignment-related systematic effects on the ATLAS Inner Detector track reconstruction, ATLAS-CONF-2012-141, URL: https://cds.cern.ch/record/1483518, 2012.
[33] ATLAS Collaboration, Muon reconstruction performance of the ATLAS detector in proton–proton collision data at $\sqrt{s} = 13$ TeV, Eur. Phys. J. C 76 (2016) 292, arXiv:1603.05598 [hep-ex].
[34] ATLAS Collaboration, Topological cell clustering in the ATLAS calorimeters and its performance in LHC Run 1, Eur. Phys. J. C 77 (2017) 490, arXiv:1603.02934 [hep-ex].
[35] ATLAS Collaboration, Measurement of the photon identification efficiencies with the ATLAS detector using LHC Run-1 data, Eur. Phys. J. C 76 (2016) 666, arXiv:1606.01813 [hep-ex].
[36] ATLAS Collaboration, Electron and photon energy calibration with the ATLAS detector using LHC Run 1 data, Eur. Phys. J. C 74 (2014) 3071, arXiv:1407.5063 [hep-ex].
[37] ATLAS Collaboration, Electron and photon energy calibration with the ATLAS detector using data collected in 2015 at $\sqrt{s} = 13$ TeV, ATL-PHYS-PUB-2016-015, URL: https://cds.cern.ch/record/2203514, 2016.
[38] ATLAS Collaboration, Electron efficiency measurements with the ATLAS detector using 2012 LHC proton–proton collision data, Eur. Phys. J. C 77 (2017) 195, arXiv:1612.01456 [hep-ex].
[39] ATLAS Collaboration, Combined search for the Standard Model Higgs boson in pp collisions at $\sqrt{s} = 7$ TeV with the ATLAS detector, Phys. Rev. D 86 (2012) 032003, arXiv:1207.0319 [hep-ex].
[40] G. Cowan, K. Cranmer, E. Gross, O. Vitells, Asymptotic formulae for likelihood-based tests of new physics, Eur. Phys. J. C 71 (2011) 1554, arXiv:1007.1727.
[41] R. Nisius, On the combination of correlated estimates of a physics observable, Eur. Phys. J. C (ISSN 1434-6052) 74 (2014) 3004, https://doi.org/10.1140/epjc/s10052-014-3004-2.
[42] L. Lyons, D. Gibaut, P. Clifford, How to combine correlated estimates of a single physical quantity, Nucl. Instrum. Methods A 270 (1988) 110.
[43] A. Valassi, Combining correlated measurements of several different physical quantities, Nucl. Instrum. Methods A 500 (2003) 391.
[44] M. Aaboud, et al., Measurement of the Higgs boson coupling properties in the $H \to ZZ^* \to 4\ell$ decay channel at $\sqrt{s} = 13$ TeV with the ATLAS detector, J. High Energy Phys. 03 (2018) 095, arXiv:1712.02304 [hep-ex].
[45] ATLAS Collaboration, Measurements of Higgs boson production and couplings in the four-lepton channel in pp collisions at center-of-mass energies of 7 and 8 TeV with the ATLAS detector, Phys. Rev. D 91 (2015) 012006, arXiv:1408.5191 [hep-ex].
[46] R. Frühwirth, Track fitting with non-Gaussian noise, Comput. Phys. Commun. 100 (1997) 1.
[47] ATLAS Collaboration, Improved electron reconstruction in ATLAS using the Gaussian Sum Filter-based model for bremsstrahlung, ATLAS-CONF-2012-047, URL: https://cds.cern.ch/record/1449796, 2012.
[48] M. Tanabashi, et al., Particle Data Group, Review of particle physics, Phys. Rev. D 98 (2018) 010001.
[49] ATLAS Collaboration, Measurement of Higgs boson production in the diphoton decay channel in pp collisions at center-of-mass energies of 7 and 8 TeV with the ATLAS detector, Phys. Rev. D 90 (2014) 112015, arXiv:1408.7084 [hep-ex].
[50] J.R. Andersen, et al., Les Houches 2015: physics at TeV colliders standard model working group report, arXiv:1605.04692 [hep-ph].
[51] ATLAS Collaboration, Search for resonances in diphoton events at $\sqrt{s} = 13$ TeV with the ATLAS detector, J. High Energy Phys. 09 (2016) 001, arXiv:1606.03833 [hep-ex].
[52] ATLAS Collaboration, ATLAS computing acknowledgements, ATL-GEN-PUB-2016-002, URL: https://cds.cern.ch/record/2202407.

The ATLAS Collaboration

M. Aaboud [34d], G. Aad [99], B. Abbott [124], O. Abdinov [13,*], B. Abeloos [128], S.H. Abidi [165], O.S. AbouZeid [143], N.L. Abraham [153], H. Abramowicz [159], H. Abreu [158], Y. Abulaiti [6], B.S. Acharya [64a,64b,o], S. Adachi [161], L. Adamczyk [81a], J. Adelman [119], M. Adersberger [112], T. Adye [141], A.A. Affolder [143], Y. Afik [158], C. Agheorghiesei [27c], J.A. Aguilar-Saavedra [136f,136a], F. Ahmadov [77,ag], G. Aielli [71a,71b], S. Akatsuka [83], T.P.A. Åkesson [94], E. Akilli [52], A.V. Akimov [108], G.L. Alberghi [23b,23a], J. Albert [174], P. Albicocco [49], M.J. Alconada Verzini [86], S. Alderweireldt [117], M. Aleksa [35], I.N. Aleksandrov [77], C. Alexa [27b], G. Alexander [159], T. Alexopoulos [10], M. Alhroob [124], B. Ali [138], G. Alimonti [66a], J. Alison [36], S.P. Alkire [145], C. Allaire [128], B.M.M. Allbrooke [153], B.W. Allen [127], P.P. Allport [21], A. Aloisio [67a,67b], A. Alonso [39], F. Alonso [86], C. Alpigiani [145], A.A. Alshehri [55], M.I. Alstaty [99], B. Alvarez Gonzalez [35], D. Álvarez Piqueras [172], M.G. Alviggi [67a,67b], B.T. Amadio [18], Y. Amaral Coutinho [78b], L. Ambroz [131], C. Amelung [26], D. Amidei [103], S.P. Amor Dos Santos [136a,136c], S. Amoroso [35], C.S. Amrouche [52], C. Anastopoulos [146], L.S. Ancu [52], N. Andari [21], T. Andeen [11], C.F. Anders [59b], J.K. Anders [20], K.J. Anderson [36], A. Andreazza [66a,66b], V. Andrei [59a], S. Angelidakis [37], I. Angelozzi [118], A. Angerami [38], A.V. Anisenkov [120b,120a], A. Annovi [69a], C. Antel [59a], M.T. Anthony [146], M. Antonelli [49], D.J.A. Antrim [169], F. Anulli [70a], M. Aoki [79], L. Aperio Bella [35], G. Arabidze [104], Y. Arai [79], J.P. Araque [136a], V. Araujo Ferraz [78b], R. Araujo Pereira [78b], A.T.H. Arce [47], R.E. Ardell [91], F.A. Arduh [86], J-F. Arguin [107], S. Argyropoulos [75],

A.J. Armbruster [35], L.J. Armitage [90], O. Arnaez [165], H. Arnold [118], M. Arratia [31], O. Arslan [24], A. Artamonov [109,*], G. Artoni [131], S. Artz [97], S. Asai [161], N. Asbah [44], A. Ashkenazi [159], E.M. Asimakopoulou [170], L. Asquith [153], K. Assamagan [29], R. Astalos [28a], R.J. Atkin [32a], M. Atkinson [171], N.B. Atlay [148], K. Augsten [138], G. Avolio [35], R. Avramidou [58a], B. Axen [18], M.K. Ayoub [15a], G. Azuelos [107,au], A.E. Baas [59a], M.J. Baca [21], H. Bachacou [142], K. Bachas [65a,65b], M. Backes [131], P. Bagnaia [70a,70b], M. Bahmani [82], H. Bahrasemani [149], A.J. Bailey [172], J.T. Baines [141], M. Bajic [39], O.K. Baker [181], P.J. Bakker [118], D. Bakshi Gupta [93], E.M. Baldin [120b,120a], P. Balek [178], F. Balli [142], W.K. Balunas [133], E. Banas [82], A. Bandyopadhyay [24], S. Banerjee [179,k], A.A.E. Bannoura [180], L. Barak [159], W.M. Barbe [37], E.L. Barberio [102], D. Barberis [53b,53a], M. Barbero [99], T. Barillari [113], M-S. Barisits [35], J. Barkeloo [127], T. Barklow [150], N. Barlow [31], R. Barnea [158], S.L. Barnes [58c], B.M. Barnett [141], R.M. Barnett [18], Z. Barnovska-Blenessy [58a], A. Baroncelli [72a], G. Barone [26], A.J. Barr [131], L. Barranco Navarro [172], F. Barreiro [96], J. Barreiro Guimarães da Costa [15a], R. Bartoldus [150], A.E. Barton [87], P. Bartos [28a], A. Basalaev [134], A. Bassalat [128], R.L. Bates [55], S.J. Batista [165], S. Batlamous [34e], J.R. Batley [31], M. Battaglia [143], M. Bauce [70a,70b], F. Bauer [142], K.T. Bauer [169], H.S. Bawa [150,m], J.B. Beacham [122], M.D. Beattie [87], T. Beau [132], P.H. Beauchemin [168], P. Bechtle [24], H.C. Beck [51], H.P. Beck [20,r], K. Becker [50], M. Becker [97], C. Becot [121], A. Beddall [12d], A.J. Beddall [12a], V.A. Bednyakov [77], M. Bedognetti [118], C.P. Bee [152], T.A. Beermann [35], M. Begalli [78b], M. Begel [29], A. Behera [152], J.K. Behr [44], A.S. Bell [92], G. Bella [159], L. Bellagamba [23b], A. Bellerive [33], M. Bellomo [158], K. Belotskiy [110], N.L. Belyaev [110], O. Benary [159,*], D. Benchekroun [34a], M. Bender [112], N. Benekos [10], Y. Benhammou [159], E. Benhar Noccioli [181], J. Benitez [75], D.P. Benjamin [47], M. Benoit [52], J.R. Bensinger [26], S. Bentvelsen [118], L. Beresford [131], M. Beretta [49], D. Berge [44], E. Bergeaas Kuutmann [170], N. Berger [5], L.J. Bergsten [26], J. Beringer [18], S. Berlendis [56], N.R. Bernard [100], G. Bernardi [132], C. Bernius [150], F.U. Bernlochner [24], T. Berry [91], P. Berta [97], C. Bertella [15a], G. Bertoli [43a,43b], I.A. Bertram [87], C. Bertsche [44], G.J. Besjes [39], O. Bessidskaia Bylund [43a,43b], M. Bessner [44], N. Besson [142], A. Bethani [98], S. Bethke [113], A. Betti [24], A.J. Bevan [90], J. Beyer [113], R.M.B. Bianchi [135], O. Biebel [112], D. Biedermann [19], R. Bielski [98], K. Bierwagen [97], N.V. Biesuz [69a,69b], M. Biglietti [72a], T.R.V. Billoud [107], M. Bindi [51], A. Bingul [12d], C. Bini [70a,70b], S. Biondi [23b,23a], T. Bisanz [51], J.P. Biswal [159], C. Bittrich [46], D.M. Bjergaard [47], J.E. Black [150], K.M. Black [25], R.E. Blair [6], T. Blazek [28a], I. Bloch [44], C. Blocker [26], A. Blue [55], U. Blumenschein [90], Dr. Blunier [144a], G.J. Bobbink [118], V.S. Bobrovnikov [120b,120a], S.S. Bocchetta [94], A. Bocci [47], C. Bock [112], D. Boerner [180], D. Bogavac [112], A.G. Bogdanchikov [120b,120a], C. Bohm [43a], V. Boisvert [91], P. Bokan [170,y], T. Bold [81a], A.S. Boldyrev [111], A.E. Bolz [59b], M. Bomben [132], M. Bona [90], J.S. Bonilla [127], M. Boonekamp [142], A. Borisov [140], G. Borissov [87], J. Bortfeldt [35], D. Bortoletto [131], V. Bortolotto [71a,61b,61c,71b], D. Boscherini [23b], M. Bosman [14], J.D. Bossio Sola [30], J. Boudreau [135], E.V. Bouhova-Thacker [87], D. Boumediene [37], C. Bourdarios [128], S.K. Boutle [55], A. Boveia [122], J. Boyd [35], I.R. Boyko [77], A.J. Bozson [91], J. Bracinik [21], N. Brahimi [99], A. Brandt [8], G. Brandt [180], O. Brandt [59a], F. Braren [44], U. Bratzler [162], B. Brau [100], J.E. Brau [127], W.D. Breaden Madden [55], K. Brendlinger [44], A.J. Brennan [102], L. Brenner [44], R. Brenner [170], S. Bressler [178], B. Brickwedde [97], D.L. Briglin [21], T.M. Bristow [48], D. Britton [55], D. Britzger [59b], I. Brock [24], R. Brock [104], G. Brooijmans [38], T. Brooks [91], W.K. Brooks [144b], E. Brost [119], J.H Broughton [21], P.A. Bruckman de Renstrom [82], D. Bruncko [28b], A. Bruni [23b], G. Bruni [23b], L.S. Bruni [118], S. Bruno [71a,71b], B.H. Brunt [31], M. Bruschi [23b], N. Bruscino [135], P. Bryant [36], L. Bryngemark [44], T. Buanes [17], Q. Buat [35], P. Buchholz [148], A.G. Buckley [55], I.A. Budagov [77], F. Buehrer [50], M.K. Bugge [130], O. Bulekov [110], D. Bullock [8], T.J. Burch [119], S. Burdin [88], C.D. Burgard [118], A.M. Burger [5], B. Burghgrave [119], K. Burka [82], S. Burke [141], I. Burmeister [45], J.T.P. Burr [131], D. Büscher [50], V. Büscher [97], E. Buschmann [51], P. Bussey [55], J.M. Butler [25], C.M. Buttar [55], J.M. Butterworth [92], P. Butti [35], W. Buttinger [35], A. Buzatu [155], A.R. Buzykaev [120b,120a], G. Cabras [23b,23a], S. Cabrera Urbán [172], D. Caforio [138], H. Cai [171], V.M.M. Cairo [2], O. Cakir [4a], N. Calace [52], P. Calafiura [18], A. Calandri [99], G. Calderini [132], P. Calfayan [63], G. Callea [40b,40a], L.P. Caloba [78b], S. Calvente Lopez [96], D. Calvet [37], S. Calvet [37], T.P. Calvet [152], M. Calvetti [69a,69b], R. Camacho Toro [36], S. Camarda [35], P. Camarri [71a,71b], D. Cameron [130], R. Caminal Armadans [100], C. Camincher [56], S. Campana [35], M. Campanelli [92], A. Camplani [66a,66b], A. Campoverde [148], V. Canale [67a,67b], M. Cano Bret [58c], J. Cantero [125], T. Cao [159], Y. Cao [171], M.D.M. Capeans Garrido [35], I. Caprini [27b], M. Caprini [27b], M. Capua [40b,40a], R.M. Carbone [38], R. Cardarelli [71a], F.C. Cardillo [50], I. Carli [139], T. Carli [35], G. Carlino [67a], B.T. Carlson [135], L. Carminati [66a,66b], R.M.D. Carney [43a,43b], S. Caron [117], E. Carquin [144b], S. Carrá [66a,66b], G.D. Carrillo-Montoya [35], D. Casadei [32b],

M.P. Casado [14,g], A.F. Casha [165], M. Casolino [14], D.W. Casper [169], R. Castelijn [118], V. Castillo Gimenez [172], N.F. Castro [136a,136e], A. Catinaccio [35], J.R. Catmore [130], A. Cattai [35], J. Caudron [24], V. Cavaliere [29], E. Cavallaro [14], D. Cavalli [66a], M. Cavalli-Sforza [14], V. Cavasinni [69a,69b], E. Celebi [12b], F. Ceradini [72a,72b], L. Cerda Alberich [172], A.S. Cerqueira [78a], A. Cerri [153], L. Cerrito [71a,71b], F. Cerutti [18], A. Cervelli [23b,23a], S.A. Cetin [12b], A. Chafaq [34a], D Chakraborty [119], S.K. Chan [57], W.S. Chan [118], Y.L. Chan [61a], P. Chang [171], J.D. Chapman [31], D.G. Charlton [21], C.C. Chau [33], C.A. Chavez Barajas [153], S. Che [122], A. Chegwidden [104], S. Chekanov [6], S.V. Chekulaev [166a], G.A. Chelkov [77,at], M.A. Chelstowska [35], C. Chen [58a], C.H. Chen [76], H. Chen [29], J. Chen [58a], J. Chen [38], S. Chen [133], S.J. Chen [15c], X. Chen [15b,as], Y. Chen [80], Y-H. Chen [44], H.C. Cheng [103], H.J. Cheng [15d], A. Cheplakov [77], E. Cheremushkina [140], R. Cherkaoui El Moursli [34e], E. Cheu [7], K. Cheung [62], L. Chevalier [142], V. Chiarella [49], G. Chiarelli [69a], G. Chiodini [65a], A.S. Chisholm [35], A. Chitan [27b], I. Chiu [161], Y.H. Chiu [174], M.V. Chizhov [77], K. Choi [63], A.R. Chomont [128], S. Chouridou [160], Y.S. Chow [118], V. Christodoulou [92], M.C. Chu [61a], J. Chudoba [137], A.J. Chuinard [101], J.J. Chwastowski [82], L. Chytka [126], D. Cinca [45], V. Cindro [89], I.A. Cioară [24], A. Ciocio [18], F. Cirotto [67a,67b], Z.H. Citron [178], M. Citterio [66a], A. Clark [52], M.R. Clark [38], P.J. Clark [48], R.N. Clarke [18], C. Clement [43a,43b], Y. Coadou [99], M. Cobal [64a,64c], A. Coccaro [53b,53a], J. Cochran [76], A.E.C. Coimbra [178], L. Colasurdo [117], B. Cole [38], A.P. Colijn [118], J. Collot [56], P. Conde Muiño [136a,136b], E. Coniavitis [50], S.H. Connell [32b], I.A. Connelly [98], S. Constantinescu [27b], F. Conventi [67a,av], A.M. Cooper-Sarkar [131], F. Cormier [173], K.J.R. Cormier [165], M. Corradi [70a,70b], E.E. Corrigan [94], F. Corriveau [101,ae], A. Cortes-Gonzalez [35], M.J. Costa [172], D. Costanzo [146], G. Cottin [31], G. Cowan [91], B.E. Cox [98], J. Crane [98], K. Cranmer [121], S.J. Crawley [55], R.A. Creager [133], G. Cree [33], S. Crépé-Renaudin [56], F. Crescioli [132], M. Cristinziani [24], V. Croft [121], G. Crosetti [40b,40a], A. Cueto [96], T. Cuhadar Donszelmann [146], A.R. Cukierman [150], M. Curatolo [49], J. Cúth [97], S. Czekierda [82], P. Czodrowski [35], M.J. Da Cunha Sargedas De Sousa [58b,136b], C. Da Via [98], W. Dabrowski [81a], T. Dado [28a,y], S. Dahbi [34e], T. Dai [103], O. Dale [17], F. Dallaire [107], C. Dallapiccola [100], M. Dam [39], G. D'amen [23b,23a], J.R. Dandoy [133], M.F. Daneri [30], N.P. Dang [179,k], N.D Dann [98], M. Danninger [173], V. Dao [35], G. Darbo [53b], S. Darmora [8], O. Dartsi [5], A. Dattagupta [127], T. Daubney [44], S. D'Auria [55], W. Davey [24], C. David [44], T. Davidek [139], D.R. Davis [47], E. Dawe [102], I. Dawson [146], K. De [8], R. De Asmundis [67a], A. De Benedetti [124], S. De Castro [23b,23a], S. De Cecco [132], N. De Groot [117], P. de Jong [118], H. De la Torre [104], F. De Lorenzi [76], A. De Maria [51,t], D. De Pedis [70a], A. De Salvo [70a], U. De Sanctis [71a,71b], A. De Santo [153], K. De Vasconcelos Corga [99], J.B. De Vivie De Regie [128], C. Debenedetti [143], D.V. Dedovich [77], N. Dehghanian [3], M. Del Gaudio [40b,40a], J. Del Peso [96], D. Delgove [128], F. Deliot [142], C.M. Delitzsch [7], M. Della Pietra [67a,67b], D. Della Volpe [52], A. Dell'Acqua [35], L. Dell'Asta [25], M. Delmastro [5], C. Delporte [128], P.A. Delsart [56], D.A. DeMarco [165], S. Demers [181], M. Demichev [77], S.P. Denisov [140], D. Denysiuk [118], L. D'Eramo [132], D. Derendarz [82], J.E. Derkaoui [34d], F. Derue [132], P. Dervan [88], K. Desch [24], C. Deterre [44], K. Dette [165], M.R. Devesa [30], P.O. Deviveiros [35], A. Dewhurst [141], S. Dhaliwal [26], F.A. Di Bello [52], A. Di Ciaccio [71a,71b], L. Di Ciaccio [5], W.K. Di Clemente [133], C. Di Donato [67a,67b], A. Di Girolamo [35], B. Di Micco [72a,72b], R. Di Nardo [35], K.F. Di Petrillo [57], A. Di Simone [50], R. Di Sipio [165], D. Di Valentino [33], C. Diaconu [99], M. Diamond [165], F.A. Dias [39], T. Dias Do Vale [136a], M.A. Diaz [144a], J. Dickinson [18], E.B. Diehl [103], J. Dietrich [19], S. Díez Cornell [44], A. Dimitrievska [18], J. Dingfelder [24], F. Dittus [35], F. Djama [99], T. Djobava [157b], J.I. Djuvsland [59a], M.A.B. Do Vale [78c], M. Dobre [27b], D. Dodsworth [26], C. Doglioni [94], J. Dolejsi [139], Z. Dolezal [139], M. Donadelli [78d], J. Donini [37], A. D'onofrio [90], M. D'Onofrio [88], J. Dopke [141], A. Doria [67a], M.T. Dova [86], A.T. Doyle [55], E. Drechsler [51], E. Dreyer [149], T. Dreyer [51], M. Dris [10], Y. Du [58b], J. Duarte-Campderros [159], F. Dubinin [108], A. Dubreuil [52], E. Duchovni [178], G. Duckeck [112], A. Ducourthial [132], O.A. Ducu [107,x], D. Duda [118], A. Dudarev [35], A.C. Dudder [97], E.M. Duffield [18], L. Duflot [128], M. Dührssen [35], C. Dülsen [180], M. Dumancic [178], A.E. Dumitriu [27b,e], A.K. Duncan [55], M. Dunford [59a], A. Duperrin [99], H. Duran Yildiz [4a], M. Düren [54], A. Durglishvili [157b], D. Duschinger [46], B. Dutta [44], D. Duvnjak [1], M. Dyndal [44], B.S. Dziedzic [82], C. Eckardt [44], K.M. Ecker [113], R.C. Edgar [103], T. Eifert [35], G. Eigen [17], K. Einsweiler [18], T. Ekelof [170], M. El Kacimi [34c], R. El Kosseifi [99], V. Ellajosyula [99], M. Ellert [170], F. Ellinghaus [180], A.A. Elliot [174], N. Ellis [35], J. Elmsheuser [29], M. Elsing [35], D. Emeliyanov [141], Y. Enari [161], J.S. Ennis [176], M.B. Epland [47], J. Erdmann [45], A. Ereditato [20], S. Errede [171], M. Escalier [128], C. Escobar [172], B. Esposito [49], O. Estrada Pastor [172], A.I. Etienvre [142], E. Etzion [159], H. Evans [63], A. Ezhilov [134], M. Ezzi [34e], F. Fabbri [23b,23a], L. Fabbri [23b,23a], V. Fabiani [117], G. Facini [92], R.M. Faisca Rodrigues Pereira [136a], R.M. Fakhrutdinov [140], S. Falciano [70a],

P.J. Falke [5], S. Falke [5], J. Faltova [139], Y. Fang [15a], M. Fanti [66a,66b], A. Farbin [8], A. Farilla [72a], E.M. Farina [68a,68b], T. Farooque [104], S. Farrell [18], S.M. Farrington [176], P. Farthouat [35], F. Fassi [34e], P. Fassnacht [35], D. Fassouliotis [9], M. Faucci Giannelli [48], A. Favareto [53b,53a], W.J. Fawcett [52], L. Fayard [128], O.L. Fedin [134,q], W. Fedorko [173], M. Feickert [41], S. Feigl [130], L. Feligioni [99], C. Feng [58b], E.J. Feng [35], M. Feng [47], M.J. Fenton [55], A.B. Fenyuk [140], L. Feremenga [8], J. Ferrando [44], A. Ferrari [170], P. Ferrari [118], R. Ferrari [68a], D.E. Ferreira de Lima [59b], A. Ferrer [172], D. Ferrere [52], C. Ferretti [103], F. Fiedler [97], A. Filipčič [89], F. Filthaut [117], M. Fincke-Keeler [174], K.D. Finelli [25], M.C.N. Fiolhais [136a,136c,b], L. Fiorini [172], C. Fischer [14], J. Fischer [180], W.C. Fisher [104], N. Flaschel [44], I. Fleck [148], P. Fleischmann [103], R.R.M. Fletcher [133], T. Flick [180], B.M. Flierl [112], L.M. Flores [133], L.R. Flores Castillo [61a], N. Fomin [17], G.T. Forcolin [98], A. Formica [142], F.A. Förster [14], A.C. Forti [98], A.G. Foster [21], D. Fournier [128], H. Fox [87], S. Fracchia [146], P. Francavilla [69a,69b], M. Franchini [23b,23a], S. Franchino [59a], D. Francis [35], L. Franconi [130], M. Franklin [57], M. Frate [169], M. Fraternali [68a,68b], D. Freeborn [92], S.M. Fressard-Batraneanu [35], B. Freund [107], W.S. Freund [78b], D. Froidevaux [35], J.A. Frost [131], C. Fukunaga [162], T. Fusayasu [114], J. Fuster [172], O. Gabizon [158], A. Gabrielli [23b,23a], A. Gabrielli [18], G.P. Gach [81a], S. Gadatsch [52], S. Gadomski [52], P. Gadow [113], G. Gagliardi [53b,53a], L.G. Gagnon [107], C. Galea [27b], B. Galhardo [136a,136c], E.J. Gallas [131], B.J. Gallop [141], P. Gallus [138], G. Galster [39], R. Gamboa Goni [90], K.K. Gan [122], S. Ganguly [178], Y. Gao [88], Y.S. Gao [150,m], C. García [172], J.E. García Navarro [172], J.A. García Pascual [15a], M. Garcia-Sciveres [18], R.W. Gardner [36], N. Garelli [150], V. Garonne [130], K. Gasnikova [44], A. Gaudiello [53b,53a], G. Gaudio [68a], I.L. Gavrilenko [108], A. Gavrilyuk [109], C. Gay [173], G. Gaycken [24], E.N. Gazis [10], C.N.P. Gee [141], J. Geisen [51], M. Geisen [97], M.P. Geisler [59a], K. Gellerstedt [43a,43b], C. Gemme [53b], M.H. Genest [56], C. Geng [103], S. Gentile [70a,70b], C. Gentsos [160], S. George [91], D. Gerbaudo [14], G. Gessner [45], S. Ghasemi [148], M. Ghneimat [24], B. Giacobbe [23b], S. Giagu [70a,70b], N. Giangiacomi [23b,23a], P. Giannetti [69a], S.M. Gibson [91], M. Gignac [143], D. Gillberg [33], G. Gilles [180], D.M. Gingrich [3,au], M.P. Giordani [64a,64c], F.M. Giorgi [23b], P.F. Giraud [142], P. Giromini [57], G. Giugliarelli [64a,64c], D. Giugni [66a], F. Giuli [131], M. Giulini [59b], S. Gkaitatzis [160], I. Gkialas [9,j], E.L. Gkougkousis [14], P. Gkountoumis [10], L.K. Gladilin [111], C. Glasman [96], J. Glatzer [14], P.C.F. Glaysher [44], A. Glazov [44], M. Goblirsch-Kolb [26], J. Godlewski [82], S. Goldfarb [102], T. Golling [52], D. Golubkov [140], A. Gomes [136a,136b,136d], R. Goncalves Gama [78a], R. Gonçalo [136a], G. Gonella [50], L. Gonella [21], A. Gongadze [77], F. Gonnella [21], J.L. Gonski [57], S. González de la Hoz [172], S. Gonzalez-Sevilla [52], L. Goossens [35], P.A. Gorbounov [109], H.A. Gordon [29], B. Gorini [35], E. Gorini [65a,65b], A. Gorišek [89], A.T. Goshaw [47], C. Gössling [45], M.I. Gostkin [77], C.A. Gottardo [24], C.R. Goudet [128], D. Goujdami [34c], A.G. Goussiou [145], N. Govender [32b,c], C. Goy [5], E. Gozani [158], I. Grabowska-Bold [81a], P.O.J. Gradin [170], E.C. Graham [88], J. Gramling [169], E. Gramstad [130], S. Grancagnolo [19], V. Gratchev [134], P.M. Gravila [27f], C. Gray [55], H.M. Gray [18], Z.D. Greenwood [93,aj], C. Grefe [24], K. Gregersen [92], I.M. Gregor [44], P. Grenier [150], K. Grevtsov [44], J. Griffiths [8], A.A. Grillo [143], K. Grimm [150], S. Grinstein [14,z], Ph. Gris [37], J.-F. Grivaz [128], S. Groh [97], E. Gross [178], J. Grosse-Knetter [51], G.C. Grossi [93], Z.J. Grout [92], A. Grummer [116], L. Guan [103], W. Guan [179], J. Guenther [35], A. Guerguichon [128], F. Guescini [166a], D. Guest [169], O. Gueta [159], R. Gugel [50], B. Gui [122], T. Guillemin [5], S. Guindon [35], U. Gul [55], C. Gumpert [35], J. Guo [58c], W. Guo [103], Y. Guo [58a,s], Z. Guo [99], R. Gupta [41], S. Gurbuz [12c], G. Gustavino [124], B.J. Gutelman [158], P. Gutierrez [124], N.G. Gutierrez Ortiz [92], C. Gutschow [92], C. Guyot [142], M.P. Guzik [81a], C. Gwenlan [131], C.B. Gwilliam [88], A. Haas [121], C. Haber [18], H.K. Hadavand [8], N. Haddad [34e], A. Hadef [99], S. Hageböck [24], M. Hagihara [167], H. Hakobyan [182,*], M. Haleem [175], J. Haley [125], G. Halladjian [104], G.D. Hallewell [99], K. Hamacher [180], P. Hamal [126], K. Hamano [174], A. Hamilton [32a], G.N. Hamity [146], K. Han [58a,ai], L. Han [58a], S. Han [15d], K. Hanagaki [79,v], M. Hance [143], D.M. Handl [112], B. Haney [133], R. Hankache [132], P. Hanke [59a], E. Hansen [94], J.B. Hansen [39], J.D. Hansen [39], M.C. Hansen [24], P.H. Hansen [39], K. Hara [167], A.S. Hard [179], T. Harenberg [180], S. Harkusha [105], P.F. Harrison [176], N.M. Hartmann [112], Y. Hasegawa [147], A. Hasib [48], S. Hassani [142], S. Haug [20], R. Hauser [104], L. Hauswald [46], L.B. Havener [38], M. Havranek [138], C.M. Hawkes [21], R.J. Hawkings [35], D. Hayden [104], C. Hayes [152], C.P. Hays [131], J.M. Hays [90], H.S. Hayward [88], S.J. Haywood [141], M.P. Heath [48], V. Hedberg [94], L. Heelan [8], S. Heer [24], K.K. Heidegger [50], J. Heilman [33], S. Heim [44], T. Heim [18], B. Heinemann [44,ap], J.J. Heinrich [112], L. Heinrich [121], C. Heinz [54], J. Hejbal [137], L. Helary [35], A. Held [173], S. Hellesund [130], S. Hellman [43a,43b], C. Helsens [35], R.C.W. Henderson [87], Y. Heng [179], S. Henkelmann [173], A.M. Henriques Correia [35], G.H. Herbert [19], H. Herde [26], V. Herget [175], Y. Hernández Jiménez [32c], H. Herr [97], G. Herten [50], R. Hertenberger [112], L. Hervas [35], T.C. Herwig [133],

G.G. Hesketh [92], N.P. Hessey [166a], J.W. Hetherly [41], S. Higashino [79], E. Higón-Rodriguez [172], K. Hildebrand [36], E. Hill [174], J.C. Hill [31], K.H. Hiller [44], S.J. Hillier [21], M. Hils [46], I. Hinchliffe [18], M. Hirose [129], D. Hirschbuehl [180], B. Hiti [89], O. Hladik [137], D.R. Hlaluku [32c], X. Hoad [48], J. Hobbs [152], N. Hod [166a], M.C. Hodgkinson [146], A. Hoecker [35], M.R. Hoeferkamp [116], F. Hoenig [112], D. Hohn [24], D. Hohov [128], T.R. Holmes [36], M. Holzbock [112], M. Homann [45], S. Honda [167], T. Honda [79], T.M. Hong [135], A. Hönle [113], B.H. Hooberman [171], W.H. Hopkins [127], Y. Horii [115], P. Horn [46], A.J. Horton [149], L.A. Horyn [36], J-Y. Hostachy [56], A. Hostiuc [145], S. Hou [155], A. Hoummada [34a], J. Howarth [98], J. Hoya [86], M. Hrabovsky [126], J. Hrdinka [35], I. Hristova [19], J. Hrivnac [128], A. Hrynevich [106], T. Hryn'ova [5], P.J. Hsu [62], S.-C. Hsu [145], Q. Hu [29], S. Hu [58c], Y. Huang [15a], Z. Hubacek [138], F. Hubaut [99], M. Huebner [24], F. Huegging [24], T.B. Huffman [131], E.W. Hughes [38], M. Huhtinen [35], R.F.H. Hunter [33], P. Huo [152], A.M. Hupe [33], N. Huseynov [77,ag], J. Huston [104], J. Huth [57], R. Hyneman [103], G. Iacobucci [52], G. Iakovidis [29], I. Ibragimov [148], L. Iconomidou-Fayard [128], Z. Idrissi [34e], P. Iengo [35], R. Ignazzi [39], O. Igonkina [118,ac], R. Iguchi [161], T. Iizawa [177], Y. Ikegami [79], M. Ikeno [79], D. Iliadis [160], N. Ilic [150], F. Iltzsche [46], G. Introzzi [68a,68b], M. Iodice [72a], K. Iordanidou [38], V. Ippolito [70a,70b], M.F. Isacson [170], N. Ishijima [129], M. Ishino [161], M. Ishitsuka [163], C. Issever [131], S. Istin [12c,an], F. Ito [167], J.M. Iturbe Ponce [61a], R. Iuppa [73a,73b], A. Ivina [178], H. Iwasaki [79], J.M. Izen [42], V. Izzo [67a], S. Jabbar [3], P. Jacka [137], P. Jackson [1], R.M. Jacobs [24], V. Jain [2], G. Jäkel [180], K.B. Jakobi [97], K. Jakobs [50], S. Jakobsen [74], T. Jakoubek [137], D.O. Jamin [125], D.K. Jana [93], R. Jansky [52], J. Janssen [24], M. Janus [51], P.A. Janus [81a], G. Jarlskog [94], N. Javadov [77,ag], T. Javůrek [50], M. Javurkova [50], F. Jeanneau [142], L. Jeanty [18], J. Jejelava [157a,ah], A. Jelinskas [176], P. Jenni [50,d], J. Jeong [44], C. Jeske [176], S. Jézéquel [5], H. Ji [179], J. Jia [152], H. Jiang [76], Y. Jiang [58a], Z. Jiang [150], S. Jiggins [50], F.A. Jimenez Morales [37], J. Jimenez Pena [172], S. Jin [15c], A. Jinaru [27b], O. Jinnouchi [163], H. Jivan [32c], P. Johansson [146], K.A. Johns [7], C.A. Johnson [63], W.J. Johnson [145], K. Jon-And [43a,43b], R.W.L. Jones [87], S.D. Jones [153], S. Jones [7], T.J. Jones [88], J. Jongmanns [59a], P.M. Jorge [136a,136b], J. Jovicevic [166a], X. Ju [179], J.J. Junggeburth [113], A. Juste Rozas [14,z], A. Kaczmarska [82], M. Kado [128], H. Kagan [122], M. Kagan [150], T. Kaji [177], E. Kajomovitz [158], C.W. Kalderon [94], A. Kaluza [97], S. Kama [41], A. Kamenshchikov [140], L. Kanjir [89], Y. Kano [161], V.A. Kantserov [110], J. Kanzaki [79], B. Kaplan [121], L.S. Kaplan [179], D. Kar [32c], M.J. Kareem [166b], E. Karentzos [10], S.N. Karpov [77], Z.M. Karpova [77], V. Kartvelishvili [87], A.N. Karyukhin [140], K. Kasahara [167], L. Kashif [179], R.D. Kass [122], A. Kastanas [151], Y. Kataoka [161], C. Kato [161], A. Katre [52], J. Katzy [44], K. Kawade [80], K. Kawagoe [85], T. Kawamoto [161], G. Kawamura [51], E.F. Kay [88], V.F. Kazanin [120b,120a], R. Keeler [174], R. Kehoe [41], J.S. Keller [33], E. Kellermann [94], J.J. Kempster [21], J. Kendrick [21], O. Kepka [137], S. Kersten [180], B.P. Kerševan [89], R.A. Keyes [101], M. Khader [171], F. Khalil-Zada [13], A. Khanov [125], A.G. Kharlamov [120b,120a], T. Kharlamova [120b,120a], A. Khodinov [164], T.J. Khoo [52], V. Khovanskiy [109,*], E. Khramov [77], J. Khubua [157b], S. Kido [80], M. Kiehn [52], C.R. Kilby [91], H.Y. Kim [8], S.H. Kim [167], Y.K. Kim [36], N. Kimura [64a,64c], O.M. Kind [19], B.T. King [88], D. Kirchmeier [46], J. Kirk [141], A.E. Kiryunin [113], T. Kishimoto [161], D. Kisielewska [81a], V. Kitali [44], O. Kivernyk [5], E. Kladiva [28b], T. Klapdor-Kleingrothaus [50], M.H. Klein [103], M. Klein [88], U. Klein [88], K. Kleinknecht [97], P. Klimek [119], A. Klimentov [29], R. Klingenberg [45,*], T. Klingl [24], T. Klioutchnikova [35], F.F. Klitzner [112], P. Kluit [118], S. Kluth [113], E. Kneringer [74], E.B.F.G. Knoops [99], A. Knue [50], A. Kobayashi [161], D. Kobayashi [85], T. Kobayashi [161], M. Kobel [46], M. Kocian [150], P. Kodys [139], T. Koffas [33], E. Koffeman [118], N.M. Köhler [113], T. Koi [150], M. Kolb [59b], I. Koletsou [5], T. Kondo [79], N. Kondrashova [58c], K. Köneke [50], A.C. König [117], T. Kono [79,ao], R. Konoplich [121,ak], N. Konstantinidis [92], B. Konya [94], R. Kopeliansky [63], S. Koperny [81a], K. Korcyl [82], K. Kordas [160], A. Korn [92], I. Korolkov [14], E.V. Korolkova [146], O. Kortner [113], S. Kortner [113], T. Kosek [139], V.V. Kostyukhin [24], A. Kotwal [47], A. Koulouris [10], A. Kourkoumeli-Charalampidi [68a,68b], C. Kourkoumelis [9], E. Kourlitis [146], V. Kouskoura [29], A.B. Kowalewska [82], R. Kowalewski [174], T.Z. Kowalski [81a], C. Kozakai [161], W. Kozanecki [142], A.S. Kozhin [140], V.A. Kramarenko [111], G. Kramberger [89], D. Krasnopevtsev [110], M.W. Krasny [132], A. Krasznahorkay [35], D. Krauss [113], J.A. Kremer [81a], J. Kretzschmar [88], K. Kreutzfeldt [54], P. Krieger [165], K. Krizka [18], K. Kroeninger [45], H. Kroha [113], J. Kroll [137], J. Kroll [133], J. Kroseberg [24], J. Krstic [16], U. Kruchonak [77], H. Krüger [24], N. Krumnack [76], M.C. Kruse [47], T. Kubota [102], S. Kuday [4b], J.T. Kuechler [180], S. Kuehn [35], A. Kugel [59a], F. Kuger [175], T. Kuhl [44], V. Kukhtin [77], R. Kukla [99], Y. Kulchitsky [105], S. Kuleshov [144b], Y.P. Kulinich [171], M. Kuna [56], T. Kunigo [83], A. Kupco [137], T. Kupfer [45], O. Kuprash [159], H. Kurashige [80], L.L. Kurchaninov [166a], Y.A. Kurochkin [105], M.G. Kurth [15d], E.S. Kuwertz [174], M. Kuze [163], J. Kvita [126], T. Kwan [174], A. La Rosa [113], J.L. La Rosa Navarro [78d], L. La Rotonda [40b,40a], F. La Ruffa [40b,40a], C. Lacasta [172],

F. Lacava [70a,70b], J. Lacey [44], D.P.J. Lack [98], H. Lacker [19], D. Lacour [132], E. Ladygin [77], R. Lafaye [5], B. Laforge [132], S. Lai [51], S. Lammers [63], W. Lampl [7], E. Lançon [29], U. Landgraf [50], M.P.J. Landon [90], M.C. Lanfermann [52], V.S. Lang [44], J.C. Lange [14], R.J. Langenberg [35], A.J. Lankford [169], F. Lanni [29], K. Lantzsch [24], A. Lanza [68a], A. Lapertosa [53b,53a], S. Laplace [132], J.F. Laporte [142], T. Lari [66a], F. Lasagni Manghi [23b,23a], M. Lassnig [35], T.S. Lau [61a], A. Laudrain [128], A.T. Law [143], P. Laycock [88], M. Lazzaroni [66a,66b], B. Le [102], O. Le Dortz [132], E. Le Guirriec [99], E.P. Le Quilleuc [142], M. LeBlanc [7], T. LeCompte [6], F. Ledroit-Guillon [56], C.A. Lee [29], G.R. Lee [144a], L. Lee [57], S.C. Lee [155], B. Lefebvre [101], M. Lefebvre [174], F. Legger [112], C. Leggett [18], G. Lehmann Miotto [35], W.A. Leight [44], A. Leisos [160,w], M.A.L. Leite [78d], R. Leitner [139], D. Lellouch [178], B. Lemmer [51], K.J.C. Leney [92], T. Lenz [24], B. Lenzi [35], R. Leone [7], S. Leone [69a], C. Leonidopoulos [48], G. Lerner [153], C. Leroy [107], R. Les [165], A.A.J. Lesage [142], C.G. Lester [31], M. Levchenko [134], J. Levêque [5], D. Levin [103], L.J. Levinson [178], D. Lewis [90], B. Li [58a,s], C-Q. Li [58a], H. Li [58b], L. Li [58c], Q. Li [15d], Q.Y. Li [58a], S. Li [58d,58c], X. Li [58c], Y. Li [148], Z. Liang [15a], B. Liberti [71a], A. Liblong [165], K. Lie [61c], S. Liem [118], A. Limosani [154], C.Y. Lin [31], K. Lin [104], S.C. Lin [156], T.H. Lin [97], R.A. Linck [63], B.E. Lindquist [152], A.L. Lionti [52], E. Lipeles [133], A. Lipniacka [17], M. Lisovyi [59b], T.M. Liss [171,ar], A. Lister [173], A.M. Litke [143], J.D. Little [8], B. Liu [76], B.L Liu [6], H.B. Liu [29], H. Liu [103], J.B. Liu [58a], J.K.K. Liu [131], K. Liu [132], M. Liu [58a], P. Liu [18], Y.L. Liu [58a], Y.W. Liu [58a], M. Livan [68a,68b], A. Lleres [56], J. Llorente Merino [15a], S.L. Lloyd [90], C.Y. Lo [61b], F. Lo Sterzo [41], E.M. Lobodzinska [44], P. Loch [7], F.K. Loebinger [98], A. Loesle [50], K.M. Loew [26], T. Lohse [19], K. Lohwasser [146], M. Lokajicek [137], B.A. Long [25], J.D. Long [171], R.E. Long [87], L. Longo [65a,65b], K.A. Looper [122], J.A. Lopez [144b], I. Lopez Paz [14], A. Lopez Solis [132], J. Lorenz [112], N. Lorenzo Martinez [5], M. Losada [22], P.J. Lösel [112], X. Lou [44], X. Lou [15a], A. Lounis [128], J. Love [6], P.A. Love [87], J.J. Lozano Bahilo [172], H. Lu [61a], N. Lu [103], Y.J. Lu [62], H.J. Lubatti [145], C. Luci [70a,70b], A. Lucotte [56], C. Luedtke [50], F. Luehring [63], I. Luise [132], W. Lukas [74], L. Luminari [70a], B. Lund-Jensen [151], M.S. Lutz [100], P.M. Luzi [132], D. Lynn [29], R. Lysak [137], E. Lytken [94], F. Lyu [15a], V. Lyubushkin [77], H. Ma [29], L.L. Ma [58b], Y. Ma [58b], G. Maccarrone [49], A. Macchiolo [113], C.M. Macdonald [146], J. Machado Miguens [133,136b], D. Madaffari [172], R. Madar [37], W.F. Mader [46], A. Madsen [44], N. Madysa [46], J. Maeda [80], S. Maeland [17], T. Maeno [29], A.S. Maevskiy [111], V. Magerl [50], C. Maidantchik [78b], T. Maier [112], A. Maio [136a,136b,136d], O. Majersky [28a], S. Majewski [127], Y. Makida [79], N. Makovec [128], B. Malaescu [132], Pa. Malecki [82], V.P. Maleev [134], F. Malek [56], U. Mallik [75], D. Malon [6], C. Malone [31], S. Maltezos [10], S. Malyukov [35], J. Mamuzic [172], G. Mancini [49], I. Mandić [89], J. Maneira [136a], L. Manhaes de Andrade Filho [78a], J. Manjarres Ramos [46], K.H. Mankinen [94], A. Mann [112], A. Manousos [74], B. Mansoulie [142], J.D. Mansour [15a], R. Mantifel [101], M. Mantoani [51], S. Manzoni [66a,66b], G. Marceca [30], L. March [52], L. Marchese [131], G. Marchiori [132], M. Marcisovsky [137], C.A. Marin Tobon [35], M. Marjanovic [37], D.E. Marley [103], F. Marroquim [78b], Z. Marshall [18], M.U.F Martensson [170], S. Marti-Garcia [172], C.B. Martin [122], T.A. Martin [176], V.J. Martin [48], B. Martin dit Latour [17], M. Martinez [14,z], V.I. Martinez Outschoorn [100], S. Martin-Haugh [141], V.S. Martoiu [27b], A.C. Martyniuk [92], A. Marzin [35], L. Masetti [97], T. Mashimo [161], R. Mashinistov [108], J. Masik [98], A.L. Maslennikov [120b,120a], L.H. Mason [102], L. Massa [71a,71b], P. Mastrandrea [5], A. Mastroberardino [40b,40a], T. Masubuchi [161], P. Mättig [180], J. Maurer [27b], B. Maček [89], S.J. Maxfield [88], D.A. Maximov [120b,120a], R. Mazini [155], I. Maznas [160], S.M. Mazza [143], N.C. Mc Fadden [116], G. Mc Goldrick [165], S.P. Mc Kee [103], A. McCarn [103], T.G. McCarthy [113], L.I. McClymont [92], E.F. McDonald [102], J.A. Mcfayden [35], G. Mchedlidze [51], M.A. McKay [41], K.D. McLean [174], S.J. McMahon [141], P.C. McNamara [102], C.J. McNicol [176], R.A. McPherson [174,ae], J.E. Mdhluli [32c], Z.A. Meadows [100], S. Meehan [145], T. Megy [50], S. Mehlhase [112], A. Mehta [88], T. Meideck [56], B. Meirose [42], D. Melini [172,h], B.R. Mellado Garcia [32c], J.D. Mellenthin [51], M. Melo [28a], F. Meloni [20], A. Melzer [24], S.B. Menary [98], L. Meng [88], X.T. Meng [103], A. Mengarelli [23b,23a], S. Menke [113], E. Meoni [40b,40a], S. Mergelmeyer [19], C. Merlassino [20], P. Mermod [52], L. Merola [67a,67b], C. Meroni [66a], F.S. Merritt [36], A. Messina [70a,70b], J. Metcalfe [6], A.S. Mete [169], C. Meyer [133], J. Meyer [158], J-P. Meyer [142], H. Meyer Zu Theenhausen [59a], F. Miano [153], R.P. Middleton [141], L. Mijović [48], G. Mikenberg [178], M. Mikestikova [137], M. Mikuž [89], M. Milesi [102], A. Milic [165], D.A. Millar [90], D.W. Miller [36], A. Milov [178], D.A. Milstead [43a,43b], A.A. Minaenko [140], I.A. Minashvili [157b], A.I. Mincer [121], B. Mindur [81a], M. Mineev [77], Y. Minegishi [161], Y. Ming [179], L.M. Mir [14], A. Mirto [65a,65b], K.P. Mistry [133], T. Mitani [177], J. Mitrevski [112], V.A. Mitsou [172], A. Miucci [20], P.S. Miyagawa [146], A. Mizukami [79], J.U. Mjörnmark [94], T. Mkrtchyan [182], M. Mlynarikova [139], T. Moa [43a,43b], K. Mochizuki [107], P. Mogg [50], S. Mohapatra [38], S. Molander [43a,43b], R. Moles-Valls [24], M.C. Mondragon [104], K. Mönig [44], J. Monk [39], E. Monnier [99],

A. Montalbano [149], J. Montejo Berlingen [35], F. Monticelli [86], S. Monzani [66a], R.W. Moore [3], N. Morange [128], D. Moreno [22], M. Moreno Llácer [35], P. Morettini [53b], M. Morgenstern [118], S. Morgenstern [35], D. Mori [149], T. Mori [161], M. Morii [57], M. Morinaga [177], V. Morisbak [130], A.K. Morley [35], G. Mornacchi [35], J.D. Morris [90], L. Morvaj [152], P. Moschovakos [10], M. Mosidze [157b], H.J. Moss [146], J. Moss [150,n], K. Motohashi [163], R. Mount [150], E. Mountricha [29], E.J.W. Moyse [100], S. Muanza [99], F. Mueller [113], J. Mueller [135], R.S.P. Mueller [112], D. Muenstermann [87], P. Mullen [55], G.A. Mullier [20], F.J. Munoz Sanchez [98], P. Murin [28b], W.J. Murray [176,141], A. Murrone [66a,66b], M. Muškinja [89], C. Mwewa [32a], A.G. Myagkov [140,al], J. Myers [127], M. Myska [138], B.P. Nachman [18], O. Nackenhorst [45], K. Nagai [131], R. Nagai [79,ao], K. Nagano [79], Y. Nagasaka [60], K. Nagata [167], M. Nagel [50], E. Nagy [99], A.M. Nairz [35], Y. Nakahama [115], K. Nakamura [79], T. Nakamura [161], I. Nakano [123], F. Napolitano [59a], R.F. Naranjo Garcia [44], R. Narayan [11], D.I. Narrias Villar [59a], I. Naryshkin [134], T. Naumann [44], G. Navarro [22], R. Nayyar [7], H.A. Neal [103], P.Y. Nechaeva [108], T.J. Neep [142], A. Negri [68a,68b], M. Negrini [23b], S. Nektarijevic [117], C. Nellist [51], M.E. Nelson [131], S. Nemecek [137], P. Nemethy [121], M. Nessi [35,f], M.S. Neubauer [171], M. Neumann [180], P.R. Newman [21], T.Y. Ng [61c], Y.S. Ng [19], H.D.N. Nguyen [99], T. Nguyen Manh [107], E. Nibigira [37], R.B. Nickerson [131], R. Nicolaidou [142], J. Nielsen [143], N. Nikiforou [11], V. Nikolaenko [140,al], I. Nikolic-Audit [132], K. Nikolopoulos [21], P. Nilsson [29], Y. Ninomiya [79], A. Nisati [70a], N. Nishu [58c], R. Nisius [113], I. Nitsche [45], T. Nitta [177], T. Nobe [161], Y. Noguchi [83], M. Nomachi [129], I. Nomidis [33], M.A. Nomura [29], T. Nooney [90], M. Nordberg [35], N. Norjoharuddeen [131], T. Novak [89], O. Novgorodova [46], R. Novotny [138], M. Nozaki [79], L. Nozka [126], K. Ntekas [169], E. Nurse [92], F. Nuti [102], F.G. Oakham [33,au], H. Oberlack [113], T. Obermann [24], J. Ocariz [132], A. Ochi [80], I. Ochoa [38], J.P. Ochoa-Ricoux [144a], K. O'Connor [26], S. Oda [85], S. Odaka [79], A. Oh [98], S.H. Oh [47], C.C. Ohm [151], H. Ohman [170], H. Oide [53b,53a], H. Okawa [167], Y. Okazaki [83], Y. Okumura [161], T. Okuyama [79], A. Olariu [27b], L.F. Oleiro Seabra [136a], S.A. Olivares Pino [144a], D. Oliveira Damazio [29], J.L. Oliver [1], M.J.R. Olsson [36], A. Olszewski [82], J. Olszowska [82], D.C. O'Neil [149], A. Onofre [136a,136e], K. Onogi [115], P.U.E. Onyisi [11], H. Oppen [130], M.J. Oreglia [36], Y. Oren [159], D. Orestano [72a,72b], E.C. Orgill [98], N. Orlando [61b], A.A. O'Rourke [44], R.S. Orr [165], B. Osculati [53b,53a,*], V. O'Shea [55], R. Ospanov [58a], G. Otero y Garzon [30], H. Otono [85], M. Ouchrif [34d], F. Ould-Saada [130], A. Ouraou [142], Q. Ouyang [15a], M. Owen [55], R.E. Owen [21], V.E. Ozcan [12c], N. Ozturk [8], K. Pachal [149], A. Pacheco Pages [14], L. Pacheco Rodriguez [142], C. Padilla Aranda [14], S. Pagan Griso [18], M. Paganini [181], G. Palacino [63], S. Palazzo [40b,40a], S. Palestini [35], M. Palka [81b], D. Pallin [37], I. Panagoulias [10], C.E. Pandini [52], J.G. Panduro Vazquez [91], P. Pani [35], L. Paolozzi [52], T.D. Papadopoulou [10], K. Papageorgiou [9,j], A. Paramonov [6], D. Paredes Hernandez [61b], B. Parida [58c], A.J. Parker [87], K.A. Parker [44], M.A. Parker [31], F. Parodi [53b,53a], J.A. Parsons [38], U. Parzefall [50], V.R. Pascuzzi [165], J.M.P. Pasner [143], E. Pasqualucci [70a], S. Passaggio [53b], F. Pastore [91], P. Pasuwan [43a,43b], S. Pataraia [97], J.R. Pater [98], A. Pathak [179,k], T. Pauly [35], B. Pearson [113], M. Pedersen [130], S. Pedraza Lopez [172], R. Pedro [136a,136b], S.V. Peleganchuk [120b,120a], O. Penc [137], C. Peng [15d], H. Peng [58a], J. Penwell [63], B.S. Peralva [78a], M.M. Perego [142], A.P. Pereira Peixoto [136a], D.V. Perepelitsa [29], F. Peri [19], L. Perini [66a,66b], H. Pernegger [35], S. Perrella [67a,67b], V.D. Peshekhonov [77,*], K. Peters [44], R.F.Y. Peters [98], B.A. Petersen [35], T.C. Petersen [39], E. Petit [56], A. Petridis [1], C. Petridou [160], P. Petroff [128], E. Petrolo [70a], M. Petrov [131], F. Petrucci [72a,72b], N.E. Pettersson [100], A. Peyaud [142], R. Pezoa [144b], T. Pham [102], F.H. Phillips [104], P.W. Phillips [141], G. Piacquadio [152], E. Pianori [176], A. Picazio [100], M.A. Pickering [131], R. Piegaia [30], J.E. Pilcher [36], A.D. Pilkington [98], M. Pinamonti [71a,71b], J.L. Pinfold [3], M. Pitt [178], M-A. Pleier [29], V. Pleskot [139], E. Plotnikova [77], D. Pluth [76], P. Podberezko [120b,120a], R. Poettgen [94], R. Poggi [68a,68b], L. Poggioli [128], I. Pogrebnyak [104], D. Pohl [24], I. Pokharel [51], G. Polesello [68a], A. Poley [44], A. Policicchio [40b,40a], R. Polifka [35], A. Polini [23b], C.S. Pollard [44], V. Polychronakos [29], D. Ponomarenko [110], L. Pontecorvo [70a], G.A. Popeneciu [27d], D.M. Portillo Quintero [132], S. Pospisil [138], K. Potamianos [44], I.N. Potrap [77], C.J. Potter [31], H. Potti [11], T. Poulsen [94], J. Poveda [35], T.D. Powell [146], M.E. Pozo Astigarraga [35], P. Pralavorio [99], S. Prell [76], D. Price [98], M. Primavera [65a], S. Prince [101], N. Proklova [110], K. Prokofiev [61c], F. Prokoshin [144b], S. Protopopescu [29], J. Proudfoot [6], M. Przybycien [81a], A. Puri [171], P. Puzo [128], J. Qian [103], Y. Qin [98], A. Quadt [51], M. Queitsch-Maitland [44], A. Qureshi [1], S.K. Radhakrishnan [152], P. Rados [102], F. Ragusa [66a,66b], G. Rahal [95], J.A. Raine [98], S. Rajagopalan [29], T. Rashid [128], S. Raspopov [5], M.G. Ratti [66a,66b], D.M. Rauch [44], F. Rauscher [112], S. Rave [97], B. Ravina [146], I. Ravinovich [178], J.H. Rawling [98], M. Raymond [35], A.L. Read [130], N.P. Readioff [56], M. Reale [65a,65b], D.M. Rebuzzi [68a,68b], A. Redelbach [175], G. Redlinger [29], R. Reece [143], R.G. Reed [32c], K. Reeves [42], L. Rehnisch [19], J. Reichert [133], A. Reiss [97], C. Rembser [35],

H. Ren [15d], M. Resciguo [70a], S. Resconi [66a], E.D. Resseguie [133], S. Rettie [173], E. Reynolds [21], O.L. Rezanova [120b,120a], P. Reznicek [139], R. Richter [113], S. Richter [92], E. Richter-Was [81b], O. Ricken [24], M. Ridel [132], P. Rieck [113], C.J. Riegel [180], O. Rifki [44], M. Rijssenbeek [152], A. Rimoldi [68a,68b], M. Rimoldi [20], L. Rinaldi [23b], G. Ripellino [151], B. Ristić [35], E. Ritsch [35], I. Riu [14], J.C. Rivera Vergara [144a], F. Rizatdinova [125], E. Rizvi [90], C. Rizzi [14], R.T. Roberts [98], S.H. Robertson [101,ae], A. Robichaud-Veronneau [101], D. Robinson [31], J.E.M. Robinson [44], A. Robson [55], E. Rocco [97], C. Roda [69a,69b], Y. Rodina [99,aa], S. Rodriguez Bosca [172], A. Rodriguez Perez [14], D. Rodriguez Rodriguez [172], A.M. Rodríguez Vera [166b], S. Roe [35], C.S. Rogan [57], O. Røhne [130], R. Röhrig [113], C.P.A. Roland [63], J. Roloff [57], A. Romaniouk [110], M. Romano [23b,23a], E. Romero Adam [172], N. Rompotis [88], M. Ronzani [121], L. Roos [132], S. Rosati [70a], K. Rosbach [50], P. Rose [143], N-A. Rosien [51], E. Rossi [67a,67b], L.P. Rossi [53b], L. Rossini [66a,66b], J.H.N. Rosten [31], R. Rosten [145], M. Rotaru [27b], J. Rothberg [145], D. Rousseau [128], D. Roy [32c], A. Rozanov [99], Y. Rozen [158], X. Ruan [32c], F. Rubbo [150], F. Rühr [50], A. Ruiz-Martinez [33], Z. Rurikova [50], N.A. Rusakovich [77], H.L. Russell [101], J.P. Rutherfoord [7], N. Ruthmann [35], E.M. Rüttinger [44,l], Y.F. Ryabov [134], M. Rybar [171], G. Rybkin [128], S. Ryu [6], A. Ryzhov [140], G.F. Rzehorz [51], P. Sabatini [51], G. Sabato [118], S. Sacerdoti [128], H.F-W. Sadrozinski [143], R. Sadykov [77], F. Safai Tehrani [70a], P. Saha [119], M. Sahinsoy [59a], M. Saimpert [44], M. Saito [161], T. Saito [161], H. Sakamoto [161], A. Sakharov [121,ak], D. Salamani [52], G. Salamanna [72a,72b], J.E. Salazar Loyola [144b], D. Salek [118], P.H. Sales De Bruin [170], D. Salihagic [113], A. Salnikov [150], J. Salt [172], D. Salvatore [40b,40a], F. Salvatore [153], A. Salvucci [61a,61b,61c], A. Salzburger [35], D. Sammel [50], D. Sampsonidis [160], D. Sampsonidou [160], J. Sánchez [172], A. Sanchez Pineda [64a,64c], H. Sandaker [130], C.O. Sander [44], M. Sandhoff [180], C. Sandoval [22], D.P.C. Sankey [141], M. Sannino [53b,53a], Y. Sano [115], A. Sansoni [49], C. Santoni [37], H. Santos [136a], I. Santoyo Castillo [153], A. Sapronov [77], J.G. Saraiva [136a,136d], O. Sasaki [79], K. Sato [167], E. Sauvan [5], P. Savard [165,au], N. Savic [113], R. Sawada [161], C. Sawyer [141], L. Sawyer [93,aj], C. Sbarra [23b], A. Sbrizzi [23b,23a], T. Scanlon [92], D.A. Scannicchio [169], J. Schaarschmidt [145], P. Schacht [113], B.M. Schachtner [112], D. Schaefer [36], L. Schaefer [133], J. Schaeffer [97], S. Schaepe [35], U. Schäfer [97], A.C. Schaffer [128], D. Schaile [112], R.D. Schamberger [152], N. Scharmberg [98], V.A. Schegelsky [134], D. Scheirich [139], F. Schenck [19], M. Schernau [169], C. Schiavi [53b,53a], S. Schier [143], L.K. Schildgen [24], Z.M. Schillaci [26], E.J. Schioppa [35], M. Schioppa [40b,40a], K.E. Schleicher [50], S. Schlenker [35], K.R. Schmidt-Sommerfeld [113], K. Schmieden [35], C. Schmitt [97], S. Schmitt [44], S. Schmitz [97], U. Schnoor [50], L. Schoeffel [142], A. Schoening [59b], E. Schopf [24], M. Schott [97], J.F.P. Schouwenberg [117], J. Schovancova [35], S. Schramm [52], N. Schuh [97], A. Schulte [97], H-C. Schultz-Coulon [59a], M. Schumacher [50], B.A. Schumm [143], Ph. Schune [142], A. Schwartzman [150], T.A. Schwarz [103], H. Schweiger [98], Ph. Schwemling [142], R. Schwienhorst [104], A. Sciandra [24], G. Sciolla [26], M. Scornajenghi [40b,40a], F. Scuri [69a], F. Scutti [102], L.M. Scyboz [113], J. Searcy [103], C.D. Sebastiani [70a,70b], P. Seema [24], S.C. Seidel [116], A. Seiden [143], J.M. Seixas [78b], G. Sekhniaidze [67a], K. Sekhon [103], S.J. Sekula [41], N. Semprini-Cesari [23b,23a], S. Senkin [37], C. Serfon [130], L. Serin [128], L. Serkin [64a,64b], M. Sessa [72a,72b], H. Severini [124], F. Sforza [168], A. Sfyrla [52], E. Shabalina [51], J.D. Shahinian [143], N.W. Shaikh [43a,43b], L.Y. Shan [15a], R. Shang [171], J.T. Shank [25], M. Shapiro [18], A.S. Sharma [1], A. Sharma [131], P.B. Shatalov [109], K. Shaw [64a,64b], S.M. Shaw [98], A. Shcherbakova [134], C.Y. Shehu [153], Y. Shen [124], N. Sherafati [33], A.D. Sherman [25], P. Sherwood [92], L. Shi [155,aq], S. Shimizu [80], C.O. Shimmin [181], M. Shimojima [114], I.P.J. Shipsey [131], S. Shirabe [85], M. Shiyakova [77], J. Shlomi [178], A. Shmeleva [108], D. Shoaleh Saadi [107], M.J. Shochet [36], S. Shojaii [102], D.R. Shope [124], S. Shrestha [122], E. Shulga [110], P. Sicho [137], A.M. Sickles [171], P.E. Sidebo [151], E. Sideras Haddad [32c], O. Sidiropoulou [175], A. Sidoti [23b,23a], F. Siegert [46], Dj. Sijacki [16], J. Silva [136a], M. Silva Jr. [179], S.B. Silverstein [43a], L. Simic [77], S. Simion [128], E. Simioni [97], B. Simmons [92], M. Simon [97], P. Sinervo [165], N.B. Sinev [127], M. Sioli [23b,23a], G. Siragusa [175], I. Siral [103], S.Yu. Sivoklokov [111], J. Sjölin [43a,43b], M.B. Skinner [87], P. Skubic [124], M. Slater [21], T. Slavicek [138], M. Slawinska [82], K. Sliwa [168], R. Slovak [139], V. Smakhtin [178], B.H. Smart [5], J. Smiesko [28a], N. Smirnov [110], S.Yu. Smirnov [110], Y. Smirnov [110], L.N. Smirnova [111], O. Smirnova [94], J.W. Smith [51], M.N.K. Smith [38], R.W. Smith [38], M. Smizanska [87], K. Smolek [138], A.A. Snesarev [108], I.M. Snyder [127], S. Snyder [29], R. Sobie [174,ae], F. Socher [46], A.M. Soffa [169], A. Soffer [159], A. Søgaard [48], D.A. Soh [155], G. Sokhrannyi [89], C.A. Solans Sanchez [35], M. Solar [138], E.Yu. Soldatov [110], U. Soldevila [172], A.A. Solodkov [140], A. Soloshenko [77], O.V. Solovyanov [140], V. Solovyev [134], P. Sommer [146], H. Son [168], W. Song [141], A. Sopczak [138], F. Sopkova [28b], D. Sosa [59b], C.L. Sotiropoulou [69a,69b], S. Sottocornola [68a,68b], R. Soualah [64a,64c,i], A.M. Soukharev [120b,120a], D. South [44], B.C. Sowden [91], S. Spagnolo [65a,65b], M. Spalla [113], M. Spangenberg [176], F. Spanò [91], D. Sperlich [19],

F. Spettel [113], T.M. Spieker [59a], R. Spighi [23b], G. Spigo [35], L.A. Spiller [102], M. Spousta [139], A. Stabile [66a,66b], R. Stamen [59a], S. Stamm [19], E. Stanecka [82], R.W. Stanek [6], C. Stanescu [72a], M.M. Stanitzki [44], B.S. Stapf [118], S. Stapnes [130], E.A. Starchenko [140], G.H. Stark [36], J. Stark [56], S.H Stark [39], P. Staroba [137], P. Starovoitov [59a], S. Stärz [35], R. Staszewski [82], M. Stegler [44], P. Steinberg [29], B. Stelzer [149], H.J. Stelzer [35], O. Stelzer-Chilton [166a], H. Stenzel [54], T.J. Stevenson [90], G.A. Stewart [55], M.C. Stockton [127], G. Stoicea [27b], P. Stolte [51], S. Stonjek [113], A. Straessner [46], J. Strandberg [151], S. Strandberg [43a,43b], M. Strauss [124], P. Strizenec [28b], R. Ströhmer [175], D.M. Strom [127], R. Stroynowski [41], A. Strubig [48], S.A. Stucci [29], B. Stugu [17], J. Stupak [124], N.A. Styles [44], D. Su [150], J. Su [135], S. Suchek [59a], Y. Sugaya [129], M. Suk [138], V.V. Sulin [108], D.M.S. Sultan [52], S. Sultansoy [4c], T. Sumida [83], S. Sun [103], X. Sun [3], K. Suruliz [153], C.J.E. Suster [154], M.R. Sutton [153], S. Suzuki [79], M. Svatos [137], M. Swiatlowski [36], S.P. Swift [2], A. Sydorenko [97], I. Sykora [28a], T. Sykora [139], D. Ta [97], K. Tackmann [44,ab], J. Taenzer [159], A. Taffard [169], R. Tafirout [166a], E. Tahirovic [90], N. Taiblum [159], H. Takai [29], R. Takashima [84], E.H. Takasugi [113], K. Takeda [80], T. Takeshita [147], Y. Takubo [79], M. Talby [99], A.A. Talyshev [120b,120a], J. Tanaka [161], M. Tanaka [163], R. Tanaka [128], R. Tanioka [80], B.B. Tannenwald [122], S. Tapia Araya [144b], S. Tapprogge [97], A. Tarek Abouelfadl Mohamed [132], S. Tarem [158], G. Tarna [27b,e], G.F. Tartarelli [66a], P. Tas [139], M. Tasevsky [137], T. Tashiro [83], E. Tassi [40b,40a], A. Tavares Delgado [136a,136b], Y. Tayalati [34e], A.C. Taylor [116], A.J. Taylor [48], G.N. Taylor [102], P.T.E. Taylor [102], W. Taylor [166b], A.S. Tee [87], P. Teixeira-Dias [91], D. Temple [149], H. Ten Kate [35], P.K. Teng [155], J.J. Teoh [129], F. Tepel [180], S. Terada [79], K. Terashi [161], J. Terron [96], S. Terzo [14], M. Testa [49], R.J. Teuscher [165,ae], S.J. Thais [181], T. Theveneaux-Pelzer [44], F. Thiele [39], J.P. Thomas [21], A.S. Thompson [55], P.D. Thompson [21], L.A. Thomsen [181], E. Thomson [133], Y. Tian [38], R.E. Ticse Torres [51], V.O. Tikhomirov [108,am], Yu.A. Tikhonov [120b,120a], S. Timoshenko [110], P. Tipton [181], S. Tisserant [99], K. Todome [163], S. Todorova-Nova [5], S. Todt [46], J. Tojo [85], S. Tokár [28a], K. Tokushuku [79], E. Tolley [122], M. Tomoto [115], L. Tompkins [150], K. Toms [116], B. Tong [57], P. Tornambe [50], E. Torrence [127], H. Torres [46], E. Torró Pastor [145], C. Tosciri [131], J. Toth [99,ad], F. Touchard [99], D.R. Tovey [146], C.J. Treado [121], T. Trefzger [175], F. Tresoldi [153], A. Tricoli [29], I.M. Trigger [166a], S. Trincaz-Duvoid [132], M.F. Tripiana [14], W. Trischuk [165], B. Trocmé [56], A. Trofymov [44], C. Troncon [66a], M. Trovatelli [174], F. Trovato [153], L. Truong [32b], M. Trzebinski [82], A. Trzupek [82], F. Tsai [44], K.W. Tsang [61a], J.C-L. Tseng [131], P.V. Tsiareshka [105], N. Tsirintanis [9], S. Tsiskaridze [14], V. Tsiskaridze [152], E.G. Tskhadadze [157a], I.I. Tsukerman [109], V. Tsulaia [18], S. Tsuno [79], D. Tsybychev [152], Y. Tu [61b], A. Tudorache [27b], V. Tudorache [27b], T.T. Tulbure [27a], A.N. Tuna [57], S. Turchikhin [77], D. Turgeman [178], I. Turk Cakir [4b,u], R. Turra [66a], P.M. Tuts [38], E. Tzovara [97], G. Ucchielli [23b,23a], I. Ueda [79], M. Ughetto [43a,43b], F. Ukegawa [167], G. Unal [35], A. Undrus [29], G. Unel [169], F.C. Ungaro [102], Y. Unno [79], K. Uno [161], J. Urban [28b], P. Urquijo [102], P. Urrejola [97], G. Usai [8], J. Usui [79], L. Vacavant [99], V. Vacek [138], B. Vachon [101], K.O.H. Vadla [130], A. Vaidya [92], C. Valderanis [112], E. Valdes Santurio [43a,43b], M. Valente [52], S. Valentinetti [23b,23a], A. Valero [172], L. Valéry [44], R.A. Vallance [21], A. Vallier [5], J.A. Valls Ferrer [172], T.R. Van Daalen [14], W. Van Den Wollenberg [118], H. Van der Graaf [118], P. Van Gemmeren [6], J. Van Nieuwkoop [149], I. Van Vulpen [118], M.C. van Woerden [118], M. Vanadia [71a,71b], W. Vandelli [35], A. Vaniachine [164], P. Vankov [118], R. Vari [70a], E.W. Varnes [7], C. Varni [53b,53a], T. Varol [41], D. Varouchas [128], A. Vartapetian [8], K.E. Varvell [154], G.A. Vasquez [144b], J.G. Vasquez [181], F. Vazeille [37], D. Vazquez Furelos [14], T. Vazquez Schroeder [101], J. Veatch [51], V. Vecchio [72a,72b], L.M. Veloce [165], F. Veloso [136a,136c], S. Veneziano [70a], A. Ventura [65a,65b], M. Venturi [174], N. Venturi [35], V. Vercesi [68a], M. Verducci [72a,72b], W. Verkerke [118], A.T. Vermeulen [118], J.C. Vermeulen [118], M.C. Vetterli [149,au], N. Viaux Maira [144b], O. Viazlo [94], I. Vichou [171,*], T. Vickey [146], O.E. Vickey Boeriu [146], G.H.A. Viehhauser [131], S. Viel [18], L. Vigani [131], M. Villa [23b,23a], M. Villaplana Perez [66a,66b], E. Vilucchi [49], M.G. Vincter [33], V.B. Vinogradov [77], A. Vishwakarma [44], C. Vittori [23b,23a], I. Vivarelli [153], S. Vlachos [10], M. Vogel [180], P. Vokac [138], G. Volpi [14], S.E. Von Buddenbrock [32c], E. Von Toerne [24], V. Vorobel [139], K. Vorobev [110], M. Vos [172], J.H. Vossebeld [88], N. Vranjes [16], M. Vranjes Milosavljevic [16], V. Vrba [138], M. Vreeswijk [118], T. Šfiligoj [89], R. Vuillermet [35], I. Vukotic [36], T. Ženiš [28a], L. Živković [16], P. Wagner [24], W. Wagner [180], J. Wagner-Kuhr [112], H. Wahlberg [86], S. Wahrmund [46], K. Wakamiya [80], J. Walder [87], R. Walker [112], W. Walkowiak [148], V. Wallangen [43a,43b], A.M. Wang [57], C. Wang [58b,e], F. Wang [179], H. Wang [18], H. Wang [3], J. Wang [154], J. Wang [59b], P. Wang [41], Q. Wang [124], R.-J. Wang [132], R. Wang [58a], R. Wang [6], S.M. Wang [155], T. Wang [38], W. Wang [155,p], W.X. Wang [58a,af], Y. Wang [58a], Z. Wang [58c], C. Wanotayaroj [44], A. Warburton [101], C.P. Ward [31], D.R. Wardrope [92], A. Washbrook [48], P.M. Watkins [21],

A.T. Watson [21], M.F. Watson [21], G. Watts [145], S. Watts [98], B.M. Waugh [92], A.F. Webb [11], S. Webb [97], C. Weber [181], M.S. Weber [20], S.A. Weber [33], S.M. Weber [59a], J.S. Webster [6], A.R. Weidberg [131], B. Weinert [63], J. Weingarten [51], M. Weirich [97], C. Weiser [50], P.S. Wells [35], T. Wenaus [29], T. Wengler [35], S. Wenig [35], N. Wermes [24], M.D. Werner [76], P. Werner [35], M. Wessels [59a], T.D. Weston [20], K. Whalen [127], N.L. Whallon [145], A.M. Wharton [87], A.S. White [103], A. White [8], M.J. White [1], R. White [144b], D. Whiteson [169], B.W. Whitmore [87], F.J. Wickens [141], W. Wiedenmann [179], M. Wielers [141], C. Wiglesworth [39], L.A.M. Wiik-Fuchs [50], A. Wildauer [113], F. Wilk [98], H.G. Wilkens [35], H.H. Williams [133], S. Williams [31], C. Willis [104], S. Willocq [100], J.A. Wilson [21], I. Wingerter-Seez [5], E. Winkels [153], F. Winklmeier [127], O.J. Winston [153], B.T. Winter [24], M. Wittgen [150], M. Wobisch [93], A. Wolf [97], T.M.H. Wolf [118], R. Wolff [99], M.W. Wolter [82], H. Wolters [136a,136c], V.W.S. Wong [173], N.L. Woods [143], S.D. Worm [21], B.K. Wosiek [82], K.W. Woźniak [82], K. Wraight [55], M. Wu [36], S.L. Wu [179], X. Wu [52], Y. Wu [58a], T.R. Wyatt [98], B.M. Wynne [48], S. Xella [39], Z. Xi [103], L. Xia [15b], D. Xu [15a], H. Xu [58a], L. Xu [29], T. Xu [142], W. Xu [103], B. Yabsley [154], S. Yacoob [32a], K. Yajima [129], D.P. Yallup [92], D. Yamaguchi [163], Y. Yamaguchi [163], A. Yamamoto [79], T. Yamanaka [161], F. Yamane [80], M. Yamatani [161], T. Yamazaki [161], Y. Yamazaki [80], Z. Yan [25], H.J. Yang [58c,58d], H.T. Yang [18], S. Yang [75], Y. Yang [161], Y. Yang [155], Z. Yang [17], W-M. Yao [18], Y.C. Yap [44], Y. Yasu [79], E. Yatsenko [5], K.H. Yau Wong [24], J. Ye [41], S. Ye [29], I. Yeletskikh [77], E. Yigitbasi [25], E. Yildirim [97], K. Yorita [177], K. Yoshihara [133], C.J.S. Young [35], C. Young [150], J. Yu [8], J. Yu [76], X. Yue [59a], S.P.Y. Yuen [24], I. Yusuff [31,a], B. Zabinski [82], G. Zacharis [10], R. Zaidan [14], A.M. Zaitsev [140,al], N. Zakharchuk [44], J. Zalieckas [17], S. Zambito [57], D. Zanzi [35], C. Zeitnitz [180], G. Zemaityte [131], J.C. Zeng [171], Q. Zeng [150], O. Zenin [140], D. Zerwas [128], M. Zgubič [131], D.F. Zhang [58b], D. Zhang [103], F. Zhang [179], G. Zhang [58a,af], H. Zhang [15c], J. Zhang [6], L. Zhang [50], L. Zhang [58a], M. Zhang [171], P. Zhang [15c], R. Zhang [58a,e], R. Zhang [24], X. Zhang [58b], Y. Zhang [15d], Z. Zhang [128], X. Zhao [41], Y. Zhao [58b,128], Z. Zhao [58a], A. Zhemchugov [77], B. Zhou [103], C. Zhou [179], L. Zhou [41], M.S. Zhou [15d], M. Zhou [152], N. Zhou [58c], Y. Zhou [7], C.G. Zhu [58b], H.L. Zhu [58a], H. Zhu [15a], J. Zhu [103], Y. Zhu [58a], X. Zhuang [15a], K. Zhukov [108], V. Zhulanov [120b,120a], A. Zibell [175], D. Zieminska [63], N.I. Zimine [77], S. Zimmermann [50], Z. Zinonos [113], M. Zinser [97], M. Ziolkowski [148], G. Zobernig [179], A. Zoccoli [23b,23a], K. Zoch [51], T.G. Zorbas [146], R. Zou [36], M. Zur Nedden [19], L. Zwalinski [35]

[1] *Department of Physics, University of Adelaide, Adelaide, Australia*
[2] *Physics Department, SUNY Albany, Albany NY, United States of America*
[3] *Department of Physics, University of Alberta, Edmonton AB, Canada*
[4] [(a)] *Department of Physics, Ankara University, Ankara;* [(b)] *Istanbul Aydin University, Istanbul;* [(c)] *Division of Physics, TOBB University of Economics and Technology, Ankara, Turkey*
[5] *LAPP, Université Grenoble Alpes, Université Savoie Mont Blanc, CNRS/IN2P3, Annecy, France*
[6] *High Energy Physics Division, Argonne National Laboratory, Argonne IL, United States of America*
[7] *Department of Physics, University of Arizona, Tucson AZ, United States of America*
[8] *Department of Physics, University of Texas at Arlington, Arlington TX, United States of America*
[9] *Physics Department, National and Kapodistrian University of Athens, Athens, Greece*
[10] *Physics Department, National Technical University of Athens, Zografou, Greece*
[11] *Department of Physics, University of Texas at Austin, Austin TX, United States of America*
[12] [(a)] *Bahcesehir University, Faculty of Engineering and Natural Sciences, Istanbul;* [(b)] *Istanbul Bilgi University, Faculty of Engineering and Natural Sciences, Istanbul;* [(c)] *Department of Physics, Bogazici University, Istanbul;* [(d)] *Department of Physics Engineering, Gaziantep University, Gaziantep, Turkey*
[13] *Institute of Physics, Azerbaijan Academy of Sciences, Baku, Azerbaijan*
[14] *Institut de Física d'Altes Energies (IFAE), Barcelona Institute of Science and Technology, Barcelona, Spain*
[15] [(a)] *Institute of High Energy Physics, Chinese Academy of Sciences, Beijing;* [(b)] *Physics Department, Tsinghua University, Beijing;* [(c)] *Department of Physics, Nanjing University, Nanjing;* [(d)] *University of Chinese Academy of Science (UCAS), Beijing, China*
[16] *Institute of Physics, University of Belgrade, Belgrade, Serbia*
[17] *Department for Physics and Technology, University of Bergen, Bergen, Norway*
[18] *Physics Division, Lawrence Berkeley National Laboratory and University of California, Berkeley CA, United States of America*
[19] *Institut für Physik, Humboldt Universität zu Berlin, Berlin, Germany*
[20] *Albert Einstein Center for Fundamental Physics and Laboratory for High Energy Physics, University of Bern, Bern, Switzerland*
[21] *School of Physics and Astronomy, University of Birmingham, Birmingham, United Kingdom*
[22] *Centro de Investigaciónes, Universidad Antonio Nariño, Bogota, Colombia*
[23] [(a)] *Dipartimento di Fisica e Astronomia, Università di Bologna, Bologna;* [(b)] *INFN Sezione di Bologna, Italy*
[24] *Physikalisches Institut, Universität Bonn, Bonn, Germany*
[25] *Department of Physics, Boston University, Boston MA, United States of America*
[26] *Department of Physics, Brandeis University, Waltham MA, United States of America*
[27] [(a)] *Transilvania University of Brasov, Brasov;* [(b)] *Horia Hulubei National Institute of Physics and Nuclear Engineering, Bucharest;* [(c)] *Department of Physics, Alexandru Ioan Cuza University of Iasi, Iasi;* [(d)] *National Institute for Research and Development of Isotopic and Molecular Technologies, Physics Department, Cluj-Napoca;* [(e)] *University Politehnica Bucharest, Bucharest;* [(f)] *West University in Timisoara, Timisoara, Romania*
[28] [(a)] *Faculty of Mathematics, Physics and Informatics, Comenius University, Bratislava;* [(b)] *Department of Subnuclear Physics, Institute of Experimental Physics of the Slovak Academy of Sciences, Kosice, Slovak Republic*
[29] *Physics Department, Brookhaven National Laboratory, Upton NY, United States of America*
[30] *Departamento de Física, Universidad de Buenos Aires, Buenos Aires, Argentina*
[31] *Cavendish Laboratory, University of Cambridge, Cambridge, United Kingdom*
[32] [(a)] *Department of Physics, University of Cape Town, Cape Town;* [(b)] *Department of Mechanical Engineering Science, University of Johannesburg, Johannesburg;* [(c)] *School of Physics, University of the Witwatersrand, Johannesburg, South Africa*
[33] *Department of Physics, Carleton University, Ottawa ON, Canada*

[34] [(a)] Faculté des Sciences Ain Chock, Réseau Universitaire de Physique des Hautes Energies - Université Hassan II, Casablanca; [(b)] Centre National de l'Energie des Sciences Techniques Nucleaires (CNESTEN), Rabat; [(c)] Faculté des Sciences Semlalia, Université Cadi Ayyad, LPHEA-Marrakech; [(d)] Faculté des Sciences, Université Mohamed Premier and LPTPM, Oujda; [(e)] Faculté des sciences, Université Mohammed V, Rabat, Morocco
[35] CERN, Geneva, Switzerland
[36] Enrico Fermi Institute, University of Chicago, Chicago IL, United States of America
[37] LPC, Université Clermont Auvergne, CNRS/IN2P3, Clermont-Ferrand, France
[38] Nevis Laboratory, Columbia University, Irvington NY, United States of America
[39] Niels Bohr Institute, University of Copenhagen, Copenhagen, Denmark
[40] [(a)] Dipartimento di Fisica, Università della Calabria, Rende; [(b)] INFN Gruppo Collegato di Cosenza, Laboratori Nazionali di Frascati, Italy
[41] Physics Department, Southern Methodist University, Dallas TX, United States of America
[42] Physics Department, University of Texas at Dallas, Richardson TX, United States of America
[43] [(a)] Department of Physics, Stockholm University; [(b)] Oskar Klein Centre, Stockholm, Sweden
[44] Deutsches Elektronen-Synchrotron DESY, Hamburg and Zeuthen, Germany
[45] Lehrstuhl für Experimentelle Physik IV, Technische Universität Dortmund, Dortmund, Germany
[46] Institut für Kern- und Teilchenphysik, Technische Universität Dresden, Dresden, Germany
[47] Department of Physics, Duke University, Durham NC, United States of America
[48] SUPA - School of Physics and Astronomy, University of Edinburgh, Edinburgh, United Kingdom
[49] INFN e Laboratori Nazionali di Frascati, Frascati, Italy
[50] Physikalisches Institut, Albert-Ludwigs-Universität Freiburg, Freiburg, Germany
[51] II. Physikalisches Institut, Georg-August-Universität Göttingen, Göttingen, Germany
[52] Département de Physique Nucléaire et Corpusculaire, Université de Genève, Genève, Switzerland
[53] [(a)] Dipartimento di Fisica, Università di Genova, Genova; [(b)] INFN Sezione di Genova, Italy
[54] II. Physikalisches Institut, Justus-Liebig-Universität Giessen, Giessen, Germany
[55] SUPA - School of Physics and Astronomy, University of Glasgow, Glasgow, United Kingdom
[56] LPSC, Université Grenoble Alpes, CNRS/IN2P3, Grenoble INP, Grenoble, France
[57] Laboratory for Particle Physics and Cosmology, Harvard University, Cambridge MA, United States of America
[58] [(a)] Department of Modern Physics and State Key Laboratory of Particle Detection and Electronics, University of Science and Technology of China, Hefei; [(b)] Institute of Frontier and Interdisciplinary Science and Key Laboratory of Particle Physics and Particle Irradiation (MOE), Shandong University, Qingdao; [(c)] School of Physics and Astronomy, Shanghai Jiao Tong University, KLPPAC-MoE, SKLPPC, Shanghai; [(d)] Tsung-Dao Lee Institute, Shanghai, China
[59] [(a)] Kirchhoff-Institut für Physik, Ruprecht-Karls-Universität Heidelberg, Heidelberg; [(b)] Physikalisches Institut, Ruprecht-Karls-Universität Heidelberg, Heidelberg, Germany
[60] Faculty of Applied Information Science, Hiroshima Institute of Technology, Hiroshima, Japan
[61] [(a)] Department of Physics, Chinese University of Hong Kong, Shatin, N.T., Hong Kong; [(b)] Department of Physics, University of Hong Kong, Hong Kong; [(c)] Department of Physics and Institute for Advanced Study, Hong Kong University of Science and Technology, Clear Water Bay, Kowloon, Hong Kong, China
[62] Department of Physics, National Tsing Hua University, Hsinchu, Taiwan
[63] Department of Physics, Indiana University, Bloomington IN, United States of America
[64] [(a)] INFN Gruppo Collegato di Udine, Sezione di Trieste, Udine; [(b)] ICTP, Trieste; [(c)] Dipartimento di Chimica, Fisica e Ambiente, Università di Udine, Udine, Italy
[65] [(a)] INFN Sezione di Lecce; [(b)] Dipartimento di Matematica e Fisica, Università del Salento, Lecce, Italy
[66] [(a)] INFN Sezione di Milano; [(b)] Dipartimento di Fisica, Università di Milano, Milano, Italy
[67] [(a)] INFN Sezione di Napoli; [(b)] Dipartimento di Fisica, Università di Napoli, Napoli, Italy
[68] [(a)] INFN Sezione di Pavia; [(b)] Dipartimento di Fisica, Università di Pavia, Pavia, Italy
[69] [(a)] INFN Sezione di Pisa; [(b)] Dipartimento di Fisica E. Fermi, Università di Pisa, Pisa, Italy
[70] [(a)] INFN Sezione di Roma; [(b)] Dipartimento di Fisica, Sapienza Università di Roma, Roma, Italy
[71] [(a)] INFN Sezione di Roma Tor Vergata; [(b)] Dipartimento di Fisica, Università di Roma Tor Vergata, Roma, Italy
[72] [(a)] INFN Sezione di Roma Tre; [(b)] Dipartimento di Matematica e Fisica, Università Roma Tre, Roma, Italy
[73] [(a)] INFN-TIFPA; [(b)] Università degli Studi di Trento, Trento, Italy
[74] Institut für Astro- und Teilchenphysik, Leopold-Franzens-Universität, Innsbruck, Austria
[75] University of Iowa, Iowa City IA, United States of America
[76] Department of Physics and Astronomy, Iowa State University, Ames IA, United States of America
[77] Joint Institute for Nuclear Research, Dubna, Russia
[78] [(a)] Departamento de Engenharia Elétrica, Universidade Federal de Juiz de Fora (UFJF), Juiz de Fora; [(b)] Universidade Federal do Rio De Janeiro COPPE/EE/IF, Rio de Janeiro; [(c)] Universidade Federal de São João del Rei (UFSJ), São João del Rei; [(d)] Instituto de Física, Universidade de São Paulo, São Paulo, Brazil
[79] KEK, High Energy Accelerator Research Organization, Tsukuba, Japan
[80] Graduate School of Science, Kobe University, Kobe, Japan
[81] [(a)] AGH University of Science and Technology, Faculty of Physics and Applied Computer Science, Krakow; [(b)] Marian Smoluchowski Institute of Physics, Jagiellonian University, Krakow, Poland
[82] Institute of Nuclear Physics Polish Academy of Sciences, Krakow, Poland
[83] Faculty of Science, Kyoto University, Kyoto, Japan
[84] Kyoto University of Education, Kyoto, Japan
[85] Research Center for Advanced Particle Physics and Department of Physics, Kyushu University, Fukuoka, Japan
[86] Instituto de Física La Plata, Universidad Nacional de La Plata and CONICET, La Plata, Argentina
[87] Physics Department, Lancaster University, Lancaster, United Kingdom
[88] Oliver Lodge Laboratory, University of Liverpool, Liverpool, United Kingdom
[89] Department of Experimental Particle Physics, Jožef Stefan Institute and Department of Physics, University of Ljubljana, Ljubljana, Slovenia
[90] School of Physics and Astronomy, Queen Mary University of London, London, United Kingdom
[91] Department of Physics, Royal Holloway University of London, Egham, United Kingdom
[92] Department of Physics and Astronomy, University College London, London, United Kingdom
[93] Louisiana Tech University, Ruston LA, United States of America
[94] Fysiska institutionen, Lunds universitet, Lund, Sweden
[95] Centre de Calcul de l'Institut National de Physique Nucléaire et de Physique des Particules (IN2P3), Villeurbanne, France
[96] Departamento de Física Teorica C-15 and CIAFF, Universidad Autónoma de Madrid, Madrid, Spain
[97] Institut für Physik, Universität Mainz, Mainz, Germany
[98] School of Physics and Astronomy, University of Manchester, Manchester, United Kingdom
[99] CPPM, Aix-Marseille Université, CNRS/IN2P3, Marseille, France
[100] Department of Physics, University of Massachusetts, Amherst MA, United States of America
[101] Department of Physics, McGill University, Montreal QC, Canada
[102] School of Physics, University of Melbourne, Victoria, Australia
[103] Department of Physics, University of Michigan, Ann Arbor MI, United States of America
[104] Department of Physics and Astronomy, Michigan State University, East Lansing MI, United States of America
[105] B.I. Stepanov Institute of Physics, National Academy of Sciences of Belarus, Minsk, Belarus

[106] Research Institute for Nuclear Problems of Byelorussian State University, Minsk, Belarus
[107] Group of Particle Physics, University of Montreal, Montreal QC, Canada
[108] P.N. Lebedev Physical Institute of the Russian Academy of Sciences, Moscow, Russia
[109] Institute for Theoretical and Experimental Physics (ITEP), Moscow, Russia
[110] National Research Nuclear University MEPhI, Moscow, Russia
[111] D.V. Skobeltsyn Institute of Nuclear Physics, M.V. Lomonosov Moscow State University, Moscow, Russia
[112] Fakultät für Physik, Ludwig-Maximilians-Universität München, München, Germany
[113] Max-Planck-Institut für Physik (Werner-Heisenberg-Institut), München, Germany
[114] Nagasaki Institute of Applied Science, Nagasaki, Japan
[115] Graduate School of Science and Kobayashi-Maskawa Institute, Nagoya University, Nagoya, Japan
[116] Department of Physics and Astronomy, University of New Mexico, Albuquerque NM, United States of America
[117] Institute for Mathematics, Astrophysics and Particle Physics, Radboud University Nijmegen/Nikhef, Nijmegen, Netherlands
[118] Nikhef National Institute for Subatomic Physics and University of Amsterdam, Amsterdam, Netherlands
[119] Department of Physics, Northern Illinois University, DeKalb IL, United States of America
[120] [(a)] Budker Institute of Nuclear Physics, SB RAS, Novosibirsk; [(b)] Novosibirsk State University Novosibirsk, Russia
[121] Department of Physics, New York University, New York NY, United States of America
[122] Ohio State University, Columbus OH, United States of America
[123] Faculty of Science, Okayama University, Okayama, Japan
[124] Homer L. Dodge Department of Physics and Astronomy, University of Oklahoma, Norman OK, United States of America
[125] Department of Physics, Oklahoma State University, Stillwater OK, United States of America
[126] Palacký University, RCPTM, Joint Laboratory of Optics, Olomouc, Czech Republic
[127] Center for High Energy Physics, University of Oregon, Eugene OR, United States of America
[128] LAL, Université Paris-Sud, CNRS/IN2P3, Université Paris-Saclay, Orsay, France
[129] Graduate School of Science, Osaka University, Osaka, Japan
[130] Department of Physics, University of Oslo, Oslo, Norway
[131] Department of Physics, Oxford University, Oxford, United Kingdom
[132] LPNHE, Sorbonne Université, Paris Diderot Sorbonne Paris Cité, CNRS/IN2P3, Paris, France
[133] Department of Physics, University of Pennsylvania, Philadelphia PA, United States of America
[134] Konstantinov Nuclear Physics Institute of National Research Centre "Kurchatov Institute", PNPI, St. Petersburg, Russia
[135] Department of Physics and Astronomy, University of Pittsburgh, Pittsburgh PA, United States of America
[136] [(a)] Laboratório de Instrumentação e Física Experimental de Partículas - LIP; [(b)] Departamento de Física, Faculdade de Ciências, Universidade de Lisboa, Lisboa; [(c)] Departamento de Física, Universidade de Coimbra, Coimbra; [(d)] Centro de Física Nuclear da Universidade de Lisboa, Lisboa; [(e)] Departamento de Física, Universidade do Minho, Braga; [(f)] Departamento de Física Teorica y del Cosmos, Universidad de Granada, Granada (Spain); [(g)] Dep Física and CEFITEC of Faculdade de Ciências e Tecnologia, Universidade Nova de Lisboa, Caparica, Portugal
[137] Institute of Physics, Academy of Sciences of the Czech Republic, Prague, Czech Republic
[138] Czech Technical University in Prague, Prague, Czech Republic
[139] Charles University, Faculty of Mathematics and Physics, Prague, Czech Republic
[140] State Research Center Institute for High Energy Physics, NRC KI, Protvino, Russia
[141] Particle Physics Department, Rutherford Appleton Laboratory, Didcot, United Kingdom
[142] IRFU, CEA, Université Paris-Saclay, Gif-sur-Yvette, France
[143] Santa Cruz Institute for Particle Physics, University of California Santa Cruz, Santa Cruz CA, United States of America
[144] [(a)] Departamento de Física, Pontificia Universidad Católica de Chile, Santiago; [(b)] Departamento de Física, Universidad Técnica Federico Santa María, Valparaíso, Chile
[145] Department of Physics, University of Washington, Seattle WA, United States of America
[146] Department of Physics and Astronomy, University of Sheffield, Sheffield, United Kingdom
[147] Department of Physics, Shinshu University, Nagano, Japan
[148] Department Physik, Universität Siegen, Siegen, Germany
[149] Department of Physics, Simon Fraser University, Burnaby BC, Canada
[150] SLAC National Accelerator Laboratory, Stanford CA, United States of America
[151] Physics Department, Royal Institute of Technology, Stockholm, Sweden
[152] Departments of Physics and Astronomy, Stony Brook University, Stony Brook NY, United States of America
[153] Department of Physics and Astronomy, University of Sussex, Brighton, United Kingdom
[154] School of Physics, University of Sydney, Sydney, Australia
[155] Institute of Physics, Academia Sinica, Taipei, Taiwan
[156] Academia Sinica Grid Computing, Institute of Physics, Academia Sinica, Taipei, Taiwan
[157] [(a)] E. Andronikashvili Institute of Physics, Iv. Javakhishvili Tbilisi State University, Tbilisi; [(b)] High Energy Physics Institute, Tbilisi State University, Tbilisi, Georgia
[158] Department of Physics, Technion, Israel Institute of Technology, Haifa, Israel
[159] Raymond and Beverly Sackler School of Physics and Astronomy, Tel Aviv University, Tel Aviv, Israel
[160] Department of Physics, Aristotle University of Thessaloniki, Thessaloniki, Greece
[161] International Center for Elementary Particle Physics and Department of Physics, University of Tokyo, Tokyo, Japan
[162] Graduate School of Science and Technology, Tokyo Metropolitan University, Tokyo, Japan
[163] Department of Physics, Tokyo Institute of Technology, Tokyo, Japan
[164] Tomsk State University, Tomsk, Russia
[165] Department of Physics, University of Toronto, Toronto ON, Canada
[166] [(a)] TRIUMF, Vancouver BC; [(b)] Department of Physics and Astronomy, York University, Toronto ON, Canada
[167] Division of Physics and Tomonaga Center for the History of the Universe, Faculty of Pure and Applied Sciences, University of Tsukuba, Tsukuba, Japan
[168] Department of Physics and Astronomy, Tufts University, Medford MA, United States of America
[169] Department of Physics and Astronomy, University of California Irvine, Irvine CA, United States of America
[170] Department of Physics and Astronomy, University of Uppsala, Uppsala, Sweden
[171] Department of Physics, University of Illinois, Urbana IL, United States of America
[172] Instituto de Física Corpuscular (IFIC), Centro Mixto Universidad de Valencia - CSIC, Valencia, Spain
[173] Department of Physics, University of British Columbia, Vancouver BC, Canada
[174] Department of Physics and Astronomy, University of Victoria, Victoria BC, Canada
[175] Fakultät für Physik und Astronomie, Julius-Maximilians-Universität Würzburg, Würzburg, Germany
[176] Department of Physics, University of Warwick, Coventry, United Kingdom
[177] Waseda University, Tokyo, Japan
[178] Department of Particle Physics, Weizmann Institute of Science, Rehovot, Israel
[179] Department of Physics, University of Wisconsin, Madison WI, United States of America
[180] Fakultät für Mathematik und Naturwissenschaften, Fachgruppe Physik, Bergische Universität Wuppertal, Wuppertal, Germany
[181] Department of Physics, Yale University, New Haven CT, United States of America
[182] Yerevan Physics Institute, Yerevan, Armenia

[a] Also at Department of Physics, University of Malaya, Kuala Lumpur; Malaysia.
[b] Also at Borough of Manhattan Community College, City University of New York, NY; United States of America.
[c] Also at Centre for High Performance Computing, CSIR Campus, Rosebank, Cape Town; South Africa.
[d] Also at CERN, Geneva; Switzerland.
[e] Also at CPPM, Aix-Marseille Université, CNRS/IN2P3, Marseille; France.
[f] Also at Département de Physique Nucléaire et Corpusculaire, Université de Genève, Genève; Switzerland.
[g] Also at Departament de Fisica de la Universitat Autonoma de Barcelona, Barcelona; Spain.
[h] Also at Departamento de Física Teorica y del Cosmos, Universidad de Granada, Granada (Spain); Spain.
[i] Also at Department of Applied Physics and Astronomy, University of Sharjah, Sharjah; United Arab Emirates.
[j] Also at Department of Financial and Management Engineering, University of the Aegean, Chios; Greece.
[k] Also at Department of Physics and Astronomy, University of Louisville, Louisville, KY; United States of America.
[l] Also at Department of Physics and Astronomy, University of Sheffield, Sheffield; United Kingdom.
[m] Also at Department of Physics, California State University, Fresno CA; United States of America.
[n] Also at Department of Physics, California State University, Sacramento CA; United States of America.
[o] Also at Department of Physics, King's College London, London; United Kingdom.
[p] Also at Department of Physics, Nanjing University, Nanjing; China.
[q] Also at Department of Physics, St. Petersburg State Polytechnical University, St. Petersburg; Russia.
[r] Also at Department of Physics, University of Fribourg, Fribourg; Switzerland.
[s] Also at Department of Physics, University of Michigan, Ann Arbor MI; United States of America.
[t] Also at Dipartimento di Fisica E. Fermi, Università di Pisa, Pisa; Italy.
[u] Also at Giresun University, Faculty of Engineering, Giresun; Turkey.
[v] Also at Graduate School of Science, Osaka University, Osaka; Japan.
[w] Also at Hellenic Open University, Patras; Greece.
[x] Also at Horia Hulubei National Institute of Physics and Nuclear Engineering, Bucharest; Romania.
[y] Also at II. Physikalisches Institut, Georg-August-Universität Göttingen, Göttingen; Germany.
[z] Also at Institucio Catalana de Recerca i Estudis Avancats, ICREA, Barcelona; Spain.
[aa] Also at Institut de Física d'Altes Energies (IFAE), Barcelona Institute of Science and Technology, Barcelona; Spain.
[ab] Also at Institut für Experimentalphysik, Universität Hamburg, Hamburg; Germany.
[ac] Also at Institute for Mathematics, Astrophysics and Particle Physics, Radboud University Nijmegen/Nikhef, Nijmegen; Netherlands.
[ad] Also at Institute for Particle and Nuclear Physics, Wigner Research Centre for Physics, Budapest; Hungary.
[ae] Also at Institute of Particle Physics (IPP); Canada.
[af] Also at Institute of Physics, Academia Sinica, Taipei; Taiwan.
[ag] Also at Institute of Physics, Azerbaijan Academy of Sciences, Baku; Azerbaijan.
[ah] Also at Institute of Theoretical Physics, Ilia State University, Tbilisi; Georgia.
[ai] Also at LAL, Université Paris-Sud, CNRS/IN2P3, Université Paris-Saclay, Orsay; France.
[aj] Also at Louisiana Tech University, Ruston LA; United States of America.
[ak] Also at Manhattan College, New York NY; United States of America.
[al] Also at Moscow Institute of Physics and Technology State University, Dolgoprudny; Russia.
[am] Also at National Research Nuclear University MEPhI, Moscow; Russia.
[an] Also at Near East University, Nicosia, North Cyprus, Mersin; Turkey.
[ao] Also at Ochadai Academic Production, Ochanomizu University, Tokyo; Japan.
[ap] Also at Physikalisches Institut, Albert-Ludwigs-Universität Freiburg, Freiburg; Germany.
[aq] Also at School of Physics, Sun Yat-sen University, Guangzhou; China.
[ar] Also at The City College of New York, New York NY; United States of America.
[as] Also at The Collaborative Innovation Center of Quantum Matter (CICQM), Beijing; China.
[at] Also at Tomsk State University, Tomsk, and Moscow Institute of Physics and Technology State University, Dolgoprudny; Russia.
[au] Also at TRIUMF, Vancouver BC; Canada.
[av] Also at Universita di Napoli Parthenope, Napoli; Italy.
[*] Deceased.

Eur. Phys. J. C (2019) 79:901
https://doi.org/10.1140/epjc/s10052-019-7399-7

THE EUROPEAN PHYSICAL JOURNAL C

Regular Article - Experimental Physics

Measurement of $W^{\pm}$-boson and Z-boson production cross-sections in pp collisions at $\sqrt{s} = 2.76$ TeV with the ATLAS detector

ATLAS Collaboration[⋆]

CERN, 1211 Geneva 23, Switzerland

Received: 9 July 2019 / Accepted: 16 October 2019 / Published online: 8 November 2019

Abstract The production cross-sections for $W^{\pm}$ and Z bosons are measured using ATLAS data corresponding to an integrated luminosity of 4.0 pb^{-1} collected at a centre-of-mass energy $\sqrt{s} = 2.76$ TeV. The decay channels $W \to \ell\nu$ and $Z \to \ell\ell$ are used, where ℓ can be an electron or a muon. The cross-sections are presented for a fiducial region defined by the detector acceptance and are also extrapolated to the full phase space for the total inclusive production cross-section. The combined (average) total inclusive cross-sections for the electron and muon channels are:

$$\sigma^{\text{tot}}_{W^+\to\ell\nu} = 2312 \pm 26\ \text{(stat.)} \pm 27\ \text{(syst.)} \pm 72\ \text{(lumi.)} \pm 30\ \text{(extr.)}\ \text{pb},$$

$$\sigma^{\text{tot}}_{W^-\to\ell\nu} = 1399 \pm 21\ \text{(stat.)} \pm 17\ \text{(syst.)} \pm 43\ \text{(lumi.)} \pm 21\ \text{(extr.)}\ \text{pb},$$

$$\sigma^{\text{tot}}_{Z\to\ell\ell} = 323.4 \pm 9.8\ \text{(stat.)} \pm 5.0\ \text{(syst.)} \pm 10.0\ \text{(lumi.)} \pm 5.5\text{(extr.)}\ \text{pb}.$$

Measured ratios and asymmetries constructed using these cross-sections are also presented. These observables benefit from full or partial cancellation of many systematic uncertainties that are correlated between the different measurements.

Contents

1 Introduction

The processes that produce W and Z bosons[1] in pp collisions via Drell–Yan annihilation are two of the simplest at hadron colliders to describe theoretically. At lowest order in quantum chromodynamics (QCD), W-boson production proceeds via $q\bar{q}' \to W$ and Z-boson production via $q\bar{q} \to Z$. Therefore, precision measurements of these production cross-sections yield important information about the parton distribution functions (PDFs) for quarks inside the proton. Factorisation theory allows PDFs to be treated separately from the perturbative QCD high-scale collision calculation as functions of the event energy scale, Q, and the momentum fraction of the parton, x, for each parton flavour. Usually PDFs are defined for a particular starting scale Q_0 and can be evolved to other scales via the DGLAP equations [1–7]. Measurements of on-shell W/Z-boson production probe the PDFs in a range of Q^2 that lies close to $m^2_{W/Z}$. The range of x that is probed depends on the centre-of-mass energy, $\sqrt{s}$, of the protons and the rapidity coverage of the detector. Each measurement of these production cross-sections at a new value of $\sqrt{s}$ thus provides information complementary to previous measurements. The combinations of initial partons participating in the production processes of W^+,W^-, and Z bosons are different, so each process provides complementary information about the products of different quark PDFs.

This paper presents the first measurements of the production cross-sections for W^+, W^- and Z bosons in pp collisions at $\sqrt{s} = 2.76$ TeV. The data were collected by the ATLAS detector at the Large Hadron Collider (LHC) [8] in 2013 and correspond to an integrated luminosity of 4.0 pb^{-1}. To provide further sensitivity to PDFs, and to reduce the systematic uncertainty in the predictions, ratios of these cross-sections and the charge asymmetry for W-boson production are also presented. The measurements are performed for leptonic (electron or muon) decays of the W and Z bosons, in

⋆ e-mail: atlas.publications@cern.ch

[1] In this paper it is implicit that Z boson refers to Z/γ^* bosons.

a defined fiducial region, and also extrapolated to the total cross-section.

Previous measurements of the W-boson and Z-boson production cross-sections in pp collisions at the LHC were performed by the ATLAS, CMS and LHCb Collaborations at $\sqrt{s} = 5.02$ TeV [9], 7 TeV [10–14], 8 TeV [15–19] and 13 TeV [20–22], and by the PHENIX and STAR Collaborations at the RHIC at $\sqrt{s} = 500$ GeV [23,24] and 510 GeV [25]. This is the first measurement at 2.76 TeV. Other measurements of these processes were performed in $p\bar{p}$ collisions at $\sqrt{s} = 1.8$ TeV and 1.96 TeV by the CDF [26–30] and D0 [31] Collaborations, and at $\sqrt{s} = 546$ GeV and 630 GeV by the UA1 [32] and UA2 [33] Collaborations.

2 ATLAS detector

The ATLAS detector [34] at the LHC covers nearly the entire solid angle around the collision point. It consists of an inner tracking detector surrounded by a thin superconducting solenoid, electromagnetic (EM) and hadronic calorimeters, and a muon spectrometer (MS) incorporating three large superconducting toroid magnets. The inner-detector system (ID) is immersed in a 2 T axial magnetic field and provides charged-particle tracking in the pseudorapidity range $|\eta| < 2.5$.[2]

The high-granularity silicon pixel detector covers the vertex region and typically provides three measurements per track. It is followed by the silicon microstrip tracker, which usually provides eight measurements from eight strip layers. These silicon detectors are complemented by the transition radiation tracker (TRT), which enables radially extended track reconstruction up to $|\eta| = 2.0$. The TRT also provides electron identification information based on the fraction of hits (typically 30 in total) above a higher energy-deposit threshold associated with the presence of transition radiation.

The calorimeter system covers the pseudorapidity range $|\eta| < 4.9$. Within the region $|\eta| < 3.2$, EM calorimetry is provided by barrel and endcap high-granularity lead/liquid-argon (LAr) sampling calorimeters, with an additional thin LAr presampler covering $|\eta| < 1.8$ that is used to correct for energy loss in material upstream of the calorimeters. Hadronic calorimetry in this region is provided by the steel/scintillator-tile calorimeter, segmented into three barrel structures with $|\eta| < 1.7$, and two copper/LAr hadronic endcap calorimeters. The solid angle coverage is completed with forward copper/LAr and tungsten/LAr calorimeter modules optimised for EM and hadronic measurements, respectively.

The muon spectrometer comprises separate trigger and high-precision tracking chambers measuring the deflection of muons in a magnetic field generated by superconducting air-core toroids. The precision chamber system covers the region $|\eta| < 2.7$ with three layers of monitored drift tubes, complemented by cathode strip chambers in the forward region, where the backgrounds are highest. The muon trigger system covers the range $|\eta| < 2.4$ with resistive plate chambers in the barrel and thin gap chambers in the endcap regions.

The ATLAS detector selected events using a three-level trigger system [35]. The first-level trigger is implemented in hardware and used a subset of detector information to reduce the event rate to a design value of at most 75 kHz. This was followed by two software-based triggers that together reduced the event rate to about 200 Hz.

3 Data and simulation samples

The data used in this measurement were collected in February 2013 during a period when proton beams at the LHC were collided at a centre-of-mass energy of 2.76 TeV. During this running period a typical value of the instantaneous luminosity was 1×10^{32} cm^{-2} s^{-1}, significantly lower than in 7, 8 and 13 TeV data-taking conditions. The typical value of the mean number of collisions per proton bunch crossing (pile-up) $\langle\mu\rangle$ was 0.3. Only data from stable collisions when the ATLAS detector was fully operational are used, yielding a data sample corresponding to an integrated luminosity of 4.0 pb^{-1}.

Samples of Monte Carlo (MC) simulated events are used to estimate the signals from W-boson and Z-boson production, and the backgrounds containing prompt leptons: electroweak-diboson production and top-quark pair ($t\bar{t}$) production. Background contributions arising from multijet events that do not contain prompt leptons are estimated directly from data, with simulated events used to cross-check these estimations in the muon channel.

Production of single W and Z bosons was simulated using POWHEG- BOX v1 r1556 [36–39]. The parton showering was performed using PYTHIA 8.17 [40]. The PDF set used for the simulation was CT10 [41], and the parton shower parameter values were those of the AU2 tune [42]. Additional quantum electrodynamics (QED) emissions from electroweak (EW) vertices and charged leptons were simulated using PHOTOS++ v3.52 [43]. Additional samples of simulated W-boson events generated with SHERPA 2.1 [44] are used to estimate uncertainties arising from the choice of event generator

[2] ATLAS uses a right-handed coordinate system with its origin at the nominal interaction point (IP) in the centre of the detector and the z-axis along the beam pipe. The x-axis points from the IP to the centre of the LHC ring, and the y-axis points upwards. Cylindrical coordinates (r, ϕ) are used in the transverse plane, ϕ being the azimuthal angle around the z-axis. The pseudorapidity is defined in terms of the polar angle θ as $\eta = -\ln\tan(\theta/2)$. Angular distance is measured in units of $\Delta R \equiv \sqrt{(\Delta\eta)^2 + (\Delta\phi)^2}$.

model. In these SHERPA samples, simulation of W-boson production in association with up to two additional partons was performed at next-to-leading order (NLO) in QCD while production of W bosons in association with three or four additional partons was performed at leading order (LO) in QCD. The sample cross-sections were normalised to next-to-next-to-leading-order (NNLO) QCD predictions for the total cross-sections described in Sect. 8.

POWHEG-BOX v1 r2330 was used to generate $t\bar{t}$ samples [45]. These samples had parton showering performed using PYTHIA 6.428 [46] with parameters corresponding to the Perugia2011C tune [47]. The CT10 PDF set was used. Additional QED final-state radiative corrections were applied using PHOTOS++ v3.52 and τ-lepton decays were performed using TAUOLA v25feb06 [48]. Single production of top quarks is a negligible contribution to this analysis, compared with $t\bar{t}$ production, so no such samples were generated.

Production of two massive electroweak bosons (WW, ZZ, WZ) was simulated using HERWIG 6.5 [49], with multiparton interactions modelled using JIMMY 4.13 [50]. The CTEQ6L1 PDF set [51] and AUET2 tune [52] were used for these samples.

Multijet production containing heavy-flavour final states, arising from the production of $b\bar{b}$ or $c\bar{c}$ pairs, were simulated using PYTHIA 8.186. The CTEQ6L1 PDF set and AU2 tune were used. Events were required to contain an electron or muon with transverse momentum $p_{\mathrm{T}} > 10$ GeV and $|\eta| < 2.8$.

The detector response to generated events was simulated by passing the events through a model of the ATLAS detector [53] based on GEANT4 [54]. Additional minimum-bias events generated using PYTHIA 8.17 and the A2 set of tuned parameters, were overlaid in such a way that the distribution of $\langle\mu\rangle$ for simulated events reproduced that in the real data. The resulting events were then passed through the same reconstruction software as the real data.

The simulated samples used for the baseline analysis are summarised in Table 1, which shows the generator used for each process together with the order in QCD at which they were generated.

4 Event selection

This section describes the selection of events consistent with the production of W bosons or Z bosons. The W-boson selection requires events to contain a single charged lepton and large missing transverse momentum. The Z-boson selection requires events to contain two charged leptons with opposite charge and the same flavour.

Events were selected by triggers that required at least one charged electron (muon) with $p_{\mathrm{T}} > 15$ GeV (10 GeV). These thresholds yield an event sample with a uniform efficiency as a function of the E_{T} and p_{T} requirements used subsequently to select the final event sample. The hard-scatter vertex, defined as the vertex with highest sum of squared track transverse momenta (for tracks with $p_{\mathrm{T}} > 400$ MeV), is required to have at least three associated tracks.

Electrons are reconstructed from clusters of energy in the EM calorimeter that are matched to a track reconstructed in the ID. The electron is required to have $p_{\mathrm{T}} > 20$ GeV and $|\eta| < 2.4$ (excluding the transition region between barrel and endcap calorimeters of $1.37 < |\eta| < 1.52$). Each electron must satisfy a set of identification criteria designed to suppress misidentified photons or jets. Electrons are required to satisfy the *medium* selection, following the definition provided in Ref. [55]. This includes requirements on the shower shape in the EM calorimeter, the leakage of the shower into the hadronic calorimeter, the number of hits measured along the track in the ID, and the quality of the cluster-track matching. A Gaussian sum filter [56] algorithm is used to re-fit the tracks and improve the estimated electron track parameters. To suppress background from misidentified objects such as jets, the electron is required to be isolated using calorimeter-based criteria. The sum of the transverse energies of clusters lying within a cone of size $\Delta R = 0.2$ around the centroid of the electron cluster and excluding the core[3] must be less than 10% of the electron p_{T}.

Muon candidates are reconstructed by combining tracks reconstructed in the ID with tracks reconstructed in the MS [57]. They are required to have $p_{\mathrm{T}} > 20$ GeV and $|\eta| < 2.4$. The muon candidates are also required to be isolated, by requiring that the scalar sum of the p_{T} of additional tracks within a cone of size $\Delta R = 0.4$ around the muon is less than 80% of the muon p_{T}.

The missing transverse momentum vector [58] ($\boldsymbol{E}_{\mathrm{T}}^{\mathrm{miss}}$) is calculated as the negative vector sum of the transverse momenta of electrons and muons, and of the transverse momentum of the recoil. The magnitude of this vector is denoted by $E_{\mathrm{T}}^{\mathrm{miss}}$. The recoil vector is obtained by summing the transverse momenta of all clusters of energy measured in the calorimeter, excluding those within $\Delta R = 0.2$ of the lepton candidate. The momentum vector of each cluster is determined by the magnitude and coordinates of the energy deposits; the cluster is assumed to be massless. Cluster energies are initially measured assuming that the energy deposition occurs only through EM interactions, and are then corrected for the different calorimeter responses to hadrons and electromagnetically interacting particles, for losses due to dead material, and for energy that is not captured by the clustering process [59]. The definition of the recoil does not make use of reconstructed jets, to avoid threshold effects. The procedure used to calibrate the recoil closely follows

[3] The core of the shower is the contribution within $\Delta\eta \times \Delta\phi = 0.125 \times 0.175$ around the cluster barycentre.

Table 1 Summary of the baseline simulated samples used

Process	Generator	Generator QCD precision
Signal samples		
$W \to \ell\nu$	POWHEG- BOX +PYTHIA 8	NLO
$Z \to \ell^+\ell^-$	POWHEG- BOX +PYTHIA 8	NLO
Background samples		
$W \to \tau\nu$	POWHEG- BOX +PYTHIA 8	NLO
$Z \to \tau^+\tau^-$	POWHEG- BOX +PYTHIA 8	NLO
$t\bar{t}$	POWHEG- BOX +PYTHIA 6	NLO
WW	HERWIG	LO
ZZ	HERWIG	LO
WZ	HERWIG	LO
$b\bar{b}$	PYTHIA 8	LO
$c\bar{c}$	PYTHIA 8	LO

that used in the recent ATLAS measurement of the W-boson mass [60], first correcting the modelling of the overall recoil in simulation and then applying corrections for residual differences in the recoil response and resolution that are derived from Z-boson data and transferred to the W-boson sample.

The W-boson selection requires events to contain exactly one lepton (electron or muon) candidate and have $E_{\mathrm{T}}^{\mathrm{miss}} > 25$ GeV. The lepton must match a lepton candidate that met the trigger criteria. The transverse mass, m_{T}, of the W-boson candidate in the event is calculated using the lepton candidate and $E_{\mathrm{T}}^{\mathrm{miss}}$ according to $m_{\mathrm{T}} = \sqrt{2p_{\mathrm{T}}^{\ell}E_{\mathrm{T}}^{\mathrm{miss}}(1-\cos(\phi_{\ell}-\phi_{E_{\mathrm{T}}^{\mathrm{miss}}}))}$. The transverse mass in W-boson production events is expected to exhibit a Jacobian peak around the W-boson mass. Thus, requiring that $m_{\mathrm{T}} > 40$ GeV suppresses background processes. After these requirements there are 3914 events in the $W \to e^+\nu$ channel, 2209 events in the $W \to e^-\bar{\nu}$ channel, 4365 events in the $W \to \mu^+\nu$ channel, and 2460 events in the $W \to \mu^-\bar{\nu}$ channel.

The Z-boson selection requires events to contain exactly two lepton candidates with the same flavour and opposite charge. At least one lepton must match a lepton candidate that met the trigger criteria. Background processes are suppressed by requiring that the invariant mass of the lepton pair satisfies $66 < m_{\ell\ell} < 116$ GeV. After these requirements there are 430 events in the $Z \to e^+e^-$ channel, and 646 events in the $Z \to \mu^+\mu^-$ channel.

5 Background estimation

The background processes that contribute to the sample of events passing the W-boson and Z-boson selections can be separated into two categories: those estimated from MC simulation and theoretical calculations, and those estimated directly from data. The main backgrounds that contribute to the event sample passing the W-boson selection are processes with a τ-lepton decaying into an electron or muon plus neutrinos, leptonic Z-boson decays where only one lepton is reconstructed, and multijet processes. The main background contribution to the event sample passing the Z-boson selection is production of two massive electroweak bosons.

The backgrounds arising from $W \to \tau\nu$, $Z \to \ell^+\ell^-$, diboson production, and $t\bar{t}$ production are estimated from the simulated samples described in Sect. 3. Predictions of the backgrounds to the W-boson and Z-boson production measurements arising from multijet production suffer from large theoretical uncertainties, and therefore the contribution to this background in the W-boson measurement is estimated from data. This is achieved by constructing a shape template for the background using a discriminating variable in a control region and then performing a template fit to the same distribution in the signal region to extract the background contribution. The choice of template variable is motivated by the difference between signal and background and by the available number of events. Previous ATLAS measurements at 7 TeV [10] and 13 TeV [21] found that multijet production makes a background contribution of less than 0.1% for Z-boson measurements; this is therefore neglected.

Electron candidates in multijet background events are typically misidentified candidates produced when jets mimic the signature of an electron, for example when a neutral pion and a charged pion overlap in the detector. Additional candidates can arise from 'non-prompt' electrons produced when a photon converts, and in decays of heavy-flavour hadrons. To construct a control region for the multijet template, a selection is used that differs from the W-boson selection described in Sect. 4 in only two respects: the medium electron identification criteria are inverted (while keeping the looser identification criteria) and the $E_{\mathrm{T}}^{\mathrm{miss}}$ requirement is removed. By construction, this control region is statistically independent of the W-boson signal region. A template for the shape of the

multijet background in the $E_{\mathrm{T}}^{\mathrm{miss}}$ distribution is then obtained from that distribution in the control region after subtraction of expected contributions from the signal and other backgrounds determined using MC samples. The normalisation of the multijet background template in the signal region is extracted by performing a χ^2 fit of the $E_{\mathrm{T}}^{\mathrm{miss}}$ distribution (applying all signal criteria except the requirement on $E_{\mathrm{T}}^{\mathrm{miss}}$) to a sum of the templates for the multijet background, the signal, and all other backgrounds. The normalisation of the signal is allowed to vary freely in the fit as is the multijet background; however, the other backgrounds are only allowed to vary from their expected values by up to 5%, corresponding to the largest level of variation in predicted electroweak-boson production cross-sections obtained from varying the choice of PDF. The normalisation from this fit can then be used together with the inverted selection to construct multijet background distributions in any other variable that is not correlated with the electron identification criteria.

Muon candidates in multijet background events are typically 'non-prompt' muons produced in the decays of hadrons. The multijet background contribution to the $W \to \mu\nu$ selection is estimated by using the same method as described for the $W \to e\nu$ selection. In this case the control region is defined by inverting the isolation requirement and removing the requirement on m_{T}. The distribution used for the fits is m_{T}.

The overall number of multijet background events is estimated from a fit to the total W-boson sample. Comparisons between the fitted distributions and data for $W \to e\nu$ and $W \to \mu\nu$ are shown in Fig. 1. Fits to the separate W^+-boson and W^--boson samples are used in the evaluation of the systematic uncertainties, as described in Sect. 7. The final estimated multijet contributions are 30 ± 11 events for $W \to e^+\nu$ and $W \to e^-\nu$ and 2.5 ± 1.9 events for $W^+ \to \mu^+\nu$ and $W^- \to \mu^-\nu$. The relative contribution of the multijet events (1%) is lower than in 13 TeV (4%) and 7 TeV (3%) data. This is in agreement with expectations for this lower pile-up running, where the resolution in $E_{\mathrm{T}}^{\mathrm{miss}}$ is improved compared to the higher pile-up running.

6 Correction for detector effects

The measurements in this paper are performed within specific fiducial regions and extrapolated to the total W-boson or Z-boson phase space. The fiducial regions are defined by the kinematic and geometric selection criteria given in Table 2; in simulations these are applied at the generator level before the emission of QED final-state radiation from the decay lepton(s) (QED Born level).

The fiducial W-boson/Z-boson production cross-section is obtained from the number of observed events meeting the selection criteria after background contributions are subtracted, $N_{W,Z}^{\mathrm{sig}}$, using the following formula:

$$\sigma^{\mathrm{fid}}_{W,Z\to\ell\nu,\ell\ell} = \frac{N^{\mathrm{sig}}_{W,Z}}{C_{W,Z}\cdot\mathcal{L}_{\mathrm{int}}},$$

where $\mathcal{L}_{\mathrm{int}}$ is the total integrated luminosity of the data samples used for the analysis. The factor $C_{W,Z}$ is the ratio of the number of generated events that satisfy the final selection criteria after event reconstruction to the number of generated events within the fiducial region. It includes the efficiency for triggering, reconstruction and identification of $W, Z \to \ell\nu, \ell^+\ell^-$ events falling within the acceptance. The different components of the efficiency are calculated using a mixture of MC simulation and measurements from data.

The total W-boson and Z-boson production cross-sections are obtained using the following formula:

$$\begin{aligned}\sigma^{\mathrm{tot}}_{W,Z\to\ell\nu,\ell\ell} &\equiv \sigma^{\mathrm{tot}} \times B(W, Z \to \ell\nu, \ell\ell)\\ &= \frac{N^{\mathrm{sig}}_{W,Z}}{A_{W,Z}\cdot C_{W,Z}\cdot\mathcal{L}_{\mathrm{int}}}.\end{aligned}$$

The factor $B(W, Z \to \ell\nu, \ell\ell)$ is the per-lepton branching fraction of the vector boson. The factor $A_{W,Z}$ is the acceptance for W/Z-boson events being studied. It is defined as the fraction of generated events that satisfy the fiducial requirements. This acceptance is determined using MC signal samples, corrected to the generator QED Born level, and is used to extrapolate the measured cross-section in the fiducial region to the full phase space. The central values of $A_{W,Z}$ are around 0.6 for these measurements, compared with 0.5 at $\sqrt{s} = 7$ TeV and 0.4 at $\sqrt{s} = 13$ TeV, so the fiducial region is closer to the full phase space in this measurement than for those at higher centre-of-mass energies. This is due to a combination of higher p_{T} thresholds for leptons in other measurements, and more-central production of vector bosons at lower $\sqrt{s}$. The values of C_W are approximately 0.67 for the $W \to e\nu$ channels and 0.75 for the $W \to \mu\nu$ channels. The values of C_Z are 0.55 for the $Z \to e^+e^-$ channel and 0.79 for $Z \to \mu^+\mu^-$. The $C_{W,Z}$ values are a little higher than for previous measurements at $\sqrt{s} = 7$ TeV and $\sqrt{s} = 13$ TeV.

7 Systematic uncertainties

The systematic uncertainty in the electron reconstruction and identification efficiency is estimated using the tag-and-probe method in 8 TeV data [55,61] and extrapolated to the 2.76 TeV dataset. The extrapolation procedure results in absolute increases of ±2%, due to uncertainties in the effect of the differing pile-up conditions in 2.76 TeV data relative to the 8 TeV data, as well as a different setting of the noise filtering in the LAr calorimeter of the 2.76 TeV data relative to the 8 TeV data. These uncertainties were estimated using a comparison between 7 TeV and 8 TeV data and MC samples,

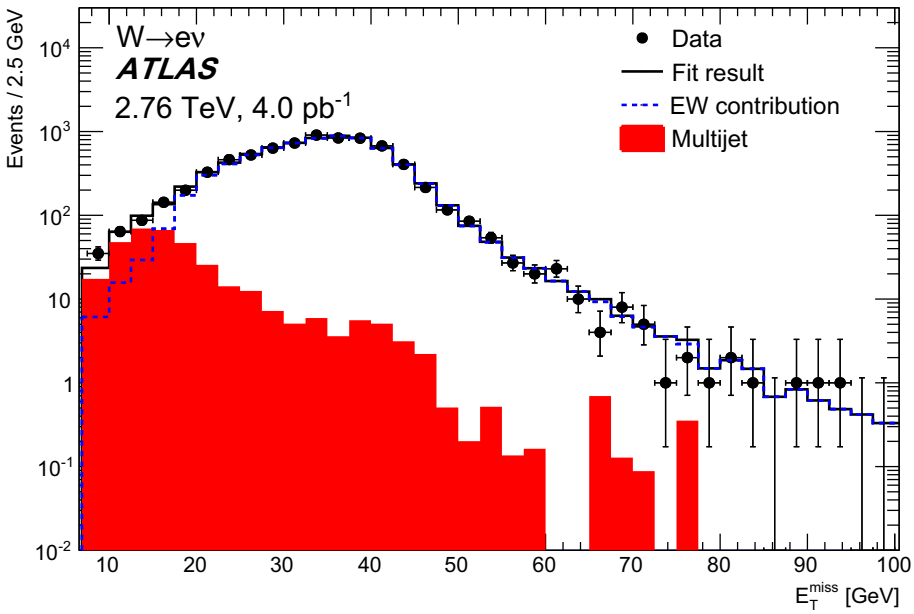

(a)

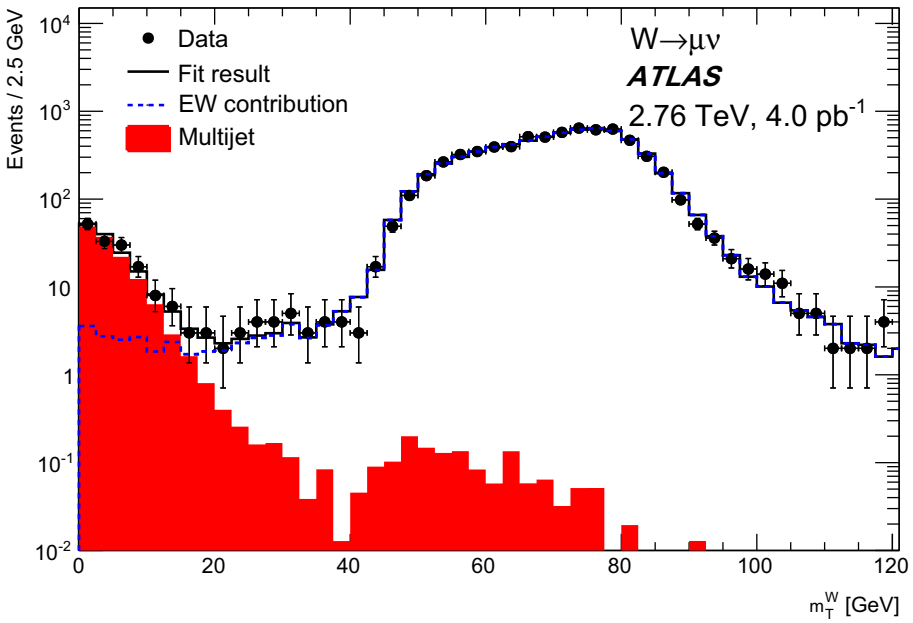

(b)

Fig. 1 Distributions used to estimate the multijet background contribution in (a) the $W \to e\nu$ channel, and (b) the $W \to \mu\nu$ channel. The data is compared to the fit result

after having established that the central values of the efficiencies are the same for different centre-of-mass energies when the same LAr filter settings are used. A similar methodology had been used for internal estimates of the electron efficiency performance at 13 TeV before the start of Run-2 data taking and was found to give a good prediction of the efficiencies in data as well as a conservative estimate of the uncertainties. Transverse-momentum-dependent isolation corrections, calculated with the tag-and-probe method in 2.76 TeV data, are very close to 1, so the systematic uncertainty in the electron isolation requirement is set to the size of the correction itself, that is $\pm 1\%$ for low p_{T} and $\pm 0.3\%$ for higher p_{T}. The electron energy scale has associated statistical uncertainties and systematic uncertainties arising from a possible bias in the calibration method, the choice of generator, the presampler energy scale, and imperfect knowledge of the material in front of the EM calorimeter [62]. The total energy-scale uncertainty is calculated as the sum in quadrature of these components.

Systematic uncertainties associated with the muon momentum can be divided into three major independent categories: momentum resolution of the MS track, momentum resolution

Table 2 Summary of the selection criteria that define the measured fiducial regions

W-boson fiducial region	Z-boson fiducial region
$p_{\mathrm{T}}^{\ell} > 20$ GeV	$p_{\mathrm{T}}^{\ell^+,-} > 20$ GeV
$\lvert\eta^{\ell}\rvert < 2.4$	$\lvert\eta^{\ell^+,-}\rvert < 2.4$
$E_{\mathrm{T}}^{\mathrm{miss}} > 25$ GeV	$66 < m_{\ell^+\ell^-} < 116$ GeV
$m_{\mathrm{T}} > 40$ GeV	

of the ID track, and an overall scale uncertainty [57]. The total momentum scale/resolution uncertainty is the sum in quadrature of these components. An η-independent uncertainty of approximately $\pm 1.1\%$ in the muon trigger efficiency, determined using the tag-and-probe method [57] in 2.76 TeV data, is taken into account. Furthermore, a p_{T}- and η- dependent uncertainty in the identification and reconstruction efficiencies of approximately $\pm 0.3\,\%$, derived using the tag-and-probe method on 8 TeV data is applied. The uncertainty in the p_{T}-dependent isolation correction in the muon channel, calculated with the tag-and-probe method in 2.76 TeV data, is about $\pm 0.6\%$ for low p_{T} and $\pm 0.5\%$ for higher p_{T}.

The luminosity uncertainty for the 2.76 TeV data is $\pm 3.1\%$. This is determined, following the same methodology as was used for the 7 TeV data recorded in 2011 [63], from a calibration of the luminosity scale derived from beam-separation scans performed during the 2.76 TeV operation of the LHC in 2013.

Systematic uncertainties in the $E_{\mathrm{T}}^{\mathrm{miss}}$ arising from the smearing and bias corrections applied to obtain satisfactory modelling of the recoil [58] affect the C_W factors in the $W \to \ell\nu$ measurement, and are taken into account.

Uncertainties arising from the choice of PDF set are evaluated using the error sets of the initial CT10 PDF set (at 90% confidence level (CL)) and from comparison with the results obtained using the central PDF sets from ABKM09 [64], NNPDF23 [65], and ATLAS-epWZ12 [66]. The effect of this uncertainty on A_{W^+} (A_{W^-}) is estimated to be $\pm 1.0\%$ (1.2%), and the effect on A_Z is estimated to be $\pm 1.4\%$. The effect on $C_{W,Z}$ is between $\pm 0.05\%$ and $\pm 0.4\%$ depending on the channel.

A summary of the systematic uncertainties in the $C_{W,Z}$ factors is shown in Table 3. The muon trigger, and electron reconstruction and identification uncertainties are dominant.

Uncertainties arising from the choice of event generator and parton shower models are estimated by comparing results obtained when using SHERPA 2.1 signal samples instead of the (nominal) POWHEG- BOX +PYTHIA 8. The effect of this uncertainty on $A_{W,Z}$ is estimated to be $\pm 0.9\%$.

The systematic uncertainty in the multijet background estimation can be divided into several components: the normalisation uncertainty from the χ^2 fit, the uncertainty in the modelling of electroweak processes by simulated samples in the fitted region, uncertainty from fit bias due to binning choice, and uncertainty from template shape. The scale normalisation uncertainty from the χ^2 fit is approximately $\pm 13\%$ for the $W \to e\nu$ channel. This uncertainty is neglected in the $W \to \mu\nu$ channel where the template bias is dominant. The mismodelling uncertainty is estimated by comparison of the fit results for ℓ^+ and ℓ^-, and for the combined $\ell^{\pm}$ candidates. The central value used is $0.5N^{\pm}$ with the uncertainties $N^+ - 0.5N^{\pm}$ and $N^- - 0.5N^{\pm}$, where N^+ is the fitted number of ℓ^+ background events, N^- is the fitted number of ℓ^- and $N^{\pm}$ is the fitted total number of $\ell^{\pm}$ background events. In the $W \to e\nu$ channel this leads to an uncertainty of $\pm 28\%$ in the multijet background. In the $W \to \mu\nu$ channel the multijet template normalisation is derived from the fit in the small-m_{T} region, where electroweak contributions are negligible and there are many data events, and this source of systematic error is found to be negligible. The fit-bias uncertainty arising from the choice of bin width is estimated by repeating the fit with different binnings. This component is negligible in the $W \to \mu\nu$ case and $\pm 15\%$ in the $W \to e\nu$ case. The uncertainty due to a potential bias from template choice is estimated by employing different template selections. For the $W \to e\nu$ channel, different inverted-isolation criteria were investigated. The overall differences are considered negligible. For the $W \to \mu\nu$ channel, template vari-

Table 3 Relative systematic uncertainties (%) in the correction factors $C_{W,Z}$ in different channels

$\delta C/C$ (%)	$W^+ \to e^+\nu$	$W^- \to e^-\nu$	$Z \to e^+e^-$	$W^+ \to \mu^+\nu$	$W^- \to \mu^-\nu$	$Z \to \mu^+\mu^-$
Lepton trigger	0.14	0.13	< 0.01	1.07	1.07	0.03
Lepton reconstr. and ident.	2.31	2.33	4.55	0.30	0.32	0.62
Lepton isolation	0.71	0.71	1.41	0.51	0.51	1.01
Lepton scale and resolution	0.44	0.43	0.34	0.05	0.05	0.04
Recoil scale and resolution	0.25	0.20	–	0.22	0.22	–
PDF	0.22	0.29	0.11	0.11	0.20	0.06
MC statistical uncertainty	0.24	0.31	0.30	0.24	0.34	0.43
Total	2.5	2.5	4.8	1.3	1.3	1.3

Table 4 The correlation model for the grouped systematic uncertainties for the measurements of W-boson and Z-boson production. The entries in different rows are uncorrelated with each other. Entries in a row with the same letter are fully correlated. Entries in a row with a starred letter are mostly correlated with the entries with the same letter (most of the individual sources of uncertainties within a group are taken as correlated). Entries with different letters in a row are either fully or mostly uncorrelated with each other

Source	Muon channel			Electron channel		
	Z	W^+	W^-	Z	W^+	W^-
Muon trigger	A	A	A	–	–	–
Muon reconstruction/ID	A	A	A	–	–	–
Muon energy scale/resolution	A	A	A	–	–	–
Muon isolation	A	A	A	–	–	–
Electron trigger	–	–	–	A*	A*	A*
Electron reconstruction/ID	–	–	–	A	A	A
Electron energy scale/resolution	–	–	–	A	A	A
Electron isolation	–	–	–	A	A	A
Recoil related	–	A	A	–	A	A
EW background	A	B	B	A	B	B
Top-quark background	A	A	A	A	A	A
Multijet background	–	A	A	–	A	A
PDF	A	A	A	A	A	A

Table 5 The numbers of observed candidate events with the estimated numbers of selected electroweak (EW) plus top, and multijet background events, together with their total uncertainty. In addition, the number of background-subtracted signal events is shown with the first uncertainty given being statistical and the second uncertainty being the total systematic uncertainty, obtained by summing in quadrature the EW+top and multijet uncertainties. Uncertainties shown as ±0.0 have a magnitude less than 0.05.

Measurement Channel	Observed candidates	Background (EW + top)	Background (multijet)	Background-subtracted data N_W^{sig}
$W^+ \to e^+\nu$	3914	108 ± 6	30 ± 11	$3776 \pm 63 \pm 12$
$W^- \to e^-\bar{\nu}$	2209	74.2 ± 3.3	30 ± 11	$2105 \pm 47 \pm 12$
$W^+ \to \mu^+\nu$	4365	152 ± 7	2.5 ± 1.9	$4210 \pm 66 \pm 7$
$W^- \to \mu^-\bar{\nu}$	2460	108 ± 4	2.5 ± 1.9	$2350 \pm 50 \pm 5$
$Z \to e^+e^-$	430	1.3 ± 0.0	–	$428.7 \pm 20.7 \pm 0.0$
$Z \to \mu^+\mu^-$	646	1.6 ± 0.1	–	$644.4 \pm 25.4 \pm 0.1$

ations were estimated from fits that use $b\bar{b} + c\bar{c}$ MC samples as the multijet templates, leading to an uncertainty of ±75%; this is the largest uncertainty in the multijet background in the $W \to \mu\nu$ channel.

Combining results and building ratios or asymmetries of results require a model for the correlations of particular systematic uncertainties between different measurements. Correlations arise mostly due to the fact that electrons, muons, and the recoil are reconstructed identically in the different measurements. Further correlations occur due to similarities in the analysis methodology such as the methods of signal and background estimation.

The systematic uncertainties from the electroweak background estimations are treated as uncorrelated between the W-boson and Z-boson measurements, and fully correlated among different flavour decay channels of the W and Z boson. The top-quark background is treated as fully correlated across all W-boson and Z-boson decay channels. The multijet background and recoil-related systematic uncertainties are also treated as fully correlated between all four W-boson decay channels despite there being an expected uncorrelated component, since the statistical uncertainty is dominant in this case.

The systematic uncertainties due to the choice of PDF are treated as fully correlated between all W-boson and Z-boson channels. The uncertainties in electron and muon selection, reconstruction and efficiency are treated as fully correlated between all W-boson and Z-boson channels.

A simplified form of the correlation model with the grouped list of the sources of systematic errors is presented in Table 4.

8 Results

The numbers of events passing the event selections described in Sect. 4 are presented in Table 5, together with the estimated background contributions described in Sect. 5. The distribution of m_{T} for $W \to \ell\nu$ candidate events is shown in Fig. 2, compared with the expected distribution for signal plus back-

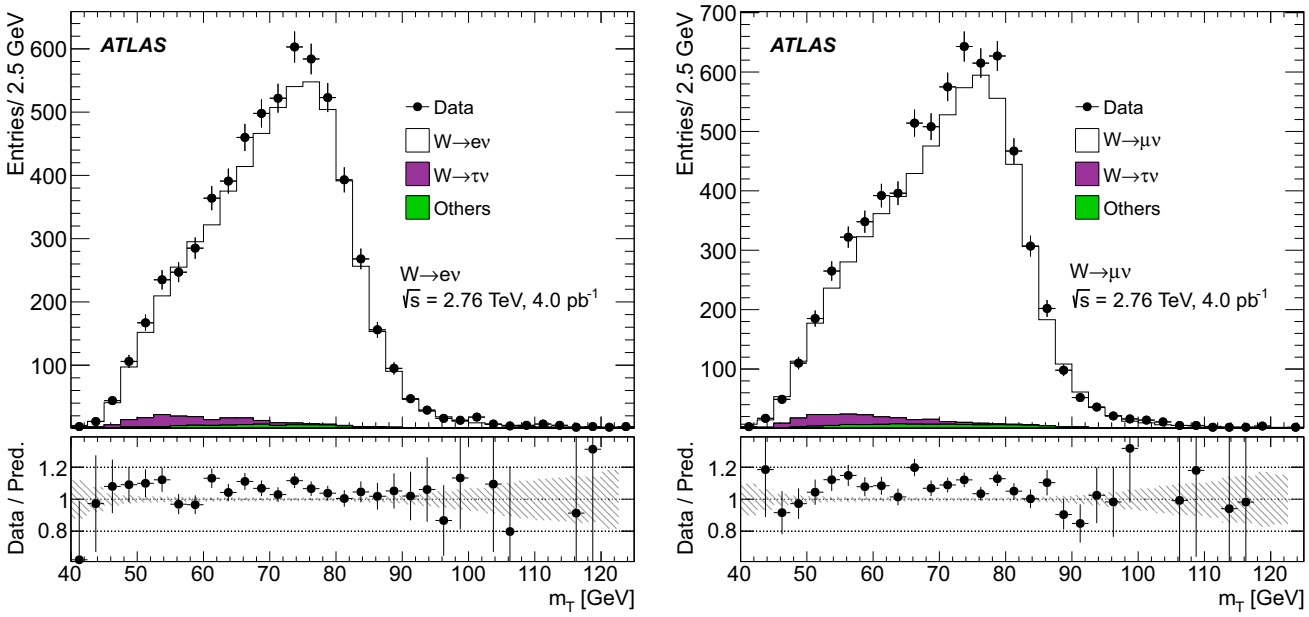

Fig. 2 The distribution of m_{T} for $W \to \ell\nu$ candidate events. The expected signal, normalised to the NNLO theoretical predictions, is shown as an unfilled histogram on top of the stacked background predictions. Backgrounds that do not originate from W production are grouped together into the 'Others' histogram. Systematic uncertainties for the signal and background distributions are combined in the shaded band. Systematic uncertainties from the measurement of the integrated luminosity are not included. The lower panel shows the ratio of the data to the prediction

grounds, where the signal is normalised to the NNLO QCD prediction. Similarly, Fig. 3 shows the distribution of $m_{\ell\ell}$ for $Z \to \ell^+\ell^-$ candidate events compared with the expectations for signal. In this case, the background contributions are not shown, because they would not be visible in the figure if included.

The measured fiducial (σ^{fid}) and total (σ^{tot}) cross-sections in the electron and muon channels are presented separately in Table 6. For these measurements, the dominant contribution to the systematic uncertainty arises from the luminosity determination.

The results obtained from the electron and muon final states are consistent. The fiducial measurements from electron and muon final states are combined following the procedure described in Ref. [67] and the result is extrapolated to the full phase space to obtain the total cross-section. The total W-boson cross-section is calculated by summing the separate W^+ and W^- cross-sections. The results are shown in Table 7.

Theoretical predictions of the fiducial and total cross-sections are computed for comparison with the measured cross-sections using DYNNLO 1.5 [68] which provides calculations at NNLO in the strong-coupling constant, $\mathcal{O}(\alpha_{\mathrm{s}}^2)$, including the boson decays into leptons ($\ell^+\nu$, $\ell^-\bar{\nu}$ or $\ell^+\ell^-$) with full spin correlations, finite width and interference effects. These calculations allow kinematic requirements to be implemented for direct comparison with experimental data. The procedure used follows that used for the previous ATLAS measurement at $\sqrt{s} = 7$ TeV [10].

Corrections for NLO EW effects are calculated with FEWZ 3.1 [69–72], for the Z bosons and with SANC [73,74] for the W bosons. The calculation was done in the G_μ EW scheme [75]. The following input parameters are taken from the Particle Data Group's Review of Particle Properties 2014 edition [76]: the Fermi constant, the masses and widths of W and Z bosons as well as the elements of the CKM matrix. The cross-sections for vector bosons decaying into these leptonic final states are calculated such that they match the definition of the measured cross-sections in the data. Thus, from complete NLO EW corrections, the following components are included: virtual QED and weak corrections, real initial-state radiation (ISR), and interference between ISR and real final-state radiation (FSR) [77]. The calculated effect of these corrections on the cross-sections is $(-0.26\pm0.02)\%$ for $\sigma^{\mathrm{fid}}_{W^+}$, $(-0.21 \pm 0.03)\%$ for $\sigma^{\mathrm{fid}}_{W^-}$, and $(-0.25 \pm 0.12)\%$ for $\sigma^{\mathrm{fid}}_{Z}$. DYNNLO is used for the central values of the predictions while FEWZ is used for the PDF variations and all other systematic variations such as QCD scale and α_{s}. The predictions are calculated using the CT14nnlo [78], NNPDF3.1 [79], MMHT14nnlo68cl [80], ABMP16 [81], HERAPDF2.0 [82],

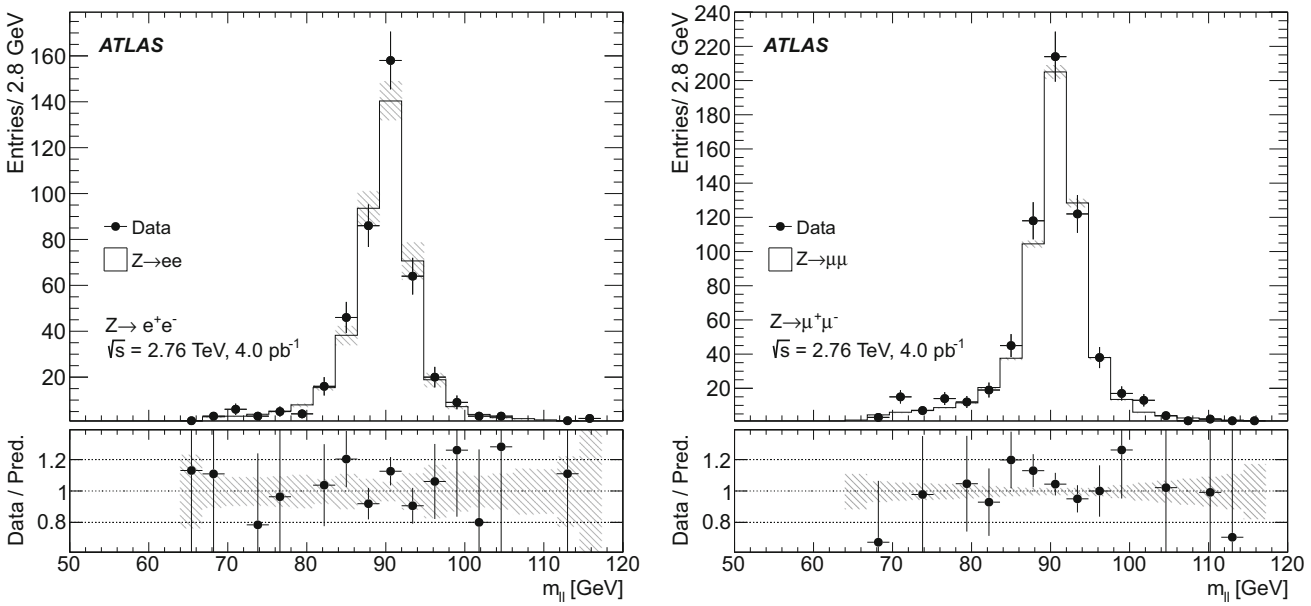

Fig. 3 The distribution of $m_{\ell\ell}$ for $Z \to \ell^+\ell^-$ candidate events. The expected signal, normalised to the NNLO theoretical predictions, is shown as an unfilled histogram. Systematic uncertainties for the signal and background distributions are combined in the shaded band. Systematic uncertainties from the measurement of the integrated luminosity are not included. The background distributions are neglected here, but would not be visible if included. The lower panel shows the ratio of the data to the prediction

Table 6 Results of the fiducial and total cross-sections measurements of the W^+-boson, W^--boson, and Z-boson production cross-sections in the electron and muon channels. The cross-sections are shown with their statistical, systematic and luminosity uncertainties (and extrapolation uncertainty for total cross-section)

	Value ± stat. ± syst. ± lumi. (± extr.)	Value ± stat. ± syst. ± lumi. (± extr.)
	$W^+ \to e\nu$	$W^+ \to \mu\nu$
$\sigma^{\text{fid}}_{W^+}$ [pb]	$1416 \pm 24 \pm 36 \pm 44$	$1438 \pm 23 \pm 19 \pm 45$
$\sigma^{\text{tot}}_{W^+}$ [pb]	$2284 \pm 38 \pm 58 \pm 71$ (±30)	$2319 \pm 36 \pm 30 \pm 72$ (±30)
	$W^- \to e\nu$	$W^- \to \mu\nu$
$\sigma^{\text{fid}}_{W^-}$ [pb]	$789 \pm 18 \pm 20 \pm 25$	$799 \pm 17 \pm 11 \pm 25$
$\sigma^{\text{tot}}_{W^-}$ [pb]	$1385 \pm 31 \pm 36 \pm 43$ (±21)	$1402 \pm 30 \pm 19 \pm 44$ (±21)
	$Z \to ee$	$Z \to \mu\mu$
σ^{fid}_{Z} [pb]	$197.6 \pm 9.6 \pm 9.5 \pm 6.1$	$205.6 \pm 8.1 \pm 2.6 \pm 6.4$
σ^{tot}_{Z} [pb]	$313.6 \pm 15.2 \pm 15.0 \pm 9.7$ (±5.3)	$326.3 \pm 12.9 \pm 4.1 \pm 10.1$ (±5.5)

Table 7 Combined fiducial and total cross-section measurements for W^+-boson, W^--boson and Z-boson production. The cross-sections are shown with their statistical, systematic and luminosity uncertainties (and extrapolation uncertainty for total cross-section)

	Value ± stat. ± syst. ± lumi. (± extr.)	Value ± stat. ± syst. ± lumi. (± extr.)
	$W^+ \to \ell\nu$	$W^- \to \ell\nu$
σ^{fid}_{W} [pb]	$1433 \pm 16 \pm 17 \pm 44$	$798 \pm 12 \pm 10 \pm 25$
σ^{tot}_{W} [pb]	$2312 \pm 26 \pm 27 \pm 72$(±30)	$1399 \pm 21 \pm 17 \pm 43$(±21)
	$W \to \ell\nu$	
σ^{fid}_{W} [pb]	$2231 \pm 20 \pm 26 \pm 69$	
σ^{tot}_{W} [pb]	$3711 \pm 34 \pm 43 \pm 115$(±51)	
	$Z \to \ell\ell$	
σ^{fid}_{Z} [pb]	$203.7 \pm 6.2 \pm 3.2 \pm 6.3$	
σ^{tot}_{Z} [pb]	$323.4 \pm 9.8 \pm 5.0 \pm 10.0$(±5.5)	

Table 8 The predictions, using the CT14nnlo PDF set, for the cross-sections measured. The calculations are performed using DYNNLO 1.5 and FEWZ 3.1 as described in the text. The errors represent the PDF and scale uncertainties

Quantity	Predicted cross-section (pb)
$\sigma^{\text{fid}}_{W^+}$	$1379\ ^{+39}_{-40}\ ^{+6}_{-6}$
$\sigma^{\text{fid}}_{W^-}$	$757.3\ ^{+20.5}_{-24.5}\ ^{+3.1}_{-3.1}$
σ^{fid}_{Z}	$196.0\ ^{+5.0}_{-5.8}\ ^{+1.1}_{-1.3}$
$\sigma^{\text{tot}}_{W^+}$	$2115\ ^{+57}_{-60}\ ^{+9}_{-11}$
$\sigma^{\text{tot}}_{W^-}$	$1266\ ^{+32}_{-38}\ ^{+5}_{-6}$
σ^{tot}_{Z}	$304.1^{+7.3}_{-8.2}\ ^{+1.1}_{-1.4}$

and ATLAS-epWZ12nnlo PDF sets. The dynamic scale, $m_{\ell\ell}$, and fixed scale, m_W, are used as the nominal renormalisation, μ_R, and factorisation, μ_F, scales for Z and W predictions, respectively.

Theoretical uncertainties in the predictions are also derived from the following sources:

PDF: these uncertainties are evaluated from the variations of the NNLO PDFs according to the recommended procedure for each PDF set. A table with all PDF uncertainties and their central values is shown in Appendix A; the PDF uncertainty from CT14nnlo was rescaled from 90% CL to 68% CL.

Scales: the scale uncertainties are defined by the envelope of the variations in which the scales are changed by factors of two subject to the constraint $0.5 \leq \mu_R/\mu_F \leq 2$.

α_s: the uncertainty due to α_s was estimated by varying the value of α_s used in the CT14nnlo PDF set by ± 0.001, corresponding to a 68% CL variation.

The statistical uncertainties in these theoretical predictions are negligible.

The numerical values of the predictions for the CT14nnlo PDF set are presented in Table 8. The predictions for the acceptance factor $A_{W,Z}$ can differ by a few percent from those derived from simulated signal samples, this may be due to a poorer description of production of low p_T W-bosons by the fixed-order calculations. The predictions are shown in comparison with the combined W-boson and Z-boson production measurements, and with results from pp and $p\bar{p}$ collisions at other centre-of-mass energies in Fig. 4. A comparison of the measurements with predictions from various different PDF sets is presented in Figs. 5 and 6. Overall there is good agreement.

Taking ratios of measurements leads to results that have significantly reduced systematic uncertainties due to full or partial cancellation of correlated systematic uncertainties, as discussed in Sect. 7. The ratios of the fiducial cross-sections

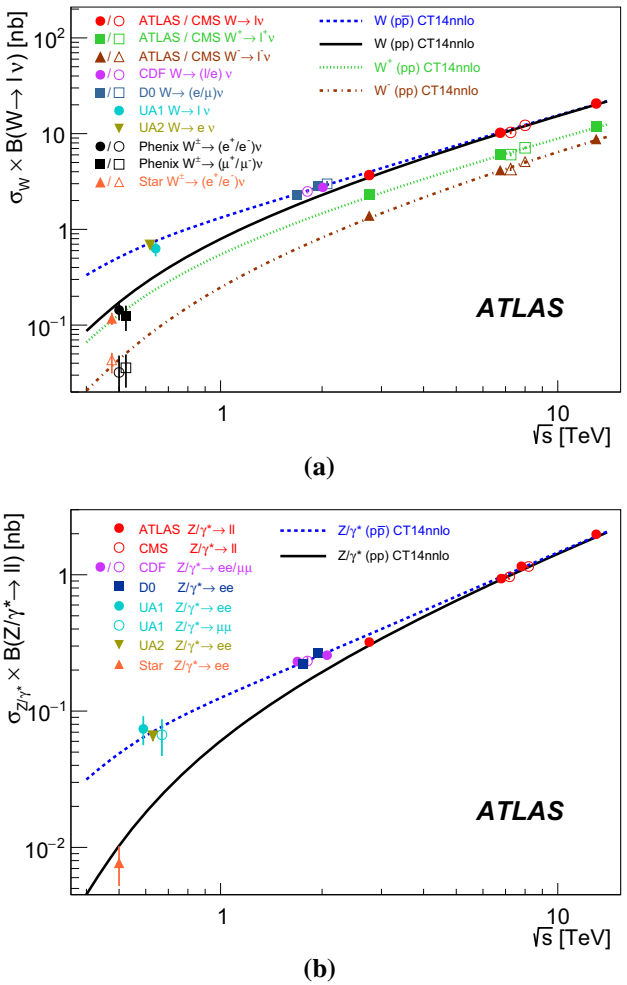

Fig. 4 The measured values of (a) $\sigma_W \times B(W \to \ell\nu)$ for W^+ bosons, W^- bosons and their sum and (b) $\sigma_{Z/\gamma^*} \times B(Z/\gamma^* \to \ell\ell)$ for proton–proton and proton–antiproton collisions as a function of $\sqrt{s}$. Data points at the same $\sqrt{s}$ are staggered to improve readability. All data points are shown together with their total uncertainty. The theoretical calculations are performed at NNLO in QCD using DYNNLO 1.5 and FEWZ 3.1 as described in the text. The theoretical uncertainties are not shown

for W-boson and Z-boson production are presented, together with the ratio for W^+-boson and W^--boson production, in Fig. 7. It can be seen that the predictions from the different PDF sets are mostly in good agreement with the measurements. There is a slight (less than two standard deviations) tension between the data and the prediction using the ABMP16 PDF set. The measured values of the ratios are:

$$R_{W/Z} = 10.95 \pm 0.35\,(\text{stat.}) \pm 0.10\,(\text{syst.});$$
$$R_{W^+/W^-} = 1.797 \pm 0.034\,(\text{stat.}) \pm 0.009\,(\text{syst.}).$$

The measurement of the ratio R_{W^+/W^-} is sensitive to the u_v and d_v valence quark distributions, while the ratio $R_{W/Z}$ can place constraints on the strange quark distributions. A common alternative way of presenting this information is in terms of the charge asymmetry, A_ℓ, in W-boson production:

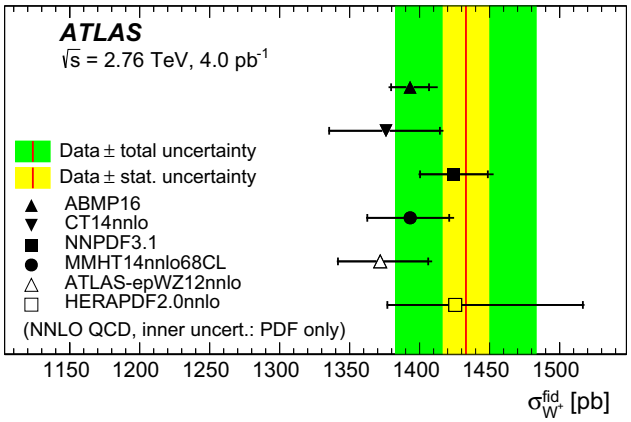

(a)

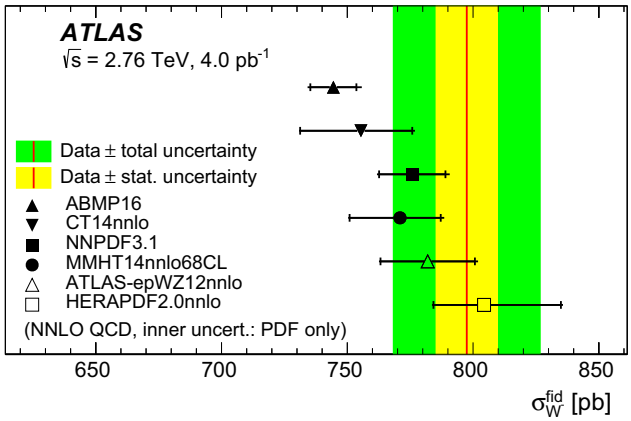

(b)

Fig. 5 NNLO predictions for the fiducial cross-section (a) $\sigma^{\text{fid}}_{W^+}$ and (b) $\sigma^{\text{fid}}_{W^-}$ for the six PDFs CT14nnlo, MMHT2014, NNPDF3.1, ATLASepWZ12, ABMP16 and, HERApdf2.0 compared with the measured fiducial cross-section as given in Table 7. The inner shaded band represents the statistical uncertainty only, the outer band corresponds to the experimental uncertainty (including the luminosity uncertainty). The theory predictions are given with the corresponding PDF (total) uncertainty shown by inner (outer) error bar

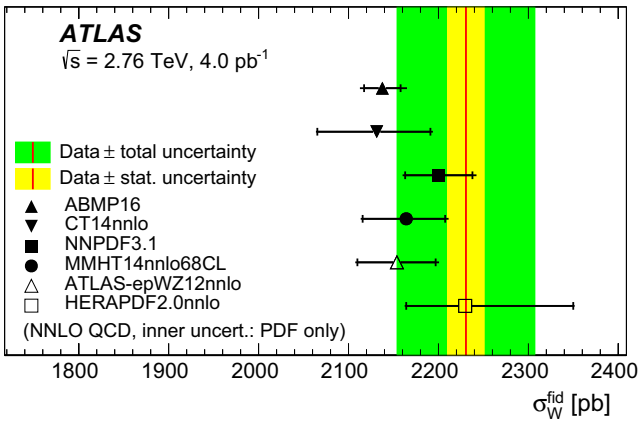

(a)

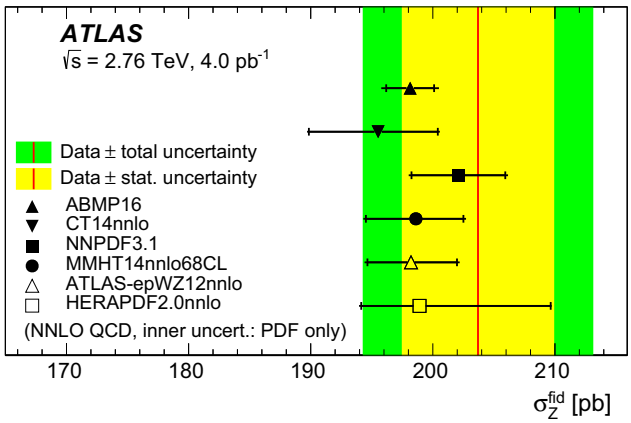

(b)

Fig. 6 NNLO predictions for the fiducial cross-sections (a) σ^{fid}_{W} and (b) σ^{fid}_{Z} for the six PDFs CT14nnlo, MMHT2014, NNPDF3.1, ATLASepWZ12, ABMP16 and HERApdf2.0 compared with the measured fiducial cross-section as given in Table 7. The inner shaded band represents the statistical uncertainty only, the outer band corresponds to the experimental uncertainty (including the luminosity uncertainty). The theory predictions are given with the corresponding PDF (total) uncertainty shown by inner (outer) error bar

$$A_\ell = \frac{\sigma^{\text{fid}}_{W^+} - \sigma^{\text{fid}}_{W^-}}{\sigma^{\text{fid}}_{W^+} + \sigma^{\text{fid}}_{W^-}}.$$

This observable also benefits from the cancellation of systematic uncertainties in the same way as the cross-section ratios. The measured value is:

$$A_\ell = 0.285 \pm 0.009(\text{stat.}) \pm 0.002(\text{syst.}).$$

The ratio of measured cross-sections in the electron and muon decay channels provides a test of lepton universality in W-boson decays. The measured ratios are:

$$R_{W^+} = \frac{\sigma^{\text{fid}}_{W^+\to e^+\nu}}{\sigma^{\text{fid}}_{W^+\to \mu^+\nu}} = 0.985 \pm 0.023\ (\text{stat.}) \pm 0.028\ (\text{syst.})$$

$$R_{W^-} = \frac{\sigma^{\text{fid}}_{W^-\to e^-\bar{\nu}}}{\sigma^{\text{fid}}_{W^-\to \mu^-\bar{\nu}}} = 0.988 \pm 0.030\ (\text{stat.}) \pm 0.028\ (\text{syst.})$$

$$R_{W} = \frac{\sigma^{\text{fid}}_{W\to e\nu}}{\sigma^{\text{fid}}_{W\to \mu\nu}} = 0.986 \pm 0.018\ (\text{stat.}) \pm 0.028\ (\text{syst.})$$

$$R_{Z} = \frac{\sigma^{\text{fid}}_{Z\to e^+e^-}}{\sigma^{\text{fid}}_{Z\to \mu^+\mu^-}} = 0.96 \pm 0.06\ (\text{stat.}) \pm 0.05\ (\text{syst.})$$

These results lie within one standard deviation of the Standard Model prediction and previous measurements by ATLAS.

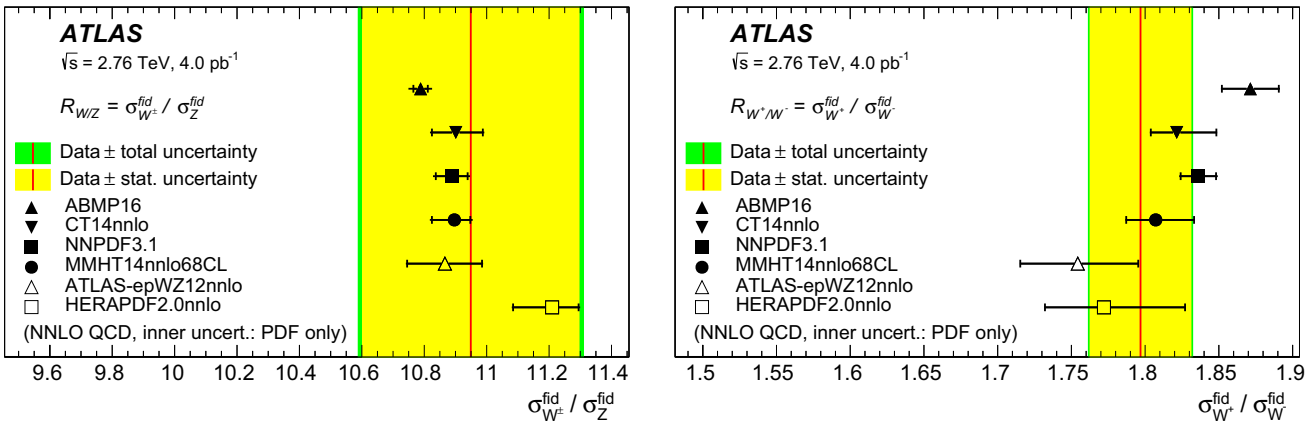

Fig. 7 The measured ratio of fiducial cross-sections for (a) W-boson production to Z-boson production, (b) W^+-boson production to W^--boson production. The measurements are compared with theoretical predictions at NNLO in QCD based on a selection of different PDF sets. The inner shaded band corresponds to statistical uncertainty while the outer band shows statistical and systematic uncertainties added in quadrature. The theory predictions are given with the corresponding PDF (total) uncertainty shown by inner (outer) error bar

9 Conclusion

This paper presents measurements of the $W \to \ell\nu$ and $Z \to \ell\ell$ production cross-sections based on about 12 400 W-boson and 1100 Z-boson candidates, after subtracting background events, reconstructed from $\sqrt{s} = 2.76$ TeV proton–proton collision data recorded by the ATLAS detector at the LHC, corresponding to integrated luminosity of 4.0 pb^{-1}. The total inclusive W-boson production cross-sections for the combined electron and muon channels are

$$\sigma^{\text{tot}}_{W^+\to\ell\nu} = 2312 \pm 26\ (\text{stat.}) \pm 27\ (\text{syst.}) \pm 72\ (\text{lumi.}) \pm 30\ (\text{extr.})\ \text{pb},$$
$$\sigma^{\text{tot}}_{W^-\to\ell\nu} = 1399 \pm 21\ (\text{stat.}) \pm 17\ (\text{syst.}) \pm 43\ (\text{lumi.}) \pm 21\ (\text{extr.})\ \text{pb},$$

and the total inclusive Z-boson cross-section in the combined electron and muon channels is:

$$\sigma^{\text{tot}}_{Z\to\ell\ell} = 323.4 \pm 9.8\ (\text{stat.}) \pm 5.0\ (\text{syst.}) \pm 10.0\ (\text{lumi.}) \pm 5.5(\text{extr.})\ \text{pb}.$$

The results obtained, and the ratios and charge asymmetries constructed from them, are in agreement with theoretical calculations based on NNLO QCD.

Acknowledgements We thank CERN for the very successful operation of the LHC, as well as the support staff from our institutions without whom ATLAS could not be operated efficiently. We acknowledge the support of ANPCyT, Argentina; YerPhI, Armenia; ARC, Australia; BMWFW and FWF, Austria; ANAS, Azerbaijan; SSTC, Belarus; CNPq and FAPESP, Brazil; NSERC, NRC and CFI, Canada; CERN; CONICYT, Chile; CAS, MOST and NSFC, China; COLCIENCIAS, Colombia; MSMT CR, MPO CR and VSC CR, Czech Republic; DNRF and DNSRC, Denmark; IN2P3-CNRS, CEA-DRF/IRFU, France; SRNSFG, Georgia; BMBF, HGF, and MPG, Germany; GSRT, Greece; RGC, Hong Kong SAR, China; ISF and Benoziyo Center, Israel; INFN, Italy; MEXT and JSPS, Japan; CNRST, Morocco; NWO, Netherlands; RCN, Norway; MNiSW and NCN, Poland; FCT, Portugal; MNE/IFA, Romania; MES of Russia and NRC KI, Russian Federation; JINR; MESTD, Serbia; MSSR, Slovakia; ARRS and MIZŠ, Slovenia; DST/NRF, South Africa; MINECO, Spain; SRC and Wallenberg Foundation, Sweden; SERI, SNSF and Cantons of Bern and Geneva, Switzerland; MOST, Taiwan; TAEK, Turkey; STFC, United Kingdom; DOE and NSF, United States of America. In addition, individual groups and members have received support from BCKDF, CANARIE, CRC and Compute Canada, Canada; COST, ERC, ERDF, Horizon 2020, and Marie Skłodowska-Curie Actions, European Union; Investissements d' Avenir Labex and Idex, ANR, France; DFG and AvH Foundation, Germany; Herakleitos, Thales and Aristeia programmes co-financed by EU-ESF and the Greek NSRF, Greece; BSF-NSF and GIF, Israel; CERCA Programme Generalitat de Catalunya, Spain; The Royal Society and Leverhulme Trust, United Kingdom. The crucial computing support from all WLCG partners is acknowledged gratefully, in particular from CERN, the ATLAS Tier-1 facilities at TRIUMF (Canada), NDGF (Denmark, Norway, Sweden), CC-IN2P3 (France), KIT/GridKA (Germany), INFN-CNAF (Italy), NL-T1 (Netherlands), PIC (Spain), ASGC (Taiwan), RAL (UK) and BNL (USA), the Tier-2 facilities worldwide and large non-WLCG resource providers. Major contributors of computing resources are listed in Ref. [83].

Data Availability Statement This manuscript has no associated data or the data will not be deposited. [Authors' comment: "All ATLAS scientific output is published in journals, and preliminary results are made available in Conference Notes. All are openly available, without restriction on use by external parties beyond copyright law and the standard conditions agreed by CERN. Data associated with journal publications are also made available: tables and data from plots (e.g. cross section values, likelihood profiles, selection efficiencies, cross section limits, ...) are stored in appropriate repositories such as HEPDATA (http://hepdata.cedar.ac.uk/). ATLAS also strives to make additional material related to the paper available that allows a reinterpretation of the data in the context of new theoretical models. For example, an extended encapsulation of the analysis is often provided for measurements in the framework of RIVET (http://rivet.hepforge.org/)". This information is taken from the ATLAS Data Access Policy, which is a public document that can be downloaded from http://opendata.cern.ch/record/413 [opendata.cern.ch].]

Table 9 The predictions at NNLO in QCD, using the MMHT14nnlo68cl, NNPDF31_nnlo_as_0118, ATLASepWZ12, HERAPDF2.0, and ABMP16 PDF sets, for the cross-sections measured in this study

Quantity	Predicted cross-section ± PDF uncertainty (pb)				
	MMHT14	NNPDF31	ATLASepWZ12	HERAPDF20	ABMP16
$\sigma^{\text{fid}}_{W^+}$	1397^{+29}_{-30}	1428^{+24}_{-24}	1375^{+34}_{-30}	1429^{+91}_{-49}	1397^{+14}_{-14}
$\sigma^{\text{fid}}_{W^-}$	773^{+17}_{-20}	778^{+14}_{-14}	784^{+19}_{-19}	806^{+31}_{-21}	746^{+9}_{-9}
σ^{fid}_{Z}	199^{+4}_{-4}	203^{+4}_{-4}	199^{+4}_{-4}	199^{+11}_{-5}	$198.6^{+2.0}_{-2.0}$
$\sigma^{\text{tot}}_{W^+}$	2138^{+43}_{-45}	2271^{+36}_{-36}	2086^{+54}_{-47}	2140^{+140}_{-70}	2214^{+21}_{-21}
$\sigma^{\text{tot}}_{W^-}$	1295^{+28}_{-33}	1330^{+22}_{-22}	1296^{+48}_{-29}	1338^{+52}_{-32}	1283^{+16}_{-16}
σ^{tot}_{Z}	308^{+6}_{-6}	313^{+5}_{-5}	308^{+6}_{-5}	312^{+16}_{-7}	$305.7^{+3.0}_{-3.0}$

Funded by SCOAP[3].

Appendix

A Theoretical predictions

This appendix presents the theoretical predictions used for comparison with the measurements in the main body of the paper. Table 9 shows the predictions using the MMHT14nnlo68cl, NNPDF31_nnlo_as_0118, ATLASep WZ12, HERAPDF2.0, and ABMP16 PDF sets with associated PDF uncertainties.

References

1. V.N. Gribov, L.N. Lipatov, Deep inelastic e p scattering in perturbation theory. Sov. J. Nucl. Phys. **15**, 438 (1972)
2. V.N. Gribov, L.N. Lipatov, Deep inelastic e p scattering in perturbation theory. Yad. Fiz. **15**, 781 (1972)
3. L.N. Lipatov, The parton model and perturbation theory. Sov. J. Nucl. Phys. **20**, 94 (1975)
4. L.N. Lipatov, The parton model and perturbation theory. Yad. Fiz. **20**, 181 (1974)
5. G. Altarelli, G. Parisi, Asymptotic freedom in parton language. Nucl. Phys. B **126**, 298 (1977)
6. Y.L. Dokshitzer, Calculation of the structure functions for deep inelastic scattering and e+ e− ennihilation by perturbation theory in quantum chromodynamics. Sov. Phys. JETP **46**, 641 (1977)
7. Y.L. Dokshitzer, Calculation of the structure functions for deep inelastic scattering and e+ e− ennihilation by perturbation theory in quantum chromodynamics. Zh. Eksp. Teor. Fiz. **73**, 1216 (1972)
8. L. Evans, P. Bryant, L.H.C. Machine, JINST **3**, S08001 (2008)
9. ATLAS Collaboration, Measurements of W and Z boson production in pp collisions at $\sqrt{s} = 5.02$ TeV with the ATLAS detector. Eur. Phys. J. C **79**, 128 (2019). arXiv:1810.08424 [hep-ex]
10. ATLAS Collaboration, Precision measurement and interpretation of inclusive W^+, W^- and Z/γ^* production cross sections with the ATLAS detector. Eur. Phys. J. C **77**, 367 (2017). arXiv:1612.03016 [hep-ex]
11. CMS Collaboration, Measurement of inclusive W and Z production cross sections in pp collisions at $\sqrt{s} = 7$ TeV. JHEP **10**, 132 (2011). arXiv:1107.4789 [hep-ex]
12. LHCb Collaboration, Measurement of the forward Z boson production cross-section in pp collisions at $\sqrt{s} = 7$ TeV. JHEP **08**, 039 (2015). arXiv:1505.07024 [hep-ex]
13. LHCb Collaboration, Measurement of the forward W boson cross-section in pp collisions at $\sqrt{s} = 7$ TeV. JHEP **12**, 079 (2014). arXiv:1408.4354 [hep-ex]
14. LHCb Collaboration, Measurement of the cross-section for $Z \to e^+e^-$ production in pp collisions at $\sqrt{s} = 7$ TeV. JHEP **02**, 106 (2013). arXiv:1212.4620 [hep-ex]
15. ATLAS Collaboration, Measurement of the transverse momentum and ϕ^*_η distributions of Drell–Yan lepton pairs in proton–proton collisions at $\sqrt{s} = 8$ TeV with the ATLAS detector. Eur. Phys. J. C **76**, 291 (2016). arXiv:1512.02192 [hep-ex]
16. CMS Collaboration, Measurement of inclusive W and Z boson production cross sections in pp collisions at $\sqrt{s} = 8$ TeV. Phys. Rev. Lett. **112**, 191802 (2014). arXiv:1402.0923 [hep-ex]
17. LHCb Collaboration, Measurement of forward W and Z boson production in pp collisions at $\sqrt{s} = 8$ TeV. JHEP **01**, 155 (2016). arXiv:1511.08039 [hep-ex]
18. LHCb Collaboration, Measurement of forward $W \to ev$ production in pp collisions at $\sqrt{s} = 8$ TeV. JHEP **10**, 030 (2016). arXiv:1608.01484 [hep-ex]
19. LHCb Collaboration, Measurement of forward $Z \to e^+e^-$ production at $\sqrt{s} = 8$ TeV. JHEP **05**, 109 (2015). arXiv:1503.00963 [hep-ex]
20. ATLAS Collaboration, Measurement of $W^\pm$ and Z-boson production cross sections in pp collisions at $\sqrt{s} = 13$ TeV with the ATLAS detector. Phys. Lett. B **759**, 601 (2016). arXiv:1603.09222 [hep-ex]
21. ATLAS Collaboration, Measurements of top-quark pair to Z-boson cross-section ratios at $\sqrt{s} = 13, 8, 7$ TeV with the ATLAS detector. JHEP **02**, 117 (2017). arXiv:1612.03636 [hep-ex]
22. LHCb Collaboration, Measurement of the forward Z boson production cross-section in pp collisions at $\sqrt{s} = 13$ TeV. JHEP **09**, 136 (2016). arXiv:1607.06495 [hep-ex]
23. PHENIX Collaboration, Cross section and parity violating spin asymmetries of $W^\pm$ boson production in polarized $p + p$ collisions at $\sqrt{s} = 500$ GeV. Phys. Rev. Lett. **106**, 062001 (2011). arXiv:1009.0505 [hep-ex]
24. STAR Collaboration, Measurement of the $W \to ev$ and $Z/\gamma^* \to e^+e^-$ production cross sections at mid-rapidity in proton-proton collisions at $\sqrt{s} = 500$ GeV. Phys. Rev. D **85**, 092010 (2012). arXiv:1112.2980 [hep-ex]
25. PHENIX Collaboration, Cross section and longitudinal single-spin asymmetry A_L for forward $W^\pm \to \mu^\pm v$ production in polarized p+p collisions at $\sqrt{s} = 510$ GeV. Phys. Rev. D **98**, 032007 (2018). arXiv:1804.04181 [hep-ex]

26. CDF Collaboration, A measurement of the production and muonic decay rate of W and Z bosons in $p\bar{p}$ collisions at $\sqrt{s} = 1.8$ TeV. Phys. Rev. Lett. **69**, 28 (1992)
27. CDF Collaboration, Measurement of $\sigma B(W \to e\nu)$ and $\sigma B(Z^0 \to e^+e^-)$ in $p\bar{p}$ Collisions at $\sqrt{s} = 1.8$ TeV. Phys. Rev. Lett. **76**, 3070 (1996). arXiv:hep-ex/9509010 [hep-ex]
28. CDF Collaboration, Measurement of Z^0 and Drell-Yan production cross section using dimuons in $p\bar{p}$ collisions at $\sqrt{s} = 1.8$ TeV. Phys. Rev. D **59**, 052002 (1999)
29. CDF Collaboration, Transverse momentum and total cross section of e^+e^- pairs in the Z-boson region from $p\bar{p}$ collisions at $\sqrt{s} = 1.8$ TeV. Phys. Rev. Lett. **84**, 845 (2000). arXiv:hep-ex/0001021 [hep-ex]
30. CDF Collaboration, Measurements of inclusive W and Z cross sections in p anti-p collisions at $\sqrt{s} = 1.96$-TeV. J. Phys. G **34**, 2457 (2007). arXiv:hep-ex/0508029 [hep-ex]
31. D0 Collaboration, W and Z boson production in $p\bar{p}$ collisions at $\sqrt{s} = 1.8$-TeV. Phys. Rev. Lett. **75**, 1456 (1995). arXiv:hep-ex/9505013 [hep-ex]
32. UA1 Collaboration, Studies of intermediate vector boson production and decay in UA1 at the CERN proton–antiproton collider. Z. Phys. C **44**, 15 (1989)
33. UA2 Collaboration, A measurement of the W and Z production cross-sections and a determination of Γ_W at the CERN $p\bar{p}$ collider. Phys. Lett. B **276**, 365 (1992)
34. ATLAS Collaboration, The ATLAS Experiment at the CERN Large Hadron Collider, JINST 3 S08003 (2008)
35. ATLAS Collaboration, Performance of the ATLAS Trigger System in 2010. Eur. Phys. J. C **72**, 1849 (2012). arXiv:1110.1530 [hep-ex]
36. P. Nason, A new method for combining NLO QCD with shower Monte Carlo algorithms. JHEP **11**, 040 (2004). arXiv:hep-ph/0409146 [hep-ph]
37. S. Frixione, P. Nason, C. Oleari, Matching NLO QCD computations with parton shower simulations: the POWHEG method. JHEP **11**, 070 (2007). arXiv:0709.2092 [hep-ph]
38. S. Alioli, P. Nason, C. Oleari, E. Re, A general framework for implementing NLO calculations in shower Monte Carlo programs: the POWHEG BOX. JHEP **06**, 043 (2010). arXiv:1002.2581 [hep-ph]
39. S. Alioli, P. Nason, C. Oleari, E. Re, NLO vector-boson production matched with shower in POWHEG. JHEP **07**, 060 (2008). arXiv:0805.4802 [hep-ph]
40. T. Sjöstrand, S. Mrenna, P.Z. Skands, A brief introduction to PYTHIA 8.1. Comput. Phys. Commun. **178**, 852 (2008). arXiv:0710.3820 [hep-ph]
41. H.-L. Lai et al., New parton distributions for collider physics. Phys. Rev. D **82**, 074024 (2010). arXiv:1007.2241 [hep-ph]
42. ATLAS Collaboration, ATLAS Pythia 8 tunes to 7 TeV data, ATL-PHYS-PUB-2014-021 (2014). https://cds.cern.ch/record/1966419
43. N. Davidson, T. Przedzinski, Z. Was, PHOTOS interface in C++: technical and physics documentation. Comput. Phys. Commun. **199**, 86 (2016). arXiv:1011.0937 [hep-ph]
44. T. Gleisberg et al., Event generation with SHERPA 1.1. JHEP **02**, 007 (2009). arXiv:0811.4622 [hep-ph]
45. S. Frixione, P. Nason, G. Ridolfi, A positive-weight next-to-leading-order Monte Carlo for heavy flavour hadroproduction. JHEP **09**, 126 (2007). arXiv:0707.3088 [hep-ph]
46. T. Sjöstrand, S. Mrenna, P.Z. Skands, PYTHIA 6.4 physics and manual. JHEP **05**, 026 (2006). arXiv:hep-ph/0603175 [hep-ph]
47. P.Z. Skands, Tuning Monte Carlo generators: the Perugia tunes. Phys. Rev. D **82**, 074018 (2010). arXiv:1005.3457 [hep-ph]
48. N. Davidson, G. Nanava, T. Przedzinski, E. Richter-Was, Z. Was, Universal interface of TAUOLA technical and physics documentation. Comput. Phys. Commun. **183**, 821 (2012). arXiv:1002.0543 [hep-ph]
49. G. Corcella et al., HERWIG 6.5 release note. arXiv: hep-ph/0210213 [hep-ph]
50. J.M. Butterworth, J.R. Forshaw, M.H. Seymour, Multiparton interactions in photoproduction at HERA. Z. Phys. C **72**, 637 (1996). arXiv:hep-ph/9601371 [hep-ph]
51. J. Pumplin et al., New generation of parton distributions with uncertainties from global QCD analysis. JHEP **07**, 012 (2002). arXiv:hep-ph/0201195 [hep-ph]
52. ATLAS Collaboration, New ATLAS event generator tunes to 2010 data, ATL-PHYS-PUB-2011-008 (2011). https://cds.cern.ch/record/1345343
53. ATLAS Collaboration, The ATLAS simulation infrastructure. Eur. Phys. J. C **70**, 823 (2010). arXiv:1005.4568 [physics.ins-det]
54. S. Agostinelli et al., GEANT4-A simulation toolkit. Nucl. Instrum. Methods A **506**, 250 (2003)
55. ATLAS Collaboration, Electron efficiency measurements with the ATLAS detector using 2012 LHC proton–proton collision data. Eur. Phys. J. C **77**, 195 (2017). arXiv:1612.01456 [hep-ex]
56. ATLAS Collaboration, Improved electron reconstruction in ATLAS using the Gaussian Sum Filterbased model for bremsstrahlung, ATLAS-CONF-2012-047 (2012). https://cds.cern.ch/record/1449796
57. ATLAS Collaboration, Measurement of the muon reconstruction performance of the ATLAS detector using 2011 and 2012 LHC proton–proton collision data. Eur. Phys. J. C **74**, 3130 (2014). arXiv:1407.3935 [hep-ex]
58. ATLAS Collaboration, Performance of algorithms that reconstruct missing transverse momentum in $\sqrt{s} = 8$ TeV proton–proton collisions in the ATLAS detector. Eur. Phys. J. C **77**, 241 (2017). arXiv:1609.09324 [hep-ex]
59. ATLAS Collaboration, Topological cell clustering in the ATLAS calorimeters and its performance in LHC Run 1. Eur. Phys. J. C **77**, 490 (2017). arXiv:1603.02934 [hep-ex]
60. ATLAS Collaboration, Measurement of the W-boson mass in pp collisions at $\sqrt{s} = 7$ TeV with the ATLAS detector. Eur. Phys. J. C **78**, 110 (2018). arXiv:1701.07240 [hep-ex]
61. ATLAS Collaboration, Measurement of differential cross sections and W^+/W^- cross-section ratios for W boson production in association with jets at $\sqrt{s} = 8$ TeV with the ATLAS detector. JHEP **05**, 077 (2018). arXiv:1711.03296 [hep-ex]
62. ATLAS Collaboration, Electron performance measurements with the ATLAS detector using the 2010 LHC proton–proton collision data. Eur. Phys. J. C **72**, 1909 (2012). arXiv:1110.3174 [hep-ex]
63. ATLAS Collaboration, Improved luminosity determination in pp collisions at p $\sqrt{s} = 7$ TeV using the ATLAS detector at the LHC. Eur. Phys. J. C **73**, 2518 (2013). arXiv:1302.4393 [hep-ex]
64. S. Alekhin, J. Bluemlein, S. Klein, S. Moch, 3-, 4-, and 5-flavor next-to-next-to-leading order parton distribution from deep-inelastic-scattering data and at hadron colliders. Phys. Rev. D **81**, 014032 (2010). arXiv:0908.2766 [hep-ph]
65. R.D. Ball et al., Parton distributions with LHC data. Nucl. Phys. B **867**, 244 (2013). arXiv:1207.1303 [hep-ph]
66. ATLAS Collaboration, Determination of the strange-quark density of the proton from ATLAS measurements of the $W \to \ell\nu$ and $Z \to \ell$ cross sections. Phys. Rev. Lett. **109**, 012001 (2012). arXiv:1203.4051 [hep-ex]
67. A. Glazov, Averaging of DIS cross section data. AIP Conf. Proc. **792**, 237 (2005)
68. S. Catani, M. Grazzini, A next-to-next-to-leading order subtraction formalism in hadron collisions and its application to Higgs–Boson production at the large hadron collider. Phys. Rev. Lett. **98**, 222002 (2007). arXiv:hep-ph/0703012 [hep-ph]
69. K. Melnikov, F. Petriello, Electroweak gauge boson production at hadron colliders through $O(\alpha_S^2)$. Phys. Rev. D **74**, 114017 (2006). arXiv:hep-ph/0609070 [hep-ph]

70. R. Gavin, Y. Li, F. Petriello, S. Quackenbush, FEWZ 2.0: a code for hadronic Z production at next-to-next-to-leading order. Comput. Phys. Commun **182**, 2388 (2011). arXiv:1011.3540 [hep-ph]
71. R. Gavin, Y. Li, F. Petriello, S. Quackenbush, W physics at the LHC with FEWZ 2.1. Comput. Phys. Commun **184**, 208 (2013). arXiv:1201.5896 [hep-ph]
72. Y. Li, F. Petriello, Combining QCD and electroweak corrections to dilepton production in the framework of the FEWZ simulation code. Phys. Rev. D **86**, 094034 (2012). arXiv:1208.5967 [hep-ph]
73. D. Bardin et al., SANC integrator in the progress: QCD and EW contributions. JETP Lett. **96**, 285 (2012). arXiv:1207.4400 [hep-ph]
74. A.B. Arbuzov, R.R. Sadykov, Z. Was, QED Bremsstrahlung in decays of electroweak bosons. Eur. Phys. J. C **73**, 2625 (2013). arXiv:1212.6783 [hep-ph]
75. W.F.L. Hollik, Radiative corrections in the standard model and their role for precision tests of the electroweak theory. Fortsch. Phys. **38**, 165 (1990)
76. K.A. Olive et al., Review of Particle Physics. Chin. Phys. C **38**, 090001 (2014)
77. S. Dittmaier, M. Huber, Radiative corrections to the neutral-current Drell–Yan process in the Standard Model and its minimal supersymmetric extension. JHEP **01**, 060 (2010). arXiv:0911.2329 [hep-ph]
78. S. Dulat et al., New parton distribution functions from a global analysis of quantum chromodynamics. Phys. Rev. D **93**, 033006 (2016). arXiv:1506.07443 [hep-ph]
79. R.D. Ball et al., Parton distributions from high-precision collider data. Eur. Phys. J. C **77**, 663 (2017). arXiv:1706.00428 [hep-ph]
80. L.A. Harland-Lang, A.D. Martin, P. Motylinski, R.S. Thorne, Parton distributions in the LHC era: MMHT 2014 PDFs. Eur. Phys. J. C **75**, 204 (2015). arXiv:1412.3989 [hep-ph]
81. S. Alekhin, J. Bluemlein, S. Moch, R. Placakyte, Parton distribution functions, α_s, and heavyquark masses for LHC Run II. Phys. Rev. D **96**, 014011 (2017). arXiv:1701.05838 [hep-ph]
82. H1 and ZEUS Collaborations, Combination of measurements of inclusive deep inelastic $e^{\pm}p$ scattering cross sections and QCD analysis of HERA data. Eur. Phys. J. C **75**, 580 (2015). arXiv:1506.06042 [hep-ex]
83. ATLAS Collaboration, ATLAS Computing Acknowledgements, ATL-GEN-PUB-2016-002. https://cds.cern.ch/record/2202407

ATLAS Collaboration

G. Aad[101], B. Abbott[128], D. C. Abbott[102], O. Abdinov[13,*], A. Abed Abud[70a,70b], K. Abeling[53], D. K. Abhayasinghe[93], S. H. Abidi[167], O. S. AbouZeid[40], N. L. Abraham[156], H. Abramowicz[161], H. Abreu[160], Y. Abulaiti[6], B. S. Acharya[66a,66b,p], B. Achkar[53], S. Adachi[163], L. Adam[99], C. Adam Bourdarios[132], L. Adamczyk[83a], L. Adamek[167], J. Adelman[121], M. Adersberger[114], A. Adiguzel[12c,ak], S. Adorni[54], T. Adye[144], A. A. Affolder[146], Y. Afik[160], C. Agapopoulou[132], M. N. Agaras[38], A. Aggarwal[119], C. Agheorghiesei[27c], J. A. Aguilar-Saavedra[140a,140f,aj], F. Ahmadov[79], W. S. Ahmed[103], X. Ai[15a], G. Aielli[73a,73b], S. Akatsuka[85], T. P. A. Åkesson[96], E. Akilli[54], A. V. Akimov[110], K. Al Khoury[132], G. L. Alberghi[23a,23b], J. Albert[176], M. J. Alconada Verzini[161], S. Alderweireldt[36], M. Aleksa[36], I. N. Aleksandrov[79], C. Alexa[27b], D. Alexandre[19], T. Alexopoulos[10], A. Alfonsi[120], M. Alhroob[128], B. Ali[142], G. Alimonti[68a], J. Alison[37], S. P. Alkire[148], C. Allaire[132], B. M. M. Allbrooke[156], B. W. Allen[131], P. P. Allport[21], A. Aloisio[69a,69b], A. Alonso[40], F. Alonso[88], C. Alpigiani[148], A. A. Alshehri[57], M. Alvarez Estevez[98], D. Álvarez Piqueras[174], M. G. Alviggi[69a,69b], Y. Amaral Coutinho[80b], A. Ambler[103], L. Ambroz[135], C. Amelung[26], D. Amidei[105], S. P. Amor Dos Santos[140a], S. Amoroso[46], C. S. Amrouche[54], F. An[78], C. Anastopoulos[149], N. Andari[145], T. Andeen[11], C. F. Anders[61b], J. K. Anders[20], A. Andreazza[68a,68b], V. Andrei[61a], C. R. Anelli[176], S. Angelidakis[38], A. Angerami[39], A. V. Anisenkov[122a,122b], A. Annovi[71a], C. Antel[61a], M. T. Anthony[149], M. Antonelli[51], D. J. A. Antrim[171], F. Anulli[72a], M. Aoki[81], J. A. Aparisi Pozo[174], L. Aperio Bella[36], G. Arabidze[106], J. P. Araque[140a], V. Araujo Ferraz[80b], R. Araujo Pereira[80b], C. Arcangeletti[51], A. T. H. Arce[49], F. A. Arduh[88], J-F. Arguin[109], S. Argyropoulos[77], J.-H. Arling[46], A. J. Armbruster[36], L. J. Armitage[92], A. Armstrong[171], O. Arnaez[167], H. Arnold[120], A. Artamonov[111,*], G. Artoni[135], S. Artz[99], S. Asai[163], N. Asbah[59], E. M. Asimakopoulou[172], L. Asquith[156], K. Assamagan[29], R. Astalos[28a], R. J. Atkin[33a], M. Atkinson[173], N. B. Atlay[151], H. Atmani[132], K. Augsten[142], G. Avolio[36], R. Avramidou[60a], M. K. Ayoub[15a], A. M. Azoulay[168b], G. Azuelos[109,az], M. J. Baca[21], H. Bachacou[145], K. Bachas[67a,67b], M. Backes[135], F. Backman[45a,45b], P. Bagnaia[72a,72b], M. Bahmani[84], H. Bahrasemani[152], A. J. Bailey[174], V. R. Bailey[173], J. T. Baines[144], M. Bajic[40], C. Bakalis[10], O. K. Baker[183], P. J. Bakker[120], D. Bakshi Gupta[8], S. Balaji[157], E. M. Baldin[122a,122b], P. Balek[180], F. Balli[145], W. K. Balunas[135], J. Balz[99], E. Banas[84], A. Bandyopadhyay[24], Sw. Banerjee[181,j], A. A. E. Bannoura[182], L. Barak[161], W. M. Barbe[38], E. L. Barberio[104], D. Barberis[55a,55b], M. Barbero[101], T. Barillari[115], M-S. Barisits[36], J. Barkeloo[131], T. Barklow[153], R. Barnea[160], S. L. Barnes[60c], B. M. Barnett[144], R. M. Barnett[18], Z. Barnovska-Blenessy[60a], A. Baroncelli[60a], G. Barone[29], A. J. Barr[135], L. Barranco Navarro[45a,45b], F. Barreiro[98], J. Barreiro Guimarães da Costa[15a], S. Barsov[138], R. Bartoldus[153], G. Bartolini[101], A. E. Barton[89], P. Bartos[28a], A. Basalaev[46], A. Bassalat[132,as], R. L. Bates[57], S. J. Batista[167], S. Batlamous[35e], J. R. Batley[32], B. Batool[151], M. Battaglia[146], M. Bauce[72a,72b], F. Bauer[145], K. T. Bauer[171], H. S. Bawa[31,n], J. B. Beacham[49], T. Beau[136], P. H. Beauchemin[170], F. Becherer[52], P. Bechtle[24], H. C. Beck[53], H. P. Beck[20,t], K. Becker[52], M. Becker[99], C. Becot[46], A. Beddall[12d], A. J. Beddall[12a], V. A. Bednyakov[79], M. Bedognetti[120], C. P. Bee[155], T. A. Beermann[76], M. Begalli[80b], M. Begel[29], A. Behera[155], J. K. Behr[46], F. Beisiegel[24], A. S. Bell[94], G. Bella[161], L. Bellagamba[23b], A. Bellerive[34], P. Bellos[9], K. Beloborodov[122a,122b],

K. Belotskiy[112], N. L. Belyaev[112], D. Benchekroun[35a], N. Benekos[10], Y. Benhammou[161], D. P. Benjamin[6], M. Benoit[54], J. R. Bensinger[26], S. Bentvelsen[120], L. Beresford[135], M. Beretta[51], D. Berge[46], E. Bergeaas Kuutmann[172], N. Berger[5], B. Bergmann[142], L. J. Bergsten[26], J. Beringer[18], S. Berlendis[7], N. R. Bernard[102], G. Bernardi[136], C. Bernius[153], T. Berry[93], P. Berta[99], C. Bertella[15a], I. A. Bertram[89], G. J. Besjes[40], O. Bessidskaia Bylund[182], N. Besson[145], A. Bethani[100], S. Bethke[115], A. Betti[24], A. J. Bevan[92], J. Beyer[115], R. Bi[139], R. M. Bianchi[139], O. Biebel[114], D. Biedermann[19], R. Bielski[36], K. Bierwagen[99], N. V. Biesuz[71a,71b], M. Biglietti[74a], T. R. V. Billoud[109], M. Bindi[53], A. Bingul[12d], C. Bini[72a,72b], S. Biondi[23a,23b], M. Birman[180], T. Bisanz[53], J. P. Biswal[161], A. Bitadze[100], C. Bittrich[48], K. Bjørke[134], K. M. Black[25], T. Blazek[28a], I. Bloch[46], C. Blocker[26], A. Blue[57], U. Blumenschein[92], G. J. Bobbink[120], V. S. Bobrovnikov[122a,122b], S. S. Bocchetta[96], A. Bocci[49], D. Boerner[46], D. Bogavac[14], A. G. Bogdanchikov[122a,122b], C. Bohm[45a], V. Boisvert[93], P. Bokan[53,172], T. Bold[83a], A. S. Boldyrev[113], A. E. Bolz[61b], M. Bomben[136], M. Bona[92], J. S. Bonilla[131], M. Boonekamp[145], H. M. Borecka-Bielska[90], A. Borisov[123], G. Borissov[89], J. Bortfeldt[36], D. Bortoletto[135], V. Bortolotto[73a,73b], D. Boscherini[23b], M. Bosman[14], J. D. Bossio Sola[103], K. Bouaouda[35a], J. Boudreau[139], E. V. Bouhova-Thacker[89], D. Boumediene[38], S. K. Boutle[57], A. Boveia[126], J. Boyd[36], D. Boye[33b,at], I. R. Boyko[79], A. J. Bozson[93], J. Bracinik[21], N. Brahimi[101], G. Brandt[182], O. Brandt[61a], F. Braren[46], B. Brau[102], J. E. Brau[131], W. D. Breaden Madden[57], K. Brendlinger[46], L. Brenner[46], R. Brenner[172], S. Bressler[180], B. Brickwedde[99], D. L. Briglin[21], D. Britton[57], D. Britzger[115], I. Brock[24], R. Brock[106], G. Brooijmans[39], W. K. Brooks[147c], E. Brost[121], J.H Broughton[21], P. A. Bruckman de Renstrom[84], D. Bruncko[28b], A. Bruni[23b], G. Bruni[23b], L. S. Bruni[120], S. Bruno[73a,73b], B. H. Brunt[32], M. Bruschi[23b], N. Bruscino[139], P. Bryant[37], L. Bryngemark[96], T. Buanes[17], Q. Buat[36], P. Buchholz[151], A. G. Buckley[57], I. A. Budagov[79], M. K. Bugge[134], F. Bührer[52], O. Bulekov[112], T. J. Burch[121], S. Burdin[90], C. D. Burgard[120], A. M. Burger[129], B. Burghgrave[8], J. T. P. Burr[46], J. C. Burzynski[102], V. Büscher[99], E. Buschmann[53], P. J. Bussey[57], J. M. Butler[25], C. M. Buttar[57], J. M. Butterworth[94], P. Butti[36], W. Buttinger[36], A. Buzatu[158], A. R. Buzykaev[122a,122b], G. Cabras[23a,23b], S. Cabrera Urbán[174], D. Caforio[56], H. Cai[173], V. M. M. Cairo[153], O. Cakir[4a], N. Calace[36], P. Calafiura[18], A. Calandri[101], G. Calderini[136], P. Calfayan[65], G. Callea[57], L. P. Caloba[80b], S. Calvente Lopez[98], D. Calvet[38], S. Calvet[38], T. P. Calvet[155], M. Calvetti[71a,71b], R. Camacho Toro[136], S. Camarda[36], D. Camarero Munoz[98], P. Camarri[73a,73b], D. Cameron[134], R. Caminal Armadans[102], C. Camincher[36], S. Campana[36], M. Campanelli[94], A. Camplani[40], A. Campoverde[151], V. Canale[69a,69b], A. Canesse[103], M. Cano Bret[60c], J. Cantero[129], T. Cao[161], Y. Cao[173], M. D. M. Capeans Garrido[36], M. Capua[41a,41b], R. Cardarelli[73a], F. Cardillo[149], G. Carducci[41a,41b], I. Carli[143], T. Carli[36], G. Carlino[69a], B. T. Carlson[139], L. Carminati[68a,68b], R. M. D. Carney[45a,45b], S. Caron[119], E. Carquin[147c], S. Carrá[46], J. W. S. Carter[167], M. P. Casado[14,f], A. F. Casha[167], D. W. Casper[171], R. Castelijn[120], F. L. Castillo[174], V. Castillo Gimenez[174], N. F. Castro[140a,140e], A. Catinaccio[36], J. R. Catmore[134], A. Cattai[36], J. Caudron[24], V. Cavaliere[29], E. Cavallaro[14], M. Cavalli-Sforza[14], V. Cavasinni[71a,71b], E. Celebi[12b], F. Ceradini[74a,74b], L. Cerda Alberich[174], K. Cerny[130], A. S. Cerqueira[80a], A. Cerri[156], L. Cerrito[73a,73b], F. Cerutti[18], A. Cervelli[23a,23b], S. A. Cetin[12b], D. Chakraborty[121], S. K. Chan[59], W. S. Chan[120], W. Y. Chan[90], J. D. Chapman[32], B. Chargeishvili[159b], D. G. Charlton[21], T. P. Charman[92], C. C. Chau[34], S. Che[126], A. Chegwidden[106], S. Chekanov[6], S. V. Chekulaev[168a], G. A. Chelkov[79,ay], M. A. Chelstowska[36], B. Chen[78], C. Chen[60a], C. H. Chen[78], H. Chen[29], J. Chen[60a], J. Chen[39], S. Chen[137], S. J. Chen[15c], X. Chen[15b,ax], Y. Chen[82], Y-H. Chen[46], H. C. Cheng[63a], H. J. Cheng[15a,15d], A. Cheplakov[79], E. Cheremushkina[123], R. Cherkaoui El Moursli[35e], E. Cheu[7], K. Cheung[64], T. J. A. Chevalérias[145], L. Chevalier[145], V. Chiarella[51], G. Chiarelli[71a], G. Chiodini[67a], A. S. Chisholm[21,36], A. Chitan[27b], I. Chiu[163], Y. H. Chiu[176], M. V. Chizhov[79], K. Choi[65], A. R. Chomont[72a,72b], S. Chouridou[162], Y. S. Chow[120], M. C. Chu[63a], X. Chu[15a], J. Chudoba[141], A. J. Chuinard[103], J. J. Chwastowski[84], L. Chytka[130], K. M. Ciesla[84], D. Cinca[47], V. Cindro[91], I. A. Cioară[27b], A. Ciocio[18], F. Cirotto[69a,69b], Z. H. Citron[180,l], M. Citterio[68a], D. A. Ciubotaru[27b], B. M. Ciungu[167], A. Clark[54], M. R. Clark[39], P. J. Clark[50], C. Clement[45a,45b], Y. Coadou[101], M. Cobal[66a,66c], A. Coccaro[55b], J. Cochran[78], H. Cohen[161], A. E. C. Coimbra[36], L. Colasurdo[119], B. Cole[39], A. P. Colijn[120], J. Collot[58], P. Conde Muiño[140a,g], E. Coniavitis[52], S. H. Connell[33b], I. A. Connelly[57], S. Constantinescu[27b], F. Conventi[69a,aaa], A. M. Cooper-Sarkar[135], F. Cormier[175], K. J. R. Cormier[167], L. D. Corpe[94], M. Corradi[72a,72b], E. E. Corrigan[96], F. Corriveau[103,af], A. Cortes-Gonzalez[36], M. J. Costa[174], F. Costanza[5], D. Costanzo[149], G. Cowan[93], J. W. Cowley[32], J. Crane[100], K. Cranmer[124], S. J. Crawley[57], R. A. Creager[137], S. Crépé-Renaudin[58], F. Crescioli[136], M. Cristinziani[24], V. Croft[120], G. Crosetti[41a,41b], A. Cueto[5], T. Cuhadar Donszelmann[149], A. R. Cukierman[153], S. Czekierda[84], P. Czodrowski[36], M. J. Da Cunha Sargedas De Sousa[60b], J. V. Da Fonseca Pinto[80b], C. Da Via[100], W. Dabrowski[83a], T. Dado[28a], S. Dahbi[35e], T. Dai[105], C. Dallapiccola[102], M. Dam[40], G. D'amen[23a,23b], V. D'Amico[74a,74b], J. Damp[99], J. R. Dandoy[137], M. F. Daneri[30], N. P. Dang[181,j], N. S. Dann[100], M. Danninger[175], V. Dao[36], G. Darbo[55b], O. Dartsi[5], A. Dattagupta[131], T. Daubney[46], S. D'Auria[68a,68b], W. Davey[24], C. David[46], T. Davidek[143], D. R. Davis[49], I. Dawson[149], K. De[8], R. De Asmundis[69a], M. De Beurs[120], S. De Castro[23a,23b], S. De Cecco[72a,72b], N. De Groot[119], P. de Jong[120], H. De la Torre[106], A. De Maria[15c], D. De Pedis[72a], A. De Salvo[72a], U. De Sanctis[73a,73b], M. De Santis[73a,73b],

A. De Santo[156], K. De Vasconcelos Corga[101], J. B. De Vivie De Regie[132], C. Debenedetti[146], D. V. Dedovich[79], A. M. Deiana[42], M. Del Gaudio[41a,41b], J. Del Peso[98], Y. Delabat Diaz[46], D. Delgove[132], F. Deliot[145,s], C. M. Delitzsch[7], M. Della Pietra[69a,69b], D. Della Volpe[54], A. Dell'Acqua[36], L. Dell'Asta[73a,73b], M. Delmastro[5], C. Delporte[132], P. A. Delsart[58], D. A. DeMarco[167], S. Demers[183], M. Demichev[79], G. Demontigny[109], S. P. Denisov[123], D. Denysiuk[120], L. D'Eramo[136], D. Derendarz[84], J. E. Derkaoui[35d], F. Derue[136], P. Dervan[90], K. Desch[24], C. Deterre[46], K. Dette[167], C. Deutsch[24], M. R. Devesa[30], P. O. Deviveiros[36], A. Dewhurst[144], S. Dhaliwal[26], F. A. Di Bello[54], A. Di Ciaccio[73a,73b], L. Di Ciaccio[5], W. K. Di Clemente[137], C. Di Donato[69a,69b], A. Di Girolamo[36], G. Di Gregorio[71a,71b], B. Di Micco[74a,74b], R. Di Nardo[102], K. F. Di Petrillo[59], R. Di Sipio[167], D. Di Valentino[34], C. Diaconu[101], F. A. Dias[40], T. Dias Do Vale[140a], M. A. Diaz[147a], J. Dickinson[18], E. B. Diehl[105], J. Dietrich[19], S. Díez Cornell[46], A. Dimitrievska[18], W. Ding[15b], J. Dingfelder[24], F. Dittus[36], F. Djama[101], T. Djobava[159b], J. I. Djuvsland[17], M. A. B. Do Vale[80c], M. Dobre[27b], D. Dodsworth[26], C. Doglioni[96], J. Dolejsi[143], Z. Dolezal[143], M. Donadelli[80d], J. Donini[38], A. D'onofrio[92], M. D'Onofrio[90], J. Dopke[144], A. Doria[69a], M. T. Dova[88], A. T. Doyle[57], E. Drechsler[152], E. Dreyer[152], T. Dreyer[53], A. S. Drobac[170], Y. Duan[60b], F. Dubinin[110], M. Dubovsky[28a], A. Dubreuil[54], E. Duchovni[180], G. Duckeck[114], A. Ducourthial[136], O. A. Ducu[109], D. Duda[115], A. Dudarev[36], A. C. Dudder[99], E. M. Duffield[18], L. Duflot[132], M. Dührssen[36], C. Dülsen[182], M. Dumancic[180], A. E. Dumitriu[27b], A. K. Duncan[57], M. Dunford[61a], A. Duperrin[101], H. Duran Yildiz[4a], M. Düren[56], A. Durglishvili[159b], D. Duschinger[48], B. Dutta[46], D. Duvnjak[1], G. I. Dyckes[137], M. Dyndal[36], S. Dysch[100], B. S. Dziedzic[84], K. M. Ecker[115], R. C. Edgar[105], T. Eifert[36], G. Eigen[17], K. Einsweiler[18], T. Ekelof[172], H. El Jarrari[35e], M. El Kacimi[35c], R. El Kosseifi[101], V. Ellajosyula[172], M. Ellert[172], F. Ellinghaus[182], A. A. Elliot[92], N. Ellis[36], J. Elmsheuser[29], M. Elsing[36], D. Emeliyanov[144], A. Emerman[39], Y. Enari[163], J. S. Ennis[178], M. B. Epland[49], J. Erdmann[47], A. Ereditato[20], M. Errenst[36], M. Escalier[132], C. Escobar[174], O. Estrada Pastor[174], E. Etzion[161], H. Evans[65], A. Ezhilov[138], F. Fabbri[57], L. Fabbri[23a,23b], V. Fabiani[119], G. Facini[94], R. M. Faisca Rodrigues Pereira[140a], R. M. Fakhrutdinov[123], S. Falciano[72a], P. J. Falke[5], S. Falke[5], J. Faltova[143], Y. Fang[15a], Y. Fang[15a], G. Fanourakis[44], M. Fanti[68a,68b], A. Farbin[8], A. Farilla[74a], E. M. Farina[70a,70b], T. Farooque[106], S. Farrell[18], S. M. Farrington[178], P. Farthouat[36], F. Fassi[35e], P. Fassnacht[36], D. Fassouliotis[9], M. Faucci Giannelli[50], W. J. Fawcett[32], L. Fayard[132], O. L. Fedin[138,q], W. Fedorko[175], M. Feickert[42], S. Feigl[134], L. Feligioni[101], A. Fell[149], C. Feng[60b], E. J. Feng[36], M. Feng[49], M. J. Fenton[57], A. B. Fenyuk[123], J. Ferrando[46], A. Ferrante[173], A. Ferrari[172], P. Ferrari[120], R. Ferrari[70a], D. E. Ferreira de Lima[61b], A. Ferrer[174], D. Ferrere[54], C. Ferretti[105], F. Fiedler[99], A. Filipčič[91], F. Filthaut[119], K. D. Finelli[25], M. C. N. Fiolhais[140a,140c,a], L. Fiorini[174], F. Fischer[114], W. C. Fisher[106], I. Fleck[151], P. Fleischmann[105], R. R. M. Fletcher[137], T. Flick[182], B. M. Flierl[114], L. Flores[137], L. R. Flores Castillo[63a], F. M. Follega[75a,75b], N. Fomin[17], J. H. Foo[167], G. T. Forcolin[75a,75b], A. Formica[145], F. A. Förster[14], A. C. Forti[100], A. G. Foster[21], M. G. Foti[135], D. Fournier[132], H. Fox[89], P. Francavilla[71a,71b], S. Francescato[72a,72b], M. Franchini[23a,23b], S. Franchino[61a], D. Francis[36], L. Franconi[20], M. Franklin[59], A. N. Fray[92], B. Freund[109], W. S. Freund[80b], E. M. Freundlich[47], D. C. Frizzell[128], D. Froidevaux[36], J. A. Frost[135], C. Fukunaga[164], E. Fullana Torregrosa[174], E. Fumagalli[55a,55b], T. Fusayasu[116], J. Fuster[174], A. Gabrielli[23a,23b], A. Gabrielli[18], G. P. Gach[83a], S. Gadatsch[54], P. Gadow[115], G. Gagliardi[55a,55b], L. G. Gagnon[109], C. Galea[27b], B. Galhardo[140a], G. E. Gallardo[135], E. J. Gallas[135], B. J. Gallop[144], P. Gallus[142], G. Galster[40], R. Gamboa Goni[92], K. K. Gan[126], S. Ganguly[180], J. Gao[60a], Y. Gao[90], Y. S. Gao[31,n], C. García[174], J. E. García Navarro[174], J. A. García Pascual[15a], C. Garcia-Argos[52], M. Garcia-Sciveres[18], R. W. Gardner[37], N. Garelli[153], S. Gargiulo[52], V. Garonne[134], K. Gasnikova[46], A. Gaudiello[55a,55b], G. Gaudio[70a], I. L. Gavrilenko[110], A. Gavrilyuk[111], C. Gay[175], G. Gaycken[24], E. N. Gazis[10], A. A. Geanta[27b], C. N. P. Gee[144], J. Geisen[53], M. Geisen[99], M. P. Geisler[61a], C. Gemme[55b], M. H. Genest[58], C. Geng[105], S. Gentile[72a,72b], S. George[93], T. Geralis[44], L. O. Gerlach[53], P. Gessinger-Befurt[99], G. Gessner[47], S. Ghasemi[151], M. Ghasemi Bostanabad[176], A. Ghosh[77], B. Giacobbe[23b], S. Giagu[72a,72b], N. Giangiacomi[23a,23b], P. Giannetti[71a], A. Giannini[69a,69b], S. M. Gibson[93], M. Gignac[146], D. Gillberg[34], G. Gilles[182], D. M. Gingrich[3,az], M. P. Giordani[66a,66c], F. M. Giorgi[23b], P. F. Giraud[145], G. Giugliarelli[66a,66c], D. Giugni[68a], F. Giuli[73a,73b], S. Gkaitatzis[162], I. Gkialas[9,i], E. L. Gkougkousis[14], P. Gkountoumis[10], L. K. Gladilin[113], C. Glasman[98], J. Glatzer[14], P. C. F. Glaysher[46], A. Glazov[46], M. Goblirsch-Kolb[26], S. Goldfarb[104], T. Golling[54], D. Golubkov[123], A. Gomes[140a,140b], R. Goncalves Gama[53], R. Gonçalo[140a,140b], G. Gonella[52], L. Gonella[21], A. Gongadze[79], F. Gonnella[21], J. L. Gonski[59], S. González de la Hoz[174], S. Gonzalez-Sevilla[54], G. R. Gonzalvo Rodriguez[174], L. Goossens[36], P. A. Gorbounov[111], H. A. Gordon[29], B. Gorini[36], E. Gorini[67a,67b], A. Gorišek[91], A. T. Goshaw[49], M. I. Gostkin[79], C. A. Gottardo[24], M. Gouighri[35b], D. Goujdami[35c], A. G. Goussiou[148], N. Govender[33b,b], C. Goy[5], E. Gozani[160], I. Grabowska-Bold[83a], E. C. Graham[90], J. Gramling[171], E. Gramstad[134], S. Grancagnolo[19], M. Grandi[156], V. Gratchev[138], P. M. Gravila[27f], F. G. Gravili[67a,67b], C. Gray[57], H. M. Gray[18], C. Grefe[24], K. Gregersen[96], I. M. Gregor[46], P. Grenier[153], K. Grevtsov[46], C. Grieco[14], N. A. Grieser[128], J. Griffiths[8], A. A. Grillo[146], K. Grimm[31,m], S. Grinstein[14,z], J.-F. Grivaz[132], S. Groh[99], E. Gross[180], J. Grosse-Knetter[53], Z. J. Grout[94], C. Grud[105], A. Grummer[118], L. Guan[105], W. Guan[181], J. Guenther[36], A. Guerguichon[132], F. Guescini[115], D. Guest[171], R. Gugel[52],

T. Guillemin[5], S. Guindon[36], U. Gul[57], J. Guo[60c], W. Guo[105], Y. Guo[60a,u], Z. Guo[101], R. Gupta[46], S. Gurbuz[12c], G. Gustavino[128], P. Gutierrez[128], C. Gutschow[94], C. Guyot[145], M. P. Guzik[83a], C. Gwenlan[135], C. B. Gwilliam[90], A. Haas[124], C. Haber[18], H. K. Hadavand[8], N. Haddad[35e], A. Hadef[60a], S. Hageböck[36], M. Hagihara[169], M. Haleem[177], J. Haley[129], G. Halladjian[106], G. D. Hallewell[101], K. Hamacher[182], P. Hamal[130], K. Hamano[176], H. Hamdaoui[35e], G. N. Hamity[149], K. Han[60a,am], L. Han[60a], S. Han[15a,15d], K. Hanagaki[81,x], M. Hance[146], D. M. Handl[114], B. Haney[137], R. Hankache[136], E. Hansen[96], J. B. Hansen[40], J. D. Hansen[40], M. C. Hansen[24], P. H. Hansen[40], E. C. Hanson[100], K. Hara[169], A. S. Hard[181], T. Harenberg[182], S. Harkusha[107], P. F. Harrison[178], N. M. Hartmann[114], Y. Hasegawa[150], A. Hasib[50], S. Hassani[145], S. Haug[20], R. Hauser[106], L. B. Havener[39], M. Havranek[142], C. M. Hawkes[21], R. J. Hawkings[36], D. Hayden[106], C. Hayes[155], R. L. Hayes[175], C. P. Hays[135], J. M. Hays[92], H. S. Hayward[90], S. J. Haywood[144], F. He[60a], M. P. Heath[50], V. Hedberg[96], L. Heelan[8], S. Heer[24], K. K. Heidegger[52], W. D. Heidorn[78], J. Heilman[34], S. Heim[46], T. Heim[18], B. Heinemann[46,au], J. J. Heinrich[131], L. Heinrich[36], C. Heinz[56], J. Hejbal[141], L. Helary[61b], A. Held[175], S. Hellesund[134], C. M. Helling[146], S. Hellman[45a,45b], C. Helsens[36], R. C. W. Henderson[89], Y. Heng[181], S. Henkelmann[175], A. M. Henriques Correia[36], G. H. Herbert[19], H. Herde[26], V. Herget[177], Y. Hernández Jiménez[33c], H. Herr[99], M. G. Herrmann[114], T. Herrmann[48], G. Herten[52], R. Hertenberger[114], L. Hervas[36], T. C. Herwig[137], G. G. Hesketh[94], N. P. Hessey[168a], A. Higashida[163], S. Higashino[81], E. Higón-Rodriguez[174], K. Hildebrand[37], E. Hill[176], J. C. Hill[32], K. K. Hill[29], K. H. Hiller[46], S. J. Hillier[21], M. Hils[48], I. Hinchliffe[18], F. Hinterkeuser[24], M. Hirose[133], S. Hirose[52], D. Hirschbuehl[182], B. Hiti[91], O. Hladik[141], D. R. Hlaluku[33c], X. Hoad[50], J. Hobbs[155], N. Hod[180], M. C. Hodgkinson[149], A. Hoecker[36], F. Hoenig[114], D. Hohn[52], D. Hohov[132], T. R. Holmes[37], M. Holzbock[114], L.B.A.H Hommels[32], S. Honda[169], T. Honda[81], T. M. Hong[139], A. Hönle[115], B. H. Hooberman[173], W. H. Hopkins[6], Y. Horii[117], P. Horn[48], L. A. Horyn[37], J-Y. Hostachy[58], A. Hostiuc[148], S. Hou[158], A. Hoummada[35a], J. Howarth[100], J. Hoya[88], M. Hrabovsky[130], J. Hrdinka[76], I. Hristova[19], J. Hrivnac[132], A. Hrynevich[108], T. Hryn'ova[5], P. J. Hsu[64], S.-C. Hsu[148], Q. Hu[29], S. Hu[60c], Y. Huang[15a], Z. Hubacek[142], F. Hubaut[101], M. Huebner[24], F. Huegging[24], T. B. Huffman[135], M. Huhtinen[36], R. F. H. Hunter[34], P. Huo[155], A. M. Hupe[34], N. Huseynov[79,ah], J. Huston[106], J. Huth[59], R. Hyneman[105], S. Hyrych[28a], G. Iacobucci[54], G. Iakovidis[29], I. Ibragimov[151], L. Iconomidou-Fayard[132], Z. Idrissi[35e], P. Iengo[36], R. Ignazzi[40], O. Igonkina[120,ab,*], R. Iguchi[163], T. Iizawa[54], Y. Ikegami[81], M. Ikeno[81], D. Iliadis[162], N. Ilic[119], F. Iltzsche[48], G. Introzzi[70a,70b], M. Iodice[74a], K. Iordanidou[168a], V. Ippolito[72a,72b], M. F. Isacson[172], M. Ishino[163], M. Ishitsuka[165], W. Islam[129], C. Issever[135], S. Istin[160], F. Ito[169], J. M. Iturbe Ponce[63a], R. Iuppa[75a,75b], A. Ivina[180], H. Iwasaki[81], J. M. Izen[43], V. Izzo[69a], P. Jacka[141], P. Jackson[1], R. M. Jacobs[24], B. P. Jaeger[152], V. Jain[2], G. Jäkel[182], K. B. Jakobi[99], K. Jakobs[52], S. Jakobsen[76], T. Jakoubek[141], J. Jamieson[57], K. W. Janas[83a], R. Jansky[54], J. Janssen[24], M. Janus[53], P. A. Janus[83a], G. Jarlskog[96], N. Javadov[79,ah], T. Javůrek[36], M. Javurkova[52], F. Jeanneau[145], L. Jeanty[131], J. Jejelava[159a,ai], A. Jelinskas[178], P. Jenni[52,c], J. Jeong[46], N. Jeong[46], S. Jézéquel[5], H. Ji[181], J. Jia[155], H. Jiang[78], Y. Jiang[60a], Z. Jiang[153,r], S. Jiggins[52], F. A. Jimenez Morales[38], J. Jimenez Pena[174], S. Jin[15c], A. Jinaru[27b], O. Jinnouchi[165], H. Jivan[33c], P. Johansson[149], K. A. Johns[7], C. A. Johnson[65], K. Jon-And[45a,45b], R. W. L. Jones[89], S. D. Jones[156], S. Jones[7], T. J. Jones[90], J. Jongmanns[61a], P. M. Jorge[140a], J. Jovicevic[36], X. Ju[18], J. J. Junggeburth[115], A. Juste Rozas[14,z], A. Kaczmarska[84], M. Kado[72a,72b], H. Kagan[126], M. Kagan[153], C. Kahra[99], T. Kaji[179], E. Kajomovitz[160], C. W. Kalderon[96], A. Kaluza[99], A. Kamenshchikov[123], L. Kanjir[91], Y. Kano[163], V. A. Kantserov[112], J. Kanzaki[81], L. S. Kaplan[181], D. Kar[33c], M. J. Kareem[168b], E. Karentzos[10], S. N. Karpov[79], Z. M. Karpova[79], V. Kartvelishvili[89], A. N. Karyukhin[123], L. Kashif[181], R. D. Kass[126], A. Kastanas[45a,45b], Y. Kataoka[163], C. Kato[60c,60d], J. Katzy[46], K. Kawade[82], K. Kawagoe[87], T. Kawaguchi[117], T. Kawamoto[163], G. Kawamura[53], E. F. Kay[176], V. F. Kazanin[122a,122b], R. Keeler[176], R. Kehoe[42], J. S. Keller[34], E. Kellermann[96], D. Kelsey[156], J. J. Kempster[21], J. Kendrick[21], O. Kepka[141], S. Kersten[182], B. P. Kerševan[91], S. Ketabchi Haghighat[167], M. Khader[173], F. Khalil-Zada[13], M. Khandoga[145], A. Khanov[129], A. G. Kharlamov[122a,122b], T. Kharlamova[122a,122b], E. E. Khoda[175], A. Khodinov[166], T. J. Khoo[54], E. Khramov[79], J. Khubua[159b], S. Kido[82], M. Kiehn[54], C. R. Kilby[93], Y. K. Kim[37], N. Kimura[66a,66c], O. M. Kind[19], B. T. King[90,*], D. Kirchmeier[48], J. Kirk[144], A. E. Kiryunin[115], T. Kishimoto[163], D. P. Kisliuk[167], V. Kitali[46], O. Kivernyk[5], E. Kladiva[28b,*], T. Klapdor-Kleingrothaus[52], M. Klassen[61a], M. H. Klein[105], M. Klein[90], U. Klein[90], K. Kleinknecht[99], P. Klimek[121], A. Klimentov[29], T. Klingl[24], T. Klioutchnikova[36], F. F. Klitzner[114], P. Kluit[120], S. Kluth[115], E. Kneringer[76], E. B. F. G. Knoops[101], A. Knue[52], D. Kobayashi[87], T. Kobayashi[163], M. Kobel[48], M. Kocian[153], P. Kodys[143], P. T. Koenig[24], T. Koffas[34], N. M. Köhler[115], T. Koi[153], M. Kolb[61b], I. Koletsou[5], T. Komarek[130], T. Kondo[81], N. Kondrashova[60c], K. Köneke[52], A. C. König[119], T. Kono[125], R. Konoplich[124,ap], V. Konstantinides[94], N. Konstantinidis[94], B. Konya[96], R. Kopeliansky[65], S. Koperny[83a], K. Korcyl[84], K. Kordas[162], G. Koren[161], A. Korn[94], I. Korolkov[14], E. V. Korolkova[149], N. Korotkova[113], O. Kortner[115], S. Kortner[115], T. Kosek[143], V. V. Kostyukhin[24], A. Kotwal[49], A. Koulouris[10], A. Kourkoumeli-Charalampidi[70a,70b], C. Kourkoumelis[9], E. Kourlitis[149], V. Kouskoura[29], A. B. Kowalewska[84], R. Kowalewski[176], C. Kozakai[163], W. Kozanecki[145], A. S. Kozhin[123], V. A. Kramarenko[113], G. Kramberger[91], D. Krasnopevtsev[60a], M. W. Krasny[136], A. Krasznahorkay[36], D. Krauss[115], J. A. Kremer[83a],

J. Kretzschmar[90], P. Krieger[167], F. Krieter[114], A. Krishnan[61b], K. Krizka[18], K. Kroeninger[47], H. Kroha[115], J. Kroll[141], J. Kroll[137], J. Krstic[16], U. Kruchonak[79], H. Krüger[24], N. Krumnack[78], M. C. Kruse[49], J. A. Krzysiak[84], T. Kubota[104], S. Kuday[4b], J. T. Kuechler[46], S. Kuehn[36], A. Kugel[61a], T. Kuhl[46], V. Kukhtin[79], R. Kukla[101], Y. Kulchitsky[107,al], S. Kuleshov[147c], Y. P. Kulinich[173], M. Kuna[58], T. Kunigo[85], A. Kupco[141], T. Kupfer[47], O. Kuprash[52], H. Kurashige[82], L. L. Kurchaninov[168a], Y. A. Kurochkin[107], A. Kurova[112], M. G. Kurth[15a,15d], E. S. Kuwertz[36], M. Kuze[165], A. K. Kvam[148], J. Kvita[130], T. Kwan[103], A. La Rosa[115], L. La Rotonda[41a,41b], F. La Ruffa[41a,41b], C. Lacasta[174], F. Lacava[72a,72b], D. P. J. Lack[100], H. Lacker[19], D. Lacour[136], E. Ladygin[79], R. Lafaye[5], B. Laforge[136], T. Lagouri[33c], S. Lai[53], S. Lammers[65], W. Lampl[7], C. Lampoudis[162], E. Lançon[29], U. Landgraf[52], M. P. J. Landon[92], M. C. Lanfermann[54], V. S. Lang[46], J. C. Lange[53], R. J. Langenberg[36], A. J. Lankford[171], F. Lanni[29], K. Lantzsch[24], A. Lanza[70a], A. Lapertosa[55a,55b], S. Laplace[136], J. F. Laporte[145], T. Lari[68a], F. Lasagni Manghi[23a,23b], M. Lassnig[36], T. S. Lau[63a], A. Laudrain[132], A. Laurier[34], M. Lavorgna[69a,69b], M. Lazzaroni[68a,68b], B. Le[104], E. Le Guirriec[101], M. LeBlanc[7], T. LeCompte[6], F. Ledroit-Guillon[58], C. A. Lee[29], G. R. Lee[17], L. Lee[59], S. C. Lee[158], S. J. Lee[34], B. Lefebvre[168a], M. Lefebvre[176], F. Legger[114], C. Leggett[18], K. Lehmann[152], N. Lehmann[182], G. Lehmann Miotto[36], W. A. Leight[46], A. Leisos[162,y], M. A. L. Leite[80d], C. E. Leitgeb[114], R. Leitner[143], D. Lellouch[180,*], K. J. C. Leney[42], T. Lenz[24], B. Lenzi[36], R. Leone[7], S. Leone[71a], C. Leonidopoulos[50], A. Leopold[136], G. Lerner[156], C. Leroy[109], R. Les[167], C. G. Lester[32], M. Levchenko[138], J. Levêque[5], D. Levin[105], L. J. Levinson[180], D. J. Lewis[21], B. Li[15b], B. Li[105], C-Q. Li[60a], F. Li[60c], H. Li[60a], H. Li[60b], J. Li[60c], K. Li[153], L. Li[60c], M. Li[15a], Q. Li[15a,15d], Q. Y. Li[60a], S. Li[60c,60d], X. Li[46], Y. Li[46], Z. Li[60b], Z. Liang[15a], B. Liberti[73a], A. Liblong[167], K. Lie[63c], S. Liem[120], C. Y. Lin[32], K. Lin[106], T. H. Lin[99], R. A. Linck[65], J. H. Lindon[21], A. L. Lionti[54], E. Lipeles[137], A. Lipniacka[17], M. Lisovyi[61b], T. M. Liss[173,aw], A. Lister[175], A. M. Litke[146], J. D. Little[8], B. Liu[78,ae], B.L Liu[6], H. B. Liu[29], H. Liu[105], J. B. Liu[60a], J. K. K. Liu[135], K. Liu[136], M. Liu[60a], P. Liu[18], Y. Liu[15a,15d], Y. L. Liu[105], Y. W. Liu[60a], M. Livan[70a,70b], A. Lleres[58], J. Llorente Merino[15a], S. L. Lloyd[92], C. Y. Lo[63b], F. Lo Sterzo[42], E. M. Lobodzinska[46], P. Loch[7], S. Loffredo[73a,73b], T. Lohse[19], K. Lohwasser[149], M. Lokajicek[141], J. D. Long[173], R. E. Long[89], L. Longo[36], K. A. Looper[126], J. A. Lopez[147c], I. Lopez Paz[100], A. Lopez Solis[149], J. Lorenz[114], N. Lorenzo Martinez[5], M. Losada[22], P. J. Lösel[114], A. Lösle[52], X. Lou[46], X. Lou[15a], A. Lounis[132], J. Love[6], P. A. Love[89], J. J. Lozano Bahilo[174], M. Lu[60a], Y. J. Lu[64], H. J. Lubatti[148], C. Luci[72a,72b], A. Lucotte[58], C. Luedtke[52], F. Luehring[65], I. Luise[136], L. Luminari[72a], B. Lund-Jensen[154], M. S. Lutz[102], D. Lynn[29], R. Lysak[141], E. Lytken[96], F. Lyu[15a], V. Lyubushkin[79], T. Lyubushkina[79], H. Ma[29], L. L. Ma[60b], Y. Ma[60b], G. Maccarrone[51], A. Macchiolo[115], C. M. Macdonald[149], J. Machado Miguens[137], D. Madaffari[174], R. Madar[38], W. F. Mader[48], N. Madysa[48], J. Maeda[82], K. Maekawa[163], S. Maeland[17], T. Maeno[29], M. Maerker[48], A. S. Maevskiy[113], V. Magerl[52], N. Magini[78], D. J. Mahon[39], C. Maidantchik[80b], T. Maier[114], A. Maio[140a,140b,140d], K. Maj[84], O. Majersky[28a], S. Majewski[131], Y. Makida[81], N. Makovec[132], B. Malaescu[136], Pa. Malecki[84], V. P. Maleev[138], F. Malek[58], U. Mallik[77], D. Malon[6], C. Malone[32], S. Maltezos[10], S. Malyukov[79], J. Mamuzic[174], G. Mancini[51], I. Mandić[91], L. Manhaes de Andrade Filho[80a], I. M. Maniatis[162], J. Manjarres Ramos[48], K. H. Mankinen[96], A. Mann[114], A. Manousos[76], B. Mansoulie[145], I. Manthos[162], S. Manzoni[120], A. Marantis[162], G. Marceca[30], L. Marchese[135], G. Marchiori[136], M. Marcisovsky[141], C. Marcon[96], C. A. Marin Tobon[36], M. Marjanovic[38], Z. Marshall[18], M.U.F Martensson[172], S. Marti-Garcia[174], C. B. Martin[126], T. A. Martin[178], V. J. Martin[50], B. Martin dit Latour[17], L. Martinelli[74a,74b], M. Martinez[14,z], V. I. Martinez Outschoorn[102], S. Martin-Haugh[144], V. S. Martoiu[27b], A. C. Martyniuk[94], A. Marzin[36], S. R. Maschek[115], L. Masetti[99], T. Mashimo[163], R. Mashinistov[110], J. Masik[100], A. L. Maslennikov[122a,122b], L. H. Mason[104], L. Massa[73a,73b], P. Massarotti[69a,69b], P. Mastrandrea[71a,71b], A. Mastroberardino[41a,41b], T. Masubuchi[163], A. Matic[114], P. Mättig[24], J. Maurer[27b], B. Maček[91], D. A. Maximov[122a,122b], R. Mazini[158], I. Maznas[162], S. M. Mazza[146], S. P. Mc Kee[105], T. G. McCarthy[115], L. I. McClymont[94], W. P. McCormack[18], E. F. McDonald[104], J. A. Mcfayden[36], M. A. McKay[42], K. D. McLean[176], S. J. McMahon[144], P. C. McNamara[104], C. J. McNicol[178], R. A. McPherson[176,af], J. E. Mdhluli[33c], Z. A. Meadows[102], S. Meehan[148], T. Megy[52], S. Mehlhase[114], A. Mehta[90], T. Meideck[58], B. Meirose[43], D. Melini[174], B. R. Mellado Garcia[33c], J. D. Mellenthin[53], M. Melo[28a], F. Meloni[46], A. Melzer[24], S. B. Menary[100], E. D. Mendes Gouveia[140a,140e], L. Meng[36], X. T. Meng[105], S. Menke[115], E. Meoni[41a,41b], S. Mergelmeyer[19], S. A. M. Merkt[139], C. Merlassino[20], P. Mermod[54], L. Merola[69a,69b], C. Meroni[68a], O. Meshkov[113,110], J. K. R. Meshreki[151], A. Messina[72a,72b], J. Metcalfe[6], A. S. Mete[171], C. Meyer[65], J. Meyer[160], J-P. Meyer[145], H. Meyer Zu Theenhausen[61a], F. Miano[156], R. P. Middleton[144], L. Mijović[50], G. Mikenberg[180], M. Mikestikova[141], M. Mikuž[91], H. Mildner[149], M. Milesi[104], A. Milic[167], D. A. Millar[92], D. W. Miller[37], A. Milov[180], D. A. Milstead[45a,45b], R. A. Mina[153,r], A. A. Minaenko[123], M. Miñano Moya[174], I. A. Minashvili[159b], A. I. Mincer[124], B. Mindur[83a], M. Mineev[79], Y. Minegishi[163], Y. Ming[181], L. M. Mir[14], A. Mirto[67a,67b], K. P. Mistry[137], T. Mitani[179], J. Mitrevski[114], V. A. Mitsou[174], M. Mittal[60c], A. Miucci[20], P. S. Miyagawa[149], A. Mizukami[81], J. U. Mjörnmark[96], T. Mkrtchyan[184], M. Mlynarikova[143], T. Moa[45a,45b], K. Mochizuki[109], P. Mogg[52], S. Mohapatra[39], R. Moles-Valls[24], M. C. Mondragon[106], K. Mönig[46], J. Monk[40], E. Monnier[101], A. Montalbano[152], J. Montejo Berlingen[36],

M. Montella[94], F. Monticelli[88], S. Monzani[68a], N. Morange[132], D. Moreno[22], M. Moreno Llácer[36], C. Moreno Martinez[14], P. Morettini[55b], M. Morgenstern[120], S. Morgenstern[48], D. Mori[152], M. Morii[59], M. Morinaga[179], V. Morisbak[134], A. K. Morley[36], G. Mornacchi[36], A. P. Morris[94], L. Morvaj[155], P. Moschovakos[36], B. Moser[120], M. Mosidze[159b], T. Moskalets[145], H. J. Moss[149], J. Moss[31,o], K. Motohashi[165], E. Mountricha[36], E. J. W. Moyse[102], S. Muanza[101], J. Mueller[139], R. S. P. Mueller[114], D. Muenstermann[89], G. A. Mullier[96], J. L. Munoz Martinez[14], F. J. Munoz Sanchez[100], P. Murin[28b], W. J. Murray[178,144], A. Murrone[68a,68b], M. Muškinja[18], C. Mwewa[33a], A. G. Myagkov[123,aq], J. Myers[131], M. Myska[142], B. P. Nachman[18], O. Nackenhorst[47], A. Nag Nag[48], K. Nagai[135], K. Nagano[81], Y. Nagasaka[62], M. Nagel[52], E. Nagy[101], A. M. Nairz[36], Y. Nakahama[117], K. Nakamura[81], T. Nakamura[163], I. Nakano[127], H. Nanjo[133], F. Napolitano[61a], R. F. Naranjo Garcia[46], R. Narayan[42], D. I. Narrias Villar[61a], I. Naryshkin[138], T. Naumann[46], G. Navarro[22], H. A. Neal[105,*], P. Y. Nechaeva[110], F. Nechansky[46], T. J. Neep[21], A. Negri[70a,70b], M. Negrini[23b], C. Nellist[53], M. E. Nelson[135], S. Nemecek[141], P. Nemethy[124], M. Nessi[36,e], M. S. Neubauer[173], M. Neumann[182], P. R. Newman[21], T. Y. Ng[63c], Y. S. Ng[19], Y. W. Y. Ng[171], H. D. N. Nguyen[101], T. Nguyen Manh[109], E. Nibigira[38], R. B. Nickerson[135], R. Nicolaidou[145], D. S. Nielsen[40], J. Nielsen[146], N. Nikiforou[11], V. Nikolaenko[123,aq], I. Nikolic-Audit[136], K. Nikolopoulos[21], P. Nilsson[29], H. R. Nindhito[54], Y. Ninomiya[81], A. Nisati[72a], N. Nishu[60c], R. Nisius[115], I. Nitsche[47], T. Nitta[179], T. Nobe[163], Y. Noguchi[85], I. Nomidis[136], M. A. Nomura[29], M. Nordberg[36], N. Norjoharuddeen[135], T. Novak[91], O. Novgorodova[48], R. Novotny[142], L. Nozka[130], K. Ntekas[171], E. Nurse[94], F. G. Oakham[34,az], H. Oberlack[115], J. Ocariz[136], A. Ochi[82], I. Ochoa[39], J. P. Ochoa-Ricoux[147a], K. O'Connor[26], S. Oda[87], S. Odaka[81], S. Oerdek[53], A. Ogrodnik[83a], A. Oh[100], S. H. Oh[49], C. C. Ohm[154], H. Oide[55a,55b], M. L. Ojeda[167], H. Okawa[169], Y. Okazaki[85], Y. Okumura[163], T. Okuyama[81], A. Olariu[27b], L. F. Oleiro Seabra[140a], S. A. Olivares Pino[147a], D. Oliveira Damazio[29], J. L. Oliver[1], M. J. R. Olsson[171], A. Olszewski[84], J. Olszowska[84], D. C. O'Neil[152], A. Onofre[140a,140e], K. Onogi[117], P. U. E. Onyisi[11], H. Oppen[134], M. J. Oreglia[37], G. E. Orellana[88], D. Orestano[74a,74b], N. Orlando[14], R. S. Orr[167], V. O'Shea[57], R. Ospanov[60a], G. Otero y Garzon[30], H. Otono[87], M. Ouchrif[35d], J. Ouellette[29], F. Ould-Saada[134], A. Ouraou[145], Q. Ouyang[15a], M. Owen[57], R. E. Owen[21], V. E. Ozcan[12c], N. Ozturk[8], J. Pacalt[130], H. A. Pacey[32], K. Pachal[49], A. Pacheco Pages[14], C. Padilla Aranda[14], S. Pagan Griso[18], M. Paganini[183], G. Palacino[65], S. Palazzo[50], S. Palestini[36], M. Palka[83b], D. Pallin[38], I. Panagoulias[10], C. E. Pandini[36], J. G. Panduro Vazquez[93], P. Pani[46], G. Panizzo[66a,66c], L. Paolozzi[54], C. Papadatos[109], K. Papageorgiou[9,i], A. Paramonov[6], D. Paredes Hernandez[63b], S. R. Paredes Saenz[135], B. Parida[166], T. H. Park[167], A. J. Parker[89], M. A. Parker[32], F. Parodi[55a,55b], E. W. P. Parrish[121], J. A. Parsons[39], U. Parzefall[52], L. Pascual Dominguez[136], V. R. Pascuzzi[167], J. M. P. Pasner[146], E. Pasqualucci[72a], S. Passaggio[55b], F. Pastore[93], P. Pasuwan[45a,45b], S. Pataraia[99], J. R. Pater[100], A. Pathak[181], T. Pauly[36], B. Pearson[115], M. Pedersen[134], L. Pedraza Diaz[119], R. Pedro[140a], T. Peiffer[53], S. V. Peleganchuk[122a,122b], O. Penc[141], H. Peng[60a], B. S. Peralva[80a], M. M. Perego[132], A. P. Pereira Peixoto[140a], D. V. Perepelitsa[29], F. Peri[19], L. Perini[68a,68b], H. Pernegger[36], S. Perrella[69a,69b], K. Peters[46], R. F. Y. Peters[100], B. A. Petersen[36], T. C. Petersen[40], E. Petit[101], A. Petridis[1], C. Petridou[162], P. Petroff[132], M. Petrov[135], F. Petrucci[74a,74b], M. Pettee[183], N. E. Pettersson[102], K. Petukhova[143], A. Peyaud[145], R. Pezoa[147c], L. Pezzotti[70a,70b], T. Pham[104], F. H. Phillips[106], P. W. Phillips[144], M. W. Phipps[173], G. Piacquadio[155], E. Pianori[18], A. Picazio[102], R. H. Pickles[100], R. Piegaia[30], D. Pietreanu[27b], J. E. Pilcher[37], A. D. Pilkington[100], M. Pinamonti[73a,73b], J. L. Pinfold[3], M. Pitt[180], L. Pizzimento[73a,73b], M.-A. Pleier[29], V. Pleskot[143], E. Plotnikova[79], D. Pluth[78], P. Podberezko[122a,122b], R. Poettgen[96], R. Poggi[54], L. Poggioli[132], I. Pogrebnyak[106], D. Pohl[24], I. Pokharel[53], G. Polesello[70a], A. Poley[18], A. Policicchio[72a,72b], R. Polifka[143], A. Polini[23b], C. S. Pollard[46], V. Polychronakos[29], D. Ponomarenko[112], L. Pontecorvo[36], S. Popa[27a], G. A. Popeneciu[27d], D. M. Portillo Quintero[58], S. Pospisil[142], K. Potamianos[46], I. N. Potrap[79], C. J. Potter[32], H. Potti[11], T. Poulsen[96], J. Poveda[36], T. D. Powell[149], G. Pownall[46], M. E. Pozo Astigarraga[36], P. Pralavorio[101], S. Prell[78], D. Price[100], M. Primavera[67a], S. Prince[103], M. L. Proffitt[148], N. Proklova[112], K. Prokofiev[63c], F. Prokoshin[79], S. Protopopescu[29], J. Proudfoot[6], M. Przybycien[83a], D. Pudzha[138], A. Puri[173], P. Puzo[132], J. Qian[105], Y. Qin[100], A. Quadt[53], M. Queitsch-Maitland[46], A. Qureshi[1], P. Rados[104], F. Ragusa[68a,68b], G. Rahal[97], J. A. Raine[54], S. Rajagopalan[29], A. Ramirez Morales[92], K. Ran[15a,15d], T. Rashid[132], S. Raspopov[5], M. G. Ratti[68a,68b], D. M. Rauch[46], F. Rauscher[114], S. Rave[99], B. Ravina[149], I. Ravinovich[180], J. H. Rawling[100], M. Raymond[36], A. L. Read[134], N. P. Readioff[58], M. Reale[67a,67b], D. M. Rebuzzi[70a,70b], A. Redelbach[177], G. Redlinger[29], K. Reeves[43], L. Rehnisch[19], J. Reichert[137], D. Reikher[161], A. Reiss[99], A. Rej[151], C. Rembser[36], M. Renda[27b], M. Rescigno[72a], S. Resconi[68a], E. D. Resseguie[137], S. Rettie[175], E. Reynolds[21], O. L. Rezanova[122a,122b], P. Reznicek[143], E. Ricci[75a,75b], R. Richter[115], S. Richter[46], E. Richter-Was[83b], O. Ricken[24], M. Ridel[136], P. Rieck[115], C. J. Riegel[182], O. Rifki[46], M. Rijssenbeek[155], A. Rimoldi[70a,70b], M. Rimoldi[46], L. Rinaldi[23b], G. Ripellino[154], B. Ristić[89], E. Ritsch[36], I. Riu[14], J. C. Rivera Vergara[176], F. Rizatdinova[129], E. Rizvi[92], C. Rizzi[36], R. T. Roberts[100], S. H. Robertson[103,af], M. Robin[46], D. Robinson[32], J. E. M. Robinson[46], C. M. Robles Gajardo[147c], A. Robson[57], E. Rocco[99], C. Roda[71a,71b], S. Rodriguez Bosca[174], A. Rodriguez Perez[14], D. Rodriguez Rodriguez[174], A. M. Rodríguez Vera[168b], S. Roe[36], O. Røhne[134], R. Röhrig[115], C. P. A. Roland[65], J. Roloff[59],

A. Romaniouk[112], M. Romano[23a,23b], N. Rompotis[90], M. Ronzani[124], L. Roos[136], S. Rosati[72a], K. Rosbach[52], G. Rosin[102], B. J. Rosser[137], E. Rossi[46], E. Rossi[74a,74b], E. Rossi[69a,69b], L. P. Rossi[55b], L. Rossini[68a,68b], R. Rosten[14], M. Rotaru[27b], J. Rothberg[148], D. Rousseau[132], G. Rovelli[70a,70b], D. Roy[33c], A. Rozanov[101], Y. Rozen[160], X. Ruan[33c], F. Rubbo[153], F. Rühr[52], A. Ruiz-Martinez[174], A. Rummler[36], Z. Rurikova[52], N. A. Rusakovich[79], H. L. Russell[103], L. Rustige[38,47], J. P. Rutherfoord[7], E. M. Rüttinger[46,k], M. Rybar[39], G. Rybkin[132], A. Ryzhov[123], G. F. Rzehorz[53], P. Sabatini[53], G. Sabato[120], S. Sacerdoti[132], H.F-W. Sadrozinski[146], R. Sadykov[79], F. Safai Tehrani[72a], B. Safarzadeh Samani[156], P. Saha[121], S. Saha[103], M. Sahinsoy[61a], A. Sahu[182], M. Saimpert[46], M. Saito[163], T. Saito[163], H. Sakamoto[163], A. Sakharov[124,ap], D. Salamani[54], G. Salamanna[74a,74b], J. E. Salazar Loyola[147c], P. H. Sales De Bruin[172], A. Salnikov[153], J. Salt[174], D. Salvatore[41a,41b], F. Salvatore[156], A. Salvucci[63a,63b,63c], A. Salzburger[36], J. Samarati[36], D. Sammel[52], D. Sampsonidis[162], D. Sampsonidou[162], J. Sánchez[174], A. Sanchez Pineda[66a,66c], H. Sandaker[134], C. O. Sander[46], I. G. Sanderswood[89], M. Sandhoff[182], C. Sandoval[22], D. P. C. Sankey[144], M. Sannino[55a,55b], Y. Sano[117], A. Sansoni[51], C. Santoni[38], H. Santos[140a,140b], S. N. Santpur[18], A. Santra[174], A. Sapronov[79], J. G. Saraiva[140a,140d], O. Sasaki[81], K. Sato[169], E. Sauvan[5], P. Savard[167,az], N. Savic[115], R. Sawada[163], C. Sawyer[144], L. Sawyer[95,an], C. Sbarra[23b], A. Sbrizzi[23a], T. Scanlon[94], J. Schaarschmidt[148], P. Schacht[115], B. M. Schachtner[114], D. Schaefer[37], L. Schaefer[137], J. Schaeffer[99], S. Schaepe[36], U. Schäfer[99], A. C. Schaffer[132], D. Schaile[114], R. D. Schamberger[155], N. Scharmberg[100], V. A. Schegelsky[138], D. Scheirich[143], F. Schenck[19], M. Schernau[171], C. Schiavi[55a,55b], S. Schier[146], L. K. Schildgen[24], Z. M. Schillaci[26], E. J. Schioppa[36], M. Schioppa[41a,41b], K. E. Schleicher[52], S. Schlenker[36], K. R. Schmidt-Sommerfeld[115], K. Schmieden[36], C. Schmitt[99], S. Schmitt[46], S. Schmitz[99], J. C. Schmoeckel[46], U. Schnoor[52], L. Schoeffel[145], A. Schoening[61b], P. G. Scholer[52], E. Schopf[135], M. Schott[99], J. F. P. Schouwenberg[119], J. Schovancova[36], S. Schramm[54], F. Schroeder[182], A. Schulte[99], H-C. Schultz-Coulon[61a], M. Schumacher[52], B. A. Schumm[146], Ph. Schune[145], A. Schwartzman[153], T. A. Schwarz[105], Ph. Schwemling[145], R. Schwienhorst[106], A. Sciandra[146], G. Sciolla[26], M. Scodeggio[46], M. Scornajenghi[41a,41b], F. Scuri[71a], F. Scutti[104], L. M. Scyboz[115], C. D. Sebastiani[72a,72b], P. Seema[19], S. C. Seidel[118], A. Seiden[146], T. Seiss[37], J. M. Seixas[80b], G. Sekhniaidze[69a], K. Sekhon[105], S. J. Sekula[42], N. Semprini-Cesari[23a,23b], S. Sen[49], S. Senkin[38], C. Serfon[76], L. Serin[132], L. Serkin[66a,66b], M. Sessa[60a], H. Severini[128], T. Šfiligoj[91], F. Sforza[170], A. Sfyrla[54], E. Shabalina[53], J. D. Shahinian[146], N. W. Shaikh[45a,45b], D. Shaked Renous[180], L. Y. Shan[15a], R. Shang[173], J. T. Shank[25], M. Shapiro[18], A. Sharma[135], A. S. Sharma[1], P. B. Shatalov[111], K. Shaw[156], S. M. Shaw[100], A. Shcherbakova[138], Y. Shen[128], N. Sherafati[34], A. D. Sherman[25], P. Sherwood[94], L. Shi[158,av], S. Shimizu[81], C. O. Shimmin[183], Y. Shimogama[179], M. Shimojima[116], I. P. J. Shipsey[135], S. Shirabe[87], M. Shiyakova[79,ac], J. Shlomi[180], A. Shmeleva[110], M. J. Shochet[37], J. Shojaii[104], D. R. Shope[128], S. Shrestha[126], E. Shulga[180], P. Sicho[141], A. M. Sickles[173], P. E. Sidebo[154], E. Sideras Haddad[33c], O. Sidiropoulou[36], A. Sidoti[23a,23b], F. Siegert[48], Dj. Sijacki[16], M. Jr. Silva[181], M. V. Silva Oliveira[80a], S. B. Silverstein[45a], S. Simion[132], E. Simioni[99], R. Simoniello[99], S. Simsek[12b], P. Sinervo[167], V. Sinetckii[113,110], N. B. Sinev[131], M. Sioli[23a,23b], I. Siral[105], S. Yu. Sivoklokov[113], J. Sjölin[45a,45b], E. Skorda[96], P. Skubic[128], M. Slawinska[84], K. Sliwa[170], R. Slovak[143], V. Smakhtin[180], B. H. Smart[144], J. Smiesko[28a], N. Smirnov[112], S. Yu. Smirnov[112], Y. Smirnov[112], L. N. Smirnova[113,v], O. Smirnova[96], J. W. Smith[53], M. Smizanska[89], K. Smolek[142], A. Smykiewicz[84], A. A. Snesarev[110], H. L. Snoek[120], I. M. Snyder[131], S. Snyder[29], R. Sobie[176,af], A. M. Soffa[171], A. Soffer[161], A. Søgaard[50], F. Sohns[53], C. A. Solans Sanchez[36], E. Yu. Soldatov[112], U. Soldevila[174], A. A. Solodkov[123], A. Soloshenko[79], O. V. Solovyanov[123], V. Solovyev[138], P. Sommer[149], H. Son[170], W. Song[144], W. Y. Song[168b], A. Sopczak[142], F. Sopkova[28b], C. L. Sotiropoulou[71a,71b], S. Sottocornola[70a,70b], R. Soualah[66a,66c,h], A. M. Soukharev[122a,122b], D. South[46], S. Spagnolo[67a,67b], M. Spalla[115], M. Spangenberg[178], F. Spanò[93], D. Sperlich[52], T. M. Spieker[61a], R. Spighi[23b], G. Spigo[36], M. Spina[156], D. P. Spiteri[57], M. Spousta[143], A. Stabile[68a,68b], B. L. Stamas[121], R. Stamen[61a], M. Stamenkovic[120], E. Stanecka[84], R. W. Stanek[6], B. Stanislaus[135], M. M. Stanitzki[46], M. Stankaityte[135], B. Stapf[120], E. A. Starchenko[123], G. H. Stark[146], J. Stark[58], S. H. Stark[40], P. Staroba[141], P. Starovoitov[61a], S. Stärz[103], R. Staszewski[84], G. Stavropoulos[44], M. Stegler[46], P. Steinberg[29], A. L. Steinhebel[131], B. Stelzer[152], H. J. Stelzer[139], O. Stelzer-Chilton[168a], H. Stenzel[56], T. J. Stevenson[156], G. A. Stewart[36], M. C. Stockton[36], G. Stoicea[27b], M. Stolarski[140a], P. Stolte[53], S. Stonjek[115], A. Straessner[48], J. Strandberg[154], S. Strandberg[45a,45b], M. Strauss[128], P. Strizenec[28b], R. Ströhmer[177], D. M. Strom[131], R. Stroynowski[42], A. Strubig[50], S. A. Stucci[29], B. Stugu[17], J. Stupak[128], N. A. Styles[46], D. Su[153], S. Suchek[61a], V. V. Sulin[110], M. J. Sullivan[90], D. M. S. Sultan[54], S. Sultansoy[4c], T. Sumida[85], S. Sun[105], X. Sun[3], K. Suruliz[156], C. J. E. Suster[157], M. R. Sutton[156], S. Suzuki[81], M. Svatos[141], M. Swiatlowski[37], S. P. Swift[2], T. Swirski[177], A. Sydorenko[99], I. Sykora[28a], M. Sykora[143], T. Sykora[143], D. Ta[99], K. Tackmann[46,aa], J. Taenzer[161], A. Taffard[171], R. Tafirout[168a], H. Takai[29], R. Takashima[86], K. Takeda[82], T. Takeshita[150], E. P. Takeva[50], Y. Takubo[81], M. Talby[101], A. A. Talyshev[122a,122b], N. M. Tamir[161], J. Tanaka[163], M. Tanaka[165], R. Tanaka[132], S. Tapia Araya[173], S. Tapprogge[99], A. Tarek Abouelfadl Mohamed[136], S. Tarem[160], G. Tarna[27b,d], G. F. Tartarelli[68a], P. Tas[143], M. Tasevsky[141], T. Tashiro[85], E. Tassi[41a,41b], A. Tavares Delgado[140a,140b], Y. Tayalati[35e], A. J. Taylor[50], G. N. Taylor[104], W. Taylor[168b],

A. S. Tee[89], R. Teixeira De Lima[153], P. Teixeira-Dias[93], H. Ten Kate[36], J. J. Teoh[120], S. Terada[81], K. Terashi[163], J. Terron[98], S. Terzo[14], M. Testa[51], R. J. Teuscher[167,af], S. J. Thais[183], T. Theveneaux-Pelzer[46], F. Thiele[40], D. W. Thomas[93], J. O. Thomas[42], J. P. Thomas[21], A. S. Thompson[57], P. D. Thompson[21], L. A. Thomsen[183], E. Thomson[137], Y. Tian[39], R. E. Ticse Torres[53], V. O. Tikhomirov[110,ar], Yu. A. Tikhonov[122a,122b], S. Timoshenko[112], P. Tipton[183], S. Tisserant[101], K. Todome[23a,23b], S. Todorova-Nova[5], S. Todt[48], J. Tojo[87], S. Tokár[28a], K. Tokushuku[81], E. Tolley[126], K. G. Tomiwa[33c], M. Tomoto[117], L. Tompkins[153,r], B. Tong[59], P. Tornambe[102], E. Torrence[131], H. Torres[48], E. Torró Pastor[148], C. Tosciri[135], J. Toth[101,ad], D. R. Tovey[149], A. Traeet[17], C. J. Treado[124], T. Trefzger[177], F. Tresoldi[156], A. Tricoli[29], I. M. Trigger[168a], S. Trincaz-Duvoid[136], W. Trischuk[167], B. Trocmé[58], A. Trofymov[145], C. Troncon[68a], M. Trovatelli[176], F. Trovato[156], L. Truong[33b], M. Trzebinski[84], A. Trzupek[84], F. Tsai[46], J.C-L. Tseng[135], P. V. Tsiareshka[107,al], A. Tsirigotis[162], N. Tsirintanis[9], V. Tsiskaridze[155], E. G. Tskhadadze[159a], M. Tsopoulou[162], I. I. Tsukerman[111], V. Tsulaia[18], S. Tsuno[81], D. Tsybychev[155], Y. Tu[63b], A. Tudorache[27b], V. Tudorache[27b], T. T. Tulbure[27a], A. N. Tuna[59], S. Turchikhin[79], D. Turgeman[180], I. Turk Cakir[4b,w], R. J. Turner[21], R. T. Turra[68a], P. M. Tuts[39], S. Tzamarias[162], E. Tzovara[99], G. Ucchielli[47], K. Uchida[163], I. Ueda[81], M. Ughetto[45a,45b], F. Ukegawa[169], G. Unal[36], A. Undrus[29], G. Unel[171], F. C. Ungaro[104], Y. Unno[81], K. Uno[163], J. Urban[28b], P. Urquijo[104], G. Usai[8], J. Usui[81], Z. Uysal[12d], L. Vacavant[101], V. Vacek[142], B. Vachon[103], K. O. H. Vadla[134], A. Vaidya[94], C. Valderanis[114], E. Valdes Santurio[45a,45b], M. Valente[54], S. Valentinetti[23a,23b], A. Valero[174], L. Valéry[46], R. A. Vallance[21], A. Vallier[36], J. A. Valls Ferrer[174], T. R. Van Daalen[14], P. Van Gemmeren[6], I. Van Vulpen[120], M. Vanadia[73a,73b], W. Vandelli[36], A. Vaniachine[166], D. Vannicola[72a,72b], R. Vari[72a], E. W. Varnes[7], C. Varni[55a,55b], T. Varol[42], D. Varouchas[132], K. E. Varvell[157], M. E. Vasile[27b], G. A. Vasquez[176], J. G. Vasquez[183], F. Vazeille[38], D. Vazquez Furelos[14], T. Vazquez Schroeder[36], J. Veatch[53], V. Vecchio[74a,74b], M. J. Veen[120], L. M. Veloce[167], F. Veloso[140a,140c], S. Veneziano[72a], A. Ventura[67a,67b], N. Venturi[36], A. Verbytskyi[115], V. Vercesi[70a], M. Verducci[74a,74b], C. M. Vergel Infante[78], C. Vergis[24], W. Verkerke[120], A. T. Vermeulen[120], J. C. Vermeulen[120], M. C. Vetterli[152,az], N. Viaux Maira[147c], M. Vicente Barreto Pinto[54], T. Vickey[149], O. E. Vickey Boeriu[149], G. H. A. Viehhauser[135], L. Vigani[135], M. Villa[23a,23b], M. Villaplana Perez[68a,68b], E. Vilucchi[51], M. G. Vincter[34], V. B. Vinogradov[79], A. Vishwakarma[46], C. Vittori[23a,23b], I. Vivarelli[156], M. Vogel[182], P. Vokac[142], S. E. von Buddenbrock[33c], E. Von Toerne[24], V. Vorobel[143], K. Vorobev[112], M. Vos[174], J. H. Vossebeld[90], M. Vozak[100], N. Vranjes[16], M. Vranjes Milosavljevic[16], V. Vrba[142], M. Vreeswijk[120], R. Vuillermet[36], I. Vukotic[37], P. Wagner[24], W. Wagner[182], J. Wagner-Kuhr[114], H. Wahlberg[88], K. Wakamiya[82], V. M. Walbrecht[115], J. Walder[89], R. Walker[114], S. D. Walker[93], W. Walkowiak[151], V. Wallangen[45a,45b], A. M. Wang[59], C. Wang[60b], F. Wang[181], H. Wang[18], H. Wang[3], J. Wang[157], J. Wang[61b], P. Wang[42], Q. Wang[128], R.-J. Wang[99], R. Wang[60a], R. Wang[6], S. M. Wang[158], W. T. Wang[60a], W. Wang[15c,ag], W. X. Wang[60a,ag], Y. Wang[60a,ao], Z. Wang[60c], C. Wanotayaroj[46], A. Warburton[103], C. P. Ward[32], D. R. Wardrope[94], N. Warrack[57], A. Washbrook[50], A. T. Watson[21], M. F. Watson[21], G. Watts[148], B. M. Waugh[94], A. F. Webb[11], S. Webb[99], C. Weber[183], M. S. Weber[20], S. A. Weber[34], S. M. Weber[61a], A. R. Weidberg[135], J. Weingarten[47], M. Weirich[99], C. Weiser[52], P. S. Wells[36], T. Wenaus[29], T. Wengler[36], S. Wenig[36], N. Wermes[24], M. D. Werner[78], M. Wessels[61a], T. D. Weston[20], K. Whalen[131], N. L. Whallon[148], A. M. Wharton[89], A. S. White[105], A. White[8], M. J. White[1], D. Whiteson[171], B. W. Whitmore[89], F. J. Wickens[144], W. Wiedenmann[181], M. Wielers[144], N. Wieseotte[99], C. Wiglesworth[40], L. A. M. Wiik-Fuchs[52], F. Wilk[100], H. G. Wilkens[36], L. J. Wilkins[93], H. H. Williams[137], S. Williams[32], C. Willis[106], S. Willocq[102], J. A. Wilson[21], I. Wingerter-Seez[5], E. Winkels[156], F. Winklmeier[131], O. J. Winston[156], B. T. Winter[52], M. Wittgen[153], M. Wobisch[95], A. Wolf[99], T. M. H. Wolf[120], R. Wolff[101], R. W. Wölker[135], J. Wollrath[52], M. W. Wolter[84], H. Wolters[140a,140c], V. W. S. Wong[175], N. L. Woods[146], S. D. Worm[21], B. K. Wosiek[84], K. W. Woźniak[84], K. Wraight[57], S. L. Wu[181], X. Wu[54], Y. Wu[60a], T. R. Wyatt[100], B. M. Wynne[50], S. Xella[40], Z. Xi[105], L. Xia[178], D. Xu[15a], H. Xu[60a,d], L. Xu[29], T. Xu[145], W. Xu[105], Z. Xu[60b], Z. Xu[153], B. Yabsley[157], S. Yacoob[33a], K. Yajima[133], D. P. Yallup[94], D. Yamaguchi[165], Y. Yamaguchi[165], A. Yamamoto[81], T. Yamanaka[163], F. Yamane[82], M. Yamatani[163], T. Yamazaki[163], Y. Yamazaki[82], Z. Yan[25], H. J. Yang[60c,60d], H. T. Yang[18], S. Yang[77], X. Yang[58,60b], Y. Yang[163], W-M. Yao[18], Y. C. Yap[46], Y. Yasu[81], E. Yatsenko[60c,60d], J. Ye[42], S. Ye[29], I. Yeletskikh[79], M. R. Yexley[89], E. Yigitbasi[25], K. Yorita[179], K. Yoshihara[137], C. J. S. Young[36], C. Young[153], J. Yu[78], R. Yuan[60b], X. Yue[61a], S. P. Y. Yuen[24], B. Zabinski[84], G. Zacharis[10], E. Zaffaroni[54], J. Zahreddine[136], A. M. Zaitsev[123,aq], T. Zakareishvili[159b], N. Zakharchuk[34], S. Zambito[59], D. Zanzi[36], D. R. Zaripovas[57], S. V. Zeißner[47], C. Zeitnitz[182], G. Zemaityte[135], J. C. Zeng[173], O. Zenin[123], T. Ženiš[28a], D. Zerwas[132], M. Zgubič[135], D. F. Zhang[15b], F. Zhang[181], G. Zhang[60a], G. Zhang[15b], H. Zhang[15c], J. Zhang[6], L. Zhang[15c], L. Zhang[60a], M. Zhang[173], R. Zhang[60a], R. Zhang[24], X. Zhang[60b], Y. Zhang[15a,15d], Z. Zhang[63a], Z. Zhang[132], P. Zhao[49], Y. Zhao[60b], Z. Zhao[60a], A. Zhemchugov[79], Z. Zheng[105], D. Zhong[173], B. Zhou[105], C. Zhou[181], M. S. Zhou[15a,15d], M. Zhou[155], N. Zhou[60c], Y. Zhou[7], C. G. Zhu[60b], H. L. Zhu[60a], H. Zhu[15a], J. Zhu[105], Y. Zhu[60a], X. Zhuang[15a], K. Zhukov[110], V. Zhulanov[122a,122b], D. Zieminska[65], N. I. Zimine[79], S. Zimmermann[52], Z. Zinonos[115], M. Ziolkowski[151], L. Živković[16], G. Zobernig[181], A. Zoccoli[23a,23b], K. Zoch[53], T. G. Zorbas[149], R. Zou[37], L. Zwalinski[36]

[1] Department of Physics, University of Adelaide, Adelaide, Australia
[2] Physics Department, SUNY Albany, Albany, NY, USA
[3] Department of Physics, University of Alberta, Edmonton, AB, Canada
[4] [(a)]Department of Physics, Ankara University, Ankara, Turkey; [(b)]Istanbul Aydin University, Istanbul, Turkey; [(c)]Division of Physics, TOBB University of Economics and Technology, Ankara, Turkey
[5] LAPP, Université Grenoble Alpes, Université Savoie Mont Blanc, CNRS/IN2P3, Annecy, France
[6] High Energy Physics Division, Argonne National Laboratory, Argonne, IL, USA
[7] Department of Physics, University of Arizona, Tucson, AZ, USA
[8] Department of Physics, University of Texas at Arlington, Arlington, TX, USA
[9] Physics Department, National and Kapodistrian University of Athens, Athens, Greece
[10] Physics Department, National Technical University of Athens, Zografou, Greece
[11] Department of Physics, University of Texas at Austin, Austin, TX, USA
[12] [(a)]Bahcesehir University, Faculty of Engineering and Natural Sciences, Istanbul, Turkey; [(b)]Istanbul Bilgi University, Faculty of Engineering and Natural Sciences, Istanbul, Turkey; [(c)]Department of Physics, Bogazici University, Istanbul, Turkey; [(d)]Department of Physics Engineering, Gaziantep University, Gaziantep, Turkey
[13] Institute of Physics, Azerbaijan Academy of Sciences, Baku, Azerbaijan
[14] Institut de Física d'Altes Energies (IFAE), Barcelona Institute of Science and Technology, Barcelona, Spain
[15] [(a)]Institute of High Energy Physics, Chinese Academy of Sciences, Beijing, China; [(b)]Physics Department, Tsinghua University, Beijing, China; [(c)]Department of Physics, Nanjing University, Nanjing, China; [(d)]University of Chinese Academy of Science (UCAS), Beijing, China
[16] Institute of Physics, University of Belgrade, Belgrade, Serbia
[17] Department for Physics and Technology, University of Bergen, Bergen, Norway
[18] Physics Division, Lawrence Berkeley National Laboratory and University of California, Berkeley, CA, USA
[19] Institut für Physik, Humboldt Universität zu Berlin, Berlin, Germany
[20] Albert Einstein Center for Fundamental Physics and Laboratory for High Energy Physics, University of Bern, Bern, Switzerland
[21] School of Physics and Astronomy, University of Birmingham, Birmingham, UK
[22] Facultad de Ciencias y Centro de Investigaciónes, Universidad Antonio Nariño, Bogota, Colombia
[23] [(a)]INFN Bologna and Universita' di Bologna, Dipartimento di Fisica, Bologna, Italy; [(b)]INFN Sezione di Bologna, Bologna, Italy
[24] Physikalisches Institut, Universität Bonn, Bonn, Germany
[25] Department of Physics, Boston University, Boston, MA, USA
[26] Department of Physics, Brandeis University, Waltham, MA, USA
[27] [(a)]Transilvania University of Brasov, Brasov, Romania; [(b)]Horia Hulubei National Institute of Physics and Nuclear Engineering, Bucharest, Romania; [(c)]Department of Physics, Alexandru Ioan Cuza University of Iasi, Iasi, Romania; [(d)]National Institute for Research and Development of Isotopic and Molecular Technologies, Physics Department, Cluj-Napoca, Romania; [(e)]University Politehnica Bucharest, Bucharest, Romania; [(f)]West University in Timisoara, Timisoara, Romania
[28] [(a)]Faculty of Mathematics, Physics and Informatics, Comenius University, Bratislava, Slovakia; [(b)]Department of Subnuclear Physics, Institute of Experimental Physics of the Slovak Academy of Sciences, Kosice, Slovak Republic
[29] Physics Department, Brookhaven National Laboratory, Upton, NY, USA
[30] Departamento de Física, Universidad de Buenos Aires, Buenos Aires, Argentina
[31] California State University, Long Beach, CA, USA
[32] Cavendish Laboratory, University of Cambridge, Cambridge, UK
[33] [(a)]Department of Physics, University of Cape Town, Cape Town, South Africa; [(b)]Department of Mechanical Engineering Science, University of Johannesburg, Johannesburg, South Africa; [(c)]School of Physics, University of the Witwatersrand, Johannesburg, South Africa
[34] Department of Physics, Carleton University, Ottawa, ON, Canada
[35] [(a)]Faculté des Sciences Ain Chock, Réseau Universitaire de Physique des Hautes Energies-Université Hassan II, Casablanca, Morocco; [(b)]Faculté des Sciences, Université Ibn-Tofail, Kénitra, Morocco; [(c)]Faculté des Sciences Semlalia, Université Cadi Ayyad, LPHEA-Marrakech, Marrakesh, Morocco; [(d)]Faculté des Sciences, Université Mohamed Premier and LPTPM, Oujda, Morocco; [(e)]Faculté des sciences, Université Mohammed V, Rabat, Morocco
[36] CERN, Geneva, Switzerland

[37] Enrico Fermi Institute, University of Chicago, Chicago, IL, USA
[38] LPC, Université Clermont Auvergne, CNRS/IN2P3, Clermont-Ferrand, France
[39] Nevis Laboratory, Columbia University, Irvington, NY, USA
[40] Niels Bohr Institute, University of Copenhagen, Copenhagen, Denmark
[41] [(a)]Dipartimento di Fisica, Università della Calabria, Rende, Italy; [(b)]INFN Gruppo Collegato di Cosenza, Laboratori Nazionali di Frascati, Frascati, Italy
[42] Physics Department, Southern Methodist University, Dallas, TX, USA
[43] Physics Department, University of Texas at Dallas, Richardson, TX, USA
[44] National Centre for Scientific Research "Demokritos", Agia Paraskevi, Greece
[45] [(a)]Department of Physics, Stockholm University, Stockholm, Sweden; [(b)]Oskar Klein Centre, Stockholm, Sweden
[46] Deutsches Elektronen-Synchrotron DESY, Hamburg and Zeuthen, Germany
[47] Lehrstuhl für Experimentelle Physik IV, Technische Universität Dortmund, Dortmund, Germany
[48] Institut für Kern- und Teilchenphysik, Technische Universität Dresden, Dresden, Germany
[49] Department of Physics, Duke University, Durham, NC, USA
[50] SUPA-School of Physics and Astronomy, University of Edinburgh, Edinburgh, UK
[51] INFN e Laboratori Nazionali di Frascati, Frascati, Italy
[52] Physikalisches Institut, Albert-Ludwigs-Universität Freiburg, Freiburg, Germany
[53] II. Physikalisches Institut, Georg-August-Universität Göttingen, Göttingen, Germany
[54] Département de Physique Nucléaire et Corpusculaire, Université de Genève, Geneva, Switzerland
[55] [(a)]Dipartimento di Fisica, Università di Genova, Genoa, Italy; [(b)]INFN Sezione di Genova, Genoa, Italy
[56] II. Physikalisches Institut, Justus-Liebig-Universität Giessen, Giessen, Germany
[57] SUPA-School of Physics and Astronomy, University of Glasgow, Glasgow, UK
[58] LPSC, Université Grenoble Alpes, CNRS/IN2P3, Grenoble INP, Grenoble, France
[59] Laboratory for Particle Physics and Cosmology, Harvard University, Cambridge, MA, USA
[60] [(a)]Department of Modern Physics and State Key Laboratory of Particle Detection and Electronics, University of Science and Technology of China, Hefei, China; [(b)]Institute of Frontier and Interdisciplinary Science and Key Laboratory of Particle Physics and Particle Irradiation (MOE), Shandong University, Qingdao, China; [(c)]School of Physics and Astronomy, Shanghai Jiao Tong University, KLPPAC-MoE, SKLPPC, Shanghai, China; [(d)]Tsung-Dao Lee Institute, Shanghai, China
[61] [(a)]Kirchhoff-Institut für Physik, Ruprecht-Karls-Universität Heidelberg, Heidelberg, Germany; [(b)]Physikalisches Institut, Ruprecht-Karls-Universität Heidelberg, Heidelberg, Germany
[62] Faculty of Applied Information Science, Hiroshima Institute of Technology, Hiroshima, Japan
[63] [(a)]Department of Physics, Chinese University of Hong Kong, Shatin, NT, Hong Kong; [(b)]Department of Physics, University of Hong Kong, Hong Kong, China; [(c)]Department of Physics and Institute for Advanced Study, Hong Kong University of Science and Technology, Clear Water Bay, Kowloon, Hong Kong, China
[64] Department of Physics, National Tsing Hua University, Hsinchu, Taiwan
[65] Department of Physics, Indiana University, Bloomington, IN, USA
[66] [(a)]INFN Gruppo Collegato di Udine, Sezione di Trieste, Udine, Italy; [(b)]ICTP, Trieste, Italy; [(c)]Dipartimento Politecnico di Ingegneria e Architettura, Università di Udine, Udine, Italy
[67] [(a)]INFN Sezione di Lecce, Lecce, Italy; [(b)]Dipartimento di Matematica e Fisica, Università del Salento, Lecce, Italy
[68] [(a)]INFN Sezione di Milano, Milan, Italy; [(b)]Dipartimento di Fisica, Università di Milano, Milan, Italy
[69] [(a)]INFN Sezione di Napoli, Naples, Italy; [(b)]Dipartimento di Fisica, Università di Napoli, Naples, Italy
[70] [(a)]INFN Sezione di Pavia, Pavia, Italy; [(b)]Dipartimento di Fisica, Università di Pavia, Pavia, Italy
[71] [(a)]INFN Sezione di Pisa, Pisa, Italy; [(b)]Dipartimento di Fisica E. Fermi, Università di Pisa, Pisa, Italy
[72] [(a)]INFN Sezione di Roma, Rome, Italy; [(b)]Dipartimento di Fisica, Sapienza Università di Roma, Rome, Italy
[73] [(a)]INFN Sezione di Roma Tor Vergata, Rome, Italy; [(b)]Dipartimento di Fisica, Università di Roma Tor Vergata, Rome, Italy
[74] [(a)]INFN Sezione di Roma Tre, Rome, Italy; [(b)]Dipartimento di Matematica e Fisica, Università Roma Tre, Rome, Italy
[75] [(a)]INFN-TIFPA, Trento, Italy; [(b)]Università degli Studi di Trento, Trento, Italy
[76] Institut für Astro- und Teilchenphysik, Leopold-Franzens-Universität, Innsbruck, Austria
[77] University of Iowa, Iowa City, IA, USA
[78] Department of Physics and Astronomy, Iowa State University, Ames, IA, USA
[79] Joint Institute for Nuclear Research, Dubna, Russia

[80] [(a)]Departamento de Engenharia Elétrica, Universidade Federal de Juiz de Fora (UFJF), Juiz de Fora, Brazil ; [(b)]Universidade Federal do Rio De Janeiro COPPE/EE/IF, Rio de Janeiro, Brazil; [(c)]Universidade Federal de São João del Rei (UFSJ), São João del Rei, Brazil; [(d)]Instituto de Física, Universidade de São Paulo, São Paulo, Brazil
[81] KEK, High Energy Accelerator Research Organization, Tsukuba, Japan
[82] Graduate School of Science, Kobe University, Kobe, Japan
[83] [(a)]AGH University of Science and Technology, Faculty of Physics and Applied Computer Science, Krakow, Poland; [(b)]Marian Smoluchowski Institute of Physics, Jagiellonian University, Krakow, Poland
[84] Institute of Nuclear Physics Polish Academy of Sciences, Krakow, Poland
[85] Faculty of Science, Kyoto University, Kyoto, Japan
[86] Kyoto University of Education, Kyoto, Japan
[87] Research Center for Advanced Particle Physics and Department of Physics, Kyushu University, Fukuoka, Japan
[88] Instituto de Física La Plata, Universidad Nacional de La Plata and CONICET, La Plata, Argentina
[89] Physics Department, Lancaster University, Lancaster, UK
[90] Oliver Lodge Laboratory, University of Liverpool, Liverpool, UK
[91] Department of Experimental Particle Physics, Jožef Stefan Institute and Department of Physics, University of Ljubljana, Ljubljana, Slovenia
[92] School of Physics and Astronomy, Queen Mary University of London, London, UK
[93] Department of Physics, Royal Holloway University of London, Egham, UK
[94] Department of Physics and Astronomy, University College London, London, UK
[95] Louisiana Tech University, Ruston, LA, USA
[96] Fysiska institutionen, Lunds universitet, Lund, Sweden
[97] Centre de Calcul de l'Institut National de Physique Nucléaire et de Physique des Particules (IN2P3), Villeurbanne, France
[98] Departamento de Física Teorica C-15 and CIAFF, Universidad Autónoma de Madrid, Madrid, Spain
[99] Institut für Physik, Universität Mainz, Mainz, Germany
[100] School of Physics and Astronomy, University of Manchester, Manchester, UK
[101] CPPM, Aix-Marseille Université, CNRS/IN2P3, Marseille, France
[102] Department of Physics, University of Massachusetts, Amherst, MA, USA
[103] Department of Physics, McGill University, Montreal, QC, Canada
[104] School of Physics, University of Melbourne, Victoria, Australia
[105] Department of Physics, University of Michigan, Ann Arbor, MI, USA
[106] Department of Physics and Astronomy, Michigan State University, East Lansing, MI, USA
[107] B.I. Stepanov Institute of Physics, National Academy of Sciences of Belarus, Minsk, Belarus
[108] Research Institute for Nuclear Problems of Byelorussian State University, Minsk, Belarus
[109] Group of Particle Physics, University of Montreal, Montreal, QC, Canada
[110] P.N. Lebedev Physical Institute of the Russian Academy of Sciences, Moscow, Russia
[111] Institute for Theoretical and Experimental Physics of the National Research Centre Kurchatov Institute, Moscow, Russia
[112] National Research Nuclear University MEPhI, Moscow, Russia
[113] D.V. Skobeltsyn Institute of Nuclear Physics, M.V. Lomonosov Moscow State University, Moscow, Russia
[114] Fakultät für Physik, Ludwig-Maximilians-Universität München, Munich, Germany
[115] Max-Planck-Institut für Physik (Werner-Heisenberg-Institut), Munich, Germany
[116] Nagasaki Institute of Applied Science, Nagasaki, Japan
[117] Graduate School of Science and Kobayashi-Maskawa Institute, Nagoya University, Nagoya, Japan
[118] Department of Physics and Astronomy, University of New Mexico, Albuquerque, NM, USA
[119] Institute for Mathematics, Astrophysics and Particle Physics, Radboud University Nijmegen/Nikhef, Nijmegen, The Netherlands
[120] Nikhef National Institute for Subatomic Physics and University of Amsterdam, Amsterdam, The Netherlands
[121] Department of Physics, Northern Illinois University, DeKalb, IL, USA
[122] [(a)]Budker Institute of Nuclear Physics and NSU, SB RAS, Novosibirsk, Russia; [(b)]Novosibirsk State University, Novosibirsk, Russia
[123] Institute for High Energy Physics of the National Research Centre, Kurchatov Institute, Protvino, Russia
[124] Department of Physics, New York University, New York, NY, USA
[125] Ochanomizu University, Otsuka, Bunkyo-ku, Tokyo, Japan

[126] Ohio State University, Columbus, OH, USA
[127] Faculty of Science, Okayama University, Okayama, Japan
[128] Homer L. Dodge Department of Physics and Astronomy, University of Oklahoma, Norman, OK, USA
[129] Department of Physics, Oklahoma State University, Stillwater, OK, USA
[130] Palacký University, RCPTM, Joint Laboratory of Optics, Olomouc, Czech Republic
[131] Center for High Energy Physics, University of Oregon, Eugene, OR, USA
[132] LAL, Université Paris-Sud, CNRS/IN2P3, Université Paris-Saclay, Orsay, France
[133] Graduate School of Science, Osaka University, Osaka, Japan
[134] Department of Physics, University of Oslo, Oslo, Norway
[135] Department of Physics, Oxford University, Oxford, UK
[136] LPNHE, Sorbonne Université, Université de Paris, CNRS/IN2P3, Paris, France
[137] Department of Physics, University of Pennsylvania, Philadelphia, PA, USA
[138] Konstantinov Nuclear Physics Institute of National Research Centre "Kurchatov Institute", PNPI, St. Petersburg, Russia
[139] Department of Physics and Astronomy, University of Pittsburgh, Pittsburgh, PA, USA
[140] [(a)]Laboratório de Instrumentação e Física Experimental de Partículas-LIP, Lisbon, Portugal; [(b)]Departamento de Física, Faculdade de Ciências, Universidade de Lisboa, Lisbon, Portugal; [(c)]Departamento de Física, Universidade de Coimbra, Coimbra, Portugal; [(d)]Centro de Física Nuclear da Universidade de Lisboa, Lisbon, Portugal; [(e)]Departamento de Física, Universidade do Minho, Braga, Portugal; [(f)]Universidad de Granada, Granada, Spain; [(g)]Dep Física and CEFITEC of Faculdade de Ciências e Tecnologia, Universidade Nova de Lisboa, Caparica, Portugal; [(h)]Instituto Superior Técnico, Universidade de Lisboa, Lisbon, Portugal
[141] Institute of Physics of the Czech Academy of Sciences, Prague, Czech Republic
[142] Czech Technical University in Prague, Prague, Czech Republic
[143] Charles University, Faculty of Mathematics and Physics, Prague, Czech Republic
[144] Particle Physics Department, Rutherford Appleton Laboratory, Didcot, UK
[145] IRFU, CEA, Université Paris-Saclay, Gif-sur-Yvette, France
[146] Santa Cruz Institute for Particle Physics, University of California Santa Cruz, Santa Cruz, CA, USA
[147] [(a)]Departamento de Física, Pontificia Universidad Católica de Chile, Santiago, Chile; [(b)]Department of Physics, Universidad Andres Bello, Santiago, Chile; [(c)]Departamento de Física, Universidad Técnica Federico Santa María, Valparaíso, Chile
[148] Department of Physics, University of Washington, Seattle, WA, USA
[149] Department of Physics and Astronomy, University of Sheffield, Sheffield, UK
[150] Department of Physics, Shinshu University, Nagano, Japan
[151] Department Physik, Universität Siegen, Siegen, Germany
[152] Department of Physics, Simon Fraser University, Burnaby, BC, Canada
[153] SLAC National Accelerator Laboratory, Stanford, CA, USA
[154] Physics Department, Royal Institute of Technology, Stockholm, Sweden
[155] Departments of Physics and Astronomy, Stony Brook University, Stony Brook, NY, USA
[156] Department of Physics and Astronomy, University of Sussex, Brighton, UK
[157] School of Physics, University of Sydney, Sydney, Australia
[158] Institute of Physics, Academia Sinica, Taipei, Taiwan
[159] [(a)]E. Andronikashvili Institute of Physics, Iv. Javakhishvili Tbilisi State University, Tbilisi, Georgia; [(b)]High Energy Physics Institute, Tbilisi State University, Tbilisi, Georgia
[160] Department of Physics, Technion, Israel Institute of Technology, Haifa, Israel
[161] Raymond and Beverly Sackler School of Physics and Astronomy, Tel Aviv University, Tel Aviv, Israel
[162] Department of Physics, Aristotle University of Thessaloniki, Thessaloniki, Greece
[163] International Center for Elementary Particle Physics and Department of Physics, University of Tokyo, Tokyo, Japan
[164] Graduate School of Science and Technology, Tokyo Metropolitan University, Tokyo, Japan
[165] Department of Physics, Tokyo Institute of Technology, Tokyo, Japan
[166] Tomsk State University, Tomsk, Russia
[167] Department of Physics, University of Toronto, Toronto, ON, Canada
[168] [(a)]TRIUMF, Vancouver, BC, Canada; [(b)]Department of Physics and Astronomy, York University, Toronto, ON, Canada
[169] Division of Physics and Tomonaga Center for the History of the Universe, Faculty of Pure and Applied Sciences, University of Tsukuba, Tsukuba, Japan

[170] Department of Physics and Astronomy, Tufts University, Medford, MA, USA
[171] Department of Physics and Astronomy, University of California Irvine, Irvine, CA, USA
[172] Department of Physics and Astronomy, University of Uppsala, Uppsala, Sweden
[173] Department of Physics, University of Illinois, Urbana, IL, USA
[174] Instituto de Física Corpuscular (IFIC), Centro Mixto Universidad de Valencia - CSIC, Valencia, Spain
[175] Department of Physics, University of British Columbia, Vancouver, BC, Canada
[176] Department of Physics and Astronomy, University of Victoria, Victoria, BC, Canada
[177] Fakultät für Physik und Astronomie, Julius-Maximilians-Universität Würzburg, Würzburg, Germany
[178] Department of Physics, University of Warwick, Coventry, UK
[179] Waseda University, Tokyo, Japan
[180] Department of Particle Physics, Weizmann Institute of Science, Rehovot, Israel
[181] Department of Physics, University of Wisconsin, Madison, WI, USA
[182] Fakultät für Mathematik und Naturwissenschaften, Fachgruppe Physik, Bergische Universität Wuppertal, Wuppertal, Germany
[183] Department of Physics, Yale University, New Haven, CT, USA
[184] Yerevan Physics Institute, Yerevan, Armenia

[a] Also at Borough of Manhattan Community College, City University of New York, New York, NY, USA
[b] Also at Centre for High Performance Computing, CSIR Campus, Rosebank, Cape Town, South Africa
[c] Also at CERN, Geneva, Switzerland
[d] Also at CPPM, Aix-Marseille Université, CNRS/IN2P3, Marseille, France
[e] Also at Département de Physique Nucléaire et Corpusculaire, Université de Genève, Geneva, Switzerland
[f] Also at Departament de Fisica de la Universitat Autonoma de Barcelona, Barcelona, Spain
[g] Also at Departamento de Física, Instituto Superior Técnico, Universidade de Lisboa, Lisbon, Portugal
[h] Also at Department of Applied Physics and Astronomy, University of Sharjah, Sharjah, United Arab Emirates
[i] Also at Department of Financial and Management Engineering, University of the Aegean, Chios, Greece
[j] Also at Department of Physics and Astronomy, University of Louisville, Louisville, KY, USA
[k] Also at Department of Physics and Astronomy, University of Sheffield, Sheffield, UK
[l] Also at Department of Physics, Ben Gurion University of the Negev, Beer Sheva, Israel
[m] Also at Department of Physics, California State University, East Bay, USA
[n] Also at Department of Physics, California State University, Fresno, USA
[o] Also at Department of Physics, California State University, Sacramento, USA
[p] Also at Department of Physics, King's College London, London, UK
[q] Also at Department of Physics, St. Petersburg State Polytechnical University, St. Petersburg, Russia
[r] Also at Department of Physics, Stanford University, Stanford, CA, USA
[s] Also at Department of Physics, University of Adelaide, Adelaide, Australia
[t] Also at Department of Physics, University of Fribourg, Fribourg, Switzerland
[u] Also at Department of Physics, University of Michigan, Ann Arbor, MI, USA
[v] Also at Faculty of Physics, M.V. Lomonosov Moscow State University, Moscow, Russia
[w] Also at Giresun University, Faculty of Engineering, Giresun, Turkey
[x] Also at Graduate School of Science, Osaka University, Osaka, Japan
[y] Also at Hellenic Open University, Patras, Greece
[z] Also at Institucio Catalana de Recerca i Estudis Avancats, ICREA, Barcelona, Spain
[aa] Also at Institut für Experimentalphysik, Universität Hamburg, Hamburg, Germany
[ab] Also at Institute for Mathematics, Astrophysics and Particle Physics, Radboud University Nijmegen/Nikhef, Nijmegen, The Netherlands
[ac] Also at Institute for Nuclear Research and Nuclear Energy (INRNE) of the Bulgarian Academy of Sciences, Sofia, Bulgaria
[ad] Also at Institute for Particle and Nuclear Physics, Wigner Research Centre for Physics, Budapest, Hungary
[ae] Also at Institute of High Energy Physics, Chinese Academy of Sciences, Beijing, China
[af] Also at Institute of Particle Physics (IPP), Vancouver, Canada
[ag] Also at Institute of Physics, Academia Sinica, Taipei, Taiwan
[ah] Also at Institute of Physics, Azerbaijan Academy of Sciences, Baku, Azerbaijan

[ai] Also at Institute of Theoretical Physics, Ilia State University, Tbilisi, Georgia
[aj] Also at Instituto de Fisica Teorica, IFT-UAM/CSIC, Madrid, Spain
[ak] Also at Department of Physics, Istanbul University, Istanbul, Turkey
[al] Also at Joint Institute for Nuclear Research, Dubna, Russia
[am] Also at LAL, Université Paris-Sud, CNRS/IN2P3, Université Paris-Saclay, Orsay, France
[an] Also at Louisiana Tech University, Ruston, LA, USA
[ao] Also at LPNHE, Sorbonne Université, Université de Paris, CNRS/IN2P3, Paris, France
[ap] Also at Manhattan College, New York, NY, USA
[aq] Also at Moscow Institute of Physics and Technology State University, Dolgoprudny, Russia
[ar] Also at National Research Nuclear University MEPhI, Moscow, Russia
[as] Also at Physics Department, An-Najah National University, Nablus, Palestine
[at] Also at Physics Dept, University of South Africa, Pretoria, South Africa
[au] Also at Physikalisches Institut, Albert-Ludwigs-Universität Freiburg, Freiburg, Germany
[av] Also at School of Physics, Sun Yat-sen University, Guangzhou, China
[aw] Also at The City College of New York, New York, NY, USA
[ax] Also at The Collaborative Innovation Center of Quantum Matter (CICQM), Beijing, China
[ay] Also at Tomsk State University, Tomsk, and Moscow Institute of Physics and Technology State University, Dolgoprudny, Russia
[az] Also at TRIUMF, Vancouver, BC, Canada
[aaa] Also at Universita di Napoli Parthenope, Naples, Italy
* Deceased

Eur. Phys. J. C (2019) 79:374
https://doi.org/10.1140/epjc/s10052-019-6870-9

THE EUROPEAN PHYSICAL JOURNAL C

Erratum

Erratum to: Measurements of W and Z boson production in pp collisions at $\sqrt{s} = 5.02$ TeV with the ATLAS detector

ATLAS Collaboration[⋆]

CERN, 1211 Geneva 23, Switzerland

Received: 3 April 2019 / Accepted: 6 April 2019 / Published online: 30 April 2019

Erratum to: Eur. Phys. J. C (2019) 79:128
https://doi.org/10.1140/epjc/s10052-019-6622-x

It has been found that the theoretical predictions for W and Z boson cross sections, and for the W boson charge asymmetry, which are labelled as NNPDF3.1 [1] have in fact been calculated using the NNPDF3.0 PDF set [2] instead. The reported experimental results are not affected.

The corrected versions of Figs. 11, 12 and 13 of the paper are presented below.

The corrected text discussing the comparison of predicted cross sections to data in Sect. 9.2 of the paper should read:

A comparison of the differential cross sections shows that the predictions obtained with the NNPDF3.1 PDF set are in good agreement with the measured values, mainly because the NNPDF3.1 global fit includes high precision LHC measurements of W/Z boson production [3,4]. On the other hand, the predictions obtained with other recent PDF sets systematically deviate from the measured values.

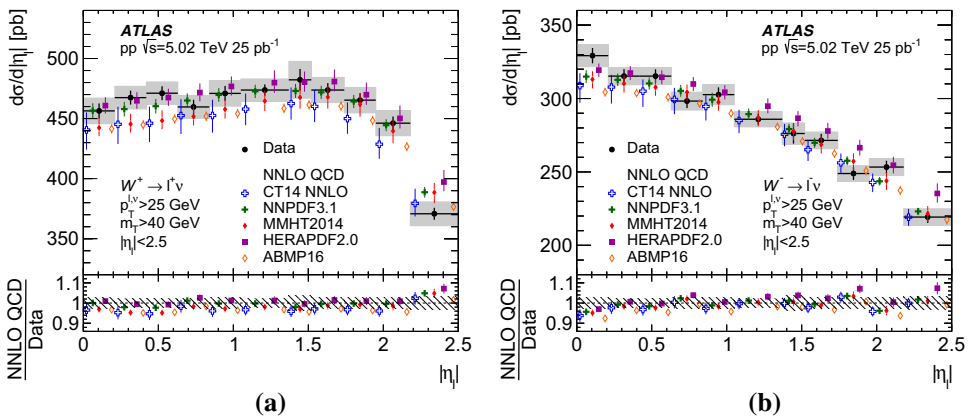

Fig. 11 Differential cross sections for **a** W^+ and **b** W^- boson production as a function of absolute decay lepton pseudorapidity compared with theoretical predictions. Statistical and systematic errors are shown as corresponding bars and shaded bands on the data points. The luminosity uncertainty is not included. Only the dominant uncertainty (PDF) is displayed for the theory. The lower panel shows the ratio of predictions to the measured differential cross section in each bin, and the shaded band shows the sum in quadrature of statistical and systematic uncertainties of the data

The original article can be found online at https://doi.org/10.1140/epjc/s10052-019-6622-x.

⋆ e-mail: atlas.publications@cern.ch

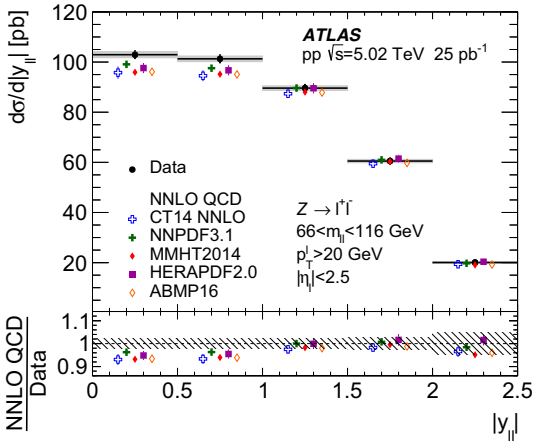

Fig. 12 Differential cross section for Z boson production as a function of absolute lepton-pair rapidity compared with theoretical predictions. Statistical and systematic errors are shown as corresponding bars and shaded bands on the data points. The luminosity uncertainty is not included. Only the dominant uncertainty (PDF) is displayed for the theory. The lower panel shows the ratio of predictions to the measured differential cross section in each bin, and the shaded band shows the sum in quadrature of statistical and systematic uncertainties of the data

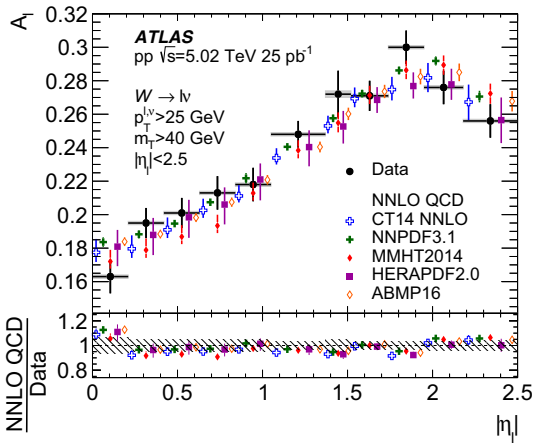

Fig. 13 Charge asymmetry for W bosons as a function of absolute decay lepton pseudorapidity compared with theoretical predictions. Statistical and systematic errors are shown as corresponding bars and shaded bands on the data points. Only the dominant uncertainty (PDF) is displayed for the theory. The lower panel shows the ratio of predictions to the measured differential cross section in each bin, and the shaded band shows the sum in quadrature of statistical and systematic uncertainties of the data

Funded by SCOAP[3].

References

1. R.D. Ball et al., Parton distributions from high-precision collider data. Eur. Phys. J. C **77**, 663 (2017). arXiv:1706.00428 [hep-ph]
2. R.D. Ball et al., Parton distributions for the LHC Run II. JHEP **04**, 040 (2015). arXiv:1410.8849 [hep-ph]
3. ATLAS Collaboration, Precision measurement and interpretation of inclusive W^+, W^- and Z/γ^* production cross sections with the ATLAS detector. Eur. Phys. J. C **77**, 367 (2017). arXiv:1612.03016 [hep-ex]
4. CMS Collaboration, Measurement of the differential cross section and charge asymmetry for inclusive $pp \to W^{\pm} + X$ production at $\sqrt{s} = 8\ TeV$. Eur. Phys. J. C **76**, 469 (2016). arXiv: 1603.01803 [hep-ex]

ATLAS Collaboration

M. Aaboud[34d], G. Aad[99], B. Abbott[125], O. Abdinov[13,*], B. Abeloos[129], D. K. Abhayasinghe[91], S. H. Abidi[164], O. S. AbouZeid[39], N. L. Abraham[153], H. Abramowicz[158], H. Abreu[157], Y. Abulaiti[6], B. S. Acharya[64a,64b,p], S. Adachi[160], L. Adamczyk[81a], J. Adelman[119], M. Adersberger[112], A. Adiguzel[12c,aj], T. Adye[141], A. A. Affolder[143], Y. Afik[157], C. Agheorghiesei[27c], J. A. Aguilar-Saavedra[137a,137f,ai], F. Ahmadov[77,ag], G. Aielli[71a,71b], S. Akatsuka[83], T. P. A. Åkesson[94], E. Akilli[52], A. V. Akimov[108], G. L. Alberghi[23a,23b], J. Albert[173], P. Albicocco[49], M. J. Alconada Verzini[86], S. Alderweireldt[117], M. Aleksa[35], I. N. Aleksandrov[77], C. Alexa[27b], T. Alexopoulos[10], M. Alhroob[125], B. Ali[139], G. Alimonti[66a], J. Alison[36], S. P. Alkire[145], C. Allaire[129], B. M. M. Allbrooke[153], B. W. Allen[128], P. P. Allport[21], A. Aloisio[67a,67b], A. Alonso[39], F. Alonso[86], C. Alpigiani[145], A. A. Alshehri[55], M. I. Alstaty[99], B. Alvarez Gonzalez[35], D. Álvarez Piqueras[171], M. G. Alviggi[67a,67b], B. T. Amadio[18], Y. Amaral Coutinho[78b], L. Ambroz[132], C. Amelung[26], D. Amidei[103], S. P. Amor Dos Santos[137a,137c], S. Amoroso[44], C. S. Amrouche[52], C. Anastopoulos[146], L. S. Ancu[52], N. Andari[142], T. Andeen[11], C. F. Anders[59b], J. K. Anders[20], K. J. Anderson[36], A. Andreazza[66a,66b], V. Andrei[59a], C. R. Anelli[173], S. Angelidakis[37], I. Angelozzi[118], A. Angerami[38], A. V. Anisenkov[120a,120b], A. Annovi[69a], C. Antel[59a], M. T. Anthony[146], M. Antonelli[49], D. J. A. Antrim[168], F. Anulli[70a], M. Aoki[79], J. A. Aparisi Pozo[171], L. Aperio Bella[35], G. Arabidze[104], J. P. Araque[137a], V. Araujo Ferraz[78b], R. Araujo Pereira[78b], A. T. H. Arce[47], R. E. Ardell[91], F. A. Arduh[86], J.-F. Arguin[107], S. Argyropoulos[75], A. J. Armbruster[35], L. J. Armitage[90], A. Armstrong[168], O. Arnaez[164], H. Arnold[118], M. Arratia[31], O. Arslan[24], A. Artamonov[109,*], G. Artoni[132], S. Artz[97], S. Asai[160], N. Asbah[57], E. M. Asimakopoulou[169], L. Asquith[153], K. Assamagan[29], R. Astalos[28a], R. J. Atkin[32a], M. Atkinson[170], N. B. Atlay[148], K. Augsten[139], G. Avolio[35], R. Avramidou[58a], M. K. Ayoub[15a], G. Azuelos[107,av], A. E. Baas[59a], M. J. Baca[21], H. Bachacou[142], K. Bachas[65a,65b], M. Backes[132], P. Bagnaia[70a,70b], M. Bahmani[82], H. Bahrasemani[149], A. J. Bailey[171], J. T. Baines[141], M. Bajic[39], C. Bakalis[10], O. K. Baker[180], P. J. Bakker[118], D. Bakshi Gupta[93], E. M. Baldin[120a,120b], P. Balek[177], F. Balli[142], W. K. Balunas[134], J. Balz[97], E. Banas[82], A. Bandyopadhyay[24], S. Banerjee[178,l], A. A. E. Bannoura[179], L. Barak[158], W. M. Barbe[37], E. L. Barberio[102], D. Barberis[53a,53b], M. Barbero[99], T. Barillari[113], M.-S. Barisits[35], J. Barkeloo[128], T. Barklow[150], R. Barnea[157], S. L. Barnes[58c], B. M. Barnett[141], R. M. Barnett[18], Z. Barnovska-Blenessy[58a], A. Baroncelli[72a], G. Barone[26], A. J. Barr[132], L. Barranco Navarro[171], F. Barreiro[96], J. Barreiro Guimarães da Costa[15a], R. Bartoldus[150], A. E. Barton[87], P. Bartos[28a], A. Basalaev[135], A. Bassalat[129], R. L. Bates[55], S. J. Batista[164], S. Batlamous[34e], J. R. Batley[31], M. Battaglia[143], M. Bauce[70a,70b], F. Bauer[142], K. T. Bauer[168], H. S. Bawa[150,n], J. B. Beacham[123], T. Beau[133], P. H. Beauchemin[167], P. Bechtle[24], H. C. Beck[51], H. P. Beck[20,s], K. Becker[50], M. Becker[97], C. Becot[44], A. Beddall[12d], A. J. Beddall[12a], V. A. Bednyakov[77], M. Bedognetti[118], C. P. Bee[152], T. A. Beermann[35], M. Begalli[78b], M. Begel[29], A. Behera[152], J. K. Behr[44], A. S. Bell[92], G. Bella[158], L. Bellagamba[23b], A. Bellerive[33], M. Bellomo[157], P. Bellos[9], K. Belotskiy[110], N. L. Belyaev[110], O. Benary[158,*], D. Benchekroun[34a], M. Bender[112], N. Benekos[10], Y. Benhammou[158], E. Benhar Noccioli[180], J. Benitez[75], D. P. Benjamin[47], M. Benoit[52], J. R. Bensinger[26], S. Bentvelsen[118], L. Beresford[132], M. Beretta[49], D. Berge[44], E. Bergeaas Kuutmann[169], N. Berger[5], L. J. Bergsten[26], J. Beringer[18], S. Berlendis[7], N. R. Bernard[100], G. Bernardi[133], C. Bernius[150], F. U. Bernlochner[24], T. Berry[91], P. Berta[97], C. Bertella[15a], G. Bertoli[43a,43b], I. A. Bertram[87], G. J. Besjes[39], O. Bessidskaia Bylund[179], M. Bessner[44], N. Besson[142], A. Bethani[98], S. Bethke[113], A. Betti[24], A. J. Bevan[90], J. Beyer[113], R. M. Bianchi[136], O. Biebel[112], D. Biedermann[19], R. Bielski[35], K. Bierwagen[97], N. V. Biesuz[69a,69b], M. Biglietti[72a], T. R. V. Billoud[107], M. Bindi[51], A. Bingul[12d], C. Bini[70a,70b], S. Biondi[23a,23b], M. Birman[177], T. Bisanz[51], J. P. Biswal[158], C. Bittrich[46], D. M. Bjergaard[47], J. E. Black[150], K. M. Black[25], T. Blazek[28a], I. Bloch[44], C. Blocker[26], A. Blue[55], U. Blumenschein[90], Dr. Blunier[144a], G. J. Bobbink[118], V. S. Bobrovnikov[120a,120b], S. S. Bocchetta[94], A. Bocci[47], D. Boerner[179], D. Bogavac[112], A. G. Bogdanchikov[120a,120b], C. Bohm[43a], V. Boisvert[91], P. Bokan[169], T. Bold[81a], A. S. Boldyrev[111], A. E. Bolz[59b], M. Bomben[133], M. Bona[90], J. S. Bonilla[128], M. Boonekamp[142], A. Borisov[121], G. Borissov[87], J. Bortfeldt[35], D. Bortoletto[132], V. Bortolotto[71a,71b], D. Boscherini[23b], M. Bosman[14], J. D. Bossio Sola[30], K. Bouaouda[34a], J. Boudreau[136], E. V. Bouhova-Thacker[87], D. Boumediene[37], C. Bourdarios[129], S. K. Boutle[55], A. Boveia[123], J. Boyd[35], D. Boye[32b], I. R. Boyko[77], A. J. Bozson[91], J. Bracinik[21], N. Brahimi[99], A. Brandt[8], G. Brandt[179], O. Brandt[59a], F. Braren[44], U. Bratzler[161], B. Brau[100], J. E. Brau[128], W. D. Breaden Madden[55], K. Brendlinger[44], L. Brenner[44], R. Brenner[169], S. Bressler[177], B. Brickwedde[97], D. L. Briglin[21], D. Britton[55], D. Britzger[59b], I. Brock[24], R. Brock[104], G. Brooijmans[38], T. Brooks[91], W. K. Brooks[144b], E. Brost[119], J. H Broughton[21], P. A. Bruckman de Renstrom[82], D. Bruncko[28b], A. Bruni[23b], G. Bruni[23b], L. S. Bruni[118], S. Bruno[71a,71b], B.H. Brunt[31], M. Bruschi[23b], N. Bruscino[136], P. Bryant[36], L. Bryngemark[44], T. Buanes[17], Q. Buat[35], P. Buchholz[148], A. G. Buckley[55], I. A. Budagov[77], M. K. Bugge[131], F. Bührer[50], O. Bulekov[110], D. Bullock[8], T. J. Burch[119], S. Burdin[88], C. D. Burgard[118], A. M. Burger[5], B. Burghgrave[119], K. Burka[82], S. Burke[141], I. Burmeister[45], J. T. P. Burr[132], V. Büscher[97], E. Buschmann[51], P. Bussey[55], J. M. Butler[25], C. M. Buttar[55], J. M. Butterworth[92], P. Butti[35],

W. Buttinger[35], A. Buzatu[155], A. R. Buzykaev[120a,120b], G. Cabras[23a,23b], S. Cabrera Urbán[171], D. Caforio[139], H. Cai[170], V. M. M. Cairo[2], O. Cakir[4a], N. Calace[52], P. Calafiura[18], A. Calandri[99], G. Calderini[133], P. Calfayan[63], G. Callea[40a,40b], L. P. Caloba[78b], S. Calvente Lopez[96], D. Calvet[37], S. Calvet[37], T. P. Calvet[152], M. Calvetti[69a,69b], R. Camacho Toro[133], S. Camarda[35], P. Camarri[71a,71b], D. Cameron[131], R. Caminal Armadans[100], C. Camincher[35], S. Campana[35], M. Campanelli[92], A. Camplani[39], A. Campoverde[148], V. Canale[67a,67b], M. Cano Bret[58c], J. Cantero[126], T. Cao[158], Y. Cao[170], M. D. M. Capeans Garrido[35], I. Caprini[27b], M. Caprini[27b], M. Capua[40a,40b], R. M. Carbone[38], R. Cardarelli[71a], F. C. Cardillo[146], I. Carli[140], T. Carli[35], G. Carlino[67a], B. T. Carlson[136], L. Carminati[66a,66b], R. M. D. Carney[43a,43b], S. Caron[117], E. Carquin[144b], S. Carrá[66a,66b], G. D. Carrillo-Montoya[35], D. Casadei[32b], M. P. Casado[14,g], A. F. Casha[164], D. W. Casper[168], R. Castelijn[118], F. L. Castillo[171], V. Castillo Gimenez[171], N. F. Castro[137a,137e], A. Catinaccio[35], J. R. Catmore[131], A. Cattai[35], J. Caudron[24], V. Cavaliere[29], E. Cavallaro[14], D. Cavalli[66a], M. Cavalli-Sforza[14], V. Cavasinni[69a,69b], E. Celebi[12b], F. Ceradini[72a,72b], L. Cerda Alberich[171], A. S. Cerqueira[78a], A. Cerri[153], L. Cerrito[71a,71b], F. Cerutti[18], A. Cervelli[23a,23b], S. A. Cetin[12b], A. Chafaq[34a], D. Chakraborty[119], S. K. Chan[57], W. S. Chan[118], Y. L. Chan[61a], J. D. Chapman[31], B. Chargeishvili[156b], D. G. Charlton[21], C. C. Chau[33], C. A. Chavez Barajas[153], S. Che[123], A. Chegwidden[104], S. Chekanov[6], S. V. Chekulaev[165a], G. A. Chelkov[77,au], M. A. Chelstowska[35], C. Chen[58a], C. H. Chen[76], H. Chen[29], J. Chen[58a], J. Chen[38], S. Chen[134], S. J. Chen[15c], X. Chen[15b,at], Y. Chen[80], Y.-H. Chen[44], H. C. Cheng[103], H. J. Cheng[15d], A. Cheplakov[77], E. Cheremushkina[121], R. Cherkaoui El Moursli[34e], E. Cheu[7], K. Cheung[62], L. Chevalier[142], V. Chiarella[49], G. Chiarelli[69a], G. Chiodini[65a], A. S. Chisholm[35,21], A. Chitan[27b], I. Chiu[160], Y. H. Chiu[173], M. V. Chizhov[77], K. Choi[63], A. R. Chomont[129], S. Chouridou[159], Y. S. Chow[118], V. Christodoulou[92], M. C. Chu[61a], J. Chudoba[138], A. J. Chuinard[101], J. J. Chwastowski[82], L. Chytka[127], D. Cinca[45], V. Cindro[89], I. A. Cioară[24], A. Ciocio[18], F. Cirotto[67a,67b], Z. H. Citron[177], M. Citterio[66a], A. Clark[52], M. R. Clark[38], P. J. Clark[48], C. Clement[43a,43b], Y. Coadou[99], M. Cobal[64a,64c], A. Coccaro[53a,53b], J. Cochran[76], H. Cohen[158], A. E. C. Coimbra[177], L. Colasurdo[117], B. Cole[38], A. P. Colijn[118], J. Collot[56], P. Conde Muiño[137a,i], E. Coniavitis[50], S. H. Connell[32b], I. A. Connelly[98], S. Constantinescu[27b], F. Conventi[67a,aw], A. M. Cooper-Sarkar[132], F. Cormier[172], K. J. R. Cormier[164], L. D. Corpe[92], M. Corradi[70a,70b], E. E. Corrigan[94], F. Corriveau[101,ae], A. Cortes-Gonzalez[35], M. J. Costa[171], F. Costanza[5], D. Costanzo[146], G. Cottin[31], G. Cowan[91], B. E. Cox[98], J. Crane[98], K. Cranmer[122], S. J. Crawley[55], R. A. Creager[134], G. Cree[33], S. Crépé-Renaudin[56], F. Crescioli[133], M. Cristinziani[24], V. Croft[122], G. Crosetti[40a,40b], A. Cueto[96], T. Cuhadar Donszelmann[146], A. R. Cukierman[150], S. Czekierda[82], P. Czodrowski[35], M. J. Da Cunha Sargedas De Sousa[58b], C. Da Via[98], W. Dabrowski[81a], T. Dado[28a,z], S. Dahbi[34e], T. Dai[103], F. Dallaire[107], C. Dallapiccola[100], M. Dam[39], G. D'amen[23a,23b], J. Damp[97], J. R. Dandoy[134], M. F. Daneri[30], N. P. Dang[178,l], N. D. Dann[98], M. Danninger[172], V. Dao[35], G. Darbo[53b], S. Darmora[8], O. Dartsi[5], A. Dattagupta[128], T. Daubney[44], S. D'Auria[55], W. Davey[24], C. David[44], T. Davidek[140], D. R. Davis[47], E. Dawe[102], I. Dawson[146], K. De[8], R. De Asmundis[67a], A. De Benedetti[125], M. De Beurs[118], S. De Castro[23a,23b], S. De Cecco[70a,70b], N. De Groot[117], P. de Jong[118], H. De la Torre[104], F. De Lorenzi[76], A. De Maria[51,u], D. De Pedis[70a], A. De Salvo[70a], U. De Sanctis[71a,71b], M. De Santis[71a,71b], A. De Santo[153], K. De Vasconcelos Corga[99], J. B. De Vivie De Regie[129], C. Debenedetti[143], D. V. Dedovich[77], N. Dehghanian[3], M. Del Gaudio[40a,40b], J. Del Peso[96], Y. Delabat Diaz[44], D. Delgove[129], F. Deliot[142], C. M. Delitzsch[7], M. Della Pietra[67a,67b], D. Della Volpe[52], A. Dell'Acqua[35], L. Dell'Asta[25], M. Delmastro[5], C. Delporte[129], P. A. Delsart[56], D. A. DeMarco[164], S. Demers[180], M. Demichev[77], S. P. Denisov[121], D. Denysiuk[118], L. D'Eramo[133], D. Derendarz[82], J. E. Derkaoui[34d], F. Derue[133], P. Dervan[88], K. Desch[24], C. Deterre[44], K. Dette[164], M. R. Devesa[30], P. O. Deviveiros[35], A. Dewhurst[141], S. Dhaliwal[26], F. A. Di Bello[52], A. Di Ciaccio[71a,71b], L. Di Ciaccio[5], W. K. Di Clemente[134], C. Di Donato[67a,67b], A. Di Girolamo[35], B. Di Micco[72a,72b], R. Di Nardo[100], K. F. Di Petrillo[57], R. Di Sipio[164], D. Di Valentino[33], C. Diaconu[99], M. Diamond[164], F. A. Dias[39], T. Dias Do Vale[137a], M. A. Diaz[144a], J. Dickinson[18], E. B. Diehl[103], J. Dietrich[19], S. Díez Cornell[44], A. Dimitrievska[18], J. Dingfelder[24], F. Dittus[35], F. Djama[99], T. Djobava[156b], J. I. Djuvsland[59a], M. A. B. Do Vale[78c], M. Dobre[27b], D. Dodsworth[26], C. Doglioni[94], J. Dolejsi[140], Z. Dolezal[140], M. Donadelli[78d], J. Donini[37], A. D'onofrio[90], M. D'Onofrio[88], J. Dopke[141], A. Doria[67a], M. T. Dova[86], A. T. Doyle[55], E. Drechsler[51], E. Dreyer[149], T. Dreyer[51], Y. Du[58b], F. Dubinin[108], M. Dubovsky[28a], A. Dubreuil[52], E. Duchovni[177], G. Duckeck[112], A. Ducourthial[133], O. A. Ducu[107,y], D. Duda[113], A. Dudarev[35], A. C. Dudder[97], E. M. Duffield[18], L. Duflot[129], M. Dührssen[35], C. Dülsen[179], M. Dumancic[177], A. E. Dumitriu[27b,e], A. K. Duncan[55], M. Dunford[59a], A. Duperrin[99], H. Duran Yildiz[4a], M. Düren[54], A. Durglishvili[156b], D. Duschinger[46], B. Dutta[44], D. Duvnjak[1], M. Dyndal[44], S. Dysch[98], B. S. Dziedzic[82], C. Eckardt[44], K. M. Ecker[113], R. C. Edgar[103], T. Eifert[35], G. Eigen[17], K. Einsweiler[18], T. Ekelof[169], M. El Kacimi[34c], R. El Kosseifi[99], V. Ellajosyula[99], M. Ellert[169], F. Ellinghaus[179], A. A. Elliot[90], N. Ellis[35], J. Elmsheuser[29], M. Elsing[35], D. Emeliyanov[141], Y. Enari[160], J. S. Ennis[175], M. B. Epland[47], J. Erdmann[45], A. Ereditato[20], S. Errede[170], M. Escalier[129], C. Escobar[171], O. Estrada Pastor[171], A. I. Etienvre[142], E. Etzion[158], H. Evans[63], A. Ezhilov[135], M. Ezzi[34e], F. Fabbri[55], L. Fabbri[23a,23b], V. Fabiani[117], G. Facini[92], R. M. Faisca Rodrigues Pereira[137a], R. M. Fakhrutdinov[121], S. Falciano[70a], P. J. Falke[5],

S. Falke[5], J. Faltova[140], Y. Fang[15a], M. Fanti[66a,66b], A. Farbin[8], A. Farilla[72a], E. M. Farina[68a,68b], T. Farooque[104], S. Farrell[18], S. M. Farrington[175], P. Farthouat[35], F. Fassi[34e], P. Fassnacht[35], D. Fassouliotis[9], M. Faucci Giannelli[48], A. Favareto[53a,53b], W. J. Fawcett[31], L. Fayard[129], O. L. Fedin[135,q], W. Fedorko[172], M. Feickert[41], S. Feigl[131], L. Feligioni[99], C. Feng[58b], E. J. Feng[35], M. Feng[47], M. J. Fenton[55], A. B. Fenyuk[121], L. Feremenga[8], J. Ferrando[44], A. Ferrari[169], P. Ferrari[118], R. Ferrari[68a], D. E. Ferreira de Lima[59b], A. Ferrer[171], D. Ferrere[52], C. Ferretti[103], F. Fiedler[97], A. Filipčič[89], F. Filthaut[117], K. D. Finelli[25], M. C. N. Fiolhais[137a,137c,a], L. Fiorini[171], C. Fischer[14], W. C. Fisher[104], N. Flaschel[44], I. Fleck[148], P. Fleischmann[103], R. R. M. Fletcher[134], T. Flick[179], B. M. Flierl[112], L. M. Flores[134], L. R. Flores Castillo[61a], F. M. Follega[73a,73b], N. Fomin[17], G. T. Forcolin[98], A. Formica[142], F. A. Förster[14], A. C. Forti[98], A. G. Foster[21], D. Fournier[129], H. Fox[87], S. Fracchia[146], P. Francavilla[69a,69b], M. Franchini[23a,23b], S. Franchino[59a], D. Francis[35], L. Franconi[131], M. Franklin[57], M. Frate[168], M. Fraternali[68a,68b], A. N. Fray[90], D. Freeborn[92], S. M. Fressard-Batraneanu[35], B. Freund[107], W. S. Freund[78b], D. C. Frizzell[125], D. Froidevaux[35], J. A. Frost[132], C. Fukunaga[161], E. Fullana Torregrosa[171], T. Fusayasu[114], J. Fuster[171], O. Gabizon[157], A. Gabrielli[23a,23b], A. Gabrielli[18], G. P. Gach[81a], S. Gadatsch[52], P. Gadow[113], G. Gagliardi[53a,53b], L. G. Gagnon[107], C. Galea[27b], B. Galhardo[137a,137c], E. J. Gallas[132], B. J. Gallop[141], P. Gallus[139], G. Galster[39], R. Gamboa Goni[90], K. K. Gan[123], S. Ganguly[177], J. Gao[58a], Y. Gao[88], Y. S. Gao[150,n], C. García[171], J. E. García Navarro[171], J. A. García Pascual[15a], M. Garcia-Sciveres[18], R. W. Gardner[36], N. Garelli[150], V. Garonne[131], K. Gasnikova[44], A. Gaudiello[53a,53b], G. Gaudio[68a], I. L. Gavrilenko[108], A. Gavrilyuk[109], C. Gay[172], G. Gaycken[24], E. N. Gazis[10], C. N. P. Gee[141], J. Geisen[51], M. Geisen[97], M. P. Geisler[59a], K. Gellerstedt[43a,43b], C. Gemme[53b], M. H. Genest[56], C. Geng[103], S. Gentile[70a,70b], S. George[91], D. Gerbaudo[14], G. Gessner[45], S. Ghasemi[148], M. Ghasemi Bostanabad[173], M. Ghneimat[24], B. Giacobbe[23b], S. Giagu[70a,70b], N. Giangiacomi[23a,23b], P. Giannetti[69a], A. Giannini[67a,67b], S. M. Gibson[91], M. Gignac[143], D. Gillberg[33], G. Gilles[179], D. M. Gingrich[3,av], M. P. Giordani[64a,64c], F. M. Giorgi[23b], P. F. Giraud[142], P. Giromini[57], G. Giugliarelli[64a,64c], D. Giugni[66a], F. Giuli[132], M. Giulini[59b], S. Gkaitatzis[159], I. Gkialas[9,k], E. L. Gkougkousis[14], P. Gkountoumis[10], L. K. Gladilin[111], C. Glasman[96], J. Glatzer[14], P. C. F. Glaysher[44], A. Glazov[44], M. Goblirsch-Kolb[26], J. Godlewski[82], S. Goldfarb[102], T. Golling[52], D. Golubkov[121], A. Gomes[137a,137b], R. Goncalves Gama[78a], R. Gonçalo[137a], G. Gonella[50], L. Gonella[21], A. Gongadze[77], F. Gonnella[21], J. L. Gonski[57], S. González de la Hoz[171], S. Gonzalez-Sevilla[52], L. Goossens[35], P. A. Gorbounov[109], H. A. Gordon[29], B. Gorini[35], E. Gorini[65a,65b], A. Gorišek[89], A. T. Goshaw[47], C. Gössling[45], M. I. Gostkin[77], C. A. Gottardo[24], C. R. Goudet[129], D. Goujdami[34c], A. G. Goussiou[145], N. Govender[32b,c], C. Goy[5], E. Gozani[157], I. Grabowska-Bold[81a], P. O. J. Gradin[169], E. C. Graham[88], J. Gramling[168], E. Gramstad[131], S. Grancagnolo[19], V. Gratchev[135], P. M. Gravila[27f], F. G. Gravili[65a,65b], C. Gray[55], H. M. Gray[18], Z. D. Greenwood[93,al], C. Grefe[24], K. Gregersen[94], I. M. Gregor[44], P. Grenier[150], K. Grevtsov[44], N. A. Grieser[125], J. Griffiths[8], A. A. Grillo[143], K. Grimm[150,b], S. Grinstein[14,aa], Ph. Gris[37], J.-F. Grivaz[129], S. Groh[97], E. Gross[177], J. Grosse-Knetter[51], G. C. Grossi[93], Z. J. Grout[92], C. Grud[103], A. Grummer[116], L. Guan[103], W. Guan[178], J. Guenther[35], A. Guerguichon[129], F. Guescini[165a], D. Guest[168], R. Gugel[50], B. Gui[123], T. Guillemin[5], S. Guindon[35], U. Gul[55], C. Gumpert[35], J. Guo[58c], W. Guo[103], Y. Guo[58a,t], Z. Guo[99], R. Gupta[41], S. Gurbuz[12c], G. Gustavino[125], B. J. Gutelman[157], P. Gutierrez[125], C. Gutschow[92], C. Guyot[142], M. P. Guzik[81a], C. Gwenlan[132], C. B. Gwilliam[88], A. Haas[122], C. Haber[18], H. K. Hadavand[8], N. Haddad[34e], A. Hadef[58a], S. Hageböck[24], M. Hagihara[166], H. Hakobyan[181,*], M. Haleem[174], J. Haley[126], G. Halladjian[104], G. D. Hallewell[99], K. Hamacher[179], P. Hamal[127], K. Hamano[173], A. Hamilton[32a], G. N. Hamity[146], K. Han[58a,ak], L. Han[58a], S. Han[15d], K. Hanagaki[79,w], M. Hance[143], D. M. Handl[112], B. Haney[134], R. Hankache[133], P. Hanke[59a], E. Hansen[94], J. B. Hansen[39], J. D. Hansen[39], M. C. Hansen[24], P. H. Hansen[39], K. Hara[166], A. S. Hard[178], T. Harenberg[179], S. Harkusha[105], P. F. Harrison[175], N. M. Hartmann[112], Y. Hasegawa[147], A. Hasib[48], S. Hassani[142], S. Haug[20], R. Hauser[104], L. Hauswald[46], L. B. Havener[38], M. Havranek[139], C. M. Hawkes[21], R. J. Hawkings[35], D. Hayden[104], C. Hayes[152], C. P. Hays[132], J. M. Hays[90], H. S. Hayward[88], S. J. Haywood[141], M. P. Heath[48], V. Hedberg[94], L. Heelan[8], S. Heer[24], K. K. Heidegger[50], J. Heilman[33], S. Heim[44], T. Heim[18], B. Heinemann[44,aq], J. J. Heinrich[112], L. Heinrich[122], C. Heinz[54], J. Hejbal[138], L. Helary[35], A. Held[172], S. Hellesund[131], S. Hellman[43a,43b], C. Helsens[35], R. C. W. Henderson[87], Y. Heng[178], S. Henkelmann[172], A. M. Henriques Correia[35], G. H. Herbert[19], H. Herde[26], V. Herget[174], Y. Hernández Jiménez[32c], H. Herr[97], M. G. Herrmann[112], G. Herten[50], R. Hertenberger[112], L. Hervas[35], T. C. Herwig[134], G. G. Hesketh[92], N. P. Hessey[165a], J. W. Hetherly[41], S. Higashino[79], E. Higón-Rodriguez[171], K. Hildebrand[36], E. Hill[173], J. C. Hill[31], K. K. Hill[29], K. H. Hiller[44], S. J. Hillier[21], M. Hils[46], I. Hinchliffe[18], M. Hirose[130], D. Hirschbuehl[179], B. Hiti[89], O. Hladik[138], D. R. Hlaluku[32c], X. Hoad[48], J. Hobbs[152], N. Hod[165a], M. C. Hodgkinson[146], A. Hoecker[35], M. R. Hoeferkamp[116], F. Hoenig[112], D. Hohn[24], D. Hohov[129], T. R. Holmes[36], M. Holzbock[112], M. Homann[45], S. Honda[166], T. Honda[79], T. M. Hong[136], A. Hönle[113], B. H. Hooberman[170], W. H. Hopkins[128], Y. Horii[115], P. Horn[46], A. J. Horton[149], L. A. Horyn[36], J.-Y. Hostachy[56], A. Hostiuc[145], S. Hou[155], A. Hoummada[34a], J. Howarth[98], J. Hoya[86], M. Hrabovsky[127], I. Hristova[19], J. Hrivnac[129], A. Hrynevich[106], T. Hryn'ova[5], P. J. Hsu[62], S.-C. Hsu[145], Q. Hu[29], S. Hu[58c], Y. Huang[15a], Z. Hubacek[139],

F. Hubaut[99], M. Huebner[24], F. Huegging[24], T. B. Huffman[132], E. W. Hughes[38], M. Huhtinen[35], R. F. H. Hunter[33], P. Huo[152], A. M. Hupe[33], N. Huseynov[77,ag], J. Huston[104], J. Huth[57], R. Hyneman[103], G. Iacobucci[52], G. Iakovidis[29], I. Ibragimov[148], L. Iconomidou-Fayard[129], Z. Idrissi[34e], P. Iengo[35], R. Ignazzi[39], O. Igonkina[118,ac], R. Iguchi[160], T. Iizawa[52], Y. Ikegami[79], M. Ikeno[79], D. Iliadis[159], N. Ilic[117], F. Iltzsche[46], G. Introzzi[68a,68b], M. Iodice[72a], K. Iordanidou[38], V. Ippolito[70a,70b], M. F. Isacson[169], N. Ishijima[130], M. Ishino[160], M. Ishitsuka[162], W. Islam[126], C. Issever[132], S. Istin[157], F. Ito[166], J. M. Iturbe Ponce[61a], R. Iuppa[73a,73b], A. Ivina[177], H. Iwasaki[79], J. M. Izen[42], V. Izzo[67a], P. Jacka[138], P. Jackson[1], R. M. Jacobs[24], V. Jain[2], G. Jäkel[179], K. B. Jakobi[97], K. Jakobs[50], S. Jakobsen[74], T. Jakoubek[138], D. O. Jamin[126], D. K. Jana[93], R. Jansky[52], J. Janssen[24], M. Janus[51], P. A. Janus[81a], G. Jarlskog[94], N. Javadov[77,ag], T. Javůrek[35], M. Javurkova[50], F. Jeanneau[142], L. Jeanty[18], J. Jejelava[156a,ah], A. Jelinskas[175], P. Jenni[50,d], J. Jeong[44], N. Jeong[44], S. Jézéquel[5], H. Ji[178], J. Jia[152], H. Jiang[76], Y. Jiang[58a], Z. Jiang[150,r], S. Jiggins[50], F. A. Jimenez Morales[37], J. Jimenez Pena[171], S. Jin[15c], A. Jinaru[27b], O. Jinnouchi[162], H. Jivan[32c], P. Johansson[146], K. A. Johns[7], C. A. Johnson[63], W. J. Johnson[145], K. Jon-And[43a,43b], R. W. L. Jones[87], S. D. Jones[153], S. Jones[7], T. J. Jones[88], J. Jongmanns[59a], P. M. Jorge[137a,137b], J. Jovicevic[165a], X. Ju[18], J. J. Junggeburth[113], A. Juste Rozas[14,aa], A. Kaczmarska[82], M. Kado[129], H. Kagan[123], M. Kagan[150], T. Kaji[176], E. Kajomovitz[157], C. W. Kalderon[94], A. Kaluza[97], S. Kama[41], A. Kamenshchikov[121], L. Kanjir[89], Y. Kano[160], V. A. Kantserov[110], J. Kanzaki[79], B. Kaplan[122], L. S. Kaplan[178], D. Kar[32c], M. J. Kareem[165b], E. Karentzos[10], S. N. Karpov[77], Z. M. Karpova[77], V. Kartvelishvili[87], A. N. Karyukhin[121], L. Kashif[178], R. D. Kass[123], A. Kastanas[151], Y. Kataoka[160], C. Kato[58c,58d], J. Katzy[44], K. Kawade[80], K. Kawagoe[85], T. Kawamoto[160], G. Kawamura[51], E. F. Kay[88], V. F. Kazanin[120a,120b], R. Keeler[173], R. Kehoe[41], J. S. Keller[33], E. Kellermann[94], J. J. Kempster[21], J. Kendrick[21], O. Kepka[138], S. Kersten[179], B. P. Kerševan[89], R. A. Keyes[101], M. Khader[170], F. Khalil-Zada[13], A. Khanov[126], A. G. Kharlamov[120a,120b], T. Kharlamova[120a,120b], E. E. Khoda[172], A. Khodinov[163], T. J. Khoo[52], E. Khramov[77], J. Khubua[156b], S. Kido[80], M. Kiehn[52], C. R. Kilby[91], Y. K. Kim[36], N. Kimura[64a,64c], O. M. Kind[19], B. T. King[88], D. Kirchmeier[46], J. Kirk[141], A. E. Kiryunin[113], T. Kishimoto[160], D. Kisielewska[81a], V. Kitali[44], O. Kivernyk[5], E. Kladiva[28b,*], T. Klapdor-Kleingrothaus[50], M. H. Klein[103], M. Klein[88], U. Klein[88], K. Kleinknecht[97], P. Klimek[119], A. Klimentov[29], R. Klingenberg[45,*], T. Klingl[24], T. Klioutchnikova[35], F. F. Klitzner[112], P. Kluit[118], S. Kluth[113], E. Kneringer[74], E. B. F. G. Knoops[99], A. Knue[50], A. Kobayashi[160], D. Kobayashi[85], T. Kobayashi[160], M. Kobel[46], M. Kocian[150], P. Kodys[140], P. T. Koenig[24], T. Koffas[33], E. Koffeman[118], N. M. Köhler[113], T. Koi[150], M. Kolb[59b], I. Koletsou[5], T. Kondo[79], N. Kondrashova[58c], K. Köneke[50], A. C. König[117], T. Kono[79], R. Konoplich[122,an], V. Konstantinides[92], N. Konstantinidis[92], B. Konya[94], R. Kopeliansky[63], S. Koperny[81a], K. Korcyl[82], K. Kordas[159], G. Koren[158], A. Korn[92], I. Korolkov[14], E. V. Korolkova[146], N. Korotkova[111], O. Kortner[113], S. Kortner[113], T. Kosek[140], V. V. Kostyukhin[24], A. Kotwal[47], A. Koulouris[10], A. Kourkoumeli-Charalampidi[68a,68b], C. Kourkoumelis[9], E. Kourlitis[146], V. Kouskoura[29], A. B. Kowalewska[82], R. Kowalewski[173], T. Z. Kowalski[81a], C. Kozakai[160], W. Kozanecki[142], A. S. Kozhin[121], V. A. Kramarenko[111], G. Kramberger[89], D. Krasnopevtsev[58a], M. W. Krasny[133], A. Krasznahorkay[35], D. Krauss[113], J. A. Kremer[81a], J. Kretzschmar[88], P. Krieger[164], K. Krizka[18], K. Kroeninger[45], H. Kroha[113], J. Kroll[138], J. Kroll[134], J. Krstic[16], U. Kruchonak[77], H. Krüger[24], N. Krumnack[76], M. C. Kruse[47], T. Kubota[102], S. Kuday[4b], J. T. Kuechler[179], S. Kuehn[35], A. Kugel[59a], F. Kuger[174], T. Kuhl[44], V. Kukhtin[77], R. Kukla[99], Y. Kulchitsky[105], S. Kuleshov[144b], Y. P. Kulinich[170], M. Kuna[56], T. Kunigo[83], A. Kupco[138], T. Kupfer[45], O. Kuprash[158], H. Kurashige[80], L. L. Kurchaninov[165a], Y. A. Kurochkin[105], M. G. Kurth[15d], E. S. Kuwertz[35], M. Kuze[162], J. Kvita[127], T. Kwan[101], A. La Rosa[113], J. L. La Rosa Navarro[78d], L. La Rotonda[40a,40b], F. La Ruffa[40a,40b], C. Lacasta[171], F. Lacava[70a,70b], J. Lacey[44], D. P. J. Lack[98], H. Lacker[19], D. Lacour[133], E. Ladygin[77], R. Lafaye[5], B. Laforge[133], T. Lagouri[32c], S. Lai[51], S. Lammers[63], W. Lampl[7], E. Lançon[29], U. Landgraf[50], M. P. J. Landon[90], M. C. Lanfermann[52], V. S. Lang[44], J. C. Lange[14], R. J. Langenberg[35], A. J. Lankford[168], F. Lanni[29], K. Lantzsch[24], A. Lanza[68a], A. Lapertosa[53a,53b], S. Laplace[133], J. F. Laporte[142], T. Lari[66a], F. Lasagni Manghi[23a,23b], M. Lassnig[35], T. S. Lau[61a], A. Laudrain[129], M. Lavorgna[67a,67b], A. T. Law[143], M. Lazzaroni[66a,66b], B. Le[102], O. Le Dortz[133], E. Le Guirriec[99], E. P. Le Quilleuc[142], M. LeBlanc[7], T. LeCompte[6], F. Ledroit-Guillon[56], C. A. Lee[29], G. R. Lee[144a], L. Lee[57], S. C. Lee[155], B. Lefebvre[101], M. Lefebvre[173], F. Legger[112], C. Leggett[18], K. Lehmann[149], N. Lehmann[179], G. Lehmann Miotto[35], W. A. Leight[44], A. Leisos[159,x], M. A. L. Leite[78d], R. Leitner[140], D. Lellouch[177], B. Lemmer[51], K. J. C. Leney[92], T. Lenz[24], B. Lenzi[35], R. Leone[7], S. Leone[69a], C. Leonidopoulos[48], G. Lerner[153], C. Leroy[107], R. Les[164], A. A. J. Lesage[142], C. G. Lester[31], M. Levchenko[135], J. Levêque[5], D. Levin[103], L. J. Levinson[177], D. Lewis[90], B. Li[103], C.-Q. Li[58a,am], H. Li[58b], L. Li[58c], Q. Li[15d], Q. Y. Li[58a], S. Li[58c,58d], X. Li[58c], Y. Li[148], Z. Liang[15a], B. Liberti[71a], A. Liblong[164], K. Lie[61c], S. Liem[118], A. Limosani[154], C. Y. Lin[31], K. Lin[104], T. H. Lin[97], R. A. Linck[63], J. H. Lindon[21], B. E. Lindquist[152], A. L. Lionti[52], E. Lipeles[134], A. Lipniacka[17], M. Lisovyi[59b], T. M. Liss[170,as], A. Lister[172], A. M. Litke[143], J. D. Little[8], B. Liu[76], B. L Liu[6], H. B. Liu[29], H. Liu[103], J. B. Liu[58a], J. K. K. Liu[132], K. Liu[133], M. Liu[58a], P. Liu[18], Y. Liu[15a], Y. L. Liu[58a], Y. W. Liu[58a], M. Livan[68a,68b], A. Lleres[56], J. Llorente Merino[15a], S. L. Lloyd[90], C. Y. Lo[61b], F. Lo Sterzo[41], E. M. Lobodzinska[44], P. Loch[7], T. Lohse[19],

K. Lohwasser[146], M. Lokajicek[138], B. A. Long[25], J. D. Long[170], R. E. Long[87], L. Longo[65a,65b], K. A. Looper[123], J. A. Lopez[144b], I. Lopez Paz[14], A. Lopez Solis[146], J. Lorenz[112], N. Lorenzo Martinez[5], M. Losada[22], P. J. Lösel[112], A. Lösle[50], X. Lou[44], X. Lou[15a], A. Lounis[129], J. Love[6], P. A. Love[87], J. J. Lozano Bahilo[171], H. Lu[61a], M. Lu[58a], N. Lu[103], Y. J. Lu[62], H. J. Lubatti[145], C. Luci[70a,70b], A. Lucotte[56], C. Luedtke[50], F. Luehring[63], I. Luise[133], L. Luminari[70a], B. Lund-Jensen[151], M. S. Lutz[100], P. M. Luzi[133], D. Lynn[29], R. Lysak[138], E. Lytken[94], F. Lyu[15a], V. Lyubushkin[77], H. Ma[29], L. L. Ma[58b], Y. Ma[58b], G. Maccarrone[49], A. Macchiolo[113], C. M. Macdonald[146], J. Machado Miguens[134,137b], D. Madaffari[171], R. Madar[37], W. F. Mader[46], A. Madsen[44], N. Madysa[46], J. Maeda[80], K. Maekawa[160], S. Maeland[17], T. Maeno[29], A. S. Maevskiy[111], V. Magerl[50], C. Maidantchik[78b], T. Maier[112], A. Maio[137a,137b,137d], O. Majersky[28a], S. Majewski[128], Y. Makida[79], N. Makovec[129], B. Malaescu[133], Pa. Malecki[82], V. P. Maleev[135], F. Malek[56], U. Mallik[75], D. Malon[6], C. Malone[31], S. Maltezos[10], S. Malyukov[35], J. Mamuzic[171], G. Mancini[49], I. Mandić[89], J. Maneira[137a], L. Manhaes de Andrade Filho[78a], J. Manjarres Ramos[46], K. H. Mankinen[94], A. Mann[112], A. Manousos[74], B. Mansoulie[142], J. D. Mansour[15a], M. Mantoani[51], S. Manzoni[66a,66b], G. Marceca[30], L. March[52], L. Marchese[132], G. Marchiori[133], M. Marcisovsky[138], C. A. Marin Tobon[35], M. Marjanovic[37], D. E. Marley[103], F. Marroquim[78b], Z. Marshall[18], M. U. F Martensson[169], S. Marti-Garcia[171], C. B. Martin[123], T. A. Martin[175], V. J. Martin[48], B. Martin dit Latour[17], M. Martinez[14,aa], V. I. Martinez Outschoorn[100], S. Martin-Haugh[141], V. S. Martoiu[27b], A. C. Martyniuk[92], A. Marzin[35], L. Masetti[97], T. Mashimo[160], R. Mashinistov[108], J. Masik[98], A. L. Maslennikov[120a,120b], L. H. Mason[102], L. Massa[71a,71b], P. Massarotti[67a,67b], P. Mastrandrea[5], A. Mastroberardino[40a,40b], T. Masubuchi[160], P. Mättig[179], J. Maurer[27b], B. Maček[89], S. J. Maxfield[88], D. A. Maximov[120a,120b], R. Mazini[155], I. Maznas[159], S. M. Mazza[143], N. C. Mc Fadden[116], G. Mc Goldrick[164], S. P. Mc Kee[103], A. McCarn[103], T. G. McCarthy[113], L. I. McClymont[92], E. F. McDonald[102], J. A. Mcfayden[35], G. Mchedlidze[51], M. A. McKay[41], K. D. McLean[173], S. J. McMahon[141], P. C. McNamara[102], C. J. McNicol[175], R. A. McPherson[173,ae], J. E. Mdhluli[32c], Z. A. Meadows[100], S. Meehan[145], T. M. Megy[50], S. Mehlhase[112], A. Mehta[88], T. Meideck[56], B. Meirose[42], D. Melini[171,h], B. R. Mellado Garcia[32c], J. D. Mellenthin[51], M. Melo[28a], F. Meloni[44], A. Melzer[24], S. B. Menary[98], E. D. Mendes Gouveia[137a], L. Meng[88], X. T. Meng[103], A. Mengarelli[23a,23b], S. Menke[113], E. Meoni[40a,40b], S. Mergelmeyer[19], C. Merlassino[20], P. Mermod[52], L. Merola[67a,67b], C. Meroni[66a], F. S. Merritt[36], A. Messina[70a,70b], J. Metcalfe[6], A. S. Mete[168], C. Meyer[134], J. Meyer[157], J.-P. Meyer[142], H. Meyer Zu Theenhausen[59a], F. Miano[153], R. P. Middleton[141], L. Mijović[48], G. Mikenberg[177], M. Mikestikova[138], M. Mikuž[89], M. Milesi[102], A. Milic[164], D. A. Millar[90], D. W. Miller[36], A. Milov[177], D. A. Milstead[43a,43b], A. A. Minaenko[121], M. Miñano Moya[171], I. A. Minashvili[156b], A. I. Mincer[122], B. Mindur[81a], M. Mineev[77], Y. Minegishi[160], Y. Ming[178], L. M. Mir[14], A. Mirto[65a,65b], K. P. Mistry[134], T. Mitani[176], J. Mitrevski[112], V. A. Mitsou[171], A. Miucci[20], P. S. Miyagawa[146], A. Mizukami[79], J. U. Mjörnmark[94], T. Mkrtchyan[181], M. Mlynarikova[140], T. Moa[43a,43b], K. Mochizuki[107], P. Mogg[50], S. Mohapatra[38], S. Molander[43a,43b], R. Moles-Valls[24], M. C. Mondragon[104], K. Mönig[44], J. Monk[39], E. Monnier[99], A. Montalbano[149], J. Montejo Berlingen[35], F. Monticelli[86], S. Monzani[66a], N. Morange[129], D. Moreno[22], M. Moreno Llácer[35], P. Morettini[53b], M. Morgenstern[118], S. Morgenstern[46], D. Mori[149], M. Morii[57], M. Morinaga[176], V. Morisbak[131], A. K. Morley[35], G. Mornacchi[35], A. P. Morris[92], J. D. Morris[90], L. Morvaj[152], P. Moschovakos[10], M. Mosidze[156b], H. J. Moss[146], J. Moss[150,o], K. Motohashi[162], R. Mount[150], E. Mountricha[35], E. J. W. Moyse[100], S. Muanza[99], F. Mueller[113], J. Mueller[136], R. S. P. Mueller[112], D. Muenstermann[87], G. A. Mullier[20], F. J. Munoz Sanchez[98], P. Murin[28b], W. J. Murray[141,175], A. Murrone[66a,66b], M. Muškinja[89], C. Mwewa[32a], A. G. Myagkov[121,ao], J. Myers[128], M. Myska[139], B. P. Nachman[18], O. Nackenhorst[45], K. Nagai[132], K. Nagano[79], Y. Nagasaka[60], M. Nagel[50], E. Nagy[99], A. M. Nairz[35], Y. Nakahama[115], K. Nakamura[79], T. Nakamura[160], I. Nakano[124], H. Nanjo[130], F. Napolitano[59a], R. F. Naranjo Garcia[44], R. Narayan[11], D. I. Narrias Villar[59a], I. Naryshkin[135], T. Naumann[44], G. Navarro[22], R. Nayyar[7], H. A. Neal[103,*], P. Y. Nechaeva[108], T. J. Neep[142], A. Negri[68a,68b], M. Negrini[23b], S. Nektarijevic[117], C. Nellist[51], M. E. Nelson[132], S. Nemecek[138], P. Nemethy[122], M. Nessi[35,f], M. S. Neubauer[170], M. Neumann[179], P. R. Newman[21], T. Y. Ng[61c], Y. S. Ng[19], H. D. N. Nguyen[99], T. Nguyen Manh[107], E. Nibigira[37], R. B. Nickerson[132], R. Nicolaidou[142], J. Nielsen[143], N. Nikiforou[11], V. Nikolaenko[121,ao], I. Nikolic-Audit[133], K. Nikolopoulos[21], P. Nilsson[29], Y. Ninomiya[79], A. Nisati[70a], N. Nishu[58c], R. Nisius[113], I. Nitsche[45], T. Nitta[176], T. Nobe[160], Y. Noguchi[83], M. Nomachi[130], I. Nomidis[133], M. A. Nomura[29], T. Nooney[90], M. Nordberg[35], N. Norjoharuddeen[132], T. Novak[89], O. Novgorodova[46], R. Novotny[139], L. Nozka[127], K. Ntekas[168], E. Nurse[92], F. Nuti[102], F. G. Oakham[33,av], H. Oberlack[113], T. Obermann[24], J. Ocariz[133], A. Ochi[80], I. Ochoa[38], J. P. Ochoa-Ricoux[144a], K. O'Connor[26], S. Oda[85], S. Odaka[79], S. Oerdek[51], A. Oh[98], S. H. Oh[47], C. C. Ohm[151], H. Oide[53a,53b], M. L. Ojeda[164], H. Okawa[166], Y. Okazaki[83], Y. Okumura[160], T. Okuyama[79], A. Olariu[27b], L. F. Oleiro Seabra[137a], S. A. Olivares Pino[144a], D. Oliveira Damazio[29], J. L. Oliver[1], M. J. R. Olsson[36], A. Olszewski[82], J. Olszowska[82], D. C. O'Neil[149], A. Onofre[137a,137e], K. Onogi[115], P. U. E. Onyisi[11], H. Oppen[131], M. J. Oreglia[36], G. E. Orellana[86], Y. Oren[158], D. Orestano[72a,72b], E. C. Orgill[98], N. Orlando[61b], A. A. O'Rourke[44], R. S. Orr[164], B. Osculati[53a,53b,*], V. O'Shea[55], R. Ospanov[58a], G. Otero y Garzon[30],

H. Otono[85], M. Ouchrif[34d], F. Ould-Saada[131], A. Ouraou[142], Q. Ouyang[15a], M. Owen[55], R. E. Owen[21], V. E. Ozcan[12c], N. Ozturk[8], J. Pacalt[127], H. A. Pacey[31], K. Pachal[149], A. Pacheco Pages[14], L. Pacheco Rodriguez[142], C. Padilla Aranda[14], S. Pagan Griso[18], M. Paganini[180], G. Palacino[63], S. Palazzo[40a,40b], S. Palestini[35], M. Palka[81b], D. Pallin[37], I. Panagoulias[10], C. E. Pandini[35], J. G. Panduro Vazquez[91], P. Pani[35], G. Panizzo[64a,64c], L. Paolozzi[52], T. D. Papadopoulou[10], K. Papageorgiou[9,k], A. Paramonov[6], D. Paredes Hernandez[61b], S. R. Paredes Saenz[132], B. Parida[163], A. J. Parker[87], K. A. Parker[44], M. A. Parker[31], F. Parodi[53a,53b], J. A. Parsons[38], U. Parzefall[50], V. R. Pascuzzi[164], J. M. P. Pasner[143], E. Pasqualucci[70a], S. Passaggio[53b], F. Pastore[91], P. Pasuwan[43a,43b], S. Pataraia[97], J. R. Pater[98], A. Pathak[178,l], T. Pauly[35], B. Pearson[113], M. Pedersen[131], L. Pedraza Diaz[117], R. Pedro[137a,137b], S. V. Peleganchuk[120a,120b], O. Penc[138], C. Peng[15d], H. Peng[58a], B. S. Peralva[78a], M. M. Perego[142], A. P. Pereira Peixoto[137a], D. V. Perepelitsa[29], F. Peri[19], L. Perini[66a,66b], H. Pernegger[35], S. Perrella[67a,67b], V. D. Peshekhonov[77,*], K. Peters[44], R. F. Y. Peters[98], B. A. Petersen[35], T. C. Petersen[39], E. Petit[56], A. Petridis[1], C. Petridou[159], P. Petroff[129], M. Petrov[132], F. Petrucci[72a,72b], M. Pettee[180], N. E. Pettersson[100], A. Peyaud[142], R. Pezoa[144b], T. Pham[102], F. H. Phillips[104], P. W. Phillips[141], M. W. Phipps[170], G. Piacquadio[152], E. Pianori[18], A. Picazio[100], M. A. Pickering[132], R. H. Pickles[98], R. Piegaia[30], J. E. Pilcher[36], A. D. Pilkington[98], M. Pinamonti[71a,71b], J. L. Pinfold[3], M. Pitt[177], M.-A. Pleier[29], V. Pleskot[140], E. Plotnikova[77], D. Pluth[76], P. Podberezko[120a,120b], R. Poettgen[94], R. Poggi[52], L. Poggioli[129], I. Pogrebnyak[104], D. Pohl[24], I. Pokharel[51], G. Polesello[68a], A. Poley[18], A. Policicchio[70a,70b], R. Polifka[35], A. Polini[23b], C. S. Pollard[44], V. Polychronakos[29], D. Ponomarenko[110], L. Pontecorvo[35], G. A. Popeneciu[27d], D. M. Portillo Quintero[133], S. Pospisil[139], K. Potamianos[44], I. N. Potrap[77], C. J. Potter[31], H. Potti[11], T. Poulsen[94], J. Poveda[35], T. D. Powell[146], M. E. Pozo Astigarraga[35], P. Pralavorio[99], S. Prell[76], D. Price[98], M. Primavera[65a], S. Prince[101], N. Proklova[110], K. Prokofiev[61c], F. Prokoshin[144b], S. Protopopescu[29], J. Proudfoot[6], M. Przybycien[81a], A. Puri[170], P. Puzo[129], J. Qian[103], Y. Qin[98], A. Quadt[51], M. Queitsch-Maitland[44], A. Qureshi[1], P. Rados[102], F. Ragusa[66a,66b], G. Rahal[95], J. A. Raine[52], S. Rajagopalan[29], A. Ramirez Morales[90], T. Rashid[129], S. Raspopov[5], M. G. Ratti[66a,66b], D. M. Rauch[44], F. Rauscher[112], S. Rave[97], B. Ravina[146], I. Ravinovich[177], J. H. Rawling[98], M. Raymond[35], A. L. Read[131], N. P. Readioff[56], M. Reale[65a,65b], D. M. Rebuzzi[68a,68b], A. Redelbach[174], G. Redlinger[29], R. Reece[143], R. G. Reed[32c], K. Reeves[42], L. Rehnisch[19], J. Reichert[134], D. Reikher[158], A. Reiss[97], C. Rembser[35], H. Ren[15d], M. Rescigno[70a], S. Resconi[66a], E. D. Resseguie[134], S. Rettie[172], E. Reynolds[21], O. L. Rezanova[120a,120b], P. Reznicek[140], E. Ricci[73a,73b], R. Richter[113], S. Richter[44], E. Richter-Was[81b], O. Ricken[24], M. Ridel[133], P. Rieck[113], C. J. Riegel[179], O. Rifki[44], M. Rijssenbeek[152], A. Rimoldi[68a,68b], M. Rimoldi[20], L. Rinaldi[23b], G. Ripellino[151], B. Ristić[87], E. Ritsch[35], I. Riu[14], J. C. Rivera Vergara[144a], F. Rizatdinova[126], E. Rizvi[90], C. Rizzi[14], R. T. Roberts[98], S. H. Robertson[101,ae], D. Robinson[31], J. E. M. Robinson[44], A. Robson[55], E. Rocco[97], C. Roda[69a,69b], Y. Rodina[99], S. Rodriguez Bosca[171], A. Rodriguez Perez[14], D. Rodriguez Rodriguez[171], A. M. Rodríguez Vera[165b], S. Roe[35], C. S. Rogan[57], O. Røhne[131], R. Röhrig[113], C. P. A. Roland[63], J. Roloff[57], A. Romaniouk[110], M. Romano[23a,23b], N. Rompotis[88], M. Ronzani[122], L. Roos[133], S. Rosati[70a], K. Rosbach[50], P. Rose[143], N.-A. Rosien[51], E. Rossi[44], E. Rossi[67a,67b], L. P. Rossi[53b], L. Rossini[66a,66b], J. H. N. Rosten[31], R. Rosten[14], M. Rotaru[27b], J. Rothberg[145], D. Rousseau[129], D. Roy[32c], A. Rozanov[99], Y. Rozen[157], X. Ruan[32c], F. Rubbo[150], F. Rühr[50], A. Ruiz-Martinez[171], Z. Rurikova[50], N. A. Rusakovich[77], H. L. Russell[101], J. P. Rutherfoord[7], E. M. Rüttinger[44,m], Y. F. Ryabov[135], M. Rybar[170], G. Rybkin[129], S. Ryu[6], A. Ryzhov[121], G. F. Rzehorz[51], P. Sabatini[51], G. Sabato[118], S. Sacerdoti[129], H. F.-W. Sadrozinski[143], R. Sadykov[77], F. Safai Tehrani[70a], P. Saha[119], M. Sahinsoy[59a], A. Sahu[179], M. Saimpert[44], M. Saito[160], T. Saito[160], H. Sakamoto[160], A. Sakharov[122,an], D. Salamani[52], G. Salamanna[72a,72b], J. E. Salazar Loyola[144b], D. Salek[118], P. H. Sales De Bruin[169], D. Salihagic[113], A. Salnikov[150], J. Salt[171], D. Salvatore[40a,40b], F. Salvatore[153], A. Salvucci[61a,61b,61c], A. Salzburger[35], J. Samarati[35], D. Sammel[50], D. Sampsonidis[159], D. Sampsonidou[159], J. Sánchez[171], A. Sanchez Pineda[64a,64c], H. Sandaker[131], C. O. Sander[44], M. Sandhoff[179], C. Sandoval[22], D. P. C. Sankey[141], M. Sannino[53a,53b], Y. Sano[115], A. Sansoni[49], C. Santoni[37], H. Santos[137a], I. Santoyo Castillo[153], A. Santra[171], A. Sapronov[77], J. G. Saraiva[137a,137d], O. Sasaki[79], K. Sato[166], E. Sauvan[5], P. Savard[164,av], N. Savic[113], R. Sawada[160], C. Sawyer[141], L. Sawyer[93,al], C. Sbarra[23b], A. Sbrizzi[23a], T. Scanlon[92], J. Schaarschmidt[145], P. Schacht[113], B. M. Schachtner[112], D. Schaefer[36], L. Schaefer[134], J. Schaeffer[97], S. Schaepe[35], U. Schäfer[97], A. C. Schaffer[129], D. Schaile[112], R. D. Schamberger[152], N. Scharmberg[98], V. A. Schegelsky[135], D. Scheirich[140], F. Schenck[19], M. Schernau[168], C. Schiavi[53a,53b], S. Schier[143], L. K. Schildgen[24], Z. M. Schillaci[26], E. J. Schioppa[35], M. Schioppa[40a,40b], K. E. Schleicher[50], S. Schlenker[35], K. R. Schmidt-Sommerfeld[113], K. Schmieden[35], C. Schmitt[97], S. Schmitt[44], S. Schmitz[97], J. C. Schmoeckel[44], U. Schnoor[50], L. Schoeffel[142], A. Schoening[59b], E. Schopf[24], M. Schott[97], J. F. P. Schouwenberg[117], J. Schovancova[35], S. Schramm[52], A. Schulte[97], H.-C. Schultz-Coulon[59a], M. Schumacher[50], B. A. Schumm[143], Ph. Schune[142], A. Schwartzman[150], T. A. Schwarz[103], Ph. Schwemling[142], R. Schwienhorst[104], A. Sciandra[24], G. Sciolla[26], M. Scornajenghi[40a,40b], F. Scuri[69a], F. Scutti[102], L. M. Scyboz[113], J. Searcy[103], C. D. Sebastiani[70a,70b], P. Seema[19], S. C. Seidel[116], A. Seiden[143], T. Seiss[36], J. M. Seixas[78b], G. Sekhniaidze[67a], K. Sekhon[103], S. J. Sekula[41], N. Semprini-Cesari[23a,23b], S. Sen[47], S. Senkin[37],

C. Serfon[131], L. Serin[129], L. Serkin[64a,64b], M. Sessa[58a], H. Severini[125], F. Sforza[167], A. Sfyrla[52], E. Shabalina[51], J. D. Shahinian[143], N. W. Shaikh[43a,43b], L. Y. Shan[15a], R. Shang[170], J. T. Shank[25], M. Shapiro[18], A. S. Sharma[1], A. Sharma[132], P. B. Shatalov[109], K. Shaw[153], S. M. Shaw[98], A. Shcherbakova[135], Y. Shen[125], N. Sherafati[33], A. D. Sherman[25], P. Sherwood[92], L. Shi[155,ar], S. Shimizu[79], C. O. Shimmin[180], M. Shimojima[114], I. P. J. Shipsey[132], S. Shirabe[85], M. Shiyakova[77], J. Shlomi[177], A. Shmeleva[108], D. Shoaleh Saadi[107], M. J. Shochet[36], S. Shojaii[102], D. R. Shope[125], S. Shrestha[123], E. Shulga[110], P. Sicho[138], A. M. Sickles[170], P. E. Sidebo[151], E. Sideras Haddad[32c], O. Sidiropoulou[35], A. Sidoti[23a,23b], F. Siegert[46], Dj. Sijacki[16], J. Silva[137a], M. Silva Jr.[178], M. V. Silva Oliveira[78a], S. B. Silverstein[43a], L. Simic[77], S. Simion[129], E. Simioni[97], M. Simon[97], R. Simoniello[97], P. Sinervo[164], N. B. Sinev[128], M. Sioli[23a,23b], G. Siragusa[174], I. Siral[103], S. Yu. Sivoklokov[111], J. Sjölin[43a,43b], P. Skubic[125], M. Slater[21], T. Slavicek[139], M. Slawinska[82], K. Sliwa[167], R. Slovak[140], V. Smakhtin[177], B. H. Smart[5], J. Smiesko[28a], N. Smirnov[110], S. Yu. Smirnov[110], Y. Smirnov[110], L. N. Smirnova[111], O. Smirnova[94], J. W. Smith[51], M. N. K. Smith[38], M. Smizanska[87], K. Smolek[139], A. Smykiewicz[82], A. A. Snesarev[108], I. M. Snyder[128], S. Snyder[29], R. Sobie[173,ae], A. M. Soffa[168], A. Soffer[158], A. Søgaard[48], D. A. Soh[155], G. Sokhrannyi[89], C. A. Solans Sanchez[35], M. Solar[139], E. Yu. Soldatov[110], U. Soldevila[171], A. A. Solodkov[121], A. Soloshenko[77], O. V. Solovyanov[121], V. Solovyev[135], P. Sommer[146], H. Son[167], W. Song[141], W. Y. Song[165b], A. Sopczak[139], F. Sopkova[28b], C. L. Sotiropoulou[69a,69b], S. Sottocornola[68a,68b], R. Soualah[64a,64c,j], A. M. Soukharev[120a,120b], D. South[44], B. C. Sowden[91], S. Spagnolo[65a,65b], M. Spalla[113], M. Spangenberg[175], F. Spanò[91], D. Sperlich[19], F. Spettel[113], T. M. Spieker[59a], R. Spighi[23b], G. Spigo[35], L. A. Spiller[102], D. P. Spiteri[55], M. Spousta[140], A. Stabile[66a,66b], R. Stamen[59a], S. Stamm[19], E. Stanecka[82], R. W. Stanek[6], C. Stanescu[72a], B. Stanislaus[132], M. M. Stanitzki[44], B. Stapf[118], S. Stapnes[131], E. A. Starchenko[121], G. H. Stark[36], J. Stark[56], S. H Stark[39], P. Staroba[138], P. Starovoitov[59a], S. Stärz[35], R. Staszewski[82], M. Stegler[44], P. Steinberg[29], B. Stelzer[149], H. J. Stelzer[35], O. Stelzer-Chilton[165a], H. Stenzel[54], T. J. Stevenson[90], G. A. Stewart[35], M. C. Stockton[128], G. Stoicea[27b], P. Stolte[51], S. Stonjek[113], A. Straessner[46], J. Strandberg[151], S. Strandberg[43a,43b], M. Strauss[125], P. Strizenec[28b], R. Ströhmer[174], D. M. Strom[128], R. Stroynowski[41], A. Strubig[48], S. A. Stucci[29], B. Stugu[17], J. Stupak[125], N. A. Styles[44], D. Su[150], J. Su[136], S. Suchek[59a], Y. Sugaya[130], M. Suk[139], V. V. Sulin[108], D. M. S. Sultan[52], S. Sultansoy[4c], T. Sumida[83], S. Sun[103], X. Sun[3], K. Suruliz[153], C. J. E. Suster[154], M. R. Sutton[153], S. Suzuki[79], M. Svatos[138], M. Swiatlowski[36], S. P. Swift[2], A. Sydorenko[97], I. Sykora[28a], T. Sykora[140], D. Ta[97], K. Tackmann[44,ab], J. Taenzer[158], A. Taffard[168], R. Tafirout[165a], E. Tahirovic[90], N. Taiblum[158], H. Takai[29], R. Takashima[84], E. H. Takasugi[113], K. Takeda[80], T. Takeshita[147], Y. Takubo[79], M. Talby[99], A. A. Talyshev[120a,120b], J. Tanaka[160], M. Tanaka[162], R. Tanaka[129], B. B. Tannenwald[123], S. Tapia Araya[144b], S. Tapprogge[97], A. Tarek Abouelfadl Mohamed[133], S. Tarem[157], G. Tarna[27b,e], G. F. Tartarelli[66a], P. Tas[140], M. Tasevsky[138], T. Tashiro[83], E. Tassi[40a,40b], A. Tavares Delgado[137a,137b], Y. Tayalati[34e], A. C. Taylor[116], A. J. Taylor[48], G. N. Taylor[102], P. T. E. Taylor[102], W. Taylor[165b], A. S. Tee[87], P. Teixeira-Dias[91], H. Ten Kate[35], P. K. Teng[155], J. J. Teoh[118], S. Terada[79], K. Terashi[160], J. Terron[96], S. Terzo[14], M. Testa[49], R. J. Teuscher[164,ae], S. J. Thais[180], T. Theveneaux-Pelzer[44], F. Thiele[39], D. W. Thomas[91], J. P. Thomas[21], A. S. Thompson[55], P. D. Thompson[21], L. A. Thomsen[180], E. Thomson[134], Y. Tian[38], R. E. Ticse Torres[51], V. O. Tikhomirov[108,ap], Yu. A. Tikhonov[120a,120b], S. Timoshenko[110], P. Tipton[180], S. Tisserant[99], K. Todome[162], S. Todorova-Nova[5], S. Todt[46], J. Tojo[85], S. Tokár[28a], K. Tokushuku[79], E. Tolley[123], K. G. Tomiwa[32c], M. Tomoto[115], L. Tompkins[150,r], K. Toms[116], B. Tong[57], P. Tornambe[50], E. Torrence[128], H. Torres[46], E. Torró Pastor[145], C. Tosciri[132], J. Toth[99,ad], F. Touchard[99], D. R. Tovey[146], C. J. Treado[122], T. Trefzger[174], F. Tresoldi[153], A. Tricoli[29], I. M. Trigger[165a], S. Trincaz-Duvoid[133], M. F. Tripiana[14], W. Trischuk[164], B. Trocmé[56], A. Trofymov[129], C. Troncon[66a], M. Trovatelli[173], F. Trovato[153], L. Truong[32b], M. Trzebinski[82], A. Trzupek[82], F. Tsai[44], J. C.-L. Tseng[132], P. V. Tsiareshka[105], A. Tsirigotis[159], N. Tsirintanis[9], V. Tsiskaridze[152], E. G. Tskhadadze[156a], I. I. Tsukerman[109], V. Tsulaia[18], S. Tsuno[79], D. Tsybychev[152,163], Y. Tu[61b], A. Tudorache[27b], V. Tudorache[27b], T. T. Tulbure[27a], A. N. Tuna[57], S. Turchikhin[77], D. Turgeman[177], I. Turk Cakir[4b,v], R. Turra[66a], P. M. Tuts[38], E. Tzovara[97], G. Ucchielli[23a,23b], I. Ueda[79], M. Ughetto[43a,43b], F. Ukegawa[166], G. Unal[35], A. Undrus[29], G. Unel[168], F. C. Ungaro[102], Y. Unno[79], K. Uno[160], J. Urban[28b], P. Urquijo[102], P. Urrejola[97], G. Usai[8], J. Usui[79], L. Vacavant[99], V. Vacek[139], B. Vachon[101], K. O. H. Vadla[131], A. Vaidya[92], C. Valderanis[112], E. Valdes Santurio[43a,43b], M. Valente[52], S. Valentinetti[23a,23b], A. Valero[171], L. Valéry[44], R. A. Vallance[21], A. Vallier[5], J. A. Valls Ferrer[171], T. R. Van Daalen[14], H. Van der Graaf[118], P. Van Gemmeren[6], J. Van Nieuwkoop[149], I. Van Vulpen[118], M. Vanadia[71a,71b], W. Vandelli[35], A. Vaniachine[163], P. Vankov[118], R. Vari[70a], E. W. Varnes[7], C. Varni[53a,53b], T. Varol[41], D. Varouchas[129], K. E. Varvell[154], G. A. Vasquez[144b], J. G. Vasquez[180], F. Vazeille[37], D. Vazquez Furelos[14], T. Vazquez Schroeder[101], J. Veatch[51], V. Vecchio[72a,72b], L. M. Veloce[164], F. Veloso[137a,137c], S. Veneziano[70a], A. Ventura[65a,65b], M. Venturi[173], N. Venturi[35], V. Vercesi[68a], M. Verducci[72a,72b], C. M. Vergel Infante[76], C. Vergis[24], W. Verkerke[118], A. T. Vermeulen[118], J. C. Vermeulen[118], M. C. Vetterli[149,av], N. Viaux Maira[144b], M. Vicente Barreto Pinto[52], I. Vichou[170,*], T. Vickey[146], O. E. Vickey Boeriu[146], G. H. A. Viehhauser[132], S. Viel[18], L. Vigani[132], M. Villa[23a,23b], M. Villaplana Perez[66a,66b],

E. Vilucchi[49], M. G. Vincter[33], V. B. Vinogradov[77], A. Vishwakarma[44], C. Vittori[23a,23b], I. Vivarelli[153], S. Vlachos[10], M. Vogel[179], P. Vokac[139], G. Volpi[14], S. E. Von Buddenbrock[32c], E. von Toerne[24], V. Vorobel[140], K. Vorobev[110], M. Vos[171], J. H. Vossebeld[88], N. Vranjes[16], M. Vranjes Milosavljevic[16], V. Vrba[139], M. Vreeswijk[118], T. Šfiligoj[89], R. Vuillermet[35], I. Vukotic[36], T. Ženiš[28a], L. Živković[16], P. Wagner[24], W. Wagner[179], J. Wagner-Kuhr[112], H. Wahlberg[86], S. Wahrmund[46], K. Wakamiya[80], V. M. Walbrecht[113], J. Walder[87], R. Walker[112], S. D. Walker[91], W. Walkowiak[148], V. Wallangen[43a,43b], A. M. Wang[57], C. Wang[58b,e], F. Wang[178], H. Wang[18], H. Wang[3], J. Wang[154], J. Wang[59b], P. Wang[41], Q. Wang[125], R.-J. Wang[133], R. Wang[58a], R. Wang[6], S. M. Wang[155], T. Wang[58a], W. Wang[15c,af], W. X. Wang[58a,af], Y. Wang[58a,am], Z. Wang[58c], C. Wanotayaroj[44], A. Warburton[101], C. P. Ward[31], D. R. Wardrope[92], A. Washbrook[48], P. M. Watkins[21], A. T. Watson[21], M. F. Watson[21], G. Watts[145], S. Watts[98], B. M. Waugh[92], A. F. Webb[11], S. Webb[97], C. Weber[180], M. S. Weber[20], S. A. Weber[33], S. M. Weber[59a], A. R. Weidberg[132], B. Weinert[63], J. Weingarten[45], M. Weirich[97], C. Weiser[50], P. S. Wells[35], T. Wenaus[29], T. Wengler[35], S. Wenig[35], N. Wermes[24], M. D. Werner[76], P. Werner[35], M. Wessels[59a], T. D. Weston[20], K. Whalen[128], N. L. Whallon[145], A. M. Wharton[87], A. S. White[103], A. White[8], M. J. White[1], R. White[144b], D. Whiteson[168], B. W. Whitmore[87], F. J. Wickens[141], W. Wiedenmann[178], M. Wielers[141], C. Wiglesworth[39], L. A. M. Wiik-Fuchs[50], A. Wildauer[113], F. Wilk[98], H. G. Wilkens[35], L. J. Wilkins[91], H. H. Williams[134], S. Williams[31], C. Willis[104], S. Willocq[100], J. A. Wilson[21], I. Wingerter-Seez[5], E. Winkels[153], F. Winklmeier[128], O. J. Winston[153], B. T. Winter[24], M. Wittgen[150], M. Wobisch[93], A. Wolf[97], T. M. H. Wolf[118], R. Wolff[99], M. W. Wolter[82], H. Wolters[137a,137c], V. W. S. Wong[172], N. L. Woods[143], S. D. Worm[21], B. K. Wosiek[82], K. W. Woźniak[82], K. Wraight[55], M. Wu[36], S. L. Wu[178], X. Wu[52], Y. Wu[58a], T. R. Wyatt[98], B. M. Wynne[48], S. Xella[39], Z. Xi[103], L. Xia[175], D. Xu[15a], H. Xu[58a,e], L. Xu[29], T. Xu[142], W. Xu[103], B. Yabsley[154], S. Yacoob[32a], K. Yajima[130], D. P. Yallup[92], D. Yamaguchi[162], Y. Yamaguchi[162], A. Yamamoto[79], T. Yamanaka[160], F. Yamane[80], M. Yamatani[160], T. Yamazaki[160], Y. Yamazaki[80], Z. Yan[25], H. J. Yang[58c,58d], H. T. Yang[18], S. Yang[75], Y. Yang[160], Z. Yang[17], W-M. Yao[18], Y. C. Yap[44], Y. Yasu[79], E. Yatsenko[58c,58d], J. Ye[41], S. Ye[29], I. Yeletskikh[77], E. Yigitbasi[25], E. Yildirim[97], K. Yorita[176], K. Yoshihara[134], C. J. S. Young[35], C. Young[150], J. Yu[8], J. Yu[76], X. Yue[59a], S. P. Y. Yuen[24], B. Zabinski[82], G. Zacharis[10], E. Zaffaroni[52], R. Zaidan[14], A. M. Zaitsev[121,ao], T. Zakareishvili[156b], N. Zakharchuk[33], J. Zalieckas[17], S. Zambito[57], D. Zanzi[35], D. R. Zaripovas[55], S. V. Zeißner[45], C. Zeitnitz[179], G. Zemaityte[132], J. C. Zeng[170], Q. Zeng[150], O. Zenin[121], D. Zerwas[129], M. Zgubič[132], D. F. Zhang[58b], D. Zhang[103], F. Zhang[178], G. Zhang[58a], H. Zhang[15c], J. Zhang[6], L. Zhang[15c], L. Zhang[58a], M. Zhang[170], P. Zhang[15c], R. Zhang[58a], R. Zhang[24], X. Zhang[58b], Y. Zhang[15d], Z. Zhang[129], P. Zhao[47], X. Zhao[41], Y. Zhao[58b,129,ak], Z. Zhao[58a], A. Zhemchugov[77], B. Zhou[103], C. Zhou[178], L. Zhou[41], M. S. Zhou[15d], M. Zhou[152], N. Zhou[58c], Y. Zhou[7], C. G. Zhu[58b], H. L. Zhu[58a], H. Zhu[15a], J. Zhu[103], Y. Zhu[58a], X. Zhuang[15a], K. Zhukov[108], V. Zhulanov[120a,120b], A. Zibell[174], D. Zieminska[63], N. I. Zimine[77], S. Zimmermann[50], Z. Zinonos[113], M. Zinser[97], M. Ziolkowski[148], G. Zobernig[178], A. Zoccoli[23a,23b], K. Zoch[51], T. G. Zorbas[146], R. Zou[36], M. Zur Nedden[19], L. Zwalinski[35]

[1] Department of Physics, University of Adelaide, Adelaide, Australia
[2] Physics Department, SUNY Albany, Albany, NY, USA
[3] Department of Physics, University of Alberta, Edmonton, AB, Canada
[4] [(a)]Department of Physics, Ankara University, Ankara, Turkey; [(b)]Istanbul Aydin University, Istanbul, Turkey; [(c)]Division of Physics, TOBB University of Economics and Technology, Ankara, Turkey
[5] LAPP, Université Grenoble Alpes, Université Savoie Mont Blanc, CNRS/IN2P3, Annecy, France
[6] High Energy Physics Division, Argonne National Laboratory, Argonne, IL, USA
[7] Department of Physics, University of Arizona, Tucson, AZ, USA
[8] Department of Physics, University of Texas at Arlington, Arlington, TX, USA
[9] Physics Department, National and Kapodistrian University of Athens, Athens, Greece
[10] Physics Department, National Technical University of Athens, Zografou, Greece
[11] Department of Physics, University of Texas at Austin, Austin, TX, USA
[12] [(a)]Faculty of Engineering and Natural Sciences, Bahcesehir University, Istanbul, Turkey; [(b)]Faculty of Engineering and Natural Sciences, Istanbul Bilgi University, Istanbul, Turkey; [(c)]Department of Physics, Bogazici University, Istanbul, Turkey; [(d)]Department of Physics Engineering, Gaziantep University, Gaziantep, Turkey
[13] Institute of Physics, Azerbaijan Academy of Sciences, Baku, Azerbaijan
[14] Institut de Física d'Altes Energies (IFAE), Barcelona Institute of Science and Technology, Barcelona, Spain
[15] [(a)]Institute of High Energy Physics, Chinese Academy of Sciences, Beijing, China; [(b)]Physics Department, Tsinghua University, Beijing, China; [(c)]Department of Physics, Nanjing University, Nanjing, China; [(d)]University of Chinese Academy of Science (UCAS), Beijing, China
[16] Institute of Physics, University of Belgrade, Belgrade, Serbia

[17] Department for Physics and Technology, University of Bergen, Bergen, Norway
[18] Physics Division, Lawrence Berkeley National Laboratory and University of California, Berkeley, CA, USA
[19] Institut für Physik, Humboldt Universität zu Berlin, Berlin, Germany
[20] Albert Einstein Center for Fundamental Physics and Laboratory for High Energy Physics, University of Bern, Bern, Switzerland
[21] School of Physics and Astronomy, University of Birmingham, Birmingham, UK
[22] Centro de Investigaciónes, Universidad Antonio Nariño, Bogotá, Colombia
[23] [(a)]Dipartimento di Fisica e Astronomia, Università di Bologna, Bologna, Italy; [(b)]INFN Sezione di Bologna, Bologna, Italy
[24] Physikalisches Institut, Universität Bonn, Bonn, Germany
[25] Department of Physics, Boston University, Boston, MA, USA
[26] Department of Physics, Brandeis University, Waltham, MA, USA
[27] [(a)]Transilvania University of Brasov, Brasov, Romania; [(b)]Horia Hulubei National Institute of Physics and Nuclear Engineering, Bucharest, Romania; [(c)]Department of Physics, Alexandru Ioan Cuza University of Iasi, Iasi, Romania; [(d)]Physics Department, National Institute for Research and Development of Isotopic and Molecular Technologies, Cluj-Napoca, Romania; [(e)]University Politehnica Bucharest, Bucharest, Romania; [(f)]West University in Timisoara, Timisoara, Romania
[28] [(a)]Faculty of Mathematics, Physics and Informatics, Comenius University, Bratislava, Slovakia; [(b)]Department of Subnuclear Physics, Institute of Experimental Physics of the Slovak Academy of Sciences, Kosice, Slovak Republic
[29] Physics Department, Brookhaven National Laboratory, Upton, NY, USA
[30] Departamento de Física, Universidad de Buenos Aires, Buenos Aires, Argentina
[31] Cavendish Laboratory, University of Cambridge, Cambridge, UK
[32] [(a)]Department of Physics, University of Cape Town, Cape Town, South Africa; [(b)]Department of Mechanical Engineering Science, University of Johannesburg, Johannesburg, South Africa; [(c)]School of Physics, University of the Witwatersrand, Johannesburg, South Africa
[33] Department of Physics, Carleton University, Ottawa, ON, Canada
[34] [(a)]Faculté des Sciences Ain Chock, Réseau Universitaire de Physique des Hautes Energies-Université Hassan II, Casablanca, Morocco; [(b)]Centre National de l'Energie des Sciences Techniques Nucleaires (CNESTEN), Rabat, Morocco; [(c)]Faculté des Sciences Semlalia, Université Cadi Ayyad, LPHEA-Marrakech, Marrakech, Morocco; [(d)]Faculté des Sciences, Université Mohamed Premier and LPTPM, Oujda, Morocco; [(e)]Faculté des sciences, Université Mohammed V, Rabat, Morocco
[35] CERN, Geneva, Switzerland
[36] Enrico Fermi Institute, University of Chicago, Chicago, IL, USA
[37] LPC, Université Clermont Auvergne, CNRS/IN2P3, Clermont-Ferrand, France
[38] Nevis Laboratory, Columbia University, Irvington, NY, USA
[39] Niels Bohr Institute, University of Copenhagen, Copenhagen, Denmark
[40] [(a)]Dipartimento di Fisica, Università della Calabria, Rende, Italy; [(b)]INFN Gruppo Collegato di Cosenza, Laboratori Nazionali di Frascati, Frascati, Italy
[41] Physics Department, Southern Methodist University, Dallas, TX, USA
[42] Physics Department, University of Texas at Dallas, Richardson, TX, USA
[43] [(a)]Department of Physics, Stockholm University, Stockholm, Sweden; [(b)]Oskar Klein Centre, Stockholm, Sweden
[44] Deutsches Elektronen-Synchrotron DESY, Hamburg and Zeuthen, Germany
[45] Lehrstuhl für Experimentelle Physik IV, Technische Universität Dortmund, Dortmund, Germany
[46] Institut für Kern- und Teilchenphysik, Technische Universität Dresden, Dresden, Germany
[47] Department of Physics, Duke University, Durham, NC, USA
[48] SUPA-School of Physics and Astronomy, University of Edinburgh, Edinburgh, UK
[49] INFN e Laboratori Nazionali di Frascati, Frascati, Italy
[50] Physikalisches Institut, Albert-Ludwigs-Universität Freiburg, Freiburg, Germany
[51] II. Physikalisches Institut, Georg-August-Universität Göttingen, Göttingen, Germany
[52] Département de Physique Nucléaire et Corpusculaire, Université de Genève, Geneva, Switzerland
[53] [(a)]Dipartimento di Fisica, Università di Genova, Genoa, Italy; [(b)]INFN Sezione di Genova, Genoa, Italy
[54] II. Physikalisches Institut, Justus-Liebig-Universität Giessen, Giessen, Germany
[55] SUPA-School of Physics and Astronomy, University of Glasgow, Glasgow, UK

[56] LPSC, Université Grenoble Alpes, CNRS/IN2P3, Grenoble INP, Grenoble, France
[57] Laboratory for Particle Physics and Cosmology, Harvard University, Cambridge, MA, USA
[58] [(a)]Department of Modern Physics and State Key Laboratory of Particle Detection and Electronics, University of Science and Technology of China, Hefei, China; [(b)]Institute of Frontier and Interdisciplinary Science and Key Laboratory of Particle Physics and Particle Irradiation (MOE), Shandong University, Qingdao, China; [(c)]School of Physics and Astronomy, Shanghai Jiao Tong University, KLPPAC-MoE, SKLPPC, Shanghai, China; [(d)]Tsung-Dao Lee Institute, Shanghai, China
[59] [(a)]Kirchhoff-Institut für Physik, Ruprecht-Karls-Universität Heidelberg, Heidelberg, Germany; [(b)]Physikalisches Institut, Ruprecht-Karls-Universität Heidelberg, Heidelberg, Germany
[60] Faculty of Applied Information Science, Hiroshima Institute of Technology, Hiroshima, Japan
[61] [(a)]Department of Physics, Chinese University of Hong Kong, Shatin, NT, Hong Kong; [(b)]Department of Physics, University of Hong Kong, Hong Kong, China; [(c)]Department of Physics and Institute for Advanced Study, Hong Kong University of Science and Technology, Clear Water Bay, Kowloon, Hong Kong, China
[62] Department of Physics, National Tsing Hua University, Hsinchu, Taiwan
[63] Department of Physics, Indiana University, Bloomington, IN, USA
[64] [(a)]INFN Gruppo Collegato di Udine, Sezione di Trieste, Udine, Italy; [(b)]ICTP, Trieste, Italy; [(c)]Dipartimento di Chimica, Fisica e Ambiente, Università di Udine, Udine, Italy
[65] [(a)]INFN Sezione di Lecce, Lecce, Italy; [(b)]Dipartimento di Matematica e Fisica, Università del Salento, Lecce, Italy
[66] [(a)]INFN Sezione di Milano, Milan, Italy; [(b)]Dipartimento di Fisica, Università di Milano, Milan, Italy
[67] [(a)]INFN Sezione di Napoli, Naples, Italy; [(b)]Dipartimento di Fisica, Università di Napoli, Naples, Italy
[68] [(a)]INFN Sezione di Pavia, Pavia, Italy; [(b)]Dipartimento di Fisica, Università di Pavia, Pavia, Italy
[69] [(a)]INFN Sezione di Pisa, Pisa, Italy; [(b)]Dipartimento di Fisica E. Fermi, Università di Pisa, Pisa, Italy
[70] [(a)]INFN Sezione di Roma, Rome, Italy; [(b)]Dipartimento di Fisica, Sapienza Università di Roma, Rome, Italy
[71] [(a)]INFN Sezione di Roma Tor Vergata, Rome, Italy; [(b)]Dipartimento di Fisica, Università di Roma Tor Vergata, Rome, Italy
[72] [(a)]INFN Sezione di Roma Tre, Rome, Italy; [(b)]Dipartimento di Matematica e Fisica, Università Roma Tre, Rome, Italy
[73] [(a)]INFN-TIFPA, Povo, Italy; [(b)]Università degli Studi di Trento, Trento, Italy
[74] Institut für Astro- und Teilchenphysik, Leopold-Franzens-Universität, Innsbruck, Austria
[75] University of Iowa, Iowa City, IA, USA
[76] Department of Physics and Astronomy, Iowa State University, Ames, IA, USA
[77] Joint Institute for Nuclear Research, Dubna, Russia
[78] [(a)]Departamento de Engenharia Elétrica, Universidade Federal de Juiz de Fora (UFJF), Juiz de Fora, Brazil; [(b)]Universidade Federal do Rio De Janeiro COPPE/EE/IF, Rio de Janeiro, Brazil; [(c)]Universidade Federal de São João del Rei (UFSJ), São João del Rei, Brazil; [(d)]Instituto de Física, Universidade de São Paulo, São Paulo, Brazil
[79] KEK, High Energy Accelerator Research Organization, Tsukuba, Japan
[80] Graduate School of Science, Kobe University, Kobe, Japan
[81] [(a)]Faculty of Physics and Applied Computer Science, AGH University of Science and Technology, Kraków, Poland; [(b)]Marian Smoluchowski Institute of Physics, Jagiellonian University, Kraków, Poland
[82] Institute of Nuclear Physics Polish Academy of Sciences, Kraków, Poland
[83] Faculty of Science, Kyoto University, Kyoto, Japan
[84] Kyoto University of Education, Kyoto, Japan
[85] Research Center for Advanced Particle Physics and Department of Physics, Kyushu University, Fukuoka, Japan
[86] Instituto de Física La Plata, Universidad Nacional de La Plata and CONICET, La Plata, Argentina
[87] Physics Department, Lancaster University, Lancaster, UK
[88] Oliver Lodge Laboratory, University of Liverpool, Liverpool, UK
[89] Department of Experimental Particle Physics, Jožef Stefan Institute and Department of Physics, University of Ljubljana, Ljubljana, Slovenia
[90] School of Physics and Astronomy, Queen Mary University of London, London, UK
[91] Department of Physics, Royal Holloway University of London, Egham, UK
[92] Department of Physics and Astronomy, University College London, London, UK
[93] Louisiana Tech University, Ruston, LA, USA
[94] Fysiska institutionen, Lunds universitet, Lund, Sweden

[95] Centre de Calcul de l'Institut National de Physique Nucléaire et de Physique des Particules (IN2P3), Villeurbanne, France
[96] Departamento de Física Teorica C-15 and CIAFF, Universidad Autónoma de Madrid, Madrid, Spain
[97] Institut für Physik, Universität Mainz, Mainz, Germany
[98] School of Physics and Astronomy, University of Manchester, Manchester, UK
[99] CPPM, Aix-Marseille Université, CNRS/IN2P3, Marseille, France
[100] Department of Physics, University of Massachusetts, Amherst, MA, USA
[101] Department of Physics, McGill University, Montreal, QC, Canada
[102] School of Physics, University of Melbourne, Parkville, VIC, Australia
[103] Department of Physics, University of Michigan, Ann Arbor, MI, USA
[104] Department of Physics and Astronomy, Michigan State University, East Lansing, MI, USA
[105] B.I. Stepanov Institute of Physics, National Academy of Sciences of Belarus, Minsk, Belarus
[106] Research Institute for Nuclear Problems of Byelorussian State University, Minsk, Belarus
[107] Group of Particle Physics, University of Montreal, Montreal, QC, Canada
[108] P.N. Lebedev Physical Institute of the Russian Academy of Sciences, Moscow, Russia
[109] Institute for Theoretical and Experimental Physics (ITEP), Moscow, Russia
[110] National Research Nuclear University MEPhI, Moscow, Russia
[111] D.V. Skobeltsyn Institute of Nuclear Physics, M.V. Lomonosov Moscow State University, Moscow, Russia
[112] Fakultät für Physik, Ludwig-Maximilians-Universität München, Munich, Germany
[113] Max-Planck-Institut für Physik (Werner-Heisenberg-Institut), Munich, Germany
[114] Nagasaki Institute of Applied Science, Nagasaki, Japan
[115] Graduate School of Science and Kobayashi-Maskawa Institute, Nagoya University, Nagoya, Japan
[116] Department of Physics and Astronomy, University of New Mexico, Albuquerque, NM, USA
[117] Institute for Mathematics, Astrophysics and Particle Physics, Radboud University Nijmegen/Nikhef, Nijmegen, The Netherlands
[118] Nikhef National Institute for Subatomic Physics, University of Amsterdam, Amsterdam, The Netherlands
[119] Department of Physics, Northern Illinois University, De Kalb, IL, USA
[120] [(a)]Budker Institute of Nuclear Physics and NSU, SB RAS, Novosibirsk, Russia; [(b)]Novosibirsk State University, Novosibirsk, Russia
[121] Institute for High Energy Physics of the National Research Centre Kurchatov Institute, Protvino, Russia
[122] Department of Physics, New York University, New York, NY, USA
[123] Ohio State University, Columbus, OH, USA
[124] Faculty of Science, Okayama University, Okayama, Japan
[125] Homer L. Dodge Department of Physics and Astronomy, University of Oklahoma, Norman, OK, USA
[126] Department of Physics, Oklahoma State University, Stillwater, OK, USA
[127] Palacký University, RCPTM, Joint Laboratory of Optics, Olomouc, Czech Republic
[128] Center for High Energy Physics, University of Oregon, Eugene, OR, USA
[129] LAL, Université Paris-Sud, CNRS/IN2P3, Université Paris-Saclay, Orsay, France
[130] Graduate School of Science, Osaka University, Osaka, Japan
[131] Department of Physics, University of Oslo, Oslo, Norway
[132] Department of Physics, Oxford University, Oxford, UK
[133] LPNHE, Sorbonne Université, Paris Diderot Sorbonne Paris Cité, CNRS/IN2P3, Paris, France
[134] Department of Physics, University of Pennsylvania, Philadelphia, PA, USA
[135] Konstantinov Nuclear Physics Institute of National Research Centre "Kurchatov Institute", PNPI, St. Petersburg, Russia
[136] Department of Physics and Astronomy, University of Pittsburgh, Pittsburgh, PA, USA
[137] [(a)]Laboratório de Instrumentação e Física Experimental de Partículas-LIP, Lisbon, Portugal; [(b)]Departamento de Física, Faculdade de Ciências, Universidade de Lisboa, Lisbon, Portugal; [(c)]Departamento de Física, Universidade de Coimbra, Coimbra, Portugal; [(d)]Centro de Física Nuclear da Universidade de Lisboa, Lisbon, Portugal; [(e)]Departamento de Física, Universidade do Minho, Braga, Portugal; [(f)]Departamento de Física Teorica y del Cosmos, Universidad de Granada, Granada, Spain; [(g)]Dep Física and CEFITEC of Faculdade de Ciências e Tecnologia, Universidade Nova de Lisboa, Caparica, Portugal
[138] Institute of Physics, Academy of Sciences of the Czech Republic, Prague, Czech Republic
[139] Czech Technical University in Prague, Prague, Czech Republic

[140] Faculty of Mathematics and Physics, Charles University, Prague, Czech Republic
[141] Particle Physics Department, Rutherford Appleton Laboratory, Didcot, UK
[142] IRFU, CEA, Université Paris-Saclay, Gif-sur-Yvette, France
[143] Santa Cruz Institute for Particle Physics, University of California Santa Cruz, Santa Cruz, CA, USA
[144] [(a)]Departamento de Física, Pontificia Universidad Católica de Chile, Santiago, Chile; [(b)]Departamento de Física, Universidad Técnica Federico Santa María, Valparaiso, Chile
[145] Department of Physics, University of Washington, Seattle, WA, USA
[146] Department of Physics and Astronomy, University of Sheffield, Sheffield, UK
[147] Department of Physics, Shinshu University, Nagano, Japan
[148] Department Physik, Universität Siegen, Siegen, Germany
[149] Department of Physics, Simon Fraser University, Burnaby, BC, Canada
[150] SLAC National Accelerator Laboratory, Stanford, CA, USA
[151] Physics Department, Royal Institute of Technology, Stockholm, Sweden
[152] Departments of Physics and Astronomy, Stony Brook University, Stony Brook, NY, USA
[153] Department of Physics and Astronomy, University of Sussex, Brighton, UK
[154] School of Physics, University of Sydney, Sydney, Australia
[155] Institute of Physics, Academia Sinica, Taipei, Taiwan
[156] [(a)]E. Andronikashvili Institute of Physics, Iv. Javakhishvili Tbilisi State University, Tbilisi, Georgia; [(b)]High Energy Physics Institute, Tbilisi State University, Tbilisi, Georgia
[157] Department of Physics, Technion, Israel Institute of Technology, Haifa, Israel
[158] Raymond and Beverly Sackler School of Physics and Astronomy, Tel Aviv University, Tel Aviv, Israel
[159] Department of Physics, Aristotle University of Thessaloniki, Thessaloníki, Greece
[160] International Center for Elementary Particle Physics and Department of Physics, University of Tokyo, Tokyo, Japan
[161] Graduate School of Science and Technology, Tokyo Metropolitan University, Tokyo, Japan
[162] Department of Physics, Tokyo Institute of Technology, Tokyo, Japan
[163] Tomsk State University, Tomsk, Russia
[164] Department of Physics, University of Toronto, Toronto, ON, Canada
[165] [(a)]TRIUMF, Vancouver, BC, Canada; [(b)]Department of Physics and Astronomy, York University, Toronto, ON, Canada
[166] Division of Physics and Tomonaga Center for the History of the Universe, Faculty of Pure and Applied Sciences, University of Tsukuba, Tsukuba, Japan
[167] Department of Physics and Astronomy, Tufts University, Medford, MA, USA
[168] Department of Physics and Astronomy, University of California Irvine, Irvine, CA, USA
[169] Department of Physics and Astronomy, University of Uppsala, Uppsala, Sweden
[170] Department of Physics, University of Illinois, Urbana, IL, USA
[171] Instituto de Física Corpuscular (IFIC), Centro Mixto Universidad de Valencia, CSIC, Valencia, Spain
[172] Department of Physics, University of British Columbia, Vancouver, BC, Canada
[173] Department of Physics and Astronomy, University of Victoria, Victoria, BC, Canada
[174] Fakultät für Physik und Astronomie, Julius-Maximilians-Universität Würzburg, Würzburg, Germany
[175] Department of Physics, University of Warwick, Coventry, UK
[176] Waseda University, Tokyo, Japan
[177] Department of Particle Physics, Weizmann Institute of Science, Rehovot, Israel
[178] Department of Physics, University of Wisconsin, Madison, WI, USA
[179] Fakultät für Mathematik und Naturwissenschaften, Fachgruppe Physik, Bergische Universität Wuppertal, Wuppertal, Germany
[180] Department of Physics, Yale University, New Haven, CT, USA
[181] Yerevan Physics Institute, Yerevan, Armenia

[a] Also at Borough of Manhattan Community College, City University of New York, NY, USA
[b] Also at California State University, East Bay, USA
[c] Also at Centre for High Performance Computing, CSIR Campus, Rosebank, Cape Town, South Africa
[d] Also at CERN, Geneva, Switzerland
[e] Also at CPPM, Aix-Marseille Université, CNRS/IN2P3, Marseille, France
[f] Also at Département de Physique Nucléaire et Corpusculaire, Université de Genève, Geneva, Switzerland

[g] Also at Departament de Fisica de la Universitat Autonoma de Barcelona, Barcelona, Spain
[h] Also at Departamento de Física Teorica y del Cosmos, Universidad de Granada, Granada (Spain), Spain
[i] Also at Departamento de Física, Instituto Superior Técnico, Universidade de Lisboa, Lisbon, Portugal
[j] Also at Department of Applied Physics and Astronomy, University of Sharjah, Sharjah, United Arab Emirates
[k] Also at Department of Financial and Management Engineering, University of the Aegean, Chios, Greece
[l] Also at Department of Physics and Astronomy, University of Louisville, Louisville, KY, USA
[m] Also at Department of Physics and Astronomy, University of Sheffield, Sheffield, UK
[n] Also at Department of Physics, California State University, Fresno, CA, USA
[o] Also at Department of Physics, California State University, Sacramento, CA, USA
[p] Also at Department of Physics, King's College London, London, UK
[q] Also at Department of Physics, St. Petersburg State Polytechnical University, St. Petersburg, Russia
[r] Also at Department of Physics, Stanford University, USA
[s] Also at Department of Physics, University of Fribourg, Fribourg, Switzerland
[t] Also at Department of Physics, University of Michigan, Ann Arbor, MI, USA
[u] Also at Dipartimento di Fisica E. Fermi, Università di Pisa, Pisa, Italy
[v] Also at Giresun University, Faculty of Engineering, Giresun, Turkey
[w] Also at Graduate School of Science, Osaka University, Osaka, Japan
[x] Also at Hellenic Open University, Patras, Greece
[y] Also at Horia Hulubei National Institute of Physics and Nuclear Engineering, Bucharest, Romania
[z] Also at II Physikalisches Institut, Georg-August-Universität Göttingen, Göttingen, Germany
[aa] Also at Institucio Catalana de Recerca i Estudis Avancats, ICREA, Barcelona, Spain
[ab] Also at Institut für Experimentalphysik, Universität Hamburg, Hamburg, Germany
[ac] Also at Institute for Mathematics, Astrophysics and Particle Physics, Radboud University Nijmegen/Nikhef, Nijmegen, The Netherlands
[ad] Also at Institute for Particle and Nuclear Physics, Wigner Research Centre for Physics, Budapest, Hungary
[ae] Also at Institute of Particle Physics (IPP), Canada
[af] Also at Institute of Physics, Academia Sinica, Taipei, Taiwan
[ag] Also at Institute of Physics, Azerbaijan Academy of Sciences, Baku, Azerbaijan
[ah] Also at Institute of Theoretical Physics, Ilia State University, Tbilisi, Georgia
[ai] Also at Instituto de Física Teórica de la Universidad Autónoma de Madrid, Spain
[aj] Also at Istanbul University, Dept. of Physics, Istanbul, Turkey
[ak] Also at LAL, Université Paris-Sud, CNRS/IN2P3, Université Paris-Saclay, Orsay, France
[al] Also at Louisiana Tech University, Ruston, LA, USA
[am] Also at LPNHE, Sorbonne Université, Paris Diderot Sorbonne Paris Cité, CNRS/IN2P3, Paris, France
[an] Also at Manhattan College, New York, NY, USA
[ao] Also at Moscow Institute of Physics and Technology State University, Dolgoprudny, Russia
[ap] Also at National Research Nuclear University MEPhI, Moscow, Russia
[aq] Also at Physikalisches Institut, Albert-Ludwigs-Universität Freiburg, Freiburg, Germany
[ar] Also at School of Physics, Sun Yat-sen University, Guangzhou, China
[as] Also at The City College of New York, New York, NY, USA
[at] Also at The Collaborative Innovation Center of Quantum Matter (CICQM), Beijing, China
[au] Also at Tomsk State University, Tomsk, and Moscow Institute of Physics and Technology State University, Dolgoprudny, Russia
[av] Also at TRIUMF, Vancouver, BC, Canada
[aw] Also at Universita di Napoli Parthenope, Naples, Italy
* Deceased

Eur. Phys. J. C (2019) 79:128
https://doi.org/10.1140/epjc/s10052-019-6622-x

THE EUROPEAN PHYSICAL JOURNAL C

Regular Article - Experimental Physics

Measurements of W and Z boson production in pp collisions at $\sqrt{s} = 5.02$ TeV with the ATLAS detector

ATLAS Collaboration[⋆]

CERN, 1211 Geneva 23, Switzerland

Received: 22 October 2018 / Accepted: 22 January 2019 / Published online: 11 February 2019

Abstract Measurements of fiducial integrated and differential cross sections for inclusive W^+, W^- and Z boson production are reported. They are based on 25.0 ± 0.5 pb^{-1} of pp collision data at $\sqrt{s} = 5.02$ TeV collected with the ATLAS detector at the CERN Large Hadron Collider. Electron and muon decay channels are analysed, and the combined W^+, W^- and Z integrated cross sections are found to be $\sigma_{W^+} = 2266 \pm 9$ (stat) ± 29 (syst) ± 43 (lumi) pb, $\sigma_{W^-} = 1401 \pm 7$ (stat) ± 18 (syst) ± 27 (lumi) pb, and $\sigma_Z = 374.5 \pm 3.4$ (stat) ± 3.6 (syst) ± 7.0 (lumi) pb, in good agreement with next-to-next-to-leading-order QCD cross-section calculations. These measurements serve as references for Pb+Pb interactions at the LHC at $\sqrt{s_{\mathrm{NN}}} = 5.02$ TeV.

1 Introduction

Measurements of $W^{\pm}$ and Z boson[1] production at hadron colliders provide a benchmark for the understanding of quantum chromodynamics (QCD) and electroweak (EW) processes. Predictions for the differential and fiducial cross sections are available up to next-to-next-to-leading-order (NNLO) accuracy in QCD and include EW corrections at next-to-leading-order (NLO) accuracy [1–3]. The rapidity distribution of EW boson production is sensitive to the underlying QCD dynamics and, in particular, to the parton distribution functions (PDFs) which define the initial kinematics of the hard process. Therefore, measurements of weak-boson production offer an excellent opportunity to test models of parton dynamics.

The ATLAS, CMS and LHCb collaborations have measured $W^{\pm}$ and Z boson production in proton–proton (pp) collisions at centre-of-mass energies of $\sqrt{s} = 7$, 8 and 13 TeV [4–7]. These measurements provide precision tests of the QCD theory and PDFs, which can be complemented with measurements at the additional centre-of-mass energy $\sqrt{s} = 5.02$ TeV.

This paper describes measurements of the production cross sections times leptonic branching ratios for the inclusive $W^+ \to \ell^+\nu$, $W^- \to \ell^-\nu$ and $Z \to \ell^+\ell^-$ ($\ell = e,\ \mu$) processes. Integrated and differential cross sections are measured in a fiducial phase space defined by detector acceptance and lepton kinematics. For $W^{\pm}$ bosons the decay lepton charge asymmetry is also determined. All measurements are performed with pp collision data corresponding to an integrated luminosity of 25.0 pb^{-1}, collected at $\sqrt{s} = 5.02$ TeV with the ATLAS detector. The data were recorded during the autumn of 2015. The peak instantaneous luminosity delivered by the LHC was $L = 3.8 \times 10^{32}$ cm^{-2} s^{-1} and the mean number of pp interactions per bunch crossing (hard scattering and pile-up events) was 1.5. Therefore, this dataset is characterised by a relatively low pile-up contribution as compared to the measurements of weak-boson production performed at higher centre-of-mass energies by ATLAS.

In addition, the measurement of $W^{\pm}$ and Z boson production in pp collisions at the centre-of-mass energy $\sqrt{s} = 5.02$ TeV is an important reference for weak-boson production in heavy-ion collisions. The LHC has provided both proton–lead (p+Pb) and lead–lead (Pb+Pb) collisions at the centre-of-mass energy per nucleon pair $\sqrt{s_{\mathrm{NN}}} = 5.02$ TeV. Published results from the ATLAS and CMS collaborations are currently available for $W^{\pm}$ and Z boson production [8–11] in Pb+Pb collisions at $\sqrt{s_{\mathrm{NN}}} = 2.76$ TeV and Z boson production [12,13] in the p+Pb system at $\sqrt{s_{\mathrm{NN}}} = 5.02$ TeV.

2 The ATLAS detector

The ATLAS experiment [14] is a multipurpose particle detector with a forward–backward symmetric cylindrical geometry.[2] It consists of an inner tracking detector surrounded by a

[1] Throughout this paper, Z/γ^* boson production is referred to as Z boson production.

⋆ e-mail: atlas.publications@cern.ch

[2] ATLAS uses a right-handed coordinate system with its origin at the nominal interaction point (IP) in the centre of the detector and the z-axis

thin superconducting solenoid, electromagnetic and hadronic calorimeters, and a muon spectrometer incorporating three large superconducting air-core toroid magnets with eight coils each.

The inner-detector system (ID) is immersed in a 2 T axial magnetic field and provides charged-particle tracking in the pseudorapidity range $|\eta| < 2.5$. At small radii, a high-granularity silicon pixel detector covers the interaction region and typically provides four measurements per track. It is followed by the silicon microstrip tracker, which usually provides eight measurement points per track. These silicon detectors are complemented by a gas-filled straw-tube transition radiation tracker, which enables track reconstruction up to $|\eta| = 2.0$. The transition radiation tracker also provides electron identification information based on the fraction of hits (out of ~ 35 in total) with an energy deposit above a threshold indicative of transition radiation.

The calorimeter system covers the pseudorapidity range $|\eta| < 4.9$. Within the region $|\eta| < 3.2$, electromagnetic (EM) calorimetry is provided by high-granularity lead/liquid-argon (LAr) calorimeters, with an additional thin LAr presampler covering $|\eta| < 1.8$ to correct for upstream energy-loss fluctuations. The EM calorimeter is divided into a barrel section covering $|\eta| < 1.475$ and two endcap sections covering $1.375 < |\eta| < 3.2$. For $|\eta| < 2.5$ it is divided into three layers in depth, which are finely segmented in η and ϕ. Hadronic calorimetry is provided by a steel/scintillator-tile calorimeter, segmented into three barrel structures within $|\eta| < 1.7$ and two copper/LAr hadronic endcap calorimeters covering $1.5 < |\eta| < 3.2$. The solid-angle coverage is completed with forward copper/LAr and tungsten/LAr calorimeter modules in $3.1 < |\eta| < 4.9$, optimised for electromagnetic and hadronic measurements, respectively.

The muon spectrometer (MS) comprises separate trigger and high-precision tracking chambers measuring the deflection of muons in the magnetic field generated by the toroid magnets. The precision chamber system covers the region $|\eta| < 2.7$ with three layers of monitored drift tubes, complemented by cathode strip chambers in the forward region. The muon trigger system covers the range $|\eta| < 2.4$ with resistive plate chambers in the barrel, and thin gap chambers in the endcap regions.

In 2015, the ATLAS detector had a two-level trigger system [15]. The level-1 trigger is implemented in hardware and uses a subset of detector information to reduce the event rate to a value of at most 75 kHz. This is followed by a software-based high-level trigger which reduces the event rate to about 1 kHz.

3 Simulated event samples

Samples of Monte Carlo (MC) simulated events are used to evaluate the selection efficiency for signal events and the contribution of several background processes to the analysed dataset. All of the samples are processed with the GEANT4-based simulation [16,17] of the ATLAS detector. Dedicated efficiency and calibration studies with data are used to derive correction factors to account for residual differences between experiment and simulation, as is subsequently described.

The processes of interest, specifically events containing $W^{\pm}$ or Z bosons, were generated with the POWHEG-BOX v2 MC program [18] interfaced to the PYTHIA 8.186 parton shower model [19]. The CT10 PDF set [20] was used in the matrix element, while the CTEQ6L1 PDF set [21] was used with the AZNLO [22] set of generator-parameter values (tune) for the modelling of non-perturbative effects in the initial-state parton shower. The PHOTOS++ v3.52 program [23] was used for QED radiation from electroweak vertices and charged leptons. Samples of top-quark pair ($t\bar{t}$) and single-top-quark production were generated with the POWHEG-BOX v2 generator, which uses NLO matrix element calculations together with the CT10f4 PDF set [24]. Top-quark spin correlations were preserved for all top-quark processes. The parton shower, fragmentation, and underlying event were simulated using PYTHIA 6.428 [25] with the CTEQ6L1 PDF set and the corresponding Perugia 2012 tune (P2012) [26]. The top-quark mass was set to 172.5 GeV. The EvtGen v1.2.0 program [27] was used to model bottom and charm hadron decays for all versions of PYTHIA. Diboson processes were simulated using the SHERPA v2.1.1 generator [28]. They were calculated for up to one (ZZ) or zero (WW, WZ) additional partons at NLO QCD accuracy and up to three additional partons at LO. In addition, the SHERPA diboson sample cross section is scaled to account for the cross section change when the G_{μ} scheme [29] is used instead of the native one for the EW parameters, resulting in an effective value of $\alpha \approx 1/132$. Multiple overlaid pp collisions were simulated with the soft QCD processes of PYTHIA v8.186 using the A2 tune [30] and the MSTW2008LO PDF set [31]. For the comparison with data in differential distributions and the evaluation of single-boson EW backgrounds for the cross-section calculations, the single-boson simulations are normalised to the results of NNLO QCD calculations obtained with a modified version of DYNNLO 1.5 [2,3] optimised for speed of computation, with uncertainties of 3%. The simulations of all other processes are normalised to the predictions of NLO QCD calculations, with uncertainties of 10% for the diboson and top-quark processes.

Footnote 2 continued
along the beam pipe. The x-axis points from the IP to the centre of the LHC ring, and the y-axis points upward. Cylindrical coordinates (r, ϕ) are used in the transverse plane, ϕ being the azimuthal angle around the z-axis. The pseudorapidity is defined in terms of the polar angle θ as $\eta = -\ln\tan(\theta/2)$, while the rapidity is defined as $y = \frac{1}{2}\ln\frac{E+p_z}{E-p_z}$.

4 Object definitions and event selection

This section describes the reconstruction of electrons, muons and hadronic recoil objects, and the selection of W and Z bosons. Candidate events are required to have at least one primary vertex reconstructed from at least three tracks with $p_{\mathrm{T}} > 400$ MeV and to pass a trigger selection, which requires a single electron or muon candidate with a p_{T} threshold of 15 GeV or 14 GeV, respectively. In addition, a loose likelihood-based identification requirement [32,33] is applied in the electron trigger.

Electron candidates are required to have $p_{\mathrm{T}} > 20$ (25) GeV in the Z (W) boson analysis and $|\eta| < 2.47$. Candidates within the transition region between barrel and endcap calorimeters ($1.37 < |\eta| < 1.52$) are rejected. In addition, medium likelihood-based identification and tight isolation requirements are applied [32,33]. Muon candidates must satisfy $p_{\mathrm{T}} > 20$ (25) GeV in the Z (W) boson analysis and $|\eta| < 2.4$ and pass the requirements of medium identification and tight isolation [34]; both criteria were optimised for 2015 analysis conditions.

Additional requirements are imposed on the significance of the transverse impact parameter, d_0, such that $|d_0|/\sigma_{d_0} < 5$ (3) for electron (muon) candidates. To ensure that lepton candidates originate from the primary vertex, a requirement is also placed on the longitudinal impact parameter, z_0, multiplied by the sine of the track polar angle, θ, such that the absolute value is smaller than 0.5 mm.

Events with Z boson candidates are selected by requiring exactly two opposite-charge electrons or muons, at least one of which is matched to a lepton selected at trigger level. The dilepton invariant mass must satisfy the fiducial requirement $66 < m_{\ell\ell} < 116$ GeV.

Events with W boson candidates are selected by requiring exactly one electron or muon that is matched to a lepton selected at trigger level. The (anti-)neutrinos from $W^{\pm} \to \ell^{\pm}\nu$ decays escape direct detection. A measure of the neutrino transverse momentum, p_{T}^{ν}, can be inferred from information about the hadronic system recoiling against the W boson. The hadronic recoil is the vector sum of all calorimeter energy clusters excluding the deposits from the decay muon or electron, and is further described below. The transverse projection of the recoil onto the r–ϕ plane, $\vec{u}_{\mathrm{T}}$, is used together with the decay lepton transverse momentum $\vec{p}_{\mathrm{T}}^{\,\ell}$ for the calculation of the missing transverse momentum vector,

$$\vec{E}_{\mathrm{T}}^{\,\mathrm{miss}} = -\left(\vec{u}_{\mathrm{T}} + \vec{p}_{\mathrm{T}}^{\,\ell}\right),$$

whose magnitude is denoted $E_{\mathrm{T}}^{\mathrm{miss}}$. The transverse mass of the lepton-$E_{\mathrm{T}}^{\mathrm{miss}}$ system is defined as $m_{\mathrm{T}} = \sqrt{2 p_{\mathrm{T}}^{\ell} E_{\mathrm{T}}^{\mathrm{miss}} \left(1 - \cos\Delta\phi_{\ell, E_{\mathrm{T}}^{\mathrm{miss}}}\right)}$ where $\Delta\phi_{\ell, E_{\mathrm{T}}^{\mathrm{miss}}}$ is the azimuthal angle between $\vec{p}_{\mathrm{T}}^{\,\ell}$ and $\vec{E}_{\mathrm{T}}^{\,\mathrm{miss}}$. The W boson candidate events are selected by requiring $E_{\mathrm{T}}^{\mathrm{miss}} > 25$ GeV and $m_{\mathrm{T}} > 40$ GeV. These event selection requirements are optimised to reduce background contributions from multi-jet processes.

The general structure of the algorithm used for hadronic recoil reconstruction is introduced in Ref. [35], where three-dimensional topological clusters [36] calibrated at the hadronic scale are used as inputs to the algorithm. In this measurement, the hadronic recoil is reconstructed using particle flow objects [37] as inputs. The ATLAS particle flow algorithm provides an improved $E_{\mathrm{T}}^{\mathrm{miss}}$ resolution compared to the algorithm using only topological clusters, and makes the measurement less sensitive to pile-up by separating the charged-hadron contribution from the neutral hadronic activity [37]. The charged activity is measured by the ID and the related tracks from charged hadrons can be matched to a vertex. From all charged hadrons, only calorimetric clusters associated with a track originating from the reconstructed primary vertex are retained as input to the hadronic recoil algorithm. The neutral hadronic activity is represented by clusters without an associated track, and is also used in the recoil algorithm.

5 Detector performance corrections

5.1 Lepton calibration and efficiency

The electron energy calibration is primarily obtained from the simulation by employing multivariate techniques [38]. The signal $Z \to ee$ MC simulation is used for deriving the data energy scale calibration and resolution corrections for the simulation. The energy resolution is corrected with additional factors no larger than about 1% in the barrel and up to 2% in the endcap region of the detector in order to account for a slightly worse resolution observed in the data. The energy scale is corrected by applying a per-electron energy scale factor to the data derived from a comparison of the electron-pair invariant mass between the simulation and the data. This procedure was found to be sensitive to the pile-up distribution in data due to different settings used for the signal readout from the EM calorimeters [39]. Therefore, a special set of scale correction factors was derived for this dataset.

Measurements of muon momenta can be biased by the detector alignment and resolution, distortions of the magnetic field or imprecise estimates of the amount of passive material in the detector. Corrections of the muon momentum scale and resolution, which are applied to the simulation, are derived as a function of the muon η and ϕ using $Z \to \mu^{+}\mu^{-}$ events [34]. The correction factors are chosen such that they minimise the χ^2 between the muon-pair invariant mass distributions in data and simulation.

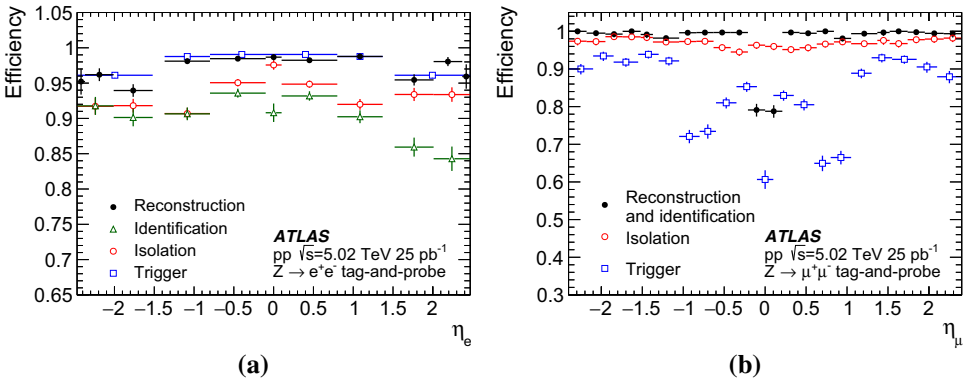

Fig. 1 Efficiencies of reconstruction, identification, isolation and trigger requirements as a function of lepton pseudorapidity for **a** electrons and **b** muons measured using the tag-and-probe method. The efficiency of each selection is defined with respect to leptons selected in the previous step

Electron candidates used for the analysis are required to satisfy selection criteria related to reconstruction, identification, isolation and trigger. For each of these requirements, the efficiency of the selection is measured in data with the tag-and-probe method in $Z \to e^+e^-$ events, as described in Ref. [33], and compared with the simulation. Data-to-simulation ratios of efficiencies are used as scale factors to correct the simulation for the observed differences. Measurements are performed as a function of the electron p_{T} and η for electrons selected in the analysis. All uncertainties related to efficiency are classified as either correlated or uncorrelated, and are propagated accordingly to the final measurement uncertainty.

The electron reconstruction efficiency is in the range 95–99% both in the data and simulation and is typically measured with a precision of 2%. The data-to-simulation ratio is up to 2% (5%) different from unity in the barrel (endcap) calorimeter and is measured typically with 2% precision for p_{T} in the range ∼30 to 50 GeV and 5% for $p_{\mathrm{T}} > 60$ GeV. The efficiency of an electron to further pass the medium identification definition varies from 85 to 95% and is measured with 2% precision. This efficiency differs from the efficiency measured in the MC simulation by up to 5%. The isolation efficiency is measured with a precision of 5% and agrees with the simulated value within 2%. Data-to-simulation correction factors for identification and isolation efficiencies are measured with a precision of 2–6%. Finally, the trigger efficiency data-to-simulation ratio is found to deviate from unity by 0.5–3% and is measured with a precision of up to 2%.

Various selection requirements related to muon trigger, reconstruction, identification and isolation are imposed on muon candidates used in the analysis. The efficiency of the selection criteria is measured in data with the tag-and-probe method in $Z \to \mu^+\mu^-$ events [15,34] and compared with the simulation. Ratios of the efficiencies determined in data and simulation are applied as scale factors to correct the simulated events. For muons with $p_{\mathrm{T}} > 20$ GeV, the correction factors measured as a function of muon p_{T} have typically an uncertainty of 1–2% and do not deviate from a constant value by more than 3%. Therefore, the p_{T} dependence of the scale factors is neglected, and they are evaluated only as a function of muon η.

The muon trigger efficiency in the endcap region of the detector ($1.05 < |\eta| < 2.4$) is measured to be around 90%, and the values obtained in data and simulation agree well. However, in the barrel region ($|\eta| < 1.05$) the trigger efficiency determined in the simulation varies from 70 to 85%, while the efficiency measured in data is lower by 5–15%, which results in sizeable scale factors. The combined reconstruction and identification efficiency for medium-quality muons typically exceeds 99% in both the data and simulation with good agreement between the two measurements. The efficiency of the isolation selection is found to be 97–98% in the MC simulation and it differs from the efficiency measured in the data by about 2% in the most central ($|\eta| < 0.6$) and most forward detector regions ($1.74 < |\eta| < 2.4$).

All measurements of lepton efficiency corrections are limited in their precision by the number of $Z \to \ell^+\ell^-$ candidates available in the $\sqrt{s} = 5.02$ TeV dataset.

Figure 1 summarises the reconstruction, identification, isolation and trigger efficiencies for electron and muon candidates obtained from the tag-and-probe method.

Figure 2 shows the invariant mass distribution of the dilepton system for electron and muon candidates from $Z \to \ell^+\ell^-$ boson decays after applying scale factors to the MC simulation. The data points are compared with simulation including Z boson signal and background components. The electron candidates in the data, shown on the left panel, are calibrated using calorimeter settings and calibration correction factors optimised for low-pile-up conditions. Good agreement between the data and the simulation is found for both channels.

5.2 Recoil calibration

In events with W or Z boson production, the hadronic recoil gives a measure of the boson transverse momentum. The calibration of the recoil is performed using dilepton

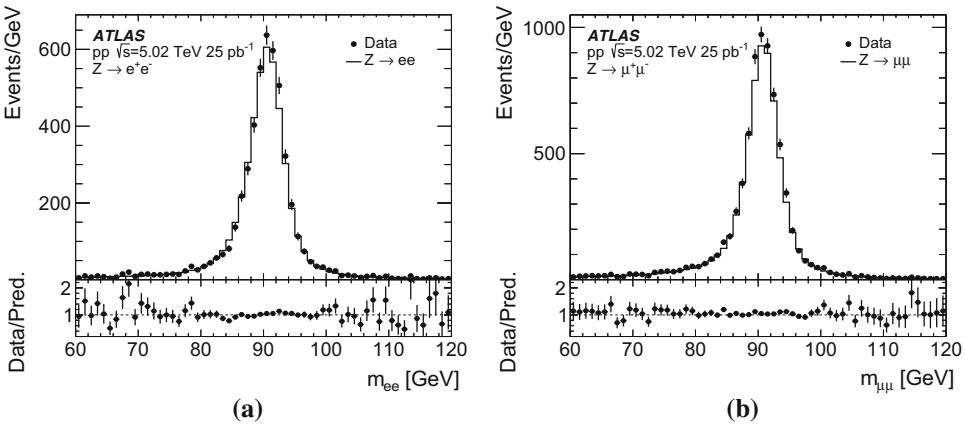

Fig. 2 Detector-level invariant mass distribution of **a** dielectron and **b** dimuon pairs from Z boson decays together with EW background contributions. Background contributions are too small to be visible on a linear scale. Only the statistical uncertainties of the data are shown

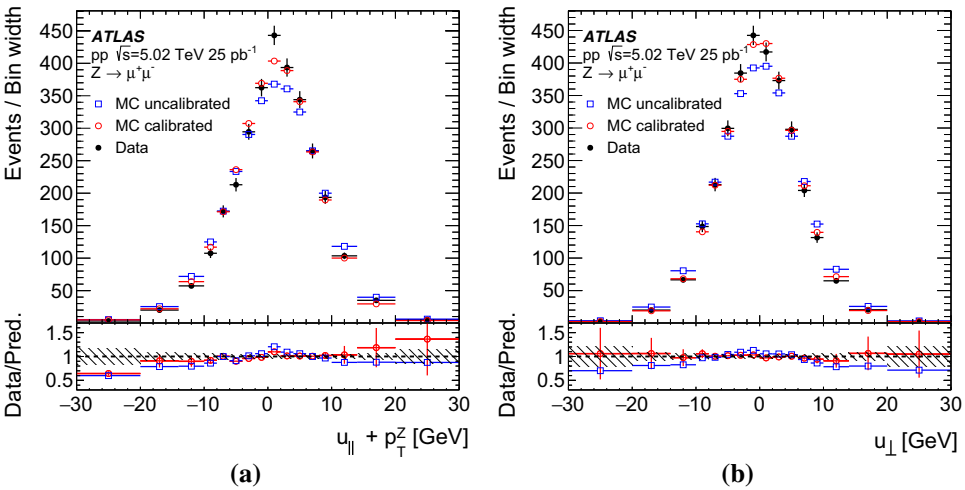

Fig. 3 Distributions of **a** $u_\parallel + p_{\mathrm{T}}^Z$ and **b** $u_\perp$ in data and $Z \to \mu^+\mu^-$ MC simulation before (squares) and after (circles) recoil calibration. The shaded band in the ratio panels represents the statistical uncertainty of the data sample, while the error bars represent the systematic uncertainty associated with the calibration procedure

events from decays of Z bosons produced in pp collisions at $\sqrt{s} = 5.02$ TeV, as information about the Z boson transverse momentum can be obtained with high precision from the measurements of lepton momenta and compared with the measurement from hadronic recoil. The recoil resolution is studied using $u_\perp$, the projection of $\vec{u}_{\mathrm{T}}$ onto the axis – in the transverse plane – perpendicular to the Z boson $\vec{p}_{\mathrm{T}}$. The resolution is given by the standard deviation of the $u_\perp$ distribution, $\sigma_{u_\perp}$. The transverse momentum scale response of the recoil can be studied using the bias defined as $u_\parallel + p_{\mathrm{T}}^Z$, where $u_\parallel$ is the projection of $\vec{u}_{\mathrm{T}}$ onto the axis defined by $\vec{p}_{\mathrm{T}}^Z$, and is quantified via the average of the bias distribution. Differences between the responses in data and simulation are less than ∼2 GeV, while up to ∼20% differences in the resolution are observed.

Following the procedure described in Ref. [35], in situ corrections to the resolution and the scale of u_{T} are obtained in Z events and are applied to the W boson event candidates, as a function of p_{T}^W. The corrections applied to the simulation are obtained as a function of p_{T}^Z:

$$u_\parallel^{W,\mathrm{corr}} = \left\langle u_\parallel^Z + p_{\mathrm{T}}^Z \right\rangle^{\mathrm{data}} - \left\langle u_\parallel^Z + p_{\mathrm{T}}^Z \right\rangle^{\mathrm{MC}} + \left\langle u_\parallel^{Z,\mathrm{data}} \right\rangle + \left(u_\parallel^{W,\mathrm{MC}} - \left\langle u_\parallel^{Z,\mathrm{data}} \right\rangle \right) \cdot \frac{\sigma_{u_\perp}^{\mathrm{data}}}{\sigma_{u_\perp}^{\mathrm{MC}}}; \quad (1)$$

$$u_\perp^{W,\mathrm{corr}} = u_\perp^{W,\mathrm{MC}} \cdot \frac{\sigma_{u_\perp}^{\mathrm{data}}}{\sigma_{u_\perp}^{\mathrm{MC}}}. \quad (2)$$

Equation (1) describes corrections applied to the recoil response in simulation. It includes a shift which brings the average value of $u_\parallel$ in the simulation closer to the one in data, taking into account differences in the bias. In addition, it corrects the response distribution for resolution differences (last term in the equation). The resolution correction is directly described by Eq. (2) where it is applied to the $u_\perp$ distribution in the simulation. The impact of the calibration on the scale and resolution in events where a Z boson decays to a dimuon pair is shown in Fig. 3. The distributions are shown for the simulation before and after applying the corrections and for data. Agreement of the distributions from simulation with data distributions is improved after applying the calibra-

tion, and residual differences are covered by the systematic uncertainties described in Sect. 8.

6 Background determination

6.1 W channels

The reported cross-section measurements correspond to inclusive Drell–Yan production of single vector bosons which decay leptonically. Background processes that contribute to the $W^{\pm}$ boson production measurement are EW processes producing $W^{\pm} \to \tau^{\pm}\nu$, $Z \to \ell^{+}\ell^{-}$, $Z \to \tau^{+}\tau^{-}$ decays, EW diboson (WW, WZ, ZZ) production, as well as top-quark production and multi-jet processes. The multi-jet background includes various processes such as semileptonic decays of heavy-flavour hadrons or in-flight decays of kaons and pions for the muon channel, as well as photon conversions or misidentified hadrons for the electron channel. The background contributions from EW and top-quark production are evaluated using simulated event samples, while the multi-jet contribution is estimated with a data-driven method similar to the one described in Ref. [5].

Although multi-jet background events are well rejected by the lepton isolation requirements, their contribution to the signal region is still sizeable because of the very large production cross sections for multi-jet processes. This contribution is estimated from template fits to data in kinematic distributions: lepton p_{T}, $E_{\mathrm{T}}^{\mathrm{miss}}$ and m_{T}. The fits are performed in a phase-space region defined by the full event selection with a looser lepton p_{T} requirement of $p_{\mathrm{T}} > 20$ GeV and with the requirements on $E_{\mathrm{T}}^{\mathrm{miss}}$ and m_{T} removed. An additional requirement on the transverse component of the hadronic recoil, $u_{\mathrm{T}} < 30$ GeV, is placed to ensure better agreement of the event kinematics between the fit region and the signal region.

Template distributions for signal, EW and top-quark background processes are constructed by applying the fit-region selection to samples of simulated events. Templates enriched in contributions from multi-jet processes are built using events in data with non-isolated leptons selected by inverting the isolation requirement described in Sect. 4. The normalisation factors of template distributions for signal, EW and top-quark backgrounds, as well as the multi-jet background, are extracted from a fit to the data. The fits are repeated with multi-jet background templates constructed from different intervals in a track-based (muon channel) or calorimeter-based (electron channel) isolation variable. Finally, a linear extrapolation to the signal region is performed as a function of the selected isolation variable, accounting also for the difference in kinematic selections between the fit region and the signal region. Examples of post-fit template $E_{\mathrm{T}}^{\mathrm{miss}}$ distributions, which are used to extract multi-jet yields in the electron and muon channels, are presented in Fig. 4.

Following this procedure, multi-jet background processes are estimated to contribute around 0.9% of the $W^{+} \to e^{+}\nu$ sample and 1.4% of the $W^{-} \to e^{-}\nu$ sample, while in the muon channel they represent around 0.1% of the $W^{+} \to \mu^{+}\nu$ sample and 0.2% of the $W^{-} \to \mu^{-}\nu$ sample.

The largest background contributions to the decay modes studied come from the production of single EW bosons decaying via other decay channels. The $Z \to e^{+}e^{-}$ background represents 0.1% of the $W^{+} \to e^{+}\nu$ sample and 0.2% of the $W^{-} \to e^{-}\nu$ sample, while the $Z \to \mu^{+}\mu^{-}$ background amounts to 2.8% and 3.8% in the $W^{+} \to \mu^{+}\nu$ and $W^{-} \to \mu^{-}\nu$ samples, respectively. The $W^{\pm} \to \tau^{\pm}\nu$ background contributes around 1.8% to the samples selected in both channels and the $Z \to \tau^{+}\tau^{-}$ background contributes approximately 0.1%. Contributions from top-quark production ($t\bar{t}$ and single top quarks) are estimated to be at the level of 0.1–0.2% in both channels. Similarly, diboson processes represent approximately 0.1% of the selected event samples.

Figures 5 and 6 show detector-level lepton pseudorapidity distributions for positive and negative electron and muon candidates from W boson decays. Good agreement is found between the data and the sum of signal and background contributions.

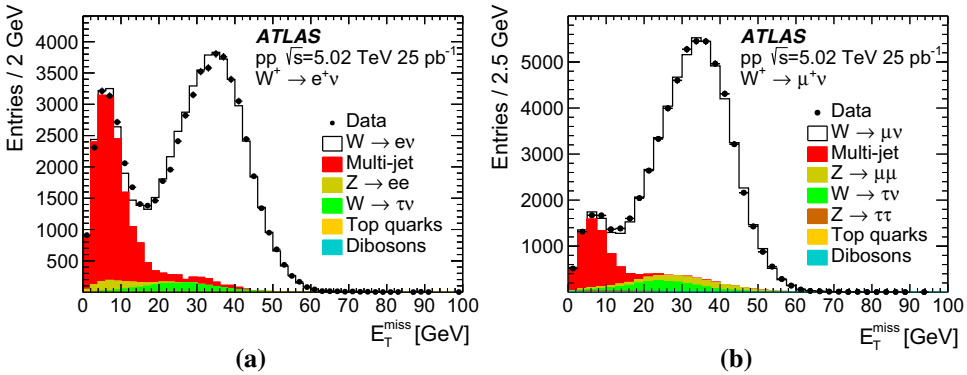

Fig. 4 Distributions of $E_{\mathrm{T}}^{\mathrm{miss}}$ used to extract multi-jet yields in the **a** electron and **b** muon channels after performing the template fits. Only the statistical uncertainties of the data are shown

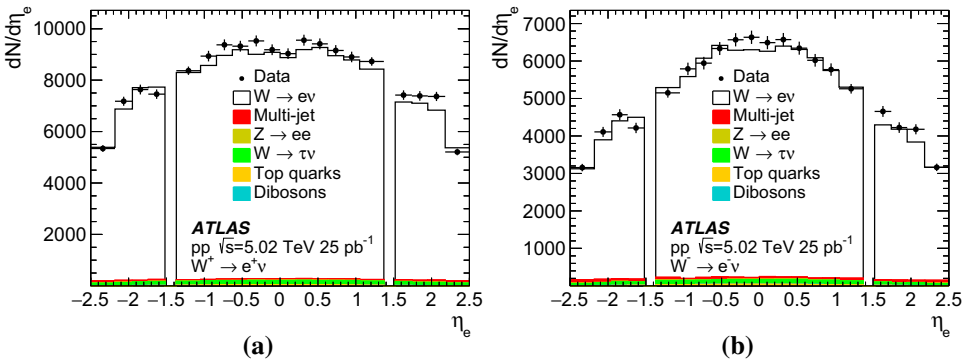

Fig. 5 Distribution of detector-level lepton pseudorapidity for **a** $W^+ \to e^+\nu$ and **b** $W^- \to e^-\nu$. Only the statistical uncertainties of the data are shown

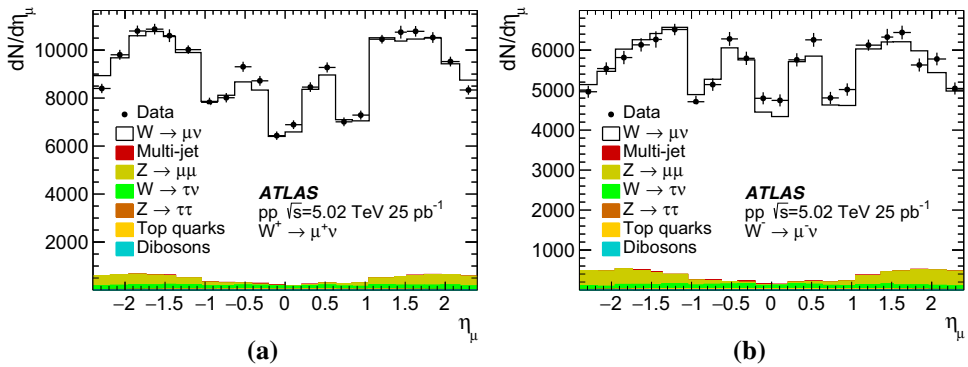

Fig. 6 Distribution of detector-level lepton pseudorapidity for **a** $W^+ \to \mu^+\nu$ and **b** $W^- \to \mu^-\nu$. Only the statistical uncertainties of the data are shown

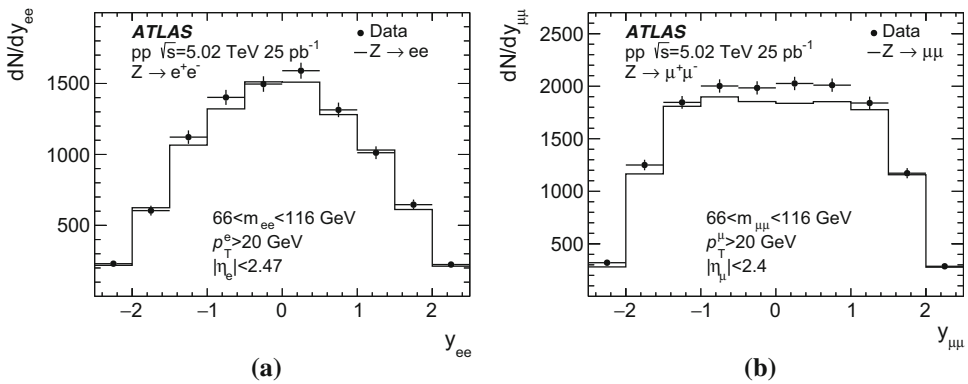

Fig. 7 Detector-level lepton-pair rapidity distributions in the **a** electron and **b** muon channels. Background contributions are negligible using a linear scale. Only the statistical uncertainties of the data are shown

6.2 Z channels

Background contributions to the Z boson sample are expected from $Z \to \tau^+\tau^-$, diboson and W boson decay processes, top-quark pair production, and the multi-jet background. The EW and top-quark contributions are evaluated from dedicated simulation samples, whereas the upper limit on the amount of the multi-jet background is estimated.

Diboson background contributes 0.08% in the muon channel and 0.14% in the electron channel. The $Z \to \tau^+\tau^-$ background is found to be at the level of 0.07% in both decay channels. The top-quark background is at the level of 0.06% in the electron channel and 0.08% in the muon channel. The W boson background is found to be below 0.01% in both channels.

The contribution of the multi-jet background in the muon channel is estimated from samples that simulate $b\bar{b}$ and $c\bar{c}$ production. The study yields an estimate at the level of $<$ 0.01%. A previous ATLAS measurement at $\sqrt{s} = 7$ TeV [4] estimated the multi-jet contribution at the level of 0.02–0.15% for the electron channel and 0.09% for the muon channel. As it is expected that this contribution increases with pile-up and since that measurement was done with higher pile-up than the current analysis, the multi-jet background is considered to be negligible in this analysis.

Figure 7 shows detector-level dilepton rapidity distributions for electron and muon candidates from Z boson decays. Good agreement is found between the data and the sum of signal and background contributions.

Table 1 summarises background contributions to the W^+, W^- and Z boson candidate samples.

Table 1 Background contributions as a percentage of the total for the W^+, W^- and Z candidate samples in the electron (muon) channels

Background	$W^+ \to e^+\nu$ ($W^+ \to \mu^+\nu$) [%]	$W^- \to e^-\nu$ ($W^- \to \mu^-\nu$) [%]	$Z \to e^+e^-$($Z \to \mu^+\mu^-$) [%]
$Z \to \ell^+\ell^-, \ell = e, \mu$	0.1 (2.8)	0.2 (3.8)	–
$W^\pm \to \ell^\pm\nu, \ell = e, \mu$	–	–	<0.01 (<0.01)
$W^\pm \to \tau^\pm\nu$	1.8 (1.8)	1.8 (1.8)	<0.01 (<0.01)
$Z \to \tau^+\tau^-$	0.1 (0.1)	0.1 (0.1)	0.07 (0.07)
Multi-jet	0.9 (0.1)	1.4 (0.2)	<0.01 (<0.01)
Top quark	0.1–0.2 (0.1–0.2)	0.1–0.2 (0.1–0.2)	0.06 (0.08)
Diboson	0.1 (0.1)	0.1 (0.1)	0.14 (0.08)

7 Measurement procedure

The integrated and differential W and Z boson production cross sections are measured within a fiducial phase space defined as follows:

- for W production: $p_{\mathrm{T}}^{\ell} > 25$ GeV, $p_{\mathrm{T}}^{\nu} > 25$ GeV, $|\eta_\ell| < 2.5$, $m_{\mathrm{T}} > 40$ GeV.
- for Z production: $p_{\mathrm{T}}^{\ell} > 20$ GeV, $|\eta_\ell| < 2.5$, $66 < m_{\ell\ell} < 116$ GeV.

Integrated fiducial cross sections in the electron and muon channels are calculated using:

$$\sigma^{\mathrm{fid}}_{W^\pm \to \ell^\pm\nu[Z\to\ell^+\ell^-]} = \frac{N_{W[Z]} - B_{W[Z]}}{C_{W[Z]} \cdot L_{\mathrm{int}}}, \tag{3}$$

where $N_{W[Z]}$ and $B_{W[Z]}$ are the number of selected events in data and the expected number of background events, respectively. The integrated luminosity of the sample is $L_{\mathrm{int}} = 25.0 \pm 0.5\,\mathrm{pb}^{-1}$, determined with the method described in Ref. [40]. A correction for the event detection efficiency is applied with the factor $C_{W[Z]}$, which is obtained from the signal simulation described in Sect. 3 as:

$$C_{W[Z]} = \frac{N^{\mathrm{MC,sel}}_{W[Z]}}{N^{\mathrm{MC,fid}}_{W[Z]}}.$$

Here, $N^{\mathrm{MC,sel}}_{W[Z]}$ is the number of events which pass the signal selection at the detector level, corrected for the observed differences between data and simulation such as in reconstruction, identification, isolation, and trigger efficiencies. The denominator $N^{\mathrm{MC,fid}}_{W[Z]}$ is computed applying the fiducial requirements to the generator-level leptons originating from W and Z boson decays. The measurement is corrected for QED final-state radiation effects by applying these requirements to the lepton momenta before photon radiation. The $C_{W[Z]}$ factors also account for the difference in acceptance between detector-level requirements on lepton $|\eta|$ and the fiducial selection of $|\eta_\ell| < 2.5$.

The procedure described above is extended to the measurement of differential cross sections as a function of the decay lepton pseudorapidity in W boson production, and as a function of the lepton-pair rapidity in Z boson production. The dependence of cross sections on these kinematic variables is particularly sensitive to the choice of PDFs. For the measurement of differential cross sections, the formula given in Eq. (3) is adjusted so that the cross sections are divided by the width of the corresponding interval in absolute pseudorapidity or rapidity. For W production, following Ref. [4], the lepton $|\eta|$ boundaries are defined as:

- 0 – 0.21 – 0.42 – 0.63 – 0.84 – 1.05 – 1.37 – 1.52 – 1.74 – 1.95 – 2.18 – 2.50;

for Z boson production, the lepton-pair $|y_{\ell\ell}|$ boundaries are defined as:

- 0 – 0.5 – 1.0 – 1.5 – 2.0 – 2.5.

For the measurement of these cross sections, the $C_{W[Z]}$ factors are computed separately for each lepton $|\eta|$ or $|y_{\ell\ell}|$ interval by applying the corresponding requirements on the reconstructed lepton kinematics in the numerator, and on the generator-level kinematics in the denominator. Migrations between rapidity intervals are negligible due to the very good angular resolution with which charged-particle tracks associated with leptons are reconstructed, and the good lepton momentum and energy resolutions. The $C_{W[Z]}$ factors for the measurements of integrated and differential cross sections are summarised in Table 2.

The uncertainty associated with the $C_{W[Z]}$ correction is dominated by experimental systematic uncertainties, described in Sect. 8. For the differential C_W factors, the relative size of statistical and systematic uncertainties added in quadrature varies in the range 1.1–2.5% (1.7–3%), while the uncertainties in differential C_Z factors are in the range 1.6–3.5% (0.9–1.2%) in the electron (muon) channel.

Table 2 Correction factors $C_{W[Z]}$ used to calculate integrated and differential W and Z boson production cross sections. The integrated $C_{W[Z]}$ factors are shown with the sum in quadrature of statistical and systematic uncertainties. For the differential $C_{W[Z]}$ factors, the spread of values across lepton $|\eta|$ or $|y_{\ell\ell}|$ intervals is shown, while their uncertainties are described in the text

Channel	C_W ($W^+ \to \ell^+\nu$)	C_W ($W^- \to \ell^-\nu$)	C_Z
Integrated cross-section measurements			
Electron channel	0.657 ± 0.006	0.667 ± 0.005	0.522 ± 0.007
Muon channel	0.723 ± 0.011	0.720 ± 0.010	0.780 ± 0.007
Differential cross-section measurements			
Electron channel	0.55–0.80		0.52–0.62
Muon channel	0.55–0.85		0.60–0.82

Uncertainties in $C_{W[Z]}$ of theoretical origin comprise uncertainties induced by the PDFs, by the description of the W and Z boson transverse momentum distributions, by the implementation of the NLO QCD matrix element and its matching to the parton shower, and by the modelling of the parton shower, hadronisation and underlying event. These uncertainties are discussed in Ref. [4], where they are evaluated to be smaller than 0.2% and thus are negligible at the present level of precision. The size of acceptance corrections included in the integrated correction factors is 7% (3%) for the W boson measurements and 14% (5%) for the Z boson measurements in the electron (muon) channel. In the case of differential W boson measurements, only the C_W factor in the interval $2.18 < |\eta_\ell| < 2.5$ includes an acceptance correction of 9% for $W^\pm \to e^\pm\nu$ processes and 40% for $W^\pm \to \mu^\pm\nu$ processes. On the other hand, all differential C_Z factors include an acceptance correction which varies from 6% to 28% for the $Z \to e^+e^-$ channel and up to 53% for the $Z \to \mu^+\mu^-$ channel.

8 Measurement uncertainties

8.1 Lepton calibration and efficiency corrections

Uncertainties in the determination of lepton trigger, reconstruction, identification and isolation efficiency scale factors affect the measurements through the correction factors $C_{W[Z]}$.

The uncertainties of the electron efficiency measurements are divided into contributions correlated across electron η and p_{T} intervals and uncorrelated ones, and are propagated to the cross-section measurements accordingly. For the $W^\pm \to e^\pm\nu$ channels the efficiency determination contributes a systematic uncertainty of 0.8% to the fiducial cross-section measurements, while for the $Z \to e^+e^-$ channel this contribution is 1.3%. Systematic effects related to the electron p_{T} scale and resolution are subdominant, yielding an uncertainty at the level of 0.3% for the $W^\pm \to e^\pm\nu$ channels and less than 0.2% for the $Z \to e^+e^-$ channel. Uncertainties in the modelling of the electron charge identification are at the level of 0.1%, and neglected for the cross section measurements. Their impact on the asymmetry measurements is however sizeable and included in the final results.

In the muon channels, the statistical components of the scale factor uncertainties are propagated to the measurements via MC pseudo-experiments, while systematic components are propagated as a single variation fully correlated across all muon $|\eta|$ intervals. The single largest contribution to the systematic uncertainty of fiducial cross-section measurements in the $W^\pm \to \mu^\pm\nu$ channels is 1.4% and comes from the determination of the muon trigger efficiency. For measurements in the $Z \to \mu^+\mu^-$ channel the largest systematic uncertainty is contributed by the muon isolation efficiency measurement and amounts to 0.7%. Uncertainties coming from the muon p_{T} scale and resolution are below 0.2% for both $W^\pm \to \mu^\pm\nu$ channels and the $Z \to \mu^+\mu^-$ channel.

8.2 Hadronic recoil corrections

The uncertainty assigned to the hadronic recoil calibration is conservatively defined from the full size of the corrections, which are derived using events with Z boson production. In these events, the impact of the correction on the $u_\perp$ and $u_\parallel + p_{\mathrm{T}}^Z$ distributions varies between a few percent and ∼20% in the range $[-15, +15]$ GeV, which dominates the reported cross-section measurements. After applying this correction to events with W^+ and W^- production, the resulting uncertainties on the cross-section measurements are at the level of 0.5% for both the muon and electron channels.

8.3 Background evaluation

Uncertainties in the evaluation of EW and top-quark backgrounds in the $W^\pm \to e^\pm\nu$ and $W^\pm \to \mu^\pm\nu$ channels are estimated by varying the respective normalisation cross sections. For single-boson production, the size of the cross-section variations is obtained from higher-order QCD calculations, while for diboson and top-quark processes the uncertainty in the cross sections is conservatively taken as

Table 3 Measured fiducial $W^+ \to \ell^+\nu$ differential and integrated cross sections for electron and muon channels

$\lvert\eta_\ell\rvert^{\min}$	$\lvert\eta_\ell\rvert^{\max}$	$W^+ \to e^+\nu$				$W^+ \to \mu^+\nu$			
		$d\sigma/d\lvert\eta_\ell\rvert$ [pb]	$\delta\sigma_{\text{stat}}$ [pb]	$\delta\sigma_{\text{syst}}$ [pb]	$\delta\sigma_{\text{lumi}}$ [pb]	$d\sigma/d\lvert\eta_\ell\rvert$ [pb]	$\delta\sigma_{\text{stat}}$ [pb]	$\delta\sigma_{\text{syst}}$ [pb]	$\delta\sigma_{\text{lumi}}$ [pb]
0.00	0.21	448	8	10	8	473	9	15	9
0.21	0.42	463	8	10	9	472	8	11	9
0.42	0.63	453	8	10	9	493	8	11	9
0.63	0.84	460	8	10	9	460	9	12	9
0.84	1.05	466	9	11	9	478	9	13	9
1.05	1.37	469	7	10	9	478	6	10	9
1.37	1.52	–	–	–	–	482	9	12	9
1.52	1.74	460	9	14	9	482	7	10	9
1.74	1.95	454	9	14	8	472	8	10	9
1.95	2.18	453	9	14	8	443	7	10	9
2.18	2.50	370	7	14	7	371	7	9	7
0.00	2.50	2243	13	27	42	2303	12	36	44

10%. The resulting uncertainties in the measurements in both the $W^\pm \to e^\pm\nu$ and $W^\pm \to \mu^\pm\nu$ channels are below 0.2%. Uncertainties related to the multi-jet background evaluation arise from the statistical precision of the multi-jet templates and uncertainty in the normalisations of the subtracted EW and top-quark contamination. These contributions are propagated through linear extrapolations over the isolation variables to the signal region. The related uncertainties in the measurements are evaluated to be 0.7–0.8% in the $W^\pm \to e^\pm\nu$ channels and not more than 0.2% in the $W^\pm \to \mu^\pm\nu$ channels.

In both the $Z \to \mu^+\mu^-$ and $Z \to e^+e^-$ channels, the uncertainty associated with the background subtraction is negligible, since all individual background contributions are below 0.2% of the selected data sample.

8.4 Luminosity calibration

Luminosity measurements in ATLAS are calibrated using dedicated van der Meer scans [40]. The analysis of data from the scan performed in pp collisions at $\sqrt{s} = 5.02$ TeV, which uses the LUCID-2 detector for the baseline luminosity measurements [41], yields a relative systematic uncertainty of 1.9% in the measured luminosity. The largest sources of uncertainty are systematic effects related to the van der Meer scan procedure and the long-term stability of the luminosity calibration

9 Results

9.1 Channel combination

Results of measurements in the electron and muon channels are summarised in Table 3 for W^+ boson production, Table 4 for W^- boson production and Table 5 for Z boson production. In these tables, the statistical uncertainty is defined from the variance of the background-subtracted number of observed events, and the systematic uncertainty includes all uncertainty components described above, except for the luminosity uncertainty, which is given separately. The systematic uncertainties coming from lepton efficiency corrections are measured as a function of lepton η and p_{T}, and include a significant statistical component due to the number of Z events used to derive the corrections. This statistical component is substantially reduced for the integrated cross sections compared to the differential ones.

The data tables provided in this paper contain compact summaries of the measurement uncertainties. A complete breakdown of systematic uncertainties and their correlated components is provided in HEPData [42].

The electron and muon channel measurements are combined using the Best Linear Unbiased Estimate (BLUE) method [43], accounting for the correlations of the systematic uncertainties across the channels and measurement bins. The $|\eta_\ell|$ and $|y_{\ell\ell}|$ distributions for the electron channel, muon channel and combined results are shown in Figs. 8 and 9 for W and Z bosons, respectively, and the results are listed in Tables 6, 7 and 8. In the interval $1.37 < |\eta_\ell| < 1.52$, only the muon channel measurements for W boson production are used. The combination yields χ^2/d.o.f= 19.3/10 for the W^+ boson results, χ^2/d.o.f= 15.1/10 for the W^- boson results, and χ^2/d.o.f= 3.0/5 for the Z boson results. A simultaneous combination of all measurements, accounting for the correlation of the experimental systematic uncertainties between the W and Z measurement results for a given lepton flavour, gives χ^2/d.o.f = 37.5/25, corresponding to a probability of 5.2%. In view of this remaining discrepancy and of the general trend of the muon channel cross sections to be higher than the electron channel ones, the systematic

Table 4 Measured fiducial $W^- \to \ell^- \nu$ differential and integrated cross sections for electron and muon channels

$\lvert\eta_\ell\rvert^{\min}$	$\lvert\eta_\ell\rvert^{\max}$	$W^- \to e^- \nu$				$W^- \to \mu^- \nu$			
		$d\sigma/d\lvert\eta_\ell\rvert$ [pb]	$\delta\sigma_{\text{stat}}$ [pb]	$\delta\sigma_{\text{syst}}$ [pb]	$\delta\sigma_{\text{lumi}}$ [pb]	$d\sigma/d\lvert\eta_\ell\rvert$ [pb]	$\delta\sigma_{\text{stat}}$ [pb]	$\delta\sigma_{\text{syst}}$ [pb]	$\delta\sigma_{\text{lumi}}$ [pb]
0.00	0.21	322	7	7	6	341	8	10	6
0.21	0.42	316	7	7	6	314	7	6	6
0.42	0.63	303	7	7	6	327	7	6	6
0.63	0.84	294	7	7	6	303	7	7	6
0.84	1.05	300	7	7	6	306	7	8	6
1.05	1.37	280	5	6	5	290	5	5	6
1.37	1.52	–	–	–	–	276	7	6	5
1.52	1.74	270	7	9	5	272	6	5	5
1.74	1.95	260	7	9	5	245	6	5	5
1.95	2.18	255	7	9	5	253	5	5	5
2.18	2.50	220	6	10	4	219	5	5	4
0.00	2.50	1393	10	17	26	1412	9	22	28

Table 5 Measured fiducial $Z \to \ell^+\ell^-$ differential and integrated cross sections for electron and muon channels

$\lvert y_{\ell\ell}\rvert^{\min}$	$\lvert y_{\ell\ell}\rvert^{\max}$	$Z \to e^+e^-$				$Z \to \mu^+\mu^-$			
		$d\sigma/d\lvert y_{\ell\ell}\rvert$ [pb]	$\delta\sigma_{\text{stat}}$ [pb]	$\delta\sigma_{\text{syst}}$ [pb]	$\delta\sigma_{\text{lumi}}$ [pb]	$d\sigma/d\lvert y_{\ell\ell}\rvert$ [pb]	$\delta\sigma_{\text{stat}}$ [pb]	$\delta\sigma_{\text{syst}}$ [pb]	$\delta\sigma_{\text{lumi}}$ [pb]
0.0	0.5	99.9	2.5	1.6	1.9	105.2	2.4	1.1	2.0
0.5	1.0	100.3	2.7	1.6	1.9	101.9	2.3	1.0	1.9
1.0	1.5	89.2	2.7	1.4	1.7	89.8	2.1	0.8	1.7
1.5	2.0	59.6	2.4	1.2	1.1	61.0	1.8	0.6	1.1
2.0	2.5	19.6	1.3	0.7	0.4	20.3	1.2	0.2	0.4
0.0	2.5	369.0	5.3	4.7	6.9	377.9	4.4	3.4	7.1

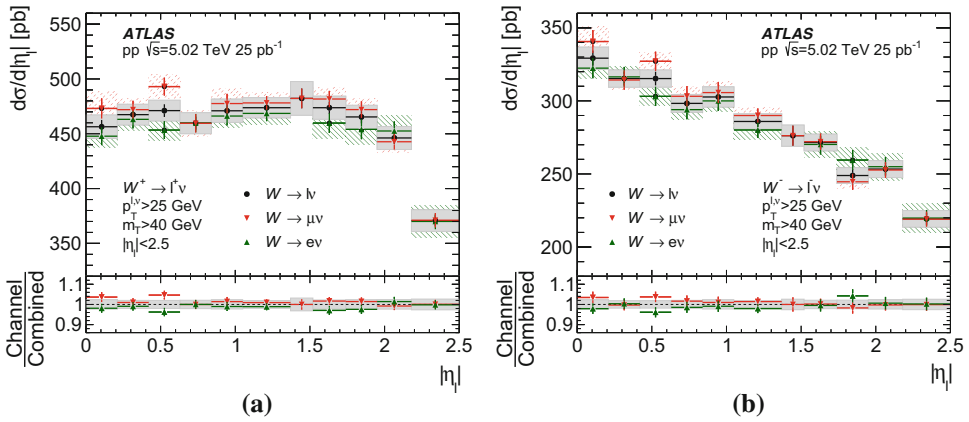

Fig. 8 Differential **a** W^+ and **b** W^- boson production cross sections as a function of absolute decay lepton pseudorapidity, for the electron, muon and combined results. Statistical and systematic errors are shown as corresponding bars and shaded bands. The luminosity uncertainty is not included. The lower panel shows the ratio of channels to the combined differential cross section in each bin. In the lower panel, error bars represent statistical uncertainties in the ratio, while the shaded band represents systematic uncertainties in the combined differential cross sections

uncertainties in the efficiency corrections are scaled such that $\chi^2/\text{d.o.f} = 1$; the correction uncertainties are scaled by a common factor, preserving the uncertainty correlations as a function of lepton p_{T} and η for this source. Tables 6, 7 and 8 include this scaling. The measured ratio of fiducial W^+ and W^- production cross sections, as well as ratios of fiducial $W^\pm$ and Z production cross sections, are summarised in Table 9.

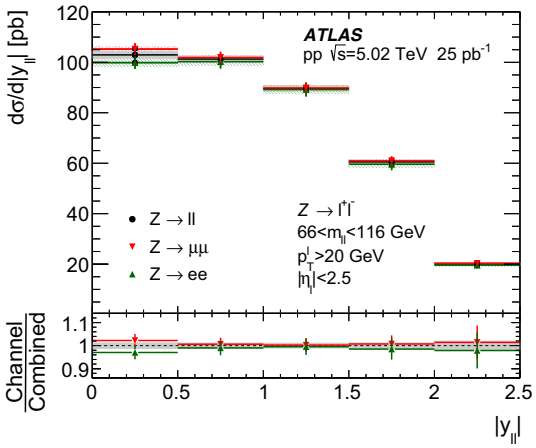

Fig. 9 Differential Z boson production cross section as a function of absolute lepton-pair rapidity, for the electron, muon and combined results. Statistical and systematic errors are shown as corresponding bars and shaded bands. The luminosity uncertainty is not included. The lower panel shows the ratio of channels to the combined differential cross section in each bin. In the lower panel, error bars represent statistical uncertainties in the ratio, while the shaded band represents systematic uncertainties in the combined differential cross sections

Table 6 Combined fiducial $W^+ \to \ell^+\nu$ differential and integrated cross sections

$\lvert\eta_\ell\rvert^{\min}$	$\lvert\eta_\ell\rvert^{\max}$	$W^+ \to \ell^+\nu$			
		$\mathrm{d}\sigma/\mathrm{d}\lvert\eta_\ell\rvert$ [pb]	$\delta\sigma_{\mathrm{stat}}$ [pb]	$\delta\sigma_{\mathrm{syst}}$ [pb]	$\delta\sigma_{\mathrm{lumi}}$ [pb]
0.00	0.21	456	6	11	9
0.21	0.42	467	6	9	9
0.42	0.63	471	6	9	9
0.63	0.84	460	6	10	9
0.84	1.05	471	6	11	9
1.05	1.37	474	5	9	9
1.37	1.52	482	9	15	9
1.52	1.74	474	6	11	9
1.74	1.95	465	6	11	9
1.95	2.18	446	6	10	9
2.18	2.50	371	5	10	7
0.00	2.50	2266	9	29	43

The measurements of differential W^+ and W^- production cross sections allow the extraction of the W boson charge asymmetry, as a function of the absolute pseudorapidity of the decay lepton:

$$A_\ell(|\eta_\ell|) = \frac{\mathrm{d}\sigma_{W^+}/\mathrm{d}|\eta_\ell| - \mathrm{d}\sigma_{W^-}/\mathrm{d}|\eta_\ell|}{\mathrm{d}\sigma_{W^+}/\mathrm{d}|\eta_\ell| + \mathrm{d}\sigma_{W^-}/\mathrm{d}|\eta_\ell|}.$$

Uncertainties in A_ℓ are calculated considering all sources of correlated and uncorrelated systematic uncertainties in the differential cross sections. The resulting dependence of A_ℓ on $|\eta_\ell|$ measured in the electron and muon channels is presented in Fig. 10 together with the combined values, while the combined results are summarised with the corresponding uncertainties in Table 10. Good agreement between the two channels is found.

Table 7 Combined fiducial $W^- \to \ell^-\nu$ differential and integrated cross sections

$\lvert\eta_\ell\rvert^{\min}$	$\lvert\eta_\ell\rvert^{\max}$	$W^- \to \ell^-\nu$			
		$\mathrm{d}\sigma/\mathrm{d}\lvert\eta_\ell\rvert$ [pb]	$\delta\sigma_{\mathrm{stat}}$ [pb]	$\delta\sigma_{\mathrm{syst}}$ [pb]	$\delta\sigma_{\mathrm{lumi}}$ [pb]
0.00	0.21	329	5	8	6
0.21	0.42	315	5	6	6
0.42	0.63	315	5	6	6
0.63	0.84	298	5	6	6
0.84	1.05	303	5	7	6
1.05	1.37	286	4	5	6
1.37	1.52	276	7	7	5
1.52	1.74	272	4	6	5
1.74	1.95	249	4	5	5
1.95	2.18	253	4	6	5
2.18	2.50	219	4	6	4
0.00	2.50	1401	7	18	27

Table 8 Combined fiducial $Z \to \ell^+\ell^-$ differential and integrated cross sections

$\lvert y_{\ell\ell}\rvert^{\min}$	$\lvert y_{\ell\ell}\rvert^{\max}$	$Z \to \ell^+\ell^-$			
		$\mathrm{d}\sigma/\mathrm{d}\lvert y_{\ell\ell}\rvert$ [pb]	$\delta\sigma_{\mathrm{stat}}$ [pb]	$\delta\sigma_{\mathrm{syst}}$ [pb]	$\delta\sigma_{\mathrm{lumi}}$ [pb]
0.0	0.5	103.0	1.7	1.2	1.9
0.5	1.0	101.3	1.8	1.1	1.9
1.0	1.5	89.6	1.7	0.9	1.7
1.5	2.0	60.5	1.4	0.7	1.1
2.0	2.5	20.0	0.9	0.4	0.4
0.0	2.5	374.5	3.4	3.6	7.0

Table 9 Ratios of integrated W and Z production cross sections

$R^{\mathrm{fid}}_{W^+/W^-}$	1.617 ± 0.012 (stat) ± 0.003 (syst)
$R^{\mathrm{fid}}_{W/Z}$	9.81 ± 0.13 (stat) ± 0.01 (syst)
$R^{\mathrm{fid}}_{W^+/Z}$	6.06 ± 0.08 (stat) ± 0.01 (syst)
$R^{\mathrm{fid}}_{W^-/Z}$	3.75 ± 0.05 (stat) ± 0.01 (syst)

9.2 Comparison with theoretical predictions

The measured cross sections are compared with theoretical predictions obtained using a modified version of DYNNLO 1.5 [2,3] optimised for speed of computation. The calculation is performed at $O(\alpha_S^2)$ in QCD and at leading order in the EW theory, with parameters set according to the G_μ scheme [29]. The input parameters (the Fermi constant

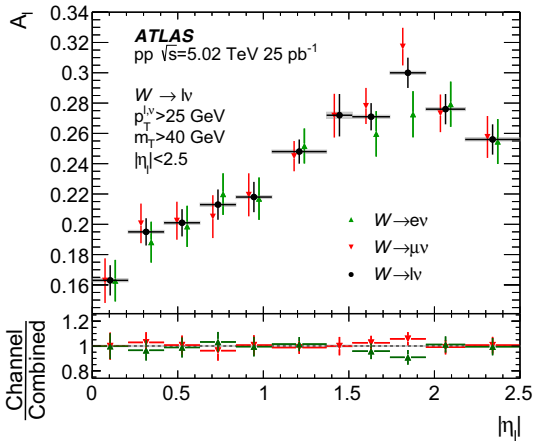

Fig. 10 Charge asymmetry for W bosons as a function of absolute decay lepton pseudorapidity, for the electron, muon and combined results. Statistical and systematic errors are shown as corresponding bars and shaded bands (not visible for most points). The lower panel shows the ratio of channels to the combined charge asymmetry in each bin. In the lower panel, error bars represent statistical uncertainties in the ratio, while the shaded band represents systematic uncertainties in the combined charge asymmetry

Table 10 Charge asymmetry for W bosons as a function of absolute pseudorapidity of the decay lepton

$\lvert\eta_\ell\rvert^{\min}$	$\lvert\eta_\ell\rvert^{\max}$	A_ℓ	δA_{stat}	δA_{syst}
0.00	0.21	0.163	0.010	0.001
0.21	0.42	0.195	0.009	0.001
0.42	0.63	0.201	0.009	0.001
0.63	0.84	0.213	0.010	0.001
0.84	1.05	0.218	0.010	0.001
1.05	1.37	0.248	0.008	0.001
1.37	1.52	0.272	0.014	0.002
1.52	1.74	0.271	0.009	0.001
1.74	1.95	0.300	0.010	0.001
1.95	2.18	0.276	0.010	0.001
2.18	2.50	0.256	0.010	0.001

G_{F}, the masses and widths of W and Z bosons, and the CKM matrix elements) are taken from Ref. [44]. The DYNNLO predictions are calculated using the NNLO PDF sets from CT14NNLO [45], NNPDF3.1 [46], MMHT14NNLO68CL [47], HERAPDF2.0 [48] and ABMP16 [49]. All considered PDF sets except HERAPDF2.0 are evaluated from global fits which include to varying extents the LHC measurements of W/Z boson, Drell–Yan, top-quark and inclusive jet production. The renormalisation and factorisation scales, respectively denoted as μ_{R} and μ_{F}, are set equal to the decay lepton-pair invariant mass, $m_{\ell\nu}$ or $m_{\ell\ell}$.

Uncertainties in these predictions are derived as follows. PDF uncertainties are evaluated from the variations of the NNLO PDFs (the PDF uncertainties of CT14NNLO are rescaled from 90% confidence level to 68% confidence level). Scale uncertainties are defined by the envelope of the variations obtained by changing μ_{R} and μ_{F} by a factor of two with respect to their nominal values and imposing $0.5 \leq \mu_{\text{R}}/\mu_{\text{F}} \leq 2$. The uncertainty induced by the strong coupling constant is estimated by varying α_{S} by ± 0.001 around the central value of $\alpha_{\text{S}}(m_Z) = 0.118$, following the prescription of Ref. [45]; the effect of these variations is estimated by comparing the CT14NNLO_AS_0117 and CT14NNLO_AS_0119 PDF sets to CT14NNLO. Finally, intrinsic limitations of the NNLO calculations for fiducial cross-section predictions lead to systematic differences between results from different programs, as explained in Ref. [50]. Therefore, an additional uncertainty of 0.7%, estimated from a comparison of predictions calculated with FEWZ 3.1 and DYNNLO, is assigned. Theory uncertainties are dominated by our knowledge of the proton PDFs.

The uncertainty of the LHC proton beam energy is estimated to be 0.1% [51] and induces typically an uncertainty of 0.1% in the cross-section predictions, which is negligible compared to other theoretical uncertainties discussed above.

Differential cross sections for W and Z boson production are shown in Figs. 11 and 12 as a function of $|\eta_\ell|$ and $|y_{\ell\ell}|$, respectively. The cross sections are compared for the combined measurement and theoretical predictions calculated with the CT14NNLO, NNPDF3.1, MMHT14NNLO68CL, HERAPDF2.0 and ABMP16 PDF sets, with uncertainties assigned as described above. In some regions of phase space, a comparison of the differential cross sections shows systematic deviations of the predictions obtained with recent PDF sets from the measured values. These deviations are largest for W^+ boson production and at central rapidity for Z boson production.

The measured lepton charge asymmetry for W bosons shown in Fig. 13 is compared with predictions calculated with the PDF sets mentioned previously. In most of the $|\eta_\ell|$ range considered, the predictions from all PDF sets tend to underestimate the measured asymmetry by a few percent.

10 Summary

Fiducial cross sections are reported for inclusive W^+, W^- and Z boson production in pp collisions at the centre-of-mass energy $\sqrt{s} = 5.02$ TeV. The measurement is based on data taken by the ATLAS detector at the LHC corresponding to an integrated luminosity of 25.0 pb^{-1}. Cross sections are reported in the electron and muon decay channels, integrated over the fiducial regions and differentially. The fiducial region is defined using lepton kinematics and detector acceptance. The differential cross sections for $W^\pm \to \ell^\pm\nu$ boson production are measured as a function of absolute lepton pseudorapidity while for $Z \to \ell^+\ell^-$ bosons they are

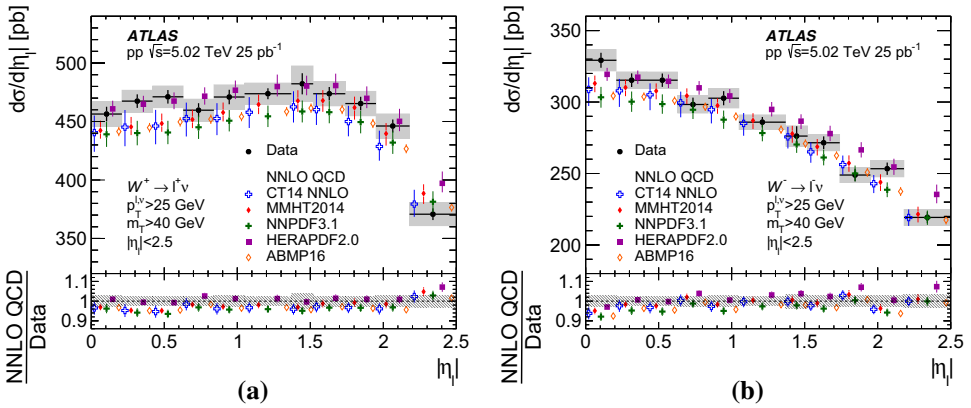

Fig. 11 Differential cross sections for **a** W^+ and **b** W^- boson production as a function of absolute decay lepton pseudorapidity compared with theoretical predictions. Statistical and systematic errors are shown as corresponding bars and shaded bands on the data points. The luminosity uncertainty is not included. Only the dominant uncertainty (PDF) is displayed for the theory. The lower panel shows the ratio of predictions to the measured differential cross section in each bin, and the shaded band shows the sum in quadrature of statistical and systematic uncertainties of the data

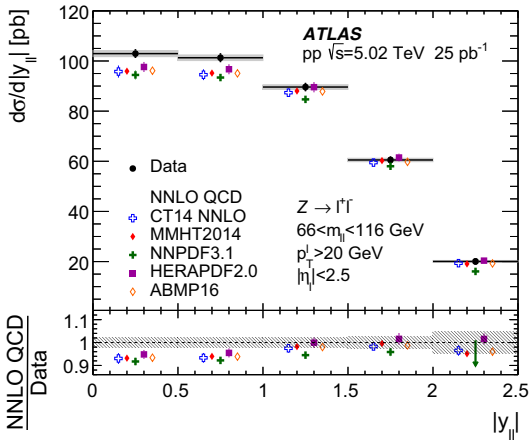

Fig. 12 Differential cross section for Z boson production as a function of absolute lepton-pair rapidity compared with theoretical predictions. Statistical and systematic errors are shown as corresponding bars and shaded bands on the data points. The luminosity uncertainty is not included. Only the dominant uncertainty (PDF) is displayed for the theory. The lower panel shows the ratio of predictions to the measured differential cross section in each bin, and the shaded band shows the sum in quadrature of statistical and systematic uncertainties of the data

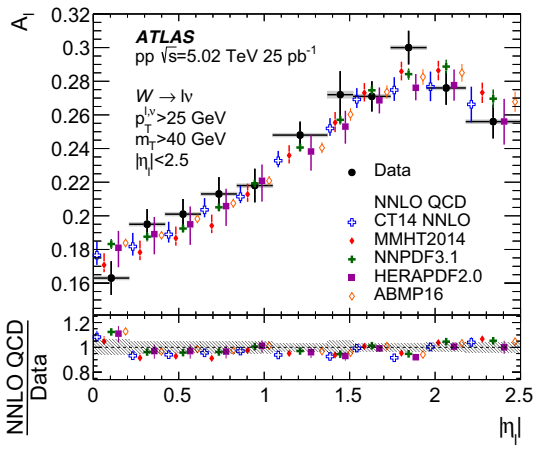

Fig. 13 Charge asymmetry for W bosons as a function of absolute decay lepton pseudorapidity compared with theoretical predictions. Statistical and systematic errors are shown as corresponding bars and shaded bands on the data points. Only the dominant uncertainty (PDF) is displayed for the theory. The lower panel shows the ratio of predictions to the measured differential cross section in each bin, and the shaded band shows the sum in quadrature of statistical and systematic uncertainties of the data

reported as a function of absolute dilepton rapidity in the mass window $66 < m_{\ell\ell} < 116$ GeV. For $W^{\pm}$ bosons the decay lepton charge asymmetry as a function of absolute lepton pseudorapidity is also measured.

The electron and muon channel results are found to agree within the measurement precision, and are therefore combined considering all sources of correlated and uncorrelated uncertainties. The combined fiducial W^+, W^-, and Z cross sections are measured with a precision of 1.2–1.7%, excluding the luminosity uncertainty. Both the integrated and differential cross sections are compared with next-to-next-to-leading-order QCD calculations using various PDF sets. A comparison of the differential cross sections shows 1–2σ deviations from the predictions obtained with many of the recent PDF sets.

These results provide the first measurement of $W^{\pm}$ and Z boson production cross sections at the centre-of-mass energy $\sqrt{s} = 5.02$ TeV and complement previous measurements at $\sqrt{s} = 7$, 8 and 13 TeV. They constitute a reference for measurements of $W^{\pm}$ and Z boson production in heavy-ion collisions collected at $\sqrt{s_{\mathrm{NN}}} = 5.02$ TeV by the LHC experiments.

Acknowledgements We thank CERN for the very successful operation of the LHC, as well as the support staff from our institutions without whom ATLAS could not be operated efficiently. We acknowledge the support of ANPCyT, Argentina; YerPhI, Armenia; ARC, Australia; BMWFW and FWF, Austria; ANAS, Azerbaijan; SSTC, Belarus; CNPq and FAPESP, Brazil; NSERC, NRC and CFI, Canada; CERN; CONICYT, Chile; CAS, MOST and NSFC, China; COLCIENCIAS, Colombia; MSMT CR, MPO CR and VSC CR, Czech Republic; DNRF and DNSRC, Denmark; IN2P3-CNRS, CEA-DRF/IRFU, France; SRNSFG, Georgia; BMBF, HGF, and MPG, Germany; GSRT, Greece; RGC, Hong Kong SAR, China; ISF and Benoziyo Center, Israel; INFN, Italy; MEXT and JSPS, Japan; CNRST, Morocco; NWO, Netherlands; RCN, Norway; MNiSW and NCN, Poland; FCT, Portugal; MNE/IFA, Romania; MES of Russia and NRC KI, Russian Federation; JINR; MESTD, Serbia; MSSR, Slovakia; ARRS and MIZŠ, Slovenia; DST/NRF, South Africa; MINECO, Spain; SRC and Wallenberg Foundation, Sweden; SERI, SNSF and Cantons of Bern and Geneva, Switzerland; MOST, Taiwan; TAEK, Turkey; STFC, United Kingdom; DOE and NSF, United States of America. In addition, individual groups and members have received support from BCKDF, CANARIE, CRC and Compute Canada, Canada; COST, ERC, ERDF, Horizon 2020, and Marie Skłodowska-Curie Actions, European Union; Investissements d' Avenir Labex and Idex, ANR, France; DFG and AvH Foundation, Germany; Herakleitos, Thales and Aristeia programmes co-financed by EU-ESF and the Greek NSRF, Greece; BSF-NSF and GIF, Israel; CERCA Programme Generalitat de Catalunya, Spain; The Royal Society and Leverhulme Trust, United Kingdom. The crucial computing support from all WLCG partners is acknowledged gratefully, in particular from CERN, the ATLAS Tier-1 facilities at TRIUMF (Canada), NDGF (Denmark, Norway, Sweden), CC-IN2P3 (France), KIT/GridKA (Germany), INFN-CNAF (Italy), NL-T1 (Netherlands), PIC (Spain), ASGC (Taiwan), RAL (UK) and BNL (USA), the Tier-2 facilities worldwide and large non-WLCG resource providers. Major contributors of computing resources are listed in Ref. [52].

Data Availability Statement This manuscript has no associated data or the data will not be deposited. [Authors' comment: All ATLAS scientific output is published in journals, and preliminary results are made available in Conference Notes. All are openly available, without restriction on use by external parties beyond copyright law and the standard conditions agreed by CERN. Data associated with journal publications are also made available: tables and data from plots (e.g. cross section values, likelihood profiles, selection efficiencies, cross section limits, ...) are stored in appropriate repositories such as HEPDATA (http://hepdata.cedar.ac.uk/). ATLAS also strives to make additional material related to the paper available that allows a reinterpretation of the data in the context of new theoretical models. For example, an extended encapsulation of the analysis is often provided for measurements in the framework of RIVET (http://rivet.hepforge.org/). This information is taken from the ATLAS Data Access Policy which is a public document that can be downloaded from http://opendata.cern.ch/record/413 [opendata.cern.ch].]

Funded by SCOAP[3].

References

1. C. Anastasiou, L. Dixon, K. Melnikov, F. Petriello, High-precision QCD at hadron colliders: electroweak gauge boson rapidity distributions at next-to-next-to-leading order. Phys. Rev. D **69**, 094008 (2004). arXiv:hep-ph/0312266
2. S. Catani, M. Grazzini, Next-to-next-to-leading order subtraction formalism in hadron collisions and its application to Higgs boson production at the large hadron collider. Phys. Rev. Lett. **98**, 222002 (2007). arXiv:hep-ph/0703012
3. S. Catani, L. Cieri, G. Ferrera, D. de Florian, M. Grazzini, Vector boson production at hadron colliders: a fully exclusive QCD calculation at next-to-next-to-leading order. Phys. Rev. Lett. **103**, 082001 (2009). arXiv:0903.2120 [hep-ph]
4. ATLAS Collaboration, Precision measurement and interpretation of inclusive W^+, W^- and Z/γ^* production cross sections with the ATLAS detector. Eur. Phys. J. C **77**, 367 (2017). arXiv:1612.03016 [hep-ex]
5. ATLAS Collaboration, Measurement of $W^\pm$ and Z-boson production cross sections in pp collisions at $\sqrt{s} = 13$ TeV with the ATLAS detector. Phys. Lett. B **759**, 601 (2016). arXiv:1603.09222 [hep-ex]
6. CMS Collaboration, Measurement of inclusive W and Z boson production cross sections in pp collisions at $\sqrt{s} = 8$ TeV. Phys. Rev. Lett. **112**, 191802 (2014). arXiv:1402.0923 [hep-ex]
7. LHCb Collaboration, Measurement of forward W and Z boson production in pp collisions at $\sqrt{s} = 8$ TeV. JHEP **01**, 155 (2016). arXiv:1511.08039 [hep-ex]
8. ATLAS Collaboration, Measurement of the production and lepton charge asymmetry of W bosons in Pb+Pb collisions at $\sqrt{s_{\rm NN}} = 2.76$ TeV with the ATLAS detector. Eur. Phys. J. C **75**, 23 (2015). arXiv:1408.4674 [hep-ex]
9. ATLAS Collaboration, Measurement of Z boson production in Pb-Pb collisions at $\sqrt{s_{NN}} = 2.76$ TeV with the ATLAS detector. Phys. Rev. Lett. **110**, 022301 (2013). arXiv:1210.6486 [hep-ex]
10. CMS Collaboration, Study of W boson production in PbPb and pp collisions at $\sqrt{s_{NN}} = 2.76$ TeV. Phys. Lett. B **715**, 66 (2012). arXiv:1205.6334 [nucl-ex]
11. CMS Collaboration, Study of Z production in PbPb and pp collisions at $\sqrt{s_{\rm NN}} = 2.76$ TeV in the dimuon and dielectron decay channels. JHEP **03**, 022 (2015). arXiv:1410.4825 [nucl-ex]
12. ATLAS Collaboration, Z boson production in $p + Pb$ collisions at $\sqrt{s_{NN}} = 5.02$ TeV measured with the ATLAS detector. Phys. Rev. C **92**, 044915 (2015). arXiv:1507.06232 [hep-ex]
13. CMS Collaboration, Study of Z boson production in pPb collisions at $\sqrt{s_{NN}} = 5.02$ TeV. Phys. Lett. B **759**, 36 (2016). arXiv:1512.06461 [hep-ex]
14. ATLAS Collaboration, The ATLAS experiment at the CERN large hadron collider. JINST **3**, S08003 (2008)
15. ATLAS Collaboration, Performance of the ATLAS trigger system in 2015. Eur. Phys. J. C **77**, 317 (2017). arXiv:1611.09661 [hep-ex]
16. S. Agostinelli et al., GEANT4—a simulation toolkit. Nucl. Instrum. Methods A **506**, 250 (2003)
17. ATLAS Collaboration, The ATLAS simulation infrastructure. Eur. Phys. J. C **70**, 823 (2010). arXiv:1005.4568 [hep-ex]
18. S. Alioli, P. Nason, C. Oleari, E. Re, A general framework for implementing NLO calculations in shower Monte Carlo programs: the POWHEG BOX. JHEP **06**, 043 (2010). arXiv:1002.2581 [hep-ph]
19. T. Sjöstrand, S. Mrenna, P. Skands, A brief introduction to PYTHIA 8.1. Comput. Phys. Commun. **178**, 852 (2008). arXiv:0710.3820 [hep-ph]
20. J. Gao, CT10 next-to-next-to-leading order global analysis of QCD. Phys. Rev. D **89**, 033009 (2014). arXiv:1302.6246 [hep-ph]

21. J. Pumplin et al., New generation of parton distributions with uncertainties from global QCD analysis. JHEP **07**, 012 (2002). arXiv:hep-ph/0201195
22. ATLAS Collaboration, Measurement of the Z/γ^* boson transverse momentum distribution in pp collisions at $\sqrt{s} = 7$ TeV with the ATLAS detector. JHEP **09**, 145 (2014). arXiv:1406.3660 [hep-ex]
23. N. Davidson, T. Przedzinski, Z. Was, PHOTOS interface in C++: technical and physics documentation. Comput. Phys. Commun. **199**, 86 (2016). arXiv:1011.0937 [hep-ph]
24. H.-L. Lai et al., New parton distributions for collider physics. Phys. Rev. D **82**, 074024 (2010). arXiv:1007.2241 [hep-ph]
25. T. Sjöstrand, S. Mrenna, P. Skands, PYTHIA 6.4 physics and manual. JHEP **05**, 026 (2006). arXiv:hep-ph/0603175
26. P.Z. Skands, Tuning Monte Carlo generators: the Perugia tunes. Phys. Rev. D **82**, 074018 (2010). arXiv:1005.3457 [hep-ph]
27. D.J. Lange, The EvtGen particle decay simulation package. Nucl. Instrum. Methods A **462**, 152 (2001)
28. T. Gleisberg et al., Event generation with SHERPA 1.1. JHEP **02**, 007 (2009). arXiv:0811.4622 [hep-ph]
29. W.F.L. Hollik, Radiative corrections in the standard model and their rôle for precision tests of the electroweak theory. Fortsch. Phys. **38**, 165 (1990)
30. ATLAS Collaboration, Summary of ATLAS Pythia 8 tunes. ATL-PHYS-PUB-2012-003. https://cds.cern.ch/record/1474107
31. A.D. Martin, W.J. Stirling, R.S. Thorne, G. Watt, Parton distributions for the LHC. Eur. Phys. J. C **63**, 189 (2009). arXiv:0901.0002 [hep-ph]
32. ATLAS Collaboration, Electron efficiency measurements with the ATLAS detector using 2012 LHC proton-proton collision data. Eur. Phys. J. C **77**, 195 (2017). arXiv:1612.01456 [hep-ex]
33. ATLAS Collaboration, Electron efficiency measurements with the ATLAS detector using the 2015 LHC proton-proton collision data. ATLAS-CONF-2016-024. https://cds.cern.ch/record/2157687
34. ATLAS Collaboration, Muon reconstruction performance of the ATLAS detector in proton-proton collision data at $\sqrt{s} = 13$ TeV. Eur. Phys. J. C **76**, 292 (2016). arXiv:1603.05598 [hep-ex]
35. ATLAS Collaboration, Measurement of the W-boson mass in pp collisions at $\sqrt{s} = 7$ TeV with the ATLAS detector. Eur. Phys. J. C **78**,110 (2018). arXiv:1701.07240 [hep-ex]
36. ATLAS Collaboration, Topological cell clustering in the ATLAS calorimeters and its performance in LHC Run 1. Eur. Phys. J. C **77** 490 (2017). arXiv:1603.02934 [hep-ex]
37. ATLAS Collaboration, Jet reconstruction and performance using particle flow with the ATLAS detector. Eur. Phys. J. C **77**, 466 (2017). arXiv:1703.10485 [hep-ex]
38. ATLAS Collaboration, Electron and photon energy calibration with the ATLAS detector using LHC run 1 data. Eur. Phys. J. C **74**, 3071 (2014). arXiv:1407.5063 [hep-ex]
39. H. Abreu et al., Performance of the electronic readout of the ATLAS liquid argon calorimeters. JINST **5**, P09003 (2010)
40. ATLAS Collaboration, Luminosity determination in pp collisions at $\sqrt{s} = 8$ TeV using the ATLAS detector at the LHC. Eur. Phys. J. C **76**, 653 (2016). arXiv:1608.03953 [hep-ex]
41. G. Avoni et al., The new LUCID-2 detector for luminosity measurement and monitoring in ATLAS. JINST **13**, P07017 (2018)
42. E. Maguire, L. Heinrich, G. Watt, HEPData: a repository for high energy physics data. J. Phys. Conf. Ser. **898**, 102006 (2017). arXiv:1704.05473 [hep-ex]
43. A. Valassi, Combining correlated measurements of several different physical quantities. Nucl. Instrum. Methods A **500**, 391 (2003)
44. Particle Data Group, K.A. Olive et al., Review of particle physics. Chin. Phys. C **38**, 090001 (2014)
45. S. Dulat et al., New parton distribution functions from a global analysis of quantum chromodynamics. Phys. Rev. D **93**, 033006 (2016). arXiv:1506.07443 [hep-ph]
46. R.D. Ball et al., Parton distributions from high-precision collider data. Eur. Phys. J. C **77**, 663 (2017). arXiv:1706.00428 [hep-ph]
47. L.A. Harland-Lang, A.D. Martin, P. Motylinski, R.S. Thorne, Parton distributions in the LHC era: MMHT 2014 PDFs. Eur. Phys. J. C **75**, 204 (2015). arXiv:1412.3989 [hep-ph]
48. H1 and ZEUS Collaborations, Combination of measurements of inclusive deep inelastic $e^{\pm}p$ scattering cross sections and QCD analysis of HERA data. Eur. Phys. J. C **75**, 580 (2015). arXiv:1506.06042 [hep-ex]
49. S. Alekhin, J. Blümlein, S. Moch, R. Plačakytė, Parton distribution functions, α_s, and heavy-quark masses for LHC Run II. Phys. Rev. D **96**, 014011 (2017). arXiv:1701.05838 [hep-ph]
50. ATLAS Collaboration, Measurements of top-quark pair to Z-boson cross-section ratios at $\sqrt{s} = 13, 8, 7$ TeV with the ATLAS detector. JHEP **02**, 117 (2017). arXiv:1612.03636 [hep-ex]
51. E. Todesco, J. Wenninger, Large hadron collider momentum calibration and accuracy. Phys. Rev. Accel. Beams **20**, 081003 (2017)
52. ATLAS Collaboration, ATLAS Computing Acknowledgements. ATL-GEN-PUB-2016-002. https://cds.cern.ch/record/2202407

ATLAS Collaboration

M. Aaboud[34d], G. Aad[99], B. Abbott[125], O. Abdinov[13,*], B. Abeloos[129], D. K. Abhayasinghe[91], S. H. Abidi[164], O. S. AbouZeid[39], N. L. Abraham[153], H. Abramowicz[158], H. Abreu[157], Y. Abulaiti[6], B. S. Acharya[64a,64b,p], S. Adachi[160], L. Adamczyk[81a], J. Adelman[119], M. Adersberger[112], A. Adiguzel[12c,aj], T. Adye[141], A. A. Affolder[143], Y. Afik[157], C. Agheorghiesei[27c], J. A. Aguilar-Saavedra[137a,137f,ai], F. Ahmadov[77,ag], G. Aielli[71a,71b], S. Akatsuka[83], T. P. A. Åkesson[94], E. Akilli[52], A. V. Akimov[108], G. L. Alberghi[23a,23b], J. Albert[173], P. Albicocco[49], M. J. Alconada Verzini[86], S. Alderweireldt[117], M. Aleksa[35], I. N. Aleksandrov[77], C. Alexa[27b], T. Alexopoulos[10], M. Alhroob[125], B. Ali[139], G. Alimonti[66a], J. Alison[36], S. P. Alkire[145], C. Allaire[129], B. M. M. Allbrooke[153], B. W. Allen[128], P. P. Allport[21], A. Aloisio[67a,67b], A. Alonso[39], F. Alonso[86], C. Alpigiani[145], A. A. Alshehri[55], M. I. Alstaty[99], B. Alvarez Gonzalez[35], D. Álvarez Piqueras[171], M. G. Alviggi[67a,67b], B. T. Amadio[18], Y. Amaral Coutinho[78b], L. Ambroz[132], C. Amelung[26], D. Amidei[103], S. P. Amor Dos Santos[137a,137c], S. Amoroso[44], C. S. Amrouche[52], C. Anastopoulos[146], L. S. Ancu[52], N. Andari[142], T. Andeen[11], C. F. Anders[59b], J. K. Anders[20], K. J. Anderson[36], A. Andreazza[66a,66b], V. Andrei[59a], C. R. Anelli[173], S. Angelidakis[37], I. Angelozzi[118], A. Angerami[38], A. V. Anisenkov[120a,120b], A. Annovi[69a], C. Antel[59a], M. T. Anthony[146], M. Antonelli[49], D. J. A. Antrim[168], F. Anulli[70a], M. Aoki[79], J. A. Aparisi Pozo[171], L. Aperio Bella[35], G. Arabidze[104], J. P. Araque[137a], V. Araujo Ferraz[78b], R. Araujo Pereira[78b], A. T. H. Arce[47], R. E. Ardell[91], F. A. Arduh[86], J.-F. Arguin[107], S. Argyropoulos[75], A. J. Armbruster[35], L. J. Armitage[90], A. Armstrong[168], O. Arnaez[164], H. Arnold[118],

M. Arratia[31], O. Arslan[24], A. Artamonov[109,*], G. Artoni[132], S. Artz[97], S. Asai[160], N. Asbah[57], E. M. Asimakopoulou[169], L. Asquith[153], K. Assamagan[29], R. Astalos[28a], R. J. Atkin[32a], M. Atkinson[170], N. B. Atlay[148], K. Augsten[139], G. Avolio[35], R. Avramidou[58a], M. K. Ayoub[15a], G. Azuelos[107,av], A. E. Baas[59a], M. J. Baca[21], H. Bachacou[142], K. Bachas[65a,65b], M. Backes[132], P. Bagnaia[70a,70b], M. Bahmani[82], H. Bahrasemani[149], A. J. Bailey[171], J. T. Baines[141], M. Bajic[39], C. Bakalis[10], O. K. Baker[180], P. J. Bakker[118], D. Bakshi Gupta[93], E. M. Baldin[120a,120b], P. Balek[177], F. Balli[142], W. K. Balunas[134], J. Balz[97], E. Banas[82], A. Bandyopadhyay[24], S. Banerjee[178,l], A. A. E. Bannoura[179], L. Barak[158], W. M. Barbe[37], E. L. Barberio[102], D. Barberis[53a,53b], M. Barbero[99], T. Barillari[113], M.-S. Barisits[35], J. Barkeloo[128], T. Barklow[150], R. Barnea[157], S. L. Barnes[58c], B. M. Barnett[141], R. M. Barnett[18], Z. Barnovska-Blenessy[58a], A. Baroncelli[72a], G. Barone[26], A. J. Barr[132], L. Barranco Navarro[171], F. Barreiro[96], J. Barreiro Guimarães da Costa[15a], R. Bartoldus[150], A. E. Barton[87], P. Bartos[28a], A. Basalaev[135], A. Bassalat[129], R. L. Bates[55], S. J. Batista[164], S. Batlamous[34e], J. R. Batley[31], M. Battaglia[143], M. Bauce[70a,70b], F. Bauer[142], K. T. Bauer[168], H. S. Bawa[150,n], J. B. Beacham[123], T. Beau[133], P. H. Beauchemin[167], P. Bechtle[24], H. C. Beck[51], H. P. Beck[20,s], K. Becker[50], M. Becker[97], C. Becot[44], A. Beddall[12d], A. J. Beddall[12a], V. A. Bednyakov[77], M. Bedognetti[118], C. P. Bee[152], T. A. Beermann[35], M. Begalli[78b], M. Begel[29], A. Behera[152], J. K. Behr[44], A. S. Bell[92], G. Bella[158], L. Bellagamba[23b], A. Bellerive[33], M. Bellomo[157], P. Bellos[9], K. Belotskiy[110], N. L. Belyaev[110], O. Benary[158,*], D. Benchekroun[34a], M. Bender[112], N. Benekos[10], Y. Benhammou[158], E. Benhar Noccioli[180], J. Benitez[75], D. P. Benjamin[47], M. Benoit[52], J. R. Bensinger[26], S. Bentvelsen[118], L. Beresford[132], M. Beretta[49], D. Berge[44], E. Bergeaas Kuutmann[169], N. Berger[5], L. J. Bergsten[26], J. Beringer[18], S. Berlendis[7], N. R. Bernard[100], G. Bernardi[133], C. Bernius[150], F. U. Bernlochner[24], T. Berry[91], P. Berta[97], C. Bertella[15a], G. Bertoli[43a,43b], I. A. Bertram[87], G. J. Besjes[39], O. Bessidskaia Bylund[179], M. Bessner[44], N. Besson[142], A. Bethani[98], S. Bethke[113], A. Betti[24], A. J. Bevan[90], J. Beyer[113], R. M. Bianchi[136], O. Biebel[112], D. Biedermann[19], R. Bielski[35], K. Bierwagen[97], N. V. Biesuz[69a,69b], M. Biglietti[72a], T. R. V. Billoud[107], M. Bindi[51], A. Bingul[12d], C. Bini[70a,70b], S. Biondi[23a,23b], M. Birman[177], T. Bisanz[51], J. P. Biswal[158], C. Bittrich[46], D. M. Bjergaard[47], J. E. Black[150], K. M. Black[25], T. Blazek[28a], I. Bloch[44], C. Blocker[26], A. Blue[55], U. Blumenschein[90], Dr. Blunier[144a], G. J. Bobbink[118], V. S. Bobrovnikov[120a,120b], S. S. Bocchetta[94], A. Bocci[47], D. Boerner[179], D. Bogavac[112], A. G. Bogdanchikov[120a,120b], C. Bohm[43a], V. Boisvert[91], P. Bokan[169], T. Bold[81a], A. S. Boldyrev[111], A. E. Bolz[59b], M. Bomben[133], M. Bona[90], J. S. Bonilla[128], M. Boonekamp[142], A. Borisov[121], G. Borissov[87], J. Bortfeldt[35], D. Bortoletto[132], V. Bortolotto[71a,71b], D. Boscherini[23b], M. Bosman[14], J. D. Bossio Sola[30], K. Bouaouda[34a], J. Boudreau[136], E. V. Bouhova-Thacker[87], D. Boumediene[37], C. Bourdarios[129], S. K. Boutle[55], A. Boveia[123], J. Boyd[35], D. Boye[32b], I. R. Boyko[77], A. J. Bozson[91], J. Bracinik[21], N. Brahimi[99], A. Brandt[8], G. Brandt[179], O. Brandt[59a], F. Braren[44], U. Bratzler[161], B. Brau[100], J. E. Brau[128], W. D. Breaden Madden[55], K. Brendlinger[44], L. Brenner[44], R. Brenner[169], S. Bressler[177], B. Brickwedde[97], D. L. Briglin[21], D. Britton[55], D. Britzger[59b], I. Brock[24], R. Brock[104], G. Brooijmans[38], T. Brooks[91], W. K. Brooks[144b], E. Brost[119], J. H Broughton[21], P. A. Bruckman de Renstrom[82], D. Bruncko[28b], A. Bruni[23b], G. Bruni[23b], L. S. Bruni[118], S. Bruno[71a,71b], B.H. Brunt[31], M. Bruschi[23b], N. Bruscino[136], P. Bryant[36], L. Bryngemark[44], T. Buanes[17], Q. Buat[35], P. Buchholz[148], A. G. Buckley[55], I. A. Budagov[77], M. K. Bugge[131], F. Bührer[50], O. Bulekov[110], D. Bullock[8], T. J. Burch[119], S. Burdin[88], C. D. Burgard[118], A. M. Burger[5], B. Burghgrave[119], K. Burka[82], S. Burke[141], I. Burmeister[45], J. T. P. Burr[132], V. Büscher[97], E. Buschmann[51], P. Bussey[55], J. M. Butler[25], C. M. Buttar[55], J. M. Butterworth[92], P. Butti[35], W. Buttinger[35], A. Buzatu[155], A. R. Buzykaev[120a,120b], G. Cabras[23a,23b], S. Cabrera Urbán[171], D. Caforio[139], H. Cai[170], V. M. M. Cairo[2], O. Cakir[4a], N. Calace[52], P. Calafiura[18], A. Calandri[99], G. Calderini[133], P. Calfayan[63], G. Callea[40a,40b], L. P. Caloba[78b], S. Calvente Lopez[96], D. Calvet[37], S. Calvet[37], T. P. Calvet[152], M. Calvetti[69a,69b], R. Camacho Toro[133], S. Camarda[35], P. Camarri[71a,71b], D. Cameron[131], R. Caminal Armadans[100], C. Camincher[35], S. Campana[35], M. Campanelli[92], A. Camplani[39], A. Campoverde[148], V. Canale[67a,67b], M. Cano Bret[58c], J. Cantero[126], T. Cao[158], Y. Cao[170], M. D. M. Capeans Garrido[35], I. Caprini[27b], M. Caprini[27b], M. Capua[40a,40b], R. M. Carbone[38], R. Cardarelli[71a], F. C. Cardillo[146], I. Carli[140], T. Carli[35], G. Carlino[67a], B. T. Carlson[136], L. Carminati[66a,66b], R. M. D. Carney[43a,43b], S. Caron[117], E. Carquin[144b], S. Carrá[66a,66b], G. D. Carrillo-Montoya[35], D. Casadei[32b], M. P. Casado[14,g], A. F. Casha[164], D. W. Casper[168], R. Castelijn[118], F. L. Castillo[171], V. Castillo Gimenez[171], N. F. Castro[137a,137e], A. Catinaccio[35], J. R. Catmore[131], A. Cattai[35], J. Caudron[24], V. Cavaliere[29], E. Cavallaro[14], D. Cavalli[66a], M. Cavalli-Sforza[14], V. Cavasinni[69a,69b], E. Celebi[12b], F. Ceradini[72a,72b], L. Cerda Alberich[171], A. S. Cerqueira[78a], A. Cerri[153], L. Cerrito[71a,71b], F. Cerutti[18], A. Cervelli[23a,23b], S. A. Cetin[12b], A. Chafaq[34a], D. Chakraborty[119], S. K. Chan[57], W. S. Chan[118], Y. L. Chan[61a], J. D. Chapman[31], B. Chargeishvili[156b], D. G. Charlton[21], C. C. Chau[33], C. A. Chavez Barajas[153], S. Che[123], A. Chegwidden[104], S. Chekanov[6], S. V. Chekulaev[165a], G. A. Chelkov[77,au], M. A. Chelstowska[35], C. Chen[58a], C. H. Chen[76], H. Chen[29], J. Chen[58a], J. Chen[38], S. Chen[134], S. J. Chen[15c], X. Chen[15b,at], Y. Chen[80], Y.-H. Chen[44], H. C. Cheng[103], H. J. Cheng[15d], A. Cheplakov[77], E. Cheremushkina[121], R. Cherkaoui El Moursli[34e], E. Cheu[7], K. Cheung[62], L. Chevalier[142], V. Chiarella[49], G. Chiarelli[69a], G. Chiodini[65a], A. S. Chisholm[35,21], A. Chitan[27b], I. Chiu[160],

Y. H. Chiu[173], M. V. Chizhov[77], K. Choi[63], A. R. Chomont[129], S. Chouridou[159], Y. S. Chow[118], V. Christodoulou[92], M. C. Chu[61a], J. Chudoba[138], A. J. Chuinard[101], J. J. Chwastowski[82], L. Chytka[127], D. Cinca[45], V. Cindro[89], I. A. Cioară[24], A. Ciocio[18], F. Cirotto[67a,67b], Z. H. Citron[177], M. Citterio[66a], A. Clark[52], M. R. Clark[38], P. J. Clark[48], C. Clement[43a,43b], Y. Coadou[99], M. Cobal[64a,64c], A. Coccaro[53a,53b], J. Cochran[76], H. Cohen[158], A. E. C. Coimbra[177], L. Colasurdo[117], B. Cole[38], A. P. Colijn[118], J. Collot[56], P. Conde Muiño[137a,i], E. Coniavitis[50], S. H. Connell[32b], I. A. Connelly[98], S. Constantinescu[27b], F. Conventi[67a,aw], A. M. Cooper-Sarkar[132], F. Cormier[172], K. J. R. Cormier[164], L. D. Corpe[92], M. Corradi[70a,70b], E. E. Corrigan[94], F. Corriveau[101,ae], A. Cortes-Gonzalez[35], M. J. Costa[171], F. Costanza[5], D. Costanzo[146], G. Cottin[31], G. Cowan[91], B. E. Cox[98], J. Crane[98], K. Cranmer[122], S. J. Crawley[55], R. A. Creager[134], G. Cree[33], S. Crépé-Renaudin[56], F. Crescioli[133], M. Cristinziani[24], V. Croft[122], G. Crosetti[40a,40b], A. Cueto[96], T. Cuhadar Donszelmann[146], A. R. Cukierman[150], S. Czekierda[82], P. Czodrowski[35], M. J. Da Cunha Sargedas De Sousa[58b], C. Da Via[98], W. Dabrowski[81a], T. Dado[28a,z], S. Dahbi[34e], T. Dai[103], F. Dallaire[107], C. Dallapiccola[100], M. Dam[39], G. D'amen[23a,23b], J. Damp[97], J. R. Dandoy[134], M. F. Daneri[30], N. P. Dang[178,l], N. D. Dann[98], M. Danninger[172], V. Dao[35], G. Darbo[53b], S. Darmora[8], O. Dartsi[5], A. Dattagupta[128], T. Daubney[44], S. D'Auria[55], W. Davey[24], C. David[44], T. Davidek[140], D. R. Davis[47], E. Dawe[102], I. Dawson[146], K. De[8], R. De Asmundis[67a], A. De Benedetti[125], M. De Beurs[118], S. De Castro[23a,23b], S. De Cecco[70a,70b], N. De Groot[117], P. de Jong[118], H. De la Torre[104], F. De Lorenzi[76], A. De Maria[51,u], D. De Pedis[70a], A. De Salvo[70a], U. De Sanctis[71a,71b], M. De Santis[71a,71b], A. De Santo[153], K. De Vasconcelos Corga[99], J. B. De Vivie De Regie[129], C. Debenedetti[143], D. V. Dedovich[77], N. Dehghanian[3], M. Del Gaudio[40a,40b], J. Del Peso[96], Y. Delabat Diaz[44], D. Delgove[129], F. Deliot[142], C. M. Delitzsch[7], M. Della Pietra[67a,67b], D. Della Volpe[52], A. Dell'Acqua[35], L. Dell'Asta[25], M. Delmastro[5], C. Delporte[129], P. A. Delsart[56], D. A. DeMarco[164], S. Demers[180], M. Demichev[77], S. P. Denisov[121], D. Denysiuk[118], L. D'Eramo[133], D. Derendarz[82], J. E. Derkaoui[34d], F. Derue[133], P. Dervan[88], K. Desch[24], C. Deterre[44], K. Dette[164], M. R. Devesa[30], P. O. Deviveiros[35], A. Dewhurst[141], S. Dhaliwal[26], F. A. Di Bello[52], A. Di Ciaccio[71a,71b], L. Di Ciaccio[5], W. K. Di Clemente[134], C. Di Donato[67a,67b], A. Di Girolamo[35], B. Di Micco[72a,72b], R. Di Nardo[100], K. F. Di Petrillo[57], R. Di Sipio[164], D. Di Valentino[33], C. Diaconu[99], M. Diamond[164], F. A. Dias[39], T. Dias Do Vale[137a], M. A. Diaz[144a], J. Dickinson[18], E. B. Diehl[103], J. Dietrich[19], S. Díez Cornell[44], A. Dimitrievska[18], J. Dingfelder[24], F. Dittus[35], F. Djama[99], T. Djobava[156b], J. I. Djuvsland[59a], M. A. B. Do Vale[78c], M. Dobre[27b], D. Dodsworth[26], C. Doglioni[94], J. Dolejsi[140], Z. Dolezal[140], M. Donadelli[78d], J. Donini[37], A. D'onofrio[90], M. D'Onofrio[88], J. Dopke[141], A. Doria[67a], M. T. Dova[86], A. T. Doyle[55], E. Drechsler[51], E. Dreyer[149], T. Dreyer[51], Y. Du[58b], F. Dubinin[108], M. Dubovsky[28a], A. Dubreuil[52], E. Duchovni[177], G. Duckeck[112], A. Ducourthial[133], O. A. Ducu[107,y], D. Duda[113], A. Dudarev[35], A. C. Dudder[97], E. M. Duffield[18], L. Duflot[129], M. Dührssen[35], C. Dülsen[179], M. Dumancic[177], A. E. Dumitriu[27b,e], A. K. Duncan[55], M. Dunford[59a], A. Duperrin[99], H. Duran Yildiz[4a], M. Düren[54], A. Durglishvili[156b], D. Duschinger[46], B. Dutta[44], D. Duvnjak[1], M. Dyndal[44], S. Dysch[98], B. S. Dziedzic[82], C. Eckardt[44], K. M. Ecker[113], R. C. Edgar[103], T. Eifert[35], G. Eigen[17], K. Einsweiler[18], T. Ekelof[169], M. El Kacimi[34c], R. El Kosseifi[99], V. Ellajosyula[99], M. Ellert[169], F. Ellinghaus[179], A. A. Elliot[90], N. Ellis[35], J. Elmsheuser[29], M. Elsing[35], D. Emeliyanov[141], Y. Enari[160], J. S. Ennis[175], M. B. Epland[47], J. Erdmann[45], A. Ereditato[20], S. Errede[170], M. Escalier[129], C. Escobar[171], O. Estrada Pastor[171], A. I. Etienvre[142], E. Etzion[158], H. Evans[63], A. Ezhilov[135], M. Ezzi[34e], F. Fabbri[55], L. Fabbri[23a,23b], V. Fabiani[117], G. Facini[92], R. M. Faisca Rodrigues Pereira[137a], R. M. Fakhrutdinov[121], S. Falciano[70a], P. J. Falke[5], S. Falke[5], J. Faltova[140], Y. Fang[15a], M. Fanti[66a,66b], A. Farbin[8], A. Farilla[72a], E. M. Farina[68a,68b], T. Farooque[104], S. Farrell[18], S. M. Farrington[175], P. Farthouat[35], F. Fassi[34e], P. Fassnacht[35], D. Fassouliotis[9], M. Faucci Giannelli[48], A. Favareto[53a,53b], W. J. Fawcett[31], L. Fayard[129], O. L. Fedin[135,q], W. Fedorko[172], M. Feickert[41], S. Feigl[131], L. Feligioni[99], C. Feng[58b], E. J. Feng[35], M. Feng[47], M. J. Fenton[55], A. B. Fenyuk[121], L. Feremenga[8], J. Ferrando[44], A. Ferrari[169], P. Ferrari[118], R. Ferrari[68a], D. E. Ferreira de Lima[59b], A. Ferrer[171], D. Ferrere[52], C. Ferretti[103], F. Fiedler[97], A. Filipčič[89], F. Filthaut[117], K. D. Finelli[25], M. C. N. Fiolhais[137a,137c,a], L. Fiorini[171], C. Fischer[14], W. C. Fisher[104], N. Flaschel[44], I. Fleck[148], P. Fleischmann[103], R. R. M. Fletcher[134], T. Flick[179], B. M. Flierl[112], L. M. Flores[134], L. R. Flores Castillo[61a], F. M. Follega[73a,73b], N. Fomin[17], G. T. Forcolin[98], A. Formica[142], F. A. Förster[14], A. C. Forti[98], A. G. Foster[21], D. Fournier[129], H. Fox[87], S. Fracchia[146], P. Francavilla[69a,69b], M. Franchini[23a,23b], S. Franchino[59a], D. Francis[35], L. Franconi[131], M. Franklin[57], M. Frate[168], M. Fraternali[68a,68b], A. N. Fray[90], D. Freeborn[92], S. M. Fressard-Batraneanu[35], B. Freund[107], W. S. Freund[78b], D. C. Frizzell[125], D. Froidevaux[35], J. A. Frost[132], C. Fukunaga[161], E. Fullana Torregrosa[171], T. Fusayasu[114], J. Fuster[171], O. Gabizon[157], A. Gabrielli[23a,23b], A. Gabrielli[18], G. P. Gach[81a], S. Gadatsch[52], P. Gadow[113], G. Gagliardi[53a,53b], L. G. Gagnon[107], C. Galea[27b], B. Galhardo[137a,137c], E. J. Gallas[132], B. J. Gallop[141], P. Gallus[139], G. Galster[39], R. Gamboa Goni[90], K. K. Gan[123], S. Ganguly[177], J. Gao[58a], Y. Gao[88], Y. S. Gao[150,n], C. García[171], J. E. García Navarro[171], J. A. García Pascual[15a], M. Garcia-Sciveres[18], R. W. Gardner[36], N. Garelli[150], V. Garonne[131], K. Gasnikova[44], A. Gaudiello[53a,53b], G. Gaudio[68a], I. L. Gavrilenko[108], A. Gavrilyuk[109], C. Gay[172], G. Gaycken[24], E. N. Gazis[10], C. N. P. Gee[141], J. Geisen[51], M. Geisen[97], M. P. Geisler[59a], K. Gellerstedt[43a,43b],

C. Gemme[53b], M. H. Genest[56], C. Geng[103], S. Gentile[70a,70b], S. George[91], D. Gerbaudo[14], G. Gessner[45], S. Ghasemi[148], M. Ghasemi Bostanabad[173], M. Ghneimat[24], B. Giacobbe[23b], S. Giagu[70a,70b], N. Giangiacomi[23a,23b], P. Giannetti[69a], A. Giannini[67a,67b], S. M. Gibson[91], M. Gignac[143], D. Gillberg[33], G. Gilles[179], D. M. Gingrich[3,av], M. P. Giordani[64a,64c], F. M. Giorgi[23b], P. F. Giraud[142], P. Giromini[57], G. Giugliarelli[64a,64c], D. Giugni[66a], F. Giuli[132], M. Giulini[59b], S. Gkaitatzis[159], I. Gkialas[9,k], E. L. Gkougkousis[14], P. Gkountoumis[10], L. K. Gladilin[111], C. Glasman[96], J. Glatzer[14], P. C. F. Glaysher[44], A. Glazov[44], M. Goblirsch-Kolb[26], J. Godlewski[82], S. Goldfarb[102], T. Golling[52], D. Golubkov[121], A. Gomes[137a,137b], R. Goncalves Gama[78a], R. Gonçalo[137a], G. Gonella[50], L. Gonella[21], A. Gongadze[77], F. Gonnella[21], J. L. Gonski[57], S. González de la Hoz[171], S. Gonzalez-Sevilla[52], L. Goossens[35], P. A. Gorbounov[109], H. A. Gordon[29], B. Gorini[35], E. Gorini[65a,65b], A. Gorišek[89], A. T. Goshaw[47], C. Gössling[45], M. I. Gostkin[77], C. A. Gottardo[24], C. R. Goudet[129], D. Goujdami[34c], A. G. Goussiou[145], N. Govender[32b,c], C. Goy[5], E. Gozani[157], I. Grabowska-Bold[81a], P. O. J. Gradin[169], E. C. Graham[88], J. Gramling[168], E. Gramstad[131], S. Grancagnolo[19], V. Gratchev[135], P. M. Gravila[27f], F. G. Gravili[65a,65b], C. Gray[55], H. M. Gray[18], Z. D. Greenwood[93,al], C. Grefe[24], K. Gregersen[94], I. M. Gregor[44], P. Grenier[150], K. Grevtsov[44], N. A. Grieser[125], J. Griffiths[8], A. A. Grillo[143], K. Grimm[150,b], S. Grinstein[14,aa], Ph. Gris[37], J.-F. Grivaz[129], S. Groh[97], E. Gross[177], J. Grosse-Knetter[51], G. C. Grossi[93], Z. J. Grout[92], C. Grud[103], A. Grummer[116], L. Guan[103], W. Guan[178], J. Guenther[35], A. Guerguichon[129], F. Guescini[165a], D. Guest[168], R. Gugel[50], B. Gui[123], T. Guillemin[5], S. Guindon[35], U. Gul[55], C. Gumpert[35], J. Guo[58c], W. Guo[103], Y. Guo[58a,t], Z. Guo[99], R. Gupta[41], S. Gurbuz[12c], G. Gustavino[125], B. J. Gutelman[157], P. Gutierrez[125], C. Gutschow[92], C. Guyot[142], M. P. Guzik[81a], C. Gwenlan[132], C. B. Gwilliam[88], A. Haas[122], C. Haber[18], H. K. Hadavand[8], N. Haddad[34e], A. Hadef[58a], S. Hageböck[24], M. Hagihara[166], H. Hakobyan[181,*], M. Haleem[174], J. Haley[126], G. Halladjian[104], G. D. Hallewell[99], K. Hamacher[179], P. Hamal[127], K. Hamano[173], A. Hamilton[32a], G. N. Hamity[146], K. Han[58a,ak], L. Han[58a], S. Han[15d], K. Hanagaki[79,w], M. Hance[143], D. M. Handl[112], B. Haney[134], R. Hankache[133], P. Hanke[59a], E. Hansen[94], J. B. Hansen[39], J. D. Hansen[39], M. C. Hansen[24], P. H. Hansen[39], K. Hara[166], A. S. Hard[178], T. Harenberg[179], S. Harkusha[105], P. F. Harrison[175], N. M. Hartmann[112], Y. Hasegawa[147], A. Hasib[48], S. Hassani[142], S. Haug[20], R. Hauser[104], L. Hauswald[46], L. B. Havener[38], M. Havranek[139], C. M. Hawkes[21], R. J. Hawkings[35], D. Hayden[104], C. Hayes[152], C. P. Hays[132], J. M. Hays[90], H. S. Hayward[88], S. J. Haywood[141], M. P. Heath[48], V. Hedberg[94], L. Heelan[8], S. Heer[24], K. K. Heidegger[50], J. Heilman[33], S. Heim[44], T. Heim[18], B. Heinemann[44,aq], J. J. Heinrich[112], L. Heinrich[122], C. Heinz[54], J. Hejbal[138], L. Helary[35], A. Held[172], S. Hellesund[131], S. Hellman[43a,43b], C. Helsens[35], R. C. W. Henderson[87], Y. Heng[178], S. Henkelmann[172], A. M. Henriques Correia[35], G. H. Herbert[19], H. Herde[26], V. Herget[174], Y. Hernández Jiménez[32c], H. Herr[97], M. G. Herrmann[112], G. Herten[50], R. Hertenberger[112], L. Hervas[35], T. C. Herwig[134], G. G. Hesketh[92], N. P. Hessey[165a], J. W. Hetherly[41], S. Higashino[79], E. Higón-Rodriguez[171], K. Hildebrand[36], E. Hill[173], J. C. Hill[31], K. K. Hill[29], K. H. Hiller[44], S. J. Hillier[21], M. Hils[46], I. Hinchliffe[18], M. Hirose[130], D. Hirschbuehl[179], B. Hiti[89], O. Hladik[138], D. R. Hlaluku[32c], X. Hoad[48], J. Hobbs[152], N. Hod[165a], M. C. Hodgkinson[146], A. Hoecker[35], M. R. Hoeferkamp[116], F. Hoenig[112], D. Hohn[24], D. Hohov[129], T. R. Holmes[36], M. Holzbock[112], M. Homann[45], S. Honda[166], T. Honda[79], T. M. Hong[136], A. Hönle[113], B. H. Hooberman[170], W. H. Hopkins[128], Y. Horii[115], P. Horn[46], A. J. Horton[149], L. A. Horyn[36], J.-Y. Hostachy[56], A. Hostiuc[145], S. Hou[155], A. Hoummada[34a], J. Howarth[98], J. Hoya[86], M. Hrabovsky[127], I. Hristova[19], J. Hrivnac[129], A. Hrynevich[106], T. Hryn'ova[5], P. J. Hsu[62], S.-C. Hsu[145], Q. Hu[29], S. Hu[58c], Y. Huang[15a], Z. Hubacek[139], F. Hubaut[99], M. Huebner[24], F. Huegging[24], T. B. Huffman[132], E. W. Hughes[38], M. Huhtinen[35], R. F. H. Hunter[33], P. Huo[152], A. M. Hupe[33], N. Huseynov[77,ag], J. Huston[104], J. Huth[57], R. Hyneman[103], G. Iacobucci[52], G. Iakovidis[29], I. Ibragimov[148], L. Iconomidou-Fayard[129], Z. Idrissi[34e], P. Iengo[35], R. Ignazzi[39], O. Igonkina[118,ac], R. Iguchi[160], T. Iizawa[52], Y. Ikegami[79], M. Ikeno[79], D. Iliadis[159], N. Ilic[117], F. Iltzsche[46], G. Introzzi[68a,68b], M. Iodice[72a], K. Iordanidou[38], V. Ippolito[70a,70b], M. F. Isacson[169], N. Ishijima[130], M. Ishino[160], M. Ishitsuka[162], W. Islam[126], C. Issever[132], S. Istin[157], F. Ito[166], J. M. Iturbe Ponce[61a], R. Iuppa[73a,73b], A. Ivina[177], H. Iwasaki[79], J. M. Izen[42], V. Izzo[67a], P. Jacka[138], P. Jackson[1], R. M. Jacobs[24], V. Jain[2], G. Jäkel[179], K. B. Jakobi[97], K. Jakobs[50], S. Jakobsen[74], T. Jakoubek[138], D. O. Jamin[126], D. K. Jana[93], R. Jansky[52], J. Janssen[24], M. Janus[51], P. A. Janus[81a], G. Jarlskog[94], N. Javadov[77,ag], T. Javůrek[35], M. Javurkova[50], F. Jeanneau[142], L. Jeanty[18], J. Jejelava[156a,ah], A. Jelinskas[175], P. Jenni[50,d], J. Jeong[44], N. Jeong[44], S. Jézéquel[5], H. Ji[178], J. Jia[152], H. Jiang[76], Y. Jiang[58a], Z. Jiang[150,r], S. Jiggins[50], F. A. Jimenez Morales[37], J. Jimenez Pena[171], S. Jin[15c], A. Jinaru[27b], O. Jinnouchi[162], H. Jivan[32c], P. Johansson[146], K. A. Johns[7], C. A. Johnson[63], W. J. Johnson[145], K. Jon-And[43a,43b], R. W. L. Jones[87], S. D. Jones[153], S. Jones[7], T. J. Jones[88], J. Jongmanns[59a], P. M. Jorge[137a,137b], J. Jovicevic[165a], X. Ju[18], J. J. Junggeburth[113], A. Juste Rozas[14,aa], A. Kaczmarska[82], M. Kado[129], H. Kagan[123], M. Kagan[150], T. Kaji[176], E. Kajomovitz[157], C. W. Kalderon[94], A. Kaluza[97], S. Kama[41], A. Kamenshchikov[121], L. Kanjir[89], Y. Kano[160], V. A. Kantserov[110], J. Kanzaki[79], B. Kaplan[122], L. S. Kaplan[178], D. Kar[32c], M. J. Kareem[165b], E. Karentzos[10], S. N. Karpov[77], Z. M. Karpova[77], V. Kartvelishvili[87], A. N. Karyukhin[121], L. Kashif[178], R. D. Kass[123], A. Kastanas[151], Y. Kataoka[160], C. Kato[58c,58d], J. Katzy[44], K. Kawade[80], K. Kawagoe[85], T. Kawamoto[160], G. Kawamura[51],

E. F. Kay[88], V. F. Kazanin[120a,120b], R. Keeler[173], R. Kehoe[41], J. S. Keller[33], E. Kellermann[94], J. J. Kempster[21], J. Kendrick[21], O. Kepka[138], S. Kersten[179], B. P. Kerševan[89], R. A. Keyes[101], M. Khader[170], F. Khalil-Zada[13], A. Khanov[126], A. G. Kharlamov[120a,120b], T. Kharlamova[120a,120b], E. E. Khoda[172], A. Khodinov[163], T. J. Khoo[52], E. Khramov[77], J. Khubua[156b], S. Kido[80], M. Kiehn[52], C. R. Kilby[91], Y. K. Kim[36], N. Kimura[64a,64c], O. M. Kind[19], B. T. King[88], D. Kirchmeier[46], J. Kirk[141], A. E. Kiryunin[113], T. Kishimoto[160], D. Kisielewska[81a], V. Kitali[44], O. Kivernyk[5], E. Kladiva[28b,*], T. Klapdor-Kleingrothaus[50], M. H. Klein[103], M. Klein[88], U. Klein[88], K. Kleinknecht[97], P. Klimek[119], A. Klimentov[29], R. Klingenberg[45,*], T. Klingl[24], T. Klioutchnikova[35], F. F. Klitzner[112], P. Kluit[118], S. Kluth[113], E. Kneringer[74], E. B. F. G. Knoops[99], A. Knue[50], A. Kobayashi[160], D. Kobayashi[85], T. Kobayashi[160], M. Kobel[46], M. Kocian[150], P. Kodys[140], P. T. Koenig[24], T. Koffas[33], E. Koffeman[118], N. M. Köhler[113], T. Koi[150], M. Kolb[59b], I. Koletsou[5], T. Kondo[79], N. Kondrashova[58c], K. Köneke[50], A. C. König[117], T. Kono[79], R. Konoplich[122,an], V. Konstantinides[92], N. Konstantinidis[92], B. Konya[94], R. Kopeliansky[63], S. Koperny[81a], K. Korcyl[82], K. Kordas[159], G. Koren[158], A. Korn[92], I. Korolkov[14], E. V. Korolkova[146], N. Korotkova[111], O. Kortner[113], S. Kortner[113], T. Kosek[140], V. V. Kostyukhin[24], A. Kotwal[47], A. Koulouris[10], A. Kourkoumeli-Charalampidi[68a,68b], C. Kourkoumelis[9], E. Kourlitis[146], V. Kouskoura[29], A. B. Kowalewska[82], R. Kowalewski[173], T. Z. Kowalski[81a], C. Kozakai[160], W. Kozanecki[142], A. S. Kozhin[121], V. A. Kramarenko[111], G. Kramberger[89], D. Krasnopevtsev[58a], M. W. Krasny[133], A. Krasznahorkay[35], D. Krauss[113], J. A. Kremer[81a], J. Kretzschmar[88], P. Krieger[164], K. Krizka[18], K. Kroeninger[45], H. Kroha[113], J. Kroll[138], J. Kroll[134], J. Krstic[16], U. Kruchonak[77], H. Krüger[24], N. Krumnack[76], M. C. Kruse[47], T. Kubota[102], S. Kuday[4b], J. T. Kuechler[179], S. Kuehn[35], A. Kugel[59a], F. Kuger[174], T. Kuhl[44], V. Kukhtin[77], R. Kukla[99], Y. Kulchitsky[105], S. Kuleshov[144b], Y. P. Kulinich[170], M. Kuna[56], T. Kunigo[83], A. Kupco[138], T. Kupfer[45], O. Kuprash[158], H. Kurashige[80], L. L. Kurchaninov[165a], Y. A. Kurochkin[105], M. G. Kurth[15d], E. S. Kuwertz[35], M. Kuze[162], J. Kvita[127], T. Kwan[101], A. La Rosa[113], J. L. La Rosa Navarro[78d], L. La Rotonda[40a,40b], F. La Ruffa[40a,40b], C. Lacasta[171], F. Lacava[70a,70b], J. Lacey[44], D. P. J. Lack[98], H. Lacker[19], D. Lacour[133], E. Ladygin[77], R. Lafaye[5], B. Laforge[133], T. Lagouri[32c], S. Lai[51], S. Lammers[63], W. Lampl[7], E. Lançon[29], U. Landgraf[50], M. P. J. Landon[90], M. C. Lanfermann[52], V. S. Lang[44], J. C. Lange[14], R. J. Langenberg[35], A. J. Lankford[168], F. Lanni[29], K. Lantzsch[24], A. Lanza[68a], A. Lapertosa[53a,53b], S. Laplace[133], J. F. Laporte[142], T. Lari[66a], F. Lasagni Manghi[23a,23b], M. Lassnig[35], T. S. Lau[61a], A. Laudrain[129], M. Lavorgna[67a,67b], A. T. Law[143], M. Lazzaroni[66a,66b], B. Le[102], O. Le Dortz[133], E. Le Guirriec[99], E. P. Le Quilleuc[142], M. LeBlanc[7], T. LeCompte[6], F. Ledroit-Guillon[56], C. A. Lee[29], G. R. Lee[144a], L. Lee[57], S. C. Lee[155], B. Lefebvre[101], M. Lefebvre[173], F. Legger[112], C. Leggett[18], K. Lehmann[149], N. Lehmann[179], G. Lehmann Miotto[35], W. A. Leight[44], A. Leisos[159,x], M. A. L. Leite[78d], R. Leitner[140], D. Lellouch[177], B. Lemmer[51], K. J. C. Leney[92], T. Lenz[24], B. Lenzi[35], R. Leone[7], S. Leone[69a], C. Leonidopoulos[48], G. Lerner[153], C. Leroy[107], R. Les[164], A. A. J. Lesage[142], C. G. Lester[31], M. Levchenko[135], J. Levêque[5], D. Levin[103], L. J. Levinson[177], D. Lewis[90], B. Li[103], C.-Q. Li[58a,am], H. Li[58b], L. Li[58c], Q. Li[15d], Q. Y. Li[58a], S. Li[58c,58d], X. Li[58c], Y. Li[148], Z. Liang[15a], B. Liberti[71a], A. Liblong[164], K. Lie[61c], S. Liem[118], A. Limosani[154], C. Y. Lin[31], K. Lin[104], T. H. Lin[97], R. A. Linck[63], J. H. Lindon[21], B. E. Lindquist[152], A. L. Lionti[52], E. Lipeles[134], A. Lipniacka[17], M. Lisovyi[59b], T. M. Liss[170,as], A. Lister[172], A. M. Litke[143], J. D. Little[8], B. Liu[76], B. L Liu[6], H. B. Liu[29], H. Liu[103], J. B. Liu[58a], J. K. K. Liu[132], K. Liu[133], M. Liu[58a], P. Liu[18], Y. Liu[15a], Y. L. Liu[58a], Y. W. Liu[58a], M. Livan[68a,68b], A. Lleres[56], J. Llorente Merino[15a], S. L. Lloyd[90], C. Y. Lo[61b], F. Lo Sterzo[41], E. M. Lobodzinska[44], P. Loch[7], T. Lohse[19], K. Lohwasser[146], M. Lokajicek[138], B. A. Long[25], J. D. Long[170], R. E. Long[87], L. Longo[65a,65b], K. A. Looper[123], J. A. Lopez[144b], I. Lopez Paz[14], A. Lopez Solis[146], J. Lorenz[112], N. Lorenzo Martinez[5], M. Losada[22], P. J. Lösel[112], A. Lösle[50], X. Lou[44], X. Lou[15a], A. Lounis[129], J. Love[6], P. A. Love[87], J. J. Lozano Bahilo[171], H. Lu[61a], M. Lu[58a], N. Lu[103], Y. J. Lu[62], H. J. Lubatti[145], C. Luci[70a,70b], A. Lucotte[56], C. Luedtke[50], F. Luehring[63], I. Luise[133], L. Luminari[70a], B. Lund-Jensen[151], M. S. Lutz[100], P. M. Luzi[133], D. Lynn[29], R. Lysak[138], E. Lytken[94], F. Lyu[15a], V. Lyubushkin[77], H. Ma[29], L. L. Ma[58b], Y. Ma[58b], G. Maccarrone[49], A. Macchiolo[113], C. M. Macdonald[146], J. Machado Miguens[134,137b], D. Madaffari[171], R. Madar[37], W. F. Mader[46], A. Madsen[44], N. Madysa[46], J. Maeda[80], K. Maekawa[160], S. Maeland[17], T. Maeno[29], A. S. Maevskiy[111], V. Magerl[50], C. Maidantchik[78b], T. Maier[112], A. Maio[137a,137b,137d], O. Majersky[28a], S. Majewski[128], Y. Makida[79], N. Makovec[129], B. Malaescu[133], Pa. Malecki[82], V. P. Maleev[135], F. Malek[56], U. Mallik[75], D. Malon[6], C. Malone[31], S. Maltezos[10], S. Malyukov[35], J. Mamuzic[171], G. Mancini[49], I. Mandić[89], J. Maneira[137a], L. Manhaes de Andrade Filho[78a], J. Manjarres Ramos[46], K. H. Mankinen[94], A. Mann[112], A. Manousos[74], B. Mansoulie[142], J. D. Mansour[15a], M. Mantoani[51], S. Manzoni[66a,66b], G. Marceca[30], L. March[52], L. Marchese[132], G. Marchiori[133], M. Marcisovsky[138], C. A. Marin Tobon[35], M. Marjanovic[37], D. E. Marley[103], F. Marroquim[78b], Z. Marshall[18], M. U. F Martensson[169], S. Marti-Garcia[171], C. B. Martin[123], T. A. Martin[175], V. J. Martin[48], B. Martin dit Latour[17], M. Martinez[14,aa], V. I. Martinez Outschoorn[100], S. Martin-Haugh[141], V. S. Martoiu[27b], A. C. Martyniuk[92], A. Marzin[35], L. Masetti[97], T. Mashimo[160], R. Mashinistov[108], J. Masik[98], A. L. Maslennikov[120a,120b], L. H. Mason[102], L. Massa[71a,71b], P. Massarotti[67a,67b], P. Mastrandrea[5], A. Mastroberardino[40a,40b], T. Masubuchi[160], P. Mättig[179], J. Maurer[27b],

B. Maček[89], S. J. Maxfield[88], D. A. Maximov[120a,120b], R. Mazini[155], I. Maznas[159], S. M. Mazza[143], N. C. Mc Fadden[116], G. Mc Goldrick[164], S. P. Mc Kee[103], A. McCarn[103], T. G. McCarthy[113], L. I. McClymont[92], E. F. McDonald[102], J. A. Mcfayden[35], G. Mchedlidze[51], M. A. McKay[41], K. D. McLean[173], S. J. McMahon[141], P. C. McNamara[102], C. J. McNicol[175], R. A. McPherson[173,ae], J. E. Mdhluli[32c], Z. A. Meadows[100], S. Meehan[145], T. M. Megy[50], S. Mehlhase[112], A. Mehta[88], T. Meideck[56], B. Meirose[42], D. Melini[171,h], B. R. Mellado Garcia[32c], J. D. Mellenthin[51], M. Melo[28a], F. Meloni[44], A. Melzer[24], S. B. Menary[98], E. D. Mendes Gouveia[137a], L. Meng[88], X. T. Meng[103], A. Mengarelli[23a,23b], S. Menke[113], E. Meoni[40a,40b], S. Mergelmeyer[19], C. Merlassino[20], P. Mermod[52], L. Merola[67a,67b], C. Meroni[66a], F. S. Merritt[36], A. Messina[70a,70b], J. Metcalfe[6], A. S. Mete[168], C. Meyer[134], J. Meyer[157], J.-P. Meyer[142], H. Meyer Zu Theenhausen[59a], F. Miano[153], R. P. Middleton[141], L. Mijović[48], G. Mikenberg[177], M. Mikestikova[138], M. Mikuž[89], M. Milesi[102], A. Milic[164], D. A. Millar[90], D. W. Miller[36], A. Milov[177], D. A. Milstead[43a,43b], A. A. Minaenko[121], M. Miñano Moya[171], I. A. Minashvili[156b], A. I. Mincer[122], B. Mindur[81a], M. Mineev[77], Y. Minegishi[160], Y. Ming[178], L. M. Mir[14], A. Mirto[65a,65b], K. P. Mistry[134], T. Mitani[176], J. Mitrevski[112], V. A. Mitsou[171], A. Miucci[20], P. S. Miyagawa[146], A. Mizukami[79], J. U. Mjörnmark[94], T. Mkrtchyan[181], M. Mlynarikova[140], T. Moa[43a,43b], K. Mochizuki[107], P. Mogg[50], S. Mohapatra[38], S. Molander[43a,43b], R. Moles-Valls[24], M. C. Mondragon[104], K. Mönig[44], J. Monk[39], E. Monnier[99], A. Montalbano[149], J. Montejo Berlingen[35], F. Monticelli[86], S. Monzani[66a], N. Morange[129], D. Moreno[22], M. Moreno Llácer[35], P. Morettini[53b], M. Morgenstern[118], S. Morgenstern[46], D. Mori[149], M. Morii[57], M. Morinaga[176], V. Morisbak[131], A. K. Morley[35], G. Mornacchi[35], A. P. Morris[92], J. D. Morris[90], L. Morvaj[152], P. Moschovakos[10], M. Mosidze[156b], H. J. Moss[146], J. Moss[150,o], K. Motohashi[162], R. Mount[150], E. Mountricha[35], E. J. W. Moyse[100], S. Muanza[99], F. Mueller[113], J. Mueller[136], R. S. P. Mueller[112], D. Muenstermann[87], G. A. Mullier[20], F. J. Munoz Sanchez[98], P. Murin[28b], W. J. Murray[141,175], A. Murrone[66a,66b], M. Muškinja[89], C. Mwewa[32a], A. G. Myagkov[121,ao], J. Myers[128], M. Myska[139], B. P. Nachman[18], O. Nackenhorst[45], K. Nagai[132], K. Nagano[79], Y. Nagasaka[60], M. Nagel[50], E. Nagy[99], A. M. Nairz[35], Y. Nakahama[115], K. Nakamura[79], T. Nakamura[160], I. Nakano[124], H. Nanjo[130], F. Napolitano[59a], R. F. Naranjo Garcia[44], R. Narayan[11], D. I. Narrias Villar[59a], I. Naryshkin[135], T. Naumann[44], G. Navarro[22], R. Nayyar[7], H. A. Neal[103,*], P. Y. Nechaeva[108], T. J. Neep[142], A. Negri[68a,68b], M. Negrini[23b], S. Nektarijevic[117], C. Nellist[51], M. E. Nelson[132], S. Nemecek[138], P. Nemethy[122], M. Nessi[35,f], M. S. Neubauer[170], M. Neumann[179], P. R. Newman[21], T. Y. Ng[61c], Y. S. Ng[19], H. D. N. Nguyen[99], T. Nguyen Manh[107], E. Nibigira[37], R. B. Nickerson[132], R. Nicolaidou[142], J. Nielsen[143], N. Nikiforou[11], V. Nikolaenko[121,ao], I. Nikolic-Audit[133], K. Nikolopoulos[21], P. Nilsson[29], Y. Ninomiya[79], A. Nisati[70a], N. Nishu[58c], R. Nisius[113], I. Nitsche[45], T. Nitta[176], T. Nobe[160], Y. Noguchi[83], M. Nomachi[130], I. Nomidis[133], M. A. Nomura[29], T. Nooney[90], M. Nordberg[35], N. Norjoharuddeen[132], T. Novak[89], O. Novgorodova[46], R. Novotny[139], L. Nozka[127], K. Ntekas[168], E. Nurse[92], F. Nuti[102], F. G. Oakham[33,av], H. Oberlack[113], T. Obermann[24], J. Ocariz[133], A. Ochi[80], I. Ochoa[38], J. P. Ochoa-Ricoux[144a], K. O'Connor[26], S. Oda[85], S. Odaka[79], S. Oerdek[51], A. Oh[98], S. H. Oh[47], C. C. Ohm[151], H. Oide[53a,53b], M. L. Ojeda[164], H. Okawa[166], Y. Okazaki[83], Y. Okumura[160], T. Okuyama[79], A. Olariu[27b], L. F. Oleiro Seabra[137a], S. A. Olivares Pino[144a], D. Oliveira Damazio[29], J. L. Oliver[1], M. J. R. Olsson[36], A. Olszewski[82], J. Olszowska[82], D. C. O'Neil[149], A. Onofre[137a,137e], K. Onogi[115], P. U. E. Onyisi[11], H. Oppen[131], M. J. Oreglia[36], G. E. Orellana[86], Y. Oren[158], D. Orestano[72a,72b], E. C. Orgill[98], N. Orlando[61b], A. A. O'Rourke[44], R. S. Orr[164], B. Osculati[53a,53b,*], V. O'Shea[55], R. Ospanov[58a], G. Otero y Garzon[30], H. Otono[85], M. Ouchrif[34d], F. Ould-Saada[131], A. Ouraou[142], Q. Ouyang[15a], M. Owen[55], R. E. Owen[21], V. E. Ozcan[12c], N. Ozturk[8], J. Pacalt[127], H. A. Pacey[31], K. Pachal[149], A. Pacheco Pages[14], L. Pacheco Rodriguez[142], C. Padilla Aranda[14], S. Pagan Griso[18], M. Paganini[180], G. Palacino[63], S. Palazzo[40a,40b], S. Palestini[35], M. Palka[81b], D. Pallin[37], I. Panagoulias[10], C. E. Pandini[35], J. G. Panduro Vazquez[91], P. Pani[35], G. Panizzo[64a,64c], L. Paolozzi[52], T. D. Papadopoulou[10], K. Papageorgiou[9,k], A. Paramonov[6], D. Paredes Hernandez[61b], S. R. Paredes Saenz[132], B. Parida[163], A. J. Parker[87], K. A. Parker[44], M. A. Parker[31], F. Parodi[53a,53b], J. A. Parsons[38], U. Parzefall[50], V. R. Pascuzzi[164], J. M. P. Pasner[143], E. Pasqualucci[70a], S. Passaggio[53b], F. Pastore[91], P. Pasuwan[43a,43b], S. Pataraia[97], J. R. Pater[98], A. Pathak[178,l], T. Pauly[35], B. Pearson[113], M. Pedersen[131], L. Pedraza Diaz[117], R. Pedro[137a,137b], S. V. Peleganchuk[120a,120b], O. Penc[138], C. Peng[15d], H. Peng[58a], B. S. Peralva[78a], M. M. Perego[142], A. P. Pereira Peixoto[137a], D. V. Perepelitsa[29], F. Peri[19], L. Perini[66a,66b], H. Pernegger[35], S. Perrella[67a,67b], V. D. Peshekhonov[77,*], K. Peters[44], R. F. Y. Peters[98], B. A. Petersen[35], T. C. Petersen[39], E. Petit[56], A. Petridis[1], C. Petridou[159], P. Petroff[129], M. Petrov[132], F. Petrucci[72a,72b], M. Pettee[180], N. E. Pettersson[100], A. Peyaud[142], R. Pezoa[144b], T. Pham[102], F. H. Phillips[104], P. W. Phillips[141], M. W. Phipps[170], G. Piacquadio[152], E. Pianori[18], A. Picazio[100], M. A. Pickering[132], R. H. Pickles[98], R. Piegaia[30], J. E. Pilcher[36], A. D. Pilkington[98], M. Pinamonti[71a,71b], J. L. Pinfold[3], M. Pitt[177], M.-A. Pleier[29], V. Pleskot[140], E. Plotnikova[77], D. Pluth[76], P. Podberezko[120a,120b], R. Poettgen[94], R. Poggi[52], L. Poggioli[129], I. Pogrebnyak[104], D. Pohl[24], I. Pokharel[51], G. Polesello[68a], A. Poley[18], A. Policicchio[70a,70b], R. Polifka[35], A. Polini[23b], C. S. Pollard[44], V. Polychronakos[29], D. Ponomarenko[110], L. Pontecorvo[35], G. A. Popeneciu[27d], D. M. Portillo Quintero[133], S. Pospisil[139], K. Potamianos[44], I. N. Potrap[77], C. J. Potter[31], H. Potti[11], T. Poulsen[94],

J. Poveda[35], T. D. Powell[146], M. E. Pozo Astigarraga[35], P. Pralavorio[99], S. Prell[76], D. Price[98], M. Primavera[65a], S. Prince[101], N. Proklova[110], K. Prokofiev[61c], F. Prokoshin[144b], S. Protopopescu[29], J. Proudfoot[6], M. Przybycien[81a], A. Puri[170], P. Puzo[129], J. Qian[103], Y. Qin[98], A. Quadt[51], M. Queitsch-Maitland[44], A. Qureshi[1], P. Rados[102], F. Ragusa[66a,66b], G. Rahal[95], J. A. Raine[52], S. Rajagopalan[29], A. Ramirez Morales[90], T. Rashid[129], S. Raspopov[5], M. G. Ratti[66a,66b], D. M. Rauch[44], F. Rauscher[112], S. Rave[97], B. Ravina[146], I. Ravinovich[177], J. H. Rawling[98], M. Raymond[35], A. L. Read[131], N. P. Readioff[56], M. Reale[65a,65b], D. M. Rebuzzi[68a,68b], A. Redelbach[174], G. Redlinger[29], R. Reece[143], R. G. Reed[32c], K. Reeves[42], L. Rehnisch[19], J. Reichert[134], D. Reikher[158], A. Reiss[97], C. Rembser[35], H. Ren[15d], M. Rescigno[70a], S. Resconi[66a], E. D. Resseguie[134], S. Rettie[172], E. Reynolds[21], O. L. Rezanova[120a,120b], P. Reznicek[140], E. Ricci[73a,73b], R. Richter[113], S. Richter[44], E. Richter-Was[81b], O. Ricken[24], M. Ridel[133], P. Rieck[113], C. J. Riegel[179], O. Rifki[44], M. Rijssenbeek[152], A. Rimoldi[68a,68b], M. Rimoldi[20], L. Rinaldi[23b], G. Ripellino[151], B. Ristić[87], E. Ritsch[35], I. Riu[14], J. C. Rivera Vergara[144a], F. Rizatdinova[126], E. Rizvi[90], C. Rizzi[14], R. T. Roberts[98], S. H. Robertson[101,ae], D. Robinson[31], J. E. M. Robinson[44], A. Robson[55], E. Rocco[97], C. Roda[69a,69b], Y. Rodina[99], S. Rodriguez Bosca[171], A. Rodriguez Perez[14], D. Rodriguez Rodriguez[171], A. M. Rodríguez Vera[165b], S. Roe[35], C. S. Rogan[57], O. Røhne[131], R. Röhrig[113], C. P. A. Roland[63], J. Roloff[57], A. Romaniouk[110], M. Romano[23a,23b], N. Rompotis[88], M. Ronzani[122], L. Roos[133], S. Rosati[70a], K. Rosbach[50], P. Rose[143], N.-A. Rosien[51], E. Rossi[44], E. Rossi[67a,67b], L. P. Rossi[53b], L. Rossini[66a,66b], J. H. N. Rosten[31], R. Rosten[14], M. Rotaru[27b], J. Rothberg[145], D. Rousseau[129], D. Roy[32c], A. Rozanov[99], Y. Rozen[157], X. Ruan[32c], F. Rubbo[150], F. Rühr[50], A. Ruiz-Martinez[171], Z. Rurikova[50], N. A. Rusakovich[77], H. L. Russell[101], J. P. Rutherfoord[7], E. M. Rüttinger[44,m], Y. F. Ryabov[135], M. Rybar[170], G. Rybkin[129], S. Ryu[6], A. Ryzhov[121], G. F. Rzehorz[51], P. Sabatini[51], G. Sabato[118], S. Sacerdoti[129], H. F.-W. Sadrozinski[143], R. Sadykov[77], F. Safai Tehrani[70a], P. Saha[119], M. Sahinsoy[59a], A. Sahu[179], M. Saimpert[44], M. Saito[160], T. Saito[160], H. Sakamoto[160], A. Sakharov[122,an], D. Salamani[52], G. Salamanna[72a,72b], J. E. Salazar Loyola[144b], D. Salek[118], P. H. Sales De Bruin[169], D. Salihagic[113], A. Salnikov[150], J. Salt[171], D. Salvatore[40a,40b], F. Salvatore[153], A. Salvucci[61a,61b,61c], A. Salzburger[35], J. Samarati[35], D. Sammel[50], D. Sampsonidis[159], D. Sampsonidou[159], J. Sánchez[171], A. Sanchez Pineda[64a,64c], H. Sandaker[131], C. O. Sander[44], M. Sandhoff[179], C. Sandoval[22], D. P. C. Sankey[141], M. Sannino[53a,53b], Y. Sano[115], A. Sansoni[49], C. Santoni[37], H. Santos[137a], I. Santoyo Castillo[153], A. Santra[171], A. Sapronov[77], J. G. Saraiva[137a,137d], O. Sasaki[79], K. Sato[166], E. Sauvan[5], P. Savard[164,av], N. Savic[113], R. Sawada[160], C. Sawyer[141], L. Sawyer[93,al], C. Sbarra[23b], A. Sbrizzi[23a], T. Scanlon[92], J. Schaarschmidt[145], P. Schacht[113], B. M. Schachtner[112], D. Schaefer[36], L. Schaefer[134], J. Schaeffer[97], S. Schaepe[35], U. Schäfer[97], A. C. Schaffer[129], D. Schaile[112], R. D. Schamberger[152], N. Scharmberg[98], V. A. Schegelsky[135], D. Scheirich[140], F. Schenck[19], M. Schernau[168], C. Schiavi[53a,53b], S. Schier[143], L. K. Schildgen[24], Z. M. Schillaci[26], E. J. Schioppa[35], M. Schioppa[40a,40b], K. E. Schleicher[50], S. Schlenker[35], K. R. Schmidt-Sommerfeld[113], K. Schmieden[35], C. Schmitt[97], S. Schmitt[44], S. Schmitz[97], J. C. Schmoeckel[44], U. Schnoor[50], L. Schoeffel[142], A. Schoening[59b], E. Schopf[24], M. Schott[97], J. F. P. Schouwenberg[117], J. Schovancova[35], S. Schramm[52], A. Schulte[97], H.-C. Schultz-Coulon[59a], M. Schumacher[50], B. A. Schumm[143], Ph. Schune[142], A. Schwartzman[150], T. A. Schwarz[103], Ph. Schwemling[142], R. Schwienhorst[104], A. Sciandra[24], G. Sciolla[26], M. Scornajenghi[40a,40b], F. Scuri[69a], F. Scutti[102], L. M. Scyboz[113], J. Searcy[103], C. D. Sebastiani[70a,70b], P. Seema[19], S. C. Seidel[116], A. Seiden[143], T. Seiss[36], J. M. Seixas[78b], G. Sekhniaidze[67a], K. Sekhon[103], S. J. Sekula[41], N. Semprini-Cesari[23a,23b], S. Sen[47], S. Senkin[37], C. Serfon[131], L. Serin[129], L. Serkin[64a,64b], M. Sessa[58a], H. Severini[125], F. Sforza[167], A. Sfyrla[52], E. Shabalina[51], J. D. Shahinian[143], N. W. Shaikh[43a,43b], L. Y. Shan[15a], R. Shang[170], J. T. Shank[25], M. Shapiro[18], A. S. Sharma[1], A. Sharma[132], P. B. Shatalov[109], K. Shaw[153], S. M. Shaw[98], A. Shcherbakova[135], Y. Shen[125], N. Sherafati[33], A. D. Sherman[25], P. Sherwood[92], L. Shi[155,ar], S. Shimizu[79], C. O. Shimmin[180], M. Shimojima[114], I. P. J. Shipsey[132], S. Shirabe[85], M. Shiyakova[77], J. Shlomi[177], A. Shmeleva[108], D. Shoaleh Saadi[107], M. J. Shochet[36], S. Shojaii[102], D. R. Shope[125], S. Shrestha[123], E. Shulga[110], P. Sicho[138], A. M. Sickles[170], P. E. Sidebo[151], E. Sideras Haddad[32c], O. Sidiropoulou[35], A. Sidoti[23a,23b], F. Siegert[46], Dj. Sijacki[16], J. Silva[137a], M. Silva Jr.[178], M. V. Silva Oliveira[78a], S. B. Silverstein[43a], L. Simic[77], S. Simion[129], E. Simioni[97], M. Simon[97], R. Simoniello[97], P. Sinervo[164], N. B. Sinev[128], M. Sioli[23a,23b], G. Siragusa[174], I. Siral[103], S. Yu. Sivoklokov[111], J. Sjölin[43a,43b], P. Skubic[125], M. Slater[21], T. Slavicek[139], M. Slawinska[82], K. Sliwa[167], R. Slovak[140], V. Smakhtin[177], B. H. Smart[5], J. Smiesko[28a], N. Smirnov[110], S. Yu. Smirnov[110], Y. Smirnov[110], L. N. Smirnova[111], O. Smirnova[94], J. W. Smith[51], M. N. K. Smith[38], M. Smizanska[87], K. Smolek[139], A. Smykiewicz[82], A. A. Snesarev[108], I. M. Snyder[128], S. Snyder[29], R. Sobie[173,ae], A. M. Soffa[168], A. Soffer[158], A. Søgaard[48], D. A. Soh[155], G. Sokhrannyi[89], C. A. Solans Sanchez[35], M. Solar[139], E. Yu. Soldatov[110], U. Soldevila[171], A. A. Solodkov[121], A. Soloshenko[77], O. V. Solovyanov[121], V. Solovyev[135], P. Sommer[146], H. Son[167], W. Song[141], W. Y. Song[165b], A. Sopczak[139], F. Sopkova[28b], C. L. Sotiropoulou[69a,69b], S. Sottocornola[68a,68b], R. Soualah[64a,64c,j], A. M. Soukharev[120a,120b], D. South[44], B. C. Sowden[91], S. Spagnolo[65a,65b], M. Spalla[113], M. Spangenberg[175], F. Spanò[91], D. Sperlich[19], F. Spettel[113], T. M. Spieker[59a], R. Spighi[23b], G. Spigo[35], L. A. Spiller[102], D. P. Spiteri[55],

M. Spousta[140], A. Stabile[66a,66b], R. Stamen[59a], S. Stamm[19], E. Stanecka[82], R. W. Stanek[6], C. Stanescu[72a], B. Stanislaus[132], M. M. Stanitzki[44], B. Stapf[118], S. Stapnes[131], E. A. Starchenko[121], G. H. Stark[36], J. Stark[56], S. H Stark[39], P. Staroba[138], P. Starovoitov[59a], S. Stärz[35], R. Staszewski[82], M. Stegler[44], P. Steinberg[29], B. Stelzer[149], H. J. Stelzer[35], O. Stelzer-Chilton[165a], H. Stenzel[54], T. J. Stevenson[90], G. A. Stewart[35], M. C. Stockton[128], G. Stoicea[27b], P. Stolte[51], S. Stonjek[113], A. Straessner[46], J. Strandberg[151], S. Strandberg[43a,43b], M. Strauss[125], P. Strizenec[28b], R. Ströhmer[174], D. M. Strom[128], R. Stroynowski[41], A. Strubig[48], S. A. Stucci[29], B. Stugu[17], J. Stupak[125], N. A. Styles[44], D. Su[150], J. Su[136], S. Suchek[59a], Y. Sugaya[130], M. Suk[139], V. V. Sulin[108], D. M. S. Sultan[52], S. Sultansoy[4c], T. Sumida[83], S. Sun[103], X. Sun[3], K. Suruliz[153], C. J. E. Suster[154], M. R. Sutton[153], S. Suzuki[79], M. Svatos[138], M. Swiatlowski[36], S. P. Swift[2], A. Sydorenko[97], I. Sykora[28a], T. Sykora[140], D. Ta[97], K. Tackmann[44,ab], J. Taenzer[158], A. Taffard[168], R. Tafirout[165a], E. Tahirovic[90], N. Taiblum[158], H. Takai[29], R. Takashima[84], E. H. Takasugi[113], K. Takeda[80], T. Takeshita[147], Y. Takubo[79], M. Talby[99], A. A. Talyshev[120a,120b], J. Tanaka[160], M. Tanaka[162], R. Tanaka[129], B. B. Tannenwald[123], S. Tapia Araya[144b], S. Tapprogge[97], A. Tarek Abouelfadl Mohamed[133], S. Tarem[157], G. Tarna[27b,e], G. F. Tartarelli[66a], P. Tas[140], M. Tasevsky[138], T. Tashiro[83], E. Tassi[40a,40b], A. Tavares Delgado[137a,137b], Y. Tayalati[34e], A. C. Taylor[116], A. J. Taylor[48], G. N. Taylor[102], P. T. E. Taylor[102], W. Taylor[165b], A. S. Tee[87], P. Teixeira-Dias[91], H. Ten Kate[35], P. K. Teng[155], J. J. Teoh[118], S. Terada[79], K. Terashi[160], J. Terron[96], S. Terzo[14], M. Testa[49], R. J. Teuscher[164,ae], S. J. Thais[180], T. Theveneaux-Pelzer[44], F. Thiele[39], D. W. Thomas[91], J. P. Thomas[21], A. S. Thompson[55], P. D. Thompson[21], L. A. Thomsen[180], E. Thomson[134], Y. Tian[38], R. E. Ticse Torres[51], V. O. Tikhomirov[108,ap], Yu. A. Tikhonov[120a,120b], S. Timoshenko[110], P. Tipton[180], S. Tisserant[99], K. Todome[162], S. Todorova-Nova[5], S. Todt[46], J. Tojo[85], S. Tokár[28a], K. Tokushuku[79], E. Tolley[123], K. G. Tomiwa[32c], M. Tomoto[115], L. Tompkins[150,r], K. Toms[116], B. Tong[57], P. Tornambe[50], E. Torrence[128], H. Torres[46], E. Torró Pastor[145], C. Tosciri[132], J. Toth[99,ad], F. Touchard[99], D. R. Tovey[146], C. J. Treado[122], T. Trefzger[174], F. Tresoldi[153], A. Tricoli[29], I. M. Trigger[165a], S. Trincaz-Duvoid[133], M. F. Tripiana[14], W. Trischuk[164], B. Trocmé[56], A. Trofymov[129], C. Troncon[66a], M. Trovatelli[173], F. Trovato[153], L. Truong[32b], M. Trzebinski[82], A. Trzupek[82], F. Tsai[44], J. C.-L. Tseng[132], P. V. Tsiareshka[105], A. Tsirigotis[159], N. Tsirintanis[9], V. Tsiskaridze[152], E. G. Tskhadadze[156a], I. I. Tsukerman[109], V. Tsulaia[18], S. Tsuno[79], D. Tsybychev[152,163], Y. Tu[61b], A. Tudorache[27b], V. Tudorache[27b], T. T. Tulbure[27a], A. N. Tuna[57], S. Turchikhin[77], D. Turgeman[177], I. Turk Cakir[4b,v], R. Turra[66a], P. M. Tuts[38], E. Tzovara[97], G. Ucchielli[23a,23b], I. Ueda[79], M. Ughetto[43a,43b], F. Ukegawa[166], G. Unal[35], A. Undrus[29], G. Unel[168], F. C. Ungaro[102], Y. Unno[79], K. Uno[160], J. Urban[28b], P. Urquijo[102], P. Urrejola[97], G. Usai[8], J. Usui[79], L. Vacavant[99], V. Vacek[139], B. Vachon[101], K. O. H. Vadla[131], A. Vaidya[92], C. Valderanis[112], E. Valdes Santurio[43a,43b], M. Valente[52], S. Valentinetti[23a,23b], A. Valero[171], L. Valéry[44], R. A. Vallance[21], A. Vallier[5], J. A. Valls Ferrer[171], T. R. Van Daalen[14], H. Van der Graaf[118], P. Van Gemmeren[6], J. Van Nieuwkoop[149], I. Van Vulpen[118], M. Vanadia[71a,71b], W. Vandelli[35], A. Vaniachine[163], P. Vankov[118], R. Vari[70a], E. W. Varnes[7], C. Varni[53a,53b], T. Varol[41], D. Varouchas[129], K. E. Varvell[154], G. A. Vasquez[144b], J. G. Vasquez[180], F. Vazeille[37], D. Vazquez Furelos[14], T. Vazquez Schroeder[101], J. Veatch[51], V. Vecchio[72a,72b], L. M. Veloce[164], F. Veloso[137a,137c], S. Veneziano[70a], A. Ventura[65a,65b], M. Venturi[173], N. Venturi[35], V. Vercesi[68a], M. Verducci[72a,72b], C. M. Vergel Infante[76], C. Vergis[24], W. Verkerke[118], A. T. Vermeulen[118], J. C. Vermeulen[118], M. C. Vetterli[149,av], N. Viaux Maira[144b], M. Vicente Barreto Pinto[52], I. Vichou[170,*], T. Vickey[146], O. E. Vickey Boeriu[146], G. H. A. Viehhauser[132], S. Viel[18], L. Vigani[132], M. Villa[23a,23b], M. Villaplana Perez[66a,66b], E. Vilucchi[49], M. G. Vincter[33], V. B. Vinogradov[77], A. Vishwakarma[44], C. Vittori[23a,23b], I. Vivarelli[153], S. Vlachos[10], M. Vogel[179], P. Vokac[139], G. Volpi[14], S. E. Von Buddenbrock[32c], E. von Toerne[24], V. Vorobel[140], K. Vorobev[110], M. Vos[171], J. H. Vossebeld[88], N. Vranjes[16], M. Vranjes Milosavljevic[16], V. Vrba[139], M. Vreeswijk[118], T. Šfiligoj[89], R. Vuillermet[35], I. Vukotic[36], T. Ženiš[28a], L. Živković[16], P. Wagner[24], W. Wagner[179], J. Wagner-Kuhr[112], H. Wahlberg[86], S. Wahrmund[46], K. Wakamiya[80], V. M. Walbrecht[113], J. Walder[87], R. Walker[112], S. D. Walker[91], W. Walkowiak[148], V. Wallangen[43a,43b], A. M. Wang[57], C. Wang[58b,e], F. Wang[178], H. Wang[18], H. Wang[3], J. Wang[154], J. Wang[59b], P. Wang[41], Q. Wang[125], R.-J. Wang[133], R. Wang[58a], R. Wang[6], S. M. Wang[155], T. Wang[58a], W. Wang[15c,af], W. X. Wang[58a,af], Y. Wang[58a,am], Z. Wang[58c], C. Wanotayaroj[44], A. Warburton[101], C. P. Ward[31], D. R. Wardrope[92], A. Washbrook[48], P. M. Watkins[21], A. T. Watson[21], M. F. Watson[21], G. Watts[145], S. Watts[98], B. M. Waugh[92], A. F. Webb[11], S. Webb[97], C. Weber[180], M. S. Weber[20], S. A. Weber[33], S. M. Weber[59a], A. R. Weidberg[132], B. Weinert[63], J. Weingarten[45], M. Weirich[97], C. Weiser[50], P. S. Wells[35], T. Wenaus[29], T. Wengler[35], S. Wenig[35], N. Wermes[24], M. D. Werner[76], P. Werner[35], M. Wessels[59a], T. D. Weston[20], K. Whalen[128], N. L. Whallon[145], A. M. Wharton[87], A. S. White[103], A. White[8], M. J. White[1], R. White[144b], D. Whiteson[168], B. W. Whitmore[87], F. J. Wickens[141], W. Wiedenmann[178], M. Wielers[141], C. Wiglesworth[39], L. A. M. Wiik-Fuchs[50], A. Wildauer[113], F. Wilk[98], H. G. Wilkens[35], L. J. Wilkins[91], H. H. Williams[134], S. Williams[31], C. Willis[104], S. Willocq[100], J. A. Wilson[21], I. Wingerter-Seez[5], E. Winkels[153], F. Winklmeier[128], O. J. Winston[153], B. T. Winter[24], M. Wittgen[150], M. Wobisch[93], A. Wolf[97], T. M. H. Wolf[118], R. Wolff[99], M. W. Wolter[82], H. Wolters[137a,137c], V. W. S. Wong[172], N. L. Woods[143], S. D. Worm[21], B. K. Wosiek[82], K. W. Woźniak[82], K. Wraight[55], M. Wu[36], S. L. Wu[178],

X. Wu[52], Y. Wu[58a], T. R. Wyatt[98], B. M. Wynne[48], S. Xella[39], Z. Xi[103], L. Xia[175], D. Xu[15a], H. Xu[58a,e], L. Xu[29], T. Xu[142], W. Xu[103], B. Yabsley[154], S. Yacoob[32a], K. Yajima[130], D. P. Yallup[92], D. Yamaguchi[162], Y. Yamaguchi[162], A. Yamamoto[79], T. Yamanaka[160], F. Yamane[80], M. Yamatani[160], T. Yamazaki[160], Y. Yamazaki[80], Z. Yan[25], H. J. Yang[58c,58d], H. T. Yang[18], S. Yang[75], Y. Yang[160], Z. Yang[17], W-M. Yao[18], Y. C. Yap[44], Y. Yasu[79], E. Yatsenko[58c,58d], J. Ye[41], S. Ye[29], I. Yeletskikh[77], E. Yigitbasi[25], E. Yildirim[97], K. Yorita[176], K. Yoshihara[134], C. J. S. Young[35], C. Young[150], J. Yu[8], J. Yu[76], X. Yue[59a], S. P. Y. Yuen[24], B. Zabinski[82], G. Zacharis[10], E. Zaffaroni[52], R. Zaidan[14], A. M. Zaitsev[121,ao], T. Zakareishvili[156b], N. Zakharchuk[33], J. Zalieckas[17], S. Zambito[57], D. Zanzi[35], D. R. Zaripovas[55], S. V. Zeißner[45], C. Zeitnitz[179], G. Zemaityte[132], J. C. Zeng[170], Q. Zeng[150], O. Zenin[121], D. Zerwas[129], M. Zgubič[132], D. F. Zhang[58b], D. Zhang[103], F. Zhang[178], G. Zhang[58a], H. Zhang[15c], J. Zhang[6], L. Zhang[15c], L. Zhang[58a], M. Zhang[170], P. Zhang[15c], R. Zhang[58a], R. Zhang[24], X. Zhang[58b], Y. Zhang[15d], Z. Zhang[129], P. Zhao[47], X. Zhao[41], Y. Zhao[58b,129,ak], Z. Zhao[58a], A. Zhemchugov[77], B. Zhou[103], C. Zhou[178], L. Zhou[41], M. S. Zhou[15d], M. Zhou[152], N. Zhou[58c], Y. Zhou[7], C. G. Zhu[58b], H. L. Zhu[58a], H. Zhu[15a], J. Zhu[103], Y. Zhu[58a], X. Zhuang[15a], K. Zhukov[108], V. Zhulanov[120a,120b], A. Zibell[174], D. Zieminska[63], N. I. Zimine[77], S. Zimmermann[50], Z. Zinonos[113], M. Zinser[97], M. Ziolkowski[148], G. Zobernig[178], A. Zoccoli[23a,23b], K. Zoch[51], T. G. Zorbas[146], R. Zou[36], M. Zur Nedden[19], L. Zwalinski[35]

[1] Department of Physics, University of Adelaide, Adelaide, Australia
[2] Physics Department, SUNY Albany, Albany, NY, USA
[3] Department of Physics, University of Alberta, Edmonton, AB, Canada
[4] [(a)]Department of Physics, Ankara University, Ankara, Turkey; [(b)]Istanbul Aydin University, Istanbul, Turkey; [(c)]Division of Physics, TOBB University of Economics and Technology, Ankara, Turkey
[5] LAPP, Université Grenoble Alpes, Université Savoie Mont Blanc, CNRS/IN2P3, Annecy, France
[6] High Energy Physics Division, Argonne National Laboratory, Argonne, IL, USA
[7] Department of Physics, University of Arizona, Tucson, AZ, USA
[8] Department of Physics, University of Texas at Arlington, Arlington, TX, USA
[9] Physics Department, National and Kapodistrian University of Athens, Athens, Greece
[10] Physics Department, National Technical University of Athens, Zografou, Greece
[11] Department of Physics, University of Texas at Austin, Austin, TX, USA
[12] [(a)]Faculty of Engineering and Natural Sciences, Bahcesehir University, Istanbul, Turkey; [(b)]Faculty of Engineering and Natural Sciences, Istanbul Bilgi University, Istanbul, Turkey; [(c)]Department of Physics, Bogazici University, Istanbul, Turkey; [(d)]Department of Physics Engineering, Gaziantep University, Gaziantep, Turkey
[13] Institute of Physics, Azerbaijan Academy of Sciences, Baku, Azerbaijan
[14] Institut de Física d'Altes Energies (IFAE), Barcelona Institute of Science and Technology, Barcelona, Spain
[15] [(a)]Institute of High Energy Physics, Chinese Academy of Sciences, Beijing, China; [(b)]Physics Department, Tsinghua University, Beijing, China; [(c)]Department of Physics, Nanjing University, Nanjing, China; [(d)]University of Chinese Academy of Science (UCAS), Beijing, China
[16] Institute of Physics, University of Belgrade, Belgrade, Serbia
[17] Department for Physics and Technology, University of Bergen, Bergen, Norway
[18] Physics Division, Lawrence Berkeley National Laboratory and University of California, Berkeley, CA, USA
[19] Institut für Physik, Humboldt Universität zu Berlin, Berlin, Germany
[20] Albert Einstein Center for Fundamental Physics and Laboratory for High Energy Physics, University of Bern, Bern, Switzerland
[21] School of Physics and Astronomy, University of Birmingham, Birmingham, UK
[22] Centro de Investigaciónes, Universidad Antonio Nariño, Bogotá, Colombia
[23] [(a)]Dipartimento di Fisica e Astronomia, Università di Bologna, Bologna, Italy; [(b)]INFN Sezione di Bologna, Bologna, Italy
[24] Physikalisches Institut, Universität Bonn, Bonn, Germany
[25] Department of Physics, Boston University, Boston, MA, USA
[26] Department of Physics, Brandeis University, Waltham, MA, USA
[27] [(a)]Transilvania University of Brasov, Brasov, Romania; [(b)]Horia Hulubei National Institute of Physics and Nuclear Engineering, Bucharest, Romania; [(c)]Department of Physics, Alexandru Ioan Cuza University of Iasi, Iasi, Romania; [(d)]Physics Department, National Institute for Research and Development of Isotopic and Molecular Technologies, Cluj-Napoca, Romania; [(e)]University Politehnica Bucharest, Bucharest, Romania; [(f)]West University in Timisoara, Timisoara, Romania

[28] [(a)]Faculty of Mathematics, Physics and Informatics, Comenius University, Bratislava, Slovakia; [(b)]Department of Subnuclear Physics, Institute of Experimental Physics of the Slovak Academy of Sciences, Kosice, Slovak Republic
[29] Physics Department, Brookhaven National Laboratory, Upton, NY, USA
[30] Departamento de Física, Universidad de Buenos Aires, Buenos Aires, Argentina
[31] Cavendish Laboratory, University of Cambridge, Cambridge, UK
[32] [(a)]Department of Physics, University of Cape Town, Cape Town, South Africa; [(b)]Department of Mechanical Engineering Science, University of Johannesburg, Johannesburg, South Africa; [(c)]School of Physics, University of the Witwatersrand, Johannesburg, South Africa
[33] Department of Physics, Carleton University, Ottawa, ON, Canada
[34] [(a)]Faculté des Sciences Ain Chock, Réseau Universitaire de Physique des Hautes Energies-Université Hassan II, Casablanca, Morocco; [(b)]Centre National de l'Energie des Sciences Techniques Nucleaires (CNESTEN), Rabat, Morocco; [(c)]Faculté des Sciences Semlalia, Université Cadi Ayyad, LPHEA-Marrakech, Marrakech, Morocco; [(d)]Faculté des Sciences, Université Mohamed Premier and LPTPM, Oujda, Morocco; [(e)]Faculté des sciences, Université Mohammed V, Rabat, Morocco
[35] CERN, Geneva, Switzerland
[36] Enrico Fermi Institute, University of Chicago, Chicago, IL, USA
[37] LPC, Université Clermont Auvergne, CNRS/IN2P3, Clermont-Ferrand, France
[38] Nevis Laboratory, Columbia University, Irvington, NY, USA
[39] Niels Bohr Institute, University of Copenhagen, Copenhagen, Denmark
[40] [(a)]Dipartimento di Fisica, Università della Calabria, Rende, Italy; [(b)]INFN Gruppo Collegato di Cosenza, Laboratori Nazionali di Frascati, Frascati, Italy
[41] Physics Department, Southern Methodist University, Dallas, TX, USA
[42] Physics Department, University of Texas at Dallas, Richardson, TX, USA
[43] [(a)]Department of Physics, Stockholm University, Stockholm, Sweden; [(b)]Oskar Klein Centre, Stockholm, Sweden
[44] Deutsches Elektronen-Synchrotron DESY, Hamburg and Zeuthen, Germany
[45] Lehrstuhl für Experimentelle Physik IV, Technische Universität Dortmund, Dortmund, Germany
[46] Institut für Kern- und Teilchenphysik, Technische Universität Dresden, Dresden, Germany
[47] Department of Physics, Duke University, Durham, NC, USA
[48] SUPA-School of Physics and Astronomy, University of Edinburgh, Edinburgh, UK
[49] INFN e Laboratori Nazionali di Frascati, Frascati, Italy
[50] Physikalisches Institut, Albert-Ludwigs-Universität Freiburg, Freiburg, Germany
[51] II. Physikalisches Institut, Georg-August-Universität Göttingen, Göttingen, Germany
[52] Département de Physique Nucléaire et Corpusculaire, Université de Genève, Geneva, Switzerland
[53] [(a)]Dipartimento di Fisica, Università di Genova, Genoa, Italy; [(b)]INFN Sezione di Genova, Genoa, Italy
[54] II. Physikalisches Institut, Justus-Liebig-Universität Giessen, Giessen, Germany
[55] SUPA-School of Physics and Astronomy, University of Glasgow, Glasgow, UK
[56] LPSC, Université Grenoble Alpes, CNRS/IN2P3, Grenoble INP, Grenoble, France
[57] Laboratory for Particle Physics and Cosmology, Harvard University, Cambridge, MA, USA
[58] [(a)]Department of Modern Physics and State Key Laboratory of Particle Detection and Electronics, University of Science and Technology of China, Hefei, China; [(b)]Institute of Frontier and Interdisciplinary Science and Key Laboratory of Particle Physics and Particle Irradiation (MOE), Shandong University, Qingdao, China; [(c)]School of Physics and Astronomy, Shanghai Jiao Tong University, KLPPAC-MoE, SKLPPC, Shanghai, China; [(d)]Tsung-Dao Lee Institute, Shanghai, China
[59] [(a)]Kirchhoff-Institut für Physik, Ruprecht-Karls-Universität Heidelberg, Heidelberg, Germany; [(b)]Physikalisches Institut, Ruprecht-Karls-Universität Heidelberg, Heidelberg, Germany
[60] Faculty of Applied Information Science, Hiroshima Institute of Technology, Hiroshima, Japan
[61] [(a)]Department of Physics, Chinese University of Hong Kong, Shatin, NT, Hong Kong; [(b)]Department of Physics, University of Hong Kong, Hong Kong, China; [(c)]Department of Physics and Institute for Advanced Study, Hong Kong University of Science and Technology, Clear Water Bay, Kowloon, Hong Kong, China
[62] Department of Physics, National Tsing Hua University, Hsinchu, Taiwan
[63] Department of Physics, Indiana University, Bloomington, IN, USA
[64] [(a)]INFN Gruppo Collegato di Udine, Sezione di Trieste, Udine, Italy; [(b)]ICTP, Trieste, Italy; [(c)]Dipartimento di Chimica, Fisica e Ambiente, Università di Udine, Udine, Italy

[65] [(a)]INFN Sezione di Lecce, Lecce, Italy; [(b)]Dipartimento di Matematica e Fisica, Università del Salento, Lecce, Italy
[66] [(a)]INFN Sezione di Milano, Milan, Italy; [(b)]Dipartimento di Fisica, Università di Milano, Milan, Italy
[67] [(a)]INFN Sezione di Napoli, Naples, Italy; [(b)]Dipartimento di Fisica, Università di Napoli, Naples, Italy
[68] [(a)]INFN Sezione di Pavia, Pavia, Italy; [(b)]Dipartimento di Fisica, Università di Pavia, Pavia, Italy
[69] [(a)]INFN Sezione di Pisa, Pisa, Italy; [(b)]Dipartimento di Fisica E. Fermi, Università di Pisa, Pisa, Italy
[70] [(a)]INFN Sezione di Roma, Rome, Italy; [(b)]Dipartimento di Fisica, Sapienza Università di Roma, Rome, Italy
[71] [(a)]INFN Sezione di Roma Tor Vergata, Rome, Italy; [(b)]Dipartimento di Fisica, Università di Roma Tor Vergata, Rome, Italy
[72] [(a)]INFN Sezione di Roma Tre, Rome, Italy; [(b)]Dipartimento di Matematica e Fisica, Università Roma Tre, Rome, Italy
[73] [(a)]INFN-TIFPA, Povo, Italy; [(b)]Università degli Studi di Trento, Trento, Italy
[74] Institut für Astro- und Teilchenphysik, Leopold-Franzens-Universität, Innsbruck, Austria
[75] University of Iowa, Iowa City, IA, USA
[76] Department of Physics and Astronomy, Iowa State University, Ames, IA, USA
[77] Joint Institute for Nuclear Research, Dubna, Russia
[78] [(a)]Departamento de Engenharia Elétrica, Universidade Federal de Juiz de Fora (UFJF), Juiz de Fora, Brazil; [(b)]Universidade Federal do Rio De Janeiro COPPE/EE/IF, Rio de Janeiro, Brazil; [(c)]Universidade Federal de São João del Rei (UFSJ), São João del Rei, Brazil; [(d)]Instituto de Física, Universidade de São Paulo, São Paulo, Brazil
[79] KEK, High Energy Accelerator Research Organization, Tsukuba, Japan
[80] Graduate School of Science, Kobe University, Kobe, Japan
[81] [(a)]Faculty of Physics and Applied Computer Science, AGH University of Science and Technology, Kraków, Poland; [(b)]Marian Smoluchowski Institute of Physics, Jagiellonian University, Kraków, Poland
[82] Institute of Nuclear Physics Polish Academy of Sciences, Kraków, Poland
[83] Faculty of Science, Kyoto University, Kyoto, Japan
[84] Kyoto University of Education, Kyoto, Japan
[85] Research Center for Advanced Particle Physics and Department of Physics, Kyushu University, Fukuoka, Japan
[86] Instituto de Física La Plata, Universidad Nacional de La Plata and CONICET, La Plata, Argentina
[87] Physics Department, Lancaster University, Lancaster, UK
[88] Oliver Lodge Laboratory, University of Liverpool, Liverpool, UK
[89] Department of Experimental Particle Physics, Jožef Stefan Institute and Department of Physics, University of Ljubljana, Ljubljana, Slovenia
[90] School of Physics and Astronomy, Queen Mary University of London, London, UK
[91] Department of Physics, Royal Holloway University of London, Egham, UK
[92] Department of Physics and Astronomy, University College London, London, UK
[93] Louisiana Tech University, Ruston, LA, USA
[94] Fysiska institutionen, Lunds universitet, Lund, Sweden
[95] Centre de Calcul de l'Institut National de Physique Nucléaire et de Physique des Particules (IN2P3), Villeurbanne, France
[96] Departamento de Física Teorica C-15 and CIAFF, Universidad Autónoma de Madrid, Madrid, Spain
[97] Institut für Physik, Universität Mainz, Mainz, Germany
[98] School of Physics and Astronomy, University of Manchester, Manchester, UK
[99] CPPM, Aix-Marseille Université, CNRS/IN2P3, Marseille, France
[100] Department of Physics, University of Massachusetts, Amherst, MA, USA
[101] Department of Physics, McGill University, Montreal, QC, Canada
[102] School of Physics, University of Melbourne, Parkville, VIC, Australia
[103] Department of Physics, University of Michigan, Ann Arbor, MI, USA
[104] Department of Physics and Astronomy, Michigan State University, East Lansing, MI, USA
[105] B.I. Stepanov Institute of Physics, National Academy of Sciences of Belarus, Minsk, Belarus
[106] Research Institute for Nuclear Problems of Byelorussian State University, Minsk, Belarus
[107] Group of Particle Physics, University of Montreal, Montreal, QC, Canada
[108] P.N. Lebedev Physical Institute of the Russian Academy of Sciences, Moscow, Russia
[109] Institute for Theoretical and Experimental Physics (ITEP), Moscow, Russia
[110] National Research Nuclear University MEPhI, Moscow, Russia
[111] D.V. Skobeltsyn Institute of Nuclear Physics, M.V. Lomonosov Moscow State University, Moscow, Russia

[112] Fakultät für Physik, Ludwig-Maximilians-Universität München, Munich, Germany
[113] Max-Planck-Institut für Physik (Werner-Heisenberg-Institut), Munich, Germany
[114] Nagasaki Institute of Applied Science, Nagasaki, Japan
[115] Graduate School of Science and Kobayashi-Maskawa Institute, Nagoya University, Nagoya, Japan
[116] Department of Physics and Astronomy, University of New Mexico, Albuquerque, NM, USA
[117] Institute for Mathematics, Astrophysics and Particle Physics, Radboud University Nijmegen/Nikhef, Nijmegen, The Netherlands
[118] Nikhef National Institute for Subatomic Physics, University of Amsterdam, Amsterdam, The Netherlands
[119] Department of Physics, Northern Illinois University, De Kalb, IL, USA
[120] [(a)]Budker Institute of Nuclear Physics and NSU, SB RAS, Novosibirsk, Russia; [(b)]Novosibirsk State University, Novosibirsk, Russia
[121] Institute for High Energy Physics of the National Research Centre Kurchatov Institute, Protvino, Russia
[122] Department of Physics, New York University, New York, NY, USA
[123] Ohio State University, Columbus, OH, USA
[124] Faculty of Science, Okayama University, Okayama, Japan
[125] Homer L. Dodge Department of Physics and Astronomy, University of Oklahoma, Norman, OK, USA
[126] Department of Physics, Oklahoma State University, Stillwater, OK, USA
[127] Palacký University, RCPTM, Joint Laboratory of Optics, Olomouc, Czech Republic
[128] Center for High Energy Physics, University of Oregon, Eugene, OR, USA
[129] LAL, Université Paris-Sud, CNRS/IN2P3, Université Paris-Saclay, Orsay, France
[130] Graduate School of Science, Osaka University, Osaka, Japan
[131] Department of Physics, University of Oslo, Oslo, Norway
[132] Department of Physics, Oxford University, Oxford, UK
[133] LPNHE, Sorbonne Université, Paris Diderot Sorbonne Paris Cité, CNRS/IN2P3, Paris, France
[134] Department of Physics, University of Pennsylvania, Philadelphia, PA, USA
[135] Konstantinov Nuclear Physics Institute of National Research Centre "Kurchatov Institute", PNPI, St. Petersburg, Russia
[136] Department of Physics and Astronomy, University of Pittsburgh, Pittsburgh, PA, USA
[137] [(a)]Laboratório de Instrumentação e Física Experimental de Partículas-LIP, Lisbon, Portugal; [(b)]Departamento de Física, Faculdade de Ciências, Universidade de Lisboa, Lisbon, Portugal; [(c)]Departamento de Física, Universidade de Coimbra, Coimbra, Portugal; [(d)]Centro de Física Nuclear da Universidade de Lisboa, Lisbon, Portugal; [(e)]Departamento de Física, Universidade do Minho, Braga, Portugal; [(f)]Departamento de Física Teorica y del Cosmos, Universidad de Granada, Granada, Spain; [(g)]Dep Física and CEFITEC of Faculdade de Ciências e Tecnologia, Universidade Nova de Lisboa, Caparica, Portugal
[138] Institute of Physics, Academy of Sciences of the Czech Republic, Prague, Czech Republic
[139] Czech Technical University in Prague, Prague, Czech Republic
[140] Faculty of Mathematics and Physics, Charles University, Prague, Czech Republic
[141] Particle Physics Department, Rutherford Appleton Laboratory, Didcot, UK
[142] IRFU, CEA, Université Paris-Saclay, Gif-sur-Yvette, France
[143] Santa Cruz Institute for Particle Physics, University of California Santa Cruz, Santa Cruz, CA, USA
[144] [(a)]Departamento de Física, Pontificia Universidad Católica de Chile, Santiago, Chile; [(b)]Departamento de Física, Universidad Técnica Federico Santa María, Valparaiso, Chile
[145] Department of Physics, University of Washington, Seattle, WA, USA
[146] Department of Physics and Astronomy, University of Sheffield, Sheffield, UK
[147] Department of Physics, Shinshu University, Nagano, Japan
[148] Department Physik, Universität Siegen, Siegen, Germany
[149] Department of Physics, Simon Fraser University, Burnaby, BC, Canada
[150] SLAC National Accelerator Laboratory, Stanford, CA, USA
[151] Physics Department, Royal Institute of Technology, Stockholm, Sweden
[152] Departments of Physics and Astronomy, Stony Brook University, Stony Brook, NY, USA
[153] Department of Physics and Astronomy, University of Sussex, Brighton, UK
[154] School of Physics, University of Sydney, Sydney, Australia
[155] Institute of Physics, Academia Sinica, Taipei, Taiwan

[156] [(a)]E. Andronikashvili Institute of Physics, Iv. Javakhishvili Tbilisi State University, Tbilisi, Georgia; [(b)]High Energy Physics Institute, Tbilisi State University, Tbilisi, Georgia
[157] Department of Physics, Technion, Israel Institute of Technology, Haifa, Israel
[158] Raymond and Beverly Sackler School of Physics and Astronomy, Tel Aviv University, Tel Aviv, Israel
[159] Department of Physics, Aristotle University of Thessaloniki, Thessaloníki, Greece
[160] International Center for Elementary Particle Physics and Department of Physics, University of Tokyo, Tokyo, Japan
[161] Graduate School of Science and Technology, Tokyo Metropolitan University, Tokyo, Japan
[162] Department of Physics, Tokyo Institute of Technology, Tokyo, Japan
[163] Tomsk State University, Tomsk, Russia
[164] Department of Physics, University of Toronto, Toronto, ON, Canada
[165] [(a)]TRIUMF, Vancouver, BC, Canada; [(b)]Department of Physics and Astronomy, York University, Toronto, ON, Canada
[166] Division of Physics and Tomonaga Center for the History of the Universe, Faculty of Pure and Applied Sciences, University of Tsukuba, Tsukuba, Japan
[167] Department of Physics and Astronomy, Tufts University, Medford, MA, USA
[168] Department of Physics and Astronomy, University of California Irvine, Irvine, CA, USA
[169] Department of Physics and Astronomy, University of Uppsala, Uppsala, Sweden
[170] Department of Physics, University of Illinois, Urbana, IL, USA
[171] Instituto de Física Corpuscular (IFIC), Centro Mixto Universidad de Valencia, CSIC, Valencia, Spain
[172] Department of Physics, University of British Columbia, Vancouver, BC, Canada
[173] Department of Physics and Astronomy, University of Victoria, Victoria, BC, Canada
[174] Fakultät für Physik und Astronomie, Julius-Maximilians-Universität Würzburg, Würzburg, Germany
[175] Department of Physics, University of Warwick, Coventry, UK
[176] Waseda University, Tokyo, Japan
[177] Department of Particle Physics, Weizmann Institute of Science, Rehovot, Israel
[178] Department of Physics, University of Wisconsin, Madison, WI, USA
[179] Fakultät für Mathematik und Naturwissenschaften, Fachgruppe Physik, Bergische Universität Wuppertal, Wuppertal, Germany
[180] Department of Physics, Yale University, New Haven, CT, USA
[181] Yerevan Physics Institute, Yerevan, Armenia

[a] Also at Borough of Manhattan Community College, City University of New York, NY, USA
[b] Also at California State University, East Bay, USA
[c] Also at Centre for High Performance Computing, CSIR Campus, Rosebank, Cape Town, South Africa
[d] Also at CERN, Geneva, Switzerland
[e] Also at CPPM, Aix-Marseille Université, CNRS/IN2P3, Marseille, France
[f] Also at Département de Physique Nucléaire et Corpusculaire, Université de Genève, Geneva, Switzerland
[g] Also at Departament de Fisica de la Universitat Autonoma de Barcelona, Barcelona, Spain
[h] Also at Departamento de Física Teorica y del Cosmos, Universidad de Granada, Granada (Spain), Spain
[i] Also at Departamento de Física, Instituto Superior Técnico, Universidade de Lisboa, Lisbon, Portugal
[j] Also at Department of Applied Physics and Astronomy, University of Sharjah, Sharjah, United Arab Emirates
[k] Also at Department of Financial and Management Engineering, University of the Aegean, Chios, Greece
[l] Also at Department of Physics and Astronomy, University of Louisville, Louisville, KY, USA
[m] Also at Department of Physics and Astronomy, University of Sheffield, Sheffield, UK
[n] Also at Department of Physics, California State University, Fresno, CA, USA
[o] Also at Department of Physics, California State University, Sacramento, CA, USA
[p] Also at Department of Physics, King's College London, London, UK
[q] Also at Department of Physics, St. Petersburg State Polytechnical University, St. Petersburg, Russia
[r] Also at Department of Physics, Stanford University, USA
[s] Also at Department of Physics, University of Fribourg, Fribourg, Switzerland
[t] Also at Department of Physics, University of Michigan, Ann Arbor, MI, USA
[u] Also at Dipartimento di Fisica E. Fermi, Università di Pisa, Pisa, Italy
[v] Also at Giresun University, Faculty of Engineering, Giresun, Turkey
[w] Also at Graduate School of Science, Osaka University, Osaka, Japan

[x] Also at Hellenic Open University, Patras, Greece
[y] Also at Horia Hulubei National Institute of Physics and Nuclear Engineering, Bucharest, Romania
[z] Also at II Physikalisches Institut, Georg-August-Universität Göttingen, Göttingen, Germany
[aa] Also at Institucio Catalana de Recerca i Estudis Avancats, ICREA, Barcelona, Spain
[ab] Also at Institut für Experimentalphysik, Universität Hamburg, Hamburg, Germany
[ac] Also at Institute for Mathematics, Astrophysics and Particle Physics, Radboud University Nijmegen/Nikhef, Nijmegen, The Netherlands
[ad] Also at Institute for Particle and Nuclear Physics, Wigner Research Centre for Physics, Budapest, Hungary
[ae] Also at Institute of Particle Physics (IPP), Canada
[af] Also at Institute of Physics, Academia Sinica, Taipei, Taiwan
[ag] Also at Institute of Physics, Azerbaijan Academy of Sciences, Baku, Azerbaijan
[ah] Also at Institute of Theoretical Physics, Ilia State University, Tbilisi, Georgia
[ai] Also at Instituto de Física Teórica de la Universidad Autónoma de Madrid, Spain
[aj] Also at Istanbul University, Dept. of Physics, Istanbul, Turkey
[ak] Also at LAL, Université Paris-Sud, CNRS/IN2P3, Université Paris-Saclay, Orsay, France
[al] Also at Louisiana Tech University, Ruston, LA, USA
[am] Also at LPNHE, Sorbonne Université, Paris Diderot Sorbonne Paris Cité, CNRS/IN2P3, Paris, France
[an] Also at Manhattan College, New York, NY, USA
[ao] Also at Moscow Institute of Physics and Technology State University, Dolgoprudny, Russia
[ap] Also at National Research Nuclear University MEPhI, Moscow, Russia
[aq] Also at Physikalisches Institut, Albert-Ludwigs-Universität Freiburg, Freiburg, Germany
[ar] Also at School of Physics, Sun Yat-sen University, Guangzhou, China
[as] Also at The City College of New York, New York, NY, USA
[at] Also at The Collaborative Innovation Center of Quantum Matter (CICQM), Beijing, China
[au] Also at Tomsk State University, Tomsk, and Moscow Institute of Physics and Technology State University, Dolgoprudny, Russia
[av] Also at TRIUMF, Vancouver, BC, Canada
[aw] Also at Universita di Napoli Parthenope, Naples, Italy
[*] Deceased

Eur. Phys. J. C (2019) 79:760
https://doi.org/10.1140/epjc/s10052-019-7199-0

THE EUROPEAN PHYSICAL JOURNAL C

Regular Article - Experimental Physics

Measurement of the cross-section and charge asymmetry of W bosons produced in proton–proton collisions at $\sqrt{s} = 8$ TeV with the ATLAS detector

ATLAS Collaboration[⋆]

CERN, 1211 Geneva 23, Switzerland

Received: 12 April 2019 / Accepted: 4 August 2019 / Published online: 12 September 2019

Abstract This paper presents measurements of the $W^+ \to \mu^+\nu$ and $W^- \to \mu^-\nu$ cross-sections and the associated charge asymmetry as a function of the absolute pseudorapidity of the decay muon. The data were collected in proton–proton collisions at a centre-of-mass energy of 8 TeV with the ATLAS experiment at the LHC and correspond to a total integrated luminosity of 20.2 fb^{-1}. The precision of the cross-section measurements varies between 0.8 and 1.5% as a function of the pseudorapidity, excluding the 1.9% uncertainty on the integrated luminosity. The charge asymmetry is measured with an uncertainty between 0.002 and 0.003. The results are compared with predictions based on next-to-next-to-leading-order calculations with various parton distribution functions and have the sensitivity to discriminate between them.

1 Introduction

Measurements of the W^+ and W^- boson cross-sections in hadron collisions are a sensitive probe of quantum chromodynamics (QCD). High-precision predictions at next-to-next-to-leading-order (NNLO) accuracy in QCD are available to compare with data. Of particular interest is the ability of such measurements to discriminate between different parton distribution functions (PDFs) [1–7], because the W boson rapidity[1] y is strongly correlated with the initial-state parton momentum fractions x. In high-energy proton–proton collisions, the main production mechanism of single W bosons is a valence quark annihilating with a sea antiquark. The W bosons are preferentially produced with a boost in the direction of the incoming valence quark, as the quark is more likely to be at a higher x than the corresponding antiquark. Since the PDFs of u and d quarks in the proton differ (largely due to there being two valence u quarks and one valence d quark), there is a production asymmetry between W^+ and W^- bosons (referred to in this paper as the W boson charge asymmetry), which also varies as a function of rapidity. The boson rapidity cannot be determined unambiguously in leptonic decays of the W boson because the decay neutrino passes through the detector unobserved. The charge asymmetry can instead be measured as a function of the decay lepton's pseudorapidity η_ℓ, which is strongly correlated with the W boson rapidity.

The W boson charge asymmetry was measured in proton–antiproton collisions by the CDF and D0 collaborations [8–10]. It was also measured, along with the individual cross-sections, in proton–proton collisions at the LHC by the ATLAS Collaboration at centre-of-mass energies of $\sqrt{s}$ = 5 TeV [11] and 7 TeV [2], by the CMS Collaboration at $\sqrt{s}$ = 7 and 8 TeV [12–14], and by the LHCb Collaboration at $\sqrt{s}$ = 7 and 8 TeV [15–17].

This paper presents measurements of the integrated fiducial cross-sections for $W^+ \to \mu^+\nu$ and $W^- \to \mu^-\bar{\nu}$, as well as the differential cross-sections, $\mathrm{d}\sigma_{W_{\mu^+}}/\mathrm{d}\eta_\mu$ and $\mathrm{d}\sigma_{W_{\mu^-}}/\mathrm{d}\eta_\mu$, as a function of $|\eta_\mu|$, where η_μ is the pseudorapidity of the decay muon. The data used were collected in proton–proton collisions at a centre-of-mass energy of $\sqrt{s} = 8$ TeV with the ATLAS experiment at the LHC and correspond to a total integrated luminosity of 20.2 fb^{-1} [18]. The muon decay channel ($W \to \mu\nu$) is particularly well suited for this measurement due to good lepton identification and small contributions from background processes. In addition, a measurement of the W boson charge asymmetry A_μ is presented, also as a function of $|\eta_\mu|$. The asymmetry is defined

[1] ATLAS uses a right-handed coordinate system with its origin at the nominal interaction point in the centre of the detector and the z-axis coinciding with the axis of the beam pipe. The x-axis points from the interaction point to the centre of the LHC ring, and the y-axis points upward. Polar coordinates (r, ϕ) are used in the transverse plane, ϕ being the azimuthal angle around the beam pipe. The pseudorapidity is defined in terms of the polar angle θ as $\eta = -\ln\tan(\theta/2)$. The rapidity y of a system is defined in terms of its energy E and its longitudinal momentum p_z as $y = (1/2)\ln[(E+p_z)/(E-p_z)]$. Angular separations between particles or reconstructed objects are measured in η–ϕ space using $\Delta R = \sqrt{(\Delta\eta)^2 + (\Delta\phi)^2}$.

⋆e-mail: atlas.publications@cern.ch

in terms of the W^+ and W^- differential cross-sections as

$$A_\mu = \frac{\mathrm{d}\sigma_{W_{\mu^+}}/\mathrm{d}\eta_\mu - \mathrm{d}\sigma_{W_{\mu^-}}/\mathrm{d}\eta_\mu}{\mathrm{d}\sigma_{W_{\mu^+}}/\mathrm{d}\eta_\mu + \mathrm{d}\sigma_{W_{\mu^-}}/\mathrm{d}\eta_\mu} \,. \quad (1)$$

The measurements are performed in a fiducial phase space, which is defined by the kinematics and geometrical acceptance of the muon. All measurements are compared with predictions from a calculation performed at NNLO accuracy using the DYNNLO program [19]. The DYNNLO predictions are produced with six different PDF sets.

2 The ATLAS detector

The ATLAS detector [20] at the LHC covers nearly the entire solid angle around the collision point. It consists of an inner tracking detector (ID) surrounded by a thin superconducting solenoid, electromagnetic and hadronic calorimeters, and a muon spectrometer (MS) incorporating three large superconducting toroid magnets. The ID is immersed in a 2 T axial magnetic field and provides charged-particle tracking in the range $|\eta| < 2.5$. A high-granularity silicon pixel detector typically provides three measurements per track and is followed by a silicon microstrip tracker, which usually provides four three-dimensional measurement points per track. These silicon detectors are complemented by a transition radiation tracker, which enables radially extended track reconstruction up to $|\eta| = 2.0$.

The calorimeter system covers the pseudorapidity range $|\eta| < 4.9$. Electromagnetic calorimetry is provided by barrel and endcap high-granularity lead/liquid-argon (LAr) sampling calorimeters in the $|\eta| < 3.2$ region. A thin LAr presampler, covering $|\eta| < 1.8$, corrects for energy loss in the material upstream of the calorimeters. Hadronic calorimetry is provided in the $|\eta| < 1.7$ region by the steel/scintillator tile calorimeter, segmented into three barrel structures, and in the endcap region by two copper/LAr calorimeters. The forward regions $3.1 < |\eta| < 4.9$ are covered by copper/LAr and tungsten/LAr calorimeter modules optimised for electromagnetic and hadronic measurements, respectively.

The MS has separate trigger and precision tracking chambers measuring the deflection of muons in a magnetic field generated by superconducting air-core toroids. The precision chamber system covers the region $|\eta| < 2.7$ with three layers of monitored drift tubes, complemented by cathode-strip chambers in the forward regions $2.0 < |\eta| < 2.7$, where the background is highest. There is a transition between the barrel and endcap muon detectors around $|\eta| = 1.05$. The muon trigger system covers the range of $|\eta| < 2.4$ with resistive-plate chambers in the barrel and thin-gap chambers in the endcap regions.

A three-level trigger system [21,22] selected candidate events in 2012. The level-1 trigger was implemented in hardware and used a subset of detector information to reduce the event rate to a design value of at most 75 kHz. This was followed by two software-based trigger levels which together reduced the event rate to about 400 Hz.

3 Analysis methodology

3.1 Description of the measurements

The integrated cross-sections for $W^+ \to \mu^+\nu$ and $W^- \to \mu^-\bar{\nu}$ production are measured in a fiducial phase space defined at the particle level by requiring the muon transverse momentum p_{T}^{μ} to be greater than 25 GeV and the neutrino transverse momentum p_{T}^{ν} to be greater than 25 GeV. The absolute muon pseudorapidity is required to be less than 2.4. The W boson transverse mass is

$$m_{\mathrm{T}} = \sqrt{2 p_{\mathrm{T}}^{\mu} p_{\mathrm{T}}^{\nu} \left(1 - \cos\left(\phi^{\mu} - \phi^{\nu}\right)\right)} \,, \quad (2)$$

where ϕ^{μ} and ϕ^{ν} are the azimuthal angles of the muon and neutrino, respectively. For this analysis, m_{T} must be at least 40 GeV, both at reconstruction and particle level. The requirements on fiducial quantities are defined before the emission of final-state photon radiation (i.e. at the 'Born level').

The differential cross-sections and charge asymmetry are measured in the same fiducial phase space as for the integrated measurement. These are measured in 11 bins of absolute muon pseudorapidity between 0 and 2.4 with bin edges at 0, 0.21, 0.42, 0.63, 0.84, 1.05, 1.37, 1.52, 1.74, 1.95, 2.18, and 2.4. The bin edges are identical to those used in the ATLAS 7 TeV measurement [2].

3.2 Data and simulated event samples

The data for this analysis comprise the entire ATLAS $\sqrt{s} = 8$ TeV data set recorded between April and December 2012, corresponding to an integrated luminosity of 20.2 fb^{-1}. The average number of proton–proton interactions per bunch crossing $\langle\mu\rangle$ was 20.7. Only events recorded with stable beams and the detector operating well are selected. The relative uncertainty of the LHC proton beam energy of $\pm 0.1\%$ [23] has no significant effect on the results.

Events from Monte Carlo (MC) simulations, including simulation of the ATLAS detector, are used for the background estimation and to correct the measured data for detector acceptance, efficiency, and resolution effects.

The $W \to \mu\nu$ signal process was simulated using POWHEG-BOX [24,25] at next-to-leading order (NLO) in perturbative QCD using the CT10 set of PDFs [26] and interfaced to PYTHIA 8.170 [27] with the AU2 set of tuned

parameters [28] to simulate the parton shower, hadronisation, and underlying event and to PHOTOS [29] to simulate final-state photon radiation (FSR). This is referred to as POWHEG+PYTHIA8 in this paper. An alternative signal sample was simulated using NLO SHERPA 1.4 [30] and the CT10 PDF set to cross-check the results obtained using POWHEG+PYTHIA8 and to evaluate systematic uncertainties in the signal modelling.

POWHEG+PYTHIA8 with the CT10 PDF set was used to simulate the background processes $W \to \tau\nu$ and $Z \to \mu\mu$ (with the AU2 tune set) and POWHEG+PYTHIA6 [31,32] also with the CT10 PDF set was used to simulate the $t\bar{t}$ process (with the P2011C tune set [33]). The $Z \to \tau\tau$ process was simulated using ALPGEN [34] with the CTEQ6L1 PDF set [35] interfaced to Herwig [36] to simulate the parton shower and JIMMY [37] to model the underlying event. The single-top process in the s-channel and Wt-channels was simulated with MC@NLO [38] interfaced to JIMMY. The t-channel was generated with ACERMC [39] interfaced to PYTHIA. The backgrounds from the diboson processes WW, WZ, and ZZ were simulated using Herwig at leading order with the CTEQ6L1 PDF set. In all cases, the GEANT4 [40] program was used to simulate the passage of particles through the ATLAS detector [41]. The multijet background is estimated using a data-driven technique, described in Sect. 3.4. A $b\bar{b} \to \mu X$ MC sample, simulated using PYTHIA8 with the AU2 tune set, is used to cross-check the data-driven estimation.

Differences in reconstruction, trigger, and isolation efficiencies for muons between MC simulations and data are evaluated using a tag-and-probe method [42] and are corrected by reweighting the MC simulated events. The muon reconstruction efficiencies are parameterised versus η and ϕ, the muon isolation efficiencies versus η and transverse momentum p_{T}, and the muon trigger efficiencies versus η, ϕ, and p_{T}. The reconstruction, trigger and isolation efficiencies are evaluated separately for positive and negative muons. This separate evaluation is particularly necessary in the case of the trigger efficiencies, which differ by up to 3% (depending on η) between positive and negative muons, much greater than the total uncertainty in the cross-section from other sources. Corrections are also applied to MC events for the description of the muon momentum scales and resolution, which are determined from fits to the observed mass distributions of $Z \to \mu\mu$ candidates in data and MC simulations [42]. To correct for charge-dependent biases of the muon momentum scale due to residual misalignments in the ID and MS, an additional momentum-dependent correction parameterised versus η and ϕ is applied. An associated uncertainty corresponding to the full size of the correction is included.

All simulated samples are normalised using their respective inclusive cross-sections at higher orders in perturbative QCD. The W and Z predictions are scaled to the NNLO calculation obtained with DYNNLO v1.5 [19,43] and the MSTW2008 PDF set [44]. The production of top quarks is normalised using the prediction at NNLO+NNLL precision from the Top++2.0 program for $t\bar{t}$ [45–51], to the calculations in Refs. [52–54] for single top quarks, and for diboson production to the NLO calculations following the procedure described in Ref. [55].

The effect of multiple interactions per bunch crossing (pile-up) is simulated by overlaying minimum-bias MC events generated with PYTHIA8 (with the A2 tune set) [41]. The simulated event samples are reweighted to describe the distribution of the number of pile-up events in the data. The MC simulations are also reweighted to better describe the distribution of the longitudinal position of the primary proton–proton collision vertex [56] in data.

3.3 Event selection

Candidate $W \to \mu\nu$ events are selected with the requirement that at least one of two single-muon triggers are satisfied. A high-threshold trigger requires muons to have $p_{\mathrm{T}} > 36$ GeV, whilst a low-threshold trigger requires $p_{\mathrm{T}} > 24$ GeV alongside the requirement that the muon must be isolated from additional nearby tracks.

Muon candidates are reconstructed by combining tracks measured in both the ID and the MS [42]. The p_{T} of the ID track is required to be greater than 25 GeV and the absolute pseudorapidity to be less than 2.4. Track quality requirements are imposed for muon identification and background suppression. The transverse impact parameter significance is required to be less than 3 to ensure that the muon candidates originate from a primary proton–proton interaction vertex. The muon candidates are also required to be isolated, satisfying $I_\mu < 0.1$, where I_μ is the scalar sum of the p_{T} of tracks within a cone of size $\Delta R = 0.4$ around the muon (excluding the muon track) divided by the p_{T} of the muon. Events are required to contain exactly one muon candidate satisfying the above criteria.

To reduce background contamination, in particular from multijet processes, events are required to have missing transverse momentum $E_{\mathrm{T}}^{\mathrm{miss}}$ greater than 25 GeV. The $E_{\mathrm{T}}^{\mathrm{miss}}$ is reconstructed using energy depositions in the calorimeters and tracks reconstructed in the inner detector and muon spectrometer [57]. It is defined as the absolute value of the negative of the vectorial sum of the transverse momenta of reconstructed objects (e.g. electrons, muons, jets) and tracks not associated with these objects. These are labelled the hard and soft terms, respectively.

The W boson transverse mass m_{T} is required to be larger than 40 GeV. This variable is defined analogously to Eq. (2) with p_{T}^{ν} replaced by $E_{\mathrm{T}}^{\mathrm{miss}}$ and ϕ^{ν} replaced by the azimuthal angle related to the $E_{\mathrm{T}}^{\mathrm{miss}}$.

3.4 Estimation of backgrounds

The backgrounds from all sources other than multijet processes are estimated using the MC samples detailed in Sect. 3.2. The $Z \to \mu\mu$ process with one of the muons not identified contributes between 1% and 8% of selected data events, depending on the value of $|\eta_\mu|$. This is the largest background for $|\eta_\mu| \gtrsim 1.4$. The contribution from $W \to \tau\nu$ where the τ-lepton decays into a muon is 2% of the selected data events and approximately constant as a function of $|\eta_\mu|$. The backgrounds from $Z \to \tau\tau$, $t\bar{t}$, and the diboson processes WW, WZ, and ZZ each amount to less than 0.3% of the selected data.

Multijet processes contribute between 2% and 4% of the selected data and are the largest sources of background for $|\eta_\mu| \lesssim 1.4$. The number and properties of the background events arising from multijet processes are estimated using a data-driven template-fit technique, similar to that used in Ref. [58]. A multijet-dominated sample is obtained from data by selecting events passing the nominal selection except that the muon fails the isolation criterion. For this purpose, events satisfying a trigger without an isolation requirement are used. Multijet templates are constructed from this sample, in a series of mutually exclusive slices in muon isolation, for each distribution of interest. The residual contribution from signal and other background sources, estimated from MC simulations, is subtracted. The normalisations of the multijet templates in the signal region are obtained by fitting the templates to data in three discriminating variables: $E_{\mathrm{T}}^{\mathrm{miss}}$, m_{T}, and the ratio $p_{\mathrm{T}}^{\mu}/m_{\mathrm{T}}$. The fits are performed in two phase-space regions (fitting regions) in which the selections on $E_{\mathrm{T}}^{\mathrm{miss}}$ and m_{T} are relaxed in order to enrich the multijet background contribution. A requirement that the W transverse momentum be less than 30 GeV is introduced in one fitting region to remove a region poorly modelled by signal MC simulations. The normalisation of the multijet template is allowed to float in each of the fits and the total MC-based signal plus background is kept constant. The multijet normalisation in the signal selection is extracted using each discriminating variable in both fitting regions (a total of six estimates). It is assumed that the normalisations of the templates in the fitting regions are the same as for the signal selection. The fits described above are performed for each muon-isolation slice (i.e. six fits per slice). The normalisation estimate extracted in each muon-isolation slice (for a particular discriminating variable and fitting region) is used to linearly extrapolate to an isolation value of 0.05, which is the average isolation of multijet events in the signal region as estimated using the $b\bar{b} \to \mu X$ MC simulation.

The central value of the multijet background is chosen to be the average of the extrapolated curves at $I_\mu = 0.05$, and the spread gives one component of the systematic uncertainty, which is estimated to be bin-to-bin correlated and 50% charge correlated. This uncertainty component includes the effects from the choice of the discriminating variable and the definition of the fitting regions. Another component arises from the effect of the cross-section uncertainty on the signal simulation contribution in the fitting regions (±5%). The fit is repeated varying this and the deviation from the nominal normalisation is taken as an uncertainty, which is again treated as being charge and bin-to-bin correlated. The fit also has a statistical uncertainty, which is treated as being uncorrelated between charges and bins. This is largely due to the limited number of data events for the multijet templates passing the signal selection in each muon-isolation slice. The size of the multijet systematic uncertainty is reported in Sect. 4. The above procedure is performed separately in each bin of muon pseudorapidity. A summary of the most important backgrounds including systematic uncertainties is given in Table 1.

Table 1 The number of data events after event selection for $W^+ \to \mu^+\nu$ and $W^- \to \mu^-\bar{\nu}$ and the percentage of selected data that each of the three major backgrounds constitutes

	$W^+ \to \mu^+\nu$	$W^- \to \mu^-\bar{\nu}$
Number of events	50 390 184	34 877 365
Percentage of data		
Multijet	2.4 ± 0.3	3.1 ± 0.3
$W \to \tau\nu$	1.9 ± 0.1	2.0 ± 0.1
$Z \to \mu\mu$	3.1 ± 0.2	4.0 ± 0.2
Others	0.62 ± 0.02	0.82 ± 0.03

Figure 1 shows the muon η, muon p_{T}, and W transverse mass distributions of selected events with positive muons (left) and with negative muons (right). The data are compared with the sum of MC and data-based estimates for the signal and the backgrounds. The predictions are normalised to the luminosity of the data, after first normalising each MC cross-section to a corresponding higher-order prediction. A normalisation shift between data and MC simulations of approximately 1% is observed for the positive muon plots. This is covered by the uncertainty in the MC signal prediction due to the cross-section uncertainty. Otherwise, the combined prediction describes the data well and within the uncertainties.

3.5 Obtaining the fiducial cross-sections

The fiducial $W^{\pm}$ differential cross-sections in bin i of pseudorapidity $(\mathrm{d}\sigma_{W_{\mu^\pm}}/\mathrm{d}\eta_\mu)_i$ are obtained from

$$\left(\frac{\mathrm{d}\sigma_{W_{\mu^\pm}}}{\mathrm{d}\eta_\mu}\right)_i = \frac{N_{\mathrm{data},i} - N_{\mathrm{bkg},i}}{\Delta\eta_i \cdot C_{W^\pm,i} \cdot \int \mathcal{L}\mathrm{d}t},$$

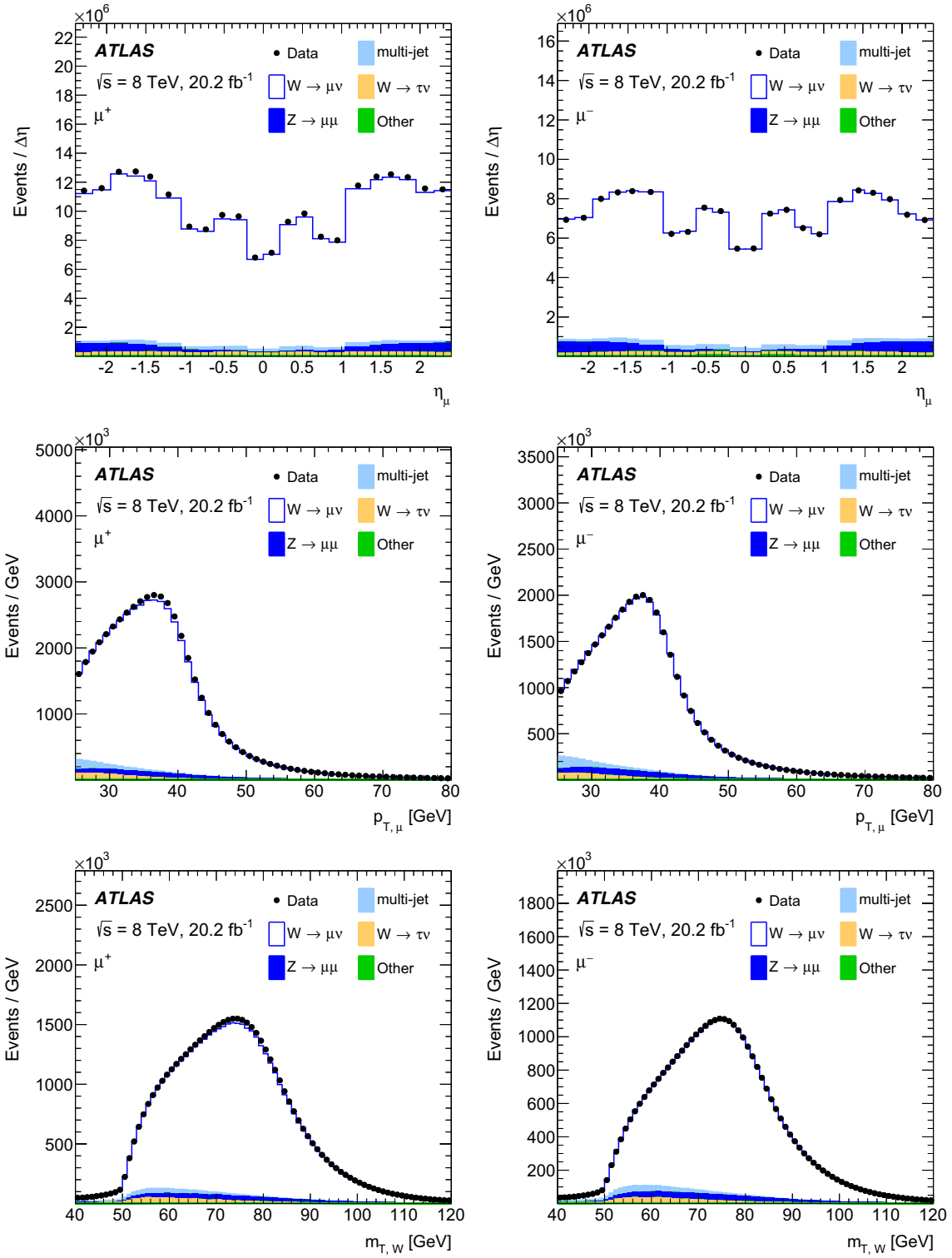

Fig. 1 The muon η (top), muon p_{T} (centre), and W boson transverse mass (bottom) distributions of selected events with positive muons (left) and negative muons (right). The statistical uncertainties of the data points are smaller than the size of the markers

where $N_{\mathrm{data},i}$ is the number of selected candidate events in data, $N_{\mathrm{bkg},i}$ is the number of background events estimated using the methods described in Sect. 3.4, $\Delta\eta_i$ is the width of bin i, and $\int \mathcal{L}\mathrm{d}t$ is the integrated luminosity. The results are provided as a function of absolute pseudorapidity, where $\Delta|\eta_i| = 2 \cdot \Delta\eta_i$. The term $C_{W^{\pm},i}$ is a factor (different for

Table 2 The $C_{W^{\pm},i}$ values with their associated systematic uncertainties as a function of $|\eta_\mu|$ and the integrated global correction factor $C_{W^{\pm}}$, each for W^+ and W^-

$\lvert\eta_\mu\rvert$	$W^+ \to \mu^+\nu$	$W^+ \to \mu^+\nu$
0.00–0.21	0.508 ± 0.004	0.505 ± 0.004
0.21–0.42	0.684 ± 0.004	0.679 ± 0.004
0.42–0.63	0.702 ± 0.005	0.702 ± 0.005
0.63–0.84	0.611 ± 0.004	0.613 ± 0.005
0.84–1.05	0.603 ± 0.004	0.601 ± 0.005
1.05–1.37	0.795 ± 0.006	0.796 ± 0.007
1.37–1.52	0.848 ± 0.008	0.845 ± 0.007
1.52–1.74	0.861 ± 0.009	0.856 ± 0.007
1.74–1.95	0.856 ± 0.009	0.855 ± 0.008
1.95–2.18	0.792 ± 0.008	0.794 ± 0.009
2.18–2.40	0.802 ± 0.008	0.812 ± 0.011
Integrated	0.736 ± 0.003	0.727 ± 0.003

positive and negative channels) which corrects for the various detector inefficiencies and resolution effects. This is estimated using $W \to \mu\nu$ signal MC simulations and defined for each bin i as the number of reconstructed events satisfying the same selection criteria as data divided by the number of generated events in the fiducial phase space. The charge asymmetry is then evaluated in each absolute pseudorapidity bin using Eq. (1). A bin-by-bin correction method is used as the purity of each bin is 99% or larger, where the bin purity is defined as the ratio of events generated and reconstructed in a certain bin to all events reconstructed in that bin (where all events are in the generator-level fiducial phase space).

The integrated fiducial cross-sections ($\sigma_{W_{\mu^\pm}}$) are obtained using one global correction factor, $C_{W^{\pm}}$, (i.e. the total number of reconstructed events satisfying the same selection criteria as data divided by the total number of generated events in the integrated fiducial phase space). The values are also obtained by summing the differential cross-sections as a function of $|\eta_\mu|$, and the results are consistent. Table 2 lists the $C_{W^{\pm},i}$ values with their associated systematic uncertainties as a function of $|\eta_\mu|$ and gives the integrated global correction factor $C_{W^{\pm}}$, each for W^+ and W^-.

4 Systematic uncertainties

This section describes the sources of systematic uncertainty considered for the cross-section and the asymmetry measurements. The size of these uncertainties as a function of $|\eta_\mu|$ is provided in Figs. 2 and 3. The data statistical uncertainties are also shown and are small compared with the total systematic uncertainty. Table 3 lists the $W^+ \to \mu^+\nu$ and $W^- \to \mu^-\bar{\nu}$ cross-sections and the asymmetry as a function of the absolute pseudorapidity of the muon, along with the data statistical uncertainties and dominant systematic uncertainties. Most sources of systematic uncertainty, described below, are treated as being correlated between the positive and negative muon channels unless otherwise noted, and therefore their relative impact is reduced for the asymmetry measurement.

Experimental sources of uncertainty are possible mismodelling of the muon momentum scale, resolution, or charge-dependent sagitta bias as well as of the reconstruction, trigger, and isolation efficiencies. Such uncertainties form a small but non-negligible fraction of the total uncertainty, 0.5% or less of the differential cross-section. A test is performed to check the compatibility of the cross-sections measured separately in positive and negative muon pseudorapidity; this is an important cross-check of the correction procedure as the detector is not forward-backward symmetric with respect to the trajectory of a charged particle. A further small uncertainty (up to 0.4% depending on the $|\eta_\mu|$ bin) is added to cover the small differences observed. This uncertainty is treated as being uncorrelated between charges and propagated to the asymmetry measurement. The above uncertainties are combined in the column labelled 'Muon

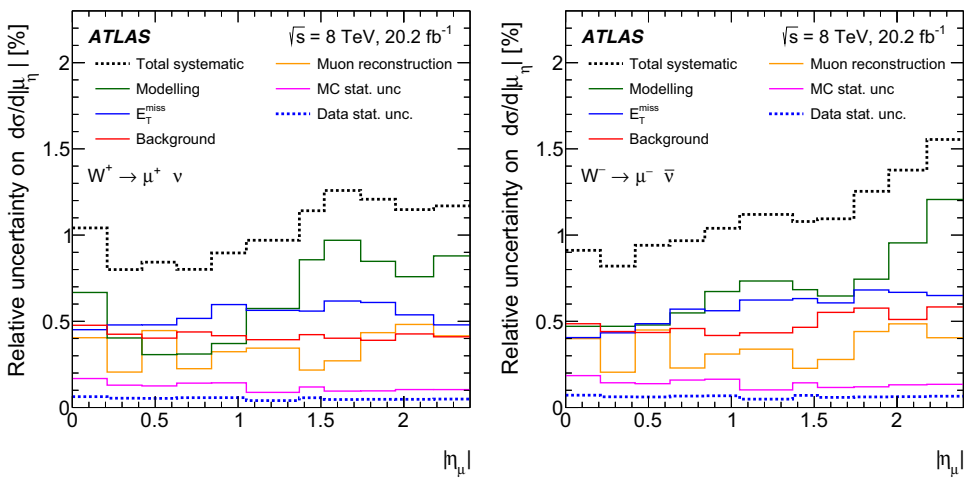

Fig. 2 The relative systematic uncertainty from each source for the W^+ (left) and W^- (right) differential cross-sections as a percentage of the differential cross-section. Also shown are the total systematic and statistical uncertainties

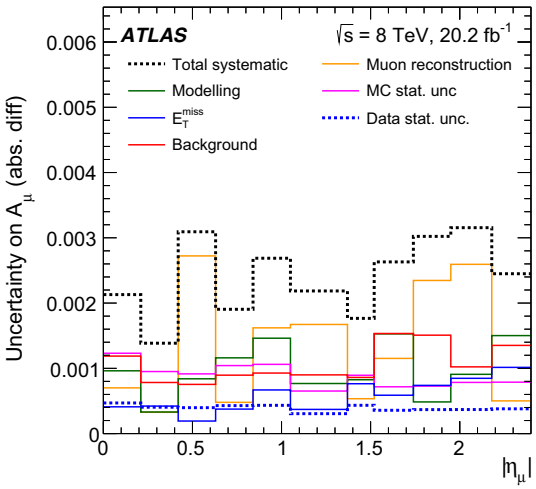

Fig. 3 The systematic uncertainty from each source for the W boson charge asymmetry as an absolute difference from the central value. Also shown are the total systematic and statistical uncertainties

Reconstruction' in Table 3. Additional sources of uncertainty are the mis-modelling of the pile-up event activity and of the primary vertex longitudinal position, both of which are small.

Uncertainties from the mis-modelling of the missing transverse momentum also contribute substantially to the total systematic uncertainty in the cross-section, although they are reduced for the asymmetry measurements. These include mis-modelling in the jet energy scale and resolution, as well as of the momentum balance between the soft term and the total transverse momentum of the hard objects in $Z \to \mu\mu$ calibration events [57]. The muon-related uncertainties in the missing transverse momentum are treated as being fully correlated with those of the signal muon and are part of the muon systematic uncertainties. The sum of all soft-term uncertainties is the largest or second largest contributor (depending on the $|\eta_\mu|$ bin) to the total uncertainty in the differential cross-sections but is significantly less important for the asymmetry measurement. The hard-term uncertainties are small for both the cross-section and asymmetry measurements. The soft-term and hard-term uncertainties are assumed to be uncorrelated with each other.

Uncertainties due to the mis-modelling of the background processes are also considered. For the backgrounds modelled with MC simulations, these are estimated by varying their normalisation within theoretical uncertainties and observing the effect on the final measurements. The cross-section uncertainty for the $Z \to \mu\mu$ process and the $W \to \tau\nu$ process is 5% [59]. The cross-section uncertainty for $t\bar{t}$ production is 6% [45–51], and for single top production 7% [52–54]. The cross-section uncertainty for diboson production is 5% for WW and ZZ production and 7% for WZ production [55].

As mentioned in Sect. 3.4, there are three components of the uncertainty in the multijet background normalisation. The two correlated uncertainties are larger for the cross-section measurements (totalling around 0.5%), whilst the effect of the statistical component is larger for the asymmetry measurement.

The statistical uncertainty due to the limited number of MC events for the other backgrounds and for the signal process is small for the cross-section measurement (less than 0.2%) but becomes significant for the asymmetry measurement (around one third of the total uncertainty), as it is completely uncorrelated between positive and negative channels.

Theoretical sources of uncertainty arise from the choice of PDF interfaced to the POWHEG+PYTHIA8 signal MC simulations (the `CT10` PDF set). This uncertainty is estimated by reweighting the POWHEG+PYTHIA8 events to the nominal values of the `CT14` [1] and `MSTW2008nlo68cl` [44] PDF sets using the LHAPDF interface [60], taking the difference to the nominal values and adding in quadrature. The PDF uncertainty is small for both the fiducial cross-section and asymmetry measurements.

The alternative SHERPA signal sample is used to estimate an uncertainty from POWHEG+PYTHIA8 related to the modelling of the matrix elements that impact kinematics, as well as the underlying event activity and hadronisation (which affects the $E_{\mathrm{T}}^{\mathrm{miss}}$ measurement). The difference between the dressed-level C_W values obtained using the POWHEG+PYTHIA8 and SHERPA simulations is statistically significant and assigned as a systematic uncertainty. This is labelled as 'Modelling' in Table 3. The dressed-level is defined by combining the four-momentum of each muon after photon FSR with that of photons radiated within a cone defined by $\Delta R = 0.1$ around the muon. This is one of the largest systematic uncertainties for both the cross-section (up to 1% at large $|\eta_\mu|$) and the asymmetry measurements. The uncertainty in the luminosity is 1.9% [18]. For the asymmetry, the uncertainty in the luminosity only affects the asymmetry measurement through negligible effects in the background estimation, and it is therefore considered fully correlated between the W^+ and W^- samples.

5 Theoretical predictions

The W^+ and W^- integrated and differential cross-sections and the W boson charge asymmetry are compared with theoretical predictions from an optimised version of the DYNNLO generator [19], which simulates initial-state QCD corrections to NNLO accuracy at leading order in the electroweak couplings with parameters set according to the G_μ scheme [61]. The input parameters (the Fermi constant G_{F}, the masses and widths of the W and Z bosons, and the CKM matrix elements) are taken from Ref. [62]. The DYNNLO predictions are calculated with the PDF sets from `CT14 NNLO` [1], `ATLASepWZ2016` [2],

Table 3 Cross-sections (differential in η_μ) and asymmetry, as a function of $|\eta_\mu|$. The central values are provided along with the statistical and dominant systematic uncertainties: the data statistical uncertainty (Data Stat.), the $E_{\mathrm{T}}^{\mathrm{miss}}$ uncertainty, the uncertainties related to muon reconstruction (Muon Reco.), those related to the background, those from MC statistics (MC Stat.), and modelling uncertainties. The uncertainties of the cross-sections are given in percent and those of the asymmetry as an absolute difference from the nominal

$\lvert\eta_\mu\rvert$		Data stat.	$E_{\mathrm{T}}^{\mathrm{miss}}$	Muon reco.	Background	MC stat.	Modelling
	$d\sigma_{W_{\mu^+}}/d\eta_\mu$ [pb]						
0.00–0.21	630.3	0.06	0.45	0.40	0.48	0.17	0.67
0.21–0.42	635.2	0.05	0.48	0.21	0.42	0.13	0.40
0.42–0.63	641.6	0.05	0.48	0.45	0.40	0.13	0.31
0.63–0.84	638.1	0.06	0.52	0.23	0.44	0.14	0.31
0.84–1.05	642.8	0.06	0.60	0.32	0.42	0.14	0.37
1.05–1.37	654.7	0.04	0.56	0.34	0.39	0.09	0.57
1.37–1.52	661.0	0.06	0.56	0.22	0.42	0.12	0.86
1.52–1.74	662.3	0.05	0.62	0.27	0.40	0.10	0.97
1.74–1.95	661.8	0.05	0.61	0.43	0.39	0.10	0.85
1.95–2.18	657.5	0.05	0.54	0.48	0.43	0.10	0.76
2.18–2.40	641.5	0.05	0.48	0.42	0.41	0.10	0.88
	$d\sigma_{W_{\mu^-}}/d\eta_\mu$ [pb]						
0.00–0.21	493.7	0.07	0.41	0.40	0.49	0.18	0.47
0.21–0.42	489.6	0.06	0.43	0.20	0.44	0.14	0.47
0.42–0.63	485.8	0.06	0.49	0.45	0.43	0.14	0.48
0.63–0.84	474.3	0.07	0.57	0.23	0.46	0.16	0.55
0.84–1.05	465.0	0.07	0.56	0.31	0.42	0.16	0.67
1.05–1.37	455.7	0.05	0.62	0.34	0.43	0.10	0.73
1.37–1.52	439.7	0.07	0.63	0.23	0.47	0.14	0.68
1.52–1.74	427.3	0.06	0.61	0.28	0.55	0.12	0.65
1.74–1.95	410.2	0.06	0.68	0.44	0.58	0.12	0.74
1.95–2.18	389.1	0.06	0.67	0.49	0.51	0.13	0.95
2.18–2.40	368.3	0.07	0.65	0.40	0.58	0.13	1.21
	A_μ						
0.00–0.21	0.1215	0.0005	0.0004	0.0007	0.0012	0.0012	0.0010
0.21–0.42	0.1294	0.0004	0.0004	0.0003	0.0008	0.0010	0.0003
0.42–0.63	0.1383	0.0004	0.0002	0.0027	0.0008	0.0009	0.0008
0.63–0.84	0.1473	0.0004	0.0004	0.0005	0.0009	0.0010	0.0012
0.84–1.05	0.1605	0.0004	0.0007	0.0016	0.0009	0.0011	0.0015
1.05–1.37	0.1792	0.0003	0.0004	0.0017	0.0009	0.0007	0.0008
1.37–1.52	0.2011	0.0004	0.0008	0.0005	0.0009	0.0009	0.0008
1.52–1.74	0.2156	0.0004	0.0006	0.0012	0.0015	0.0007	0.0015
1.74–1.95	0.2347	0.0004	0.0007	0.0023	0.0015	0.0007	0.0005
1.95–2.18	0.2565	0.0004	0.0008	0.0026	0.0010	0.0008	0.0009
2.18–2.40	0.2706	0.0004	0.0010	0.0005	0.0014	0.0008	0.0015

HERAPDF2.0 [3], NNPDF3.1 [4], PDF4LHC15 [5] and MMHT2014 NNLO [6]. The renormalisation and factorisation scales are set equal to the invariant mass of the muon–neutrino pair.

Uncertainties in the DYNNLO prediction due the choice of scales are evaluated by varying the factorisation and renormalisation scales independently by factors of 0.5 and 2 from their nominal values. The uncertainty on the CT14 NNLO prediction is evaluated using the corresponding PDF error sets.

6 Results

The measured integrated fiducial cross-sections multiplied by the branching fraction for the decay into a muon and a neutrino are listed in Table 4, along with the associated uncertainties which are dominated by the 1.9% uncertainty in the luminosity. Also provided is the sum of the $W^+ \to \mu^+\nu$ and $W^- \to \mu^-\bar{\nu}$ integrated cross-sections and their ratio, the total uncertainties on which are 2.1% and 0.3% respectively. The data are compared with the NNLO predictions from DYNNLO, the total uncertainties on which are dom-

Table 4 The measured fiducial production cross-sections times branching ratio for $W^+ \to \mu^+\nu$ and $W^- \to \mu^-\bar{\nu}$, their sum, and their ratio for both data and the predictions from DYNNLO (CT14 NNLO PDF set)

Data	
$\sigma\ (W^+ \to \mu^+\nu)$ [pb]	3110 ± 0.5 (stat.) ± 28 (syst.) ± 59 (lumi.)
$\sigma\ (W^- \to \mu^-\bar{\nu})$ [pb]	2137 ± 0.4 (stat.) ± 21 (syst.) ± 41 (lumi.)
Sum [pb]	5247 ± 0.6 (stat.) ± 49 (syst.) ± 100 (lumi.)
Ratio	1.4558 ± 0.0004 (stat.) ± 0.0040 (syst.)
DYNNLO (CT14 NNLO PDF set)	
$\sigma\ (W^+ \to \mu^+\nu)$ [pb]	3015 ± 92 (PDF) ± 15 (scale)
$\sigma\ (W^- \to \mu^-\bar{\nu})$ [pb]	2105 ± 53 (PDF) ± 10 (scale)
Sum [pb]	5120 ± 140 (PDF) ± 23 (scale)
Ratio	1.4320 ± 0.0100 (PDF) ± 0.0007 (scale)

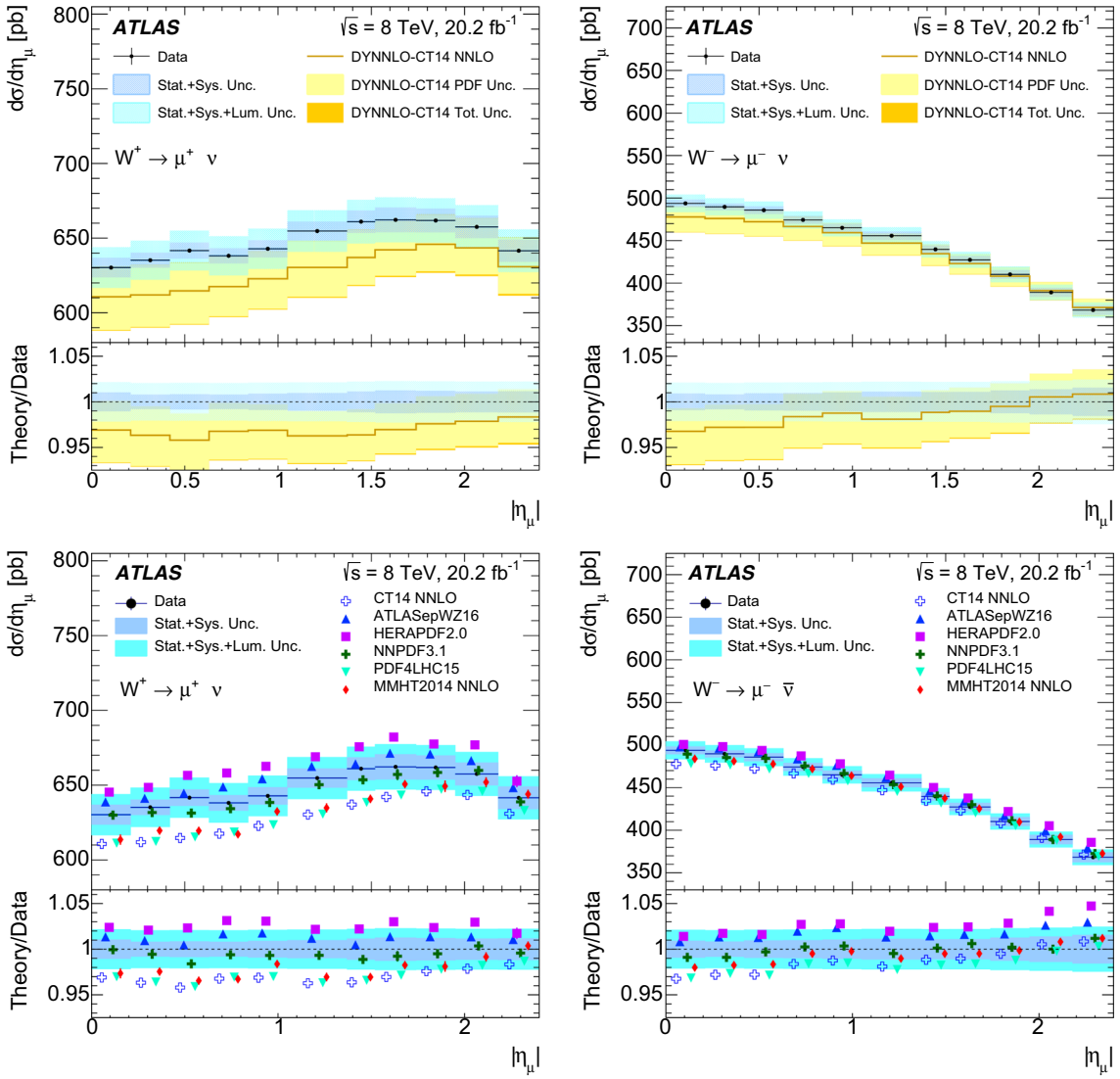

Fig. 4 The W^+ (left) and W^- (right) fiducial cross-sections, differential in muon pseudorapidity multiplied by the branching fraction for the decay into a muon and a neutrino are shown as a function of the absolute muon pseudorapidity. The data are presented with systematic and total uncertainties (the data statistical uncertainties are smaller than the size of the markers) and are compared with the predictions from DYNNLO. In the top two plots, the CT14 NNLO PDF set is used, and DYNNLO is shown with its associated total theoretical uncertainty. In the bottom two plots, the data are compared with the central values of six different PDF sets described in the text. The statistical uncertainties of the DYNNLO predictions are indicated by error bars. The ratios of the data to the corresponding prediction are shown in the lower panels

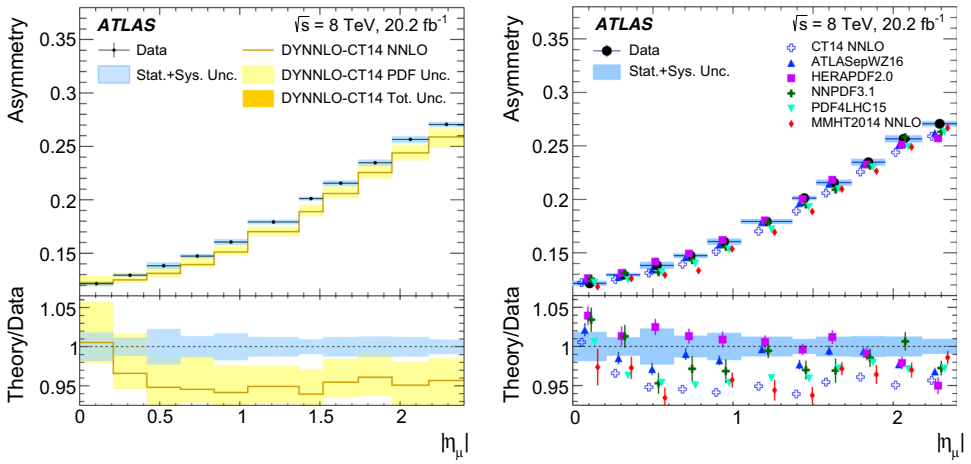

Fig. 5 The W boson charge asymmetry as a function of absolute muon pseudorapidity. The data are presented with systematic and total uncertainties (the data statistical uncertainties are smaller than the size of the markers). In the left plot, the data are compared with the prediction from DYNNLO in which the `CT14 NNLO` PDF set is used. The DYNNLO prediction is also shown with its associated total theoretical uncertainty, along with the component from the PDF set. In the right plot, the data are compared with the central prediction from DYNNLO produced using a selection of PDFs. The statistical uncertainties of the DYNNLO predictions are indicated by error bars. The ratios of the data to the corresponding prediction are shown in the lower panels

inated by the component from the PDF uncertainty. Data and theory agree well and within the uncertainties, although the ratio measurements differ by approximately two standard deviations. The results presented in Table 4 are consistent, within about one standard deviation, with those measured using W boson decays in the electron channel in data at a centre-of-mass energy of 8 TeV [63].

The W^+ and W^- fiducial cross-sections, differential in muon pseudorapidity, multiplied by the branching fraction for the decay into a muon and a neutrino, are shown as a function of absolute muon pseudorapidity in Fig. 4. These are presented with systematic and total uncertainties. The data statistical uncertainties are smaller than the size of the markers. The cross-section values are detailed in Table 3. The measured cross-sections are compared with theoretical predictions obtained using DYNNLO.

In the top plots of Fig. 4, DYNNLO is shown with its associated total theoretical uncertainty, and from the PDF uncertainty (evaluated with the `CT14 NNLO` error sets). The component from the PDF uncertainty dominates the total and is shown separately. The data precision is similar to the intrinsic theoretical uncertainty from scale variations but is much higher than the uncertainty from the PDF. Therefore the data are useful for constraining and evaluating the performance of different PDF sets. In the bottom plots the data are compared with the central values of each PDF set described above. The statistical uncertainties of the DYNNLO predictions are indicated by error bars.

The measured W boson charge asymmetry as a function of absolute muon pseudorapidity is presented in Fig. 5. The values are detailed in Table 3. Again the data are shown with its total systematic uncertainty. In Fig. 5 (left) the data are compared with the prediction from DYNNLO in which the `CT14 NNLO` PDF set is used. The DYNNLO prediction is also shown with its associated total theoretical uncertainty, along with the component from the PDF set, which dominates. In Fig. 5 (right) the data are compared with the central prediction from the six PDF sets considered. The statistical uncertainties of the DYNNLO predictions are indicated by error bars. The ratios of the data to the corresponding prediction are shown in the lower panels. The comparison with `ATLASepWZ2016` and `NNPDF3.1` is of particular interest as both include information from the ATLAS 7 TeV measurement [2], which is expected to be largely uncorrelated with the current data being presented. It is observed that its central value is generally closer to the data than the alternatives, other than `HERAPDF2.0` which performs about as well.

7 Conclusion

Fiducial cross-sections for $W^+ \to \mu^+\nu$ and $W^- \to \mu^-\bar{\nu}$ and the W boson charge asymmetry are measured differentially as a function of the absolute muon pseudorapidity using 20.2 fb^{-1} of data from proton–proton collisions at a centre-of-mass energy of 8 TeV with the ATLAS experiment at the LHC. The muon and neutrino transverse momenta are required to be greater than 25 GeV and the W boson transverse mass to be greater than 40 GeV. A precision of 0.8–1.5% is achieved for the cross-section values, depending on the pseudorapidity, whilst an uncertainty between 0.002 and 0.003 (in absolute units) is obtained for the asymmetry. The

integrated fiducial $W^{\pm}$ production cross-sections are also determined. The measurements are compared to predictions at NNLO accuracy in QCD computed with the DYNNLO program. The precision of the measurement is better than both the uncertainties on the PDF sets as well as the spread between different sets, showing the sensitivity of the measurement to discriminate between them and serve as input to improve the knowledge on the proton structure.

Acknowledgements We thank CERN for the very successful operation of the LHC, as well as the support staff from our institutions without whom ATLAS could not be operated efficiently. We acknowledge the support of ANPCyT, Argentina; YerPhI, Armenia; ARC, Australia; BMWFW and FWF, Austria; ANAS, Azerbaijan; SSTC, Belarus; CNPq and FAPESP, Brazil; NSERC, NRC and CFI, Canada; CERN; CONICYT, Chile; CAS, MOST and NSFC, China; COLCIENCIAS, Colombia; MSMT CR, MPO CR and VSC CR, Czech Republic; DNRF and DNSRC, Denmark; IN2P3-CNRS, CEA-DRF/IRFU, France; SRNSFG, Georgia; BMBF, HGF, and MPG, Germany; GSRT, Greece; RGC, Hong Kong SAR, China; ISF and Benoziyo Center, Israel; INFN, Italy; MEXT and JSPS, Japan; CNRST, Morocco; NWO, Netherlands; RCN, Norway; MNiSW and NCN, Poland; FCT, Portugal; MNE/IFA, Romania; MES of Russia and NRC KI, Russian Federation; JINR; MESTD, Serbia; MSSR, Slovakia; ARRS and MIZŠ, Slovenia; DST/NRF, South Africa; MINECO, Spain; SRC and Wallenberg Foundation, Sweden; SERI, SNSF and Cantons of Bern and Geneva, Switzerland; MOST, Taiwan; TAEK, Turkey; STFC, UK; DOE and NSF, USA. In addition, individual groups and members have received support from BCKDF, CANARIE, CRC and Compute Canada, Canada; COST, ERC, ERDF, Horizon 2020, and Marie Skłodowska-Curie Actions, European Union; Investissements d' Avenir Labex and Idex, ANR, France; DFG and AvH Foundation, Germany; Herakleitos, Thales and Aristeia programmes co-financed by EU-ESF and the Greek NSRF, Greece; BSF-NSF and GIF, Israel; CERCA Programme Generalitat de Catalunya, Spain; The Royal Society and Leverhulme Trust, United Kingdom.
The crucial computing support from all WLCG partners is acknowledged gratefully, in particular from CERN, the ATLAS Tier-1 facilities at TRIUMF (Canada), NDGF (Denmark, Norway, Sweden), CC-IN2P3 (France), KIT/GridKA (Germany), INFN-CNAF (Italy), NL-T1 (Netherlands), PIC (Spain), ASGC (Taiwan), RAL (UK) and BNL (USA), the Tier-2 facilities worldwide and large non-WLCG resource providers. Major contributors of computing resources are listed in Ref. [64].

Data Availability Statement This manuscript has no associated data or the data will not be deposited [Authors' comment: All ATLAS scientific output is published in journals, and preliminary results are made available in Conference Notes. All are openly available, without restriction on use by external parties beyond copyright law and the standard conditions agreed by CERN. Data associated with journal publications are also made available: tables and data from plots (e.g. cross section values, likelihood profiles, selection efficiencies, cross section limits,...) are stored in appropriate repositories such as HEPDATA (http://hepdata.cedar.ac.uk/). ATLAS also strives to make additional material related to the paper available that allows a reinterpretation of the data in the context of new theoretical models. For example, an extended encapsulation of the analysis is often provided for measurements in the framework of RIVET (http://rivet.hepforge.org/)." This information is taken from the ATLAS Data Access Policy, which is a public document that can be downloaded from http://opendata.cern.ch/record/413.]

Funded by SCOAP[3].

References

1. S. Dulat et al., New parton distribution functions from a global analysis of quantum chromodynamics. Phys. Rev. D **93**, 033006 (2016). arXiv:1506.07443 [hep-ph]
2. ATLAS Collaboration, Precision measurement and interpretation of inclusive W^+, W^- and Z/γ^* production cross sections with the ATLAS detector, Eur. Phys. J. C 77 (2017) 367. arXiv:1612.03016 [hep-ex]
3. H1 and ZEUS Collaborations, Combination of measurements of inclusive deep inelastic $e^{\pm}p$ scattering cross sections and QCD analysis of HERA data. Eur. Phys. J. C **75**, 580 (2015). arXiv:1506.06042 [hep-ex]
4. R.D. Ball et al., Parton distributions from high-precision collider data. Eur. Phys. J. C **77**, 663 (2017). arXiv:1706.00428 [hep-ph]
5. J. Butterworth et al., PDF4LHC recommendations for LHC Run II. J. Phys. G **43**, 023001 (2016). arXiv:1510.03865 [hep-ph]
6. L.A. Harland-Lang, A.D. Martin, P. Motylinski, R.S. Thorne, Parton distributions in the LHC era: MMHT 2014 PDFs. Eur. Phys. J. C **75**, 204 (2015). arXiv:1412.3989 [hep-ph]
7. S. Alekhin, J. Blümlein, S. Moch, R. Plačakytė, Parton distribution functions, α_s, and heavy-quark masses for LHC Run II. Phys. Rev. D **96**, 014011 (2017). arXiv:1701.05838 [hep-ph]
8. CDF Collaboration, Direct Measurement of the W Production Charge Asymmetry in $p\bar{p}$ Collisions at $\sqrt{s} = 1.96$ TeV, Phys. Rev. Lett. **102**, 181801 (2009). arXiv:0901.2169 [hep-ex]
9. D0 Collaboration, Measurement of the muon charge asymmetry in $p\bar{p} \to$ W+X $\to \mu\nu$ + X events at $\sqrt{s} = 1.96$ TeV, Phys. Rev. D **88**, 091102 (2013). arXiv:1309.2591 [hep-ex]
10. D0 Collaboration, Measurement of the electron charge asymmetry in $p\bar{p} \to W + X \to e\nu + X$ decays in $p\bar{p}$ collisions at $\sqrt{s} = 1.96$ TeV, Phys. Rev. D **91**, 032007 (2015). arXiv:1412.2862 [hep-ex] (Erratum: Phys. Rev. D 91 (2015) 079901)
11. ATLAS Collaboration, Measurements of W and Z boson production in pp collisions at $\sqrt{s} = 5.02$ TeV with the ATLAS detector, Eur. Phys. J. C **79**, 128 (2019). arXiv:1810.08424 [hep-ex]
12. CMS Collaboration, Measurement of the electron charge asymmetry in inclusive W production in pp collisions at $\sqrt{s} = 7$ TeV. Phys. Rev. Lett. **109**, 111806 (2012). arXiv:1206.2598 [hep-ex]
13. CMS Collaboration, Measurement of the muon charge asymmetry in inclusive $pp \to W + X$ production at $\sqrt{s} = 7$ TeV and an improved determination of light parton distribution functions. Phys. Rev. D **90**, 032004 (2014). arXiv:1312.6283 [hep-ex]
14. CMS Collaboration, Measurement of the differential cross section and charge asymmetry for inclusive $pp \to W^{\pm} + X$ production at $\sqrt{s} = 8$ TeV. Eur. Phys. J. C **76**, 469 (2016). arXiv:1603.01803 [hep-ex]
15. LHCb Collaboration, Measurement of the forward W boson cross-section in pp collisions at $\sqrt{s} = 7$ TeV, JHEP **12**, 079 (2014). arXiv:1408.4354 [hep-ex]
16. LHCb Collaboration, Measurement of forward W and Z boson production in pp collisions at $\sqrt{s} = 8$ TeV, JHEP **01**, 155 (2016). arXiv:1511.08039 [hep-ex]
17. LHCb Collaboration, Measurement of forward $W \to e\nu$ production in pp collisions at $\sqrt{s} = 8$ TeV, JHEP **10**, 030 (2016). arXiv:1608.01484 [hep-ex]
18. ATLAS Collaboration, Luminosity determination in pp collisions at $\sqrt{s} = 8$ TeV using the ATLAS detector at the LHC, Eur. Phys. J. C **76**, 653 (2016). arXiv:1608.03953 [hep-ex]

19. S. Catani, L. Cieri, G. Ferrera, D. de Florian, M. Grazzini, Vector boson production at hadron colliders: a fully exclusive QCD calculation at next-to-next-to-leading order. Phys. Rev. Lett. **103**, 082001 (2009). arXiv:0903.2120 [hep-ph]
20. ATLAS Collaboration, The ATLAS Experiment at the CERN Large Hadron Collider, JINST **3**, S08003 (2008)
21. ATLAS Collaboration, Performance of the ATLAS Trigger System in 2010, Eur. Phys. J. C **72**, 1849 (2012). arXiv:1110.1530 [hep-ex]
22. ATLAS Collaboration, Performance of the ATLAS muon trigger in pp collisions at $\sqrt{s} = 8$ TeV, Eur. Phys. J. C **75**, 120 (2015). arXiv:1408.3179 [hep-ex]
23. E. Todesco, J. Wenninger, Large hadron collider momentum calibration and accuracy. Phys. Rev. Accel. Beams **20**, 081003 (2017)
24. S. Alioli, P. Nason, C. Oleari, E. Re, NLO vector-boson production matched with shower in POWHEG. JHEP **07**, 060 (2008). arXiv:0805.4802 [hep-ph]
25. S. Alioli, P. Nason, C. Oleari, E. Re, A general framework for implementing NLO calculations in shower Monte Carlo programs: the POWHEG BOX. JHEP **06**, 043 (2010). arXiv:1002.2581 [hep-ph]
26. H.-L. Lai et al., New parton distributions for collider physics. Phys. Rev. D **82**, 074024 (2010). arXiv:1007.2241 [hep-ph]
27. T. Sjöstrand, S. Mrenna, P.Z. Skands, A brief introduction to PYTHIA 8.1, Comput. Phys. Commun. **178**, 852 (2008). arXiv:0710.3820 [hep-ph]
28. ATLAS Collaboration, Summary of ATLAS Pythia 8 tunes, ATL-PHYS-PUB-2012-003 (2012), https://cds.cern.ch/record/1474107
29. P. Golonka, Z. Was, PHOTOS Monte Carlo: a precision tool for QED corrections in Z and W decays. Eur. Phys. J. C **45**, 97 (2006). arXiv:hep-ph/0506026
30. T. Gleisberg et al., Event generation with SHERPA 1.1. JHEP **02**, 007 (2009). arXiv:0811.4622 [hep-ph]
31. S. Frixione, P. Nason, G. Ridolfi, A Positive-weight next-to-leading-order Monte Carlo for heavy flavour hadroproduction. JHEP **09**, 126 (2007). arXiv:0707.3088 [hep-ph]
32. T. Sjöstrand, S. Mrenna, P.Z. Skands, PYTHIA 6.4 physics and manual. JHEP **05**, 026 (2006). arXiv:hep-ph/0603175
33. ATLAS Run 1 Pythia8 tunes, tech. rep. ATL-PHYS-PUB-2014-021, CERN (2014), https://cds.cern.ch/record/1966419
34. M.L. Mangano, M. Moretti, F. Piccinini, R. Pittau, A.D. Polosa, ALPGEN, a generator for hard multiparton processes in hadronic collisions. JHEP **07**, 001 (2003). arXiv:hep-ph/0206293
35. J. Pumplin et al., New generation of parton distributions with uncertainties from global QCD analysis. JHEP **07**, 012 (2002). arXiv:hep-ph/0201195
36. G. Corcella et al., HERWIG 6: an event generator for hadron emission reactions with interfering gluons (including supersymmetric processes). JHEP **01**, 010 (2001). arXiv:hep-ph/0011363
37. J. Butterworth, J.R. Forshaw, M. Seymour, Multiparton interactions in photoproduction at HERA. Z. Phys. C **72**, 637 (1996). arXiv:hep-ph/9601371
38. S. Frixione, B.R. Webber, Matching NLO QCD computations and parton shower simulations. JHEP **06**, 029 (2002). arXiv:hep-ph/0204244
39. B.P. Kersevan, E. Richter-Was, The Monte Carlo event generator AcerMC versions 2.0 to 3.8 with interfaces to PYTHIA 6.4, HERWIG 6.5 and ARIADNE 4.1. Comput. Phys. Commun. **184**, 919 (2013). arXiv:hep-ph/0405247
40. S. Agostinelli et al., GEANT4—a simulation toolkit. Nucl. Instrum. Methods Phys. Res. A **506**, 250 (2003)
41. ATLAS Collaboration, The ATLAS Simulation Infrastructure, Eur. Phys. J. C **70**, 823 (2010). arXiv:1005.4568 [physics.ins-det]
42. ATLAS Collaboration, Measurement of the muon reconstruction performance of the ATLAS detector using 2011 and 2012 LHC proton–proton collision data, Eur. Phys. J. C **74**, 3130 (2014). arXiv:1407.3935 [hep-ex]
43. S. Catani, M. Grazzini, Next-to-next-to-leading-order subtraction formalism in hadron collisions and its application to Higgs-boson production at the LHC. Phys. Rev. Lett. **98**, 222002 (2007). arXiv:hep-ph/0703012
44. A.D. Martin, W.J. Stirling, R.S. Thorne, G. Watt, Parton distributions for the LHC. Eur. Phys. J. C **63**, 189 (2009). arXiv:0901.0002 [hep-ph]
45. M. Cacciari, M. Czakon, M. Mangano, A. Mitov, P. Nason, Top-pair production at hadron colliders with next-to-next-to-leading logarithmic soft-gluon resummation. Phys. Lett. B **710**, 612 (2012). arXiv:1111.5869 [hep-ph]
46. M. Beneke, P. Falgari, S. Klein, C. Schwinn, Hadronic top-quark pair production with NNLL threshold resummation. Nucl. Phys. B **855**, 695 (2012). arXiv:1109.1536 [hep-ph]
47. P. Bärnreuther, M. Czakon, A. Mitov, Percent-level-precision physics at the tevatron: first genuine next-to-next-to-leading order QCD corrections to $q\bar{q} \to t\bar{t} + X$. Phys. Rev. Lett. **109**, 132001 (2012). arXiv:1204.5201 [hep-ph]
48. M. Czakon, A. Mitov, NNLO corrections to top-pair production at hadron colliders: the all-fermionic scattering channels. JHEP **12**, 054 (2012). arXiv:1207.0236 [hep-ph]
49. M. Czakon, A. Mitov, NNLO corrections to top pair production at hadron colliders: the quark-gluon reaction. JHEP **01**, 080 (2013). arXiv:1210.6832 [hep-ph]
50. M. Czakon, P. Fiedler, A. Mitov, Total top-quark pair-production cross section at hadron colliders through $O(\alpha_S^4)$. Phys. Rev. Lett. **110**, 252004 (2013). arXiv:1303.6254 [hep-ph]
51. M. Czakon, A. Mitov, Top++: a program for the calculation of the top-pair cross-section at hadron colliders. Comput. Phys. Commun. **185**, 2930 (2014). arXiv:1112.5675 [hep-ph]
52. N. Kidonakis, Next-to-next-to-leading logarithm resummation for s-channel single top quark production. Phys. Rev. D **81**, 054028 (2010). arXiv:1001.5034 [hep-ph]
53. N. Kidonakis, Next-to-next-to-leading-order collinear and soft gluon corrections for t-channel single top quark production. Phys. Rev. D **83**, 091503 (2011). arXiv:1103.2792 [hep-ph]
54. N. Kidonakis, Two-loop soft anomalous dimensions for single top quark associated production with a W^- or H^-. Phys. Rev. D **82**, 054018 (2010). arXiv:1005.4451 [hep-ph]
55. ATLAS Collaboration, Multi-Boson Simulation for 13 TeV ATLAS Analyses, ATL-PHYS-PUB- 2017-005, (2017), https://cds.cern.ch/record/2261933
56. ATLAS Collaboration, Performance of primary vertex reconstruction in proton–proton collisions at $\sqrt{s} = 7$ TeV in the ATLAS experiment, ATLAS-CONF-2010-069, (2010), https://cds.cern.ch/record/1281344
57. ATLAS Collaboration, Performance of algorithms that reconstruct missing transverse momentum in $\sqrt{s} = 8$ TeV proton–proton collisions in the ATLAS detector, Eur. Phys. J. C **77**, 41 (2017). arXiv:1609.09324 [hep-ex]
58. ATLAS Collaboration, Measurement of the W-boson mass in pp collisions at $\sqrt{s} = 7$ TeV with the ATLAS detector, Eur. Phys. J. C **78**, 110 (2018). arXiv:1701.07240 [hep-ex]
59. ATLAS Collaboration, ATLAS simulation of boson plus jets processes in Run 2, ATL-PHYS-PUB- 2017-006, (2017), https://cds.cern.ch/record/2261937
60. M. Whalley, D. Bourilkov, R. Group, The Les Houches Accord PDFs (LHAPDF) and LHAGLUE, (2005), arXiv:hep-ph/0508110
61. W.F.L. Hollik, Radiative corrections in the standard model and their role for precision tests of the electroweak theory. Fortsch. Phys. **38**, 165 (1990)
62. C. Patrignani et al., Review of particle physics. Chin. Phys. C **40**, 100001 (2016)
63. ATLAS Collaboration, Measurement of differential cross sections and W^+/W^- cross-section ratios for W boson production in asso-

ATLAS Collaboration

G. Aad[101], B. Abbott[128], D. C. Abbott[102], O. Abdinov[13,*], A. Abed Abud[70a,70b], K. Abeling[53], D. K. Abhayasinghe[93], S. H. Abidi[167], O. S. AbouZeid[40], N. L. Abraham[156], H. Abramowicz[161], H. Abreu[160], Y. Abulaiti[6], B. S. Acharya[66a,66b,n], B. Achkar[53], S. Adachi[163], L. Adam[99], C. Adam Bourdarios[132], L. Adamczyk[83a], L. Adamek[167], J. Adelman[121], M. Adersberger[114], A. Adiguzel[12c,ah], S. Adorni[54], T. Adye[144], A. A. Affolder[146], Y. Afik[160], C. Agapopoulou[132], M. N. Agaras[38], A. Aggarwal[119], C. Agheorghiesei[27c], J. A. Aguilar-Saavedra[140f,140a,ag], F. Ahmadov[79], X. Ai[15a], G. Aielli[73a,73b], S. Akatsuka[85], T. P. A. Åkesson[96], E. Akilli[54], A. V. Akimov[110], K. Al Khoury[132], G. L. Alberghi[23a,23b], J. Albert[176], M. J. Alconada Verzini[88], S. Alderweireldt[119], M. Aleksa[36], I. N. Aleksandrov[79], C. Alexa[27b], D. Alexandre[19], T. Alexopoulos[10], A. Alfonsi[120], M. Alhroob[128], B. Ali[142], G. Alimonti[68a], J. Alison[37], S. P. Alkire[148], C. Allaire[132], B. M. M. Allbrooke[156], B. W. Allen[131], P. P. Allport[21], A. Aloisio[69a,69b], A. Alonso[40], F. Alonso[88], C. Alpigiani[148], A. A. Alshehri[57], M. Alvarez Estevez[98], B. Alvarez Gonzalez[36], D. Álvarez Piqueras[174], M. G. Alviggi[69a,69b], Y. Amaral Coutinho[80b], A. Ambler[103], L. Ambroz[135], C. Amelung[26], D. Amidei[105], S. P. Amor Dos Santos[140a], S. Amoroso[46], C. S. Amrouche[54], F. An[78], C. Anastopoulos[149], N. Andari[145], T. Andeen[11], C. F. Anders[61b], J. K. Anders[20], A. Andreazza[68a,68b], V. Andrei[61a], C. R. Anelli[176], S. Angelidakis[38], A. Angerami[39], A. V. Anisenkov[122a,122b], A. Annovi[71a], C. Antel[61a], M. T. Anthony[149], M. Antonelli[51], D. J. A. Antrim[171], F. Anulli[72a], M. Aoki[81], J. A. Aparisi Pozo[174], L. Aperio Bella[36], G. Arabidze[106], J. P. Araque[140a], V. Araujo Ferraz[80b], R. Araujo Pereira[80b], C. Arcangeletti[51], A. T. H. Arce[49], F. A. Arduh[88], J-F. Arguin[109], S. Argyropoulos[77], J.-H. Arling[46], A. J. Armbruster[36], L. J. Armitage[92], A. Armstrong[171], O. Arnaez[167], H. Arnold[120], A. Artamonov[111,*], G. Artoni[135], S. Artz[99], S. Asai[163], N. Asbah[59], E. M. Asimakopoulou[172], L. Asquith[156], K. Assamagan[29], R. Astalos[28a], R. J. Atkin[33a], M. Atkinson[173], N. B. Atlay[151], H. Atmani[132], K. Augsten[142], G. Avolio[36], R. Avramidou[60a], M. K. Ayoub[15a], A. M. Azoulay[168b], G. Azuelos[109,av], M. J. Baca[21], H. Bachacou[145], K. Bachas[67a,67b], M. Backes[135], F. Backman[45a,45b], P. Bagnaia[72a,72b], M. Bahmani[84], H. Bahrasemani[152], A. J. Bailey[174], V. R. Bailey[173], J. T. Baines[144], M. Bajic[40], C. Bakalis[10], O. K. Baker[183], P. J. Bakker[120], D. Bakshi Gupta[8], S. Balaji[157], E. M. Baldin[122a,122b], P. Balek[180], F. Balli[145], W. K. Balunas[135], J. Balz[99], E. Banas[84], A. Bandyopadhyay[24], Sw. Banerjee[181,i], A. A. E. Bannoura[182], L. Barak[161], W. M. Barbe[38], E. L. Barberio[104], D. Barberis[55a,55b], M. Barbero[101], T. Barillari[115], M-S. Barisits[36], J. Barkeloo[131], T. Barklow[153], R. Barnea[160], S. L. Barnes[60c], B. M. Barnett[144], R. M. Barnett[18], Z. Barnovska-Blenessy[60a], A. Baroncelli[60a], G. Barone[29], A. J. Barr[135], L. Barranco Navarro[174], F. Barreiro[98], J. Barreiro Guimarães da Costa[15a], R. Bartoldus[153], G. Bartolini[101], A. E. Barton[89], P. Bartos[28a], A. Basalaev[46], A. Bassalat[132], R. L. Bates[57], S. J. Batista[167], S. Batlamous[35e], J. R. Batley[32], B. Batool[151], M. Battaglia[146], M. Bauce[72a,72b], F. Bauer[145], K. T. Bauer[171], H. S. Bawa[31,l], J. B. Beacham[126], T. Beau[136], P. H. Beauchemin[170], F. Becherer[52], P. Bechtle[24], H. C. Beck[53], H. P. Beck[20,q], K. Becker[52], M. Becker[99], C. Becot[46], A. Beddall[12d], A. J. Beddall[12a], V. A. Bednyakov[79], M. Bedognetti[120], C. P. Bee[155], T. A. Beermann[76], M. Begalli[80b], M. Begel[29], A. Behera[155], J. K. Behr[46], F. Beisiegel[24], A. S. Bell[94], G. Bella[161], L. Bellagamba[23b], A. Bellerive[34], P. Bellos[9], K. Beloborodov[122a,122b], K. Belotskiy[112], N. L. Belyaev[112], D. Benchekroun[35a], N. Benekos[10], Y. Benhammou[161], D. P. Benjamin[6], M. Benoit[54], J. R. Bensinger[26], S. Bentvelsen[120], L. Beresford[135], M. Beretta[51], D. Berge[46], E. Bergeaas Kuutmann[172], N. Berger[5], B. Bergmann[142], L. J. Bergsten[26], J. Beringer[18], S. Berlendis[7], N. R. Bernard[102], G. Bernardi[136], C. Bernius[153], F. U. Bernlochner[24], T. Berry[93], P. Berta[99], C. Bertella[15a], I. A. Bertram[89], G. J. Besjes[40], O. Bessidskaia Bylund[182], N. Besson[145], A. Bethani[100], S. Bethke[115], A. Betti[24], A. J. Bevan[92], J. Beyer[115], R. Bi[139], R. M. Bianchi[139], O. Biebel[114], D. Biedermann[19], R. Bielski[36], K. Bierwagen[99], N. V. Biesuz[71a,71b], M. Biglietti[74a], T. R. V. Billoud[109], M. Bindi[53], A. Bingul[12d], C. Bini[72a,72b], S. Biondi[23a,23b], M. Birman[180], T. Bisanz[53], J. P. Biswal[161], A. Bitadze[100], C. Bittrich[48], K. Bjørke[134], K. M. Black[25], T. Blazek[28a], I. Bloch[46], C. Blocker[26], A. Blue[57], U. Blumenschein[92], G. J. Bobbink[120], V. S. Bobrovnikov[122a,122b], S. S. Bocchetta[96], A. Bocci[49], D. Boerner[46], D. Bogavac[14], A. G. Bogdanchikov[122a,122b], C. Bohm[45a], V. Boisvert[93], P. Bokan[53,172], T. Bold[83a], A. S. Boldyrev[113], A. E. Bolz[61b], M. Bomben[136], M. Bona[92], J. S. Bonilla[131], M. Boonekamp[145], H. M. Borecka-Bielska[90], A. Borisov[123], G. Borissov[89], J. Bortfeldt[36], D. Bortoletto[135], V. Bortolotto[73a,73b], D. Boscherini[23b], M. Bosman[14], J. D. Bossio Sola[103], K. Bouaouda[35a], J. Boudreau[139], E. V. Bouhova-Thacker[89], D. Boumediene[38], S. K. Boutle[57], A. Boveia[126], J. Boyd[36], D. Boye[33b,ap], I. R. Boyko[79], A. J. Bozson[93], J. Bracinik[21], N. Brahimi[101], G. Brandt[182], O. Brandt[61a], F. Braren[46], U. Bratzler[164], B. Brau[102], J. E. Brau[131], W. D. Breaden Madden[57], K. Brendlinger[46], L. Brenner[46], R. Brenner[172], S. Bressler[180], B. Brickwedde[99], D. L. Briglin[21], D. Britton[57], D. Britzger[115], I. Brock[24], R. Brock[106], G. Brooijmans[39], W. K. Brooks[147b], E. Brost[121], J. H. Broughton[21], P. A. Bruckman de Renstrom[84], D. Bruncko[28b], A. Bruni[23b], G. Bruni[23b], L. S. Bruni[120], S. Bruno[73a,73b], B. H. Brunt[32], M. Bruschi[23b], N. Bruscino[139], P. Bryant[37], L. Bryngemark[96], T. Buanes[17], Q. Buat[36], P. Buchholz[151], A. G. Buckley[57], I. A. Budagov[79], M. K. Bugge[134], F. Bührer[52], O. Bulekov[112], T. J. Burch[121], S. Burdin[90], C. D. Burgard[120], A. M. Burger[129], B. Burghgrave[8], K. Burka[84],

J. T. P. Burr[46], V. Büscher[99], E. Buschmann[53], P. J. Bussey[57], J. M. Butler[25], C. M. Buttar[57], J. M. Butterworth[94], P. Butti[36], W. Buttinger[36], A. Buzatu[158], A. R. Buzykaev[122a,122b], G. Cabras[23a,23b], S. Cabrera Urbán[174], D. Caforio[56], H. Cai[173], V. M. M. Cairo[153], O. Cakir[4a], N. Calace[36], P. Calafiura[18], A. Calandri[101], G. Calderini[136], P. Calfayan[65], G. Callea[57], L. P. Caloba[80b], S. Calvente Lopez[98], D. Calvet[38], S. Calvet[38], T. P. Calvet[155], M. Calvetti[71a,71b], R. Camacho Toro[136], S. Camarda[36], D. Camarero Munoz[98], P. Camarri[73a,73b], D. Cameron[134], R. Caminal Armadans[102], C. Camincher[36], S. Campana[36], M. Campanelli[94], A. Camplani[40], A. Campoverde[151], V. Canale[69a,69b], A. Canesse[103], M. Cano Bret[60c], J. Cantero[129], T. Cao[161], Y. Cao[173], M. D. M. Capeans Garrido[36], M. Capua[41a,41b], R. Cardarelli[73a], F. C. Cardillo[149], I. Carli[143], T. Carli[36], G. Carlino[69a], B. T. Carlson[139], L. Carminati[68a,68b], R. M. D. Carney[45a,45b], S. Caron[119], E. Carquin[147b], S. Carrá[68a,68b], J. W. S. Carter[167], M. P. Casado[14,e], A. F. Casha[167], D. W. Casper[171], R. Castelijn[120], F. L. Castillo[174], V. Castillo Gimenez[174], N. F. Castro[140a,140e], A. Catinaccio[36], J. R. Catmore[134], A. Cattai[36], J. Caudron[24], V. Cavaliere[29], E. Cavallaro[14], D. Cavalli[68a], M. Cavalli-Sforza[14], V. Cavasinni[71a,71b], E. Celebi[12b], F. Ceradini[74a,74b], L. Cerda Alberich[174], A. S. Cerqueira[80a], A. Cerri[156], L. Cerrito[73a,73b], F. Cerutti[18], A. Cervelli[23a,23b], S. A. Cetin[12b], D. Chakraborty[121], S. K. Chan[59], W. S. Chan[120], W. Y. Chan[90], J. D. Chapman[32], B. Chargeishvili[159b], D. G. Charlton[21], T. P. Charman[92], C. C. Chau[34], S. Che[126], A. Chegwidden[106], S. Chekanov[6], S. V. Chekulaev[168a], G. A. Chelkov[79,au], M. A. Chelstowska[36], B. Chen[78], C. Chen[60a], C. H. Chen[78], H. Chen[29], J. Chen[60a], J. Chen[39], S. Chen[137], S. J. Chen[15c], X. Chen[15b,at], Y. Chen[82], Y-H. Chen[46], H. C. Cheng[63a], H. J. Cheng[15a,15d], A. Cheplakov[79], E. Cheremushkina[123], R. Cherkaoui El Moursli[35e], E. Cheu[7], K. Cheung[64], T. J. A. Chevalérias[145], L. Chevalier[145], V. Chiarella[51], G. Chiarelli[71a], G. Chiodini[67a], A. S. Chisholm[21,36], A. Chitan[27b], I. Chiu[163], Y. H. Chiu[176], M. V. Chizhov[79], K. Choi[65], A. R. Chomont[132], S. Chouridou[162], Y. S. Chow[120], M. C. Chu[63a], J. Chudoba[141], A. J. Chuinard[103], J. J. Chwastowski[84], L. Chytka[130], K. M. Ciesla[84], D. Cinca[47], V. Cindro[91], I. A. Cioară[27b], A. Ciocio[18], F. Cirotto[69a,69b], Z. H. Citron[180], M. Citterio[68a], D. A. Ciubotaru[27b], B. M. Ciungu[167], A. Clark[54], M. R. Clark[39], P. J. Clark[50], C. Clement[45a,45b], Y. Coadou[101], M. Cobal[66a,66c], A. Coccaro[55b], J. Cochran[78], H. Cohen[161], A. E. C. Coimbra[36], L. Colasurdo[119], B. Cole[39], A. P. Colijn[120], J. Collot[58], P. Conde Muiño[140a,f], E. Coniavitis[52], S. H. Connell[33b], I. A. Connelly[57], S. Constantinescu[27b], F. Conventi[69a,aw], A. M. Cooper-Sarkar[135], F. Cormier[175], K. J. R. Cormier[167], L. D. Corpe[94], M. Corradi[72a,72b], E. E. Corrigan[96], F. Corriveau[103,ac], A. Cortes-Gonzalez[36], M. J. Costa[174], F. Costanza[5], D. Costanzo[149], G. Cowan[93], J. W. Cowley[32], J. Crane[100], K. Cranmer[124], S. J. Crawley[57], R. A. Creager[137], S. Crépé-Renaudin[58], F. Crescioli[136], M. Cristinziani[24], V. Croft[120], G. Crosetti[41a,41b], A. Cueto[5], T. Cuhadar Donszelmann[149], A. R. Cukierman[153], S. Czekierda[84], P. Czodrowski[36], M. J. Da Cunha Sargedas De Sousa[60b], J. V. Da Fonseca Pinto[80b], C. Da Via[100], W. Dabrowski[83a], T. Dado[28a], S. Dahbi[35e], T. Dai[105], C. Dallapiccola[102], M. Dam[40], G. D'amen[23a,23b], V. D'Amico[74a,74b], J. Damp[99], J. R. Dandoy[137], M. F. Daneri[30], N. P. Dang[181], N. D. Dann[100], M. Danninger[175], V. Dao[36], G. Darbo[55b], O. Dartsi[5], A. Dattagupta[131], T. Daubney[46], S. D'Auria[68a,68b], W. Davey[24], C. David[46], T. Davidek[143], D. R. Davis[49], E. Dawe[104], I. Dawson[149], K. De[8], R. De Asmundis[69a], M. De Beurs[120], S. De Castro[23a,23b], S. De Cecco[72a,72b], N. De Groot[119], P. de Jong[120], H. De la Torre[106], A. De Maria[15c], D. De Pedis[72a], A. De Salvo[72a], U. De Sanctis[73a,73b], M. De Santis[73a,73b], A. De Santo[156], K. De Vasconcelos Corga[101], J. B. De Vivie De Regie[132], C. Debenedetti[146], D. V. Dedovich[79], A. M. Deiana[42], M. Del Gaudio[41a,41b], J. Del Peso[98], Y. Delabat Diaz[46], D. Delgove[132], F. Deliot[145], C. M. Delitzsch[7], M. Della Pietra[69a,69b], D. Della Volpe[54], A. Dell'Acqua[36], L. Dell'Asta[73a,73b], M. Delmastro[5], C. Delporte[132], P. A. Delsart[58], D. A. DeMarco[167], S. Demers[183], M. Demichev[79], G. Demontigny[109], S. P. Denisov[123], D. Denysiuk[120], L. D'Eramo[136], D. Derendarz[84], J. E. Derkaoui[35d], F. Derue[136], P. Dervan[90], K. Desch[24], C. Deterre[46], K. Dette[167], C. Deutsch[24], M. R. Devesa[30], P. O. Deviveiros[36], A. Dewhurst[144], S. Dhaliwal[26], F. A. Di Bello[54], A. Di Ciaccio[73a,73b], L. Di Ciaccio[5], W. K. Di Clemente[137], C. Di Donato[69a,69b], A. Di Girolamo[36], G. Di Gregorio[71a,71b], B. Di Micco[74a,74b], R. Di Nardo[102], K. F. Di Petrillo[59], R. Di Sipio[167], D. Di Valentino[34], C. Diaconu[101], F. A. Dias[40], T. Dias Do Vale[140a], M. A. Diaz[147a], J. Dickinson[18], E. B. Diehl[105], J. Dietrich[19], S. Díez Cornell[46], A. Dimitrievska[18], W. Ding[15b], J. Dingfelder[24], F. Dittus[36], F. Djama[101], T. Djobava[159b], J. I. Djuvsland[17], M. A. B. Do Vale[80c], M. Dobre[27b], D. Dodsworth[26], C. Doglioni[96], J. Dolejsi[143], Z. Dolezal[143], M. Donadelli[80d], J. Donini[38], A. D'onofrio[92], M. D'Onofrio[90], J. Dopke[144], A. Doria[69a], M. T. Dova[88], A. T. Doyle[57], E. Drechsler[152], E. Dreyer[152], T. Dreyer[53], Y. Duan[60b], F. Dubinin[110], M. Dubovsky[28a], A. Dubreuil[54], E. Duchovni[180], G. Duckeck[114], A. Ducourthial[136], O. A. Ducu[109], D. Duda[115], A. Dudarev[36], A. C. Dudder[99], E. M. Duffield[18], L. Duflot[132], M. Dührssen[36], C. Dülsen[182], M. Dumancic[180], A. E. Dumitriu[27b], A. K. Duncan[57], M. Dunford[61a], A. Duperrin[101], H. Duran Yildiz[4a], M. Düren[56], A. Durglishvili[159b], D. Duschinger[48], B. Dutta[46], D. Duvnjak[1], G. I. Dyckes[137], M. Dyndal[36], S. Dysch[100], B. S. Dziedzic[84], K. M. Ecker[115], R. C. Edgar[105], T. Eifert[36], G. Eigen[17], K. Einsweiler[18], T. Ekelof[172], M. El Kacimi[35c], R. El Kosseifi[101], V. Ellajosyula[172], M. Ellert[172], F. Ellinghaus[182], A. A. Elliot[92], N. Ellis[36], J. Elmsheuser[29], M. Elsing[36], D. Emeliyanov[144], A. Emerman[39], Y. Enari[163], J. S. Ennis[178], M. B. Epland[49], J. Erdmann[47], A. Ereditato[20], M. Errenst[36], M. Escalier[132], C. Escobar[174], O. Estrada Pastor[174], E. Etzion[161], H. Evans[65], A. Ezhilov[138], F. Fabbri[57], L. Fabbri[23a,23b], V. Fabiani[119], G. Facini[94],

R. M. Faisca Rodrigues Pereira[140a], R. M. Fakhrutdinov[123], S. Falciano[72a], P. J. Falke[5], S. Falke[5], J. Faltova[143], Y. Fang[15a], Y. Fang[15a], G. Fanourakis[44], M. Fanti[68a,68b], A. Farbin[8], A. Farilla[74a], E. M. Farina[70a,70b], T. Farooque[106], S. Farrell[18], S. M. Farrington[178], P. Farthouat[36], F. Fassi[35e], P. Fassnacht[36], D. Fassouliotis[9], M. Faucci Giannelli[50], W. J. Fawcett[32], L. Fayard[132], O. L. Fedin[138,o], W. Fedorko[175], M. Feickert[42], S. Feigl[134], L. Feligioni[101], A. Fell[149], C. Feng[60b], E. J. Feng[36], M. Feng[49], M. J. Fenton[57], A. B. Fenyuk[123], J. Ferrando[46], A. Ferrante[173], A. Ferrari[172], P. Ferrari[120], R. Ferrari[70a], D. E. Ferreira de Lima[61b], A. Ferrer[174], D. Ferrere[54], C. Ferretti[105], F. Fiedler[99], A. Filipčič[91], F. Filthaut[119], K. D. Finelli[25], M. C. N. Fiolhais[140a], L. Fiorini[174], F. Fischer[114], W. C. Fisher[106], I. Fleck[151], P. Fleischmann[105], R. R. M. Fletcher[137], T. Flick[182], B. M. Flierl[114], L. F. Flores[137], L. R. Flores Castillo[63a], F. M. Follega[75a,75b], N. Fomin[17], G. T. Forcolin[75a,75b], A. Formica[145], F. A. Förster[14], A. C. Forti[100], A. G. Foster[21], M. G. Foti[135], D. Fournier[132], H. Fox[89], P. Francavilla[71a,71b], S. Francescato[72a,72b], M. Franchini[23a,23b], S. Franchino[61a], D. Francis[36], L. Franconi[20], M. Franklin[59], A. N. Fray[92], B. Freund[109], W. S. Freund[80b], E. M. Freundlich[47], D. C. Frizzell[128], D. Froidevaux[36], J. A. Frost[135], C. Fukunaga[164], E. Fullana Torregrosa[174], E. Fumagalli[55a,55b], T. Fusayasu[116], J. Fuster[174], A. Gabrielli[23a,23b], A. Gabrielli[18], G. P. Gach[83a], S. Gadatsch[54], P. Gadow[115], G. Gagliardi[55a,55b], L. G. Gagnon[109], C. Galea[27b], B. Galhardo[140a], G. E. Gallardo[135], E. J. Gallas[135], B. J. Gallop[144], P. Gallus[142], G. Galster[40], R. Gamboa Goni[92], K. K. Gan[126], S. Ganguly[180], J. Gao[60a], Y. Gao[90], Y. S. Gao[31,l], C. García[174], J. E. García Navarro[174], J. A. García Pascual[15a], C. Garcia-Argos[52], M. Garcia-Sciveres[18], R. W. Gardner[37], N. Garelli[153], S. Gargiulo[52], V. Garonne[134], A. Gaudiello[55a,55b], G. Gaudio[70a], I. L. Gavrilenko[110], A. Gavrilyuk[111], C. Gay[175], G. Gaycken[24], E. N. Gazis[10], A. A. Geanta[27b], C. N. P. Gee[144], J. Geisen[53], M. Geisen[99], M. P. Geisler[61a], C. Gemme[55b], M. H. Genest[58], C. Geng[105], S. Gentile[72a,72b], S. George[93], T. Geralis[44], D. Gerbaudo[14], L. O. Gerlach[53], P. Gessinger-Befurt[99], G. Gessner[47], S. Ghasemi[151], M. Ghasemi Bostanabad[176], M. Ghneimat[24], A. Ghosh[77], B. Giacobbe[23b], S. Giagu[72a,72b], N. Giangiacomi[23a,23b], P. Giannetti[71a], A. Giannini[69a,69b], S. M. Gibson[93], M. Gignac[146], D. Gillberg[34], G. Gilles[182], D. M. Gingrich[3,av], M. P. Giordani[66a,66c], F. M. Giorgi[23b], P. F. Giraud[145], G. Giugliarelli[66a,66c], D. Giugni[68a], F. Giuli[73a,73b], S. Gkaitatzis[162], I. Gkialas[9,h], E. L. Gkougkousis[14], P. Gkountoumis[10], L. K. Gladilin[113], C. Glasman[98], J. Glatzer[14], P. C. F. Glaysher[46], A. Glazov[46], M. Goblirsch-Kolb[26], S. Goldfarb[104], T. Golling[54], D. Golubkov[123], A. Gomes[140a,140b], R. Goncalves Gama[53], R. Gonçalo[140a,140b], G. Gonella[52], L. Gonella[21], A. Gongadze[79], F. Gonnella[21], J. L. Gonski[59], S. González de la Hoz[174], S. Gonzalez-Sevilla[54], G. R. Gonzalvo Rodriguez[174], L. Goossens[36], P. A. Gorbounov[111], H. A. Gordon[29], B. Gorini[36], E. Gorini[67a,67b], A. Gorišek[91], A. T. Goshaw[49], C. Gössling[47], M. I. Gostkin[79], C. A. Gottardo[24], M. Gouighri[35b], D. Goujdami[35c], A. G. Goussiou[148], N. Govender[33b,a], C. Goy[5], E. Gozani[160], I. Grabowska-Bold[83a], E. C. Graham[90], J. Gramling[171], E. Gramstad[134], S. Grancagnolo[19], M. Grandi[156], V. Gratchev[138], P. M. Gravila[27f], F. G. Gravili[67a,67b], C. Gray[57], H. M. Gray[18], C. Grefe[24], K. Gregersen[96], I. M. Gregor[46], P. Grenier[153], K. Grevtsov[46], N. A. Grieser[128], J. Griffiths[8], A. A. Grillo[146], K. Grimm[31,k], S. Grinstein[14,w], J.-F. Grivaz[132], S. Groh[99], E. Gross[180], J. Grosse-Knetter[53], Z. J. Grout[94], C. Grud[105], A. Grummer[118], L. Guan[105], W. Guan[181], J. Guenther[36], A. Guerguichon[132], F. Guescini[168a], D. Guest[171], R. Gugel[52], B. Gui[126], T. Guillemin[5], S. Guindon[36], U. Gul[57], J. Guo[60c], W. Guo[105], Y. Guo[60a,r], Z. Guo[101], R. Gupta[46], S. Gurbuz[12c], G. Gustavino[128], P. Gutierrez[128], C. Gutschow[94], C. Guyot[145], M. P. Guzik[83a], C. Gwenlan[135], C. B. Gwilliam[90], A. Haas[124], C. Haber[18], H. K. Hadavand[8], N. Haddad[35e], A. Hadef[60a], S. Hageböck[36], M. Hagihara[169], M. Haleem[177], J. Haley[129], G. Halladjian[106], G. D. Hallewell[101], K. Hamacher[182], P. Hamal[130], K. Hamano[176], H. Hamdaoui[35e], G. N. Hamity[149], K. Han[60a,aj], L. Han[60a], S. Han[15a,15d], K. Hanagaki[81,u], M. Hance[146], D. M. Handl[114], B. Haney[137], R. Hankache[136], P. Hanke[61a], E. Hansen[96], J. B. Hansen[40], J. D. Hansen[40], M. C. Hansen[24], P. H. Hansen[40], E. C. Hanson[100], K. Hara[169], A. S. Hard[181], T. Harenberg[182], S. Harkusha[107], P. F. Harrison[178], N. M. Hartmann[114], Y. Hasegawa[150], A. Hasib[50], S. Hassani[145], S. Haug[20], R. Hauser[106], L. B. Havener[39], M. Havranek[142], C. M. Hawkes[21], R. J. Hawkings[36], D. Hayden[106], C. Hayes[155], R. L. Hayes[175], C. P. Hays[135], J. M. Hays[92], H. S. Hayward[90], S. J. Haywood[144], F. He[60a], M. P. Heath[50], V. Hedberg[96], L. Heelan[8], S. Heer[24], K. K. Heidegger[52], J. Heilman[34], S. Heim[46], T. Heim[18], B. Heinemann[46,aq], J. J. Heinrich[131], L. Heinrich[36], C. Heinz[56], J. Hejbal[141], L. Helary[61b], A. Held[175], S. Hellesund[134], C. M. Helling[146], S. Hellman[45a,45b], C. Helsens[36], R. C. W. Henderson[89], Y. Heng[181], S. Henkelmann[175], A. M. Henriques Correia[36], G. H. Herbert[19], H. Herde[26], V. Herget[177], Y. Hernández Jiménez[33c], H. Herr[99], M. G. Herrmann[114], T. Herrmann[48], G. Herten[52], R. Hertenberger[114], L. Hervas[36], T. C. Herwig[137], G. G. Hesketh[94], N. P. Hessey[168a], A. Higashida[163], S. Higashino[81], E. Higón-Rodriguez[174], K. Hildebrand[37], E. Hill[176], J. C. Hill[32], K. K. Hill[29], K. H. Hiller[46], S. J. Hillier[21], M. Hils[48], I. Hinchliffe[18], F. Hinterkeuser[24], M. Hirose[133], S. Hirose[52], D. Hirschbuehl[182], B. Hiti[91], O. Hladik[141], D. R. Hlaluku[33c], X. Hoad[50], J. Hobbs[155], N. Hod[180], M. C. Hodgkinson[149], A. Hoecker[36], F. Hoenig[114], D. Hohn[52], D. Hohov[132], T. R. Holmes[37], M. Holzbock[114], L. B. A. H Hommels[32], S. Honda[169], T. Honda[81], T. M. Hong[139], A. Hönle[115], B. H. Hooberman[173], W. H. Hopkins[6], Y. Horii[117], P. Horn[48], A. J. Horton[152], L. A. Horyn[37], J-Y. Hostachy[58], A. Hostiuc[148], S. Hou[158], A. Hoummada[35a], J. Howarth[100], J. Hoya[88], M. Hrabovsky[130], J. Hrdinka[76],

I. Hristova[19], J. Hrivnac[132], A. Hrynevich[108], T. Hryn'ova[5], P. J. Hsu[64], S.-C. Hsu[148], Q. Hu[29], S. Hu[60c], Y. Huang[15a], Z. Hubacek[142], F. Hubaut[101], M. Huebner[24], F. Huegging[24], T. B. Huffman[135], M. Huhtinen[36], R. F. H. Hunter[34], P. Huo[155], A. M. Hupe[34], N. Huseynov[79,ae], J. Huston[106], J. Huth[59], R. Hyneman[105], S. Hyrych[28a], G. Iacobucci[54], G. Iakovidis[29], I. Ibragimov[151], L. Iconomidou-Fayard[132], Z. Idrissi[35e], P. I. Iengo[36], R. Ignazzi[40], O. Igonkina[120,y], R. Iguchi[163], T. Iizawa[54], Y. Ikegami[81], M. Ikeno[81], D. Iliadis[162], N. Ilic[119], F. Iltzsche[48], G. Introzzi[70a,70b], M. Iodice[74a], K. Iordanidou[39], V. Ippolito[72a,72b], M. F. Isacson[172], N. Ishijima[133], M. Ishino[163], M. Ishitsuka[165], W. Islam[129], C. Issever[135], S. Istin[160], F. Ito[169], J. M. Iturbe Ponce[63a], R. Iuppa[75a,75b], A. Ivina[180], H. Iwasaki[81], J. M. Izen[43], V. Izzo[69a], P. Jacka[141], P. Jackson[1], R. M. Jacobs[24], V. Jain[2], G. Jäkel[182], K. B. Jakobi[99], K. Jakobs[52], S. Jakobsen[76], T. Jakoubek[141], J. Jamieson[57], K. W. Janas[83a], R. Jansky[54], J. Janssen[24], M. Janus[53], P. A. Janus[83a], G. Jarlskog[96], N. Javadov[79,ae], T. Javůrek[36], M. Javurkova[52], F. Jeanneau[145], L. Jeanty[131], J. Jejelava[159a,af], A. Jelinskas[178], P. Jenni[52,b], J. Jeong[46], N. Jeong[46], S. Jézéquel[5], H. Ji[181], J. Jia[155], H. Jiang[78], Y. Jiang[60a], Z. Jiang[153,p], S. Jiggins[52], F. A. Jimenez Morales[38], J. Jimenez Pena[174], S. Jin[15c], A. Jinaru[27b], O. Jinnouchi[165], H. Jivan[33c], P. Johansson[149], K. A. Johns[7], C. A. Johnson[65], K. Jon-And[45a,45b], R. W. L. Jones[89], S. D. Jones[156], S. Jones[7], T. J. Jones[90], J. Jongmanns[61a], P. M. Jorge[140a], J. Jovicevic[36], X. Ju[18], J. J. Junggeburth[115], A. Juste Rozas[14,w], A. Kaczmarska[84], M. Kado[132], H. Kagan[126], M. Kagan[153], T. Kaji[179], E. Kajomovitz[160], C. W. Kalderon[96], A. Kaluza[99], A. Kamenshchikov[123], L. Kanjir[91], Y. Kano[163], V. A. Kantserov[112], J. Kanzaki[81], L. S. Kaplan[181], D. Kar[33c], M. J. Kareem[168b], E. Karentzos[10], S. N. Karpov[79], Z. M. Karpova[79], V. Kartvelishvili[89], A. N. Karyukhin[123], L. Kashif[181], R. D. Kass[126], A. Kastanas[45a,45b], Y. Kataoka[163], C. Kato[60c,60d], J. Katzy[46], K. Kawade[82], K. Kawagoe[87], T. Kawaguchi[117], T. Kawamoto[163], G. Kawamura[53], E. F. Kay[176], V. F. Kazanin[122a,122b], R. Keeler[176], R. Kehoe[42], J. S. Keller[34], E. Kellermann[96], D. Kelsey[156], J. J. Kempster[21], J. Kendrick[21], O. Kepka[141], S. Kersten[182], B. P. Kerševan[91], S. Ketabchi Haghighat[167], M. Khader[173], F. Khalil-Zada[13], M. K. Khandoga[145], A. Khanov[129], A. G. Kharlamov[122a,122b], T. Kharlamova[122a,122b], E. E. Khoda[175], A. Khodinov[166], T. J. Khoo[54], E. Khramov[79], J. Khubua[159b], S. Kido[82], M. Kiehn[54], C. R. Kilby[93], Y. K. Kim[37], N. Kimura[66a,66c], O. M. Kind[19], B. T. King[90,*], D. Kirchmeier[48], J. Kirk[144], A. E. Kiryunin[115], T. Kishimoto[163], D. P. Kisliuk[167], V. Kitali[46], O. Kivernyk[5], E. Kladiva[28b,*], T. Klapdor-Kleingrothaus[52], M. H. Klein[105], M. Klein[90], U. Klein[90], K. Kleinknecht[99], P. Klimek[121], A. Klimentov[29], T. Klingl[24], T. Klioutchnikova[36], F. F. Klitzner[114], P. Kluit[120], S. Kluth[115], E. Kneringer[76], E. B. F. G. Knoops[101], A. Knue[52], D. Kobayashi[87], T. Kobayashi[163], M. Kobel[48], M. Kocian[153], P. Kodys[143], P. T. Koenig[24], T. Koffas[34], N. M. Köhler[115], T. Koi[153], M. Kolb[61b], I. Koletsou[5], T. Komarek[130], T. Kondo[81], N. Kondrashova[60c], K. Köneke[52], A. C. König[119], T. Kono[125], R. Konoplich[124,am], V. Konstantinides[94], N. Konstantinidis[94], B. Konya[96], R. Kopeliansky[65], S. Koperny[83a], K. Korcyl[84], K. Kordas[162], G. Koren[161], A. Korn[94], I. Korolkov[14], E. V. Korolkova[149], N. Korotkova[113], O. Kortner[115], S. Kortner[115], T. Kosek[143], V. V. Kostyukhin[24], A. Kotwal[49], A. Koulouris[10], A. Kourkoumeli-Charalampidi[70a,70b], C. Kourkoumelis[9], E. Kourlitis[149], V. Kouskoura[29], A. B. Kowalewska[84], R. Kowalewski[176], C. Kozakai[163], W. Kozanecki[145], A. S. Kozhin[123], V. A. Kramarenko[113], G. Kramberger[91], D. Krasnopevtsev[60a], M. W. Krasny[136], A. Krasznahorkay[36], D. Krauss[115], J. A. Kremer[83a], J. Kretzschmar[90], P. Krieger[167], F. Krieter[114], A. Krishnan[61b], K. Krizka[18], K. Kroeninger[47], H. Kroha[115], J. Kroll[141], J. Kroll[137], J. Krstic[16], U. Kruchonak[79], H. Krüger[24], N. Krumnack[78], M. C. Kruse[49], T. Kubota[104], S. Kuday[4b], J. T. Kuechler[46], S. Kuehn[36], A. Kugel[61a], T. Kuhl[46], V. Kukhtin[79], R. Kukla[101], Y. Kulchitsky[107,ai], S. Kuleshov[147b], Y. P. Kulinich[173], M. Kuna[58], T. Kunigo[85], A. Kupco[141], T. Kupfer[47], O. Kuprash[52], H. Kurashige[82], L. L. Kurchaninov[168a], Y. A. Kurochkin[107], A. Kurova[112], M. G. Kurth[15a,15d], E. S. Kuwertz[36], M. Kuze[165], A. K. Kvam[148], J. Kvita[130], T. Kwan[103], A. La Rosa[115], L. La Rotonda[41a,41b], F. La Ruffa[41a,41b], C. Lacasta[174], F. Lacava[72a,72b], D. P. J. Lack[100], H. Lacker[19], D. Lacour[136], E. Ladygin[79], R. Lafaye[5], B. Laforge[136], T. Lagouri[33c], S. Lai[53], S. Lammers[65], W. Lampl[7], C. Lampoudis[162], E. Lançon[29], U. Landgraf[52], M. P. J. Landon[92], M. C. Lanfermann[54], V. S. Lang[46], J. C. Lange[53], R. J. Langenberg[36], A. J. Lankford[171], F. Lanni[29], K. Lantzsch[24], A. Lanza[70a], A. Lapertosa[55a,55b], S. Laplace[136], J. F. Laporte[145], T. Lari[68a], F. Lasagni Manghi[23a,23b], M. Lassnig[36], T. S. Lau[63a], A. Laudrain[132], A. Laurier[34], M. Lavorgna[69a,69b], M. Lazzaroni[68a,68b], B. Le[104], O. Le Dortz[136], E. Le Guirriec[101], M. LeBlanc[7], T. LeCompte[6], F. Ledroit-Guillon[58], C. A. Lee[29], G. R. Lee[17], L. Lee[59], S. C. Lee[158], S. J. Lee[34], B. Lefebvre[168a], M. Lefebvre[176], F. Legger[114], C. Leggett[18], K. Lehmann[152], N. Lehmann[182], G. Lehmann Miotto[36], W. A. Leight[46], A. Leisos[162,v], M. A. L. Leite[80d], R. Leitner[143], D. Lellouch[180,*], K. J. C. Leney[42], T. Lenz[24], B. Lenzi[36], R. Leone[7], S. Leone[71a], C. Leonidopoulos[50], A. Leopold[136], G. Lerner[156], C. Leroy[109], R. Les[167], C. G. Lester[32], M. Levchenko[138], J. Levêque[5], D. Levin[105], L. J. Levinson[180], D. J. Lewis[21], B. Li[15b], B. Li[105], C-Q. Li[60a], F. Li[60c], H. Li[60a], H. Li[60b], J. Li[60c], K. Li[153], L. Li[60c], M. Li[15a], Q. Li[15a,15d], Q. Y. Li[60a], S. Li[60c,60d], X. Li[46], Y. Li[46], Z. Li[60b], Z. Liang[15a], B. Liberti[73a], A. Liblong[167], K. Lie[63c], S. Liem[120], C. Y. Lin[32], K. Lin[106], T. H. Lin[99], R. A. Linck[65], J. H. Lindon[21], A. L. Lionti[54], E. Lipeles[137], A. Lipniacka[17], M. Lisovyi[61b], T. M. Liss[173,as], A. Lister[175], A. M. Litke[146], J. D. Little[8], B. Liu[78,ab], B. L. Liu[6], H. B. Liu[29], H. Liu[105], J. B. Liu[60a], J. K. K. Liu[135], K. Liu[136], M. Liu[60a], P. Liu[18], Y. Liu[15a,15d], Y. L. Liu[105], Y. W. Liu[60a],

M. Livan[70a,70b], A. Lleres[58], J. Llorente Merino[15a], S. L. Lloyd[92], C. Y. Lo[63b], F. Lo Sterzo[42], E. M. Lobodzinska[46], P. Loch[7], S. Loffredo[73a,73b], T. Lohse[19], K. Lohwasser[149], M. Lokajicek[141], J. D. Long[173], R. E. Long[89], L. Longo[36], K. A. Looper[126], J. A. Lopez[147b], I. Lopez Paz[100], A. Lopez Solis[149], J. Lorenz[114], N. Lorenzo Martinez[5], M. Losada[22], P. J. Lösel[114], A. Lösle[52], X. Lou[46], X. Lou[15a], A. Lounis[132], J. Love[6], P. A. Love[89], J. J. Lozano Bahilo[174], M. Lu[60a], Y. J. Lu[64], H. J. Lubatti[148], C. Luci[72a,72b], A. Lucotte[58], C. Luedtke[52], F. Luehring[65], I. Luise[136], L. Luminari[72a], B. Lund-Jensen[154], M. S. Lutz[102], D. Lynn[29], R. Lysak[141], E. Lytken[96], F. Lyu[15a], V. Lyubushkin[79], T. Lyubushkina[79], H. Ma[29], L. L. Ma[60b], Y. Ma[60b], G. Maccarrone[51], A. Macchiolo[115], C. M. Macdonald[149], J. Machado Miguens[137], D. Madaffari[174], R. Madar[38], W. F. Mader[48], N. Madysa[48], J. Maeda[82], K. Maekawa[163], S. Maeland[17], T. Maeno[29], M. Maerker[48], A. S. Maevskiy[113], V. Magerl[52], N. Magini[78], D. J. Mahon[39], C. Maidantchik[80b], T. Maier[114], A. Maio[140a,140b,140d], O. Majersky[28a], S. Majewski[131], Y. Makida[81], N. Makovec[132], B. Malaescu[136], Pa. Malecki[84], V. P. Maleev[138], F. Malek[58], U. Mallik[77], D. Malon[6], C. Malone[32], S. Maltezos[10], S. Malyukov[36], J. Mamuzic[174], G. Mancini[51], I. Mandić[91], L. Manhaes de Andrade Filho[80a], I. M. Maniatis[162], J. Manjarres Ramos[48], K. H. Mankinen[96], A. Mann[114], A. Manousos[76], B. Mansoulie[145], I. Manthos[162], S. Manzoni[120], A. Marantis[162], G. Marceca[30], L. Marchese[135], G. Marchiori[136], M. Marcisovsky[141], C. Marcon[96], C. A. Marin Tobon[36], M. Marjanovic[38], F. Marroquim[80b], Z. Marshall[18], M.U.F Martensson[172], S. Marti-Garcia[174], C. B. Martin[126], T. A. Martin[178], V. J. Martin[50], B. Martin dit Latour[17], L. Martinelli[74a,74b], M. Martinez[14,w], V. I. Martinez Outschoorn[102], S. Martin-Haugh[144], V. S. Martoiu[27b], A. C. Martyniuk[94], A. Marzin[36], L. Masetti[99], T. Mashimo[163], R. Mashinistov[110], J. Masik[100], A. L. Maslennikov[122a,122b], L. H. Mason[104], L. Massa[73a,73b], P. Massarotti[69a,69b], P. Mastrandrea[71a,71b], A. Mastroberardino[41a,41b], T. Masubuchi[163], A. Matic[114], P. Mättig[24], J. Maurer[27b], B. Maček[91], S. J. Maxfield[90], D. A. Maximov[122a,122b], R. Mazini[158], I. Maznas[162], S. M. Mazza[146], S. P. Mc Kee[105], T. G. McCarthy[115], L. I. McClymont[94], W. P. McCormack[18], E. F. McDonald[104], J. A. Mcfayden[36], G. Mchedlidze[53], M. A. McKay[42], K. D. McLean[176], S. J. McMahon[144], P. C. McNamara[104], C. J. McNicol[178], R. A. McPherson[176,ac], J. E. Mdhluli[33c], Z. A. Meadows[102], S. Meehan[148], T. Megy[52], S. Mehlhase[114], A. Mehta[90], T. Meideck[58], B. Meirose[43], D. Melini[174], B. R. Mellado Garcia[33c], J. D. Mellenthin[53], M. Melo[28a], F. Meloni[46], A. Melzer[24], S. B. Menary[100], E. D. Mendes Gouveia[140a,140e], L. Meng[36], X. T. Meng[105], S. Menke[115], E. Meoni[41a,41b], S. Mergelmeyer[19], S. A. M. Merkt[139], C. Merlassino[20], P. Mermod[54], L. Merola[69a,69b], C. Meroni[68a], O. Meshkov[113,110], J. K. R. Meshreki[151], A. Messina[72a,72b], J. Metcalfe[6], A. S. Mete[171], C. Meyer[65], J. Meyer[160], J-P. Meyer[145], H. Meyer Zu Theenhausen[61a], F. Miano[156], R. P. Middleton[144], L. Mijović[50], G. Mikenberg[180], M. Mikestikova[141], M. Mikuž[91], H. Mildner[149], M. Milesi[104], A. Milic[167], D. A. Millar[92], D. W. Miller[37], A. Milov[180], D. A. Milstead[45a,45b], R. A. Mina[153,p], A. A. Minaenko[123], M. Miñano Moya[174], I. A. Minashvili[159b], A. I. Mincer[124], B. Mindur[83a], M. Mineev[79], Y. Minegishi[163], Y. Ming[181], L. M. Mir[14], A. Mirto[67a,67b], K. P. Mistry[137], T. Mitani[179], J. Mitrevski[114], V. A. Mitsou[174], M. Mittal[60c], A. Miucci[20], P. S. Miyagawa[149], A. Mizukami[81], J. U. Mjörnmark[96], T. Mkrtchyan[184], M. Mlynarikova[143], T. Moa[45a,45b], K. Mochizuki[109], P. Mogg[52], S. Mohapatra[39], R. Moles-Valls[24], M. C. Mondragon[106], K. Mönig[46], J. Monk[40], E. Monnier[101], A. Montalbano[152], J. Montejo Berlingen[36], M. Montella[94], F. Monticelli[88], S. Monzani[68a], N. Morange[132], D. Moreno[22], M. Moreno Llácer[36], P. Morettini[55b], M. Morgenstern[120], S. Morgenstern[48], D. Mori[152], M. Morii[59], M. Morinaga[179], V. Morisbak[134], A. K. Morley[36], G. Mornacchi[36], A. P. Morris[94], L. Morvaj[155], P. Moschovakos[36], B. Moser[120], M. Mosidze[159b], T. Moskalets[145], H. J. Moss[149], J. Moss[31,m], K. Motohashi[165], E. Mountricha[36], E. J. W. Moyse[102], S. Muanza[101], J. Mueller[139], R. S. P. Mueller[114], D. Muenstermann[89], G. A. Mullier[96], J. L. Munoz Martinez[14], F. J. Munoz Sanchez[100], P. Murin[28b], W. J. Murray[178,144], A. Murrone[68a,68b], M. Muškinja[18], C. Mwewa[33a], A. G. Myagkov[123,an], J. Myers[131], M. Myska[142], B. P. Nachman[18], O. Nackenhorst[47], A.Nag Nag[48], K. Nagai[135], K. Nagano[81], Y. Nagasaka[62], M. Nagel[52], E. Nagy[101], A. M. Nairz[36], Y. Nakahama[117], K. Nakamura[81], T. Nakamura[163], I. Nakano[127], H. Nanjo[133], F. Napolitano[61a], R. F. Naranjo Garcia[46], R. Narayan[11], D. I. Narrias Villar[61a], I. Naryshkin[138], T. Naumann[46], G. Navarro[22], H. A. Neal[105,*], P. Y. Nechaeva[110], F. Nechansky[46], T. J. Neep[21], A. Negri[70a,70b], M. Negrini[23b], C. Nellist[53], M. E. Nelson[135], S. Nemecek[141], P. Nemethy[124], M. Nessi[36,d], M. S. Neubauer[173], M. Neumann[182], P. R. Newman[21], T. Y. Ng[63c], Y. S. Ng[19], Y. W. Y. Ng[171], H. D. N. Nguyen[101], T. Nguyen Manh[109], E. Nibigira[38], R. B. Nickerson[135], R. Nicolaidou[145], D. S. Nielsen[40], J. Nielsen[146], N. Nikiforou[11], V. Nikolaenko[123,an], I. Nikolic-Audit[136], K. Nikolopoulos[21], P. Nilsson[29], H. R. Nindhito[54], Y. Ninomiya[81], A. Nisati[72a], N. Nishu[60c], R. Nisius[115], I. Nitsche[47], T. Nitta[179], T. Nobe[163], Y. Noguchi[85], M. Nomachi[133], I. Nomidis[136], M. A. Nomura[29], M. Nordberg[36], N. Norjoharuddeen[135], T. Novak[91], O. Novgorodova[48], R. Novotny[142], L. Nozka[130], K. Ntekas[171], E. Nurse[94], F. G. Oakham[34,av], H. Oberlack[115], J. Ocariz[136], A. Ochi[82], I. Ochoa[39], J. P. Ochoa-Ricoux[147a], K. O'Connor[26], S. Oda[87], S. Odaka[81], S. Oerdek[53], A. Ogrodnik[83a], A. Oh[100], S. H. Oh[49], C. C. Ohm[154], H. Oide[55a,55b], M. L. Ojeda[167], H. Okawa[169], Y. Okazaki[85], Y. Okumura[163], T. Okuyama[81], A. Olariu[27b], L. F. Oleiro Seabra[140a], S. A. Olivares Pino[147a], D. Oliveira Damazio[29], J. L. Oliver[1], M. J. R. Olsson[171], A. Olszewski[84], J. Olszowska[84], D. C. O'Neil[152], A. Onofre[140a,140e], K. Onogi[117],

P. U. E. Onyisi[11], H. Oppen[134], M. J. Oreglia[37], G. E. Orellana[88], Y. Oren[161], D. Orestano[74a,74b], N. Orlando[14], R. S. Orr[167], V. O'Shea[57], R. Ospanov[60a], G. Otero y Garzon[30], H. Otono[87], M. Ouchrif[35d], F. Ould-Saada[134], A. Ouraou[145], Q. Ouyang[15a], M. Owen[57], R. E. Owen[21], V. E. Ozcan[12c], N. Ozturk[8], J. Pacalt[130], H. A. Pacey[32], K. Pachal[49], A. Pacheco Pages[14], C. Padilla Aranda[14], S. Pagan Griso[18], M. Paganini[183], G. Palacino[65], S. Palazzo[50], S. Palestini[36], M. Palka[83b], D. Pallin[38], I. Panagoulias[10], C. E. Pandini[36], J. G. Panduro Vazquez[93], P. Pani[46], G. Panizzo[66a,66c], L. Paolozzi[54], C. Papadatos[109], K. Papageorgiou[9,h], A. Paramonov[6], D. Paredes Hernandez[63b], S. R. Paredes Saenz[135], B. Parida[166], T. H. Park[167], A. J. Parker[89], M. A. Parker[32], F. Parodi[55a,55b], E. W. P. Parrish[121], J. A. Parsons[39], U. Parzefall[52], L. Pascual Dominguez[136], V. R. Pascuzzi[167], J. M. P. Pasner[146], E. Pasqualucci[72a], S. Passaggio[55b], F. Pastore[93], P. Pasuwan[45a,45b], S. Pataraia[99], J. R. Pater[100], A. Pathak[181], T. Pauly[36], B. Pearson[115], M. Pedersen[134], L. Pedraza Diaz[119], R. Pedro[140a], T. Peiffer[53], S. V. Peleganchuk[122a,122b], O. Penc[141], H. Peng[60a], B. S. Peralva[80a], M. M. Perego[132], A. P. Pereira Peixoto[140a], D. V. Perepelitsa[29], F. Peri[19], L. Perini[68a,68b], H. Pernegger[36], S. Perrella[69a,69b], K. Peters[46], R. F. Y. Peters[100], B. A. Petersen[36], T. C. Petersen[40], E. Petit[101], A. Petridis[1], C. Petridou[162], P. Petroff[132], M. Petrov[135], F. Petrucci[74a,74b], M. Pettee[183], N. E. Pettersson[102], K. Petukhova[143], A. Peyaud[145], R. Pezoa[147b], L. Pezzotti[70a,70b], T. Pham[104], F. H. Phillips[106], P. W. Phillips[144], M. W. Phipps[173], G. Piacquadio[155], E. Pianori[18], A. Picazio[102], R. H. Pickles[100], R. Piegaia[30], D. Pietreanu[27b], J. E. Pilcher[37], A. D. Pilkington[100], M. Pinamonti[73a,73b], J. L. Pinfold[3], M. Pitt[180], L. Pizzimento[73a,73b], M.-A. Pleier[29], V. Pleskot[143], E. Plotnikova[79], D. Pluth[78], P. Podberezko[122a,122b], R. Poettgen[96], R. Poggi[54], L. Poggioli[132], I. Pogrebnyak[106], D. Pohl[24], I. Pokharel[53], G. Polesello[70a], A. Poley[18], A. Policicchio[72a,72b], R. Polifka[143], A. Polini[23b], C. S. Pollard[46], V. Polychronakos[29], D. Ponomarenko[112], L. Pontecorvo[36], S. Popa[27a], G. A. Popeneciu[27d], D. M. Portillo Quintero[58], S. Pospisil[142], K. Potamianos[46], I. N. Potrap[79], C. J. Potter[32], H. Potti[11], T. Poulsen[96], J. Poveda[36], T. D. Powell[149], G. Pownall[46], M. E. Pozo Astigarraga[36], P. Pralavorio[101], S. Prell[78], D. Price[100], M. Primavera[67a], S. Prince[103], M. L. Proffitt[148], N. Proklova[112], K. Prokofiev[63c], F. Prokoshin[147b], S. Protopopescu[29], J. Proudfoot[6], M. Przybycien[83a], A. Puri[173], P. Puzo[132], J. Qian[105], Y. Qin[100], A. Quadt[53], M. Queitsch-Maitland[46], A. Qureshi[1], P. Rados[104], F. Ragusa[68a,68b], G. Rahal[97], J. A. Raine[54], S. Rajagopalan[29], A. Ramirez Morales[92], K. Ran[15a,15d], T. Rashid[132], S. Raspopov[5], M. G. Ratti[68a,68b], D. M. Rauch[46], F. Rauscher[114], S. Rave[99], B. Ravina[149], I. Ravinovich[180], J. H. Rawling[100], M. Raymond[36], A. L. Read[134], N. P. Readioff[58], M. Reale[67a,67b], D. M. Rebuzzi[70a,70b], A. Redelbach[177], G. Redlinger[29], K. Reeves[43], L. Rehnisch[19], J. Reichert[137], D. Reikher[161], A. Reiss[99], A. Rej[151], C. Rembser[36], M. Renda[27b], M. Rescigno[72a], S. Resconi[68a], E. D. Resseguie[137], S. Rettie[175], E. Reynolds[21], O. L. Rezanova[122a,122b], P. Reznicek[143], E. Ricci[75a,75b], R. Richter[115], S. Richter[46], E. Richter-Was[83b], O. Ricken[24], M. Ridel[136], P. Rieck[115], C. J. Riegel[182], O. Rifki[46], M. Rijssenbeek[155], A. Rimoldi[70a,70b], M. Rimoldi[20], L. Rinaldi[23b], G. Ripellino[154], B. Ristić[89], E. Ritsch[36], I. Riu[14], J. C. Rivera Vergara[147a], F. Rizatdinova[129], E. Rizvi[92], C. Rizzi[36], R. T. Roberts[100], S. H. Robertson[103,ac], M. Robin[46], D. Robinson[32], J. E. M. Robinson[46], A. Robson[57], E. Rocco[99], C. Roda[71a,71b], S. Rodriguez Bosca[174], A. Rodriguez Perez[14], D. Rodriguez Rodriguez[174], A. M. Rodríguez Vera[168b], S. Roe[36], O. Røhne[134], R. Röhrig[115], C. P. A. Roland[65], J. Roloff[59], A. Romaniouk[112], M. Romano[23a,23b], N. Rompotis[90], M. Ronzani[124], L. Roos[136], S. Rosati[72a], K. Rosbach[52], N-A. Rosien[53], G. Rosin[102], B. J. Rosser[137], E. Rossi[46], E. Rossi[74a,74b], E. Rossi[69a,69b], L. P. Rossi[55b], L. Rossini[68a,68b], R. Rosten[14], M. Rotaru[27b], J. Rothberg[148], D. Rousseau[132], G. Rovelli[70a,70b], D. Roy[33c], A. Rozanov[101], Y. Rozen[160], X. Ruan[33c], F. Rubbo[153], F. Rühr[52], A. Ruiz-Martinez[174], A. Rummler[36], Z. Rurikova[52], N. A. Rusakovich[79], H. L. Russell[103], L. Rustige[38,47], J. P. Rutherfoord[7], E. M. Rüttinger[46,j], Y. F. Ryabov[138], M. Rybar[39], G. Rybkin[132], A. Ryzhov[123], G. F. Rzehorz[53], P. Sabatini[53], G. Sabato[120], S. Sacerdoti[132], H.F-W. Sadrozinski[146], R. Sadykov[79], F. Safai Tehrani[72a], B. Safarzadeh Samani[156], P. Saha[121], S. Saha[103], M. Sahinsoy[61a], A. Sahu[182], M. Saimpert[46], M. Saito[163], T. Saito[163], H. Sakamoto[163], A. Sakharov[124,am], D. Salamani[54], G. Salamanna[74a,74b], J. E. Salazar Loyola[147b], P. H. Sales De Bruin[172], D. Salihagic[115,*], A. Salnikov[153], J. Salt[174], D. Salvatore[41a,41b], F. Salvatore[156], A. Salvucci[63a,63b,63c], A. Salzburger[36], J. Samarati[36], D. Sammel[52], D. Sampsonidis[162], D. Sampsonidou[162], J. Sánchez[174], A. Sanchez Pineda[66a,66c], H. Sandaker[134], C. O. Sander[46], I. G. Sanderswood[89], M. Sandhoff[182], C. Sandoval[22], D. P. C. Sankey[144], M. Sannino[55a,55b], Y. Sano[117], A. Sansoni[51], C. Santoni[38], H. Santos[140a,140b], S. N. Santpur[18], A. Santra[174], A. Sapronov[79], J. G. Saraiva[140a,140d], O. Sasaki[81], K. Sato[169], E. Sauvan[5], P. Savard[167,av], N. Savic[115], R. Sawada[163], C. Sawyer[144], L. Sawyer[95,ak], C. Sbarra[23b], A. Sbrizzi[23a], T. Scanlon[94], J. Schaarschmidt[148], P. Schacht[115], B. M. Schachtner[114], D. Schaefer[37], L. Schaefer[137], J. Schaeffer[99], S. Schaepe[36], U. Schäfer[99], A. C. Schaffer[132], D. Schaile[114], R. D. Schamberger[155], N. Scharmberg[100], V. A. Schegelsky[138], D. Scheirich[143], F. Schenck[19], M. Schernau[171], C. Schiavi[55a,55b], S. Schier[146], L. K. Schildgen[24], Z. M. Schillaci[26], E. J. Schioppa[36], M. Schioppa[41a,41b], K. E. Schleicher[52], S. Schlenker[36], K. R. Schmidt-Sommerfeld[115], K. Schmieden[36], C. Schmitt[99], S. Schmitt[46], S. Schmitz[99], J. C. Schmoeckel[46], U. Schnoor[52], L. Schoeffel[145], A. Schoening[61b], E. Schopf[135], M. Schott[99], J. F. P. Schouwenberg[119], J. Schovancova[36], S. Schramm[54], F. Schroeder[182], A. Schulte[99], H-C. Schultz-Coulon[61a],

M. Schumacher[52], B. A. Schumm[146], Ph. Schune[145], A. Schwartzman[153], T. A. Schwarz[105], Ph. Schwemling[145], R. Schwienhorst[106], A. Sciandra[146], G. Sciolla[26], M. Scodeggio[46], M. Scornajenghi[41a,41b], F. Scuri[71a], F. Scutti[104], L. M. Scyboz[115], C. D. Sebastiani[72a,72b], P. Seema[19], S. C. Seidel[118], A. Seiden[146], T. Seiss[37], J. M. Seixas[80b], G. Sekhniaidze[69a], K. Sekhon[105], S. J. Sekula[42], N. Semprini-Cesari[23a,23b], S. Sen[49], S. Senkin[38], C. Serfon[76], L. Serin[132], L. Serkin[66a,66b], M. Sessa[60a], H. Severini[128], F. Sforza[170], A. Sfyrla[54], E. Shabalina[53], J. D. Shahinian[146], N. W. Shaikh[45a,45b], D. Shaked Renous[180], L. Y. Shan[15a], R. Shang[173], J. T. Shank[25], M. Shapiro[18], A. S. Sharma[1], A. Sharma[135], P. B. Shatalov[111], K. Shaw[156], S. M. Shaw[100], A. Shcherbakova[138], Y. Shen[128], N. Sherafati[34], A. D. Sherman[25], P. Sherwood[94], L. Shi[158,ar], S. Shimizu[81], C. O. Shimmin[183], Y. Shimogama[179], M. Shimojima[116], I. P. J. Shipsey[135], S. Shirabe[87], M. Shiyakova[79,z], J. Shlomi[180], A. Shmeleva[110], M. J. Shochet[37], S. Shojaii[104], D. R. Shope[128], S. Shrestha[126], E. Shulga[180], P. Sicho[141], A. M. Sickles[173], P. E. Sidebo[154], E. Sideras Haddad[33c], O. Sidiropoulou[36], A. Sidoti[23a,23b], F. Siegert[48], Dj. Sijacki[16], M. Silva Jr.[181], M. V. Silva Oliveira[80a], S. B. Silverstein[45a], S. Simion[132], E. Simioni[99], R. Simoniello[99], P. Sinervo[167], N. B. Sinev[131], M. Sioli[23a,23b], I. Siral[105], S. Yu. Sivoklokov[113], J. Sjölin[45a,45b], E. Skorda[96], P. Skubic[128], M. Slawinska[84], K. Sliwa[170], R. Slovak[143], V. Smakhtin[180], B. H. Smart[144], J. Smiesko[28a], N. Smirnov[112], S. Yu. Smirnov[112], Y. Smirnov[112], L. N. Smirnova[113,s], O. Smirnova[96], J. W. Smith[53], M. Smizanska[89], K. Smolek[142], A. Smykiewicz[84], A. A. Snesarev[110], H. L. Snoek[120], I. M. Snyder[131], S. Snyder[29], R. Sobie[176,ac], A. M. Soffa[171], A. Soffer[161], A. Søgaard[50], F. Sohns[53], C. A. Solans Sanchez[36], E. Yu. Soldatov[112], U. Soldevila[174], A. A. Solodkov[123], A. Soloshenko[79], O. V. Solovyanov[123], V. Solovyev[138], P. Sommer[149], H. Son[170], W. Song[144], W. Y. Song[168b], A. Sopczak[142], F. Sopkova[28b], C. L. Sotiropoulou[71a,71b], S. Sottocornola[70a,70b], R. Soualah[66a,66c,g], A. M. Soukharev[122a,122b], D. South[46], S. Spagnolo[67a,67b], M. Spalla[115], M. Spangenberg[178], F. Spanò[93], D. Sperlich[52], T. M. Spieker[61a], R. Spighi[23b], G. Spigo[36], M. Spina[156], D. P. Spiteri[57], M. Spousta[143], A. Stabile[68a,68b], B. L. Stamas[121], R. Stamen[61a], M. Stamenkovic[120], E. Stanecka[84], R. W. Stanek[6], B. Stanislaus[135], M. M. Stanitzki[46], M. Stankaityte[135], B. Stapf[120], E. A. Starchenko[123], G. H. Stark[146], J. Stark[58], S. H. Stark[40], P. Staroba[141], P. Starovoitov[61a], S. Stärz[103], R. Staszewski[84], G. Stavropoulos[44], M. Stegler[46], P. Steinberg[29], A. L. Steinhebel[131], B. Stelzer[152], H. J. Stelzer[139], O. Stelzer-Chilton[168a], H. Stenzel[56], T. J. Stevenson[156], G. A. Stewart[36], M. C. Stockton[36], G. Stoicea[27b], M. Stolarski[140a], P. Stolte[53], S. Stonjek[115], A. Straessner[48], J. Strandberg[154], S. Strandberg[45a,45b], M. Strauss[128], P. Strizenec[28b], R. Ströhmer[177], D. M. Strom[131], R. Stroynowski[42], A. Strubig[50], S. A. Stucci[29], B. Stugu[17], J. Stupak[128], N. A. Styles[46], D. Su[153], S. Suchek[61a], Y. Sugaya[133], V. V. Sulin[110], M. J. Sullivan[90], D. M. S. Sultan[54], S. Sultansoy[4c], T. Sumida[85], S. Sun[105], X. Sun[3], K. Suruliz[156], C. J. E. Suster[157], M. R. Sutton[156], S. Suzuki[81], M. Svatos[141], M. Swiatlowski[37], S. P. Swift[2], T. Swirski[177], A. Sydorenko[99], I. Sykora[28a], M. Sykora[143], T. Sykora[143], D. Ta[99], K. Tackmann[46,x], J. Taenzer[161], A. Taffard[171], R. Tafirout[168a], E. Tahirovic[92], H. Takai[29], R. Takashima[86], K. Takeda[82], T. Takeshita[150], E. P. Takeva[50], Y. Takubo[81], M. Talby[101], A. A. Talyshev[122a,122b], N. M. Tamir[161], J. Tanaka[163], M. Tanaka[165], R. Tanaka[132], B. B. Tannenwald[126], S. Tapia Araya[173], S. Tapprogge[99], A. Tarek Abouelfadl Mohamed[136], S. Tarem[160], G. Tarna[27b,c], G. F. Tartarelli[68a], P. Tas[143], M. Tasevsky[141], T. Tashiro[85], E. Tassi[41a,41b], A. Tavares Delgado[140a,140b], Y. Tayalati[35e], A. J. Taylor[50], G. N. Taylor[104], W. Taylor[168b], A. S. Tee[89], R. Teixeira De Lima[153], P. Teixeira-Dias[93], H. Ten Kate[36], J. J. Teoh[120], S. Terada[81], K. Terashi[163], J. Terron[98], S. Terzo[14], M. Testa[51], R. J. Teuscher[167,ac], S. J. Thais[183], T. Theveneaux-Pelzer[46], F. Thiele[40], D. W. Thomas[93], J. O. Thomas[42], J. P. Thomas[21], A. S. Thompson[57], P. D. Thompson[21], L. A. Thomsen[183], E. Thomson[137], Y. Tian[39], R. E. Ticse Torres[53], V. O. Tikhomirov[110,ao], Yu. A. Tikhonov[122a,122b], S. Timoshenko[112], P. Tipton[183], S. Tisserant[101], K. Todome[23a,23b], S. Todorova-Nova[5], S. Todt[48], J. Tojo[87], S. Tokár[28a], K. Tokushuku[81], E. Tolley[126], K. G. Tomiwa[33c], M. Tomoto[117], L. Tompkins[153,p], K. Toms[118], B. Tong[59], P. Tornambe[102], E. Torrence[131], H. Torres[48], E. Torró Pastor[148], C. Tosciri[135], J. Toth[101,aa], D. R. Tovey[149], C. J. Treado[124], T. Trefzger[177], F. Tresoldi[156], A. Tricoli[29], I. M. Trigger[168a], S. Trincaz-Duvoid[136], W. Trischuk[167], B. Trocmé[58], A. Trofymov[132], C. Troncon[68a], M. Trovatelli[176], F. Trovato[156], L. Truong[33b], M. Trzebinski[84], A. Trzupek[84], F. Tsai[46], J.C-L. Tseng[135], P. V. Tsiareshka[107,ai], A. Tsirigotis[162], N. Tsirintanis[9], V. Tsiskaridze[155], E. G. Tskhadadze[159a], M. Tsopoulou[162], I. I. Tsukerman[111], V. Tsulaia[18], S. Tsuno[81], D. Tsybychev[155], Y. Tu[63b], A. Tudorache[27b], V. Tudorache[27b], T. T. Tulbure[27a], A. N. Tuna[59], S. Turchikhin[79], D. Turgeman[180], I. Turk Cakir[4b,t], R. J. Turner[21], R. T. Turra[68a], P. M. Tuts[39], S Tzamarias[162], E. Tzovara[99], G. Ucchielli[47], K. Uchida[163], I. Ueda[81], M. Ughetto[45a,45b], F. Ukegawa[169], G. Unal[36], A. Undrus[29], G. Unel[171], F. C. Ungaro[104], Y. Unno[81], K. Uno[163], J. Urban[28b], P. Urquijo[104], G. Usai[8], J. Usui[81], L. Vacavant[101], V. Vacek[142], B. Vachon[103], K. O. H. Vadla[134], A. Vaidya[94], C. Valderanis[114], E. Valdes Santurio[45a,45b], M. Valente[54], S. Valentinetti[23a,23b], A. Valero[174], L. Valéry[46], R. A. Vallance[21], A. Vallier[36], J. A. Valls Ferrer[174], T. R. Van Daalen[14], P. Van Gemmeren[6], I. Van Vulpen[120], M. Vanadia[73a,73b], W. Vandelli[36], A. Vaniachine[166], D. Vannicola[72a,72b], R. Vari[72a], E. W. Varnes[7], C. Varni[55a,55b], T. Varol[42], D. Varouchas[132], K. E. Varvell[157], M. E. Vasile[27b], G. A. Vasquez[176], J. G. Vasquez[183], F. Vazeille[38], D. Vazquez Furelos[14], T. Vazquez Schroeder[36], J. Veatch[53], V. Vecchio[74a,74b], M. J. Veen[120], L. M. Veloce[167],

F. Veloso[140a,140c], S. Veneziano[72a], A. Ventura[67a,67b], N. Venturi[36], A. Verbytskyi[115], V. Vercesi[70a], M. Verducci[74a,74b], C. M. Vergel Infante[78], C. Vergis[24], W. Verkerke[120], A. T. Vermeulen[120], J. C. Vermeulen[120], M. C. Vetterli[152,av], N. Viaux Maira[147b], M. Vicente Barreto Pinto[54], T. Vickey[149], O. E. Vickey Boeriu[149], G. H. A. Viehhauser[135], L. Vigani[135], M. Villa[23a,23b], M. Villaplana Perez[68a,68b], E. Vilucchi[51], M. G. Vincter[34], V. B. Vinogradov[79], A. Vishwakarma[46], C. Vittori[23a,23b], I. Vivarelli[156], M. Vogel[182], P. Vokac[142], S. E. von Buddenbrock[33c], E. Von Toerne[24], V. Vorobel[143], K. Vorobev[112], M. Vos[174], J. H. Vossebeld[90], N. Vranjes[16], M. Vranjes Milosavljevic[16], V. Vrba[142], M. Vreeswijk[120], T. Šfiligoj[91], R. Vuillermet[36], I. Vukotic[37], T. Ženiš[28a], L. Živković[16], P. Wagner[24], W. Wagner[182], J. Wagner-Kuhr[114], H. Wahlberg[88], K. Wakamiya[82], V. M. Walbrecht[115], J. Walder[89], R. Walker[114], S. D. Walker[93], W. Walkowiak[151], V. Wallangen[45a,45b], A. M. Wang[59], C. Wang[60b], F. Wang[181], H. Wang[18], H. Wang[3], J. Wang[157], J. Wang[61b], P. Wang[42], Q. Wang[128], R.-J. Wang[99], R. Wang[60a], R. Wang[6], S. M. Wang[158], W. T. Wang[60a], W. Wang[15c,ad], W. X. Wang[60a,ad], Y. Wang[60a,al], Z. Wang[60c], C. Wanotayaroj[46], A. Warburton[103], C. P. Ward[32], D. R. Wardrope[94], A. Washbrook[50], A. T. Watson[21], M. F. Watson[21], G. Watts[148], B. M. Waugh[94], A. F. Webb[11], S. Webb[99], C. Weber[183], M. S. Weber[20], S. A. Weber[34], S. M. Weber[61a], A. R. Weidberg[135], J. Weingarten[47], M. Weirich[99], C. Weiser[52], P. S. Wells[36], T. Wenaus[29], T. Wengler[36], S. Wenig[36], N. Wermes[24], M. D. Werner[78], P. Werner[36], M. Wessels[61a], T. D. Weston[20], K. Whalen[131], N. L. Whallon[148], A. M. Wharton[89], A. S. White[105], A. White[8], M. J. White[1], D. Whiteson[171], B. W. Whitmore[89], F. J. Wickens[144], W. Wiedenmann[181], M. Wielers[144], N. Wieseotte[99], C. Wiglesworth[40], L. A. M. Wiik-Fuchs[52], F. Wilk[100], H. G. Wilkens[36], L. J. Wilkins[93], H. H. Williams[137], S. Williams[32], C. Willis[106], S. Willocq[102], J. A. Wilson[21], I. Wingerter-Seez[5], E. Winkels[156], F. Winklmeier[131], O. J. Winston[156], B. T. Winter[52], M. Wittgen[153], M. Wobisch[95], A. Wolf[99], T. M. H. Wolf[120], R. Wolff[101], R. W. Wölker[135], J. Wollrath[52], M. W. Wolter[84], H. Wolters[140a,140c], V. W. S. Wong[175], N. L. Woods[146], S. D. Worm[21], B. K. Wosiek[84], K. W. Woźniak[84], K. Wraight[57], S. L. Wu[181], X. Wu[54], Y. Wu[60a], T. R. Wyatt[100], B. M. Wynne[50], S. Xella[40], Z. Xi[105], L. Xia[178], D. Xu[15a], H. Xu[60a,c], L. Xu[29], T. Xu[145], W. Xu[105], Z. Xu[60b], Z. Xu[153], B. Yabsley[157], S. Yacoob[33a], K. Yajima[133], D. P. Yallup[94], D. Yamaguchi[165], Y. Yamaguchi[165], A. Yamamoto[81], T. Yamanaka[163], F. Yamane[82], M. Yamatani[163], T. Yamazaki[163], Y. Yamazaki[82], Z. Yan[25], H. J. Yang[60c,60d], H. T. Yang[18], S. Yang[77], X. Yang[58,60b], Y. Yang[163], Z. Yang[17], W-M. Yao[18], Y. C. Yap[46], Y. Yasu[81], E. Yatsenko[60c,60d], J. Ye[42], S. Ye[29], I. Yeletskikh[79], M. R. Yexley[89], E. Yigitbasi[25], E. Yildirim[99], K. Yorita[179], K. Yoshihara[137], C. J. S. Young[36], C. Young[153], J. Yu[78], R. Yuan[60b], X. Yue[61a], S. P. Y. Yuen[24], B. Zabinski[84], G. Zacharis[10], E. Zaffaroni[54], J. Zahreddine[136], R. Zaidan[14], A. M. Zaitsev[123,an], T. Zakareishvili[159b], N. Zakharchuk[34], S. Zambito[59], D. Zanzi[36], D. R. Zaripovas[57], S. V. Zeißner[47], C. Zeitnitz[182], G. Zemaityte[135], J. C. Zeng[173], O. Zenin[123], D. Zerwas[132], M. Zgubič[135], D. F. Zhang[15b], F. Zhang[181], G. Zhang[60a], G. Zhang[15b], H. Zhang[15c], J. Zhang[6], L. Zhang[15c], L. Zhang[60a], M. Zhang[173], R. Zhang[60a], R. Zhang[24], X. Zhang[60b], Y. Zhang[15a,15d], Z. Zhang[63a], Z. Zhang[132], P. Zhao[49], Y. Zhao[60b], Z. Zhao[60a], A. Zhemchugov[79], Z. Zheng[105], D. Zhong[173], B. Zhou[105], C. Zhou[181], M. S. Zhou[15a,15d], M. Zhou[155], N. Zhou[60c], Y. Zhou[7], C. G. Zhu[60b], H. L. Zhu[60a], H. Zhu[15a], J. Zhu[105], Y. Zhu[60a], X. Zhuang[15a], K. Zhukov[110], V. Zhulanov[122a,122b], D. Zieminska[65], N. I. Zimine[79], S. Zimmermann[52], Z. Zinonos[115], M. Ziolkowski[151], G. Zobernig[181], A. Zoccoli[23a,], K. Zoch[53], T. G. Zorbas[149], R. Zou[37], L. Zwalinski[36]

[1] Department of Physics, University of Adelaide, Adelaide, Australia
[2] Physics Department, SUNY Albany, Albany, NY, USA
[3] Department of Physics, University of Alberta, Edmonton, AB, Canada
[4] [(a)]Department of Physics, Ankara University, Ankara, Turkey; [(b)]Istanbul Aydin University, Istanbul, Turkey; [(c)]Division of Physics, TOBB University of Economics and Technology, Ankara, Turkey
[5] LAPP, Université Grenoble Alpes, Université Savoie Mont Blanc, CNRS/IN2P3, Annecy, France
[6] High Energy Physics Division, Argonne National Laboratory, Argonne, IL, USA
[7] Department of Physics, University of Arizona, Tucson, AZ, USA
[8] Department of Physics, University of Texas at Arlington, Arlington, TX, USA
[9] Physics Department, National and Kapodistrian University of Athens, Athens, Greece
[10] Physics Department, National Technical University of Athens, Zografou, Greece
[11] Department of Physics, University of Texas at Austin, Austin, TX, USA
[12] [(a)]Bahcesehir University, Faculty of Engineering and Natural Sciences, Istanbul, Turkey; [(b)]Istanbul Bilgi University, Faculty of Engineering and Natural Sciences, Istanbul, Turkey; [(c)]Department of Physics, Bogazici University, Istanbul, Turkey; [(d)]Department of Physics Engineering, Gaziantep University, Gaziantep, Turkey
[13] Institute of Physics, Azerbaijan Academy of Sciences, Baku, Azerbaijan
[14] Institut de Física d'Altes Energies (IFAE), Barcelona Institute of Science and Technology, Barcelona, Spain

[15] [(a)]Institute of High Energy Physics, Chinese Academy of Sciences, Beijing, China; [(b)]Physics Department, Tsinghua University, Beijing, China; [(c)]Department of Physics, Nanjing University, Nanjing, China; [(d)]University of Chinese Academy of Science (UCAS), Beijing, China
[16] Institute of Physics, University of Belgrade, Belgrade, Serbia
[17] Department for Physics and Technology, University of Bergen, Bergen, Norway
[18] Physics Division, Lawrence Berkeley National Laboratory and University of California, Berkeley, CA, USA
[19] Institut für Physik, Humboldt Universität zu Berlin, Berlin, Germany
[20] Albert Einstein Center for Fundamental Physics and Laboratory for High Energy Physics, University of Bern, Bern, Switzerland
[21] School of Physics and Astronomy, University of Birmingham, Birmingham, UK
[22] Facultad de Ciencias y Centro de Investigaciónes, Universidad Antonio Nariño, Bogota, Colombia
[23] [(a)]INFN Bologna and Universita' di Bologna, Dipartimento di Fisica, Italy; [(b)]INFN Sezione di Bologna, Bologna, Italy
[24] Physikalisches Institut, Universität Bonn, Bonn, Germany
[25] Department of Physics, Boston University, Boston, MA, USA
[26] Department of Physics, Brandeis University, Waltham, MA, USA
[27] [(a)]Transilvania University of Brasov, Brasov, Romania; [(b)]Horia Hulubei National Institute of Physics and Nuclear Engineering, Bucharest, Romania; [(c)]Department of Physics, Alexandru Ioan Cuza University of Iasi, Iasi, Romania; [(d)]National Institute for Research and Development of Isotopic and Molecular Technologies, Physics Department, Cluj-Napoca, Romania; [(e)]University Politehnica Bucharest, Bucharest, Romania; [(f)]West University in Timisoara, Timisoara, Romania
[28] [(a)]Faculty of Mathematics, Physics and Informatics, Comenius University, Bratislava, Slovak Republic; [(b)]Department of Subnuclear Physics, Institute of Experimental Physics of the Slovak Academy of Sciences, Kosice, Slovak Republic
[29] Physics Department, Brookhaven National Laboratory, Upton, NY, USA
[30] Departamento de Física, Universidad de Buenos Aires, Buenos Aires, Argentina
[31] California State University, Long Beach, CA, USA
[32] Cavendish Laboratory, University of Cambridge, Cambridge, UK
[33] [(a)]Department of Physics, University of Cape Town, Cape Town, South Africa; [(b)]Department of Mechanical Engineering Science, University of Johannesburg, Johannesburg, South Africa; [(c)]School of Physics, University of the Witwatersrand, Johannesburg, South Africa
[34] Department of Physics, Carleton University, Ottawa, ON, Canada
[35] [(a)]Faculté des Sciences Ain Chock, Réseau Universitaire de Physique des Hautes Energies - Université Hassan II, Casablanca, Morocco; [(b)]Faculté des Sciences, Université Ibn-Tofail, Kenitra, Morocco; [(c)]Faculté des Sciences Semlalia, Université Cadi Ayyad, LPHEA, Marrakech, Morocco; [(d)]Faculté des Sciences, Université Mohamed Premier and LPTPM, Oujda, Morocco; [(e)]Faculté des sciences, Université Mohammed V, Rabat, Morocco
[36] CERN, Geneva, Switzerland
[37] Enrico Fermi Institute, University of Chicago, Chicago, IL, USA
[38] LPC, Université Clermont Auvergne, CNRS/IN2P3, Clermont-Ferrand, France
[39] Nevis Laboratory, Columbia University, Irvington, NY, USA
[40] Niels Bohr Institute, University of Copenhagen, Copenhagen, Denmark
[41] [(a)]Dipartimento di Fisica, Università della Calabria, Rende, Italy; [(b)]INFN Gruppo Collegato di Cosenza, Laboratori Nazionali di Frascati, Frascati, Italy
[42] Physics Department, Southern Methodist University, Dallas, TX, USA
[43] Physics Department, University of Texas at Dallas, Richardson, TX, USA
[44] National Centre for Scientific Research "Demokritos", Agia Paraskevi, Greece
[45] [(a)]Department of Physics, Stockholm University, Stockholm, Sweden; [(b)]Oskar Klein Centre, Stockholm, Sweden
[46] Deutsches Elektronen-Synchrotron DESY, Hamburg and Zeuthen, Germany
[47] Lehrstuhl für Experimentelle Physik IV, Technische Universität Dortmund, Dortmund, Germany
[48] Institut für Kern- und Teilchenphysik, Technische Universität Dresden, Dresden, Germany
[49] Department of Physics, Duke University, Durham, NC, USA
[50] SUPA-School of Physics and Astronomy, University of Edinburgh, Edinburgh, UK
[51] INFN e Laboratori Nazionali di Frascati, Frascati, Italy
[52] Physikalisches Institut, Albert-Ludwigs-Universität Freiburg, Freiburg, Germany
[53] II. Physikalisches Institut, Georg-August-Universität Göttingen, Göttingen, Germany

[54] Département de Physique Nucléaire et Corpusculaire, Université de Genève, Geneva, Switzerland
[55] [(a)]Dipartimento di Fisica, Università di Genova, Genoa, Italy; [(b)]INFN Sezione di Genova, Genoa, Italy
[56] II. Physikalisches Institut, Justus-Liebig-Universität Giessen, Giessen, Germany
[57] SUPA-School of Physics and Astronomy, University of Glasgow, Glasgow, UK
[58] LPSC, Université Grenoble Alpes, CNRS/IN2P3, Grenoble INP, Grenoble, France
[59] Laboratory for Particle Physics and Cosmology, Harvard University, Cambridge, MA, USA
[60] [(a)]Department of Modern Physics and State Key Laboratory of Particle Detection and Electronics, University of Science and Technology of China, Hefei, China; [(b)]Institute of Frontier and Interdisciplinary Science and Key Laboratory of Particle Physics and Particle Irradiation (MOE), Shandong University, Qingdao, China; [(c)]School of Physics and Astronomy, Shanghai Jiao Tong University, KLPPAC-MoE, SKLPPC, Shanghai, China; [(d)]Tsung-Dao Lee Institute, Shanghai, China
[61] [(a)]Kirchhoff-Institut für Physik, Ruprecht-Karls-Universität Heidelberg, Heidelberg, Germany; [(b)]Physikalisches Institut, Ruprecht-Karls-Universität Heidelberg, Heidelberg, Germany
[62] Faculty of Applied Information Science, Hiroshima Institute of Technology, Hiroshima, Japan
[63] [(a)]Department of Physics, Chinese University of Hong Kong, Shatin, N.T. Hong Kong, China; [(b)]Department of Physics, University of Hong Kong, Hong Kong, China; [(c)]Department of Physics and Institute for Advanced Study, Hong Kong University of Science and Technology, Clear Water Bay, Kowloon, Hong Kong, China
[64] Department of Physics, National Tsing Hua University, Hsinchu, Taiwan
[65] Department of Physics, Indiana University, Bloomington, IN, USA
[66] [(a)]INFN Gruppo Collegato di Udine, Sezione di Trieste, Udine, Italy; [(b)]ICTP, Trieste, Italy; [(c)]Dipartimento Politecnico di Ingegneria e Architettura, Università di Udine, Udine, Italy
[67] [(a)]INFN Sezione di Lecce, Lecce, Italy; [(b)]Dipartimento di Matematica e Fisica, Università del Salento, Lecce, Italy
[68] [(a)]INFN Sezione di Milano, Milan, Italy; [(b)]Dipartimento di Fisica, Università di Milano, Milan, Italy
[69] [(a)]INFN Sezione di Napoli, Naples, Italy; [(b)]Dipartimento di Fisica, Università di Napoli, Naples, Italy
[70] [(a)]INFN Sezione di Pavia, Pavia, Italy; [(b)]Dipartimento di Fisica, Università di Pavia, Pavia, Italy
[71] [(a)]INFN Sezione di Pisa, Pisa, Italy; [(b)]Dipartimento di Fisica E. Fermi, Università di Pisa, Pisa, Italy
[72] [(a)]INFN Sezione di Roma, Rome, Italy; [(b)]Dipartimento di Fisica, Sapienza Università di Roma, Rome, Italy
[73] [(a)]INFN Sezione di Roma Tor Vergata, Rome, Italy; [(b)]Dipartimento di Fisica, Università di Roma Tor Vergata, Rome, Italy
[74] [(a)]INFN Sezione di Roma Tre, Rome, Italy; [(b)]Dipartimento di Matematica e Fisica, Università Roma Tre, Rome, Italy
[75] [(a)]INFN-TIFPA, Povo, Italy; [(b)]Università degli Studi di Trento, Trento, Italy
[76] Institut für Astro- und Teilchenphysik, Leopold-Franzens-Universität, Innsbruck, Austria
[77] University of Iowa, Iowa City, IA, USA
[78] Department of Physics and Astronomy, Iowa State University, Ames, IA, USA
[79] Joint Institute for Nuclear Research, Dubna, Russia
[80] [(a)]Departamento de Engenharia Elétrica, Universidade Federal de Juiz de Fora (UFJF), Juiz de Fora, Brazil; [(b)]Universidade Federal do Rio De Janeiro COPPE/EE/IF, Rio de Janeiro, Brazil; [(c)]Universidade Federal de São João del Rei (UFSJ), São João del Rei, Brazil; [(d)]Instituto de Física, Universidade de São Paulo, São Paulo, Brazil
[81] KEK, High Energy Accelerator Research Organization, Tsukuba, Japan
[82] Graduate School of Science, Kobe University, Kobe, Japan
[83] [(a)]AGH University of Science and Technology, Faculty of Physics and Applied Computer Science, Kraków, Poland; [(b)]Marian Smoluchowski Institute of Physics, Jagiellonian University, Kraków, Poland
[84] Institute of Nuclear Physics Polish Academy of Sciences, Kraków, Poland
[85] Faculty of Science, Kyoto University, Kyoto, Japan
[86] Kyoto University of Education, Kyoto, Japan
[87] Research Center for Advanced Particle Physics and Department of Physics, Kyushu University, Fukuoka, Japan
[88] Instituto de Física La Plata, Universidad Nacional de La Plata and CONICET, La Plata, Argentina
[89] Physics Department, Lancaster University, Lancaster, UK
[90] Oliver Lodge Laboratory, University of Liverpool, Liverpool, UK
[91] Department of Experimental Particle Physics, Jožef Stefan Institute and Department of Physics, University of Ljubljana, Ljubljana, Slovenia
[92] School of Physics and Astronomy, Queen Mary University of London, London, UK
[93] Department of Physics, Royal Holloway University of London, Egham, UK

[94] Department of Physics and Astronomy, University College London, London, UK
[95] Louisiana Tech University, Ruston, LA, USA
[96] Fysiska institutionen, Lunds universitet, Lund, Sweden
[97] Centre de Calcul de l'Institut National de Physique Nucléaire et de Physique des Particules (IN2P3), Villeurbanne, France
[98] Departamento de Física Teorica C-15 and CIAFF, Universidad Autónoma de Madrid, Madrid, Spain
[99] Institut für Physik, Universität Mainz, Mainz, Germany
[100] School of Physics and Astronomy, University of Manchester, Manchester, UK
[101] CPPM, Aix-Marseille Université, CNRS/IN2P3, Marseille, France
[102] Department of Physics, University of Massachusetts, Amherst, MA, USA
[103] Department of Physics, McGill University, Montreal, QC, Canada
[104] School of Physics, University of Melbourne, Melbourne, VIC, Australia
[105] Department of Physics, University of Michigan, Ann Arbor, MI, USA
[106] Department of Physics and Astronomy, Michigan State University, East Lansing, MI, USA
[107] B.I. Stepanov Institute of Physics, National Academy of Sciences of Belarus, Minsk, Belarus
[108] Research Institute for Nuclear Problems of Byelorussian State University, Minsk, Belarus
[109] Group of Particle Physics, University of Montreal, Montreal, QC, Canada
[110] P.N. Lebedev Physical Institute of the Russian Academy of Sciences, Moscow, Russia
[111] Institute for Theoretical and Experimental Physics of the National Research Centre Kurchatov Institute, Moscow, Russia
[112] National Research Nuclear University MEPhI, Moscow, Russia
[113] D.V. Skobeltsyn Institute of Nuclear Physics, M.V. Lomonosov Moscow State University, Moscow, Russia
[114] Fakultät für Physik, Ludwig-Maximilians-Universität München, Munich, Germany
[115] Max-Planck-Institut für Physik (Werner-Heisenberg-Institut), Munich, Germany
[116] Nagasaki Institute of Applied Science, Nagasaki, Japan
[117] Graduate School of Science and Kobayashi-Maskawa Institute, Nagoya University, Nagoya, Japan
[118] Department of Physics and Astronomy, University of New Mexico, Albuquerque, NM, USA
[119] Institute for Mathematics, Astrophysics and Particle Physics, Radboud University Nijmegen/Nikhef, Nijmegen, The Netherlands
[120] Nikhef National Institute for Subatomic Physics and University of Amsterdam, Amsterdam, The Netherlands
[121] Department of Physics, Northern Illinois University, DeKalb, IL, USA
[122] [(a)]Budker Institute of Nuclear Physics and NSU, SB RAS, Novosibirsk, Russia; [(b)]Novosibirsk State University Novosibirsk, Novosibirsk, Russia
[123] Institute for High Energy Physics of the National Research Centre Kurchatov Institute, Protvino, Russia
[124] Department of Physics, New York University, New York, NY, USA
[125] Ochanomizu University, Otsuka, Bunkyo-ku, Tokyo, Japan
[126] Ohio State University, Columbus, OH, USA
[127] Faculty of Science, Okayama University, Okayama, Japan
[128] Homer L. Dodge Department of Physics and Astronomy, University of Oklahoma, Norman, OK, USA
[129] Department of Physics, Oklahoma State University, Stillwater, OK, USA
[130] Palacký University, RCPTM, Joint Laboratory of Optics, Olomouc, Czech Republic
[131] Center for High Energy Physics, University of Oregon, Eugene, OR, USA
[132] LAL, Université Paris-Sud, CNRS/IN2P3, Université Paris-Saclay, Orsay, France
[133] Graduate School of Science, Osaka University, Osaka, Japan
[134] Department of Physics, University of Oslo, Oslo, Norway
[135] Department of Physics, Oxford University, Oxford, UK
[136] LPNHE, Sorbonne Université, Paris Diderot Sorbonne Paris Cité, CNRS/IN2P3, Paris, France
[137] Department of Physics, University of Pennsylvania, Philadelphia, PA, USA
[138] Konstantinov Nuclear Physics Institute of National Research Centre "Kurchatov Institute", PNPI, St. Petersburg, Russia
[139] Department of Physics and Astronomy, University of Pittsburgh, Pittsburgh, PA, USA
[140] [(a)]Laboratório de Instrumentação e Física Experimental de Partículas-LIP, Coimbra, Portugal; [(b)]Departamento de Física, Faculdade de Ciências, Universidade de Lisboa, Lisboa, Portugal; [(c)]Departamento de Física, Universidade de Coimbra, Coimbra, Portugal; [(d)]Centro de Física Nuclear da Universidade de Lisboa, Lisboa, Portugal; [(e)]Departamento

de Física, Universidade do Minho, Braga, Portugal; [f]Universidad de Granada, Granada (Spain), Portugal; [g]Dep Física and CEFITEC of Faculdade de Ciências e Tecnologia, Universidade Nova de Lisboa, Caparica, Portugal
[141] Institute of Physics of the Czech Academy of Sciences, Prague, Czech Republic
[142] Czech Technical University in Prague, Prague, Czech Republic
[143] Charles University, Faculty of Mathematics and Physics, Prague, Czech Republic
[144] Particle Physics Department, Rutherford Appleton Laboratory, Didcot, UK
[145] IRFU, CEA, Université Paris-Saclay, Gif-sur-Yvette, France
[146] Santa Cruz Institute for Particle Physics, University of California Santa Cruz, Santa Cruz, CA, USA
[147] [a]Departamento de Física, Pontificia Universidad Católica de Chile, Santiago, Chile; [b]Departamento de Física, Universidad Técnica Federico Santa María, Valparaiso, Chile
[148] Department of Physics, University of Washington, Seattle, WA, USA
[149] Department of Physics and Astronomy, University of Sheffield, Sheffield, UK
[150] Department of Physics, Shinshu University, Nagano, Japan
[151] Department Physik, Universität Siegen, Siegen, Germany
[152] Department of Physics, Simon Fraser University, Burnaby, BC, Canada
[153] SLAC National Accelerator Laboratory, Stanford, CA, USA
[154] Physics Department, Royal Institute of Technology, Stockholm, Sweden
[155] Departments of Physics and Astronomy, Stony Brook University, Stony Brook, NY, USA
[156] Department of Physics and Astronomy, University of Sussex, Brighton, UK
[157] School of Physics, University of Sydney, Sydney, Australia
[158] Institute of Physics, Academia Sinica, Taipei, Taiwan
[159] [a]E. Andronikashvili Institute of Physics, Iv. Javakhishvili Tbilisi State University, Tbilisi, Georgia; [b]High Energy Physics Institute, Tbilisi State University, Tbilisi, Georgia
[160] Department of Physics, Technion, Israel Institute of Technology, Haifa, Israel
[161] Raymond and Beverly Sackler School of Physics and Astronomy, Tel Aviv University, Tel Aviv, Israel
[162] Department of Physics, Aristotle University of Thessaloniki, Thessaloniki, Greece
[163] International Center for Elementary Particle Physics and Department of Physics, University of Tokyo, Tokyo, Japan
[164] Graduate School of Science and Technology, Tokyo Metropolitan University, Tokyo, Japan
[165] Department of Physics, Tokyo Institute of Technology, Tokyo, Japan
[166] Tomsk State University, Tomsk, Russia
[167] Department of Physics, University of Toronto, Toronto, ON, Canada
[168] [a]TRIUMF, Vancouver, BC, Canada; [b]Department of Physics and Astronomy, York University, Toronto, ON, Canada
[169] Division of Physics and Tomonaga Center for the History of the Universe, Faculty of Pure and Applied Sciences, University of Tsukuba, Tsukuba, Japan
[170] Department of Physics and Astronomy, Tufts University, Medford, MA, USA
[171] Department of Physics and Astronomy, University of California Irvine, Irvine, CA, USA
[172] Department of Physics and Astronomy, University of Uppsala, Uppsala, Sweden
[173] Department of Physics, University of Illinois, Urbana, IL, USA
[174] Instituto de Física Corpuscular (IFIC), Centro Mixto Universidad de Valencia - CSIC, Valencia, Spain
[175] Department of Physics, University of British Columbia, Vancouver, BC, Canada
[176] Department of Physics and Astronomy, University of Victoria, Victoria, BC, Canada
[177] Fakultät für Physik und Astronomie, Julius-Maximilians-Universität Würzburg, Würzburg, Germany
[178] Department of Physics, University of Warwick, Coventry, UK
[179] Waseda University, Tokyo, Japan
[180] Department of Particle Physics, Weizmann Institute of Science, Rehovot, Israel
[181] Department of Physics, University of Wisconsin, Madison, WI, USA
[182] Fakultät für Mathematik und Naturwissenschaften, Fachgruppe Physik, Bergische Universität Wuppertal, Wuppertal, Germany
[183] Department of Physics, Yale University, New Haven, CT, USA
[184] Yerevan Physics Institute, Yerevan, Armenia

[a] Also at Centre for High Performance Computing, CSIR Campus, Rosebank, Cape Town, South Africa
[b] Also at CERN, Geneva, Switzerland

[c] Also at CPPM, Aix-Marseille Université, CNRS/IN2P3, Marseille, France
[d] Also at Département de Physique Nucléaire et Corpusculaire, Université de Genève, Geneva, Switzerland
[e] Also at Departament de Fisica de la Universitat Autonoma de Barcelona, Barcelona, Spain
[f] Also at Departamento de Física, Instituto Superior Técnico, Universidade de Lisboa, Lisbon, Portugal
[g] Also at Department of Applied Physics and Astronomy, University of Sharjah, Sharjah, United Arab Emirates
[h] Also at Department of Financial and Management Engineering, University of the Aegean, Chios, Greece
[i] Also at Department of Physics and Astronomy, University of Louisville, Louisville, KY, USA
[j] Also at Department of Physics and Astronomy, University of Sheffield, Sheffield, UK
[k] Also at Department of Physics, California State University, East Bay, USA
[l] Also at Department of Physics, California State University, Fresno, USA
[m] Also at Department of Physics, California State University, Sacramento, USA
[n] Also at Department of Physics, King's College London, London, UK
[o] Also at Department of Physics, St. Petersburg State Polytechnical University, St. Petersburg, Russia
[p] Also at Department of Physics, Stanford University, Stanford CA, USA
[q] Also at Department of Physics, University of Fribourg, Fribourg, Switzerland
[r] Also at Department of Physics, University of Michigan, Ann Arbor MI, USA
[s] Also at Faculty of Physics, M.V. Lomonosov Moscow State University, Moscow, Russia
[t] Also at Giresun University, Faculty of Engineering, Giresun, Turkey
[u] Also at Graduate School of Science, Osaka University, Osaka, Japan
[v] Also at Hellenic Open University, Patras, Greece
[w] Also at Institucio Catalana de Recerca i Estudis Avancats, ICREA, Barcelona, Spain
[x] Also at Institut für Experimentalphysik, Universität Hamburg, Hamburg, Germany
[y] Also at Institute for Mathematics, Astrophysics and Particle Physics, Radboud University Nijmegen/Nikhef, Nijmegen, The Netherlands
[z] Also at Institute for Nuclear Research and Nuclear Energy (INRNE) of the Bulgarian Academy of Sciences, Sofia, Bulgaria
[aa] Also at Institute for Particle and Nuclear Physics, Wigner Research Centre for Physics, Budapest, Hungary
[ab] Also at Institute of High Energy Physics, Chinese Academy of Sciences, Beijing, China
[ac] Also at Institute of Particle Physics (IPP), Canada
[ad] Also at Institute of Physics, Academia Sinica, Taipei, Taiwan
[ae] Also at Institute of Physics, Azerbaijan Academy of Sciences, Baku, Azerbaijan
[af] Also at Institute of Theoretical Physics, Ilia State University, Tbilisi, Georgia
[ag] Also at Instituto de Fisica Teorica, IFT-UAM/CSIC, Madrid, Spain
[ah] Also at Istanbul University, Dept. of Physics, Istanbul, Turkey
[ai] Also at Joint Institute for Nuclear Research, Dubna, Russia
[aj] Also at LAL, Université Paris-Sud, CNRS/IN2P3, Université Paris-Saclay, Orsay, France
[ak] Also at Louisiana Tech University, Ruston LA, USA
[al] Also at LPNHE, Sorbonne Université, Paris Diderot Sorbonne Paris Cité, CNRS/IN2P3, Paris, France
[am] Also at Manhattan College, New York NY, USA
[an] Also at Moscow Institute of Physics and Technology State University, Dolgoprudny, Russia
[ao] Also at National Research Nuclear University MEPhI, Moscow, Russia
[ap] Also at Physics Dept, University, of South Africa, Pretoria, South Africa
[aq] Also at Physikalisches Institut, Albert-Ludwigs-Universität Freiburg, Freiburg, Germany
[ar] Also at School of Physics, Sun Yat-sen University, Guangzhou, China
[as] Also at The City College of New York, New York NY, USA
[at] Also at The Collaborative Innovation Center of Quantum Matter (CICQM), Beijing, China
[au] Also at Tomsk State University, Tomsk, and Moscow Institute of Physics and Technology State University, Dolgoprudny, Russia
[av] Also at TRIUMF, Vancouver BC, Canada
[aw] Also at Universita di Napoli Parthenope, Naples, Italy
*Deceased

Eur. Phys. J. C (2019) 79:847
https://doi.org/10.1140/epjc/s10052-019-7321-3

THE EUROPEAN PHYSICAL JOURNAL C

Regular Article - Experimental Physics

Measurement of the inclusive cross-section for the production of jets in association with a Z boson in proton–proton collisions at 8 TeV using the ATLAS detector

ATLAS Collaboration[⋆]

CERN, 1211 Geneva 23, Switzerland

Received: 17 July 2019 / Accepted: 18 September 2019 / Published online: 14 October 2019

Abstract The inclusive cross-section for jet production in association with a Z boson decaying into an electron–positron pair is measured as a function of the transverse momentum and the absolute rapidity of jets using 19.9 fb^{-1} of $\sqrt{s} = 8$ TeV proton–proton collision data collected with the ATLAS detector at the Large Hadron Collider. The measured Z + jets cross-section is unfolded to the particle level. The cross-section is compared with state-of-the-art Standard Model calculations, including the next-to-leading-order and next-to-next-to-leading-order perturbative QCD calculations, corrected for non-perturbative and QED radiation effects. The results of the measurements cover final-state jets with transverse momenta up to 1 TeV, and show good agreement with fixed-order calculations.

Contents

1 Introduction

The measurement of the production cross-section of jets, a collimated spray of hadrons, in association with a Z boson (Z + jets), is an important process for testing the predictions of perturbative quantum chromodynamics (pQCD). It provides a benchmark for fixed-order calculations and predictions from Monte Carlo (MC) simulations, which are often used to estimate the Z + jets background in the measurements of Standard Model processes, such as Higgs boson production, and in searches for new physics beyond the Standard Model.

Various properties of Z + jets production have been measured in proton–antiproton collisions at $\sqrt{s} = 1.96$ TeV at the Tevatron [1–4]. The differential Z + jets cross-section is measured as functions of the Z boson transverse momentum and the jets' transverse momenta and rapidities, and as a function of the angular separation between the Z boson and jets in final states with different jet multiplicities. The experiments at the Large Hadron Collider (LHC) [5] have an increased phase space compared to previous measurements by using proton–proton collision data at $\sqrt{s} = 7, 8$ and 13 TeV [6–15]. The measurements at the LHC allow state-of-the-art theoreti-

⋆ e-mail: atlas.publications@cern.ch

cal Z + jets predictions to be tested. These have recently been calculated to next-to-next-to-leading-order (NNLO) accuracy in pQCD [16,17].

This paper studies the double-differential cross-section of inclusive jet production in association with a Z boson which decays into an electron–positron pair. The cross-section is measured as a function of absolute jet rapidity, $|y_{\text{jet}}|$, and jet transverse momentum, $p_{\text{T}}^{\text{jet}}$, using the proton–proton (pp) collision data at $\sqrt{s} = 8$ TeV collected by the ATLAS experiment. The measured cross-section is unfolded to the particle level.

The cross-section calculated at fixed order for Z + jets production in pp collisions at $\sqrt{s} = 8$ TeV is dominated by quark–gluon scattering. The Z + jets cross-section is sensitive to the gluon and sea-quark parton distribution functions (PDFs) in the proton. In the central $|y_{\text{jet}}|$ region the Z + jets cross-section probes the PDFs in the low x range, where x is the proton momentum fraction, while in the forward $|y_{\text{jet}}|$ region it examines the intermediate and high x values. The scale of the probe is set by $p_{\text{T}}^{\text{jet}}$.

The measured cross-section is compared with the next-to-leading-order (NLO) and NNLO Z + jets fixed-order calculations, corrected for hadronisation and the underlying event. In addition, the data are compared with the predictions from multi-leg matrix element (ME) MC event generators supplemented with parton shower simulations.

The structure of the paper is as follows. The ATLAS detector is briefly described in Sect. 2. This is followed by a description of the data in Sect. 3 and the simulated samples in Sect. 4. The definition of the object reconstruction, calibration and identification procedures and a summary of the selection criteria are given in Sect. 5. The Z + jets backgrounds are discussed in Sect. 6. The correction of the measured spectrum to the particle level is described in Sect. 7. The experimental uncertainties are discussed in Sect. 8. The fixed-order calculations together with parton-to-particle-level corrections are presented in Sect. 9. Finally, the measured cross-section is presented and compared with the theory predictions in Sect. 10. The quantitative comparisons with the fixed-order pQCD predictions are summarised in Sect. 11.

2 The ATLAS detector

The ATLAS experiment [18] at the LHC is a multipurpose particle detector with a forward–backward symmetric cylindrical geometry and nearly 4π coverage in solid angle.[1] It consists of an inner tracking detector surrounded by a thin superconducting solenoid, electromagnetic and hadronic calorimeters, and a muon spectrometer incorporating three large superconducting toroidal magnets.

The inner-detector system (ID) is immersed in a 2 T axial magnetic field and provides charged-particle tracking in the range $|\eta| < 2.5$. A high-granularity silicon pixel detector covers the pp interaction region and typically provides three measurements per track. It is followed by a silicon microstrip tracker (SCT), which usually provides four two-dimensional measurement points per track. These silicon detectors are complemented by a transition radiation tracker (TRT), which provides electron identification information.

The calorimeter system covers the pseudorapidity range $|\eta| < 4.9$. In the region $|\eta| < 3.2$, electromagnetic calorimetry is provided by barrel and endcap high-granularity lead/liquid-argon (LAr) electromagnetic calorimeters, with an additional thin LAr presampler covering $|\eta| < 1.8$ to correct for energy loss in material upstream of the calorimeters. Hadronic calorimetry is provided by a steel/scintillator-tile calorimeter, segmented into three barrel structures for $|\eta| < 1.7$, and two copper/LAr hadronic endcap calorimeters in the range $1.5 < |\eta| < 3.2$. The calorimetry in the forward pseudorapidity region, $3.1 < |\eta| < 4.9$, is provided by the copper-tungsten/LAr calorimeters.

The muon spectrometer surrounds the calorimeters and contains three large air-core toroidal superconducting magnets with eight coils each. The field integral of the toroids ranges between 2.0 and 6.0 T m across most of the detector. The muon spectrometer includes a system of precision tracking chambers and fast detectors for triggering.

A three-level trigger [19] was used to select events for offline analysis. The first-level trigger is implemented in hardware and used a subset of the detector information to reduce the accepted rate to at most 75 kHz. This was followed by two software-based trigger levels that together reduced the average accepted event rate to 400 Hz.

3 Data sample

The data used for this analysis are from proton–proton collisions at $\sqrt{s} = 8$ TeV that were collected by the ATLAS detector in 2012 during stable beam conditions. Events recorded when any of the ATLAS subsystems were defective or non-operational are excluded. Data were selected with a dielectron trigger, which required two reconstructed electron candidates with transverse momenta greater than 12 GeV. Only

[1] ATLAS uses a right-handed coordinate system with its origin at the nominal interaction point (IP) in the centre of the detector and the z-axis along the beam pipe. The x-axis points from the IP to the centre of the LHC ring, and the y-axis points upwards. Cylindrical coordinates (r, ϕ) are used in the transverse plane, ϕ being the azimuthal angle around the z-axis. The pseudorapidity is defined in terms of the polar angle θ as $\eta = -\ln\tan(\theta/2)$. Angular distance is measured in units of $\Delta R \equiv \sqrt{(\Delta\eta)^2 + (\Delta\phi)^2}$.

events with electron energy leakage of less than 1 GeV into the hadronic calorimeter were accepted. The trigger required that reconstructed electron candidates were identified using the 'loose1' criteria [20], which are discussed in Sect. 5.1.

The integrated luminosity of the analysis data sample after the trigger selection is 19.9 fb^{-1} measured with an uncertainty of $\pm 1.9\%$ [21]. The average number of simultaneous proton–proton interactions per bunch crossing is 20.7.

In addition, a special data sample was selected for a data-driven study of multijet and W+ jets backgrounds. For this purpose, the analysis data sample was enlarged by including auxiliary events selected by a logical OR of two single-electron triggers.

The first single-electron trigger required events with at least one reconstructed electron candidate with a transverse momentum greater than 24 GeV and hadronic energy leakage less than 1 GeV. The electron candidate satisfied the 'medium1' identification criteria [20], a tightened subset of 'loose1'. The reconstructed electron track was required to be isolated from other tracks in the event. The isolation requirement rejected an event if the scalar sum of reconstructed track transverse momenta in a cone of size $\Delta R = 0.2$ around the electron track exceeded 10% of the electron track's transverse momentum.

The second single-electron trigger accepted events with at least one electron candidate with a transverse momentum greater than 60 GeV and identified as 'medium1'. This trigger reduced inefficiencies in events with high-p_{T} electrons that resulted from the isolation requirement used in the first trigger.

Events selected by single-electron triggers include a large number of background events that are normally rejected by the Z + jets selection requirements, but these events are used in the data-driven background studies.

4 Monte Carlo simulations

Simulated Z + jets signal events were generated using the Sherpa v. 1.4 [22] multi-leg matrix element MC generator. The MEs were calculated at NLO accuracy for the inclusive Z production process, and additionally with LO accuracy for up to five partons in the final state, using Amegic++ [23]. Sherpa MEs were convolved with the CT10 [24] PDFs. Sherpa parton showers were matched to MEs following the CKKW scheme [25]. The MENLOPS [26] prescription was used to combine different parton multiplicities from matrix elements and parton showers. Sherpa predictions were normalised to the inclusive Z boson production cross-section calculated at NNLO [27–29] and are used for the unfolding to particle level and for the evaluation of systematic uncertainties.

An additional Z + jets signal sample with up to five partons in the final state at LO was generated using Alpgen v. 2.14 [30]. The parton showers were generated using Pythia v. 6.426 [31] with the Perugia 2011C [32] set of tuned parameters to model the underlying event's contribution. The Alpgen MEs were matched to the parton showers following the MLM prescription [30]. The proton structure was described by the CTEQ6L1 [33] PDF. Referred to as the Alpgen+Pythia sample, these predictions were normalised to the NNLO cross-section. This sample is used in the analysis for the unfolding uncertainty evaluation and for comparisons with the measurement.

The five-flavour scheme with massless quarks was used in both the Sherpa and Alpgen+Pythia predictions.

Backgrounds from the $Z \to \tau\tau$, diboson (WW, WZ and ZZ), $t\bar{t}$ and single-top-quark events are estimated using MC simulations. The $Z \to \tau\tau$ events were generated using Powheg- Box v. 1.0 [34,35] interfaced to Pythia v. 8.160 [36] for parton showering using the CT10 PDFs and the AU2 [37] set of tuned parameters. The $Z \to \tau\tau$ prediction was normalised to the NNLO cross-section [27–29]. The WW, WZ and ZZ events were generated using Herwig v. 6.520.2 [38] with the CTEQ6L1 PDFs and the AUET2 [39] set of tuned parameters. The diboson predictions were normalised to the NLO cross-sections [40,41]. Samples of single-top-quark events, produced via the s-, t- and Wt-channels, and $t\bar{t}$ events were generated with Powheg- Box v. 1.0 interfaced to Pythia v. 6.426, which used the CTEQ6L1 PDFs and the Perugia 2011C set of tuned parameters. The prediction for single-top-quark production in s-channel were normalised to the NNLO calculations matched to the next-to-next-to-leading-logarithm (NNLL) calculations (NNLO+NNLL) [42], while predictions in t- and Wt-channel are normalised to the NLO+NNLL calculations [43,44]. The $t\bar{t}$ samples were normalised to the NNLO+NNLL calculations [45].

The Photos [46] and Tauola [47] programs were interfaced to the MC generators, excluding Sherpa, to model electromagnetic final-state radiation and τ-lepton decays, respectively.

Additional proton–proton interactions, generally called pile-up, were simulated using the Pythia v. 8.160 generator with the MSTW2008 [48] PDFs and the A2 [37] set of tuned parameters. The pile-up events were overlaid onto the events from the hard-scattering physics processes. MC simulated events were reweighted to match the distribution of the average number of interactions per bunch crossing in data.

All MC predictions were obtained from events processed with the ATLAS detector simulation [49] that is based on Geant 4 [50].

5 Object definitions and event selection

The measured objects are the electrons and jets reconstructed in ATLAS. The methods used to reconstruct, identify and calibrate electrons are presented in Sect. 5.1. The reconstruction of jets, their calibration, and background suppression methods are discussed in Sect. 5.2. Finally, all selection requirements are summarised in Sect. 5.3.

5.1 Electron reconstruction and identification

Electron reconstruction in the central region, $|\eta| < 2.5$, starts from energy deposits in calorimeter cells. A sliding-window algorithm scans the central volume of the electromagnetic calorimeter in order to seed three-dimensional clusters. The window has a size of 3×5 in units of 0.025×0.025 in η–ϕ space. Seeded cells have an energy sum of the constituent calorimeter cells greater than 2.5 GeV. An electron candidate is reconstructed if the cluster is matched to at least one track assigned to the primary vertex, as measured in the inner detector. The energy of a reconstructed electron candidate is given by the energy of a cluster that is enlarged to a size of 3×7 (5×5) in η–ϕ space in the central (endcap) electromagnetic calorimeter in order to take into account the shape of electromagnetic shower energy deposits in different calorimeter regions. The η and ϕ coordinates of a reconstructed electron candidate are taken from the matched track. The details of the electron reconstruction are given in Ref. [51].

A multistep calibration is used to correct the electron energy scale to that of simulated electrons [52]. Cluster energies in data and in MC simulation are corrected for energy loss in the material upstream of the electromagnetic calorimeter, energy lost outside of the cluster volume and energy leakage beyond the electromagnetic calorimeter. The reconstructed electron energy in data is corrected as a function of electron pseudorapidity using a multiplicative scale factor obtained from a comparison of $Z \to ee$ mass distributions between data and simulation. In addition, the electron energy in the MC simulation is scaled by a random number taken from a Gaussian distribution with a mean value of one and an η-dependent width, equal to the difference between the electron energy resolution in data and MC simulation, determined in situ using $Z \to ee$ events.

A set of cut-based electron identification criteria, which use cluster shape and track properties, is applied to reconstructed electrons to suppress the residual backgrounds from photon conversions, jets misidentified as electrons and semileptonic heavy-hadron decays. There are three types of identification criteria, listed in the order of increasing background-rejection strength but diminishing electron selection efficiency: 'loose', 'medium' and 'tight' [51]. The 'loose' criteria identify electrons using a set of thresholds applied to cluster shape properties measured in the first and second LAr calorimeter layers, energy leakage into the hadronic calorimeter, the number of hits in the pixel and SCT detectors, and the angular distance between the cluster position in the first LAr calorimeter layer and the extrapolated track. The 'medium' selection tightens 'loose' requirements on shower shape variables. In addition, the 'medium' selection sets conditions on the energy deposited in the third calorimeter layer, track properties in the TRT detector and the vertex position. The 'tight' selection tightens the 'medium' identification criteria thresholds, sets conditions on the measured ratio of cluster energy to track momentum and rejects reconstructed electron candidates matched to photon conversions.

Each MC simulated event is reweighted by scale factors that make the trigger, reconstruction and identification efficiencies the same in data and MC simulation. The scale factors are generally close to one and are calculated in bins of electron transverse momenta and pseudorapidity [20,51].

5.2 Jet reconstruction, pile-up suppression and quality criteria

Jets are reconstructed using the anti-k_t algorithm [53] with a radius parameter $R = 0.4$, as implemented in the FastJet software package [54]. Jet reconstruction uses topologically clustered cells from both the electromagnetic and hadronic calorimeters [55]. The topological clustering algorithm groups cells with statistically significant energy deposits as a method to suppress noise. The energy scale of calorimeter cells is initially established for electromagnetic particles. The local cell weighting (LCW) [56] calibration is applied to topological clusters to correct for the difference between the detector responses to electromagnetic and hadronic particles, energy losses in inactive material and out-of-cluster energy deposits. The LCW corrections are derived using the MC simulation of the detector response to single pions.

The jet energy scale (JES) calibration [57] corrects the energy scale of reconstructed jets to that of simulated particle-level jets. The JES calibration includes origin correction, pile-up correction, MC-based correction of the jet energy and pseudorapidity (MCJES), global sequential calibration (GSC) and residual in situ calibration.

The origin correction forces the four-momentum of the jet to point to the hard-scatter primary vertex rather than to the centre of the detector, while keeping the jet energy constant.

Pile-up contributions to the measured jet energies are accounted for by using a two-step procedure. First, the reconstructed jet energy is corrected for the effect of pile-up by using the average energy density in the event and the area of the jet [58]. Second, a residual correction is applied to remove the remaining dependence of the jet energy on the number of

reconstructed primary vertices, N_{PV}, and the expected average number of interactions per bunch crossing, $\langle\mu\rangle$.

The MCJES corrects the reconstructed jet energy to the particle-level jet energy using MC simulation. In addition, a correction is applied to the reconstructed jet pseudorapidity to account for the biases caused by the transition between different calorimeter regions and the differences in calorimeter granularity.

Next, the GSC corrects the jet four-momenta to reduce the response's dependence on the flavour of the parton that initiates the jet. The GSC is determined using the number of tracks assigned to a jet, the p_{T}-weighted transverse distance in the η–ϕ space between the jet axis and all tracks assigned to the jet (track width), and the number of muon track segments assigned to the jet.

Finally, the residual in situ correction makes the jet response the same in data and MC simulation as a function of detector pseudorapidity by using dijet events (η-intercalibration), and as a function of jet transverse momentum by using well-calibrated reference objects in Z/γ and multijet events.

Jets originating from pile-up interactions are suppressed using the jet vertex fraction (JVF) [58]. The JVF is calculated for each jet and each primary vertex in the event as a ratio of the scalar sum of p_{T} of tracks, matched to a jet and assigned to a given vertex, to the scalar sum of p_{T} of all tracks matched to a jet.

Applying jet quality criteria suppresses jets from non-collision backgrounds that arise from proton interactions with the residual gas in the beam pipe, beam interactions with the collimator upstream of the ATLAS detector, cosmic rays overlapping in time with the proton–proton collision and noise in the calorimeter. Jet quality criteria are used to distinguish jets by using the information about the quality of the energy reconstruction in calorimeter cells, the direction of the shower development and the properties of tracks matched to jets. There are four sets of selection criteria that establish jet quality: 'looser', 'loose', 'medium' and 'tight'. They are listed in the order of increasing suppression of non-collision jet background but decreasing jet selection efficiency. The 'medium' jet selection is used in the paper due to its high background rejection rate together with about 100% jet selection efficiency in the $p_{\mathrm{T}}^{\mathrm{jet}} > 60\,\mathrm{GeV}$ region [57].

5.3 Event selection

Events are required to have a primary vertex with at least three assigned tracks that have a transverse momentum greater than 400 MeV. When several reconstructed primary vertices satisfy this requirement, the hard-scatter vertex is taken to be the one with the highest sum of the squares of the transverse momenta of its assigned tracks.

Each event is required to have exactly two reconstructed electrons, each with transverse momentum greater than 20 GeV and an absolute pseudorapidity less than 2.47, excluding the detector transition region, $1.37 < |\eta_e| < 1.52$, between barrel and endcap electromagnetic calorimeters. The electrons are required to have opposite charges, be identified using the 'medium' [51] criteria and be matched to electron candidates that were selected by the trigger. The 'medium' identification ensures the electrons originate from the hard-scatter vertex. The electron-pair invariant mass, m_{ee}, is required to be in the $66\,\mathrm{GeV} < m_{ee} < 116\,\mathrm{GeV}$ range.

Jets are required to have a transverse momentum greater than 25 GeV and an absolute jet rapidity less than 3.4. Jets with $p_{\mathrm{T}}^{\mathrm{jet}} < 50\,\mathrm{GeV}$, $|\eta_{\mathrm{det}}| < 2.4$, where η_{det} is reconstructed relative to the detector centre, and $|\mathrm{JVF}| < 0.25$ are considered to be from pile-up. Jets originating from pile-up are removed from the measurement. MC simulations poorly describe the effects of high pile-up in the $p_{\mathrm{T}}^{\mathrm{jet}} < 50\,\mathrm{GeV}$ and $|y_{\mathrm{jet}}| > 2.4$ region, so this region is not included in the measurement. Jets reconstructed within $\Delta R = 0.4$ of selected electrons are rejected in order to avoid overlap. Jets are required to satisfy the 'medium' [57] quality criteria. In addition, jets in regions of the detector that are poorly modelled are rejected in data and MC simulations in order to avoid biasing the measured jet energy [57]. Each jet that meets the selection requirements is used in the measurement.

As a result, 1,486,415 events with two electrons and at least one jet were selected for the analysis.

6 Backgrounds

The majority of irreducible backgrounds in this measurement are studied using MC samples that simulate $Z \to \tau\tau$, diboson, $t\bar{t}$ and single top-quark production. The $Z \to \tau\tau$ process is a background if both τ-leptons decay into an electron and neutrino. Diboson production constitutes a background to the Z + jets signal if the W and/or Z boson decays into electrons. Since the top-quark decays predominantly via $t \to Wb$, the $t\bar{t}$ and single top-quark constitute a background to the Z + jets signal when W bosons decay into an electron or jets are misidentified as electrons.

Multijet production constitutes a background to the Z + jets signal when two jets are misidentified as electrons. The W+ jets background is due to an electron from W boson decay and a jet misidentified as electron. A combined background from multijet and W+ jets events is studied using a data-driven technique, thus providing a model-independent background estimate.

A background-enriched data sample is used for the combined multijet and W+ jets background control region. Its selection requires two reconstructed electrons with at least

one electron that satisfies the 'medium' identification criteria, but not the 'tight' ones. This allows selection of events with at least one jet misidentified as an electron. No identification criteria are applied to the second reconstructed electron, in order to allow for the possibility of W+ jets events with a genuine electron from W boson decay, and multijet events with a jet misidentified as another electron. Both selected electrons are required to have the same charge to suppress the Z + jets signal events. The combined multijet and W+ jets background template is constructed by subtracting the MC simulated Z + jets signal events and $Z \to \tau\tau$, diboson, $t\bar{t}$ and single-top-quark background events in the control region from data.

The purity of the template is calculated as the fraction of multijet and W+ jets events in the data control region. The purity is about 98% in the tails of the m_{ee} distribution and is about 80% near the m_{ee} peak at 91 GeV. The template purity is above 90% in all $|y_{\text{jet}}|$ and $p_{\text{T}}^{\text{jet}}$ bins.

The combined multijet and W+ jets background template is normalised to data using the invariant mass distribution of reconstructed electron pairs. A maximum-likelihood fit is used to adjust the normalisation of the combined multijet and W+ jets background template relative to the measured Z + jets distribution. The normalisations of MC simulated samples are fixed in the fit: the $Z \to \tau\tau$, diboson, $t\bar{t}$ and single-top-quark distributions are normalised by their fixed-order cross-sections, whereas the normalisation of the MC simulated Z + jets signal events is scaled to data to give the same total number of events near the peak of the Z mass spectrum in the $90\,\text{GeV} < m_{ee} < 92\,\text{GeV}$ range. The combined multijet and W+ jets background is fit to data in an extended m_{ee} region, $60\,\text{GeV} < m_{ee} < 140\,\text{GeV}$, excluding the bins under the Z peak within the $80\,\text{GeV} < m_{ee} < 100\,\text{GeV}$ region. The extended m_{ee} region is used for the normalisation extraction only, as it allows more background events in the tails of the Z mass spectrum. The normalisation of the multijet and W+ jets background template, calculated in the fit, is used to adjust the templates, obtained in the $|y_{\text{jet}}|$ and $p_{\text{T}}^{\text{jet}}$ bins, to the Z + jets signal region.

The total number of jets in Z + jets events are shown as a function of $|y_{\text{jet}}|$ and $p_{\text{T}}^{\text{jet}}$ bins in Fig. 1. Data are compared with the sum of signal MC events and all backgrounds.

The SHERPA Z + jets simulation, normalised to the NNLO cross-section, is lower than data by about 10% in the $p_{\text{T}}^{\text{jet}} <$ 200 GeV region. These differences are mostly covered by the variations within electron and jet uncertainties introduced in Sect. 8. In the $p_{\text{T}}^{\text{jet}} > 200\,\text{GeV}$ region, agreement with data is within the statistical uncertainties.

The ALPGEN+PYTHIA predictions are in agreement with data within 10% for jets with transverse momenta below 100 GeV. However, the level of disagreement increases as a function of the jet transverse momenta, reaching 30% in the $400\,\text{GeV} < p_{\text{T}}^{\text{jet}} < 1050\,\text{GeV}$ region.

The dominant background in the measurement is from $t\bar{t}$ events. It is 0.3–0.8% in the $25\,\text{GeV} < p_{\text{T}}^{\text{jet}} < 50\,\text{GeV}$ region and 1–2.5% in the $50\,\text{GeV} < p_{\text{T}}^{\text{jet}} < 100\,\text{GeV}$ region, with the largest contribution in the central rapidity region. In the $100\,\text{GeV} < p_{\text{T}}^{\text{jet}} < 200\,\text{GeV}$ region, this background is approximately 3%, while in the $200\,\text{GeV} < p_{\text{T}}^{\text{jet}} < 1050\,\text{GeV}$ region it is 1.8–8%, increasing for forward rapidity jets.

The combined multijet and W+ jets background and the diboson background are similar in size. The contributions of these backgrounds are 0.5–1%.

The $Z \to \tau\tau$ and single-top-quark backgrounds are below 0.1%.

7 Unfolding of detector effects

The experimental measurements are affected by the detector resolution and reconstruction inefficiencies. In order to compare the measured cross-sections with the theoretical Z + jets predictions at the particle level, the reconstructed spectrum is corrected for detector effects using the iterative Bayesian unfolding method [59]. The unfolding is performed using the SHERPA Z + jets simulation.

The particle-level phase space in the MC simulation is defined using two dressed electrons and at least one jet. For the dressed electron, the four-momenta of any photons within a cone of $\Delta R = 0.1$ around its axis are added to the four-momentum of the electron. Electrons are required to have $|\eta| < 2.47$ and $p_{\text{T}} > 20\,\text{GeV}$. The electron pair's invariant mass is required to be within the range $66\,\text{GeV} < m_{ee} < 116\,\text{GeV}$.

Jets at the particle level are built by using the anti-k_t jet algorithm with a radius parameter $R = 0.4$ to cluster stable final-state particles with a decay length of $c\tau > 10$ mm, excluding muons and neutrinos. Jets are selected in the $|y_{\text{jet}}| < 3.4$ and $p_{\text{T}}^{\text{jet}} > 25\,\text{GeV}$ region. Jets within $\Delta R = 0.4$ of electrons are rejected.

The closest reconstructed and particle-level jets are considered matched if ΔR between their axes satisfies $\Delta R < 0.4$.

The input for the unfolding is the transfer matrix, which maps reconstructed jets to the particle-level jets in the $|y_{\text{jet}}|$–$p_{\text{T}}^{\text{jet}}$ plane, taking into account the bin-to-bin migrations that arise from limited detector resolution. An additional $p_{\text{T}}^{\text{jet}}$ bin, $17\,\text{GeV} < p_{\text{T}}^{\text{jet}} < 25\,\text{GeV}$, is included in the reconstructed and particle-level jet spectra to account for the migrations from the low $p_{\text{T}}^{\text{jet}}$ range. This bin is not reported in the measurement.

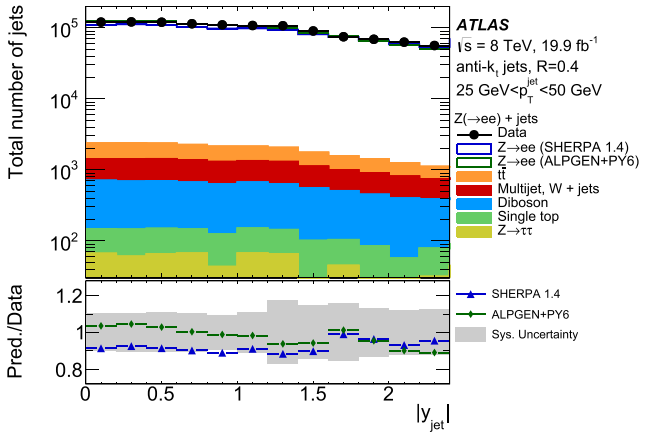

(a) 25 GeV $< p_{\mathrm{T}}^{\mathrm{jet}} <$ 50 GeV

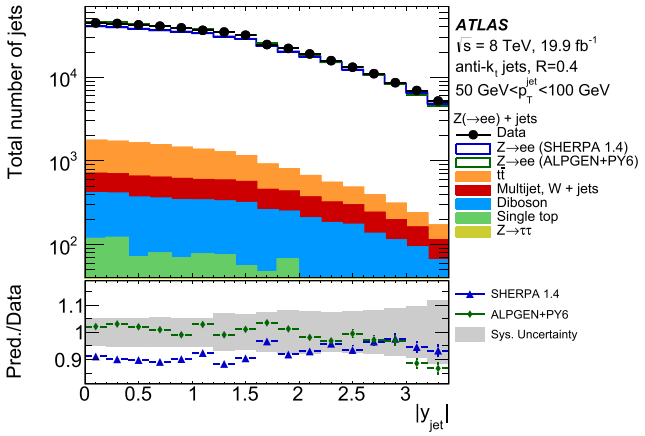

(b) 50 GeV $< p_{\mathrm{T}}^{\mathrm{jet}} <$ 100 GeV

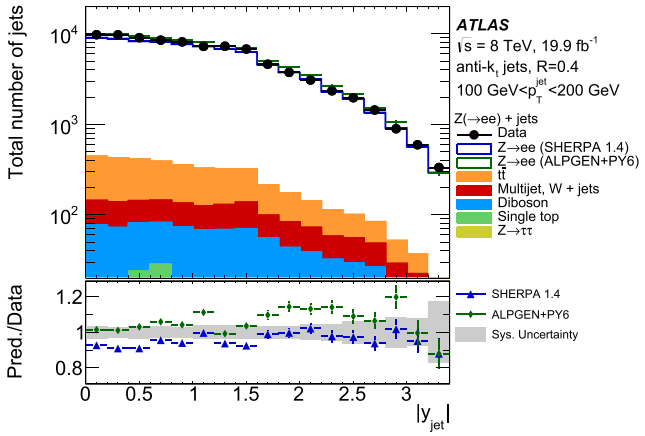

(c) 100 GeV $< p_{\mathrm{T}}^{\mathrm{jet}} <$ 200 GeV

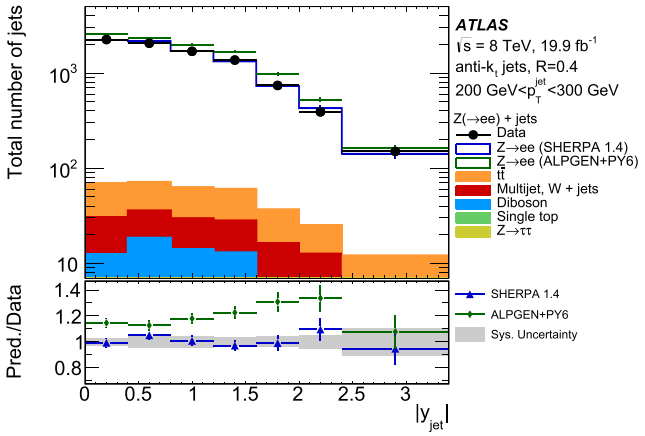

(d) 200 GeV $< p_{\mathrm{T}}^{\mathrm{jet}} <$ 300 GeV

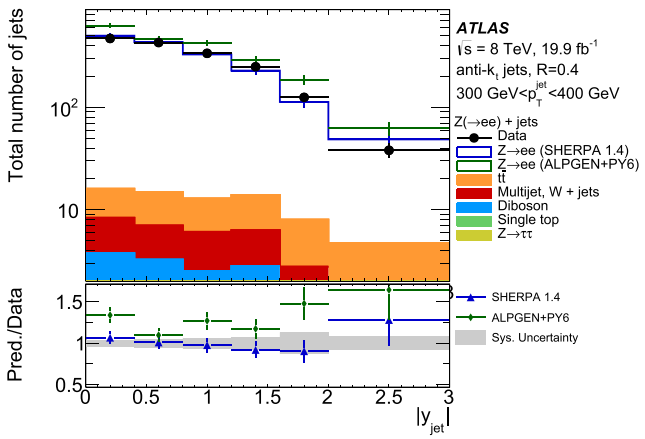

(e) 300 GeV $< p_{\mathrm{T}}^{\mathrm{jet}} <$ 400 GeV

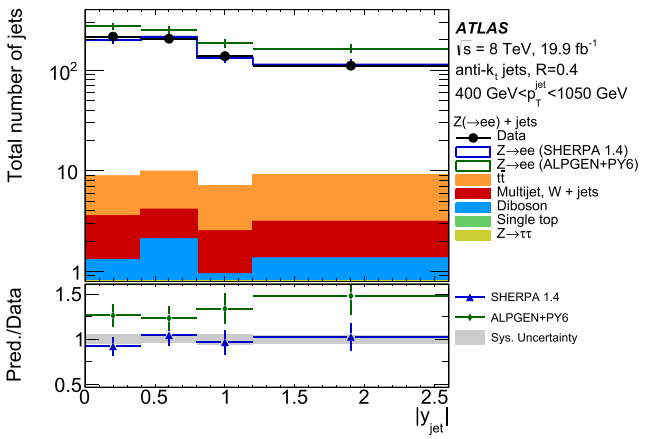

(f) 400 GeV $< p_{\mathrm{T}}^{\mathrm{jet}} <$ 1050 GeV

Fig. 1 The total number of jets in Z + jets events as a function of $|y_{\mathrm{jet}}|$ in $p_{\mathrm{T}}^{\mathrm{jet}}$ bins for the integrated luminosity of 19.9 fb^{-1}. Data are presented with markers. The filled areas correspond to the backgrounds stacked. All backgrounds are added to the Z + jets SHERPA and ALPGEN+PYTHIA predictions. Lower panels show ratios of MC predictions to data. The grey band shows the sum in quadrature of the electron and jet uncertainties. The statistical uncertainties are shown with vertical error bars. In the lower panels the total data + MC statistical uncertainty is shown

Given the significant amount of migration between jet transverse momentum bins, the unfolding is performed in all $|y_{\text{jet}}|$ and $p_{\text{T}}^{\text{jet}}$ bins simultaneously. The migration between adjacent $|y_{\text{jet}}|$ bins is found to be small.

The transfer matrix is defined for matched jets. Therefore, the reconstructed jet spectrum must be corrected to account for matching efficiencies prior to unfolding. The reconstruction-level matching efficiency is calculated as the fraction of reconstructed jets matching particle-level jets. This efficiency is 80–90% in the $25\,\text{GeV} < p_{\text{T}}^{\text{jet}} < 100\,\text{GeV}$ region and is above 99% in the $p_{\text{T}}^{\text{jet}} > 100\,\text{GeV}$ region. The particle-level jet matching efficiency is calculated as the fraction of particle-level jets matching reconstructed jets. This efficiency is 45–55% in all bins of the measurement due to the inefficiency of the Z boson reconstruction.

The backgrounds are subtracted from data prior to unfolding. The unfolded number of jets in data, $N_i^{\mathcal{P}}$, in each bin i of the measurement is obtained as

$$N_i^{\mathcal{P}} = \frac{1}{\mathcal{E}_i^{\mathcal{P}}} \sum_j U_{ij} \mathcal{E}_j^{\mathcal{R}} N_j^{\mathcal{R}}, \tag{1}$$

where $N_j^{\mathcal{R}}$ is the number of jets reconstructed in bin j after the background subtraction, U_{ij} is an element of the unfolding matrix, and $\mathcal{E}_j^{\mathcal{R}}$ and $\mathcal{E}_i^{\mathcal{P}}$ are the reconstruction-level and particle-level jet matching efficiencies, respectively.

The transfer matrix and the matching efficiencies are improved using three unfolding iterations to reduce the impact of the particle-level jet spectra mis-modelling on the unfolded data.

8 Experimental uncertainties

8.1 Electron uncertainties

The electron energy scale has associated statistical uncertainties and systematic uncertainties arising from a possible bias in the calibration method, the choice of generator, the presampler energy scale, and imperfect knowledge of the material in front of the EM calorimeter. The total energy-scale uncertainty is calculated as the sum in quadrature of these components. It is varied by $\pm 1\sigma$ in order to propagate the electron energy scale uncertainty into the measured Z + jets cross-sections.

The electron energy resolution has uncertainties associated to the extraction of the resolution difference between data and simulation using $Z \to ee$ events, to the knowledge of the sampling term of the calorimeter energy resolution and to the pile-up noise modelling. These uncertainties are evaluated in situ using the $Z \to ee$ events, and the total uncertainty is calculated as the sum in quadrature of the different uncertainties. The scale factor for electron energy resolution in MC simulation is varied by $\pm 1\sigma$ in the total uncertainty in order to propagate this uncertainty into the Z + jets cross-section measurements.

The uncertainties in calculations of the electron trigger, reconstruction and identification efficiencies are propagated into the measurements by $\pm 1\sigma$ variations of the scale factors, used to reweight the MC simulated events, within the total uncertainty of each efficiency [20,51].

For each systematic variation a new transfer matrix and new matching efficiencies are calculated, and data unfolding is performed. The deviation from the nominal unfolded result is assigned as the systematic uncertainty in the measurements.

8.2 Jet uncertainties

The uncertainty in the jet energy measurement is described by 65 uncertainty components [57]. Of these, 56 JES uncertainty components are related to detector description, physics modelling and sample sizes of the Z/γ and multijet MC samples used for JES in situ measurements. The single-hadron response studies are used to describe the JES uncertainty in high-p_{T} jet regions, where the in situ studies have few events. The MC non-closure uncertainty takes into account the differences in the jet response due to different shower models used in MC generators. Four uncertainty components are due to the pile-up corrections of the jet kinematics, and take into account mis-modelling of N_{PV} and $\langle\mu\rangle$ distributions, the average energy density and the residual p_{T} dependence of the N_{PV} and $\langle\mu\rangle$ terms. Two flavour-based uncertainties take into account the difference between the calorimeter responses to the quark- and gluon-initiated jets. One uncertainty component describes the correction for the energy leakage beyond the calorimeter ('punch-through' effect). All JES uncertainties are treated as bin-to-bin correlated and independent of each other.

A reduced set of uncertainties, which combines the uncertainties of the in situ methods into six components with a small loss of correlation information, is used in this measurement. The JES uncertainties are propagated into the measurements in the same way as done for electron uncertainties.

The uncertainty that accounts for the difference in JVF requirement efficiency between data and MC simulation is evaluated by varying the nominal JVF requirement in MC simulation to represent a few percent change in efficiency [60]. The unfolding transfer matrix and the matching efficiencies are re-derived, and the results of varying the JVF requirement are propagated to the unfolded data. The deviations from the nominal results are used as the systematic uncertainty.

Pile-up jets are effectively suppressed by the selection requirements. The jet yields in events with low $\langle\mu\rangle$ and

high $\langle\mu\rangle$ are compared with the jet yields in events without any requirements on $\langle\mu\rangle$. These jet yields agree with each other within the statistical uncertainties. The same result is achieved by comparing the jet yields in events that have low or high numbers of reconstructed primary vertices with the jet yields in events from the nominal selection. Consequently, no additional pile-up uncertainty is introduced.

The jet energy resolution (JER) uncertainty accounts for the mis-modelling of the detector jet energy resolution by the MC simulation. To evaluate the JER uncertainty in the measured Z + jets cross-sections, the energy of each jet in MC simulation is smeared by a random number taken from a Gaussian distribution with a mean value of one and a width equal to the quadratic difference between the varied resolution and the nominal resolution [61]. The smearing is repeated 100 times and then averaged. The transfer matrix determined from the averaged smearing is used for unfolding. The result is compared with the nominal measurement and the symmetrised difference is used as the JER uncertainty.

The uncertainty that accounts for the mis-modelling of the 'medium' jet quality criteria is evaluated using jets, selected with the 'loose' and 'tight' criteria. The data-to-MC ratios of the reconstructed Z + jets distributions, obtained with different jet quality criteria, is compared with the nominal. An uncertainty of 1%, which takes the observed differences into account, is assigned to the measured Z + jets cross-section in all bins of $|y_{\text{jet}}|$ and $p_{\text{T}}^{\text{jet}}$.

8.3 Background uncertainties

The uncertainties in each background estimation are propagated to the measured Z + jets cross-sections.

The data contamination by the $Z \to \tau\tau$, diboson, $t\bar{t}$ and single-top-quark backgrounds is estimated using simulated spectra scaled to the corresponding total cross-sections. Each of these background cross-sections has an uncertainty. The normalisation of each background is independently varied up and down by its uncertainty and propagated to the final result. The MC simulation of the dominant $t\bar{t}$ background describes the shapes of the jet $p_{\text{T}}^{\text{jet}}$ and y_{jet} distributions in data to within a few percent [62], such that possible shape mis-modellings of the jet kinematics in $t\bar{t}$ events are covered by the uncertainty in the total $t\bar{t}$ cross-section. The shape mis-modellings in other backgrounds have negligible effect on the final results. Therefore, no dedicated uncertainties due to the background shape mis-modelling are assigned.

The uncertainties in the combined multijet and W+ jets background arise from assumptions about the template shape and normalisation. The shape of the template depends on the control region selection and the control region contaminations by the other backgrounds. The template normalisation depends on the m_{ee} range, used to fit the template to the measured Z + jets events, due to different amounts of background contamination in the tails of the m_{ee} distribution.

To evaluate the template shape uncertainty due to the control region selection, a different set of electron identification criteria is used to derive a modified template. The selection requires two reconstructed electrons with at least one electron that satisfies the 'loose' identification criteria, but not the 'medium' ones. The difference between the nominal and modified templates is used to create a symmetric template to provide up and down variations of this systematic uncertainty.

To estimate the template shape uncertainty due to the control region contaminations by the other backgrounds, the $Z \to \tau\tau$, diboson, $t\bar{t}$ and single-top-quark cross-sections are varied within their uncertainties. The dominant change in the template shape is due to $t\bar{t}$ cross-section variation, while the contributions from the variation of the other background cross-sections are small. The templates varied within the $t\bar{t}$ cross-section uncertainties are used to propagate this uncertainty into the measurement.

The uncertainty in the multijet and W+ jets background template normalisation to the measured Z + jets events is evaluated by fitting the template in the $66\,\text{GeV} < m_{ee} < 140\,\text{GeV}$ and $60\,\text{GeV} < m_{ee} < 116\,\text{GeV}$ regions, excluding the bins under the Z boson peak within the $80\,\text{GeV} < m_{ee} < 100\,\text{GeV}$ region, and in the $60\,\text{GeV} < m_{ee} < 140\,\text{GeV}$ region, excluding the bins within the $70\,\text{GeV} < m_{ee} < 110\,\text{GeV}$. As a result, the normalisation varies up and down depending on the number of background events in both tails of the m_{ee} distribution. The templates with the largest change in the normalisation are used to propagate this uncertainty into the measurement.

The data unfolding is repeated for each systematic variation of the backgrounds. The differences relative to the nominal Z + jets cross-section are used as the systematic uncertainties.

8.4 Unfolding uncertainty

The accuracy of the unfolding procedure depends on the quality of the description of the measured spectrum in the MC simulation used to build the unfolding matrix. Two effects are considered in order to estimate the influence of MC modelling on the unfolding results: the shape of the particle-level spectrum and the parton shower description.

The impact of the particle-level shape mis-modelling on the unfolding is estimated using a data-driven closure test. For this test, the particle-level $(|y_{\text{jet}}|, p_{\text{T}}^{\text{jet}})$ distribution in SHERPA is reweighted using the transfer matrix, such that the shape of the matched reconstructed $(|y_{\text{jet}}|, p_{\text{T}}^{\text{jet}})$ distribution agrees with the measured spectrum corrected for the matching efficiency. The reweighted reconstructed $(|y_{\text{jet}}|, p_{\text{T}}^{\text{jet}})$ distribu-

tions are then unfolded using the nominal SHERPA transfer matrix. The results are compared with the reweighted particle-level ($|y_{\text{jet}}|$, $p_{\text{T}}^{\text{jet}}$) spectrum and the relative differences are assigned as the uncertainty.

The impact of the differences in the parton shower description between SHERPA and ALPGEN+PYTHIA on the unfolding results is estimated using the following test. The ALPGEN+PYTHIA particle-level ($|y_{\text{jet}}|$, $p_{\text{T}}^{\text{jet}}$) spectrum is reweighted using the ALPGEN+PYTHIA transfer matrix, such that its reconstruction-level distribution agrees with the one in SHERPA. The original reconstructed ($|y_{\text{jet}}|$, $p_{\text{T}}^{\text{jet}}$) distribution in SHERPA is then unfolded using the reweighted ALPGEN+PYTHIA transfer matrix. The results are compared with the original particle-level ($|y_{\text{jet}}|$, $p_{\text{T}}^{\text{jet}}$) spectrum in SHERPA and the differences are assigned as the uncertainty.

Both unfolding uncertainties are symmetrised at the cross-section level.

8.5 Reduction of statistical fluctuations in systematic uncertainties

The systematic uncertainties suffer from fluctuations of a statistical nature.

The statistical components in the electron and jet uncertainties are estimated using toy MC simulations with 100 pseudo-experiments. Each Z + jets event in the systematically varied configurations is reweighted by a random number taken from a Poisson distribution with a mean value of one. As a result, 100 replicas of transfer matrix and matching efficiencies are created for a given systematic uncertainty variation, and are used to unfold the data. The replicas of unfolded spectra are then divided by the nominal Z + jets distributions to create an ensemble of systematic uncertainty spectra. The statistical component in the systematic uncertainties is calculated as the RMS across all replicas in an ensemble.

The pseudo-experiments are not performed for the JER systematic uncertainty. The statistical errors in the JER systematic uncertainty are calculated, considering the unfolded data in the nominal and JER varied configurations to be independent of each other.

Each component of the unfolding uncertainty is derived using 100 pseudo-experiments to calculate the statistical error.

To reduce the statistical fluctuations, the bins are combined iteratively starting from both the right and left sides of each systematic uncertainty spectrum until their significance satisfies $\sigma > 1.5$. The result with the most bins remaining is used as the systematic uncertainty. A Gaussian kernel is then applied to regain the fine binning and smooth out any additional statistical fluctuations.

If up and down systematic variations within a bin result in uncertainties with the same sign, then the smaller uncertainty is set to zero.

8.6 Statistical uncertainties

Statistical uncertainties are derived using toy MC simulations with 100 pseudo-experiments performed in both data and MC simulation. The data portion of the statistical uncertainty is evaluated by unfolding the replicas of the data using the nominal transfer matrix and matching efficiencies. The MC portion is calculated using the replicas of the transfer matrix and matching efficiencies to unfold the nominal data. To calculate the total statistical uncertainty in the measurement, the Z + jets distributions, obtained from pseudo-experiments drawn from the data yields, are unfolded using the transfer matrices and efficiency corrections, calculated using pseudo-experiments in the MC simulation. The covariance matrices between bins of the measurement are computed using the unfolded results. The total statistical uncertainties are calculated using the diagonal elements of the covariance matrices.

8.7 Summary of experimental uncertainties

The Z + jets cross-section measurement has 39 systematic uncertainty components. All systematic uncertainties are treated as being uncorrelated with each other and fully correlated among $|y_{\text{jet}}|$ and $p_{\text{T}}^{\text{jet}}$ bins.

The systematic uncertainties in the electron energy scale, electron energy resolution, and electron trigger, reconstruction and identification efficiencies are found to be below 1%.

The JES in situ methods uncertainty is 2–5% in most bins of the measurement. The η-intercalibration uncertainty is below 1% in the $|y_{\text{jet}}| < 1.0$ and $p_{\text{T}}^{\text{jet}} < 200\,\text{GeV}$ regions, but it increases with $|y_{\text{jet}}|$, reaching 6–14% in the most forward rapidity bins. The η-intercalibration uncertainty is below 1.5% for jets with $p_{\text{T}}^{\text{jet}} > 200\,\text{GeV}$. The flavour-based JES uncertainties are below 3%. The pile-up components of the JES uncertainty are 0.5–1.5%. Other components of the JES uncertainty are below 0.2%.

The JVF uncertainty is below 1%.

The JER is the dominant source of uncertainty in the Z + jets cross-section in the $25\,\text{GeV} < p_{\text{T}}^{\text{jet}} < 50\,\text{GeV}$ region with a 3–10% contribution. In the $50\,\text{GeV} < p_{\text{T}}^{\text{jet}} < 100\,\text{GeV}$ region the JER uncertainty is 1–3%, and below 1% for jets with higher transverse momenta.

The jet quality uncertainty is set constant at 1%, as discussed in Sect. 8.2.

The unfolding uncertainty due to the shape of the particle-level spectrum is 2–5% in the first $p_{\text{T}}^{\text{jet}}$ bin, $25\,\text{GeV} < p_{\text{T}}^{\text{jet}} < 50\,\text{GeV}$. In the $50\,\text{GeV} < p_{\text{T}}^{\text{jet}} < 200\,\text{GeV}$ region, this uncertainty is about 1.5% for central jets below $|y_{\text{jet}}| = 2$,

while for forward jets this uncertainty increases to 5%. In the $p_{\mathrm{T}}^{\mathrm{jet}} > 200\,\mathrm{GeV}$ region, this uncertainty is below 1.5%. The unfolding uncertainty due to the parton shower description is 0.7% in the $400\,\mathrm{GeV} < p_{\mathrm{T}}^{\mathrm{jet}} < 1050\,\mathrm{GeV}$ region, while for jets with smaller transverse momenta this uncertainty is negligible.

The $t\bar{t}$ background uncertainty is 0.02–0.6% in all bins of the measurement. The $Z \to \tau\tau$, diboson and single-top-quark background uncertainties are below 0.05%.

The multijet and W+ jets background uncertainty is 0.1–1.2% depending on $|y_{\mathrm{jet}}|$ and $p_{\mathrm{T}}^{\mathrm{jet}}$. The uncertainty in the background template normalisation is asymmetric due to different background contributions in the tails of the m_{ee} distribution in the background normalisation evaluation procedure. This uncertainty is $^{+0.1}_{-0.4}$% in the low $p_{\mathrm{T}}^{\mathrm{jet}}$ bins, increasing to $^{+0.4}_{-1.2}$% in the high $p_{\mathrm{T}}^{\mathrm{jet}}$ bins. The uncertainty in the multijet and W+ jets background control region selection increases from 0.03% to 0.6% as a function of $p_{\mathrm{T}}^{\mathrm{jet}}$. The contribution of the $t\bar{t}$ cross-section variation to the multijet and W+ jets background uncertainty is below 0.1%.

The statistical uncertainties are 0.5–4% in the $p_{\mathrm{T}}^{\mathrm{jet}} < 100\,\mathrm{GeV}$ region, 2–14% in the $100\,\mathrm{GeV} < p_{\mathrm{T}}^{\mathrm{jet}} < 300\,\mathrm{GeV}$ region, 8–39% in the $300\,\mathrm{GeV} < p_{\mathrm{T}}^{\mathrm{jet}} < 400\,\mathrm{GeV}$ region and 11–18% in the last $p_{\mathrm{T}}^{\mathrm{jet}}$ bin, $400\,\mathrm{GeV} < p_{\mathrm{T}}^{\mathrm{jet}} < 1050\,\mathrm{GeV}$. The smallest statistical uncertainty corresponds to central rapidity regions, while the largest uncertainty corresponds to forward rapidity regions.

The experimental uncertainties are shown in Fig. 2. The largest total systematic uncertainty of 7–12% is in the $25\,\mathrm{GeV} < p_{\mathrm{T}}^{\mathrm{jet}} < 50\,\mathrm{GeV}$ region, where the uncertainty increases from central rapidity jets to the forward rapidity jets, and up to 15% for the forward rapidity jets in the $100\,\mathrm{GeV} < p_{\mathrm{T}}^{\mathrm{jet}} < 200\,\mathrm{GeV}$ region. The total systematic uncertainty decreases with increasing $p_{\mathrm{T}}^{\mathrm{jet}}$. In the $400\,\mathrm{GeV} < p_{\mathrm{T}}^{\mathrm{jet}} < 1050\,\mathrm{GeV}$ region the total systematic uncertainty is 2–5%. The luminosity uncertainty of 1.9% is not shown and not included in the total uncertainty and its components.

9 Fixed-order predictions and theoretical uncertainties

9.1 Fixed-order calculations

Theoretical Z + jets predictions at NLO are calculated using MCFM [40] interfaced to APPLgrid [63] for fast convolution with PDFs. The renormalisation and factorisation scales, μ_{R} and μ_{F}, are set to

$$\mu_{\mathrm{R}} = \mu_{\mathrm{F}} = \frac{\sqrt{m_{ee}^2 + p_{\mathrm{T},Z}^2} + \sum p_{\mathrm{T,\,partons}}}{2},$$

where m_{ee} is the electron pair's invariant mass, $p_{\mathrm{T},Z}$ is the transverse momentum of the Z boson and $\sum p_{\mathrm{T,\,partons}}$ is the sum of the transverse momenta of the partons.

The NLO Z + jets predictions are obtained using the CT14 NLO [64], NNPDF3.1 [65], JR14 NLO [66], HERAPDF2.0 [67], MMHT2014 [68], ABMP16 [69] and ATLAS-epWZ16 [70] PDF sets. The PDFs are determined by various groups using the experimental data and are provided with the uncertainties. The PDF uncertainties in the Z + jets cross-sections are calculated at the 68% confidence level according to the prescription recommended by the PDF4LHC group [71].

The following variations of factorisation and renormalisation scales are performed to assess the uncertainty due to missing higher-order terms: $\{\mu_{\mathrm{R}}/2, \mu_{\mathrm{F}}\}$, $\{2\mu_{\mathrm{R}}, \mu_{\mathrm{F}}\}$, $\{\mu_{\mathrm{R}}, \mu_{\mathrm{F}}/2\}$, $\{\mu_{\mathrm{R}}, 2\mu_{\mathrm{F}}\}$, $\{\mu_{\mathrm{R}}/2, \mu_{\mathrm{F}}/2\}$, $\{2\mu_{\mathrm{R}}, 2\mu_{\mathrm{F}}\}$. The envelope of the cross-sections calculated with different scales is used as the uncertainty.

The uncertainty due to the strong coupling is estimated using additional PDF sets, calculated with $\alpha_{\mathrm{S}}(m_Z^2) = 0.116$ and $\alpha_{\mathrm{S}}(m_Z^2) = 0.120$. The resulting uncertainty is scaled to the uncertainty of the world average $\alpha_{\mathrm{S}}(m_Z^2) = 0.118 \pm 0.0012$, as recommended by the PDF4LHC group [71].

The state-of-the-art NNLO Z + jets cross-section is calculated by the authors of Ref. [16] using NNLOJET [72]. The NNLO predictions are convolved with the CT14 PDF. The renormalisation and factorisation scales are set similarly to those in NLO calculations.

9.2 Non-perturbative correction

The fixed-order predictions are obtained at the parton level. Bringing fixed-order predictions to the particle level for comparisons with the measured Z + jets cross-sections requires a non-perturbative correction (NPC) that accounts for both the hadronisation and underlying-event effects.

The NPCs are studied using several MC generators to account for differences in the modelling of hadronisation and the underlying event. The studies are done using the leading-logarithm parton shower MC generators Pythia v. 8.210 with the A14 [73] underlying-event tune and Herwig++ v. 2.7.1 with the UE-EE5 tune [74], and the multi-leg matrix element MC generators Sherpa v. 1.4.5 with the CT10 PDF, Sherpa v. 2.2.0 with NNPDF 2.3 [75] and MadGraph v. 2.2.3 [76], supplemented with parton showers from Pythia v. 8.210 with the A14 tune.

The NPCs are calculated using the ratios of Z + jets cross-sections obtained at the particle level to those at the parton level. The correction derived using Sherpa v. 1.4.5 is the nominal one in this analysis. The envelope of the non-perturbative corrections, calculated with other MC generators, is used as the systematic uncertainty. The NPCs in different MC generators are shown in Fig. 3. The nominal

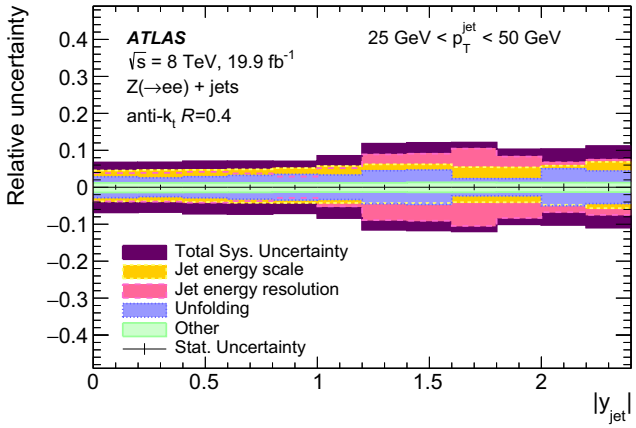

(a) 25 GeV $< p_{\mathrm{T}}^{\mathrm{jet}} <$ 50 GeV

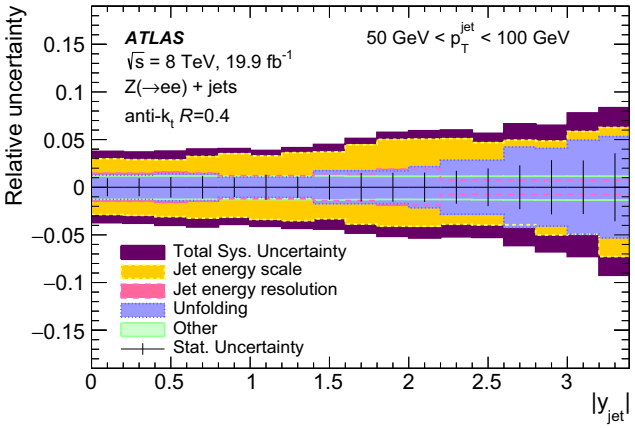

(b) 50 GeV $< p_{\mathrm{T}}^{\mathrm{jet}} <$ 100 GeV

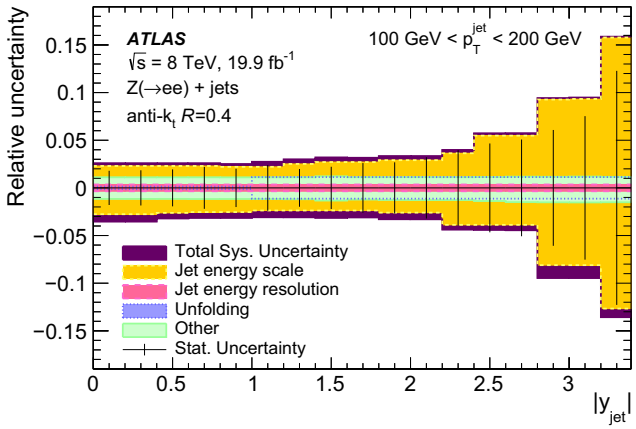

(c) 100 GeV $< p_{\mathrm{T}}^{\mathrm{jet}} <$ 200 GeV

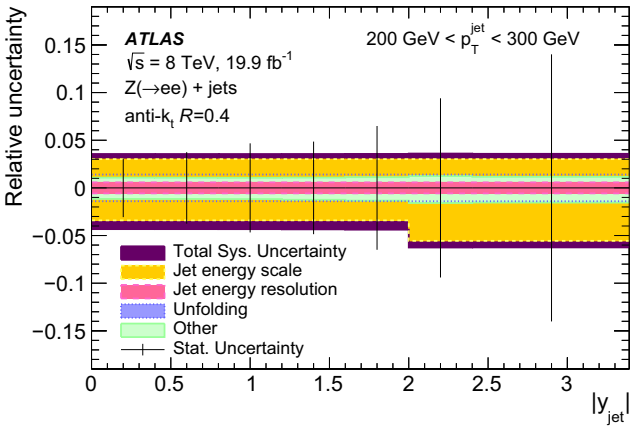

(d) 200 GeV $< p_{\mathrm{T}}^{\mathrm{jet}} <$ 300 GeV

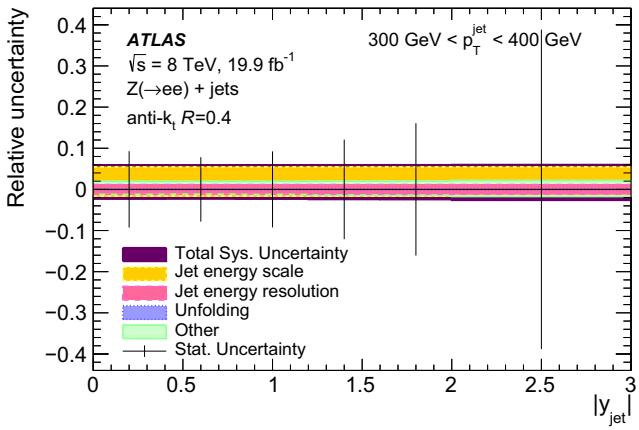

(e) 300 GeV $< p_{\mathrm{T}}^{\mathrm{jet}} <$ 400 GeV

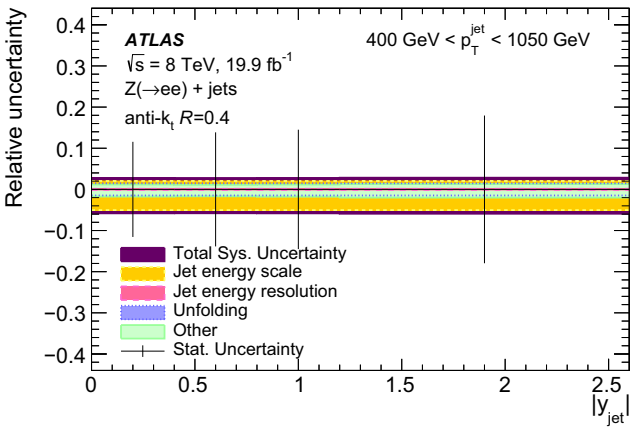

(f) 400 GeV $< p_{\mathrm{T}}^{\mathrm{jet}} <$ 1050 GeV

Fig. 2 Experimental uncertainties in the measured double-differential Z + jets production cross-section as a function of $|y_{\mathrm{jet}}|$ in $p_{\mathrm{T}}^{\mathrm{jet}}$ bins. The jet energy scale, jet energy resolution, unfolding, 'other' and total systematic uncertainties are shown with different colours overlaid. The jet energy scale uncertainty is the sum in quadrature of the jet energy scale uncertainty components. The unfolding uncertainty is the sum in quadrature of two unfolding uncertainties. The 'other' systematic uncertainty is the sum in quadrature of the electron uncertainties, background uncertainties, JVF and jet quality uncertainties. The total systematic uncertainty is the sum in quadrature of all systematic uncertainty components except for the luminosity uncertainty of 1.9%. The total statistical uncertainties are shown with vertical error bars

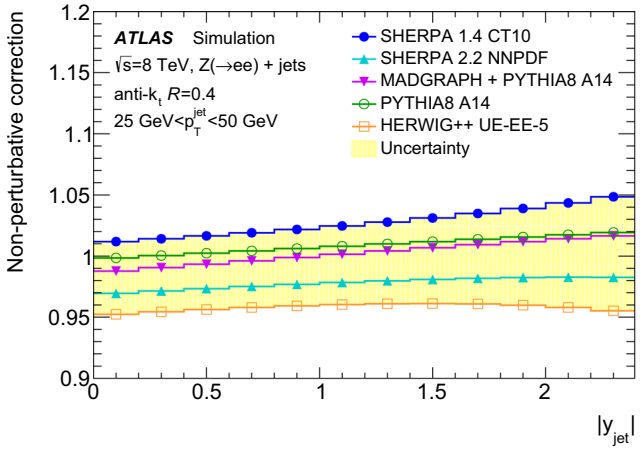

(a) 25 GeV < $p_{\mathrm{T}}^{\mathrm{jet}}$ < 50 GeV

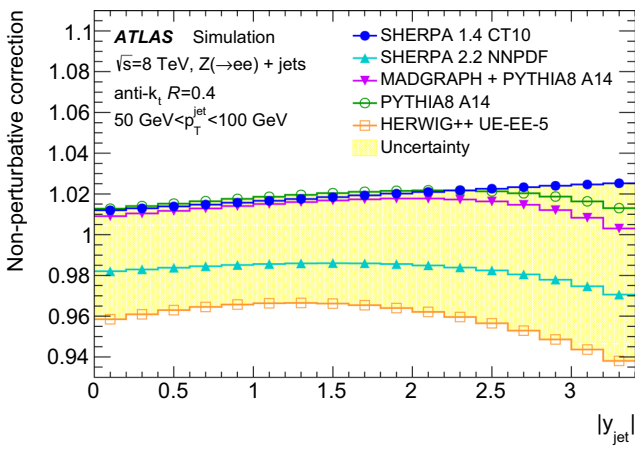

(b) 50 GeV < $p_{\mathrm{T}}^{\mathrm{jet}}$ < 100 GeV

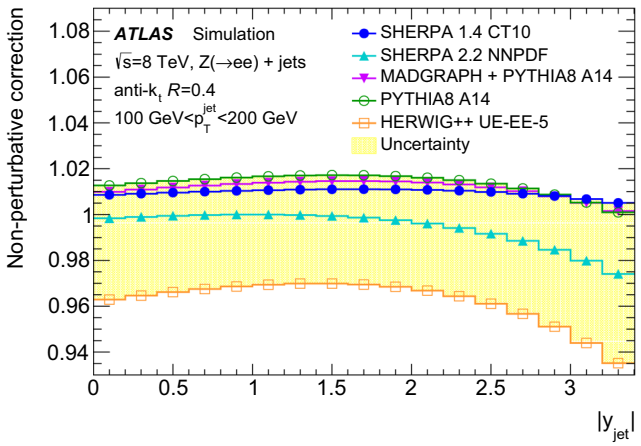

(c) 100 GeV < $p_{\mathrm{T}}^{\mathrm{jet}}$ < 200 GeV

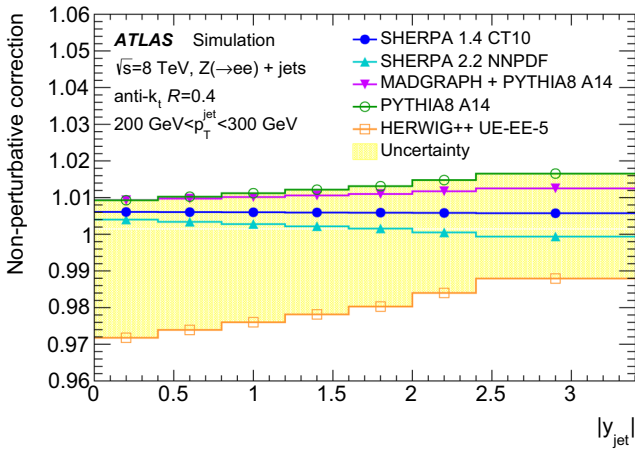

(d) 200 GeV < $p_{\mathrm{T}}^{\mathrm{jet}}$ < 300 GeV

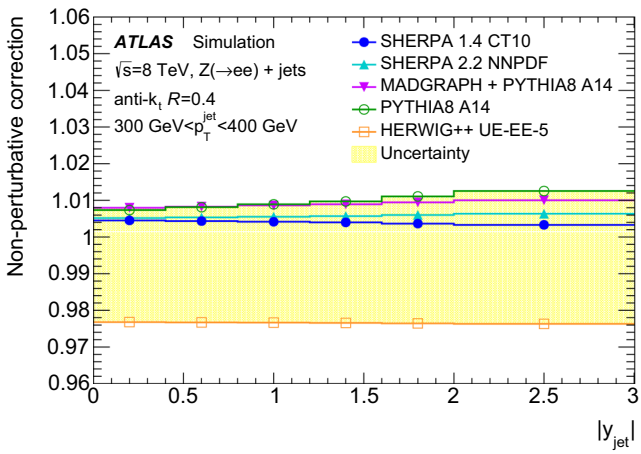

(e) 300 GeV < $p_{\mathrm{T}}^{\mathrm{jet}}$ < 400 GeV

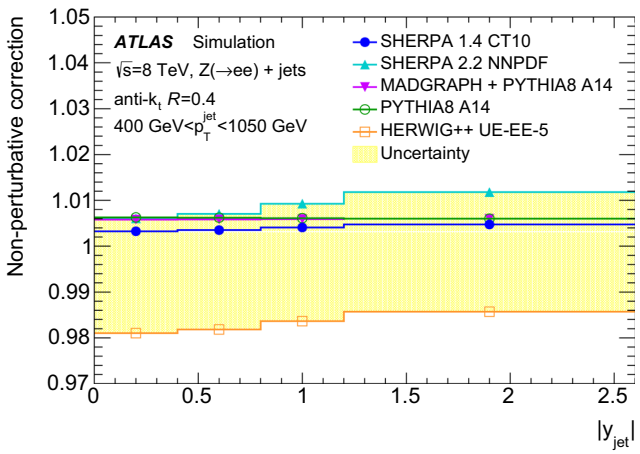

(f) 400 GeV < $p_{\mathrm{T}}^{\mathrm{jet}}$ < 1050 GeV

Fig. 3 The non-perturbative correction for the Z + jets production cross-section as a function of $|y_{\mathrm{jet}}|$ in $p_{\mathrm{T}}^{\mathrm{jet}}$ bins. The spread of predictions represents the uncertainty

correction for jets with low transverse momenta, $25\,\text{GeV} < p_{\text{T}}^{\text{jet}} < 50\,\text{GeV}$, in the central rapidity regions, $|y_{\text{jet}}| < 1.5$, is small, but it increases to 5% in the forward rapidity bins. The nominal correction for jets with higher transverse momenta is below 2%. These corrections together with uncertainties are provided in HEPData [77].

9.3 QED radiation correction

The fixed-order Z + jets cross-section predictions must be corrected for the QED radiation in order to be compared with data. The correction is determined as the ratio of two Z + jets cross-sections, one calculated using dressed electrons after QED final-state radiation (FSR), with all photons clustered within a cone of $\Delta R = 0.1$ around the electron axis, and the other calculated using Born-level electrons at the lowest order in the electromagnetic coupling α_{QED} prior to QED FSR radiation. The baseline correction is calculated using the SHERPA MC samples, while the correction calculated using ALPGEN+PYTHIA is used to estimate the uncertainty. The uncertainty is calculated as the width of the envelope of corrections obtained with these two MC generators. The results are shown in Fig. 4. The QED correction is largest in the $25\,\text{GeV} < p_{\text{T}}^{\text{jet}} < 50\,\text{GeV}$ region. It is about 5% for jets in the central absolute rapidity regions. In the $p_{\text{T}}^{\text{jet}} > 50\,\text{GeV}$ regions the QED correction is 1.5–2.5%, decreasing as a function of jet transverse momentum. The QED corrections calculated using ALPGEN+PYTHIA are in good agreement with those from SHERPA. These corrections together with uncertainties are provided in HEPData.

9.4 Summary of theoretical uncertainties

The total theoretical uncertainties are calculated as the sum in quadrature of the effects of the PDF, scale, and α_{S} uncertainties, and the uncertainties due to non-perturbative and QED radiation effects.

The uncertainties for the Z + jets cross-section calculated at NLO using the CT14 PDF as a function of $|y_{\text{jet}}|$ in $p_{\text{T}}^{\text{jet}}$ bins are shown in Fig. 5. The total uncertainties are dominated by the scale and NPC uncertainties in the $p_{\text{T}}^{\text{jet}} < 100\,\text{GeV}$ region, where they reach $\pm 15\%$ and -10%, respectively. In the $p_{\text{T}}^{\text{jet}} > 100\,\text{GeV}$ region, the scale uncertainty alone dominates, as the NPC uncertainty decreases for high jet transverse momenta. The total uncertainty in this region is 10–20%. Other uncertainties are below 5%.

The NNLO uncertainties are shown in Fig. 6. The scale uncertainty at NNLO is significantly reduced. This uncertainty is below 1% in the $25\,\text{GeV} < p_{\text{T}}^{\text{jet}} < 50\,\text{GeV}$ bin, increasing to 5% in the $400\,\text{GeV} < p_{\text{T}}^{\text{jet}} < 1050\,\text{GeV}$ bin. In the $p_{\text{T}}^{\text{jet}} < 200\,\text{GeV}$ region, the negative part of the total uncertainty is dominated by the NPC uncertainty and its absolute value reaches 7–15% depending on the jet rapidity. The positive part of the total uncertainty is within 5%, with about equal contributions from PDF, scale and α_{S} uncertainties. In the $p_{\text{T}}^{\text{jet}} > 200\,\text{GeV}$ region, both the negative and positive parts of the total uncertainty are within 6% in most bins.

The uncertainty in the QED correction is below 0.5% and is negligible in the fixed-order theory predictions.

10 Results

The double-differential Z + jets cross-section as a function of $|y_{\text{jet}}|$ and $p_{\text{T}}^{\text{jet}}$ is calculated as

$$\frac{\mathrm{d}^2\sigma}{\mathrm{d}p_{\text{T}}^{\text{jet}}\mathrm{d}|y_{\text{jet}}|} = \frac{1}{\mathcal{L}}\frac{N_i^{\mathcal{P}}}{\Delta p_{\text{T}}^{\text{jet}}\,\Delta|y_{\text{jet}}|},$$

where $\mathcal{L}$ is the integrated luminosity, $N_i^{\mathcal{P}}$ is the number of jets in data at the particle level as given in Eq. (1), and $\Delta p_{\text{T}}^{\text{jet}}$ and $\Delta|y_{\text{jet}}|$ are the widths of the jet transverse momentum and absolute jet rapidity ranges for bin i, respectively. The backgrounds are subtracted before data unfolding is performed to obtain $N_i^{\mathcal{P}}$.

The measured Z + jets cross-section covers five orders of magnitude and falls steeply as a function of $|y_{\text{jet}}|$ and $p_{\text{T}}^{\text{jet}}$. A summary of measured cross-sections, together with the systematic and statistical uncertainties, is provided in Appendix A. The measured cross-sections with the full breakdown of all uncertainties are provided in HEPData.

The comparisons with the theoretical predictions are shown in Figs. 7, 8, 9, 10, 11 and 12. The fixed-order theoretical predictions are corrected for the non-perturbative and QED radiation effects. The NLO predictions are lower than the data by approximately 5–10%. However, this difference is covered by the uncertainties. The NNLO calculations compensate for the NLO-to-data differences in most bins of the measurement and show better agreement with the central values of the cross-sections in data. The SHERPA v. 1.4 and ALPGEN+PYTHIA MC-to-data ratios are approximately constant across all $|y_{\text{jet}}|$ bins, but a dependence on $p_{\text{T}}^{\text{jet}}$ is observed. The SHERPA v. 1.4 predictions are lower than the data by about 10% in the $25\,\text{GeV} < p_{\text{T}}^{\text{jet}} < 200\,\text{GeV}$ region, but in the $p_{\text{T}}^{\text{jet}} > 200\,\text{GeV}$ region they agree within a few percent. The ALPGEN+PYTHIA predictions agree with data in the $25\,\text{GeV} < p_{\text{T}}^{\text{jet}} < 100\,\text{GeV}$ region, but exceed the data as a function of $p_{\text{T}}^{\text{jet}}$, the largest difference being about 20% in the highest $p_{\text{T}}^{\text{jet}}$ bin, $400\,\text{GeV} < p_{\text{T}}^{\text{jet}} < 1050\,\text{GeV}$.

Additionally, data is compared to the SHERPA v. 2.2 prediction. In this prediction, the matrix elements are calculated with NLO accuracy for the inclusive Z production process up to two additional partons in the final state, and

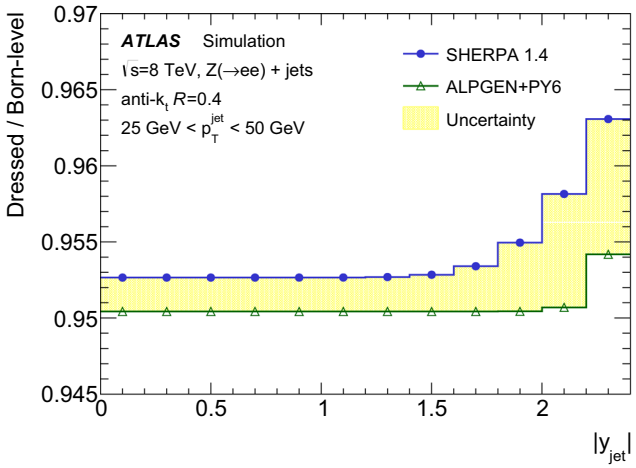

(a) 25 GeV $< p_{\mathrm{T}}^{\mathrm{jet}} <$ 50 GeV

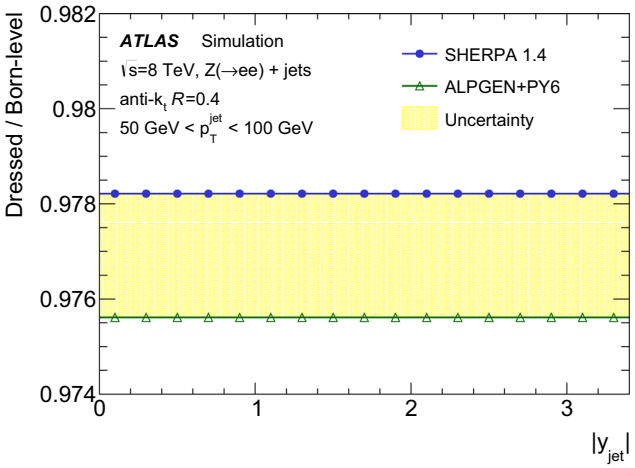

(b) 50 GeV $< p_{\mathrm{T}}^{\mathrm{jet}} <$ 100 GeV

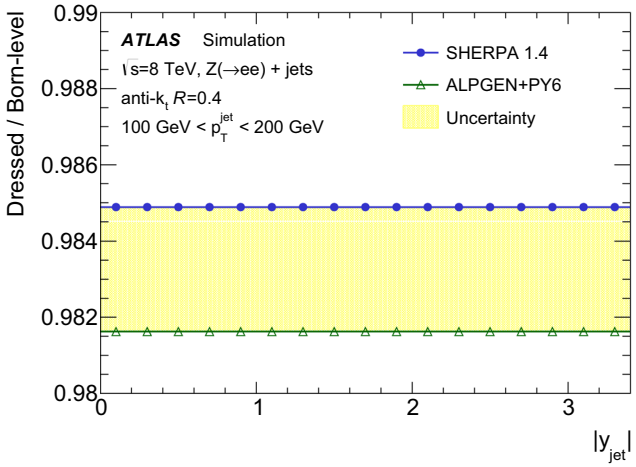

(c) 100 GeV $< p_{\mathrm{T}}^{\mathrm{jet}} <$ 200 GeV

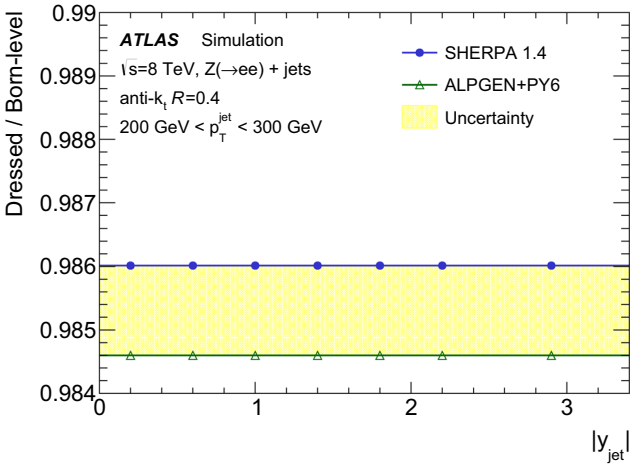

(d) 200 GeV $< p_{\mathrm{T}}^{\mathrm{jet}} <$ 300 GeV

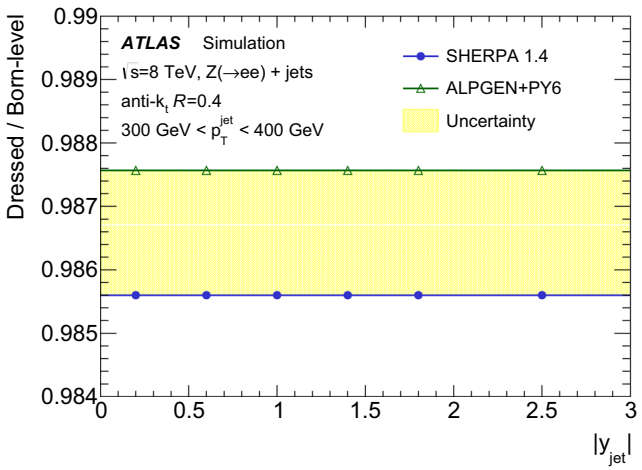

(e) 300 GeV $< p_{\mathrm{T}}^{\mathrm{jet}} <$ 400 GeV

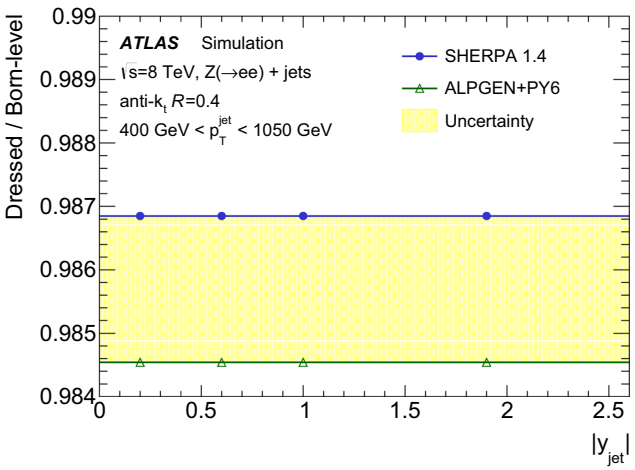

(f) 400 GeV $< p_{\mathrm{T}}^{\mathrm{jet}} <$ 1050 GeV

Fig. 4 The correction for QED radiation effects for the Z + jets production cross-section as a function of $|y_{\mathrm{jet}}|$ in $p_{\mathrm{T}}^{\mathrm{jet}}$ bins. The spread of predictions represents the uncertainty

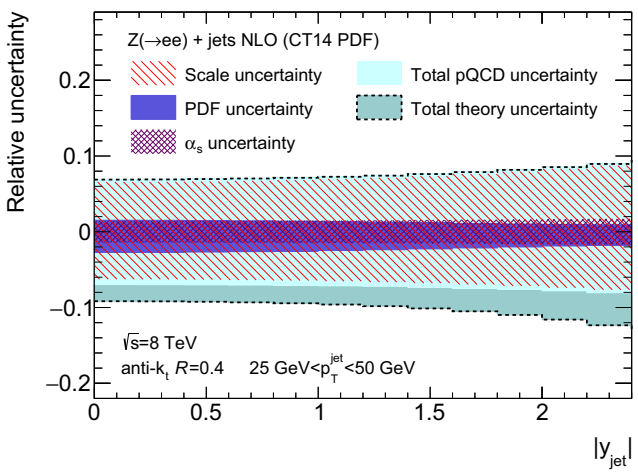

(a) 25 GeV < $p_{\mathrm{T}}^{\mathrm{jet}}$ < 50 GeV

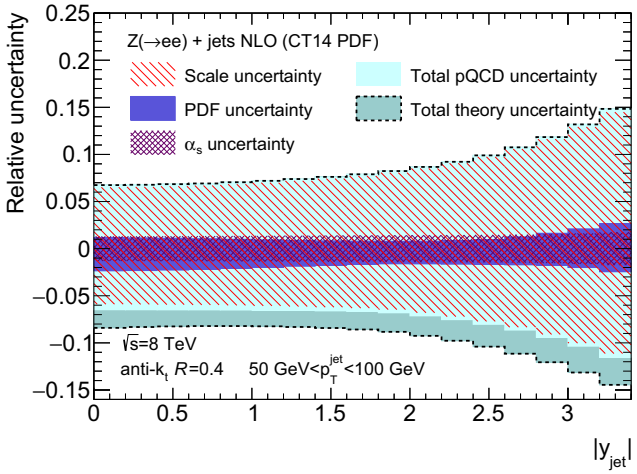

(b) 50 GeV < $p_{\mathrm{T}}^{\mathrm{jet}}$ < 100 GeV

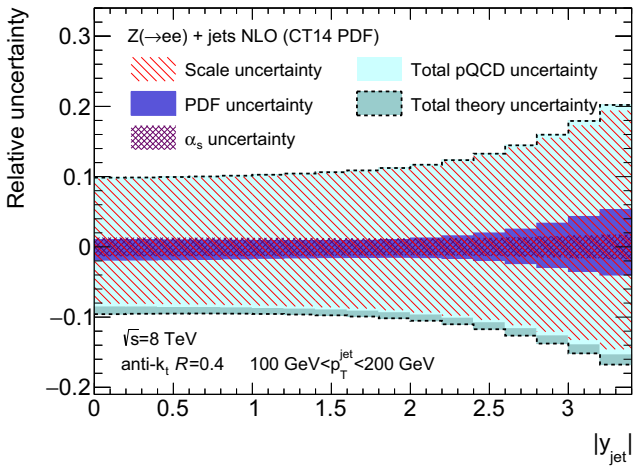

(c) 100 GeV < $p_{\mathrm{T}}^{\mathrm{jet}}$ < 200 GeV

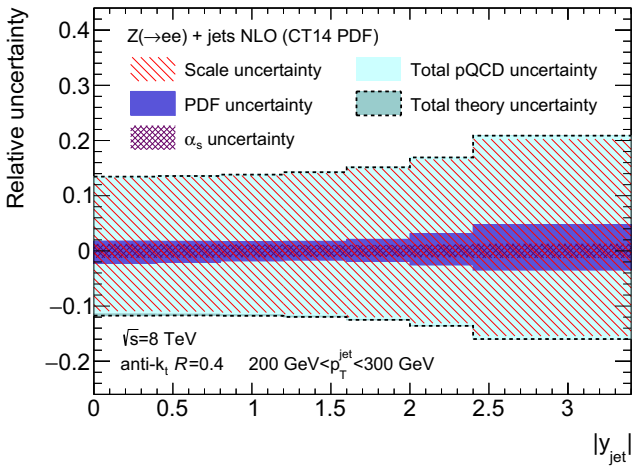

(d) 200 GeV < $p_{\mathrm{T}}^{\mathrm{jet}}$ < 300 GeV

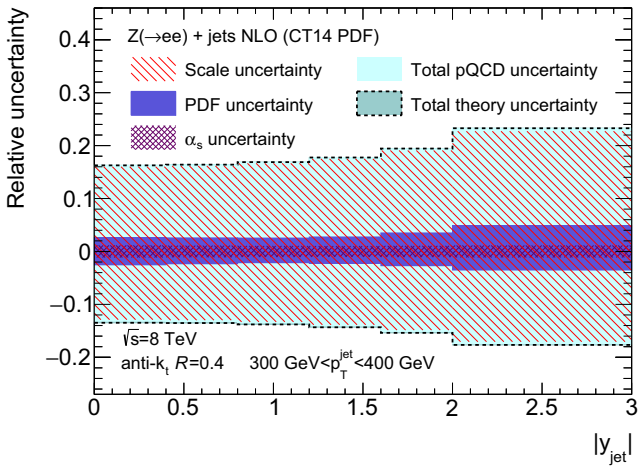

(e) 300 GeV < $p_{\mathrm{T}}^{\mathrm{jet}}$ < 400 GeV

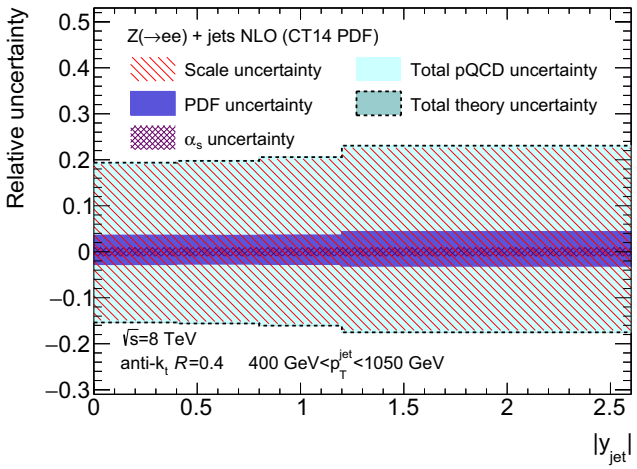

(f) 400 GeV < $p_{\mathrm{T}}^{\mathrm{jet}}$ < 1050 GeV

Fig. 5 The uncertainties in NLO pQCD predictions as a function of $|y_{\mathrm{jet}}|$ in $p_{\mathrm{T}}^{\mathrm{jet}}$ bins. Total pQCD uncertainty is the sum in quadrature of the PDF, scale and α_{S} uncertainties. Total theory uncertainty is the sum in quadrature of the total pQCD uncertainty and the uncertainties from the non-perturbative and QED radiation corrections. The CT14 PDF is used in the calculations

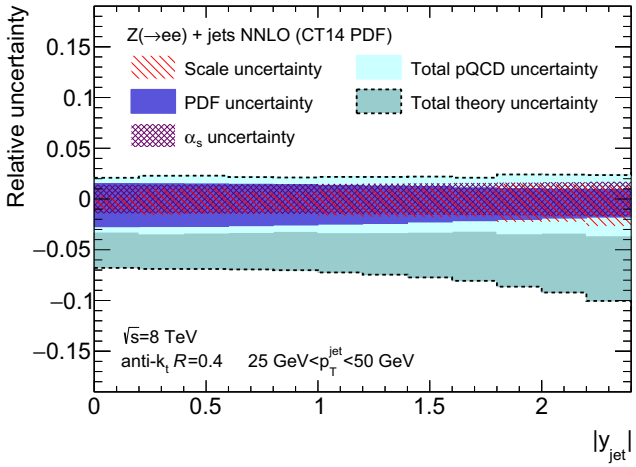

(a) 25 GeV < $p_{\mathrm{T}}^{\mathrm{jet}}$ < 50 GeV

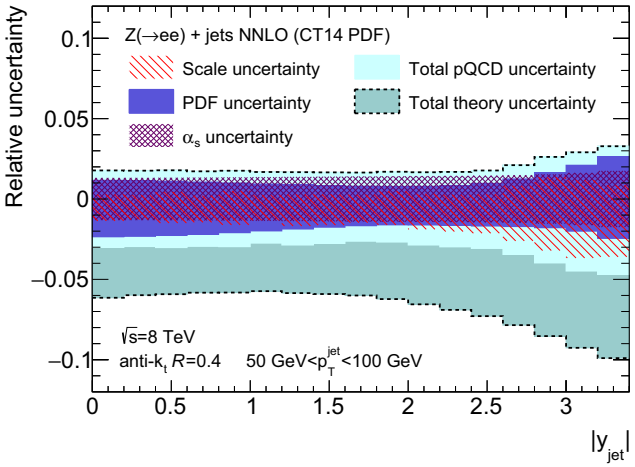

(b) 50 GeV < $p_{\mathrm{T}}^{\mathrm{jet}}$ < 100 GeV

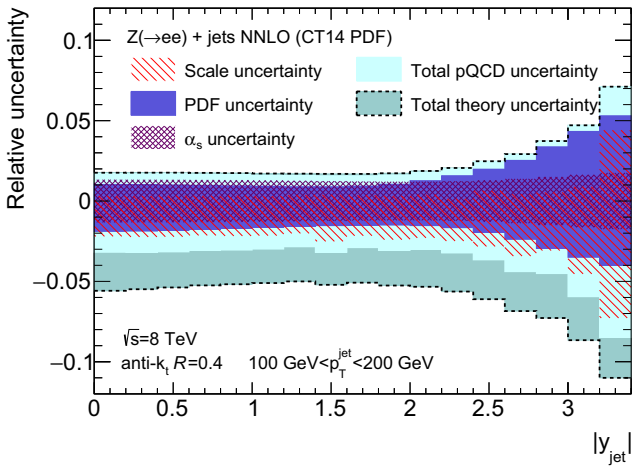

(c) 100 GeV < $p_{\mathrm{T}}^{\mathrm{jet}}$ < 200 GeV

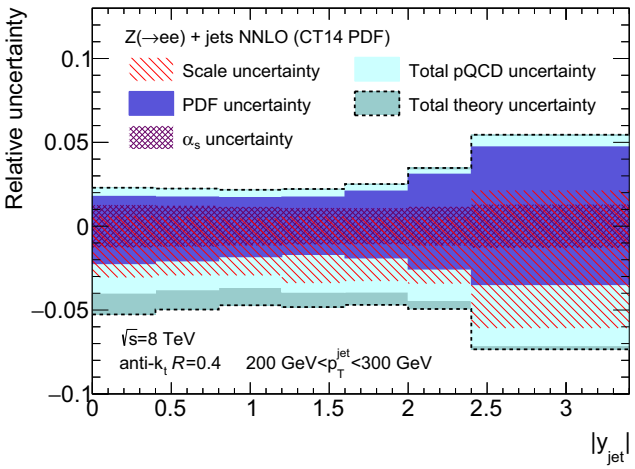

(d) 200 GeV < $p_{\mathrm{T}}^{\mathrm{jet}}$ < 300 GeV

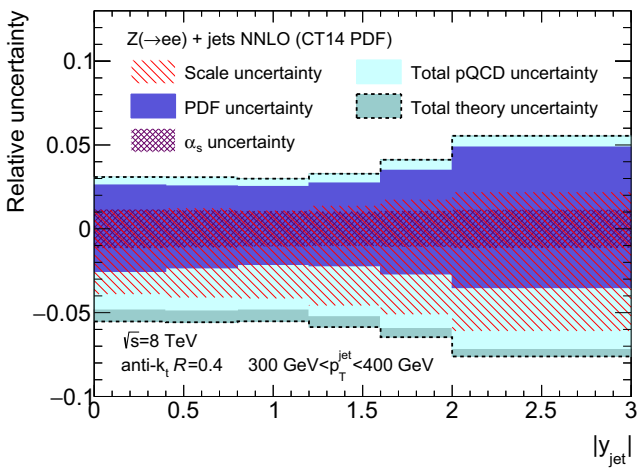

(e) 300 GeV < $p_{\mathrm{T}}^{\mathrm{jet}}$ < 400 GeV

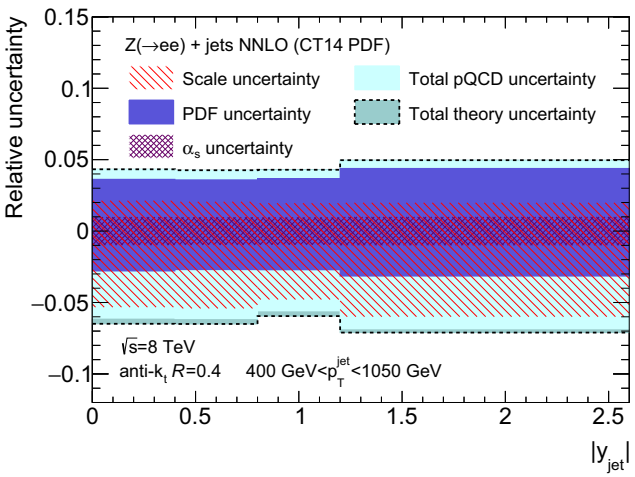

(f) 400 GeV < $p_{\mathrm{T}}^{\mathrm{jet}}$ < 1050 GeV

Fig. 6 The uncertainties in NNLO pQCD predictions as a function of $|y_{\mathrm{jet}}|$ in $p_{\mathrm{T}}^{\mathrm{jet}}$ bins. Total pQCD uncertainty is the sum in quadrature of the PDF, scale and α_{S} uncertainties. Total theory uncertainty is the sum in quadrature of the total pQCD uncertainty and the uncertainties from the non-perturbative and QED radiation corrections. The CT14 PDF is used in the calculations

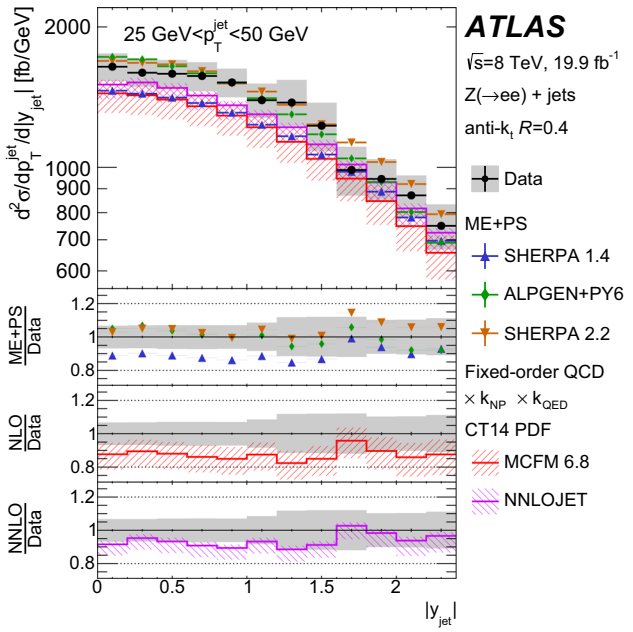

Fig. 7 The double-differential Z + jets production cross-section as a function of $|y_{\text{jet}}|$ in the 25 GeV $< p_{\text{T}}^{\text{jet}} <$ 50 GeV range. The data are compared with the SHERPA v. 1.4, SHERPA v. 2.2 and ALPGEN+PYTHIA parton shower MC generator predictions and with the fixed-order theory predictions. The fixed-order theory predictions are corrected for the non-perturbative and QED radiation effects. The fixed-order calculations are performed using the CT14 PDF. The total statistical uncertainties are shown with error bars. The total uncertainties in the measurement and in the fixed-order theory predictions are represented with shaded bands. The total uncertainty in the measurement is the sum in quadrature of the statistical and systematic uncertainties except for the luminosity uncertainty of 1.9%. The total uncertainty in the fixed-order theory predictions is the sum in quadrature of the effects of the PDF, scale, and α_{S} uncertainties, and the uncertainties from the non-perturbative and QED radiation corrections. Lower panels show the ratios of predictions to data

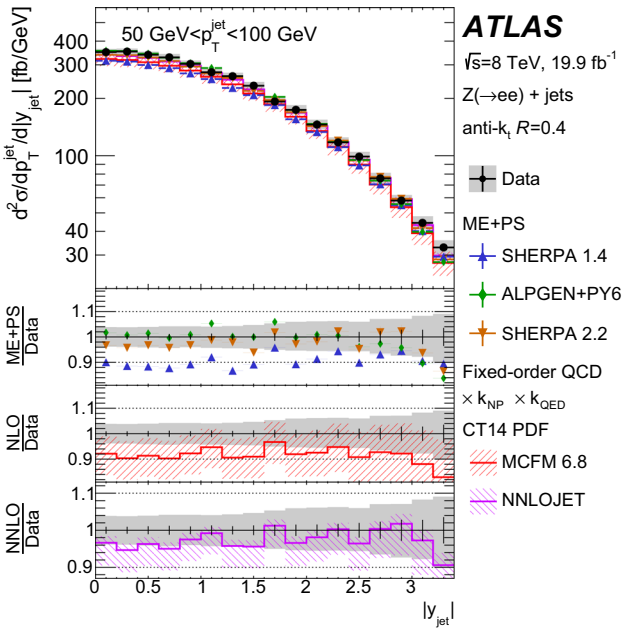

Fig. 8 The double-differential Z + jets production cross-section as a function of $|y_{\text{jet}}|$ in the 50 GeV $< p_{\text{T}}^{\text{jet}} <$ 100 GeV range. The data are compared with the SHERPA v. 1.4, SHERPA v. 2.2 and ALPGEN+PYTHIA parton shower MC generator predictions and with the fixed-order theory predictions. The fixed-order theory predictions are corrected for the non-perturbative and QED radiation effects. The fixed-order calculations are performed using the CT14 PDF. The total statistical uncertainties are shown with error bars. The total uncertainties in the measurement and in the fixed-order theory predictions are represented with shaded bands. The total uncertainty in the measurement is the sum in quadrature of the statistical and systematic uncertainties except for the luminosity uncertainty of 1.9%. The total uncertainty in the fixed-order theory predictions is the sum in quadrature of the effects of the PDF, scale, and α_{S} uncertainties, and the uncertainties from the non-perturbative and QED radiation corrections. Lower panels show the ratios of predictions to data

with LO accuracy in the final states with up to four partons. SHERPA v. 2.2 MEs are convolved with the NNPDF 3.0 [65] PDFs. The MEs are merged with SHERPA parton shower using the ME+PS@NLO [78] prescription. This prediction shows a good agreement with data in all bins of the measurement.

The ratios between the measured Z + jets production cross-sections and the NLO predictions, calculated with various PDF sets, are shown in Figs. 13, 14 and 15. The calculations with MMHT2014 and NNPDF3.1 predict 1–2% larger cross-sections compared to those using the CT14 PDF. The cross-sections calculated with ATLAS-epWZ16 PDF are larger by 2–3%. The ABMP16 and HERAPDF2.0 cross-section predictions in the $|y_{\text{jet}}| < 2.0$ and $p_{\text{T}}^{\text{jet}} < 100$ GeV regions are 3–5% larger than those from the CT14 PDF, while in other bins of the measurement their predictions are up to 5% lower than those obtained with the CT14 PDF. The JR14 PDF predictions are 2–5% lower than those from the CT14 PDF in the 25 GeV $< p_{\text{T}}^{\text{jet}} <$ 200 GeV region and higher by 2% in the $p_{\text{T}}^{\text{jet}} >$ 200 GeV region. The differences between the cross-sections calculated at NLO accuracy with various PDF sets are covered by the theoretical uncertainties. In the NNLO calculations, the difference between CT14 PDF and NNPDF3.1 predictions is 2–5%, which is comparable to the size of the theoretical uncertainties, as shown in Fig. 16.

11 Quantitative data and theory comparison

The fixed-order pQCD predictions at NNLO accuracy, corrected for electroweak and non-perturbative effects, are quantitatively compared with the measured cross-section using a χ^2 function that accounts for both the experimental and theoretical uncertainties

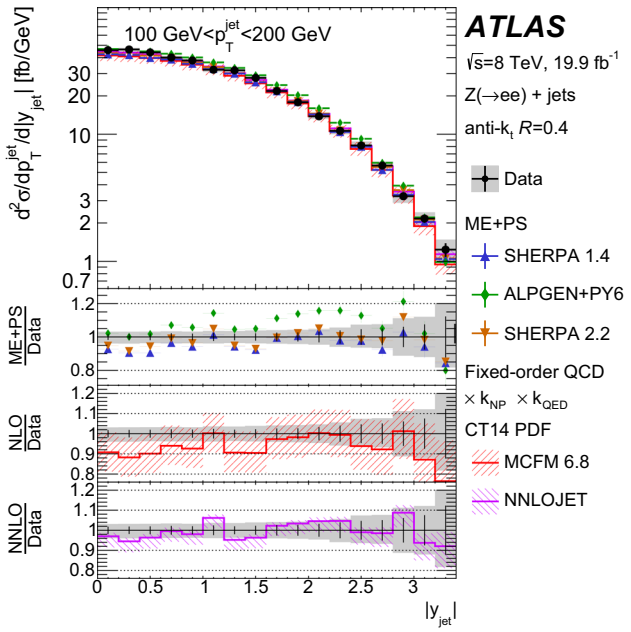

Fig. 9 The double-differential Z + jets production cross-section as a function of $|y_{\text{jet}}|$ in the 100 GeV $< p_{\text{T}}^{\text{jet}} <$ 200 GeV range. The data are compared with the SHERPA v. 1.4, SHERPA v. 2.2 and ALPGEN+PYTHIA parton shower MC generator predictions and with the fixed-order theory predictions. The fixed-order theory predictions are corrected for the non-perturbative and QED radiation effects. The fixed-order calculations are performed using the CT14 PDF. The total statistical uncertainties are shown with error bars. The total uncertainties in the measurement and in the fixed-order theory predictions are represented with shaded bands. The total uncertainty in the measurement is the sum in quadrature of the statistical and systematic uncertainties except for the luminosity uncertainty of 1.9%. The total uncertainty in the fixed-order theory predictions is the sum in quadrature of the effects of the PDF, scale, and α_{S} uncertainties, and the uncertainties from the non-perturbative and QED radiation corrections. Lower panels show the ratios of predictions to data

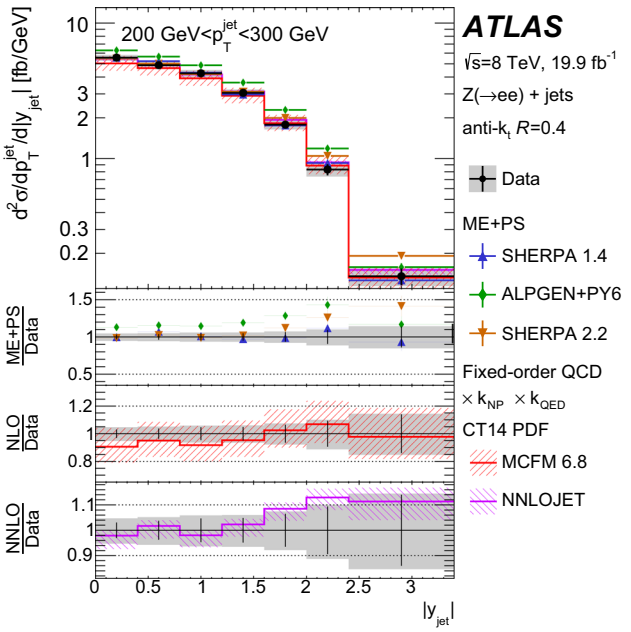

Fig. 10 The double-differential Z + jets production cross-section as a function of $|y_{\text{jet}}|$ in the 200 GeV $< p_{\text{T}}^{\text{jet}} <$ 300 GeV range. The data are compared with the SHERPA v. 1.4, SHERPA v. 2.2 and ALPGEN+PYTHIA parton shower MC generator predictions and with the fixed-order theory predictions. The fixed-order theory predictions are corrected for the non-perturbative and QED radiation effects. The fixed-order calculations are performed using the CT14 PDF. The total statistical uncertainties are shown with error bars. The total uncertainties in the measurement and in the fixed-order theory predictions are represented with shaded bands. The total uncertainty in the measurement is the sum in quadrature of the statistical and systematic uncertainties except for the luminosity uncertainty of 1.9%. The total uncertainty in the fixed-order theory predictions is the sum in quadrature of the effects of the PDF, scale, and α_{S} uncertainties, and the uncertainties from the non-perturbative and QED radiation corrections. Lower panels show the ratios of predictions to data

$$\chi^2\left(\beta^{\text{data}}, \beta^{\text{theory}}\right) = \sum_{i=1}^{N_{\text{bins}}} \frac{\left(\sigma_i^{\text{data}} + \sum_\mu \Gamma_{i;\mu}^{\text{data}} \beta_\mu^{\text{data}} - \sigma_i^{\text{theory}} - \sum_\nu \Gamma_{i;\nu}^{\text{theory}} \beta_\nu^{\text{theory}}\right)^2}{\Delta_i^2} + \sum_\mu \left(\beta_\mu^{\text{data}}\right)^2 + \sum_\nu \left(\beta_\nu^{\text{theory}}\right)^2, \quad (2)$$

where experimental (theoretical) uncertainties are included in the calculation using the nuisance parameter vectors β^{data} $\left(\beta^{\text{theory}}\right)$ and their influence on the data and the theory predictions is described by the respective $\Gamma_{l;\rho}$ matrices. The Latin indices run over bins of measurements and the Greek indices render sources of uncertainties. The measured cross-sections and their theory predictions in each bin are represented by σ_i^{data} and σ_i^{theory}, respectively. Uncorrelated uncertainties in data are denoted by Δ_i. The theoretical uncertainties include those arising from renormalisation and factorisation scales variations, PDF uncertainties, uncertainties in calculations of non-perturbative and electroweak effects as well as from the $\alpha_{\text{S}}(m_Z)$ uncertainty. All experimental and theoretical systematic uncertainties are assumed to be independent of each other, and fully correlated across the bins of the measurement. The negligible correlations of statistical uncertainties are not included in the χ^2 tests presented here.

The minimisation of Eq. (2), for the case of symmetric systematic uncertainties, results in a system of linear equations for the shifts of systematic uncertainties, β_ρ. The asymmetries in systematic uncertainties are accounted for using an iterative procedure. Here, the influences $\Gamma_{l;\rho}$ are recalculated as

$$\Gamma_{l;\rho} \rightarrow \Gamma_{l;\rho} + \Omega_{l;\rho}\beta_\rho,$$

where $\Gamma_{l;\rho} = \frac{1}{2}\left(\Gamma_{l;\rho}^+ - \Gamma_{l;\rho}^-\right)$ and $\Omega_{l;\rho} = \frac{1}{2}\left(\Gamma_{l;\rho}^+ + \Gamma_{l;\rho}^-\right)$, after each iteration using the shifts β_ρ from the previous iteration. The $\Gamma_{l;\rho}^+$ and $\Gamma_{l;\rho}^-$ are positive and negative components

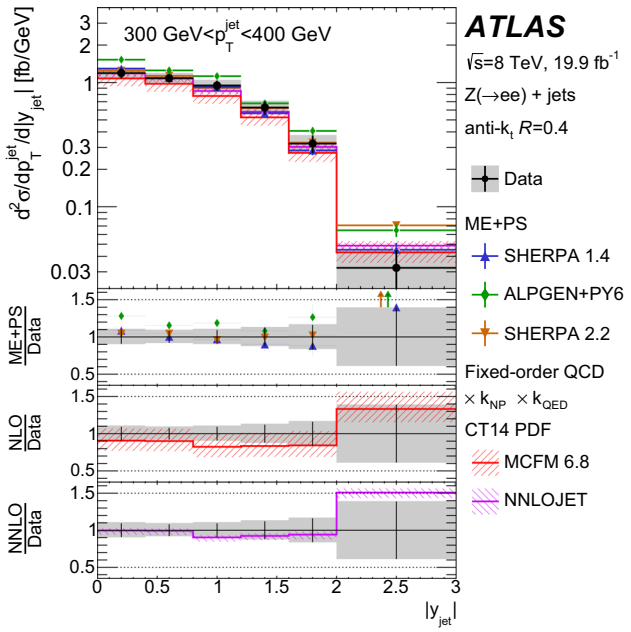

Fig. 11 The double-differential Z + jets production cross-section as a function of $|y_{\text{jet}}|$ in the 300 GeV $< p_{\text{T}}^{\text{jet}} <$ 400 GeV range. The data are compared with the SHERPA v. 1.4, SHERPA v. 2.2 and ALPGEN+PYTHIA parton shower MC generator predictions and with the fixed-order theory predictions. The fixed-order theory predictions are corrected for the non-perturbative and QED radiation effects. The fixed-order calculations are performed using the CT14 PDF. The total statistical uncertainties are shown with error bars. The total uncertainties in the measurement and in the fixed-order theory predictions are represented with shaded bands. The total uncertainty in the measurement is the sum in quadrature of the statistical and systematic uncertainties except for the luminosity uncertainty of 1.9%. The total uncertainty in the fixed-order theory predictions is the sum in quadrature of the effects of the PDF, scale, and α_{S} uncertainties, and the uncertainties from the non-perturbative and QED radiation corrections. Lower panels show the ratios of predictions to data

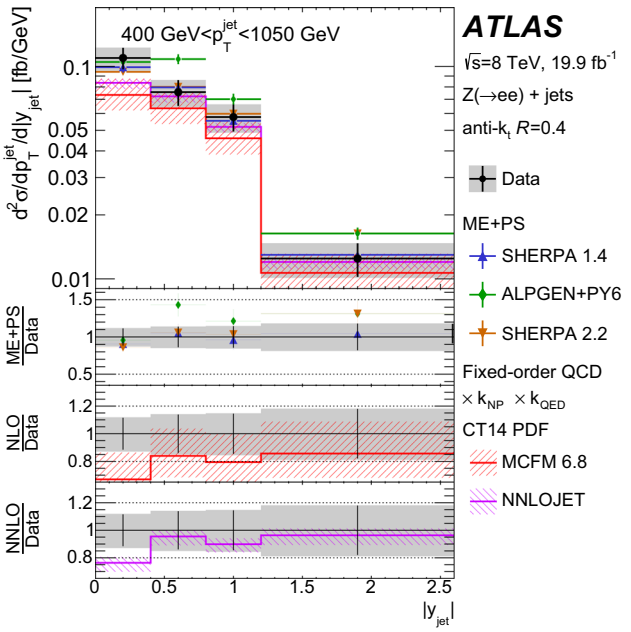

Fig. 12 The double-differential Z + jets production cross-section as a function of $|y_{\text{jet}}|$ in the 400 GeV $< p_{\text{T}}^{\text{jet}} <$ 1050 GeV range. The data are compared with the SHERPA v. 1.4, SHERPA v. 2.2 and ALPGEN+PYTHIA parton shower MC generator predictions and with the fixed-order theory predictions. The fixed-order theory predictions are corrected for the non-perturbative and QED radiation effects. The fixed-order calculations are performed using the CT14 PDF. The total statistical uncertainties are shown with error bars. The total uncertainties in the measurement and in the fixed-order theory predictions are represented with shaded bands. The total uncertainty in the measurement is the sum in quadrature of the statistical and systematic uncertainties except for the luminosity uncertainty of 1.9%. The total uncertainty in the fixed-order theory predictions is the sum in quadrature of the effects of the PDF, scale, and α_{S} uncertainties, and the uncertainties from the non-perturbative and QED radiation corrections. Lower panels show the ratios of predictions to data

of systematic uncertainties, respectively. The χ^2 values at the minimum provide a measure of the probability of compatibility between the measurements and the predictions.

Table 1 shows a summary of the calculated χ^2_{uncorr}, the first term in Eq. (2), together with χ^2_{corr}, the sum of squared shifts of nuisance parameters, for each $p_{\text{T}}^{\text{jet}}$ bin separately. A good agreement between measurements and theory is seen for the fits in individual $p_{\text{T}}^{\text{jet}}$ bins in the $p_{\text{T}}^{\text{jet}} > 50$ GeV range, with not so good agreement in the 25 $< p_{\text{T}}^{\text{jet}} <$ 50 GeV range. The level of agreement between data and predictions is very similar for different PDF sets.

In addition to fits of the predictions to measured cross-sections in the individual $p_{\text{T}}^{\text{jet}}$ bins, all measured data points are fitted simultaneously. Several ranges of $p_{\text{T}}^{\text{jet}}$ are considered. The results of the global fits are presented in Table 2. Very good agreement between measurement and calculation is observed when using the $p_{\text{T}}^{\text{jet}} > 50$ GeV bins, while not so good agreement is observed when the 25 $< p_{\text{T}}^{\text{jet}} <$ 50 GeV bin is included in the global fit.

The results of the χ^2 tests strongly depend on what is assumed about the correlation of systematic uncertainties. In general, the correlations of uncertainties related to detector measurements are carefully studied and well known [57,79]. In contrast, the assumption of 100% correlations of uncertainties resulting from simple comparisons of two (or more) different MC simulations (two-point systematic uncertainties) are less justified. In order to investigate the impact of these assumptions on the results of χ^2 tests performed in this section, the uncertainties that are derived from comparisons of two different MC models, namely uncertainties in the jet flavour composition and jet flavour response, were split into two subcomponents [80,81]. The first subcomponent is derived by multiplying the original nuisance parameter with a linear function of $p_{\text{T}}^{\text{jet}}$ and jet absolute rapidity and the second subcomponent is constructed such that the sum

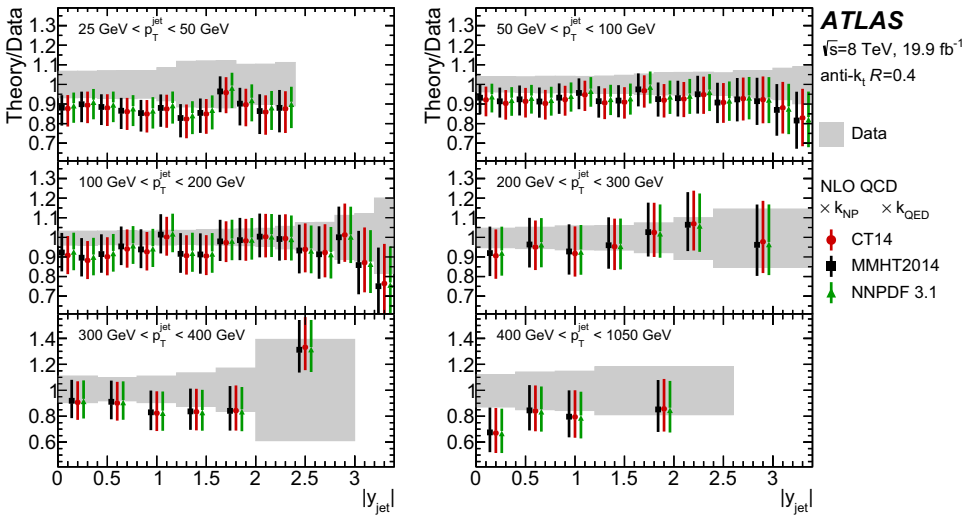

Fig. 13 Ratio of the measured Z + jets production cross-section and the NLO QCD predictions, obtained using MCFM, corrected for the non-perturbative and QED radiation effects as a function of $|y_{\text{jet}}|$ and $p_{\text{T}}^{\text{jet}}$ bins. Theoretical predictions are calculated using various PDF sets. The coloured error bars represent the sum in quadrature of the effects of the PDF, scale, and α_{S} uncertainties, and the uncertainties from the non-perturbative and QED radiation corrections. The grey band shows the sum in quadrature of the statistical and systematic uncertainties in the measurement except for the luminosity uncertainty of 1.9%

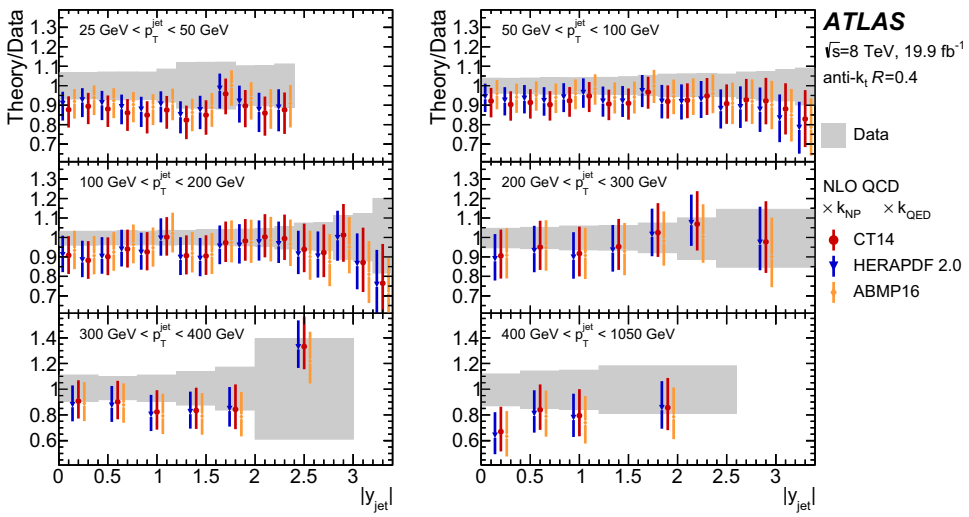

Fig. 14 Ratio of the measured Z + jets production cross-section and the NLO QCD predictions, obtained using MCFM, corrected for the non-perturbative and QED radiation effects as a function of $|y_{\text{jet}}|$ and $p_{\text{T}}^{\text{jet}}$ bins. Theoretical predictions are calculated using various PDF sets. The coloured error bars represent the sum in quadrature of the effects of the PDF, scale, and α_{S} uncertainties, and the uncertainties from the non-perturbative and QED radiation corrections. The grey band shows the sum in quadrature of the statistical and systematic uncertainties in the measurement except for the luminosity uncertainty of 1.9%

in quadrature of both subcomponents is equal to the original nuisance parameter. These decorrelations did not result in a large improvement in the χ^2 values.

12 Conclusions

The double-differential Z + jets cross-section, with the Z boson decaying into an electron–positron pair, is measured using proton–proton collision data with an integrated luminosity 19.9 fb^{-1} collected by the ATLAS experiment at the LHC in 2012 at $\sqrt{s} = 8$ TeV centre-of-mass energy. The measurement is performed as a function of the absolute jet rapidity and the jet transverse momentum.

The measured cross-section is corrected for detector effects and the results are provided at the particle level. The measurements are compared with theory predictions, calculated using the multi-leg matrix element MC genera-

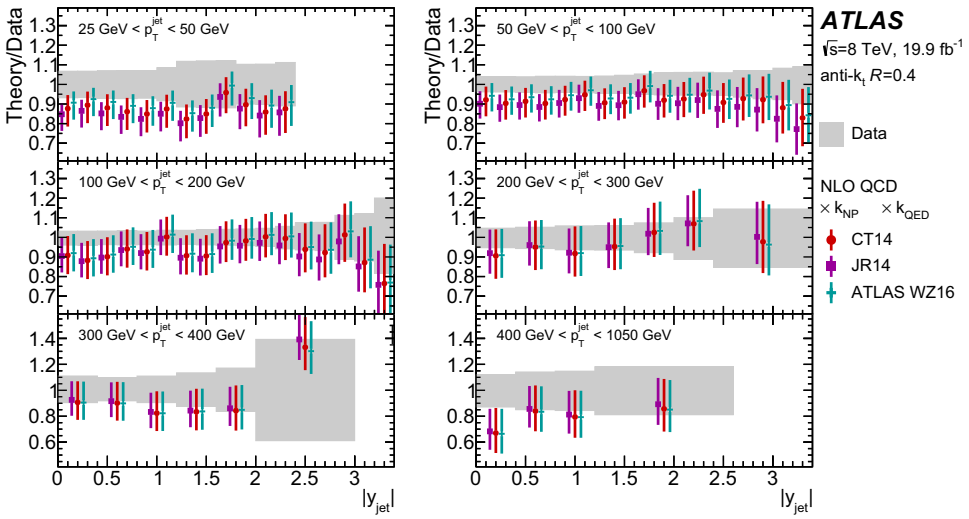

Fig. 15 Ratio of the measured Z + jets production cross-section and the NLO QCD predictions, obtained using MCFM, corrected for the non-perturbative and QED radiation effects as a function of $|y_{\text{jet}}|$ and $p_{\text{T}}^{\text{jet}}$ bins. Theoretical predictions are calculated using various PDF sets. The coloured error bars represent the sum in quadrature of the effects of the PDF, scale, and α_{S} uncertainties, and the uncertainties from the non-perturbative and QED radiation corrections. The grey band shows the sum in quadrature of the statistical and systematic uncertainties in the measurement except for the luminosity uncertainty of 1.9%

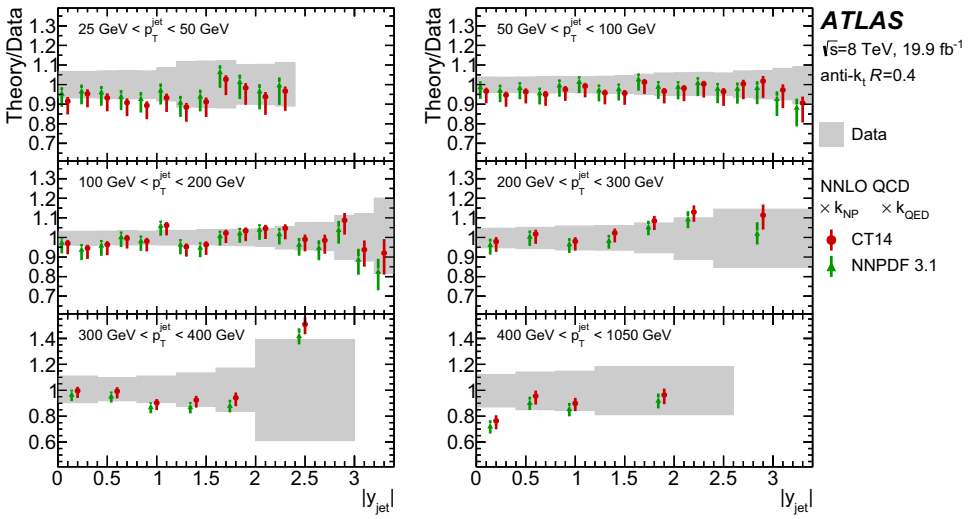

Fig. 16 Ratio of the measured Z + jets production cross-section and the NNLO QCD predictions, obtained using NNLOJET, corrected for the non-perturbative and QED radiation effects as a function of $|y_{\text{jet}}|$ and $p_{\text{T}}^{\text{jet}}$ bins. Theoretical predictions are calculated using various PDF sets. The coloured error bars represent the sum in quadrature of the effects of the PDF, scale, and α_{S} uncertainties, and the uncertainties from the non-perturbative and QED radiation corrections. The grey band shows the sum in quadrature of the statistical and systematic uncertainties in the measurement except for the luminosity uncertainty of 1.9%

tors SHERPA and ALPGEN+PYTHIA, supplemented with parton shower simulations. SHERPA v. 1.4 and ALPGEN+PYTHIA describe well the shape of the Z + jets distribution as a function of $|y_{\text{jet}}|$, but not so well as a function of $p_{\text{T}}^{\text{jet}}$. SHERPA v. 2.2 is in good agreement with data in all bins of the measurement.

The parton-level fixed-order Z + jets predictions, corrected for hadronisation, underlying-event and QED radiation effects, agree with the data within the uncertainties.

The uncertainties in the measured cross-sections are about half of the theoretical uncertainties in the NLO calculations in most bins of the measurement and are approximately similar to the uncertainties in the NNLO calculations.

The measured double-differential Z + jets cross-section provides a precision input to constrain the parton distribution functions.

Table 1 Values of χ^2_{uncorr} and χ^2_{corr} evaluated for theory predictions corrected for non-perturbative and electroweak effects and measured Z + jets cross-sections. The total χ^2 is equal to the sum of χ^2_{uncorr} and χ^2_{corr}. The fits are performed individually in each $p_{\text{T}}^{\text{jet}}$ bin. The predictions are calculated using several NNLO QCD PDF sets and one NLO QCD PDF set, CT14nlo

$p_{\text{T}}^{\text{jet}}$ range (GeV)	n_{bins}	CT14nlo		CT14		NNPDF3.1		MMHT2014		ABMP16	
		χ^2_{uncorr}	χ^2_{corr}	χ^2_{uncorr}	χ^2_{corr}	χ^2_{uncorr}	χ^2_{corr}	χ^2_{uncorr}	χ^2_{corr}	χ^2_{uncorr}	χ^2_{corr}
$25 < p_{\text{T}}^{\text{jet}} < 50$	12	31.5	14.7	32.2	15.6	33.6	15.7	32.7	15.9	31.8	13.8
$50 < p_{\text{T}}^{\text{jet}} < 100$	17	23.6	2.6	24.2	2.3	27.1	2.3	26.3	2.1	24.9	2.5
$100 < p_{\text{T}}^{\text{jet}} < 200$	17	24.9	3.6	24.8	2.5	26.1	1.8	27.2	2.8	22.6	1.5
$200 < p_{\text{T}}^{\text{jet}} < 300$	7	3.1	0.9	2.9	0.7	3.6	0.1	4.5	0.5	2.7	0.2
$300 < p_{\text{T}}^{\text{jet}} < 400$	6	2.7	0.1	2.7	0.1	2.9	0.1	3.2	0.0	2.5	0.3
$400 < p_{\text{T}}^{\text{jet}} < 1050$	4	1.9	0.4	1.9	0.4	1.9	0.5	2.0	0.3	1.7	0.8

Table 2 Values of χ^2 evaluated from the comparison of theory predictions corrected for non-perturbative and electroweak effects with the measured Z + jets cross-sections. The fits are performed globally in all bins of the measurement within several $p_{\text{T}}^{\text{jet}}$ ranges. The predictions are calculated using several NNLO QCD PDF sets and one NLO QCD PDF set, CT14nlo

	$p_{\text{T}}^{\text{jet}}$ range (GeV)	CT14nlo	CT14	NNPDF3.1	MMHT2014	ABMP16
		$p_{\text{T}}^{\text{jet}} > 25$ GeV				
χ^2_{uncorr}	$25 < p_{\text{T}}^{\text{jet}} < 50$	38.9	40.5	42.3	41.3	38.7
	$50 < p_{\text{T}}^{\text{jet}} < 100$	32.1	33.0	37.5	39.2	31.6
	$100 < p_{\text{T}}^{\text{jet}} < 200$	26.4	27.8	31.0	31.7	27.8
	$200 < p_{\text{T}}^{\text{jet}} < 300$	6.3	6.3	5.1	5.6	4.1
	$300 < p_{\text{T}}^{\text{jet}} < 400$	2.9	3.0	2.9	3.1	2.5
	$400 < p_{\text{T}}^{\text{jet}} < 1050$	2.2	2.4	2.2	2.3	1.7
χ^2_{corr}		21.2	19.8	19.3	18.7	17.8
χ^2/n_{bins}		129.9/63	132.6/63	140.0/63	141.9/63	124.3/63
		$p_{\text{T}}^{\text{jet}} > 50$ GeV				
χ^2_{uncorr}	$50 < p_{\text{T}}^{\text{jet}} < 100$	24.4	24.8	26.9	27.1	24.8
	$100 < p_{\text{T}}^{\text{jet}} < 200$	24.4	24.6	26.6	27.7	22.7
	$200 < p_{\text{T}}^{\text{jet}} < 300$	4.4	4.2	4.4	4.7	3.4
	$300 < p_{\text{T}}^{\text{jet}} < 400$	2.7	2.8	3.0	3.1	2.5
	$400 < p_{\text{T}}^{\text{jet}} < 1050$	3.6	4.0	3.8	3.9	2.9
χ^2_{corr}		6.5	4.7	4.3	5.1	4.1
χ^2/n_{bins}		66.1/51	65.2/51	69.0/51	71.6/51	60.4/51
		$p_{\text{T}}^{\text{jet}} > 100$ GeV				
χ^2_{uncorr}	$100 < p_{\text{T}}^{\text{jet}} < 200$	24.8	25.0	25.9	26.6	22.4
	$200 < p_{\text{T}}^{\text{jet}} < 300$	3.2	3.3	4.1	4.4	3.3
	$300 < p_{\text{T}}^{\text{jet}} < 400$	2.7	2.8	3.0	3.1	2.6
	$400 < p_{\text{T}}^{\text{jet}} < 1050$	3.4	3.8	3.6	3.6	3.3
χ^2_{corr}		4.9	3.7	2.7	4.1	2.3
χ^2/n_{bins}		39.0/34	38.5/34	39.3/34	41.8/34	33.8/34

Acknowledgements We thank CERN for the very successful operation of the LHC, as well as the support staff from our institutions without whom ATLAS could not be operated efficiently. We acknowledge the support of ANPCyT, Argentina; YerPhI, Armenia; ARC, Australia; BMWFW and FWF, Austria; ANAS, Azerbaijan; SSTC, Belarus; CNPq and FAPESP, Brazil; NSERC, NRC and CFI, Canada; CERN; CONICYT, Chile; CAS, MOST and NSFC, China; COLCIENCIAS, Colombia; MSMT CR, MPO CR and VSC CR, Czech Republic; DNRF and DNSRC, Denmark; IN2P3-CNRS, CEA-DRF/IRFU, France; SRNSFG, Georgia; BMBF, HGF, and MPG, Germany; GSRT, Greece; RGC, Hong Kong SAR, China; ISF and Benoziyo Center, Israel; INFN, Italy; MEXT and JSPS, Japan; CNRST, Morocco; NWO, Netherlands; RCN, Norway; MNiSW and NCN, Poland; FCT, Portugal; MNE/IFA, Romania; MES of Russia and NRC KI, Russian Federation; JINR; MESTD, Serbia; MSSR, Slovakia; ARRS and MIZŠ, Slovenia; DST/NRF, South Africa; MINECO, Spain; SRC and Wallenberg Foundation, Sweden; SERI, SNSF and Cantons of Bern and Geneva, Switzerland; MOST, Taiwan; TAEK, Turkey; STFC, UK; DOE and NSF, USA.

In addition, individual groups and members have received support from BCKDF, CANARIE, CRC and Compute Canada, Canada; COST, ERC, ERDF, Horizon 2020, and Marie Skłodowska-Curie Actions, European Union; Investissements d' Avenir Labex and Idex, ANR, France; DFG and AvH Foundation, Germany; Herakleitos, Thales and Aristeia programmes co-financed by EU-ESF and the Greek NSRF, Greece; BSF-NSF and GIF, Israel; CERCA Programme Generalitat de Catalunya, Spain; The Royal Society and Leverhulme Trust, UK. The crucial computing support from all WLCG partners is acknowledged gratefully, in particular from CERN, the ATLAS Tier-1 facilities at TRIUMF (Canada), NDGF (Denmark, Norway, Sweden), CC-IN2P3 (France), KIT/GridKA (Germany), INFN-CNAF (Italy), NL-T1 (Netherlands), PIC (Spain), ASGC (Taiwan), RAL (UK) and BNL (USA), the Tier-2 facilities worldwide and large non-WLCG resource providers. Major contributors of computing resources are listed in Ref. [82].

Data Availability Statement This manuscript has no associated data or the data will not be deposited. [Authors' comment: "All ATLAS scientific output is published in journals, and preliminary results are made available in Conference Notes. All are openly available, without restriction on use by external parties beyond copyright law and the standard conditions agreed by CERN. Data associated with journal publications are also made available: tables and data from plots (e.g. cross section values, likelihood profiles, selection efficiencies, cross section limits, ...) are stored in appropriate repositories such as HEPDATA (http://hepdata.cedar.ac.uk/). ATLAS also strives to make additional material related to the paper available that allows a reinterpretation of the data in the context of new theoretical models. For example, an extended encapsulation of the analysis is often provided for measurements in the framework of RIVET (http://rivet.hepforge.org/)." This information is taken from the ATLAS Data Access Policy, which is a public document that can be downloaded from http://opendata.cern.ch/record/413.]

Funded by SCOAP[3].

Appendix

A Tables of measured cross-sections

Table 3 The measured double-differential Z + jets production cross-sections as a function of $|y_{\text{jet}}|$ in the 25 GeV $< p_{\text{T}}^{\text{jet}} <$ 50 GeV range. $\delta_{\text{data}}^{\text{stat}}$ and $\delta_{\text{MC}}^{\text{stat}}$ are the statistical uncertainties in data and MC simulation, respectively. $\delta_{\text{tot}}^{\text{sys}}$ is the total systematic uncertainty and includes the following components: uncertainties due to electron reconstruction ($\delta_{\text{rec}}^{\text{el}}$), identification ($\delta_{\text{ID}}^{\text{el}}$) and trigger ($\delta_{\text{trig}}^{\text{el}}$) efficiencies; electron energy scale ($\delta_{\text{scale}}^{\text{el}}$) and energy resolution ($\delta_{\text{res}}^{\text{el}}$) uncertainties; sum in quadrature of the uncertainties from JES in situ methods ($\delta_{\text{in situ}}^{\text{JES}}$); sum in quadrature of the uncertainties from JES η-intercalibration methods ($\delta_{\eta\text{-int}}^{\text{JES}}$); an uncertainty of the measured single-hadron response ($\delta_{\text{hadron}}^{\text{JES}}$); MC non-closure uncertainty ($\delta_{\text{closure}}^{\text{JES}}$); sum in quadrature of the uncertainties due to pile-up corrections of the jet kinematics ($\delta_{\text{pile-up}}^{\text{JES}}$); sum in quadrature of the flavour-based uncertainties ($\delta_{\text{flavour}}^{\text{JES}}$); punch-through uncertainty ($\delta_{\text{pthrough}}^{\text{JES}}$); JER uncertainty ($\delta^{\text{JER}}$); JVF uncertainty ($\delta^{\text{JVF}}$); sum in quadrature of the unfolding uncertainties (δ^{unf}); sum in quadrature of the uncertainties due to MC generated backgrounds normalisation ($\delta_{\text{MC}}^{\text{bg}}$); sum in quadrature of the uncertainty due to combined multijet and W+ jets backgrounds ($\delta_{\text{mult}}^{\text{bg}}$); uncertainty due to jet quality selection (δ^{qual}). All uncertainties are given in %. The luminosity uncertainty of 1.9% is not shown and not included in the total uncertainty and its components

$\lvert y_{\text{jet}}\rvert$	$\frac{d^2\sigma}{d\lvert y_{\text{jet}}\rvert dp_{\text{T}}^{\text{jet}}}$ (fb/GeV)	$\delta_{\text{data}}^{\text{stat}}$ (%)	$\delta_{\text{MC}}^{\text{stat}}$ (%)	$\delta_{\text{tot}}^{\text{sys}}$ (%)	$\delta_{\text{rec}}^{\text{el}}$ (%)	$\delta_{\text{ID}}^{\text{el}}$ (%)	$\delta_{\text{trig}}^{\text{el}}$ (%)	$\delta_{\text{scale}}^{\text{el}}$ (%)	$\delta_{\text{res}}^{\text{el}}$ (%)	$\delta_{\text{in situ}}^{\text{JES}}$ (%)	$\delta_{\eta-\text{int}}^{\text{JES}}$ (%)
0.0–0.2	1643.603	0.42	0.51	$+6.70$	$+0.08$	$+0.23$	$+0.31$	-0.16	$+0.01$	$+3.04$	$+0.30$
				-6.80	-0.08	-0.27	-0.44	$+0.14$	-0.01	-3.04	-0.49
0.2–0.4	1595.690	0.34	0.60	$+6.72$	$+0.08$	$+0.23$	$+0.31$	-0.16	$+0.01$	$+3.16$	$+0.30$
				-6.70	-0.08	-0.27	-0.44	$+0.14$	-0.01	-3.02	-0.49
0.4–0.6	1587.440	0.37	0.60	$+7.01$	$+0.08$	$+0.23$	$+0.31$	-0.16	$+0.01$	$+3.17$	$+0.30$
				-7.14	-0.08	-0.27	-0.44	$+0.14$	-0.01	-3.14	-0.49
0.6–0.8	1569.884	0.38	0.60	$+7.02$	$+0.08$	$+0.23$	$+0.31$	-0.16	$+0.01$	$+3.19$	$+0.30$
				-7.24	-0.08	-0.27	-0.44	$+0.14$	-0.01	-3.25	-0.49
0.8–1.0	1520.883	0.36	0.59	$+6.98$	$+0.08$	$+0.23$	$+0.31$	-0.16	$+0.01$	$+3.33$	$+0.30$
				-7.04	-0.08	-0.27	-0.33	$+0.14$	-0.01	-3.25	-0.49
1.0–1.2	1393.139	0.38	0.64	$+8.49$	$+0.08$	$+0.23$	$+0.31$	-0.16	$+0.01$	$+3.60$	$+0.76$
				-8.32	-0.08	-0.27	-0.33	$+0.14$	-0.01	-3.35	-0.49
1.2–1.4	1377.328	0.47	0.57	$+11.78$	$+0.08$	$+0.23$	$+0.31$	-0.16	$+0.01$	$+3.69$	$+0.76$
				-11.50	-0.08	-0.27	-0.33	$+0.14$	-0.01	-3.29	-0.69
1.4–1.6	1228.213	0.42	0.60	$+12.01$	$+0.08$	$+0.23$	$+0.31$	-0.16	$+0.01$	$+3.65$	$+1.44$
				-11.69	-0.08	-0.27	-0.33	$+0.14$	-0.01	-3.22	-1.14
1.6–1.8	987.654	0.48	0.64	$+12.09$	$+0.08$	$+0.23$	$+0.31$	-0.16	$+0.01$	$+3.37$	$+1.42$
				-11.95	-0.08	-0.27	-0.33	$+0.14$	-0.01	-3.10	-1.25

Table 3 continued

$\lvert y_{\text{jet}}\rvert$	$\frac{d^2\sigma}{d\lvert y_{\text{jet}}\rvert dp_{\text{T}}^{\text{jet}}}$ (fb/GeV)	$\delta_{\text{data}}^{\text{stat}}$ (%)	$\delta_{\text{MC}}^{\text{stat}}$ (%)	$\delta_{\text{tot}}^{\text{sys}}$ (%)	$\delta_{\text{rec}}^{\text{el}}$ (%)	$\delta_{\text{ID}}^{\text{el}}$ (%)	$\delta_{\text{trig}}^{\text{el}}$ (%)	$\delta_{\text{scale}}^{\text{el}}$ (%)	$\delta_{\text{res}}^{\text{el}}$ (%)	$\delta_{\text{in situ}}^{\text{JES}}$ (%)	$\delta_{\eta-\text{int}}^{\text{JES}}$ (%)
1.8–2.0	944.560	0.45	0.65	+10.24	+0.08	+0.23	+0.40	−0.16	+0.01	+3.38	+1.58
				−10.02	−0.08	−0.27	−0.33	+0.14	−0.01	−3.09	−1.25
2.0–2.2	871.035	0.49	0.85	+10.30	+0.08	+0.23	+0.40	−0.16	+0.01	+3.65	+1.96
				−10.18	−0.08	−0.27	−0.33	+0.14	−0.01	−3.41	−1.74
2.2–2.4	749.498	0.54	0.80	+11.14	+0.08	+0.23	+0.40	−0.16	+0.01	+4.23	+2.57
				−10.92	−0.08	−0.27	−0.33	+0.14	−0.01	−3.95	−2.33

$\lvert y_{\text{jet}}\rvert$	$\delta_{\text{hadron}}^{\text{JES}}$ (%)	$\delta_{\text{closure}}^{\text{JES}}$ (%)	$\delta_{\text{pile-up}}^{\text{JES}}$ (%)	$\delta_{\text{flavour}}^{\text{JES}}$ (%)	$\delta_{\text{pthrough}}^{\text{JES}}$ (%)	δ^{JER} (%)	δ^{JVF} (%)	δ^{unf} (%)	$\delta_{\text{MC}}^{\text{bg}}$ (%)	$\delta_{\text{mult}}^{\text{bg}}$ (%)	δ^{qual} (%)
0.0–0.2	+0.00	+0.01	+1.63	+2.95	+0.00	−3.83	+0.47	+2.84	+0.06	+0.14	+1.00
	−0.01	−0.01	−1.68	−3.04	−0.02	+3.83	−0.72	−2.84	−0.05	−0.38	−1.00
0.2–0.4	+0.00	+0.01	+1.65	+3.04	+0.00	−3.89	+0.47	+2.55	+0.06	+0.14	+1.00
	−0.01	−0.01	−1.60	−3.05	−0.02	+3.89	−0.72	−2.55	−0.05	−0.39	−1.00
0.4–0.6	+0.00	+0.01	+1.59	+3.08	+0.00	−4.17	+0.46	+2.86	+0.06	+0.15	+1.00
	−0.01	−0.01	−1.72	−3.23	−0.02	+4.17	−0.67	−2.86	−0.05	−0.39	−1.00
0.6–0.8	+0.00	+0.01	+1.62	+3.26	+0.00	−3.74	+0.46	+3.22	+0.05	+0.15	+1.00
	−0.01	−0.01	−1.82	−3.46	−0.02	+3.74	−0.67	−3.22	−0.05	−0.40	−1.00
0.8–1.0	+0.00	+0.01	+1.80	+3.54	+0.00	−2.88	+0.46	+3.48	+0.05	+0.15	+1.00
	−0.01	−0.01	−1.88	−3.61	−0.02	+2.88	−0.56	−3.48	−0.05	−0.39	−1.00
1.0–1.2	+0.00	+0.01	+1.97	+3.93	+0.00	−5.18	+0.46	+3.32	+0.05	+0.16	+1.00
	−0.01	−0.01	−1.81	−3.87	−0.02	+5.18	−0.56	−3.32	−0.05	−0.41	−1.00
1.2–1.4	+0.00	+0.01	+2.04	+4.49	+0.00	−8.88	+0.46	+4.47	+0.05	+0.17	+1.00
	−0.01	−0.01	−1.78	−4.14	−0.02	+8.88	−0.56	−4.47	−0.05	−0.41	−1.00
1.4–1.6	+0.00	+0.01	+2.00	+4.37	+0.00	−9.07	+0.71	+4.67	+0.05	+0.18	+1.00
	−0.01	−0.01	−1.74	−4.02	−0.02	+9.07	−0.69	−4.67	−0.05	−0.42	−1.00
1.6–1.8	+0.00	+0.01	+1.83	+3.60	+0.00	−10.46	+0.71	+2.32	+0.06	+0.17	+1.00
	−0.01	−0.01	−1.62	−3.51	−0.02	+10.46	−0.69	−2.32	−0.05	−0.43	−1.00
1.8–2.0	+0.00	+0.01	+1.90	+3.38	+0.00	−8.31	+0.55	+2.32	+0.05	+0.16	+1.00
	−0.01	−0.01	−1.66	−3.23	−0.02	+8.31	−0.55	−2.32	−0.05	−0.43	−1.00
2.0–2.2	+0.00	+0.01	+2.05	+3.56	+0.00	−6.74	+0.55	+5.01	+0.05	+0.17	+1.00
	−0.01	−0.01	−1.94	−3.60	−0.02	+6.74	−0.55	−5.01	−0.05	−0.43	−1.00
2.2–2.4	+0.00	+0.01	+2.70	+3.91	+0.00	−7.48	+0.55	+4.42	+0.05	+0.18	+1.00
	−0.01	−0.01	−2.50	−3.85	−0.02	+7.48	−0.55	−4.42	−0.05	−0.42	−1.00

Table 4 The measured double-differential Z + jets production cross-sections as a function of $|y_{\text{jet}}|$ in the 50 GeV $< p_{\text{T}}^{\text{jet}} <$ 100 GeV range. $\delta_{\text{data}}^{\text{stat}}$ and $\delta_{\text{MC}}^{\text{stat}}$ are the statistical uncertainties in data and MC simulation, respectively. $\delta_{\text{tot}}^{\text{sys}}$ is the total systematic uncertainty and includes the following components: uncertainties due to electron reconstruction ($\delta_{\text{rec}}^{\text{el}}$), identification ($\delta_{\text{ID}}^{\text{el}}$) and trigger ($\delta_{\text{trig}}^{\text{el}}$) efficiencies; electron energy scale ($\delta_{\text{scale}}^{\text{el}}$) and energy resolution ($\delta_{\text{res}}^{\text{el}}$) uncertainties; sum in quadrature of the uncertainties from JES in situ methods ($\delta_{\text{in situ}}^{\text{JES}}$); sum in quadrature of the uncertainties from JES η-intercalibration methods ($\delta_{\eta\text{-int}}^{\text{JES}}$); an uncertainty of the measured single-hadron response ($\delta_{\text{hadron}}^{\text{JES}}$); MC non-closure uncertainty ($\delta_{\text{closure}}^{\text{JES}}$); sum in quadrature of the uncertainties due to pile-up corrections of the jet kinematics ($\delta_{\text{pile-up}}^{\text{JES}}$); sum in quadrature of the flavour-based uncertainties ($\delta_{\text{flavour}}^{\text{JES}}$); punch-through uncertainty ($\delta_{\text{pthrough}}^{\text{JES}}$); JER uncertainty ($\delta^{\text{JER}}$); JVF uncertainty ($\delta^{\text{JVF}}$); sum in quadrature of the unfolding uncertainties (δ^{unf}); sum in quadrature of the uncertainties due to MC generated backgrounds normalisation ($\delta_{\text{MC}}^{\text{bg}}$); sum in quadrature of the uncertainty due to combined multijet and W+ jets backgrounds ($\delta_{\text{mult}}^{\text{bg}}$); uncertainty due to jet quality selection (δ^{qual}). All uncertainties are given in %. The luminosity uncertainty of 1.9% is not shown and not included in the total uncertainty and its components

$\lvert y_{\text{jet}}\rvert$	$\frac{d^2\sigma}{d\lvert y_{\text{jet}}\rvert dp_{\text{T}}^{\text{jet}}}$ (fb/GeV)	$\delta_{\text{data}}^{\text{stat}}$ (%)	$\delta_{\text{MC}}^{\text{stat}}$ (%)	$\delta_{\text{tot}}^{\text{sys}}$ (%)	$\delta_{\text{rec}}^{\text{el}}$ (%)	$\delta_{\text{ID}}^{\text{el}}$ (%)	$\delta_{\text{trig}}^{\text{el}}$ (%)	$\delta_{\text{scale}}^{\text{el}}$ (%)	$\delta_{\text{res}}^{\text{el}}$ (%)	$\delta_{\text{in situ}}^{\text{JES}}$ (%)	$\delta_{\eta-\text{int}}^{\text{JES}}$ (%)
0.0–0.2	349.964	0.56	0.80	+3.75	+0.03	+0.15	+0.24	−0.25	+0.00	+2.67	+0.31
				−3.71	−0.08	−0.21	−0.29	+0.19	−0.05	−2.61	−0.26
0.2–0.4	352.217	0.71	0.80	+3.68	+0.03	+0.15	+0.24	v0.25	+0.00	+2.56	+0.31
				−3.77	−0.08	−0.21	−0.29	+0.19	−0.05	−2.70	−0.26
0.4–0.6	338.924	0.74	0.81	+3.78	+0.03	+0.15	+0.24	−0.25	+0.00	+2.52	+0.31
				−3.99	−0.08	−0.21	−0.29	+0.19	−0.05	−2.86	−0.26
0.6–0.8	328.606	0.72	0.93	+3.99	+0.03	+0.15	+0.24	−0.25	+0.00	+2.75	+0.31
				−4.15	−0.08	−0.21	−0.29	+0.19	−0.05	−2.86	−0.26
0.8–1.0	303.475	0.69	0.87	+4.05	+0.03	+0.15	+0.24	−0.25	+0.00	+2.98	+0.31
				−3.89	−0.08	−0.21	−0.29	+0.19	−0.05	−2.76	−0.26
1.0–1.2	274.407	0.71	1.05	+3.85	+0.03	+0.15	+0.24	−0.25	+0.00	+2.74	+0.31
				−4.09	−0.08	−0.21	−0.29	+0.19	−0.05	−2.83	−0.96
1.2–1.4	261.553	0.81	0.84	+4.14	+0.03	+0.15	+0.24	−0.25	+0.00	+2.86	+1.25
				−4.31	−0.08	−0.21	−0.29	+0.19	−0.05	−2.86	−0.96
1.4–1.6	233.170	0.75	1.02	+4.48	+0.03	+0.15	+0.24	−0.25	+0.00	+2.82	+1.25
				−4.38	−0.08	−0.21	−0.29	+0.19	−0.05	−2.74	−0.96
1.6–1.8	192.405	0.92	1.16	+5.11	+0.03	+0.15	+0.24	−0.25	+0.00	+3.09	+2.10
				−4.80	−0.08	−0.21	−0.29	+0.19	−0.05	−2.92	−1.97
1.8–2.0	174.081	0.90	1.18	+5.75	+0.03	+0.15	+0.24	−0.25	+0.00	+3.38	+2.61
				−5.14	−0.08	−0.21	−0.29	+0.19	−0.05	−3.05	−2.27
2.0–2.2	145.578	0.94	1.11	+5.92	+0.03	+0.15	+0.24	−0.25	+0.00	+3.48	+2.80
				−5.31	−0.08	−0.21	−0.29	+0.19	−0.05	−3.02	−2.36
2.2–2.4	117.333	1.08	1.37	+5.99	+0.03	+0.15	+0.24	−0.25	+0.00	+3.56	+2.78
				−5.18	−0.08	−0.21	−0.29	+0.19	−0.05	−2.83	−2.23
2.4–2.6	98.813	1.31	1.42	+5.65	+0.03	+0.15	+0.24	−0.25	+0.00	+3.32	+2.56
				−5.25	−0.08	−0.21	−0.29	+0.19	−0.05	−2.87	−2.20
2.6–2.8	75.900	1.47	1.67	+6.65	+0.03	+0.15	+0.24	−0.25	+0.00	+3.21	+2.88
				−6.11	−0.08	−0.21	−0.29	+0.19	−0.05	−2.85	−2.20
2.8–3.0	58.038	1.59	2.21	+6.49	+0.03	+0.15	+0.24	−0.25	+0.00	+3.08	+2.88
				−6.76	−0.08	−0.21	−0.29	+0.19	−0.05	−2.85	−3.79
3.0–3.2	44.324	1.58	2.56	+7.78	+0.03	+0.15	+0.24	−0.25	+0.00	+3.08	+4.36
				−7.26	−0.08	−0.21	−0.29	+0.19	−0.05	−2.72	−3.79
3.2–3.4	32.909	2.09	2.91	+8.34	+0.03	+0.15	+0.24	−0.25	+0.00	+3.08	+4.91
				−9.23	−0.08	−0.21	−0.29	+0.19	−0.05	−2.72	−6.55

Table 4 continued

$\lvert y_{\text{jet}}\rvert$	$\delta^{\text{JES}}_{\text{hadron}}$ (%)	$\delta^{\text{JES}}_{\text{closure}}$ (%)	$\delta^{\text{JES}}_{\text{pile-up}}$ (%)	$\delta^{\text{JES}}_{\text{flavour}}$ (%)	$\delta^{\text{JES}}_{\text{pthrough}}$ (%)	δ^{JER} (%)	δ^{JVF} (%)	δ^{unf} (%)	$\delta^{\text{bg}}_{\text{MC}}$ (%)	$\delta^{\text{bg}}_{\text{mult}}$ (%)	δ^{qual} (%)
0.0–0.2	+0.00	+0.00	+1.02	+0.81	+0.00	−1.47	−0.46	+1.28	+0.17	+0.15	+1.00
	−0.03	−0.02	−0.92	−0.77	−0.02	+1.47	+0.49	−1.28	−0.15	−0.42	−1.00
0.2–0.4	+0.00	+0.00	+1.02	+0.81	+0.00	−1.47	−0.46	+1.28	+0.16	+0.15	+1.00
	−0.03	−0.02	−0.92	−0.77	−0.02	+1.47	+0.49	−1.28	−0.15	−0.42	−1.00
0.4–0.6	+0.00	+0.00	+1.07	+0.81	+0.00	−1.60	−0.46	+1.43	+0.16	+0.15	+1.00
	−0.03	−0.02	−0.92	−0.77	−0.02	+1.60	+0.49	−1.43	−0.15	−0.43	−1.00
0.6–0.8	+0.00	+0.00	+1.07	+1.28	+0.00	−1.47	−0.46	+1.41	+0.16	+0.16	+1.00
	−0.03	−0.02	−1.08	−1.44	−0.02	+1.47	+0.49	−1.41	−0.14	−0.43	−1.00
0.8–1.0	+0.00	+0.00	+1.07	+1.50	+0.00	−1.21	−0.46	+1.07	+0.15	+0.17	+1.00
	−0.03	−0.02	−1.08	−1.44	−0.02	+1.21	+0.49	−1.07	−0.14	−0.45	−1.00
1.0–1.2	+0.00	+0.00	+1.01	+1.49	+0.00	−1.21	−0.46	+1.07	+0.15	+0.19	+1.00
	−0.03	−0.02	−1.19	−1.44	−0.02	+1.21	+0.49	−1.07	−0.14	− 0.46	−1.00
1.2–1.4	+0.00	+0.00	+1.01	+1.54	+0.00	−1.21	−0.46	+1.07	+0.14	+0.21	+1.00
	−0.03	−0.02	−1.19	−1.94	−0.02	+1.21	+0.49	−1.07	−0.13	−0.49	−1.00
1.4–1.6	+0.00	+0.00	+1.01	+1.78	+0.00	−1.42	−0.46	+1.73	+0.13	+0.37	+1.00
	−0.03	−0.02	−1.05	−1.69	−0.02	+1.42	+0.40	−1.73	−0.12	−0.60	−1.00
1.6–1.8	+0.00	+0.00	+1.34	+2.01	+0.00	−1.42	−0.46	+1.73	+0.13	+0.19	+1.00
	−0.03	−0.02	−1.05	−1.69	−0.02	+1.42	+0.40	−1.73	−0.12	−0.51	−1.00
1.8–2.0	+0.00	+0.00	+1.34	+2.25	+0.00	−1.89	−0.34	+1.73	+0.12	+0.20	+1.00
	−0.03	−0.02	−1.05	−1.66	−0.02	+1.89	+0.40	−1.73	−0.11	−0.55	−1.00
2.0–2.2	+0.00	+0.00	+1.40	+1.91	+0.00	−1.89	−0.34	+2.16	+0.11	+0.20	+1.00
	−0.03	−0.02	−0.92	−1.66	−0.02	+1.89	+0.40	−2.16	−0.10	−0.56	−1.00
2.2–2.4	+0.00	+0.00	+1.40	+1.91	+0.00	−0.76	−0.34	+2.83	+0.11	+0.21	+1.00
	−0.03	−0.02	−0.92	−1.66	−0.02	+0.76	+0.40	−2.83	−0.10	−0.58	−1.00
2.4–2.6	+0.00	+0.00	+0.87	+1.91	+0.00	−0.76	−0.34	+2.83	+0.11	+0.23	+1.00
	−0.03	−0.02	−0.92	−1.82	−0.02	+0.76	+0.40	−2.83	−0.10	−0.64	−1.00
2.6–2.8	+0.00	+0.00	+0.87	+2.25	+0.00	−0.76	−0.34	+4.23	+0.10	+0.24	+1.00
	−0.03	−0.02	−0.92	−1.82	−0.02	+0.76	+0.40	−4.23	−0.10	−0.67	−1.00
2.8–3.0	+0.00	+0.00	+0.87	+2.25	+0.00	−0.76	−0.34	+4.08	+0.10	+0.25	+1.00
	−0.03	−0.02	−0.92	−1.82	−0.02	+0.76	+0.40	−4.08	−0.09	−0.69	−1.00
3.0–3.2	+0.00	+0.00	+0.87	+2.25	+0.00	−0.76	−0.34	+4.94	+0.09	+0.26	+1.00
	−0.03	−0.02	−0.92	−1.82	−0.02	+0.76	+0.40	−4.94	−0.09	−0.70	−1.00
3.2–3.4	+0.00	+0.00	+0.87	+2.25	+0.00	−0.76	−0.34	+5.32	+0.09	+0.25	+1.00
	−0.03	−0.02	−0.92	−1.82	−0.02	+0.76	+0.40	−5.32	−0.09	−0.70	−1.00

Table 5 The measured double-differential Z + jets production cross-sections as a function of $|y_{\text{jet}}|$ in the 100 GeV $< p_{\text{T}}^{\text{jet}} <$ 200 GeV range. $\delta_{\text{data}}^{\text{stat}}$ and $\delta_{\text{MC}}^{\text{stat}}$ are the statistical uncertainties in data and MC simulation, respectively. $\delta_{\text{tot}}^{\text{sys}}$ is the total systematic uncertainty and includes the following components: uncertainties due to electron reconstruction ($\delta_{\text{rec}}^{\text{el}}$), identification ($\delta_{\text{ID}}^{\text{el}}$) and trigger ($\delta_{\text{trig}}^{\text{el}}$) efficiencies; electron energy scale ($\delta_{\text{scale}}^{\text{el}}$) and energy resolution ($\delta_{\text{res}}^{\text{el}}$) uncertainties; sum in quadrature of the uncertainties from JES in situ methods ($\delta_{\text{in situ}}^{\text{JES}}$); sum in quadrature of the uncertainties from JES η-intercalibration methods ($\delta_{\eta\text{-int}}^{\text{JES}}$); an uncertainty of the measured single-hadron response ($\delta_{\text{hadron}}^{\text{JES}}$); MC non-closure uncertainty ($\delta_{\text{closure}}^{\text{JES}}$); sum in quadrature of the uncertainties due to pile-up corrections of the jet kinematics ($\delta_{\text{pile-up}}^{\text{JES}}$); sum in quadrature of the flavour-based uncertainties ($\delta_{\text{flavour}}^{\text{JES}}$); punch-through uncertainty ($\delta_{\text{pthrough}}^{\text{JES}}$); JER uncertainty ($\delta^{\text{JER}}$); JVF uncertainty ($\delta^{\text{JVF}}$); sum in quadrature of the unfolding uncertainties (δ^{unf}); sum in quadrature of the uncertainties due to MC generated backgrounds normalisation ($\delta_{\text{MC}}^{\text{bg}}$); sum in quadrature of the uncertainty due to combined multijet and W+ jets backgrounds ($\delta_{\text{mult}}^{\text{bg}}$); uncertainty due to jet quality selection (δ^{qual}). All uncertainties are given in %. The luminosity uncertainty of 1.9% is not shown and not included in the total uncertainty and its components

$\lvert y_{\text{jet}}\rvert$	$\frac{d^2\sigma}{d\lvert y_{\text{jet}}\rvert dp_{\text{T}}^{\text{jet}}}$ (fb/GeV)	$\delta_{\text{data}}^{\text{stat}}$ (%)	$\delta_{\text{MC}}^{\text{stat}}$ (%)	$\delta_{\text{tot}}^{\text{sys}}$ (%)	$\delta_{\text{rec}}^{\text{el}}$ (%)	$\delta_{\text{ID}}^{\text{el}}$ (%)	$\delta_{\text{trig}}^{\text{el}}$ (%)	$\delta_{\text{scale}}^{\text{el}}$ (%)	$\delta_{\text{res}}^{\text{el}}$ (%)	$\delta_{\text{in situ}}^{\text{JES}}$ (%)	$\delta_{\eta-\text{int}}^{\text{JES}}$ (%)
0.0–0.2	45.769	1.28	1.29	+2.58	−0.04	+0.02	+0.11	−0.29	+0.06	+1.44	+0.50
				−3.54	+0.00	−0.08	−0.15	+0.38	+0.00	−2.11	−0.67
0.2–0.4	46.342	1.22	1.39	+2.58	−0.04	+0.02	+0.11	−0.29	+0.06	+1.44	+0.50
				−3.54	+0.00	−0.08	−0.15	+0.38	+0.00	−2.11	−0.67
0.4–0.6	43.964	1.25	1.47	+2.58	−0.04	+0.02	+0.11	−0.29	+0.06	+1.44	+0.50
				−3.21	+0.00	−0.08	−0.15	+0.38	+0.00	−1.93	−0.67
0.6–0.8	40.076	1.40	1.67	+2.58	−0.04	+0.02	+0.11	−0.29	+0.06	+1.44	+0.50
				−3.15	+0.00	−0.08	−0.15	+0.38	+0.00	−1.93	−0.67
0.8–1.0	37.981	1.40	1.38	+2.50	−0.04	+0.02	+0.11	−0.29	+0.06	+1.44	+0.50
				−3.15	+0.00	−0.08	−0.15	+0.38	+0.00	−1.93	−0.67
1.0–1.2	32.122	1.63	1.68	+2.74	−0.04	+0.02	+0.11	−0.29	+0.06	+1.44	+0.50
				−3.08	+0.00	−0.08	−0.15	+0.38	+0.00	−1.82	−0.67
1.2–1.4	31.772	1.33	1.53	+2.99	−0.04	+0.02	+0.11	−0.29	+0.06	+1.87	+0.50
				−3.09	+0.00	−0.08	−0.15	+0.38	+0.00	−1.82	−0.67
1.4–1.6	27.737	1.34	1.85	+3.19	−0.04	+0.02	+0.11	−0.29	+0.06	+1.87	+0.50
				−3.15	+0.00	−0.08	−0.15	+0.38	+0.00	−1.82	−0.67
1.6–1.8	21.873	1.85	2.01	+3.16	−0.04	+0.02	+0.11	−0.29	+0.06	+1.87	+0.50
				−3.10	+0.00	−0.08	−0.15	+0.38	+0.00	−1.82	−0.67
1.8–2.0	17.806	1.88	2.00	+3.33	−0.04	+0.02	+0.11	−0.29	+0.06	+1.98	+0.50
				−3.29	+0.00	−0.08	−0.15	+0.38	+0.00	−1.95	−0.67
2.0–2.2	13.820	2.26	2.26	+3.33	−0.04	+0.02	+0.11	−0.29	+0.06	+1.98	+0.50
				−3.30	+0.00	−0.08	−0.15	+0.38	+0.00	−1.95	−0.67
2.2–2.4	10.613	2.55	2.81	+3.98	−0.04	+0.02	+0.11	−0.29	+0.06	+2.23	+0.50
				−4.38	+0.00	−0.08	−0.15	+0.38	+0.00	−1.95	−2.96
2.4–2.6	8.152	3.12	2.94	+5.72	−0.04	+0.02	+0.11	−0.29	+0.06	+2.23	+4.14
				−4.41	+0.00	−0.08	−0.15	+0.38	+0.00	−1.95	−2.96
2.6–2.8	5.663	3.22	3.91	+5.73	−0.04	+0.02	+0.11	−0.29	+0.06	+2.23	+4.14
				−4.45	+0.00	−0.08	−0.15	+0.38	+0.00	−1.95	−2.96
2.8–3.0	3.248	3.91	4.78	+9.42	−0.04	+0.02	+0.11	−0.29	+0.06	+2.23	+8.54
				−9.46	+0.00	−0.08	−0.15	+0.38	+0.00	−1.95	−7.71
3.0–3.2	2.169	5.43	5.73	+9.48	−0.04	+0.02	+0.11	−0.29	+0.06	+2.47	+8.54
				−9.46	+0.00	−0.08	−0.15	+0.38	+0.00	−1.95	−7.71
3.2–3.4	1.234	7.36	9.27	+15.87	−0.04	+0.02	+0.11	−0.29	+0.06	+2.47	+15.33
				−13.57	+0.00	−0.08	−0.15	+0.38	+0.00	−1.95	−12.42

Table 5 continued

$\lvert y_{\text{jet}}\rvert$	$\delta^{\text{JES}}_{\text{hadron}}$ (%)	$\delta^{\text{JES}}_{\text{closure}}$ (%)	$\delta^{\text{JES}}_{\text{pile-up}}$ (%)	$\delta^{\text{JES}}_{\text{flavour}}$ (%)	$\delta^{\text{JES}}_{\text{pthrough}}$ (%)	δ^{JER} (%)	δ^{JVF} (%)	δ^{unf} (%)	$\delta^{\text{bg}}_{\text{MC}}$ (%)	$\delta^{\text{bg}}_{\text{mult}}$ (%)	δ^{qual} (%)
0.0–0.2	+0.00	+0.00	+0.83	+1.51	+0.00	−0.36	−0.04	+0.14	+0.19	+0.18	+1.00
	−0.06	−0.03	−1.13	−2.20	−0.06	+0.36	+0.00	−0.14	−0.18	−0.43	−1.00
0.2–0.4	+0.00	+0.00	+0.83	+1.51	+0.00	−0.36	−0.04	+0.14	+0.18	+0.18	+1.00
	−0.06	−0.03	−1.13	−2.20	−0.06	+0.36	+0.00	−0.14	−0.17	−0.44	−1.00
0.4–0.6	+0.00	+0.00	+0.83	+1.51	+0.00	−0.36	−0.04	+0.14	+0.19	+0.17	+1.00
	−0.06	−0.03	−1.13	−1.84	−0.06	+0.36	+0.00	−0.14	−0.17	−0.43	−1.00
0.6–0.8	+0.00	+0.00	+0.83	+1.51	+0.00	−0.36	−0.04	+0.14	+0.18	+0.20	+1.00
	−0.06	−0.03	−1.13	−1.73	−0.06	+0.36	+0.00	−0.14	−0.17	−0.47	−1.00
0.8–1.0	+0.00	+0.00	+0.83	+1.37	+0.00	−0.36	−0.04	+0.14	+0.17	+0.17	+1.00
	−0.06	−0.03	−1.13	−1.73	−0.06	+0.36	+0.00	−0.14	−0.16	−0.46	−1.00
1.0–1.2	+0.00	+0.00	+0.83	+1.37	+0.00	−0.36	−0.04	+1.13	+0.18	+0.18	+1.00
	−0.06	−0.03	−0.92	−1.45	−0.06	+0.36	+0.00	−1.13	−0.16	−0.48	−1.00
1.2–1.4	+0.00	+0.00	+0.83	+1.37	+0.00	−0.36	−0.04	+1.13	+0.17	+0.19	+1.00
	−0.06	−0.03	−0.92	−1.45	−0.06	+0.36	+0.00	−1.13	−0.15	−0.53	−1.00
1.4–1.6	+0.00	+0.00	+0.83	+1.70	+0.00	−0.36	−0.04	+1.13	+0.17	+0.52	+1.00
	−0.06	−0.03	−0.92	−1.45	−0.06	+0.36	+0.00	−1.13	−0.16	−0.79	−1.00
1.6–1.8	+0.00	+0.00	+0.83	+1.70	+0.00	−0.36	−0.04	+1.13	+0.16	+0.24	+1.00
	−0.06	−0.03	−0.92	−1.45	−0.06	+0.36	+0.00	−1.13	−0.15	−0.60	−1.00
1.8–2.0	+0.00	+0.00	+1.17	+1.70	+0.00	−0.36	−0.04	+1.13	+0.15	+0.26	+1.00
	−0.06	−0.03	−0.92	−1.66	−0.06	+0.36	+0.00	−1.13	−0.14	−0.68	−1.00
2.0–2.2	+0.00	+0.00	+1.17	+1.70	+0.00	−0.36	−0.04	+1.13	+0.15	+0.26	+1.00
	−0.06	−0.03	−0.92	−1.66	−0.06	+0.36	+0.00	−1.13	−0.14	−0.70	−1.00
2.2–2.4	+0.00	+0.00	+1.17	+2.57	+0.00	−0.36	−0.04	+1.13	+0.15	+0.25	+1.00
	−0.06	−0.03	−0.92	−1.66	−0.06	+0.36	+0.00	−1.13	−0.14	−0.70	−1.00
2.4–2.6	+0.00	+0.00	+1.17	+2.57	+0.00	−0.36	−0.04	+1.13	+0.15	+0.32	+1.00
	−0.06	−0.03	−0.92	−1.66	−0.06	+0.36	+0.00	−1.13	−0.14	−0.87	−1.00
2.6–2.8	+0.00	+0.00	+1.17	+2.57	+0.00	−0.36	−0.04	+1.13	+0.17	+0.44	+1.00
	−0.06	−0.03	−0.92	−1.66	−0.06	+0.36	+0.00	−1.13	−0.16	−1.04	−1.00
2.8–3.0	+0.00	+0.00	+1.17	+2.57	+0.00	−0.36	−0.04	+1.13	+0.18	+0.40	+1.00
	−0.06	−0.03	−0.92	−4.65	−0.06	+0.36	+0.00	−1.13	−0.17	−1.07	−1.00
3.0–3.2	+0.00	+0.00	+1.17	+2.57	+0.00	−0.36	−0.04	+1.13	+0.18	+0.46	+1.00
	−0.06	−0.03	−0.92	−4.65	−0.06	+0.36	+0.00	−1.13	−0.17	−1.09	−1.00
3.2–3.4	+0.00	+0.00	+1.17	+2.57	+0.00	−0.36	−0.04	+1.13	+0.15	+0.41	+1.00
	−0.06	−0.03	−0.92	−4.65	−0.06	+0.36	+0.00	−1.13	−0.13	−1.07	−1.00

Table 6 The measured double-differential Z + jets production cross-sections as a function of $|y_{\text{jet}}|$ in the 200 GeV $< p_{\text{T}}^{\text{jet}} <$ 300 GeV range. $\delta_{\text{data}}^{\text{stat}}$ and $\delta_{\text{MC}}^{\text{stat}}$ are the statistical uncertainties in data and MC simulation, respectively. $\delta_{\text{tot}}^{\text{sys}}$ is the total systematic uncertainty and includes the following components: uncertainties due to electron reconstruction ($\delta_{\text{rec}}^{\text{el}}$), identification ($\delta_{\text{ID}}^{\text{el}}$) and trigger ($\delta_{\text{trig}}^{\text{el}}$) efficiencies; electron energy scale ($\delta_{\text{scale}}^{\text{el}}$) and energy resolution ($\delta_{\text{res}}^{\text{el}}$) uncertainties; sum in quadrature of the uncertainties from JES in situ methods ($\delta_{\text{in situ}}^{\text{JES}}$); sum in quadrature of the uncertainties from JES η-intercalibration methods ($\delta_{\eta\text{-int}}^{\text{JES}}$); an uncertainty of the measured single-hadron response ($\delta_{\text{hadron}}^{\text{JES}}$); MC non-closure uncertainty ($\delta_{\text{closure}}^{\text{JES}}$); sum in quadrature of the uncertainties due to pile-up corrections of the jet kinematics ($\delta_{\text{pile-up}}^{\text{JES}}$); sum in quadrature of the flavour-based uncertainties ($\delta_{\text{flavour}}^{\text{JES}}$); punch-through uncertainty ($\delta_{\text{pthrough}}^{\text{JES}}$); JER uncertainty ($\delta^{\text{JER}}$); JVF uncertainty ($\delta^{\text{JVF}}$); sum in quadrature of the unfolding uncertainties (δ^{unf}); sum in quadrature of the uncertainties due to MC generated backgrounds normalisation ($\delta_{\text{MC}}^{\text{bg}}$); sum in quadrature of the uncertainty due to combined multijet and W+ jets backgrounds ($\delta_{\text{mult}}^{\text{bg}}$); uncertainty due to jet quality selection (δ^{qual}). All uncertainties are given in %. The luminosity uncertainty of 1.9% is not shown and not included in the total uncertainty and its components

$\lvert y_{\text{jet}}\rvert$	$\frac{d^2\sigma}{d\lvert y_{\text{jet}}\rvert dp_{\text{T}}^{\text{jet}}}$ (fb/GeV)	$\delta_{\text{data}}^{\text{stat}}$ (%)	$\delta_{\text{MC}}^{\text{stat}}$ (%)	$\delta_{\text{tot}}^{\text{sys}}$ (%)	$\delta_{\text{rec}}^{\text{el}}$ (%)	$\delta_{\text{ID}}^{\text{el}}$ (%)	$\delta_{\text{trig}}^{\text{el}}$ (%)	$\delta_{\text{scale}}^{\text{el}}$ (%)	$\delta_{\text{res}}^{\text{el}}$ (%)	$\delta_{\text{in situ}}^{\text{JES}}$ (%)	$\delta_{\eta-\text{int}}^{\text{JES}}$ (%)
0.0–0.4	5.561	2.50	2.63	+3.55	−0.05	+0.12	+0.10	−0.18	−0.06	+2.62	+0.39
				−4.33	+0.04	+0.00	−0.01	+0.18	+0.05	−3.10	−0.77
0.4–0.8	4.889	2.36	2.93	+3.55	−0.05	+0.12	+0.10	−0.18	−0.06	+2.62	+0.39
				−4.33	+0.04	+0.00	−0.01	+0.18	+0.05	−3.10	−0.77
0.8–1.2	4.260	3.18	3.41	+3.54	−0.05	+0.12	+0.10	−0.18	−0.06	+2.62	+0.39
				−4.33	+0.04	+0.00	−0.01	+0.18	+0.05	−3.10	−0.77
1.2–1.6	3.055	3.61	3.17	+3.55	−0.05	+0.12	+0.10	−0.18	−0.06	+2.62	+0.39
				−4.35	+0.04	+0.00	−0.01	+0.18	+0.05	−3.10	−0.77
1.6–2.0	1.780	4.43	4.42	+3.56	−0.05	+0.12	+0.10	−0.18	−0.06	+2.62	+0.39
				−4.38	+0.04	+0.00	−0.01	+0.18	+0.05	−3.10	−0.77
2.0–2.4	0.831	6.45	7.17	+3.60	−0.05	+0.12	+0.10	−0.18	−0.06	+2.62	+0.39
				−6.26	+0.04	+0.00	−0.01	+0.18	+0.05	−5.37	−0.77
2.4–3.4	0.136	9.48	11.75	+3.58	−0.05	+0.12	+0.10	−0.18	−0.06	+2.62	+0.39
				−6.25	+0.04	+0.00	−0.01	+0.18	+0.05	−5.37	−0.77

$\lvert y_{\text{jet}}\rvert$	$\delta_{\text{hadron}}^{\text{JES}}$ (%)	$\delta_{\text{closure}}^{\text{JES}}$ (%)	$\delta_{\text{pile-up}}^{\text{JES}}$ (%)	$\delta_{\text{flavour}}^{\text{JES}}$ (%)	$\delta_{\text{pthrough}}^{\text{JES}}$ (%)	δ^{JER} (%)	δ^{JVF} (%)	δ^{unf} (%)	$\delta_{\text{MC}}^{\text{bg}}$ (%)	$\delta_{\text{mult}}^{\text{bg}}$ (%)	δ^{qual} (%)
0.0–0.4	+0.04	+0.15	+0.36	+1.40	+0.20	−0.58	−0.04	+1.40	+0.09	+0.28	+1.00
	+0.00	+0.00	−0.75	−2.08	−0.06	+0.58	+0.09	−1.40	−0.08	−0.54	−1.00
0.4–0.8	+0.04	+0.15	+0.36	+1.40	+0.20	−0.58	−0.04	+1.40	+0.10	+0.25	+1.00
	+0.00	+0.00	−0.75	−2.08	−0.06	+0.58	+0.09	−1.40	−0.09	−0.55	−1.00
0.8–1.2	+0.04	+0.15	+0.36	+1.40	+0.20	−0.58	−0.04	+1.40	+0.11	+0.21	+1.00
	+0.00	+0.00	−0.75	−2.08	−0.06	+0.58	+0.09	−1.40	−0.10	−0.57	−1.00
1.2–1.6	+0.04	+0.15	+0.36	+1.40	+0.20	−0.58	−0.04	+1.40	+0.14	+0.27	+1.00
	+0.00	+0.00	−0.75	−2.08	−0.06	+0.58	+0.09	−1.40	−0.13	−0.71	−1.00
1.6–2.0	+0.04	+0.15	+0.36	+1.40	+0.20	−0.58	−0.04	+1.40	+0.17	+0.39	+1.00
	+0.00	+0.00	−0.75	−2.08	−0.06	+0.58	+0.09	−1.40	−0.16	−0.84	−1.00
2.0–2.4	+0.04	+0.15	+0.36	+1.40	+0.20	−0.58	−0.04	+1.40	+0.22	+0.65	+1.00
	+0.00	+0.00	−0.75	−2.08	−0.06	+0.58	+0.09	−1.40	−0.20	−1.19	−1.00
2.4–3.4	+0.04	+0.15	+0.36	+1.40	+0.20	−0.58	−0.04	+1.40	+0.32	+0.42	+1.00
	+0.00	+0.00	−0.75	−2.08	−0.06	+0.58	+0.09	−1.40	−0.29	−1.12	−1.00

Table 7 The measured double-differential Z + jets production cross-sections as a function of $|y_{\text{jet}}|$ in the 300 GeV $< p_{\text{T}}^{\text{jet}} <$ 400 GeV range. $\delta_{\text{data}}^{\text{stat}}$ and $\delta_{\text{MC}}^{\text{stat}}$ are the statistical uncertainties in data and MC simulation, respectively. $\delta_{\text{tot}}^{\text{sys}}$ is the total systematic uncertainty and includes the following components: uncertainties due to electron reconstruction ($\delta_{\text{rec}}^{\text{el}}$), identification ($\delta_{\text{ID}}^{\text{el}}$) and trigger ($\delta_{\text{trig}}^{\text{el}}$) efficiencies; electron energy scale ($\delta_{\text{scale}}^{\text{el}}$) and energy resolution ($\delta_{\text{res}}^{\text{el}}$) uncertainties; sum in quadrature of the uncertainties from JES in situ methods ($\delta_{\text{in situ}}^{\text{JES}}$); sum in quadrature of the uncertainties from JES η-intercalibration methods ($\delta_{\eta\text{-int}}^{\text{JES}}$); an uncertainty of the measured single-hadron response ($\delta_{\text{hadron}}^{\text{JES}}$); MC non-closure uncertainty ($\delta_{\text{closure}}^{\text{JES}}$); sum in quadrature of the uncertainties due to pile-up corrections of the jet kinematics ($\delta_{\text{pile-up}}^{\text{JES}}$); sum in quadrature of the flavour-based uncertainties ($\delta_{\text{flavour}}^{\text{JES}}$); punch-through uncertainty ($\delta_{\text{pthrough}}^{\text{JES}}$); JER uncertainty ($\delta^{\text{JER}}$); JVF uncertainty ($\delta^{\text{JVF}}$); sum in quadrature of the unfolding uncertainties (δ^{unf}); sum in quadrature of the uncertainties due to MC generated backgrounds normalisation ($\delta_{\text{MC}}^{\text{bg}}$); sum in quadrature of the uncertainty due to combined multijet and W+ jets backgrounds ($\delta_{\text{mult}}^{\text{bg}}$); uncertainty due to jet quality selection (δ^{qual}). All uncertainties are given in %. The luminosity uncertainty of 1.9% is not shown and not included in the total uncertainty and its components

$\lvert y_{\text{jet}}\rvert$	$\frac{d^2\sigma}{d\lvert y_{\text{jet}}\rvert dp_{\text{T}}^{\text{jet}}}$ [fb/GeV]	$\delta_{\text{data}}^{\text{stat}}$ (%)	$\delta_{\text{MC}}^{\text{stat}}$ (%)	$\delta_{\text{tot}}^{\text{sys}}$ (%)	$\delta_{\text{rec}}^{\text{el}}$ (%)	$\delta_{\text{ID}}^{\text{el}}$ (%)	$\delta_{\text{trig}}^{\text{el}}$ (%)	$\delta_{\text{scale}}^{\text{el}}$ (%)	$\delta_{\text{res}}^{\text{el}}$ (%)	$\delta_{\text{in situ}}^{\text{JES}}$ (%)	$\delta_{\eta-\text{int}}^{\text{JES}}$ (%)
0.0–0.4	1.190	5.83	6.75	+5.95	+0.74	+0.56	+0.00	+0.00	+0.76	+4.03	+1.41
				−2.33	+0.00	+0.00	+0.51	+0.72	+0.00	−1.63	+0.00
0.4–0.8	1.083	5.52	5.50	+5.94	+0.74	+0.56	+0.00	+0.00	+0.76	+4.03	+1.41
				−2.30	+0.00	+0.00	+0.51	+0.72	+0.00	−1.63	+0.00
0.8–1.2	0.946	6.68	6.87	+5.95	+0.74	+0.56	+0.00	+0.00	+0.76	+4.03	+1.41
				−2.34	+0.00	+0.00	+0.51	+0.72	+0.00	−1.63	+0.00
1.2–1.6	0.628	8.15	8.34	+5.96	+0.74	+0.56	+0.00	+0.00	+0.76	+4.03	+1.41
				−2.43	+0.00	+0.00	+0.51	+0.72	+0.00	−1.63	+0.00
1.6–2.0	0.322	11.56	11.42	+5.97	+0.74	+0.56	+0.00	+0.00	+0.76	+4.03	+1.41
				−2.46	+0.00	+0.00	+0.51	+0.72	+0.00	−1.63	+0.00
2.0–3.0	0.032	26.98	24.63	+6.01	+0.74	+0.56	+0.00	+0.00	+0.76	+4.03	+1.41
				−2.64	+0.00	+0.00	+0.51	+0.72	+0.00	−1.63	+0.00

$\lvert y_{\text{jet}}\rvert$	$\delta_{\text{hadron}}^{\text{JES}}$ (%)	$\delta_{\text{closure}}^{\text{JES}}$ (%)	$\delta_{\text{pile-up}}^{\text{JES}}$ (%)	$\delta_{\text{flavour}}^{\text{JES}}$ (%)	$\delta_{\text{pthrough}}^{\text{JES}}$ (%)	δ^{JER} (%)	δ^{JVF} (%)	δ^{unf} (%)	$\delta_{\text{MC}}^{\text{bg}}$ (%)	$\delta_{\text{mult}}^{\text{bg}}$ (%)	δ^{qual} (%)
0.0–0.4	+0.68	+0.46	+2.42	+2.24	+0.54	−1.16	+0.79	+0.08	+0.10	+0.30	+1.00
	+0.00	+0.00	−0.13	+0.00	+0.00	+1.16	+0.00	−0.08	−0.09	−0.65	−1.00
0.4–0.8	+0.68	+0.46	+2.42	+2.24	+0.54	−1.16	+0.79	+0.08	+0.11	+0.23	+1.00
	+0.00	+0.00	−0.13	+0.00	+0.00	+1.16	+0.00	−0.08	−0.10	−0.55	−1.00
0.8–1.2	+0.68	+0.46	+2.42	+2.24	+0.54	−1.16	+0.79	+0.08	+0.12	+0.30	+1.00
	+0.00	+0.00	−0.13	+0.00	+0.00	+1.16	+0.00	−0.08	−0.11	−0.68	−1.00
1.2–1.6	+0.68	+0.46	+2.42	+2.24	+0.54	−1.16	+0.79	+0.08	+0.19	+0.45	+1.00
	+0.00	+0.00	−0.13	+0.00	+0.00	+1.16	+0.00	−0.08	−0.17	−0.95	−1.00
1.6–2.0	+0.68	+0.46	+2.42	+2.24	+0.54	−1.16	+0.79	+0.08	+0.26	+0.51	+1.00
	+0.00	+0.00	−0.13	+0.00	+0.00	+1.16	+0.00	−0.08	−0.24	−1.00	−1.00
2.0–3.0	+0.68	+0.46	+2.42	+2.24	+0.54	−1.16	+0.79	+0.08	+0.69	+0.63	+1.00
	+0.00	+0.00	−0.13	+0.00	+0.00	+1.16	+0.00	−0.08	−0.63	−1.25	−1.00

Table 8 The measured double-differential Z + jets production cross-sections as a function of $|y_{\text{jet}}|$ in the 400 GeV $< p_{\text{T}}^{\text{jet}} <$ 1050 GeV range. $\delta_{\text{data}}^{\text{stat}}$ and $\delta_{\text{MC}}^{\text{stat}}$ are the statistical uncertainties in data and MC simulation, respectively. $\delta_{\text{tot}}^{\text{sys}}$ is the total systematic uncertainty and includes the following components: uncertainties due to electron reconstruction ($\delta_{\text{rec}}^{\text{el}}$), identification ($\delta_{\text{ID}}^{\text{el}}$) and trigger ($\delta_{\text{trig}}^{\text{el}}$) efficiencies; electron energy scale ($\delta_{\text{scale}}^{\text{el}}$) and energy resolution ($\delta_{\text{res}}^{\text{el}}$) uncertainties; sum in quadrature of the uncertainties from JES in situ methods ($\delta_{\text{in situ}}^{\text{JES}}$); sum in quadrature of the uncertainties from JES η-intercalibration methods ($\delta_{\eta\text{-int}}^{\text{JES}}$); an uncertainty of the measured single-hadron response ($\delta_{\text{hadron}}^{\text{JES}}$); MC non-closure uncertainty ($\delta_{\text{closure}}^{\text{JES}}$); sum in quadrature of the uncertainties due to pile-up corrections of the jet kinematics ($\delta_{\text{pile-up}}^{\text{JES}}$); sum in quadrature of the flavour-based uncertainties ($\delta_{\text{flavour}}^{\text{JES}}$); punch-through uncertainty ($\delta_{\text{pthrough}}^{\text{JES}}$); JER uncertainty ($\delta^{\text{JER}}$); JVF uncertainty ($\delta^{\text{JVF}}$); sum in quadrature of the unfolding uncertainties (δ^{unf}); sum in quadrature of the uncertainties due to MC generated backgrounds normalisation ($\delta_{\text{MC}}^{\text{bg}}$); sum in quadrature of the uncertainty due to combined multijet and W+ jets backgrounds ($\delta_{\text{mult}}^{\text{bg}}$); uncertainty due to jet quality selection (δ^{qual}). All uncertainties are given in %. The luminosity uncertainty of 1.9% is not shown and not included in the total uncertainty and its components

$\lvert y_{\text{jet}}\rvert$	$\frac{d^2\sigma}{d\lvert y_{\text{jet}}\rvert dp_{\text{T}}^{\text{jet}}}$ [fb/GeV]	$\delta_{\text{data}}^{\text{stat}}$ (%)	$\delta_{\text{MC}}^{\text{stat}}$ (%)	$\delta_{\text{tot}}^{\text{sys}}$ (%)	$\delta_{\text{rec}}^{\text{el}}$ (%)	$\delta_{\text{ID}}^{\text{el}}$ (%)	$\delta_{\text{trig}}^{\text{el}}$ (%)	$\delta_{\text{scale}}^{\text{el}}$ (%)	$\delta_{\text{res}}^{\text{el}}$ (%)	$\delta_{\text{in situ}}^{\text{JES}}$ (%)	$\delta_{\eta-\text{int}}^{\text{JES}}$ (%)
0.0–0.4	0.110	6.84	8.88	+2.79	−0.34	+0.00	+0.00	−0.82	−0.41	+2.01	+0.22
				−5.82	+0.00	−0.26	−0.43	+0.00	+0.00	−4.74	−0.50
0.4–0.8	0.076	9.45	9.66	+2.76	−0.34	+0.00	+0.00	−0.82	−0.41	+2.01	+0.22
				−5.81	+0.00	−0.26	−0.43	+0.00	+0.00	−4.74	−0.50
0.8–1.2	0.058	11.67	11.68	+2.78	−0.34	+0.00	+0.00	−0.82	−0.41	+2.01	+0.22
				−5.83	+0.00	−0.26	−0.43	+0.00	+0.00	−4.74	−0.50
1.2–2.6	0.012	12.84	13.36	+2.84	−0.34	+0.00	+0.00	−0.82	−0.41	+2.01	+0.22
				−5.90	+0.00	−0.26	−0.43	+0.00	+0.00	−4.74	−0.50

$\lvert y_{\text{jet}}\rvert$	$\delta_{\text{hadron}}^{\text{JES}}$ (%)	$\delta_{\text{closure}}^{\text{JES}}$ (%)	$\delta_{\text{pile-up}}^{\text{JES}}$ (%)	$\delta_{\text{flavour}}^{\text{JES}}$ (%)	$\delta_{\text{pthrough}}^{\text{JES}}$ (%)	δ^{JER} (%)	δ^{JVF} (%)	δ^{unf} (%)	$\delta_{\text{MC}}^{\text{bg}}$ (%)	$\delta_{\text{mult}}^{\text{bg}}$ (%)	δ^{qual} (%)
0.0–0.4	+0.00	+0.00	+0.10	+0.33	+0.13	−0.14	+0.01	+1.47	+0.15	+0.59	+1.00
	−0.36	−0.33	−0.91	−2.13	−0.58	+0.14	−0.32	−1.47	−0.14	−0.84	−1.00
0.4–0.8	+0.00	+0.00	+0.10	+0.33	+0.13	−0.14	+0.01	+1.47	+0.18	+0.42	+1.00
	−0.36	−0.33	−0.91	−2.13	−0.58	+0.14	−0.32	−1.47	−0.16	−0.71	−1.00
0.8–1.2	+0.00	+0.00	+0.10	+0.33	+0.13	−0.14	+0.01	+1.47	+0.21	+0.54	+1.00
	−0.36	−0.33	−0.91	−2.13	−0.58	+0.14	−0.32	−1.47	−0.20	−0.86	−1.00
1.2–2.6	+0.00	+0.00	+0.10	+0.33	+0.13	−0.14	+0.01	+1.47	+0.37	+0.73	+1.00
	−0.36	−0.33	−0.91	−2.13	−0.58	+0.14	−0.32	−1.47	−0.34	−1.24	−1.00

References

1. CDF Collaboration, Measurement of Inclusive Jet Cross Sections in $Z/\gamma^*(\rightarrow e^+e^-)$+jets Production in $p\bar{p}$ Collisions at $\sqrt{s}$ = 1.96 TeV. Phys. Rev. Lett **100**, 102001 (2008). arXiv:0711.3717 [hep-ex]
2. D0 Collaboration, Measurement of differential cross section of $Z/\gamma^* + jets + X$ events in $p\bar{p}$ collisions at $\sqrt{s}$ = 1.96 TeV. Phys. Lett. B **678**, 45 (2009). arXiv:0903.1748 [hep-ex]
3. D0 Collaboration, Measurement of $Z/\gamma^* + jets + X$ angular distributions in $p\bar{p}$ collisions at $\sqrt{s}$ = 1.96 TeV. Phys. Lett. B **682**, 370 (2010). arXiv:0907.4286 [hep-ex]
4. CDF Collaboration, Measurement of differential production cross sections for Z/γ^* bosons in association with jets in $p\bar{p}$ collisions at $\sqrt{s}$ = 1.96 TeV. Phys. Rev. D **91**, 012002 (2015). arXiv:1409.4359 [hep-ex]
5. L. Evans, P. Bryant, LHC Machine, JINST **3**, S08001 (2008)
6. ATLAS Collaboration, Measurement of the production cross section for Z/γ^* in association with jets in pp collisions at $\sqrt{s}$ = 7 TeV with the ATLAS detector. Phys. Rev. D **85**, 032009 (2012). arXiv:1111.2690 [hep-ex]
7. ATLAS Collaboration, Measurement ofthe production cross section of jets in association with a Z boson in pp collisions at $\sqrt{s}$ = 7 TeV with the ATLAS detector. JHEP **07**, 032 (2013). arXiv:1304.7098 [hep-ex]
8. ATLAS Collaboration, Measurements of the production cross section of a Z boson in association with jets in pp collisions at $\sqrt{s}$ = 13 TeV with the ATLAS detector. Eur. Phys. J. C **77** , 361 (2017). arXiv:1702.05725 [hep-ex]
9. CMS Collaboration, Rapidity distributions in exclusive $Z + jet$ and $\gamma + jet$ events in pp collisions at $\sqrt{s}$ = 7 TeV. Phys. Rev. D **88**, 112009 (2013). arXiv:1310.3082 [hep-ex]
10. CMS Collaboration, Measurements of jet multiplicity and differential production cross sections of $Z + jets$ events in proton-proton collisions at $\sqrt{s}$ = 7 TeV. Phys. Rev. D **91**, 052008 (2015). arXiv:1408.3104 [hep-ex]

11. CMS Collaboration, Measurements of the differential production cross sections for a Z boson in association with jets in pp collisions at $\sqrt{s} = 8$ TeV. JHEP **04**, 022 (2017). arXiv:1611.03844 [hep-ex]
12. CMS Collaboration, Measurement of differential cross sections for Z boson production in association with jets in proton-proton collisions at $\sqrt{s} = 13$ TeV. Eur. Phys. J. C **78**, 965 (2018). arXiv:1804.05252 [hep-ex]
13. CMS Collaboration, Measurement of differential cross sections for Z boson pair production in association with jets at $\sqrt{s} = 8TeV$ and 13 TeV. Phys. Lett. B **789**, 19 (2019). arXiv:1806.11073 [hep-ex]
14. LHCb Collaboration, Study of forward $Z + jet$ production in pp collisions at $\sqrt{s} = 7$ TeV. JHEP **01**, 033 (2014). arXiv:1310.8197 [hep-ex]
15. LHCb Collaboration, Measurement of forward W and Z boson production in association with jets in proton–proton collisions at $\sqrt{s} = 8$ TeV. JHEP **05** , 131 (2016). arXiv:1605.00951 [hep-ex]
16. A. Gehrmann-De Ridder, T. Gehrmann, E.W.N. Glover, A. Huss, T.A. Morgan, Precise QCD predictions for the production of a Z Boson in association with a hadronic jet. Phys. Rev. Lett **117**, 022001 (2016). arXiv:1507.02850 [hep-ph]
17. R. Boughezal et al., Z-Boson production in association with a jet at next-to-next-to-leading order in perturbative QCD. Phys. Rev. Lett **116**, 152001 (2016). arXiv:1512.01291 [hep-ph]
18. ATLAS Collaboration, The ATLAS Experiment at the CERN Large Hadron Collider, JINST **3**, S08003 (2008)
19. ATLAS Collaboration, Performance of the ATLAS Trigger System in 2010. Eur. Phys. J. C **72**, 1849 (2012). arXiv:1110.1530 [hep-ex]
20. ATLAS Collaboration, Performance of the ATLAS Electron and Photon Trigger in $p-p$ Collisions at $\sqrt{s} = 7$ TeV in 2011, ATLAS-CONF-2012-048, 2012. https://cds.cern.ch/record/1450089
21. ATLAS Collaboration, Luminosity determination in pp collisions at $\sqrt{s} = 8$ TeV using the ATLAS detector at the LHC. Eur. Phys. J. C **76**, 653 (2016). arXiv:1608.03953 [hep-ex]
22. T. Gleisberg et al., Event generation with SHERPA 1.1. JHEP **02**, 007 (2009). arXiv:0811.4622 [hep-ph]
23. F. Krauss, R. Kuhn, G. Soff, AMEGIC++ 1.0, a matrix element generator in C++. JHEP **02**, 044 (2002). arXiv:hep-ph/0109036 [hep-ph]
24. H.-L. Lai et al., New parton distributions for collider physics. Phys. Rev. D **82**, 074024 (2010). arXiv:1007.2241 [hep-ph]
25. S. Catani, F. Krauss, R. Kuhn, B.R. Webber, QCD matrix elements + parton showers. JHEP **11**, 063 (2001). arXiv:hep-ph/0109231 [hep-ph]
26. K. Hamilton, P. Nason, Improving NLO-parton shower matched simulations with higher order matrix elements. JHEP **06**, 039 (2010). arXiv:1004.1764 [hep-ph]
27. C. Anastasiou, L. Dixon, K. Melnikov, F. Petriello, High-precision QCD at hadron colliders: electroweak gauge boson rapidity distributions at next-to-next-to leading order. Phys. Rev. D **69**, 094008 (2004). arXiv:hep-ph/0312266 [hep-ph]
28. K. Melnikov, F. Petriello, Electroweak gauge boson production at hadron colliders through $O(\alpha_s^2)$. Phys. Rev. D **74**, 114017 (2006). arXiv:hep-ph/0609070
29. F.P.R. Gavin, Y. Li, S. Quackenbush, FEWZ 2.0: A code for hadronic Z production at next-to-next-to-leading order. Comput. Phys. Commun. **182**, 2388 (2011). arXiv:1011.3540 [hep-ph]
30. M.L. Mangano, M. Moretti, F. Piccinini, R. Pittau, A.D. Polosa, ALPGEN, a generator for hard multiparton processes in hadronic collisions. JHEP **07**, 001 (2003). arXiv:hep-ph/0206293 [hep-ph]
31. T. Sjöstrand, S. Mrenna, P.Z. Skands, PYTHIA 6.4 physics and manual. JHEP **05**, 026 (2006). arXiv:hep-ph/0603175
32. P.Z. Skands, Tuning Monte Carlo generators: the Perugia tunes. Phys. Rev. D **82**, 074018 (2010). arXiv:1005.3457 [hep-ph]
33. J. Pumplin et al., New generation of parton distributions with uncertainties from global QCD analysis. JHEP **07**, 012 (2002). arXiv:hep-ph/0201195 [hep-ph]
34. S. Frixione, P. Nason, C. Oleari, Matching NLO QCD computations with parton shower simulations: the POWHEG method. JHEP **11**, 070 (2007). arXiv:0709.2092 [hep-ph]
35. S. Alioli, P. Nason, C. Oleari, E. Re, NLO vector-boson production matched with shower in POWHEG. JHEP **0807**, 060 (2008). arXiv:0805.4802 [hep-ph]
36. T. Sjöstrand, S. Mrenna, P.Z. Skands, A brief introduction to PYTHIA 8.1. Comput. Phys. Commun. **178**, 852 (2008). arXiv:0710.3820 [hep-ph]
37. ATLAS Collaboration, Summary of ATLAS Pythia 8 tunes, ATL-PHYS-PUB-2012-003 (2012). http://cds.cern.ch/record/1474107
38. G. Corcella et al., HERWIG 6: an event generator for hadron emission reactions with interfering gluons (including supersymmetric processes). JHEP **01**, 010 (2001). arXiv:hep-ph/0011363
39. ATLAS Collaboration, New ATLAS event generator tunes to 2010 data, ATL-PHYS-PUB-2011-008 (2011). https://cds.cern.ch/record/1345343
40. J.M. Campbell, R.K. Ellis, MCFM for the TeVatron and the LHC. Nucl. Phys. Proc. Suppl **205–206**, 10 (2010). arXiv:1007.3492 [hep-ph]
41. J.M. Campbell, R.K. Ellis, Update on vector boson pair production at hadron colliders. Phys. Rev. D **60**, 113006 (2006). arXiv:hep-ph/9905386
42. N. Kidonakis, Next-to-next-to-leading logarithm resummation for s-channel single top quark production. Phys. Rev. D **81**, 054028 (2010). arXiv:1001.5034 [hep-ph]
43. N. Kidonakis, Next-to-next-to-leading-order collinear and soft gluon corrections for t-channel single top quark production. Phys. Rev. D **83**, 091503 (2011). arXiv:1103.2792 [hep-ph]
44. N. Kidonakis, Two-loop soft anomalous dimensions for single top quark associated production with a W^- or H^-. Phys. Rev. D **82**, 054018 (2010). arXiv:1005.4451 [hep-ph]
45. M. Czakon, A. Mitov, Top++: a program for the calculation of the top-pair cross-section at hadron colliders. Comput. Phys. Commun. **185**, 2930 (2014). arXiv:1112.5675 [hep-ph]
46. P. Golonka, Z. Was, PHOTOS Monte Carlo: a precision tool for QED corrections in Z and W decays. Eur. Phys. J. C **45**, 97 (2006). arXiv:hep-ph/0506026 [hep-ph]
47. S. Jadach, Z. Was, R. Decker, J.H. Kühn, The τ decay library TAUOLA, version 2.4. Comput. Phys. Commun. **76**, 361 (1993)
48. A.D. Martin, W.J. Stirling, R.S. Thorne, G. Watt, Parton distributions for the LHC. Eur. Phys. J. C **63**, 1072 (2009). arXiv:0901.0002 [hep-ph]
49. ATLAS Collaboration, The ATLAS Simulation Infrastructure. Eur. Phys. J. C **70**, 823 (2010). arXiv:1005.4568 [physics.ins-det]
50. S. Agostinelli et al., Geant4—a simulation toolkit. Nucl. Instrum. Methods A **506**, 250 (2003)
51. ATLAS Collaboration, Electron efficiency measurements with the ATLAS detector using 2012 LHC proton–proton collision data. Eur. Phys. J. C **77**, 195 (2017). arXiv:1612.01456 [hep-ex]
52. ATLAS Collaboration, Electron performance measurements with the ATLAS detector using the 2010 LHC proton–proton collision data, Eur. Phys. J. C **72**, 1909 (2012). arXiv:1110.3174 [hep-ex]
53. M. Cacciari, G.P. Salam, G. Soyez, The anti-k_t jet clustering algorithm. JHEP **04**, 063 (2008). arXiv:0802.1189 [hep-ph]
54. M. Cacciari, G.P. Salam, G. Soyez, FastJet user manual. Eur. Phys. J. C **72**, 1896 (2012). arXiv:1111.6097 [hep-ph]
55. ATLAS collaboration, Topological cell clustering in the ATLAS calorimeters and its performance in LHC Run 1. Eur. Phys. J. C **77**, 490 (2017). arXiv:1603.02934 [hep-ex]
56. ATLAS Collaboration, Local Hadronic Calibration, ATL-LARG-PUB-2009-001-2 (2008). https://cds.cern.ch/record/1112035
57. ATLAS Collaboration, Jet energy measurement and its systematic uncertainty in proton–proton collisions at $\sqrt{s} = 7$ TeV with the ATLAS detector. Eur. Phys. J. C **75**, 17 (2015). arXiv:1406.0076 [hep-ex]

58. ATLAS Collaboration, Performance of pile-up mitigation techniques for jets in pp collisions at $\sqrt{s} = 8$ TeV using the ATLAS detector. Eur. Phys. J. C **76**, 581 (2016). arXiv:1510.03823 [hep-ex]
59. G. D'Agostini, A multidimensional unfolding method based on Bayes' theorem. Nucl. Instrum. Methods A **362**, 487 (1995)
60. ATLAS Collaboration, Pile-up subtraction and suppression for jets in ATLAS, ATLAS-CONF-2013-083 (2013). https://cds.cern.ch/record/1570994
61. ATLAS Collaboration, Jet energy resolution in proton–proton collisions at $\sqrt{s} = 7$ TeV recorded in 2010 with the ATLAS detector. Eur. Phys. J. C **73**, 2306 (2013). arXiv:1210.6210 [hep-ex]
62. ATLAS Collaboration, Measurement of the $t\bar{t}$ production cross-section using e μ events with b-tagged jets in pp collisions at $\sqrt{s} = 7$ and 8 TeV with the ATLAS detector. Eur. Phys. J. C **74**, 3109 (2014). arXiv:1406.5375 [hep-ex]
63. T. Carli et al., A posteriori inclusion of parton density functions in NLO QCD final-state calculations at hadron colliders: the APPLGRID Project. Eur. Phys. J. C **66**, 503 (2010). arXiv:0911.2985 [hep-ph]
64. T.-J. Hou et al., Reconstruction of Monte Carlo replicas from Hessian parton distributions. JHEP **03**, 099 (2017). arXiv:1607.06066 [hep-ph]
65. R.D. Ball et al., Parton distributions for the LHC run II. JHEP **04**, 040 (2015). arXiv:1410.8849 [hep-ph]
66. P. Jimenez-Delgado, E. Reya, Delineating parton distributions and the strong coupling. Phys. Rev. D **89**, 074049 (2014). arXiv:1403.1852 [hep-ph]
67. H1 and ZEUS Collaborations, Combination of measurements of inclusive deep inelastic $e^{\pm}p$ scattering cross sections and QCD analysis of HERA data. Eur. Phys. J. C **75**, 580 (2015). arXiv:1506.06042 [hep-ex]
68. L.A. Harland-Lang, A.D. Martin, P. Motylinski, R.S. Thorne, Parton distributions in the LHC era: MMHT 2014 PDFs. Eur. Phys. J. C **75**, 204 (2015). arXiv:1412.3989 [hep-ph]
69. S. Alekhin, J. Bluemlein, S. Moch, R. Placakyte, Parton distribution functions, α_s and heavy-quark masses for LHC run II. Phys. Rev. D **96**, 014011 (2017). arXiv:1701.05838 [hep-ph]
70. ATLAS Collaboration, Precision measurement and interpretation of inclusive W^+, W^- and Z/γ^* production cross sections with the ATLAS detector. Eur. Phys. J. C **77**, 367 (2017). arXiv:1612.03016 [hep-ex]
71. J. Butterworth et al., PDF4LHC recommendations for LHC run II. J. Phys. G **43**, 023001 (2016). arXiv:1510.03865 [hep-ph]
72. R. Gauld, A. Gehrmann-De Ridder, T. Gehrmann, E.W.N. Glover, A. Huss, Precise predictions for the angular coefficients in Z-boson production at the LHC. JHEP **11**, 003 (2017). arXiv:1708.00008 [hep-ph]
73. ATLAS Collaboration, ATLAS Pythia 8 tunes to 7 TeV data, ATL-PHYS-PUB-2014-021 (2014). https://cds.cern.ch/record/1966419
74. M.H. Seymour, A. Siodmok, Constraining MPI models using σ_{eff} and recent TeVatron and LHC underlying event data. JHEP **10**, 113 (2013). arXiv:1307.5015 [hep-ph]
75. R.D. Ball et al., Parton distributions with LHC data. Nucl. Phys. B **867**, 244 (2013). arXiv:1207.1303 [hep-ph]
76. J. Alwall, M. Herquet, F. Maltoni, O. Mattelaer, T. Stelzer, MadGraph 5: going beyond. JHEP **06**, 128 (2011). arXiv:1106.0522 [hep-ph]
77. The Durham High-Energy Physics Database. https://www.hepdata.net
78. S. Höche, F. Krauss, M. Schönherr, F. Siegert, QCD matrix elements + parton showers: The NLO case. JHEP **04**, 027 (2013). arXiv:1207.5030 [hep-ph]
79. ATLAS Collaboration, Jet energy scale measurements and their systematic uncertainties in proton–proton collisions at $\sqrt{s} = 13$ TeV with the ATLAS detector. Phys. Rev. D **96**, 072002 (2017). arXiv: 1703.09665 [hep-ex]
80. ATLAS Collaboration, Measurement of the inclusive jet cross-sections in proton–proton collisions at $\sqrt{s} = 8$ TeV with the ATLAS detector. JHEP **09**, 020 (2017). arXiv:1706.03192 [hep-ex]
81. ATLAS Collaboration, Measurement of inclusive jet and dijet cross-sections in proton–proton collisions at $\sqrt{s} = 13$ TeV with the ATLAS detector. JHEP **05**, 195 (2018). arXiv:1711.02692 [hep-ex]
82. ATLAS Collaboration, ATLAS Computing Acknowledgements, ATL-GEN-PUB-2016-002 (2016). https://cds.cern.ch/record/2202407

ATLAS Collaboration

G. Aad[101], B. Abbott[128], D. C. Abbott[102], O. Abdinov[13,*], A. Abed Abud[70a,70b], K. Abeling[53], D. K. Abhayasinghe[93], S. H. Abidi[167], O. S. AbouZeid[40], N. L. Abraham[156], H. Abramowicz[161], H. Abreu[160], Y. Abulaiti[6], B. S. Acharya[66a,66b,n], B. Achkar[53], S. Adachi[163], L. Adam[99], C. Adam Bourdarios[132], L. Adamczyk[83a], L. Adamek[167], J. Adelman[121], M. Adersberger[114], A. Adiguzel[12c,ai], S. Adorni[54], T. Adye[144], A. A. Affolder[146], Y. Afik[160], C. Agapopoulou[132], M. N. Agaras[38], A. Aggarwal[119], C. Agheorghiesei[27c], J. A. Aguilar-Saavedra[140a,ah,140f], F. Ahmadov[79], W. S. Ahmed[103], X. Ai[15a], G. Aielli[73a,73b], S. Akatsuka[85], T. P. A. Åkesson[96], E. Akilli[54], A. V. Akimov[110], K. Al Khoury[132], G. L. Alberghi[23a,23b], J. Albert[176], M. J. Alconada Verzini[88], S. Alderweireldt[36], M. Aleksa[36], I. N. Aleksandrov[79], C. Alexa[27b], D. Alexandre[19], T. Alexopoulos[10], A. Alfonsi[120], M. Alhroob[128], B. Ali[142], G. Alimonti[68a], J. Alison[37], S. P. Alkire[148], C. Allaire[132], B. M. M. Allbrooke[156], B. W. Allen[131], P. P. Allport[21], A. Aloisio[69a,69b], A. Alonso[40], F. Alonso[88], C. Alpigiani[148], A. A. Alshehri[57], M. Alvarez Estevez[98], D. Álvarez Piqueras[174], M. G. Alviggi[69a,69b], Y. Amaral Coutinho[80b], A. Ambler[103], L. Ambroz[135], C. Amelung[26], D. Amidei[105], S. P. Amor Dos Santos[140a], S. Amoroso[46], C. S. Amrouche[54], F. An[78], C. Anastopoulos[149], N. Andari[145], T. Andeen[11], C. F. Anders[61b], J. K. Anders[20], A. Andreazza[68a,68b], V. Andrei[61a], C. R. Anelli[176], S. Angelidakis[38], A. Angerami[39], A. V. Anisenkov[122a,122b], A. Annovi[71a], C. Antel[61a], M. T. Anthony[149], M. Antonelli[51], D. J. A. Antrim[171], F. Anulli[72a], M. Aoki[81], J. A. Aparisi Pozo[174], L. Aperio Bella[36], G. Arabidze[106], J. P. Araque[140a], V. Araujo Ferraz[80b], R. Araujo Pereira[80b], C. Arcangeletti[51], A. T. H. Arce[49], F. A. Arduh[88], J-F. Arguin[109], S. Argyropoulos[77], J.-H. Arling[46], A. J. Armbruster[36], A. Armstrong[171], O. Arnaez[167], H. Arnold[120], A. Artamonov[111,*], G. Artoni[135], S. Artz[99], S. Asai[163], N. Asbah[59], E. M. Asimakopoulou[172], L. Asquith[156], K. Assamagan[29], R. Astalos[28a], R. J. Atkin[33a], M. Atkinson[173], N. B. Atlay[19], H. Atmani[132], K. Augsten[142], G. Avolio[36], R. Avramidou[60a], M. K. Ayoub[15a], A. M. Azoulay[168b], G. Azuelos[109,ax], M. J. Baca[21], H. Bachacou[145], K. Bachas[67a,67b], M. Backes[135], F. Backman[45a,45b], P. Bagnaia[72a,72b], M. Bahmani[84], H. Bahrasemani[152], A. J. Bailey[174], V. R. Bailey[173], J. T. Baines[144], M. Bajic[40], C. Bakalis[10], O. K. Baker[183], P. J. Bakker[120], D. Bakshi Gupta[8], S. Balaji[157], E. M. Baldin[122a,122b], P. Balek[180], F. Balli[145], W. K. Balunas[135], J. Balz[99], E. Banas[84], A. Bandyopadhyay[24], Sw. Banerjee[181,i], A. A. E. Bannoura[182], L. Barak[161], W. M. Barbe[38], E. L. Barberio[104], D. Barberis[55a,55b], M. Barbero[101], T. Barillari[115], M-S. Barisits[36], J. Barkeloo[131], T. Barklow[153], R. Barnea[160], S. L. Barnes[60c], B. M. Barnett[144], R. M. Barnett[18], Z. Barnovska-Blenessy[60a], A. Baroncelli[60a], G. Barone[29], A. J. Barr[135], L. Barranco Navarro[45a,45b], F. Barreiro[98], J. Barreiro Guimarães da Costa[15a], S. Barsov[138], R. Bartoldus[153], G. Bartolini[101], A. E. Barton[89], P. Bartos[28a], A. Basalaev[46], A. Bassalat[132,aq], R. L. Bates[57], S. J. Batista[167], S. Batlamous[35e], J. R. Batley[32], B. Batool[151], M. Battaglia[146], M. Bauce[72a,72b], F. Bauer[145], K. T. Bauer[171], H. S. Bawa[31,l], J. B. Beacham[49], T. Beau[136], P. H. Beauchemin[170], F. Becherer[52], P. Bechtle[24], H. C. Beck[53], H. P. Beck[20,r], K. Becker[52], M. Becker[99], C. Becot[46], A. Beddall[12d], A. J. Beddall[12a], V. A. Bednyakov[79], M. Bedognetti[120], C. P. Bee[155], T. A. Beermann[76], M. Begalli[80b], M. Begel[29], A. Behera[155], J. K. Behr[46], F. Beisiegel[24], A. S. Bell[94], G. Bella[161], L. Bellagamba[23b], A. Bellerive[34], P. Bellos[9], K. Beloborodov[122a,122b], K. Belotskiy[112], N. L. Belyaev[112], D. Benchekroun[35a], N. Benekos[10], Y. Benhammou[161], D. P. Benjamin[6], M. Benoit[54], J. R. Bensinger[26], S. Bentvelsen[120], L. Beresford[135], M. Beretta[51], D. Berge[46], E. Bergeaas Kuutmann[172], N. Berger[5], B. Bergmann[142], L. J. Bergsten[26], J. Beringer[18], S. Berlendis[7], N. R. Bernard[102], G. Bernardi[136], C. Bernius[153], T. Berry[93], P. Berta[99], C. Bertella[15a], I. A. Bertram[89], G. J. Besjes[40], O. Bessidskaia Bylund[182], N. Besson[145], A. Bethani[100], S. Bethke[115], A. Betti[24], A. J. Bevan[92], J. Beyer[115], R. Bi[139], R. M. Bianchi[139], O. Biebel[114], D. Biedermann[19], R. Bielski[36], K. Bierwagen[99], N. V. Biesuz[71a,71b], M. Biglietti[74a], T. R. V. Billoud[109], M. Bindi[53], A. Bingul[12d], C. Bini[72a,72b], S. Biondi[23a,23b], M. Birman[180], T. Bisanz[53], J. P. Biswal[161], D. Biswas[181], A. Bitadze[100], C. Bittrich[48], K. Bjørke[134], K. M. Black[25], T. Blazek[28a], I. Bloch[46], C. Blocker[26], A. Blue[57], U. Blumenschein[92], G. J. Bobbink[120], V. S. Bobrovnikov[122a,122b], S. S. Bocchetta[96], A. Bocci[49], D. Boerner[46], D. Bogavac[14], A. G. Bogdanchikov[122a,122b], C. Bohm[45a], V. Boisvert[93], P. Bokan[53,172], T. Bold[83a], A. S. Boldyrev[113], A. E. Bolz[61b], M. Bomben[136], M. Bona[92], J. S. Bonilla[131], M. Boonekamp[145], H. M. Borecka-Bielska[90], A. Borisov[123], G. Borissov[89], J. Bortfeldt[36], D. Bortoletto[135], V. Bortolotto[73a,73b], D. Boscherini[23b], M. Bosman[14], J. D. Bossio Sola[103], K. Bouaouda[35a], J. Boudreau[139], E. V. Bouhova-Thacker[89], D. Boumediene[38], S. K. Boutle[57], A. Boveia[126], J. Boyd[36], D. Boye[33b,ar], I. R. Boyko[79], A. J. Bozson[93], J. Bracinik[21], N. Brahimi[101], G. Brandt[182], O. Brandt[32], F. Braren[46], U. Bratzler[164], B. Brau[102], J. E. Brau[131], W. D. Breaden Madden[57], K. Brendlinger[46], L. Brenner[46], R. Brenner[172], S. Bressler[180], B. Brickwedde[99], D. L. Briglin[21], D. Britton[57], D. Britzger[115], I. Brock[24], R. Brock[106], G. Brooijmans[39], W. K. Brooks[147b], E. Brost[121], J. H. Broughton[21], P. A. Bruckman de Renstrom[84], D. Bruncko[28b], A. Bruni[23b], G. Bruni[23b], L. S. Bruni[120], S. Bruno[73a,73b], B. H. Brunt[32], M. Bruschi[23b], N. Bruscino[139], P. Bryant[37], L. Bryngemark[96], T. Buanes[17], Q. Buat[36], P. Buchholz[151], A. G. Buckley[57], I. A. Budagov[79], M. K. Bugge[134], F. Bührer[52], O. Bulekov[112], T. J. Burch[121], S. Burdin[90], C. D. Burgard[120], A. M. Burger[129], B. Burghgrave[8], K. Burka[84], J. T. P. Burr[46], J. C. Burzynski[102],

V. Büscher[99], E. Buschmann[53], P. J. Bussey[57], J. M. Butler[25], C. M. Buttar[57], J. M. Butterworth[94], P. Butti[36], W. Buttinger[36], A. Buzatu[158], A. R. Buzykaev[122a,122b], G. Cabras[23a,23b], S. Cabrera Urbán[174], D. Caforio[56], H. Cai[173], V. M. M. Cairo[153], O. Cakir[4a], N. Calace[36], P. Calafiura[18], A. Calandri[101], G. Calderini[136], P. Calfayan[65], G. Callea[57], L. P. Caloba[80b], S. Calvente Lopez[98], D. Calvet[38], S. Calvet[38], T. P. Calvet[155], M. Calvetti[71a,71b], R. Camacho Toro[136], S. Camarda[36], D. Camarero Munoz[98], P. Camarri[73a,73b], D. Cameron[134], R. Caminal Armadans[102], C. Camincher[36], S. Campana[36], M. Campanelli[94], A. Camplani[40], A. Campoverde[151], V. Canale[69a,69b], A. Canesse[103], M. Cano Bret[60c], J. Cantero[129], T. Cao[161], Y. Cao[173], M. D. M. Capeans Garrido[36], M. Capua[41a,41b], R. Cardarelli[73a], F. C. Cardillo[149], G. Carducci[41a,41b], I. Carli[143], T. Carli[36], G. Carlino[69a], B. T. Carlson[139], L. Carminati[68a,68b], R. M. D. Carney[45a,45b], S. Caron[119], E. Carquin[147b], S. Carrá[46], J. W. S. Carter[167], M. P. Casado[14,d], A. F. Casha[167], D. W. Casper[171], R. Castelijn[120], F. L. Castillo[174], V. Castillo Gimenez[174], N. F. Castro[140a,140e], A. Catinaccio[36], J. R. Catmore[134], A. Cattai[36], J. Caudron[24], V. Cavaliere[29], E. Cavallaro[14], M. Cavalli-Sforza[14], V. Cavasinni[71a,71b], E. Celebi[12b], F. Ceradini[74a,74b], L. Cerda Alberich[174], K. Cerny[130], A. S. Cerqueira[80a], A. Cerri[156], L. Cerrito[73a,73b], F. Cerutti[18], A. Cervelli[23a,23b], S. A. Cetin[12b], Z. Chadi[35a], D. Chakraborty[121], S. K. Chan[59], W. S. Chan[120], W. Y. Chan[90], J. D. Chapman[32], B. Chargeishvili[159b], D. G. Charlton[21], T. P. Charman[92], C. C. Chau[34], S. Che[126], A. Chegwidden[106], S. Chekanov[6], S. V. Chekulaev[168a], G. A. Chelkov[79,aw], M. A. Chelstowska[36], B. Chen[78], C. Chen[60a], C. H. Chen[78], H. Chen[29], J. Chen[60a], J. Chen[39], S. Chen[137], S. J. Chen[15c], X. Chen[15b,av], Y. Chen[82], Y-H. Chen[46], H. C. Cheng[63a], H. J. Cheng[15a,15d], A. Cheplakov[79], E. Cheremushkina[123], R. Cherkaoui El Moursli[35e], E. Cheu[7], K. Cheung[64], T. J. A. Chevalérias[145], L. Chevalier[145], V. Chiarella[51], G. Chiarelli[71a], G. Chiodini[67a], A. S. Chisholm[36,21], A. Chitan[27b], I. Chiu[163], Y. H. Chiu[176], M. V. Chizhov[79], K. Choi[65], A. R. Chomont[72a,72b], S. Chouridou[162], Y. S. Chow[120], M. C. Chu[63a], X. Chu[15a], J. Chudoba[141], A. J. Chuinard[103], J. J. Chwastowski[84], L. Chytka[130], K. M. Ciesla[84], D. Cinca[47], V. Cindro[91], I. A. Cioară[27b], A. Ciocio[18], F. Cirotto[69a,69b], Z. H. Citron[180], M. Citterio[68a], D. A. Ciubotaru[27b], B. M. Ciungu[167], A. Clark[54], M. R. Clark[39], P. J. Clark[50], C. Clement[45a,45b], Y. Coadou[101], M. Cobal[66a,66c], A. Coccaro[55b], J. Cochran[78], H. Cohen[161], A. E. C. Coimbra[36], L. Colasurdo[119], B. Cole[39], A. P. Colijn[120], J. Collot[58], P. Conde Muiño[140a,e], E. Coniavitis[52], S. H. Connell[33b], I. A. Connelly[57], S. Constantinescu[27b], F. Conventi[69a,ay], A. M. Cooper-Sarkar[135], F. Cormier[175], K. J. R. Cormier[167], L. D. Corpe[94], M. Corradi[72a,72b], E. E. Corrigan[96], F. Corriveau[103,ad], A. Cortes-Gonzalez[36], M. J. Costa[174], F. Costanza[5], D. Costanzo[149], G. Cowan[93], J. W. Cowley[32], J. Crane[100], K. Cranmer[124], S. J. Crawley[57], R. A. Creager[137], S. Crépé-Renaudin[58], F. Crescioli[136], M. Cristinziani[24], V. Croft[120], G. Crosetti[41a,41b], A. Cueto[5], T. Cuhadar Donszelmann[149], A. R. Cukierman[153], S. Czekierda[84], P. Czodrowski[36], M. J. Da Cunha Sargedas De Sousa[60b], J. V. Da Fonseca Pinto[80b], C. Da Via[100], W. Dabrowski[83a], T. Dado[28a], S. Dahbi[35e], T. Dai[105], C. Dallapiccola[102], M. Dam[40], G. D'amen[23a,23b], V. D'Amico[74a,74b], J. Damp[99], J. R. Dandoy[137], M. F. Daneri[30], N. P. Dang[181], N. D. Dann[100], M. Danninger[175], V. Dao[36], G. Darbo[55b], O. Dartsi[5], A. Dattagupta[131], T. Daubney[46], S. D'Auria[68a,68b], W. Davey[24], C. David[46], T. Davidek[143], D. R. Davis[49], I. Dawson[149], K. De[8], R. De Asmundis[69a], M. De Beurs[120], S. De Castro[23a,23b], S. De Cecco[72a,72b], N. De Groot[119], P. de Jong[120], H. De la Torre[106], A. De Maria[15c], D. De Pedis[72a], A. De Salvo[72a], U. De Sanctis[73a,73b], M. De Santis[73a,73b], A. De Santo[156], K. De Vasconcelos Corga[101], J. B. De Vivie De Regie[132], C. Debenedetti[146], D. V. Dedovich[79], A. M. Deiana[42], M. Del Gaudio[41a,41b], J. Del Peso[98], Y. Delabat Diaz[46], D. Delgove[132], F. Deliot[145,q], C. M. Delitzsch[7], M. Della Pietra[69a,69b], D. Della Volpe[54], A. Dell'Acqua[36], L. Dell'Asta[73a,73b], M. Delmastro[5], C. Delporte[132], P. A. Delsart[58], D. A. DeMarco[167], S. Demers[183], M. Demichev[79], G. Demontigny[109], S. P. Denisov[123], D. Denysiuk[120], L. D'Eramo[136], D. Derendarz[84], J. E. Derkaoui[35d], F. Derue[136], P. Dervan[90], K. Desch[24], C. Deterre[46], K. Dette[167], C. Deutsch[24], M. R. Devesa[30], P. O. Deviveiros[36], A. Dewhurst[144], S. Dhaliwal[26], F. A. Di Bello[54], A. Di Ciaccio[73a,73b], L. Di Ciaccio[5], W. K. Di Clemente[137], C. Di Donato[69a,69b], A. Di Girolamo[36], G. Di Gregorio[71a,71b], B. Di Micco[74a,74b], R. Di Nardo[102], K. F. Di Petrillo[59], R. Di Sipio[167], D. Di Valentino[34], C. Diaconu[101], F. A. Dias[40], T. Dias Do Vale[140a], M. A. Diaz[147a], J. Dickinson[18], E. B. Diehl[105], J. Dietrich[19], S. Díez Cornell[46], A. Dimitrievska[18], W. Ding[15b], J. Dingfelder[24], F. Dittus[36], F. Djama[101], T. Djobava[159b], J. I. Djuvsland[17], M. A. B. Do Vale[80c], M. Dobre[27b], D. Dodsworth[26], C. Doglioni[96], J. Dolejsi[143], Z. Dolezal[143], M. Donadelli[80d], B. Dong[60c], J. Donini[38], A. D'onofrio[92], M. D'Onofrio[90], J. Dopke[144], A. Doria[69a], M. T. Dova[88], A. T. Doyle[57], E. Drechsler[152], E. Dreyer[152], T. Dreyer[53], A. S. Drobac[170], Y. Duan[60b], F. Dubinin[110], M. Dubovsky[28a], A. Dubreuil[54], E. Duchovni[180], G. Duckeck[114], A. Ducourthial[136], O. A. Ducu[109], D. Duda[115], A. Dudarev[36], A. C. Dudder[99], E. M. Duffield[18], L. Duflot[132], M. Dührssen[36], C. Dülsen[182], M. Dumancic[180], A. E. Dumitriu[27b], A. K. Duncan[57], M. Dunford[61a], A. Duperrin[101], H. Duran Yildiz[4a], M. Düren[56], A. Durglishvili[159b], D. Duschinger[48], B. Dutta[46], D. Duvnjak[1], G. I. Dyckes[137], M. Dyndal[36], S. Dysch[100], B. S. Dziedzic[84], K. M. Ecker[115], R. C. Edgar[105], M. G. Eggleston[49], T. Eifert[36], G. Eigen[17], K. Einsweiler[18], T. Ekelof[172], H. El Jarrari[35e], M. El Kacimi[35c], R. El Kosseifi[101], V. Ellajosyula[172], M. Ellert[172], F. Ellinghaus[182], A. A. Elliot[92], N. Ellis[36], J. Elmsheuser[29], M. Elsing[36], D. Emeliyanov[144], A. Emerman[39], Y. Enari[163], M. B. Epland[49], J. Erdmann[47], A. Ereditato[20], M. Errenst[36], M. Escalier[132],

C. Escobar[174], O. Estrada Pastor[174], E. Etzion[161], H. Evans[65], A. Ezhilov[138], F. Fabbri[57], L. Fabbri[23a,23b], V. Fabiani[119], G. Facini[94], R. M. Faisca Rodrigues Pereira[140a], R. M. Fakhrutdinov[123], S. Falciano[72a], P. J. Falke[5], S. Falke[5], J. Faltova[143], Y. Fang[15a], Y. Fang[15a], G. Fanourakis[44], M. Fanti[68a,68b], M. Faraj[66a,66c], A. Farbin[8], A. Farilla[74a], E. M. Farina[70a,70b], T. Farooque[106], S. Farrell[18], S. M. Farrington[50], P. Farthouat[36], F. Fassi[35e], P. Fassnacht[36], D. Fassouliotis[9], M. Faucci Giannelli[50], W. J. Fawcett[32], L. Fayard[132], O. L. Fedin[138,o], W. Fedorko[175], M. Feickert[42], S. Feigl[134], L. Feligioni[101], A. Fell[149], C. Feng[60b], E. J. Feng[36], M. Feng[49], M. J. Fenton[57], A. B. Fenyuk[123], J. Ferrando[46], A. Ferrante[173], A. Ferrari[172], P. Ferrari[120], R. Ferrari[70a], D. E. Ferreira de Lima[61b], A. Ferrer[174], D. Ferrere[54], C. Ferretti[105], F. Fiedler[99], A. Filipčič[91], F. Filthaut[119], K. D. Finelli[25], M. C. N. Fiolhais[140a], L. Fiorini[174], F. Fischer[114], W. C. Fisher[106], I. Fleck[151], P. Fleischmann[105], R. R. M. Fletcher[137], T. Flick[182], B. M. Flierl[114], L. F. Flores[137], L. R. Flores Castillo[63a], F. M. Follega[75a,75b], N. Fomin[17], J. H. Foo[167], G. T. Forcolin[75a,75b], A. Formica[145], F. A. Förster[14], A. C. Forti[100], A. G. Foster[21], M. G. Foti[135], D. Fournier[132], H. Fox[89], P. Francavilla[71a,71b], S. Francescato[72a,72b], M. Franchini[23a,23b], S. Franchino[61a], D. Francis[36], L. Franconi[20], M. Franklin[59], A. N. Fray[92], B. Freund[109], W. S. Freund[80b], E. M. Freundlich[47], D. C. Frizzell[128], D. Froidevaux[36], J. A. Frost[135], C. Fukunaga[164], E. Fullana Torregrosa[174], E. Fumagalli[55a,55b], T. Fusayasu[116], J. Fuster[174], A. Gabrielli[23a,23b], A. Gabrielli[18], G. P. Gach[83a], S. Gadatsch[54], P. Gadow[115], G. Gagliardi[55a,55b], L. G. Gagnon[109], C. Galea[27b], B. Galhardo[140a], G. E. Gallardo[135], E. J. Gallas[135], B. J. Gallop[144], G. Galster[40], R. Gamboa Goni[92], K. K. Gan[126], S. Ganguly[180], J. Gao[60a], Y. Gao[50], Y. S. Gao[31,l], C. García[174], J. E. García Navarro[174], J. A. García Pascual[15a], C. Garcia-Argos[52], M. Garcia-Sciveres[18], R. W. Gardner[37], N. Garelli[153], S. Gargiulo[52], V. Garonne[134], A. Gaudiello[55a,55b], G. Gaudio[70a], I. L. Gavrilenko[110], A. Gavrilyuk[111], C. Gay[175], G. Gaycken[46], E. N. Gazis[10], A. A. Geanta[27b], C. N. P. Gee[144], J. Geisen[53], M. Geisen[99], M. P. Geisler[61a], C. Gemme[55b], M. H. Genest[58], C. Geng[105], S. Gentile[72a,72b], S. George[93], T. Geralis[44], L. O. Gerlach[53], P. Gessinger-Befurt[99], G. Gessner[47], S. Ghasemi[151], M. Ghasemi Bostanabad[176], M. Ghneimat[24], A. Ghosh[132], A. Ghosh[77], B. Giacobbe[23b], S. Giagu[72a,72b], N. Giangiacomi[23a,23b], P. Giannetti[71a], A. Giannini[69a,69b], G. Giannini[14], S. M. Gibson[93], M. Gignac[146], D. Gillberg[34], G. Gilles[182], D. M. Gingrich[3,ax], M. P. Giordani[66a,66c], F. M. Giorgi[23b], P. F. Giraud[145], G. Giugliarelli[66a,66c], D. Giugni[68a], F. Giuli[73a,73b], S. Gkaitatzis[162], I. Gkialas[9,g], E. L. Gkougkousis[14], P. Gkountoumis[10], L. K. Gladilin[113], C. Glasman[98], J. Glatzer[14], P. C. F. Glaysher[46], A. Glazov[46], M. Goblirsch-Kolb[26], S. Goldfarb[104], T. Golling[54], D. Golubkov[123], A. Gomes[140a,140b], R. Goncalves Gama[53], R. Gonçalo[140a,140b], G. Gonella[52], L. Gonella[21], A. Gongadze[79], F. Gonnella[21], J. L. Gonski[59], S. González de la Hoz[174], S. Gonzalez-Sevilla[54], G. R. Gonzalvo Rodriguez[174], L. Goossens[36], P. A. Gorbounov[111], H. A. Gordon[29], B. Gorini[36], E. Gorini[67a,67b], A. Gorišek[91], A. T. Goshaw[49], C. Gössling[47], M. I. Gostkin[79], C. A. Gottardo[119], M. Gouighri[35b], D. Goujdami[35c], A. G. Goussiou[148], N. Govender[33b], C. Goy[5], E. Gozani[160], I. Grabowska-Bold[83a], E. C. Graham[90], J. Gramling[171], E. Gramstad[134], S. Grancagnolo[19], M. Grandi[156], V. Gratchev[138], P. M. Gravila[27f], F. G. Gravili[67a,67b], C. Gray[57], H. M. Gray[18], C. Grefe[24], K. Gregersen[96], I. M. Gregor[46], P. Grenier[153], K. Grevtsov[46], C. Grieco[14], N. A. Grieser[128], J. Griffiths[8], A. A. Grillo[146], K. Grimm[31,k], S. Grinstein[14,x], J.-F. Grivaz[132], S. Groh[99], E. Gross[180], J. Grosse-Knetter[53], Z. J. Grout[94], C. Grud[105], A. Grummer[118], L. Guan[105], W. Guan[181], J. Guenther[36], A. Guerguichon[132], J. G. R. Guerrero Rojas[174], F. Guescini[115], D. Guest[171], R. Gugel[52], T. Guillemin[5], S. Guindon[36], U. Gul[57], J. Guo[60c], W. Guo[105], Y. Guo[60a,s], Z. Guo[101], R. Gupta[46], S. Gurbuz[12c], G. Gustavino[128], P. Gutierrez[128], C. Gutschow[94], C. Guyot[145], C. Gwenlan[135], C. B. Gwilliam[90], A. Haas[124], C. Haber[18], H. K. Hadavand[8], N. Haddad[35e], A. Hadef[60a], S. Hageböck[36], M. Hagihara[169], M. Haleem[177], J. Haley[129], G. Halladjian[106], G. D. Hallewell[101], K. Hamacher[182], P. Hamal[130], K. Hamano[176], H. Hamdaoui[35e], G. N. Hamity[149], K. Han[60a,ak], L. Han[60a], S. Han[15a,15d], K. Hanagaki[81,v], M. Hance[146], D. M. Handl[114], B. Haney[137], R. Hankache[136], P. Hanke[61a], E. Hansen[96], J. B. Hansen[40], J. D. Hansen[40], M. C. Hansen[24], P. H. Hansen[40], E. C. Hanson[100], K. Hara[169], A. S. Hard[181], T. Harenberg[182], S. Harkusha[107], P. F. Harrison[178], N. M. Hartmann[114], Y. Hasegawa[150], A. Hasib[50], S. Hassani[145], S. Haug[20], R. Hauser[106], L. B. Havener[39], M. Havranek[142], C. M. Hawkes[21], R. J. Hawkings[36], D. Hayden[106], C. Hayes[155], R. L. Hayes[175], C. P. Hays[135], J. M. Hays[92], H. S. Hayward[90], S. J. Haywood[144], F. He[60a], M. P. Heath[50], V. Hedberg[96], L. Heelan[8], S. Heer[24], K. K. Heidegger[52], W. D. Heidorn[78], J. Heilman[34], S. Heim[46], T. Heim[18], B. Heinemann[46,as], J. J. Heinrich[131], L. Heinrich[36], C. Heinz[56], J. Hejbal[141], L. Helary[61b], A. Held[175], S. Hellesund[134], C. M. Helling[146], S. Hellman[45a,45b], C. Helsens[36], R. C. W. Henderson[89], Y. Heng[181], S. Henkelmann[175], A. M. Henriques Correia[36], G. H. Herbert[19], H. Herde[26], V. Herget[177], Y. Hernández Jiménez[33c], H. Herr[99], M. G. Herrmann[114], T. Herrmann[48], G. Herten[52], R. Hertenberger[114], L. Hervas[36], T. C. Herwig[137], G. G. Hesketh[94], N. P. Hessey[168a], A. Higashida[163], S. Higashino[81], E. Higón-Rodriguez[174], K. Hildebrand[37], E. Hill[176], J. C. Hill[32], K. K. Hill[29], K. H. Hiller[46], S. J. Hillier[21], M. Hils[48], I. Hinchliffe[18], F. Hinterkeuser[24], M. Hirose[133], S. Hirose[52], D. Hirschbuehl[182], B. Hiti[91], O. Hladik[141], D. R. Hlaluku[33c], X. Hoad[50], J. Hobbs[155], N. Hod[180], M. C. Hodgkinson[149], A. Hoecker[36], F. Hoenig[114], D. Hohn[52], D. Hohov[132], T. R. Holmes[37], M. Holzbock[114], L. B. A. H. Hommels[32], S. Honda[169], T. Honda[81], T. M. Hong[139],

A. Hönle[115], B. H. Hooberman[173], W. H. Hopkins[6], Y. Horii[117], P. Horn[48], L. A. Horyn[37], A. Hostiuc[148], S. Hou[158], A. Hoummada[35a], J. Howarth[100], J. Hoya[88], M. Hrabovsky[130], J. Hrdinka[76], I. Hristova[19], J. Hrivnac[132], A. Hrynevich[108], T. Hryn'ova[5], P. J. Hsu[64], S.-C. Hsu[148], Q. Hu[29], S. Hu[60c], D. P. Huang[94], Y. Huang[15a], Z. Hubacek[142], F. Hubaut[101], M. Huebner[24], F. Huegging[24], T. B. Huffman[135], M. Huhtinen[36], R. F. H. Hunter[34], P. Huo[155], A. M. Hupe[34], N. Huseynov[79,af], J. Huston[106], J. Huth[59], R. Hyneman[105], S. Hyrych[28a], G. Iacobucci[54], G. Iakovidis[29], I. Ibragimov[151], L. Iconomidou-Fayard[132], Z. Idrissi[35e], P. I. Iengo[36], R. Ignazzi[40], O. Igonkina[120,z,*], R. Iguchi[163], T. Iizawa[54], Y. Ikegami[81], M. Ikeno[81], D. Iliadis[162], N. Ilic[119], F. Iltzsche[48], G. Introzzi[70a,70b], M. Iodice[74a], K. Iordanidou[168a], V. Ippolito[72a,72b], M. F. Isacson[172], M. Ishino[163], M. Ishitsuka[165], W. Islam[129], C. Issever[135], S. Istin[160], F. Ito[169], J. M. Iturbe Ponce[63a], R. Iuppa[75a,75b], A. Ivina[180], H. Iwasaki[81], J. M. Izen[43], V. Izzo[69a], P. Jacka[141], P. Jackson[1], R. M. Jacobs[24], B. P. Jaeger[152], V. Jain[2], G. Jäkel[182], K. B. Jakobi[99], K. Jakobs[52], S. Jakobsen[76], T. Jakoubek[141], J. Jamieson[57], K. W. Janas[83a], R. Jansky[54], J. Janssen[24], M. Janus[53], P. A. Janus[83a], G. Jarlskog[96], N. Javadov[79,af], T. Javůrek[36], M. Javurkova[52], F. Jeanneau[145], L. Jeanty[131], J. Jejelava[159a,ag], A. Jelinskas[178], P. Jenni[52,a], J. Jeong[46], N. Jeong[46], S. Jézéquel[5], H. Ji[181], J. Jia[155], H. Jiang[78], Y. Jiang[60a], Z. Jiang[153,p], S. Jiggins[52], F. A. Jimenez Morales[38], J. Jimenez Pena[115], S. Jin[15c], A. Jinaru[27b], O. Jinnouchi[165], H. Jivan[33c], P. Johansson[149], K. A. Johns[7], C. A. Johnson[65], K. Jon-And[45a,45b], R. W. L. Jones[89], S. D. Jones[156], S. Jones[7], T. J. Jones[90], J. Jongmanns[61a], P. M. Jorge[140a], J. Jovicevic[36], X. Ju[18], J. J. Junggeburth[115], A. Juste Rozas[14,x], A. Kaczmarska[84], M. Kado[72a,72b], H. Kagan[126], M. Kagan[153], C. Kahra[99], T. Kaji[179], E. Kajomovitz[160], C. W. Kalderon[96], A. Kaluza[99], A. Kamenshchikov[123], L. Kanjir[91], Y. Kano[163], V. A. Kantserov[112], J. Kanzaki[81], L. S. Kaplan[181], D. Kar[33c], M. J. Kareem[168b], S. N. Karpov[79], Z. M. Karpova[79], V. Kartvelishvili[89], A. N. Karyukhin[123], L. Kashif[181], R. D. Kass[126], A. Kastanas[45a,45b], Y. Kataoka[163], C. Kato[60c,60d], J. Katzy[46], K. Kawade[82], K. Kawagoe[87], T. Kawaguchi[117], T. Kawamoto[163], G. Kawamura[53], E. F. Kay[176], V. F. Kazanin[122a,122b], R. Keeler[176], R. Kehoe[42], J. S. Keller[34], E. Kellermann[96], D. Kelsey[156], J. J. Kempster[21], J. Kendrick[21], O. Kepka[141], S. Kersten[182], B. P. Kerševan[91], S. Ketabchi Haghighat[167], M. Khader[173], F. Khalil-Zada[13], M. Khandoga[145], A. Khanov[129], A. G. Kharlamov[122a,122b], T. Kharlamova[122a,122b], E. E. Khoda[175], A. Khodinov[166], T. J. Khoo[54], E. Khramov[79], J. Khubua[159b], S. Kido[82], M. Kiehn[54], C. R. Kilby[93], Y. K. Kim[37], N. Kimura[66a,66c], O. M. Kind[19], B. T. King[90,*], D. Kirchmeier[48], J. Kirk[144], A. E. Kiryunin[115], T. Kishimoto[163], D. P. Kisliuk[167], V. Kitali[46], O. Kivernyk[5], E. Kladiva[28b,*], T. Klapdor-Kleingrothaus[52], M. Klassen[61a], M. H. Klein[105], M. Klein[90], U. Klein[90], K. Kleinknecht[99], P. Klimek[121], A. Klimentov[29], T. Klingl[24], T. Klioutchnikova[36], F. F. Klitzner[114], P. Kluit[120], S. Kluth[115], E. Kneringer[76], E. B. F. G. Knoops[101], A. Knue[52], D. Kobayashi[87], T. Kobayashi[163], M. Kobel[48], M. Kocian[153], P. Kodys[143], P. T. Koenig[24], T. Koffas[34], N. M. Köhler[36], T. Koi[153], M. Kolb[61b], I. Koletsou[5], T. Komarek[130], T. Kondo[81], N. Kondrashova[60c], K. Köneke[52], A. C. König[119], T. Kono[125], R. Konoplich[124,an], V. Konstantinides[94], N. Konstantinidis[94], B. Konya[96], R. Kopeliansky[65], S. Koperny[83a], K. Korcyl[84], K. Kordas[162], G. Koren[161], A. Korn[94], I. Korolkov[14], E. V. Korolkova[149], N. Korotkova[113], O. Kortner[115], S. Kortner[115], T. Kosek[143], V. V. Kostyukhin[24], A. Kotwal[49], A. Koulouris[10], A. Kourkoumeli-Charalampidi[70a,70b], C. Kourkoumelis[9], E. Kourlitis[149], V. Kouskoura[29], A. B. Kowalewska[84], R. Kowalewski[176], C. Kozakai[163], W. Kozanecki[145], A. S. Kozhin[123], V. A. Kramarenko[113], G. Kramberger[91], D. Krasnopevtsev[60a], M. W. Krasny[136], A. Krasznahorkay[36], D. Krauss[115], J. A. Kremer[83a], J. Kretzschmar[90], P. Krieger[167], F. Krieter[114], A. Krishnan[61b], K. Krizka[18], K. Kroeninger[47], H. Kroha[115], J. Kroll[141], J. Kroll[137], J. Krstic[16], U. Kruchonak[79], H. Krüger[24], N. Krumnack[78], M. C. Kruse[49], J. A. Krzysiak[84], T. Kubota[104], O. Kuchinskaia[166], S. Kuday[4b], J. T. Kuechler[46], S. Kuehn[36], A. Kugel[61a], T. Kuhl[46], V. Kukhtin[79], R. Kukla[101], Y. Kulchitsky[107,aj], S. Kuleshov[147b], Y. P. Kulinich[173], M. Kuna[58], T. Kunigo[85], A. Kupco[141], T. Kupfer[47], O. Kuprash[52], H. Kurashige[82], L. L. Kurchaninov[168a], Y. A. Kurochkin[107], A. Kurova[112], M. G. Kurth[15a,15d], E. S. Kuwertz[36], M. Kuze[165], A. K. Kvam[148], J. Kvita[130], T. Kwan[103], A. La Rosa[115], L. La Rotonda[41a,41b], F. La Ruffa[41a,41b], C. Lacasta[174], F. Lacava[72a,72b], D. P. J. Lack[100], H. Lacker[19], D. Lacour[136], E. Ladygin[79], R. Lafaye[5], B. Laforge[136], T. Lagouri[33c], S. Lai[53], S. Lammers[65], W. Lampl[7], C. Lampoudis[162], E. Lançon[29], U. Landgraf[52], M. P. J. Landon[92], M. C. Lanfermann[54], V. S. Lang[46], J. C. Lange[53], R. J. Langenberg[36], A. J. Lankford[171], F. Lanni[29], K. Lantzsch[24], A. Lanza[70a], A. Lapertosa[55a,55b], S. Laplace[136], J. F. Laporte[145], T. Lari[68a], F. Lasagni Manghi[23a,23b], M. Lassnig[36], T. S. Lau[63a], A. Laudrain[132], A. Laurier[34], M. Lavorgna[69a,69b], M. Lazzaroni[68a,68b], B. Le[104], O. Le Dortz[136], E. Le Guirriec[101], M. LeBlanc[7], T. LeCompte[6], F. Ledroit-Guillon[58], C. A. Lee[29], G. R. Lee[17], L. Lee[59], S. C. Lee[158], S. J. Lee[34], B. Lefebvre[168a], M. Lefebvre[176], F. Legger[114], C. Leggett[18], K. Lehmann[152], N. Lehmann[182], G. Lehmann Miotto[36], W. A. Leight[46], A. Leisos[162,w], M. A. L. Leite[80d], C. E. Leitgeb[114], R. Leitner[143], D. Lellouch[180,*], K. J. C. Leney[42], T. Lenz[24], B. Lenzi[36], R. Leone[7], S. Leone[71a], C. Leonidopoulos[50], A. Leopold[136], G. Lerner[156], C. Leroy[109], R. Les[167], C. G. Lester[32], M. Levchenko[138], J. Levêque[5], D. Levin[105], L. J. Levinson[180], D. J. Lewis[21], B. Li[15b], B. Li[105], C-Q. Li[60a], F. Li[60c], H. Li[60a], H. Li[60b], J. Li[60c], K. Li[153], L. Li[60c], M. Li[15a], Q. Li[15a,15d], Q. Y. Li[60a], S. Li[60c,60d], X. Li[46], Y. Li[46], Z. Li[60b], Z. Liang[15a], B. Liberti[73a], A. Liblong[167], K. Lie[63c], S. Liem[120], C. Y. Lin[32],

K. Lin[106], T. H. Lin[99], R. A. Linck[65], J. H. Lindon[21], A. L. Lionti[54], E. Lipeles[137], A. Lipniacka[17], M. Lisovyi[61b], T. M. Liss[173,au], A. Lister[175], A. M. Litke[146], J. D. Little[8], B. Liu[78,ac], B. L. Liu[6], H. B. Liu[29], H. Liu[105], J. B. Liu[60a], J. K. K. Liu[135], K. Liu[136], M. Liu[60a], P. Liu[18], Y. Liu[15a,15d], Y. L. Liu[105], Y. W. Liu[60a], M. Livan[70a,70b], A. Lleres[58], J. Llorente Merino[15a], S. L. Lloyd[92], C. Y. Lo[63b], F. Lo Sterzo[42], E. M. Lobodzinska[46], P. Loch[7], S. Loffredo[73a,73b], T. Lohse[19], K. Lohwasser[149], M. Lokajicek[141], J. D. Long[173], R. E. Long[89], L. Longo[36], K. A. Looper[126], J. A. Lopez[147b], I. Lopez Paz[100], A. Lopez Solis[149], J. Lorenz[114], N. Lorenzo Martinez[5], M. Losada[22], P. J. Lösel[114], A. Lösle[52], X. Lou[46], X. Lou[15a], A. Lounis[132], J. Love[6], P. A. Love[89], J. J. Lozano Bahilo[174], M. Lu[60a], Y. J. Lu[64], H. J. Lubatti[148], C. Luci[72a,72b], A. Lucotte[58], C. Luedtke[52], F. Luehring[65], I. Luise[136], L. Luminari[72a], B. Lund-Jensen[154], M. S. Lutz[102], D. Lynn[29], R. Lysak[141], E. Lytken[96], F. Lyu[15a], V. Lyubushkin[79], T. Lyubushkina[79], H. Ma[29], L. L. Ma[60b], Y. Ma[60b], G. Maccarrone[51], A. Macchiolo[115], C. M. Macdonald[149], J. Machado Miguens[137], D. Madaffari[174], R. Madar[38], W. F. Mader[48], N. Madysa[48], J. Maeda[82], K. Maekawa[163], S. Maeland[17], T. Maeno[29], M. Maerker[48], A. S. Maevskiy[113], V. Magerl[52], N. Magini[78], D. J. Mahon[39], C. Maidantchik[80b], T. Maier[114], A. Maio[140a,140b,140d], O. Majersky[28a], S. Majewski[131], Y. Makida[81], N. Makovec[132], B. Malaescu[136], Pa. Malecki[84], V. P. Maleev[138], F. Malek[58], U. Mallik[77], D. Malon[6], C. Malone[32], S. Maltezos[10], S. Malyukov[36], J. Mamuzic[174], G. Mancini[51], I. Mandić[91], L. Manhaes de Andrade Filho[80a], I. M. Maniatis[162], J. Manjarres Ramos[48], K. H. Mankinen[96], A. Mann[114], A. Manousos[76], B. Mansoulie[145], I. Manthos[162], S. Manzoni[120], A. Marantis[162], G. Marceca[30], L. Marchese[135], G. Marchiori[136], M. Marcisovsky[141], C. Marcon[96], C. A. Marin Tobon[36], M. Marjanovic[38], F. Marroquim[80b], Z. Marshall[18], M. U. F. Martensson[172], S. Marti-Garcia[174], C. B. Martin[126], T. A. Martin[178], V. J. Martin[50], B. Martin dit Latour[17], L. Martinelli[74a,74b], M. Martinez[14,x], V. I. Martinez Outschoorn[102], S. Martin-Haugh[144], V. S. Martoiu[27b], A. C. Martyniuk[94], A. Marzin[36], S. R. Maschek[115], L. Masetti[99], T. Mashimo[163], R. Mashinistov[110], J. Masik[100], A. L. Maslennikov[122a,122b], L. H. Mason[104], L. Massa[73a,73b], P. Massarotti[69a,69b], P. Mastrandrea[71a,71b], A. Mastroberardino[41a,41b], T. Masubuchi[163], D. Matakias[10], A. Matic[114], P. Mättig[24], J. Maurer[27b], B. Maček[91], S. J. Maxfield[90], D. A. Maximov[122a,122b], R. Mazini[158], I. Maznas[162], S. M. Mazza[146], S. P. Mc Kee[105], T. G. McCarthy[115], L. I. McClymont[94], W. P. McCormack[18], E. F. McDonald[104], J. A. Mcfayden[36], M. A. McKay[42], K. D. McLean[176], S. J. McMahon[144], P. C. McNamara[104], C. J. McNicol[178], R. A. McPherson[176,ad], J. E. Mdhluli[33c], Z. A. Meadows[102], S. Meehan[148], T. Megy[52], S. Mehlhase[114], A. Mehta[90], T. Meideck[58], B. Meirose[43], D. Melini[174], B. R. Mellado Garcia[33c], J. D. Mellenthin[53], M. Melo[28a], F. Meloni[46], A. Melzer[24], S. B. Menary[100], E. D. Mendes Gouveia[140a,140e], L. Meng[36], X. T. Meng[105], S. Menke[115], E. Meoni[41a,41b], S. Mergelmeyer[19], S. A. M. Merkt[139], C. Merlassino[20], P. Mermod[54], L. Merola[69a,69b], C. Meroni[68a], O. Meshkov[110,113], J. K. R. Meshreki[151], A. Messina[72a,72b], J. Metcalfe[6], A. S. Mete[171], C. Meyer[65], J. Meyer[160], J-P. Meyer[145], H. Meyer Zu Theenhausen[61a], F. Miano[156], M. Michetti[19], R. P. Middleton[144], L. Mijović[50], G. Mikenberg[180], M. Mikestikova[141], M. Mikuž[91], H. Mildner[149], M. Milesi[104], A. Milic[167], D. A. Millar[92], D. W. Miller[37], A. Milov[180], D. A. Milstead[45a,45b], R. A. Mina[153,p], A. A. Minaenko[123], M. Miñano Moya[174], I. A. Minashvili[159b], A. I. Mincer[124], B. Mindur[83a], M. Mineev[79], Y. Minegishi[163], Y. Ming[181], L. M. Mir[14], A. Mirto[67a,67b], K. P. Mistry[137], T. Mitani[179], J. Mitrevski[114], V. A. Mitsou[174], M. Mittal[60c], O. Miu[167], A. Miucci[20], P. S. Miyagawa[149], A. Mizukami[81], J. U. Mjörnmark[96], T. Mkrtchyan[184], M. Mlynarikova[143], T. Moa[45a,45b], K. Mochizuki[109], P. Mogg[52], S. Mohapatra[39], R. Moles-Valls[24], M. C. Mondragon[106], K. Mönig[46], J. Monk[40], E. Monnier[101], A. Montalbano[152], J. Montejo Berlingen[36], M. Montella[94], F. Monticelli[88], S. Monzani[68a], N. Morange[132], D. Moreno[22], M. Moreno Llácer[36], C. Moreno Martinez[14], P. Morettini[55b], M. Morgenstern[120], S. Morgenstern[48], D. Mori[152], M. Morii[59], M. Morinaga[179], V. Morisbak[134], A. K. Morley[36], G. Mornacchi[36], A. P. Morris[94], L. Morvaj[155], P. Moschovakos[36], B. Moser[120], M. Mosidze[159b], T. Moskalets[145], H. J. Moss[149], J. Moss[31,m], K. Motohashi[165], E. Mountricha[36], E. J. W. Moyse[102], S. Muanza[101], J. Mueller[139], R. S. P. Mueller[114], D. Muenstermann[89], G. A. Mullier[96], J. L. Munoz Martinez[14], F. J. Munoz Sanchez[100], P. Murin[28b], W. J. Murray[144,178], A. Murrone[68a,68b], M. Muškinja[18], C. Mwewa[33a], A. G. Myagkov[123,ao], J. Myers[131], M. Myska[142], B. P. Nachman[18], O. Nackenhorst[47], A.Nag Nag[48], K. Nagai[135], K. Nagano[81], Y. Nagasaka[62], M. Nagel[52], E. Nagy[101], A. M. Nairz[36], Y. Nakahama[117], K. Nakamura[81], T. Nakamura[163], I. Nakano[127], H. Nanjo[133], F. Napolitano[61a], R. F. Naranjo Garcia[46], R. Narayan[42], I. Naryshkin[138], T. Naumann[46], G. Navarro[22], H. A. Neal[105,*], P. Y. Nechaeva[110], F. Nechansky[46], T. J. Neep[21], A. Negri[70a,70b], M. Negrini[23b], C. Nellist[53], M. E. Nelson[135], S. Nemecek[141], P. Nemethy[124], M. Nessi[36,c], M. S. Neubauer[173], M. Neumann[182], P. R. Newman[21], Y. S. Ng[19], Y. W. Y. Ng[171], B. Ngair[35e], H. D. N. Nguyen[101], T. Nguyen Manh[109], E. Nibigira[38], R. B. Nickerson[135], R. Nicolaidou[145], D. S. Nielsen[40], J. Nielsen[146], N. Nikiforou[11], V. Nikolaenko[123,ao], I. Nikolic-Audit[136], K. Nikolopoulos[21], P. Nilsson[29], H. R. Nindhito[54], Y. Ninomiya[81], A. Nisati[72a], N. Nishu[60c], R. Nisius[115], I. Nitsche[47], T. Nitta[179], T. Nobe[163], Y. Noguchi[85], I. Nomidis[136], M. A. Nomura[29], M. Nordberg[36], N. Norjoharuddeen[135], T. Novak[91], O. Novgorodova[48], R. Novotny[142], L. Nozka[130], K. Ntekas[171], E. Nurse[94], F. G. Oakham[34,ax], H. Oberlack[115], J. Ocariz[136], A. Ochi[82], I. Ochoa[39], J. P. Ochoa-Ricoux[147a], K. O'Connor[26], S. Oda[87], S. Odaka[81], S. Oerdek[53], A. Ogrodnik[83a], A. Oh[100],

S. H. Oh[49], C. C. Ohm[154], H. Oide[55a,55b], M. L. Ojeda[167], H. Okawa[169], Y. Okazaki[85], Y. Okumura[163], T. Okuyama[81], A. Olariu[27b], L. F. Oleiro Seabra[140a], S. A. Olivares Pino[147a], D. Oliveira Damazio[29], J. L. Oliver[1], M. J. R. Olsson[171], A. Olszewski[84], J. Olszowska[84], D. C. O'Neil[152], A. Onofre[140a,140e], K. Onogi[117], P. U. E. Onyisi[11], H. Oppen[134], M. J. Oreglia[37], G. E. Orellana[88], Y. Oren[161], D. Orestano[74a,74b], N. Orlando[14], R. S. Orr[167], V. O'Shea[57], R. Ospanov[60a], G. Otero y Garzon[30], H. Otono[87], P. S. Ott[61a], M. Ouchrif[35d], J. Ouellette[29], F. Ould-Saada[134], A. Ouraou[145], Q. Ouyang[15a], M. Owen[57], R. E. Owen[21], V. E. Ozcan[12c], N. Ozturk[8], J. Pacalt[130], H. A. Pacey[32], K. Pachal[49], A. Pacheco Pages[14], C. Padilla Aranda[14], S. Pagan Griso[18], M. Paganini[183], G. Palacino[65], S. Palazzo[50], S. Palestini[36], M. Palka[83b], D. Pallin[38], I. Panagoulias[10], C. E. Pandini[36], J. G. Panduro Vazquez[93], P. Pani[46], G. Panizzo[66a,66c], L. Paolozzi[54], C. Papadatos[109], K. Papageorgiou[9,g], S. Parajuli[43], A. Paramonov[6], D. Paredes Hernandez[63b], S. R. Paredes Saenz[135], B. Parida[166], T. H. Park[167], A. J. Parker[89], M. A. Parker[32], F. Parodi[55a,55b], E. W. P. Parrish[121], J. A. Parsons[39], U. Parzefall[52], L. Pascual Dominguez[136], V. R. Pascuzzi[167], J. M. P. Pasner[146], E. Pasqualucci[72a], S. Passaggio[55b], F. Pastore[93], P. Pasuwan[45a,45b], S. Pataraia[99], J. R. Pater[100], A. Pathak[181], T. Pauly[36], B. Pearson[115], M. Pedersen[134], L. Pedraza Diaz[119], R. Pedro[140a], T. Peiffer[53], S. V. Peleganchuk[122a,122b], O. Penc[141], H. Peng[60a], B. S. Peralva[80a], M. M. Perego[132], A. P. Pereira Peixoto[140a], D. V. Perepelitsa[29], F. Peri[19], L. Perini[68a,68b], H. Pernegger[36], S. Perrella[69a,69b], K. Peters[46], R. F. Y. Peters[100], B. A. Petersen[36], T. C. Petersen[40], E. Petit[101], A. Petridis[1], C. Petridou[162], P. Petroff[132], M. Petrov[135], F. Petrucci[74a,74b], M. Pettee[183], N. E. Pettersson[102], K. Petukhova[143], A. Peyaud[145], R. Pezoa[147b], L. Pezzotti[70a,70b], T. Pham[104], F. H. Phillips[106], P. W. Phillips[144], M. W. Phipps[173], G. Piacquadio[155], E. Pianori[18], A. Picazio[102], R. H. Pickles[100], R. Piegaia[30], D. Pietreanu[27b], J. E. Pilcher[37], A. D. Pilkington[100], M. Pinamonti[73a,73b], J. L. Pinfold[3], M. Pitt[180], L. Pizzimento[73a,73b], M.-A. Pleier[29], V. Pleskot[143], E. Plotnikova[79], P. Podberezko[122a,122b], R. Poettgen[96], R. Poggi[54], L. Poggioli[132], I. Pogrebnyak[106], D. Pohl[24], I. Pokharel[53], G. Polesello[70a], A. Poley[18], A. Policicchio[72a,72b], R. Polifka[143], A. Polini[23b], C. S. Pollard[46], V. Polychronakos[29], D. Ponomarenko[112], L. Pontecorvo[36], S. Popa[27a], G. A. Popeneciu[27d], D. M. Portillo Quintero[58], S. Pospisil[142], K. Potamianos[46], I. N. Potrap[79], C. J. Potter[32], H. Potti[11], T. Poulsen[96], J. Poveda[36], T. D. Powell[149], G. Pownall[46], M. E. Pozo Astigarraga[36], P. Pralavorio[101], S. Prell[78], D. Price[100], M. Primavera[67a], S. Prince[103], M. L. Proffitt[148], N. Proklova[112], K. Prokofiev[63c], F. Prokoshin[79], S. Protopopescu[29], J. Proudfoot[6], M. Przybycien[83a], D. Pudzha[138], A. Puri[173], P. Puzo[132], J. Qian[105], Y. Qin[100], A. Quadt[53], M. Queitsch-Maitland[46], A. Qureshi[1], P. Rados[104], F. Ragusa[68a,68b], G. Rahal[97], J. A. Raine[54], S. Rajagopalan[29], A. Ramirez Morales[92], K. Ran[15a,15d], T. Rashid[132], S. Raspopov[5], D. M. Rauch[46], F. Rauscher[114], S. Rave[99], B. Ravina[149], I. Ravinovich[180], J. H. Rawling[100], M. Raymond[36], A. L. Read[134], N. P. Readioff[58], M. Reale[67a,67b], D. M. Rebuzzi[70a,70b], A. Redelbach[177], G. Redlinger[29], K. Reeves[43], L. Rehnisch[19], J. Reichert[137], D. Reikher[161], A. Reiss[99], A. Rej[151], C. Rembser[36], M. Renda[27b], M. Rescigno[72a], S. Resconi[68a], E. D. Resseguie[137], S. Rettie[175], E. Reynolds[21], O. L. Rezanova[122a,122b], P. Reznicek[143], E. Ricci[75a,75b], R. Richter[115], S. Richter[46], E. Richter-Was[83b], O. Ricken[24], M. Ridel[136], P. Rieck[115], C. J. Riegel[182], O. Rifki[46], M. Rijssenbeek[155], A. Rimoldi[70a,70b], M. Rimoldi[46], L. Rinaldi[23b], G. Ripellino[154], B. Ristić[89], I. Riu[14], J. C. Rivera Vergara[176], F. Rizatdinova[129], E. Rizvi[92], C. Rizzi[36], R. T. Roberts[100], S. H. Robertson[103,ad], M. Robin[46], D. Robinson[32], J. E. M. Robinson[46], C. M. Robles Gajardo[147b], A. Robson[57], E. Rocco[99], C. Roda[71a,71b], S. Rodriguez Bosca[174], A. Rodriguez Perez[14], D. Rodriguez Rodriguez[174], A. M. Rodríguez Vera[168b], S. Roe[36], O. Røhne[134], R. Röhrig[115], C. P. A. Roland[65], J. Roloff[59], A. Romaniouk[112], M. Romano[23a,23b], N. Rompotis[90], M. Ronzani[124], L. Roos[136], S. Rosati[72a], K. Rosbach[52], G. Rosin[102], B. J. Rosser[137], E. Rossi[46], E. Rossi[74a,74b], E. Rossi[69a,69b], L. P. Rossi[55b], L. Rossini[68a,68b], R. Rosten[14], M. Rotaru[27b], J. Rothberg[148], D. Rousseau[132], G. Rovelli[70a,70b], A. Roy[11], D. Roy[33c], A. Rozanov[101], Y. Rozen[160], X. Ruan[33c], F. Rubbo[153], F. Rühr[52], A. Ruiz-Martinez[174], A. Rummler[36], Z. Rurikova[52], N. A. Rusakovich[79], H. L. Russell[103], L. Rustige[38,47], J. P. Rutherfoord[7], E. M. Rüttinger[46,j], Y. F. Ryabov[138], M. Rybar[39], G. Rybkin[132], E. B. Rye[134], A. Ryzhov[123], G. F. Rzehorz[53], P. Sabatini[53], G. Sabato[120], S. Sacerdoti[132], H.F-W. Sadrozinski[146], R. Sadykov[79], F. Safai Tehrani[72a], B. Safarzadeh Samani[156], P. Saha[121], S. Saha[103], M. Sahinsoy[61a], A. Sahu[182], M. Saimpert[46], M. Saito[163], T. Saito[163], H. Sakamoto[163], A. Sakharov[124,an], D. Salamani[54], G. Salamanna[74a,74b], J. E. Salazar Loyola[147b], P. H. Sales De Bruin[172], A. Salnikov[153], J. Salt[174], D. Salvatore[41a,41b], F. Salvatore[156], A. Salvucci[63a,63b,63c], A. Salzburger[36], J. Samarati[36], D. Sammel[52], D. Sampsonidis[162], D. Sampsonidou[162], J. Sánchez[174], A. Sanchez Pineda[66a,66c], H. Sandaker[134], C. O. Sander[46], I. G. Sanderswood[89], M. Sandhoff[182], C. Sandoval[22], D. P. C. Sankey[144], M. Sannino[55a,55b], Y. Sano[117], A. Sansoni[51], C. Santoni[38], H. Santos[140a,140b], S. N. Santpur[18], A. Santra[174], A. Sapronov[79], J. G. Saraiva[140a,140d], O. Sasaki[81], K. Sato[169], E. Sauvan[5], P. Savard[167,ax], N. Savic[115], R. Sawada[163], C. Sawyer[144], L. Sawyer[95,al], C. Sbarra[23b], A. Sbrizzi[23a], T. Scanlon[94], J. Schaarschmidt[148], P. Schacht[115], B. M. Schachtner[114], D. Schaefer[37], L. Schaefer[137], J. Schaeffer[99], S. Schaepe[36], U. Schäfer[99], A. C. Schaffer[132], D. Schaile[114], R. D. Schamberger[155], N. Scharmberg[100], V. A. Schegelsky[138], D. Scheirich[143], F. Schenck[19], M. Schernau[171], C. Schiavi[55a,55b], S. Schier[146], L. K. Schildgen[24], Z. M. Schillaci[26], E. J. Schioppa[36], M. Schioppa[41a,41b], K. E. Schleicher[52], S. Schlenker[36], K. R. Schmidt-Sommerfeld[115],

K. Schmieden[36], C. Schmitt[99], S. Schmitt[46], S. Schmitz[99], J. C. Schmoeckel[46], U. Schnoor[52], L. Schoeffel[145], A. Schoening[61b], P. G. Scholer[52], E. Schopf[135], M. Schott[99], J. F. P. Schouwenberg[119], J. Schovancova[36], S. Schramm[54], F. Schroeder[182], A. Schulte[99], H-C. Schultz-Coulon[61a], M. Schumacher[52], B. A. Schumm[146], Ph. Schune[145], A. Schwartzman[153], T. A. Schwarz[105], Ph. Schwemling[145], R. Schwienhorst[106], A. Sciandra[146], G. Sciolla[26], M. Scodeggio[46], M. Scornajenghi[41a,41b], F. Scuri[71a], F. Scutti[104], L. M. Scyboz[115], C. D. Sebastiani[72a,72b], P. Seema[19], S. C. Seidel[118], A. Seiden[146], T. Seiss[37], J. M. Seixas[80b], G. Sekhniaidze[69a], K. Sekhon[105], S. J. Sekula[42], N. Semprini-Cesari[23a,23b], S. Sen[49], S. Senkin[38], C. Serfon[76], L. Serin[132], L. Serkin[66a,66b], M. Sessa[60a], H. Severini[128], F. Sforza[170], A. Sfyrla[54], E. Shabalina[53], J. D. Shahinian[146], N. W. Shaikh[45a,45b], D. Shaked Renous[180], L. Y. Shan[15a], R. Shang[173], J. T. Shank[25], M. Shapiro[18], A. Sharma[135], A. S. Sharma[1], P. B. Shatalov[111], K. Shaw[156], S. M. Shaw[100], A. Shcherbakova[138], M. Shehade[180], Y. Shen[128], N. Sherafati[34], A. D. Sherman[25], P. Sherwood[94], L. Shi[158,at], S. Shimizu[81], C. O. Shimmin[183], Y. Shimogama[179], M. Shimojima[116], I. P. J. Shipsey[135], S. Shirabe[87], M. Shiyakova[79,aa], J. Shlomi[180], A. Shmeleva[110], M. J. Shochet[37], S. Shojaii[104], D. R. Shope[128], S. Shrestha[126], E. M. Shrif[33c], E. Shulga[180], P. Sicho[141], A. M. Sickles[173], P. E. Sidebo[154], E. Sideras Haddad[33c], O. Sidiropoulou[36], A. Sidoti[23a,23b], F. Siegert[48], Dj. Sijacki[16], M. Silva Jr.[181], M. V. Silva Oliveira[80a], S. B. Silverstein[45a], S. Simion[132], E. Simioni[99], R. Simoniello[99], S. Simsek[12b], P. Sinervo[167], V. Sinetckii[110,113], N. B. Sinev[131], M. Sioli[23a,23b], I. Siral[105], S. Yu. Sivoklokov[113], J. Sjölin[45a,45b], E. Skorda[96], P. Skubic[128], M. Slawinska[84], K. Sliwa[170], R. Slovak[143], V. Smakhtin[180], B. H. Smart[144], J. Smiesko[28a], N. Smirnov[112], S. Yu. Smirnov[112], Y. Smirnov[112], L. N. Smirnova[113,t], O. Smirnova[96], J. W. Smith[53], M. Smizanska[89], K. Smolek[142], A. Smykiewicz[84], A. A. Snesarev[110], H. L. Snoek[120], I. M. Snyder[131], S. Snyder[29], R. Sobie[176,ad], A. Soffer[161], A. Søgaard[50], F. Sohns[53], C. A. Solans Sanchez[36], E. Yu. Soldatov[112], U. Soldevila[174], A. A. Solodkov[123], A. Soloshenko[79], O. V. Solovyanov[123], V. Solovyev[138], P. Sommer[149], H. Son[170], W. Song[144], W. Y. Song[168b], A. Sopczak[142], F. Sopkova[28b], C. L. Sotiropoulou[71a,71b], S. Sottocornola[70a,70b], R. Soualah[66a,66c,f], A. M. Soukharev[122a,122b], D. South[46], S. Spagnolo[67a,67b], M. Spalla[115], M. Spangenberg[178], F. Spanò[93], D. Sperlich[52], T. M. Spieker[61a], R. Spighi[23b], G. Spigo[36], M. Spina[156], D. P. Spiteri[57], M. Spousta[143], A. Stabile[68a,68b], B. L. Stamas[121], R. Stamen[61a], M. Stamenkovic[120], E. Stanecka[84], B. Stanislaus[135], M. M. Stanitzki[46], M. Stankaityte[135], B. Stapf[120], E. A. Starchenko[123], G. H. Stark[146], J. Stark[58], S. H. Stark[40], P. Staroba[141], P. Starovoitov[61a], S. Stärz[103], R. Staszewski[84], G. Stavropoulos[44], M. Stegler[46], P. Steinberg[29], A. L. Steinhebel[131], B. Stelzer[152], H. J. Stelzer[139], O. Stelzer-Chilton[168a], H. Stenzel[56], T. J. Stevenson[156], G. A. Stewart[36], M. C. Stockton[36], G. Stoicea[27b], M. Stolarski[140a], P. Stolte[53], S. Stonjek[115], A. Straessner[48], J. Strandberg[154], S. Strandberg[45a,45b], M. Strauss[128], P. Strizenec[28b], R. Ströhmer[177], D. M. Strom[131], R. Stroynowski[42], A. Strubig[50], S. A. Stucci[29], B. Stugu[17], J. Stupak[128], N. A. Styles[46], D. Su[153], S. Suchek[61a], V. V. Sulin[110], M. J. Sullivan[90], D. M. S. Sultan[54], S. Sultansoy[4c], T. Sumida[85], S. Sun[105], X. Sun[3], K. Suruliz[156], C. J. E. Suster[157], M. R. Sutton[156], S. Suzuki[81], M. Svatos[141], M. Swiatlowski[37], S. P. Swift[2], T. Swirski[177], A. Sydorenko[99], I. Sykora[28a], M. Sykora[143], T. Sykora[143], D. Ta[99], K. Tackmann[46,y], J. Taenzer[161], A. Taffard[171], R. Tafirout[168a], H. Takai[29], R. Takashima[86], K. Takeda[82], T. Takeshita[150], E. P. Takeva[50], Y. Takubo[81], M. Talby[101], A. A. Talyshev[122a,122b], N. M. Tamir[161], J. Tanaka[163], M. Tanaka[165], R. Tanaka[132], S. Tapia Araya[173], S. Tapprogge[99], A. Tarek Abouelfadl Mohamed[136], S. Tarem[160], G. Tarna[27b,b], G. F. Tartarelli[68a], P. Tas[143], M. Tasevsky[141], T. Tashiro[85], E. Tassi[41a,41b], A. Tavares Delgado[140a,140b], Y. Tayalati[35e], A. J. Taylor[50], G. N. Taylor[104], W. Taylor[168b], A. S. Tee[89], R. Teixeira De Lima[153], P. Teixeira-Dias[93], H. Ten Kate[36], J. J. Teoh[120], S. Terada[81], K. Terashi[163], J. Terron[98], S. Terzo[14], M. Testa[51], R. J. Teuscher[167,ad], S. J. Thais[183], T. Theveneaux-Pelzer[46], F. Thiele[40], D. W. Thomas[93], J. O. Thomas[42], J. P. Thomas[21], A. S. Thompson[57], P. D. Thompson[21], L. A. Thomsen[183], E. Thomson[137], E. J. Thorpe[92], Y. Tian[39], R. E. Ticse Torres[53], V. O. Tikhomirov[110,ap], Yu. A. Tikhonov[122a,122b], S. Timoshenko[112], P. Tipton[183], S. Tisserant[101], K. Todome[23a,23b], S. Todorova-Nova[5], S. Todt[48], J. Tojo[87], S. Tokár[28a], K. Tokushuku[81], E. Tolley[126], K. G. Tomiwa[33c], M. Tomoto[117], L. Tompkins[153,p], K. Toms[118], B. Tong[59], P. Tornambe[102], E. Torrence[131], H. Torres[48], E. Torró Pastor[148], C. Tosciri[135], J. Toth[101,ab], D. R. Tovey[149], A. Traeet[17], C. J. Treado[124], T. Trefzger[177], F. Tresoldi[156], A. Tricoli[29], I. M. Trigger[168a], S. Trincaz-Duvoid[136], W. Trischuk[167], B. Trocmé[58], A. Trofymov[132], C. Troncon[68a], M. Trovatelli[176], F. Trovato[156], L. Truong[33b], M. Trzebinski[84], A. Trzupek[84], F. Tsai[46], J. C.-L. Tseng[135], P. V. Tsiareshka[107,aj], A. Tsirigotis[162], N. Tsirintanis[9], V. Tsiskaridze[155], E. G. Tskhadadze[159a], M. Tsopoulou[162], I. I. Tsukerman[111], V. Tsulaia[18], S. Tsuno[81], D. Tsybychev[155], Y. Tu[63b], A. Tudorache[27b], V. Tudorache[27b], T. T. Tulbure[27a], A. N. Tuna[59], S. Turchikhin[79], D. Turgeman[180], I. Turk Cakir[4b,u], R. J. Turner[21], R. T. Turra[68a], P. M. Tuts[39], S Tzamarias[162], E. Tzovara[99], G. Ucchielli[47], K. Uchida[163], I. Ueda[81], M. Ughetto[45a,45b], F. Ukegawa[169], G. Unal[36], A. Undrus[29], G. Unel[171], F. C. Ungaro[104], Y. Unno[81], K. Uno[163], J. Urban[28b], P. Urquijo[104], G. Usai[8], J. Usui[81], Z. Uysal[12d], L. Vacavant[101], V. Vacek[142], B. Vachon[103], K. O. H. Vadla[134], A. Vaidya[94], C. Valderanis[114], E. Valdes Santurio[45a,45b], M. Valente[54], S. Valentinetti[23a,23b], A. Valero[174], L. Valéry[46], R. A. Vallance[21], A. Vallier[36], J. A. Valls Ferrer[174], T. R. Van Daalen[14], P. Van Gemmeren[6], I. Van Vulpen[120], M. Vanadia[73a,73b], W. Vandelli[36], A. Vaniachine[166], D. Vannicola[72a,72b], R. Vari[72a], E. W. Varnes[7],

C. Varni[55a,55b], T. Varol[42], D. Varouchas[132], K. E. Varvell[157], M. E. Vasile[27b], G. A. Vasquez[176], J. G. Vasquez[183], F. Vazeille[38], D. Vazquez Furelos[14], T. Vazquez Schroeder[36], J. Veatch[53], V. Vecchio[74a,74b], M. J. Veen[120], L. M. Veloce[167], F. Veloso[140a,140c], S. Veneziano[72a], A. Ventura[67a,67b], N. Venturi[36], A. Verbytskyi[115], V. Vercesi[70a], M. Verducci[71a,71b], C. M. Vergel Infante[78], C. Vergis[24], W. Verkerke[120], A. T. Vermeulen[120], J. C. Vermeulen[120], M. C. Vetterli[152,ax], N. Viaux Maira[147b], M. Vicente Barreto Pinto[54], T. Vickey[149], O. E. Vickey Boeriu[149], G. H. A. Viehhauser[135], L. Vigani[61b], M. Villa[23a,23b], M. Villaplana Perez[68a,68b], E. Vilucchi[51], M. G. Vincter[34], V. B. Vinogradov[79], G. S. Virdee[21], A. Vishwakarma[46], C. Vittori[23a,23b], I. Vivarelli[156], M. Vogel[182], P. Vokac[142], S. E. von Buddenbrock[33c], E. Von Toerne[24], V. Vorobel[143], K. Vorobev[112], M. Vos[174], J. H. Vossebeld[90], M. Vozak[100], N. Vranjes[16], M. Vranjes Milosavljevic[16], V. Vrba[142], M. Vreeswijk[120], T. Šfiligoj[91], R. Vuillermet[36], I. Vukotic[37], T. Ženiš[28a], L. Živković[16], P. Wagner[24], W. Wagner[182], J. Wagner-Kuhr[114], S. Wahdan[182], H. Wahlberg[88], K. Wakamiya[82], V. M. Walbrecht[115], J. Walder[89], R. Walker[114], S. D. Walker[93], W. Walkowiak[151], V. Wallangen[45a,45b], A. M. Wang[59], C. Wang[60c], C. Wang[60b], F. Wang[181], H. Wang[18], H. Wang[3], J. Wang[157], J. Wang[61b], P. Wang[42], Q. Wang[128], R.-J. Wang[99], R. Wang[60a], R. Wang[6], S. M. Wang[158], W. T. Wang[60a], W. Wang[15c,ae], W. X. Wang[60a,ae], Y. Wang[60a,am], Z. Wang[60c], C. Wanotayaroj[46], A. Warburton[103], C. P. Ward[32], D. R. Wardrope[94], N. Warrack[57], A. Washbrook[50], A. T. Watson[21], M. F. Watson[21], G. Watts[148], B. M. Waugh[94], A. F. Webb[11], S. Webb[99], C. Weber[183], M. S. Weber[20], S. A. Weber[34], S. M. Weber[61a], A. R. Weidberg[135], J. Weingarten[47], M. Weirich[99], C. Weiser[52], P. S. Wells[36], T. Wenaus[29], T. Wengler[36], S. Wenig[36], N. Wermes[24], M. D. Werner[78], M. Wessels[61a], T. D. Weston[20], K. Whalen[131], N. L. Whallon[148], A. M. Wharton[89], A. S. White[105], A. White[8], M. J. White[1], D. Whiteson[171], B. W. Whitmore[89], W. Wiedenmann[181], M. Wielers[144], N. Wieseotte[99], C. Wiglesworth[40], L. A. M. Wiik-Fuchs[52], F. Wilk[100], H. G. Wilkens[36], L. J. Wilkins[93], H. H. Williams[137], S. Williams[32], C. Willis[106], S. Willocq[102], J. A. Wilson[21], I. Wingerter-Seez[5], E. Winkels[156], F. Winklmeier[131], O. J. Winston[156], B. T. Winter[52], M. Wittgen[153], M. Wobisch[95], A. Wolf[99], T. M. H. Wolf[120], R. Wolff[101], R. W. Wölker[135], J. Wollrath[52], M. W. Wolter[84], H. Wolters[140a,140c], V. W. S. Wong[175], N. L. Woods[146], S. D. Worm[21], B. K. Wosiek[84], K. W. Woźniak[84], K. Wraight[57], S. L. Wu[181], X. Wu[54], Y. Wu[60a], T. R. Wyatt[100], B. M. Wynne[50], S. Xella[40], Z. Xi[105], L. Xia[178], X. Xiao[105], D. Xu[15a], H. Xu[60a,b], L. Xu[29], T. Xu[145], W. Xu[105], Z. Xu[60b], Z. Xu[153], B. Yabsley[157], S. Yacoob[33a], K. Yajima[133], D. P. Yallup[94], D. Yamaguchi[165], Y. Yamaguchi[165], A. Yamamoto[81], F. Yamane[82], M. Yamatani[163], T. Yamazaki[163], Y. Yamazaki[82], Z. Yan[25], H. J. Yang[60c,60d], H. T. Yang[18], S. Yang[77], X. Yang[58,60b], Y. Yang[163], W-M. Yao[18], Y. C. Yap[46], Y. Yasu[81], E. Yatsenko[60c,60d], J. Ye[42], S. Ye[29], I. Yeletskikh[79], M. R. Yexley[89], E. Yigitbasi[25], K. Yorita[179], K. Yoshihara[137], C. J. S. Young[36], C. Young[153], J. Yu[78], R. Yuan[60b,h], X. Yue[61a], S. P. Y. Yuen[24], B. Zabinski[84], G. Zacharis[10], E. Zaffaroni[54], J. Zahreddine[136], A. M. Zaitsev[123,ao], T. Zakareishvili[159b], N. Zakharchuk[34], S. Zambito[59], D. Zanzi[36], D. R. Zaripovas[57], S. V. Zeißner[47], C. Zeitnitz[182], G. Zemaityte[135], J. C. Zeng[173], O. Zenin[123], D. Zerwas[132], M. Zgubič[135], D. F. Zhang[15b], F. Zhang[181], G. Zhang[15b], H. Zhang[15c], J. Zhang[6], L. Zhang[15c], L. Zhang[60a], M. Zhang[173], R. Zhang[24], X. Zhang[60b], Y. Zhang[15a,15d], Z. Zhang[63a], Z. Zhang[132], P. Zhao[49], Y. Zhao[60b], Z. Zhao[60a], A. Zhemchugov[79], Z. Zheng[105], D. Zhong[173], B. Zhou[105], C. Zhou[181], M. S. Zhou[15a,15d], M. Zhou[155], N. Zhou[60c], Y. Zhou[7], C. G. Zhu[60b], H. L. Zhu[60a], H. Zhu[15a], J. Zhu[105], Y. Zhu[60a], X. Zhuang[15a], K. Zhukov[110], V. Zhulanov[122a,122b], D. Zieminska[65], N. I. Zimine[79], S. Zimmermann[52], Z. Zinonos[115], M. Ziolkowski[151], G. Zobernig[181], A. Zoccoli[23a,23b], K. Zoch[53], T. G. Zorbas[149], R. Zou[37], L. Zwalinski[36]

[1] Department of Physics, University of Adelaide, Adelaide, Australia
[2] Physics Department, SUNY Albany, Albany, NY, USA
[3] Department of Physics, University of Alberta, Edmonton, AB, Canada
[4] [(a)]Department of Physics, Ankara University, Ankara, Turkey; [(b)]Istanbul Aydin University, Istanbul, Turkey; [(c)]Division of Physics, TOBB University of Economics and Technology, Ankara, Turkey
[5] LAPP, Université Grenoble Alpes, Université Savoie Mont Blanc, CNRS/IN2P3, Annecy, France
[6] High Energy Physics Division, Argonne National Laboratory, Argonne, IL, USA
[7] Department of Physics, University of Arizona, Tucson, AZ, USA
[8] Department of Physics, University of Texas at Arlington, Arlington, TX, USA
[9] Physics Department, National and Kapodistrian University of Athens, Athens, Greece
[10] Physics Department, National Technical University of Athens, Zografou, Greece
[11] Department of Physics, University of Texas at Austin, Austin, TX, USA
[12] [(a)]Bahcesehir University, Faculty of Engineering and Natural Sciences, Istanbul, Turkey; [(b)]Istanbul Bilgi University, Faculty of Engineering and Natural Sciences, Istanbul, Turkey; [(c)]Department of Physics, Bogazici University, Istanbul, Turkey; [(d)]Department of Physics Engineering, Gaziantep University, Gaziantep, Turkey
[13] Institute of Physics, Azerbaijan Academy of Sciences, Baku, Azerbaijan
[14] Institut de Física d'Altes Energies (IFAE), Barcelona Institute of Science and Technology, Barcelona, Spain

[15] [(a)]Institute of High Energy Physics, Chinese Academy of Sciences, Beijing, China; [(b)]Physics Department, Tsinghua University, Beijing, China; [(c)]Department of Physics, Nanjing University, Nanjing, China; [(d)]University of Chinese Academy of Science (UCAS), Beijing, China
[16] Institute of Physics, University of Belgrade, Belgrade, Serbia
[17] Department for Physics and Technology, University of Bergen, Bergen, Norway
[18] Physics Division, Lawrence Berkeley National Laboratory and University of California, Berkeley, CA, USA
[19] Institut für Physik, Humboldt Universität zu Berlin, Berlin, Germany
[20] Albert Einstein Center for Fundamental Physics and Laboratory for High Energy Physics, University of Bern, Bern, Switzerland
[21] School of Physics and Astronomy, University of Birmingham, Birmingham, UK
[22] Facultad de Ciencias y Centro de Investigaciónes, Universidad Antonio Nariño, Bogota, Colombia
[23] [(a)]Dipartimento di Fisica, INFN Bologna and Universita' di Bologna, Bologna, Italy; [(b)]INFN Sezione di Bologna, Bologna, Italy
[24] Physikalisches Institut, Universität Bonn, Bonn, Germany
[25] Department of Physics, Boston University, Boston, MA, USA
[26] Department of Physics, Brandeis University, Waltham, MA, USA
[27] [(a)]Transilvania University of Brasov, Brasov, Romania; [(b)]Horia Hulubei National Institute of Physics and Nuclear Engineering, Bucharest, Romania; [(c)]Department of Physics, Alexandru Ioan Cuza University of Iasi, Iasi, Romania; [(d)]Physics Department, National Institute for Research and Development of Isotopic and Molecular Technologies, Cluj-Napoca, Romania; [(e)]University Politehnica Bucharest, Bucharest, Romania; [(f)]West University in Timisoara, Timisoara, Romania
[28] [(a)]Faculty of Mathematics, Physics and Informatics, Comenius University, Bratislava, Slovak Republic; [(b)]Department of Subnuclear Physics, Institute of Experimental Physics of the Slovak Academy of Sciences, Kosice, Slovak Republic
[29] Physics Department, Brookhaven National Laboratory, Upton, NY, USA
[30] Departamento de Física, Universidad de Buenos Aires, Buenos Aires, Argentina
[31] California State University, Long Beach, CA, USA
[32] Cavendish Laboratory, University of Cambridge, Cambridge, UK
[33] [(a)]Department of Physics, University of Cape Town, Cape Town, South Africa; [(b)]Department of Mechanical Engineering Science, University of Johannesburg, Johannesburg, South Africa; [(c)]School of Physics, University of the Witwatersrand, Johannesburg, South Africa
[34] Department of Physics, Carleton University, Ottawa, ON, Canada
[35] [(a)]Faculté des Sciences Ain Chock, Réseau Universitaire de Physique des Hautes Energies-Université Hassan II, Casablanca, Morocco; [(b)]Faculté des Sciences, Université Ibn-Tofail, Kenitra, Morocco; [(c)]Faculté des Sciences Semlalia, Université Cadi Ayyad, LPHEA-Marrakech, Marrakesh, Morocco; [(d)]Faculté des Sciences, Université Mohamed Premier and LPTPM, Oujda, Morocco; [(e)]Faculté des sciences, Université Mohammed V, Rabat, Morocco
[36] CERN, Geneva, Switzerland
[37] Enrico Fermi Institute, University of Chicago, Chicago, IL, USA
[38] LPC, Université Clermont Auvergne, CNRS/IN2P3, Clermont-Ferrand, France
[39] Nevis Laboratory, Columbia University, Irvington, NY, USA
[40] Niels Bohr Institute, University of Copenhagen, Copenhagen, Denmark
[41] [(a)]Dipartimento di Fisica, Università della Calabria, Rende, Italy; [(b)]INFN Gruppo Collegato di Cosenza, Laboratori Nazionali di Frascati, Frascati, Italy
[42] Physics Department, Southern Methodist University, Dallas, TX, USA
[43] Physics Department, University of Texas at Dallas, Richardson, TX, USA
[44] National Centre for Scientific Research "Demokritos", Agia Paraskevi, Greece
[45] [(a)]Department of Physics, Stockholm University, Stockholm, Sweden; [(b)]Oskar Klein Centre, Stockholm, Sweden
[46] Deutsches Elektronen-Synchrotron DESY, Hamburg and Zeuthen, Germany
[47] Lehrstuhl für Experimentelle Physik IV, Technische Universität Dortmund, Dortmund, Germany
[48] Institut für Kern- und Teilchenphysik, Technische Universität Dresden, Dresden, Germany
[49] Department of Physics, Duke University, Durham, NC, USA
[50] SUPA-School of Physics and Astronomy, University of Edinburgh, Edinburgh, UK
[51] INFN e Laboratori Nazionali di Frascati, Frascati, Italy
[52] Physikalisches Institut, Albert-Ludwigs-Universität Freiburg, Freiburg, Germany

[53] II. Physikalisches Institut, Georg-August-Universität Göttingen, Göttingen, Germany
[54] Département de Physique Nucléaire et Corpusculaire, Université de Genève, Geneva, Switzerland
[55] [(a)]Dipartimento di Fisica, Università di Genova, Genoa, Italy; [(b)]INFN Sezione di Genova, Genoa, Italy
[56] II. Physikalisches Institut, Justus-Liebig-Universität Giessen, Giessen, Germany
[57] SUPA-School of Physics and Astronomy, University of Glasgow, Glasgow, UK
[58] LPSC, Université Grenoble Alpes, CNRS/IN2P3, Grenoble INP, Grenoble, France
[59] Laboratory for Particle Physics and Cosmology, Harvard University, Cambridge, MA, USA
[60] [(a)]Department of Modern Physics and State Key Laboratory of Particle Detection and Electronics, University of Science and Technology of China, Hefei, China; [(b)]Institute of Frontier and Interdisciplinary Science and Key Laboratory of Particle Physics and Particle Irradiation (MOE), Shandong University, Qingdao, China; [(c)]School of Physics and Astronomy, Shanghai Jiao Tong University, KLPPAC-MoE, SKLPPC, Shanghai, China; [(d)]Tsung-Dao Lee Institute, Shanghai, China
[61] [(a)]Kirchhoff-Institut für Physik, Ruprecht-Karls-Universität Heidelberg, Heidelberg, Germany; [(b)]Physikalisches Institut, Ruprecht-Karls-Universität Heidelberg, Heidelberg, Germany
[62] Faculty of Applied Information Science, Hiroshima Institute of Technology, Hiroshima, Japan
[63] [(a)]Department of Physics, Chinese University of Hong Kong, Shatin, N.T., Hong Kong, China; [(b)]Department of Physics, University of Hong Kong, Hong Kong, China; [(c)]Department of Physics and Institute for Advanced Study, Hong Kong University of Science and Technology, Clear Water Bay, Kowloon, Hong Kong, China
[64] Department of Physics, National Tsing Hua University, Hsinchu, Taiwan
[65] Department of Physics, Indiana University, Bloomington, IN, USA
[66] [(a)]INFN Gruppo Collegato di Udine, Sezione di Trieste, Udine, Italy; [(b)]ICTP, Trieste, Italy; [(c)]Dipartimento Politecnico di Ingegneria e Architettura, Università di Udine, Udine, Italy
[67] [(a)]INFN Sezione di Lecce, Lecce, Italy; [(b)]Dipartimento di Matematica e Fisica, Università del Salento, Lecce, Italy
[68] [(a)]INFN Sezione di Milano, Milan, Italy; [(b)]Dipartimento di Fisica, Università di Milano, Milan, Italy
[69] [(a)]INFN Sezione di Napoli, Naples, Italy; [(b)]Dipartimento di Fisica, Università di Napoli, Naples, Italy
[70] [(a)]INFN Sezione di Pavia, Pavia, Italy; [(b)]Dipartimento di Fisica, Università di Pavia, Pavia, Italy
[71] [(a)]INFN Sezione di Pisa, Pisa, Italy; [(b)]Dipartimento di Fisica E. Fermi, Università di Pisa, Pisa, Italy
[72] [(a)]INFN Sezione di Roma, Rome, Italy; [(b)]Dipartimento di Fisica, Sapienza Università di Roma, Rome, Italy
[73] [(a)]INFN Sezione di Roma Tor Vergata, Rome, Italy; [(b)]Dipartimento di Fisica, Università di Roma Tor Vergata, Rome, Italy
[74] [(a)]INFN Sezione di Roma Tre, Rome, Italy; [(b)]Dipartimento di Matematica e Fisica, Università Roma Tre, Rome, Italy
[75] [(a)]INFN-TIFPA, Povo, Italy; [(b)]Università degli Studi di Trento, Trento, Italy
[76] Institut für Astro- und Teilchenphysik, Leopold-Franzens-Universität, Innsbruck, Austria
[77] University of Iowa, Iowa City, IA, USA
[78] Department of Physics and Astronomy, Iowa State University, Ames, IA, USA
[79] Joint Institute for Nuclear Research, Dubna, Russia
[80] [(a)]Departamento de Engenharia Elétrica, Universidade Federal de Juiz de Fora (UFJF), Juiz de Fora, Brazil; [(b)]Universidade Federal do Rio De Janeiro COPPE/EE/IF, Rio de Janeiro, Brazil; [(c)]Universidade Federal de São João del Rei (UFSJ), São João del Rei, Brazil; [(d)]Instituto de Física, Universidade de São Paulo, São Paulo, Brazil
[81] KEK, High Energy Accelerator Research Organization, Tsukuba, Japan
[82] Graduate School of Science, Kobe University, Kobe, Japan
[83] [(a)]AGH University of Science and Technology, Faculty of Physics and Applied Computer Science, Kraków, Poland; [(b)]Marian Smoluchowski Institute of Physics, Jagiellonian University, Kraków, Poland
[84] Institute of Nuclear Physics Polish Academy of Sciences, Kraków, Poland
[85] Faculty of Science, Kyoto University, Kyoto, Japan
[86] Kyoto University of Education, Kyoto, Japan
[87] Research Center for Advanced Particle Physics and Department of Physics, Kyushu University, Fukuoka, Japan
[88] Instituto de Física La Plata, Universidad Nacional de La Plata and CONICET, La Plata, Argentina
[89] Physics Department, Lancaster University, Lancaster, UK
[90] Oliver Lodge Laboratory, University of Liverpool, Liverpool, UK
[91] Department of Experimental Particle Physics, Jožef Stefan Institute and Department of Physics, University of Ljubljana, Ljubljana, Slovenia
[92] School of Physics and Astronomy, Queen Mary University of London, London, UK

[93] Department of Physics, Royal Holloway University of London, Egham, UK
[94] Department of Physics and Astronomy, University College London, London, UK
[95] Louisiana Tech University, Ruston, LA, USA
[96] Fysiska institutionen, Lunds universitet, Lund, Sweden
[97] Centre de Calcul de l'Institut National de Physique Nucléaire et de Physique des Particules (IN2P3), Villeurbanne, France
[98] Departamento de Física Teorica C-15 and CIAFF, Universidad Autónoma de Madrid, Madrid, Spain
[99] Institut für Physik, Universität Mainz, Mainz, Germany
[100] School of Physics and Astronomy, University of Manchester, Manchester, UK
[101] CPPM, Aix-Marseille Université, CNRS/IN2P3, Marseille, France
[102] Department of Physics, University of Massachusetts, Amherst, MA, USA
[103] Department of Physics, McGill University, Montreal, QC, Canada
[104] School of Physics, University of Melbourne, Melbourne, VIC, Australia
[105] Department of Physics, University of Michigan, Ann Arbor, MI, USA
[106] Department of Physics and Astronomy, Michigan State University, East Lansing, MI, USA
[107] B.I. Stepanov Institute of Physics, National Academy of Sciences of Belarus, Minsk, Belarus
[108] Research Institute for Nuclear Problems of Byelorussian State University, Minsk, Belarus
[109] Group of Particle Physics, University of Montreal, Montreal, QC, Canada
[110] P.N. Lebedev Physical Institute of the Russian Academy of Sciences, Moscow, Russia
[111] Institute for Theoretical and Experimental Physics of the National Research Centre Kurchatov Institute, Moscow, Russia
[112] National Research Nuclear University MEPhI, Moscow, Russia
[113] D.V. Skobeltsyn Institute of Nuclear Physics, M.V. Lomonosov Moscow State University, Moscow, Russia
[114] Fakultät für Physik, Ludwig-Maximilians-Universität München, Munich, Germany
[115] Max-Planck-Institut für Physik (Werner-Heisenberg-Institut), Munich, Germany
[116] Nagasaki Institute of Applied Science, Nagasaki, Japan
[117] Graduate School of Science and Kobayashi-Maskawa Institute, Nagoya University, Nagoya, Japan
[118] Department of Physics and Astronomy, University of New Mexico, Albuquerque, NM, USA
[119] Institute for Mathematics, Astrophysics and Particle Physics, Radboud University Nijmegen/Nikhef, Nijmegen, The Netherlands
[120] Nikhef National Institute for Subatomic Physics and University of Amsterdam, Amsterdam, The Netherlands
[121] Department of Physics, Northern Illinois University, DeKalb, IL, USA
[122] [(a)]Budker Institute of Nuclear Physics and NSU, SB RAS, Novosibirsk, Russia; [(b)]Novosibirsk State University Novosibirsk, Novosibirsk, Russia
[123] Institute for High Energy Physics of the National Research Centre Kurchatov Institute, Protvino, Russia
[124] Department of Physics, New York University, New York, NY, USA
[125] Ochanomizu University, Otsuka, Bunkyo-ku, Tokyo, Japan
[126] Ohio State University, Columbus, OH, USA
[127] Faculty of Science, Okayama University, Okayama, Japan
[128] Homer L. Dodge Department of Physics and Astronomy, University of Oklahoma, Norman, OK, USA
[129] Department of Physics, Oklahoma State University, Stillwater, OK, USA
[130] Palacký University, RCPTM, Joint Laboratory of Optics, Olomouc, Czech Republic
[131] Center for High Energy Physics, University of Oregon, Eugene, OR, USA
[132] LAL, Université Paris-Sud, CNRS/IN2P3, Université Paris-Saclay, Orsay, France
[133] Graduate School of Science, Osaka University, Osaka, Japan
[134] Department of Physics, University of Oslo, Oslo, Norway
[135] Department of Physics, Oxford University, Oxford, UK
[136] LPNHE, Sorbonne Université, Paris Diderot Sorbonne Paris Cité, CNRS/IN2P3, Paris, France
[137] Department of Physics, University of Pennsylvania, Philadelphia, PA, USA
[138] Konstantinov Nuclear Physics Institute of National Research Centre "Kurchatov Institute", PNPI, St. Petersburg, Russia
[139] Department of Physics and Astronomy, University of Pittsburgh, Pittsburgh, PA, USA
[140] [(a)]Laboratório de Instrumentação e Física Experimental de Partículas-LIP, Lisbon, Portugal; [(b)]Departamento de Física, Faculdade de Ciências, Universidade de Lisboa, Lisbon, Portugal; [(c)]Departamento de Física, Universidade de Coimbra, Coimbra, Portugal; [(d)]Centro de Física Nuclear da Universidade de Lisboa, Lisbon, Portugal; [(e)]Departamento de Física,

Universidade do Minho, Braga, Portugal; [f]Universidad de Granada, Granada, Spain; [g]Dep Física and CEFITEC of Faculdade de Ciências e Tecnologia, Universidade Nova de Lisboa, Caparica, Portugal
[141] Institute of Physics of the Czech Academy of Sciences, Prague, Czech Republic
[142] Czech Technical University in Prague, Prague, Czech Republic
[143] Charles University, Faculty of Mathematics and Physics, Prague, Czech Republic
[144] Particle Physics Department, Rutherford Appleton Laboratory, Didcot, UK
[145] IRFU, CEA, Université Paris-Saclay, Gif-sur-Yvette, France
[146] Santa Cruz Institute for Particle Physics, University of California Santa Cruz, Santa Cruz, CA, USA
[147] [a]Departamento de Física, Pontificia Universidad Católica de Chile, Santiago, Chile; [b]Departamento de Física, Universidad Técnica Federico Santa María, Valparaiso, Chile
[148] Department of Physics, University of Washington, Seattle, WA, USA
[149] Department of Physics and Astronomy, University of Sheffield, Sheffield, UK
[150] Department of Physics, Shinshu University, Nagano, Japan
[151] Department Physik, Universität Siegen, Siegen, Germany
[152] Department of Physics, Simon Fraser University, Burnaby, BC, Canada
[153] SLAC National Accelerator Laboratory, Stanford, CA, USA
[154] Physics Department, Royal Institute of Technology, Stockholm, Sweden
[155] Departments of Physics and Astronomy, Stony Brook University, Stony Brook, NY, USA
[156] Department of Physics and Astronomy, University of Sussex, Brighton, UK
[157] School of Physics, University of Sydney, Sydney, Australia
[158] Institute of Physics, Academia Sinica, Taipei, Taiwan
[159] [a]E. Andronikashvili Institute of Physics, Iv. Javakhishvili Tbilisi State University, Tbilisi, Georgia; [b]High Energy Physics Institute, Tbilisi State University, Tbilisi, Georgia
[160] Department of Physics, Technion, Israel Institute of Technology, Haifa, Israel
[161] Raymond and Beverly Sackler School of Physics and Astronomy, Tel Aviv University, Tel Aviv, Israel
[162] Department of Physics, Aristotle University of Thessaloniki, Thessaloniki, Greece
[163] International Center for Elementary Particle Physics and Department of Physics, University of Tokyo, Tokyo, Japan
[164] Graduate School of Science and Technology, Tokyo Metropolitan University, Tokyo, Japan
[165] Department of Physics, Tokyo Institute of Technology, Tokyo, Japan
[166] Tomsk State University, Tomsk, Russia
[167] Department of Physics, University of Toronto, Toronto, ON, Canada
[168] [a]TRIUMF, Vancouver, BC, Canada; [b]Department of Physics and Astronomy, York University, Toronto, ON, Canada
[169] Division of Physics and Tomonaga Center for the History of the Universe, Faculty of Pure and Applied Sciences, University of Tsukuba, Tsukuba, Japan
[170] Department of Physics and Astronomy, Tufts University, Medford, MA, USA
[171] Department of Physics and Astronomy, University of California Irvine, Irvine, CA, USA
[172] Department of Physics and Astronomy, University of Uppsala, Uppsala, Sweden
[173] Department of Physics, University of Illinois, Urbana, IL, USA
[174] Instituto de Física Corpuscular (IFIC), Centro Mixto Universidad de Valencia-CSIC, Valencia, Spain
[175] Department of Physics, University of British Columbia, Vancouver, BC, Canada
[176] Department of Physics and Astronomy, University of Victoria, Victoria, BC, Canada
[177] Fakultät für Physik und Astronomie, Julius-Maximilians-Universität Würzburg, Würzburg, Germany
[178] Department of Physics, University of Warwick, Coventry, UK
[179] Waseda University, Tokyo, Japan
[180] Department of Particle Physics, Weizmann Institute of Science, Rehovot, Israel
[181] Department of Physics, University of Wisconsin, Madison, WI, USA
[182] Fakultät für Mathematik und Naturwissenschaften, Fachgruppe Physik, Bergische Universität Wuppertal, Wuppertal, Germany
[183] Department of Physics, Yale University, New Haven, CT, USA
[184] Yerevan Physics Institute, Yerevan, Armenia

[a] Also at CERN, Geneva, Switzerland
[b] Also at CPPM, Aix-Marseille Université, CNRS/IN2P3, Marseille, France

[c] Also at Département de Physique Nucléaire et Corpusculaire, Université de Genève, Geneva, Switzerland
[d] Also at Departament de Fisica de la Universitat Autonoma de Barcelona, Barcelona, Spain
[e] Also at Departamento de Física, Instituto Superior Técnico, Universidade de Lisboa, Lisbon, Portugal
[f] Also at Department of Applied Physics and Astronomy, University of Sharjah, Sharjah, United Arab Emirates
[g] Also at Department of Financial and Management Engineering, University of the Aegean, Chios, Greece
[h] Also at Department of Physics and Astronomy, Michigan State University, East Lansing MI, USA
[i] Also at Department of Physics and Astronomy, University of Louisville, Louisville, KY, USA
[j] Also at Department of Physics and Astronomy, University of Sheffield, Sheffield, UK
[k] Also at Department of Physics, California State University, East Bay, USA
[l] Also at Department of Physics, California State University, Fresno, USA
[m] Also at Department of Physics, California State University, Sacramento, USA
[n] Also at Department of Physics, King's College London, London, UK
[o] Also at Department of Physics, St. Petersburg State Polytechnical University, St. Petersburg, Russia
[p] Also at Department of Physics, Stanford University, Stanford CA, USA
[q] Also at Department of Physics, University of Adelaide, Adelaide, Australia
[r] Also at Department of Physics, University of Fribourg, Fribourg, Switzerland
[s] Also at Department of Physics, University of Michigan, Ann Arbor MI, USA
[t] Also at Faculty of Physics, M.V. Lomonosov Moscow State University, Moscow, Russia
[u] Also at Giresun University, Faculty of Engineering, Giresun, Turkey
[v] Also at Graduate School of Science, Osaka University, Osaka, Japan
[w] Also at Hellenic Open University, Patras, Greece
[x] Also at Institucio Catalana de Recerca i Estudis Avancats, ICREA, Barcelona, Spain
[y] Also at Institut für Experimentalphysik, Universität Hamburg, Hamburg, Germany
[z] Also at Institute for Mathematics, Astrophysics and Particle Physics, Radboud University Nijmegen/Nikhef, Nijmegen, Netherlands
[aa] Also at Institute for Nuclear Research and Nuclear Energy (INRNE) of the Bulgarian Academy of Sciences, Sofia, Bulgaria
[ab] Also at Institute for Particle and Nuclear Physics, Wigner Research Centre for Physics, Budapest, Hungary
[ac] Also at Institute of High Energy Physics, Chinese Academy of Sciences, Beijing, China
[ad] Also at Institute of Particle Physics (IPP), Canada
[ae] Also at Institute of Physics, Academia Sinica, Taipei, Taiwan
[af] Also at Institute of Physics, Azerbaijan Academy of Sciences, Baku, Azerbaijan
[ag] Also at Institute of Theoretical Physics, Ilia State University, Tbilisi, Georgia
[ah] Also at Instituto de Fisica Teorica, IFT-UAM/CSIC, Madrid, Spain
[ai] Also at Istanbul University, Dept. of Physics, Istanbul, Turkey
[aj] Also at Joint Institute for Nuclear Research, Dubna, Russia
[ak] Also at LAL, Université Paris-Sud, CNRS/IN2P3, Université Paris-Saclay, Orsay, France
[al] Also at Louisiana Tech University, Ruston LA, USA
[am] Also at LPNHE, Sorbonne Université, Paris Diderot Sorbonne Paris Cité, CNRS/IN2P3, Paris, France
[an] Also at Manhattan College, New York NY, USA
[ao] Also at Moscow Institute of Physics and Technology State University, Dolgoprudny, Russia
[ap] Also at National Research Nuclear University MEPhI, Moscow, Russia
[aq] Also at Physics Department, An-Najah National University, Nablus, Palestine
[ar] Also at Physics Dept, University of South Africa, Pretoria, South Africa
[as] Also at Physikalisches Institut, Albert-Ludwigs-Universität Freiburg, Freiburg, Germany
[at] Also at School of Physics, Sun Yat-sen University, Guangzhou, China
[au] Also at The City College of New York, New York NY, USA
[av] Also at The Collaborative Innovation Center of Quantum Matter (CICQM), Beijing, China
[aw] Also at Tomsk State University, Tomsk, and Moscow Institute of Physics and Technology State University, Dolgoprudny, Russia
[ax] Also at TRIUMF, Vancouver BC, Canada
[ay] Also at Universita di Napoli Parthenope, Napoli, Italy
* Deceased

Eur. Phys. J. C (2020) 80:616
https://doi.org/10.1140/epjc/s10052-020-8001-z

THE EUROPEAN PHYSICAL JOURNAL C

Regular Article - Experimental Physics

Measurement of the transverse momentum distribution of Drell–Yan lepton pairs in proton–proton collisions at $\sqrt{s} = 13$ TeV with the ATLAS detector

ATLAS Collaboration[⋆]

CERN, 1211 Geneva 23, Switzerland

Received: 9 December 2019 / Accepted: 4 May 2020 / Published online: 10 July 2020

Abstract This paper describes precision measurements of the transverse momentum $p_{\mathrm{T}}^{\ell\ell}$ ($\ell = e, \mu$) and of the angular variable ϕ_{η}^{*} distributions of Drell–Yan lepton pairs in a mass range of 66–116 GeV. The analysis uses data from 36.1 fb^{-1} of proton–proton collisions at a centre-of-mass energy of $\sqrt{s} = 13$ TeV collected by the ATLAS experiment at the LHC in 2015 and 2016. Measurements in electron-pair and muon-pair final states are performed in the same fiducial volumes, corrected for detector effects, and combined. Compared to previous measurements in proton–proton collisions at $\sqrt{s} = 7$ and 8 TeV, these new measurements probe perturbative QCD at a higher centre-of-mass energy with a different composition of initial states. They reach a precision of 0.2% for the normalized spectra at low values of $p_{\mathrm{T}}^{\ell\ell}$. The data are compared with different QCD predictions, where it is found that predictions based on resummation approaches can describe the full spectrum within uncertainties.

Contents

1 Introduction

In high-energy hadron–hadron collisions, the vector bosons W and Z/γ^{*} are produced via quark–antiquark annihilation [1], and can be observed with very small backgrounds by using their leptonic decay modes. The vector bosons have non-zero momentum transverse to the beam direction due to the emission of quarks and gluons from the initial-state partons as well as to the intrinsic transverse momentum of the initial-state partons in the proton. Phenomenologically, the spectrum at low transverse momentum of the Z boson, $p_{\mathrm{T}}^{\ell\ell}$, reconstructed through the decay into a pair of charged leptons, can be described using soft-gluon resummation [2–7] and non-perturbative models to account for the intrinsic transverse momentum of partons. At high $p_{\mathrm{T}}^{\ell\ell}$ the spectrum can be calculated by fixed-order perturbative quantum chromodynamics (QCD) predictions [8–12], and next-to-leading-order electroweak (NLO EW) effects are expected to be important [13–15]. Parton-shower models [16–18] or resummation may be matched to fixed-order calculations to describe the full spectrum.

A precise measurement of the $p_{\mathrm{T}}^{\ell\ell}$ spectrum provides an important input to the background prediction in searches for beyond the Standard Model (SM) processes, e.g. in the monojet signature [19], as well as to SM precision measurements. In particular, the measurement of the mass of the W boson [20] relies on the measurement of the $p_{\mathrm{T}}^{\ell\ell}$ distribution to constrain the transverse momentum spectrum of the W boson, p_{T}^{W}, since a direct measurement of the transverse momentum distribution of W bosons is experimentally challenging [21]. The $p_{\mathrm{T}}^{\ell\ell}$ spectrum was measured previously in proton–proton (pp) collisions at the Large Hadron Collider (LHC) by the ATLAS Collaboration at centre-of-mass energies of $\sqrt{s} = 7$ TeV and 8 TeV [22,23], including several mass regions near and away from the Z-boson resonance. Related measurements were also made by the CMS [24–28] and the LHCb [29–31] collaborations at the LHC and by the

⋆ e-mail: atlas.publications@cern.ch

CDF [32] and D0 [33,34] collaborations in $p\bar{p}$ collisions at the TeVatron.

Compared to measurements at lower $\sqrt{s}$, Z-boson production at 13 TeV is characterized by a smaller parton momentum fraction of the colliding protons, leading to a different flavour composition and a larger phase space for hard QCD radiation. A precise measurement will test this energy dependence and play an important role in future studies of the W-boson mass using the 13 TeV data.

The granularity of the measurement in the low-$p_{\mathrm{T}}^{\ell\ell}$ domain is limited by the lepton momentum resolution. To overcome this limitation, the ϕ_η^* observable was introduced [35] as an alternative probe of $p_{\mathrm{T}}^{\ell\ell}$. It is defined as

$$\phi_\eta^* = \tan\left(\frac{\pi - \Delta\phi}{2}\right) \times \sin(\theta_\eta^*)\,,$$

where $\Delta\phi$ is the azimuthal angle in radians between the two leptons. The angle θ_η^* is a measure of the scattering angle of the leptons relative to the proton beam direction in the rest frame of the dilepton system and is defined by $\cos(\theta_\eta^*) = \tanh[(\eta^- - \eta^+)/2]$, where η^- and η^+ are the pseudorapidities[1] of the negatively and positively charged lepton, respectively. Therefore, ϕ_η^* depends exclusively on the directions of the two leptons, which are measured more precisely than their momenta.

In this paper, measurements of the $p_{\mathrm{T}}^{\ell\ell}$ and the ϕ_η^* spectra are presented using pp collision data at $\sqrt{s} = 13$ TeV collected in 2015 and 2016 with the ATLAS detector, corresponding to an integrated luminosity of 36.1 fb^{-1}. Both the dielectron and dimuon final states $Z/\gamma^* \to \ell\ell$ ($\ell = e$ or μ) are analysed in a dilepton mass window of $m_{\ell\ell} = 66$–116 GeV. The measurement is performed in a fiducial phase space that is close to the detector acceptance for leptons in transverse momentum p_{T}^{ℓ} and pseudorapidity η_ℓ.

2 The ATLAS detector

The ATLAS experiment uses a multipurpose detector [36–38] with a cylindrical geometry and almost 4π coverage in solid angle. The collision point is surrounded by tracking detectors, collectively referred to as the inner detector (ID), followed by a superconducting solenoid providing a 2 T axial magnetic field, a calorimeter system and a muon spectrometer. The ID provides precise measurements of charged-particle tracks in the pseudorapidity range $|\eta| < 2.5$. It consists of three subdetectors arranged in a coaxial geometry around the beam axis: a silicon pixel detector, a silicon microstrip detector and a transition radiation tracker.

The electromagnetic calorimeter covers the region $|\eta| < 3.2$ and is based on a high-granularity, lead/liquid- argon (LAr) sampling technology. The hadronic calorimeter uses a steel/scintillator-tile detector in the region $|\eta| < 1.7$ and a copper/LAr detector in the region $1.5 < |\eta| < 3.2$. The forward calorimeter (FCAL) covers the range $3.2 < |\eta| < 4.9$ and also uses LAr as the active material and copper or tungsten absorbers for the EM and hadronic sections, respectively.

The muon spectrometer (MS) consists of separate trigger and high-precision tracking chambers to measure the deflection of muons in a magnetic field generated by three large superconducting toroids arranged with an eightfold azimuthal coil symmetry around the calorimeters. The high-precision chambers cover a range of $|\eta| < 2.7$. The muon trigger system covers the range $|\eta| < 2.4$ with resistive-plate chambers in the barrel and thin-gap chambers in the endcap regions.

A two-level trigger system is used to select events in real time [39]. It consists of a hardware-based first-level trigger and a software-based high-level trigger. The latter employs algorithms similar to those used offline and is used to identify electrons and muons.

3 Analysis methodology

3.1 Description of the measurements

The Z-boson differential cross-sections are measured as a function of $p_{\mathrm{T}}^{\ell\ell}$ and ϕ_η^* separately for the dielectron and dimuon decay channels. Only small background contributions are expected. The results are reported within a fiducial phase space chosen to be close to the experimental acceptance defined by the lepton transverse momenta $p_{\mathrm{T}}^{\ell} > 27$ GeV, the absolute lepton pseudorapidity $|\eta_\ell| < 2.5$ and the dilepton invariant mass $m_{\ell\ell} = 66$–116 GeV.

The lepton kinematics can be described at different levels regarding the effects of final-state photon radiation (QED FSR). Cross-sections at *Born* level employ the lepton kinematics before QED FSR, while the *bare* level is defined by leptons after emission of QED FSR. A *dressed* lepton is defined by combining the bare four-momenta of each lepton with that of QED FSR photons radiated from the lepton within a cone of size $\Delta R = 0.1$ around the lepton. The results in this paper are reported at the dressed and Born levels.

The differential cross-sections in $p_{\mathrm{T}}^{\ell\ell}$ and ϕ_η^* are measured and their normalized spectra derived. The total systematic

[1] ATLAS uses a right-handed coordinate system with its origin at the nominal interaction point (IP) in the centre of the detector and the z-axis along the beam pipe. The x-axis points from the IP to the centre of the LHC ring, and the y-axis points upwards. Cylindrical coordinates (r, ϕ) are used in the transverse plane, ϕ being the azimuthal angle around the z-axis. The pseudorapidity is defined in terms of the polar angle θ as $\eta = -\ln\tan(\theta/2)$. Angular distance is measured in units of $\Delta R = \sqrt{(\Delta\eta)^2 + (\Delta\phi)^2}$.

uncertainty of the latter is significantly reduced due to large correlations in many sources of uncertainty between the measurement bins.

3.2 Simulated event samples

Events simulated by Monte Carlo (MC) generators are used to predict the detector response to the signal process in order to correct the data for detector inefficiencies and resolution as well as to estimate most of the background from processes other than $Z/\gamma^* \to \ell\ell$ in the selected data sample.

The $Z/\gamma^* \to \ell\ell$ signal process was generated with the POWHEG-BOX V1 MC event generator [40–43] at next-to-leading order in α_S interfaced to PYTHIA 8.186 [17] for the modelling of the parton shower, hadronization, and underlying event, with parameters set according to the AZNLO tune [22]. The CT10 (NLO) set of parton distribution functions (PDF) [44] was used for the hard-scattering processes, whereas the CTEQ6L1 PDF set [45] was used for the parton shower. The effect of final-state photon radiation was simulated with Photos++ v3.52 [46,47]. The EVTGEN v1.2.0 program [48] was used to decay bottom and charm hadrons.

POWHEG+PYTHIA8 was also used to simulate the majority of the background processes considered. The $Z \to \tau\tau$ and the diboson processes WW, WZ and ZZ [49] (requiring $m_{\ell\ell} > 4$ GeV for any pair of same-flavour opposite-charge leptons) used the same tune and PDF as the signal process. The $t\bar{t}$ and single-top-quark [50,51] backgrounds to the dielectron channel were simulated with POWHEG+PYTHIA6 [52] with the P2012 tune [53] and CT10 PDF, while for the dimuon channel POWHEG+PYTHIA8 with the A14 tune [54] and the NNPDF3.0 PDF [55] was used. It was found that the prediction of the $t\bar{t}$ background is in very good agreement for both generators. The photon-induced background $\gamma\gamma \to \ell\ell$ was generated with PYTHIA8 using the NNPDF2.3 QED PDF [56].

The effect of multiple interactions in the same and neighbouring bunch crossings (pile-up) was modelled by overlaying the hard-scattering event with simulated minimum-bias events generated with PYTHIA 8.186 using the MSTW2008LO set of PDFs [57] and the A2 tune [58]. The simulated event samples were reweighted to describe the distribution of the number of pile-up interactions in the data, and further reweighted such that the distribution of the longitudinal position of the primary pp collision vertex matches that in data. The primary vertex is defined as the vertex with at least two reconstructed tracks with $p_T > 0.4$ GeV and with the highest sum of squared transverse momenta of associated tracks. The GEANT4 program was used to simulate the passage of particles through the ATLAS detector [59,60]. The simulated events are reconstructed with the same analysis procedure as the data. The reconstruction, trigger and isolation efficiencies as well as lepton momentum scale and resolution in the MC simulation are corrected to match those determined in data [61–63].

3.3 Event selection

Candidate $Z \to ee$ events are triggered requiring at least one identified electron with $p_T > 24$ GeV in 2015 and $p_T > 26$ GeV in 2016 data [64]. In addition to the increased p_T threshold, the electron also has to satisfy isolation criteria in the 2016 data. Candidate $Z \to \mu\mu$ events were recorded with triggers that require at least one isolated muon with $p_T > 20$ GeV in 2015 and $p_T > 26$ GeV in 2016 data.

Electron candidates are reconstructed from clusters of energy in the electromagnetic calorimeter matched to ID tracks [62]. They are required to have $p_T > 27$ GeV and $|\eta| < 2.47$ (excluding the transition regions between the barrel and the endcap electromagnetic calorimeters, $1.37 < |\eta| < 1.52$). Electron candidates are required to pass the 'medium' identification requirement, and are also required to be isolated according to the 'gradient' isolation criterion [62].

Muon candidates are reconstructed by combining tracks reconstructed in the inner detector with tracks reconstructed in the MS [61]. They are required to have $p_T > 27$ GeV and $|\eta| < 2.5$ and satisfy identification criteria corresponding to the 'medium' working point [61]. Track quality requirements are imposed to suppress backgrounds, and the muon candidates are required to be isolated according to the 'gradient' isolation criterion [61], which is p_T- and η-dependent and based on the calorimeter and track information.

Electron and muon candidates are required to originate from the primary vertex. Thus, the significance of the track's transverse impact parameter calculated relative to the beam line, $|d_0/\sigma_{d_0}|$, must be smaller than 3.0 for muons and less than 5.0 for electrons. Furthermore, the longitudinal impact parameter, z_0 (the difference between the z-coordinate of the point on the track at which d_0 is defined and the longitudinal position of the primary vertex), is required to satisfy $|z_0 \cdot \sin(\theta)| < 0.5$ mm.

Events are required to contain exactly two same-flavour leptons passing the lepton selection. The two leptons must be of opposite electric charge and their invariant mass must satisfy $66 < m_{\ell\ell} < 116$ GeV. No additional veto on the presence of leptons of different flavour is applied. Table 1 shows the number of events satisfying the above selection criteria in the electron channel and the muon channel. Also given are the estimated contributions from the background sources described below in Sect. 3.4.

3.4 Estimation of backgrounds

The backgrounds from all sources other than multijet processes are estimated using the MC samples detailed in Sect. 3.2. The number and properties of the background

Table 1 Selected signal candidate events in data for both decay channels as well as the expected background contributions including their total uncertainties

	$Z/\gamma^* \to ee$	$Z/\gamma^* \to \mu\mu$
Two reconstructed leptons within fiducial volume	13 649 239	18 162 641
Electroweak background ($Z \to \tau\tau, WW, WZ, ZZ$)	40 000 ± 2000	50 000 ± 2500
Photon-induced background	2900 ± 140	4100 ± 200
Top-quark background	38 000 ± 1900	45 400 ± 2200
Multijet background	8500 ± 4900	1000 ± 200
Total background	89 400 ± 5600	100 500 ± 3300

events where one or two reconstructed lepton candidates originate from hadrons or hadron decay products, i.e. multijet processes as well as W+jets, are estimated using the data-driven techniques described in the following for both decay channels.

In the electron channel, a multijet-dominated sample is selected from data with two same-charge electron candidates satisfying the 'loose' identification criteria, but not the 'medium' criteria [62], i.e. they are more likely to be caused by misidentified jets. This sample is collected by a di-electron trigger without isolation criteria [64]. In the muon channel, a multijet sample is obtained by selecting two same-charge muons. The residual contamination from processes with prompt leptons is estimated using the simulation and subtracted.

The normalization of the multijet template in the electron channel is determined in a fit to the distribution of the electron isolation using all event-selection criteria except those for the isolation variables. Systematic uncertainties in the normalization are estimated by varying the fit range on the electron isolation distribution.

In the muon channel, the normalization is obtained using the ratio of number of opposite-charge dimuon events to the number of same-charge dimuon events where the muons fail to satisfy the isolation criterion. Assuming no correlation between the isolation of muons in multijet events and their charge, this ratio can be applied to a control sample, defined by pairs of isolated same-charge muons passing the signal-kinematic selection, to determine the multijet contamination in the signal region. The systematic uncertainty in the estimate is obtained by varying the isolation criterion for the muons.

The total fraction of selected data events originating from background processes is about 0.6% in both the electron and muon channels. The background is dominated by contributions from diboson and $t\bar{t}$ processes. An overview of the estimated number of background events is given in Table 1, together with the corresponding total uncertainties.

Figure 1 shows the dilepton invariant mass and the lepton pseudorapidity distribution, for the electron and muon channels separately. The predictions are in fair agreement with the data. The impact of the residual differences between these distributions on the $p_{\mathrm{T}}^{\ell\ell}$ and ϕ_η^* measurements is estimated by reweighting the MC signal sample to data and then repeating the measurement procedure. Figure 2 compares the measured $p_{\mathrm{T}}^{\ell\ell}$ and ϕ_η^* distributions for both channels with the signal MC predictions. The disagreement between the data and the predictions for large values of $p_{\mathrm{T}}^{\ell\ell}$ and ϕ_η^* is expected because POWHEG+PYTHIA8 is effectively a computation at leading-order in α_{S} in this region.

3.5 Correction for detector effects

The production cross-section times the branching ratio for decays into a single lepton flavour are measured in fiducial volumes as defined in Sect. 3.1. Integrated fiducial cross-sections in the electron and muon channels are computed following the equation

$$\sigma^{\mathrm{fid}}_{Z/\gamma^*\to\ell\ell} = \frac{N_{\mathrm{Data}} - N_{\mathrm{Bkg}}}{C_Z \cdot L},$$

where N_{Data} is the number of observed signal candidates and N_{Bkg} is the number of background events expected in the selected sample. The integrated luminosity of the sample is $L = 36.1\,\mathrm{fb}^{-1}$. A correction for the event detection efficiency is applied with the factor C_Z, which is obtained from the simulation of signal events as the ratio of the sum of event weights after simulation, reconstruction and selection, to the sum of MC event weights for events satisfying the fiducial requirements. The factor C_Z is affected by experimental uncertainties, described in Sect. 4, while theory and modelling uncertainties are negligible.

The differential distributions within the fiducial volume are corrected for detector effects and bin-to-bin migrations using an iterative Bayesian unfolding method [65–67]. First, the data are corrected for events that pass the detector-level selection but not the particle-level selection. Then, the iterative Bayesian unfolding technique is used as a regularized way to correct for the detector resolution in events that pass both the detector-level and particle-level selections. The method is applied with four iterations implemented in the RooUnfold framework [67]. After the application of the response matrix, a final correction is applied to account for events that pass the particle-level but not detector-level selec-

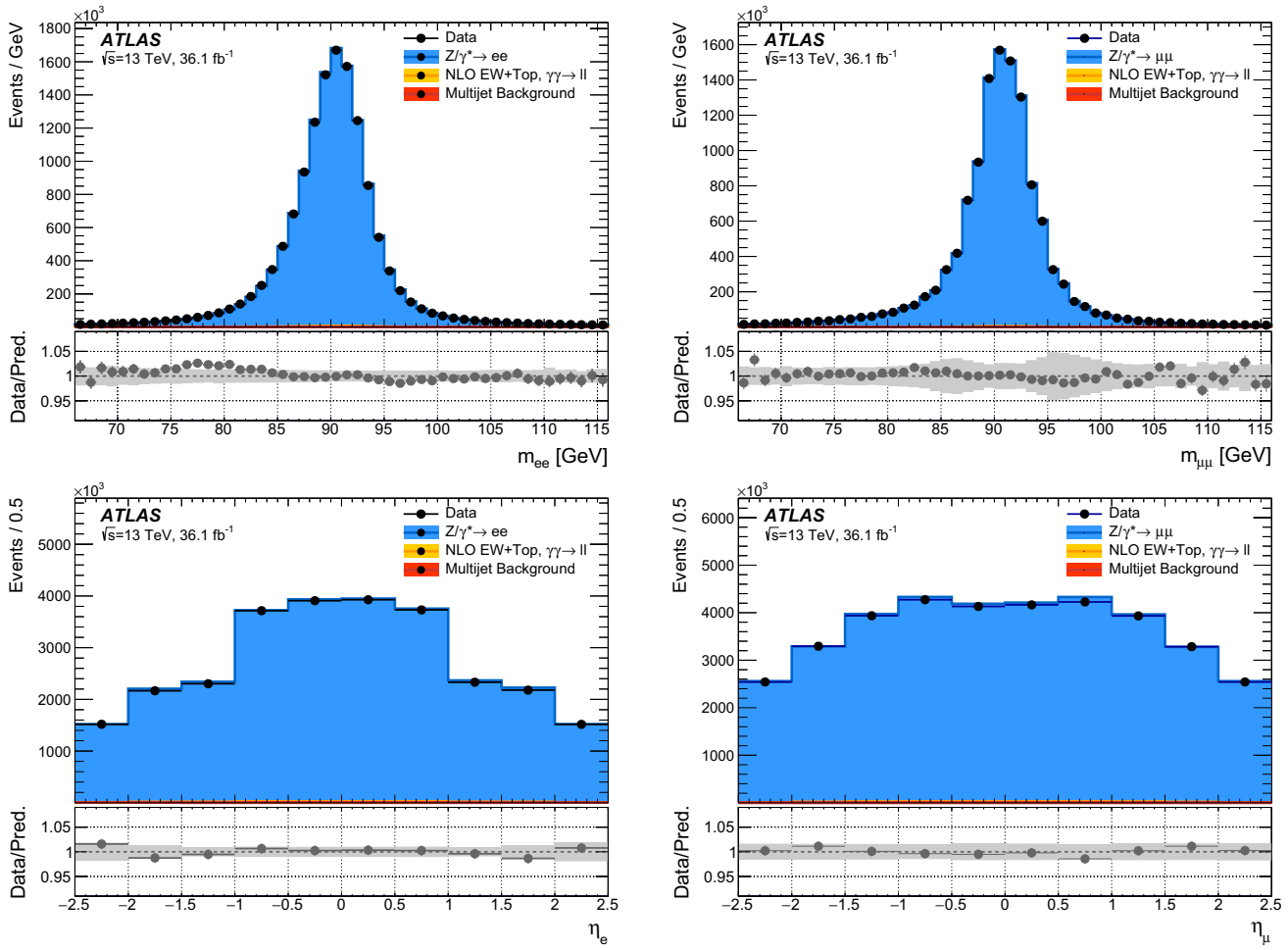

Fig. 1 The distribution of events passing the selection requirements in the electron channel (left) and muon channel (right) as a function of dilepton invariant mass $m_{\ell\ell}$ (upper row) and lepton pseudorapidity η (lower row), the latter with one entry for each lepton per event. The MC signal sample is simulated using POWHEG+PYTHIA8. The statistical uncertainties of the data points are generally smaller than the size of the markers. The predictions of the MC signal sample together with the MC background samples are normalized to the integral of the data and the total experimental uncertainty of the predicted values is shown as a grey band in the ratio of the prediction to data

tion, resulting in unfolded distributions on Born and dressed particle level. The response matrices, which connect the distributions at reconstruction and particle level, as well as the correction factors are derived using the POWHEG+PYTHIA signal MC sample.

4 Statistical and systematic uncertainties

Uncertainties in the measurement are assessed for each aspect of the analysis, including the background subtraction, event detection efficiencies, response matrix, and unfolding method. The entire analysis procedure is repeated for each systematic uncertainty. Each source of uncertainty is varied to estimate the effect on the final result.

The effect on the measurement from the size of the data and MC samples is estimated by generating pseudo-experiment variations of the respective samples. The resulting statistical uncertainties are considered as uncorrelated between bins and between channels.

Uncertainties in the scale and resolution of the electron energy scale [63] and muon momentum scale [61] are among the dominant uncertainties in the $p_{\mathrm{T}}^{\ell\ell}$ measurement. Furthermore, uncertainties related to lepton reconstruction and selection efficiencies are considered [39,61,62,64], covering the lepton identification, reconstruction, isolation, triggering and track-to-vertex matching processes. The lepton related systematic uncertainties have only a small statistical component. There is an additional uncertainty in the muon channel to cover charge-dependent biases in the muon momentum measurement. The majority of these experimental uncertain-

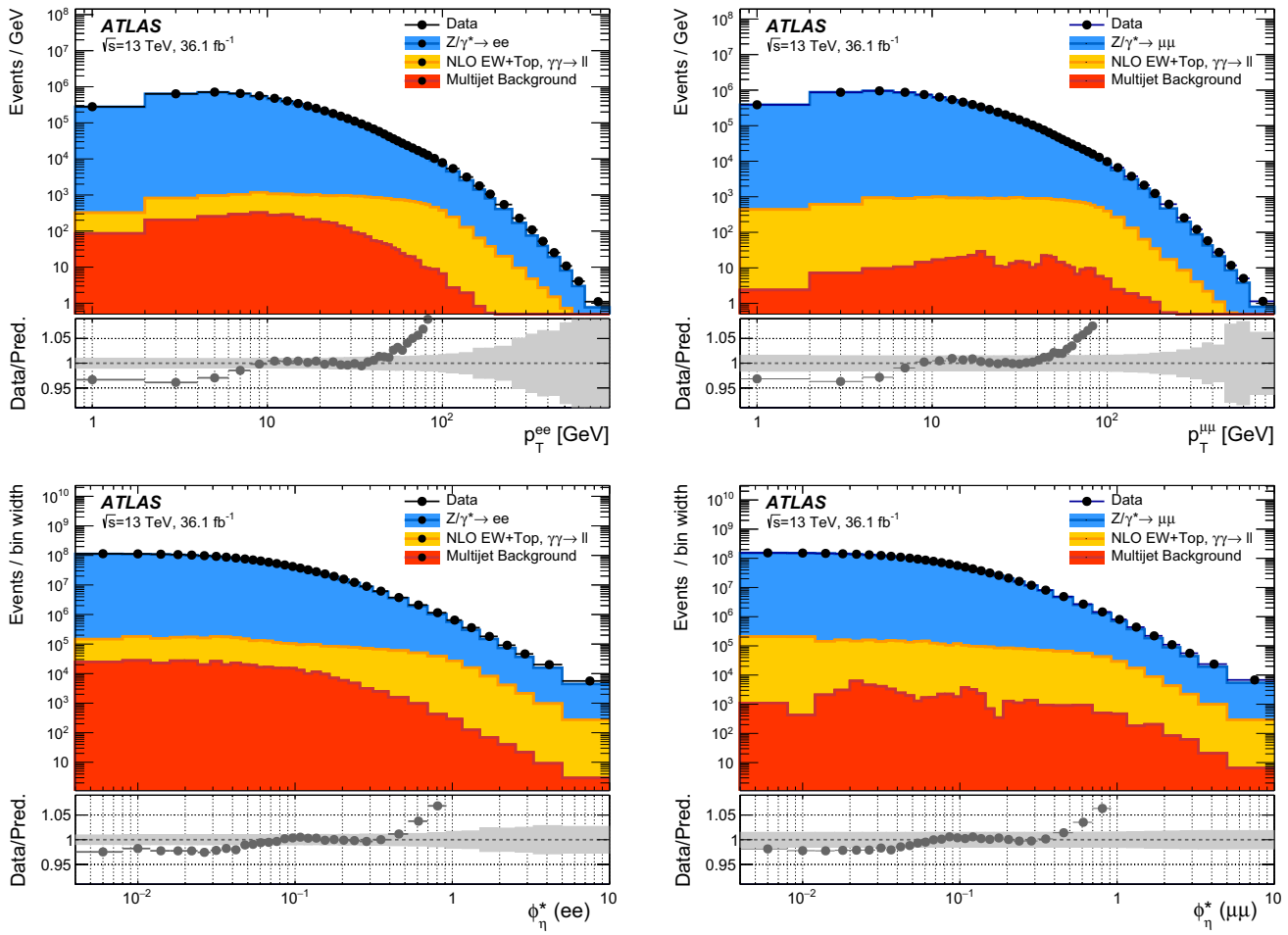

Fig. 2 The distribution of events passing the selection requirements in the electron channel (left) and muon channel (right) as a function of dilepton transverse momentum (upper row) and ϕ^*_η (lower row). The MC signal sample is simulated using POWHEG+PYTHIA8. The statistical uncertainties of the data points are generally smaller than the size of the markers. The predictions are normalized to the integral of the data and the total experimental uncertainty of the predicted values is shown as a grey band in the ratio of the prediction to data

ties are considered correlated between bins of $p_{\mathrm{T}}^{\ell\ell}$ and ϕ^*_η. An exception are the components of the reconstruction and identification efficiencies which have a significant statistical component due to the limited number of events in the data samples used to derive the efficiency corrections. Uncertainties related to electron or muon reconstruction and identification are always assumed to be uncorrelated with each other. They dominate the uncertainty in the fiducial cross-section measurement.

The uncertainties in the MC background estimates are obtained by independently varying the theory cross-sections used to normalize the corresponding samples and observing the effect on the measured $p_{\mathrm{T}}^{\ell\ell}$ and ϕ^*_η cross-sections. These background uncertainties are considered correlated between bins of $p_{\mathrm{T}}^{\ell\ell}$ and ϕ^*_η and between the electron and muon channels. As described in Sect. 3.4, the uncertainty in the multijet background in the electron channel is obtained by changing the input range of the template used to estimate the multijet background. For the muon channel, the measurement is performed again with a modified isolation variable used in the normalization procedure. The differences between the nominal and modified measurements are used as uncertainty. The estimated multijet backgrounds are assumed to be uncorrelated between the channels.

An uncertainty is derived to cover the mis-modelling of the simulated pile-up activity following the measurement of the cross-section of inelastic pp collisions [68]. Also, the uncertainty in modelling the distribution of the longitudinal position of the primary vertex is considered. These uncertainties are treated as correlated between the electron channel and muon channel.

The uncertainty from the unfolding method is determined by repeating the procedure with a different simulation where the nominal particle-level spectrum is reweighted so that the simulated detector-level spectrum is in good agreement with the data. The modified detector-level distribution is unfolded

Table 2 Overview of the detector efficiency correction factors, C_Z, for the electron and muon channels and their systematic uncertainty contributions

	Electron channel		Muon channel	
	Born	Dressed	Born	Dressed
C_Z	0.509 ± 0.005	0.522 ± 0.005	0.685 ± 0.011	0.702 ± 0.011
Trigger efficiencies	± 0.0004		± 0.0004	
Identification & reconstruction efficiencies	± 0.0049		± 0.0102	
Isolation efficiencies	± 0.0009		± 0.0029	
Energy/momentum scale and resolution	± 0.0014		± 0.0010	
Pile-up	± 0.0011		± 0.0019	
Model uncertainties	± 0.0001		± 0.0001	

with the nominal response matrix and the difference between the result and the reweighted particle-level spectrum is taken as the bias of the unfolding method due to the choice of prior. The closure of the unfolding procedure is also tested using the generator-level distributions of the SHERPA MC sample described in Sect. 5.2, where consistent results within the assigned unfolding uncertainties are found.

The uncertainty from the choice of PDF used in the signal MC generator is evaluated by reweighting the signal MC simulation to the 52 error sets of the CT10 PDF set and computing the resulting variation of the results [44,69]. The differences found in this way are negligible, similar to scale-choice uncertainties. The uncertainty in the combined 2015–2016 integrated luminosity is 2.1% [70], obtained using the LUCID-2 detector [71] for the primary luminosity measurements. This uncertainty only applies to the absolute cross-section measurements.

The experimental uncertainties of C_Z for the integrated fiducial cross-section measurements in the electron and muon channels are summarized in Table 2. The electron identification efficiency and muon reconstruction efficiency contribute a large fraction of the total systematic uncertainty for both the integrated and absolute differential measurements. These uncertainties are greatly reduced for the normalized measurement of differential distributions. A summary of the uncertainties in the normalized differential cross-section measurements is provided in Fig. 3 as a function of $p_{\mathrm{T}}^{\ell\ell}$ and ϕ_η^* for both decay channels. The statistical uncertainties for the electron and muon channel measurements are a combination of the uncertainties due to limited data and MC sample sizes. The systematic uncertainties are divided into categories and originate from lepton scales and resolutions, reconstruction and identification efficiencies, as well as the MC signal modelling in the unfolding procedure and further smaller uncertainty sources such as the subtraction of background contributions. These smaller contributions are summarized as "other" uncertainties.

5 Results and discussion

5.1 Combination

The fiducial cross-sections measured in the $Z/\gamma^* \to ee$ and $Z/\gamma^* \to \mu\mu$ channels are presented in Table 3 including statistical, systematic and luminosity uncertainties. When correcting for the more restrictive fiducial volume definition, these results are in good agreement with the previous ATLAS measurements at 13 TeV [72]. The electron- and muon-channel cross-sections are combined using χ^2 minimization, following the best linear unbiased estimator prescription (BLUE) [73–75]. The combination is performed on Born level, resulting in a combined cross-section of $\sigma_{\mathrm{fid}}(pp \to Z/\gamma^* \to \ell\ell) = 736.2 \pm 0.2(\mathrm{stat}) \pm 6.4(\mathrm{sys}) \pm 14.7\ (\mathrm{lumi})$ pb (Table 3).[2] There is a reduction of the uncertainty compared to individual electron- and muon-channel measurements since the dominant detector-related systematic uncertainty sources are largely uncorrelated. The uncertainties due to pile-up, physics modelling and luminosity are treated as correlated between the two decay channels.

The normalized differential cross-sections $1/\sigma_{\mathrm{fid}} \times \mathrm{d}\sigma_{\mathrm{fid}}/\mathrm{d}p_{\mathrm{T}}^{\ell\ell}$ and $1/\sigma_{\mathrm{fid}} \times \mathrm{d}\sigma_{\mathrm{fid}}/\mathrm{d}\phi_\eta^*$ measured in the two decay channels as well as their combination are illustrated in Fig. 4. When building the χ^2 for combination procedure, the measurement uncertainties are separated into those from bin-to-bin uncorrelated sources and those from bin-to-bin correlated sources, the latter largely reduced due to the normalization by the fiducial cross-section. The normalized differential measurements are combined at Born level following the BLUE prescription. The resulting $\chi^2/N_{\mathrm{dof}} = 47/44$ for the combination for $p_{\mathrm{T}}^{\ell\ell}$ and the $\chi^2/N_{\mathrm{dof}} = 32/36$ for ϕ_η^* indicate good agreement between the two chan-

[2] The results on dressed level are about 2.4% lower compared to the Born level definition

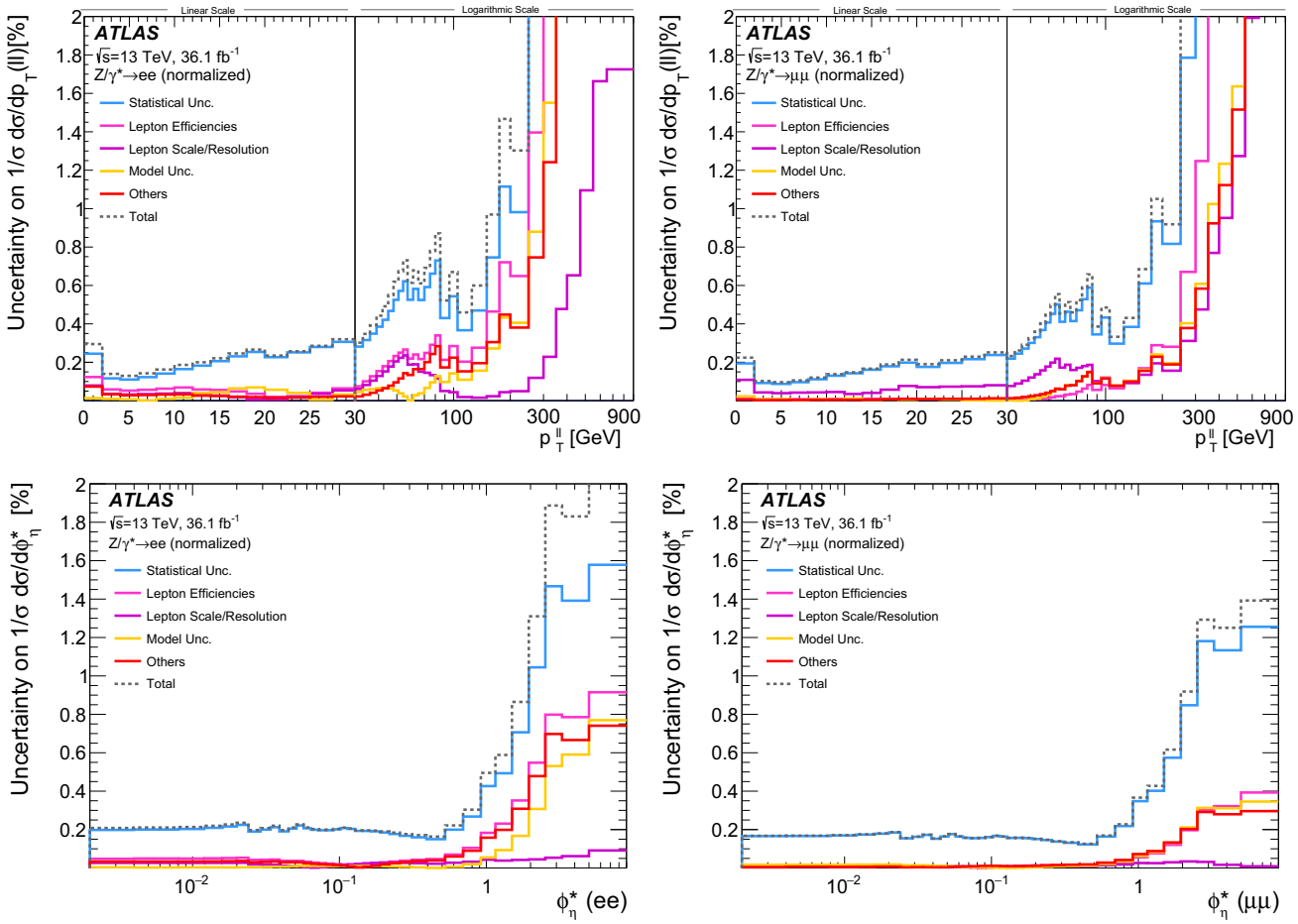

Fig. 3 The systematic uncertainties for the electron channel measurement (left) and muon channel measurement (right) for the normalized $p_{\mathrm{T}}^{\ell\ell}$ (upper row) and normalized ϕ_{η}^{*} (lower row). The statistical uncertainties are a combination of the uncertainties due to limited data and MC sample sizes. The $p_{\mathrm{T}}^{\ell\ell}$ distribution is split into linear and logarithmic scales at 30 GeV. Some uncertainties are larger than 2% for $p_{\mathrm{T}}^{\ell\ell} > 200$ GeV and hence cannot be displayed. The corresponding uncertainties are also summarized in Table 4

Table 3 Measured integrated cross-section in the fiducial volume in the electron and muon decay channels at Born level and their combination as well as the theory prediction at NNLO in α_{S} using the CT14 PDF set

Channel	Measured cross-section × $\mathcal{B}(Z/\gamma^* \to \ell\ell)$ (value ± stat. ± syst. ± lumi.)	Predicted cross-section × $\mathcal{B}(Z/\gamma^* \to \ell\ell)$ (value ± PDF ± α_{S} ± scale ± intrinsic)
$Z/\gamma^* \to ee$	$738.3 \pm 0.2 \pm 7.7 \pm 15.5$ pb	
$Z/\gamma^* \to \mu\mu$	$731.7 \pm 0.2 \pm 11.3 \pm 15.3$ pb	
$Z/\gamma^* \to \ell\ell$	$736.2 \pm 0.2 \pm 6.4 \pm 15.5$ pb	$703^{+19}_{-24}{}^{+6}_{-8}{}^{+4}_{-6}{}^{+5}_{-5}$ pb [72]

nels.[3] The combined precision is between 0.1% and 0.5% for $p_{\mathrm{T}}^{\ell\ell} < 100$ GeV, rising to 10% towards the high end of the spectrum, where the overall precision is limited by the data and MC sample size. The combined results for both distributions are presented in Table 4 including statistical and bin-to-bin uncorrelated and correlated systematic uncertainties. The measurement results are reported at Born level and factors k_{dr}, the binwise ratio of dressed and born level results, are given to transfer to the dressed particle level.

5.2 Comparison with predictions

The integrated fiducial cross-section is compared with a fixed-order theory prediction that is computed in the same way as in Ref. [76]. The speed-optimized DYTURBO [77] version of the DYNNLO 1.5 [10] program with the CT14 NNLO set of PDFs [78] is used to obtain a prediction at next-to-next-to-leading order (NNLO) in α_{S} in the G_{μ} EW

[3] The χ^2/N_{dof} is still good when taking into account only bins with $p_{\mathrm{T}}^{\ell\ell} > 50$ GeV.

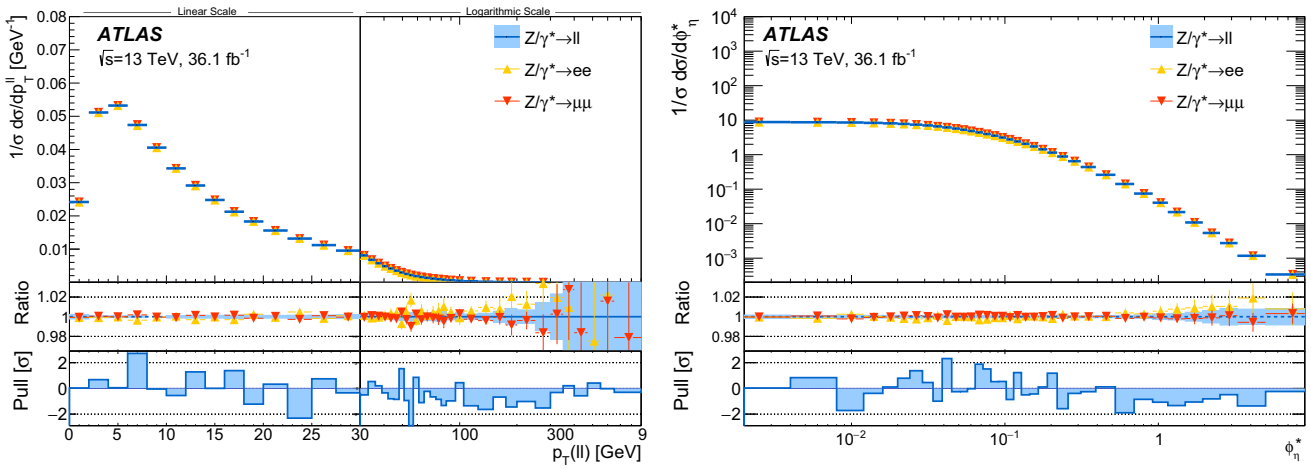

Fig. 4 The measured normalized cross section as a function of $p_{\mathrm{T}}^{\ell\ell}$ (left) and ϕ_{η}^{*} (right) for the electron and muon channels and the combined result as well as their ratio together with the total uncertainties, shown as a blue band. The pull distribution between the electron and muon channels, defined as the difference between the two channels divided by the combined uncorrelated uncertainty, is also shown. The $p_{\mathrm{T}}^{\ell\ell}$ distribution is split into linear and logarithmic scales at 30 GeV

Table 4 The measured combined normalized differential cross-sections, divided by the bin-width, in the fiducial volume at Born level as well as a factor k_{dr} to translate from the Born particle level to the dressed particle level

Bin [GeV]	$1/\sigma_{\mathrm{fid}} \times \mathrm{d}\sigma/\mathrm{d}p_{\mathrm{T}}^{\ell\ell}$ [1/GeV]	Corr. uncert.	Uncorr. uncert.	k_{dr}	Bin	$1/\sigma_{\mathrm{fid}} \times \mathrm{d}\sigma/\mathrm{d}\phi_{\eta}^{*}$	Corr. uncert.	Uncorr. uncert.	k_{dr}
0–2	0.024189	± 0.15%	± 0.18%	0.978	0–0.004	8.8053	± 0.03%	± 0.13%	0.992
2–4	0.051144	± 0.06%	± 0.08%	0.985	0.004–0.008	8.6969	± 0.03%	± 0.13%	0.993
4–6	0.053232	± 0.05%	± 0.08%	0.994	0.008–0.012	8.5624	± 0.02%	± 0.13%	0.993
6–8	0.047383	± 0.05%	± 0.08%	1.000	0.012–0.016	8.3378	± 0.02%	± 0.13%	0.994
8–10	0.040568	± 0.04%	± 0.09%	1.010	0.016–0.02	8.0881	± 0.03%	± 0.14%	0.994
10–12	0.034317	± 0.06%	± 0.11%	1.010	0.02–0.024	7.7920	± 0.03%	± 0.14%	0.995
12–14	0.029157	± 0.07%	± 0.12%	1.010	0.024–0.029	7.4174	± 0.02%	± 0.12%	0.995
14–16	0.024804	± 0.06%	± 0.14%	1.010	0.029–0.034	7.0360	± 0.02%	± 0.13%	0.996
16–18	0.021268	± 0.05%	± 0.15%	1.010	0.034–0.039	6.5989	± 0.02%	± 0.13%	0.998
18–20	0.018325	± 0.04%	± 0.16%	1.010	0.039–0.045	6.1608	± 0.02%	± 0.12%	0.998
20–22.5	0.015605	± 0.03%	± 0.14%	1.010	0.045–0.051	5.7085	± 0.01%	± 0.13%	0.999
22.5–25	0.013180	± 0.03%	± 0.15%	1.000	0.051–0.057	5.2791	± 0.02%	± 0.14%	1.000
25–27.5	0.011207	± 0.04%	± 0.17%	1.000	0.057–0.064	4.8488	± 0.02%	± 0.13%	1.000
27.5–30	0.0095568	± 0.05%	± 0.19%	0.999	0.064–0.072	4.4139	± 0.01%	± 0.12%	1.000
30–33	0.0081029	± 0.06%	± 0.17%	0.998	0.072–0.081	3.9705	± 0.01%	± 0.12%	1.000
33–36	0.0067881	± 0.08%	± 0.19%	0.996	0.081–0.091	3.5515	± 0.01%	± 0.12%	1.000
36–39	0.0057563	± 0.09%	± 0.21%	0.994	0.091–0.102	3.1421	± 0.02%	± 0.13%	1.000
39–42	0.0048769	± 0.12%	± 0.23%	0.993	0.102–0.114	2.7659	± 0.01%	± 0.13%	1.000
42–45	0.0041688	± 0.12%	± 0.25%	0.992	0.114–0.128	2.4125	± 0.01%	± 0.13%	1.000
45–48	0.0035213	± 0.14%	± 0.28%	0.993	0.128–0.145	2.0648	± 0.01%	± 0.12%	1.000
48–51	0.0029751	± 0.17%	± 0.31%	0.991	0.145–0.165	1.7299	± 0.02%	± 0.13%	1.000
51–54	0.0025433	± 0.18%	± 0.35%	0.992	0.165–0.189	1.4282	± 0.02%	± 0.13%	1.000
54–57	0.0021832	± 0.20%	± 0.38%	0.994	0.189–0.219	1.1469	± 0.02%	± 0.12%	1.000
57–61	0.0018779	± 0.15%	± 0.31%	0.994	0.219–0.258	0.8848	± 0.02%	± 0.12%	1.000
61–65	0.0015932	± 0.17%	± 0.35%	0.994	0.258–0.312	0.6470	± 0.03%	± 0.11%	1.000
65–70	0.0013519	± 0.16%	± 0.32%	0.995	0.312–0.391	0.4387	± 0.03%	± 0.11%	1.000
70–75	0.0011323	± 0.17%	± 0.37%	0.995	0.391–0.524	0.2610	± 0.03%	± 0.10%	1.000

Table 4 continued

Bin [GeV]	$1/\sigma_{\text{fid}} \times \mathrm{d}\sigma/\mathrm{d}p_{\mathrm{T}}^{\ell\ell}$ [1/GeV]	Corr. uncert.	Uncorr. uncert.	k_{dr}	Bin	$1/\sigma_{\text{fid}} \times \mathrm{d}\sigma/\mathrm{d}\phi_{\eta}^{*}$	Corr. uncert.	Uncorr. uncert.	k_{dr}
75–80	0.0009574	± 0.20%	± 0.43%	0.995	0.524–0.695	0.1414	± 0.04%	± 0.13%	1.000
80–85	0.0008150	± 0.22%	± 0.49%	0.995	0.695–0.918	0.07462	± 0.07%	± 0.17%	1.000
85–95	0.0006537	± 0.14%	± 0.29%	0.996	0.918–1.153	0.04047	± 0.12%	± 0.27%	1.000
95–105	0.0004849	± 0.18%	± 0.37%	0.995	1.153–1.496	0.02167	± 0.14%	± 0.30%	1.000
105–125	0.0003291	± 0.12%	± 0.25%	0.996	1.496–1.947	0.01084	± 0.18%	± 0.42%	1.000
125–150	0.0001861	± 0.16%	± 0.32%	0.994	1.947–2.522	0.005386	± 0.23%	± 0.59%	1.000
150–175	0.0001050	± 0.24%	± 0.51%	0.993	2.522–3.277	0.002738	± 0.31%	± 0.79%	1.000
175–200	$6.1279 \cdot 10^{-5}$	± 0.30%	± 0.78%	0.992	3.277–5.000	0.0011730	± 0.29%	± 0.72%	1.000
200–250	$3.0584 \cdot 10^{-5}$	± 0.22%	± 0.66%	0.995	5.000–10.00	0.0003372	± 0.30%	± 0.78%	0.997
250–300	$1.2211 \cdot 10^{-5}$	± 0.34%	± 1.4%	0.997					
300–350	$5.9026 \cdot 10^{-6}$	± 0.56%	± 2.3%	0.994					
350–400	$2.7742 \cdot 10^{-6}$	± 0.90%	± 3.8%	0.991					
400–470	$1.2513 \cdot 10^{-6}$	± 0.82%	± 4.9%	0.991					
470-550	$5.5219 \cdot 10^{-7}$	± 1.2%	± 7.9%	0.994					
550–650	$2.0165 \cdot 10^{-7}$	± 1.5%	± 13%	0.995					
650–900	$5.1153 \cdot 10^{-8}$	± 1.8%	± 16%	0.990					
900–2500	$1.5735 \cdot 10^{-9}$	± 6.3%	± 60%	0.964					

scheme [79]. The FEWZ 3.1 [9] program is used to compute next-to-leading-order (NLO) electroweak corrections and to cross-check the DYNNLO calculation. The prediction is shown in Table 3 together with its uncertainties estimated as follows. The dominant uncertainty is from limited knowledge of the proton PDFs and is estimated using the eigenvectors of the respective CT14 PDF set, rescaled from 90% to 68% confidence level. The uncertainties due to the strong coupling constant are estimated by varying α_{S} by ± 0.001. Missing higher-order QCD corrections are estimated by variations of the renormalization (μ_{R}) and factorization (μ_{F}) scales by factors of two with an additional constraint of $0.5 \leq \mu_{\mathrm{R}}/\mu_{\mathrm{F}} \leq 2$ around the nominal value of $m_{\ell\ell}$. The deviation from the FEWZ calculation is taken as an intrinsic uncertainty in the NNLO QCD calculation. A more detailed discussion of the agreement with theory predictions using different PDF sets is given in Ref. [72].

The differential measurements are compared with a variety of predictions of the $p_{\mathrm{T}}^{\ell\ell}$ and ϕ_{η}^{*} spectra that are based on different theoretical approaches to take into account both the soft and hard emissions from the initial state (ISR). Unless stated otherwise, the predictions do not consider NLO EW effects. The comparisons between the combined result corrected to QED Born level and the various predictions are shown in Figs. 5 and 6. Systematic uncertainties in the theoretical predictions are evaluated for this comparison where feasible.

The first prediction is obtained from PYTHIA8 with matrix elements at LO in α_{S} supplemented with a parton shower with the AZ set of tuned parameters [22]. The AZ tune optimized the intrinsic k_{T} and parton shower ISR parameters to optimally describe the ATLAS 7 TeV $p_{\mathrm{T}}^{\ell\ell}$ and ϕ_{η}^{*} data [22,80]. It was later used in the measurement of the W-boson mass using 7 TeV data [20], which requires a high-precision description of the W-boson transverse momentum spectrum at low p_{T}.

The second prediction is based on POWHEG+PYTHIA8 using NLO matrix elements with the PYTHIA8 parton shower parameters set according to the AZNLO tune [22] derived using the same data as the PYTHIA8 AZ tune. The predictions using the AZ and AZNLO tunes describe the 13 TeV data to within 2–4% in the region of low $p_{\mathrm{T}}^{\ell\ell} < 40$ GeV and $\phi_{\eta}^{*} < 0.5$, and in this region the prediction using the PYTHIA8 AZ tune is the one that agrees best with the data. This shows that predictions based on tunes to 7 TeV collision data can also provide a good description at significantly higher centre-of-mass energies for low $p_{\mathrm{T}}^{\ell\ell}$. At high $p_{\mathrm{T}}^{\ell\ell}$ these predictions are well below the data due to missing higher-order matrix elements, similar to the situation observed at lower $\sqrt{s}$.

The third prediction is simulated with the SHERPA v2.2.1 [18] generator. In this set-up, NLO-accurate matrix elements for up to two partons, and LO-accurate matrix elements for up to four partons are calculated with the Comix [81] and OpenLoops [82,83] libraries. The default SHERPA parton shower [84] based on Catani–Seymour dipole factorisation and the cluster hadronization model [85] is used with the dedicated set of tuned parameters developed by the authors for the NNPDF3.0nnlo PDF set [55]. The NLO matrix elements of a given parton multiplicity are matched to the parton

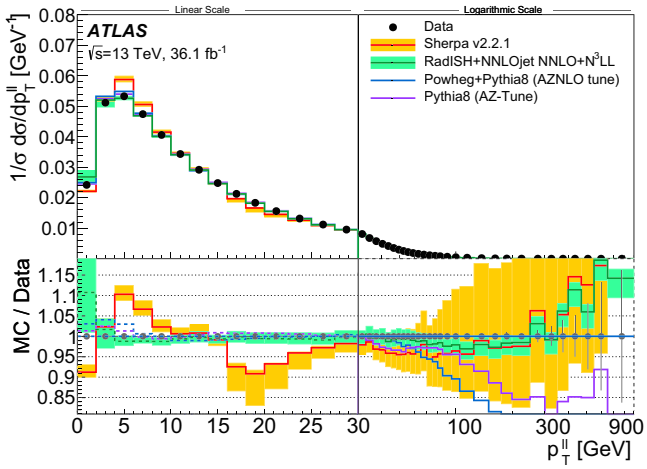

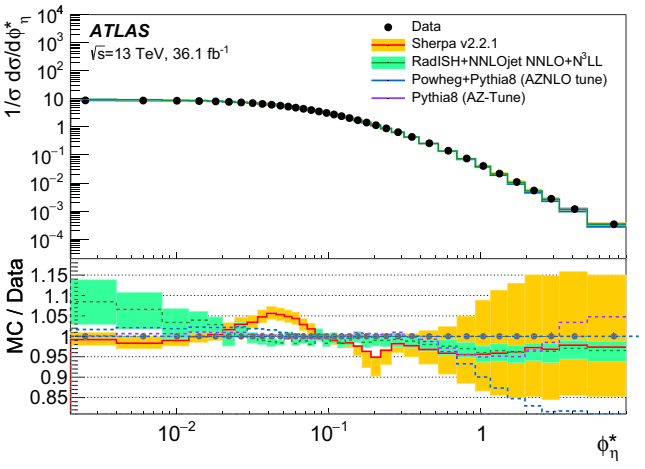

Fig. 5 Comparison of the normalized $p_{\mathrm{T}}^{\ell\ell}$ (left) and ϕ_{η}^{*} (right) distributions predicted by different computations: PYTHIA8 with the AZ tune, POWHEG+PYTHIA8 with the AZNLO tune, SHERPA v2.2.1 and RADISH with the Born level combined measurement. The uncertainties of the measurement are shown as vertical bars and uncertainties of the SHERPA and RADISH predictions are indicated by the coloured bands

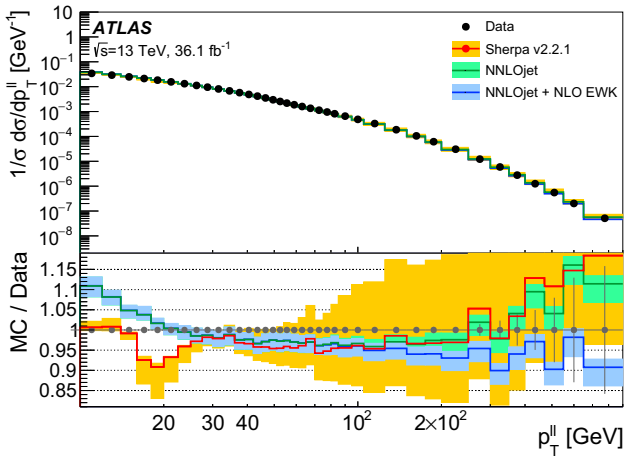

Fig. 6 Comparison of the normalized $p_{\mathrm{T}}^{\ell\ell}$ distribution in the range $p_{\mathrm{T}}^{\ell\ell} > 10$ GeV. The Born level combined measurement is compared with predictions by SHERPA v2.2.1, fixed-order NNLOJET and NNLOJET supplied with NLO electroweak corrections. The uncertainties in the measurement are shown as vertical bars and the uncertainties in the predictions are indicated by the coloured bands

shower using a colour-exact variant of the MC@NLO algorithm [86]. Different parton multiplicities are then merged into an inclusive sample using an improved CKKW matching procedure [87,88] which is extended to NLO accuracy using the MEPS@NLO prescription [89]. The merging threshold is set to 20 GeV. Uncertainties from missing higher orders are evaluated [90] using seven variations of the QCD factorization and renormalization scales in the matrix elements by factors of 0.5 and 2, avoiding variations in opposite directions. For the computation of uncertainties in the normalized spectra the effect of a certain variation is fully correlated across the full spectrum and an envelope of all variations is taken at the end, which results in uncertainties of 3–4% at low $p_{\mathrm{T}}^{\ell\ell}$ and up to 25% at high $p_{\mathrm{T}}^{\ell\ell}$. The effects of uncertainties in the PDF set are evaluated using 100 replica variations and are found to be very small, typically $< 1\%$ up to $p_{\mathrm{T}}^{\ell\ell} < 100$ GeV and a few percent above. SHERPA does describe the data in the high $p_{\mathrm{T}}^{\ell\ell} > 30$ GeV and $\phi_{\eta}^{*} > 0.1$ region to within about 4% up to the point where statistical uncertainties in the data exceed that level, which is better than the uncertainty estimate obtained from scale variations. On the other hand, the SHERPA prediction disagrees with the shape of the data at low $p_{\mathrm{T}}^{\ell\ell} < 25$ GeV and somewhat less with the ϕ_{η}^{*} distribution. The data may be useful in improving the parton shower settings in this regime.

Finally a prediction based on the RADISH program [91,92] is presented that combines a fixed-order NNLO prediction of Z+jet production ($O(\alpha_{\mathrm{S}}^{3})$) from NNLOJET [93] with resummation of $\log(m_{\ell\ell}/p_{\mathrm{T}}^{\ell\ell})$ terms at next-to-next-to-next-to-leading-logarithm ($\mathrm{N^3LL}$) accuracy [7]. The NNPDF3.1nnlo set of PDFs [94] is used with QCD scales set to $\mu_{\mathrm{R}} = \mu_{\mathrm{F}} = \sqrt{(m_{\ell\ell})^2 + (p_{\mathrm{T}}^{\ell\ell})^2}$ and the resummation scale set to $Q = m_{\ell\ell}/2$. Uncertainties in this prediction are derived from variations of μ_{R} and μ_{F} in the same way as for the SHERPA prediction described above and, in addition, two variations of Q by a factor of two up and down, assuming that the effects of scale variations are fully correlated across the full spectrum. Within the uncertainties of typically 1–3% the RADISH prediction agrees with the data over the full spectrum of $p_{\mathrm{T}}^{\ell\ell}$ and ϕ_{η}^{*}, apart from a small tension in the very low $p_{\mathrm{T}}^{\ell\ell}$ and ϕ_{η}^{*} region where non-perturbative effects are relevant, highlighting the benefits of this state-of-the-art prediction.

Figure 6 compares the $p_{\mathrm{T}}^{\ell\ell}$ measurement with predictions in the range of $p_{\mathrm{T}}^{\ell\ell} > 10$ GeV. In addition to the SHERPA prediction described above, the data are compared with the

fixed-order NNLOJET prediction described above both with and without NLO EW corrections [13]. The NNLOJET prediction is only expected to describe the data at sufficiently large $p_{\mathrm{T}}^{\ell\ell} \gtrsim 15$ GeV, while deviations for smaller values are expected due to large logarithms $\ln(m_{\ell\ell}/p_{\mathrm{T}}^{\ell\ell})$ [93]. At the highest $p_{\mathrm{T}}^{\ell\ell}$ values probed, the application of NLO EW leads to a suppression of up to 20% due to large Sudakov logarithms. The theoretical uncertainties on these corrections are not shown, but have been elsewhere estimated to be up to 5% for $p_{\mathrm{T}}^{\ell\ell} \approx 1$ TeV [15]. In this region, NNLOJET without NLO EW corrections is generally above the data, and when including these corrections it tends to be lower than the data. However, the difference is not significantly larger than the uncertainties in the measurements.

6 Conclusion

Measurements of the $Z/\gamma^* \to ee$ and $Z/\gamma^* \to \mu\mu$ cross-sections, differential in the transverse momentum and ϕ_η^*, have been performed in a fiducial volume defined by $p_{\mathrm{T}}^{\ell} > 27$ GeV, $|\eta_\ell| < 2.5$ and $66 < m_{\ell\ell} < 116$ GeV, using 36.1 fb^{-1} of data from proton–proton collisions recorded in 2015 and 2016 at a centre-of-mass energy of 13 TeV with the ATLAS experiment at the LHC. This data-set allows coverage of a kinematic range up to the TeV-range. The cross-section results from the individual channels were combined and good agreement between the two was observed. The relative precision of the combined result is better than 0.2% for $p_{\mathrm{T}}^{\ell\ell} < 30$ GeV, which provides crucial information to validate and tune MC event generators and will constrain models of vector-boson production in future measurements of the W-boson mass.

The integrated fiducial cross-section measurements are compared with fixed-order perturbative QCD predictions. Differential spectra in $p_{\mathrm{T}}^{\ell\ell}$ and ϕ_η^* are compared with a selection of calculations implementing resummation and non-perturbative effects through parton showers or analytic calculations. The predictions based on the PYTHIA8 parton shower with parameters tuned to 7 TeV data are found to describe the 13 TeV data well at low $p_{\mathrm{T}}^{\ell\ell}$ and ϕ_η^*. The SHERPA prediction based on merging of higher-order, high-multiplicity matrix elements gives an excellent description of the data at high $p_{\mathrm{T}}^{\ell\ell}$, while the very accurate RADISH NNLO+N^{3}LL prediction agrees with data for the full spectrum. The fixed-order NNLOJET prediction with and without NLO EW effects describes the data well for high $p_{\mathrm{T}}^{\ell\ell}$.

Acknowledgements We thank CERN for the very successful operation of the LHC, as well as the support staff from our institutions without whom ATLAS could not be operated efficiently. We acknowledge the support of ANPCyT, Argentina; YerPhI, Armenia; ARC, Australia; BMWFW and FWF, Austria; ANAS, Azerbaijan; SSTC, Belarus; CNPq and FAPESP, Brazil; NSERC, NRC and CFI, Canada; CERN; CONICYT, Chile; CAS, MOST and NSFC, China; COLCIENCIAS, Colombia; MSMT CR, MPO CR and VSC CR, Czech Republic; DNRF and DNSRC, Denmark; IN2P3-CNRS and CEA-DRF/IRFU, France; SRNSFG, Georgia; BMBF, HGF and MPG, Germany; GSRT, Greece; RGC and Hong Kong SAR, China; ISF and Benoziyo Center, Israel; INFN, Italy; MEXT and JSPS, Japan; CNRST, Morocco; NWO, The Netherlands; RCN, Norway; MNiSW and NCN, Poland; FCT, Portugal; MNE/IFA, Romania; MES of Russia and NRC KI, Russia Federation; JINR; MESTD, Serbia; MSSR, Slovakia; ARRS and MIZŠ, Slovenia; DST/NRF, South Africa; MINECO, Spain; SRC and Wallenberg Foundation, Sweden; SERI, SNSF and Cantons of Bern and Geneva, Switzerland; MOST, Taiwan; TAEK, Turkey; STFC, UK; DOE and NSF, USA. In addition, individual groups and members have received support from BCKDF, CANARIE, Compute Canada and CRC, Canada; ERC, ERDF, Horizon 2020, Marie Skłodowska-Curie Actions and COST, European Union; Investissements d'Avenir Labex, Investissements d'Avenir Idex and ANR, France; DFG and AvH Foundation, Germany; Herakleitos, Thales and Aristeia programmes co-financed by EU-ESF and the Greek NSRF, Greece; BSF-NSF and GIF, Israel; CERCA Programme Generalitat de Catalunya and PROMETEO Programme Generalitat Valenciana, Spain; Göran Gustafssons Stiftelse, Sweden; The Royal Society and Leverhulme Trust, UK. The crucial computing support from all WLCG partners is acknowledged gratefully, in particular from CERN, the ATLAS Tier-1 facilities at TRIUMF (Canada), NDGF (Denmark, Norway, Sweden), CC-IN2P3 (France), KIT/GridKA (Germany), INFN-CNAF (Italy), NL-T1 (Netherlands), PIC (Spain), ASGC (Taiwan), RAL (UK) and BNL (USA), the Tier-2 facilities worldwide and large non-WLCG resource providers. Major contributors of computing resources are listed in Ref. [95].

Data Availability Statement This manuscript has no associated data or the data will not be deposited. [Authors' comment: All ATLAS scientific output is published in journals, and preliminary results are made available in Conference Notes. All are openly available, without restriction on use by external parties beyond copyright law and the standard conditions agreed by CERN. Data associated with journal publications are also made available: tables and data from plots (e.g. cross section values, likelihood profiles, selection efficiencies, cross section limits, ...) are stored in appropriate repositories such as HEPDATA (http://hepdata.cedar.ac.uk/). ATLAS also strives to make additional material related to the paper available that allows a reinterpretation of the data in the context of new theoretical models. For example, an extended encapsulation of the analysis is often provided for measurements in the framework of RIVET (http://rivet.hepforge.org/). This information is taken from the ATLAS Data Access Policy, which is a public document that can be downloaded from http://opendata.cern.ch/record/413 [opendata.cern.ch].]

Funded by SCOAP^3.

References

1. S.D. Drell, T.-M. Yan, Massive lepton pair production in hadron–hadron collisions at high-energies. Phys. Rev. Lett. **25**, 316 (1970)
2. J.C. Collins, D.E. Soper, G.F. Sterman, Transverse momentum distribution in Drell–Yan pair and W and Z boson Production. Nucl. Phys. B **250**, 199 (1985)
3. C. Balázs, C.-P. Yuan, Soft gluon effects on lepton pairs at hadron colliders. Phys. Rev. D **56**, 5558 (1997). arXiv:hep-ph/9704258
4. T. Becher, M. Neubert, Drell–Yan production at small q_T, transverse parton distributions and the collinear anomaly. Eur. Phys. J. C **71**, 1665 (2011). arXiv:1007.4005 [hep-ph]
5. S. Catani, D. de Florian, G. Ferrera, M. Grazzini, Vector boson production at hadron colliders: transverse-momentum resummation and leptonic decay. JHEP **12**, 047 (2015). arXiv:1507.06937 [hep-ph]
6. M.A. Ebert, F.J. Tackmann, Resummation of transverse momentum distributions in distribution space. JHEP **02**, 110 (2017). arXiv:1611.08610 [hep-ph]
7. W. Bizon, P.F. Monni, E. Re, L. Rottoli, P. Torrielli, Momentum-space resummation for transverse observables and the Higgs $p_\perp$ at $N^3LL+NNLO$. JHEP **02**, 108 (2018). arXiv:1705.09127 [hep-ph]
8. K. Melnikov, F. Petriello, Electroweak gauge boson production at hadron colliders through $\mathcal{O}(\alpha_s^2)$. Phys. Rev. D **74**, 114017 (2006). arXiv:hep-ph/0609070
9. Y. Li, F. Petriello, Combining QCD and electroweak corrections to dilepton production in FEWZ. Phys. Rev. D **86**, 094034 (2012). arXiv:1208.5967 [hep-ph]
10. S. Catani, L. Cieri, G. Ferrera, D. de Florian, M. Grazzini, Vector Boson production at hadron colliders: a fully exclusive QCD calculation at next-to-next-to-leading order. Phys. Rev. Lett. **103**, 082001 (2009). arXiv:0903.2120 [hep-ph]
11. R. Boughezal et al., Z-boson production in association with a jet at next-to-next-to-neading order in perturbative QCD. Phys. Rev. Lett. **116**, 152001 (2016). arXiv:1512.01291 [hep-ph]
12. A. Gehrmann-De Ridder, T. Gehrmann, E.W.N. Glover, A. Huss, T.A. Morgan, Precise QCD predictions for the production of a Z boson in association with a hadronic jet. Phys. Rev. Lett. **117**, 022001 (2016). arXiv:1507.02850 [hep-ph]
13. A. Denner, S. Dittmaier, T. Kasprzik, A. Mück, Electroweak corrections to dilepton + jet production at hadron colliders. JHEP **06**, 069 (2011). arXiv:1103.0914 [hep-ph]
14. S. Kallweit, J.M. Lindert, P. Maierhöfer, S. Pozzorini, M. Schönherr, NLO QCD+EW predictions for V + jets including off-shell vector-boson decays and multijet merging. JHEP **04**, 021 (2016). arXiv:1511.08692 [hep-ph]
15. J.M. Lindert et al., Precise predictions for V+jets dark matter backgrounds. Eur. Phys. J. C **77**, 829 (2017). arXiv:1705.04664 [hep-ph]
16. J. Bellm et al., Herwig 7.0/Herwig++ 3.0 release note. Eur. Phys. J. C **76**, 196 (2016). arXiv:1512.01178 [hep-ph]
17. T. Sjöstrand et al., An introduction to PYTHIA 8.2. Comput. Phys. Commun. **191**, 159 (2015). arXiv:1410.3012 [hep-ph]
18. E. Bothmann et al., Event generation with Sherpa 2.2. Sci. Post Phys. **7**, 034 (2019). arXiv:1905.09127 [hep-ph]
19. ATLAS Collaboration, Search for dark matter and other new phenomena in events with an energetic jet and large missing transverse momentum using the ATLAS detector. JHEP **01**, 126 (2018). arXiv:1711.03301 [hep-ex]
20. ATLAS Collaboration, Measurement of the W-boson mass in pp collisions at $\sqrt{s} = 7$ TeV with the ATLAS detector. Eur. Phys. J. C **78**, 110 (2018). arXiv:1701.07240 [hep-ex]. Erratum: Eur. Phys. J. C 78 (2018) 898
21. ATLAS Collaboration, Measurement of the transverse momentum distribution of W bosons in pp collisions at $\sqrt{s} = 7$ TeV with the ATLAS detector. Phys. Rev. D **85**, 012005 (2012). arXiv:1108.6308 [hep-ex]
22. ATLAS Collaboration, Measurement of the Z/γ^* boson transverse momentum distribution in pp collisions at $\sqrt{s} = 7$ TeV with the ATLAS detector. JHEP **09**, 145 (2014). arXiv:1406.3660 [hep-ex]
23. ATLAS Collaboration, Measurement of the transverse momentum and ϕ_η^* distributions of Drell-Yan lepton pairs in proton–proton collisions at $\sqrt{s} = 8$ TeV with the ATLAS detector. Eur. Phys. J. C **76**, 291 (2016). arXiv:1512.02192 [hep-ex]
24. CMS Collaboration, Measurements of differential Z boson production cross sections in proton–proton collisions at $\sqrt{s} = 13$ TeV. JHEP **12**, 061 (2019). arXiv:1909.04133 [hep-ex]
25. CMS Collaboration, Measurement of differential cross sections in the kinematic angular variable ϕ^* for inclusive Z boson production in pp collisions at $\sqrt{s} = 8$ TeV. JHEP **03**, 172 (2018). arXiv:1710.07955 [hep-ex]
26. CMS Collaboration, Measurement of the transverse momentum spectra of weak vector bosons produced in proton-proton collisions at $\sqrt{s} = 8$ TeV. JHEP **02**, 096 (2017). arXiv:1606.05864 [hep-ex]
27. CMS Collaboration, Measurement of the Z boson differential cross section in transverse momentum and rapidity in proton-proton collisions at 8 TeV. Phys. Lett. B **749**, 187 (2015). arXiv:1504.03511 [hep-ex]
28. CMS Collaboration, Measurement of the rapidity and transverse momentum distributions of Z bosons in pp collisions at $\sqrt{s} = 7$ TeV. Phys. Rev. D **85**, 032002 (2012). arXiv:1110.4973 [hep-ex]
29. LHCb Collaboration, Measurement of the forward Z boson production cross-section in pp collisions at $\sqrt{s} = 7$ TeV. JHEP **08**, 039 (2015). arXiv:1505.07024 [hep-ex]
30. LHCb Collaboration, Measurement of forward W and Z boson production in association with jets in proton-proton collisions at $\sqrt{s} = 8$ TeV. JHEP **05**, 131 (2016). arXiv:1605.00951 [hep-ex]
31. LHCb Collaboration, Measurement of the forward Z boson production cross-section in pp collisions at $\sqrt{s} = 13$ TeV. JHEP **09**, 136 (2016). arXiv:1607.06495 [hep-ex]
32. T. Aaltonen et al., Transverse momentum cross section of e^+e^- pairs in the Z-boson region from $p\bar{p}$ collisions at $\sqrt{s} = 1.96$ TeV. Phys. Rev. D **86**, 052010 (2012). arXiv:1207.7138 [hep-ex]
33. V.M. Abazov et al., Measurement of the normalized $Z/\gamma^* \to \mu^+\mu^-$ transverse momentum distribution in $p\bar{p}$ collisions at $\sqrt{s} = 1.96$ TeV. Phys. Lett. B **693**, 522 (2010). arXiv:1006.0618 [hep-ex]
34. V.M. Abazov et al., Precise study of the Z/γ^* Boson transverse momentum distribution in $p\bar{p}$ collisions using a novel technique. Phys. Rev. Lett. **106**, 122001 (2011). arXiv:1010.0262 [hep-ex]
35. A. Banfi, S. Redford, M. Vesterinen, P. Waller, T.R. Wyatt, Optimisation of variables for studying dilepton transverse momentum distributions at hadron colliders. Eur. Phys. J. C **71**, 1600 (2011). arXiv:1009.1580 [hep-ex]
36. ATLAS Collaboration, The ATLAS Experiment at the CERN Large Hadron Collider, JINST **3**, S08003 (2008)
37. B. Abbott et al., Production and integration of the ATLAS Insertable B-Layer. JINST **13**, T05008 (2018). arXiv:1803.00844 [physics.ins-det]
38. ATLAS Collaboration, ATLAS Insertable B-Layer Technical Design Report, ATLAS-TDR-19, (2010), https://cds.cern.ch/record/1291633, Addendum: ATLAS-TDR-19-ADD-1, (2012), https://cds.cern.ch/record/1451888
39. ATLAS Collaboration, Performance of the ATLAS trigger system in 2015. Eur. Phys. J. C **77**, 317 (2017). arXiv:1611.09661 [hep-ex]
40. P. Nason, A new method for combining NLO QCD with shower Monte Carlo algorithms. JHEP **11**, 040 (2004). arXiv:hep-ph/0409146
41. S. Frixione, P. Nason, C. Oleari, Matching NLO QCD computations with parton shower simulations: the POWHEG method. JHEP **11**, 070 (2007). arXiv:0709.2092 [hep-ph]

42. S. Alioli, P. Nason, C. Oleari, E. Re, A general framework for implementing NLO calculations in shower Monte Carlo programs: the POWHEG BOX. JHEP **06**, 043 (2010). arXiv:1002.2581 [hep-ph]
43. S. Alioli, P. Nason, C. Oleari, E. Re, NLO vector-boson production matched with shower in POWHEG. JHEP **07**, 060 (2008). arXiv:0805.4802 [hep-ph]
44. H.-L. Lai et al., New parton distributions for collider physics. Phys. Rev. D **82**, 074024 (2010). arXiv:1007.2241 [hep-ph]
45. J. Pumplin et al., New Generation of Parton Distributions with Uncertainties from Global QCD Analysis. JHEP **07**, 012 (2002). arXiv:hep-ph/0201195
46. P. Golonka, Z. Was, PHOTOS Monte Carlo: a precision tool for QED corrections in Z and W decays. Eur. Phys. J. C **45**, 97 (2006). arXiv:hep-ph/0506026
47. N. Davidson, T. Przedzinski, Z. Was, PHOTOS Interface in C++: Technical and Physics Documentation. Comput. Phys. Commun. **199**, 86 (2016). arXiv:1011.0937 [hep-ph]
48. D.J. Lange, The EvtGen particle decay simulation package. Nucl. Instrum. Methods A **462**, 152 (2001)
49. P. Nason, G. Zanderighi, W^+W^-, WZ and ZZ production in the POWHEG-BOX-V2. Eur. Phys. J. C **74**, 2702 (2014). arXiv:1311.1365 [hep-ph]
50. S. Frixione, P. Nason, G. Ridolfi, A positive-weight next-to-leading-order Monte Carlo for heavy flavour hadroproduction. JHEP **09**, 126 (2007). arXiv:0707.3088 [hep-ph]
51. E. Re, Single-top W_t-channel production matched with parton showers using the POWHEG method. Eur. Phys. J. C **71**, 1547 (2011). arXiv:1009.2450 [hep-ph]
52. T. Sjöstrand, S. Mrenna, P.Z. Skands, PYTHIA 6.4 Physics and Manual. JHEP **05**, 026 (2006). arXiv:hep-ph/0603175
53. P.Z. Skands, Tuning Monte Carlo generators: The Perugia tunes. Phys. Rev. D **82**, 074018 (2010). arXiv:1005.3457 [hep-ph]
54. ATLAS Collaboration, ATLAS Pythia 8 tunes to 7 TeV data, ATL-PHYS-PUB-2014-021 (2014). https://cds.cern.ch/record/1966419
55. R.D. Ball et al., Parton distributions for the LHC Run II. JHEP **04**, 040 (2015). arXiv:1410.8849 [hep-ph]
56. R.D. Ball et al., Parton distributions with QED corrections. Nucl. Phys. B **877**, 290 (2013). arXiv:1308.0598 [hep-ph]
57. A.D. Martin, W.J. Stirling, R.S. Thorne, G. Watt, Parton distributions for the LHC. Eur. Phys. J. C **63**, 189 (2009). arXiv:0901.0002 [hep-ph]
58. ATLAS Collaboration, Summary of ATLAS Pythia 8 tunes, ATL-PHYS-PUB-2012-003 (2012). https://cds.cern.ch/record/1474107
59. S. Agostinelli et al., GEANT4 - a simulation toolkit. Nucl. Instrum. Methods A **506**, 250 (2003)
60. ATLAS Collaboration, The ATLAS simulation infrastructure. Eur. Phys. J. C **70**, 823 (2010). arXiv:1005.4568 [physics.ins-det]
61. ATLAS Collaboration, Muon reconstruction performance of the ATLAS detector in proton–proton collision data at $\sqrt{s} = 13$ TeV. Eur. Phys. J. C **76**, 292 (2016). arXiv:1603.05598 [hep-ex]
62. ATLAS Collaboration, Electron reconstruction and identification in the ATLAS experiment using the 2015 and 2016 LHC proton–proton collision data at $\sqrt{s} = 13$ TeV. Eur. Phys. J. C **79**, 639 (2019). arXiv:1902.04655 [hep-ex]
63. ATLAS Collaboration, Electron and photon energy calibration with the ATLAS detector using 2015–2016 LHC proton–proton collision data. JINST **14**, P03017 (2019). arXiv:1812.03848 [hep-ex]
64. ATLAS Collaboration, Performance of electron and photon triggers in ATLAS during LHC Run 2 (2019). arXiv:1909.00761 [hep-ex]
65. G. D'Agostini, A multidimensional unfolding method based on Bayes' theorem. Nucl. Instrum. Meth. Phys. Res. A **A362**, 487 (1995)
66. G. D'Agostini, Improved iterative Bayesian unfolding (2010). arXiv:1010.0632 [physics.data-an]
67. T. Adye, Unfolding algorithms and tests using RooUnfold (2011). arXiv:1105.1160 [physics.data-an]
68. ATLAS Collaboration, Measurement of the Inelastic Proton–Proton Cross Section at $\sqrt{s} = 13$ TeV with the ATLAS Detector at the LHC. Phys. Rev. Lett. **117**, 182002 (2016). arXiv:1606.02625 [hep-ex]
69. A. Buckley et al., LHAPDF6: parton density access in the LHC precision era. Eur. Phys. J. C **75**, 132 (2015). arXiv:1412.7420 [hep-ph]
70. ATLAS Collaboration, Luminosity determination in pp collisions at $\sqrt{s} = 13$ TeV using the ATLAS detector at the LHC, ATLAS-CONF-2019-021 (2019). https://cds.cern.ch/record/2677054
71. G. Avoni et al., The new LUCID-2 detector for luminosity measurement and monitoring in ATLAS. JINST **13**, P07017 (2018)
72. ATLAS Collaboration, Measurements of top-quark pair to Z-boson cross-section ratios at $\sqrt{s} = 13$, 8, 7 TeV with the ATLAS detector. JHEP **02**, 117 (2017). arXiv:1612.03636 [hep-ex]
73. L. Lyons, D. Gibaut, P. Clifford, How to combine correlated estimates of a single physical quantity. Nucl. Instrum. Methods A **270**, 110 (1988)
74. A. Valassi, Combining correlated measurements of several different physical quantities. Nucl. Instrum. Methods A **500**, 391 (2003)
75. R. Nisius, On the combination of correlated estimates of a physics observable. Eur. Phys. J. C **74**, 3004 (2014). arXiv:1402.4016 [physics.data-an]
76. ATLAS Collaboration, Measurement of $W^{\pm}$ and Z-boson production cross sections in pp collisions at $\sqrt{s} = 13$ TeV with the ATLAS detector. Phys. Lett. B **759**, 601 (2016). arXiv:1603.09222 [hep-ex]
77. S. Camarda et al., DYTurbo: Fast predictions for Drell–Yan processess(2019).arXiv:1910.07049 [hep-ph]
78. S. Dulat et al., New parton distribution functions from a global analysis of quantum chromodynamics. Phys. Rev. D **93**, 033006 (2016). arXiv:1506.07443 [hep-ph]
79. W.F.L. Hollik, Radiative corrections in the standard model and their role for precision tests of the electroweak theory. Fortsch. Phys. **38**, 165 (1990)
80. ATLAS Collaboration, Measurement of angular correlations in Drell-Yan lepton pairs to probe Z/γ^* boson transverse momentum at $\sqrt{s} = 7$ TeV with the ATLAS detector.Phys. Lett. B **720**, 32 (2013). arXiv:1211.6899 [hep-ex]
81. T. Gleisberg, S. Höche, Comix, a new matrix element generator. JHEP **12**, 039 (2008). arXiv:0808.3674 [hep-ph]
82. F. Cascioli, P. Maierhofer, S. Pozzorini, Scattering amplitudes with open loops. Phys. Rev. Lett. **108**, 111601 (2012). arXiv:1111.5206 [hep-ph]
83. A. Denner, S. Dittmaier, L. Hofer, Collier: a fortran-based complex one-loop library in extended regularizations. Comput. Phys. Commun. **212**, 220 (2017). arXiv:1604.06792 [hep-ph]
84. S. Schumann, F. Krauss, A parton shower algorithm based on Catani-Seymour dipole factorisation. JHEP **03**, 038 (2008). arXiv:0709.1027 [hep-ph]
85. J.-C. Winter, F. Krauss, G. Soff, A modified cluster-hadronisation model. Eur. Phys. J. C **36**, 381 (2004). arXiv:hep-ph/0311085 [hep-ph]
86. S. Höche, F. Krauss, M. Schönherr, F. Siegert, A critical appraisal of NLO+PS matching methods. JHEP **09**, 049 (2012). arXiv:1111.1220 [hep-ph]
87. S. Catani, F. Krauss, R. Kuhn, B.R. Webber, QCD matrix elements + parton showers. JHEP **11**, 063 (2001). arXiv:hep-ph/0109231
88. S. Höche, F. Krauss, S. Schumann, F. Siegert, QCD matrix elements and truncated showers. JHEP **05**, 053 (2009). arXiv:0903.1219 [hep-ph]
89. S. Höche, F. Krauss, M. Schönherr, F. Siegert, QCD matrix elements + parton showers: the NLO case. JHEP **04**, 027 (2013). arXiv:1207.5030 [hep-ph]

90. E. Bothmann, M. Schönherr, S. Schumann, Reweighting QCD matrix-element and parton-shower calculations. Eur. Phys. J. C **76**, 590 (2016). arXiv:1606.08753 [hep-ph]
91. W. Bizon et al., The transverse momentum spectrum of weak gauge bosons at N^{3}LL+NNLO. Eur. Phys. J. C **79**, 868 (2019). arXiv:1905.05171 [hep-ph]
92. W. Bizon et al., Fiducial distributions in Higgs and Drell-Yan production at N^{3}LL+NNLO. JHEP **12**, 132 (2018). arXiv:1805.05916 [hep-ph]
93. A. Gehrmann-De Ridder, T. Gehrmann, E.W.N. Glover, A. Huss, T.A. Morgan, NNLO QCD corrections for Drell-Yan p_T^Z and ϕ^* observables at the LHC. JHEP **11**, 094 (2016). arXiv:1610.01843 [hep-ph].Erratum: JHEP 10 (2018) 126
94. R.D. Ball et al., Parton distributions from high-precision collider data. Eur. Phys. J. C **77**, 663 (2017). arXiv:1706.00428 [hep-ph]
95. ATLAS Collaboration, ATLAS Computing Acknowledgements, ATL-GEN-PUB-2016-002.https://cds.cern.ch/record/2202407

ATLAS Collaboration

G. Aad[102], B. Abbott[129], D. C. Abbott[103], A. Abed Abud[36], K. Abeling[53], D. K. Abhayasinghe[94], S. H. Abidi[167], O. S. AbouZeid[40], N. L. Abraham[156], H. Abramowicz[161], H. Abreu[160], Y. Abulaiti[6], B. S. Acharya[67a,67b,n], B. Achkar[53], S. Adachi[163], L. Adam[100], C. Adam Bourdarios[5], L. Adamczyk[84a], L. Adamek[167], J. Adelman[121], M. Adersberger[114], A. Adiguzel[12c], S. Adorni[54], T. Adye[144], A. A. Affolder[146], Y. Afik[160], C. Agapopoulou[65], M. N. Agaras[38], A. Aggarwal[119], C. Agheorghiesei[27c], J. A. Aguilar-Saavedra[140f,140a,ag], F. Ahmadov[80], W. S. Ahmed[104], X. Ai[18], G. Aielli[74a,74b], S. Akatsuka[86], T. P. A. Åkesson[97], E. Akilli[54], A. V. Akimov[111], K. Al Khoury[65], G. L. Alberghi[23a,23b], J. Albert[176], M. J. Alconada Verzini[161], S. Alderweireldt[36], M. Aleksa[36], I. N. Aleksandrov[80], C. Alexa[27b], T. Alexopoulos[10], A. Alfonsi[120], F. Alfonsi[23a,23b], M. Alhroob[129], B. Ali[142], M. Aliev[166], G. Alimonti[69a], S. P. Alkire[148], C. Allaire[65], B. M. M. Allbrooke[156], B. W. Allen[132], P. P. Allport[21], A. Aloisio[70a,70b], F. Alonso[89], C. Alpigiani[148], A. A. Alshehri[57], E. Alunno Camelia[74a,74b], M. Alvarez Estevez[99], M. G. Alviggi[70a,70b], Y. Amaral Coutinho[81b], A. Ambler[104], L. Ambroz[135], C. Amelung[26], D. Amidei[106], S. P. Amor Dos Santos[140a], S. Amoroso[46], C. S. Amrouche[54], F. An[79], C. Anastopoulos[149], N. Andari[145], T. Andeen[11], C. F. Anders[61b], J. K. Anders[20], A. Andreazza[69a,69b], V. Andrei[61a], C. R. Anelli[176], S. Angelidakis[38], A. Angerami[39], A. V. Anisenkov[122a,122b], A. Annovi[72a], C. Antel[54], M. T. Anthony[149], E. Antipov[130], M. Antonelli[51], D. J. A. Antrim[171], F. Anulli[73a], M. Aoki[82], J. A. Aparisi Pozo[174], L. Aperio Bella[15a], J. P. Araque[140a], V. Araujo Ferraz[81b], R. Araujo Pereira[81b], C. Arcangeletti[51], A. T. H. Arce[49], F. A. Arduh[89], J.-F. Arguin[110], S. Argyropoulos[78], J.-H. Arling[46], A. J. Armbruster[36], A. Armstrong[171], O. Arnaez[167], H. Arnold[120], Z. P. Arrubarrena Tame[114], G. Artoni[135], S. Artz[100], S. Asai[163], T. Asawatavonvanich[165], N. Asbah[59], E. M. Asimakopoulou[172], L. Asquith[156], J. Assahsah[35d], K. Assamagan[29], R. Astalos[28a], R. J. Atkin[33a], M. Atkinson[173], N. B. Atlay[19], H. Atmani[65], K. Augsten[142], G. Avolio[36], R. Avramidou[60a], M. K. Ayoub[15a], A. M. Azoulay[168b], G. Azuelos[110,ar], H. Bachacou[145], K. Bachas[68a,68b], M. Backes[135], F. Backman[45a,45b], P. Bagnaia[73a,73b], M. Bahmani[85], H. Bahrasemani[152], A. J. Bailey[174], V. R. Bailey[173], J. T. Baines[144], M. Bajic[40], C. Bakalis[10], O. K. Baker[183], P. J. Bakker[120], D. Bakshi Gupta[8], S. Balaji[157], E. M. Baldin[122a,122b], P. Balek[180], F. Balli[145], W. K. Balunas[135], J. Balz[100], E. Banas[85], A. Bandyopadhyay[24], Sw. Banerjee[181,i], A. A. E. Bannoura[182], L. Barak[161], W. M. Barbe[38], E. L. Barberio[105], D. Barberis[55a,55b], M. Barbero[102], G. Barbour[95], T. Barillari[115], M.-S. Barisits[36], J. Barkeloo[132], T. Barklow[153], R. Barnea[160], S. L. Barnes[60c], B. M. Barnett[144], R. M. Barnett[18], Z. Barnovska-Blenessy[60a], A. Baroncelli[60a], G. Barone[29], A. J. Barr[135], L. Barranco Navarro[45a,45b], F. Barreiro[99], J. Barreiro Guimarães da Costa[15a], S. Barsov[138], R. Bartoldus[153], G. Bartolini[102], A. E. Barton[90], P. Bartos[28a], A. Basalaev[46], A. Basan[100], A. Bassalat[65,am], M. J. Basso[167], R. L. Bates[57], S. Batlamous[35e], J. R. Batley[32], B. Batool[151], M. Battaglia[146], M. Bauce[73a,73b], F. Bauer[145], K. T. Bauer[171], H. S. Bawa[31], J. B. Beacham[49], T. Beau[136], P. H. Beauchemin[170], F. Becherer[52], P. Bechtle[24], H. C. Beck[53], H. P. Beck[20,r], K. Becker[178], C. Becot[46], A. Beddall[12d], A. J. Beddall[12a], V. A. Bednyakov[80], M. Bedognetti[120], C. P. Bee[155], T. A. Beermann[182], M. Begalli[81b], M. Begel[29], A. Behera[155], J. K. Behr[46], F. Beisiegel[24], A. S. Bell[95], G. Bella[161], L. Bellagamba[23b], A. Bellerive[34], P. Bellos[9], K. Beloborodov[122a,122b], K. Belotskiy[112], N. L. Belyaev[112], D. Benchekroun[35a], N. Benekos[10], Y. Benhammou[161], D. P. Benjamin[6], M. Benoit[54], J. R. Bensinger[26], S. Bentvelsen[120], L. Beresford[135], M. Beretta[51], D. Berge[46], E. Bergeaas Kuutmann[172], N. Berger[5], B. Bergmann[142], L. J. Bergsten[26], J. Beringer[18], S. Berlendis[7], G. Bernardi[136], C. Bernius[153], F. U. Bernlochner[24], T. Berry[94], P. Berta[100], C. Bertella[15a], I. A. Bertram[90], O. Bessidskaia Bylund[182], N. Besson[145], A. Bethani[101], S. Bethke[115], A. Betti[42], A. J. Bevan[93], J. Beyer[115], D. S. Bhattacharya[177], P. Bhattarai[26], R. Bi[139], R. M. Bianchi[139], O. Biebel[114], D. Biedermann[19], R. Bielski[36], K. Bierwagen[100], N. V. Biesuz[72a,72b], M. Biglietti[75a], T. R. V. Billoud[110], M. Bindi[53], A. Bingul[12d], C. Bini[73a,73b], S. Biondi[23a,23b], M. Birman[180], T. Bisanz[53], J. P. Biswal[161], D. Biswas[181,i], A. Bitadze[101], C. Bittrich[48], K. Bjørke[134], K. M. Black[25], T. Blazek[28a], I. Bloch[46], C. Blocker[26], A. Blue[57], U. Blumenschein[93], G. J. Bobbink[120], V. S. Bobrovnikov[122a,122b], S. S. Bocchetta[97], A. Bocci[49], D. Boerner[46],

D. Bogavac[14], A. G. Bogdanchikov[122a,122b], C. Bohm[45a], V. Boisvert[94], P. Bokan[53,172], T. Bold[84a], A. S. Boldyrev[113], A. E. Bolz[61b], M. Bomben[136], M. Bona[93], J. S. Bonilla[132], M. Boonekamp[145], C. D. Booth[94], H. M. Borecka-Bielska[91], A. Borisov[123], G. Borissov[90], J. Bortfeldt[36], D. Bortoletto[135], D. Boscherini[23b], M. Bosman[14], J. D. Bossio Sola[104], K. Bouaouda[35a], J. Boudreau[139], E. V. Bouhova-Thacker[90], D. Boumediene[38], S. K. Boutle[57], A. Boveia[127], J. Boyd[36], D. Boye[33c,an], I. R. Boyko[80], A. J. Bozson[94], J. Bracinik[21], N. Brahimi[102], G. Brandt[182], O. Brandt[32], F. Braren[46], B. Brau[103], J. E. Brau[132], W. D. Breaden Madden[57], K. Brendlinger[46], L. Brenner[46], R. Brenner[172], S. Bressler[180], B. Brickwedde[100], D. L. Briglin[21], D. Britton[57], D. Britzger[115], I. Brock[24], R. Brock[107], G. Brooijmans[39], W. K. Brooks[147c], E. Brost[121], J. H. Broughton[21], P. A. Bruckman de Renstrom[85], D. Bruncko[28b], A. Bruni[23b], G. Bruni[23b], L. S. Bruni[120], S. Bruno[74a,74b], M. Bruschi[23b], N. Bruscino[73a,73b], P. Bryant[37], L. Bryngemark[97], T. Buanes[17], Q. Buat[36], P. Buchholz[151], A. G. Buckley[57], I. A. Budagov[80], M. K. Bugge[134], F. Bührer[52], O. Bulekov[112], T. J. Burch[121], S. Burdin[91], C. D. Burgard[120], A. M. Burger[130], B. Burghgrave[8], J. T. P. Burr[46], C. D. Burton[11], J. C. Burzynski[103], V. Büscher[100], E. Buschmann[53], P. J. Bussey[57], J. M. Butler[25], C. M. Buttar[57], J. M. Butterworth[95], P. Butti[36], W. Buttinger[36], C. J. Buxo Vazquez[107], A. Buzatu[158], A. R. Buzykaev[122a,122b], G. Cabras[23a,23b], S. Cabrera Urbán[174], D. Caforio[56], H. Cai[173], V. M. M. Cairo[153], O. Cakir[4a], N. Calace[36], P. Calafiura[18], A. Calandri[102], G. Calderini[136], P. Calfayan[66], G. Callea[57], L. P. Caloba[81b], A. Caltabiano[74a,74b], S. Calvente Lopez[99], D. Calvet[38], S. Calvet[38], T. P. Calvet[155], M. Calvetti[72a,72b], R. Camacho Toro[136], S. Camarda[36], D. Camarero Munoz[99], P. Camarri[74a,74b], D. Cameron[134], R. Caminal Armadans[103], C. Camincher[36], S. Campana[36], M. Campanelli[95], A. Camplani[40], A. Campoverde[151], V. Canale[70a,70b], A. Canesse[104], M. Cano Bret[60c], J. Cantero[130], T. Cao[161], Y. Cao[173], M. D. M. Capeans Garrido[36], M. Capua[41a,41b], R. Cardarelli[74a], F. Cardillo[149], G. Carducci[41a,41b], I. Carli[143], T. Carli[36], G. Carlino[70a], B. T. Carlson[139], L. Carminati[69a,69b], R. M. D. Carney[45a,45b], S. Caron[119], E. Carquin[147c], S. Carrá[46], J. W. S. Carter[167], M. P. Casado[14,e], A. F. Casha[167], D. W. Casper[171], R. Castelijn[120], F. L. Castillo[174], L. Castillo Garcia[14], V. Castillo Gimenez[174], N. F. Castro[140a,140e], A. Catinaccio[36], J. R. Catmore[134], A. Cattai[36], V. Cavaliere[29], E. Cavallaro[14], M. Cavalli-Sforza[14], V. Cavasinni[72a,72b], E. Celebi[12b], L. Cerda Alberich[174], K. Cerny[131], A. S. Cerqueira[81a], A. Cerri[156], L. Cerrito[74a,74b], F. Cerutti[18], A. Cervelli[23a,23b], S. A. Cetin[12b], Z. Chadi[35a], D. Chakraborty[121], W. S. Chan[120], W. Y. Chan[91], J. D. Chapman[32], B. Chargeishvili[159b], D. G. Charlton[21], T. P. Charman[93], C. C. Chau[34], S. Che[127], S. Chekanov[6], S. V. Chekulaev[168a], G. A. Chelkov[80,aq], M. A. Chelstowska[36], B. Chen[79], C. Chen[60a], C. H. Chen[79], H. Chen[29], J. Chen[60a], J. Chen[39], J. Chen[26], S. Chen[137], S. J. Chen[15c], X. Chen[15b], Y.-H. Chen[46], H. C. Cheng[63a], H. J. Cheng[15a], A. Cheplakov[80], E. Cheremushkina[123], R. Cherkaoui El Moursli[35e], E. Cheu[7], K. Cheung[64], T. J. A. Chevalérias[145], L. Chevalier[145], V. Chiarella[51], G. Chiarelli[72a], G. Chiodini[68a], A. S. Chisholm[21], A. Chitan[27b], I. Chiu[163], Y. H. Chiu[176], M. V. Chizhov[80], K. Choi[66], A. R. Chomont[73a,73b], S. Chouridou[162], Y. S. Chow[120], M. C. Chu[63a], X. Chu[15a,15d], J. Chudoba[141], A. J. Chuinard[104], J. J. Chwastowski[85], L. Chytka[131], D. Cieri[115], K. M. Ciesla[85], D. Cinca[47], V. Cindro[92], I. A. Cioară[27b], A. Ciocio[18], F. Cirotto[70a,70b], Z. H. Citron[180,j], M. Citterio[69a], D. A. Ciubotaru[27b], B. M. Ciungu[167], A. Clark[54], M. R. Clark[39], P. J. Clark[50], C. Clement[45a,45b], Y. Coadou[102], M. Cobal[67a,67c], A. Coccaro[55b], J. Cochran[79], H. Cohen[161], A. E. C. Coimbra[36], L. Colasurdo[119], B. Cole[39], A. P. Colijn[120], J. Collot[58], P. Conde Muiño[140a,140h], S. H. Connell[33c], I. A. Connelly[57], S. Constantinescu[27b], F. Conventi[70a,as], A. M. Cooper-Sarkar[135], F. Cormier[175], K. J. R. Cormier[167], L. D. Corpe[95], M. Corradi[73a,73b], E. E. Corrigan[97], F. Corriveau[104,ae], A. Cortes-Gonzalez[36], M. J. Costa[174], F. Costanza[5], D. Costanzo[149], G. Cowan[94], J. W. Cowley[32], J. Crane[101], K. Cranmer[125], S. J. Crawley[57], R. A. Creager[137], S. Crépé-Renaudin[58], F. Crescioli[136], M. Cristinziani[24], V. Croft[170], G. Crosetti[41a,41b], A. Cueto[5], T. Cuhadar Donszelmann[149], A. R. Cukierman[153], W. R. Cunningham[57], S. Czekierda[85], P. Czodrowski[36], M. J. Da Cunha Sargedas De Sousa[60b], J. V. Da Fonseca Pinto[81b], C. Da Via[101], W. Dabrowski[84a], F. Dachs[36], T. Dado[28a], S. Dahbi[35e], T. Dai[106], C. Dallapiccola[103], M. Dam[40], G. D'amen[29], V. D'Amico[75a,75b], J. Damp[100], J. R. Dandoy[137], M. F. Daneri[30], N. P. Dang[181,i], N. S. Dann[101], M. Danninger[175], V. Dao[36], G. Darbo[55b], O. Dartsi[5], A. Dattagupta[132], T. Daubney[46], S. D'Auria[69a,69b], C. David[168b], T. Davidek[143], D. R. Davis[49], I. Dawson[149], K. De[8], R. De Asmundis[70a], M. De Beurs[120], S. De Castro[23a,23b], S. De Cecco[73a,73b], N. De Groot[119], P. de Jong[120], H. De la Torre[107], A. De Maria[15c], D. De Pedis[73a], A. De Salvo[73a], U. De Sanctis[74a,74b], M. De Santis[74a,74b], A. De Santo[156], K. De Vasconcelos Corga[102], J. B. De Vivie De Regie[65], C. Debenedetti[146], D. V. Dedovich[80], A. M. Deiana[42], J. Del Peso[99], Y. Delabat Diaz[46], D. Delgove[65], F. Deliot[145,q], C. M. Delitzsch[7], M. Della Pietra[70a,70b], D. Della Volpe[54], A. Dell'Acqua[36], L. Dell'Asta[74a,74b], M. Delmastro[5], C. Delporte[65], P. A. Delsart[58], D. A. DeMarco[167], S. Demers[183], M. Demichev[80], G. Demontigny[110], S. P. Denisov[123], L. D'Eramo[136], D. Derendarz[85], J. E. Derkaoui[35d], F. Derue[136], P. Dervan[91], K. Desch[24], C. Deterre[46], K. Dette[167], C. Deutsch[24], M. R. Devesa[30], P. O. Deviveiros[36], A. Dewhurst[144], F. A. Di Bello[54], A. Di Ciaccio[74a,74b], L. Di Ciaccio[5], W. K. Di Clemente[137], C. Di Donato[70a,70b], A. Di Girolamo[36], G. Di Gregorio[72a,72b], B. Di Micco[75a,75b], R. Di Nardo[75a,75b], K. F. Di Petrillo[59], R. Di Sipio[167], D. Di Valentino[34], C. Diaconu[102], F. A. Dias[40], T. Dias Do Vale[140a], M. A. Diaz[147a], J. Dickinson[18], E. B. Diehl[106],

J. Dietrich[19], S. Díez Cornell[46], A. Dimitrievska[18], W. Ding[15b], J. Dingfelder[24], F. Dittus[36], F. Djama[102], T. Djobava[159b], J. I. Djuvsland[17], M. A. B. Do Vale[81c], M. Dobre[27b], D. Dodsworth[26], C. Doglioni[97], J. Dolejsi[143], Z. Dolezal[143], M. Donadelli[81d], B. Dong[60c], J. Donini[38], A. D'onofrio[15c], M. D'Onofrio[91], J. Dopke[144], A. Doria[70a], M. T. Dova[89], A. T. Doyle[57], E. Drechsler[152], E. Dreyer[152], T. Dreyer[53], A. S. Drobac[170], D. Du[60b], Y. Duan[60b], F. Dubinin[111], M. Dubovsky[28a], A. Dubreuil[54], E. Duchovni[180], G. Duckeck[114], A. Ducourthial[136], O. A. Ducu[110], D. Duda[115], A. Dudarev[36], A. C. Dudder[100], E. M. Duffield[18], L. Duflot[65], M. Dührssen[36], C. Dülsen[182], M. Dumancic[180], A. E. Dumitriu[27b], A. K. Duncan[57], M. Dunford[61a], A. Duperrin[102], H. Duran Yildiz[4a], M. Düren[56], A. Durglishvili[159b], D. Duschinger[48], B. Dutta[46], D. Duvnjak[1], G. I. Dyckes[137], M. Dyndal[36], S. Dysch[101], B. S. Dziedzic[85], K. M. Ecker[115], R. C. Edgar[106], M. G. Eggleston[49], T. Eifert[8], G. Eigen[17], K. Einsweiler[18], T. Ekelof[172], H. El Jarrari[35e], R. El Kosseifi[102], V. Ellajosyula[172], M. Ellert[172], F. Ellinghaus[182], A. A. Elliot[93], N. Ellis[36], J. Elmsheuser[29], M. Elsing[36], D. Emeliyanov[144], A. Emerman[39], Y. Enari[163], M. B. Epland[49], J. Erdmann[47], A. Ereditato[20], M. Errenst[36], M. Escalier[65], C. Escobar[174], O. Estrada Pastor[174], E. Etzion[161], H. Evans[66], A. Ezhilov[138], F. Fabbri[57], L. Fabbri[23a,23b], V. Fabiani[119], G. Facini[95], R. M. Faisca Rodrigues Pereira[140a], R. M. Fakhrutdinov[123], S. Falciano[73a], P. J. Falke[5], S. Falke[5], J. Faltova[143], Y. Fang[15a], Y. Fang[15a], G. Fanourakis[44], M. Fanti[69a,69b], M. Faraj[67a,67c,t], A. Farbin[8], A. Farilla[75a], E. M. Farina[71a,71b], T. Farooque[107], S. Farrell[18], S. M. Farrington[50], P. Farthouat[36], F. Fassi[35e], P. Fassnacht[36], D. Fassouliotis[9], M. Faucci Giannelli[50], W. J. Fawcett[32], L. Fayard[65], O. L. Fedin[138,o], W. Fedorko[175], A. Fehr[20], M. Feickert[173], L. Feligioni[102], A. Fell[149], C. Feng[60b], M. Feng[49], M. J. Fenton[57], A. B. Fenyuk[123], S. W. Ferguson[43], J. Ferrando[46], A. Ferrante[173], A. Ferrari[172], P. Ferrari[120], R. Ferrari[71a], D. E. Ferreira de Lima[61b], A. Ferrer[174], D. Ferrere[54], C. Ferretti[106], F. Fiedler[100], A. Filipčič[92], F. Filthaut[119], K. D. Finelli[25], M. C. N. Fiolhais[140a,140c,a], L. Fiorini[174], F. Fischer[114], W. C. Fisher[107], I. Fleck[151], P. Fleischmann[106], R. R. M. Fletcher[137], T. Flick[182], B. M. Flierl[114], L. Flores[137], L. R. Flores Castillo[63a], F. M. Follega[76a,76b], N. Fomin[17], J. H. Foo[167], G. T. Forcolin[76a,76b], A. Formica[145], F. A. Förster[14], A. C. Forti[101], A. G. Foster[21], M. G. Foti[135], D. Fournier[65], H. Fox[90], P. Francavilla[72a,72b], S. Francescato[73a,73b], M. Franchini[23a,23b], S. Franchino[61a], D. Francis[36], L. Franconi[20], M. Franklin[59], A. N. Fray[93], P. M. Freeman[21], B. Freund[110], W. S. Freund[81b], E. M. Freundlich[47], D. C. Frizzell[129], D. Froidevaux[36], J. A. Frost[135], C. Fukunaga[164], E. Fullana Torregrosa[174], E. Fumagalli[55a,55b], T. Fusayasu[116], J. Fuster[174], A. Gabrielli[23a,23b], A. Gabrielli[18], S. Gadatsch[54], P. Gadow[115], G. Gagliardi[55a,55b], L. G. Gagnon[110], C. Galea[27b], B. Galhardo[140a], G. E. Gallardo[135], E. J. Gallas[135], B. J. Gallop[144], G. Galster[40], R. Gamboa Goni[93], K. K. Gan[127], S. Ganguly[180], J. Gao[60a], Y. Gao[50], Y. S. Gao[31,l], C. García[174], J. E. García Navarro[174], J. A. García Pascual[15a], C. Garcia-Argos[52], M. Garcia-Sciveres[18], R. W. Gardner[37], N. Garelli[153], S. Gargiulo[52], C. A. Garner[167], V. Garonne[134], S. J. Gasiorowski[148], P. Gaspar[81b], A. Gaudiello[55a,55b], G. Gaudio[71a], I. L. Gavrilenko[111], A. Gavrilyuk[124], C. Gay[175], G. Gaycken[46], E. N. Gazis[10], A. A. Geanta[27b], C. M. Gee[146], C. N. P. Gee[144], J. Geisen[53], M. Geisen[100], C. Gemme[55b], M. H. Genest[58], C. Geng[106], S. Gentile[73a,73b], S. George[94], T. Geralis[44], L. O. Gerlach[53], P. Gessinger-Befurt[100], G. Gessner[47], S. Ghasemi[151], M. Ghasemi Bostanabad[176], M. Ghneimat[151], A. Ghosh[65], A. Ghosh[78], B. Giacobbe[23b], S. Giagu[73a,73b], N. Giangiacomi[23a,23b], P. Giannetti[72a], A. Giannini[70a,70b], G. Giannini[14], S. M. Gibson[94], M. Gignac[146], D. Gillberg[34], G. Gilles[182], D. M. Gingrich[3,ar], M. P. Giordani[67a,67c], P. F. Giraud[145], G. Giugliarelli[67a,67c], D. Giugni[69a], F. Giuli[74a,74b], S. Gkaitatzis[162], I. Gkialas[9,g], E. L. Gkougkousis[14], P. Gkountoumis[10], L. K. Gladilin[113], C. Glasman[99], J. Glatzer[14], P. C. F. Glaysher[46], A. Glazov[46], G. R. Gledhill[132], M. Goblirsch-Kolb[26], D. Godin[110], S. Goldfarb[105], T. Golling[54], D. Golubkov[123], A. Gomes[140a,140b], R. Goncalves Gama[53], R. Gonçalo[140a], G. Gonella[52], L. Gonella[21], A. Gongadze[80], F. Gonnella[21], J. L. Gonski[39], S. González de la Hoz[174], S. Gonzalez-Sevilla[54], G. R. Gonzalvo Rodriguez[174], L. Goossens[36], N. A. Gorasia[21], P. A. Gorbounov[124], H. A. Gordon[29], B. Gorini[36], E. Gorini[68a,68b], A. Gorišek[92], A. T. Goshaw[49], M. I. Gostkin[80], C. A. Gottardo[119], M. Gouighri[35b], A. G. Goussiou[148], N. Govender[33c], C. Goy[5], E. Gozani[160], I. Grabowska-Bold[84a], E. C. Graham[91], J. Gramling[171], E. Gramstad[134], S. Grancagnolo[19], M. Grandi[156], V. Gratchev[138], P. M. Gravila[27f], F. G. Gravili[68a,68b], C. Gray[57], H. M. Gray[18], C. Grefe[24], K. Gregersen[97], I. M. Gregor[46], P. Grenier[153], K. Grevtsov[46], C. Grieco[14], N. A. Grieser[129], A. A. Grillo[146], K. Grimm[31,k], S. Grinstein[14,z], J.-F. Grivaz[65], S. Groh[100], E. Gross[180], J. Grosse-Knetter[53], Z. J. Grout[95], C. Grud[106], A. Grummer[118], L. Guan[106], W. Guan[181], C. Gubbels[175], J. Guenther[36], A. Guerguichon[65], J. G. R. Guerrero Rojas[174], F. Guescini[115], D. Guest[171], R. Gugel[52], T. Guillemin[5], S. Guindon[36], U. Gul[57], J. Guo[60c], W. Guo[106], Y. Guo[60a,s], Z. Guo[102], R. Gupta[46], S. Gurbuz[12c], G. Gustavino[129], M. Guth[52], P. Gutierrez[129], C. Gutschow[95], C. Guyot[145], C. Gwenlan[135], C. B. Gwilliam[91], A. Haas[125], C. Haber[18], H. K. Hadavand[8], A. Hadef[60a], S. Hageböck[36], M. Haleem[177], J. Haley[130], G. Halladjian[107], G. D. Hallewell[102], K. Hamacher[182], P. Hamal[131], K. Hamano[176], H. Hamdaoui[35e], M. Hamer[24], G. N. Hamity[50], K. Han[60a,y], L. Han[60a], S. Han[15a], Y. F. Han[167], K. Hanagaki[82,w], M. Hance[146], D. M. Handl[114], B. Haney[137], R. Hankache[136], E. Hansen[97], J. B. Hansen[40], J. D. Hansen[40], M. C. Hansen[24], P. H. Hansen[40], E. C. Hanson[101], K. Hara[169], T. Harenberg[182], S. Harkusha[108], P. F. Harrison[178], N. M. Hartmann[114], Y. Hasegawa[150], A. Hasib[50], S. Hassani[145], S. Haug[20], R. Hauser[107], L. B. Havener[39],

M. Havranek[142], C. M. Hawkes[21], R. J. Hawkings[36], D. Hayden[107], C. Hayes[106], R. L. Hayes[175], C. P. Hays[135], J. M. Hays[93], H. S. Hayward[91], S. J. Haywood[144], F. He[60a], M. P. Heath[50], V. Hedberg[97], L. Heelan[8], S. Heer[24], K. K. Heidegger[52], W. D. Heidorn[79], J. Heilman[34], S. Heim[46], T. Heim[18], B. Heinemann[46,ao], J. J. Heinrich[132], L. Heinrich[36], J. Hejbal[141], L. Helary[61b], A. Held[175], S. Hellesund[134], C. M. Helling[146], S. Hellman[45a,45b], C. Helsens[36], R. C. W. Henderson[90], Y. Heng[181], L. Henkelmann[61a], S. Henkelmann[175], A. M. Henriques Correia[36], H. Herde[26], V. Herget[177], Y. Hernández Jiménez[33e], H. Herr[100], M. G. Herrmann[114], T. Herrmann[48], G. Herten[52], R. Hertenberger[114], L. Hervas[36], T. C. Herwig[137], G. G. Hesketh[95], N. P. Hessey[168a], A. Higashida[163], S. Higashino[82], E. Higón-Rodriguez[174], K. Hildebrand[37], J. C. Hill[32], K. K. Hill[29], K. H. Hiller[46], S. J. Hillier[21], M. Hils[48], I. Hinchliffe[18], F. Hinterkeuser[24], M. Hirose[133], S. Hirose[52], D. Hirschbuehl[182], B. Hiti[92], O. Hladik[141], D. R. Hlaluku[33e], X. Hoad[50], J. Hobbs[155], N. Hod[180], M. C. Hodgkinson[149], A. Hoecker[36], D. Hohn[52], D. Hohov[65], T. Holm[24], T. R. Holmes[37], M. Holzbock[114], L. B. A. H. Hommels[32], S. Honda[169], T. M. Hong[139], J. C. Honig[52], A. Hönle[115], B. H. Hooberman[173], W. H. Hopkins[6], Y. Horii[117], P. Horn[48], L. A. Horyn[37], S. Hou[158], A. Hoummada[35a], J. Howarth[101], J. Hoya[89], M. Hrabovsky[131], J. Hrdinka[77], I. Hristova[19], J. Hrivnac[65], A. Hrynevich[109], T. Hryn'ova[5], P. J. Hsu[64], S.-C. Hsu[148], Q. Hu[29], S. Hu[60c], Y. F. Hu[15a,15d], D. P. Huang[95], Y. Huang[60a], Y. Huang[15a], Z. Hubacek[142], F. Hubaut[102], M. Huebner[24], F. Huegging[24], T. B. Huffman[135], M. Huhtinen[36], R. F. H. Hunter[34], P. Huo[155], N. Huseynov[80,af], J. Huston[107], J. Huth[59], R. Hyneman[106], S. Hyrych[28a], G. Iacobucci[54], G. Iakovidis[29], I. Ibragimov[151], L. Iconomidou-Fayard[65], P. Iengo[36], R. Ignazzi[40], O. Igonkina[120,ab,*], R. Iguchi[163], T. Iizawa[54], Y. Ikegami[82], M. Ikeno[82], D. Iliadis[162], N. Ilic[119,167,ae], F. Iltzsche[48], G. Introzzi[71a,71b], M. Iodice[75a], K. Iordanidou[168a], V. Ippolito[73a,73b], M. F. Isacson[172], M. Ishino[163], W. Islam[130], C. Issever[19,46], S. Istin[160], F. Ito[169], J. M. Iturbe Ponce[63a], R. Iuppa[76a,76b], A. Ivina[180], H. Iwasaki[82], J. M. Izen[43], V. Izzo[70a], P. Jacka[141], P. Jackson[1], R. M. Jacobs[24], B. P. Jaeger[152], V. Jain[2], G. Jäkel[182], K. B. Jakobi[100], K. Jakobs[52], T. Jakoubek[141], J. Jamieson[57], K. W. Janas[84a], R. Jansky[54], J. Janssen[24], M. Janus[53], P. A. Janus[84a], G. Jarlskog[97], N. Javadov[80,af], T. Javůrek[36], M. Javurkova[103], F. Jeanneau[145], L. Jeanty[132], J. Jejelava[159a], A. Jelinskas[178], P. Jenni[52,b], J. Jeong[46], N. Jeong[46], S. Jézéquel[5], H. Ji[181], J. Jia[155], H. Jiang[79], Y. Jiang[60a], Z. Jiang[153,p], S. Jiggins[52], F. A. Jimenez Morales[38], J. Jimenez Pena[115], S. Jin[15c], A. Jinaru[27b], O. Jinnouchi[165], H. Jivan[33e], P. Johansson[149], K. A. Johns[7], C. A. Johnson[66], K. Jon-And[45a,45b], R. W. L. Jones[90], S. D. Jones[156], S. Jones[7], T. J. Jones[91], J. Jongmanns[61a], P. M. Jorge[140a], J. Jovicevic[36], X. Ju[18], J. J. Junggeburth[115], A. Juste Rozas[14,z], A. Kaczmarska[85], M. Kado[73a,73b], H. Kagan[127], M. Kagan[153], A. Kahn[39], C. Kahra[100], T. Kaji[179], E. Kajomovitz[160], C. W. Kalderon[97], A. Kaluza[100], A. Kamenshchikov[123], M. Kaneda[163], N. J. Kang[146], L. Kanjir[92], Y. Kano[117], V. A. Kantserov[112], J. Kanzaki[82], L. S. Kaplan[181], D. Kar[33e], K. Karava[135], M. J. Kareem[168b], S. N. Karpov[80], Z. M. Karpova[80], V. Kartvelishvili[90], A. N. Karyukhin[123], L. Kashif[181], R. D. Kass[127], A. Kastanas[45a,45b], C. Kato[60c,60d], J. Katzy[46], K. Kawade[150], K. Kawagoe[88], T. Kawaguchi[117], T. Kawamoto[145], G. Kawamura[53], E. F. Kay[176], V. F. Kazanin[122a,122b], R. Keeler[176], R. Kehoe[42], J. S. Keller[34], E. Kellermann[97], D. Kelsey[156], J. J. Kempster[21], J. Kendrick[21], K. E. Kennedy[39], O. Kepka[141], S. Kersten[182], B. P. Kerševan[92], S. Ketabchi Haghighat[167], M. Khader[173], F. Khalil-Zada[13], M. Khandoga[145], A. Khanov[130], A. G. Kharlamov[122a,122b], T. Kharlamova[122a,122b], E. E. Khoda[175], A. Khodinov[166], T. J. Khoo[54], E. Khramov[80], J. Khubua[159b], S. Kido[83], M. Kiehn[54], C. R. Kilby[94], Y. K. Kim[37], N. Kimura[95], O. M. Kind[19], B. T. King[91,*], D. Kirchmeier[48], J. Kirk[144], A. E. Kiryunin[115], T. Kishimoto[163], D. P. Kisliuk[167], V. Kitali[46], O. Kivernyk[5], T. Klapdor-Kleingrothaus[52], M. Klassen[61a], M. H. Klein[106], M. Klein[91], U. Klein[91], K. Kleinknecht[100], P. Klimek[121], A. Klimentov[29], T. Klingl[24], T. Klioutchnikova[36], F. F. Klitzner[114], P. Kluit[120], S. Kluth[115], E. Kneringer[77], E. B. F. G. Knoops[102], A. Knue[52], D. Kobayashi[88], T. Kobayashi[163], M. Kobel[48], M. Kocian[153], P. Kodys[143], P. T. Koenig[24], T. Koffas[34], N. M. Köhler[36], T. Koi[153], M. Kolb[145], I. Koletsou[5], T. Komarek[131], T. Kondo[82], K. Köneke[52], A. X. Y. Kong[1], A. C. König[119], T. Kono[126], R. Konoplich[125,aj], V. Konstantinides[95], N. Konstantinidis[95], B. Konya[97], R. Kopeliansky[66], S. Koperny[84a], K. Korcyl[85], K. Kordas[162], G. Koren[161], A. Korn[95], I. Korolkov[14], E. V. Korolkova[149], N. Korotkova[113], O. Kortner[115], S. Kortner[115], T. Kosek[143], V. V. Kostyukhin[149,166], A. Kotsokechagia[65], A. Kotwal[49], A. Koulouris[10], A. Kourkoumeli-Charalampidi[71a,71b], C. Kourkoumelis[9], E. Kourlitis[149], V. Kouskoura[29], A. B. Kowalewska[85], R. Kowalewski[176], C. Kozakai[163], W. Kozanecki[145], A. S. Kozhin[123], V. A. Kramarenko[113], G. Kramberger[92], D. Krasnopevtsev[60a], M. W. Krasny[136], A. Krasznahorkay[36], D. Krauss[115], J. A. Kremer[84a], J. Kretzschmar[91], P. Krieger[167], F. Krieter[114], A. Krishnan[61b], K. Krizka[18], K. Kroeninger[47], H. Kroha[115], J. Kroll[141], J. Kroll[137], K. S. Krowpman[107], J. Krstic[16], U. Kruchonak[80], H. Krüger[24], N. Krumnack[79], M. C. Kruse[49], J. A. Krzysiak[85], T. Kubota[105], O. Kuchinskaia[166], S. Kuday[4b], J. T. Kuechler[46], S. Kuehn[36], A. Kugel[61a], T. Kuhl[46], V. Kukhtin[80], R. Kukla[102], Y. Kulchitsky[108,ah], S. Kuleshov[147c], Y. P. Kulinich[173], M. Kuna[58], T. Kunigo[86], A. Kupco[141], T. Kupfer[47], O. Kuprash[52], H. Kurashige[83], L. L. Kurchaninov[168a], Y. A. Kurochkin[108], A. Kurova[112], M. G. Kurth[15a,15d], E. S. Kuwertz[36], M. Kuze[165], A. K. Kvam[148], J. Kvita[131], T. Kwan[104], A. La Rosa[115], L. La Rotonda[41a,41b], F. La Ruffa[41a,41b], C. Lacasta[174], F. Lacava[73a,73b], D. P. J. Lack[101], H. Lacker[19], D. Lacour[136], E. Ladygin[80], R. Lafaye[5], B. Laforge[136], T. Lagouri[33e], S. Lai[53], I. K. Lakomiec[84a],

S. Lammers[66], W. Lampl[7], C. Lampoudis[162], E. Lançon[29], U. Landgraf[52], M. P. J. Landon[93], M. C. Lanfermann[54], V. S. Lang[46], J. C. Lange[53], R. J. Langenberg[103], A. J. Lankford[171], F. Lanni[29], K. Lantzsch[24], A. Lanza[71a], A. Lapertosa[55a,55b], S. Laplace[136], J. F. Laporte[145], T. Lari[69a], F. Lasagni Manghi[23b,23a], M. Lassnig[36], T. S. Lau[63a], A. Laudrain[65], A. Laurier[34], M. Lavorgna[70a,70b], S. D. Lawlor[94], M. Lazzaroni[69a,69b], B. Le[105], E. Le Guirriec[102], M. LeBlanc[7], T. LeCompte[6], F. Ledroit-Guillon[58], A. C. A. Lee[95], C. A. Lee[29], G. R. Lee[17], L. Lee[59], S. C. Lee[158], S. J. Lee[34], S. Lee[79], B. Lefebvre[168a], H. P. Lefebvre[94], M. Lefebvre[176], C. Leggett[18], K. Lehmann[152], N. Lehmann[182], G. Lehmann Miotto[36], W. A. Leight[46], A. Leisos[162,x], M. A. L. Leite[81d], C. E. Leitgeb[114], R. Leitner[143], D. Lellouch[180,*], K. J. C. Leney[42], T. Lenz[24], R. Leone[7], S. Leone[72a], C. Leonidopoulos[50], A. Leopold[136], C. Leroy[110], R. Les[167], C. G. Lester[32], M. Levchenko[138], J. Levêque[5], D. Levin[106], L. J. Levinson[180], D. J. Lewis[21], B. Li[15b], B. Li[106], C.-Q. Li[60a], F. Li[60c], H. Li[60a], H. Li[60b], J. Li[60c], K. Li[153], L. Li[60c], M. Li[15a,15d], Q. Li[15a,15d], Q. Y. Li[60a], S. Li[60c,60d], X. Li[46], Y. Li[46], Z. Li[60b], Z. Liang[15a], B. Liberti[74a], A. Liblong[167], K. Lie[63c], S. Lim[29], C. Y. Lin[32], K. Lin[107], T. H. Lin[100], R. A. Linck[66], J. H. Lindon[21], A. L. Lionti[54], E. Lipeles[137], A. Lipniacka[17], T. M. Liss[173,ap], A. Lister[175], J. D. Little[8], B. Liu[79], B. L. Liu[6], H. B. Liu[29], H. Liu[106], J. B. Liu[60a], J. K. K. Liu[37], K. Liu[136], M. Liu[60a], P. Liu[18], Y. Liu[15a,15d], Y. L. Liu[106], Y. W. Liu[60a], M. Livan[71a,71b], A. Lleres[58], J. Llorente Merino[152], S. L. Lloyd[93], C. Y. Lo[63b], F. Lo Sterzo[42], E. M. Lobodzinska[46], P. Loch[7], S. Loffredo[74a,74b], T. Lohse[19], K. Lohwasser[149], M. Lokajicek[141], J. D. Long[173], R. E. Long[90], L. Longo[36], K. A. Looper[127], J. A. Lopez[147c], I. Lopez Paz[101], A. Lopez Solis[149], J. Lorenz[114], N. Lorenzo Martinez[5], A. M. Lory[114], M. Losada[22], P. J. Lösel[114], A. Lösle[52], X. Lou[46], X. Lou[15a], A. Lounis[65], J. Love[6], P. A. Love[90], J. J. Lozano Bahilo[174], M. Lu[60a], Y. J. Lu[64], H. J. Lubatti[148], C. Luci[73a,73b], A. Lucotte[58], C. Luedtke[52], F. Luehring[66], I. Luise[136], L. Luminari[73a], B. Lund-Jensen[154], M. S. Lutz[103], D. Lynn[29], H. Lyons[91], R. Lysak[141], E. Lytken[97], F. Lyu[15a], V. Lyubushkin[80], T. Lyubushkina[80], H. Ma[29], L. L. Ma[60b], Y. Ma[60b], G. Maccarrone[51], A. Macchiolo[115], C. M. Macdonald[149], J. Machado Miguens[137], D. Madaffari[174], R. Madar[38], W. F. Mader[48], M. Madugoda Ralalage Don[130], N. Madysa[48], J. Maeda[83], T. Maeno[29], M. Maerker[48], A. S. Maevskiy[113], V. Magerl[52], N. Magini[79], D. J. Mahon[39], C. Maidantchik[81b], T. Maier[114], A. Maio[140a,140b,140d], K. Maj[84a], O. Majersky[28a], S. Majewski[132], Y. Makida[82], N. Makovec[65], B. Malaescu[136], Pa. Malecki[85], V. P. Maleev[138], F. Malek[58], U. Mallik[78], D. Malon[6], C. Malone[32], S. Maltezos[10], S. Malyukov[80], J. Mamuzic[174], G. Mancini[51], I. Mandić[92], L. Manhaes de Andrade Filho[81a], I. M. Maniatis[162], J. Manjarres Ramos[48], K. H. Mankinen[97], A. Mann[114], A. Manousos[77], B. Mansoulie[145], I. Manthos[162], S. Manzoni[120], A. Marantis[162], G. Marceca[30], L. Marchese[135], G. Marchiori[136], M. Marcisovsky[141], L. Marcoccia[74a,74b], C. Marcon[97], C. A. Marin Tobon[36], M. Marjanovic[129], Z. Marshall[18], M. U. F. Martensson[172], S. Marti-Garcia[174], C. B. Martin[127], T. A. Martin[178], V. J. Martin[50], B. Martin di t Latour[17], L. Martinelli[75a,75b], M. Martinez[14,z], V. I. Martinez Outschoorn[103], S. Martin-Haugh[144], V. S. Martoiu[27b], A. C. Martyniuk[95], A. Marzin[36], S. R. Maschek[115], L. Masetti[100], T. Mashimo[163], R. Mashinistov[111], J. Masik[101], A. L. Maslennikov[122a,122b], L. Massa[23a,23b], P. Massarotti[70a,70b], P. Mastrandrea[72a,72b], A. Mastroberardino[41a,41b], T. Masubuchi[163], D. Matakias[10], A. Matic[114], N. Matsuzawa[163], P. Mättig[24], J. Maurer[27b], B. Maček[92], D. A. Maximov[122a,122b], R. Mazini[158], I. Maznas[162], S. M. Mazza[146], S. P. Mc Kee[106], T. G. McCarthy[115], W. P. McCormack[18], E. F. McDonald[105], J. A. Mcfayden[36], G. Mchedlidze[159b], M. A. McKay[42], K. D. McLean[176], S. J. McMahon[144], P. C. McNamara[105], C. J. McNicol[178], R. A. McPherson[176,ae], J. E. Mdhluli[33e], Z. A. Meadows[103], S. Meehan[36], T. Megy[52], S. Mehlhase[114], A. Mehta[91], T. Meideck[58], B. Meirose[43], D. Melini[160], B. R. Mellado Garcia[33e], J. D. Mellenthin[53], M. Melo[28a], F. Meloni[46], A. Melzer[24], S. B. Menary[101], E. D. Mendes Gouveia[140a,140e], L. Meng[36], X. T. Meng[106], S. Menke[115], E. Meoni[41a,41b], S. Mergelmeyer[19], S. A. M. Merkt[139], C. Merlassino[135], P. Mermod[54], L. Merola[70a,70b], C. Meroni[69a], G. Merz[106], O. Meshkov[113,111], J. K. R. Meshreki[151], A. Messina[73a,73b], J. Metcalfe[6], A. S. Mete[171], C. Meyer[66], J.-P. Meyer[145], H. Meyer Zu Theenhausen[61a], F. Miano[156], M. Michetti[19], R. P. Middleton[144], L. Mijović[50], G. Mikenberg[180], M. Mikestikova[141], M. Mikuž[92], H. Mildner[149], M. Milesi[105], A. Milic[167], D. A. Millar[93], D. W. Miller[37], A. Milov[180], D. A. Milstead[45a,45b], R. A. Mina[153], A. A. Minaenko[123], M. Miñano Moya[174], I. A. Minashvili[159b], A. I. Mincer[125], B. Mindur[84a], M. Mineev[80], Y. Minegishi[163], L. M. Mir[14], A. Mirto[68a,68b], K. P. Mistry[137], T. Mitani[179], J. Mitrevski[114], V. A. Mitsou[174], M. Mittal[60c], O. Miu[167], A. Miucci[20], P. S. Miyagawa[149], A. Mizukami[82], J. U. Mjörnmark[97], T. Mkrtchyan[61a], M. Mlynarikova[143], T. Moa[45a,45b], K. Mochizuki[110], P. Mogg[52], S. Mohapatra[39], R. Moles-Valls[24], M. C. Mondragon[107], K. Mönig[46], J. Monk[40], E. Monnier[102], A. Montalbano[152], J. Montejo Berlingen[36], M. Montella[95], F. Monticelli[89], S. Monzani[69a], N. Morange[65], D. Moreno[22], M. Moreno Llácer[174], C. Moreno Martinez[14], P. Morettini[55b], M. Morgenstern[120], S. Morgenstern[48], D. Mori[152], M. Morii[59], M. Morinaga[179], V. Morisbak[134], A. K. Morley[36], G. Mornacchi[36], A. P. Morris[95], L. Morvaj[155], P. Moschovakos[36], B. Moser[120], M. Mosidze[159b], T. Moskalets[145], H. J. Moss[149], J. Moss[31,m], E. J. W. Moyse[103], S. Muanza[102], J. Mueller[139], R. S. P. Mueller[114], D. Muenstermann[90], G. A. Mullier[97], D. P. Mungo[69a,69b], J. L. Munoz Martinez[14], F. J. Munoz Sanchez[101], P. Murin[28b], W. J. Murray[178,144], A. Murrone[69a,69b], M. Muškinja[18], C. Mwewa[33a], A. G. Myagkov[123,ak], A. A. Myers[139], J. Myers[132], M. Myska[142],

B. P. Nachman[18], O. Nackenhorst[47], A.Nag Nag[48], K. Nagai[135], K. Nagano[82], Y. Nagasaka[62], J. L. Nagle[29], E. Nagy[102], A. M. Nairz[36], Y. Nakahama[117], K. Nakamura[82], T. Nakamura[163], I. Nakano[128], H. Nanjo[133], F. Napolitano[61a], R. F. Naranjo Garcia[46], R. Narayan[42], I. Naryshkin[138], T. Naumann[46], G. Navarro[22], P. Y. Nechaeva[111], F. Nechansky[46], T. J. Neep[21], A. Negri[71a,71b], M. Negrini[23b], C. Nellist[53], M. E. Nelson[45a,45b], S. Nemecek[141], P. Nemethy[125], M. Nessi[36,d], M. S. Neubauer[173], M. Neumann[182], R. Newhouse[175], P. R. Newman[21], C. W. Ng[139], Y. S. Ng[19], Y. W. Y. Ng[171], B. Ngair[35e], H. D. N. Nguyen[102], T. Nguyen Manh[110], E. Nibigira[38], R. B. Nickerson[135], R. Nicolaidou[145], D. S. Nielsen[40], J. Nielsen[146], N. Nikiforou[11], V. Nikolaenko[123,ak], I. Nikolic-Audit[136], K. Nikolopoulos[21], P. Nilsson[29], H. R. Nindhito[54], Y. Ninomiya[82], A. Nisati[73a], N. Nishu[60c], R. Nisius[115], I. Nitsche[47], T. Nitta[179], T. Nobe[163], Y. Noguchi[86], I. Nomidis[136], M. A. Nomura[29], M. Nordberg[36], N. Norjoharuddeen[135], T. Novak[92], O. Novgorodova[48], R. Novotny[142], L. Nozka[131], K. Ntekas[171], E. Nurse[95], F. G. Oakham[34,ar], H. Oberlack[115], J. Ocariz[136], A. Ochi[83], I. Ochoa[39], J. P. Ochoa-Ricoux[147a], K. O'Connor[26], S. Oda[88], S. Odaka[82], S. Oerdek[53], A. Ogrodnik[84a], A. Oh[101], S. H. Oh[49], C. C. Ohm[154], H. Oide[165], M. L. Ojeda[167], H. Okawa[169], Y. Okazaki[86], M. W. O'Keefe[91], Y. Okumura[163], T. Okuyama[82], A. Olariu[27b], L. F. Oleiro Seabra[140a], S. A. Olivares Pino[147a], D. Oliveira Damazio[29], J. L. Oliver[1], M. J. R. Olsson[171], A. Olszewski[85], J. Olszowska[85], D. C. O'Neil[152], A. P. O'neill[135], A. Onofre[140a,140e], P. U. E. Onyisi[11], H. Oppen[134], M. J. Oreglia[37], G. E. Orellana[89], D. Orestano[75a,75b], N. Orlando[14], R. S. Orr[167], V. O'Shea[57], R. Ospanov[60a], G. Otero y Garzon[30], H. Otono[88], P. S. Ott[61a], M. Ouchrif[35d], J. Ouellette[29], F. Ould-Saada[134], A. Ouraou[145], Q. Ouyang[15a], M. Owen[57], R. E. Owen[21], V. E. Ozcan[12c], N. Ozturk[8], J. Pacalt[131], H. A. Pacey[32], K. Pachal[49], A. Pacheco Pages[14], C. Padilla Aranda[14], S. Pagan Griso[18], M. Paganini[183], G. Palacino[66], S. Palazzo[50], S. Palestini[36], M. Palka[84b], D. Pallin[38], I. Panagoulias[10], C. E. Pandini[36], J. G. Panduro Vazquez[94], P. Pani[46], G. Panizzo[67a,67c], L. Paolozzi[54], C. Papadatos[110], K. Papageorgiou[9,g], S. Parajuli[43], A. Paramonov[6], D. Paredes Hernandez[63b], S. R. Paredes Saenz[135], B. Parida[166], T. H. Park[167], A. J. Parker[31], M. A. Parker[32], F. Parodi[55a,55b], E. W. Parrish[121], J. A. Parsons[39], U. Parzefall[52], L. Pascual Dominguez[136], V. R. Pascuzzi[167], J. M. P. Pasner[146], F. Pasquali[120], E. Pasqualucci[73a], S. Passaggio[55b], F. Pastore[94], P. Pasuwan[45a,45b], S. Pataraia[100], J. R. Pater[101], A. Pathak[181,i], J. Patton[91], T. Pauly[36], J. Pearkes[153], B. Pearson[115], M. Pedersen[134], L. Pedraza Diaz[119], R. Pedro[140a], T. Peiffer[53], S. V. Peleganchuk[122a,122b], O. Penc[141], H. Peng[60a], B. S. Peralva[81a], M. M. Perego[65], A. P. Pereira Peixoto[140a], D. V. Perepelitsa[29], F. Peri[19], L. Perini[69a,69b], H. Pernegger[36], S. Perrella[140a], A. Perrevoort[120], K. Peters[46], R. F. Y. Peters[101], B. A. Petersen[36], T. C. Petersen[40], E. Petit[102], A. Petridis[1], C. Petridou[162], P. Petroff[65], M. Petrov[135], F. Petrucci[75a,75b], M. Pettee[183], N. E. Pettersson[103], K. Petukhova[143], A. Peyaud[145], R. Pezoa[147c], L. Pezzotti[71a,71b], T. Pham[105], F. H. Phillips[107], P. W. Phillips[144], M. W. Phipps[173], G. Piacquadio[155], E. Pianori[18], A. Picazio[103], R. H. Pickles[101], R. Piegaia[30], D. Pietreanu[27b], J. E. Pilcher[37], A. D. Pilkington[101], M. Pinamonti[67a,67c], J. L. Pinfold[3], M. Pitt[161], L. Pizzimento[74a,74b], M.-A. Pleier[29], V. Pleskot[143], E. Plotnikova[80], P. Podberezko[122a,122b], R. Poettgen[97], R. Poggi[54], L. Poggioli[65], I. Pogrebnyak[107], D. Pohl[24], I. Pokharel[53], G. Polesello[71a], A. Poley[18], A. Policicchio[73a,73b], R. Polifka[143], A. Polini[23b], C. S. Pollard[46], V. Polychronakos[29], D. Ponomarenko[112], L. Pontecorvo[36], S. Popa[27a], G. A. Popeneciu[27d], L. Portales[5], D. M. Portillo Quintero[58], S. Pospisil[142], K. Potamianos[46], I. N. Potrap[80], C. J. Potter[32], H. Potti[11], T. Poulsen[97], J. Poveda[36], T. D. Powell[149], G. Pownall[46], M. E. Pozo Astigarraga[36], P. Pralavorio[102], S. Prell[79], D. Price[101], M. Primavera[68a], S. Prince[104], M. L. Proffitt[148], N. Proklova[112], K. Prokofiev[63c], F. Prokoshin[80], S. Protopopescu[29], J. Proudfoot[6], M. Przybycien[84a], D. Pudzha[138], A. Puri[173], P. Puzo[65], J. Qian[106], Y. Qin[101], A. Quadt[53], M. Queitsch-Maitland[36], A. Qureshi[1], M. Racko[28a], F. Ragusa[69a,69b], G. Rahal[98], J. A. Raine[54], S. Rajagopalan[29], A. Ramirez Morales[93], K. Ran[15a,15d], T. Rashid[65], S. Raspopov[5], D. M. Rauch[46], F. Rauscher[114], S. Rave[100], B. Ravina[149], I. Ravinovich[180], J. H. Rawling[101], M. Raymond[36], A. L. Read[134], N. P. Readioff[58], M. Reale[68a,68b], D. M. Rebuzzi[71a,71b], A. Redelbach[177], G. Redlinger[29], K. Reeves[43], L. Rehnisch[19], J. Reichert[137], D. Reikher[161], A. Reiss[100], A. Rej[151], C. Rembser[36], M. Renda[27b], M. Rescigno[73a], S. Resconi[69a], E. D. Resseguie[137], S. Rettie[175], B. Reynolds[127], E. Reynolds[21], O. L. Rezanova[122a,122b], P. Reznicek[143], E. Ricci[76a,76b], R. Richter[115], S. Richter[46], E. Richter-Was[84b], O. Ricken[24], M. Ridel[136], P. Rieck[115], O. Rifki[46], M. Rijssenbeek[155], A. Rimoldi[71a,71b], M. Rimoldi[46], L. Rinaldi[23b], G. Ripellino[154], I. Riu[14], J. C. Rivera Vergara[176], F. Rizatdinova[130], E. Rizvi[93], C. Rizzi[36], R. T. Roberts[101], S. H. Robertson[104,ae], M. Robin[46], D. Robinson[32], J. E. M. Robinson[46], C. M. Robles Gajardo[147c], M. Robles Manzano[100], A. Robson[57], A. Rocchi[74a,74b], E. Rocco[100], C. Roda[72a,72b], S. Rodriguez Bosca[174], A. Rodriguez Perez[14], D. Rodriguez Rodriguez[174], A. M. Rodríguez Vera[168b], S. Roe[36], O. Røhne[134], R. Röhrig[115], R. A. Rojas[147c], B. Roland[52], C. P. A. Roland[66], J. Roloff[29], A. Romaniouk[112], M. Romano[23a,23b], N. Rompotis[91], M. Ronzani[125], L. Roos[136], S. Rosati[73a], G. Rosin[103], B. J. Rosser[137], E. Rossi[46], E. Rossi[75a,75b], E. Rossi[70a,70b], L. P. Rossi[55b], L. Rossini[69a,69b], R. Rosten[14], M. Rotaru[27b], J. Rothberg[148], B. Rottler[52], D. Rousseau[65], G. Rovelli[71a,71b], A. Roy[11], D. Roy[33e], A. Rozanov[102], Y. Rozen[160], X. Ruan[33e], F. Rühr[52], A. Ruiz-Martinez[174], A. Rummler[36], Z. Rurikova[52], N. A. Rusakovich[80], H. L. Russell[104], L. Rustige[38,47], J. P. Rutherfoord[7], E. M. Rüttinger[149], M. Rybar[39],

G. Rybkin[65], E. B. Rye[134], A. Ryzhov[123], J. A. Sabater Iglesias[46], P. Sabatini[53], G. Sabato[120], S. Sacerdoti[65], H. F.-W. Sadrozinski[146], R. Sadykov[80], F. Safai Tehrani[73a], B. Safarzadeh Samani[156], M. Safdari[153], P. Saha[121], S. Saha[104], M. Sahinsoy[61a], A. Sahu[182], M. Saimpert[46], M. Saito[163], T. Saito[163], H. Sakamoto[163], A. Sakharov[125,aj], D. Salamani[54], G. Salamanna[75a,75b], J. E. Salazar Loyola[147c], A. Salnikov[153], J. Salt[174], D. Salvatore[41a,41b], F. Salvatore[156], A. Salvucci[63a,63b,63c], A. Salzburger[36], J. Samarati[36], D. Sammel[52], D. Sampsonidis[162], D. Sampsonidou[162], J. Sánchez[174], A. Sanchez Pineda[67a,36,67c], H. Sandaker[134], C. O. Sander[46], I. G. Sanderswood[90], M. Sandhoff[182], C. Sandoval[22], D. P. C. Sankey[144], M. Sannino[55a,55b], Y. Sano[117], A. Sansoni[51], C. Santoni[38], H. Santos[140a,140b], S. N. Santpur[18], A. Santra[174], A. Sapronov[80], J. G. Saraiva[140a,140d], O. Sasaki[82], K. Sato[169], F. Sauerburger[52], E. Sauvan[5], P. Savard[167,ar], R. Sawada[163], C. Sawyer[144], L. Sawyer[96,ai], C. Sbarra[23b], A. Sbrizzi[23a], T. Scanlon[95], J. Schaarschmidt[148], P. Schacht[115], B. M. Schachtner[114], D. Schaefer[37], L. Schaefer[137], J. Schaeffer[100], S. Schaepe[36], U. Schäfer[100], A. C. Schaffer[65], D. Schaile[114], R. D. Schamberger[155], N. Scharmberg[101], V. A. Schegelsky[138], D. Scheirich[143], F. Schenck[19], M. Schernau[171], C. Schiavi[55a,55b], S. Schier[146], L. K. Schildgen[24], Z. M. Schillaci[26], E. J. Schioppa[36], M. Schioppa[41a,41b], K. E. Schleicher[52], S. Schlenker[36], K. R. Schmidt-Sommerfeld[115], K. Schmieden[36], C. Schmitt[100], S. Schmitt[46], S. Schmitz[100], J. C. Schmoeckel[46], U. Schnoor[52], L. Schoeffel[145], A. Schoening[61b], P. G. Scholer[52], E. Schopf[135], M. Schott[100], J. F. P. Schouwenberg[119], J. Schovancova[36], S. Schramm[54], F. Schroeder[182], A. Schulte[100], H.-C. Schultz-Coulon[61a], M. Schumacher[52], B. A. Schumm[146], Ph. Schune[145], A. Schwartzman[153], T. A. Schwarz[106], Ph. Schwemling[145], R. Schwienhorst[107], A. Sciandra[146], G. Sciolla[26], M. Scodeggio[46], M. Scornajenghi[41a,41b], F. Scuri[72a], F. Scutti[105], L. M. Scyboz[115], C. D. Sebastiani[73a,73b], P. Seema[19], S. C. Seidel[118], A. Seiden[146], B. D. Seidlitz[29], T. Seiss[37], J. M. Seixas[81b], G. Sekhniaidze[70a], K. Sekhon[106], S. J. Sekula[42], N. Semprini-Cesari[23a,23b], S. Sen[49], C. Serfon[77], L. Serin[65], L. Serkin[67a,67b], M. Sessa[60a], H. Severini[129], S. Sevova[153], T. Šfiligoj[92], F. Sforza[55a,55b], A. Sfyrla[54], E. Shabalina[53], J. D. Shahinian[146], N. W. Shaikh[45a,45b], D. Shaked Renous[180], L. Y. Shan[15a], J. T. Shank[25], M. Shapiro[18], A. Sharma[135], A. S. Sharma[1], P. B. Shatalov[124], K. Shaw[156], S. M. Shaw[101], M. Shehade[180], Y. Shen[129], A. D. Sherman[25], P. Sherwood[95], L. Shi[158], S. Shimizu[82], C. O. Shimmin[183], Y. Shimogama[179], M. Shimojima[116], I. P. J. Shipsey[135], S. Shirabe[165], M. Shiyakova[80,ac], J. Shlomi[180], A. Shmeleva[111], M. J. Shochet[37], J. Shojaii[105], D. R. Shope[129], S. Shrestha[127], E. M. Shrif[33e], E. Shulga[180], P. Sicho[141], A. M. Sickles[173], P. E. Sidebo[154], E. Sideras Haddad[33e], O. Sidiropoulou[36], A. Sidoti[23a,23b], F. Siegert[48], Dj. Sijacki[16], M. Jr. Silva[181], M. V. Silva Oliveira[81a], S. B. Silverstein[45a], S. Simion[65], R. Simoniello[100], S. Simsek[12b], P. Sinervo[167], V. Sinetckii[113], N. B. Sinev[132], S. Singh[152], M. Sioli[23a,23b], I. Siral[132], S. Yu. Sivoklokov[113], J. Sjölin[45a,45b], E. Skorda[97], P. Skubic[129], M. Slawinska[85], K. Sliwa[170], R. Slovak[143], V. Smakhtin[180], B. H. Smart[144], J. Smiesko[28a], N. Smirnov[112], S. Yu. Smirnov[112], Y. Smirnov[112], L. N. Smirnova[113,u], O. Smirnova[97], J. W. Smith[53], M. Smizanska[90], K. Smolek[142], A. Smykiewicz[85], A. A. Snesarev[111], H. L. Snoek[120], I. M. Snyder[132], S. Snyder[29], R. Sobie[176,ae], A. Soffer[161], A. Søgaard[50], F. Sohns[53], C. A. Solans Sanchez[36], E. Yu. Soldatov[112], U. Soldevila[174], A. A. Solodkov[123], A. Soloshenko[80], O. V. Solovyanov[123], V. Solovyev[138], P. Sommer[149], H. Son[170], W. Song[144], W. Y. Song[168b], A. Sopczak[142], A. L. Sopio[95], F. Sopkova[28b], C. L. Sotiropoulou[72a,72b], S. Sottocornola[71a,71b], R. Soualah[67a,67c,f], A. M. Soukharev[122a,122b], D. South[46], S. Spagnolo[68a,68b], M. Spalla[115], M. Spangenberg[178], F. Spanò[94], D. Sperlich[52], T. M. Spieker[61a], G. Spigo[36], M. Spina[156], D. P. Spiteri[57], M. Spousta[143], A. Stabile[69a,69b], B. L. Stamas[121], R. Stamen[61a], M. Stamenkovic[120], E. Stanecka[85], B. Stanislaus[135], M. M. Stanitzki[46], M. Stankaityte[135], B. Stapf[120], E. A. Starchenko[123], G. H. Stark[146], J. Stark[58], S. H. Stark[40], P. Staroba[141], P. Starovoitov[61a], S. Stärz[104], R. Staszewski[85], G. Stavropoulos[44], M. Stegler[46], P. Steinberg[29], A. L. Steinhebel[132], B. Stelzer[152], H. J. Stelzer[139], O. Stelzer-Chilton[168a], H. Stenzel[56], T. J. Stevenson[156], G. A. Stewart[36], M. C. Stockton[36], G. Stoicea[27b], M. Stolarski[140a], S. Stonjek[115], A. Straessner[48], J. Strandberg[154], S. Strandberg[45a,45b], M. Strauss[129], P. Strizenec[28b], R. Ströhmer[177], D. M. Strom[132], R. Stroynowski[42], A. Strubig[50], S. A. Stucci[29], B. Stugu[17], J. Stupak[129], N. A. Styles[46], D. Su[153], S. Suchek[61a], V. V. Sulin[111], M. J. Sullivan[91], D. M. S. Sultan[54], S. Sultansoy[4c], T. Sumida[86], S. Sun[106], X. Sun[3], K. Suruliz[156], C. J. E. Suster[157], M. R. Sutton[156], S. Suzuki[82], M. Svatos[141], M. Swiatlowski[37], S. P. Swift[2], T. Swirski[177], A. Sydorenko[100], I. Sykora[28a], M. Sykora[143], T. Sykora[143], D. Ta[100], K. Tackmann[46,aa], J. Taenzer[161], A. Taffard[171], R. Tafirout[168a], H. Takai[29], R. Takashima[87], K. Takeda[83], T. Takeshita[150], E. P. Takeva[50], Y. Takubo[82], M. Talby[102], A. A. Talyshev[122a,122b], N. M. Tamir[161], J. Tanaka[163], M. Tanaka[165], R. Tanaka[65], S. Tapia Araya[173], S. Tapprogge[100], A. Tarek Abouelfadl Mohamed[136], S. Tarem[160], K. Tariq[60b], G. Tarna[27b,c], G. F. Tartarelli[69a], P. Tas[143], M. Tasevsky[141], T. Tashiro[86], E. Tassi[41a,41b], A. Tavares Delgado[140a], Y. Tayalati[35e], A. J. Taylor[50], G. N. Taylor[105], W. Taylor[168b], A. S. Tee[90], R. Teixeira De Lima[153], P. Teixeira-Dias[94], H. Ten Kate[36], J. J. Teoh[120], S. Terada[82], K. Terashi[163], J. Terron[99], S. Terzo[14], M. Testa[51], R. J. Teuscher[167,ae], S. J. Thais[183], T. Theveneaux-Pelzer[46], F. Thiele[40], D. W. Thomas[94], J. O. Thomas[42], J. P. Thomas[21], P. D. Thompson[21], L. A. Thomsen[183], E. Thomson[137], E. J. Thorpe[93], R. E. Ticse Torres[53], V. O. Tikhomirov[111,al], Yu. A. Tikhonov[122a,122b], S. Timoshenko[112], P. Tipton[183], S. Tisserant[102], K. Todome[23a,23b], S. Todorova-Nova[5],

S. Todt[48], J. Tojo[88], S. Tokár[28a], K. Tokushuku[82], E. Tolley[127], K. G. Tomiwa[33e], M. Tomoto[117], L. Tompkins[153,p], B. Tong[59], P. Tornambe[103], E. Torrence[132], H. Torres[48], E. Torró Pastor[148], C. Tosciri[135], J. Toth[102,ad], D. R. Tovey[149], A. Traeet[17], C. J. Treado[125], T. Trefzger[177], F. Tresoldi[156], A. Tricoli[29], I. M. Trigger[168a], S. Trincaz-Duvoid[136], D. T. Trischuk[175], W. Trischuk[167], B. Trocmé[58], A. Trofymov[145], C. Troncon[69a], M. Trovatelli[176], F. Trovato[156], L. Truong[33c], M. Trzebinski[85], A. Trzupek[85], F. Tsai[46], J. C.-L. Tseng[135], P. V. Tsiareshka[108,ah], A. Tsirigotis[162,x], V. Tsiskaridze[155], E. G. Tskhadadze[159a], M. Tsopoulou[162], I. I. Tsukerman[124], V. Tsulaia[18], S. Tsuno[82], D. Tsybychev[155], Y. Tu[63b], A. Tudorache[27b], V. Tudorache[27b], T. T. Tulbure[27a], A. N. Tuna[59], S. Turchikhin[80], D. Turgeman[180], I. Turk Cakir[4b,v], R. J. Turner[21], R. T. Turra[69a], P. M. Tuts[39], S. Tzamarias[162], E. Tzovara[100], G. Ucchielli[47], K. Uchida[163], I. Ueda[82], F. Ukegawa[169], G. Unal[36], A. Undrus[29], G. Unel[171], F. C. Ungaro[105], Y. Unno[82], K. Uno[163], J. Urban[28b], P. Urquijo[105], G. Usai[8], Z. Uysal[12d], V. Vacek[142], B. Vachon[104], K. O. H. Vadla[134], A. Vaidya[95], C. Valderanis[114], E. Valdes Santurio[45a,45b], M. Valente[54], S. Valentinetti[23a,23b], A. Valero[174], L. Valéry[46], R. A. Vallance[21], A. Vallier[36], J. A. Valls Ferrer[174], T. R. Van Daalen[14], P. Van Gemmeren[6], I. Van Vulpen[120], M. Vanadia[74a,74b], W. Vandelli[36], M. Vandenbroucke[145], E. R. Vandewall[130], A. Vaniachine[166], D. Vannicola[73a,73b], R. Vari[73a], E. W. Varnes[7], C. Varni[55a,55b], T. Varol[158], D. Varouchas[65], K. E. Varvell[157], M. E. Vasile[27b], G. A. Vasquez[176], F. Vazeille[38], D. Vazquez Furelos[14], T. Vazquez Schroeder[36], J. Veatch[53], V. Vecchio[75a,75b], M. J. Veen[120], L. M. Veloce[167], F. Veloso[140a,140c], S. Veneziano[73a], A. Ventura[68a,68b], N. Venturi[36], A. Verbytskyi[115], V. Vercesi[71a], M. Verducci[72a,72b], C. M. Vergel Infante[79], C. Vergis[24], W. Verkerke[120], A. T. Vermeulen[120], J. C. Vermeulen[120], M. C. Vetterli[152,ar], N. Viaux Maira[147c], M. Vicente Barreto Pinto[54], T. Vickey[149], O. E. Vickey Boeriu[149], G. H. A. Viehhauser[135], L. Vigani[61b], M. Villa[23a,23b], M. Villaplana Perez[3], E. Vilucchi[51], M. G. Vincter[34], G. S. Virdee[21], A. Vishwakarma[46], C. Vittori[23a,23b], I. Vivarelli[156], M. Vogel[182], P. Vokac[142], S. E. von Buddenbrock[33e], E. Von Toerne[24], V. Vorobel[143], K. Vorobev[112], M. Vos[174], J. H. Vossebeld[91], M. Vozak[101], N. Vranjes[16], M. Vranjes Milosavljevic[16], V. Vrba[142], M. Vreeswijk[120], R. Vuillermet[36], I. Vukotic[37], P. Wagner[24], W. Wagner[182], J. Wagner-Kuhr[114], S. Wahdan[182], H. Wahlberg[89], V. M. Walbrecht[115], J. Walder[90], R. Walker[114], S. D. Walker[94], W. Walkowiak[151], V. Wallangen[45a,45b], A. M. Wang[59], A. Z. Wang[181], C. Wang[60c], F. Wang[181], H. Wang[18], H. Wang[3], J. Wang[63a], J. Wang[61b], P. Wang[42], Q. Wang[129], R.-J. Wang[100], R. Wang[60a], R. Wang[6], S. M. Wang[158], W. T. Wang[60a], W. Wang[15c], W. X. Wang[60a], Y. Wang[60a], Z. Wang[60c], C. Wanotayaroj[46], A. Warburton[104], C. P. Ward[32], D. R. Wardrope[95], N. Warrack[57], A. Washbrook[50], A. T. Watson[21], M. F. Watson[21], G. Watts[148], B. M. Waugh[95], A. F. Webb[11], S. Webb[100], C. Weber[183], M. S. Weber[20], S. A. Weber[34], S. M. Weber[61a], A. R. Weidberg[135], J. Weingarten[47], M. Weirich[100], C. Weiser[52], P. S. Wells[36], T. Wenaus[29], T. Wengler[36], S. Wenig[36], N. Wermes[24], M. D. Werner[79], M. Wessels[61a], T. D. Weston[20], K. Whalen[132], N. L. Whallon[148], A. M. Wharton[90], A. S. White[106], A. White[8], M. J. White[1], D. Whiteson[171], B. W. Whitmore[90], W. Wiedenmann[181], C. Wiel[48], M. Wielers[144], N. Wieseotte[100], C. Wiglesworth[40], L. A. M. Wiik-Fuchs[52], H. G. Wilkens[36], L. J. Wilkins[94], H. H. Williams[137], S. Williams[32], C. Willis[107], S. Willocq[103], J. A. Wilson[21], I. Wingerter-Seez[5], E. Winkels[156], F. Winklmeier[132], O. J. Winston[156], B. T. Winter[52], M. Wittgen[153], M. Wobisch[96], A. Wolf[100], T. M. H. Wolf[120], R. Wolff[102], R. Wölker[135], J. Wollrath[52], M. W. Wolter[85], H. Wolters[140a,140c], V. W. S. Wong[175], N. L. Woods[146], S. D. Worm[21], B. K. Wosiek[85], K. W. Woźniak[85], K. Wraight[57], S. L. Wu[181], X. Wu[54], Y. Wu[60a], T. R. Wyatt[101], B. M. Wynne[50], S. Xella[40], Z. Xi[106], L. Xia[178], X. Xiao[106], I. Xiotidis[156], D. Xu[15a], H. Xu[60a], L. Xu[29], T. Xu[145], W. Xu[106], Z. Xu[60b], Z. Xu[153], B. Yabsley[157], S. Yacoob[33a], K. Yajima[133], D. P. Yallup[95], N. Yamaguchi[88], Y. Yamaguchi[165], A. Yamamoto[82], M. Yamatani[163], T. Yamazaki[163], Y. Yamazaki[83], Z. Yan[25], H. J. Yang[60c,60d], H. T. Yang[18], S. Yang[60a], X. Yang[58,60b], Y. Yang[163], W.-M. Yao[18], Y. C. Yap[46], Y. Yasu[82], E. Yatsenko[60c,60d], H. Ye[15c], J. Ye[42], S. Ye[29], I. Yeletskikh[80], M. R. Yexley[90], E. Yigitbasi[25], K. Yorita[179], K. Yoshihara[137], C. J. S. Young[36], C. Young[153], J. Yu[79], R. Yuan[60b,h], X. Yue[61a], S. P. Y. Yuen[24], M. Zaazoua[35e], B. Zabinski[85], G. Zacharis[10], E. Zaffaroni[54], J. Zahreddine[136], A. M. Zaitsev[123,ak], T. Zakareishvili[159b], N. Zakharchuk[34], S. Zambito[59], D. Zanzi[36], D. R. Zaripovas[57], S. V. Zeißner[47], C. Zeitnitz[182], G. Zemaityte[135], J. C. Zeng[173], O. Zenin[123], T. Ženiš[28a], D. Zerwas[65], M. Zgubič[135], B. Zhang[15c], D. F. Zhang[15b], G. Zhang[15b], H. Zhang[15c], J. Zhang[6], L. Zhang[15c], L. Zhang[60a], M. Zhang[173], R. Zhang[181], S. Zhang[106], X. Zhang[60b], Y. Zhang[15a,15d], Z. Zhang[63a], Z. Zhang[65], P. Zhao[49], Y. Zhao[60b], Z. Zhao[60a], A. Zhemchugov[80], Z. Zheng[106], D. Zhong[173], B. Zhou[106], C. Zhou[181], M. S. Zhou[15a,15d], M. Zhou[155], N. Zhou[60c], Y. Zhou[7], C. G. Zhu[60b], C. Zhu[15a,15d], H. L. Zhu[60a], H. Zhu[15a], J. Zhu[106], Y. Zhu[60a], X. Zhuang[15a], K. Zhukov[111], V. Zhulanov[122a,122b], D. Zieminska[66], N. I. Zimine[80], S. Zimmermann[52], Z. Zinonos[115], M. Ziolkowski[151], L. Živković[16], G. Zobernig[181], A. Zoccoli[23a,23b], K. Zoch[53], T. G. Zorbas[149], R. Zou[37], L. Zwalinski[36]

[1] Department of Physics, University of Adelaide, Adelaide, Australia
[2] Physics Department, SUNY Albany, Albany, NY, USA
[3] Department of Physics, University of Alberta, Edmonton, AB, Canada

[4] [(a)]Department of Physics, Ankara University, Ankara, Turkey; [(b)]Istanbul Aydin University, Istanbul, Turkey; [(c)]Division of Physics, TOBB University of Economics and Technology, Ankara, Turkey
[5] LAPP, Université Grenoble Alpes, Université Savoie Mont Blanc, CNRS/IN2P3, Annecy, France
[6] High Energy Physics Division, Argonne National Laboratory, Argonne, IL, USA
[7] Department of Physics, University of Arizona, Tucson, AZ, USA
[8] Department of Physics, University of Texas at Arlington, Arlington, TX, USA
[9] Physics Department, National and Kapodistrian University of Athens, Athens, Greece
[10] Physics Department, National Technical University of Athens, Zografou, Greece
[11] Department of Physics, University of Texas at Austin, Austin, TX, USA
[12] [(a)]Bahcesehir University, Faculty of Engineering and Natural Sciences, Istanbul, Turkey; [(b)]Istanbul Bilgi University, Faculty of Engineering and Natural Sciences, Istanbul, Turkey; [(c)]Department of Physics, Bogazici University, Istanbul, Turkey; [(d)]Department of Physics Engineering, Gaziantep University, Gaziantep, Turkey
[13] Institute of Physics, Azerbaijan Academy of Sciences, Baku, Azerbaijan
[14] Institut de Física d'Altes Energies (IFAE), Barcelona Institute of Science and Technology, Barcelona, Spain
[15] [(a)]Institute of High Energy Physics, Chinese Academy of Sciences, Beijing, China; [(b)]Physics Department, Tsinghua University, Beijing, China; [(c)]Department of Physics, Nanjing University, Nanjing, China; [(d)]University of Chinese Academy of Science (UCAS), Beijing, China
[16] Institute of Physics, University of Belgrade, Belgrade, Serbia
[17] Department for Physics and Technology, University of Bergen, Bergen, Norway
[18] Physics Division, Lawrence Berkeley National Laboratory and University of California, Berkeley, CA, USA
[19] Institut für Physik, Humboldt Universität zu Berlin, Berlin, Germany
[20] Albert Einstein Center for Fundamental Physics and Laboratory for High Energy Physics, University of Bern, Bern, Switzerland
[21] School of Physics and Astronomy, University of Birmingham, Birmingham, UK
[22] Facultad de Ciencias y Centro de Investigaciónes, Universidad Antonio Nariño, Bogota, Colombia
[23] [(a)]Dipartimento di Fisica, INFN Bologna and Universita' di Bologna, Fisica, Italy; [(b)]INFN Sezione di Bologna, Bologna, Italy
[24] Physikalisches Institut, Universität Bonn, Bonn, Germany
[25] Department of Physics, Boston University, Boston, MA, USA
[26] Department of Physics, Brandeis University, Waltham, MA, USA
[27] [(a)]Transilvania University of Brasov, Brasov, Romania; [(b)]Horia Hulubei National Institute of Physics and Nuclear Engineering, Bucharest, Romania; [(c)]Department of Physics, Alexandru Ioan Cuza University of Iasi, Iasi, Romania ; [(d)]National Institute for Research and Development of Isotopic and Molecular Technologies, Physics Department, Cluj-Napoca, Romania; [(e)]University Politehnica Bucharest, Bucharest, Romania; [(f)]West University in Timisoara, Timisoara, Romania
[28] [(a)]Faculty of Mathematics, Physics and Informatics, Comenius University, Bratislava, Slovak Republic; [(b)]Department of Subnuclear Physics, Institute of Experimental Physics of the Slovak Academy of Sciences, Kosice, Slovak Republic
[29] Physics Department, Brookhaven National Laboratory, Upton, NY, USA
[30] Departamento de Física, Universidad de Buenos Aires, Buenos Aires, Argentina
[31] California State University, CA, USA
[32] Cavendish Laboratory, University of Cambridge, Cambridge, UK
[33] [(a)]Department of Physics, University of Cape Town, Cape Town, South Africa; [(b)]iThemba Labs, Western Cape, South Africa; [(c)]Department of Mechanical Engineering Science, University of Johannesburg, Johannesburg, South Africa ; [(d)]University of South Africa, Department of Physics, Pretoria, South Africa; [(e)]School of Physics, University of the Witwatersrand, Johannesburg, South Africa
[34] Department of Physics, Carleton University, Ottawa, ON, Canada
[35] [(a)]Faculté des Sciences Ain Chock, Réseau Universitaire de Physique des Hautes Energies - Université Hassan II, Casablanca, Morocco; [(b)]Faculté des Sciences, Université Ibn-Tofail, Kénitra, Morocco; [(c)]Faculté des Sciences Semlalia, Université Cadi Ayyad, LPHEA-Marrakech, Morocco; [(d)]Faculté des Sciences, Université Mohamed Premier and LPTPM, Oujda, Morocco; [(e)]Faculté des sciences, Université Mohammed V, Rabat, Morocco
[36] CERN, Geneva, Switzerland
[37] Enrico Fermi Institute, University of Chicago, Chicago, IL, USA
[38] LPC, Université Clermont Auvergne, CNRS/IN2P3, Clermont-Ferrand, France

[39] Nevis Laboratory, Columbia University, Irvington, NY, USA
[40] Niels Bohr Institute, University of Copenhagen, Copenhagen, Denmark
[41] [(a)]Dipartimento di Fisica, Università della Calabria, Rende, Italy; [(b)]INFN Gruppo Collegato di Cosenza, Laboratori Nazionali di Frascati, Italy
[42] Physics Department, Southern Methodist University, Dallas, TX, USA
[43] Physics Department, University of Texas at Dallas, Richardson, TX, USA
[44] National Centre for Scientific Research "Demokritos", Agia Paraskevi, Greece
[45] [(a)]Department of Physics, Stockholm University, Stockholm, Sweden; [(b)]Oskar Klein Centre, Stockholm, Sweden
[46] Deutsches Elektronen-Synchrotron DESY, Hamburg and Zeuthen, Germany
[47] Lehrstuhl für Experimentelle Physik IV, Technische Universität Dortmund, Dortmund, Germany
[48] Institut für Kern- und Teilchenphysik, Technische Universität Dresden, Dresden, Germany
[49] Department of Physics, Duke University, Durham, NC, USA
[50] SUPA - School of Physics and Astronomy, University of Edinburgh, Edinburgh, UK
[51] INFN e Laboratori Nazionali di Frascati, Frascati, Italy
[52] Physikalisches Institut, Albert-Ludwigs-Universität Freiburg, Freiburg, Germany
[53] II. Physikalisches Institut, Georg-August-Universität Göttingen, Göttingen, Germany
[54] Département de Physique Nucléaire et Corpusculaire, Université de Genève, Geneva, Switzerland
[55] [(a)]Dipartimento di Fisica, Università di Genova, Genova, Italy; [(b)]INFN Sezione di Genova, Genova, Italy
[56] II. Physikalisches Institut, Justus-Liebig-Universität Giessen, Giessen, Germany
[57] SUPA - School of Physics and Astronomy, University of Glasgow, Glasgow, UK
[58] LPSC, Université Grenoble Alpes, CNRS/IN2P3, Grenoble INP, Grenoble, France
[59] Laboratory for Particle Physics and Cosmology, Harvard University, Cambridge, MA, USA
[60] [(a)]Department of Modern Physics and State Key Laboratory of Particle Detection and Electronics, University of Science and Technology of China, Hefei, China; [(b)]Institute of Frontier and Interdisciplinary Science and Key Laboratory of Particle Physics and Particle Irradiation (MOE), Shandong University, Qingdao, China; [(c)]School of Physics and Astronomy, Shanghai Jiao Tong University, KLPPAC-MoE, SKLPPC, Shanghai, China; [(d)]Tsung-Dao Lee Institute, Shanghai, China
[61] [(a)]Kirchhoff-Institut für Physik, Ruprecht-Karls-Universität Heidelberg, Heidelberg, Germany; [(b)]Physikalisches Institut, Ruprecht-Karls-Universität Heidelberg, Heidelberg, Germany
[62] Faculty of Applied Information Science, Hiroshima Institute of Technology, Hiroshima, Japan
[63] [(a)]Department of Physics, Chinese University of Hong Kong, Shatin, N.T., Hong Kong, China; [(b)]Department of Physics, University of Hong Kong, Hong Kong, China; [(c)]Department of Physics and Institute for Advanced Study, Hong Kong University of Science and Technology, Clear Water Bay, Kowloon, Hong Kong, China
[64] Department of Physics, National Tsing Hua University, Hsinchu, Taiwan
[65] IJCLab, Université Paris-Saclay, CNRS/IN2P3, 91405 Orsay, France
[66] Department of Physics, Indiana University, Bloomington, IN, USA
[67] [(a)]INFN Gruppo Collegato di Udine, Sezione di Trieste, Udine, Italy; [(b)]ICTP, Trieste, Italy; [(c)]Dipartimento Politecnico di Ingegneria e Architettura, Università di Udine, Udine, Italy
[68] [(a)]INFN Sezione di Lecce, Lecce, Italy; [(b)]Dipartimento di Matematica e Fisica, Università del Salento, Lecce, Italy
[69] [(a)]INFN Sezione di Milano, Milan, Italy; [(b)]Dipartimento di Fisica, Università di Milano, Milan, Italy
[70] [(a)]INFN Sezione di Napoli, Naples, Italy; [(b)]Dipartimento di Fisica, Università di Napoli, Naples, Italy
[71] [(a)]INFN Sezione di Pavia, Pavia, Italy; [(b)]Dipartimento di Fisica, Università di Pavia, Pavia, Italy
[72] [(a)]INFN Sezione di Pisa, Pisa, Italy; [(b)]Dipartimento di Fisica E. Fermi, Università di Pisa, Pisa, Italy
[73] [(a)]INFN Sezione di Roma, Rome, Italy; [(b)]Dipartimento di Fisica, Sapienza Università di Roma, Rome, Italy
[74] [(a)]INFN Sezione di Roma Tor Vergata, Rome, Italy; [(b)]Dipartimento di Fisica, Università di Roma Tor Vergata, Rome, Italy
[75] [(a)]INFN Sezione di Roma Tre, Rome, Italy; [(b)]Dipartimento di Matematica e Fisica, Università Roma Tre, Rome, Italy
[76] [(a)]INFN-TIFPA, Rome, Italy; [(b)]Università degli Studi di Trento, Trento, Italy
[77] Institut für Astro- und Teilchenphysik, Leopold-Franzens-Universität, Innsbruck, Austria
[78] University of Iowa, Iowa City, IA, USA
[79] Department of Physics and Astronomy, Iowa State University, Ames, IA, USA
[80] Joint Institute for Nuclear Research, Dubna, Russia

[81] [(a)]Departamento de Engenharia Elétrica, Universidade Federal de Juiz de Fora (UFJF), Juiz de Fora, Brazil ; [(b)]Universidade Federal do Rio De Janeiro COPPE/EE/IF, Rio de Janeiro, Brazil; [(c)]Universidade Federal de São João del Rei (UFSJ), São João del Rei, Brazil; [(d)]Instituto de Física, Universidade de São Paulo, São Paulo, Brazil
[82] KEK, High Energy Accelerator Research Organization, Tsukuba, Japan
[83] Graduate School of Science, Kobe University, Kobe, Japan
[84] [(a)]AGH University of Science and Technology, Faculty of Physics and Applied Computer Science, Krakow, Poland ; [(b)]Marian Smoluchowski Institute of Physics, Jagiellonian University, Krakow, Poland
[85] Institute of Nuclear Physics Polish Academy of Sciences, Krakow, Poland
[86] Faculty of Science, Kyoto University, Kyoto, Japan
[87] Kyoto University of Education, Kyoto, Japan
[88] Research Center for Advanced Particle Physics and Department of Physics, Kyushu University, Fukuoka , Japan
[89] Instituto de Física La Plata, Universidad Nacional de La Plata and CONICET, La Plata, Argentina
[90] Physics Department, Lancaster University, Lancaster, UK
[91] Oliver Lodge Laboratory, University of Liverpool, Liverpool, UK
[92] Department of Experimental Particle Physics, Jožef Stefan Institute and Department of Physics, University of Ljubljana, Ljubljana, Slovenia
[93] School of Physics and Astronomy, Queen Mary University of London, London, UK
[94] Department of Physics, Royal Holloway University of London, Egham, UK
[95] Department of Physics and Astronomy, University College London, London, UK
[96] Louisiana Tech University, Ruston, LA, USA
[97] Fysiska institutionen, Lunds universitet, Lund, Sweden
[98] Centre de Calcul de l'Institut National de Physique Nucléaire et de Physique des Particules (IN2P3), Villeurbanne, France
[99] Departamento de Física Teorica C-15 and CIAFF, Universidad Autónoma de Madrid, Madrid, Spain
[100] Institut für Physik, Universität Mainz, Mainz, Germany
[101] School of Physics and Astronomy, University of Manchester, Manchester, UK
[102] CPPM, Aix-Marseille Université, CNRS/IN2P3, Marseille, France
[103] Department of Physics, University of Massachusetts, Amherst, MA, USA
[104] Department of Physics, McGill University, Montreal, QC, Canada
[105] School of Physics, University of Melbourne, Victoria, Australia
[106] Department of Physics, University of Michigan, Ann Arbor, MI, USA
[107] Department of Physics and Astronomy, Michigan State University, East Lansing, MI, USA
[108] B.I. Stepanov Institute of Physics, National Academy of Sciences of Belarus, Minsk, Belarus
[109] Research Institute for Nuclear Problems of Byelorussian State University, Minsk, Belarus
[110] Group of Particle Physics, University of Montreal, Montreal, QC, Canada
[111] P.N. Lebedev Physical Institute of the Russian Academy of Sciences, Moscow, Russia
[112] National Research Nuclear University MEPhI, Moscow, Russia
[113] D.V. Skobeltsyn Institute of Nuclear Physics, M.V. Lomonosov Moscow State University, Moscow, Russia
[114] Fakultät für Physik, Ludwig-Maximilians-Universität München, Munich, Germany
[115] Max-Planck-Institut für Physik (Werner-Heisenberg-Institut), Munich, Germany
[116] Nagasaki Institute of Applied Science, Nagasaki, Japan
[117] Graduate School of Science and Kobayashi-Maskawa Institute, Nagoya University, Nagoya, Japan
[118] Department of Physics and Astronomy, University of New Mexico, Albuquerque, NM, USA
[119] Institute for Mathematics, Astrophysics and Particle Physics, Radboud University Nijmegen/Nikhef, Nijmegen, The Netherlands
[120] Nikhef National Institute for Subatomic Physics and University of Amsterdam, Amsterdam, The Netherlands
[121] Department of Physics, Northern Illinois University, DeKalb, IL, USA
[122] [(a)]Budker Institute of Nuclear Physics and NSU, SB RAS, Novosibirsk, Russia; [(b)]Novosibirsk State University Novosibirsk, Novosibirsk, Russia
[123] Institute for High Energy Physics of the National Research Centre Kurchatov Institute, Protvino, Russia
[124] Institute for Theoretical and Experimental Physics named by A.I. Alikhanov of National Research Centre "Kurchatov Institute", Moscow, Russia
[125] Department of Physics, New York University, New York, NY, USA

[126] Ochanomizu University, Otsuka, Bunkyo-ku, Tokyo, Japan
[127] Ohio State University, Columbus, OH, USA
[128] Faculty of Science, Okayama University, Okayama, Japan
[129] Homer L. Dodge Department of Physics and Astronomy, University of Oklahoma, Norman, OK, USA
[130] Department of Physics, Oklahoma State University, Stillwater, OK, USA
[131] Palacký University, RCPTM, Joint Laboratory of Optics, Olomouc, Czech Republic
[132] Center for High Energy Physics, University of Oregon, Eugene, OR, USA
[133] Graduate School of Science, Osaka University, Osaka, Japan
[134] Department of Physics, University of Oslo, Oslo, Norway
[135] Department of Physics, Oxford University, Oxford, UK
[136] LPNHE, Sorbonne Université, Université de Paris, CNRS/IN2P3, Paris, France
[137] Department of Physics, University of Pennsylvania, Philadelphia, PA, USA
[138] Konstantinov Nuclear Physics Institute of National Research Centre "Kurchatov Institute", PNPI, St. Petersburg, Russia
[139] Department of Physics and Astronomy, University of Pittsburgh, Pittsburgh, PA, USA
[140] [(a)]Laboratório de Instrumentação e Física Experimental de Partículas - LIP, Lisbon, Portugal; [(b)]Departamento de Física, Faculdade de Ciências, Universidade de Lisboa, Lisbon, Portugal; [(c)]Departamento de Física, Universidade de Coimbra, Coimbra, Portugal; [(d)]Centro de Física Nuclear da Universidade de Lisboa, Lisboa, Portugal; [(e)]Departamento de Física, Universidade do Minho, Braga, Portugal; [(f)]Departamento de Física Teórica y del Cosmos, Universidad de Granada, Granada (Spain), Portugal; [(g)]Dep Física and CEFITEC of Faculdade de Ciências e Tecnologia, Universidade Nova de Lisboa, Caparica, Portugal; [(h)]Instituto Superior Técnico, Universidade de Lisboa, Lisboa, Portugal
[141] Institute of Physics of the Czech Academy of Sciences, Prague, Czech Republic
[142] Czech Technical University in Prague, Prague, Czech Republic
[143] Charles University, Faculty of Mathematics and Physics, Prague, Czech Republic
[144] Particle Physics Department, Rutherford Appleton Laboratory, Didcot, UK
[145] IRFU, CEA, Université Paris-Saclay, Gif-sur-Yvette, France
[146] Santa Cruz Institute for Particle Physics, University of California Santa Cruz, Santa Cruz, CA, USA
[147] [(a)]Departamento de Física, Pontificia Universidad Católica de Chile, Santiago, Chile; [(b)]Universidad Andres Bello, Department of Physics, Santiago, Chile; [(c)]Departamento de Física, Universidad Técnica Federico Santa María, Valparaíso, Chile
[148] Department of Physics, University of Washington, Seattle, WA, USA
[149] Department of Physics and Astronomy, University of Sheffield, Sheffield, UK
[150] Department of Physics, Shinshu University, Nagano, Japan
[151] Department Physik, Universität Siegen, Siegen, Germany
[152] Department of Physics, Simon Fraser University, Burnaby, BC, Canada
[153] SLAC National Accelerator Laboratory, Stanford, CA, USA
[154] Physics Department, Royal Institute of Technology, Stockholm, Sweden
[155] Departments of Physics and Astronomy, Stony Brook University, Stony Brook, NY, USA
[156] Department of Physics and Astronomy, University of Sussex, Brighton, UK
[157] School of Physics, University of Sydney, Sydney, Australia
[158] Institute of Physics, Academia Sinica, Taipei, Taiwan
[159] [(a)]E. Andronikashvili Institute of Physics, Iv. Javakhishvili Tbilisi State University, Tbilisi, Georgia; [(b)]High Energy Physics Institute, Tbilisi State University, Tbilisi, Georgia
[160] Department of Physics, Technion, Israel Institute of Technology, Haifa, Israel
[161] Raymond and Beverly Sackler School of Physics and Astronomy, Tel Aviv University, Tel Aviv, Israel
[162] Department of Physics, Aristotle University of Thessaloniki, Thessaloniki, Greece
[163] International Center for Elementary Particle Physics and Department of Physics, University of Tokyo, Tokyo, Japan
[164] Graduate School of Science and Technology, Tokyo Metropolitan University, Tokyo, Japan
[165] Department of Physics, Tokyo Institute of Technology, Tokyo, Japan
[166] Tomsk State University, Tomsk, Russia
[167] Department of Physics, University of Toronto, Toronto, ON, Canada
[168] [(a)]TRIUMF, Vancouver, BC, Canada; [(b)]Department of Physics and Astronomy, York University, Toronto, ON, Canada
[169] Division of Physics and Tomonaga Center for the History of the Universe, Faculty of Pure and Applied Sciences, University of Tsukuba, Tsukuba, Japan

[170] Department of Physics and Astronomy, Tufts University, Medford, MA, USA
[171] Department of Physics and Astronomy, University of California Irvine, Irvine, CA, USA
[172] Department of Physics and Astronomy, University of Uppsala, Uppsala, Sweden
[173] Department of Physics, University of Illinois, Urbana, IL, USA
[174] Instituto de Física Corpuscular (IFIC), Centro Mixto Universidad de Valencia - CSIC, Valencia, Spain
[175] Department of Physics, University of British Columbia, Vancouver, BC, Canada
[176] Department of Physics and Astronomy, University of Victoria, Victoria, BC, Canada
[177] Fakultät für Physik und Astronomie, Julius-Maximilians-Universität Würzburg, Würzburg, Germany
[178] Department of Physics, University of Warwick, Coventry, UK
[179] Waseda University, Tokyo, Japan
[180] Department of Particle Physics, Weizmann Institute of Science, Rehovot, Israel
[181] Department of Physics, University of Wisconsin, Madison, WI, USA
[182] Fakultät für Mathematik und Naturwissenschaften, Fachgruppe Physik, Bergische Universität Wuppertal, Wuppertal, Germany
[183] Department of Physics, Yale University, New Haven, CT, USA

[a] Also at Borough of Manhattan Community College, City University of New York, New York NY, USA
[b] Also at CERN, Geneva, Switzerland
[c] Also at CPPM, Aix-Marseille Université, CNRS/IN2P3, Marseille, France
[d] Also at Département de Physique Nucléaire et Corpusculaire, Université de Genève, Genève, Switzerland
[e] Also at Departament de Fisica de la Universitat Autonoma de Barcelona, Barcelona, Spain
[f] Also at Department of Applied Physics and Astronomy, University of Sharjah, Sharjah, United Arab Emirates
[g] Also at Department of Financial and Management Engineering, University of the Aegean, Chios, Greece
[h] Also at Department of Physics and Astronomy, Michigan State University, East Lansing MI, USA
[i] Also at Department of Physics and Astronomy, University of Louisville, Louisville, KY, USA
[j] Also at Department of Physics, Ben Gurion University of the Negev, Beer Sheva, Israel
[k] Also at Department of Physics, California State University, East Bay, USA
[l] Also at Department of Physics, California State University, Fresno, USA
[m] Also at Department of Physics, California State University, Sacramento, USA
[n] Also at Department of Physics, King's College London, London, UK
[o] Also at Department of Physics, St. Petersburg State Polytechnical University, St. Petersburg, Russia
[p] Also at Department of Physics, Stanford University, Stanford CA, USA
[q] Also at Department of Physics, University of Adelaide, Adelaide, Australia
[r] Also at Department of Physics, University of Fribourg, Fribourg, Switzerland
[s] Also at Department of Physics, University of Michigan, Ann Arbor MI, USA
[t] Also at Dipartimento di Matematica, Informatica e Fisica, Università di Udine, Udine, Italy
[u] Also at Faculty of Physics, M.V. Lomonosov Moscow State University, Moscow, Russia
[v] Also at Giresun University, Faculty of Engineering, Giresun, Turkey
[w] Also at Graduate School of Science, Osaka University, Osaka, Japan
[x] Also at Hellenic Open University, Patras, Greece
[y] Also at IJCLab, Université Paris-Saclay, CNRS/IN2P3, 91405, Orsay, France
[z] Also at Institucio Catalana de Recerca i Estudis Avancats, ICREA, Barcelona, Spain
[aa] Also at Institut für Experimentalphysik, Universität Hamburg, Hamburg, Germany
[ab] Also at Institute for Mathematics, Astrophysics and Particle Physics, Radboud University Nijmegen/Nikhef, Nijmegen, Netherlands
[ac] Also at Institute for Nuclear Research and Nuclear Energy (INRNE) of the Bulgarian Academy of Sciences, Sofia, Bulgaria
[ad] Also at Institute for Particle and Nuclear Physics, Wigner Research Centre for Physics, Budapest, Hungary
[ae] Also at Institute of Particle Physics (IPP), Vancouver, Canada
[af] Also at Institute of Physics, Azerbaijan Academy of Sciences, Baku, Azerbaijan
[ag] Also at Instituto de Fisica Teorica, IFT-UAM/CSIC, Madrid, Spain
[ah] Also at Joint Institute for Nuclear Research, Dubna, Russia
[ai] Also at Louisiana Tech University, Ruston LA, USA

[aj] Also at Manhattan College, New York NY, USA
[ak] Also at Moscow Institute of Physics and Technology State University, Dolgoprudny, Russia
[al] Also at National Research Nuclear University MEPhI, Moscow, Russia
[am] Also at Physics Department, An-Najah National University, Nablus, Palestine
[an] Also at Physics Dept, University of South Africa, Pretoria, South Africa
[ao] Also at Physikalisches Institut, Albert-Ludwigs-Universität Freiburg, Freiburg, Germany
[ap] Also at The City College of New York, New York NY, USA
[aq] Also at Tomsk State University, Tomsk, and Moscow Institute of Physics and Technology State University, Dolgoprudny, Russia
[ar] Also at TRIUMF, Vancouver BC, Canada
[as] Also at Universita di Napoli Parthenope, Napoli, Italy
*Deceased

Published for SISSA by Springer

Received: *March 27, 2020*
Accepted: *June 15, 2020*
Published: *July 7, 2020*

Measurements of the production cross-section for a Z boson in association with b-jets in proton-proton collisions at $\sqrt{s} = 13$ TeV with the ATLAS detector

The ATLAS collaboration

E-mail: atlas.publications@cern.ch

Abstract: This paper presents a measurement of the production cross-section of a Z boson in association with b-jets, in proton-proton collisions at $\sqrt{s} = 13\,\text{TeV}$ with the ATLAS experiment at the Large Hadron Collider using data corresponding to an integrated luminosity of $35.6\,\text{fb}^{-1}$. Inclusive and differential cross-sections are measured for events containing a Z boson decaying into electrons or muons and produced in association with at least one or at least two b-jets with transverse momentum $p_{\text{T}} > 20\,\text{GeV}$ and rapidity $|y| < 2.5$. Predictions from several Monte Carlo generators based on leading-order (LO) or next-to-leading-order (NLO) matrix elements interfaced with a parton-shower simulation and testing different flavour schemes for the choice of initial-state partons are compared with measured cross-sections. The 5-flavour number scheme predictions at NLO accuracy agree better with data than 4-flavour number scheme ones. The 4-flavour number scheme predictions underestimate data in events with at least one b-jet.

Keywords: Hadron-Hadron scattering (experiments)

ArXiv ePrint: 2003.11960

https://doi.org/10.1007/JHEP07(2020)044

JHEP07(2020)044

Contents

1 Introduction

The measurement of the production rate of a Z boson in association with jets originating from b-quarks[1] ($Z + b$-jets) in proton-proton (pp) collisions provides an important test of perturbative quantum chromodynamics (pQCD). Current predictions for $Z+b$-jets production are known at next-to-leading-order (NLO) accuracy in pQCD, and they can be derived in either a 4-flavour number scheme (4FNS) or a 5-flavour number scheme (5FNS) [1–4].

[1] Unless otherwise mentioned, it is implicitly assumed that b-quark refers to both b-quark and $\bar{b}$-antiquark.

JHEP07(2020)044

In the 4FNS, b-quarks do not contribute to the parton distribution functions (PDFs) of the proton and, in QCD, they only appear in a massive final state due to gluon splitting ($g \to b\bar{b}$). In the 5FNS, b-quark density is allowed in the initial state via a b-quark PDF, with the b-quark typically being massless. Therefore, in the 5FNS the $Z + b$-jets cross-section is sensitive to the b-quark PDF and can be used to constrain it. The ambiguity among the schemes is an intrinsic property of the calculation and is expected to reduce with the inclusion of higher order perturbative corrections [3].

Furthermore, the measurement of $Z + b$-jets production provides a benchmark to test predictions from Monte Carlo (MC) simulations. These are commonly used to estimate the background contribution of $Z + b$-jet events to other topologies, such as the production of a Higgs boson decaying into a b-quark pair in association with a Z boson, or in searches for physics beyond the SM with signatures containing leptons and b-jets in the final state.

The $Z + b$-jets processes occur more rarely than the production of Z-boson events with inclusive jets (Z+jets) and they are more challenging to measure. The b-jets are identified by exploiting the long lifetime of b-hadrons produced in the quark hadronisation, and a higher level of background affects the measurement. The background is mainly composed of events with a Z boson associated with light-flavour jets or c-jets,[2] misidentified as b-jets, and events from the dileptonic decay of a $t\bar{t}$ pair.

Inclusive and differential cross-sections of $Z + b$-jets production have been measured in proton-antiproton collisions at the centre-of-mass energy of $\sqrt{s} = 1.96$ TeV by the CDF and D0 experiments [5–8] and at the Large Hadron Collider (LHC) [9] in $\sqrt{s} = 7$ TeV pp collisions by the ATLAS and CMS experiments [10–15], as well as in $\sqrt{s} = 8$ TeV pp collisions by the CMS experiment [16, 17]. The CMS experiment also recently released a measurement of the ratio of $Z + b$-jets to Z+jets cross-sections and the ratio of $Z + c$-jets to $Z + b$-jets cross-sections for events with at least one b-jet or one c-jet in $\sqrt{s} = 13$ TeV pp collisions [18].

This paper presents a measurement of the inclusive and differential production cross-sections of a Z boson, decaying into electrons or muons, in association with at least one or at least two b-jets using $35.6\,\text{fb}^{-1}$ of pp collision data collected by the ATLAS experiment at $\sqrt{s} = 13$ TeV in 2015 and 2016. For events with at least one b-jet, the differential cross-sections are presented as a function of the transverse momentum[3] (p_{T}) and the absolute value of the rapidity ($|y|$) of the leading b-jet, the p_{T} and the $|y|$ of the Z boson (Z p_{T} and Z $|y|$), and as a function of observables correlating the Z boson with the leading b-jet, namely the azimuthal angle between them ($\Delta\phi_{Zb}$), the absolute value of their rapidity difference (Δy_{Zb}), and their angular separation (ΔR_{Zb}). For events with at least two b-jets, the differential cross-sections are presented as a function of the p_{T} of the Z boson

[2] A c-jet is a jet originating from a c-quark.

[3] ATLAS uses a right-handed coordinate system with its origin at the nominal interaction point (IP) in the centre of the detector and the z-axis along the beam pipe. The x-axis points from the IP to the centre of the LHC ring, and the y-axis points upwards. Cylindrical coordinates (r, ϕ) are used in the transverse plane, ϕ being the azimuthal angle around the z-axis. The pseudorapidity is defined in terms of the polar angle θ as $\eta = -\ln\tan(\theta/2)$. Angular separation is measured in units of $\Delta R \equiv \sqrt{(\Delta\eta)^2 + (\Delta\phi)^2}$. When dealing with massive jets and particles, the rapidity $y = \frac{1}{2}\ln\frac{E+p_z}{E-p_z}$ is used, in which E is the jet or particle energy and p_z is the z-component of the jet or particle momentum.

JHEP07(2020)044

and as a function of observables built using the two leading b-jets, namely their p_{T} ($p_{\mathrm{T},bb}$), their invariant mass (m_{bb}), $p_{\mathrm{T},bb}$ divided by their invariant mass ($p_{\mathrm{T},bb}/m_{bb}$), the azimuthal angle between them ($\Delta\phi_{bb}$), the absolute value of their rapidity difference (Δy_{bb}), and their angular separation (ΔR_{bb}). The higher $\sqrt{s}$ leads to a large increase in the measured cross-section in comparison with previous ATLAS publications. This allows more extreme regions of phase space to be explored and new measurements to be performed in the rare two-b-jets configuration (i.e. $p_{\mathrm{T},bb}$ and $p_{\mathrm{T},bb}/m_{bb}$). Previous ATLAS measurements were compared with MC predictions based on leading-order matrix elements interfaced with a parton-shower simulation, which showed substantial mismodelling. Recent advances in this field permit this paper to compare the data with the latest MC predictions using next-to-leading-order matrix elements, which are expected to provide a better description of the data.

The experimental apparatus is described in section 2, and details of the data sample and the MC simulations are provided in section 3. The object definitions and the event selection at detector level are presented in section 4. Backgrounds that do not contain a real Z boson are estimated via MC simulations and validated in control regions in data or via data-driven techniques, while backgrounds containing a real Z boson and jets not originating from b-quarks are estimated with a fit to data distributions sensitive to the flavour of the jet (flavour fit); both are described in section 5. Distributions of the kinematic variables are presented in section 6. After background subtraction, the data are unfolded to particle level in a fiducial phase space, which is detailed in section 7. Systematic uncertainties in the unfolded data are discussed in section 8. The results are presented in section 9, and conclusions are drawn in section 10.

2 The ATLAS detector

The ATLAS detector [19] at the LHC covers nearly the entire solid angle around the collision point. It consists of an inner tracking detector surrounded by a thin superconducting solenoid, electromagnetic and hadronic calorimeters, and a muon spectrometer incorporating three large superconducting toroidal magnets.

The inner-detector system (ID) is immersed in a 2 T axial magnetic field and provides charged-particle tracking in the range $|\eta| < 2.5$. The high-granularity silicon pixel detector covers the vertex region and provides four measurements for most tracks, the first hit normally being in the insertable B-layer [20, 21]. It is followed by the silicon microstrip tracker, which provides eight measurements per track. These silicon detectors are complemented by the transition radiation tracker (TRT), which enables radially extended track reconstruction up to $|\eta| = 2.0$. The TRT also provides electron identification information based on the fraction of hits (typically 30 in total) with an energy deposit above the transition-radiation threshold.

The calorimeter system covers the pseudorapidity range $|\eta| < 4.9$. Within the region $|\eta| < 3.2$, electromagnetic calorimetry is provided by barrel and endcap high-granularity lead/liquid-argon (LAr) calorimeters, with an additional thin LAr presampler covering $|\eta| < 1.8$ to correct for energy loss in material upstream of the calorimeters. Hadronic

JHEP07(2020)044

calorimetry is provided by the steel/scintillator-tile calorimeter, segmented into three barrel structures within $|\eta| < 1.7$, and two copper/LAr hadronic endcap calorimeters. The solid angle coverage is completed with forward copper/LAr and tungsten/LAr calorimeter modules optimised for electromagnetic and hadronic measurements, respectively.

The muon spectrometer (MS) comprises separate trigger and high-precision tracking chambers measuring the deflection of muons in a magnetic field generated by the superconducting air-core toroid magnets. The field integral of the toroid magnets ranges between 2.0 and 6.0 T m across most of the detector. The precision chambers cover the region $|\eta| < 2.7$ with three layers of monitored drift tubes, complemented by cathode-strip chambers in the forward region, where the background is highest. The muon trigger system covers the range $|\eta| < 2.4$ with resistive-plate chambers in the barrel, and thin-gap chambers in the endcap regions.

Interesting events are accepted by the first-level trigger system implemented in custom hardware, followed by selections made by algorithms implemented in software in the high-level trigger [22]. The first-level trigger accepts events from the 40 MHz bunch crossings at a rate below 100 kHz, which the high-level trigger further reduces in order to record events to disk at about 1 kHz rate.

3 Data set and simulated event samples

3.1 Data set description

The data used in this measurement were recorded in 2015 and 2016 with the ATLAS detector at the LHC in pp collisions at $\sqrt{s} = 13$ TeV. The candidate events were selected by either a single-electron or single-muon trigger that imposed a minimum transverse energy (transverse momentum) threshold for the electron (muon) channel and quality and isolation requirements, which depended on the LHC running conditions. The threshold in 2015 was 24 (20) GeV for the electrons (muons), satisfying loose isolation requirements. Due to the higher instantaneous luminosity in 2016, the threshold was increased to 26 GeV for both the electrons and the muons, and a more restrictive isolation requirement was imposed on both leptons along with more restrictive identification requirements for electrons. Triggers with higher thresholds but with no isolation requirement or with loosened identification criteria were also used to increase the efficiency. Crossings of proton bunches occurred every 25 ns, the collisions achieved a peak instantaneous luminosity of 1.37×10^{34} cm^{-2}s^{-1}, and the mean number of pp interactions per bunch crossing (pile-up) was $\langle\mu\rangle = 24$. After applying criteria to ensure good ATLAS detector operation, the total integrated luminosity amounts to 35.6 fb^{-1}. The uncertainty in the combined 2015-2016 integrated luminosity is 2.1% [23], obtained using the LUCID-2 detector [24] for the primary luminosity measurements.

3.2 Simulated event samples for signal and background processes

MC simulations are used to describe signal events, to estimate the contribution of background processes, to unfold the data yield to the particle level, to estimate systematic uncertainties, and to compare predictions with the unfolded data distributions.

JHEP07(2020)044

An overview of all signal and background processes and the generators used for the production of nominal results is given in table 1 together with the theory uncertainty in the normalisation cross-sections corresponding to PDFs and scale variations.

Inclusive $Z(\to \ell\ell, \ell = e, \mu)$ production in association with both light- and heavy-flavour jets was simulated using the Sherpa v2.2.1 [25] generator. In this set-up, matrix elements at NLO for up to two partons, and matrix elements at LO for up to four partons, were calculated with the Comix [26] and OpenLoops [27, 28] libraries. They were matched with the Sherpa parton shower [29] using the MEPS@NLO prescription [30–33]. Sherpa uses the 5FNS with massless b- and c-quarks in the matrix element, but massive quarks in the parton shower. Samples were generated using the NNPDF3.0nnlo PDF set [34], along with the dedicated set of tuned parton-shower parameters developed by the Sherpa authors. In section 9, where several predictions are compared with the unfolded data, these samples are shown with their uncertainties and are referred to as Sherpa 5FNS (NLO). The uncertainties account for missing higher orders and are evaluated [35] using seven variations of the QCD factorisation and renormalisation scales in the matrix elements by factors of 0.5 and 2 and avoiding variations in opposite directions.

Additional $Z(\to \ell\ell)$ samples were produced with the LO matrix-element generator Alpgen v2.14 [36], interfaced with Pythia v6.426 [37] to model parton showers, using the parameter values of the Perugia2011C tune [38] for simulating the underlying event, and the CTEQ6L1 PDF set [39]. Matrix elements were calculated for up to five partons, and merged using the MLM prescription [40] with a matching scale of 15 GeV. Alpgen uses the 4FNS with massive b- and c-quarks in the matrix element and in the parton shower of Pythia. The matrix elements for the production of $Z + b\bar{b}$ and $Z + c\bar{c}$ events are explicitly included and a heavy-flavour overlap procedure is used to remove the double counting, between the matrix element and the parton shower, of heavy quarks from gluon splitting. The properties of b- and c-hadron decays were simulated with EvtGen v1.2.0 [41], as was done in all generated samples where the parton shower was simulated with Pythia. Photos++ v3.52 [42, 43] was used to simulate QED final-state radiation (FSR). The Alpgen samples are used in the analysis to estimate systematic uncertainties in the unfolding procedure and in backgrounds containing a genuine Z boson. In section 9 these samples are referred to as Alpgen + Py6 4FNS (LO). Samples of $Z(\to \tau\tau)$, $W(\to \ell\nu)$, and $W(\to \tau\nu)$ events were simulated with Sherpa, using the same set-up adopted for the signal samples.

The Z-boson and W-boson samples are normalised to the inclusive next-to-next-to-leading-order (NNLO) cross-section predictions provided by the FEWZ 3.1 program [44–47] with the CT14 PDF set. The K-factor applied to the Z samples to match the NNLO prediction is 0.975 for Sherpa and 1.196 for Alpgen.

The production of $t\bar{t}$ events with at least one W boson decaying leptonically was modelled using the Powheg-Box [48–51] v2 generator at NLO with the NNPDF3.0NLO [34] PDF set. The h_{damp} parameter, which regulates the high-p_{T} emissions against which the $t\bar{t}$ system recoils, is set to 1.5 m_{top} [52]. The events were interfaced with Pythia v8.230 [53] using the A14 tune [54]. The $t\bar{t}$ sample is normalised to the theory prediction at NNLO in QCD including the resummation of next-to-next-to-leading logarithmic (NNLL) soft-gluon terms [55–61]. Four additional $t\bar{t}$ samples were simulated to evaluate the un-

JHEP07(2020)044

certainty in this process, as described in [52]. One sample was produced with MadGraph5_aMC@NLO [62] and the same parton-shower model of the nominal $t\bar{t}$ sample in order to estimate the uncertainty due to the modelling of the hard scattering process. A second Powheg-Box sample showered with Herwig 7.13 [63, 64] was generated to evaluate the uncertainty due to the modelling of the parton shower and hadronization processes. A third sample was produced to simulate higher energy radiation with the factorisation and renormalisation scales changed by a factor of 0.5 while simultaneously increasing the h_{damp} value to 3.0 m_{top} and using the upper variation of the initial state radiation (ISR) from the A14 tune. The last sample simulates the lower energy radiation. It was generated with the renormalisation and factorisation scales varied by a factor of 2.0 while keeping the h_{damp} value at 1.5 m_{top} and using the ISR downward variation in the parton shower. The last two samples are also used to estimate the impact of FSR with parton-shower weights that vary the renormalisation scale for QCD emission in the FSR by factors of 0.5 and 2.0.

Single-top-quark events in the Wt-, s- and t-channels were generated using the Powheg-Box v1 generator interfaced with Pythia v6.4 [37]; the latter simulates parton showers, fragmentation, and the underlying event using the Perugia 2012 tune [38]. The CT10 PDF set was used [65]. The single-top samples for the t- and s-channels are normalised to cross-sections from NLO predictions [66, 67], while the Wt-channel sample is normalised to cross-sections from approximate NNLO predictions [68].

Diboson processes (WW, WZ, and ZZ) with one of the bosons decaying hadronically and the other leptonically were generated using Sherpa v2.2.1 with the CT10nlo PDF set. The matrix element includes up to one parton at NLO and up to three additional partons at LO. The samples are normalised to the NLO predictions [69].

Simulated events for $qq \to VH(\to b\bar{b})$ with $V = W$ or Z plus zero or one jet production at NLO were generated with the Powheg-Box v2 + GoSam + MiNLO generator [51, 70–72] with the NNPDF3.0NLO PDF set. The contribution from $gg \to ZH(\to b\bar{b})$ production was simulated using the LO Powheg-Box v2 matrix-element generator. The samples of simulated events include all final states where the Higgs boson decays into $b\bar{b}$ and the vector boson into a leptonic final state. The mass of the Higgs boson is set to 125 GeV and the $H \to b\bar{b}$ branching fraction is set to 58%. The $qq \to VH(\to b\bar{b})$ cross-section is calculated at NNLO (QCD) and NLO (EW), while the $gg \to ZH$ cross-section is calculated at NLO+NLL (QCD).

Generated events were processed with the ATLAS detector simulation [76], based on Geant4 [77], to simulate the detector response to final-state particles. To account for the effects of pile-up, multiple overlaid pp collisions were simulated with the soft QCD processes of Pythia v8.186 using the A2 tune [78] and the MSTW2008LO PDF set [79]. The distribution of the average number of interactions per bunch crossing in the simulation is weighted to reflect that in the data. Simulated events are processed with the same reconstruction algorithms as for the data.

3.3 Theoretical predictions

In addition to particle-level predictions from the fully simulated Sherpa and Alpgen samples described above, unfolded results from data are compared with six other predictions listed in table 2.

JHEP07(2020)044

Process	Generator	Order of cross-section calculation	Reference normalisation	Normalisation cross-section uncertainty
$Z \to \ell\ell$ ($\ell = e, \mu, \tau$) with $66 < m_{\ell\ell} < 116$ GeV	Sherpa	NNLO	[44–47]	5%
$W \to \ell\nu$ ($\ell = e, \mu, \tau$)	Sherpa	NNLO	[44–47]	5%
$t\bar{t}$	Powheg-Box	NNLO + NNLL ($m_{\text{top}} = 172.5$ GeV)	[55–61]	6%
Single top (t-, Wt-, s-channel)	Powheg-Box ($m_{\text{top}} = 172.5$ GeV)	NLO		6%
Dibosons $Z(\to \ell\ell) + Z(\to qq)$, $W(\to \ell\nu) + W(\to qq)$)	Sherpa	NLO	[69]	5%
Higgs $qq \to Z(\to \ell\ell) + H(\to b\bar{b})$ $gg \to Z(\to \ell\ell) + H(\to b\bar{b})$ $qq \to W(\to \ell\nu) + H(\to b\bar{b})$	Powheg-Box	NNLO QCD + NLO EW NLO + NLL NNLO QCD + NLO EW	[73–75]	3%

Table 1. Signal and background MC samples: the generator programs used in the simulation are listed in the second column, the order of the QCD calculation and the reference used for the calculations of the normalisation cross section are reported in the third and fourth columns. The normalisation cross-section uncertainty in the final column corresponds to PDFs and scale variations.

Two particle-level predictions (using specific parton-shower and matching predictions) were produced with the Sherpa v2.2.7 generator using NLO matrix elements [80]. The first sample, referred to as Sherpa Zbb 4FNS (NLO), includes $Z + b\bar{b}$ events generated in the 4FNS at NLO with massive b-quarks. It is interesting to compare this sample, which contains two b-quarks in the matrix elements, with the unfolded data even in the case of distributions with at least one b-jet, to understand if there are regions of the phase space that can be described with such a configuration. The second sample, referred to as Sherpa Fusing 4FNS+5FNS (NLO), contains the matrix elements at NLO for up to two partons, and matrix elements at LO for up to three partons. It includes both $Z + b\bar{b}$ events generated in the 4FNS at NLO with massive b-quarks, and Z+jets events generated in the 5FNS at NLO. They are combined according to the procedure described in ref. [81]. The combination is achieved by means of a dedicated heavy-flavour overlap removal procedure, the fusing technique, that acts as an additional step after the multijet merging algorithms. This procedure combines the advantages of inclusive 5FNS calculations with the higher precision of 4FNS calculations in regions of phase space where the b-quark mass sets a relevant scale. The two Sherpa samples use the NNPDF3.0nnlo PDF set with $\alpha_{\text{S}}(m_Z) = 0.118$ and the corresponding number of active quark flavours. Masses of c- and b-quarks are taken into account in the parton shower in all Sherpa samples.

Results are also compared with predictions from the LO matrix-element generator MadGraph5_aMC@NLO v2.2.2 [62] interfaced with Pythia v8.186 [53] with the A14 tune [54] to model the parton shower and underlying event. The matrix element includes up

JHEP07(2020)044

Generator	$N_{\text{max}}^{\text{partons}}$		FNS	PDF	Parton
	NLO	LO		set	Shower
Z+jets (including Z+b and Z+bb)					
Sherpa 5FNS (NLO)	2	4	5	NNPDF3.0nnlo	Sherpa
Sherpa Fusing 4FNS+5FNS (NLO)	2	3	5 (*)	NNPDF3.0nnlo	Sherpa
Alpgen + Py6 4FNS (LO)	—	5	4	CTEQ6L1	Pythia v6.426
Alpgen + Py6 (rew. NNPDF3.0lo)	—	5	4	NNPDF3.0lo	Pythia v6.426
MGaMC + Py8 5FNS (LO)	—	4	5	NNPDF3.0nlo	Pythia v8.186
MGaMC + Py8 5FNS (NLO)	1	—	5	NNPDF3.0nnlo	Pythia v8.186
Z+bb					
Sherpa Zbb 4FNS (NLO)	2	—	4	NNPDF3.0nnlo	Sherpa
MGaMC + Py8 Zbb 4FNS (NLO)	2	—	4	NNPDF3.0nnlo	Pythia v8.186

Table 2. Summary of theoretical predictions for the signal, including the maximum number of partons at each order in α_{S}, the flavour number scheme (FNS), the PDFs set and the parton shower. (*) Details of the merging between 4FNS and 5FNS in Sherpa Fusing 4FNS+5FNS (NLO) are available in ref. [81].

to four partons. Additional jets are produced by the parton shower, which uses the CKKW-L merging procedure [82], with a matching scale of 30 GeV. MadGraph5_aMC@NLO uses the 5FNS with massless b- and c-quarks in the matrix element, and massive quarks in the parton shower. The NNPDF3.0nlo PDF set is used with $\alpha_{\text{S}}(m_Z) = 0.118$. This prediction is referred to as MGaMC + Py8 5FNS (LO).

Two additional predictions were produced with MadGraph5_aMC@NLO v2.6.2, using matrix-element calculations with NLO accuracy. The first sample includes Z+jets events generated in the 5FNS with up to one parton at NLO, and massless b- and c-quarks; the second sample includes $Z + b\bar{b}$ events generated in the 4FNS at NLO, and massive b-quarks. Both samples were generated using the NNPDF3.0nnlo PDF set with $\alpha_{\text{S}} = 0.118$. They were interfaced to the Pythia v8.186 parton shower using the FxFx merging scheme [83], with a matching scale of 25 GeV. As in the previous case, massive c- and b-quarks are produced in the parton shower. The first sample is referred to as MGaMC + Py8 5FNS (NLO); the second is referred to as MGaMC + Py8 Zbb 4FNS (NLO).

An additional Alpgen prediction is used to test the sensitivity of the measurements to the parton structure of the proton. The Alpgen samples presented in section 3.2 are reweighted to the NNPDF3.0lo PDF set, using the prescriptions reported in ref. [84]. These predictions are referred to as Alpgen + Py6 (rew. NNPDF3.0lo). The predictions of LO MC generators, such as Alpgen + Py6 4FNS (LO) and MGaMC + Py8 5FNS (LO), with up to four or five partons in the matrix element, are still an interesting case to study as they allow comparison with the predictions of MC generators at NLO accuracy and with a smaller number of partons in the matrix element. Furthermore, they provide a benchmark in common with past analyses, such as in ref. [11].

JHEP07(2020)044

4 Event selection

Events selected in this analysis are required to have a signature consistent with a Z boson, decaying into two electrons or two muons, in association with at least one or at least two b-jets. Candidate events are required to have a primary vertex (PV), defined as the vertex with the highest sum of track p_{T}^2 with at least two associated tracks measured in the ID (ID tracks), each with $p_{\mathrm{T}} > 400$ MeV.

Electron candidates are reconstructed by matching a cluster of energy deposited in the EM calorimeter to a well-reconstructed ID track. Electrons are identified using a likelihood function based on variables describing the shape of the electromagnetic showers in the calorimeter, track properties, and track-to-cluster matching quantities [85]. Electrons must satisfy the 'tight' likelihood requirement. Electron candidates are required to have $p_{\mathrm{T}} > 27$ GeV and $|\eta| < 2.47$. Candidates in the transition region between the barrel and endcap electromagnetic calorimeters, $1.37 < |\eta| < 1.52$, are excluded.

Muon candidates are reconstructed by fitting a unique trajectory through the hits associated with a pair of matching tracks which are reconstructed separately in the ID and the MS; the energy loss in the calorimeter is taken into account in the combination procedure. Muons must satisfy the 'medium' identification criterion based on requirements on the number of hits and on the quality of the combined fit [86]. Muon candidates are required to have $p_{\mathrm{T}} > 27$ GeV and $|\eta| < 2.5$.

To select leptons originating from the primary pp interaction, the lepton tracks are required to have a longitudinal impact parameter (z_0) satisfying $|z_0 \sin(\theta)| < 0.5$ mm relative to the PV. The transverse impact parameter significance (d_0/σ_{d_0}) of the electron (muon) candidates must satisfy $d_0/\sigma_{d_0} < 5$ (3). In order to further suppress leptons from non-prompt processes or leptons from hadrons in jets, both the electron and muon candidates are required to satisfy p_{T}-dependent cone-based isolation requirements [86], which use information from ID tracks. The isolation requirements are set so that the scalar sum of the transverse momenta of the tracks in the isolation cone[4] around the lepton is less than 6% of the lepton p_{T}.

Jets are reconstructed, using the anti-k_t algorithm [87, 88] with radius parameter $R = 0.4$, from topological clusters of energy deposits in the calorimeter [89]. Jets are calibrated using a simulation-based calibration scheme, followed by in situ corrections to account for differences between simulation and data [90]. Events with jets arising from detector noise or other non-collision sources are discarded [91]. Furthermore, to eliminate jets containing a large energy contribution from pile-up, jets with $p_{\mathrm{T}} < 60$ GeV and $|\eta| < 2.4$ are required to have a significant fraction of their tracks with origin compatible with the primary vertex, as defined by a jet vertex tagger discriminant (JVT) [92]. Selected jets must have $p_{\mathrm{T}} > 20$ GeV and rapidity $|y| < 2.5$.

An overlap removal procedure is applied to electron, muon and jet candidates to prevent double counting. Any jet whose axis lies within $\Delta R = 0.2$ of an electron is removed. If a jet is reconstructed within $\Delta R = 0.2$ of a muon and the jet has fewer than three associ-

[4]The ΔR parameter of the isolation cone is defined by $\Delta R = \min(10\ \mathrm{GeV}/p_{\mathrm{T}}, 0.3)$ where p_{T} is the transverse momentum of the lepton candidate.

JHEP07(2020)044

ated tracks or the muon energy constitutes most of the jet energy, then the jet is removed. Any electron or muon of a given p_{T} reconstructed within $\Delta R = \min(0.4, 0.04 + 10\ \mathrm{GeV}/p_{\mathrm{T}})$ of the axis of any surviving jet is removed. Jets that survive the overlap removal procedure are removed if they are within $\Delta R = 0.4$ of the selected leptons.

The b-jets, defined as the jets containing at least one b-hadron, are identified using a multivariate algorithm, MV2c10 [93, 94]. This algorithm uses the impact parameter and reconstructed secondary vertex information of the tracks associated with the jets. Its output lies in the range $[-1, +1]$. A value close to $+1$ denotes a higher probability for the jet to be a b-jet. The b-jet candidates are selected if their MV2c10 output is greater than 0.8244. This selection corresponds to an efficiency of 70% for selecting jets containing b-hadrons, and misidentification rates of 0.26% and 8.3%, respectively, for light-flavour (u-, d-, s-quark and gluon) jets and c-jets, as estimated from a sample of simulated $t\bar{t}$ events. Other working points are defined by different b-tagging discriminant output thresholds; they are used to define control regions and to define the bins used in the flavour fit, as detailed in section 5.1.

In simulation, reconstructed jets are labelled as b-jets if they lie within $\Delta R = 0.3$ of one or more weakly decaying b-hadrons with $p_{\mathrm{T}} > 5$ GeV. Reconstructed jets not identified as b-jets are considered to be c-jets if they lie within $\Delta R = 0.3$ of any c-hadron with $p_{\mathrm{T}} > 5$ GeV. All other jets are classified as light-jets. Simulated Z+jets events are sequentially categorised depending on the labels of the jets, starting from b-jets, as follows: $Z+b$ when they have exactly one b-jet, $Z+bb$ when they have at least two b-jets, $Z+c$ when they have at least one c-jet, $Z+l$ when they have only light-jets. A similar classification is adopted for simulated W+jets events. In the distributions with at least one b-jet, the sum of $Z+b$ and $Z+bb$ samples is used to define the signal, and the Z+jets background is constituted by the sum of the $Z+c$ and $Z+l$ samples. In the distributions with at least two b-jets, the $Z+bb$ samples alone constitute the signal, while the sum of the $Z+b$, $Z+c$, and $Z+l$ samples form the Z+jets background.

The missing transverse momentum ($E_{\mathrm{T}}^{\mathrm{miss}}$), which may correspond to a neutrino escaping interaction with the detector, is defined as the negative vector sum of the transverse momentum of all identified hard physics objects (electrons, muons, jets), as well as an additional track-based soft term defined in ref. [95].

Events are required to have exactly two leptons[5] of the same flavour (ee or $\mu\mu$) but of opposite charge with their dilepton invariant mass in the range $76\,\mathrm{GeV} < m_{\ell\ell} < 106\,\mathrm{GeV}$. Events with $p_{\mathrm{T}}^{\ell\ell} < 150$ GeV must also have $E_{\mathrm{T}}^{\mathrm{miss}} < 60\,\mathrm{GeV}$. The requirement on the $E_{\mathrm{T}}^{\mathrm{miss}}$ value reduces by about 55% the background from $t\bar{t}$ events with dileptonic decay, while the signal is reduced by about 5%. Events passing the above selection and having at least one or at least two jets belong to the region referred to as the pre-tag region. The signal region is a subset of the pre-tag region. Events belonging to the signal region are assigned to two regions: those with at least one b-jet, referred to as the 1-tag region; and those with at least two b-jets, referred to as the 2-tag region, which is a subset of the 1-tag region.

A summary of the object selection and the event selection used in the analysis to define

[5] At least one of the lepton candidates is required to match the lepton that triggered the event.

JHEP07(2020)044

	Electron channel	Muon channel
Trigger	Single electron	Single muon
Leptons	Tight Isolated PV association: $\lvert d_0/\sigma_{d_0}\rvert < 5$, $\lvert z_0 \sin\theta\rvert < 0.5$ mm $p_{\mathrm{T}} > 27$ GeV $\lvert\eta\rvert < 1.37$ or $1.52 < \lvert\eta\rvert < 2.47$	Medium Isolated PV association: $\lvert d_0/\sigma_{d_0}\rvert < 3$, $\lvert z_0 \sin\theta\rvert < 0.5$ mm $p_{\mathrm{T}} > 27$ GeV $\lvert\eta\rvert < 2.5$
Jets	$p_{\mathrm{T}} > 20$ GeV and $\lvert y\rvert < 2.5$ $\Delta R(\text{jet}, \ell) > 0.4$	
b-jet	$p_{\mathrm{T}} > 20$ GeV and $\lvert y\rvert < 2.5$	

Regions				
	Pre-tag region	Signal regions	Z+jets Validation Region	$t\bar{t}$ Validation Region
Leptons	2 same-flavour, opposite-charge			1 e, 1 μ, opposite-charge
$m_{\ell\ell}$	76 GeV $< m_{\ell\ell} <$ 106 GeV			
$E_{\mathrm{T}}^{\mathrm{miss}}$	$E_{\mathrm{T}}^{\mathrm{miss}} <$ 60 GeV if $p_{\mathrm{T}}^{\ell\ell} <$ 150 GeV			
Jets	≥ 1 or ≥ 2 jets			
b-tagging efficiency working point selection	—	70%	≥ 1 b-jet at 77%–70%	70%
Number of b-jets	—	≥ 1 b-jets (1-tag region) ≥ 2 b-jets (2-tag region)	≥ 1 b-jets	≥ 2 b-jets

Table 3. Summary of object and event selections defining the signal regions and the validation regions for the main backgrounds of the analysis at detector level.

the signal regions and the validation regions for the main backgrounds, which are presented in section 5, is given in table 3.

4.1 Correction factors applied to simulation and corresponding uncertainties

Corrections are applied to simulated samples in order to ensure that the object selection efficiencies and the energy and momentum calibrations agree with data within the uncertainties associated with the corrections.

The electron and muon trigger efficiencies are estimated in data and simulation in order to determine simulation-to-data correction factors and their corresponding uncertainties. The average per-event correction factor is about 0.98 (0.93) for electron (muon) triggers; they are known with an uncertainty below 1% [85, 86]. Corrections to efficiencies for lepton reconstruction, identification, isolation and association with the PV in simulated samples are derived from data. Each per-lepton correction factor is close to unity and known with a precision that is better than 1% in the kinematic range considered [85, 86].

The energy scale of the electrons and the momentum scale of the muons in simulation are adjusted with correction factors that deviate from unity at the per-mil level and the resolutions are adjusted with correction factors that deviate from unity at the per-cent level in order to match lepton p_{T} and $m_{\ell\ell}$ distributions in data; the corresponding uncertainties are negligible.

JHEP07(2020)044

The jet energy scale (JES) is calibrated on the basis of the simulation including in situ corrections obtained from data [90]. The JES uncertainties are estimated using a decorrelation scheme comprising a set of 21 independent parameters, the largest of which may reach several per cent in specific corners of the phase space. The jet energy resolution (JER) uncertainty is derived by over-smearing the jet energy in the simulation by about 4% at $p_{\mathrm{T}} = 20$ GeV to about 0.5% at a p_{T} of several hundred GeV [96]. Simulation-to-data corrections and relative uncertainties are also applied to adjust the efficiency of the JVT requirement following the prescriptions of ref. [97]. The uncertainty in the scale and resolution of $E_{\mathrm{T}}^{\mathrm{miss}}$ is estimated by propagating the uncertainties in the transverse momenta of reconstructed objects and an uncertainty to account for soft hadronic activity in the event, as described in ref. [95].

Flavour-tagging efficiencies in simulation are scaled to match those measured in data for jets of all flavours as a function of the different b-tagging discriminant output thresholds, and of the jet p_{T} (and η for light-jets), using weights derived from control samples enriched in jets of each flavour [98]. In the case of b-jets, correction factors and their uncertainties are estimated from data using dileptonic $t\bar{t}$ events [98]. The correction factors for b-jets are close to unity. The uncertainties, described by a set of 28 independent parameters, are as low as 3% for jet p_{T} of about 60 GeV, but reach 10% for jet p_{T} of about 20 GeV and up to 20% beyond 300 GeV. In the case of c-jets, correction factors are derived using jets from W-boson decays in $t\bar{t}$ events [99]. The correction factors for c-jets range from about 1.2 to about 1.6. Their uncertainties, described by a set of 28 independent parameters, are about 20%–30% in the bulk of the phase space, but up to 100% for large jet p_{T} and for the b-tagging discriminant output threshold closest to +1. In the case of light-flavour jets, correction factors are derived using dijet events [100]. The correction factors for light-jets range from about 2 to about 3, with uncertainties described by a set of 36 independent parameters and ranging from 50% to 100%. An additional uncertainty of 30% is applied to the efficiency of b-tagging for simulated jets originating from pile-up interactions, which are less than 1% of the selected jets.

A variation in the pile-up reweighting of simulated events (referred to as pile-up uncertainty) is included to account for the uncertainty in the ratio of the predicted and measured inelastic cross-sections in the fiducial volume [101].

5 Background estimation

The main background in the 1-tag region is constituted by events with a Z boson produced in association with jets, where either a light-jet or a c-jet is misidentified as a b-jet; it is determined using a fit to data as detailed in section 5.1. Dileptonic $t\bar{t}$ events dominate in the 2-tag region. Smaller background contributions from the production of dibosons, a Higgs boson, a single top quark, a $Z \to \tau\tau$, or a $W \to \ell\nu$ are estimated using simulation, as described in section 3.2. Uncertainties in the normalisation cross-section of these predictions range from 4% to 6% depending on the process, as detailed in table 1. Background contributions from multijet events are estimated with a data-driven technique and found to be negligible, as described below.

JHEP07(2020)044

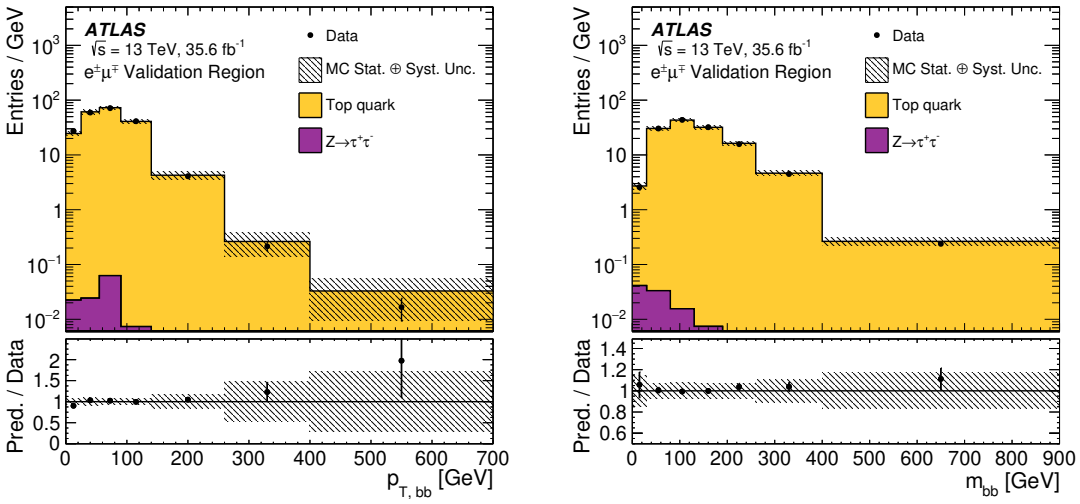

Figure 1. Transverse momentum (left) and invariant mass (right) of the di-b-jet system built with the two highest-p_{T} b-jets for events with at least two b-jets in the $t\bar{t}$ validation region. Systematic uncertainties of the predicted distributions are combined with the statistical ones in the hatched band, and the statistical uncertainty of the data is shown as error bars. The systematic uncertainties for the predictions account only for the yield and the shape of $t\bar{t}$ events.

The $t\bar{t}$ contribution is estimated using simulated events generated with Powheg-Box + Pythia normalised to the theoretically predicted cross-section, as discussed in section 3.2. An uncertainty of about 6% is assigned to the inclusive $t\bar{t}$ cross-section (see table 1), following the variation of the renormalisation and factorisation scales by a factor of 2.0, and the variation of the PDFs within their uncertainties. In addition, uncorrelated systematic uncertainties in the modelling of the distributions are derived by comparing the predictions from the nominal $t\bar{t}$ sample with the ones from the alternative samples described in section 3.2.

The modelling of $t\bar{t}$ production in the simulation is validated using a $t\bar{t}$-enriched region, which is selected by requiring that events have two leptons of different flavour ($e\mu$); all other selections are the same as in the signal region. As an example, figure 1 shows the $p_{\mathrm{T},bb}$ and the m_{bb} distributions for events with at least two b-jets. The total background from top quarks is the sum of $t\bar{t}$ and single-top events, where the latter are about 3% of the $t\bar{t}$ component in the validation region, and other backgrounds are negligible. Data and simulation agree well within the uncertainties which account for both the yield and shape uncertainties of simulated $t\bar{t}$ events and the statistical uncertainties of predictions and data.

Background contributions from multijet events in the electron and muon channels are estimated using a data-driven technique. Multijet-enriched control regions without b-tag and $m_{\ell\ell}$ requirements are used to derive the expected shape of this background. In the electron channel, the multijet-enriched control region is defined by applying the full signal event selection except for the electron identification and the d_0/σ_{d_0} cuts, and inverting the isolation selection for both electron candidates. In the muon channel, the multijet-enriched control region is defined by applying the full signal event selection but requiring

JHEP07(2020)044

both muon candidates to have the same charge. In both channels, contributions from non-multijet sources in the control regions are estimated from simulation and subtracted from the data, with the remaining distributions used as shape templates. A fit of the $m_{\ell\ell}$ distribution to data is then performed within the window of 60 GeV $< m_{\ell\ell} <$ 160 GeV in the one-jet and two-jets pre-tag regions separately and leaving the normalisation of the signal and of the multijet background templates free to float in the fit, while the normalisation of the other processes is fixed in the fit. The multijet background estimate in the pre-tag region is then extrapolated to the two signal regions using normalisation factors equal to the fraction of events in the multijet control region that satisfy the 1-tag and 2-tag requirements. Contributions from non-multijet processes are subtracted before estimating this fraction. Systematic uncertainties are assessed by varying the $m_{\ell\ell}$ range and the binning of the fit, excluding the Z-boson peak from the fit, performing the fit in the tagged regions in place of the pre-tag ones, and by allowing the other processes to be varied independently in the fit. The estimated size of the multijet background is consistent with zero within the statistical uncertainty even after considering all sources of systematic uncertainty. It is therefore neglected in the analysis.

5.1 Extraction of the cross-section for Z-boson production in association with light-jets and c-jets

The flavour fit used for the extraction of the yields of Z + light-jets and Z + c-jets backgrounds for the 1-tag and 2-tag selections is a maximum-likelihood fit to data based on flavour-sensitive distributions. The fit is done simultaneously in the electron and muon channels with templates derived from simulation.

In the 1-tag region, the b-tagging discriminant output of the leading b-jet is used as the flavour-sensitive distribution. This observable for events belonging to the signal region is distributed into three intervals that define the bins of the discriminant output distribution. Each bin corresponds to a certain range of b-tagging efficiency. The bins are numbered from 1 to 3, corresponding respectively to efficiencies of 60%–70% (bin 1), 50%–60% (bin 2) and <50% (bin 3) as estimated from simulated $t\bar{t}$ events. The light-flavour jet (c-jet) misidentification rates for the three bins are respectively 0.195% (5.4%), 0.048% (1.96%), and <0.017% (<0.94%). The signal template is built with simulated $Z+ \geq 1b$ events. The template shapes of the $Z+l$ and $Z+c$ samples are very similar (as shown in figure 2), hence those samples are combined to form a single template. All non-Z+jets backgrounds are combined into a single template, determined from the sum of their predicted contributions. The normalisations of the signal and of the Z+jets background are free to float in the fit, while the normalisation of the sum of the non-Z+jets backgrounds is fixed to their estimate.

In the 2-tag region the combination of the three bins of the b-tagging discriminant outputs of the leading and sub-leading b-jets produces a distribution with six bins that is used for the fit to data. The signal template is built with simulated $Z + bb$ events. Templates built with $Z + b$, $Z + c$ and $Z + l$ simulated events are combined into a single template. Because of the large rejection of light-flavour jets achieved in the 2-tag selection, the simulated $Z + l$ events in this region are not subjected to the b-tagging requirement. Instead they are weighted by a per-event probability that the jets pass the two-b-tags

JHEP07(2020)044

Generator	Signal SF	Z+jets background SF	Signal post-fit yield	Z+jets background post-fit yield	Signal + Z+jets post-fit yield
Sherpa	1.109 ± 0.003	0.861 ± 0.004	309 650 ± 810	166 640 ± 650	476 290 ± 750
Alpgen	1.480 ± 0.004	1.015 ± 0.002	297 670 ± 740	178 100 ± 400	475 810 ± 480

Table 4. Scale factors obtained for the fitted signal and Z+jet background for Sherpa and Alpgen fits, the total post-fit yields, and the statistical uncertainty, estimated with pseudo-experiments, from the fit for the 1-tag signal region.

Generator	Signal SF	Z+ jets background SF	Signal post-fit yield	Z+ jets background post-fit yield	Signal + Z+jets post-fit yield
Sherpa	1.18 ± 0.01	1.08 ± 0.04	23 440 ± 250	4780 ± 180	28 220 ± 200
Alpgen	1.18 ± 0.01	1.30 ± 0.05	23 650 ± 240	4550 ± 180	28 200 ± 200

Table 5. Scale factors obtained for the fitted signal and Z+jet background for Sherpa and Alpgen fits, the total post-fit yields, and the statistical uncertainty, estimated with pseudo-experiments, from the fit for the 2-tag signal region.

selection (procedure referred to as the *truth*-tagging). This probability is computed on the basis of the per-jet probabilities, which are assumed to be independent of each other [102]. As for the fit in the 2-tag region, the normalisations of the signal and of the Z+jets background are also free to float, while the normalisation of the other backgrounds is fixed to their estimate.

Tables 4 and 5 show the normalisation scale factors in the 1- and 2-tag regions obtained from the fit, together with the post-fit yields for the signal and Z+jet background samples generated with Sherpa or Alpgen. There is good agreement between the sum of the signal and background post-fit yields of Sherpa and Alpgen. The differences between Sherpa and Alpgen in the modelling of the Z+jet backgrounds after the flavour fit are taken into account in the systematic uncertainties as described below. The statistical uncertainty is estimated with pseudo-experiments.

Figure 2 shows the b-tagging discriminant bins after the fit in the 1-tag and 2-tag regions. In the upper panel of each figure, data are compared with the fit results obtained using templates derived from Sherpa samples for signal and Z+jet backgrounds. The lower panel shows the ratio of post-fit predictions to data using the Sherpa or Alpgen samples for signal and Z+jet backgrounds.

The Z+jets backgrounds predicted by Sherpa and corrected for the normalisation factor obtained from the fit are used as the nominal estimate in this analysis. Systematic uncertainties due to the object selection efficiencies and calibrations, discussed in section 4.1, affect the normalisation and the shape of Z+jets backgrounds. They are assessed by repeating the fit with the templates varied according to each of the systematic uncertainties. The fit is also repeated for each of the uncertainties affecting the $t\bar{t}$ and other backgrounds detailed above. An additional systematic uncertainty (referred to as the flavour fit uncertainty) in the normalisation of the Z+jets backgrounds is estimated by repeating the fit after separating the $Z + c$ from the $Z + l$ template in the 1-tag region,

JHEP07(2020)044

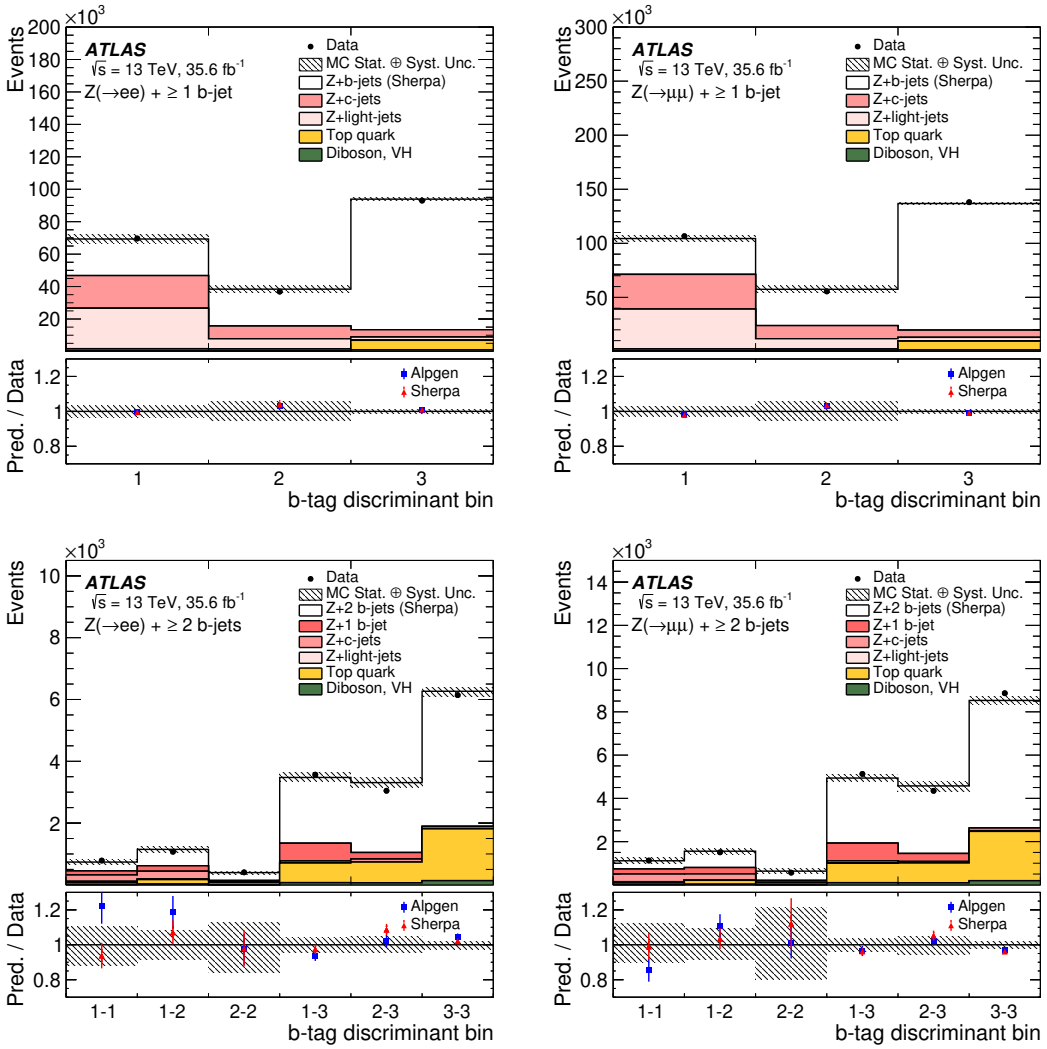

Figure 2. Post-fit b-tagging discriminant distributions for the electron (left) and muon (right) channels in the 1-tag (top) and 2-tag (bottom) signal regions. The lower panels display the ratios of the predictions to data using the signal and Z+jet background simulation either from SHERPA (red) or ALPGEN (blue). Systematic and statistical uncertainties for the predicted distributions are combined in the hatched band, and the statistical uncertainty, estimated with pseudo-experiments, is shown on the data points. The systematic uncertainties account for both the detector-level uncertainties and the theory uncertainty of the non-Z backgrounds.

and after separating the $Z + b$ from the $Z + c$ and $Z + l$ templates in the 2-tag region. An uncertainty affecting the shape and rate of the Z+jets background is derived by taking the difference between the post-fit Z+jets background evaluations using SHERPA and ALPGEN samples. Another uncertainty accounts for potential jet-jet correlations that are not covered by the *truth*-tagging procedure which mitigates the large statistical fluctuations in the 2-tag region for $Z + l$. A 20% uncertainty is derived by taking the largest difference between the double-tagged event yields obtained with or without the weighting procedure

JHEP07(2020)044

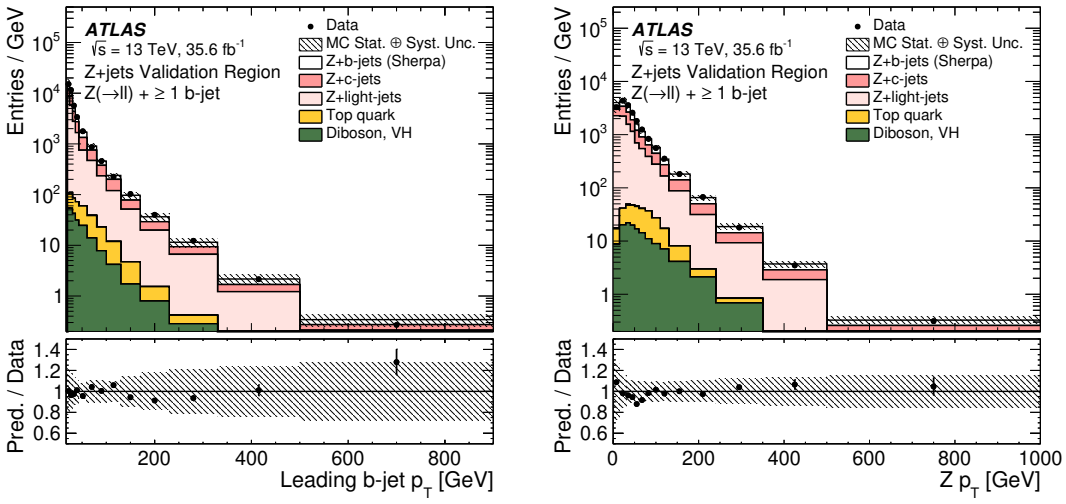

Figure 3. The p_{T} of the leading b-jet (left) and of the Z boson (right) for events with at least one b-jet in the Z+jets validation region defined in table 3. Post-fit distributions for signal and Z + jets backgrounds are shown. Systematic and statistical uncertainties for the predicted distributions are combined in the hatched band, and the statistical uncertainty is shown on the data points. The uncertainty in the predictions includes only the flavour-tagging efficiency uncertainty and flavour-fit uncertainty.

being applied to simulated samples of $Z + bb$, $Z + cc$, $W + bb$, and $W + cc$.[6] These samples suffer less from statistical limitations. The test is done with both the Sherpa and Alpgen samples.

The post-fit estimate of the Sherpa Z+jets background is validated in a region defined by applying the full signal event selection with the exception of b-tagging requirements. Events with at least one b-jet, with the b-tagging discriminant output in the b-jet efficiency range of 70%–77% and light-flavour jet (c-jet) misidentification rates of 0.51% (7.7%), are selected to provide a sample enriched in c-jets and light-flavour jets. As an example, figure 3 shows the p_{T} of the leading b-jet and the p_{T} of the Z boson in this region. The $Z + l$ and $Z + c$ backgrounds constitute 50% and 28% of the total prediction, respectively. Agreement between data and estimated backgrounds is observed within uncertainties. These include the uncertainties due to the flavour fit and b-tagging efficiency, and the statistical uncertainties of the predictions and data.

The normalisation factors of the signal samples, shown in tables 4 and 5, are applied in figures 2 and 3 in this section to demonstrate the robustness of this procedure, while in the following sections, post-fit normalisation factors are applied only to Z+jets background.

6 Kinematic distributions

After the signal selection criteria are applied, the measured and expected distributions are compared at the detector level. The Z+jets background is shown for the normalisation factors derived from the flavour fit. Pre-fit distributions are used for the signal samples.

[6]Simulated Z+jets events are categorised as $Z + cc$ ($W + cc$) if they belong to the $Z + c$ ($W + c$) category and have at least two c-jets.

JHEP07(2020)044

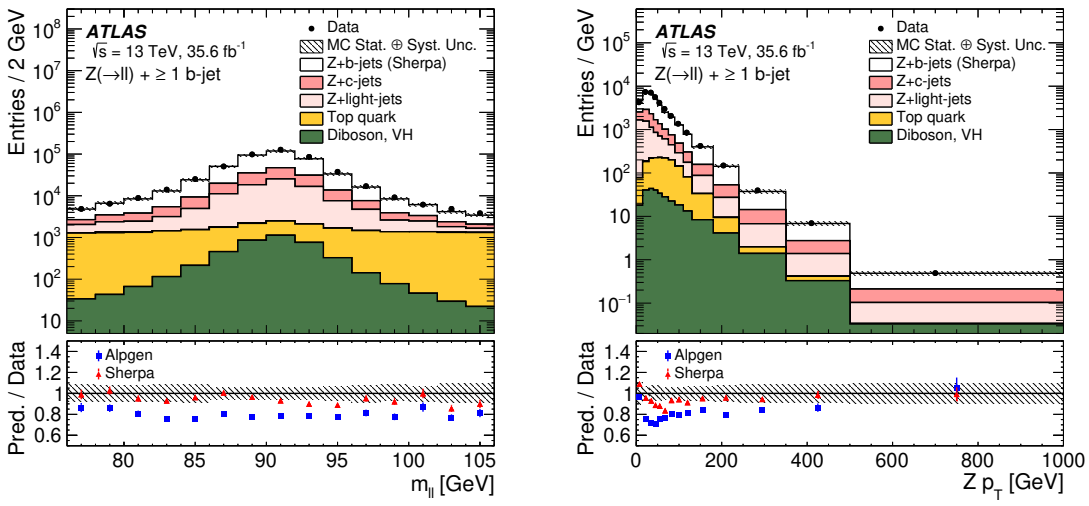

Figure 4. Distribution of events passing the signal selection as a function of $m_{\ell\ell}$ (left) and $p_{\mathrm{T},Z}$ (right) for events with at least one b-jet. The lower panels display the ratio of the predictions for signal plus background to data using either Sherpa (red) or Alpgen + Pythia6 (blue) as the signal simulation. The statistical uncertainty of the data is shown as black error bars and the total uncertainty of the prediction as a hatched band. The latter consists of the statistical uncertainty and all systematic uncertainties from the predictions.

Figure 4 shows, as an example, the distributions of the $m_{\ell\ell}$ and p_{T} of the Z boson for events in the 1-tag region. Figure 5 shows the p_{T} of the Z boson and the ΔR_{bb} distributions for events in the 2-tag region. The uncertainty bands include the statistical uncertainties of the simulated sample, the event-selection uncertainties described in section 4 (omitting the common luminosity uncertainty), and the background uncertainties described in section 5. Both generators do not describe precisely the data in the full range of the measurement, although the Sherpa generator provides the best agreement with data.

The total numbers of selected events in data and in predictions are presented in table 6, together with the prediction of each process, expressed as a fraction of the total number of predicted events.

7 Correction to particle level

The signal event yields are determined by subtracting the estimated background contributions from the data. The resulting distributions are corrected for detector-level effects to the fiducial phase space at particle level defined in table 7. The procedure, based on simulated samples, corrects for Z-boson, jet, and b-jet selection efficiencies, resolution effects, and small differences between the fiducial and detector-level phase spaces. The pre-fit distributions of the Sherpa signal samples are used to perform the unfolding procedure. The signal samples for the simulation of Z events with at least one or at least two b-jets are defined in section 4. Particle-level objects are selected with requirements close to the corresponding requirements for reconstructed signal candidate objects, in order to limit

JHEP07(2020)044

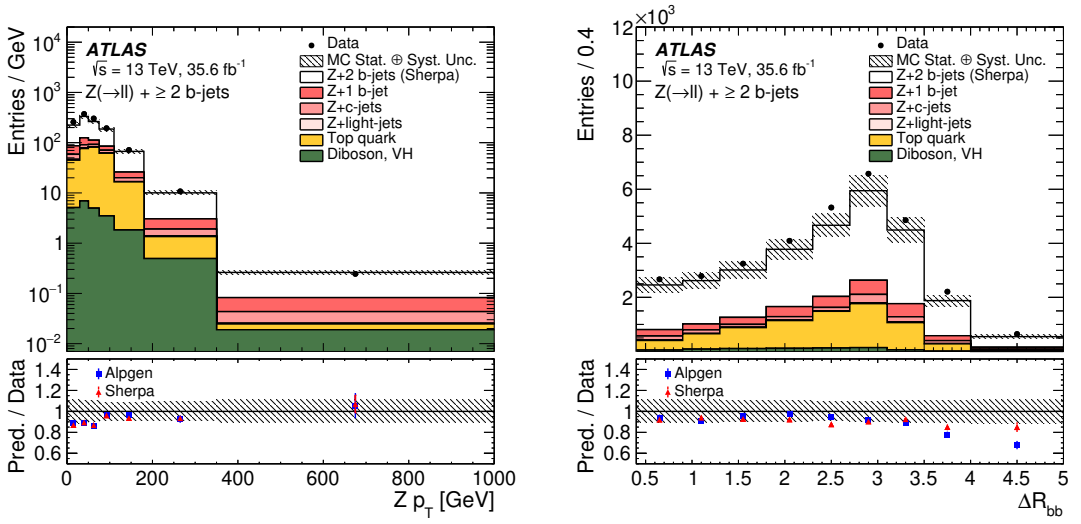

Figure 5. Distribution of events passing the signal selection as a function of $p_{\mathrm{T},Z}$ (left) and ΔR_{bb} (right) for events with at least two b-jets. The lower panels display the ratio of the predictions for signal plus background to data using either Sherpa (red) or Alpgen + Pythia6 (blue) as the signal simulation. The statistical uncertainty of the data is shown as black error bars and the total uncertainty of the prediction as the hatched band. The latter consists of the statistical uncertainty and all systematic uncertainties from the predictions.

1-tag region	
Signal	
$Z + b$, $Z + bb$	59%
Backgrounds	
$Z + c$	18%
$Z + l$	18%
Top	4%
Diboson, VH	1%
Others	$< 1\%$
Total predicted	470 000 ± 650
Data	499 645

2-tag region	
Signal	
$Z + bb$	60%
Backgrounds	
$Z + b$	9%
$Z + c$	5%
$Z + l$	$< 1\%$
Top	23%
Diboson, VH	2%
Others	1%
Total predicted	33 070 ± 180
Data	36 548

Table 6. The expected size of the signal and backgrounds, expressed as a fraction of the total number of predicted events for inclusive b-jet multiplicities for the signal selection. The signal and Z+jets background predictions are from the Sherpa generator, with the Z+jets background estimate obtained after applying the normalisation scale factors obtained from the flavour fit. The total numbers of predicted and observed events are also shown. The uncertainty in the total predicted number of events is statistical only.

the dependence of the measurement on theoretical predictions. In this definition, the lepton kinematic variables are computed using final-state leptons from the Z-boson decay. Photons radiated by the boson decay products within a cone of size $\Delta R = 0.1$ around the direction of a final-state lepton are added to the lepton, and the sum is referred to as the 'dressed' lepton. Particle-level jets are identified by applying the anti-k_t algorithm with

JHEP07(2020)044

Kinematic variable	Acceptance cut
Lepton p_{T}	$p_{\mathrm{T}} > 27$ GeV
Lepton η	$\lvert\eta\rvert < 2.5$
$m_{\ell\ell}$	$m_{\ell\ell} = 91 \pm 15$ GeV
b-jet p_{T}	$p_{\mathrm{T}} > 20$ GeV
b-jet rapidity	$\lvert y\rvert < 2.5$
b-jet-lepton angular distance	$\Delta R(b\text{-jet}, \ell) > 0.4$

Table 7. Kinematic criteria defining the fiducial phase space of the measurement at particle level.

$R = 0.4$ to all final-state particles with a lifetime longer than 30 ps, excluding the dressed Z-boson decay products. A jet is identified as b-tagged if it lies within $\Delta R = 0.3$ of one or more weakly decaying b-hadrons with $p_{\mathrm{T}} > 5$ GeV. If a b-hadron matches more than one jet, only the closest jet in ΔR is labelled as a b-jet.

The correction of differential distributions is implemented using an iterative Bayesian method of unfolding [103] with two iterations. Simulated events are used to generate a response matrix for each distribution to account for bin-to-bin migration effects between the detector-level and particle-level distributions. The matrix is filled with the events that pass both the detector-level and particle-level selections. The particle-level prediction is used as the initial prior to determine the first estimate of the unfolded data distribution. For the second iteration, the new estimate of unfolded data is obtained using the background-subtracted data and an unfolding matrix, which is derived on the basis of the Bayes' theorem from the response matrix and the current prior. The background-subtracted data are corrected for the expected fraction of events which pass the detector-level selection, but not the particle-level one (unmatched-events), before entering the iterative unfolding. For each bin of each differential distribution, the unfolded event yields are divided by the integrated luminosity of the data sample and by the bin width, to obtain the cross-section measurement. The differential cross-section measurement of a given observable in the i-th bin is given by:

$$\sigma_i = \frac{1}{\epsilon_i L} \sum U_{ij} f_j N_j^{\mathrm{bsD}},$$

where L is the integrated luminosity, ϵ_i is the reconstruction efficiency in i-th bin, N_j^{bsD} is the number of background-subtracted data events in the j-th bin, f_j is the factor that corrects for unmatched events in the j-th bin, and U_{ij} is the element (i, j) of the unfolding matrix calculated after two iterations, using the updated prior from the first iteration and the response matrix.

The measurement of the inclusive cross-section for Z-boson events with at least one or at least two b-jets is obtained by applying a particle-level correction to the number of events in data with at least one or at least two b-jets, after background subtraction. The correction, which is applied as a divisor of the background-subtracted data, is derived from the ratio of the total number of reconstructed events in the detector-level phase space to the number of particle-level events in the fiducial phase space. It is 0.399 ± 0.001 for Z-

JHEP07(2020)044

Source of uncertainty	$Z(\to \ell\ell) + \geq 1$ b-jet [%]	$Z(\to \ell\ell) + \geq 2$ b-jets [%]
b-jet tagging efficiency	7.0	14
b-jet mistag rate	2.4	1.1
Jet	2.4	5.0
Lepton	0.8	1.2
$E_{\mathrm{T}}^{\mathrm{miss}}$	0.6	1.3
$Z + c$ and $Z + l$ backgrounds	4.5	1.1
Top background	0.5	3.8
Other backgrounds	< 0.1	0.1
Pile-up	1.7	2.6
Unfolding	3.8	4.1
Luminosity	2.3	2.9
Total [%]	10	16

Table 8. Relative systematic uncertainties in the measured production cross-sections of $Z(\to \ell\ell) + \geq 1$ b-jet and $Z(\to \ell\ell) + \geq 2$ b-jets events. The "Jet" term includes the JES, JER and JVT uncertainties. The "Lepton" term includes the lepton trigger, efficiency, scale and resolution uncertainties. The "$Z + c$ and $Z + l$ backgrounds" term also includes the $Z + 1b$ background in the $Z + \geq 2$ b-jets measurement.

boson events with at least one b-jet and 0.258 ± 0.002 for Z-boson events with at least two b-jets, using Sherpa signal samples and quoting the statistical error.

Since the electron and muon decay channels are combined to increase the precision of the signal fits to data, the corrections and response matrices are made using electron and muon signal samples to obtain combined particle-level yields. To validate this procedure, the analysis is performed for each of the two lepton channels separately. The results obtained from the individual channels are compatible within 1.4σ and 1.6σ with the inclusive cross-section of Z-boson events with at least one b-jet and at least two b-jets, respectively. This comparison uses only the sum in quadrature of the statistical and uncorrelated systematic uncertainties. The differential cross-section measurements in the two channels also agree over the full range of each distribution.

8 Uncertainties in the cross-section measurements

Table 8 summarises the systematic uncertainties of the inclusive $Z + b$-jets cross-sections in the one- and two-b-tag regions. Figure 6 shows as an example the breakdown of the systematic uncertainties in the cross-section as a function of Z-boson p_{T} for events with at least one b-jet and as a function of ΔR_{bb} for events with at least two b-jets.

The systematic uncertainties in the cross-sections associated with the detector-level uncertainty sources described in section 4.1 are derived for each observable by propagating systematic shifts from each source through both the response matrices (unfolding factor) and the subtracted background contributions into the unfolded data for the differential (in-

JHEP07(2020)044

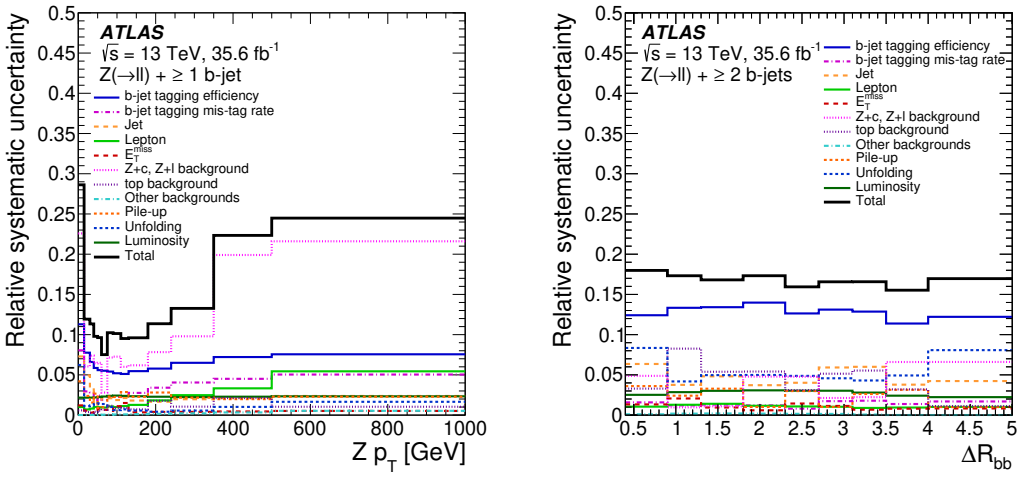

Figure 6. Relative systematic uncertainties in the fiducial cross-section as a function of the Z-boson p_{T} in events with at least one b-jet (left) and as a function of the ΔR between the two leading b-jets in events with at least two b-jets (right). The total uncertainty is shown in black while the different components listed in table 8 are shown in different colours.

clusive) cross-section measurements. The dominant source of uncertainty is the modelling of the b-tagging efficiency. Its impact on the inclusive cross-section ranges from 7.0% for Z-boson events with at least one b-jet to 14% for Z-boson events with at least two b-jets. Its effect on differential cross-section measurements ranges from 5% to 10% for Z-boson events with at least one b-jet and from 10% to 15% for Z-boson events with at least two b-jets. The impact of the mistag rate of c- and light-jets is smaller; it is 2.4% for Z-boson events with at least one b-jet and 1% for Z-boson events with at least two b-jets.

The uncertainty from each background source is determined by applying shifts to the subtracted background contributions and to the nominal response matrices or unfolding factors. The sources of uncertainty considered for $Z + l$ and $Z + c$ (and $Z + 1b$ in the $Z + \geq 2b$-jets measurement), $t\bar{t}$ and single-top, diboson and other minor backgrounds are described in section 5. The dominant uncertainty in the background to events with at least one b-jet originates from Z+jets events. This uncertainty contributes 4.5% to the uncertainty in the inclusive cross-section. An uncertainty of 3.7% derives from the difference between the modelling in Alpgen and Sherpa, while 2.6% is due to the flavour fit uncertainty. The impact of this uncertainty on the differential cross-sections ranges from a few per cent up to 25% in the extreme corners of the phase space. For a Z-boson p_{T} value of about 500 GeV, the difference between the modelling in Alpgen and Sherpa contributes 18% to this uncertainty, and the flavour fit uncertainty is 12%.

In contrast, the uncertainty in the estimation of background from $t\bar{t}$ events is the dominant source of uncertainty in the background to Z-boson events with at least two b-jets. It contributes 3.8% to the inclusive cross-section and ranges from 1% to 9% in the differential cross-sections.

The uncertainty due to modelling of the $Z + b$-jets signal samples in the events with at least one and at least two b-jets are also accounted for. This is evaluated for each observable

JHEP07(2020)044

by reweighting the generator-level distribution in the SHERPA samples to provide a better description of the data at detector level. The modified SHERPA samples are then used to emulate data and are unfolded with the nominal simulated sample. An additional source accounts for the possible mismodelling of an observable that is not one of the unfolded observables (i.e. a hidden variable). This uncertainty is evaluated by reweighting, in the SHERPA samples, the generator-level distribution of the leading lepton's p_{T}, which is one of the observables showing the largest mismodelling, to provide a better description of the data at detector level. The modified SHERPA samples are used to unfold the data. The effect of the hidden variable's mismodelling is negligible for all considered variables and all bins. A third uncertainty source accounts for the different hadronisation and parton-shower models used for the signal simulation. This uncertainty is evaluated by unfolding the ALPGEN signal samples, which emulate the background-subtracted data, with the SHERPA signal samples. The generator-level distributions from the ALPGEN samples are first reweighted to agree with SHERPA in order to remove effects related to shape differences. The difference between the generator-level distribution and the unfolded ALPGEN reweighted distribution is taken as the uncertainty. For the inclusive cross-section, the modelling uncertainty is estimated by replacing the unfolding factor computed with SHERPA with the one computed with ALPGEN. The dependence on the size of the simulated sample is derived using pseudo-experiments, and the spread of the results is taken as an uncertainty. The statistical term is typically less than a few per cent. It reaches 5% in the last bin of the ΔR_{bb} distribution and 15% only in the last bin of the Δy_{bb} distribution.

The total unfolding uncertainty in the inclusive cross-sections is at the level of 4% in each of the two signal regions. In the differential distributions it is less than 5% in the 1-tag region and at a level of 5%–10% in the 2-tag region, except in some bins of the angular variables and in the tail of the p_{T} and m_{bb} distributions, where it reaches 20%.

9 Results

The inclusive and differential cross-section measurements for $Z + \geq 1$ b-jet and $Z + \geq 2$ b-jets are shown in figures 7–15. The statistical uncertainty of the data is propagated through the unfolding by using 1000 pseudo-experiments, repeating the flavour fit for each of them. The statistical uncertainty in the inclusive cross-sections of $Z + \geq 1$ b-jet and $Z + \geq 2$ b-jets is 0.3% and 0.8% respectively. As mentioned in section 8, the systematic uncertainties are propagated through the unfolding via the response matrices or the unfolding factors and via the variation of the subtracted background. The measurements are compared with the predictions from SHERPA 5FNS (NLO), ALPGEN + PY6 4 FNS (LO), SHERPA FUSING 4FNS+5FNS (NLO), SHERPA ZBB 4FNS (NLO), MGAMC + PY8 5FNS (LO), MGAMC + PY8 ZBB 4FNS (NLO) and MGAMC + PY8 5FNS (NLO). Theoretical uncertainties of SHERPA 5FNS (NLO), computed as described in section 3, are shown in the comparison with data. In this section, all predictions are normalised to their own cross-section to allow an unbiased comparison among different generators.[7]

[7]The NNLO cross-section K-factor applied to the inclusive ALPGEN and SHERPA samples in previous sections is removed.

JHEP07(2020)044

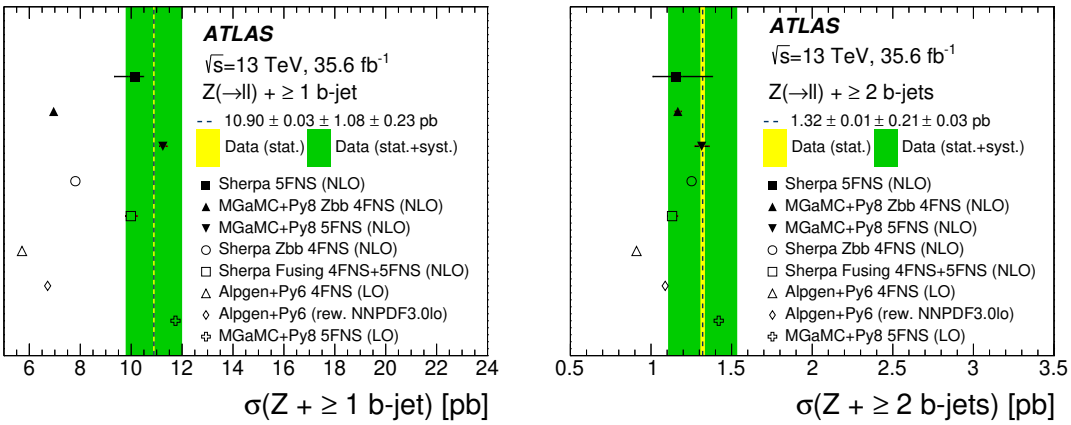

Figure 7. Measured cross-sections for $Z + \geq 1$ b-jet (left) and $Z + \geq 2$ b-jets (right). The data are compared with the predictions from Sherpa 5FNS (NLO), Alpgen + Py6 4 FNS (LO), Sherpa Fusing 4FNS+5FNS (NLO), Sherpa Zbb 4FNS (NLO), MGaMC + Py8 5FNS (LO), MGaMC + Py8 Zbb 4FNS (NLO) and MGaMC + Py8 5FNS (NLO). The yellow band corresponds to the statistical uncertainty of the data, and the green band to statistical and systematic uncertainties of the data, added in quadrature. The error bars on the Sherpa 5FNS (NLO) predictions correspond to the statistical and theoretical uncertainties added in quadrature. Only statistical uncertainties are shown for the other predictions.

9.1 Inclusive cross-sections

The measured inclusive cross-sections for $Z + \geq 1$ b-jet and $Z + \geq 2$ b-jets, shown in figure 7, are $10.90 \pm 0.03(\text{stat.}) \pm 1.08(\text{syst.}) \pm 0.25(\text{lumi.})$ pb and $1.32 \pm 0.01(\text{stat.}) \pm 0.21(\text{syst.}) \pm 0.04(\text{lumi.})$ pb, respectively. The 4FNS MC predictions are systematically lower than data in the inclusive one-b-jet case, both for MC generators with LO matrix elements, as implemented in Alpgen + Py6 4FNS (LO), and for Zbb predictions at NLO, as implemented in Sherpa Zbb 4FNS (NLO) and MGaMC + Py8 Zbb 4FNS (NLO). The 4FNS predictions agree well with data in the inclusive two-b-jet case. Even though the LO Alpgen + Py6 4FNS (LO) underestimates the data, the predictions and data agree within two standard deviations (2σ) of the experimental uncertainty. Use of the NNPDF3.0lo PDF set in Alpgen predictions gives better agreement with data because of a higher acceptance in the fiducial region. The 5FNS simulations, in general, adequately predict the inclusive cross-sections for both $Z + \geq 1$ b-jet and $Z + \geq 2$ b-jets. Overall, this is consistent with the results presented in the ATLAS measurement at $\sqrt{s} = 7$ TeV [11].

9.2 Differential cross-sections for $Z + \geq 1$ b-jet

The differential cross-section measurements for the $Z + \geq 1$ b-jet process are shown in figures 8–11. Each distribution is presented and discussed in detail in this section.

The distributions of the transverse momentum of the Z boson and of the jets probe pQCD over a wide range of scales and provide important input to the background prediction for other SM processes, including Higgs boson production and searches beyond the SM. The differential cross-section as a function of the Z-boson p_{T} for events with at least one b-jet is shown in figure 8 (left). In the low p_{T} region, up to 100 GeV, where soft radiative effects

JHEP07(2020)044

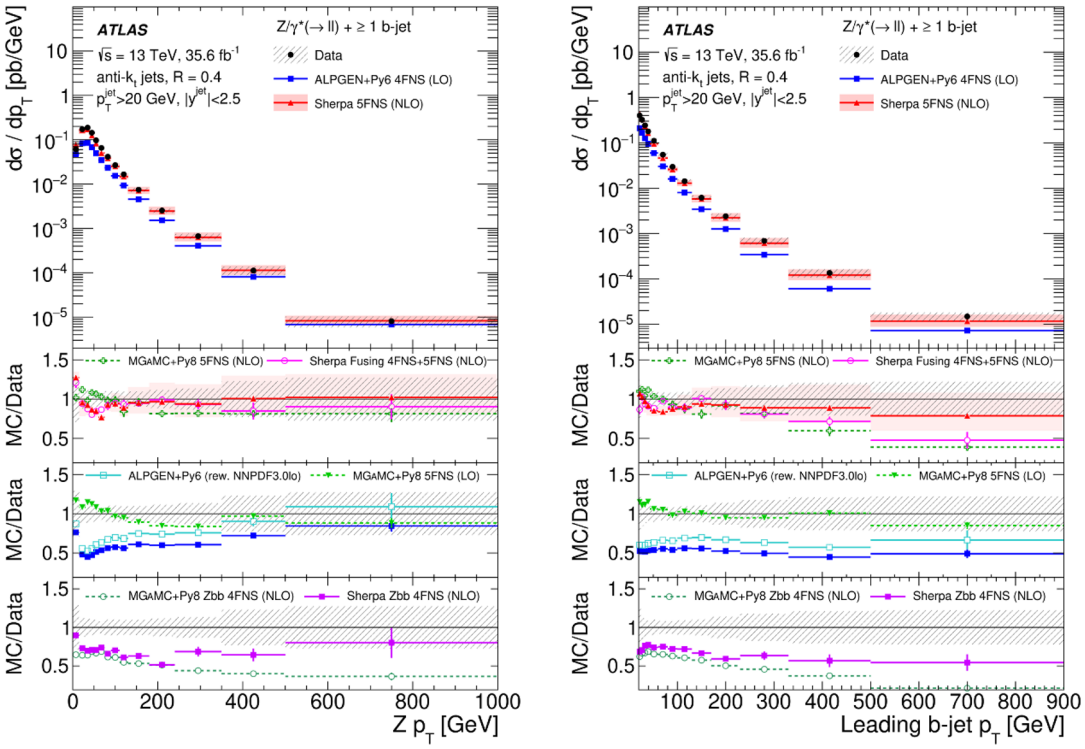

Figure 8. Measured cross-section as a function of Z-boson p_{T} (left) and leading b-jet p_{T} (right) in events with at least one b-jet. The data are compared with the predictions from Sherpa 5FNS (NLO), Alpgen + Py6 4 FNS (LO), Sherpa Fusing 4FNS+5FNS (NLO), Sherpa Zbb 4FNS (NLO), MGaMC + Py8 5FNS (LO), MGaMC + Py8 Zbb 4FNS (NLO) and MGaMC + Py8 5FNS (NLO). The error bars correspond to the statistical uncertainty, and the hatched bands to the data statistical and systematic uncertainties added in quadrature. The red band corresponds to the statistical and theoretical uncertainties of Sherpa 5FNS (NLO) added in quadrature. Only statistical uncertainties are shown for the other predictions.

play a role, all the predicted shapes except that of MGaMC + Py8 Zbb 4FNS (NLO) exhibit trends different from those in the data. Overall, the predictions from Sherpa 5FNS (NLO) and Sherpa Fusing 4FNS+5FNS (NLO) show the best agreement with data. Predictions from MGaMC + Py8 5FNS (LO) and MGaMC + Py8 5FNS (NLO) are within the experimental uncertainty band for most of the bins. The harder Z-boson p_{T} in Alpgen predictions than in data has already been reported by ATLAS for data collected at $\sqrt{s} = 7$ TeV [11]. Figure 8 (right) shows the leading b-jet p_{T}. MGaMC + Py8 5FNS (LO) provides a satisfactory description within the uncertainty of the data, while MGaMC + Py8 5FNS (NLO) underestimates the data in the high p_{T} region. This region is populated by additional hard radiation, which in MGaMC + Py8 5FNS (NLO) is simulated only via parton shower. Sherpa 5FNS (NLO) exhibits the best agreement with data. The contrasting behaviour of Sherpa Fusing 4FNS+5FNS (NLO), which underestimates the data at high p_{T}, may be interesting to investigate further in the future. The NLO 4FNS predictions of Zbb, as implemented in Sherpa and MGaMC, show a softer leading b-jet p_{T}, while the inclusive LO 4FNS prediction, as implemented in Alpgen, describes

JHEP07(2020)044

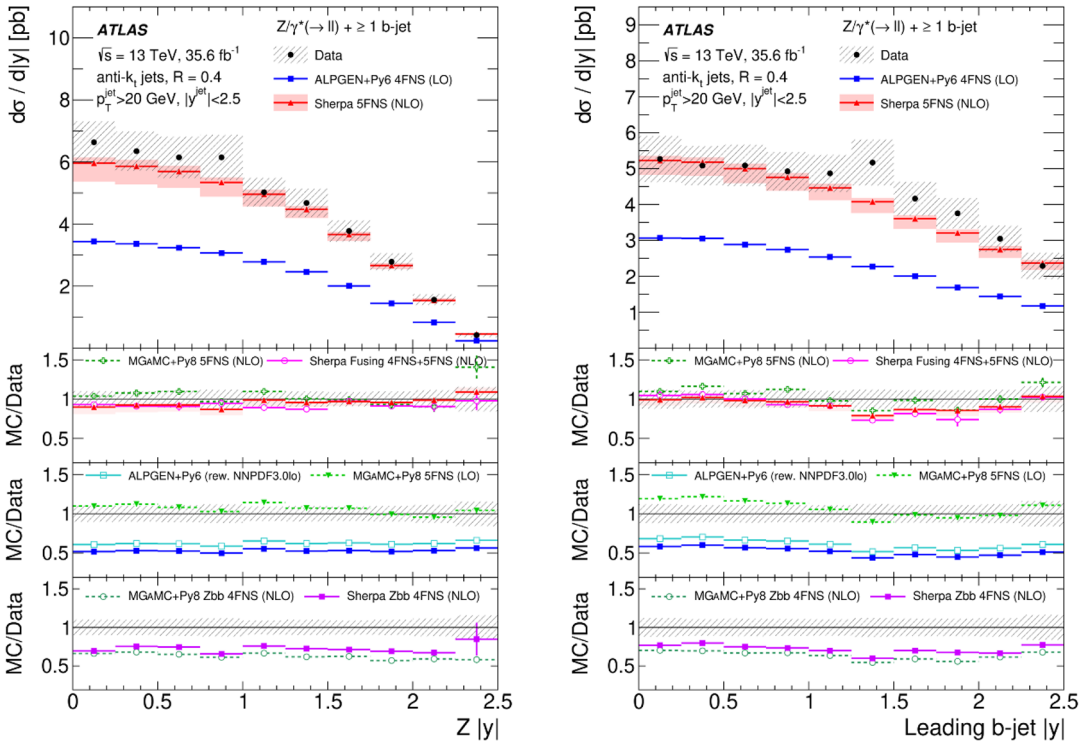

Figure 9. Measured cross-section as a function of Z-boson $|y|$ (left) and leading b-jet $|y|$ (right) in events with at least one b-jet. The data are compared with the predictions from Sherpa 5FNS (NLO), Alpgen + Py6 4 FNS (LO), Sherpa Fusing 4FNS+5FNS (NLO), Sherpa Zbb 4FNS (NLO), MGaMC + Py8 5FNS (LO), MGaMC + Py8 Zbb 4FNS (NLO) and MGaMC + Py8 5FNS (NLO). The error bars correspond to the statistical uncertainty, and the hatched bands to the data statistical and systematic uncertainties added in quadrature. The red band corresponds to the statistical and theoretical uncertainties of Sherpa 5FNS (NLO) added in quadrature. Only statistical uncertainties are shown for the other predictions.

the shape of the data quite well despite the large underestimation of the normalisation already discussed for figure 7.

The distributions of the Z-boson rapidity, the leading b-jet rapidity, and their separation, Δy_{Zb}, are directly sensitive to the b-quark PDFs and to higher-order diagram contributions, and they may show differences for different flavour schemes. The differential cross-sections as a function of the Z-boson rapidity and of the leading b-jet rapidity for events with at least one b-jet are shown in figure 9. All MC predictions provide a satisfactory description of the shape of the data. Some modulation relative to data is observed in the leading b-jet $|y|$ distribution, in some cases beyond the experimental uncertainty. Figure 10 (right) shows the differential cross-section as a function of Δy_{Zb}. Sherpa 5FNS (NLO) and Sherpa Fusing 4FNS+5FNS (NLO) describe the data quite well, while all other predictions exhibit a slightly smaller rapidity separation than data, even if within the uncertainty of the data. Use of a different PDF set as in Alpgen predictions leads to a change in the distribution, but the differences are small compared with the experimental uncertainties.

JHEP07(2020)044

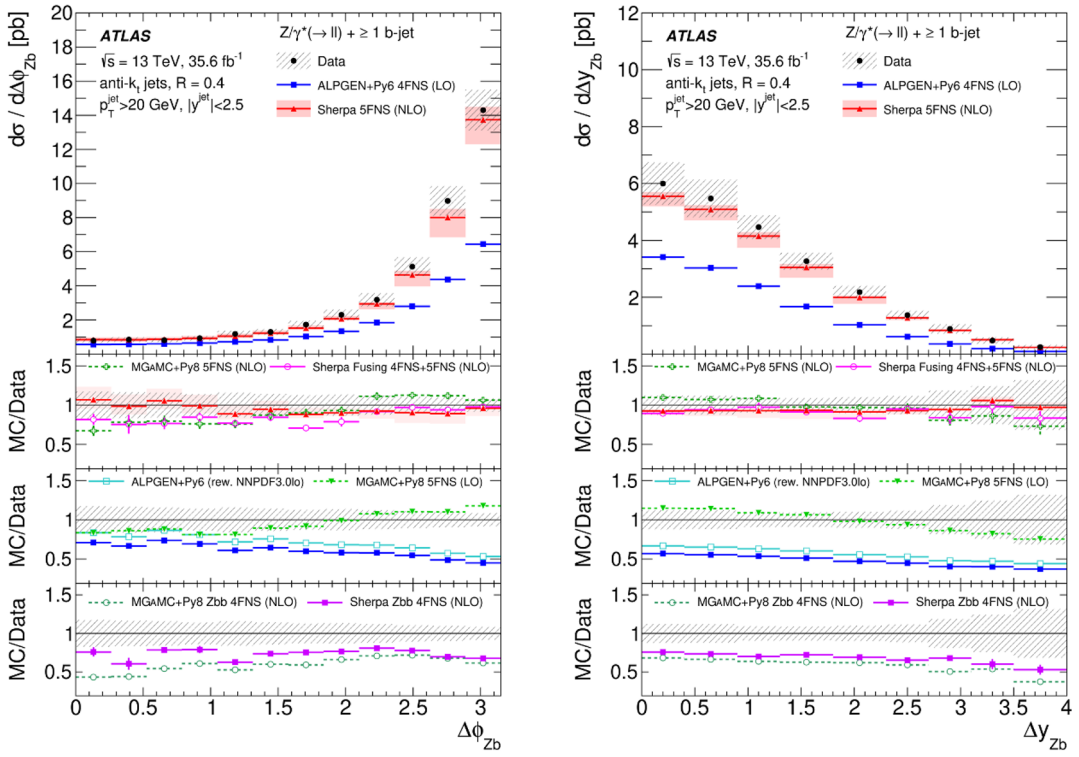

Figure 10. Measured cross-section as a function of $\Delta\phi$ (left) and Δy between the Z-boson candidate and the leading b-jet (right) in events with at least one b-jet. The data are compared with the predictions from Sherpa 5FNS (NLO), Alpgen + Py6 4 FNS (LO), Sherpa Fusing 4FNS+5FNS (NLO), Sherpa Zbb 4FNS (NLO), MGaMC + Py8 5FNS (LO), MGaMC + Py8 Zbb 4FNS (NLO) and MGaMC + Py8 5FNS (NLO). The error bars correspond to the statistical uncertainty, and the hatched bands to the data statistical and systematic uncertainties added in quadrature. The red band corresponds to the statistical and theoretical uncertainties of Sherpa 5FNS (NLO) added in quadrature. Only statistical uncertainties are shown for the other predictions.

The distribution of $\Delta\phi_{Zb}$ is sensitive to the presence of additional radiation in the event. In fixed order calculations of the $Z + 1b$ process, the LO matrix element provides contributions only for $\Delta\phi_{Zb} = \pi$, while the NLO matrix element is the first order which populates the region of $\Delta\phi_{Zb} < \pi$. In MC simulations the region below π is populated via parton shower and via merging of parton shower with multi-parton matrix elements. Therefore the region of small azimuthal separation between the Z boson and the leading b-jet is the most sensitive to additional QCD radiation and soft corrections. It is also sensitive to the presence of boosted particles decaying into a Z boson and b-quarks. The differential cross-section as a function of $\Delta\phi_{Zb}$ for events with at least one b-jet is shown in figure 10 (left). The Sherpa 5FNS (NLO) generator provides the best agreement with data. Sherpa Fusing 4FNS+5FNS (NLO) is still consistent with data within the experimental uncertainty in most of the bins, but a small difference between the two simulations is observed for small values. This result is highly correlated with the difference observed in the leading b-jet p_{T} distribution. It confirms that the current performance

JHEP07(2020)044

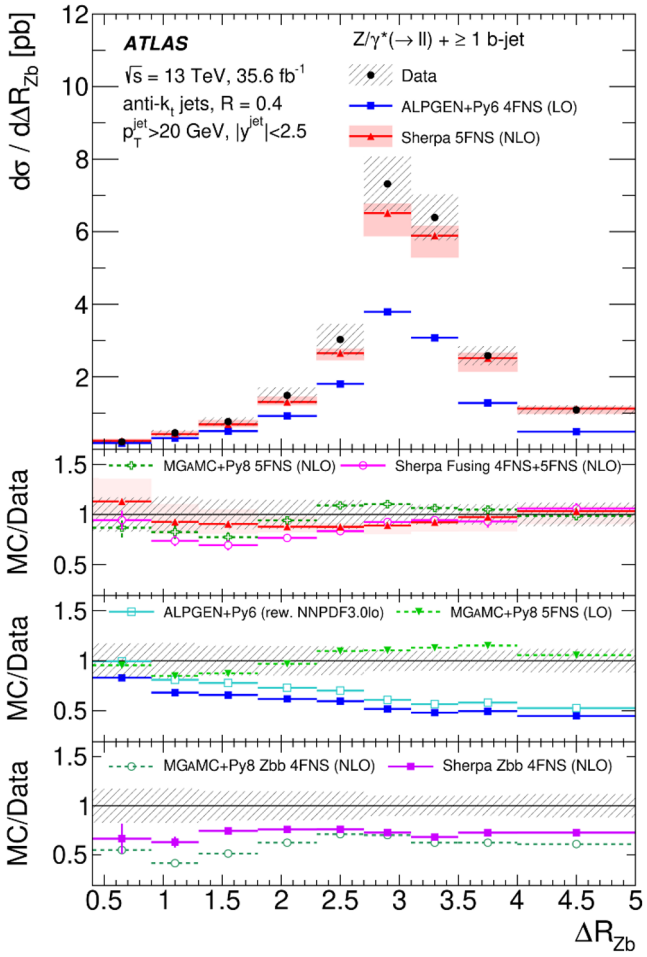

Figure 11. Measured cross-section as a function of the ΔR between the Z-boson candidate and the leading b-jet in events with at least one b-jet. The data are compared with the predictions from Sherpa 5FNS (NLO), Alpgen + Py6 4 FNS (LO), Sherpa Fusing 4FNS+5FNS (NLO), Sherpa Zbb 4FNS (NLO), MGaMC + Py8 5FNS (LO), MGaMC + Py8 Zbb 4FNS (NLO) and MGaMC + Py8 5FNS (NLO). The error bars correspond to the statistical uncertainty, and the hatched bands to the statistical and systematic uncertainties of the data, added in quadrature. The red band corresponds to the statistical and theoretical uncertainties of Sherpa 5FNS (NLO) added in quadrature. Only statistical uncertainties are shown for the other predictions.

of Sherpa Fusing 4FNS+5FNS (NLO) in the regime of high-p_{T} jets with a Z boson emitted collinearly is slightly worse than the Sherpa 5FNS (NLO) configuration. All MGaMC simulations predict too many large azimuthal separations, with a consequent deficit at small angles. Also, in this case the modelling in MGaMC + Py8 5FNS (NLO) is slightly worse than in MGaMC + Py8 5FNS (LO). The differential cross-section as a function of ΔR_{Zb}, as shown in figure 11, contains the convolution of effects discussed for the Δy_{Zb} and $\Delta\phi_{Zb}$ distributions.

JHEP07(2020)044

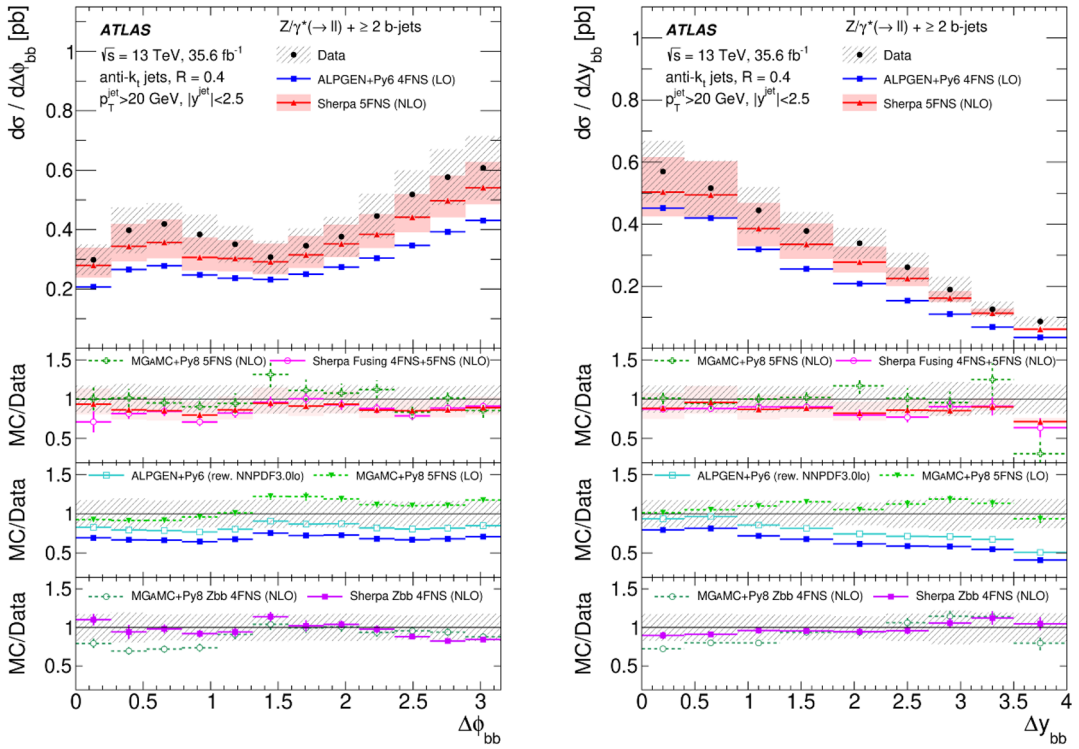

Figure 12. Measured cross-section as a function of $\Delta\phi$ (left) and Δy between the two leading b-jets (right) in events with at least two b-jets. The data are compared with the predictions from Sherpa 5FNS (NLO), Alpgen + Py6 4 FNS (LO), Sherpa Fusing 4FNS+5FNS (NLO), Sherpa Zbb 4FNS (NLO), MGaMC + Py8 5FNS (LO), MGaMC + Py8 Zbb 4FNS (NLO) and MGaMC + Py8 5FNS (NLO). The error bars correspond to the statistical uncertainty, and the hatched bands to the data statistical and systematic uncertainties added in quadrature. The red band corresponds to the statistical and theoretical uncertainties of Sherpa 5FNS (NLO) added in quadrature. Only statistical uncertainties are shown for the other predictions.

9.3 Differential cross-sections for $Z + \geq 2$ b-jets

Events with a Z boson produced in association with two b-jets constitute an important background to other SM and beyond-SM processes. Furthermore, they probe the mechanism of a gluon splitting into heavy quarks. The differential cross-section measurements for $Z + \geq 2$ b-jet are shown in figures 12–15. Each distribution is presented and discussed in detail in this section.

The distributions of angular separation between the two leading b-jets allow characterisation of the hard radiation at large angles and the soft radiation for collinear emissions. The differential cross-sections as a function of $\Delta\phi_{bb}$ and of Δy_{bb} are shown in figure 12. Most of the predictions provide satisfactory descriptions of the data within the large experimental uncertainties. Disagreement between data and MGaMC + Py8 Zbb 4FNS (NLO) is observed at low values of $\Delta\phi_{bb}$. Mismodelling of Δy_{bb} is observed for Alpgen. This observable has some sensitivity to PDFs, but that is below the experimental uncertainties. The ΔR_{bb} observable is sensitive to the various production mechanisms of the Zbb

JHEP07(2020)044

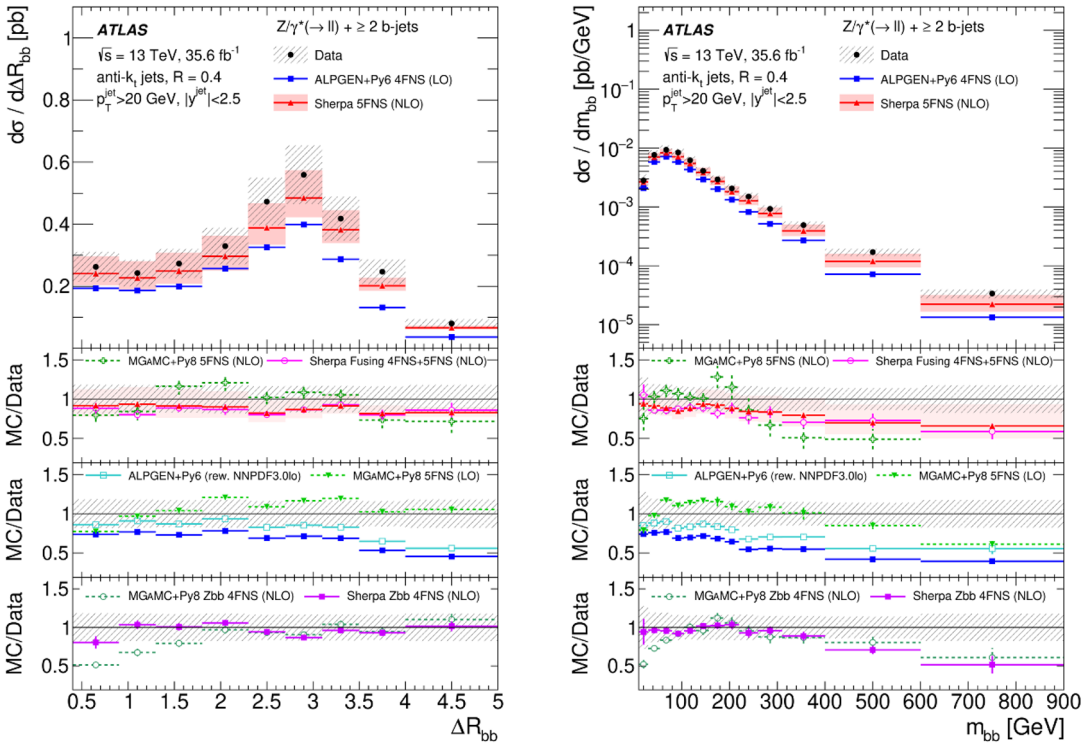

Figure 13. Measured cross-section as a function of ΔR between the two leading b-jets (left) and invariant mass of the two leading b-jets (right) in events with at least two b-jets. The data are compared with the predictions from Sherpa 5FNS (NLO), Alpgen + Py6 4 FNS (LO), Sherpa Fusing 4FNS+5FNS (NLO), Sherpa Zbb 4FNS (NLO), MGaMC + Py8 5FNS (LO), MGaMC + Py8 Zbb 4FNS (NLO) and MGaMC + Py8 5FNS (NLO). The error bars correspond to the statistical uncertainty, and the hatched bands to the data statistical and systematic uncertainties added in quadrature. The red band corresponds to the statistical and theoretical uncertainties of Sherpa 5FNS (NLO) added in quadrature. Only statistical uncertainties are shown for the other predictions.

final state. The region at low ΔR_{bb} is dominated by the production of two b-jets from gluon splitting. Probing this region requires two b-jets in the final state, so it is not sensitive to very small angles of the splitting. The interplay of the modelling of $\Delta\phi_{bb}$ and Δy_{bb} in Alpgen + Py6 4 FNS (LO) influences the prediction of the ΔR_{bb} distribution shown in figure 13 (left). All Sherpa predictions describe the shape of this observable quite well, featuring a substantial improvement at low ΔR_{bb} relative to the LO version reported by ATLAS using data at $\sqrt{s} = 7$ TeV. Overall, this is consistent with the results presented in the ATLAS measurement of gluon-splitting properties at $\sqrt{s} = 13$ TeV [11]. MGaMC + Py8 Zbb 4FNS (NLO) presents a large mismodelling at low ΔR_{bb}, which is the part of the phase space dominated by gluon splitting.

The invariant mass of the two leading b-jets is an important observable in the measurement of associated ZH production with Higgs boson decays into $b\bar{b}$, and in searches for physics beyond the SM in the same final state. The differential cross-section as a function of m_{bb} for events with at least two b-jets is shown in figure 13 (right). All Sherpa

JHEP07(2020)044

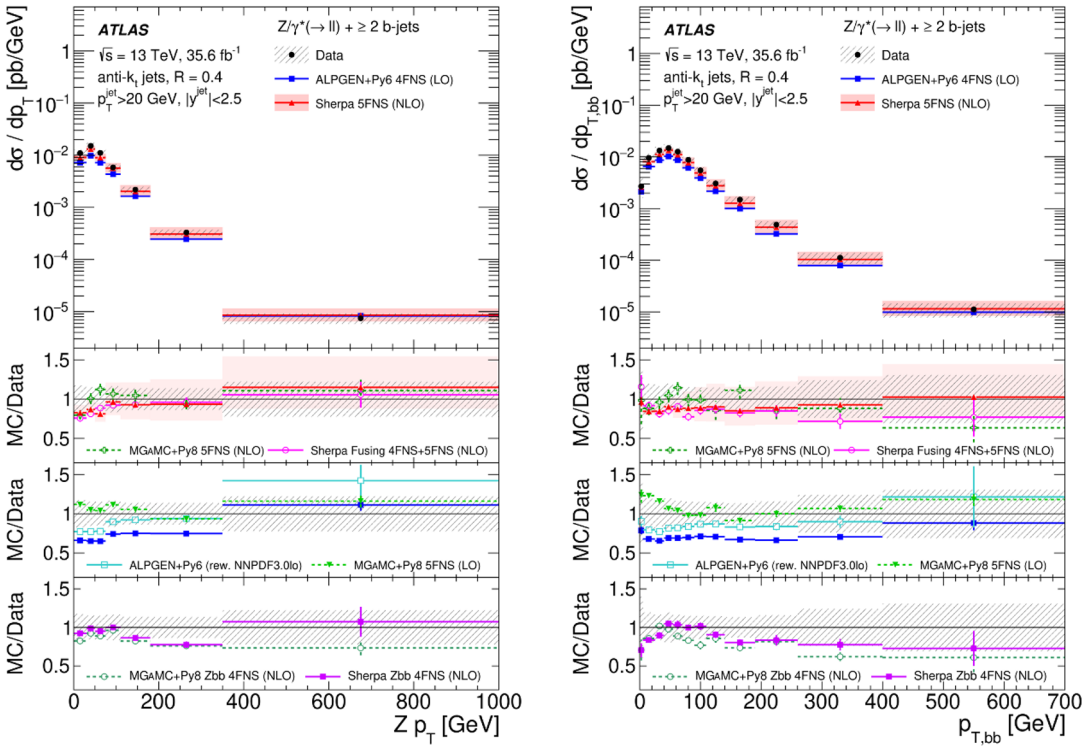

Figure 14. Measured cross-section as a function of p_{T} of the Z boson (left) and of the di-b-jet system ($p_{\mathrm{T},bb}$) (right) in events with at least two b-jets. The data are compared with the predictions from Sherpa 5FNS (NLO), Alpgen + Py6 4 FNS (LO), Sherpa Fusing 4FNS+5FNS (NLO), Sherpa Zbb 4FNS (NLO), MGaMC + Py8 5FNS (LO), MGaMC + Py8 Zbb 4FNS (NLO) and MGaMC + Py8 5FNS (NLO). The error bars correspond to the statistical uncertainty, and the hatched bands to the data statistical and systematic uncertainties added in quadrature. The red band corresponds to the statistical and theoretical uncertainties of Sherpa 5FNS (NLO) added in quadrature. Only statistical uncertainties are shown for the other predictions.

predictions provide a quite good model of the shape of this observable's distribution up to about 300 GeV, while the other predictions show various discrepancies in this region. This is particularly evident for MGaMC + Py8 Zbb 4FNS (NLO), and it is consistent with the mismodelling observed at low ΔR_{bb}, the region dominated by gluon splitting. In the high mass range all predictions underestimate the data, resulting in a sizeable mismodelling. Hence the use of these predictions for the background estimate in searches for physics beyond the SM in this final state could be problematic.

The differential cross-sections as a function of the Z-boson p_{T} and of the p_{T} of the di-b-jet system ($p_{\mathrm{T},bb}$) for events with at least two b-jets are shown in figure 14. Most of the predictions agree with data within the large experimental uncertainties, which are about 25% in most of the bins, and large statistical uncertainties of the predictions, which for some MC samples reach 25% in the highest bins. Alpgen shows a harder Z-boson p_{T} spectrum than data, as was observed in the distribution of events with at least one b-jet. The Zbb simulation at NLO with 4FNS, as implemented in MGaMC + Py8 Zbb 4FNS (NLO) and Sherpa Zbb 4FNS (NLO), shows better agreement with data with respect

JHEP07(2020)044

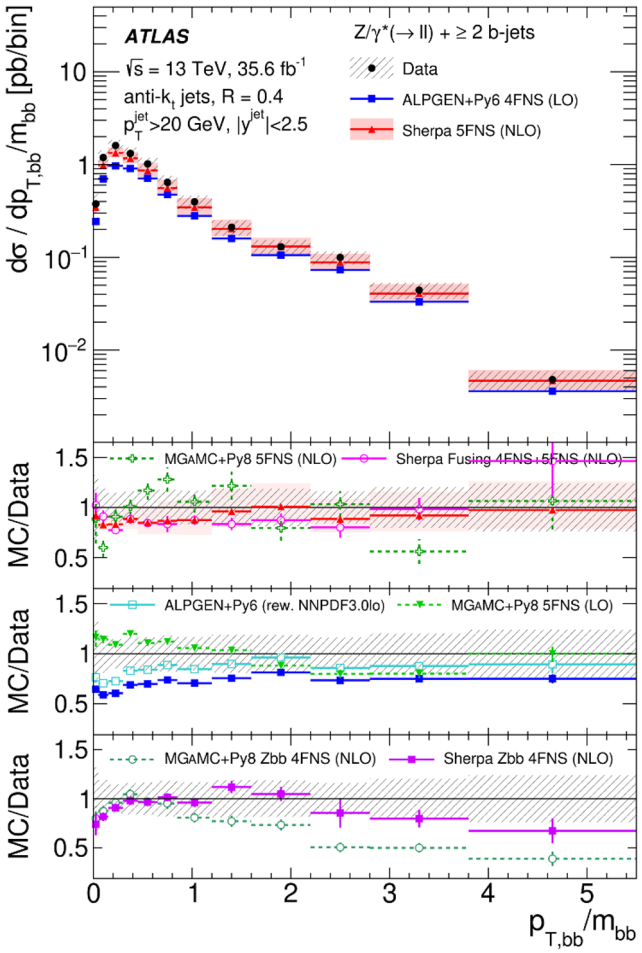

Figure 15. Measured cross-section as a function of the p_{T} of the di-b-jet system divided by its invariant mass ($p_{\mathrm{T},bb}/m_{bb}$) in events with at least two b-jets. The data are compared with the predictions from Sherpa 5FNS (NLO), Alpgen + Py6 4 FNS (LO), Sherpa Fusing 4FNS+5FNS (NLO), Sherpa Zbb 4FNS (NLO), MGaMC + Py8 5FNS (LO), MGaMC + Py8 Zbb 4FNS (NLO) and MGaMC + Py8 5FNS (NLO). The error bars correspond to the statistical uncertainty, and the hatched bands to the statistical and systematic uncertainties of the data, added in quadrature. The red band corresponds to the statistical and theoretical uncertainties of Sherpa 5FNS (NLO) added in quadrature. Only statistical uncertainties are shown for the other predictions.

to the p_{T} distributions for events with at least one b-jet, but significant disagreement is still observed.

Finally, the ratio of the p_{T} of the di-b-jet system to its invariant mass ($p_{\mathrm{T},bb}/m_{bb}$) is sensitive to gluon splitting: a small value indicates a hard splitting and a large value is a consequence of soft splitting. The differential cross-section as a function of $p_{\mathrm{T},bb}/m_{bb}$ is shown in figure 15. Sherpa 5FNS (NLO) and Sherpa Fusing 4FNS+5FNS (NLO) show quite good agreement with data, while MGaMC + Py8 Zbb 4FNS (NLO) agrees less well.

JHEP07(2020)044

10 Conclusion

This paper presents a measurement of the cross-sections for Z-boson production in association with one or more b-jets in pp collisions at $\sqrt{s} = 13$ TeV. The analysed data correspond to an integrated luminosity of $35.6\,\text{fb}^{-1}$ recorded by the ATLAS detector at the LHC.

The cross-sections are measured using the electron and muon decay modes of the Z boson in a fiducial phase space. In addition to the inclusive cross-sections, differential cross-sections of several kinematic observables are measured, extending the range of jet transverse momenta to higher values than reported in previous ATLAS publications, which used data at lower centre-of-mass energies.

The measurements are compared with predictions from a variety of Monte Carlo generators. In general, 5-flavour number scheme (5FNS) calculations at NLO accuracy predict the inclusive cross-sections well, while inclusive 4-flavour number scheme (4FNS) LO calculations largely underestimate the data. Predictions of Zbb at NLO accuracy agree with data only in the two-b-jets case, and underestimate the data in the case of events with at least one b-jet. Overall, Sherpa 5FNS (NLO), a 5FNS generator with matrix elements at NLO for up to two partons and matrix elements at LO for up to four partons, describes the various differential distributions within the experimental uncertainties. A significant discrepancy, common to all generators, is found for large values of m_{bb}. The Sherpa Fusing 4FNS+5FNS (NLO) simulation, which combines 4FNS with 5FNS at NLO accuracy using a novel technique, agrees with Sherpa 5FNS (NLO), showing that in general at the scales tested by this measurement the effects of this merging are minor. A disagreement of about 20 30% is observed for large values of the leading b-jet transverse momentum, and for small angular separations between the Z boson and the leading b-jet.

The 5FNS simulation with matrix elements for up to four partons at LO, as implemented in MGaMC + Py8 (LO), describes the data within the experimental uncertainties in most cases. In some cases this simulation is even better than predictions from MGaMC + Py8 5FNS (NLO), which has matrix elements with only one parton at NLO. This indicates the importance of simulations with several partons in the matrix element for a fair description of the data. The pure Zbb simulation at NLO in the 4FNS, as generated by Sherpa and MGaMC, shows significant deviations from the data even in the two-b-jets configuration, and this is more pronounced in MGaMC.

This measurement provides essential input for the improvement of theoretical predictions and Monte Carlo generators of Z-boson production in association with b-jets, allowing a better quantitative understanding of perturbative QCD.

Acknowledgments

We thank CERN for the very successful operation of the LHC, as well as the support staff from our institutions without whom ATLAS could not be operated efficiently.

We acknowledge the support of ANPCyT, Argentina; YerPhI, Armenia; ARC, Australia; BMWFW and FWF, Austria; ANAS, Azerbaijan; SSTC, Belarus; CNPq and FAPESP, Brazil; NSERC, NRC and CFI, Canada; CERN; CONICYT, Chile; CAS, MOST

JHEP07(2020)044

and NSFC, China; COLCIENCIAS, Colombia; MSMT CR, MPO CR and VSC CR, Czech Republic; DNRF and DNSRC, Denmark; IN2P3-CNRS and CEA-DRF/IRFU, France; SRNSFG, Georgia; BMBF, HGF and MPG, Germany; GSRT, Greece; RGC and Hong Kong SAR, China; ISF and Benoziyo Center, Israel; INFN, Italy; MEXT and JSPS, Japan; CNRST, Morocco; NWO, Netherlands; RCN, Norway; MNiSW and NCN, Poland; FCT, Portugal; MNE/IFA, Romania; MES of Russia and NRC KI, Russia Federation; JINR; MESTD, Serbia; MSSR, Slovakia; ARRS and MIZŠ, Slovenia; DST/NRF, South Africa; MINECO, Spain; SRC and Wallenberg Foundation, Sweden; SERI, SNSF and Cantons of Bern and Geneva, Switzerland; MOST, Taiwan; TAEK, Turkey; STFC, United Kingdom; DOE and NSF, United States of America. In addition, individual groups and members have received support from BCKDF, CANARIE, Compute Canada and CRC, Canada; ERC, ERDF, Horizon 2020, Marie Skłodowska-Curie Actions and COST, European Union; Investissements d'Avenir Labex, Investissements d'Avenir Idex and ANR, France; DFG and AvH Foundation, Germany; Herakleitos, Thales and Aristeia programmes co-financed by EU-ESF and the Greek NSRF, Greece; BSF-NSF and GIF, Israel; CERCA Programme Generalitat de Catalunya and PROMETEO Programme Generalitat Valenciana, Spain; Göran Gustafssons Stiftelse, Sweden; The Royal Society and Leverhulme Trust, United Kingdom.

The crucial computing support from all WLCG partners is acknowledged gratefully, in particular from CERN, the ATLAS Tier-1 facilities at TRIUMF (Canada), NDGF (Denmark, Norway, Sweden), CC-IN2P3 (France), KIT/GridKA (Germany), INFN-CNAF (Italy), NL-T1 (Netherlands), PIC (Spain), ASGC (Taiwan), RAL (U.K.) and BNL (U.S.A.), the Tier-2 facilities worldwide and large non-WLCG resource providers. Major contributors of computing resources are listed in ref. [104].

References

[1] F. Febres Cordero, L. Reina and D. Wackeroth, *W- and Z-boson production with a massive bottom-quark pair at the Large Hadron Collider*, *Phys. Rev. D* **80** (2009) 034015 [arXiv:0906.1923] [INSPIRE].

[2] J.M. Campbell, R. Ellis, F. Maltoni and S. Willenbrock, *Associated production of a Z boson and a single heavy quark jet*, *Phys. Rev. D* **69** (2004) 074021 [hep-ph/0312024] [INSPIRE].

[3] F. Maltoni, G. Ridolfi and M. Ubiali, *b-initiated processes at the LHC: a reappraisal*, *JHEP* **07** (2012) 022 [*Erratum ibid.* **04** (2013) 095] [arXiv:1203.6393] [INSPIRE].

[4] G. Ridolfi, M. Ubiali and M. Zaro, *A fragmentation-based study of heavy quark production*, *JHEP* **01** (2020) 196 [arXiv:1911.01975] [INSPIRE].

[5] CDF collaboration, *Measurement of cross sections for b jet production in events with a Z boson in $p\bar{p}$ collisions at $\sqrt{s} = 1.96$ TeV*, *Phys. Rev. D* **79** (2009) 052008 [arXiv:0812.4458] [INSPIRE].

JHEP07(2020)044

[6] D0 collaboration, *Measurement of the ratio of differential cross sections $\sigma(p\bar{p} \to Z + bjet)/\sigma(p\bar{p} \to Z + jet)$ in $p\bar{p}$ collisions at $\sqrt{s} = 1.96$ TeV*, *Phys. Rev. D* **87** (2013) 092010 [arXiv:1301.2233] [INSPIRE].

[7] CDF collaboration, *First measurement of the b-jet cross section in events with a W boson in $p\bar{p}$ collisions at $\sqrt{s} = 1.96$ TeV*, *Phys. Rev. Lett.* **104** (2010) 131801 [arXiv:0909.1505] [INSPIRE].

[8] D0 collaboration, *Measurement of the $p\bar{p} \to W + b + X$ production cross section at $\sqrt{s} = 1.96$ TeV*, *Phys. Lett. B* **718** (2013) 1314 [arXiv:1210.0627] [INSPIRE].

[9] *LHC Machine*, 2008 *JINST* **3** S08001 [INSPIRE].

[10] ATLAS collaboration, *Measurement of the cross-section for W boson production in association with b-jets in pp collisions at $\sqrt{s} = 7$ TeV with the ATLAS detector*, *JHEP* **06** (2013) 084 [arXiv:1302.2929] [INSPIRE].

[11] ATLAS collaboration, *Measurement of differential production cross-sections for a Z boson in association with b-jets in 7 TeV proton-proton collisions with the ATLAS detector*, *JHEP* **10** (2014) 141 [arXiv:1407.3643] [INSPIRE].

[12] CMS collaboration, *Measurement of the production cross sections for a Z boson and one or more b jets in pp collisions at $\sqrt{s} = 7$ TeV*, *JHEP* **06** (2014) 120 [arXiv:1402.1521] [INSPIRE].

[13] CMS collaboration, *Measurement of the cross section and angular correlations for associated production of a Z Boson with b hadrons in pp collisions at $\sqrt{s} = 7$ TeV*, *JHEP* **12** (2013) 039 [arXiv:1310.1349] [INSPIRE].

[14] CMS collaboration, *Measurement of the production cross section for a W boson and two b jets in pp collisions at $\sqrt{s} = 7$ TeV*, *Phys. Lett. B* **735** (2014) 204 [arXiv:1312.6608] [INSPIRE].

[15] CMS collaboration, *Measurement of the Z/γ^*+b-jet cross section in pp collisions at $\sqrt{s} = 7$ TeV*, *JHEP* **06** (2012) 126 [arXiv:1204.1643] [INSPIRE].

[16] CMS collaboration, *Measurement of the production cross section of a W boson in association with two b jets in pp collisions at $\sqrt{s} = 8$ TeV*, *Eur. Phys. J. C* **77** (2017) 92 [arXiv:1608.07561] [INSPIRE].

[17] CMS collaboration, *Measurements of the associated production of a Z boson and b jets in pp collisions at $\sqrt{s} = 8$ TeV*, *Eur. Phys. J. C* **77** (2017) 751 [arXiv:1611.06507] [INSPIRE].

[18] CMS collaboration, *Measurement of the associated production of a Z boson with charm or bottom quark jets in proton-proton collisions at $\sqrt{s} = 13$ TeV*, arXiv:2001.06899 [INSPIRE].

[19] ATLAS collaboration, *The ATLAS experiment at the CERN Large Hadron Collider*, 2008 *JINST* **3** S08003 [INSPIRE].

[20] ATLAS collaboration, *ATLAS Insertable B-layer technical design report*, ATLAS-TDR-19 (2010).

[21] ATLAS IBL collaboration, *Production and integration of the ATLAS insertable B-layer*, 2018 *JINST* **13** T05008 [arXiv:1803.00844] [INSPIRE].

[22] ATLAS collaboration, *Performance of the ATLAS trigger system in 2015*, *Eur. Phys. J. C* **77** (2017) 317 [arXiv:1611.09661] [INSPIRE].

JHEP07(2020)044

[23] ATLAS collaboration, *Luminosity determination in pp collisions at $\sqrt{s} = 13$ TeV using the ATLAS detector at the LHC*, ATLAS-CONF-2019-021 (2019).

[24] G. Avoni et al., *The new LUCID-2 detector for luminosity measurement and monitoring in ATLAS*, 2018 *JINST* **13** P07017 [INSPIRE].

[25] SHERPA collaboration, *Event generation with Sherpa 2.2*, *SciPost Phys.* **7** (2019) 034 [arXiv:1905.09127] [INSPIRE].

[26] T. Gleisberg and S. Hoeche, *Comix, a new matrix element generator*, *JHEP* **12** (2008) 039 [arXiv:0808.3674] [INSPIRE].

[27] F. Cascioli, P. Maierhofer and S. Pozzorini, *Scattering amplitudes with open loops*, *Phys. Rev. Lett.* **108** (2012) 111601 [arXiv:1111.5206] [INSPIRE].

[28] A. Denner, S. Dittmaier and L. Hofer, *Collier: a Fortran-based Complex One-Loop LIbrary in Extended Regularizations*, *Comput. Phys. Commun.* **212** (2017) 220 [arXiv:1604.06792] [INSPIRE].

[29] S. Schumann and F. Krauss, *A parton shower algorithm based on Catani-Seymour dipole factorisation*, *JHEP* **03** (2008) 038 [arXiv:0709.1027] [INSPIRE].

[30] S. Hoeche, F. Krauss, M. Schonherr and F. Siegert, *A critical appraisal of NLO+PS matching methods*, *JHEP* **09** (2012) 049 [arXiv:1111.1220] [INSPIRE].

[31] S. Hoeche, F. Krauss, M. Schonherr and F. Siegert, *QCD matrix elements + parton showers: the NLO case*, *JHEP* **04** (2013) 027 [arXiv:1207.5030] [INSPIRE].

[32] S. Catani, F. Krauss, R. Kuhn and B.R. Webber, *QCD matrix elements + parton showers*, *JHEP* **11** (2001) 063 [hep-ph/0109231] [INSPIRE].

[33] S. Hoeche, F. Krauss, S. Schumann and F. Siegert, *QCD matrix elements and truncated showers*, *JHEP* **05** (2009) 053 [arXiv:0903.1219] [INSPIRE].

[34] NNPDF collaboration, *Parton distributions for the LHC Run II*, *JHEP* **04** (2015) 040 [arXiv:1410.8849] [INSPIRE].

[35] E. Bothmann, M. Schönherr and S. Schumann, *Reweighting QCD matrix-element and parton-shower calculations*, *Eur. Phys. J. C* **76** (2016) 590 [arXiv:1606.08753] [INSPIRE].

[36] M.L. Mangano et al., *ALPGEN, a generator for hard multiparton processes in hadronic collisions*, *JHEP* **07** (2003) 001 [hep-ph/0206293] [INSPIRE].

[37] T. Sjöstrand, S. Mrenna and P.Z. Skands, *PYTHIA 6.4 physics and manual*, *JHEP* **05** (2006) 026 [hep-ph/0603175] [INSPIRE].

[38] P.Z. Skands, *Tuning Monte Carlo generators: the Perugia tunes*, *Phys. Rev. D* **82** (2010) 074018 [arXiv:1005.3457] [INSPIRE].

[39] J. Pumplin et al., *New generation of parton distributions with uncertainties from global QCD analysis*, *JHEP* **07** (2002) 012 [hep-ph/0201195] [INSPIRE].

[40] J. Alwall et al., *Comparative study of various algorithms for the merging of parton showers and matrix elements in hadronic collisions*, *Eur. Phys. J. C* **53** (2008) 473 [arXiv:0706.2569] [INSPIRE].

[41] D.J. Lange, *The EvtGen particle decay simulation package*, *Nucl. Instrum. Meth. A* **462** (2001) 152 [INSPIRE].

JHEP07(2020)044

[42] P. Golonka and Z. Was, *PHOTOS Monte Carlo: a precision tool for QED corrections in Z and W decays*, *Eur. Phys. J. C* **45** (2006) 97 [hep-ph/0506026] [INSPIRE].

[43] N. Davidson, T. Przedzinski and Z. Was, *PHOTOS interface in C++: technical and physics documentation*, *Comput. Phys. Commun.* **199** (2016) 86 [arXiv:1011.0937] [INSPIRE].

[44] C. Anastasiou, L.J. Dixon, K. Melnikov and F. Petriello, *High precision QCD at hadron colliders: electroweak gauge boson rapidity distributions at NNLO*, *Phys. Rev. D* **69** (2004) 094008 [hep-ph/0312266] [INSPIRE].

[45] R. Gavin, Y. Li, F. Petriello and S. Quackenbush, *FEWZ 2.0: a code for hadronic Z production at next-to-next-to-leading order*, *Comput. Phys. Commun.* **182** (2011) 2388 [arXiv:1011.3540] [INSPIRE].

[46] R. Gavin, Y. Li, F. Petriello and S. Quackenbush, *W physics at the LHC with FEWZ 2.1*, *Comput. Phys. Commun.* **184** (2013) 208 [arXiv:1201.5896] [INSPIRE].

[47] Y. Li and F. Petriello, *Combining QCD and electroweak corrections to dilepton production in FEWZ*, *Phys. Rev. D* **86** (2012) 094034 [arXiv:1208.5967] [INSPIRE].

[48] S. Frixione, P. Nason and G. Ridolfi, *A positive-weight next-to-leading-order Monte Carlo for heavy flavour hadroproduction*, *JHEP* **09** (2007) 126 [arXiv:0707.3088] [INSPIRE].

[49] P. Nason, *A new method for combining NLO QCD with shower Monte Carlo algorithms*, *JHEP* **11** (2004) 040 [hep-ph/0409146] [INSPIRE].

[50] S. Frixione, P. Nason and C. Oleari, *Matching NLO QCD computations with parton shower simulations: the POWHEG method*, *JHEP* **11** (2007) 070 [arXiv:0709.2092] [INSPIRE].

[51] S. Alioli, P. Nason, C. Oleari and E. Re, *A general framework for implementing NLO calculations in shower Monte Carlo programs: the POWHEG BOX*, *JHEP* **06** (2010) 043 [arXiv:1002.2581] [INSPIRE].

[52] ATLAS collaboration, *Studies on top-quark Monte Carlo modelling for Top2016*, ATL-PHYS-PUB-2016-020 (2016).

[53] T. Sjöstrand et al., *An introduction to PYTHIA 8.2*, *Comput. Phys. Commun.* **191** (2015) 159 [arXiv:1410.3012] [INSPIRE].

[54] ATLAS collaboration, *ATLAS PYTHIA 8 tunes to 7 TeV datas*, ATL-PHYS-PUB-2014-021 (2014).

[55] M. Beneke, P. Falgari, S. Klein and C. Schwinn, *Hadronic top-quark pair production with NNLL threshold resummation*, *Nucl. Phys. B* **855** (2012) 695 [arXiv:1109.1536] [INSPIRE].

[56] M. Cacciari, M. Czakon, M. Mangano, A. Mitov and P. Nason, *Top-pair production at hadron colliders with next-to-next-to-leading logarithmic soft-gluon resummation*, *Phys. Lett. B* **710** (2012) 612 [arXiv:1111.5869] [INSPIRE].

[57] P. Bärnreuther, M. Czakon and A. Mitov, *Percent level precision physics at the Tevatron: first genuine NNLO QCD corrections to $q\bar{q} \to t\bar{t} + X$*, *Phys. Rev. Lett.* **109** (2012) 132001 [arXiv:1204.5201] [INSPIRE].

[58] M. Czakon and A. Mitov, *NNLO corrections to top-pair production at hadron colliders: the all-fermionic scattering channels*, *JHEP* **12** (2012) 054 [arXiv:1207.0236] [INSPIRE].

[59] M. Czakon and A. Mitov, *NNLO corrections to top pair production at hadron colliders: the quark-gluon reaction*, *JHEP* **01** (2013) 080 [arXiv:1210.6832] [INSPIRE].

JHEP07(2020)044

[60] M. Czakon, P. Fiedler and A. Mitov, *Total top-quark pair-production cross section at hadron colliders through $O(\alpha_S^4)$*, *Phys. Rev. Lett.* **110** (2013) 252004 [arXiv:1303.6254] [INSPIRE].

[61] M. Czakon and A. Mitov, *Top++: a program for the calculation of the top-pair cross-section at hadron colliders*, *Comput. Phys. Commun.* **185** (2014) 2930 [arXiv:1112.5675] [INSPIRE].

[62] J. Alwall et al., *The automated computation of tree-level and next-to-leading order differential cross sections and their matching to parton shower simulations*, *JHEP* **07** (2014) 079 [arXiv:1405.0301] [INSPIRE].

[63] M. Bahr et al., *HERWIG++ physics and manual*, *Eur. Phys. J. C* **58** (2008) 639 [arXiv:0803.0883] [INSPIRE].

[64] J. Bellm et al., *HERWIG 7.0/HERWIG++ 3.0 release note*, *Eur. Phys. J. C* **76** (2016) 196 [arXiv:1512.01178] [INSPIRE].

[65] H.-L. Lai et al., *New parton distributions for collider physics*, *Phys. Rev. D* **82** (2010) 074024 [arXiv:1007.2241] [INSPIRE].

[66] M. Aliev et al., *HATHOR: HAdronic Top and Heavy quarks crOss section calculatoR*, *Comput. Phys. Commun.* **182** (2011) 1034 [arXiv:1007.1327] [INSPIRE].

[67] P. Kant et al., *HatHor for single top-quark production: Updated predictions and uncertainty estimates for single top-quark production in hadronic collisions*, *Comput. Phys. Commun.* **191** (2015) 74 [arXiv:1406.4403] [INSPIRE].

[68] N. Kidonakis, *Two-loop soft anomalous dimensions for single top quark associated production with a W- or H-*, *Phys. Rev. D* **82** (2010) 054018 [arXiv:1005.4451] [INSPIRE].

[69] T. Gleisberg et al., *Event generation with SHERPA 1.1*, *JHEP* **02** (2009) 007 [arXiv:0811.4622] [INSPIRE].

[70] G. Cullen et al., *Automated one-loop calculations with GoSam*, *Eur. Phys. J. C* **72** (2012) 1889 [arXiv:1111.2034] [INSPIRE].

[71] K. Hamilton, P. Nason and G. Zanderighi, *MINLO: Multi-scale Improved NLO*, *JHEP* **10** (2012) 155 [arXiv:1206.3572] [INSPIRE].

[72] G. Luisoni, P. Nason, C. Oleari and F. Tramontano, *$HW^{\pm}/HZ + 0$ and 1 jet at NLO with the POWHEG BOX interfaced to GoSam and their merging within MiNLO*, *JHEP* **10** (2013) 083 [arXiv:1306.2542] [INSPIRE].

[73] O. Brein, A. Djouadi and R. Harlander, *NNLO QCD corrections to the Higgs-strahlung processes at hadron colliders*, *Phys. Lett. B* **579** (2004) 149 [hep-ph/0307206] [INSPIRE].

[74] A. Denner, S. Dittmaier, S. Kallweit and A. Mück, *Electroweak corrections to Higgs-strahlung off W/Z bosons at the Tevatron and the LHC with HAWK*, *JHEP* **03** (2012) 075 [arXiv:1112.5142] [INSPIRE].

[75] L. Altenkamp et al., *Gluon-induced Higgs-strahlung at next-to-leading order QCD*, *JHEP* **02** (2013) 078 [arXiv:1211.5015] [INSPIRE].

[76] ATLAS collaboration, *The ATLAS simulation infrastructure*, *Eur. Phys. J. C* **70** (2010) 823 [arXiv:1005.4568] [INSPIRE].

[77] GEANT4 collaboration, *GEANT4 — a simulation toolkit*, *Nucl. Instrum. Meth. A* **506** (2003) 250 [INSPIRE].

JHEP07(2020)044

[78] ATLAS collaboration, *Summary of ATLAS Pythia 8 tunes*, ATLAS-PHYS-PUB-2012-003 (2012).

[79] A.D. Martin, W.J. Stirling, R.S. Thorne and G. Watt, *Parton distributions for the LHC*, *Eur. Phys. J. C* **63** (2009) 189 [arXiv:0901.0002] [INSPIRE].

[80] https://sherpa.hepforge.org/doc/SHERPA-MC-2.2.6.html

[81] S. Höche, J. Krause and F. Siegert, *Multijet merging in a variable flavor number scheme*, *Phys. Rev. D* **100** (2019) 014011 [arXiv:1904.09382] [INSPIRE].

[82] ATLAS collaboration, *Monte Carlo generators for the production of a W or Z/γ^* boson in association with jets at ATLAS in Run 2*, ATL-PHYS-PUB-2016-003 (2016).

[83] R. Frederix and S. Frixione, *Merging meets matching in MC@NLO*, *JHEP* **12** (2012) 061 [arXiv:1209.6215] [INSPIRE].

[84] J. Butterworth et al., *PDF4LHC recommendations for LHC Run II*, *J. Phys. G* **43** (2016) 023001 [arXiv:1510.03865] [INSPIRE].

[85] ATLAS collaboration, *Electron reconstruction and identification in the ATLAS experiment using the 2015 and 2016 LHC proton-proton collision data at $\sqrt{s} = 13$ TeV*, *Eur. Phys. J. C* **79** (2019) 639 [arXiv:1902.04655] [INSPIRE].

[86] ATLAS collaboration, *Muon reconstruction performance of the ATLAS detector in proton–proton collision data at $\sqrt{s} = 13$ TeV*, *Eur. Phys. J. C* **76** (2016) 292 [arXiv:1603.05598] [INSPIRE].

[87] M. Cacciari, G.P. Salam and G. Soyez, *The anti-k_t jet clustering algorithm*, *JHEP* **04** (2008) 063 [arXiv:0802.1189] [INSPIRE].

[88] M. Cacciari, G.P. Salam and G. Soyez, *FastJet user manual*, *Eur. Phys. J. C* **72** (2012) 1896 [arXiv:1111.6097] [INSPIRE].

[89] ATLAS collaboration, *Topological cell clustering in the ATLAS calorimeters and its performance in LHC Run 1*, *Eur. Phys. J. C* **77** (2017) 490 [arXiv:1603.02934] [INSPIRE].

[90] ATLAS collaboration, *Jet energy scale measurements and their systematic uncertainties in proton-proton collisions at $\sqrt{s} = 13$ TeV with the ATLAS detector*, *Phys. Rev. D* **96** (2017) 072002 [arXiv:1703.09665] [INSPIRE].

[91] ATLAS collaboration, *Selection of jets produced in 13TeV proton-proton collisions with the ATLAS detector*, ATLAS-CONF-2015-029 (2015).

[92] ATLAS collaboration, *Performance of pile-up mitigation techniques for jets in pp collisions at $\sqrt{s} = 8$ TeV using the ATLAS detector*, *Eur. Phys. J. C* **76** (2016) 581 [arXiv:1510.03823] [INSPIRE].

[93] ATLAS collaboration, *Performance of b-jet identification in the ATLAS experiment*, 2016 *JINST* **11** P04008 [arXiv:1512.01094] [INSPIRE].

[94] ATLAS collaboration, *Optimisation of the ATLAS b-tagging performance for the 2016 LHC Run*, ATL-PHYS-PUB-2016-012 (2016).

[95] ATLAS collaboration, *Performance of missing transverse momentum reconstruction with the ATLAS detector using proton-proton collisions at $\sqrt{s} = 13$ TeV*, *Eur. Phys. J. C* **78** (2018) 903 [arXiv:1802.08168] [INSPIRE].

JHEP07(2020)044

[96] ATLAS collaboration, *Jet energy resolution in proton-proton collisions at $\sqrt{s} = 7$ TeV recorded in 2010 with the ATLAS detector*, *Eur. Phys. J. C* **73** (2013) 2306 [arXiv:1210.6210] [INSPIRE].

[97] ATLAS collaboration, *Identification and rejection of pile-up jets at high pseudorapidity with the ATLAS detector*, *Eur. Phys. J. C* **77** (2017) 580 [*Erratum ibid.* **77** (2017) 712] [arXiv:1705.02211] [INSPIRE].

[98] ATLAS collaboration, *Measurements of b-jet tagging efficiency with the ATLAS detector using $t\bar{t}$ events at $\sqrt{s} = 13$ TeV*, *JHEP* **08** (2018) 089 [arXiv:1805.01845] [INSPIRE].

[99] ATLAS collaboration, *Measurement of b-tagging efficiency of c-jets in $t\bar{t}$ events using a likelihood approach with the ATLAS detector*, ATLAS-CONF-2018-001 (2018).

[100] ATLAS collaboration, *Calibration of light-flavour b-jet mistagging rates using ATLAS proton-proton collision data at $\sqrt{s} = 13$ TeV*, ATLAS-CONF-2018-006 (2018).

[101] ATLAS collaboration, *Measurement of the inelastic proton-proton cross section at $\sqrt{s} = 13$ TeV with the ATLAS detector at the LHC*, *Phys. Rev. Lett.* **117** (2016) 182002 [arXiv:1606.02625] [INSPIRE].

[102] ATLAS collaboration, *Evidence for the $H \to b\bar{b}$ decay with the ATLAS detector*, *JHEP* **12** (2017) 024 [arXiv:1708.03299] [INSPIRE].

[103] G. D'Agostini, *A multidimensional unfolding method based on Bayes' theorem*, *Nucl. Instrum. Meth. A* **362** (1995) 487 [INSPIRE].

[104] ATLAS collaboration, *ATLAS computing acknowledgements*, ATL-GEN-PUB-2016-002 (2016).

JHEP07(2020)044

The ATLAS collaboration

G. Aad[102], B. Abbott[128], D.C. Abbott[103], A. Abed Abud[36], K. Abeling[53], D.K. Abhayasinghe[94], S.H. Abidi[166], O.S. AbouZeid[40], N.L. Abraham[155], H. Abramowicz[160], H. Abreu[159], Y. Abulaiti[6], B.S. Acharya[67a,67b,n], B. Achkar[53], L. Adam[100], C. Adam Bourdarios[5], L. Adamczyk[84a], L. Adamek[166], J. Adelman[121], M. Adersberger[114], A. Adiguzel[12c], S. Adorni[54], T. Adye[143], A.A. Affolder[145], Y. Afik[159], C. Agapopoulou[65], M.N. Agaras[38], A. Aggarwal[119], C. Agheorghiesei[27c], J.A. Aguilar-Saavedra[139f,139a,ae], A. Ahmad[36], F. Ahmadov[80], W.S. Ahmed[104], X. Ai[18], G. Aielli[74a,74b], S. Akatsuka[86], T.P.A. Åkesson[97], E. Akilli[54], A.V. Akimov[111], K. Al Khoury[65], G.L. Alberghi[23b,23a], J. Albert[175], M.J. Alconada Verzini[160], S. Alderweireldt[36], M. Aleksa[36], I.N. Aleksandrov[80], C. Alexa[27b], T. Alexopoulos[10], A. Alfonsi[120], F. Alfonsi[23b,23a], M. Alhroob[128], B. Ali[141], S. Ali[157], M. Aliev[165], G. Alimonti[69a], C. Allaire[36], B.M.M. Allbrooke[155], B.W. Allen[131], P.P. Allport[21], A. Aloisio[70a,70b], F. Alonso[89], C. Alpigiani[147], A.A. Alshehri[57], E. Alunno Camelia[74a,74b], M. Alvarez Estevez[99], M.G. Alviggi[70a,70b], Y. Amaral Coutinho[81b], A. Ambler[104], L. Ambroz[134], C. Amelung[26], D. Amidei[106], S.P. Amor Dos Santos[139a], S. Amoroso[46], C.S. Amrouche[54], F. An[79], C. Anastopoulos[148], N. Andari[144], T. Andeen[11], C.F. Anders[61b], J.K. Anders[20], S.Y. Andrean[45a,45b], A. Andreazza[69a,69b], V. Andrei[61a], C.R. Anelli[175], S. Angelidakis[38], A. Angerami[39], A.V. Anisenkov[122b,122a], A. Annovi[72a], C. Antel[54], M.T. Anthony[148], E. Antipov[129], M. Antonelli[51], D.J.A. Antrim[170], F. Anulli[73a], M. Aoki[82], J.A. Aparisi Pozo[173], M.A. Aparo[155], L. Aperio Bella[15a], V. Araujo Ferraz[81b], R. Araujo Pereira[81b], C. Arcangeletti[51], A.T.H. Arce[49], F.A. Arduh[89], J-F. Arguin[110], S. Argyropoulos[52], J.-H. Arling[46], A.J. Armbruster[36], A. Armstrong[170], O. Arnaez[166], H. Arnold[120], Z.P. Arrubarrena Tame[114], G. Artoni[134], S. Artz[100], S. Asai[162], T. Asawatavonvanich[164], N. Asbah[59], E.M. Asimakopoulou[171], L. Asquith[155], J. Assahsah[35d], K. Assamagan[29], R. Astalos[28a], R.J. Atkin[33a], M. Atkinson[172], N.B. Atlay[19], H. Atmani[65], K. Augsten[141], G. Avolio[36], M.K. Ayoub[15a], G. Azuelos[110,am], H. Bachacou[144], K. Bachas[161], M. Backes[134], F. Backman[45a,45b], P. Bagnaia[73a,73b], M. Bahmani[85], H. Bahrasemani[151], A.J. Bailey[173], V.R. Bailey[172], J.T. Baines[143], C. Bakalis[10], O.K. Baker[182], P.J. Bakker[120], D. Bakshi Gupta[8], S. Balaji[156], E.M. Baldin[122b,122a], P. Balek[179], F. Balli[144], W.K. Balunas[134], J. Balz[100], E. Banas[85], M. Bandieramonte[138], A. Bandyopadhyay[24], Sw. Banerjee[180,i], L. Barak[160], W.M. Barbe[38], E.L. Barberio[105], D. Barberis[55b,55a], M. Barbero[102], G. Barbour[95], T. Barillari[115], M-S. Barisits[36], J. Barkeloo[131], T. Barklow[152], R. Barnea[159], B.M. Barnett[143], R.M. Barnett[18], Z. Barnovska-Blenessy[60a], A. Baroncelli[60a], G. Barone[29], A.J. Barr[134], L. Barranco Navarro[45a,45b], F. Barreiro[99], J. Barreiro Guimarães da Costa[15a], U. Barron[160], S. Barsov[137], F. Bartels[61a], R. Bartoldus[152], G. Bartolini[102], A.E. Barton[90], P. Bartos[28a], A. Basalaev[46], A. Basan[100], A. Bassalat[65,aj], M.J. Basso[166], R.L. Bates[57], S. Batlamous[35e], J.R. Batley[32], B. Batool[150], M. Battaglia[145], M. Bauce[73a,73b], F. Bauer[144], K.T. Bauer[170], H.S. Bawa[31], J.B. Beacham[49], T. Beau[135], P.H. Beauchemin[169], F. Becherer[52], P. Bechtle[24], H.C. Beck[53], H.P. Beck[20,q], K. Becker[177], C. Becot[46], A. Beddall[12d], A.J. Beddall[12a], V.A. Bednyakov[80], M. Bedognetti[120], C.P. Bee[154], T.A. Beermann[181], M. Begalli[81b], M. Begel[29], A. Behera[154], J.K. Behr[46], F. Beisiegel[24], M. Belfkir[5], A.S. Bell[95], G. Bella[160], L. Bellagamba[23b], A. Bellerive[34], P. Bellos[9], K. Beloborodov[122b,122a], K. Belotskiy[112], N.L. Belyaev[112], D. Benchekroun[35a], N. Benekos[10], Y. Benhammou[160], D.P. Benjamin[6], M. Benoit[54], J.R. Bensinger[26], S. Bentvelsen[120], L. Beresford[134], M. Beretta[51], D. Berge[19], E. Bergeaas Kuutmann[171], N. Berger[5], B. Bergmann[141], L.J. Bergsten[26], J. Beringer[18], S. Berlendis[7], G. Bernardi[135], C. Bernius[152], F.U. Bernlochner[24], T. Berry[94], P. Berta[100], C. Bertella[15a], A. Berthold[48], I.A. Bertram[90], O. Bessidskaia Bylund[181], N. Besson[144],

JHEP07(2020)044

A. Bethani[101], S. Bethke[115], A. Betti[42], A.J. Bevan[93], J. Beyer[115], D.S. Bhattacharya[176], P. Bhattarai[26], R. Bi[138], R.M. Bianchi[138], O. Biebel[114], D. Biedermann[19], R. Bielski[36], K. Bierwagen[100], N.V. Biesuz[72a,72b], M. Biglietti[75a], T.R.V. Billoud[110], M. Bindi[53], A. Bingul[12d], C. Bini[73a,73b], S. Biondi[23b,23a], M. Birman[179], T. Bisanz[53], J.P. Biswal[3], D. Biswas[180,i], A. Bitadze[101], C. Bittrich[48], K. Bjørke[133], T. Blazek[28a], I. Bloch[46], C. Blocker[26], A. Blue[57], U. Blumenschein[93], G.J. Bobbink[120], V.S. Bobrovnikov[122b,122a], S.S. Bocchetta[97], A. Bocci[49], D. Boerner[46], D. Bogavac[14], A.G. Bogdanchikov[122b,122a], C. Bohm[45a], V. Boisvert[94], P. Bokan[53,171], T. Bold[84a], A.E. Bolz[61b], M. Bomben[135], M. Bona[93], J.S. Bonilla[131], M. Boonekamp[144], C.D. Booth[94], H.M. Borecka-Bielska[91], L.S. Borgna[95], A. Borisov[123], G. Borissov[90], J. Bortfeldt[36], D. Bortoletto[134], D. Boscherini[23b], M. Bosman[14], J.D. Bossio Sola[104], K. Bouaouda[35a], J. Boudreau[138], E.V. Bouhova-Thacker[90], D. Boumediene[38], S.K. Boutle[57], A. Boveia[127], J. Boyd[36], D. Boye[33c], I.R. Boyko[80], A.J. Bozson[94], J. Bracinik[21], N. Brahimi[102], G. Brandt[181], O. Brandt[32], F. Braren[46], B. Brau[103], J.E. Brau[131], W.D. Breaden Madden[57], K. Brendlinger[46], L. Brenner[46], R. Brenner[171], S. Bressler[179], B. Brickwedde[100], D.L. Briglin[21], D. Britton[57], D. Britzger[115], I. Brock[24], R. Brock[107], G. Brooijmans[39], W.K. Brooks[146d], E. Brost[29], P.A. Bruckman de Renstrom[85], D. Bruncko[28b], A. Bruni[23b], G. Bruni[23b], L.S. Bruni[120], S. Bruno[74a,74b], M. Bruschi[23b], N. Bruscino[73a,73b], L. Bryngemark[97], T. Buanes[17], Q. Buat[36], P. Buchholz[150], A.G. Buckley[57], I.A. Budagov[80], M.K. Bugge[133], F. Bührer[52], O. Bulekov[112], B.A. Bullard[59], T.J. Burch[121], S. Burdin[91], C.D. Burgard[120], A.M. Burger[129], B. Burghgrave[8], J.T.P. Burr[46], C.D. Burton[11], J.C. Burzynski[103], V. Büscher[100], E. Buschmann[53], P.J. Bussey[57], J.M. Butler[25], C.M. Buttar[57], J.M. Butterworth[95], P. Butti[36], W. Buttinger[36], C.J. Buxo Vazquez[107], A. Buzatu[157], A.R. Buzykaev[122b,122a], G. Cabras[23b,23a], S. Cabrera Urbán[173], D. Caforio[56], H. Cai[172], V.M.M. Cairo[152], O. Cakir[4a], N. Calace[36], P. Calafiura[18], G. Calderini[135], P. Calfayan[66], G. Callea[57], L.P. Caloba[81b], A. Caltabiano[74a,74b], S. Calvente Lopez[99], D. Calvet[38], S. Calvet[38], T.P. Calvet[154], M. Calvetti[72a,72b], R. Camacho Toro[135], S. Camarda[36], D. Camarero Munoz[99], P. Camarri[74a,74b], M.T. Camerlingo[75a,75b], D. Cameron[133], C. Camincher[36], S. Campana[36], M. Campanelli[95], A. Camplani[40], A. Campoverde[150], V. Canale[70a,70b], A. Canesse[104], M. Cano Bret[78], J. Cantero[129], T. Cao[160], Y. Cao[172], M.D.M. Capeans Garrido[36], M. Capua[41b,41a], R. Cardarelli[74a], F. Cardillo[148], G. Carducci[41b,41a], I. Carli[142], T. Carli[36], G. Carlino[70a], B.T. Carlson[138], E.M. Carlson[175,167a], L. Carminati[69a,69b], R.M.D. Carney[152], S. Caron[119], E. Carquin[146d], S. Carrá[46], J.W.S. Carter[166], T.M. Carter[50], M.P. Casado[14,e], A.F. Casha[166], F.L. Castillo[173], L. Castillo Garcia[14], V. Castillo Gimenez[173], N.F. Castro[139a,139e], A. Catinaccio[36], J.R. Catmore[133], A. Cattai[36], V. Cavaliere[29], E. Cavallaro[14], V. Cavasinni[72a,72b], E. Celebi[12b], F. Celli[134], L. Cerda Alberich[173], K. Cerny[130], A.S. Cerqueira[81a], A. Cerri[155], L. Cerrito[74a,74b], F. Cerutti[18], A. Cervelli[23b,23a], S.A. Cetin[12b], Z. Chadi[35a], D. Chakraborty[121], J. Chan[180], W.S. Chan[120], W.Y. Chan[91], J.D. Chapman[32], B. Chargeishvili[158b], D.G. Charlton[21], T.P. Charman[93], C.C. Chau[34], S. Che[127], S. Chekanov[6], S.V. Chekulaev[167a], G.A. Chelkov[80,ah], B. Chen[79], C. Chen[60a], C.H. Chen[79], H. Chen[29], J. Chen[60a], J. Chen[39], J. Chen[26], S. Chen[136], S.J. Chen[15c], X. Chen[15b], Y. Chen[60a], Y-H. Chen[46], H.C. Cheng[63a], H.J. Cheng[15a], A. Cheplakov[80], E. Cheremushkina[123], R. Cherkaoui El Moursli[35e], E. Cheu[7], K. Cheung[64], T.J.A. Chevalérias[144], L. Chevalier[144], V. Chiarella[51], G. Chiarelli[72a], G. Chiodini[68a], A.S. Chisholm[21], A. Chitan[27b], I. Chiu[162], Y.H. Chiu[175], M.V. Chizhov[80], K. Choi[11], A.R. Chomont[73a,73b], S. Chouridou[161], Y.S. Chow[120], L.D. Christopher[33e], M.C. Chu[63a], X. Chu[15a,15d], J. Chudoba[140], J.J. Chwastowski[85], L. Chytka[130], D. Cieri[115], K.M. Ciesla[85], D. Cinca[47], V. Cindro[92], I.A. Cioară[27b], A. Ciocio[18], F. Cirotto[70a,70b], Z.H. Citron[179,j], M. Citterio[69a], D.A. Ciubotaru[27b], B.M. Ciungu[166], A. Clark[54], M.R. Clark[39], P.J. Clark[50], S.E. Clawson[101], C. Clement[45a,45b], Y. Coadou[102], M. Cobal[67a,67c], A. Coccaro[55b], J. Cochran[79],

JHEP07(2020)044

R. Coelho Lopes De Sa[103], H. Cohen[160], A.E.C. Coimbra[36], B. Cole[39], A.P. Colijn[120], J. Collot[58], P. Conde Muiño[139a,139h], S.H. Connell[33c], I.A. Connelly[57], S. Constantinescu[27b], F. Conventi[70a,an], A.M. Cooper-Sarkar[134], F. Cormier[174], K.J.R. Cormier[166], L.D. Corpe[95], M. Corradi[73a,73b], E.E. Corrigan[97], F. Corriveau[104,ac], M.J. Costa[173], F. Costanza[5], D. Costanzo[148], G. Cowan[94], J.W. Cowley[32], J. Crane[101], K. Cranmer[125], S.J. Crawley[57], R.A. Creager[136], S. Crépé-Renaudin[58], F. Crescioli[135], M. Cristinziani[24], V. Croft[169], G. Crosetti[41b,41a], A. Cueto[5], T. Cuhadar Donszelmann[170], A.R. Cukierman[152], W.R. Cunningham[57], S. Czekierda[85], P. Czodrowski[36], M.M. Czurylo[61b], M.J. Da Cunha Sargedas De Sousa[60b], J.V. Da Fonseca Pinto[81b], C. Da Via[101], W. Dabrowski[84a], F. Dachs[36], T. Dado[28a], S. Dahbi[33e], T. Dai[106], C. Dallapiccola[103], M. Dam[40], G. D'amen[29], V. D'Amico[75a,75b], J. Damp[100], J.R. Dandoy[136], M.F. Daneri[30], N.S. Dann[101], M. Danninger[151], V. Dao[36], G. Darbo[55b], O. Dartsi[5], A. Dattagupta[131], T. Daubney[46], S. D'Auria[69a,69b], C. David[167b], T. Davidek[142], D.R. Davis[49], I. Dawson[148], K. De[8], R. De Asmundis[70a], M. De Beurs[120], S. De Castro[23b,23a], S. De Cecco[73a,73b], N. De Groot[119], P. de Jong[120], H. De la Torre[107], A. De Maria[15c], D. De Pedis[73a], A. De Salvo[73a], U. De Sanctis[74a,74b], M. De Santis[74a,74b], A. De Santo[155], K. De Vasconcelos Corga[102], J.B. De Vivie De Regie[65], C. Debenedetti[145], D.V. Dedovich[80], A.M. Deiana[42], J. Del Peso[99], Y. Delabat Diaz[46], D. Delgove[65], F. Deliot[144,p], C.M. Delitzsch[7], M. Della Pietra[70a,70b], D. Della Volpe[54], A. Dell'Acqua[36], L. Dell'Asta[74a,74b], M. Delmastro[5], C. Delporte[65], P.A. Delsart[58], D.A. DeMarco[166], S. Demers[182], M. Demichev[80], G. Demontigny[110], S.P. Denisov[123], L. D'Eramo[121], D. Derendarz[85], J.E. Derkaoui[35d], F. Derue[135], P. Dervan[91], K. Desch[24], C. Deterre[46], K. Dette[166], C. Deutsch[24], M.R. Devesa[30], P.O. Deviveiros[36], F.A. Di Bello[73a,73b], A. Di Ciaccio[74a,74b], L. Di Ciaccio[5], W.K. Di Clemente[136], C. Di Donato[70a,70b], A. Di Girolamo[36], G. Di Gregorio[72a,72b], B. Di Micco[75a,75b], R. Di Nardo[75a,75b], K.F. Di Petrillo[59], R. Di Sipio[166], C. Diaconu[102], F.A. Dias[40], T. Dias Do Vale[139a], M.A. Diaz[146a], F.G. Diaz Capriles[24], J. Dickinson[18], E.B. Diehl[106], J. Dietrich[19], S. Díez Cornell[46], A. Dimitrievska[18], W. Ding[15b], J. Dingfelder[24], F. Dittus[36], F. Djama[102], T. Djobava[158b], J.I. Djuvsland[17], M.A.B. Do Vale[81c], M. Dobre[27b], D. Dodsworth[26], C. Doglioni[97], J. Dolejsi[142], Z. Dolezal[142], M. Donadelli[81d], B. Dong[60c], J. Donini[38], A. D'onofrio[15c], M. D'Onofrio[91], J. Dopke[143], A. Doria[70a], M.T. Dova[89], A.T. Doyle[57], E. Drechsler[151], E. Dreyer[151], T. Dreyer[53], A.S. Drobac[169], D. Du[60b], T.A. du Pree[120], Y. Duan[60b], F. Dubinin[111], M. Dubovsky[28a], A. Dubreuil[54], E. Duchovni[179], G. Duckeck[114], O.A. Ducu[110], D. Duda[115], A. Dudarev[36], A.C. Dudder[100], E.M. Duffield[18], L. Duflot[65], M. Dührssen[36], C. Dülsen[181], M. Dumancic[179], A.E. Dumitriu[27b], A.K. Duncan[57], M. Dunford[61a], A. Duperrin[102], H. Duran Yildiz[4a], M. Düren[56], A. Durglishvili[158b], D. Duschinger[48], B. Dutta[46], D. Duvnjak[1], G.I. Dyckes[136], M. Dyndal[36], S. Dysch[101], B.S. Dziedzic[85], K.M. Ecker[115], M.G. Eggleston[49], T. Eifert[8], G. Eigen[17], K. Einsweiler[18], T. Ekelof[171], H. El Jarrari[35e], R. El Kosseifi[102], V. Ellajosyula[171], M. Ellert[171], F. Ellinghaus[181], A.A. Elliot[93], N. Ellis[36], J. Elmsheuser[29], M. Elsing[36], D. Emeliyanov[143], A. Emerman[39], Y. Enari[162], M.B. Epland[49], J. Erdmann[47], A. Ereditato[20], P.A. Erland[85], M. Errenst[36], M. Escalier[65], C. Escobar[173], O. Estrada Pastor[173], E. Etzion[160], H. Evans[66], M.O. Evans[155], A. Ezhilov[137], F. Fabbri[57], L. Fabbri[23b,23a], V. Fabiani[119], G. Facini[177], R.M. Faisca Rodrigues Pereira[139a], R.M. Fakhrutdinov[123], S. Falciano[73a], P.J. Falke[24], S. Falke[36], J. Faltova[142], Y. Fang[15a], Y. Fang[15a], G. Fanourakis[44], M. Fanti[69a,69b], M. Faraj[67a,67c,r], A. Farbin[8], A. Farilla[75a], E.M. Farina[71a,71b], T. Farooque[107], S.M. Farrington[50], P. Farthouat[36], F. Fassi[35e], P. Fassnacht[36], D. Fassouliotis[9], M. Faucci Giannelli[50], W.J. Fawcett[32], L. Fayard[65], O.L. Fedin[137,o], W. Fedorko[174], A. Fehr[20], M. Feickert[172], L. Feligioni[102], A. Fell[148], C. Feng[60b], M. Feng[49], M.J. Fenton[170], A.B. Fenyuk[123], S.W. Ferguson[43], J. Ferrando[46], A. Ferrante[172], A. Ferrari[171], P. Ferrari[120], R. Ferrari[71a], D.E. Ferreira de Lima[61b], A. Ferrer[173], D. Ferrere[54],

JHEP07(2020)044

C. Ferretti[106], F. Fiedler[100], A. Filipčič[92], F. Filthaut[119], K.D. Finelli[25], M.C.N. Fiolhais[139a,139c,a], L. Fiorini[173], F. Fischer[114], W.C. Fisher[107], I. Fleck[150], P. Fleischmann[106], T. Flick[181], B.M. Flierl[114], L. Flores[136], L.R. Flores Castillo[63a], F.M. Follega[76a,76b], N. Fomin[17], J.H. Foo[166], G.T. Forcolin[76a,76b], A. Formica[144], F.A. Förster[14], A.C. Forti[101], E. Fortin[102], M.G. Foti[134], D. Fournier[65], H. Fox[90], P. Francavilla[72a,72b], S. Francescato[73a,73b], M. Franchini[23b,23a], S. Franchino[61a], D. Francis[36], L. Franco[5], L. Franconi[20], M. Franklin[59], A.N. Fray[93], P.M. Freeman[21], B. Freund[110], W.S. Freund[81b], E.M. Freundlich[47], D.C. Frizzell[128], D. Froidevaux[36], J.A. Frost[134], M. Fujimoto[126], C. Fukunaga[163], E. Fullana Torregrosa[173], T. Fusayasu[116], J. Fuster[173], A. Gabrielli[23b,23a], A. Gabrielli[18], S. Gadatsch[54], P. Gadow[115], G. Gagliardi[55b,55a], L.G. Gagnon[110], B. Galhardo[139a], G.E. Gallardo[134], E.J. Gallas[134], B.J. Gallop[143], G. Galster[40], R. Gamboa Goni[93], K.K. Gan[127], S. Ganguly[179], J. Gao[60a], Y. Gao[50], Y.S. Gao[31,l], C. García[173], J.E. García Navarro[173], J.A. García Pascual[15a], C. Garcia-Argos[52], M. Garcia-Sciveres[18], R.W. Gardner[37], N. Garelli[152], S. Gargiulo[52], C.A. Garner[166], V. Garonne[133], S.J. Gasiorowski[147], P. Gaspar[81b], A. Gaudiello[55b,55a], G. Gaudio[71a], I.L. Gavrilenko[111], A. Gavrilyuk[124], C. Gay[174], G. Gaycken[46], E.N. Gazis[10], A.A. Geanta[27b], C.M. Gee[145], C.N.P. Gee[143], J. Geisen[97], M. Geisen[100], C. Gemme[55b], M.H. Genest[58], C. Geng[106], S. Gentile[73a,73b], S. George[94], T. Geralis[44], L.O. Gerlach[53], P. Gessinger-Befurt[100], G. Gessner[47], S. Ghasemi[150], M. Ghasemi Bostanabad[175], M. Ghneimat[150], A. Ghosh[65], A. Ghosh[78], B. Giacobbe[23b], S. Giagu[73a,73b], N. Giangiacomi[23b,23a], P. Giannetti[72a], A. Giannini[70a,70b], G. Giannini[14], S.M. Gibson[94], M. Gignac[145], D. Gillberg[34], G. Gilles[181], D.M. Gingrich[3,am], M.P. Giordani[67a,67c], P.F. Giraud[144], G. Giugliarelli[67a,67c], D. Giugni[69a], F. Giuli[74a,74b], S. Gkaitatzis[161], I. Gkialas[9,g], E.L. Gkougkousis[14], P. Gkountoumis[10], L.K. Gladilin[113], C. Glasman[99], J. Glatzer[14], P.C.F. Glaysher[46], A. Glazov[46], G.R. Gledhill[131], I. Gnesi[41b], M. Goblirsch-Kolb[26], D. Godin[110], S. Goldfarb[105], T. Golling[54], D. Golubkov[123], A. Gomes[139a,139b], R. Goncalves Gama[53], R. Gonçalo[139a], G. Gonella[131], L. Gonella[21], A. Gongadze[80], F. Gonnella[21], J.L. Gonski[39], S. González de la Hoz[173], S. Gonzalez Fernandez[14], C. Gonzalez Renteria[18], R. Gonzalez Suarez[171], S. Gonzalez-Sevilla[54], G.R. Gonzalvo Rodriguez[173], L. Goossens[36], N.A. Gorasia[21], P.A. Gorbounov[124], H.A. Gordon[29], B. Gorini[36], E. Gorini[68a,68b], A. Gorišek[92], A.T. Goshaw[49], M.I. Gostkin[80], C.A. Gottardo[119], M. Gouighri[35b], A.G. Goussiou[147], N. Govender[33c], C. Goy[5], E. Gozani[159], I. Grabowska-Bold[84a], E.C. Graham[91], J. Gramling[170], E. Gramstad[133], S. Grancagnolo[19], M. Grandi[155], V. Gratchev[137], P.M. Gravila[27f], F.G. Gravili[68a,68b], C. Gray[57], H.M. Gray[18], C. Grefe[24], K. Gregersen[97], I.M. Gregor[46], P. Grenier[152], K. Grevtsov[46], C. Grieco[14], N.A. Grieser[128], A.A. Grillo[145], K. Grimm[31,k], S. Grinstein[14,x], J.-F. Grivaz[65], S. Groh[100], E. Gross[179], J. Grosse-Knetter[53], Z.J. Grout[95], C. Grud[106], A. Grummer[118], J.C. Grundy[134], L. Guan[106], W. Guan[180], C. Gubbels[174], J. Guenther[36], A. Guerguichon[65], J.G.R. Guerrero Rojas[173], F. Guescini[115], D. Guest[170], R. Gugel[52], T. Guillemin[5], S. Guindon[36], U. Gul[57], J. Guo[60c], W. Guo[106], Y. Guo[60a], Z. Guo[102], R. Gupta[46], S. Gurbuz[12c], G. Gustavino[128], M. Guth[52], P. Gutierrez[128], C. Gutschow[95], C. Guyot[144], C. Gwenlan[134], C.B. Gwilliam[91], A. Haas[125], C. Haber[18], H.K. Hadavand[8], A. Hadef[60a], M. Haleem[176], J. Haley[129], J.J. Hall[148], G. Halladjian[107], G.D. Hallewell[102], K. Hamacher[181], P. Hamal[130], K. Hamano[175], H. Hamdaoui[35e], M. Hamer[24], G.N. Hamity[50], K. Han[60a,w], L. Han[60a], S. Han[15a], Y.F. Han[166], K. Hanagaki[82,u], M. Hance[145], D.M. Handl[114], B. Haney[136], M.D. Hank[37], R. Hankache[135], E. Hansen[97], J.B. Hansen[40], J.D. Hansen[40], M.C. Hansen[24], P.H. Hansen[40], E.C. Hanson[101], K. Hara[168], T. Harenberg[181], S. Harkusha[108], P.F. Harrison[177], N.M. Hartman[152], N.M. Hartmann[114], Y. Hasegawa[149], A. Hasib[50], S. Hassani[144], S. Haug[20], R. Hauser[107], L.B. Havener[39], M. Havranek[141], C.M. Hawkes[21], R.J. Hawkings[36], S. Hayashida[117], D. Hayden[107], C. Hayes[106], R.L. Hayes[174], C.P. Hays[134], J.M. Hays[93], H.S. Hayward[91],

JHEP07(2020)044

S.J. Haywood[143], F. He[60a], M.P. Heath[50], V. Hedberg[97], S. Heer[24], A.L. Heggelund[133], K.K. Heidegger[52], W.D. Heidorn[79], J. Heilman[34], S. Heim[46], T. Heim[18], B. Heinemann[46,ak], J.J. Heinrich[131], L. Heinrich[36], J. Hejbal[140], L. Helary[61b], A. Held[125], S. Hellesund[133], C.M. Helling[145], S. Hellman[45a,45b], C. Helsens[36], R.C.W. Henderson[90], Y. Heng[180], L. Henkelmann[32], A.M. Henriques Correia[36], H. Herde[26], Y. Hernández Jiménez[33e], H. Herr[100], M.G. Herrmann[114], T. Herrmann[48], G. Herten[52], R. Hertenberger[114], L. Hervas[36], T.C. Herwig[136], G.G. Hesketh[95], N.P. Hessey[167a], H. Hibi[83], A. Higashida[162], S. Higashino[82], E. Higón-Rodriguez[173], K. Hildebrand[37], J.C. Hill[32], K.K. Hill[29], K.H. Hiller[46], S.J. Hillier[21], M. Hils[48], I. Hinchliffe[18], F. Hinterkeuser[24], M. Hirose[132], S. Hirose[52], D. Hirschbuehl[181], B. Hiti[92], O. Hladik[140], D.R. Hlaluku[33e], J. Hobbs[154], N. Hod[179], M.C. Hodgkinson[148], A. Hoecker[36], D. Hohn[52], D. Hohov[65], T. Holm[24], T.R. Holmes[37], M. Holzbock[114], L.B.A.H. Hommels[32], T.M. Hong[138], J.C. Honig[52], A. Hönle[115], B.H. Hooberman[172], W.H. Hopkins[6], Y. Horii[117], P. Horn[48], L.A. Horyn[37], S. Hou[157], A. Hoummada[35a], J. Howarth[57], J. Hoya[89], M. Hrabovsky[130], J. Hrdinka[77], I. Hristova[19], J. Hrivnac[65], A. Hrynevich[109], T. Hryn'ova[5], P.J. Hsu[64], S.-C. Hsu[147], Q. Hu[29], S. Hu[60c], Y.F. Hu[15a,15d], D.P. Huang[95], Y. Huang[60a], Y. Huang[15a], Z. Hubacek[141], F. Hubaut[102], M. Huebner[24], F. Huegging[24], T.B. Huffman[134], M. Huhtinen[36], R.F.H. Hunter[34], P. Huo[154], N. Huseynov[80,ad], J. Huston[107], J. Huth[59], R. Hyneman[106], S. Hyrych[28a], G. Iacobucci[54], G. Iakovidis[29], I. Ibragimov[150], L. Iconomidou-Fayard[65], P. Iengo[36], R. Ignazzi[40], O. Igonkina[120,z,*], R. Iguchi[162], T. Iizawa[54], Y. Ikegami[82], M. Ikeno[82], D. Iliadis[161], N. Ilic[119,166,ac], F. Iltzsche[48], H. Imam[35a], G. Introzzi[71a,71b], M. Iodice[75a], K. Iordanidou[167a], V. Ippolito[73a,73b], M.F. Isacson[171], M. Ishino[162], W. Islam[129], C. Issever[19,46], S. Istin[159], F. Ito[168], J.M. Iturbe Ponce[63a], R. Iuppa[76a,76b], A. Ivina[179], H. Iwasaki[82], J.M. Izen[43], V. Izzo[70a], P. Jacka[140], P. Jackson[1], R.M. Jacobs[46], B.P. Jaeger[151], V. Jain[2], G. Jäkel[181], K.B. Jakobi[100], K. Jakobs[52], T. Jakoubek[140], J. Jamieson[57], K.W. Janas[84a], R. Jansky[54], M. Janus[53], P.A. Janus[84a], G. Jarlskog[97], A.E. Jaspan[91], N. Javadov[80,ad], T. Javůrek[36], M. Javurkova[103], F. Jeanneau[144], L. Jeanty[131], J. Jejelava[158a], A. Jelinskas[177], P. Jenni[52,b], N. Jeong[46], S. Jézéquel[5], H. Ji[180], J. Jia[154], H. Jiang[79], Y. Jiang[60a], Z. Jiang[152], S. Jiggins[52], F.A. Jimenez Morales[38], J. Jimenez Pena[115], S. Jin[15c], A. Jinaru[27b], O. Jinnouchi[164], H. Jivan[33e], P. Johansson[148], K.A. Johns[7], C.A. Johnson[66], R.W.L. Jones[90], S.D. Jones[155], S. Jones[7], T.J. Jones[91], J. Jongmanns[61a], P.M. Jorge[139a], J. Jovicevic[36], X. Ju[18], J.J. Junggeburth[115], A. Juste Rozas[14,x], A. Kaczmarska[85], M. Kado[73a,73b], H. Kagan[127], M. Kagan[152], A. Kahn[39], C. Kahra[100], T. Kaji[178], E. Kajomovitz[159], C.W. Kalderon[29], A. Kaluza[100], A. Kamenshchikov[123], M. Kaneda[162], N.J. Kang[145], S. Kang[79], Y. Kano[117], J. Kanzaki[82], L.S. Kaplan[180], D. Kar[33e], K. Karava[134], M.J. Kareem[167b], I. Karkanias[161], S.N. Karpov[80], Z.M. Karpova[80], V. Kartvelishvili[90], A.N. Karyukhin[123], A. Kastanas[45a,45b], C. Kato[60d,60c], J. Katzy[46], K. Kawade[149], K. Kawagoe[88], T. Kawaguchi[117], T. Kawamoto[144], G. Kawamura[53], E.F. Kay[175], S. Kazakos[14], V.F. Kazanin[122b,122a], R. Keeler[175], R. Kehoe[42], J.S. Keller[34], E. Kellermann[97], D. Kelsey[155], J.J. Kempster[21], J. Kendrick[21], K.E. Kennedy[39], O. Kepka[140], S. Kersten[181], B.P. Kerševan[92], S. Ketabchi Haghighat[166], M. Khader[172], F. Khalil-Zada[13], M. Khandoga[144], A. Khanov[129], A.G. Kharlamov[122b,122a], T. Kharlamova[122b,122a], E.E. Khoda[174], A. Khodinov[165], T.J. Khoo[54], G. Khoriauli[176], E. Khramov[80], J. Khubua[158b], S. Kido[83], M. Kiehn[54], C.R. Kilby[94], E. Kim[164], Y.K. Kim[37], N. Kimura[95], O.M. Kind[19], B.T. King[91,*], D. Kirchmeier[48], J. Kirk[143], A.E. Kiryunin[115], T. Kishimoto[162], D.P. Kisliuk[166], V. Kitali[46], C. Kitsaki[10], O. Kivernyk[24], T. Klapdor-Kleingrothaus[52], M. Klassen[61a], C. Klein[34], M.H. Klein[106], M. Klein[91], U. Klein[91], K. Kleinknecht[100], P. Klimek[121], A. Klimentov[29], T. Klingl[24], T. Klioutchnikova[36], F.F. Klitzner[114], P. Kluit[120], S. Kluth[115], E. Kneringer[77], E.B.F.G. Knoops[102], A. Knue[52], D. Kobayashi[88], T. Kobayashi[162], M. Kobel[48], M. Kocian[152], T. Kodama[162], P. Kodys[142],

JHEP07(2020)044

D.M. Koeck[155], P.T. Koenig[24], T. Koffas[34], N.M. Köhler[36], M. Kolb[144], I. Koletsou[5], T. Komarek[130], T. Kondo[82], K. Köneke[52], A.X.Y. Kong[1], A.C. König[119], T. Kono[126], V. Konstantinides[95], N. Konstantinidis[95], B. Konya[97], R. Kopeliansky[66], S. Koperny[84a], K. Korcyl[85], K. Kordas[161], G. Koren[160], A. Korn[95], I. Korolkov[14], E.V. Korolkova[148], N. Korotkova[113], O. Kortner[115], S. Kortner[115], V.V. Kostyukhin[148,165], A. Kotsokechagia[65], A. Kotwal[49], A. Koulouris[10], A. Kourkoumeli-Charalampidi[71a,71b], C. Kourkoumelis[9], E. Kourlitis[148], V. Kouskoura[29], A.B. Kowalewska[85], R. Kowalewski[175], W. Kozanecki[101], A.S. Kozhin[123], V.A. Kramarenko[113], G. Kramberger[92], D. Krasnopevtsev[60a], M.W. Krasny[135], A. Krasznahorkay[36], D. Krauss[115], J.A. Kremer[100], J. Kretzschmar[91], P. Krieger[166], F. Krieter[114], A. Krishnan[61b], K. Krizka[18], K. Kroeninger[47], H. Kroha[115], J. Kroll[140], J. Kroll[136], K.S. Krowpman[107], U. Kruchonak[80], H. Krüger[24], N. Krumnack[79], M.C. Kruse[49], J.A. Krzysiak[85], T. Kubota[105], O. Kuchinskaia[165], S. Kuday[4b], J.T. Kuechler[46], S. Kuehn[36], A. Kugel[61a], T. Kuhl[46], V. Kukhtin[80], Y. Kulchitsky[108,af], S. Kuleshov[146b], Y.P. Kulinich[172], M. Kuna[58], T. Kunigo[86], A. Kupco[140], T. Kupfer[47], O. Kuprash[52], H. Kurashige[83], L.L. Kurchaninov[167a], Y.A. Kurochkin[108], A. Kurova[112], M.G. Kurth[15a,15d], E.S. Kuwertz[36], M. Kuze[164], A.K. Kvam[147], J. Kvita[130], T. Kwan[104], L. La Rotonda[41b,41a], F. La Ruffa[41b,41a], C. Lacasta[173], F. Lacava[73a,73b], D.P.J. Lack[101], H. Lacker[19], D. Lacour[135], E. Ladygin[80], R. Lafaye[5], B. Laforge[135], T. Lagouri[146b], S. Lai[53], I.K. Lakomiec[84a], S. Lammers[66], W. Lampl[7], C. Lampoudis[161], E. Lançon[29], U. Landgraf[52], M.P.J. Landon[93], M.C. Lanfermann[54], V.S. Lang[52], J.C. Lange[53], R.J. Langenberg[103], A.J. Lankford[170], F. Lanni[29], K. Lantzsch[24], A. Lanza[71a], A. Lapertosa[55b,55a], S. Laplace[135], J.F. Laporte[144], T. Lari[69a], F. Lasagni Manghi[23b,23a], M. Lassnig[36], T.S. Lau[63a], A. Laudrain[65], A. Laurier[34], M. Lavorgna[70a,70b], S.D. Lawlor[94], M. Lazzaroni[69a,69b], B. Le[101], E. Le Guirriec[102], A. Lebedev[79], M. LeBlanc[7], T. LeCompte[6], F. Ledroit-Guillon[58], A.C.A. Lee[95], C.A. Lee[29], G.R. Lee[17], L. Lee[59], S.C. Lee[157], S. Lee[79], B. Lefebvre[167a], H.P. Lefebvre[94], M. Lefebvre[175], C. Leggett[18], K. Lehmann[151], N. Lehmann[20], G. Lehmann Miotto[36], W.A. Leight[46], A. Leisos[161,v], M.A.L. Leite[81d], C.E. Leitgeb[114], R. Leitner[142], D. Lellouch[179,*], K.J.C. Leney[42], T. Lenz[24], R. Leone[7], S. Leone[72a], C. Leonidopoulos[50], A. Leopold[135], C. Leroy[110], R. Les[166], C.G. Lester[32], M. Levchenko[137], J. Levêque[5], D. Levin[106], L.J. Levinson[179], D.J. Lewis[21], B. Li[15b], B. Li[106], C-Q. Li[60a], F. Li[60c], H. Li[60a], H. Li[60b], J. Li[60c], K. Li[147], L. Li[60c], M. Li[15a,15d], Q. Li[15a,15d], Q.Y. Li[60a], S. Li[60d,60c], X. Li[46], Y. Li[46], Z. Li[60b], Z. Li[104], Z. Liang[15a], M. Liberatore[46], B. Liberti[74a], A. Liblong[166], K. Lie[63c], S. Lim[29], C.Y. Lin[32], K. Lin[107], T.H. Lin[100], R.A. Linck[66], R.E. Lindley[7], J.H. Lindon[21], A. Linss[46], A.L. Lionti[54], E. Lipeles[136], A. Lipniacka[17], T.M. Liss[172,al], A. Lister[174], J.D. Little[8], B. Liu[79], B.L. Liu[6], H.B. Liu[29], H. Liu[106], J.B. Liu[60a], J.K.K. Liu[37], K. Liu[60d], M. Liu[60a], P. Liu[15a], Y. Liu[46], Y. Liu[15a,15d], Y.L. Liu[106], Y.W. Liu[60a], M. Livan[71a,71b], A. Lleres[58], J. Llorente Merino[151], S.L. Lloyd[93], C.Y. Lo[63b], E.M. Lobodzinska[46], P. Loch[7], S. Loffredo[74a,74b], T. Lohse[19], K. Lohwasser[148], M. Lokajicek[140], J.D. Long[172], R.E. Long[90], L. Longo[36], K.A. Looper[127], I. Lopez Paz[101], A. Lopez Solis[148], J. Lorenz[114], N. Lorenzo Martinez[5], A.M. Lory[114], P.J. Lösel[114], A. Lösle[52], X. Lou[46], X. Lou[15a], A. Lounis[65], J. Love[6], P.A. Love[90], J.J. Lozano Bahilo[173], M. Lu[60a], Y.J. Lu[64], H.J. Lubatti[147], C. Luci[73a,73b], A. Lucotte[58], C. Luedtke[52], F. Luehring[66], I. Luise[135], L. Luminari[73a], B. Lund-Jensen[153], M.S. Lutz[160], D. Lynn[29], H. Lyons[91], R. Lysak[140], E. Lytken[97], F. Lyu[15a], V. Lyubushkin[80], T. Lyubushkina[80], H. Ma[29], L.L. Ma[60b], Y. Ma[95], G. Maccarrone[51], A. Macchiolo[115], C.M. Macdonald[148], J. Machado Miguens[136], D. Madaffari[173], R. Madar[38], W.F. Mader[48], M. Madugoda Ralalage Don[129], N. Madysa[48], J. Maeda[83], T. Maeno[29], M. Maerker[48], V. Magerl[52], N. Magini[79], J. Magro[67a,67c,r], D.J. Mahon[39], C. Maidantchik[81b], T. Maier[114], A. Maio[139a,139b,139d], K. Maj[84a], O. Majersky[28a], S. Majewski[131], Y. Makida[82], N. Makovec[65], B. Malaescu[135], Pa. Malecki[85], V.P. Maleev[137], F. Malek[58], U. Mallik[78], D. Malon[6], C. Malone[32],

JHEP07(2020)044

S. Maltezos[10], S. Malyukov[80], J. Mamuzic[173], G. Mancini[51], I. Mandić[92], L. Manhaes de Andrade Filho[81a], I.M. Maniatis[161], J. Manjarres Ramos[48], K.H. Mankinen[97], A. Mann[114], A. Manousos[77], B. Mansoulie[144], I. Manthos[161], S. Manzoni[120], A. Marantis[161], G. Marceca[30], L. Marchese[134], G. Marchiori[135], M. Marcisovsky[140], L. Marcoccia[74a,74b], C. Marcon[97], C.A. Marin Tobon[36], M. Marjanovic[128], Z. Marshall[18], M.U.F. Martensson[171], S. Marti-Garcia[173], C.B. Martin[127], T.A. Martin[177], V.J. Martin[50], B. Martin dit Latour[17], L. Martinelli[75a,75b], M. Martinez[14,x], P. Martinez Agullo[173], V.I. Martinez Outschoorn[103], S. Martin-Haugh[143], V.S. Martoiu[27b], A.C. Martyniuk[95], A. Marzin[36], S.R. Maschek[115], L. Masetti[100], T. Mashimo[162], R. Mashinistov[111], J. Masik[101], A.L. Maslennikov[122b,122a], L. Massa[23b,23a], P. Massarotti[70a,70b], P. Mastrandrea[72a,72b], A. Mastroberardino[41b,41a], T. Masubuchi[162], D. Matakias[29], A. Matic[114], N. Matsuzawa[162], P. Mättig[24], J. Maurer[27b], B. Maček[92], D.A. Maximov[122b,122a], R. Mazini[157], I. Maznas[161], S.M. Mazza[145], J.P. Mc Gowan[104], S.P. Mc Kee[106], T.G. McCarthy[115], W.P. McCormack[18], E.F. McDonald[105], J.A. Mcfayden[36], G. Mchedlidze[158b], M.A. McKay[42], K.D. McLean[175], S.J. McMahon[143], P.C. McNamara[105], C.J. McNicol[177], R.A. McPherson[175,ac], J.E. Mdhluli[33e], Z.A. Meadows[103], S. Meehan[36], T. Megy[38], S. Mehlhase[114], A. Mehta[91], B. Meirose[43], D. Melini[159], B.R. Mellado Garcia[33e], J.D. Mellenthin[53], M. Melo[28a], F. Meloni[46], A. Melzer[24], S.B. Menary[101], E.D. Mendes Gouveia[139a,139e], L. Meng[36], X.T. Meng[106], S. Menke[115], E. Meoni[41b,41a], S. Mergelmeyer[19], S.A.M. Merkt[138], C. Merlassino[134], P. Mermod[54], L. Merola[70a,70b], C. Meroni[69a], G. Merz[106], O. Meshkov[113,111], J.K.R. Meshreki[150], A. Messina[73a,73b], J. Metcalfe[6], A.S. Mete[6], C. Meyer[66], J-P. Meyer[144], H. Meyer Zu Theenhausen[61a], F. Miano[155], M. Michetti[19], R.P. Middleton[143], L. Mijović[50], G. Mikenberg[179], M. Mikestikova[140], M. Mikuž[92], H. Mildner[148], M. Milesi[105], A. Milic[166], C.D. Milke[42], D.W. Miller[37], A. Milov[179], D.A. Milstead[45a,45b], R.A. Mina[152], A.A. Minaenko[123], M. Miñano Moya[173], I.A. Minashvili[158b], A.I. Mincer[125], B. Mindur[84a], M. Mineev[80], Y. Minegishi[162], L.M. Mir[14], M. Mironova[134], A. Mirto[68a,68b], K.P. Mistry[136], T. Mitani[178], J. Mitrevski[114], V.A. Mitsou[173], M. Mittal[60c], O. Miu[166], A. Miucci[20], P.S. Miyagawa[148], A. Mizukami[82], J.U. Mjörnmark[97], T. Mkrtchyan[61a], M. Mlynarikova[142], T. Moa[45a,45b], S. Mobius[53], K. Mochizuki[110], P. Mogg[114], S. Mohapatra[39], R. Moles-Valls[24], M.C. Mondragon[107], K. Mönig[46], E. Monnier[102], A. Montalbano[151], J. Montejo Berlingen[36], M. Montella[95], F. Monticelli[89], S. Monzani[69a], N. Morange[65], D. Moreno[22a], M. Moreno Llácer[173], C. Moreno Martinez[14], P. Morettini[55b], M. Morgenstern[159], S. Morgenstern[48], D. Mori[151], M. Morii[59], M. Morinaga[178], V. Morisbak[133], A.K. Morley[36], G. Mornacchi[36], A.P. Morris[95], L. Morvaj[154], P. Moschovakos[36], B. Moser[120], M. Mosidze[158b], T. Moskalets[144], H.J. Moss[148], J. Moss[31,m], E.J.W. Moyse[103], S. Muanza[102], J. Mueller[138], R.S.P. Mueller[114], D. Muenstermann[90], G.A. Mullier[97], D.P. Mungo[69a,69b], J.L. Munoz Martinez[14], F.J. Munoz Sanchez[101], P. Murin[28b], W.J. Murray[177,143], A. Murrone[69a,69b], M. Muškinja[18], C. Mwewa[33a], A.G. Myagkov[123,ah], A.A. Myers[138], J. Myers[131], M. Myska[141], B.P. Nachman[18], O. Nackenhorst[47], A.Nag Nag[48], K. Nagai[134], K. Nagano[82], Y. Nagasaka[62], J.L. Nagle[29], E. Nagy[102], A.M. Nairz[36], Y. Nakahama[117], K. Nakamura[82], T. Nakamura[162], H. Nanjo[132], F. Napolitano[61a], R.F. Naranjo Garcia[46], R. Narayan[42], I. Naryshkin[137], T. Naumann[46], G. Navarro[22a], P.Y. Nechaeva[111], F. Nechansky[46], T.J. Neep[21], A. Negri[71a,71b], M. Negrini[23b], C. Nellist[119], M.E. Nelson[45a,45b], S. Nemecek[140], M. Nessi[36,d], M.S. Neubauer[172], F. Neuhaus[100], M. Neumann[181], R. Newhouse[174], P.R. Newman[21], C.W. Ng[138], Y.S. Ng[19], Y.W.Y. Ng[170], B. Ngair[35e], H.D.N. Nguyen[102], T. Nguyen Manh[110], E. Nibigira[38], R.B. Nickerson[134], R. Nicolaidou[144], D.S. Nielsen[40], J. Nielsen[145], N. Nikiforou[11], V. Nikolaenko[123,ah], I. Nikolic-Audit[135], K. Nikolopoulos[21], P. Nilsson[29], H.R. Nindhito[54], Y. Ninomiya[82], A. Nisati[73a], N. Nishu[60c], R. Nisius[115], I. Nitsche[47], T. Nitta[178], T. Nobe[162], D.L. Noel[32], Y. Noguchi[86], I. Nomidis[135], M.A. Nomura[29],

JHEP07(2020)044

M. Nordberg[36], J. Novak[92], T. Novak[92], O. Novgorodova[48], R. Novotny[141], L. Nozka[130], K. Ntekas[170], E. Nurse[95], F.G. Oakham[34,am], H. Oberlack[115], J. Ocariz[135], A. Ochi[83], I. Ochoa[39], J.P. Ochoa-Ricoux[146a], K. O'Connor[26], S. Oda[88], S. Odaka[82], S. Oerdek[53], A. Ogrodnik[84a], A. Oh[101], S.H. Oh[49], C.C. Ohm[153], H. Oide[164], M.L. Ojeda[166], H. Okawa[168], Y. Okazaki[86], M.W. O'Keefe[91], Y. Okumura[162], T. Okuyama[82], A. Olariu[27b], L.F. Oleiro Seabra[139a], S.A. Olivares Pino[146a], D. Oliveira Damazio[29], J.L. Oliver[1], M.J.R. Olsson[170], A. Olszewski[85], J. Olszowska[85], D.C. O'Neil[151], A.P. O'neill[134], A. Onofre[139a,139e], P.U.E. Onyisi[11], H. Oppen[133], R.G. Oreamuno Madriz[121], M.J. Oreglia[37], G.E. Orellana[89], D. Orestano[75a,75b], N. Orlando[14], R.S. Orr[166], V. O'Shea[57], R. Ospanov[60a], G. Otero y Garzon[30], H. Otono[88], P.S. Ott[61a], G.J. Ottino[18], M. Ouchrif[35d], J. Ouellette[29], F. Ould-Saada[133], A. Ouraou[144], Q. Ouyang[15a], M. Owen[57], R.E. Owen[21], V.E. Ozcan[12c], N. Ozturk[8], J. Pacalt[130], H.A. Pacey[32], K. Pachal[49], A. Pacheco Pages[14], C. Padilla Aranda[14], S. Pagan Griso[18], M. Paganini[182], G. Palacino[66], S. Palazzo[50], S. Palestini[36], M. Palka[84b], D. Pallin[38], P. Palni[84a], I. Panagoulias[10], C.E. Pandini[36], J.G. Panduro Vazquez[94], P. Pani[46], G. Panizzo[67a,67c], L. Paolozzi[54], C. Papadatos[110], K. Papageorgiou[9,g], S. Parajuli[42], A. Paramonov[6], C. Paraskevopoulos[10], D. Paredes Hernandez[63b], S.R. Paredes Saenz[134], B. Parida[165], T.H. Park[166], A.J. Parker[31], M.A. Parker[32], F. Parodi[55b,55a], E.W. Parrish[121], J.A. Parsons[39], U. Parzefall[52], L. Pascual Dominguez[135], V.R. Pascuzzi[18], J.M.P. Pasner[145], F. Pasquali[120], E. Pasqualucci[73a], S. Passaggio[55b], F. Pastore[94], P. Pasuwan[45a,45b], S. Pataraia[100], J.R. Pater[101], A. Pathak[180,i], J. Patton[91], T. Pauly[36], J. Pearkes[152], B. Pearson[115], M. Pedersen[133], L. Pedraza Diaz[119], R. Pedro[139a], T. Peiffer[53], S.V. Peleganchuk[122b,122a], O. Penc[140], H. Peng[60a], B.S. Peralva[81a], M.M. Perego[65], A.P. Pereira Peixoto[139a], L. Pereira Sanchez[45a,45b], D.V. Perepelitsa[29], F. Peri[19], L. Perini[69a,69b], H. Pernegger[36], S. Perrella[139a], A. Perrevoort[120], K. Peters[46], R.F.Y. Peters[101], B.A. Petersen[36], T.C. Petersen[40], E. Petit[102], A. Petridis[1], C. Petridou[161], P. Petroff[65], F. Petrucci[75a,75b], M. Pettee[182], N.E. Pettersson[103], K. Petukhova[142], A. Peyaud[144], R. Pezoa[146d], L. Pezzotti[71a,71b], T. Pham[105], F.H. Phillips[107], P.W. Phillips[143], M.W. Phipps[172], G. Piacquadio[154], E. Pianori[18], A. Picazio[103], R.H. Pickles[101], R. Piegaia[30], D. Pietreanu[27b], J.E. Pilcher[37], A.D. Pilkington[101], M. Pinamonti[67a,67c], J.L. Pinfold[3], C. Pitman Donaldson[95], M. Pitt[160], L. Pizzimento[74a,74b], M.-A. Pleier[29], V. Pleskot[142], E. Plotnikova[80], P. Podberezko[122b,122a], R. Poettgen[97], R. Poggi[54], L. Poggioli[135], I. Pogrebnyak[107], D. Pohl[24], I. Pokharel[53], G. Polesello[71a], A. Poley[18], A. Policicchio[73a,73b], R. Polifka[142], A. Polini[23b], C.S. Pollard[46], V. Polychronakos[29], D. Ponomarenko[112], L. Pontecorvo[36], S. Popa[27a], G.A. Popeneciu[27d], L. Portales[5], D.M. Portillo Quintero[58], S. Pospisil[141], K. Potamianos[46], I.N. Potrap[80], C.J. Potter[32], H. Potti[11], T. Poulsen[97], J. Poveda[173], T.D. Powell[148], G. Pownall[46], M.E. Pozo Astigarraga[36], P. Pralavorio[102], S. Prell[79], D. Price[101], M. Primavera[68a], S. Prince[104], M.L. Proffitt[147], N. Proklova[112], K. Prokofiev[63c], F. Prokoshin[80], S. Protopopescu[29], J. Proudfoot[6], M. Przybycien[84a], D. Pudzha[137], A. Puri[172], P. Puzo[65], J. Qian[106], Y. Qin[101], A. Quadt[53], M. Queitsch-Maitland[36], A. Qureshi[1], M. Racko[28a], F. Ragusa[69a,69b], G. Rahal[98], J.A. Raine[54], S. Rajagopalan[29], A. Ramirez Morales[93], K. Ran[15a,15d], T. Rashid[65], D.M. Rauch[46], F. Rauscher[114], S. Rave[100], B. Ravina[148], I. Ravinovich[179], J.H. Rawling[101], M. Raymond[36], A.L. Read[133], N.P. Readioff[58], M. Reale[68a,68b], D.M. Rebuzzi[71a,71b], G. Redlinger[29], K. Reeves[43], L. Rehnisch[19], J. Reichert[136], D. Reikher[160], A. Reiss[100], A. Rej[150], C. Rembser[36], A. Renardi[46], M. Renda[27b], M. Rescigno[73a], S. Resconi[69a], E.D. Resseguie[18], S. Rettie[95], B. Reynolds[127], E. Reynolds[21], O.L. Rezanova[122b,122a], P. Reznicek[142], E. Ricci[76a,76b], R. Richter[115], S. Richter[46], E. Richter-Was[84b], O. Ricken[24], M. Ridel[135], P. Rieck[115], O. Rifki[46], M. Rijssenbeek[154], A. Rimoldi[71a,71b], M. Rimoldi[46], L. Rinaldi[23b], G. Ripellino[153], I. Riu[14], P. Rivadeneira[46], J.C. Rivera Vergara[175], F. Rizatdinova[129], E. Rizvi[93], C. Rizzi[36], R.T. Roberts[101], S.H. Robertson[104,ac], M. Robin[46], D. Robinson[32], C.M. Robles Gajardo[146d],

JHEP07(2020)044

M. Robles Manzano[100], A. Robson[57], A. Rocchi[74a,74b], E. Rocco[100], C. Roda[72a,72b], S. Rodriguez Bosca[173], D. Rodriguez Rodriguez[173], A.M. Rodríguez Vera[167b], S. Roe[36], O. Røhne[133], R. Röhrig[115], R.A. Rojas[146d], B. Roland[52], C.P.A. Roland[66], J. Roloff[29], A. Romaniouk[112], M. Romano[23b,23a], N. Rompotis[91], M. Ronzani[125], L. Roos[135], S. Rosati[73a], G. Rosin[103], B.J. Rosser[136], E. Rossi[46], E. Rossi[75a,75b], E. Rossi[70a,70b], L.P. Rossi[55b], L. Rossini[69a,69b], R. Rosten[14], M. Rotaru[27b], B. Rottler[52], D. Rousseau[65], G. Rovelli[71a,71b], A. Roy[11], D. Roy[33e], A. Rozanov[102], Y. Rozen[159], X. Ruan[33e], F. Rühr[52], A. Ruiz-Martinez[173], A. Rummler[36], Z. Rurikova[52], N.A. Rusakovich[80], H.L. Russell[104], L. Rustige[38,47], J.P. Rutherfoord[7], E.M. Rüttinger[148], M. Rybar[39], G. Rybkin[65], E.B. Rye[133], A. Ryzhov[123], J.A. Sabater Iglesias[46], P. Sabatini[53], S. Sacerdoti[65], H.F-W. Sadrozinski[145], R. Sadykov[80], F. Safai Tehrani[73a], B. Safarzadeh Samani[155], M. Safdari[152], P. Saha[121], S. Saha[104], M. Sahinsoy[61a], A. Sahu[181], M. Saimpert[36], M. Saito[162], T. Saito[162], H. Sakamoto[162], D. Salamani[54], G. Salamanna[75a,75b], J.E. Salazar Loyola[146d], A. Salnikov[152], J. Salt[173], A. Salvador Salas[14], D. Salvatore[41b,41a], F. Salvatore[155], A. Salvucci[63a,63b,63c], A. Salzburger[36], J. Samarati[36], D. Sammel[52], D. Sampsonidis[161], D. Sampsonidou[161], J. Sánchez[173], A. Sanchez Pineda[67a,36,67c], H. Sandaker[133], C.O. Sander[46], I.G. Sanderswood[90], M. Sandhoff[181], C. Sandoval[22a], D.P.C. Sankey[143], M. Sannino[55b,55a], Y. Sano[117], A. Sansoni[51], C. Santoni[38], H. Santos[139a,139b], S.N. Santpur[18], A. Santra[173], A. Sapronov[80], J.G. Saraiva[139a,139d], O. Sasaki[82], K. Sato[168], F. Sauerburger[52], E. Sauvan[5], P. Savard[166,am], R. Sawada[162], C. Sawyer[143], L. Sawyer[96,ag], C. Sbarra[23b], A. Sbrizzi[23a], T. Scanlon[95], J. Schaarschmidt[147], P. Schacht[115], B.M. Schachtner[114], D. Schaefer[37], L. Schaefer[136], J. Schaeffer[100], S. Schaepe[36], U. Schäfer[100], A.C. Schaffer[65], D. Schaile[114], R.D. Schamberger[154], E. Schanet[114], N. Scharmberg[101], V.A. Schegelsky[137], D. Scheirich[142], F. Schenck[19], M. Schernau[170], C. Schiavi[55b,55a], L.K. Schildgen[24], Z.M. Schillaci[26], E.J. Schioppa[68a,68b], M. Schioppa[41b,41a], K.E. Schleicher[52], S. Schlenker[36], K.R. Schmidt-Sommerfeld[115], K. Schmieden[36], C. Schmitt[100], S. Schmitt[46], S. Schmitz[100], J.C. Schmoeckel[46], L. Schoeffel[144], A. Schoening[61b], P.G. Scholer[52], E. Schopf[134], M. Schott[100], J.F.P. Schouwenberg[119], J. Schovancova[36], S. Schramm[54], F. Schroeder[181], A. Schulte[100], H-C. Schultz-Coulon[61a], M. Schumacher[52], B.A. Schumm[145], Ph. Schune[144], A. Schwartzman[152], T.A. Schwarz[106], Ph. Schwemling[144], R. Schwienhorst[107], A. Sciandra[145], G. Sciolla[26], M. Scodeggio[46], M. Scornajenghi[41b,41a], F. Scuri[72a], F. Scutti[105], L.M. Scyboz[115], C.D. Sebastiani[73a,73b], P. Seema[19], S.C. Seidel[118], A. Seiden[145], B.D. Seidlitz[29], T. Seiss[37], C. Seitz[46], J.M. Seixas[81b], G. Sekhniaidze[70a], S.J. Sekula[42], N. Semprini-Cesari[23b,23a], S. Sen[49], C. Serfon[29], L. Serin[65], L. Serkin[67a,67b], M. Sessa[60a], H. Severini[128], S. Sevova[152], F. Sforza[55b,55a], A. Sfyrla[54], E. Shabalina[53], J.D. Shahinian[145], N.W. Shaikh[45a,45b], D. Shaked Renous[179], L.Y. Shan[15a], M. Shapiro[18], A. Sharma[134], A.S. Sharma[1], P.B. Shatalov[124], K. Shaw[155], S.M. Shaw[101], M. Shehade[179], Y. Shen[128], A.D. Sherman[25], P. Sherwood[95], L. Shi[157], S. Shimizu[82], C.O. Shimmin[182], Y. Shimogama[178], M. Shimojima[116], I.P.J. Shipsey[134], S. Shirabe[164], M. Shiyakova[80,aa], J. Shlomi[179], A. Shmeleva[111], M.J. Shochet[37], J. Shojaii[105], D.R. Shope[128], S. Shrestha[127], E.M. Shrif[33e], E. Shulga[179], P. Sicho[140], A.M. Sickles[172], E. Sideras Haddad[33e], O. Sidiropoulou[36], A. Sidoti[23b,23a], F. Siegert[48], Dj. Sijacki[16], M.Jr. Silva[180], M.V. Silva Oliveira[81a], S.B. Silverstein[45a], S. Simion[65], R. Simoniello[100], C.J. Simpson-allsop[21], S. Simsek[12b], P. Sinervo[166], V. Sinetckii[113], S. Singh[151], M. Sioli[23b,23a], I. Siral[131], S.Yu. Sivoklokov[113], J. Sjölin[45a,45b], A. Skaf[53], E. Skorda[97], P. Skubic[128], M. Slawinska[85], K. Sliwa[169], R. Slovak[142], V. Smakhtin[179], B.H. Smart[143], J. Smiesko[28b], N. Smirnov[112], S.Yu. Smirnov[112], Y. Smirnov[112], L.N. Smirnova[113,s], O. Smirnova[97], J.W. Smith[53], M. Smizanska[90], K. Smolek[141], A. Smykiewicz[85], A.A. Snesarev[111], H.L. Snoek[120], I.M. Snyder[131], S. Snyder[29], R. Sobie[175,ac], A. Soffer[160], A. Søgaard[50], F. Sohns[53], C.A. Solans Sanchez[36], E.Yu. Soldatov[112], U. Soldevila[173], A.A. Solodkov[123], A. Soloshenko[80],

JHEP07(2020)044

O.V. Solovyanov[123], V. Solovyev[137], P. Sommer[148], H. Son[169], W. Song[143], W.Y. Song[167b], A. Sopczak[141], A.L. Sopio[95], F. Sopkova[28b], C.L. Sotiropoulou[72a,72b], S. Sottocornola[71a,71b], R. Soualah[67a,67c,f], A.M. Soukharev[122b,122a], D. South[46], S. Spagnolo[68a,68b], M. Spalla[115], M. Spangenberg[177], F. Spanò[94], D. Sperlich[52], T.M. Spieker[61a], G. Spigo[36], M. Spina[155], D.P. Spiteri[57], M. Spousta[142], A. Stabile[69a,69b], B.L. Stamas[121], R. Stamen[61a], M. Stamenkovic[120], E. Stanecka[85], B. Stanislaus[134], M.M. Stanitzki[46], M. Stankaityte[134], B. Stapf[120], E.A. Starchenko[123], G.H. Stark[145], J. Stark[58], P. Staroba[140], P. Starovoitov[61a], S. Stärz[104], R. Staszewski[85], G. Stavropoulos[44], M. Stegler[46], P. Steinberg[29], A.L. Steinhebel[131], B. Stelzer[151], H.J. Stelzer[138], O. Stelzer-Chilton[167a], H. Stenzel[56], T.J. Stevenson[155], G.A. Stewart[36], M.C. Stockton[36], G. Stoicea[27b], M. Stolarski[139a], S. Stonjek[115], A. Straessner[48], J. Strandberg[153], S. Strandberg[45a,45b], M. Strauss[128], T. Strebler[102], P. Strizenec[28b], R. Ströhmer[176], D.M. Strom[131], R. Stroynowski[42], A. Strubig[50], S.A. Stucci[29], B. Stugu[17], J. Stupak[128], N.A. Styles[46], D. Su[152], W. Su[60c], S. Suchek[61a], V.V. Sulin[111], M.J. Sullivan[91], D.M.S. Sultan[54], S. Sultansoy[4c], T. Sumida[86], S. Sun[106], X. Sun[101], K. Suruliz[155], C.J.E. Suster[156], M.R. Sutton[155], S. Suzuki[82], M. Svatos[140], M. Swiatlowski[167a], S.P. Swift[2], T. Swirski[176], A. Sydorenko[100], I. Sykora[28a], M. Sykora[142], T. Sykora[142], D. Ta[100], K. Tackmann[46,y], J. Taenzer[160], A. Taffard[170], R. Tafirout[167a], R. Takashima[87], K. Takeda[83], T. Takeshita[149], E.P. Takeva[50], Y. Takubo[82], M. Talby[102], A.A. Talyshev[122b,122a], K.C. Tam[63b], N.M. Tamir[160], J. Tanaka[162], R. Tanaka[65], S. Tapia Araya[172], S. Tapprogge[100], A. Tarek Abouelfadl Mohamed[107], S. Tarem[159], K. Tariq[60b], G. Tarna[27b,c], G.F. Tartarelli[69a], P. Tas[142], M. Tasevsky[140], T. Tashiro[86], E. Tassi[41b,41a], A. Tavares Delgado[139a], Y. Tayalati[35e], A.J. Taylor[50], G.N. Taylor[105], W. Taylor[167b], H. Teagle[91], A.S. Tee[90], R. Teixeira De Lima[152], P. Teixeira-Dias[94], H. Ten Kate[36], J.J. Teoh[120], S. Terada[82], K. Terashi[162], J. Terron[99], S. Terzo[14], M. Testa[51], R.J. Teuscher[166,ac], S.J. Thais[182], N. Themistokleous[50], T. Theveneaux-Pelzer[46], F. Thiele[40], D.W. Thomas[94], J.O. Thomas[42], J.P. Thomas[21], E.A. Thompson[46], P.D. Thompson[21], E. Thomson[136], E.J. Thorpe[93], R.E. Ticse Torres[53], V.O. Tikhomirov[111,ai], Yu.A. Tikhonov[122b,122a], S. Timoshenko[112], P. Tipton[182], S. Tisserant[102], K. Todome[23b,23a], S. Todorova-Nova[142], S. Todt[48], J. Tojo[88], S. Tokár[28a], K. Tokushuku[82], E. Tolley[127], R. Tombs[32], K.G. Tomiwa[33e], M. Tomoto[117], L. Tompkins[152], P. Tornambe[103], E. Torrence[131], H. Torres[48], E. Torró Pastor[147], C. Tosciri[134], J. Toth[102,ab], D.R. Tovey[148], A. Traeet[17], C.J. Treado[125], T. Trefzger[176], F. Tresoldi[155], A. Tricoli[29], I.M. Trigger[167a], S. Trincaz-Duvoid[135], D.A. Trischuk[174], W. Trischuk[166], B. Trocmé[58], A. Trofymov[65], C. Troncon[69a], F. Trovato[155], L. Truong[33c], M. Trzebinski[85], A. Trzupek[85], F. Tsai[46], J.C-L. Tseng[134], P.V. Tsiareshka[108,af], A. Tsirigotis[161,v], V. Tsiskaridze[154], E.G. Tskhadadze[158a], M. Tsopoulou[161], I.I. Tsukerman[124], V. Tsulaia[18], S. Tsuno[82], D. Tsybychev[154], Y. Tu[63b], A. Tudorache[27b], V. Tudorache[27b], T.T. Tulbure[27a], A.N. Tuna[59], S. Turchikhin[80], D. Turgeman[179], I. Turk Cakir[4b,t], R.J. Turner[21], R.T. Turra[69a], P.M. Tuts[39], S. Tzamarias[161], E. Tzovara[100], G. Ucchielli[47], K. Uchida[162], F. Ukegawa[168], G. Unal[36], A. Undrus[29], G. Unel[170], F.C. Ungaro[105], Y. Unno[82], K. Uno[162], J. Urban[28b], P. Urquijo[105], G. Usai[8], Z. Uysal[12d], V. Vacek[141], B. Vachon[104], K.O.H. Vadla[133], A. Vaidya[95], C. Valderanis[114], E. Valdes Santurio[45a,45b], M. Valente[54], S. Valentinetti[23b,23a], A. Valero[173], L. Valéry[46], R.A. Vallance[21], A. Vallier[36], J.A. Valls Ferrer[173], T.R. Van Daalen[14], P. Van Gemmeren[6], I. Van Vulpen[120], M. Vanadia[74a,74b], W. Vandelli[36], M. Vandenbroucke[144], E.R. Vandewall[129], A. Vaniachine[165], D. Vannicola[73a,73b], R. Vari[73a], E.W. Varnes[7], C. Varni[55b,55a], T. Varol[157], D. Varouchas[65], K.E. Varvell[156], M.E. Vasile[27b], G.A. Vasquez[175], F. Vazeille[38], D. Vazquez Furelos[14], T. Vazquez Schroeder[36], J. Veatch[53], V. Vecchio[101], M.J. Veen[120], L.M. Veloce[166], F. Veloso[139a,139c], S. Veneziano[73a], A. Ventura[68a,68b], N. Venturi[36], A. Verbytskyi[115], V. Vercesi[71a], M. Verducci[72a,72b], C.M. Vergel Infante[79], C. Vergis[24],

JHEP07(2020)044

W. Verkerke[120], A.T. Vermeulen[120], J.C. Vermeulen[120], C. Vernieri[152], M.C. Vetterli[151,am], N. Viaux Maira[146d], T. Vickey[148], O.E. Vickey Boeriu[148], G.H.A. Viehhauser[134], L. Vigani[61b], M. Villa[23b,23a], M. Villaplana Perez[3], E.M. Villhauer[50], E. Vilucchi[51], M.G. Vincter[34], G.S. Virdee[21], A. Vishwakarma[46], C. Vittori[23b,23a], I. Vivarelli[155], M. Vogel[181], P. Vokac[141], S.E. von Buddenbrock[33e], E. Von Toerne[24], V. Vorobel[142], K. Vorobev[112], M. Vos[173], J.H. Vossebeld[91], M. Vozak[101], N. Vranjes[16], M. Vranjes Milosavljevic[16], V. Vrba[141], M. Vreeswijk[120], R. Vuillermet[36], I. Vukotic[37], S. Wada[168], P. Wagner[24], W. Wagner[181], J. Wagner-Kuhr[114], S. Wahdan[181], H. Wahlberg[89], R. Wakasa[168], V.M. Walbrecht[115], J. Walder[90], R. Walker[114], S.D. Walker[94], W. Walkowiak[150], V. Wallangen[45a,45b], A.M. Wang[59], A.Z. Wang[180], C. Wang[60c], F. Wang[180], H. Wang[18], H. Wang[3], J. Wang[63a], J. Wang[61b], P. Wang[42], Q. Wang[128], R.-J. Wang[100], R. Wang[60a], R. Wang[6], S.M. Wang[157], W.T. Wang[60a], W. Wang[15c], W.X. Wang[60a], Y. Wang[60a], Z. Wang[60c], C. Wanotayaroj[46], A. Warburton[104], C.P. Ward[32], D.R. Wardrope[95], N. Warrack[57], A. Washbrook[50], A.T. Watson[21], M.F. Watson[21], G. Watts[147], B.M. Waugh[95], A.F. Webb[11], C. Weber[29], M.S. Weber[20], S.A. Weber[34], S.M. Weber[61a], A.R. Weidberg[134], J. Weingarten[47], M. Weirich[100], C. Weiser[52], P.S. Wells[36], T. Wenaus[29], T. Wengler[36], S. Wenig[36], N. Wermes[24], M.D. Werner[79], M. Wessels[61a], T.D. Weston[20], K. Whalen[131], N.L. Whallon[147], A.M. Wharton[90], A.S. White[106], A. White[8], M.J. White[1], D. Whiteson[170], B.W. Whitmore[90], W. Wiedenmann[180], C. Wiel[48], M. Wielers[143], N. Wieseotte[100], C. Wiglesworth[40], L.A.M. Wiik-Fuchs[52], H.G. Wilkens[36], L.J. Wilkins[94], H.H. Williams[136], S. Williams[32], C. Willis[107], S. Willocq[103], P.J. Windischhofer[134], I. Wingerter-Seez[5], E. Winkels[155], F. Winklmeier[131], B.T. Winter[52], M. Wittgen[152], M. Wobisch[96], A. Wolf[100], T.M.H. Wolf[120], R. Wolff[102], R. Wölker[134], J. Wollrath[52], M.W. Wolter[85], H. Wolters[139a,139c], V.W.S. Wong[174], N.L. Woods[145], S.D. Worm[46], B.K. Wosiek[85], K.W. Woźniak[85], K. Wraight[57], S.L. Wu[180], X. Wu[54], Y. Wu[60a], T.R. Wyatt[101], B.M. Wynne[50], S. Xella[40], Z. Xi[106], L. Xia[177], X. Xiao[106], X. Xie[60a], I. Xiotidis[155], D. Xu[15a], H. Xu[60a], H. Xu[60a], L. Xu[29], T. Xu[144], W. Xu[106], Z. Xu[60b], Z. Xu[152], B. Yabsley[156], S. Yacoob[33a], K. Yajima[132], D.P. Yallup[95], N. Yamaguchi[88], Y. Yamaguchi[164], A. Yamamoto[82], M. Yamatani[162], T. Yamazaki[162], Y. Yamazaki[83], J. Yan[60c], Z. Yan[25], H.J. Yang[60c,60d], H.T. Yang[18], S. Yang[60a], T. Yang[63c], X. Yang[60b,58], Y. Yang[162], Z. Yang[60a], W-M. Yao[18], Y.C. Yap[46], Y. Yasu[82], E. Yatsenko[60c,60d], H. Ye[15c], J. Ye[42], S. Ye[29], I. Yeletskikh[80], M.R. Yexley[90], E. Yigitbasi[25], P. Yin[39], K. Yorita[178], K. Yoshihara[79], C.J.S. Young[36], C. Young[152], J. Yu[79], R. Yuan[60b,h], X. Yue[61a], M. Zaazoua[35e], B. Zabinski[85], G. Zacharis[10], E. Zaffaroni[54], J. Zahreddine[135], A.M. Zaitsev[123,ah], T. Zakareishvili[158b], N. Zakharchuk[34], S. Zambito[59], D. Zanzi[36], D.R. Zaripovas[57], S.V. Zeißner[47], C. Zeitnitz[181], G. Zemaityte[134], J.C. Zeng[172], O. Zenin[123], T. Ženiš[28a], D. Zerwas[65], M. Zgubič[134], B. Zhang[15c], D.F. Zhang[15b], G. Zhang[15b], J. Zhang[6], Kaili. Zhang[15a], L. Zhang[15c], L. Zhang[60a], M. Zhang[172], R. Zhang[180], S. Zhang[106], X. Zhang[60c], X. Zhang[60b], Y. Zhang[15a,15d], Z. Zhang[63a], Z. Zhang[65], P. Zhao[49], Z. Zhao[60a], A. Zhemchugov[80], Z. Zheng[106], D. Zhong[172], B. Zhou[106], C. Zhou[180], H. Zhou[7], M.S. Zhou[15a,15d], M. Zhou[154], N. Zhou[60c], Y. Zhou[7], C.G. Zhu[60b], C. Zhu[15a,15d], H.L. Zhu[60a], H. Zhu[15a], J. Zhu[106], Y. Zhu[60a], X. Zhuang[15a], K. Zhukov[111], V. Zhulanov[122b,122a], D. Zieminska[66], N.I. Zimine[80], S. Zimmermann[52], Z. Zinonos[115], M. Ziolkowski[150], L. Živković[16], G. Zobernig[180], A. Zoccoli[23b,23a], K. Zoch[53], T.G. Zorbas[148], R. Zou[37], L. Zwalinski[36]

[1] *Department of Physics, University of Adelaide, Adelaide; Australia*

[2] *Physics Department, SUNY Albany, Albany NY; United States of America*

[3] *Department of Physics, University of Alberta, Edmonton AB; Canada*

[4] *Department of Physics[(a)], Ankara University, Ankara; Istanbul Aydin University[(b)], Application and Research Center for Advanced Studies, Istanbul; Division of Physics[(c)], TOBB University of Economics and Technology, Ankara; Turkey*

JHEP07(2020)044

[5] LAPP, Université Grenoble Alpes, Université Savoie Mont Blanc, CNRS/IN2P3, Annecy; France
[6] High Energy Physics Division, Argonne National Laboratory, Argonne IL; United States of America
[7] Department of Physics, University of Arizona, Tucson AZ; United States of America
[8] Department of Physics, University of Texas at Arlington, Arlington TX; United States of America
[9] Physics Department, National and Kapodistrian University of Athens, Athens; Greece
[10] Physics Department, National Technical University of Athens, Zografou; Greece
[11] Department of Physics, University of Texas at Austin, Austin TX; United States of America
[12] Bahcesehir University[(a)], Faculty of Engineering and Natural Sciences, Istanbul; Istanbul Bilgi University[(b)], Faculty of Engineering and Natural Sciences, Istanbul; Department of Physics[(c)], Bogazici University, Istanbul; Department of Physics Engineering[(d)], Gaziantep University, Gaziantep; Turkey
[13] Institute of Physics, Azerbaijan Academy of Sciences, Baku; Azerbaijan
[14] Institut de Física d'Altes Energies (IFAE), Barcelona Institute of Science and Technology, Barcelona; Spain
[15] Institute of High Energy Physics[(a)], Chinese Academy of Sciences, Beijing; Physics Department[(b)], Tsinghua University, Beijing; Department of Physics[(c)], Nanjing University, Nanjing; University of Chinese Academy of Science (UCAS)[(d)], Beijing; China
[16] Institute of Physics, University of Belgrade, Belgrade; Serbia
[17] Department for Physics and Technology, University of Bergen, Bergen; Norway
[18] Physics Division, Lawrence Berkeley National Laboratory and University of California, Berkeley CA; United States of America
[19] Institut für Physik, Humboldt Universität zu Berlin, Berlin; Germany
[20] Albert Einstein Center for Fundamental Physics and Laboratory for High Energy Physics, University of Bern, Bern; Switzerland
[21] School of Physics and Astronomy, University of Birmingham, Birmingham; United Kingdom
[22] Facultad de Ciencias y Centro de Investigaciónes[(a)], Universidad Antonio Nariño, Bogotá; Departamento de Física[(b)], Universidad Nacional de Colombia, Bogotá, Colombia; Colombia
[23] INFN Bologna and Università di Bologna[(a)], Dipartimento di Fisica; INFN Sezione di Bologna[(b)]; Italy
[24] Physikalisches Institut, Universität Bonn, Bonn; Germany
[25] Department of Physics, Boston University, Boston MA; United States of America
[26] Department of Physics, Brandeis University, Waltham MA; United States of America
[27] Transilvania University of Brasov[(a)], Brasov; Horia Hulubei National Institute of Physics and Nuclear Engineering[(b)], Bucharest; Department of Physics[(c)], Alexandru Ioan Cuza University of Iasi, Iasi; National Institute for Research and Development of Isotopic and Molecular Technologies[(d)], Physics Department, Cluj-Napoca; University Politehnica Bucharest[(e)], Bucharest; West University in Timisoara[(f)], Timisoara; Romania
[28] Faculty of Mathematics[(a)], Physics and Informatics, Comenius University, Bratislava; Department of Subnuclear Physics[(b)], Institute of Experimental Physics of the Slovak Academy of Sciences, Kosice; Slovak Republic
[29] Physics Department, Brookhaven National Laboratory, Upton NY; United States of America
[30] Departamento de Física, Universidad de Buenos Aires, Buenos Aires; Argentina
[31] California State University, CA; United States of America
[32] Cavendish Laboratory, University of Cambridge, Cambridge; United Kingdom
[33] Department of Physics[(a)], University of Cape Town, Cape Town; [(b)]iThemba Labs, Western Cape; Department of Mechanical Engineering Science[(c)], University of Johannesburg, Johannesburg; University of South Africa[(d)], Department of Physics, Pretoria; School of Physics[(e)], University of the Witwatersrand, Johannesburg; South Africa
[34] Department of Physics, Carleton University, Ottawa ON; Canada
[35] Faculté des Sciences Ain Chock[(a)], Réseau Universitaire de Physique des Hautes Energies - Université Hassan II, Casablanca; Faculté des Sciences[(b)], Université Ibn-Tofail, Kénitra; Faculté des Sciences Semlalia[(c)], Université Cadi Ayyad, LPHEA-Marrakech; Faculté des Sciences[(d)], Université Mohamed Premier and LPTPM, Oujda; Faculté des sciences[(e)], Université Mohammed V, Rabat; Morocco

JHEP07(2020)044

[36] CERN, Geneva; Switzerland
[37] Enrico Fermi Institute, University of Chicago, Chicago IL; United States of America
[38] LPC, Université Clermont Auvergne, CNRS/IN2P3, Clermont-Ferrand; France
[39] Nevis Laboratory, Columbia University, Irvington NY; United States of America
[40] Niels Bohr Institute, University of Copenhagen, Copenhagen; Denmark
[41] Dipartimento di Fisica[(a)], Università della Calabria, Rende; INFN Gruppo Collegato di Cosenza[(b)], Laboratori Nazionali di Frascati; Italy
[42] Physics Department, Southern Methodist University, Dallas TX; United States of America
[43] Physics Department, University of Texas at Dallas, Richardson TX; United States of America
[44] National Centre for Scientific Research "Demokritos", Agia Paraskevi; Greece
[45] Department of Physics[(a)], Stockholm University; Oskar Klein Centre[(b)], Stockholm; Sweden
[46] Deutsches Elektronen-Synchrotron DESY, Hamburg and Zeuthen; Germany
[47] Lehrstuhl für Experimentelle Physik IV, Technische Universität Dortmund, Dortmund; Germany
[48] Institut für Kern- und Teilchenphysik, Technische Universität Dresden, Dresden; Germany
[49] Department of Physics, Duke University, Durham NC; United States of America
[50] SUPA - School of Physics and Astronomy, University of Edinburgh, Edinburgh; United Kingdom
[51] INFN e Laboratori Nazionali di Frascati, Frascati; Italy
[52] Physikalisches Institut, Albert-Ludwigs-Universität Freiburg, Freiburg; Germany
[53] II. Physikalisches Institut, Georg-August-Universität Göttingen, Göttingen; Germany
[54] Département de Physique Nucléaire et Corpusculaire, Université de Genève, Genève; Switzerland
[55] Dipartimento di Fisica[(a)], Università di Genova, Genova; INFN Sezione di Genova[(b)]; Italy
[56] II. Physikalisches Institut, Justus-Liebig-Universität Giessen, Giessen; Germany
[57] SUPA - School of Physics and Astronomy, University of Glasgow, Glasgow; United Kingdom
[58] LPSC, Université Grenoble Alpes, CNRS/IN2P3, Grenoble INP, Grenoble; France
[59] Laboratory for Particle Physics and Cosmology, Harvard University, Cambridge MA; United States of America
[60] Department of Modern Physics and State Key Laboratory of Particle Detection and Electronics[(a)], University of Science and Technology of China, Hefei; Institute of Frontier and Interdisciplinary Science and Key Laboratory of Particle Physics and Particle Irradiation (MOE)[(b)], Shandong University, Qingdao; School of Physics and Astronomy[(c)], Shanghai Jiao Tong University, KLPPAC-MoE, SKLPPC, Shanghai; Tsung-Dao Lee Institute[(d)], Shanghai; China
[61] Kirchhoff-Institut für Physik[(a)], Ruprecht-Karls-Universität Heidelberg, Heidelberg; Physikalisches Institut[(b)], Ruprecht-Karls-Universität Heidelberg, Heidelberg; Germany
[62] Faculty of Applied Information Science, Hiroshima Institute of Technology, Hiroshima; Japan
[63] Department of Physics[(a)], Chinese University of Hong Kong, Shatin, N.T., Hong Kong; Department of Physics[(b)], University of Hong Kong, Hong Kong; Department of Physics and Institute for Advanced Study[(c)], Hong Kong University of Science and Technology, Clear Water Bay, Kowloon, Hong Kong; China
[64] Department of Physics, National Tsing Hua University, Hsinchu; Taiwan
[65] IJCLab, Université Paris-Saclay, CNRS/IN2P3, 91405, Orsay; France
[66] Department of Physics, Indiana University, Bloomington IN; United States of America
[67] INFN Gruppo Collegato di Udine[(a)], Sezione di Trieste, Udine; ICTP[(b)], Trieste; Dipartimento Politecnico di Ingegneria e Architettura[(c)], Università di Udine, Udine; Italy
[68] INFN Sezione di Lecce[(a)]; Dipartimento di Matematica e Fisica[(b)], Università del Salento, Lecce; Italy
[69] INFN Sezione di Milano[(a)]; Dipartimento di Fisica[(b)], Università di Milano, Milano; Italy
[70] INFN Sezione di Napoli[(a)]; Dipartimento di Fisica[(b)], Università di Napoli, Napoli; Italy
[71] INFN Sezione di Pavia[(a)]; Dipartimento di Fisica[(b)], Università di Pavia, Pavia; Italy
[72] INFN Sezione di Pisa[(a)]; Dipartimento di Fisica E. Fermi[(b)], Università di Pisa, Pisa; Italy
[73] INFN Sezione di Roma[(a)]; Dipartimento di Fisica[(b)], Sapienza Università di Roma, Roma; Italy
[74] INFN Sezione di Roma Tor Vergata[(a)]; Dipartimento di Fisica[(b)], Università di Roma Tor Vergata, Roma; Italy

JHEP07(2020)044

[75] *INFN Sezione di Roma Tre[(a)]; Dipartimento di Matematica e Fisica[(b)], Università Roma Tre, Roma; Italy*
[76] *INFN-TIFPA[(a)]; Università degli Studi di Trento[(b)], Trento; Italy*
[77] *Institut für Astro- und Teilchenphysik, Leopold-Franzens-Universität, Innsbruck; Austria*
[78] *University of Iowa, Iowa City IA; United States of America*
[79] *Department of Physics and Astronomy, Iowa State University, Ames IA; United States of America*
[80] *Joint Institute for Nuclear Research, Dubna; Russia*
[81] *Departamento de Engenharia Elétrica[(a)], Universidade Federal de Juiz de Fora (UFJF), Juiz de Fora; Universidade Federal do Rio De Janeiro COPPE/EE/IF[(b)], Rio de Janeiro; Universidade Federal de São João del Rei (UFSJ)[(c)], São João del Rei; Instituto de Física[(d)], Universidade de São Paulo, São Paulo; Brazil*
[82] *KEK, High Energy Accelerator Research Organization, Tsukuba; Japan*
[83] *Graduate School of Science, Kobe University, Kobe; Japan*
[84] *AGH University of Science and Technology[(a)], Faculty of Physics and Applied Computer Science, Krakow; Marian Smoluchowski Institute of Physics[(b)], Jagiellonian University, Krakow; Poland*
[85] *Institute of Nuclear Physics Polish Academy of Sciences, Krakow; Poland*
[86] *Faculty of Science, Kyoto University, Kyoto; Japan*
[87] *Kyoto University of Education, Kyoto; Japan*
[88] *Research Center for Advanced Particle Physics and Department of Physics, Kyushu University, Fukuoka; Japan*
[89] *Instituto de Física La Plata, Universidad Nacional de La Plata and CONICET, La Plata; Argentina*
[90] *Physics Department, Lancaster University, Lancaster; United Kingdom*
[91] *Oliver Lodge Laboratory, University of Liverpool, Liverpool; United Kingdom*
[92] *Department of Experimental Particle Physics, Jožef Stefan Institute and Department of Physics, University of Ljubljana, Ljubljana; Slovenia*
[93] *School of Physics and Astronomy, Queen Mary University of London, London; United Kingdom*
[94] *Department of Physics, Royal Holloway University of London, Egham; United Kingdom*
[95] *Department of Physics and Astronomy, University College London, London; United Kingdom*
[96] *Louisiana Tech University, Ruston LA; United States of America*
[97] *Fysiska institutionen, Lunds universitet, Lund; Sweden*
[98] *Centre de Calcul de l'Institut National de Physique Nucléaire et de Physique des Particules (IN2P3), Villeurbanne; France*
[99] *Departamento de Física Teorica C-15 and CIAFF, Universidad Autónoma de Madrid, Madrid; Spain*
[100] *Institut für Physik, Universität Mainz, Mainz; Germany*
[101] *School of Physics and Astronomy, University of Manchester, Manchester; United Kingdom*
[102] *CPPM, Aix-Marseille Université, CNRS/IN2P3, Marseille; France*
[103] *Department of Physics, University of Massachusetts, Amherst MA; United States of America*
[104] *Department of Physics, McGill University, Montreal QC; Canada*
[105] *School of Physics, University of Melbourne, Victoria; Australia*
[106] *Department of Physics, University of Michigan, Ann Arbor MI; United States of America*
[107] *Department of Physics and Astronomy, Michigan State University, East Lansing MI; United States of America*
[108] *B.I. Stepanov Institute of Physics, National Academy of Sciences of Belarus, Minsk; Belarus*
[109] *Research Institute for Nuclear Problems of Byelorussian State University, Minsk; Belarus*
[110] *Group of Particle Physics, University of Montreal, Montreal QC; Canada*
[111] *P.N. Lebedev Physical Institute of the Russian Academy of Sciences, Moscow; Russia*
[112] *National Research Nuclear University MEPhI, Moscow; Russia*
[113] *D.V. Skobeltsyn Institute of Nuclear Physics, M.V. Lomonosov Moscow State University, Moscow; Russia*
[114] *Fakultät für Physik, Ludwig-Maximilians-Universität München, München; Germany*
[115] *Max-Planck-Institut für Physik (Werner-Heisenberg-Institut), München; Germany*

JHEP07(2020)044

[116] *Nagasaki Institute of Applied Science, Nagasaki; Japan*
[117] *Graduate School of Science and Kobayashi-Maskawa Institute, Nagoya University, Nagoya; Japan*
[118] *Department of Physics and Astronomy, University of New Mexico, Albuquerque NM; United States of America*
[119] *Institute for Mathematics, Astrophysics and Particle Physics, Radboud University Nijmegen/Nikhef, Nijmegen; Netherlands*
[120] *Nikhef National Institute for Subatomic Physics and University of Amsterdam, Amsterdam; Netherlands*
[121] *Department of Physics, Northern Illinois University, DeKalb IL; United States of America*
[122] *Budker Institute of Nuclear Physics and NSU[(a)], SB RAS, Novosibirsk; Novosibirsk State University Novosibirsk[(b)]; Russia*
[123] *Institute for High Energy Physics of the National Research Centre Kurchatov Institute, Protvino; Russia*
[124] *Institute for Theoretical and Experimental Physics named by A.I. Alikhanov of National Research Centre "Kurchatov Institute", Moscow; Russia*
[125] *Department of Physics, New York University, New York NY; United States of America*
[126] *Ochanomizu University, Otsuka, Bunkyo-ku, Tokyo; Japan*
[127] *Ohio State University, Columbus OH; United States of America*
[128] *Homer L. Dodge Department of Physics and Astronomy, University of Oklahoma, Norman OK; United States of America*
[129] *Department of Physics, Oklahoma State University, Stillwater OK; United States of America*
[130] *Palacký University, RCPTM, Joint Laboratory of Optics, Olomouc; Czech Republic*
[131] *Institute for Fundamental Science, University of Oregon, Eugene, OR; United States of America*
[132] *Graduate School of Science, Osaka University, Osaka; Japan*
[133] *Department of Physics, University of Oslo, Oslo; Norway*
[134] *Department of Physics, Oxford University, Oxford; United Kingdom*
[135] *LPNHE, Sorbonne Université, Université de Paris, CNRS/IN2P3, Paris; France*
[136] *Department of Physics, University of Pennsylvania, Philadelphia PA; United States of America*
[137] *Konstantinov Nuclear Physics Institute of National Research Centre "Kurchatov Institute", PNPI, St. Petersburg; Russia*
[138] *Department of Physics and Astronomy, University of Pittsburgh, Pittsburgh PA; United States of America*
[139] *Laboratório de Instrumentação e Física Experimental de Partículas - LIP[(a)], Lisboa; Departamento de Física[(b)], Faculdade de Ciências, Universidade de Lisboa, Lisboa; Departamento de Física[(c)], Universidade de Coimbra, Coimbra; Centro de Física Nuclear da Universidade de Lisboa[(d)], Lisboa; Departamento de Física[(e)], Universidade do Minho, Braga; Departamento de Física Teórica y del Cosmos[(f)], Universidad de Granada, Granada (Spain); Dep Física and CEFITEC of Faculdade de Ciências e Tecnologia[(g)], Universidade Nova de Lisboa, Caparica; Instituto Superior Técnico[(h)], Universidade de Lisboa, Lisboa; Portugal*
[140] *Institute of Physics of the Czech Academy of Sciences, Prague; Czech Republic*
[141] *Czech Technical University in Prague, Prague; Czech Republic*
[142] *Charles University, Faculty of Mathematics and Physics, Prague; Czech Republic*
[143] *Particle Physics Department, Rutherford Appleton Laboratory, Didcot; United Kingdom*
[144] *IRFU, CEA, Université Paris-Saclay, Gif-sur-Yvette; France*
[145] *Santa Cruz Institute for Particle Physics, University of California Santa Cruz, Santa Cruz CA; United States of America*
[146] *Departamento de Física[(a)], Pontificia Universidad Católica de Chile, Santiago; Universidad Andres Bello[(b)], Department of Physics, Santiago; Instituto de Alta Investigación[(c)], Universidad de Tarapacá; Departamento de Física[(d)], Universidad Técnica Federico Santa María, Valparaíso; Chile*
[147] *Department of Physics, University of Washington, Seattle WA; United States of America*
[148] *Department of Physics and Astronomy, University of Sheffield, Sheffield; United Kingdom*
[149] *Department of Physics, Shinshu University, Nagano; Japan*

JHEP07(2020)044

[150] Department Physik, Universität Siegen, Siegen; Germany
[151] Department of Physics, Simon Fraser University, Burnaby BC; Canada
[152] SLAC National Accelerator Laboratory, Stanford CA; United States of America
[153] Physics Department, Royal Institute of Technology, Stockholm; Sweden
[154] Departments of Physics and Astronomy, Stony Brook University, Stony Brook NY; United States of America
[155] Department of Physics and Astronomy, University of Sussex, Brighton; United Kingdom
[156] School of Physics, University of Sydney, Sydney; Australia
[157] Institute of Physics, Academia Sinica, Taipei; Taiwan
[158] E. Andronikashvili Institute of Physics[(a)], Iv. Javakhishvili Tbilisi State University, Tbilisi; High Energy Physics Institute[(b)], Tbilisi State University, Tbilisi; Georgia
[159] Department of Physics, Technion, Israel Institute of Technology, Haifa; Israel
[160] Raymond and Beverly Sackler School of Physics and Astronomy, Tel Aviv University, Tel Aviv; Israel
[161] Department of Physics, Aristotle University of Thessaloniki, Thessaloniki; Greece
[162] International Center for Elementary Particle Physics and Department of Physics, University of Tokyo, Tokyo; Japan
[163] Graduate School of Science and Technology, Tokyo Metropolitan University, Tokyo; Japan
[164] Department of Physics, Tokyo Institute of Technology, Tokyo; Japan
[165] Tomsk State University, Tomsk; Russia
[166] Department of Physics, University of Toronto, Toronto ON; Canada
[167] TRIUMF[(a)], Vancouver BC; Department of Physics and Astronomy[(b)], York University, Toronto ON; Canada
[168] Division of Physics and Tomonaga Center for the History of the Universe, Faculty of Pure and Applied Sciences, University of Tsukuba, Tsukuba; Japan
[169] Department of Physics and Astronomy, Tufts University, Medford MA; United States of America
[170] Department of Physics and Astronomy, University of California Irvine, Irvine CA; United States of America
[171] Department of Physics and Astronomy, University of Uppsala, Uppsala; Sweden
[172] Department of Physics, University of Illinois, Urbana IL; United States of America
[173] Instituto de Física Corpuscular (IFIC), Centro Mixto Universidad de Valencia - CSIC, Valencia; Spain
[174] Department of Physics, University of British Columbia, Vancouver BC; Canada
[175] Department of Physics and Astronomy, University of Victoria, Victoria BC; Canada
[176] Fakultät für Physik und Astronomie, Julius-Maximilians-Universität Würzburg, Würzburg; Germany
[177] Department of Physics, University of Warwick, Coventry; United Kingdom
[178] Waseda University, Tokyo; Japan
[179] Department of Particle Physics, Weizmann Institute of Science, Rehovot; Israel
[180] Department of Physics, University of Wisconsin, Madison WI; United States of America
[181] Fakultät für Mathematik und Naturwissenschaften, Fachgruppe Physik, Bergische Universität Wuppertal, Wuppertal; Germany
[182] Department of Physics, Yale University, New Haven CT; United States of America

[a] Also at Borough of Manhattan Community College, City University of New York, New York NY; United States of America
[b] Also at CERN, Geneva; Switzerland
[c] Also at CPPM, Aix-Marseille Université, CNRS/IN2P3, Marseille; France
[d] Also at Département de Physique Nucléaire et Corpusculaire, Université de Genève, Genève; Switzerland
[e] Also at Departament de Fisica de la Universitat Autonoma de Barcelona, Barcelona; Spain
[f] Also at Department of Applied Physics and Astronomy, University of Sharjah, Sharjah; United Arab Emirates

JHEP07(2020)044

[g] Also at Department of Financial and Management Engineering, University of the Aegean, Chios; Greece
[h] Also at Department of Physics and Astronomy, Michigan State University, East Lansing MI; United States of America
[i] Also at Department of Physics and Astronomy, University of Louisville, Louisville, KY; United States of America
[j] Also at Department of Physics, Ben Gurion University of the Negev, Beer Sheva; Israel
[k] Also at Department of Physics, California State University, East Bay; United States of America
[l] Also at Department of Physics, California State University, Fresno; United States of America
[m] Also at Department of Physics, California State University, Sacramento; United States of America
[n] Also at Department of Physics, King's College London, London; United Kingdom
[o] Also at Department of Physics, St. Petersburg State Polytechnical University, St. Petersburg; Russia
[p] Also at Department of Physics, University of Adelaide, Adelaide; Australia
[q] Also at Department of Physics, University of Fribourg, Fribourg; Switzerland
[r] Also at Dipartimento di Matematica, Informatica e Fisica, Università di Udine, Udine; Italy
[s] Also at Faculty of Physics, M.V. Lomonosov Moscow State University, Moscow; Russia
[t] Also at Giresun University, Faculty of Engineering, Giresun; Turkey
[u] Also at Graduate School of Science, Osaka University, Osaka; Japan
[v] Also at Hellenic Open University, Patras; Greece
[w] Also at IJCLab, Université Paris-Saclay, CNRS/IN2P3, 91405, Orsay; France
[x] Also at Institucio Catalana de Recerca i Estudis Avancats, ICREA, Barcelona; Spain
[y] Also at Institut für Experimentalphysik, Universität Hamburg, Hamburg; Germany
[z] Also at Institute for Mathematics, Astrophysics and Particle Physics, Radboud University Nijmegen/Nikhef, Nijmegen; Netherlands
[aa] Also at Institute for Nuclear Research and Nuclear Energy (INRNE) of the Bulgarian Academy of Sciences, Sofia; Bulgaria
[ab] Also at Institute for Particle and Nuclear Physics, Wigner Research Centre for Physics, Budapest; Hungary
[ac] Also at Institute of Particle Physics (IPP), Vancouver; Canada
[ad] Also at Institute of Physics, Azerbaijan Academy of Sciences, Baku; Azerbaijan
[ae] Also at Instituto de Fisica Teorica, IFT-UAM/CSIC, Madrid; Spain
[af] Also at Joint Institute for Nuclear Research, Dubna; Russia
[ag] Also at Louisiana Tech University, Ruston LA; United States of America
[ah] Also at Moscow Institute of Physics and Technology State University, Dolgoprudny; Russia
[ai] Also at National Research Nuclear University MEPhI, Moscow; Russia
[aj] Also at Physics Department, An-Najah National University, Nablus; Palestine
[ak] Also at Physikalisches Institut, Albert-Ludwigs-Universität Freiburg, Freiburg; Germany
[al] Also at The City College of New York, New York NY; United States of America
[am] Also at TRIUMF, Vancouver BC; Canada
[an] Also at Universita di Napoli Parthenope, Napoli; Italy

[*] Deceased

JHEP07(2020)044